

Inamuddin · Sabu Thomas
Raghvendra Kumar Mishra
Abdullah M. Asiri *Editors*

Sustainable Polymer Composites and Nanocomposites

 Springer

Sustainable Polymer Composites and Nanocomposites

Inamuddin · Sabu Thomas
Raghvendra Kumar Mishra
Abdullah M. Asiri
Editors

Sustainable Polymer Composites and Nanocomposites

 Springer

Editors

Inamuddin
Department of Applied Chemistry
Aligarh Muslim University
Aligarh, India

Sabu Thomas
School of Chemical Sciences
Mahatma Gandhi University
Kottayam, Kerala, India

Raghvendra Kumar Mishra
Mahatma Gandhi University
Kottayam, Kerala, India

Abdullah M. Asiri
Chemistry Department, Faculty of Science
King Abdulaziz University
Jeddah, Saudi Arabia

ISBN 978-3-030-05398-7

ISBN 978-3-030-05399-4 (eBook)

<https://doi.org/10.1007/978-3-030-05399-4>

Library of Congress Control Number: 2018963283

© Springer Nature Switzerland AG 2019, corrected publication 2019

This work is subject to copyright. All rights are reserved by the Publisher, whether the whole or part of the material is concerned, specifically the rights of translation, reprinting, reuse of illustrations, recitation, broadcasting, reproduction on microfilms or in any other physical way, and transmission or information storage and retrieval, electronic adaptation, computer software, or by similar or dissimilar methodology now known or hereafter developed.

The use of general descriptive names, registered names, trademarks, service marks, etc. in this publication does not imply, even in the absence of a specific statement, that such names are exempt from the relevant protective laws and regulations and therefore free for general use.

The publisher, the authors and the editors are safe to assume that the advice and information in this book are believed to be true and accurate at the date of publication. Neither the publisher nor the authors or the editors give a warranty, express or implied, with respect to the material contained herein or for any errors or omissions that may have been made. The publisher remains neutral with regard to jurisdictional claims in published maps and institutional affiliations.

This Springer imprint is published by the registered company Springer Nature Switzerland AG
The registered company address is: Gewerbestrasse 11, 6330 Cham, Switzerland

Contents

Processing, Characterization and Application of Micro and Nanocellulose Based Environmentally Friendly Polymer Composites	1
Adriana de Campos, Ana Carolina Corrêa, Pedro Ivo Cunha Claro, Eliangela de Moraes Teixeira and José Manoel Marconcini	
Extraction of Cellulose Nanofibers and Their Eco/Friendly Polymer Composites	37
Stephen C. Agwuncha, Chioma G. Anusionwu, Shesan J. Owonubi, E. Rotimi Sadiku, Usman A. Busuguma and I. David Ibrahim	
Synthesis, Characterization and Applications of Polyolefin Based Eco-Friendly Polymer Composites	65
Akash Deep, Deepanshu Bhatt, Vishal Shrivastav, Sanjeev K. Bhardwaj and Poonma Malik	
Spectroscopy and Microscopy of Eco-friendly Polymer Composites	105
Ashish K. Shukla, Chandni Sharma, Syed M. S. Abidi and Amitabha Acharya	
Biocompatible and Biodegradable Chitosan Composites in Wound Healing Application: In Situ Novel Photo-Induced Skin Regeneration Approach	143
Amr A. Essawy, Hassan Hefni and A. M. El-Nggar	
Mechanical, Thermal and Viscoelastic Properties of Polymer Composites Reinforced with Various Nanomaterials	185
T. H. Mokhothu, A. Mtibe, T. C. Mokhena, M. J. Mochane, O. Ofosu, S. Muniyasamy, C. A. Tshifularo and T. S. Motsoeneng	

Preparation and Characterization of Antibacterial Sustainable Nanocomposites	215
T. C. Mokhena, M. J. Mochane, T. H. Mokhothu, A. Mtibe, C. A. Tshifularo and T. S. Motsoeneng	
Extraction of Nano Cellulose Fibres and Their Eco-friendly Polymer Composite	245
Bashiru Kayode Sodipo and Folahan Abdul Wahab Taiwo Owolabi	
Static and Dynamic Mechanical Properties of Eco-friendly Polymer Composites	259
Bernardo Zuccarello	
Synthesis, Characterization, and Applications of Hemicellulose Based Eco-friendly Polymer Composites	293
Busra Balli, Mehmet Harbi Calimli, Esra Kuyuldar and Fatih Sen	
Impact of Nanoparticle Shape, Size, and Properties of the Sustainable Nanocomposites	313
Thandapani Gomathi, K. Rajeshwari, V. Kanchana, P. N. Sudha and K. Parthasarathy	
Polymeric Composites as Catalysts for Fine Chemistry	337
P. SundarRajan, K. GracePavithra, D. Balaji and K. P. Gopinath	
Fabrication Methods of Sustainable Hydrogels	355
Cédric Delattre, Fiona Louis, Mitsuru Akashi, Michiya Matsusaki, Philippe Michaud and Guillaume Pierre	
Application of Sustainable Nanocomposites for Water Purification Process	387
Hayelom Dargo Beyene and Tekilt Gebregiorgs Ambaye	
Sustainable Nanocomposites in Food Packaging	413
H. Anuar, F. B. Ali, Y. F. Buys, M. A. Siti Nur E'zzati, A. R. Siti Munirah Salimah, M. S. Mahmud, N. Mohd Nordin and S. A. Adli	
Mechanical Techniques for Enhanced Dispersion of Cellulose Nanocrystals in Polymer Matrices	437
Jamileh Shojaeiarani, Dilpreet S. Bajwa and Kerry Hartman	
Processing and Industrial Applications of Sustainable Nanocomposites Containing Nanofillers	451
Khadija Zadeh, Sadiya Waseem, Kishor Kumar Sadasivuni, Kalim Deshmukh, Aqib Muzaffar, M. Basheer Ahamed and Mariam Al-Ali AlMaadeed	

Recent Advances in Paper-Based Analytical Devices: A Pivotal Step Forward in Building Next-Generation Sensor Technology	479
Charu Agarwal and Levente Csóka	
Polymers and Polymer Composites for Adsorptive Removal of Dyes in Water Treatment	519
Weiya Huang, Shuhong Wang and Dan Li	
Current Scenario of Nanocomposite Materials for Fuel Cell Applications	557
Raveendra M. Hegde, Mahaveer D. Kurkuri and Madhuprasad Kigga	
Rubber Clay Nanocomposites	593
Mariajose Cova Sanchez, Alejandro Bacigalupe, Mariano Escobar and Marcela Mansilla	
Organic/Silica Nanocomposite Membranes Applicable to Green Chemistry	629
Mashallah Rezakazemi, Amir Dashti, Nasibeh Hajilary and Saeed Shirazian	
Extraction of Cellulose Nanofibers and Their Eco-friendly Polymer Composites	653
M. Hazwan Hussin, Djalal Trache, Caryn Tan Hui Chuin, M. R. Nurul Fazita, M. K. Mohamad Haafiz and Md. Sohrab Hossain	
Recyclable and Eco-friendly Single Polymer Composite	693
Mohd Azmuddin Abdullah, Muhammad Afzaal, Safdar Ali Mirza, Sakinatu Almustapha and Hanaa Ali Hussein	
Processing Aspects and Biomedical and Environmental Applications of Sustainable Nanocomposites Containing Nanofillers	727
Mohd Azmuddin Abdullah, Muhammad Shahid Nazir, Zaman Tahir, Yasir Abbas, Majid Niaz Akhtar, Muhammad Rafi Raza and Hanaa Ali Hussein	
Smart Materials, Magnetic Graphene Oxide-Based Nanocomposites for Sustainable Water Purification	759
Janardhan Reddy Koduru, Rama Rao Karri and N. M. Mubarak	
Functionalized Carbon Nanomaterial for Artificial Bone Replacement as Filler Material	783
Fahad Saleem Ahmed Khan, N. M. Mubarak, Mohammad Khalid and Ezzat Chan Abdullah	
Inorganic Nanocomposite Hydrogels: Present Knowledge and Future Challenge	805
Nasrin Moini, Arash Jahandideh and Gary Anderson	

Processing, Characterization and Application of Natural Rubber Based Environmentally Friendly Polymer Composites	855
Nayan Ranjan Singha, Manas Mahapatra, Mrinmoy Karmakar and Pijush Kanti Chattopadhyay	
Electrical Properties of Sustainable Nano-Composites Containing Nano-Fillers: Dielectric Properties and Electrical Conductivity	899
Sabzoi Nizamuddin, Sabzoi Maryam, Humair Ahmed Baloch, M. T. H. Siddiqui, Pooja Takkalkar, N. M. Mubarak, Abdul Sattar Jatoi, Sadaf Aftab Abbasi, G. J. Griffin, Khadija Qureshi and Nhol Kao	
Thermal Properties of Sustainable Thermoplastics Nanocomposites Containing Nanofillers and Its Recycling Perspective	915
Pooja Takkalkar, Sabzoi Nizamuddin, Gregory Griffin and Nhol Kao	
Application of Sustainable Nanocomposites in Membrane Technology	935
Pravin G. Ingole	
Reliable Natural-Fibre Augmented Biodegraded Polymer Composites	961
Ritu Payal	
An Overview on Plant Fiber Technology: An Interdisciplinary Approach	977
Alan Miguel Brum da Silva, Sandra Maria da Luz, Irulappasamy Siva, Jebas Thangiah Winowlin Jappes and Sandro Campos Amico	
Nanocellulose-Reinforced Adhesives for Wood-Based Panels	1001
Elaine Cristina Lengowski, Eraldo Antonio Bonfatti Júnior, Marina Mieko Nishidate Kumode, Mayara Elita Carneiro and Kestur Gundappa Satyanarayana	
Nanocellulose in the Paper Making	1027
Elaine Cristina Lengowski, Eraldo Antonio Bonfatti Júnior, Marina Mieko Nishidate Kumode, Mayara Elita Carneiro and Kestur Gundappa Satyanarayana	
Impact of Nanoparticle Shape, Size, and Properties of Silver Nanocomposites and Their Applications	1067
Arpita Hazra Chowdhury, Rinku Debnath, Sk. Manirul Islam and Tanima Saha	
Toxicological Evaluations of Nanocomposites with Special Reference to Cancer Therapy	1093
Arpita Hazra Chowdhury, Arka Bagchi, Arunima Biswas and Sk. Manirul Islam	

Synthesis, Characterization and Application of Bio-based Polyurethane Nanocomposites	1121
Sonalee Das, Sudheer Kumar, Smita Mohanty and Sanjay Kumar Nayak	
Clay Based Biopolymer Nanocomposites and Their Applications in Environmental and Biomedical Fields	1159
K. Sangeetha, P. Angelin Vinodhini and P. N. Sudha	
Thermal Behaviour and Crystallization of Green Biocomposites	1185
Vasile Cristian Grigoras	
Eco-friendly Polymer Composite: State-of-Arts, Opportunities and Challenge	1233
V. S. Aigbodion, E. G. Okonkwo and E. T. Akinlabi	
Synthesis, Characterization, and Applications of Hemicelluloses Based Eco-friendly Polymer Composites	1267
Xinwen Peng, Fan Du and Linxin Zhong	
Self-healing Bio-composites: Concepts, Developments, and Perspective	1323
Zeinab Karami, Sara Maleki, Armaghan Moghaddam and Arash Jahandideh	
Chemical Modification of Lignin and Its Environmental Application	1345
Zhili Li, Yuanyuan Ge, Jiubing Zhang, Duo Xiao and Zijun Wu	
Synthesis and Characterization and Application of Chitin and Chitosan-Based Eco-friendly Polymer Composites	1365
Aneela Sabir, Faizah Altaf and Muhammad Shafiq	
Nanocomposites for Environmental Pollution Remediation	1407
Anjali Bajpai, Maya Sharma and Laxmi Gond	
Correction to: Extraction of Nano Cellulose Fibres and Their Eco-friendly Polymer Composite	C1
Bashiru Kayode Sodipo and Folahan Abdul Wahab Taiwo Owolabi	

Processing, Characterization and Application of Micro and Nanocellulose Based Environmentally Friendly Polymer Composites



Adriana de Campos, Ana Carolina Corrêa, Pedro Ivo Cunha Claro, Eliangela de Moraes Teixeira and José Manoel Marconcini

1 Introduction

The demands for biodegradable products, made from renewable and sustainable resources, and present low environmental impact are increasing by the consumers, industry, and the government [112]. The use of these polymer-based materials is important because of the growing need for using renewable and environmentally friendly resources. Collagen, chitin, starch, poly (hydroxybutyrates) (PHB), poly (hydroxyalkanoates) (PHA), polylact acid (PLA) and polycaprolactones (PCL) are examples of biodegradable polymers of high interest [104].

However, many of these materials have their use limited by high cost, poor physical properties, such as humidity sensibility, structure instability and low mechanical properties [6]. In order to improve these properties, natural fibers such as cellulose in micro and nano scale may be used, maintaining the all bio-based character of the material. Furthermore, since they are renewable, inexpensive and environmentally friendly resource, cellulose fibers and its micro e nanocomponents such as microfibrils and nanocellulose are used to manufacturing biodegradable nanocomposites either as nanofiller in a polymer matrix or as an all cellulose-based component film.

There is a wide variety of cellulose sources that can be applied in composites and nanocomposites field, such as kenaf [28, 61], sisal [20, 21, 29, 30, 31, 110, 114], sugar cane bagasse [54, 85, 96], oil palm [8, 32, 33, 43, 53, 66, 75, 93, 109], cotton [20, 21, 35, 46, 87], curaua [5, 23, 118], etc.

A. de Campos (✉) · A. C. Corrêa · P. I. C. Claro · J. M. Marconcini
Embrapa Instrumentation, São Carlos, SP, Brazil
e-mail: dridecampos@yahoo.com.br

P. I. C. Claro
Federal University of São Carlos, São Carlos, Brazil

E. de Moraes Teixeira
Barra do Garças Unit, Federal University of São Carlos, São Carlos, Brazil

According to ISO standards(ISO/TS 20477:2017), cellulosic nanomaterials can be subdivided into two classes:

1. cellulose nano-objects: “discrete piece of material with one, two or three external dimensions in the nanoscale” (1–100 nm). It involves cellulose nano-fibers as cellulose nanocrystals (CNCs) and cellulose nanofibrils (CNFs);
2. cellulose nano-structured materials: a material having an internal composition of inter-related constituent parts in which one or more of those parts is in nanoscale. Its includes cellulose microcrystals (CMCs) and microcrystalline cellulose (MCCs), cellulose microfibrils (CMFs) or Microfibrillated Cellulose (MFC), and bacterial cellulose (BCs). They also can be aggregated cellulose nanostructures.

The cellulose nanostructures can be distinguished by their different chemical and physical properties, source, obtaining method and morphology [70]. By adding these nanoscale compounds as filler into polymers even in small quantities, the properties of polymers can be improved, depending on the type of nanocellulose, the dispersion throughout the matrix and interfacial interactions between the nanocellulose and polymeric matrix.

In this chapter, we will first make a brief description of the definition, terminology, and methods of obtaining cellulose nanostructures. Next, we will present procedures used in the functionalization of the cellulose surface to improve the hydrophilic character and the compatibility with polymer matrices. We then present studies of all-cellulosic nanostructured films, types of processing involving the production of bionanocomposites and other important applications of them in non-biocomposite areas.

2 Micro and Nano-cellulose

2.1 *Brief Description*

Cellulose fibers can be extracted from a variety of sources such as wood pulp, residues of some industrial process (sugar cane bagasse, cassava bagasse, coconut, rice, oil palm, soy, etc.), that can be used for nanocellulose production (see Fig. 1 and Table 1) and plant fibers (sisal, cotton, curaua, hemp, flax, ramie, jute, etc.). They have been widely applied in several fields such as reinforcement in material sciences, catalysis, biomedical engineering, paints, cosmetics and electronic applications due to their sustainability, biocompatibility and good mechanical properties [103].

In nature, the cellulose chains are packaged in such an orderly manner that compact nanocrystals are formed, which are stabilized by inter and intramolecular hydrogen bonding [4, 67, 88]. These hydrogen bonding make the nanocrystals completely insoluble in water and in most organic solvents and lead to a material with mechanical strength only limited by the forces of adjacent atoms [69]. In the cell wall structures of vegetable plants, those cellulose nanocrystals are joined by segments of amorphous holocellulose to form the micro/nanofibrils that constitute the individual cellulose fibers [41].

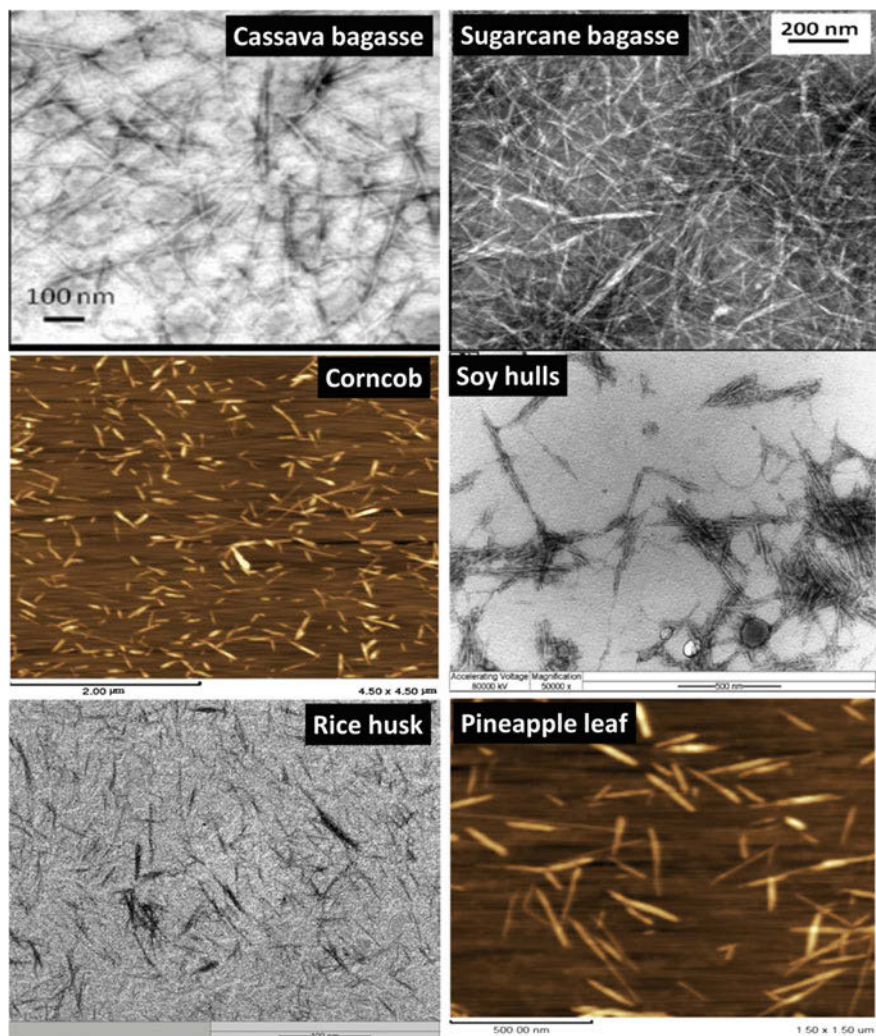


Fig. 1 Cellulose nanofibers extracted from a variety agro- residue

The loss of the hierarchical structure of the cellulose fibers can occur by mechanical, chemical, physical and biological treatments, or by a combination of them, releasing the microfibrils [68, 92]. Depending on these factors, different cellulose nanostructures (or a mix of them) are obtained. These nanostructures present high aspect ratio, with diameters and lengths ranging from units to several microns, excellent mechanical properties, high specific surface area, biodegradability, and biocompatibility [130].

The term *nanocellulose* describes the cellulose fibril or crystallite containing at least one dimension in the nanoscale (1–100 nm). There are many different types of terminologies used for describing nanocelluloses as will be seen next.

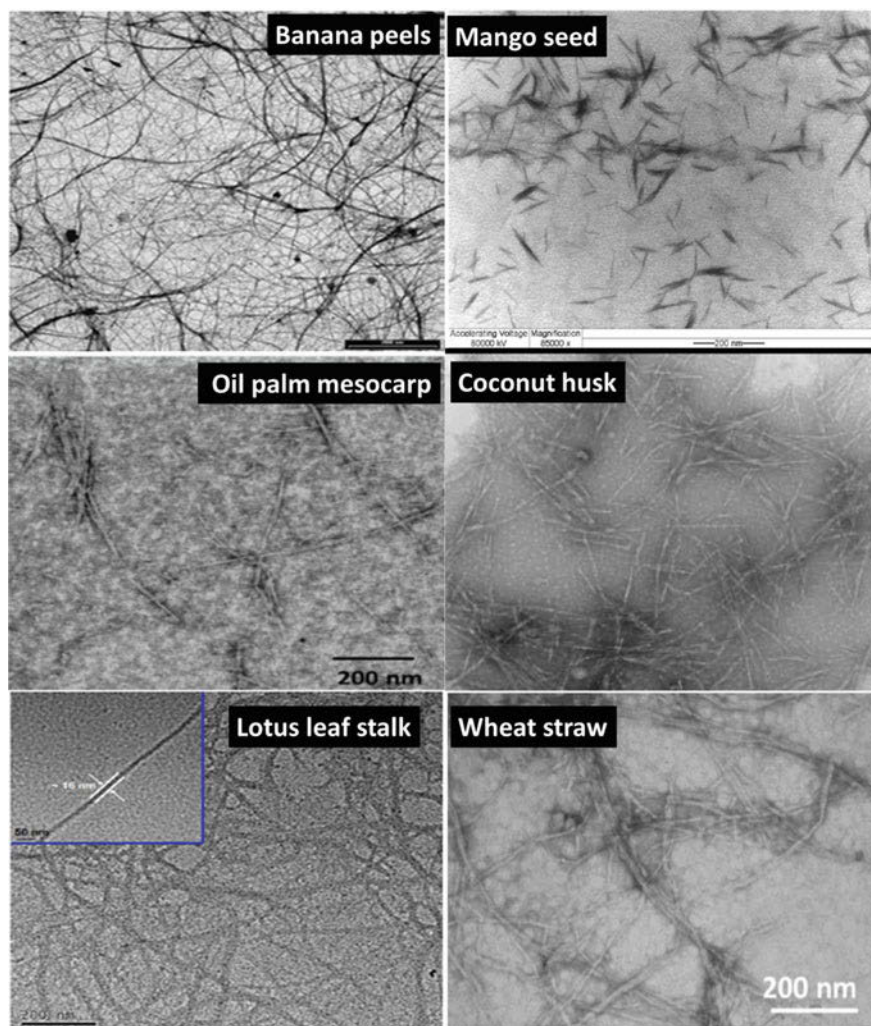


Fig. 1 (continued)

The cellulose fibers disintegrated into micro dimensions are designed as cellulose microfibrils or microfibrillated cellulose (MFC). They are nanofibrils aggregates (bundles) (30–100 cellulose molecules) forming a nanostructured material with diameters of around 3–30 nm and length higher than 1 μm [39, 80]. The MFCs appear as interconnected, nano-fibrillar structure. The MFCs are obtained by mechanical disintegration of fibers which generally involves a combination of processes such as high-pressure homogenization, grinding, ultrasonication and steam explosion, obtaining an aqueous suspension displaying a gel-like behaviour [116].

During the disassembly process, the microfibrils can release more or less their individual constituents, called nanofibrillated cellulose (NFCs), cellulose nanofibers

Table 1 Dimensions characteristics of nanocellulose from agro- residue

Vegetal source	Length (L)/nm	Diameter (D)/nm	L/D	References
Cassava bagasse	1700–360	2–11	76	[34]
Sugarcane bagasse	256 ± 55	4 ± 2	64	[36]
Corn cob	211 ± 44	4 ± 1	53 ± 16	[113]
Soy hulls	123 ± 39	2.8 ± 0.7	44	[45]
Rice husk	–	15–20	10–15	[65]
Pineapple leaf	250 ± 52	4.4 ± 1.4	60	[38]
Banana peels	500–330	8–26	50–12	[97]
Mango seed	123 ± 22	4.6 ± 2.2	34 ± 19	[56]
Oil palm mesocarp	104 ± 52	9.00 ± 4.00	12	[32, 33]
Coconut husk	194 ± 70	5.5 ± 1.5	39 ± 14	[107]
Lotus leaf stalk	Microns	20 ± 15	40	[16]
Wheat straw	400	5	80	[82]

or nanofibrils (CNFs). These are composed of long and entanglement cellulosic chains and, as well as CMFs, maintain both, their amorphous and crystalline domains. The CNFs present a diameter of the 3–5 nm and length of 500–1000 nm [89]. Khalil et al. [72] disagreed with the “microfibril” term because it does not reflect the real dimensions of the fibril. Nechyporchuk and colleagues [92] reported that both cellulose, microfibrils (bundles) and elementary fibrils are referred to as cellulose nanofibrils. Depending on the production process, both CMFs and CNFs are obtained, and their morphologies also strongly depend on the cellulose source. In both cases, hemicellulose and lignin generally are removed before their productions. These nanostructures maintain the amorphous and crystalline phase of cellulose. They can aggregate to some extent during the drying process. Suspensions of CNFs can also present gel properties even at low cellulose concentrations forming an entangled network structure [92].

Microcrystalline celluloses (MCCs) are also aggregates of multi-sizes cellulose microfibrils. It is found as a fine powder and they are commonly known under the brand name Avicel®. It has a diameter of around 10–50 µm. MCCs are obtained from partially depolymerized pure cellulose, synthesized from the α-cellulose precursor. The MCC can be synthesized by different processes such as reactive extrusion, enzyme-mediated, steam explosion and acid hydrolysis. The MCC is a valuable additive in the pharmaceutical, food, cosmetic and other industries [57, 89]. MCC is characterized by a high degree of crystallinity, typically ranging between 55 and 80% [125]. CCNs can also be prepared from MCCs using NaOH/urea dissolution method and followed by regeneration, neutralization, and ultrasonication [112].

Bacterial cellulose (BCs) or microbial cellulose is a type of cellulose microfibrils produced extracellularly by specific bacteria. The *Acetobacter xylinum* is the most efficient producer of bacterial cellulose and this occurs in a culture medium containing carbon and nitrogen sources [2, 68, 91]. Bacterial cellulose result from direct synthesis, and not from the destruction of the primary structure of cellulose

fibers, as in case of CNFs and CNCs. BCs present an average diameter of 20–100 nm and lengths in micrometre, they entangle to form a stable network structured as ribbon-shaped fibrils. BCs do not require any pre-treatment to remove impurities or contaminants such as lignin, pectin, and hemicellulose, i.e. the bacteria produce high-purity cellulose material with a distinct crystallinity of 80–90%. These peculiar properties of BCs make them an attractive material for use in biomedical applications [2, 70, 76, 80, 92].

Cellulose nanocrystals (CNCs) are also called nanocrystalline cellulose (NNCs), cellulose whiskers and rod-like cellulose, the area high crystalline cellulosic material resulting from acid hydrolysis of native cellulose with mineral acids, removing the amorphous phase of cellulose and leaving intact the crystalline phase. In order to obtain CNCs, the native lignocellulosic fibers should be previously submitted to a treatment of delignification process prior to the hydrolysis. CNCs present elongated rod-like aspect and their surface can be negatively charged when sulfuric acid (the most utilized acid) is employed for extraction. The charged surface of CNCs prevents the aggregation in aqueous suspension due to electrostatic repulsion between particles. They are considered a rigid and no defect crystal. Their diameter and length depends on the cellulose source: CNCs present diameters of around 5–30 nm and length of 100–500 nm for plants source, of around 100 nm to several microns for CNCs from tunicate and algae cellulose [2, 80, 92]. Lin and Dufresne [80] have reported several studies that showed the values of CNCs' elastic modulus ranging from 100–206 GPa, values similar to Kevlar and potentially stronger than steel.

Figure 2 shows some examples of nanostructures obtained from bleached sugarcane bagasse. As it can be observed, the type of treatment applied to the same fiber results in different nanostructures, with different crystallinities and thermal behaviour.

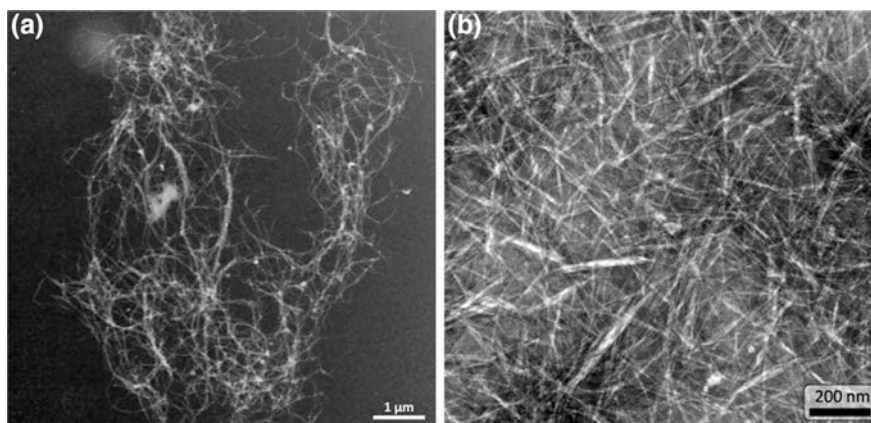


Fig. 2 TEM micrographs showing the morphology of nanostructures from bleached sugar cane bagasse. **a** After enzymatic hydrolysis (10 mg of Enzyme Viscozyme (1000 FBG/g) and 33 mg of Enzyme FiberCare (5000 ECU/g)/g of biomass and reaction time of 3 days at 45 °C) [29]; **b** after acid hydrolysis with sulfuric acid solution (6 M) for 45 min at 45 °C

The thermal properties of these cellulosic materials are important to determine their processing temperature range and use. The thermal degradation of lignocellulosic materials begins with an initial decomposition of the hemicelluloses, followed by lignin pyrolysis, depolymerization, combustion and oxidation of carbides. Thus, the MFCs and NFCs had a thermal degradation temperature higher than the fibers (350 °C) due to the removal of much of the amorphous material. The thermal degradation of CNCs usually starts at temperatures lower than MFCs and NFCs (200–300 °C), due to the presence of sulfate groups in the obtaining of the nanocrystals. The CNCs with lower sulfate content on their surface present higher thermal stability [23, 29, 34, 89, 105]. The combination of sulfuric and hydrochloric acids during the hydrolyses to obtain the CNCs generates nanoparticles with better thermal stability due to the reduced presence of sulfate groups on their surface, also causing a decrease in the stability of CNCs in suspension [105]. Studies have found that CNC obtained by enzymatic hydrolysis exhibited superior thermal stability, compared to CNC obtained by chemical hydrolysis using sulfuric acid [13]. Uschanov et al. [128] studied the esterification of MCCs, CNCs and regenerated cellulose with different kind of long-chain fatty acid as oleic, decanoic, linoleic and tall oil fatty acids (TOFA), a product of a mixture of 10% or less of saturated fatty acids and 90% or more of unsaturated octadecanoic (C18) acids. Thermal stability of CNCs was poorer than that of MCC or regenerated cellulose. They concluded that the modification weakened the thermal stability and the degradation temperature seemed to be dependent on the nature of the fatty acid used. Fatty acid chain length and double bond content affected the reactivity between cellulose and fatty acid; a longer chain length and the increase on double bond content decreased the degree of substitution (DS). Lee and colleagues [77] modified the surface of BC using organic acids (acetic, hexanoic and dodecanoic acids) via esterification reactions. As well as Uschavov et al. [128], they observed that the thermal degradation behaviour of organic acid modified BC sheets decrease with the increase of carbon chain length of the organic acids used. Agustin et al. [3] produced BC esters using different chloride acids and showed that the temperature at maximum weight loss rate (T_{max}) increased after esterification. The thermal stability of CNCs from white and coloured cotton was investigated in dynamic and isothermal (180 °C) conditions under an oxidizing atmosphere [35]. The thermal stability of white cotton CNCs, under dynamic conditions, was slightly higher than of coloured cotton CNCs. However, the colored-CNCs were more thermally stable, in isothermal conditions, than white-CNCs. This behaviour was attributed to lower sulfonation on coloured cotton CNCs surfaces than on white cotton CNCs surface.

Cellulose nanostructures or nanocellulose in general, have gained attention from researchers and industry because of their high Young modulus (130 GPa) [18], which is higher than that of the S-glass (86–90 GPa) and comparable to Kevlar (131 GPa), rendering them good reinforcement in natural and synthetic polymer matrices [103]. The inherent hydrophilic nature of nanocellulose limited its widespread application. Surface modifications of nanocellulose diminish its hydrophilicity which will be briefly discussed further ahead.

2.2 Obtaining Different Types of Micro and Nano-cellulose by the Mechanical, Chemical and Enzymatic Process

The nanocellulose materials can be obtained by different processes with the result in specific or a mix of morphologies, physical properties, and consequently different applications.

The mechanical process for extraction involves refining or high shear homogenization, microfluidization and sonication, which result in microfibrils and nanofibrils. Refining and homogenization are performed in the presence of water, producing microfibrils (MFCs)/nanofibrils (CNFs) through a relatively narrow space of a disk apparatus between the rotor and the stator. In the microfluidization process, the suspension is subjected to high pressure to pass through a Y or Z type geometry interaction chamber [132]. Sonication is performed on a fiber suspension to separate the microfibrils or nanofibrils beams from the cell wall of the fibers through cavitation [99]. The cavitation leads to a formation of powerful oscillating high intensive waves. These microscopic gas bubbles expand and implode breaking down cellulose fibers to microfibrils/nanofibrils [105].

The chemical treatment involves strong acid hydrolysis applied to cellulosic fibers allowing dissolution of amorphous domains and therefore longitudinal cutting of the microfibrils which generate cellulose nanocrystals (CNCs) also known as whiskers. During the acid hydrolysis process, the hydronium ions penetrate the cellulose chains in the amorphous regions promoting the hydrolytic cleavage of the glycosidic bonds, under a controlled period of time and temperature, keeping the crystallites intact [35, 40, 124]. Sulfuric acid (H_2SO_4) is generally used as a hydrolyzing agent because its reaction with the surface hydroxyl groups via an esterification process allows the grafting of anionic sulfate ester groups. The presence of these negatively charged groups induces the formation of a negative electrostatic layer covering the nanocrystals and promoting their better dispersion in water [40]. CNCs prepared using hydrochloric (HCl) acid or a mix of HCl/ H_2SO_4 for hydrolysis exhibit good thermal but tend to aggregate in water [23]. Their geometrical dimensions depend on the origin of the cellulose source and hydrolysis conditions, but the length is usually in the range of a few hundred nanometers, and the width or diameter is in the range of a few nanometers. An important parameter for cellulose nanocrystals (CNCs) is the aspect ratio, which is defined as the ratio of the length to the diameter (L/d) [40].

Organic acids or a mix of them with mineral acid have been used to extract CNCs and concomitantly to produce carboxylated CNFs and CNCs [17, 64, 119] using mechanical assistance (ultrasound or micro fluidics).

The enzymatic process usually involves bulk of enzymes that act synergistically in the hydrolysis of cellulose since a single enzyme is not able to degrade cellulose [44, 80, 117, 130]. The most used bulks for enzymatic hydrolysis contains predominantly endoglucanase and/or exoglucanase [44, 55, 101, 117]. Celobiohydrolases or exoglucanases are a type of cellulase able to attack cellulose by the end of chains, resulting in cellobiose units. Endoglucanases randomly hydrolyze the amorphous

regions, resulting in cellulose nanocrystals, in the single crystal range, since most of the fibers are in the form of crystalline structure entwined in an amorphous cellulose phase.

Both ethanol and nanocelluloses (CNFs and CNCs) were produced using eucalyptus cellulose pulp as raw material for enzymatic hydrolysis route [13]. The solid residues from ethanol production after 24 h of hydrolysis at 50 °C was characterized as CNFs. If the hydrolysis time was increased to 144 h and the temperature reduced to 35–40 °C, CNCs with a crystallinity index of 83%, length of 260 nm and diameter of 15 nm were found in this solid residue. Yarbrough et al. [130] studied the production of nanocellulose of different sizes and aspect ratios using enzymatic treatments (endo- and exoglucanases) with mechanical refinement and acid hydrolysis. The authors related that the majority of commercial cellulase cocktails are optimized for the highest conversion of cellulose to sugars, which is not desired to obtain cellulose nanocrystals. Then, they compared nanocellulose production using *T. reesei*, a classic fungal cellulase system containing predominantly exoglucanases, with that of *C. bescii*, a bacterial enzyme system that contains complex multifunctional enzymes. They showed that CNC produced by *C. bescii* system is more uniform than that produced by the *T. reesei*, after a reaction time of 48 h, due to the difference between the cellulases excreted by *C. bescii* and the cellulolytic agents in fungal excretion of *T. reesei*.

Bacterial celluloses (BCs) are produced by fermentation of low molecular weight sugars using bacteria from *Acetobacter* species. Therefore they are biosynthetic products. *Acetobacter xylinum* produces extracellular cellulose microfibrils to provide a firm floating matrix, allowing the embedded bacteria to stay in close contact with the atmosphere [100]. During the biosynthesis, the glucose chains are produced inside the bacterial body and outgrowth through tiny pores present on the cell envelope. By joining several glucose units, microfibrils are formed and further aggregate as ribbons. BCs are commonly regarded as a material with better biocompatibility than other types of nanocellulose, but their production is a little limited due to high synthesis cost and low yield [80].

In Table 2 is presented morphology and thermal properties of a variety of sources obtained from the different process and its classification.

2.3 Functionalization or Surface Modification of Micro and Nano-cellulose

The chemical modification on the cellulose surface can improve their interaction with apolar matrices, in addition to reducing their hydrophobicity. Esterifications and silanizations are most commonly used in the preparation of cellulose for composite applications [60, 90].

Cellulose can also be modified by the formation of ionic groups on its surface. The oxidation of the cellulose surface, by plasma or corona treatment, can generate carboxylic acids groups that improve their interaction with the matrix in the

Table 2 Morphology and thermal properties of variety of sources of cellulose


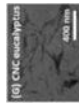
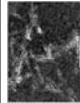
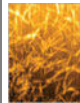

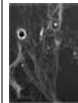
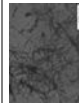

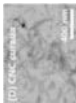
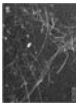
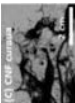




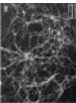
Source	Process obtaining	Nanocellulose classification	Morphology	Diameter (nm)	Length (nm)	Crystallinity (%)	Thermal Stability/ atmosphere (°C)	References
Eucalyptus pulp	Mineral acid hydrolysis	CNC		10–30	50–100	82	180/air	[123]
		CNC		23 ± 5	200 ± 50	–	163/N ₂	[19]
	Enzymatic hydrolysis	CNC		15 ± 6	–	–	323/air	[13]
		CNC		15	275–380	80–82	322/N ₂	[17]
	Mechanical grinding	CNF		17 ± 4	1100 ± 50	–	292/N ₂	[19]
	Sonification	CNF		30–40	200–250	33	310/air	[123, 124]
	Enzymatic hydrolysis	CNF		21 ± 3	216 ± 86	83	323/air	[13]
	(continued)							

Table 2 (continued)

Source	Process obtaining	Nanocellulose classification	Morphology	Diameter (nm)	Length (nm)	Crystallinity (%)	Thermal Stability/ atmosphere (°C)	References
Curaua	Mineral acid hydrolysis	CNC		6–10	80–170	81 (H ₂ SO ₄) 83 (H ₂ SO ₄ / HCl) 87 (HCl)	254/air 285/air 295/air	[23]
				34 ± 5	400 ± 100	–	158/air	[19]
Sugarcane bagasse	Enzymatic hydrolysis + sonification	CNF		3.8 ± 1.3	1280 ± 670	78.5	–	[29]
	Mechanical grinding	CNF		36 ± 8	–	–	303/N ₂	[19]
	Mineral acid hydrolysis	CNC		37.84	220	–	249/N ₂	[85]
		CNC		8 ± 3	255 ± 55	70.5	210/air	[36]
Sugarcane bagasse	Mineral acid hydrolysis	CNC		9.8 ± 6.3	280.1 ± 73.3	68.54 ± 1.30	250/N ₂	[74]
		CNF-sheet		39 ± 13	–	72.9	179/N ₂	[50]
		CNF		30 ± 7	255 ± 83	72	–	[29]

composites [62]. Modifications by sulfonation, carboxylation or graphitization, in addition to modification by acetylation/alkylation and treatment with silane agents, can also be used. In sulfonation treatments, sulfuric acid solutions in moderate concentration are used, obtaining partial sulfonation on the cellulose surface in aqueous suspension with colloidal appearance, due to repulsive forces of the sulfate groups adhered to the surface of the cellulose. Carboxylation can result in more hydrophilic cellulose surfaces. An effective way of inducing controlled oxidation on the cellulose surface, in order to create carboxylic groups, involves treatment with 2,2,6,6-tetramethylpiperidine-1-oxyl (TEMPO) radical where the hydroxyl groups are selectively converted into carboxylic groups, generating a negative charge on cellulose surface, not aggregating when dispersed in water, forming bi-refringent suspensions [62]. Among methods of modifying polymers, grafting is a versatile method for promoting the polymer in a variety of functional groups. Polymeric materials with good properties can be obtained by grafting, and changing parameters such as polymer type, degree of polymerization and dispersibility in the main and in the side chains, in addition to the density and uniformity of grafts, it can be combined the best properties of two or more polymers in a physical unit, in this case, the cellulose [108].

Lignocellulosic fibers from sugarcane bagasse were chemically modified by Pasquini et al. [95] using dodecanoyl chloride and pyridine, and toluene, octadecanoyl chloride, and pyridine. The modified fibers were incorporated into low-density polyethylene (LDPE) with improved dispersion and surface adhesion to the matrix. However, in spite of the better compatibility of the modified fibers with the matrix, these composites did not present improvements in the mechanical properties than those whose fibers were not treated; this fact can be due to the degradation that the chemical treatment caused to the fibers, reducing its degree of polymerization (DP).

The chemical modification of cellulose nanofibers or nanocrystals follows the same principles as those applied to the fibers, Ljungberg et al. [83, 84] modified the surface of cellulose nanocrystals (CNCs) obtained from tunicates in order to incorporate them in atactic [83] and isotactic polypropylene (PP) [84]. In both cases, the surface treatments in the CNCs were the same; the neutral suspension of CNCs was first dried and redispersed in toluene using ultra Turrax equipment; however, the CNCs did not stand in suspension and decanted. A grafting of PP-g-MA on CNCs surface was also made, but redispersing these grafted CNCs in toluene also precipitated due to the agglomerations. Finally, the aqueous suspension of CNCs was mixed to the surfactant polyoxyethylenenonylphenyl ether phosphate ester (BNA-Ceca ATO Co.) in the ratio of 4:1 surfactant: CNCs, the pH was adjusted to 8 with KOH and the suspension was lyophilized and redispersed in toluene, and this suspension did not precipitate. Subsequently, these suspensions of whiskers in toluene were mixed to the PP solubilized in toluene and films were prepared by casting with the evaporation of the toluene in a vacuum oven. Transparent nanocomposite films were obtained with the introduction of surfactant, resulting in good CNCs dispersion in PP and higher mechanical properties than pure PP films.

Uschanov et al. [128] obtained dispersed CNCs in toluene by modifying their surface with pyridine and toluene sulfonyl chloride (TsCl) solution in an inert atmosphere and adding fatty acids in the same molar concentration of TsCl. The final product was filtered, washed with methanol and ethanol and finally dried in a vacuum oven. However, such modifications have caused a decrease in thermal stability since the degradation temperature depends on the nature of the fatty acid and its degree of substitution on the cellulose surface.

Lif et al. [79] prepared hydrophobic microfibrillated cellulose (MFCs) by adding sodium periodate in the aqueous suspension at room temperature for 1 h. After MFCs were washed with water, they were dispersed in methanol. Octadecylamine and sodium cyanoborohydride was added to the MFCs in methanol, and the solid was washed with methanol, acetone and redispersed in octane. However, in order to disperse these hydrophobic MFCs in an organic solvent, neutral surfactants (without ions) were also used, which gave MFCs dispersed in diesel for up to 30 days.

Stenstad et al. [120] also modified MFCs with cerium-induced grafting; coating with hexamethylenediisocyanate by the introduction of glycidyl methacrylate (GMA) and graphitization of anhydrides. Cerium grafting reactions were carried out in suspensions of MFCs dispersed in HNO_3 solution under an inert atmosphere and adding ceric (IV) ammonium nitrate $(\text{NH}_4)_2\text{Ce}(\text{NO}_3)_6$, followed by the addition of GMA for the polymerization. Cerium (IV) ions are strong oxidizing agents for alcohols with 1,2-glycol groups, forming chelating complexes that decompose forming free radicals in the cellulose, and in the presence of GMA monomers, these radicals enable the formation of grafted polymers on the surface of the fibers, and for each added GMA monomer, an ester group is introduced. The coating with hexamethylenediisocyanate was performed in MFCs dispersed in THF under an inert atmosphere. Hexamethylenediisocyanate and catalyst 1,4-diazabicyclo[2, 2, 2] octane (DABCO) were added and the mixture was stirred for 2 h at 50 °C. Samples were washed with THF and to the isocyanate-coated MFCs suspension, bis-3-amino propylamine and 3-diethylamino propylamine solubilized in THF were added. Grafting diisocyanates promote the formation of a hydrophobic layer on the surface of the microfibril. Isocyanates rapidly react with hydroxyls forming urethane bonds. So reactions must occur in dry solvents and any further reaction should occur immediately after the isocyanate graphitization. The amines were added to the isocyanate-functionalized MFCs to introduce positive charges to its surface because amines readily react with isocyanate forming urea bonds. For grafting anhydrides, diisopropylamine a catalyst was added to the isocyanate-coated MFCs dispersed in THF, under an inert atmosphere. Succinic or maleic anhydrides were dissolved in dry THF (0.8 M concentration) and these solutions were added to the MFCs suspension. With the introduction of anhydrides, vinyl groups were formed on the surface of the fiber and could be a starting point for the polymerization of water-insoluble monomers as an alternative to cerium-induced GMA graphitization.

Siqueira et al. [115, 117] modified the CNCs and MFCs surfaces using a long-chain isocyanate by different methods. After the chemical modification,

crystalline structure destruction was not observed. Compared to CNCs, a higher grafting density was necessary to disperse MFCs in a nonpolar liquid medium.

Lin and colleagues [81] extracted CNCs from linter by acid hydrolysis with sulfuric acid (30% v/v) at 60 °C for 6 h, followed by centrifugation and neutralization with ammonia. These whiskers were acetylated with acetic anhydride solution and pyridine. After the reaction, the acetylated cellulose was washed, purified and dried. Subsequently, films were prepared by casting from a mechanical mixture of PLA solubilized in chloroform and acetylated cellulose. The nanocomposite films showed improvement in the mechanical properties of up to 61% at the maximum tensile (with 6% acetylated cellulose) and 40% in the elastic modulus (with 10% acetylated cellulose), when compared to the matrix, due to introduction of filler with high stiffness and good interfacial adhesion with PLA. Improvements in the thermal properties of nanocomposites and increase in crystallinity index were also observed. van der Berg et al. [11] isolated CNCs from tunicates via hydrolysis with sulfuric acid and with hydrochloric acid. The CNCs were dried by lyophilization and redispersed in water and organic solvents such as dimethyl sulfoxide, formic acid, m-cresol, dimethylformamide and dimethyl pyrrolidone. The CNCs were not superficially treated, and even then, they showed good dispersion in these solvents, especially those extracted with sulfuric acid and in the proportion of 1 mg/1 mL of CNCs in the solvent. However, an excessive time was used in the ultrasound to disperse the CNCs in the solvents, being able to cause breakage in the cellulosic chains, reducing their length and, consequently, the aspect ratio (L/D).

Qu and co-workers [102] extracted CNCs from wood pulp with sulfuric acid solution (15%) at 80 °C for 4 h, the mixture was filtered and washed until neutrality, the filtrate was placed in a flask with ethyl alcohol, and acetic acid was added to adjust the pH between 4 and 5. MEMO (3-Methacryloxypropyltrimethoxysilane) was added to modify the cellulose surface with silane agent and to enable its incorporation into PLA by casting. The modified CNCs presented lower thermal stability than the unmodified CNCs because the MEMO modifier presented lower stability than the CNCs, but the morphological integrity of them was maintained. The obtained nanocomposites presented higher tensile strength with 1% by mass of CNCs and 1% of v/v MEMO.

CNCs of ramie fibers were modified by Fischer esterification HCl-catalyzed reaction using di- and tricarboxylic organic acids (malonic, malic and citric acids) [119]. Some properties of modified CNCs were compared to respective CNCs obtained by acid hydrolysis using only HCl. Contrary to what the researchers supposed, a little effect of organic acid pKa was found. The functionality of the free carboxylic acid was introduced to the CNCs surface. The morphology and crystallinity of unmodified and modified CNCs were similar. The results showed that modifying CNCs with bio-based organic acids proved to be an efficient way to introduce carboxylic acid functionality on CNCs surface.

Pommet et al. [100] found a preferential growth of BCs on the surface of the natural fiber than freely in the culture medium composed by fructose, yeast extract, peptone, Na₂HPO₄ and citric acid. They proposed a *green* way to modify natural

fibers by attaching bacterial cellulose nanofibers to the surface of these fibers using them as a substrate during the fermentation process of bacterial cellulose. The fermentation process in presence of natural fibers led to the formation of pellicles based on bacterial cellulose, preferably around the natural fibers. An increase in the mechanical strength of the BCs coated fibers was also observed due to the strong hydrogen bonding between the hydroxyl groups present in the BCs and the natural lignocellulosic fibers [48, 68]. So, the coating of bacterial cellulose onto cellulose fibers was considered a new form of controlling the interactions between fibers and polymer matrices because facilitates the good distribution of BCs within the matrix and improve interfacial adhesion between the fibers and the polymer matrix through mechanical interlocking.

The hydrophilic surface of BCs became hydrophobic via esterification reaction with organic acids (acetic, hexanoic and dodecanoic acids) [77]. The authors verified that the degree of surface hydroxyl group substitution decrease with the increase of carbon chain length of the organic acids used.

BCs were acetylated with acetic anhydride in the presence of iodine as a catalyst [58]. The substitution degree (DS) increased when the iodine concentration increased. They verified that the nanostructural morphology preservation is limited by conditions of temperature, time and iodine amount. The better conditions of reaction were 80 °C for 60 min and the amount of catalyst must be less than 0.125 mM. The acetylated BCs showed hydrophobic surface and good mechanical properties which favour the interactions of modified BC and the hydrophobic non-polar polymer matrix. For more drastic reactions conditions, the crystalline structure of BCs was lost.

Thus, there are different types of cellulose/nanocellulose modification reactions as described above. The following three main strategies can be observed: (i) use of a surfactant to functionalize the cellulose/nanocellulose; (ii) chemical reaction and modification of cellulose/nanocellulose in aqueous media and (iii) chemical reaction and modification of cellulose/nanocellulose in an organic solvent.

2.4 All-Based Micro and Nano-cellulose Films

In the literature, there are reported lots of studies of films obtained by casting and still few studies about continuous casting with MFCs, NFCs or CNCs.

Iwamoto et al. [63] studied CNFs films and acrylic composites reinforced with CNFs obtained by casting and extracted from Pinus commercial cellulose pulp. The fibrillation process occurred in the grinder mill with the following numbers of passes: 1; 3; 5; 9; 15 and 30. After 30 passes, the elastic modulus and mechanical tensile strength of CNFs films and acrylic nanocomposites containing CNFs decreased, indicating the decrease of CNFs aspect ratio. CNFs showed a decrease in the crystallinity and in the degree of polymerization with the increase of passes through the grinder, indicating that mechanical shear process causes degradation of cellulose. Therefore, it is necessary to ensure the effective fibrillation of fibers

through the grinder, but without cellulose degradation and a decrease of CNFs aspect ratio due to mechanical shearing. In this way, it is necessary to control the fibrillation parameters and consider that each lignocellulosic fiber needs different procedures to obtain the desired final structure.

Siqueira et al. [115] addressed the study of films structured with MFCs by microfluidizer and CNCs by acid hydrolysis obtained from the loofah (*Luffa cylindrical*). The films were obtained by casting, i.e. by water evaporation of aqueous suspension. CNCs had a length of 242 ± 86 nm, the diameter of 5 ± 1 nm and aspect ratio of 47. MFCs had a diameter of 55 ± 15 nm and the length could not be measured. CNCs films achieved a tensile strength of 68 ± 24 MPa and elastic modulus of 2.4 ± 0.2 GPa, while MFCs films showed a tensile strength of 53 ± 19 MPa and elastic modulus of 3 ± 1 GPa. They concluded that CNCs films present greater mechanical resistance than CMFs films.

Sisal CNCs and MFCs were used to prepared cellulosic membranes. The films were obtained by casting at room temperature for five days followed by drying at 60 °C overnight [10]. The water vapour sorption and gas barrier (carbon dioxide, nitrogen, and oxygen) properties of films were evaluated. It was observed that the water diffusion coefficients were higher for CNCs films than for CMFs. This behaviour was associated with the presence of residual lignin, extractive and fatty acids at the surface of MFCs based films. The CNFs films were also much more permeable to gases than MFCs, indicating that gas molecules penetrate slower in CMFs films because of longer diffusion path. Additionally, it was supposed that the entanglements of these long flexible nanoparticles and lower porosity of the films acted as barrier domains, leading to the tortuosity of the diffusion pathway.

Bufalino [14] developed CNFs films from sawdust residues of three Amazonian species (*C. goeldiana*, *B. parinarioides*, and *P. gigantocarpa*) and eucalyptus (*E. grandis*). The fibers were pretreated with sodium hydroxide and peroxide to remove lignin and hemicelluloses. Films were produced by conventional casting from CNFs obtained with the following passes in grinder: 10; 20; 30 and 40 passes. There was observed an improvement in tensile strength and elastic modulus on CNFs films obtained from the largest number of passes in the grinder. A decrease in the opacity with the increase in the number of passes through grinder was also observed. The colour of the films varied among the species and was related to the residual lignin, different for each species. Figure 3 shows the colour variation index and transparency of the CNFs films according to the number of passes through the grinder and according to the four species studied. It is concluded that the number of passes through the grinder and the plant species influence the mechanical and optical properties of CNFs films.

Recent works report the use of continuous casting for a scale up production of nanocellulose based films. Claro et al. [19] investigated the morphological structure, thermal and mechanical properties of CNCs and CNFs films from curaua leaf fiber and eucalyptus pulp, obtained by continuous casting. The process of continuous casting produced 6 m of dry nanocellulose film per hour and allows the films to not crack. Figure 4 showed the continuous casting scheme and CNCs/CNFs films obtained by this method.

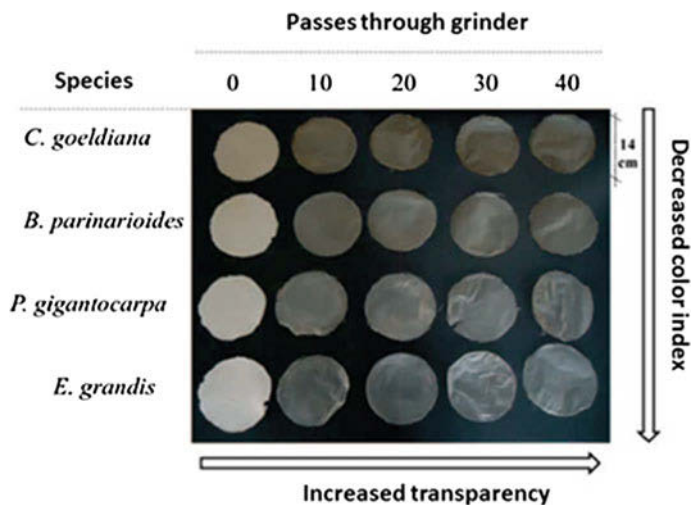


Fig. 3 Variation of color aspect index and transparency of CNFs films in relation to vegetable origin and the number of passes through grinder [111]

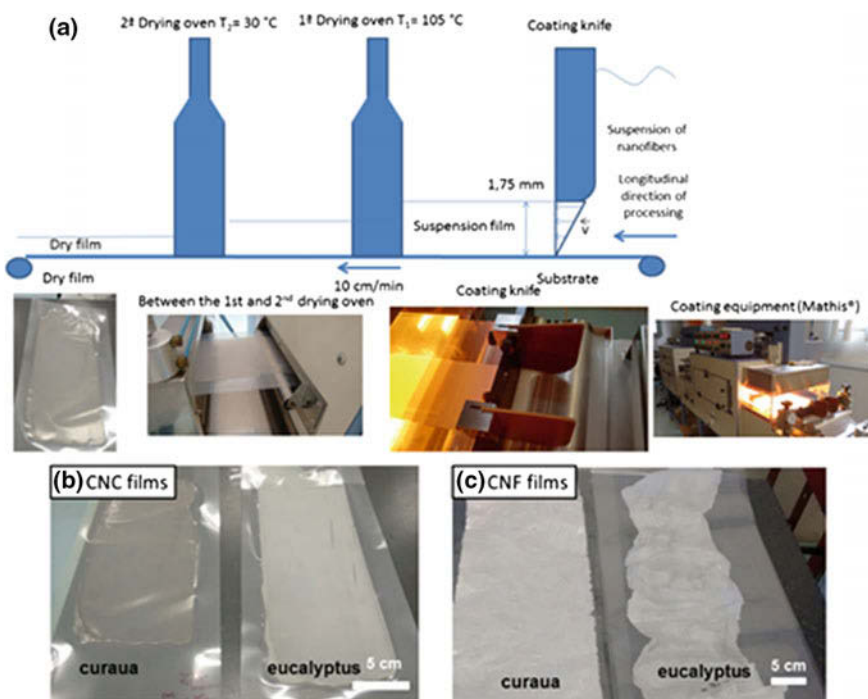


Fig. 4 a Scheme of the continuous casting process, curaua and eucalyptus, b CNCs films and, c CNFs films [19]

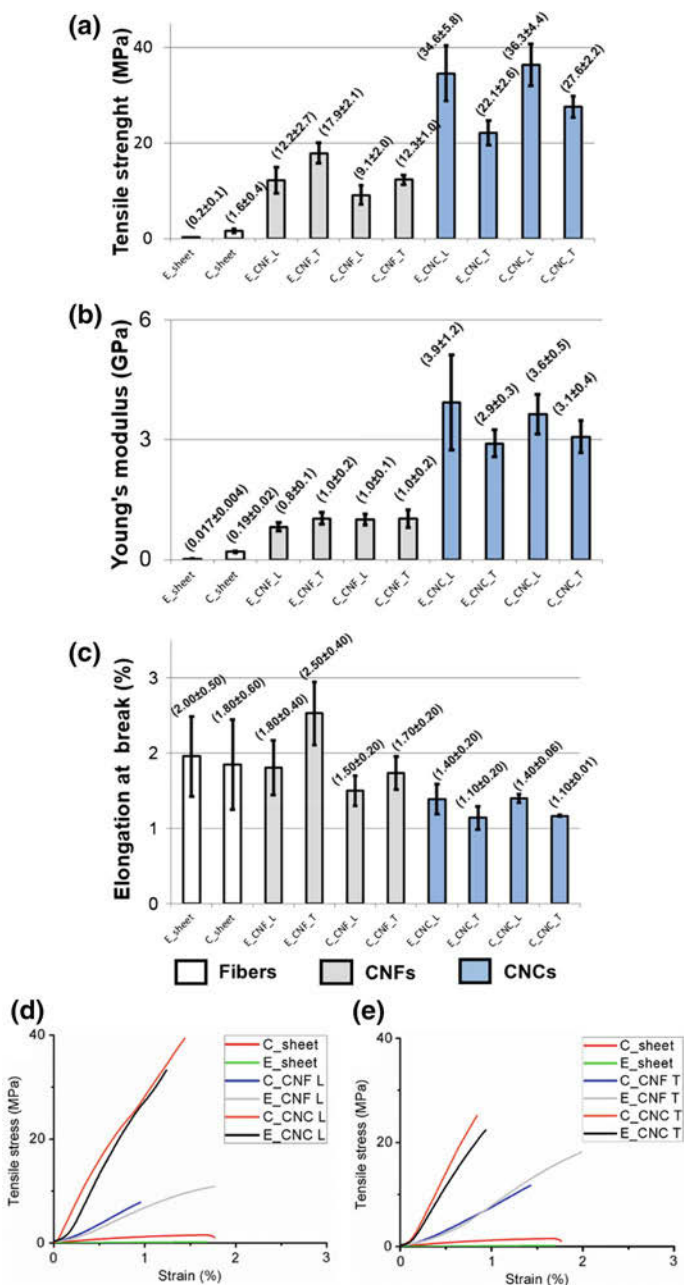


Fig. 5 Mechanical properties under tensile test of fibers sheets and films of CNFs and CNCs from curaua (C) and eucalyptus pulp (E): **a** tensile strength; **b** Young's modulus; **c** elongation at break; **d** stress-strain curve of machine direction (L) and **e** cross direction (T) [19]

CNCs and CNFs suspensions were slowly deposited on a polyester substrate. The coating knife regulates the thickness of the sample and disperses the suspension on a polyester substrate in a pulling speed of 10 cm/min. The equipment presents two drying ovens; the first was set at 105 °C and the second at 30 °C, where the sample undergoes a rapid drying process. CNFs and CNCs films presented mechanical anisotropy due to the orientation of the nanofibers in suspension towards the continuous processing, as shown in Fig. 5.

CNCs films presented higher mechanical resistance (34–36 MPa) in the longitudinal direction of processing and orientation of the nanocrystals. On the other hand, CNFs films presented higher mechanical resistance (12–18 MPa) in the transversal direction of processing and the orientation of the nanofibrils. Therefore, the continuous casting process becomes a viable process for CNCs and CNFs films with different properties and structural morphology than in conventional casting, which is due to the orientation of nanofibers and the rapid drying process.

3 Processing and Applications of Micro and Nano-cellulose Based on Biodegradable Polymers

Micro and nano-cellulose present relative high mechanical properties showing great potential as reinforcement in new biocomposites, innovative bioplastics, and advanced reinforced composite materials [98]. They also present high stiffness, strength, low density and excellent biodegradability and they can be used as a reinforcing material for different polymers, especially biodegradable ones.

Micro and nanocellulose are obtained as dilute suspension and they can be applied to polymer matrix in aqueous solution or freeze-dried aiming better dispersion. CNFs or CNCs are usually dispersed in water, thus, the simplest processing method consists of mixing the cellulose nanostructures in aqueous suspension with water-soluble polymers. This mixture can be cast and the liquid evaporated, resulting in films of nanocomposites, the conventional casting process. This method frequently results in well-dispersed nanostructures, as this avoids the aggregation of the nanomaterial due to the intercalation of the matrix and nanocellulose, preserving its individualized state. This wet casting/evaporation processing method can be extended to other liquids to cover a broader range of polymer matrices [39], but it will be necessary a solvent exchange from water to the polymer solvent, in order to guarantee the dispersion of CNC or CNF through the polymer matrix. However, when it is necessary for high-volume production, the casting or wet processing can be difficult to scale up. The dilute suspension presents stability when it is surface charged by sulfate groups, resulted from acid hydrolysis (CNCs) or from the presence of residual hemicelluloses (CNFs) [39]. But the use of micro/nano cellulose as reinforcement in polymer nanocomposites still presents some challenges and limitations due to their low thermal stability compared to the polymers, their hydrophilicity, the strong hydrogen bonds between adjacent cellulose fibrils, and poor dispersion and compatibility with nonpolar solvents and nonpolar matrices.

In order to overcome some of these problems of dispersion in hydrophobic polymers, the nanocellulose structures can be dispersed in an organic solvent, chemically modified, or grafted with nonpolar molecules. However, the use of them as reinforcements in a wide variety of bio-based polymers, obtained from polysaccharides and proteins, resulted in an increase in the moisture, mechanical and barrier resistance of these materials without compromising their biodegradability [15]. The efficiency of micro/nanocellulose as reinforcement depends on several factors, such as the good interaction between the polymer and the cellulose, good dispersion, addition of the appropriate amount of filler, among others.

The good interaction between the polymer matrix and the cellulose nanostructures, that is, the good interfacial adhesion or compatibility, together with a good dispersion, are characteristics that provide a more efficient tensile transfer from the polymer matrix to the rigid dispersed phase, resulting in an increase in the mechanical strength of the obtained nanocomposite. The compatibility between the polymer and the micro/nanocellulose can be more easily achieved when nanocomposites are prepared with polar polymers, i.e. polymers that present polar groups in their chains, such as polyesters, polyether, polyamides, etc., which could be more compatible with the hydroxyls present in the cellulose chains, thus generating higher interfacial adhesion, resulting in much more efficient stress transfer. This good adhesion, allied to randomly dispersed micro/nanocellulose, may also provide a decrease in the permeability of water or other solvents through the polymer as it would hinder the path to be covered by the solvent molecules throughout the nanocomposite.

An important parameter to control is the amount of CNCs that should be introduced to the polymer in order to obtain nanocomposites with improved properties. For fillers with fiber aspects, the percolation threshold is related to the aspect ratio of nanofibres according to the following expression:

$$\Phi_c = \frac{0.7}{L/d}$$

where (L/d) is the aspect ratio of the nanofiber, assuming a cylindrical shape, and (Φ_c) is the percolation threshold in a volumetric fraction. If it is necessary to obtain the massic fraction, Φ_c should be multiplied by the density, which for cellulose is 1.5 g/cm^3 [47]. Below the percolation threshold, few improvements in the properties are observed, but when slightly larger amounts than the percolation threshold are incorporated, a three-dimensional network of nanostructures is formed, where statistically a nanocrystal will touch each other randomly, causing significant improvements in properties, especially in mechanical.

Different techniques have been utilized to produce micro- or nanocellulose-polymer composites: casting-evaporation, melt compounding, electrospinning and solution blow spinning among others.

The processing of materials reinforced with micro/nanocellulose by traditional methods in the molten state is vulnerable and susceptible to agglomeration and poor dispersion of them in the polymeric matrix. In the specified case of CNCs,

most studies only found interesting results when they were dispersed in a solvent, and this suspension was mixed with the polymer solubilized in the same solvent, i.e. via casting. Thus, most studies use diluted suspension because lyophilized cellulose nanomaterials aggregate through hydrogen bonding and nanoscale is lost. Normally, lyophilized cellulose nanomaterials incorporated in polymer material request a new dilute suspension by sonication system. The simplest method consists of mixing the dilute suspension of CNC with a polymer material such as starch, for example, making the CNCs well dispersed in the polymer matrix.

Starches are abundant, cheap, biodegradable and a renewable resource material, which makes them attractive, and when together with a plasticizer, under suitable conditions of temperature and shear, the TPS (thermoplastic starch) is formed, which can be molded or mixed with other resins. The major drawback of TPS is its hydrophilicity, in addition to its poor mechanical properties. However, its use, besides reducing costs, can also improve the compatibility of cellulose nanostructures with the polymer matrix, due to the similarity of its chemical structures, which would increase the mechanical properties of the nanocomposite, that is, a compensation of losses due to the use of TPS.

CNCs extracted from cassava bagasse were investigated as reinforcement agent in natural rubber (NR) matrix. The nanoparticles in aqueous suspension were mixed with the NR latex emulsion in fraction varying from 0 to 10 wt% (dry basis). The films were obtained by casting of the mixtures. The favourable interactions between the NR matrix and CNCs filler were confirmed by the relatively high reinforcing effect. An increase from 2.2 MPa for the unfilled matrix to 102 and 154 MPa for the NR film reinforced with the nanofiller was observed [96].

The CNFs were extracted from wheat straw using steam explosion, acidic treatment and high shear mechanical treatment [71]. These nanofibrils were dispersed in regular maize starch (TPS) using glycerol as a plasticizer and high shear mixer. The films were obtained by casting. The results revealed improvement in crystallinity with the addition of CNFs. Mechanical properties increased with the increase of CNFs concentration. Barrier properties also improved with the addition of CNFs up to 10%, but further addition decreased properties due to possible CNFs agglomeration because caused reduction in matrix homogeneity and cohesion. The authors proposed that the increase in CNFs content led to the formation of denser microcrystal network, thereby increasing the mechanical properties. This dense network should decrease the diffusivity through the sample. But this increase in CNFs content may compromise the adhesion level between the nanofiller and the matrix, and the mechanical performance, also causes an increase in the diffusivity of water.

Waxy maize starch nanocrystal (WSNC) and cellulose nanocrystals (CNCs) extracted by acid hydrolysis from microcrystalline cellulose (MCC) were united in order to investigate possible synergistic effects on the normal maize starch matrix plasticized by glycerol [51]. A homogeneous distribution of the nanofillers was demonstrated and the use of CNCs and WSNC upgraded mechanical results, but no significant differences in barrier properties were obtained as compared to the use of only WSNC.

Thomas et al. [122] report another series of studies involving the use of cellulose nanostructures (MFCs) reinforcing natural rubber (NR) latex matrix. In their specific study, ultra-fine nanocellulose from jute fibers was prepared by steam explosion method and it was used as the reinforcing agent in NR latex along with cross-linking agents, as Zinc-based and sulfur were used during the processing. The nanocomposite films were prepared from pre-vulcanized latex by casting on a glass plate followed by drying at room temperature. The mixture of the aqueous suspension in various proportions of MFCs (0–3 wt%), the latex and the cross-linking agents were done by ball milling, followed by ultra-sonication and drying. The results revealed that the distribution of the filler among the matrix was homogeneous for all the compositions. By adding 2% MFCs, a network by H-bonding interaction was created. The increase of MFCs content in the NR matrix caused a substantial increase in the mechanical properties of the nanocomposite. The vulcanizing agents used for the crosslinking in the NR matrix created a kind of Zn/cellulose complex, forming a network between the layers of NR matrix, improving the dispersion of the MFCs in the NR matrix.

Reports regarding the environmental biodegradability of the starch/CNFs nanocomposites were performed by Babae et al. [7]. Their study investigated the effect of the addition of unmodified and acetylated CNFs extracted from the kenaf bast fibers (*Hibiscus cannabinus*) in starch glycerol/matrix. The nanofibers were acetylated with acetic anhydride and pyridine under reflux. The nanocomposites were prepared using the solution casting method. The influence of acetylation of CNFs on its biodegradation by white rot fungus (*T. versicolor*) and physicomechanical properties of nanocomposites into the matrix were investigated.

This study showed that both acetylated and non-acetylated CNFs can be used to produce a starch nanocomposite. The mechanical tests showed that the tensile strength and elastic modulus of both nanocomposites increased, in comparison to the matrix, but these improvements were lower for the acetylated ones. The storage modulus and the $\tan \delta$ peak position of both nanocomposites showed improvement when compared to the matrix. Regardless of the type CNFs, their addition resulted in an increase in the T_g of the nanocomposites. Besides that, the moisture absorption of the nanocomposites reduced by addition of the acetylated nanofibers compared to the non-acetylated one. Furthermore, the fungal biodegradability results showed a longer decomposition period for nanocomposites. But, the acetylated nanocomposite needs a longer time for degradation, and it became more sustainable by replacing the hydroxyl groups with acetyl groups.

Palm oil industry generates a large amount of cellulose-rich residues as oil palm mesocarp fiber (OPMF). Targeting the use of agro-residues as raw materials for cellulose nanocrystals (CNCs) production, de Campos et al. [32, 33] obtained these CNCs from oil palm mesocarp fiber via sulfuric acid hydrolysis and microfluidization, obtaining a stable aqueous suspension and increase in cellulose crystallinity (Fig. 6). The influence of CNCs on properties of cassava starch plasticized with glycerol films was investigated. The reinforcing effect of the CNCs was significant only for loading of up to 6 wt% of CNCs, increasing the elastic modulus. Below percolation threshold, elongation at break was even higher than neat starch

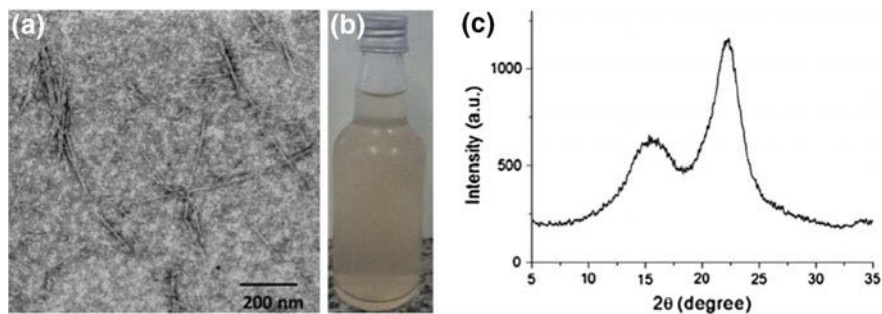


Fig. 6 **a** Scanning transmission electron (STEM) micrograph of cellulose nanocrystals from oil palm mesocarp fibers (OPMF); **b** stable aqueous suspension of CNC-OPMF; **c** XRD patterns of OPMF [32, 33]

films. Above the percolation threshold, there was a formation of a percolating network, leading to CNCs agglomeration and decreasing the mechanical properties of the starch bionanocomposites.

Nanocomposites of chitosan with cellulose are environmentally friendly and the films presented improved physical properties. The CNFs-Chitosan nanocomposites resulted in materials with improved functional properties, in which a wide range of applicability in the field of food packaging, biomedical, water treatment, etc. could be developed. In general, the nanocomposites are obtained by a solvent casting method, electrospinning, and sol-gel transition. Chitosan (cationic) and CNCs (anionic) can be mixed to produce polyelectrolyte complexes using titration. Besides, a two-phase (chitosan and cellulose) based nanocomposites were achieved, and researchers also successfully developed a multi phase material with a high capacity of heavy metal absorption. Furthermore, blends of chitosan and cellulose/nanocellulose resulted in a material with antibacterial activity, metal ions adsorption, odour treatment properties etc. Other commonly used methods for blending are electrospinning, casting and sol-gel transition [1].

Bionanocomposites were developed by casting/evaporation wheat gluten (WG) and (CNCs) from bagasse pulp and TiO_2 nanoparticles [42]. The results demonstrated that CNCs and titanium dioxide nanoparticles improved the mechanical and water vapour barrier properties of gluten films. An optimal content of 7.5% of CNCs and 0.6% of TiO_2 nanoparticles improved the functional properties of WG based materials, according to tensile tests and water resistance of the bionanocomposites. The molecular mobility of amorphous WG chains was not affected by the cellulosic nanofiller. But an increment in T_g of WG/CNC could be verified with TiO_2 nanoparticles incorporation. This behaviour ascribed the strong interfacial interaction between the TiO_2 nanoparticles and the matrix, without disruption in the regularity of the WG chains. Paper sheets coated with the aforementioned nanocomposite exhibited excellent antimicrobial activities i.e. 100, 100 and 98.5% against *S. cerevisiae*, *E. coli*, and *S. aureus* respectively, for 3 layers coated paper after 2 h of exposure to UVA light illumination.

On the other hand, there are some studies demonstrating that it is possible and feasible to incorporate CNC into TPS matrices in the molten state on a torque rheometer at 140 °C, and also using a twin screw extruder [32, 34, 36]. It was observed that the CNCs improved the mechanical properties of TPS in addition to decreasing their sensitivity to moisture, and any modification of these materials was necessary due to their compatibilities and chemical similarities. Lyophilization of CNCs has been the technique most used to ensure the effective dispersion of the nanoparticles through the polymeric matrix obtained by extrusion, but there are still agglomerations of nanofibers in a polymer matrix [59].

Thus, another way of incorporating cellulose nanostructures into polymers is by the melt processing of polymer nanocomposites. Extrusion and injection-moulding processes are industrially common methods; they are cheap, fast and solvent-free techniques. Due to the hydroxyl groups of cellulose, better results were obtained when cellulose nanostructures were incorporated in polar polymers or starch because strong nanofiller-matrix interactions are expected. The use of polar polymers, such as polyamides, to obtain nanocomposites with CNCs showed promising results in the increase of mechanical properties, however, it was necessary a previous treatment of CNCs, with surface coating with polyamide 6, to increase their thermal resistance in order to support the processing temperatures of polyamides [22]. There are also several studies of poly (lactic acid) (PLA) or poly (ϵ -caprolactone) to obtain fully biodegradable nanocomposites, because they are polar and biodegradable polymers [29, 37], but they are still more expensive than commodities polymers, such as polyethylene or polypropylene. About the dispersion of hydrophilic cellulose nanostructures in conventional hydrophobic polymers by the extrusion process, it is generally necessary to match the surface properties of the filler and the matrix, i.e. modify the cellulose surface using a surfactant or covalently graft hydrophobic chains with hydroxyls, or also coating the cellulose nanomaterial with chains compatible with the matrix.

In this way, the main issues to overcome for an efficient melt processing of cellulose nanostructures reinforcing polymer nanocomposites are the aggregation of nanocellulose due to the drying process prior to melt processing, the irregular dispersion within the matrix, the low thermal stability, structural integrity after shear pressure of melt processing and orientation towards processing [39].

Film extrusion is a process in which the melt polymer is forced through a planar matrix, in which the film can be formed by blowing or not [59]. When cellulose nanofibers are added to the melt polymer to form films, some problems may arise: film breakdown; thermal degradation of the polymer matrix and/or nanocellulose; alignment of the nanocellulose and increase in viscosity due to the high aspect ratio of the particles [59]. Many studies have shown that the challenge of obtaining extruded polymeric films reinforced with nanocellulose, with improvement on mechanical and barrier properties, is the good dispersion of the nanocellulose throughout the polymer matrix [59]. Martínez-Sanz et al. [86] prepared PLA films reinforced with CNCs by extrusion and observed an elastic modulus of 2.2 GPa and mechanical tensile strength of 61 MPa, much better results than for pure polymer.

Thermoplastic starch (TPS) reinforced with microfibrillated cellulose (MFCs) were prepared via extrusion. The yield strength was improved by $\sim 50\%$ and stiffness by $\sim 250\%$ upon adding 20 wt% MFC compared to neat TPS [78].

de Campos et al. [29] dispersed CNCs in TPS and PCL nanocomposites by the aqueous suspension. The authors first obtained CNCs from sisal by alkali treatment followed by sulfuric acid hydrolysis. The CNCs neutral suspension was dispersed in starch prior to extrusion to obtain TPS and TPS/PCL nanocomposite. They observed greater dispersibility of the CNC with lower concentration. High concentration of CNC in nanocomposite presented agglomeration and compromised mechanical performance, while lower CNC concentration improved the mechanical properties. The displacement and narrowing of the carbonyl band of the blend with 5% CNC showed the interaction between carbonyl groups of PCL with OH groups of CNC, and avoided the interaction between CNCs, preventing their aggregation.

Electrospinning is a technology widely used for fibers formation. This technique uses electrical forces to produce polymer fibers with diameters ranging from 2 nm to several micrometres using bio-based polymer solutions or synthetic polymers is a process that offers capabilities for producing nanofibers and fabrics with controllable pore structure [12]. Electrospun fibers have been applied in various areas, such as, nanocatalysis, tissue engineering scaffolds, protective clothing, filtration, biomedical, pharmaceutical, optical electronics, healthcare, biotechnology, defense and security, and environmental engineering, due to its smaller pores and higher surface area than regular fibers [12]. The technique consists of feeding a polymer solution into a stream of pressurized air using a concentric nozzle. When the aerodynamic forces overcome the solution surface tension, a solution jet jettisons towards a collector and the solvent is evaporated forming polymer fibers that are collected as non-woven mats [27].

Recent studies showed that the use of poly (ethylene oxide) (PEO) as a matrix to obtain nanocomposite fibers containing CNCs and CNFs by electrospinning [73]. The incorporation of CNCs increased the elastic modulus in two times and mechanical tensile strength in 2.5 times in relation to pure PEO [131]. The incorporation of CNFs also increased the elastic modulus and mechanical tensile strength in more than two times in relation to neat PEO, indicating the potential use of cellulose nanofibers as reinforcement in nanocomposites obtained by electrospinning [129].

Solution Blow Spinning (SBS) is a technique for commercial-scale nanofiber production, with lower cost compared to electrospinning [27]. The SBS process is compatible with a wider variety of solvents than electrospinning and eliminates the necessity of using high voltages [26, 94] and it is a great advantage to be more portable, because with the commercial airbrush systems, depositing fibers on a broad range of collectors and surfaces are facilitated [9, 126]. The applications for SBS include their use in sensors and biosensors, wound dressings, tissue sutures, drug delivery materials, filter membranes and adsorbents [27, 94]. da Silva Parize et al. [27] prepared bio-based nanocomposites of PLA and CNCs by SB-Spinning (Fig. 7). CNCs were obtained from Eucalyptus kraft pulp by sulfuric acid hydrolysis (CNC) and esterified with maleic anhydride (CNC_{AM}), they were

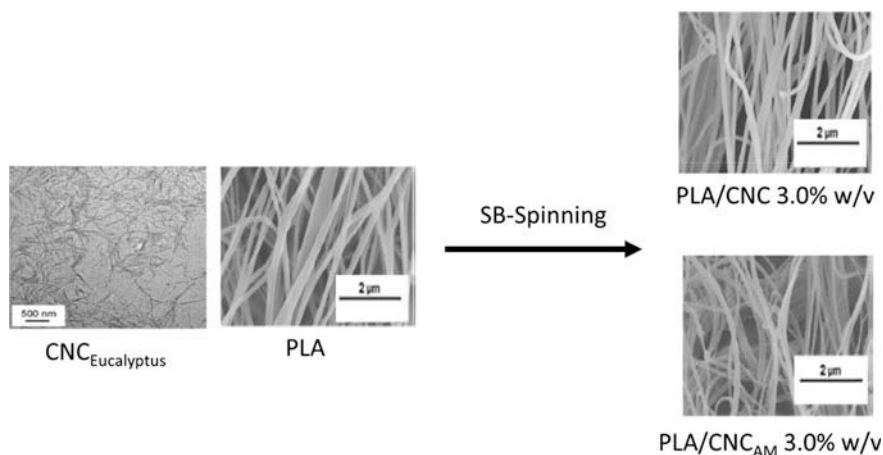


Fig. 7 CNCs from Eucalyptus kraft pulp applied in PLA nanofibers. Adapted from da Parize et al. [27]

applied in PLA solubilized into dimethyl carbonate (DMC) as a solvent. The authors observed that CNCs of both sulfate groups and modified with maleic anhydride acted as nucleating agents and tends to favour the formation of PLA crystals of higher stability since the CNCs of both methods presented crystallinity of around 64%. It is assumed that a fraction of the CNCs are on the surface of the PLA fibers since the hydrophilicity of the composite films increased significantly.

4 General Applications

Nanocellulose and cellulose microfibrils present various potential applications and have the advantage of being derived from natural sources and often a vegetal residue. There are several potential applications, such as barrier [6] for liquid and gaseous materials, reinforcement of plastics and cement, sensors of oil and gas industry, medical devices as special dressings and prostheses [25, 80], in paints, coatings, films and foams, cosmetics, photonics and in electrical as field effect transistors (FET) [49] and electronic industries, solar cells, etc. [24].

The use of nanocellulose as reinforcement is already well understood. Both microfibrils, nanofibrils and cellulose nanocrystals improve especially the mechanical properties as well as thermal properties. The mechanical reinforcement is related to cellulose hydrogen bonding network within the polymer matrix.

MFCs-, CNFs- and CNCs-based polymer nanocomposites provide improvements in barrier properties. These characteristics are dependent on the fibrils morphology of cellulose because their morphology can act as a barrier for the penetration, as well as diffusion of liquid and even gaseous materials into the cellulose-based film [89].

Cellulose-based composite has been applied also as sensor materials. The gas-sensing material can be fabricated from inorganic semiconductor metal oxides, inserting a small amount of metal atom or organic conducting polymer [127]. However, in both systems, they are not entirely satisfactory. The mixture of both and the cellulose can result in a flexible and conductive material. Because cellulose can hold inorganic particles and consequently gain flexibility, being suitable for use as a gas sensor [127].

Lin and Dufresne [80] reported a series of applications of nanocellulose as biomedical materials. They highlighted these nanostructures as a “gift” provided by Nature. Its physical properties, special surface chemistry, biocompatibility, biodegradability and low toxicity make the nanocellulose a potential source of production of diverse biomedical materials as tissue bioscaffolds for cellular culture, drug excipient and drug delivery, immobilization and recognition of enzyme/protein and development in substitutes/medical materials like blood vessel, cartilage and tissue repair.

Nanocellulose applied to photonics has the main interest related to having the liquid crystalline behaviour of CNCs which gives rise to iridescent films of defined optical character and because both CNCs and CNFs may form optically transparent stand-alone films. The evaporation of aqueous suspensions from CNCs can form chiral nematic, iridescent and coloured films which depends on polydispersity of the CNC sizes [2].

Another topic of great interest is a nanocellulose-based coating for controlled release of drugs, in the form of membranes. In addition, modified CNC can be used with aromatic groups, which can control the release of amino acids, being a promising candidate in the immobilization of proteins, preserving the structural integrity of the protein and increasing the activity and long-term storage stability [121].

In food industry nanocellulose acts as a food stabilizer. They have a better affinity with water than with oil and in some cases, nanocellulose may be substituted for oil in some cases to produce low-calorie foods acting as a functional food ingredient [52]. The barrier properties increase the protection and preservation of products and can increase the shelf-life of food [76].

5 Conclusions

Microfibrils and cellulose nanofibers can be obtained by several methods and their performance in determined applications depends on the extraction methodology and their dispersion in the matrix. In this way, the improvements that the microfibrils and nanocellulose could give to the polymer nanocomposite depend upon their type and dispersion and also the good interface interactions or compatibility between the microfibrils and nanocellulose and polymer. These are characteristics that provide a more efficient tensile transfer from the polymer matrix to the rigid dispersed phase, resulting in the mechanical improvement of the obtained composites.

References

1. Abdul Khalil HPS, Saurabh CK, Adnan AS et al (2016) A review on chitosan-cellulose blends and nanocellulose reinforced chitosan biocomposites: Properties and their applications. *Carbohydr Polym* 150:216–226
2. Abitbol T, Rivkin A, Cao Y et al (2016) Nanocellulose, a tiny fiber with huge applications. *Curr Opin Biotechnol* 39:76–88
3. Agustin MB, Nakatsubo F, Yano H (2016) Products of low-temperature pyrolysis of nanocellulose esters and implications for the mechanism of thermal stabilization. *Cellulose* 23:2887–2903. <https://doi.org/10.1007/s10570-016-1004-0>
4. Alemdar A, Sain M (2008) Biocomposites from wheat straw nanofibers: morphology, thermal and mechanical properties. *Compos Sci Technol* 68:557–565. <https://doi.org/10.1016/j.compscitech.2007.05.044>
5. Araujo MAM, Sena Neto AR, Hage E et al (2015) Curaua leaf fiber (*Ananas comosus* var. *erectifolius*) reinforcing poly(lactic acid) biocomposites: formulation and performance. *Polym Compos* 36:1520–1530. <https://doi.org/10.1002/pc.23059>
6. Azeredo HMC, Rosa MF, Mattoso LHC (2017) Nanocellulose in bio-based food packaging applications. *Ind Crops Prod* 97:664–671. <https://doi.org/10.1016/j.indcrop.2016.03.013>
7. Babae M, Jonoobi M, Hamzeh Y, Ashori A (2015) Biodegradability and mechanical properties of reinforced starch nanocomposites using cellulose nanofibers. *Carbohydr Polym* 132:1–8. <https://doi.org/10.1016/j.carbpol.2015.06.043>
8. Bahrin EK, Baharuddin AS, Ibrahim MF et al (2012) Physicochemical property changes and enzymatic hydrolysis enhancement of oil palm empty fruit bunches treated with superheated steam. *BioResources* 7:1784–1801. <https://doi.org/10.15376/biores.7.2.1784-1801>
9. Behrens AM, Casey BJ, Sikorski MJ et al (2014) In situ deposition of PLGA nanofibers via solution blow spinning. *ACS Macro Lett* 3:249–254. <https://doi.org/10.1021/mz500049x>
10. Belbekhouche S, Bras J, Siqueira G et al (2011) Water sorption behavior and gas barrier properties of cellulose whiskers and microfibrils films. *Carbohydr Polym* 83:1740–1748. <https://doi.org/10.1016/j.carbpol.2010.10.036>
11. van der Berg O, Capadona JR, Weder C (2007) Preparation of homogeneous dispersions of tunicate cellulose whiskers in organic solvents. *Biomacromol* 8:1353–1357. <https://doi.org/10.1021/bm061104q>
12. Bhardwaj N, Kundu SC (2010) Electrospinning: A fascinating fiber fabrication technique. *Biotechnol Adv* 28:325–347. <https://doi.org/10.1016/j.biotechadv.2010.01.004>
13. Bondancia TJ, Mattoso LHC, Marconcini JM, Farinas CS (2017) A new approach to obtain cellulose nanocrystals and ethanol from eucalyptus cellulose pulp via the biochemical pathway. *Biotechnol Prog* 33:1085–1095. <https://doi.org/10.1002/btpr.2486>
14. Bufalino L (2014) Filmes de nanocelulose a partir de resíduos madeireiros da Amazônia. UFLA 106
15. Carmona VB, Corrêa AC, Marconcini JM, Mattoso LHC (2015) Properties of a biodegradable ternary blend of thermoplastic starch (TPS), Poly(ϵ -Caprolactone) (PCL) and Poly(Lactic Acid) (PLA). *J Polym Environ* 23:83–89. <https://doi.org/10.1007/s10924-014-0666-7>
16. Chen Y, Wu Q, Huang B et al (2015) Isolation and characteristics of cellulose and nanocellulose from lotus leaf stalk agro-wastes. *BioResources* 10:684–696
17. Chen L, Zhu JY, Baez C et al (2016) Highly thermal-stable and functional cellulose nanocrystals and nanofibrils produced using fully recyclable organic acids. *Green Chem* 18:3835–3843. <https://doi.org/10.1039/C6GC00687F>
18. Chin KM, Sung Ting S, Ong HL, Omar M (2018) Surface functionalized nanocellulose as a veritable inclusionary material in contemporary bioinspired applications: a review. *J Appl Polym Sci* 135. <https://doi.org/10.1002/app.46065>

19. Claro PIC, Corrêa AC, de Campos A et al (2018) Curaua and eucalyptus nanofibers films by continuous casting: mechanical and thermal properties. *Carbohydr Polym* 181:1093–1101. <https://doi.org/10.1016/j.carbpol.2017.11.037>
20. Corradini E, Teixeira EM, Paladin PD et al (2009) Thermal stability and degradation kinetic study of white and colored cotton fibers by thermogravimetric analysis. *J Therm Anal Calorim* 97:415–419
21. Corradini E, Imam SH, Agnelli JM, Mattoso LHC (2009a) Effect of coconut, sisal and jute fibers on the properties of starch/gluten/glycerol matrix. *J Polym Environ* 17:1–9. <https://doi.org/10.1007/s10924-009-0115-1>
22. Corrêa AC, de Moraes Teixeira E, Carmona VB et al (2014) Obtaining nanocomposites of polyamide 6 and cellulose whiskers via extrusion and injection molding. *Cellulose* 21:311–322. <https://doi.org/10.1007/s10570-013-0132-z>
23. Corrêa AC, de Teixeira EM, Pessan LA, Mattoso LHC (2010) Cellulose nanofibers from curaua fibers. *Cellulose* 17:1183–1192. <https://doi.org/10.1007/s10570-010-9453-3>
24. Costa SV, Pingel P, Janietz S, Nogueira AF (2016) Inverted organic solar cells using nanocellulose as substrate. *J Appl Polym Sci* 133. <https://doi.org/10.1002/app.43679>
25. Czaja WK, Young DJ, Kawecki M, Brown RM (2007) The future prospects of microbial cellulose in biomedical applications. *Biomacromol* 8:1–12
26. da Silva Parize DD, Foschini MM, de Oliveira JE et al (2016) Solution blow spinning: parameters optimization and effects on the properties of nanofibers from poly(lactic acid)/dimethyl carbonate solutions. *J Mater Sci* 51:4627–4638. <https://doi.org/10.1007/s10853-016-9778-x>
27. da Silva Parize DD, de Oliveira JE, Williams T et al (2017) Solution blow spun nanocomposites of poly(lactic acid)/cellulose nanocrystals from Eucalyptus kraft pulp. *Carbohydr Polym* 174:923–932. <https://doi.org/10.1016/j.carbpol.2017.07.019>
28. Davoodi MM, Sapuan SM, Ahmad D et al (2010) Mechanical properties of hybrid kenaf/glass reinforced epoxy composite for passenger car bumper beam. *Mater Des* 31:4927–4932. <https://doi.org/10.1016/j.matdes.2010.05.021>
29. de Campos A, Teodoro KBR, Teixeira EM et al (2013) Properties of thermoplastic starch and TPS/polycaprolactone blend reinforced with sisal whiskers using extrusion processing. *Polym Eng Sci* 53:800–808. <https://doi.org/10.1002/pen.23324>
30. de Campos A, Correa AC, Cannella D et al (2013) Obtaining nanofibers from curaua and sugarcane bagasse fibers using enzymatic hydrolysis followed by sonication. *Cellulose* 20:1491–1500. <https://doi.org/10.1007/s10570-013-9909-3>
31. de Campos A, Tonoli GHD, Marconcini JM et al (2013) TPS/PCL composite reinforced with treated sisal fibers: property, biodegradation and water-absorption. *J Polym Environ* 21:1–7. <https://doi.org/10.1007/s10924-012-0512-8>
32. de Campos A, de Neto ARS, Rodrigues VB et al (2017a) Production of cellulose nanowhiskers from oil palm mesocarp fibers by acid hydrolysis and microfluidization. *J Nanosci Nanotechnol* 17:4970–4976. <https://doi.org/10.1166/jnn.2017.13451>
33. de Campos A, Sena Neto AR, Rodrigues VB et al (2017b) Bionanocomposites produced from cassava starch and oil palm mesocarp cellulose nanowhiskers. *Carbohydr Polym* 175:330–336. <https://doi.org/10.1016/j.carbpol.2017.07.080>
34. de Moraes Teixeira E, Pasquini D, Curvelo AAS et al (2009) Cassava bagasse cellulose nanofibrils reinforced thermoplastic cassava starch. *Carbohydr Polym* 78:422–431. <https://doi.org/10.1016/j.carbpol.2009.04.034>
35. de Moraes Teixeira E, Corrêa AC, Manzoli A et al (2010) Cellulose nanofibers from white and naturally colored cotton fibers. *Cellulose* 17:595–606. <https://doi.org/10.1007/s10570-010-9403-0>
36. de Moraes Teixeira E, Bondancia TJ, Teodoro KBR et al (2011) Sugarcane bagasse whiskers: Extraction and characterizations. *Ind Crops Prod* 33:63–66. <https://doi.org/10.1016/j.indcrop.2010.08.009>

37. de Morais Teixeira E, de Campos A, Marconcini JM et al (2014) Starch/fiber/poly(lactic acid) foam and compressed foam composites. *RSC Adv* 4:6616. <https://doi.org/10.1039/c3ra47395c>
38. dos Santos RM, Flauzino Neto WP, Silvério HA et al (2013) Cellulose nanocrystals from pineapple leaf, a new approach for the reuse of this agro-waste. *Ind Crops Prod* 50:707–714. <https://doi.org/10.1016/j.indcrop.2013.08.049>
39. Dufresne A (2018) Cellulose nanomaterials as green nanoreinforcements for polymer nanocomposites. *Philos Trans R Soc A Math Phys Eng Sci* 376:20170040. <https://doi.org/10.1098/rsta.2017.0040>
40. Dufresne A, Castaño J (2016) Polysaccharide nanomaterial reinforced starch nanocomposites: a review. *Starch/Staerke* 1–19. <https://doi.org/10.1002/star.201500307>
41. Eichhorn SJ, Dufresne A, Aranguren M et al (2010) Review: current international research into cellulose nanofibres and nanocomposites. *J Mater Sci* 45:1–33. <https://doi.org/10.1007/s10853-009-3874-0>
42. El-Wakil NA, Hassan EA, Abou-Zeid RE, Dufresne A (2015) Development of wheat gluten/nanocellulose/titanium dioxide nanocomposites for active food packaging. *Carbohydr Polym* 124:337–346. <https://doi.org/10.1016/j.carbpol.2015.01.076>
43. Fahma F, Iwamoto S, Hori N et al (2010) Isolation, preparation, and characterization of nanofibers from oil palm empty-fruit-bunch (OPEFB). *Cellulose* 17:977–985. <https://doi.org/10.1007/s10570-010-9436-4>
44. Filson PB, Dawson-Andoh BE (2009) Characterization of sugars from model and enzyme-mediated pulp hydrolyzates using high-performance liquid chromatography coupled to evaporative light scattering detection. *Bioresour Technol* 100:6661–6664. <https://doi.org/10.1016/j.biortech.2008.12.067>
45. Flauzino Neto WP, Silvério HA, Dantas NO, Pasquini D (2013) Extraction and characterization of cellulose nanocrystals from agro-industrial residue—Soy hulls. *Ind Crops Prod* 42:480–488. <https://doi.org/10.1016/j.indcrop.2012.06.041>
46. Forsman N, Lozhechnikova A, Khakalo A et al (2017) Layer-by-layer assembled hydrophobic coatings for cellulose nanofibril films and textiles, made of polylysine and natural wax particles. *Carbohydr Polym* 173:392–402. <https://doi.org/10.1016/j.carbpol.2017.06.007>
47. Garcia de Rodriguez NL, Thielemans W, Dufresne A (2006) Sisal cellulose whiskers reinforced polyvinyl acetate nanocomposites. *Cellulose* 13:261–270. <https://doi.org/10.1007/s10570-005-9039-7>
48. Gardner DJ, Oporto GS, Mills R, Samir MASA (2008) Adhesion and Surface Issues in Cellulose and Nanocellulose. *J Adhesion Sci Technol* 22:545–567. <https://doi.org/10.1163/156856108X295509>
49. Gaspar D, Fernandes SN, De Oliveira AG et al (2014) Nanocrystalline cellulose applied simultaneously as the gate dielectric and the substrate in flexible field effect transistors. *Nanotechnology* 25. <https://doi.org/10.1088/0957-4484/25/9/094008>
50. Ghaderi M, Mousavi M, Yousefi H, Labbafi M (2014) All-cellulose nanocomposite film made from bagasse cellulose nanofibers for food packaging application. *Carbohydr Polym* 104:59–65. <https://doi.org/10.1016/j.carbpol.2014.01.013>
51. González K, Retegi A, González A et al (2015) Starch and cellulose nanocrystals together into thermoplastic starch bionanocomposites. *Carbohydr Polym* 117:83–90. <https://doi.org/10.1016/j.carbpol.2014.09.055>
52. Gómez HC, Serpa A, Velásquez-Cock J et al (2016) Vegetable nanocellulose in food science: a review. *Food Hydrocoll.* 57:178–186
53. Harmaen AS, Khalina A, Azowa I et al (2015) Thermal and biodegradation properties of poly(lactic acid)/fertilizer/oil palm fibers blends biocomposites. *Polym Compos* 36:576–583. <https://doi.org/10.1002/pc.22974>

54. Hassan ML, Bras J, Hassan EA, et al (2012) Polycaprolactone/ Modified Bagasse Whisker Nanocomposites with Improved Moisture-Barrier and Biodegradability Properties. *J Appl Polym Sci* 1–10. <https://doi.org/10.1002/app>
55. Henriksson M, Henriksson G, Berglund LA, Lindström T (2007) An environmentally friendly method for enzyme-assisted preparation of microfibrillated cellulose (MFC) nanofibers. *Eur Polym J* 43:3434–3441. <https://doi.org/10.1016/j.eurpolymj.2007.05.038>
56. Henrique MA, Silvério HA, Flauzino Neto WP, Pasquini D (2013) Valorization of an agro-industrial waste, mango seed, by the extraction and characterization of its cellulose nanocrystals. *J Environ Manage* 121:202–209. <https://doi.org/10.1016/j.jenvman.2013.02.054>
57. Hindi SSZ (2017) Microcrystalline cellulose: the inexhaustible treasure for pharmaceutical industry. *Nanosci Nanotechnol Res* 4:17–24. <https://doi.org/10.12691/nnr-4-1-3>
58. Hu W, Chen S, Xu Q, Wang H (2011) Solvent-free acetylation of bacterial cellulose under moderate conditions. *Carbohydr Polym* 83:1575–1581. <https://doi.org/10.1016/j.carbpol.2010.10.016>
59. Hubbe MA, Ferrer A, Tyagi P et al (2017) Nanocellulose in thin films, coatings, and plies for packaging applications: a review. *BioResources* 12:2143–2233
60. Hubbe M, Rojas OJ, Lucia L, Sain M (2008) Cellulosic Nanocomposites: a review. *BioResources* 3:929–980. <https://doi.org/10.15376/biores.3.3.929-980>
61. Ibrahim Nor Azowa, Hadithon Kamarul Arifin, Abdan K (2010) Effect of fiber treatment on mechanical properties of kenaf fiber-Ecoflex composites. *J Reinf Plast Compos* 29:2192–2198. <https://doi.org/10.1177/0731684409347592>
62. Isogai A, Saito T, Fukuzumi H (2011) TEMPO-oxidized cellulose nanofibers. *Nanoscale* 3:71–85. <https://doi.org/10.1039/C0NR00583E>
63. Iwamoto S, Nakagaito AN, Yano H (2007) Nano-fibrillation of pulp fibers for the processing of transparent nanocomposites. *Appl Phys A Mater Sci Process* 89:461–466. <https://doi.org/10.1007/s00339-007-4175-6>
64. Jia C, Chen L, Shao Z et al (2017) Using a fully recyclable dicarboxylic acid for producing dispersible and thermally stable cellulose nanomaterials from different cellulosic sources. *Cellulose* 24:2483–2498. <https://doi.org/10.1007/s10570-017-1277-y>
65. Johar N, Ahmad I, Dufresne A (2012) Extraction, preparation and characterization of cellulose fibres and nanocrystals from rice husk. *Ind Crops Prod* 37:93–99. <https://doi.org/10.1016/j.indcrop.2011.12.016>
66. Kaisangsri N, Kerdchoechuen O, Laohakunjit N (2014) Characterization of cassava starch based foam blended with plant proteins, kraft fiber, and palm oil. *Carbohydr Polym* 110:70–77. <https://doi.org/10.1016/j.carbpol.2014.03.067>
67. Kalia S, Boufi S, Celli A, Kango S (2014) Nanofibrillated cellulose: surface modification and potential applications. *Colloid Polym Sci* 292:5–31. <https://doi.org/10.1007/s00396-013-3112-9>
68. Kalia S, Dufresne A, Cherian BM t al (2011) Cellulose-based bio- and nanocomposites: a review. *Int J Polym Sci* 2011
69. Kamel S (2007) Nanotechnology and its applications in lignocellulosic composites, a mini review. *Express Polym Lett* 1:546–575
70. Kargarzadeh H, Mariano M, Huang J et al (2017) Recent developments on nanocellulose reinforced polymer nanocomposites: a review. *Polym (United Kingdom)* 132:368–393
71. Kaushik A, Singh M, Verma G (2010) Green nanocomposites based on thermoplastic starch and steam exploded cellulose nanofibrils from wheat straw. *Carbohydr Polym* 82:337–345. <https://doi.org/10.1016/j.carbpol.2010.04.063>
72. Khalil HPSA, Davoudpour Y, Aprilia NAS, Mustapha A, Hossain S, Islam N, Dungani R (2014) Nanocellulose-based polymer nanocomposite: isolation, characterization and applications. In: *nanocellulose polymer nanocomposites*. John Wiley & Sons, Inc., p 273–309. ISBN: 978-1-118-87190-4

73. Kim JH, Shim BS, Kim HS et al (2015) Review of nanocellulose for sustainable future materials. *Int J Precis Eng. Manuf Green Technol* 2:197–213
74. Lam NT, Chollakup R, Smitthipong W et al (2017) Characterization of cellulose nanocrystals extracted from sugarcane bagasse for potential biomedical materials. *Sugar Tech* 19:539–552. <https://doi.org/10.1007/s12355-016-0507-1>
75. Lamaming J, Hashim R, Sulaiman O et al (2015) Cellulose nanocrystals isolated from oil palm trunk. *Carbohydr Polym* 127:202–208. <https://doi.org/10.1016/j.carbpol.2015.03.043>
76. Lavoine N, Desloges I, Dufresne A, Bras J (2012) Microfibrillated cellulose—its barrier properties and applications in cellulosic materials: a review. *Carbohydr Polym* 90:735–764
77. Lee KY, Quero F, Blaker JJ et al (2011) Surface only modification of bacterial cellulose nanofibres with organic acids. *Cellulose* 18:595–605. <https://doi.org/10.1007/s10570-011-9525-z>
78. Lendvai L, Karger-Kocsis J, Kmetty Á, Drakopoulos SX (2016) Production and characterization of microfibrillated cellulose-reinforced thermoplastic starch composites. *J Appl Polym Sci* 133. <https://doi.org/10.1002/app.42397>
79. Lif A, Stenstad P, Syverud K et al (2010) Fischer-Tropsch diesel emulsions stabilised by microfibrillated cellulose and nonionic surfactants. *J Colloid Interface Sci* 352:585–592. <https://doi.org/10.1016/j.jcis.2010.08.052>
80. Lin N, Dufresne A (2014) Nanocellulose in biomedicine: current status and future prospect. *Eur Polym J* 59:302–325. <https://doi.org/10.1016/j.eurpolymj.2014.07.025>
81. Lin N, Huang J, Chang PR et al (2011) Surface acetylation of cellulose nanocrystal and its reinforcing function in poly(lactic acid). *Carbohydr Polym* 83:1834–1842. <https://doi.org/10.1016/j.carbpol.2010.10.047>
82. Liu Q, Lu Y, Aguedo M et al (2017) Isolation of high-purity cellulose nanofibers from wheat straw through the combined environmentally friendly methods of steam explosion, microwave-assisted hydrolysis, and microfluidization. *ACS Sustain Chem Eng* 5:6183–6191. <https://doi.org/10.1021/acssuschemeng.7b01108>
83. Ljungberg N, Bonini C, Bortolussi F et al (2005) New nanocomposite materials reinforced with cellulose whiskers in atactic polypropylene: effect of surface and dispersion characteristics. *Biomacromol* 6:2732–2739. <https://doi.org/10.1021/bm050222v>
84. Ljungberg N, Cavaillé JY, Heux L (2006) Nanocomposites of isotactic polypropylene reinforced with rod-like cellulose whiskers. *Polymer (Guildf)* 47:6285–6292. <https://doi.org/10.1016/j.polymer.2006.07.013>
85. Mandal A, Chakrabarty D (2011) Isolation of nanocellulose from waste sugarcane bagasse (SCB) and its characterization. *Carbohydr Polym* 86:1291–1299. <https://doi.org/10.1016/j.carbpol.2011.06.030>
86. Martínez-Sanz M, Lopez-Rubio A, Lagaron JM (2012) Optimization of the dispersion of unmodified bacterial cellulose nanowhiskers into polylactide via melt compounding to significantly enhance barrier and mechanical properties. *Biomacromol* 13:3887–3899. <https://doi.org/10.1021/bm301430j>
87. Miao X, Lin J, Tian F et al (2016) Cellulose nanofibrils extracted from the byproduct of cotton plant. *Carbohydr Polym* 136:841–850. <https://doi.org/10.1016/j.carbpol.2015.09.056>
88. El Miri N, Abdelouahdi K, Barakat A et al (2015) Bio-nanocomposite films reinforced with cellulose nanocrystals: rheology of film-forming solutions, transparency, water vapor barrier and tensile properties of films. *Carbohydr Polym* 129:156–167. <https://doi.org/10.1016/j.carbpol.2015.04.051>
89. Mishra RK, Sabu A, Tiwari SK (2018) Materials chemistry and the futurist eco-friendly applications of nanocellulose: status and prospect. *J Saudi Chem Soc* 22:949. <https://doi.org/10.1016/j.jscs.2018.02.005>
90. Moon RJ, Martini A, Nairn J et al (2011) Cellulose nanomaterials review: structure, properties and nanocomposites
91. Nakagaito AN, Iwamoto S, Yano H (2005) Bacterial cellulose: the ultimate nano-scalar cellulose morphology for the production of high-strength composites. *Appl Phys A Mater Sci Process* 80:93–97. <https://doi.org/10.1007/s00339-004-2932-3>

92. Nechyporchuk O, Belgacem MN, Bras J (2016) Production of cellulose nanofibrils: a review of recent advances. *Ind Crops Prod* 93:2–25
93. Nikmatin S, Syafiuddin A, Irwanto DAY (2017) Properties of oil palm empty fruit bunch-filled recycled acrylonitrile butadiene styrene composites: effect of shapes and filler loadings with random orientation. *BioResources* 12:1090–1101. <https://doi.org/10.15376/biores.12.1.1090-1101>
94. Oliveira JE, Moraes EA, Costa RGF et al (2011) Nano and submicrometric fibers of poly(D, L-lactide) obtained by solution blow spinning: process and solution variables. *J Appl Polym Sci* 122:3396–3405. <https://doi.org/10.1002/app.34410>
95. Pasquini D, de Teixeira EM, da Curvelo AA et al (2008) Surface esterification of cellulose fibres: processing and characterisation of low-density polyethylene/cellulose fibres composites. *Compos Sci Technol* 68:193–201. <https://doi.org/10.1016/j.compscitech.2007.05.009>
96. Pasquini D, de Teixeira EM, da Curvelo AA S et al (2010) Extraction of cellulose whiskers from cassava bagasse and their applications as reinforcing agent in natural rubber. *Ind Crops Prod* 32:486–490. <https://doi.org/10.1016/j.indcrop.2010.06.022>
97. Pelissari FM, Sobral PJDA, Menegalli FC (2014) Isolation and characterization of cellulose nanofibers from banana peels. *Cellulose* 21:417–432. <https://doi.org/10.1007/s10570-013-0138-6>
98. Peng Y, Gardner DJ, Han Y et al (2013) Influence of drying method on the material properties of nanocellulose I: thermostability and crystallinity. *Cellulose* 20:2379–2392. <https://doi.org/10.1007/s10570-013-0019-z>
99. Petersson L, Oksman K (2006) Preparation and properties of biopolymer-based nanocomposite films using microcrystalline cellulose. In: *ACS Symposium Series*. pp 132–150
100. Pommet M, Juntaro J, Heng JYY et al (2008) Surface modification of natural fibers using bacteria: depositing bacterial cellulose onto natural fibers to create hierarchical fiber reinforced nanocomposites. *Biomacromol* 9:1643–1651. <https://doi.org/10.1021/bm800169g>
101. Pääkko M, Ankerfors M, Kosonen H et al (2007) Enzymatic hydrolysis combined with mechanical shearing and high-pressure homogenization for nanoscale cellulose fibrils and strong gels. *Biomacromol* 8:1934–1941. <https://doi.org/10.1021/bm061215p>
102. Qu P, Zhou Y, Zhang X et al (2012) Surface modification of cellulose nanofibrils for poly (lactic acid) composite application. *J Appl Polym Sci* 125:3084–3091. <https://doi.org/10.1002/app.36360>
103. Ran F, Tan Y (2018) *Polyaniline-based composites and nanocomposites*. Elsevier, Amsterdam
104. Rodrigues APH, de Souza SD, Gil CSB et al (2017) Biobased nanocomposites based on collagen, cellulose nanocrystals, and plasticizers. *J Appl Polym Sci* 134: <https://doi.org/10.1002/app.44954>
105. Rojas J, Bedoya M, Ciro Y (2015) World’ s largest science, technology & medicine open access book publisher current trends in the production of cellulose nanoparticles and nanocomposites for biomedical applications. *Cellul Asp Curr Trends* 193–228. <https://doi.org/10.5772/61334>
106. Roman M, Winter WT (2004) Effect of sulfate groups from sulfuric acid hydrolysis on the thermal degradation behavior of bacterial cellulose. *Biomacromol* 5:1671. <https://doi.org/10.1021/bm034519+>
107. Rosa MF, Medeiros ES, Malmonge J a., et al (2010) Cellulose nanowhiskers from coconut husk fibers: effect of preparation conditions on their thermal and morphological behavior. *Carbohydr Polym* 81:83–92. <https://doi.org/10.1016/j.carbpol.2010.01.059>
108. Roy D, Semsarilar M, Guthrie JT, Perrier S (2009) Cellulose modification by polymer grafting: a review. *Chem Soc Rev* 38:2046. <https://doi.org/10.1039/b808639g>
109. Salehudin MH, Salleh E, Muhamad II, Mamat SNH (2014) Starch-based biofilm reinforced with empty fruit bunch cellulose nanofibre. *Mater Res Innov* 18:S6-322–S6-325. <https://doi.org/10.1179/1432891714z.000000000977>

110. Santana JS, do Rosário JM, Pola CC et al (2017) Cassava starch-based nanocomposites reinforced with cellulose nanofibers extracted from sisal. *J Appl Polym Sci* 134:1–9. <https://doi.org/10.1002/app.44637>
111. Scatolino MV, Bufalino L, Mendes LM et al (2017) Impact of nanofibrillation degree of eucalyptus and Amazonian hardwood sawdust on physical properties of cellulose nanofibril films. *Wood Sci Technol* 51:1095–1115. <https://doi.org/10.1007/s00226-017-0927-4>
112. Shankar S, Rhim JW (2016) Preparation of nanocellulose from micro-crystalline cellulose: the effect on the performance and properties of agar-based composite films. *Carbohydr Polym* 135:18–26. <https://doi.org/10.1016/j.carbpol.2015.08.082>
113. Silvério HA, Flauzino Neto WP, Dantas NO, Pasquini D (2013) Extraction and characterization of cellulose nanocrystals from corncob for application as reinforcing agent in nanocomposites. *Ind Crops Prod* 44:427–436. <https://doi.org/10.1016/j.indcrop.2012.10.014>
114. Siqueira G, Bras J, Dufresne A (2009) Cellulose whiskers versus microfibrils: influence of the nature of the nanoparticle and its surface functionalization on the thermal and mechanical properties of nanocomposites. *Biomacromol* 10:425–432. <https://doi.org/10.1021/bm801193d>
115. Siqueira G, Bras J, Dufresne A (2010) *Luffa cylindrica* as a lignocellulosic source of fiber, microfibrillated cellulose, and cellulose nanocrystals. *BioResources* 5:727–740. <https://doi.org/10.15376/biores.5.2.727-740>
116. Siqueira G, Fraschini C, Bras J et al (2011) Impact of the nature and shape of cellulosic nanoparticles on the isothermal crystallization kinetics of poly(ϵ -caprolactone). *Eur Polym J* 47:2216–2227. <https://doi.org/10.1016/j.eurpolymj.2011.09.014>
117. Siqueira G, Tapin-Lingua S, Bras J et al (2010) Morphological investigation of nanoparticles obtained from combined mechanical shearing, and enzymatic and acid hydrolysis of sisal fibers. *Cellulose* 17:1147–1158. <https://doi.org/10.1007/s10570-010-9449-z>
118. Souza SF, Lopez A, Cai JHUI, Wu C (2010) Nanocellulose from curava fibers and their nanocomposites. *Mol Cryst Liq Cryst* 522:342–352. <https://doi.org/10.1080/15421401003722955>
119. Spinella S, Maiorana A, Qian Q et al (2016) Concurrent cellulose hydrolysis and esterification to prepare a surface-modified cellulose nanocrystal decorated with carboxylic acid moieties. *ACS Sustain Chem Eng* 4:1538–1550. <https://doi.org/10.1021/acssuschemeng.5b01489>
120. Stenstad P, Andresen M, Tanem BS, Stenius P (2008) Chemical surface modifications of microfibrillated cellulose. *Cellulose* 15:35–45. <https://doi.org/10.1007/s10570-007-9143-y>
121. Tan L, Mandley SJ, Peijnenburg W et al (2018) Combining ex-ante LCA and EHS screening to assist green design: a case study of cellulose nanocrystal foam. *J Clean Prod* 178:494–506. <https://doi.org/10.1016/j.jclepro.2017.12.243>
122. Thomas MG, Abraham E, Jyotishkumar P et al (2015) Nanocelluloses from jute fibers and their nanocomposites with natural rubber: preparation and characterization. *Int J Biol Macromol* 81:768–777. <https://doi.org/10.1016/j.ijbiomac.2015.08.053>
123. Tonoli GHD, de Moraes Teixeira E, Corrêa C et al (2012a) Cellulose micro/nanofibres from Eucalyptus kraft pulp: preparation and properties. *Carbohydr Polym*. <https://doi.org/10.1016/j.carbpol.2012.02.052>
124. Tonoli GHD, de Moraes Teixeira E, Corrêa CC et al (2012b) Cellulose micro/nanofibres from Eucalyptus kraft pulp: Preparation and properties. *Carbohydr Polym* 89:80–88. <https://doi.org/10.1016/j.carbpol.2012.02.052>
125. Trache D, Hussin MH, Hui Chuin CT et al (2016) Microcrystalline cellulose: Isolation, characterization and bio-composites application—a review. *Int J Biol Macromol* 93:789–804
126. Tutak W, Sarkar S, Lin-Gibson S et al (2013) The support of bone marrow stromal cell differentiation by airbrushed nanofiber scaffolds. *Biomaterials* 34:2389–2398. <https://doi.org/10.1016/j.biomaterials.2012.12.020>

127. Ummartyotin S, Manuspiya H (2015) A critical review on cellulose: from fundamental to an approach on sensor technology. *Renew Sustain Energy Rev* 41:402–412. <https://doi.org/10.1016/j.rser.2014.08.050>
128. Uschanov P, Johansson LS, Maunu SL, Laine J (2011) Heterogeneous modification of various celluloses with fatty acids. *Cellulose* 18:393–404. <https://doi.org/10.1007/s10570-010-9478-7>
129. Xu X, Liu F, Jiang L et al (2013) Cellulose nanocrystals vs. cellulose nano fibrils: a comparative study on their microstructures and effects as polymer reinforcing agents. *ACS Appl Mater Interfaces* 5:2999–3009. <https://doi.org/10.1021/am302624t>
130. Yarbrough JM, Zhang R, Mittal A et al (2017) Multifunctional cellulolytic enzymes outperform processive fungal cellulases for coproduction of nanocellulose and biofuels. *ACS Nano* 11:3101–3109. <https://doi.org/10.1021/acsnano.7b00086>
131. Zhou C, Chu R, Wu R, Wu Q (2011) Electrospun polyethylene oxide/cellulose nanocrystal composite nanofibrous mats with homogeneous and heterogeneous microstructures. *Biomacromol* 12:2617–2625. <https://doi.org/10.1021/bm200401p>
132. Zimmermann T, Bordeanu N, Strub E (2010) Properties of nanofibrillated cellulose from different raw materials and its reinforcement potential. *Carbohydr Polym* 79:1086–1093. <https://doi.org/10.1016/j.carbpol.2009.10.045>

Extraction of Cellulose Nanofibers and Their Eco/Friendly Polymer Composites



Stephen C. Agwuncha, Chioma G. Anusionwu, Shesan J. Owonubi, E. Rotimi Sadiku, Usman A. Busuguma and I. David Ibrahim

1 Introduction

According to Lee et al. [1], cellulose nanoparticles are rod-like particles that have a diameter in the nanoscale and consist of multiple cellulose chains that are combined with intra- and intermolecular hydrogen bonds. The long discussions that are still on-going about the preservation of our natural resources globally, has led to renewed interest in the natural material [2–10]. The push for renewable materials through researches is not unconnected to the fact that traditional materials like metals, glass, and synthetic polymer increases environmental problems [11–13]. These problems are already viewed as a disaster in waiting and if not checked properly may consume the globe. Problems associated with the usage of these traditional materials include, but not limited to; health problems, waste management issues, land degradation, groundwater contamination etc. [14–16].

To solve these problems, researchers are now focusing on materials from renewable resources. Cellulose, a semi-crystalline polycarbohydrate compound, is

S. C. Agwuncha (✉)

Department of Chemistry, Ibrahim Badamasi Babangida University,
Lapai, Nigeria

e-mail: acsjanil22@gmail.com; agwunchas@ibbu.edu.ng

C. G. Anusionwu

Department of Applied Chemistry, University of Johannesburg, Johannesburg, RSA

S. J. Owonubi

Department of Chemistry, University of Zululand, Kwadlangezwa,
Kwazulu Natal, RSA

E. R. Sadiku · I. D. Ibrahim

Department of Chemical, Metallurgical and Material Engineering,
Tshwane University of Technology, Pretoria, RSA

U. A. Busuguma

Department of Remedial Science, Ramat Polytechnic, Maiduguri, Nigeria

© Springer Nature Switzerland AG 2019

Inamuddin et al. (eds.), *Sustainable Polymer Composites and Nanocomposites*,
https://doi.org/10.1007/978-3-030-05399-4_2

the most abundant natural polymer on the earth [17–25]. It is derived from ligno-cellulosic biomass [26–29]. It is relatively available in abundance, renewable, biodegradable, eco-friendly, cost-effective and energy efficient [24, 30–32]. It is a biocompatible material obtained from plants, bacteria, algae, and animals too [25, 31–34]. It is composed of anhydroglucose units linked by chemical β -1,4-glycosidic bonds [35–38].

Basically, cellulose fibers consist of other components like lignin hemicellulose, waxes, oil, and water-soluble inorganic salts [9, 30]. However, the cellulose content remains the main component with its percentage of natural materials ranging from 45 to 90% [40, 41]. In cellulose fibers, the cellulose forms microfibrils and are surrounded by lignin and hemicellulose, which are acting as cement in the fibers. A helically cellular cellulose microfibril embedded in cementing material is formed from long-chain cellulose molecules [25, 42]. Through natural biosynthesis, it has been established that about 30–100 individual cellulose molecules come together through the chain extended conformation to form the basic unit in the cellulose fibers [43–45]. These fibers are primarily at Nano-scale [39, 46]. This chapter will be discussing the extraction and isolation of these nanoscale materials and their applications in today's world. The various extractable nanoscale materials will be referred to as cellulose nanoparticles (CNPs).

2 Nano-Scale Structure in Cellulose Fibers

Various types of Nano-scale cellulosic structures have been extracted from cellulose fibers and are classified into different groups based on their shapes, dimensions, functions and preparation methods. These also depend largely on the source of cellulose and the conditioning used in processing the nano-scale structures [3–10, 20–25]. Based on the proposed classification by the technical association of pulp and paper industry (TAPPI), the following nomenclatures are used [35, 47–53]

2.1 *Microcrystalline Cellulose*

Microcrystalline cellulose (MCC) consists of a large multi-sized aggregate of nanocrystals which are bonded to one another. The commercially available MCC have been found to have spherical or rod-like shapes with sizes ranging from 10 to 200 μm

2.2 *Cellulose Microfibrils*

Cellulose microfibrils [CMF] is said to be made up of multiple aggregates of elementary nanofibrils with width ranging between 20 and 100 nm and a length of

0.5–2.0 μm . CMF is produced via the use of intensive mechanical refinement of purified cellulose pulp [54–56]

2.3 Cellulose Nanofibrils

Cellulose nanofibers (CNF) are those parts that are made up of stretched bundles of elementary nanofibers made of alternating crystalline and amorphous domains. CNF has dimensions ranged from 20 to 50 nm for the width and 0.5 to 2 μm in length. CNF and CMF have been used interchangeably in many kinds of literature.

2.4 Cellulose Nanocrystals

Cellulose nanocrystals (CNC) are rod-like in shape. They are more rigid when compared to CNF. This may be adduced to its high crystalline nature [3, 22, 24]. CNC is also referred to as monocrystalline cellulose, nanowhiskers, nanorods or rod-like cellulose crystals. CNC can vary widely in their geometrical dimension diameter ranging from 5 to 50 nm and 100 to 500 nm in length. This is because CNC is generated by splitting the amorphous domains as well as the breaking of local crystalline contact between the nanofibers done by hydrolysis using highly concentrated acid [57–60].

2.5 Amorphous Nanocellulose

Amorphous nanocelluloses (ANC) are obtained by acid hydrolysis of regenerated cellulose followed by ultrasound is integration [61–63]. ANC particles are found to have elliptical shapes with diameters of 50–200 nm. ANC is said to exhibit high accessibility due to their porosity with its irregular pattern, enhanced sorption and thickening ability. However, it has poor mechanical property.

2.6 Cellulose Nanoyarn

Cellulose nanoyarn (CNY) is prepared by electrospinning a solution of cellulose or cellulose derivatives [64–66]. Although, knowledge and understanding of CNY are still limited to date because the study on CNY has been very low. However, the majority of the obtained CNY have diameters of 500–800 nm. CNY has low crystalline with very low thermal stability.

3 Source of Cellulose Nanofibers

The different types of nanocellulose particles that were described earlier, in the last section, are all derived from cellulose fibers. It is the mode of preparation that determines the final products. Cellulose fibers are extracted from different sources including plants, animals and bacteria. The source of the cellulose is very important because it influences the type of treatment required and by extension, the size and properties of the extracted cellulose [67–70].

Studies have shown that plant materials vary widely, and so, are the cellulose extracted from them. For example, cellulose from woods has porous antistrophic structure and exhibits a unique combination of high strength, stiffness, toughness and low density [71].

Algae are another source of cellulose. It varies in species. There are green, red, grey and brown types [72]. CMF from an algae cell wall was successfully extracted using a combination of hydrolysis and mechanical refining [4]. Although, other methods have also been used [72–75].

Tunicates are marine invertebrates. Although, research focus has largely been channelled towards Sea squirts (*Ascidiacea*) which is just one of the classes of tunicates. The tunicates produce cellulose in the outer tissue referred to as tunic. It is from the tunic that the tunicin, a fraction of cellulose is extracted [76–81].

Bacterial cellulose is produced from the primary metabolism in certain types of bacteria [7, 14]. *Gluconacetobacter xylinus* is the most widely used species for bacterial cellulose. All these are viable sources of cellulose fibres, emphasizing the bioavailability and renewability of these natural materials [6, 9, 14].

4 Extraction and Isolation of Cellulose Nanoparticle

The extraction method for CNPs can be classified into three main groups, namely mechanical, chemical and biological methods. For the purpose of this chapter, we will concentrate more on the chemical methods and procedures. However, some very important mechanical methods available will be mentioned passively. Such mechanical methods include high-pressure homogenization, microfluidization, grinding cryocrushing and ultra-sonication.

High-pressure Homogenization involves the use of force to push a suspension of the cellulose pulp through a very narrow channel using a piston, under a high pressure. It is widely used for large-scale production of CNP. However, this method is associated with problems such as high energy consumption, excessive mechanical damage to the crystalline structure of the CNP and incomplete disintegration of the pulp fibers [35].

Micro fluidization is a mechanical method that uses the application of the constant shear rate to prepare CNPs. Morphological characterization of CNPs from microfluidization showed that it produced more homogeneous size distribution than high-pressure homogenization [82]. However, both methods have similar problems.

Grinding involves the passing of the cellulose slurry through two grindstones. One static and the other rotating at approximately 1500 rpm. This helps to apply a shearing stress to the fibers to separating cellulose fiber into nano-sized particles [35].

Cryocrushing involves the freezing and subsequent crushing of water-swollen cellulose fibers using liquid nitrogen. The cryocrushed fibers are then dispersed uniformly in water using disintegrator [35].

5 Chemicals Methods

Chemical method of extraction and isolation of CNPs can be categorized into three steps. These do not involve the mechanical size reduction of the fibers. Step one involves the purification of the raw fiber material to remove the non-cellulosic components, step two involves a controlled chemical treatment to isolate nanocrystals and step three involves the use of chemical or ultrasound treatment to concentrate and dry the CNP. These steps have been summarized in the following order of chemical processes: extractives pre-alkalization, alkalization, acetylation/bleaching and acid hydrolysis [2]. Whichever theory is adopted, the same processes are involved chemically. We will take the extraction processes step by step.

Step one—removal of non-cellulosic components

This step is mostly carried out using alkali solution containing 1–5% sodium hydroxide at elevated temperature, ranging between 30 and 70 °C for 1–4 h, depending on the concentration of the NaOH Solution been used. The alkali treatment removes a certain amount of lignin, hemicellulose, wax and oil. The alkali treatment also helps in depolymerizing the native cellulose structure, defibrillating the external cellulose micro fibrils and by extension exposing the short length crystallites of the cellulose material [45].

Different authors have approached the alkalization of the raw fibers in different ways. This is due to the fact that different plant fibers contain these components in different proportions [17, 24, 26, 29, 35, 83–86]. Therefore, factors such as fiber source, plant history and weather and soil type are very important considerations. In addition, some authors have carried out pre-alkalization using ethanol and water (in the ratio of 1:1, v/v), to remove grease and oil stains on the fibers before the actual alkalization procedure. Table 1 presents different methods used by different authors to carry out the alkalization process [87–95].

Under this step, the bleaching or acetylation of the fibers is done too. The bleaching process is done to further purify the alkaline treated fibers, so as to remove the lignin and hemicellulose left to a large extent, if not completely. These components act as the cementing material in the fibers. Hemicellulose is a water-soluble polysaccharide while lignin is a complex organic compound soluble in alkali medium. Therefore, the bleaching is to improve the quality of the cellulose. Published works have shown that authors have used the different chemical

Table 1 Different methods of alkali treatments of cellulose fibers as published by different authors [24]

Sources	Chemicals/ equipment	Conditions	References
Coconut husk fibers	2 wt% NaOH solution	80 °C, 2 h, mechanical stirring, 2 times	[88]
Kenaf fibers	4 wt% NaOH solution	80 °C, 3 h, mechanical stirring, 3 times	[89]
Kenaf fibers	NaOH-AQ (anthraquinone)	Cook in a digester for 45 min at 160 °C	[90]
Kenaf fibers	12% NaOH, 0.15% AQ	Cook in a digester for 45 min at 120 °C	[91]
Rice husk	Alkali solution (4 wt % NaOH)	Reflux mixture at 120 °C for 1 h in a round bottom flask	[92]
H. sabdariffa fiber	2 wt% NaOH solution	120 °C, 1 h, 15 lbs for	[93]
Soy hull, Wheat straw	17.5% w/w NaOH solution	2 h	[94]
Wood fiber	3 wt% potassium hydroxide	80 °C, 2 h,	[95]
	6 wt% potassium hydroxide	80 °C, 2 h,	

combination to achieve the desired results [3, 6, 8, 25, 26, 31, 83, 84, 90–95]. Some have used sodium chlorite (NaClO_2), others have used hydrogen peroxide (H_2O_2), TEMP (2,2,6,6, tetramethylpiperidine-1-oxidant)

Ng et al. [24] listed some various bleaching treatments on fibers after alkalization (Table 2). This table shows that conditions can vary widely, even with the same type of chemical combination. However, bleaching is carried out by heating the alkali-treated fibers in a solution of sodium chlorite to the boiling point under acidic condition [87]. Such conditions (acidic) are created by the use of buffer which can be prepared using NaOH and acetic acid and diluted appropriately. In the presence of the acetic buffer, the NaClO_2 is broken down to form chlorine dioxide (ClO_2) leading to the liberation of chlorine dioxide throughout the duration of the bleaching. The use of H_2O_2 had improved the removal of lignin and hemicellulose. This is because H_2O_2 is able to break the linkage formed between the lignin and hemicellulose during the alkalization process which led to the ineffective removal of the lignin. The bleaching can be repeated several times to ensure the complete removal of the cementing components. The resulting white colour fiber after bleaching is an indication that the bleaching process is complete and successful. Literature has shown that the number of times the bleaching steps were repeated has a significant effect on the final properties of the CNP obtained [24]. CNP with more bleaching steps gives CNP that are slightly more thermally stable, better morphologies with higher crystallinity [88]

Table 2 Different methods used for the bleaching process of cellulose fibers [24]

Fiber sources	Chemicals requirement	Temperature/time requirements	References
Coconut	Sodium chlorite, glacial acetic acid	60–70 °C, 1 h, mechanical stirring, 1 and 4 times	[88]
Kenaf	2% NaClO ₂ and 3% acetic acid	70 °C, 180 min	[90]
	1.5% NaOH and 1% H ₂ O ₂	70 °C, 90 min	
	1.25% NaClO ₂ and 3% acetic acid	70 °C, 90 min,	
Kenaf	2% NaClO ₂ and 3% acetic acid	70 °C, 90 min	[91]
	1.2% NaOCl	25 °C, 60 min	
Rice husk	Acetic acidic buffer, aqueous 1.7 wt% NaClO ₂ and distilled water	Reflux in a silicon oil bath at 100–130 °C for 4 h, four times	[92]
H. <i>sabdariffa</i>	A solution of NaOH/acetic acid/sodium hypochlorite mixture	25 °C, one hour	[93]
Wood	Acidified aqueous NaClO ₂	75 °C, 1 h, 5 times	[95]

Step two—Isolation of CNP

After the alkali and bleaching processes, the new material obtained is referred to as cellulose fibrils (CF). The CF has improved crystalline structures that appeared to be very compact in the nanocrystal form and kept in hydrogen bond interaction among cellulose chains adjacent to each other. The cellulose crystals as a whole are bonded together by the presence of disordered amorphous sections which exhibit imperfect orientation along the axis (as shown in Fig. 1). Therefore, to obtain an isolate with high crystallinity and purity CNP, the disordered amorphous region has to be removed selectively. This is done by the use of chemical and mechanical methods. For the chemical methods, the most common method adopted is the acidic hydrolysis [87, 91, 95, 96]

The acidic hydrolysis method is a very convenient process that has been used in time past and is still being used to obtain single and well-defined cellulose nanocrystals (CNC). The acid attacks the amorphous region preferentially, leaving the crystalline region insoluble [24, 35, 93, 97]. However as reported by some author, the conditions of the acid hydrolysis, may determine to a large extent the properties of the final CNC obtained. These conditions include time, temperature and concentration of the acidic reagents. Table 3 listed some of the commonly used chemicals that have been employed to carry out this hydrolysis process [94, 98–101]. Chemically speaking, by subjecting the bleached cellulose fibrils to the concentrated acid solution, the hydronium ions attacked the oxygen on the glycoside bonds between the two anhydroglucose units through the amorphous region which is seen as structural defects. Hence, a hydrolytic cleavage of the glycosidic bond along the amorphous chain [94, 102]. Also, the glycosidic bond can be cleaved away from the oxygen element. This is followed by two anhydroglucose units of separation and splitting into fragments of shorter chains [90, 97]. The H₂SO₄ acid solution is most preferred because it forms charged stable crystallites that remain intact and can be easily isolated. If HCl acid solution is used the uncharged CNP

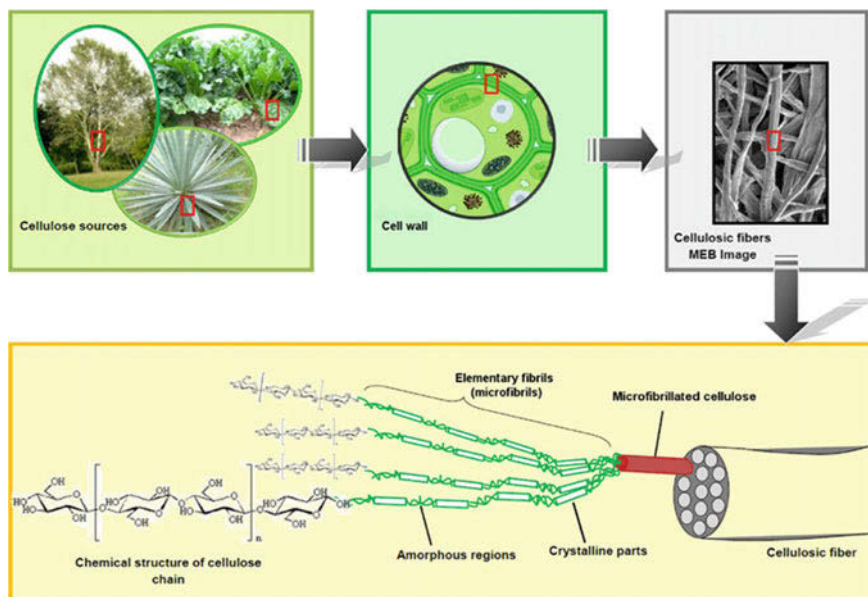


Fig. 1 Schematic diagram emphasizing the sources of cellulose fibers and the nanostructural arrangement of their unit molecules [39]

tend to flocculate in aqueous dispersion making it difficult to isolate from the acidic solution. For H_2SO_4 , it reacts with surface hydroxyl groups leading to the formation of the negatively large sulfonic group [103–111]. The condition used for the acidic hydrolysis vary widely and depends largely on the precursors. Ng et al. [24] listed some acidic hydrolysis methods with the condition used by various authors shown in Table 3.

Step three—Mechanical Dialysis and Drying of Isolated CNPs

This stage involves the concentration, isolation and drying of the CNPs obtained from the acid hydrolysis process. Once the hydrolysis process is assumed to be completed, the process needs to be rapidly stopped. Many authors have applied a different method to achieve this objective at this stage. No matter the method employed or condition used, the most important thing here, is to recover most CNP isolated. So authors have argued that hydrolysis alone may not give CNP of uniform sizes. Therefore, additional step mechanical agitation or homogenization may be used to improve uniformity in size [115–117]. To stop the hydrolysis reaction, a large quantity of water or iceberg is added to the reaction to stop any further reaction on the cellulose. Then the solution formed is centrifuge repeated to remove the acidic solution and isolate the CNPs. This is done repeatedly until the supernatant becomes turbid. The supernatant is then homogenized using homogenizer or micro-fluidizer or microfluidics. The aggregate CNPs can also be homogenized using mechanical shearing. However, removing water from the CNP suspensions is

Table 3 Selected procedure used for acid hydrolysis of cellulose nanoparticles isolation [24]

Fiber sources	Chemicals/equipment	Conditions	References
Cotton	47% H ₂ SO ₄ solutions	60 °C, 2 h, strong agitation	[98]
	64–65% (w/w) H ₂ SO ₄ solutions	10 mL/g cellulose at 45 °C for 1 h,	[102]
	Conc HCl	20 mL/g cellulose at 45 °C for 1 h	[112]
Kenaf	30% H ₂ SO ₄ solutions	80 °C, 4 h, with strong agitation	[101]
	65% H ₂ SO ₄ solutions (preheated)	50 °C, 60 min, constantly mixing using magnetic stirring	[113]
	2.5 M HCl solution	105 °C, 20 min, stirring	[113]
Corn-cob	9.17 M H ₂ SO ₄ solutions 15 mL of H ₂ SO ₄ solutions per grams of fibers,	45 °C, 60 min	[114]
<i>H. sabdariffa</i> fiber	Oxalic acid	3 h in an autoclave at 20 lbs	[94]
Coconut husk fiber	HNO ₃ (0.05 N nitric acid solution)	70 °C for 1 h	[88]
	Concentrated sulfuric acid solution (64 wt%)	10 mL/g cellulose at 45 °C for 120, 150, and 180 min	
Rice husk	10.0 mol L ⁻¹ of sulfuric acid (pre-heated)	strong agitation with a fibre content of 4–6 wt% at 50 °C for 40 min	[93]
<i>L. cylindrica</i>	65 wt% sulfuric acid (pre-heated)	mechanical agitation at 50 °C for 40 min	[115]

a delicate process. Therefore, drying the aqueous suspensions and understanding the drying process is highly necessary. The major drying process include

- (i) oven drying
- (ii) freeze drying
- (iii) supercritical drying and
- (iv) spray drying [24, 118, 119]

In summary, the process of extracting CNPs from cellulose can be given in the following steps as below and as exemplified in Fig. 2:

- i. reduction of the cellulose fiber size into 2–5 mm by suitable mechanical process
- ii. alkalization of the chopped fibers using alkaline solution which may be repeated as desired
- iii. bleaching of the alkaline treated fibrils, this process may be repeated as desired
- iv. acid hydrolysis of the bleached fibrils to isolate CNPs
- v. mechanical centrifuge of an acid solution containing the isolated CNPs
- vi. drying of the isolated CNPs

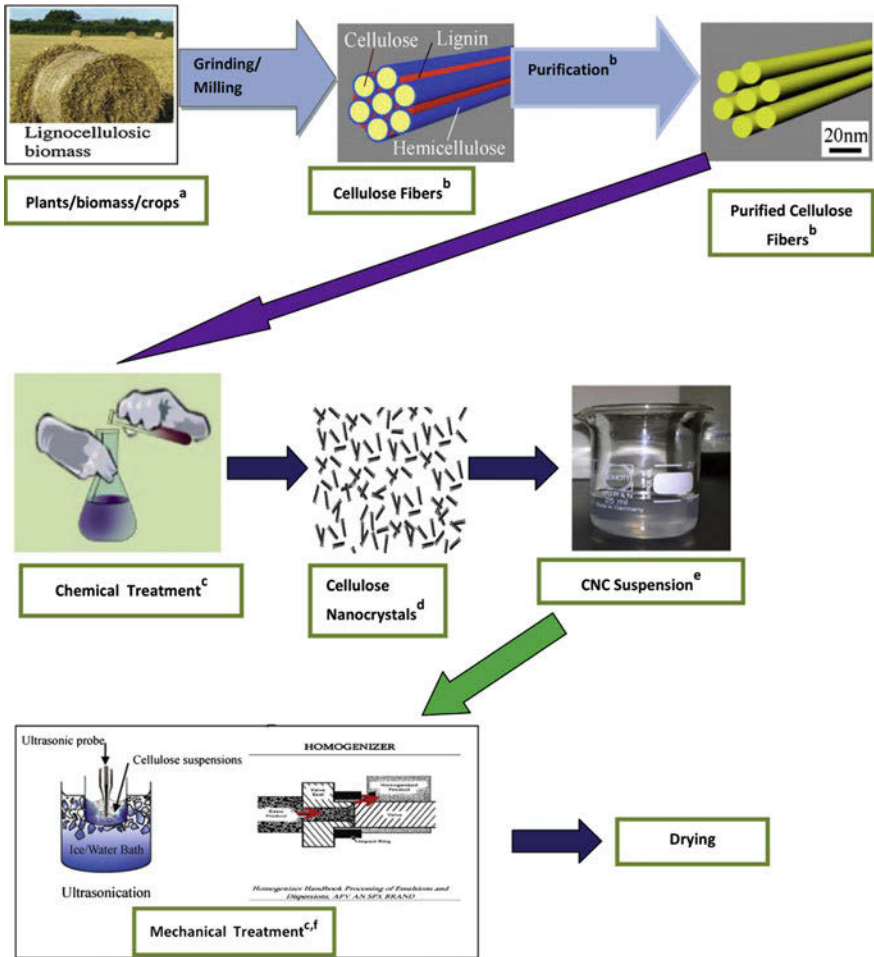


Fig. 2 Schematic diagram showing the main steps in the isolation of CNPs [24]

Feng et al. [83] extracted cellulose nanofibrils from sugarcane bagasse (SCB) and described the method used as environmentally friendly. According to their work, the SCB fibers were treated in a laboratory designed continuous steam explosion extruder [83]. 5 kg of the SCB was wetted with deionized water until the moisture content reached 45% before being transferred to the steam explosion extruder where it was treated four times at 120–130 °C temperature and 1.1–1.5 MPa pressure and then allowed to dry in air. This step was followed by alkali-catalyzed hydrothermal treatment and bleaching with H₂O₂ at 80 °C for 3 h. The bleached fibers were separated, the washed unit it attains pH ≈ 7 before it was freeze dried. The freeze-dried bleached fibers were further blended to disintegrate the nanofibrils. This was done by first forming a suspension of the freeze-dried fiber and then blended using a blender at 4800 rpm for 5 min. The suspension is then treated with

ultra-sonication in an ice/water bath for 40 min. From the SEM and TEM results obtained, the morphology of the nanofibrils showed uniform diameters, although the CNPs were slightly agglomerate due to the presence of hydrogen bonding on the surface of the CNPs. Also, the thermal analysis showed that the CNP prepared had improved the thermal stability of about 14% increase. They concluded that dilute solution of NaOH at 200 °C elevated temperature was able to remove most, if not all, of the hemicellulose and destroyed the structure of the lignin. The CNPs was obtained with the high-speed dispersion coupled with ultra-sonication. This method completely eliminated the acid hydrolysis step and still gave CNF of uniform diameter.

Neto et al. [120] extracted CNPs from agro-industrial waste using Soya hulls. In their work, the soya hulls were first treated with a diluted solution of NaOH for 4 h at 100 °C under mechanical stirring the treated fiber was washed to remove the alkali solution completely and then dried at 50 °C for 12 h. The alkali treated fibers were then bleached using acetate buffer (prepared with 27 g NaOH and 75 ml glacial acetic acid and diluted to 1L) and sodium chlorite. The bleaching was carried out at 80 °C for 4 h. At the end process, the fibers were washed until it was neutral and then dried at 50 °C. CNPs isolation was done by first blending the bleached fibers and sieved through a 35-mesh before the acid hydrolysis step. The hydrolysis was performed at 40 °C for 30 min under vigorous and constant stirring. On completion, the mixture was diluted with cold water to 10-fold. This is to stop the reaction, then the diluted mixture is centrifuged twice for 10 min at 7000 rpm to remove the excess acid and the precipitated was dialyzed until it is neutral (pH \approx 5–7). Subsequently, the resulting suspension was treated using a disperser for 5 min at 20,000 rpm and sonicated for 5 min before the colloidal suspension was stored in the refrigerator at 4 °C with the addition of some drop of chloroform. From their results, they concluded that the extraction process gave stable CNPs with a high content of cellulose and fairly uniform diameter and aspect ratio.

In other work, Nascimento and Rezende [13] used a combined approach to obtain cellulose nanocrystals (CNC) and nanofibrils (CNF) from elephant grass. Their methods involved repeated alkali and bleaching treatment on the same fibers and using a different concentration of reagents. Furthermore, the isolation temperature, using 60% (w/w) H₂SO₄ solution, was varied from 20 to 60 °C with a 1:30 (g/cm³) fiber to solution ratio. The results showed that the amount of CNPs obtained decreased as the number of repetition is increased. Also, as the concentration of the chemical reagent was increased, the CNP yield decreases. Furthermore, the extraction time of 20 min was grossly inadequate to isolate the CNP. This is because in all the reagent combination used, none was able to isolate CNP within 20 min. However, with a minimum of 40 min, CNP was isolated. This is dependent on other parameters such as concentration and reagent mixture.

Whether the solution is a concentrated or diluted alkali or acidic solution, the issue of environmental pollution is always there. Therefore, some authors have tagged the use of steam explosion as a green method that is more environmentally friendly [36, 37, 43, 83, 121–125]. In these cases, the fibers were placed in a reactor (e.g. autoclave) at high pressure and temperature of 20 lb and 110 °C respectively

for 1 h. Most fibers treated with steam explosion are bleached with a combination of NaOH/acetic acid and sodium hypochlorite solutions [43]. The attempt to avoid the use of chlorite (NaClO_2) is due to health and safety concerns.

Many of the focus in cellulose nanocrystal extraction are targeting nonwoody plants such as sugarcane [13, sugar palm [19], rice husk [50], sisal [126–128]. However, the extraction process still remains the same since the extraction process is all about the removal of lignin (i.e. delignification), hemicellulose and all another non-cellulose component.

6 Applications of CNPs

CNPs have unique properties that are very useful to man. Properties like low density, large surface area, high stiffness and crystallinity, high aspect ratio, biocompatibility, biodegradability and renewability [127]. These properties have enabled its application in many industries including medicals, pharmaceuticals, packaging, water treatment, built and construction, and many others [40, 128, 129].

7 Medicals

So many medicals devices are now manufactured using polymer blends, composites and nanocomposites. Some two decades ago, these devices were prepared using only polymer materials. However, the health and environmental risk associated with this practice have necessitated the development of more health and environmentally friendly material. Research has shown that compounding the polymer blends has made these devices, not only environmentally friendly but also biocompatible and biodegradable [22, 26, 40].

Different types of medical devices have been made possible with the use of cellulose nanocrystals. Achaby et al. [26] compounded some selected biopolymers, namely chitosan, alginates and K-carrageenan, with CNC to evaluate their effect on the tensile properties of the polymer film. Although the selected polymers are considered as water-soluble polysaccharides, hence their treatment with water is made easier. Also, CNC hydrolyzed with sulfuric acid has free OH^- and anionic sulfate groups on their surfaces. This made the CNC highly dispersible nanomaterial in water. The compatibility between CNC and biopolymers makes the CNC dispersity in the biopolymer uniform [26]. Therefore, films of CNC and biopolymers such as chitosan, alginates and K-carrageenan can be prepared more easily, if all conditions are controlled. In their work, Achaby et al. [26], utilized their properties to prepare a film of CNC and their biopolymer. The CNC-biopolymer composites were found to have smooth faces and good flexibility.

Biopolymer-based composite films are usually known to have low tensile properties. This has limited their possible applications. These drawbacks have been

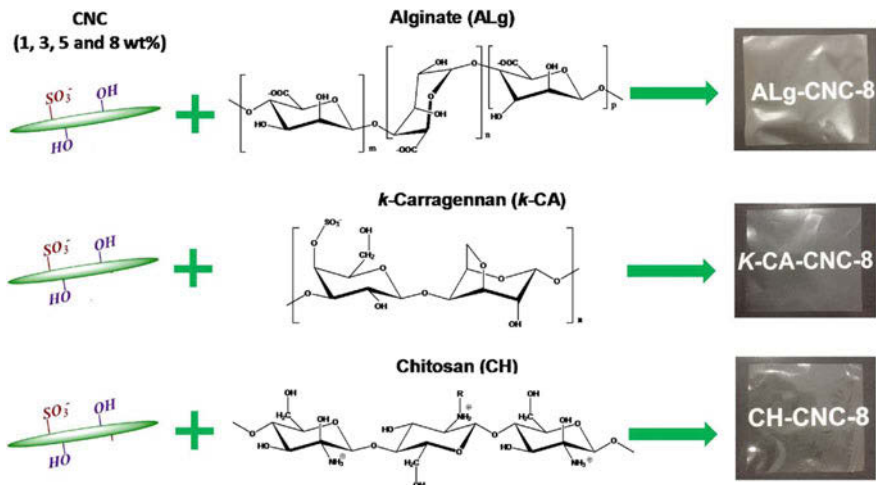


Fig. 3 A schematic representation of nanocomposite films based on CNC as nanofillers and alginate, k-carrageenan and chitosan biopolymer materials [26]

overcome with the compounding of the biopolymers using CNCs as shown by the number of literature on this issue [123–126, 130]. CNC has been reported to have a significantly reinforcing impact on the mechanical properties of the biopolymer. Figure 3 shows samples of films prepared by compounding chitosan, alginate and K-carrageenan with CNC intended for medical applications. This was made possible due to their relatively high aspect ratio and elastic modulus. Base on the application of CNC various medical devices are fabricated using biopolymer-based nanocomposites. For example screen and pin for orthopaedic surgery [131], a scaffold for tissue engineering [35] and many more.

8 Drug Delivery Systems

Drug delivery is a modern technology in which drugs are loaded on special materials and when administrated, are made to gradually release the drug depending on the design condition. Drug delivery system improves the bioavailability of the drug, preventing premature degradation, enhancing uptake, maintain drug concentration and reduce the side effect by treating disease site target cell [132–135]. The uploading of the drugs can be physical if it was just absorbed by the material or chemical if there was any chemical bond formed. Many of the drug delivery materials are pre-design to have these properties for specific target [132, 133]. One of the properties of these materials is hydrophilicity and ability to chemically modify the surface of the selected materials. Cellulose nanocrystals have been found to meet all these requirements.

CNC are hydrophilic materials that are rich in OH groups on their surface. They can be chemically modified with ease and still maintain their biodegradability (50, 34, 36, 22, 41, (1)). The CNC is able to bind and release water-solution molecules through ionic interaction and this enables them to act as drug delivery materials [32, 136–138]. Below are some reported applications of CNCs in drug delivery and release technology.

According to [139], who studied the chemically conjugated molecules to CNCs through the covalent and noncovalent bond, so as to functionalize the CNC. Tetracycline and doxorubicin which are both water soluble and ionizable drugs were found to have bound significantly in large amount to functionalized CNCs and were also released within a period of one day.

Furthermore, cetyl trimethyl ammonium bromide (CTAB) was used to functionalize the surface of CNC in order to make the material more hydrophobic. This led to an increase in the Zeta potential value of the CNC functionalized material (i.e. from -55 to 0 mv). The functionalized CNC were found to bound large quantities of some anticancer drugs namely docetaxel paclitaxel and etoposide. These drugs are hydrophobic and were found to be released in a regular pattern for a period of two days [139].

CTAB was also used to modify the surface of torispherical CNCs. This was to improve the loading capacity for anti-cancer drugs that are water insoluble such as Luteolin and luteoside [140]. CTAB is commonly used in conjugating nanomaterials in order to improve the hydrophobicity which will eventually lead to improving loading of hydrophobic drugs such as most anticancer drugs [141]. However, this method should be used with caution as it has been shown that CTAB can interact with the phospholipid bilayers of cells [32].

Again, CNCs was modified using cationic porphyrin (por) by [142]. This interesting conjugation which forms suspended particles in aqueous systems was found to be very effective for photodynamic inactivation of staphylococcus aureus and mycobacteriumsmegmatis. However, it showed discrete activity against Escherichia coli. In addition, [143] showed that CNC-Por was also very effective on microorganisms such as Acinetobacterbaumannii.

Curcumin (CUR), an anticancer drug for treating prostate cancer was conjugated to CNC (CNC-CUR) [144]. This particle which was found to be in the nanosize range (5.2 nm) showed a high level of cellular uptake. This led to a maximum ultrastructural change on apoptosis. When the CNC-CUR was compared to the efficacy of CUR alone, The CNC-CUR drug showed increased efficacy in its anticancer activity better than the free CUR. The results obtained showed that conjugating CUR with CNCs improved the drug's availability and also its suitability for the treatment of prostate cancer [144].

Also, [145] described a similar approach for the preparation of drug carrier nanosize CNC for animated biologically active molecules and drugs. A spacer molecule (gamma-aminobutyric acid) was grafted on CNCs through periodate oxidation and Schiff base condensation reaction. However, due to fast releases of the targeting moiety, syringyl alcohol (a releasable linker) was attached to CNC to help control the release to the targeting moiety.

Furthermore, [146] carried out three-step covalent binding procedures that convert CNC into fluorescent labelling nanoparticles. The fluorescent labelling nanoparticles were prepared by conjugating CNC with pyrene (Py-CNC). The prepared nanomaterial was found to be highly selective toward Fe^{3+} . Based on the selectivity, it was suggested that the material might be useful as a chemosensor for Fe^{3+} for applications in chemical, biological and ecological systems. [147] prepared water-soluble photosensitizer-CNC (PS-CNC) by combining CNC with polyaminated chlorine p6. This improved greatly the cancer cell targeting potential of the drug, indicating possible biomedical applications. Subsequently [148], used Chitosan polysaccharide to react with CNC that was modified using TEMPO. This modification helps introduced carboxyl moieties on the CNC surface.

In a review by [138], it was reported that 5-(4,6-dichlorotriazinyl) aminofluorescein (DTAF) was grafted onto cotton-derived CNCs (DTAF-CNCs). This helped to create different charge densities on the surface of the CNC. These Charges influenced the labelling efficacy which was observed to be within nmol/g range. Although, the amount of DTAF bound to the CNCs was found to depend on the surface charge density the amount increases with decreased charge density.

Folic acid (FA) link to CNCs drug delivery system which was observed in an in vitro experiment to have good mediated uptake by rat brain tumour was prepared by [149].

Tosufloxacin osylate (TFLX) was covalently attached to maleate-modified CNC (MA-CNC) surface to prepare a prodrug using L-leucine as a spacer molecule [150]. The investigation was conducted to evaluate the release behaviour in stimulated fluids of the colon, gastric and intestine. Based on the results obtained, the MA-CNC was effective in entrapping the drug with very good release behaviour for colon specificity. Although more research may be required in this area, the MA-CNC has shown good properties for it to be used as a drug delivery system for a colon-treatment.

In all the examples provided above, it can be said that CNPs are finding good application in medicine and medical related fields. The drug delivery system is one of such active area that a lot of researches are ongoing. However, a lot of caution is required at the moment. Many of the drug-related researches are on cancer, HIV/AIDS, tuberculosis and diabetes [151]. Therefore, there is still a lot to be done. The good news here is that it is possible with the right commitment.

9 Industrial Application

Functionalized CNPs have been utilized greatly in the area of filtration for water treatment. Water treatment goal is to improve the aesthetic qualities of domestic and industrial water. Contaminants can be organic or inorganic particulate matters [152, 153]. However, molecular pollutants have defiled the traditional methods of filtration. Hence, the introduction of functionalized materials that can interact chemically with the contaminants at molecular level becomes very important [12, 18].

This method has been used for the removal of organic persistent pollutants. Today domestic water filtration systems are fitted with candles made of functionalized CNPs composites that can remove organic pollutants as well as heavy metals (Fig. 4ai, aii). Also, industrial water treatment system has filtration column too that are packed with nanocellulose materials, functionalized to remove chemicals impurities (Fig. 4b). The presence of OH group on the surface of cellulose nanocrystals has made it possible to modify the CNPs for different functionality [152–154].

Zhang et al. [31] prepared cellulose beads (CBs) with the amino functional group and porous structure for the removal of the active ingredient by adsorption as a new application for nanocellulose particles. The CBs were prepared by the inverse suspension, coupled with a water-in-oil thermal regeneration method. The CBs were then modified using epichlorohydrin, diethylenetriamine and triethylenetetramine. The CBs and modified CBs (MCBs) were then used for adsorption of hyperin (Hy) and 2-o-galloylhyperin (Ga), the active ingredient of pyrola (*pyrola incarnata*), a medicinal plant that is traditional to China. The adsorption capacity of the MCBs and ten other commercial resins for Hy and Ga were investigated. From the results obtained, the adsorption capacities of the MCBs were much higher than all the commercial resins. The investigation showed that some of the MCBs had adsorption capacity that were three times higher when compared to the commercial resins. Based on their explanation, the effective interaction between the MCBs and the active ingredient were due to the ability to form chemical bonds such as van de

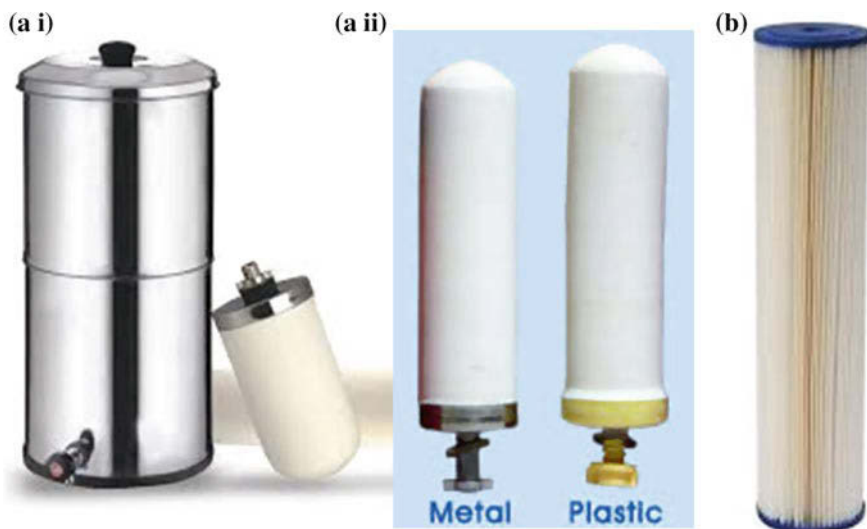


Fig. 4 Typical examples of candles (ai and aii) and column (b) for domestic and industrial water filtration respectively, researched are on-going to replace these materials with nanocellulose composites [155–157]. Image source: Adapted from google image

Waal forces, hydrogen bonding and electrostatic interactions. Furthermore, the 3D porous structure of the MCBs enhanced the surface area significantly, thereby, providing more sites for adsorption of the active compounds [158–161].

Application of CNPs as adsorption material has aroused interest due to multiple hydroxyl functionalities on the surface of the nanocellulose. These sites offer many active sites for chemical modification. Based on this, CNPs materials have been successfully used in various fields [31]. In recent time, cellulose have been modified with alkenes [162, 163], Oxiranes [164], Amines [165] and carbonyls [166, 167]. Such modification has improved the adsorption efficiencies and physical stability of the CNPs. Reported works have shown that these modified CNPs have been successfully applied to the adsorption of metal ions [168, 169] and organic compounds [170, 171].

10 Preparation of Polymer Composites

The compounding of polymers, either neat or blends of polymers, with CNPs has helped to diversify their possible application. Many polymer materials suffer from water permeability limitation. Some polymers suffer from poor mechanical and thermal properties [172]. However, the addition of CNPs to such polymeric matrix as the filter has helped improved the wettability, or water permeability, mechanical properties (Youngs modulus and impact strength) and thermal stability.

Furthermore, the compounding of polymer with CNPs filters has been shown to improve the degradability of the polymers [30, 36, 55], thereby increasing the possibility of wider applications with little fear of environmental pollution issues. In the building and construction industry concrete waste generated pose a serious disposal problem. However, the substitution of the concrete with biodegradables composites has greatly reduced the problem [173]. This is because many biodegradable composites can either be reused, recycled or compose as manure on farmland.

The aspect ratio for these CNPs has led to improved mechanical properties [88, 129]. The surface area, which is in range of nano, has been reported to be responsible for the improvement in the mechanical properties of the composites. However, the compounding of the polymer matrixes with CNP fillers have conferred on the composites many other properties including oxygen permeability, water absorption and permeability, wettability, e.t.c [7, 14, 17, 20, 24, 25]

10.1 Packaging

The formation of films and preparation of composites using CNPs has revolutionized the packaging industry. The problems of the packaging industry in the past include waste management and environmental pollution [30, 32, 173]. The polymer

materials in use then do not undergo degradation easily. Therefore their disposal becomes a serious issue. However, the replacement of these materials with the ones prepared using cellulose fiber extracts, especially CNPs, has solved many of the associated problems [1, 2, 24, 25].

CNP films and composites are applied in different packaging industries. These include (i) film for food and fruit wrapping, which also improve the shelf life of the food items; (ii) multi-layer functionalized packaging items for food extracts like juice extract; (iii) easy-to-serve or take-away pack used in fast food centers and shopping malls; (iv) drug and medical packages.

Nanopaper structure is one of the important applications of MFC suspension which are mainly converted films of MFC [174]. Cellulose gels which are also obtained from MFC can be converted into a film by different methods. Among them are casting method and vacuum filtration. The removal of the water content of the MFC gel leads to the formation of a cellulose nanofiber network. This is made possible because of the inter-fibrillar hydrogen bond formed inside the material. The process involved in the film formation and the quality of MFC used will greatly affect the quality of the film produced. A number of these processes have been developed in order to obtain more uniform films from the MFC. Films prepared by the vacuum filtration method have been observed to have a thickness which varies widely from 60 to 80 μm . However, using the dynamic sheet former, films with homogenous thickness have been obtained [175, 176]. The method is said to be fast and leads to the formation of highly transparent films if the appropriate instrument is used. Solvent exchange process has also been used to prepare a film of good qualities. Such films have displayed porosities of varying thickness ranging between 70 and 90 μm [174]. Other methods used in the preparation of MFC film is the spraying or the classical solvent casting method [177–180]. In all these methods, the concentration of the MFC in the solvents is left below 1 wt%. In whichever method is employed, the objective is to remove the solvent in a controlled manner that combines different conditions of temperature, relative humidity and time. This process often last for 2 h regardless of the method used [181, 182].

10.2 Emulsifiers and Solvent Thickner

CNPs are been used as emulsifiers for so many products these days [179]. CNPs have been used in the preparation of products like paints, liquid detergents and many more [109]. The neutral nature of the CNPs has made their utilization for these purposes very possible. Also, CNPs forms a stable colloid when dissolved in water or suitable solvents. Although, this may depend on the process by which the CNPs were prepared.

11 Conclusion

Cellulose is the most common natural raw material available on earth with a biosynthesis production of 10^{11} – 10^{12} tons per year. It has many benefits which include low cost, lightweight, renewable, biodegradable and environmentally friendly. They can be extracted from plants and animals. The extraction and isolation of cellulose nanoparticles (CNPs) from cellulose fibers has led to the discovery of these new renewable, biocompatible, biodegradable, nanosize materials of different kinds and shapes. The processes used in the isolation determine the final properties of these materials. The processes can be categorized as follows: fiber size reduction, alkalization, bleaching, hydrolysis and mechanical isolation. The extraction of nanocellulose particles has led to the isolation of such materials as cellulose nanocrystals, cellulose nanofibrils (CNF) and cellulose microfibrils (CMF). These nanosize materials have different shapes which also affect their chemical properties. In recent time, the CNPs have found very useful applications in our society. They are used as fillers for composites preparation, film formation, biomedical and industrial materials.

References

1. Lee HR, Kim K, Mun SC, Chang YK, Choi SQ (2018) A new method to produce cellulose nanofibrils from microalgae and the measurement of their mechanical strength. *Carbohydr Polym* 180:276–285
2. Mondragon G, Fernandes S, Retegi A, Pena C, Algar I, Eceiza A, Arbelaiz A (2014) A common strategy to extracting cellulose nanoentities from different plants. *Ind Crops Prod* 55:140–148
3. Liu Z, Li X, Xie W, Deng H (2017) Extraction, isolation and characterization of nanocrystalline cellulose from industrial kelp (*Laminaria japonica*) waste. *Carbohydr Polym* 173:353–359
4. Wang M, Bi W, Huang X, Chen DDY (2016) Ball mill assisted rapid mechanochemical extraction method for natural products from plants. *J Chromatogr A* 1449:8–16
5. Ling Z, Zhang X, Yang G, Takabe K, Xu F (2018) Nanocrystals of cellulose allomorphs have different adsorption of cellulase and subsequent degradation. *Ind Crops Prod* 112:541–549
6. Robles E, Fernández-Rodríguez J, Barbosa AM, Gordobil O, Carreno NLV, Labidi J (2018) Production of cellulose nanoparticles from blue agave waste treated with environmentally friendly processes. *Carbohydr Polym*. Available online 6 Jan 2018. ISSN 0144-8617
7. Das AM, Hazarika MP, Goswami M, Yadav A, Khound P (2016) Extraction of cellulose from agricultural waste using Montmorillonite K-10/LiOH and its conversion to renewable energy: Biofuel by using *Myrothecium gramineum*. *Carbohydr Polym* 141:20–27
8. Guerrero LC, Guzmán SS, Mendoza JS, Flores CA, Camacho OP (2018) Eco-friendly isolation of cellulose nanoplatelets through oxidation under mild conditions. *Carbohydr Polym* 181:642–649
9. Manzato L, Rabelo LCA, de Souza SM, da Silva CG, Sanches EA, Rabelo D, Mariuba LAM, Simonsen J (2017) New approach for extraction of cellulose from *tucumã's* endocarp and its structural characterization. *J Mol Struct* 1143:229–234

10. Liu L, Ju M, Li W, Jiang Y (2014) Cellulose extraction from *Zoysia japonica* pretreated by alumina-doped MgO in AMIMCl. *Carbohydr Polym* 113:1–8
11. Harini K, Mohan CC, Ramya K, Karthikeyan K, Sukumar M (2018) Effect of *Punica granatum* peel extracts on antimicrobial properties in Walnut shell cellulose reinforced Bio-thermoplastic starch films from cashew nut shells. *Carbohydr Polym* 184:231–242
12. Bali G, Khunsupat R, Akinosho H, Payyavula RS, Samuel R, Tuskan GA, Kalluri UC, Ragauskas AJ (2016) Characterization of cellulose structure of *Populus* plants modified in candidate cellulose biosynthesis genes. *Biomass Bioenerg* 94:146–154
13. Nascimento SA, Rezende CA (2018) Combined approaches to obtain cellulose nanocrystals, nanofibrils and fermentable sugars from elephant grass. *Carbohydr Polym* 180:38–45
14. Faruk O, Bledzki AK, Fink HP (2012) Biocomposites reinforced with natural fibers: 2000–2010. *Prog Polym Sci* 37:1552–1596
15. Dufresne A (2013) Nanocellulose: a new ageless bionanomaterial. *Mater Today* 16(6): 220–227
16. Rezende CA, de Lima MA, Maziero P, de Azevedo ER, Garcia W, Polikarpov I (2011) Chemical and morphological characterization of sugarcane bagasse submitted to a delignification process for enhanced enzymatic digestibility. *Biotechnol Biofuels* 4:54
17. Wang Z, Yao Z, Zhou J, Zhang J (2017) Reuse of waste cotton cloth for the extraction of cellulose nanocrystals. *Carbohydr Polym* 157:945–952
18. Luo J, Semenikhin N, Chang H, Moon RJ, Kumar S (2018) Post-sulfonation of cellulose nanofibrils with a one-step reaction to improve dispersibility. *Carbohydr Polym* 181:247–255
19. Ilyas RA, Sapuan SM, Ishak MR (2018) Isolation and characterization of nanocrystalline cellulose from sugar palm fibres (*Arenga Pinnata*). *Carbohydr Polym* 181:1038–1051
20. Xu S, Hossain MM, Lau BBY, To TQ, Rawal R, Aldous L (2017) Total quantification and extraction of shikimic acid from star anise (*Illicium verum*) using solid-state NMR and cellulose-dissolving aqueous hydroxide solutions. *Sustain Chem Pharm* 5:115–121
21. Smyth M, Garcia A, Rader C, Foster EJ, Bras J (2017) Extraction and process analysis of high aspect ratio cellulose nanocrystals from corn (*Zea mays*) agricultural residue. *Ind Crops Prod* 108:257–266
22. Ilangovan M, Guna V, Hu C, Nagananda GS, Reddy N (2018) *Curcuma longa* L. plant residue as a source for natural cellulose fibers with antimicrobial activity. *Ind Crops Prod* 112:556–560
23. Alila S, Besbes I, Vilar MR, Mutje P, Boufi S (2013) Non-woody plants as raw materials for production of microfibrillated cellulose (MFC): a comparative study. *Ind Crops Prod* 41:250–259
24. Ng HM, Sin LT, Tee TT, Bee ST, Hui D, Low CY, Rahmat AR (2015) Extraction of cellulose nanocrystals from plant sources for application as reinforcing agent in polymers. *Compos B Eng* 75:176–200
25. Zhang K, Sun P, Liu H, Shang S, Song J, Wang D (2016) Extraction and comparison of carboxylated cellulose nanocrystals from bleached sugarcane bagasse pulp using two different oxidation methods. *Carbohydr Polym* 138:237–243
26. El Achaby M, Kassab Z, Barakat A, Aboulkas A (2018) Alfa fibers as viable sustainable source for cellulose nanocrystals extraction: Application for improving the tensile properties of biopolymer nanocomposite films. *Ind Crops Prod* 112:499–510
27. Chien CH, Zhou C, Wei HC, Sing SY, Theodore A, Wu CY, Hsu YM, Birky B (2018) Feasibility test of cellulose filter for collection of sulfuric acid mists. *Sep Purif Technol* 195:398–403
28. Vinayaka DL, Guna V, Madhavi D, Arpitha M, Reddy N (2017) *Ricinus communis* plant residues as a source for natural cellulose fibers potentially exploitable in polymer composites. *Ind Crops Prod* 100:126–131
29. Sobolciak P, Tanvir A, Popelka A, Moffat J, Mahmoud KA, Krupa I (2017) The preparation, properties and applications of electrospun co-polyamide 6,12 membranes modified by cellulose nanocrystals. *Mater Des* 132:314–323

30. Khoathane MC, Sadiku ER, Agwuncha SC (2015) Chapter 14—Surface modification of natural fiber composites and their potential applications. In: Thakur VK, Singha AS (eds) *Surface modification of biopolymers*. Wiley, USA, pp 370–400
31. Zhang DY, Zhang N, Song P, Hao JY, Wan Y, Yao XH, Chen T, Li L (2018) Functionalized cellulose beads with three dimensional porous structure for rapid adsorption of active constituents from *Pyrola incarnate*. *Carbohydr Polym* 181:560–569
32. Seabra AB, Bernardes JS, Fávoro WJ, Paula AJ, Durán N (2018) Cellulose nanocrystals as carriers in medicine and their toxicities: a review. *Carbohydr Polym* 181:514–527
33. Moon RJ, Martini A, Nairn J, Simonsen J, Youngblood J (2011) Cellulose nanomaterials review: structure, properties and nanocomposites. *Chem Soc Rev* 40(7):3941–3994
34. Tingaut P, Zimmermann T, Sebe G (2012) Cellulose nanocrystals and microfibrillated cellulose as building blocks for the design of hierarchical functional materials. *J Mater Chem* 22(38):20105–20111
35. Kargarzadeh H, Loelovich M, Ahmad I, Thomas S, Dufresne A (2017) Methods for extraction of nanocellulose from various sources. In: Kargarzadeh H, Ahmad I, Thomas S, Dufresne A (eds) *Handbook of nanocellulose and cellulose nano composite*, 1st edn. Wiley VCH
36. Nascimento DM, Almeida JS, Dias AF, Figueirêdo MCB, Morais JPS, Feitosa JPA, Rosa MF (2014) A novel green approach for the preparation of cellulose nanowhiskers from white coir. *Carbohydr Polym* 110(2014):456–463
37. Deepa B, Abraham E, Cherian BM, Bismarck A, Blaker JJ, Pothan LA, Leao AL, de Souza SF, Kottaisamy M (2011) Structure, morphology and thermal characteristics of banana nano fibers obtained by steam explosion. *Biores Technol* 102(2011):1988–1997
38. Lin J, Miao X, Zhang X, Bian F (2017) Controllable generation of renewable nanofibrils from green materials and their application in nanocomposites. In: Thakur VK, Thakur MK, Kessler MR (eds) *Handbook of composites from renewable materials*. Wiley-Scrivener publishing, 8, pp 61–102
39. Lavoine N, Desloges I, Dufresne A, Bras J (2012) Microfibrillated cellulose—its barrier properties and applications in cellulosic materials: a review. *Carbohydr Polym* 90(2):735–764
40. Cherian BM, Leao AL, de Souza SF, Costa LMM, de Olyveira GM, Kottaisamy M, Nagarajan ER, Thomas S (2011) Cellulose nanocomposites with nanofibres isolated from pineapple leaf fibers for medical applications. *Carbohydr Polym* 86(2011):1790–1798
41. Nascimento DM, Dias AF, Junior CPA, Rosa MF, Morais JPS, Figueiredo MCB (2016) A comprehensive approach for obtaining cellulose nanocrystal from coconut fiber. Part II: environment assessment of technological pathways. *Ind Crops and Prod*
42. Kalia S, Dufresne A, Cherian BM, Kaith BS, Averous L, Njuguna J et al (2011) Cellulose-based bio- and nanocomposites: a review. *Int J Polym Sci* 1–35
43. Cherian BM, Leao AL, De Souza SF, Thomas S, Pothan LA, Kottaisamy M (2010) Isolation of nanocellulose from pineapple leaf by steam explosion. *Carbohydr Polym* 81:720–725
44. Costa LMM, de Olyveira GM, Cherian BM, Leao AL, de Souza SF, Ferreira M (2013) Bionanocomposites from electrospun PVA/pineapple nanofibers/Stryphnodendron adstringens bark extract for medical applications. *Ind Crops Prod* 41(2013):198–202
45. Abraham E, Deepa B, Pothan LA, Jacob M, Thomas S, Cvelbar U, Anandjiwala R (2014) Extractio of nanocellulose fibrils from lignocellulosic fibres: a novel approach. *Carbohydr Polym* 86:1468–1475
46. Wang B, Sain M (2007) Isolation of nanofibers from soybean source and their reinforcing capability on synthetic polymers. *Compos Sci Technol* 67:2521–2527
47. Mariano M, El Kissi N, Dufresne A (2014) Cellulose nanocrystals and related nanocomposites: review of some properties and challenges. *J Polym Sci Part B: Polym Phys* 52:791–806
48. Li Y, Liu Y, Chen W, Wang Q, Liu Y, Li J, Yu H (2015) Facile extraction of cellulose nanocrystals from wood using ethanol and peroxide solvothermal pretreatment followed by ultrasonic nanofibrillation. *Green Chem* 00:1–8

49. Luzia F, Fortunati E, Pugliaa D, Lavorgna M, Santulli C, Kenny JM, Torre L (2014) Optimized extraction of cellulose nanocrystals from pristine and carded hemp fibres. *Ind Crops Prod* 56:175–186
50. Cao Y, Wang WH, Wang QW (2013) Application of mechanical models to flax fiber/wood fiber/plastic composites. *BioResources* 8(3):3276–3288
51. Jonooobi M, Mathew AP, Oksman K (2012) Producing low-cost cellulose nanofiber from sludge as new source of raw materials. *Ind Crop Prod* 40:232–238
52. Chen W, Yu H, Liu Y, Hai Y, Zhang M, Chen P (2011) Isolation and characterization of cellulose nanofibers from four plant cellulose fibers using a chemical-ultrasonic process. *Cellulose* 18:433–442
53. Eichhorn SJ, Dufresne A, Aranguren M, Marcovich NE, Capadona JR, Rowan S J, Weder C, Thielemans W, Toman M, Renneckar S et al (2010) Review: current international research into cellulose nanofibres and nanocomposites. *J Mater Sci* 45:1–33
54. Ahola S, Turon X, Osterberg M, Laine J, Rojas O (2008) Enzymatic hydrolysis of native cellulose nanofibrils and other cellulose model films: effect of surface structure. *Langmuir* 24(20):11592–11599
55. Teixeira EM, Bondancia TJ, Teodoro KR, Corrêa AC, Marconcini JM, Mattoso LHC (2011) Sugarcane bagasse whiskers: extraction and characterizations. *Ind Crops Prod* 33(1):63–66
56. Abe K, Iwamoto S, Yano H (2007) Obtaining cellulose nanofibers with a uniform width of 15 nm from wood. *Biomacromol* 8(10):3276–3278
57. Li MC, Wu Q, Song K, Lee S, Qing Y, Wu Y (2015) Cellulose nanoparticles: structure–morphology–rheology relationships. *ACS Sustain Chem Eng* 3(5):821–832
58. Li MC, Wu Q, Song K, Qing Y, Wu Y (2015) Cellulose nanoparticles as modifiers for rheology and fluid loss in bentonite water-based fluids. *ACS Appl Mater Interface* 7(8):5006–5016
59. Li W, Yue JQ, Liu SX (2012) Preparation of nanocrystalline cellulose via ultrasound and its reinforcement capability for poly(vinyl alcohol) composites. *Ultrason Sonochem* 19(3):479–485
60. Chen WS, Yu HP, Li Q, Liu YX, Li J (2011) Ultralight and highly flexible aerogels with long cellulose I nanofibers. *Soft Matter* 7(21):10360–10368
61. Ioelovich M (2013) Nanoparticles of amorphous cellulose and their properties. *Am J Nanosci Nanotechnol* 1(1):41–45
62. Ioelovich M (2014) Cellulose-nanostructured natural polymer. Lambert Academic Publishing, Saarbrücken
63. Ioelovich M (2014) Peculiarities of cellulose nanoparticles. *Tappi J* 13(5):45–52
64. Kim CW, Kim DS, Kang SY, Marquez M, Joo YL (2006) Structural studies of electrospun cellulose nanofibers. *Polymer* 47(14):5097–5107
65. Quan SL, Kang SG, Chin IJ (2010) Characterization of cellulose fibers electrospun using ionic liquid. *Cellulose* 17(2):223–230
66. Stylianopoulos T, Kokonou M, Michael S, Tryfonos A, Rebholz C, Odysseos AD, Dumanidis C (2012) Tensile mechanical properties and hydraulic permeabilities of electrospun cellulose acetate fiber meshes. *J Biomed Mater Res* 100(8):2222–2230
67. Abdul Khalil HPS, Bhat AH, Yusra AF (2012) Green composites from sustainable cellulose nanofibrils: a review. *Carbohydr Polym* 87(2):963–979
68. Abdul Khalil HPS, Davoudpour Y, Islam MN, Mustapha A, Sudesh K, Dungani R et al (2014) Production and modification of nanofibrillated cellulose using various mechanical processes: a review. *Carbohydr Polym* 99:649–665
69. Samir MAS, Alloin F, Dufresne A (2005) Review of recent research into cellulosic whiskers, their properties and their application in nanocomposite field. *Biomacromol* 6(2):612–626
70. Morais JPS, Rosa MF, de Souza FMM, Nascimento LD, do Nascimento DM, Cassales AR (2013) Extraction and characterization of nanocellulose structures from raw cotton linter. *Carbohydr Polym* 91(1):229–235

71. Emanuel MF, Ricardo AP, Mano JF, Reisa RL (2013) Bionanocomposites from lignocellulosic resources: properties, applications and future trends for their use in the biomedical field. *Prog Polym Sci* 38(10–11):1415–1441
72. Imai T, Sugiyama J (1998) Nanodomains of I α and I β cellulose in algal microfibrils. *Macromolecules* 31(18):6275–6279
73. Kim NH, Herth W, Vuong R, Chanzy H (1996) The cellulose system in the cell wall of microsterias. *J Struct Biol* 117(3):195–203
74. Sugiyama J, Harada H, Fujiyoshi Y, Uyeda N (1985) Lattice images from ultrathin sections of cellulose microfibrils in the cell wall of *Valonia macrophysa* Kütz. *Planta* 166(2):161–168
75. Hua K, Stromme M, Mihrayam A, Ferraz N (2015) Nanocellulose from green algae modulates the in vitro inflammatory response of monocytes/macrophages. *Cellulose* 22:3673–3688
76. Elazzouzi-Hafraoui S, Nishiyama Y, Putaux JL, Heux L, Dubreuil F, Rochas C (2008) The shape and size distribution of crystalline nanoparticles prepared by acid hydrolysis of native cellulose. *Biomacromol* 9(1):57–65
77. Iwamoto S, Isogai A, Iwata T (2011) Structure and mechanical properties of wet-spun fibers made from natural cellulose nanofibers. *Biomacromol* 12(3):831–836
78. Kimura S, Itoh T (1996) New cellulose synthesizing complexes (terminal complexes) involved in animal cellulose biosynthesis in the tunicate *Metandrocarpa uedai*. *Protoplasma* 194(3–4):151–163
79. Peng BL, Dhar N, Liu HL, Tam KC (2011) Chemistry and applications of nanocrystalline cellulose and its derivatives: a nanotechnology perspective. *Can J Chem Eng* 89(5):1191–1206
80. Sturcová A, Davies GR, Eichhorn SJ (2005) Elastic modulus and stress-transfer properties of tunicate cellulose whiskers. *Biomacromol* 6(2):1055–1061
81. Zhao Y, Zhang Y, Lindström ME, Li J (2014) Tunicate cellulose nanocrystals: preparation, neat films and nanocomposite films with glucomannans. *Carbohydr Polym* 117:286–296
82. Ferrer A, Filpponen I, Rodríguez A, Laine J, Rojas OJ (2012) Valorization of residual Empty palm fruit bunch fibers (EPFBF) by microfluidization: production of nanofibrillated cellulose and EPFBF nanopaper. *Bioresour Technol* 125:249–255
83. Feng YH, Cheng TY, Yang WG, Ma PT, He HZ, Yin XC, Yu XX (2018) Characteristics and environmentally friendly extraction of cellulose nanofibrils from sugarcane bagasse. *Ind Crops Prod* 111:285–291
84. Abdullah MA, Nazir MS, Raza MR, WahjoediB A, Yussof AW (2016) Autoclave and ultra-sonication treatments of oil palm empty fruit bunch fibers for cellulose extraction and its polypropylene composite properties. *J Clean Prod* 126:686–697
85. Miao X, Lin J, Tian F, Li X, Bian F, Wang J (2016) Cellulose nanofibrils extracted from the byproduct of cotton plant. *Carbohydr Polym* 136:841–850
86. Trovatti E, Fernandes SCM, Rubatat L, da-Silva-Perez D, Freire CSR, Silvestre AJD et al (2012) Pullulane nanofibrillated cellulose composite films with improved thermal and mechanical properties. *Compos Sci Technol* 72:1556–1561
87. Besbesa I, Vilar MR, Boufi S (2011) Nanofibrillated cellulose from alfa, eucalyptus and pine fibres: preparation, characteristics and reinforcing potential. *Carbohydr Polym* 86:1198–1206
88. Rosa MF, Medeiros ES, Malmonge JA, Gregorski KS, Wood DF, Mattoso LHC et al (2010) Cellulose nanowhiskers from coconut husk fibers: effect of preparation conditions on their thermal and morphological behavior. *Carbohydr Polym* 81:83–92
89. Kargarzadeh H, Ahmad I, Abdullah I, Dufresne A, Zainudin SY, Sheltami RM (2012) Effects of hydrolysis conditions on the morphology, crystallinity, and thermal stability of cellulose nanocrystals extracted from kenaf bast fibers. *Cellulose* 19:855–866
90. Jonoobi M, Harun J, Shakeri A, Misra M, Oksman K (2009) Chemical composition, crystallinity, and thermal degradation of bleached and unbleached kenaf bast (*Hibiscus cannabinus*) pulp and nanofibers. *BioResources* 4(2):626–639
91. Shin HK, Jeun JP, Kim HB, Kang PH (2012) Isolation of cellulose fibers from kenaf using electron beam. *Radiat Phys Chem* 81:936–940

92. Johar N, Ahmad I, Dufresne A (2012) Extraction, preparation and characterization of cellulose fibres and nanocrystals from rice husk. *Ind Crops Prod* 37:93–99
93. Sonia A, Dasan KP, Alex R (2013) Celluloses microfibrils (CMF) reinforced poly (ethylene-co-vinyl acetate) (EVA) composites: dynamic mechanical, gamma and thermal ageing studies. *Eng Chem* 228:1214–1222
94. Alemdar A, Sain M (2008) Biocomposites from wheat straw nanofibers: morphology, thermal and mechanical properties. *Compos Sci Technol* 68:557–565
95. Chen WS, Yu HP, Liu YX, Chen P, Zhang MX, Hai YF (2011) Individualization of cellulose nanofibers from wood using high-intensity ultrasonication combined with chemical pretreatments. *Carbohydr Polym* 2011:1804–1811
96. Zimmermann T, Bordeanu N, Strub E (2010) Properties of nanofibrillated cellulose from different raw materials and its reinforcement potential. *Carbohydr Polym* 79:1086–1093
97. Zainuddin SYZ, Ahmad I, Kargazadeh H, Abdullah I, Dufresne A (2013) Potential of using multiscale kenaf fibers as reinforcing filler in cassava starch-kenaf biocomposites. *Carbohydr Polym* 92:2299–2305
98. Maiti S, Jayaramudu J, Dasa K, Reddy SM, Sadiku R, Ray SS et al (2012) Preparation and characterization of nano-cellulose with new shape from different precursor. *Carbohydr Polym* 98:562–567
99. Aranguren MI, Marcovich NE, Salgueiro W, Somoza A (2013) Effect of the nanocellulose content on the properties of reinforced polyurethanes. A study using mechanical tests and positron annihilation spectroscopy. *Polym Test* 32:115–122
100. Tee TT, Sin LT, Gobinath R, Bee ST, Hui D, Rahmat AR et al (2013) Investigation of nano-size montmorillonite on enhancing polyvinyl alcohol-starch blends prepared via solution cast approach. *Compos Part B* 47:238–247
101. Shi J, Shi SQ, Barnes HM, Pittman JCU (2011) A chemical process for preparing cellulosic fibers hierarchically from kenaf bast fibers. *BioResources* 6(1):879–890
102. Lu P, Hsieh YL (2010) Preparation and properties of cellulose nanocrystals: rods, spheres, and network. *Carbohydr Polym* 82:329–336
103. Bai W, Holbery J, Li KC (2009) A technique for production of nanocrystalline cellulose with a narrow size distribution. *Cellulose* 16(3):455–465
104. Filson PB, Dawson-Andoh BE (2009) Sono-chemical preparation of cellulose nanocrystals from lignocellulose derived materials. *Bioresour Technol* 100(7):2259–2264
105. Araki J, Wada M, Kuga S, Okano T (1998) Low properties of microcrystalline cellulose suspension prepared by acid treatment of native cellulose. *Colloids Surf A* 142(1):75–82
106. Yu H, Qin Z, Liang B, Liu N, Zhou Z, Chen L (2013) Facile extraction of thermally stable cellulose nanocrystals with a high yield of 93% through hydrochloric acid hydrolysis under hydrothermal conditions. *J Mater Chem A* 1(12):3938–3944
107. Acharya SK, Mishra P, Mehar SK (2011) Effect of surface treatment on the mechanical properties of bagasse fiber reinforced polymer composite. *Bio-Resources* 6(3):3155–3165
108. Karimi S, Tahir P, Karimi A, Dufresne A, Abdulkhani A (2014) Kenaf bast cellulosic fibers hierarchy: a comprehensive approach from micro to nano. *Carbohydr Polym* 101:878–885
109. Habibi Y, Lucia LA, Rojas OJ (2010) Cellulose nanocrystals: chemistry, self-assembly, and applications. *Chem Rev* 110:3479–3500
110. Ruiz E, Cara C, Manzanares P, Ballesteros M, Castro E (2008) Evaluation of steam explosion pre-treatment for enzymatic hydrolysis of sunflower stalks. *Enzyme Microb Technol* 42(2):160–166
111. de Souza Lima MM, Borsali R (2002) Static and dynamic light scattering from polyelectrolyte microcrystal cellulose. *Langmuir* 18(4):992–996
112. Spagnol C, Rodrigues FHA, Pereira AGB, Fajardo AR, Rubira AF, Muniz EC (2012) Superabsorbent hydrogel composite made of cellulose nanofibrils and chitosan-graft-poly (acrylic acid). *Carbohydr Polym* 87:2038–2045
113. Zaini LH, Jonoobi M, Tahir PMD, Karimi S (2013) Isolation and characterization of cellulose whiskers from kenaf (*Hibiscus cannabinus* L.) bast fibers. *J Biomater Nanobiotechnol* 4: 37–44

114. Silverio HA, Neto WPF, Dantas NO, Pasquini D (2013) Extraction and characterization of cellulose nanocrystals from corncob for application as reinforcing agent in nanocomposites. *Ind Crops Prod* 44:427–436
115. Follain N, Belbekhouche S, Bras J, Siqueira G, Marais S, Dufresne A (2013) Water transport properties of bio-nanocomposites reinforced by Luffa cylindrical cellulose nanocrystals. *Membr Sci* 427:218–229
116. Liu HY, Liu D, Yao F, Wu QL (2010) Fabrication and properties of transparent polymethylmethacrylate/cellulose nanocrystals composites. *Bioresour Technol* 101:5685–5692
117. Espino-Perez E, Bras J, Ducruet V, Guinault A, Dufresne A, Domenek S (2013) Influence of chemical surface modification of cellulose nanowhiskers on thermal, mechanical, and barrier properties of poly(lactide) based bionanocomposites. *Eur Polym J* 49:3144–3154
118. Peng YC, Gardner DJ, Han YS (2012) Drying cellulose nanofibrils: in search of a suitable method. *Cellulose* 19:91–102
119. Jiang SH, Duan GG, Scheobel J, Agarwal S, Greiner A (2013) Short electrospun polymeric nanofibers reinforced polyimide nanocomposites. *Compos Sci Technol* 88:57–61
120. Neto WPF, Silvério HA, Dantas NO, Pasquini D (2013) Extraction and characterization of cellulose nanocrystals from agro-industrial residue—Soy hulls. *Ind Crops Prod* 42:480–488
121. Besbes I, Rei Vilar M, Boufi S (2011) Nanofibrillated cellulose from alfa, eucalyptus and pine fibres: preparation, characteristics and reinforcing potential. *Carbohydr Polym* 86:1198–1206
122. Besbes I, Alila S, Boufi S (2011) Nanofibrillated cellulose from TEMPO-oxidized eucalyptus fibres: effect of the carboxyl content. *Carbohydr Polym* 84:975–983
123. El Achaby M, El Miri N, Aboulkas A, Zahouily M, Bilal E, Barakat A, Solhy A (2017) Processing and properties of eco-friendly bio-nanocomposite films filled with cellulose nanocrystals from sugarcane bagasse. *Int J Biol Macromol* 96:340–352
124. El Miri N, Abdelouahdi K, Barakat A, Zahouily M, Fihri A, Solhy A, El Achaby M (2015) Bio-nanocomposite films reinforced with cellulose nanocrystals: rheology of film-forming solutions, transparency, water vapor barrier and tensile properties of films. *Carbohydr Polym* 129:156–167
125. El Miri N, El Achaby M, Fihri A, Larzek M, Zahouily M, Abdelouahdi K, Barakat A, Solhy A (2016) Synergistic effect of cellulose nanocrystals/graphene oxide nanosheets as functional hybrid nanofiller for enhancing properties of PVA nanocomposites. *Carbohydr Polym* 137:239–248
126. Teodoro KBR, Teixeira EM, Corrêa AC, Campos A, Marconcini JM, Mattoso LHC (2011) Whiskers from sisal fibers obtained under different acid hydrolysis conditions: effect of time and temperature of extraction. *Polímeros* 21(4):280–285
127. Siqueira G, Abdillahi H, Bras J, Dufresne A (2010) High reinforcing capability cellulose nanocrystals extracted from *Syngonanthus nitens* (Capim Dourado). *Cellulose* 17(2): 289–298
128. Silvério HA, Neto WPF, Dantas NO, Pasquini D (2013) Extraction and characterization of cellulose nanocrystals from corncob for application as reinforcing agent in nanocomposites. *Ind Crops Prod* 44:427–436
129. Islam MT, Alam MM, Zoccola M (2013) Review on modification of nanocellulose for application in composites. *Int J Innovative Res Sci Eng Technol* 2(10):5451
130. Gandolfi S, Ottolina G, Riva S, Fantoni GP, Patel I (2013) Complete chemical analysis of carmaghola hemp hurds and structural features of its components. *BioResources* 8:2641–2656
131. Klemm D, Schumann D, Udhardt U, Marsch S (2001) Bacterial synthesized cellulose—artificial blood vessels for microsurgery. *Prog Polym Sci* 26(9):1561–1603
132. Owonubi SJ, Agwuncha SC, Mukwevho E, Aderibigbe BA, Sadiku ER, Biotidara OF, Varaprasad K (2017) Application of hydrogel biocomposites for multiple drug delivery. In: *Handbook of composites from renewable materials*, vol 6: *Nanocomposites: advance applications*. Scrivener Publishing, pp 139–166

133. Anirudhan TS, Rejeena SR (2015) Biopolymer-based stimuli-sensitive functionalized graft copolymers as controlled drug delivery systems. In: Thakur VK, Singha AS (eds) *Surface modification of biopolymers*. Wiley, USA, pp 291–334
134. Zhao Q, Li B (2008) pH-controlled drug loading and release from biodegradable micro capsules. *Nanomedicine* 4:302–310
135. Tsukagoshi T, Kondo Y, Yoshino N (2007) Preparation of thin polymer film with controlled drug release. *Colloids Surf B Biointerfaces* 57:219–225
136. Charreau H, Foresti ML, Vázquez A (2013) Nanocellulose patents trends: a comprehensive review on patents on cellulose nanocrystals, microfibrillated and bacterial cellulose. *Recent Pat Nanotechnol* 7:56–80
137. Plackett DV, Letchford K, Jackson JK, Burt HM (2014) A review of nanocellulose as a novel vehicle for drug delivery. *Nord Pulp Pap Res J* 29:105–118
138. Abitbol T, Palermo A, Moran-Mirabal JM, Cranston ED (2013) Fluorescent labeling and characterization of cellulose nanocrystals with varying charge contents. *Biomacromol* 14:3278–3284
139. Jackson JK, Letchford K, Wasserman BZ, Ye L, Hamad WY, Burt HM (2011) The use of nanocrystalline cellulose for the binding and controlled release of drugs. *Int J Nanomed* 6:321–330
140. Qing WX, Wang Y, Wang YY, Zhao DB, Liu XH, Zhu JH (2016) The modified nanocrystalline cellulose for hydrophobic drug delivery. *Appl Surf Sci* 366:404–409
141. Alkilany AM, Murphy C (2010) Toxicity and cellular uptake of gold nanoparticles: what we have learned so far? *J Nanopart Res* 12:2313
142. Feese E, Sadeghifar H, Gracz HS, Argyropoulos DS, Ghiladi RA (2011) Photobactericidal porphyrin-cellulose nanocrystals: synthesis, characterization: and antimicrobial properties. *Biomacromol* 12:3528–3539
143. Carpenter BL, Feese E, Sadeghifar H, Argyropoulos DS, Ghiladi RA (2012) Porphyrin-cellulose nanocrystals: a photobactericidal material that exhibits broad spectrum antimicrobial activity. *J Photochem Photobiol* 88:527–536
144. Yallapu MM, Dobberpuhl MR, Maher DM, Jaggi M, Chauhan SC (2012) Design of curcumin loaded cellulose nanoparticles for prostate cancer. *Curr Drug Metab* 13:120–128
145. Dash R, Ragauskas AJ (2012) Synthesis of a novel cellulose nanowhisker-based drug delivery system. *RCS Adv* 2:3403–3409
146. Zhang L, Li Q, Zhou J, Zhang L (2012) Synthesis and photophysical behavior of pyrene-bearing cellulose nanocrystals for Fe³⁺ sensing. *Macromol Chem Phys* 212:1612–1617
147. Drogat N, Granet R, Le Morvan C, Bégaud-Grimaud G, Krausz P, Sol V (2012) Chlorin-PEI-labeled cellulose nanocrystals: synthesis: characterization and potential application in PDT. *Bioorg Med Chem Lett* 22:3648–3652
148. Akhlaghi SP, Berry RC, Tam KC (2013) Surface modification of cellulose nanocrystal with chitosan oligosaccharide for drug delivery applications. *Cellulose* 20:1746–1747
149. Dong S, Cho HJ, Lee YW, Roman M (2014) Synthesis and cellular uptake of folic acid-conjugated cellulose nanocrystals for cancer targeting. *Biomacromol* 15:1560–1567
150. Tang L, Huang B, Li T, Lu Q, Chen X (2014) Functionalized cellulose nanocrystals as a carrier for colon-targeted drug delivery system. *Supercond Sci Technol* 32:22–28
151. Colacino KR, Arena CB, Dong S, Roman M, Davalos RV, Lee YW (2015) Folate conjugated cellulose nanocrystals potentiate irreversible electroporation-induced cytotoxicity for the selective treatment of cancer cells. *Technol Cancer Res Treat* 14:757–766
152. Lahiji RR, Boluk Y, McDermott M (2012) Adhesive surface interactions of cellulose nanocrystals from different sources. *J Mater Sci* 47:3961–3970
153. Cao J, Peng LQ, Du LJ, Zhang QD, Xu JJ (2017) Ultrasound-assisted ionic liquid-based micellar extraction combined with microcrystalline cellulose as sorbent in dispersive microextraction for the determination of phenolic compounds in propolis. *Anal Chim Acta* 963:24–32

154. Siaueira G, Bras J, Dufresne A (2009) Cellulose whiskers versus microfibrils: Influence of the nature of the nanoparticle and its surface functionalization on the thermal and mechanical properties of nanocomposites. *Biomacromol* 10(2):425–432
155. Mcallister S (2005) Analysis and comparison of sustainable water filters. United Nations, 22
156. Hassan E, Hassan M, Abou-zeid R, Berglund L, Oksman K (2017) Use of bacterial cellulose and crosslinked cellulose nanofibers membranes for removal of oil from oil-in-water emulsions. *Polymers* 9(9). <https://doi.org/10.3390/polym9090388>
157. Voisin H, Bergström L, Liu P, Mathew A (2017) Nanocellulose-based materials for water purification. *Nanomaterials* 7(3):57. <https://doi.org/10.3390/nano7030057>
158. El-Nahas AM, Salaheldin TA, Zaki T, El-Maghrabi HH, Marie AM, Morsy SM et al (2017) Functionalized cellulose-magnetite nanocomposite catalysts for efficient biodiesel production. *Chem Eng J* 322:167–180
159. Lee M, Heo MH, Lee HH, Kim YW, Shin J (2017) Tunable softening and toughening of individualized cellulose nanofibers-polyurethane urea elastomer composites. *Carbohydr Polym* 159:125–135
160. Xu D, Xiao X, Cai J, Zhou J, Zhang L (2015) Highly rate and cycling stable electrode materials constructed from polyaniline/cellulose nanoporous microspheres. *J Mater Chem A* 3:16424–16429
161. Zhang J, Li L, Li Y, Yang C (2017) Microwave-assisted synthesis of hierarchical mesoporous nano-TiO₂/cellulose composites for rapid adsorption of Pb²⁺. *Chem Eng J* 313:1132–1141
162. Chesney A, Barnwell P, Stonehouse DF, Steel PG (2000) Amino-derivatised beaded cellulose gels: novel accessible and biodegradable scavenger resins for solution phase combinatorial synthesis. *Green Chem* 2:57–62
163. Chesney A, Steel PG, Stonehouse DF (2000) High loading cellulose based poly (alkenyl) resins for resin capture applications in halogenation reactions. *J Comb Chem* 2:434–437
164. Weber V, Linsberger I, Etenauer M, Loth F, Höyhty M, Falkenhagen D (2005) Development of specific adsorbents for human tumor necrosis factor- α : influence of antibody immobilization on performance and biocompatibility. *Biomacromol* 6:1864–1870
165. Heinze T, Liebert T (2001) Unconventional methods in cellulose functionalization. *Prog Polym Sci* 26:1689–1762
166. Korecká L, Bílková Z, Holápek M, Královský J, Benes M, Lenfeld J et al (2004) Utilization of newly developed immobilized enzyme reactors for preparation and study of immunoglobulin G fragments. *J Chromatogr B* 808:15–24
167. Volkert B, Wolf B, Fischer S, Li N, Lou C (2009) Application of modified bead cellulose as a carrier of active ingredients. *Macromol Symp* 280:130–135
168. He Z, Song H, Cui Y, Zhu W, Du K, Yao S (2014) Porous spherical cellulose carrier modified with polyethyleneimine and its adsorption for Cr(III) and Fe(III) from aqueous solutions. *Chin J Chem Eng* 22:984–990
169. Monier M, Akl MA, Ali WM (2014) Modification and characterization of cellulose cotton fibers for fast extraction of some precious metal ions. *Int J Biol Macromol* 66:125–134
170. Wang L, Li J (2013) Adsorption of C. I. reactive red 228 dye from aqueous solution by modified cellulose from flax shive: Kinetics, equilibrium, and thermodynamics. *Ind Crops Prod* 42:153–158
171. Zhou Y, Min Y, Qiao H, Huang Q, Wang E, Ma T (2015) Improved removal of malachite green from aqueous solution using chemically modified cellulose by anhydride. *Int J Biol Macromol* 74:271–277
172. Saito T, Kuramae R, Wohlert J, Berglund LA, Isogai A (2013) An ultrastrong nanofibrillar biomaterial: the strength of single cellulose nanofibrils revealed via sonication-induced fragmentation. *Biomacromol* 14(1):248–253
173. John MJ, Thomas S (2008) Biofibres and biocomposites. *Carbohydr Polym* 71:343–364
174. Henriksson M, Berglund LA, Isaksson P, Lindström T, Nishino T (2008) Cellulose nanopaper structures of high toughness. *Biomacromol* 9(6):1579–1585

175. Rodionova G, Lenes M, Eriksen O, Gregersen O (2010) Surface chemical modification of microfibrillated cellulose: Improvement of barrier properties for packaging applications. *Cellulose* 18(1):127–134
176. Sehaqui H, Liu A, Zhou Q, Berglund LA (2010) Fast preparation procedure for large, flat cellulose and cellulose/inorganic nanopaper structures. *Biomacromolecules* 11(9):2195–2198
177. Aulin C, Gällstedt M, Lindström T (2010) Oxygen and oil barrier properties of microfibrillated cellulose films and coatings. *Cellulose* 17(3):559–574
178. Aulin C, Netrval J, Wågberg L, Lindström T (2010) Aerogels from nanofibrillated cellulose with tunable oleophobicity. *Soft Matter* 6(14):3298–3305
179. Spence KL, Venditti RA, Habibi Y, Rojas OJ, Pawlak JJ (2010) The effect of chemical composition on microfibrillar cellulose films from wood pulps: mechanical processing and physical properties. *Biores Technol* 101(15):5961–5968
180. Spence KL, Venditti RA, Rojas OJ, Habibi Y, Pawlak JJ (2010) The effect of chemical composition on microfibrillar cellulose films from wood pulps: water interactions and physical properties for packaging applications. *Cellulose* 17(4):835–848
181. Chinga-Carrasco G, Syverud K (2010) Computer-assisted quantification of the multi-scale structure of films made of nanofibrillated cellulose. *J Nanopart Res* 12:841–851
182. Blaker JJ, Lee KY, Li X, Menner A, Bismarck A (2009) Renewable nanocomposite polymer foams synthesized from Pickering emulsion templates. *Roy Soc Chem* 11(9):1321–1326

Synthesis, Characterization and Applications of Polyolefin Based Eco-Friendly Polymer Composites



Akash Deep, Deepanshu Bhatt, Vishal Shrivastav, Sanjeev K. Bhardwaj and Poonma Malik

1 Introduction to Polyolefins

Polyolefins are the term for polymeric materials which ensembles polyethylene plastics of different types including low-density polyethylene (LDPE), linear low-density polyethylene (LLDPE), high-density polyethylene (HDPE), and polypropylene (PP). In another word, polyolefins are the class of synthetic polymers which are formed by polymerization of olefin monomer units. They are commonly produced from the carbon-rich resources such as coal, oil and natural gas. These polymers are prevalently used in a wide array of applications such as food industry, hygiene, medical instrumentation, toys manufacturing, agricultural sector, geotextiles, electronics (as an insulator), apparels and household accessories, sports items, transport systems, ropes and twines, packaging material, etc. Their properties and applicability are highly influenced by molecular properties and branching. In general, Polyolefins can be without any polar group (non-functionalised polymers) or with polar groups (functionalized polymers). Almost all the polyolefin manufacturing processes involve the use of either free radical initiators or coordination catalysts. Currently, polymers bearing polar functionalized side groups are highly desirable materials compared to non-functionalised ones as the former category offers beneficial properties of strong adhesion, toughness, easy print/paintability, good miscibility and favourable rheological properties [1].

A. Deep (✉) · D. Bhatt · V. Shrivastav · S. K. Bhardwaj
Nanotechnology Lab, CSIR-Central Scientific Instrument Organisation (CSIR-CSIO),
Chandigarh 160030, India
e-mail: dr.akashdeep@csio.res.in

P. Malik
CSIR-Central Scientific Instrument Organisation (CSIR-CSIO), C-92, CSIO Colony,
Chandigarh 160030, India

2 Non-functionalised Polyolefins

Non-functionalised Polyolefins or simply Polyolefins are one of the most essential polymers in modern life. It is impressive to consider that Polyolefins, made from simple monomers containing only carbon and hydrogen, can be used in a wide variety of applications [2]. Polyolefins can be manufactured by the injection molding and extrusion method and they are characterized by excellent rigidity, toughness, and temperature resistance. At present, Polyolefins are the most significant commodity plastics. The large impact of Polyolefins in the market has been created because of their low production costs, relatively low environmental impact, and flexible and tunable physical and mechanical properties [3].

Polyolefins can be broadly classified into two main types, polyethylene, and polypropylene. Polyethylene (PE) are further categorized according to their short and long chain branch (LCB) structure in three major types: low-density polyethylene (LDPE), linear low-density polyethylene (LLDPE), and high-density polyethylene (HDPE) [4].

3 Synthesis of Polyolefins

Low-density polyethylene (LDPE) is produced commonly by free radical polymerization. The manufacturing is carried out in reactors at pressures of 1000–3000 atm and temperatures of 200–275 °C. Under these extreme conditions, the starting material ethylene becomes a supercritical fluid with a density of 0.4–0.5 g/mL. Initiation of reaction can be carried out either by oxygen or peroxides. Here, branching controls the density of high-pressure polyethylenes. In general, as the branching of polymeric chain increases, it leads to reduce the density of the polymer. The rate of propagation steps increases by increasing the pressure and controls the termination and branching steps. Commonly, high pressure favours the production of higher densities, less branching and high molecular weight of polymers.

The synthesis of HDPE and LLDPE is achieved with the help of coordination catalysts [4]. This process is known as coordination polymerization. Most HDPE and LLDPE resins are prepared with either Ziegler-Natta or Phillips catalysts. The use of coordination catalysts is very common for olefin polymerization. Here, the catalytic property depends on the type of transition metal and the geometry and electronic character of the ligands. In most cases, the activation of the catalyst is carried out by some sort of complexes (known as precatalyst or catalyst precursor). The activation is made just prior to the injection of catalyst in the polymerization reactor or inside the reactor itself. The activator further alkylates the pre-catalyst complex to form the active sites and stabilizes the resulting cationic active site. Besides activation, the precursor also works as a Lewis acid (electron acceptor) which helps to scavenge the polar impurities (e.g., oxygen, sulfur, nitrogen compounds) from the reactor.

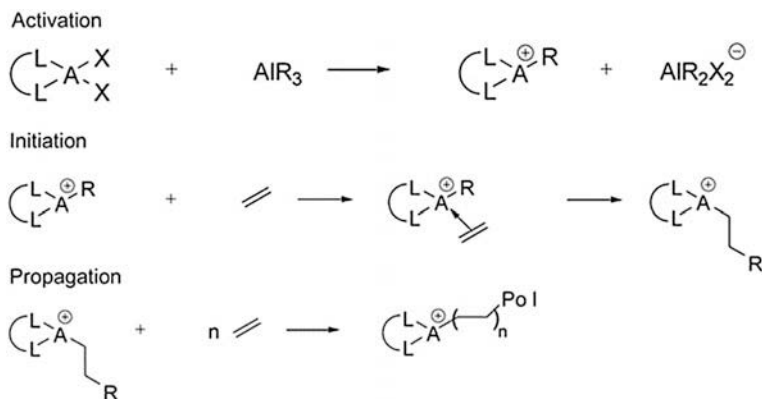


Fig. 1 Activation, initiation and propagation steps for coordination polymerization. Reproduced from Soares et al. [5]

The polymerization process involves two main steps (Fig. 1). The monomer coordination takes place to the active site followed by its insertion into the growing polymer chain.

Prior to insertion, the double bond in the monomer coordinates to the active site of the transition metal. After the insertion into the polymer chain, another olefin monomer can coordinate to the vacant site and the process continues at a fast frequency until a chain transfer reaction takes place. In the case of copolymerization, there is a competition between comonomers for the coordination site and their insertion into the growing polymer chains.

4 Polypropylene

Polypropylene can be produced in a variety of stereochemical configurations (Fig. 2). The isotactic polypropylene has the methyl groups on the same side of the backbone; the syndiotactic candidate carries on alternating sides, and the atactic polypropylene possesses the methyl groups in a random fashion along the chain. Among these, the atactic polypropylene is amorphous and has little commercial value. Both isotactic and syndiotactic polypropylene are semi-crystalline in morphology with high melting temperatures. Isotactic polypropylene is the most dominant material of its class in the market. It is easily produced with the application of heterogeneous Ziegler–Natta, and metallocene catalysts. In comparison to isotactic polypropylene, the syndiotactic polypropylene can be produced only with the help of metallocene catalysts and has much less commercial value.

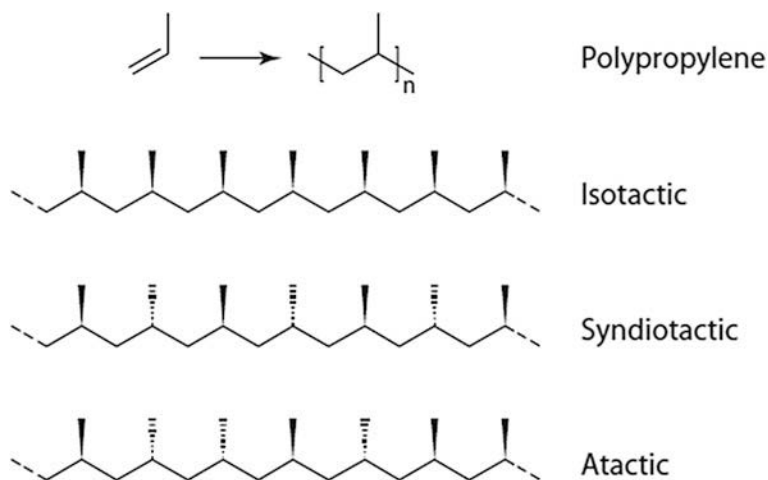


Fig. 2 Main polypropylene types: isotactic, syndiotactic, and atactic. Reproduced from Koltzenburg et al. (2017), [6]

4.1 Controlled Polymerisation of Polyolefins

In comparison to the early generation of multi-site Ziegler-Natta catalysts, modern metallocene catalysts have only one type of catalytically active center, which can readily be fine-tuned to produce some uniform homo- and copolymers with extraordinary properties. These metallocene structures, especially ligand substitution patterns, can then be tailored to control the final polymer microstructure, their molecular weights, end groups, and morphology with utmost precision [7, 8]. The use of metallocene catalysts for the production of Polyolefins became significant since the 1980s. Metallocenes function very actively for olefin polymerization when activated with methyl aluminoxane (MAO), instead of trimethylaluminum (TMA) which was commonly used in a case with Ziegler-Natta catalysts. The presence of MAO in the process enhances the activity of metallocenes by a factor of about 1000 [9–11].

4.1.1 Future of Metallocenes or Single-Site Catalysts

As describes earlier, metallocenes have some unique advantages over conventional Ziegler-Natta catalysts. They allow the realization of tailor-made polymers which were not possible by conventional catalysts. The innovation of single-site catalyst by metallocenes and some other organometallic catalysts from multi-site catalysts was a remarkable event in polyolefin industry. It is estimated that metallocenes will overpass all the other kind of catalytic processes in next few years. However, more

varieties of tailored multi-site catalysts should be discovered in near future to catalyze the production of next-generation eco-friendly highly functionalized homopolymers and copolymers.

5 Synthesis of Functionalised Polyolefins with Better Eco-Friendliness

The recent research in the area of Polyolefins has been focussed on making their functionalized forms, e.g., complex, mixtures, block copolymers, and micro-and nanocomposites with inorganic and organic fillers. Such approaches are helpful to realize the development of more efficient and environmentally friendly Polyolefins. Functionalized polyolefins play a fundamental role in improving the properties of morphology and thermal and mechanical behaviours. The functionalized Polyolefins also help in discovering new materials which were otherwise difficult to be obtained by conventional synthesis approaches.

The starting material for the synthesis of polar functionalized polymers is simple polyolefins (e.g., polyethylene or polypropylene). An introduction of small amounts of polar functionalities into the alkene chain makes a tremendous effect on the surface properties of resulting polymers [12, 13]. The functionalised Polyolefins, on the basis of their structure, can be classified into four categories (Fig. 3): (a) randomly functionalized copolymers that exist as either branched, (b) linear structures, (c) end-functionalised copolymers, (d) block copolymers, and (e) graft copolymers [14, 15].

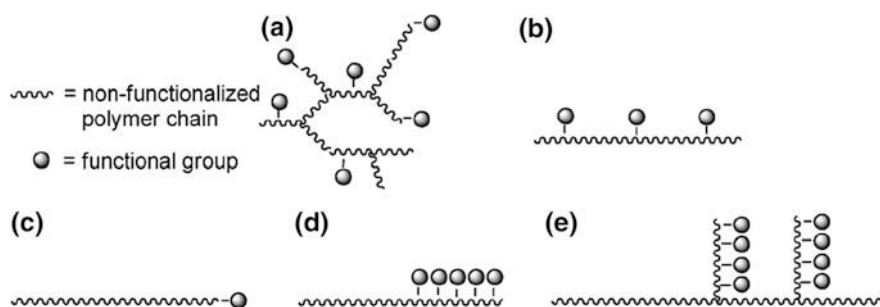


Fig. 3 a Randomly functionalized copolymers that exist as either branched, b linear structures, c end-functionalized copolymers, d block copolymers, and e graft copolymers. Reproduced from Franssen et al. (2013), [16]

5.1 Randomly Functionalised Copolymers

Randomly functionalized Polyolefins, as the name indicates, have functional groups in an unsystematic way. A slight change in their structure allows the introduction of new properties. Such copolymers can be synthesized in a variety of ways as depicted in Fig. 4.

5.1.1 Polymer Post-functionalization

Polymer post-functionalization is currently one of the most favored approaches. The post-functionalization of polymeric structures can be carried out in the bulk as well as on the surface [12]. For instance, the reaction of free radicals with C–H bonds of a polymer backbone can result in the H abstraction and the subsequent formation of a polymeric radical. In a different approach, insertions of carbenes or nitrenes into the C–H bonds of the polymer backbone is practised. In an industrial setting, surface modification is also processed via plasma, corona and flame treatment [17]. Non-functionalised polyolefins have no reactive groups and therefore their chemical modifications (inert C–H bonds) may generally require harsh conditions [17, 18]. Note that such treatments can also cause many undesirable side reactions to happen; for example, cross-linking or chain scission. This can lead to severely alter the properties of the polymer.

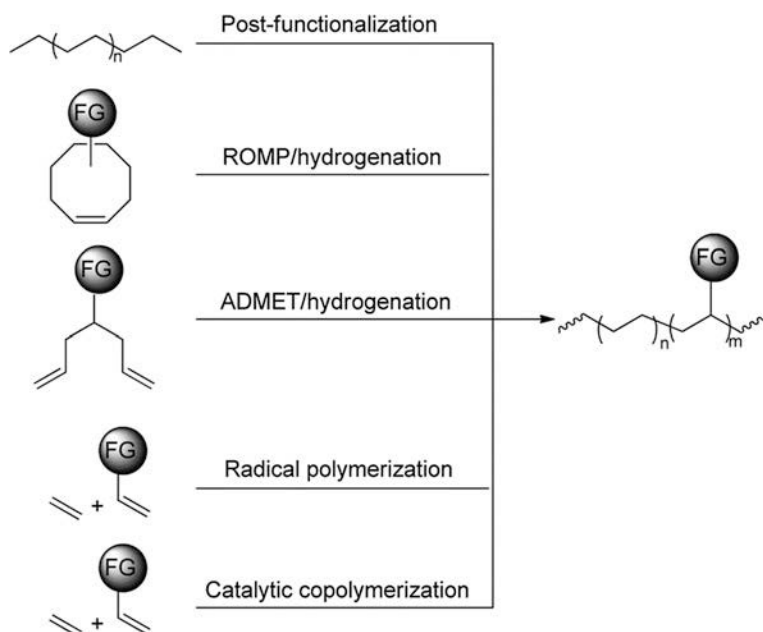


Fig. 4 Different synthesis pathways for the synthesis of randomly functionalized copolymers. Reproduced from Franssen et al. (2013), [16]

5.1.2 Ring-Opening Metathesis Polymerization (ROMP)

ROMP of the functionalized cyclic alkenes, followed by subsequent hydrogenation of the resulting polyalkenamers offer a viable approach to obtain functionalized Polyolefins. The development of more efficient and polar-tolerant catalysts (mainly based on ruthenium) has sparked the growth of ROMP based treatments [19]. The method provides controlled sequence distributions of copolymers which in turn has a major effect on the crystallinity and physical properties of the produced polymers.

5.1.3 Acyclic Diene Metathesis Polycondensation (ADMET)

ADMET process is very much similar to ROMP synthetic route. However, ADMET requires the use of special symmetrically functionalized a,o-diene monomers instead of cyclic monomers. The presence of polar functionalities in monomers leads to catalyst poisoning. As a result, the protection of the functional group is often required prior to polymerization [20, 21]. The recent discovery of certain metal complexes has allowed the production of a wide variety of side group (e.g., alcohol, acetate, ether, ester, amine/amide, halide, etc.) containing functional polymers. ADMET allows gaining precise control over the polymeric microstructure. Hence, it can function as a complementary technique to another process like radical polymerization.

5.1.4 Radical Polymerization

Radical polymerization of olefins and polar vinyl monomers (e.g. acrylates, vinyl acetate and acrylic acid) is a widely applied approach on commercial scales. The resulting copolymers find many applications in our daily life. The radical polymerization of non-polar olefins and polar vinyl monomers is not necessarily feasible due to the poor reactivity of olefins and lack of stability of the generated radicals for smooth polymerization. The product formation is often dependent upon harsh polymerization conditions (such as high temperatures and pressures). Consequently, the formation of highly branched Polyolefins is realized with these processes [22, 23].

5.1.5 Catalytic Routes

Transition-metal (TM) catalyzed routes facilitate the synthesis of functionalized copolymers. These processes allow control over the number of polar functionalities and their distribution along the polymer backbone which is a special advantage of TM catalyzed methods over the radical polymerization reactions [24]. The TM catalyzed routes involve either early transition-metal catalysis or late transition-metal catalysis with both of the methods having their own pros and cons.

5.2 Chain-End Functionalized Copolymers

Chain-end functionalization is a key step in the synthesis of Polyolefins. This is, in fact, the starting point for constructing more complex macromolecular architectures including block copolymers and graft copolymers from otherwise unreactive polyolefin chains. Polyolefins bearing a terminal functional group at either one end or both ends (i.e. telechelic polymers) can be prepared by different chain-end functionalization routes. These strategies may contain controlled end-capping of living TM-catalysed polymerization, in situ chain transfer reactions during TM catalyzed coordination polymerization, and modification of preformed unsaturated chain ends [25, 26].

5.2.1 End-Capping of Living Polymerizations

The end-capping of living polymerization is a classical approach for the introduction of terminal functionalities. This approach is rather less suitable for end-functionalization of Polyolefins with polar groups. The process is metal-consuming and requires the use of specific catalysts [27].

5.2.2 Chain-Transfer Reactions

End-functionalisation via chain transfer is a fairly efficient approach because of it being very metal-efficient and attainment of desired end functionality of Polyolefins. The chain-transfer reactions can be carried out in a variety of ways as elaborated in Fig. 5.

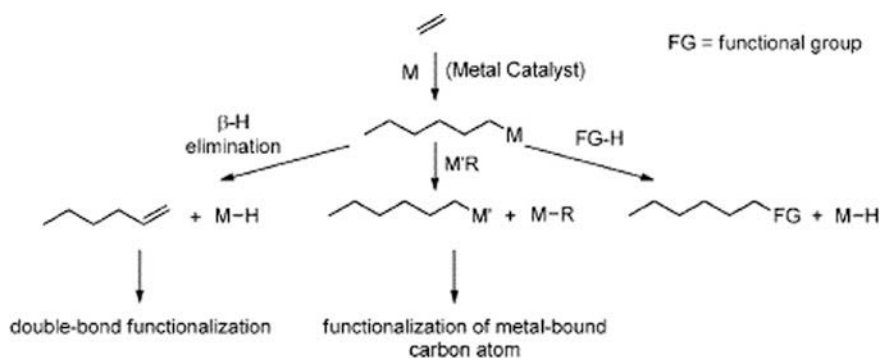


Fig. 5 Overview of chain-transfer reactions used for the end-functionalization of Polyolefins. Reproduced from Franssen et al. (2013), [16]

5.2.3 Functionalisation of Unsaturated Chain Ends

The chemical modification of preformed unsaturated chain-ends of Polyolefins has been used for the introduction of several functionalities. The associated process may involve hydroboration, hydrosilylation and hydroalumination reactions [26]. This approach is not free from certain limitations which ultimately undermine its utility for the synthesis of end-functionalised Polyolefins. As such, the chain-end unsaturation of the preformed Polyolefins should be nearly to quantitative amounts to guarantee complete functionalization.

5.3 *Segmented Copolymers: Block and Graft Copolymers*

The segmented copolymers can bear a large quantity of functional groups with simultaneous preservation of the original properties of precursors (i.e. non-functionalised polyolefin chains). In this way, the crystallinity, melting point and hydrophobicity of the original Polyolefins are retained even after the functionalization. Both block and graft copolymers are ideally suited to act as compatibilisers in polymer blends. The functionalised segments can ensure desired adhesion to the polar surfaces whereas the non-polar segment can interpenetrate into Polyolefin homopolymer domains [28].

5.3.1 Synthesis of Block Copolymers

The synthesis of polyolefin-based block copolymers is often processed in a multi-step manner that involves the application of two or more mechanistically distinct polymerisation techniques [29]. Most of the popularly used synthesis pathways for block copolymers involve transformation reactions, which are processed via cross-over between distinct polymerization mechanisms. Figure 6 gives an overview of the transformation reactions used for synthesis of block copolymers.

Mechanistic transformations are performed in various living/controlled polymerization for the synthesis of block copolymers. In Fig. 6, the solid lines are indicative of pathways which are suitable for the synthesis of functional Polyolefins. The dashed pathways do not provide desired results.

5.3.2 Synthesis of Graft Copolymers

Graft copolymers can commonly be prepared via transformation reactions. Such reactions involve two mechanistically distinct polymerization mechanisms. The modification of one chain end is more or less straightforward in the of block copolymers. In contrast, the synthesis conditions for graft copolymers are more challenging. These methods require modifications on multiple sites along the

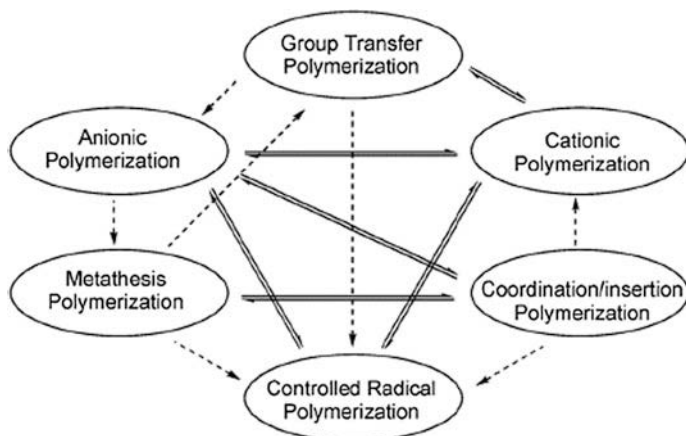


Fig. 6 An overview of different transformation reactions used in the synthesis of block copolymers. Reproduced from Franssen et al. (2013), [16]

backbone of the polymer. In summary, three major routes are used for the synthesis of graft copolymers which include grafting onto, grafting from, and grafting through approaches (as described in Fig. 7) [30, 31].

The “grafting onto” method requires the polymer backbone to be synthesized with randomly placed functionalities. A subsequent step for the coupling of the two functionalities then allows the formation of graft copolymers which have end-functionalized polymers as branches of the main chain. The “grafting from” methods involves the synthesis of a polymer backbone through ETM-catalysed insertion polymerization. The functionalities are thereafter incorporated via direct copolymerization of selected functional monomers in the presence of either ethene or propene (or both) [25, 32]. In the “grafting through” or macro-monomer method, a polymer–oligomer chain (containing a polymerizable end group) is formed which can subsequently be copolymerized to yield graft copolymers [16, 33]. The variations of the degree of polymerization of the side chains and polymer backbone can allow the selection of the length of the grafts and the final grafting density, respectively. At the time, incompatibility of the monomers (e.g., in their viscosities) may pose some difficulties in the grafting though processes. In such cases, the multi-step reaction must be carried out to ensure the desired success.

Overall, a remarkable volume of research work has been carried out over the past decade to prepare functional Polyolefins. As can be expected in the world of chemistry, each method (described above) has its own advantages and limitations. The synthesis of functional Polyolefins in a controlled way with the tuneable amount of functionalities still remains a challenge despite many recent advances in this field. Researchers are working in the direction of improving the quality of new catalysts.

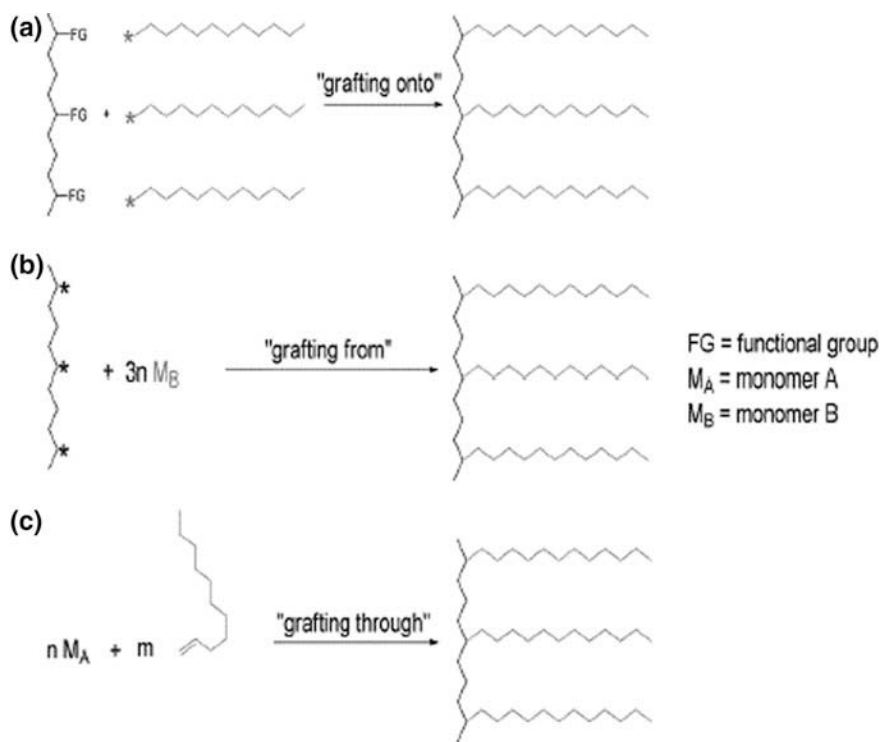


Fig. 7 General methods for the synthesis of graft copolymers. Reproduced from Franssen et al. (2013), [16]

6 Synthesis of Eco-Friendly Polyolefin Composites

With the functionalization of Polyolefins, they become amenable towards the formation of composites with other materials, e.g. natural fibers. The constituent materials define the properties (e.g., strength and stiffness) of the composite. In recent decades, there a great interest has generated toward the development of green composites which shows the advantages of being fully sustainable, biodegradable, and environment-friendly. The addition of biodegradable additives in Polyolefins at the time of their manufacturing may allow the resulting composites to undergo faster degradation after their use. During recycling of such composites, the bacterial action leads to the release of additive and breakage of the long chain of Polyolefin molecules into smaller ones. Thus, it becomes possible to degrade Polyolefins composites with the help of naturally occurring bacteria.

Researchers have proposed the formation of Polyolefin composites with natural materials like wood and natural fibers, wood flour, wood waste, sugar cane, rice hulls, paper waste and industrial fibers. The above mentioned natural sources are easily available and their addition helps in the realization of biodegradation and

disposable polyolefins. The next few paragraphs of information are devoted to the discussion on different industrial synthesis methods employed to produce polyolefin composites.

Industry uses different synthesis methods to prepare the composites of polyolefin inefficient and cost-effective manner. The condition, such as processing temperature, the rate of cooling, pressure, and the steps in general influence the properties and shape of the final product to a large extent. In this way, one can control the materials' mechanical stability, crystallinity, elastic modulus, tensile strength, etc. For example, the extrusion method is one of the simplest and oldest methods which is used to mix two or more polymers or elastomers (e.g. wood-thermoplastic composites). The same product having a lighter weight and more complicated shape can be obtained by injection or compression molding methods [34].

6.1 Extrusion and Pultrusion

Extrusion is the process in which plasticized polymers are forced to pass through a die under pre-optimized conditions of temperature, pressure, and dosing. The materials of the desired shape such as tubing, pipes, hose, sheet and film, continuous filaments, or coated electrical wire are obtained. Currently, this technique is used in many industries for the production of polyolefin composites because of cost-effectiveness and continuous working characteristics [35–38]. This process allows the formation of a variety of plastic products like bags, pipes, thin sheet, etc. Pultrusion is a technique similar to extrusion with the major difference that the workpiece is pulled from the die. Nowadays it is the most cost-efficient technique for the production of Polyolefins composites. It can also yield continuous production of products with constant and straight cross-sectional profile. The instrument for pultrusion has a heating die, in which the materials get cross-linked with each other and then are released with a desired cross-sectional profile.

6.2 Injection Molding

Though extrusion process is one of the oldest techniques and successful to produce Polyolefin composites, it is limited to form a simple basic structure in forms of pipes, cylinders, sheets, and so on. For complex geometry, alternative techniques have to be used. The injection molding technique overcomes such limitations and is used to produce complex 3D structures. The injection molding is considered as one of the best “net shape” (i.e., the production of desired products using only one process) manufacturing processes. This technique offers the advantages of simplicity, reliability, versatility, and efficiency [39]. One-third of total polymer production is processed by injection molding. The injection molding technology gives advantages like complex structure production and automation. However, some

drawbacks are also observed at times. For instance, it is not necessarily suitable for low production purposes due to high-cost of tool, and requirements of auxiliary equipment and mold.

6.3 Calendering

The calendering process to prepared Polyolefin composites involves the passage of two or more materials through a series of heated rollers. Thus, it decreases the thickness of the material and provides the production of thin sheets of about 1 mm thickness. The cost of calendering equipment is high but it can work continuously once the production starts. Calendaring is used to make Polyolefin composites with paper, wool, silk and other natural fibers [40].

6.4 Compression Molding and Thermoforming

Compression molding and thermoforming are also used for the preparation of Polyolefin composites. Compression machine mimics a press oriented vertically with top and bottom halves wholly interlocked with each other. The materials are placed between the above two halves and then compressed under the influence of heat and pressure. Thermoforming is similar to compression molding. The only difference being the presence of additional holes that can be used to alter the air pressure.

7 Improvement of Composite Compatibility Between Polyolefins and Natural Additives

As a common problem, polyolefins are incompatible with other constituents like the natural fiber with which they are going to be blended for the formation of eco-friendly composites. Such a situation can be countered with the application of compatibilizers. For instance, polylactide (PLA)/polyethylene (PE) composites have been prepared with the application of E-GMA and EMA-GMA (glycidyl methacrylate groups) as compatibilizer [41]. PLA's role is to maintain a good mechanical strength and toughness, whereas GMA increases the elastic modulus of the final product [42]. The above technique is useful method when nature fibers (containing -OH group) are used for the Polyolefin composite preparation. The natural fibers are hydrophilic while Polyolefins are hydrophobic, which leads to incompatibility. As another example, bio-polyethene/curaua fiber composite can be processed in presence of hydroxyl-terminated polybutadiene (LHPB) as a

compatibility agent. Note that bio-Polyolefins are the biodegradable materials whose olefin monomers are extracted from naturally available sources.

The Polyolefin composites can be modified (stabilized) by various physical, chemical, physical-chemical and mechanical methods. The selection of the appropriate method depends upon the nature of both Polyolefin and the additive as well as the processing conditions deployed during the formation of the composite.

7.1 Chemical Methods

The use of the chemical can stabilize the composite. As already discussed by few examples, surface modification or compatibilization can be achieved by chemical reactions utilizing the hydroxyl groups. Besides this, copolymerization can also be an option. Silanes can couple with a hydroxyl group to form a layer of hydrocarbon which is hydrophobic. Hence the use of silanization chemistry is helpful to reduce wettability of the fiber and improve the stability of composites [43–46]. Similarly, isocyanates also react with the hydroxyl group of natural fibers to form the urethane linkage [47–49]. Since the presence of acetyl group can also decrease the water content or absorption, the acetylation of materials can also stabilize the composites by increasing the hydrophobic behaviour. For example, acetylation of wood increases its interfacial compatibility with polypropylene [50].

Chemical compatibilizers help to stabilize the composites while also simultaneously enhancing certain other properties, such as tensile and mechanical strengths. The processing of natural fibers by benzylation and maleic acid are some useful examples wherein not only the hydrophobicity of the fiber could be improved but better mechanical strength and thermal stability of the composite (e.g., benzyolated wood/HDPE composites) are realized [51, 52]. The treatment of Jute with succinic acid followed by the composite formation with PP was found to be useful in yielding composites of improved toughness [53].

7.2 Physical Methods

Physical methods have also been demonstrated for improving the compatibility between Polyolefins and natural additives. The treatment with gamma-rays, laser, and plasma cause the polarity of the surface to change. The change in polarity of the surface results in the modification of hydrophobicity nature of constituents. Likewise, the use of enzymes coating and steam explosion process is much simpler and less costly than the chemical methods. However, the composite property can get greatly affected by the treatment condition and duration. The enzyme modification of Abaca and Palm fiber was suggested during its composite preparation with PP [54]. This treatment improved the tensile strength and hydrophobic nature of the composite. Steam explosion process is also helpful to improve the adhesion of

fibers with Polyolefin matrices. Furthermore, vibratory ball milling and compression milling are primarily used mechanical means to enhance the compatibility between thermoplastic and lignocellulosic fiber.

8 Characterization of Polyolefins and Composites

8.1 *Microstructural Properties*

The microstructural properties of Polyolefins and their composites are characterized by their chemical composition, molecular weight, and long or short chain branching. Gel permeation chromatography (GPC) [55], differential scanning calorimetry (DSC) [56], nuclear magnetic resonance spectroscopy (NMR) [57], Viscometry [58], Fourier-transform infrared spectroscopy (FTIR) [4], Osmometry [58], temperature rising elution fractionation (TREF) [59, 60], crystallization analysis fractionation (CRYSTAF) [59, 60], crystallization elution fractionation (CEF) [59, 60], and Raman analysis [61] are some of the techniques used to characterize Polyolefins. These techniques are briefly discussed in the subsequent subsections.

8.1.1 Gel Permeation Chromatography (GPC)

Gel permeation chromatography (GPC), also known as molecular sieving or size exclusion chromatography, is a widely used analytical method for measurement of the molecular weight distribution of olefins and other polymers. It is a fractionation technique where polymer molecules are fractionated according to their molecular size. The instrument for chromatographic procedure usually consists of columns connected in series along with a pump, a sample injection port, and a detector. The columns are packed with a bed of porous particles, also referred to as stationary phase through which the mobile phase containing the mixture of polymers is passed. The column packings have different pore sizes that allow the separation of the molecules by the mechanism of size exclusion. Short chains of molecules penetrate the pores of the packing material, while the larger molecules diffuse through the voids and thus get fractionated faster on the basis of their retention time. Consequently, chains with higher molecular weights will take a shorter time to exit the column set than chains with lower molecular weights. The column elutions are then passed through various detectors intended for monitoring either concentration, viscosity, refractive index or light scattering of the polymer. Finally, the elution times or elution volumes are converted to molecular weight distribution (MWD) using a calibration curve obtained using polystyrene standards. The efficiency of this technique is governed by various factors such as the type of polymer,

concentration and molecular weight of the polymer, branching of polymers, type of mobile phase used and the working temperature [4, 62].

High-temperature GPC (HT-GPC) technique based on simplified triple detection can be used for the determination of long chain branching and molar mass distribution in Polyolefins and their composites [55]. An example is given in Fig. 8 to show the overlay of GPC chromatographs of PyO-PP, PyO-POPP40 and distilled pyrolyzed oil PyO-POPP40-A [63]. These samples are of pyrolyzed oil from neat polypropylene, potato-peel powder/polypropylene, and distillate (200 °C fraction) of potato-peel powder/polypropylene components, respectively. A difference in the molecular weight range of PyO-PP and PyO-POPP40 would help confirm the formation of an eco-friendly composite of PP. The average molecular weight (M_w) of PyO-PP, PyO-POPP40 and PyO-POPP40-A oils were estimated as 341, 263 and 248 daltons, respectively. The shift in molecular weight was ascribed to the presence of higher molecular weight oligomers in PyO-PP compared to PyO-POPP40 (presence of 40% potato-peel powder). This addition led to chemical reactions which in turn resulted in the cleavage of high molecular weight oligomers.

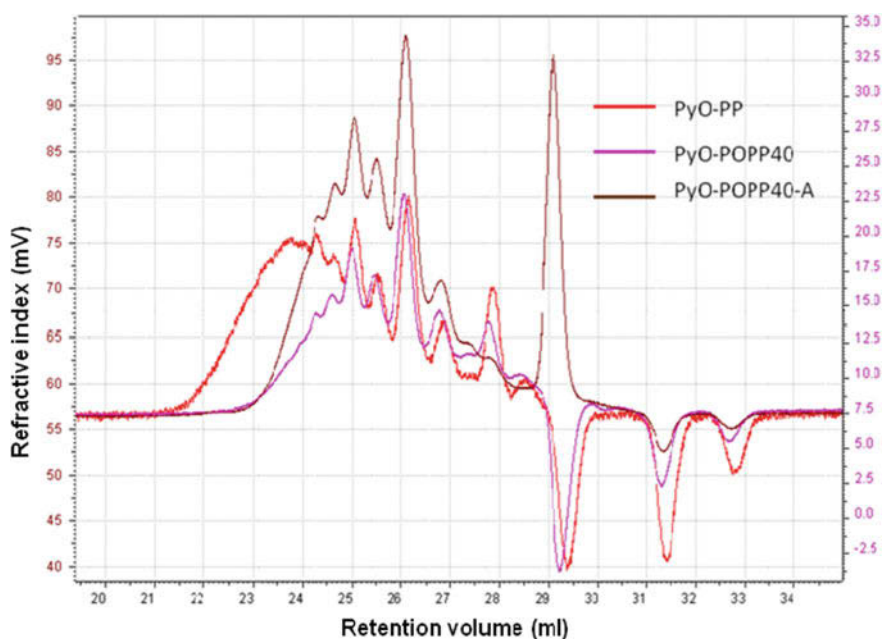


Fig. 8 Overlay GPC chromatogram of pyrolyzed products of polyolefin composites—PyO-PP, PyO-POPP40, and PyO-POPP40-A (Pyrolysed oil from neat PP and POPP40 biocomposite (potato-peel powder/polypropylene) designated as PyO-PP and PyO-POPP40 respectively. A distillate of boiling point up to 200 °C obtained from of PyO-POPP40 designated as PyO-POPP40-A. Reproduced from Sugumaran et al. (2017), [63]

8.1.2 Differential Scanning Calorimetry (DSC)

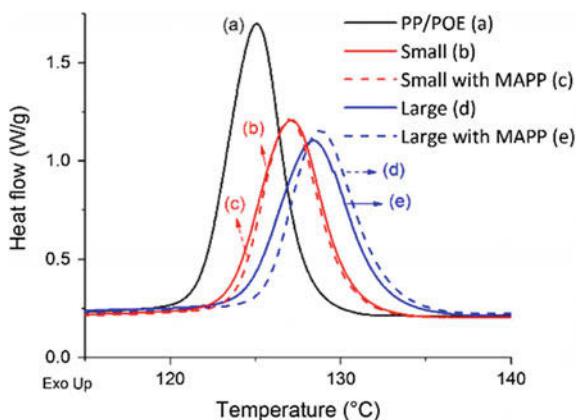
Differential scanning calorimetry (DSC) is a thermo-analytical technique and was developed by Watson and O'Neill in 1962. DSC thermal fractionation technique is used for the calculation of short-chain branching distribution (SCBD) in olefins. The DSC instrument determines the change in heat flow by measuring the temperature difference between the reference and the sample as a function of temperature. During the DSC analysis, the weighed sample is placed in a sample crucible pan against a reference pan. The sample cell is either heated or cooled at a controlled rate to obtain the melting or the crystallization/glass transition temperature. The heat flow difference between the sample and the reference cells is continuously monitored and displayed as a function of temperature/time. DSC is frequently used to calculate glass transition temperatures, the heat of fusion, crystallization temperatures, and degradation temperatures of various polymeric materials. Further, the integration of the area under the melting peak gives the heat of fusion from which the degree of crystallinity can also be derived [4, 118].

As an example, the DSC properties of a new class of toughened Polyolefin biocomposites (composite of pyrolyzed miscanthus based biocarbon, poly(octene ethylene) (POE) elastomer, and polypropylene (PP)) have been elaborated in Fig. 9 [64]. The DSC curves of composite samples were characterized with the shift in the crystallization peak of PP toward higher temperatures. The effect is found more pronounced with larger biocarbon particles.

8.1.3 Nuclear Magnetic Resonance (NMR)

Nuclear magnetic resonance (NMR) is a commonly used technique for the determination of chemical structures of a variety of polymers. Among different types of NMR, ^1H and ^{13}C MNR are frequently utilized for characterization of olefins. These studies determine branching types and help in the identification of

Fig. 9 DSC graph of the first cooling cycle for the Polyolefin matrix and biocomposites. Reproduced from Behazin et al. (2017), [64]



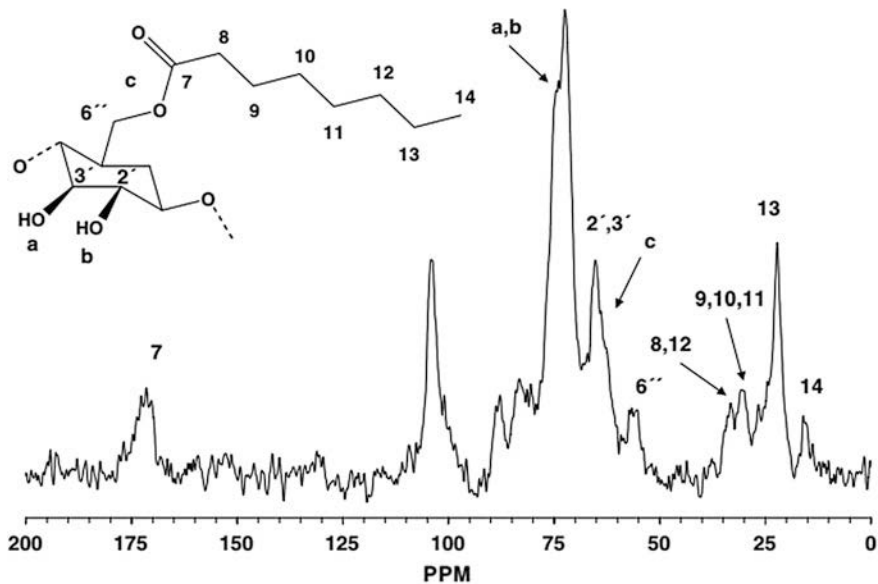


Fig. 10 CP/MAS ^{13}C NMR spectrum for blue agave fiber after esterification. Reproduced from Tronc et al. (2007), [66]

comonomers in the polymeric structures [4]. The change in the number, relative position, number and kind of branching can result in entirely different properties of olefins, and thus the determination of such change becomes very significant. ^1H NMR is used for the characterization of copolymers, such as ethylene-1-butene (EBR) and ethylene 1-octene copolymer (EOR). ^{13}C NMR can be used for the quantification of monomer distribution in olefin plastomers/elastomers [65]. Note that ^{13}C NMR may require long analysis durations. Alternatively, high magnetic field coupled improved proton NMR technique provide rapid analysis of complex spectra (1-olefin comonomer) within 1–2 min. The application of NMR in Polyolefin composites can be understood by the example of blue agave fibers which were used to enhance the fiber/HDPE interfacial interaction after their modification by acetylation with acetic anhydride in octanoic acid [66]. The fibers were characterized with a peak at 172 ppm to provide a useful indication of a successful modification (Fig. 10).

8.1.4 Fourier Transform Infrared Spectroscopy (FTIR)

Fourier transform infrared (FTIR) spectrum is produced by a sample when it is exposed to varying IR frequency. During the process of analysis, some frequencies are absorbed while other frequencies pass through and get transmitted. The IR spectrum denotes the absorption and transmission data of sample molecule

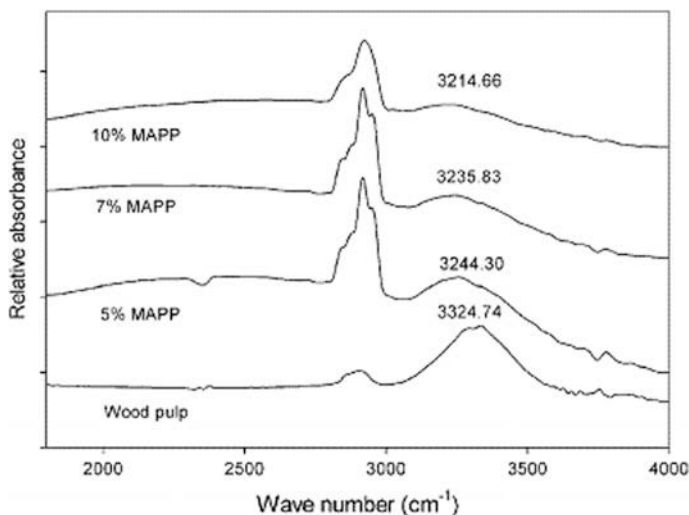


Fig. 11 FTIR spectra of 100% wood pulp and 30% wood pulp-PP bio-composite fiber with varying fractions of MAPP. Reproduced from Awal et al. (2009), [68]

corresponding to frequencies of vibrations between the bonds of the atoms. Since no two compounds reflect exactly similar infrared spectrum, the vibration frequency spectra become fingerprint for a particular compound [4]. FTIR is a very rapid analytical technique for the determination of short chain branching type in olefins. Small dissimilarities in the region of $1300\text{--}1400\text{ cm}^{-1}$ have been studied for the identification of different polyethylene types. Researchers have reported a linear relationship between the absorptions ratio at 1378 cm^{-1} (arising from methyl groups deformation) and the branching length in the copolymer [67]. As such, the FTIR ASTM test methods can be used for the quantification of the methyl group content in α -olefin copolymers [4].

Figure 11 shows FTIR spectra of samples of 100% wood pulp and 30% wood pulp-PP bio-composite fiber bearing different fractions of MAPP (maleated polypropylene) [68]. The C–H stretching vibrations ($2800\text{--}3000\text{ cm}^{-1}$) were observed in all the samples of pure wood pulp and bio-composite fibers. Particularly, the FTIR spectra of bio-composite fibers were significantly more intensive because of the reason that PP and MAPP would react with pure wood pulp. This reaction influenced the peak intensity of C–H stretching in the bio-composite fibers.

8.1.5 Crystallization Analysis Fractionation (CRYSTAF) and Temperature Rising Elution Fractionation (TREF)

Crystallization analysis fractionation (CRYSTAF) and temperature rising elution fractionation (TREF) are used for the determination of chemical composition

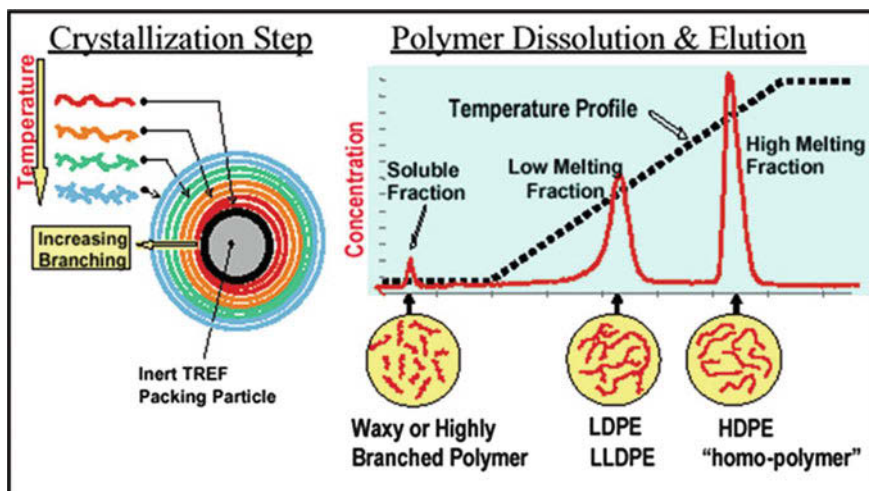


Fig. 12 Schematic presentation of the TREF process which involves crystallization and the dissolution/elution steps. Reproduced from Pasch et al. 2016, [60]

distribution (CCD) and comonomer distribution in olefins. Both the methods study the crystallization temperatures distribution [69, 70]. TREF works on the principle of measuring crystallization and elution temperature cycles followed by computation of the distribution of copolymers in the composition [60] (schematic of the process shown in Fig. 12). The olefins sample is first dissolved in a solvent (maintained at high temperature) and subsequently injected into a column composed of an inert support. The column is then cooled at a very slow rate to achieve crystallization. The chains crystallize in order of their increasing crystallinity. In the next step, elution temperature cycle is introduced to isolate the fractions physically. For this, the temperature of the column is gradually increased while the solvent is passing through. With the increasing temperature, the fractions are dissolved corresponding to their branching. The technique is frequently used to validate the presence of copolymers during the polymerization of olefins [71, 72].

CRYSTAF with simpler hardware design was introduced as a new analytical technique that avoids the additional elution temperature cycle step and physical separation of fractions. It helped to accelerate the CCD analysis of Polyolefins. The process works on crystallization based separation like TREF, but the fractionation takes place during the crystallization step itself. The instrument for CRYSTAF is composed of a filter containing crystallization vessel and an infrared detector [60, 73]. The latter component monitors the concentration of polymer solution after filtration and crystallization of olefins as induced by the decrease in temperature (normally used cooling rate of 0.1 °C/ min) [69, 73]. The presence of alike copolymers in olefins can lead to co-crystallization at a same cooling rate during CRYSTAF analysis. In such cases, TREF is preferred for analyzing copolymers because it is least affected by co-crystallization [4].

8.1.6 Crystallization Elution Fractionation (CEF)

Based on the similar principles of crystallizability, another separation technique was discovered in 2006. This approach comprised the use of a packed column and physical segregation of fractions in the crystallization step (like TREF and CRYSTAF technique). This new analytical approach is known as crystallization elution fractionation (CEF) and is relatively faster while offering higher resolution quantification of the CCD of semicrystalline polymers compared to TREF and CRYSTAF [4, 74]. The instrument of CEF is composed of an injection valve, a packed column, a pump and an IR detector. The sample is injected into the column through a pump flow and then dynamic crystallization process starts at a previously set cooling rate (generally 3 °C/min) and crystallization flow rate. The flow and cooling rates need adjustments such that the column temperature should be equal to room temperature when sample arrives to end of the column. The oven begins the heating program at the end of crystallization process and then the elution flow starts. Finally, the concentration and composition of species are determined through a dual wavelength IR detector attached at the end of the column [60, 75].

8.1.7 Osmometry

Polyolefin molecules are normally comprised of an asymmetric distribution of chain lengths. Some of them may have chains of very high molecular weight. Osmometry technique is used routinely for the assessment of molar mass of Polyolefins. This technique evaluates the number average molecular weight (M_n) [76]. Membrane osmometry (MO) [77] and vapour pressure osmometry (VPO) [58, 76] are the two types of osmometries used for the evaluation of the kinetic data during polymerization and copolymerization reactions. The membrane osmometer analyses the osmotic pressure by employing a pressure transducer. It is commonly used for high molecular weight polymers. However, problems with membrane permeation and polydispersity if polymer samples limit the usage of this technique [59, 77]. Vapour pressure osmometry, on the other hand, can be used for the determination of molecular weight of polymers with M_n less than 20,000 g/mol [58, 76].

8.1.8 Viscometry

Viscometry is a conventional method for the characterization of polymers. The analysis is used to measure the intrinsic viscosity which is related to molecular mass. Viscometry technique uses the universal calibration method to determine the molecular weight distribution, Mark-Houwink coefficients, and branching/structural information of the olefins and copolymers. Viscosity index so obtained, are also used to assign the class type to the olefins [58]. The technique can additionally detect the presence of oligomers and other small molecules. The above points make Viscometry as a preferable option over light scattering methods. Two types of

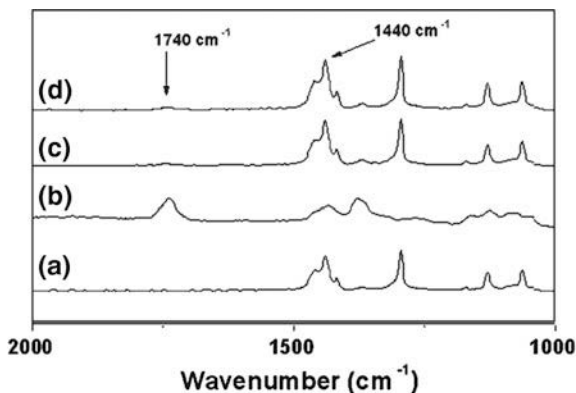
technique, i.e. Ubbelohde viscometer [78] and capillary viscometer [79] are most commonly used. In the former technique, the melted solution is allowed to pass through a vertical capillary under gravity, opposed by capillary forces. The time needed for some defined volume of solution to pass through the capillary is measured [80]. In the capillary viscometer, the solution is passed using inlet pressure at either side of a capillary and the difference in pressure is measured [81].

8.1.9 Raman Spectroscopic Analysis

Raman spectroscopy is a powerful chemical analysis technique owing to unique advantages of being a non-invasive and non-destructive method. Raman spectra of materials are their fingerprint characteristics. As such, it requires no sample preparation and only a small amount of material is sufficient for the analysis. Furthermore, Raman analysis is completed in a short period of time (e.g. few seconds to few minutes). Thus, Raman analysis is highly useful for real time monitoring of chemical reactions. With reference to plastic materials characterization, Raman spectroscopy can be profitably utilized for the following purposes: in real-time monitoring of polymerization reactions to control the processing time, quantitative compositional analysis of polymer melt streams, and waste plastic characterization in the recycling sector, especially for Polypropylene (PP) and Polyethylene (PE) identification [61].

As such, the initial use of real-time Raman spectroscopy for the estimation of crystallinity of Polyolefins was realized during blown film extrusion process [82–84]. The study established Raman spectroscopy as a robust and non-destructive technique to monitor crystallinity evolution in industrial settings. This analysis offers remote sampling capabilities when coupled via fibre optics. Raman spectroscopic systems (real-time polarized Raman spectroscopy) can also be used to analyze the molecular orientation evolution of trans C–C bond during the blown film extrusion of low-density polyethylene (LDPE). Spectra can be obtained at different locations along the blown film line, starting from the molten state and extending up to the solidified state [82]. In a study, composites of linear low-density poly(ethylene-co-butene) (PE) or maleated linear low-density poly(ethylene-co-butene) (M-PE) and cellulose (CEL), cellulose acetate (CA), cellulose acetate propionate (CAP), or cellulose acetate butyrate (CAB) were synthesized [85]. Raman spectra analysis was used to investigate the extraction of one phase with a selective solvent. Figure 13 shows the collected Raman spectra for M-PE, CAP, and the M-PE-CAP composite before and after extraction with acetone. The samples of PE-CEL and M-PE-CEL composites, for which the polyolefin chains are extracted, show intensity ratio of I_{1373}/I_{1440} in an increasing order increase after extraction. Whereas, the composites prepared with M-PE and CAP or CAB show practically same intensity ratio of I_{1740}/I_{1440} after extraction. The composites prepared with PE were characterized with a decrease in the intensity ratio of I_{1740}/I_{1440} after extraction to reveal that cellulose esters can be more easily removed in the absence of MA.

Fig. 13 Raman spectra obtained for **a** M-PE **b** CAP **c** M-PE-CAP composite before extraction with acetone, **d** M-PE-CAP composite after extraction with acetone. Reproduced from Kosaka et al. (2007), [85]



Some researchers have utilized Raman Spectroscopy for the characterization and identification of Polyolefins from the post-consumer plastic waste. The data procured was set up to define quality control logic that could be applied at industrial plant level for Polyolefins recycling [86].

8.2 Morphological Properties

8.2.1 Optical Microscopy

Optical microscopy of Polyolefins is frequently used for investigating the details of olefins microstructures. For instance, Fig. 14a, b show the optical microscopic image of a sample of polypropylene particles embedded with catalyst particles. As this example highlight, one can study and assess the completion of the polymerization process [87].

Similarly, an optical photograph of polyolefin biocomposites prepared with waste cardboard (CB) is shown in Fig. 8c [89]. This simple analysis reveals that large shear and compressive forces imparted to the material during the solid-state processing has resulted in major filler size reduction in the polymer composite.

8.2.2 Scanning Electron Microscopy (SEM)

Scanning electron microscope (SEM) technique probes the sample with high-intensity electrons. The collection of subsequently generated secondary electrons allow the study of surface morphology and measurement of particle sizes. Note that secondary electrons are emitted from the surface. SEM images provide useful information on the surface of relatively thicker and bigger samples. At times, SEM is used to produce a good representation of the 3-D structure of the sample

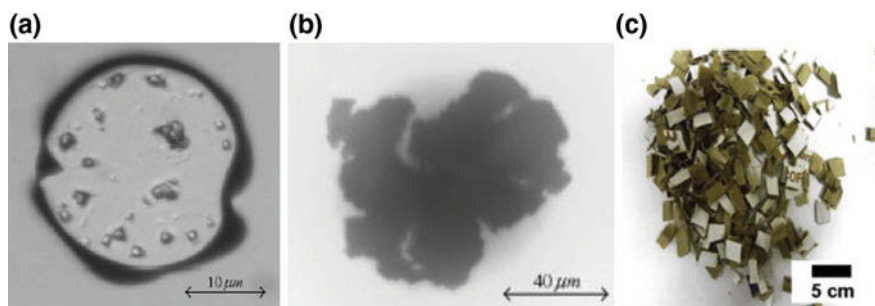


Fig. 14 Optical microscopic images of molten poly(propylene) particles showing catalyst fragments inside the polymer melt: **a** polymer particle produced by reaction of 10 min **b** polymer particle produced after 30 s. Reproduced from Abboud et al. (2005), [88]. **c** Optical photographs of 2–3 cm size waste cardboard (CB) pieces employed in the preparation of a polyolefin/CB composite [87, 89]. Reproduced from Iyer et al. (2015), [89]

and also have some major advantages of higher magnification and greater depth of field over conventional microscopes [90].

SEM is used to analyze the phase morphology of Polyolefins and their composite materials. These analyses can include the study of surface roughness and fracture toughness [91]. SEM can also reveal interface adhesion between the polymer fiber and matrix in which it is used. The measurement of adhesion allows assessing the stress transfer from matrix to fiber. The analysis of phase adherence between fibers and polymeric matrix can also reveal the propagation of the cracks generated during impact tests [92–94]. In some studies, SEM has been used to analyze the effects of addition of organo-montmorillonite and maleated Polyolefins on the phase morphology of the PP/HDPE blend. Such analysis was used to evaluate the change in two-phased morphology of the PP/HDPE blend [95]. As an example of SEM analysis of Polyolefin biocomposite, the investigations on the samples of low-density polypropylene (LDPP) with microcrystalline cellulose (MCC) and PP with cardboard (CB) are shown in Fig. 15 [89]. The fractured surfaces showed no signs of pull-out, highlighting that the filler did not agglomerate during the composite formation process. MCC, as such, can show strong inter-particle affinity due to the presence of numerous hydroxyl groups on the cellulose surface but SEM investigations of LDPE/MCC composites showed very good dispersion.

8.2.3 Atomic Force Microscopy (AFM)

Since its invention in 1986, the atomic force microscopy (AFM) has assumed a paramount significance for probing the samples at the nanoscale [96]. Different variations of AFM-based methods have been developed to generate information about electrical, magnetic, morphological, and mechanical parameters from various

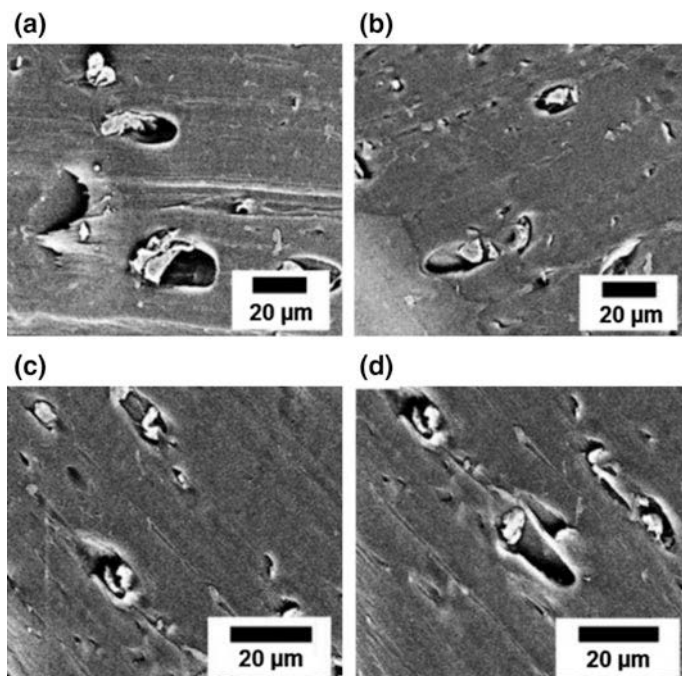


Fig. 15 SEM images of **a** 90/10 wt% LDPE/CB, **b** 85/15 wt% PP/CB, **c** 90/10 wt% LDPE/MCC, **d** 90/10 wt% PP/MCC. Reproduced from Iyer et al. (2015), [89]

materials. AFM has the ability to generate images based on mechanical properties which makes it particularly significant for the analysis of polymers (including Polyolefins). In such analyses, AFM can be operated in tapping mode (or amplitude modulation mode) phase imaging which is one of the most popular and routinely used mode the study of polymers [97]. Some other AFM based techniques used for the quantitative nanomechanical characterizations, include force modulation [97, 98], peak force quantitative nanomechanical mapping (QNM) [99], intermodulation spectroscopy [100], pulsed force mode [97, 101], contact resonance (CR) techniques [97], and force volume imaging [102]. In particular, the contact resonance (CR) techniques (or dynamic contact modes of AFM) were developed to study the elastic properties of stiff materials, such as polymer nanotubes [103, 104]. CR-FM can also be utilized for the study of viscoelastic properties of materials and storage [105, 106] and loss moduli of individual components in blends [99, 107].

The application of AFM studies on polymer composites can be elaborated by citing the example of a novel class of injection-moulded, toughened biocomposites which was engineered from pyrolyzed miscanthus based biocarbon, poly(octene ethylene) (POE) elastomer, and polypropylene (PP) [64]. The addition of maleic anhydride grafted PP (MAPP) controlled the morphology and adhesion between the filler and the matrix. AFM scans of the biocarbon interface in the presence and

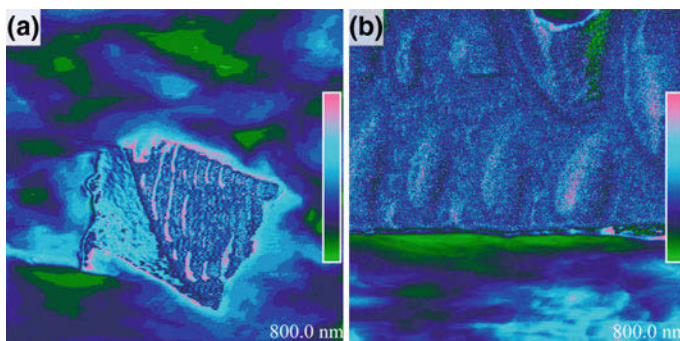


Fig. 16 AFM modulus mapping of a biocarbon–matrix interface in the small particle composites: **a** with 5% MAPP and **b** uncompatibilized. Reproduced from Behazin et al. (2017), [64]

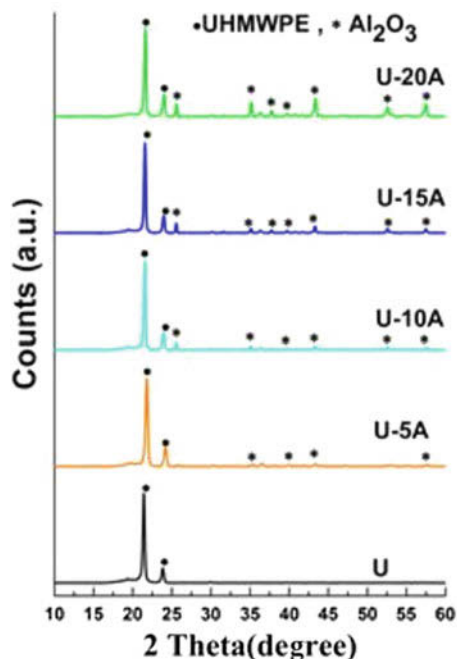
absence of MAPP (Fig. 16) are highlighted by few specific observations. The green colour in both the images represents the phase with the lowest modulus (i.e. POE phase). The blue and pink colours attribute to stiffer phases, i.e. PP, MAPP, and biocarbon particles. Biocarbon particles in the composites are found surrounded mainly by the blue phases in a compatibilized sample, whereas interphase mostly consists of the green phases in uncompatibilized composite. Thus, AFM studies helped to confirm that rubber was dispersed separately from biocarbon in the presence of MAPP.

8.2.4 X-Ray Diffraction (XRD)

XRD studies are used to elaborate crystal forms and dispersibility of different Polyolefins, such as PP and HDPE in the polyolefin blends/composites. XRD analysis can resolve both iso- and syndiotactic crystallinity. The small-angle X-ray scattering (SAXS) has been found useful to determine the lamellar thickness of Polyolefins and crystalline fibril morphology [108]. Whereas, the wide-angle X-ray scattering (SAXS) investigations can reveal the degree of crystallinity and discrimination between crystalline and amorphous phases [108]. SAXS also enables a direct access to the morphology and can quantitatively determine the thicknesses of alternating layers between the crystalline and amorphous regions of the lamellae morphology. The temperature-dependent SAXS measurements are used to verify the location of the order-disorder transition temperatures. SAXS also reveals critical information about the hydrophilic and hydrophobic phase separations in polyolefin composites [39, 109].

The application of XRD analysis for the characterization of ultrahigh molecular weight polyethylene (UHMWPE), which is considered as one of the best options for biopolymer materials, is shown in Fig. 17 [110]. The application of UHMWPE as biomaterial implants of human bone can be processed via surface plasma treatment, UV curing, chemical and physical surface treatment, and reinforcements.

Fig. 17 XRD spectra of UHMWPE- Al_2O_3 composites pellets [110]



Specifically, the reinforcement of metal nanoparticles (Fe, Cu, Ag, Zn), ceramics (Fe_3O_4 , Al_2O_3 , ZrO_3 , ZnO, AgO, MgO, Si_3N_4) or natural materials serve the purpose well. Figure 17 shows the XRD patterns of one such sample, i.e., Al_2O_3 reinforced UHMWPE compression-moulded composites. The dominant involvement of UHMWPE has suppressed the peaks of Al_2O_3 . The presence of UHMWPE is evident with two main characteristic peaks, i.e. at 21.9° and 24.18° . The involvement of Al_2O_3 is suggested with peaks observed at 35 , 37.9 and 43.58° . Thus, it can be concluded with XRD analysis that starting phases did not experience any degradation during the compression molding of UHMWPE- Al_2O_3 composites.

8.2.5 Transmission Electron Microscopy (TEM)

TEM also uses electrons like SEM, but here electrons are allowed to pass through a sample. As electrons strongly interact with the sample and need to pass through the sample, the samples are needed to prepare as very thin sections [90]. TEM is used to determine the lamellar thickness of polymers [111]. For instance, the morphology of isotactic polypropylene (iPP) as studied by TEM is shown in Fig. 18. The structure of iPP after non-isothermal melt-crystallization and melt-crystallized at a rate of cooling of 750 K/s have been shown as examples. It is clear that one can study the effect of the application of temperature programs during the annealing process of iP [111]. Similarly, TEM can be applied to study the biodegradation of Polyolefin composites.

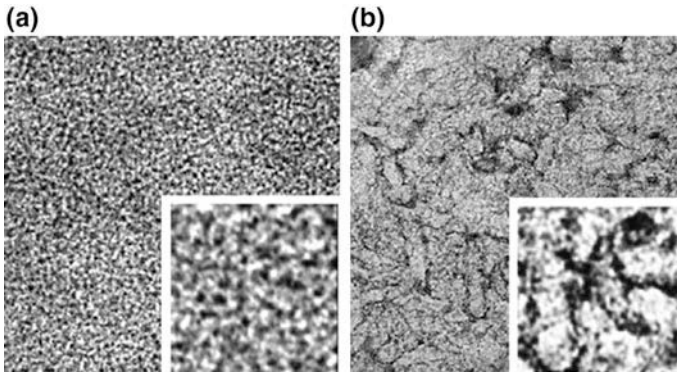


Fig. 18 TEM analysis of iPP, melt-crystallized at 750 K/s, and annealed **a** for a period of 60 min at 393 K; **b** for a period of 60 min at 433 K. Reproduced from Zia et al. [111]

8.3 Mechanical Properties

Mechanical characterization of Polyolefins is important to understand the material behaviour under the influence of applied loading. Mechanical testing machine (e.g. from MTS, Instron) can be used for this purpose, where the material is loaded in its bulk form to evaluate its various mechanical properties, such as yield strength, fracture stress or ultimate strength, elastic modulus or stiffness, Poisson's ratio and elongation [112].

8.3.1 Three-Point Flexural Test

Bending tests or flexural tests determine the mechanical properties of uni-directional composite materials. Flexural modulus and strength are obtained through three-point or four-point test configurations. In the former example, the contact zone between the specimen and cylindrical supports is changed as a result of the rotation of the cross sections in the deformation process. The four-point bending test involves contact between cylindrical loading noses and specimen [113]. For brittle polymers, the study of flexural strength is an essential parameter. The analysis of modulus of elasticity (i.e., the rigidity of the material) is also revealed during the flexural test. The three-point flexural test is a preferred option to evaluate the flexural strength of Polyolefins because of low values of data variation and less procedural complicity [114, 115].

8.3.2 Tensile Test

Tensile properties of Polyolefins are measured before their applications in actual designs [116]. For instance, the tensile test method is useful to assess the improvement in the in-plane tensile properties of polyolefin matrix composite materials when they are reinforced by the high-modulus fibers. The measurement of tensile properties is important from the point of view of material specifications and quality assurance. The tensile tests can yield information about the ultimate tensile strain, ultimate tensile strength, Poisson's ratio, tensile chord modulus of elasticity and transition strain [117].

8.3.3 Dynamic Mechanical Analysis

Viscoelastic property of Polyolefins can be assessed by dynamic mechanical techniques which are among the most popular one of different available methods. The dynamic mechanical analysis (DMA) can be readily applied to both polymeric solids and liquid samples. In this method, a small cyclic strain is applied to a sample followed by the measurement of the resultant stress response, or sometimes vice-versa [118]. DMA can be used to determine polymer properties like molecular relaxation processes, inherent mechanical or flow properties with respect to time and temperature, viscoelastic transitions or relaxations, glass transition temperature, (T_g), and secondary transitions in amorphous and crystalline polymers [118].

9 Degradation of Polyolefins and Composites

9.1 Ageing and Corrosion

Ageing of plastics is a relatively complex process. Under the influence of harsh and aggressive environments, polymers may experience a change in their material properties due to the involvement of physical and/or chemical processes [119]. Such ageing of polymers can be accounted by the action of sunlight, oxygen, temperature, or other harmful atmospheric emissions [120]. Therefore, the Polyolefins and their composites can also reflect sudden changes in their macroscopic properties after a certain induction period. The ageing of Polyolefins can also result in their catastrophic failure in form of embrittlement and sometimes total disintegration [121, 122].

The corrosion type of degradation of Polyolefins can happen because of their unavoidable interaction with air pollutants (e.g, particulate matter, SO_2 , hydrocarbons, N_xO_y , atomic oxygen, ozone, singlet oxygen, etc.). The corrosion can lead to affect the material properties like loss of gloss by abrasion, loss of reinforcement and breakup, crazing and cracking, and or leaching [8]. Sometimes, the

electrochemical corrosion can also be observed in the polymer (e.g., in EVA, PE, Butyl Rubber coated metal surfaces) [123–125].

9.2 Chemical Degradation

Stereoregular Polyolefins are often inert toward the attack of chemical reagents. The reagents like alkalis, aqueous acid and basic salts, inorganic and organic acids; or even KMnO_4 , $\text{K}_2\text{Cr}_2\text{O}_7$, and KNO_3 do not necessarily have much effect on stereoregular Polyolefins [8]. Their chemical degradation is achieved by strong oxidizing agents, such as H_2SO_4 [126]. For example, H_2SO_4 can cause rapid deterioration of the mechanical properties of PE through acidolysis [127]. Likewise, it can also be achieved through the action of liquid or gaseous chlorine or fluorine [128, 129]. Specifically, the use of dry chlorine may not cause embrittlement of LDPE but bromine or iodine can get absorbed and diffused through polyethylene (PE) to cause serious harm to the mechanical integrity of Polyolefins [8].

9.3 Biodegradation

The microbial attack does not normally affect the properties of Polyolefins as the associated action limits only to the chain ends. Nonetheless, the paraffin with $\text{MW} \leq 450$ can show some biodegradability, while low MW Polyolefins could be partially degraded [130, 131]. Therefore, strategies have been suggested to first reduce the MW of the Polyolefins with some additional process, which can then follow the action of microbes under suitable conditions [8, 132].

Apart from the other degradation methods, Polyolefins can also be subjected to mechanical [133–135], ultrasonic [136], radiation-induced [137], oxidative [132], photolysis [132], and thermolytic degradation [138] approaches.

10 Applications of Polyolefins and Eco-Friendly Composites

Polyolefins are used in a wide range of applications, ranging from our daily-life materials to high-end industrial products. Among all, Polyethylene is one of the most widely used commodity thermoplastic. The consumption of HDPE is extremely large in many sectors followed by LLDPE and LDPE. They are very commonly employed in the building and construction, electronics, electrical, consumer goods, automotive industries, etc. [139–143]. The application of PE in the manufacturing of various consumer goods includes the production of items like pipes,

toys, containers, lids, plastic bags, buckets, covers, plastic wraps, sheets, films, stretch wraps, bottles and extrusion coated paper cartons [144–147]. Isotactic polypropylene (i-PP) is probably the second most important Polyolefin finding applications in many industries just like PE. It is a competitor of HDPE in various areas [148, 149]. When compared with HDPE, i-PP has characteristics of the higher melting point, improved crack resistance, an increased heat deflection temperature, and improved tensile strength. Nonetheless, HDPE is superior to i-PP with regard to thermal stability, exposure to light (UV) and susceptibility toward oxidative degradation. As far as application areas are concerned, i-PP enjoys better acceptability in case of more demanding applications. HDPE is more useful when material specification requires high resistance against thermooxidative degradation.

Another Polyolefin, Polyisobutene (PIB) is not produced on high production scale but is particularly employed in applications like sealants, chewing gum, adhesives, cable filling, synthetic rubber (butyl rubber), roofing membranes, and lubricants. Its low molecular grades variants are viscous oily liquids in nature, while the mid-range is more sticky materials. The high molecular grades PIBs are generated as elastic rubbery materials. Polybutene-1 (PB-1) is a low volume polyolefin which is highly compatible with polypropylene as both of them bear similar molecular structures. Their composites help in to improve the mechanical properties at elevated temperatures. PB-1 is used in applications like the pressure pipes for the supply of hot and cold (drinking) water, and consumer and medical packaging. Its low molecular weight variants are used in the production of paper laminates, adhesives, and sealants to manage tack and peel strength. They are also compatible with a variety of nonpolar resins including PP, PE, SIS, EVA, and SBS. A summary of applications of Polyolefins is presented in Table 1.

The applications of thermoplastic natural fibre-containing eco-friendly composites include their deployment in door and window frames, railings for the parapet wall systems, and decking and furniture material. The applications of eco-friendly composites are expected to increase significantly in near future. The favourable economics of natural fiber composites seems to popularize their use to a great extent as such types of composites can facilitate sustainable development of cost-effective and ecological technologies. The demand for lighter and strong polymer materials is increasing in many sectors, such as environmental friendly

Table 1 Summarized of applications of major categories of Polyolefins

Type	Applications
Low-density polyethylene (LDPE)	Shrink film, carry bags, heavy-duty refuse bags
High-density polyethylene (HDPE)	Crates and boxes, bottles (used in food products, detergents, cosmetics), food containers, industrial wrappings, carry bags, drums for food, beverages, and chemicals
Linear low-density polyethylene (LLDPE)	Stretch film, industrial packaging film, thin-walled containers, heavy-duty medium and small bags
Polypropylene (PP)	Food packaging (e.g. yoghurt and margarine tubs)

automotive components. For instance, the hemp mats in glass-fibre reinforced thermosets have been reported more ecoefficient than the conventional glass-fibre alternative. Likewise, the life cycle of the wood-fibre reinforced PP composites suggests better environmental protection than PP. The addition of biodegradable waste (e.g., rice husks, cotton linter) during the formation of composite materials can also present a viable way of solving the problem of waste disposal.

11 Conclusion

Traditionally used polymers involved synthesis approaches which posed serious health hazards and evolution of toxic gases. Their recycling was also not environmentally sustainable and complete. In this particular context, various classes of polyolefins have enabled an environmentally sustainable use of polymers. Polyolefins synthesized from natural resins generate fewer waste products during production while also helping in safer disposal. The enormous physical properties of polyolefins, such as mechanical strength, durability, elasticity, etc. can be tailored via selection of suitable synthesis conditions and optimized functionalization. Polyolefins support the addition of biodegradable materials (e.g., natural fiber and waste) in them to make composites having features of low-cost, strength, low density, and more importantly, an ecological efficiency. Future development of polyolefins is more focused on achieving lightweight designs, and even better recyclability, reusability.

References

1. Boffa LS, Novak BM (2000) Copolymerization of polar monomers with olefins using transition-metal complexes. *Chem Rev* 100:1479–1494
2. Soares JB (2007) An overview of important microstructural distributions for polyolefin analysis. In: *Macromolecular symposia*. Wiley Online Library, pp 1–12
3. Pasch H (2001) Recent developments in polyolefin characterization. In: *Macromolecular symposia*. Wiley Online Library, pp 91–98
4. Alkhazal A (2011) Characterization of ethylene/ α -olefin copolymers made with a single-site catalyst using crystallization elution fractionation. University of Waterloo
5. Soares JB, McKenna T, Cheng C (2007) Coordination polymerization. *Polym React Eng* 29–117
6. Koltzenburg S, Maskos M, Nuyken O (2017) Introduction and basic concepts. In: *Polymer chemistry*. Springer, pp 1–16
7. Storr A, Jones K, Laubengayer A (1968) The partial hydrolysis of ethylalane compounds. *J Am Chem Soc* 90:3173–3177
8. Vasile C, Seymour RB (2000) *Handbook of polyolefins*. Marcel Dekker, New York
9. Sinn H (1995) Proposals for structure and effect of methylalumoxane based on mass balances and phase separation experiments. In: *Macromolecular symposia*. Wiley Online Library, pp 27–52

10. Kaminsky W (1998) Highly active metallocene catalysts for olefin polymerization. *J Chem Soc Dalton Trans* 1413–1418
11. Bubeck R (2002) Structure–property relationships in metallocene polyethylenes. *Mater Sci Eng R Rep* 39:1–28
12. Patil AO (2000) Functional polyolefins. *Chem Inno* 30:19–24
13. Novák I, Borsig E, Hřčková LU, Fiedlerova A, Kleinova A, Pollak V (2007) Study of surface and adhesive properties of polypropylene grafted by maleic anhydride. *Polym Eng Sci* 47:1207–1212
14. Dong J-Y, Hu Y (2006) Design and synthesis of structurally well-defined functional polyolefins via transition metal-mediated olefin polymerization chemistry. *Coord Chem Rev* 250:47–65
15. Nakamura A, Ito S, Nozaki K (2009) Coordination-insertion copolymerization of fundamental polar monomers. *Chem Rev* 109:5215–5244
16. Franssen NM, Reek JN, de Bruin B (2013) Synthesis of functional ‘polyolefins’: state of the art and remaining challenges. *Chem Soc Rev* 42:5809–5832
17. Chung TM (2002) Functionalization of polyolefins. Elsevier
18. Boen NK, Hillmyer MA (2005) Post-polymerization functionalization of polyolefins. *Chem Soc Rev* 34:267–275
19. Bielawski CW, Grubbs RH (2007) Living ring-opening metathesis polymerization. *Prog Polym Sci* 32:1–29
20. Opper KL, Fassbender B, Brunklaus G, Spiess HW, Wagener KB (2009) Polyethylene functionalized with precisely spaced phosphonic acid groups. *Macromolecules* 42:4407–4409
21. Opper KL, Markova D, Klapper M, Müllen K, Wagener KB (2010) Precision phosphonic acid functionalized polyolefin architectures. *Macromolecules* 43:3690–3698
22. Ouchi M, Terashima T, Sawamoto M (2009) Transition metal-catalyzed living radical polymerization: toward perfection in catalysis and precision polymer synthesis. *Chem Rev* 109:4963–5050
23. Finch C (1985) Encyclopedia of polymer science and engineering, volume 2, anionic polymerisation to cationic polymerisation editor-in-chief Jacqueline I. Kroschwitz. In: Mark HF, Bikales NM, Overberger CG, Menges G (eds) Wiley-Interscience, New York, pp xxiv+ 814, subscription price £ 175.00 (US 205.00) single volume price £210.00 (US 240.00). ISBN 0-471-88786-2 (vol 2), *British Polymer Journal*, vol 17, pp 377–377
24. Berkefeld A, Mecking S (2008) Coordination copolymerization of polar vinyl monomers H₂C=CHX. *Angew Chem Int Ed* 47:2538–2542
25. Lopez RG, D’Agosto F, Boisson C (2007) Synthesis of well-defined polymer architectures by successive catalytic olefin polymerization and living/controlled polymerization reactions. *Prog Polym Sci* 32:419–454
26. Yanjarappa M, Sivaram S (2002) Recent developments in the synthesis of functional poly (olefin)s. *Prog Polym Sci* 27:1347–1398
27. Amin SB, Marks TJ (2008) Versatile pathways for in situ polyolefin functionalization with heteroatoms: catalytic chain transfer. *Angew Chem Int Ed* 47:2006–2025
28. Matsugi T, Kojoh SI, Kawahara N, Matsuo S, Kaneko H, Kashiwa N (2003) Synthesis and morphology of polyethylene-block-poly (methyl methacrylate) through the combination of metallocene catalysis with living radical polymerization. *J Polym Sci Part A: Polym Chem* 41:3965–3973
29. Yagci Y, Tasdelen MA (2006) Mechanistic transformations involving living and controlled/living polymerization methods. *Prog Polym Sci* 31:1133–1170
30. Rezakazemi M, Sadrzadeh M, Matsuura T (2018) Thermally stable polymers for advanced high-performance gas separation membranes. *Prog Energy Combust Sci* 66:1–41
31. Rezakazemi M, Ebadi Amooghin A, Montazer-Rahmati MM, Ismail AF, Matsuura T (2014) State-of-the-art membrane based CO₂ separation using mixed matrix membranes (MMMs): an overview on current status and future directions. *Prog Polym Sci* 39:817–861

32. Chung T, Janvikul W (1999) Borane-containing polyolefins: synthesis and applications. *J Organomet Chem* 581:176–187
33. Kaneyoshi H, Inoue Y, Matyjaszewski K (2005) Synthesis of block and graft copolymers with linear polyethylene segments by combination of degenerative transfer coordination polymerization and atom transfer radical polymerization. *Macromolecules* 38:5425–5435
34. White JL, Kim EK (1991) *Twin screw extrusion: technology and principles*. Hanser, Munich
35. Salleh FM, Hassan A, Yahya R, Azzahari AD (2014) Effects of extrusion temperature on the rheological, dynamic mechanical and tensile properties of kenaf fiber/HDPE composites. *Compos B Eng* 58:259–266
36. Mulinari DR, Voorwald HJ, Cioffi MOH, Da Silva MLC, da Cruz TG, Saron C (2009) Sugarcane bagasse cellulose/HDPE composites obtained by extrusion. *Compos Sci Technol* 69:214–219
37. Mano B, Araújo J, Spinacé M, De Paoli M-A (2010) Polyolefin composites with curaua fibres: effect of the processing conditions on mechanical properties, morphology and fibres dimensions. *Compos Sci Technol* 70:29–35
38. AlMaadeed MA, Nogellova Z, Mičušík M, Novak I, Krupa I (2014) Mechanical, sorption and adhesive properties of composites based on low density polyethylene filled with date palm wood powder. *Mater Des* 53:29–37
39. Zhang M, Shan C, Liu L, Liao J, Chen Q, Zhu M, Wang Y, An L, Li N (2016) Facilitating anion transport in polyolefin-based anion exchange membranes via bulky side chains. *ACS Appl Mater Interfaces* 8:23321–23330
40. Rao S, Jayaraman K, Bhattacharyya D (2012) Micro and macro analysis of sisal fibre composites hollow core sandwich panels. *Compos B Eng* 43:2738–2745
41. Brito GF, Agrawal P, Araújo EM, de Mélo TJ (2012) Polylactide/biopolyethylene bioblends. *Polímeros* 22:427–429
42. Castro D, Ruvolo-Filho A, Frollini E (2012) Materials prepared from biopolyethylene and curaua fibers: Composites from biomass. *Polym Testing* 31:880–888
43. Jacob M, Francis B, Varughese K, Thomas S (2006) The effect of silane coupling agents on the viscoelastic properties of rubber biocomposites. *Macromol Mater Eng* 291:1119–1126
44. Donath S, Militz H, Mai C (2004) Wood modification with alkoxysilanes. *Wood Sci Technol* 38:555–566
45. Fang L, Chang L, Guo W-J, Chen Y, Wang Z (2014) Influence of silane surface modification of veneer on interfacial adhesion of wood–plastic plywood. *Appl Surf Sci* 288:682–689
46. Xie Y, Krause A, Militz H, Steuernagel L, Mai C (2013) Effects of hydrophobation treatments of wood particles with an amino alkylsiloxane co-oligomer on properties of the ensuing polypropylene composites. *Compos A Appl Sci Manuf* 44:32–39
47. Spiridon I, Darie RN, Bodîrlău R, Teacă C-A, Doroftei F (2013) Polypropylene-based composites reinforced by toluene diisocyanate modified wood. *J Compos Mater* 47:3451–3464
48. Bodîrlău R, Teacă C-A, Resmerita A-M, Spiridon I (2012) Investigation of structural and thermal properties of different wood species treated with toluene-2, 4-diisocyanate. *Cellul Chem Technol* 46:381
49. Kabir M, Wang H, Lau K, Cardona F (2012) Chemical treatments on plant-based natural fibre reinforced polymer composites: an overview. *Compos B Eng* 43:2883–2892
50. Li Y (2014) Characterization of acetylated eucalyptus wood fibers and its effect on the interface of eucalyptus wood/polypropylene composites. *Int J Adhes Adhes* 50:96–101
51. Li X, Tabil LG, Panigrahi S (2007) Chemical treatments of natural fiber for use in natural fiber-reinforced composites: a review. *J Polym Environ* 15:25–33
52. Wei L, McDonald AG, Freitag C, Morrell JJ (2013) Effects of wood fiber esterification on properties, weatherability and biodurability of wood plastic composites. *Polym Degrad Stab* 98:1348–1361
53. Ahmed AS, Islam MS, Hassan A, Haafiz MM, Islam KN, Arjmandi R (2014) Impact of succinic anhydride on the properties of jute fiber/polypropylene biocomposites. *Fibers Polym* 15:307

54. Mamun AA, Heim H-P, Beg DH, Kim TS, Ahmad SH (2013) PLA and PP composites with enzyme modified oil palm fibre: a comparative study. *Compos A Appl Sci Manuf* 53:160–167
55. Ortín A, López E, del Hierro P, Sancho-Tello J, Yau WW (2018) Simplified robust triple detection methods for high temperature GPC analysis of polyolefins. In: *Macromolecular symposia*. Wiley Online Library, pp 1700044
56. Song S, Fu Z, Xu J, Fan Z (2017) Synthesis of functional polyolefins via ring-opening metathesis polymerization of ester-functionalized cyclopentene and its copolymerization with cyclic comonomers. *Polym Chem* 8:5924–5933
57. Jung M, Lee Y, Kwak S, Park H, Kim B, Kim S, Lee KH, Cho HS, Hwang KY (2016) Analysis of chain branch of polyolefins by a new proton NMR approach. *Anal Chem* 88:1516–1520
58. Liu Y, Wang Z, Zhang X (2012) Characterization of supramolecular polymers. *Chem Soc Rev* 41:5922–5932
59. Monrabal B (2013) Polyolefin characterization: recent advances in separation techniques. In: *Polyolefins: 50 years after Ziegler and Natta*. Springer, pp 203–251
60. Pasch H, Malik MI (2016) *Advanced separation techniques for polyolefins*. Springer
61. Serranti S, Bonifazi G (2010) Post-consumer polyolefins (PP-PE) recognition by combined spectroscopic sensing techniques. *Open Waste Manag J* 3(1):35–45
62. Soares JB (2004) Polyolefins with long chain branches made with single-site coordination catalysts: a review of mathematical modeling techniques for polymer microstructure. *Macromol Mater Eng* 289:70–87
63. Sugumaran V, Prakash S, Arora AK, Kapur GS, Narula AK (2017) Thermal cracking of potato-peel powder-polypropylene biocomposite and characterization of products—pyrolysed oils and bio-char. *J Anal Appl Pyrol* 126:405–414
64. Behazin E, Misra M, Mohanty AK (2017) Sustainable biocomposites from pyrolyzed grass and toughened polypropylene: structure-property relationships. *ACS Omega* 2:2191–2199
65. Ndiripo A, Albrecht A, Monrabal B, Wang J, Pasch H (2018) Chemical composition fractionation of olefin plastomers/elastomers by solvent and thermal gradient interaction chromatography. *Macromol Rapid Commun* 39(6):1700703
66. Tronc E, Hernandez-Escobar C, Ibarra-Gomez R, Estrada-Monje A, Navarrete-Bolanos J, Zaragoza-Contreras E (2007) Blue agave fiber esterification for the reinforcement of thermoplastic composites. *Carbohyd Polym* 67:245–255
67. Zhang Q, Chen P, Xie X, Cao X (2009) An effective method to identify the type and content of α -olefin in polyolefine copolymer by fourier transform infrared-differential scanning calorimetry. *J Appl Polym Sci* 113:3027–3032
68. Awal A, Ghosh S, Sain M (2009) Thermal properties and spectral characterization of wood pulp reinforced bio-composite fibers. *J Therm Anal Calorim* 99:695–701
69. Monrabal B (2006) Microstructure characterization of polyolefins. TREF and CRYSTAF. In: *Studies in surface science and catalysis*. Elsevier, pp 35–42
70. Monrabal B (2015) Separation of ethylene-propylene copolymers by crystallization and adsorption mechanisms. A journey inside the analytical techniques. In: *Macromolecular symposia*. Wiley Online Library, pp 147–166
71. Takeuchi D, Chiba Y, Takano S, Kurihara H, Kobayashi M, Osakada K (2017) Ethylene polymerization catalyzed by dinickel complexes with a double-decker structure. *Polym Chem* 8:5112–5119
72. Xue Y-H, Bo S-Q, Ji X-L (2015) Comparison of chain structures between high-speed extrusion coating polyethylene resins by preparative temperature rising elution fractionation and cross-fractionation. *Chin J Polym Sci* 33:1586–1597
73. Albrecht A, Jayaratne K, Jeremic L, Sumerin V, Pakkanen (2016) Describing and quantifying the chemical composition distribution in unimodal and multimodal ZN-polyethylene using CRYSTAF. *J Appl Polym Sci* 133(9):43089 (3–8)

74. Monrabal B, Sancho-Tello J, Mayo N, Romero L (2007) Crystallization elution fractionation. A new separation process for polyolefin resins. In: *Macromolecular symposia*. Wiley Online Library, pp 71–79
75. Monrabal B, Romero L, Mayo N, Sancho-Tello J (2009) Advances in crystallization elution fractionation. In: *Macromolecular symposia*. Wiley Online Library, pp 14–24
76. Fadeeva V, Tikhova V, Nikulicheva O, Oleynik I, Oleynik I (2010) Composition determination of post-metallocene olefin polymerization catalysts. *J Struct Chem* 51:186–191
77. Young RJ, Lovell PA (2011) *Introduction to polymers*. CRC Press
78. Mialon L, Pemba AG, Miller SA (2010) Biorenewable polyethylene terephthalate mimics derived from lignin and acetic acid. *Green Chem* 12:1704–1706
79. Prut E, Nedorezova P, Klyamkina A, Medintseva T, Zhorina L, Kuznetsova O, Chapurina A, Aladyshev A (2013) Blend polyolefin elastomers based on a stereoblock elastomeric PP. *Polym Sci Ser A* 55:177–185
80. Yi J, Liu Y, Pan D, Cai X (2013) Synthesis, thermal degradation, and flame retardancy of a novel charring agent aliphatic—aromatic polyamide for intumescent flame retardant polypropylene. *J Appl Polym Sci* 127:1061–1068
81. Jukić A, Faraguna F, Franjić I, Kuzmić S (2017) Molecular interaction and viscometric behavior of mixtures of polyolefin and poly (styrene-co-dodecyl methacrylate-co-octadecyl methacrylate) rheology modifiers in solution of lubricating base oil. *J Ind Eng Chem* 56:270–276
82. Gururajan G, Ogale AA (2009) Molecular orientation evolution during low-density polyethylene blown film extrusion using real-time Raman spectroscopy. *J Raman Spectrosc* 40:212–217
83. Cherukupalli S, Ogale A (2004) Integrated experimental–modelling study of microstructural development and kinematics in a blown film extrusion process: I. Real-time Raman spectroscopy measurements of crystallinity. *Plast Rubber Compos* 33:367–371
84. Cherukupalli SS, Ogale AA (2004) Online measurements of crystallinity using Raman spectroscopy during blown film extrusion of a linear low-density polyethylene. *Polym Eng Sci* 44:1484–1490
85. Kosaka P, Kawano Y, Petri H, Fantini M, Petri D (2007) Structure and properties of composites of polyethylene or maleated polyethylene and cellulose or cellulose esters. *J Appl Polym Sci* 103:402–411
86. Serranti S, Gargiulo A, Bonifazi G (2011) Characterization of post-consumer polyolefin wastes by hyperspectral imaging for quality control in recycling processes. *Waste Manag* 31:2217–2227
87. McKenna TF, Di Martino A, Weickert G, Soares JB (2010) Particle growth during the polymerisation of olefins on supported catalysts, 1–nascent polymer structures. *Macromol React Eng* 4:40–64
88. Abboud M, Denifl P, Reichert KH (2005) Fragmentation of Ziegler-Natta catalyst particles during propylene polymerization. *Macromol Mater Eng* 290:558–564
89. Iyer KA, Flores AM, Torkelson JM (2015) Comparison of polyolefin biocomposites prepared with waste cardboard, microcrystalline cellulose, and cellulose nanocrystals via solid-state shear pulverization. *Polymer* 75:78–87
90. McMahon G (2008) *Analytical instrumentation: a guide to laboratory, portable and miniaturized instruments*. Wiley
91. Fang C, Nie L, Liu S, Yu R, An N, Li S (2013) Characterization of polypropylene–polyethylene blends made of waste materials with compatibilizer and nano-filler. *Compos B Eng* 55:498–505
92. Spiridon I (2014) I. Natural fiber-polyolefin composites. Mini-review. *Cellul Chem Technol* 48:599–611
93. Fávoro SL, Lopes MS, de Carvalho Neto AGV, de Santana RR, Radovanovic E (2010) Chemical, morphological, and mechanical analysis of rice husk/post-consumer polyethylene composites. *Compos A Appl Sci Manuf* 41:154–160

94. May-Pat A, Valadez-González A, Herrera-Franco PJ (2013) Effect of fiber surface treatments on the essential work of fracture of HDPE-continuous henequen fiber-reinforced composites. *Polym Test* 32:1114–1122
95. Chiu F-C, Yen H-Z, Lee C-E (2010) Characterization of PP/HDPE blend-based nanocomposites using different maleated polyolefins as compatibilizers. *Polym Test* 29:397–406
96. Binnig G, Quate CF, Gerber C (1986) Atomic force microscope. *Phys Rev Lett* 56:930
97. Yablon DG, Gannepalli A, Proksch R, Killgore J, Hurley DC, Grabowski J, Tsou AH (2012) Quantitative viscoelastic mapping of polyolefin blends with contact resonance atomic force microscopy. *Macromolecules* 45:4363–4370
98. Radmacher M, Tillmann R, Gaub H (1993) Imaging viscoelasticity by force modulation with the atomic force microscope. *Biophys J* 64:735–742
99. Young T, Monclus M, Burnett T, Broughton W, Ogin S, Smith P (2011) The use of the PeakForce™ quantitative nanomechanical mapping AFM-based method for high-resolution Young's modulus measurement of polymers. *Meas Sci Technol* 22:125703
100. Platz D, Tholén EA, Pesen D, Haviland DB (2008) Intermodulation atomic force microscopy. *Appl Phys Lett* 92:153106
101. Rosa-Zeiser A, Weilandt E, Hild S, Marti O (1997) The simultaneous measurement of elastic, electrostatic and adhesive properties by scanning force microscopy: pulsed-force mode operation. *Meas Sci Technol* 8:1333
102. Wang D, Fujinami S, Liu H, Nakajima K, Nishi T (2010) Investigation of reactive polymer-polymer interface using nanomechanical mapping. *Macromolecules* 43:5521–5523
103. Hurley DC (2009) Contact resonance force microscopy techniques for nanomechanical measurements. In: *Applied scanning probe methods*, vol XI. Springer, pp 97–138
104. Cuenot S, Frétiigny C, Demoustier-Champagne S, Nysten B (2003) Measurement of elastic modulus of nanotubes by resonant contact atomic force microscopy. *J Appl Phys* 93:5650–5655
105. Gannepalli A, Yablon D, Tsou A, Proksch R (2011) Mapping nanoscale elasticity and dissipation using dual frequency contact resonance AFM. *Nanotechnology* 22:355705
106. Killgore JP, Yablon D, Tsou A, Gannepalli A, Yuya P, Turner J, Proksch R, Hurley D (2011) Viscoelastic property mapping with contact resonance force microscopy. *Langmuir* 27:13983–13987
107. Proksch R, Yablon DG (2012) Loss tangent imaging: theory and simulations of repulsive-mode tapping atomic force microscopy. *Appl Phys Lett* 100:073106
108. Deplace F, Wang Z, Lynd NA, Hotta A, Rose JM, Hustad PD, Tian J, Ohtaki H, Coates GW, Shimizu F (2010) Processing-structure-mechanical property relationships of semicrystalline polyolefin-based block copolymers. *J Polym Sci Part B: Polym Phys* 48:1428–1437
109. Mahanthappa MK, Lim LS, Hillmyer MA, Bates FS (2007) Control of mechanical behavior in polyolefin composites: integration of glassy, rubbery, and semicrystalline components. *Macromolecules* 40:1585–1593
110. Patel AK, Trivedi P, Balani K (2014) Processing and mechanical characterization of compression-molded ultrahigh molecular weight polyethylene biocomposite reinforced with aluminum oxide. *J Nanosci Nanoeng Appl* 4:1–11
111. Zia Q, Androsch R, Radosch H-J, Ingoliç E (2008) Crystal morphology of rapidly cooled isotactic polypropylene: a comparative study by TEM and AFM. *Polym Bull* 60:791
112. S.R. Hartshorn, *Structural adhesives: chemistry and technology*, Springer Science & Business Media, 2012
113. Mujika F (2006) On the difference between flexural moduli obtained by three-point and four-point bending tests. *Polym Test* 25:214–220
114. Junior R, Adalberto S, Zanchi CH, Carvalho RVD, Demarco FF (2007) Flexural strength and modulus of elasticity of different types of resin-based composites. *Braz Oral Res* 21:16–21
115. Chung S, Yap A, Chandra S, Lim C (2004) Flexural strength of dental composite restoratives: comparison of biaxial and three-point bending test. *J Biomed Mater Res B Appl Biomater* 71:278–283

116. Carlsson LA, Adams DF, Pipes RB (2014) Experimental characterization of advanced composite materials. CRC press
117. Standard AS (2008) Standard test method for tensile properties of polymer matrix composite materials. ASTM D3039/D M 3039:2008
118. Menczel JD, Prime RB (2014) Thermal analysis of polymers: fundamentals and applications. Wiley
119. Rowe RK, Islam M, Hsuan Y (2009) Effects of thickness on the aging of HDPE geomembranes. *J Geotech Geoenvironmental Eng* 136:299–309
120. Corti A, Muniyasamy S, Vitali M, Imam SH, Chiellini E (2010) Oxidation and biodegradation of polyethylene films containing pro-oxidant additives: synergistic effects of sunlight exposure, thermal aging and fungal biodegradation. *Polym Degrad Stab* 95:1106–1114
121. Dehbi A, Mourad A, Bouaza A (2011) Ageing effect on the properties of tri-layer polyethylene film used as greenhouse roof. *Procedia Eng* 10:466–471
122. Baldwin FP, Strate GV (1972) Polyolefin elastomers based on ethylene and propylene. *Rubber Chem Technol* 45(3):709–881
123. Samimi A (2012) Study an analysis and suggest new mechanism of 3 layer polyethylene coating corrosion cooling water pipeline in oil refinery in Iran. *Int J Innov Appl Stud ISSR J* 1(2):216–225
124. Castaneda H, Benetton XD (2008) SRB-biofilm influence in active corrosion sites formed at the steel-electrolyte interface when exposed to artificial seawater conditions. *Corros Sci* 50:1169–1183
125. Kempe M (2011) Overview of scientific issues involved in selection of polymers for PV applications. In: *Photovoltaic Specialists Conference (PVSC), 2011 37th IEEE, IEEE*, pp 000085–000090
126. Czop M, Biegańska J Impact of selected chemical substances on the degradation of the polyolefin materials 66(4):307–314
127. Pant D (2011) Degradation of various low density polyethylene products on alumina surface with sulphuric acid—DTS technique. *J Solid Waste Technol Manag* 37:47–54
128. Rubino M, Netramai S, Auras R, Annous BA (2010) Effect of chlorine dioxide gas on physical, thermal, mechanical, and barrier properties of polymeric packaging materials. *J Appl Polym Sci* 115:1742–1750
129. Eng J, Sassi T, Steele T, Vitarelli G (2011) The effects of chlorinated water on polyethylene pipes. *Plast Eng* 67:18
130. Shah AA, Hasan F, Hameed A, Ahmed S (2008) Biological degradation of plastics: a comprehensive review. *Biotechnol Adv* 26:246–265
131. Sheik S, Chandrashekar K, Swaroop K, Somashekarappa H (2015) Biodegradation of gamma irradiated low density polyethylene and polypropylene by endophytic fungi. *Int Biodeterior Biodegradation* 105:21–29
132. Ammala A, Bateman S, Dean K, Petinakis E, Sangwan P, Wong S, Yuan Q, Yu L, Patrick C, Leong K (2011) An overview of degradable and biodegradable polyolefins. *Prog Polym Sci* 36:1015–1049
133. Badia J, Strömberg E, Karlsson S, Ribes-Greus A (2012) Material valorisation of amorphous polylactide. Influence of thermo-mechanical degradation on the morphology, segmental dynamics, thermal and mechanical performance. *Polym Degrad Stab* 97:670–678
134. Badia J, Strömberg E, Ribes-Greus A, Karlsson S (2011) A statistical design of experiments for optimizing the MALDI-TOF-MS sample preparation of polymers. An application in the assessment of the thermo-mechanical degradation mechanisms of poly (ethylene terephthalate). *Anal Chim Acta* 692:85–95
135. Badia J, Vilaplana F, Karlsson S, Ribes-Greus A (2009) Thermal analysis as a quality tool for assessing the influence of thermo-mechanical degradation on recycled poly (ethylene terephthalate). *Polym Test* 28:169–175
136. Desai V, Shenoy M, Gogate P (2008) Ultrasonic degradation of low-density polyethylene. *Chem Eng Process* 47:1451–1455

137. Yoshiga A, Otaguro H, Parra DF, Lima LFC, Lugao AB (2009) Controlled degradation and crosslinking of polypropylene induced by gamma radiation and acetylene. *Polym Bull* 63:397–409
138. Panda AK, Singh R, Mishra D (2010) Thermolysis of waste plastics to liquid fuel: a suitable method for plastic waste management and manufacture of value added products—a world prospective. *Renew Sustain Energy Rev* 14:233–248
139. Shen L, Haufe J, Patel MK (2009) Product overview and market projection of emerging bio-based plastics PRO-BIP 2009, Report for European polysaccharide network of excellence (EPNOE) and European bioplastics 243
140. Bilici MK, Yüklér Aİ, Kurtulmuş M (2011) The optimization of welding parameters for friction stir spot welding of high density polyethylene sheets. *Mater Des* 32:4074–4079
141. Sanchis R, Fenollar O, García D, Sanchez L, Balart R (2008) Improved adhesion of LDPE films to polyolefin foams for automotive industry using low-pressure plasma. *Int J Adhes Adhes* 28:445–451
142. Kanbur Y, Irimia-Vladu M, Głowacki ED, Voss G, Baumgartner M, Schwabegger G, Leonat L, Ullah M, Sarica H, Erten-Ela S (2012) Vacuum-processed polyethylene as a dielectric for low operating voltage organic field effect transistors. *Org Electron* 13:919–924
143. Siddique R, Khatib J, Kaur I (2008) Use of recycled plastic in concrete: a review. *Waste Manag* 28:1835–1852
144. Joseph SC, Douglas MF, Butler AF, Bastow DR, Salhus JE, Hartfel MA, inventors; 3M Innovative Properties Co, assignee (2014) Apparatus for spraying liquids, and disposable containers and liners suitable for use therewith. United States patent US 8,628,026.
145. Pace GV, Hartman TG (2010) Migration studies of 3-chloro-1, 2-propanediol (3-MCPD) in polyethylene extrusion-coated paperboard food packaging. *Food Addit Contam* 27:884–891
146. Kirwan MJ, Plant S, Strawbridge JW (2011) *Plastics in food packaging*, Food and Beverage Packaging Technology, 2nd edn. pp 157–212
147. Kriegel R, Huang X, Schultheis MW, Bippert DA, Insolia GE, Kolls B, Summerville S (2010) Bio-based polyethylene terephthalate packaging and method of making thereof. Google Patents
148. Yuan X, Matsuyama Y, Chung TM (2010) Synthesis of functionalized isotactic polypropylene dielectrics for electric energy storage applications. *Macromolecules* 43:4011–4015
149. Arutchelvi J, Sudhakar M, Arkatkar A, Doble M, Bhaduri S, Uppara PV (2008) Biodegradation of polyethylene and polypropylene. *Indian J Biotechnol* 07(1)

Spectroscopy and Microscopy of Eco-friendly Polymer Composites



Ashish K. Shukla, Chandni Sharma, Syed M. S. Abidi
and Amitabha Acharya

List of Abbreviations

AFM	Atomic force microscopy
AT	Nano-Attapulgit
BC	Bacterial cellulose
CASN	Citric acid modified starch nanoparticle
CD	Circular dichroism
CdS QD	Cadium sulfide quantum dot
CHNS	Carbon-hydrogen-nitrogen-sulfur
CNCs	Cellulose nanocrystals
CNS	Cellulose Nanosphere
CPC	Cetylpyridinium chloride
CT/CG	Chitin/cashew gum
DLS	Dynamic light scattering
DMC	Dry-milled corn
DSC	Differential scanning calorimetry
DTPA	Diethylenetriaminepentaacetic acid
EDS	Energy dispersive X-ray spectroscopy
EFPNC	Eco-friendly polymer nanocompositess
FCNTs	Functionalized Carbon nanotube
FESEM	Field emission scanning electron microscope
FTIR	Fourier-transform infrared spectroscopy
GA	Gum arabic
GO	Graphene oxide
HA	Hyaluronan
HRTEM	High resolution transmission electron microscope

A. K. Shukla · C. Sharma · S. M. S. Abidi · A. Acharya (✉)
Biotechnology Division, CSIR-Institute of Himalayan Bioresource Technology,
Palampur 176061, Himachal Pradesh, India
e-mail: amitabha@ihbt.res.in

A. K. Shukla · C. Sharma · S. M. S. Abidi · A. Acharya
Academy of Scientific & Innovative Research (AcSIR), CSIR- Institute of Himalayan
Bioresource Technology, Palampur 176061, Himachal Pradesh, India

ICP-MS	Inductive coupled plasma mass spectroscopy
kDa	Kilodalton
LOX	Lipoxygenase
MCC	Microcrystalline cellulose
MPa	Megapascal
MPTMS	3-(trimethoxysilyl)-propyl methacrylate
NDs	Nanodiamonds
NF	Nanofibrils
NMR	Nuclear magnetic resonance
NPs	Nanoparticles
PBAT	Poly(butylene adipate-co-terephthalate)
PCL	Poly-caprolactone
PDDF	Pair distance distribution function
PGA	Poly-glycolite
PHA	Polyhydroxyalkanoate
PHBV	(3-hydroxybutyrate-co-3-hydroxyvalerate)
PLA	Poly(lactic acid)
PLGA	Poly(D,L-lactide-co-glycolide)
PVA	Polyvinyl alcohol
RChi	Regenerated chitin
SAXS	Small angle X-ray scattering
SCC	Spherical cellulose container
SEM	Scanning electron microscopy
SLRP	Sequential liquid-lignin recovery and purification
SPI/CNTs	Soy protein isolate-carbon nanotube
SPI-MMT	Soy protein isolate-montmorillonite
SPIONs	Superparamagnetic iron oxide
TEM	Transmission electron microscopy
Tg	Glass-rubber transition
TGA	Thermogravimetric analysis
TG-MS	Thermogravimetric-Mass Spectroscopy
Tm	Melting point
UP	Unsaturated polyester
UV-Vis	Ultraviolet-visible spectroscopy
XRD	X-ray diffraction

1 Introduction

The eco-friendly polymers which are also known as green polymers comprise the materials which are either biodegradable or derived from biobased renewable sources. Therefore, these polymers and their corresponding composites trim down the negative human footprint on the environment. In the current scenario, due to the growing

environmental issues; it is indeed necessary to put together the great importance for developing “green materials” in both R&D as well as in industries [1]. Photosynthetic components extracted from plants and wood biomass; such as starch, cellulose, hemicellulose, lignin produced from atmospheric carbon dioxide, can be used as renewable carbon resources [2]. Based on the concept of “carbon neutrality”; when biodegradable polymers such as polylactic acid (PLA), polyhydroxyalkanoate (PHA), polysaccharide derivatives are burnt, they are considered as green materials, because the liberated carbon dioxide is again transformed into biomass [3].

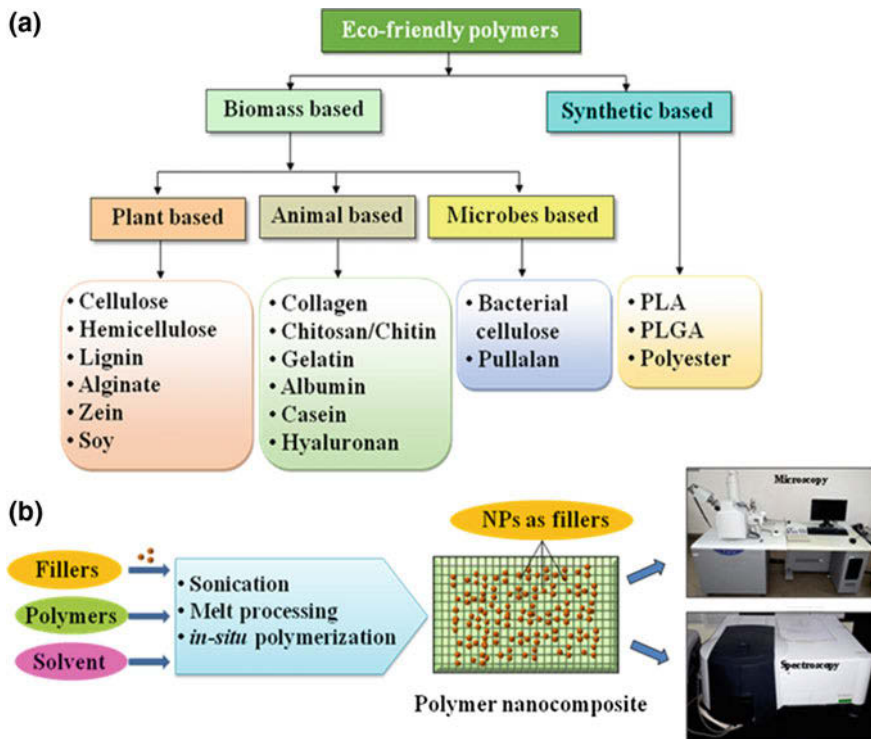
NCs are known as the materials of the 21st century; having a unique design and different properties which are lacking in conventional composites [4]. A number of biodegradable polymers and their layered silicate NCs are widely being used for different applications. NCs, as the term indicates are the composites in which at least one of the dimensions falls under nanometre range (1–100 nm). NCs consist of one or more discontinuous phases which are distributed over single continuous phase. The continuous phase is known as matrix whereas discontinuous phase as reinforcing material. Mechanically, NCs are having high aspect ratio and high surface to volume ratio of the reinforcing material. Green composites are made from both renewable sources based on biopolymers and biofillers (including nano-type fillers), with a positive environmental impact.

NCs are the alternative materials for overcoming the lacunae of microcomposites and monolithic; however, NCs may go through the formulation challenges related to the control of elemental composition in nanocluster. NCs possess multifunctional advantages due to some unique properties like smaller filler size, improved ductility with the same strength, light transmission characteristics, flame retardancy, thermal stability and chemical resistance. Three different techniques are usually followed to prepare eco-friendly polymer NCs (EFPNC) which include solution casting, in situ polymerization, and melt processing. Additionally, as dimension reaches the nanometre level, interactions at phase interfaces improved significantly, and this is important to enhance the properties of the material [1].

Polymers which are used as NCs can be classified based on their (a) native biomass such as plants, animals, microbial and synthetic based and (b) chemical structure (polysaccharide and polypeptide based). Eco-friendly polymers can be extracted from the natural sources mainly by chemical treatment and mechanical method including grinding, milling, sonication, and ultrasonication. The prepared polymer NCs are very useful in making lightweight sensors, producing structural components with a high strength to weight ratio, aerospace, automotive, electronics, biotech, and pharmaceutical industries [3].

2 Isolation of Eco-friendly Polymers

This part of the chapter briefly describes different processes used for the isolation of eco-friendly polymers from their natural sources. The described eco-friendly polymers were classified according to their origin viz., plant, animal, microbial and synthetic based (Scheme 1).



Scheme 1 **a** Pictorial representation of different eco-friendly polymers classified according to their source. **b** Schematic representation of different components of polymer nanocomposites and their characterization techniques

2.1 Eco-friendly Polymers of Plant Origin

Plant-based polymers have gained tremendous attention in recent years due to their high sustainability. In the next section, attempts have been made to concisely report different extraction techniques available in the literature for isolation of plant-based biopolymers.

2.1.1 Cellulose Extraction

Cellulose, with $\sim 10^{11}$ tons of annual turnover, is the most abundant natural polymer, containing vital skeletal polysaccharide component, composed of the $\beta(1-4)$ glycosidic bond [5]. The biosynthesis of cellulose takes place not only in the plant but also in bacteria viz. *Acetobacter*, *Acanthamoeba*, *Achromobacter* and fungi [6, 7]. Cellulose is an extensive linear-chain polymer with a large number of hydroxy groups (three per anhydroglucose unit). Cellulose from its natural precursor sources

can be isolated in two stages. The first stage involves pretreatment of raw material for purification and homogenization depending on the source material and desired morphology of cellulose particles. The pretreatments for plant biomass involve the complete or partial removal of matrix materials (hemicellulose, lignin etc.) and the isolation of individual complete fibers. Detailed descriptions of several of these pretreatment methods are already available in literature [8, 9]. The plant cellulose extraction methods include chemical and mechanical treatment as well as a combination of both. The chemical treatment involves acid hydrolysis [8, 10, 11] whereas the mechanical treatment includes high pressure homogenization [12, 13], grinding, cryo-crushing [14] and sonication [15]. Appropriate treatment of cellulose fibers leads to increase in the inner surface, alters degree of crystallinity, breaks hydrogen bonding and increases the reactivity of the cellulose to further facilitate the process of nanocellulose formation [10].

2.1.2 Hemicellulose Extraction

The hemicelluloses usually comprise off 20–30% of the dry weight of wood. It is the monomer of mixed sugar of short polymer length, consist mainly of mannose along with xylose, glucose, galactose and arabinose, where the main chain is connected to $\beta(1-4)$ glycosidic bonds. The presence of hydroxyl group on the backbone of hemicellulose creates an opportunity for the chemical modification and can lead to the development of new nanobiocomposite. Lignin content was removed from plant biomass using concentrated NaOH and ethanol, and the resulting holocellulose solids were then extracted using NaOH (10%) to provide a filtrate rich in hemicellulose. After the addition of ethanol, the precipitates were collected which predominantly contain xylose based hemicellulose [16, 17].

2.1.3 Lignin Extraction

Lignin is one of the abundant biopolymers after cellulose which is derived from plants and their wastes [18] and acts as connecting bridge between cellulose and hemicellulose. Lignin with cellulose combines to form large lignocellulosic biomass which has a high potential for production of biomaterials and chemicals [18–20]. Lignin can be isolated via different techniques viz., physical and chemical pretreatments and oxidation [21], enzymatic cellulose hydrolysis [22], acidification of black liquors (liquid-lignin) through sequential liquid lignin recovery process (SLRP) [23], pre-hydrolysis using kraft pulping [24] and microwave-assisted acidolysis [25]. Lignin has also been isolated from reed straw via thermomechanical process through attritor-type laboratory ball mill [26].

2.1.4 Starch Extraction

Starch is one of the major dietary sources of carbohydrates and it is found abundantly in the form of polysaccharide in plants. This is an important polymer, formed from long chains of α -glucose units joined together by glycosidic linkages containing two types of molecules i.e. amylose and amylopectin [27]. It is commonly found in roots, tubers, cereal grains and also occurs in a variety of foods, fruits and vegetable tissues etc. Starch and its derivatives have been used as capping and reducing agents for the synthesis of many metallic nanoparticles [28]. Starch is mostly isolated from white rice through alkali extraction method [27]. Acid hydrolysis at 37 °C was used to extract starch from peas to form pea starch nanocomposite [29]. Similarly, starch nanocrystals were also prepared from native pea granules through acid hydrolysis using mild stirring [30]. Enzymatic treatment of waxy maize through α -amylase hydrolysis was also one of the approaches used for starch isolation [31]. Few other techniques include ultrasonication [32], combined enzymatic hydrolysis couple with chemical or physical treatment and acidic treatment was also used for starch isolation [33, 34].

2.1.5 Alginate Extraction

Alginate is the derivative of alginic acid widely distributed in the cell wall of brown algae in the form of calcium, magnesium and sodium salt of alginic acid. These are anionic linear polysaccharides containing β -D mannuronic and α -L-guluronic acid residues linked by β 1–4 glycosidic bond forming homo- and heteropolymeric structures. Alginate biopolymer and its NCs are biocompatible and inexpensive which allows them to be used for various biomedical applications [35]. Alginate extraction was done using broken seaweed pieces, which was then stirred with a hot solution of an alkali, usually sodium carbonate. Alginate nanocomposite can be prepared in a two-step procedure based on the ionotropic pre-gelation of polyanion with calcium chloride salt followed by polycationic crosslinking [36].

2.1.6 Zein Extraction

Maize, a major cereal grain throughout the world, is being used for the isolation of zein. Zein is a protein that is exclusively found in corn. However, there are some other proteins with similar prolamin characteristics, which can be isolated from common cereals such as wheat, barley, rye, and sorghum [37]. Zein extractions require a complex balance between yield, quality, and purity. Dry-milled corn (DMC), acts as a good material to extract zein. Wet milling of corns can also be used to create a co-product that is rich in zein [38].

2.1.7 Soy Extraction

The consumption of soy has gained popularity in the world during recent decades due to (i) increased awareness of the consumer, (ii) drive for a healthier lifestyle, (iii) predominance of lactose intolerance cases and (iv) improved processing of soybeans with reduced off-flavors. Common process of soy extraction steps involves soaking of the soybeans, followed by grinding of the materials in cold water. Subsequently, these materials were then filtered and cooked at 100 °C for 30 min. This method can be further modified by grinding the soy extracts in hot water, which has the advantage of lipoxygenase (LOX) inactivation in the final extract [39].

2.2 *Animal-Based Eco-friendly Polymers*

This section includes different biopolymers isolated from animal origin viz., collagen, gelatin, chitin and chitosan, casein and hyaluronan.

2.2.1 Collagen Extraction

Collagen is a fibrous protein which is predominantly present in the connective tissues of animals. It offers a wide range of applications in the food, pharmaceuticals, cosmeceuticals and photographic industries. Before the extraction of collagen, a pretreatment is performed using an acid or alkaline process which depends on the origin of the raw material. Collagen can be extracted by both chemical and enzymatic hydrolysis process. Although, chemical hydrolysis is frequently used in many industries, enzymatic hydrolysis shows more potential in obtaining products having high nutritional significance and improved functionality. Furthermore, the enzymatic processes require less processing time and have the advantage of minimal waste generation [40].

2.2.2 Gelatin Extraction

Gelatin is a fibrous denatured polymer derived from collagen protein. It is an important biodegradable polymer having a broad range of applications in food and pharmaceutical industries. Due to its inherent cross-linking property, it has been widely used for nanoparticle synthesis [41]. There are mainly two types of gelatin viz., Type A and Type B which can be obtained via acid and base treatment [42] respectively in combination with thermomechanical process [43].

2.2.3 Chitin Extraction

Chitin is the second most abundant naturally occurring polysaccharide after cellulose and mostly found in crustaceous shell or in cell walls of fungi. Chitin is consisted of repeated homopolymeric $\beta(1\rightarrow4)$ linked *N*-acetyl-D-glucosamine units [44]. It has limited industrial application due to its insolubility in commonly used solvents. Further, the isolation of pure chitin from natural sources is difficult. The general methodologies for isolation of chitin involves three main processes viz., demineralization, decolourisation followed by deacetylation. After initial washing and drying, the raw scales were soaked in HCl (1%) solution for 36 h. These were then washed, dried in oven and kept in NaOH (2N) solution for 36 h to complete demineralization. Finally, these scales were immersed in potassium permanganate solution for 1 h, followed by addition of oxalic acid to achieve decolorization. Chitin isolated from the above process was further subjected to NaOH treatment (50% w/v) to obtain deacetylated chitin [45].

2.2.4 Casein Extraction

Casein is an essential protein which approximately counts for 80% of the total protein content of cow milk. Casein is also termed as globular protein, because it generally forms globules in the milk, and is mainly responsible for white color of the milk. Casein in its native form exists as calcium salt, hence termed as calcium caseinate. Casein can be extracted from reconstituted nonfat powdered milk using acetic acid treatment. This procedure allows the extraction of casein in the form of precipitated mass [46].

2.2.5 Hyaluronan (HA) Extraction

HA is a high-molecular-weight unsulfated polysaccharide. HA is mainly composed of subunits of D-glucuronic acid and *N*-acetyl glucosamine which is coupled by $\beta(1\rightarrow3)$ and $\beta(1\rightarrow4)$ glycosidic linkages. High water-retention capacity, mucoadhesion property, viscoelasticity, non-immunogenicity and biocompatibility make it an ideal candidate for healthcare applications [47]. HA can be obtained from various animal sources, such as umbilical cords, rooster combs, bovine submaxillary glands and zones of maturing chondrocytes. Muscle and skeleton comprises off $\sim 35\%$ of human HA. Extraction procedure of HA mainly includes dissection of bigeye tuna, followed by repeated thawing and filtration of vitreous at 4 °C to isolate the carbohydrate content which was further precipitated by adding cetylpyridinium chloride (CPC) to the filtrate. The HA-CPC complex was separated by re-suspending the precipitated mass in sodium chloride solution followed by centrifugation. Using a series of continued chemical followed by centrifugation process HA was finally isolated as freeze-dried material [48].

2.3 Bacterial-Based Eco-friendly Polymers

2.3.1 Bacterial Cellulose Extraction

Bacterial cellulose shares almost identical chemical structure as that of plant-derived cellulose, though it possesses high degree of polymerization, purity, crystallinity, water holding capacity compared to the later one [49]. This interesting biopolymer has been widely used in food, pharma, paper industry etc. [50]. For the successful production and isolation of BC, several factors such as physiological and nutritional conditions, temperature, incubation time, agitation etc. plays an important role. Standard static condition of bacterial growth is required for the isolation of bacterial cellulose. Glycerol improved the dry mass production of bacterial cellulose approximately 2–3 times as compared to when mannitol and glycerol in combination was used as carbon source [51].

2.3.2 Pullulan Extraction

Pullulan is an extracellular hydrophilic polysaccharide produced by different strains of yeast-like fungus e.g., *Aureobasidium pullulans*. It is synthesized intracellularly at the cell wall and secreted out to the cell surface to form a loose and slimy layer. It comprises of mixed linear linkage of α -D-glucan which consist mainly maltotriose units coupled by α -(1→6) linkages [52]. Pullulanase, is an enzyme belonging to the α -amylase family, identified as glycoside hydrolase and breaks α -(1→6) linkages present in various biopolymers like pullulan, starch and amylopectin [53]. Extraction of pullulan involves the use of fermenter; in which production medium was inoculated with 10% seed culture. Finally, the fermentation was performed at an optimized temperature (27 °C) and air flow condition under optimized revolution (~210 rpm) for one week to isolate pullulan [52].

2.4 Synthetic Eco-friendly Polymers

2.4.1 PLA Synthesis

PLA is a synthetic biodegradable polymer of lactic acid with two optically active stereoisomers viz., L(+) and D(-). Isolation of lactic acid in industry is mainly accomplished by fermentation process using bacterial strains of *Lactobacillus* genus viz., *Lactobacillus delbrueckii*, *L. amylophilus*, *L. bulgaricus* and *L. leichmanii* at a pH range between 5.4–6.4 and temperature range of 38–42 °C. PLA can be subsequently produced from lactic acid through polymerization process [54].

2.4.2 PLGA Synthesis

Poly(D,L-lactide-co-glycolide) (PLGA) is amongst the most widely used FDA approved biodegradable polymer for bio-applications since it produces metabolite monomers lactic acid and glycolic acid, after its hydrolysis. This copolymer can be synthesized by treating D, L-lactide and glycolide at 175 °C in the presence of stannous octoate and lauryl alcohol. PLGA-nanoparticles are internalized in cells partly through fluid phase pinocytosis and also through clathrin-mediated endocytosis process [55, 56].

2.4.3 Polyesters Synthesis

Polyesters are a class of polymers which can be synthesized as a result of polycondensation (step-growth polymerization) reaction between dialcohol and diacid/ or diester. Unsaturated polyester (UP) resin is widely used in various industrial applications such as marine, automotive, coatings, storage tanks, piping and construction [57].

3 Spectroscopic and Microscopic Characterization of Biopolymers and Their NCs

This part of the chapter includes different spectroscopic and microscopic techniques which were used for the characterization of the described eco-friendly polymers and their corresponding NCs. For the ease of understanding, the discussion in this section was classified based on the chemical structure of the polymers viz., polysaccharide, polypeptide and synthetic based materials.

3.1 Polysaccharide-Based Biopolymers

Polysaccharide-based biopolymers are composed of long chains of monosaccharide units, which are connected by glycosidic bonds. Polysaccharide NCs have become increasingly important materials over the past decade, since these offer a green alternative to synthetic polymers. These have also been used as composites with hard nanomaterials, such as metal nanoparticles and carbon-based nanomaterials (Fig. 1).

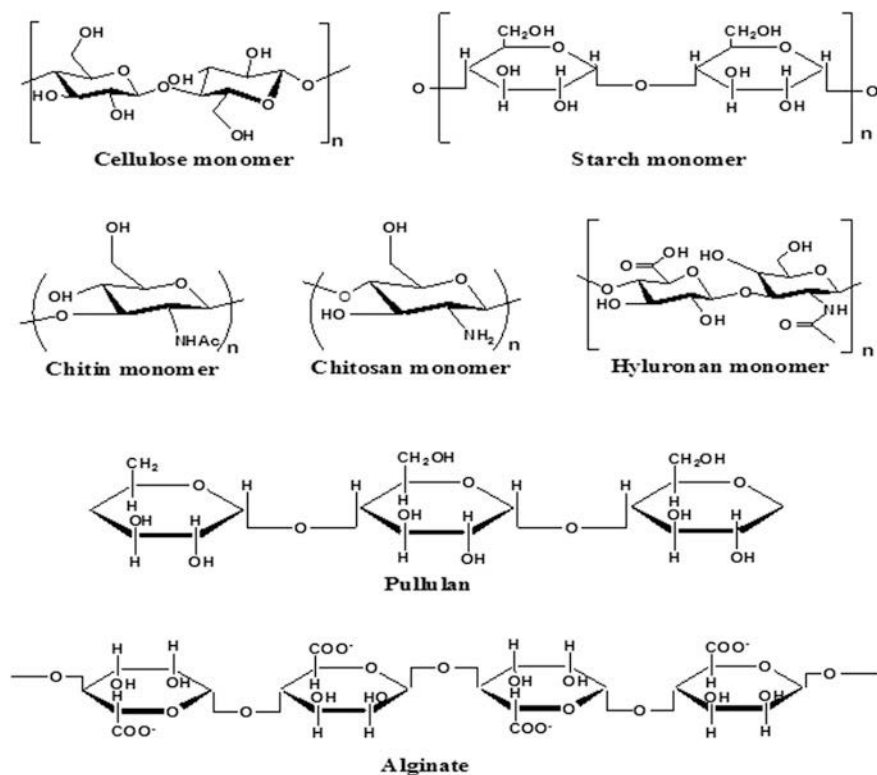


Fig. 1 Chemical structures of different polysaccharide based biopolymers

3.1.1 CHNS Analysis

The elemental analysis of lignin suggested that organosolv and kraft lignin have higher percentage of carbon and lower percentage of nitrogen content compared to other sources of lignin. However, the nitrogen content was higher for aminated lignin of epoxy resin polymer [58]. It was also reported that corn straw and wheat straw contains approximately equal amount carbon, hydrogen, nitrogen, and sulfur [59]. CHNS analysis of modified nanocrystalline cellulose (CNC) revealed higher amount of carbon content and less amount of sulphur and oxygen content as compared to native CNC [60].

3.1.2 FT-IR Spectroscopy

FT-IR has been one of the most common spectroscopic techniques that were used for the identification of different chemical functional groups present in the biopolymers. Numerous studies were already performed on natural fibers by FT-IR

[61]. The peak observed at 3349 cm^{-1} represents the stretching vibration of O–H, related to hydroxyl groups present in lignin, hemicelluloses and cellulose [10]. The C–H stretching vibrations in cellulose, hemicelluloses and lignin were identified at the spectrum range of $\sim 2900\text{ cm}^{-1}$. The transmittance peak observed at $\sim 1645\text{ cm}^{-1}$ was attributed to the O–H bending vibration which resulted from the interaction between cellulose and the absorbed water molecules [62]. The peak position at $\sim 1462\text{ cm}^{-1}$ present in the spectrum was attributed to the symmetric bending of $-\text{CH}_2$ present in sugar backbone whereas the peak at $\sim 1313\text{ cm}^{-1}$ was due to the existence of bending vibration from C–H and C–O bonds in the polysaccharide aromatic rings of cellulose. The peaks observed at $\sim 1216\text{ cm}^{-1}$ and 1157 cm^{-1} were assigned to C–O–C of arylalkyl ether present in lignin and C–H rocking vibration, respectively. The characteristic anhydroglucose chains showed peak at $\sim 1047\text{ cm}^{-1}$ due to C–O stretching. Further, the peak at $\sim 898\text{ cm}^{-1}$ was identified as C–H glycosidic deformation or β -glycosidic linkage and was also known as the amorphous band [10]. Spiridonov et al. [63] reported decrease in $-\text{COO}-$ peak in presence of Fe^{3+} coordination for maghemite carboxymethylcellulose NCs. Further, FT-IR studies were also used to evaluate cellulose stability for TiO_2 -cellulose nanocomposite prepared by microwave solvothermal process [64]. In another report, a hemicellulose-diethylenetriaminepentaacetic acid (DTPA)-chitosan nanocomposite was characterized by FT-IR studies. The corresponding spectra showed new peaks at ~ 3030 and 2780 cm^{-1} which indicated the carboxylic acids present in DTPA [65]. The FT-IR spectra of bacterial cellulose almost correspond to the peaks already mentioned for other cellulose species [66]. Foong et al. [67] reported appearance of new IR peaks at ~ 1720 and 1449 cm^{-1} which corresponds to acetyl and CH_3 groups of PLA and indicated conjugation of PLA on bacterial cellulose surface. A mixed nanocomposite of chitosan and alginate nanoparticles was prepared in presence of glutaraldehyde and characterized using FT-IR. The bands obtained at ~ 3360 – 3440 cm^{-1} were assigned as N–H and O–H stretching modes of vibrations for chitosan/alginate NCs. Further, the broadening of IR band confirmed the formation of intermolecular hydrogen bonding for chitosan/alginate NCs [68]. FT-IR spectroscopic analysis of chitin/chitosan revealed that the absorption bands of chitosan were similar to those for standard chitin. IR bands observed in the range of ~ 3425 – 2881 cm^{-1} were assigned to N–H stretching for primary amines whereas the bands at ~ 3425 – 3422 cm^{-1} were indicative of different vibrations of N–H, O–H and NH_2 , present in chitin. When chitin undergoes deacetylation, a higher intensity peak was observed at $\sim 1597\text{ cm}^{-1}$ which suggested effective deacetylation and prevalence of NH_2 group [45]. The chitin and chitosan isolated from *Fusarium solani* present in marine soil revealed the presence of amide I region (~ 1657 – 1642 cm^{-1}), amide II stretching with C–O group (~ 1560 – 1550 cm^{-1}) and amide III region (1381 – 1375 cm^{-1}) [69]. The herbal nanocomposite of chitosan showed IR peaks of lower intensity at $\sim 3474/3468\text{ cm}^{-1}$ and $1745/1654\text{ cm}^{-1}$, possibly due to the presence of intermolecular hydrogen bonding between chitosan and corresponding active ingredients [70]. Pullulan nanocomposite prepared using lysozyme nanofibres (LNF) and polysaccharide solutions were characterized by FT-IR and showed characteristic bands for

both the reactants [71]. The existence of both α -(1 \rightarrow 4) and α -(1 \rightarrow 6) glycosidic linkages in the pullulan structure was confirmed by the presence of IR band at 935 cm^{-1} [72]. Chemometric analysis of lignin isolated from different sources was also studied using infrared spectroscopy [73]. Although there are various sources of lignin or lignocellulosic biomass, the best quality material can be screened by monitoring characteristic FT-IR spectra [74, 75]. IR peaks at ~ 800 , 1350, 1540 and $3300\text{--}3500\text{ cm}^{-1}$ were assigned for N–H vibration, C–N vibration, N–H bending vibration, and N–H stretching vibration of aminated lignin respectively. Further, the peak at $\sim 3400\text{ cm}^{-1}$ was assigned for O–H stretching of demethylated lignin [58] while the peak at $\sim 1270\text{ cm}^{-1}$ was designated for aromatic ring vibration of guaiacyl lignin [74, 76].

Similarly, FT-IR spectra were used for the chemical characterization of corn starch, starch nanoparticles (SN) and citric acid modified starch nanoparticles (CASN). The key difference between CASN compared to corn starch and SN was the appearance of a new peak at $\sim 1738\text{ cm}^{-1}$ for an ester group and at $\sim 1017\text{ cm}^{-1}$ for C–O bond stretching of the C–O–C group of the anhydroglucose ring which was exclusively present in CASN. It was being inferred that in corn starch and SN, the oxygen of the C–O–C group could form the hydrogen-bond with the hydroxyl groups and the ester bonds in CASN, shifting C–O bond stretching of the C–O–C group to 1026 cm^{-1} [77].

3.1.3 Powder XRD

Powder XRD technique has been used widely for the identification of crystalline and amorphous nature of the concerned polymers and their composites. The XRD was used to investigate the crystalline structure of the raw fibers, mercerized cellulose, and CNS. It was observed that the XRD patterns of raw fibers and commercial cellulose were clearly different compared to the mercerized cellulose and cellulose nanoparticles. For the raw fibers, a characteristic 2θ band between 13° (101), 17° (101) along with a broad peak at 22.5° (002) were observed, which corresponds to the cellulose-I structure. These results were in agreement with those observed for native cellulose [78]. It was also observed that the peaks for the amorphous region at 14° and 16° were hard to distinguish due to their close proximity [79]. Further, it was found that in case of mercerized cellulose and CNS, the corresponding peaks were shifted to 12° , 20° , and 22° and were related to same crystal planes mentioned earlier. The crystallinity index for raw material, mercerized cellulose and CNS were found to be ~ 68 , 64 and 88%, respectively [80]. In case of TiO_2 -cellulose nanocomposite additional peaks at 34.3° (004), 38.2° (004), 48.0° (200) and 70.11° (220) were observed corresponding to the tetragonal structure of TiO_2 and reflected no change in the crystalline structure of the wood cellulose fibers [64]. Observation of a broad peak at 19° in powder XRD indicated the conversion of hemicellulose to xylitol [81]. Xylan hemicellulose (XH)/cellulose fiber NCs showed the presence of crystalline peaks whereas freeze-dried XH powder showed no distinct crystalline peaks [82]. Bacterial cellulose showed three

characteristic peaks of cellulose at $2\theta = 14.7^\circ$ [39], 16.4° [39] and 22.6° (200) which were attributed to the elementary cellulose crystalline structure. Carbon sources used for bacterial growth can also affect the degree of crystallinity in bacterial cellulose. Further, the crystallinity of bacterial cellulose produced in agitated condition was found to be lower than the static culture due to the presence of structural disorder [83]. XRD studies of the bacterial cellulose (BC) and drug-loaded BC matrices were carried out by varying the scanning angle in the range of 10° to 60° . The distinct peaks observed in the diffractogram for BC at 14.12° , 16.8° , and 22.72° demonstrated the crystalline structure of BC. The surface modified BC showed peak pattern similar to as-synthesized BC with lower intensity, indicating a reduction in the crystallinity as a result of acetylation. Apart from the peaks at 26.90° , 28.54° and 29.82° , BC-famotidine matrices have strong peaks at 11.58° and 17.76° , confirming the entrapment of drug into matrices. The appearance of distinct peaks in the pattern for BC-tizanidine matrices at 25.06° and 26.46° showed lower crystal growth of the drug nanocomposite [84]. XRD patterns of calcium alginate/graphene oxide NCs revealed an amorphous structure, whereas those of barium alginate/graphene oxide composites indicated the presence of semi-crystalline structure which might have resulted from the preferential binding of barium ions to mannuronic acid blocks [85]. The XRD patterns of chitin and hydrolyzed chitosan confirmed that all chitin samples exhibited strong reflections at a 2θ value between 9 and 10° . XRD spectra further suggested that chitin is amorphous in nature whereas chitosan is crystalline [45]. Chitin/cashew gum (CT/CG) nanocomposite showed sharp peaks at $2\theta = 9.28^\circ$ and 17.54° corresponding to diffractions of CT and CG segments respectively when blended with metal oxide nanoparticles. Furthermore, peaks at 2θ corresponding to 21.65° and 26.13° , indicated the semi-crystalline nature of the blend matrix [86]. The XRD patterns of carbonized lignin showed peaks at 26.7° (002), 43.2° (100/101), 54.7° (004) and 78.1° (110) confirming the structural changes happened in lignin after carbonization whereas untreated lignin did not show above-mentioned peaks, which revealed its non-crystalline nature [87]. Pure pullulan has no crystalline peaks implying that the material is fully amorphous [88]. Unfilled glycerol plasticized and non-plasticized pullulan films were characterized by a broad peak centered at around 19° , typical of fully amorphous materials [89]. Rice starch showed A-type diffraction pattern peaks at a 2θ value of 9.9° , 15.0° , 17.0° , 18.1° and 23.5° . Extensive hydrolysis of rice starch showed less intensity diffraction patterns which indicated that hydrolysis occurred in the amorphous region [31]. A native starch granule was pre-treated with β -amylase and glucoamylase and found that pretreated starch granules have semi-crystalline nature as compared to native starch [33].

3.1.4 NMR

NMR is a one of the strongest technique which is used for characterization of chemical moiety present in most of the compounds. Microcrystalline cellulose (MCC) biopolymer was converted into spherical cellulose container (SCC) by the

sonochemical method and investigated by ^{13}C MAS NMR. The spectra depicted that peak of different carbon atoms of the glucose pyranose repeating unit in MCC and SCC were quite similar [90]. ^1H -NMR spectra of acetylated and demethylated lignin showed peaks corresponding to 6.0 and 8.0 ppm for two of its important aromatic precursor's viz., syringyl and guaiacyl respectively. Further, the peak at 6.96 ppm was assigned for a proton of C5 position in the 9 carbon units of lignin while 3.82 ppm peak was designated for a proton of methoxy group of the same material [91]. ^{13}C NMR spectrum of the aminated lignin was observed and showed a peak around 130 ppm which corresponds to ortho- and para- positions of the aromatic ring. Further, peaks were observed at δ value 16.5, 17.8, 59.5, 82.2, 136.8 and 137.3 ppm for methyl groups, CH group of the aromatic ring and amine, CH connected to oxygen and amine connected aromatic carbon atoms respectively [58]. 2D NMR analysis of mild wood lignin showed typical lignin substructures such as β -O-4, β - β , β -5, benzaldehyde and cinnamaldehyde units [92]. ^{31}P NMR is a powerful tool for hydroxyl group analysis in lignin biomass. Softwood lignin showed characteristic peaks of hydroxyl groups present in an aromatic moiety of lignin [93].

3.1.5 DLS and Zeta Potential

The stability of CNS is mainly related to the ions present during the acid hydrolysis. For sulfuric acid treatment, the formation of sulfate ester groups allows water dispersion of CNSs and prevents aggregation. The zeta potential of 0.1% CNS in water indicated an average zeta potential of -23.3 ± 3.2 mV [94]. The DLS size of CNSs was found to be in the broad range 30 nm to 1 μm which indicated the anisotropic properties of the CNS suspension which were attributed to the different aggregate states CNSs in solution [95]. Similarly, for hemicellulose broad particle size distribution ranging from 50 to 400 nm was observed. Further, hemicellulose showed negative zeta potential value which can be due to the presence of pectic substances (anionic polysaccharides) and oxidized lignin structure on hemicellulose surface [96]. Silver-chitosan nanocomposite showed particle diameter of ~ 1553 nm whereas, simple chitosan showed the diameter of 78.8 nm. The zeta potential analysis of silver chitosan nanocomposite revealed that the prepared nanocomposite was negatively charged (-3.4 mV at neutral pH) [97]. Zeta potential and particle size of chitin nanocomposite was found to increase as the amount of chitin (wt%) were enhanced in the corresponding NCs [98]. The hydrodynamic diameter of magnetic nanoparticles coated by a series of carboxymethylated polysaccharides, such as dextran, cellulose, and pullulan was found to be 229, 719, and 330 nm, respectively. The ζ potential in all of these cases had slightly negative values, which increased with increasing magnetite content present in the composite [99].

3.1.6 UV-Vis

The formation of gold-carboxymethylcellulose (CMC) NCs was confirmed by UV-Vis spectroscopy by monitoring the appearance of Au surface plasmon band at 522 nm which was otherwise absent in case of both the precursors [100]. The absorption intensity of Au was found to gradually increase with increasing CMC concentrations in NCs. Moreover, absorption peak width became narrower suggesting uniform size distribution of synthesized Au nanoparticles in presence of carboxymethyl cellulose [101]. The absorption peak of chitosan ZnO nanocomposite was observed at 360 nm, which was having lesser intensity than macrocrystalline ZnO absorption found at 372 nm. This was attributed to the quantum size effect of chitosan-ZnO nanoparticles [102].

3.1.7 SAXS

SAXS was used to determine pair distances distribution function (PDDF) profile related to the shape and the conformational arrangement of macromolecules. The PDDF profile of the CNS before sonication (CNS-BS) and after sonication (CNS-AS) showed different geometries. Interestingly, the non-sonicated CNS exhibited an elongated curve due to agglomerated particles, whereas the CNS-AS exhibited a Gaussian curve corresponding to spherical particles [103].

3.1.8 TGA

TGA was used to characterize the thermal behaviour of raw fibers, mercerized cellulose and CNS and the values were found to be dependent on components present in the plant cell wall. In fact, the cellulose decomposition was reported in the range of 315–400 °C whereas for hemicellulose and lignin it was found to be between 200–315 °C and 160–900 °C respectively [104]. For the raw fiber, mercerized cellulose and CNS, decomposition started at 218, 223 and 209 °C and the maximum degradation was observed at 346, 342 and 326 °C respectively. It was found that compared to the CNS, the thermal stability of raw fibers and mercerized cellulose was higher, possibly because of the presence of sulfate group at the surface of the CNS. The difference in thermal behaviour between mercerized cellulose and raw fibers was explained based on the presence of hemicellulose and lignin material in the raw fibers [105]. Further, it was found that TiO₂-cellulose nanocomposite was more stable than pure cellulose [64]. Xylan-rich hemicellulose (XH) and cellulose nanocomposite showed good thermal stability than freeze-dried XH powder because of the presence of crystal structure [82]. Further, hemicellulose Fe₃O₄ hydrogel NCs were also studied using TGA [106]. Similarly, bacterial cellulose and its NCs were also evaluated for their thermal stability using TGA studies and found that it resembles quite well with the thermal properties of the plant cellulose. Literature reports suggested that the presence of mineral phase has

changed the thermal degradation profiles of the bimetallic–alginate nanocomposite samples when compared with the non-mineralized composite. This might have resulted from the presence of mineral phase which improved the thermal stability of the NCs by lowering the rate of alginate decomposition [107]. TGA thermogram of AgCl/chitin nanocomposite suggested a reduction in the area under endothermic peak in DSC and weight loss in TGA; thus confirming better stability for NCs [108]. The aminated lignins were studied in detail to evaluate their thermal stability [58]. TGA curves for freeze-dried raw starch samples suggested that the maximum loss of mass happened around 260–330 °C and for the same composite, it was noticed at ~300 °C [32].

3.1.9 TGMS

Thermogravimetric- mass spectroscopy (TGMS) has been used to understand the pyrolysis mechanism for hemicellulose. Under inert atmosphere and elevated temperature condition carbonaceous material undergo aromatization. The decomposition of the hemicellulose was observed between 200 and 580 °C and the mass spectroscopy (MS) result showed peaks for CO₂ ($m/z = 44$), CO ($m/z = 28$), CH₄ ($m/z = 16$), and H₂O ($m/z = 18$) [109].

3.1.10 DSC

DSC is one of the best analytical techniques to find the polymer crystallinity. The same technique can also be used to study oxidation reaction as well as other chemical reactions. DSC thermogram of chitosan-alginate (CS-AL) NCs prepared with glutaraldehyde showed one broad endothermic peak at ~112.1 °C for crystallization temperature whereas the glass transition temperature was found to be ~350 °C. The studies suggested that the crosslinker increases the thermal stability of the corresponding NCs [110]. In a different study, glass-rubber transition (T_g), melting point (T_m), and the degree of crystallinity for the synthetic poly (caprolactone) (PCL) was found to be around ~60, 69 °C, and 58%, respectively. For the developed chitin whiskers/PCL composites, it was found that both T_g and T_m was almost independent of the whiskers concentration [111]. Thermal analysis of developed lignin-epoxy resin suggested enthalpy values were directly proportional to the amine content present in the composites [58]. Further, it was also observed that the enthalpy values of lignin may vary depending on their biomass [18].

3.1.11 ICP-MS

Inductive coupled plasma mass spectroscopy is used to determine the concentration of metallic nanoparticles absorbed on the surface of the nanocomposite. In case of silver/cellulose NCs, prepared by different concentration of silver nitrate in presence

of α -cellulose, carboxymethyl cellulose and amino-cellulose as stabilizers, showed that the quantity of silver nanocluster present on cellulose sample was directly proportional to the concentration of silver nitrate in the precursor solution [112].

3.1.12 SEM

SEM was used to understand the surface morphology of raw fibers before and after each treatment for cellulose extraction. The morphology of the fibers changed due to the purification process. In general, the raw fibers are constituted by bundles of cellulose microfibrils and are covered by different layers. The structural morphology of microfibrils cannot be visualized, as they are still buried inside lignin and hemicellulose [113]. For mercerized cellulose, the surface was found to be more clean, smooth and the available microfibrils can be clearly seen. Thus, SEM characterization clearly distinct between raw fibers and the mercerized cellulose. Similarly, CNSs obtained after the acid hydrolysis showed a narrow size distribution of particle size in the range of 46 ± 17 nm. SEM image revealed the three-dimensional structure of hemicellulose/chitosan nanocomposite having continuous cell pore structure [106]. Similarly, the SEM studies on BC showed structure composed of a random network of cellulose nanofibers. It was reported that the outer surface consists of dense layers covering an internal microstructure in the shape of honeycombs whereas the inner region is composed of fibers forming large pores [114]. SEM images of the alginate-zinc oxide NCs appeared to be rough which may have resulted from the interaction between the nanoparticles and the alginate matrix. The presence of ZnO-NPs in the alginate matrix was observed as bright spots with a moderate degree of agglomeration. The presence of elemental Zn was also confirmed by EDS analysis. [115]. The diameter of chitin nanowisker determined by SEM was found to be much higher compared to the actual whiskers diameter. This resulted from a charge concentration effect due to the emergence of chitin whiskers [116]. Drug-loaded pullulan films appeared to have a random distribution of drug particles with no sign of complete phase separation, thus indicating a nanocomposite structure in the films [117]. Carbon microparticles derived from lignin were analyzed using SEM and the data were compared with untreated lignin, thermo-stabilised lignin and carbonized lignin. The average particle size for untreated, thermostabilised and carbonized lignin was found to be 9.1, 7.0 and 5.3 μm respectively [87]. SEM analysis of dilute acid pretreated corn stover revealed the formation of semispherical and spherical structures on its surface which led to the hypothesis that the droplet formations evolved from the lignocellulosic matrix of corn stover during pre-acid treatment [118]. The microstructures of maize, mango, and banana starch granules were observed by SEM imaging. Mango starch granules were found to be spherical and domeshaped with some non-uniform growth and spotting having 5–10 μm particles size, which clearly indicated that the starch particles may have collapsed during drying. In case of maize and starch granules, regular spherical shaped particles were observed. Banana starch granules were elongated and lenticular in shape, and the average

longitudinal dimension was found to be 40 μm with a radius around 20 μm [34]. Citric acid modified starch nanoparticles (CASN) and native starch nanoparticles (SN) was found to have a size range between 50–100 nm and 50–300 nm respectively [77]. In one of the reports, the fractured structure of lamella indicated the homogenous dispersity of SN on soy protein matrix [30].

3.1.13 TEM

In TEM, CNS samples showed mainly the presence of aggregates created during the slow drying process [119]. Interestingly, white regions were observed inside the particles and have been related to the entanglement or local twist of the crystalline regions [120]. TEM studies were performed for alginate-ZnO nanocomposite to monitor size, morphology and dispersion of ZnO NPs on the nanocomposite. It was observed that the polymer conjugated ZnO NPs represented an irregular spherical shape with size variations between 20 and 100 nm which was almost comparable to the bare ZnO NPs [115]. Interfacial adhesion between lignin nanoparticles and PVA matrix was observed through TEM. Lignin nanoparticles showed no change in aggregation states even after incorporation of PVA matrix which suggested an interaction of lignin hydroxyl groups with PVA [121]. The TEM images of superparamagnetic nanoparticles coated by pullulan revealed that the average size for all of the samples varied between 3.4 and 9 nm depending on the amount of magnetite present in the nanocomposite [99]. TEM image of chitosan-ZnO NCs revealed that the particles possess mostly rod-like structure with a size close to 100 nm [102]. HRTEM studies were also used for such characterization [86]. TEM images of pea starch nanoparticles suggested aggregated NPs having a length of ~ 60 –150 nm and width of 15–30 nm [30]. Another report suggested the formation of well dispersed and spherical shaped starch colloids of sizes ~ 200 nm [32].

3.1.14 AFM

AFM is an imaging technique used for characterizing the surface topology of solid materials. AFM based morphological studies reflected the existence of absorbed nanoparticles on the surface of hemicellulose NCs [96]. Films formed by xylan hemicellulose and chitosan showed a very smooth surface with few nodules. Studies further suggested that cellulose nanofilm have higher roughness factor as compared to cellulose nanofibers [82, 122]. AFM images of GO-alginate biopolymer suggested an average thickness of the sheets was about 1.0 nm, which indicated the formation of single-layered exfoliated GO for the nanocomposite [123]. AFM has been directly applied for the surface analysis of lignin and its polymer composites. The AFM images of hydrothermally pretreated wheat straw and corn stover revealed that the parenchyma cell lining has an aggregate of cellulose fibers and the integrity of microfibrils remained intact. The AFM images of pullulan nanocomposite of magnetite nanoparticles revealed that the magnetite

nanoparticles had a strong tendency to form agglomerate in the dry state. The magnetite nanoparticles were found uniformly distributed throughout the samples; whereas the aggregation was observed at a higher concentration of magnetite [99]. The AFM images of cross-linked chitosan/chitin NCs showed well isolated nanometer-scale crystals of chitin. The diameter of chitin nanocrystals was found to vary between 13 and 20 nm [124]. In another literature report, the homogeneity of regenerated chitin (RChi) films was investigated by AFM [125].

3.2 Polypeptide-Based Biopolymers

Peptides are emerging as a new class of biomaterials due to their unique chemical, physical, and biological properties. The development of peptide-based biomaterials is driven by the convergence of protein engineering and macromolecular self-assembly. The next section focuses on different spectroscopic and microscopic techniques used for characterization of polypeptide-based polymers (Fig. 2).

3.2.1 CHNS Analysis

Elemental analysis of the collagen waste from goat skins revealed the % of C, N, H and S to be approximately 41.5, 14.7, 7.1 and 0.2%, respectively. Further, XPS and

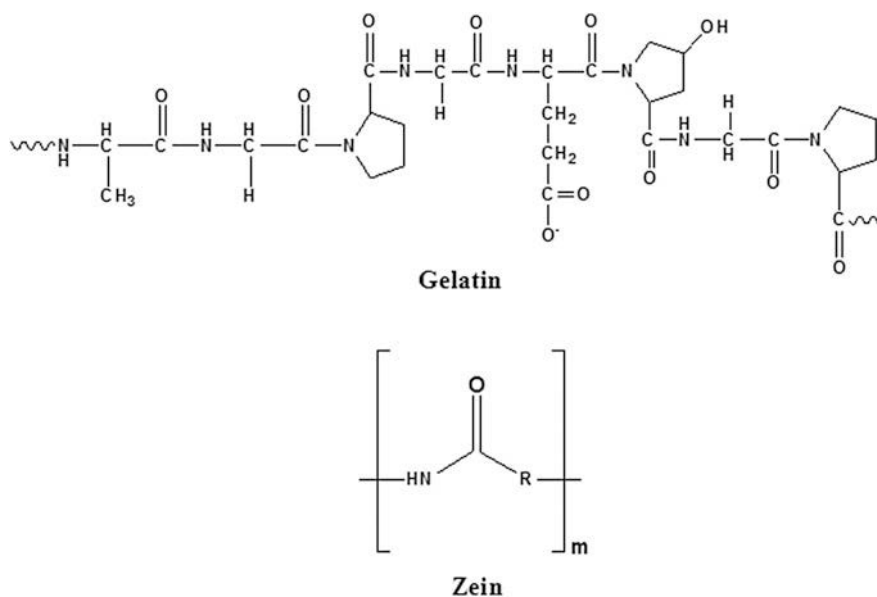


Fig. 2 Chemical structures of different polypeptide based biopolymers

CHNS analysis of carbon materials derived from collagen waste at elevated temperature abundantly showed the presence of carbon, oxygen and nitrogen in the range of 72–82, 6.2–15.4 and 2.9–13.6%, respectively [126]. The amount of zein adsorbed on the surface of montmorillonite (MMT) was determined by CHNS analysis; and it was found that biohybrids based on extracted phase (EXT) showed a lower amount of adsorbed protein than those prepared from precipitate [127].

3.2.2 FT-IR

Collagen is the principal structural constituent present in tissues; found most abundantly in the body. FT-IR spectra of type 1 collagen obtained from bone and skin tissues showed peaks of amide I at 1690, 1660, 1630 cm^{-1} corresponding to stretching vibration of C=O and amide III peak at 1235 cm^{-1} corresponding to stretching vibration of C–N and bending of N–H. Carbohydrate moieties present in collagen exhibited stretching vibration of C–O and C–O–C at 1100–1005 cm^{-1} [128, 129]. In another literature report, it was observed that the collagen-immobilized poly (3-hydroxybutyrate-co-3-hydroxyvalerate) (PHBV) and hydroxyapatite nanocomposite scaffolds showed IR peak at $\sim 1722 \text{ cm}^{-1}$ corresponding to vibrational bands of C=O present in PHBV whereas a peak at $\sim 1039 \text{ cm}^{-1}$ suggested the presence of PO_4^{3-} group exists in hydroxyapatite. In the same, characteristic peaks were observed at ~ 1640 and 1572 cm^{-1} for both amide I and amide II bonds of collagen, respectively [130]. The hybrid polymer/inorganic NCs of hyaluronan can be prepared either by in situ or ex situ method using both chemical and physical methods. The FTIR spectrum of HA/ZnO nanocomposite showed the peaks at ~ 3412 , ~ 1616 , ~ 1411 , ~ 1149 , ~ 1066 , ~ 946 , and $\sim 661 \text{ cm}^{-1}$; thus confirming the presence of HA in the nanocomposite. The formation of ZnO nanoparticles was confirmed by distinct peak obtained at 441 cm^{-1} . The asymmetric sulfate stretching vibration band was observed at 1270 cm^{-1} and the peak at 1066 cm^{-1} was attributed to symmetric C–O vibration related to C–O–SO₃ or due to the weak C–OH stretching resulting from ZnO coordination. On the other hand, the peaks at ~ 1632 and 1433 cm^{-1} corresponded to stretching of (NH) C=O and –COO[–] or –OH groups, respectively. These peaks became strong and shifted slightly in the presence of ZnO nanoparticles, indicating that interactions between the (NH)C=O, –COOH, and OH groups of HA and ZnO nanoparticles [47]. Major peaks in FT-IR spectra of gelatin isolated from scales and bones of fish were observed in amide region. Scales gelatin showed amide-I and amide-III peaks along with phosphate stretching peaks which indicated the presence of calcium salts in scales gelatin sample. Interestingly, bone gelatin samples showed N–H stretching vibration of amide A at $\sim 3340 \text{ cm}^{-1}$ along with the amide-I, amide-II, and amide-III peaks [131]. FT-IR of glutaraldehyde-crosslinked gelatin nanoparticles showed a peak at 2927 cm^{-1} for asymmetric stretching of –CH₂ groups present in gelatin [132]. The FT-IR spectra of casein-acrylate TiO₂ nanocomposite suggested the successful grafting of acrylate monomers on the casein matrix.

Similar spectroscopic studies were also performed for hollow casein nanospheres [46] or poly(*n*-butyl acrylate)–casein NCs [133, 134]. Zein-based biodegradable nanopesticide containing geraniol and citronellal as active ingredients were synthesized and characterized using FT-IR. The spectra of zein showed bands between 3100 and 2800 cm^{-1} , which corresponds to $-\text{C}-\text{H}$ groups present in fatty acids and amino acids. The spectrum of the geraniol loaded zein nanoparticles showed characteristic zein amides I and II peaks along with minimal shifts which may have resulted from the interactions of zein nanoparticles with the corresponding essential oil [135]. Similar FT-IR studies were also performed for soy protein isolate-carbon nanotube (SPI/CNTs) composites [136].

3.2.3 Powder XRD

XRD patterns for silica nanoparticles doped in hydroxyapatite/collagen and hydroxyapatite/gelatin showed crystalline planes for hydroxyapatite which was independent of doping material. Further, the crystallite size of hydroxyapatite gelatin silica nanocomposite and hydroxyapatite collagen silica composite was found to be 10.73 and 4.19 nm respectively [137]. In the X-ray diffraction pattern of HA/ZnO nanocomposite, prominent peaks were observed and assigned to the hexagonal wurtzite structure of nanometer ZnO particles with a degree of crystallinity [47]. The main peak in the XRD diffractogram of zein films with and without oleic acid appeared at the 2θ value of 19° which was susceptible to the number of cellulose nanofibrils (NF) present in the composite [138]. XRD patterns of raw zein and zein nanoparticles suggested amorphous nature for both the material which was further reduced in presence of high flow rate of CO_2 [139]. XRD pattern of gelatin and its corresponding drug loaded counterpart was found to show peaks at $2\theta = 20$ and 22° respectively, suggesting increase in the crystalline nature upon drug entrapment [132]. The XRD pattern for casein calcium phosphate nanocomposite revealed amorphous nature for the material [140].

3.2.4 NMR

Conformational study of a collagen peptide by ^1H NMR spectroscopy revealed an interesting temperature dependant 1:1:1 pattern of sharp resonance bands and slightly broader peak at ~ 6.95 ppm, which was found to become even more broader with decreased temperature conditions. Further, $^{14}\text{N}-^1\text{H}$ spin-spin couplings were also observed because of quadrupolar relaxation which induces severe resonance broadening [141]. In another study, NMR spectra of collagen were investigated to compare between native and collagen present in biological tissues, such as bone, cartilage and skin. Characteristic signals from all collagen amino acids were obtained with a unique signal at 71.1 ppm, which can be assigned to the C_γ carbon of hydroxyproline. The ^{13}C MAS NMR spectra provided supports to resolve the fingerprint region of collagen whereas, ^{31}P cross polarization magic angle spinning

(CPMAS) studies on bone and bone implants have allowed to depict the biomineralization process [142]. $^1\text{H-NMR}$ spectra of methacrylic acid modified gelatin composite showed δ values between ~ 0.86 and 3.57 ppm which indicated characteristic peaks of methyl groups present in the amino acid residue of gelatin [143].

3.2.5 DLS and Zeta Potential

The particle size of zein nanoparticles was found to be ~ 300 nm which showed a constant decrease with increase in homogenization speed [144]. The zeta potential of zein nanoparticles coupled with gum arabic (GA) was found to be negative because of the presence of carboxylate groups in GA [145]. The DLS measurements revealed that the casein NCs showed the diameter of ~ 40 – 65 nm at pH 7.0 and the net charge was found to be negative [46].

3.2.6 UV-Vis and Fluorescence Studies

The presence of characteristic ZnO absorption band at 344 nm confirmed incorporation of ZnO into HA [47]. It was found that with increasing zein concentration, the plasmon resonance band of silver nanoparticles shifted from 458 to 428 nm and confirmed the formation of small size zein-silver nanoparticles [146]. The fluorescence of electrospun zein nanofibers conjugated with CdS QD (Quantum dot) showed emission at 561 nm. The emission intensity was found to be directly proportional to the CdS QD concentration. Further, the uniform fluorescence emission profile confirmed that the nanohybrid structure was stable in nature [147].

3.2.7 Circular Dichroism (CD) Spectroscopy

CD studies were carried out to confirm the presence of triple helix structure for type I collagen obtained from bovine calf skin [148]. Again, collagen obtained from streptococcal proteins showed unfolding of helix structure at 220 nm after denaturation [149]. CD spectroscopy studies were also carried out for gelatin composites [150].

3.2.8 TGA

The thermal stability of collagen was tested using TGA and results indicated that beyond denaturation temperature (T_d) collagen mostly converts into lower molecular weights elements. The specific viscosities started decreasing between 25 and 30 °C for skin collagen and between 30 and 35 °C for bone and muscle collagens [151]. TGA analysis showed that the in situ prepared silver/hyaluronan bio-nanocomposite increased the thermal and mechanical stability of resultant fibres [152].

Again, the TGA profile for the synthesized soy carbon nanotubes showed a weight loss of about 2% when the temperature was varied from 25 to 450 °C [136].

3.2.9 DSC

Collagen extracted from bovine tendon showed higher denaturation temperature for crosslinked collagen scaffolds due to highly stable triple helix conformation [153]. Collagen helix and their crosslinking nanocomposite showed changes in enthalpy and also in melting temperature [154]. Similar studies were also performed for casein and its developed composites [134].

3.2.10 SEM

SEM characterization of type I collagen extracted from equine tendon has been carried out to observe microscopic changes on the polymer surface [155]. Collagen obtained from bovine tendon suggested the presence of 50–150 μm pores on the nanocomposite surface [153]. FESEM image of HA/ZnO nanocomposite showed that ZnO nanoparticles of 3–8 nm size were present on the HA surface [47]. The majority of zein particles obtained via liquid-liquid dispersion was spherical in shape and possess particles size of less than 200 nm [144]. SEM images of prepared functionalized carbon nanotubes (FCNTs) showed homogeneous dispersion in the modified SPI adhesive, although individual CNTs could be observed as agglomerates [136]. Similar SEM studies were also carried out for SPI–MMT (montmorillonite) bio-nanocomposite [156] and casein NCs [46].

3.2.11 TEM

TEM studies were successfully carried out for HA-ZnO composites which showed the presence of 10–12 nm ZnO particles on the HA surface [47]. Similarly, gelatin nanoparticles of ~ 100 nm size were also observed [132]. Both zein and its corresponding silver-zein nanocomposite were characterized using TEM and size of the nanoparticles were found to be ~ 60 nm [146]. Similar studies were also carried out for casein and casein/calcium phosphate NCs [134, 140].

3.2.12 AFM

The AFM studies of collagen isolated from bovine vertebrae showed fibrils having a diameter in the range of 50–200 nm [157]. In another AFM study, the surface morphology of type I collagen showed thin film formation on nanocomposite surface [158]. Similar AFM studies were also performed for Zein–GA composites which suggested the formation of uniform spherical particles with average size of

143 nm and height of 43.8 nm [145]. AFM images revealed that casein nanospheres were spherical in shape with an average height of 21.0 ± 1.3 nm [134]. Further data on roughness factor for different casein NCs indicated that higher casein concentration allows homogeneous and smooth film formation [133]. The microstructure of the nanocomposite prepared from CNCs and soyabean oil was also characterized via AFM [159].

3.3 Synthetic Based Polymers

Eco-friendly synthetic based polymers have gained a lot of attention in current scenario due to their versatile nature and various applications in different fields. Different types of green NCs have been derived from modified synthetic polymers such as polylactic acid, poly(D,L-lactide-co-glycolide) (PLA, PLGA) and polyesters. This section draws the attention towards various techniques available for characterization of above mentioned synthetic biodegradable polymers (Fig. 3).

3.3.1 FT-IR

The FT-IR spectrum of PLGA-superparamagnetic iron oxide (SPIONs) nanocomposite with and without BSA showed prominent peak at ~ 2950 – 2850 cm^{-1} , assigned to C–H stretching of oleic acid on the SPIONs' surface whereas carboxylic acid present in PLGA showed sharp peaks at 1765 – 1750 cm^{-1} (C=O stretching), 1300 – 1090 cm^{-1} (C–C–O stretching), 1190 – 1085 cm^{-1} (C–O–C stretching) and 3100 – 2950 cm^{-1} (O–H stretching). However, BSA protein exhibited small signalling peaks at ~ 1650 cm^{-1} (C–O stretching of amide) and ~ 1540 cm^{-1} (N–H bending of amide) due to its lower concentration in the corresponding nanocomposite [160]. In another study, FT-IR spectra of PLA NCs showed peaks at ~ 2992 , ~ 1373 , and ~ 1454 cm^{-1} for stretching vibration, symmetric and asymmetric bending vibration of $-\text{CH}_3$ groups respectively. The nanocomposite of PLA poly (butylene adipate-co-terephthalate) nano-attapulgit (PLA/PBAT/AT) exhibited native PLA peak for stretching vibration of C=O group confirming the presence of

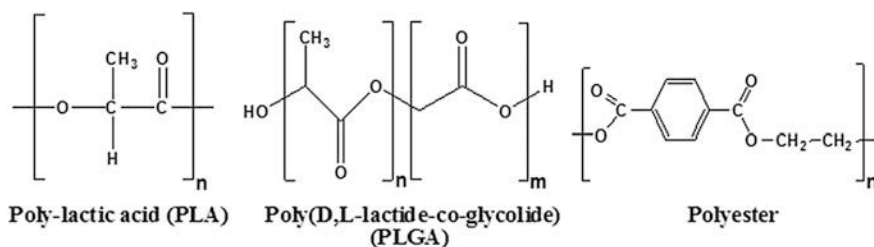


Fig. 3 Chemical structures of different synthetic biopolymers

PLA in the composite. Moreover, peaks at ~ 3057 and 740 cm^{-1} were attributed for stretching and bending vibrations of C–H present in benzene [25]. FT-IR spectra were observed for unsaturated polyester/styrene (UP) nanocomposite filled with nanodiamonds (NDs) containing carboxyl and methacrylate functional groups and exhibited a peak at 980 cm^{-1} which was assigned to the C–H out-of-plane bending in polyester molecules. Whereas, peak at 1730 cm^{-1} corresponds to C=O group which remained unchanged in UP/NDs nanocomposite [57].

3.3.2 Powder XRD

XRD pattern of pristine montmorillonite (Mt) and insulin-Mt-PLGA NCs showed a characteristic peak at a 2θ value of 6.4° (001) with a corresponding d spacing of 13.6 \AA . However, no XRD pattern was observed for Mt due to its low concentration. Besides this, a hump corresponding to amorphous PLGA matrix also appeared at a 2θ value between 10 and 25° . XRD data depicted that Mt concentration could not influence the encapsulation efficiency of insulin in the composite [91]. XRD pattern observed for PLA and polylactic acid/poly-caprolactone (PLA/PCL) nanocomposite revealed their crystallinity indices to be 31.43 , and 17.34% respectively. Further, two peaks of PLA at a 2θ value of $\sim 16.4^\circ$ and $\sim 22.6^\circ$ were observed from the same studies [161].

3.3.3 NMR

^{13}C solid-state NMR spectra of chitosan-PLA modified CNT NCs showed peaks at 65 and between 20 and 22 ppm for chitosan-CNTs and the composite respectively [162]. In another literature report, ^1H NMR spectra suggested chemical shift in poly (D,L-lactide-co-glycolide) (PLGA) copolymer with δ value between 1.46 – 1.68 , 4.67 – 4.90 and 5.13 – 5.30 ppm assigned to $-\text{CH}_3$, $-\text{CH}_2$, and $-\text{CH}$ functional groups respectively [56]. ^1H NMR of unsaturated polyester-styrene cured resin showed the integration of the broad bands at ~ 6.8 and 0.8 – 4.0 ppm which were assigned to the ring protons of styrene and esterified fumarate residues of aliphatic chain [163].

3.3.4 TGA

It was found that carbon dot (CD) conjugation improved the thermostability of polyesters by shifting the initial degradation temperature of the nanocomposite towards higher temperature. The increased thermostability of the NCs can be ascribed to high cross-linking density and secondary interactions imparted by CD with the polyester chains [164].

3.3.5 DSC

The positive influence of CNTs on the thermo-mechanical properties of unsaturated polyester NCs (UP) was studied using DSC. DSC thermogram provided the information of chain intercalation and thermal transition for the studied NCs. Interestingly, the NCs exhibited a split in the melting endotherm whereas the corresponding polyester showed a single peak, suggesting bond formation between CNT and UP for the former case [57].

3.3.6 SEM

SEM analysis of the nanocomposite prepared using iron oxide and lysine/BSA modified PLGA were studied and was used for protein antigen delivery and immune stimulation in dendritic cells [160]. The surface morphology of the fractured PLA nanocomposite (PLA/PBAT/AT) was observed by SEM studies [25]. In a separate study, the native PLA showed irregular microfibril structure compared to PLA nanocomposite (PLA/PCL) when both were dissolved in the phosphate saline buffer [161].

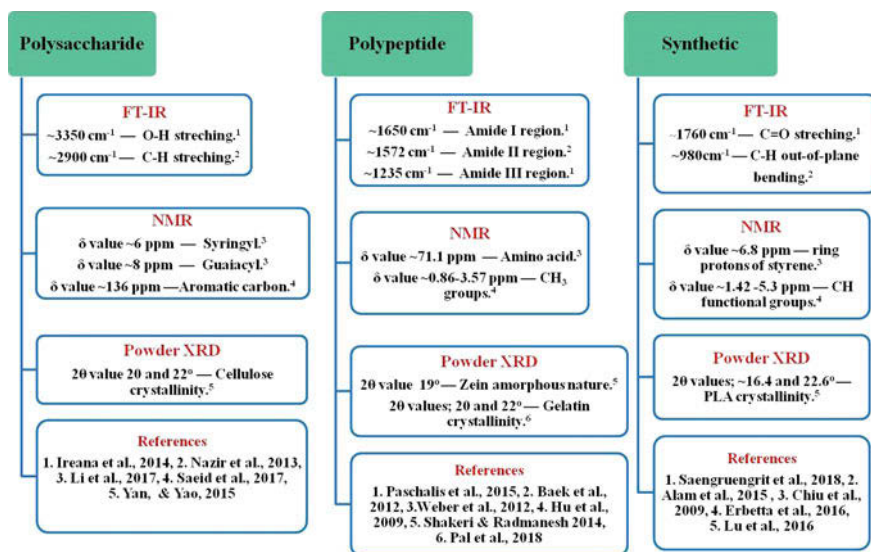
3.3.7 TEM

The TEM studies suggested that the mean particle size of Fe_3O_4 and Fe_3O_4 -3-(trimethoxysilyl)-propyl methacrylate (MPTMS) was 8.8 ± 1.8 and 8.7 ± 1.8 nm respectively. Further, TEM images of Fe_3O_4 -MPTMS-PLGA NCs showed 1–2 nm polymer coating thickness [165]. The surface morphology of PLA and PLA nanocomposite (PLA/PBAT/AT) were also studied using TEM [25].

The signature peaks for the described eco-friendly polymers have been summarized in Scheme 2.

4 Future Perspectives

For the sustainable development of the society, next-generation eco-friendly polymer composites are required to produce from renewable sources which possess superior physicochemical and biological properties. Globally BASF, Nature Works, Arkema, Novamont, and Plantic has been found to be the major player which governs the mass production of different polymers like- polylactic acid, starch-based polymer etc. contributing in several industries like—food, healthcare, and agriculture. Moreover, it is expected that this area will witness an increase in the CAGR by a significant amount at the end of 2021. Thus industries are changing their focus toward exploring the possibilities of biodegradable polymers. NCs offer



Scheme 2 Illustrative representation of the characteristic FT-IR, NMR and powder XRD peaks observed for different eco-friendly polymers

some great advantages over microcomposites because these possess improved strength and hardness. For the best utilization of the isolated eco-friendly polymers and their corresponding composites, proper characterization needs to be done.

Acknowledgements The authors would like to thank Director, CSIR-IHBT for his constant support and encouragement. AA acknowledges financial assistance in the form of project grant MLP-0201 from CSIR and GAP-0214 (EMR/2016/003027) from DST, Government of India. AKS, CS, SMSA acknowledge Academy of Scientific and Innovative Research (AcSIR) and CSIR-GATE and DBT for their respective JRF fellowship. AKS, CS and SMSA have contributed equally to this book chapter. The CSIR-IHBT communication number of this manuscript is 4254.

References

1. Camargo PHC, Satyanarayana KG, Wypych F (2009) Nanocomposites: synthesis, structure, properties and new application opportunities. *Mater Res* 12(1):1–39
2. Davidson S (2008) Sustainable bioenergy: genomics and biofuels development. *Nat Edu* 1(1):175–181
3. Iwata T (2015) Biodegradable and bio-based polymers: future prospects of eco-friendly plastics. *Angew Chem Int Ed* 54(11):3210–3215
4. Ray SS, Bousmina M (2005) Biodegradable polymers and their layered silicate nanocomposites: in greening the 21st century materials world. *Prog Mater Sci* 50(8):962–1079
5. Joshi G, Naithani S, Varshney VK, Bisht SS, Rana V, Gupta PK (2015) Synthesis and characterization of carboxymethyl cellulose from office waste paper: a greener approach towards waste management. *Waste Manag* 38:33–40

6. Singhsa P, Narain R, Manuspiya H (2018) Physical structure variations of bacterial cellulose produced by different *Komagataeibacter xylinus* strains and carbon sources in static and agitated conditions. *Cellulose* 25(3):1571–1581
7. Tuli M, Gurumayum S, Kaur S, Nagal S, Attri I (2015) Isolation and screening of cellulolytic fungi by baiting method from soils of Jalandhar. *Res J Pharm Biol Chem Sci* 6(2):375–380
8. Singla R, Soni S, Kulurkar PM, Kumari A, Mahesh S, Patial V, Yadav SK (2017) In situ functionalized nanobiocomposites dressings of bamboo cellulose nanocrystals and silver nanoparticles for accelerated wound healing. *Carbohydr Polym* 155:152–162
9. Phanthong P, Reubroycharoen P, Hao X, Xu G, Abudula A, Guan G (2018) Nanocellulose: extraction and application. *CRC* 1(1):32–43
10. Fatah IYA, Khalil HPS, Hossain MS, Aziz AA, Davoudpour Y, Dungani R, Bhat A (2014) Exploration of a chemo-mechanical technique for the isolation of nanofibrillated cellulosic fiber from oil palm empty fruit bunch as a reinforcing agent in composites materials. *Polymers* 6(10):2611–2624
11. Shao C, Wang M, Chang H, Xu F, Yang J (2017) A self-healing cellulose nanocrystal-poly(ethylene glycol) nanocomposite hydrogel via diels-alder click reaction. *ACS Sustain Chem Eng* 5(7):6167–6174
12. Li J, Wei X, Wang Q, Chen J, Chang G, Kong L, Liu Y (2012) Homogeneous isolation of nanocellulose from sugarcane bagasse by high pressure homogenization. *Carbohydr Polym* 90(4):1609–1613
13. Wang W, Mozuch MD, Sabo RC, Kersten P, Zhu JY, Jin Y (2015) Production of cellulose nanofibrils from bleached eucalyptus fibers by hyperthermostable endoglucanase treatment and subsequent microfluidization. *Cellulose* 22(1):351–361
14. Alemdar A, Sain M (2008) Isolation and characterization of nanofibers from agricultural residues—wheat straw and soy hulls. *Bioresour Technol* 99(6):1664–1671
15. Chen L, Wang Q, Hirth K, Baez C, Agarwal UP, Zhu JY (2015) Tailoring the yield and characteristics of wood cellulose nanocrystals (CNC) using concentrated acid hydrolysis. *Cellulose* 22(3):1753–1762
16. Lindblad Soderqvist M, Albertsson AC, Ranucci E, Laus M, Giani E (2005) Biodegradable polymers from renewable sources: rheological characterization of hemicellulose-based hydrogels. *Biomacromolecules* 6(2):684–690
17. Muchlisyam JS, Harahap U (2016) Hemicellulose: Isolation and its application in pharmacy. *Handbook of sustainable polymers: Processing and applications*, p 305–339
18. Dereca W, Nuruddin Md, Mahesh H, Alfred T-N, Shaik J (2015) Extraction and characterization of lignin from different biomass resources. *JMRT* 4(1):26–32
19. Hu L, Pan H, Zhou Y, Zhang M (2011) Methods to improve lignin's reactivity as a phenol substitute and as a replacement for other phenolic compounds: a brief review. *BioResources* 6(3):3515–3525
20. Kuhad R, Singh A (2007) *Lignocellulose biotechnology: future prospects*. I.K. International Publishing House, Delhi
21. Harmsen PFH, Huijgen WJJ, Bermúdez López LM, Bakker RRC (2010) Literature review of physical and chemical pretreatment processes for lignocellulosic biomass. Energy Research Centre of the Netherlands (ECN), ECN-E-10-013
22. Lee SH, Doherty TV, Linhardt RJ, Dordick JS (2009) Ionic liquid-mediated selective extraction of lignin from wood leading to enhanced enzymatic cellulose hydrolysis. *Biotechnol Bioeng* 102(5):1368–1376
23. Velez J, Thies MC (2016) Liquid lignin from the SLRP process: the effect of process conditions and black liquor properties. *J Wood Chem Technol* 36:27–41
24. Shi H, Fatehi P, Xiao H, Ni Y (2012) A process for isolating lignin of pre-hydrolysis liquor of Kraft pulping process based on surfactant and calcium oxide treatments. *Biochem Eng J* 68:19–24

25. Zhou L, Santomauro F, Fan J, Macquarrie D, Clark J, Chuck CJ, Budarin V (2017) Fast microwave-assisted acidolysis: a new biorefinery approach for the zero-waste utilisation of lignocellulosic biomass to produce high quality lignin and fermentable saccharides. *Faraday Discuss* 202:351–370
26. Bychkov AL, Podgorbunskikh EM, Ryabchikova EI, Lomovsky OI (2018) The role of mechanical action in the process of the thermomechanical isolation of lignin. *Cellulose* 25:1–5
27. Reddy DK, Bhotmange MG (2013) Isolation of starch from rice (*Oryza sativa* L.) and its morphological study using scanning electron microscopy. *IJAFST* 4(9): 859–866
28. El-Sheikh Manal A (2017) New technique in starch nanoparticles synthesis. *Carbohydr Polym* 176:214–219
29. Chen Y, Liu C, Chang PR, Anderson DP, Huneault MA (2009) Pea starch-based composite films with pea hull fibers and pea hull fiber-derived nanowhiskers. *Polym Eng Sci* 49(2): 369–378
30. Zheng H, Ai F, Chang PR, Huang J, Dufresne A (2009) Structure and properties of starch nanocrystal-reinforced soy protein plastics. *Polym Composite* 30(4):474–480
31. Kim J-Y, Park D-J, Lim S-T (2008) Fragmentation of waxy rice starch granules by enzymatic hydrolysis. *Cereal Chem* 85(2):182–187
32. Liu D, Wu Q, Chen H, Chang RR (2009) Transitional properties of starch colloid with particle size reduction from micro to nanometer. *J Colloid Interface Sci* 339(1):117–124
33. LeCorre D, Vahanian E, Dufresne A, Bras J (2012) Enzymatic pretreatment for preparing starch nanocrystals. *Biomacromolecules* 13(1):132–137
34. Espinosa Solis V, Jane J, Bello Perez LA (2009) Physicochemical characteristics of starches from unripe fruits of mango and banana. *Starke* 61(5):291–299
35. Haque S, Md S, Sahni JK, Ali J, Baboota S (2014) Development and evaluation of brain targeted intranasal alginate nanoparticles for treatment of depression. *J Psychiatr Res* 48(1): 1–12
36. Xu X, Qu T, Fan L, Chen X, Gao M, Zhang J, Guo T (2016) Preparation of pH-and magnetism-responsive sodium alginate/Fe₃O₄@ HNTs nanocomposite beads for controlled release of granulysin. *RSC Adv* 6(113):111747–111753
37. Anderson TJ, Lamsal BP (2011) Zein extraction from corn, corn products, and coproducts and modifications for various applications: a review. *Cereal Chem* 88(2):159–173
38. Dickey LC, Parris N, Craig JC, Kurantz MJ (2001) Ethanol extraction of zein from maize. *Ind Crops Prod* 13(1):67–76
39. Preece KE, Hooshyar N, Zuidam NJ (2017) Whole soybean protein extraction processes: a review. *Innovative Food Sci Emerg Technol* 43:163–172
40. Schmidt MM, Dornelles RCP, Mello RO, Kubota EH, Mazutti MA, Kempka AP, Demiate IM (2016) Collagen extraction process. *Int Food Res J* 23(3):913–922
41. Shyni K, Hema GS, Ninan G, Mathew S, Joshy CG, Lakshmanan PT (2014) Isolation and characterization of gelatin from the skins of skipjack tuna (*Katsuwonus pelamis*), dog shark (*Scoliodon sorrakowah*), and rohu (*Labeo rohita*). *Food Hydrocoll* 39:68–76
42. Anchana D, Kamatchi P, Leela K (2016) Extraction, characterization and application of gelatin from *Carcharhinus amblyrhyncho* and *Sphyrna barracuda*. *IOSR-JBB* 2(6):40–49
43. Du L, Keplová L, Khiari Z, Betti M (2014) Preparation and characterization of gelatin from collagen biomass obtained through a pH-shifting process of mechanically separated turkey meat. *Poult Sci* 93(4):989–1000
44. Fernando LAT, Poblete MRS, Ongkiko AGM, Diaz LJJ (2016) Chitin extraction and synthesis of chitin-based polymer films from Philippine Blue Swimming Crab (*Portunus pelagicus*) shells. *Procedia Chem* 19:462–468
45. Kumari S, Rath PK (2014) Extraction and characterization of chitin and chitosan from (*Labeo rohita*) fish scales. *Procedia Materials Science* 6:482–489
46. Xiao-Zhou S, Hong-Ru W, Mian H (2014) Characterization of the casein/keratin self-assembly nanomicelles. *J Nanomater* 2014(183815):1–7

47. Namvar F, Azizi S, Rahman HS, Mohamad R, Rasedee A, Soltani M, Rahim RA (2016) Green synthesis, characterization, and anticancer activity of hyaluronan/zinc oxide nanocomposite. *OncoTargets Ther* 9:4549
48. Amagai I, Tashiro Y, Ogawa H (2009) Improvement of the extraction procedure for hyaluronan from fish eyeball and the molecular characterization. *Fish Sci* 75(3):805–810
49. Guhados G, Wan W, Hutter JL (2005) Measurement of the elastic modulus of single bacterial cellulose fibers using atomic force microscopy. *Langmuir* 21(14):6642–6646
50. Huang HC, Chen LC, Lin SB, Hsu CP, Chen HH (2010) In situ modification of bacterial cellulose network structure by adding interfering substances during fermentation. *Bioresour Technol* 101(15):6084–6091
51. Zeng X, Small DP, Wan W (2011) Statistical optimization of culture conditions for bacterial cellulose production by *Acetobacter xylinum* BPR 2001 from maple syrup. *Carbohydr Polym* 85(3):506–513
52. Sheoran SK, Dubey KK, Tiwari DP, Singh BP (2012) Directive production of pullulan by altering cheap source of carbons and nitrogen at 5l bioreactor level. *ISRN Chemical Engineering* 2012:1–5
53. Shehata AN, Darwish DA, Masoud HM (2016) Extraction, purification and characterization of endo-acting pullulanase Type I from white edible mushrooms. *J Appl Pharm Sci* 6(01): 147–152
54. Jamshidian M, Tehrani EA, Imran M, Jacquot M, Desobry S (2010) Poly-lactic acid: production, applications, nanocomposites, and release studies. *Compr Rev Food Sci Food Saf* 9(5):552–571
55. Danhier F, Ansorena E, Silva JM, Coco R, Le Breton A, Preat V (2012) PLGA-based nanoparticles: an overview of biomedical applications. *J Control Release* 161(2):505–522
56. Erbetta CDAC, Alves RJ, Resende JM, de Souza Freitas RF, de Sousa RG (2012) Synthesis and characterization of poly(D, L-lactide-co-glycolide) copolymer. *J Biomater Nanobiotechnol* 3(02):208
57. Beg MDH, Alam AM, Yunus RM, Mina MF (2015) Improvement of interaction between pre-dispersed multi-walled carbon nanotubes and unsaturated polyester resin. *J Nanopart Res* 17(1):53
58. Saeid N, Omid Z, Yousef Mojtaba, Saba A, Minoo N (2017) Catalyzed synthesis characterization of a novel lignin-based curing agent for the curing of high-performance epoxy resin. *Polymers* 9(7):266
59. Le DM, Nielsen AD, Sørensen HR, Meyer AS (2017) Characterisation of authentic lignin biorefinery samples by Fourier transform infrared spectroscopy and determination of the chemical formula for lignin. *BioEnerg Res* 10(4):1025–1035
60. Abraham E, Kam D, Nevo Y, Slattegard R, Rivkin A, Lapidot S, Shoseyov O (2016) Highly modified cellulose nanocrystals and formation of epoxy-nanocrystalline cellulose (CNC) nanocomposites. *ACS Appl Mater Interfaces* 8(41):28086–28095
61. Luduena LN, Vecchio A, Stefani PM, Alvarez VA (2013) Extraction of cellulose nanowhiskers from natural fibers and agricultural byproducts. *Fibers Polym* 14(7):1118–1127
62. Haafiz MM, Eichhorn SJ, Hassan A, Jawaid M (2013) Isolation and characterization of microcrystalline cellulose from oil palm biomass residue. *Carbohydr Polym* 93(2):628–634
63. Spiridonov VV, Panova IG, Afanasov MI, Zezin SB, Sybachin AV, Yaroslavov AA (2018) Water-Soluble magnetic nanocomposites based on carboxymethyl cellulose and iron (III) oxide. *Polym Sci Ser B* 60(1):116–121
64. Cardoso GV, Mello LRDS, Zanatta P, Cava S, Raubach CW, Moreira ML (2018) Physico-chemical description of titanium dioxide–cellulose nanocomposite formation by microwave radiation with high thermal stability. *Cellulose* 25(4):2331–2341
65. Ayoub A, Venditti RA, Pawlak JJ, Salam A, Hubbe MA (2013) Novel hemicellulose–chitosan biosorbent for water desalination and heavy metal removal. *ACS Sustain Chem Eng* 1(9):1102–1109

66. Badshah M, Ullah H, Khan AR, Khan S, Park JK, Khan T (2018) Surface modification and evaluation of bacterial cellulose for drug delivery. *Int J Biol Macromol* 113:526–533
67. Foong CY, Hamzah MSA, Razak SIA, Saidin S, Nayan NHM (2018) Influence of poly (lactic acid) layer on the physical and antibacterial properties of dry bacterial cellulose sheet for potential acute wound healing materials. *Fibers Polym* 19(2):263–271
68. Vijayalakshmi K, Gomathi T, Sudha PN (2014) Preparation and characterization of nanochitosan/sodium alginate/microcrystalline cellulose beads. *Der Pharmacia Lettre* 6(4): 65–77
69. Krishnaveni B, Ragunathan R (2015) Extraction and Characterization of chitin and chitosan from *F. solani* CBNR BKRR, synthesis of their bionanocomposites and study of their productive application. *J Pharm Sci Res* 7(4):197–205
70. Shanathi P, Kothai S (2015) Synthesis and characterization of chitosan with incorporated herb—a novel bionano composite. *Int J Chemtech Res* 8(8):208–214
71. Silva NH, Vilela C, Almeida A, Marrucho IM, Freire CS (2018) Pullulan-based nanocomposite films for functional food packaging: exploiting lysozyme nanofibers as antibacterial and antioxidant reinforcing additives. *Food Hydrocoll* 77:921–930
72. Mitić Ž, Cakić M, Nikolić GM, Nikolić R, Nikolić GS, Pavlović R, Santaniello E (2011) Synthesis, physicochemical and spectroscopic characterization of copper (II)-polysaccharide pullulan complexes by UV–vis, ATR-FTIR, and EPR. *Carbohydr Res* 346(3):434–441
73. Xu F, Yu J, Tesso T, Dowell F, Wang D (2013) Qualitative and quantitative analysis of lignocellulosic biomass using infrared techniques: a mini-review. *Appl Energy* 104:801–809
74. Sills DL, Gossett JM (2012) Using FTIR to predict saccharification from enzymatic hydrolysis of alkali-pretreated biomasses. *Biotechnol Bioeng* 109(2):353–362
75. Tian X, Rehmann L, Xu CC, Fang Z (2016) Pretreatment of eastern white pine (*Pinus strobes* L.) for enzymatic hydrolysis and ethanol production by organic electrolyte solutions. *ACS Sustain Chem Eng* 4(5):2822–2829
76. Kubo S, Kadla JF (2005) Hydrogen bonding in lignin: a Fourier transform infrared model compound study. *Biomacromolecules* 6(5):2815–2821
77. Ma X, Jian R, Chang PR, Yu J (2008) Fabrication and characterization of citric acid-modified starch nanoparticles/plasticized-starch composites. *Biomacromolecules* 9(11): 3314–3320
78. Poletto M, Pistor V, Zattera AJ (2013) Structural characteristics and thermal properties of native cellulose. In: *Cellulose-fundamental aspects*. InTech, p 45–68
79. El Oudiani A, Chaabouni Y, Msahli S, Sakli F (2011) Crystal transition from cellulose I to cellulose II in NaOH treated *Agave americana* L. fibre. *Carbohydr Polym* 86(3):1221–1229
80. Huang HD, Liu CY, Zhou D, Jiang X, Zhong GJ, Yan DX, Li ZM (2015) Cellulose composite aerogel for highly efficient electromagnetic interference shielding. *J Mater Chem A* 3(9):4983–4991
81. Dietrich K, Hernandez-Mejia C, Verschuren P, Rothenberg G, Shiju NR (2017) One-pot selective conversion of hemicellulose to xylitol. *Org Process Res Dev* 21(2):165–170
82. Peng XW, Ren JL, Zhong LX, Sun RC (2011) Nanocomposite films based on xylan-rich hemicelluloses and cellulose nanofibers with enhanced mechanical properties. *Biomacromolecules* 12(9):3321–3329
83. Zhong C, Zhang GC, Liu M, Zheng XT, Han PP, Jia SR (2013) Metabolic flux analysis of *Gluconacetobacter xylinus* for bacterial cellulose production. *Appl Microbiol Biotechnol* 97 (14):6189–6199
84. Ramírez JAÁ, Hoyos CG, Arroyo S, Cerrutti P, Foresti ML (2016) Acetylation of bacterial cellulose catalyzed by citric acid: use of reaction conditions for tailoring the esterification extent. *Carbohydr Polym* 153:686–695
85. Chen K, Ling Y, Cao C, Li X, Chen X, Wang X (2016) Chitosan derivatives/reduced graphene oxide/alginate beads for small-molecule drug delivery. *Mater Sci Eng C* 69:1222–1228

86. Ramesan MT, Siji C, Kalaprasad G, Bahuleyan BK, Al-Maghrabi MA (2018) Effect of silver doped zinc oxide as nanofiller for the development of biopolymer nanocomposites from chitin and cashew gum. *J Polym Environ* 26(7):2983–2991
87. Köhnke J, Fürst C, Unterweger C, Rennhofer H, Lichtenegger HC, Keckes J, Emsenhuber G, Liebner F, Gindl-Altmutter W (2016) Carbon microparticles from organosolv lignin as filler for conducting poly(lactic acid). *Polymers* 8(6):205
88. Shivananda CS, Rao BL, Madhukumar R, Sarojini BK, Somashekhar R, Asha, S, Sangappa Y (2016) Silk fibroin/pullulan blend films: preparation and characterization. In: AIP conference proceedings, vol 1731(1). AIP Publishing, p 070013
89. Trovatti E, Fernandes SC, Rubatat L, Freire CS, Silvestre AJ, Neto CP (2012) Sustainable nanocomposite films based on bacterial cellulose and pullulan. *Cellulose* 19(3):729–737
90. Tzhayik O, Pulidindi IN, Gedanken A (2014) Forming nanospherical cellulose containers. *Ind Eng Chem Res* 53(36):13871–13880
91. Lal S, Perwez A, Rizvi MA, Datta M (2017) Design and development of a biocompatible montmorillonite PLGA nanocomposites to evaluate in vitro oral delivery of insulin. *Appl Clay Sci* 147:69–79
92. Goundalkar MJ, Corbett DB, Bujanovic BM (2014) Comparative analysis of milled wood lignins (MWLs) isolated from sugar maple (SM) and hot water extracted sugar maple (ESM). *Energies* 7(3):1363–1375
93. Pu Y, Cao S, Ragauskas AJ (2011) Application of quantitative ³¹P NMR in biomass lignin and biofuel precursors characterization. *Energy Environ Sci* 4(9):3154–3166
94. Mascheroni E, Rampazzo R, Orteni MA, Piva G, Bonetti S, Piergiorgio L (2016) Comparison of cellulose nanocrystals obtained by sulfuric acid hydrolysis and ammonium persulfate, to be used as coating on flexible food-packaging materials. *Cellulose* 23(1):779–793
95. Astruc J, Nagalakshmaiah M, Laroche G, Grandbois M, Elkoun S, Robert M (2017) Isolation of cellulose-II nanospheres from flax stems and their physical and morphological properties. *Carbohydr Polym* 178:352–359
96. Kishani S, Vilaplana F, Xu W, Xu C, Wagberg (2018) Solubility of softwood hemicelluloses. *Biomacromolecules* 19(4):1245–1255
97. Madhusudhan KN, Meghana PB, Vinaya Rani G, Moorthy SM, Mary-Josepha AV (2017) Extraction and characterization of chitin and chitosan from *Aspergillus niger*, synthesis of silver-chitosan nanocomposites and evaluation of their antimicrobial potential. *Journal of Advances in Biotechnology* 6(3):939–945
98. Mushi NE, Utsel S, Berglund LA (2014) Nanostructured biocomposite films of high toughness based on native chitin nanofibers and chitosan. *Front Chem* 2(99):1–11
99. Coseri S, Spatareanu A, Sacarescu L, Socoliuc V, Sorin Stratulat I, Harabagiu V (2016) Pullulan: a versatile coating agent for superparamagnetic iron oxide nanoparticles. *J Appl Polym Sci* 133(5):42926(1–9)
100. Li G, Sun Y, Liu H (2018) Gold-carboxymethyl cellulose nanocomposites greenly synthesized for fluorescent sensitive detection of Hg(II). *J Cluster Sci* 29(1):177–184
101. Li J, Zhang J, Zha S, Gao Q, Li J, Zhang Q (2017) Fast curing biobased phenolic resins via lignin demethylated under mild reaction condition. *Polymers* 9(9):428
102. Anandhavelu S, Thambidurai S (2012) Preparation of chitosan-ZnO nanocomposite from chitin polymer. *Adv Mat Res* 584:234–238
103. Putnam CD, Hamme M, Hura GL, Tainer JA (2007) X-ray solution scattering (SAXS) combined with crystallography and computation: defining accurate macromolecular structures, conformations and assemblies in solution. *Q Rev Biophys* 40(3):191–285
104. Yang H, Yan R, Chen H, Lee DH, Zheng C (2007) Characteristics of hemicellulose, cellulose and lignin pyrolysis. *Fuel* 86(12–13):1781–1788
105. Nagalakshmaiah M, Mortha G, Dufresne A (2016) Structural investigation of cellulose nanocrystals extracted from chili leftover and their reinforcement in cariflex-IR rubber latex. *Carbohydr Polym* 136:945–954

106. Zhao W, Odelius K, Edlund U, Zhao C, Albertsson AC (2015) In situ synthesis of magnetic field-responsive hemicellulose hydrogels for drug delivery. *Biomacromolecules* 16(8):2522–2528
107. Malagurski I, Levic S, Mitric M, Pavlovic V, Dimitrijevic-Brankovic S (2018) Bimetallic alginate nanocomposites: new antimicrobial biomaterials for biomedical application. *Mater Lett* 212:32–36
108. Praveen P, Rao V (2014) Synthesis and thermal studies of chitin/AgCl nanocomposite. *Procedia Materials Science* 5(2014):1155–1159
109. Deng J, Xiong T, Wang H, Zheng A, Wang Y (2016) Effects of cellulose, hemicellulose, and lignin on the structure and morphology of porous carbons. *ACS Sustain Chem Eng* 4(7):3750–3756
110. Gokila S, Gomathi T, Sudha PN, Anil S (2017) Removal of the heavy metal ion chromium (VI) using chitosan and alginate nanocomposites. *Int J Biol Macromol* 104:1459–1468
111. Morin A, Dufresne A (2002) Nanocomposites of chitin whiskers from *Riftia* tubes and poly (caprolactone). *Macromolecules* 35(6):2190–2199
112. Alahmadi NS, Betts JW, Heinze T, Kelly SM, Koschella A, Wadhawan JD (2018) Synthesis and antimicrobial effects of highly dispersed, cellulose-stabilized silver/cellulose nanocomposites. *RSC Adv* 8(7):3646–3656
113. Mathew L, Joshy MK, Joseph R (2011) Isora fibre: a natural reinforcement for the development of high performance engineering materials. In: *Cellulose fibers: bio-and nano-polymer composites*. Springer, Berlin, Heidelberg, p 291–324
114. Uraki Y, Nemoto J, Otsuka H, Tamai Y, Sugiyama J, Kishimoto T, Shimomura M (2007) Honeycomb-like architecture produced by living bacteria, *Gluconacetobacter xylinus*. *Carbohydr Polym* 69(1):1–6
115. Motshekgga SC, Ray SS, Maity A (2018) Synthesis and characterization of alginate beads encapsulated zinc oxide nanoparticles for bacteria disinfection in water. *J Colloid Interface Sci* 512:686–692
116. PM V, Thomas S (2011) Preparation and characterization of chitin nanowhiskers and their polymer nanocomposites. *Int J Polym Technol* 3(1):35–44
117. Krull SM, Ma Z, Li M, Davé RN, Bilgili E (2016) Preparation and characterization of fast dissolving pullulan films containing BCS class II drug nanoparticles for bioavailability enhancement. *Drug Dev Ind Pharm* 42(7):1073–1085
118. Selig MJ, Viamajala S, Decker SR, Tucker MP, Himmel ME, Vinzant TB (2007) Deposition of lignin droplets produced during dilute acid pretreatment of maize stems retards enzymatic hydrolysis of cellulose. *Biotechnol Prog* 23(6):1333–1339
119. Yan CF, Yu HY, Yao JM (2015) One-step extraction and functionalization of cellulose nanospheres from lyocell fibers with cellulose II crystal structure. *Cellulose* 22(6):3773–3788
120. Parambath Kanoth B, Claudino M, Johansson M, Berglund LA, Zhou Q (2015) Biocomposites from natural rubber: synergistic effects of functionalized cellulose nanocrystals as both reinforcing and cross-linking agents via free-radical thiol–ene chemistry. *ACS Appl Mater Interfaces* 7(30):16303–16310
121. Tian D, Hu J, Bao J, Chandra RP, Saddler JN, Canhui Lu (2017) Lignin valorization: lignin nanoparticles as high-value bio-additive for multifunctional nanocomposites. *Biotechnol Biofuels* 10(1):192
122. Geng L, Peng X, Zhan C, Naderi A, Sharma PR, Mao Y, Hsiao BS (2017) Structure characterization of cellulose nanofiber hydrogel as functions of concentration and ionic strength. *Cellulose* 24(12):5417–5429
123. Vilcinskas K, Zlopassa J, Jansen K, Mulder FM, Picken SJ, Koper GJ (2016) Water sorption and diffusion in (reduced) graphene oxide-alginate biopolymer nanocomposites. *Macromol Mater Eng* 301(9):1049–1063
124. Mathew AP, Laborie MPG, Oksman K (2009) Cross-linked chitosan/chitin crystal nanocomposites with improved permeation selectivity and pH stability. *Biomacromolecules* 10(6):1627–1632

125. Kittle JD, Wang C, Qian C, Zhang Y, Zhang M, Roman M, Esker AR (2012) Ultrathin chitin films for nanocomposites and biosensors. *Biomacromolecules* 13(3):714–718
126. Ashokkumar M, Narayanan NT, Reddy ALM, Gupta BK, Chandrasekaran B, Talapatra S, Thanikaivelan P (2012) Transforming collagen wastes into doped nanocarbons for sustainable energy applications. *Green Chem* 14(6):1689–1695
127. Alcântara AC, Darder M, Aranda P, Ruiz-Hitzky E (2016) Effective intercalation of zein into Na-montmorillonite: role of the protein components and use of the developed biointerfaces. *Beilstein J Nanotechnol* 7:1772
128. Belbachir K, Noreen R, Gouspillou G, Petibois C (2009) Collagen types analysis and differentiation by FTIR spectroscopy. *Anal Bioanal Chem* 395(3):829–837
129. Paschalis EP, Gamsjaeger S, Tatakis DN, Hassler N, Robins SP, Klaushofer K (2015) Fourier transform infrared spectroscopic characterization of mineralizing type I collagen enzymatic trivalent cross-links. *Calcif Tissue Int* 96(1):18–29
130. Baek JY, Xing ZC, Kwak G, Yoon KB, Park SY, Park LS, Kang IK (2012) Fabrication and characterization of collagen-immobilized porous PHBV/HA nanocomposite scaffolds for bone tissue engineering. *J Nanomater* 2012:1–11
131. Zakaria S, Bakar NHA (2015) Extraction and characterization of gelatin from Black tilapia (*Oreochromis niloticus*) scales and bones. In: International conference on advances in science, engineering, technology & natural resources (ICASETNR-15), Kota Kinabalu (Malaysia), p 77–80
132. Pal A, Bajpai J, Bajpai AK (2018) Easy fabrication and characterization of gelatin nanocarriers and in vitro investigation of swelling controlled release dynamics of paclitaxel. *Polym Bull* 75(10):4691–4711
133. Picchio ML, Ronco LI, Passeggi MC, Minari RJ, Gugliotta LM (2017) Poly (n-butyl acrylate)-casein nanocomposites as promising candidates for packaging films. *J Polym Environ* 26(6):2579–2587
134. Zhang F, Ma J, Xu Q, Zhou J, Simion D, Carmen G, Li Y (2016) Correction to hollow casein-based polymeric nanospheres for opaque coatings. *ACS Appl Mater Interfaces* 8(24):15856–15856
135. Oliveira JL, Campos EVR, Pereira ADES, Pasquoto T, Lima R, Grillo R, Fraceto LF (2018) Zein nanoparticles as eco-friendly carrier systems for botanical repellents aiming sustainable agriculture. *J Agric Food Chem* 66(6):1330–1340
136. Sadare OO, Daramola MO, Afolabi AS (2015) Preparation and characterization of nanocomposite soy-carbon nanotubes (SPI/CNTs) adhesive from soy protein isolate. In: Proceedings of the world congress on engineering, vol 2. London, U.K., p 1–3
137. Najafizadeha F, Sadjadia MAS, Fatemib SJ, Mobarakehc MK, Afshard RM (2016) A comparison between biocompatibilities of nanocomposites of silica doped in HA/collagen and those doped in HA/gelatin. *OJC* 32(3):1551–1557
138. Shakeri A, Radmanesh S (2014) Preparation of cellulose nanofibrils by high-pressure homogenizer and Zein composite films. *Adv Mat Res* 829:534–538
139. Li S, Zhao Y (2017) Preparation of zein nanoparticles by using solution-enhanced dispersion with supercritical CO₂ and elucidation with computational fluid dynamics. *Int J Nanomedicine* 12:3485
140. Ding GJ, Zhu YJ, Cheng GF, Ruan YJ, Qi C, Lu BQ, Wu J (2016) Porous microspheres of casein/amorphous calcium phosphate nanocomposite: room temperature synthesis and application in drug delivery. *Curr Nanosci* 12(1):70–78
141. Consonni R, Santomo L, Tenni R, Longhi R, Zetta L (1998) Conformational study of a collagen peptide by 1H NMR spectroscopy: observation of the 14N–1H spin-spin coupling of the Arg guanidinium moiety in the triple-helix structure. *FEBS Lett* 436(2):243–246
142. Weber F, Böhme J, Scheidt HA, Gründer W, Rammelt S, Hacker M, Huster D (2012) 31P and 13C solid-state NMR spectroscopy to study collagen synthesis and biomineralization in polymer-based bone implants. *NMR Biomed* 25(3):464–475

143. Hu X, Ma L, Wang C, Gao C (2009) Gelatin hydrogel prepared by photo-initiated polymerization and loaded with TGF- β 1 for cartilage tissue engineering. *Macromol Biosci* 9(12):1194–1201
144. Zhong Q, Jin M (2009) Zein nanoparticles produced by liquid–liquid dispersion. *Food Hydrocoll* 23(8):2380–2387
145. Chen H, Zhong Q (2015) A novel method of preparing stable zein nanoparticle dispersions for encapsulation of peppermint oil. *Food Hydrocoll* 43:593–602
146. Ghazy OA, Nabih S, Abdel-Moneam YK, Senna MM (2015) Synthesis and characterization of silver/zein nanocomposites and their application. *Polym Composite* 38(S1):E9–E15
147. Dhandayuthapani B, Poulouse AC, Nagaoka Y, Hasumura T, Yoshida Y, Maekawa T, Kumar DS (2012) Biomimetic smart nanocomposite: in vitro biological evaluation of zein electrospun fluorescent nanofiber encapsulated CdS quantum dots. *Biofabrication* 4(2): 025008
148. Consonni R, Zetta L, Longhi R, Toma L, Zanaboni G, Tenni R (2000) Conformational analysis and stability of collagen peptides by CD and by ^1H - and ^{13}C -NMR spectroscopies. *Biopolymers* 53(1):99–111
149. Xu Y, Keene DR, Bujnicki JM, Höök M, Lukomski S (2002) Streptococcal Scl1 and Scl2 proteins form collagen-like triple helices. *J Biol Chem* 277(30):27312–27318
150. Ahsan SM, Mohan Rao Ch (2016) Structural studies on aqueous gelatin solutions: implications in designing a thermo-responsive nanoparticulate formulation. *Int J Biol Macromol* 95:1126–1134
151. Muralidharan N, Shakila RJ, Sukumar D, Jeyasekaran G (2013) Skin, bone and muscle collagen extraction from the trash fish, leather jacket (*Odonus niger*) and their characterization. *J Food Sci Technol* 50(6):1106–1113
152. Abdel-Mohsen AM, Jancar J, Abdel-Rahman RM, Vojtek L, Hyršl P, Dušková M, Nejezchlebová H (2017) A novel in situ silver/hyaluronan bio-nanocomposite fabrics for wound and chronic ulcer dressing: in vitro and in vivo evaluations. *Int J Pharm* 520(1–2): 241–253
153. Zhang L, Ma D, Wang F, Zhang Q (2002) The modification of scaffold material in building artificial dermis. *Artif Cells Blood Substit Biotechnol* 30(4):319–332
154. Mizuno K, Hayashi T, Peyton DH, Bächinger HP (2004) Hydroxylation-induced stabilization of the collagen triple helix acetyl-(glycyl-4 (r)-hydroxypropyl-4 (r)-hydroxypropyl) 10-nh2 forms a highly stable triple helix. *J Biol Chem* 279(36):38072–38078
155. Tampieri A, Celotti G, Landi E, Sandri M, Roveri N, Falini G (2003) Biologically inspired synthesis of bone-like composite: self-assembled collagen fibers/hydroxyapatite nanocrystals. *J Biomed Mater Res Part A* 67(2):618–625
156. Kumar P, Sandeep KP, Alavi S, Truong VD, Gorga RE (2010) Preparation and characterization of bio-nanocomposite films based on soy protein isolate and montmorillonite using melt extrusion. *J Food Eng* 100(3):480–489
157. Hassenkam T, Fantner GE, Cutroni JA, Weaver JC, Morse DE, Hansma PK (2004) High-resolution AFM imaging of intact and fractured trabecular bone. *Bone* 35(1), 4–10
158. Zhang J, Senger B, Vautier D, Picart C, Schaaf P, Voegel JC, Lavalle P (2005) Natural polyelectrolyte films based on layer-by layer deposition of collagen and hyaluronic acid. *Biomaterials* 26(16):3353–3361
159. Song L, Wang Z, Lamm ME, Yuan L, Tang C (2017) Supramolecular polymer nanocomposites derived from plant oils and cellulose nanocrystals. *Macromolecules* 50 (19):7475–7483
160. Saengruengrit C, Ritprajak P, Wanichwecharungruang S, Sharma A, Salvan G, Zahn DR, Insin N (2018) The combined magnetic field and iron oxide-PLGA composite particles: effective protein antigen delivery and immune stimulation in dendritic cells. *J Colloid Interface Sci* 520:101–111
161. Lu Y, Chen Y-C, Zhang P-H (2016) Preparation and characterisation of polylactic acid (PLA)/polycaprolactone (PCL) composite microfibre membranes. *Fibres Text East Eur* 3(117):17–21

162. Carson L, Kelly-Brown C, Stewart M, Oki A, Regisford G, Luo Z, Bakhmutov VI (2009) Synthesis and characterization of chitosan–carbon nanotube composites. *Mater Lett* 63(6–7): 617–620
163. Chiu HT, Chen SC (2001) Curing reaction of unsaturated polyester resin modified by dicyclopentadiene. *J Polym Res* 8(3):183–190
164. Hazarika D, Karak N (2016) Biodegradable tough waterborne hyperbranched polyester/carbon dot nanocomposite: approach towards an eco-friendly material. *Green Chem* 18(19): 5200–5211
165. Atila Dinçer C, Yıldız N, Karakeçili A, Aydoğan N, Çalimli A (2017) Synthesis and characterization of Fe₃O₄-MPTMS-PLGA nanocomposites for anticancer drug loading and release studies. *Artif Cells Nanomed Biotechnol* 45(7):1408–1414

Biocompatible and Biodegradable Chitosan Composites in Wound Healing Application: In Situ Novel Photo-Induced Skin Regeneration Approach



Amr A. Essawy, Hassan Hefni and A. M. El-Nggar

List of Abbreviations

Aw	Water absorbency
CCNC	Chitosan-based copper nanocomposite
CF	Chitosan-fibrin
CFU	Colony-forming unit
CMCS	Carboxymethyl chitosan
COX-2	Cyclooxygenase-2
CS-Ag	Chitosan-Ag
CSNPs	Chitosan nanoparticles
CZBs	Chitosan hydrogel/nano-ZnO nanocomposite bandages
DA	Deacetylation
DC	Decoloration
DM	Demineralization
DP	Degree of polymerization
DP	Deproteinization
ECM	Extracellular matrix
FDA	American Food and Drug Administration
FTIR	Fourier transform infrared
IL	Interleukin

A. A. Essawy (✉)
Chemistry Department, Faculty of Science,
Fayoum University, Fayoum 63514, Egypt
e-mail: aae01@fayoum.edu.eg

A. A. Essawy
Chemistry Department, College of Science, Jouf University,
P.O. Box 2014, Sakaka, Aljouf, Kingdom of Saudi Arabia

H. Hefni
Petrochemicals Department, Egyptian Petroleum Research Institute (EPRI),
Cairo, Egypt

A. M. El-Nggar
Chemistry Department, Faculty of Science, Al-Azhar University,
Cairo 11751, Egypt

LPS	Lipopolysaccharide
Mel/CS MS	Melatonin-loaded chitosan-based microspheres
MW	Molecular weight
MyD88	Myeloid differentiation primary-response protein 88
NF- κ B	Nuclear factor-kappa
NMR	Nuclear magnetic resonance
nT/COL-CS	Nano-titania/collagen-chitosan
PVA	Polyvinyl alcohol
Q-CF	Quercetin-loaded chitosan-fibrin
ROS	Reactive oxygen species
SSD	Silver sulfadiazine
TLR-4	Toll-like receptor 4
TMC	<i>N,N,N</i> -Trimethyl chitosan
TNF- α	Tumor necrosis factor-alpha

1 Introduction

Many types of polymers have diverse biomedical applications since they have unique properties and can be easily tailored. Polymeric materials include natural biopolymers, especially proteins, polysaccharides, polynucleotides, and natural rubber as well as synthetic polymers like polyethers, polyalkenes, polycarbonates, polyesters, and polyamides. The biocompatibility and biodegradability of the polymers is the main reason for their usage in biomedical applications. Biocompatibility term referred to the ability of materials to interact with a living system without revealing the undesirable degree of harm to the living system and biodegradability can be defined as the capability of materials in being degraded by biological activity. Biodegradable polymers are biocompatible; i.e. they do not rise an inflammatory response, and they degrade *in vivo* by hydrolysis and possible enzyme reactions, afterword they are removed from the body through regular metabolic processes [1]. Biocompatible and biodegradable materials should have important properties to consider when they are used for the medical purpose, in brief; do not trigger inflammatory or toxic response to the body, acceptable shelf life, the degradation period match to the healing or regeneration process, non-toxicity of degraded products, easily released from the body, permeability, appropriate molecular weight, solubility, suitable structure, surface charge and water absorption [2].

Wounds are an abnormal defect in the skin, vary to many types, and each category needs peculiar caring to achieve healing objective [3]. This fact was inspired researchers to develop suitable wound dressings, by considering the use of biocompatible natural and synthetic polymers and their composites as the bases of wound dressings. These polymers overcome the disadvantages of classical dressing materials [4].

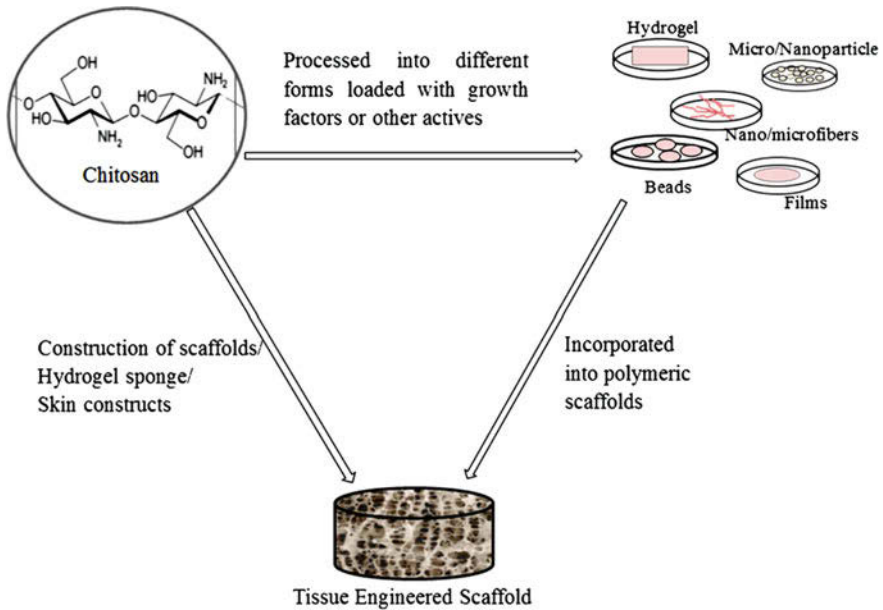


Fig. 1 Schematic representation of the possibilities of processing chitosan into different forms [5]. Copyright 2014. Reproduced with permission from Springer Nature

Recent reports are aiming to develop dressing alternatives to accelerate the wound repairing process. Naturally, derived materials like chitosan and its composites could be used to achieve this target. Chitosan is a renewable basic polysaccharide emerges as a viable structure that can be massively modified to diverse types of bio-based composites have a great potential in biomedical engineering. Chitosan has an interesting capability to be processed into gels, nanofibers, membranes, scaffolds, sponge-like forms, beads, microparticles and nanoparticles (Fig. 1) [5].

The different decorated forms of chitosan take into consideration the adaptation with the requirements of wound healing applications. The dried forms of chitosan have possibly to be hydrated via absorption of wounds exudates forming a hydrogel layer over the wounded area. Chitosan exhibits excellent biocompatibility, biodegradability, nontoxicity, anti-microbial and be used as hydrating agents [6]. Also, chitosan has an adhesive nature, antifungal, bactericidal feature, and oxygen permeability. Because of these immense activities, chitosan and its composites show good positive impacts on wound healing. Earlier reports indicated that chitosan-based dressings can accelerate the repair of diverse tissues and facilitates contraction of wounds. It stimulates cell proliferation. Hemostatic properties of chitosan aids to natural blood thrombosis as well as blocking of nerve endings that reduce pain. Moreover, gradual depolymerization of chitosan releases *N*-acetyl-glucosamine, which initiates fibroblast proliferation, deposits collagen

regularly, and induces the synthesis of a desirable amount of natural hyaluronic acid at the wound site. This leads to higher rate of wound repairing within a minimal scar [7]. Several studies enumerate the chitosan functionality in promoting the polymorphonuclear neutrophils migration, and induction of granulation by promoting dermal fibroblasts proliferation [8] that accelerate wound healing. The polymer, chitosan possess basic amino groups and thus acquires an overall positive charge at acidic pH. In common with many cationic polymers, chitosan has pronounced antimicrobial effects due to destabilization of the external membrane of bacteria via interaction between chitosan positive charges and negative charges of the microbial cell membrane. This causes the disruption of the microbial membrane, and subsequent infiltration of intracellular constituents. Studies proposed an alteration in cell permeability via the interaction between the cell membrane and chitosan [9].

Reports conclude that lower concentrations of chitosan exhibit a considerable antibacterial activity against various pathogens like *Escherichia coli* or *Staphylococcus aureus* [7]. Therefore, it finds rich use in the medical field in promoting wound healing. Furthermore, chitosan dressings reveal minimal side effects and provide microbial disinfection. Chitosan is appropriate for wound healing because of its ease of administration, wound protection, water retention that produces a moist environment on the wound beds, without drawbacks of accumulating exudates. In addition, its permeable nature provides appropriate oxygen required for reparative processes.

2 Biodegradable Polymers

Biodegradable materials take a great attention of the researchers aiming to the better suited medical application which will stay inside the body until the healing process is finished and then gradually decomposed. Polymers degradation process is dependent on the polymer properties and its site in the body.

Both synthetic and natural polymers have been widely investigated as biodegradable materials that showed controllable chemical breakdown into non-toxic degradation products. Classification of biodegradable polymers can be explained as illustrated in Fig. 2 [10].

Biodegradation of polymeric biomaterials involves cleavage of hydrolytically or enzymatically sensitive bonds in the polymer leading to polymer decomposition. Polymeric biomaterials could be classified according to degradation mode into enzymatically- and hydrolytically degradable polymers. Enzymatic degradation takes place to almost natural polymers. Natural polymers are the firstly used biodegradable biomaterials in clinical applications. On the other hand, hydrolytically degradable polymers contain in their backbone hydrolytically labile functional groups such as amides, anhydrides, acetal, carbonates, urethanes, esters, orthoesters etc. that have hydrolytic susceptibility [2].

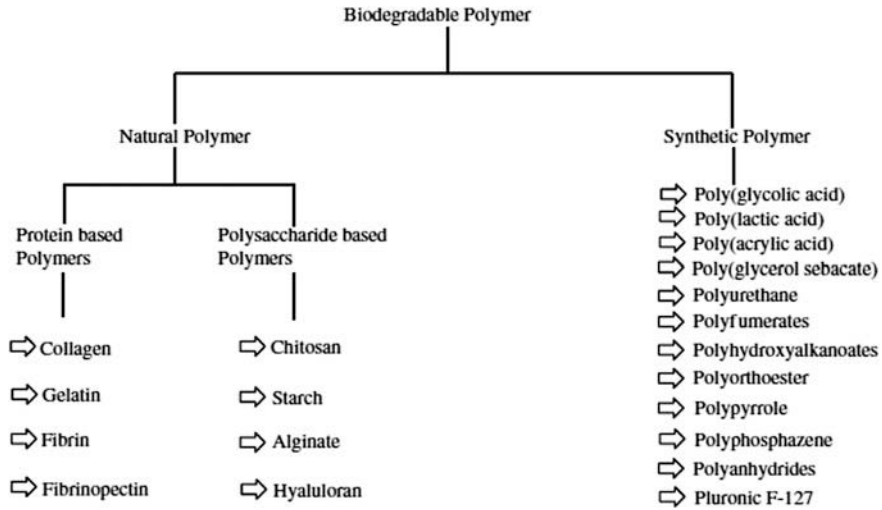


Fig. 2 Classification of biodegradable polymers [10]. Copyright 2016. Reprinted with permission from Springer Nature

The degradation of polymers can go into the different process depending on the polymer structure. The polymer that contains hydrolyzable units directly incorporated in the backbone of the polymer chain slowly degraded to smaller units and can be eliminated from the body. The polymer that has degradable side chains can be a breakdown in the body providing residual polymers with hydroxyl, carboxyl or other hydrating groups making the polymer water-soluble and excreted from the body. Another way depend on a hydrolysable cross-linking unit in the cross-linking polymer where a water-soluble polymer is exerted due to the cleavage of cross-links in polymeric networks (Fig. 3) [1].

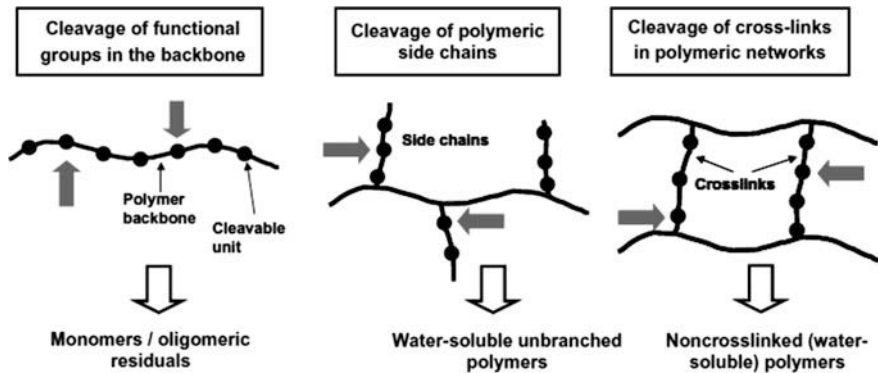


Fig. 3 Degradation routes for biodegradable polymers [1]. Copyright 2017. Reprinted with permission from Springer Nature

Substances like superoxide anion, hydrogen peroxide, macrophages, hypochlorite and foreign bodies can induce chemical changes causing degradation of the polymers. Throughout the process of wound healing, hydrolysis can be catalyzed by physiological ions, such as PO_4^{3-} , or by secreted enzymes. Processes of chemical changes such as hydrolysis can cause the breakdown of polymer macromolecular chains [1].

3 Biocompatible Polymers

Enormous polymeric frameworks can be utilized in medicine, but many of these materials failed to interact with biological systems, wherefore the researchers develop new materials in order to overcome this problem. The most important and precondition properties of any biomaterial is good biocompatibility. There are extensive materials that are, very desirable, but unfortunately rejected by the human tissues, so the biocompatible materials must have an appropriate response for a specific application [11]. Among these biomaterials, polymers are the most widely used for biomedical applications. The features of flexibility and biocompatibility of polymeric biomaterials enable its usage in the wide range of applications. Biocompatible polymers are necessary for repairing, retrieving tissues functionality, delivery of bioactive agents, and tissue engineering [1].

The Physical and chemical properties of the biomaterials; -hydrophilicity, hydrophobicity, ionic groups, the multi-component frame of structurally amorphous and crystalline morphology as well as and the topography, i.e. the surface roughness have a great influence in their compatibility (Fig. 4) [11].

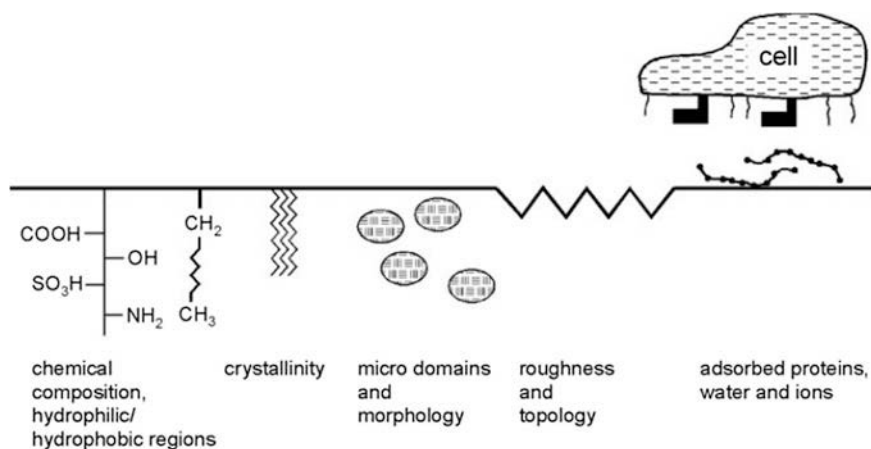


Fig. 4 Interactions of the biomaterial and the bio-system [11]. Copyright 2017. Reprinted with permission from Springer Nature

Biocompatibility examinations of materials perform *in vitro* and *in vivo* in order to examine the systematic and local effects of the material on the human body. Evaluation of biocompatibility of biomaterials *in vivo* includes the assessment of physiologic effects of the body on material and material on the body, that can be achieved by testing the overall biocompatibility of biomaterials; its potential toxicity, biodegradability, the reaction between the tissue and biomaterials and mutagenicity of degraded products, etc. [1]. Biocompatibility of biomaterials can be detected *in vitro* cell cultures to evaluate their toxicity by measuring the activity of cellular enzymes via colourimetric assays (e.g. MTT assay) or fluorescent measurement [12].

4 Wounds

Wounds are the damage or distraction in the normal anatomical structure and function, and it can be a simple cut in the superficial layer of skin or more deep to extend into subcutaneous tissue. This causes a damage to other structures, for example, tendons, muscles, vessels, nerves, and even bone. Wounds can be resulting from an accidental or surgical operation or they can be a secondary result of the specific disease. Wounds are a principal cause of morbidity that impaired quality of life and acquires a lot of healthcare resources [13]. Different classifications of wounds are based on diverse criteria. Elapsed time is a crucial factor in wound classification. Thus, from a clinical point of view, wounds can be viewed as acute and chronic depending on the consumed time for healing [3]. Acute wounds originate from superficial scratches to deep injuries and heal completely with minimal or no scar formation within a time frame of three weeks [14]. Chronic wounds are those that have failed to proceed through an efficient, convenient and timely reparative procedure to create anatomic and functional integrity of the injured site. Chronic wounds represent a silent epidemic that influences a substantial division of the world population. Patients of chronic wounds oftentimes suffer from “highly branded” diseases for example, certain types of ulcers, diabetes and overweight [15].

Healing wounds early, has a great benefit in reduced or no scar formation, whereas delayed treatment leads to severe hypertrophic scarring directly proportional to the wound closure delay time. Earlier wound healing is also accompanied by lower mortality and high patient compliance [16].

Both chronic and acute skin wounds are susceptible to infection because of sterile loss of the natural hindrance function of the skin, facilitating the development of microbial contamination, inside the wound environment. Microbial contamination is involved in the infection of wounds and hence the failure of those wounds to be healed. Therefore researchers concentrated on the investigation of wound healing materials that can be lead to upgrade in the wound management strategies [17].

The percentage of wound contraction could be measured by tracing the margins of wounds on a transparent paper by a fine tip permanent marker. By taking the traced boundaries, the wound area in square millimetres (mm^2) could be determined plan metrically. At a predetermined time interval, the wounded area of each animal on 0 days starting at 3 h post wounding. Wilson's formula shown below gives an estimate of percent wound contraction for a given wound healed area:

$$\% \text{ wound contraction} = \frac{\text{0 day wound area} - \text{unhealed wound}}{\text{0 day wound area}} \times 100$$

4.1 *Insights to the Wound Healing Process*

Skin is the biggest body organ, working as a hindrance to harmful media, preventing pathogens from penetration into the body. Therefore the early repair of injured skin is a major objective for medical-care experts. Effective wound healing prompts to the rebuilding of tissue integrity and takes place through an organized multistage prepare including a multitude cell types. Skin wound healing is a complicated and dynamic natural process including coordinated interactions between different immunological and biological systems, the typical healing reaction starts quickly after tissue damage and takes several steps.

Some researchers consider that wound healing involves three phases: Inflammation, proliferation and tissue remodelling [18], whereas other researchers believe there are four stages in wound healing: Hemostasis, inflammation, proliferation and tissue remodelling. However, everyone agrees that these phases are connected, suggesting that the wound-healing process is a connected series (Fig. 5) [19]. Normal wound healing timeframe is presented in Fig. 6 [20].

4.1.1 **Coagulation and Hemostasis Phase**

Firstly hemostasis and a blood coagulation, start immediately after the injury to prevent bleeding when the blood segments spill into the site of injury, the platelets trigger vasoconstriction, to reduce blood loss and come into contact with exposed collagen and different components of the extracellular matrix. This contact triggers the platelets to release clotting factors as well as essential growth factors and cytokines, which provide wound healing cascade via activating the attraction of neutrophils and monocytes into the clot [13].

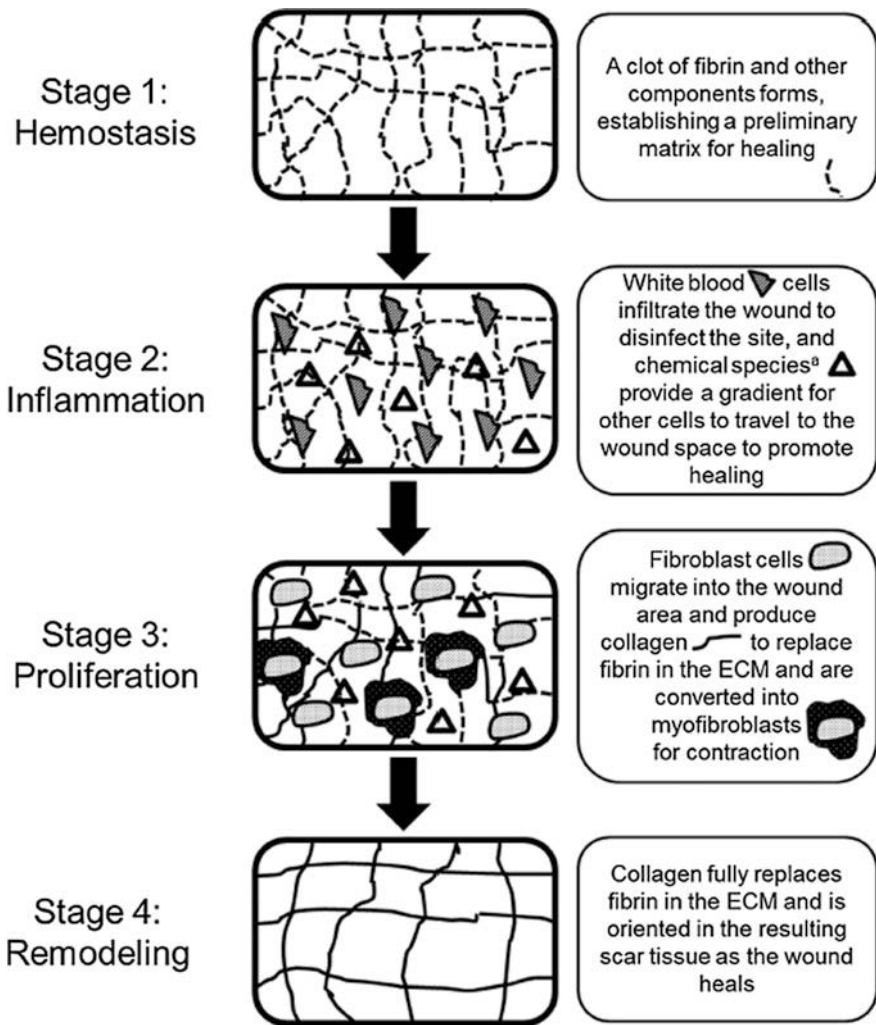


Fig. 5 Wound healing process [19]. Copyright 2016. Reproduced with permission from Springer Nature

4.1.2 Inflammatory Phase

Shortly after hemostasis, the inflammation stage sets in close to a skin injury; the primary inflammatory response is stimulated by chemotactic substances, which attract leukocytes (neutrophils) and monocytes, that its main function is to prevent infection. Neutrophils are white blood cells that migrate across endothelia from local blood vessels and start the debridement via phagocytosis to destroy and expel foreign materials, bacteria and damaged tissue in the wounded area. Monocytes are

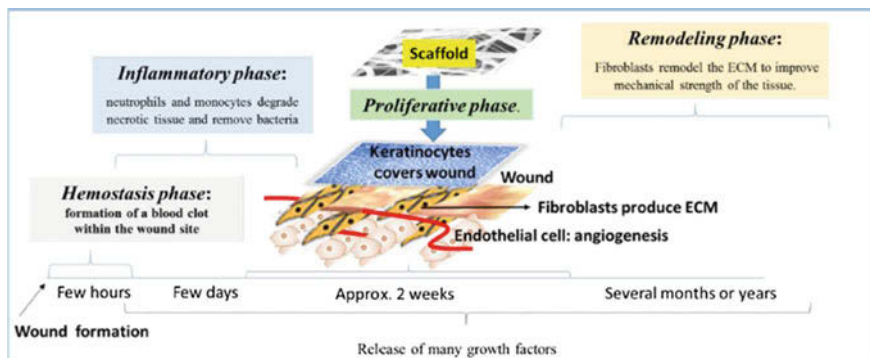


Fig. 6 Timeframe of wound healing phases [20]. Copyright 2017. Reproduced with permission from Springer Nature

white blood cells that develop into macrophages and provide immunological defences against many infectious organisms. The cells of remainders were phagocytosed by macrophages. Phagocytic activity is vital for the subsequent processes because no healing will happen for acute wounds suffering from bacterial imbalance [13].

4.1.3 Proliferation Phase

The proliferative stage in wound healing is distinguished by wound contraction, epithelialization, and angiogenesis, granulation tissue formation. Granulated tissue mainly consists of fibroblast and new blood vessels (Angiogenesis). Once the injury site is scoured, the inflammatory response is followed by proliferation and matrix synthesis, in order to fill the wound gap and reestablish the skin barrier. Fibroblasts migrate into the wound and secrete collagen to start the proliferative stage and deposit new extracellular matrix (ECM). Forming and establishing alternate blood vessels is vital in wound healing [13]. Angiogenesis is one of a critical component of normal wound healing and is stimulated by a vascular endothelial growth factor, resulting in increased vascular permeability, endothelial cell migration, and capillary formation [21]. The proliferation phase includes the initial repair processes for both the epidermal and dermal layers. Fibroblasts, macrophages and vascular tissues coordinately enter the wound to start the formation of a new dermal composite, the granulation tissue. Simultaneously, in a process named re-epithelialization, keratinocytes at the wound edge migrate over the granulation tissue to differentiate the new external layer of the epidermis [22–24].

4.1.4 Remodelling Phase

In remodelling phase, the new collagen matrix becomes more cross-linked and organized due to the wound contraction which brings the wound edge close together and increases the wound tensile strength [13]. During the remodelling phase, fibroblasts organize the collagen matrix and activate the transformation of fibroblasts to myofibroblasts to facilitate wound contraction. The healed wound, at last, enters the maturation phase, and granulation tissue continues to be remodelled and restoration of skin style [25].

Wound healing depends on the right selection of a material for a particular wound to achieve faster healing. These materials are focused to insulate wound from dehydration and promote healing. Different materials can be employed as dressing for healing wounds depending on the cause and kind of wound. Both natural and synthetic materials used in wound healing process can be passive, interactive and bioactive dressings. Passive dressings are permeable materials, such as gauze and tulle dressings, used to cover the wound to renovate its function. Interactive materials are semi-permeable or non-permeable, available in the forms of films, foam, hydrogel, and hydrocolloids. The ideal wound healing materials should achieve a fast cure rate at a reasonable cost with minimal annoyance to the patient [26, 27].

4.2 *Classical Wound Healing*

Classical wound healing agents include topical liquid and semi-solid preparations as well as dry classical dressings. These agents have still had some preferred standpoint in certain clinical settings for wound healing [28]. Classical wound healing dressings provide cover over the wound, including gauze, plasters, bandages (natural or synthetic) and cotton wool, their primary function is to maintain dryness of wounded area by possible evaporation of wound exudates, thus prevent entrance of hazard bacteria into the wound. Gauze dressings produced from cotton fibres, rayon, polyesters give some of the protection against bacterial infection. Different types of sterile gauze dressings are used for absorbing exudates and fluid in an open wound. These dressings need to consecutive change. Gauze dressings are less cost-effective. Because of excrement wound drainage, dressings become moistened and have a tendency to become adherent to the wound making it painful when removing. Bandages that are produced from natural cotton wool and cellulose differ from synthetic bandages which made out of polyamide in its functions. Tulle dressings, impregnated dressings with paraffin that not adhere to wound surface and suitable for the superficial clean wound. Generally, classical dressings are used for the clean and dry wounds with mild exudate levels or used as secondary dressings. Since classical dressings have some of the limitation such as fail in providing a moist environment to the wound, they have been replaced by modern dressings with more advanced formulations [26]. In topical liquid formulations, for example,

the povidone-iodine system is of paramount influence in the initial treatment of wounds as it reduces bacterial infection, thus its incorporation into dressing systems results in controlling or preventing infection. Next treatment of wounded areas by physiological saline solution shows a dual cleansing by removing either the dead tissue or washing the possibly dissolved polymeric dressings adsorbed onto the wounded sites. Saline solution is likewise used to immerse dry wounds during dressing change to help removal with little or no pain. Semi-solid preparations such as silver nitrate used to treat bacterial contamination stay on the surface of the wound for a more extended timeframe compared with solutions [28]. There are a large number of antiseptic agents have cytotoxic properties, but if utilized correctly they can be very effective. Recent reports show that antiseptics can be used selectively as the first line of treatment of infected wounds [29]. The commonly used antiseptics are hydrogen peroxide and iodine-based preparations. Due to the extensive use of the antimicrobial, the incidence of resistance had been increased. In general, topical antimicrobial agents are indicated early in wound management to control contamination and decrease microbial burden [30].

5 Bioactive Materials and Their Progress in Treating Wounds

Bioactive materials are materials which have been designed to induce specific biological activity [31]. Bioactive materials that engaged in wound treatment are developed to facilitate the healing of wounds instead of just to cover it. These materials are focused to insulate the wound from dehydration and promote healing. Bioactive materials play a vital role in the healing process. Biodegradability and biocompatibility are among distinguishable features for bioactive materials processed as dressing agents [4]. These agents are obtained generally from natural tissues like collagen, hyaluronic acid, chitosan, gelatin and alginate. Their usage in healing wounds can be singly or in combination. The collagen basic structure is protein, and because of its unique properties, it has been examined by numerous scientists for its active function in healing wounds. Upon contacting collagen to the wounded tissue, formation of fibroblast and promotion of endothelial migration is achieved. Hyaluronic acid is a glycosaminoglycan segment of extracellular matrix and has unique biological and physicochemical properties. The biocompatibility and biodegradability of collagen and hyaluronic acid are quite similar. Chitosan helps in forming granulated tissue throughout the wound healing proliferative stage. In many ways it was reported that the bioactive materials have superiority to other types of wound healing materials [26]. Perfect wound healing materials ought to keep up a wet domain at the wound interface, allow gaseous exchange, act as a barrier to microorganisms and remove excess exudates. It is necessary for the bioactive wound healing agents to fulfill many requirements such as: safety, non-allergenic, non-adherent to be easily removed, and availability of the raw

biomaterials used in their constitution within a minimal processing. In addition, they have antimicrobial properties and promotes wound healing. Recently, many of scientists are dedicate in producing a unique bioactive, wound healing materials, by synthesizing and modifying biocompatible materials helps in promotion of wound healing process. Among these materials, chitosan and its derivatives, of controlled efficacy in repairing wounds are directed to promote healing at the molecular, cellular, and systemic levels. Chitosan is a cost-effective and naturally abundant biological material extracted from invertebrate's skeleton as well as the cell wall of fungi.

Chitosan is non-toxic biodegradable and antimicrobial agents has good biocompatibility, thus it shows positive impacts on wound healing [7]. Naturally originated materials are being widely used in wound healing because of their similarities to the extracellular matrix, typically good bio-characteristics, and cellular interaction. Also, it can be easily formulated to get better cell adhesion and tissue growth. In this way, natural polymers and their applications in wounds for support and healing have attracted much consideration throughout the most recent decade [32]. Using chitosan as an accelerator for wound healing is reported in many studies where chitosan can profitably affect every step of wound healing. Chitosan and its derivatives could accelerate wound healing by improving the functions of inflammatory cells, such as polymorphonuclear leukocytes [33], macrophages, and fibroblasts [34].

6 Chitosan

Chitosan is a linear polysaccharide obtained by deacetylation of chitin. It is a copolymer composed from $\beta(1\rightarrow4)$ 2-amino-2-deoxy-D-glucose and $\beta(1\rightarrow4)$ N-acetyl-2-amino-2-deoxy-D-glucose. Chitin is the abundant component of the skeletal structure of many classes such as the group of invertebrates that include arthropods, molluscs, and annelids. But in animals, chitin is associated with other constituents, such as lipids, calcium carbonate, proteins, and pigments. It has been estimated that the crustacean chitin present in the sea amounts to 1560 million tons [35]. Chitin is also found as a major polymeric component of the cell wall of fungi and algae. Chitin structure is similar to cellulose as shown in Fig. 7 but it has an acetamide group in a position of C-2 instead of a hydroxyl group. Chitosan structure is a deacetylated form of chitin [1].

6.1 Properties of Chitosan

Chitosan has several properties that control its activity, such as solubility, the degree of deacetylation, molecular weight, the degree of crystallinity, and degree of polymerization.

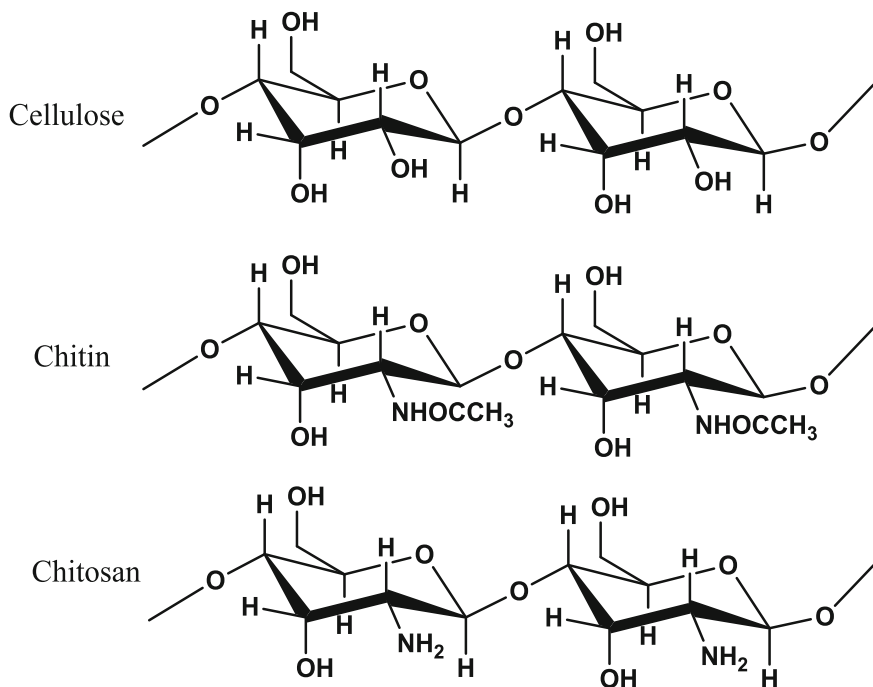


Fig. 7 Chemical structures of cellulose, chitin and chitosan [1]. Copyright 2017. Reproduced with permission from Springer Nature

6.1.1 Solubility of Chitosan

Chitosan is the poly-glucosamine, have a basic nature. It forms salts with acids and produces polyelectrolyte. Chemical modification of chitosan or formulating it as film or fiber is mainly correlated to its solubility in nature. Chitosan easily dissolves in dilute organic or mineral acids via the protonation of free amino groups at $\text{pH} < 6.5$, but it is insoluble in water due to the presence of intra and inter-hydrogen bonds in its structure. Acetic and formic acids are widely used for research and applications of chitosan. On the other hand, chitosan solubility decreases with an increase in molecular weight. Oligomers of chitosan with a degree of polymerization (DP) of 8 or less are water soluble regardless of pH [36].

6.1.2 Degree of N-Deacetylation

Studying the degree of N-deacetylation in chitosan, i.e. the ratio of 2-acetamido-2-deoxy-D-glucopyranose to 2-amino-2-deoxy-D-glucopyranose structural units is important. This ratio has a strong effect on solubility and solution properties of chitosan. Chitin is insoluble in dilute acetic acid. But when chitin is deacetylated to a

certain degree (approximately 60% deacetylation) whereupon it becomes soluble in acid, it is referred to as chitosan. Chitosan is the fully or partially N-deacetylated derivative of chitin with a typical degree of acetylation less than 40% [37]. For measuring this ratio, a several methods have been used, such as FTIR spectroscopy [38], H^1 NMR spectroscopy [39], C^{13} solid-state NMR spectroscopy [40], elemental analysis, and thermal analysis [38].

6.1.3 The Molecular Weight (MW)

It is important to mention that the applications of chitosan are correlated with its molecular weight (MW). The chitosan molecular weight depends on its source and deacetylation conditions (time, temperature and NaOH concentration), respectively. Chitosan produced from deacetylation of chitin with a MW over 100,000. Consequently, it is required to reduce the MW by chemical methods to a much lower MW for easy application as a textile finish [38]. The MW of chitosan can be measured by several methods, such as light scattering spectrophotometry [41], gel permeation chromatography [39] and viscometry [41].

Viscometry is the simplest and most rapid methods for determining the molecular weights of polymers [41]. The most commonly used equation relating limiting viscosity values to MW is the Mark-Houwink equation as follows [35]:

$$[\eta] = K \cdot M^\alpha$$

where $[\eta]$ is the limiting viscosity number and K , α are constants independent of MW over a wide range of MW. They are dependent on the polymer, temperature, solvent, and, in case of polyelectrolytes, the nature and concentration of the added low-molecular-weight electrolyte.

6.2 Chitosan Sources and Production

There are many natural sources to extract chitosan such as mushroom, insects, yeast, the cell wall of fungi and marine shellfish such as lobster, crab, krill, cuttlefish, shrimp, and squid pens. Chitin is the outer protective coating for shellfish, that consists of covalently bound network with some metals, proteins and carotenoids. Crustacean shells composed of 30–50% calcium carbonate, 20–30% chitin, 30–40% proteins and also contain pigments (astaxanthin, canthaxanthin, lutein, and β -carotene), and these percentages change according to species or seasons. Chitin and chitosan are commercially produced from the shrimp, prawn, and crab wastes [42].

Different techniques have been reported for chitosan production. Preceding preparation of chitosan from the crustacean generally consists of four basic steps: demineralization, deproteinization, decolouration, and deacetylation [42].

Before starting, shells were washed by warming water to remove soluble organics, adherent proteins, and other impurities. The shells were then dried in the oven at 70 °C for a period of 24 h until completely dried shells were obtained. Then, the shells are ready to chitosan production [43].

6.2.1 Demineralization (DM)

Demineralization is generally carried out using acids such as hydrochloric acid, nitric acid, acetic acid, or formic acid (up to 10%) at ambient temperature with stirring to dissolve calcium carbonate as calcium chloride [42]. However, hydrochloric acid is the preferred acid and is used at a concentration of 0.2–2 M for 1–48 h at temperatures ranging from 0 to 100 °C with solid-to-solvent ratio of 1:15 (w/v) is usually used and then filtered under vacuum [39].

6.2.2 Deproteinization (DP)

Chitin is combined naturally with protein via covalent bonds, and deproteinization of demineralized shells is usually carried out by alkaline treatment. The shells are treated with sodium or potassium hydroxide (65–100 °C) at the shell to alkali ratio of 1:4 for times ranging from 1 to 12 h. Accordingly, a detachment of protein occurs from the shrimp waste solid component. Relatively high ratios of a solid-to-alkali solution of 1/10 or 1/20 are used with stirring to increase the deproteinization efficiency. After complete deproteinization, simple filtration can easily separate the protein hydrolysate from the solids in the protein slurry [42].

6.2.3 Decoloration (DC)

The deproteinized chitin is a coloured product. For commercial suitability, chitin is decolorized to yield white chitin powder. It is important to assure the inertness of chemicals towards physicochemical or functional properties during the discolouration process of chitin. Discolouration firstly starts with the treatment of chitin with acetone and then dried for 2 h at ambient temperature, then a bleaching step using 0.315% (v/v) sodium hypochlorite (NaOCl) solution for 5 min at ambient temperature with a solid to solvent ratio of 1:10 (w/v). Samples were then washed with water and dried in an oven at 60 °C for 2–3 h.

6.2.4 Deacetylation (DA)

The production of chitosan from chitin could be achieved by removing the acetyl groups from chitin in a process known as deacetylation. Various factors that affect the deacetylation process, including temperature, prior treatments applied to chitin

isolation, time of deacetylation, alkali concentration, the ratio of chitin to alkali solution, prior treatments applied to chitin isolation, atmosphere (air or nitrogen), the density of chitin, and the particle size. The N-acetyl groups cannot be removed by acidic reagents without hydrolysis of the polysaccharide, thus, alkaline methods must be applied for N-deacetylation. It is generally achieved by treatment with concentrated potassium or sodium hydroxide solution (40–60%) usually at 80–140 °C for 30 min or longer using a solid to solvent ratio of 1:10 (w/v) to remove some or all of the acetyl groups from the polymer. In that process, sodium hydroxide is noted to be the preferred alkali. The resulting chitosan was washed to neutrality with running tap water, rinsed with distilled water, filtered, and dried at 60 °C for 24 h in the oven [42].

6.3 Modified Chitosan

The physicochemical properties of chitosan can be amended to more desirable features that meet various applications. Fortunately, the various functional groups in the polymeric domain of chitosan enable its modification (Fig. 8) [42]. Alteration of chitosan properties could be subjected chemically under mild conditions via the reactive hydroxyl and amino groups distributed in chitosan structure. Below, we report on promising examples of amended chitosan that recently take an eminent position in advanced research and have special markets [44].

6.3.1 Thiolated Chitosan

Thiolated chitosans could be formed by the interaction of thiols with the chitosans' primary amino group. There are three types of thiolated chitosans have been formed: chitosan–cysteine conjugates, chitosan–thioglycolic acid conjugates and chitosan–4-thio-butyl-amidine conjugates. The immobilized thiol groups improve

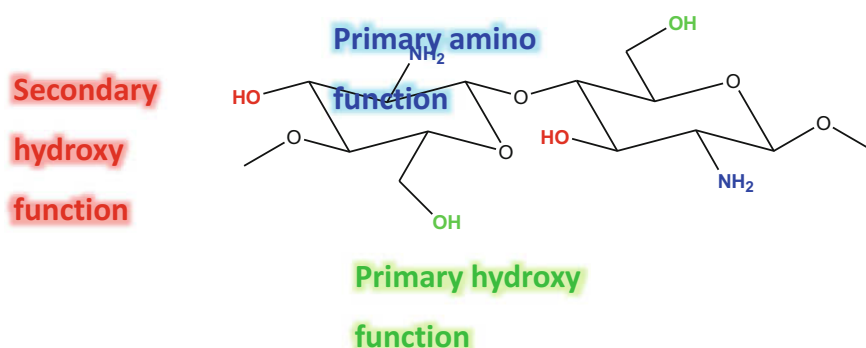


Fig. 8 Functional groups in chitosan that can be modified

many properties of chitosan. Due to the formation of disulfide bonds with mucus glycoproteins, the mucoadhesiveness is aggrandized [6]. For example, the thiolated chitosan rather plain chitosan reveals enhancement by (1.6–3 folds) in the permeation of paracellular markers through intestinal mucosa. Moreover, the thiol groups may react with thiol groups, thus decreases the release rate and maintains the peptide release for a longer time.

6.3.2 *O*, *N*-Carboxymethyl Chitosan

Another type of modified chitosan is the carboxymethyl chitosan (CMCS) that shows greatly enhanced antimicrobial activity than chitosan. This could be attributed to the inter- and intra-molecular interactions between the carboxyl and amino groups that increase the increased cationic groups [45]. *N*-carboxymethyl chitosan is a glucan type of chitosan carrying pendant glycine groups formed when using glyoxalic acid in the preparation course [46]. The film-forming ability of *N*-carboxymethyl chitosan assists in imparting a pleasant feeling of smoothness to the skin and in protecting it from adverse environmental conditions and consequences of the use of detergents.

6.3.3 Highly Cationic Chitosan

N,N,N-Trimethyl chitosan (TMC) and *N*-[(2-hydroxy-3-trimethylammonium) propyl] chitosan chloride are quaternary soluble derivatives that show effective enhancing properties of transport the peptide, protein, and drugs through mucosal membranes. They have been used as an absorption enhancer, antibacterial agent and gene vector due to its ability to form complexes with anionic gels or macromolecules [47]. TMC was synthesized by reductive methylation of chitosan in an alkaline media at elevated temperature as can be seen in Fig. 9 [48].

6.3.4 PEGylated Chitosan Derivatives

Modification of chitosan and chitosan derivatives through PEGylation reveals novel physicochemical properties, especially towards their solubility and their use in gene and drug delivery. As has been published [49], the PEG-g-chitosan derivative was

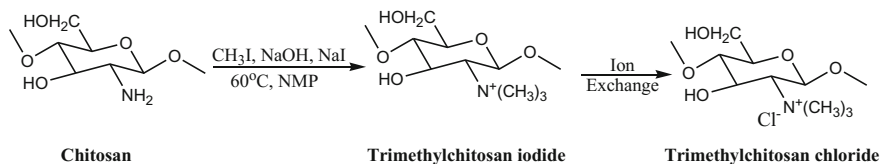


Fig. 9 The preparation methods of TMC

synthesized by functionalizing chitosan using a PEG-aldehyde. Chitosan was first modified with a PEG-aldehyde to yield an imine (Schiff base), which was then reduced to PEG-g-chitosan using sodium borohydride (NaBH_4). In recent years many applications, have been suggested for PEGylated chitosans. For example, uses of PEG-g-chitosan for cell adhesion applications and application in wound healing and tissue engineering [50].

7 Chitosan Composites and Their Inherent Biological Properties

Chitosan is a natural cationic copolymer of *N*-acetyl glucosamine and *D*-glucosamine. There are appropriate properties for chitosan making it suitable for use in several biological fields such as drug delivery and wound healing [51]. The main advantage of chitosan that it can be easily modified or make it in combination via a simple procedure. A new class of biomaterials were obtained from chitosan composites with good mechanical, physicochemical characteristics and useful properties, which can't be accomplished either by chitosan or the combined material alone [52]. Chitosan naturally exists as a composite with proteins and minerals in invertebrates, that keep the integrity of its structural shells [53]. Thus combining of chitosan and protein to form chitosan-protein composites make those composites have biocompatibility. Many such composite scaffolds, for example, chitosan-collagen and chitosan-gelatin [54] have been tested for their ability to promote cells adhesion and proliferation. In the same pattern, chitosan and another glycosaminoglycan such as heparin and hyaluronic acid have been combined to form composites that provide specific cellular adhesion [52]. Chitosan-based wound healing materials, which prepared by combining chitosan with synthetic or natural materials is an effective way to prepare new wound healing materials for enhancing its versatile property. Poly(vinyl alcohol), poly(vinyl pyrrolidone), poly(ethylene oxide), and polyglutamic acid are an example of chitosan composites with synthetic polymers that tested for wound healing applications. Different inorganic materials can be combined with chitosan and give a good benefit in biological applications. Wound healing materials that are prepared from chitosan and nanoparticles, can interact at molecular and cellular level. This gives better antibacterial activity and rapid healing action for the wound [10]. Biocompatibility, biodegradability, hemostatic, bio-adhesion, antimicrobial activity, anti-inflammatory and non-toxicity are inherent biological properties of chitosan and chitosan composites, that give it a great attention in wound healing process [55, 56].

7.1 *Non-toxicity*

In vivo, administration route affects the extent of chitosan toxicity. Arai et al. reported that oral administration of chitosan within 16 g/kg resulted in lethal dose in mice, whereas it amounts to >15 g/kg in rats. While intra-peritoneal administration shows higher lethal dosage of 30 g/kg in rats and 52 g/kg in mice. Upon subcutaneous administration, the lethal dose amounts to >100 g/kg in mice [57]. However, low toxicity (e.g., loss of appetite) may be the side effect when administering chitosan orally to rabbits or hens during 34 weeks at doses of 700–800 mg/kg/day. As reported by Rao and Sharma [58], there is no pyrogenic effects, no toxicity in mice and no irritation detected for either skin or eyes in rabbits. In addition, almost studies presented chitosan as a safe material that may induce low or minimal toxic effects. Moreover, chitosan shows considerable suitability and safety in food applications and as a pharmaceutical excipient for the parenteral route [59]. Furthermore, concluded data about chitosan toxicity based on human studies are quite limited. A daily dose of 4.5 g from chitosan took by human volunteers did not result in toxic effects [60]. In addition, human trials up to twelve weeks showed no toxic effects, no allergies, and only nausea symptoms and constipation in 2.6–5.4% of subjects [61]. Accordingly, chitosan does not show significant acute toxicity.

7.2 *Antimicrobial Activity*

The antimicrobial activity of chitosan is influenced by several inherent structural factors including chitosan molecular weight, the degree of deacetylation and consequently the number of available free amine groups. The antimicrobial activity of chitosan increases by decreasing pH as it is correlated to the glucosamine amino group [62]. Nevertheless, the presence of some ions (e.g. Ca^{2+} , Mg^{2+}) [63] could significantly affect the antimicrobial activity of chitosan. Unfortunately, it is difficult to compare the estimated antimicrobial characteristics of chitosans reported in the literature, indeed there is no a reference efficacy [64]. Because of the mutations of microorganisms, a challenge in addressing modified chitosan formulations of increased antimicrobial activity is a continuous demand. Chemically modified chitosan of amended antimicrobial activity could be referred to the primary (C-6) and secondary (C-3) hydroxyl groups on each repeating unit in addition to the amino groups (C-2) on each deacetylated unit. Two mechanisms could be engaged in the antimicrobial action of chitosan [65]. They firstly propose an interaction between the positively charged chitosan and the negatively charged surface groups of the cells. This could affect the permeability and cause a shortage in the fundamental solutes necessary for the cell. The second mechanism refers to inhibition of synthesizing the microbial RNA as a result of interacting with the protonated amino groups of chitosan with the cell DNA and thus inhibit the synthesis of microbial RNA.

7.3 *Anti-inflammatory Nature*

Anti-inflammatory drugs with high efficiency and fewer side effects are a great target for a large number of researchers. Therefore, it draws attention to the anti-inflammatory drugs from plants that have better effects, fewer side effects and rich resources. Chitosan is one of the most abundant on the earth and naturally occur. Chitosan and chitosan composites used to reduces inflammatory and pain with high efficiency and fewer side effects [66]. Many reports show that the inflammatory response is resulting from lipopolysaccharide, one of the components of the cell wall of gram-negative bacteria. Lipopolysaccharide (LPS) is known to stimulate the production of many local factors, including tumour necrosis factor-alpha (TNF- α), interleukin, and prostaglandin E2, from immune cells (macrophages) and fibroblasts cells in inflamed tissues [67]. It is known that prostaglandin E2 considers a main inflammatory mediator in the inflammatory response. Several researchers show that lipopolysaccharide (LPS) activates macrophages and stimulate the production of proinflammatory cyclooxygenase-2 (COX-2) enzyme, leading to the synthesis of large amounts of Prostaglandin E2 at inflammatory sites [68, 69]. Another pro-inflammatory product that has a critical role in inflammation is the nuclear factor-kappa (NF- κ B) that is activated by lipopolysaccharide (LPS) via stimulation of Toll-like receptor 4 (TLR-4) on immune cells. Lipopolysaccharide immune cell activation is facilitated by two proteins known as CD14 and MD-2 on the cell surface, then Toll-like receptor 4 (TLR-4) triggers a reaction with the adaptor molecule MyD88 (myeloid differentiation primary-response protein 88). The MyD88-depending signaling cascade leads to the activation of nuclear factor-kappa (NF- κ B), that regulates proinflammatory genes that release pro-inflammatory cytokines such as tumor necrosis factor-alpha (TNF- α), interleukin (IL-1, IL-6), which exaggerate the inflammatory response. So, the suppression of nuclear factor-kappa (NF- κ B) activation via inactivation of lipopolysaccharide, is a potent strategy for the treatment of inflammation [70, 71].

It is reported in many papers, that chitosan suppresses the production of nuclear factor-kappa (NF- κ B) and significantly inhibited Prostaglandin E2 without cytotoxicity [69, 72]. Chitosan as a cationic polymer exhibits an anti-inflammatory effect due to ionic bonding and electrostatic interaction between its positive centers and the highly anionic lipopolysaccharide. However, the therapeutic potential of chitosan, depending on lipopolysaccharide-binding, need to increase the efficiency of interaction between chitosan and lipopolysaccharide. Based on this concept, chemical modification of chitosan was performed to increase the affinity of lipopolysaccharide-chitosan binding [73]. *N*-acetylglucosamine, an anti-inflammatory agent, is the monomer of chitosan and also already exists in the body as hyaluronic acid that plays important role in wound repair. Furthermore, chitosan has a physical analgesic effect on the wound by giving a cooling and soothing effect when applied to an open wound. Therefore, chitosan shows a high anti-inflammatory effect even when comparing it with the synthetic non-steroidal

anti-inflammatory drug, such as indomethacin. Due to anti-inflammatory effects of chitosan, these are beneficial for the treatment of acute and chronic inflammation of wounds [66].

7.4 Biocompatibility

This propriety results from the interaction of the positive charge in pure chitosan or chitosan composites with the negatively charged cell membranes due to ionic exchange between the intercellular and extracellular medium [74]. Chitosan and its composites have been investigated in numerous studies in a biological field and in general, they showed high biocompatibility [75]. It was reported in human trials of up to 12 weeks showed no significant clinical symptoms, with no evidence of an adverse response of chitosan indicating to its biocompatibility [61]. Chitosan has been approved by the American Food and Drug Administration (FDA) as a wound dressing material, confirming its biocompatibility [76].

7.5 Biodegradability

An important aspect of the use of polymers in biological systems is their biodegradation process in the body. Many reports illustrated, that chitosan and its composites can be degraded by enzymes such as lysozyme, chitinase, lipases and not produce any harmful byproducts, because these products are oligosaccharides that are either incorporated into glycosaminoglycan and glycoprotein metabolic pathways or easily excreted in urine directly [77, 78]. Chitosan can be degraded by lysozyme via hydrolysis process and the degradation products are nontoxic [59]. The degradation rate of chitosan depends on its physical characterization and the preparation methods. It is important to clear up that rapid degradation of chitosan, may cause an accumulation of amino sugars, resulting in an inflammatory response and, thus, affecting chitosan biocompatibility [74].

7.6 Hemostatic Properties

Chitosan hemostatic dressing is most promising in wound healing process due to an effective response to stop bleeding and its regeneration advantages. Properties of chitosan facilitate attracting red blood cells to chitosan, leading to rapidly blood coagulation, and this was a reason for its approval in the USA for use it in wound healing process [79]. Chitosan as a hemostatic agent would induce clot formation via an interaction between the cell membrane of blood cells and free amino groups chitosan. The positive surfaces of chitosan attract the negative charge of the

membranes of erythrocytes and platelets, leading to platelet activation and blood coagulation that reduce bleeding and enhance hemostasis [59]. It is reported recently that chitosan promotes coagulation in vitro, with reducing the time of blood clotting by 40% compared to blood alone, that suggest chitosan can induce blood coagulation because of the interactions between acidic groups of blood cells and free amino groups of chitosan [80]. The hemostatic mechanism of chitosan may be due to three possible actions to stop bleeding, absorption of plasma, coagulation of red blood cells, and platelet aggregation. Absorption features of chitosan is a prominent factor that helps to act as a hemostatic via plasma absorption. In addition to plasma absorption, coagulation of erythrocytes also is one important hemostatic way of chitosan. The clotting of erythrocytes was enhanced in the presence of chitosan due to crosslinking of the erythrocytes with chitosan polymer chains. When chitosan attached to blood, resulting in a change in morphology of erythrocytes. They loss typical shape and seemed to have an unusual affinity towards one another. The main cause of hemostatic effect of chitosan is its ability to the aggregation and activation of platelet, forming an aggregated bloc in irregular shapes [81, 82].

7.7 *Mucoadhesivity*

Mucus surfaces are the moist surfaces, which major components are mucin glycoproteins, lipids, inorganic salts and water, the latter, consists more than 95% of their weight, making them a highly hydrated system. The mucoadhesive molecules have features make them, interact chemically and mechanically with the glycoproteins of the mucus. The favoured of mucoadhesive features are an anionic surface charge, high molecular weight, flexible chains, surface-active properties and affinity to build hydrogen bond, which helps in spreading throughout the mucus layer [83]. The cationic polymers such as chitosan can be absorbed on the mucus surfaces via electrostatic interaction. Several types of polymers have been reported as mucoadhesive due to their ability to interact physically and/or chemically with the mucus surfaces. Moreover, the chitosan muco adhesive properties may be attributable to its cationic character [74]. Chitosan and its composites have a high adhesive force that will promote binding to the negative surface of the mucus surfaces and cover different epithelial surfaces [84]. The mucoadhesion of chitosan can be illustrated by the interaction between negatively charged residues in the mucin glycoprotein and chitosan positively charged amino groups [85]. Mucoadhesion of chitosan and its composites is one of the important characters that promote to improve the wound healing via interaction with the negatively charged cell membranes, thus chitosan can stay close to the wound and prohibits the growth of microorganisms.

8 Modified Chitosan and the Biomedical Engineering of Wound Healings

Over decades, materials applied in wound healing processes are originated from diverse naturally occurring polymers. Moreover, those materials arisen from polysaccharides like chitosan have received the great attention from the worldwide researchers because of its important biological properties. Chitosan helps in every step of wound healing via accelerating the infiltration of inflammatory cells like neutrophils, absorbing exudates, making a barrier against microbes and helps in healing without scar formation. However, the tenuous behaviour of chitosan delimits its usage in a pristine form and pave the way for its modification in many forms such as gels, films, fibers, and scaffolds or blending with other materials to get a more suitable tissue engineering material. Blending of chitosan or its combination either with natural or synthetic polymers reduce cost, improve its handling. Moreover, this enhances the wettability, gas permeability and mechanical properties. The nanoparticles and growth factors blended into chitosan also exhibit better antibacterial activity and minimize the time span for wound healing [10]. Chitosan and modified chitosan activate macrophages, stimulate cell proliferation and tissue organization. Hemostatic properties of chitosan aids to natural blood thrombosis as well as blocking of nerve endings that reduces pain. Gradual depolymerization of chitosan releases *N*-acetyl- β -D-glucosamine, which initiates fibroblast proliferation, deposits of collagen and stimulates synthesis of a higher level from natural hyaluronic acid at the wound site. This plays a pivotal role in wound healing [7]. Chitosan stimulates neutrophil in the inflammatory stage, to clean out the wound site from bacteria. Chitosan activates the inflammatory cells, macrophages, and fibroblasts which helps in wound healing without forming stigma [10].

8.1 Wound Healing Using Chitosan Impregnated Drug

Healing of chronic wounds necessitates a durability in regular drug administration. Prolonged drug release continuously exposes the wounded area to the action of the drug and thus reduce the used dose [86]. Recently, few reports conclude an antibiotic-medicated chitosan dressing to get a controlled drug release system. In this system, optimization of the amount of impregnated drug that provides the controlled and sustained antibiotic action is a demand to be achieved.

8.1.1 Wound Dressing Using Sulfadiazine Loaded Chitosan Nanoparticles

El-Feky et al. [87] reports for silver sulfadiazine (SSD) loaded chitosan nanoparticles (CSNPs) for the controlled-release of SSD into burn wound to control

bacterial growth. This work aimed to combine the advantages of the potent antimicrobial and antifungal SSD drug with the advantages of chitosan nanoparticles as drug carrier systems and effective fabric coating material. Generally, the chemical bonding of SSD to textile dressings is not possible. Therefore, no specific concentration or release rate of the sulfadiazine drug from the dressing to the wounded area is precisely identified. Thus, the followed strategy was to encapsulate SSD on a suitable hydrophilic nano-carrier has the possibility to be a coater for the wound. By this way, the drug cytotoxic effect might be prevented and the effective controlled application of SSD on healing wound is enhanced [88].

Water absorbency (A_w) of the wound-dresser is a crucial parameter in the healing process and could be determined by the following equation:

$$A_w = \frac{m_{wet} - m_{dry}}{m_{dry}} \times 100$$

where m_{dry} and m_{wet} are the weights of the dry and wet samples, respectively.

A_w , could be estimated by immersing the investigated dresser in water until reaching an equilibrium where the excess water on the surface of wet samples was drained for 1 h through a calibrated sieve.

The continuous delivery of SSD in its loaded chitosan formulation that could extend over 24 h help to improve patients' compliance by removing the need for multi-daily drug administration and is expected to offer an effective treatment due to the longer undisrupted contact time between the drug and the wounded area.

8.1.2 Wound Dressing Using Simvastatin—Chitosan Microparticles Loaded Polyvinyl Alcohol Hydrogels

Yasasvini et al. [89] prepared a simvastatin—chitosan microparticles loaded with polyvinyl alcohol (PVA) hydrogels via a chemical cross-linking method. The simvastatin loaded chitosan are firstly developed followed by the incorporation of the particles in hydrogels. Depending on the in vitro release profile of the plain drug, the preparative route optimizes the percent composition of the chitosan microparticles and loaded PVA hydrogels. Optimized composition results in high entrapment of simvastatin drug as estimated by the following formula:

$$EE(\%) = \frac{\text{Total amount of drug} - \text{Amount of drug the in supernatant}}{\text{Total amount of drug}} \times 100$$

Adaptation of the composition percent of the constituents of this system provided prolonged release with a minimum amount of drug loaded in the formulation. This reduces the used dose of the drug and maintains its required therapeutic concentration in plasma. Thus, topical wound healing of high efficiency is improved. The simvastatin loaded chitosan revealed a granulated tissue with complete epithelialization was obtained in case of animals treated with the lowest

dose hydrogels. On the other side, control animals are in the late fibroblastic state after 21 days whereas the animals treated with the lowest dose of hydrogel acquires a contracted wound profile [89].

8.1.3 Wound Dressing Using Scaffolds of Chitosan-Fibrin (CF) Loaded with Quercetin

Scaffolds composed of quercetin-loaded chitosan–fibrin (Q-CF) due to dry-freeze method were presented by Vedakumari et al. [90]. These scaffolds are non-toxic and showed suitable biocompatibility in tissue engineering applications. Quercetin is found in plants and belongs to flavonoids. It exhibits antiviral, antiulcer, anti-cancer, antibacterial, anti-allergic and anti-inflammatory properties [91]. Moreover, quercetin potentially scavenges oxygen free radicals and shows efficient in vitro and in vivo inhibition of lipids peroxidation. It has been reported that wounds medicated with free radical scavenging drugs showed enhanced healing [92]. The developed Q-CF scaffolds show quick water uptake and consequently quercetin dissolution at the scaffold surface. This leads to an initial rapid release of quercetin for up to 3 h. After that, a slow rate of quercetin release for up to 48 h is further estimated. The slower step could be ascribed to a gradual degradation of chitosan resulting in the formation of interconnected pores on the surface of the scaffolds [90].

Since microbial infection is a major problem during the process of wound healing, hence antimicrobial activity is significant parameter required to be dealt. The Q-CF scaffold demonstrated a higher potential for bactericidal activity against *Escherichia coli* and *Staphylococcus aureus* compared to quercetin free (CF) scaffolds. The noticeable difference in the bactericidal activity of CF and Q-CF scaffolds may be due to a synergistic effect of quercetin and chitosan. The earlier holds strong antibacterial activity against *E. coli* and *S. aureus* [93], whereas the positive charges on the latter interact with the negatively charged microbial cell wall causing discharge of proteinaceous and other intracellular components. It also binds to the nuclear DNA and inhibits the synthesis of mRNA and proteins [94].

Furthermore, a time-dependent monitoring of a group of biochemical parameters due to investigation of the granulation tissues from the Q-CF treated group in comparison to the CF group revealed the following conclusions: Q-CF treated group showed significant increase in the quantity of collagen that causes improved migration of fibroblasts and epithelial cells to the wound site for effective healing. The content of hexosamine was reduced referring to an increase in the extracellular matrix formation. Nevertheless, a prominent difference is noticed among all the three groups. A higher level of total protein content, representing the efficient synthesis and accumulation of proteins in the granulation tissues and a significant increase in the level of uronic acid [95]. These observations highlight the combined role between quercetin, chitosan and fibrin in the induction of fibroblast proliferation and quickness of healing in Q-CF treated wounds.

8.1.4 Wound Dressing Using Melatonin-Loaded Chitosan-Based Microspheres (Mel/CS MS)

Another dry powder formulation of Mel/CS MS was developed by Romić et al. [96] using a spray drying method. Melatonin is a neurotransmitter hormone and biological modifier has pleiotropic bioactivities [97]. Melatonin stimulates antioxidant enzymes, efficient free radical scavenging, and anti-inflammatory properties [98]. Also, melatonin has antibacterial effects that enhance wound healing via its influences on the phases of inflammation, glycosaminoglycan and collagen accumulation in addition to cell proliferation at the wounded site [99]. Moreover, melatonin reduces endothelial dysfunction in burns treatment owing to reactive oxygen species antagonizing and thus, shortens the healing time [100, 101]. In contact with wound exudates, the Mel/CS MS powder renders into the hydrogel. Pluronic-F127 was incorporated in the microspheres matrix to enhance melatonin amorphization and release rate. Furthermore, the entrapped melatonin has potentiated chitosan antimicrobial activity towards *Staphylococcus aureus* and five clinical isolates *S. aureus* MRSA strains. The microspheres within relevant concentrations for antimicrobial activity against planktonic bacteria show considerable biocompatibility to skin keratinocytes and fibroblasts.

8.2 Wound Healing Due to Chitosan Composites with Metal or Metal Oxide Nanoparticles

Wound healing could be influenced by copper nanoparticles. The latter could efficiently affect the complex phenomenon of healing involving various cells, cytokines and growth factors. It was found that metallic copper nanoparticles rather than copper ions show better modulation of cells, cytokines and growth factors involved in the process of wound healing. Copper plays role in activating endothelial cells as it stimulates their proliferation and migration. It induces the direct in vitro proliferation of human endothelial cells directly in vitro and it is also considered as a cofactor for many angiogenic mediators. As mentioned before, chitosan due to its biocompatibility, antifungal/antibacterial properties, and biodegradability is viewed as a beneficial polymeric candidate in healing.

Gopal et al. [102] presented for a chitosan-based copper nanocomposite (CCNC). In their synthetic route, chitosan powder was slowly added to the acetic acid solution (1%) in a normal saline and stirred for 8 h to get (10%) colloidal solution of chitosan. After that, CCNC of 0.3% was prepared by slow addition of an ethanolic dispersion of copper nanoparticles to the chitosan colloidal solution under continuous stirring followed by sonication for 5 min. The healing efficacy of the as-prepared CCNC nanocomposite was tested in the topical treatment of an open excision wound in adult Wistar rats. The relatively fastest wound contraction was detected in the CCNC-treated group during the monitored time frame compared to chitosan and control treated groups.

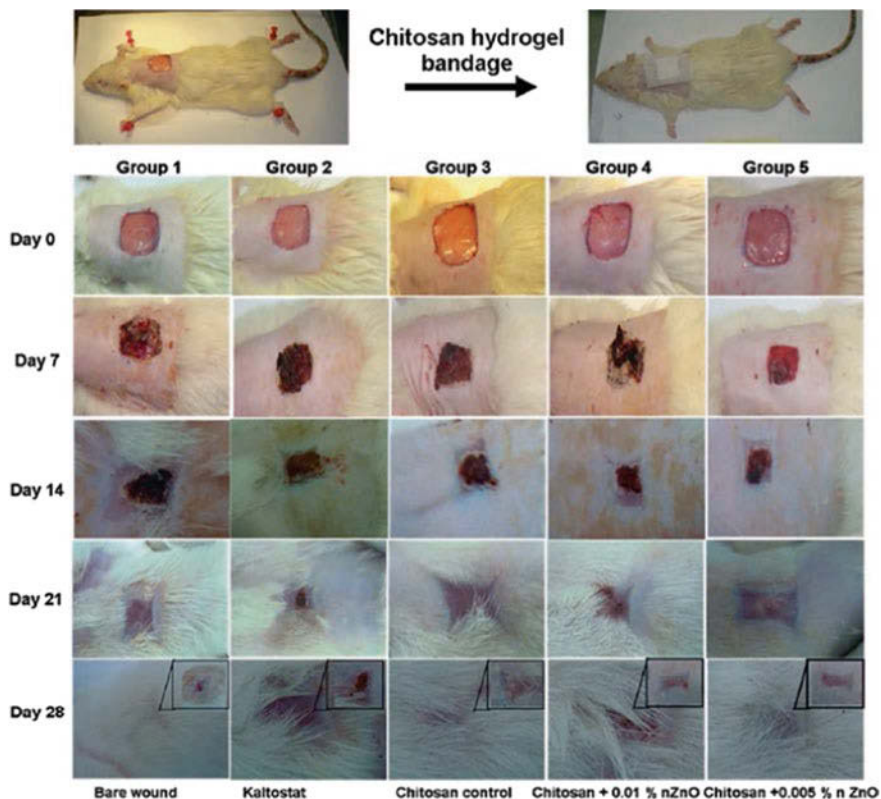


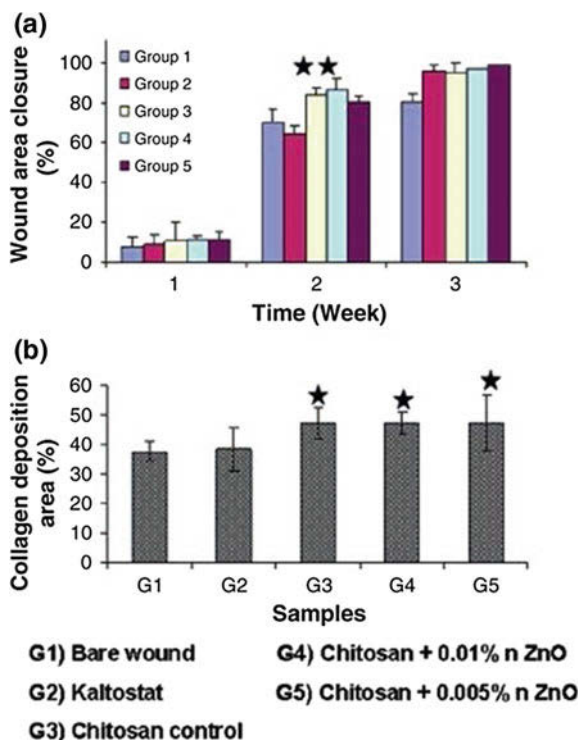
Fig. 10 Photographs of wound healing study [10]. Copyright 2016. Reprinted with permission from Springer Nature

Further composites prepared depending on chitosan and nano-ZnO, that can be used in wound healing. Sudheesh Kumar et al. developed chitosan hydrogel/nano-ZnO nanocomposite bandages (CZBs) via the mingling of ZnO nanoparticle (nZnO) with chitosan hydrogel, and study the wound healing ability of the as-prepared CZBs on rats. Figure 10 illustrates that chitosan nanocomposites bandages “control group” show excellent healing after 1 and 2 weeks, compared to Kaltostat and bare wound. Wounds treated with chitosan control and CZBs achieved significant closure to $\sim 90\%$ after 2 weeks as compared to Kaltostat treated the wound and bare wounds, which showed 70% closure (Fig. 11a). The chitosan controls and CZBs show enhancing collagen deposition in the wound healing after 4 weeks. CZBs showed controlled degradation, enhanced blood clotting, excellent platelet activation ability, cytocompatibility, and antibacterial activity. All these properties indicate that advanced CZBs can be used for wound healing [10].

Another recent study presented by Fan et al. [103] developed a nano-titania/collagen-chitosan (nT/COL-CS) scaffolds. The stability, safety, and broadens in spectrum antibiosis of TiO₂ making it promising additive in decorating matrices used in biomedical applications. Only the nano-TiO₂ of anatase crystallinity has been reported to have the antimicrobial property [104]. The employed synthetic route implies at first, the preparation of TiO₂ hydrosol as reported by Macwan et al. [105] from tetrabutyl titanate precursor added to distilled water, ethanol, and hydrochloric acid within a molar ratio 1:200:16:0.3. A second step to finally produce nT/COL-CS was carried out through this technique: 20 mL of COL and CS solution (5 mg/mL) using 0.5 M acetic acid. After that, isovolumetric COL and CS solutions were mixed at 4 °C followed by the addition of appropriate amounts of TiO₂ hydrosol to get (COL-CS/TiO₂) of ratios 1–4. The mixtures were homogenized under continuous stirring at 4 °C for 2 h, then kept for 4 h at 37 °C bath. Then, the mixtures were poured into similar good culture plate and frozen at –30 °C, subjected to vacuum freeze-dried at –50 °C and stored at –20 °C while not in use. The added nano-TiO₂ further binds to collagen and chitosan via hydrogen bonding and serves as a bridge between their molecular chains resulting in an increase in the density of the mesh structure.

The nT-COL/CS reveals a remarkable aggregation of red blood cells on the nT-COL/CS surface that develop into clumps. Therefore, the nT-COL/CS scaffolds

Fig. 11 **a** Evaluation of the wound area closure and **b** study of the collagen deposition area (in both graphs, the star symbols represent the *p* 0.05 level, indicating that the means are significantly different, compared with the control) [10]



may be conducive to the hemostatic of the wound and may reduce the time of wound repairing. Moreover, the images indicate that the red blood cell aggregation is independent of the content of nano-TiO₂.

Therefore, the biomedical studies on these scaffolds conclude their cleaning and sterilizing effect for the wounded area, as well as, their high swelling property that reduces the wound exudates and the aggregation of red blood cell. These characteristics achieve the requirements of a viable candidate for wound repairing dressing.

Beer et al. [106] and Lara et al. [107] report for silver composites of considerable antimicrobial efficiency and propose a mechanism for this action. However, incorporating Ag to host matrices could enhance the antimicrobial effect. A biocomposite of chitosan/ZnO containing Ag (CS/ZnO/Ag) showed potent antimicrobial, antibacterial, and antifungal properties without any toxic side effects. This may offer a new promising generation from wound healing dressings whereas the blended ZnO nanoparticles have antimicrobial, antibacterial properties in either micro- or nanocomposites that could be beneficial in preventing infectious diseases [2, 108]. However, the higher antibacterial efficiency of ZnO is correlated to the optimum amount of Zn ions precursor during the sol-cast preparation route [109].

Ding et al. [110] developed a bilayer dressing sponge consists of cross-linked chitosan-oxidized Bletillastrata polysaccharide as a base layer with chitosan-Ag (CS-Ag) as the upper layer. The upper layer (CS-Ag) prohibits the bacterial proliferation and avoids direct contact with wound area whereas the lower layer showed less gelling time, more uniform aperture distribution, higher water retention, preferable mechanical strength and improved cell proliferation ability. Additionally, this double layered system provides excellent gas permeation and water retention ability. Therefore, significant acceleration of cutaneous wounds healing rate was achieved where a good mature epidermization with less inflammatory cells reached on day 7.

8.3 Wound Healing Based on Hydrogels and Growth Factor Delivery

Hydrogels are polymers with cross-linked networks, that have hydrophilic functional groups in their polymeric structure such as an amine (NH₂), hydroxyl (–OH), amide (–CONH–, –CONH₂) and sulfate (–SO₃H) that make them have a high affinity for water absorption. In biological and medical fields there are great interests to hydrogels because of a large number of convenient properties and preparation methods in medical and pharmaceutical industries. Different types of polymers (natural and synthetic) have been examined in hydrogel preparation. Chitosan is a natural cationic polymer, that has vast benefits at hydrogel modification. This polysaccharide has hydrophilic nature and can be degraded via human enzymes which result in biocompatibility [111]. Chitosan hydrogels are convenient for wound healing due to ease of application, wound protection, water retention, oxygen permeability and flexibility in acquiring the wound geometry.

Chitosan hydrogel was used as dressing to accelerate wound healing [14]. Chitosan hydrogels may be used as a vehicle to deliver proteins such as growth factors into wounds to accelerate healing [112]. Sustained release of growth factors in wounds has some delay, but when using chitosan hydrogels as a carrier, it gives prolonging the period of activity. Growth factors strongly promote cell division, migration, differentiation, and proliferation, and its combination with chitosan hydrogels give the advantages in wound healing process [113].

8.4 Wound Healing via Bioactive Modified Chitosan Based on Photodynamic Therapy

The abuse of antibiotics cause high incidence of bacterial resistance, and therefore, result in a serious problem which threatens the public health. Photodynamic therapy has arisen as a promising and important way in many fields of medical therapy. Recently, many study on photodynamic therapy for wound healing give interesting results that open door for wound healing [114]. Photodynamic therapy technique, depend on photosensitizer, that has been activated by exposure to illumination of suitable wavelength, and in the presence of oxygen produce highly reactive oxygen species that are able to damage the plasma membranes and DNA, leading to bacterial death. Prevention and treatment via photodynamic therapy, has a great advantage comparing to ordinary antimicrobials, because of the dual antimicrobials action of the photosensitizer, that can be attack the infected area via producing reactive oxygen species, and moreover, photosensitizer can be bind directly to cell wall and membranes of bacteria resulting in direct damage to its structures. Thus, bacteria cells have not chance to create resistance [115, 116]. The ideal photosensitizer should be easily synthesized, stable composition, non-toxic, photostable, cost-effective and have eradication power against pathogens [117]. The susceptibility of photosensitizer to eradicate bacteria has been shown to be dependent upon the type of bacteria (Gram-positive or gram-negative). Gram-positive bacteria have a permeable cell membrane which facilitate penetration of neutral, anionic, or cationic photosensitizers into the cell, and otherwise, gram-negative bacteria have an outer membrane that hinder regulate movement of molecules through the cell wall. Therefore, the photosensitizers with cationic charge or using cationic carrier are able to enter through the membrane and penetrate the cell and hence increase the efficacy of photosensitizers against gram-negative and yeast. Thus, negatively charged antimicrobial photosensitizers have narrow spectrum in the treatment of mixed infections, while positively charged photosensitizers such as conjugating polymers or those loaded on a cationic polymer such as chitosan are generally highly effective photosensitizer. Modified chitosan has been chosen, as a suitable delivery system for photosensitizers based on their advantages (e.g. biodegradable, biocompatibility, less toxicity, anti-microbial and hemostatic properties). Also, chitosan has a synergistic effect with photosensitizers, which potentiate their action in Photodynamic therapy [115].

9 Study Case for the Anti-bacterial Activity of Chitosan Grafted Poly(*N*-Methylaniline) Nanoparticles

Antibacterial activity of Chitosan-graft-poly(*N*-Methylaniline) nanoparticle [118] against *Escherichia coli* (Gram-negative) and *Staphylococcus aureus* (Gram-positive) as a wound-causing bacteria model was investigated via determination of the growth inhibitory effect of chitosan-graft-poly(*N*-Methylaniline) in broth bacterial suspension with concentration of 10^8 CFU ml^{-1} as a reference for initial colony quantification, that determined by using the plate counting method. To attain this situation, from a fresh bacterial agar plate, transfer the growth bacteria into a sterile capped glass tube containing an appropriate amount of sterile broth solution to make suspension of isolate overnight colonies into broth sterile media. Decimal serial dilutions were made from bacterial suspension, and each of these serial dilutions was cultured in sterile Petri plates. The plates were incubated for 24 h at 37 °C. The plates containing between 30 and 300 colonies were counted, and the colony-forming unit (CFU) was calculated. CFU can be assessed by comparing the optical absorbance of known CFU and unknown CFU via a spectrophotometer at 625 nm. The absorbance will be adjusted to the same range of the McFarland standard 0.5 ($1-2 \times 10^8$ CFU ml^{-1}) with optical absorbance in range (0.08–0.13). Adjust the suspension to be in balance with McFarland Standard 0.5 by adding sterile distilled water or broth. After adjusting the bacterial suspension to a concentration of 10^8 CFU ml^{-1} with sterilized distilled water, the preparing bacterial cell suspension was directly used for the antibacterial tests for Chitosan-graft-poly(*N*-Methylaniline). In each test, 10 ml of the bacterial suspension and 0.1 g of the Chitosan-graft-poly(*N*-Methylaniline) copolymer sample were placed in a sterilized Erlenmeyer flask and carried out in triplicate. The Erlenmeyer flask was shaken (250 rpm), after for 2 h, 1 ml of this suspension was pipetted out from the flask and the change in optical absorbance was recorded [119, 120]. The percentage of inhibition was counted as follows:

$$\text{Inhibition \%} = (\text{Control conc.} - \text{Taste conc.}) / \text{Control conc.} \times 100$$

E. coli and *S. aureus*, widely used as a pathogenic for wounds, were chosen as the standard bacterium for determining the antibacterial properties of the Chitosan-graft-poly(*N*-Methylaniline) nanoparticle. Growth inhibitory effect (Inhibition %) were used to determine the antibacterial activity of the Chitosan-graft-poly(*N*-Methylaniline) nanoparticle, which is 91.6 and 87.2% for *E. coli* and *S. aureus* respectively. This result indicated to a good antibacterial activity of tested polymer. It was observed that Chitosan-graft-poly(*N*-Methylaniline) nanoparticle showed good antibacterial activity due to the synergistic effect between chitosan and conducting polymer chains grafted onto the chitosan backbone [121, 122].

10 A Case Study in Wound Healing Due to Chitosan Grafted Poly(*N*-Methylaniline) Nanoparticles of Photo-Driven Skin Regeneration

Photodynamic therapy means the combination of a light source with a photosensitizing agent and hence produce reactive oxidizing species able to disinfect microorganisms and promote the process of tissues repairing and regeneration. A promising technique in repairing or treating wounds may ascribe when photodynamic therapy, applied topically to the wounds and the used photoactive dressings irradiated with light of appropriate energy corresponds to the optimum response. The development of nano-polymeric system photosensitizer has a great attention because of the biocompatibility and the accessibility for multi-functionalization of the nanoparticle. Nano-polymeric system based in photodynamic therapy offers several advantages such as the ability to deliver a large amount of photosensitizer to the target area, flexibility toward surface modification for better efficiency, and prevention from microorganisms in the living biological system. Many nano-polymeric systems have been used in photodynamic therapy like chitosan, collagen, albumin and alginate are grouped as natural polymers. Also, synthetic polymers like polyacrylamide and polylactide-polyglycolide co-polymers could be utilized [117]. The copolymer Chitosan-graft-poly(*N*-Methylaniline) is a modified chitosan by grafting with photoactive conducting polymer [118] acting as a potential photosensitizer, that absorbs Ultra violet and visible light, in turn, able to generate reactive oxygen species (ROS). This can reveal an environmentally desirable polymeric photosensitizer. To emphasize the effect of photodynamic therapy based on Chitosan-graft-poly(*N*-Methylaniline) nanoparticles, we applied it in wound creation in animals and investigate the wound repairing output. The effect of Chitosan-graft-poly(*N*-Methylaniline) nanoparticles on wound healing process was tested in dark and in presence of fluorescent lamp illumination with distance 1.5 m, as a visible light source (photodynamic therapy). The wound healing evaluation carried based on rat wound model, a single full-thickness skin excision wounds of 1 cm² in diameter was created on the back of each rat. Before wound creation in rats, the skin of the rats was shaved and disinfected using 70% (v/v) ethanol. Then the wounds were treated by Chitosan-graft-poly(*N*-Methylaniline) nanoparticles, and subsequently changed at different time intervals 3, 6, and 9 days after the surgery. The wounds diameters were serially measured using a caliper, and the appearance of the wound was examined visually. The percentage of the remaining wound areas were calculated as area before treatment (A_0) minus area contracted after treatment (A_t), divided by area before treatment (A_0), multiplied by 100% as follows:

$$\text{Remaining wound areas(\%)} = [(A_0) - (A_t)] / (A_0) \times 100$$

The test was carried out on three groups, each one consists of four rats, which photodynamic therapy group, dark group, and control (untreated) group. The percentage of the remaining wound areas after the application of Chitosan-graft-poly

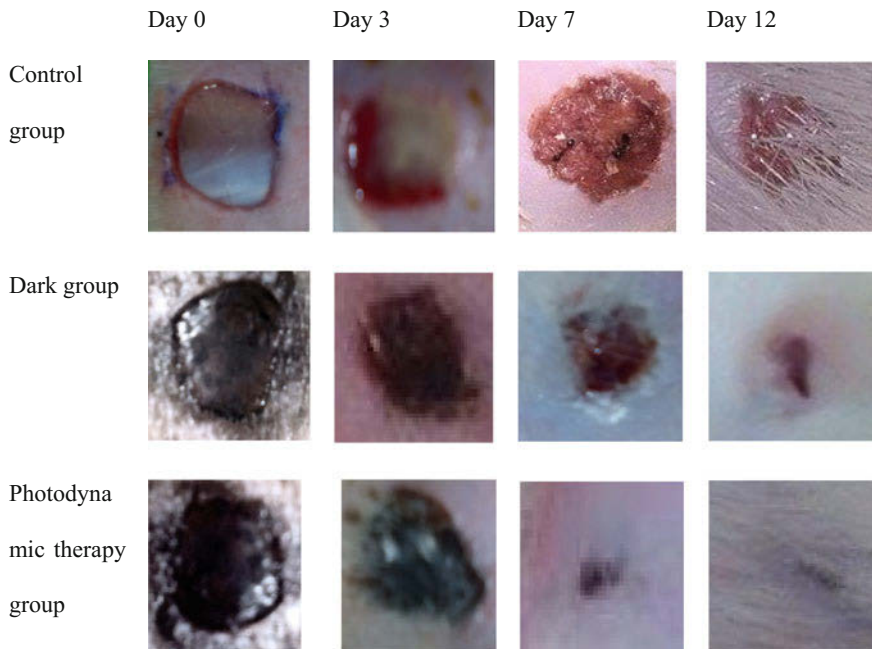


Fig. 12 Images of wounds from authors study case on the back of the rats at different time intervals

(*N*-Methylaniline) nanoparticles was found to decrease in a time-dependent manner in all the groups (Fig. 12). The wounds showed progressive healing up to 12 days for photodynamic therapy group and dark group versus control group. The healing was much better for photodynamic therapy group due to the synergistic effect of, killing bacteria via producing reactive oxygen species after light excitation and the native antibacterial action of chitosan-graft-poly(*N*-methyl aniline) nanoparticles, indicating to its importance in caring of wounds. Photodynamic therapy group and the dark group showed obvious activity in comparison with the control. It was encouraging that results showed significant differences only after 3 days versus control group, and the healing rate of photodynamic therapy was markedly higher than the dark group. After 12 days, the percentage of the remaining wound areas were 43.6, 8.9, and 1.0% for photodynamic therapy group, dark group, and control group, respectively. It suggested that the wound could be healed after treatment by chitosan-graft-poly(*N*-methyl aniline) nanoparticles. And the healing effect of chitosan-graft-poly(*N*-methyl aniline) was significantly better than that of control (untreated) group. It was probably because that photodynamic therapy group and the dark group could available prevent bacterial invasion and wound moisture to evaporate, which was advantageous for wound healing. Chitosan-graft-poly(*N*-methylaniline) may promote the cell migration and angiogenesis in various stages of wound healing. Moreover, it should be noted that the healing rate of

the control group was the slowest by visual monitoring from Fig. 12. After application of chitosan-graft-poly(*N*-methylaniline) nanoparticles in the photodynamic therapy group and dark group, wounds were turned softer due to rapid absorption of wound secretion and adjoined with the wound closely. And at the same time, bacterial infection was prevented by the outer barrier. Moreover, as early as in the 3rd day, new tissue appeared on the wound and granulation tissue was formed, which suggested that wound was in the proliferative phase. By day 12, wound disappeared and hair was seen, which suggested that the generation of hair follicles appeared.

11 Future Prospective

This chapter presents a detailed overview of biocompatible and biodegradable polymeric formulations and their correlation to wounds as well as the insights of wound healing process. Also, highlighting the recent progress in the biomedical treatment of wounds especially the current progress of chitosan-based composites and their applications in the biomedical engineering/management of wound healing. Additionally, the chapter describes the clinical findings that affect the appearance and functionality of the restored tissues taking into consideration the cost and time consumed for wound closure. Despite, a lot of chitosan-based formulations for wound healing purposes was developed, presenting a more decorated chitosan composite with greenly synthesized metallic and metal oxides of immense activity towards wounding areas is still infrequent and represents a novel perspective need to be increasingly dealt. These chitosan-based composites should fulfil many requirements in terms of effectiveness in microorganism disinfection, biocompatibility, and safety. Furthermore, our novel insights in developing chitosan nanografts as an advanced photoactive dressing for wound healing pave the way and opens the door to formulate photostable chitosan-based dressings. In this unconventional strategy, the developed photoactive dressings should safely produce reactive oxygen species able to disinfect microorganisms, promote repair and regeneration of wounded tissues. In this context, future criteria are recommended to investigate in-depth, the in vitro-in vivo correlation, and to conduct trials to human models [2].

References

1. Zivic F et al (2017) Biomaterials in clinical practice: advances in clinical research and medical devices. Springer, Berlin
2. Nair LS, Laurencin CT (2007) Biodegradable polymers as biomaterials. *Prog Polym Sci* 32(8–9):762–798
3. Mir M et al (2018) Synthetic polymeric biomaterials for wound healing: a review. *Progress Biomater* 1–21
4. Yudanova TN, Reshetov IV (2006) Modern wound dressings: manufacturing and properties. *Pharm Chem J* 40(2):85

5. Pandey AR, Singh US, Momin M, Bhavsar C (2017) Chitosan: application in tissue engineering and skin grafting. *J Polym Res* 24(8):125
6. Liu X et al (2016) In vitro BMP-2 peptide release from thiolated chitosan based hydrogel. *Int J Biol Macromol* 93:314–321
7. Jayakumar R et al (2011) Biomaterials based on chitin and chitosan in wound dressing applications. *Biotechnol Adv* 29(3):322–337
8. Howling GI et al (2001) The effect of chitin and chitosan on the proliferation of human skin fibroblasts and keratinocytes in vitro. *Biomaterials* 22(22):2959–2966
9. Li P et al (2011) A polycationic antimicrobial and biocompatible hydrogel with microbe membrane suctioning ability. *Nat Mater* 10(2):149
10. Dutta PK (2016) Chitin and chitosan for regenerative medicine. Springer, Berlin
11. Klee D, Höcker H (2000) Polymers for biomedical applications: improvement of the interface compatibility. In: *Biomedical applications polymer blends*. Springer, pp 1–57
12. Rickert D et al (2006) Biocompatibility testing of novel multifunctional polymeric biomaterials for tissue engineering applications in head and neck surgery: an overview. *Eur Arch Oto-Rhino-Laryngol Head Neck* 263(3):215–222
13. Velnar T, Bailey T, Smrkolj V (2009) The wound healing process: an overview of the cellular and molecular mechanisms. *J Int Med Res* 37(5):1528–1542
14. Patrulea V, Ostafe V, Borchard G, Jordan O (2015) Chitosan as a starting material for wound healing applications. *Eur J Pharm Biopharm* 97:417–426
15. Sen CK et al (2009) Human skin wounds: a major and snowballing threat to public health and the economy. *Wound Repair Regeneration* 17(6):763–771
16. Shevchenko RV, James SL, James SE (2009) A review of tissue-engineered skin bioconstructs available for skin reconstruction. *J Royal Soc Interface* rsif20090403
17. Percival SL et al (2012) A review of the scientific evidence for biofilms in wounds. *Wound Repair Regeneration* 20(5):647–657
18. Li X, Mohan S, Gu W, Baylink DJ (2001) Analysis of gene expression in the wound repair/regeneration process. *Mamm Genome* 12(1):52–59
19. Jorgensen SN, Sanders JR (2016) Mathematical models of wound healing and closure: a comprehensive review. *Med Biol Eng Compu* 54(9):1297–1316
20. Kennedy KM, Bhaw-Luximon A, Jhurry D (2017) Skin tissue engineering: biological performance of electrospun polymer scaffolds and translational challenges. *Regenerative Eng Transl Med* 3(4):201–214
21. Fitzmaurice GJ et al (2014) Do statins have a role in the promotion of postoperative wound healing in cardiac surgical patients? *Ann Thorac Surg* 98(2):756–764
22. Braiman-Wiksman L, Solomonik I, Spira R, Tennenbaum T (2007) Novel insights into wound healing sequence of events. *Toxicol Pathol* 35(6):767–779
23. Diegelmann RF, Evans MC et al (2004) Wound healing: an overview of acute, fibrotic and delayed healing. *Front Biosci* 9(1):283–289
24. Muzzarelli RAA (2009) Chitins and chitosans for the repair of wounded skin, nerve, cartilage and bone. *Carbohydr Polym* 76(2):167–182
25. Fonder MA et al (2008) Treating the chronic wound: a practical approach to the care of nonhealing wounds and wound care dressings. *J Am Acad Dermatol* 58(2):185–206
26. Dhivya S, Padma VV, Santhini E (2015) Wound dressings—a review. *Biomedicine* 5(4)
27. Rivera AE, Spencer JM (2007) Clinical aspects of full-thickness wound healing. *Clin Dermatol* 25(1):39–48
28. Boateng JS, Matthews KH, Stevens HNE, Eccleston GM (2008) Wound healing dressings and drug delivery systems: a review. *J Pharm Sci* 97(8):2892–2923
29. Sarabahi S (2012) Recent advances in topical wound care. *Indian J Plast Surg: Official Publ Assoc Plast Surg India* 45(2):379
30. Lio PA, Kaye ET (2009) Topical antibacterial agents. *Infect Dis Clin North Am* 23(4): 945–963

31. Vert M et al (2012) Terminology for biorelated polymers and applications (IUPAC recommendations 2012). *Pure Appl Chem* 84(2):377–410
32. Huang S, Fu X (2010) Naturally derived materials-based cell and drug delivery systems in skin regeneration. *J Controlled Release* 142(2):149–159
33. Santos TC et al (2007) In vitro evaluation of the behaviour of human polymorphonuclear neutrophils in direct contact with chitosan-based membranes. *J Biotechnol* 132(2):218–226
34. Ueno H, Mori T, Fujinaga T (2001) Topical formulations and wound healing applications of chitosan. *Adv Drug Deliv Rev* 52(2):105–115
35. Peniche C, Argüelles-Monal W, Goycoolea FM (2008) Chitin and chitosan: major sources, properties and applications. Monomers, polymers and composites from renewable resources. Elsevier, Amsterdam, pp 517–542
36. Kumar MNVR (2000) A review of chitin and chitosan applications. *React Funct Polym* 46(1):1–27
37. Pillai CKS, Paul Willi, Sharma CP (2009) Chitin and chitosan polymers: chemistry, solubility and fiber formation. *Prog Polym Sci* 34(7):641–678
38. Hussein MHM et al (2013) Preparation of some eco-friendly corrosion inhibitors having antibacterial activity from sea food waste. *J Surfactants Deterg* 16(2):233–242
39. El-Fattah MA et al (2016) Improvement of corrosion resistance, antimicrobial activity, mechanical and chemical properties of epoxy coating by loading chitosan as a natural renewable resource. *Prog Org Coat* 101:288–296
40. de Velde K, Kiekens P (2004) Structure analysis and degree of substitution of chitin, chitosan and dibutrylchitin by FT-IR spectroscopy and solid state ¹³C NMR. *Carbohydr Polym* 58(4):409–416
41. Wasikiewicz JM, Yeates SG (2013) ‘Green’ molecular weight degradation of chitosan using microwave irradiation. *Polym Degrad Stab* 98(4):863–867
42. Ramawat KP, Mérillon J-M (2015) Polysaccharides: bioactivity and biotechnology. Springer, Heidelberg
43. Negm NA et al (2015) Treatment of industrial wastewater containing copper and cobalt ions using modified chitosan. *J Ind Eng Chem* 21:526–534
44. Muzzarelli RAA, Muzzarelli C (2005) Chitosan chemistry: relevance to the biomedical sciences. In: Polysaccharides I. Springer, Berlin, pp 151–209
45. Vo D-T, Sabrina S, Lee C-K (2017) Silver deposited carboxymethyl chitosan-grafted magnetic nanoparticles as dual action deliverable antimicrobial materials. *Mater Sci Eng, C* 73:544–551
46. Muzzarelli R, Delben F, Ilari P, Tomasetti M (1994) N-(Carboxymethyl) chitosan, a versatile chitin derivative. *Agro-Food-Industry Hi-Tech*
47. Wu M, Long Z, Xiao H, Dong C (2016) Recent research progress on preparation and application of N,N,N-trimethyl chitosan. *Carbohydr Res* 434:27–32
48. Mourya VK, Inamdar NN (2009) Trimethyl chitosan and its applications in drug delivery. *J Mater Sci Mater Med* 20(5):1057
49. Casettari L et al (2012) PEGylated chitosan derivatives: synthesis, characterizations and pharmaceutical applications. *Prog Polym Sci* 37(5):659–685
50. Hefni HHH et al (2016) Synthesis, characterization and anticorrosion potentials of Chitosan-g-PEG assembled on silver nanoparticles. *Int J Biol Macromol* 83:297–305
51. Huaixan LN et al (2016) Macroscopic, histochemical, and immunohistochemical comparison of hysterorrhaphy using catgut and chitosan suture wires. *J Biomed Mater Res B Appl Biomater* 104(1):50–57
52. Hein S, Wang K, Stevens WF, Kijems J (2008) Chitosan composites for biomedical applications: status, challenges and perspectives. *Mater Sci Technol* 24(9):1053–1061
53. Raabe D et al (2006) Microstructure and crystallographic texture of the chitin-protein network in the biological composite material of the exoskeleton of the Lobster *Homarus americanus*. *Mater Sci Eng A* 421(1–2):143–153

54. Arpornmaeklong P, Suwatwirote N, Pripatnanont P, Oungbho K (2007) Growth and differentiation of mouse osteoblasts on chitosan-collagen sponges. *Int J Oral Maxillofac Surg* 36(4):328–337
55. Silva D et al (2013) Chitosan and platelet-derived growth factor synergistically stimulate cell proliferation in gingival fibroblasts. *J Periodontol Res* 48(6):677–686
56. Zhao R et al (2014) Electrospun chitosan/sericin composite nanofibers with antibacterial property as potential wound dressings. *Int J Biol Macromol* 68:92–97
57. Costa EM et al (2014) Chitosan mouthwash: toxicity and in vivo validation. *Carbohydr Polym* 111:385–392
58. Rao SB, Sharma CP (1997) Use of chitosan as a biomaterial: studies on its safety and hemostatic potential. *J Biomed Mater Res* 34(1):21–28
59. Baldrick P (2010) The safety of chitosan as a pharmaceutical excipient. *Regul Toxicol Pharmacol* 56(3):290–299
60. Gades MD, Stern JS (2003) Chitosan supplementation and fecal fat excretion in men. *Obesity* 11(5):683–688
61. Ylitalo R et al (2002) Cholesterol-lowering properties and safety of chitosan. *Arzneimittelforschung* 52(01):1–7
62. Tamer TM, Valachová K, Mohyeldin MS, Soltes L (2016) Free radical scavenger activity of cinnamyl chitosan Schiff base. *J Appl Pharm Sci* 6:130
63. Fujita M et al (2004) Inhibition of vascular prosthetic graft infection using a photocrosslinkable chitosan hydrogel. *J Surg Res* 121(1):135–140
64. Eldin MSM, Soliman EA, Hashem AI, Tamer TM (2008) Antibacterial activity of chitosan chemically modified with new technique. *J Trends Biomater Artif Organs* 22(3):121–133
65. Chung Y-C, Chen C-Y (2008) Antibacterial characteristics and activity of acid-soluble chitosan. *Biores Technol* 99(8):2806–2814
66. Ahmed S, Ikram S (2016) Chitosan based scaffolds and their applications in wound healing. *Achievements Life Sci* 10(1):27–37
67. Shoji M et al (2006) Lipopolysaccharide stimulates the production of prostaglandin E2 and the receptor Ep4 in osteoblasts. *Life Sci* 78(17):2012–2018
68. Grishin AV et al (2006) Lipopolysaccharide induces cyclooxygenase-2 in intestinal epithelium via a noncanonical P38 MAPK pathway. *J Immunol* 176(1):580–88 (Baltimore, Md. : 1950)
69. Yang E-J et al (2010) Anti-inflammatory effect of chitosan oligosaccharides in RAW 264.7 cells. *Open Life Sci* 5:95
70. Van Amersfoort ES, Van Berkel TJC, Kuiper J (2003) Receptors, mediators, and mechanisms involved in bacterial sepsis and septic shock. *Clin Microbiol Rev* 16(3):379–414
71. Ma L et al (2016) Anti-inflammatory activity of chitosan nanoparticles carrying NF-KappaB/P65 antisense oligonucleotide in RAW264.7 macrophage stimulated by lipopolysaccharide. *Colloids Surf B* 142:297–306
72. Tu J et al (2016) Chitosan nanoparticles reduce LPS-induced inflammatory reaction via inhibition of NF-KappaB pathway in Caco-2 cells. *Int J Biol Macromol* 86:848–856
73. Naberezhnykh GA et al (2008) Interaction of chitosans and their N-acylated derivatives with lipopolysaccharide of gram-negative bacteria. *Biochem Biokhim* 73(4):432–441
74. Rodrigues S, Dionisio M, Lopez CR, Grenha Ana (2012) Biocompatibility of chitosan carriers with application in drug delivery. *J Funct Biomater* 3(3):615–641
75. Xu C et al (2012) Chitosan as a barrier membrane material in periodontal tissue regeneration. *J Biomed Mater Res Part B Appl Biomater* 100:1435–1443
76. Kean T, Thanou M (2010) Biodegradation, biodistribution and toxicity of chitosan. *Adv Drug Deliv Rev* 62(1):3–11
77. Leite ÁJ, Caridade SG, Mano JF (2016) Synthesis and characterization of bioactive biodegradable chitosan composite spheres with shape memory capability. *J Non-Cryst Solids* 432:158–166

78. Mollah MZI et al (2016) Biodegradable colour polymeric film (starch-chitosan) development: characterization for packaging materials. *Open J Org Polym Mater* 06:11–24
79. Kozen BG et al (2008) An alternative hemostatic dressing: comparison of CELOX, HemCon, and QuikClot. *Acad Emerg Med: Official J Soc Acad Emerg Med* 15(1):74–81
80. Balan V, Verestiuc L (2014) Strategies to improve chitosan hemocompatibility: a review. *Eur Polym J* 53
81. Pogorielov MV, Sikora VZ (2015) Chitosan as a hemostatic agent: current state. *Eur J Med. Series B* 2(1):24–33
82. Whang HS et al (2005) Hemostatic agents derived from chitin and chitosan. *J Macromol Sci Part C* 45(4):309–323
83. Boddupalli B, Mohammed Z, Nath R, Banji D (2010) Mucoadhesive drug delivery system: an overview. *J Adv Pharm Technol Res* 1(4):381–387
84. Perchyonok VT et al (2014) Evaluation of nystatin containing chitosan hydrogels as potential dual action bio-active restorative materials: In: Puoci F (ed) *Vitro approach*. *J Funct Biomater* 5(4):259–72. <http://www.ncbi.nlm.nih.gov/pmc/articles/PMC4285406/>
85. Croisier F, Jérôme C (2013) Chitosan-based biomaterials for tissue engineering. *Eur Polym J* 49(4):780–92. <http://www.sciencedirect.com/science/article/pii/S0014305712004181>
86. Frykberg RG, Banks J (2015) Challenges in the treatment of chronic wounds. *Adv Wound Care* 4(9):560–582
87. El-Feky GS, Sharaf SS, El Shafei A, Hegazy AA (2017) Using chitosan nanoparticles as drug carriers for the development of a silver sulfadiazine wound dressing. *Carbohydr Polym* 158:11–19
88. Agnihotri S, Bajaj G, Mukherji S, Mukherji Soumyo (2015) Arginine-assisted immobilization of silver nanoparticles on ZnO nanorods: an enhanced and reusable antibacterial substrate without human cell cytotoxicity. *Nanoscale* 7(16):7415–7429
89. Yasasvini S et al (2017) Topical hydrogel matrix loaded with simvastatin microparticles for enhanced wound healing activity. *Mater Sci Eng C Mater Biol Appl* 72:160–167
90. Vedakumari WS et al (2017) Quercetin impregnated chitosan-fibrin composite scaffolds as potential wound dressing materials—fabrication, characterization and in vivo analysis. *Eur J Pharm Sci: Official J Eur Fed Pharm Sci* 97:106–112
91. Gomathi K, Gopinath D, Rafiuddin Ahmed M, Jayakumar R (2003) Quercetin incorporated collagen matrices for dermal wound healing processes in rat. *Biomaterials* 24(16):2767–2772
92. Veerapandian M, Seo Y-T, Yun K, Lee M-H (2014) Graphene oxide functionalized with silver@silica-polyethylene glycol hybrid nanoparticles for direct electrochemical detection of quercetin. *Biosens Bioelectron* 58:200–204
93. Metwally AM, Omar AA, Harraz FM, El Sohafy SM (2010) Phytochemical investigation and antimicrobial activity of *Psidium guajava* L. leaves. *Pharmacognosy Magazine* 6(23): 212–218
94. Bhardwaj N, Kundu S (2011) Silk fibroin protein and chitosan polyelectrolyte complex porous scaffolds for tissue engineering applications. *Carbohydr Polym* 85:325–333
95. Noorjahan SE, Sastry TP (2004) An in vivo study of hydrogels based on physiologically clotted fibrin-gelatin composites as wound-dressing materials. *J Biomed Mater Res B Appl Biomater* 71(2):305–312
96. Romić MD et al (2016) Melatonin-loaded chitosan/Pluronic® F127 microspheres as in situ forming hydrogel: an innovative antimicrobial wound dressing. *Eur J Pharm Biopharm* 107:67–79. <http://www.sciencedirect.com/science/article/pii/S0939641116302223>
97. Reiter RJ, Tan D-X, Fuentes-Broto L (2010) Melatonin: a multitasking molecule. *Prog Brain Res* 181:127–151
98. Gomez-Florit M, Ramis JM, Monjo M (2013) Anti-fibrotic and anti-inflammatory properties of melatonin on human gingival fibroblasts in vitro. *Biochem Pharmacol* 86(12):1784–1790

99. Drobnik J (2012) Wound healing and the effect of pineal gland and melatonin. *J Exp Integr Med* 2(1):3–14
100. Sahib AS, Al-Jawad FH, Al-Kaisy AA (2009) Burns, endothelial dysfunction, and oxidative stress: the role of antioxidants. *Annals Burns Fire Disasters* 22(1):6–11. <http://www.ncbi.nlm.nih.gov/pmc/articles/PMC3188210/>
101. Sahib AS, Al-Jawad FH, Alkaisy AA (2010) Effect of antioxidants on the incidence of wound infection in burn patients. *Ann Burns Fire Disasters* 23(4):199–205
102. Gopal A, Kant V, Gopalakrishnan A, Tandan SK, Kumar D (2014) Chitosan-based copper nanocomposite accelerates healing in excision wound model in rats. *Eur J Pharmacol* 731:8–19
103. Fan X et al (2016) Nano-TiO₂/collagen-chitosan porous scaffold for wound repairing. *Int J Biol Macromol* 91:15–22
104. Verdier T, Coutand M, Bertron A, Roques C (2014) Antibacterial activity of TiO₂ photocatalyst alone or in coatings on *E. coli*: the influence of methodological aspects. *Coatings* 4:670–686
105. Macwan DP, Dave P, Chaturvedi S (2011) A review on nano-TiO₂ sol–gel type syntheses and its applications. *J Mater Sci* 46:3669–3686
106. Beer C et al (2012) Toxicity of silver nanoparticles—nanoparticle or silver ion? *Toxicol Lett* 208(3):286–292
107. Lara HH, Ayala-Nunez NV, Ixtapan-Turrent L, Rodriguez-Padilla C (2010) Mode of antiviral action of silver nanoparticles against HIV-1. *J Nanobiotechnol* 8:1
108. Wang X, Du Y, Liu H (2004) Preparation, characterization and antimicrobial activity of chitosan-Zn complex. *Carbohydr Polym* 56:21–26
109. Darder M, Aranda P, Ruiz-Hitzky E (2007) Bionanocomposites: a new concept of ecological, bioinspired, and functional hybrid materials. *Adv Mater* 19:1309–1319
110. Ding L et al (2017) Spongy bilayer dressing composed of chitosan–Ag nanoparticles and Chitosan-*Bletilla striata* polysaccharide for wound healing applications. *Carbohydr Polym* 157:1538–1547
111. Ahmadi F, Oveisi Z, Samani SM, Amoozgar Z (2015) Chitosan based hydrogels: characteristics and pharmaceutical applications. *Res Pharm Sci* 10(1):1–16
112. Luca L et al (2011) Injectable RhBMP-2-loaded chitosan hydrogel composite: osteoinduction at ectopic site and in segmental long bone defect. *J Biomed Mater Res Part A* 96:66–74
113. Dai T, Tanaka M, Huang Y-Y, Hamblin MR (2011) Chitosan preparations for wounds and burns: antimicrobial and wound-healing effects. *Expert Rev Anti-Infect Ther* 9(7):857–879
114. Chatterjee DK, Fong LS, Zhang Y (2008) Nanoparticles in photodynamic therapy: an emerging paradigm. *Adv Drug Deliv Rev* 60(15):1627–1637
115. Chen C-P, Chen C-T, Tsai T (2012) Chitosan nanoparticles for antimicrobial photodynamic inactivation: characterization and in vitro investigation. *Photochem Photobiol* 88(3):570–576
116. Chien H-F et al (2013) The use of chitosan to enhance photodynamic inactivation against *Candida albicans* and its drug-resistant clinical isolates. *Int J Mol Sci* 14(4):7445–7456. <http://www.ncbi.nlm.nih.gov/pmc/articles/PMC3645695/>
117. Gupta A et al (2013) Shining light on nanotechnology to help repair and regeneration. *Biotechnol Adv* 31(5):607–631
118. Sayyah SM, Essawy AA, El-Nggar AM (2015) Kinetic studies and grafting mechanism for methyl aniline derivatives onto chitosan: highly adsorptive copolymers for dye removal from aqueous solutions. *React Funct Polym* 96:50–60. <http://www.sciencedirect.com/science/article/pii/S1381514815300249>
119. Singh G, Joyce E, Beddow J, Mason T (2012) Evaluation of antibacterial activity of ZnO nanoparticles coated sonochemically onto textile fabrics. *World J Microbiol Biotechnol* 2:106–120
120. Wiegand I, Hilpert K, Hancock REW (2008) Agar and broth dilution methods to determine the minimal inhibitory concentration (MIC) of antimicrobial substances. *Nat Protoc* 3(2):163–175

121. Çabuk M, Yusuf A, Yavuz M, Unal H (2014) Synthesis, characterization and antimicrobial activity of biodegradable conducting polypyrrole-graft-chitosan copolymer. *Appl Surf Sci* 318:168–175
122. Shanmugam A, Kathiresan K, Nayak L (2016) Preparation, characterization and antibacterial activity of chitosan and phosphorylated chitosan from cuttlebone of *Sepia kobeensis* (Hoyle, 1885). *Biotechnol Rep* 9:25–30

Mechanical, Thermal and Viscoelastic Properties of Polymer Composites Reinforced with Various Nanomaterials



T. H. Mokhothu, A. Mtibe, T. C. Mokhena, M. J. Mochane, O. Ofosu, S. Muniyasamy, C. A. Tshifularo and T. S. Motsoeneng

1 Introduction

Nanotechnology has attracted a considerable attention in science community due to the growing demand to develop high-performance materials for medical, sensors, computing, packaging, textiles, automotive, membrane-based separation, water purification, etc. to make our lives more comfortable. Various nanomaterials such as carbon nanotubes, graphite, metal oxide nanoparticles, clay nanoparticles, and nanocellulose have been extensively investigated due to their good physical, antimicrobial, electrical, thermal, chemical and mechanical properties. In recent years, nanomaterials have been used in applications that require elevated

T. H. Mokhothu
Department of Chemistry, Durban University of Technology,
Durban, South Africa

A. Mtibe (✉) · T. C. Mokhena (✉) · O. Ofosu · S. Muniyasamy
C. A. Tshifularo
CSIR Materials Science and Manufacturing, Polymers and Composites
Competence Area, Nonwovens and Composites Research Group,
Port Elizabeth, South Africa
e-mail: mtibe.asanda@gmail.com

T. C. Mokhena
e-mail: mokhenateboho@gmail.com

T. C. Mokhena · C. A. Tshifularo
Department of Chemistry, Nelson Mandela University, Port Elizabeth, South Africa

M. J. Mochane
Department of Life Sciences, Central University of Technology Free State,
Bloemfontein, South Africa

T. S. Motsoeneng
Department of Polymer Technology, Tshwane University of Technology,
Pretoria, South Africa

mechanical performance such as polymer nanocomposites as a reinforcing element. Polymer nanocomposite is a combination of the polymer matrix and nanomaterials with one, two and/or three dimensions.

Polymers are widely used in various applications due to their low cost, flexibility and easy processing. However, they have inherited some drawbacks such as low tensile properties and poor fracture toughness which limits their applications [20]. Therefore, to address these drawbacks nanomaterials have to be compounded with the polymer matrix. To develop polymer nanocomposites with the required properties depends on the filler properties and dispersion of the filler within the polymer matrix. For instance, to formulate polymer nanocomposites with high conductivity, carbon nanotubes should be used as filler due to its high conductivity [4]. However, it is widely accepted that poor dispersibility causes agglomeration of filler which led to poor interfacial adhesion between a filler and polymer matrix and therefore results in the poor mechanical performance of the resultant material [20]. To improve the dispersion of fillers in a polymer matrix, modification of either filler or polymer should be considered to alter the functional groups of the materials in order to achieve a good interaction between polymer and filler which enhances properties of the resultant materials [95, 96].

Many researchers have investigated the effect of nanomaterials on the properties of polymer nanocomposites [14, 87–89, 93, 94]. However, many studies indicated that the incorporation of nanomaterials enhanced the properties of the resultant polymer nanocomposites [90–92, 101]. For example, [67] reported that the incorporation of nanocellulose enhanced tensile and thermal properties of polyvinyl alcohol (PVA) nanocomposites. It was also widely noticed that the increase in loading showed a positive effect on mechanical properties of nanocomposites.

This book chapter reviews the effect of nanomaterials on the properties of polymer nanocomposites. It is also highlighting the hybridization of fillers and studied their effect on the properties of nanocomposites. Lastly, this chapter highlights the incorporation of nanomaterials in biopolymers and investigated their properties.

2 Mechanical Properties of Nanocomposites

2.1 Mechanical Properties of Polymer Reinforced with Cellulose-Based Nanofillers

Cellulose-based nanofillers are categorized into cellulose nanocrystals (CNCs) and cellulose nanofibres (CNFs). CNFs consist of crystalline and amorphous region whereas CNCs consist of the only crystalline region. In addition, CNFs are web-shaped [58] bundles stabilized by hydrogen bonds while CNCs are rod-like shaped [75]. The diameters of both CNFs and CNCs are in nanoscale and their lengths in microscale [77]. It was also reported that the tensile strength and modulus of CNCs were 14.3–28.6 and 143 GPa, respectively [19]. In addition, CNCs have a

low elongation at break, high aspect ratio, and large surface area. CNFs have similar characteristics with CNCs.

Due to the aforementioned extraordinary properties of cellulose-based nanofillers, they have attracted a considerable attention in polymer nanocomposites field as suitable reinforcement using low loading amount. The study reported by Chen et al. [25] revealed that the addition of 10 wt% of CNCs extracted from pea hull fiber in pea starch polymer enhanced tensile strength and elongation at break of the pea starch nanocomposites due to their high aspect ratio. The authors added that the strong adhesion between the two materials led to the improvement of mechanical properties of the resultant nanocomposites. Similar observations were reported in the case of CNFs [13, 45, 48, 49]. In addition, [49] indicated that the increase in CNFs loading in polylactic acid (PLA) led to the enhancement of tensile strength and modulus but, elongation at break was reduced. This was attributed to the good mechanical properties of CNFs and the interaction between CNFs and PLA. In contrast, [47] reported that no significant alterations in tensile properties were observed in melt-spun PLA reinforced with CNCs.

The hydrophilic nature of cellulose-based nanofillers led to poor interaction between nanofillers and the hydrophobic polymer matrix. Hence, the surface modification of these materials is crucial to improving their hydrophobicity, dispersion, and interaction between them and the polymer matrix. The incorporation of acetylated CNCs up to 4.5 wt% resulted in an overall increase in tensile strength and modulus as well as elongation at break. The further increase above that resulted in a decrease in tensile properties. This can be explained by the fact that when loading was less than 4.5 wt%, the distance between CNCs was big and therefore the interaction was weak to form percolation network. However, at higher loadings, a decrease in tensile properties was observed due to agglomeration [114]. On the other hand, [13], reported that the enhancement of tensile properties in thermoplastic starch (TPS) reinforced with unmodified CNFs was due to the formation of hydrogen-bonded nanofibres network, entanglement and strong interfacial adhesion between TPS and CNFs. The authors also reported that tensile properties of TPS reinforced with acetylated CNFs were lower than those of unmodified CNFs reinforced TPS. This was attributed to the lack of fibers-to fibers and fibers-to-polymer matrix interactions due to the surface hydrophobicity in modified CNFs.

2.2 Mechanical Properties of Polymer Nanocomposites Reinforced with Carbonaceous Nanofillers

Carbonaceous nanofillers such as carbon nanotubes (CNTs) and graphite have exhibited extraordinary tensile strength and modulus, electrical properties, large surface area, high aspect ratio and low density. Given these extraordinary properties, CNTs can be regarded as ideal candidates for reinforcement in polymer nanocomposites to enhance the mechanical properties, thermal conductivity and electrical properties of the resultant polymer nanocomposites. Considering the

properties of CNTs, [20] developed epoxy nanocomposites reinforced with multi-wall carbon nanotubes (MWNTs). The results suggested that the incorporation of pristine MWNTs in epoxy led to a slight increase in tensile modulus but decrease tensile strength. However, incorporation of functionalized MWNTs with polystyrene sulfonate (PSS) and poly(4-amino styrene) (PAS) in epoxy resulted in an increase in both tensile modulus and strength. Similar findings were also reported by Mashhadzadeh et al. [69]. It was also reported that the addition of CNTs in high-density polyethylene (HDPE) resulted in the improvement of its hardness [35]. In contrast, other authors reported that the addition of carbonaceous fillers without modification in polymer matrix results in improvement of tensile properties [4, 74, 109, 111]. Moreover, it is worth noting that the increase in filler loading enhanced mechanical properties of the resultant polymer nanocomposites [4]. In addition, the addition of carbonaceous nanofillers in polymer matrix induce the electrical properties of nanocomposites [50]. Lopez-manchado et al. [63] investigated the effect of thermal reduced graphene oxide on the mechanical properties of plasticized natural rubber with dodecyltrimethylammonium bromide (DTAB). The addition of thermal reduced graphene oxide enhanced the stiffness of plasticised natural rubber.

Numerous researchers have investigated the effect of loading of carbonaceous nanofillers in polymer matrices [2, 50]. For instance, [50] investigated the effect of large aspect ratios and exceptional high mechanical strength MWNTs loading on the mechanical properties of acrylonitrile butadiene styrene. Both tensile strength and modulus increased with increase in loading but, in the case of tensile strength it increased up to 7 wt% and decreased with further increase in loading. The enhancement of mechanical properties was due to the uniform dispersion of MWNTs throughout the polymer matrix. Above 7 wt% loading, the agglomeration of MWNTs was clearly observed which could be the reason for the decline in the tensile strength of the nanocomposites. On the other hand, elongation at break decreased with an increase in loading. In addition, the addition of MWNTs at different loading also improved the electrical conductivity. Liao et al. [60] tested the impact strength of polypropylene (PP) nanocomposites reinforced with MWNTs and hydroxyapatite designed for bone implants. The authors reported in their extensively investigated study that the impact strength of PP reinforced with hydroxyapatite decreases with increasing hydroxyapatite loading. However, the incorporation of MWNTs in PP nanocomposites reinforced with hydroxyapatite enhanced the impact strength due to their flexibility and large strain to failure. Also, it was reported that the inclusion of MWNTs increases the degree of crystallinity of PP nanocomposites which lead to the enhancement of tensile properties and impact strength. Younesi et al. [116] investigated flexural behaviour of low-density polyethylene (LDPE) reinforced with single wall carbon nanotubes (SWNTs) and wood flour. The addition of SWNTs and the modification of LDPE with maleic anhydride enhanced the flexural modulus. However, the flexural modulus increased with increasing loading (1–3 wt%) of SWNTs. The enhancement of flexural properties was due to the high aspect ratio of SWNTs. It was also reported that SWNTs were well dispersed in the polymer and therefore improved the interfacial adhesion between polymer and SWNTs which result in improvement of flexural properties. Furthermore, impact strength also improved when SWNTs were added.

2.2.1 Mechanical Properties of Biopolymers Reinforced with Carbonaceous Fillers

Much research is focusing on the development of biobased and biodegradable products due to their eco-friendliness, sustainability, and biodegradability. Biopolymers are among the materials that have been extensively investigated. Biopolymers which are widely studied include polylactic PLA, TPS, poly(hydroxybutyrate-co-hydroxyvalerate) PHBV, poly(butylene succinate) (PBS), polysaccharides and proteins. Like any other material, biopolymers have inherited some drawbacks such as moisture absorption, difficulty in processability and low properties in comparison to traditional petroleum-based polymers. To address these drawbacks, biopolymers are blended with other polymers or reinforced with stiffer nanofillers. For instance, [97] reported that the addition of 1 wt% CNTs in PHBV reduced water uptake

Table 1 Biopolymers reinforced with carbonaceous nanofillers

Biodegradable polymer	Filler	Publication year	References
Larch lignocellulose	MWNTs	2017	Huang et al. [46]
Poly(butylene succinate-co-adipate) (PBSA)	Halloysite nanotube	2016	Chiu [27]
Polycaprolactone (PCL)	MWNTs	2010	Sanchez-garcia et al. [97]
Hydroxyapatite	MWNTs	2017	Khan et al. [52]
PBSA/maleated polyethylene blend	Halloysite nanotube	2017	Chiu [28]
Poly(lactic-co-glycolic acid)	Carboxylation MWNTs	2011	Lin et al. [61]
Epoxidized natural rubber	MWNTs	2018	Krainoi et al. [55]
Poly lactide/poly(ϵ -caprolactone)	Thermally exfoliated graphene oxide (GO)	2018	Botlhoko et al. [17]
Poly(3-hydroxyalkanoate)	Grafted MWNTs	2015	Mangeon et al. [68]
PLA	Kenaf fibre/ MWNTs	2017	Chen et al. [22]
Poly(l-lactide) (PLLA)/poly(3-hydroxybutyrate-co-4-hydroxybutyrate) (P(3HB-co-4HB)) blend	MWNTs	2017	Gao et al. [38]
TPS	Oxidized MWNTs	2013	Cheng et al. [26]
PLA	CNT	2016	Wang et al. [112]

whereas at increased CNTs loading an increase in water uptake was observed. Similar results were observed in the case of PHBV reinforced with carbon nanofibres. Other studies that investigated the mechanical properties of biopolymers reinforced with carbonaceous nanofillers are summarized in Table 1.

Incorporation of carbonaceous nanofillers into biodegradable polymers improves the mechanical properties of the resultant polymer nanocomposites [55, 97]. For example, the incorporation of MWNTs in epoxidized natural rubber nanocomposites led to enhancement of mechanical properties as shown in Fig. 1.

It was also reported that mechanical properties of epoxidized natural rubber nanocomposites increased with increasing MWNTs loading. It was seen that at 5 wt% MWNTs loading reinforced epoxidized had the highest tensile strength, further increase in loading above 5 wt% MWNTs led to a decrease in tensile strength while modulus was constantly improving. The decrease in tensile strength after 5 wt% MWNTs could be due to CNTs aggregation in the polymer matrix. Conversely, the elongation at break decreased with MWNTs loading [55]. Similar results were reported by Wang et al. [112], in their case they discovered that 3 wt% CNTs loading was the optimum and further increase in CNTs loading led to decrease in tensile properties.

Other researchers [18, 26, 61, 68] incorporated functionalized carbonaceous nanofillers in biopolymers to further enhance mechanical properties of the nanocomposites. Lin et al. [61] incorporated carboxylated MWNTs in poly (lactic-co-glycolic acid) for bone tissue engineering. Morphological properties indicated that the treatment shortened the length of CNTs which tend to avoid agglomeration. This led to enhancement of tensile properties of the resultant nanocomposites by nearly three-fold in comparison to the virgin polymer and by nearly two-fold in comparison to those of polymer reinforced with untreated MWNTs. In addition, functionalized MWNTs based nanocomposites degrade faster than both unfunctionalized MWNTs based nanocomposites and virgin polymer. Similar results were observed in the case of PHBV reinforced with 3 wt% grafted CNTs [68]. In contrast, the addition of functionalized graphene oxide in polylactide/poly(ϵ -caprolactone) blend led to the decrease in tensile properties. However, tensile properties slightly improved with the increase in loading.

A global research is now moving towards hybridizing two or more fillers to enhance the performance of the material for diversified applications [22, 60, 116]. Chen et al. [22] fabricated PLA nanocomposites reinforced with a combined functionalized kenaf fibres and MWNTs by melt mixing and compression moulding techniques. They reported that tensile properties of the resultant nanocomposites increased due to the interfacial interaction between modified kenaf fibres by 3-glycidoxypropyltrimethoxysilane and PLA which improved the stress transfer and thus, lead to increase in tensile properties. Impact strength results were correlating well with those of tensile properties. The authors reported that the enhancement of impact strength was attributed to the structure of cellulose which tolerates higher deformation under impact.

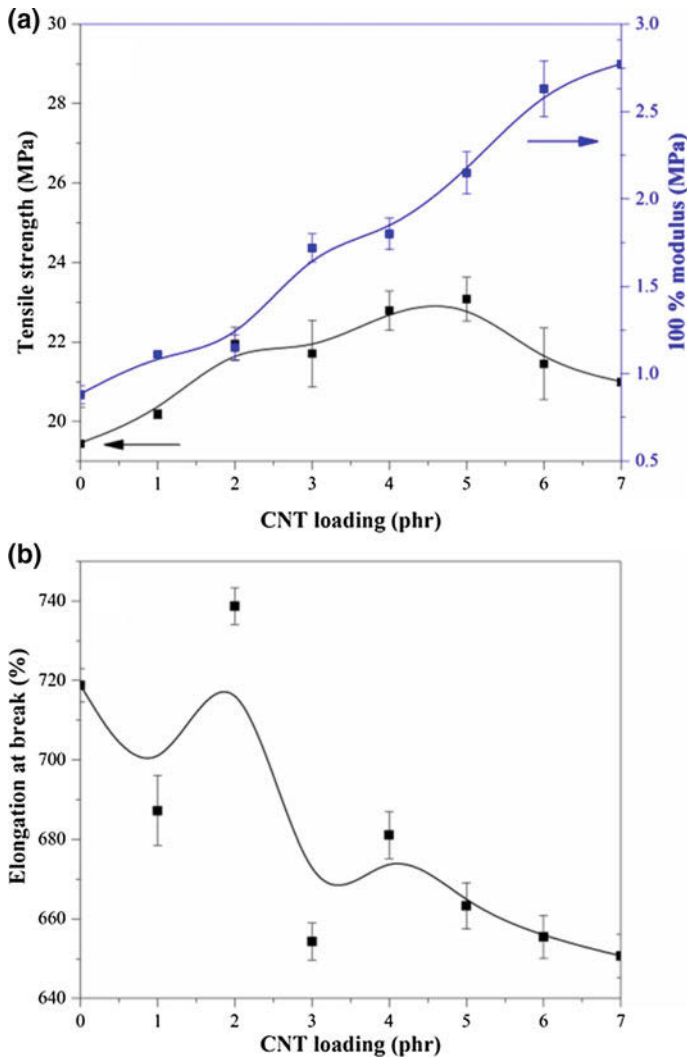


Fig. 1 Tensile strength and modulus of epoxidized natural rubber and their nanocomposites (a) and elongation at break of epoxidized natural rubber and their nanocomposites [55], copyright with the permission from Elsevier

2.3 Mechanical Properties of Polymer Reinforced with Nanoclays

In recent years, nanoclays have received considerable attention as reinforcing element in polymer nanocomposites due to their extraordinary properties such as high mechanical properties, large surface area and high aspect ratio, good thermal,

optical, magnetic and electrical properties. Other properties of nanoclays include environmental friendliness, abundantly available and non-toxic which make them suitable for food packaging applications. Most recent, nanoclays have been utilized to develop active packaging materials with improved tensile strength, modulus, and elongation at break. It was also reported in the same study that the incorporation of nanoclays reduced the diffusion of water vapour across the polymer matrix [85].

Montmorillonite, bentonite, and sepiolite are the most commonly used nanoclays and they were successfully applied in various polymer nanocomposite systems as nanofillers. These materials are hydrophilic in nature which makes them miscible with hydrophilic polymer matrices. In the case of hydrophobic polymeric matrices, the miscibility of nanoclays and matrix can be achieved by modifying nanoclays by exchanging interlayer of cationic galleries of silicate layer with organic component [86]. Shah et al. [100] reported a study on organoclays modified with quaternary ammonium substituents. They reported that the d-spacing, interlayer spacing and hydrophobicity (parameters that determine compatibility between nanoclays and polymer matrix) of nanoclays increased with increasing chain length and benzyl substituents which result in an increase in exfoliation. This study also discovered that the incorporation of organoclays enhances tensile strength and modulus, flexural strength, hardness and elongation at break of the resultant nanocomposites. However, the incorporation of organoclays showed an inverse effect on impact strength.

Other critical issues affecting mechanical properties of nanocomposites reinforced with nanoclays are higher phase separation and particles aggregation in a polymer matrix which should be prevented to achieve proper reinforce effect of nanoclays. These shortcomings can be mitigated by modifying nanoclays. In one study, transmission electron microscopy (TEM) and scanning electron microscopy (SEM) revealed that the addition of pristine nanoclays in polymer matrix resulted to disordered structures which indicate poor dispersion of nanoclays in the polymer matrix. On the other hand, nanocomposites reinforced with organoclays displayed some fine exfoliated and individual un-exfoliated layers of clay and therefore dispersion of clay in polymer matrix was evident [100]. Malkappa et al. [66] reported that the surface roughness increases with increasing in organoclays loading while; agglomeration was evident and became more visible when organoclays loading was increasing as shown in Fig. 2. Also, tensile strength and modulus increased with increasing organoclays loading whereas elongation at break showed inversely effect. Similar observations were evident in Alcântara et al. [6] study, they also reported that water resistance, biocompatibility, and biodegradation were improved when fibrous nanoclays were incorporated in polysaccharides. In another study, it was reported that tensile strength and modulus (as shown in Fig. 3) of biopolymer blends reinforced with expanded organoclay (EOC) increased linearly with increasing nanoclays loading. However, elongation at break was inversely proportional to nanoclays loading [76].

Recently, [72] fabricated PP/LDPE blends reinforced with organoclays by twin screw extruder and injection moulding and investigated their effect on mechanical properties. They discovered that the impact strength of PP decreased after blending

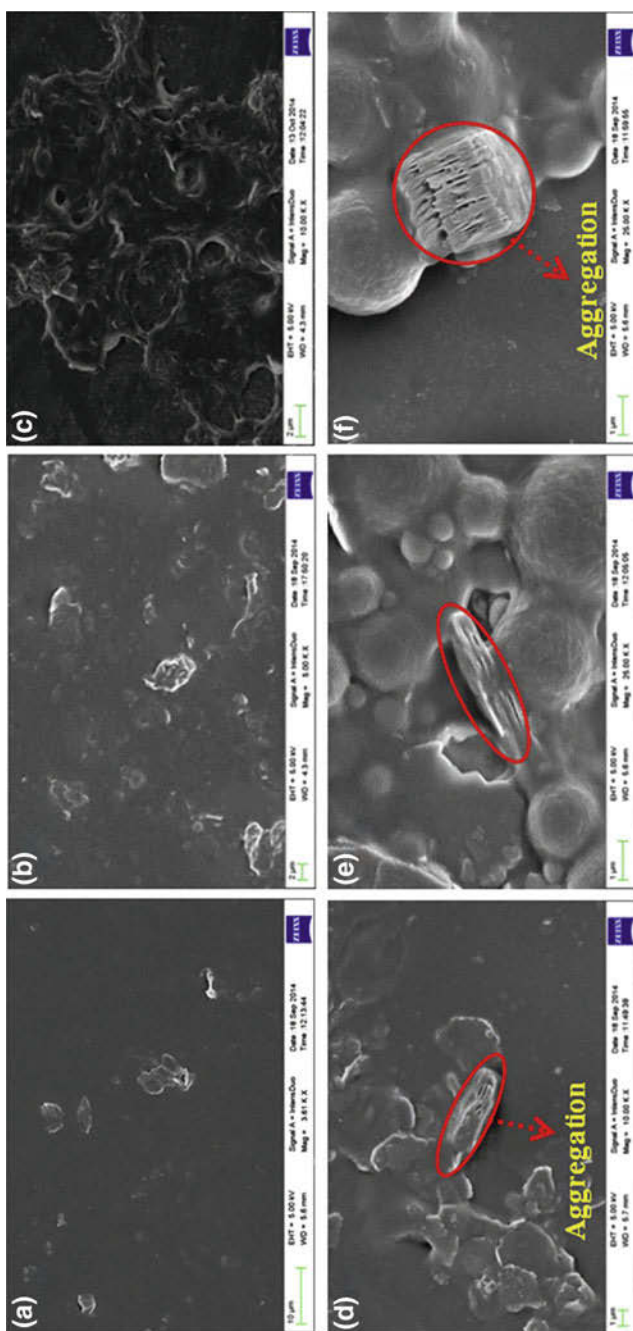
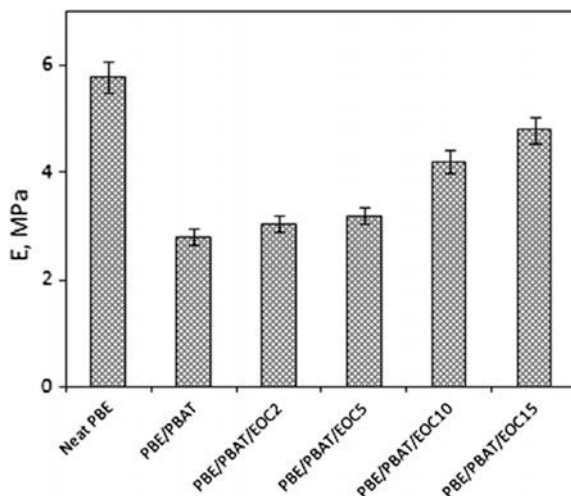


Fig. 2 Field emission electron microscopy (FESEM) images of: **a** water dispersible polyurethane (WDPUs)/Cloisite-30B-1 wt%, **b** WDPUs/Cloisite-30B-3 wt%, **c** WDPUs/Cloisite-30B-5 wt%, **d** WDPUs/OKao-3 wt% and **f** WDPUs/OKao-5 wt% [66], copyright with the permission from Elsevier

Fig. 3 tensile modulus of neat Natureplast PBE 003 (PBE), PBE/PBAT blend and its nanocomposites reinforced with expanded organoclay (EOC) [54], copyright with the permission from Elsevier



it with 20 wt% LDPE due to poor compatibility between the two polymers. However, the addition of organoclays in the blend led to the deterioration of impact strength which could be due to the restriction of chain mobility. In the same study, they investigated the effect of organoclays on tensile strength, tensile modulus, and elongation at break of polymer blends. The values of tensile strength, tensile modulus, and elongation of the blend were intermediates in comparison to those of neat polymers. The incorporation of organoclays in polymer blends enhanced tensile modulus and elongation at break while tensile strength was deteriorating. Moreover, a similar trend was also observed when the combination of organoclays and the compatibilizers were added to the blend. The highest elongation at break was observed when the combination of organoclays and the compatibilizers were added to the blend this was due to the miscibility of the materials. This indicates that nanoclays were well dispersed in the blend and the interaction between them and both polymers in the blend was improved.

Numerous researchers have reported the effect of hybrid of nanoclays together with other nanofillers such as metal oxide nanoparticles, nanotubes and natural fibres on the mechanical properties of nanocomposites [1, 9, 23, 51, 81, 117]. For instance, [23] reported that the incorporation of fillers (organoclays and rice husk) in recycled HDPE and polyethylene terephthalate (PET) blend enhanced the mechanical performance of nanocomposites. They suggested that the improvement of tensile properties could be due to the presence of organoclays which might carry much load and the fact that clay is stiffer than polymer matrix. The further enhancement was observed when compatibilizers were incorporated in polymer matrix reinforced with organoclays and rice husk. These results were in agreement with the results reported by other researchers [1, 9, 33] and they also reported that the mechanical performance was further improved when natural fibers were alkali treated. Other researchers [51, 117] investigated the effect of hybrid of nanoclays

and metal oxide nanoparticles (zinc and silver) on mechanical properties of nanocomposites. They reported that incorporation of nanoparticles enhanced the tensile strength and modulus. In addition, the inclusion of nanoparticles reduced water vapour permeability but, increased water content and density. Moreover, the inclusion of nanoparticles improved the antibacterial activity against Gram-positive *S. aureus*, Gram-negative *E. Coli*, and foodborne pathogens.

2.3.1 Mechanical Properties of Biopolymers Reinforced with Nanoclays

In recent years, nanocomposites from biopolymers reinforced with nanoclays have been extensively studied due to their low toxicity and biodegradability. Aliphatic polyesters have attracted tremendous attention for diversified applications. Polybutylene succinate (PBS) is among the widely studied aliphatic polyester. Phua et al. [84] investigated the impact of nanoclays on mechanical performance of polybutylene succinate (PBS) nanocomposites. In their study, they investigated mechanical properties to determine the biodegradation behaviour of nanocomposites. Before soil burial, they observed that the mechanical properties improved when organoclays were incorporated. The mechanical properties of nanocomposites deteriorated after soil burial and further reduced with soil burial time. In another study, the incorporation of nanoclays improved the mechanical performance of PLA. It was also reported that the increase in nanoclays loading increased linearly the tensile modulus while inversely effect was observed for elongation at break [43]. In contrast, the inclusion of organoclays in PHBV did not reinforce as anticipated due to the aggregation of clay in a polymer matrix [30]. Thereafter, numerous researchers fabricated nanocomposites from blended aliphatic polyesters with other biodegradable polymers and nanoclays. One of the limitations of biodegradable polymers is low mechanical properties which are not suitable for other applications such as packaging. The poor mechanical properties can be enhanced by blending biopolymers with other polymers or reinforced with stiffer fillers. Ayana et al. [11] and Lendvai et al. [59] blended thermoplastic starch with PLA and PBAT, respectively and subsequently reinforced with nanoclays. Ayana et al. [11] reported that the introduction of nanoclays enhanced tensile properties of the blends with an increase in loading. On the other hand, in the case of TPS/PBAT blend the inclusion of nanoclays did not show any effect on the tensile strength and modulus [59].

Agro-polymers such as starch, cellulose, protein, chitin and chitosan-based nanocomposites have recently attracted more interest due to their renewability, biocompatibility, biodegradability and non-toxicity with outstanding adsorption properties. The major drawbacks of agro-polymers are moisture absorption, difficulty processability, and poor mechanical properties. The inclusion of nanoclays in agro-polymers could result in the reduction of moisture absorption as well as enhance mechanical performance of nanocomposites. Numerous researchers [5, 34] are investigating efforts to overcome the drawbacks of agro-polymers.

The inclusion of nanoclays reduced water absorption and a further increase in nanoclays loading showed a decrease in water absorption [5]. They also reported that tensile strength and elongation at break decreased with increasing loading of nanoclays. Farahnaky et al. [34] prepared gelatin nanocomposites reinforced with nanoclays by a solvent casting method. They showed that tensile modulus increased linearly with increasing nanoclays loading while elongation at break decreased with increasing loading. A similar trend was observed in the case of chitosan nanocomposites reinforced with nanoclays [39, 40].

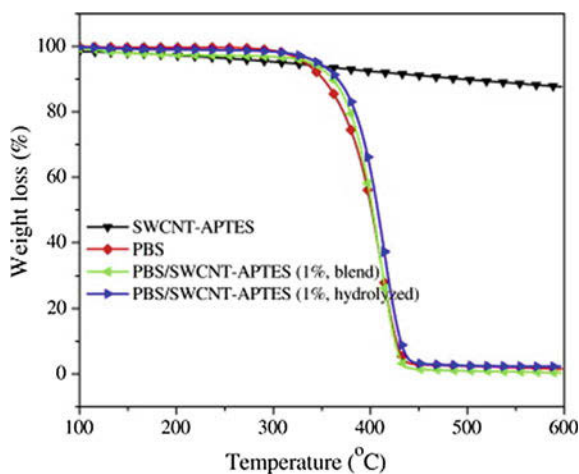
3 Thermal Properties

3.1 Thermogravimetric Analysis (TGA)

Thermogravimetric analysis is widely used to investigate the thermal degradation of polymer nanocomposites. A typical thermogram of polymer nanocomposite shows a material subjected to heat will suffer mass loss, followed by a sharp drop in mass over a narrow range and subsequently back to the flat slope as reactant is exhausted [12]. TGA and derivative thermogravimetric (DTG) are used to determine the mass loss and degradation of the material at a certain temperature as well as the remaining char content. Typical TGA curves are shown in Fig. 4.

In the published literature, it has been reported that the improvement in thermal stabilities of the nanocomposites is mainly attributed to the reinforcement effect of nanomaterials on polymers [57, 97, 119]. For instance, [3] investigated the effect of CNCs on thermal properties of polyfurfuryl alcohol (PFA) nanocomposites. They reported that the incorporation of CNCs improved the thermal stability of the PFA. Both the neat PFA and the nanocomposites showed two degradation steps at above

Fig. 4 TGA curves of SWNTs functionalized with acyl aminopropyltriethoxysilane (APTES), neat PBS, PBS/SWNTs-APTES (1%, hydrolyzed) [108], copyright with the permission from Elsevier



200 °C and in the temperature range of 320–400 °C which involves the scission of the weaker chemical bonds. According to Sanchez-garcia et al. [97], high thermal stabilities of PCL was achieved when 1 and 3 wt% of CNTs were incorporated, though increasing CNTs loading above 5 wt% result in filler agglomeration which reduced thermal stabilities of resultant nanocomposites. Similar behaviour was observed in the case of PHBV nanocomposites. Lai et al. [57] reported that the thermal stabilities of PLA nanocomposites increased with increasing in nanoclays loading. Interestingly, char content also increased with increasing in nanoclays loading. Other studies on thermal properties of nanocomposites are listed in Table 2.

Other researchers reported that the functionalization of either filler or polymer matrix enhances thermal stabilities of the resultant materials. For instance, [119] investigated the effect of unmodified and modified CNCs with phthalic anhydride on thermal stabilities of PBSA. They reported that degradation temperature of neat PBSA was above 300 °C due to chain scission and inter and intramolecular transesterification reactions. PBSA reinforced with CNCs modified with phthalic anhydride exhibited higher degradation temperature in comparison to those of PBSA reinforced with unmodified CNCs and neat PBSA. This enhancement was due to the addition of phthalic anhydride. Similar observations were reported in the case epoxy reinforced with GO modified with silane [111]. Majeed et al. [64] studied the incorporation of CNTs in neat LDPE and maleic anhydride grafted polyethylene (MAPE). They reported that MAPE reinforced with CNTs was thermally more stable in comparison to LDPE reinforced with CNTs and neat LDPE. The improved thermal stability with the inclusion of MAPE could result in improved compatibility and better dispersion of CNTs. In another study, they investigated thermal properties of rHDPE/rPET blend mixed with 3 wt% MAPE and 5 wt% ethylene-glycidyl methacrylate and subsequently reinforced with 3 wt% nanoclays and 70 wt% rice husk. Nanocomposites of polymer blends reinforced with nanoclays only exhibited a single step degradation pattern with improved thermal stability. However, the addition of rice husk resulted in three degradation steps which represent moisture evaporation at temperatures ranging from 135 to 145 °C, depolymerisation of hemicellulose and decomposition of cellulose at temperatures ranging from 230 to 370 °C and decomposition of nanocomposites and slightly decomposition of lignin at temperatures ranging from 476 to 482 °C. Incorporation of rice husk and nanoclays in compatibilizing matrix resulted in improvement of thermal stability in comparison to uncompatibilizing matrix.

Nanomaterials have been reported in numerous studies to enhance the thermal stabilities of polymer matrices. In contrast, [112] reported that the inclusion of CNTs did not affect the single stage decomposition pattern of PLA and remain unaltered. However, the incorporation of 1 wt% CNTs in PLA exhibited no alterations in thermal stability in comparison to neat PLA. However, the incorporation of 10 wt% CNTs in PLA resulted in a decrease in thermal stability but, the char content was higher in comparison to that of neat PLA and PLA reinforced with 1 wt% CNTs. The decrease in thermal stabilities after incorporation 10 wt% CNTs was due to the agglomeration of CNTs in PLA. Therefore, they reported that excessive CNTs prevent stress transfer and other superior properties to PLA.

Table 2 TGA degradation temperatures of polymers and nanocomposites

Sample	Degradation temperature (°C)	References
PCL	413	Sanchez-garcia et al. [97]
PCL + 10 wt% carbon nanofibres (CNF)	412	
PHBV	286	Sanchez-garcia et al. [97]
PCL + 10 wt% CNF	293	
Poly (acrylic acid) grafted onto amylose (PAA-g-amylose)	311	Abdollahi et al. [2]
PAA-g-amylose + 5 wt% graphene oxide (GO)	385	
Epoxy	341	Wan et al. [111]
Epoxy + 0.5 wt% pristine GO	354	
LDPE	479	Majeed et al. [64]
LDPE + 3 wt% CNTs	390	
Epoxidized natural rubber	430	Krainoi et al. [55]
Epoxidized natural rubber + 7 wt% CNTs	448	
PLA	385	Wang et al. [112]
PLA + 10 wt% CNTs	370	
rHDPE/rPET (75/25)	472	Chen and Ahmad [23]
rHDPE/rPET + 3 wt% clay	478	
rHDPE/rPET + 3 wt% clay + 70 wt% rice husk	481	
PLA	308	Fukushima et al. [37]
PLA + 7 wt% nanoclays	324	
PP/LDPE (80/20)	350	Mofokeng et al. [72]
PP/LDPE + 4 wt% nanoclays	380	
Whey protein isolate	301	Azevedo et al. [10]
Whey protein isolate + 3 wt% nanoclays	307	
Poly(methylmethacrylate) (PMMA)	367	Dong et al. [31]
PMMA + 41 wt% CNCs	384	
Thermoplastic polyurethane (TPU)	307	Floros et al. [36]
TPU + 2.5 wt% CNCs	334	
PMMA	183	Liu et al. [62]
PMMA + 8 wt% CNCs	192	
Epoxy	384	Xu et al. [113]
Epoxy + 15 wt% CNCs	388	
PLA	351	Shi et al. [102]
PLA + 10 wt% CNCs	356	

3.2 Differential Scanning Calorimetry (DSC)

Differential scanning calorimetry is a thermal analysis technique that assesses quantitative information on thermal transitions of materials through changes in heat capacity (C_p) by temperature. A sample of known weight (5–10 mg) is subjected to

Table 3 DSC analysis of polymer nanocomposites reinforced with various nanoparticles

Sample	$T_m/^\circ\text{C}$	$\Delta H_m/\text{J g}^{-1}$	$T_c/^\circ\text{C}$	$\Delta H_c/\text{J g}^{-1}$	$\chi_c/\%$	References
PE	138.6	186.06	113.3	–	63.5	Nikkhah et al. [80]
In situ PECN-3%	139.8	174.80	118.8	–	59.6	
In situ PECN-5%	140.2	155.38	122.6	–	53.03	
PP	168.8	95.0	109.7	–	46.8	Baniasadi et al. [15]
In situ PPCN-3%	168.4	90.4	119.7	–	44.5	
In situ PPCN-5%	167.5	89.15	122.5	–	43.9	
PLA	148	27.2	110 ^a	16.14 ^b	12	Valapa et al. [110]
PLA-GR-0.3wt%	152.8	27.8	113 ^a	9.8 ^b	19.2	
PLA-GR-0.5wt%	152.6	23.3	110 ^a	6.84 ^b	17.5	
PP	165.1	–	–	102	48.8	Pedrazzoli et al. [82]
PP-xGnP-3wt%	165.3	–	–	102.1	50.4	
PP-xGnP-5wt%	165.9	–	–	100.4	50.6	
PBS	114.5	79.7	80.1	–	–	Han et al. [44]
PBSSi-3	112.0	77.2	64.3	–	–	
PBSSi-5	110.7	63.5	55.8	–	–	

T_m melting temperature, T_c crystallization temperature, ΔH_m and ΔH_c melting and crystallization enthalpy, χ_c percentage of crystallinity

^acold crystallization temperature (T_{cc})

^benthalpy of cold crystallization (ΔH_{cc})

heating and cooling through programmed temperature conditions and changes in its heat capacity are tracked as changes in the heat flow. This allows the detection of thermal transitions such as melting temperature (T_m), melt crystallization/cooling temperature (T_c), melting enthalpy (ΔH_m), melt crystallization/cooling enthalpy (ΔH_c), a glass transition (T_g), curing and phase changes. Various studies on polymer matrices reinforced with different nanomaterials/nanoparticles/nanofillers (nanoclays, carbonaceous (carbon nanotubes and graphene), nanocellulose and inorganic oxide) have used DSC analysis to investigate the influence of nanoparticles on their thermal transitions [8, 21, 24, 29, 41, 42, 53, 56, 79, 80, 83, 98, 103–106, 110, 115, 118]. The melting and crystallization behaviours of polymer matrices which affect morphology, mechanical and thermal properties of the resulting nanocomposites are well documented in the literature and some of the undertaken studies investigated the influence of nanoparticles in polymer matrices are summarised in Table 3. Furthermore, the performance of polymer nanocomposites does not only depend on their molecular weight and chemical structure but significantly influenced by their crystallization properties such as crystallization rate, crystallization temperature and crystallinity [118]. In addition, it also reported in the literature that polymer crystallization is usually preceded by heterogeneous or homogeneous nucleation, or self-nucleation and then by crystal growth with respect to crystallization time [106]. These properties can be determined by using various mathematical models reported in literature to determine the crystallization kinetics [41], and the degree of

crystallinity (χ_c) which is the most used parameter [8, 16, 21, 24, 98, 107, 118], and is calculated according to Eq. 1.

$$\chi_c = \left(\frac{\Delta H_m / w_p}{\Delta H_m^o} \right) \times 100\% \quad (1)$$

where ΔH_m is the experiment of melting enthalpy of the nanocomposite, w_p is the weight fraction of the polymer in the nanocomposite and ΔH_m^o is the melting enthalpy of 100% crystalline polymer.

Studies on reinforcing polymers such as linear low-density polyethylene (LLDPE), polypropylene (PP), ethylene vinyl acetate (EVA) and poly(lactic acid) with exfoliated or expanded graphite and functionalized graphite nanoplatelets were investigated on their influence on thermal behaviour in polymer nanocomposites [8, 56, 71, 83, 98, 105, 110]. From these studies, incorporation of graphite nanoplatelets in polymer matrices enhanced the melting and crystallization temperature, melting endotherm and the crystallinity of the nanocomposites. For instance, improvement in the crystallinity for graphene (GR)/PLA composite samples were observed up to 0.3 wt% loading in comparison to neat PLA [110], while in binary PP nanocomposites the addition of exfoliated graphite nanoplatelets (xGnP) resulted in a significant increase in the crystallization temperature up to 5 wt% xGnP content [83]. A similar observation was recorded on poly(butylene succinate)/carbon nanotubes nanocomposites (PBS/CNT) [7] and poly(ϵ -caprolactone) (PCL) blended with a polycarbonate/multi-wall carbon nanotubes masterbatch (PC/MWCNT) [41]. This has demonstrated that the graphene/exfoliated graphite nanoplatelets, MWCNT and CNT dispersed in the composites can facilitate the polymer's crystallization process or act as nucleating agent [8, 98, 105]. On the other hand, slight decreases in the enthalpy and crystallinity were also observed when graphite or carbon nanotubes loadings were increased and this was attributed to agglomeration and poor dispersion of the nanoparticles which restricted polymer chain mobility and reduced the extent of crystallization [41, 70, 83].

In clay reinforced polymer nanocomposites, it has been reported that the presence of small amount of well-dispersed clay nanolayers can act as effective nucleating agents to accelerate crystallization in the polymer, thereby slightly increasing the melting and crystallization temperatures of the polymer composite [15]. On the other hand, the inclusion of clay nanolayers in polymer matrices has been observed to decrease the degree of crystallinity and does not significantly change the thermal transitions of the resulting nanocomposites. This is mainly attributed to the following observations (i) the additions of organoclays into crystalline polymer matrices do not ensure the enhancement of the polymer matrix crystallization rate [29, 103], (ii) that presence of clay nanolayers can form strong polymer-clay network which can limit the mobility of polymer chains and as a result decrease the degree of crystallinity especially at high clay concentration [15, 80, 104]. On the other hand, [73] recently investigated the effects of clay localization and its distribution in an immiscible blend of PP/LDPE on the non-isothermal crystallization and degradation kinetics. The authors observed that

the non-isothermal crystallisation analysis for the localization of clay particles in the blend composites had two opposing effects, (i) the poorly dispersed clay particles at the PP/LDPE interface in the non-compatibilized blend composite had no significant effect on the crystallisation temperature of PP but allowed the free movement of PP chains, which resulted in a higher crystallinity of PP than that of PP in the neat blend; (ii) the well-dispersed clay particles in the compatibilized blend composites disrupted the free movement of PP chains, resulting in a lower crystallisation temperature and crystallinity than that of PP in the neat blend.

In the case of inorganic oxides reinforced polymer composites, a heterogeneous nucleation effect was observed to play a significant role in polymer crystallization which can be exploited for the shortening of cycle time during processing [99]. The nanoparticles turn to increasing the crystallization temperature and the rate of the polymer composite, while in other cases the heterogeneous nucleation becomes dominating with increasing filler concentration [106], but was seen to decrease the crystallization activation energy and crystallinity of the polymer with the addition of hydroxyapatite nanorods (HAP) by Zhan et al. [118]. The authors investigated the crystallization and melting properties of PBS composites with titanium dioxide nanotubes (TNTs) or (HAP). This was caused by strong hydrogen bonding interaction that exists between HAP and PBS, which reduced the transport of the PBS macromolecules and as a result lowered the crystallization rate of PBS/HAP composite than that of pure PBS.

On the other hand, PBS/nano-CaCO₃ composites showed independence of the crystallization behaviour with increasing nano-CaCO₃ content. Furthermore, the nanoparticles had little influence on the crystallization and melting behaviour of PBS. This implied that the nano-CaCO₃ might not have played an active role in the heterogeneous nucleation of PBS matrix. For natural fiber reinforced polymer composites, natural fibers were observed to act as nucleating agents promoting crystallization of polymer matrices [16, 32, 107]. For instance, [32] prepared poly (3-hydroxy butyrate) (PHB)/poly lactic acid (PLLA)/Tributyl citrate (TBC) blend reinforced with CNCs to increase the elongation at break of PLLA for food packaging. The well dispersed CNCs and PHB in PLLA matrix acted as bio-nuclei in PLLA matrix to help the crystallization rate and reduce the size of spherulites and thereby improving the elongation at break from 6% for pure PLLA to 40–190% for the composites with CNCs. It is also worth noting that reinforcing with natural fibers could lead to different nucleation activity due to the different surface structure of the fibers [16].

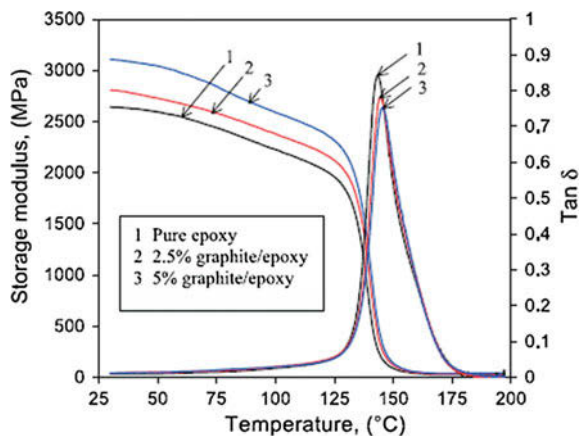
4 Dynamic Mechanical Analysis (DMA)

The dynamic mechanical analysis is a technique that determines the viscous modulus (loss modulus, G''), elastic modulus (storage modulus, G') and damping coefficient ($\tan\delta$) as a function of temperature, time or frequency. The DMA is used to identify transition regions in polymer materials, such as the glass transition

temperature (T_g) and to recognize transitions corresponding to other molecular motions which are beyond the resolution of DSC. The viscoelastic properties of the polymer matrices reinforced with various nanofillers have been investigated from the measurements of storage modulus and the loss factor using dynamic mechanical analysis to evaluate the effect polymer/nanofiller interface with changing polymer mobility. These measurements provide indications about the increase in the storage or decrease in modulus of the resulting nanocomposites, shift in the glass transition temperature due to the polymer chain restriction or mobility [44, 65, 82].

Song et al. [105] fabricated exfoliated graphene-based polypropylene nanocomposites with enhanced mechanical and thermal properties prepared by melt blending technique. The exfoliated graphene nanosheets were varied from 0.1 to 5 wt% to evaluate the influence of graphene loading on polypropylene. The storage modulus of the PP/graphene nanocomposites increased with increasing graphene loading up to 1 wt%, while further increases in graphene loading led to a slight decrease in the storage modulus in the entire temperature range (-50 – 150 °C). The results were in agreement with their tensile modulus and the reduction in the storage modulus was attributed to the plasticization effect of low modulus of PP matrix. The glass transition temperature of PP improved by ~ 2.5 °C at 0.1 wt% (0.041 vol.%) graphene content, which indicated a restriction in chain mobility of PP. Similar observation was recorded in the study on mechanical and thermal properties of graphite platelet/epoxy composites [115]. At 2.5 and 5 wt%, graphite platelet/epoxy composites showed increased storage modulus (about 8 and 18%) higher than the pure epoxy matrix. As the temperature was increased, both pure epoxy and its composites showed a gradual drop in storage modulus followed by a sudden drop at the glass transition temperature. The drop in modulus is associated with the material transition from a glassy state to a rubbery state as seen in Fig. 5. Furthermore, with increasing graphite contents of 0, 2.5 and 5 wt% the T_g gradually increased to 143, 145 and 146.8 °C, respectively. This was attributed to the good adhesion between the polymer and graphite platelets, which restrict the segmental motion of cross-links under loading.

Fig. 5 Dynamic mechanical properties of pure epoxy and its composites [115], copyright with the permission from Elsevier



In a comparison of the effect of expanded graphite (EG) and modified graphite flakes (i-MG) on the physical and thermo-mechanical properties of styrene butadiene rubber/polybutadiene rubber (SBR/BR) blends [65]. A drastic increase in the storage modulus of EG and i-MG loaded SBR/BR composites in the presence of carbon black (CB) was observed in a wide range of temperature compared to the BR based nanocomposites. This was attributed to good dispersion of nanofillers in the rubber blend which increased its stiffness, and as a result, increased the storage modulus of SBR/BR based nanocomposites. In addition, as a result of isocyanate surface modification on graphite sheets (i-MG), higher basal spacing and exfoliated structure of i-MG sheets than EG flakes was achieved. Exfoliated graphite i-MG sheets were uniformly dispersed in different rubber matrices in the presence of CB, and resulted in superior mechanical, dynamic mechanical and thermal properties compared to the EG filled rubber composites. Surface modification of graphite sheets prior to nanocomposite preparation is one of the significant aspects that facilitate the compatibility between the polymer matrix and the nanofiller to form a homogeneous dispersion of nanoparticles and enhance adhesion in the polymer composites. Modification of graphene/graphite sheets by a range of techniques employing various organo modifying agents to improve mechanical properties of polymer nanocomposites are reported in the literature [20, 56, 69]. Among these reported techniques, the nucleophilic addition of organic molecules to the surface of graphene/graphite is an effective way to the bulk production of surface-modified graphene.

Analysis of thermomechanical properties for polymer matrices reinforced with nanomaterials is important in ascertaining the performance of the nanocomposite under stress and temperature. In polypropylene/clay nanocomposites (PPCNs) prepared by in situ polymerization [15], the presence of clay nanolayers dispersed in PP matrix resulted in a significant increase in stiffness (storage modulus) for all nanocomposites with increasing clay content and temperature. The reinforcing effect was at a maximum in the region above the glass transition temperature of the matrix, primarily due to the larger difference in mechanical properties between the filler and the matrix as it changes from the glassy to the rubbery state. Moreover, a marginal increase in T_g with increasing clay concentration (between 1 and 5 wt%) was observed. This was attributed to the interactions between polymer and filler which delay the segmental motion of the chains. Better dispersion of clay particles in a polymer provides greater reinforcement and higher chain immobility, thereby resulting in high storage modulus values [72]. Similar observations were recorded in the extraction of CNCs from flax fibers and their reinforcing effect on poly (furfuryl) alcohol (PFA) [78]. Incorporation of CNCs into PFA matrix resulted in increased storage modulus over the whole temperature range, the loss modulus peak shifted to higher temperatures and the magnitude of the peak decreased due to the presence of CNCs, the glass transition temperature values increased after the inclusion of CNCs into PFA. The overall results implied that the presence of CNCs in PFA improved the stiffness of the composite, restricted polymer chain mobility as a result of good interaction between the polymer and the filler.

5 Melt Rheology Properties

The study on melt rheological properties for polymer materials is very important from the processing point of view. In addition, information on the microstructure of the polymer materials in the melted state can be provided from the melt rheology [7]. Rheological properties are known as mechanical properties of the material that undergoes deformation and flow in the presence of stress. The melt rheology is usually measured from the melt phase of the polymer from its melting temperature at the desired strain that is well within the linear viscoelastic range. Viscoelastic properties of thermoplastic and nanofiller reinforced composites can be measured over a range of frequencies to gauge the rate of the viscosity changes with shear rate. Various studies on the effect of the nanofiller addition, such as carbonaceous [7, 17], natural fibers/cellulose [53], inorganic oxides [24, 82, 106] and nanoclays [72] on the isothermal frequency dependence of the dynamic shear storage modulus (G') and complex viscosity (η^*) were investigated. For instance, [7] prepared PBS/CNTs nanocomposites fabricated by melt mixing and investigated the rheological properties. The viscoelastic properties of PBS/CNTs composites at high frequencies behaved the same while low frequencies the nanocomposites were frequency independent (Fig. 6a, b). The nanocomposites showed gradual changes in the

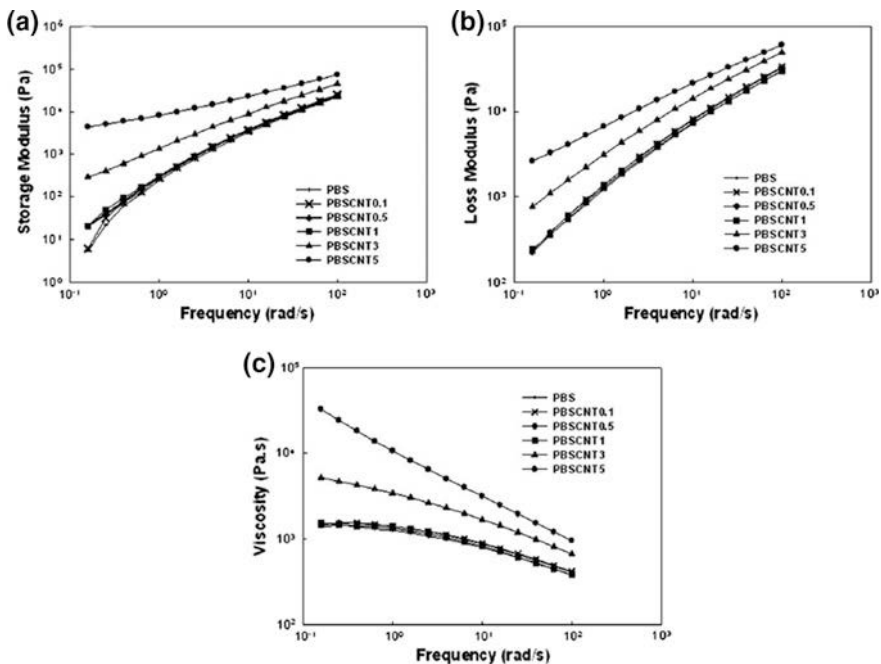


Fig. 6 Viscoelastic properties of PBS and PBS/CNTs composites in the melted state **a** Storage modulus of **b** loss modulus and **c** complex viscosity [7], copyright with the permission from Elsevier

composites from liquid-like to solid-like behaviour, especially for PBS/CNT3 and PBS/CNT5 samples. This was attributed to interactions between nanotubes which formed interconnected structures of CNTs in the PBS/CNTs composites, thereby enhancing the relaxation behaviour and increased the storage modulus. In addition, improvement in the complex viscosity was also observed due to the flow restriction of the polymer by filler in the melted state (Fig. 6c). On contrary, the G' and G'' of pure PBS and PBS/nano-CaCO₃ composites with various nano-CaCO₃ loadings as a function of frequency exhibited a liquid-like a behaviour for both PBS and CaCO₃ filled composites [24]. The results implied that the nano-CaCO₃ particles had little influence on the microstructure of PBS; the relaxation mechanism and the microstructure of the PBS/nano-CaCO₃ composites mainly depended on the PBS matrix than on nano-CaCO₃ content. Furthermore, a similar decrease in G' and η^* was observed for linear-low-density polyethylene reinforced boehmite alumina (LLDPE-BA) [82]. The observation was attributed to the highly branched LLDPE whose chains would tend to get entangled; apparently even poorly bonded plain BA particles fill in the spaces between chain branches and enable an easier flow. Khumalo et al. [54] in a similar study suggested that there was no strong interaction between the BA and LDPE in the nanocomposites.

6 Conclusions

In this chapter, the mechanical, thermal, dynamic mechanical and rheological properties of polymer nanocomposites reinforced with nanomaterials were presented. It can be concluded that nanomaterials have the power to alter the properties of polymer nanocomposites which can be exploited in a variety of applications. By combining nanomaterials with the polymer matrix, novel materials with multi-properties can be achieved. The development of polymer nanocomposite with multi-properties depends on various factors such as filler particle size, surface area, aspect ratio, compositions, purity, crystallinity, shape, properties (mechanical, antibacterial, thermal, electrical etc.), dispersion, filler loading and interaction between filler and polymer matrix. Nanomaterials which were reviewed in this study are nanocellulose, carbonaceous fillers, and nanoclays and they have received significant attention globally particularly due to their extraordinary properties. The major drawback of polymer nanocomposites is a homogeneous dispersion of nanomaterials in the polymer matrix. To address such drawback, functionalization of either filler or polymer is the effective approach to alter the functional groups of the material, thus improving the interfacial adhesion between filler and polymer matrix which enhances the properties of the resultant material. In this chapter, it was noticed that loading nanomaterials in polymer matrix improved their properties and further increase filler loading to threshold amount enhanced the properties polymer. Many researchers indicated that adding filler after threshold amount deteriorates the properties of the material due to agglomeration which led to poor interaction between filler and polymer matrix and therefore, this result in poor properties of the

resultant material [55, 112]. The novel polymer nanocomposites with multi-properties can be used in medical, agricultural, food packaging, automotive etc. Much research is required to further develop the commercially available polymer nanocomposites and develop other novel materials.

References

1. Abdellaoui H, Bensalah H, Raji M, Rodrigue D, Bouhfid R, Quaiss AK (2017) Laminated epoxy biocomposites based on clay and jute fibers. *J Bionic Eng* 14:379–389. [https://doi.org/10.1016/S1672-6529\(16\)60406-7](https://doi.org/10.1016/S1672-6529(16)60406-7)
2. Abdollahi R, Taghizadeh MT, Savani S (2018) Thermal and mechanical properties of graphene oxide nanocomposite hydrogel based on poly (acrylic acid) grafted onto amylose. *Polym Degrad Stab* 147:151–158. <https://doi.org/10.1016/j.polymdegradstab.2017.11.022>
3. Ahmad EEM, Luyt AS, Djoković V (2013) Thermal and dynamic mechanical properties of bio-based poly(furfuryl alcohol)/sisal whiskers nanocomposites. *Polym Bull* 70:1265–1276. <https://doi.org/10.1007/s00289-012-0847-2>
4. Al-saleh MH (2015) Electrically conductive carbon nanotube/polypropylene nanocomposite with improved mechanical properties. *JMADE* 85:76–81. <https://doi.org/10.1016/j.matdes.2015.06.162>
5. Alboofetileh M, Rezaei M, Hosseini H, Abdollahi M (2013) Effect of montmorillonite clay and biopolymer concentration on the physical and mechanical properties of alginate nanocomposite films. *J Food Eng* 117:26–33. <https://doi.org/10.1016/j.jfoodeng.2013.01.042>
6. Alcântara ACS, Darder M, Aranda P, Ruiz-hitzky E (2014) Polysaccharide–fibrous clay bionanocomposites. *Appl Clay Sci* 96:2–8. <https://doi.org/10.1016/j.clay.2014.02.018>
7. Ali FB, Mohan R (2010) Thermal, mechanical, and rheological properties of biodegradable polybutylene succinate/carbon nanotubes nanocomposites. 1–6. <https://doi.org/10.1002/pc.20913>
8. An JE, Jeon GW, Jeong YG (2012) Preparation and properties of polypropylene nanocomposites reinforced with exfoliated graphene. *Fibers Polym* 13:507–514. <https://doi.org/10.1007/s12221-012-0507-z>
9. Arrakhiz FZ, Benmoussa K, Bouhfid R, Quaiss A (2013) Pine cone fiber/clay hybrid composite: mechanical and thermal properties. *Mater Des* 50:376–381. <https://doi.org/10.1016/j.matdes.2013.03.033>
10. Azevedo VM, Silva EK, Pereira CFG, Costa JMG, Borges SV (2015) Whey protein isolate biodegradable films: Influence of the citric acid and montmorillonite clay nanoparticles on the physical properties. *Food Hydrocoll* 43:252–258. <https://doi.org/10.1016/j.foodhyd.2014.05.027>
11. Ayana B, Suin S, Khatua BB (2014) Highly exfoliated eco-friendly thermoplastic starch (TPS)/ poly (lactic acid)(PLA)/clay nanocomposites using unmodified nanoclay. *Carbohydr Polym* 110:430–439. <https://doi.org/10.1016/j.carbpol.2014.04.024>
12. Azwa ZN, Yousif BF, Manalo AC, Karunasena W (2013) A review on the degradability of polymeric composites based on natural fibres. *Mater Des* 47:424–442. <https://doi.org/10.1016/j.matdes.2012.11.025>
13. Babaee M, Jonoobi M, Hamzeh Y, Ashori A (2015) Biodegradability and mechanical properties of reinforced starch nanocomposites using cellulose nanofibers. *Carbohydr Polym* 132:1–8. <https://doi.org/10.1016/j.carbpol.2015.06.043>
14. Baheri B, Shahverdi M, Rezakazemi M, Motaee E, Mohammadi T (2015) Performance of PVA/NaA mixed matrix membrane for removal of water from ethylene glycol solutions by pervaporation. *Chem Eng Commun* 202:316–321. <https://doi.org/10.1080/00986445.2013.841149>

15. Baniasadi H, Ramazani A, Javan Nikkiah S (2010) Investigation of in situ prepared polypropylene/clay nanocomposites properties and comparing to melt blending method. *Mater Des* 31:76–84. <https://doi.org/10.1016/j.matdes.2009.07.014>
16. Běhálek L, Maršálková M, Lenfeld P, et al (2013) Study of crystallization of polylactic acid composites and nanocomposites with natural fibres by DSC method. 1–6
17. Botlhoko OJ, Ramontja J, Ray SS (2017) Thermal, mechanical, and rheological properties of graphite- and graphene oxide-filled biodegradable polylactide/poly (E-caprolactone) blend composites. 45373:1–14. <https://doi.org/10.1002/app.45373>
18. Botlhoko JO, Ramontja J, Sinha S (2018) Morphological development and enhancement of thermal, mechanical, and electronic properties of thermally exfoliated graphene oxide- filled biodegradable polylactide/poly (ϵ -caprolactone) blend composites. *Polymer (Guildf)* 139:188–200. <https://doi.org/10.1016/j.polymer.2018.02.005>
19. Cao X, Xu C, Wang Y, Liu Y, Liu Y, Chen Y (2013) New nanocomposite materials reinforced with cellulose nanocrystals in nitrile rubber. *Polym Test* 32:819–826. <https://doi.org/10.1016/j.polymertesting.2013.04.005>
20. Cha J, Jin S, Hun J, Park CS, Ryu HJ, Hong SH (2016) Functionalization of carbon nanotubes for fabrication of CNT/ epoxy nanocomposites. *JMADE* 95:1–8. <https://doi.org/10.1016/j.matdes.2016.01.077>
21. Cheewawuttipong W, Fuoka D, Tanoue S, Uematsu H, Lemoto Y (2013) Thermal and mechanical properties of polypropylene/boron nitride composites. *Energy Proc* 34:808–817. <https://doi.org/10.1016/j.egypro.2013.06.817>
22. Chen PY, Lian HY, Shih YF, Chen-Wei SM, Jeng RJ (2017) Preparation, characterization and crystallization kinetics of Kenaf fiber/multi-walled carbon nanotube/polylactic acid (PLA) green composites. *Mater Chem Phys* 196:249–255. <https://doi.org/10.1016/j.matchemphys.2017.05.006>
23. Chen RS, Ahmad S (2017) Mechanical performance and flame retardancy of rice husk/ organoclay-reinforced blend of recycled plastics. *Mater Chem Phys* 198:57–65. <https://doi.org/10.1016/j.matchemphys.2017.05.054>
24. Chen RY, Zou W, Zhang HC, Zhang GZ, Yang ZT, Jin G, Qu JP (2015) Thermal behavior, dynamic mechanical properties and rheological properties of poly(butylene succinate) composites filled with nanometer calcium carbonate. *Polym Test* 42:160–167. <https://doi.org/10.1016/j.polymertesting.2015.01.015>
25. Chen Y, Liu C, Chang PR, Cao X, Anderson DP (2009) Bionanocomposites based on pea starch and cellulose nanowhiskers hydrolyzed from pea hull fibre: effect of hydrolysis time. *Carbohydr Polym* 76:607–615. <https://doi.org/10.1016/j.carbpol.2008.11.030>
26. Cheng J, Zheng P, Zhao F, Ma X (2013) The composites based on plasticized starch and carbon nanotubes. *Int J Biol Macromol* 59:13–19. <https://doi.org/10.1016/j.ijbiomac.2013.04.010>
27. Chiu F (2016) Fabrication and characterization of biodegradable poly (butylene succinate-co-adipate) nanocomposites with halloysite nanotube and organo-montmorillonite as nano fillers. *Polym Test* 54:1–11. <https://doi.org/10.1016/j.polymertesting.2016.06.018>
28. Chiu F (2017) Halloysite nanotube- and organoclay- filled biodegradable poly (butylene succinate-co-adipate)/ maleated polyethylene blend- based nanocomposites with enhanced rigidity. *Compos Part B* 110:193–203. <https://doi.org/10.1016/j.compositesb.2016.10.091>
29. Chiu FC, Chu PH (2006) Characterization of solution-mixed polypropylene/clay nanocomposites without compatibilizers. *J Polym Res* 13:73–78. <https://doi.org/10.1007/s10965-005-9009-7>
30. Daitx TS, Carli LN, Crespo JS, Mauler RS (2015) Effects of the organic modification of different clay minerals and their application in biodegradable polymer nanocomposites of PHBV. *Appl Clay Sci* 115:157–164. <https://doi.org/10.1016/j.clay.2015.07.038>
31. Dong H, Strawhecker KE, Snyder JF, Orlicki JA, Reiner RS, Rudie AW (2012) Cellulose nanocrystals as a reinforcing material for electrospun poly(methyl methacrylate) fibers: Formation, properties and nanomechanical characterization. *Carbohydr Polym* 87:2488–2495. <https://doi.org/10.1016/j.carbpol.2011.11.015>

32. El-hadi AM (2017) Increase the elongation at break of poly (lactic acid) composites for use in food packaging films. *Nat Publ Gr* 1–14. <https://doi.org/10.1038/srep46767>
33. Essabir H, Boujmal R, Bensalah MO, Rodrigue D, Bouhfid R, Qaiss AK (2016) Mechanical and thermal properties of hybrid composites: oil-palm fiber/clay reinforced high density polyethylene. *Mech Mater* 98:36–43. <https://doi.org/10.1016/j.mechmat.2016.04.008>
34. Farahnaky A, Dadfar SMM, Shahbazi M (2014) Physical and mechanical properties of gelatin–clay nanocomposite. *J Food Eng* 122:78–83. <https://doi.org/10.1016/j.jfoodeng.2013.06.016>
35. Ferreira FV, Francisco W, Menezes BRC, Brito FS, Coutinho AS, Cividanes LS, Coutinho AR, Thim GP (2016) Correlation of surface treatment, dispersion and mechanical properties of HDPE/CNT nanocomposites. *Appl Surf Sci* 389:921–929. <https://doi.org/10.1016/j.apsusc.2016.07.164>
36. Floros M, Hojabri L, Abraham E, Jose J, Thomas S, Pothan L, Leao AL, Marine S (2012) Enhancement of thermal stability, strength and extensibility of lipid-based polyurethanes with cellulose-based nanofibers. *Polym Degrad Stab* 97:1970–1978. <https://doi.org/10.1016/j.polymdegradstab.2012.02.016>
37. Fukushima K, Tabuani D, Camino G (2012) Poly (lactic acid)/clay nanocomposites: effect of nature and content of clay on morphology, thermal and thermo-mechanical properties. *Mater Sci Eng, C* 32:1790–1795. <https://doi.org/10.1016/j.msec.2012.04.047>
38. Gao T, Li Y, Bao R, Liu ZY, Xie BH, Yang MB, Yang W (2017) Tailoring co-continuous like morphology in blends with highly asymmetric composition by MWCNTs: towards biodegradable high-performance electrical conductive poly (l-lactide) poly (3-hydroxybutyrate- co-4-hydroxybutyrate) blends. *Compos Sci Technol* 152:111–119. <https://doi.org/10.1016/j.compscitech.2017.09.014>
39. Giannakas A, Grigoriadi K, Leontiou A, Barkoula NM, Lavados A (2014) Preparation, characterization, mechanical and barrier properties investigation of chitosan–clay nanocomposites. *Carbohydr Polym* 108:103–111. <https://doi.org/10.1016/j.carbpol.2014.03.019>
40. Giannakas A, Vlacha M, Salmas C, Leontiou A, Katapodis P, Stamatis H, Barkoula NM, Ladavos A (2016) Preparation, characterization, mechanical, barrier and antimicrobial properties of chitosan/PVOH/clay nanocomposites. *Carbohydr Polym* 140:408–415. <https://doi.org/10.1016/j.carbpol.2015.12.072>
41. Gumedde TP, Luyt AS, Hassan MK, Pérez-Camargo RA, Tercjak A, Müller AJ (2017) Morphology, nucleation, and isothermal crystallization kinetics of poly(ϵ -caprolactone) mixed with a polycarbonate/MWCNTs masterbatch. *Polymers* <https://doi.org/10.3390/polym9120709>
42. Gumedde TP, Luyt AS, Pérez-Camargo RA, Müller AJ (2017) The influence of paraffin wax addition on the isothermal crystallization of LLDPE. *J App Poly Sci* 44398:1–7. <https://doi.org/10.1002/app.44398>
43. Guo Y, Yang K, Zuo X et al (2016) Effects of clay platelets and natural nanotubes on mechanical properties and gas permeability of Poly (lactic acid) nanocomposites. *Polymer (Guildf)* 83:246–259. <https://doi.org/10.1016/j.polymer.2015.12.012>
44. Il HS, Im SS, Kim DK (2003) Dynamic mechanical and melt rheological properties of sulfonated poly(butylene succinate) ionomers. *Polymer (Guildf)* 44:7165–7173. [https://doi.org/10.1016/S0032-3861\(03\)00673-6](https://doi.org/10.1016/S0032-3861(03)00673-6)
45. Hietala M, Mathew AP, Oksman K (2013) Bionanocomposites of thermoplastic starch and cellulose nanofibers manufactured using twin-screw extrusion. *Eur Polym J* 49:950–956. <https://doi.org/10.1016/j.eurpolymj.2012.10.016>
46. Huang J, Zhang S, Zhang F, Guo Z, Jin L, Pan Y, Wang Y, Guo T (2017) Enhancement of lignocellulose-carbon nanotubes composites by lignocellulose grafting. *Carbohydr Polym* 160:115–122. <https://doi.org/10.1016/j.carbpol.2016.12.053>
47. John MJ, Anandjiwala R, Oksman K, Mathew AP (2013) Melt-spun polylactic acid fibers: effect of cellulose nanowhiskers on processing and properties. *J Appl Polym Sci* 127:274–281. <https://doi.org/10.1002/app.37884>

48. Jonoobi M, Aitomäki Y, Mathew AP, Oksman K (2014) Thermoplastic polymer impregnation of cellulose nanofibre networks: morphology, mechanical and optical properties. *Compos Part A Appl Sci Manuf* 58:30–35. <https://doi.org/10.1016/j.compositesa.2013.11.010>
49. Jonoobi M, Harun J, Mathew AP, Oksman K (2010) Mechanical properties of cellulose nanofiber (CNF) reinforced polylactic acid (PLA) prepared by twin screw extrusion. *Compos Sci Technol* 70:1742–1747. <https://doi.org/10.1016/j.compscitech.2010.07.005>
50. Jyoti J, Basu S, Pratap B, Dhakate SR (2015) Superior mechanical and electrical properties of multiwall carbon nanotube reinforced acrylonitrile butadiene styrene high performance composites. *Compos Part B* 83:58–65. <https://doi.org/10.1016/j.compositesb.2015.08.055>
51. Kanmani P, Rhim J (2014) Physical, mechanical and antimicrobial properties of gelatin based active nanocomposite films containing AgNPs and nanoclay. *Food Hydrocoll* 35:644–652. <https://doi.org/10.1016/j.foodhyd.2013.08.011>
52. Khan AS, Hussain AN, Sidra L, Sarfraz Z, Khalid H, Khan M, Manzoor F, Shahzadi L, Yar M, Rehman IU (2017) Fabrication and in vivo evaluation of hydroxyapatite/carbon nanotube electrospun fibers for biomedical/dental application. *Mater Sci Eng, C* 80:387–396. <https://doi.org/10.1016/j.msec.2017.05.109>
53. Khoshkava V, Kamal MR (2014) Effect of cellulose nanocrystals (CNC) particle morphology on dispersion and rheological and mechanical properties of polypropylene/CNC nanocomposites. <https://doi.org/10.1021/am500577e>
54. Khumalo VM, Karger-Kocsis J, Thomann R (2010) Polyethylene/synthetic boehmite alumina nanocomposites: structure, thermal and rheological properties. *eXPRES Poly Lett* 4: 264–274. <https://doi.org/10.3144/expresspolymlett.2010.34>
55. Krainoi A, Kummerlöwe C, Nakaramontri Y, Vennemann N, Pichaiyut S, Wisunthorn S, Nakason C (2018) Influence of critical carbon nanotube loading on mechanical and electrical properties of epoxidized natural rubber nanocomposites. *Polym Test* 66:122–136. <https://doi.org/10.1016/j.polymertesting.2018.01.003>
56. Kuila T, Bose S, Mishra AK, Khanra P, Kim NH, Lee JH (2012) Effect of functionalized graphene on the physical properties of linear low density polyethylene nanocomposites. *Polym Test* 31:31–38. <https://doi.org/10.1016/j.polymertesting.2011.09.007>
57. Lai S, Wu S, Lin G, Don T (2014) Unusual mechanical properties of melt-blended poly (lactic acid) (PLA)/clay nanocomposites. *Eur Polym J* 52:193–206. <https://doi.org/10.1016/j.eurpolymj.2013.12.012>
58. Lekha P, Mtibe A, Motaung T., Andrew JE, Sithole BB, Gibril M (2016) Effect of mechanical treatment on properties of cellulose nanofibrils produced from bleached hardwood and softwood pulps. *Maderas Cienc y Tecnol* 18:0–0. <https://doi.org/10.4067/s0718-221x2016005000041>
59. Lendvai L, Apostolov A, Karger-kocsis J (2017) Characterization of layered silicate-reinforced blends of thermoplastic starch (TPS) and poly (butylene adipate-co-terephthalate). *Carbohydr Polym* 173:566–572. <https://doi.org/10.1016/j.carbpol.2017.05.100>
60. Liao CZ, Li K, Wong HM, Tong WY, Yeung KWK, Tjong SC (2013) Novel polypropylene biocomposites reinforced with carbon nanotubes and hydroxyapatite nanorods for bone replacements. *Mater Sci Eng, C* 33(3):1380–1388
61. Lin C, Wang Y, Lai Y, Yang W, Jiao F, Zhang H, Ye S, Zhang Q (2011) Colloids and surfaces B: biointerfaces Incorporation of carboxylation multiwalled carbon nanotubes into biodegradable poly (lactic-co-glycolic acid) for bone tissue engineering. *Colloids Surf B Biointerfaces* 83:367–375. <https://doi.org/10.1016/j.colsurfb.2010.12.011>
62. Liu H, Liu D, Yao F, Wu Q (2010) Fabrication and properties of transparent polymethylmethacrylate/cellulose nanocrystals composites. *Bioresour Technol* 101:5685–5692. <https://doi.org/10.1016/j.biortech.2010.02.045>

63. Lopez-manchado MA, Brasero J, Avil F (2016) Effect of the morphology of thermally reduced graphite oxide on the mechanical and electrical properties of natural rubber nanocomposites. *Compos Part B: Eng* 87:350–356. <https://doi.org/10.1016/j.compositesb.2015.08.079>
64. Majeed K, Al M, Almaadeed A, Zagho MM (2018) Comparison of the effect of carbon, halloysite and titania nanotubes on the mechanical and thermal properties of LDPE based nanocomposite films. *Chinese J Chem Eng* 26:428–435. <https://doi.org/10.1016/j.cjche.2017.09.017>
65. Malas A, Pal P, Das CK (2014) Effect of expanded graphite and modified graphite flakes on the physical and thermo-mechanical properties of styrene butadiene rubber/polybutadiene rubber (SBR/BR) blends. *Mater Des* 55:664–673. <https://doi.org/10.1016/j.matdes.2013.10.038>
66. Malkappa K, Rao BN, Jana T (2016) Functionalized polybutadiene diol based hydrophobic, water dispersible polyurethane nanocomposites: role of organo-clay structure. *Polymer (Guildf)* 99:404–416. <https://doi.org/10.1016/j.polymer.2016.07.039>
67. Mandal A, Chakrabarty D (2014) Journal of industrial and engineering chemistry studies on the mechanical, thermal, morphological and barrier properties of nanocomposites based on poly (vinyl alcohol) and nanocellulose from sugarcane bagasse. *J Ind Eng Chem* 20:462–473. <https://doi.org/10.1016/j.jiec.2013.05.003>
68. Mangeon C, Mahouche-Chergui S, Versace DL, Guerrouache M, Carbonnier B, Langlois V, Renard E (2015) Reactive & functional polymers poly (3-hydroxyalkanoate)-grafted carbon nanotube nanofillers as reinforcing agent for PHAs-based electrospun mats. *React Funct Polym* 89:18–23. <https://doi.org/10.1016/j.reactfunctpolym.2015.03.001>
69. Mashhadzadeh AH, Fereidoon A, Ahangari MG (2017) Surface modification of carbon nanotubes using 3-aminopropyltriethoxysilane to improve mechanical properties of nanocomposite based polymer matrix: experimental and density functional theory study. *Appl Surf Sci* 420:167–179. <https://doi.org/10.1016/j.apsusc.2017.05.148>
70. Mochane MJ (2014) Thermal and mechanical properties of polyolefins/Wax Pcm blends prepared with and without expanded graphite
71. Mochane MJ, Luyt AS (2015) The Effect of expanded graphite on the thermal stability, latent heat, and flammability properties of EVA/Wax phase change blends. *Polym Eng Sci* <https://doi.org/10.1002/pen>
72. Mofokeng TG, Ray SS, Ojijo V (2018a) Structure—property relationship in PP/LDPE blend composites : The role of nanoclay localization. 46193:1–12. <https://doi.org/10.1002/app.46193>
73. Mofokeng TG, Ray SS, Ojijo V (2018b) Influence of selectively localised nanoclay particles on non-isothermal crystallisation and degradation behaviour of PP/LDPE blend composites. <https://doi.org/10.3390/polym10030245>
74. Moradi M, Mohandesi JA, Haghshenas DF (2015) Mechanical properties of the poly (vinyl alcohol) based nanocomposites at low content of surfactant wrapped graphene sheets. *Polymer (Guildf)* 60:207–214. <https://doi.org/10.1016/j.polymer.2015.01.044>
75. Motaung TE, Mtibe A (2015) Alkali treatment and cellulose nanowhiskers extracted from maize stalk residues. *Mater Sci App* 6:1022–1032. <https://doi.org/10.4236/msa.2015.611102>
76. Moustafa H, Galliard H, Vidal L, Dufresne A (2017) Facile modification of organoclay and its effect on the compatibility and properties of novel biodegradable PBE/PBAT nanocomposites. *Eur Polym J* 87:188–199. <https://doi.org/10.1016/j.eurpolymj.2016.12.009>
77. Mtibe A, Liganiso LZ, Mathew AP, Oksman K, John MJ, Anandjiwala RD (2015a) A comparative study on properties of micro and nanopapers produced from cellulose and cellulose nanofibres. *Carbohydr Polym* 118:1–8. <https://doi.org/10.1016/j.carbpol.2014.10.007>
78. Mtibe A, Mandlevu Y, Liganiso LZ, Anandjiwala RD (2015b) Extraction of cellulose nanowhiskers from flax fibres and their reinforcing effect on poly (furfuryl) alcohol. 9:1–9. <https://doi.org/10.1166/jbmb.2015.1531>

79. Murariu M, Dechief AL, Bonnaud L, Paint Y, Gallos A, Fontaine G, Bourbigot S, Dubois P (2010) The production and properties of polylactide composites filled with expanded graphite. *Polym Degrad Stab* 95:889–900. <https://doi.org/10.1016/j.polymdegradstab.2009.12.019>
80. Nikkhhah SJ, Ramazani A, Baniyasi H, Tavakolzadeh F (2009) Investigation of properties of polyethylene/clay nanocomposites prepared by new in situ Ziegler-Natta catalyst. *Mater Des* 30:2309–2315. <https://doi.org/10.1016/j.matdes.2008.11.019>
81. Ortiz AV, Teixeira JG, Gomes MG, Oliveira RR, Díaz FRV, Moura EAB (2014) Preparation and characterization of electron-beam treated HDPE composites reinforced with rice husk ash and Brazilian clay. *Appl Surf Sci* 310:331–335. <https://doi.org/10.1016/j.apsusc.2014.03.075>
82. Pedrazzoli D, Ceccato R, Karger-Kocsis J, Pegoretti A (2013) Viscoelastic behaviour and fracture toughness of linear-low-density polyethylene reinforced with synthetic boehmite alumina nanoparticles. *Express Polym Lett* 7:652–666. <https://doi.org/10.3144/expresspolymlett.2013.62>
83. Pedrazzoli D, Pegoretti A (2014) Expanded graphite nanoplatelets as coupling agents in glass fiber reinforced polypropylene composites. *Compos Part A Appl Sci Manuf* 66:25–34. <https://doi.org/10.1016/j.compositesa.2014.06.016>
84. Phua YJ, Lau NS, Sudesh K, Chow WS, Ishak ZAM (2012) Biodegradability studies of poly (butylene succinate)/organo-montmorillonite nanocomposites under controlled compost soil conditions: effects of clay loading and compatibiliser. *Polym Degrad Stab* 97:1345–1354. <https://doi.org/10.1016/j.polymdegradstab.2012.05.024>
85. Ranjan N, Roy I, Sarkar G, Bhattacharyya A, Das R, Rana D, Banerjee R, Paul AK, Mishra R, Chattopadhyay D (2018) Development of active packaging material based on cellulose acetate butyrate/polyethylene glycol/aryl ammonium cation modified clay. *Carbohydr Polym* 187:8–18. <https://doi.org/10.1016/j.carbpol.2018.01.065>
86. Reddy MM, Vivekanandhan S, Misra M, Bhatia SK, Mohanty AK (2013) Biobased plastics and bionanocomposites: current status and future opportunities. *Prog Polym Sci* 38:1653–1689. <https://doi.org/10.1016/j.progpolymsci.2013.05.006>
87. Rezakazemi M, Dashti A, Asghari M, Shirazian S (2017) H₂-selective mixed matrix membranes modeling using ANFIS, PSO-ANFIS, GA-ANFIS. *Int J Hydrogen Energy* 42:15211–15225. <https://doi.org/10.1016/j.ijhydene.2017.04.044>
88. Rezakazemi M, Ebadi Amooghin A, Montazer-Rahmati MM, Ismail AF, Matsuura T (2014) State-of-the-art membrane based CO₂ separation using mixed matrix membranes (MMMs): an overview on current status and future directions. *Prog Polym Sci* 39:817–861. <https://doi.org/10.1016/j.progpolymsci.2014.01.003>
89. Rezakazemi M, Mohammadi T (2013) Gas sorption in H₂-selective mixed matrix membranes: experimental and neural network modeling. *Int J Hydrogen Energy* 38:14035–14041. <https://doi.org/10.1016/j.ijhydene.2013.08.062>
90. Rezakazemi M, Razavi S, Mohammadi T, Nazari AG (2011) Simulation and determination of optimum conditions of pervaporative dehydration of isopropanol process using synthesized PVA-APTEOS/TEOS nanocomposite membranes by means of expert systems. *J Memb Sci* 379:224–232. <https://doi.org/10.1016/j.memsci.2011.05.070>
91. Rezakazemi M, Sadrzadeh M, Matsuura T (2018) Thermally stable polymers for advanced high-performance gas separation membranes. *Prog Energy Combust Sci* 66:1–41. <https://doi.org/10.1016/j.peccs.2017.11.002>
92. Rezakazemi M, Sadrzadeh M, Mohammadi T, Matsuura T (2017b) Methods for the preparation of organic-inorganic nanocomposite polymer electrolyte membranes for fuel cells
93. Rezakazemi M, Shahidi K, Mohammadi T (2012a) Sorption properties of hydrogen-selective PDMS/zeolite 4A mixed matrix membrane. *Int J Hydrogen Energy* 37:17275–17284. <https://doi.org/10.1016/j.ijhydene.2012.08.109>

94. Rezakazemi M, Shahidi K, Mohammadi T (2012b) Hydrogen separation and purification using crosslinkable PDMS/zeolite A nanoparticles mixed matrix membranes. *Int J Hydrogen Energy* 37:14576–14589. <https://doi.org/10.1016/j.ijhydene.2012.06.104>
95. Rezakazemi M, Vatani A, Mohammadi T (2015) Synergistic interactions between POSS and fumed silica and their effect on the properties of crosslinked PDMS nanocomposite membranes. *RSC Adv* 5:82460–82470. <https://doi.org/10.1039/c5ra13609a>
96. Rezakazemi M, Vatani A, Mohammadi T (2016) Synthesis and gas transport properties of crosslinked poly(dimethylsiloxane) nanocomposite membranes using octatrimethylsiloxy POSS nanoparticles. *J Nat Gas Sci Eng* 30:10–18. <https://doi.org/10.1016/j.jngse.2016.01.033>
97. Sanchez-garcia MD, Lagaron JM, Hoa SV (2010) Effect of addition of carbon nanofibers and carbon nanotubes on properties of thermoplastic biopolymers. *Compos Sci Technol* 70:1095–1105. <https://doi.org/10.1016/j.compscitech.2010.02.015>
98. Sefadi JS, Luyt AS, Pionteck J, Gohs U (2015) Effect of surfactant and radiation treatment on the morphology and properties of PP/EG composites. *J Mater Sci* 50:6021–6031. <https://doi.org/10.1007/s10853-015-9149-z>
99. Shafiq M, Yasin T, Saeed S (2012) Synthesis and characterization of linear low-density polyethylene/sepiolite nanocomposites. *J Appl Polym Sci* 123:1718–1723. <https://doi.org/10.1002/app.34633>
100. Shah KJ, Shukla AD, Shah DO, Imae T (2016) Effect of organic modifiers on dispersion of organoclay in polymer nanocomposites to improve mechanical properties. *Polymer (Guildf)* 97:525–532. <https://doi.org/10.1016/j.polymer.2016.05.066>
101. Shahverdi M, Baheri B, Rezakazemi M, Motaei E, Mohammadi T (2013) Pervaporation study of ethylene glycol dehydration through synthesized (PVA-4A)/polypropylene mixed matrix composite membranes. *Polym Eng Sci* 53:1487–1493. <https://doi.org/10.1002/pen.23406>
102. Shi Q, Zhou C, Yue Y, Guo W, Wu Y, Wu Q (2012) Mechanical properties and in vitro degradation of electrospun bio-nanocomposite mats from PLA and cellulose nanocrystals. *Carbohydr Polym* 90:301–308. <https://doi.org/10.1016/j.carbpol.2012.05.042>
103. Sibeko MA, Luyt AS (2013) Preparation and characterization of vinylsilane crosslinked high-density polyethylene composites filled with nanoclays. *Polym Compos* 34:1720–1727. <https://doi.org/10.1002/pc.22575>
104. Silva BL, Nack FC, Lepienski CM, Coelho LAF, Becker D (2014) Influence of intercalation methods in properties of clay and carbon nanotube and high density polyethylene nanocomposites. *Mater Res* 17:1628–1636. <https://doi.org/10.1590/1516-1439.303714>
105. Song P, Cao Z, Cai Y, Zhao L, Fang Z, Fu S (2011) Fabrication of exfoliated graphene-based polypropylene nanocomposites with enhanced mechanical and thermal properties. *Polymer (Guildf)* 52:4001–4010. <https://doi.org/10.1016/j.polymer.2011.06.045>
106. Song X, Zhou S, Wang Y, Kang W, Cheng B (2012) Mechanical properties and crystallization behavior of polypropylene non-woven fabrics reinforced with POSS and SiO₂ nanoparticles. 13:1015–1022. <https://doi.org/10.1007/s12221-012-1015-x>
107. Sullivan EM, Moon RJ, Kalaitzidou K (2015) Processing and characterization of cellulose nanocrystals/poly(lactic acid) nanocomposite films. *Mater* 2015:8106–8116. <https://doi.org/10.3390/ma8125447>
108. Tan L, Chen Y, Zhou W, Ye S, Wei J (2011) Novel approach toward poly(butylene succinate)/single-walled carbon nanotubes nanocomposites with interfacial-induced crystallization behaviors and mechanical strength. *Polymer* 52:3587–3596. <https://doi.org/10.1016/j.polymer.2011.06.006>
109. Tarfaoui M, Lafdi K, El MA (2016) Mechanical properties of carbon nanotubes based polymer composites. *Compos Part B* 103:113–121. <https://doi.org/10.1016/j.compositesb.2016.08.016>
110. Valapa RB, Pugazhenth G, Katiyar V (2015) Effect of graphene content on the properties of poly(lactic acid) nanocomposites. *RSC Adv* 5:28410–28423. <https://doi.org/10.1039/C4RA15669B>

111. Wan Y, Gong L, Tang L, Wu LB, Jiang JX (2014) Mechanical properties of epoxy composites filled with silane-functionalized graphene oxide. *Compos PART A* 64:79–89. <https://doi.org/10.1016/j.compositesa.2014.04.023>
112. Wang L, Qiu J, Sakai E, Wei X (2016) The relationship between microstructure and mechanical properties of carbon nanotubes/poly(lactic acid) nanocomposites prepared by twin-screw extrusion. *Compos Part A* 89:18–25. <https://doi.org/10.1016/j.compositesa.2015.12.016>
113. Xu S, Girouard N, Schueneman G, Shofner ML, Meredith JC (2013) Mechanical and thermal properties of waterborne epoxy composites containing cellulose nanocrystals. *Polymer (Guildf)* 54:6589–6598. <https://doi.org/10.1016/j.polymer.2013.10.011>
114. Yang ZY, Wang WJ, Shao ZQ, Zhu HD, Li YH, Wang FJ (2013) The transparency and mechanical properties of cellulose acetate nanocomposites using cellulose nanowhiskers as fillers. *Cellulose* 20:159–168. <https://doi.org/10.1007/s10570-012-9796-z>
115. Yasmin A, Daniel IM (2004) Mechanical and thermal properties of graphite platelet/epoxy composites. *Polymer (Guildf)* 45:8211–8219. <https://doi.org/10.1016/j.polymer.2004.09.054>
116. Younesi H, Farsi M, Rezazadeh Z (2013) Physical, mechanical and morphological properties of polymer composites manufactured from carbon nanotubes and wood flour. *Compos Part B* 44:750–755. <https://doi.org/10.1016/j.compositesb.2012.04.023>
117. Zahedi Y, Fathi-achachlouei B, Yousefi AR (2017) Physical and mechanical properties of hybrid montmorillonite/zinc oxide reinforced carboxymethyl cellulose nanocomposites. *Int J Biol Macromol*. <https://doi.org/10.1016/j.ijbiomac.2017.10.185>
118. Zhan J, Chen Y, Tang G, Pan H, Zhang Q, Song L, Hu Y (2014) Crystallization and melting properties of poly (butylene succinate) composites with titanium dioxide nanotubes or hydroxyapatite nanorods. *J App Poly Sci* 40335:1–10. <https://doi.org/10.1002/app.40335>
119. Zhang X, Zhang Y (2015) Poly(butylene succinate-co-butylene adipate)/cellulose nanocrystal composites modified with phthalic anhydride. *Carbohydr Polym* 134:52–59. <https://doi.org/10.1016/j.carbpol.2015.07.078>

Preparation and Characterization of Antibacterial Sustainable Nanocomposites



T. C. Mokhena, M. J. Mochane, T. H. Mokhothu, A. Mtibe,
C. A. Tshifularo and T. S. Motsoeneng

1 Introduction

Pathogenic infections have been the major problem in different fields such as agriculture, healthcare, packaging, and wastewater treatment [26, 38]. These infections are known to cause many deaths more than any other cause. Pathogenic infections result from germs which are found at different places such as air, soil, and water. Because germs are found everywhere it is possible to come in contact with them through touching, eating, drinking or breathing something that contains germs. Germs can be categorized into four: bacteria, viruses, fungi, and protozoa. In this chapter, we limit our discussion to bacteria as a form of germs encountered by humans and animals. Currently, different antibiotics are often used to treat an infection caused by various bacteria. It is recognized that bacteria can mutate their genes in such that they become resistant to the commonly used antimicrobial

T. C. Mokhena (✉) · A. Mtibe (✉) · C. A. Tshifularo
CSIR Materials Science and Manufacturing, Polymers and Composites Competence Area,
Nonwovens and Composites Research Group, Port Elizabeth, South Africa
e-mail: mokhenateboho@gmail.com

A. Mtibe
e-mail: mtibe.asanda@gmail.com

T. C. Mokhena · C. A. Tshifularo
Department of Chemistry, Nelson Mandela University, Port Elizabeth 6301, South Africa

M. J. Mochane
Department of Life Sciences, Central University of Technology,
Free State Private Bag X20539, Bloemfontein, South Africa

T. H. Mokhothu
Department of Chemistry, Durban University of Technology, Durban, South Africa

T. S. Motsoeneng
Chemistry Department, University of South Africa (UNISA), Florida Park,
Roodepoort, Johannesburg, South Africa

agents. Thus, these infections can be combated by potent or specific antimicrobial agents that can mitigate, combat and/or eradicate these bacteria.

In recent years, there has been growing interest in employing a wide variety of nanoparticles as new antimicrobial agents [46, 47]. Unlike conventional antibacterial agents, nanoparticles are extremely toxic towards various bacteria and stable in different conditions found in various industries. Different nanoparticles such as silver, copper, and zinc were reported to be exceptionally effective in eradicating various bacteria at fairly low concentrations. This opened doors for their application in different fields such as agriculture, healthcare, packaging, wastewater treatment, textile, and clothing. Although these nanoparticles show high antibacterial efficiency, their use in industrial applications presents several challenges which brought concerns with regard to their impact on the environment. For example metal copper, even though is cheaper than silver, corrode at standard conditions. On the other hand, if these nanoparticles are used alone their release, recovery, and reuse, cost and long-term effect on health and/or environment limit their success in various fields. A suitable solution is to immobilize and control their release to overcome these limitations [48].

Over the past years, research has escalated in employing polymers as a host matrix for nanoparticles [7, 54, 58, 70, 75] in order to control their release and/or to protect these particles. Polymers have attractive properties such as lightweight, low cost, and mold-ability into various shapes which afford their application in different fields foams, structural adhesives and composites, fillers, fibres, films, emulsions, coatings, rubbers, sealing materials, adhesive resins, membranes [53, 55–57, 59–66, 69, 71]. The properties of the resulting nanocomposite material especially antibacterial activity and release rate were found to be directly dependent on the properties of the polymers (e.g. hydrophilicity, crystallinity and molecular weight). Generally, traditional petroleum-based polymers dominate almost all fields; however, their long-term environmental sustainability is now being questioned. This spurred much interest to utilize biodegradable and compostable polymers as alternative replacement owing to their unique properties such as renewability, biodegradability, and their abundant availability. Thus, these polymers mitigate the environmental impact. They are classified into three categories based on their origin: (i) natural polymers such as proteins (e.g. gelatin, soy protein, silk, and collagen), polysaccharides (e.g. hyaluronic acid, chitin and cellulose) and lipids; (ii) chemically synthesized natural raw materials e.g. polylactic acid (PLA), and microbiological produced or genetically modified bacteria (e.g. polyhydroxyalkanoates (PHA) family); and (iii) chemically synthesized from petrochemical products (e.g. aliphatic-co-polyester (PBSA), aromatic-co-polyester (PBSA) polyester amides (PEA), and polycaprolactone (PCL)) [42]. In this chapter, these polymers will all be denoted as biopolymers to avoid any confusion.

The incorporation of the nanoparticles into biopolymers is of significant importance not only with regards to their antibacterial efficiency but also to improve the overall properties of the resulting nanocomposite materials. Different strategies have been employed to prepare anti biocidal biopolymers which can be classified into two, namely wet and dry methods. A wet method involves the addition of the

nanoparticles precursor into the biopolymer solution followed by synthesizing of the nanoparticles. Another route is to dissolve a polymer in a suitable solvent and then add nanoparticles into the polymer solution followed by casting and drying. Dry method involves the addition of the nanoparticles into melted polymer followed by mixing under high shear. This method received a considerable interest because it can easily be adopted in the industry since these units are already installed and being used to prepare particulate filled polymer composites.

In this chapter, we review the current development and recent advances in the preparation and characterization of sustainable antimicrobial nanocomposites, the strategies to enhance their antibacterial activity as well as future prospects of these interesting materials. We also highlight the preparation of different antibacterial nanoparticles and recent developments.

2 Synthesis of Different Nanoparticles

Over the past decades, the synthesis of nanoparticles garnered much interest owing to their unique properties such as large surface-to-volume ratio, modified structure and increased activity as compared to macromolecules. Nanoparticles have seen tremendous success in various fields such as optical, electronic, medicine, textile and clothing and drug delivery. Nanoparticles are present in nature, where they are synthesized by natural processes like biodegradation and biomineralization. They are classified according to their origin as either natural-occurring or man-made.

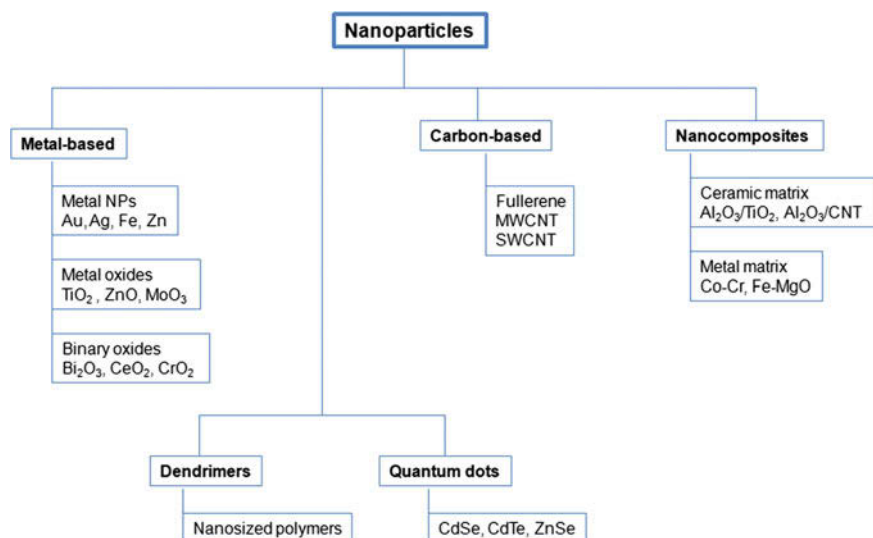


Fig. 1 Classification of nanoparticles by composition

They can further be categorized according to their composition i.e. metal-based, carbon-based, and nanocomposites as well as dendrimers and quantum dots as shown in Fig. 1. In general, there are two approaches used to synthesize various nanoparticles i.e. bottom-up and top-down approach. In a top-down approach, the large macroscopic particles are milled into nano-sized particles. In this case, the synthesized macroscale patterns are reduced into nanoscale particles through plastic deformation. The main disadvantage of this approach is that it cannot be employed for large-scale production since it is an expensive and slow process [2].

2.1 Different Methods Used to Synthesise Nanoparticles

Various nanoparticles synthesis methods have been developed, including physical, chemical and green approaches [9, 39, 40]. The main disadvantages of the physical method are expensive equipment, high temperature and pressure, large area for installation of machines. It involves physical forces which are responsible for the attraction of nano-sized particles to yield large, stable, well-defined nanostructures. The examples of the physical method include colloidal dispersion and basic techniques such as vapour condensation, amorphous crystallization, and physical fragmentation to mention few. Chemical methods involve the use of different toxic chemicals which can be hazardous to the environment and the person handling them. It is recognized that the chemicals employed in chemical approach can bind onto and/or reside in the synthesized nanoparticles (NPs) which can be hazardous especially in medical and packaging applications. In case of food packaging, these chemicals may migrate into the food which can be dangerous to human health. Moreover, the same scenario is often a concern for the physical approach. Chemical methods include chemical emulsion, wet chemical, spray pyrolysis, electrodeposition, chemical and direct precipitation and microwave assisted combustion, while physical include the use of high vacuum in processes such as pulsed laser deposition, molecular beam epitaxy and thermal evaporation. Irrespective of the method used to synthesize the nanoparticles, reducing and stabilizing agents are required in order to control the size (or shape) and the dispersion of the NPs in the medium. Green method involves the use of plants extracts, algae, fungi and bacteria. For instance, the extracts from the plants parts such as roots, leaves, stems, seed and fruits have phytochemicals which can act as reducing and stabilizing agent for the synthesis of different nanoparticles. Green methods are contamination-free since there are no intermediate chemicals involved. The possibility of the large-scale production makes this method the most interesting for future nanoparticles production. The disadvantages of this process are limited to each technique used. For example, the use of micro-organism is time-consuming and expensive. This process involves different steps such as (i) the screening of the bacteria which is the time-consuming process; and (ii) monitoring of culture broth and entire synthesis process to avoid contamination. Moreover, the lack of control over the size and shape of the resulting nanoparticles as well as the cost associated with the media used to grow bacteria add

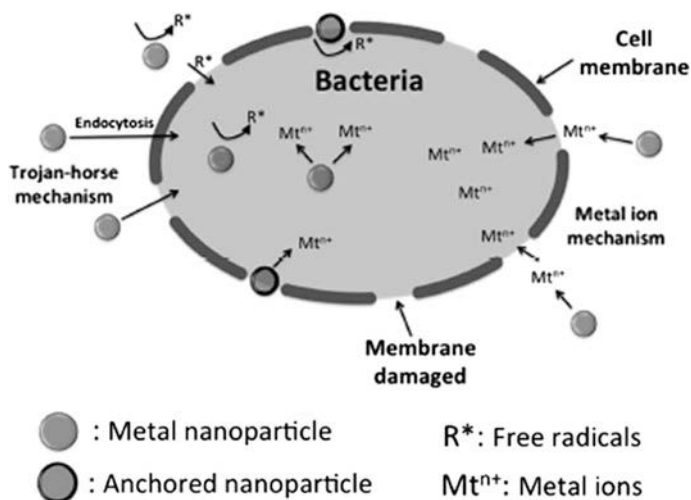


Fig. 2 Schematic presentation based on a summary of the mechanism associated with the antibacterial behaviour of metal nanoparticles (1) “Trojan-horse effect” due to endocytosis processes; (2) attachment to the membrane surface; (3) catalyzed radical formation; and (4) release of metal ions. Redrawn from [46]

to the drawback of this method. However in next sections only synthesis of antibacterial nanoparticles will be discussed. On the other hand, the antibacterial activities of metal nanoparticles are often not well understood. A summary of a possible mechanisms associated with the antibacterial activity of the metal nanoparticles against pathogenic microbes is schematically presented in Fig. 2.

2.2 Preparation and Antibacterial Mechanisms of the NPs

2.2.1 Silver Nanoparticles (AgNPs)

The antibacterial properties of silver nanoparticles have been known for more than 2000 years ago. It is highly toxic towards microbes with a wide variety of products that are commercially available because of its broad spectrum of antibacterial activity. It is found in these products in ionic or metallic form. The nanosilver (AgNPs) exhibits high surface area to volume ratio with exceptional antibacterial efficiency towards more than 650 types of bacteria, as well as various viruses and fungi. Moreover, there are 3 proposed mechanisms for the antibacterial activity of AgNPs: (i) the NPs attachment to the cell wall which disturbs the cell membrane permeability or disrupt the cell membrane, (ii) NPs penetration through the cell wall and reacting with thiol and phosphorus-containing compounds which disturbs the respiration and replication processes, and (iii) the release of silver ions by

nanoparticles [42–44]. All these mechanisms are often associated with the bacteriostatic and bactericidal effects of AgNPs. There are various methods to prepare silver nanoparticles such as electrochemical, chemical, optical, thermal decomposition, microwave, hydrogel method, sonochemical, UV and gamma radiation. These methods involve reducing an ionic silver salt to metallic silver in an appropriate medium. The most commonly used method in the industry is a chemical reduction due to high production efficiency and control over the shape and size of the resulting nanoparticles. In recent years, there has been growing interest in the synthesis of silver nanoparticles in the presence of polymers to avoid the agglomeration of the nanoparticles after synthesis, especially natural-based polymers. The stability and dispersion of these particles are mostly influenced by the presence of the functional groups along the polymer chain which act as either reducing or stabilizing agent and in other cases as both reducing and stabilizing agent e.g. Chitosan. Chitosan has amino and hydroxyl groups along the polymer chains. The amino groups can coordinate with metal ions when mixed with silver salts while reduction

Table 1 Summary of the synthesise antibacterial nanoparticles

Salt precursor	Synthesize route	Comments	References
<i>AgNPs</i>			
Chemical synthesis			
Silver nitrate	AgNO ₃ (1 mM, 80 ml) was added drop-wise to an ice-cold NaBH ₄ 2 mM solution (240 ml) under vigorous stirring	Ag nanoparticles with an average size around 38 nm were obtained and this was confirmed by UV-vis absorption peak at 433 nm for bacterial cellulose/AgNPs and 425 nm for Vegetable Cellulose/AgNPs	[49]
Silver nitrate	AgNPs were prepared by sodium citrate reduction of AgNO ₃ followed by heating in a furnace at 200 °C for an hour	The resulting AgNPs were a mainly spherical shape with the size of about 50 nm	[83]
Green synthesis			
Silver nitrate	For the first set -the supernatant from soil derived <i>Pseudomonas putida</i> MVP2 was mixed with AgNO ₃ and the second set <i>P. putida</i> was directly mixed with AgNO ₃ to adjust the final concentration of 1 mM and monitored for the reduction of silver solution into AgNPs	For the first step, AgNPs had the size ranging between 5 and 16 nm, while for the second set the AgNO ₃ treated bacteria showed the number of black spots on the bacterial membrane and cytoplasm which strongly proved that AgNPs were mostly synthesized in the outer membrane of the bacteria	[22]

(continued)

Table 1 (continued)

Salt precursor	Synthesize route	Comments	References
Silver nitrate	A mixture of silver nitrate microcrystalline cellulose was sonicated for 10 min followed by addition of curry leaves (<i>Murraya koenigii</i>) extract to reduce silver ions into AgNPs	UV-vis spectra showed Plasmon peak vibration at 430 nm confirming the formation of AgNPs and the resulting spherical AgNPs had a diameter of 10–25 nm with a spherical shape	[87]
Silver nitrate	<i>Rhizopus stolonifer</i> aqueous mycelial extract was mixed with AgNO ₃ solution (1 mM AgNO ₃ final concentration) and incubated on orbital shaker 180 rpm at 40 °C for two days	AgNPs have a spherical form and diameter about 6.04 nm which was confirmed by UV-vis absorption peak at 420 nm	[1]
ZnNPs			
Zinc nitrate	Mixing crude form with zinc nitrate and heated at 450 ± 10 °C for 30 min followed by calcination at 750 °C	<i>Euphorbia Jatropha</i> was used as reducing agent and the resulting hexagonal nanoparticles had a size ranging between 6 and 21 nm	[21]
Zinc nitrate	aloe leaf extracts were mixed with zinc nitrate and heated at 150 °C for 5–6 h. The resulting pale white precipitate was centrifuged for 15 min and dried at 80 °C for 7–8 h Chemical synthesis- Zinc nitrate was dissolved in distilled water and NaOH was added dropwise and then the solution was left overnight. The obtained white precipitate was centrifuge for 10 min and then dried at 80 °C for 6 h. During drying, complete conversion of Zn(OH) ₂ into ZnO takes place. All the obtained white precipitate were ground	The sizes of the prepared green and chemical ZnO nanoparticles were 40 and 25 nm	[24]
Zinc nitrate hexahydrate	Moringa <i>Oleifera</i> extracts as an effective chelating agent. A mixture of the extract and zinc nitrate hexahydrate was left for 18 h then heated at 100 °C and the resulting powder was washed with water to remove any extracts followed by heating at 500 °C for an hour	TEM results showed that highly crystalline zinc oxide nanoparticles with particle size varying from 12.27 and 30.51 nm were obtained.	[37]

(continued)

Table 1 (continued)

Salt precursor	Synthesize route	Comments	References
Chemical synthesis			
Zinc acetate	Chemical synthesis- a mixture of zinc acetate and NaOH (added dropwise) was then calcinated at 300 °C for 6 h	Zinc nanoparticles having an average size of 60 nm was obtained	[85]
<i>CuNPs</i>			
Chemical synthesis			
Cu (NO ₃) ₂ ·3H ₂ O	Synthesized ligand benzildiethylenetriamine was used to synthesize the nanoparticles	By reducing the concentration of the reducing agent (ligand) led to an increase in nanoparticles size. The size of the particles ranged between 15 and 63 nm depending on the concentration of the ligand	[12]
CuSO ₄ ·5H ₂ O	Ascorbic acid was used as a reducing agent while starch was used as a stabilizing agent	The obtained Cu and Cu ₂ O nanoparticles were cubic in shape with a mean size of 28.73 and 25.19 nm, respectively	[30]
Green synthesis			
CuSO ₄	A Gram-negative bacterium belonging to the genus <i>Serratia</i> was isolated from the midgut of <i>Stibara</i> sp., an insect of the Cerambycidae family of beetles and used to synthesis CuNPs from 1–48 h	The resulting nanoparticles were polydispersed and vary from 10–30 nm in diameter	[25]
CuSO ₄ ·5H ₂ O	Native cyclodextrins as a stabilizing agent and ascorbic acid reducing agent	The resulting pattern from selected area electron diffraction (SAED) and lattice Fringes confirmed that crystalline structure of Cu-NPs with face-centred cubic (FCC) with a (111), (200) and (220) lattice planes of Cu. The Cu-NPs depends on the type of native cyclodextrin (NCD) and the obtained nanoparticles were spherical with a size between 2 and 33 nm. The smaller Cu-NPs were obtained with α-NCD (viz. 4 nm), while the nanoparticles obtained with β-NCD showed narrow size distribution having a size of 6.5 nm	[20]

(continued)

Table 1 (continued)

Salt precursor	Synthesize route	Comments	References
Cu(NO ₃) ₂	<i>Garcinia mangostana</i> leaf extract as a reducing agent was mixed with copper nitrate and heated at 70 °C for an hour	Cu nanoparticles with the mean particle size of 28.9 nm were obtained	[50]
Cu(NO ₃) ₂	The extracts of <i>E. prostrate</i> was mixed with copper acetate and stirred for 24 h at room temperature without external energy	Monodisperse and spherical particles with sizes ranging from 28 to 45 nm and (mean, 36 ± 1.2 nm) were obtained	[15]

of silver ion is coupled with oxidation of hydroxyl group. Table 1 highlights recent studies based on the production of the silver nanoparticles.

2.2.2 Zinc Nanoparticles

Zinc oxide received a lot of attention owing to its special characteristics such as anti-corrosion, antibacterial, and has low electrons conductivity and excellent heat resistance. It has been prepared via physical and chemical methods [2, 28]. The chemical methods include the reaction of zinc with alcohol, vapour transport, hydrothermal synthesis and precipitation method. In order to avoid the complications that are bound to physical and chemical methods, the green synthesis of zinc oxide has been employed for the past years. There is still a lot of controversy about the mechanism behind the antibacterial activity displayed by zinc nanoparticles [2, 28]. It was postulated that the toxicity mechanism result from intercellular reactive oxygen species (ROS) generation and Zn²⁺ release. ROS-include superoxide anion, hydrogen peroxide and hydroxide-are harmful to bacterial cells, while the released Zn²⁺ disrupts important metabolic pathways. Since the morphology of the zinc nanoparticles-which depends on the synthesis technique-plays significant role in their antibacterial activity. There has been a lot of interest in recent years towards the development of novel synthesis methods and applications. Green synthesis methods received more interest because of their unique attractive properties-including environmentally friendlier, cost-effective, biocompatible and safe. Plants, algae, fungi and bacteria have been employed as a green method to produce zinc nanoparticles. Figure 3 illustrate the synthesis of zinc oxide nanoparticles by using different sources. Recent studies based on the use of different bacteria, fungi, and plants parts that have been used to prepare zinc nanoparticles are summarized in Table 1.

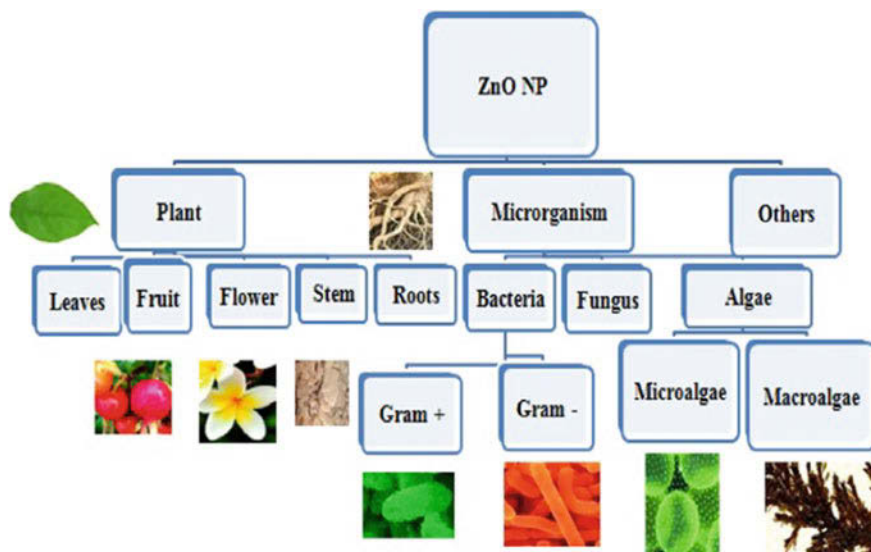


Fig. 3 Zinc oxide nanoparticles synthesis by using different sources [2]

2.2.3 Gold Nanoparticles (AuNPs)

Gold nanoparticles garnered much interest in different fields such as wastewater treatment, catalysis, biosensing, optics and therapeutic applications owing to its unique features which include good antibacterial activity, optical and photothermal properties. There are two proposed mechanisms with regard to antibacterial activity of AuNPs (i) a change in the membrane potential and prevention of ATPase activities resulting in a decline in cellular metabolism, and (ii) inhibiting the binding of subunits of the ribosomes of tRNA resulting in a collapsing in biological processes [86]. There is a paradigm shift towards green, cost-effective and controllable methods to synthesize gold nanoparticles. Similarly to other nanoparticles, the use of plants extracts, bacteria and fungi have been employed to synthesize gold nanoparticles. For an example, typical fresh leaves of *Piper guineense* (Fig. 4) were used for the synthesise of gold nanoparticles [79]. On the other hand, natural polymers were also employed as stabilizing and reducing agents to synthesize gold nanoparticles. Gold nanoparticles having diameters ranging between 50 and 200 nm were synthesized by Shih et al. [78] using chitosan as stabilizing and reducing agent, while carboxymethyl chitosan was used by Laudenslager et al. [72]. The resulting gold nanoparticles had an average size of 22.9 nm.

Fig. 4 Leaf and fruit of *Piper guineense* [79]



2.2.4 Copper Nanoparticles

Copper is the most important element due to its role in living organisms. It plays an important role in the transportation of oxygen during electron transport chain and iron homeostasis. Its antibacterial activity is associated with cellular damage after contact between Cu^{2+} and bacteria membrane [18]. This led to the development of novel synthesis techniques for producing nano-sized copper particles. The electrochemical is the widely used method to produce copper nanoparticles (CuNPs) [27]. This is as a result of the efficiency of this method to produce large quantities of the nanoparticles at a short period of time. CuNPs can also be synthesized through several techniques such as chemical reduction, laser ablation, sol-gel processing, and thermal reduction [18]. The nanoparticles synthesized from these techniques have different antibacterial activity. Furthermore, the reaction medium composition and stabilizers had an effect on the size of the resultant nanoparticles. Satyvaldiev et al. [74] investigated the synthesis and biological activity of copper nanoparticles under different medium (alkaline and ammonia) and in the presence of a stabilizer (gelatin). The FESEM images (Figs. 5 and 6) in both media with and without gelatin were found to be spherical in shape. However, the insets in Fig. 5a, b showed that Cu nanoparticles in an alkaline medium had smaller particle size than in ammonia medium. The addition of gelatin reduced the particle size more, which was associated with an increase of nanoparticle stability in the presence of gelatin. The recent studies based on the synthesis of the CuNPs and their properties are summarized in Table 1.

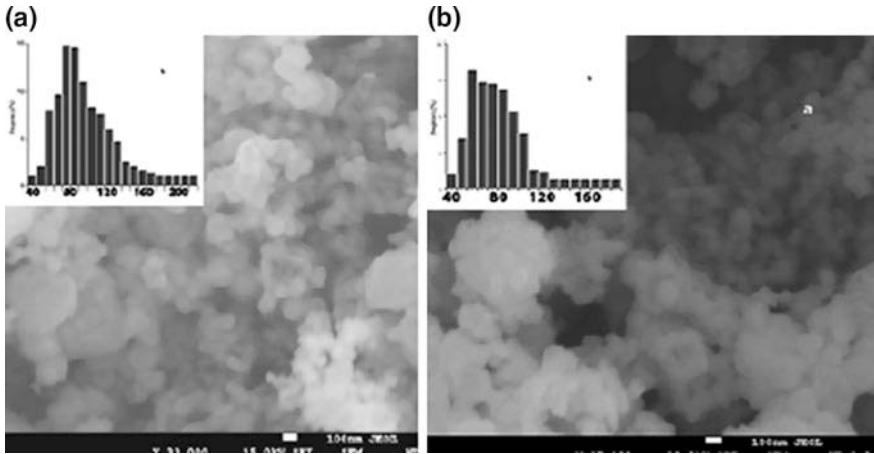


Fig. 5 SEM images of Cu nanopowders produced in an alkaline medium (a) and Cu nanopowders obtained in an alkaline medium in the presence of gelatin (b) with their particle size histograms in their insets [74]

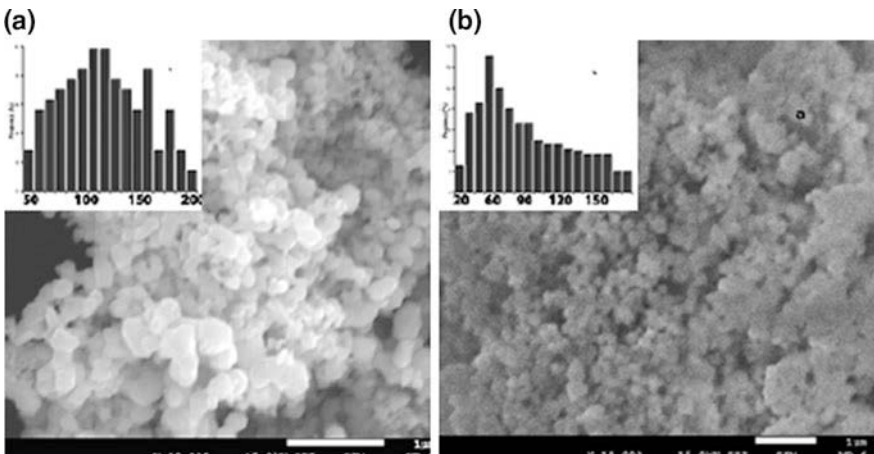


Fig. 6 SEM images of Cu nanoparticles obtained in an ammonia medium (a) and Cu nanoparticles obtained in the presence of gelatin in an ammonia medium (b) with their particle size histograms in their insets [74]

2.2.5 Carbon-Based Nanoparticles

Carbon nanotubes have attractive properties such as high mechanical strength, large surface area, high thermal stability (>700 °C), high aspect ratio (length to diameter) and electrical conductivity [16, 52]. They have been used in wide variety of industrial applications such as energy storage, construction, and entertainment.

They also have excellent antimicrobial activity [13, 29, 35]. The antibacterial activity of carbon nanotubes is still unknown. It is proposed that the antibacterial activity is induced by physical membrane perturbation and oxidative stress. It is reported that the antibacterial activity is influenced by CNT distribution, diameter, length, and electronic structure [13, 29]. CNT are classified into single and multi-wall carbon nanotubes depending on the number of graphite layers. Single-walled CNT is composed of graphene sheet wrapped into a cylinder, while multi-walled CNT consists of two or more concentric mixed cylinders. Large-scale production of CNT is achieved through chemical vapour deposition. Other techniques employed to produce CNTs include electric arc discharge and laser ablation. Three most important aspects of the synthesis of CNT are carbon source, energy, and a metal catalyst.

Graphite nanosheets-known as graphene is one of the promising carbonaceous materials with exceptional properties such as electrical; thermal; mechanical; barrier and flame retardant properties [8, 33, 73, 90]. It is obtained from expandable natural graphite by different exfoliation process such as chemical or electrochemical, mechanical, and thermal and/or chemical. The mechanical technique includes the use of scotch/adhesive tape to repeatedly peel off graphene layer from graphite crystal until individual atomic planes are obtained. Beside scotch tape, epitaxial growth of graphene on silicon carbide was also reported. In this case, silicon carbides heated to high temperatures above 1100 °C to reduce it into graphene. Yet another method to produce graphene includes CVD of hydrocarbons on a metal or metal-coated substrates such as Ni films and Cu foil. Large-scale graphene production involves exfoliation of graphite via acid oxidation (e.g. nitric acid/sulphuric acid) into expandable graphite oxide (GO), followed by reduction of GO (e.g. by hydrazine, NaBH₄) and annealing in argon/hydrogen to yield graphene sheets. The disadvantage of the exfoliation using oxidation/reduction from GO is the quality of the resulting graphene as compared to scotch tape, epitaxially grown on SiC and CVD. The solution methods, however, have been employed for the production of graphene ribbons through cutting open nanotubes in the presence of potassium permanganate and sulphuric acid. The solution methods such as filtration, solution casting, electrophoretic deposition and Langmuir-Blodgett deposition afford the formation of graphene-based functionalized films.

2.2.6 Clay Minerals

Clay minerals are also known as layered silicates because of their stacked structure of 1 nm silicate sheets which are in nanoscale with a variable basal distance. They often used in human and health formulations like excipients or active substances because of the unique features which include chemical inertness and low or zero toxicity [35]. Clay is classified into various classes: smectites, vermiculite, montmorillonite, halloysite, palygorskite and many more. Smectites are planar dioctahedral and trioctahedral 2:1 clay minerals having a layer charge between -0.2 and -0.6 per formula unit which contains hydrate exchangeable cations. Smectite 2:1

layer unit is made up of one alumina octahedral sheets sandwiched between two silica tetrahedral sheets. Montmorillonite is generally defined as dioctahedral smectites. The term vermiculite is used to define planar dioctahedral and trioctahedral with a layer charge between -0.6 and -0.9 per formula unit which contains hydrated exchangeable cations. Halloysite is commonly defined as a 1:1 aluminosilicate structure with its size depending on the deposit, while palygorskite is 2:1 layered structure consists of two-dimensional tetrahedral sheets. The antibacterial activity of clay is proposed to take place through clay permeation into the cell membrane, damage the cell wall, and disturbs the natural processes of the cell which results in eradication of microorganisms.

3 Preparation of Antibacterial Nanocomposites

Depending on the intended application several processing techniques such as melt compounding, solution casting, in situ polymerization and electrospinning were employed to prepare antibacterial nanocomposites. Solution casting involves dissolving the polymer and antibacterial agent in a suitable solvent, casting and drying or evaporation of the solvent [85, 88]. This process is often limited to laboratory-scale and/or polymers which are soluble in available solvents. The heat-sensitive polymers and/or antibacterial agents are usually prepared via solution casting. Melt compounding involves mixing the antibacterial agent and polymer at the temperature above melting temperature of the polymer under high shear. These techniques include single/twin screw extruder, injection moulding, melt mixer and hot melt presser. They can be used either alone or in combination in order to prepare the resulting nanocomposite product [10]. The melt compounding is limited to polymers that can melt with antibacterial agents which are not sensitive to high temperatures. In most cases, the antibacterial agent ends up in the amorphous part of the polymer, thus the crystallinity of the polymer plays a major role on the dispersion as well as the release rate of the antibacterial agent from the system. Nevertheless, these techniques are most significant importance from the commercial viewpoint. The other interesting preparation method of the antibacterial nanocomposites is electrospinning. This technique is cheaper and has a potential for large-scale production. Electrospinning is capable of producing multifunctional nanofibre from natural and synthetic polymers, polymer blends and composites [10]. The resulting fibres have unique properties such as high surface area, inter- and intrafibrous pores as well as strong adhesive force, good air filtration, high adhesion barrier activity and heat resistance which rare of significant importance towards biomedical applications. The resulting electrospun scaffolds have a similar shape to human skin tissues; hence they are often employed in tissue engineering. However, the above-mentioned properties render these fibers opportunity to be applied in other fields such as water and air filtration, energy storage and packaging. Coating of the antibacterial agents onto the polymeric matrix has also been adopted by several authors [23, 41]. All these preparation techniques result in different morphologies

and thus, influence the antibacterial efficiency of the resulting nanocomposite material. In this case, the contact between the nanoparticles with the microbes is of significance in order to promote the antibacterial activity of the resulting composite material. It is recognized that in case of metal nanoparticles the ions release is the main contributor to the eradication of the microbes [46]. However, for nanoparticles such as carbon nanotubes, the main contribution comes from the contact with microbes by piercing the membrane of the microbe. Thus the preparation method plays a major role in the antibacterial behaviour of the resulting composites as well as the type of polymer. In summary the antibacterial behavior of the antibacterial nanocomposites is directly dependent on these factors: (i) adsorption of microbes on the polymer surface; (ii) polymer-type to allow water penetration to reach the embedded nanoparticles to allow their dissolution and realization; (iii) contact between nanoparticles with available microbes; and (iv) physical and structural properties of the nanoparticles.

4 Antibacterial Nanocomposites

4.1 Silver/Biopolymer Nanocomposites

Silver nanoparticles nanocomposites are often prepared by either ex situ or in situ [17]. In situ involves the inclusion of silver ionic solution, reducing agent and polymeric material into one system followed by reduction of silver ionic solution into silver nanoparticles, while ex situ involves the synthesis of particles beforehand followed by addition of AgNPs into the polymeric material. In situ preparation of silver nanoparticles was carried out by mixing AgNO_3 (1 mM, 80 ml) and an ice-cold NaBH_4 2 mM solution (240 ml) drop-wise to under vigorous stirring in the presence of bacterial cellulose (BC) as well as vegetable cellulose (VC) [49]. A significant antibacterial activity for nanocomposite samples against both gram-negative (*K. pneumonia*) and gram-positive (*S. aureus* and spore-forming *B. subtilis*) tested bacteria, by the action of both BC- and VC-based Ag nanocomposite samples. [31] prepared cellulose/AgNPs nanocomposite by in situ method. In this case, ethylene glycol, cellulose and silver nitrate were mixed together and exposed to microwave radiation. The resulting nanocomposite material displayed high antimicrobial efficiency (Fig. 7) against tested bacteria viz. *Escherichia coli* and *Staphylococcus aureus*.

Ex situ was used to prepare PBAT/AgNPs nanocomposites for packaging applications via solution casting [84]. AgNPs were prepared by chemical synthesis using sodium citrate as reducing agent. It was reported that increase in nanofiller wt% improves mechanical, oxygen permeability, and antimicrobial properties, but at a higher loading the films become stiff. [76] reported on the synthesis of AgNPs using tocopherol as reducing and capping agents in order to prepare PBAT/AgNPs composite films for food packaging. The films were prepared through solution casting

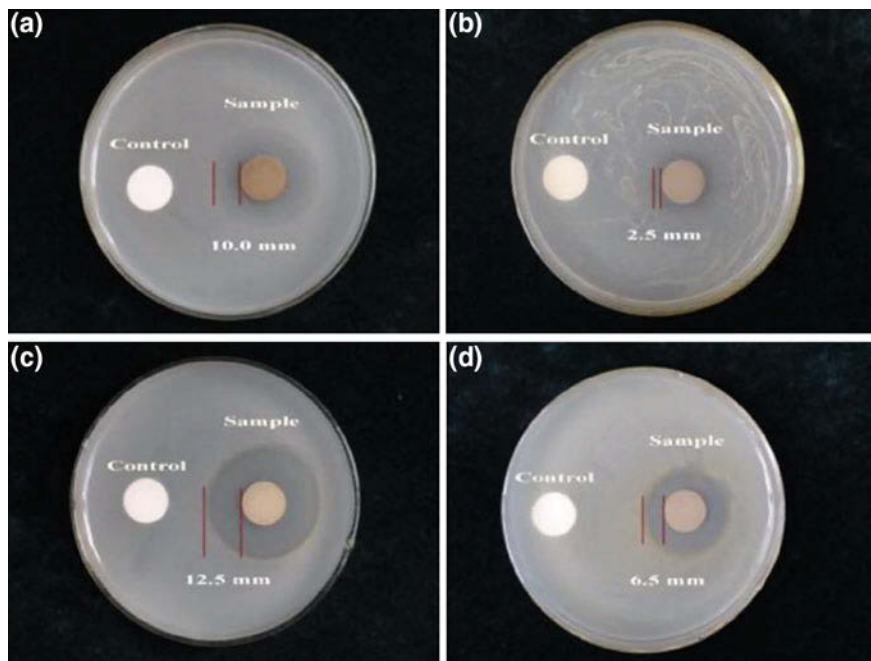


Fig. 7 Antimicrobial activities of the cellulose–Ag nanocomposites: **a, c** *Escherichia coli* and **b, d** *Staphylococcus aureus* [31]

method and the addition of AgNPs leading to rougher surfaces as compared to smooth PBAT. However, the synthesized AgNPs were spherical with a diameter of 10–50 nm. It was found that the PBAT/AgNPs exhibited good antibacterial activity against both food-borne pathogenic bacteria (i.e. *E. coli* and *L. monocytogenes*), but showed stronger antibacterial activity towards *E. coli* than *L. monocytogenes* since the Gram-negative bacteria are more vulnerable to AgNPs than Gram-positive ones. On the other hand, mechanical strength, water vapour barrier property, and water contact angle of the PBAT films improved significantly after addition of AgNPs making this material a good candidate for the potential for food packaging especially looking at the concentration of silver used in this case i.e. 10 mg silver in 4 g PBAT. [77] studied the effect of silver nanoparticles obtained from different synthesis routes viz. metallic silver (AgM) or silver zeolite (AgZ) prepared under vigorous stirring for 12 h, trisodium reduced (AgNP^C) and laser ablated (AgNP^{LA}) on the properties of alginate as host matrix. The resulting silver zeolite (AgZ) nanoparticles were cubical in shape with the size of 2–5 μm, whereas the shapes of AgNP^C, AgNP^{LA}, and AgM were almost spherical, and the size was in the range of 50–200 nm. It was found that the prepared composites via solution casting were flexible, smooth, and free-standing, but the composites were rougher than pristine alginate films. The minimum inhibitory concentration (MIC) or minimum bactericidal concentration (MBC) of AgNP^C, AgZ, AgNO₃, AgNP^{LA}, and AgM against *E. coli* were

3.125/6.25, 3.125/12.5, 1.562/6.25, >50/>50, >50/>50 $\mu\text{g/mL}$, respectively, and those against *L. monocytogenes* were 6.25/12.5, 6.25/12.5, 3.25/6.25, >50/>50, >50/>50 $\mu\text{g/mL}$, respectively. The degree of antimicrobial activity was greatly influenced by the type of silver particles. It was found that among the silver particles included groups, alginate/AgNP^C, alginate/AgZ, and alginate/AgNO₃ composite films exhibited potent antibacterial activity against both foodborne pathogenic bacteria, however, alginate/AgNP^{LA} and alginate/AgM composite films did not show distinctive antibacterial activity. It was postulated that the low or negligible antibacterial activity of alginate/AgNP^{LA} and alginate/AgM composite films may be regarded to the AgNP^{LA} strongly capped with poly vinyl pyrrolidone (PVP) and interacting tightly with the alginate resulting in the prevention of oxidation of AgNPs to form Ag ions, and that the stable metallic silver of AgM was not oxidized easily to release silver ions.

4.2 Zinc/Biopolymer Nanocomposites

Zinc nanoparticles have been used to reinforce different biopolymers, especially for packaging applications. Poly(butylenes adipate-co-terephthalate) PBAT is one of the biopolymers that has been reinforced with zinc nanoparticles for different applications. PBAT is an aliphatic/aromatic copolyester synthesis from 1,4-butanediol, adipic acid, and terephthalic acid. It is a biodegradable polymer having excellent compatibility with other biodegradable polymers such as aliphatic polyesters and starch-based polymers. Due to its unique properties which include biodegradability and biocompatibility, PBAT has been used in packaging films, agricultural films and compost bags. In the case of packaging, different fillers are often added to improve their properties such as barrier properties, and mechanical properties. One of the most important aspects of food packaging is the antibacterial efficiency of the polymer being used. Different antibacterial nanoparticles are often added not only to improve the antibacterial activity but also the barrier properties [85]. Venkatesan and Rajeswari [85] prepared PBAT/ZnO nanocomposites through solution casting using chloroform as a solvent. ZnO was prepared using a chemical method whereby zinc acetate was mixed with NaOH (by adding NaOH drop by drop) followed by calcination at 300 °C for 6 h in a furnace. The antibacterial activity was tested using *E. coli* and *S. aureus*. It was reported that the inhibition zone increased with increase in zinc nanoparticles content regardless of bacteria type. The diameter of the inhibition zones for nanocomposites containing 1, 3, 5 and 10 wt of ZnO nanoparticles were 11.0, 11.8, 12.7, 13.3, and 14.1 mm for *E. coli* and 11.0, 12.0, 13.5, 13.9, and 15.1 mm against *S. aureus*, respectively.

Zinc nanoparticles were also incorporated into PHBV for packaging application by Ana and Angel [4]. Nanocomposites were prepared through solution casting. In this case, the nanoparticles were firstly dispersed in chloroform and then mixed with polymer solution also dissolved in chloroform followed by sonication, casting and drying. Using TEM and SEM, it was found that the ZnNP were well dispersed in

the polymer matrix. This was ascribed to the interactions between the –OH groups of the ZnO surface and the polar moieties of the biopolymer preventing nanoparticle aggregation while improving the compatibility between the filler and matrix phases. However, at the higher content of the nanoparticles well-dispersed clusters were obtained. This was also confirmed by an increase in mechanical properties up to 4 wt% of the filler with Young modulus reaching ~ 1.7 GPa and tensile strength of ~ 30 MPa, whereas elongation at break decreased from 4% (for neat polymer) to $\sim 2.9\%$. The nanocomposites exhibited antibacterial activity against human pathogenic bacteria, and the effect on *E. coli* was stronger than on *S. aureus* due to their difference in thickness of their membranes. Gram-positive bacteria usually have one cytoplasmic membrane and a thick wall composed of multilayers of peptidoglycan, whereas the Gram-negative have a more complex cell wall structure, with a layer of peptidoglycan between the outer membrane and the cytoplasmic membrane. Hence *E. coli* is more susceptible to antibacterial agents than *S. aureus*.

Augustine et al. [6] prepared electrospun polycaprolactone/ZnNPs nanocomposite membrane as biomaterials with antibacterial and cell adhesion properties. The incorporation of ZnNPs reduced the size of resulting electrospun nanofibers and these nanofibers became ore rougher with an increase in ZnNPs content due to their agglomeration. At a low content of ZnNPs viz. up to 1 wt%, tensile strength and modulus increased linearly, while further increase in ZnNPs content led to a decrease in tensile strength and modulus of the nanocomposite membrane. This was attributed to the agglomeration of the nanoparticles because of their high surface energy resulting in their agglomerate and thus led to poor dispersion. It was also reported that the nanocomposite membrane had good antibacterial activity against *E. coli* and *S. aureus*, but at low NPs content i.e. below 5 wt% the antibacterial activity was statistically insignificant. Strong antibacterial activity was recognized at 5 and 6 wt% of the nanoparticles. This was ascribed to the fact that at low NPs content, the NPs are trapped within the polymeric matrix and thus, those in direct contact with bacterial cells are very few in number. Interestingly, the nanocomposites membranes showed 100% cell viability. Agustin and Padmawijaya [5] investigated the effect of glycerol and zinc oxide on the antibacterial activity of biodegradable bioplastics from chitosan-kepok banana peel starch. It was reported that the biodegradability rates decreased (Table 2) as the zinc oxide concentration in banana peel starch-chitosan bioplastic, thus composite bioplastic material will inhibit bacterial growth. The resultant biocomposites have a significant potential to be used for food packaging by having the biodegradable properties and also inhibit bacterial growth.

Table 2 Biodegradable test of chitosan-starch bioplastics [5]

Zinc oxide (%)	Degradation time (minutes)
1	35
3	42
5	72

4.3 Gold/Biopolymer Nanocomposites

Mendoza et al. [38] exploited the reductive and stabilizing action of chitosan to prepare gold/chitosan nanocomposites. In this case, the precursor was introduced dropwise into chitosan solution (with chitosan as a stabilizing and reducing agent) and stirred for 4 h at 60 °C. Spherical gold nanoparticles embedded in chitosan were obtained as confirmed by maximum surface Plasmon resonance at ~525 nm. The authors reported that the size of the nanoparticles increased with an increase in precursor' concentration i.e. 1 mM yielded spherical NPs with a diameter of 14 ± 5 nm while for 2 mM was 14 ± 3 nm. They found that the composite exhibited superior bactericidal ability against both bacteria (*S. aureus* and *E. coli*) models without showing cytotoxicity on human cells at the concentrations tested.

4.4 Copper/Biopolymer Nanocomposites

[11] investigated antimicrobial nanocomposites and electrospun coatings based on poly(3-hydroxybutyrate-co-3-hydroxyvalerate) and copper oxide nanoparticles for active packaging and coating applications. A blend of poly (hydroxybutyrate-co-hydroxyvalerate (PHBV) composed of PHBV3 (3 mol valerate) and PHBV18 (18 mol valerate) was prepared by melt mixing and used as a control. On the other hand, the nanocomposites were prepared via two different coating technology: (i) two different content of CuNPs (i.e. 0.1 and 0.05%) were melt mixed with the blend of PHBV3 pellet (86 wt%) and unpurified PHBV18 powder (14 wt%) followed by melt-pressing at 180 °C for 3 min, (ii) PHBV3 film was coated with PHBV18/CuNPs electrospun ultrathin fibers mats containing 0.05% followed by hot-pressing at 150 °C for 2 min (without pressing) (denoted ES-0.05%). Mechanical properties for all prepared samples were not significantly influenced by the addition of NPs. Water Vapour Permeability (WVP), however, increased by the addition of the NPs, more especially where fiber mats were put as an antibacterial coating onto PHBV3 matrix. This was ascribed to the more hydrophilic character of the electrospun mats with PHBV/CuNPs as compared to neat PHBV3 film used as a substrate in the coated system. In the case of oxygen permeability (OP), the addition of 0.05% NPs reduced OP by 34.2% which was related to the additional tortuous path created by the well-distributed and dispersed NPs. The OP of the ES-0.05% was higher than its counterpart prepared by melt compounding. This was ascribed to the lower crystallinity of ES-0.05%. For antibacterial activity, a reduction of about 5 log colony-forming unit/mL of *S. enterica* was recorded for those films prepared with 0.05% CuO by melt-mixing and no viable count of bacteria were recorded either for nanocomposites films containing 0.1% CuO or the 0.05% ES coating structure after 24 h of exposure. No viable counts of *L. monocytogenes* were recorded in any of the samples after 24 h of exposure. The effectiveness for inactivation of *L. monocytogenes* was attributed to structural and chemical

compositional differences between cell surfaces of Gram-positive and Gram-negative bacteria. Bio-disintegration tests showed that the coated structures were fully biodegraded in a period of 35 days at the composting condition.

Mary et al. [36] coated cellulose with copper (II) ions and CuNPs to evaluate their release from the system. Cellulose was chemically modified by periodate-induced oxidation followed by covalent attachment of biopolymer chitosan (CAC). The Cu(II) was immobilized to CAC by its immersion in Cu(II) solution (CBCAC), while CuNPs were produced by borohydride-induced reduction of Cu(II). In this case, CAC was immersed in Cu(II) solution followed by immersion in sodium borohydride solution for 24 h and then dried in a vacuum chamber at 50 °C (NCLCAC). It was reported that the release of Cu(II) from all prepared samples was depended on the concentration of Cu(II) in the system i.e. high release was recorded for higher Cu(II) and/or CuNPs concentration. Similarly, the antibacterial activity against *E. coli* was found to be dependent on the concentration of Cu(II) and CuNPs. The radius of inhibition zone increases with an increase in the copper and CuNPs contents of loading solutions. This was attributed to the biocidal action of Cu(II) ions, which are released from the fibers which can be related to the copper content in the loading solutions increasing, with the amount bound to fibers also increases and thus, the antibacterial action of resulting fibers becomes more effective, thus resulting in the formation of “zone of inhibition” with greater area (or radius).

4.5 Carbon-Based/Biopolymer Nanocomposites

[19] prepared antibacterial carboxymethyl chitosan (CMC)/carbon nanotubes (CNT) nanocomposites via solution casting. CMC-CNTs 20 recorded highest antibacterial efficacy as compared to other composites with inhibition zone diameter of 22.3 ± 0.21 mm against *S. aureus* and of 21.3 ± 0.72 mm against *E. coli* corresponding to 23.2 ± 0.12 mm and 22.5 ± 0.63 mm for ampicillin and gentamicin, respectively. The MIC value for CMC-CNT20 was 1.95 µg/mL against both *S. aureus* and *E. coli* corresponding to 0.98 and 1.95 µg/mL for antibiotics ampicillin and gentamicin, respectively. It was postulated that the highly hydrophilic composite potent result from penetration inside the microbe and cause osmotic imbalances, which enhanced the mode of growth inhibition. Moreover, the presence of CNTs has a synergistic effect in destroying the microbial cell membrane and suppressing the microbial growth. Elsewhere in the literature, it was reported that functionalization of CNT and polymer led to the formation of ester linkages from the condensation of the carboxylic acid of acrylic acid-grafted poly(butylene adipate-co-terephthalate) (PBAT-g-AA) with the hydroxyl groups of multi-hydroxyl functionalized multi-walled carbon nanotubes (MWCNT-OH) [89]. This resulted in strong antibacterial activity against *E. coli* (BCRC 10239) when compared to poly(butylene adipate-co-terephthalate) (PBAT)/multiwalled carbon nanotubes (MWCNTs) nanocomposites. This was attributed to electrostatic

interactions between the composite and bacterial strains since *E. coli* with an extracellular capsule carry a less negative charge and are less prone to adsorption on the positively charged surface of PBAT-g-AA/MWCNT-OH. An et al. [3] prepared composite blend of polylactic acid/polyurethane (PLA/PU) reinforced with graphene oxide (GO) through solution mixing. In this case, the authors prepared composites based on two different concentration of GO i.e. 3wt% (PLA/PU3) and 5wt% (PLA/PU5) to evaluate their antibacterial efficiency against gram-negative and gram-positive bacteria. It was reported the incorporation of 5 wt% of GO into PLA/PU reduced *E. coli* and *S. aureus* growth up to 100%, while 3 wt% reduced *E. coli* growth up to 100% and *S. aureus* growth up to 99% after 24 h of incubation. Moreover, after 4 h of incubation with PLA/PU3 and PLA/PU5 composites at 37 °C, the antibacterial activity for *E. coli* was 54 and 91%, whereas 54 and 89% were recorded for *S. aureus*, respectively. This confirms the antibacterial efficacy of GO which was dependent on its content as shown in Fig. 8. It can be seen that after 4 h of incubation of both bacteria (viz. *E. coli* and *S. aureus*) lost their original appearance. This was attributed to the effect of either oxidative stress or physical disruption related to the carbon nanomaterials. Despite the antibacterial efficiency of graphene nanosheets, it can also serve as substrate or matrix for the antimicrobial agent [91].

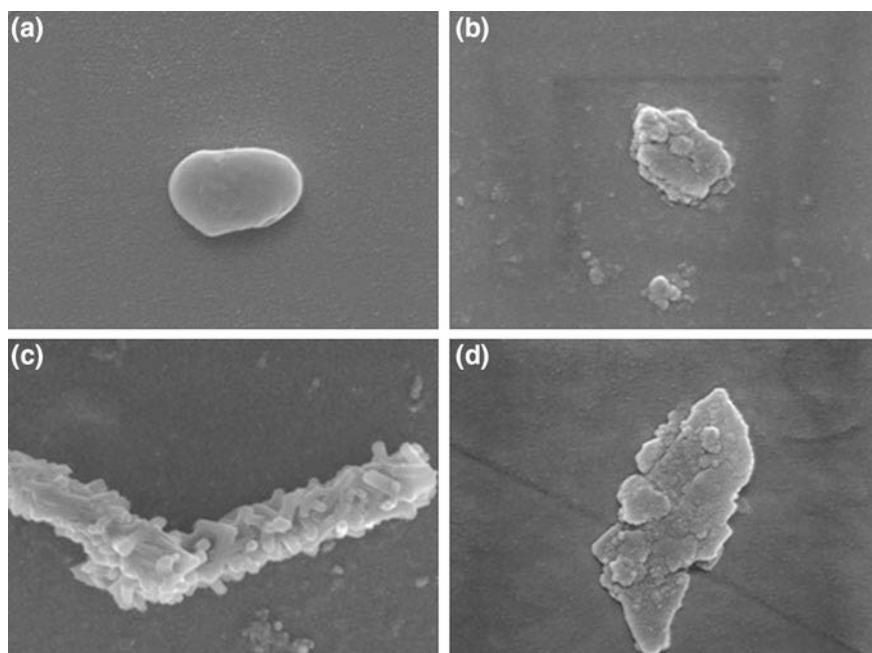


Fig. 8 SEM images of *S. aureus* attached to **a** glass plate and **b** PLA/PU/G5 for 4 h incubation at 37 °C SEM images of *E. coli* attached on **c** glass plate and **d** PLA/PU/GO (5%) for 4 h incubation at 37 °C. Reprinted from [3]

4.6 Clay Minerals/Biopolymer Nanocomposites

In most cases, clay is usually added to different polymeric materials to improve the mechanical and thermal properties of the resulting nanocomposite product. In case of packaging, clay minerals were found to improve the barrier property which is one of the important aspects [17]. The most used method of preparation is solution intercalation. It is recognized that the modification of clay minerals plays an important role in their antibacterial activity especially the presence of quaternary ammonium groups [67, 68]. On contrary, [51] reported that unmodified montmorillonite displayed good antibacterial activity against *S. aureus* and *E. faecalis* antibacterial. The authors mentioned that this scenario could be related to the preparation method of the composites and composites. The nanocomposites were prepared through solution casting. Despite unmodified MMT not showing any antibacterial activity, the nanocomposites showed good antibacterial activity towards *S. aureus* and *E. faecalis* as well as lactose-positive bacteria from *Enterobacteriaceae* family. This was attributed to a very good homogeneity obtained from the preparation method. A comparison between three nanoclays i.e. Cloisite 20A (dimethyl di(hydrogenated tallowalkyl) quaternary ammonium), Cloisite 30B (bis-(2-hydroxyethyl) methyl(hydrogenated tallowalkyl) quaternary ammonium) and unmodified Cloisite Na⁺ was reported by Sothornvit et al. [80]. PLA/nanoclay composites were prepared via solution casting using chloroform as a solvent. On contrary to the previous study, it was reported in this study that the unmodified-based composites showed no antibacterial activity towards gram negative and gram-positive bacteria. Despite Cloisite 30B nanoclay showing antibacterial activity towards both gram negative and gram positive bacteria, its composites showed bacteriostatic against *L. monocytogenes*, while Cloisite 20 A based composites displayed no antibacterial activity. However, it is worth mentioning that the antibacterial activity of the nanoclays also depends on the polymer properties especially hydrophilicity which plays a major role for the bacteria to enter the composite material. Rhim et al. [67] reported that Cloisite 30B showed good antibacterial activity towards gram negative and positive bacteria when using chitosan as host matrix. This was attributed to the hydrophilicity of chitosan and the solvent used to prepare the composites i.e. acetic acid. [45] modified clay with cetyl trimethylammonium bromide (CTAB) to improve its antibacterial efficiency. It was found that the CTAB modified clay composites exhibited good antibacterial activity against *B. subtilis* and *S. aureus*. This was attributed to the presence of long chain hydrophobic alkyl and cationic charge of a quaternary ammonium group in modified clay. Zones of inhibition diameter of PBAT/modified nanoclay nanocomposites were 11.2, 13.7, 12.0 mm against *B. subtilis* and 11.1, 13.5, 11.5 mm against *S. aureus* with loading 2, 4, and 8 wt%, respectively. Besides good antibacterial efficacy, PBAT/modified nanoclay composites showed the greater degree of property enhancement of water vapor transmission rate as well as low degradation rate when compared to unmodified clay composites. The latter was attributed to the smooth surfaces obtained from modified clay composites.

The antibacterial activity for nanoclay (rectorite modified with CTAB) under different conditions i.e. weak acid, under weak acid, water, and weak basic condition was reported by Wang et al. [88]. It was reported that the nanocomposites displayed good antibacterial activity against both gram negative and positive bacteria in all media. This was ascribed to high affinity and the strong interaction between host matrix and modified nanoclay resulting in adsorption and immobilization capacity of modified nanoclay and the antimicrobial activity of host matrix i.e. quaternized chitosan.

5 Hybrid Biopolymer Nanocomposites

A combination of two or more nanoparticles is often introduced into polymeric materials with the aim of overcoming the limitations of one filler by other filler [32]. In some cases, the introduction of the second nanofiller may also improve the antibacterial efficiency of the resulting nanocomposite material. Li et al. [32] developed green nanocomposites material based on PLA/silver/titanium nanoparticles hybrid composite. It reported that the hybrid composites showed a significant improvement in the thermal stability and mechanical properties, while the antibacterial efficiency increased with increase in the concentration of silver nanoparticles as second filler. Vasile et al. [82] recently reported on the preparation of PLA reinforced with Cu-doped ZnO powder functionalized with AgNPs nanocomposites with melt compounding method. It was stated that the optimum composition was PLA/ZnO: Cu/Ag 0.5 to give suitable mechanical and thermal properties, good barrier properties to ultraviolet light, water vapour, oxygen and carbon dioxide, antibacterial activity and low migration amount of nanoparticles into food simulants. These results suggested that the prepared nanocomposites have potential to be used in food packaging.

In situ preparation of silver nanoparticles was carried out by mixing silver ionic solution with cellulose nanocrystals and then introduced into a blend of PLA/PBAT [34]. The antibacterial activity of the PLA/PBAT/NCC-Ag nanocomposite films was studied by using a testing protocol similar to Kirby-Bauer disc diffusion test and it was reported that thickness of the inhibition rings in the growth of *Gram-negative Escherichia coli* and *Gram-positive Staphylococcus aureus* is around 2.6 and 1.8 mm, respectively. On the other hand, the killing efficiency of the composites against *Escherichia coli* was determined to be 99.7% obtained from plate count method. [81] investigated the antibacterial property of a poly (lactic acid) nanosilver-doped multiwall carbon nanotube nanocomposite. It was reported that the antibacterial activity (Fig. 9) declined with increasing in MWCNT-Ag content in the nanocomposites. Furthermore, the authors claimed that the MWCNT-Ag synergy was able to transfer the antimicrobial properties of the PLA.

Fig. 9 Antibacterial activity of the PLA and PLA/MWCNT-Ag nanocomposites particles in the PLA matrix [81]

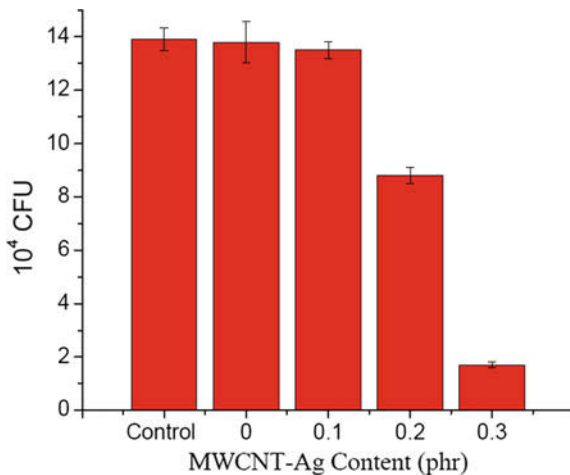
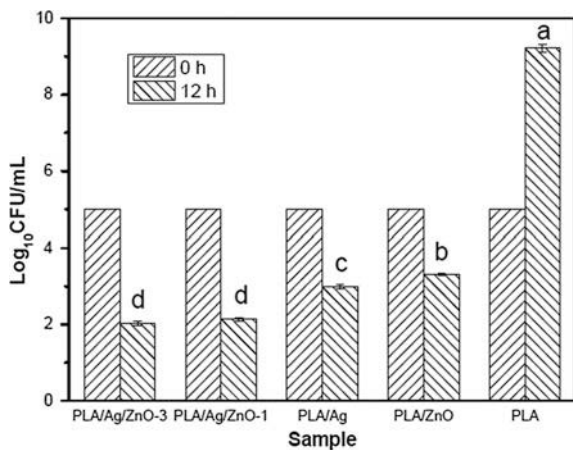


Fig. 10 Antimicrobial activity of pure PLA and PLA nano-composite films. Values followed by different superscript letters (a–e) in the same column were significantly different ($p < 0.05$), where a is the highest value[14]



Solvent volatilizing method was used for the preparation of antimicrobial active based on PLA with nanosilver (Ag) and nano-zinc oxide (ZnO) [14]. The antimicrobial properties of both nanoparticles and their synergy were investigated for inhibition of *E. coli* growth. It was noted by the authors that the control film, neat PLA film, had no antimicrobial activity (Fig. 10) to inhibit the growth of *E. coli*. The addition of two nanoparticles separately reduced the \log_{10} CFU/mL values (Fig. 10) of the PLA nano-composite. This was attributed to the nanoparticle being able to release the surface of the films through the micro-voids, formed in the PLA nanocomposites film by nanoparticles and restrained the growth of *E. coli*. The synergy between ZnO and Ag decreased the \log_{10} CFU/ML values further in comparison to single nano.

6 Conclusion and Future Recommendations

It can be concluded that the use of nanoparticles as antibacterial agents not only improve the antibacterial efficacy but contribute to the overall properties of the resulting nanocomposites. Amongst all synthesized routes for antibacterial nanoparticles, green methods using abundantly available natural products is of significant importance from biomedical and packaging point of view. These techniques avoid the use of toxic chemicals which can reside within nanoparticles that can be hazardous to human and animals. The possibility of large-scale production using green methods makes this technique one of the most interesting for future research. Even though nanoparticles possess high antibacterial properties with low toxicity towards mammalian cells, general concerns about the potential hazard to the environment and human beings need to be addressed. At the current moment, very little information is available to assess the migration of nanoparticles and possible hazard to human beings and the environment despite the claims that nanoparticles synthesized from green routes have a lower impact on the environment. Among all metallic nanoparticles, silver nanoparticles are the most studied which calls for more research on other cheaper metals having similar properties as silver nanoparticles. Hybridization or combination of two or more nanoparticles incorporated into the common polymer and/or polymer blends serve as one of the promising subjects for the future especially in biomedical in order to eradicate multidrug resistant bacteria.

References

1. Abdel Rahim K, Mahmoud SY, Ali AM et al (2017) Extracellular biosynthesis of silver nanoparticles using *Rhizopus stolonifer*. Saudi J Biol Sci. <https://doi.org/10.1016/j.sjbs.2016.02.025>
2. Agarwal H, Venkat Kumar S, Rajeshkumar S (2017) A review on green synthesis of zinc oxide nanoparticles—An eco-friendly approach. Resour Technol. <https://doi.org/10.1016/j.refit.2017.03.002>
3. An X, Ma H, Liu B, Wang J (2013) Graphene oxide reinforced polylactic acid/polyurethane antibacterial composites. J Nanomater. <https://doi.org/10.1155/2013/373414>
4. Ana MD, Angel LD (2014) ZnO-reinforced poly (3-hydroxybutyrate- co -3-hydroxyvalerate) bionanocomposites with antimicrobial function for food packaging. J Mol Sci, Int. <https://doi.org/10.3390/ijms150610950>
5. Agustin YE, Padmawijara (2017) Effect of glycerol and zinc oxide addition on antibacterial activity of biodegradable bioplastics from chitosan-kepok banana peel starch. <https://doi.org/10.1088/1757-899x/223/1/012046>
6. Augustine R, Malik HN, Singhal DK, et al (2014) Electrospun polycaprolactone/ZnO nanocomposite membranes as biomaterials with antibacterial and cell adhesion properties. J Polym Res. <https://doi.org/10.1007/s10965-013-0347-6>
7. Baheri B, Shahverdi M, Rezakazemi M et al (2015) Performance of PVA/NaA Mixed matrix membrane for removal of water from ethylene glycol solutions by pervaporation. Chem Eng Commun 202:316–321. <https://doi.org/10.1080/00986445.2013.841149>

8. Bayer IS (2017) Thermomechanical properties of polylactic review for biomedical applications. <https://doi.org/10.3390/ma10070748>
9. Bothoko OJ, Ramontja J, Ray SS (2017) Thermally shocked graphene oxide-containing biocomposite for thermal management applications. *RSC Adv* 7:33751–33756. <https://doi.org/10.1039/c7ra05421a>
10. Castro-Mayorga J, Fabra M, Cabedo L, Lagaron J (2016) On the use of the electrospinning coating technique to produce antimicrobial polyhydroxyalkanoate materials containing in situ-stabilized silver nanoparticles. *Nanomaterials*. <https://doi.org/10.3390/nano7010004>
11. Castro Mayorga JL, Fabra Rovira MJ, Cabedo Mas L et al (2018) Antimicrobial nanocomposites and electrospun coatings based on poly(3-hydroxybutyrate-co-3-hydroxyvalerate) and copper oxide nanoparticles for active packaging and coating applications. *J Appl Polym Sci*. <https://doi.org/10.1002/app.45673>
12. Chandra S, Kumar A, Tomar PK (2014) Synthesis and characterization of copper nanoparticles by reducing agent. *J Saudi Chem Soc* 18:149–153. <https://doi.org/10.1016/j.jscs.2011.06.009>
13. Chen H, Wang B, Gao D et al (2013) Broad-spectrum antibacterial activity of carbon nanotubes to human gut bacteria. 2735–2746. <https://doi.org/10.1002/sml.201202792>
14. Chu Z, Zhao T, Li L et al (2017) Characterization of antimicrobial poly (lactic acid)/ nano-composite films with silver and zinc oxide nanoparticles. *Materials* (Basel). <https://doi.org/10.3390/ma10060659>
15. Chung IM, Rahuman AA, Marimuthu S et al (2017) Green synthesis of copper nanoparticles using *Eclipta prostrata* leaves extract and their antioxidant and cytotoxic activities. 18–24. <https://doi.org/10.3892/etm.2017.4466>
16. De Azeredo HMC (2009) Nanocomposites for food packaging applications. *Food Res. Int*. <https://doi.org/10.1016/j.foodres.2009.03.019>
17. De Azeredo HMC (2013) Antimicrobial nanostructures in food packaging. *Trends Food Sci Technol* <https://doi.org/10.1016/j.tifs.2012.11.006>
18. Din MI, Arshad F, Hussain Z, Mukhtar M (2017) Green adeptness in the synthesis and stabilization of copper nanoparticles : catalytic, antibacterial, cytotoxicity, and antioxidant activities. <https://doi.org/10.1186/s11671-017-2399-8>
19. El-ghany NAA (2017) Antimicrobial activity of new carboxymethyl chitosan–carbon nanotube biocomposites and their swell ability in different pH media. *J Carbohydr Chem* 0:1–14. <https://doi.org/10.1080/07328303.2017.1353610>
20. Espinoza-go H, Alonso-nu G, Sua J (2017) A green synthesis of copper nanoparticles using native cyclodextrins as stabilizing agents. *J Saudi Chem Soc* 341–348. <https://doi.org/10.1016/j.jscs.2016.10.005>
21. Geetha MS, Nagabhushana H, Shivananjaiah HN (2016) Green mediated synthesis and characterization of ZnO nanoparticles using *Euphorbia Jatropha* latex as reducing agent. *J Sci Adv Mater Devices*. <https://doi.org/10.1016/j.jsamd.2016.06.015>
22. Gopinath V, Priyadarshini S, Loke MF et al (2017) Biogenic synthesis, characterization of antibacterial silver nanoparticles and its cell cytotoxicity. *Arab J Chem*. <https://doi.org/10.1016/j.arabjc.2015.11.011>
23. Gopiraman M, Jatoti AW, Hiromichi S et al (2016) Silver coated anionic cellulose nanofiber composites for an efficient antimicrobial activity. *Carbohydr Polym*. <https://doi.org/10.1016/j.carbpol.2016.04.084>
24. Gunalan S, Sivaraj R, Rajendran V (2012) Green synthesized ZnO nanoparticles against bacterial and fungal pathogens. *Prog Nat Sci Mater Int*. <https://doi.org/10.1016/j.pnsc.2012.11.015>
25. Hasan SS, Singh S, Parikh RY, Dharne MS (2008) Bacterial synthesis of copper/copper oxide nanoparticles bacterial synthesis of copper/copper oxide nanoparticles. <https://doi.org/10.1166/jnn.2008.095>
26. Huang KS, Yang CH, Huang SL et al (2016) Recent advances in antimicrobial polymers: a mini-review. *Int J Mol Sci* 17(9):1578. <https://doi.org/10.3390/ijms17091578>

27. José De Andrade C, Maria De Andrade L, Mendes MA, Oller Do Nascimento CA (2017) An overview on the production of microbial copper nanoparticles by bacteria, fungi and algae. *Glob J Res Eng*
28. Judith P, Espitia P (2012) Zinc oxide nanoparticles : synthesis, antimicrobial activity and food packaging applications. *Food Bioprocess Technol* 1447–1464. <https://doi.org/10.1007/s11947-012-0797-6>
29. Kang S, Pinault M, Pfefferle LD et al (2007) Single-walled carbon nanotubes exhibit strong antimicrobial activity. *Langmuir* 23(17):8670–8673. <https://doi.org/10.1021/la701067r>
30. Khan A, Rashid A, Younas R, Chong R (2015) A chemical reduction approach to the synthesis of copper nanoparticles. *Int Nano Lett.* <https://doi.org/10.1007/s40089-015-0163-6>
31. Li SM, Jia N, Ma MG, et al (2011) Cellulose-silver nanocomposites: Microwave-assisted synthesis, characterization, their thermal stability, and antimicrobial property. *Carbohydr Polym.* <https://doi.org/10.1016/j.carbpol.2011.04.060>
32. Li W, Zhang C, Chi H et al (2017) Development of antimicrobial packaging film made from poly(lactic acid) incorporating titanium dioxide and silver nanoparticles. *Molecules.* <https://doi.org/10.3390/molecules22071170>
33. Li X, Xiao Y, Bergeret A, et al (2014) Preparation of polylactide/graphene composites from liquid-phase exfoliated graphite sheets. <https://doi.org/10.1002/pc.22673>
34. Ma P, Jiang L, Yu M et al (2016) Green antibacterial nanocomposites from Poly (lactide)/ Poly (butylene adipate -co-terephthalate)/nanocrystal cellulose-silver nanohybrids
35. Martynková GS, Valášková M (2014) Antimicrobial nanocomposites based on natural modified materials: a review of carbons and clays. *J Nanosci Nanotechnol.* <https://doi.org/10.1166/jnn.2014.8903>
36. Mary G, Bajpai SK, Chand N (2009) Copper (II) Ions and copper nanoparticles-loaded chemically modified cotton cellulose fibers with fair antibacterial properties. <https://doi.org/10.1002/app>
37. Matinise N, Fuku XG, Kaviyarasu K et al (2017) Applied Surface Science ZnO nanoparticles via *Moringa oleifera* green synthesis: Physical properties & mechanism of formation. *Appl Surf Sci* 406:339–347. <https://doi.org/10.1016/j.apsusc.2017.01.219>
38. Mendoza G, Regiel-Futyr A, Andreu V et al (2017) Bactericidal effect of gold-chitosan nanocomposites in coculture models of pathogenic bacteria and human macrophages. *ACS Appl Mater Interfaces* 9:17693–17701. <https://doi.org/10.1021/acsami.6b15123>
39. Mochane MJ, Luyt AS (2015) Synergistic effect of expanded graphite, diammonium phosphate and Cloisite 15A on flame retardant properties of EVA and EVA/wax phase-change blends. *J Mater Sci* 50:3485–3494. <https://doi.org/10.1007/s10853-015-8909-0>
40. Mochane MJ, Luyt AS (2015) The effect of expanded graphite on the thermal stability, latent heat, and flammability properties of EVA/wax phase change blends. *Polym Eng Sci* 55:1255–1262. <https://doi.org/10.1002/pen.24063>
41. Mokhena TC, Jacobs NV, Luyt AS (2018) Nanofibrous alginate membrane coated with cellulose nanowhiskers for water purification. *Cellulose* 25. <https://doi.org/10.1007/s10570-017-1541-1>
42. Mokhena TC, Jacobs V, Luyt AS (2015) A review on electrospun bio-based polymers for water treatment. *Express Polym Lett* 9. <https://doi.org/10.3144/expresspolymlett.2015.79>
43. Mokhena TC, Luyt AS (2017) Development of multifunctional nano/ultrafiltration membrane based on a chitosan thin film on alginate electrospun nanofibres. *J Clean Prod* 156:. <https://doi.org/10.1016/j.jclepro.2017.04.073>
44. Mokhena TC, Luyt AS (2017) Electrospun alginate nanofibres impregnated with silver nanoparticles: preparation, morphology and antibacterial properties. *Carbohydr Polym* 165. <https://doi.org/10.1016/j.carbpol.2017.02.068>
45. Mondal D, Bhowmick B, Mollick MMR et al (2014) Antimicrobial activity and biodegradation behavior of poly(butylene adipate-co-terephthalate)/clay nanocomposites. *J Appl Polym Sci.* <https://doi.org/10.1002/app.40079>
46. Palza H (2015) Antimicrobial polymers with metal nanoparticles. *Int J Mol, Sci*

47. Palza H, Quijada R, Delgado K (2015) Antimicrobial polymer composites with copper micro- and nanoparticles: effect of particle size and polymer matrix. *J Bioact Compat Polym*. <https://doi.org/10.1177/0883911515578870>
48. Phogat N, Khan SA, Shankar S, et al (2016) Fate of inorganic nanoparticles in agriculture. *Adv. Mater. Lett*
49. Pinto RJB, Marques PAAP, Neto CP, et al (2009) Antibacterial activity of nanocomposites of silver and bacterial or vegetable cellulosic fibers. *Acta Biomater*. <https://doi.org/10.1016/j.actbio.2009.02.003>
50. Prabhu YT, Rao KV, Sai VS, Pavani T (2017) ORIGINAL ARTICLE A facile biosynthesis of copper nanoparticles: a micro-structural and antibacterial activity investigation. *J Saudi Chem Soc* 21:180–185. <https://doi.org/10.1016/j.jscs.2015.04.002>
51. Rapacz-Kmita A, Pierchała MK, Tomas-Trybuś A et al (2017) The wettability, mechanical and antimicrobial properties of polylactide/montmorillonite nanocomposite films. *Acta Bioeng Biomech*. <https://doi.org/10.5277/abb-00820-2017-02>
52. Review CNA, Gonçalves C (2017) Poly (lactic acid) composites containing. 1–37. <https://doi.org/10.3390/polym9070269>
53. Rezakazemi M, Dashti A, Riasat Harami H et al (2018) Fouling-resistant membranes for water reuse. *Environ Chem Lett* 1–49. <https://doi.org/10.1007/s10311-018-0717-8>
54. Rezakazemi M, Ebadi Amooghin A, Montazer-Rahmati MM et al (2014) State-of-the-art membrane based CO₂ separation using mixed matrix membranes (MMMs): an overview on current status and future directions. *Prog Polym Sci* 39:817–861. <https://doi.org/10.1016/j.progpolymsci.2014.01.003>
55. Rezakazemi M, Khajeh A, Meshbah M (2017) Membrane filtration of wastewater from gas and oil production. *Environ Chem Lett* 1–22. <https://doi.org/10.1007/s10311-017-0693-4>
56. Rezakazemi M, Mohammadi T (2013) Gas sorption in H₂-selective mixed matrix membranes: experimental and neural network modeling. *Int J Hydrogen Energy* 38:14035–14041. <https://doi.org/10.1016/j.ijhydene.2013.08.062>
57. Rezakazemi M, Razavi S, Mohammadi T, Nazari AG (2011) Simulation and determination of optimum conditions of pervaporative dehydration of isopropanol process using synthesized PVA-APTEOS/TEOS nanocomposite membranes by means of expert systems. *J Memb Sci* 379:224–232. <https://doi.org/10.1016/j.memsci.2011.05.070>
58. Rezakazemi M, Sadrzadeh M, Matsuura T (2018) Thermally stable polymers for advanced high-performance gas separation membranes. *Prog Energy Combust Sci* 66:1–41. <https://doi.org/10.1016/j.peccs.2017.11.002>
59. Rezakazemi M, Sadrzadeh M, Mohammadi T (2017b) Separation via pervaporation techniques through polymeric membranes
60. Rezakazemi M, Sadrzadeh M, Mohammadi T, Matsuura T (2017) Methods for the preparation of organic-inorganic nanocomposite polymer electrolyte membranes for fuel cells
61. Rezakazemi M, Shahidi K, Mohammadi T (2012) Sorption properties of hydrogen-selective PDMS/zeolite 4A mixed matrix membrane. *Int J Hydrogen Energy* 37:17275–17284. <https://doi.org/10.1016/j.ijhydene.2012.08.109>
62. Rezakazemi M, Shahidi K, Mohammadi T (2012) Hydrogen separation and purification using crosslinkable PDMS/zeolite A nanoparticles mixed matrix membranes. *Int J Hydrogen Energy* 37:14576–14589. <https://doi.org/10.1016/j.ijhydene.2012.06.104>
63. Rezakazemi M, Shahidi K, Mohammadi T (2015) Synthetic PDMS composite membranes for pervaporation dehydration of ethanol. *Desalin Water Treat* 54:1542–1549. <https://doi.org/10.1080/19443994.2014.887036>
64. Rezakazemi M, Shahverdi M, Shirazian S et al (2011) CFD simulation of water removal from water/ethylene glycol mixtures by pervaporation. *Chem Eng J* 168:60–67. <https://doi.org/10.1016/j.cej.2010.12.034>
65. Rezakazemi M, Vatani A, Mohammadi T (2015) Synergistic interactions between POSS and fumed silica and their effect on the properties of crosslinked PDMS nanocomposite membranes. *RSC Adv* 5:82460–82470. <https://doi.org/10.1039/c5ra13609a>

66. Rezakazemi M, Vatani A, Mohammadi T (2016) Synthesis and gas transport properties of crosslinked poly(dimethylsiloxane) nanocomposite membranes using octatrimethylsiloxy POSS nanoparticles. *J Nat Gas Sci Eng* 30:10–18. <https://doi.org/10.1016/j.jngse.2016.01.033>
67. Rhim J-W, Hong S-K, Park H-M, N.g PKW (2006) Preparation and Characterization of Chitosan-Based Nanocomposite Films with Antimicrobial Activity. *J. Agric. Food Chem.* 54, 16, 5814–5822. <https://doi.org/10.1021/jf060658h>
68. Rhim JW, Park HM, Ha CS (2013) Bio-nanocomposites for food packaging applications. *Prog Polym Sci.* <https://doi.org/10.1016/j.progpolymsci.2013.05.008>
69. Rostamizadeh M, Rezakazemi M, Shahidi K, Mohammadi T (2013) Gas permeation through H₂-selective mixed matrix membranes: experimental and neural network modeling. *Int J Hydrogen Energy* 38:1128–1135. <https://doi.org/10.1016/j.ijhydene.2012.10.069>
70. Sadeghi A, Nazem H, Rezakazemi M, Shirazian S (2018) Predictive construction of phase diagram of ternary solutions containing polymer/solvent/nonsolvent using modified Flory-Huggins model. *J Mol Liq* 263:282–287. <https://doi.org/10.1016/j.molliq.2018.05.015>
71. Sadrzadeh M, Rezakazemi M, Mohammadi T (2017) Fundamentals and measurement techniques for gas transport in polymers
72. Laudenslager MJ, Schiffman JD, Schauer CL (2008) Carboxymethyl chitosan as a matrix material for platinum, gold, and silver nanoparticles. 2682–2685. <https://doi.org/10.1021/bm800835e>
73. Sengupta R, Bhattacharya M, Bandyopadhyay S, Bhowmick AK (2011) A review on the mechanical and electrical properties of graphite and modified graphite reinforced polymer composites. *Prog Polym Sci* 36:638–670. <https://doi.org/10.1016/j.progpolymsci.2010.11.003>
74. Satyvvaldiev AS, Zhasnakunov ZK, Omurzak E, Doolotkeldieva TD, Bobusheva ST, Orozmatova GT, Kelgenbaeva Z (2018) Copper nanoparticles : synthesis and biological activity. <https://doi.org/10.1088/1757-899x/302/1/012075>
75. Shahverdi M, Baheri B, Rezakazemi M et al (2013) Pervaporation study of ethylene glycol dehydration through synthesized (PVA-4A)/polypropylene mixed matrix composite membranes. *Polym Eng Sci* 53:1487–1493. <https://doi.org/10.1002/pen.23406>
76. Shankar S, Rhim J (2016) LWT—food science and technology tocopherol-mediated synthesis of silver nanoparticles and preparation of antimicrobial pbat/silver nanoparticles composite films. *LWT - Food Sci Technol* 72:149–156. <https://doi.org/10.1016/j.lwt.2016.04.054>
77. Shankar S, Wang LF, Rhim JW (2016) Preparations and characterization of alginate/silver composite films: effect of types of silver particles. *Carbohydr Polym.* <https://doi.org/10.1016/j.carbpol.2016.03.026>
78. Shih CM, Shieh YT, Twu YK (2009) Preparation of gold nanopowders and nanoparticles using chitosan suspensions. *Carbohydr Polym* 78:309–315. <https://doi.org/10.1016/j.carbpol.2009.04.008>
79. Shittu KO, Bankole MT, Abdulkareem AS et al (2017) Application of gold nanoparticles for improved drug efficiency
80. Sothornvit R, Rhim JW, Hong SI (2009) Effect of nano-clay type on the physical and antimicrobial properties of whey protein isolate/clay composite films. *J Food Eng.* <https://doi.org/10.1016/j.jfoodeng.2008.09.026>
81. Tsou CH, Yao WH, Lu YC, et al (2017) Antibacterial property and cytotoxicity of a poly (lactic acid)/nanosilver-doped multiwall carbon nanotube nanocomposite. *Polymers (Basel)* 9. <https://doi.org/10.3390/polym9030100>
82. Vasile C, Răpă M, Ștefan M et al (2017) New PLA/ ZnO: Cu/ Ag bionanocomposites for food packaging. 11:531–544
83. Venkatesan R, Rajeswari N (2017) TiO₂ nanoparticles/poly(butylene adipate-co-terephthalate) bionanocomposite films for packaging applications. <https://doi.org/10.1002/pat.4042>
84. Venkatesan R, Rajeswari N, Tamilselvi A (2018) Antimicrobial, mechanical, barrier, and thermal properties of bio-based poly (butylene adipate-co-terephthalate) (PBAT)/Ag₂O nanocomposite films for packaging application. <https://doi.org/10.1002/pat.4089>
85. Venkatesan R, Rajeswari N (2016) ZnO/PBAT nanocomposite films : investigation on the mechanical and biological activity for food packaging. <https://doi.org/10.1002/pat.3847>

86. Vimbela GV, Ngo SM, Frazee C, Yang L, David A Stout DA (2017) Antibacterial properties and toxicity from metallic nanomaterials. *Int J Nanomedicine* 12:3941–3965. <https://doi.org/10.2147/ijn.s134526>
87. Vivekanandhan S, Christensen L, Misra M, Kumar Mohanty A (2012) Green process for impregnation of silver nanoparticles into microcrystalline cellulose and their antimicrobial bionanocomposite films. *J Biomater Nanobiotechnol*. <https://doi.org/10.4236/jbnb.2012.33035>
88. Wang X, Du Y, Luo J, et al (2009) A novel biopolymer/rectorite nanocomposite with antimicrobial activity. *Carbohydr Polym*. <https://doi.org/10.1016/j.carbpol.2009.01.015>
89. Wu CS (2009) Antibacterial and static dissipating composites of poly(butylene adipate-co-terephthalate) and multi-walled carbon nanotubes. *Carbon N Y* 47:3091–3098. <https://doi.org/10.1016/j.carbon.2009.07.023>
90. Wu D, Cheng Y, Feng S, et al (2013) Crystallization behavior of polylactide/graphene composites crystallization behavior of polylactide/graphene composites. <https://doi.org/10.1021/ie4004199>
91. Yan X, Li F, Di Hu K et al (2017) Nacre-mimic reinforced Ag@reduced graphene oxide-sodium alginate composite film for wound healing. *Sci Rep*. <https://doi.org/10.1038/s41598-017-14191-5>

Extraction of Nano Cellulose Fibres and Their Eco-friendly Polymer Composite



Bashiru Kayode Sodipo and Folahan Abdul Wahab Taiwo Owolabi

1 Introduction

Global green revolution aimed at mitigating the negative ecological effect of polymeric materials has led to research and development into various sustainable and renewable eco-friendly materials to replace petroleum-based materials [1–3].

Nano fibre cellulose (NFC) is one of the most attractive renewable materials for advanced applications. This is due to its mechanical and physical properties. NFC consists of flexible cellulosic nano-material with lateral dimensions of about 10–100 nm diameter and several micrometres long [4]. They are described as long flexible nanofilaments composed of a crystalline and amorphous portion [5]. Nanocellulose can be divided into three types of materials: (I) nano-fiber cellulose (NFC), (II) nanocrystals cellulose (NCC) or cellulose nanowhiskers (CNWs), and (III) bacterial cellulose (BC). However, a report in this book chapter covers only that of NFC and typical TEM micrograph of NFC is shown in Fig. 1.

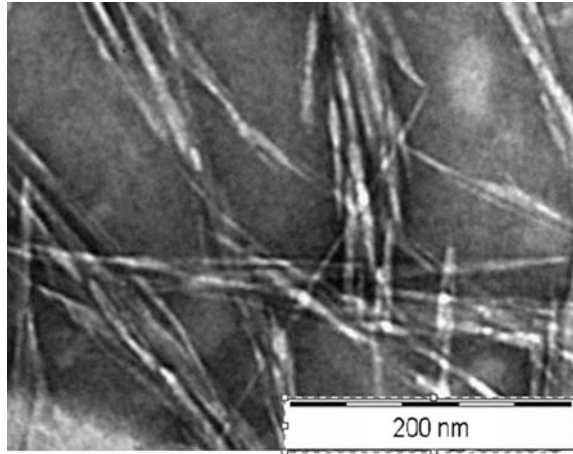
Unlike Petroleum based and synthetic polymer nanocomposite, NFC polymer nanocomposite has many advantages due to low weight, reduced tool wearing, recyclable and biodegradable properties [6]. Moreover, in order to develop a fully eco-friendly polymer nanocomposite, the use of a reinforcement derived from renewable biomass is needed. Petroleum-based polymers have gained attention due to a variety

The original version of this chapter was inadvertently published with the incorrect author sequence and corresponding author. The correction to this chapter is available at https://doi.org/10.1007/978-3-030-05399-4_48

B. K. Sodipo (✉)
Department of Physics, Kaduna State University, Kaduna, Nigeria
e-mail: bashirsodipo@gmail.com

F. A. W. T. Owolabi
Pulp and Paper division, Federal Institute of Industrial Research Oshodi, Oshodi, Nigeria
e-mail: fathok2375@gmail.com

Fig. 1 TEM micrograph of typical nano fiber cellulose



of products, e.g. plastic materials having several superior properties (e.g. water repellence and formability). Despite the wide acceptability of the petroleum-based polymers, there are major disadvantages associated with petroleum-based polymers. These include; crude oil as a non-renewable resource, the products are not bio-degradable, increasing oil prices, dwindling oil resources and a high focus on sustainability.

Similar to the petroleum-based polymer, the global concern towards the potential hazard of the use of the synthetic fibres such as glass (or carbon, aramid, etc.) fibres result in release of CO_2 into the atmosphere (global warming), along with some other health hazardous gases like NO_x and SO_x and dust [7, 8]. In addition, dust and fragments are generated when recycling conventional plastic composites by grinding them down and constitute disposal problem either to landfill or by incineration [9].

All these factors have motivated a renewed interest in bio-based polymers. For the past two decades, research and development on the utilization of the most abundant biopolymer on earth, such as cellulose have resulted in a variety of products, e.g. cellophane, rayon, nitrocellulose (used in gunpowder), adhesives and lacquer [10]. Substantial breakthrough is recorded through the production of the biodegradable composite. The exceptional breakthrough recorded from the properties of the biopolymers has attracted more research findings due to the growing environmental awareness among the consumers. In addition, the natural fibres have high specific strength and modulus, high sound attenuation of lignocellulosic-based composites, non-food agricultural based economy, relatively reactive surface comparatively, easy processability and economical [4].

Previous use of a cellulose-based polymer as ropes, paper, timber for housing structures and its recent use in the field of biopolymers, has proven the ubiquitous and abundant nature of cellulose fibers. The global annual biomass production of cellulose has been reported as about 1.5×10^{12} tons [11]. Natural fibers otherwise referred to as cellulosic fibers are everywhere throughout the world in plants such as grasses, seeds, stalks, and woody vegetation. Apart from the massive availability of cellulose source of NFC, its application in polymer composite has been gaining

universal attention for its environmentally friendly nature and its mechanical reinforcement property [12]. Apart from wood which has been widely exploited commercially as cellulose-based natural bio-resource, other cellulosic materials gaining wide attention include, plants, bacteria, non-wood such as hemp, flax, jute, ramie, cotton and agro-industrial wastes because they contain a natural polyphenolic polymer, lignin, in their structure. The fiber of the cellulose bio-polymers composed of bundles of microfibrils stabilized laterally by inter and intra-molecular hydrogen bonding. In contrast, the use of natural fibers can minimize harmful pollutants, and their eventual breakdown is environmentally benign.

Despite the fact that natural fibers, come from renewable animal or plant sources, they usually lack the high-performance characteristics of many synthetic fibers [13] (Khalil et al. 2016). However, natural fibers fillers or reinforcement in polymeric matrix composites provides positive environmental benefits with respect to ultimate disposability and raw material use [14]. Bio-composites which could be micro or nano-based composite are a family of materials consisting of a polymeric matrix reinforced derived from renewable sources or biodegradables.

2 Production of Cellulose Nanofibrils

NFC can be manufactured basically from Pulping processes which include; Mechanical pulping, Homogenization, Chemical pulping, Steam explosion, High-intensity ultrasonication etc. Furthermore, they can be prepared from a number of different cellulosic sources through an energy-dependent process entailing three major pathways as shown in Fig. 2.

NFC is obtained after a strong mechanical shearing applied on cellulose slurry which is pumped through a homogenizer or grinder device. NFC displayed higher specific area which leads to a higher amount of hydrogen interactions compared with other cellulose fiber-based suspension, and they give gel-like structure at solid content as low as between 2 and 5% [15]. So far, several devices based on a high-pressure homogenizing system such as homogenizer system, micro fluidizer, grinder and recently refiners' devices have been developed to increase the production yield and the quality of the NFC [16].

Several pre-treatments schemes needed in order to obtain fibers with decreased fibrillation energy have been proposed. This include, enzymatic pre-treatment [15], TEMPO-mediated oxidation pre-treatment [17], Carboxymethylation and acetylation [18] and alkaline peroxide pre-treatment [14]. The pre-treatment methods are aimed



Fig. 2 Nanofibrillated cellulose production flow chat

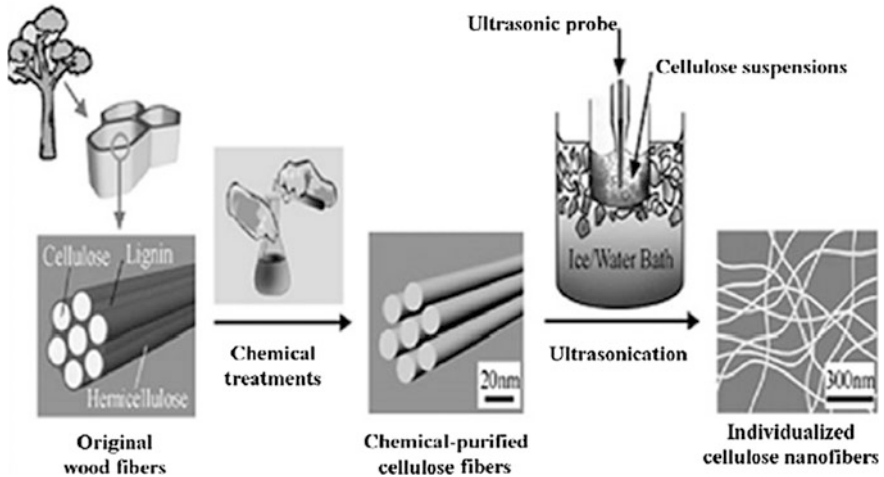


Fig. 3 Schematic process for cellulose nanofibres production [68] copyright permission

at: (a) limiting the hydrogen bonding, (b) increasing the repulsive charge, and (c) decrease the degree of polymerization DP or the amorphous link between individual MFCs. The first and the most common mechanical treatments for NFC production include Gaulin homogenizer and micro fluidizer, grinding process, cryocrushing, electrospinning, energy consumption and new processes. The common mechanical devices used in NFC production are shown in Fig. 3.

According to Syyerud and coworkers (2011) the less energy that is utilized, the less the fibrillation of cellulose fibres and the amount of nanofibrils produced. Since the first successful isolation of cellulose microfibrils was reported by Turbak et al. [19] with the aid of Gaulin laboratory homogenizer, several pathways have been successfully proposed for producing cellulose nanofibrils [15, 17].

All of these methods comprise, Mechanical treatments, e.g. cryocrushing, grinding, high pressure homogenizing, chemical treatments and enzyme-assisted hydrolysis [20]. Other processes include TEMPO-mediated oxidation on the surface of microfibrils with mild mechanical treatment, electrospinning methods and ultrasonic technique. In addition, cellulose fibers are subjected to homogenization, steam explosion, and high-intensity ultra-sonication to disperse the agglomeration of the microfibrils [12]. These methods lead to different types of nanofibrillar materials, depending on the cellulose raw material and its pre-treatment and more importantly, depending on the disintegration process itself.

3 NFC Polymer Composite

Due to the ease of nanofibre dispersal in water, cellulose nano fibre composites have explored primarily solvent casting as means of processing nanocomposites. In another development, Oksman et al. [21] reported the processing of cellulose

Table 1 Summary of recent nano fibrilated cellulose-thermoplastic composites and their applications [69]

Polymer component	Manufacturing technique	Applications
Polyethylene glycol	PEG-g-CNF ribbons by stretching hydrogel	Ultra-high tensile strength and modulus for optoelectronic and medical devices
Amorphous dialcohol cellulose	Oxidation + reduction of CNF surface	Barrier films
Polyethylene	Extrusion	High-performance cellulose environmentally friendly HDPE, Evaluation of cotton filler in LDPE
Thermoplastic starch	Solution casting	Decreased water sensitivity, thermally stable starch
Maize amylopectin	Solution casting	Continuous papermaking
Polyvinyl amine	Layer by layer	Self-healing polymer films
Polyacrylamide	Solution casting	Films with good mechanical, optical thermal and oxygen barrier properties
PVA	Solution casting	Flexible displays, optical devices, packaging and automobile windows, food packaging
Carboxymethyl cellulose	Solution casting	Edible coatings and packaging materials
Poly(butylene adipate-co-terephthalate)	Injection molding	Light-weight and high-performance materials for defense, infrastructure, and energy

nanocomposites using twin-screw extrusion to produce different thermoplastic polymers composite with cellulose nanofibres. Researchers have successfully exploited the use of NFC as biodegradable polymers with improved brittleness, low thermal stability and poor barrier properties [22]. NFC has been successfully used in the field of engineering, biomaterials and medical care. The potential of NFC in research and development of novel research in engineering reinforcement, medical devices and applications in healthcare and veterinary medicine have also been reported. Significant improvements in properties, disposal and recycling problems, combined with environmental and societal concerns have further revealed the potential of NFC [4].

The common nano fibrilated cellulose-thermoplastic composites and their applications are tabulated in Table 1.

4 Challenges of NFC Polymer Composite

In spite of the global trends in the use of NFC in polymer composite, their application as fillers and strength reinforcement in polymer composite has been saddled with a lot of challenges which borders on the intrinsic physical properties.

These physical properties including a high number of hydroxyl groups, leading to strong hydrogen interactions between two nanofibrils and to the gel-like structure once produced [23]. In addition, the high hydrophilicity of this material makes it vulnerable to form agglomerates in petrochemical polymers.

As the dispersal of cellulose NFC in organic solvents is essential, consequently, surface modification of NFC is of utmost importance in order to improve compatibility with a wider variety of matrices. The reactivity of NFC in polymer composite is achievable by its surface modification chemically, to reduce the number of hydroxyl interactions and also to increase the compatibility with several matrices. So, many methods have been proposed for cellulose surface modification [24], which consist of corona or plasma discharges [25], surface derivatization [26], graft copolymerization [27] and use of surfactant [28]. Some approaches aiming at surface modification in order to hydrophobize nanocellulosic include: Acetylation [29], Silylation [30], Grafting [31], grafting in situ catalyzed ring-opening polymerization [32] and the use of coupling agents [33]. Due to strong hydrogen bonding interactions between cellulose hydroxyl groups, it is challenging to obtain well separated NFC in organic solvents, especially for non-polar solvents.

5 Poly-lactic Acid (PLA) Based Nanocellulosic Composites

PLA is biodegradable, thermoplastic and aliphatic polyester derived from renewable resources such as starch. Also, it appears as one of the best sustainable alternatives to petrochemical-derived products [34]. PLA has been found to have good stiffness and strength. It can be processed with conventional plastic processing machinery and is being used in several applications, such as food packaging, water, and milk bottles, and degradable plastic bags as well as in automotive applications [35]. Products made from PLA are biodegradable, eco-friendly and potentially compostable [36, 37]. The performance of PLA can be greatly enhanced by the addition of nano-reinforcements.

Recent studies on PLA had shown that the biopolymer has good mechanical properties, thermal plasticity, and biocompatibility, and is readily fabricated, thus being a promising polymer for various end-use applications [38–40]. However, PLA, similar to polystyrene, is a comparatively brittle and stiff polymer with low deformation at the break and low impact strength. Dufresne et al. [41], reported that the overall mechanical performance of nanocomposites, depends on six factors: (a) Crystallinity of the matrix (b) aspect ratio of additive, (c) volume fraction of additive (d) adhesion and compatibility between the polymer matrix and additives, (e) the orientation of additives (f) stress transfer efficiency of additives. The potential reinforcement efficacy of nanofibre was carried out with PLA using mechanically fibrillated nanofibres [34]. The result shows that Young's modulus and tensile strength of the PLA was increased by 40 and 25%, respectively with the addition of micro-fibrillated cellulose (MFC), without a reduction of yield strain at a fibre content of 10 wt% [13].

Ali Abdulkhali et al. [42] investigated the effect of morphological, thermal, mechanical and barrier properties of PLA based biocomposites prepared with embedded CNF-Ac using a solvent casting procedure. The report has it that, the tensile strength (TS), elastic modulus (EM) and elongation percentage (E) were significantly increased for the prepared cellulose nanocomposites with 3 and 5 wt% CNF-Ac. The reinforcement of PLA with CNF-Ac caused a slight increase in glass transition and melting temperatures. The mechanical tests of PLA and its nanocomposite films results in an improvement in the mechanical properties of PLA composites by the addition of acetylated cellulose nanofibers [34]. This observation is born out of the fact that there was an increase incompatibility between the moieties.

Meanwhile, NFC has shown to be a promising reinforcement of PLA composites. Their contribution to the biodegradability with improved barrier properties has been of immense advantage. The application of PLA as a potential biopolymer to substitute the conventional petroleum-based plastics is gradually gaining the interest of researchers in the area of polymer biocomposite. PLA products are used in packaging films (for textiles and non-wovens), packaging with good barrier properties and low heat-seals. Other areas of interest are a paper coating, fibres, and a host of moulded articles [4].

6 Polyhydroxyalkanoate (PHA) Based Nanocellulosic Composites

PHA are polyesters produced naturally by numerous microorganisms. Different monomers of PHA can be combined to give materials various properties. The availability of PHAs has necessitated much research in the area of biosynthesis, microstructure, thermal and mechanical properties. Research focuses on the application of PHAs in recent years has been driven by its renewable resources and the similarity of PHA physical properties to those of conventional plastics [43, 44]. In the bid to reducing their hydrophilicity, cellulose nanocrystals from microfibrils cellulose were successfully topochemically trimethylsilylated. PHAs are used in packaging films like bags, containers and paper coatings [45]. Analogous applications in conventional commodity plastics include disposable items such as razors, utensils, nappies, feminine hygiene products, cosmetic containers, shampoo bottles and cups [46].

7 Starch-Based Nanocellulosic Composites

Starch-based nanocellulosic as biodegradable thermoplastic materials has offered great potential application in food packaging or biomedical industry. Among the advantages of starch, films are its application as excellent intermediates for

transporting antimicrobials and antioxidants. Different starch sources for starch-based nanocellulose composite have been reported. Polysaccharide sources for starch nanofillers and nanocomposites include flax, ramie, cassava bagasse, wheat straws, regular maize, and chitin, chitosan, among others. Starch comprises of a linear polymer amylose, and a branched polymer amylopectin, with α -(1–6)-linked branch points [49]. Starch sourced from variety of crops such as corn, wheat, rice and potato can be blended with biodegradable polymers such as PHB [50], PLA [51], PCL [52] and chitosan [53]. Apart from its wide availability, starch is a source of biodegradable biopolymer which is readily available at low cost when compared with most synthetic plastics [54]. It has been reported that MFC and biodegradable cellulose have also been reported as promising candidates for starch reinforcement [55]. Some different methods for processing both starch matrix and nanocomposites include solution casting method [56] and extrusion technique [57].

8 NFC Polymer Composite in Thermoplastics Materials

Thermoplastic polymers were compounded with biomaterials to reduce production costs while maintaining original properties. The development of environmentally friendly plastics for production of composites and nanocomposites is ultimately promising. Aliphatic biodegradable polyesters, such as polylactic acid (PLA), polycaprolactone (PCL), poly(3-hydroxybutyrate) (PHB), and polyglycolic acid (PGA), have been widely compounded with different materials to produce green composites. PLA is one of the most promising alternatives to typical plastics and has gained much attention mainly due to its biodegradability. The advantages of cellulose nanocomposite materials in polymer composite compared with conventional composites is that at low reinforcement levels, there is superior thermal, mechanical and barrier properties as well as their improved recyclability, transparency and low weight [21, 22]. Researchers have explored the concept of bio-derived nanocomposites as a route to the development of bioplastics or bioreins with better properties [21, 58]. There is some common eco-friendly nanocomposite which includes: PLA, PHB, and Starch based nanocellulosic composites. This recent shift to “green” composites have necessitated the coupling of various kinds of natural fibers to biodegradable resins such as PLA and modified starch to reinforce plant-derived, polymeric matrix materials and improve their mechanical properties [59].

The fundamental compatibility challenges in the nanocomposite preparations are polymer matrix is hydrophobic while natural fibers are generally hydrophilic. Hence this barrier usually causes non-uniform dispersion of the fibers within the matrix and poor mechanical properties have to be broken to allow for proper coupling of the two or more composite fragments. To overcome this challenges of compatibility and grafting between fibers and thermoplastic matrices in composites production, surface treatment by the use of additives is adopted [9]. The common additives used include chemical coupling agents or compatibilizers Maleated

polyethylene (MAPE) [60], carboxylated polyethylene (CAPE) [61], titanium derived mixture (TDM), Maleic anhydride polypropylene (MAPP), [62], calendaring, [63] thermal treatment [64], reaction with methanol melamine, isocyanates, triazine, silane [65] and mercerization of the matrix [66]. Despite all these possibilities, a better understanding of the molecular structure and interfacial interaction between the matrix and the fibres and the relationship between the structure and property is very important in this area of research [48].

9 NFC Polymer Composite in Automotive

Khalfallah et al. [67] reported that automotive parts industry is highly selective in terms of the matrix characteristics. This means that matrices with good visco-elastic properties, high thermal stability is required for meeting automotive specifications. Nanocomposites have been used in several applications in automotive industries such as various vehicle types of door handles, door panels, instrument panels, parcel shelves, headrests, roofs, upholstery and engine covers and intake manifolds and timing belt covers [68]. The use of green nanocomposite in impellers and blades for vacuum cleaners, power tool housings, mower hoods and covers for portable electronic equipment such as mobile phones are receiving interesting attention [60, 69]. In addition, the recycling by combustion of lignocellulosics filled composites is easier in comparison with inorganic fillers systems. Therefore, the possibility of using lignocellulosic fillers in the plastic industry has received considerable interest. Automotive applications display strong promise for natural fibre reinforcements. 2–5 Potential applications of agrofibre based composites in railways, aircraft, irrigation systems, furniture industries, and sports and leisure items are currently being investigated [35, 70].

10 Conclusions

Cellulose nanofibres have been seen as stimulating potential reinforcements in nanocomposites. Their potential application in medicine, automobile, and construction has been attributed to their size and the ability to undergo surface chemical modification. Several methods channelled towards cellulose nanofibres extraction from cellulose sources have been categorized as chemical and mechanical treatment. In order to reduce the mechanical energy, enzymatic or chemical pre-treatment methods are inevitable. The strength properties of cellulose nanofibres composite compete favourably with other engineering materials, hence, could be useful in high-end technological applications. This study revealed that dispersion of NFC is a very critical step to promote remarkable percolation of NFC by interacting with each other, and with the surrounding matrix, in a way that greatly enhances the mechanical properties of the resultant material. Due to compatibility

problems of nanocellulosic materials and hydrophobic matrices, it can be anticipated that nanocomposites based on hydrophilic matrix polymers will be easier to commercialize. In order to achieve improved mechanical properties in polymer nanocomposites, good filler-matrix interaction is essential. Moreover, in order to develop a fully eco-friendly polymer nanocomposite, the use of a reinforcement derived from renewable biomass is needed. However, by combining the mechanical treatment with certain pre-treatments, various works have shown that it can decrease energy consumption significantly.

Acknowledgements The authors are thankful to the Federal Institute of Industrial Research Oshodi Nigeria and the Kaduna State University, Nigeria for their role in the successful completion of this book chapter.

References

1. Brown TD, Dalton PD, Hutmacher DW (2016) Melt electrospinning today: an opportune time for an emerging polymer process. *Prog Polym Sci* 56:116–166
2. He K, Huo H, Zhang Q, He D, An F, Wang M, Walsh MP (2005a) Oil consumption and CO₂ emissions in China's road transport: current status, future trends, and policy implications. *Energy Policy* 33(12):1499–1507
3. He MC, Xie HP, Peng SP, Jiang YD (2005b) Study on rock mechanics in deep mining engineering. *Chin J Rock Mechan Eng* 24(16):2803–2813
4. Trache D, Hussin MH, Chuin CTH, Sabar S, Fazita MN, Taiwo OF, Hassan TM, Haafiz MM (2016) Microcrystalline cellulose: isolation, characterization and bio-composites application—a review. *Int J Biol Macromole* 93:789–804
5. Abe K, Iwamoto S, Yano H (2007) Obtaining cellulose nanofibers with a uniform width of 15 nm from wood. *Biomacromolecules* 8(10):3276–3278
6. Cheung HY, Ho MP, Lau KT, Cardona F, Hui D (2009) Natural fibre-reinforced composites for bioengineering and environmental engineering applications. *Compos B Eng* 40(7):655–663
7. Mansor MR, Sapuan SM, Zainudin ES, Nuraini AA, Hambali A (2013) Hybrid natural and glass fibres reinforced polymer composites material selection using analytical hierarchy process for automotive brake lever design. *Mater Des* 51:484–492
8. Marsh G (2003) Next step for automotive materials. *Mater Today* 6(4):36–43 (Elsevier)
9. Balakrishnan H, Hassan A, Imran M, Wahit MU (2012) Toughening of polylactic acid nanocomposites: a short review. *Polym-Plast Technol Eng* 51(2):175–192
10. Abe K, Nakatsubo F, Yano H (2009) High-strength nanocomposite based on fibrillated chemi-thermomechanical pulp. *Compos Sci Technol* 69(14):2434–2437
11. Klemm D, Kramer F, Moritz S et al (2011) Nanocelluloses: a new family of nature-based materials. *Angewandte Chemie Int Ed* 50:5438–5466
12. Abdul Khalil HPS, Bhat AH, Ireana Yusra AF (2012) Green composites from sustainable cellulose nanofibrils: a review. *Carbohydr Polym* 87:963–979
13. Haafiz MM, Hassan A, HPS AK, Owolabi AF, Marliana MM, Arjmandi R, Inuwa IM, Fazita MR, Nurul MR (2017) Cellulose nanowhiskers from oil palm empty fruit bunch biomass as green fillers. *Cellulose-Reinforced Nanofibre Compos* 241
14. Owolabi AWT, Ghazali A, Wanrosli WD, Abbas FMA (2016) Effect of alkaline peroxide pre-treatment on microfibrillated cellulose from oil palm fronds rachis amenable for pulp and paper and bio-composite production. *BioResources* 11(2):3013–3026

15. Paakko M, Ankerfors M, Kosonen H, Nykanen A, Ahola S, Osterberg M (2007) Enzymatic hydrolysis combined with mechanical shearing and high-pressure homogenization for nanoscale cellulose fibrils and strong gels. *Biomacromolecules* 8(6):1934–1941
16. Pandey JK, Kumar AP, Misra M, Mohanty AK, Drzal LT, Singh RP (2005) Recent advances in biodegradable nanocomposites. *J Nanosci Nanotechnol* 5:497–526
17. Saito T, Nishiyama Y, Putaux JL, Vignon M, Isogai A (2006) Homogeneous suspensions of individualized microfibrils from TEMPO-catalyzed oxidation of native cellulose. *Biomacromolecules* 7(6):1687–1691
18. Aulin C, Ahola S, Josefsson P, Nishino T, Hirose Y, Österberg M et al (2009) Nanoscale cellulose films with different crystallinities and mesostructures—their surface properties and interaction with water. *Langmuir* 25(13):7675–7685
19. Turbak AF, Snyder FW, Sandberg KR (1983) Microfibrillated cellulose, a new cellulose product: properties, uses, and commercial potential. *J Appl Polym Sci* 28:815–827
20. Wang YX, Tian HF, Zhang LN (2010) Role of starch nanocrystals and cellulose whiskers in synergistic reinforcement of waterborne polyurethane. *Carbohydr Polym* 80(3):665–671
21. Oksman K, Mathew AP, Bondeson D, Kvien I (2006) Manufacturing process of cellulose whiskers/poly(lactic acid) nanocomposites. *Compos Sci Technol* 66:2776–2784
22. Sorrentino A, Vittoria GGV (2007) Potential perspectives of bionanocomposites for food packaging applications. *Trends Food Sci Technol* 18:84–95
23. Lamaming J, Hashim R, Sulaiman O, Leh CP, Sugimoto T, Nordin NA (2015) Cellulose nanocrystals isolated from oil palm trunk. *Carbohydr Polym* 127:202–208
24. John MJ, Thomas S (2008) Biofibres and biocomposites. *Carbohydr Polym* 71(3):343–364
25. Bataille P, Ricard L, Sapiéha S (1989) Effects of cellulose fibers in polypropylene composites. *Polym Compos* 10:103–108
26. Hafren J, Zou WB, Cordova A (2006) Heterogeneous ‘organoclick’ derivatization of polysaccharides. *Macromol Rapid Commun* 27:1362–1366
27. Gruber E, Granzow C (1996) Preparing cationic pulp by graft copolymerisation. 1. Synthesis and characterization. *Papier* 50:293
28. Bonini C, Heux L, Cavaille JY, Lindner P, Dewhurst C, Terech P (2002) Rodlike cellulose whiskers coated with surfactant: a small-angle neutron scattering characterization. *Langmuir* 18:3311–3314
29. Kim DY, Nishiyama Y, Kuga S (2002) Surface acetylation of bacterial cellulose. *Cellulose* 9:361–367
30. Gousse C, Chanzy H, Cerrada ML, Fleury E (2004) Surface silylation of cellulose microfibrils: preparation and rheological properties. *Polymer* 45:1569–1575
31. Stenstad P, Andresen M, Tanem BS, Stenius P (2008) Chemical surface modifications of microfibrillated cellulose. *Cellulose* 15:35–45
32. Habibi Y, Heux L, Mahrouz M, Vignon MR (2008) Morphological and structural study of seed pericarp of *Opuntia ficus-indica* prickly pear fruits. *Carbohydr Polym* 72(1):102–112
33. Lu J, Askeland P, Drzal LT (2008) Surface modification of microfibrillated cellulose for epoxy composite applications. *Polymer* 49:1285–1296
34. Iwatake A, Nogi M, Yano H (2008) Cellulose nanofibre-reinforced poly(lactic acid). *Compos Sci Technol* 68(9):2103–2106
35. Behrens BA, Doege E, Reinsch S, Telkamp K, Daehndel H, Specker A (2007) Precision forging processes for high-duty automotive components. *J Mater Process Technol* 185(1):139–146
36. Kosior E, Braganca RM, Fowler P (2006) Lightweight compostable packaging: literature review. *Waste Resour Action Program* 26:1–48
37. Kyrikou I, Briassoulis D (2007) Biodegradation of agricultural plastic films: a critical review. *J Polym Environ* 15(2):125–150
38. Haafiz MM, Eichhorn SJ, Hassan A, Jawaid M (2013) Isolation and characterization of microcrystalline cellulose from oil palm biomass residue. *Carbohydr Polym* 93(2):628–634

39. Haafiz MM, Hassan A, Khalil HA, Fazita MN, Islam MS, Inuwa IM, Marliana MM, Hussin MH (2016) Exploring the effect of cellulose nanowhiskers isolated from oil palm biomass on polylactic acid properties. *Int J Biol Macromol* 85:370–378
40. Ray SS, Yamada K, Okamoto M, Fujimoto Y, Ogami A, Ueda K (2003) New polylactide/layered silicate nanocomposites. 5. Designing of materials with desired properties. *Polymer* 44(21):6633–6646
41. Dufresne A, Kellerhals MB, Witholt B (1999) Transcrystallization in mcl-PHAs/cellulose whiskers composites. *Macromolecules* 32(22):7396–7401
42. Abdulkhani A, Hosseinzadeh J, Dadashi S, Mousavi M (2015) A study of morphological, thermal, mechanical and barrier. properties of PLA based biocomposites prepared with micro and nano sized cellulosic fibers. *Cell Chem Technol* 49(7–8):597–605
43. Evans JD, Sikdar SK (1990) Biodegradable plastics: an idea whose time has come? *Chem Technol* 20:38–42
44. Plackett D, Vázquez A (2004) Natural polymer sources. In: Baillie Caroline (ed) *Green composites polymer composites and the environment*. Woodhead Publishing Ltd/CRC Press LLC, Cambridge, pp 123–153
45. Kunioka M, Tamaki A, Doi Y (1989) Crystalline and thermal properties of bacterial copolyesters: poly(3-hydroxybutyrate-co-3-hydroxyvalerate) and poly(3-hydroxybutyrate-co-4-hydroxybutyrate). *Macromolecules* 22:694
46. Ma X, Yu J, Ma Y (2005) Urea and formamide as a mixed plasticizer for thermoplastic wheat flour. *Carbohydr Polym* 60:111. Yang J-H, Yu J-G, Ma X (2006) Preparation and properties of ethylenebisformamide. *Carbohydr Polym* 63(2006):218
47. Abdul Khalil HPS, Hanida S, Kang SCW, NikFuaad NA (2007) Agro-hybrid composite: the effects on mechanical and physical properties of oil palm fiber (EFB)/glass hybrid reinforced polyester composites. *J Reinf Plast Compos* 26:203–218
48. Adeosun SO, Lawal GI, Balogun SA, Akpan EI (2012) Review of green polymer nanocomposites. *J Miner Mater Charact Eng* 11(04):385
49. Dufresne A (2003) Interfacial phenomena in nanocomposites based on polysaccharide nanocrystals. *Compos Interfaces* 10(4–5):369–388
50. Lai SM, Don TM, Huang YC (2006) Preparation and properties of biodegradable thermoplastic starch/poly(hydroxyl butyrate) blends. *J Appl Polym Sci* 100:2371–2379
51. Jang WY, Shin BY, Lee TX, Narayan R (2007) Thermal properties and morphology of biodegradable PLA/starch compatibilized blends. *J Ind Eng Chem* 13:457–464
52. Sarazin P, Li G, Orts WJ, Favis BD (2008) Binary and ternary blends of polylactide, polycaprolactone and thermoplastic starch. *Polymer* 49:599–609
53. Durango AM, Soares NFF, Benevides S, Teixeira J, Carvalho M, Wobeto C et al (2006) Development and evaluation of an edible antimicrobial film based on yam starch and chitosan. *Packaging Technol Sci* 19:55–59
54. Ma PC, Siddiqui NA, Marom G, Kim JK (2010) Dispersion and functionalization of carbon nanotubes for polymer-based nanocomposites: a review. *Compos A Appl Sci Manuf* 41(10):1345–1367
55. Mondragón M, Arroyo K, Romero-García J (2008) Biocomposites of thermoplastic starch with surfactant. *Carbohydr Polym* 74:201–208
56. Piyada K, Waranyou S, Thawien W (2013) Mechanical, thermal and structural properties of rice starch films reinforced with rice starch nanocrystals. *Int Food Res J* 20:439–449
57. Hietala M, Mathew AP, Oksman K (2013) Bionanocomposites of thermoplastic starch and cellulose nanofibers manufactured using twin-screw extrusion. *Eur Polym J* 49:950–956
58. Plackett D, Andersen TL, Pedersen WB, Nielsen L (2003) Biodegradable composites based on L-polylactide and jute fibres. *Compos Sci Technol* 63:1287–1296
59. Ray SS, Okamoto M (2003) Polymer/layered silicate nanocomposites: a review from preparation to processing. *Prog Polym Sci* 28(11):1539–1641
60. Pandey JK, Ahn SH, Lee CS, Mohanty AK, Misra M (2010) Recent advances in the application of natural fibre based composites. *Macromol Mater Eng* 295(11):975–989

61. Lee SY, Kang IA, Doh GH, Yoon HG, Park BD, Wu Q (2008) Thermal and mechanical properties of wood flour/talc-filled polylactic acid composites: effect of filler content and coupling treatment. *J Thermoplast Compos Mater* 21(3):209–223
62. Qu P, Gao Y, Wu G, Zhang L (2010) Nanocomposites of poly (lactic acid) reinforced with cellulose nanofibrils. *BioResources* 5(3):1811–1823
63. Okubo K, Fujii T, Thostenson ET (2009) Multi-scale hybrid biocomposite: processing and mechanical characterization of bamboo fibre reinforced PLA with microfibrillated cellulose. *Compos A Appl Sci Manuf* 40(4):469–475
64. Kim JP, Yoon T-H, Mun SP, Rhee JM, Lee JS (2006) Wood-polyethylene composites using ethylene-vinyl alcohol copolymer as adhesion promoter. *Bioresour Biotechnol* 97:494–499
65. Rong MZ, Zhang MQ, Liu Y, Yang GC, Zeng HM (2001) The effect of fibre treatment on the mechanical properties of unidirectional sisal-reinforced epoxy composites. *Compos Sci Technol* 61:1437–1447
66. Qin C, Soykeabkaew N, Xiuyuan N, Peijs T (2008) The effect of fibre volume fraction and mercerization on the properties of all cellulose composites. *Carbohydr Polym* 71:458–467
67. Khalfallah M, Abbès B, Abbès F, Guo Y, Marcel V, Duval A, Vanfleteren F, Rousseau F (2014) Innovative flax tapes reinforced acrodur biocomposites: a new alternative for automotive applications. *Mater Des* 64:116–126
68. Chen W, Yu H, Liu Y, Chen P, Zhang M, Yunfei H (2011) Individualization of cellulose nanofibers from wood using high-intensity ultrasonication combined with chemical pre-treatments. *Carbohydr Polym* 83:1804–1811
69. Tiffany A, Rivkin A, Cao Y, Nevo Y, Abraham E, Ben-Shalom T, Lapidot S, Shoseyov O (2016) Nanocellulose, a tiny fiber with huge applications. *Curr Opin Biotechnol* 39:76–88
70. Herrera N, Salaberria AM, Mathew AP, Oksman K (2016) Plasticized polylactic acid nanocomposite films with cellulose and chitin nanocrystals prepared using extrusion and compression molding with two cooling rates: effects on mechanical, thermal and optical properties. *Compos A Appl Sci Manuf* 83:89–97

Static and Dynamic Mechanical Properties of Eco-friendly Polymer Composites



Bernardo Zuccarello

1 Introduction

The increasing sensitivity to environmental protection and the recent laws against environmental pollution that were implemented because of the production of high amounts of synthetic materials based on petroleum chemistry, have led to a widespread attention toward biocomposites, i.e. to eco-friendly polymer composites produced by an eco-sustainable or renewable matrix reinforced by natural fibres. If properly combined with 'green' matrixes or biopolymers, natural fibres could enable for partially or completely renewable biocomposites to be produced. These biocomposites can be easily biodegraded at their end of life by composting and are therefore used as improver/fertilizer in agriculture terrains. Biodegradable polymers and natural fibres are extremely attractive because they can substitute the synthetic matrix obtained by the petroleum industry, and can produce composite materials with interesting mechanical properties such as good tensile strength, sufficient stiffness, and high toughness. Moreover, many natural fibres exhibit other properties that are highly regarded in the industrial field, e.g., low damageability, good thermal and acoustic insulation, low skin irritability, high availability in the current market, low embodied energy, and extremely low cost. Natural fibres have been used to reinforce thermoplastic matrixes (polypropylene, polyethylene, polyurethane, polystyrene, PVC, etc.) that are characterized by higher toughness and easier recyclability, and thermosetting matrixes (polyester, phenolic, and epoxy resins, etc.) that exhibit better mechanical characteristics, but lower recyclability and environmental compatibility.

Despite such interesting properties, biocomposites are hitherto used only for non-structural applications (filling material, soundproofing, thermal insulation, packaging etc.) in various fields of industrial production, packaging and automotive

B. Zuccarello (✉)
Viale delle Scienze, 90128 Palermo, Italy
e-mail: bernardo.zuccarello@unipa.it

(large manufacturers such as BMW, Volvo, Mercedes-Benz, Ford, GM, Toyota, etc., increasingly use of biocomposites for the manufacturing of dashboards, insulating elements, doors, backs, etc.), naval industry, and civil constructions (panels, sandwich etc.), where their lightness and low cost, both inferior to that of any composite material reinforced by synthetic fibres, are particularly appreciated. In typical non-structural applications, such biocomposites are constituted by green thermosetting (partially bio-based) or thermoplastic (recyclable and/or renewable) matrixes, reinforced by short or discontinuous randomly oriented natural fibres; they are typically manufactured by moulding or extrusion processes, and are characterized by relatively low mechanical strength combined with sufficient stiffness.

Although various recent works have been devoted to the implementation of high-performance biocomposites that can be used for structural applications (self-bearing or load-bearing panels, etc.), and also by the preliminary improvement of the fibre properties [1–18], the development of eco-friendly or renewable high-performance biocomposites reinforced by natural fibres is an objective expected by the scientific community; however, it has not yet been fully achieved.

The interesting synthesis of biocomposites hitherto are reported in various review articles published in high-quality journals devoted to materials and composites [18–34]. The primary objective of this chapter is to present both the static and dynamic mechanical properties of eco-friendly polymer composites described in literature, as well as to present the reader some scientific background to correctly evaluate the matrix/fibre adhesion and interpret the mechanical behaviour of such materials. This can also be achieved using recent micromechanical models developed for particular biocomposites; further, it can be extended to the entire family of eco-friendly polymer composites reinforced by natural fibres. Therefore, the reader will have sufficient knowledge on biocomposites and their capacity to substitute traditional materials as metals and fiberglass.

2 Constituent Materials: Polymer Matrixes and Natural Fibres

As mentioned above, eco-friendly polymer composites can be obtained using several types of matrixes and various reinforcing natural fibres. Obviously the static and the dynamic properties of such biocomposites are strictly related to the mechanical characteristics of the constituent materials as well as to the primary functional parameters such as the matrix–fibre adhesion, manufacturing process, and fibre volume fraction. Considering the materials used as the matrix, the analysis of the numerous research works reported in literature shows that they have considered both thermosetting and thermoplastic polymers characterized by variable environmental impact, from green matrixes obtained using an eco-friendly manufacturing process [1, 2, 35–39], to partially bio-based matrixes [40–44], to completely renewable matrixes obtained using proper biopolymers, such as PLA and the like [45–47].

Consequently, the environmental impact of a composite included in the wide family of the polymer matrix biocomposites reinforced by natural fibre can vary in a wide range; in practice, the renewability can vary from approximately 20–30% (biocomposite produced by 20–30% of the weight of natural fibres mixed to traditional synthetic matrixes) to approximately 100% (biocomposites produced by renewable matrix reinforced by natural fibres obtained by renewable extraction processes).

2.1 Static Mechanical Properties

The static mechanical properties of the material that constitute biocomposites are generally performed using tensile strength, although various researchers have also used the proper flexural tests on the matrixes. In general, the matrixes and fibres exhibit an elasto-plastic behaviour with variable plastic phase; in terms of experimental scattering, the matrixes show values aligned with those of typical plastics with standard deviations less than 3–5%, whereas a higher scattering characterizes the single fibre tests used for the fibre characterization. As an example, Fig. 1 shows the results of champagne tensile tests performed on one lot containing 10 fibres of agave sisalana [36, 37].

This case shows an almost ideal linear elastic behaviour with the ultimate stresses that vary from approximately 600 MPa to approximately 1150 MPa; the tensile modulus varies instead from approximately 20 GPa to approximately 60 GPa. Considering that the experimental evidence regarding the tensile test results show a good accordance with the Gaussian distribution, we can conclude that the tensile strength (having in this case a mean value of approximately 690 MPa) is typically characterized by the standard deviation of approximately 10%, i.e. 2–3 times that of polymer matrix materials. Such relatively higher experimental scattering of the fibre characteristics forewarned researchers that it can lead to components with variable mechanical characteristics, although this

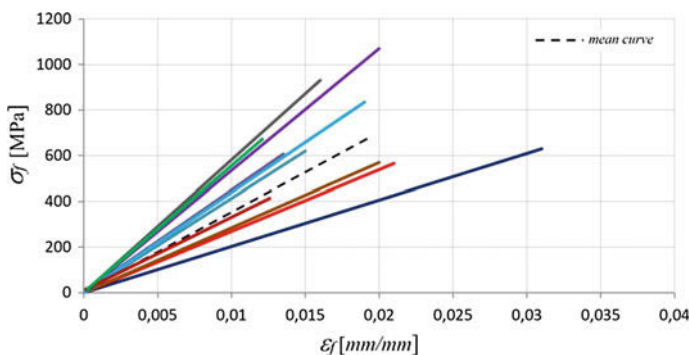


Fig. 1 Tensile tests results on single fibre of agave sisalana, and relative mean curve

conjecture is not true because its presence in a generic component of thousands of fibres leads to an obvious statistical mean such that, as widely confirmed by the experimental evidence, the mechanical properties of different biocomposite specimens have standard deviations comparable with those of other composite materials.

Synthetically, Table 1 shows the mechanical characteristics of the primary polymer matrixes used in literature [25, 35, 36, 45–48] for the manufacturing of biocomposites reinforced by various natural fibres.

Table 1 shows that the tensile strength and relative tensile modulus of various thermosetting matrixes (epoxy, polyester, vinylester, phenolic, etc.) are within a relatively small range: the tensile strength from 35 to 100 MPa; the Young modulus from 2.0 to 4.8 GPa. The failure strain, however, is within a wider range, with variations of approximately one order of magnitude: from 1 to 8%, approximately.

Regarding the synthetic thermoplastic matrixes (PP, LDPE, HDPE, PS, and Nylon), Table 2 shows that the tensile strength varies from approximately 10–95 MPa, whereas more significant variations affect the tensile modulus that varies from approximately 0.1 GPa (LDPE) to approximately 3.9 GPa (Nylon 6.6). As shown, the failure strain for thermoplastic resins can become extremely high; in practice, it can vary from 1% (PS) to extremely high values of approximately 600–800% (PP, LDPE).

Regarding the primary biodegradable matrixes in Table 3, except for PCL, PEA, SPI and starch, the tensile mechanical properties of such polymers are comparable with those of the synthetic thermosetting resins: tensile strength from approximately 25 MPa to approximately 60 MPa; tensile modulus from 0.35 GPa to approximately 6 GPa; failure strain from 1.4 to 9%. Unlike these, PCL, PEA, SPI, and starch exhibit relative low tensile strength (5–20 MPa), low tensile modulus (0.1–0.85 GPa), and high failure strain (approximately 30–235%). It is noteworthy that although the failure strain is often neglected by various authors in the prediction of the mechanical performance of biocomposites, as it has been clearly observed in [1, 2, 35–39], it influences significantly the damage mechanisms of the biocomposites and, consequently, the actual mechanical strength. As an example, in a unidirectional biocomposite laminate, a matrix failure strain less than that of the reinforcing fibres leads to a premature damage of the biocomposite that occurs prior the tensile fibre failure, by diffuse matrix/fibre debonding and possible delamination; consequently, the biocomposite tensile strength can be much lower than that can be obtained by the full utilization of the fibre tensile strength using a matrix having a failure strain higher than that of the fibres.

Regarding the reinforcing fibres, Table 4 shows the primary natural fibres extracted from plants, used for the implementation of interesting biocomposites reported in literature. For a useful comparison, the primary synthetic fibres (glass, aramid, and carbon) used to reinforce polymer matrix composites, have been reported as well.

Table 4 shows that the tensile strength of such natural fibres can vary in two orders of magnitude, from the values comparable or inferior to those of the thermosetting matrixes, as shown by the alfa fibres (tensile strength of approximately) to values comparable with that of the synthetic fibres. This is also shown by the

Table 1 Mechanical properties of thermosetting polymers used as matrix in biocomposites

Polymer	Density (g/cm ³)	Tensile strength (MPa)	Tensile modulus (GPa)	Elongation (%)	Impact strength (J/m ²)	References
Polyester resin	1.2-1.5	40-90	2.0-4.5	2.0	0.2-3.2	[25]
Polyester resin	1.0-1.4	41-90	2.1-4.4	2.0-2.6	0.9	[47]
Vinyl ester resin	1.2-1.4	69-83	3.1-3.8	4.0-7.0	2.5	[25]
Epoxy resin	1.1-1.4	35-100	3.0-6.0	1.0-6.0	0.3	[25]
Epoxy resin	1.1-1.4	45-90	2.3-3.1	2.0-8.0	0.4	[47]
Phenolyc resin	1.3	35-62	2.8-4.8	1.5-2.0	0.35	[25]
Green epoxy	1.1	50	2.5	2.5	-	[35, 36]

Table 2 Mechanical properties of thermoplastic polymers used as matrix in biocomposites

Polymer	Density (g/cm ³)	Tensile strength (MPa)	Tensile modulus (GPa)	Elongation (%)	Impact strength (J/m ²)	References
PP	0.9	26–41	0.9–1.8	15–700	21.4–267.0	[25, 47, 48]
LDPE	0.9	8–78	0.4	90–800	>854.0	[25, 48]
HDPE	0.9	14–38	0.4–1.5	2–130	26.7–1068.0	[25]
PS	1.0–1.1	25–69	2.8–5.0	1.0–2.5	1.1	[25, 48]
Nylon 6	1.1	43–79	2.9	20–150	42.7–160.0	[25]
Nylon 6,6	1.1	12–94	2.5–3.9	35–100	16.0–654.0	[25]

Table 3 Mechanical properties of biodegradable polymers used as matrix in biocomposites

Polymer	Density (g/cm ³)	Tensile strength (MPa)	Tensile modulus (GPa)	Elongation (%)	References
PLA	0.9–1.3	21–60	0.3–3,8	2.5–8.0	[45–48]
PHB	1.1–1.3	21–40	0.9–4.0	5.0–8.4	[45–48]
PHBV	1.2	26	1.0–2.4	1.4–25	[46, 48]
PGA	1.5	60	6.0	1.5	[45]
PCL	1.1	21	0.2	300.0	[45]
PEA	1.2	16	0.4	85.0–119.0	[46]
SPI	1.2–1.5	6	0.1	170.0–236.0	[46]
Starch	1.0–1.4	5–6	0.1–0.8	31.0–44.0	[45–47]

curaua fibres (tensile strength of approximately 3000 MPa). Similarly, the tensile modulus varies in the two orders of magnitude range, from approximately 1.44 GPa for pineapple to approximately 128 GPa for ramie. Regarding the failure strain, it varies from approximately 1% for ‘rigid’ fibres such as flax, hemp, jute, abaca, and bagasse; approximately 8–50% for “deformable” fibres such as oil palm, piassava, and coir. Consequently, we can conclude that this wide family of natural fibres includes (a) “high failure strain” fibres that cannot be used to reinforce thermosetting matrixes (having strain failures of less than 10%, see Table 1), the rigid polystyrene (PS, see Table 2), the most biodegradable resins such as PLA, PHB, PHBV, and PGA, as well as “low modulus” fibres that cannot be used to reinforce polymer matrixes having relatively high modulus. Therefore, a fibre classification more useful than the classical one based on the vegetable component from which they are extracted (seed, fruit, bast, stem, leaf, etc.), is one that is based on the tensile modulus that governs the reinforcing effects and, consequently, the failure strain and subsequently the tensile strength.

To obtain high-performance biocomposites, two basic requirements must be satisfied: (1) a good fibre reinforcing effect where the fibres should have a tensile modulus at least 10 times higher than that of the matrix, (2) the failure strain of the fibre should be inferior to that of the matrix to fully exploit the fibre strength without premature matrix failure. Considering these requirements, similar to synthetic fibres, natural fibres can be divided into three classes: low modulus (LM) fibres that include fibres with a tensile modulus less than 10 GPa (coir, low modulus sisal, cotton, low modulus pineapple, oil palm, low modulus palf, piassava), intermediate modulus (IM) fibres that include fibres with a tensile modulus in the range of 10–40 GPa (jute, bamboo, low modulus flax, bagasse, low modulus kenaf, low modulus ramie, sisal, and low-modulus curaua), high modulus (HM) fibres that include fibres with a modulus higher than 40 GPa (high-modulus pineapple, high-modulus flax, high-modulus hemp, high-modulus jute, high-modulus kenaf, high-modulus ramie, high-modulus palf, high-modulus curaua). The LM natural fibres can be used to reinforce low-modulus polymer matrixes such as PE, PP, low-modulus PLA, low-modulus PHB, PCL, PEA, SPI, and starch, whereas the IM natural fibres can reinforce most polymer matrixes except those

Table 4 Mechanical properties of the various natural fibres used to reinforce biocomposites

Origin	Fiber	Density (g/cm ³)	Tensile strenght (MPa)	Tensile modulus (GPa)	Elongation (%)	References
Seed or fruit	Cotton	1.5–1.6	287–800	5.5–12.6	3.0–12.0	[25, 45–47]
	Coir	1.1–1.5	95–593	2.8–6.0	15.0–51.4	[25, 45–47, 49]
	Pineapple	0.8–0.6	180–627	1.4–82.0	3.2–14.5	[2, 6]
Bast or stem	Oil palm	0.7–1.5	248	3.2	25.0	[5]
	Flax	1.4–1.5	343–2000	27.6–103.0	1.0–3.5	[25, 45–47, 49]
	Hemp	1.4–1.5	270–920	23.5–90.0	1.0–4.0	[25, 46, 47, 49]
	Jute	1.3–1.5	320–860	10.0–60.0	1.0–1.8	[25, 45–47, 49]
	Kenaf	1.4–1.5	195–930	14.5–66.0	1.3–5.5	[25, 46, 47, 49]
	Ramie	1.0–1.6	400–1000	24.5–128.0	1.2–4.0	[25, 45–47, 49]
	Sisal	1.3–1.5	363–790	9.0–39.5	2.0–7.0	[25, 35, 45–47, 49]
	Abaca	1.5	400–980	6.2–20.0	1.0–10.0	[46, 49]
	Henequen	1.2	430–570	10.1–16.3	3.7–5.9	[46]
	Banana	1.3	500–800	12.0–32.0	1.5–9.0	[45, 46]
Cane, grass and reed	Palf	0.8–1.6	180–1627	1.4–82.5	1.6–14.5	[46]
	Curauá	1.4	87–3000	10.5–96.0	1.3–6.0	[45, 46, 49]
	Bamboo	0.6–1.1	140–800	11.0–32.0	2.5–3.7	[46, 47, 49]
	Bagasse	1.3	222–290	17.0–27.1	1.1–10.0	[45, 46, 49]
	Softwood	1.5	1000	40.0	4.4	[25]
	Wood	2.5–2.6	1000–3500	70.0–85.0	0.5–4.8	[25, 46, 47]
	Glass	2.5	4570	86.0	2.8	[25, 46]
	S	1.4	3000–3150	63.0–67.0	3.3–3.7	[25, 46]
	Aramid	1.4	4000	230.0–240.0	1.4–1.8	[25, 46]
	Carbon	1.8	4400–4800	225.0–260.0	1.8–1.9	[47]
Carbon	1.9	3600–3900	390–410	0.9–1.0	[47]	

having a modulus higher than 4–5 GPa such as some PSs, thermosetting matrixes, and biodegradable PGA. Obviously, the HM natural fibres can reinforce any polymer matrix except those having a lower failure strain. As an example, the coir fibres (LM), having a modulus in the range of 3–6 GPa and a strain failure in the range of 15–51% (see Table 4), can be used advantageously to reinforce the LDPE that has a tensile modulus less than 0.2 GPa (less than 1/10 of the fibre modulus, see Table 1) and a failure strain that is always higher than 90% (approximately 2–6 times the failure strain of the fibres); however, it cannot be used to reinforce a green epoxy having comparable stiffness and a lower failure strain (approximately 2%, see Table 1). Unfortunately, such elementary rules are not always adhered to in literature, as can be observed from Ref. [1] that reported coir fibre being used to reinforce PP having a tensile modulus of approximately 1–2 GPa, i.e. comparable with that of the fibres, and a failure strain of less than 15%; consequently, it is not surprising if the relative biocomposite has mechanical properties (tensile strength in the range of 25–30 MPa, and tensile modulus in the range of 1.1–1.25 GPa) that are comparable with those of the simple matrix (tensile strength in the range of 26–34 MPa, and tensile modulus of approximately 1–2 GPa). Further, as mentioned above, a rigid fibre cannot be always advantageously used to reinforce a relatively deformable matrix; for example, an epoxy resin having a tensile modulus of 3 GPa and a strain failure of approximately 2% can be reinforced advantageously by flax, jute, hemp, kenaf, ramie, banana, and curaua with a mean tensile modulus higher than 30 GPa and a failure strain of less than 2%, but cannot be reinforced by sisal, bamboo, isora, alfa, piassava, and softwood because they always show a strain failure higher than 2%. An exemplary demonstration of such important feature is reported in Ref. [1], where the authors considered agave *Marginata* fibres extracted by rolling (without any fibre treatment), and clearly showed how the substitution to the green epoxy (having strain failure of 2%) with a PLA matrix (having strain failure of approximately 5%) allowed a biocomposite having a tensile strength of 103.6 MPa to be transformed into a biocomposite having a tensile strength of 188.3 MPa, i.e. to obtain a strength increment of approximately 83%.

Finally, the density of the polymer matrixes used for the manufacturing of biocomposites vary in an extremely limited range, from approximately 0.9–1.5 g/cm³ whereas the density of the natural fibres falls within the range of 0.6 (low density pineapple)–1.6 g/cm³ (cotton and palf), and is always significantly inferior to the density of synthetic glass fibres (approximately 2.6 g/cm³); consequently, polymer biocomposites reinforced by natural fibres are always lighter than the fibre glass composites that they intend to substitute in several fields of industrial production: automotive, construction, nautical, packaging, etc.

2.2 *Dynamic Mechanical Properties*

Unlike the static properties that can be defined for both matrixes and fibres, the dynamic properties, i.e. impact and fatigue strength, can be analysed only for the

polymer matrixes that can be subjected to both impact and fatigue tests; such particular service loadings, in fact, cannot be applied to a single fibre. Tables 1, 2 and 3 show how the impact strength, determined typically by Charpy or Izod test, is relatively low for the thermosetting matrixes (from 0.15 to approximately 3 J/m²) that, as it is well known, exhibit brittle behaviour. The impact strength is instead significantly higher, from one to three orders of magnitude, for thermoplastic matrixes (from 20 to approximately 1000 J/m²) that exhibit a ductile behaviour with higher ultimate strains. As expected by considering the experimental evidence for synthetic composites, the reinforcing by natural fibres allow a user to increase significantly the impact strength of the thermosetting matrixes, being more limited to the reinforcing fibre contribution for thermoplastic resins (unlike the thermosetting matrices, the stress concentration effect prevails on the reinforcing effect).

Similarly, the fatigue strength that is relatively low for a generic polymer matrix (fatigue ratio of less than 0.25), can be increased significantly by the introduction of natural fibres, especially in the cases of high module fibres. Obviously, the actual improvement in the dynamical properties is strictly related to various parameters, e.g., fibre length (short/long fibre) and its orientation (random or aligned), fibre volume fraction, laminate setup, etc.

3 Fibre/Matrix Adhesion

As mentioned above and widely shown in literature, the mechanical properties of generic biocomposites are strictly related to the fibre/matrix adhesion; in fact, it influences significantly the load transmission, from matrix to fibres, as well as the peculiar damage mechanisms that in many cases can include the premature phenomena of fibre/matrix debonding, pull-out, and delamination, with important consequence on the mechanical strength of the biocomposites in the static and dynamic loading conditions. As it is well known, for short fibre composites, a low matrix-adhesion can lead to the easy debonding of the transversal fibres along with the possible pull-out of the longitudinal fibres. In the long fibre composite, instead, a poor fibre-matrix adhesion can lead to the debonding phenomena, but only when significant and diffuse matrix defects appear [49]. Unfortunately, little research has been devoted to the accurate analysis of the actual fibre/matrix adhesion of biocomposites. Typically, the low adhesion has been summarily deduced from the observed low mechanical performance of the analysed biocomposites, ad also when they were actually related to the low quality of the manufacturing process (presence of diffuse voids and/or direct contact between adjacent fibres, etc.), or to a low reinforcing effect owing to a low fibre/matrix elastic modulus mismatch. However, many studies have been devoted to the improving of the fibre/matrix adhesion by proposing various surface fibre treatments such as NaOH treatment (mercerization) [18], the addition of nanomaterials [50], and the addition of a silane coupling agent [14]. As it is well known, the fibre/matrix adhesion is typically analysed through the pull-out test that comprises the measurement of the load that lead to the pull-out of a

single fibre partially embedded on the matrix. In general, such a test is performed by embedding partially a single fibre into a cylinder of matrix having the proper diameter, and by computing the mean shear stress at the fibre/matrix interface by dividing the relieved pull-out load to the interface area. The ratio between the computing mean shear stress and the ultimate shear stress of the matrix is considered, as well as the goodness index of the matrix/fibre adhesion. Unfortunately, as widely demonstrated in [1], such an approach yields an underestimated evaluation of the fibre/matrix adhesion because the interface shear stress distribution is not uniform and, most importantly, such nonuniformity tends to increase significantly in the pull-out tests with the stiffness mismatch between the fibre and the surrounding matrix cylinder. Consequently, considering this in the pull-out test, the ratio of the transversal sections of the fibre and matrix can be extremely different from that of the analysed biocomposite. subsequently, the interface shear stress distribution can be extremely different, and the matrix/fibre adhesion evaluation performed by considering the mean shear stress will not be reliable. As explained in [1], a reliable evaluation can be instead obtained by considering the ratio r_a between the maximum shear stress τ_{max} that occurs at the fibre/matrix interface free point in the pull-out incipient condition, and the matrix ultimate shear stress $\tau_{m,u}$. Such a ratio is an index that varies from 0 (null adhesion) to 1 (perfect adhesion), and it is related to the pull-out load $P_{pull-out}$ experimentally detected, by the simple formula [1]:

$$r_a = \frac{\tau_{max}}{\tau_{m,R}} = \frac{P_{pull-out}\lambda}{2\pi d\tau_{m,R}} \left[\frac{1-S}{1+S} \cdot \text{Tanh}\left(\lambda \frac{l}{2}\right) + \frac{(d/D)}{\text{Tanh}(\lambda l/2)} \right] \quad (1)$$

where d is the fibre diameter, D is the diameter of the matrix cylinder as shown in Fig. 2, S is the well-known stiffness unbalancing defined by the ratio between the fibre stiffness and the surrounding matrix cylinder stiffness, whereas λ is the base parameter of the bi-material couple analysed, related to the geometry and the elastic moduli of the coupled materials [1].

Equation 1 shows that the maximum shear stresses are proportional with the fibre stiffness, and inversely proportional to the matrix stiffness. For a given matrix, the fibre stiffness has a noticeable influence on the pull-out strength of the biocomposite, as shown in Fig. 3. The latter shows the influence of the tensile modulus of various agave fibres (it increases from the MDN type to MPN type) on the interface shear stress distribution of a green epoxy (Fig. 3a) and a PLA (Fig. 3b) matrix biocomposite.

Figure 3a shows that for the green epoxy matrix, the maximum specific shear stresses vary from 1.85 to 2.87 N/mm, an increase of approximately +55%, corresponding to the transition from the stiffest MPN fibres to the less stiff MDN fibres. Figure 3b shows that by substituting green epoxy with PLA, the maximum shear stresses decrease (by approximately 40%), being included between 1.09 for the stiffer MPN fibres to 1.74 N/mm for the less stiff MDN fibres.

The values of the index r_a reported in Table 5 for the abovementioned agave fibres reinforcing epoxy and PLA, corroborate clearly how, in accordance with the

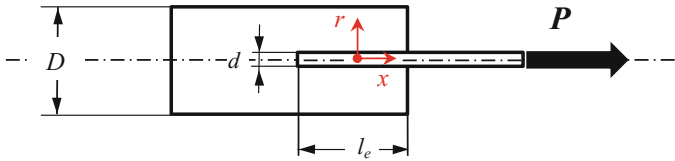


Fig. 2 Experimental layout of single-fiber pull-out test

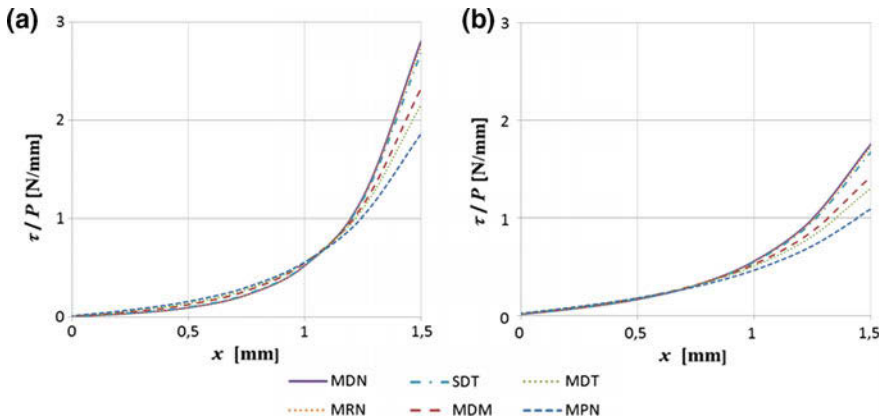


Fig. 3 Fibre-matrix interface shear stress distribution for **a** green epoxy and **b** PLA matrix reinforced by various agave fibres

findings above, the increase in the pull-out load does not correspond necessarily to an increase in the fibre-matrix adhesion, but a significant increase can be also be associated with the increase in the fibre stiffness (and subsequently the unbalancing of S that compares with Eq. 1).

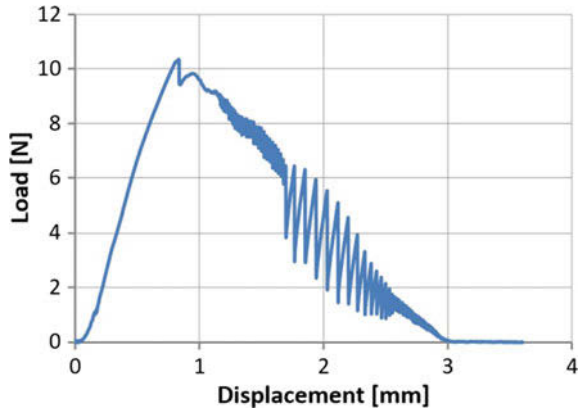
Table 5 shows that for a given fibre, i.e., the PLA, the pull-out loads are always higher than the epoxy ones. Such a result has caused several authors to erroneously state that the PLA/agave adhesion is better than that of the epoxy/agave combination [35], whereas the higher pull-out load observed is solely due to the lower stiffness of the PLA compared to the epoxy. Further, Table 5 shows that particular fibre treatments such as mercerization (MDT and SDT fibres) lead to improvements in the fibre-matrix adhesion (increasingly higher for the PLA), although significant pull-out strength increments are obtained by increasing the fibre stiffness, as shown in the stiffer MPN fibres that are not subjected to any fibre treatment.

As an example, Fig. 4 shows the typical trend of the pull-out test curve, observed for natural fibres: a first elastic-linear step, corresponding to the loading phase of the embedded fibre, followed by a second decreasing step characterized by the fibre sliding that occurs in a discontinuous manner until the complete extraction.

Table 5 Results of the pull-out tests on green epoxy and PLA reinforced by various agave fibres

Fiber	Matrix	E_f (GPa)	$P_{pull-out}$ (N)	τ_{max} (MPa)	r_a	$\bar{\tau}_m$ (MPa)	$r_a^{(*)}$
MDN	Epoxy	9.2	8.1	23.12	0.64	6.44	0.17
MRN	Epoxy	9.3	9.2	28.09	0.72	7.88	0.21
MPN	Epoxy	18.7	13.7	26.26	0.73	10.90	0.30
MDM	Epoxy	12.7	13.5	32.28	0.89	10.74	0.29
MDT	Epoxy	14.5	14.2	31.52	0.87	11.30	0.31
SDT	Epoxy	9.8	10.1	27.85	0.77	8.04	0.22
MDN	PLA	9.2	10.3	17.61	0.46	8.20	0.21
MRN	PLA	9.3	10.5	17.83	0.46	8.36	0.22
MPN	PLA	18.7	16.1	16.75	0.44	12.81	0.33
MDM	PLA	12.7	21.9	30.26	0.79	17.43	0.45
MDT	PLA	14.5	23.2	29.20	0.76	18.47	0.48
SDT	PLA	9.8	18.3	30.06	0.79	14.57	0.38

Fig. 4 Typical single fibre pull-out curve observed from test on natural fibres



4 Static Mechanical Properties

One of the primary objectives of the abundant research works reported in literature regarding polymer matrix composites is the analysis of the mechanical properties, primarily the tensile properties, although when the biocomposite is considered for sandwich and/or structural panels, the flexural properties have also been analysed. As mentioned above, the mechanical properties of a polymer matrix biocomposite are strictly related to the particular type and distribution of the fibres; hence, in the following, the static properties are reported and discussed by separating the biocomposites into three different classes: short fibres of randomly oriented biocomposites, MAT discontinuous fibres biocomposites, and long fibre biocomposites. The so-called class of woven biocomposites is neglected because the use of coarse woven fabrics typically manufactured for the production of craft items is

not adequate for the manufacturing of good quality biocomposites to be used in the industrial field.

4.1 Random Short Fibres Biocomposites

Natural short fibres of polymer matrix composites are the class of biocomposites that are used more in the industrial field, owing to its particular properties of low cost, easy manufacturing, and sufficient stiffness; in general, they are manufactured by low-cost extrusion or injection/compression moulding processes and are used for non-structural applications in various industrial fields, in which they are particularly appreciated for their light weight, low cost, and high renewability that allow the environmental problems related to their final disposal to be overcome. As demonstrated in [37], a three-dimensional (3D) random distribution of the reinforcing fibres leads to better mechanical properties with respect to a two-dimensional (2D) random distribution that, therefore, should be avoided. However, the manufacturing process is an important parameter that can influence significantly the quality of such biocomposites, because the presence of internal defects as voids and/or the direct contact between the fibres (i.e. fibre wetting defects) can lead to a significant decrease in the mechanical strength, affected by the easy propagation of local damage mechanisms. Hence, several research works devoted to the optimization of the manufacturing process have been published [1, 2, 35–38]. In general, such short fibre biomaterials exhibit a tensile strength comparable or inferior to that of the simple matrix, along with a tensile modulus that, instead, can be significantly superior to the matrix one. In other words, the reinforcing by randomly oriented short fibres overcomes the limitation of plastics related to their low stiffness, although improvements in terms of mechanical strength are again expected from the industrial users to extend the use of such materials to semi-structural and structural applications. As explained in [37], the mechanical strength of such materials can be potentially improved by four distinct actions:

- (1) increase the fibre-matrix adhesion to contrast both the debonding phenomena affecting the transverse fibres (occurring at the initial phase of the local damage), and the partial pull-out of longitudinal fibres occurring in the final phase of the damage process;
- (2) increase the fibres length (l), assuring that it is greater than the critical length (l_c): in this case, the composite failure should be caused by fibre failure and not by premature pull-out;
- (3) increase the stiffness of the fibres to increment the load fraction supported by the fibres themselves, and decrease the mean stress supported by the matrix, with a consequent reduction of both the transverse debonding and the subsequent matrix failure phenomena;
- (4) increase the fibre volume fraction, to decrease, as in the previous action (3), the mean stress on the matrix, with the same advantages.

Action (1) has been considered in literature by various authors, as it is corroborated by the large number of research works [3, 4, 6, 7, 13–19] devoted to the fibre surface treatments aimed to improve the fibre-matrix adhesion. Unfortunately, this approach leads to limited increases in the biocomposite strength (always less than approximately 10–20%), because the strength to the transverse debonding, that is the local damage mechanism with which the damage of short fibre biocomposite starts (see Fig. 5), is always limited by the relatively low matrix strength that is also significantly influenced by the overall quality of the composite, i.e. by voids and the direct contacts between the fibres, and are equivalent to microcracks in the matrix and fibre-matrix interface, respectively.

In detail, the SEM micrograph of Fig. 5b corroborates that after the initial debonding of transverse fibres, the typical damage mechanism involves both the pull-out and tensile failure of the fibres aligned with the applied load.

Unfortunately, action (2) is not effective for natural fibre biocomposites because, owing to the viscosity of the matrix, the manufacturing processes used for the thermosetting (simple matrix-fibres mixing) and thermoplastic matrix (extrusion or similar processes), yields a fibre curvature that increases with fibre length and leads to a significant reduction in the biocomposite strength. Hence, the experimental evidence shows that the maximum strength of the biocomposites is achieved using a fibre length in the range of 3–6 mm [1, 2, 17, 21, 35–38].

Regarding action (3), it is noteworthy that increasing the fibre stiffness by fibre treatment yields limited results with non-negligible increase in the environmental impact; therefore, such an action is not advisable.

For the abovementioned reasons, the only potentially effective action that can increase the strength of the natural short fibre biocomposites is the increment of the fibre volume fraction (action 4), by the contemporary use of a proper manufacturing process that permits the defects concentration to be limited, which tends to increase with V_f . Consequently, as demonstrated in [37], similar results can be obtained by implementing the proper compression moulding process characterized by a curing cycle under a suitable combined pressure. In practice, such an optimized process

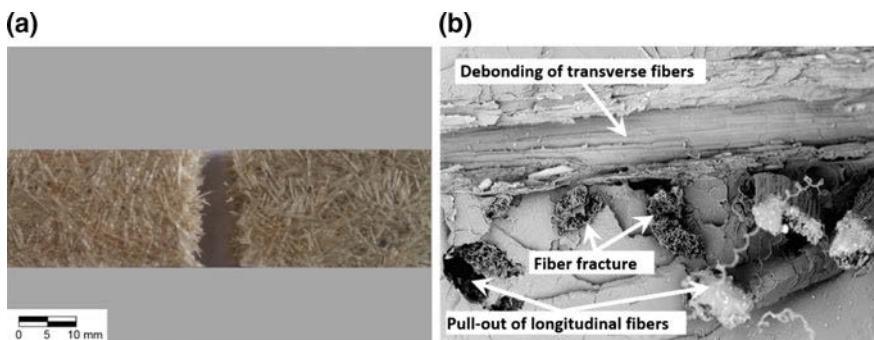


Fig. 5 a Typical failure of short fibre biocomposites subject to tensile load and b SEM micrograph of the relative fracture surface

should allow the increase in V_f above the typical values (10–20%) of literature, without significant increases in the defects concentration.

As an example, Fig. 6 shows the optimal curing processes (p_c and t_g are the curing pressure and gelling time, respectively) versus V_f , for a green epoxy matrix biocomposite reinforced by sisal fibres [37].

Table 6 shows the static mechanical characteristic of the most random short fibre biocomposites reported in literature.

By varying the fibre type (agave, hemp, jute, sisal, coir, abaca, flax), the maximum tensile strength corresponds to the critical fibre volume fraction $V_{f,crit}$ that falls within the range of 20–35%. In practice, the tensile strength varies with V_f as indicated in Fig. 7. Although it refers to agave fibres [37], it can be qualitatively applied to any short natural fibre biocomposites.

Figure 7 shows that the ultimate tensile stress $\sigma_{b,u}$ decreases in the range $0 < V_f < V_{f,min}$, obeying to the simple relationship:

$$\sigma_{b,u} = \sigma_{m,R} \cdot (1 - V_f) \tag{2}$$

whereas for $V_f \geq V_{f,min}$, the tensile strength follows the relationships obtained by considering a $[0/\pm 60]$ quasi-isotropic laminate model [37]:

$$\sigma_{b,u} = \left\{ [C_\sigma \cdot \sigma_{pull-out} \cdot V_f + \sigma_{m,u} \cdot (1 - V_f)]^{0^\circ} + 2[(\sigma_{m,u} \cdot r_a/K)]^{\pm 60^\circ} \right\} / 3 \tag{3}$$

in which C is a calibration coefficient introduced to consider the biocomposite defects (primarily owing to the incomplete wetting of the free fibres), whereas the subscripts f and m refer to the fibre and matrix, respectively.

The optimization of the manufacturing process can lead to an appreciable improvement in the tensile strength, up to approximately 50% higher than that of the simple matrix, as shown in Fig. 8 for the particular case of epoxy-sisal biocomposite manufactured by an optimized compression moulding [37].

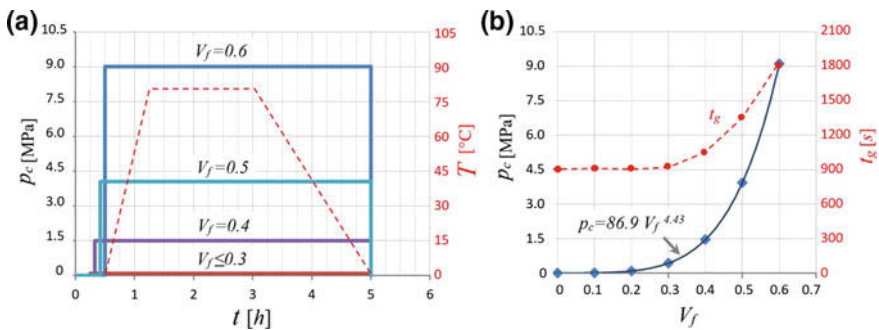


Fig. 6 a optimal thermo-mechanical curing processes for short agave fibre biocomposites and b relative optimal relationship between p_c and t_g parameters versus V_f

Table 6 Mechanical properties of the short fibre biocomposites reported in literature (matrix property in brackets)

Matrix	Fiber	V _f (%)	Tensile strength (MPa)	Tensile modulus (GPa)	Elongation (%)	Manufacturing process	Impact strength (kJ/m ²)	References
PP	Agave C	10–30	23–27	1.7–2.2	4–8	Extrusion	2.8–4.1	[55]
PP	Abaca	30	41(30)	5(1.8)	–	Extrusion/injection	–	[49]
PP + PPgMA5%	Agave C	10–30	30–32	1.9–2.5	4–9	Extrusion	2.8	[55]
PP	Agave R	10–30	23–28	1.8–2.2	5–8	Extrusion	2.7–4.2	
PP + PPgMA5%	Agave R	10–30	25–28	1.8–2.3	4–8	Extrusion	3.2	
MAPP 5%	Coir	30	25–31	1.1–1.25	–	Compression moulding	–	[25]
PLA	Hemp	40	45–55(32)	57–74	–	Compression moulding	9–25	
PLA	Abaca	30	79(65)	3.8	–	Extrusion coating and injection moulding	–	[49]
PBS	Jute	20	27(17)	1.9	4.3	Compression moulding	–	[25]
LLDPE	Flax	10	13–14(13)	–	–	Hand layup	–	
HDPE	Flax	10	20(19)	–	–	Hand layup	–	
HDPE	Hemp	20–40	37–30(22)	3.2–7	–	Twin-screw	–	
Starch	Jute	30	25	2.5	–	Extrusion	–	[35]
PLA	Ramie	30	72	–	–	Injection moulding	–	
	Jute	30	78	9	–	Injection moulding	–	
	Flax	30	50	8	–	Injection moulding	–	
	Hemp treated	52	–	–	–	Injection moulding	–	
PTB	Hemp	30	60	7	–	Extrusion	–	
PTP	Hemp	25	62	9.5	–	Extrusion	–	
PHBV	Jute	30	35	7	–	Extrusion	–	
PLLA	Flax	30	99	8	–	Extrusion	–	

(continued)

Table 6 (continued)

Matrix	Fiber	V _f (%)	Tensile strength (MPa)	Tensile modulus (GPa)	Elongation (%)	Manufacturing process	Impact strength (kJ/m ²)	References
PHB	Flax	30	38	–	–	Extrusion	–	
Epoxy	Optimized agave	35	75	6	1.2	Hand lay-up	–	
PP	Jute	30	50	6	–	Compression moulding	–	
	Glass	30	80	4.8	–	Compression moulding	–	
	Hemp	40	52	6	–	Compression moulding	–	
	Kenaf	40	28	–	–	Compression moulding	–	
	Flax	30	38	5	–	Compression moulding	88	
Epoxy	Agave opt	50	62	8	–	Hand lay-up	–	
Epoxy	Agave americana	35	37	2.6	1.2	Extrusion	–	[37]
Polyester	Sisal	30	60	2	–	Compression moulding	–	
HDPE	Agave	20	27	0.9	–	Compression moulding	–	
Epoxy	Sisal	10	67	2.5	2.2	Extrusion	–	
Epoxy	Sisal	35	77	10.5	1.2	Compression moulding	–	
HDPE	Flax	20–40	39–32(23)	3.5–6.5	5.2–5.0	Hand lay-up	–	[25]
Epoxy	Agave MPN	30	36	1.9	1.9	Extrusion	–	[2]
PLA	Agave MPN	30	46	2.9	2.1	Extrusion	–	
PP	Hemp + glass	15/5	52–60(30)	3.7–4.4(1.1)	–	Injection moulding	–	[49]
Polyester	Glass/Sisal	/	176	–	–	Compression moulding	–	[9]
Polyester	Glass/Jute	/	229	–	–	Compression moulding	–	[9]
Polyester	Glass/Sisal/Jute	/	200	–	–	Compression moulding	–	[9]

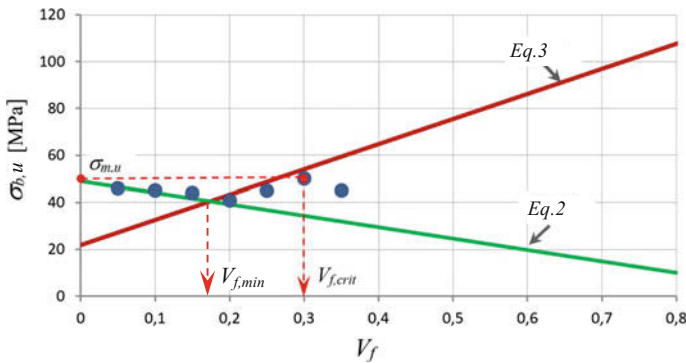


Fig. 7 Strength of short agave fibre biocomposites versus V_f and comparison with theoretical models

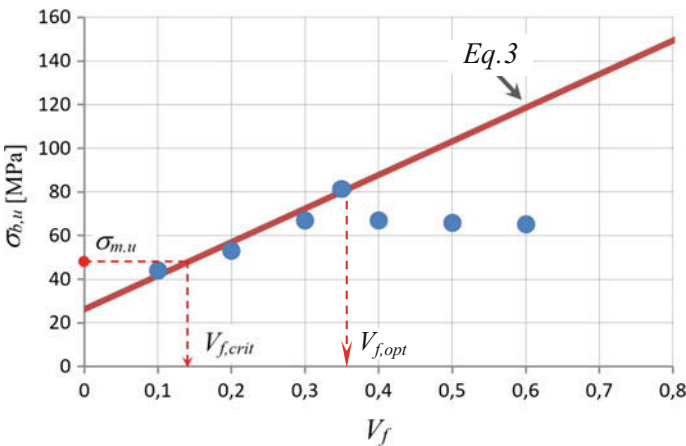


Fig. 8 Strength of short agave fibre biocomposites obtained by an optimized manufacturing process, versus V_f and comparison with the theoretical model of Eq. 3

As shown, using an optimized compression moulding manufacturing process allows the tensile strength to increment significantly; further, in the range $V_{f,crit} < V_f < V_{f,opt}$, the tensile strength obeys again the abovementioned quasi-isotropic model (Eq. 3).

In terms of the tensile modulus, Table 6 shows that the maximum stiffness corresponds to the higher volume fractions that fall within the range of 30–60%. In other words, the maximum tensile strength and the maximum tensile modulus corresponds to different fibre volume fractions that have to be properly chosen if the primary reinforcing objective is to increase the matrix strength or, in turn, increase the matrix stiffness. In general, the tensile modulus varies with V_f in good accordance with the following modified Halpin–Tsai model [37]:

$$E_b = \frac{3}{8}E_L + \frac{5}{8}E_T \quad (4)$$

$$\text{with } E_L = E_m \frac{1 + 2(l/d)\eta_L V_f}{1 - \eta_L V_f} \quad \text{and} \quad E_T = E_m \frac{1 + 2\eta_T V_f}{1 - \eta_T V_f} \quad (5-6)$$

$$\eta_L = \frac{(C_E E_f / E_m) - 1}{(E_f / E_m) + 2(l/d)}; \quad \eta_T = \frac{(C_E E_f / E_m) - 1}{(E_f / E_m) + 2} \quad (7-8)$$

in which C_E is a proper calibration coefficient introduced to consider the curvature of the free fibres that leads to a decrease in the actual fibre stiffness. As an example, Fig. 9 shows the tensile modulus of the biocomposites reinforced by short agave fibres versus V_f along with Eq. 4 and the non-modified Halpin–Tsai model.

As shown, the introduction of the calibration coefficient C_E allows a reliable theoretical relationship to be obtained that can be used for the prediction of the tensile stiffness at the design stage.

Finally, hybrid biocomposites reinforced by natural and synthetic fibres have been proposed in literature by various authors, as sisal/glass, jute/glass, and sisal/jute/glass (see the last rows of Table 6) to improve the mechanical performance of biocomposites reinforced by only natural fibres. The examination of the results shows that the hybridization allows appreciable increments (up to approximately 25%) of the tensile strength, although more interesting results are obtained in terms of the tensile modulus because the significant elastic modulus mismatch of the fibres do not lead to a contemporary failure of the different reinforcing fibres.

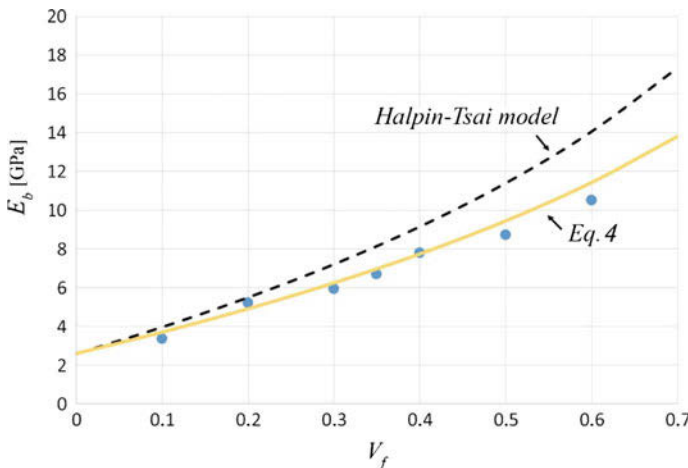


Fig. 9 Tensile modulus of short agave biocomposites and comparison with the theoretical model of Eq. 4

4.2 *MAT Biocomposites*

With the term ‘MAT biocomposites’, most authors refer to biocomposites reinforced by 2D MAT fabrics composed of discontinuous and randomly oriented natural fibres. The use of such fabrics enables the user to manufacture biocomposites laminate using hand lay-up or similar processes (hot pressed, etc.). Interesting results have been reported in [25] that consider polypropylene-hemp biocomposites, and in [37] that consider green epoxy/sisal biocomposites (see Table 7).

From such works, it is shown that although using MAT fabrics allows for an easy manufacturing process and a laminate of relatively high dimensions, it produces biocomposites with mechanical strength inferior to that obtained by 3D randomly oriented short fibres (in general, slightly inferior tensile strength compared to that of the simple matrix). This is attributable to the higher defect concentration, especially to the partial fibre wetting owing to the preliminary mutual fibre contact that occurs during the MAT fabric manufacturing. Further studies are required to implement new manufacturing processes that would overcome such drawbacks.

4.3 *Long Fibre Biocomposites*

As it is well known from micromechanics [51, 52], reinforcement with aligned long fibres is a unique method that can potentially yield high-performance biocomposites. Using such method, biocomposites having tensile strength 3–10 times that of the simple matrix, and tensile modulus that obeys the modified rule of mixture can be obtained. However, a good fibre alignment is an important feature, such that high-quality natural long fibre biocomposites can be obtained only using unidirectional fabrics with well-aligned fibres [35]. Further, limited misalignment can yield significant mechanical properties reduction. Hence, the mechanical properties of similar biocomposites reported in literature vary often in a wide range; for example, as shown in Table 8, the tensile strength of unidirectional epoxy/sisal biocomposites with a high volume fraction can vary from 150 to approximately 470 MPa according to the accuracy of the manufacturing process and fibre alignment.

The influence of the matrix/fibre adhesion on the mechanical properties of long fibre biocomposites is relatively negligible, except for a high percentage of matrix defects or significant delamination [5]. As mentioned above, the ratio between the failure strain of the matrix and fibres, along with the fibre alignment are basic parameters that govern the tensile strength. Unfortunately, accurate unidirectional fabrics of natural fibres are not available in the current market; therefore, the practical exploitation of high-performance biocomposites depends on the future industrial production of such products; for example, Fig. 10 shows the accurate ‘stitched’ unidirectional fabrics properly produced in laboratory [35].

Table 7 Mechanical properties of MAT biocomposites reported in literature

Matrix	Fiber	V_f (%)	Tensile strength (MPa)	Tensile modulus (GPa)	Elongation (%)	Manufacturing process	Impact strength (kJ/m ²)	References
PP	Hemp	40–50	51–57(60)	6–7(2.7)	–	Hot pressed	–	[25]
Green epoxy	Optimized agave	30	50(50)	6(3)	0.8	Optimized compression molding	–	[37]
Green epoxy	Optimized agave	35	45(50)	7(3)	0.7	Optimized compression molding	–	[37]

Table 8 Mechanical properties of long fibre biocomposites reported in literature

Matrix	Fiber	V _f (%)	Tensile strength (MPa)	Tensile modulus (GPa)	Elongation (%)	Manufacturing process	Impact strength (kJ/m ²)	References
PP	Glass	20	64	4.1	-	Hand lay-up	14	[55]
Epoxy	Sisal	47-52	157-180	13.0-15.0	-	Vertical/axial injection	40-47	[56]
Comstarch	Curaua	69.3	216	13.0	1.5	Compr. moulding DM	-	[57]
		67.0	275	29.0	1.2	Compr. moulding PF	-	
		69.9	327	36.0	1.2	Compr. moulding PS	-	
Epoxy	Jute	40	179			Compression moulding	-	[58]
Epoxy	Sisal	40	177			Compression moulding	-	
Epoxy	Banana	40	102			Compression moulding	-	
PP	Jute	40	38(33)	1.3(0.9)	-	Carding/hot pressing	-	[25]
PP	Kenaf	30-40	32(32)	1.2(0.9)	-	Carding/hot pressing	-	
Epoxy	ArcticFlax	54	275	39.0	-	Hand lay-up	-	[35]
	Sisal treated	73	412	6.0	-	Hand lay-up	-	
	Sisal untreated	77	327	10.0	-	Hand lay-up	-	
Soy protein	Sisal	50	180	3.5	-	Hand lay-up	-	
Polyester	Flax	60	310	28.0	-	Hand lay-up	-	
PCL	Curaua	70	220	13.5	-	Hand lay-up	-	
Green epoxy	Agave	30-70	210-470	13-30	1.8-2.1	Opt. compr. molding	-	
Green epoxy	Agave MPN	30	230	11.1	1.9	Hand lay-up	-	[2]
PLA	Agave MPN	30	241	10.0	2.1	Compression molding	-	

Fig. 10 a unidirectional ‘stitched’ fabric of agave fibre obtained in laboratory



Figure 11 shows the primary parameter of the optimized compression moulding process used to manufacture high-performance unidirectional epoxy/sisal biocomposites.

The experimental analysis performed in [35] has shown that the use of accurate manufacturing processes leads to high-quality biocomposites whose tensile characteristics obey the modified rule of mixture (MRoM). The longitudinal tensile strength is expressed by the well-known formulas:

$$\sigma_{L,R} = C_d \sigma_{f,u} V_f + \sigma_m (\varepsilon_{f,u}) (1 - V_f) \quad (9)$$

in which C_d is the correction coefficient that primarily considers fibre damage and residual misalignment. Figure 12 shows the good accordance between Eq. 9 and the experimental evidence, with deviation of less than 10%.

Figure 13 shows the good accordance between the longitudinal Young modulus and the value predicted by a ROM properly corrected by introducing a corrective calibration coefficient for the fibre modulus [35].

Finally, the example of fracture surface and the SEM micrograph reported in Fig. 14 corroborates how the damage mechanism of high-quality unidirectional biocomposites involves the fracture orthogonal to the longitudinal axis and the expected fibre tensile failure without premature damage mechanisms as pull-out and/or debonding.

Finally, it is remarkable to observe how high-performance biocomposites exhibit tensile strengths of up to approximately 500 MPa (see Fig. 10 as an example or Table 8), i.e. comparable with that of typical construction materials such as steels (400–500 MPa) and good GFRP (≈ 500 MPa). Further, such a maximum strength is higher than that of many aluminium alloys widely used in the aeronautics and automotive industry (260–410 MPa), and of typical epoxy-glass short fibre composites (50–150 MPa). In terms of the specific tensile strength, it is noteworthy that

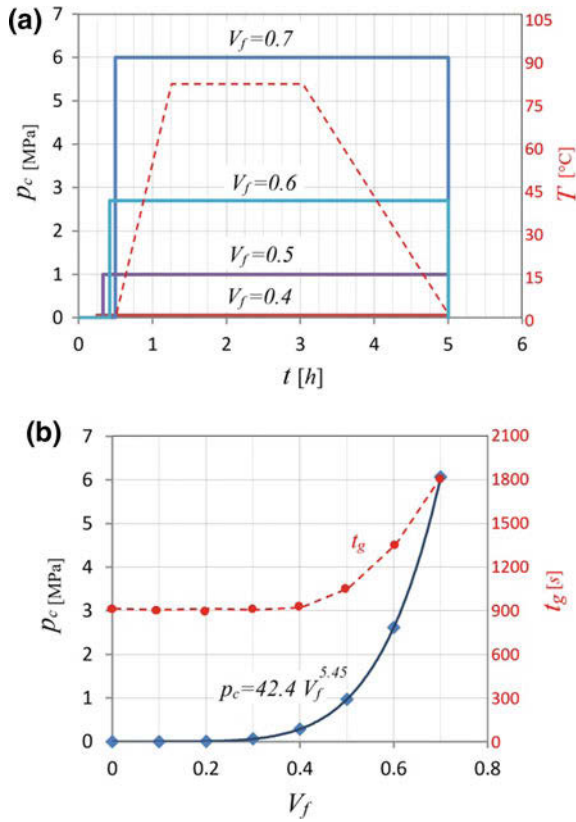


Fig. 11 a Diagrams of an optimal curing process for long fibre biocomposites and b optimal curing parameters versus V_f

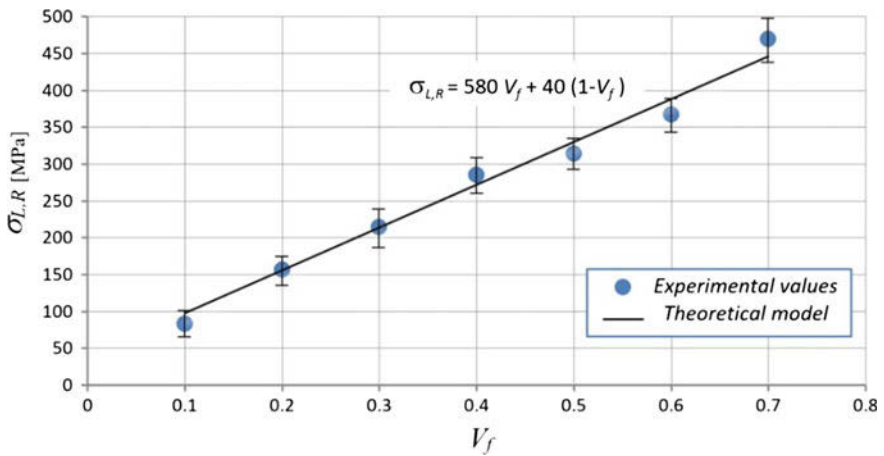


Fig. 12 Tensile strength of long agave fibre biocomposites versus V_f and theoretical model (MROM)

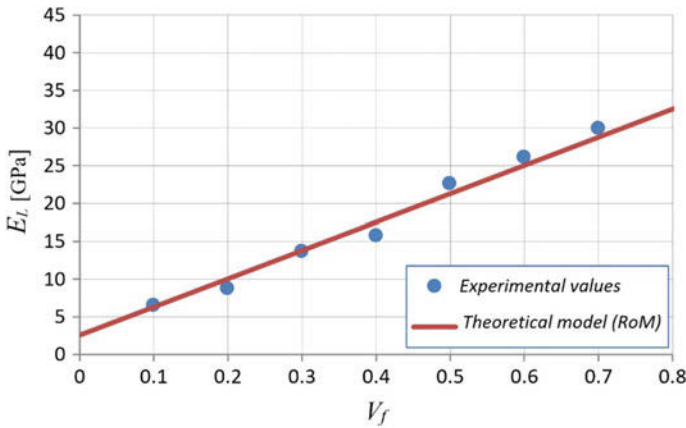


Fig. 13 Longitudinal young modulus of the green epoxy/sisal fibre biocomposites versus fibre volume fraction

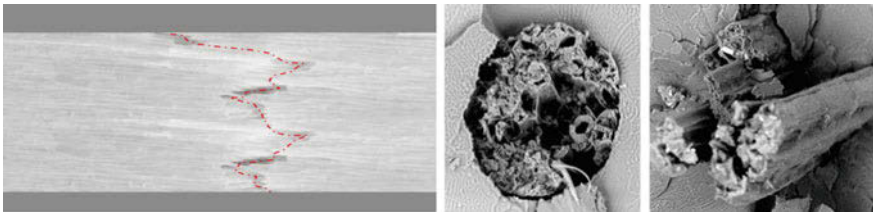


Fig. 14 Typical fracture surface and relative SEM micrographs of the long fibre biocomposites under tensile load

the strength index of approximately $\sigma_{L,R}/\rho = 35 \times 10^3$ m are reached, i.e. values superior not only to that of typical steels (between 5.8×10^3 m and 10.6×10^3 m), but also to that of good aluminium (15×10^3 m approximately). It is also comparable to that of good unidirectional GFRP (approximately 35×10^3 m with $V_f = 50\text{--}60\%$). Therefore, such high performance unidirectional biocomposites [35] can replace both traditional metals (steel, aluminium) and glass fibre reinforced composites (GFRP) in static structural applications. Considering the low cost of natural fibres, such a replacement can lead not only to a significant reduction in the environmental impact and the weight, but also a remarkable reduction in the costs in many fields of industrial production.

5 Dynamic Mechanical Properties

The need to extend the use of biocomposites for semi-structural and structural applications has led to an increased interest in the analysis and optimization of the dynamic mechanical performance of such materials, especially in the presence of

fatigue and impact loading. Considering the impact strength, the research works reported in literature (see also Tables 6, 7 and 8) show that the natural fibres have a relatively high strength to impact, especially the fibres (agave, etc.) constituted by subfibers that, like aramidic fibres, lead to high fracture energy. In more detail, the reinforcing by natural fibres yields appreciable increments of the impact strength of the thermosetting matrixes (see Tables 6, 7 and 8), up to one order of magnitude, whereas negligible improvements are obtained for the thermoplastics matrixes. Further studies are however necessary for a more reliable analysis of the impact strength of most biocomposites, by varying the primary parameters as fibre volume fraction, manufacturing process, etc.

Considering the fatigue strength, a few research works have been reported hitherto, and further studies are necessary to deeply understand the fatigue behaviour of biocomposites. However, the research activities reported in literature, has shown firstly that, as expected, the fatigue behaviour of the polymer matrix biocomposites is strictly related to various parameters such as matrix fatigue strength, fibre orientation, laminate lay-up, and manufacturing process. As observed from Table 9, the fatigue properties of good quality short fibre biocomposites is relatively good with respect to metal and other technical materials, which exhibits a fatigue ratio of approximately 0.5; the fatigue ratio of the analysed biocomposites, in fact, varies in the range of 0.7–0.8. Owing to the high fatigue ratio, we can conclude that the reinforcing of polymeric matrixes with natural fibres allows the user to increment significantly the fatigue strength of the matrixes; considering that the fatigue ratio of the matrixes varies in the range of 0.15–0.30 (typical plastics), whereas the fatigue ratio of the biocomposites varies in the range of 0.70–0.80. It follows that for a typical biocomposite having static strength equal to that of the matrix, the fibre reinforcing leads to a significant improvement in the fatigue strength, from 3 to 5 times the value of the simple matrix. As an example, the HDPE matrix shown in Table 6 exhibits a fatigue limit of approximately 5 MPa whereas the corresponding biocomposite exhibits a fatigue limit of approximately 20–24 MPa, i.e. approximately 4–5 times the value of the simple matrix. Low quality biocomposites obtained by compression moulding, lead instead to low fatigue strength with fatigue ratio less than 0.55 (see last rows of Table 9). Therefore, it is possible to state that although the reinforcing polymer matrixes by the natural fibres do not lead in general to appreciable improvements in the static strength, good quality biocomposites leads to interesting strength increments in terms of fatigue strength.

Regarding the long fibre biocomposites, only a few authors have performed fatigue analysis and further studies are necessary to gain a complete knowledge of the fatigue behaviour of such materials. As an example, Table 10 shows some data relative to polyester and epoxy reinforced by sisal, with and without alkali treatment [53], and by hemp, jute, kenaf and flax with different lay-ups.

As shown in Table 10, the unidirectional (UD) long natural sisal fibre biocomposites exhibit fatigue ratio in the range of 0.40–0.58, i.e. lower than that of good-quality short fibre biocomposites; similar results are shown for jute, flax and kenaf, whereas better results are obtained for good quality biocomposites reinforced

Table 9 Fatigue properties of short fibre biocomposites reported in literature

Matrix	Fiber	V_f (%)	Tensile strength (MPa)	Fatigue limit 10^6 cycles (MPa)	Manufacturing process	References
HDPE	Hemp	20–40	29–30(28)	22–24(0.80)	Injection moulding	[59]
HDPE (moisture)	Hemp	20	27.5	19.5(0.70)	Injection moulding	
Polyester (Al_2O_3)	Hemp/Jute	0	24–41(23)	16.5–31(0.75)	Injection moulding	[60]
PBT	Glass 0°	30	80(60)	40(0.5)	Injection moulding	[61]
PBT	Glass 18°	30	78(60)	35(0.45)	Injection moulding	
PBT	Glass 45°	30	50(60)	25(0.50)	Injection moulding	
PBT	Glass 90°	30	48(60)	24(0.50)	Injection moulding	
PA6 + rubber 10%	Glass0°	35	55(150)	27(0.50)	Injection moulding	
PA6 + rubber 10%	Glass 18°	35	50(150)	25(0.50)	Injection moulding	
PA6 + rubber 10%	Glass 45°	35	33(150)	19(0.55)	Injection moulding	
PA6 + rubber 10%	Glass 90°	35	30(150)	16(0.50)	Injection moulding	
PA6 + rubber 10%	Short birch	40	55(35)	22(0.45)	Injection moulding	[62]
HDPE	Short birch	50	37(30)	15(0.40)	Compres. moulding	[63]
Polyester	Hemp	55	50(32)	19(0.38)	Compres. moulding	[64]
Polyester	Glass	55	200(32)	50(0.25)	Compres. moulding	[64]
Polyester	Jute	40	47(32)	23.5(0.50)	Compres. moulding	[70]

Table 10 Fatigue properties of long fibre biocomposites reported in literature

Matrix	Fiber	V _f (%)	Tensile strength (MPa)	Fatigue limit 10 ⁶ cycles (MPa)	Manufacturing process	References
Polyester	Sisal (UD)	68.2	255(89)	100(0.40)	Moulding hot press	[53]
Polyester	Sisal (UD)	64.4	225(89)	120(0.54)	Moulding hot press	
Epoxy	Sisal (UD)	71.5	350(95)	139(0.40)	Moulding hot press	
Epoxy	Sisal (UD)	68.5	340(95)	159(0.47)	Moulding hot press	
Epoxy	Flax [± 45] _{1,6}	55	75(60)	44(0.58)	Hand lay-up	[66]
Polyester	Sisal [0/90] _{1s}	50	102(32)	56(0.55)	Low press. moulding	[67]
Polyester	Hemp	40	170(32)	130(0.76)	Compress. moulding	[68]
Polyester	Jute	40	225(32)	110(0.48)	Compress. moulding	[68]
Epoxy	Flax	40	150(60)	65(0.43)	Compress. moulding	[68]
Epoxy	Kenaf/Kevlar	35	216(73)	130(0.60)	Compress. moulding	[71]

by hemp. However, owing to the high static strength increment from the long fibre, it is possible to state that the reinforcement with long natural fibres leads to significant fatigue strength increment of the polymer matrix that is always higher than that obtained by short fibre biocomposites. Considering that the static strength of good-quality long fibre biocomposites is in general 3–5 times that of the matrix one, it is possible to state that the reinforcing by long natural fibre leads to an increment in the fatigue life of the matrix by approximately one order of magnitude. As an example, the reinforcing by sisal of a polyester matrix [53] having a fatigue strength of approximately 12 MPa, leads to a biocomposite with a fatigue strength of 120 MPa (see also Table 10). Further, in the fatigue load condition, the scattering of the experimental data of biocomposites are comparable with those of other materials such as metals or synthetic composites, and a statistical approach involving simple models such as the normal or Weibull distribution, can be used for a better prediction of the fatigue behaviour [54]. Finally, it is noteworthy that such results are extremely attractive especially by considering the low cost of the natural fibres; unlike synthetic composites, the cost of the biocomposites is lower than that of the simple matrix, i.e. unlike synthetic fibres, the fatigue properties increment obtained by natural fibres is not associated with a significant cost increment.

6 Conclusions

The critical analysis of the static and dynamic mechanical properties of polymer matrix composites reported in literature has shown that such properties are strictly affected by the corresponding properties of the matrix and fibre, as well as by the actual fibre/matrix adhesion whose correct estimation requires the consideration of the nonuniform shear stress distribution that occurs at the fibre/matrix interface. Such a distribution is significantly influenced by the fibre/matrix stiffness ratio such that the pull-out load increases with the fibre stiffness, and such a parameter is not a reliable parameter to the correct estimation of the fibre/matrix adhesion.

In general, the mechanical strength of the short fibre biocomposites is comparable with that of the simple matrix and an appreciable increment can be obtained only by using the proper manufacturing processes that allow the user to increase the fibre volume fraction (until approximately 35% at least) without increasing the typical defects such as voids and incomplete wetting of the free fibres. Hence, recent research activities have shown that a strength increment of approximately 60% can be obtained, as it has been demonstrated for green epoxy/sisal biocomposites. Further, a 3D random distribution of the fibres is always better than a 2D random distribution; therefore, the latter should be avoided during the biocomposite manufacturing. Moreover, although the use of MAT fabrics (2D discontinuous random fibres) allows the user to manufacture high-dimension laminates with hand lay-up or similar manufacturing processes, the diffuse wetting defects lead to mechanical strength that is always less than that of the randomly oriented short fibre biocomposites. Consequently, this configuration is not advisable if the maximum

mechanical strength is the primary objective of the reinforcement. However, the best static and dynamic mechanical performances are shown by the long fibre biocomposites. Such configuration is less affected by the limited matrix/fibre adhesion and, if an optimized manufacturing process is used along with the appropriate matrix/fibre couple (having a sufficient stiffness mismatch and adequate failure strains), it can lead to unidirectional high-performance biocomposites with a tensile strength up to approximately 500 MPa, with a tensile modulus of approximately 30 GPa or higher. In this case, an important influence parameter is the fibre alignment and the use of free fibre must be avoided; instead, it should be substituted by high-quality unidirectional fabrics. The low specific weight of the natural fibres (always less than that of the synthetic fibres) leads to long fibre biocomposites with a strength index superior to that of typical steels, aluminium alloys, and GFRP; consequently, these biocomposites can replace such materials (metals and composites) in various industrial applications.

References

1. Zuccarello B, Zingales M (2017) Toward high performance renewable agave reinforced biocomposite: optimization of fiber performance and fiber-matrix adhesion analysis. *Compos B* 122:109–120
2. Zuccarello B, Scaffaro R (2017) Experimental analysis and micromechanical models of high performance renewable agave reinforced biocomposites. *Compos Part B* 119:141–152
3. Herrera-Franco PJ, Valadez-Gonzalez A (2005) A study of the mechanical properties of short natural-fiber reinforced composites. *Compos B* 36:597–608
4. Sreekumar PA, Joseph K, Unnikrishnan G, Thomas S (2007) A comparative study on mechanical properties of sisal-leaf fiber reinforced polyester composites prepared by resin transfer and compression moulding techniques. *Compos Sci Technol* 67:453461
5. Cirello A, Zuccarello B (2006) On the effects of a crack propagating toward the interface of a bimaterial system. *Eng Fract Mech* 73:1264–1277
6. Murherjee PS, Satyanarayana KG (1987) Structure and properties of some vegetable fibres, part 1. Sisal fibres. *J Mater Sci* 19:3925–3934
7. Belaadi A, Bezazi A, Bouchak M, Scarpa F, Boba K (2014) Novel extraction techniques, chemical and mechanical characterization of agave Americana L. natural fibres. *Compos Part B* 66:194–203
8. Chand N, Hashimi SAR (1993) Mechanical properties of sisal fibres at elevated temperatures. *J Mater Sci* 28:6724–6728
9. Chan N, Verma S, Khazanchi AC (1989) SEM and strength characteristic of acetylated sisal fiber. *J Mater Sci Lett* 8:1307–1309
10. Silva FA, Chawla N, Filho RDT (2008) Tensile behavior of high performance natural (sisal) fibers. *Compos Sci Technol* 68:3438–3443
11. Thomason JL, Carruthers J, Kelly J, Johnson G (2008) Fibre cross-section determination and variability in sisal and lax and its effects on fibre performance characterization. *Compos Sci Technol* 71:1008–1015
12. Belaadi A, Bezazi A, Bouchak M, Scarpa F, Zhu C (2008) Thermochemical and statistical mechanical properties of natural sisal fibres. *Compos Part B* 67:481–489
13. Kaewkuk S, Sutapun W, Jarukmjorn K (2013) Effects of interfacial modification and fiber content on physical properties of sisal fiber/polypropylene composites. *Compos Part B* 45:544–549

14. Bisanda ETN, Ansell MO (1999) The effect of silane treatment on the mechanical and physical properties of sisal-epoxy composites. *Compos Sci Technol* 41:165–168
15. Joseph K, Thomas S, Pavithran C (1996) Effect of chemical treatment on the tensile properties of short sisal fiber-reinforced poly-ethylene composites. *Polymer* 37:5139–5149
16. Singh B, Gupta M, Verma A (1996) Influence of fibre surface treatment on the properties of sisal-polyester composites. *Polym Compos* 17:910–918
17. Mysamy K, Rajendran I (2011) Influence of alkali treatment and fibre length on mechanical properties of short agave fibre reinforced epoxy composites. *Mater Des* 32:4629–4640
18. Kim JT, Netravali AN (2010) Mercerization of sisal fibers: effect of tension on mechanical properties of sisal fiber and fiber-reinforced composites. *Compos Part A* 41:1245–1252
19. Sood M, Dwivedi G (2017) Effect of fiber treatment on flexural properties of natural fiber reinforced composites: a review. *Egypt J Pet* <https://doi.org/10.1016/j.ejpe.2017.11.005>
20. Furqan A, Heung SC, Myung KP (2015) A review: natural fiber composites selection in view of mechanical, light weight, and economic properties. *Macromol Mater Eng* 300:10–24
21. Li Y, Mai Y-W, Ye L (2000) Sisal fibre and its composites: a review of recent developments. *Compos Sci Technol* 60:2037–2055
22. Omrani E, Menezes PL, Rohatgi PK (2015) State of the art on tribological behavior of polymer matrix composites reinforced with natural fibers in the green materials world. *Eng Sci Technol* 21:165–175
23. Koronis G, Silva A, Fontul M (2013) Green composites: a review of adequate materials for automotive applications. *Compos Part B* 44:120–127
24. Nabi D, Jog JP (2017) Natural fiber polymer composites: a review. *Adv Polym Technol* 18 (4):351–363
25. Ku H, Wang H, Pattarachaiyakoo N (2011) A review on the ensile properties of natural fiber reinforced polymer composites. *Compos Part B* 42:856–873
26. Jagadeesh D, Kanny K, Prashantha, K (2017) A review on research and development of green composites from plant protein-based polymers. *Polym Compos* 38:1505–1518
27. Bharath KK, Basavarajappa S (2015) Applications of biocomposite materials based on natural fibers from renewable resources: a review. *Sci Eng Compos Mater* 23:1–10
28. Ramesha M, Palanikumarb K, Hemachandra Reddy KK (2017) Plant fibre based bio-composites: sustainable and renewable green materials. *Renew Sustain Energy Rev* 79:558–584
29. Sharath Shekar HS, Ramachandra M (2018) Green composites: a review. *Mater Today Proc* 5:2518–2526
30. Benzait Z, Trabzon L (2018) A review of recent research on materials used in polymer-matrix composites for body armor application. *J Compos Mater*, pp 1–23 <https://doi.org/10.1177/0021998318764002>
31. Sanjay MR, Madhu P, Jawaid M, Sentamaraikannan P, Senthil S, Pradeep S (2018) Characterization and properties of natural fiber polymer composites: a comprehensive review. *J Clean Prod* 172:566–581
32. Khan T, Sultan MTBH, Ariffin AH (2018) The challenges of natural fiber in manufacturing, material selection, and technology application: a review. *J Reinf Plast Compos* 37:770–779
33. Layth M, Ansari NMN, Pua G, Jawaid M, Saiful Islam M (2015) A review on natural fiber reinforced polymer composite and its applications. *Int J Polymer Sci*, 15 <https://doi.org/10.1155/2015/243947>
34. Nunna S, Chandra PR, Shrivastava S, Jalan A (2012) A review on mechanical behaviour of natural fiber based hybrid composites. *Reinf Palstics Compos* 31(11):759–769
35. Zuccarello B, Marannano G, Mancino A (2018) Optimal manufacturing of high performance biocomposites reinforced by sisal fibers. *Compos Struct* 194:575–583
36. Mancino A, Marannano G, Zuccarello B (2017) Analisi del comportamento meccanico di diverse varietà di fibre di agave e dei relativi biocompositi ecosostenibili. In: *Proceedings of the 46° Aias national congress 2017*
37. Zuccarello B, Marannano G (2018) Random short fiber biocomposites: optimal manufacturing process and reliable theoretical models. *Mater Des* 149:87–100

38. Zuccarello B, Mancino A, Marannano G (2017) Implementation of eco-sustainable biocomposite materials reinforced by optimized agave fibers. *Struct Int Proc* 8:526–538
39. Pantano A, Zuccarello B (2017) Numerical model for the characterization of biocomposites reinforced by sisal fibers. *Struct Int Proc* 8:517–525
40. Di Landro L, Janszen G (2014) Composites with hemp reinforcement and bio-based epoxy matrix. *Compos B Eng* 67:220–226
41. Chang KH (2015) Development of a bio-based composite material from soybean oil and keratin fibers. *J Polym Sci* 95:1524–1538
42. Haq M, Burgueño R, Mohanty AK, Misra M (2008) Hybrid bio-based composites from blends of unsaturated polyester and soybean oil reinforced with nanoclay and natural fibers. *Compos Sci* 68(15):3344–3351
43. Feldman M, Bledzki K (2014) Bio-based polyamides reinforced with cellulosic fibres—processing and properties. *Compos Sci Technol* 100:113–120
44. Patel M, Marini L (2015) Life-cycle assessment of bio-based polymers and natural fiber composites. Wiley Online Publications. <https://doi.org/10.1002/3527600035>
45. Satyanarayana KG, Arizaga GGC, Wypych F (2009) Biodegradable composites based on lignocellulosic fibers—an overview. *Prog Polym Sci* 34:982–1201
46. Yan Libo, Kasal Bohumil, Huang Liang (2016) A review of recent research on the use of cellulose fibers, their fibre fabric reinforced cementitious, geo-polymer and polymer composites in civil engineering. *Compos B* 92:94–132
47. Dicker MPM, Duckworth PF, Baker AB, Francois G, Hazard MK, Weaver PM (2014) Green composites: a review of material attributes and complementary applications. *Compos Part A* 56:280–289
48. Mohanty AK, Misra M, Drzal LT (2005) Natural fibers, biopolymers and biocomposites. CRC Press
49. Faruk O, Bledzki AK, Fink HP, Sain M (2012) Biocomposites reinforced with natural fibers: 2000-2010. *Progr Polim Sci* 37:1552–1596
50. Ramzy A, Beermann D, Steuernagel L, Meiners D, Ziegmann G (2014) Developing a new generation of sisal composite fibers for use in industrial application. *Compos Part B* 66:287–298
51. Agarwal BD, Broutman LJ (1998) Analysis and performance of fiber composites. Wiley, New York
52. Barbero EJ (1999) Introduction to composite materials design. Taylor & Francis, Ann Arbor, MI
53. Towo AN, Ansell MP (2008) Fatigue and evaluation and dynamic mechanical thermal analysis of sisal fibre-thermosetting resin composites. *Compos Sci Technol* 68:925–932
54. Torres JP, Vandi LJ, Deidt M, Heitzmann MT (2017) The mechanical properties of natural fibre composite laminates: a statistical study. *Compos Part A* 98:99–104
55. Langhorst AE, Burkholder J, Long J, Thomas R, Kiziltas A, Mielewski D (2017) Blue-agave fiber-reinforced polypropylene composites for automotive applications. *Bioresources* 13:820–835
56. Yan L, Hao M, Yiou S, Qian L, Zhuoyuan Z (2015) Effect of resin inside fiber lumen on the mechanical properties of sisal fiber reinforced composites. *Compos Sci Technol* 108:32–40
57. Gomes A, Matsuo T, Goda K, Ohgi J (2007) Development and effect of alkali treatment on tensile properties of curaua fiber green composites. *Compos Part A* 38:1811–1820
58. Singh JIP, Dhawan V, Singh S, Jangid K (2017) Study of effect of surface treatment on mechanical properties of natural fiber reinforced composites. *Mater Today* 4:2793–2799
59. Fotouh A, Wolodko JD, Lipsett MG (2014) Fatigue of natural fiber thermoplastic composites. *Compos B* 62:175–182
60. Bendigeri C, Jwalesh HN (2016) Review on fatigue behavior of polymeric biomaterials with natural fibers. *Int J Adv Eng Res Sci* 3(2):2349–6495
61. Mortazavian S, Fatemi A (2017) Fatigue of short fiber thermoplastic composites: a review of recent experimental results analysis. *Int J Fatigue* 102:171–183

62. Mejri M, Toubal L, Cuillière JC, Francois V (2017) Fatigue life and residual strength of a short-natural-fiber-reinforced plastic vs. nylon. *Compos B* 110:429–441
63. Bravo A, Toubal L, Koffi D, Erchiqui F (2018) Gear fatigue life and thermomechanical behavior of novel green and bio-composite materials VS high-performance thermoplastics. *Polym Testing* 66:403–414
64. Shahzad A, Isaac DH (2014) Fatigue properties of hemp and fiber composites. *Polym Compos* 35:1926–1934
65. Belkacemi C, Bezzazi B (2014) Quasi-static mechanical characterization and fatigue of a composites laminates. *Adv Appl Sci Res* 5(3):328–335
66. Boughera B, Sawi IE, Fawaz Z, Maraghni F (2015) Investigation and modeling of the fatigue damage in natural fiber composites. In: TMS middle east—mediterranean materials congress on energy and infrastructure systems 2015, Doha, Qatar
67. Belaadi A, Bezazi A, Maache A, Scarpa F (2014) Fatigue in sisal fiber reinforced polyester composites: hysteresis and energy dissipation. *Proc Eng Part B* 74:325–328; 67:481–489
68. Mahboob Z, Bougherara H (2018) Fatigue of flax-epoxy and other plant fibre composites: critical review and analysis. *Compos Part A* 109:440–462
69. Saman S, Sahrba MJ, Leman Z, Sultan MTH, Ishak MR, Cardona F (2016) Tension-compression fatigue behaviour of plain woven kenaf/Kevlar hybrid composites. *BioResource* 11(2):3575–3586
70. Milanese AC, Cioffi MOH, Woorwald HJC (2012) Thermal and mechanical behavior of sisal/phenolic composites. *Compos Part B* 43:2843–2850
71. Etaati A, Pather S, Fang Z, Wang H (2014) The study of fiber/matrix bond strength in short hemp polypropylene composites from dynamic mechanical analysis. *Compos B* 62:19–28

Synthesis, Characterization, and Applications of Hemicellulose Based Eco-friendly Polymer Composites



Busra Balli, Mehmet Harbi Calimli, Esra Kuyuldar and Fatih Sen

1 Introduction

Generally, composites offer very promising solutions to the ongoing problems of the world [1–90]. Fuel cells [30–32, 90] materials for catalysis [79, 33–35, 80–86, 90–96], capacitors [20], solar cells [25, 26], thermopower applications [2], sensors [9, 10, 13, 42, 90, 94] are some examples of these solutions. Materials are also used corporately in combining their superior properties. Metal-metal combinations, polymer-metal combinations and their some hybrids with carbon-based materials are used for variety of nanomaterial applications [6, 7, 14–17, 23, 55, 78–84].

Composite materials are also widely used in developing appropriate materials for various applications as conductive polymer and other electronically active material composites. Graphene and graphene oxide [4, 27, 45–47], carbon nanotubes (CNTs) [14–17, 45–47, 79–85, 93, 95], activated carbon (AC) [14–17, 33], vulcanized carbon (VC) [30–32], carbon black [9, 10] and graphene derived materials which have different structure and morphologies as reduced graphene oxide [3, 30–32, 37, 45–47], graphene nanosheets, graphene nanoribbons, graphene nanoplatelets may thought as active materials for different applications. Also, a wide variety of nanoparticles are utilized in composite systems [34, 35, 73, 74, 85–89, 91–93, 95, 96]. Besides, biodegradable polymers or polymer composites (PCs) produced using renewable materials are referred to as eco-friendly polymer composites (EFPCs). Since they have a carbon-neutral lifecycle, their use as an alternative to petroleum-based materials can result in the reduction of carbon dioxide emissions. Having a net zero carbon footprint, EFPCs are also good materials for the envi-

B. Balli · E. Kuyuldar · F. Sen (✉)

Sen Research Group, Biochemistry Department, Faculty of Arts and Science, Dumlupınar University, Evliya Çelebi Campus, 43100 Kütahya, Turkey
e-mail: fatih.sen@dpu.edu.tr

M. H. Calimli

Tuzluca Vocational School, Iğdir University, Iğdir, Turkey

ronment and surrounding eco-systems [97–109]. It is an unavoidable fact that the world is currently facing serious challenges with regard to the environmental, social and political crisis. Another pressing issue that needs to be tackled by people is that of energy. Today, a large part of the world depends on fossil fuels to meet the demand for energy [110–115]. However, fossil-based energy sources are becoming exhausted at a great speed. Therefore, it is imperative that not only scientific organizations but also public and private sectors focus on the innovation of eco-friendly materials, also referred to as “green materials.” This research area has recently witnessed important accomplishments thanks to scientists and engineers who have realized that making environmentally responsible decisions is the ultimate way to protect the environment and to prevent energy crises [108]. Figure 1 shows the world energy consumption according to energy sources.

Production of environmentally friendly materials requires different fields to participate in the process. These fields engage in sustainable chemistry and work on biodegradable and bio-based materials structurally, chemically, and physically [116–120]. They also pay close attention to make sure that environmentally hazardous substances are not included in any stage of the design and production process. The fields with which we are concerned are EFPCs, sustainable chemistry, natural resources and eco-friendly engineering processes, etc. Animal and plant products can be used to manufacture many natural polymers. These materials have various appealing features. They are ubiquitous, do not contain synthetic substances, can be recycled and consumed by microorganisms. In the last ten years, numerous studies have been carried out on the production of polymeric materials (blends, composites, and nanocomposites). These studies mostly conducted experiments polymers and fillers were mixed. When resin systems are integrated with reinforcing materials, EFPCs achieve excellent features. The combination of resin systems and reinforcing fiber/filler particles results in the composite material integrating the features of resin features and of fibers/fillers. In a composite material, the resin matrix distributes the load on the composite between fiber/filler particles.

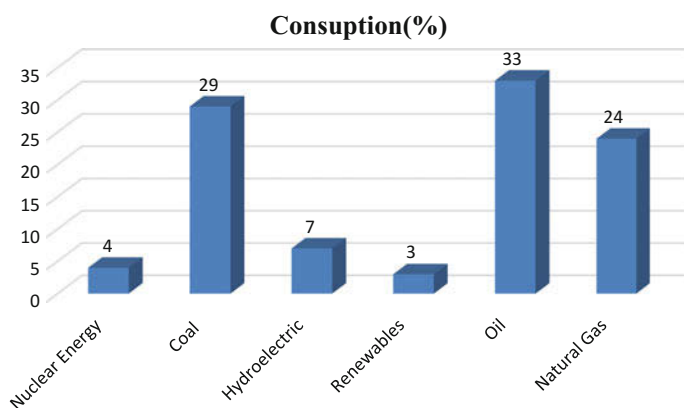


Fig. 1 The primary energy consumption in the world

In addition, it prevents fibers from being damaged due to abrasion and impact and enhances the load-bearing capacity of the composite. The resulting composite has high hardness and resistance and low density and is easy to use. Therefore, it is a better material than metals to be used in the manufacture of various products.

EFPCs have the high specific strength and specific stiffness, high fracture, abrasion, impact, corrosion and fatigue resistance, and low cost.

The greatest appeal of eco-friendly composites is that they are environmentally friendly, completely degradable and sustainable. Baillie addressed the construction and biorhythm evaluation of green composites in detail [8]. EFPCs might be employed effectively for various purposes such as short life-cycle goods manufactured in large quantities and disposable goods. Cellulose, NR, polysaccharides, starch, chitin, proteins, collagens/gelatin, and lignin are natural and biodegradable chemical compounds while polyamides, polyvinyl alcohol, polyvinyl acetate, polyglycolic acid, and polylactic acid are synthetic compounds. New fibre-reinforced materials are made from renewable resources and used in almost all areas [107].

Being superior to synthetic raw materials, EFPCs can play a significant role in the elimination of environmental problems, especially caused by plastic waste, and in the sustainable development of eco-friendly and cost-effective technologies [69]. Numerous studies are conducted on EFPCs to find innovative ways to manufacture eco-friendly materials from biodegradable polymers and renewable sources.

Eco-friendly Polymer Nanocomposites (EPNs) have also drawn enormous attention owing to their potential application in the field of agriculture such as product waste management [118]. EPNs can also be employed to improve the environmental compatibility of recycling processes.

There is the classification of six types of the most common EPN, including (i) EPN with Green Fillers and (ii) EPN with Green-Base-Composite such as—EPN from Cellulose,—EPN from Thermoplastic Starch,—EPN from Polylactic Acid,—EPN from Polymer Mixture,—EPN from Others (Gelatin, PHB, Chitosan).

2 Definitions About Hemicellulose and Derivatives

Of natural polymers, lignocellulosic is likely to be a very important material as it can be converted into biofuels and bioproducts. Mainly found in lignocellulose, hemicelluloses are the second most abundant renewable material in nature, easy to use, has film-forming features, good biocompatibility, and biodegradability [118, 119]. Hemicelluloses contain a very large quantity of free hydroxyl groups, which are perfect for chemical modification. Materials with exclusive features can be manufactured using chemically modified hemicelluloses in order to improve the biopolymers [39, 75, 101]. In recent years, hemicelluloses-based biocompatible films have been popular owing to reduced cost, oxygen barrier features and ease of access [18, 51].

Natural biopolymers are superior to synthetic ones in the sense that the former is more cost-effective, biocompatible, harmless and biodegradable. Being the non-cellulose cell-wall polysaccharides of agricultural and forest plants, hemicelluloses are regarded as unlimited and sustainable materials for the manufacturing of biopolymers and biomaterials [29, 70].

However, hemicelluloses contain a very large amount of hydroxyl groups distributed along the central and terminal region. In addition, these hydroxyl groups generate intermolecular and intramolecular hydrogen bonds [70, 77]. Hemicellulosic materials are non-hydrophobic, semi-crystalline and hygroscopic and have low mechanical features [36]. Due to these disadvantages, hemicelluloses films cannot be used widely. Plasticizers are generally used to enhance the mechanical features of films consist of hemicellulose [43, 44, 120].

As the main hemicelluloses in hardwood and annuals, xylan-type hemicelluloses are regarded as appropriate sources to achieve films. Emulsification and coating processes were employed to achieve arabinoxylan-based films [71, 72]. Lignin or glycerol was used to produce pure xylan, yet, self-supporting films [43, 44]. Table 1 shows the content of some lignocellulosic materials.

Plasticized films from aspen glucuronoxylan exhibit low oxygen permeability and therefore might be ideal for food packaging materials [49]. Up to 40% xylan in wheat gluten was used to produce composite films [57]. In addition, chemical modifications were performed in order to reduce the moisture sensitivity of

Table 1 Some lignocellulosic materials and their contents

Natural fibre	Cellulose (wt %)	Hemicellulose (wt %)	Lignin (wt %)	Total (wt %)
Cotton	89.7	1.0	2.7	93.4
Flax	80	13	2	95
Hemp	74.1	7.6	2.2	83.9
Sugar cane	51.8	27.6	10.7	90.1
Bamboo	54.6	11.4	21.7	87.7
Coconut	51.3	11.7	30.7	93.7
Wheat straw	38	36	22	96
	38.0	29.0	15.0	82
	33.2	24.0	15.1	72.3
	28.8	39.1	18.6	86.5
Rape straw	36	37	24	97
	37.6	31.4	21.3	90.3
Spruce + bark	42	27	26	95
	41.0	24.3	30.0	95.3
	50.8	21.2	27.5	99.5
Poplar wood	50	30	≤ 20	≤ 100

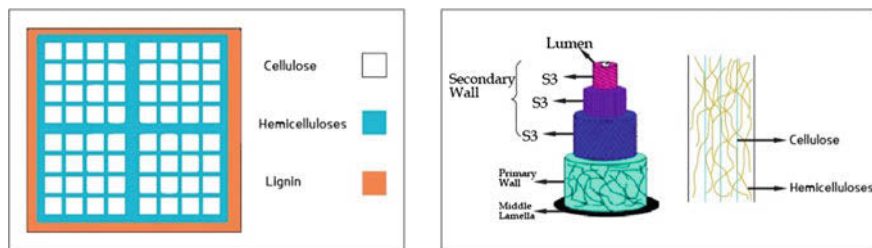


Fig. 2 The schematic representation of hierarchical structure of wood cell

hemicellulose-based films [50, 52]. The molecular structure of hemicelluloses had a large effect on film formation, structure, mechanical features, and moisture content. Side groups separated the xylan or mannan chains, and therefore, hemicellulose where the backbone was least substituted with arabinose or galactose was the most interactive one [29, 53, 66, 102].

Hemicelluloses can also be described in more detail and seen schematically in Fig. 2. They are the second most abundant polysaccharides in biomass. They are biosynthesized by trees and terrestrial plants. Despite the fact that they are in large quantity, hemicelluloses are little used by industries. Hemicelluloses are not completely degraded in most of the lignocellulosic refining processes, but they are removed or further used as feed raw material. Nevertheless, some methods have been developed to separate and isolate high molar mass hemicelluloses. Alkalines are used to extract hemicelluloses from plants. Water is also used to extract some parts of hemicelluloses. Forests and agricultural areas provide a large number of raw materials and studies have been and are being conducted to find potential application areas for it. Potential areas of use of hemicelluloses are paper, packaging, coatings, hydrogels, absorbents, and emulsifiers. As a group of polysaccharides, hemicelluloses have a positive effect on cell wall flexibility by cross-linking cellulose and lignin. They compose the hydrophilic component of the cell wall. They have categorized into different groups according to their structure: xylans, mannans, galactans, arabinans, and β -glucans. Xylans and mannans, the two most common ones, are used as components of polymer blends, PCs, and nanocomposites. As plant mannan gums have similar chemical features to that of hemicelluloses, they have also been categorized as hemicelluloses [73].

2.1 Properties

Most hemicelluloses support cell walls as do celluloses [100]. Thanks to the ability of hemicelluloses to absorb a large body of water, cell walls become less brittle and, more elastic and resistant to bending. Hemicelluloses also form absorbent molecular networks around cellulose crystallites, which enable the cell walls to transfer

intermediate products and sources of nourishment [54]. In addition, it is reported that some fundamental properties of arabinoxylans allow intermolecular alignment between arabinoxylans and polysaccharides, which enables the composition of gels with several components in the wall matrix. Furthermore, ferulic acid residues on arabinoxylan chains allow for covalent interaction between polysaccharide–polysaccharide, polysaccharide–protein, or polysaccharide–lignin [40].

Having less degree of structural order and polymerization, hemicelluloses are chemically and thermally less stable than celluloses. Another difference between hemicelluloses and celluloses is that the former is soluble in alkalines, the feature of which is widely used to section various polysaccharides in samples which do not contain lignin. Nevertheless, this process leads to the removal of ester groups and decrease in solubility. Some hemicelluloses are able to be dissolved in water partially or completely [5]. Hemicelluloses gain hydrophilic property thanks to various free hydroxyl groups in them [38]. The more stable hemicelluloses are, the more they are dissolved in water and less tightly bind to cellulose. On the other hand, the more sporadic the side chains of molecules are, the less they are dissolved in water and more tightly bind to cellulose [60]. A reduction in polymerization generally leads to an increase in solubility [105]. Acetylated hemicelluloses can also be dissolved in dimethyl sulfoxide, formamide, and *N,N*-dimethylformamide. Almost all plants contain hemicelluloses, which are, therefore, found in diets. Cell-wall polysaccharides are important as dietary fibers and contribute to lipid metabolism. Therefore, their consumption helps feces pass through the digestive tract [5, 99, 108]. There is a classification of hemicelluloses such as (i) Softwood hemicelluloses;—Galactoglucomannan (Mannans),—Arabinoglucuronoxylan (Xylans),—Arabinogalactan,—Pectins (ii) Hardwood hemicelluloses such as—Glucuronoxylan,—Glucomanan, (iii) Grasses like -Arabinoxylan-main.

3 Hemicellulose Based Composites and Their Applications

Environmentally friendly polymer composites (EFPCs) are used in the manufacture of packaging materials, films, sanitation products, bottles, fishing nets, cutlery, trays and various other products; sensing, adsorbing and many other applications [1, 19, 24, 28, 41, 61, 64, 99, 106, 109].

Expanding their areas of application, most eco-friendly polymers possess perfect features. Hemicelluloses contain a very large quantity of free hydroxyl groups distributed along the backbone and side chains, which are perfect for chemical modification. Materials with exclusive features can be manufactured using chemically modified hemicelluloses in order to improve the biopolymers [39, 101, 119]. In recent years, hemicellulose-based nanocomposite films (HBNCFs) have been popular owing to reduced cost, oxygen barrier features and ease of access [75]. In addition, these hydroxyl groups generate intermolecular and intramolecular

hydrogen bonds [70, 77]. Hemicelluloses are hydrophilic and HBNCFs are semicrystalline and hygroscopic and have low mechanical features [36]. Due to these disadvantages, hemicelluloses films cannot be used widely. Plasticizers are generally used to improve the mechanical features of hemicellulose films [43, 44, 51, 120].

Owing to the fact that hemicellulose-based biomaterials are biocompatible, harmless and biodegradable, they have become of great interest for the manufacture of pharmaceutical, tissue engineering, and food packaging products. HBNCFs have attracted the greatest attention due to their oxygen barrier properties. However, they are not very good at forming films and have low performance. Plasticizers or hydrophobization is generally needed to turn hemicelluloses into appropriate materials for packaging products. Rather than concentrating on materials themselves, most studies on hemicelluloses address converting polymers into sugars [109]. Peng et al. suggested an efficient and feasible technique to manufacture superior HBNCFs. He combined cellulose nanofibers (CNFs) and xylan (XH) films as plasticizers were also included in the process. Sugar composition was xylose (89.38%), arabinose (5.75%), glucose (1.87%), galactose (0.66%) glucuronic acid (1.78%) and galacturonic acid (0.55%). Morphological tests indicated that XH film surface and CNF-reinforced NCF consisted mainly of nodules (10–70 nm) and that CNFs were embedded in the XH matrix. Aggregates started to develop in an interval of arabinose/xylose ranging from 0.23 to 0.31 in an aqueous solution and when the arabinose substituents were exhausted, unsubstituted xylan chains formed a steady connection, which shows that the intermolecular interaction could be adjusted by manipulating the substituted groups or by including a second component that establishes an interaction with the molecular chains of hemicelluloses. Film formation was better, and the tensile strength improved greatly due to high aspect ratio and strong interactions between CNF and the XH matrix. Fang et al. [39] employed the freeze-thaw method in order to use hemicelluloses from bamboo holocellulose, PVA, and chitin nanowhiskers to manufacture a hybrid hydrogel. FTIR and NMR results showed that the gelation process witnessed physical crosslinking instead of a chemical reaction. PVA functioned as a hydrogel scaffold while hemicelluloses were firmly hydrophilic and showed hydrogen-bonding features when chitin nanowhiskers functioned as a cross-linker. According to atomic force microscopy (AFM) images of chitin, whisker size was about 200 nm in length and 40 nm in width. The mechanical features of hydrogels were greatly enhanced by an increase in the rate of chitin nanowhiskers. The hydrogels are potential materials to be utilized in the manufacture of tissue engineering products. Laminated films, one layer of which is polyester and the other of which is made of carbon nanotubes and hemicellulose, have been patented in Japan [58]. Polymers were supplied by removing hemicellulose from *Abelmoschus manihot* or *Hydrangea paniculata*. The homogenous distribution of carbon nanotubes in hemicellulose films was leading to obtaining mechanically strong films [109].

3.1 Composite Formation and Characterization with Layered Silicates

For nanocomposite formation, polymer chains should be dispersed in the galleries between silicate layers in order to obtain two distinct classes of lamellar nanocomposites; intercalated and exfoliated as represented schematically in Fig. 3. Intercalation takes place with a little polymer permeating into the galleries, which leads to silicate layers expanding in a limited manner. This way, a systematic structure with multiple layers separated by several nanometers is obtained. Large-scale polymer diffusion causes silicate layers to exfoliate or delaminate. An exfoliated nanocomposite contains nanometer thick platelets that are uniformly dispersed all over the polymer matrix. On the contrary, when the polymer and silicate do not form a homogeneous mixture when mixed, the layers do not apart, and they function as agglomerates or tactoids.

Total diffusion of clay platelets in a polymer increases the number of usable reinforcing materials to carry an applied load and to avert the formation of cracks. The pairing of the enormous surface area of the clay and the polymer matrix enables stress to be shifted to the reinforcement stage, which leads to mechanical improvement. Furthermore, the impenetrable clay layers require a convoluted track for a permeant to travel across the nanocomposites as seen in Fig. 4. Thanks to obstructed diffusion tracks along nanocomposites, the barrier property and flame retardancy of polymer-clay nanocomposites are improved, and they are more resistant to chemicals and uptake less solvent [104].

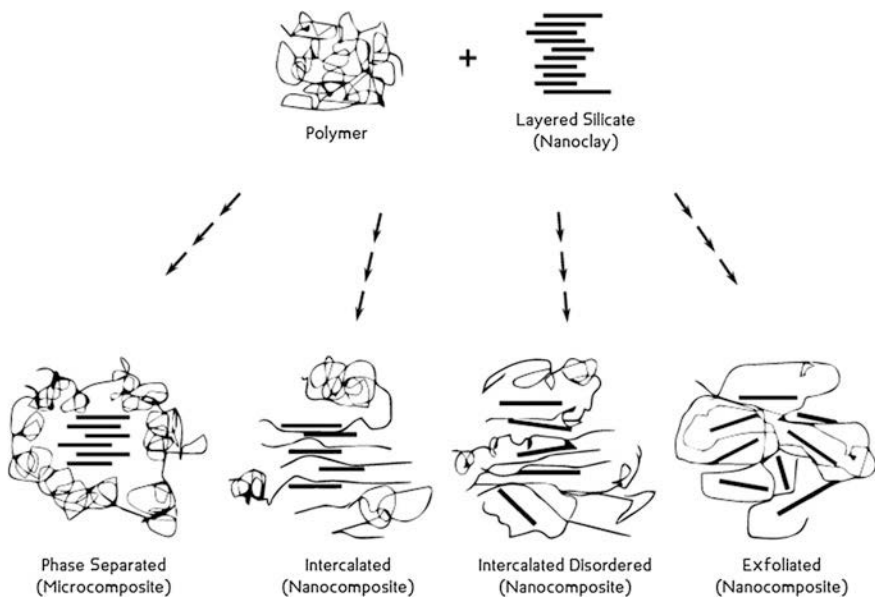
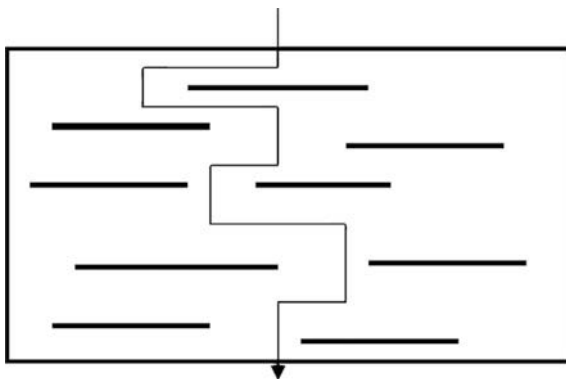


Fig. 3 Possible structures of nanocomposites

Fig. 4 Proposed model for the tortuous zigzag diffusion path in a polymer-clay nanocomposite when used as a gas barrier



3.2 Packaging Materials

The food producers have a wide range of natural recipes that are used in packaging applications and have a variety of needs that ensure the quality and safety of food. The first goal of this industry is assuring the protection of food products from the many factors related to the environment, gases, water etc. The most important factor in food packages is oxygen since oxygen has a very important material in the various chemical industries because oxygen mostly affects the expiration date of foods, fruits, vegetables, microbial growth etc. Nowadays, in order to cancel this effect of oxygen, Al plates and/or foil and some of the polymers such as polyethylene vinyl alcohol (EVOH), polyvinylidene chloride (PVDC) etc. are mainly used as packaging materials. Water, then again, is one of most important material, the catalyst that affects the chemical reactions and/or enzymatic changes and known as the principal food ingredient.

Biomass has become of greater interest for food packaging applications. The aim of most studies is to alter hemicelluloses and enhance the mechanical features of HBNCFs converted into a quaternary form. To this end, those studies focus on assuming an environmentally friendly and feasible approach. Chen et al. Integrated quaternized hemicelluloses, chitosan, and MMT to produce films. They analyzed the morphological structure and optical, physical, mechanical and thermal features of the films. Another aim of the study was to determine the ideal ratio in order to produce HBNCFs. The principal endeavour will present chitosan-based materials.

Peng et al. [70] reported that the molecular makeup of hemicelluloses had a great effect on film formation, mechanical features, and moisture content. The side groups made xylan or mannan chains separate, indicating that the hemicellulose which had the biggest interaction was the one in which arabinose or galactose substituted the backbone the least [53, 100, 102]. This was a pioneer study in the sense that it aimed to incorporate cellulose nanofibers into XH in order to manufacture mechanically improved nanocomposite films. SEM and AFM images pointed out that surface of XH and CNF-reinforced nanocomposite films consisted

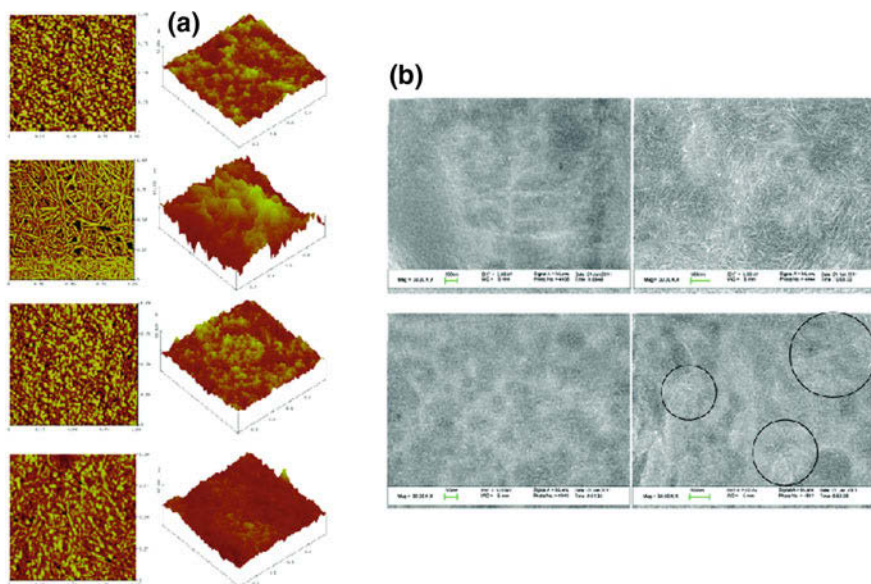


Fig. 5 Properties of CNF-reinforced nanocomposite films

mainly of nodules with a diameter of 10–70 nm and that CNFs were embedded in the XH matrix as shown in Fig. 5. The XH film had a peak at $2\theta = \sim 18^\circ$, indicating that it was semicrystalline. The thermal stability of the nanocomposite film was better than that of the XH film. Film formation was better, and the tensile strength improved greatly due to high aspect ratio and strong interactions between CNF and the XH matrix, which points to an efficient and feasible technique for the manufacturing of superior HBNCFs [77].

3.3 Other Applications

Xylan is used in a wide variety of medical applications. Glyceronoxylylene, xylitol or sorbitol-based films are widely used in the field of food packaging because their oxygen permeability is very low and there is a potential for further spread in the future [49]. Xylooligosaccharides (XOS) would hydrolysis results from claiming xylan-type hemicelluloses for guaranteeing possibility to a significant number of fields including chemical, sustenance and pharmaceutical commercial enterprises. For case, in the nourishment industry, XOS has an assortment of incredible physiological properties such as bringing down cholesterol levels, moving forward gastrointestinal function and the organic accessibility of calcium, and decreasing the risk of colon cancer [62, 76].

In order to make further improvements on the properties of the all-cellulose composites, it is recommended to use cellulose nanofibers that extracted from Napier grass fibers as reinforcement in cellulose matrix in further studies. According to the properties of composite films, it can be concluded that all these cellulose composites are suitable for using in warping, mulching and sorbent applications [97]. Another example of using natural fibers as reinforcement was seen in the study of Maniraman et al. [65]. *Furcraea foetida* (FF) plant was extracted and investigated. The structure of natural fibers generally longer, they have smaller diameter values and low spiral angle of the cellulose arrangement [56]. That quality of a bio-composite relies on the properties of the fiber and the resin and additionally on the quality from claiming their interfacial holding. So, to in front of fabricating bio-composites, additionally, it is a necessity to learn about those properties of fibers. There are many kinds of literature about natural fibers and their properties. They enlighten that celluloses, hemicelluloses and non-cellulosic components (lignin, wax, and pectin) are constructed in the natural fibers. But, the bio-fiber yielding plants grow only in particular regions based on environmental circumstances [11]. New assortments of fibers have appropriate properties for use as reinforcement are needed to be identified and developed. A lot of leaf fibers, such as those mined from *Artisditahystrix*, *Sansevieria cylindrica*, *Tamarindus Indica* L and *sansevieria ehrenbergii* have been used as an unsurpassed reinforcement for polymeric matrices [65].

Also, Kozłowski and Przybylak carried out a research and review to collect fire performance data for several types of eco-friendly polymer composites reinforced by cellulosic fibers [59].

Glucomannan type's materials can be seen as hemicellulosic materials which have film-forming properties. It is generally used in wooden as a "green" absorption material (gels, etc.) and it can be isolated from various method turbines or production fibreboard. Modification of new materials including non-hydrophilic and thermal character also can bring about the xylan which has high molecular weight displaying a stepped forward capability to form films. Film-forming is essential so as for xylan if you want to form self-supporting barrier films to be used in food packaging.

3.4 Basic Components of Composite Materials

The composites consist essentially of the matrix and reinforcing materials that give it physicochemical properties. The matrix part is the basic component of the composite and supports the physicochemical and biological properties of the reinforcing material. Matrixes are the main component to protect the reinforcements of the composites from abrasion and environmental influences. At the same time, it provides composites stability by allowing the matrix fibers and filler materials to coexist. A reaction with synergistic effect occurs by the matrix loading of the reinforcing materials. Thus, thanks to the reinforcement material and matrix, composite materials with the desired properties are prepared. Due to the

physicomechanical properties of the polymer composites, they are of great interest because they have a much higher application area than the individual polymeric structures. The main materials reinforced with composite matrices are metallic oxides, clay, fiber constructions and carbonates. These reinforcing materials give physicomechanical and biological properties to the composites [12, 98].

The structure of lignocellulosic stocks forms polysaccharide and lignin. When lignocellulosic raw materials are introduced into biorefinery and subjected to a series of treatments, products such as cellulose, hemicellulose and lignin are formed. Cellulose, hemicellulose and lignin products are raw materials of lignocellulosic composites. These substances are the main components of animal feed and lumber resources. Cellulose is naturally present as a composition of lignin and hemicellulose fibers. Lignin protects carbohydrates from biological attack and is infectious by very few microorganisms [22, 68].

3.5 The Effect of Fibers on Composite Materials

Fibers play a very important role in the development of multifunctional composite materials. The shrinking the size of any composite material causes a reduction in material defects. The fibrous materials have a higher surface area, a larger surface area, compared to bulk materials. Many studies have shown that multifunctional composite properties depend on properties such as fiber length, volume, fiber type, fiber orientation, etc. These features can be briefly summarized as follows:

- Composite materials composed of long fiber structures have higher mechanical resistance than short fibers. Whereas short fiber composites are less costly and easier to process than long fibers [117].
- Increasing the amount of fiber loading to a certain amount of composite material, resulting in an increase in composite material properties. However, after this particular value, there is a decrease in the composite properties due to the interlocking between the matrix and fibers [63].
- Fiber loading method make a significant impact on composite material properties. The lowest value of Young's modulus was found to be 45° and 60° in the fibers and there have been seen discrepancies between theoretical and experimental values [48].
- Generally, the fibers are made of beeswax, gelatin starch and oily materials to improve adhesion and retention properties [67].

4 Conclusions

In this chapter; the synthesis and characterization of Eco-friendly polymer composites (EFPCs) and their usage in various applications such as food packaging, medical applications, gas barriers etc. have been examined in detail and as it can be

seen these polymer composites are getting more and more attention to science and technology due to their superior properties such as biodegradability, renewability, high strength and stiffness, low cost and ecologically friendly formation. Eco-friendly polymer composites (EFPCs) from natural components provide a potential alternative to other commercial composite materials without compromising strength, stiffness and abrasion resistance properties to a variety of industrial and other applications.

References

1. Abdelwahab NA, Al-Ashkar EA, Abdel-Ghaffara MA (2015) Preparation and characterization of eco-friendly poly(p-phenylenediamine) and its composite with chitosan for removal of copper ions from aqueous solutions. *Trans Nonferrous Met Soc China* 25:3808–3819
2. Abrahamson JT, Sen F, Sempere B et al (2013) Excess thermopower and the theory of thermopower waves. *ACS Nano* 7(8):6533–6544
3. Aday B, Yıldız Y, Ulus R et al (2016) One-pot, efficient and green synthesis of acridinedione derivatives using highly monodisperse platinum nanoparticles supported with reduced graphene oxide. *New J Chem* 40:748–754
4. Akocak S, Sen B, Lolak N et al (2017) One-pot three-component synthesis of 2-amino-4H-chromene derivatives by using monodisperse Pd nanomaterials anchored graphene oxide as highly efficient and recyclable catalyst. *Nano-Struct Nano-Objects* 11:25–31
5. Alén R (2000) Structure and chemical composition of wood. In: Stenius P (ed) *Forest products chemistry*. Fapet Oy, Helsinki, pp 12–57
6. Ayranci R, Baskaya G, Guzel M et al (2017) Carbon-based nanomaterials for high-performance optoelectrochemical systems. *Chem Select* 2(4):1548–1555
7. Ayranci R, Baskaya G, Guzel M et al (2017) Enhanced optical and electrical properties of PEDOT via nanostructured carbon materials: a comparative investigation. *Nano-Struct Nano-Objects* 11:13–19
8. Baillie C (2004) Polymer composites and the environment. *Green Compos* 1–8
9. Baskaya G, Esirden I, Erken E et al (2017) Synthesis of 5-substituted-1H-tetrazole derivatives using monodisperse carbon black decorated Pt nanoparticles as heterogeneous nanocatalysts. *J Nanosci Nanotechnol* 17:1992–1999
10. Baskaya G, Yıldız Y, Savk A et al (2017) Rapid, sensitive, and reusable detection of glucose by highly monodisperse nickel nanoparticles decorated functionalized multi-walled carbon nanotubes. *Biosens Bioelectron* 91:728–733
11. Batra SK (1985) *Handbook of fiber science and technology*. In: Lewin M, Pearce EM (eds) *Fiber chemistry*, vol IV. Marcel Dekker, New York, pp 727–808
12. Bloor D, Donnelly K, Hands PJ, Laughlin P, Lussey D (2005) A metal–polymer composite with unusual properties. *J Phys D Appl Phys* 38:2851–2860
13. Bozkurt S, Tosun B, Sen B et al (2017) A hydrogen peroxide sensor based on TNM functionalized reduced graphene oxide grafted with highly monodisperse Pd nanoparticles. *Anal Chim Acta* 989C:88–94
14. Celik B, Baskaya G, Karatepe O et al (2016) Monodisperse Pt(0)/DPA@GO nanoparticles as highly active catalysts for alcohol oxidation and dehydrogenation of DMAB. *Int J Hydrogen Energy* 41:5661–5669

15. Celik B, Erken E, Eris S et al (2016) Highly monodisperse Pt(0)@AC NPs as highly efficient and reusable catalysts: the effect of the surfactant on their catalytic activities in room temperature dehydrocoupling of DMAB. *Catal Sci Technol* 6:1685–1692
16. Celik B, Kuzu S, Erken E et al (2016) Nearly monodisperse carbon nanotube furnished nanocatalysts as highly efficient and reusable catalyst for dehydrocoupling of DMAB and C1 to C3 alcohol oxidation. *Int J Hydrogen Energy* 41:3093–3101
17. Celik B, Yildiz Y, Erken E et al (2016) Monodisperse palladium-cobalt alloy nanoparticles assembled on poly (*N*-vinyl-pyrrolidone) (PVP) as highly effective catalyst for the dimethylamine borane (DMAB) dehydrocoupling. *RSC Adv* 6:24097–24102
18. Chen GG, Qi XM, Guan Y et al (2016) High strength hemicellulose-based nanocomposite film for food packaging applications. *ACS Sustain Chem Eng* 4:1985–1993
19. Chen L, Wu P, Chen M et al (2018) Preparation and characterization of the eco-friendly chitosan/vermiculite biocomposite with excellent removal capacity for cadmium and lead. *Appl Clay Sci* <https://doi.org/10.1016/j.clay.2017.12.050>
20. Chen T, Dai L (2013) Carbon nanomaterials for high-performance supercapacitors. *Mater Today* 16:272–280
21. Ciolacu D, Popa VI (2011) Cellulose allomorphs: structure. Accessibility and reactivity. Nova Science Publisher, New York, pp 1–3 (Chapter 1)
22. Clark J, Deswarte F (2008) Introduction to chemicals from biomass. Wiley, UK
23. Dasdelen Z, Yildiz Y, Eris S et al (2017) Enhanced electrocatalytic activity and durability of Pt nanoparticles decorated on GO-PVP hybride material for methanol oxidation reaction. *Appl Catal B* 219C:511–516
24. Davachi SM, Shekarabi AS (2018) Preparation and characterization of antibacterial, eco-friendly edible nanocomposite films containing *Salvia macrosiphon* and nanoclay. *Int J Biol Macromol* 113:66–72
25. Demir E, Savk A, Sen B et al (2017) A novel monodisperse metal nanoparticles anchored graphene oxide as counter electrode for dye-sensitized solar cells. *Nano-Struct Nano-Objects* 12:41–45
26. Demir E, Sen B, Sen F (2017) Highly efficient nanoparticles and f-MWCNT nanocomposites-based counter electrodes for dye-sensitized solar cells. *Nano-Struct Nano-Objects* 11:39–45
27. Demirci T, Celik B, Yildiz Y et al (2016) One-pot synthesis of hantzsch dihydropyridines using highly efficient and stable PdRuNi@GO catalyst. *RSC Adv* 6:76948–76956
28. Divsalar E, Tajik H, Moradi M et al (2018) Characterization of cellulosic paper coated with chitosan-zinc oxidenanocomposite containing nisin and its application in packaging of UF cheese. *Int J Biol Macromol* 109:1311–1318
29. Ebringerova A, Hromadkova Z, Heinze T (2005) Hemicellulose. *Adv Polym Sci* 186:1–67
30. Eris S, Daşdelen Z, Sen F (2018) Enhanced electrocatalytic activity and stability of monodisperse Pt nanocomposites for direct methanol fuel cells. *J Colloid Interface Sci* 513:767–773
31. Eris S, Daşdelen Z, Sen F (2018) Investigation of electrocatalytic activity and stability of Pt@f-VC catalyst prepared by in-situ synthesis for methanol electrooxidation. *Int J Hydrogen Energy* 43(1):385–390
32. Eris S, Daşdelen Z, Yıldız Y et al (2018) Nanostructured polyaniline-rGO decorated platinum catalyst with enhanced activity and durability for methanol oxidation. *Int J Hydrogen Energy* 43(3):1337–1343
33. Erken E, Esirden İ, Kaya M et al (2015) A rapid and novel method for the synthesis of 5-substituted 1H-tetrazole catalyzed by exceptional reusable monodisperse Pt NPs@AC under the microwave irradiation. *RSC Adv* 5:68558–68564
34. Erken E, Pamuk H, Karatepe O et al (2016) New Pt(0) nanoparticles as highly active and reusable catalysts in the C1–C3 alcohol oxidation and the room temperature dehydrocoupling of dimethylamine-borane (DMAB). *J Cluster Sci* 27:9

35. Erken E, Yıldız Y, Kilbas B et al (2016) Synthesis and characterization of nearly monodisperse Pt nanoparticles for C1 to C3 alcohol oxidation and dehydrogenation of dimethylamine-borane (DMAB). *J Nanosci Nanotechnol* 16:5944–5950
36. Escalante A, Gonçalves A, Bodi A et al (2012) Flexible oxygen barrier films from spruce xylan. *Carbohydr Polym* 87:2381–2387
37. Esirden İ, Erken E, Kaya M et al (2015) Monodisperse Pt NPs@rGO as highly efficient and reusable heterogeneous catalysts for the synthesis of 5-substituted 1H-tetrazole derivatives. *Catal Sci Technol* 5:4452–4457
38. Fang JM, Sun RC, Fowler P et al (1999) Esterification of wheat straw hemicelluloses in the *N,N*-dimethylformamide/lithium chloride homogeneous system. *J Appl Polym Sci* 74:2301–2311
39. Fang JM, Sun RC, Tomkinson J et al (2000) Acetylation of wheat straw hemicellulose B in a new non-aqueous swelling system. *Carbohydr Polym* 41:379–387
40. Fincher GB, Stone BA (1986) Cell walls and their components in cereal grain technology. In: Pomeranz Y (ed) *Advances in cereal science and technology*. American Association of Cereal Chemists Inc., St Paul, pp 207–295
41. Galindo-Rosales FJ, Martínez-Aranda S, Campo-Deaño L (2015) CorkSTFfluidics—a novel concept for the development of eco-friendly light-weight energy absorbing composites. *Mater Des* 82:326–334
42. Giraldo JP, Landry MP, Faltermeier SM et al (2014) A nanobionic approach to augment plant photosynthesis and biochemical sensing using targeted nanoparticles. *Nat Mater* 13:400–408
43. Goksu EI, Karamanlioglu M, Bakir U et al (2007) Production and characterization of films from cotton stalk xylan. *J Agric Food Chem* 55:10685–10691
44. Goksu EI, Karamanlioglu M, Bakir U et al (2007) Production and characterization of films from cotton stalk xylan. *J Agric Food Chem* 55(26):10685–10691
45. Goksu H, Celik B, Yıldız Y et al (2016) Superior monodisperse CNT-supported CoPd (CoPd@CNT) nanoparticles for selective reduction of nitro compounds to primary amines with NaBH₄ in aqueous medium. *Chem Select* 1(10):2366–2372
46. Goksu H, Yıldız Y, Celik B et al (2016) Eco-friendly hydrogenation of aromatic aldehyde compounds by tandem dehydrogenation of dimethylamine-borane in the presence of reduced graphene oxide furnished platinum nanocatalyst. *Catal Sci Technol* 6:2318–2324
47. Goksu H, Yıldız Y, Celik B et al (2016) Highly efficient and monodisperse graphene oxide furnished Ru/Pd nanoparticles for the dehalogenation of aryl halides via ammonia borane. *Chem Select* 1(5):953–958
48. Graupner N, Ziegmann G, Wilde F et al (2016) Procedural influences on compression and injection moulded cellulose fibre-reinforced polylactide (PLA) composites: influence of fibre loading, fibre length, fibre orientation and voids. *Compos Part an Appl Sci Manuf* 81:158–171
49. Grondahl M, Eriksson L, Gatenholm P (2004) Material properties of plasticized hardwood xylns for potential application as oxygen barrier films. *Biomacromol* 5(4):1528–1535
50. Grondahl M, Gustafsson A, Gatenholm P (2006) Surface- and bulk-modified galactoglucomannan hemicellulose films and film laminates for versatile oxygen barriers. *Macromolecules* 39:2718–2721
51. Hansen NM, Plackett D (2008) Sustainable films and coatings from hemicelluloses: a review. *Biomacromol* 9:1493–1505
52. Hartman J, Albertsson AC, Sjöberg J (2006) Surface- and bulk-modified galactoglucomannan hemicellulose films and film laminates for versatile oxygen barriers. *Biomacromol* 7:1983–1989
53. Hoijs A, Sternemalm E, Heikkinen S et al (2008) Material properties of films from enzymatically tailored arabinoxylns. *Biomacromol* 9:2042–2047
54. Izydorczyk MS, Biliaderis CG (1995) Cereal arabinoxylnase: advances in structure and physicochemical properties. *Carbohydr Polym* 28:33–48

55. Karatepe O, Yildiz Y, Pamuk H et al (2016) Enhanced electro catalytic activity and durability of highly mono disperse Pt@PPy-PANI nanocomposites as a novel catalyst for electro-oxidation of methanol. *RSC Adv* 6:50851–50857
56. Kathiresan M, Pandiarajan P, Senthamaraiannan P et al (2016) Physicochemical properties of new cellulosic artisditahystrix leaf fiber. *Int J Polym Anal Charact* 21(6):663–668
57. Kayserilolu BS, Bakir U, Yilmaz L et al (2003) Use of xylan, an agricultural by-product, in wheat gluten based biodegradable films: mechanical, solubility and water vapor transfer rate properties. *Bioresour Technol* 87:239–246
58. Khalil HPSA, Davoudpour Y, Islam MN et al (2014) Production and modification of nanofibrillated cellulose using various mechanical processes: a review. *Carbohydr Polym* 99:649–665
59. Kozłowski R, Władysław-Przybylak M (2008) Flammability and fire resistance of composites reinforced by natural fibers. *Polym Adv Technol* 19:446–453
60. Lawther JM, Sun RC, Banks WB (1995) Extraction, fractionation, and characterization of structural polysaccharides from wheat straw. *J Agric Food Chem* 43:667–675
61. Li Y, Liu H, Dai K et al (2015) Tuning of vapor sensing behaviors of eco-friendly conductive polymercomposites utilizing ramie fiber. *Sens Actuators B* 221:1279–1289
62. Lin Q, Li H, Ren J (2017) Production of xylooligosaccharides by microwave-induced, organic acid-catalyzed hydrolysis of different xylan-type hemicelluloses: optimization by response surface methodology. *Carbohydr Polym* 157:214–225
63. Liu W, Luo L, Xu S, Zhao H (2014) Effect of fiber volume fraction on crack propagation rate of ultra-high toughness cementitious composites. *Eng Fract Mech* 124:52–63
64. Luo Z, Zhang J, Zhuang C et al (2016) An eco-friendly composite adsorbent for efficient removal of Cu²⁺ from aqueous solution. *J Taiwan Inst Chem Eng* 60:479–487
65. Manimaran P, Senthamaraiannan P, Sanjay MR et al (2018) Study on characterization of *Furcraea foetida* new natural fiber as composite reinforcement for lightweight applications. *Carbohydr Polym* 181:650–658
66. Mikkonen KS, Rita H, Helen H et al (2007) Effect of polysaccharide structure on mechanical and thermal properties of galactomannan-based films. *Biomacromol* 8(10):3198–3205
67. Mittal G, Rhee K, Mišković-Stanković V, Hui D (2018) Reinforcements in multi-scale polymer composites: processing, properties, and applications. *Compos B Eng* 138:122–139
68. Mukrimin SG (2013) Utilization of hazelnut husk as biomass. *Sustain Energy Technol Assess* 4:72–77
69. Okamoto M (2004) Biodegradable polymer/layered silicate nanocomposites: a review. *J Ind Eng Chem* 10(7):1156–1181
70. Peng XW, Ren JL, Zhong LX (2011) Nanocomposite films based on xylan-rich hemicelluloses and cellulose nanofibers with enhanced mechanical properties. *Biomacromol* 12:3321–3329
71. Peroval C, Debeaufort F, Despre D et al (2002) Edible arabinoxylan-based films. 1. Effects of lipid type on water vapor permeability, film structure, and other physical characteristics. *J Agric Food Chem* 50(14):3977–3983
72. Phan TD, Debeaufort F, Peroval C et al (2002) Arabinoxylan–lipid-based edible films and coatings. 3. Influence of drying temperature on film structure and functional properties. *J Agric Food Chem* 50(8):2423–2428
73. Sahin B, Aygün A, Gündüz H et al (2018) Cytotoxic effects of platinum nanoparticles obtained from pomegranate extract by the green synthesis method on the MCF-7 cell line. *Colloids Surf B* 163:119–124
74. Sahin B, Demir E, Aygün A et al (2017) Investigation of the effect of pomegranate extract and monodisperse silver nanoparticle combination on MCF-7 cell line. *J Biotechnol* 260C:79–83
75. Salam A, Pawlak JJ, Venditti RA et al (2011) Incorporation of carboxyl groups into xylan for improved absorbency. *Cellulose* 18:1033–1041

76. Samanta AK, Jayapal N, Jayaram C et al (2015) Xylooligosaccharides as prebiotics from agricultural by-products: production and applications. *Bioact Carbohydr Dietary Fibre* 5 (1):62–71
77. Schroeter J, Felix F (2005) Melting cellulose. *Cellulose* 12:159–165
78. Sen B, Akdere EH, Savk A et al (2018) A novel thiocarbamide functionalized graphene oxide supported bimetallic monodisperse Rh-Pt nanoparticles (RhPt/TC@GO NPs) for Knoevenagel condensation of aryl aldehydes together with malononitrile. *Appl Catal B* 225 (5):148–153
79. Sen B, Kuzu S, Demir E et al (2017) Highly efficient catalytic dehydrogenation of dimethyl ammonia borane via monodisperse palladium-nickel alloy nanoparticles assembled on PEDOT. *Int J Hydrogen Energy* 42(36):23307–23314
80. Sen B, Kuzu S, Demir E et al (2017) Highly monodisperse RuCo nanoparticles decorated on functionalized multiwalled carbon nanotube with the highest observed catalytic activity in the dehydrogenation of dimethylamine borane. *Int J Hydrogen Energy* 42(36):23292–23298
81. Sen B, Kuzu S, Demir E et al (2017) Hydrogen liberation from the dehydrocoupling of dimethylamine-borane at room temperature by using novel and highly monodispersed RuPtNi nanocatalysts decorated with graphene oxide. *Int J Hydrogen Energy* 42(36):23299–23306
82. Sen B, Kuzu S, Demir E et al (2017) Monodisperse palladium-nickel alloy nanoparticles assembled on graphene oxide with the high catalytic activity and reusability in the dehydrogenation of dimethylamine-borane. *Int J Hydrogen Energy* 42(36):23276–23283
83. Sen B, Kuzu S, Demir E et al (2017) Polymer-Graphene hybride decorated Pt nanoparticles as highly efficient and reusable catalyst for the dehydrogenation of dimethylamine-borane at room temperature. *Int J Hydrogen Energy* 42(36):23284–23291
84. Sen B, Lolak N, Paralı Ö et al (2017) Bimetallic PdRu/graphene oxide-based catalysts for one-pot three-component synthesis of 2-amino-4H-chromene derivatives. *Nano-Struct Nano-Objects* 12:33–40
85. Sen F, Boghossian AA, Sen S et al (2013) Application of nanoparticle antioxidants to enable hyperstable chloroplasts for solar energy harvesting. *Adv Energy Mater* 3(7):881–893
86. Sen F, Ertan S, Sen S et al (2012) Platinum nanocatalysts prepared with different surfactants for C1 to C3 alcohol oxidations and their surface morphologies by AFM. *J Nanopart Res* 14:922–926
87. Sen F, Gokagac G (2007) Different sized platinum nanoparticles supported on carbon: an XPS study on these methanol oxidation catalysts. *J Phys Chem C* 111:5715–5720
88. Sen F, Gokagac G (2007) The activity of carbon supported platinum nanoparticles towards methanol oxidation reaction—role of metal precursor and a new surfactant, *tert*-octanethiol. *J Phys Chem C* 111:1467–1473
89. Sen F, Gokagac G (2014) Pt nanoparticles synthesized with new surfactants: improvement in C1–C3 alcohol oxidation catalytic activity. *J Appl Electrochem* 44(1):199–207
90. Sen F, Karataş Y, Gülcan M et al (2014) Amylamine stabilized platinum (0) nanoparticles: active and reusable nanocatalyst in the room temperature dehydrogenation of dimethylamine-borane. *RSC Adv* 4(4):1526–1531
91. Sen F, Ozturk Z, Sen S et al (2012) The preparation and characterization of nano-sized Pt–Pd alloy catalysts and comparison of their superior catalytic activities for methanol and ethanol oxidation. *J Mater Sci* 47:8134–8144
92. Sen F, Sen S, Gokagac G (2011) Efficiency enhancement in the methanol/ethanol oxidation reactions on Pt nanoparticles prepared by a new surfactant, 1,1-dimethyl heptanethiol, and surface morphology by AFM. *Phys Chem Chem Phys* 13:1676–1684
93. Sen F, Sen S, Gokagac G (2013) High performance Pt nanoparticles prepared by new surfactants for C1 to C3 alcohol oxidation reactions. *J Nanopart Res* 15:1979
94. Sen F, Ulissi ZW, Gong X et al (2014) Spatiotemporal intracellular nitric oxide signaling captured using internalized, near-infrared fluorescent carbon nanotube nanosensors. *Nano Lett* 14(8):4887–4894

95. Sen S, Sen F, Boghossian AA et al (2013) The effect of reductive dithiothreitol and trolox on nitric oxide quenching of single walled carbon nanotubes. *J Phys Chem C* 117(1):593–602
96. Sen S, Sen F, Gokagac G (2011) Preparation and characterization of nano-sized Pt–Ru/C catalysts and their superior catalytic activities for methanol and ethanol oxidation. *Phys Chem Chem Phys* 13:6784–6792
97. Senthil Muthu Kumar T, Rajini N, Obi Reddy K et al (2018) All-cellulose composite films with cellulose matrix and Napier grass cellulose fibril fillers. *Int J Biol Macromol* 112:1310–1315
98. Shah N, Ul-Islam M, Khattak WA, Park WJ (2013) Overview of bacterial cellulose composites: a multipurpose advanced material. *Carbohydr Polym* 98(2):1585–1598
99. Sinha Ray S (2013) Environmentally friendly polymer nanocomposites. Woodhead Publishing Limited, p 2856
100. Sjöström E (1993) Wood chemistry fundamentals and applications. Academic Press Inc., San Diego, p 293
101. Söderqvist Lindblad M, Ranucci E, Albertsson AC (2001) Biodegradable polymers from renewable sources. New hemicellulose-based hydrogels. *Macromol Rapid Commun* 22:962–967
102. Sternemalm E, Höije A, Gatenholm P (2008) Effect of arabinose substitution on the material properties of arabinoxyran films. *Carbohydr Res* 343:753–757
103. Sun RC, Sun XF, Tomkinson J (2004) Hemicelluloses and their derivatives. In: Gatenholm P, Tenkanen M (eds) *Hemicelluloses: science and technology*. ACS symposium series, vol 864. American Chemical Society, Washington, pp 2–22
104. Tang XZ, Kumar P, Alavi S (2012) Recent advances in biopolymers and biopolymer-based nanocomposites for food packaging materials. *Crit Rev Food Sci Nutr* 52:426–442
105. Tenkanen M (2004) Enzymatic tailoring of hemicelluloses. In: Gatenholm P, Tenkanen M (eds) *Hemicelluloses: science and technology*. ACS symposium series, vol 864. American Chemical Society, Washington, pp 292–311
106. Tersur Orasugh J, Ranjan Saha N, Rana D et al (2018) Jute cellulose nano-fibrils/hydroxypropylmethylcellulose nanocomposite: a novel material with potential for application in packaging and transdermal drug delivery system. *Ind Crops Prod* 112:633–643
107. Thakur VK, Thakur MK (2015) Eco-friendly polymer nanocomposites. *Process Prop* 75:579
108. Thomas S, Visakh Aji PM, Mathew P (ed) (2012) *Advances in natural polymers: composites and nanocomposites*, vol 18. Springer Science & Business Media, p 426
109. Won JP, Kang HB, Lee SJ et al (2012) Eco-friendly fireproof high-strength polymer cementitious composites. *Constr Build Mater* 30:406–412
110. Yildiz Y, Erken E, Pamuk H et al (2016) Monodisperse Pt nanoparticles assembled on reduced graphene oxide: highly efficient and reusable catalyst for methanol oxidation and dehydrocoupling of dimethylamine-borane (DMAB). *J Nanosci Nanotechnol* 16:5951–5958
111. Yildiz Y, Esirden İ, Erken E et al (2016) Microwave (Mw)-assisted synthesis of 5-substituted 1H-tetrazoles via [3 + 2] cycloaddition catalyzed by Mw–Pd/Co nanoparticles decorated on multi-walled carbon nanotubes. *Chem Select* 1(8):1695–1701
112. Yildiz Y, Kuzu S, Sen B et al (2017) Different ligand based monodispersed metal nanoparticles decorated with rGO as highly active and reusable catalysts for the methanol oxidation. *Int J Hydrogen Energy* 42(18):13061–13069
113. Yildiz Y, Onal Okyay T, Gezer B et al (2016) Monodisperse Mw–Pt NPs@VC as highly efficient and reusable adsorbents for methylene blue removal. *J Cluster Sci* 27:1953–1962
114. Yildiz Y, Onal Okyay T, Sen B et al (2017) Highly monodisperse Pt/Rh nanoparticles confined in the graphene oxide for highly efficient and reusable sorbents for methylene blue removal from aqueous solutions. *Chem Select* 2(2):697–701
115. Yildiz Y, Pamuk H, Karatepe O et al (2016) Carbon black hybride material furnished monodisperse platinum nanoparticles as highly efficient and reusable electrocatalysts for formic acid electro-oxidation. *RSC Adv* 6:32858–32862

116. Yıldız Y, Ulus R, Eris S et al (2016) Functionalized multi-walled carbon nanotubes (f-MWCNT) as highly efficient and reusable heterogeneous catalysts for the synthesis of acridinedione derivatives. *Chem Select* 1(13):3861–3865
117. Zhang D, He M, Qin S, Yu J (2017) Effect of fiber length and dispersion on properties of long glass fiber reinforced thermoplastic composites based on poly(butylene terephthalate). *RSC Adv* 7:15439–15454
118. Zhang Y, Pitkänen L, Douglade J et al (2011) Wheat bran arabinoxylans: chemical structure and film properties of three isolated fractions. *Carbohydr Polym* 86:852–859
119. Zhong LX, Peng XW, Yang D et al (2013) Longchain anhydride modification: a new strategy for preparing xylan films. *J Agric Food Chem* 61:655–661
120. Zhu Ryberg Y, Edlund U, Albertsson AC (2011) Conceptual approach to renewable barrier film design based on wood hydrolysate. *Biomacromol* 12:1355–1362

Impact of Nanoparticle Shape, Size, and Properties of the Sustainable Nanocomposites



Thandapani Gomathi, K. Rajeshwari, V. Kanchana, P. N. Sudha and K. Parthasarathy

1 Introduction

Nanotechnology has imposed a hopeful approach to resolve many technological impasses incurred in various the branches of science and technology. The field of nanotechnology is an interdisciplinary area and it is one of the most popular areas of current research and development basically in all disciplines. It obviously includes polymer science and technology [78]. It can be defined as “the design, characterization, production and application of structures, devices and systems by controlling shape and size at the nanoscale” (<100 nm) [108]. According to Drexler, “Nanotechnology is the principle of manipulation of the structure of matter at the molecular level. It entails the ability to build molecular systems with atom-by-atom precision, yielding a variety of nanomachines [131, 72].”

In the past decades, major research on the production of nanocomposites includes the use of synthetic polymeric materials, which have become a present dispute [85, 37, 135]. The dispute is because of the shortage of the natural resources and also the environmental concerns for their non-biocompatibility, cross contaminations and toxicity risks [4, 22, 63, 101, 129]. Renewable and sustainable

T. Gomathi (✉) · P. N. Sudha

Department of Chemistry, D.K.M. College for Women, Vellore, Tamil Nadu, India

e-mail: drgoms1@gmail.com; chemist.goms@gmail.com

K. Rajeshwari

Department of Chemistry, Adhi College of Engineering, Walajabad, Tamilnadu, India

V. Kanchana

Department of Chemistry, Sree Sastha Institute of Engineering and Technology, Chennai, Tamil Nadu, India

K. Parthasarathy

Siddha Central Research Institute, Central Council for Research in Siddha, Ministry of AYUSH, Arumbakkam, Chennai, Tamil Nadu, India

© Springer Nature Switzerland AG 2019

Inamuddin et al. (eds.), *Sustainable Polymer Composites and Nanocomposites*,

https://doi.org/10.1007/978-3-030-05399-4_11

materials are of great concern in scientific research and industry which has overcome the disputes over the use of synthetic materials. These materials include biomass as industrial and agricultural residues and energy crops. The preparation of polymer composites using natural polymers has advantages over synthetic sources, particularly as a solution to the environmental problems [109]. Also, the green chemistry explores chemistry techniques and methodologies so as to reduce or eliminate the use of hazardous materials to human health or to the environment [116].

Therefore, sustainable green nanocomposites are these days broadly researched due to the want for transformation to nanocomposites from biodegradable polymers, complete eco-friendly conservation and reduction of carbon dioxide release [2]. The nanocomposite is the term, which is extensively used to describe a broad range of materials with one of the dimension is in nano range. Blends of polymers and nanoparticles, commonly called “polymer nanocomposites” (PNC), have garnered much attention due to the possibility of dramatic improvement of polymeric properties with the addition of a relatively small fraction of nanoparticles [49, 157, 122, 32, 145, 146, 132]. The use of agricultural wastes has attracted many researchers for the production of nanocomposites [128]. Polymer nanocomposites (PNCs) are made by dispersing nanoparticles (NPs) into polymer matrices [112]. The use of PNCs is anticipated to enhance producing speed and utilization with increased biocompatibility [109]. This chapter will provide the physicochemical and biological importance of sustainable nanocomposites in various fields of applications with the impact of its properties.

2 Composites

Composites, the wonder materials composed of matrix phase and dispersed phase and have become an essential part of today’s material. They are widely used in diverse areas of applications such as transportation, construction, electronics and consumer products. Composites are the materials that consist of two or more chemically and physically different phases separated by a distinct interface. Matrix phase is the primary phase having a continuous character, usually more ductile and less hard phase. Dispersed (reinforcing) phase is the second phase which is embedded in the matrix and it is usually stronger than the matrix. When this different phases combined, it will lead to the material with more useful structural or functional properties non-attainable by any of the constituent alone [45]. They also offer unusual combinations of properties such as stiffness, strength, and weight which was difficult to attain separately by the individual components [48, 49]. The progress in the field of materials science has taken a new led since the advent of nanocomposites.

2.1 *Nanocomposites*

Nanocomposites are a relatively new class of materials with ultrafine phase dimensions, typically of the order of a few nanometers. Nanocomposites are the composites which are size dependent with at least one of the phases shows dimensions in the nanometer range [123] and are different from those of the atomic and bulk counterparts [45]. The size plays a vital role in the nanocomposites with unique properties typically not shared by their microcomposite and, therefore, offer new technology and business opportunities [48, 49]. According to the type of matrix materials that are used for the preparation of nanocomposites, the nanocomposites are classified into following three classes [34]: Polymer Matrix Nanocomposites, Ceramic Matrix Nanocomposites and Metal Matrix Nanocomposites.

In the current economic and environmental climate, it is more critical to develop sustainable composites utilizing nanotechnology. But the polymers which have excellent properties such as low cost, lightweight, easy processing, corrosion resistance, ductility and high durability the productions of sustainable nanocomposites are achievable. These properties can arrive from the polymer more over than ceramics and metals. Also on comparing with metals and ceramics, polymers have poor electrical, thermal and mechanical properties, low coordination number and lightweight atoms, poor gas barrier, heat resistance and fire performance properties. Therefore, polymers can find many more applications as engineered materials [141].

2.2 *Sustainable Polymeric Nanocomposites*

Polymer nanocomposites (PNCs) are two-phase materials with high industrial importance, in which the polymers are reinforced by nanoscale fillers. All thermoplastics, thermosets, and elastomers have been used to make sustainable polymer nanocomposites. As a result of increasing focus concerning on the environment, the development of new environmentally friendly or biodegradable polymers has come on the role and these materials are called environmentally friendly PNCs (EFPNCs). The field of applications EFPNCs is immense [118, 13], because of their lightweight, high chemical resistance, and low dielectric constant, high interfacial area, unique shape- and size-dependent, tunable properties [110]. Also, PNCs have to provide the scope for the improvement of various mechanical, thermal, optical, rheological, magnetic, and electrical [95] even at a very low loading of nanoparticles. Due to the advantage of nanotechnology nowadays, nanoscale materials have been used as fillers instead of conventional microscale materials and also provide better properties [110].

Nanoparticles, such as nanochitosan, nanocellulose, carbon nanotubes, clays or layered silicates, nano silica, graphene, and nano calcium carbonate are widely used in the polymer nanocomposites in the development of sustainable polymer

nanocomposites to alter the chemical, electrical, mechanical, optical, and thermal properties of biodegradable polymer matrices [94]. However, nanocomposites prepared using biodegradable polymers and clays materials are much attractive and impressive because of its enhancements in the physicochemical properties.

3 Preparation Methods

There is a great challenge over the past decade in preparing the uniform nanocomposite using hydrophobic (water repelling) polymer matrix and hydrophilic (water absorbing) fibers. Because this combination resulted in the non-uniform dispersion of fibers within the matrix with poor mechanical properties [11, 66]. Traditionally, there are three methods available for the preparation of nanocomposites. The methods are solution casting, melt blending, and in-situ polymerization.

Nowadays, nanocomposites are engineered with a variety of sizes, shapes, and chemistries. Also, for preparing nanocomposites, initially the nanoparticles are synthesized and modified for its surface area and exposed to the physical and biological application in our current research paradigm. In the literature reports, many researchers adopted various techniques for the fabrication and modification of nanomaterials. In the case of biomedical application, the nanostructures material to be capable of navigating the body, infecting and transforming cells, or detecting and repairing diseased cells. Therefore to engineer such kind of biocompatible material, the better understanding of the size, shape, surface area and functional properties of the nanomaterials and its interaction with the system are needed. Hence the fabrication methods include solvent casting, phase separation, drawing-processing, template-assisted synthesis, self-assembly, and electrospinning techniques.

3.1 *Electrospinning*

Recently, electrospinning methods have achieved widespread attention as an easy, leading and adaptable technique for the fabrication of fibers matrix in nanometer scale. Electrospinning technique is a preferred technique because of the delivering of nanofibers with the high surface area to volume ratio and a large number of inter-/intra fibrous voids capable for various applications over solvent casting and phase-separation [120]. From the literature, it was reported that the electrospinning technique has helped for the advancements in many applicable areas like bio-engineering, environmental protection, electronics, optics, sensors and catalysis [24, 28, 70, 74].

Especially in biomedical applications, nanofibers fabricated via electrospinning methods leads to the materials with high surface area which is essential for surface interchanges and highly interconnected porous structure for the diffusion and

transport of fluid, essential nutrients and drugs for tissue engineering applications to achieve a great success in that field [130]. This type of fibrous mats can be produced using electrospinning method by electrically charging a suspended droplet of polymer melt or solution and control over physical nature of the fibrous mats with suitable thickness and composition along with the porosity of the (nano) fibrous mesh [125] which is available in the electrospinning instrument. The physico-chemical properties such as large surface-to-volume ratio, flexibility, surface functionality, mechanical properties, and the freedom on materials' design [51, 59] are possessed by the resulting ideal membranes for the above specified important applications.

3.2 One Step in-Situ Polymerization Method

Zou et al. [165], reported one step in-situ polymerization method for the preparation of polymeric nanocomposites. This technique involves the dispersion followed by bulk polymerization. During dispersion of nanofillers in the monomer(s), the nanofillers was always modified initially to increase the interaction or good dispersion between the polymers. Easy handling and better performance are the important advantages of this method. Using this method, [54], synthesized graphene, GO, and functionalized GO—Epoxy nanocomposites, Dash et al. [33] synthesized poly(anthranilic acid) (PAnA)/MWCNT composites and Wu and Liu [158] prepared PS/MWCNTs.

3.3 Thermal Spray Synthesis

Thermal spray processing is a well-proven technique for the development of nanostructured coating [64]. This thermal spray technique is considered as an effective method for the preparation of nanocomposites because agglomerated nanocrystalline powders formed during synthesis of nanomaterials are melted, accelerated and quenched very rapidly in a single step. Due to rapid melting and solidification process, there will be the retention of a nanocrystalline phase and even amorphous structure. This retention of the nanocrystalline structure leads to enhanced wear behaviour, greater hardness, and reduced coefficient of friction compared to other conventional coatings methods.

3.4 Sol-Gel Method

It is a bottom-up approach using for the preparation of polymeric nanocomposites. The term sol-gel is associated with two relations steps, sol (a colloidal suspension)

and gel (3D interconnecting network formed between phases) [119]. During engineering the nanostructured material using this technique, the solid nanoparticles is dispersed initially in the monomer solution. The resulting colloidal suspension (sol) from polymerization reactions forms an interconnecting 3D network which extends throughout the liquid between phases (gel followed by the hydrolysis procedure [137]. Here, the polymer serves as a nucleating agent and promotes the growth of layered crystals. As the crystals grow, the polymer seeps between layers and hence nanocomposite is formed.

4 Biophysical Properties

Polymer nanocomposites always exhibit enhanced physical properties than individual materials [80]. These properties do not depend solely on the chemical structure of the matrix but also on other factors like processing steps which determine the orientation of the molecules in the final morphology and the effect of fillers. The enhanced of properties can be arrived even at small amounts of nanoparticles loadings in the matrix and were browbeaten at the economic degree for decades already [13].

Many parameters of the nanoparticles can also play a position inside the reinforcement of the polymer matrix. The parameters are nanoparticle shape and size, loading and dispersion, interaction, mobility, temperature, entanglement of the polymers, diploma of polymerization, elasticity, surface chemistry, and biopersistence [75]. The effect of particle morphology is the main parameter during synthesis and for the synthesis of nanoparticles, the solutions of polymeric materials used should contain size-confined, nanosized pools of inter- and intramolecular origin. Also for optimizing the ultimate properties of the nanocomposites for various application the understanding of the relationship between processing, morphology and functional properties of nanocomposites will be very helpful for predicting properties of nanocomposite systems.

4.1 Structure

As structural members, composite materials are used as crashworthiness, protective armours in air and space vehicles. Nanocomposites materials can be produced both by complex and simple processes. For preparing the nanocomposites with the preferred structure the first essential condition is the formation of homogeneous phase by the nanoparticles in the polymer matrix [71]. The complexity of structure and the factors figuring out it trade from one nanocomposite to the other, consequently the structure is mentioned according to the kind of reinforcement. The nanostructure phases of nanocomposite structure can be defined as:

zero-dimensional (embedded cluster), 1D (one-dimension; e.g. nanotubes), 2D (nanoscale coatings) and 3D (embedded network).

Particulate reinforcements have dimensions which might be about same in all guidelines. Large particle and dispersion-strengthened composites are the 2 subclasses of particle-reinforced composites [136]. Depending upon the reinforcements, the PNCs have structures like molecular layers, films, membranes, plates, particles, network, nanotubes and nanofibers, ribbon, tape, rosette, cage-like and tubular morphologies have been synthesized [71, 50].

4.2 *Shape*

Numerous attempts had been made to distribute spherical nanoparticles in a polymer matrix with the maximum one of a kind strategy, due to the fact that aggregation is the main issue in those composites. The most regularly used method is the use of conventional technologies to homogenize the previously organized particles into the matrix polymer. According to the shape of the crystallites or grains, the nanomaterials are broadly classified into four categories such as (1) Three dimensional (3D) nanomaterials like zeolites or molecular sieves with cage-like nanopores, (2) Two dimensional (2D) nanomaterials such as thin films, quantum well, (3) One dimensional (1D) nanomaterials such as quantum wire/quantum rod etc., (4) Zero-dimensional (0D) nanomaterials such as quantum dots [134]. In 3D, nanomaterials are composed of equiaxed nanometer-sized grains. In this case, the electrons are delocalized and move freely in all directions (x, y and z). In 2D, the electrons are delocalized in two directions (x and y) and confined in one direction (z). In 1D, the electrons are delocalized in one direction (z) and confined into two directions (x and y). Zero dimension exhibits confinement in all three spatial directions and there is no delocalization. Usually, particles don't have any preferred directions and are specially used to improve properties or lower the cost of isotropic materials [17]. The shape of the reinforcing particles can be spherical, cubic, platelet, or regular or irregular geometry.

4.3 *Size*

Lately, there has been an extremely good deal of attempt to use both the shape and the size of nanoparticles to goal precise cell uptake mechanisms, biodistribution styles, and pharmacokinetics [75]. Even though the physicochemical properties of nanosized complexes and structures have an effect on their function [40], it will likely be critical to apprehend how the physicochemical properties relate to biological interactions and functions in order to appropriately materialize the capability of nanotechnology. For instance, the shape at once impacts uptake into cells: rods display the best uptake, followed with the aid of spheres, cylinders, and cubes [53].

NP size may additionally have an effect on the uptake efficiency and kinetics, the internalization mechanism and additionally the subcellular distribution. A size-dependent uptake in different cell lines has been reported for Au [10, 30, 156], mesoporous silica [91], polystyrene [147] and iron oxide NPs [61], with the maximum cellular uptake at a NP core size in the range of 30–50 nm, which suggests that there is an optimal size for active uptake. Gratton et al. [53] determined this ordering using synthesized nanoparticles larger than 100 nm. In studies with sub-100-nm nanoparticles, spheres show an appreciable advantage over rods [30, 114].

4.4 Surface Area/Morphology

Surface area is the important parameter to enhance the applications of nanocomposites. The surface area of the nanoparticles is more essential for the improvements of the properties, although, the high surface area and surface attraction can also result in agglomeration. The nanofillers may not give expected results if they exist as micrometre-sized agglomerates. The two main aspects of mixing viz, dispersion and distribution, facilitate the breakdown of the filler agglomerates into aggregates and particles, as well as distributing the particles uniformly throughout the polymeric matrix, without affecting the particle size and final properties. The improved properties can be obtained if there is a relatively better dispersion of nanoparticles in the polymer matrix. A good dispersion enhances the number of possible interaction between the polymer and the filler. Although, the introduction of nanoparticles into polymer or polymer blends have benefited in improving various properties, the polymer that interacts with the nanofiller plays the determining role in the final property. The high specific area associated with nanoparticles enhance the chances of adsorption of the macromolecular chains onto their surfaces and influences the structural evolution and phase separation. The effective dispersion of the fillers in the polymer matrix and the improvement of polymer-filler interactions are two key challenges in the field of polymer nanocomposites.

4.5 Applications

Size, shape, and surface morphology play pivotal roles in controlling the physical, chemical, biological, optical, and electronic properties of nanoscopic materials. The high surface energy of these particles makes them extremely reactive, and most systems undergo aggregation without protection or passivation of their surfaces [44, 155, 32, 144]. The use of nanoparticles (NPs) in the biomedical field is one of the most important branches of nanobiotechnology.

4.6 *Biological Applications*

The biological applications of nanocomposites mainly depend on the specific structure–activity relationships between NP shape and certain common biological endpoints [154, 152]. The variables such as size, shape, composition, ligand chemistry and coverage can influence the toxicity of nanoparticles to organisms. This can be avoided by analyzing the unique effects shown by each variable. It is a highly challenging job to study the impact of each parameter, but it can be studied by changing one variable and keeping others as constant [19].

From the biological viewpoint, the majority of microorganisms such as bacteria and virus appears in different shapes. The majority of bacterias and viruses appears to be spherical in shape. The other shapes such as filamentous, crescent, twisted, bullet- and rod-shaped forms have also been observed in nature [75]. Khatamiana et al. [73] has worked on binary hybrids of chitosan-zeolite nanocomposites various medical applications such as tissue engineering and industrial applications such as antimicrobial food packaging, which exhibit dose-dependent toxicity to cells and very low toxicity was observed up to 0.25 and 0.1 mg/mL concentrations.

Lifeng et al. [113] and Ma and Lim [93] reported that the nanochitosan exhibited higher antibacterial activity and antifungal activity. The antibacterial activity is due to the fact that the negatively charged surface of the bacterial cell wall interacts effectively to a greater degree with the polycationic nanochitosan (NH_3^+) and hinder the growth of the microorganism [164]. This suggested also suggested that chitosan nanoparticles might also be able to diffuse into a fungal cell and hence disrupt the synthesis of DNA as well as RNA. This interaction caused disruption of the microbial cells, which then changed their metabolism and led to cell death [83].

4.7 *Drug Delivery/Gene Delivery*

The use of nanocomposite in drug delivery application depends on many factors such as size, shape, surface morphology and its composition [87]. The particle size is the prime factor which determines the half-life of drug clearance in tissues [65]. To arrive at a tumour-specific nanoparticle design, it is first essential to understand the relationships between nanoparticle size and shape with its transport. The remarkable factor in the competence of most of the drug delivery system is particle size and surface area. These factors will enhance the solubility and bioavailability, an additional capability to cross the blood-brain barrier (BBB), go through the pulmonary system and be absorbed through the endothelial cells of the skin [76]. The effect of particle size on nanoparticle pharmacokinetics, margination, extravasation, and binding has been comprehensively studied. Early studies evaluating the effect of liposome size on pharmacokinetics have identified the size range of 60–100 nm to be ideal for maximizing blood circulation half-life [88, 100, 104].

When the particles size of the nanoparticles gets smaller, the surface area of the nanoparticles gets larger, which results in the adherence of the drug molecules to the surface of the particles. The above literature assessment and discussion leads to the importance of size optimization of nanoparticles composites for the effective delivery of the drug molecules. It was predicted that approximately 100 nm size of drug carrier will be effective. Due to the high diffusive component of transport for smaller nanoparticles, there may be significant particle washout from a tumour over time [142]. On the other hand, larger nanoparticles have higher long-term tumour accumulation. Therefore caution must be taken with size selection, however, as pharmacokinetic and margination performance does not necessarily correlate to faster extravasation kinetics. For instance, the apparent permeability of a nanoparticle to the vascular endothelial wall decreases as the radius of the particle increases [162]. The particle size and distribution of nanoparticles can be controlled by different synthesis method and modified various synthesis parameters for example by adjusting the pH and ionic strength in coprecipitation, a commonly used method [68].

The shape also plays a major role in not only nanoparticle pharmacokinetics, but also intravascular transport, binding, and accumulation at the site of a tumour. Hence, the basic ideas about nano-bio interactions will be helpful in engineering the nanostructured material for the specific design of carrier to ensure the highest possible delivery efficiency. In many cases, nanoparticles enter the cell after binding to the receptor target. Once bound, several factors can dictate the behaviour of nanomaterials at the nano-bio interface.

Li et al. [87] reported that effect of nanoparticles shapes using a coarse grain model with self-consistent field theory and Flory theory. They developed PEGylated in different shapes such as nanospheres, nanorods, nanocubes, and nanodisks with the same surface area of 201 nm² to ensure an equal number of PEG molecules on the surface regardless of shape [87], polyethylene glycol (PEG) coating improves the biocompatibility and circulation time [150].

Veisheh et al. [148] studied the effect of surface charge on internalization on different cell lines by MNPs. The report tells that the material can bind with non-targeted cells, resulting in a specific internalization which was due to the surface phenomenon of the MNPs. [98], utilized Chitosan functionalized magnetite doped luminescent rare earth nanoparticles (Fe₃O₄@LaF₃: Ce³⁺, Tb³⁺/chitosan nanoparticles) in targeted delivery of paclitaxel for lung cancer.

An et al. [6], used glycopolymer modified magnetic mesoporous silica nanoparticles for Magnetic resonance imaging (MRI) scan and controlled drug delivery of anticancer drug 5-fluorouracil. The hybrid Fe₃O₄⁻ carboxymethyl chitosan nanoparticles [87] finds the medical application of tumor-targeted delivery of rapamycin.

The other, nanoparticles coated with polymers or surfactants like polyethylene glycol polyethylene oxide, polyoxamer, poloxamine, and polysorbate 80 [8], single-walled carbon nanotubes (SWCNTs) and multiwalled carbon nanotubes

(MWCNTs) [115, 124] have been confirmed valuable in drug delivery applications. [25, 103] applied Buckminsterfullerene C60 (spherical molecule) and its derivatives are utilized for the treatment of cancer [69].

4.8 Wound Healing

Wound healing is a multifaceted and major biological response that helps in the restoration of tissue consistency and body functions [3]. The main point in wound healing is a physiological situation favourable to tissue repair and rejuvenation in the shortest time with less pain, restlessness, and scarring to the patient. Wound healing follows a complex sequence of events at the cellular level, which replaces the devitalized tissues and restores the natural characteristics of the skin that are conciliation by an injury (Matthews and Rawlings [99]). A recent study of biomaterials on wound healing has gained special interest because of their inimitable chemical, physical, and biological properties.

Nanofibers are key materials for wound healing applications because of their surface area. There are several methods for producing nanofibers such as drawing, template synthesis, phase separation, self-assembly, and electrospinning. A range of polymeric, metallic, and ceramic nanomaterials are investigated for wound healing applications.

Silver has been used as an antimicrobial since the 1800s but in the last two decades, interest in silver for wound treatment resurged [42]. Silver nanoparticles impregnated in the biocompatible polymeric matrix were therefore utilized for antimicrobial wound healing material [97]. TiO₂ and ZnO nanoparticles are extensively used in the cosmetic and pharmaceutical industry as UV shield and also as a wound healing material (Murphy and Evans [102]). Antimicrobial peptides formulated with gold Nanodots inhibit the multiplication of multidrug-resistant bacteria pathogen and also promotes wound healing in an animal model [86]. The drug delivery of curcumin using various nanomaterial-based vehicles has been studied in wound healing acting as anti-biotic, anti-viral and antioxidant properties [21].

The size and concentration of nanoparticles will influence the wound healing characteristics. Graphene oxide is used as antibacterial in the field of biomedicine. Graphene related materials have shown potential results in the area of tissue engineering and wound healing [6].

4.9 Tissue Engineering

Tissue engineering (TE) is a multidisciplinary field focused on the development and application of knowledge in chemistry, physics, engineering, life and clinical

sciences to the solution of critical medical problems, as tissue loss and organ failure [82]. In tissue engineering, the scaffold prepares a three-dimensional (3D) construct for cell attachment and migration, proliferation, and formation of an extracellular matrix (ECM), deliver and retain cells and biochemical factors enable diffusion of vital cell nutrients, as well as a carrier of growth factors or other biomolecular signals [9]. Many biomedical applications require nanoparticles with low toxicity, biocompatibility, and stability with high preferential accumulation in the target tissue or organ [79].

Scaffolds for tissue engineering should have good mechanical properties, suitable biodegradability, and most importantly good biocompatibility [9, 117]. Particularly, the surface properties of the material define the interactions between the cells and the material and, consequently, affect cell adhesion [36].

Nanomaterials and nanotechnology are being progressively integrated into tissue engineering to ease the development of various tissue treatment and substitutes to restore missing, damaged and injured tissues and organs (Fig. 1). The triumph of nanomaterials in tissue engineering is contingent upon the inflammatory responses they elicit *in vivo* [96] and also be utilized for a number of biomedical and biotechnological applications such as drug delivery, enzyme immobilization and DNA transfection etc. [84]. Nanotechnology offers hybrid materials with potentials at the molecular level [35].

Yadav et al [161] suggested that Graphene-based chitosan nanocomposites have been used in tissue engineering application for wound healing purpose. A nano-HAp/collagen composite was fabricated into a three-dimensional scaffold from nano-HA powders and natural collagen by simply blending the two

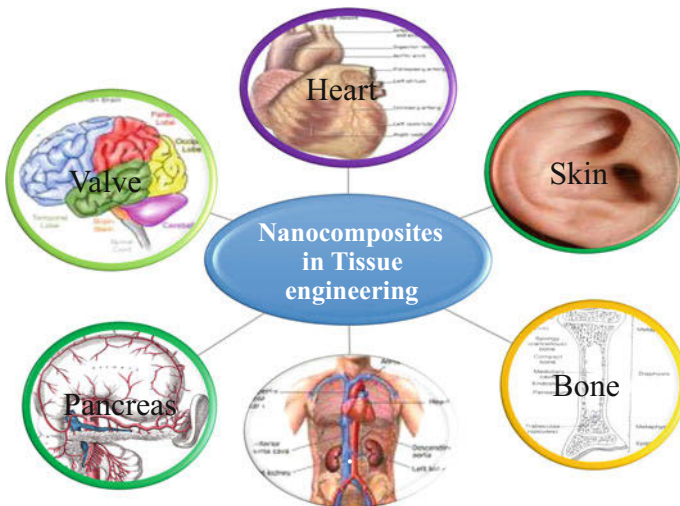


Fig. 1 Polymer nanocomposites in tissue engineering applications

components together. The composite of CNPs has also been generated for bone tissue engineering.

The naturally derived silk fibroin nanoparticles find numerous applications in various application mainly in bone regeneration and dentistry nanospheres and nanofibrous scaffolds [111, 153, 57]. Fonseca-Santos and Chorilli [43] reported the faster cell attachment on graphene/CS nanocomposite films displaying good biocompatibility and non-cytotoxicity. Similarly, [29, 151], prepared CS/GO nanocomposites containing nano-hydroxyapatite composites with improved mechanical properties. These materials can show high cell proliferation rate [133] and [149]. Chitosan-gold nanoparticles have managed to supplement osseointegration of dental implants. Nanomaterials enhance the wound healing and burn curing. Gold and silver metal nanoparticles prove to be a marvellous property such as low toxicity in vivo, bacteriostatic and bactericidal activities [107].

Silver nanoparticles based bandage supports the recovery of severe partial thickness burns. The benefit of silver nanoparticles-based dressings, even for a prolonged period, does not have a negative effect on the proliferation of fibroblasts and keratinocytes, which leads the healing of the wound [58]. The implant of Collagen with silver nanoparticles proves to have the antibacterial activity and makes it an appropriate component for wound dressing material.

According to [52], Gold nanoparticles are biocompatible, cell viable, hence used in drug delivery and wound healing process. The cross-linking of collagen with gold nanoparticles which allowed the ease assimilation of biomolecules like growth factors, peptides, cell adhesion molecules by their immobilization at the Gold surface without altering of collagen structure. The combination of gelatin chitosan with gold nanoparticles shows safe and excellent wound healing property. [143], suggested that bio-composite scaffolds containing chitosan/ nanohydroxyapatite/ nano-copper-zinc have appropriate morphological and physical quality in Bone Tissue Engineering (BTE).

4.10 Water Treatment

Wastewater usually contains several poisonous and unsafe contaminants, such as heavy metals, organic impurities, dyes, pesticides, and inorganic salts etc., that being discharged from various industrial effluents and domestic resources [5]. The water reservoirs containing these substances causes many chronic or acute diseases, therefore these contaminants must be removed and discarded from the wastewater before being discharged into the nearest water bodies [1]. The methods for removing pollutants from the wastewater was given in Fig. 2. Many researchers suggested that the nanocomposites have excellent adsorption capability, selectivity, and steadiness than nanoparticles. So, they find a range of applications in multiple areas.

The adsorption of different pollutants such as heavy metal ions, dyes, and pesticides from the polluted water with the help of nanocomposites has alarmed

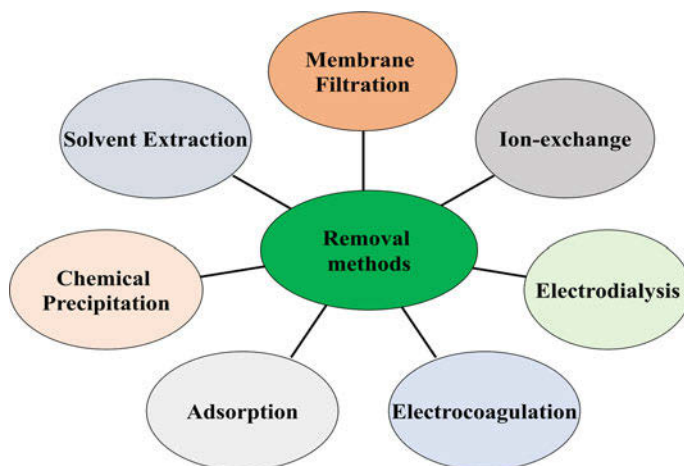


Fig. 2 Removal methods for wastewater treatment

important interest. In this chapter, various nanocomposites and its blends utilized for treatment of wastewater have been highlighted such as graphene, CNT, nanoclays [41, 126], nanochitosan [89], nano alginate [20, 38]. Bai et al. [12] suggested that the Graphene with certain polysaccharides (such as alginates, starch, cellulose, chitosan) forms nanocomposites with improved mechanical properties. Starch/graphene nanocomposite films with 0.2–3.0 wt% graphene platelets were prepared via aqueous solutions casting which was used as an adsorbent. Apart from this, it was also utilized to use in the selective determination of iodide in seafood samples. The heavy metals like Au(III) and Pd(II) were adsorbed on cross-linked CS/GO nanocomposites, with maximum adsorption capacities were observed [127].

Long and Yang [90], has found CNTs to be exceptional adsorbent for the removal of lead, cadmium and organic 1, 2- DCB from water, being a potential medium in wastewater treatment. Nanoclays also find applications in remediating heavy metals from the effluents which are readily available, eco-friendly, economical chemical substances and recent studies reveal the above findings [77]. The nanoclay combination with cationic starch was studied to relate the relationship between polymer and nanoclay in atrazine reduction.

The nano adsorption technique, have been effectively used to investigate the removal of pollutants. Remediation of wastewater using several nano-materials and nano-adsorbent is being concentrated recently [163]. Nano-adsorbent has high adsorption capacity on the surface of the nano-material [81].

Recently development on carbon-based nano-materials (CNMs) in the form of carbon nanotubes, carbon nanoparticles and carbon nanosheets has gained more attention for treatment of wastewater [26]. Other than this silicon, nanoclays, polymer-based nano-materials, nanofibers and aerogels nano-material is also used as nano-adsorbents which are discussed in the various literature. [47] reported that oxide based nano-particles have high surface area for the effective wastewater

treatment applications [46], cerium oxides, Titanium oxide/dendrimers composites [15, 14] zinc oxides, magnesium oxide [55], manganese oxides, copper oxides, Zinc oxides [39] and ferric oxides [160, 159]. Gupta et al. [56] done Surface modification of Fe_2O_3 nanoparticles with 3-aminopropyltrimethoxysilane. According to Gupta et al. [56], the modification of these nano-adsorbents shows high affinity for the removal of different pollutants such as Cr^{3+} , Co^{2+} , Ni^{2+} , Cu^{2+} , Cd^{2+} , Pb^{2+} , and As^{3+} simultaneously from wastewater.

The nanoparticles of manganese oxide show high adsorption ability due to their morphological and polymorphic structure [92]. Generally, they were used for the removal of various heavy metals such as arsenic from wastewater [154, 152].

Ihsanullah Al-Khalidi et al. [62] used widely Carbon-based nanomaterials organic materials in the field of removing heavy metals in recent decades, due to its nontoxic nature and high sorption abilities. Earlier activated carbon was used as sorbents, but its drawback to remove heavy metals at micro levels other nanoparticles such as carbon nanotubes, fullerene, and graphene are synthesized and used as nanosorbents [6].

By using CNT such as MWCNT [60] and SWCNT were used to several studies reported the removal of heavy metals such as Pb(II) and Mn(II) [139], alumina supported on CNT adsorbed Cu(II) Pb(II) from its aqueous solution [55, 138].

Chen et al [24, 28] and [27], synthesized Inorganic nano-adsorbent the highly ordered $\text{Mg}(\text{OH})_2$ nanotube arrays inside the pores anodic alumina membranes to form $\text{Mg}(\text{OH})_2/\text{Al}_2\text{O}_3$ composite membranes. And these membranes are used to adsorb Nickel ions from wastewater with high efficiency. Chandra et al. [23] accounted magnetite-graphene adsorbents with a particle size of ~ 10 nm which gives a high binding capacity of different oxidation states As^{3+} and As^{5+} , and the rate of binding capacity increases with increase in adsorption sites in the graphene composite.

Therefore nanocomposites have enormous characteristics predominantly for the effective removal of pollutant from wastewater even at micro level concentration, with high selectivity, sensitivity and adsorption capability.

4.11 Agriculture

Nanotechnology applications in the agriculture could play a fundamental role. The main application of nanocomposites in agricultural is to reduce the application of plant protection products, minimize nutrient losses in fertilization and increase yields through optimized nutrient management. Nanoparticles technology is a fast-growing strategy to tackle [106] specific treatment in the agricultural field. The goal of this imaging nanoparticles is to reduce the number of unnecessary troubles in agriculture sectors [140].

The new nanosensors such as active carbon nanotubes, nanofibers, and fullerenes also relevant implications for application in agriculture in particular for soil analysis, easy biochemical sensing and control, water management and

delivery, pesticide and nutrient delivery. Research peoples are concentrating in the field of biopolymer composites in order to improve the properties of individual polymers. Generally, silicate, clay and titanium dioxide (TiO_2) added to biopolymers to improve mechanical, barrier properties, other functions, and applications, thereby acts as an antimicrobial agent, biosensors and oxygen scavenger [121]. Antifungal activities of polymers based copper nanocomposites against pathogenic fungi have been reported [31]. A functional hybrid nanocomposite based on the intercalation of two herbicides anions (2,4-dichlorophenoxy acetate and 4-chlorophenoxy acetate) with zinc – aluminium layered double hydroxide [16].

A number of studies reported that the nanoparticles mediated plant transformation has the potential for genetic modification in plants by observed plant reactions after contact. Specifically in specific agricultural problems in plant-pathogen interactions and provide new ways for the crop protection [105]. Nanosilver is widely in agriculture field because of its specific properties [67]. Nanotechnology develops effectiveness, safety, patient adherence, as well as reducing health care costs [7]. Nanoparticles not only influence the health agricultural plant growth, it also associated with null use of hazardous insecticides and pesticides by acting as the alternative product [18].

The application of nanotechnology would be highly promising in agricultural research to put forward not only the detection of plant diseases and also in the analysis and assessment of the use of nanoparticles in plant tissues.

5 Conclusion

Nanostructured materials have a greater impact in various fields. The ability to engineer nanostructured materials has already demonstrated great value. In the next decade, it will be important to elucidate how the physicochemical properties of nanomaterials and their by-products interact with biological systems. This chapter will substantially have an effect on our capacity to engineer new generations nanomaterials with nontoxic and specified properties for various applications. This chapter also provides the essential ideas on basic concepts of structural properties of the material successful nanomaterials to design.

References

1. Abdullahassan MA, Souabi S, Yaacoubi A, Baudu M (2006) Removal of surfactant from industrial wastewaters by coagulation flocculation process. *Int J Environ Sci Technol* 3(4): 327–332
2. Adeosun SO, Lawal GI, Balogun Sambo A, Akpan Emmanuel I (2012) Review of green polymer nanocomposites. *J Miner Mater Charact Eng* 11(4):483–514
3. Ajayan PM, Schadler LS, Braun PV (2006) *Nanocomposite science and technology*, Wiley, New York, NY, USA

4. Amass W, Amass A, Tighe BA (1998) Review of biodegradable polymers: Uses, current developments in the synthesis and characterization of biodegradable polyesters, blends of biodegradable polymers and recent advances in biodegradation studies. *Polym Int* 47: 89–144
5. Amuda OS, Amoo IA, Ajayi OO (2006) Performance optimization of coagulation/flocculation process in the treatment of beverage industrial wastewater. *J Hazard Mater* 129:69–72
6. An J, Zhang X, Guo Q, Zhao Y, Wu Z, Li C (2015) Glycopolymer modified magnetic mesoporous silica nanoparticles for MR imaging and targeted drug delivery. *Colloids and Surfaces A. Physicochemical Eng Aspects* 482:98–108
7. Anwunobi AP, Emeje MO (2011) Recent application of natural polymers in nanodrug delivery. *J Nanomedic Nanotechnol. S* 4:002
8. Araujo L, Lobenberg R et al (1999) Influence of the surfactant concentration on the body distribution of nanoparticles. *J Drug Target* 6:373–385
9. Armentano I, Dottori M, Fortunati E, Mattioli S, Kenny JM (2010) Biodegradable polymer matrix nanocomposites for tissue engineering : a review. *Polym Degrad Stab* 95:2126–2146. <https://doi.org/10.1016/j.polyimdegradstab.2010.06.007>
10. Arnida, Malugin A, Ghandehari H (2010) Cellular uptake and toxicity of gold nanoparticles in prostate cancer cells: a comparative study of rods and spheres. *J Appl Toxicol* 30(3): 212–217
11. Ashori A (2008) Wood-plastic composites as promising green-composites for automotive industries. *Bioresour Biotechnol* 99:4661–4667
12. Bai J, Zhong X, Jiang S, Huang Y, Duan X, (2010) Graphene nanomesh nature nanotechnology (5)3:190–194
13. Balazs AC, Emrick T, Russell TP (2006) Nanoparticle polymer composites: where two small worlds meet. *Science*, 314(5802), 1107–1110 <https://doi.org/10.1126/science.1130557>
14. Barakat MA, Al-Hutailah RI, Hashim MH, Qayyum E, Kuhn JN (2013) Titania supported silver-based bimetallic nanoparticles as photocatalysts. *Environ Sci Pollut Res* 20(6):3751–3759
15. Barakat MA, Ramadan MH, Alghamdi MA, Al-Garny SS, Woodcock HL, Kuhn JN (2013) Remediation of Cu (II), Ni (II), and Cr (III) ions from simulated wastewater by dendrimer/titania composites. *J Environ Manage* 117:50–57
16. Bashi AM, Haddawi SM, Dawood AH (2011) Synthesis and characterizations of two herbicides with Zn/Al layered double hydroxide nanohybrides. *J Kerbala Univ* 9(1):9–16
17. Bednarczyk BA (2003) *Compos B* 34:175–197
18. Begum N, Sharma B, Pandey RS (2010) Evaluation of insecticidal efficacy of calotropis procera and annona squamosa ethanol extracts against musca domestica. *J Biofertil Biopestici* 1:101
19. Buchman JT, Miranda J, Gallagher, Chi-Ta Yang, Xi Zhang, Miriam O P, Krausee Rigoberto, Hernandez. Galya Orr, (2016) Research highlights: examining the effect of shape on nanoparticle interactions with organisms. *Environ Sci Nano* <https://doi.org/10.1039/c6en90015a>
20. Cao K, Jiang Z, Zhao J, Zhao C, Gao C, Pan F, Wang B, Cao X, Yang J (2014) Enhanced water permeation through sodium alginate membranes by incorporating graphene oxides. *J Membr Sci* 469:272–283
21. Castangia I, Nacher A, Caddeo C, Valenti D, Fadda AM, Díez-Sales O, Ruiz-Saurí A, Manconi M (2014) Fabrication of quercetin and curcumin bionanovesicles for the prevention and rapid regeneration of full-thickness skin defects on mice. *Acta Biomater* 10(3):1292–1300
22. Chandra R, Rustgi R (1998) Biodegradable polymers. *Prog Polym Sci* 23:1273–1335
23. Chandra V, Park J, Chun Y, Lee JW, Hwang IC, Kim KS (2010) Water-dispersible magnetite-reduced graphene oxide composites for arsenic removal. *ACS Nano* 4:3979–3986
24. Chen L, Bromberg L, Hatton TA, Rutledge GC (2007) Catalytic hydrolysis of p-nitrophenyl acetate by electrospun polyacrylamidoxime nanofibers. *Polymer* 48(16):4675–4682

25. Chen Z, Mao R et al (2012) Fullerenes for cancer diagnosis and therapy: preparation, biological and clinical perspectives. *Curr Drug Metab* 13(8):1035–1045
26. Chen GC, Shan XQ, Wang YS, Wen B, Pei ZG, Xie YN, Liu T, Pignatello JJ (2009) Adsorption of 2,4,6-trichlorophenol by multiwalled carbon nanotubes as affected by Cu(II). *Water Res* 43(9):2409–2418
27. Chen CZ, Zhou ZW (2004) The preparation of nano-ZnO and its middle infrared-ultraviolet-visible light absorption properties. *J Funct Mater* 35:97–98
28. Chen X, Mao SS (2007) Titanium dioxide nanomaterials: synthesis, properties, modifications and applications. *Chem. Rev* 107:2891–2959
29. Cheung RC, Ng TB, Wong JH, Chan WY (2015) Chitosan: an update on potential biomedical and pharmaceutical applications. *Mar Drugs* 13:5156–5186
30. Chithrani BD, Ghazani AA, Chan WC (2006) Determining the size and shape dependence of gold nanoparticle uptake into mammalian cells. *Nano Lett* 6(4):662–8
31. Cioffi N, Torsi L, Ditaranto N et al (2004) Antifungal activity of polymer- based copper nanocomposite coatings. *Appl Phys Lett* 85(12):2417–2419
32. Crandall BC (ed) (1996) *Nanotechnology* MIT Press, Cambridge
33. Dash MP, Tripathy M, Sasmal A, Mohanty GC, Nayak P (2010) Poly(anthranilic acid)/ multi-walled carbon nanotube composites: spectral, morphological, and electrical properties. *J Mater Sci* 45(14) 3858–3865
34. Deborah DL, Chung (2002) *Composite materials, functional materials for modern technologies*, Springer-Verlag London Ltd, UK
35. Deepachitra R, Nigam R, Prohit SD, et al (2014) In vitro study of hydroxyapatite coatings on fibrin functionalized/pristine graphene oxide for bone grafting. *Mater Manuf Process* 30(6): 804–811
36. Dobkowski J, Kołos R, Kamiński J, Kowalczyńska HM (1999) Cell adhesion to polymeric surfaces: experimental study and simple theoretical approach. *J Biomed Mater Res* 47: 234–242
37. Drzal LT (2010) Sustainable biodegradable green nanocomposites from bacterial bioplastic for automotive applications. <http://www.egr.msu.edu/cmssc/biomaterials/index.html> (accessed on 20 August 2010)
38. Fan J, Shi Z, Lian M, Li H, Yin J (2013) Mechanically strong graphene oxide/sodium alginate/polyacrylamide nanocomposite hydrogel with improved dye adsorption capacity. *J Mater Chem A* 1. 51:7433–7443
39. Fang J, Fan H, Ma Y, Wang Z, Chang Q (2015) Surface defects control for ZnO nanorods synthesized by quenching and their anti-recombination in photocatalysis. *Appl Surface Sci* 332:47–54
40. Feldherr CM, Lanford RE, Akin D (1992) Signal-mediated nuclear transport in simian virus 40-transformed cells is regulated by large tumor antigen. *Proc Natl Acad Sci USA* 15:11002–11005
41. Floody MC, Theng B, Reyes P, Mora M (2009) Natural nanoclays: applications and future trends—a Chilean perspective. *Clay Miner* 44:161–176
42. Fong J, Wood F (2006) Nanocrystalline silver dressings in wound management: a review. *Int J Nanomed* 1(4):441–449
43. Fonseca-Santos B, Chorilli M (2017) An overview of carboxymethyl derivatives of chitosan: Their use as biomaterials and drug delivery systems. *Mater Sci Eng C Mater Biol Appl* 77:1349–1362
44. Freeman RG, Grabar KC, Allison KJ, Bright RM, Davis JA, Guthrie AP, Hommer MB, Jackson MA, Smith PC, Walter DG, Natan MJ (1995). SERS Substrates. *Science* 267
45. Gangopadhyay R, De A (2000) Conducting polymer nanocomposites: a brief overview 608–622
46. Gao C, Zhang W, Li H, Lang L, Xu Z (2008) Controllable fabrication of mesoporous MgO with various morphologies and their absorption performance for toxic pollutants in water. *Cryst Growth Des* 8:3785–3790

47. Geng B, Jin Z, Li T, Qi X (2009) Kinetics of hexavalent chromium removal from water by chitosan-Fe₀ nanoparticles. *Chemosphere* 75(6):825–830
48. Giannes BEP (1996). Polymer layered silicate nanocomposites. 29–35
49. Giannelis EP (1996) *Adv Mater* 8:29
50. Gleiter H (2000) Nanostructured materials: basic concepts and microstructure. *Acta Mater* 48:1
51. Graham K, Schreuder-gibson H, Gogins M (2003) Incorporation of electrospun nanofibers into functional structures. *Tech Assos Pulp Pap Ind* 1–16
52. Grant SA, Spradling CS, Grant DN (2014) Assessment of the biocompatibility and stability of a gold nanoparticle collagen bioscaffold. *J Biomed Mater Res, Part A* 102:332–339
53. Gratton SE, Ropp PA, Pohlhaus PD, Luft JC, Madden VJ et al (2008) The effect of particle design on cellular internalization pathways. *Proc Natl Acad Sci USA* 105:11613–11618
54. Guo Y, Bao C, Song L, Yuan B, Hu Y (2011) In situ polymerization of graphene, graphite oxide, and functionalized graphite oxide into epoxy resin and comparison study of on-the-flame behavior. *Ind Eng Chem Res* 50:7772–7783
55. Gupta VK, Agarwal S, Saleh TA (2011) Synthesis and characterization of alumina-coated carbon nanotubes and their application for lead removal. *J Hazard Mater* 185:17–23
56. Gupta VK, Tyagi I, Sadegh H, Shahryari-Ghoshekand R, Makhlof ASH, Maazinejad B (2015) Nanoparticles as adsorbent; a positive approach for removal of noxious metal ions: a review. *Sci Technol Dev* 34:195
57. He P, Sahoo S, Ng KS, Chen K, Toh SL, Goh JC (2013) Enhanced osteoinductivity and osteoconductivity through hydroxyapatite coating of silk-based tissue-engineered ligament scaffold. *J Biomed Mater Res A* 101:555–566
58. Heydarnejad MS, Rahnama S, Mobini-Dehkordi M, Yarmohammadi P, Aslnai H (2014) Sliver nanoparticles accelerate skin wound healing in mice (*Mus musculus*) through suppression of innate immune system. *Nanomed J* 1(2):79–87
59. Huang Z, Zhang Y, Kotaki M, Ramakrishna S (2003) A review on polymer nanofibers by electrospinning and their applications in nanocomposites. *Compos Sci Technol* 63:2223–2253. [https://doi.org/10.1016/S0266-3538\(03\)00178-7](https://doi.org/10.1016/S0266-3538(03)00178-7)
60. Huang ZN, Wang XL, Yang DS (2015) Adsorption of Cr(VI) in wastewater using magnetic multi-wall carbon nanotubes. *Water Sci Eng* 8(3):226–232
61. Huang J, Bu L, Xie J, Chen K, Cheng Z, Li X, Chen X (2010) Effects of nanoparticle size on cellular uptake and liver MRI with polyvinylpyrrolidone-coated iron oxide nanoparticles. *ACS Nano* 4(12):7151–60
62. Ihsanullah Al-Khaldi FA, Abusharkh B, Khaled M, Atieh MA, Nasser MS, Saleh TA, Agarwal S, Tyagi I, Gupta VK (2015) Adsorptive removal of cadmium (II) ions from liquid phase using acid modified carbon-based adsorbents. *J Molecul Liq* 204:255–263
63. Jamshidian M, Tehrani EA, Imran M et al (2010) Poly-lactic acid: Production, applications, nanocomposites, and release studies. *Compr Rev Food Sci Food Saf* 9:552–571
64. Jiang H, Lau M, Tellkamp VL, Lavernia EJ (2000) Synthesis of nanostructured coatings by high velocity oxygen-fuel thermal spraying. In: Nalwa HS (ed) *Handbook of nanostructured materials and nanotechnology*, Academic Press, San Diego, CA, USA
65. Jin R, Lin B, Li D, Ai H (2014) Super paramagnetic iron oxide nanoparticles for MR imaging and therapy: design considerations and clinical applications. *Curr Opin Pharmacol* 18:18–27
66. John MJ, Thomas S (2008) Biofibres and biocomposites. *Carbohydr Polym* 71:343–364
67. Jolanta P, Marcin B, Zygmunt K (2011) Nanosilver—making difficult decisions. *Ecol Chem Eng* 18(2)
68. Jolivet JP, Henry M, Livage J (2000) *Metal oxide chemistry and synthesis: from solution to solid state*. Wiley, New York
69. Kaminskas LM, Boyd BJ et al (2011) Dendrimer pharmacokinetics: the effect of size, structure and surface characteristics on ADME properties. *Nanomedicine* 6(6):1063–1084

70. Katepalli H, Bikshapathi M, Sharma CS, Verma N, Sharma A (2011) Synthesis of hierarchical fabrics by electrospinning of PAN nanofibers on activated carbon microfibers for environmental remediation applications. *Chem Eng J* 171(3):1194–1200
71. Keledi G, Hari J, Pukanszky B (2012) Polymer nanocomposites: structure, interaction, and functionality. *Nanoscale* 4:1919
72. Khan WS, Ceylan M, Asmatulu R (2012) Effects of nanotechnology on global warming. In: ASEE midwest section conference, Rollo, MO, 19–21, Sep 2012, p 13
73. Khatamiana M, Divband B, Daryana M (2016) Preparation, characterization and antimicrobial property of Ag⁺- nano Chitosan/ZSM-5: novel Hybrid Biocomposites. *Nanomed J* 3(4):268–279
74. Kijeńska E, Prabhakaran MP, Swieszkowski W, Kurzydowski KJ, Ramakrishna S (2012) Electrospun bio-composite P (LLACL)/ collagen I/collagen III scaffolds for nerve tissue engineering. *J Biomed Mater Res B Appl Biomater* 100(4):1093–1102
75. Kinnear C, Moore Thomas L, Rodriguez-Lorenzo L, Rothen-Rutishauser B, Petri-Fink A (2017) Form follows function. Nanoparticle shape and its implications for nanomedicine. *Chem Rev* 117:11476–11521
76. Kohane DS (2007) Microparticles and nanoparticles for drug delivery. *Biotechnol Bioeng* 96(2):203–209
77. Kokabi M, Sirousazar M, Hassan ZM (2007) PVA–clay nanocomposite hydrogels for wound dressing. *Eur Polym J* 43:773–781
78. Kudumula KK (2016) Scope of polymer nano-composite in bio-medical applications. *IOSR-JMCE* 13(5):18–21
79. Kumar A, Gupta M (2005) Synthesis and surface engineering of iron oxide nanoparticles for biomedical applications. *Biomaterials* 26:3995–4021. <https://doi.org/10.1016/j.biomaterials.2004.10.012>
80. Kumar SK, Krishnamoorti R (2010) *Annu Rev Chem Biomol Eng* 1:37
81. Kyzas GZ, Bikiaris DN, Seredych M, Bandosz TJ, Deliyanni EA (2014) Removal of dorzolamide from biomedical wastewaters with adsorption onto graphite oxide/ poly (acrylic acid) grafted chitosan nanocomposite. *Bioresour Technol* 152:399–406
82. Langer R, Vacanti J (1993) *Tissue engineering science* (80) 260:920–6
83. Leceta I, Guerrero P, Ibarburu I, Duenas MT, de la Caba K (2013) Characterization and antimicrobial analysis of chitosan based films. *J Food Engineering* 116(4):889– 899
84. Lee KY, Mooney DJ (2012) Alginate: properties and biomedical applications. *Prog Polym Sci* 37:106–126
85. Leja K, Lewandowicz G (2010) Polymer biodegradation and biodegradable polymers—a review. *Polish J Environ Stud* 19:255–266
86. Leu JG, Chen SA, Chen HM, Wu WM, Hung CF, Yao YD, Tu CS, Liang YJ (2012) The effects of gold nanoparticles in wound healing with antioxidant epigallocatechin gallate and α -lipoic acid. *Nanomedicine*. 8(5):767–775
87. Li et al (2015) *Nanoscale* 7:16631–16646. <https://doi.org/10.1039/C5NR02970H>
88. Litzinger DC et al (1994) Effect of liposome size on the circulation time and intraorgan distribution of amphipathic poly (ethylene glycol)-containing liposomes. *Biochim Biophys Acta* 1190(1):99–107
89. Liu D, Zhu Y, Li Z, Tian D, Chen L, Chen P (2013) Chitin nanofibrils for rapid and efficient removal of metal ions from water system. *Carbohydr Polym* 98:483–489
90. Long RQ, Yang RT (2001) Carbon nanotubes as superior sorbent for dioxin removal. *J Am Chem Soc* 123(9):2058–2059
91. Lu F, Wu SH, Hung Y, Mou CY (2009) Size effect on cell uptake in well-suspended, uniform mesoporous silica nanoparticles. *Small Jun* 5(12):1408–1413
92. Luo T, Cui J, Hu S, Huang Y, Jing C (2010) Arsenic removal and recovery from copper smelting wastewater using TiO₂. *Environ Sci Technol* 44(23):9094–9098
93. Ma Z, Lim LY (2003) Uptake of chitosan and associated insulin in Caco-2 cell monolayers: a comparison between chitosan molecules and chitosan nanoparticles. *Pharm Res* 20(11): 1812–1819

94. Mago G, Jana SC, Ray SS, McNally T, McNally T (2012) Polymer nanocomposite processing, characterization, and applications. <https://doi.org/10.1155/2012/924849>
95. Mago G, Ray SS, Shofner ML, Wang S, Zhang J (2013) Polymer nanocomposite processing, characterization, and applications. *J Nanomater* <https://doi.org/10.1155/2014/403492>
96. Malafaya PB, Silva GA, Reis RL (2007) Natural-origin polymers as carriers and scaffolds for biomolecules and cell delivery in tissue engineering applications. *Adv Drug Deliv Rev* 59:207–233
97. Maneerung T, Tokura S, Rujiravanit R (2008) Impregnation of silver nanoparticles into bacterial cellulose for antimicrobial wound dressing. *Carbohydr Polym* 72:43–51
98. Mangaiyarkarasi R, Chinnathambi S, Karthikeyan S, Aruna P, Ganesan S (2016) Paclitaxel conjugated $\text{Fe}_3\text{O}_4\text{-LaF}_3\text{:Ce}^{3+}\text{,Tb}^{3+}$ nanoparticles as bifunctional targeting carriers for Cancer theranostics application. *J Magn Magn Mater* 399:207–215
99. Matthews FL, Rawlings RD (1999) *Composite materials: engineering and science*: Elsevier, Amsterdam, The Netherland
100. Mayer LD et al (1989) Influence of vesicle size, lipid composition, and drug-to-lipid ratio on the biological activity of liposomal doxorubicin in mice. *Cancer Res* 49(21):5922–5930
101. Mohanty AK, Misra M, Hinrichsen G (2000) Biofibres, biodegradable polymers and biocomposites: an overview. *Macromol Mater Eng* 276(277):1–24
102. Murphy PS, Evans GRD (2012) Advances in wound healing: a review of current wound healing products. *Plast Sur Int* 190436:1–8
103. Murugesan S, Mousa SA et al (2007) Carbon inhibits vascular endothelial growth factor- and fibroblast growth factor-promoted angiogenesis. *FEBS Lett* 581:1157–1160
104. Nagayasu A, Uchiyama K, Kiwada H (1999) The size of liposomes: a factor which affects their targeting efficiency to tumors and therapeutic activity of liposomal antitumor drugs. *Adv Drug Deliv Rev* 40(1–2):75–87
105. Nair R, Varghese SH, Nair BG, Maekawa T, Yoshida Y et al (2010) Nanoparticulate material delivery to plants. *Plant Sci* 179:154–163
106. Nanjwade BK, Derkar GK, Bechra HM, Nanjwade VK, Manvi FV (2011) Design and characterization of nanocrystals of lovastatin for solubility and dissolution enhancement. *J Nanomedic Nanotechnol* 2:107
107. Okamoto M, John B (2013) Synthetic biopolymer nanocomposites for tissue engineering scaffolds. *Prog Polym Sci* 38:1487–1503
108. Ovissipour M, Roopesh SM, Rasco BA, Sablani SS (2014) Engineered nanoparticles (ENPs): applications, risk assessment, and risk management in the agriculture and food sectors, In: Wang S (ed) *Food chemical hazard detection: development and application of new technologies* Wiley, Chichester, UK. <https://doi.org/10.1002/9781118488553.ch7>
109. Pandey JK, Chu WS, Lee CS et al (2007) Preparation characterization and performance evaluation of nanocomposites from natural fiber reinforced biodegradable polymer matrix for automotive applications. Presented at the international symposium on polymers and the environment: emerging technology and science, bioenvironmental polymer society (BEPS), Vancouver, WA, USA, 17–20 October 2007
110. Panupakorn P, Chaichana E, Praserttham P, Jongsomjit B (2013) Polyethylene/clay nanocomposites produced by in situ polymerization with zirconocene/MAO catalyst. *J Nanomater* <https://doi.org/10.1155/2013/154874>
111. Park KE, Jung SY, Lee SJ, Min BM, Park WH (2006) Biomimetic nanofibrous scaffolds: preparation and characterization of chitin/silk fibroin blend nanofibers. *Int J Biol Macromol* 38:165–173
112. Paul DR, Robeson LM (2008) *Polymer* 49:3187
113. Qi L, Xu Z, Jiang X, Hu C, Zou X (2004) Preparation and antibacterial activity of chitosan nanoparticles. *Carbohydr Res* 339(15):2693–2700
114. Qiu Y, Liu Y, Wang LM, Xu LG, Bai R et al (2010) Surface chemistry and aspect ratio mediated cellular uptake of Au nanorods. *Biomaterials* 31:7606–7619
115. Rastogi V, Yadav P et al (2014) Carbon nanotubes: an emerging drug carrier for targeting cancer cells. *J Drug Deliv* 670815

116. Raveendran P, Fu J, Wallen SL (2003) Completely green synthesis and stabilization of metal nanoparticles. *J Am Chem Soc* 125:13940–13941. <https://doi.org/10.1021/ja029267j>
117. Ravichandran R, Sundarajan S, Venugopal JR, Mukherjee S, Ramakrishna S (2012) Advances in polymeric systems for tissue engineering and biomedical applications. *Macromol Biosci* 12:286–311. <https://doi.org/10.1002/mabi.201100325>
118. Ray SS (2013) Environmentally friendly polymer nanocomposites, types, processing and properties. Woodhead Publishing Series in Composites Science and Engineering. 44, Woodhead Publishing Ltd
119. Reddy RJ (2010) Preparation, characterization and properties of injection molded graphene nanocomposites, Master's thesis, Mechanical Engineering, Wichita State University, Wichita, Kansas, USA
120. Reneker DH, Fong H (2006) Polymeric nanofiber. American Chemical Society Publishers, Washington. 1–6
121. Rhim J, Park HM, Ha CS (2013) Bionanocomposites for food packaging application. *Prog Polym Sci* 38:1629–1652
122. Roco MC, Williams S, Alivisatos P (eds) (2000) nanotechnology research directions: IWGN workshop report vision for nanotechnology in the next decade, Kluwer Academic Publishers, Dordrecht
123. Roy R, Roy R, Roy D (1986) Alternative perspectives on “quasi-crystallinity”, non-uniformity and nanocomposites. *Mater Lett* 4:323–328
124. Sanginario A, Miccoli B et al (2017) Carbon nanotubes as an effective opportunity for cancer diagnosis and treatment. *Biosensors* 7(1):9
125. Savva I, Krekos G, Taculescu A, Marinica O, Vekas L, Krasia-christoforu T (2012) Fabrication and characterization of magneto-responsive electrospun nanocomposite membranes based on methacrylic random copolymers and magnetite nanoparticles. *J Nanomater* 9. <https://doi.org/10.1155/2012/578026>
126. Shahidi S, Ghoranneviss M (2014) Effect of plasma pretreatment followed by nanoclay loading on flame retardant properties of cotton fabric. *J. Fusion Energ* 33:88
127. Singh V, Joung D, Zhai L, Das S, Khondaker SI, Seal S (2011) Graphene based materials: past, present and future. *Prog Mater Sci* 56:1178–1271
128. Sinha SR, Bousmina M, Mai Y Yu Z (2006) Eds Biodegradable polymer/layered silicate nanocomposites. Polymer nanocomposites. Woodhead Publishing and Maney Publishing, Cambridge, England, pp 57–129
129. Siracusa V, Rocculi P, Romani S et al (2008) Biodegradable polymers for food packaging: a review. *Trends Food Sci Technol* 19:634–643
130. Stamatialis DF, Papenburg BJ, Giron M, Bettahalli SM, Schmitmeier S, Wessling M (2008) Medical applications of membranes. *Drug Delivery Artif Organs Tissue Eng* 308:1–34. <https://doi.org/10.1016/j.memsci.2007.09.059>
131. Stander L, Theodore L (2011) Environmental implications of nanotechnology—an update. *Int J Environ Res Public Health* 8:470–479
132. Starr FW, Glotzer SC, Dutcher JR, Marangoni AG (eds) (2004) Soft materials, structure and dynamics, Marcel Dekker, New York
133. Sultana N, Mokhtar M, Hassan MI, Jin RM, Roobahani F, Khan TH (2015) Chitosan-based nanocomposite scaffolds for tissue engineering applications. *Mater Manuf Process* 30: 273–278
134. Suryanarayana C (1994) Structure and properties of nanocrystalline materials. *Bull Mater Sci* 17:307
135. TPA Plast global engineering nanocomposite polymers. http://www.tpacomponents.com/uploads/pdf/en/0305_EN.pdf (accessed on 20 August 2010)
136. Tabiei A, Aminjikai SB (2009) *Compos Struct* 88:65–82
137. Tanaka (2004) Polymer nanocomposites as dielectrics and electrical insulation—perspectives for processing technologies material characterization and future applications, *IEEE Trans Dielectr Electr Insul* 11:5

138. Tang X, Zhang Q, Liu Z, Pan K, Dong Y, Li Y (2014) Removal of Cu (II) by loofah fibers as a natural and low-cost adsorbent from aqueous solutions. *J Mol Liq* 199:401–407
139. Tarigh GD, Shemirani F (2013) Magnetic multi-wall carbon nanotube nanocomposite as an adsorbent for preconcentration and determination of lead (II) and manganese (II) in various matrices. *Talanta* 115:744–750
140. Thomas S, Waterman P, Chen S, Marinelli B, Seaman M et al (2011) Development of secreted protein and acidic and rich in cysteine (SPARC) targeted nanoparticles for the prognostic molecular imaging of metastatic prostate cancer. *J Nanomedic Nanotechnol* 2:112
141. Thostenson ET, Li C, Chou TW (2005) Nanocomposites in context. *Compos Sci Technol* 65:491–516
142. Toy R et al (2013) Multimodal in vivo imaging exposes the voyage of nanoparticles in tumor microcirculation. *ACS Nano* 7(4):3118–3129
143. Tripathi A, Saravanan S, Pattnaik S, Moorthi A, Partridge NC, Selvamurugan N (2012) Bio-composite scaffolds containing chitosan/nano-hydroxyapatite/nano-copper-zinc for bone tissue engineering. *Int J Biol Macromol* 50:294–299
144. Ulman A (1996) Formation and structure of self-assembled monolayers. *Chem Rev* 96 1533–1554. <https://doi.org/10.1021/cr9502357>
145. Vaia RA, Giannelis EP (2001) *MRS Bull* 26:394
146. Vaia RA, Giannelis EP (eds) (2001) *Polymer nanocomposites*. American Chemical Society, Washington
147. Varela JA, Bexiga MG, Åberg C, Simpson JC, Dawson KA (2012) Quantifying size-dependent interactions between fluorescently labeled polystyrene nanoparticles and mammalian cells. *J Nanobiotechnol* 10(1):39
148. Veiseh O, Gunn JW, Zhang M (2010) Design and fabrication of magnetic nanoparticles for targeted drug delivery and imaging. *Adv Drug Deliv Rev* 62(3):284–304
149. Venkatesan J, Kim SK (2014) Nano-hydroxyapatite composite biomaterials for bone tissue engineering—a review. *J Biomed Nanotechnol* 10:3124–3140
150. Villasaliu et al (2014) *Expert Opin. Drug Delivery* 11:139–154. <https://doi.org/10.1517/17425247.2014.866651>
151. Wan Y, Chen X, Xiong G, Guo R, Luo H (2014) Synthesis and characterization of three-dimensional porous graphene oxide/sodium alginate scaffolds with enhanced mechanical properties. *Mater Express* 4:429–434
152. Wang J, Byrne JD, Napier ME, De Simone JM (2011) More effective nanomedicines through particle design. *Small* 7:1919–1931
153. Wang X, Wenk E, Matsumoto A, Meinel L, Li C, Kaplan DL (2007) Silk microspheres for encapsulation and controlled release. *J Control Release* 117:360–370
154. Wang HQ, Yang GF, Li QY, Zhong XX, Wang FP, LiZ S, Li YH (2011) Porous nano-MnO₂ Large scale synthesis via a facile quick-redox procedure and application in a supercapacitor. *New J Chem* 35:469–475
155. Wang R, Yang J, Zheng Z, Carducci MD, Jiao J, Seraphin S, (2001) Dendron-Controlled Nucleation and Growth of Gold Nanoparticles. *Angew Chem Int Edi* 40(3) 549–552
156. Wang SH, Lee CW, Chiou A, Wei PK (2010) Size-dependent endocytosis of gold nanoparticles studied by three-dimensional mapping of plasmonic scattering images. *J Nanobiotechnol* 8(1):33
157. Wypych G (1999) *Handbook of fillers*, 4th edn. ChemTec Publishing, Toronto
158. X Wu, P Liu (2010) Polymer grafted multiwalled carbon nanotubes via facile in-situ solution radical polymerisation. *J Exp Nanosci* 5(5):383–389. <https://doi.org/10.1080/17458080903583956>
159. Xu Z, Gu Q, Hu H, Li F (2008) A novel electrospun polysulfone fiber membrane: application to advanced treatment of secondary bio-treatment sewage. *Environ Technol* 29:13–21
160. Xu D, Tan X, Chen C, Wang X (2008) Removal of Pb (II) from aqueous solution by oxidized multiwalled carbon nanotubes. *J Hazard Mater* 154:407–416

161. Yadav M, Rhee KY, Park SJ (2014) Synthesis and characterization of grapheneoxide/carboxymethylcellulose/alginate composite blend films. *Carbohydr Polym* 110:18–25
162. Yaehne K et al (2013) Nanoparticle accumulation in angiogenic tissues: towards predictable pharmacokinetics. *Small* 9(18):3118–3127
163. Zhang Y, Shen Z, Dai C, Zhou X (2014) Removal of selected pharmaceuticals from aqueous solution using magnetic chitosan: Sorption behaviour and mechanism. *Environ Sci Pollut Res* 21:12780–12789
164. Zheng L, Abhyankar W, Ouwerling N, Dekker HL, van Veen H, van der Wel NN, Roseboom W, de Koning LJ, Brul S, de Koster CG (2016) *Bacillus subtilis* spore inner membrane proteome. *J Proteome Res* 15:585–594
165. Zou H, Wu SS, Shen J (2008) Polymer/silica nanocomposites: preparation, characterization, properties, and applications. *Chem Rev* 108:3893–3957

Polymeric Composites as Catalysts for Fine Chemistry



P. SundarRajan, K. GracePavithra, D. Balaji and K. P. Gopinath

1 Introduction

For the past three decades, conjugated polymers (CPs) have been studied intensively ever since the discovery of the conducting polyacetylene (PAC) in 1976 [41]. Among CPs, Polypyrrole (PPy) and polyaniline (PANI) are often studied. Later, a variety of CPs has been developed and extensively used due to their high conductivity, as listed in Table 1. These CPs are normally stable in air, widespread availability, cheap, chemically inert, and can be effectively prepared as a host for incorporating various catalysts which having intriguing properties. New generations of these materials find its application in the various sectors such as chemical sensors, biosensors, energy storage (super capacitors, dielectric capacitors, batteries, solar cells, fuel cells), biomedical devices, optical devices, electromagnetic interference shielding, anticorrosion and antistatic coatings, electro active devices and catalysis.

In recent times, these CPs was recognized as suitable candidate for supporting heterogeneous catalysts (e.g., noble metals) as well as for basic research and practical applications owing to their intrinsic properties, for example, chemical stability, superior electrical conductivity, special optical properties, better carrier mobility, enhanced electrochemical activity, reusability, high accessible surface area, chemical functionalities (like solvation, templating effect, wettability and so on) and bio-compatibility [14, 28]. Most of the catalytic processes which are

P. SundarRajan · K. GracePavithra · D. Balaji · K. P. Gopinath (✉)
Department of Chemical Engineering, Sri Sivasubramaniya Nadar College of Engineering,
Rajiv Gandhi Salai (OMR), Kalavakkam 603110, Tamil Nadu, India
e-mail: gopinathkp@ssn.edu.in

P. SundarRajan
e-mail: ksundarp@gmail.com

Table 1 Some reported conducting polymers [1, 12]

Polymer	Label	Band gap (eV)	Conductivity (S cm ⁻¹)	Year ^a
Polyacetylene	Pac	1.5	10 ³ to 1.7 × 10 ⁵	1977
Poly(p-phenylene)	PPP	–	500	1979
Poly(p-phenylenevinylene)	PPV	2.5	3 to 5 × 10 ³	1979
Polypyrrole	PPy	3.1	10 ² to 7.5 × 10 ³	1979
Polyaniline	PAni	3.2	0–200	1980
Polythiophene	PT	2.0	10 to 10 ³	1981
Polyfurane	PF	–	–	1981

^aReported for the first time (in the year) as conducting polymer

followed in industrial applications are found to be so complex because individual catalysts cannot meet the demand in terms of catalytic activity, selectivity and resistance towards deactivation. Hence, the introduction of composite catalyst, which has at least two components clubbed together attracted many researchers [60]. Among composite catalyst, CPs based composites show outstanding performance as an effect of synergistic performance which is derived from individual component anchored on them. Therefore, in this chapter, the applications of polymer composite as a catalyst in wider fields such as fuel cells, cross-coupling reaction, photocatalysis and 4-nitrophenol reduction are discussed briefly.

2 Electrocatalytic Activity of Polymer Composite

Low-temperature fuel cells are receiving substantial interest due to an eco-friendly approach of direct electrochemical oxidation of hydrogen/alcohols (mostly, low molecular weight) into either H₂O or CO₂ or both, which produces electricity in the fuel cell. For oxidative and reduction reactions in a fuel cell, platinum or platinum catalysts supported on a conductive material are frequently utilized as electrode materials [4, 7]. In those catalysts, the surface to volume ratio of metal particles is very high which promotes the accessible area for the reactions. The cost of fuel cell operation usually relies upon the morphology and dispersal behaviour of these metal particles because they are assumed as a key part in decreasing the loading rate of the catalyst. The main prerequisites of a proper catalyst support to be used in a fuel cell are

- (a) appropriate void fractions for supporting gas flow,
- (b) high stability during fuel cell working environments,
- (c) high surface to volume ratio, for achieving high metal dispersion, and
- (d) high specific conductance.

Currently, in low-temperature fuel cells, carbon, specifically Vulcan XC-72 carbon blacks, is usually preferred for supporting electrocatalyst nanoparticles because of its substantial specific conductance and surface area [3]. A primary issue associated with the utilization of carbon blacks as a cathode catalyst support in a fuel cell is their less resistivity towards corrosion due to the electrochemical oxidation of carbon surface. The carbon support instability leads to platinum particle coalesce and platinum detachment which results in reducing platinum surface area. On the other hand, the similar corrosion was to be found higher in the anode catalyst, during the reversal of the cell voltage caused by fuel starvation. Likewise, platinum catalysts appear to stimulate the carbon corrosion rate [4, 42, 49].

In addition, the existence of more numbers of micropores will leads to the low accessible surface area for the dispersion of particles and uneven transport of the fuel to the surface. Thus, carbon blacks having a huge surface area comprising mainly micropores (<1 nm) becomes a burden to act as a catalyst support. Eventually, carbon does not conduct protons that restricts the performance achievements. A proton-conducting polymer (e.g., Nafion[®]) is typically blended with a catalyst for the maximum usage of the catalyst because it mainly assists the transport of protons within the catalyst layer. In response to that, several substitutes of electrocatalyst supports are being investigated. Among them, mesoporous carbon and carbon gels received a greater attention as a fuel catalyst supports due to the presence of high quantity of mesopores and high surface area, which permits for high flow of reactant and metal dispersion [4].

Catalysts deposited on aforementioned carbons exhibited catalytic activity much higher than similar catalyst deposited on carbon black support. Their stability during fuel cell operational condition is nearly the same as that of carbon blacks. Lately, carbon-based nanostructures, for example, carbon nanofibers (CNFs) and carbon nanotubes (CNTs) were explored as a supporting material for a catalyst in fuel cells. Platinum/bimetallic Pt-based catalysts deposited on CNT and CNF exhibited catalytic activity much higher than similar catalysts deposited on carbon blacks support, because of the exceptional morphology and features like high chemical stability, high accessible surface area and high electrical conductivity [3]. Investigations performed using carbon-based nanostructures in polymer electrolyte membrane fuel cell (PEMFCs) conditions demonstrated that these nanostructures can be more robust and can replace the traditional carbon black [54]. Though, these supporting materials do not inhibit corrosion due to the oxidation of carbon surface instead merely reduce the rate.

In such a case, non-carbon materials have been explored as a support for the catalyst. Conducting oxides are developing as a suitable candidate for catalyst support due to their oxidative resistance. Additionally, during fuel cell operation, these materials exhibited electrochemical and thermal stability and delivered remarkable resistance towards corrosion in different electrolytic media. Unlike carbon, conducting oxides cease to improve electro-catalysis, but rather acts just as a mechanical support, in some cases several metal oxide supports will be able to serve as co-catalysts. Certainly, it is notable that several metal oxides, for example, SnO₂, WO₃, and RuO₂ can able to enrich the catalysis of platinum for oxidation of

alcohol [20, 37, 40]. However, a major issue associated with the ceramic oxides is their low surface area, which influences the metal dispersion and, thereby resulting in a reduced catalytic activity. Additionally, the electrical conductivity of some metal oxides, for example, TiO_2 and SnO_2 are low at temperatures beneath $200\text{ }^\circ\text{C}$.

Depending on the morphology features, conducting polymers (CPs) have been employed in a fuel cell as a supporting material for catalysts. Normally, CPs satisfies the main prerequisites of a proper catalyst support to be used in a fuel cell that is mentioned earlier. Some of the CPs are proton- as well as electron-conducting materials, so they can be alternative to catalyst incorporated with Nafion[®] and deliver improved performance. The most commonly used CPs are heterocyclic polymers such as polypyrrole (PPy), polythiophene (PTh), polyaniline (PAni) and their derivatives. Table 1 shows the conductivities of some common conjugated polymers. The catalyst activity seems to be higher in PPy and PAni that is mainly due to the synergistic effect of the host matrix and the metal particles [3, 14]. Under fuel cell environment, polymer-supported catalyst usually exhibits a satisfactory stability (e.g., catalytic activity and film integrity). But, in both PAni and PPy, chemical degradation was found during metal doping and the catalysis. In addition, under both oxidizing and reducing conditions, the deposition of the catalyst particles resulted in the degradation of electrical conductivity of the polypyrrole.

And the intermediate products (aldehydes) formed during alcohol oxidation degraded the polyaniline. Furthermore, the use of PAni and PPy as electrocatalyst supports are limited due to loss of electrical conductivity [4].

In summary, the utilization of either carbon or ceramic or polymer materials as a catalyst support in a fuel cell is not totally satisfactory. Accordingly, composite of polymer-carbon, ceramic-carbon and polymer-ceramic materials have been proposed in the most recent years as catalyst supports in fuel cells. These composite may have more reasonable properties than the individual materials when used as a supporting material for the catalyst. Gomez-Romero [12] divided them into two major categories, as per the inherent features of the host and guest phases. Thus, organic-inorganic (OI) materials signify composites with organic hosts and inorganic guests, whereas in inorganic-organic (IO) materials, the organic phase is guest to an inorganic host. In OI hybrids, generally, the inorganic molecules will contribute their chemical activity and requires the structural support from CPs to form a useful solid material. On the other hand, in IO hybrids, the inorganic phase will be providing the structural task even though embedded CPs can also imprint their polymeric nature onto the materials acquired.

2.1 Composite Polymer-Carbon Black Supports

Usually, the electrochemical activity of catalysts supported on composite polymer-carbon blacks (normally Vulcan XC-72), is higher than that of the similar catalysts supported on either carbon or polymer. This enhancement is mainly due to the

higher accessible surface area and electrical conductivity of the support and the polymer/electrolyte interface with simpler charge-transfer which permitting the use of almost all the deposited metal nanoparticles. Xu et al. [61] basically examined the influence of PANi on carbon characteristics (IO material) and found the optimum mass ratio of PANi to C (PANi: C = 0.25:1). An excess amount of PANi will reduce the conductivity of the composite, whereas a limited amount of PANi will reduce the anti-poisoning ability of the catalyst. Subsequently, the produced CO poisoning intermediate compound contributes 61.5% of the reduction in methanol oxidation current on the Pt/C catalyst, after 200 potential cycles, however, just 20% reduction is observed while using the Pt/PANi–C composite catalyst. This implies that the anti-poisoning ability of Pt/PANi–C was three folds greater than the Pt/C. In addition, the presence of PANi encourages ability of the catalyst to absorb more water and generates an active oxy-compound (Pt–OH), which elevates oxidation of carbon monoxide into carbon dioxide.

The work of Wu et al. [55] addressed the impact of using conventional carbon particles (Vulcan XC-72) along with CP (PANi) (OI material). They demonstrated that the integration of carbon particles into PANi film not just increases the electron conductivity, yet additionally reduces charge-transfer resistance across PANi/electrolyte interfaces. In both cases, for methanol oxidation, the activity of platinum supported on PANi–C (polymer-carbon) composite was considerably higher than that of the single host component.

Mokrane et al. [35] synthesized conducting polypyrrole (PPy)/C (Vulcan XC-72) composite material with different PPy/C ratios via chemical polymerization method. They noticed that the composite firmly affected the electrochemical activity of supported platinum toward the oxygen reduction reaction (ORR) in acid medium. The variation of the PPy/C ratio decides the so-called substrate effect for electrocatalysis. Thus, ORR is indirectly proportional to PPy content in the composite.

2.2 Composite Polymer-CNT Supports

Among many varieties of carbons, carbon nanotubes were commonly used as the carbon material in polymer-carbon composite due to their attracting features. To understand the different characteristics of polymer–CNT composites, comprehensive knowledge of the morphology, properties, and chemistry of CNT is significant. CNTs are prepared by single sheets of hexagonally arranged carbon atoms, called graphene and represented in the form of 3D cylindrical nanostructures. There are two basic classifications of CNT, that is, single-walled carbon nanotubes (SWCNTs) and multi-walled carbon nanotubes (MWCNTs) [4]. SWCNT can be pictured as a rolled-up graphene sheet (tubular), which comprises of benzene molecules, including hexagonal rings of carbon atoms, whereas MWCNT contains

a stack of graphene sheets that are rolled up into concentric cylinders. The unique properties related with CNT is usually influenced by various parameters, such as nanotube synthetic method, quality of nanotubes, chirality, size, shape, alignment of nanotubes, defect density, and degree of crystallinity [36]. In most cases, polymer–CNT composites are OI materials, where CNT are dispersed in the polymer matrix to enhance the electrical and mechanical properties of the polymer. The probability of attaining high conductivity at low CNT content makes them a suitable candidate for many potential applications. Moreover, in order to achieve the desired CNT properties, the system is designed in such a manner to create a uniform dispersion of CNT in the composites with high stability.

The major problems associated with the synthesis of polymer–CNT composites exist in the effective integration of CNT into a polymer matrix, the control over the alignment of CNT in the matrix and the evaluation of the dispersion. Accordingly, several techniques have been proposed for the incorporation of CNT in the polymer matrix includes melt mixing, in situ polymerization, electrospinning, chemical functionalization of the carbon nanotubes and solution mixing [43]. Besides, at existing phase of technology growth, CNT production methods are too expensive and not reasonable for manufacturing at pilot scale. Additionally, because of the complex synthesis approach, the quality of CNT differs from one supplier then onto the next and even with the same vendors at various times, making them unreliable for pilot-scale use [31].

Baikeri and Maimaitiyiming [5] revealed that poly(9,9-dioctyl fluorine-alt-2-amino-4,6-pyrimidine) (oligomer) acts as an effective dispersant for SWCNTs. Pt particle was doped on the Py-SWCNT films by H_2PtCl_6 via coordination reaction. Furthermore, the incorporation of SWCNT also lead to higher catalytic activity due to the higher accessible surface area and the electrical conductivity of Py-SWCNT composite was considerably higher. Zhu et al. [68] prepared homogeneous PANi-MWNT nanocomposites by functionalizing the MWNT by the means of diazotization reaction. The 4-carboxylicbenzene group was altered on MWNT surface via a C–C covalent bond, which helps the dispersion of carbon nanotubes in aniline. Later, electrochemical polymerization was performed by cyclic voltammetry in sulphuric acid containing aniline and 0.8 wt% MWNT. The functionalization of the MWNT can prevent separation of microscopic phase in the nanocomposite and thereby ensure the adaptability of CNTs in the PANi matrix. Compared to pure PANi film, the Pt-modified PANi–MWNT composite exhibited long-term stability with a higher activity for formic acid oxidation. On this basis, the Polymer–CNT composites can serve as excellent host matrices for fuel cell catalysts.

2.3 Composite Polymer-Ceramic Supports

A recently developing field of materials, so-called “nanohybrid” or “nanocomposite” materials, produced by coordinating interactions of different organic and

inorganic materials at the molecular level to obtain new materials with enhanced features and unique functions. This strategy has been effectively utilized currently for the production of new nanocomposite materials by a redox intercalation approach to get hybrid lamellar transition-metal oxides possessing improved synergistic activity. It is renowned that intercalation prompts alteration in the spacing between the layered structures. For instance, a few conducting polymers, for example, PANi, PPy, and PTh are known to oxidatively polymerize in presence of strong oxidizing transition-metal oxides (like V_2O_5).

In low-temperature fuel cells, ceramic materials (includes carbides and metal oxides which acts as a carbon-alternative) have been studied as oxidation resistant supports for catalysts [4]. During fuel cell operational condition, these materials are highly stable and exhibited exceptional resistance towards corrosion (under different electrolytic medium). In some cases, various metal oxide supports also acted as co-catalysts. Mesoporous ceramic materials are effectively utilized as a support of fuel cell catalyst because they possess high accessible surface area, large pore volumes with controllable sizes. On these bases, PANI-doped mesoporous metal oxides have been studied as anode materials in fuel cell applications.

Maiyalagan and Viswanathan [30] prepared a stable conducting PEDOT- V_2O_5 nanocomposite material via the intercalation of poly(3,4ethylenedioxythiophene) (PEDOT) in V_2O_5 matrix. PEDOT- V_2O_5 was used as the support for Pt in formaldehyde reduction method. For methanol oxidation, the electrochemical activity and stability of the Pt/PEDOT- V_2O_5 electrode were greater than that of Pt/C electrode, under the electrochemical operating conditions. Pang et al. [39] synthesized PANi- SnO_2 composites via chemical polymerization of aniline in presence of SnO_2 . The Pt has supported the PANi- SnO_2 matrix and on SnO_2 for comparative study. The characterization study using XRD (X-ray diffraction) indicated that the nanoparticles Pt were evenly deposited on PANi- SnO_2 than the other one. In comparison with the Pt/ SnO_2 electrode, the Pt supported-PANI- SnO_2 electrode exhibited better electrochemical characteristics (larger electrochemical surface area (ESA), better anti-poisoning ability and higher electrocatalytic activity for methanol oxidation) under the same operating parameters.

3 Catalysing Cross-Coupling Reactions

In the coupling reactions like Mizoroki-Heck, Suzuki-Miyaura and Sonogashira-Hahihara reactions, homogeneous palladium catalysis has garnered vast significance. This kind of catalysis offers high turnover numbers (TON), high reactivity and frequently provides high yields and selectivity. With the help of ligands (such as phosphines, amines, carbenes, dibenzylideneacetone (dba), etc.), the Pd catalysts properties can be enhanced.

Recent development in ligand-free Pd catalysts has replaced ligand assisted techniques. In another aspect, homogeneous catalysis has various disadvantages, such as difficulty in reuse or recycling the catalyst. This resulted in the loss of precious metal and ligands. Additionally, the impurities and the residual metals in the end-products have to be expelled [11]. These issues are to be resolved in order to catalyse the coupling reactions in the industry using homogeneous Pd-catalyst which are still an as challenging task. Heterogeneous Pd catalysis was found to be a feasible alternative. In this technique, Pd is attached to a solid support, such as zeolites and molecular sieves, activated carbon, metal oxides (mainly alumina or silica and also ZnO, MgO, ZrO₂, TiO₂), alkali, clays and alkaline earth salts (BaSO₄, CaCO₃, SrCO₃, BaCO₃), organic polymers, porous glass or polymers implanted in porous glass. In another aspect, Pd can also be converted to composite material by attaching it directly to a solid support; or by covalently bounding Pd to the supports with the help of ligands. These two methods of solid support permits to reuse or recover the heterogeneous catalyst after the process until the catalyst get deactivated. However, heterogeneous catalysis requires more extreme reaction conditions than homogeneous catalysis without causing a problem to the stability of the catalysts, because Pd catalyst is often thermally stable.

3.1 Suzuki-Miyaura Reactions

For the modern synthetic organic chemistry especially in the synthesis of biaryl compounds, Suzuki-Miyaura reaction was turned into the backbone. In recent times, the biaryl compounds are synthesized by catalysing arylation through Suzuki-Miyaura reaction using Pd/C catalyst and they also exist in heterocyclic. Furthermore, Suzuki-Miaura reactions can utilize for coupling variety of organic compounds which are different from aryl compounds (such as alkynes, alenes or alkenes). Marck et al [32] reported about the Pd/C catalysed Suzuki reaction for the first time in 1994.

Generally, in catalytic applications, some of the expected outcomes are evenly dispersion of nanoparticles, easy recovery and reusability, and control in particle size. However, nanoparticles often get aggregated and influenced the selectivity and catalytic activity of the catalyst. Hence, these nanoparticles should be anchored on a host complex such as macromolecular organic ligands or polymer. Esmailpour et al. [10] investigated the Suzuki-Miyaura reactions using Fe₃O₄@SiO₂-polymer-imid-Pd magnetic nanocatalyst without added phosphine ligands. So-produced Pd nanoparticles provided better accessibility for reactants without getting aggregated. In addition, they offered the easy separation of the catalyst using a magnetic field, short reaction times, easy purification, higher product yields and reduced Pd leaching. Sun et al. [46] prepared the magnetic polymer-supported catalyst by dispersing of Pd on the surface of the orange-like Fe₃O₄/polypyrrole (PPy) composite and investigated their application in Suzuki cross-coupling reaction in water. The PPy provided two functions: (i) protection of the magnetic

particles against corruption and oxidation by acids and oxygen; (ii) presence of numbers of functional groups ($-\text{NH}-$) on the surface facilitated the immobilization of catalytic active species. Furthermore, the easy separation of magnetic Fe_3O_4 (seeds in composite) was achieved and reused for 6 times during a reaction turn without any loss.

3.2 Heck Cross-Coupling Reactions

The first Mizoroki-Heck cross-coupling reactions were discovered separately by Mizoroki et al. [33] and Heck and Nolley [15] where the palladium-catalysed arylation of olefins. In presence of palladium catalyst, an aryl (pseudo) halide reacts with an alkene along with a base to form an arylated alkene. This reaction has been employed in many fields, including fine chemicals syntheses, bioactive compounds, drug intermediates, natural products, antioxidants, UV absorbers, and other industrial applications Esmailpour et al. [10].

For Heck cross-coupling reactions, soluble palladium compounds such as phosphine palladium complexes are found to be the effective catalyst [21, 45]. The advancement of the catalyst with non-phosphine ligands [18, 29] gathered the attention of many researchers as phosphine ligands are found to be unfit to our environment due to its cost, toxicity, sensitivity to air and moisture. In recent studies, several efficient eco-friendly matrices were reported for supporting heterogeneous catalysts (Palladium) such as carbon nanotubes/nanofibers, clay, ionic liquids, silica, zeolites, metal oxides, graphene, d-glucosamine, magnetic materials and polymers. For the efficient separation of catalyst for recycling and organic end-products, immobilization of metal catalyst on solid matrix considered to be an efficient tool. In most cases, polymers are used a solid matrix because it provides different combinations of metal bonding to the matrix of the polymer by a non-covalent or covalent bonding, through hydrogen bridges, hydrophobic or specific fluorous interactions as well as ionic bonding.

Many types of research recently reported that under phosphine-free conditions polymer-anchored palladium composites were active for the Heck reaction. Under the phosphine-free condition, Islam et al. [18] examined the catalytic activity of Pd (II) supported on poly (N-vinyl carbazole) in the heck reaction (cross-coupling reaction) of terminal alkenes with aryl halides. The polymer-anchored metal complex found to be air-stable, non-polluting and active under different reaction parameters while optimization of the reaction conditions. The simple reaction conditions and in operation, higher yield, easy regeneration of the catalyst and rapid conversion makes them a suitable candidate for industrial application. Sarkar et al. [44] prepared a heterogeneous poly(hydroxamic acid) Pd(II) complex by utilizing corn-cob cellulose waste as a solid matrix with a reusable ability. Cellulose (biopolymer) is considered as a supporting material due to various attracting features such as low-density, inexpensive, insolubility, better stability while using organic solvents and wide availability. Under ambient reaction conditions, the

cellulose-poly(hydroxamic acid)-Pd(II) catalysed the reaction of aryl/heteroaryl halides and arenediazonium tetrafluoroborate with a different olefins and without a loss during recycling of the catalyst.

3.3 *Sonogashira-Hagihara Reaction*

The sonogashira cross-coupling reaction is well-known for the construction of c-c bonds, especially for the formation of alkynes. Generally, the catalyst used for this type of transformation includes Pd/C, CELL-Pd(0), Pd(dmba)Cl(PTA), PdCl₂(PCy₃)₂, PdCl₂/PPh₃ and PdCl₂(PPh₃)₂ together with CuI as co-catalyst [25, 34]. In recent decades, modification in the conventional Sonogashira protocol has been done. Notable among them are phase transfer and copper-free condition; and catalyst utilization, which includes N-heterocyclic carbene (NHC) ligands mostly used for reaction with less reactive bromo- and chloroarenes. The consequence of various solvent such as ionic liquids, aqueous-organic solvent mixtures in presence of water-soluble phosphine ligands is explored. (Bhattacharya and Sengupta [6].

Tamami et al. [48] developed a catalytic system by anchoring palladium nanoparticle on poly (N-vinyl imidazole) (PVI) grafted silica through an eco-friendly approach. This catalytic system showed exceptional activity in copper-free Sonogashira-Hagihara reaction of phenylacetylene with aryl halides, under short reaction times with high yields. Furthermore, seven consequence cycles demonstrated that the polymer-supported catalyst retained its activity and recyclability without any loss. Heravi et al. [17] combined copper- and solvent-free Sonogashira coupling for the different reaction of alkynes with several aryl halides in presence of recyclable and reusable PdCl₂ catalyst which is supported on modified poly(styrene-co-maleic anhydride). In addition to higher activity, the catalyst also produced a wide variety of coupling products with remarkable yields. Moreover, without any pre-activation steps, the catalyst was reused for a minimum of five consecutive cycles.

4 Photocatalytic Degradation of the Pollutant

Due to the properties like higher catalytic activity, structure-based optical and electronic property, rapid reaction rate, and higher surface area, nanoparticles have high in potential as catalyst as well as redox active media, which attracted many researchers in designing of photo/chem-catalytic materials with greater efficiency especially for the purification of water and gases which are contaminated. Nanosized semiconductor materials such as nano-TiO₂ [24, 50], ZnO [38], CdS [67], and CdO [47], zero-valence metals such as Cu⁰ [27, 57] and Fe⁰ [51, 52] and bimetallic nanoparticles such as Fe/Pd [53], Fe/Ni [56], and Pd/Sn [26] are commonly used catalytic nanoparticles. For a variety of contaminants which includes polychlorinated

biphenyls (PCBs), halogenated aliphatics, organochlorine pesticides, azo dyes [66], halogenated herbicides and nitroaromatics are degraded using a catalyst or redox reagents. But the limitations are seen in the segregation of fine particles from the aqueous suspensions and in catalyst recovering. This limit has been rectified by immobilizing the nanoparticles onto polymer support (such as porous resins [26], polymeric membranes [9, 47, 50] and ion exchangers [27]) with minimum particle loss and coalesce. Table 2 summarizes some polymer-supported nanocomposites for photocatalytic degradation of pollutants from the various aqueous environment.

In degradation of organic pollutants, nano-TiO₂ usually plays as a catalyst. Ameen et al. [2] done a research on degradation of methylene blue (MB) dye by poly 1-naphthylamine (PNA)/TiO₂ nanocomposite prepared by in situ polymerization, where enhanced photocatalytic activity was observed. The photodegradation efficiency of MB colour might be due to the effective charge separation of the electrons (e⁻) and hole (h⁺) pairs at the interfaces of PAN and TiO₂. Some bimetals (such as Cu⁰, Fe⁰, Fe/Pd, Pd/Sn, Ni/Fe, etc.) and nanoscale metals are found to be very efficient in degradation of different organic pollutants (such as brominated methanes, chlorinated methanes, trihalomethanes, chlorinated benzenes, chlorinated ethenes, other polychlorinated hydrocarbons, dyes and pesticides) [26, 51–53, 56, 57]. The aforementioned metal nanoparticles are found to be very higher in reactivity, for example, self-ignition of nZVI is possible when exposed to air. Hence, oxidation is inhibited in order to preserve the nature of the chemical until they are exposed to the targeted contaminants.

Lin et al. [27] done a research using cation exchanger resin doped with nanoscale zero-valent copper (nZVC) which increases the accessible surface area of the catalyst by reducing aggregation of nZVC particles. During the reaction between CCl₄ and Cu⁰, the Cu ion produced is recycled back by simultaneous cation exchange resin. The combination of sorption due to host resin and degradation by means of nZVC resulted in declination of the quantity of pollutant (CCl₄) available in aqueous solution.

Dong et al. [8] researched a composite made by intercalating sodium carboxymethylcellulose (CMC) (serves as a stabilizer) into parallelized iron (Fe/Pd) nanoparticles. When comparing to CMC-stabilized nanoparticles, the pristine Fe/Pd particles, showed less stability against agglomeration, soil transport and chemical reactivity. It is concluded from batch dichlorination tests that CMC-stabilized nanoparticles photodegraded trichloroethene (TCE) which is found to be 17-folds faster than the non-stabilized nanoparticles.

5 Catalytic Reduction of 4-Nitrophenol

Recently, for the degradation of aromatic dye and nitro-compounds, various metal nanocatalysts has been developed in order to attain sustainable environment. Since 4-nitrophenol was found to be toxic, it has to be reduced to 4-aminophenol which is important in application aspect. Comparing to 4-nitrophenol, 4-aminophenol find its

Table 2 Summary of polymer-supported nanocomposites for photocatalysts

NPs	Polymer support	Pollutant	Preparation method	Results	References
TiO ₂	Polyaniline (PAni)	Phenol	Aniline polymerization in presence of TiO ₂	Under visible light, illumination phenol was degraded after 5 h in an aqueous solution	Li et al. [24]
TiO ₂	Poly (3-hexylthiophene) (PHT)	Methyl orange (MO)	Dispersion of TiO ₂ nanoparticles onto the polymer matrix	Under optimum molar ratio of TiO ₂ /PHT (75:1), the removal efficiency of MO reached 88.5% under 10 h illumination	Wang et al. [50]
TiO ₂	Poly (1-naphthylamine) (PNA)	Methylene blue (MB)	In situ polymerization of 1-naphthylamine monomer with TiO ₂	Under visible light illumination, MB was degraded nearly 60%	Ameen et al. [2]
Au/TiO ₂	Poly(methyl methacrylate) (PMMA)	Trypan blue (TB)	PMMA was first dissolved in tetrahydrofuran and TiO ₂ powder suspended in a dissolved polymer	Degradation efficiency was 90% by Au-TiO ₂ /PMMA thin film under sunlight	Elfeky and Al-Sherbini [9]
ZnO	PAni	Methylene blue (MB)	In situ polymerization method	% removal of MB after 1 h irradiation was 28% under UV and 82% under visible light	[38]
CdS	Chitosan	Congo red (CR)	Bio-mineralization simulation	85.9% of 0.02 g/L CR was degraded using 1.5 g/L composite catalyst under 180 min of illumination	Zhu et al. [67]
CdO	PAni	MB and Malachite green (MG)	Chemical oxidative polymerization	MB and MG dyes were photocatalytically degraded with removal efficiency of 99% under natural sunlight irradiation	Tadjarodi et al. [47]
Fe ⁰	Poly(methyl methacrylate) (PMMA)	Trichloroethene (TCE)	In situ synthesis with MMA and FeSO ₄ ·7H ₂ O as a precursor	The observed degradation rate of TCE was 0.0034 h ⁻¹ and dechlorination efficiency was 62.3%	Wang et al. [51, 52]
Fe ⁰	Carboxymethyl cellulose (CMC)	Cr(VI)	In situ synthesis with FeSO ₄ ·7H ₂ O as a precursor	After 1 h, higher removal efficiency was found in CMC/Fe ⁰ (94%) when compared with Fe ⁰ (22%)	Wang et al. [51, 52]

(continued)

Table 2 (continued)

NPs	Polymer support	Pollutant	Preparation method	Results	References
Cu ⁰	Chitosan	Cr(VI)	In situ synthesis with CU(SO ₄) ₂ ·5H ₂ O as a precursor	The concentration of Cr(VI) reduced from 50 to 2.21 mgL ⁻¹ in presence of 1 g composite after 24 h	Wu et al. [57]
Fe/Pd	Poly(vinylidene fluoride) (PVDF)	Trichloroacetic acid (TCAA)	Reduction deposition	Dechlorination of TCAA was observed within 180 min	Wang et al. [53]
Ni/Fe	Cellulose acetate	Trichloroethylene	Solvent-cast	Observed that reduction rate was proportional to the Ni content (0–14.3 wt%)	Wu and Ritchie [56]
Pd/Sn	Resin	Trichloroethylene	In situ reduction of Sn ²⁺ to Sn ⁰ and the deposited Pb ⁰ via reduction of Pb ⁴⁺	When compared to commercial Sn, the rate of dechlorination in Resin-Pd/Sn was promoted by ~2 orders of magnitude	Lin et al. [26]

footprint as intermediate in the hair-dyeing agent, antipyretic drugs, anticorrosion lubricant and photographic developers etc. Hence, conversion of 4-nitrophenol (4-NP) by borohydride ions (BH_4^-) using metal nanocatalysts into 4-aminophenol (4-AP) via catalytic reduction became more significant. Various novel metal (such as Ag, Au, Pd, Pt etc.), metal oxide (such as Cu_2O) and bimetal (such as Au/Ag, Au/Pt, Pd/Ag, Pd/ ZnO_2 and Pt/ CeO_2 , etc.) nanostructures were considered as catalyst for the reduction of 4-NP using NaBH_4 , which is a pollutant in industrial wastewaters and non-biodegradable material, can be harmful to environment and human health [63].

For the enhancement of the activity of these type of catalysts, the particle morphology and size can be altered. Moreover, the catalytic performance is found higher while using bimetallic nanomaterials (such as Pt/Au alloy nanoparticles (NPs)) [62], Ag/Pd bimetallic NPs [19], and Au/Ag alloy nanoclusters [58]. Therefore, the important key variable for catalytic activity is considered as low-coordination sites and the elevated range of surface-to-volume ratio in nanocatalysts. In any case, these variables have the potential to reduce the surface energy of nanocatalyst and thereby increases the chance of agglomeration which influences the catalytic activity of nanocatalysts. In response to above problem, a promising technique has been proposed, that is anchoring of nanocatalyst on the support matrix, such as cellulose nanofibers [16], silica nanotubes [64], carbon nanotubes [22, 23], polymer-type matrices [13, 59], and graphene [22, 23]. Among these support materials, polymer-type carriers have received great interest for practical application because these materials contain various functional groups which act as anchor sites for loading nanoparticles (catalyst) and thereby improves the properties of nanoparticles, dispersibility and recyclability. Wu et al. [59] fabricated a composite particle of polystyrene/reduced graphene oxide@gold nanoparticles by a facile and controllable method and reported that as-prepared PS/RGO@AuNP composite has good dispersibility in water and additionally, showed excellent catalytic activity in the reduction of p-nitrophenol by sodium borohydride in aqueous solution. In Heidari [16] work, cost-effective biopolymer (nanofibrillated cellulose (NFC)) was used as support for silver nanoparticles and achieved shorter reduction period. Zhang et al. [65] immobilized silver nanoparticles in sulfhydryl functionalized poly(glycidyl methacrylate) microspheres for enhancing monodispersity and recyclability. Moreover, Ag NPs@PGMA-SH composite showed higher catalytic activity during the reduction of 4-NP, which was 1.3–1.32 times higher than reported in the literature. This catalyst also exhibited excellent reusability as a conversion higher than 92% (after 10 consecutive cycles).

6 Conclusions

Many researchers dedicated their work on CPs ever since the discovery of conducting polyacetylene in the 1970s and published more number of research results in this relevant field. The rapid development in the field of science and technology

has led to the advancement in the CPs and their composite materials in nanoscale. The application of these polymer-based composites is found to be interesting. The well-known use of polymer-based composites in catalytic applications such as fuel cells, cross-coupling reaction, photocatalysis degradation and reduction of pollutants are discussed briefly. Among them, polymer composite as a catalyst in fuel cell and photocatalysis are often studied. Moreover, the interaction behaviour between the host polymers and the immobilized catalyst are highlighted. Others issues regarding the technology limitation and challenging tasks are also discussed.

References

1. Abdelhamid ME, O'Mullane AP, Snook GA (2015) Storing energy in plastics: a review on conducting polymers & their role in electrochemical energy storage. *RSC Adv* 5:11611–11626
2. Ameen S, Akhtar MS, Kim YS et al (2011) Nanocomposites of poly (1-naphthylamine)/SiO₂ and poly (1-naphthylamine)/TiO₂: Comparative photocatalytic activity evaluation towards methylene blue dye. *Appl Catal B Environ* 103(1–2):136–142
3. Antolini E (2009) Carbon supports for low-temperature fuel cell catalysts. *Appl Catal B* 88:1–24
4. Antolini E (2010) Composite materials: an emerging class of fuel cell catalyst supports. *Appl Catal B-Environ* 100:413–426
5. Baikeri S, Maimaitiyiming X (2017) Polypyrimidine/SWCNTS composite comprising Pt nanoparticles: possible electrocatalyst for fuel cell. *Polym Sci Ser A* 59(5):734–740
6. Bhattacharya S, Sengupta S (2004) Palladium catalyzed alkynylation of aryl halides (Sonogashira reaction) in water. *Tetrahedron Lett* 45(47):8733–8736
7. Costamagna P, Srinivasan S (2001) Quantum jumps in the PEMFC science and technology from the 1960s to the year 2000: part I. Fundamental scientific aspects. *J Power Sources* 102:242–252
8. Dong T, Luo H, Wang Y et al (2011) Stabilization of Fe–Pd bimetallic nanoparticles with sodium carboxymethyl cellulose for catalytic reduction of para-nitrochlorobenzene in water. *Desalination* 271(1–3):11–19
9. Elfeky SA, Al-Sherbini ASA (2011) Photocatalytic decomposition of trypan blue over nanocomposite thin films. *Kinet Catal* 52(3):391–396
10. Esmaeilpourv M, Javidi J, Dodeji FN, Hassannezhad H (2014) Fe₃O₄@SiO₂-polymer-imid-Pd magnetic porous nanosphere as magnetically separable catalyst for Mizoroki-Heck and Suzuki-Miyaura coupling reactions. *J Iran Chem Soc* 11(6):1703–1715
11. Garrett CE, Prasad K (2004) The art of meeting palladium specifications in active pharmaceutical ingredients produced by Pd-catalyzed reactions. *Adv Synth Catal* 346:889–900
12. Gomez-Romero P (2001) Hybrid organic–inorganic materials—in search of synergic activity. *Adv Mater* 13:163–174
13. Harish S, Mathiyarasu J, Phani KLN et al (2009) Synthesis of conducting polymer supported Pd nanoparticles in aqueous medium and catalytic activity towards 4-nitrophenol reduction. *Catal Lett* 128(1–2):197
14. Hasik M, Turek W, Nyczyk A et al (2009) Application of conjugated polymer–platinum group metal composites as heterogeneous catalysts. *Catal Lett* 127:304–311
15. Heck RF, Nolley JP Jr (1972) Palladium-catalyzed vinylic hydrogen substitution reactions with aryl, benzyl, and styryl halides. *J Org Chem* 37:2320–2322

16. Heidari H (2018) Ag nanoparticle/nanofibrillated cellulose composite as an effective and green catalyst for reduction of 4-nitrophenol. *J Clust Sci*:1–7
17. Heravi MM, Hashemi E, Beheshtiha YS et al (2014) PdCl₂ on modified poly (styrene-co-maleic anhydride): A highly active and recyclable catalyst for the Suzuki-Miyaura and Sonogashira reactions. *J Mol Catal A Chem* 394:74–82
18. Islam M, Mondal P, Roy AS et al (2010) Use of a recyclable poly (N-vinyl carbazole) palladium (II) complex catalyst: Heck cross-coupling reaction under phosphine-free and aerobic conditions. *Transition Met Chem* 35(4):491–499
19. Jing H, Wang H (2015) Structural evolution of Ag–Pd bimetallic nanoparticles through controlled Galvanic replacement: effects of mild reducing agents. *Chem Mater* 27:2172–2180
20. Kumar A, Ramani VK (2013) RuO₂–SiO₂ mixed oxides as corrosion-resistant catalyst supports for polymer electrolyte fuel cells. *Appl Catal B* 138–139:43–50
21. Lauer MG, Thompson MK, Shaughnessy KH (2014) Controlling Olefin isomerization in the Heck reaction with neopentyl phosphine ligands. *J Org Chem* 79(22):10837–10848
22. Li H, Han L, Cooper-White J et al (2012) Palladium nanoparticles decorated carbon nanotubes: facile synthesis and their applications as highly efficient catalysts for the reduction of 4-nitrophenol. *Green Chem* 14(3):586–591
23. Li J, Liu CY, Liu Y (2012) Au/graphene hydrogel: synthesis, characterization and its use for catalytic reduction of 4-nitrophenol. *J Mater Chem* 22(17):8426–8430
24. Li X, Wang D, Cheng G et al (2008) Preparation of polyaniline modified TiO₂ nanoparticles and their photocatalytic activity under visible light illumination. *Appl Catal B Environ* 81(3–4):267–273
25. Liang Y, Xie YX, Li JH (2006) Modified palladium-catalyzed Sonogashira cross-coupling reactions under copper-, amine-, and solvent-free conditions. *J Org Chem* 71(1):379–381
26. Lin CJ, Liou YH, Lo SL (2009) Supported Pd/Sn bimetallic nanoparticles for reductive dechlorination of aqueous trichloroethylene. *Chemosphere* 74(2):314–319
27. Lin CJ, Lo SL, Liou YH (2005) Degradation of aqueous carbon tetrachloride by nanoscale zerovalent copper on a cation resin. *Chemosphere* 59(9):1299–1307
28. Lin Z, Wenya D, Nautiyal A et al (2018) Recent progress on nanostructured conducting polymers and composites: synthesis, application, and future aspects. *Sci China Mater* 61(3):303–352
29. Luo C, Zhang Y, Wang Y (2005) Palladium nanoparticles in poly (ethyleneglycol): the efficient and recyclable catalyst for Heck reaction. *J Mol Catal A: Chem* 229(1–2):7–12
30. Maiyalagan T, Viswanathan B (2010) Synthesis, characterization and electrocatalytic activity of Pt supported on poly(3,4-ethylenedioxythiophene)–V₂O₅ nanocomposites electrodes for methanol oxidation. *Mater Chem Phys* 121:165–171
31. Mansor NB (2014) Development of catalysts and catalyst supports for polymer electrolyte fuel cells. Dissertation for the degree of Doctor of Philosophy, University College London, London
32. Marck G, Villiger A, Buchecker R (1994) Aryl couplings with heterogeneous palladium catalysts. *Tetrahedron Lett* 35:3277–3280
33. Mizoroki T, Mori K, Ozaki A (1971) Arylation of olefin with aryl iodide catalyzed by palladium. *Bull Chem Soc Jpn* 44:581–584
34. Mohsen E, Jaber J, Mehdi MA et al (2014) Synthesis and characterization of Fe₃O₄@ SiO₂–polymer-imid–Pd magnetic porous nanospheres and their application as a novel recyclable catalyst for Sonogashira-Hagihara coupling reactions. *J Iran Chem Soc* 11(2):499–510
35. Mokrane S, Makhloufi L, Alonso-Vante N (2008) Electrochemistry of platinum nanoparticles supported in polypyrrole (PPy)/C composite materials. *J Solid State Electrochem* 12:569–574
36. Moniruzzaman M, Winey KI (2006) Polymer nanocomposites containing carbon nanotubes. *Macromol* 39(16):5194–5205
37. Muthuraman N, Guruvaiah PK, Agneeswara PG (2012) High performance carbon supported Pt–WO₃ nanocomposite electrocatalysts for polymer electrolyte membrane fuel cell. *Mater Chem Phys* 133:924–931

38. Olad A, Nosrati R (2012) Preparation, characterization, and photocatalytic activity of polyaniline/ZnO Nano composite. *Res Chem Intermed* 38:323–336
39. Pang H, Huang C, Chen J et al (2010) Preparation of polyaniline–tin dioxide composites and their application in methanol electro-oxidation. *J Solid State Electrochem* 14:169–174
40. Peng F, Zhou C, Wang H et al (2009) The role of RuO₂ in the electrocatalytic oxidation of methanol for direct methanol fuel cell. *Catal Commun* 10:533–537
41. Qu L, Dai L, Sun SS (2016) Conjugated polymers, fullerene C60, and carbon nanotubes for optoelectronic devices. In: Sun S-S, Dalton LR (eds) *Introduction to organic electronic and optoelectronic materials and devices*, 2nd edn. Taylor & Francis, CRC Press, Boca Raton
42. Roen LM, Paik CH, Jarvi TD (2004) Electrocatalytic corrosion of carbon support in PEMFC cathodes. *Electrochem Sol State Lett* 7:19–22
43. Sahoo NG, Rana S, Cho JW et al (2010) Polymer nanocomposites based on functionalized carbon nanotubes. *Prog Polym Sci* 35:837–867
44. Sarkar SM, Rahman ML, Chong KF et al (2017) Poly (hydroxamic acid) palladium catalyst for heck reactions and its application in the synthesis of Ozagrel. *J Catal* 350:103–110
45. Sharma S, Sarkar BR (2018) Efficient Mizoroki–Heck coupling reactions using phosphine-modified Pd (II)–picolinate complex. *Synth Commun*:1–9
46. Sun X, Zheng Y, Sun (2015) Pd nanoparticles immobilized on orange-like magnetic polymer-supported Fe₃O₄/PPy nanocomposites: a novel and highly active catalyst for suzuki reaction in water. *Catal Lett* 145(4):1047–1053
47. Tadjarodi A, Imani M, Kerdari H (2013) Experimental design to optimize the synthesis of CdO cauliflower-like nanostructure and high performance in photodegradation of toxic azo dyes. *Mater Res Bull* 48:935–942
48. Tamami B, Allahyari H, Farjadian F et al (2011) Synthesis and applications of poly (N-vinylimidazole) grafted silica-containing palladium nanoparticles as a new re-cyclable catalyst for Heck, Sonogashira and Suzuki coupling reactions. *Iran Polym J* 20:699–712
49. Taniguchi A, Akita T, Yasuda K et al (2004) Analysis of electrocatalyst degradation in PEMFC caused by cell reversal during fuel starvation. *J Power Sources* 130:42–49
50. Wang DS, Zhang J, Luo Q et al (2009) Characterization and photocatalytic activity of poly (3-hexylthiophene)-modified TiO₂ for degradation of methyl orange under visible light. *J Hazard Mater* 169(1–3):546–550
51. Wang Q, Qian H, Yang Y et al (2010) Reduction of hexavalent chromium by carboxymethyl cellulose-stabilized zero-valent iron nanoparticles. *J Contam Hydrol* 114(1–4):35–42
52. Wang W, Zhou M, Jin Z (2010) Reactivity characteristics of poly(methyl methacrylate) coated nanoscale iron particles for trichloroethylene remediation. *J Hazard Mater* 173(1–3):724–730
53. Wang X, Chen C, Liu H et al (2008) Preparation and characterization of PAA/PVDF membrane-immobilized Pd/Fe nanoparticles for dechlorination of trichloroacetic acid. *Water Res* 42(18):4656–4664
54. Wang X, Li W, Chen Z et al (2006) Durability investigation of carbon nanotube as catalyst support for proton exchange membrane fuel cell. *J Power Sources* 158:154–159
55. Wu G, Li L, Li JH et al (2005) Polyaniline-carbon composite films as supports of Pt and PtRu particles for methanol electrooxidation. *Carbon* 43:2579–2587
56. Wu LF, Ritchie SMC (2006) Removal of trichloroethylene from water by cellulose acetate supported bimetallic Ni/Fe nanoparticles. *Chemosphere* 63(2):285–292
57. Wu SJ, Liou TH, Mi FL (2009) Synthesis of zero-valent copper-chitosan nanocomposites and their application for treatment of hexavalent chromium. *Bioresour Technol* 100(19):4348–4353
58. Wu T, Zhang L, Gao J et al (2013) Fabrication of graphene oxide decorated with Au–Ag alloy nanoparticles and its superior catalytic performance for the reduction of 4-nitrophenol. *J Mater Chem A* 1(25):7384–7390
59. Wu Z, Wang L, Hu Y et al (2016) Facile synthesis of PS/RGO@ AuNP composite particles as highly active and reusable catalyst for catalytic reduction of p-nitrophenol. *Colloid Polym Sci* 294(7):1165–1172

60. Xie Z, Liu Z, Wang Y et al (2010) An overview of recent development in composite catalysts from porous materials for various reactions and processes. *Int J Mol Sci* 11(5):2152–2187
61. Xu Y, Peng X, Zeng H et al (2008) Study of an anti-poisoning catalyst for methanol electro-oxidation based on PAN-C composite carriers. *C Chim* 11:147–151
62. Ye W, Yu J, Zhou Y et al (2016) Green synthesis of Pt–Au dendrimer-like nanoparticles supported on polydopamine-functionalized graphene and their high performance toward 4-nitrophenol reduction. *Appl Catal B Environ* 181:371–378
63. You JG, Shanmugam C, Liu YW et al (2017) Boosting catalytic activity of metal nanoparticles for 4-nitrophenol reduction: modification of metal nanoparticles with poly(diallyldimethylammonium chloride). *J Hazard Mater* 324:420–427
64. Zhang S, Gai S, He F et al (2014) In situ assembly of well-dispersed Ni nanoparticles on silica nanotubes and excellent catalytic activity in 4-nitrophenol reduction. *Nanoscale* 6(19):11181–11188
65. Zhang W, Sun Y, Zhang L (2015) In situ synthesis of monodisperse silver nanoparticles on sulfhydryl-functionalized poly (glycidyl methacrylate) microspheres for catalytic reduction of 4-nitrophenol. *Ind Eng Chem Res* 54(25):6480–6488
66. Zhao X, Lv L, Pan B et al (2011) Polymer-supported nanocomposites for environmental application: a review. *Chem Eng J* 170(2–3):381–394
67. Zhu H, Jiang R, Xiao L et al (2009) Photocatalytic decolorization and degradation of Congo red on innovative crosslinked chitosan/nano-CdS composite catalyst under visible light irradiation. *J Hazard Mater* 169(1–3):933–940
68. Zhu ZZ, Wang Z, Li HL (2008) Functional multi-walled carbon nanotube/polyaniline composite films as supports of platinum for formic acid electrooxidation. *Appl Surf Sci* 254(10):2934–2940

Fabrication Methods of Sustainable Hydrogels



Cédric Delattre, Fiona Louis, Mitsuru Akashi, Michiya Matsusaki,
Philippe Michaud and Guillaume Pierre

List of Abbreviations

2D	Two dimensions
3D	Three dimensions/three dimensional
4D	Four dimensional
AA	Acrylic acid
AD	Adipocytes
ADSC	Adipose-derived stem cells
BMP-2	Bone morphogenetic proteins 2
CC	Cell coating
CLSM	Confocal laser scanning microscopy
DMEM	Dulbecco's modified eagle medium
ECM(s)	Extracellular matrices
EDC	Ethyl carbodiimide
EG	Ethylene glycol
EGDMA	Ethylene glycol dimethacrylate

C. Delattre · P. Michaud · G. Pierre (✉)
Institut Pascal, Université Clermont Auvergne, CNRS, SIGMA Clermont,
63000 Clermont-Ferrand, France

F. Louis · M. Matsusaki
Joint Research Laboratory (TOPPAN) for Advanced Cell Regulatory Chemistry,
Graduate School of Engineering, Osaka University, 2-1 Yamadaoka, Suita,
Osaka 565-0871, Japan

M. Akashi
Department of Frontier Biosciences, Graduate School of Frontier Biosciences,
Osaka University, 1-3 Yamadaoka, Suita, Osaka 565-0871, Japan

M. Matsusaki
Department of Applied Chemistry, Graduate School of Engineering,
Osaka University, 2-1 Yamadaoka, Suita, Osaka 565-0871, Japan

M. Matsusaki
JST-PRESTO, Kawaguchi, Japan

FBS	Fetal bovine serum
FN	Fibronectin
G	Gelatin
HEMA	Hydroxyethyl methacrylate
HUVECs	Human umbilical vein endothelial cells
IPN	Interpenetrating polymeric
iPS-CMs	Induced pluripotent stem cell-derived cardiomyocytes
LbL	Layer-by-layer
LCA	Life-cycle assessment
LECs	Lymph epithelial cells
MBSCs	Bone marrow stromal cells
MCS	Maleic chitosan derivatives
MMT	Montmorillonite
NHDFs	Normal human dermal fibroblasts
PAAm	Polyacrylamide
PBS	Phosphate buffer saline
PEG	Poly(ethylene glycol)
PEGDA	Poly(ethylene glycol) diacrylate
PLGA	Poly(lactic-co-glycolic acid)
PPGs	Polyacrylamide particle gels
PPO-PEO	Poly(propylene oxide)-poly(ethylene oxide)
PVA	Poly (vinyl) alcohol
PVP	Poly (vinyl pyrrolidone)
PVSA	Poly-vinylsulfonic acid
RGD	Arginine-glycine-aspartic acid
TPVA	Thiol-terminated poly (vinyl alcohol)
VAc	Vinyl acetate

1 Introduction

What is a hydrogel? Answering this seemingly simple question could appear easy but this is not the case. Using the SciFinder portal (<https://scifinder.cas.org>), the word “hydrogels” led to 114,105 references (70% published between 2007 and 2017) including 28 book chapters, 6761 reviews, 24,324 patents and 83,187 articles (Fig. 1). Except for book chapters, the number of research articles, reviews and patents per year has doubled in less than 10 years. Basically, hydrogels are three-dimensional, smart and/or hungry polymer networks extensively swollen with water. Their sizes are variable, and they are named recently micro- and nanohydrogels when their sizes are reduced to 1 μm and 1 nm respectively [1]. Depending upon the pore size between polymer networks, the structure of hydrogel can be classified as nonporous, microporous, or superporous [2]. These complex structures

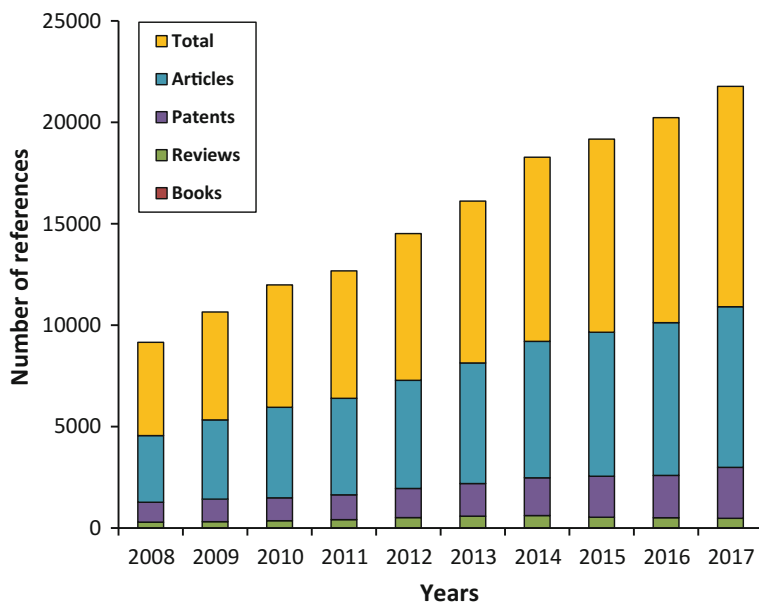


Fig. 1 Evolution of the scientific production relative to hydrogels between 2008 and 2017

are capable to absorb large quantities of water or other fluids such as biological liquids, but they do not dissolve in them. Owing to their varying compositions, hydrogels are classified into three categories for biomedical applications depending on their physical properties, i.e. liquid, semi-solid and solid [3]. They should be biocompatible, and non-toxic and can be biodegraded (or not) for specific applications. The most common hydrogels are cross-linked polymers generated by the polymerization of one or several monomers [4]. They can be also formed by the reticulation of synthetic or natural polymers [5]. Their hydrophilicity is mainly due to the presence of hydrophilic groups such as $-\text{OH}$, $-\text{CONH}_2$, $-\text{COOH}$, $-\text{CONH}-$ or others [5]. Their ionic nature can be neutral, cationic or anionic, some of them having ampholytic behaviour. Hydrogels are sometimes named ‘reversible’ or ‘physical’ gels if molecular entanglements (ionic interactions, hydrophobic forces or hydrogen-bonding) play the main role in forming the network. It is sometimes possible to dissolve them by changing physicochemical environmental conditions, such as the ionic strength of the solution, light, magnetic field, pH, or temperature [6]. Hydrogels are non-reversible when a cross-linker leads to the formation of covalent bonds to build the network. All these families of hydrogels may have natural or synthetic origins. Novel hydrogels with specific properties made of natural and biodegradable polymers are in great demand. Nonetheless, during the 50 last years of scientific literature and patents speaking of hydrogels, the natural hydrogels have been gradually replaced by synthetic ones. Synthetic hydrogels are described in the literature as homopolymeric, copolymeric or multipolymeric

hydrogels. They have been found more versatile and diverse for biomedical applications owing to their tailorable designs or modifications. Hydrogels based on polyethylene glycol (PEG), poly (vinyl) alcohol (PVA), poly (vinyl pyrrolidone) (PVP) are examples of synthetic hydrogels. Natural hydrogels are produced using polymers (mainly polysaccharides and proteins) extracted from various biomass. Despite their “green” nature and biocompatibility, they have some disadvantages such as insufficient mechanical properties but also some variations depending on the production batch. The polysaccharides currently used in natural hydrogels are dextran, hyaluronic acid, alginate or chitosan [7–9] whereas the main protein employed is collagen [10].

The success of hydrogels in tissue engineering, agriculture, drug delivery, superabsorbent, wound dressing, sealing, coal dewatering, artificial snow, separation of biomolecules or cells, antiadhesive compound, biosensors, contact lenses and other is linked to their characteristics including gas (such as O₂) permeability, stability, biocompatibility, excellent mechanical properties, wettability and permeability to water, refractive index and light transmittance [3, 4].

This book chapter intends to clarify the classification of hydrogels, to describe the methodologies for making them and to synthesize all their applications in several scientific and industrial areas.

2 Classifying Hydrogel: What’s the Bottom Line?

Fabrication methodology of sustainable firstly requires a strong and comprehensive understanding of hydrogel products involved in the preparation. Recently, Varaprasad et al. [11] published a decent mini review describing an updated hydrogels classification, regarding their cross-linking and physical states but also some associated developments in miscellaneous applications. Based on different aspects (Fig. 2), hydrogels can be classified in many ways, depending on (i) source, which is of main importance for a sustainable point of view, (ii) polymeric composition, (iii) physicochemical composition, (iv) type of cross-linkers used, (v) network electrical charge and finally (vi) physical appearance [4]. Today, life-cycle assessment (LCA) of hydrogels should be also considered as a seventh item. In an eco-designing point of view, the good knowledge of the environmental effect and generated hydrogels is of first importance. LCA should be considered here as a comprehensive methodology to estimate and evaluate the environmental impact of the whole fabrication methodology of hydrogels, but also all over its whole life cycle according to ISO 14044. This notion implicated not only one single parameter but a succession of analyses throughout the product lifecycle. Thus, the best typical crop of the environmental impact of a product must consider the environmental courses all over the whole product’s life, including the emission to land, water and air as well as the energy and material balance of product resources [12–14]. A complete LCA from the extraction of polymers/materials following by their modification/transformation/designing/manufacturing into a “sustainable”

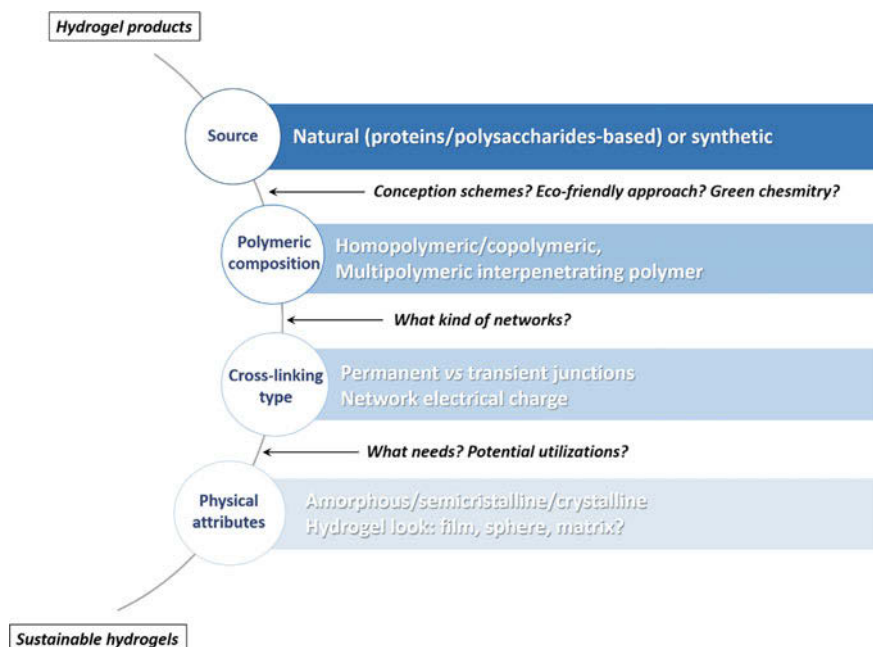


Fig. 2 The overall bottom line for classifying hydrogels

hydrogel, through the practical use of the product and finally the end of life circumstances, such as disposal or recycling, should be considered [15]. It was found that engineered bio-sourced materials should prospectively play an increasingly major role in our consumer society which is in perpetual search of sustainable and environmentally friendly materials. It was particularly reported that in comparison to petroleum-based materials, biopolymer materials could significantly reduce the energy/environmental balance impact. The use of biomass feedstocks and byproducts (polysaccharide-based composition for example) for making hydrogels is also not negligible and could contribute to trapping carbon thanks to this concept.

Hydrogels can be separated depending on their natural or synthetic origins. Thus, the hydrogel can contain natural polysaccharides and/or proteins such as chitosan, cellulose, alginate, starch, gelatin, or collagen. The list of synthetic polymers is longer, and the most common synthetic monomers used, especially in the pharmaceutical field, are probably PEG and its derivatives (PEG acrylate, methacrylate, diacrylate, dimethacrylate), ethylene glycol (EG), acrylic acid (AA) or hydroxyethyl methacrylate (HEMA). Table 1 gives an overview of these polymers commonly used for the preparation of hydrogels.

The type of polymer network generating during the fabrication method also greatly affects the classes of hydrogels [16]. From a single species of monomer, it is possible to obtain homopolymeric hydrogels which may have cross-linked skeletal structure, as reported by Takashi et al. [17]. The use of two or more different

Table 1 Some natural and synthetic monomers used for making hydrogels

Natural polymers	Number of publications ^a	Synthetic polymers	Number of publications
Chitosan/chitin	218/82	Poly(ethylene glycol) (PEG)	370
Alginate	336	PEG-acrylate	27
		PEG methacrylate	38
		PEG diacrylate	118
		PEG dimethacrylate	33
Dextran	55	Methacrylic acid	72
Cellulose	105	Ethylene glycol (EG)	319
Gelatin	262	Hydroxyethyl methacrylate (HEMA) and derivatives	59
Fibrin	72	Ethylene glycol dimethacrylate (EGDMA)	29
Collagen	252	Vinyl acetate (VAc)	2
		Polyvinyl alcohol (PVA)	101
		Acrylic acid (AA)	141

^aBased on Scopus, with the keywords combination “polymer name AND hydrogel AND fabrication”

monomer species can be used to prepare copolymeric hydrogels, which needs at least a hydrophilic component and are characterized by a specific configuration in the chain of the polymer network [18]. Note that this kind of hydrogel can include a natural polymer in its structure [19]. The last type according to polymeric composition classification, i.e. the so-called multipolymer interpenetrating polymeric (IPN) hydrogels, is made of two independent natural and/or cross-linked synthetic polymers. The semi-ipn hydrogel is also reported in the literature and is composed of a cross-linked and a non-cross-linked polymer [20]. The kind of cross-linked interactions is also considered since it is possible to prepare hydrogels with chemically cross-linked networks (e.g. grafting, radical polymerization, condensation/enzymatic reaction, high-energy radiation) but also physically cross-linked networks. The cohesion of the last one is in general based on ionic and/or hydrophobic interactions, hydrogens bonds, polymer chain entanglements, stereo-complex formation, thermo-reversible gels, maturation due to heat-inducing aggregation, freeze-thawing [4, 11, 21]. The physical and chemical structure plus the physical appearance of hydrogels give birth to supplementary classes, e.g. non-crystalline, semi-crystalline, crystalline as well as gels (macro/micro/nano), matrix, film or microsphere. Generally speaking, some authors also report three main classes based on physical properties, i.e. solid, bio-adhesive and liquid-based hydrogels [11]. The preparation process is mainly involved for obtaining these looks (see Sect. 3). Finally, as reported by Ahmed [4], four groups describe the importance of electrical charge into hydrogel network on the cross-linked chains, i.e. neutral, ionic, amphoteric electrolyte and zwitterionic.

3 Methodology for Making Hydrogels and Sustainable Hydrogels

3.1 Goals and Technical Features

As described above, talking about hydrogels involves working on highly hydrophilic polymer networks presenting high swollen properties with water and aqueous media. Lot of works in the literature described hydrogels as a hydrocolloid gels material in which one, the dispersion medium is water [4, 22]. One of the most important applications of hydrogels largely described during the last decade is probably their uses as polymeric matrices for: (i) controlled releases of pharmaceuticals drugs and and (ii) living cells entrapment/encapsulation [23–25]. Therefore, from the past 30 years, hydrogels continue to be a technology booming thank to their very high flexibility degree closely like human tissues [4, 26, 27]. A lot of studies was published for the optimization of hydrogels synthesis aiming to increase the technical features and improve their efficiency in pharmaceutical and biomedical applications [3, 4, 28]. In fact, the perpetual search for new biomaterials (e.g. artificial organs or tissues, filling materials, pharmaceutical release, diagnostic system) such as hydrogel is a fundamental notion in the biomedical sector. This requires a multidisciplinary approach involving physicians, biologists, chemists, and physicochemical. Hydrogels thus constitute a group of polymeric biomaterials having a hydrophilic structure allowing them to retain large quantities of water per area unit in a complex three-dimensional network. Moreover, thanks to the cross-links between the chains of the network, these biomaterials are highly resistant to dissolution in aqueous media. Consequently, as related by lot of authors [22, 23, 29, 30] we can easily list different functional features to characterize a most favorable hydrogel material for industrial applications such as: (i) highest biocompatibility, (ii) lowest solubility, (iii) highest swelling properties in water and in saline media, (iv) highest re-wetting ability depending on the desired applications, (v) highest biodegradability, (vi) highest stability and robustness in swelling surrounding, (vii) highest durability during storage before use, (viii) lowest releaser of toxic compound, (ix) odorless and/or colorlessness, (x) highest temperature, pH and photostability before and after swelling formation and, (xi) highest porosity to allow the fluid circulation and the best swelling properties. In general, it is well established that according to the use of the hydrogels, the main technical features to be developed must be optimized to consider a genius balance between the properties of the biomaterials and the targeted applications [3, 30]. Moreover, as very well related by Ahmed [4], it was clearly established that according to the nature, the intrinsic properties, the distribution and the density of compounds used (e.g. natural or synthetic polymers, cross-linkers, adhesives, adjuvants, extracellular matrices), hydrogel macrostructures could include diverse amount of water in swelling state in the application medium leading to higher water mass fraction in scaffold than polymers mass fraction itself. Therefore, if we focus particularly on the case of entrapment living cell application, another innovative technology is the cell coating

(CC). Generally, classic *in vitro* cultures in two dimensions (2D) can only present monolayer structures even after reaching cells confluency in the culture dish. One of the explanations might be the lack of extracellular matrices (ECMs) expressed by cells when they are maintained in 2D culture, which is necessary to switch into three-dimensional (3D) structure tissues. To overcome this issue, artificial addition of ECM surrounding the cells can be performed. This is called CC, which means nanometer- or micrometre-sized polymer thin films around cells, to induce their biological activities. This coating is performed using protein or polymer and can control for instance cell adhesion [31], growth direction [32, 33], or even killing specific bacteria [34]. Different coating methods exist, one of them is called “Layer-by-Layer” (LbL) formerly developed by Decher in 1981 to coat polymer and proteins onto substrate surfaces by dipping or spraying [35, 36]. This approach has been more and more used for cell surface modification, due to its easy preparation and tunable composition on cell surfaces under physiological conditions. The aim is to use specific ECM as coating components, known for their interactions with integrin receptor on the cell membranes. Many different types of ECM are found in our body, the most represented being collagen, laminin, hyaluronic acid, fibronectin or elastin. By selecting appropriate natural ECM components cytotoxicity is avoided while inducing specific cell-adhesive properties on molecules like RGD (arginine-glycine-aspartic acid) [37]. Among the cell membrane proteins, integrin receptors are important, determining the specificity for extracellular ligands as well as inducing intracellular signaling processes [38, 39]. Specifically, the $\alpha 5 \beta 1$ integrin receptors can recognize the ECM component fibronectin (FN) since it contains the RGD sequence [40]. Gelatin (G) is a mixture of peptides and proteins produced from partial hydrolysis of collagen extracted from the skin, bones, and connective tissues. FN and G can interact with each other due to the collagen-binding domain found in FN, leading to nanometer-sized cell-adhesive surface films on cell surfaces, like the natural ECMs for multilayered structures without any cytotoxicity.

3.2 Technologies Developed for Their Preparation

A lot of strategies has been described in the literature to synthesize diverse forms of hydrogels. As recently mentioned in a very interesting review [30], hydrogels can be prepared by using several methodologies such as (i) polymerization grafting; (ii) chemical or physical cross-linking and (iii) radical cross-linking (Fig. 3). Conventionally, polymerization and radical processes are well defined as a good technology to generate varied hydrogels with controlled size, composition, particles distribution and morphologies [41–43]. Generally, the chemical method is the most common process related in literature for the preparation of hydrogel biomaterials with very good mechanical strength [23]. Nevertheless, the main drawback of chemical cross-linking is the use of toxic cross-linker such as for example

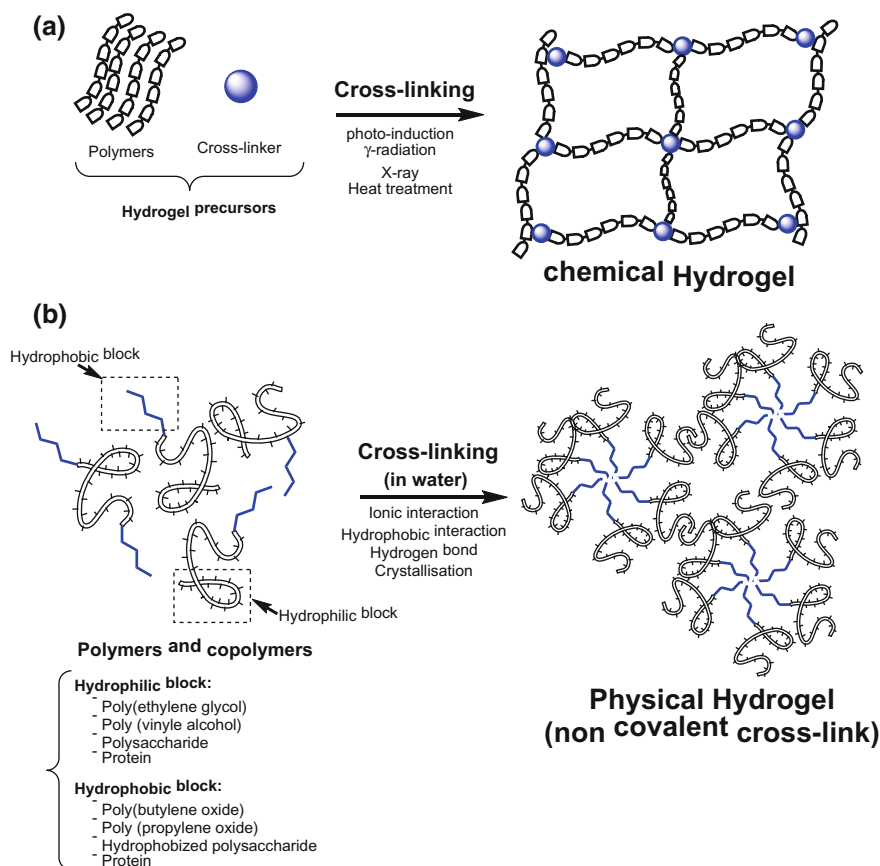


Fig. 3 The main strategies to prepare hydrogels. **a** Chemical cross-linked polymers, **b** physically cross-linked polymers

glutaraldehyde and epichlorohydrin which must be removed for industrial and/or human applications. Consequently, a healthier alternative is the physical cross-link method [4, 22].

In a classic way, for the production of hydrogels (from macro- to nanogel 3D-networks) lot of cross-linking reactions have been performed (Table 2) such as: (1) the photo-induction reaction, (2) the Schiff-base reaction, (3) the thiol/disulfide reaction, (4) the carboxyl/amine reaction, (5) the amide/amine reaction and, (6) the click chemistry reaction [4, 23]. Furthermore, to perform the best hydrogel synthesis with controlled cross-link density and molecular sizes, studies traditionally recommend multi-steps procedure from polymerization to cross-link multifunctional mono/polymers having very reactive groups/functions [3, 4, 23]. As clearly mentioned by Mahinroosta et al. [30], the most important challenge for the preparation of hydrogels is the crucial control of the particle size distribution

Table 2 Examples of cross-linking reaction performed to prepare hydrogels

Methods	Mechanisms/cross-linker	Polymers/blocks	References
Chemical cross-linking	Gamma radiation	Cellulose, tara gum, acrylic acid	Alla et al. [81], Amin et al. [82]
	Aldehyde-amine reaction/ glutaraldehyde	Chitosan, polyvinyl alcohol	Zu et al. [83]
	Addition reaction/ 1,6-hexanedibromide	Scleroglucan	Coviello et al. [84]
	Condensation reaction/ <i>N,N</i> -(3-dimethylaminopropyl)- <i>N</i> -ethyl carbodiimide (EDC)	Gelatin	Kuijpers et al. [85]
	Photo-polymerization	Acrylated lactic acid, poly (ethylene glycol)	Hubbell [86]
Physical cross-linking	Photo-clickable polymerization	Maleilated chitosan, poly (vinyl alcohol)	Zhou et al. [52]
	Amphiphilic graft	Polystyrene, poly (vinylpyridine)	Forster and Antonietti [87]
	Hydrophobic modification; self-aggregation	Cholesteryl, modified pullulan	Taniguchi et al. [88]
	Ionic interaction/calcium ions (Ca^{2+})	Alginate	Gacesa [89]
	Melt polycondensation	Poly(butylene terephthalate); Poly (ethylene glycol)	Bezemer et al. [90]
Enzymatic cross-linking	Transglutaminase reaction	Lysine-containing protein, poly-(ethylene glycol) glutaminamide	Sperinde and Griffith [44]
	Horseradish peroxidase reaction	Silk fibroin proteins, hyaluronic acid	Raia et al. [46]
	Alcalase reaction	Sucrose, acrylate, metacrylate	Chen et al. [45]
	Transglutaminase reaction	Hyaluronan	Brogiere et al. [54]
	Transglutaminase reaction	Gelatin	Yang et al. [91]

modulated by synthesis processes such as the regulation of monomer/polymer/cross-linker ratio, the perfect adjustment of experimental conditions (e.g. pH, ionic strength, temperature). To accomplish this aim, other cross-linking alternative methods using enzymes were proposed to generate specific hydrogels [23]. As for example, Sperinde and Griffith [44] synthesized original hydrogels with cross-linking between a lysine-containing protein and a functionalized PEG by using transglutaminase (a human tissue enzyme). In their study, authors showed the catalyzed reaction between the amine group of lysine and the γ -carboxamide group

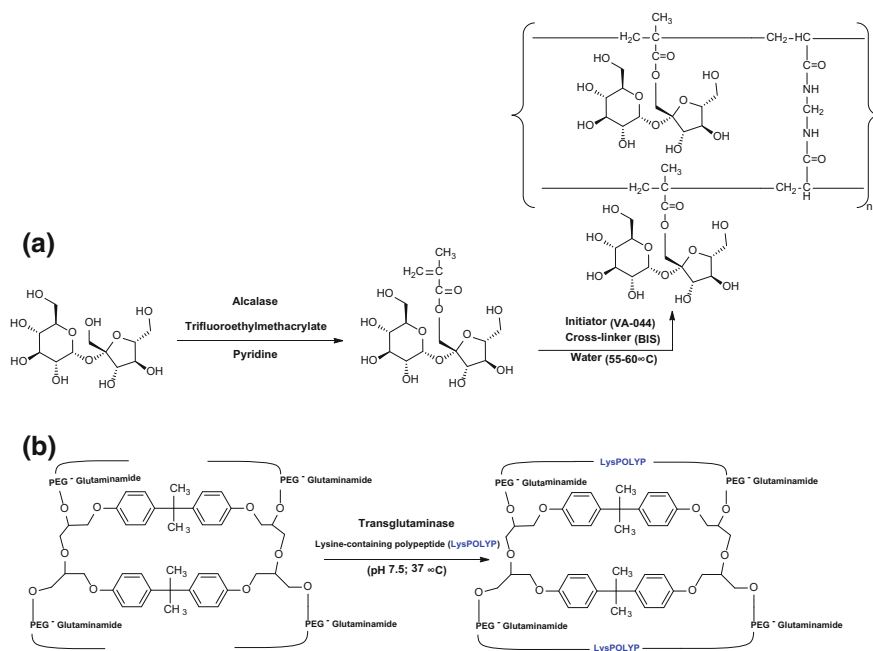


Fig. 4 Two main examples of enzymatic cross-linking for the preparation of hydrogels. **a** Chemoenzymatic synthesis of poly-sucrose-methacrylate-hydrogel (adapted from Chen et al. [45]), **b** enzymatic cross-linking of glutaminamide polyethylene glycol (PEG) with lysine-containing polypeptide using transglutaminase

of PEG resulting in an attractive biomaterial allowing highly hydrated 3D-networks for living cells. In another enzymatic strategy, Chen et al. [45] developed chemo-enzymatic and enzymatic approaches to prepare a sugar-based hydrogel such as poly-sugar acrylate/methacrylate with highly water absorbents and drug delivery systems properties. As a final point, not to mention that recently, an enzymatic crosslinked silk fibroin proteins-hyaluronic acid hydrogel was produced by using horseradish peroxidase resulting in a highly elastic hydrogel with the application as scaffolds in tissue engineering [46]. The main enzymatic cross-linking way to prepare hydrogels are presented in Fig. 4.

Concerning the LbL coating (see Sect. 3.1), this “cell accumulation technique” technology provide around 6 nm thick FN-G films around cell surface, fabricated by FN and G coatings alternatively for 9 steps. Till now, over 100 μm thick 3D-tissue models with capillary networks [47, 48] were successfully constructed for further advanced studies as drug delivery systems, cancer cell invasion mechanism observation, or even manufacturing a biosensor chip [49]. Some tissues, for example, cartilage tissues [50], require a higher amount of ECMs, cell-cell distance in the tissues being in micrometre-sized level, and LbL FN-G coating methodology providing only nanometer-sized level. Another novel approach called “collagen

coating method” and “multiple coating methods” was thus developed to construct 3D-tissue models with lower cell density and more ECM content using micro-coating technologies [51]. For this method, collagen type I, the most widely used material in biomedical and tissue engineering, was directly used. The method lies in the specific recognition abilities between another integrin receptor, $\alpha 2\beta 1$, and the collagen I fibers.

3.3 Preparation and Optimization: Few Examples

In view of the above concerning the technologies used (chemical, physical and enzymatic cross-linking) to prepare hydrogels, a lot of optimization processes have been recently developed in order to synthesize improving hydrogel biomaterials with higher application performances. As for example, in their study, Zhou et al. [52] produce a very interesting maleilated chitosan/thiol-terminated PVA hydrogel by using photo-clickable thiol-ene polymerization process with and thiol-terminated poly (vinyl alcohol) (TPVA) and maleic chitosan derivatives (MCS) activated under UV light source (60 mW/cm^2) by a photo-initiator such as the 2-hydroxy-1-[4-(hydroxyethoxy) phenyl]-2-methyl-1-propanone (Darocur 2959). In this case, the author has clearly shown the potential of this new photocrosslinked MCS/TPVA hydrogels as tissue engineering scaffolds biomaterial due to the efficient L929 cells attachment and proliferation.

Moreover, we can mention the work of Lu et al. [53] on the specific preparation of a new tissue adhesive phenolic glycol chitosan hydrogel using an optimized photo-cross-linkage process activated by blue-light illumination. In this study, author particularly showed that this biomaterial possesses hemostatic properties and very good tissue adhesiveness. Moreover, the encapsulation of antibiotic such as gentamycin into these hydrogels gave very advantageous antibacterial ability.

Recently, Brogiere et al. [54], proposed a new hyaluronan hydrogel synthesized by an optimized enzymatic cross-linking strategy using a transglutaminase activity from the activated blood coagulation factor XIII. Authors related that this hydrogel possesses higher significant ability for 3D neuronal network tissue engineering (strong synaptic connection, dendritic and axonal specification, faster neurite out-growth) than classical hyaluronan gels. Last technological advances in the hydrogel biomaterial fields were performed lately (Fig. 5). First, we can cite Yan et al. [55] who developed a multiscale modeling approach to synthesize an extracellular matrix mimetic hydrogel with sequestered recombinant human bone morphogenetic protein-2 (rhBMP-2). This novel synthetic bone scaffold prepared by an optimized carbonylhydrazide/aldehyde cross-linking strategy was efficiently validated as by in vivo assay with rat ectopic model. Secondly, Kim et al. [56] designed a very smart heparin mimetic hydrogel to improve and stabilize bone morphogenetic proteins 2 (BMP-2) properties which are well known as one of the most important bone formation stimulators. In this study, authors prepared a hydrogel biomaterial surface model with an efficient photo-crosslink process using heparin and

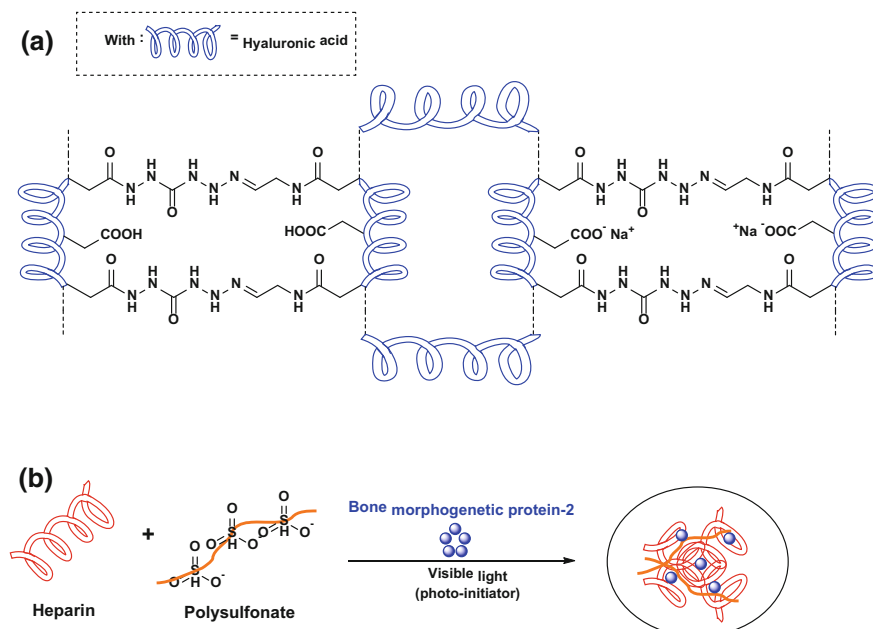


Fig. 5 Last technological advances in the hydrogel biomaterial fields. **a** An extracellular matrix mimetic hydrogel with cross-linked hyaluronic acid (adapted from Yan et al. [55]), **b** a new hydrogel biomaterial surface model with an efficient photo-crosslinking process using heparin and polysulfonate derivatives to encapsulate bone morphogenetic protein-2 (adapted from Kim et al. [56])

polysulfonate derivatives such as poly-4-styrenesulfonic acid (PSS) and poly-vinylsulfonic acid (PVSA). These sulfonated hydrogels were successful used to bind/encapsulate BMP-2 to increase osteogenesis and osteoinductive properties of bone marrow stromal cells (MBSCs) for bone tissue engineering.

Finally, other optimizations were done in the case of CC methodology, in order to evaluate coating effect on the construction of 3D-tissue models, cells without coating, cells coated with FN-G nanofilms or cells coated with collagen microfilms were seeded. Cells coated with collagen microfilms resulted at least 2-fold higher tissue than nano-coating (Fig. 6), with about 1/3 the cell number sufficient to fabricate equal-thick 3D-tissues. Collagen micro-coated cells led to tissues thickness up to 1871 μm . Also, cell-cell distances in these 3D-tissues were calculated as 15.6 ± 4.0 and 8.8 ± 3.1 μm , respectively. In comparison, cells without any coating resulted in compact distribution in some area and the very near distance between cells, about 3 times smaller than a cell with collagen micro-coating (data not shown). The difference in cell number also showed that the thickness of all samples increased according to the seeded cell number. The next step was the construction of functional 3D-tissue models. The development of 3D-vascularized thick tissues possessing high-density blood capillary networks is still an important

issue for tissue engineering. To get a vascularized model, a sandwich culture with one layer of Human Umbilical Vein Endothelial Cells (HUVECs) seeded between 4 or 10-layers of FN-G nanofilm coated Normal Human Dermal Fibroblasts (NHDFs) was used. After 1 week, a highly developed homogenous capillary network with the tubular morphology of HUVECs was observed (Fig. 6B1, B2). With micrometre-sized collagen fiber-coated cells, vascularized network structures were also observed, suggesting that collagen coating method can be used to construct vascularized thick 3D-tissues (Fig. 6A1, A2). Other functional tissue models with FN-G nanofilm coated cells, as induced pluripotent stem cell-derived cardiomyocytes (iPS-CMs) or lymph epithelial cells (LECs), were also successfully constructed. Strong beating phenomenon was assessed during incubation [57]. When using collagen microfilm coating method, the constructed 3D tissues showed stable and strong beating (80 times/min) and high cell viability (>90%) after 4 days of incubation in 800 μm thick 3D tissues. Immunostaining assays such like actinin antibody, troponin T antibody, connexin antibody, and Azan stains were also performed to confirm the good functionality of cardiac myoblasts in the 3D iPS-CM tissues [24]. The collagen microfilm coating method can thus be applied to various types of cells and different purposes.

4 Innovative Sustainable Hydrogels: What's New?

4.1 Utilization of Current and Classical Hydrogel Products

Also known as smart and hungry three-dimensional networks, hydrogels are still subject of numerous papers and patents because of their high-tech potential for applications in a large range of fields, from the biomedical, biotechnology, agriculture to the pharmaceutical, microelectronics industry, oil recovery or cosmetic [30, 58]. Today, hydrogels must respond to physicochemical parameters (electric/magnetic field, solvent, pH, ionic strength, temperature) in their surroundings, change their physicochemical properties and be able to return to their initial states. Thus, the use of hydrogel products is obviously reliant on their technical features. Overall, the following items correctly characterize the functional properties that hydrogels should achieve [4], i.e. (i) the lowest soluble content and residual monomer, (ii) the lowest price, (iii) most eco-friendly approach (LCA concept), (iv) the highest stability and durability in the swelling environment, (v) the highest behavior against storage, (vi) the best potential for biodegradation without formation of toxic species, (vii) a light-stability without any color, odor and toxicity, (viii) a re-wetting capacity, that is, the ability to release or maintain solution trapped in the hydrogel (high flexibility), (ix) the highest absorbency under load, (x) the highest absorption capacity but also the possibility to correctly control a desired rate of absorption. Different items and levels in these features must be considered for making an "ideal" hydrogel. Nevertheless, authors recognize that no hydrogel can

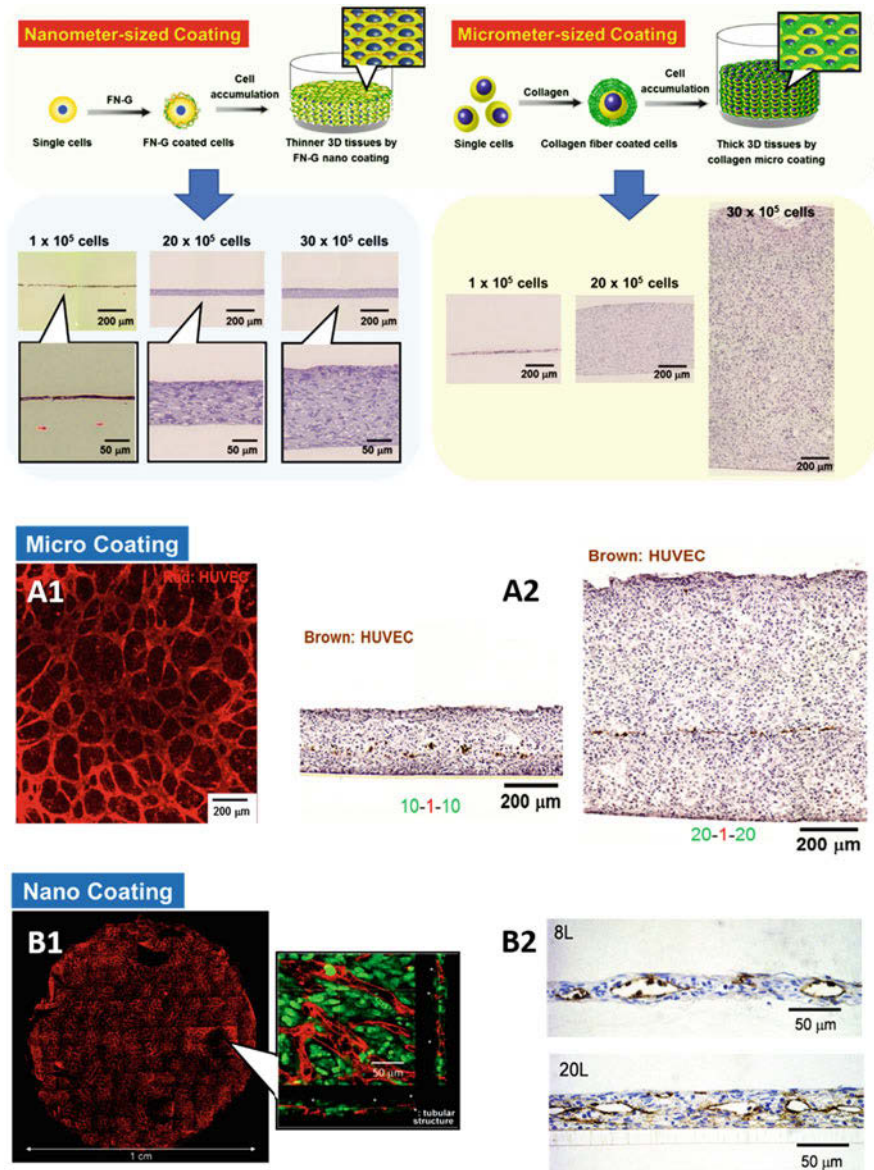


Fig. 6 Schematic illustration of fabrication of ECM layers on cell surfaces by (top left) nanometer-sized FN/G films and (top right) micrometre-sized collagen nanofiber matrices for construction of 3D-tissue models with higher and lower cell densities. Images of confocal laser scanning microscopy (CLSM) of vascularized 3D-tissue models constructed by **A1** nano- and **A2** micro-coatings by sandwich culture. Immunohistological staining images using anti-CD31 antibody of the 3D-tissue models by **B1** nano- and **B2** micro coating methods, adapted from Liu et al. [80]

simultaneously (and at maximum level) fulfil to each item. Thus, the applicative goals of hydrogels strongly impact the way for their fabrication, leading sometimes to porous hydrogel/aerogel (delivery drug system) [59] or superabsorbent capacity for (blood, hygienic) compress use [60] for example. Table 3 gives an overview of applications and performance of hydrogels in various fields before 2015.

4.2 *An Innovative Strategy for Making Hydrogel Products*

Since 2015, recent developments have been made in miscellaneous application fields. These works actually address few classes of hydrogels even if we can consider the growing interest for natural and sustainable hydrogels, i.e. (i) natural-based hydrogels, (ii) synthetic-based hydrogels, (iii) superabsorbent hybrid hydrogels or (iv) conducting polymer hydrogels. The properties of these innovative hydrogels will depend on several parameters such as concentration, type, and a number of ionizable groups, medium (and associated counter ion), hydrophilic/hydrophobic balance, charge, etc. As reported by Mahinroosta et al. [30], new intelligent hydrogels (Fig. 7) should be (i) sensitive to a wide range of external stimuli, such as temperature [61], enzymes [62], light [63] or pH (Aycañ and Alemdar 2018), (ii) able to change their volumetric shape (expansion/contraction), (iii) swell and deswell (swelling ratio) biological fluids in particular for drug delivery applications and/or medical devices, etc. Recent developments especially involve the use of 3D printing for the fabrication of intelligent scaffolds. Tan et al. [64] published a cryogenic 3D printing method using the liquid to a solid phase change of a composite hydrogel. They successfully produced specific geometrical structures with compressive stiffness of $O(1)$ kPa (0.49 ± 0.04 kPa stress at 30% compressive strain). Collagen type I, gelatin and other molecules were used to coat the 3D printed material before testing the systems on human dermal fibroblasts and other biomedical contexts, e.g. surgical training and tissue engineering. Besides, cross-linkable multi-stimuli responsive hydrogels were also prepared by direct-write 3D printing [65]. The behaviors of the new hydrogels were particularly interesting since they responded to shear-thinning, UV light but also temperature. This robust scaffold were made of poly(allyl glycidyl ether)-stat-poly(alkyl glycidyl ether)-block-poly(ethylene glycol)-block-poly(allyl glycidyl ether)-stat-poly(alkyl glycidyl ether) and synthesized by polymerization of glycidyl ethers. Bioelectronics platforms also gain attention and their fabrication can be performed using simple, flexible route by 3D bioprinting [66]. The authors confirmed the biocompatibility of the system against C2C12 murine myoblasts cell line. 3D printed hydrogels are in general programmable and responsive to environmental and fields signals, repeatable and stable over cycle/time, as reported by Lv et al. [67] for poly(ethylene glycol) diacrylate hydrogel microstructures which have excellent humidity responsiveness. New startups also try to take control of the cell microenvironment, e.g. Alvéole (<http://alveolab.com>, France) which develops innovative photopatterning solution (PRIMO) for 3D scaffold designing. This tool, using pseudo

Table 3 Overview of some hydrogel applications (before 2015)

Applications	Type of hydrogel	Properties/uses	References
Biomedical Biotechnology Pharmaceutical	Dextrin-based hydrogel/nanogel	Cell encapsulation and injectable nano/hydrogel	Silva et al. [92]
	Dextrin-based hydrogel/urinary bladder matrix		
	Ionically cross-linkable (alginate) hyaluronate-based hydrogels	Drug (primary chondrocytes) delivery system for in vivo cartilage regeneration	Park et al. [93]
	Polyvinyl alcohol hydrogel/dextran copolymerization	Vascular grafting, high bio and hemocompatibility	Alexandre et al. [94]
	DNA hydrogel, DNA-capped gold nanoparticles	Enzymatic tool kit, adapter for protein detection, thermostable, plasmonics	Yang et al. [95]
	Fe3O4 nanoparticle/hydrogel magnetic nanocomposite	Excellent catalytic activity, sensitive toward H ₂ O ₂ detection, environmental chelation	Gao et al. [96]
	Collagen/b-sodium glycerophosphate-carbodiimide hydrogel	Chitosan human-like assemblage, soft tissue defect filling, delivery system properties	Li et al. [97]
	TiO ₂ /PEGDA hybrid hydrogel	Photodynamic therapy on tumour cells	Zhang et al. [98]
	Chitosan highly hydrated collagen hydrogel	Scaffold mimicking native extracellular matrix	Chicaturu et al. [99]
	PVA/chitosan hydrogel	Swelling activity and antimicrobial potential, drug (sparfloxacin) delivery system	Abdel-Mohsen et al. [100]
	Poly(lactic acid)-poly(ethylene oxide) block copolymers	Nanoclusters as biosensors, enhance elastic modulus of the hydrogel, tissue engineering scaffold	Saffer et al. [101]
	PVA hydrogel	Arterial biomodelling	Kosukegawa et al. [102]
	Poly(<i>N</i> -isopropylacrylamide)/iron oxide magnetic hydrogel nanocomposites	Drug delivery system, hyperthermia for cancer treatment	Meenach et al. [103]
	Carboxy-methylated cellulose/chitosan hydrogel (irradiation)	Adsorption of heavy metal ions, water treatment	Zhao and Mitomo [104]
Poly(acrylamide-co-acrylic acid)/chitosan nanostructured hydrogel	Drug (ascorbic acid) delivery system	Becerra-Bracamontes et al. [105]	

(continued)

Table 3 (continued)

Applications	Type of hydrogel	Properties/uses	References
Food packaging	Poly(ethylene glycol)/poly(e (open)-caprolactone)-based hydrogel	Cell delivery application, scaffold for cartilage formation (tissue collagen type II, aggrecan, SOX9, COMP gene expression)	Park et al. [106]
	PEG-PLGA graft copolymeric hydrogel	Molecular recognition for cancer treatment/imaging	Jeong and Gutowska [107]
	Methylcellulose-10%PEG	Skin irritation (atopic eczema), a delivery system for allergens	Darsow et al. [108]
	Petrolatum-10%isopropyl myristate	Wound dressing and implant materials. Fill the spaces in a wound, isolate the area from bacterial infection	Corkhill and Hamilton [109]
	PPO-PEO	Sensitive food packaging, heat capacity, delivery system, usable in w/o system	Fuciños et al. [110]
	Poly(N-isopropylacrylamide) nanohydrogel	Water and mechanical barrier properties, biohydrogel, antifogging, respiring hydrogel, antimicrobial property	Rhim and Wang [111]
	Agar/k-carrageenan/konjac glucomannan	Delivery system (pimaricin), antifungal, resistant to acidic conditions, thermal resistance	Fuciños et al. [112]
	Poly(N-isopropylacrylamide) nanohydrogel	Biodegradable, eco-friendly material	Roy et al. [113]
	Poly(N-isopropylacrylamide)/carboxymethylcellulose hydrogel	Delivery system (by enzymes degradation), tool for detecting bacteria and fungi	Schneider et al. [114]
	Poly(N-isopropylacrylamide)(80%)/acrylic acid(20%)	Controlling microbial proliferation	Incoronato et al. [115]
Cosmetic	Poly(vinylpyrrolidone)/carboxymethylcellulose hydrogel	Thermo-(ir)reversible gel, biodegradable, from waste proteins	Langmaier et al. [116]
	Carboxymethylcellulose hydrogel	Injectable, soft tissue filler, tunable hydrogel	Varma et al. [117]
	Poly(vinyl alcohol)/hyaluronic acid blends	Gelation time performance, high mechanical properties, blend hydrogel	Kodavaty and Deshpande [118]
			(continued)

Table 3 (continued)

Applications	Type of hydrogel	Properties/uses	References
Agriculture	Nanostructured lipid carriers-based hydrogel	Skin hydration, entrapment of oil (argan), easy formulated	Tichota et al. [119]
	Polyacrylamide-based hydrogel	Lip enhancement, widespread facial infections, potentially risky for health	Wang et al. [120, 121]
	Calcium hydroxylapatite-based hydrogel	Injectable, long-lasting un-permanent filler, highly biocompatible, dermal filler, potential body reactions (risk)	Pavicic [122]
	Palmitoyl glycol chitosan hydrogel	The delivery system (magnesium ascorbyl phosphate), UV protection, an inhibitor of tyrosinase	Wang et al. [120, 121]
	P(MAA-co-EGMA) hydrogel microparticles	Smart carrier, high skin permeability, pH-sensitive release behaviour	Lee and Kim [123]
	Xanthan/lignin hydrogel-epichlorohydrine	Thermal stability, hydrophobicity, decent biocompatibility	Raschup et al. [124]
	Xyloglucan-chitosan complex hydrogel	Non-toxic, antimicrobial and texture properties, thermal stability	Simi and Abraham [125]
	Guar gum-g-polyacrylate-based hydrogel	Water retention and swelling behavior, application in moisture stress agriculture, pH-sensitive	Chandrika et al. [126]
	Fertilizing hydrogel	Work for establishing poplar	Böhlenius and Overgaard [127]
	ι/k-carrageenan-agar/xanthan hydrogel blends	Coating seed, increase water holding capacity, increase gel strength	Hotta et al. [128]
	Chitin hydrogel	Biodegradable, plant growth regulator, excellent water uptake ability	Tang et al. [129]
	Nanocomposite PAAm/methyl cellulose/montmorillonite hydrogel	Nutrient carrier vehicle, increase water absorption speed	Bortolin et al. [130]
	Poly(acrylamide-co-acrylic acid)/AlZnFe ₂ O ₄ hydrogel	Superabsorbent, improve wheat plant growth and establishment, enhance the moisture retention	Shahid et al. [131]
Pectin-based polymer hydrogel	Remover of Cu ²⁺ and Pb ²⁺ , the release of fertilizers, help to conserve water, able to macromolecular relaxation	Guilherme et al. [132]	

(continued)

Table 3 (continued)

Applications	Type of hydrogel	Properties/uses	References
Separation Oil recovery	Crosslinked dextran hydrogel-epichlorohydrin-toluene	Separation of liposome and drugs, water swelling property, high separation performance, decent sphericity and distribution	Bao et al. [133, 134]
	Dimethylamino ethyl methacrylate hydrogel	Thermo and pH-controllable, superhydrophilicity, superoleophobicity, o/w separation	Cao et al. [135]
	Clay nanosheets, <i>N,N</i> -dimethylacrylamide and 2-acrylamide-2-methylpropanesulfonic acid	The high-strength freestanding elastic hydrogel, selectively separation of Pb^{2+} and Cu^{2+} , recycle membrane	Bao et al. [133, 134]
	PEG-laponite XLG-acrylamide particle gels (PPGs)	3D dense network, mobility control, fracture-plugging applications, long-term thermal stability	Tongwa and Bai [136]
	Polyacrylamide/montmorillonite (Na-MMT)-chromium hydrogel	Enhance oil recovery, in-depth profile modifier, oil displacing agent, strong thermal stability	Zolfaghari et al. [137]
	Polyacrylamide/poly(vinyl alcohol)-chromium triacetate hydrogel	Gelation and swelling behaviour, enhance oil recovery	Aalaie et al. [138]
	PAM inverse emulsion/acrylamide	In-depth permeability control, fluid diverting, oil driving, increase oil productivity	Lei et al. [139]
	Xanthan/ Zr^{4+} flowing gel	Enhance oil recovery, strongly resistant to shearing	Wang and Zhang [140]
	Conventional bilayer lipid membranes-hydrogel salt-bridge	pH and ion sensors, sensors for ligand-reception interactions, drug testing, enhance oil recovery	Tiena and Ottovaab [141]

hydrogel solution, allows the absorption of specific proteins on illuminated areas then cells to these proteins, respecting a defined micropattern, and thus 3D construction, for biomedical and tissue engineering for example. Finally, recent works highlighted 4D fabrication using shape-morphing hydrogel [68]. Alginate and hyaluronic acid were used as biopolymers for the conception of the hydrogel, and mouse bone marrow stromal cells for the biocompatibility tests. The authors were able to generate average internal tube diameters (20 μm), comparable to the smallest blood vessels without any loss of cell viability. Their statements are strong since this 4D (four-dimensional) biofabrication strategy aims to produce dynamically reconfigurable architectures, with tunable functionalities, as reported in Fig. 7. Wang et al. [69] recently published a comprehensive review concerning new development and biomedical applications of these hydrogels. This paper illustrates the work already done but mainly to perform in the fabrication processes which absolutely need to be (i) inexpensive, (ii) from and/or using nontoxic/non-hazardous materials and techniques and (iii) fine and easily-tuning possibilities. Thus, a wide range of papers are nowadays available in the literature and natural polymer (DNA, protein, polysaccharide) based-hydrogels take benefit from the situation [70–72].

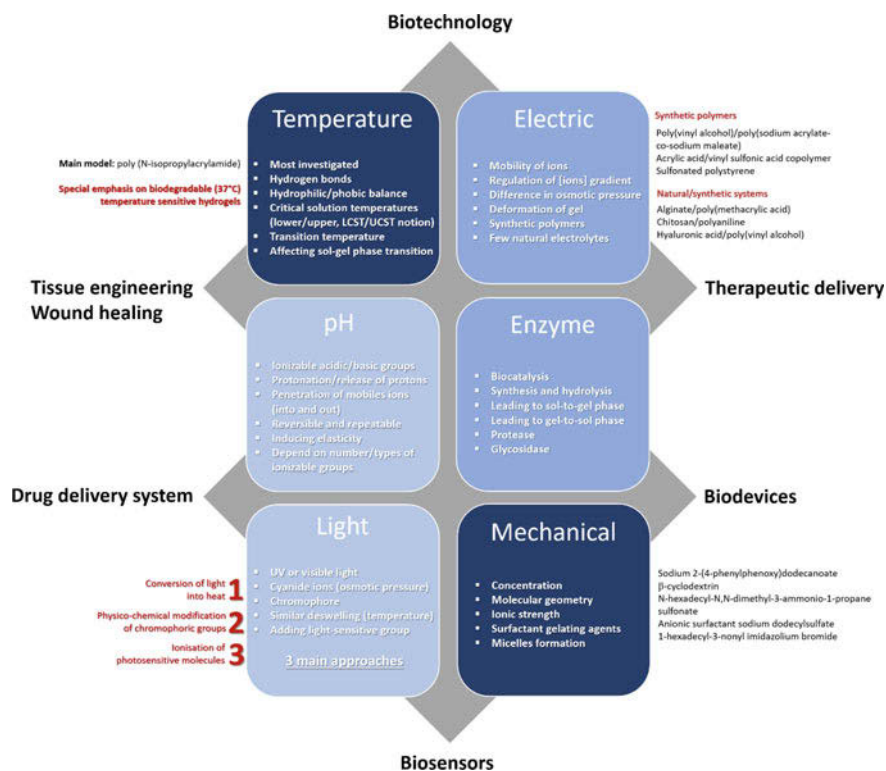
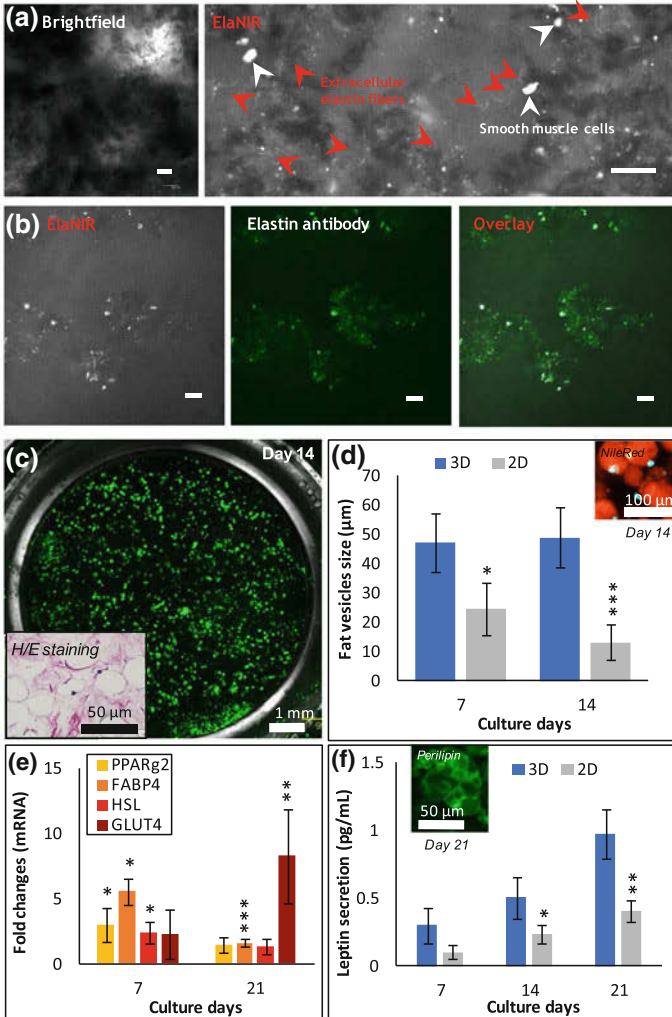
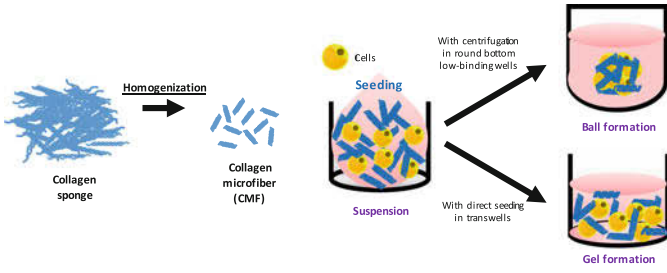


Fig. 7 Main strategies for the conception of new smart hydrogels and recently associated polymers



◀**Fig. 8** Schematic illustration of collagen microfiber hydrogels model construction. **a** Bright field (left) and ElaNIR signal in NIR channel (right). **b** ElaNIR signal was detected in NIR channel (left), the signal from an anti-elastin antibody (middle) and overlay imaging (right). Scale bar: 100 μm . **c** Live/dead assay attesting the good viability of mature adipocytes after 14 days in collagen microfibers hydrogels. **d** Adipose vesicles diameters measured each week using Nile red specific lipids staining. **e** Adipogenesis gene expression assessed by RT-qPCR on total RNA of ADSC (PPAR γ 2, FABP4, GLUT4 and HSL genes) expressed in fold changes regarding 2D condition. **f** Leptin secretion measurement by ELISA in the culture medium every week and normalized by DNA content. Perilipin immunostaining performed at day 21. Error bars represent SD. Tukey multiple comparison test (double-way ANOVA) was used with $*p < 0.05$, $**p < 0.01$, and $***p < 0.001$

4.3 Focus on the Nano to Micro ECM Gel Coating System

Classic collagen hydrogels are still widely used for tissue engineering despite its limited collagen content of maximum 0.3%, remaining far away from the in vivo conditions. In this context, the use of collagen microfibers instead of classic collagen dilution can achieve higher density (until 20–30 wt%). The method relies on the immersion of porcine type I collagen in $\times 10$ PBS (Phosphate buffer saline), followed by its homogenization for 2 min to create the microfibers (VH-10 homogenizer, As One Corp., Osaka, Japan). After centrifugation, the microfibers were washed in DMEM (Dulbecco's modified eagle medium) without FBS (Fetal bovine serum) before being mixed with the cells suspension.

4.3.1 Live-Staining of Secreted Elastin by Smooth Muscle Cells in All Tissues

Elastin is one of the major components of the extracellular and thus often assessed during tissue regeneration. For example, the aorta wall is constructed with an arrangement of elastin in concentric lamellae presenting smooth muscle cells between them [73]. A new fluorescent ElaNIR probe was used to visualize specific elastin secretion in smooth muscle cells 3D-tissue models. Human umbilical artery smooth muscle cells were seeded in ball microfibers collagen tissues. These ball tissues were made by centrifuging the mix cells-collagen microfibers in round bottom low-binding plate wells. Smooth muscle cells ball tissues displayed an increase of extracellular elastin fibers as stained by ElaNIR probes (Fig. 8a), confirmed by consistent elastin antibody staining (Fig. 8b). Overall, the specific ElaNIR probe along with the in vivo like smooth muscle tissue can be used as a model for observation of elastin production during tissue regeneration or for the screening of elastin-enhancing chemicals in cosmetics products [74].

4.3.2 Adipose Tissue Regeneration Inducing and Maintaining the Functionality of Both Pre and Mature Adipocytes in Long-Term Cultures

Adipose tissue regeneration is currently a competitive challenge for either cosmetic/ pharmaceutical assays or plastic surgery purposes. Conventional *in vitro* two-dimensional (2D) cell cultures using directly mature adipocytes (AD) showed limited culture time by quickly dedifferentiating [75] while getting sufficiency matured AD by differentiating adipose-derived stem cells (ADSC) usually required more than one month [76]. The existing three-dimensional (3D) models accelerated the ADSC adipogenesis, but the mature AD still cannot be maintained more than one-week *in vitro* cultures [77]. In this context, the construction of a biomimetic 3D-tissue is determinant. Using collagen microfibers, high-density collagen (until 20–30 wt%, see H/E staining (Fig. 8c), similar to *in vivo* [78] artificial adipose tissues were performed mixing the homogenized type I collagen with a mature AD or ADSC and seeding in 24 well transwells. These 3D-tissues ensured the long-term maintenance of unilocular mature AD with a good viability of 95% at day 14 (Live/Dead image Fig. 8c). On the contrary, the 2D mature AD showed significantly 4 times smaller multiple vesicles (Fig. 8d). Concerning ADSC, 3D adipogenic genes expression was found at least significantly doubled throughout the differentiation (even 8.3 times higher for GLUT4 at day 21, Fig. 8e), along with up to almost 4 times bigger fat vesicles observed at day 14 (data not shown). Perilipin immunostaining, the protein stabilizing the fat vesicles, and leptin secretion, the well-known safety protein, finally attested the up to the twice better functionality of 3D adipocytes (Fig. 5e). The obtained long-term functional maintenance and the faster adipogenesis made this model relevant for screening assays and reconstructive surgery.

5 Conclusions

More and more hydrogels have been published and patented these last years for their specific properties leading to various applications. Some of them are widely present in commercial products. Their success is linked to their ability to swell in aqueous solutions or suspensions. This book chapter has done the state of the art of the different natural or synthetic hydrogels available and described the obtaining processes for different uses in numerous industrial fields. The potential of these macromolecular networks has not been fully explored at this time notably in therapy for tissue engineering and drug delivery, two fields where only a few products are on the market. Covalently cross-linked hydrogels made in the absence of solvents are the more popular for this kind of applications. Undoubtedly, methods from supramolecular chemistry applied to the synthesis in aqueous environments of new hydrogels having modifiable properties could open the way of new possibilities. Supramolecular chemistry is a domain of chemistry that focuses

on the building of macromolecular systems made up of non-covalently assembled molecular subunits. Current researches focusing on hydrogels for multidrug delivery by a single system and/or sequential delivery on demand with a high level of control by stimuli highlight also new opportunities. Another way of hydrogel improvement, notably for application in the human body, could be the control of their swelling capacity. Indeed, the swelling of hydrogels and/or their degradation after their implantation can alter surrounding tissues. This disadvantage can be limited by decreasing the polymer concentration but in this case, the time to form the hydrogel is too long. An interesting article recently published in *Nature Biomedical Engineering* proposed an original solution of a two-step gelation process of PEG hydrogels at low concentration [79]. In a first step, branched polymers clusters were generated but the crosslinking reaction was intentionally stopped just before the full gelation. The solution was then injected into the body at the required place and the clusters present in the co-crosslinked solution to form a gel in ten minutes. These hydrogels have low cytotoxicity and can act as an artificial vitreous body. So, the future of hydrogels in the therapeutic area will be probably linked to the development of innovative properties such as those described above but also to the reduction of costs for their obtaining.

Acknowledgements This research was supported by JST-PRESTO (15655131) and a Grant-in-Aid for Scientific Research (B) (26282138 and 17H02099). The authors also thank the program “Exploration Japon 2018” from Campus France, SST and SCAC (Ambassade de France au Japon).

References

1. Ganguly K, Chaturvedi K, More UA, Nadagouda MN, Aminabhavi TM (2014) Polysaccharide-based micro/nanohydrogels for delivering macromolecular therapeutics. *J Control Release* 193:162–173
2. Mastropietro DJ, Omidian H, Park K (2012) Drug delivery applications for superporous hydrogels. *Expert Opin Drug Deliv* 9:71–89
3. Calo E, Khutoryanskiy VV (2015) Biomedical applications of hydrogels: a review of patents and commercial products. *Euro Polym J* 65:252–267
4. Ahmed EM (2015) Hydrogels: preparation, characterizations and applications: a review. *J Adv Res* 6:105–121
5. Singhal R, Gupta K (2016) A review: tailor-made hydrogel structures (classifications and synthesis parameters). *Polym Plast Technol Eng* 55:54–70
6. Chai Q, Jiao Y, Yu X (2017) Hydrogels for biomedical applications: their characteristics and the mechanisms behind them. *Gels* 3, 6. <https://doi.org/10.3390/gels3010006>
7. Bescrades IG, Demirtas TT, Durukan MD et al (2015) Microwave-assisted fabrication of chitosan-hydroxyapatite superporous hydrogel composites as bone scaffold. *J Tissue Eng Regen Med* 9:1233–1246
8. Salimi-Kenari H, Mollaie F, Dashtimoghadam E et al (2018) Effects of chain length of the cross-linking agent on rheological and swelling characteristics of dextran hydrogels. *Carbohydr Polym* 181:141–149
9. Tavsanli B, Okay O (2017) Mechanically strong hyaluronic acid hydrogels with an interpenetrated network structure. *Euro Polym J* 94:185–195

10. Maisani M, Ziane S, Ehret C et al (2018) A new composite hydrogel combining the biological properties of collagen with the mechanical properties of a supramolecular scaffold for bone tissue engineering. *J Tissue Eng Regen Med* 12:1489–1500
11. Varaprasad K, Rahavendra GM, Jayaramudu T et al (2017) A mini review on hydrogels classification and recent developments in miscellaneous applications. *Mat Sci Eng C* 79:958–971
12. Mati-Baouche N, Elchinger PH, de Baynast H, Pierre G, Delattre C, Michaud P (2014) Chitosan as an adhesive. *Eur Polym J* 60:198–213
13. Shonnard DR, Kicherer A, Saling P (2003) Industrial applications using BASF ecoefficiency analysis: perspectives on green engineering principles. *Environ Sci Technol* 37:5340–5348
14. Vink ETH, Rábago KR, Glassner DA, Gruber P (2003) Applications of life cycle assessment to nature works polylactide (PLA) production. *Polym Degr Stab* 80:403–19
15. Clark JH (2008) Green chemistry: today (and tomorrow). *Green Chem* 8:17–21
16. Tian H, Tang Z, Zhuang X et al (2012) Biodegradable synthetic polymers: preparation, functionalization and biomedical application. *Prog Polym Sci* 37:237–280
17. Takashi L, Hatsumi T, Makoto M et al (2007) Synthesis of porous poly (N-isopropylacrylamide) gel beads by sedimentation polymerization and their morphology. *J Appl Polym Sci* 104:842
18. Yang L, Chu JS, Fix JA (2002) Colon-specific drug delivery: new approaches and in vitro/in vivo evaluation. *Int J Pharm* 235:1–15
19. Zuluaga M, Gregnanin G, Cencetti C, Di Meo C, Gueguen V, Letourneur D, Meddahi-Pelle A, Pavon-Djavid G, Matricardi P (2018) PVA/dextran hydrogel patches as delivery system of antioxidant astaxanthin: a cardiovascular approach. *Biomed Mater* 13:1–13
20. Maolin Z, Jun L, Min Y et al (2000) The swelling behaviour of radiation prepared semi-interpenetrating polymer networks composed of polyNIPAAm and hydrophilic polymers. *Radiat Phys Chem* 58:397–400
21. Hacker MC, Mikos AG (2011) Synthetic polymers. In: Atala A, Lanza R, Thomson JA, Nerem RM (eds) *Principles of regenerative medicine*, 2nd edn. Academic Press, USA, pp 587–622
22. Ahmed EM, Aggor FS, Awad AM et al (2013) An innovative method for preparation of nanometal hydroxide superabsorbent hydrogel. *Carbohydr Polym* 91(2):693–698
23. Akhtar MF, Hanif M, Ranjha NM (2016) Methods of synthesis of hydrogels: a review. *Saudi Pharm J* 24(5):554–559
24. Liu CY, Matsusaki M, Akashi M (2015) Control of cell-cell distance and cell densities in millimeter-sized 3D tissues constructed by collagen nanofiber coating techniques. *ACS Biomater Sci Eng* 1:639–645
25. Yuangang Z, Ying Z, Xiuhua Z et al (2012) Preparation and characterization of chitosan–polyvinyl alcohol blend hydrogels for the controlled release of nano-insulin. *Int J Biol Macromol* 50(1):82–87
26. Brannon-Peppas L, Harland RS (1991) Absorbent polymer technology. *J Control Release* 17(3):297–298
27. Li Y, Huang G, Zhang X et al (2013) Magnetic hydrogels and their potential biomedical applications. *Adv Funct Mater* 23(6):660–672
28. Matsusaki M, Yoshida H, Akashi M (2007) The construction of 3D-engineered tissues composed of cells and extracellular matrices by hydrogel template approach. *Biomaterials* 28:2729–2737
29. Gobbi A, Whyte GP (2016) One-stage cartilage repair using a hyaluronic acid-based scaffold with activated bone marrow-derived mesenchymal stem cells compared with microfracture: five-year follow-up. *Am J Sports Med* 44(11):2846–2854
30. Mahinroosta M, Farsangi ZJ, Allahverdi A et al (2018) Hydrogels as intelligent materials: a brief review of synthesis, properties and applications. *Mat Tod Chem* 8:42–55
31. Pierschbacher MD, Ruoslahti E (1987) Influence of stereochemistry of the sequence Arg-Gly-Asp-Xaa on binding specificity in cell adhesion. *J Biol Chem* 262:17294–17298

32. Chang PC, Liu BY, Liu CM et al (2007) Bone tissue engineering with novel rhBMP2-PLLA composite scaffolds. *J Biomed Mater Res A* 81:771–780. <https://doi.org/10.1002/jbm.a.31031>
33. Recknor JB, Sakaguchi DS, Mallapragada SK (2006) Directed growth and selective differentiation of neural progenitor cells on micropatterned polymer substrates. *Biomaterials* 27:4098–4108. <https://doi.org/10.1016/j.biomaterials.2006.03.029>
34. Liss M, Petersen B, Wolf H et al (2002) An aptamer-based quartz crystal protein biosensor. *Anal Chem* 74:4488–4495
35. Decher G (1997) Fuzzy nanoassemblies: Toward layered polymeric multicomposites. *Science* 277:1232–1237. <https://doi.org/10.1126/science.277.5330.1232>
36. Decher G, Hong JD (2011) Buildup of ultrathin multilayer films by a self-assembly process, 1 consecutive adsorption of anionic and cationic bipolar amphiphiles on charged surfaces. *Makromol Chem Macromol Symp* 46:321–327. <https://doi.org/10.1002/masy.19910460145>
37. Ruoslahti E, Pierschbacher MD (1987) New perspectives in cell adhesion: RGD and integrins. *Science* 238:491–497
38. Arnaout MA, Mahalingam B, Xiong J-P (2005) Integrin structure, allostery, and bidirectional signaling. *Annu Rev Cell Dev Biol* 21:381–410
39. Campbell ID, Humphries MJ (2011) Integrin structure, activation, and interactions. *Cold Spring Harb Perspect Biol* 3:1–15. <https://doi.org/10.1101/cshperspect.a004994>
40. Nagae M, Re S, Mihara E et al (2012) Crystal structure of $\alpha 5 \beta 1$ integrin ectodomain: atomic details of the fibronectin receptor. *J Cell Biol* 197:131–140. <https://doi.org/10.1083/jcb.201111077>
41. Liu P, Zhai M, Li J et al (2002) Radiation preparation and swelling behavior of sodium carboxymethyl cellulose hydrogels. *Radiat Phys Chem* 63(3–6):525–528
42. Said HM, Alla SGA, El-Naggar AWM (2004) Synthesis and characterization of novel gels based on carboxymethyl cellulose/acrylic acid prepared by electron beam irradiation. *React Funct Polym* 61(3):397–404
43. Sanson N, Rieger J (2010) Synthesis of nanogels/microgels by conventional and controlled radical crosslinking copolymerization. *Polym Chem* 1:965–977
44. Sperinde JJ, Griffith LG (1997) Synthesis and characterization of enzymatically-crosslinked-poly(ethylene glycol) hydrogels. *Macromolecules* 30:5255–5264
45. Chen X, Martin BD, Neubauer TK et al (1995) Enzymatic and chemoenzymatic approaches to synthesis of sugar-based polymer and hydrogels. *Carbohydr Polym* 28:15–21
46. Raia NR, Partlow BP, McGill M et al (2017) Enzymatically crosslinked silk-hyaluronic acid hydrogels. *Biomaterials* 131:58–67
47. Nishiguchi A, Matsusaki M, Asano Y et al (2014) Effects of angiogenic factors and 3D-microenvironments on vascularization within sandwich cultures. *Biomaterials* 35:4739–4748. <https://doi.org/10.1016/j.biomaterials.2014.01.079>
48. Nishiguchi A, Yoshida H, Matsusaki M et al (2011) Rapid construction of three-dimensional multilayered tissues with endothelial tube networks by the cell-accumulation technique. *Adv Mater* 23:3506–3510. <https://doi.org/10.1002/adma.201101787>
49. Matsusaki M, Akashi M (2014) Control of extracellular microenvironments using polymer/protein nanofilms for the development of three-dimensional human tissue chips. *Polym J* 46:524–536. <https://doi.org/10.1038/pj.2014.20>
50. Stockwell RA (1967) The cell density of human articular and costal cartilage. *J Anat* 101:753–763
51. Liu CY, Matsusaki M, Akashi M (2014) The construction of cell-density controlled three-dimensional tissues by coating micrometer-sized collagen fiber matrices on single cell surfaces. *RSC Adv* 4:46141–46144. <https://doi.org/10.1039/C4RA09085C>
52. Zhou Y, Zhao S, Zhang C et al (2018) Photopolymerized maleilated chitosan/thiol-terminated poly (vinyl alcohol) hydrogels as potential tissue engineering scaffolds. *Carbohydr Polym* 184:383–389
53. Lu M, Liu Y, Huang YC et al (2018) Fabrication of photo-crosslinkable glycol chitosan hydrogel as a tissue adhesive. *Carbohydr Polym* 181:668–674

54. Broguiere N, Isenmann L, Zenobi-Wong M (2016) Novel enzymatically cross-linked hyaluronan hydrogels support the formation of 3D neuronal networks. *Biomaterials* 99:47–55
55. Yan HJ, Casalini T, Hulsart-Billström G et al (2018) Synthetic design of growth factor sequestering extracellular matrix mimetic hydrogel for promoting *in vivo* bone formation. *Biomaterials* 161:190–202
56. Kim S, Cui ZK, Kim PJ, Jung LY, Lee M (2018) Design of hydrogels to stabilize and enhance bone morphogenetic protein activity by heparin mimetics. *Acta Biomater* (in press). <https://doi.org/10.1016/j.actbio.2018.03.034>
57. Amano Y, Nishiguchi A, Matsusaki M et al (2016) Development of vascularized iPSC derived 3D-cardiomyocyte tissues by filtration Layer-by-Layer technique and their application for pharmaceutical assays. *Acta Biomater* 33:110–121
58. Ullah F, Othman MBH, Javed F et al (2015) Classification, processing and application of hydrogels: a review. *Mat Sci Eng C* 57:414–433
59. Pierre G, Punta C, Delattre C et al (2017) TEMPO-mediated oxidation of polysaccharides: an ongoing story. *Carbohydr Polym* 165:71–85
60. Anisha S, Kumar SP, Kumar GV et al (2010) Hydrogels: a review. *Int J Pharmaceut Sci Rev Res* 4(2):97
61. Tylman M, Piekarczyk K, Owczarż P et al (2018) Structure of chitosan thermosensitive gels containing graphene oxide. *J Mol Struct* 1161:530–535. <https://doi.org/10.1016/j.molstruc.2018.02.065>
62. Alshememry AK, El-Tokhy SS, Unsworth LD (2017) Using properties of tumor microenvironments for controlling local, on-demand delivery from biopolymer-based nanocarriers. *Curr Pharm Des* 23:5358–5391. <https://doi.org/10.2174/1381612823666170522100545>
63. Qin XH, Wang X, Rottmar M et al (2018) Near-infrared light-sensitive polyvinyl alcohol hydrogel photoresist for spatiotemporal control of cell-instructive 3D microenvironments. *Adv Mat* 30(1705564). <https://doi.org/10.1002/adma.201705564>
64. Tan Z, Parisi C, Di Silvio L et al (2017) Cryogenic 3D Printing of super soft hydrogels. *Sci Reports* 7(16668). <https://doi.org/10.1038/s41598-017-16668-9>
65. Karis DG, Ono RJ, Zhang M et al (2017) Cross-linkable multi-stimuli responsive hydrogel inks for direct-write 3D printing. *Polym Chem* 8:4199–4206
66. Agarwala S, Lee JM, Ng WL (2018) A novel 3D bioprinted flexible and biocompatible hydrogel bioelectronic platform. *Biosens Bioelec* 102:365–371
67. Lv C, Sun XC, Xia H et al (2018) Humidity-responsive actuation of programmable hydrogel microstructures based on 3D printing. *Sens Act B: Chem* 259:736–744. <https://doi.org/10.1016/j.snb.2017.12.053>
68. Kirillova A, Maxson R, Stoychev G et al (2017) 4D Biofabrication using shape-morphing hydrogels. *Adv Mat* 29(1703443). <https://doi.org/10.1002/adma.201703443>
69. Wang Y, Adokoh CK, Narain R (2018) Recent development and biomedical applications of self-healing hydrogels. *Exp Opin Drug Deliv* 15:77–91. <https://doi.org/10.1080/17425247.2017.1360865>
70. Aljohani W, Ullah MW, Li W et al (2018) Three-dimensional printing of alginate-gelatin-agar scaffolds using free-form motor assisted microsyringe extrusion system. *J Polym Res* 25 (62). <https://doi.org/10.1007/s10965-018-1455-0>
71. Azizi S, Mohamad R, Abdul Rahim R et al (2017) Hydrogel beads bio-nanocomposite based on Kappa-Carrageenan and green synthesized silver nanoparticles for biomedical applications. *Int J Biol Macromol* 104:423–431
72. Tedesco MT, Di Lisa D, Massobrio P (2018) Soft chitosan microbeads scaffold for 3D functional neuronal networks. *Biomaterials* 156:159–171
73. O'Connell MK, Murthy S, Phan S et al (2008) The three-dimensional micro- and nanostructure of the aortic medial lamellar unit measured using 3D confocal and electron microscopy imaging. *Matrix Biol J Int Soc Matrix Biol* 27:171–181. <https://doi.org/10.1016/j.matbio.2007.10.008>

74. Su D et al (2018) Elastin: a near-infrared zwitterionic fluorescent probe for in vivo elastin imaging. *Chem J* (accepted)
75. Lessard J, Pelletier M, Biertho L et al (2015) Characterization of dedifferentiating human mature adipocytes from the visceral and subcutaneous fat compartments: fibroblast-activation protein alpha and dipeptidyl peptidase 4 as major components of matrix remodeling. *PLoS ONE* 10:e0122065. <https://doi.org/10.1371/journal.pone.0122065>
76. Louis F, Pannetier P, Souguir Z et al (2017) A biomimetic hydrogel functionalized with adipose ECM components as a microenvironment for the 3D culture of human and murine adipocytes. *Biotechnol Bioeng* 114:1813–1824. <https://doi.org/10.1002/bit.26306>
77. Toda S, Uchihashi K, Aoki S et al (2009) Adipose tissue-organotypic culture system as a promising model for studying adipose tissue biology and regeneration. *Organogenesis* 5:50–56
78. Choi JS, Kim BS, Kim JY et al (2011) Decellularized extracellular matrix derived from human adipose tissue as a potential scaffold for allograft tissue engineering. *J Biomed Mater Res A* 97A:292–299. <https://doi.org/10.1002/jbm.a.33056>
79. Hayashi K, Okamoto F, Hoshi S et al (2017) Fast-forming hydrogel with ultralow polymeric content as an artificial vitreous body. *Nat Biomed Eng* 1:0044
80. Liu CY, Matsusaki M, Akashi M (2016) Three-dimensional tissue models constructed by cells with nanometer- or micrometer-sized films on the surfaces. *Chem Rec* 16:783–796
81. Alla SG, Sen M, El-Naggar AW (2012) Swelling and mechanical properties of superabsorbent hydrogels based on Tara gum/acrylic acid synthesized by gamma radiation. *Carbohydr Polym* 89(2):478–485
82. Amin MCI, Ahmad N, Halib N et al (2012) Synthesis and characterization of thermo- and pH-responsive bacterial cellulose/acrylic acid hydrogels for drug delivery. *Carbohydr Polym* 88(2):465–473
83. Zu Y, Zhang Y, Zhao X et al (2012) Preparation and characterization of chitosan polyvinyl alcohol blend hydrogels for the controlled release of nano-insulin. *Int J Biol Macromol* 50:82–87
84. Coviello T, Grassi M, Rambone G et al (1999) Novel hydrogel system from scleroglucan: synthesis and characterization. *J Control Release* 60(2–3):367–378
85. Kuijpers AJ, Van Wachem PB, Van Luyn MJ et al (2000) *In vivo* and *in vitro* release of lysozyme from cross-linked gelatin hydrogels: a model system for the delivery of antibacterial proteins from prosthetic heart valves. *J Control Release* 67:323–336
86. Hubbell JA (1996) Hydrogel systems for barriers and local drug delivery in the control of wound healing. *J Control Release* 39:305–313
87. Forster S, Antonietti M (1998) Amphiphilic block copolymers in structure-controlled nanomaterial hybrids. *Adv Mater* 10:195–217
88. Taniguchi I, Akiyoshi K, Sunamoto J (1999) Self-aggregate nanoparticles of cholesteryl and galactoside groups-substituted pullulan and their specific binding to galactose specific lectin, RCA120. *Macromol Chem Phys* 200:1555–1560
89. Gacesa P (1988) Alginates. *Carbohydr Polym* 8:161–182
90. Bezemer JM, Radersma R, Grijpma DW et al (2000) Zero-order release of lysozyme from (poly)ethylene glycol/poly(butylene terephthalate) matrices. *J Control Release* 64(1–3):179–192
91. Yang G, Xiao Z, Ren X, Long H et al (2016) Enzymatically crosslinked gelatin hydrogel promotes the proliferation of adipose tissue-derived stromal cells. *PeerJ* 4:e2497
92. Silva DM, Nunes C, Pereira I et al (2014) Structural analysis of dextrans and characterization of dextrin-based biomedical hydrogels. *Carbohydr Polym* 114:458–466
93. Park H, Woo EK, Lee KY (2014) Ionically cross-linkable hyaluronate-based hydrogels for injectable cell delivery. *J Control Release: Off J Control Release Soc* 196:146–153
94. Alexandre N, Ribeiro J, Gärtner A et al (2014) Biocompatibility and hemocompatibility of polyvinyl alcohol hydrogel used for vascular grafting—in vitro and in vivo studies. *J Biomed Mater Res* 102:4262–4275
95. Yang D, Hartman MR, Derrien TL et al (2014) DNA materials: bridging nanotechnology and biotechnology. *Acc Chem Res* 47:1902–1911

96. Gao Y, Wei Z, Li F et al (2014) Synthesis of a morphology controllable Fe₃O₄ nanoparticle/hydrogel magnetic nanocomposite inspired by magnetotactic bacteria and its application in H₂O₂ detection. *Green Chem* 16:1255–1261
97. Li X, Fan DD, Deng JJ et al (2013) Synthesis and characterization of chitosan human like collagen/ β -sodium glycerophosphate-carbodiimide hydrogel. *Asian J Chem* 25:9613–9616
98. Zhang H, Shi R, Xie A et al (2013) Novel TiO₂/PEGDA hybrid hydrogel prepared in situ on tumor cells for effective photodynamic therapy. *ACS Appl Mater Interfaces* 5:12317–12322
99. Chicatun F, Muja N, Serpooshan V et al (2013) Effect of chitosan incorporation on the consolidation process of highly hydrated collagen hydrogel scaffolds. *Soft Matter* 9:10811–10821
100. Abdel-Mohsen AM, Aly AS, Hrdina R et al (2011) Eco-synthesis of PVA/chitosan hydrogels for biomedical application. *J Polym Env* 19:1005–1012
101. Saffer EM, Tew GN, Bhatia SR (2011) Poly(lactic acid)-poly(ethylene oxide) block copolymers: new directions in self-assembly and biomedical applications. *Curr Med Chem* 18:5676–5686
102. Kosukegawa H, Mamada K, Kuroki K et al (2009) Evaluation of compliance of poly (vinyl alcohol) hydrogel for development of arterial biomodeling. In: *Proceedings of the 13th international conference on biomedical engineering, IFMBE*, pp 1993–1995
103. Meenach S, Anderson AA, Suthar M et al (2009) Biocompatibility analysis of magnetic hydrogel nanocomposites based on poly(N-isopropylacrylamide) and iron oxide. *J Biomed Mar Res Part A* 91A:903–909
104. Zhao L, Mitomo H (2008) Adsorption of heavy metal ions from aqueous solution onto chitosan entrapped CM-cellulose hydrogels synthesized by irradiation. *J Appl Polym Sci* 110:1388–1395
105. Becerra-bracamontes F, Sanchez-Diaz JC, Gonzalez-Alvarez A et al (2007) Design of a drug delivery system based on poly(acrylamide-co-acrylic acid)/chitosan nanostructured hydrogels. *J Appl Polym Sci* 106:3939–3944
106. Park JS, Woo DG, Sun BK et al (2007) In vitro and in vivo test of PEG/PCL-based hydrogel scaffold for cell delivery application. *J Control Release* 124:51–59
107. Jeong B, Gutowska A (2002) Lessons from nature: stimuli-responsive polymers and their biomedical applications. *Trends Biotechnol* 20:305–311
108. Darsow U, Vieluf D, Ring J (1995) Atopy patch test with different vehicles and allergen concentrations: an approach to standardization. *J Allergy Clin Immunol* 95:677–684
109. Corkhill PH, Hamilton CJ, Tighe BJ (1989) Synthetic hydrogels. VI. Hydrogel composites as wound dressings and implant materials. *Biomaterials* 10:3–10
110. Fuciños C, Fuciños P, Miguez M et al (2014) Temperature- and pH-sensitive nanohydrogels of poly(N-Isopropylacrylamide) for food packaging applications: modelling the swelling-collapse behavior. *PLoS ONE* 9:e87190. <https://doi.org/10.1371/journal.pone.0087190>
111. Rhim JW, Wang LF (2013) Mechanical and water barrier properties of agar/ κ -carrageenan/konjac glucomannan ternary blend biohydrogel films. *Carbohydr Polym* 96:71–81
112. Fuciños C, Guerra NP, Teijon JM et al (2012) Use of poly(N-isopropylacrylamide) nanohydrogels for the controlled release of pimaricin in active packaging. *J Food Sci* 77: N21–28. <https://doi.org/10.1111/j.1750-3841.2012.02781.x>
113. Roy N, Saha N, Kitano T et al (2012) Biodegradation of PVP-CMC hydrogel film: a useful food packaging material. *Carbohydr Polym* 89:346–353
114. Schneider KP, Gewessler U, Flock T et al (2012) Signal enhancement in polysaccharide-based sensors for infections by incorporation of chemically modified laccase. *N Biotechnol* 29:502–509
115. Incoronato AL, Conte A, Buonocore GG et al (2011) Agar hydrogel with silver nanoparticles to prolong the shelf life of Fior di Latte cheese. *J Dairy Sci* 94:1697–1704
116. Langmaier F, Mokrejs P, Kolomaznik K et al (2008) Biodegradable packing materials from hydrolysates of collagen waste proteins. *Waste Manag* 28:549–556

117. Varma DM, Gold GT, Taub PJ et al (2014) Injectable carboxymethylcellulose hydrogels for soft tissue filler applications. *Acta Biomater* 10:4996–5004
118. Kodavaty J, Deshpande AP (2014) Regimes of microstructural evolution as observed from rheology and surface morphology of crosslinked poly(vinyl alcohol) and hyaluronic acid blends during gelation. *J Appl Polym Sci* 131:1–10. <https://doi.org/10.1002/APP.41081>
119. Tichota DM, Silva AC, Sousa Lobo JM et al (2014) Design, characterization, and clinical evaluation of argan oil nanostructured lipid carriers to improve skin hydration. *Int J Nanomed* 9:3855–3864
120. Wang PC, Huang YL, Hou SS et al (2013a) Lauroyl/palmitoyl glycol chitosan gels enhance skin delivery of magnesium ascorbyl phosphate. *J Cosmet Sci* 64:273–286
121. Wang Y, Du R, Yu T (2013b) Systematical method for polyacrylamide and residual acrylamide detection in cosmetic surgery products and example application. *Sci Justice* 53:350–357
122. Pavavic T (2013) Calcium hydroxylapatite filler: an overview of safety and tolerability. *J Drugs Dermatol* 12:996–1002
123. Lee E, Kim B (2011) Smart delivery system for cosmetic ingredients using pH-sensitive polymer hydrogel particles. *Korean J Chem Eng* 28:1347. <https://doi.org/10.1007/s11814-010-0509-8>
124. Raschip IE, Hitruc EG, Vasile C (2011) Semi-interpenetrating polymer networks containing polysaccharides. II. Xanthan/lignin networks: a spectral and thermal characterization. *High Perf Polym* 23:219–229. <https://doi.org/10.1177/09544008311399112>
125. Simi CK, Abraham TE (2010) Transparent xyloglucan–chitosan complex hydrogels for different applications. *Food Hydrocoll* 24:72–80
126. Chandrika KSVP, Singh A, Sarkar DJ et al (2014) pH-sensitive crosslinked guar gum-based superabsorbent hydrogels: swelling response in simulated environments and water retention behavior in plant growth media. *J Appl Polym Sci* 131:1–12. <https://doi.org/10.1002/APP.41060>
127. Böhlenius H, Overgaard R (2014) Effects of direct application of fertilizers and hydrogel on the establishment of poplar cuttings. *Forests* 5:2967–2979
128. Hotta M, Kennedy J, Higginbotham CL et al (2014) Synthesis and characterisation of novel ι-Carrageenan hydrogel blends for agricultural seed coating application. *Appl Mech Mat* 679:81–91
129. Tang H, Zhang L, Hu L et al (2014) Application of chitin hydrogels for seed germination, seedling growth of rapeseed. *J Plant Growth Regul* 33:195–201
130. Bortolin A, Aouada FA, Mattoso LH et al (2013) Nanocomposite PAAm/methyl cellulose/montmorillonite hydrogel: evidence of synergistic effects for the slow release of fertilizers. *J Agric Food Chem* 61:7431–7439
131. Shahid SA, Qidwai AA, Anwar F et al (2012) Improvement in the water retention characteristics of sandy loam soil using a newly synthesized poly(acrylamide-co-acrylic acid)/AlZnFe₂O₄ superabsorbent hydrogel nanocomposite material. *Molecules* 17:9397–9412
132. Guilherme MR, Reis AV, Paulino AT et al (2010) Pectin-based polymer hydrogel as a carrier for release of agricultural nutrients and removal of heavy metals from wastewater. *J Appl Polym Sci* 117:3146–3154
133. Bao JM, Wang YZ, Li YX (2014a) Preparation of crosslinked dextran hydrogel microspheres by inverse suspension polymerization and its application in separation of liposome and drug. *Xiandai Huagong/Modern Chem Indus* 34:55–58, 60. ISSN: 02534320
134. Bao S, Wu D, Wang Q et al (2014b) Functional elastic hydrogel as recyclable membrane for the adsorption and degradation of methylene blue. *PLoS One* 9(2):e88802. <https://doi.org/10.1371/journal.pone.0088802>
135. Cao Y, Lui N, Fu C et al (2014) Thermo and pH dual-responsive materials for controllable oil/water separation. *ACS Appl Mater Interfaces* 6:2026–2030
136. Tongwa P, Bai B (2014) Degradable nanocomposite preformed particle gel for chemical enhanced oil recovery applications. *J Petrol Sci Eng* 124:35–45

137. Zolfaghari R, Katlab AA, Nabavizadeh J et al (2006) Preparation and characterization of nanocomposite hydrogels based on polyacrylamide for enhanced oil recovery applications. *J Appl Polym Sci* 100:2096–2103
138. Aalaie J, Vasheghani-Farahani E, Semsarzadeh MA et al (2008) Gelation and swelling behavior of semi-interpenetrating polymer network hydrogels based on polyacrylamide and poly(vinyl alcohol). *J Macromol Sci Part B* 47:1017–1027
139. Lei ZX, Chen YM, Chen YW et al (2006) Preliminary results of pilot test on indepth permeability profile control/emulsion flood by using PAM inverse emulsion. *Oilfield Chem* 23:81–84
140. Wang XM, Zhang DS (2003) A preliminary study on xanthan/zirconium flowable gel as flooding fluid. *Oilfield Chem* 20:157–159
141. Tiena HT, Ottovaab AL (1998) Supported planar lipid bilayers (s-BLMs) as electrochemical biosensors. *Electrochim Acta* 43:3587–3610

Application of Sustainable Nanocomposites for Water Purification Process



Hayelom Dargo Beyene and Tekilt Gebregiorgs Ambaye

1 Introduction

Water is one of the most vital bases for the living system and is used in daily life activities. Due to rapid industrial growth, natural water resources are affected by several water pollutants. The World Health Organization (WHO) 2014 report on water supply and sanitation estimated that 748 million people still lack safe drinking water, 2.5 billion peoples without access sanitation and 3900 children die every day due to poor quality water and communicable diseases [1]. These statistics indicated that water pollution by numerous pollutants becomes an alarming issue worldwide. Consequently, competent water treatment technologies have been established to raise the potential of water resources and to decline the challenges and concerns associated with water pollution. In this regard, nanocomposite has to play a significant role in the water purification technology including potable water treatment, wastewater desalination, and treatment in order to deliver the real technology to clean water at a lower price using less energy by decreasing further ecological impacts.

Nanomaterials are materials which have the structural components sized from 1 to 100 nm [2]. They have unique properties when compared with other conventional materials, such as mechanical, electrical, optical, and magnetic properties due to their the small size and higher specific surface area, nanomaterials [2]. In recent years, nanomaterials have been effectively applied to numerous perspectives as catalysis [3], medicine [3], sensing, and biology [4]. They have extensive applications to prevent several environmental problems like water and wastewater

H. D. Beyene (✉)

Department of Chemistry, Adigrat University, P.O. Box: 50, Adigrat, Ethiopia
e-mail: hayeda21@gmail.com

T. G. Ambaye

Department of Chemistry, Mekelle University, Mekelle, Ethiopia

treatment. Because, nanomaterials have the potential to eliminate different toxins, for instance, heavy metals, organic pollutants, inorganic anions, and pathogens [5]. Zero-valent metal nanoparticles (nZVI), metal oxides nanoparticles, carbon nanotubes (CNTs) and nanocomposites are the most recent appropriate nanomaterials for water and wastewater treatment [6].

The nZVI is one of the most useful nanomaterials for water purification [7–9]. The nZVI has a role in water purification as an electron subscriber which encourages the conversion toxic metals to safe forms (the reduction of chromium from hexavalent into trivalent form), adsorption, co-precipitation processes and strong reducing ability [10]. The nZVI has discovered real application for eliminating various organic and inorganic pollutants such as polychlorinated compounds [11, 12], Nitrates, phosphates and perchlorates [13, 14], nitroaromatic compounds [15], organic dyes [16], phenols [17], heavy metals [18], metalloids [19], and radio elements [6, 20].

Other nanoparticles like silver (Ag), titanium oxide (TiO₂), zinc oxide (ZnO), iron oxides and CNT are applied in water treatment technology. Silver nanoparticles (AgNPs) are very noxious to microbes and hence have solid antibacterial effects for an extensive variety of microorganisms (viruses, bacteria, and fungi) [21]. AgNPs are the promising antimicrobial agents, which have been extensively used for water disinfection [21]. AgNPs have the removal potential for bacteria's like methicillin-resistant *Staphylococcus aureus*, ampicillin resistant *E. coli*, a common water contaminant, erythromycin resistant *Streptococcus pyogenes* and vancomycin-resistant *Staphylococcus aureus* [22], *Pseudomonas aeruginosa*, *Vibrio cholera* [23], *Bacillus subtilis* [24]. There are different ways of Nanosilver disinfection mechanisms such as the interaction of AgNPs with DNA, altering the membrane and altering the enzymatic activity and thus destroy it [25–28], the dissolution of AgNPs that able to react through the thiol sets of enzymes disable, and interrupt usual services the cell [29].

In nanocomposites (NCs), there is no a previous documented review of their application in water and wastewater treatment perspectives. NCs are formed through the combination of more than two materials having various physical and chemical properties and unique interface [28], [30]. Composites have many advantages than other compounds due to their unique characteristics such as high durability, high rigidity, high strength, gas-barrier features, corrosion resistance, low density, and heat resistance. The combination of the matrix (continuous phase) and the reinforced materials (dispersed) is known as composite materials. They are materials of the 21st century which are multiple phase materials a minimum one of the phase's displays sizes from the range 10–100 nm [31]. Today, NC materials have developed as appropriate choices to overwhelmed restrictions of various manufacturing tools. NCs have wide practice in various fields such as life sciences, drug distribution schemes, and wastewater treatment. In NCs, the nanoparticles were merged within diverse functionalized materials like multiwall CNT, activated carbon, cheap graphene oxide, and polymeric media. NCs have a number of application in the area of food packaging [32–34], anti-corrosion barrier protection [31], biomedical [31, 35] and coating [36]. This chapter focuses on the exciting NC

types and their current application in water purifications. Besides, the future perspective of nanocomposites in water treatment also addressed.

2 Conventional Water Purifications Technologies

Surface water (spring, rivers, and lakes) and unconventional water resources (which are not available for direct use. For example, wastewater, seawater and brackish water) are the major universal water resources potentials [37]. Globally, the upsurge in industrialization and urbanization with a quick population growth and weather change contributes to the pollution of freshwater resources [38–40]. Table 1 shows the available conventional water purification technologies such as coagulation and flocculation, air flotation and advanced oxidation processes. These methods are very quiet in removing the contaminants efficiently. However, these methods possess several challenges related to the formation of either secondary pollution or higher energy requirement. Therefore, a massive attention should be given to the improvement/innovation of technologies having ecologically friendly, low energy consumption and economical feasible treatments perspectives applicable to the feasible water sanitization systems. To meet the demand for clean water standards, many authors have been focused on the suitable and economically viable water purification approaches including water remediation, reclamation, and desalination [41].

Table 1 Water purification methods [24, 41]

Water purification technologies	Contaminate removed
Coagulation and flocculation	Turbidity, dissolved organic carbon, bacteria and chemical contaminants such as cyanide compounds, phosphorus, fluorides, arsenic etc
Boiling	Kill the bacterial cultures
Distillation	To destroy microbial cells and unwanted chemicals such as calcium, lead, magnesium
Ultraviolet treatment	Can achieve disinfection of about 99.99%
Ultrasound	Damage cellular structures of bacteria
Ozone	It is effective in eradicating tastes, odour, colour, iron, and manganese; and not affected by pH and temperature
Chlorine	Kills several waterborne pathogens
Catalytic process	Applied to breakdown down an extensive diversity of organic materials like organic acids, estrogens, pesticides, dyes, crude oil and microbes
Bioremediation	Eradicating heavy metals, organic toxins, pesticides and dyes by plant extracts and microbes.

3 Types of Nanocomposites and Its Application in Water Purification

The use of nanoparticles in water management has associated with some practical problems, such as accumulation, tough separation, drainage into the contact water, possess environmental and human health [30]. One capable approach to improve the application of nano-particulate materials is to develop NC materials that take advantages of both the hosts and impregnated nanoparticles (Fig. 1) [42]. NCs have the potential to mitigate the discharge of nanoparticles into the environment, and improves the suitability of nanotechnology with current infrastructures. The NCs are essentially multiphase solid material, including porous media, colloids, gels, and copolymers in a broad sense. The selection of hosts for nanocomposites is of great significance, and even dominates the performance of the resultant nanocomposites. Compared with free nanomaterials, the performance and usability of nanocomposites were significantly improved, in terms of nanoparticle dispersion, stability, and recyclability. Hence, nanocomposite materials could bond the gap between nanoscopic and mesoscopic scale. Till now, nanocomposites were believed to be the most likely way to forward water nanotechnology from laboratory up to the large-scale applications [41].

3.1 Metal Nanocomposite

Polymer-supported nanosilver has recognized antibacterial properties of polyurethane and cellulose acetate impregnated nanosilver-fiber composites have good inhibition activity for Gram-positive and negative bacteria. The dispersion

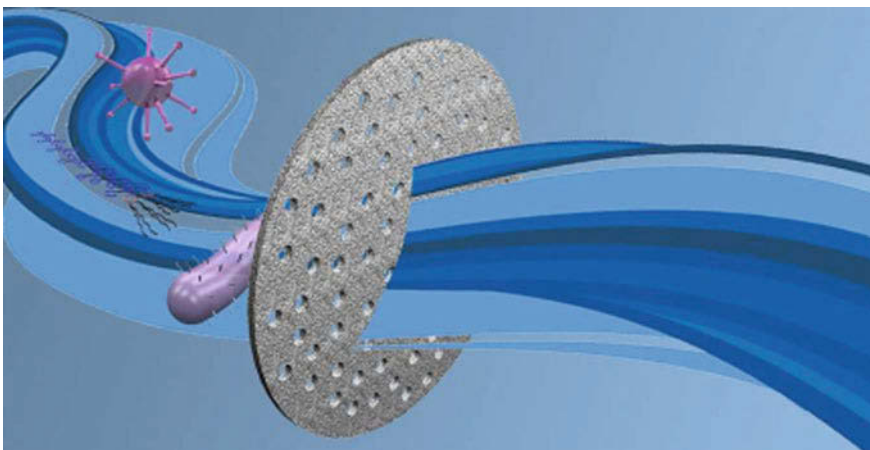


Fig. 1 Application of nanocomposite for water purification [42]

nanoparticle in polyurethane foam has gained effective antibacterial filters [43]. Once announced in polymeric membranes, a decrease of biofouling as well as good pathogen eradication efficiency was perceived. Nanosilver was also used in the making of economically feasible microfilters for handling drinking water which is mainly preferred in unreachable regions [44].

Silver-alginate composite beads were effectively prepared using three different methods. Specifically, the adsorption-reduction (AR), hydraulic retention time (HRT) and simultaneous gelation-reduction (SGR) composite beads were talented to succeed a disinfection effectiveness for portable water purifying. Those Composite beads equipped using diverse methods were established effective cleaning in the *E. coli* to various degrees. Both SGR and the AR beads confirmed equivalent disinfection efficiency but, the SGR beads released knowingly more Ag than the AR beads fix, indicating that the SGR beads may have a higher lifespan than the AR beads without losing sterilization success. These results weight the significance of improving the synthesis method in yielding material configurations that lead to the essential physical properties of numerous aspects [45].

The synthesized novel NC containing AgNPs and mesoporous alumina have been used for the elimination of dye compounds like methyl orange, bromothymol blue, and reactive yellow from synthetic waste. The results display that the silver/mesoporous alumina nanocomposite (Ag/OMA NC) was noble adsorbent for the elimination of anionic dyes from aqueous solution, and also this NCs had an antibacterial activity against both Gram-negative and Gram-positive bacteria [46].

The addition of AgNPs and *Moringa oleifera* seed powder were improved graphene structure which improves the removal efficiency of pollutants from liquid industrial waste like textile, tannery, and paper mill. The adsorption study of the adsorbents clearly revealed that the graphene loaded with AgNPs and seed powder of *Moringa oleifera* composite (GAM) designated superior results compared to normal adsorbents due to the configuration of GAM sorbent which is recognized by the high surface area, biocidal action, adsorption activity AgNPs, and coagulation property of *Moringa oleifera*. Thus motivated the composite to be novel, economically feasible, and environmental suitable and promising adsorbent for water treatment [47].

Bimetallic nanocomposites supported on carbon are of great interest. Carbon supported bimetallic nanoparticles have reduced surface area which enhances their properties to a large extent. Nowadays, Water pollution is crucial problem happen due to existence contaminates like chemicals, microbes (fungi, bacteria, and virus) in water by human activities. Nanotechnology offers an alternative to the water purification. The bimetallic nanoparticles like ruthenium-palladium are used as reinforce to develop NC on the surface carbon matrix which had successfully helped in wastewater treatment having perchlorate as the main pollutant [31]. Others like, NCs of Au/Pd nanoparticles reinforced on TO₂ have been synthesis by microemulsion means and being used as an efficient photocatalyst due to their high light absorption ability. Bimetallic NCs of Fe/Ni-K have the capacity to remove DBG from the wastewater. The degree of eliminating DBG in the NC (Ni/Fe-K) is greater than that of separate kaolin and the bimetallic nanoparticles (Ni/Fe) [31, 48].

3.2 *Metal Oxide Nanocomposite*

The Metal oxide nanocomposite (MONC) are often used as adsorbents, photocatalyst, and devices to challenge environmental pollution problems. MONC are used merging with graphene, silica, other oxides, carbon nanotube (CNT), polymers for the removal of various organic and inorganic of pollutants [49]. Currently, removal of organic pollutants from wastewater is one of the most significant alarms in water pollution control. In last decade, the interest in solving global water pollution by means of photocatalysis is increased rapidly using metal oxide nanoparticles (TiO_2 and ZnO). However, the use of basic TiO_2 and ZnO nanoparticles are limited because of their extensive band gap and the high recombination rate of photo produced charges. Coupling is developing an approach to increase the destroying degree of organic contaminants under visible light conditions. MONC provide a current technique to modify the properties of semiconductor metal oxide photocatalyst through encouraging charge transfer processes and improving charge separation [50].

The alumina composite reinforced by CNTs was produced by rising CNT above Fe and Ni-doped energetic alumina. The composite was influenced by numerous factors able to initiated high capacity synthesis which is factors includes activated alumina, CNT, amorphous carbon and various surface functional groups such as carboxyl, carbonyl and hydroxyl present in the clusters [51]. Ihsanullah et al. [52] deliberated that the consequence CNT/ Al_2O_3 for actual elimination of chlorophenol and phenol from aqueous solutions. Alumina ornamented onto the exterior of multi-well carbon nanotube (MWCNT) was an inspiring adsorbent for immediate removal of Cd^{+2} and trichloroethylene (TCE) from poisoned groundwater. Electrostatic interactions, the hydrogen bond interactions and the protonation or hydroxylation of Al_2O_3 are the adsorption mechanism of Al_2O_3 /MWCNTs to remove Cd^{+2} and TCE from the polluted water Fig. 2 [53, 54].

TiO_2 is the new greater type of composites based Metal oxide. TiO_2 nanocomposite has received more attention in water purification due to its nontoxicity, and the ability for the photo-oxidative degradation contaminates such as MB [55], benzene derivatives [56], and carbamazepine [57] were powerfully photodegraded by CNT/ TiO_2 composites. Researchers described that the bond of carbon-oxygen-titanium can enlarge the light absorption to longer wavelengths and hence potentially improvement of the photocatalytic action [53]. Senusi et al. [40] also indicated that synthesized TiO_2 -zeolite NCs for the innovative water treatment of industrial dyes. The results indicated that the nanocomposite followed an adsorption concerned with photocatalytic degradation, which is mainly effective for eradicating trace dye compounds [40]. A novel Cu- TiO_2 - SiO_2 NCs synthesized by a sol-gel method and used to degrade Rhodamine Blue in water modelling the dyes wastewater under both UV and visible light irradiation. Studies revealed that the Cu- TiO_2 - SiO_2 nanocomposite has smaller crystalline size, higher surface area, and slight agglomeration by judging from the characteristic analysis. The Cu- TiO_2 - SiO_2 nanocomposite exhibited higher photocatalytic activity than TiO_2 for the

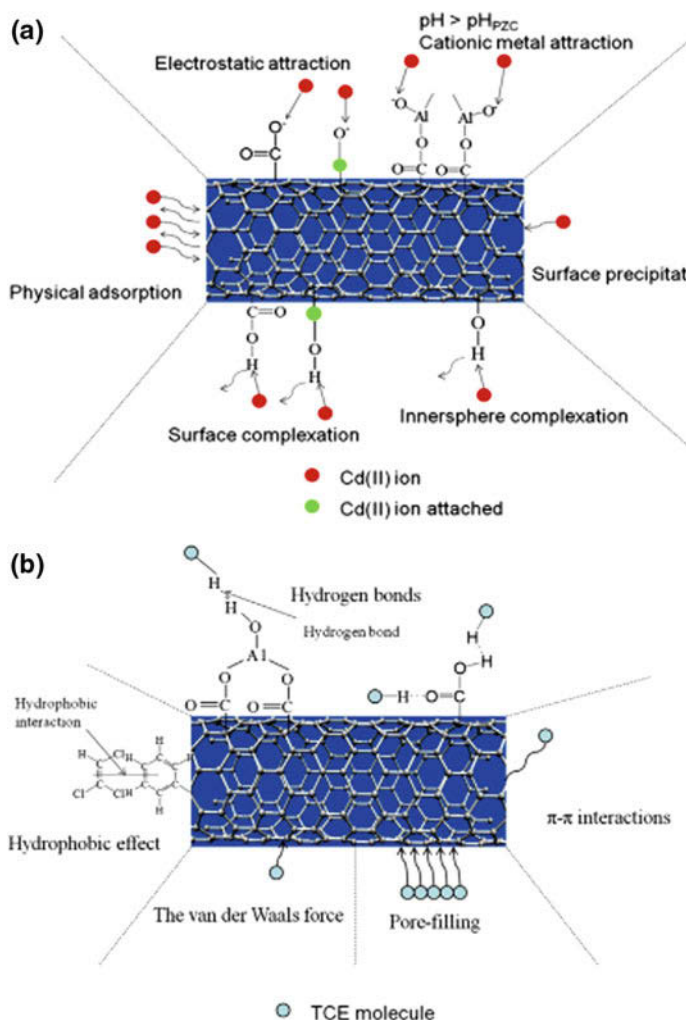


Fig. 2 The diagram representation of Cd(II) ion (a) and TCE (b) interface with Al₂O₃/MWCNTs [53]

degradation of Rhodamine Blue under both UV and visible light irradiation. The increase in the photocatalytic activity may be due to the lower recombination rate of electron-hole and the high dispersion of SiO₂ [58].

Iron oxides (i.e. Fe₂O₃ and Fe₃O₄) are unique and talented magnetic constituents which create a new composite with CNTs, and graphene. This is one of the greatest smart magnetic metallic oxides and has established extensive consideration due to its exceptional physical and chemical properties and several benefits such as high reversible capacity, rich abundance, cheap, and environmentally friend [54]. Magnetic nanoparticles are highly advantageous than nonmagnetic nanoparticles

since they can simply isolate from water via a magnetic field. Magnetic field separation is a practice also allows simple isolation and recycled the adsorbents. Magnetic nanocomposites can be fabricated using magnetite (Fe_3O_4), maghemite (Fe_2O_3), and jacobite (MnFe_2O_4) nanoparticles as reinforcer filling on a polymer matrix which permits easy separation of the composite from the aqueous solutions after the sorption process [29].

Researchers were investigated series of magnetic alginate polymers prepared and batch trials were shown to examine their capacity to eliminate heavy metal ions such as Co^{+2} , Cr^{+6} , Ni^{+4} , Pb^{+2} , Cu^{+2} , Mn^{+2} , La^{+3} and organic dyes (MB and MO) from aqueous solutions. Different types of iron oxide magnetic composites have been positively useful as an adsorbent for the elimination of various targets of impurities from water and wastewater such as naphthylamine [59], metals [59], phenol [59], and tetracycline [60], As^{+3} , As^{+5} [61], dyes [62]. Moreover, graphene-based iron oxide NCs have confirmed an exceptional adsorption capacity to fix extra heavy metals and organic dyes such as Cr^{+6} , Pb^{+2} , Co^{+2} , neutral red, MB etc. due to magnetic properties, high surface to volume ratio and rapid diffusion rate [59].

In addition to the above, Currently, many researchers have studied also on the practice of metal oxide NCs for water and wastewater purification. Currently, many scientists focus on the heavy metals removal due to their strong influence on health and environment. The Saad et al. [63] was to manufacture ZnO@Chitosan nanocomposite (ZONC) to eliminate Pb^{+2} , Cd^{+2} and Cu^{+2} ions from unclean water with optimal removal efficiency for Pb^{+2} , Cd^{+2} and Cu^{+2} ions at pH 4, 6 and 6.5 with adsorption capacity were 476.1, 135.1 and 117.6 mg/g, respectively. The researchers also studied nonstop adsorption-desorption cyclic outcomes established that ZONC can be reused after recovery of ions by EDTA solution, and the regenerate ZOCS used over without significant efficiency loss [63].

Singh et al. [64] investigated that BC_4/SnO_2 NCs was an effective catalyst for the degradation of industrial dyes such as Novacron red Huntsman (NRH) and MB. This composite is also discovered for catalysis destruction of industrial dyes. The Degradation study displays that 1 g/L catalyst concentration of BC_4/SnO_2 destroys NRH and MB dye up to nearly 97.38 and 79.41%, respectively, in 20 min using sun radiation. The catalyst can be recycled and recovered [64].

Zr-magnetic metal-organic frameworks composites (Zr-MFCs) are an amino-rich prepared by a facile and efficient strategy. The achieved Zr-MFCs were confirmed to be effective adsorbents with feasible adsorption ability and fast adsorption kinetics for metal ions and organic dyes removal from water. The amine-decorated MFCs were very efficient for metal ions and dyes elimination than row MFC-O. MFC-N confirmed the maximum ability for Pb^{2+} (102 mg g^{-1}) and MB (128 mg g^{-1}), while MFC-O revealed the maximum ability for MB (219 mg g^{-1}). Furthermore, Zr-MFCs have also good removal efficiency for anionic and cationic dyes from the miscellaneous solution by adjusting pH. Zr-MFC adsorbents can be simply improved by removing metal ions and/or organic dyes from the adsorbents with appropriate reagents without change adsorption capacity up to 6 generations. The attained results confirmed the prepared MFCs have the great application perspective as interesting adsorbents for water treatment [65].

Saad et al. [63] investigated a facile method for in situ fabrication of ZnO@Chitosan nanocomposite (ZONS), and the attained composite demonstrated noble ability and rapid kinetics for Pb^{+2} , Cd^{+2} and Cu^{+2} ions adsorption. The main advantage of this product is the recovery of metal ions and the significant ability for adsorption after many series of recycling. The ZONC demonstrations important feasibility in ecological remediation for wastewater treatment and can attain the increasing need for the purification of water resources [63].

3.3 Carbon Nanocomposite

A magnetic multi-wall carbon nanotube (MMWCNT) nanocomposite was used as an adsorbent for removal of cationic dyes from aqueous solutions. The MMWCNT nanocomposite was composed of viable multi-wall CNT and IONPs. The elimination of MB, neutral red and brilliant cresyl blue was deliberate using MMWCNT nanocomposite adsorbent. Investigations were carried out to study adsorption kinetics, the adsorption capacity of the sorbent and the effect of sorption dosage and pH values on the elimination of cationic dyes [66].

Mesoporous carbon with entrenched iron carbide nanoparticles (ICNPs) was effectively synthesized via a facile impregnation-carbonization method. Biomass was used as a carbon basis and an iron pioneer was rooted to create mesopores through a catalytic graphitization reaction. The pore conformation of the NCs structured by the iron pioneer loadings and the immovable ICNPs support as a dynamic component of magnetic isolation next sorption. The newly produced mesopores were established as a critical feature to increase the adsorption capacity of organic dyes while immovable ICNPs are responsible for the careful removal of heavy metal ions (Zn^{2+} , Cu^{2+} , Ni^{2+} , Cr^{6+} , and Pb^{2+}). Composed with the desirable elimination of extra noxious heavy metal species (Cr^{6+} and Pb^{2+}), these mesoporous NCs show favourable applications in impurity removal from water. The facile material preparation permits appropriate scale-up production with economical feasible and lowest ecological impact [67].

Advanced technologies integrating with engineered nanoparticles into biochar fabrication schemes might increase the roles of biochar for numerous uses comprising soil fertility upgrading, carbon sequestration, and wastewater treatment. Inyang et al. [68], investigated that removal ability MB was evaluated in batch sorption using untreated hickory biochars (HC), bagasse biochars (BC) and CNT-biochar composites (HC-CNT and BC-CNT, respectively). The addition of CNTs considerably enriched the physiochemical properties of HC-CNT and BC-CNT such as extreme thermal stabilities, surface areas, and pore volumes. These results recommend that electrostatic magnetism was the principal devices for the removal of MB onto the biochar-nanocomposite. Hybridized CNT-biochar NC can be considered as capable, cheap adsorbent material for eliminating dyes and organic contaminants from water [68].

Carbon-nanocomposites (CNCs) are constituents that have two or more elements prepared to form a composite mixture with CNTs as the primary host synthesized the poly 1,8-diaminonaphthalene/MWCNTs COOH hybrid material which could be used as an active sorbent for the separation Cd^{+2} and Pb^{+2} at trace levels [40]. Muneeb et al. [69] was primed a new NCs from biomass used for the removal of selected heavy metals (As, Cr, Cu, Pd and Zn) from the wastewater. With the increase in pH, there was a decline in percentage adsorption of the metals [70].

Tian et al. [70] stated an eco-friendly, effective and synergistic nanocomposite development for new antibacterial agents using both iron oxide nanoparticles (IONPs) and AgNPs on the surface of graphene oxide (GO), resulted in novel GO-IONP-Ag nanocomposite. When associated with pure AgNPs, GO-IONP-Ag offers deliberately improved bacteriocidal action to both Gram-negative bacteria and Gram-positive bacteria. GO has the beautiful benefit through GO-IONP-Ag composite to kill Gram-positive bacteria at small agent concentration. Moreover, GO-IONP-Ag nanocomposite can simply reprocess by magnetic separation, low cost, and environmentally. In the account of those exceptional benefits, the developed GO-IONP-Ag nanocomposite can use for prospective requests as a multifunctional sterile agent in the diverse area [71].

3.4 Polymer Nanocomposite

Polymer nanocomposites (PNCs) are a superior type of tools which nanoparticles spread in a polymer matrix resulting in novel materials having unique physical and chemical properties [70]. Polymers are special supports for nanomaterials as they usually possess tunable porous structures, excellent mechanical properties, and chemically bounded functional groups. PNCs are prospecting materials for their sound performance in water and wastewater treatment. Adsorption of contaminant through PNC is among various treatment technologies, which is considered as an advanced tool in water treatment technology. PNCs often integrate the essential advantages of both the nanoparticles and the polymeric matrix [72]. PNCs could be synthesis by either joining nanoparticles into polymer structures or by fixing polymers to nanoparticles. Direct compounding and in situ synthesis are two leading approaches used in the manufacture of several PNCs as shown in Fig. 3 [41]. PNC has of great potential for pollutants removal including heavy metals (Cu, Pb, Cr (III), Ni), As, F, and P. The pollutants were often removed through multiple mechanisms including surface complexation, electrostatic attraction and co-precipitation [73].

These PNCs are avoided challenging issues such as nanoparticle dissolution, which is common when using free nanoparticles [72]. Some of the nanocomposites were also responsive to regeneration and recycle without significant capacity loss, which is critical from economic outlook. Since of the large size of the PNCs, they could be simply isolated from treated water.

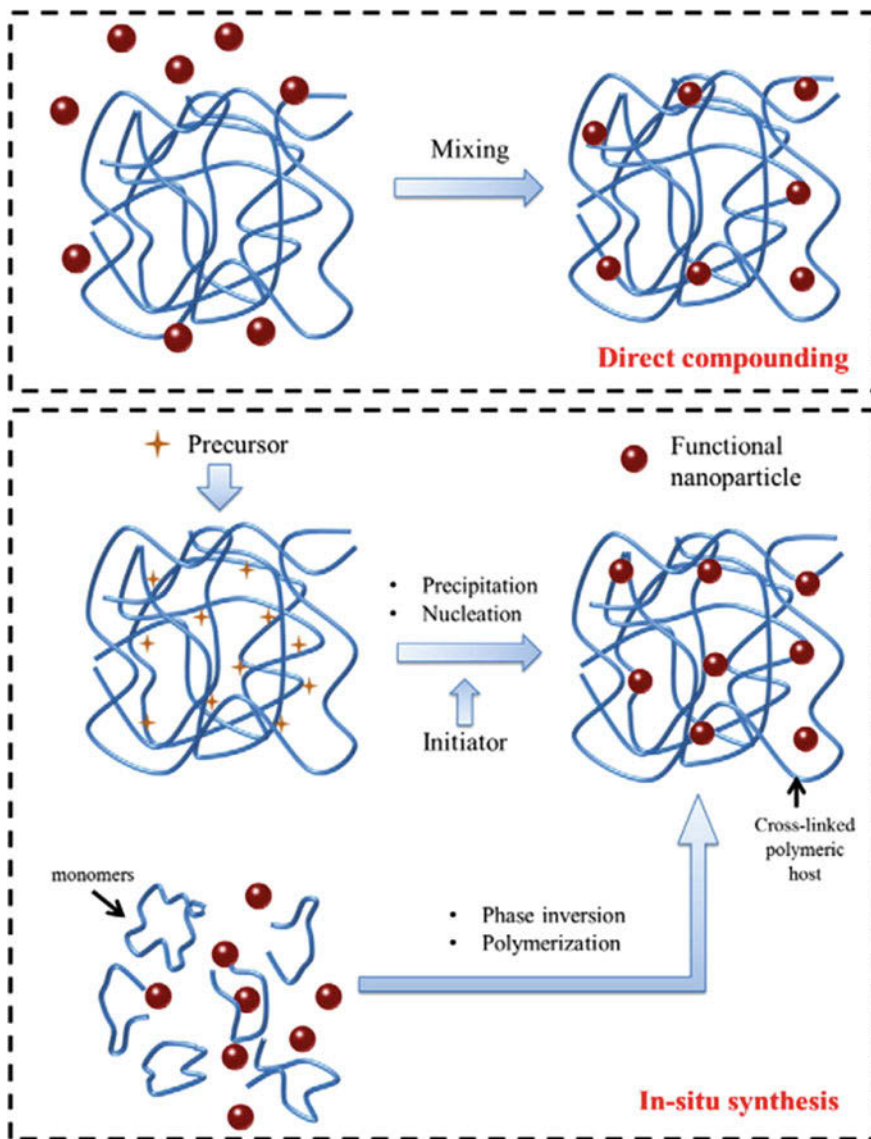


Fig. 3 Graphic of fusion methods for PNCs. Adapted with permission [41]

Alginate [74], macromolecule (polypyrrole) [75] polyaniline [76], porous resins [77] and ion-exchangers [41] are most extensively used polymeric hosts. New types of polymeric hosts are essentially bio-polymers such as chitosan and cellulose. They are plentiful in nature and eco-friendly. However, they could suffer a serious biodegradation problem in the long-term application. cellulose showed good chemical stability and mechanical strength, due to its densely and systematic

aligned, hydrogen-bonded molecules, sound swelling resistance and its characteristics such as hydrophilicity and chirality. Chitosan is the another most naturally rich polysaccharide next to cellulose. Chitosan has exceptional features such as high reactivity, excellent complexation behaviour, and chemical stability. The amino and hydroxyl groups of chitosan aid as energetic sites for water pollutants [78]. Generally, cross-linked chitosan was insoluble even at low pHs, so that they might be applicable over a wide pH range. Djerahov et al. [78] prepared a steady CS-AgNPs colloid by diffusing the AgNPs sol in chitosan medium and additional recycled it to attain a cast film with high steadiness under packing and good mechanical strength. It showed efficient isolation and extraction of Al^{+3} , Cd^{+2} , Cu^{+2} , Co^{+2} , Fe^{+3} , Ni^{+2} , Pb^{+2} and Zn^{+2} [40, 78].

Saxena and Saxena [79] developed Bimetal oxide fixed PNC by means of Alumina and IONPs with Nylon-6,6 and Poly (sodium-4-,styrenesulphonate) as polymer medium for pollutants elimination from the water. The prepared NCs have maximum pollutant removal capacities for all factors. The exclusion of total alkalinity, total hardness, calcium, magnesium, chloride, nitrate, fluoride, TDS and EC was 66.67, 42.85, 66.67, 25, 58.66, 34.78, 63.85, 41.27 and 41.37% respectively by this composite. This is an indication period towards emerging multi-functional and profitable PNCs for water remediation requests [79].

CNTs powerfully sorb varied polar organic compounds attributable to the stuff miscellaneous interfaces together with hydrophobic impact, peppiness interactions, covalent bonding, valence bonding, and electrical connections. The π -electron wealthy CNT apparent allows energy exchanges with carbon-based molecules with C=C bonds. Organic compounds that have used functional groups like $-\text{COOH}$, $-\text{OH}$, $-\text{NH}_2$ might additionally kind a bond with the graphitic CNT exterior that pays electrons. Electricity magnetism enables the surface assimilation of exciting carbon-based chemicals like some antibiotics at appropriate pH range. PNCs are sorbents tailored adsorbents which are talented for eliminating different types of pollutants. Their internal shells can be hydrophobic for sorption of organic compounds while the exterior channels can be tailored (e.g., $-\text{OH}$ or $-\text{NH}_2$) for sorption of inorganic pollutants like heavy metals. complexation, electrostatic interactions, hydrophobic effect, and hydrogen bonding are the mechanism established during sorption process [80].

Carboxymethyl-cyclodextrin polymer adapted Fe_3O_4 nanoparticles (Copolymers) was manufactured for selective elimination of Pb^{2+} , Cd^{2+} , Ni^{2+} ions from wastewater. The adsorption efficiency of metallic ions was influenced by the factors like contact time, a dose of copolymers pH, ionic strength, and temperature. At equilibrium condition in single sorption way, the optimum uptakes of the adsorbent for Pb^{2+} , Cd^{2+} , and Ni^{2+} were 64.5, 27.7 and 13.2 mg g^{-1} respectively at 45 min and 25 °C. The PNC improved the sorption capacity since of the chelating abilities of the several hydroxyl and carboxyl sets in polymer support with metal ions. In mixed adsorption experiments, CDpoly-MNPs might favorably high sorption of Pb^{2+} ions with an attraction order of $\text{Pb}^{2+} \gg \text{Cd}^{2+} > \text{Ni}^{2+}$ [81].

Khaydarov. et al. [82] studies a new technique for emerging nanocarbon-conjugated polymer nanocomposites (NCPC) by means of carbon colloids as

nanoparticle and polyethyleneimine as a matrix for metal ions removal from water. The researchers have been examined the efficiency of NCPC depends on size carbon colloids, synthesis NCPC and its chemical features, the ratio of carbon colloids and polyethyleneimine, the speed of coagulation NCPC, interaction mechanism, removal potential NCPC against pH. The bonding capacity adsorbent was 4.0–5.7 mmol/g with divalent metal ions at pH 6 which sorption has above 99% removal efficiency for Zn^{2+} , Cd^{2+} , Cu^{2+} , Hg^{2+} , Ni^{2+} , Cr^{6+} [82].

Clay can found the suitable matrix for varnish of polyaniline. The characterization outcomes of NC established that the clay sheet was develop layered in the synthesis NC. Parameters like contact time, pH, and concentration were determined the adsorption capacity of modified adsorbent. The researchers were announced new clay NC which use of polyaniline improved clay nanocomposite as an adsorbent for water purification of lead ions. It can be used as talented sorption scheme incoming water and wastewater treatment in order to eliminate lead ion [83].

Nithya and Sudha [84] studied using chitosan-g-poly(butyl acrylate)/bentonite NC as an adsorbent for chromium, lead and other significant physicochemical water quality parameters such as total solids (TS), biological oxygen demand (BOD), chemical oxygen demand (COD), total hardness, salinity, turbidity and conductivity from the tannery wastewater. The effect of some parameters, such as contact time, pH and dose adsorbent was assessed. The outcomes showed that NC can be used tannery wastewater treatment containing heavy metals powerfully [84].

3.5 Membranes Nanocomposite

In membrane technology, porous materials are plays capturing role to trap pollutants. Inclusive, numerous forms of membranes with diverse pore sizes engaged in water treatment process including microfiltration, ultrafiltration, reverse osmosis and nanofiltration membranes which depend on their shared materials that would be clean out through each process as shown Fig. 4 [42]. The existing membranes have numerous challenges for water purification, such as the exchange link between permeability, selectivity and low resistance to fouling. Recent progress in nanotechnology have offered the growth of the new generation membrane for water purification [40]. Nanocomposite membrane (NCM) has a great role in water purification and reuses for several bases of water such as drinking water, brackish, seawater, and wastewater treatment. NCM is an innovative type of membranes prepared by merging complex constituents with nanomaterials that are developing as a promising tool to answer membrane separation problems. The innovative NCM can be deliberate to fulfil exact water purification uses by calibration their assembly and chemical characters (e.g., water-heating, porousness, charge density, and thermal and mechanical stability) and announcing distinctive functionalities (e.g., medicinal drug, photocatalytic or adsorbent capabilities). The advance of membranes with high permeability, rejection and smart protective property is way

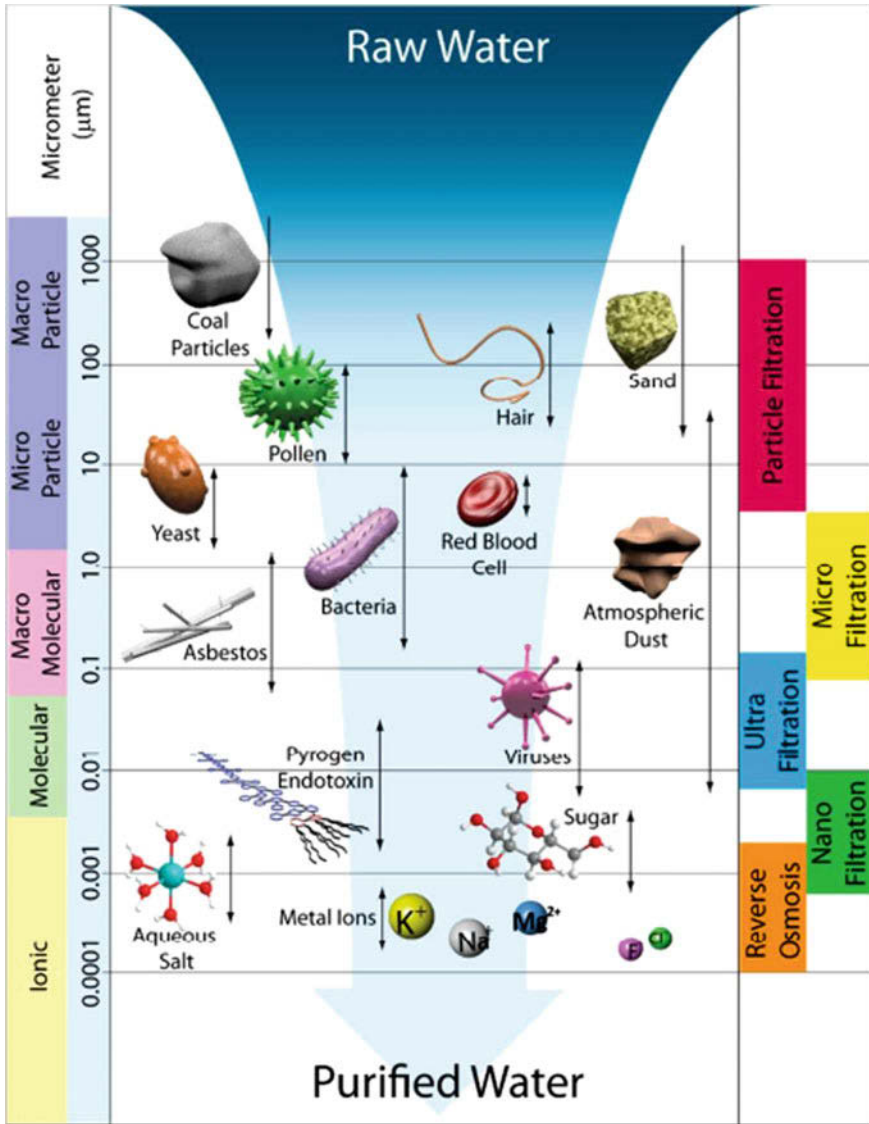


Fig. 4 Schematic illustration of membrane filtration [42]

required for water purification beneath the context of energy potency and cost-effectiveness. According to membrane assembly and position of nanomaterials, they can be classified into four groups: (1) conventional nanocomposite, (2) thin-film nanocomposite (TFN), (3) thin-film composite (TFC) with nanocomposite substrate, and (4) surface-located nanocomposite [85].

In water treatment applications, membranes have to significantly determine hydrophilicity, surface structure, and high toughness with respect to physico-chemical and mechanical stability. Pore size and porosity have also strong significant in membrane separation practices. NCM is a mixture of material that can have nanoscale inorganic and/or organic solid phases in a porous structure. These nanoscale constituents enrich membrane assets that would other not be fulfilled by the polymer only [85]. Nanomaterials can improve numerous characteristics of mechanical strength, thermal stability, antifouling properties, permeability, and selectivity which have enhanced membrane separations process. Various constituents such as CNTs, graphene and GO, silica and zeolites, metal and metal oxides, polymers, dendrimers and biological nanomaterials are used in NCM to improve water purification performance [86, 87].

NCM able to reflect as a novel class of filtration tools containing hybrid medium membranes and surface active membranes. Hybrid medium membranes use nanofillers, which are auxiliary to a medium material. In most cases, the nanofillers are inanimate and fixed in a polymeric or inorganic oxide medium. These nanofibers article has larger specific surface area leading to a higher surface-to-mass ratio [88]. NCMs are materials which have no single application of separating pollutants from water. They are also introducing new functionalities such as adsorption [89], photocatalysis [90], antimicrobial activity [91] and surface modification [91] which promoted adsorbing, degrading, and/or deactivating contaminates.

Most of the researchers have confirmed that the integration of nanomaterials into polymers besides to adjust assembly and physicochemical assets like hydrophilicity, porosity, and charge density, chemical, the thermal and mechanical stability of membranes, they are also announced exceptional characteristics such as bactericidal and photocatalytic features into the membranes. The effects of nanofiller on the performance of on the 3 type's NCMs are explained as follows.

3.5.1 Conventional Nanocomposite Membranes

Synthesis of CNM is commonly built on phase inversion (PI) technique in which nanofibers are discrete in polymer solution previous to the PI method as shown Fig. 5 [85]. It can be synthesised in either flat area or deep fiber arrangements. CNM is mostly applied in microfiltration or Ultrafiltration methods because it's typical porous arrangement.

It is known to join nanoparticles inside the polymer medium to create efficient membranes with an exact ability to adsorb heavy metals from water. For instance, incorporated PANI/Fe₃O₄ NPs inside polyethersulfone (PES) [92] and chitosan drops inside ethylene vinyl alcohol (EVAL) medium [93] had to remove Cu (II) water. Both outlooks have confirmed the opportunity of making CNM for the adsorptive elimination of impurities from water.

In the CNM research area, TiO₂ has also merged into numerous membrane mediums to deliver membrane with photocatalytic actions. TiO₂ has been extensively used for water treatment since its exceptional photocatalytic action, solidity,

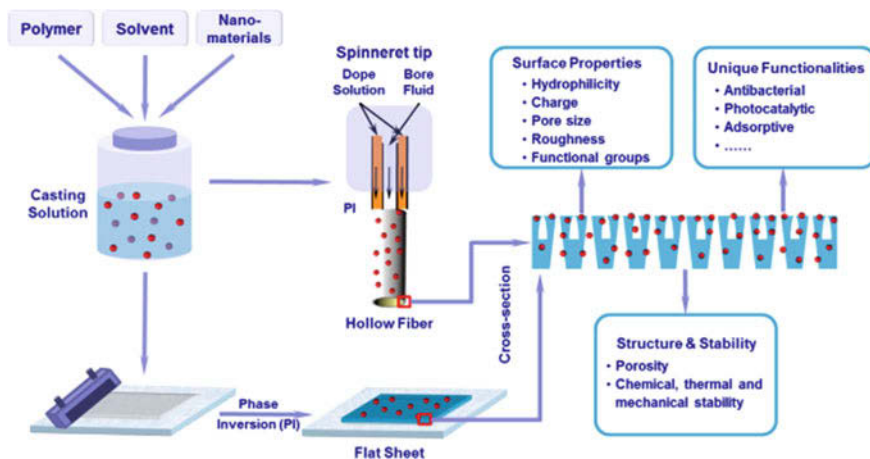


Fig. 5 Production of conventional CNM through the PI process [85]

and simplicity for its fabrication [84]. Evolving antimicrobial membranes will be expected to increase membrane efficiency and lifespan meaningfully which benefits to deliver microbes free clean water. For example, Ag is an excellent biocidal that usually used as an antimicrobial agent in CNM [85, 94]. AgNPs introduced into various metrics such as cellulose acetate [84], PSU [84], and PES [95] enhanced the membrane anti-bacterial activity, virus removal, and biofouling resistance respectively. The efficiency of CNM can be improved by the role reinforcement as indicated in Table 2.

Table 2 Type and role of reinforcement for conventional nanocomposite membrane [84, 91, 96–101]

Type of Reinforcement	Role of Reinforcement
Carbon Nanotube	Incorporation for improved properties such as anti-biofouling and good strength
metal oxide (TiO ₂ , ZnO, SiO ₂ , Al ₂ O ₃ , Fe ₃ O ₄)	Adjusts the assembly and physicochemical assets, such as hydrophilicity, Porosity, charge density, and chemical, thermal, and mechanical stability of membranes. Introduces the unique characteristics such as antifouling, and photocatalytic action into the membranes.
Metals (Ag, Cu, Se)	Antimicrobial functionality
Nano clay	Improvement in abrasion resistance
Organic Material	Enhance in hydrophilicity, upgrading sorption capacity, and anti-compaction, the antifouling performance of resultant membranes.
AgNPs	Reduce biofouling
Zeolite	Improvement hydrophilicity, advance cross-linking property and increase membrane inflexibility
Biomaterial	Water-channel membrane proteins
Hybrid material	Synergistic effect

3.5.2 Thin-Film Nanocomposites

Thin film nanocomposites (TFNs) membrane contains an extreme tinny wall sheet above a more permeable assistant material. TFN is interfacially synthesized by reverse osmosis or nanofiltration membrane which is extensively applied to remove heavy metals, desalinate seawater/brackish water, hardness causing salts, organic contaminants like pesticides, insecticides and disinfection intermediates. Researchers have been focused to advance water flux, toxin elimination, and antifouling characteristics of TFC I (1) to adapt the auxiliary film thus the linkage among the wall layer and the second layer might be improved, and (2) to enhance the wall layer by changing the IP settings, i.e. exchanging monomers, applying physical layering [102]. Materials like zeolites, CNTs, silica, Ag, and TiO₂ used for CNM synthesis have also been discovered to make TFN membranes [85, 101].

In general technologies yield NCs, a novel theory has been projected centred on diffusing nanomaterials into the extremely tinny wall to increase membrane efficiency for water purification [84]. The known production method is done the in situ IP course among aqueous phenylenediamine (MPD) and trimesoylchloride (TMC) organic solution as shown in Fig. 6. The nanofiller able to spread either in aqueous or an organic phase.

The additions nanoparticle make ready the thin films membranes to yield benefit of the properties of the nanomaterials. Adding of nanoparticles to in between polymerization routes or exterior accessory by self-assembly has announced the concept of TFN, which offer possible profits of improved separation efficiency, reduction fouling, antimicrobial action, and other novel properties. Like TFC membranes, TFN membrane performance can be achieved with nanoparticle

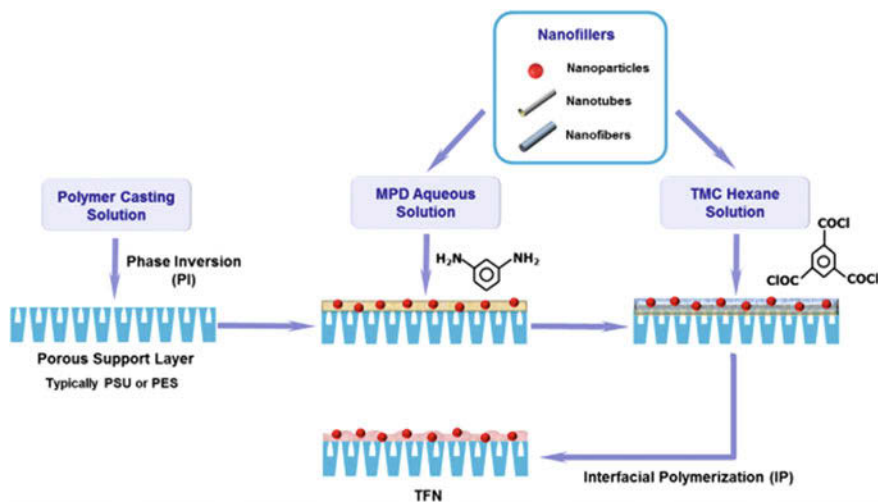


Fig. 6 Production of TFN membranes through the IP method [85]

Table 3 Summary of TFN membranes with nanocomposite substrate [85, 103]

Type of reinforcement	Role of reinforcement
Carboxylic MWNTs	Better antifouling and anti-oxidative properties
Zeolite	Salt elimination; Fighting to physical compaction
MWNTs	Increase the flexible strength of substrate and salt elimination
Ag-zeolite/PA-PSf	Improved water penetrability, Reduced tendency for biofouling
Titania/PA-PES	Reduced porousness and improved elimination at small unit additions, Improved permeability and reduced salt refusal beyond 5 wt%
Zeolite/PA-PSf	Improved interaction with water and superficial charge, Reduced superficial irregularity, Improved water penetrability by 80%
Zeolite/PA-PSf	Improved interaction with water, Increased water penetrability, Improved salt removal in RO testing

Note PA Polyamide, PSf Polysulfone, PES polyethersulfone

additions to the preserve membrane the coating film, or both. Like CNM, The efficiency of TFN can be improved by the role reinforcement as indicated in Table 3.

3.5.3 TFC with Nanocomposite Substrate

This membrane has been established to look at the consequences of nanofiller on membrane compaction manners. During this category, oxide nanoparticles were entrenched into the postscript substrate [104] that utilized at IP process to arrange TFC film. The ready membrane displays a better primary porousness and minor flux failure throughout the compaction related with the first TFC one. The nanoparticles deliver necessary automated care to moderate the failure of permeable arrangement and resist thickness decline. Membranes with NC substrate tolerate so much less physical compaction and show a vital role in sustaining high water porousness [96].

Nanocomposite membrane coated with nano-TiO₂ shown higher catalytic and/or photo activity properties. For instance, TiO₂ imbedded PES membrane showed enhanced antifouling capability while a novel anatase/titanate nanocomposite membrane simultaneously remove Cr (VI) and 4-chlorophenol through adsorption and photocatalytic oxidation. Impregnation of AgNPs into the membrane would allow fabricating thin-film nanocomposite with an excellent antibacterial performance for water treatment [41].

An important number of articles on membrane nanoscience has motivated on production of multipurpose membranes by addition of nanoparticles into polymeric or inorganic membranes. Hydrophilic metal oxides (e.g., Al₂O₃, TiO₂, and zeolite), antimicrobials (e.g., AgNPs and CNTs), and photocatalytic nanomaterials (e.g., bi-metallic nanomaterials, TiO₂) are the nanomaterials used this application.

The additional water loving metal oxide nanoparticles played a great role to decline fouling by improving the membrane hydrophilicity while the adding of metal oxide nanoparticles such as alumina [105], silica, zeolite [79] and TiO_2 has contributed to increasing membrane surface hydrophilicity, water permeability, or fouling resistance to polymeric ultrafiltration membranes. Besides to this, this metal and/or metal oxide nanoparticles also aid to improve the mechanical and thermal solidity of polymeric membranes, decreasing the destructive influence of compression and heat on membrane porousness [79, 106].

Qin et al. [107] investigated that handling the wastewater effluent generated from oil refinery and shell gas was difficult since this type of waste effluent was contaminated by contents of oils and salts. This type of wastewater was difficult to treat using conventional membranes because the membrane was severe fouling or failure by salts. The researchers developed another NCFO membrane for succeeding direct oil/water isolation and desalination. This NCFO membrane was accumulated an oil preventing and salt eliminating hydrogel separating layer on surface GO nanosheets imparted polymeric sustenance layer. The hydrogel separating layer governs strong water heating that leads to superior antifouling competency under several oil/, water emulsions, and the imparted GO in support layer can considerably moderate interior concentration polarization by decreasing FO membrane. Compared with viable FO membrane, the new membrane establishes triple water flux, higher eliminations for oil (>99.9%) and salts (>99.7%) and pointedly worse fouling attraction when examined with replicated shale gas wastewater as shown the Fig. 7. These combined benefits will validate this new NCFO membrane with wide requests in handling highly salty and oily effluents [107].

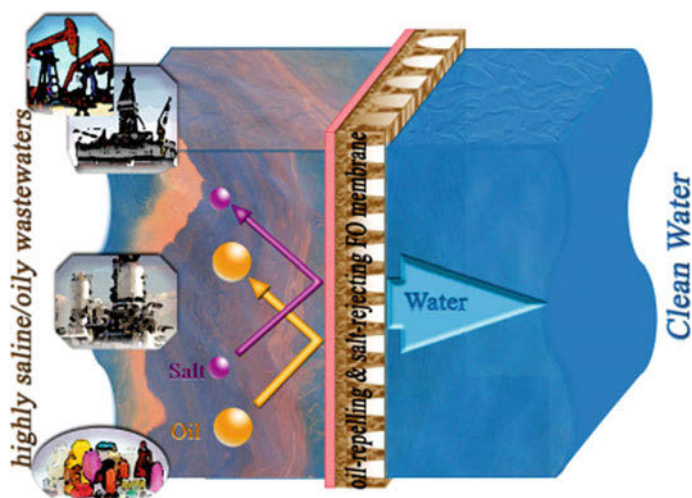


Fig. 7 Illustration of immediate oil/water separation and desalination by Hydrogel/GOFO membrane [107]

4 Future Outlooks

In this chapter, the most extensively studied nanocomposite, Metal nanocomposite, nanocomposite zero-valent metals (Ag, Pb, and Zn), MONCs (TiO₂, ZnO, and iron oxides), PNCs and MNCs were highlighted. Moreover, their applications in water purification were discussed in detail. Since the current rapid water demand development and sustainable application, NC look exceptionally favourable materials for water purification.

However, more studies are quiet required to solve the NC encounters. Still, now, insufficient types of nanocomposite are available commercially. Meanwhile, less production price is critical to confirm their extensive requests for water purification, future research has to devote to developing the commercial competence of NCs. Moreover, with progressively widespread applications of the NCs in water treatment, there are increasing alarms about their potential noxiousness to the environment and human health. Existing evidence in the literature has discovered that numerous NCs. However, principles for evaluating the noxiousness of NCs are somewhat inadequate at present-day. Hence, widespread assessment of the toxicity of NC is the crucial necessity to confirm their real applications. What is more, the assessment and contrast of the performance of numerous NC in water purification are recognized standards. It is hard to relate the performances of diverse nanoparticles and figure out talented NC that merits extra application. Consequently, the performance assessment tool of the NC in water purification ought to be perfected in the future.

5 Conclusion

Growing demand and deficiency of clean water as a result of rapid urbanization, population growth, and climate disruption have become unparalleled urgent global issues. Globally, Water purification is a priority issue for human use, ecosystem management, agriculture, and industry. The water sanitization process using nanoparticles are quite efficient. However, these are linked with some weakness such as aggregation, tough separation, and leakage into the contact water, environmental impact and human health. Therefore, to improve water treatment process system, researchers have been paid to develop eco-friendly, energy efficient and low price for sustainable water purification. The nanocomposites are basically multiphase solid materials, including porous media, colloids, gels, and copolymers in a broad sense. The selection of hosts for nanocomposites have a great consequence, and even controls the performance of nanocomposites in water purification. Compared with free nanomaterials, the efficiency and usability of nanocomposites were significantly improved, in terms of nanoparticle dispersion, stability, and recyclability. Nowadays, nanocomposites were supposed to be the supreme likely way of advancing water nanotechnology from lab study to large-scale application.

A number of the researcher was investigated nanocomposites synthesis from metal, metal oxide, carbon, polymer and membrane are the common materials used for water purification. Polymer nanocomposites (PNCs) are a superior class of materials which nanoparticles (NPs) dispersed in a polymer matrix resulting in novel materials having unique physical and chemical properties [74]. Polymers are special supports for nanomaterials as they usually possess tunable porous structures, excellent mechanical properties, and chemically bounded functional groups. Polymer-based nanocomposites (PNCs) are prospecting materials for their sound performance in water and wastewater treatment. Nanocomposite membrane has a great role in water purification and reuses for various sources of water such as drinking water, brackish, seawater, and wastewater treatment. Nanocomposite membranes is an innovative type of membranes prepared by merging polymeric materials with nanoparticles are developing as an encouraging solution to above challenges.

References

1. WHO/UNICEF (2014) Progress on drinking water and sanitation. Monitoring Programme update, WHO report, pp 1–18
2. Dargo H, Ayaliew A, Kassa H (2017) Synthesis paradigm and applications of silver nanoparticles (AgNPs), a review. *Sustain Mater Technol* 13:18–23
3. Liang XJ, Kumar A, Shi D, Cui D (2012) Nanostructures for medicine and pharmaceuticals. *J Nanomaterials* 2012:2012–2014
4. Kusior A, Klich-Kafel J, Trenczek-Zajac A, Swierczek K, Radecka M, Zakrzewska K (2013) TiO₂-SnO₂ nanomaterials for gas sensing and photocatalysis. *J Eur Ceram Soc* 33(12): 2285–2290
5. Diana S, Luigi R, Vincenzo V (2017) Progress in Nanomaterials Applications for Water Purification, In: Lofrano, Gi, Libralato, Giovanni, Brown, Jeanette (Eds) *Nanotechnologies for Environmental Remediation, Applications and Implications*, 1st ed, pp 1–24. Springer International Publishing AG
6. Lu H et al (2014) An overview of nanomaterials for water and wastewater treatment. *J Environ Anal Chem* 2016(2):10–12
7. Mueller NC et al (2012) Application of nanoscale zero valent iron (NZVI) for groundwater remediation in Europe. *Environ Sci Pollut Res* 19(2):550–558
8. Karn B, Kuiken T, Otto M (2009) Nanotechnology and in situ remediation: a review of the benefits and potential risks. *Environ Health Perspect* 117(12):1823–1831
9. Kumar D, Parashar A, Chandrasekaran N, Mukherjee A (2017) The stability and fate of synthesized zero-valent iron nanoparticles in freshwater microcosm system. *3 Biotech* 7(3): 1–9
10. Fu F, Dionysiou DD, Liu H (2014) The use of zero-valent iron for groundwater remediation and wastewater treatment: a review. *J Hazard Mater* 267:194–205
11. Amin MT, Alazba AA, Manzoor U (2014) A review on removal of pollutants from water/wastewater using different types of nanomaterials. *Adv Mater Sci Eng* vol 2014:ID 825910
12. Ghasemzadeh G, Momenpour M, Omid F, Hosseini MR, Ahani M, Barzegari A (2014) Applications of nanomaterials in water treatment and environmental remediation. *Front Environ Sci Eng* 8(4):471–482
13. Marková Z et al (2013) Air stable magnetic bimetallic Fe-Ag nanoparticles for advanced antimicrobial treatment and phosphorus removal. *Environ Sci Technol* 47(10):5285–5293

14. Muradova GG, Gadjeva SR, Di L, Vilardi G (2016) Nitrates removal by bimetallic nanoparticles in water. *Chem Eng Trans* 47:205–210
15. Xiong Z, Lai B, Yang P, Zhou Y, Wang J, Fang S (2015) Comparative study on the reactivity of Fe/Cu bimetallic particles and zero valent iron (ZVI) under different conditions of $N < \inf > 2 < /inf >$ air or without aeration. *J Hazard Mater* 297:261–268
16. Hoag GE, Collins JB, Holcomb JL, Hoag JR, Nadagouda MN, Varma RS (2009) Degradation of bromothymol blue by ‘greener’ nano-scale zero-valent iron synthesized using tea polyphenols. *J Mater Chem* 19(45):8671–8677
17. Sun Z, Song G, Du R, Hu X (2017) Modification of a Pd-loaded electrode with a carbon nanotubes-polypyrrole interlayer and its dechlorination performance for 2,3-dichlorophenol. *RSC Adv* 7(36):22054–22062
18. Arancibia-Miranda N et al (2016) Nanoscale zero valent supported by zeolite and montmorillonite: template effect of the removal of lead ion from an aqueous solution. *J Hazard Mater* 301:371–380
19. Ling L, Pan B, Zhang WX (2014) Removal of selenium from water with nanoscale zero-valent iron: mechanisms of intraparticle reduction of Se (IV). *Water Res* 71(34):274–281
20. Ling L, Zhang WX (2015) Enrichment and encapsulation of uranium with iron nanoparticle. *J Am Chem Soc* 137(8):2788–2791
21. Mahmoudi M, Serpooshan V (2012) Silver-coated engineered magnetic nanoparticles are promising for the success in the fight against antibacterial resistance threat. *ACS Nano* 6(3):2656–2664
22. Lara HH, Romero-Urbina DG, Pierce C, Lopez-Ribot JL, Arellano-Jiménez MJ, Jose-Yacaman M (2015) Effect of silver nanoparticles on *Candida albicans* biofilms: an ultrastructural study. *J Nanobiotechnol* 13(1):1–12
23. Morones JR et al (2005) The bactericidal effect of silver nanoparticles. *Nanotechnology* 16(10):2346–2353
24. Surendhiran D, Sirajunnisa A, Tamilselvam K (2017) Silver–magnetic nanocomposites for water purification. *Environ Chem Lett* 15(3):367–386
25. Kim JS et al (2007) Antimicrobial effects of silver nanoparticles. *Nanomed Nanotechnol Biol Med* 3(1):95–101
26. Xiu Z-M, Ma J, Alvarez PJJ (2011) Differential effect of common ligands and molecular oxygen on antimicrobial activity of silver nanoparticles versus silver ions. *Environ Sci Technol* 45(20):9003–9008
27. Mlalila NG, Swai HS, Hilonga A, Kadam DM (2017) Antimicrobial dependence of silver nanoparticles on surface plasmon resonance bands against *Escherichia coli*. *Nanotechnol Sci Appl* 10:1–9
28. Ishida H, Campbell S, Blackwell J (2000) General approach to nanocomposite preparation. *Chem Mater* 12(5):1260–1267
29. Tapas RS (2017) Polymer Nanocomposites for Environmental Applications. In: Deba KT, Bibhu PS (Eds) *Properties and Applications of Polymer Nanocomposites, Clay and Carbon Based Polymer Nanocomposites*, 1st ed, pp 77–99. Springer-Verlag GmbH Germany
30. Gehrke I, Geiser A, Somborn-Schulz A (2015) Innovations in nanotechnology for water treatment. *Nanotechnol Sci Appl* 8:1–17
31. Sharma G, Amit K, Shweta, Mu N, Ram PD, Zeid AA, Gene TM (2017) Novel development of nanoparticles to bimetallic nanoparticles and their composites: a review. *J King Saud Univ Sci*. <https://doi.org/10.1016/j.jksus.2017.06.012>
32. Rhim JW, Park HM, Ha CS (2013) Bio-nanocomposites for food packaging applications. *Prog Polym Sci* 38(10–11):1629–1652
33. de Azeredo HMC (2009) Nanocomposites for food packaging applications. *Food Res Int* 42(9):1240–1253
34. Othman SH (2014) Bio-nanocomposite materials for food packaging applications: types of biopolymer and nano-sized filler. *Agric Agric Sci Procedia* 2:296–303

35. Zare Y, Shabani I (2016) Polymer/metal nanocomposites for biomedical applications. *Mater Sci Eng C* 60:195–203
36. Veprek S, Veprek-Heijman MJG (2008) Industrial applications of superhard nanocomposite coatings. *Surf Coat Technol* 202(21):5063–5073
37. Zhang R et al (2016) Antifouling membranes for sustainable water purification: strategies and mechanisms. *Chem Soc Rev* 45(21):5888–5924
38. Galiano F et al (2015) A step forward to a more efficient wastewater treatment by membrane surface modification via polymerizable bicontinuous microemulsion. *J Membr Sci* 482: 103–114
39. Manawi Y, Kochkodan V, Hussein MA, Khaleel MA, Khraisheh M, Hilal N (2016) Can carbon-based nanomaterials revolutionize membrane fabrication for water treatment and desalination? *Desalination* 391:69–88
40. Senusi F, Shahadat M, Ismail S, Hamid SA (2018) Recent advancement in membrane technology for water purification, In : Oves M (ed) *Modern age environmental problems and their remediation, Recent Advancement*, 1st edn. Springer International Publishing AG, pp 1–237
41. Zhang Y et al (2016) Nanomaterials-enabled water and wastewater treatment. *NanoImpact* 3–4:22–39
42. Lee A, Elam JW, Darling SB (2016) Membrane materials for water purification: design, development, and application. *Environ Sci Water Res Technol* 2(1):17–42
43. Botes M, Cloete TE (2010) The potential of nanofibers and nanobiocides in water purification. *Crit Rev Microbiol* 36(1):68–81
44. Peter-Varbanets M, Zurbrügg C, Swartz C, Pronk W (2009) Decentralized systems for potable water and the potential of membrane technology. *Water Res* 43(2):245–265
45. Lin S, Huang R, Cheng Y, Liu J, Lau BLT, Wiesner MR (2013) Silver nanoparticle-alginate composite beads for point-of-use drinking water disinfection. *Water Res* 47(12):3959–3965
46. Yahyaei B, Azizian S, Mohammadzadeh A, Pajohi-Alamoti M (2015) Chemical and biological treatment of waste water with a novel silver/ordered mesoporous alumina nanocomposite. *J Iran Chem Soc* 12(1):167–174
47. Firdhouse MJ, Lalitha P (2016) Nanosilver-decorated nanographene and their adsorption performance in waste water treatment. *Bioresour Bioprocess* 3(1):12
48. Liu X, Chen Z, Chen Z, Megharaj M, Naidu R (2013) Remediation of direct black G in wastewater using kaolin-supported bimetallic Fe/Ni nanoparticles. *Chem Eng J* 223:764–771
49. Lateef A, Nazir R (2017) Metal nanocomposites : synthesis, characterization and their applications, In: P. DS, (ed) *Science and applications of tailored nanostructures*, 1st edn. One central press, Italy, pp 239–240
50. Ray C, Pal T (2017) Recent advances of metal-metal oxide nanocomposites and their tailored nanostructures in numerous catalytic applications. *J Mater Chem A* 5(20):9465–9487
51. Sankaramakrishnan N, Jaiswal M, Verma N (2014) Composite nanofloral clusters of carbon nanotubes and activated alumina: an efficient sorbent for heavy metal removal. *Chem Eng J* 235:1–9
52. Ihsanullah, Asmaly HA, Saleh TA, Laoui T, Gupta VK, Atieh MA (2015) Enhanced adsorption of phenols from liquids by aluminum oxide/carbon nanotubes: comprehensive study from synthesis to surface properties. *J Mol Liq* 206(February):176–182
53. Liang J et al (2015) Facile synthesis of alumina-decorated multi-walled carbon nanotubes for simultaneous adsorption of cadmium ion and trichloroethylene. *Chem Eng J* 273:101–110
54. Mallakpour S, Khadem E (2016) Carbon nanotube–metal oxide nanocomposites: fabrication, properties and applications. *Chem Eng J* 302(May):344–367
55. Ming-Zheng G, Chun-Yan C, Jian-Ying H, Shu-Hui L, Song-Nan Z, Shu D, Qing-Song L, Ke-Qin Z, Yue-Kun L (2016) Synthesis, modification, and photo/photoelectrocatalytic degradation applications of TiO₂ nanotube arrays: a review. *Nanotechnol Rev* 5(1). <https://doi.org/10.1515/ntrrev-2015-0049>

56. Silva CG, Faria JL (2010) Photocatalytic oxidation of benzene derivatives in aqueous suspensions: synergic effect induced by the introduction of carbon nanotubes in a TiO₂ matrix. *Appl Catal B Environ* 101(1–2):81–89
57. Martínez C, Canle LM, Fernández MI, Santaballa JA, Faria J (2011) Kinetics and mechanism of aqueous degradation of carbamazepine by heterogeneous photocatalysis using nanocrystalline TiO₂, ZnO and multi-walled carbon nanotubes-anatase composites. *Appl Catal B Environ* 102(3–4):563–571
58. Li J, Zhen D, Sui G, Zhang C, Deng Q, Jia L (2012) Nanocomposite of Cu-TiO₂ < SUB > 2</SUB > -SiO₂ < SUB > 2</SUB > with high photoactive performance for degradation of rhodamine B dye in aqueous wastewater. *J Nanosci Nanotechnol* 12(8): 6265–6270
59. Khan M et al (2015) Graphene based metal and metal oxide nanocomposites: synthesis, properties and their applications. *J Mater Chem A* 3(37):18753–18808
60. Ma J, Zhang J, Xiong Z, Yong Y, Zhao XS (2011) Preparation, characterization and antibacterial properties of silver-modified graphene oxide. *J Mater Chem* 21(10):3350–3352
61. Chandra V, Park J, Chun Y, Lee JW, Hwang IC, Kim KS (2010) Water-dispersible magnetite-reduced graphene oxide composites for arsenic removal. *ACS Nano* 4(7):3979–3986
62. Geng Z et al (2012) Highly efficient dye adsorption and removal: a functional hybrid of reduced graphene oxide-Fe₃O₄ nanoparticles as an easily regenerative adsorbent. *J Mater Chem* 22(8):3527–3535
63. Saad AHA, Azzam AM, El-Wakeel ST, Mostafa BB, Abd El-latif MB (2018) Removal of toxic metal ions from wastewater using ZnO@Chitosan core-shell nanocomposite. *Environ Nanotechnol Monit Manag* 9(August):67–75
64. Singh P et al (2018) Specially designed B₄C/SnO₂ nanocomposite for photocatalysis: traditional ceramic with unique properties. *Appl Nanosci* 8(1–2):1–9
65. Huang L, He M, Chen B, Hu B (2018) Magnetic Zr-MOFs nanocomposites for rapid removal of heavy metal ions and dyes from water. *Chemosphere* 199:435–444
66. Gong JL et al (2009) Removal of cationic dyes from aqueous solution using magnetic multi-wall carbon nanotube nanocomposite as adsorbent. *J Hazard Mater* 164(2–3):1517–1522
67. Chen L et al (2016) Facile synthesis of mesoporous carbon nanocomposites from natural biomass for efficient dye adsorption and selective heavy metal removal. *RSC Adv* 6(3): 2259–2269
68. Inyang M, Gao B, Zimmerman A, Zhang M, Chen H (2014) Synthesis, characterization, and dye sorption ability of carbon nanotube-biochar nanocomposites. *Chem Eng J* 236:39–46
69. Muneeb M, Zahoor M, Muhammad B, AliKhan F, Ullah R, AbdEl-Salam NM (2017) Removal of heavy metals from drinking water by magnetic carbon nanostructures prepared from biomass. *J Nanomater* 2017:10
70. Tian T et al (2014) Graphene-based nanocomposite as an effective, multifunctional, and recyclable antibacterial agent. *ACS Appl Mater Interfaces* 6(11):8542–8548
71. Zarei M (2017) Application of nanocomposite polymer hydrogels for ultra-sensitive fluorescence detection of proteins in gel electrophoresis. *TrAC - Trends Anal Chem* 93:7–22
72. Zhao S et al (2012) Performance improvement of polysulfone ultrafiltration membrane using well-dispersed polyaniline-poly(vinylpyrrolidone) nanocomposite as the additive. *Ind Eng Chem Res* 51(12):4661–4672
73. Pan B, Xu J, Wu B, Li Z, Liu X (2013) Enhanced removal of fluoride by polystyrene anion exchanger supported hydrous zirconium oxide nanoparticles. *Environ Sci Technol* 47(16): 9347–9354
74. Settanni, G, Zhou, J, Suo, T, Schöttler, S, Landfester, K, Schmid, F, Mailänder, V (2017) Protein corona composition of poly (ethylene glycol)- and poly (phosphoester)-coated nanoparticles correlates strongly with the amino acid composition of the protein surface. *Nanoscale* 9(6):2138–2144

75. Kelta B, Tadesse AM, Yadav OP, Diaz I, Mayoral Á (2017) Nano-crystalline titanium (IV) tungstomolybdate cation exchanger: Synthesis, characterization and ion exchange properties. *J Environ Chem Eng* 5(1):1004–1014
76. Zhang L, Liu J, Guo X (2018) Investigation on mechanism of phosphate removal on carbonized sludge adsorbent. *J Environ Sci (China)* 64:335–344
77. Vunain E, Mishra AK, Mamba BB (2016) Dendrimers, mesoporous silicas and chitosan-based nanosorbents for the removal of heavy-metal ions: a review. *Int J Biol Macromol* 86:570–586
78. Djerahov L, Vasileva P, Karadjova I, Kurakalva RM, Aradhi KK (2016) Chitosan film loaded with silver nanoparticles - Sorbent for solid phase extraction of Al (III), Cd (II), Cu (II), Co (II), Fe (III), Ni (II), Pb (II) and Zn (II). *Carbohydr Polym* 147(March):45–52
79. Saxena S, Saxena U (2016) Development of bimetal oxide doped multifunctional polymer nanocomposite for water treatment. *Int Nano Lett* 6(4):223–234
80. Qu X, Alvarez PJJ, Li Q (2013) Applications of nanotechnology in water and wastewater treatment. *Water Res* 47(12):3931–3946
81. Zayed A et al (2013) Fe₃O₄/cyclodextrin polymer nanocomposites for selective heavy metals removal from industrial wastewater. *Carbohydr Polym* 91(1):322–332
82. Khaydarov RA, Khaydarov RR, Gapurova O (2010) Water purification from metal ions using carbon nanoparticle-conjugated polymer nanocomposites. *Water Res* 44(6):1927–1933
83. Piri S, Zanjani ZA, Piri F, Zamani A, Yaftian M, Davari M (2016) Potential of polyaniline modified clay nanocomposite as a selective decontamination adsorbent for Pb (II) ions from contaminated waters; kinetics and thermodynamic study. *J Environ Health Sci Eng* 14(1): 1–10
84. Nithya R, Sudha PN (2017) Removal of heavy metals from tannery effluent using chitosan-g-poly (butyl acrylate)/bentonite nanocomposite as an adsorbent. *Text Cloth Sustain* 2(1):7
85. Yin J, Deng B (2015) Polymer-matrix nanocomposite membranes for water treatment. *J Membr Sci* 479:256–275
86. Shen YX, Saboe PO, Sines IT, Erbakan M, Kumar M (2014) Biomimetic membranes: a review. *J Memb Sci* 454:359–381
87. Hernández S, Saad A, Ormsbee L, Bhattacharyya D (2016) Nanocomposite and responsive membranes for water treatment, In: Hankins NP, Singh R (ed) *Emerging membrane technology for sustainable water treatment*, 1st edn. Elsevier B.V., USA, pp 389–431
88. Nasreen SAAN, Sundarrajan S, Nizar SAS, Balamurugan R, Ramakrishna S (2013) Advancement in electrospun nanofibrous membranes modification and their application in water treatment. *Membr (Basel)* 3(4):266–284
89. Fard AK et al (2018) Inorganic membranes: preparation and application for water treatment and desalination. *Mater (Basel)* 11(1):74
90. Razzaq H, Nawaz H, Siddiq A, Siddiq M, Qaisar S (2016) Madridge a brief review on nanocomposites based on PVDF with nanostructured TiO₂ as filler. *J Nanotechnol* 1(1): 29–35
91. Pant HR et al (2014) One-step fabrication of multifunctional composite polyurethane spider-web-like nanofibrous membrane for water purification. *J Hazard Mater* 264:25–33
92. Daraei P et al (2012) Novel polyethersulfone nanocomposite membrane prepared by PANI/Fe₃O₄ nanoparticles with enhanced performance for Cu (II) removal from water. *J Membr Sci* 415–416:250–259
93. Tetala KKR, Stamatialis DF (2013) Mixed matrix membranes for efficient adsorption of copper ions from aqueous solutions. *Sep Purif Technol* 104:214–220
94. Lopez Goerne TM (2011) Study of Bacterial Sensitivity to Ag-TiO₂ Nanoparticles. *J Nanomed Nanotechnol* 5(01):2
95. Liu S, Fang F, Wu J, Zhang K (2015) The anti-biofouling properties of thin-film composite nanofiltration membranes grafted with biogenic silver nanoparticles. *Desalination* 375(November):121–128

96. Tewari PK (2016) Nanocomposite membrane technology, 1st edn. CRC Press Taylor & Francis Group, Boca Raton
97. Ladewig B, Al-Shaeli MNZ (2017) Fundamental of membrane process. In: Ladewig B, Al-Shaeli MNZ (eds) Fundamentals of membrane bioreactors, 1st edn. Springer Nature Singapore, Singapore, pp 13–38
98. Jamshidi Gohari R, Halakoo E, Nazri NAM, Lau WJ, Matsuura T, Ismail AF (2014) Improving performance and antifouling capability of PES UF membranes via blending with highly hydrophilic hydrous manganese dioxide nanoparticles. *Desalination* 335(1):87–95
99. Jamshidi Gohari R, Lau WJ, Matsuura T, Ismail AF (2013) Fabrication and characterization of novel PES/Fe-Mn binary oxide UF mixed matrix membrane for adsorptive removal of as (III) from contaminated water solution. *Sep Purif Technol* 118:64–72
100. Akar N, Asar B, Dizge N, Koyuncu I (2013) Investigation of characterization and biofouling properties of PES membrane containing selenium and copper nanoparticles. *J Membr Sci* 437:216–226
101. Manjarrez Nevárez L et al (2011) Biopolymers-based nanocomposites: membranes from propionated lignin and cellulose for water purification. *Carbohydr Polym* 86(2):732–741
102. Jeong BH et al (2007) Interfacial polymerization of thin film nanocomposites: a new concept for reverse osmosis membranes. *J Membr Sci* 294(1–2):1–7
103. Pendergast MM, Hoek EMV (2011) A review of water treatment membrane nanotechnologies. *Energy Environ Sci* 4(6):1946–1971
104. Lind ML, Suk DE, Nguyen TV, Hoek EMV (2010) Tailoring the structure of thin film nanocomposite membranes to achieve seawater RO membrane performance. *Environ Sci Technol* 44(21):8230–8235
105. Maximous N, Nakhla G, Wong K, Wan W (2010) Optimization of Al₂O₃/PES membranes for wastewater filtration. *Sep Purif Technol* 73(2):294–301
106. Pendergast MTM, Nygaard JM, Ghosh AK, Hoek EMV (2010) Using nanocomposite materials technology to understand and control reverse osmosis membrane compaction. *Desalination* 261(3):255–263
107. Qin D, Liu Z, Delai Sun D, Song X, Bai H (2015) A new nanocomposite forward osmosis membrane custom-designed for treating shale gas wastewater. *Sci Rep* 5(January):1–14

Sustainable Nanocomposites in Food Packaging



H. Anuar, F. B. Ali, Y. F. Buys, M. A. Siti Nur E'zzati,
A. R. Siti Munirah Salimah, M. S. Mahmud,
N. Mohd Nordin and S. A. Adli

List of Abbreviations

APs	Alkyl phenols
CNCs	Cellulose nanocrystals
CNT	Carbon nanotube
CNW	Cellulose nanowhisker
CO ₂ PC	Carbon dioxide permeability coefficient
CO ₂ TR	Carbon dioxide transmission rate
DSC	Differential scanning calorimetry
DMF	N, N-dimethylformamide
EVOH	Ethylene vinyl alcohol copolymer
HDPE	High-density polyethylene
HPMC	Hydroxyl propyl methyl cellulose
HT	Hydroxytyrosol
HV	Hydroxyl-valerate
LDPE	Low-density polyethylene
MgO	Magnesium oxide
MMT	Montmorillonite
MWNT	Multi-walled carbon nanotube
OPC	Oxygen permeability coefficient
OTR	Oxygen transmission rate
PANI	Polyaniline
PCL	Poly(ϵ -caprolactone)
PEG	Polyethylene glycol
PEGME	Polyethylene glycol methyl ether

H. Anuar (✉) · Y. F. Buys · M. A. Siti Nur E'zzati · A. R. Siti Munirah Salimah ·
M. S. Mahmud · N. Mohd Nordin
Department of Manufacturing and Materials Engineering, Faculty of Engineering,
International Islamic University Malaysia, Jalan Gombak, 53100 Kuala Lumpur, Malaysia
e-mail: hazleen@iium.edu.my

F. B. Ali · S. A. Adli
Department of Biotechnology Engineering, Faculty of Engineering, International Islamic
University Malaysia, Jalan Gombak, 53100 Kuala Lumpur, Malaysia

PET	Polyethylene terephthalate
PHA	Poly hydroxyalkanoate
PHB	Polyhydroxy butyrate
PHBV	Polyhydroxybutyrate-co-hydroxyvalerate
PLA	Polylactic acid
PP	Polypropylene
PVA	Polyvinyl alcohol
ROP	Ring-opening polymerization
SEM	Scanning electron microscopy
TGA	Thermogravimetric analysis
WHO	World health organization
WSC	Water-soluble chitosan
WVPC	Water vapour permeability coefficient
WVTR	Water vapour transmission rate

1 Introduction

Human activities have already brought about changes to the ecological system worldwide, thereby giving rise to global warming and pollution. These problems have led to increased environmental degradation, which is destroying many things. Many plastic packaging industries are trying to minimize their reliance on synthetic materials in order to reduce toxicity levels [47]. Therefore, new environmental guidelines are forcing the exploration of novel packaging materials that are compatible with the environment. Such materials are currently being developed from various natural resources, among which biopolymers are the most popular. Biopolymers have many advantages compared to petroleum-based plastics in terms of performance, processability, and biodegradability [82]. There are several types of biopolymer matrices including polylactic acid (PLA), polyvinyl alcohol (PVA), polyhydroxy butyrate (PHB) and starch-based polymers. The poor gas and water barrier properties, unstable mechanical properties and weak resistivity of plastics have limited their use in various applications [55]. Therefore, to improve their mechanical and barrier properties, and to impart novel features to them, biopolymers are reinforced with various nanofillers for the development of nanocomposites.

1.1 Nanocomposites

Various terms have been used for advanced multifunctional packaging such as smart, active, and intelligent packaging. The idea behind using such terms for this

technology is to describe the selected reaction of a certain type of packaging when located in different environments. This reaction allows the smart or active packaging to sense changes in certain properties of food products and report them to the customer [40]. Active food packaging materials encompassing nanocomposites play several roles, including those of protecting food products from the outside environment, as well as increasing their shelf life by preserving their value for a longer period of time [79]. Other than that, smart packaging materials prevent oxidation of the food item from taking place, hence delaying its deterioration. They also function as a moisture controller, anti-microbial agent and freshness indicator [40]. Thus, active and intelligent packaging systems also deal with nanocomposite materials when they show ideal properties of smart packaging through their features.

Nanocomposites have been used in recent years in many industries such as in textiles, home decorations, packaging, furnishings, and agriculture. The application of natural fibers in nanocomposite materials is not a serious concern due to new technologies on the fabrication of synthetic fibers [79]. These synthetic fibers are mass produced for application in various industries. However, during the fabrication of these fibers, pollutants are produced that have an effect on the environment. The structure of biopolymer plastics tends to limit their application when there is a lack of reinforcement such as nanofillers or nanofibers [55]. Synthetic fibers are improved by reinforcement with nanofibers to enable them to be used in packaging applications. During this phase, the load is transferred by the matrix to the nanofibers. Apart from the mechanical and thermal properties, permeability is considered to be the most important parameter in the selection of materials for food packaging applications [40]. A high resistance to vapour and moisture is important when choosing a suitable polymer-based plastic. Bio-nanocomposites provide an excellent balance in mechanical, thermal and barrier properties.

The incorporation of nanofillers from inorganic and organic natural fibers can lead to green food packaging [43]. Natural fibers are more compatible with the environment than other fibers because they are biodegradable and renewable. In addition, these materials are cheap and have a low level of toxicity [49]. Nanofibers are measured in nanometres (10^{-9} m), and the term 'nano' relates to a range of nanoparticles. The measurement of the diameter of nanoparticles changes to nanometres following the shrinkage of micrometre materials. Deepa et al. [13] mentioned that the nanometre measurement of constituents is equivalent to being 80,000 times thinner than that of the hair of a person. However, this depends on whether the nanocomposite materials originated from material or fiber sources. Sometimes, they may become tiny particles but do not reach the nano-size range. The unique properties of nanocomposite materials are that they enhance the properties of composites, they have more attractive features in terms of their mechanical properties, they have flexible surfaces, and high surface area ratios [75]. Their surface area ratios are 10^3 times more than those of micrometre materials [48].

Nanofillers play a potential role in improving or altering the properties of the material in nanocomposites. Nanocomposite materials have a more acceptable demand due to the specific advantages that they have over non-biodegradable

products. Being more environmentally friendly, nanomaterials are used in many applications like the aerospace, automotive, electronics and biotechnology sectors [63]. Nanofibers and their composites offer a highly attractive contemporary to the research line. Nanocomposites show an outstanding improvement due to the nano-reinforcement. Basically, nanofibers are extracted for the stiffness that they provide to the reinforcement in nanocomposite materials [48]. Unlike natural fibers, synthetic fibers are produced from petrochemicals, while natural fibers originate from farm or agricultural crops. Due to environmental processes, biopolymer nanocomposite packaging is subject to degradation when exposed to environmental conditions such as moisture, sunlight, temperature or different pH solutions [77].

In nanoclay composites, the barrier properties depend on the orientation of the nanofiller, and its dispersion condition in the polymer matrix. The clay layers are able to create a barrier to delay the diffusion of molecules through the food packaging. According to Majeed et al. [40], nanoclay composites have gained a lot of attention from packaging manufacturers due to their cost-effectiveness, wide availability and simple processability. Nanoclay-based composites are usually reinforced with a polymeric starch-based material. Talegaonkar et al. [79] and his group identified the reason behind the successful use of nanoclay composites as a nanofiller in food packaging materials. According to them, the nanoclay that is used as a nanofiller improves the barrier properties of the biocomposite, possibly by increasing the tortuosity of the diffusive path for permeants, such as gas, moisture, and vapour. Li et al. [36] also added that the addition of 60 wt% of nanoclay in agarose starch increases the elastic modulus by five times than that of neat agarose starch at 2.4 GPa. It has been proven that the mechanical behaviour of bio-nanocomposites can be improved with the presence of nanoclay in it.

Smart or active packaging plays the most important role in the security of food products by preserving their integrity throughout their shelf life. The use of nanocomposite materials in food packaging industries is a new green technology aimed at attaining markedly enhanced packaging properties like improved mechanical properties and water resistance, increased thermal stability and barrier properties, and decreased migration activity. In addition, nanocomposites also offer an environmental approach, where they can be degraded within a few months. There are various types of nanofiller-based natural fibers that are suitable for preparation as nanocomposite materials. Thus, the nanocomposite materials are remarkably incorporated as packaging materials and also provide smart properties to the packaging system, thereby ultimately increasing the shelf life of food products and improving product quality.

2 Nanocomposite Preparation

The properties of nanocomposites heavily depend on the dispersion states of the reinforcement phase in the matrix. In order to optimize the properties of nanocomposites, it is necessary to disperse the particles in homogeneous

“nano-level” dispersion. For the cases of clay reinforced nanocomposites, there are three possible polymer/clay nanocomposite structures, i.e. flocculated, intercalated, and exfoliated [71], with exfoliation structure, followed by intercalation are the preferred ones. It also should be noted that in preparing nanocomposites specimens, degradation of the matrices should be avoided.

Various procedures to disperse the nanoparticles inside the polymeric matrices have been reported, and mainly can be classified into three classes, i.e. solution casting, melt mixing and in situ polymerization.

2.1 *Polymer Solution Casting*

Solvent casting technology, for the production of high-quality flexible films, has attracted widespread interest from plastic manufacturers. Driven by the requirements of the photographic industry well over a century ago, the solvent casting method has gradually declined due to the development of new film extrusion technology. However, due to the existence of certain limitations which constrain the applicability of conventional polymer processing methods, researchers' have adopted several measures to develop and modify polymer processing methods to suit natural polymers [53]. Solution casting is known as solvent casting or the wet processing method and is used for forming polymer thin films. Polymer films have many technological applications and advantages in industries such as packaging, medical devices, and photography tools and are also used in the coating industry. Notably, uniformity is the main characteristic for any of these applications.

Solution casting is a unique process where it is not reliant upon conventional extrusion and injection moulding machines, yet it incorporates well-mixed constituents like those produced by more traditional methods [30]. Solution casting is a manufacturing process that involves mixing of the solubilized polymer matrix and filler under continuous agitation via stirring, which is then followed by casting into a flat mould and solution drying. Moreover, it is often referred to as the evaporation method where the film is left for one day [58]. Salehifar et al. [65] stated in their findings that the solvent casting process is used in industrial food packaging for a broad range of applications. Accordingly, each polymer matrix has its own co-solvent to assist in dissolving the polymer. Notably, alcohol, chemical solvent, water or dissolving solutions are used in this kind of process as co-solvent [38]. Moreover, the dissolved polymer process can be improved using applied heat or via a readjusted PH condition which will enhance the formation of properties of the thin film matrix.

For the raw materials in the solvent casting method, several prerequisites are required. First, the polymer matrix should be soluble in the inorganic solvent or PH water. Also, the solution needs to be stable with suitable minimum solid substance and viscosity to achieve satisfactory performance [57]. The second prerequisite is the opportunity to produce a homogeneous thin film and removing the film after the drying process [66]. Figure 1 illustrates the solvent casting process to produce

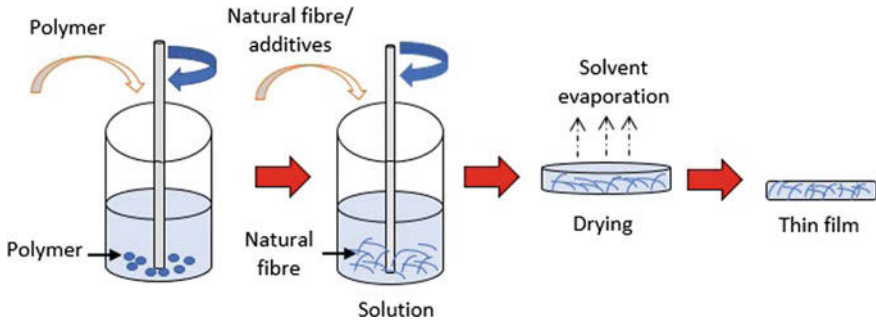


Fig. 1 Process to produce polymer nanocomposites film

biocomposite film. Notably, basic film applications are produced using different polymer and solvent combinations. During the casting process, the solid polymer matrix of various shapes (i.e. granules, powder or pellet size) is gradually dissolved in pure co-solvent. As a precautionary measure, the material type and geometry of the paddle or magnetic stirrer needs to be carefully selected due to the significant difference in viscosity between the polymer and co-solvent which may affect the mixture solvent [69]. Therefore, the temperature and mechanical stirring rate need to be carefully controlled given it affects the quality of solvent evaporation, polymer chain and skin formation of the polymer film. Typically, the induced temperature is varied between room temperature and the boiling point of the solvent [30]. Also, the dissolution time usually takes several iterations which are dependent on the type of solvent and method used.

The advantages of the manufacturing process of polymer solution casting over traditional film extrusion methods are mainly due to the unique approach and without the need to apply thermal or mechanical stress. Therefore, the degradation process or adverse side reaction is considered to be significant. Accordingly, solution casting is becoming an attractive process where the production of film offers uniform thickness distribution, maximum optical purity and extremely low toxicity [69]. Additionally, the process is conducted at a low temperature where it is relevant for thermally activated films although, in some circumstances, it may be temperature sensitive with active constituents. According to Salit et al. [66], due to the process being conducted at low temperature, the thin film shelf life can be extended to incorporate a much longer period. Furthermore, the non-melting process from soluble raw materials will possibly produce high-temperature resistant films. Notably, the main advantages of solvent casting are primarily due to the total cost of manufacturing prototypes and production volumes, which are much less than in extrusion blending. Also, this includes an inexpensive mould with a standard manufacturing/production line [57].

Next, a case study is used to examine nanocellulose reinforced with biodegradable polymer matrix where the focus is on the polymer process and to achieve outcomes. Jiang et al. [27] reported on cellulose nanowhisker

(CNW) reinforced poly(3-hydroxybutyrate) (PHB) by solvent casting and extrusion blending. Polyethylene glycol (PEG) acts as a compatibiliser or dispersion agent, and N, N-dimethylformamide (DMF) is co-solvent for this composite. Firstly, CNW/PEG was dissolved in a DMF stable suspension for 4 h of sonication at 258 °C. PHBV was also dissolved in DMF, and the mixture continued to be sonicated further for 2 h for complete homogeneity, followed by the solvent mixture casted on a glass plate. The film PHBV/CNW composite was formed following the complete evaporation of DMF. Finally, the sample was removed from the glass plate and kept in a desiccator to maintain a constant humidity. The homogeneous dispersion of CNW posed a significant challenge in preparing the nanocomposite, due to the possibility of hydrogen bonding inducing agglomeration on the sample.

The solvent casting technique demonstrated better dispersion of CNW in the nanocomposite compared to the extrusion method in which good dispersion significantly improved the properties of the PHBV nanocomposite [27]. PEG was also added to increase the dispersion in the nanocomposite. The addition of CNW also enhanced the PLA molecular mobility. Whisker content from 0 to 30 wt% also increased the tensile strength and Young's modulus obtained. Therefore, the enhanced tensile properties indicate good dispersion and strong interfacial adhesion between the fiber and the polymer matrix. The water resistance of the composite also increases with whisker content. By comparing the preparation method, the result for the composite prepared via extrusion showed lower tensile properties as compared to solution casting. Agglomeration of cellulose nanowhisker was reported to be observed under the scanning electron microscopy (SEM) micrograph and no intimate contact between cellulose nanowhisker and polymer matrix even though with the presence of a compatibilizer. Notably, the influences of agglomeration decreased the performance of the composite.

In conclusion, solution casting has numerous benefits compared to other fabrication methods due to lower production temperature required and no mechanical stress. Medical manufacturers are producing materials such as silicone urethane, via solution casting to produce breakthrough products subsequently excel in manufacturing performance and shorter lead times in supplying the demands. Solution casting as a manufacturing process depends only on the reaction between the co-solvent and polymer or the natural fiber mixture [53]. One of the primary reasons is due to solvent casting requiring lower energy, thereby reducing costs in recovering the solvent, and only a small investment is necessary for installing the facilities needed in handling the solvents and dope solutions which differs from other manufacturing methods [30]. Therefore, high quality of the thin film can only be achieved using the solvent casting methods and not using other methods.

2.2 Polymerization

Polymers are basically made of a large number of repeating unit of monomers. There are various methods that can be used to produce the polymers; step-growth

polymerization method (condensation polymer) and chain growth polymerization method (cationic polymerization and anionic polymerization). Depends on the constituents of the monomer, homopolymer and copolymers can be prepared. For an example, homopolymer polypropylene (PP) has been used extensively in food packaging industry as this polymer is known for its' exceptional properties [8]. PP is polymerized from its monomer which is propylene through Ziegler-Natta polymerization and by metallocene catalysis polymerization. Despite its low impact strength at low temperatures and high gas permeability, PP is reinforced with other components such as fillers, inorganic materials and many more in order to improve its properties. Previous studies show significant improvement in gas barrier properties of PP when blended with montmorillonite (MMT) by a twin-screw extruder [11, 93] and coating with corn zein nanocomposite [34].

Another polymer extensively used as packaging material is polyethylene terephthalate (PET). PET is produced by a step-growth polymerization of ethylene glycol and terephthalic acid or dimethyl terephthalate [20]. PET exhibit exceptional properties such as strength, permeability, chemical resistance and high transparency making it suitable for many applications. PET is also blended with other components such as clay by stretch blow molding machine in order to study the migration of aluminium and silicon from the composite into acidic food simulant bottle [20]. The study shows that the migration of aluminium and silicon is dependent on storage time and temperature. Another study had produced a nanocomposite by blending PET with layered double hydroxide by using high energy ball milling process and the results obtained showed that the oxygen diffusion and permeability are lower than that of neat PET [80].

Both PP and PET are known as non-degradable polymers. Despite its non-degradability, they are extensively used as food packaging material as they possess suitable properties for application in packaging. Nowadays, the biopolymer is emerging to substitute this conventional plastic as they can degrade naturally into the environment [20]. Biopolymers are categorized into their synthesis process namely from biomass product, microorganism, biotechnology and oil-products. Starch can be used to form a biodegradable film and different sources of starch can be obtained from plant biomass such as corn or sugarcane [81]. A study done by Heydari et al. [23] prepared corn starch film with glycerol by casting method where with increasing glycerol content, the tensile strength decreases. Chitosan is another polymer synthesized from chitin which is the most abundant agro-polymer in nature next to cellulose. Chitosan nanocellulose is developed in previous studies in order to improve its anti-microbial properties in food packaging, for extending the shelf life of meat in particular [14].

Poly hydroxyalkanoate (PHA) is a biopolymer synthesized from a microorganism. The homopolymer of PHA, poly(3-hydroxybutyrate) (PHB) and copolymer hydroxyl-valerate (HV) have been extensively studied to improve their properties [81]. From a previous study, PHA is combined with nano keratin by using two methods, direct melt compounding and pre-incorporated into an electrospun masterbatch of PHA and also solution casting [31]. Barrier properties are enhanced by both methods while sample prepared by solvent casting shows good adhesion.

Another study had been done by incorporating polyhydroxybutyrate-co-hydroxyvalerate (PHBV) with cellulose nanowhiskers using electrospinning techniques and showed improve barrier properties despite the extreme brittleness [31]. In another study, PHB had also been fabricated with cellulose nanocrystal by using solution casting technique and the results from the study show enhance gas barrier and migration properties [67]. Previous studies had also blended Poly (3-hydroxybutyrate-co-3-hydroxyvalerate) with other components such as clay [31], zinc oxide [15] and cellulose nanocrystal [92].

PLA is a polymer formed by ring opening polymerization of lactic acid [81]. PLA is considered a renewable material as it is manufactured by fermentation of renewable agriculture resources. Despite the attention towards PLA for its commercialization towards substituting conventional plastic, PLA brittleness and high cost limit its application. Many research had been done to modify PLA in order to widen its applications. PLA/zinc oxide film prepared by twin-screw extruder proven to improve PLA mechanical properties [44]. Other than that, PLA had also been blended with MMT by using a twin-screw extruder to form a nanocomposite. Comparing to neat PLA, the study shows that PLA/MMT exhibit good mechanical and oxygen barrier properties. Another study had been done by Pinto et al. [59] where PLA is incorporated with graphene by using solvent casting method. This study also shows improvement in mechanical and oxygen barrier properties.

Poly(ϵ -caprolactone) (PCL) is a synthetic biopolymer that can be synthesized either by ring opening polymerization from ϵ -caprolactone (monomer) or by free radical ring opening polymerization of 2-methylene-1-3-dioxepane [6]. Because of its high cost and brittleness, PCL applications is limited to medical purpose. However, many researchers have attempted to modify PCL by blending it with other components in order to widen its applications to other fields such as in food packaging sector. Beltrán et al. [6] had done a study on blending PCL with hydroxytyrosol (HT) and a commercial montmorillonite by melt blending method. The presence of montmorillonite decrease oxygen permeability but enhance the elasticity PCL. Another study had developed an antimicrobial PCL/clay nanocomposite films by melt blending method [90]. Results obtained from the study shows that mechanical water vapour barrier properties and antimicrobial properties improved for the nanocomposite, showing that it is suitable for the application in food packaging.

PVA is another type of synthetic biopolymer. Unlike other polymers, PVA is not synthesized from its monomer, instead, PVA is prepared by partial or complete hydrolysis of polyvinyl acetate to remove acetate groups [10]. According to Butnaru et al. [10], for PVA to be used in applications such as food sector and pharmaceutical, PVA need to be cross-linked first by the freeze-thawing method. Butnaru et al. [10] also had done a study to prepare a nanocomposite by blending PVA with chitosan and clay. The study shows enhanced properties in terms of thermal stability, mechanical and antimicrobial properties. A previous study had also been done where PVA had been blended with cellulose nanocrystal by a solvent casting method and the result proven to improve its mechanical properties [18] (Table 1).

Table 1 Summary of nanocomposites preparation in food packaging industry

No.	Nanocomposite	Processing method	References	Remarks
1	Polypropylene blended with montmorillonite (MMT) (PP/MMT)	Polypropylene (PP); Ziegler-Natta polymerization and by metallocene catalysis polymerization	Zehetmeyer et al. [93]	Improve gas barrier properties
2	Polypropylene/Organoclay Nanocomposites	Polypropylene (PP); in situ polymerization supported Ziegler-Natta catalysts	Almeida et al. [1]	Improve thermal degradation
3	PET blended with clay	Polyethylene terephthalate (PET); step-growth polymerization of ethylene glycol and terephthalic acid or dimethyl terephthalate	Galotto and Ulloa [20]	Migration of aluminium and silicon is dependent on storage time and temperature
4	PET blended with layered double hydroxide (PET/LDH)		Tammamo et al. [80]	Oxygen diffusion and permeability is lower than that of neat PET
5	Com starch film with glycerol	Casting method	Heydari et al. [23]	With increasing glycerol content, the tensile strength decreases
6	Chitosan nanocellulose	Casting method	Dehmad et al. [14]	Improve its anti-microbial properties in food packaging (extending the shelf life of meat)
7	PHA combined with nano keratin	Poly hydroxyalkanoate (PHA); synthesized from a microorganism (fermentation)	Lagarón et al. [31]	Barrier properties are enhanced by both methods while sample prepared by solvent casting shows good adhesion
8	PHB fabricated with cellulose nanocrystal	Poly(3-hydroxybutyrate) (PHB); synthesize from a microorganism (fermentation)	Sengupta et al. [67]	Enhance gas barrier and migration properties

(continued)

Table 1 (continued)

No.	Nanocomposite	Processing method	References	Remarks
9	Polyhydroxybutyrate-co-hydroxyvalerate (PHBV) with cellulose nanowhiskers	Polyhydroxybutyrate-co-hydroxyvalerate (PHBV): synthesized from mixed microbial cultures	Lagarón et al. [31]	Improve barrier properties despite the extreme brittleness
10	Poly (3-hydroxybutyrate-co-3-hydroxyvalerate) blended with clay		Lagarón et al. [31]	Improve thermal stability
11	Poly (3-hydroxybutyrate-co-3-hydroxyvalerate) blended with zinc oxide		Diez-Pascual and Diez-Vicente [15]	Improve stiffness, strength, toughness, and glass transition Temperature as well as a reduction in water uptake and oxygen and water vapour permeability
12	Poly (3-hydroxybutyrate-co-3-hydroxyvalerate) blended with cellulose nanocrystal		Yu et al. [92]	Improve mechanical performance, thermal stability, barrier, and migration properties, improve PLA mechanical properties
13	PLA/ZnO film	Poly(lactic acid (PLA): Ring-opening polymerization (ROP) of lactic acid	Marra et al. [44]	
14	PLA blended with montmorillonite (MMT) (PLA/MMT) PLA blended with graphene		Pinto et al. [59]	PLA/MMT exhibit good mechanical and oxygen barrier properties Improvement in mechanical and oxygen barrier properties
	PCL blended with hydroxytyrosol (HT) and a commercial montmorillonite PCL/clay nanocomposite films	Poly(ϵ -caprolactone) (PCL): ring opening polymerization from ϵ -caprolactone (monomer) or by free radical ring opening polymerization of 2-methylene-1-3-dioxepane	Beltrán et al. [6]	Presence of montmorillonite decrease oxygen permeability but enhance the elasticity PCL
15	PVA blended with cellulose nanocrystal	Poly(vinyl alcohol) (PVA): partial or complete hydrolysis of poly(vinyl acetate) to remove acetate groups	Yahiaoui et al. [90] Fortunati et al. [18]	Mechanical, water vapour barrier properties and antimicrobial properties improved Improve its mechanical properties
16	Polyaniline/poly(vinyl alcohol)/Ag (PANI/PVA/Ag)	Poly(vinyl alcohol) (PVA): in situ chemical oxidation polymerization of aniline monomer	Ghaffari-Moghaddam and Eslah [21]	Improve antibacterial properties

2.3 Melt Mixing

Amongst the three methods, melt mixing is the most economically attractive and scalable method for dispersing nanoparticles into polymers. To some extent, this method is also preferable over other two methods because it aligns well with the currently established industrial processing routes. This method also can be considered as environmentally benign, due to the unnecessary to use organic solvents. Melt mixing process involves melting of the thermoplastic polymer matrix to form viscous liquid followed by incorporation of nanoparticles.

In order to ensure proper dispersion of the nanoparticles during melt processing, two key factors need to be considered, i.e. (i) favourable interaction between the polymer matrix and the nanoparticle, and (ii) suitable processing conditions [50]. The favourable enthalpic interaction between particles and the matrix is necessary, because, in the absence of such favourable interactions, the dispersion of the nanoparticles within the matrix becomes difficult, and may only result in the formation of micro-composites instead of nanocomposites. Meanwhile, the processing conditions are also needed to be controlled carefully. Although high shear mixing in principle can improve the dispersion states of the particles, too high mechanical shearing, combined with high temperature and possible oxidation, may degrade certain types of polymers, especially biopolymers [50].

There are numerous works that reported successful attempts in preparing PLA based nanocomposites by melt mixing method. PLA nanocomposites reinforced with various types of particles such as silica [32, 86, 94], clay [33, 72], carbon nanotube [87], graphene [28, 46], titanium dioxide (TiO₂) [17] and nanocellulose [2, 22] have been successfully prepared by melt mixing process. In most cases, nanoparticles were surface modified to facilitate favourable interaction with the polymer matrix, which leads to better dispersion states. For example, -COOH surface modified multi-walled carbon nanotube (MWNTs) displayed better dispersion in the PLA matrix than the unmodified MWNTs [87], or polyethylene glycol methyl ether (PEGME)-modified nanosilica exhibited better dispersion states in the PLA matrix compared to pristine nanosilica.

Beside surface modification of nanoparticles, processing conditions in melt mixing method also affect the dispersion state of the particles in PLA nanocomposites. Villmow et al. [83] showed that higher rotating speed (500 rpm compared to 100 rpm), more mixing elements in extruder screw configuration, and temperature profile with raising value towards the extruder die contributed to better dispersion of CNT inside PLA matrix. Okubo et al. [52] exhibited that dispersion of cellulosenano- or microfibers was improved with decreased gap distance in roll-milling, while Oksman et al. [51] also pointed out that the type of screw in extruder influence the dispersion states of nanoparticles inside the matrix, i.e. in case of nanocellulose processing, the co-rotating twin-screw extruders are preferred over counter-rotating, because they are better for mixing and dispersing. In principle, higher mechanical shearing may lead to better dispersion of nanoparticles inside the matrix.

Preparation of PHA family based nanocomposites by melt mixing method has also been reported. The examples include PHBV reinforced with carbon nanotube (CNT) [68], PHBV reinforced with hydroxyapatite [54], PHB/clay nanocomposites [9, 39], etc. Similar to PLA based nanocomposites, surface chemistry of nanoparticles play a critical role in helping good dispersion. Organo-modified MMT dispersed better compared pristine MMT inside PHB matrix [9]. In PHBV matrix, hydroxyapatite treated with silane coupling agent exhibited better dispersion states and mechanical properties compared to untreated hydroxyapatite particles [54]. However, since many of PHA are sensitive to thermo-mechanical degradation, the melt-processing of PHA nanocomposites occurred within a short window and caution should be taken to avoid degradation during processing [9, 50].

3 Characterization of Nanocomposites

3.1 Mechanical Property

Mechanical characteristic is one of the crucial factors in nanocomposite especially in designing food packaging. Chemical resistance of the product can be affected by its process-ability and mechanical properties such as tensile strength, tear strength, elongation, toughness, softness and puncture resistance [5]. So, it is mandatory to perform the suitability test for nanocomposite food packaging stored with food as a function of duration. For example, the tensile test is conducted to determine the tensile strength, Young's modulus, yield stress and elongation at break of the nanocomposite. Generally, this testing is carried out according to the ASTM D88 standard testing method for tensile properties of thin plastic sheeting and ASTM D638 for testing materials up to 14 mm of thickness.

Moreover, impact properties test is also conducted to determine the amount of energy needed for the plastic deformation at certain condition according to ASTM D1709 for plastic film. Impact test consists of Charpy and IZOD specimen configuration according to ASTM D256 and ASTM 6110, respectively. The flexural test measures the force required to bend the sample under three-point loading conditions according to ASTM D790. This test is conducted as an indication of a material's stiffness when flexed. The sample lies on a support span and the load is applied to the centre by the loading nose producing three-point bending.

The modification of polymer content leads to increase in tensile performance up to 50% of the original value [5]. Nanocomposite film with the addition of water-soluble chitosan (WSC) increased the tensile strength of the polymer [78]. Relative elongation is also an important mechanical property as it could affect the biodegradable rate during the degradation process. As studied by Mostafa et al. [45], the percentage of elongation values for starch blend film was reduced in inoculated soil faster than in non-inoculated soil. Elongation of starch blend film dropped rapidly by 56% in inoculated soil compared to 12% decrement in elongation within

the fixed time basis. Therefore, mechanical stability properties help to improve the new innovations in biobased food packaging for commercial use.

3.2 Thermal Property

Addition of nanoparticles into polymeric materials also may enhance the thermal properties. Higher thermal stability is important in food packaging application to withstand a wide range of temperature exposure during food processing, transportation, and storage [55]. A recent report by De Silva et al. [12] showed that incorporation of magnesium oxide (MgO) into chitosan exhibited higher thermal stability and fire retardancy, due to the high thermal stability of MgO along with the homogeneous distribution of MgO nanoparticles in chitosan films. Kim and Cha [29] also reported that addition of organically modified MMT nanoclays into ethylene vinyl alcohol copolymer (EVOH) resulted in enhancement of thermal stability as indicated by thermogravimetric analysis (TGA), as well as shifting the crystallization temperature of EVOH as displayed by differential scanning calorimetry (DSC) result.

3.3 Degradation Behaviour

Development of new food packaging materials that capable to be degraded in a controlled manner has been a focus of interest of researchers nowadays. Incorporation of nanoparticles into degradable polymeric matrix may affect the degradation behaviour of the composites. Addition of cellulose nanocrystals (CNCs) into PLA helps to enhance the disintegrability rate of PLA since this nanocellulose is equipped with hydrophilic nature [3, 19]. However, different observation has been found when PLA is added with coated CNC with surface surfactant (s-CNC). Even though s-CNC accelerate the disintegration process of PLA, however, water diffusion is slightly restricted due to the improvement in barrier properties and therefore slowdowns the hydrolysis process and delays the degradation process [19]. It can be concluded that the addition of appropriate plasticizers will help to improve the disintegration of PLA in composting conditions [3, 35], which indirectly speed up the disintegration of PLA-plasticizer nanocomposites.

In other literature reported by Pandey et al. [56], the addition of addition of nano-layered silicate into PLA matrix increased the biodegradation rate of the materials. The increment was predicted due to the presence of terminal hydroxylated edge groups in the silicate layers. Addition of 4% of nano-layered silicate lead to the good dispersion of silicate layer in PLA matrix and these hydroxy groups begin the heterogeneous hydrolysis of PLA matrix by absorbing water from compost. Up to one month, the weight loss and hydrolysis of PLA and PLA with 4% filler is about the same, however, after one month, the degradation of nanocomposites increased significantly.

3.4 Migration Testing

Migration is the process where chemicals are transferred from nanocomposites to food as they come in contact with each other. The term “migration”, according to Icoz and Eker [26], is used to define the diffusion of substances from high concentration regions to low concentration regions within the food and the packaging material. The chemical substances that are added to polymeric materials to enhance the characteristics of a composite may interact with the food components and move into the food during the processing, storage, and distribution. The quality, such as taste and odour, as well as safety of the food will be affected and cause significant health problems to the consumer. There are various factors that influence the rate of migration, such as the contact time, temperature, structure of the nanocomposite (thickness for plastics), chemical properties (molecular size, polarity, vapor pressure, etc.) of the migrants, and the types of materials that come in contact with the food [7, 26]. Migration can occur in different ways such as contact migration, gas phase migration, penetration migration, set-off migration, and condensation or distillation migration [26].

Generally, this testing is carried out according to the EN 1186 standard testing method, and several types of food simulants are used to analyze the overall migration testing. These food simulants are chosen as they are less chemically complex than foods [7] according to the regulations by EU 10/2011. The recommended simulants, as stated by Bhunia et al. [7], are: ethanol (10% v/v) (simulant A) to simulate aqueous foods (pH > 4.5); acetic acid (3% v/v) (simulant B) to simulate acidic foods; ethanol (20% v/v) (simulant C) to simulate alcoholic products; ethanol (50% v/v) (simulant D1) and vegetable oil (simulant D2) to simulate fatty foods, and lastly, Tenax (PPPO) (simulant E) to simulate dry food. The overall migration is limited to 10 mg/dm² on a contact area basis or 60 mg/kg in the stimulant or food (for plastics).

The food contact material or migration testing is important especially in producing food packaging as it affects the quality and shelf life of food and has a bad impact on human health. The substances that migrate into food can transform to become toxic and hazardous to consumers, especially babies and children. The composition of the materials that come in contact with food, such as additives and plasticizers, may affect the safety and quality of food. They affect the human reproductive system and are carcinogenic as both of them are described as endocrine disruptors. Phthalate esters, alkyl phenols (APs) and 2,2-bis (4-hydroxyphenyl) propane, also known as bisphenol A, are examples of hazardous chemicals that have serious toxic effects if exposed to the human body even at low concentrations [85].

Therefore, migration testing is very important in food packaging applications in order to maintain the safety and quality of the food and also consumer health. It is necessary to choose carefully the materials and their properties to protect the quality and safety of food.

3.5 *Antimicrobial Testing*

Nanomaterial has revealed many benefits in various fields. As the uses of nanomaterials have been increasing, it has been found to be a promising advancement for the food packaging productions in the global market. However, the use of nanomaterials in food packaging could be challenging due to the method in reducing particle size and the fact that characteristic of nanoparticles material is quite different from microparticles [24]. Food packaging offers to maintain the quality of food taste, prolong shelf life and protect food from contamination. However, food security is an excessive problem due to increasing disease from contamination adverse from food packaging materials. World Health Organization (WHO) stated the spoilage of food arise at any time during production of food to consume. Pathogens bacterial are to blame in many cases because it easily grows on food surface [84]. This leads to the introduction of nanocomposite as an active antimicrobial packaging and particularly designed to control the bacteria from adversely affect health. By using active packaging, the internal environment is modified via constant interaction with the food over the specified shelf life [41].

Nanoscale materials consist of a high surface to volume ratio than micro-size particles which make them easier to attach with a numerous number of the molecule and increased the efficiency [88]. Nanoparticles such as copper, silver and zinc oxide usually used in the retarded growth of microorganism due to strong antibacterial or antifungal activities. The reinforcement of this kind nanoparticles in biocomposite may overcome the problem of food spoilage. So, the main goal of active packaging enhances the packaging products quality by guarantee food security and improve sensory properties of food while sustaining food quality [61]. Active antimicrobial packaging may be described as a structure that alters the environment inside the plastic package by modifying the condition of the packaged food system. Food spoilage can be formed when it is exposed to air via processing, production, and packaging of food [70]. Generally, active food packaging is divided into two categories; biodegradables and non-biodegradable materials. Petroleum-based packaging has particularly benefit of high mechanical strength, low cost of raw material, availability, ease production process, good barrier properties but not biodegradable [84]. They cause environmental pollution as they can take hundreds of years to completely degrade.

Besides, petroleum-based packaging material can also preserve food over the particular period but, currently, consumers do prefer products made of biodegradable resources [76]. Besides, those packaging have chemical additives diffused through the plastic barrier into food products thus provides a negative effect on the health. Biopolymer materials have attracted widespread industries because they can be decomposed easily. Therefore, utilization of antimicrobial material in biopolymer packaging can provide significant enhancement of property which can help to increase health security and shelf life of food. It is one of the methods that effectively kill or inhibit pathogenic microorganism from growth in infected food [62]. Hence, a good food packaging able to reduce contamination over the food [44, 64].

The improvement of biopolymer-based nanocomposites with antibacterial agent presents interesting potentials because the bio-based polymer can be varied according to specific technology requirements and also fulfil the nanostructures with envisaged applications [60]. The antimicrobial elements most commonly introduced into packaging products can be characterized into many types such as plant oil extract, enzymes, bacteriocin, preservation, chemical substance and others [76, 84]. Previous literature have recognized the potential application of antimicrobial nanocomposite for wound dressing [89], bactericides [60] and medical devices [16].

Nanoparticles have different activities depending on pathogenic and spoilage microorganism species [44]. Pinto et al. [60] reported based on their finding in antimicrobial activity test, the presence of nanoparticle copper (0.93–4.95%) can against *K. pneumoniae* (Gram-negative bacteria) in cellulose nanocomposite specimens. The inhibition of bacteria depends on the nanofiller content in the specimens, where increasing copper content gave significant inhibited bacteria growth. This study believed that Gram-negative bacteria can be affected by copper-based material as they have a strong antimicrobial action against peptidoglycan layer. The interaction of nanoparticles could cause in changing its permeability and the structures promote the membrane degradation which ultimately causing the death of bacteria [25]. According to Lai et al. [33], the incorporated nanoclay into PVA film showed strong antimicrobial activity against Gram-positive bacteria (*L. monocytogenes* and *S.aureus*). Nanoclay was known as an active agent due to its highly dispersed in biocomposite and increased their exposure toward microorganism [37]. These may result in deteriorated bacterial cell membranes and cause cell lysis. Current food technology used antimicrobial in covering substances because this method will make sure food product are safe and lead to extend shelf life [61]. Therefore, selection of removal of any microorganism should be identified for selection of an appropriate antimicrobial agent.

The main function of nanomaterials to act as an antioxidant agent is, it consists of microbial cidal effects and microbial static effects on the microorganism. Microbial static effects related to the active function of substance to enhance the concentration below minimal inhibitory during preserved or storage process of food product [41]. This state may reduce perishable to occur by contamination. The main concept permitted in this packaging are wrapping system with presence of antimicrobial agent either natural or synthetic agents. The existence of an antimicrobial agent in packaging product is more significant than adding antimicrobial agent directly onto food, the fact of covered product that consists antimicrobial agent could not diffuse into food product as well as can be thrown away after its' usage [25]. The major challenge in food packaging is the design of nanocomposite material with active antimicrobial products. Lately, many customers concern about potential health risks when chemical additives are added to packaging products. The achievement by scientists with the new formulation of reinforced nanoparticles verified the potential of bio-nanocomposites as an active food packaging, can be considered as an alternative to conventional composites used in the packaging material.

3.6 Optical Behaviour

Greater lightness and transparency in food packaging are vital as they are in high demand by consumers. Most non-composite foods packaging are colourless and transparent. These characteristics, however, are slightly affected by the addition of other materials, which in the end influence the aesthetic value of the food packaging. Arrieta et al. [4] revealed that the lightness of PLA is 94.08 ± 0.07 , while that of PLA/limonene is 93.86 ± 0.10 . Both PLA and PLA/limonene have high brightness characteristics, but their lightness is reduced once additives are added. In other researches, the lightness and transparency of coated films for food packaging were affected in the presence of proteins and plasticizers.

Lee et al. [34] stated that the transparency of protein-coated films was increased from 16.9 to 19.7 for corn zein, 13.3 to 30.3 for soy protein isolate and 17.8 to 28.6 for whey protein isolate. Moreover, the transparency of protein-coated films also increased with the addition of plasticizers. Yoo and Krochta [91] compared the transparencies of biopolymer, biopolymer blended and synthetic polymer films. The results indicated that the percentage of transparency of biopolymers like hydroxyl propyl methyl cellulose (HPMC) films was higher compared to synthetic polymers such as low-density polyethylene (LDPE), high-density polyethylene (HDPE) and polypropylene (PP) films.

Generally, the optical properties of nanocomposites are evaluated according to the *CIELAB* colour system. In this system, the colour coordinates L^* , a^* and b^* represent lightness, red-green and yellow-blue, respectively. An increase in the L^* value indicates that the nanocomposite specimen is lightening. The colour is switching to red if the a^* value is increasing, while it is turning green if the value is decreasing. The increase in the value of b^* shows that the colour is switching towards yellow, and a decreasing value indicates that it is turning to blue. Therefore, the total colour difference (ΔE) can be determined by using Eq. 1.

$$\Delta E = (\Delta L^2 + \Delta a^2 + \Delta b^2)^{1/2} \quad (1)$$

Transparency and opacity are essential properties in food packaging application as they improve the appearance of a product. Opacity is the degree to which light is not allowed to travel through. Products with high transparency, especially in packaging, have become more popular in the market as consumers prefer see-through rather than opaque packaging. Thus, nanocomposites with high transparency and lightness are important in food packaging applications as there is a high demand for them from consumers.

3.7 Permeability and Barrier Properties

The determination of the barrier properties of the nanocomposite is important as it determines the shelf-life of the product. Various factors may affect the barrier properties to gases and vapours on the nanocomposite such as environmental conditions like temperature and relative humidity. Permeability according to Siracusa [73], stated that the ability of the gas or vapour transmits through a resisting material. Permeates diffusion is influenced by the structure of the nanocomposite, permeability to specific gases or vapour, area, thickness, temperature, the difference in pressure or concentration gradient across the nanocomposite.

Oxygen transmission rate (OTR), water vapour transmission rate (WVTR) and carbon dioxide transmission rate (CO₂TR) are main examples of the barrier properties that used in food packaging application [74]. The oxygen permeability coefficient (OPC) exhibits the amount of oxygen that permeates into packaging materials in term of per unit area and time (kg m/m² s Pa) [73, 74]. When the nanocomposite film packaging has lower oxygen permeability coefficients, it prolongs the product's lifespan as the pressure of the oxygen inside the packaging decrease to the point where it slows down the oxidation. The OPC is correlated to the OTR by using Eq. (2)

$$OPC = \frac{OTR \cdot l}{\Delta P} \quad (2)$$

For water vapour permeability coefficient (WVPC) and carbon dioxide permeability coefficient (CO₂PC), both indicate the amount of water vapour and carbon dioxide, respectively that permeates per unit area and time as well (kg m/m² s Pa). The WVPC and CO₂PC are correlated to the WVTR and CO₂TR by using Eqs. (3) and (4), respectively.

$$WVPC = \frac{WVTR \cdot l}{\Delta P} \quad (3)$$

$$CO_2PC = \frac{CO_2TR \cdot l}{\Delta P} \quad (4)$$

where l is the thickness of the nanocomposite film and ΔP is $P_1 - P_2$, P_1 is the gas partial pressure at the temperature test on the test side and P_2 is equal to zero on detector side.

In order to improve barrier properties to gasses, vapour and aromas due to the sensitivity of various food products to oxygen degradation, microbial growth stimulated by moisture and aroma for keeping the food quality, nano or microfilters can be incorporated into biopolymers food packaging. Mali et al. [42] stated that the oxygen permeability was decreased while mechanical and heal seal properties were improved in bio-nanocomposite films from sago starch and bovine gelatin with nanorod-rich zinc oxide as the nanofillers.

Thus, oxygen and water vapour permeabilities in nanocomposite are essential properties as they give a major impact on the shelf-life of fresh and processed foods. It is important to know if there is an interaction between food and packaging and factors that influence the transport mechanism through the material.

Acknowledgements The authors wish to thank Ministry of Education Malaysia for the Fundamental Research Grant Scheme, FRGS14-105-0346, FRGS14-108-0349, FRGS16-003-0502 and RIGS16-085-0249 for the financial support and International Islamic University Malaysia for the facilities and equipment in making these studies a success.

References

1. Almeida LA, Marques MDFV, Dahmouche K (2015) Synthesis of polypropylene/organoclay nanocomposites via in situ polymerization with improved thermal and dynamic-mechanical properties. *J Nanosci Nanotechnol* 15(3):2514–2522
2. Arias A, Heuzey MC, Huneault MA et al (2015) Enhanced dispersion of cellulose nanocrystals in melt-processed polylactide-based nanocomposites. *Cellulose* 22(1):483–498
3. Arrieta MP, Fortunati E, Dominici F et al (2014) PLA-PHB/cellulose based films: mechanical, barrier and disintegration properties. *Polym Degrad Stab* 107:139–149
4. Arrieta MP, Lopez J, Ferrandiz S et al (2013) Characterization of PLA-limonene blends for food packaging applications. *Polym Testing* 32(4):760–768
5. Badmus AA, Gauri S, Ali NI et al (2015) Mechanical stability of biobased food packaging materials. *Food Sci Q Manag* 39:41–47
6. Beltrán A, Valente AJM, Jiménez A et al (2014) Characterization of poly(ϵ -caprolactone)-based nanocomposites containing hydroxytyrosol for active food packaging. *J Agric Food Chem* 62(10):2244–2252
7. Bhunia K, Sablani S, Tang J et al (2013) Migration of chemical compounds from packaging polymers during microwave, conventional heat treatment and storage. *Compr Rev Food Sci Food Saf* 12:523–545
8. Boone Lox F, Pottie S (1993) Deficiencies of polypropylene in its use as a food-packaging material—a review. *Packag Technol Sci* 6(June):277–281
9. Bordes P, Pollet E, Bourbigot S et al (2008) Structure and properties of PHA/clay nano-biocomposites prepared by melt intercalation. *Macromol Chem Phys* 209(14):1473–1484
10. Butnaru E, Cheaburu CN, Yilmaz O et al (2016) Poly(vinyl alcohol)/chitosan/montmorillonite nanocomposites for food packaging applications: influence of montmorillonite content. *High Perform Polym* 28(10):1124–1138
11. Choi RN, Cheigh CI, Lee SY et al (2011) Preparation and properties of polypropylene/clay nanocomposites for food packaging. *J Food Sci* 76(8):62–67
12. De Silva RT, Mantilaka MMMGPG, Ratnayake SP et al (2017) Nano-MgO reinforced chitosan nanocomposites for high performance packaging applications with improved mechanical, thermal and barrier properties. *Carbohydr Polym* 157:739–747
13. Deepa B, Abraham E, Cherian BM et al (2011) Structure, morphology and thermal characteristics of banana nanofibers obtained by steam explosion. *Bioresour Technol* 102(2): 1988–1997
14. Dehnad D, Mirzaei H, Emam-Djomeh Z et al (2014) Thermal and antimicrobial properties of chitosan-nanocellulose films for extending shelf life of ground meat. *Carbohydr Polym* 109:148–154

15. Diez-Pascual AM, Diez-Vicente, Angel L (2014) ZnO-reinforced poly (3-hydroxybutyrate-co -3-hydroxyvalerate) bionanocomposites with antimicrobial function for food packaging. *Appl Mater Interf* 9:822–9834
16. Feldman D (2016) Review-polymer nanocomposites in medicine. *J Macromol Sci, Part A: Pure and Appl Chem* 53(1):55–62
17. Fonseca C, Ochoa A, Ulloa MT et al (2015) Poly (lactic acid)/TiO₂ nanocomposites as alternative biocidal and antifungal materials. *Mater Sci Eng* 57:314–320
18. Fortunati E, Puglia D, Monti M et al (2012) Cellulose nanocrystals extracted from okra fibers in PVA nanocomposites. *J Appl Polym Sci* 128(5):3220–3230
19. Fortunati E, Rinaldi S, Peltzer M et al (2014) Nano-biocomposite films with modified cellulose nanocrystals and synthesized silver nanoparticles. *Carbohydr Polym* 101:1122–1133
20. Galotto M, Ulloa P (2010) Effect of high-pressure food processing on the mass transfer properties of selected packaging materials. *Packag Technol Sci* 23(May):253–266
21. Ghaffari-Moghaddam M, Eslahi H (2014) Synthesis, characterization and antibacterial properties of a novel nanocomposite based on polyaniline/polyvinyl alcohol/Ag. *Arab J Chem* 7(5):846–855
22. Herrera N, Mathew AP, Oksman K (2015) Plasticized polylactic acid/cellulose nanocomposites prepared using melt-extrusion and liquid feeding: mechanical, thermal and optical properties. *Compos Sci Technol* 106:149–155
23. Heydari A, Alemzadeh I, Vossoughi M (2013) Functional properties of biodegradable corn starch nanocomposites for food packaging applications. *Mater Des* 50:954–961
24. Honarvar Z, Hadian Z, Mashayekh M (2016) Nanocomposites in food packaging applications and their risk assessment for health. *Electr Phys* 8(6):2531–2538
25. Hu W, Chen S, Yang J et al (2014) Functionalized bacterial cellulose derivatives and nanocomposites. *Carbohydr Polym* 101(1):1043–1060
26. Icoz A, Eker B (2016) Selection of food packaging material, migration and its effects on food quality. In: 1st international conference on quality of life, Center for Quality, Faculty of Engineering, University of Kragujevac, June 2016
27. Jiang L, Morelius E, Zhang J et al (2008) Study of the Poly(3-hydroxybutyrate-co-3-hydroxyvalerate)/Cellulose Nanowhisker composites prepared by solution casting and melt processing. *J Compos Mater* 42(24):2629–2645
28. Kim IH, Jeong YG (2010) Polylactide/exfoliated graphite nanocomposites with enhanced thermal stability, mechanical modulus, and electrical conductivity. *J Polym Sci, Part B: Polym Phys* 48(8):850–858
29. Kim SW, Cha SH (2014) Thermal, mechanical, and gas barrier properties of ethylene–vinyl alcohol copolymer-based nanocomposites for food packaging films: Effects of nanoclay loading. *J Appl Polym Sci* 131(11):40289
30. Kong I, Tshai KY, Hoque ME (2015) Manufacturing of natural fibre-reinforced polymer composites by solvent casting method. In: Salit MS (ed) *Manufacturing of natural fibre reinforced polymer composites*. Springer International Publishing, Switzerland, pp 331–349
31. Lagarón JM, López-Rubio A, José Fabra M (2015) Bio-based packaging. *J Appl Polym Sci* 133(2):42971
32. Lai SM, Hsieh YT (2016) Preparation and properties of polylactic acid (PLA)/silica nanocomposites. *J Macromol Sci, Part B* 55(3):211–228
33. Lai SM, Wu SH, Lin GG et al (2014) Unusual mechanical properties of melt-blended poly (lactic acid)(PLA)/clay nanocomposites. *Eur Polym J* 52:193–206
34. Lee JW, Son SM, Hong SI (2008) Characterization of protein-coated polypropylene films as a novel composite structure for active food packaging application. *J Food Eng* 86(4):484–493
35. Lemmouchi Y, Murariu M, Santos DAM et al (2009) Plasticization of poly(lactide) with blends of tributyl citrate and low molecular weight poly(D, L-lactide)-B-poly(ethylene glycol) copolymers. *Eur Polym J* 45(10):2839–2848
36. Li X, Gao H, Scrivens WA et al (2005) Structural and mechanical characterization of nanoclay-reinforced agarose nanocomposites. *Nanotechnology* 16(10):2020–2029

37. Liu G, Song Y, Wang J et al (2014) Effects of nanoclay type on the physical and antimicrobial properties of PVOH-based nanocomposite films. *LWT-Food Sci Technol* 57(2):562–568
38. Lunineau G, Rahaman A (2012) A review of strategies for improving the degradation properties of laminated continuous-fiber/epoxy composites with carbon-basednanoreinforcements. *Carbon* 50:2377–2395
39. Maiti P, Batt CA, Giannelis EP (2007) New biodegradable polyhydroxybutyrate/layered silicate nanocomposites. *Biomacromol* 8(11):3393–3400
40. Majeed K, Jawaid M, Hassan A et al (2013) Potential materials for food packaging from nanoclay/natural fibres filled hybrid composites. *Mater Des* 46:341–410
41. Malhotra B, Anu K, Harsha K (2015) Review-antimicrobial food packaging: potential and pitfalls. *Front Microbiol* 6(611):1–9
42. Mali S, Victoria EM, Garcia M et al (2004) Barrier, mechanical and optical properties of plasticized Yam starch films. *Carbohydr Polym* 56:129–135
43. Marina R, Alfonso J, Mercedes P et al (2014) Development of novel nano-biocomposite antioxidant films based on poly (lactic acid) and thymol for active packaging. *Food Chem* 1–31
44. Marra A, Silvestre C, Duraccio D et al (2016) Polylactic acid/zinc oxide biocomposite films for food packaging application. *Int J Biol Macromol* 88:254–262
45. Mostafa HM, Sourell H, Bockisch FJ (2010) The mechanical properties of some bioplastics under different soil types for use as a biodegradable drip tubes. *CIGR Ejournal* 12:1–8
46. Murariu M, Dechief AL, Bonnaud L et al (2010) The production and properties of polylactide composites filled with expanded graphite. *Polym Degrad Stab* 95(5):889–900
47. Mushy NE, Utsel S, Berglund LA (2014) Nanostructured biocomposite films of high toughness based on native chitin nanofibers and chitosan. *Front Chem* 2:99
48. Nascimento P, Marim R, Carvalho G et al (2016) Nanocellulose produced from rice hulls and its effect on the properties of biodegradable starch films. *Mater Res* 19(1):167–174
49. Neelamana IK, Thomas S, Parameswaranpillai J (2013) Characteristics of banana fibers and banana fiber reinforced phenol formaldehyde composites-macroscale to nanoscale. *J Appl Polym Sci* 130(2):1239–1246
50. Ojijo V, Sinha Ray S (2013) Processing strategies in bionanocomposites. *Prog Polym Sci* 38 (10–11):1543–1589
51. Oksman K, Aitomäki Y, Mathew AP et al (2016) Review of the recent developments in cellulose nanocomposite processing. *Compos Part A: Appl Sci Manuf* 83:2–18
52. Okubo K, Fujii T, Thostenson ET (2009) Multi-scale hybrid biocomposite: processing and mechanical characterization of bamboo fiber reinforced PLA with microfibrillated cellulose. *Compos Part A: Appl Sci Manuf* 40(4):469–475
53. Olatunji O, Richard O (2016) Processing and characterization of natural polymers. In: Olatunji O (ed) *Natural polymers*. Springer International Publishing, Switzerland, pp 19–34
54. Öner M, İlhan B (2016) Fabrication of poly (3-hydroxybutyrate-co-3-hydroxyvalerate) biocomposites with reinforcement by hydroxyapatite using extrusion processing. *Mater Sci Eng, C* 65:19–26
55. Othman SH (2014) Bio-nanocomposite materials for food packaging applications: types of biopolymer and nano-sized filler. *Agric Agric Sci Proc* 2:296–303
56. Pandey JK, Reddy KR, Kumar AP et al (2005) An overview on the degradability of polymer nanocomposites. *Polym Degrad Stab* 88:234–250
57. Pazourkova L, Martynkova G, Placha D (2015) Preparation and mechanical properties of polymeric nanocomposites with hydroxyapatite and hydroxyapatite/clay mineral fillers—review. *J Nanotechnol: Nanomed Nanobiotechnol* 2(007):1–8
58. Petersson L, Kvien I, Oksman K (2007) Structure and thermal properties of poly (lactic acid)/cellulose Whiskers nanocomposites. *Compos Sci Technol* 67:2535–2544
59. Pinto AM, Cabral J, Tanaka DAP et al (2012) Effect of incorporation of graphene oxide and graphene nanoplatelets on mechanical and gas permeability properties of poly(lactic acid) films. *Polym Int* 62(1):33–40
60. Pinto RJB, Daina S, Sadocco P et al (2013) Antibacterial activity of nanocomposites of copper and cellulose. *BioMed Res Int*, 1–6

61. Qin Y, Yang J, Xue J (2015) Characterization of antimicrobial poly(lactic acid)/ poly (trimethylene carbonate) films with cinnamaldehyde. *J Mater Sci* V50(3):1150–1158
62. Ramos M, Jiménez A, Peltzer M et al (2014) Development of novel nano-composite antioxidants films based on poly (lactic acid) and tymol for active packaging. *Food Chem* 162:149–155
63. Saba N, Paridah MT, Mohammad J (2014) Potentiality of nano filler/natural fiber filled polymer hybrid composites. A review. *Polymers* 2014(6): 2247–2273
64. Saeedeh SA, Hosseini H, Mohammadifar MA et al (2014) Characterization of k-carrageenan films incorporated plant essential oils with improved antimicrobial activity. *Carbohydr Polym* 101:582–591
65. Salehifar M, Mohammad Hadi BN, Reza A et al (2013) Effect of LDPE/MWCNT films on the shelf life of Iranian Lavash bread. *Eur J Exp Biol* 3(6):183–188
66. Salit MS, Jawaid M, Yusoff NB, Hoque ME (2015) Manufacturing of natural fibre reinforced polymer composites. Springer, Switzerland
67. Sengupta R, Chakraborty S, Bandyopadhyay S et al (2007) A short review on rubber/ clay nanocomposites with emphasis on mechanical properties. *Engineering* 47:21–25
68. Shan GF, Gong X, Chen WP et al (2011) Effect of multi-walled carbon nanotubes on crystallization behavior of poly (3-hydroxybutyrate-co-3-hydroxyvalerate). *Coll Polym Sci* 289(9):1005–1014
69. Siemann U (2005) Solvent cast technology—a versatile tool for thin film production. *Prog Coll Polym Sci* 130:1–14
70. Singh P, Ali AW, Sven S (2011) Active packaging of food products: recent trends. *Nutr Food Sci* 41(4):249–260
71. Sinha RS, Bousmina M (2005) Biodegradable polymers and their layered silicate nanocomposites: in greening the 21st century materials world. *Prog Mater Sci* 50:962–1079
72. Sinha RS, Maiti P, Okamoto M et al (2002) New polylactide/layered silicate nanocomposites. 1. Preparation, characterization, and properties. *Macromolecules* 35(8):3104–3110
73. Siracusa V (2012) Food packaging permeability behaviour: a report. *Int J Polym Sci* 2012:1–11
74. Siracusa V, Rocculi P, Romani S et al (2008) Biodegradable polymers for food packaging: a review. *Trends Food Sci Technol* 19(12):634–643
75. Siti Nur E'zzati MA, Anuar H, Siti Munirah Salimah, AR (2018) Effect of coupling agent on durian skin fibre nanocomposite reinforced polypropylene. In: IOP conference series: materials science and engineering, University Islamic University Malaysia, Malaysia, 8–9 August 2017
76. Souza AC, Souza C, Dias AMA et al (2014) Impregnation of cinnamaldehyde into cassava starch biocomposite films using supercritical fluid technology for the development of food active packaging. *Carbohydr Polym* 102:830–837
77. Sriupayoa J, Supaphola P, Blackwell J et al (2005) Preparation and characterization of alpha-Chitin Whisker-reinforced poly (vinyl alcohol) nanocomposite films with or without heat treatment. *Polymer* 46(15):5637–5644
78. Suzuki S, Shimahashi K, Takahara J et al (2005) Effect of addition of water-soluble chitin on amylose film. *Biomacromol* 6:3238–3242
79. Talegaonkar S, Sharma H, Pandey S et al (2017) Chapter 3: Bionanocomposites: smart biodegradable packaging material for food preservation. In: Grumezescu AM (ed) *Food Packaging, Nanotechnology in the Agri-Food Industry* 7. Elsevier, United Kingdom, pp 79–110
80. Tammaro L, Vittoria V, Bugatti V (2014) Dispersion of modified layered double hydroxides in poly(ethylene terephthalate) by high energy ball milling for food packaging applications. *Eur Polym J* 52(1):172–180
81. Tang XZ, Kumar P, Alavi S et al (2012) Recent advances in biopolymers and biopolymer-based nanocomposites for food packaging materials. *Cri Rev Food Sci Nut* 52(5):426–442
82. Valdés A, Mellinas AC, Ramos M et al (2014) Natural additives and agricultural wastes in biopolymer formulations for food packaging. *Front Chem* 2(6):10

83. Villmow T, Pötschke P, Pegel S et al (2008) Influence of twin-screw extrusion conditions on the dispersion of multi-walled carbon nanotubes in a poly (lactic acid) matrix. *Polymer* 49 (16):3500–3509
84. Vodnar DV, Oana LP, Francisc VD (2015) Antimicrobial efficiency of edible films in food industry. *Notule Botanicae Horti Agrobotamici* 3(2):302–312
85. Wagner M, Oehlmann J (2009) Endocrine disruptors in bottled mineral water: total estrogenic burden and migration from plastic bottles. *Environ Sci Pollut Res* 16(3):278–286
86. Wen X, Lin Y, Han C et al (2009) Thermomechanical and optical properties of biodegradable poly(L-lactide)/silica nanocomposites by melt compounding. *J Appl Polym Sci* 114:3379–3388
87. Wu D, Wu L, Zhang M et al (2008) Viscoelasticity and thermal stability of polylactide composites with various functionalized carbon nanotubes. *Polym Degrad Stab* 93(8):1577–1584
88. Wu J, Yu C, Li Q (2017) Novel regenerable antimicrobial nanocomposite membranes: effect of silver loading and valence state. *J Membr Sci* 531:68–76
89. Wu J, Zheng Y, Song W et al (2014) In situ synthesis of silver-nanoparticles/bacterial cellulose composites for slow-released antimicrobial wound dressing. *Carbohydr Polym* 104(1):762–771
90. Yahiaoui F, Benhacine F, Ferfera-Harrar H et al (2014) Development of antimicrobial PCL/nanoclay nanocomposite films with enhanced mechanical and water vapor barrier properties for packaging applications. *Polym Bull* 72(2): 235–254
91. Yoo S, Krochta JM (2011) Whey protein–polysaccharide blended edible film formation and barrier, tensile, thermal and transparency properties. *J Sci Food Agric* 91(14):2628–2636
92. Yu H, Yan C, Yao J (2014) Fully biodegradable food packaging materials based on functionalized cellulose nanocrystals/poly(3-hydroxybutyrate-co-3-hydroxyvalerate) nanocomposites. *RSC Adv* 4(104):59792–59802
93. Zehetmeyer G, Soares RMD, Brandelli A et al (2012) Evaluation of polypropylene/montmorillonite nanocomposites as food packaging material. *Polym Bull* 68(8):2199–2217
94. Zheng Y, Yan K, Zhao Y et al (2016) Preparation and characterization of poly (L-lactic acid)/hollow silica nanospheres nanocomposites. *Fibers Polym* 17(12):2020–2026

Mechanical Techniques for Enhanced Dispersion of Cellulose Nanocrystals in Polymer Matrices



Jamileh Shojaeiarani, Dilpreet S. Bajwa and Kerry Hartman

1 Introduction

The growing concern regarding the impact of petroleum-based polymers on the environment and the development of biopolymers call for a transition from petroleum-based polymers to sustainable biopolymers. However, such a transition possess a substantial challenge for scientists and industries, requiring innovative materials and the applicable methods for improving the potential application of new materials.

Among all different types of biopolymers, cellulose is one of the most abundant organic compound available on the earth and it is the primary structural component of the cell wall of various plants, many forms of algae and the oomycetes. It is also present in different species of fungi, bacteria, and some sea animals such as tunicates [1]. Cellulose crystallites contain highly ordered, crystalline portions along with some disordered (amorphous) domains [2]; crystallinity index of the celluloses indicates the ratio between the area of the crystalline regions and the total area. Cellulose can be transformed into micro or nano-scale products with different shape and crystallinity using different methods such as acid hydrolysis, combined with mechanical shearing and enzymatic hydrolysis [3–7]. During the process, the amorphous or disordered regions of cellulose are hydrolyzed, and the crystalline regions with higher resistance to acid attack remain intact [8–10]. The resulting crystalline segments with the dimensions of nanometer is called nanocellulose (NC); generally, the family of NC can be classified as cellulose nanocrystals (CNCs), cellulose nanofiber (CNF), and cellulose nanowhisiker (CNW) [11].

J. Shojaeiarani (✉) · D. S. Bajwa
Department of Mechanical Engineering, North Dakota State University,
Fargo, ND 58102, USA
e-mail: jamileh.shojaeiarani@ndsu.edu

K. Hartman
Department of sciences, Nueta Hidatsa Sahnish College, New Town, ND 58763, USA
e-mail: khartm@nhsc.edu

In general, CNCs with a strength over 10 GPa and the elastic modulus of 150 GPa [12] has attracted wide attention as a reinforcing agent and have been employed in the nanocomposite, soft-tissue replacement, and food packaging industry for several decades [7, 13, 14]. The specific structure of CNCs contains several free hydroxyl groups on the surface (Fig. 1). The strong hydrophilic character of CNCs due to the presence of free hydroxyl groups on the surface of CNCs restricts the application of different solvents processing as the medium for solution blending [15].

The hydroxyl group located at C₆ is primary alcohol and at C₂ and C₃ are secondary alcohols. It has been reported that the hydroxyl group located at 6 positions has reactivity ten times higher than the other hydroxyl group [16]. The high reactivity of the hydroxyl groups to form hydrogen bonds strongly influence the overall properties of cellulose such as the reactivity of the hydroxyl groups, hierarchical organization, crystallinity, and limited solubility in most solvents [17, 18].

There are plenty of studied highlighting the optimum characteristics of CNCs as reinforcing agent. It is reported that the homogeneous dispersion of CNCs within the polymeric matrix is an essential step for achieving the superior properties of CNCs in composite materials [19, 20]. In addition, the dispersion of CNCs into the hydrophobic polymer with water-insoluble nature is a big issue. Therefore, several techniques have been experimented to decrease the affinity for moisture of the CNCs and improve the compatibility with a nonpolar polymer. The presence of hydroxyl groups on the surface of CNCs provides an opportunity for application of different surface modification techniques to alter the hydrophilicity and improve the compatibility with different nonpolar polymer matrices [21, 22]. Much research has been devoted to moderate the hydrophilicity of cellulose nanocrystals using physical and chemical modifications [23].

The application of different chemical-oriented surface modification methods is the most common method to alter the hydrophobicity nature of CNCs and enhance the compatibility between CNCs and nonpolar polymer. However, the need for developing new manufacturing processes capable of scaling up motivated the academia to find out innovative processing techniques. In the literature, two innovative manufacturing processes can be found: the application of liquid feeding and the application of masterbatch approach. This chapter contains contributions to the field of cellulose nanocomposites in the area of mechanical processing reporting new advances of the emerging ideas about manufacturing processes, which mainly focus on the achieved mechanical improvement.

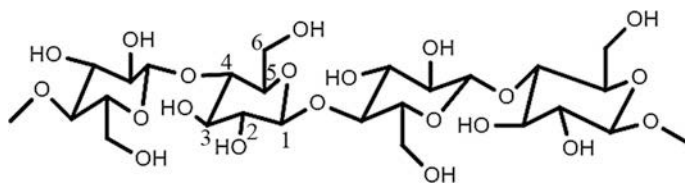


Fig. 1 Schematic representation of a cellulose molecule

2 Liquid Feeding

The application of extruder to shape thermoplastic materials dates back to 1935 when the first extruder machine was built by Paul Troester [24]. Since then, it has become the most broadly used processing technique through the development of different types of extruders capable of serving in different fields. The dramatic growth in plastic processing industry makes it essential to feed solid and liquid phases into extruders. In solid feeding extruders, the forces generated from rotating the screw and the stationary barrel move the materials down in the screw channel. In Liquid feeding extruders, the liquid can be fed into an extruder through a liquid injection nozzle.

It is reported that the drying process of cellulose nanocrystals results in the formation of irreversible aggregates which cannot be re-dispersed through an extrusion process. The application of liquid feeding seems to be a possible option to limit the formation of cellulose nanocrystal agglomerates. The incorporation of liquid and solid phase in an extruder could be difficult and the liquid feed rate, as well as liquid temperature, need to be monitored carefully, since the liquid temperature can strongly influence the viscosity and the change in liquid viscosity can result in pellet slippage on the barrel wall and consequently form undesirable product [25].

The first report of liquid feeding application of cellulose nanofillers into a polymer was by Oksman [26]. The extrusion process was implemented using an extruder equipped with a peristaltic pump which controlled the liquid feeding rate. Two different feeding methods were used: the dry materials were fed into the extruder from a top mounted hopper into the barrel taking advantage from gravimetric feeding and the aqueous cellulose nanowhisker suspension was fed into the extruder using a vacuum pump to ensure the constant liquid feeding rate. In the extrusion process, the existing solvent in the liquid phase was removed by atmospheric venting (Zones 7 and 8) as well as vacuum venting (zone 10) (Fig. 2).

The elaboration of achieving uniformly dispersed cellulose nanowhisker in this work resulted in the generation of the high amount of solvent vapour during the extrusion process. TEM analysis of the composite samples exhibited partly dispersed cellulose nanowhisker into the matrix as well as thermal degradation of cellulose nanowhisker [26].

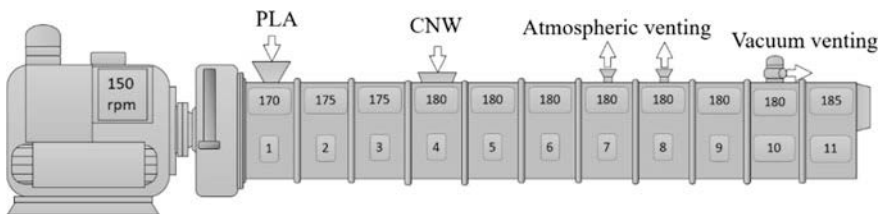


Fig. 2 Schematic image of extrusion process with liquid feeding [26]

In another work similar to cellulose nanowhisker liquid feeding, cellulose nanofibers were fed into PLA in a liquid phase. The high viscosity of cellulose nanofiber suspension reduced the uniform dispersion thorough composite samples [27]. The need for a specific extruder capable of feeding liquid and dry matter was reported as an essential need for incorporating liquid cellulose nanofiber into the polymer matrix.

3 Masterbatch Approach

The incorporation of cellulose nanocrystals into the different polymer matrix in a step-wise manner is one of the most commonly used preprocessing techniques in nanocomposites preparation. It is reported that the application of masterbatch can maximize the dispersion of cellulose nanocrystals in a polymer matrix, however, the time-consuming nature is the main weakness of the masterbatch approach [28, 29]. In masterbatch approach, a selective polymer is employed as a carrier for cellulose nanocrystals. The polymer can be either the same or different than the host polymer in the nanocomposite [30–34]. The highly concentrated masterbatches can be diluted in the extrusion process by adding polymer using the let-down ratio or mixing ratio (CNCs: polymer, generally between 1:14 and 1:20). The let-down ratio is of paramount importance since high mixing ratio might limit the uniform dispersion of CNCs in the polymer matrix [35]. Solvent casting and spin-coating are two methods employed in preparing CNCs masterbatches in literature.

3.1 Solvent Casting

Solvent casting has a widespread use in different applications owing to its simplicity and low-cost processing [36–39]. Solvent casting technique contains solubilization, casting, and solvent evaporation steps [40–45]. In solvent casting method, a polymer melt or polymer solution is applied on a flat surface, the solvent is then evaporated leaving a solid film. The evaporation rate of the solvent depends on the boiling point of the solvent, the viscosity of the solution, the pressure and the ambient temperature [46]. The rheological properties of the polymeric solution are of huge importance since the film thickness and the roughness of the film depends on the viscosity of the solution.

The solvent casting is a century-old method for nanocomposite films production [47–49] and is the most common method for preparing highly concentrated masterbatches. The application of solvent casting in composites manufacturing was reported for the first time by Favier et al. [50]. In that study, a tunicin-based nanocrystal in a latex matrix of poly(styrene-*co*-butyl acrylate) was studied and the competitive mechanical properties in corresponding composites confirmed the capability of solvent casting technique in composite films preparation.

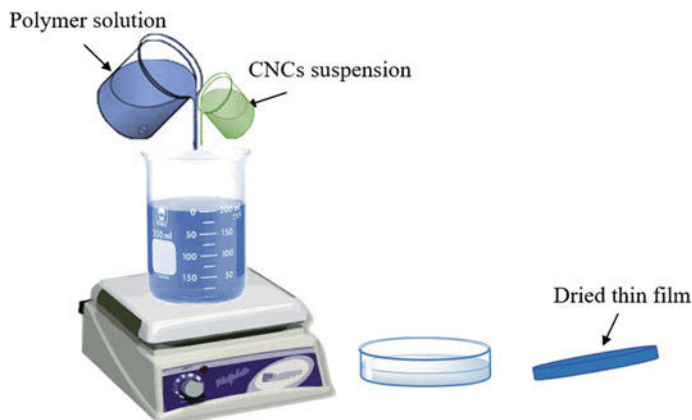


Fig. 3 Schematic depicting of solvent casting method

The preparation of thin films with uniform thickness, maximum optical clarity, and low haze were some advantages reported for solvent casting technology [51–53]. In general, the literature regarding the preparation of cellulose nanoparticles masterbatches involves the solvent casting as the main technique [20, 30, 54].

In solvent casting method, a polymer is first dissolved in a selective solvent either at room temperature or at elevated temperatures [55, 56]. The nanocelluloses are dispersed in either same or different solvent separately. The application of sonication and homogenization techniques can be used to increase the dispersion of nanoparticles through the solvent prior to the addition to the polymer solution [57]. The solution of polymer and CNCs suspension are then mixed together using magnetic stirrer and then poured into a flat-bottomed glass Petri-dishes and the solvent is evaporated and consolidate the films (Fig. 3).

3.1.1 Formation of Aggregates in Masterbatch Films

The morphology of thin film masterbatches generally affects the mechanical properties of final composites since the high concentration of CNCs in masterbatches tends to form CNCs' aggregates [35]. The time-intensive drying process in solvent casting method can intensify the formation of micro-sized cellulose aggregates in the masterbatch. The slow evaporation rate in solvent casting permits solvent molecules to exclude the nanoparticles and pushing them into closer proximity and leading to the formation of unavoidable CNC aggregates [35, 58]. In a recently published work, the formation of CNC aggregates in the masterbatch films was explored. In the aforementioned work, chloroform was used as the solvent and the percentage of CNCs in masterbatch films was 15% and the ultimate thickness was kept constant at 1.12 mm. Figure 4 illustrated the SEM image from a cross-section of the masterbatch.

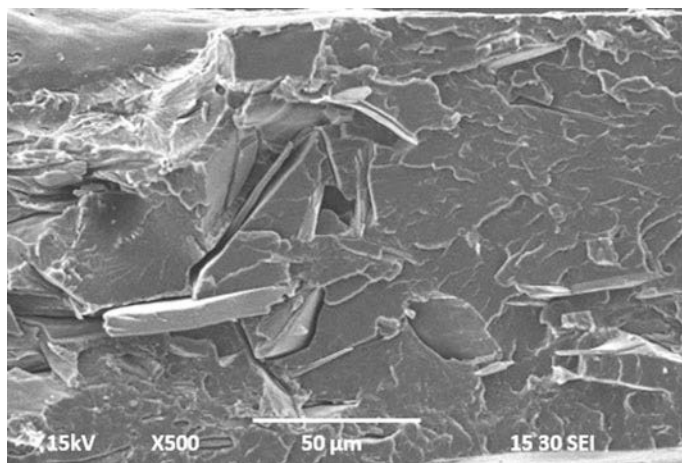


Fig. 4 Cross-sectional SEM image of solvent cast masterbatch film [35]

The formation of permanent CNC aggregates with relatively large effective size suggested strong aggregation in solvent cast masterbatches. It was reported that CNC aggregates formed during masterbatch preparation are difficult to separate during the extrusion process and those aggregates might result in poor adhesion between cellulose nanocrystals and polymer matrix [59].

3.2 *Spin-Coating*

Spin-coating is a common method employed to prepare thin films with thickness in the order of micrometre to nanometers. In this method, a liquid is deposited on a substrate, which can either be static or rotate at a specific angular velocity [60–62]. The deposited liquid generally consists of volatile solvents and non-volatile solute, and the non-volatile solute forms a thin film after solvent evaporation. Spin-coating involves four consecutive stages: deposition, spin-up, spin-off, and evaporation with some overlap in spin-off and evaporation steps [63]. During spin-off state, a film of liquid tends to spread with a uniform thickness, and after reaching a uniform thickness it tends to remain the uniform thickness. This behaviour suggests that mixture viscosity does not depend on shear and it would be constant throughout the substrate [64]. The equilibrium between centrifugal force generated from rotating substrate and the hydrodynamic (viscous) force evolving from the viscosity of mixture governs the efficiency of the formation of thin films with desirable thickness [35, 65]. In another word, the solution viscosity and the spinning speed mainly influence the film forming procedure. In general, the uniformity of thin film depends on the spinning speed, the concentration of mixture, and the volatility of

the solvent [66]. The desired film thickness can be achieved by adjusting the spinning time and speed [67].

The most common application of spin-coating method is in the field of micro-electronic thin films preparation. This method was first used by Emil et al., who studied the thin film formation of Newtonian fluid on a rotating substrate [68]. The application of this method in polymer films has been investigated in several theoretical and experimental studies [65, 69, 70].

A recently published work introduced an efficient spin-coating method for masterbatch preparation [35]. In this study, thin films with the thickness of the order of micrometres were spread evenly over the glass substrate using a combination of centrifugal force and the surface tension of the solution (Fig. 5).

In this work, the PLA-CNCs mixture was loaded in a syringe and injected through a needle (diameter = 500 μm) onto the centre of the rotating glass substrate with 100 mm diameter. The solvent evaporates simultaneously as the solution is applied to the substrate [62]. The spinning speed was kept constant at 400 rpm. The PLA-CNC mixture was loaded onto the centre of rotating substrate for 180 s.

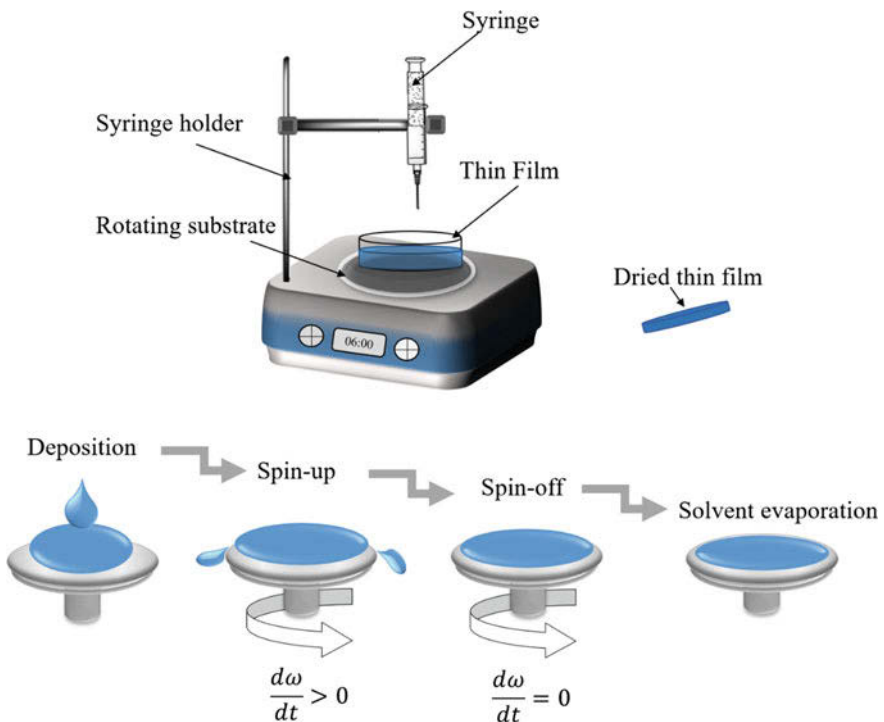


Fig. 5 Schematic illustration of the spin-coating method and four consecutive stages of the spin-coating method

3.2.1 Formation of Aggregates in Masterbatch Films

The volatile solvents used in spin-coating technique with a high evaporation rate can influence the formation of CNC aggregates through the polymer matrix. In fact, the high evaporation rate and low vaporizing time of the solvent from thin films in spin-coating method limit the movement of CNCs through the matrix and inhibits their assembly into micro-sized aggregates [35]. In fact, the rapid increase in the viscosity of solution as a result of the high evaporation rate of solvent kinetically traps the CNCs in the polymer matrix and hinder their movement for making more CNCs bundles. In the spin-coating method, thin film masterbatches are effectively dried out during spinning step. It is reported that in the spin-coating process as the solution is injected onto rotating substrate, the solvent evaporates and this, in turn, results in trapping the individual cellulose nanocrystals from forming big aggregates (Fig. 6).

The SEM micrograph of the free surface of spin-coated masterbatch exhibits that the high evaporation rate results in the formation of widespread voids on the free surface of masterbatches (Fig. 7).

3.3 Variation of Aggregates in Masterbatch Along the Cross-Sectional Thickness

The CNCs concentration and the formation of CNC aggregate through the thickness of the thin film masterbatches are shown in Fig. 8 (CNCs aggregates are pointed by arrow). In the solvent cast masterbatch, since the solvent evaporation occurs at a

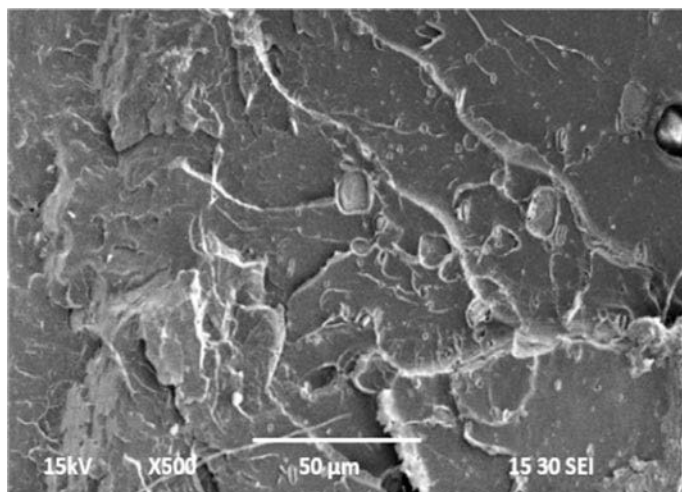


Fig. 6 Cross-sectional SEM image of solvent cast masterbatch film [35]

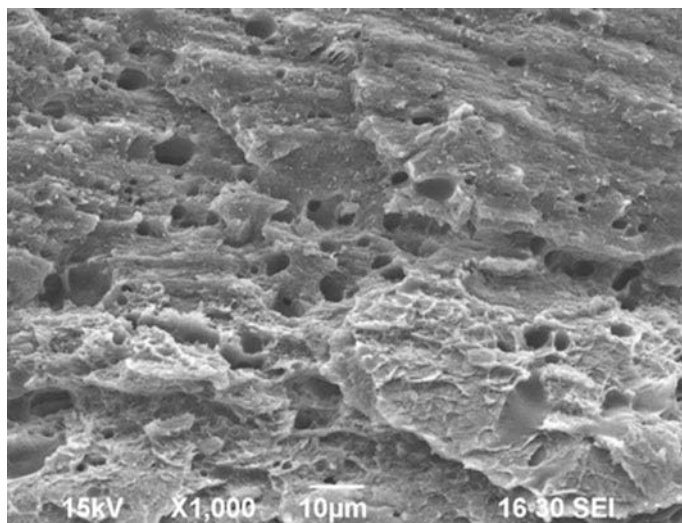


Fig. 7 The presence of voids on cross-sectional SEM image of spin-coat masterbatch film

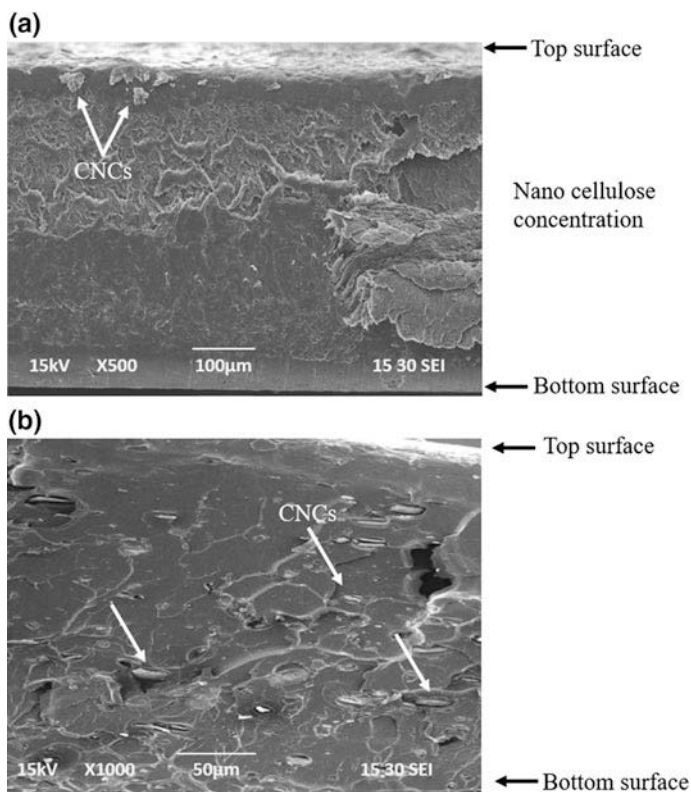


Fig. 8 The comparison of CNCs aggregates formation in the masterbatches: **a** solvent cast, **b** spin-coated

relatively low rate from the free surface of the film, the concentration of CNCs varies vertically along with the thickness of the thin film and the highest solute concentration happens close to the free surface. The increasing CNCs concentration can lead to the formation of CNC aggregates (Fig. 5a), however, in the spin-coated masterbatch, the CNC aggregates with perpendicular orientation with respect to the film thickness are scattered throughout the masterbatch thickness (Fig. 5b). These observations confirm the lower CNCs mobility in the spin-coated masterbatch as a result of the high evaporation rate of the solvent as well as the centrifugal force generated from rotating substrate [35].

4 Conclusion

The potential of nanocellulose to improve material properties has been widely accepted, however, application of nanocellulose in commercial polymer products has been lacking. One of the main hurdles is a uniform dispersion of nanocellulose material through polymer matrices. This review shows clearly that besides surface modification treatment, the application of mechanical pre-processing techniques has a great potential for improving the dispersion of nanocellulose through polymer matrices. This, in turn, results in higher compatibility between the polymer matrix and cellulose nanocrystals. The different techniques discussed in this chapter demonstrated an improvement in the performance characteristics of corresponding nanocomposites. All these techniques are expected to widen the domain of different mechanical pre-processing techniques for using nanocellulose materials.

Acknowledgements This work is based upon works supported by the National Science Foundation, ND EPSCoR under grant No. 11A1355466.

References

1. Klemm D, Heublein B, Fink HP, Bohn A (2005) Cellulose: fascinating biopolymer and sustainable raw material. *Angew Chem Int Ed* 44(22):3358–3393
2. Akhlaghi SP, Berry RC, Tam KC (2013) Surface modification of cellulose nanocrystal with chitosan oligosaccharide for drug delivery applications. *Cellulose* 20(4):1747–1764
3. Gozdecki C, Wilczyn A (2015) Effects of wood particle size and test specimen size on mechanical and water resistance properties of injected wood–high density polyethylene composite. *Wood Fiber Sci* 47(4):365–374
4. Siqueira G, Tapin-Lingua S, Bras J, da Silva Perez D, Dufresne A (2010) Morphological investigation of nanoparticles obtained from combined mechanical shearing, and enzymatic and acid hydrolysis of sisal fibers. *Cellulose* 17(6):1147–1158
5. Wang Q, Zhao X, Zhu J (2014) Kinetics of strong acid hydrolysis of a bleached kraft pulp for producing cellulose nanocrystals (CNCs). *Ind Eng Chem Res* 53(27):11007–11014
6. Filson PB, Dawson-Andoh BE, Schwegler-Berry D (2009) Enzymatic-mediated production of cellulose nanocrystals from recycled pulp. *Green Chem* 11(11):1808–1814

7. Ahola S, Turon X, Osterberg M, Laine J, Rojas O (2008) Enzymatic hydrolysis of native cellulose nanofibrils and other cellulose model films: effect of surface structure. *Langmuir* 24(20):11592–11599
8. Angles MN, Dufresne A (2001) Plasticized starch/tunicin whiskers nanocomposite materials. 2. Mechanical behavior. *Macromolecules* 34(9):2921–2931
9. Turbak AF, Snyder FW, Sandberg KR (1983) Microfibrillated cellulose, a new cellulose product: properties, uses, and commercial potential. *J Appl Polym Sci: Appl Polym Symp (United States)*, vol 37, No. CONF-8205234-Vol. 2. ITT Rayonier Inc., Shelton, WA
10. Dong XM, Revol J-F, Gray DG (1998) Effect of microcrystallite preparation conditions on the formation of colloid crystals of cellulose. *Cellulose* 5(1):19–32
11. Hindi SS (2017) Differentiation and synonyms standardization of amorphous and crystalline cellulosic products. *Nanosci Nanotechnol* 4(3):73–85
12. Iwamoto S, Kai W, Isogai A, Iwata T (2009) Elastic modulus of single cellulose microfibrils from tunicate measured by atomic force microscopy. *Biomacromol* 10(9):2571–2576
13. Miao C, Hamad WY (2013) Cellulose reinforced polymer composites and nanocomposites: a critical review. *Cellulose* 20(5):2221–2262
14. Abitbol T, Rivkin A, Cao Y, Nevo Y, Abraham E, Ben-Shalom T, Lapidot S, Shoseyov O (2016) Nanocellulose, a tiny fiber with huge applications. *Curr Opin Biotechnol* 39:76–88
15. Nagalakshmaiah M (2016) Melt processing of cellulose nanocrystals: thermal, mechanical and rheological properties of polymer nanocomposites. Grenoble Alpes
16. Hebeish A, Guthrie J (2012) The chemistry and technology of cellulosic copolymers, vol 4. Springer Science & Business Media
17. Habibi Y, Lucia LA, Rojas OJ (2010) Cellulose nanocrystals: chemistry, self-assembly, and applications. *Chem Rev* 110(6):3479–3500
18. Popa V (2011) Polysaccharides in medicinal and pharmaceutical applications. *Smithers Rapra*
19. Sokolova Y, Shubanov S, Kandyrin L, Kalugina E (2009) Polymer nanocomposites and their structure and properties. A review. *Plast Massy* 3:18–23
20. Shojaeiarani J, Bajwa DS, Stark NM (2018) Green esterification: A new approach to improve thermal and mechanical properties of poly(lactic acid) composites reinforced by cellulose nanocrystals. *J Appl Polym Sci*
21. Eyley S, Thielemans W (2014) Surface modification of cellulose nanocrystals. *Nanoscale* 6(14):7764–7779
22. Lucia LA, Rojas O (2009) The nanoscience and technology of renewable biomaterials. Wiley
23. Thakur VK (2014) Nanocellulose polymer nanocomposites: fundamentals and applications. Wiley
24. Rauwendaal C (2014) Polymer extrusion: Carl Hanser Verlag GmbH Co KG
25. Giles Jr HF, Mount III EM, Wagner Jr JR (2004) Extrusion: the definitive processing guide and handbook. William Andrew
26. Oksman K, Mathew AP, Bondeson D, Kvien I (2006) Manufacturing process of cellulose whiskers/poly(lactic acid) nanocomposites. *Compos sci technol* 66(15):2776–2784
27. Herrera N, Mathew AP, Oksman K (2015) Plasticized poly(lactic acid)/cellulose nanocomposites prepared using melt-extrusion and liquid feeding: mechanical, thermal and optical properties. *Compos Sci Technol* 106:149–155
28. Pracella M, Haque MM-U, Puglia D (2014) Morphology and properties tuning of PLA/cellulose nanocrystals bio-nanocomposites by means of reactive functionalization and blending with PVAc. *Polymer* 55(16):3720–3728
29. Mariano M, El Kissi N, Dufresne A (2015) Melt processing of cellulose nanocrystal reinforced polycarbonate from a masterbatch process. *Eur Polym J* 69:208–223
30. Jonoobi M, Harun J, Mathew AP, Oksman K (2010) Mechanical properties of cellulose nanofiber (CNF) reinforced poly(lactic acid) (PLA) prepared by twin screw extrusion. *Compos Sci Technol* 70(12):1742–1747
31. Gong G, Mathew AP, Oksman K (2011) Toughening effect of cellulose nanowhiskers on poly(vinyl acetate): fracture toughness and viscoelastic analysis. *Polym Compos* 32(10):1492–1498

32. Corrêa AC, de Moraes Teixeira E, Carmona VB, Teodoro KBR, Ribeiro C, Mattoso LHC, Marconcini JM (2014) Obtaining nanocomposites of polyamide 6 and cellulose whiskers via extrusion and injection molding. *Cellulose* 21(1):311–322
33. Lee S-H, Teramoto Y, Endo T (2011) Cellulose nanofiber-reinforced polycaprolactone/polypropylene hybrid nanocomposite. *Compos A Appl Sci Manuf* 42(2):151–156
34. Yang W, Fortunati E, Dominici F, Giovanale G, Mazzaglia A, Balestra G, Kenny J, Puglia D (2016) Synergic effect of cellulose and lignin nanostructures in PLA based systems for food antibacterial packaging. *Eur Polymer J* 79:1–12
35. Shojaeiarani J, Bajwa D, Stark N (2018) Spin-coating: a new approach for improving dispersion of cellulose nanocrystals and mechanical properties of poly(lactic acid) composites. *Carbohydr Polym*
36. Rezakazemi M, Sadrzadeh M, Mohammadi T, Matsuura T (2017) Methods for the preparation of organic-inorganic nanocomposite polymer electrolyte membranes for fuel cells. In: Inamuddin D, Mohammad A, Asiri AM (eds) *Organic-inorganic composite polymer electrolyte membranes*. Springer International Publishing, Cham, pp 311–325
37. Rezakazemi M, Ebadi Amooghin A, Montazer-Rahmati MM, Ismail AF, Matsuura T (2014) State-of-the-art membrane based CO₂ separation using mixed matrix membranes (MMMs): an overview on current status and future directions. *Prog Polym Sci* 39(5):817–861
38. Baheri B, Shahverdi M, Rezakazemi M, Motaee E, Mohammadi T (2014) Performance of PVA/NaA mixed matrix membrane for removal of water from Ethylene Glycol solutions by pervaporation. *Chem Eng Commun* 202(3):316–321
39. Shahverdi M, Baheri B, Rezakazemi M, Motaee E, Mohammadi T (2013) Pervaporation study of ethylene glycol dehydration through synthesized (PVA-4A)/polypropylene mixed matrix composite membranes. *Polym Eng Sci* 53(7):1487–1493
40. Dashti A, Harami HR, Rezakazemi M (2018) Accurate prediction of solubility of gases within H₂-selective nanocomposite membranes using committee machine intelligent system. *Int J Hydrogen Energy* 43(13):6614–6624
41. Rezakazemi M, Dashti A, Asghari M, Shirazian S (2017) H₂-selective mixed matrix membranes modeling using ANFIS, PSO-ANFIS, GA-ANFIS. *Int J Hydrogen Energy* 42(22):15211–15225
42. Rostamizadeh M, Rezakazemi M, Shahidi K, Mohammadi T (2013) Gas permeation through H₂-selective mixed matrix membranes: experimental and neural network modeling. *Int J Hydrogen Energy* 38(2):1128–1135
43. Rezakazemi M, Mohammadi T (2013) Gas sorption in H₂-selective mixed matrix membranes: experimental and neural network modeling. *Int J Hydrogen Energy* 38(32):14035–14041
44. Rezakazemi M, Shahidi K, Mohammadi T (2012) Sorption properties of hydrogen-selective PDMS/zeolite 4A mixed matrix membrane. *Int J Hydrogen Energy* 37(22):17275–17284
45. Rezakazemi M, Shahidi K, Mohammadi T (2012) Hydrogen separation and purification using crosslinkable PDMS/zeolite A nanoparticles mixed matrix membranes. *Int J Hydrogen Energy* 37(19):14576–14589
46. Chinaglia DL, Gregorio R, Stefanello JC, Pisani Altafim RA, Wirges W, Wang F, Gerhard R (2010) Influence of the solvent evaporation rate on the crystalline phases of solution-cast poly(vinylidene fluoride) films. *J Appl Polym Sci* 116(2):785–791
47. Rezakazemi M, Vatani A, Mohammadi T (2016) Synthesis and gas transport properties of crosslinked poly(dimethylsiloxane) nanocomposite membranes using octatrimethylsiloxy POSS nanoparticles. *J Nat Gas Sci Eng* 30:10–18
48. Rezakazemi M, Vatani A, Mohammadi T (2015) Synergistic interactions between POSS and fumed silica and their effect on the properties of crosslinked PDMS nanocomposite membranes. *RSC Adv* 5(100):82460–82470
49. Farno E, Rezakazemi M, Mohammadi T, Kasiri N (2014) Ternary gas permeation through synthesized pdms membranes: experimental and CFD simulation based on sorption-dependent system using neural network model. *Polym Eng Sci* 54(1):215–226
50. Favier V, Canova G, Cavallé J, Chanzy H, Dufresne A, Gauthier C (1995) Nanocomposite materials from latex and cellulose whiskers. *Polym Adv Technol* 6(5):351–355

51. Siemann U (2005) Solvent cast technology—A versatile tool for thin film production. In: Scattering methods and the properties of polymers, pp 307–316
52. Anbukarasu P, Sauvageau D, Elias A (2015) Tuning the properties of polyhydroxybutyrate films using acetic acid via solvent casting. *Sci Rep* 5:17884
53. Hsu S-T, Yao YL (2014) Effect of film formation method and annealing on morphology and crystal structure of Poly (L-Lactic Acid) films. *J Manuf Sci Eng* 136(2):021006
54. Jonoobi M, Mathew AP, Abdi MM, Makinejad MD, Oksman K (2012) A comparison of modified and unmodified cellulose nanofiber reinforced polylactic acid (PLA) prepared by twin screw extrusion. *J Polym Environ* 20(4):991–997
55. Rezakazemi M, Sadrzadeh M, Matsuura T (2018) Thermally stable polymers for advanced high-performance gas separation membranes. *Progr Energy Combust Sci* 66:1–41
56. Sadeghi A, Nazem H, Rezakazemi M, Shirazian S (2018) Predictive construction of phase diagram of ternary solutions containing polymer/solvent/nonsolvent using modified Flory-Huggins model. *J Mol Liq* 263:282–287
57. Dufresne A (2013) Nanocellulose: a new ageless bionanomaterial. *Mater Today* 16(6): 220–227
58. Bruckner JR, Kuhnhold A, Honorato-Rios C, Schilling T, Lagerwall JP (2016) Enhancing self-assembly in cellulose nanocrystal suspensions using high-permittivity solvents. *Langmuir* 32(38):9854–9862
59. Mathew AP, Oksman K, Sain M (2005) Mechanical properties of biodegradable composites from poly lactic acid (PLA) and microcrystalline cellulose (MCC). *J Appl Polym Sci* 97(5): 2014–2025
60. Mellbring O, Kihlman Øiseth S, Krozer A, Lausmaa J, Hjertberg T (2001) Spin coating and characterization of thin high-density polyethylene films. *Macromolecules* 34(21):7496–7503
61. Norrman K, Ghanbari-Siahkali A, Larsen N (2005) 6 Studies of spin-coated polymer films. *Annu Rep Sect “C” (Physical Chemistry)* 101:174–201
62. Hall DB, Underhill P, Torkelson JM (1998) Spin coating of thin and ultrathin polymer films. *Polym Eng Sci* 38(12):2039–2045
63. Syed JA, Lu H, Tang S, Meng X (2015) Enhanced corrosion protective PANI-PAA/PEI multilayer composite coatings for 316SS by spin coating technique. *Appl Surf Sci* 325:160–169
64. Brinker C, Hurd A, Schunk P, Frye G, Ashley C (1992) Review of sol-gel thin film formation. *J Non-Cryst Solids* 147:424–436
65. Danglad-Flores J, Eickelmann S, Riegler H (2018) Deposition of polymer films by spin casting: a quantitative analysis. *Chem Eng Sci*
66. Sahu N, Parija B, Panigrahi S (2009) Fundamental understanding and modeling of spin coating process: a review. *Indian J Phys* 83(4):493–502
67. Lien S-Y, Wu D-S, Yeh W-C, Liu J-C (2006) Tri-layer antireflection coatings (SiO₂/SiO₂–TiO₂/TiO₂) for silicon solar cells using a sol-gel technique. *Sol Energy Mater Sol Cells* 90(16):2710–2719
68. Emslie AG, Bonner FT, Peck LG (1958) Flow of a viscous liquid on a rotating disk. *J Appl Phys* 29(5):858–862
69. Herrera MA, Sirviö JA, Mathew AP, Oksman K (2016) Environmental friendly and sustainable gas barrier on porous materials: nanocellulose coatings prepared using spin-and dip-coating. *Mater Des* 93:19–25
70. Zabihi F, Xie Y, Gao S, Eslamian M (2015) Morphology, conductivity, and wetting characteristics of PEDOT: PSS thin films deposited by spin and spray coating. *Appl Surf Sci* 338:163–177

Processing and Industrial Applications of Sustainable Nanocomposites Containing Nanofillers



Khadija Zadeh, Sadiya Waseem, Kishor Kumar Sadasivuni, Kalim Deshmukh, Aqib Muzaffar, M. Basheer Ahamed and Mariam Al-Ali AlMaadeed

List of Abbreviations

3D	Three dimensional
Ag NWs	Silver nanowires
BNCs	Bionanocomposites
BOEA	Battery operated portable handheld electrospinning apparatus
CS	Chitosan
CaCO ₃	Calcium carbonate
CNTs	Carbon nanotubes
ESO	Epoxidized soybean oil
FTIR	Fourier transform infrared spectroscopy
HNTs	Halloysite nanotubes
GO	Graphene oxide
GNFs	Graphite nanoflakes
GNPs	Graphene nanoplatelets
GBR	Guide bone regeneration
GTR	Guide tissue regeneration
HA	Hyaluronic acid
LBL	Layer By layer
MWCNTs	Multiwalled carbon nanotubes
NPs	Nanoparticles
NFs	Nanofillers

K. Zadeh · K. K. Sadasivuni (✉)
Center for Advanced Materials, Qatar University, PO Box 2713, Doha, Qatar
e-mail: kishor_kumars@yahoo.com

S. Waseem
Advanced Carbon Products, CSIR-NPL, New Delhi 110012, India

K. Deshmukh · A. Muzaffar · M. Basheer Ahamed
Department of Physics, B.S. Abdur Rahman Crescent Institute of Science and Technology,
Chennai 600048, Tamil Nadu, India

M. A.-A. AlMaadeed
Materials Science and Technology Program, Qatar University, PO Box 2713, Doha, Qatar

NF	Nanofiller
NMs	Nanomaterials
NCs	Nanocomposites
PNCs	Polymer nanocomposites
PVA	Polyvinylalcohol
PEG	Polyethylene glycol
PANI	Polyaniline
PCO	Poly (cyclooctene)
P3HT	Poly (3-hexylthiophene)
PLA	Poly (lactic acid)
POMA	Poly (O-methoxyaniline)
PCL	Poly (caprolactone)
PTAA	Poly (3-thiophene acetic acid)
PLGA	Poly (lactic-co-glycolic acid)
SWCNTs	Single-walled carbon nanotubes
SiO ₂	Silicon dioxide
SMPs	Shape memory polymers
TiO ₂	Titanium dioxide
WVP	Water vapour permeability
ZnO	Zinc oxide
Zn	Zinc

1 Introduction

In the scientific research field, nanotechnology is a hugely popular area which covers polymer science and technology, micro and nanoelectronics, biomaterials etc. [1–3]. Polymer nanocomposites (PNCs) for industrial applications belong to a certain category of reinforced polymers having a lesser amount of effectively dispersed nanoparticles (NPs) [4, 5]. These PNCs are more beneficial than micro composites due to their size and interaction capability at the low filler loadings [6, 7]. The NPs in the form of fillers possess large specific surface area and higher surface energy when added to polymeric matrix which leads to changes in the morphological surfaces of the overall nanocomposites (NCs) [8–10]. The interaction of nanofillers (NFs) with the polymer matrix alters the chain mobility of the polymer and generates new trap centres in the NCs thereby changing desirable properties [11–13]. The analysis based on the use of materials in nanosize range provides an opportunity to design and produce new materials with enhanced bending, flexibility and improved physical properties for various interdisciplinary fields [14–16]. Since the NCs consist of different constituents having different structures compositions and properties, therefore, it leads to the development of materials with multi-functionality [17, 18]. The evolution of technology regarding the synthesis of new materials to be served

for various applications has been diverted towards the development of synthetic strategies for production of NCs [19, 20]. The technologically advanced synthetic strategies provide various advantages over conventional procedures like the technique used to procure homogenous large grained materials [21]. The evolution of NCs in the recent times is solely attributed to their new, desirable and advanced properties compared to the conventional materials [22].

PNCs comprise an essentially important class of commercial materials with applications including electrical insulators, thermal conductors, damping, and aerospace. In the composites having micrometre-scale dimensions, the properties are limited due to lack of optimization of micrometre-scale composite fillers [23–26]. The fillers provide optimization of one property at the expense of other like stiffness at expense of toughness and toughness is achieved at the expense of optical clarity etc. [27]. The presence of defects adds to the limitations of the conventional composites arising as a result of regions of the high or low volume fraction of micrometer-scale fillers which in turn ultimately leads to the failure of the composite [28, 29]. These limitations associated with such types of composites led to the development of NFs based PNCs. In NCs, unprecedented advantages of combined properties were observed like the insertion of equiaxed NPs in thermoplastics leads to increase in the tensile strength, stress yield and Young's modulus in contrast to the pure polymer [30–32]. The development of chemical and in situ processing pertaining to NPs and NCs respectively has provided control over the morphology of such materials [33–37]. In addition to that, the advancement in the development process has provided the capability to manage the control over the interface between the matrix and the filler [35, 38]. Besides, the NCs are exciting materials due to their unique feature to attain a combination of properties pertaining to their potential as industrial and commercial materials [36]. The technical community has made substantial progress in the processing of NCs [39, 40]. However, the progress is still under the initial or basic phase embracing the understanding of NCs, their tailoring and optimization of properties [41]. The optimization achieved so far yields the ability to change the size, shape, volume fraction and degree of dispersion.

Most commercial materials used nowadays, are based on petroleum or their derived products and plastics. Both of these are used in various fields like packaging industry, petroleum industries which produce a negative impact on the environment. Their constant use has led to issues like pollution of air, water, and soil which ultimately leads to the global warming. Their toxic behaviour and non-degrading or long degrading periods lead to an enormous rise in the concentration of CO₂ [42]. As such there arises a need for alternative materials which are degradable and sustainable. The examples of such sustainable alternatives include biopolymers and clay NCs as renewable sources to develop inventive green materials like polymer blends containing NFs and bio-nanocomposites (BNCs) [31]. Pectin, a sustainable polymer is used to develop smart green materials for specific applications. A blend of pectin and Chitosan (CS) are predicted to be used as carriers in pharmaceutical industry [43]. In another study, it was reported that the NCs developed using pectin and starch is expected to serve for the conservative cause in food packaging industry owing to the enhanced mechanical properties and

oxygen barrier tendencies [44]. The bio-films based on gelatin and pectin as sustainable and biocompatible NCs displayed improved tensile strength and water-resistant characteristics presenting an alternative material for fragile and watertight packing [45]. In a similar study, graphene oxide (GO) reinforced polyvinyl alcohol (PVA)/polyethylene glycol (PEG) blend composites were reported as high-performance dielectric material [46]. PEG is biocompatible, non-toxic and exhibits enriched water solubility. It acts as an efficient plasticizer for many biopolymers and NCs. The addition of a suitable amount of PEG to CS as per reports enhances the mechanical properties of the overall NCs [47]. The amount of PEG is significant due to the dependence of effectiveness of plasticization, variation in glass transition temperature on concentration [48]. The sustainability of polymers filled with nanoclay is well investigated for unique properties from both physical and chemical point of view [49]. The most promising NFs among nanoclay materials are the halloysite nanotubes (HNTs) due to their size and biocompatibility which makes it an ideal material for use in the biotechnology field, for water decontamination, as anti-corrosive coatings on metals, for humidity control and packaging [49–52].

The polymers sometimes do not display the desired properties. In such circumstances, NFs are added to the polymer matrix or blended with another suitable polymer to achieve the desired properties [53, 54]. The addition of small quantity of NPs is intended to facilitate new properties of the composites. However, the attainment of new properties is proportional to the surface treatment of the NFs and the processing technique applied. In polymer nanocomposites, the presence of NFs does not create large stress concentrations or do not alter ductility of the polymer [55]. Generally, the NFs with optical clarity (not scattering light) are added to the polymer matrix which subsequently changes the electrical and mechanical properties. For example, the addition of carbon nanotubes (CNTs) to polymer matrix greatly enhances the strength of the overall NCs. This type of interaction has been reported in the polymer matrix and single-walled carbon nanotubes (SWCNTs) wherein filler displays higher optical gain and large interfacial area [56]. In the formation of the NCs, the prime concern remains the credibility of NFs integration with polymers to display desired properties pertaining to the particular application.

In the industrial field, there is an urgency to seek new functional materials acquiring unique properties which can meet the difficult challenges concerning this field. As far as nanotechnology is concerned, there is no guideline pertaining to the mixing of NPs with polymers in composite structure to achieve the required properties [57]. The main challenges for NCs are to display and maintain the unique and multiple properties on a large scale through the use of conventional chemicals and materials [58]. For an industrial purpose, it is essential to establish a method or model to determine which nanofiller (NF) can be incorporated effectively for the formation of NCs and what new and improved properties can be achieved by following such procedures [59]. This can be achieved by determining the extent of effectiveness of dispersion of NPs in the matrix and its impact on the structure of polymer to yield desired properties [60]. Once the basic model is established, it is imperative to determine how the mixing of various NPs in polymer matrix

influences the structure and properties of the NCs [61, 62]. In addition to the basic processing models, the interaction between NFs and polymer matrix also requires prime focus due to which the consequences on the overall NCs can be attained. Therefore, it requires a combination and optimum utilization of numerical modelling, characterization, and informatics towards the formation of particular NCs encompassing desired properties [63, 64]. It is noteworthy, that the nanocomposite exhibits properties which are significantly different from the NFs and the polymer.

The processing technique has a huge impact on the electrical, thermal and mechanical properties of NCs to a great extent [65]. In case of NCs, just like the composites at the macroscale, the properties are dictated by the distribution, orientation, and interaction between the polymer matrix and NF [66]. At the nanoscale, the biggest challenge is presented by the dispersion of NFs like CNTs in the polymer matrices to attain considerable interfacial adhesion between the NF and polymer matrix [67, 68]. This is because the propensity of NFs like CNT's for the reinforcement to aggregate endures unless high shear forces are applied for homogeneous dispersion of the polymer and NF. However, it is important to control the intensity of the mixing, as over mixing often leads to structural damage of NF [69]. In addition to that, the viscosity parameter requires prime attention due to vicious nature of polymer and NF solution and as such, there arises difficulty in the moulding of NCs [70]. The other issue in the processing of NCs is the compatibility of NFs with polymer and solvents. To overcome these issues, several approaches have been devised and implemented to achieve desired mixing of NFs and polymers in solvents [71]. These approaches include dry powder mixing; melt mixing and surfactant-assisted mixing [72–77]. However, there is still room for more creative and advanced processing techniques for better results.

Nanocomposite technology has implications of exceptionally wide range like in medical field for the surgical purpose, in the agriculture sector for effective crop treatment, in construction for high tensile strength materials [74–78]. The development of sustainable nanocomposite technology can lead to processing of advanced materials and devices having applications devoted towards better living, safety and eco-friendly in nature [79]. As such the development of novel NCs with suitable NFs has seen enormous growth in the recent times. The rise of NCs can be attributed to their value-added properties which are obtained without altering the basic properties of their components [80, 81]. The integration of graphene with the polymer leads to enhancement of electrical, physical, mechanical and barrier properties of the polymer composite at exceptionally low filler loadings.

The NCs for industrial applications are still under developing stage although a lot of success has been achieved in understanding their properties. The conceptual analysis and proofs of concepts have been consistently made, however, the optimization of nanocomposite materials is still obscure [82]. The optimization of nanocomposite materials is achievable only when the physics behind the control of improved properties are appropriately and thoroughly understood along with the establishment of the routes of processing to get the desired structures is obtained [79, 83]. This is because the fabrication of the new NCs, the optimization through modelling provides the material response and structural property linkages [84].

After the establishment of the nanocomposite structure through modelling, assistance in the development of material processing is provided. This chapter provides an insight of processing of sustainable NCs containing NFs used in industrial applications.

2 Fabrication Techniques of Nanocomposites

In the industrial field, the fabrication techniques regarding the development of composites based on nanomaterials (NMs) play a pivotal role in determining the properties and applications of the nanocomposite material. The composite material is composed of at least two different types of material phases which are interconnected by means of inherent interfaces. The formation of stable NCs requires the compatibility and reduction of interfacial tension involving different material phases [85]. When it comes to nanocomposite materials, they contain NPs of nanoscale dimensions dispersed with even small interfacial separations. In contrast to that, the NCs are inherited with a large surface area due to which there is a substantial enhancement in many of its properties [86]. Therefore, it is important to consider a proper fabrication technique to form stable NCs without aggregation and phase separation [87]. For fabrication of NCs containing NFs, there are several conventional techniques like intercalation method including in situ polymerization, solution mixing, melt compounding. Additionally, other techniques like sol-gel, molecular composite and direct dispersion are also quite vividly used. In order to get a nanocomposite which exhibits unique properties, it is essential that the interaction between the components is strong in nature [88]. By using proper fabrication, the intended interaction can be achieved and therefore the nanocomposite will exhibit unique characteristics. In general, for stable nanocomposite formation containing NFs, the interfacial tension should be lower than 5×10^{-4} N/m [89]. In the above-listed techniques, the most exploited method used in the fabrication of PNCs includes layer exfoliation and intercalation [90]. The other commonly used fabricating methods comprise the flexible polymerization process and cost friendly melt compound process. For industrial manufacture line, it is essential to develop techniques which produce sustainable, cost-effective and eco-friendly NCs. In this chapter, some of the technical features of the fabrication methods developed for the industrial purpose are described.

2.1 Intercalation Method

Considering the fabrication of NCs containing NFs, intercalation method is the most popular method. This method comprises of a top-down approach in which the fillers are downsized to nano-dimensions [90]. In this method, the polymer or monomers layers are intercalated between layers of inorganic layered substances

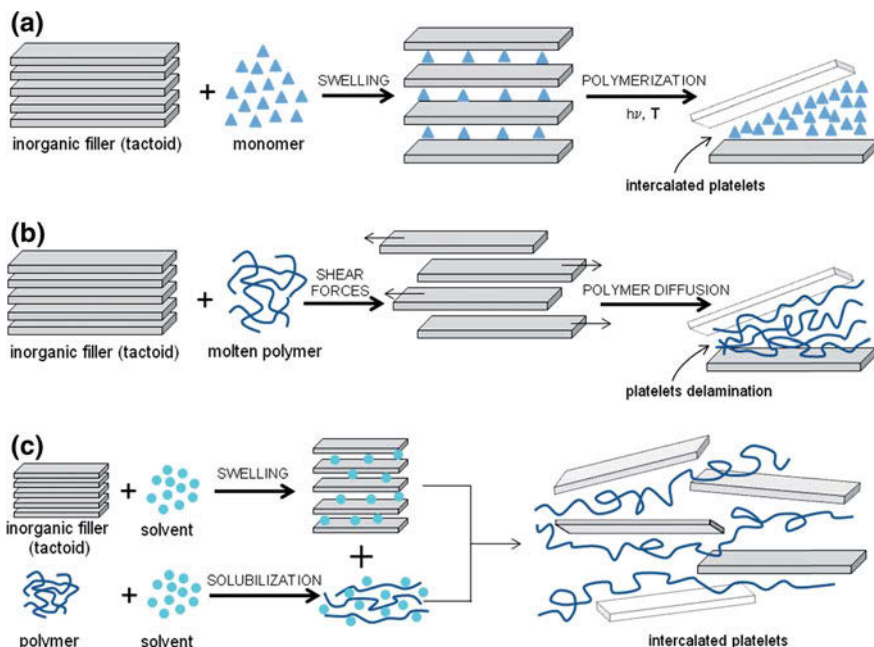


Fig. 1 Schematic representation of different intercalation methods: **a** in situ polymerization, **b** melt processing, and **c** solution casting [93]. Copyright 2010. Reproduced with permission from The Royal Society of Chemistry (RSC)

[91]. Within the polymer matrix, the inorganic substance is dispersed during the process of polymerization or melt-compounding thereby exfoliating the layered inorganic substance through each layer causing uniform dispersion of NFs [92]. The intercalation consist of three methods as shown schematically in Fig. 1 comprising of in situ polymerization, melt compounding and solution casting [93].

In the first method called as in situ polymerization, the layered substance like nanoclay is inflated within a liquid monomer or monomer solution as shown in Fig. 1a for the formation of polymer in between the intercalated layers. The polymerization commences on the application of either heat, an organic initiator or via the use of a catalyst [93]. The catalyst is fixed by means of cation exchange within the layered substance prior to inflation. However, the disadvantage of this method is the quick affinity of the inorganic substance towards sediment from the organic polymer and how rapid the phase separation occurs [94]. The interaction between solvent and NFs at the solvent-filler interface can be enhanced by incorporation of specific groups which are linked with the interface in order to stabilize the NPs dispersion [95].

The second method called melt intercalation method or melt processing as shown in Fig. 1b comprises annealing occurring statically or under application of shear [96]. The shear is necessary for delamination of the layered substance in order

to allow the polymer chains to diffuse into interlayers of NF to achieve exfoliated morphology [97]. In this method, the polymer and organically modified layered substance (silicates) are mixed above the softening point of the polymer i.e. the polymer is in the molten state prior to mixing. This fabrication method is eco-friendly as it does not involve organic solvents. This method is also highly compatible with the current industrial process like extrusion and injection moulding. This method can be applied to those NCs for which the other methods are not suitable. In melt processing, the extent of intercalation is affected by several factors like the thermodynamic interaction between the components and the diffusion of polymer from the melt into the silicate interlayers [98]. In order to achieve proper dispersion of polymer and NFs, there are two main considerations including the favourable enthalpic interaction between the components and appropriate fabricating conditions [99].

The final method termed, is the solution casting as shown in Fig. 1c the intercalation of polymer or pre-polymer from solution dependent on the solvent system where the polymer is soluble, and the layered substance is swellable (silicate fillers) [73]. The layered substance is dispersed in a solvent like chloroform or toluene causing the substance inflation. The polymer is also dispersed in a solvent to form a polymer solution. The polymer solution and inorganic NF solution are mixed leading to the displacement of solvent within the layers of NFs and ultimately the displaced sites are occupied by the polymer chains due to intercalation [100]. The mixing of the polymer solution with the delaminated nanoparticles causes strong interaction between the components of the composite [81]. The intercalation is attributed to the entropy resulting from desorption of the solvent molecules thereby balancing the decrease in entropy of the confined intercalated chains [101]. From the intercalated structure, when the solvent is removed, a nanocomposite comprising NF layer with the polymer is formed. The advantage of this method is quick rapid exfoliation of the stacked layers by application of an appropriate solvent [102]. On the other hand, the usage of organic solvents is strongly discarded as it makes the method unsafe and hazardous to the environment [103].

2.2 *Sol-Gel Method*

The sol-gel method comprises of a bottom-up approach in which NCs are formed using combined in situ NF formation and polymerization. In the sol-gel method, the NCs are made at relatively low temperature comprising of hydrolysis of the constituent molecular precursors followed by polycondensation to a glass-like form [104]. The sol-gel method allocates incorporation of organic and inorganic additives during the glassy network formation taking place at room temperature [105, 106]. Due to this reason, sol-gel has been conventionally used in the fabrication of glasses, polycrystals, porous composites, organic and inorganic NCs and ceramic materials. The process is initiated using metal alkoxide, melted using water, alcohol, ammonia or an acid for homogeneous dispersion. The metal alkoxide

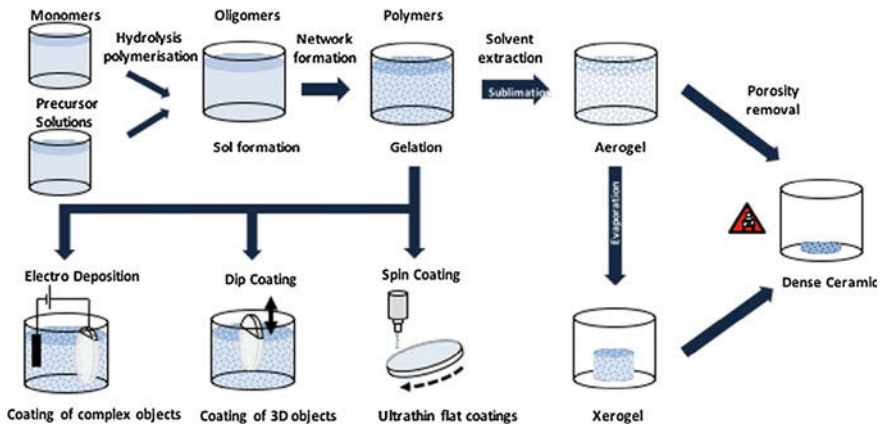


Fig. 2 Schematic representation of sol-gel synthesis routes [108]. Reproduced with permission from The Elsevier Ltd.

undergoes hydrolysis on reaction with water to form metal hydroxide and alcohol [107]. The sol-gel method is expected to be one of the key technologies in future for fabrication of NMs. The sol-gel method for processing of composite films is shown in Fig. 2. The process is initiated with the selection of appropriate precursors reacting at various steps to form colloidal particles or polymeric gels [108]. However, the prime requirements for this method for thin film deposition by spin coating or drop casting is stable sol and this sol is converted into a polymeric gel.

The metal ions bordered by ligands are mainly used as precursors for sol-gel reaction due to radial reaction mode. For the synthesis of zinc oxide (ZnO) thin film, the precursors used were zinc acetate dihydrate; $Zn(CH_3COO)_2 \cdot (H_2O)_2$ and ethanol were used as solvent [96]. The zinc (Zn) precursor and the dopant element were first dissolved in an appropriate solvent. This was followed by the addition of stabilizing agent (Monoethanolamine) to avoid premature precipitation and quick conversion of the sol into the gel. The solution of precursor material and the stabilizer is constantly kept on magnetic hot plate bath under constant stirring while maintaining the temperature at 25–80 °C in an oil bath leading to the formation of sol. The sol after attaining stability is aged for 24 h at room temperature. This is followed by post heat treatment where the parameters including drying time and temperature are altered. The procedure is continued several times to yield homogeneous, crystalline and single phase ZnO films after annealing.

2.3 Direct Dispersion Method

This method of nanocomposite fabrication is a top-down approach and comprises of surface modification of NFs aiding to the usage of chemicals to improve their

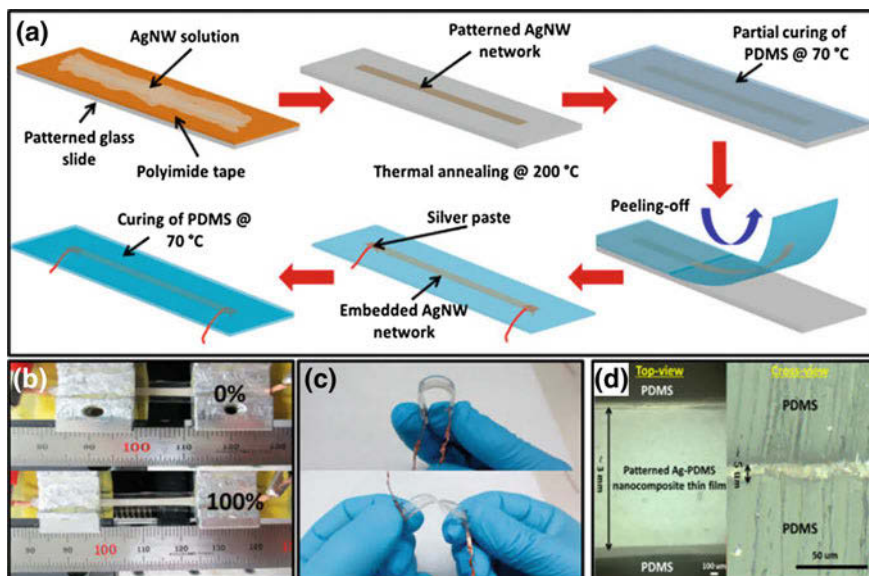


Fig. 3 **a** Fabrication process of sandwich-structured PDMS/AgNW/PDMS based strain sensors, **b** Strain sensor before and after 100% stretching, **c** strain sensor under bending and twisting, **d** optical microscopy images on top and cross-section of the strain sensor [111]. Reproduced with permission from. The American Chemical Society

compatibility with polymers [109]. The surface modified NFs are dispersed homogeneously in the polymer solution. The NCs fabricated by this method include fabrication of stretchable sensors, coating agents which are photo-hardened using functionalized silica NPs, comb-shaped block copolymers which are silver (Ag) protected, polyamide nanocomposite with silica nano-particles surface treated aminobutyric acid etc. [110–113]. The schematic representation for fabrication of stretchable sensors [111] is shown in Fig. 3. It can be seen that the fabricated sandwich-structured strain sensors exhibit excellent flexibility, stretching and bending ability. The top and cross-sectional optical images of the samples demonstrated the fabrication of well-patterned silver nanowires (AgNWs)-PNCs film with an average thickness of 5 μm .

Direct dispersion method is suitable for fabrication of polymer-based composites containing NFs or micro-fillers [42]. Generally, the polymer and the fillers are mixed in two ways i.e. either in presence of a solvent or without solvent [43]. The first case involves melting of the constituents while the second case involves mixing of the constituents in a solution [45]. Besides the above methods, there are several other methods used in the fabrication of NCs, which are listed in Table 1.

Table 1 Various techniques for fabrication of nanocomposites

Fabrication technique	Nanocomposites	Properties	References
Intercalation	<ul style="list-style-type: none"> • Polyethylene/ clay nanocomposites • Conducting polyaniline (PANI) and montmorillonite (Mmt) 	<ul style="list-style-type: none"> • Reduction in heat release rate by 32% • Enhanced thermal stability 	[114, 115]
Solvent casting	<ul style="list-style-type: none"> • Poly (3-hexylthiophene) (P3HT) • Gelatin and bioactive glass 	<ul style="list-style-type: none"> • Higher mechanical strength and conductivity • Improved biocompatibility and porosity 	[116, 117]
Melt compounding	<ul style="list-style-type: none"> • Cellulose whiskers-Polylactic acid • Polyethylene terephthalate/graphene 	<ul style="list-style-type: none"> • Improvement in material elongation • Low percolation threshold and superior electrical conductivity 	[118, 119]
In-situ polymerization	<ul style="list-style-type: none"> • LiFePO₄-carbon • Graphene oxide-epoxy 	<ul style="list-style-type: none"> • High power and long cycling life • Increased storage modulus, electrical conductivity and thermal stability 	[120, 121]
Doctor blade	<ul style="list-style-type: none"> • Graphene nanoplatelet-Liquid crystalline polymer • TiO₂ -SiO₂ nanocomposite 	<ul style="list-style-type: none"> • Better electrical conductivity and improvement shear modulus • Superior crystallinity, photocurrent density and photovoltaic performance 	[122, 123]
Compression molding	<ul style="list-style-type: none"> • Exfoliated graphite-polypropylene • Polyethylene-layered silicate 	<ul style="list-style-type: none"> • Enhanced flexibility and lower percolation threshold • Thermodynamic stability and improvement in tensile strength 	[124, 125]
Sol-gel	<ul style="list-style-type: none"> • Ag-TiO₂ nanocomposite • Carbon nanotubes—TiO₂ 	<ul style="list-style-type: none"> • Exhibition of antimicrobial properties • Improvement in photo-catalytic properties 	[126, 127]
Direct dispersion	<ul style="list-style-type: none"> • TiO₂-graphene nanocomposite • Graphene metal nanocomposite films 	<ul style="list-style-type: none"> • Decrease in lateral resistance and increase in photo-activity • Enhanced optical, electrical and mechanical properties 	[109, 128]

3 Applications of Sustainable Nanocomposites

Consistent efforts have been made in the last two decades in the area of nanotechnology in order to get NMs with determined functionality and promising prospects of sustainable materials [129]. Tailoring the properties of sustainable

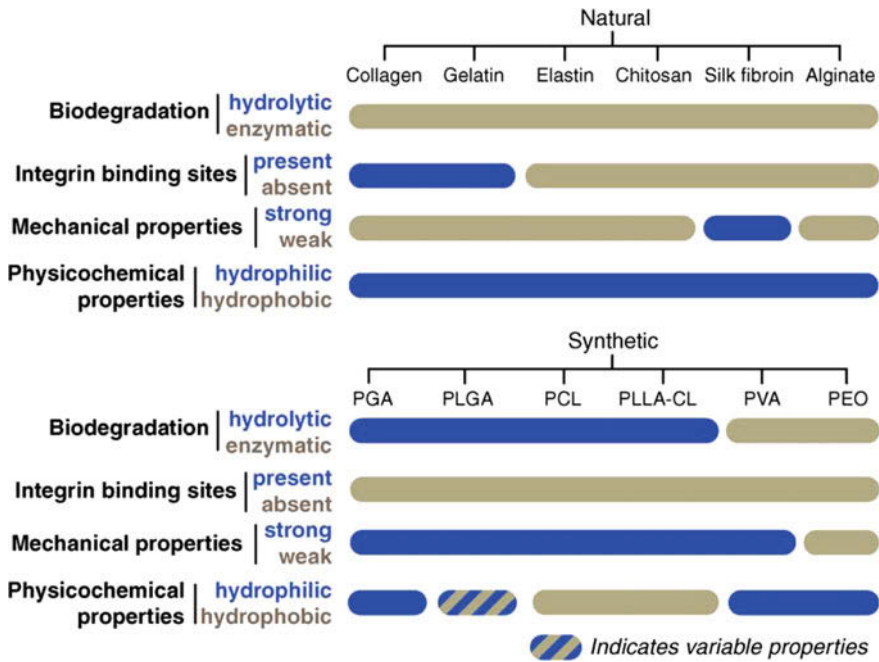


Fig. 4 Natural and synthetic polymers commonly used in the preparation of polyblend nanofibers with their key biological, mechanical and physicochemical properties [131]. Reproduced with permission from The Elsevier Ltd.

Table 2 Several polymer nanocomposites with their specific applications

Nanocomposites	Application	Properties	References
PCL/CNC/PEG	Shape memory polymer	Nanocomposites possessed good cytocompatibility and enhance mechanical properties	[132]
PLA/MWCNT	Electronics	Highly efficient nanocomposites as anti-static agents and can be applied for coating of electronic devices	[133]
PLA/CNC	Food packaging	Enhancement of stiffness, strength, and it is also easily processed to make a film for use in industrial packaging	[134]
PCL/lignin	Biomedical “tissue engineering”	Electrospun PCL-Lig scaffold enhanced the biological response	[135]

nanocomposite required biopolymer matrices. Biopolymers are polymers that biodegrade with different properties including renewability, sustainability, non-toxicity, and biodegradability [130]. Figure 4 illustrates classes of biodegradable polymers from different resources as sustainable matrices for the NFs [131].

The selection of NFs depends entirely on the application field of biological, mechanical and physicochemical properties. There is tremendous interest in the development of sustainable NCs for a wide range of commercial applications and many of these applications are already sought after for industrial applications. Table 2 shows several applications of sustainable NCs.

3.1 *Electronic Applications*

The behaviour of NCs in terms of electrical conductivity by large depends on the properties of NMs. For instance, some polymeric materials are considered poor electrical conductor due to the existence of high bandgap but, in the nano revolution researchers focused on sustainable polymeric nanomaterials having many advantages such as flexibility, inexpensive, non-corrosive and conductive materials in order to fabricate biodegradable and transient electronic devices for biomedical and other important applications [136]. Mai et al. [137] developed an intelligent sustainable nanocomposite sensor system comprising of Polylactic acid (PLA)/CNTs that can sense the degrading levels of the biopolymer which is correlated with the changes in electrical resistivity of the PLA/CNT NCs. Today the researchers mainly concentrate on the synthesis and development of new smart materials. These materials react with externally applied force like, thermal, light or magnetic. Piezoelectric is an example of such smart materials.

Piezoelectric materials convert mechanical energy (force) to an electrical signal. Thus, it can be seen that indeed the smart materials act as sensor component. Poly (vinylidene fluoride) is an example of smart polymer matrix; however, the addition of nanomaterials such as (SWNTs) is used as NF to tailor the sensing and power harvesting with enhanced performance [138, 139]. The use of smart materials as sensing and shape changing devices has been enhanced due to increase emphasis on nanocomposite materials. A typical smart material assembly contains:

- Sensor components: containing smart materials that monitor changes in pressure, temperature, light current or magnetic field.
- A communication network that relays changes detected by sensor component
- Actuator part that react to the command, it could be also smart materials such as piezoelectric.

Biopolymers and biopolymer NCs are desired materials for supercapacitor applications. These materials should possess low cost, high conductivity, high voltage window and high storage capacity in order to find application as a supercapacitor electrode. Higher conductivity can be achieved by using suitable electrode material through negative or positive “doping” with ions either by oxidation or reduction process. Christinelli et al. [140] reported the fabrication of supercapacitors with layer-by-layer (LBL) technique using poly (o-methoxyaniline) (POMA) and poly (3-thiophene acetic acid) (PTAA). The results were compared with POMA

casting film. The film behaviour with increasing bilayer numbers through a self-doping process which initiated each layer to act as a capacitor in parallel resulting in an increase in the overall capacitance of the film and the surface area. Hence, in this proposition, it is reasonable to expect an increase in the active area of the film with an increase in the number of bilayers [140].

In recent years, highly flexible and planar supercapacitor electrodes have been prepared using graphite nanoflakes (GNFs) on polymer lapping films as a flexible substrate. Botta et al. [141] reported the effect of the addition of GNFs into PLA matrix and evaluated the effect of reprocessing on the properties of PLA filled with graphene nanoplatelets (GNPs). In particular, the morphological analyses, intrinsic viscosity measurements, thermal, rheological and mechanical tests were carried out on the materials reprocessed using five subsequent extrusion cycles. It was found that addition of GNPs in the PLA matrix resulted in the decrease of the degradation rate as a function of the reprocessing cycles. Biodegradable polymers with high crystallinity, high hydrophobicity, and facile processing are used to maintain the functionality of electronic devices that are exposed to aqueous solutions, high salinity environments, and elevated temperature. Alam et al. [142] reported a technically benign procedure to combine vermiculite nanoplatelets with nanocellulose fiber dispersions to form functional biohybrid films. The unique combination of excellent oxygen-barrier properties and optical transparency of these biohybrid materials suggests their potential as an alternative in the flexible packaging of oxygen-sensitive devices such as in the displays of a light emitting diode, gas-storage and as barrier coatings in large volume-packaging.

3.2 Shape Memory and Biomedical Applications

Shape-memory polymers (SMPs) have attracted significant attention due to their fascinating applications. CNTs possess attractive properties such as high thermal and electrical conductivity which encourages towards utilizing them as the functional filler in PNCs. Wang et al. [143] reported the development of a chemically cross-linked polycyclooctene (PCO), multiwall carbon nanotubes (MWCNTs) and polyethylene based shape memory NCs with co-continuous structure and selective distribution of MWCNTs in the PCO matrix. It was noted that the selective distribution of MWCNTs in the PCO matrix reduces the conductivity. The shape memory composites with thermally responsive thicknesses could be employed as an artificial tendon [144] as shown in Fig. 5. The biodegradable polymers are proposed to provide temporary assisting support for cell growth which otherwise gets degraded with time in a controlled way into nontoxic products [145]. In tissue engineering, the methods from materials engineering and life science are employed to create artificial constructs for regeneration of new tissue.

One of the most promising approaches toward cells growth is Scaffold, carried via application of temporary support for regrowth of the targeted tissues without the loss of the three-dimensional stable structure [146]. In the biomedical application,

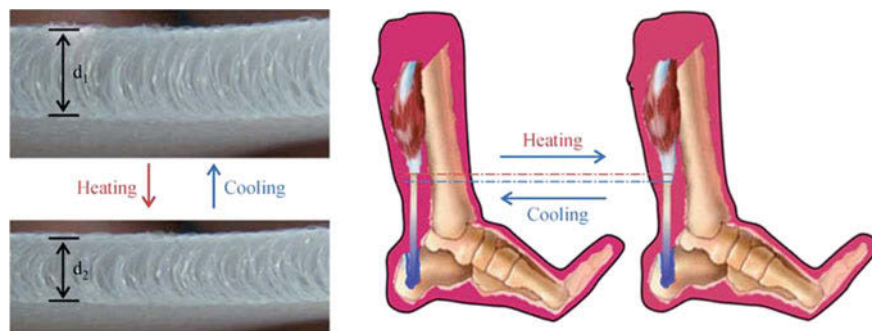


Fig. 5 Shape memory application sustainable polymer composite in biomedical field [144]. Reproduced with permission from The Springer Nature

the tissue engineering scaffold is one of the massive fields of research in recent years because of its potential in the repair or replacement of damaged tissues and organs. Tissue engineering scaffolds are three dimensional (3D) backbones that can be used for cell proliferation migration and differentiation which ultimately aid in the formation of the extracellular matrix [147].

Biopolymer scaffolds is a major part of tissue engineering which becomes helpful through cell seeding, proliferation, and formation of new tissues providing great scopes in the research field of engineering. The diversity of tissues depends majorly on 3 factors such as pore size, porosity and surface area which are widely recognized in the field of tissue engineering scaffold [148]. For example, PLA/CNTs have been extensively investigated for biomedical and other applications. It has a potential use in biomedical scaffolds for tissue engineering. The electrical conductivity of the carbon-based nanostructures plays a vital role in direct cell growth as they are capable of conducting and stimulating an electric field in the process of healing of tissues [149].

Fujihara et al. [150] developed guided bone regeneration (GBR) membranes by reinforcing calcium carbonate (CaCO_3) NPs into polycaprolactone (PCL) matrix to synthesize nanofibers with the help of electrospinning technique. The nanofibrous membrane was fabricated by developing two layers. These layers are called mechanical support layer and PCL/ CaCO_3 nanocomposite as a functional layer. Figure 6 shows the membrane supported osteoblast attachment and proliferation of a battery operated portable handheld electrospinning apparatus (BOEA) which has potential application in rapid hemostatic treatments [151].

Biodegradable NCs has fascinating application in dental field Such as periodontal and alveolar bone regeneration. Both Guided tissue regeneration (GTR) and GBR works on the principle of placement of a barrier membrane with the motive of preventing epithelial migration into the defective area, thus allowing sufficient and prolonged time for periodontal ligament, cementum and bone regeneration. Park et al. [152] developed a membrane of biodegradable poly (lactic-co-glycolic acid) (PLGA) and hyaluronic acid (HA) to obtain HA-PLGA NPs used for bone and

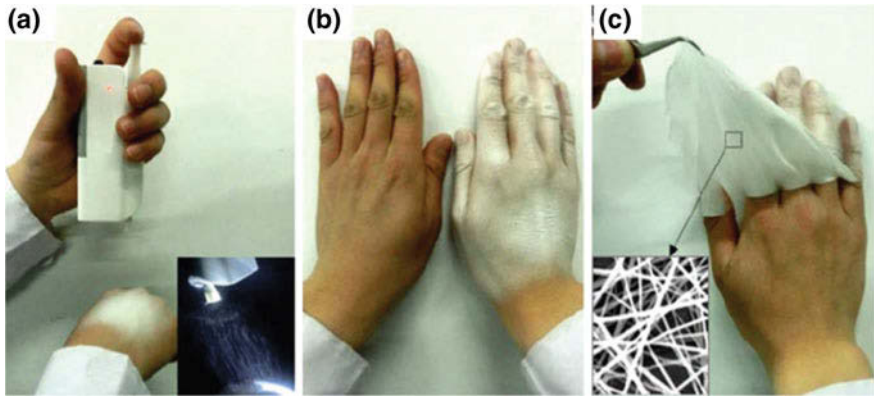


Fig. 6 **a** The BOEA spinning process on hand, **b** fabricated PLA fibrous membrane on another hand in 2 min, **c** fibrous membrane showing good flexibility and compactness [151]. Reproduced with permission from The Elsevier Ltd.

periodontal regeneration as shown in Fig. 7. Several biomedical applications of CS composites [154] have been reported as shown in Fig. 8. CS is the potential material to be used as artificial kidney membrane, hypocholesterolemic agents, drug delivery systems, absorbable sutures and supports for immobilized enzymes. CS has some unique characteristic advantages due to its nontoxicity and biodegradability which doesn't damage the environment. Being a biocompatible material, CS breaks down slowly into harmless products that are absorbed completely by the body.

3.3 Mechanical Applications

NFs are used to improve the mechanical properties of biopolymers as reinforcement materials. Example of such NMs is nanocellulose which is one of the most abundant biomass materials extracted from cellulose. It has been showed to be an environmentally friendly material with excellent mechanical properties owing to its unique nano-structure. Nanocellulose has been extensively used as functional materials in a variety of applications [155]. To induce a wide range of bending and geometries in the surfaces of such materials, the prototype can be laminated with a wood veneer surface from either side. The flexible fireboard can be fixed with desired geometry by fixing another veneer layer on the other side of it which produces sandwich panels as shown in Fig. 9. Similarly, flat or curved sandwich panels can be fabricated from the same materials which are developed following the same production process with different post-production processes. When the veneer is applied from both the sides of the panel, the form is fixed and no geometrical variations are required [156].

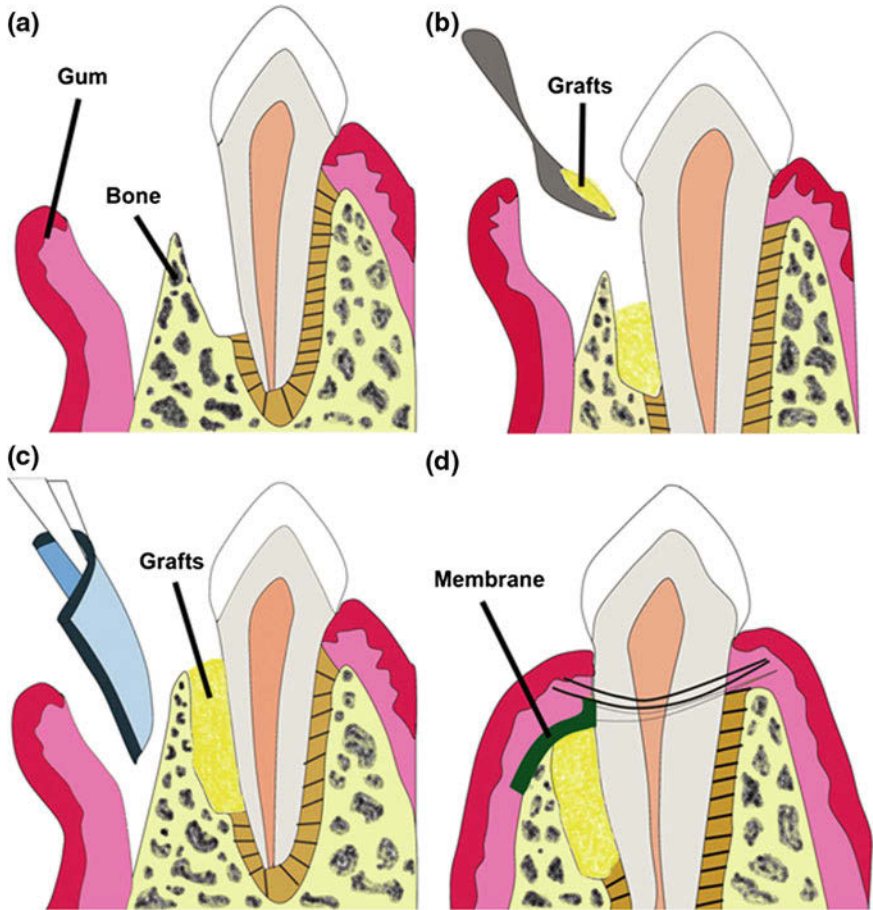


Fig. 7 Schematic representation of a combination therapy of bone grafts and GTR membrane for periodontal regeneration. Reprinted from Ref. [153]. Reproduced with permission from The Elsevier Ltd.

The great biocompatibility and biodegradability, in particular, render nanocellulose is seen as promising sustainable NF. Bulota et al. [157] introduced acetylated micro-fibrillo cellulose to PLA with fiber contents 2–20% using solution casting method. The maximum tensile strength was observed with fiber content over 10% whereas Young's modulus was increased by approximately 15%. However, no improvement was observed in case of tensile strength. The strain recorded in the materials at the time of fracture improved from 8.4% to 76.1% with 5% fiber loading. Miao et al. [158] reported preparation of epoxidized soybean oil (ESO) based paper cellulose composites. The study demonstrated the good compatibility between ESO and cellulose paper. Boron trifluoride diethyl etherate was used as catalyst and ESO was in situ polymerized on the morphological surface of

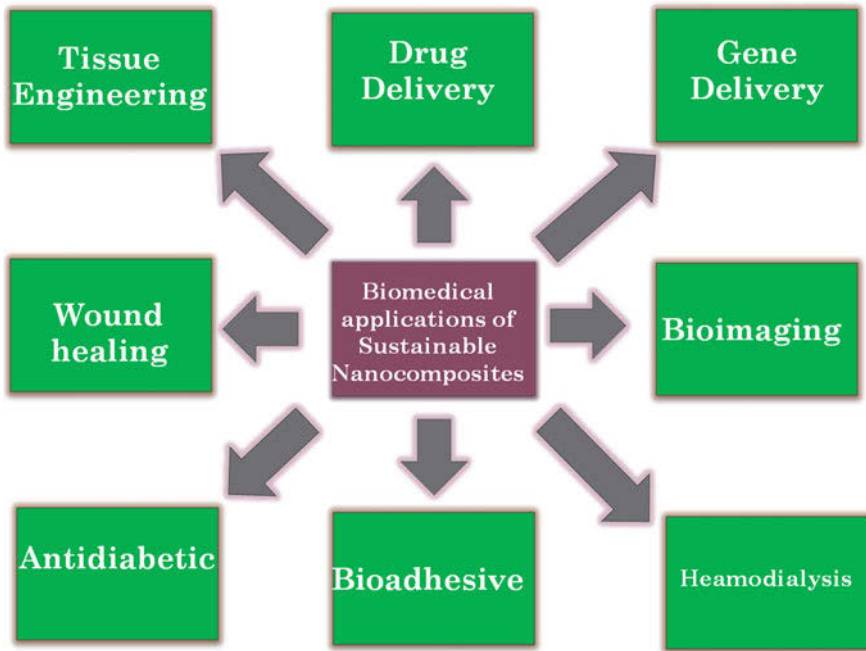


Fig. 8 Various biomedical applications of Chitosan

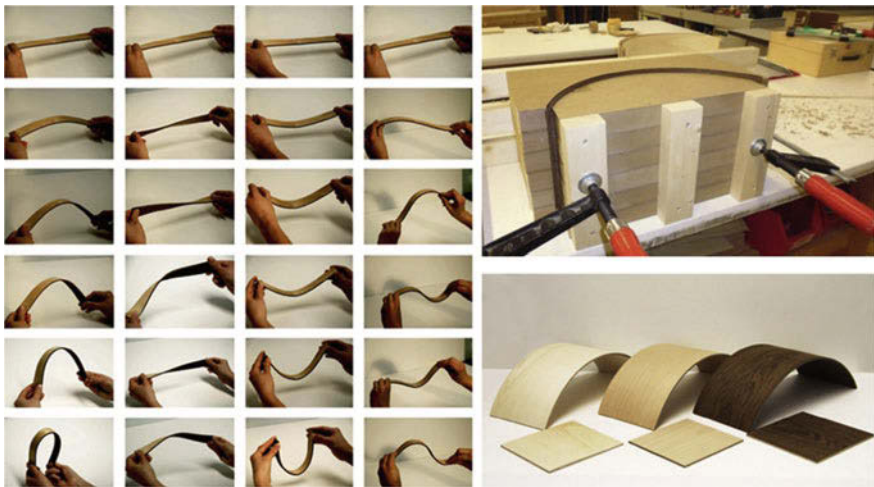


Fig. 9 Illustration of a wood veneer surface with excellent flexibility and a wide range of geometries [156]. Reproduced with permission from The Elsevier Ltd.

the cellulose. The long alkyl chain of the ESO is assumed to improve fiber dispersion in PLA matrix. The polymerization of ESO was confirmed using Fourier transform infrared spectroscopy (FTIR). Water vapour permeability (WVP) measurements revealed that these composites can be used as the potential water resistant material. Majeed et al. [159] reviewed a work on natural fiber/nanoclay reinforced polymeric materials for food packaging application. The biodegradable hybrid material obtained by mixing natural fibers with nanoclay exhibits improved barrier properties. At some optimum proportion, this combination can show excellent dispersion along with good compatibility with the matrix. This combination of hybrid materials has excellent mechanical strength at very low cost. This material has most suitable application as vapour sensitive materials to be used in electronic goods and pharmaceutical packaging.

4 Conclusions

This chapter discussed the significant progress in the processing of sustainable NCs containing NFs. The sustainable NCs formation requires polymer which is as bio-based polymer matrix along with NFs. In this chapter, some of the technical features of the fabrication methods were described for the industrial purposes. The processing technique greatly influences the electrical, biological and mechanical properties of sustainable NCs to a great extent. Biodegradable polymers enhanced by NFs are attractive and befitting candidates for applications in several fields such as biomedical, especially as drug delivery, tissue engineering and in, electronic such as supercapacitors, piezoelectric materials, and biosensors. Mechanical and barrier properties of the Biopolymer NCs can be greatly improved by reinforcing them with various NFs. The resultant BNCs maintains their vital essence of biodegradability even after infusion. Biopolymer composites with anticipated properties have the ample potential to replace conventional materials presently used in various field of applications.

References

1. Mrlik M, Sobolciak P, Krupa I, Kasak P (2018) Light-controllable viscoelastic properties of a photolabile carboxybetaine ester-based polymer with mucus and cellulose sulfate. *Emergent Mater* 1(1–2):1–1
2. Meng T, Yi C, Liu L, Karim A, Gong X (2018) Enhanced thermoelectric properties of two-dimensional conjugated polymers. *Emergent Mater* 1(1–2):1
3. Popelka A, Sobolciak P, Mrlik M, Nogellova Z, Chodák I, Ouederni M, Al-Maadeed MA, Krupa I (2018) Foamy phase change materials based on linear low-density polyethylene and paraffin wax blends. *Emergent Mater* 1(1–2):1–8

4. Deshmukh K, Ahamed MB, Deshmukh RR, Pasha SKK, Bhagat PR, Chidambaram K (2016) Biopolymer composites with high dielectric performance: interface engineering. In: Sadasivuni KK, Ponnamma D, Kim J, Cabibihan JJ, AlMaadeed MAA (eds) Biopolymer composites in electronics. Elsevier, Amsterdam, pp 27–128
5. Deshmukh K, Sankaran S, Ahamed MB, Sadasivuni KK, Pasha SKK, Ponnamma D, Sreekanth PSR, Chidambaram K (2017) Dielectric spectroscopy. In: Thomas S, Mishra RK, Thomas R, Zachariah AK (eds) Instrumental techniques to the characterizations of nanomaterials. Elsevier, Amsterdam, pp 237–299
6. Thangamani GJ, Deshmukh K, Chidambaram K, Ahamed MB, Sadasivuni KK, Ponnamma D, Faisal M, Nambiraj NA, Pasha SKK (2018) Influence of CuO nanoparticles and graphene nanoplatelets on the sensing behavior of poly (vinylalcohol) nanocomposites for the detection of ethanol and propanol vapors. *J Mater Sci Mater Electron* 29(6):5186–5205
7. Badgayan ND, Samanta S, Sahu SK, Venkata Siva SB, Sadasivuni KK, Sahu D, Rama Sreekanth PS (2017) Tribological behaviour of 1D and 2D nanofiller based high density polyethylene nanocomposites: a run in and steady state phase analysis. *Wear* 376–377:1379–1390
8. Thangamani GJ, Deshmukh K, Sadasivuni KK, Chidambaram K, Ahamed MB, Ponnamma D, AlMaadeed MAA, Pasha SKK (2017) Recent advances in electrochemical biosensors and gas sensors based on graphene and carbon nanotubes (CNT): a review. *Ad Mater Lett* 8(3):196–205
9. Sathapathy KD, Deshmukh K, Ahamed MB, Sadasivuni KK, Ponnamma D, Pasha SKK, AlMaadeed MAA, Ahmad J (2017) High quality factor poly (vinylidene fluoride) based novel nanocomposites filled with graphene nanoplatelets and vanadium pentoxide for high-Q capacitor applications. *Ad Mater Lett* 8(3):288–294
10. Mohanapriya MK, Deshmukh K, Chidambaram K, Ahamed MB, Sadasivuni KK, Ponnamma D, AlMaadeed MAA, Deshmukh RR, Pasha SKK (2017) Polyvinyl alcohol (PVA)/Polystyrene sulfonic acid (PSSA)/carbon black nanocomposites for flexible energy storage device applications. *J Mater Sci Mater Electron* 28(8):6099–6111
11. Abdullah N, Yusof N, Ismail AF, Othman FE, Jaafar J, Jye LW, Salleh WN, Aziz F, Misdan N (2018) Effects of manganese (VI) oxide on polyacrylonitrile-based activated carbon nanofibers (ACNFs) and its preliminary study for adsorption of lead (II) ions. *Emergent Mater* 1(1–2):1–6
12. Mohanapriya MK, Deshmukh K, Ahamed MB, Chidambaram K, Pasha SKK (2016) Zeolite 4A filled poly (3, 4-ethylenedioxythiophene): (polystyrenesulfonate) and polyvinyl alcohol blend nanocomposites as high-k dielectric materials for embedded capacitor applications. *Ad Mater Lett* 7(12):996–1002
13. Muzaffar A, Ahamed MB, Deshmukh K, Faisal M, Pasha SKK (2018) Enhanced electromagnetic absorption in NiO and BaTiO₃ based polyvinylidene fluoride nanocomposites. *Mater Lett* 218:217–220
14. Ponnamma D, Sadasivuni KK, Strankowski M, Moldenaers P, Thomas S, Grohens Y (2013) Interrelated shape memory and Payne effect in polyurethane/graphene oxide nanocomposites. *RSC Adv* 3(36):16068–16079
15. Ponnamma D, Sadasivuni KK, Strankowski M, Guo Q, Thomas S (2013) Synergistic effect of multiwalled carbon nanotubes and reduced graphene oxide in natural rubber for sensing applications. *Soft Matter* 9(43):10343–10353
16. Sadasivuni KK, Castro M, Saiter A, Delbreilh L, Feller JF, Thomas S, Grohens Y (2013) Development of poly(isobutylene-co-isoprene)/reduced graphene oxide nanocomposites for barrier, dielectric and sensing applications. *Mater Lett* 96:109–112
17. Mohanapriya MK, Deshmukh K, Ahamed MB, Chidambaram K, Pasha SKK (2016) Influence of cerium oxide (CeO₂) nanoparticles on the structural, morphological, mechanical and dielectric properties of PVA/PPy blend nanocomposites. *Mater Today Proc* 3(6):1864–1873
18. Sadasivuni KK, Saiter A, Gautier N, Thomas S, Grohens Y (2013) Effect of molecular interaction on the performance of poly (isobutylene-co-isoprene)/graphene and clay nanocomposites. *Colloids Polymer Sci* 291(7):1729–1740

19. Fayyad EM, Abdullah AM, Hassan MK, Mohamed AM, Jarjoura G, Farhat Z (2018) Recent advances in electroless-plated Ni-P and its composites for erosion and corrosion applications: a review. *Emergent Mater* 1(1–2):1–22
20. Illa MP, Khandelwal M, Sharma CS (2018) Bacterial cellulose-derived carbon nanofibers as anode for lithium-ion batteries. *Emergent Mater* 1(3–4):1–6
21. Nisar U, Amin R, Shakoor A, Essehli R, Al-Qaradawi S, Kahraman R, Belharouak I (2018) Synthesis and electrochemical characterization of Cr-doped lithium-rich Li 1.2 Ni 0.16 Mn 0.56 Co 0.08-x Cr x O 2 cathodes. *Emergent Mater* 1(3–4):1–0
22. Reddy YG, Awasthi AM, Chary AS, Reddy SN (2018) Characterization and ion transport studies through impedance spectroscopy on (1-x) Pb (NO 3) 2: xAl 2 O 3 composite solid electrolytes. *Emergent Mater* 1(3–4):1–0
23. Fadiran OO, Girouard N, Meredith JC (2018) Pollen fillers for reinforcing and strengthening of epoxy composites. *Emergent Mater* 1(1–2):95–103
24. Selmy AE, Soliman M, Allam NK (2018) Refractory plasmonics boost the performance of thin-film solar cells. *Emergent Mater* 1(3–4):1–7
25. Ponnamma D, Erturk A, Parangusan H, Deshmukh K, Ahamed MB, Al-Maadeed MA (2018) Stretchable quaternary phasic PVDF-HFP nanocomposite films containing graphene-titania-SrTiO₃ for mechanical energy harvesting. *Emergent Mater* 1(1–2):55–65
26. Ponnamma D, Sadasivuni KK, Grohens Y, Guo Q, Thomas S (2014) Carbon nanotube based elastomer composites-an approach towards multifunctional materials. *J Mater Chem C* 2(40):8446–8485
27. Fujiyama-Novak JH, Rufino V, Amaral RA, Habert AC, Borges CP, Mano B (2016) Oxygen permeability of nanocomposite-based polyolefin films. *Macromol Symp* 368(1):19–23
28. Sadasivuni KK, Ponnamma D, Kumar B, Strankowski M, Cardinaels R, Moldenaers P, Thomas S, Grohens Y (2014) Dielectric properties of modified graphene oxide filled polyurethane nanocomposites and its correlation with rheology. *Compos Sci Technol* 104:18–25
29. Deshmukh K, Ahamed MB, Sadasivuni KK, Ponnamma D, AlMaadeed MAA, Pasha SKK, Deshmukh RR, Chidambaram K (2017) Graphene oxide reinforced poly (4-styrenesulfonic acid)/polyvinyl alcohol blend composites with enhanced dielectric properties for portable and flexible electronics. *Mater Chem Phys* 186:188–201
30. Cooke KO, Khan TI (2018) Effect of thermal processing on the tribology of nanocrystalline Ni/TiO₂ coatings. *Emergent Mater* 1(3–4):1–9
31. Rahman M, Hamdan S, Hashim DM, Islam M, Takagi H (2015) Bamboo fiber polypropylene composites: effect of fiber treatment and nano clay on mechanical and thermal properties. *J Vinyl Add Tech* 21(4):253–258
32. Chen T, Xie Y, Wei Q, Wang XA, Hagman O, Karlsson O, Liu J, Lin M (2016) Improving the mechanical properties of ultra-low density plant fiber composite (ULD_PFC) by refining treatment. *BioResources* 11(4):8558–8569
33. Chen RS, Ahmad S (2017) Mechanical performance and flame retardancy of rice husk/organoclay-reinforced blend of recycled plastics. *Mater Chem Phys* 198:57–65
34. Tasdemir M (2017) Effects of olive pit and almond shell powder on polypropylene. *Key Eng Mater Trans Tech* 733:65–68
35. Arjmandi R, Hassan A, Majeed K, Zakaria Z (2015) Rice husk filled polymer composites. *Int J Polymer Sci* 32. Article ID 501471
36. Majeed K, Hassan A, Bakar AA, Jawaid M (2016) Effect of montmorillonite (MMT) content on the mechanical, oxygen barrier, and thermal properties of rice husk/MMT hybrid filler-filled low-density polyethylene nanocomposite blown films. *J Thermoplast Compos Mater* 29(7):1003–1019
37. Ahmad J, Deshmukh K, Habib M, Hägg MB (2013) Influence of TiO₂ on the chemical, mechanical and gas separation properties of polyvinylalcohol-titanium dioxide (PVA/TiO₂) nanocomposite membrane. *Int J Polym Anal Charact* 18(4):287–296

38. Mohanapriya MK, Deshmukh K, Ahamed MB, Chidambaram K, Pasha SKK (2015) Structural, morphological and dielectric properties of multiphase nanocomposites consisting of polycarbonate, barium titanate and carbon black nanoparticles. *Int J Chem Tech Res* 8(5): 32–41
39. Feller JF, Sadasivuni KK, Castro M, Bellegou H, Pillin I, Thomas S, Grohens Y (2015) Gas barrier efficiency of clay and graphene-poly(isobutylene-co-isoprene) nanocomposite membranes evidenced by a quantum resistive vapour sensor cell. *Nanocomposites* 1(4): 96–105
40. Kafy A, Sadasivuni KK, Akther A, Min SK, Kim J (2015) Cellulose/graphene nanocomposites as multifunctional electronic and solvent sensor material. *Mater Lett* 159:20–23
41. Akhtar MN, Sulong AB, Nazir MS, Majeed K, Radzi MK, Ismail NF, Raza MR (2017) Kenaf-biocomposites: manufacturing, characterization, and applications. In: *Green biocomposites*. Springer International Publication, Berlin, pp 225–254
42. Cavallaro G, Lazzara G, Milioto S (2013) Sustainable nanocomposites based on halloysite nanotubes and pectin/polyethylene glycol blend. *Polym Degrad Stab* 98(12):2529–2536
43. Ghaffari A, Navaee K, Oskoui M, Bayati K, Rafiee-Tehrani M (2007) Preparation and characterization of free mixed-film of pectin/chitosan/Eudragit® RS intended for sigmoidal drug delivery. *Eur J Pharm Biopharm* 67(1):175–186
44. Miyamoto H, Yamane C, Seguchi M, Okajima K (2010) Comparison between cellulose blend films prepared from aqueous sodium hydroxide solution and edible films of biopolymers with possible application for new food materials. *Food Sci Technol Res* 17(1): 21–30
45. Mishra RK, Majeed AB, Banthia AK (2011) Development and characterization of pectin/gelatin hydrogel membranes for wound dressing. *Int J Plas Technol* 15(1):82–95
46. Deshmukh K, Ahamed MB, Sadasivuni KK, Ponnamma D, Deshmukh RR, Pasha SK, AlMaadeed MA, Chidambaram K (2016) Graphene oxide reinforced polyvinyl alcohol/polyethylene glycol blend composites as high-performance dielectric material. *J Polym Res* 23:159
47. Gunbas ID, Aydemir SU, GülceİZ S, Deliloğlu Gürhan I, Hasirci N (2012) Semi-IPN chitosan/PEG microspheres and films for biomedical applications: characterization and sustained release optimization. *Ind Eng Chem Res* 51(37):11946–11954
48. Altinisik A, Yurdakoc K (2011) Synthesis, characterization, and enzymatic degradation of chitosan/PEG hydrogel films. *J Appl Polym Sci* 122(3):1556–1563
49. Ruiz-Hitzky E, Sobral MM, Gómez-Avilés A, Nunes C, Ruiz-García C, Ferreira P, Aranda P (2016) Clay-graphene nanoplatelets functional conducting composites. *Adv Func Mater* 26(41):7394–7405
50. Liu M, Wu C, Jiao Y, Xiong S, Zhou C (2013) Chitosan–halloysite nanotubes nanocomposite scaffolds for tissue engineering. *J Mater Chem B* 1:2078–2089
51. Abdullayev E, Lvov Y (2010) Clay nanotubes for corrosion inhibitor encapsulation: release control with end stoppers. *J Mater Chem* 20:6681–6687
52. Lvov Y, Abdullayev E (2013) Functional polymer–clay nanotube composites with sustained release of chemical agents. *Prog Polym Sci* 38(10–11):1690–1719
53. Deshmukh K, Ahamed MB, Sadasivuni KK, Ponnamma D, Deshmukh RR, Trimukhe AM, Pasha SK, Polu AR, AlMaadeed MA, Chidambaram K (2017) Solution-processed white graphene-reinforced ferroelectric polymer nanocomposites with improved thermal conductivity and dielectric properties for electronic encapsulation. *J Polym Res* 24:27
54. Deshmukh K, Ahmad J, Hägg MB (2014) Fabrication and characterization of polymer blends consisting of cationic polyallylamine and anionic polyvinyl alcohol. *Ionics* 20: 957–967
55. Deshmukh K, Ahamed MB, Deshmukh RR, Sadasivuni KK, Ponnamma D, Pasha SK, AlMaadeed MA, Polu AR, Chidambaram K (2017) Eeonomer 200F®: a high-performance nanofiller for polymer reinforcement-Investigation of the structure, morphology and dielectric properties of polyvinyl alcohol/Eeonomer-200F® nanocomposites for embedded capacitor applications. *J Electron Mater* 46(4):2406–2418

56. Spitalsky Z, Tasis D, Papagelis K, Galiotis C (2010) Carbon nanotube–polymer composites: chemistry, processing, mechanical and electrical properties. *Prog Polym Sci* 35(3):357–401
57. Deshmukh K, Ahamed MB, Deshmukh RR, Pasha SK, Sadasivuni KK, Ponnamma D, Chidambaram K (2016) Synergistic effect of vanadium pentoxide and graphene oxide in polyvinyl alcohol for energy storage application. *Eur Polymer J* 76:14–27
58. Lau WJ, Gray S, Matsuura T, Emadzadeh D, Chen JP, Ismail AF (2015) A review on polyamide thin film nanocomposite (TFN) membranes: history, applications, challenges and approaches. *Water Res* 80:306–824
59. Janson A, Minier-Matar J, Al-Shamari E, Hussain A, Sharma R, Rowley D, Adham S (2018) Evaluation of new ion exchange resins for hardness removal from boiler feedwater. *Emergent Mater* 1(1–2):1–1
60. Nagaraj A, Govindaraj D, Rajan M (2018) Magnesium oxide entrapped Polypyrrole hybrid nanocomposite as an efficient selective scavenger for fluoride ion in drinking water. *Emergent Mater* 1(1–2):1–9
61. Hegab HM, Zou L (2015) Graphene oxide-assisted membranes: fabrication and potential applications in desalination and water purification. *J Membr Sci* 484:95–106
62. Deshmukh K, Ahamed MB, Sadasivuni KK, Ponnamma D, AlMaadeed MAA, Deshmukh RR, Pasha SKK, Polu AR, Chidambaram K (2017) Fumed SiO₂ nanoparticle reinforced biopolymer blend nanocomposites with high dielectric constant and low dielectric loss for flexible organic electronics. *J Appl Polym Sci* 134(5):44427
63. Basavaiah K, Kahsay MH, Rama Devi D (2018) Green synthesis of magnetite nanoparticles using aqueous pod extract of *Dolichos lablab* L for an efficient adsorption of crystal violet. *Emergent Mater* 1(3–4):1–2
64. Deshmukh K, Ahamed MB, Deshmukh RR, Pasha SKK, Sadasivuni KK, Polu AR, Ponnamma D, AlMaadeed MAA, Chidambaram K (2017) Newly developed biodegradable polymer nanocomposites of cellulose acetate and Al₂O₃ nanoparticles with enhanced dielectric performance for embedded passive applications. *J Mater Sci Mater Electron* 28(1):973–986
65. Parambath SV, Ponnamma D, Sadasivuni KK, Thomas S, Stephen R (2017) Effect of polyhedral oligomeric silsesquioxane on the physical properties of polyvinyl alcohol. *J Appl Polym Sci* 134(43):45447
66. Ponnamma D, Chamakh MM, Deshmukh K, Ahamed MB, Alper E, Sharma P, AlMaadeed MAA (2017) Ceramic based polymer nanocomposites as piezoelectric materials. In: Ponnamma D, Sadasivuni KK, Cabibihan JJ, AlMaadeed MAA (eds) the Book “Smart polymer nanocomposites. Springer Publications, Berlin, pp 77–94
67. Kim H, Macosko CW (2008) Morphology and properties of polyester/exfoliated graphite nanocomposites. *Macromolecules* 41(9):3317–3327
68. Andrews R, Jacques D, Minot M, Rantell T (2002) Fabrication of carbon multiwall nanotube/polymer composites by shear mixing. *Macromol Mater Eng* 287(6):395–403
69. Hou Y, Cheng Y, Hobson T, Liu J (2010) Design and synthesis of hierarchical MnO₂ nanospheres/carbon nanotubes/conducting polymer ternary composite for high performance electrochemical electrodes. *Nano Lett* 10(7):2727–2733
70. Ajayan PM, Tour JM (2007) Materials science: nanotube composites. *Nature* 447(7148):1066–1068
71. Thakur VK, Kessler MR (2015) Self-healing polymer nanocomposite materials: a review. *Polymer* 69:369–383
72. Deshmukh K, Ahamed MB, Pasha SK, Deshmukh RR, Bhagat PR (2015) Highly dispersible graphene oxide reinforced polypyrrole/polyvinyl alcohol blend nanocomposites with high dielectric constant and low dielectric loss. *RSC Adv* 5:61933–61945
73. Potts JR, Dreyer DR, Bielawski CW, Ruoff RS (2011) Graphene-based polymer nanocomposites. *Polymer* 52:5–25
74. El Achaby M, Arrakhiz FE, Vaudreuil S, Kacem Qaiss A, Bousmina M, Fassi-Fehri O (2012) Mechanical, thermal, and rheological properties of graphene-based polypropylene nanocomposites prepared by melt mixing. *Polym Compos* 33(5):733–744

75. Tang QY, Chan YC, Wong NB, Cheung R (2010) Surfactant-assisted processing of polyimide/multiwall carbon nanotube nanocomposites for microelectronics applications. *Polym Int* 59(9):1240–1245
76. Inam F, Heaton A, Brown P, Peijs T, Reece MJ (2014) Effects of dispersion surfactants on the properties of ceramic–carbon nanotube (CNT) nanocomposites. *Ceram Int* 40(1): 511–516
77. Tkalya EE, Ghislandi M, de With G, Koning CE (2012) The use of surfactants for dispersing carbon nanotubes and graphene to make conductive nanocomposites. *Curr Opin Colloid Inter Sci* 17(4):225–232
78. Veprek S, Veprek-Heijman MJ (2008) Industrial applications of superhard nanocomposite coatings. *Surf Coat Technol* 202(21):5063–5073
79. Fukushima K, Wu MH, Bocchini S, Rasyida A, Yang MC (2012) PBAT based nanocomposites for medical and industrial applications. *Mater Sci Eng C* 32:1331–1351
80. Ponnamma D, Saiter A, Saiter JM, Thomas S, Grohens Y, AlMaadeed MAA, Sadasivuni KK (2016) Influence of temperature on the confinement effect of micro and nanolevel graphite filled poly(isoprene-co-isobutylene) composites. *J Polym Res* 23:125
81. Stankovich S, Dikin DA, Dommett GH, Kohlhaas KM, Zimney EJ, Stach EA, Piner RD, Nguyen ST, Ruoff RS (2006) Graphene-based composite materials. *Nature* 442:282–286
82. Deshmukh K, Ahamed MB, Deshmukh RR, Pasha SKK, Chidambaram K, Sadasivuni KK, Ponnamma D, AlMaadeed MA (2016) Ecofriendly synthesis of graphene oxide reinforced hydroxypropyl methyl cellulose/polyvinylalcohol blend nanocomposites filled with zinc oxide nanoparticles for high-k capacitor applications. *Polymer-Plastics Technol Eng* 55(12): 1240–1253
83. Deshmukh K, Ahamed MB, Polu AR, Sadasivuni KK, Pasha SK, Ponnamma D, AlMaadeed MA, Deshmukh RR, Chidambaram K (2016) Impedance spectroscopy, ionic conductivity and dielectric studies of new Li + ion conducting polymer blend electrolytes based on biodegradable polymers for solid state battery applications. *J Mater Sci Mater Electron* 27(11):11410–11424
84. Stephenson T, Li Z, Olsen B, Mitlin D (2014) Lithium ion battery applications of molybdenum disulfide (MoS₂) nanocomposites. *Energy Environ Sci* 7:209–231
85. Pfaendner R (2010) Nanocomposites: industrial opportunity or challenge? *Polym Degrad Stab* 95(3):369–373
86. Ahmad R, Griffete N, Lamouri A, Felidj N, Chehimi MM, Mangeney C (2015) Nanocomposites of gold nanoparticles@ molecularly imprinted polymers: chemistry, processing, and applications in sensors. *Chem Mater* 27(16):5464–5478
87. Siqueira G, Mathew AP, Oksman K (2011) Processing of cellulose nanowhiskers/cellulose acetate butyrate nanocomposites using sol–gel process to facilitate dispersion. *Compos Sci Technol* 71(16):1886–1892
88. Biswas M, Ray SS (2001) Recent progress in synthesis and evaluation of polymer-montmorillonite nanocomposites. *Adv Polym Sci* 155:167–222
89. Deshmukh K, Ahamed MB, Deshmukh RR, Pasha SK, Sadasivuni KK, Ponnamma D, AlMaadeed MA (2017) Striking multiple synergies in novel three-phase fluoropolymer nanocomposites by combining titanium dioxide and graphene oxide as hybrid fillers. *J Mater Sci Mater Electron* 28(1):559–575
90. Deshmukh K, Ahamed MB, Deshmukh RR, Bhagat PR, Pasha SK, Bhagat A, Shirbhate R, Telare F, Lakhani C (2016) Influence of K₂CrO₄ doping on the structural, optical and dielectric properties of polyvinyl alcohol/K₂CrO₄ composite films. *Polymer-Plastics Technol Eng* 55(3):231–241
91. Parry S, Pancoast J, Mildenhall S (2015) Chemical and bonding effects of exposing uncured PBI-NBR insulation to ambient conditions. *J Appl Polym Sci* 132(40):42636
92. Balachandran M, Devanathan S, Muraleekrishnan R, Bhagawan SS (2012) Optimizing properties of nanoclay–nitrile rubber (NBR) composites using face centred central composite design. *Mater Des* 35:854–862

93. Unalan IU, Cerri G, Marcuzzo E, Cozzolino CA, Farris S (2014) Nanocomposite films and coatings using inorganic nanobuilding blocks (NBB): current applications and future opportunities in the food packaging sector. *RSC Adv* 4(56):29393–29428
94. Liu L, Jia D, Luo Y, Guo B (2006) Preparation, structure and properties of nitrile–butadiene rubber–organoclay nanocomposites by reactive mixing intercalation method. *J Appl Polym Sci* 100(3):1905–1913
95. Fuentes-Alventosa JM, Introzzi L, Santo N, Cerri G, Brundu A, Farris S (2013) Self-assembled nanostructured biohybrid coatings by an integrated sol–gel/intercalation’ approach. *RSC Adv* 3(47):25086–25096
96. Kim H, Abdala AA, Macosko CW (2010) Graphene/polymer nanocomposites. *Macromolecules* 43(16):6515–6530
97. Ramanathan T, Abdala AA, Stankovich S, Dikin DA, Herrera-Alonso M, Piner RD, Adamson DH, Schniepp HC, Chen XR, Ruoff RS, Nguyen ST (2008) Functionalized graphene sheets for polymer nanocomposites. *Nat Nanotechnol* 3:327–331
98. Dennis H, Hunter DL, Chang D, Kim S, White JL, Cho JW, Paul DR (2001) Effect of melt processing conditions on the extent of exfoliation in organoclay-based nanocomposites. *Polymer* 42(23):9513–9522
99. Njuguna J, Pieliowski K, Desai S (2008) Nanofiller-reinforced polymer nanocomposites. *Polym Adv Technol* 19(8):947–959
100. Capadona JR, Van Den Berg O, Capadona LA, Schroeter M, Rowan SJ, Tyler DJ, Weder C (2007) A versatile approach for the processing of polymer nanocomposites with self-assembled nanofibre templates. *Nat Nanotechnol* 2:765–769
101. Moniruzzaman M, Winey KI (2006) Polymer nanocomposites containing carbon nanotubes. *Macromolecules* 39(16):5194–5205
102. Roth SV, Herzog G, Körstgens V, Buffet A, Schwartzkopf M, Perlich J, Kashem MA, Döhrmann R, Gehrke R, Rothkirch A, Stassig K (2011) In situ observation of cluster formation during nanoparticle solution casting on a colloidal film. *J Phys Condens Matter* 23(25):254208
103. Al-Hussein M, Schindler M, Ruderer MA, Perlich J, Schwartzkopf M, Herzog G, Heidmann B, Buffet A, Roth SV, Müller-Buschbaum P (2013) In situ X-ray study of the structural evolution of gold nano-domains by spray deposition on thin conductive P3HT films. *Langmuir* 29(8):2490–2497
104. Klein LC (2013) Sol-gel optics: processing and applications. Springer Publications, Berlin
105. Zhang J, Zhang M, Lin L, Wang X (2015) Sol processing of conjugated carbon nitride powders for thin-film fabrication. *Angew Chem Int Ed* 54(21):6297–6301
106. Neena D, Shah AH, Deshmukh K, Ahmad H, Fu DJ, Kondamareddy KK, Kumar P, Dwivedi RK, Sing V (2016) Influence of (Co-Mn)co-doping on the microstructures, optical properties of sol gel derived ZnO nanoparticles. *Eur Phys J D* 70:53
107. Zhang J, Chen Y, Wang X (2015) Two-dimensional covalent carbon nitride nanosheets: synthesis, functionalization, and applications. *Energy Environ Sci* 8(11):3092–3108
108. Owens Gareth J, Singh Rajendra K, Foroutan Farzad, Alqaysi Mustafa, Han Cheol-Min, Mahapatra Chinmaya, Kim Hae-Won, Knowles Jonathan C (2016) Sol–gel based materials for biomedical applications. *Prog Mater Sci* 77:1–79
109. Williams G, Seger B, Kamat PV (2008) TiO₂-graphene nanocomposites. UV-assisted photocatalytic reduction of graphene oxide. *ACS Nano* 2(7):1487–1491
110. Vatani M, Lu Y, Lee KS, Kim HC, Choi JW (2013) Direct-write stretchable sensors using single-walled carbon nanotube/polymer matrix. *J Electron Packag* 135(1):011009
111. Morteza A, Aekachan P, Sangjun L, Seunghwa R, Park I (2014) Highly stretchable and sensitive strain sensor based on silver nanowire elastomer nanocomposite. *ACS Nano* 8(5): 5154–5163
112. Lu Y, Vatani M, Choi JW (2013) Direct-write/cure conductive polymer nanocomposites for 3D structural electronics. *J Mech Sci Technol* 27(10):2929–2934

113. Vatani M, Engeberg ED, Choi JW (2014) Detection of the position, direction and speed of sliding contact with a multi-layer compliant tactile sensor fabricated using direct-print technology. *Smart Mater Struct* 23(9):095008
114. Wang S, Hu Y, Zhongkai Q, Wang Z, Chen Z, Fan W (2003) Preparation and flammability properties of polyethylene/clay nanocomposites by melt intercalation method from Na⁺-montmorillonite. *Mater Lett* 57:2675–2678
115. Yoshimoto S, Ohashi F, Ohnishi Y, Nonami T (2004) Synthesis of polyaniline–montmorillonite nanocomposites by the mechanochemical intercalation method. *Synth Met* 145(2–3):265–270
116. Kuila BK, Nandi AK (2004) Physical, mechanical, and conductivity properties of poly(3-hexylthiophene)-montmorillonite clay nanocomposites produced by the solvent casting method. *Macromolecules* 37(23):8577–8584
117. Mozafari M, Moztarzadeh F, Rabiee M, Azami M, Maleknia S, Tahriri M, Moztarzadeh Z, Nezafati N (2010) Development of macroporous nanocomposite scaffolds of gelatin/bioactive glass prepared through layer solvent casting combined with lamination technique for bone tissue engineering. *Ceram Int* 36(8):2431–2439
118. Oksman K, Mathew AP, Bondeson D, Kvien I (2006) Manufacturing process of cellulose whiskers/poly(lactic acid) nanocomposites. *Compos Sci Technol* 66(15):2776–2784
119. Zhang HB, Zheng WG, Yan Q, Yang Y, Wang JW, Lu ZH, Ji GY, Yu ZZ (2010) Electrically conductive polyethylene terephthalate/graphene nanocomposites prepared by melt compounding. *Polymer* 51(5):1191–1196
120. Wang Y, Wang Y, Hosono E, Wang K, Zhou H (2008) The design of a LiFePO₄/carbon nanocomposite with a core–shell structure and its synthesis by an in situ polymerization restriction method. *Angew Chem Int Ed* 47(39):7461–7465
121. Bao C, Guo Y, Song L, Kan Y, Qian X, Hu Y (2011) In situ preparation of functionalized graphene oxide/epoxy nanocomposites with effective reinforcements. *J Mater Chem* 21(35):13290–13298
122. Biswas S, Fukushima H, Drzal LT (2011) Mechanical and electrical property enhancement in exfoliated graphene nanoplatelet/liquid crystalline polymer nanocomposites. *Compos A Appl Sci Manuf* 42(4):371–375
123. Hussain I, Tran HP, Jaksik J, Moore J, Islam N, Uddin MJ (2018) Functional materials, device architecture, and flexibility of perovskite solar cell. *Emergent Mater* 1(3–4):1–22
124. Kalaitzidou K, Fukushima H, Drzal LT (2007) A new compounding method for exfoliated graphite–polypropylene nanocomposites with enhanced flexural properties and lower percolation threshold. *Compos Sci Technol* 67(10):2045–2051
125. Alexandre M, Dubois P, Sun T, Garces JM, Jérôme R (2002) Polyethylene-layered silicate nanocomposites prepared by the polymerization-filling technique: synthesis and mechanical properties. *Polymer* 43(8):2123–2132
126. Zhang H, Chen G (2009) Potent antibacterial activities of Ag/TiO₂ nanocomposite powders synthesized by a one-pot sol-gel method. *Environ Sci Technol* 43(8):2905–2910
127. Jitianu A, Cacciaguerra T, Benoit R, Delpoux S, Beguin F, Bonnamy S (2004) Synthesis and characterization of carbon nanotubes–TiO₂ nanocomposites. *Carbon* 42(5–6):1147–1151
128. Liu C, Wang K, Luo S, Tang Y, Chen L (2011) Direct electrodeposition of graphene enabling the one step synthesis of graphene–metal nanocomposite films. *Small* 7(9):1203–1206
129. Belgacem MN, Gandini A (2008) Monomers, polymers and composites from renewable resources. Elsevier Publications, Amsterdam
130. Abdul Khalil HPS, Bhat AH, Ireana Yusra AF (2012) Green composites from sustainable cellulose nanofibrils: a review. *Carbohydr Polym* 87(2):963–979
131. Jonathan G, Zhang M (2010) Polyblend nanofibers for biomedical applications: perspectives and challenges. *Trends Biotechnol* 28(4):189–197
132. Liu Y, Li Y, Yang G, Zheng X, Zhou S (2015) Multi-stimulus-responsive shape-memory polymer nanocomposite network cross-linked by cellulose nanocrystals. *ACS Appl Mater Inter* 7(7):4118–4126

133. Yeom J, Oh EJ, Reddy M (2009) Guided bone regeneration by poly (lactic-*co*-glycolic acid) grafted hyaluronic acid bi-layer films for periodontal barrier applications. *Acta Biomaterialia* 5(9):3394–3403
134. Reddy MM, Vivekanandhan S, Misra M, Bhatia SK, Mohanty AK (2013) Biobased plastics and bionanocomposites: current status and future opportunities. *Progress Polymer Sci* 38 (10):1653–1689
135. Salami M, Kaveian F, Rafienia M, Saber-Samandari S, Khandan A, Naeimi M (2017) Electrospun polycaprolactone/lignin-based nanocomposite as a novel tissue scaffold for biomedical applications. *J Med Signals Sens* 7(4):228–238
136. Sadasivuni KK, Ponnamma D, Kim J, Cabibihan JJ, AlMaadeed MAA (2017) Introduction of biopolymer composites. In: Ponnamma D (ed) *Biopolymer Composites in electronics*. Elsevier, Amsterdam
137. Mai F, Habibi Y, Jean-Marie R, Philippe D, Feller JF, Ton P, Emiliano B (2013) Poly (lactic acid)/carbon nanotube nanocomposites with integrated degradation sensing. *Polymer* 54(25): 6818–6823
138. Sadasivuni KK Ponnamma D, Cabibihan JJ, AlMaadeed MAA (2016) Electronic applications of polydimethylsiloxane and its composites. In: Ponnamma D, Sadasivuni KK, Wan C, Thomas S, AlMaadeed MAA (eds) *Flexible and stretchable electronic composites*. Springer Publication, Berlin, pp 199–228
139. Okonkwo PC, Collins E, Okonkwo E (2017) Application of biopolymer composites in super capacitor. In: Sadasivuni KK Cabibihan JJ, Ponnamma D, AlMaadeed MAA (eds) *Biopolymer composites in electronics*. Springer Publication, Berlin, pp 487–503
140. Christinelli WA, Gonçalves R, Pereira EC (2016) A new generation of electrochemical supercapacitors based on layer-by-layer polymer films. *J Power Sources* 303:73–80
141. Botta L, Scaffaro R, Sutura F, Mistretta MC (2018) Reprocessing of PLA/graphene nanoplatelets nanocomposites. *Polymers* 10:18
142. Alam J, Alam M, Raja M, Abduljaleel Z, Dass LA (2014) MWCNTs-reinforced epoxidized linseed oil plasticized polylactic acid nanocomposite and its electroactive shape memory behaviour. *Int J Mol Sci* 15(11):19924–19937
143. Wang ZW, Zhao J, Chen M, Yang MH, Tang LY, Dang ZM, Chen FH, Huang MM, Dong X (2014) Dually actuated triple shape memory polymers of cross-linked polycyclooctene-carbon nanotube/polyethylene nanocomposites. *ACS Appl Mater Interfaces* 6(22):20051–20059
144. Wang K, Strandman S, Zhu XX (2017) A mini review: shape memory polymers for biomedical applications. *Front Chem Sci Technol* 11(2):143–153
145. Ikada Y (2006) Scope of tissue engineering. *Tissue engineering: fundamentals and applications*. *Inter Sci Technol* 8:1–90
146. Wei G, Ma PX (2004) Structure and properties of nano-hydroxyapatite/polymer composite scaffolds for bone tissue engineering. *Biomaterials* 25(19):4749–4757
147. Salgado AJ, Coutinho OP, Reis RL (2004) Bone tissue engineering: state of the art and future trends. *Macromol Biosci* 4(8):743–765
148. McCullen SD, Stevens DR, Roberts WA, Clarke LI, Bernacki SH, Gorga RE, Lobo EG (2007) Characterization of electrospun nanocomposite scaffolds and biocompatibility with adipose-derived human mesenchymal stem cells. *Int J Nanomed* 2(2):253–263
149. Sowmya S, Bumgardener JD, Chennazhi KP, Nair SV, Jayakumara R (2013) Role of nanostructured biopolymers and bioceramics in enamel, dentin and periodontal tissue regeneration. *Progress Polymer Sci* 38(10–11):1748–1772
150. Fujihara K, Kotaki M, Ramakrishna S (2005) Guided bone regeneration membrane made of polycaprolactone/calcium carbonate composite nano-fibers. *Biomaterials* 26(19):4139–4147
151. Minghuan L, Xiao-Peng D, Ye-Ming L, Da-Peng Y, Yun-Ze L (2017) Electrospun nanofibers for wound healing. *Mater Sci Eng C* 76:1413–1423

152. Park JK, Yeom J, Oh EJ, Reddy M, Kim JY, Cho DW, Lim HP, Kim NS, Park SW, Shin HI, Yang DJ, Park KB, Hahn SK (2009) Guided bone regeneration by poly(lactic-co-glycolic acid) grafted hyaluronic acid bi-layer films for periodontal barrier applications. *Acta Biomaterialia* 5(9):3394–3403
153. Chen FM, Zhang J, Zhang M, An Y, Chen F, Wu ZF (2010) A review on endogenous regenerative technology in periodontal regenerative medicine. *Biomaterials* 31(31):7892–7927
154. Shakeel A, Saiqa I (2016) Chitosan based scaffolds and their applications in wound healing. *Achieve Life Sci* 10(1):27–37
155. Zadeh KM, Ponnamma D, Al-Maadeed MAA (2017) Date palm fibre filled recycled ternary polymer blend composites with enhanced flame retardancy. *Polymer Test* 61:341–348
156. Dahy H (2017) Biocomposite materials based on annual natural fibres and biopolymers—design, fabrication and customized applications in architecture. *Construct Build Mater* 147:212–220
157. Bulota M, Kreitsmann K, Hughes M, Paltakari J (2012) Acetylated microfibrillated cellulose as a toughening agent in poly (lactic acid). *J Appl Polymer Sci* 126(S1):E448–E457
158. Miao S, Liu K, Wang P, Su Z, Zhang S (2015) Preparation and characterization of epoxidized soybean oil-based paper composite as potential water-resistant materials. *J Appl Polymer Sci* 132(10):41575
159. Majeed K, Jawaid M, Hassan A, Abu Bakar A, Khalil HPSA, Salema AA, Inuwa I (2013) Potential materials for food packaging from nanoclay/natural fibers filled hybrid composites. *Mater Des* 46:391–410

Recent Advances in Paper-Based Analytical Devices: A Pivotal Step Forward in Building Next-Generation Sensor Technology



Charu Agarwal and Levente Csóka

List of Abbreviations

μ PADs	Microfluidic paper-based analytical devices
Ab	Antibody
ABTS	2,2'-azino-bis(3-ethylbenzothiazoline-6-sulfonic acid)
ACV	Alternating current voltammetry
AEC	3-amino-9-ethylcarbazole
AFP	α -fetoprotein
AKD	Alkyl ketene dimer
AP	Absorbent pad
BA	Biogenic amines
BDDE	Boron-doped diamond electrode
BHB	β -hydroxybutyrate
BPA	Bisphenol A
CA125	Carcinoma antigen 125
CA199	Carcinoma antigen 199
CB	Carbon black
CBM	Carbohydrate binding molecule
CEA	Carcinoembryonic antigen
CFU	Colony forming units
CNCs	Carbon nanocrystals
CPRG	Chlorophenol red β -galactopyranoside
Cy3	Cyanine 3
DAB	3,3'-diaminobenzidine
DAP	1,8-diaminonaphthalene
ECL	Electrochemiluminescent
eGFP	Enhanced green fluorescent protein

C. Agarwal · L. Csóka (✉)
Institute of Wood Based Products and Technologies,
University of Sopron, Sopron 9400, Hungary
e-mail: levente.csoka@skk.nyme.hu

C. Agarwal
e-mail: charu.agarwal3@gmail.com

ELISA	Enzyme linked immunosorbent assay
FRET	Förster resonance energy transfer
GA	Glucoamylase
GNPs	Gold nanoparticles
GNRs	Gold nanorods
GO	Graphene oxide
GOx	Glucose oxidase
GQDs	Graphene quantum dots
HPV	Human papillomavirus
HRP	Horseradish peroxidase
IgG	Immunoglobulin G
LFIA	Lateral flow immunoassay
LRET	Luminescence resonance energy transfer
LSPR	Localized surface plasmon resonance
MEMS	Micro-electro-mechanical systems
MIP	Molecularly imprinted polymers
MNPs	Magnetic nanoparticles
NPs	Nanoparticles
NQS	Sodium 1,2-naphthoquinone-4-sulfonate
OTB	<i>O</i> -toluidine blue
PATP	<i>P</i> -aminothiophenol
PB	Prussian blue
PBS	Phosphate buffered saline
PC	Phycocyanin
PC-paper	Parylene C-coated paper
PEC	Photoelectrochemical
PEDOT:PSS	Poly(3,4-ethylenedioxythiophene):poly(styrenesulfonate)
PL	Photoluminescence
POC	Point-of-care
poly(DAB)	Poly-3,3'-diaminobenzidine
PVP	Polyvinylpyrrolidone
QDs	Quantum dots
R6G	Rhodamine-6G
RDX	1,3,5-trinitroperhydro-1,3,5-triazine
RGO	Reduced graphene oxide
SCO	Spin-crossover
SEM	Scanning electron micrographs
SERS	Surface-enhanced Raman spectroscopy
SP	Sample pad
SPCE	Screen-printed carbon electrode
SWV	Square wave voltammetry
TA	Thioctic acid
TBPB	Tetrabromophenol blue
TG	Thioguanine

Thi	Thionine
TMB	3,3',5,5'-tetramethylbenzidine
TMPyP	5,10,15,20-tetrakis(1-methyl-4-pyridinio)porphyrin tetraiodide
TNT	2,4,6-trinitrotoluene
TPA	Tri- <i>n</i> -propylamine
ubi	Ubiquitin
UV-Vis	Ultraviolet-visible
WHO	World health organization

1 Introduction

The term “point-of-care (POC) testing” has gained immense popularity since the last decade especially in connection to the diagnostic applications. It has offered the fascinating possibility of providing rapid results in places with limited availability of resources [1]. Lately, the paper has attracted the significant attention of the global research community as a substrate for the development of dip-sticks, lateral flow immunoassays (LFIAs) and microfluidic paper-based analytical devices (μ PADs) [2–4]. The interest in making use of paper stemmed from the belief that the conventional devices were too complicated and expensive to be used on a large scale in developing countries. The low cost of paper and its ability to wick fluids by capillary action due to hydrophilicity, thus eliminating the need for pumps or external power to transfer fluids, were the primary motivating factors inspiring researchers to work with paper as a new generation material for sensing devices [5]. Additionally, the porosity and high surface-to-volume ratio of paper are advantageous for assays wherein the reagents are bound on the paper surface and its flammable nature allows for easy disposal of paper devices via incineration. The μ PADs are extremely promising for POC diagnostic devices for use in resource-limited settings owing to their ease of operation, low cost and ability to work without external power supply or supporting equipment [6]. In addition, μ PADs are generally easy to fabricate, user-friendly and offer simple readouts of analytical assay results [7]. Further, paper substrates are easily compatible with printing processes like ink-jet printing, screen printing and flexographic printing [8]. Finally, being environmentally friendly, the paper is a sustainable material, which enables it to stand out amongst its peers as a pathway for “green” sensors [9].

Since the last decade, the focus has shifted towards quantitative sensings such as that required for glucose and tumour markers than mere qualitative analysis as in case of pH and pregnancy test strips. Following the seminal work on microfluidic paper-based analytical devices by Whitesides’ group in 2007 [10], a myriad of works have been published on sensing devices using paper as a substrate for the detection of a plethora of analytes. Paper substrates have been functionalized with biomolecules [11], metal and metal oxide nanoparticles [12], quantum dots [13],

aptamers [14], spin-crossover particles [15] and metamaterials [9] to develop a range of sensors. These sensors find major applications in clinical diagnostics and therapeutics [16–18], environmental monitoring and analysis [19], food and water quality [20, 21] and forensics [22]. For instance, visual detection of DNA on paper chips has been reported which have the ability to identify and distinguish dog and human genomic and mitochondrial samples for forensic purposes [23]. Similarly, paper-based electrochemical sensors have shown potential for the detection of K-562 cells, one of the most aggressive human chronic myelogenous leukaemia cell lines, based on the release of hydrogen peroxide (H_2O_2) from cells [24]. This development has been made possible by the multiple attributes of paper-based sensors as per the “ASSURED” criteria of the World Health Organization (WHO) for effective POC testing devices that stands for affordable, sensitive, specific, user-friendly, rapid and robust, equipment-free, delivered to end-users [25, 26].

This chapter presents a concise review of paper-based analytical devices used for sensing in various sectors comprising of biomedical diagnostics, environmental monitoring, food and water safety as well as forensics and security, in the ongoing decade with a focus on the discussion of sensing principle or the mechanism of detection (Fig. 1). The various analytes have been broadly grouped based on the classical detection principles of colorimetry, electrochemistry, and luminescence-based sensing.

2 Sensing in the Physical World

Paper-based sensors have been used to measure some of the most fundamental parameters in basic and applied sciences such as temperature [27], pH [28] and humidity [29, 30]. Precise measurement of these physical quantities is required in areas as diverse as medicine, biotechnology, environmental science, and meteorology to name a few. An optical temperature sensor was fabricated by soaking the paper in a temperature sensitive luminescent indicator dichlorotris(1,10-phenanthroline)ruthenium(II) hydrate ($Ru(phen)_3$) [31]. The dried paper was subsequently laminated to eliminate oxygen cross-sensitivity by preventing its diffusion. A linear response to temperature was obtained with phase fluorimetry and ratio imaging. In another study, paper thermometers with an ultrafast response and high stability were developed using an ionic liquid (1-ethyl-3-methyl imidazolium bis(trifluoromethylsulfonyl)imide) deposited on paper by means of pen writing or inkjet printing [27]. The low viscosity and hydrophobic nature of the ionic ink facilitated easy writing while resisting the hydration by moisture in the atmosphere (Fig. 2a). The sensing ability of the paper chip was quantified by the relative change in conductivity against temperature change. The conductivity was contributed solely by the ionic liquid since paper itself is electrically insulated with a very high resistance. The thermal response of the paper thermometer reached over 60% by raising the ambient temperature and remained the

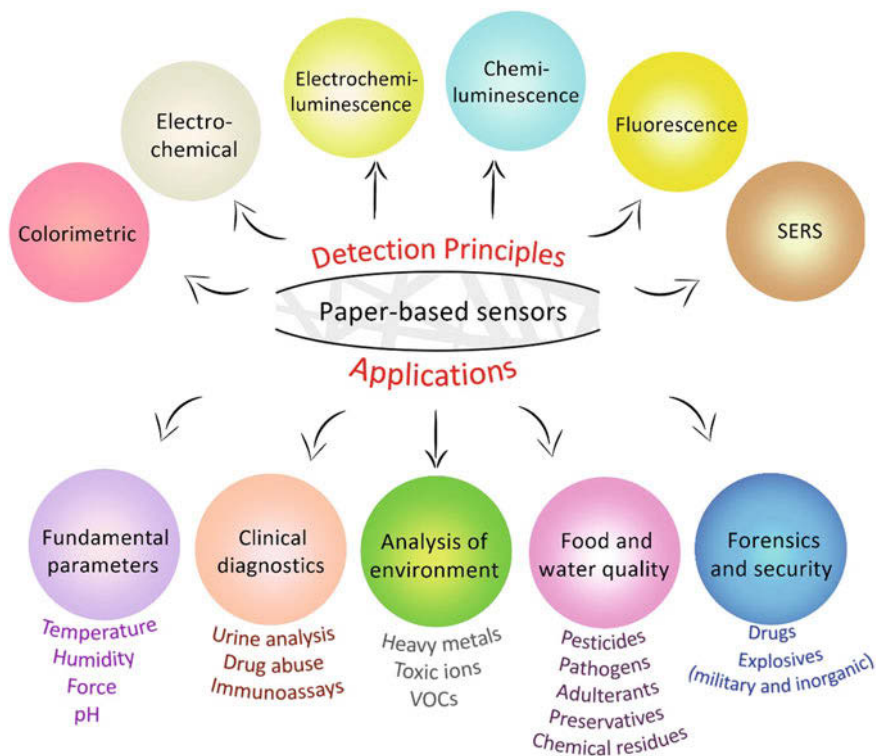


Fig. 1 Sensing approaches of paper-based analytical devices for various applications

same after multiple heating and cooling cycles (Fig. 2b) [27]. Cellulose nanocomposites showing spin-crossover phenomena and having thermochromic properties have been fabricated by adsorption of spin-crossover (SCO) nanoparticles onto linter fibres [32, 33]. The $[\text{Fe}(\text{hptrz})_3](\text{OTs})_2$ (hptrz = 4-heptyl-1,2,4-triazole, OTs = *p*-toluenesulfonyl) SCO particles are known to display an abrupt spin transition with a hysteresis loop close to room temperature, a characteristic which is highly relevant for potential application in paper thermometry. The curves for the temperature dependence on the optical reflectance revealed that the reflectance changes occurred rather abruptly in the heating and cooling modes, thus unambiguously relating to the spin transition process of the SCO particle complex [32].

Taking advantage of the hydrophilicity of paper, humidity sensors with good stability and reproducibility were developed by simply “writing” the carbon electrodes by pencils and ink marker consisting of oxidized multi-walled carbon nanotubes [34]. Similarly, pH sensors were fabricated using phenol red and chlorophenol red indicators on paper. The indicators produced selective colour changes, which were captured by a smartphone camera and processed to extract the hue from the colour space [35]. Similarly, a graphene-based paper sensor fabricated by vacuum filtration process was reported for sensing the pH of the analyte by

Table 1 Detection of various biomedical analytes

Target	Sensing agents/sensor components	Limit of detection	Linear range	References
<i>Colorimetric sensing</i>				
Glucose	GOx, HRP	3×10^{-4} M	1.0×10^{-3} – 11.0×10^{-3} M	Zhu et al. [152]
Urease enzyme	Hexamethyldisilazane, tetra-ethylorthosilicate	1 unit mL ⁻¹	1–20 units mL ⁻¹	Malekghasemi et al. [153]
Lactate dehydrogenase	Pullulan coating to immobilize reagents	13 U L ⁻¹	0–450 U L ⁻¹	Kannan et al. [154]
Zika virus RNA genome	CRISPR-based tool	–	–	Pardee et al. [155]
Antioxidants	Ceria nanoparticles	–	20–400 µM	Sharpe et al. [156]
Blood typing	Antibodies	–	–	Guan et al. [157], Khatri et al. [158]
Procaine	Reagents	0.9 µmol L ⁻¹	5–60 µmol L ⁻¹	Silva et al. [39]
<i>Electrochemical sensing</i>				
Glucose	Plasma isolation membranes	3.4 mM	0–33.1 mM	Noiphung et al. [159]
Adenosine triphosphate	Paper-based electrode	0.08 µM	0.3–450 µM	Wang et al. [160]
Rabbit immunoglobulin G	Protein probes immobilized on ZnO nanowires grown on paper	60 fg mL ⁻¹ 300 fg mL ⁻¹	–	Li and Liu [161]
Butyrylcholinesterase activity in serum	Carbon black/Prussian blue	0.5 IU mL ⁻¹	1–12 IU mL ⁻¹	Scordo et al. [162]
Acetaminophen	AuNPs-polyglutamic acid/single-walled carbon nanotube	15.0 µM	50–300 µM	Lee et al. [163]
p-aminophenol	Au & Pt microwire electrodes	31 µM	–	Adkins et al. [164]
Fe ²⁺	Carbon nanotube electrodes	10 µM 10 µM	10–200 µM 10–100 µM	da Costa et al. [165]
Dopamine	Carbon black/Prussian blue	3 µg/L	3–25 µg/L	Cinti et al. [166]

(continued)

Table 1 (continued)

Target	Sensing agents/sensor components	Limit of detection	Linear range	References
Norepinephrine	Boron doped diamond paste electrodes	2.5 μM	2.5–100 μM	Nantaphol et al. [167]
Serotonin		0.5 μM	0.5–7.5 μM	
<i>Luminescence-based sensing</i>				
Polynucleotide kinase activity	λ exonuclease assisted fluorescence quenching	0.0001 U mL^{-1}	–	Zhang et al. [168]
Immunoglobulin E (IgE)	Upconversion nanoparticles & carbon nanoparticles leading to LRET	–	0.5–80 ng mL^{-1}	Jiang et al. [169]
<i>Other types</i>				
Cancer cells: MCF-7 HL-60 K562	Graphene oxide & aptamer leading to FRET	62 cells mL^{-1} 70 cells mL^{-1} 65 cells mL^{-1}	180–8 $\times 10^7$ cells mL^{-1} 210–7 $\times 10^7$ cells mL^{-1} 200–7 $\times 10^7$ cells mL^{-1}	Liang et al. [170]
Pulse and motion of body	Strain/deforming angle measurement using RGO	–	–	Saha et al. [171]
Hepatitis B virus DNA	Nafion-coated paper for ion concentration polarization	150 copies mL^{-1}	–	Gong et al. [172]
Glucose/DNA/protein	Resistive temperature detector (RTD) for calorimetric determination	–	–	Davaji et al. [173]

Table 2 Detection of various environmental analytes

Target	Sensing agents/sensor components	Limit of detection	Linear range	References
<i>Colorimetric sensing</i>				
Hg ²⁺ ion	AuNPs with oligonucleotide sequences	50 nM	25–100 nM	Chen et al. [174]
Organophosphate pesticides	Acetylcholinesterase	–	–	Sicard et al. [175]
Nitrite ion	Mixed indicator (N-(1-naphthyl)-ethylenediamine & p-amino benzenesulfonamide)	–	0.156–1.25 mmol L ⁻¹	Wang et al. [176]
Metals	Reagents and buffer	0.75 µg (Fe) 0.75 µg (Ni) 0.75 µg (Cu) 0.12 µg (Cr)	1.5–15 µg (Fe) 1.5–15 µg (Ni) 3.0–15 µg (Cu) 0.38–6.0 µg (Cr)	Rattanarat et al. [177]
Dissolved ammonia in water	Reagents for modified Berthelot's reaction	10 mg L ⁻¹	10–200 mg L ⁻¹	Cho et al. [178]
<i>Electrochemical sensing</i>				
Ferricyanide	UV curable screen printing & ink-jet inks	8 µM	0.05–1 mM	Lamas-Ardisana et al. [179]
Chlorine	poly(3,4-ethylenedioxythiophene): poly(styrenesulfonate)	0.5 ppm	0.5–500 ppm	Qin et al. [180]
Phosphate	Reagents screen-printed on electrodes	4 µM	0–300 µM	Cinti et al. [181]
Bisphenol A	AuNPs with multi-walled carbon nanotubes	0.03 mg L ⁻¹	0.2–20 mg L ⁻¹	Li et al. [182]
Pb ²⁺ Cd ²⁺	Boron doped diamond paste electrodes	1 ppb 25 ppb	1–200 ppb 25–200 ppb	Nantaphol et al. [167]
Formaldehyde	Microbial fuel cell-based paper sensor	–	–	Chouler et al. [183]
<i>Luminescence-based sensing</i>				
Formaldehyde	Fluorescence quenching using acetoacetamide reagent	0.2 ppm	0–8 ppm	Liu et al. [132]
Hydrazine	Fluorescence quenching of fluorogens with aggregation-induced emission	143 ppb	0–60 µM	Zhang et al. [184]
<i>Other types</i>				
Volatile organic compounds	Measurement of mechanical deflection angle of thin polymers adhered to paper	–	–	Fraitwan et al. [185]
Titania (TiO ₂) nanoparticles	Photocatalytic effect of TiO ₂ on methylene blue	–	0–5000 ppm	Bulbul et al. [186]



Fig. 2 a Fabrication process showing ionic liquid (IL) paper chip written with a pen, b thermal response with on-off cycles of the paper chip between 45 and 25 °C. Adapted with permission from Ref. [27] © 2017 ACS publisher

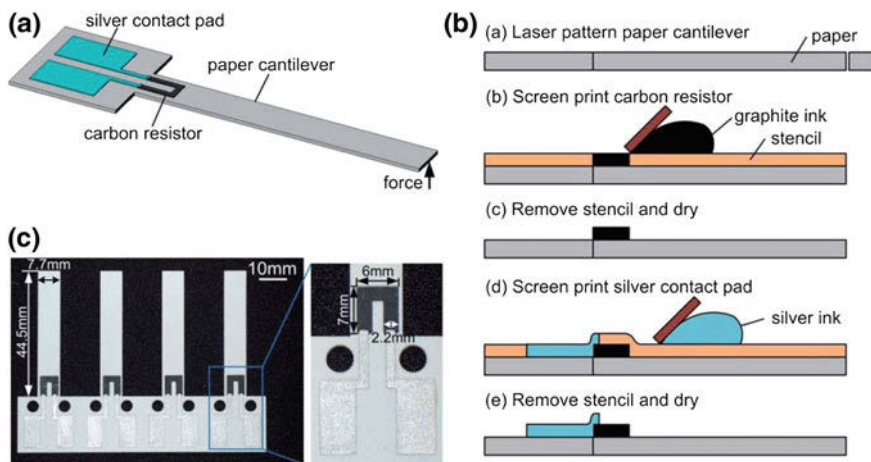


Fig. 3 a Schematic showing a paper-based piezoresistive force sensor with a carbon resistor as the sensing component, b fabrication of the sensor by laser cutting of paper and screen printing of carbon and silver inks, c picture of an array of four devices. Adapted with permission from Ref. [37] © 2011 RSC publisher

directly measuring the resistance across the sensor [36]. The sensor showed a sensitivity of $30.8 \Omega/\text{pH}$ and a high linearity. Another study developed a MEMS (micro-electro-mechanical systems) sensor for the measurement of forces based on the piezoresistive effect of conducting materials patterned on paper [37]. Paper was preferred over commonly used silicon for the construction of the sensor primarily due to its low cost, lightweight, disposability, and ease of fabrication. As shown in Fig. 3a, the carbon resistor experienced a mechanical strain/stress when a force was applied to the cantilever beam. This induced a change in resistance of the resistor, which allowed quantification of the applied force. The carbon resistors used high-resistivity graphite ink, while the contact pads used low-resistivity silver ink (Fig. 3b, c). The sensor had a resolution of $120 \mu\text{N}$, a measurement range of $\pm 16 \text{ mN}$ and a sensitivity of 0.84 mV mN^{-1} [37].

3 Sensing in Biomedical Health Care and Clinical Diagnostics

3.1 Colorimetric Sensing

Colorimetric spot tests using paper are rapid, inexpensive and can be done in locations with limited infrastructure. Further, the white paper provides a strong contrast against a coloured substrate that allows direct checking of the results with the naked eye [38, 39]. This has immensely facilitated the use of paper in a number of colorimetric assays for diagnostics and therapeutics. For example, colorimetric test strips prepared using a chromogen (2,4,6-tribromo-3-hydroxybenzoic acid) have been used for glucose detection by measuring their colour intensity as the differential diffusive reflectance [40]. The sensing of hydrogen sulfide (H_2S) gas from live cancer cell lines (LNCaP and PC-3) was demonstrated using paper coated with a polyvinylpyrrolidone (PVP) membrane containing silver/Nafion. The silver in the coating zones reacted with sulfide, giving a brown colour of silver sulfide (Ag_2S). The assay showed a high sensitivity, selectivity and reproducibility with a limit of detection of $1.4 \mu M$ Na_2S in phosphate buffered saline (PBS) [38]. A text-displaying assay for urinary protein was fabricated by using printing techniques and combining the classical colorimetric indicator system with an inert colourant [41]. As shown in Fig. 4a, tetrabromophenol blue (TBPB), a colorimetric indicator, which was inkjet-deposited in the form of symbols on paper underwent colour changes in a concentration-dependent manner. A transparent coloured layer served to screen TBPB deposited on the paper. After the colorimetric response, a

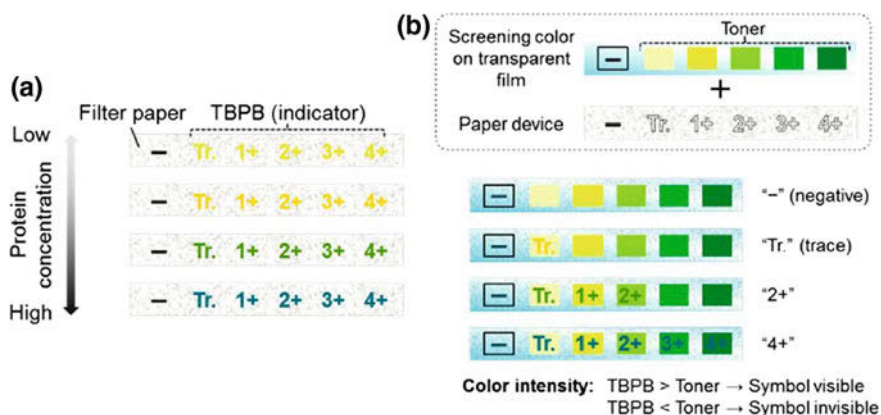


Fig. 4 Schematic showing the principle of the paper device utilizing a TBPB-based colorimetric indicator system for protein: **a** inkjet-deposited TBPB symbols exhibiting colorimetric response depending on the sample concentration, **b** response after the colorimetric reaction, where transparent film with screening color is overlaid on the paper device. Adapted with permission from Ref. [41] © 2017 ACS publisher

series of screening colours served to shield the indicator symbols with weaker colour intensity than that of the respective screening colour, making the symbols invisible to the human eye, as shown in Fig. 4b. In order to improve the sensitivity of bioassays on μ PADs, a bienzyme system was combined with a drying method to achieve signal amplification and reduction of the background signal, respectively for the detection of glucose and uric acid [42].

Paper-based immunoassays with antibody-antigen interaction are gaining popularity in resource-limited settings due to their simplicity and affordability. In a paper-based enzyme-linked immunosorbent assay (ELISA), paper modified with chitosan and glutaraldehyde to enhance antigen (ubiquitin or ubi & enhanced green fluorescent protein or eGFP) immobilization was used to detect targeted antibodies (anti-ubi & anti-eGFP). The cationic chitosan was bonded to anionic cellulose forming a layer on the surface of the paper, while glutaraldehyde served as a cross-linker to facilitate the covalent attachment of chitosan with the protein groups. The assay used a drinking straw for washing and incubation to avoid the need of pipettes and shakers. A visible green colour resulted on catalysis of the 2,2'-azino-bis(3-ethylbenzothiazoline-6-sulfonic acid) (ABTS) substrate by protein L HRP in the presence of targeted antibodies with a detection limit of 0.5 nM [43]. Similar immunoassay for the detection of anti-*Leishmania* antibodies was achieved using a paper-based 96-well ELISA [44].

Aptamers, single-stranded oligonucleotides, have been widely used in μ PADs for the selective and sensitive detection of a large number of analytes such as proteins, cells ions and microbes due to their ability to specifically recognize and interact with targets. The advantage of aptamer-based assays is that by simply changing the aptamer, sensing of different targets can be done by synthesizing the respective target-responsive hydrogels [45]. An aptamer-crosslinked hydrogel was used for detection of cocaine in urine taking advantage of their ability to bind to a specific target molecule [46]. As shown in Fig. 5, the hydrogel collapsed in presence of the target due to aptamer sequence (L-Apt) dissociating from polymer chains (P-SA and P-SB), thereby releasing the trapped glucoamylase (GA) and generating glucose. The capillary action caused glucose to flow in solution along the channel, where it was subsequently converted into H_2O_2 by glucose oxidase (GOx) already present on the substrate. Similarly, 3,3'-diaminobenzidine (DAB) was converted into a brown-coloured bar of poly-3,3'-diaminobenzidine (poly(DAB)) by horseradish peroxidase (HRP), whose length could be positively correlated to the amount of target to achieve visual distance-base quantitative detection. The cascade of enzymatic steps for signal amplification made it possible to achieve highly sensitive detection of targets [46]. Earlier, the same group reported the simultaneous detection of multiple analytes such as cocaine, adenosine and Pb^{2+} in urine using target-induced phase-transformation of the aptamer hydrogel to mediate fluid flow and signal readout in the μ PAD [47]. Another group used DNA-triggered hybridization chain reaction to capture hairpin probes and bind GOx tags via biotin-streptavidin interactions, where its quantity could be positively related to the adenosine analyte [48].

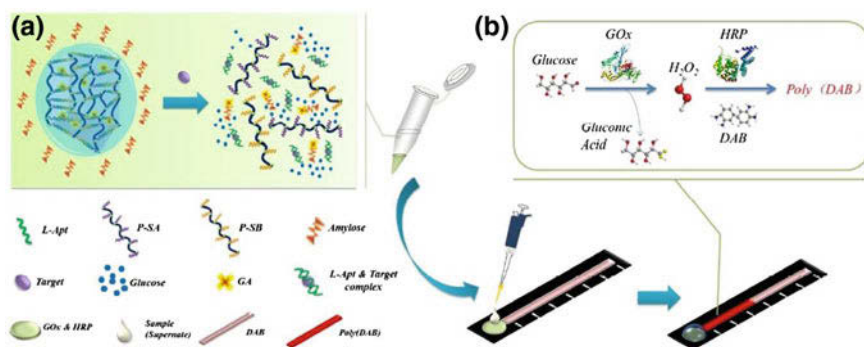


Fig. 5 Schematic of aptamer-based μ PAD for distance-based visual quantitative analysis of cocaine in urine: **a** target-induced dissolution of hydrogel releasing GA to catalyse the production of glucose, **b** conversion of glucose to gluconic acid catalysed by GOx generating H_2O_2 , which reacts with DAB catalysed by HRP to yield a brown stripe of poly(DAB) for signal readout. Adapted with permission from Ref. [46] © 2016 ACS publisher

3.2 Electrochemical Sensing

The detection of simple and complex analytes of clinical significance has been achieved based on the concept of electrochemistry including glucose [49], uric acid [50], drugs such as diazepam [51] and ketamine [52], tumor markers [53] and DNA viruses such as human papillomavirus (HPV) [54]. Detection of carcinoembryonic antigen was performed by a label-free electrochemical immunosensor fabricated by coating nanocomposites of amino functional graphene (NH_2 -G)/thionine (Thi)/gold nanoparticles (AuNPs) on the screen-printed working electrode [55]. The concept was based on the fact that the decreased response currents of Thi were proportional to the concentrations of corresponding antigens due to the formation of antibody-antigen immunocomplex. The cyclic voltammetry and differential pulse voltammetry results revealed the stability of peak currents, thus indicating that the electroactive material was tightly bound to the electrode. The determination of antigen solutions showed linear working ranges of 50 pg mL^{-1} – 500 ng mL^{-1} with the limit of detection as 10 pg mL^{-1} [55]. Another study reported the use of conducting paper modified by poly(3,4-ethylenedioxythiophene):poly(styrenesulfonate) (PEDOT:PSS) and reduced graphene oxide (RGO) for the detection of carcinoembryonic antigen. There was a significant increase in the electrical conductivity of the paper due to conformational rearrangement in the polymer and strong non-covalent interactions between PEDOT and cellulose [56].

In order to eliminate the need for enzymatic amplification and to improve the sensitivity, the analyte (biotin/streptavidin) was labelled with silver nanoparticles (AgNPs) and magnetic microbeads. Detection limit as low as 767 fM could be achieved by magnetic preconcentration of AgNP labels followed by their oxidation to Ag^+ by slipping a piece of paper to deliver the oxidizing agent at a specific time and

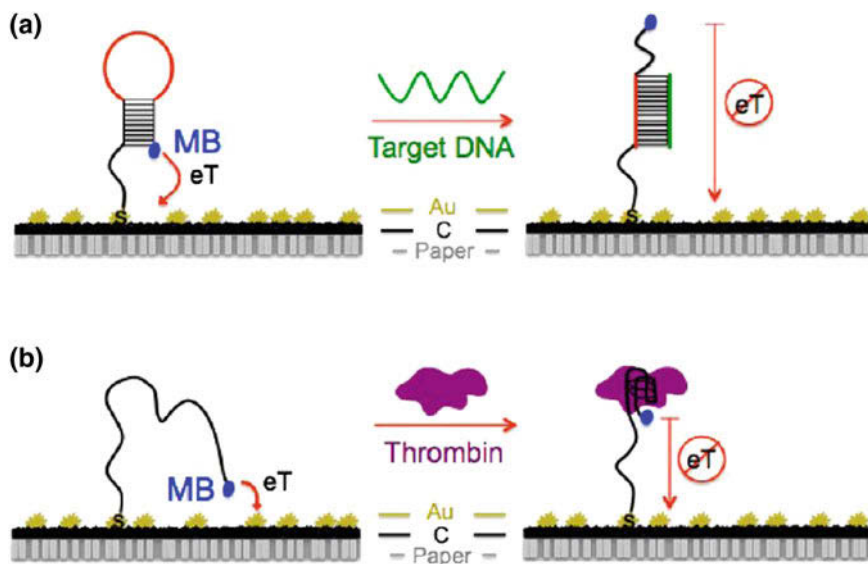


Fig. 6 Sensing mechanism of DNA and thrombin on a PAD. Adapted with permission from Ref. [61] © 2014 ACS publisher

point in the device [57]. In another work, a “pop-up” sensor fabricated from paper folded into a 3D structure enabled electrochemical detection of β -hydroxybutyrate (BHB), a biomarker for diabetic ketoacidosis, using a glucometer [58]. Similarly, amperometric detection of troponin, a cardiovascular biomarker, was done using conducting paper electrodes formed by coating a layer of polyaniline. The change in the oxidation current of polyaniline was proportional to the analyte concentration. The assay showed a sensitivity of $5.5 \mu\text{A}/\text{ng mL}^{-1} \text{cm}^{-2}$ over a wide physiological range of $1\text{--}100 \text{ ng mL}^{-1}$ [59]. Parylene C-coated newspaper acted as a sensing electrode for the detection of pathogenic *E. coli* based on DNA hybridization, showing excellent performance in the cyclic voltammetry and electrochemical impedance spectroscopy experiments with a detection limit of 0.16 nM [60].

Based on target-induced folding or unfolding of an aptamer linked to an electrochemical label, the detection of DNA and thrombin down to limits of 30 and 16 nM, respectively was achieved [61]. The oligonucleotide probes had a pendant redox reporter (methylene blue) at the distal end and a thiol at the proximal end for easy attachment to a gold electrode. On binding of the analyte, the probe underwent a conformational change that altered the location of the redox reporter relative to the electrode, as shown in Fig. 6. The sensor was “on” if the redox reporter moved closer to the electrode and “off” if, it moved away. This conformational change resulted in a change in faradaic current that was easily detected using alternating current voltammetry (ACV) or square wave voltammetry (SWV).

3.3 Luminescence-Based Sensing

Various luminescence-based techniques viz. fluorescence, chemiluminescence, electrochemiluminescence have been used to sense a range of biomedical analytes on paper platforms [62]. They offer the advantages of being highly sensitive, non-invasive, rapid and easy to implement. Recent studies have employed chemiluminescence, i.e., the generation of light via a chemical reaction, for the detection of L-cysteine [63], DNA fragments [64], carcinoembryonic antigen [65] and cotinine biomarker [66]. Similarly, electrochemiluminescence, which is the luminescence produced by relaxation of excited state molecules during electron-transfer occurring at the surface of an electrode, has been adopted for sensing of hepatitis B virus surface antigen in serum [67]. A 3D paper-based electrochemiluminescent (ECL) device was fabricated by screen printing eight carbon electrodes on paper for detecting a panel of tumor markers- α -fetoprotein (AFP), carcinoma antigen 125 (CA125), carcinoma antigen 199 (CA199) and carcinoembryonic antigen (CEA) in clinical serum samples using tris-(bipyridine)-ruthenium (II) ($\text{Ru}(\text{bpy})_3^{2+}$) and tri-*n*-propylamine (TPA) [68]. As evident from Fig. 7, the capture antibodies were immobilized on the working electrodes through chitosan coating and glutaraldehyde cross-linking. $\text{Ru}(\text{bpy})_3^{2+}$ -labeled signal antibodies were added to corresponding electrodes to carry out the

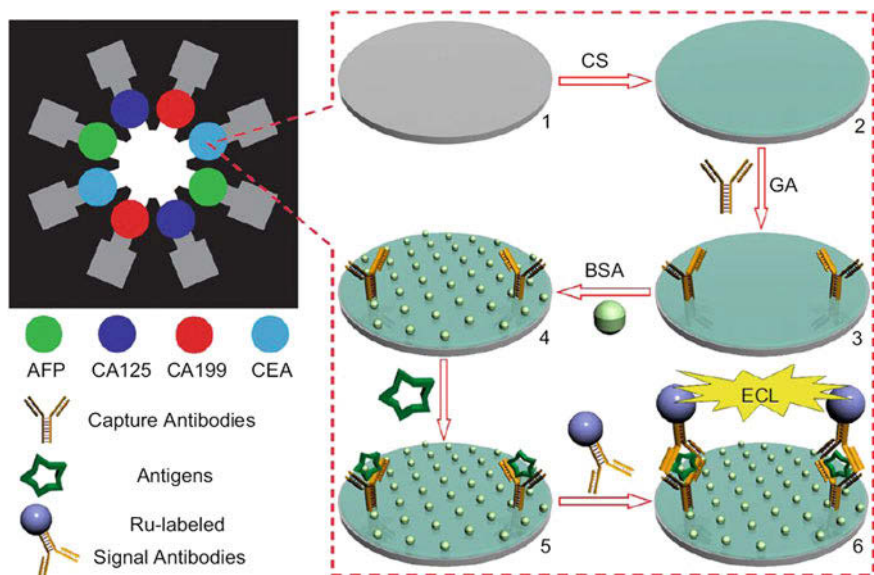


Fig. 7 Fabrication and detection principle for paper-based ECL device: (1) screen-printed carbon working electrode; (2) after chitosan modification; (3) after immobilization of capture antibodies; (4) after blocking & washing; (5) after capturing and washing; (6) after incubation with signal antibodies, washing & ECL reaction. Adapted with permission from Ref. [68] © 2012 Elsevier publisher

immunoreactions and ECL detections. The sandwich immunocomplexes were found to give much higher ECL response than the nonspecific adsorption of signal antibodies without antigen. Moreover, since the ECL intensity rose with antigen concentration, the immune device could be for the determination of sensitive antigens. The limits of detection for the four markers were 0.15 ng mL^{-1} , 0.6 U mL^{-1} , 0.17 U mL^{-1} and 0.5 ng mL^{-1} , respectively [68]. Another study fabricated a photoelectrochemical (PEC) immunosensor using CdS quantum dots (QDs) deposited on a paper working electrode modified with zinc oxide nanorods grown on reduced graphene oxide as the photoactive matrix and chemiluminescence reagent/enzyme/antibody bioconjugate as the label for sensitive detection of cancer antigen 125 [69].

Fluorescence, which is by far the most widely employed optical detection technique, has been used for sensing numerous targets including aluminium (Al^{3+}) detection in living cells [70], Cu^{2+} in human urine [71], sulfur dioxide derivative (SO_3^{2-}) in mitochondria [72], β -D-galactosidase enzyme [73], peptide, protein and DNA [74]. In order to overcome the limitations of conventional methods of attaching biomolecules onto the cellulose surface, a chemo-enzymatic method for activating cellulose with functional groups by click chemistry was proposed using propargylated xyloglucan as a molecular anchor [75]. They demonstrated the detection of esterase with a biosensor fabricated by tethering a chromogenic moiety/fluorophore to the cellulose substrate, instead of a biomolecular entity, thus simultaneously addressing the issues of signal attenuation and potential toxicity due to chromophore diffusion after substrate cleavage. The sensitivity and selectivity of fluorescence-based sensing with a quick response time makes them preferred over other detection techniques in a number of bioassays [72]. Fluorescent probes have successfully been employed to detect antibiotic-resistant genes from various bacteria [76]. Another study used fluorescence emission of fluorescein-labeled DNA probe to detect hybridization of DNA strands captured on antibodies via CBM-ZZ (carbohydrate binding molecule with high affinity for cellulose and double Z fragment of staphylococcal protein A, which recognizes IgG antibodies). The antibodies anchored via CBM-ZZ fusions were combined with wax printed μPADs for capturing and detecting DNA hybrids [77]. Other studies reporting nucleic acid assays have employed chemiluminescence [78] and luminescence resonance energy transfer (LRET) [79].

3.4 Other Sensor Types

Surface-enhanced Raman spectroscopy (SERS) is a non-destructive and sensitive technique used in molecular detection, which combines the specificity of Raman spectroscopy with the metal nanostructure-induced sensitivity provided by plasmon assisted scattering [80]. Detection of rhodamine-6G at ppb level was achieved using office paper as a SERS substrate taking advantage of its low porosity and the better ink retaining the capacity to obtain a uniform distribution of silver nanostars along with higher values for the enhancement factor [80]. A SERS paper strip fabricated

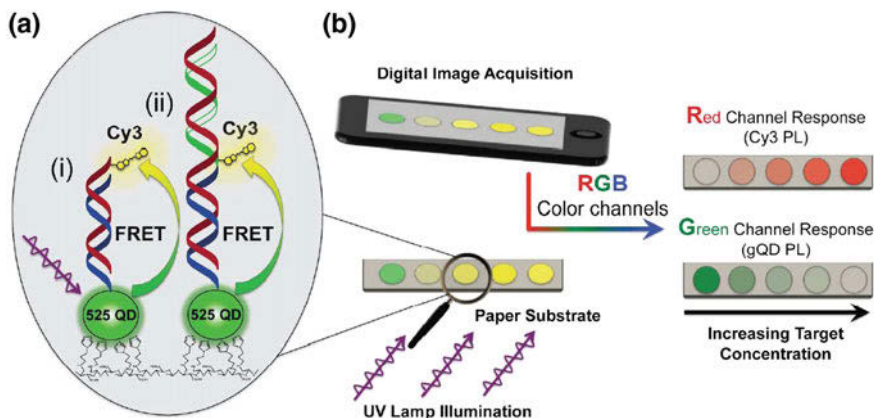


Fig. 8 **a** Design of paper-based QD-FRET nucleic acid hybridization assay. Modified paper-substrates immobilized with QD-probe conjugates, and hybridization assays in (i) a direct format or (ii) a sandwich format provided the proximity for FRET sensitized emission from the acceptor dye when the substrate was illuminated with a UV lamp, **b** digital imaging of paper substrates showing increase in Cy3 PL with corresponding decrease in gQD PL as target concentration increases, associated with R and G channels, respectively. Adapted with permission from Ref. [88] © 2014 ACS publisher

by in situ synthesis of AuNPs on cellulose fibers could detect a cancer marker in a whole blood sample [81]. The nanoparticles not only generated condensed hot spots on the fibres but also enhanced the size exclusion effect of paper. Several other studies have reported SERS-based paper sensors [82–86].

Similarly, localized surface plasmon resonance (LSPR)-based biosensors, where the bulk refractive index sensitivity and the electromagnetic decay length of the metal nanostructures are employed as optical transducers, have been used to detect contagious biomolecules [8] and cardiac biomarkers [87]. The strong electric fields thus created around the nanoparticles improved the signal intensity dramatically and allowed for extremely sensitive detection with only a small amount of analyte required. The Au and Ag NPs deposited on a paper substrate by the laser-induced annealing technique showed a rapid colour change on binding with cysteine, which could be observed by the naked eye and measured spectroscopically [8].

A nucleic acid hybridization assay was developed using green-emitting QDs (gQDs) immobilized on imidazole-modified paper, as donors in Förster resonance energy transfer (FRET) (Fig. 8a). A hybridization event brought the Cyanine 3 (Cy3) acceptor dye in close proximity to the immobilized gQDs and was responsible for a FRET sensitized emission from the dye, which served as an analytical signal. The photoluminescence (PL) intensities of gQDs and Cy3 were associated with the green (G) and red (R) imaging channels of an iPad camera after R-G-B splitting of the acquired images, as shown in Fig. 8b. The use of dry paper substrates for data acquisition offered 10-fold higher sensitivity and 10-fold lower limit of detection for the assay as compared to the hydrated paper substrates [88].

Table 1 lists some of the major biomedical analytes detected using different sensing mechanisms.

4 Sensing for Environmental Monitoring

4.1 Colorimetric Sensing

There has been a growing interest in the colorimetric detection of heavy metals and toxic compounds, which is an instrumental part of the rapid on-site environmental analysis and its real-time monitoring. The detection of toxic ions such as cobalt (Co^{2+}) [89], silver (Ag^+) [90], chloride (Cl^-) [91] and copper (Cu^{2+}) [92] in aquatic environments such as wastewater or groundwater has been reported on paper-based sensing platforms. A multiplexed patterned sensor for the detection of heavy metals was fabricated by ink-jet printing of sol-gel based bio-inks that allowed colorimetric visualization of the enzymatic activity of β -galactosidase [93]. As shown in Fig. 9a, the chromogenic substrate, chlorophenol red β -galactopyranoside (CPRG), is hydrolyzed by the β -galactosidase enzyme to give a red-magenta product. It is printed as a substrate zone and is moved to the sensing zone by lateral flow of a sample along the paper sensor. The presence of heavy metals in the sample causes a loss of the red-magenta colour in a concentration-dependent manner (Fig. 9b). In order to identify the different metals such as Hg^{2+} , Cu^{2+} , Cr^{4+} and Ni^{2+} in the mixture, a multiplexed sensor was made with two assay arms as controls, one for testing a mixture of metal ions using the β -galactosidase assay, and four additional assay arms that had different colorimetric reagents (Fig. 9c). Interestingly, time-programmable assays for metal ion determination have been developed, where the acceleration or delay of fluid transport can be controlled by adjusting capillary and laminar flow on paper without active pumping [94]. This was achieved by razor-crafting open channels on the paper using a cutting blade in a perpendicular or longitudinal directions to the direction of flow.

In order to eliminate the need for on-spot calibration using standard solutions and reduce the influence of paper inhomogeneity, matrix effects and environmental conditions on the results, a generic approach using calibrant-loaded paper was developed for multiple-point standard addition calibration [95]. The sensing areas were pre-loaded with an excess of colorimetric reagents and known amounts of the analyte; thus, a coloured product was developed before analysis. During analysis, the excess of reagents present in the sensing zone reacted with the analyte in the sample generating a combined colorimetric signal corresponding to the total concentration of the analyte in the sensing area. The combined analytical signals were used to generate a multiple standard additions curve and calculate the analyte concentration [95].

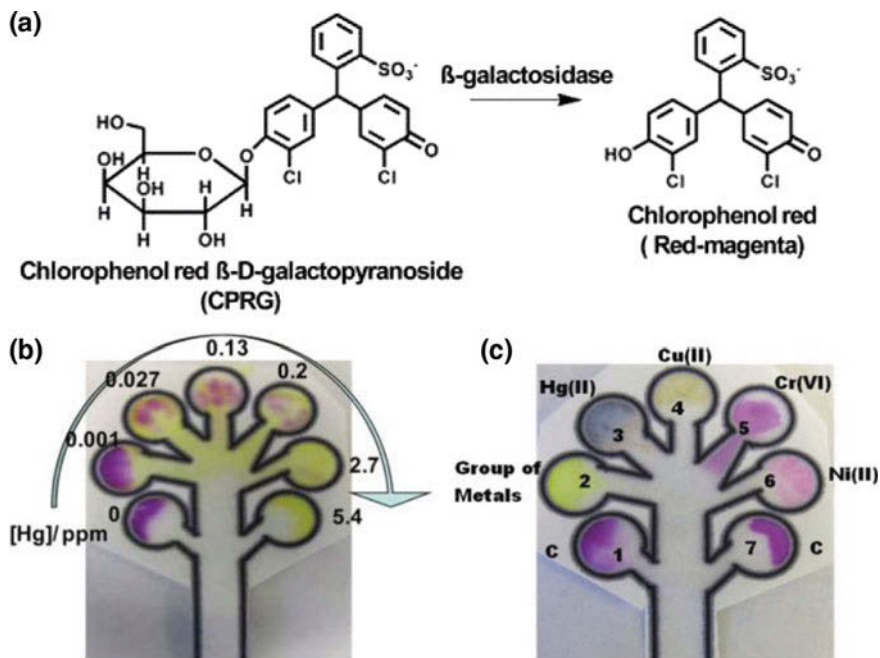


Fig. 9 a Detection principle for sensing of heavy metal ions, b dose-dependent color intensity of Hg^{2+} on the β -galactosidase-immobilized paper sensor, c detection of individual metals from a mixture on the multiplexed patterned sensor. Adapted with permission from Ref. [93] © 2011 ACS publisher

4.2 Electrochemical Sensing

Coulometric sensors were developed for the detection of halides in water samples using thin-layer coulometry, where the target ions are preferentially and exhaustively transported through an ion-selective membrane [96]. The sequential oxidation/plating of the halide at the silver wire and its subsequent regeneration with an inverted potential was monitored by cyclic voltammetry. The paper served the dual function of transporting the sample by capillarity as well as the making of an exhaustive electrochemical process. Confinement of the sample between a silver element and a Nafion membrane facilitated the resolution of a mixture of halides in a wide concentration range- from $10^{-4.8}$ to 0.1 M for iodide and bromide and from $10^{-4.5}$ to 0.6 M for chloride, with a detection limit of 10^{-5} M [96].

There have been studies based on the principle of potentiometric sensing of ions such as sodium and potassium [97]. Potentiometric ion sensors were fabricated using a newspaper and coating it with parylene C (PC-paper) to impart hydrophobicity along with improved mechanical properties and chemical stability [98]. A two-electrode configuration containing ion-selective and reference electrodes was achieved by depositing polyaniline and chloride on pre-patterned gold

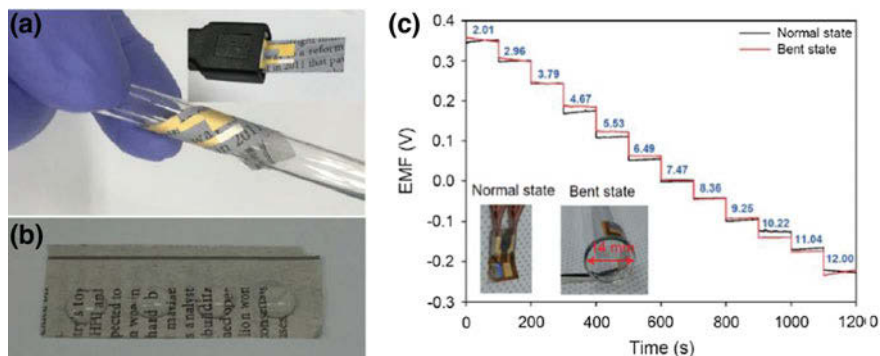


Fig. 10 **a** Image showing USB-type sensing platform and flexibility of ion sensor, **b** water droplets on PC-paper, **c** response of pH sensors with increasing pH in normal and bent states, while inset shows pH sensors in normal and bent states. Adapted with permission from Ref. [98] © 2017 Elsevier publisher

and silver layers on the sensors, respectively. These pH sensors were tested by increasing the pH levels from 2 to 12, as shown in Fig. 10c. A plot of EMF signals against the pH generated a line indicating behaviour according to Nernst equation. Moreover, this response remained the unaffected on sing bent electrodes, thus confirming the mechanical resistance of the sensors. Further, they showed good repeatability and a low potential drift [98].

4.3 Luminescence-Based Sensing

Recently, a photoluminescent nanopaper was fabricated by embedding nitrogen-doped carbon quantum dots (N-CQDs) into bacterial cellulose nanofibers for the selective detection of iodide (I^-) down to 6.1 ppm [99]. The blue emission of N-CQDs embedded paper remarkably quenched in the presence of I^- . On the contrary, hardly any change could be observed for other tested anions like chloride, fluoride, bromide, acetate, sulfate and nitrate. The quenching effect resulted from the photo-induced electron transfer between N-CQDs in the nanopaper and iodide ions in the sample [99]. Another work demonstrated the use of photoluminescent copper nanoclusters for sensing of H_2S in spring-water down to 650 nM [100]. The sensing was based on the strong Cu–S interaction resulting in the formation of non-luminescent CuS particles and subsequent photoluminescence quenching effect. The simultaneous detection of toxic heavy metal pollutants using a paper-based oligonucleotide ECL sensor was developed with carbon nanocrystals (CNCs) capped silica nanoparticles (Si@CNCs) and $Ru(bpy)_3^{2+}$ -AuNPs clusters (Ru@AuNPs) as ECL labels (Fig. 11) [101]. The immobilized Si@CNCs-tagged DNA showed an ECL signal in the cathodic potential for Pb^{2+} detection, while the Ru@AuNPs modified one exhibited the signal in the anodic potential for Hg^{2+}

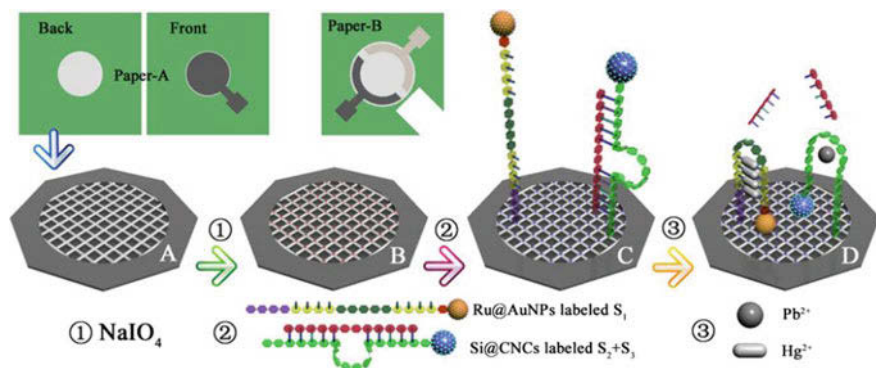


Fig. 11 Schematic illustration of a paper-based ECL device. The immunoassay was on the back of wax-patterned paper working zone: (1) the paper was spotted with NaIO₄; (2) after immobilized with Ru@AuNPs labeled DNA strands for Hg²⁺ and Si@CNCs labeled DNA strands for Pb²⁺; (3) after capturing with Pb²⁺ and Hg²⁺. Adapted with permission from Ref. [101] © 2013 Elsevier publisher

detection. The Pb²⁺ and Hg²⁺ ions induced a conformational change of DNA strands through the formation of G-quadruplex and T–Hg–T complex with detection limits of 10 pM and 0.2 nM, respectively.

Very recently, a “turn-off” fluorescence sensor was fabricated by immobilizing a cationic porphyrin, 5,10,15,20-tetrakis(1-methyl-4-pyridinio)porphyrin tetraiodide (TMPyP), onto a pre-patterned paper for the detection of Cu²⁺ [102]. The fluorescence signal of TMPyP (with two distinct maxima at 674 and 711 nm), which was easily visible to naked eyes under illumination, showed selective and substantial quenching effect in the presence of 20 mM Cu²⁺ against other metal ions. In contrast, a “turn-on” fluorescence sensor was developed to detect cyanide ion (CN⁻) in water with a detection limit of 39.9 nM [103]. The sensing was based on the nucleophilic addition of CN⁻ to the β-conjugated position of the barbituric acid moiety of the sensor, thus disrupting the π-conjugation and hampering the intramolecular charge transfer to produce a colorimetric and fluorescent response. Similar fluorescence-based sensing of phycocyanin (PC), a pigment-protein occurring in water bodies, has been demonstrated using QDs with molecularly imprinted polymers (MIP) deposited on paper [104]. As shown in the Fig. 12, in the absence of template molecule on the surface of QDs, the electrons of QDs absorb the UV energy and get excited. Subsequently, the QDs emit green fluorescence when the excited electrons return to the ground state. If the energy level of phycocyanin is higher than that of QDs, when the excited electrons of QDs return to the ground state, they will not generate fluorescence. Thus, adsorption of more phycocyanin onto the surface imprinting sites results in greater fluorescence quenching. Similarly, a ratiometric oxygen sensor based on fluorescence-phosphorescence was designed to detect as low as 0.01% of oxygen [105].

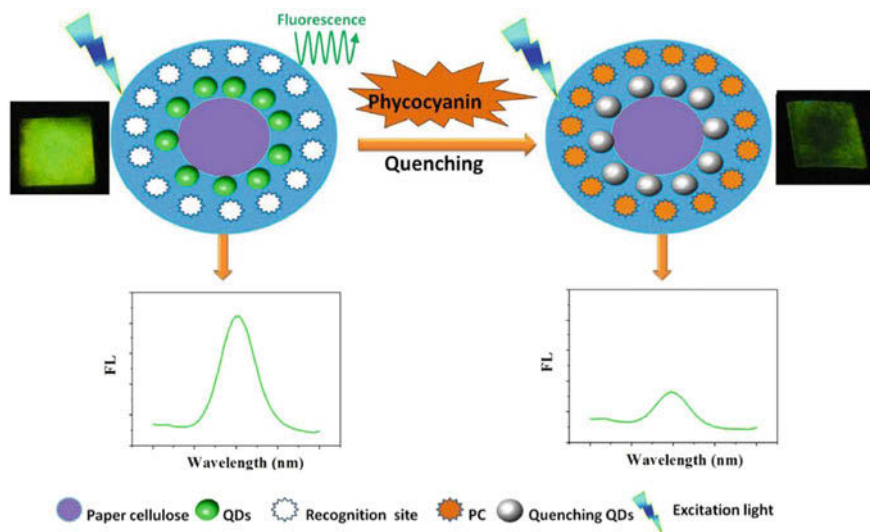


Fig. 12 Sensing principle of paper@QDs@PC-MIPs. Adapted with permission from Ref. [104] © 2017 ACS publisher

4.4 Other Sensor Types

Very recently, graphene quantum dots (GQDs) were immobilized on a paper substrate as a screening tool for organic pollutants such as 4-nitrophenol and paraoxon in seawater [13]. The luminescent blue GQDs were quenched in the presence of the target based on the phenomenon of FRET. Likewise, FRET was exploited on a paper-based sensor strip containing carbon nanodots (C-dots) conjugated to rhodamine for the detection of Al^{3+} ions [106]. As evident from Fig. 13, the hybrid system showed blue emission at 410 nm from C-dots since the unopened rhodamine could not absorb the energy from the blue emission of C-dots, leading to no FRET. On exposure to Al^{3+} , the metal ions induced ring-opening of rhodamine on C-dots through the chelation of the rhodamine-6G (R6G) moiety with metal ions, leading to a spectral overlap of the absorption of the donor (C-dots) and the emission of the ring-opened acceptor (rhodamine), finally emitting yellow. The addition of Al^{3+} to C-dots-R6G solution led to a gradual decrease in emission intensity at 410 nm with concomitant increase in emission at 560 nm, thus exhibiting a change in emission from blue to yellow (inset of Fig. 13).

SERS was exploited on a filter paper for the sensing of thiram and ferbam as model pesticides in trace amounts with detection limits of 0.46 and 0.49 mM, respectively [107]. In order to improve the retention of AgNPs on paper, the hydrophilic hydroxyl groups were converted to hydrophobic alkyl groups by the application of alkyl ketene dimer (AKD). This led to an increased contact angle with a reduced contact area and longer retention time of the aqueous dispersion due

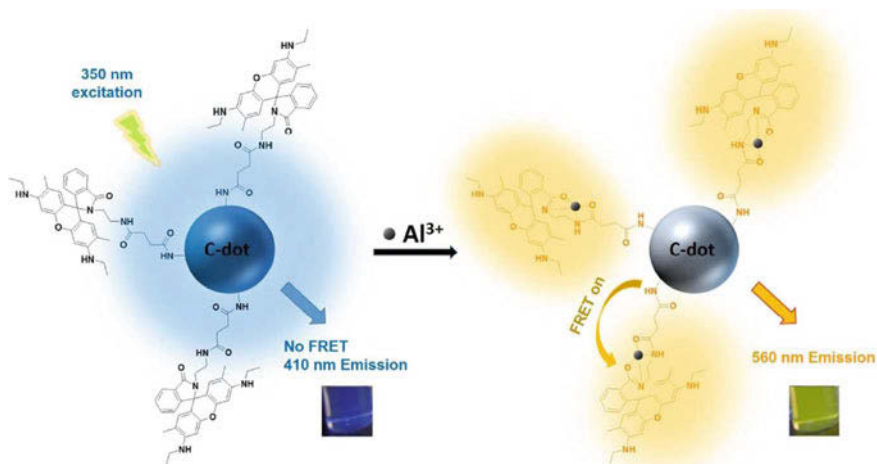


Fig. 13 FRET-based sensing mechanism of the C-dots-R6G in response to Al^{3+} . Photographs in the inset are under 365 nm UV light. Adapted with permission from Ref. [106] © 2015 ACS publisher

to lower absorption, thus concentrating the nanoparticles on paper. The SERS signal was strongly intensified by the increased number of SERS hot spots owing to the increased density of the nanoparticles on a small contact area of the paper surface [107]. In a similar fashion, SERS was implemented on a paper biosensor to enhance the low intensity of Raman signals for detecting wastewater components [108] and organic pollutants [109]. Table 2 lists the various environmental analytes detected by different sensing principles.

5 Sensing for Food and Water Quality

5.1 Colorimetric Sensing

Paper-based sensors have shown immense potential for monitoring and detecting various contaminants such as bacteria and chemical residues present in food, which holds utmost significance to ensure “food safety”. Foodborne pathogens like *E. coli*, *Salmonella typhimurium*, and *L. monocytogenes* have been detected in food samples by measuring the colour change when an enzyme associated with the pathogen of interest reacts with a chromogenic substrate [110]. A colorimetric assay for the detection of *L. monocytogenes* consisted of magnetic nanoparticles conjugated with protease specific substrate to be selectively cleaved by the *L. monocytogenes* proteases with a limit of detection of 2.17×10^2 CFU/mL [111]. The ability of the protease to break the peptide bonds in a protein substrate led to a colour change from black to golden. Gas sensors using diatomite on paper for detecting volatile

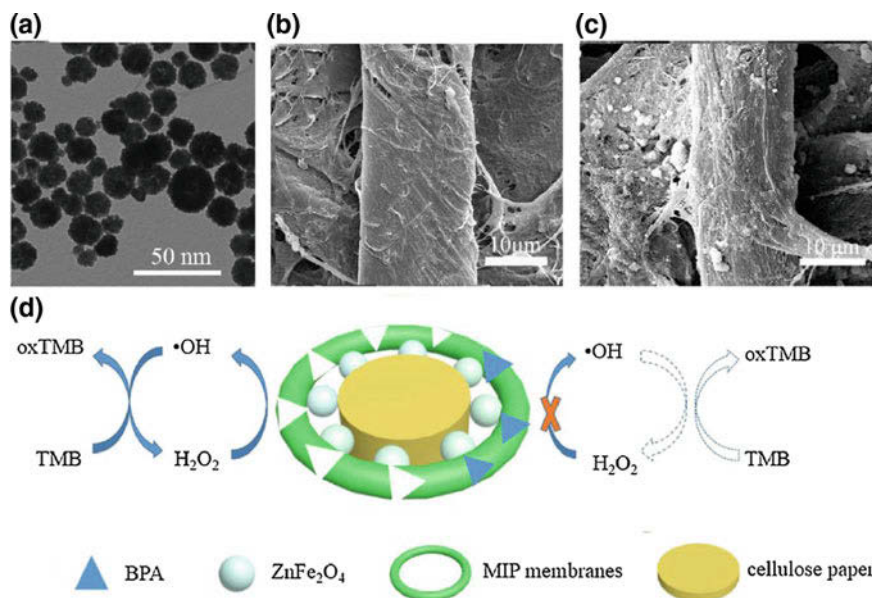
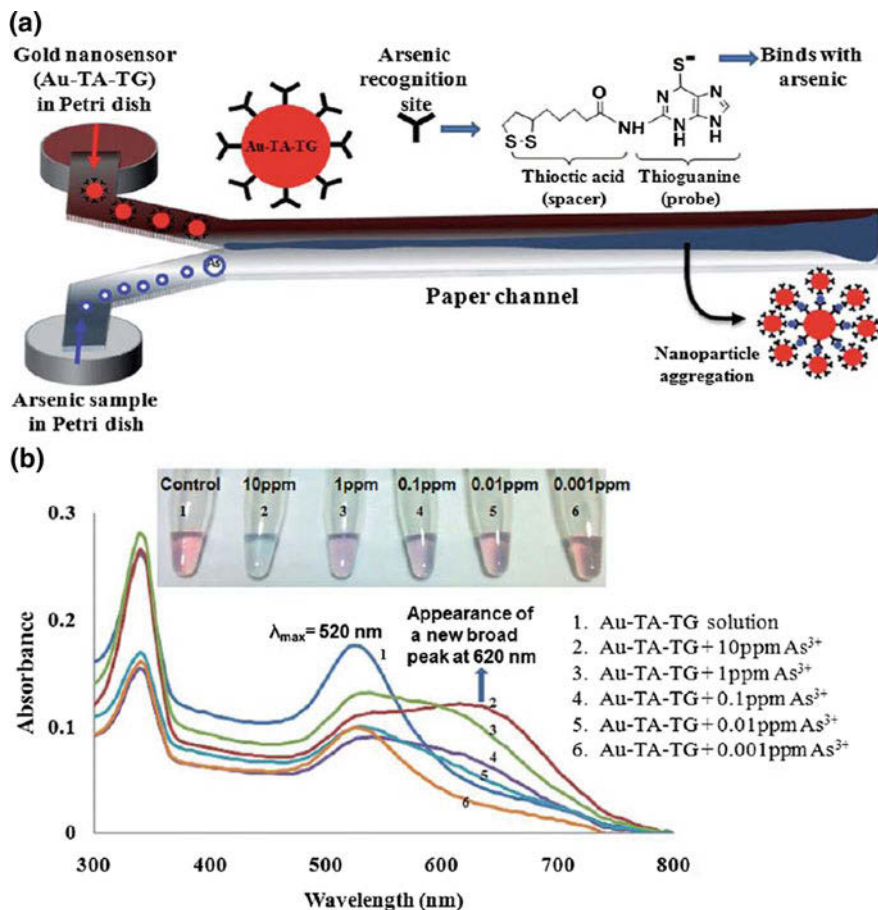


Fig. 14 a TEM of the synthesized ZnFe₂O₄ MNPs, SEM images of b synthesized MIP membranes and c MIP membranes@ZnFe₂O₄, d mechanism for the detection of BPA. Adapted with permission from Ref. [114] © 2017 Elsevier publisher

nitrogenous compounds such as ammonia as an indicating factor for meat spoilage [112]. The colour change of a pH-sensitive dye like bromophenol blue coated on paper occurs in presence of ammonia, which acts as a Lewis base and induces the colour change due to the release of hydrogen. Another work used the metachromasy of a dye, *o*-toluidine blue (OTB) to detect charged macromolecules, indicated by a characteristic colour change from blue to pink. On coming in contact with ionic molecules, the dye molecules align with the charges on the molecules, resulting in a shift in the wavelength of maximum absorbance of the dye [113].

The colorimetric sensing technique has been used to detect several toxic chemical contaminants in food such as bisphenol A [114], benzoic acid [115], clenbuterol [116], melamine [117], residual antibiotics [118] and estrogens [119]. Bisphenol A (BPA) has been widely used in food packaging such as the plastic beverage bottles and causes contamination of food as well as the environment [114]. A sensor was developed for the detection of BPA combining the intrinsic peroxidase activity and the colorimetric potential of ZnFe₂O₄ magnetic nanoparticles (ZnFe₂O₄ MNPs) and the adsorption capacity of molecularly imprinted polymer (MIP) membranes. Figure 14 shows the morphology of the MNPs and their binding on the membranes. As can be seen from Fig. 14d, in the absence of BPA, H₂O₂ was adsorbed on the ZnFe₂O₄ MNPs and activated by the ferric ions to generate ·OH, which subsequently oxidized 3,3',5,5'-tetramethylbenzidine (TMB) to form a blue complex due to the transfer of charge. In contrast, no ·OH



could be generated when BPA was anchored on the membrane surface. The assay was linear over the range 10–1000 nM with a limit of detection of 6.18 nM [114]. Other studies have also reported the detection of pesticides [120], food preservatives such as sulfur dioxide [121] and foodborne carcinogens such as aflatoxin B₁ [122]. Similarly, studies have reported the detection of cadmium (Cd²⁺) [123] and nitrite [35] toxic ions in drinking water.

The very low concentration of arsenic (As) has been detected in water, 1 ppb which is lower than the WHO's reference standard for drinking water, using a microfluidic paper nanosensor fabricated by anchoring gold nanoparticles (Au) to thioctic acid (TA) and thioguanine (TG). As shown in Fig. 15a, when the two

extended arms of the Y-channel are touched into the Au-TA-TG and As solutions, the fluids started flowing into the channel due to capillary action and rapidly interacts to form a visible bluish-black precipitate. TA acts as a spacer arm to increase the detection ability by reducing the steric hindrance. During detection, TG probes interact with As^{3+} ions leading to aggregation of nanoparticles. This causes a visual colour change due to inter-particles coupled plasmon resonance from aggregated Au nanoparticles. Figure 15b shows the shift in UV-Vis spectra wavelength (from λ_{max} 520 nm to λ_{max} 620 nm) indicating As binding with Au-TA-TG and formation of aggregates in various concentrations of As solutions [124].

5.2 Electrochemical Sensing

Electrochemical detection of ethanol in beer has been reported using screen-printed electrodes on office paper modified with Carbon Black and Prussian Blue (CB/PBNPs) nanocomposite [125]. Ethanol was quantified indirectly from the concentration of H_2O_2 , which was produced by the enzymatic reaction between alcohol oxidase (bio-recognition element) and ethanol. A quick response was obtained in just 40 s with a sensitivity of $9.13 \mu\text{A}/\text{mM cm}^2$ and a detection limit of 0.52 mM. The presence of lead and cadmium ions in rice and fish was sensed with bismuth-modified, boron-doped diamond electrode (Bi-BDDE) [126]. The Bi-BDDE increased the sensitivity of ion detection; exhibiting sharp and well-defined peaks in the stripping voltammograms, which were significantly higher than the stripping peak current observed in case of bismuth-modified screen-printed carbon electrode (Bi-SPCE). The superior performance of BDDE was attributed to the fact that bismuth could form “fused” alloys with ions, which rendered them ready to be reduced.

The detection of cadmium in rice was performed by a double-sided conductive carbon tape coated with a thin layer of gold for stripping analysis of Cd^{2+} coupled with in situ electrodeposition of bismuth [127]. Likewise, resistive sensors on paper with copper acetate were developed for monitoring the quality of raw broiler meat where H_2S was detected as an end product of microbial metabolism by replicating the aerobic and anaerobic conditions of modified atmosphere packaging in the laboratory [128]. Similarly, capacitive humidity sensors built for smart packaging showed a logarithmic response on paper [129].

5.3 Luminescence-Based Sensing

The photoluminescent quenching ability of graphene oxide (GO) was demonstrated for the detection of the pathogen (*E. coli*) using an LFIA with a limit of detection as low as 10 CFU mL^{-1} [130]. As shown in Fig. 16a, test, and control lines were

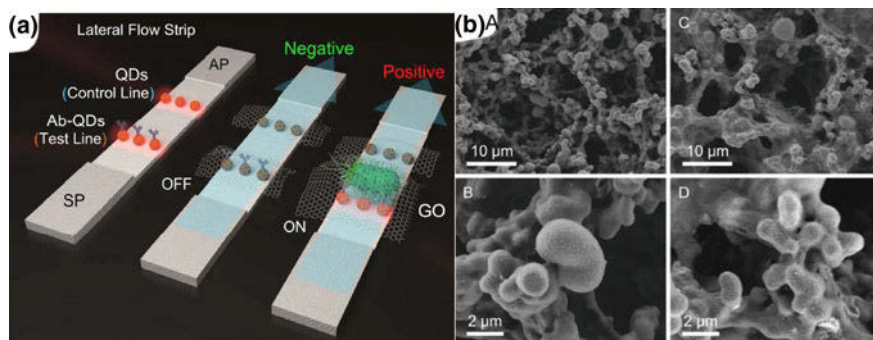


Fig. 16 **a** Photoluminescent lateral flow assay revealed by graphene oxide (GO) for *E. coli* detection, **b** SEM images of the paper-based sensing platform: (A & B) Bare detection line, (C & D) Graphene oxide coated detection line. Adapted with permission from Ref. [130] © 2015 ACS publisher

printed on a nitrocellulose substrate with antibody decorated CdSe@ZnS quantum dots (Ab-QDs) and bare QDs, respectively. Capillary forces caused the sample flow from the sample pad (SP) to the absorbent pad (AP). In the absence of target pathogen, the test line is quenched by GO. On the contrary, when the target is present, it is selectively captured by the Ab-QDs and the test line is not significantly quenched compared to the control line due to hindered resonance energy transfer caused by the increased distance between the donor and the acceptor. The control line, with no pathogen-binding molecules, is always quenched thus ensuring the correctness of the assay. The scanning electron micrographs (SEM) of the biosensing platform are shown in Fig. 16b [130]. Other studies have employed the fluorescence-based sensing approach for the determination of chemical contaminants in food such as formaldehyde [131, 132], Hg^{2+} , Ag^+ and aminoglycoside antibiotic residues [133].

Another immunoassay developed for the detection of *Salmonella*, a common foodborne pathogen, was based on chemiluminescent reaction indicated by the quantification of adenosine triphosphate (ATP) [134]. The wax-printed μPAD was Z-folded for liquid handling without external driving force. As shown in Fig. 17, the μPAD was divided into two separate functional zones- reagent zone A and testing zone B by the folding area. Each functional zone possessed humped circles that were opposite. For testing, the reagent and tested samples were put into the corresponding zones; then the hump of the two circles was connected in order to allow the liquid to flow through the Z-folding. The ATP aptamer, immobilized on the reagent zone, bonded to the target and released the HRP tagged DNA associated with the aptamer. The released HRP tagged DNA then went through the micro-channel humps and arrived at the testing zone B via Z-folding of the μPAD . Eventually, H_2O_2 was added to lead to a colour change (since 3-amino-9-ethylcarbazole (AEC) coated on the testing zone was oxidized by HRP/ H_2O_2), thus determining the concentration of ATP. The detection limit was $1 \mu\text{M}$ for ATP and around 2.6×10^7 CFU/mL for *Salmonella* [134]. Another work

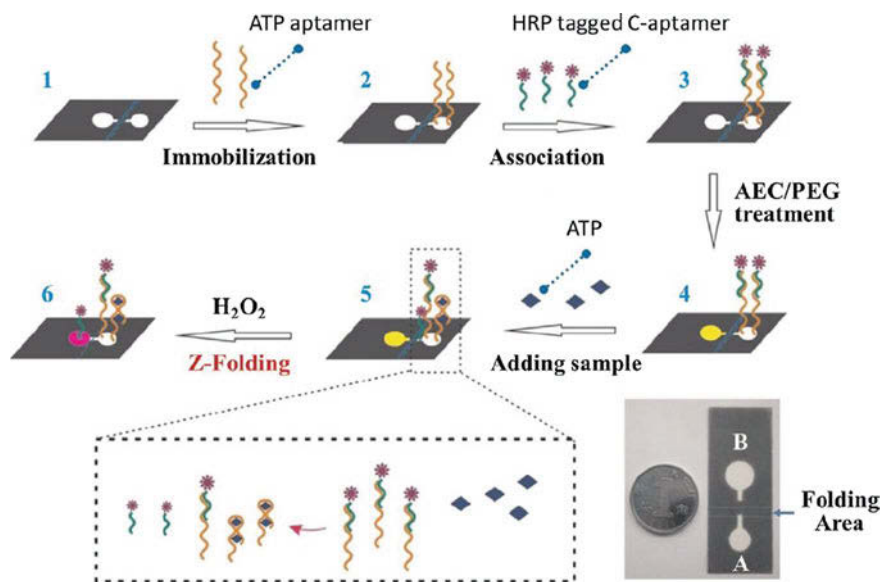


Fig. 17 Schematic showing the fabrication of Z-folded μ PAD for *Salmonella* detection via ATP quantification. Adapted with permission from Ref. [134] © 2015 Elsevier publisher

developed an LFIA based on enzyme-catalyzed chemiluminescence for the detection of fumonisins, which is produced by *Fusarium* mould species, in maize with a detection limit of $2.5 \mu\text{g L}^{-1}$ [135]. The immunological and chemiluminescence reactions were conducted sequentially in the LFIA strip and the HRP-labeled tracer antibody was revealed by chemiluminescence to achieve the quantification. In a similar way, chemiluminescence-based sensing has been exploited on paper platforms for the detection of dichlorvos pesticides in vegetables [136, 137].

5.4 Other Sensor Types

A triple-mode colorimetric, fluorescent, and SERS sensor was developed for detecting nitrite ion, a widely used meat preservative, based on the hybrid assembly of gold nanorods (GNRs)-azo-gold nanoparticles (GNPs) (GNRs-Azo-GNPs) on a paper strip [138]. A quantitative colorimetric response resulted on the addition of nitrite by the Griess reaction between *p*-aminothiophenol (PATP) and 1,8-diaminonaphthalene (DAP), causing a drop in the fluorescence intensities due to FRET from DAP to azo-moiety. The sensor with a limit of detection of $0.01 \mu\text{M}$ also served as a SERS substrate for quantitative analysis of nitrite [138]. A filter paper with AgNPs served as a rag to collect pesticide residues from the peels of apples, bananas, and tomatoes [139]. The thiram and paraoxon residues could be collected by simply swabbing the paper substrate across a wide surface area of the peels. The

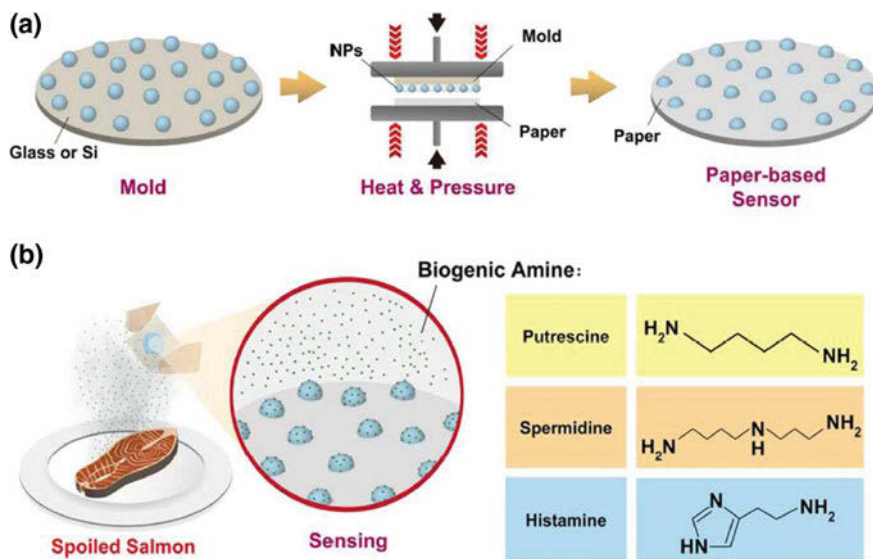


Fig. 18 Schematic representations showing **a** metal nanoparticles imprinted onto a paper, **b** nanoparticle-embedded paper to detect volatile biogenic amines released from spoiled salmon. Adapted with permission from Ref. [140] © 2017 ACS publisher

AgNP-decorated filter paper with ‘dynamic SERS’ provided not only the hot spots from nanostructures and concentrated target molecules but also a high sensitivity and reproducibility pesticide detection. Based on plasmonic refractometric sensing, gas sensors were fabricated by imprinting nanoparticles on inkjet paper [140]. Refractometric sensing is based on the adsorption of the analyte on the surface of the nanoparticles resulting in a red-shift in the wavelength and an extinction increase of the LSPR peak. Plasmonic nanoparticles such as gold and silver were deposited on paper using reversal lithography (Fig. 18a). The high reflectance and smoothness of inkjet papers were exploited for sensing of biogenic amines (BA) released from spoiled fish. The levels of BA, generated through microbial action, were used as an indicator of food freshness. During detection, the volatile BAs attached spontaneously onto the nanoparticle surface via their amino groups forming a dense layer (Fig. 18b). This led to a change in the local refractive index around the nanoparticles, resulting in the red-shift of the LSPR wavelength [140].

6 Sensing for Forensics and Security

Lately, sensing high-energy materials has gained immense importance in security and forensics in view of their potential toxicity and environmental risks. The modern methods for their detection such as gas chromatography coupled with mass

spectrometry, ion mobility spectrometry and energy dispersive X-ray spectroscopy are all infrastructure-intensive and cannot be implemented outside a laboratory setting [141, 142]. This motivated the development of complementary techniques for rapid, straightforward and on-site detection of explosives. Several sensing approaches including colorimetry [143], luminescence quenching [141], fluorescence quenching [144], SERS [145] and others [146] have been implemented on paper platforms to achieve these goals. The detection of improvised explosives has been demonstrated by μ PADs containing reagents capable of reacting with explosives and resulting in a specific colorimetric reaction [143, 147]. A single eluent reservoir was used to extract the explosives and transport them to the testing zones by capillary action. Inorganic explosives with nitrate, nitrite, ammonium, chlorate and perchlorate oxidizers, as well as military explosives such as 2,4,6-trinitrotoluene (TNT) and 1,3,5-trinitroperhydro-1,3,5-triazine (RDX), along with urea nitrate and organic peroxides could be detected with limits of detection between 0.39 and 19.8 μg [143]. Another study detected TNT down to 14 ng/cm^2 based on the photothermal effect of the complex formed by charge transfer between an electron-rich group in polyaniline and an electron-deficient nitro group in TNT, which led to a near infra-red absorption at 800 nm, inducing a temperature rise proportional to the concentration of TNT upon irradiation [148].

Detection of drugs is of paramount significance for crime scene investigations. Using an office paper, a simple colorimetric sensor was fabricated for sensing of phenacetin, an analgesic and antipyretic drug, widely used as a cutting agent by traffickers for illicit drugs such as cocaine to increase profits [149]. The sensing mechanism involved hydrolysis of the adulterant in the presence of an acid followed by reaction of the formed compound with sodium 1,2-naphthoquinone-4-sulfonate (NQS) to yield a reddish-orange product, which could be read by a smartphone camera. Likewise, the electrochemical detection of alprazolam, a psychotropic drug, was performed by methylene blue doped silver core-shell palladium nano-hybrids (Ag@Pd nano-hybrids) on a chip. The cyclic voltammetry tests showed that Ag@Pd nano-hybrids generated a strong electrochemical signal in PBS. Due to the redox transition of methylene blue, the drug was reduced to its corresponding dihydro derivative on the modified surface of the biosensor chip [150].

7 Summary, Challenges and Future Perspectives

The present chapter has reviewed the developments in the paper-based sensing devices with an emphasis on the fundamental sensing approaches. Considering the multitude of striking features of paper, it is no surprise that there has been a dramatic increase in the number of research groups working on analytical devices using paper as a substrate. The hydrophilicity and low-cost of paper are the two key attributes that have made it a versatile sensing platform in virtually every sector from healthcare to security. The paper-based sensing technology has come a long way from simple qualitative test strips to the 3D complex assays that have the

potential to carry out multiple chemical reactions in a simple format without the need for any external equipment. Although paper-based sensing technology has seen immense development since the last decade and is undoubtedly the dawn of a new day in building a next-generation sensor technology, there are still a number of concerns that need to be addressed. The clinical performance of the existing devices needs to be improved as varying specificity and sensitivity may lead to false-positive or false-negative results [26]. Since different detection methods could also cause varying performance, it would be imperative to assess them to reach an optimal sensitivity and specificity as well as to reduce cost. Especially in case of colorimetric assays, there exists the possibility of subjective judgement among the users in interpreting the results with the naked eye in different illumination environments, which could lead to controversial readouts. The reagents used in the assay, particularly the biomolecules such as enzymes and antibodies, being highly susceptible to the surrounding environment, may degrade in extreme conditions thus affecting the robustness of the assay and having a detrimental influence on its performance. Additionally, the changes in temperature and humidity may affect the long-term stability of the immobilized reagents, leading to varying signals. Furthermore, batch-to-batch variation may also have an impact on the reproducibility of testing [151]. Eventually, the extent of commercialization into the market, outside the research laboratories will be the deciding factor for the ultimate success of paper-based sensing devices.

Acknowledgements CA is grateful to the Tempus Public Foundation (TPF) for providing financial assistance under the *Stipendium Hungaricum Programme*. This chapter was also made in frame of the “EFOP-3.6.1-16-2016-00018—Improving the role of research + development + innovation in the higher education through institutional developments assisting intelligent specialization in Sopron and Szombathely.”

References

1. Nayak S, Blumenfeld NR, Laksanasopin T, Sia SK (2017) Point-of-care diagnostics: recent developments in a connected age. *Anal Chem* 89:102–123
2. Gong MM, Sinton D (2017) Turning the page: advancing paper-based microfluidics for broad diagnostic application. *Chem Rev* 117:8447–8480
3. Sher M, Zhuang R, Demirci U, Asghar W (2017) Paper-based analytical devices for clinical diagnosis: recent advances in the fabrication techniques and sensing mechanisms. *Expert Rev Mol Diagn* 17:351–366
4. Zarei M (2017) Portable biosensing devices for point-of-care diagnostics: recent developments and applications. *Trends Anal Chem* 91:26–41
5. Martinez AW (2011) Microfluidic paper-based analytical devices: from POCKET to paper-based ELISA. *Bioanalysis* 3:2589–2592
6. Martinez AW, Phillips ST, Whitesides GM, Carrilho E (2010) Diagnostics for the developing world: Microfluidic paper-based analytical devices. *Anal Chem* 82:3–10
7. Morbioli GG, Mazzu-Nascimento T, Stockton AM, Carrilho E (2017) Technical aspects and challenges of colorimetric detection with microfluidic paper-based analytical devices (mPADs)—a review. *Anal Chim Acta* 970:1–22

8. Tseng SC et al (2012) Eco-friendly plasmonic sensors: using the photothermal effect to prepare metal nanoparticle-containing test papers for highly sensitive colorimetric detection. *Anal Chem* 84:5140–5145
9. Tao H et al (2011) Metamaterials on paper as a sensing platform. *Adv Mater* 23:3197–3201
10. Martinez AW, Phillips ST, Butte MJ, Whitesides GM (2007) Patterned paper as a platform for inexpensive, low-volume, portable bioassays. *Angew Chem Int Ed* 46:1318–1320
11. Parolo C, Merkoci A (2013) Paper-based nanobiosensors for diagnostics. *Chem Soc Rev* 42:450–457
12. Ge S, Zhang L, Zhang Y, Lan F, Yan M, Yu J (2017) Nanomaterials-modified cellulose paper as a platform for biosensing applications. *Nanoscale* 9:4366–4382
13. Alvarez-Diduk R, Orozco J, Merkoci A (2017) Paper strip-embedded graphene quantum dots: a screening device with a smartphone readout. *Sci Rep* 7:976–984
14. Carrasquilla C, Little JR, Li Y, Brennan JD (2015) Patterned paper sensors printed with long-chain DNA aptamers. *Chemistry* 21:7369–7373
15. Rat S et al (2016) Elastic coupling between spin-crossover particles and cellulose fibers. *Chem Commun* 52:11267–11269
16. Lim WY, Goh BT, Khor SM (2017) Microfluidic paper-based analytical devices for potential use in quantitative and direct detection of disease biomarkers in clinical analysis. *J Chromatogr B* 1060:424–442
17. Mahato K, Srivastava A, Chandra P (2017) Paper based diagnostics for personalized health care: emerging technologies and commercial aspects. *Biosens Bioelectron* 96:246–259
18. Wang S, Chinnasamy T, Lifson MA, Inci F, Demirci U (2016) Flexible substrate-based devices for point-of-care diagnostics. *Trends Biotechnol* 34:909–921
19. Meredith NA, Quinn C, Cate DM, Reilly TH 3rd, Volckens J, Henry CS (2016) Paper-based analytical devices for environmental analysis. *Analyst* 141:1874–1887
20. Bulbul G, Hayat A, Andreescu S (2015) Portable nanoparticle-based sensors for food safety assessment. *Sensors* 15:30736–30758
21. Hua M, Li S, Wang S, Lu X (2018) Detecting chemical hazards in foods using microfluidic paper-based analytical devices (μ PADs): The real-world application. *Micromachines* 9:32–45
22. Ansari N, Lodha A, Pandya A, Menon SK (2017) Determination of cause of death using paper-based microfluidic device as a colorimetric probe. *Anal Methods* 9:5632–5639
23. Song Y, Gyarmati P, Araujo AC, Lundeberg J, Brumer H 3rd, Stahl PL (2014) Visual detection of DNA on paper chips. *Anal Chem* 86:1575–1582
24. Ge S, Zhang L, Zhang Y, Liu H, Huang J, Yan M, Yu J (2015) Electrochemical K-562 cells sensor based on origami paper device for point-of-care testing. *Talanta* 145:12–19
25. Nilghaz A, Guan L, Tan W, Shen W (2016) Advances of paper-based microfluidics for diagnostics—the original motivation and current status. *ACS Sens* 1:1382–1393
26. Yamada K, Shibata H, Suzuki K, Citterio D (2017) Toward practical application of paper-based microfluidics for medical diagnostics: state-of-the-art and challenges. *Lab Chip* 17:1206–1249
27. Tao X, Jia H, He Y, Liao S, Wang Y (2017) Ultrafast paper thermometers based on a green sensing ink. *ACS Sens* 2:449–454
28. Yang J, Kwak TJ, Zhang X, McClain R, Chang WJ, Gunasekaran S (2016) Iridium oxide-reduced graphene oxide nanohybrid thin film modified screen-printed electrodes as disposable electrochemical paper microfluidic pH sensors. *J Vis Exp* 117:e53339–e53345
29. Balde M, Vena A, Sorli B (2015) Fabrication of porous anodic aluminium oxide layers on paper for humidity sensors. *Sens Actuators B Chem* 220:829–839
30. Yuan Y, Zhang Y, Liu R, Liu J, Li Z, Liu X (2016) Humidity sensor fabricated by inkjet-printing photosensitive conductive inks PEDOT:PVMA on a paper substrate. *RSC Adv* 6:47498–47508
31. Koren K, Kühl M (2015) A simple laminated paper-based sensor for temperature sensing and imaging. *Sens Actuators B Chem* 210:124–128

32. Nagy V et al (2014) Cellulose fiber nanocomposites displaying spin-crossover properties. *Colloids Surf A Physicochem Eng Asp* 456:35–40
33. Nagy V, Suleimanov I, Molnár G, Salmon L, Bousseksou A, Csóka L (2015) Cellulose–spin crossover particle composite papers with reverse printing performance: a proof of concept. *J Mater Chem C* 3:7897–7905
34. Zhao H, Zhang T, Qi R, Dai J, Liu S, Fei T (2017) Drawn on paper: a reproducible humidity sensitive device by handwriting. *ACS Appl Mater Interfaces* 9:28002–28009
35. Lopez-Ruiz N, Curto VF, Erenas MM, Benito-Lopez F, Diamond D, Palma AJ, Capitan-Vallvey LF (2014) Smartphone-based simultaneous pH and nitrite colorimetric determination for paper microfluidic devices. *Anal Chem* 86:9554–9562
36. Lee C-Y, Lei KF, Tsai S-W, Tsang N-M (2016) Development of graphene-based sensors on paper substrate for the measurement of pH value of analyte. *BioChip J* 10:182–188
37. Liu X, Mwangi M, Li X, O'Brien M, Whitesides GM (2011) Paper-based piezoresistive MEMS sensors. *Lab Chip* 11:2189–2196
38. Lee J, Lee YJ, Ahn YJ, Choi S, Lee G-J (2018) A simple and facile paper-based colorimetric assay for detection of free hydrogen sulfide in prostate cancer cells. *Sens Actuators B Chem* 256:828–834
39. Silva TG, de Araujo WR, Munoz RA, Richter EM, Santana MH, Coltro WK, Paixao TR (2016) Simple and sensitive paper-based device coupling electrochemical sample pretreatment and colorimetric detection. *Anal Chem* 88:5145–5151
40. Cha R, Wang D, He Z, Ni Y (2012) Development of cellulose paper testing strips for quick measurement of glucose using chromogen agent. *Carbohydr Polym* 88:1414–1419
41. Yamada K, Suzuki K, Citterio D (2017) Text-displaying colorimetric paper-based analytical device. *ACS Sens* 2:1247–1254
42. Chen X, Chen J, Wang F, Xiang X, Luo M, Ji X, He Z (2012) Determination of glucose and uric acid with bienzyme colorimetry on microfluidic paper-based analysis devices. *Biosens Bioelectron* 35:363–368
43. Chan SK, Lim TS (2016) A straw-housed paper-based colorimetric antibody–antigen sensor. *Anal Methods* 8:1431–1436
44. Costa MN et al (2014) A low cost, safe, disposable, rapid and self-sustainable paper-based platform for diagnostic testing: lab-on-paper. *Nanotechnology* 25:094006–094017
45. Tian T et al (2016) Integration of target responsive hydrogel with cascaded enzymatic reactions and microfluidic paper-based analytic devices (mPADs) for point-of-care testing (POCT). *Biosens Bioelectron* 77:537–542
46. Wei X et al (2016) Microfluidic distance readout sweet hydrogel integrated paper-based analytical device (μ DiSH-PAD) for visual quantitative point-of-care testing. *Anal Chem* 88:2345–2352
47. Wei X et al (2015) Target-responsive DNA hydrogel mediated “stop-flow” microfluidic paper-based analytic device for rapid, portable and visual detection of multiple targets. *Anal Chem* 87:4275–4282
48. Zhang Y et al (2016) Naked-eye quantitative aptamer-based assay on paper device. *Biosens Bioelectron* 78:538–546
49. Santhiago M, Kubota LT (2013) A new approach for paper-based analytical devices with electrochemical detection based on graphite pencil electrodes. *Sens Actuators B Chem* 177:224–230
50. Yao Y, Zhang C (2016) A novel screen-printed microfluidic paper-based electrochemical device for detection of glucose and uric acid in urine. *Biomed Microdevices* 18:92–100
51. Narang J et al (2017) Lab on paper chip integrated with Si@GNRs for electroanalysis of diazepam. *Anal Chim Acta* 980:50–57
52. Narang J, Malhotra N, Singhal C, Mathur A, Chakraborty D, Ingle A, Pundir CS (2017) Point of care with micro fluidic paper based device incorporated with nanocryst of Zeolite-GO for electrochemical sensing of date rape drug. *Proc Technol* 27:91–93

53. Wang P, Ge L, Yan M, Song X, Ge S, Yu J (2012) Paper-based three-dimensional electrochemical immunodevice based on multi-walled carbon nanotubes functionalized paper for sensitive point-of-care testing. *Biosens Bioelectron* 32:238–243
54. Teengam P, Siangproh W, Tuantranont A, Henry CS, Vilaivan T, Chailapakul O (2017) Electrochemical paper-based peptide nucleic acid biosensor for detecting human papillomavirus. *Anal Chim Acta* 952:32–40
55. Wang Y et al (2016) A novel label-free microfluidic paper-based immunosensor for highly sensitive electrochemical detection of carcinoembryonic antigen. *Biosens Bioelectron* 83:319–326
56. Kumar S et al (2015) Reduced graphene oxide modified smart conducting paper for cancer biosensor. *Biosens Bioelectron* 73:114–122
57. Scida K, Cunningham JC, Renault C, Richards I, Crooks RM (2014) Simple, sensitive, and quantitative electrochemical detection method for paper analytical devices. *Anal Chem* 86:6501–6507
58. Wang CC et al (2016) A paper-based “pop-up” electrochemical device for analysis of beta-hydroxybutyrate. *Anal Chem* 88:6326–6333
59. Jagadeesan KK, Kumar S, Sumana G (2012) Application of conducting paper for selective detection of troponin. *Electrochem Commun* 20:71–74
60. Yang M et al (2016) Flexible and disposable sensing platforms based on newspaper. *ACS Appl Mater Interfaces* 8:34978–34984
61. Cunningham JC, Brenes NJ, Crooks RM (2014) Paper electrochemical device for detection of DNA and thrombin by target-induced conformational switching. *Anal Chem* 86:6166–6170
62. Mirasoli M, Guardigli M, Michelini E, Roda A (2014) Recent advancements in chemical luminescence-based lab-on-chip and microfluidic platforms for bioanalysis. *J Pharm Biomed Anal* 87:36–52
63. Liu W, Luo J, Guo Y, Kou J, Li B, Zhang Z (2014) Nanoparticle coated paper-based chemiluminescence device for the determination of L-cysteine. *Talanta* 120:336–341
64. Liu F, Zhang C (2015) A novel paper-based microfluidic enhanced chemiluminescence biosensor for facile, reliable and highly-sensitive gene detection of *Listeria monocytogenes*. *Sens Actuators B Chem* 209:399–406
65. Zhao M, Li H, Liu W, Guo Y, Chu W (2016) Plasma treatment of paper for protein immobilization on paper-based chemiluminescence immunodevice. *Biosens Bioelectron* 79:581–588
66. Liu W, Cassano CL, Xu X, Fan ZH (2013) Laminated paper-based analytical devices (LPAD) with origami-enabled chemiluminescence immunoassay for cotinine detection in mouse serum. *Anal Chem* 85:10270–10276
67. Chen Y, Wang J, Liu Z, Wang X, Li X, Shan G (2018) A simple and versatile paper-based electrochemiluminescence biosensing platform for hepatitis B virus surface antigen detection. *Biochem Eng J* 129:1–6
68. Ge L, Yan J, Song X, Yan M, Ge S, Yu J (2012) Three-dimensional paper-based electrochemiluminescence immunodevice for multiplexed measurement of biomarkers and point-of-care testing. *Biomaterials* 33:1024–1031
69. Ge S, Liang L, Lan F, Zhang Y, Wang Y, Yan M, Yu J (2016) Photoelectrochemical immunoassay based on chemiluminescence as internal excited light source. *Sens Actuators B Chem* 234:324–331
70. Shi L, Li L, Li X, Zhang G, Zhang Y, Dong C, Shuang S (2017) Excitation-independent yellow-fluorescent nitrogen-doped carbon nanodots for biological imaging and paper-based sensing. *Sens Actuators B Chem* 251:234–241
71. Cai Y, You J, You Z, Dong F, Du S, Zhang L (2018) Profuse color-evolution-based fluorescent test paper sensor for rapid and visual monitoring of endogenous Cu^{2+} in human urine. *Biosens Bioelectron* 99:332–337

72. Samanta S, Halder S, Dey P, Manna U, Ramesh A, Das G (2018) A ratiometric fluorogenic probe for the real-time detection of SO_3^{2-} in aqueous medium: Application in a cellulose paper based device and potential to sense SO_3^{2-} in mitochondria. *Analyst* 143:250–257
73. Thom NK, Lewis GG, Yeung K, Phillips ST (2014) Quantitative fluorescence assays using a self-powered paper-based microfluidic device and a camera-equipped cellular phone. *RSC Adv* 4:1334–1340
74. Mei Q, Zhang Z (2012) Photoluminescent graphene oxide ink to print sensors onto microporous membranes for versatile visualization bioassays. *Angew Chem Int Ed* 51:5602–5606
75. Derikvand F, Yin DT, Barrett R, Brumer H (2016) Cellulose-based biosensors for esterase detection. *Anal Chem* 88:2989–2993
76. Li B, Zhou X, Liu H, Deng H, Huang R, Xing D (2018a) Simultaneous detection of antibiotic resistance genes on paper-based chip using $[\text{Ru}(\text{phen})_2\text{dppz}]^{2+}$ turn-on fluorescence probe. *ACS Appl Mater Interfaces*. <https://doi.org/10.1021/acsami.7b17653>
77. Rosa AM, Louro AF, Martins SA, Inacio J, Azevedo AM, Prazeres DM (2014) Capture and detection of DNA hybrids on paper via the anchoring of antibodies with fusions of carbohydrate binding modules and ZZ-domains. *Anal Chem* 86:4340–4347
78. Wang Y, Wang S, Ge S, Wang S, Yan M, Zang D, Yu J (2013) Facile and sensitive paper-based chemiluminescence DNA biosensor using carbon dots dotted nanoporous gold signal amplification label. *Anal Methods* 5:1328–1336
79. Zhou F, Noor MO, Krull UJ (2014) Luminescence resonance energy transfer-based nucleic acid hybridization assay on cellulose paper with upconverting phosphor as donors. *Anal Chem* 86:2719–2726
80. Oliveira MJ et al (2017) Office paper decorated with silver nanostars—an alternative cost effective platform for trace analyte detection by SERS. *Sci Rep* 7:2480–2493
81. Hu SW, Qiao S, Pan JB, Kang B, Xu JJ, Chen HY (2018) A paper-based SERS test strip for quantitative detection of Mucin-1 in whole blood. *Talanta* 179:9–14
82. Abbas A, Brimer A, Slocik JM, Tian L, Naik RR, Singamaneni S (2013) Multifunctional analytical platform on a paper strip: separation, preconcentration, and subattomolar detection. *Anal Chem* 85:3977–3983
83. Banaei N, Foley A, Houghton JM, Sun Y, Kim B (2017) Multiplex detection of pancreatic cancer biomarkers using a SERS-based immunoassay. *Nanotechnology* 28:455101–455111
84. Kim W-S, Shin J-H, Park H-K, Choi S (2016) A low-cost, monometallic, surface-enhanced Raman scattering-functionalized paper platform for spot-on bioassays. *Sens Actuators B Chem* 222:1112–1118
85. Liu Q et al (2014) Paper-based plasmonic platform for sensitive, noninvasive, and rapid cancer screening. *Biosens Bioelectron* 54:128–134
86. Ngo YH, Li D, Simon GP, Garnier G (2012) Gold nanoparticle-paper as a three-dimensional surface enhanced Raman scattering substrate. *Langmuir* 28:8782–8790
87. Tadepalli S et al (2015) Peptide functionalized gold nanorods for the sensitive detection of a cardiac biomarker using plasmonic paper devices. *Sci Rep* 5:16206–16216
88. Noor MO, Krull UJ (2014) Camera-based ratiometric fluorescence transduction of nucleic acid hybridization with reagentless signal amplification on a paper-based platform using immobilized quantum dots as donors. *Anal Chem* 86:10331–10339
89. Liu X, Yang Y, Li Q, Wang Z, Xing X, Wang Y (2018c) Portably colorimetric paper sensor based on ZnS quantum dots for semi-quantitative detection of Co^{2+} through the measurement of grey level. *Sens Actuators B Chem*. <https://doi.org/10.1016/j.snb.2018.01.121>
90. Dhavamani J, Mujawar LH, El-Shahawi MS (2018) Hand drawn paper-based optical assay plate for rapid and trace level determination of Ag^+ in water. *Sens Actuators B Chem* 258:321–330
91. Yakoh A, Rattanarat P, Siangproh W, Chailapakul O (2018) Simple and selective paper-based colorimetric sensor for determination of chloride ion in environmental samples using label-free silver nanoprisms. *Talanta* 178:134–140

92. Chaiyo S, Siangproh W, Apilux A, Chailapakul O (2015) Highly selective and sensitive paper-based colorimetric sensor using thiosulfate catalytic etching of silver nanoplates for trace determination of copper ions. *Anal Chim Acta* 866:75–83
93. Hossain SM, Brennan JD (2011) *b*-Galactosidase-based colorimetric paper sensor for determination of heavy metals. *Anal Chem* 83:8772–8778
94. Giokas DL, Tsogas GZ, Vlessidis AG (2014) Programming fluid transport in paper-based microfluidic devices using razor-crafted open channels. *Anal Chem* 86:6202–6207
95. Kappi FA, Tsogas GZ, Christodouleas DC, Giokas DL (2017) Calibrant-loaded paper-based analytical devices for standard addition quantitative assays. *Sens Actuators B Chem* 253:860–867
96. Cuartero M, Crespo GA, Bakker E (2015) Paper-based thin-layer coulometric sensor for halide determination. *Anal Chem* 87:1981–1990
97. Ruecha N, Chailapakul O, Suzuki K, Citterio D (2017) Fully inkjet-printed paper-based potentiometric ion-sensing devices. *Anal Chem* 89:10608–10616
98. Yoon JH et al (2017) Fabrication of newspaper-based potentiometric platforms for flexible and disposable ion sensors. *J Colloid Interface Sci* 508:167–173
99. Zor E, Alpaydin S, Arici A, Saglam ME, Bingol H (2018) Photoluminescent nanopaper-based microcuvette for iodide detection in seawater. *Sens Actuators B Chem* 254:1216–1224
100. Chen PC, Li YC, Ma JY, Huang JY, Chen CF, Chang HT (2016) Size-tunable copper nanocluster aggregates and their application in hydrogen sulfide sensing on paper-based devices. *Sci Rep* 6:24882–24890
101. Zhang M, Ge L, Ge S, Yan M, Yu J, Huang J, Liu S (2013) Three-dimensional paper-based electrochemiluminescence device for simultaneous detection of Pb^{2+} and Hg^{2+} based on potential-control technique. *Biosens Bioelectron* 41:544–550
102. Prabhath J, Vilaivan T, Praneenararat T (2018) Fabrication of a paper-based turn-off fluorescence sensor for Cu^{2+} ion from a pyridinium porphyrin. *ChemistrySelect* 3:894–899
103. Sun T, Niu Q, Li Y, Li T, Hu T, Wang E, Liu H (2018) A novel oligothiophene-based colorimetric and fluorescent “turn on” sensor for highly selective and sensitive detection of cyanide in aqueous media and its practical applications in water and food samples. *Sens Actuators B Chem* 258:64–71
104. Li B, Zhang Z, Qi J, Zhou N, Qin S, Choo J, Chen L (2017) Quantum dot-based molecularly imprinted polymers on three-dimensional origami paper microfluidic chip for fluorescence detection of phycoerythrin. *ACS Sens* 2:243–250
105. Zhao H, Zang L, Wang L, Qin F, Zhang Z, Cao W (2015) Luminescence ratiometric oxygen sensor based on gadolinium labeled porphyrin and filter paper. *Sens Actuators B Chem* 215:405–411
106. Kim Y, Jang G, Lee TS (2015) New fluorescent metal-ion detection using a paper-based sensor strip containing tethered rhodamine carbon nanodots. *ACS Appl Mater Interfaces* 7:15649–15657
107. Lee M, Oh K, Choi HK, Lee SG, Youn HJ, Lee HL, Jeong DH (2018) Subnanomolar sensitivity of filter paper-based SERS sensor for pesticide detection by hydrophobicity change of paper surface. *ACS Sens* 3:151–159
108. Lee J-C, Kim W, Choi S (2017) Fabrication of a SERS-encoded microfluidic paper-based analytical chip for the point-of-assay of wastewater. *Int J Precis Eng Manuf-Green Tech* 4:221–226
109. Bharadwaj S, Pandey A, Yagci B, Ozguz V, Qureshi A (2018) Graphene nano-mesh-Ag-ZnO hybrid paper for sensitive SERS sensing and self-cleaning of organic pollutants. *Chem Eng J* 336:445–455
110. Jokerst JC, Adkins JA, Bisha B, Mentele MM, Goodridge LD, Henry CS (2012) Development of a paper-based analytical device for colorimetric detection of select foodborne pathogens. *Anal Chem* 84:2900–2907

111. Alhogail S, Suaifan G, Zourob M (2016) Rapid colorimetric sensing platform for the detection of *Listeria monocytogenes* foodborne pathogen. *Biosens Bioelectron* 86:1061–1066
112. Hakovirta M, Aksoy B, Hakovirta J (2015) Self-assembled micro-structured sensors for food safety in paper based food packaging. *Mater Sci Eng, C* 53:331–335
113. Swerin A, Mira I (2014) Ink-jettable paper-based sensor for charged macromolecules and surfactants. *Sens Actuators B Chem* 195:389–395
114. Kong Q, Wang Y, Zhang L, Ge S, Yu J (2017) A novel microfluidic paper-based colorimetric sensor based on molecularly imprinted polymer membranes for highly selective and sensitive detection of bisphenol A. *Sens Actuators B Chem* 243:130–136
115. Liu C-C, Wang Y-N, Fu L-M, Chen K-L (2018) Microfluidic paper-based chip platform for benzoic acid detection in food. *Food Chem* 249:162–167
116. Ma L, Nilghaz A, Choi JR, Liu X, Lu X (2018) Rapid detection of clenbuterol in milk using microfluidic paper-based ELISA. *Food Chem* 246:437–441
117. Gao N, Huang P, Wu F (2018) Colorimetric detection of melamine in milk based on Triton X-100 modified gold nanoparticles and its paper-based application. *Spectrochim Acta A Mol Biomol Spectrosc* 192:174–180
118. Ha N-R, Jung I-P, Kim S-H, Kim AR, Yoon M-Y (2017) Paper chip-based colorimetric sensing assay for ultra-sensitive detection of residual kanamycin. *Process Biochem* 62:161–168
119. Xiao L, Zhang Z, Wu C, Han L, Zhang H (2017) Molecularly imprinted polymer grafted paper-based method for the detection of 17 β -Estradiol. *Food Chem* 221:82–86
120. Nouanthavong S, Nacapricha D, Henry CS, Sameenoi Y (2016) Pesticide analysis using nanoceria-coated paper-based devices as a detection platform. *Analyst* 141(5):1837–1846
121. Liu C-C, Wang Y-N, Fu L-M, Yang D-Y (2017) Rapid integrated microfluidic paper-based system for sulfur dioxide detection. *Chem Eng J* 316:790–796
122. Busa LS, Mohammadi S, Maeki M, Ishida A, Tani H, Tokeshi M (2016) A competitive immunoassay system for microfluidic paper-based analytical detection of small size molecules. *Analyst* 141:6598–6603
123. Lopez Marzo AM, Pons J, Blake DA, Merkoci A (2013) All-integrated and highly sensitive paper based device with sample treatment platform for Cd²⁺ immunodetection in drinking/tap waters. *Anal Chem* 85:3532–3538
124. Nath P, Arun RK, Chanda N (2014) A paper based microfluidic device for the detection of arsenic using a gold nanosensor. *RSC Adv* 4:59558–59561
125. Cinti S, Basso M, Moscone D, Arduini F (2017) A paper-based nanomodified electrochemical biosensor for ethanol detection in beers. *Anal Chim Acta* 960:123–130
126. Chaiyo S, Apiluk A, Siangproh W, Chailapakul O (2016) High sensitivity and specificity simultaneous determination of lead, cadmium and copper using μ PAD with dual electrochemical and colorimetric detection. *Sens Actuators B Chem* 233:540–549
127. Bi X-M, Wang H-R, Ge L-Q, Zhou D-M, Xu J-Z, Gu H-Y, Bao N (2018) Gold-coated nanostructured carbon tape for rapid electrochemical detection of cadmium in rice with in situ electrodeposition of bismuth in paper-based analytical devices. *Sens Actuators B Chem*. <https://doi.org/10.1016/j.snb.2018.01.007>
128. Koskela J et al (2015) Monitoring the quality of raw poultry by detecting hydrogen sulfide with printed sensors. *Sens Actuators B Chem* 218:89–96
129. Mraovic M, Muck T, Pivar M, Trontelj J, Pletersek A (2014) Humidity sensors printed on recycled paper and cardboard. *Sensors* 14:13628–13643
130. Morales-Narváez E, Naghdi T, Zor E, Merkoçi A (2015) Photoluminescent lateral-flow immunoassay revealed by graphene oxide: highly sensitive paper-based pathogen detection. *Anal Chem* 87:8573–8577
131. Guzman JMCC, Tayo LL, Liu C-C, Wang Y-N, Fu L-M (2018) Rapid microfluidic paper-based platform for low concentration formaldehyde detection. *Sens Actuators B Chem* 255:3623–3629

132. Liu C-C, Wang Y-N, Fu L-M, Huang Y-H (2018) Microfluidic paper-based chip platform for formaldehyde concentration detection. *Chem Eng J* 332:695–701
133. Zhang Y, Zuo P, Ye BC (2015) A low-cost and simple paper-based microfluidic device for simultaneous multiplex determination of different types of chemical contaminants in food. *Biosens Bioelectron* 68:14–19
134. Jin SQ, Guo SM, Zuo P, Ye BC (2015) A cost-effective Z-folding controlled liquid handling microfluidic paper analysis device for pathogen detection via ATP quantification. *Biosens Bioelectron* 63:379–383
135. Mirasoli M, Buragina A, Dolci LS, Simoni P, Anfossi L, Giraudi G, Roda A (2012) Chemiluminescence-based biosensor for fumonisins quantitative detection in maize samples. *Biosens Bioelectron* 32:283–287
136. Liu W, Guo Y, Luo J, Kou J, Zheng H, Li B, Zhang Z (2015) A molecularly imprinted polymer based a lab-on-paper chemiluminescence device for the detection of dichlorvos. *Spectrochim Acta A Mol Biomol Spectrosc* 141:51–57
137. Liu W, Kou J, Xing H, Li B (2014) Paper-based chromatographic chemiluminescence chip for the detection of dichlorvos in vegetables. *Biosens Bioelectron* 52:76–81
138. Li D, Ma Y, Duan H, Deng W, Li D (2018) Griess reaction-based paper strip for colorimetric/fluorescent/SERS triple sensing of nitrite. *Biosens Bioelectron* 99:389–398
139. Zhu Y, Li M, Yu D, Yang L (2014) A novel paper rag as ‘D-SERS’ substrate for detection of pesticide residues at various peels. *Talanta* 128:117–124
140. Tseng SY, Li SY, Yi SY, Sun AY, Gao DY, Wan D (2017) Food quality monitor: Paper-based plasmonic sensors prepared through reversal nanoimprinting for rapid detection of biogenic amine odorants. *ACS Appl Mater Interfaces* 9:17307–17317
141. Gonzalez CM, Iqbal M, Dasog M, Piercey DG, Lockwood R, Klapotke TM, Veinot JG (2014) Detection of high-energy compounds using photoluminescent silicon nanocrystal paper based sensors. *Nanoscale* 6:2608–2612
142. Sablok K, Bhalla V, Sharma P, Kaushal R, Chaudhary S, Suri CR (2013) Amine functionalized graphene oxide/CNT nanocomposite for ultrasensitive electrochemical detection of trinitrotoluene. *J Hazard Mater* 248–249:322–328
143. Peters KL, Corbin I, Kaufman LM, Zreibe K, Blanes L, McCord BR (2015) Simultaneous colorimetric detection of improvised explosive compounds using microfluidic paper-based analytical devices (μ PADs). *Anal Methods* 7:63–70
144. Aparna RS, Anjali Devi JS, Sachidanandan P, George S (2018) Polyethylene imine capped copper nanoclusters-fluorescent and colorimetric onsite sensor for the trace level detection of TNT. *Sens Actuators B Chem* 254:811–819
145. Nergiz SZ, Gandra N, Farrell ME, Tian L, Pellegrino PM, Singamaneni S (2013) Biomimetic SERS substrate: peptide recognition elements for highly selective chemical detection in chemically complex media. *J Mater Chem A* 1:6543–6549
146. Hughes S, Dasary SS, Begum S, Williams N, Yu H (2015) Meisenheimer complex between 2,4,6-trinitrotoluene and 3-aminopropyltriethoxysilane and its use for a paper-based sensor. *Sens Biosensing Res* 5:37–41
147. Pesenti A, Taudte RV, McCord B, Doble P, Roux C, Blanes L (2014) Coupling paper-based microfluidics and lab on a chip technologies for confirmatory analysis of trinitro aromatic explosives. *Anal Chem* 86:4707–4714
148. Huang S, He Q, Xu S, Wang L (2015) Polyaniline-based photothermal paper sensor for sensitive and selective detection of 2,4,6-trinitrotoluene. *Anal Chem* 87:5451–5456
149. da Silva GO, de Araujo WR, Paixao T (2018) Portable and low-cost colorimetric office paper-based device for phenacetin detection in seized cocaine samples. *Talanta* 176:674–678
150. Narang J, Malhotra N, Singhal C, Mathur A, Pn AK, Pundir CS (2017) Detection of alprazolam with a lab on paper economical device integrated with urchin like Ag@ Pd shell nano-hybrids. *Mater Sci Eng, C* 80:728–735
151. Hu J, Wang S, Wang L, Li F, Pingguan-Murphy B, Lu TJ, Xu F (2014) Advances in paper-based point-of-care diagnostics. *Biosens Bioelectron* 54:585–597

152. Zhu W-J, Feng D-Q, Chen M, Chen Z-D, Zhu R, Fang H-L, Wang W (2014) Bienzyme colorimetric detection of glucose with self-calibration based on tree-shaped paper strip. *Sens Actuators B Chem* 190:414–418
153. Malekghasemi S, Kahveci E, Duman M (2016) Rapid and alternative fabrication method for microfluidic paper based analytical devices. *Talanta* 159:401–411
154. Kannan B, Jahanshahi-Anbuhı S, Pelton RH, Li Y, Filipe CD, Brennan JD (2015) Printed paper sensors for serum lactate dehydrogenase using pullulan-based inks to immobilize reagents. *Anal Chem* 87:9288–9293
155. Pardee K et al (2016) Rapid, low-cost detection of Zika virus using programmable biomolecular components. *Cell* 165:1255–1266
156. Sharpe E, Frasco T, Andreescu D, Andreescu S (2013) Portable ceria nanoparticle-based assay for rapid detection of food antioxidants (NanoCerac). *Analyst* 138:249–262
157. Guan L, Tian J, Cao R, Li M, Cai Z, Shen W (2014) Barcode-like paper sensor for smartphone diagnostics: an application of blood typing. *Anal Chem* 86:11362–11367
158. Khatri V, Halasz K, Trandafilovic LV, Dimitrijevic-Brankovic S, Mohanty P, Djokovic V, Csoka L (2014) ZnO-modified cellulose fiber sheets for antibody immobilization. *Carbohydr Polym* 109:139–147
159. Noiphung J, Songjaroen T, Dungchai W, Henry CS, Chailapakul O, Laiwattanapaisal W (2013) Electrochemical detection of glucose from whole blood using paper-based microfluidic devices. *Anal Chim Acta* 788:39–45
160. Wang P, Cheng Z, Chen Q, Qu L, Miao X, Feng Q (2018) Construction of a paper-based electrochemical biosensing platform for rapid and accurate detection of adenosine triphosphate (ATP). *Sens Actuators B Chem* 256:931–937
161. Li X, Liu X (2016) A microfluidic paper-based origami nanobiosensor for label-free, ultrasensitive immunoassays. *Adv Healthc Mater* 5:1326–1335
162. Scordo G, Moscone D, Palleschi G, Arduini F (2018) A reagent-free paper-based sensor embedded in a 3D printing device for cholinesterase activity measurement in serum. *Sens Actuators B Chem* 258:1015–1021
163. Lee SH, Lee JH, Tran V-K, Ko E, Park CH, Chung WS, Seong GH (2016) Determination of acetaminophen using functional paper-based electrochemical devices. *Sens Actuators B Chem* 232:514–522
164. Adkins JA, Noviana E, Henry CS (2016) Development of a quasi-steady flow electrochemical paper-based analytical device. *Anal Chem* 88:10639–10647
165. da Costa TH, Song E, Tortorich RP, Choi J-W (2015) A paper-based electrochemical sensor using inkjet-printed carbon nanotube electrodes. *ECS J Solid State Sci Technol* 4:S3044–S3047
166. Cinti S, Minotti C, Moscone D, Palleschi G, Arduini F (2017) Fully integrated ready-to-use paper-based electrochemical biosensor to detect nerve agents. *Biosens Bioelectron* 93:46–51
167. Nantaphol S, Channon RB, Kondo T, Siangproh W, Chailapakul O, Henry CS (2017) Boron doped diamond paste electrodes for microfluidic paper-based analytical devices. *Anal Chem* 89:4100–4107
168. Zhang H, Zhao Z, Lei Z, Wang Z (2016) Sensitive detection of polynucleotide kinase activity by paper-based fluorescence assay with I exonuclease-assistance. *Anal Chem* 88:11358–11363
169. Jiang P, He M, Shen L, Shi A, Liu Z (2017) A paper-supported aptasensor for total IgE based on luminescence resonance energy transfer from upconversion nanoparticles to carbon nanoparticles. *Sens Actuators B Chem* 239:319–324
170. Liang L et al (2016) Aptamer-based fluorescent and visual biosensor for multiplexed monitoring of cancer cells in microfluidic paper-based analytical devices. *Sens Actuators B Chem* 229:347–354
171. Saha B, Baik S, Lee J (2017) Highly sensitive bendable and foldable paper sensors based on reduced graphene oxide. *ACS Appl Mater Interfaces* 9:4658–4666
172. Gong MM, Nosrati R, San Gabriel MC, Zini A, Sinton D (2015) Direct DNA analysis with paper-based ion concentration polarization. *J Am Chem Soc* 137:13913–13919

173. Davaji B, Lee CH (2014) A paper-based calorimetric microfluidics platform for bio-chemical sensing. *Biosens Bioelectron* 59:120–126
174. Chen GH, Chen WY, Yen YC, Wang CW, Chang HT, Chen CF (2014) Detection of mercury (II) ions using colorimetric gold nanoparticles on paper-based analytical devices. *Anal Chem* 86:6843–6849
175. Sicard C et al (2015) Tools for water quality monitoring and mapping using paper-based sensors and cell phones. *Water Res* 70:360–369
176. Wang B, Lin Z, Wang M (2015) Fabrication of a paper-based microfluidic device to readily determine nitrite ion concentration by simple colorimetric assay. *J Chem Educ* 92:733–736
177. Rattanarat P, Dungchai W, Cate D, Volckens J, Chailapakul O, Henry CS (2014) Multilayer paper-based device for colorimetric and electrochemical quantification of metals. *Anal Chem* 86:3555–3562
178. Cho YB, Jeong SH, Chun H, Kim YS (2018) Selective colorimetric detection of dissolved ammonia in water via modified Berthelot's reaction on porous paper. *Sens Actuators B Chem* 256:167–175
179. Lamas-Ardisana PJ et al (2017) Disposable electrochemical paper-based devices fully fabricated by screen-printing technique. *Electrochem Commun* 75:25–28
180. Qin Y, Pan S, Howlader MM, Ghosh R, Hu NX, Deen MJ (2016) Paper-based, hand-drawn free chlorine sensor with poly(3,4-ethylenedioxythiophene):poly(styrenesulfonate). *Anal Chem* 88:10384–10389
181. Cinti S, Talarico D, Palleschi G, Moscone D, Arduini F (2016) Novel reagentless paper-based screen-printed electrochemical sensor to detect phosphate. *Anal Chim Acta* 919:78–84
182. Li H, Wang W, Lv Q, Xi G, Bai H, Zhang Q (2016) Disposable paper-based electrochemical sensor based on stacked gold nanoparticles supported carbon nanotubes for the determination of bisphenol A. *Electrochem Commun* 68:104–107
183. Chouler J, Cruz-Izquierdo A, Rengaraj S, Scott JL, Di Lorenzo M (2018) A screen-printed paper microbial fuel cell biosensor for detection of toxic compounds in water. *Biosens Bioelectron* 102:49–56
184. Zhang R, Zhang C-J, Song Z, Liang J, Kwok RTK, Tang BZ, Liu B (2016) AIEgens for real-time naked-eye sensing of hydrazine in solution and on a paper substrate: structure-dependent signal output and selectivity. *J Mater Chem C* 4:2834–2842
185. Fraiwan A, Lee H, Choi S (2016) A paper-based cantilever array sensor: monitoring volatile organic compounds with naked eye. *Talanta* 158:57–62
186. Bulbul G, Eskandarloo H, Abbaspourrad A (2018) A novel paper based colorimetric assay for the detection of TiO₂ nanoparticles. *Anal Methods* 10:275–280

Polymers and Polymer Composites for Adsorptive Removal of Dyes in Water Treatment



Weiya Huang, Shuhong Wang and Dan Li

List of Abbreviations

AB 25	Acid blue 25
AF	Acid fuchsin
AB	Amido black 10B
AS	Almond shell waste
APT	Attapulgite
BY 28	Basic yellow 28
BF	Basic fuchsin
BV 14	Basic violet 14
CFA	Coal fly ash
CNT	Carbon nanotube
CMC	Carboxymethyl cellulose
mCS/CNT	Magnetic chitosan-decorated carbon nanotube
CR	Congo red
CV	Crystal violet
Bent/CMC-g-P (DMAEMA)	Carboxymethyl cellulose grafted by poly(2-(dimethylamino)ethyl methacrylate) modified bentonite
DB	Direct blue 199
ES	Emeraldine salt
EB	Emeraldine base
EY	Eosin Y
GV	Gentian violet
HA-Am-PAA-B	Humic acid-immobilized amine modified polyacrylamide/bentonite composite
TRGO/PVA	Hydrothermally reduced graphene oxide/poly (vinyl alcohol)

W. Huang · S. Wang

School of Metallurgy and Chemical Engineering, Jiangxi University of Science and Technology, Ganzhou, China

D. Li (✉)

School of Engineering and Information Technology, Murdoch University, Murdoch, Australia

e-mail: L.Li@murdoch.edu.au

© Springer Nature Switzerland AG 2019

Inamuddin et al. (eds.), *Sustainable Polymer Composites and Nanocomposites*,
https://doi.org/10.1007/978-3-030-05399-4_19

hPEI-CE	Hyperbranched polyethyleneimine functionalized cellulose
IC	Indigo carmine
MNPs	Magnetic nanoparticles
MS	Mesoporous silica
MB	Methylene blue
MG	Methylene green
MO	Methyl orange
NR	Neutral red
OVS	Octavinylsilsesquioxane
OR	Oil red O
PAM	Polyacrylamide
PVI	Poly(1-vinyl imidazole)
PSSMA	Poly(4-styrenesulfonic acid-co-maleic acid) sodium
PSSMA/M-rGO	Poly(4-styrenesulfonic acid-co-maleic acid) sodium modified magnetic reduced graphene oxide nanocomposite
Mt	Montmorillonite
Pal	Palygorskite
poly(AN-co-ST)	Poly(acrylonitrile-co-styrene)
PAMAM	Polyamidoamine
PANI	Polyaniline
PANI -FP	Polyaniline-coated filter papers
PANI-MS@Fe ₃ O ₄	Polyaniline functionalized magnetic mesoporous silica composite
PEI	Polyethyleneimine
PmPD	Poly(m-phenylenediamine)
PGA	Poly(γ -glutamic acid)
PVA	Poly (vinyl alcohol)
PV	Proflavine
r-GO-PIL	PVI polymer functionalized reduced graphene oxide
RB5	Reactive black 5
RR228	Reactive red 228
RB	Rhodamine B
RB2	Rose Bengal
TC	Tetracycline
TPE	Tetraphenylethylene
PAmABAmPD	Terpolymer of aniline/m-aminobenzoic acid/m-phenylenediamine
TCAS	Thiacalix[4]arene tetrasulfonate
β -CD	β -cyclodextrin
20CMC-Bent	20% of CMC in the total amount of CMC + Bent composite
RR2	Reactive red 2
MDI	4,4'-diphenylmethane diisocyanate
TAT	1,3,5-triacryloylhexahydro-1,3,5-triazine

1 Introduction

Natural and synthetic dyes have been commonly used to colour substrates, including food, drugs, cosmetics, paper, leather, plastics and textile products. Synthetic dyes play the dominating role particularly in the fabric and textile industry as compared with natural dyes, which insufficiently meet the industrial demand and therefore are more often used in the food industry [1]. It is estimated that more than 10,000 types of dyes are being used in various industrial applications. According to the literature, more than 8×10^5 tons of synthetic dyes are produced annually worldwide, in which 10–15% is released into natural water environment [2, 3]. Synthetic dyes often exhibit resistance to biodegradation and their persistence in the environment results in pollution, which has become a severe problem worldwide [4]. In particular, many of the synthetic dyes are toxic, carcinogenic and mutagenic. Therefore, dyes in wastewater, even in a small amount, are undesirable and should be properly removed before they enter the environment [5].

According to the applications of dyes, they are classified into groups of acidic, basic, reactive, direct, dispersed, and sulphur dyes; whilst based on the chemical structure of dyes, they are classified as nitro, azo, indigoid, anthraquinone, tri-arylmethane and nitroso dyes [6]. The most common way is to classify them as anionic (e.g. acid, reactive, and direct dyes), cationic (basic dyes), and nonionic dyes (dispersed dyes), depending on the ionic charge of dye molecules [6]. Cationic dyes were reported with greater toxicity than anionic dyes, because of their easy interaction with negatively charged cell membrane surfaces and entry into cells [5]. The commonly used dyes with their molecular structure, molecular weight, classification and λ_{max} were summarized in Table 4.

In order to remove dyes from wastewater, several biological, chemical and physical methods have been developed, including coagulation, adsorption, membrane separation, precipitation, chemical oxidation, and aerobic or anaerobic treatment [6–8]. Among them, adsorption seems to be the favourite technique because of low cost and diversity of adsorbents, easy operation, environmental and economic sustainability [7, 8]. Various adsorbents have been investigated for dye removal, such as activated carbon, carbon nanotubes, graphene, clay minerals, metal oxides, polymers, non-conventional low-cost adsorbents (e.g. agricultural and industrial waste or by-products), etc. [1, 4, 6, 9–11]. Several parameters, including high adsorption capacity, fast adsorption rate, good selectivity, wide availability, low cost, easy regeneration and feasible reusability, are intensively concerned when designing and selecting a suitable adsorbent to target dye removal. In general, hydrophilic adsorbents are preferable for use, which attract the dye molecules via electrostatic interaction, van der Waals force, π - π interaction, and hydrogen bonding [12].

Recently, polymers and polymer composites have attracted tremendous attention as adsorbents for dye treatments [4, 12–14]. Polymers exhibit a number of excellent properties [13], such as high strength, good flexibility, chemical inertness,

hydrophilic surface chemistry, which are able to act as matrix materials to fabricate polymer composites with inorganics. Their properties can be tuned via functionalization with chemical groups, crosslinking or blending with organic materials which are capable to interact with dye pollutants. Therefore, polymers and polymer composites serve as promising adsorbent materials for high-performance dye removal from water.

The current development of polymers or polymer composites as adsorbents concentrates on the use of nanostructures, such as nanosized particles, which provided great external surface area and exhibited high adsorption to dyes. For example, the nano-sized poly(*m*-phenylenediamine) (PmPD) exhibited enhanced adsorption capacity, which was calculated by the Langmuir model (387.6 mg/g) towards Orange G (OG), as compared with that of micro-sized PmPD (163.9 mg/g) [15]. However, the nanoparticles might suffer from aggregation, affecting adsorption capacity and kinetics. To improve application potential, polymers and their composites were synthesized in the form of nanofibers, which can be successfully produced by an electrospinning method. These one-dimensional (1D) nanoscale adsorbents, due to their great surface-to-volume ratios, were widely studied for the enhanced properties [16–19]. In addition, porous structures are highly desirable, because they can facilitate the diffusion of dyes into the adsorbents, resulting in fast and efficient adsorption [20]. The porous structure is also favourable to increase the swelling rate of the polymers; however, their mechanic strength would be reduced with increasing porosity. This can be solved by fabricating composite with other inorganic materials, e.g. bentonite [20]. Polymeric adsorbents, in the forms of hydrogels or xerogels which are three-dimensionally crosslinked hydrophilic polymers, were synthesized, functionalized and used as super-adsorbents to remove dyes from aqueous solution, ascribed to their high physicochemical stability and good regeneration property [21–24].

2 Modified or Functionalized Polymers and Polymer Composites

The surface chemistry of adsorbents, such as surface acidity/basicity and points of zero charge, significantly affects the adsorption of dyes. For targeting the removal of anionic dyes, surface properties of adsorbents were modified to minimize negative charge and increase positive charge on surfaces. Since that adsorption takes place on the surfaces of polymer adsorbents, another important factor for consideration is the density of functional groups on surfaces [14, 25]. For example, Qiu et al. synthesized three polystyrene resins with significantly different surface functionality and studied their adsorption performance for an anionic dye Reactive Black 5 dye (RB5), as shown in Fig. 1a [14]. As compared with commercial polymer XAD-4 of a low-degree functionality, NG-8, which was synthesized in the laboratory, had primarily acidic functional groups; and its aminated product MN-8

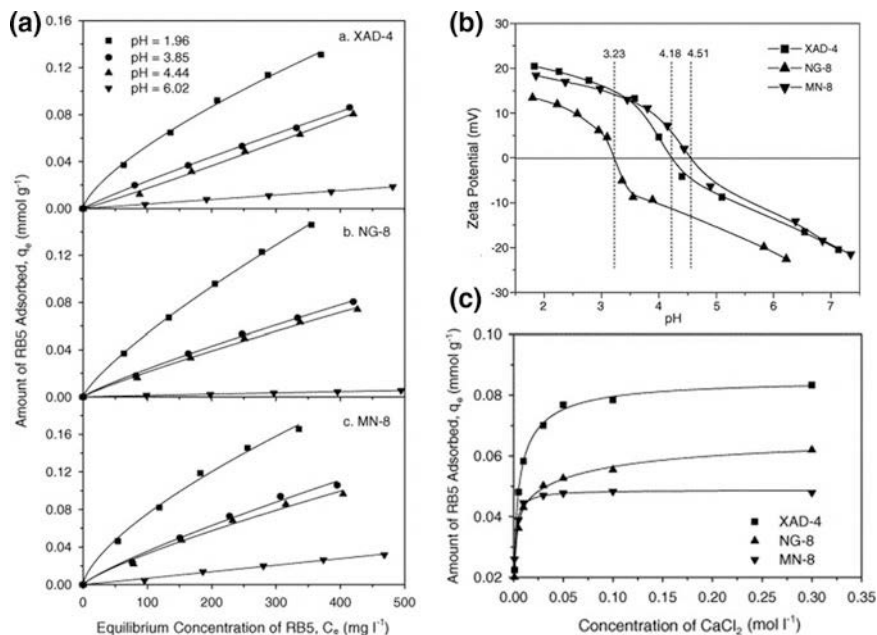


Fig. 1 **a** Adsorption of RB5 by three different polymers (XAD-4, NG-8, and MN-8) at pH = 1.96, 3.85, 4.44, and 6.02; **b** zeta potentials of XAD-4, NG-8, and MN-8 as a function of solution pH and determined points of zero charge; **c** effect of CaCl_2 concentration with initial RB5 concentration of 100 mg/L (reprinted from [14] with permission from Elsevier)

possessed mainly basic amino groups. It was found that XAD-4 exhibited non-polar nature; however moderate polarity was seen for NG-8 and MN-8. Their corresponding point of zero charge was 4.18, 3.23, and 4.51, respectively, as shown in Fig. 1b. The equilibrium adsorption capacity of RB5 for XAD-4, NG-8 and MN-8 was recorded as 115.05, 129.94 and 158.69 mg/g, accordingly, at pH = 1.90 and RB5 equilibrium concentration of 300 mg/L (Table 1). Moreover, the adsorption decreased at high solution pH for all adsorbents. MN-8 was the most effective adsorbent in RB5 removal at all tested pH values; which might probably lie in its increasing basicity caused by the protonation of amine groups and in turn creation of more positive charges on the surface. It was noted that the enhanced adsorption was observed in the presence of CaCl_2 , as shown in Fig. 1c, possibly ascribed to the neutralization of negative surface charge by Ca^{2+} and RB5-Ca^{2+} pairings [14].

Some biopolymers, such as chitosan, have a large number of functional groups in their molecules, such as hydroxyl ($-\text{OH}$) and primary amine ($-\text{NH}_2$), which can be utilized as functional groups for treatment of dyes due to the electrostatic interaction or hydrogen bonding force [26, 27]. Due to the presence of some groups, such as sulfate ($-\text{SO}_3\text{H}$) or carboxyl ($-\text{COOH}$), some biopolymers are negatively charged and have potential application for adsorption of cationic dyes [5, 28]. For example, κ -carrageenan is a highly negatively charged natural polysaccharide and was used

Table 1 Dye removal by modified or functionalized polymer composites

Adsorbent	Dye	Adsorption capacity (mg g ⁻¹)	pH	Temperature (°C)	Initial concentration (mg L ⁻¹)	References
EDTA-EDA-PAN nanofibers ^h	Methyl orange (MO)	99.15 ^a	4	25	5–300	[18]
	Reactive red (RR)	110.0 ^a	4	25	5–300	
Ti(IV) functionalized chitosan molecularly imprinted polymer (Ti-CSMIP)	Active brilliant red X-3B	161.1 ^a	6.0–7.0	20	/	[27]
	Basic violet 14 (BV 14)	67.11 ^a	6.2	25	1–100	[17]
Carboxylated functionalized acrylonitrile-styrene co-polymer nanofibers	Rhodamine B (RB)	1666 ^a	/	/	/	[34]
	Congo red (CR)	1040 ^a				
Silsesquioxane-based tetraphenylethene-linked nanoporous polymers	Crystal violet (CV)	862 ^a				
	Methylene blue (MB)	144 ^a				
	Methyl orange (MO)	67 ^a				
	Methylene blue (MB)	4.537 ^b	/	room temperature	11	[66]
	Reactive black 5 (RB5)	115.05 ^b /153.73 ^b	1.90/6.05 ^f	30 ± 0.5	300	[14]
XAD-4 ^c		129.94 ^b	1.90	30 ± 0.5	300	
		158.69 ^b	1.90	30 ± 0.5	300	
NG-8 ^d		858.28 ^b	5.0	40	/	[31]
MN-8 ^e						
Crosslinked chitosan with TAT ^g	Acid orange 7					(continued)

Table 1 (continued)

Adsorbent	Dye	Adsorption capacity (mg g ⁻¹)	pH	Temperature (°C)	Initial concentration (mg L ⁻¹)	References
Hydrothermally reduced graphene oxide/poly (vinyl alcohol) (TRGO/PVA) aerogels	Acid red 88	640.61 ^b	6.0	40	/	
	Neutral red (NR)	306.2 ^a	7	30	/	[12]
	Indigo carmine (IC)	250.0 ^a	2	30	/	
Functional poly(m-phenylenediamine) nanoparticles	Orange G (OG)	387.6 ^a	/	30	/	[15]
	Basic fuchsin (BF)	295 ^b	6.5 ± 0.1	25	20–350	[32]
	Methylene blue (MB)	528 ^b	6.5 ± 0.1	25	20–350	
Poly(1-vinylimidazole) (PVI) -modified graphene sheets	Methyl blue	1910 ^a	/	room temperature	100–700	[36]
Cellulose functionalized with hyperbranched Polyethylenimine	Congo red (CR)	2107 ^a /2100 ^b	5.0	25	100–1000	[25]
	Basic yellow 28 (BY28)	1865 ^a /1860 ^b	9.0	25	100–1000	

^aMaximum adsorption capacities calculated by Langmuir model

^bEquilibrium adsorption capacity

^cA representative St-DVB resin developed by Rohm & Haas, displays an excellent adsorptive affinity for small organic compounds (e.g., phenols), was purchased from Rohm & Haas (Philadelphia, PA)

^dWas synthesized using the Friedel-Crafts reaction through self-crosslinking of a chloromethylated copolymer of St-DVB

^eWas obtained by aminating swollen NG-8 using 40% dimethylamine solution at 45 °C for 10 h

^fpH = 6.05 solution with 0.01 mol l⁻¹ CaCl₂

^gChitosan crosslinked with 1,3,5-triaicyloylhexahydro-1,3,5-triazine (TAT)

^hEthylenediaminetetraacetic acid (EDTA) and ethylenediamine (EDA) crosslinker modified electrospon polyacrylonitrile (PAN) nanofibers

to modify carbon nanotubes to improve the adsorption performance for cationic dye methylene blue (MB) [5]. The magnetite nanoparticles decorated with poly (γ -glutamic acid) (PGA), which is an anionic polypeptide with α -carboxyl groups and synthesized by *Bacillus* species in a fermentation process, had the Langmuir maximum adsorption capacity of 78.67 mg/g for MB [28].

To enhance their adsorption performance for dye removal, it is an effective way by introducing new functional groups or increasing the density of surface functionality. For example, Wang et al. chemically modified biopolymer chitosan via carboxymethylation, which introduced different amounts of active $-\text{OH}$, $-\text{COOH}$, and $-\text{NH}_2$ groups onto the chitosan by controlling the degree of substitution. The resulting N, O-carboxymethyl chitosan showed enhanced adsorption capacity to remove cationic dye MB, with the Langmuir maximum adsorption capacity of 351 mg/g [29]. It is also a good method to fabricate bifunctional materials, which show applications in not only dye decolorization, but also other areas, such as heavy metal ion removal and bacterial capturing [30, 31]. Functional groups, such as amine, can be protonated to be positively charged and adsorb negatively charged dye molecules via electrostatic attraction. For example, the cellulose functionalized with quaternary ammonium groups had an enhanced adsorption of 190 mg/g at pH = 3 for reactive red 228 (RR228), due to the electrostatic attraction (cellulose-R-N⁺ (C₂H₅)₃...SO₃⁻) between the positive quaternary ammonium group and SO₃H group from negatively charged dye molecules RR228 [3]. Other functional groups, e.g. carboxylic, can improve the polarity of adsorbent to enhance its sorption affinity to cationic dyes [17, 32]. For example, the carboxylated poly (acrylonitrile-co-styrene) nanofiber showed the Langmuir-derived maximum dye adsorption capacity, 67.11 mg/g, when removing basic violet 14 dye (BV 14) (as shown in Table 1). Its adsorption equilibrium was achieved within 30 min and the dye adsorption followed the pseudo-second-order model, suggesting chemisorption [17]. In addition to carboxyl functional groups, the internal hydrophobic cavity in the functional molecule β -cyclodextrin (β -CD), which is a torus-shaped cyclic oligosaccharide made up of seven α -1,4-linked-D-glucopyranose units, formed inclusion complexes with dye organic molecules through host-guest interactions. As a result, the β -CD functionalized poly (styrene-alt-maleic anhydride) adsorbent showed a high equilibrium adsorption quantity of 272.56 and 366.35 mg/g for basic fuchsin (BF) and MB (at pH = 6.5, and initial BF and MB concentration of 95.7 and 93.6 mg/L) (Table 1), respectively; which was one magnitude greater than that of the unfunctionalized adsorbent [32]. In addition, the adsorption capacities increased with increasing initial dyes concentrations from 20 to 350 mg/L, and their Langmuir maximum adsorption capacity for BF and MB reached 298.5 and 531.9 mg/g, respectively [32].

The fabrication of polymers consisting of different organic segments can improve their physical and chemical properties [4, 22]. It would endow new properties to the resulting polymeric materials for dye decolorization applications [17, 33]. Chitosan is a copolymer of D-glucosamine and N-acetyl-D-glucosamine units with a large number of $-\text{OH}$ and $-\text{NH}_2$ groups; it is prepared by the N-deacetylation of chitin in an aqueous alkaline solution [4]. These functional

groups on chitosan chains work as sites for electrostatic interaction and coordination in dye adsorptive removal. However, the disadvantage of ready dissolution in an acidic medium makes the phase separation very difficult, thus limiting its application for dye removal. Chemical modification by crosslinking, grafting and/or other methods can improve its stability in acidic solution and enhance its mechanical strength [4]. After introducing a hexahydrotriazine ring into the crosslinked structure of chitosan with 1,3,5-triacryloylhexahydro-1,3,5-triazine (TAT), the crosslinked chitosan showed the promising adsorption of 858.28 mg/g towards CI Acid Orange 7 at pH 5.0, while that of 640.61 mg/g to Acid Red 88 at pH 6.0, as shown in Table 1 [31]. Besides, the flexibility of the structure of the modified polymer materials might have some certain effect on the adsorption process [31]. Poly(acrylonitrile-co-styrene) (poly(AN-co-ST)), as an important random copolymer of acrylonitrile and styrene, exhibits high resistance to heat, chemicals and oil, accompanied with other features, e.g. high rigidity and superior transparency [17]. The carboxylated functionalized poly(AN-co-ST) nanofibers exhibited a good adsorption capacity to BV 14, with the maximum capacity of 67.11 mg/g, as shown in Table 1. Liu et al. fabricated a series of hybrid polymers after the Friedel–Crafts reaction of tetraphenylethylene (TPE) and octavinylsilsesquioxane (OVS) (Fig. 2a, b) [34]. In addition to the high luminescence properties ascribed to TPE, the resulting silsesquioxane based TPE-bridged polymers had found adsorption use in gas, dye and metal ion detection. Particularly, the adsorption capacity of hybrid polymer for cationic dye rhodamine B (RB), anionic dye congo red (CR) and crystal violet (CV) was 1666, 1042 and 862 mg/g, respectively, as shown in Table 1. The adsorption process was mainly governed by size-selective mechanism ascribed to the unique bimodal pore structure in the hybrid polymers with micropores centring at ~ 1.4 nm and mesopores centring at ~ 4.5 nm, as well as the high surface area of up to 1910 cm^2/g [34]. Zhu et al. modified cellulose with cationic hyperbranched polyethyleneimine (hPEI) via forming Schiff base structure between the amino groups of hPEI and the aldehyde groups on the chemically oxidized cellulose surface (Fig. 2c, d). Because of a large number of amino groups, the resulting functionalized hPEI-CE copolymers displayed the high Langmuir-derived adsorption capacity of 2107 mg/g to anionic dye CR at pH 5.0 and that of 1865 mg/g to cationic basic yellow 28 (BY28) at pH 9.0, since the pH_{pzc} of the copolymer was recorded at pH 8.6 [25].

Recently, the combination of organic and inorganic materials has become an important strategy to modify properties of adsorbents. The resulting adsorbents may not only take advantage of the characteristic of each material, but also improve adsorption performance [27, 35]. Several inorganic compounds or materials, such as mesoporous silica or carbon, carbon nanotubes, graphene, clay, fly ash, metal oxides, and inorganic salts, etc, have been widely used to fabricate inorganic-organic materials as adsorbents. Among them, graphene has drawn significant research interest [12, 36], which can form covalent bonds with a polymer, e.g. as shown in Fig. 3a, by utilizing a diazonium addition reaction and the subsequent grafting of poly(1-vinyl imidazole) (PVI) onto the graphene via a quaternarization reaction. The resulting PVI polymer functionalized reduced graphene

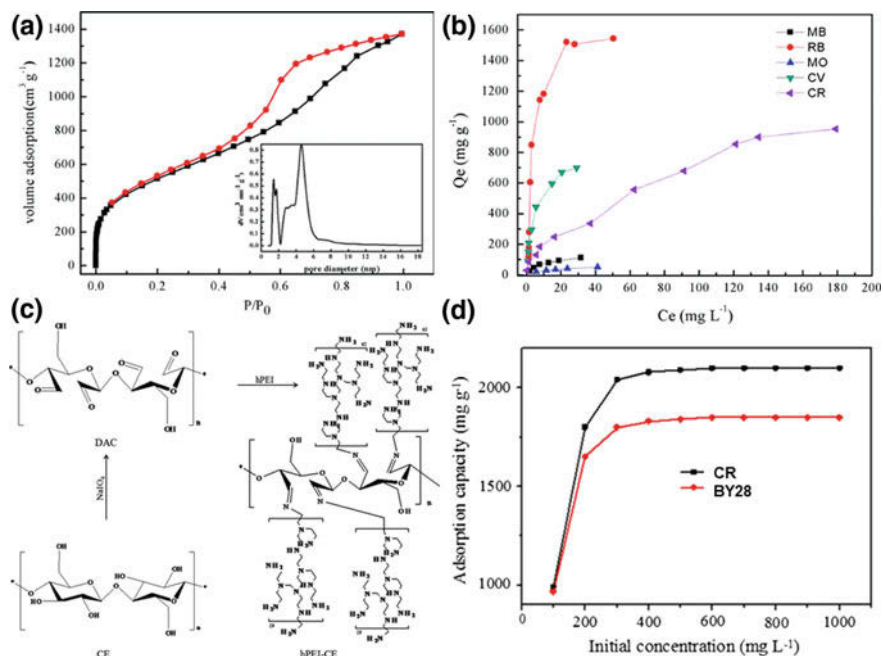


Fig. 2 **a** N_2 adsorption-desorption isotherm (inset: pore-size distribution) and **b** equilibrium adsorption capacity of silsesquioxane based TPE-bridged polymers (reproduced from [34] with permission of The Royal Society of Chemistry); **c** synthesis of cationic hyperbranched polyethyleneimine (hPEI) functionalized cellulose (hPEI-CE) and **d** initial concentration on the adsorption capacity of hPEI-CE for CR and BY28 (reproduced from [25])

oxide (r-GO-PIL) displayed enhanced adsorption efficiency towards anionic dyes methyl blue as compared to the unmodified graphene (r-GO), as shown in Fig. 3b. The adsorption equilibrium was almost reached after 1120 min, as shown in Fig. 3c. The adsorption process fitted well with the Langmuir isotherm model and the maximum adsorption capacity was 1910 mg/g; such highly effective adsorption was explained by the van der Waals forces and electrostatic interactions between r-GO-PIL and dye [36]. Xiao and co-workers fabricated hydrothermally reduced graphene oxide/poly(vinyl alcohol) (TRGO/PVA) in the form of aerogels via an in situ hydrothermal reduction followed by direct sol-aerogel transformation strategy (Fig. 4a–d). The resulting materials showed an attractive adsorption of various cationic, anionic and nonionic dyes. Their Langmuir-derived maximum adsorption capacity for cationic neutral red (NR) and anionic indigo carmine (IC) dye was 306.2 and 250.0 mg/g (Table 1), respectively (Fig. 4e). Noticeably, other common cationic, anionic or nonionic dyes were also able to be removed by the TRGO/PVA aerogel (Fig. 4f). This attractive adsorption capacity was mostly due to the $\pi - \pi$ interactions between aromatic or heterocyclic structures of dyes and graphene sheets; whilst the additional electrostatic attraction contributes to

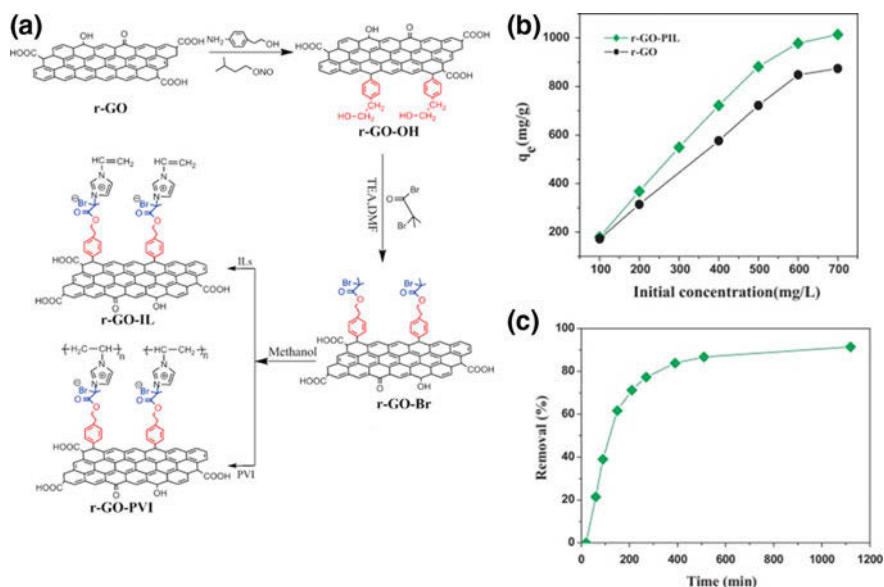


Fig. 3 a Grafting of poly(1-vinylimidazole) onto the surface of the chemically reduced graphene oxide; b adsorption capacity of r-GO and r-GO-PIL for the methyl blue at room temperature; c Removal of MB by r-GO-PIL as a function of time (initial concentration of dye: 350 mg/L, solution volume: 30 mL, amount of r-GO-PIL: 5 mg) (reprinted from [36] with permission from Elsevier)

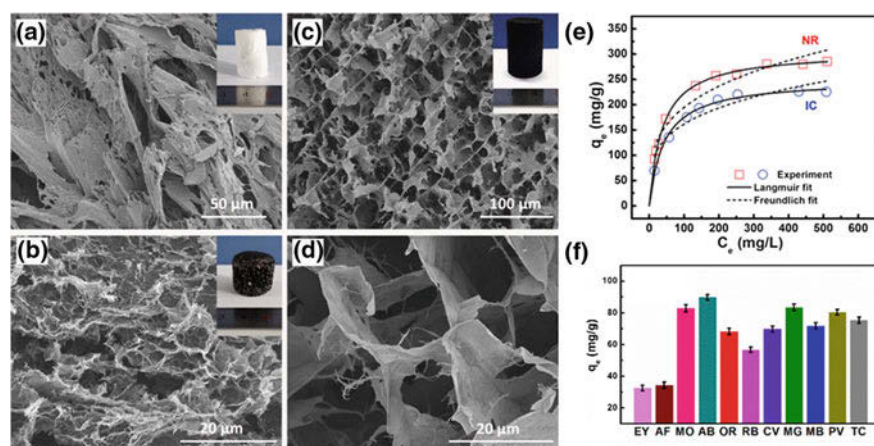


Fig. 4 SEM images of poly(vinyl alcohol) (PVA) a, TRGO b, and TRGO/PVA (0.5 wt%/1.0 wt%) (c): low magnification, d: high magnification aerogels (insets: optical photographs of aerogels); e adsorption isotherms using TRGO/PVA (0.5 wt%/1.0 wt%) aerogel fitted by the Langmuir and Freundlich models; f adsorption of anionic dyes, eosin Y(EY), acid fuchsin (AF), methyl orange (MO) and amido black 10B (AB) (at pH = 2), as well as the adsorption of nonionic dye, oil red O (OR), cationic dyes, RB, CV, methylene green (MG) and MB, and aromatic drugs, proflavine (PV) and tetracycline (TC) (at pH = 7) (reprinted from [12] with permission from Elsevier)

higher adsorption of cationic dye NR than anionic dye IC [12]. More progress on the development of inorganic-organic adsorbents has been reviewed in the following sections.

3 Polyaniline and Its Composites

Polyaniline (PANI) is one of the amine-containing conjugated polymers, which has been extensively investigated during the last two decades. Many merits have been realized in related to its properties, such as good environmental stability, low-cost monomers for synthesis, high conductivity, instant redox property, air and moisture stability, water insolubility and flexibility [37–39]. It has been found applications for different purposes, including anti-corrosion coating, batteries and sensors, supercapacitor and optoelectronic devices [15, 37, 39, 40]. Especially, PANI has incredible potential in treating dye-polluted water, because of the presence of amine and imine functional groups, which can act as the chelating and adsorbing sites through electrostatic interaction or hydrogen bond [8, 24]. When these nitrogen-containing functional groups are protonated, PANI is present in its emeraldine salt (ES) state; whilst those are deprotonated, PANI exhibits in its form of emeraldine base (EB). This conversion can be easily achieved by the treatment using acid or base [41]. It is notable that the deprotonated PANI-EB favours the selective adsorption of cationic dyes; whilst the PANI-ES preferentially adsorbs anionic dyes due to the electrostatic interactions. This was supported by Majumdar's research [42], that the polyaniline-coated filter papers in both PANI (ES)-FP and PANI (EB)-FP forms were synthesized to remove seven different anionic dyes and cationic dyes. The Langmuir adsorption capacity of Eosin yellow (EY) (as an anionic model dye) on PANI (ES)-FP was 4.3 mg/g and that of MB (as a cationic model dye) on PANI (EB)-FP was 1.3 mg/g at neutral pH. Figure 5a schematically shows the adsorption of dyes by PANI (ES)-FP and PANI (EB)-FP.

It is noted that the use of PANI powders as adsorbent could be limited by its surface area [43]. Research interest was attracted at the fabrication of PANI into various nanostructures, i.e. nanoparticles and nanotubes [38, 44], or its composite with the incorporation of nanosized inorganics [8, 40, 45]. Various inorganic materials, such as mesoporous silica, carbon nanotubes, nanosized metal or metal oxide (e.g. Ag, γ -Al₂O₃, MgO, and ZrO₂), as well as metal salts (e.g. cupric chloride, α -zirconium phosphate, et al.), have been explored; the summary of those works is shown in Table 2 [8, 37, 38, 41, 43, 45–47]. For example, PANI/ γ -Al₂O₃ nanocomposite was fabricated by in situ polymerization of aniline in the presence of γ -Al₂O₃ nanoparticles, as shown in Fig. 5b. The PANI/ γ -Al₂O₃ nanocomposite showed a high adsorption capacity of 1000 mg/g for cationic dye Direct blue 199 (DB) at pH 2, calculated by the Langmuir isotherm model. The adsorption process was proceeded via electrostatic attraction between the protonated ammonia groups in PANI (R-NH₃⁺) and sulfonic groups from anionic dye ions (D-SO₃⁻), in the form of (R-NH₃⁺ ··· O₃S-D) [8].

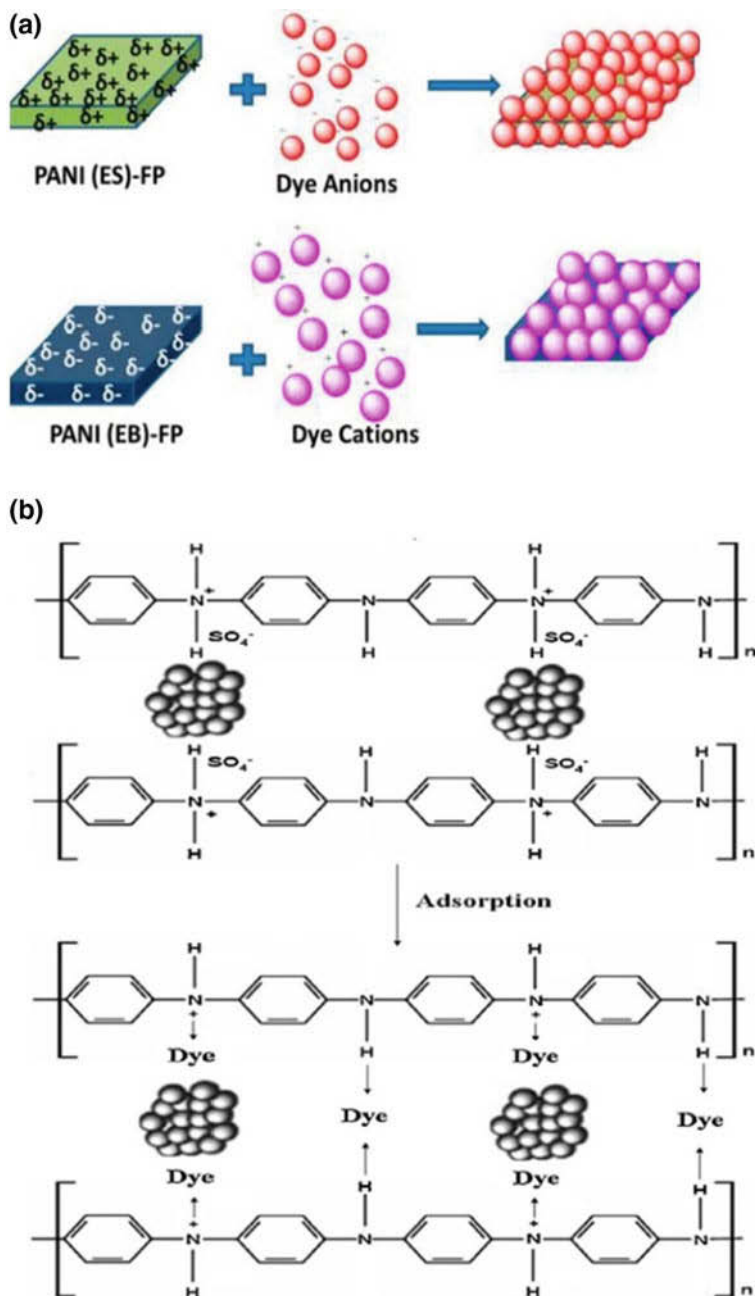


Fig. 5 a Schematic of adsorption of anionic and cationic dyes by PANI (ES)-FP and PANI (EB)-FP; b adsorption of anionic dyes by PANI/ γ - Al_2O_3 nanocomposite (modified & reprinted with permission from [42, 8])

Table 2 Dye removal by polyaniline (PANI) composites

Adsorbent	Dye	Adsorption capacity (mg g^{-1})	pH	Temperature ($^{\circ}\text{C}$)	Initial concentration (mg L^{-1})	References
PANI/zirconium oxide	Methylene blue (MB)	77.51 ^a	/	26 \pm 1	10–40	[37]
PANI/MgO	Reactive orange 16 (RO)	558.4 ^a	7	30	50–250	[43]
PANI/ γ - Al_2O_3	Reactive red 194	71.9 ^a	2	25	/	[8]
	Acid blue 62	222.2 ^a	2	25	/	
	Direct blue 199	1000 ^a	2	25	/	
PANI doped with 8% CuCl_2	Cibacron navy P-2R-01	99.83% ^b	6	25	60	[47]
PANI/Ag nanocomposite	Brilliant green (BG)	23.66 ^a	/	30	/	[45]
PANI/ α -zirconium phosphate	Methyl orange (MO)	377.46 ^a	4	/	/	[38]
PANI nanotube	Methyl orange (MO)	254.15 ^a	4	/	/	[38]
Carbon nanotube/PANI	Malachite green (MG)	13.95 ^c /88% ^b	7	20	16	[41]
	Folic Acid-PANI	Eosin yellow (EY)	247.5 ^a	3	25	100–230
Eosin yellow (EY)		239 ^c	3	25	200	
Rose Bengal (RB2)		206 ^c	3	25	200	
Methyl orange (MO)		173 ^c	3	25	200	

(continued)

Table 2 (continued)

Adsorbent	Dye	Adsorption capacity (mg g^{-1})	pH	Temperature ($^{\circ}\text{C}$)	Initial concentration (mg L^{-1})	References
Fe_3O_4 @AmABAmPD-TCAS ^c	Methylene blue (MB)	31.64 ^a	8	30	5–50	[33]
	Malachite green (MG)	29.07 ^a	8	30	5–50	
PANI-MS@ Fe_3O_4 ^d	Methyl orange (MO)	55.74 ^a	4	0	4–32	[48]
	PANI emeraldine salt (ES)-coated filter paper	4.26 ^a	7	/	1–25	
	Methylene blue (MB)	1.26 ^a	7	/	1–25	[42]

^aMaximum adsorption capacity calculated by Langmuir isotherm model^bRemoval rate %^cThe adsorbent is composed of a Fe_3O_4 core and polyamine–aminobenzoic acid–phenylenediamine terpolymer shell functionalized with thiacalix(4)arene tetrasulfonate as the internal dopant^dPolyamine functionalized magnetic mesoporous silica iron oxide (MS@ Fe_3O_4) nanoparticles^eEquilibrium adsorption capacity

A synergistic effect of PANI and inorganic materials was seen on improving the adsorptive removal of dyes from the literature [37, 40, 43]. For example, the carbon nanotube (CNT)/PANI composites fabricated by Zeng et al. had an equilibrium adsorption capacity of 13.95 mg/g for cationic dye malachite green (MG) at an initial MG concentration of 16 mg/L, which was 15% higher than that of neat PANI. This was probably due to the strong interaction of CNT-PANI, as well as its high porosity and large surface area [41]. Wang and co-workers synthesized PANI and α -zirconium phosphate composite (PANI/ α -ZrP) via in situ oxidative polymerization reaction. The resulting PANI/ α -ZrP exhibited BET surface area of 30.40 m²/g, showing plate-like α -ZrP structures decorated by PANI thin layer of small and uniform fibrillar nanostructure (Fig. 6b); this differed from the structure of PANI nanotube (Fig. 6a). Thanks to this unique structure, the PANI/ α -ZrP composites showed the Langmuir-derived maximum methyl orange (MO) adsorption of 377.46 mg/g, which was greater than that of PANI nanotubes (254.15 mg/g), as shown in Fig. 6c. In the kinetic study (Fig. 6d), the fast adsorption in first 60 min was probably ascribed to the electrostatic interactions between sorption sites of PANI/ α -ZrP, i.e. amine and imine functional groups,

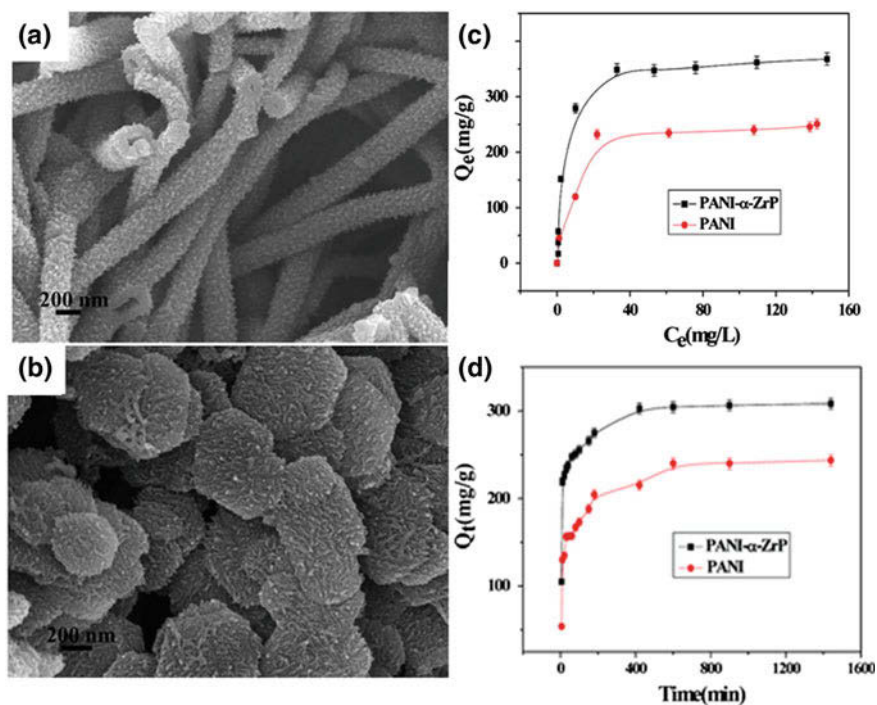


Fig. 6 SEM images of **a** PANI, **b** PANI/ α -ZrP (α -ZrP/aniline mol ratio = 1:30); **c** adsorption isotherms of MO on PANI nanotubes and PANI/ α -ZrP nanocomposites; **d** adsorption kinetics curves for the adsorption of MO with initial concentration of 100.0 mg/L by PANI nanotubes and PANI/ α -ZrP nanocomposites (reprinted with permission from [38])

and MO molecule; after that, the adsorption process slowed down and reached equilibrium [38].

Organic functional materials, such as folic acid, aminobenzoic acid, phenylenediamine, etc., and other materials, e.g. low-cost filter paper, have been used to improve the properties of PANI for dye-containing water purification, as shown in Table 2 [24, 33, 42]. For example, Das et al. fabricated a novel porous folic acid/PANI hydrogel, in which folic acid was used as a cross-linker to PANI. The as-synthesized folic acid/PANI hydrogel exhibited high specific surface area with 3D interconnected pores. The folic acid/PANI xerogels were found efficient in removing anionic dyes, such as EY, Rose Bengal (RB2), MO, ascribed to the electrostatic attraction between anionic dyes and positively charged PANI, which was presented in emeraldine salt (ES) state [24]. Moreover, magnetic nanoparticles, such as Fe_3O_4 , were introduced to PANI composites for efficient magnetic separation and reuse [33, 48]; this has been covered in the following section.

4 Magnetic Polymer Composites

The development of magnetic polymer composites is of importance for recycling and reusing in practical application. The magnetic separation offers the ability to recover and reuse the suspended adsorbents after multiple cycles of adsorption, which is of great significance for sustainable process management. In particular, the magnetic separation is believed to be more efficient than conventional centrifugation and filtration, which might be subject to the risk of blockage of filters and loss of adsorbents [5, 49].

In the past decades, the adsorbents combined with magnetic nanoparticles (MNPs) have attracted great research interest, ascribed to their good adsorption capacity, high adsorption rate and convenient recycling of solids by employing an external magnetic field. Fe_3O_4 MNPs are most commonly used as magnetic particles due to their unique property such as low toxicity, biocompatibility and easy handling of magnetic separation [5, 50, 51]. Fe_3O_4 MNPs can be synthesized by precipitation in a fine mixture of Fe(II) and Fe(III) solution with ammonium hydroxide under nitrogen atmosphere [28], or via a solvothermal route under heating [26]. However, the practical application of bare Fe_3O_4 MNPs has seen several limitations, such as the leaching of iron in strong acid solution and a high tendency to aggregate [28]. Therefore, an effective surface coating of Fe_3O_4 MNPs with appropriate coating materials, such as inorganic silica or polymer is necessary to enhance the stabilization of MNPs.

The combination of polymer with MNPs resulted in magnetic polymer composite; it benefits from both abundant functional groups of the polymer, which endows high affinity towards dyes, and magnetic properties of MNPs. So far, such materials have been widely studied on the removal of dyes from aqueous solution, as shown in Table 3. The presence of nitrogen-containing groups in the polymers, i.e. polyethyleneimine, poly 1, 4-phenylenediamine, and polyaniline, etc., makes them

Table 3 Dye removal by magnetic polymer composites

Polymers and composites	Magnetic particles	Dye	Adsorption capacity (mg g ⁻¹)	pH	Temperature (°C)	References
Poly 1, 4-phenylenediamine	Fe ₃ O ₄ nanoparticles	Direct red 81 (DR81)	144.92 ^a	4.0	/	[52]
Cross-linked polyethylenimine	Fe ₃ O ₄ -NH ₂ cubic crystalline	Alizarin red S (ARS)	256.1 ^a	3.0	30	[51]
		Methyl orange (MO)	244.4 ^a	3.0	30	
		Methyl blue	172.1 ^a	3.0	30	
		Nuclear fast red (NFR)	138.8 ^a	3.0	30	
		Sunset yellow FCF (SY)	145.8 ^a	3.0	30	
		Alizarin green (AG)	134.6 ^a	3.0	30	
Chitosan/poly(vinyl alcohol) hydrogel beads	Fe ₃ O ₄ nanoparticles	Congo red (CR)	467.3 ^a	/	25 ± 0.2	[22]
Oxidized multiwalled carbon nanotube (OMWCNT)- κ-carrageenan	Fe ₃ O ₄ (10–25 nm)	Methylene blue (MB)	396.63 ^a	6.5	25	[5]
		Methylene blue (MB)	78.67 ^a	6.0	28	[28]
Poly(γ-glutamic acid) (PGA)	Fe ₃ O ₄ (8.3 nm)	Methylene blue (MB)	31.64 ^a	8.0	30	[33]
Terpolymer of aniline/m-aminobenzoic acid/m-phenylenediamine	Fe ₃ O ₄ (39 nm)	Methylene blue (MB)	29.07 ^a	8.0	30	
		Malachite green (MG)				

(continued)

Table 3 (continued)

Polymers and composites	Magnetic particles	Dye	Adsorption capacity (mg g ⁻¹)	pH	Temperature (°C)	References
Carboxymethyl chitosan-g-poly(acrylamide) (CMC-g-PAAm).	Fe ₃ O ₄ (<3 nm)/ Iaponite RD	Crystal violet (CV)	120 ^a	/	24	[55]
Polyaniline (PANI)/mesoporous silica	Fe ₃ O ₄ (110– 130 nm)	Methyl orange (MO)	55.74 ^a	4.0	0	[48]
Poly(4-styrenesulfonic acid-co-maleic acid) sodium (PSSMA)	Fe ₃ O ₄ (~ 50 nm)	Basic fuchsin (BF)	588.2 ^a	7.0	25	[54]
		Crystal violet (CV)	384.6 ^a	7.0	25	
Chitosan/carbon nanotube	Fe ₃ O ₄ (~ 65 nm)	Methylene blue (MB)	270.3 ^a	7.0	25	
		Acid red 18 (AR18)	691.0 ^a	3.0	30	[26]
Titania-polyaniline	CoFe ₂ O ₄	Methyl orange (MO)	168.57 ^a	/	/	[40]
Polysaccharide resin	CuFe ₂ O ₄	Methylene blue (MB)	366.6 ^a	8.0	/	[30]
		Methylene blue (MB)	1990 ^a	8	30	[53]
Polyacrylamide microspheres	γ-Fe ₂ O ₃	Neutral red	1937 ^b	/	30	
		Gentian violet	1850 ^b	/	30	

^aMaximum adsorption capacity calculated by Langmuir isotherm model^bAt C₀ of 100 mg/L, the equilibrium adsorption capacities for GV and NR are 1850 and 1937 mg/g

easily be positively charged in an acidic medium and in turn, facilitates the adsorption of negatively charged dyes, such as Direct red 81, and Acid Red 18 (AR18), etc., via strong electrostatic attraction, which is considered to be the dominant adsorption mechanism [48, 50–52]. The maximum adsorption capacity calculated by the Langmuir model was in the range of 55.7–256.1 mg/g at pH = 3.0 or 4.0, as shown in Table 3 [48, 51, 52]. With anionic functional groups (e.g. $-\text{COO}^-$, $-\text{SO}_3^-$), the polymers such as natural polysaccharides, poly(γ -glutamic acid) (PGA) and poly(4-styrenesulfonic acid-co-maleic acid) sodium (PSSMA) are highly negatively charged at pH 6.0–8.0 [5, 28, 33]; therefore, electrostatic interaction formed between polymers and cationic dyes, as shown in Fig. 7a [28]. In addition, other mechanisms, such as π - π interaction, hydrogen bonding, ion exchange and hydrophobic interaction are recommended in the adsorption process of dyes onto some magnetic polymer composites [30, 33, 39]. For example, in addition to electrostatic interactions between the functional groups ($-\text{SO}_3$, $-\text{OH}$ and $-\text{NH}$) in the polymer with the cationic dyes (MB and MG), dye was captured via π - π interactions between hydrophobic residues of dyes and aromatic cavity from the polymer backbone of magnetic polymer nanocomposite, as shown in Fig. 7b [33]. More importantly, magnetic polymer nanocomposite with porous structure or surface is believed to have extraordinary adsorption performance, i.e. a high sorption capacity as well as a fast adsorption process. For example, the porous magnetic polyacrylamide (PAM) microspheres reached an equilibrium adsorption for MB in about 200 min, and the maximum adsorption capacity calculated by Langmuir model was 1990 mg/g. Their equilibrium adsorption capacities for gentian violet (GV) and neutral red (NR) at an initial concentration of 100 mg/L, were 1850 and 1937 mg/g, respectively, as shown in Table 3 [53]. The equilibrium adsorption capacity of MB onto porous magnetic PAM microspheres increased from 263 to 1977 mg/g, when initial dye concentration was changed from 5 to 300 mg/L [53].

The internal architectures of these magnetic polymer nanocomposites were examined by TEM. Two were distinguished, MNPs embedded in cross-linked polymer and core-shell structured polymer@MNPs, as shown in Fig. 8 [33, 54]. Several methods were used to fabricate magnetic polymer composites with the former structure. For example, a two-step strategy included the synthesis of MNPs

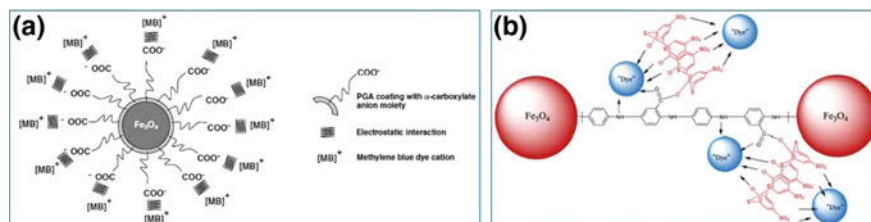


Fig. 7 Schematic diagram of proposed mechanism of **a** MB dye adsorption on PGA-MNPs (MNPs, magnetite nanoparticles; PGA, poly(γ -glutamic acid)); and **b** cationic dye adsorption on to Fe_3O_4 @PAmABAmPD-TCAS nano adsorbent (PAmABAmPD, terpolymer of aniline/m-aminobenzoic acid/m-phenylenediamine; TCAS, Thiocalix(4)arene tetrasulfonate) (reprinted with permission from [28, 33])

and their dispersion in monomer-containing solution, followed by polymerization. In addition, a simple and facile one-pot solvothermal method was developed [54] and a dispersing route, in which porous PAM microspheres were dispersed in Fe(II) and Fe(III) solution and then in NaOH solution at 100 °C [53], was adopted. On the other side, core-shell structured polymer@ MNPs could be fabricated by firstly coating a dense silica and subsequently mesoporous silica, which generated pores on the surface of magnetic nanoparticles (Fe_3O_4) and allowed the PANI conjugated into the pores of mesoporous silica (MS), and finally to obtain PANI-MS@ Fe_3O_4 nanocomposites [48]. Other ways to fabricate the core-shell structure were by directly coating the MNPs with a water-soluble polymer in deionized water [28], or via in situ coprecipitation method in which the synthesis started from a fine mixture of Fe(II) and Fe(III) salts and doped copolymer [33].

The reusability is considered as a key performance for investigation. The desorption of dye-loaded adsorbent was conducted by adjusting the pH of the aqueous solution since the tendency of maximum dye recovery was in general inversely proportional to the trend observed for the dye adsorption at different pHs. The adsorption of anionic dyes onto magnetic polymer composites is unfavourable at the alkaline medium, thus, NaOH or ammonium solution could be selected as effective dye desorption eluent to regenerate the spent adsorbents [51]. On the other side,

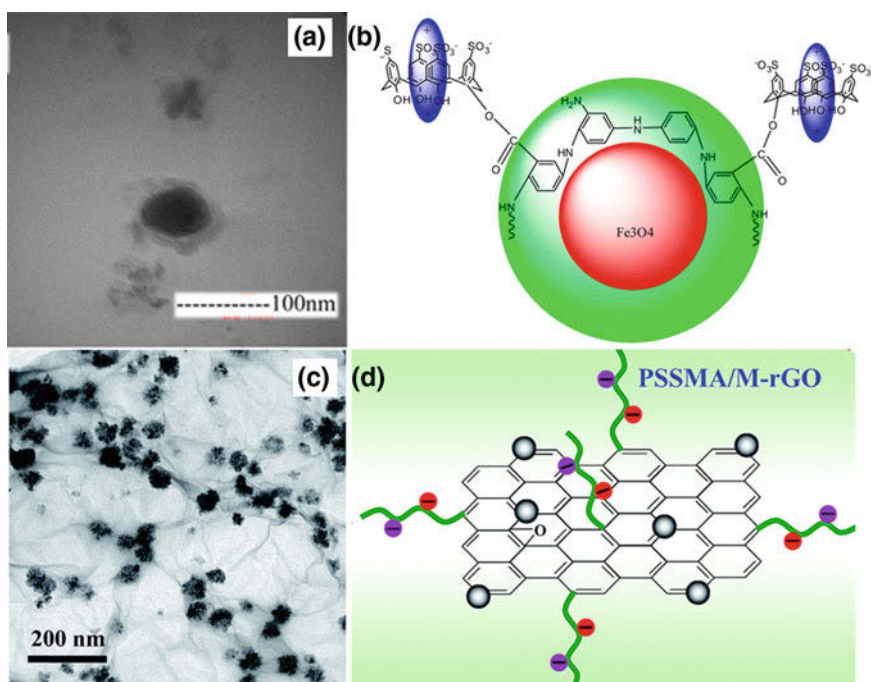


Fig. 8 TEM image and structural schematic of (a, b) Fe_3O_4 @PAMABAmPD-TCAS and (c, d) poly(4-styrenesulfonic acid-co-maleic acid) sodium (PSSMA) modified magnetic reduced graphene oxide nanocomposite (PSSMA/M-rGO) (reprinted with permission from [33, 54])

desorption of cationic dyes was usually favoured in acid solution, e.g. 100–91% of the MB recovered from PGA-MNPs at pH = 1–3 [28]. The MB adsorbed onto montmorillonite/polyaniline/ Fe_3O_4 (Mt/PANI/ Fe_3O_4) nanocomposite could be successfully desorbed using 0.5 M HCl as the desorbing agent, and almost no decrease in the adsorption ratio was observed upon five cycles, as shown in Fig. 9a [39].

With the aid of a solvent, such as methanol or ethanol, solvent desorption technique was used to enhance the regeneration of the exhausted magnetic adsorbents [26, 48, 53]. The pH of solvent solution affected the surface charge and functional groups of adsorbent, the properties of dye molecule and in turn the desorption process [26, 48, 53]. The cationic dye MB saturated magnetic PAM microspheres could be completely regenerated (100% desorption) with acid methanol-water solution (50 v/v%, 10 mL) of pH 2 as the desorption solvent; while another cationic dye neutral red (NR) adsorbed magnetic PAM microspheres could be regenerated by neutral methanol-water solution as desorption solvent for three cycles of repeating washing process [53]. This is probably due to the difference in the charge of dye molecules, that the molecule of NR is less positively charged than MB [53]. To desorb anionic dye AR18 from the saturated magnetic chitosan-decorated carbon nanotube (mCS/CNT), which formed by compositing MNPs in chitosan-decorated carbon nanotube (CS/CNT), basic solvent solution, i.e. ammonia/ethanol (v/v, 2:3) was applied as desorption solution. The removal rate of anionic dye AR18 using regenerated mCS/CNT could be largely maintained even after 10 consecutive cycles (99.11–99.76%), indicating the excellent stability, regeneration, and reusability, as shown in Fig. 9b [26]. Such an excellent reusability might be attributed to OH^- in ammonia/ethanol elution enabling the release of anionic AR18 from the adsorbent surface; the regenerated mCS/CNT adsorbent could be magnetically recycled and reused [26]. To remove anionic dye MO from polyaniline functionalized magnetic mesoporous silica composite (PANI-MS@ Fe_3O_4), methanol solution containing 4% acetic acid was used as desorption eluent, in which electrostatic repulsion occurred between the protonated MO molecule and the positively charged nanocomposites adsorbent, due to the presence

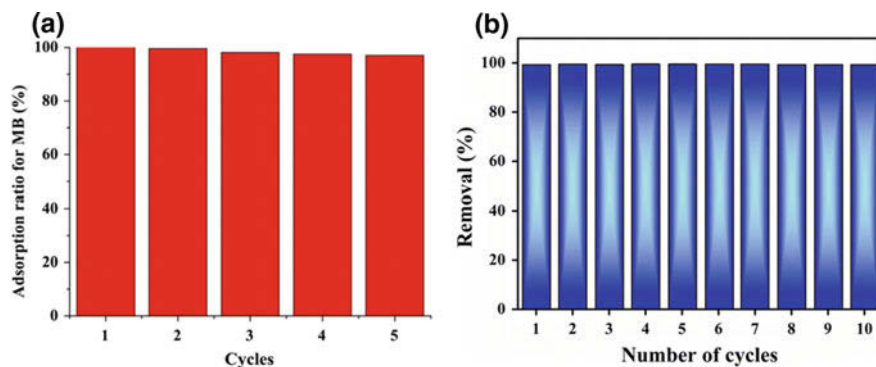


Fig. 9 **a** Adsorption cycles of MB onto Mt/PANI/ Fe_3O_4 composites; **b** AR18 onto magnetic chitosan-decorated carbon nanotube (mCS/CNT) (reprinted with permission from [26, 39])

of nitrogen-containing functionalities (imine and amine groups) in PANI. Thus, there was still 80.25% of the anionic dye MO adsorbed onto the regenerated PANI-MS@Fe₃O₄ after three cycles of adsorption-desorption [48]. Other desorption solution, e.g. ethanol/water with 0.5 M KCl, was used to desorb cationic dye CV efficiently (desorption rate >97%) [55]. Taking the merit of magnetic separation, the spent magnetic polymer composites can be easily recycled and potentially reused.

5 Polymer/Clay Composites

The economic efficiency, as well as adsorption performance, are of extra importance when selecting a suitable adsorbent for practical application. Natural clays are hydrated layered aluminosilicates, which are widely available and low-cost, thus may be more viable and inexpensive for use as adsorbents to remove dyes from wastewater. Because of abundant silicon hydroxyls, negative surface charges and exchangeable cations (usually Na⁺ and Ca²⁺), clay minerals, e.g. attapulgite, are capable to adsorb cation dyes (e.g. MB) from water [56]. However, the relatively low adsorption capacity especially for anionic dyes due to the negatively charged surface limited their application. Organo-modification of clays with polymers is an essential way to fabricate effective adsorbents with enhanced adsorption capacity toward cationic or anionic dyes pollutants [7, 56]. Due to the presence of reactive –OH groups on their surfaces, clays can interact with reactive sites of polymers and monomers leading to the generation of polymer/clay composites [57]. In the last decades, significant research interest has been attracted on the development of polymer composites as adsorbents by incorporating inorganic clays such as attapulgite, montmorillonite, vermiculite, palygorskite and bentonite into polymeric matrices [20, 39, 57, 58]. The blending of clays not only potentially reduced fabrication cost, but also improved some properties, e.g. mechanical and thermal stability or swelling ability [20].

Among different clay minerals, bentonite is known for its good specific surface area and source abundance. The carboxymethyl cellulose (CMC) grafted by poly(2-(dimethylamino) ethyl methacrylate) modified bentonite (Bent/CMC-g-P(DMAEMA)) showed a maximum adsorption of 110.7 mg/g toward anionic MO (operation conditions: pH 6.86, 298 K and 50 min), and its removal rate was almost doubled in compared with bentonite [7]. In addition to ionic interaction, the hydrogen bonding interactions between the hydroxyl group (Si-OH, Al-OH, Fe-OH, and Mg-OH) in parent Bent and –O, –N in dye molecular greatly contributed to the observed good adsorption performance. By changing weight % of Bent in the polymer/clay composites, the surface characteristic of Bent/CMC-g-P(DMAEMA) was tuned; the resulting adsorption capacity was optimized when prepared using 20% CMC in the total amount of CMC + Bent [7]. Besides, humic acid-immobilized amine modified polyacrylamide/bentonite composite (HA-Am-PAA-B) was capable to remove cationic dyes (MG, MB, and CV) from

their single and binary component solutions, as a result of the negative surface charge of the adsorbent [59]. The carrageenan-graft-poly (acrylamide)/bentonite exhibited a maximum MB adsorption capacity up to 156.25 mg/g and its adsorption was well fitted by the Langmuir isotherm model [20].

Attapulgite (APT) and palygorskite (Pal) are another two available clays, which exist in fibrous/rod morphology [56, 58]. Featured with one-dimensional nanoscale and a large number of silanol groups, APT and Pal are good inorganic candidate materials for composite fabrication. The APT/Fe₃O₄/PANI nanocomposites showed a much higher adsorption ratio, 96.0%, for CR at pH of 7, as compared with that of APT, 14.5% (298 K, contact time: 60 min) [56]. The adsorption capacity of Reactive Red 3BS onto the polyamidoamine (PAMAM) dendrimer-functionalized Pal adsorbents markedly increased from 34.2 to 322.6 mg/g (293 K, contact time: 20 min) by increasing addition of PAMAM, which contains amino-terminated groups. The anionic dyes could be trapped and then stabilized in the cavities of PAMAM dendrimers due to the host-guest affinity [58].

Temperature is one of the factors affecting equilibrium capacity of adsorbents, which correlates with the exothermicity or endothermicity nature of adsorption. Mostly, the adsorption capacity increased by increasing of temperature during the endothermic adsorption of dyes onto polymer/clay composites, which could be confirmed by the positive values of enthalpy change (ΔH°) [57, 60]. The diffusion rate of dye molecules from solution to the adsorbent surface was also enhanced with increasing temperature, thus, adsorption capacity was improved [20, 57]. In the case of MO adsorption onto 20CMC-Bent (20% of CMC in the total amount of CMC + Bent composite), the negative ΔH° value indicated an exothermic adsorption process [7].

The adsorption capacity of cationic dye onto polymer/clay composites was observed to increase at higher pH [20, 57]; this was explained by the stronger electrostatic attraction formed between deprotonated functional groups of the adsorbents and positively-charged dye molecules. The maximum removal rate % of MG, MB, and CV onto the HA-Am-PAA-B was 99.7, 99.3, and 98.8%, respectively, at pH 6.0 with an initial dye concentration of 200 $\mu\text{mol/L}$ [59]. The optimized adsorption pH was observed in the range of 6.0–8.0, under which the carboxylic and phenolic groups were deprotonated and the surface charge of adsorbent was negative (pH_{pzc} 4.8) [59].

Interestingly, at pH = 6.3, the Mt/PANI/Fe₃O₄ composite, which was protonated via treating with 0.1 M HCl, displayed a maximum adsorption ratio of 98.1% toward anionic dye CR; whilst the dedoped Mt/PANI/Fe₃O₄ showed excellent adsorption ratio of 99.6 and 96.2% to cationic dyes MB and Brilliant green (BG), respectively (298 K, contact time: 60 min) [39]. This difference resulted from the variation on the surface charge, that the dedoped Mt/PANI/Fe₃O₄ was negatively charged, as compared to positively charged Mt/PANI/Fe₃O₄ after acid treatment. The resulting clay/polymer composite showed excellent adsorption capacity to both cationic dyes and anionic dyes, in relative to the original Mt adsorbent [39]. Moreover, by introducing magnetic particles, such as Fe₃O₄ and CoFe₂O₄, the clay/polymer composites were able to be recovered by magnetic separation for reuse [39, 56, 60]. For example, via magnetic separation, no decrease in the adsorption ratio of

MB onto the dedoped Mt/PANI/Fe₃O₄ composite was observed upon five successive cycles [39].

6 Polymer/by-Products or Waste Composites

Recently, there has been increasing research interest in exploring polymer composites synthesized with industrial or agricultural by-products or waste, such as coir pith, fly ash, flax shive, sawdust, sugarcane molasses, and almond shell waste, etc., due to the biodegradability, low cost and great availability [2, 3, 61–65]. By-products or waste materials may have a certain affinity to cationic dyes, because of the presence of surface hydroxyl groups; however, the adsorption capacity of anionic dyes was usually found to be low [63]. For example, the use of flax shive cellulose exhibited only ~0.5 mg/g adsorption towards RR228 [3]; whilst that of almond shell waste (AS) to acid blue 25 (AB25) was less than 2.4 mg/g [63]. Benefited from functional groups of polymers, their incorporated polymer composites exhibited enhanced dye adsorption capacity.

In order to achieve good adsorption property, the physical or chemical modification is usually adopted to increase surface groups of waste/by-products for functionalization with polymers and in turn improve their adhesion with the polymer matrix. For example, after heat and alkali treatment, the surface area of coal fly ash (CFA), a coal combustion by-product, increased from 66.78 to 102.89 m²/g, accompanied with greater total pore volume and average pore size; these features were believed to contribute in enhancing adsorption capacity. Moreover, the modified CFA possessed a greater amount of surface silanol groups (Si–OH), which could be functionalized with polyethyleneimine (PEI) to fabricate composite adsorbents. Thanks to the amine group at the end of the PEI chain as well as the high amine density, the Langmuir maximum adsorption capacity of CFA/PEI composite was found to be 316.75 mg/g for reactive red 2 (RR2) (pH = 3, 313 K) and 174.83 mg/g for MG (pH = 8, 308 K), respectively [61]. Goes and co-workers chemically modified cellulose with 4,4'-diphenylmethane diisocyanate (MDI); the resulting material showed enhanced adsorption capacity [2]. The equilibrium adsorption capacities of MB onto polyurethane foams with unmodified cellulose was 1.57 mg/g; that on polyurethane with chemically modified cellulose increased to 1.83 mg/g under the same operating conditions. This difference might result from the structural changes caused by the reaction of MDI on cellulose surface [2].

7 Conclusions

Adsorption has been investigated as an effective approach for the treatment of dye-containing wastewater. Polymers and polymer composites exhibited attractive features of high strength, good flexibility, and ease of modification or

functionalization, thus as potential adsorbents with high adsorption capacity, fast adsorption rate and good reusability. Recent advances in polymers and polymer composites, such as PANI composites, magnetic polymer composites, polymer/clay composites and polymer/by-products or waste composites, were reviewed in terms of their properties and adsorption. The regeneration of spent polymers and polymer composites and subsequent reuse was also discussed, which potentially improved the cost efficiency of adsorbents.

Both the properties of adsorbents and dyes were considered as the key factors tuning adsorptive dye removal from aqueous solution. Generally, polymers and polymer composites attract the dye molecules via electrostatic interaction, van der Waals forces, π - π interaction, and hydrogen bonding. Electrostatic interaction and hydrogen bonding are two of the most commonly underlying mechanisms governing the sorption process, which were found to be affected by the complex physicochemical natures of dyes (e.g. cationic, anionic and nonionic dyes) and the properties of adsorbents (such as surface acidity or charge, zeta potential, pore size and its distribution, and surface area). The polymer sorbents with enhanced positively charged surface sites via modification or functionalization were found to favour the removal of anionic dyes and vice versa. By combining with inorganic materials, e.g. graphene, the resulting polymer composites exhibited a broad-spectrum adsorption performance, which was explained by the π - π interactions between aromatic or heterocyclic structures of dyes and graphene sheets.

Polymers and polymer composites with special characteristics, such as the presence of an internal hydrophobic cavity, in the forms of nanosized particles or 1D nanofibers, and the introduction of 3D porous structure (i.e. nanopores or mesopores), could facilitate the adsorption. The selectivity during adsorption could be achieved via tuning the pore size in the porous polymers or polymer composites, which was suggested as being governed by the size-selective mechanism.

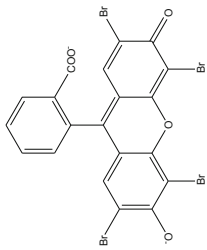
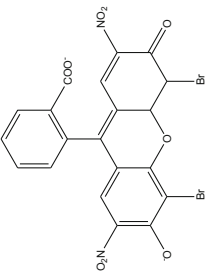
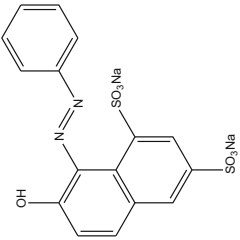
Note that the adsorption performance was significantly affected by a number of operating conditions, including solution pH, temperature, initial dye concentration, and equilibrium time. For example, the solution pH would vary both solution chemistry and surface binding sites of adsorbents. Therefore, it is necessary for optimization of operation conditions towards enhanced adsorptive dye removal from water.

Acknowledgements The authors gratefully acknowledge funding from the National Natural Science Foundation of China (No.21607064, No.21263005 and No.21567008), and Qingjiang youth Talent program of Jiangxi University of Science and Technology (No. JXUSTQJYX20170005).

Appendix

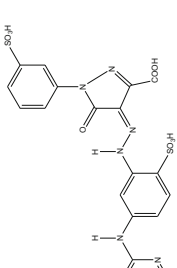

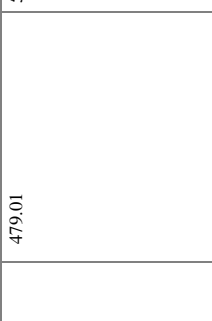
See Table 4.

Table 4 Molecular structure/weight, abbreviation, species and λ_{max} of dyes in reports

Dye	Abbreviation	Molecular weight (g mol^{-1})	λ_{max} (nm)	Ionic species	Molecular structure	References
Eosin yellow	EY	645.89	517	Anionic		[42]
Eosin blue	EB	578.09	516	Anionic		[42]
Orange G	OG	452.37	480	Anionic		[42]

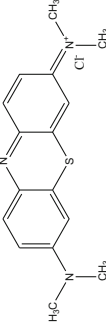
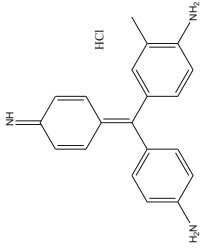
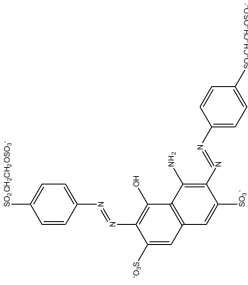
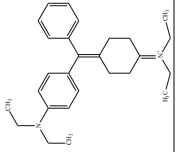
(continued)

Table 4 (continued)

Dye	Abbreviation	Molecular weight (g mol ⁻¹)	λ_{max} (nm)	Ionic species	Molecular structure	References
Reactive orange-14	RO	631.383	420	Anionic		[42]
OrangeII (C I Acid orange 7)	/	350.32	483	Anionic		[31, 42]
Rhodamine B	RHB	479.01	554	Cationic		[42]

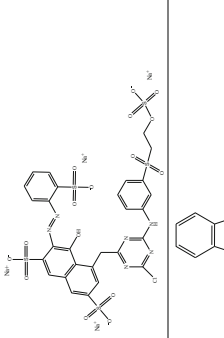
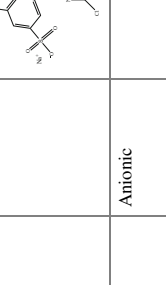
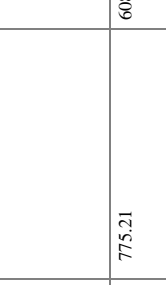
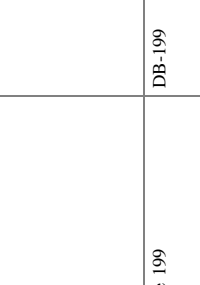
(continued)

Table 4 (continued)

Dye	Abbreviation	Molecular weight (g mol ⁻¹)	λ_{max} (nm)	Ionic species	Molecular structure	References
Methylene blue	MB	373.9	663	Cationic		[28]
Basic violet 14	BV	337.85	545	Cationic		[17]
Reactive black 5	RB5	991.82	597	Anionic		[14]
Brilliant green	BG	482.63	625	Cationic		[45]

(continued)

Table 4 (continued)

Dye	Abbreviation	Molecular weight (g mol^{-1})	λ_{max} (nm)	Ionic species	Molecular structure	References
Reactive red 194	RR-194	984.2062	542	Anionic		[8]
Direct blue 199	DB-199	775.21	608	Anionic		[8]
Acid blue 62	AB-62	400.45	620	Anionic		[8]
CI Acid red 88	AR 88	400.38	505	Anionic		[31]

(continued)

Table 4 (continued)

Dye	Abbreviation	Molecular weight (g mol^{-1})	λ_{max} (nm)	Ionic species	Molecular structure	References
Alizarin red S	ARS	342.26	423	Anionic		[51]
Nuclear fast red	NFR	357.28	518	Anionic		[51]
Alizarin green	AG	622.58	642	Anionic		[51]
Methyl orange	MO	327.33	463	Anionic		[51]
Sunset yellow FCF	SY	452.37	482	Anionic		[51]

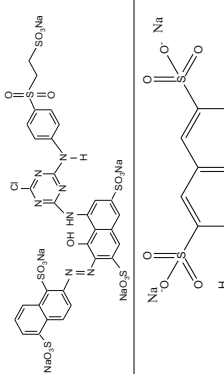
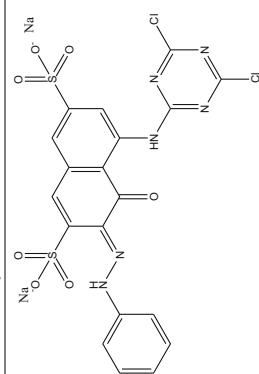
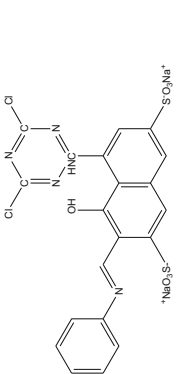
(continued)

Table 4 (continued)

Dye	Abbreviation	Molecular weight (g mol ⁻¹)	λ_{max} (nm)	Ionic species	Molecular structure	References
Methyl blue	/	799.80	600	Anionic		[51]
Congo red	CR	696.68	497/500	Anionic		[14, 34]
Malachite green	MG	364.92	617	Cationic		[41]
Acid red 18	AR18	604.47	507	Anionic		[26, 65]

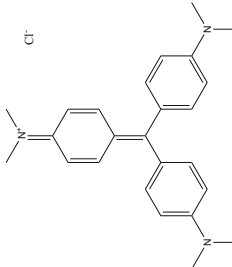
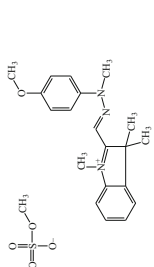
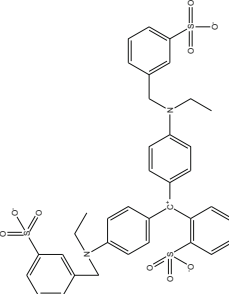
(continued)

Table 4 (continued)

Dye	Abbreviation	Molecular weight (g mol ⁻¹)	λ_{max} (nm)	Ionic species	Molecular structure	References
Reactive red 3BS (C.I. reactive red 195)	/	1118.83	546	Anionic		[58]
Reactive red	RR	613.92	547	Anionic		[25]
Active brilliant red X-3B	/	615.33	540.5	Anionic		[27]

(continued)

Table 4 (continued)

Dye	Abbreviation	Molecular weight (g mol^{-1})	λ_{max} (nm)	Ionic species	Molecular structure	References
Crystal violet (methyl violet 10B)	CV	407.99	595	Cationic		[55]
Basic yellow 28	BY28	433.52	420	Cationic		[25]
Brilliant blue 133	BB133	792.85	609.5	Anionic		[25]

References

1. Ngulube T et al (2017) An update on synthetic dyes adsorption onto clay based minerals: a state-of-art review. *J Environ Manag* 191:35–57
2. Goes MM et al (2016) Polyurethane foams synthesized from cellulose-based wastes: kinetics studies of dye adsorption. *Ind Crops Prod* 85:149–158
3. Wang L, Li J (2013) Adsorption of C.I. reactive red 228 dye from aqueous solution by modified cellulose from flax shive: kinetics, equilibrium, and thermodynamics. *Ind Crops Prod* 42(Supplement C):153–158
4. Kanmani P et al (2017) Environmental applications of chitosan and cellulosic biopolymers: a comprehensive outlook. *Bioresour Technol* 242:295–303
5. Duman O et al (2016) Synthesis of magnetic oxidized multiwalled carbon nanotube-kappa-carrageenan-Fe₃O₄ nanocomposite adsorbent and its application in cationic methylene blue dye adsorption. *Carbohydr Polym* 147:79–88
6. Rajabi M, Mahanpoor K, Moradi O (2017) Removal of dye molecules from aqueous solution by carbon nanotubes and carbon nanotube functional groups: critical review. *Rsc Adv* 7(74):47083–47090
7. Li W et al (2017) Tunable adsorption properties of bentonite/carboxymethyl cellulose-g-poly (2-(dimethylamino) ethyl methacrylate) composites toward anionic dyes. *Chem Eng Res Des* 124:260–270
8. Javadian H, Angaji MT, Naushad M (2014) Synthesis and characterization of polyaniline/gamma-alumina nanocomposite: a comparative study for the adsorption of three different anionic dyes. *J Ind Eng Chem* 20(5):3890–3900
9. Ezzatahmadi N et al (2017) Clay-supported nanoscale zero-valent iron composite materials for the remediation of contaminated aqueous solutions: a review. *Chem Eng J* 312:336–350
10. Pandey S (2017) A comprehensive review on recent developments in bentonite-based materials used as adsorbents for wastewater treatment. *J Mol Liq* 241:1091–1113
11. Sulyman M, Namiesnik J, Gierak A (2017) Low-cost adsorbents derived from agricultural by-products/wastes for enhancing contaminant uptakes from wastewater: a review. *Polish J Environ Stud* 26(2):479–510
12. Xiao J et al (2017) Multifunctional graphene/poly(vinyl alcohol) aerogels: in situ hydrothermal preparation and applications in broad-spectrum adsorption for dyes and oils. *Carbon* 123:354–363
13. Voisin H et al (2017) Nanocellulose-based materials for water purification. *Nanomaterials* 7(3):19
14. Qiu Y, Ling F (2006) Role of surface functionality in the adsorption of anionic dyes on modified polymeric sorbents. *Chemosphere* 64(6):963–971
15. Zhang L et al (2012) Facile and large-scale synthesis of functional poly(m-phenylenediamine) nanoparticles by Cu²⁺ + -assisted method with superior ability for dye adsorption. *J Mater Chem* 22(35):18244–18251
16. Gezici O et al (2016) Humic-makeup approach for simultaneous functionalization of polyacrylonitrile nanofibers during electrospinning process, and dye adsorption study. *Soft Mater* 14(4):278–287
17. Elkady MF, El-Aassar MR, Hassan HS (2016) Adsorption profile of basic dye onto novel fabricated carboxylated functionalized co-polymer nanofibers. *Polymers* 8(5):177
18. Chauque EFC et al (2017) Electrospun polyacrylonitrile nanofibers functionalized with EDTA for adsorption of ionic dyes. *Phys Chem Earth* 100:201–211
19. Almasian A, Olya ME, Mahmoodi NM (2015) Preparation and adsorption behavior of diethylenetriamine/polyacrylonitrile composite nanofibers for a direct dye removal. *Fibers Polym* 16(9):1925–1934
20. Pourjavadi A et al (2016) Porous Carrageenan-g-polyacrylamide/bentonite superabsorbent composites: swelling and dye adsorption behavior. *J Polym Res* 23(3)

21. Ekici S, Isikver Y, Saraydin D (2006) Poly(acrylamide-sepiolite) composite hydrogels: preparation, swelling and dye adsorption properties. *Polym Bull* 57(2):231–241
22. Zhu HY et al (2012) Novel magnetic chitosan/poly(vinyl alcohol) hydrogel beads: preparation, characterization and application for adsorption of dye from aqueous solution. *Bioresour Technol* 105:24–30
23. Zhu L et al (2017) Adsorption of dyes onto sodium alginate graft poly(acrylic acid-co-2-acrylamide-2-methyl propane sulfonic acid)/kaolin hydrogel composite. *Polym Polymer Compos* 25(8):627–634
24. Das S et al (2017) Folic acid-polyaniline hybrid hydrogel for adsorption/reduction of chromium(VI) and selective adsorption of anionic dye from water. *Acs Sustain Chem Eng* 5(10):9325–9337
25. Zhu W et al (2016) Functionalization of cellulose with hyperbranched polyethylenimine for selective dye adsorption and separation. *Cellulose* 23(6):3785–3797
26. Wang S et al (2014) Highly efficient removal of acid Red 18 from aqueous solution by magnetically retrievable Chitosan/carbon nanotube: batch study, isotherms, kinetics, and thermodynamics. *J Chem Eng Data* 59(1):39–51
27. Deng H, Wei Z, Wang X (2017) Enhanced adsorption of active brilliant red X-3B dye on chitosan molecularly imprinted polymer functionalized with Ti(IV) as Lewis acid. *Carbohydr Polym* 157:1190–1197
28. Inbaraj BS, Chen BH (2011) Dye adsorption characteristics of magnetite nanoparticles coated with a biopolymer poly(γ -glutamic acid). *Bioresour Technol* 102(19):8868–8876
29. Wang L, Li Q (2010) Wang A Adsorption of cationic dye on N,O-carboxymethyl-chitosan from aqueous solutions: equilibrium, kinetics, and adsorption mechanism. *Polym Bull* 65(9):961–975
30. Beyki MH et al (2017) Clean approach to synthesis of graphene like CuFe₂O₄@polysaccharide resin nanohybrid: bifunctional compound for dye adsorption and bacterial capturing. *Carbohydr Polym* 174:128–136
31. Shimizu Y, Saito Y, Nakamura T (2006) Crosslinking of chitosan with a trifunctional crosslinker and the adsorption of acid dyes and metal ions onto the resulting polymer. *Adsorpt Sci Technol* 24(1):29–39
32. Zhang X et al (2015) Adsorption of basic dyes on beta-cyclodextrin functionalized poly(styrene-alt-maleic anhydride). *Sep Sci Technol* 50(7):947–957
33. Lakouraj MM, Norouzi R-S, Balo S (2015) Preparation and cationic dye adsorption of novel Fe₃O₄ supermagnetic/thiacalix 4 arene tetrasulfonate self-doped/polyaniline nanocomposite: kinetics, isotherms, and thermodynamic study. *J Chem Eng Data* 60(8):2262–2272
34. Liu H, Liu H (2017) Selective dye adsorption and metal ion detection using multifunctional silsesquioxane-based tetraphenylethene-linked nanoporous polymers. *J Mater Chem A* 5(19):9156–9162
35. Liu J et al (2017) Preparation of polyhedral oligomeric silsesquioxane based cross-linked inorganic-organic nanohybrid as adsorbent for selective removal of acidic dyes from aqueous solution. *J Coll Interf Sci* 497:402–412
36. Zhao W et al (2015) Functionalized graphene sheets with poly(ionic liquid)s and high adsorption capacity of anionic dyes. *Appl Surf Sci* 326:276–284
37. Agarwal S et al (2016) Synthesis and characteristics of polyaniline/zirconium oxide conductive nanocomposite for dye adsorption application. *J Mol Liq* 218:494–498
38. Wang L et al (2012) Stable organic-inorganic hybrid of polyaniline/ α -zirconium phosphate for efficient removal of organic pollutants in water environment. *ACS Appl Mater Interf* 4(5):2686–2692
39. Mu B et al (2016) Preparation, characterization and application on dye adsorption of a well-defined two-dimensional superparamagnetic clay/polyaniline/Fe₃O₄ nanocomposite. *Appl Clay Sci* 132:7–16
40. Xiong P et al (2013) Ternary titania-cobalt ferrite-polyaniline nanocomposite: a magnetically recyclable hybrid for adsorption and photodegradation of dyes under visible light. *Ind Eng Chem Res* 52(30):10105–10113

41. Zeng Y et al (2013) Enhanced adsorption of malachite green onto carbon nanotube/polyaniline composites. *J Appl Polym Sci* 127(4):2475–2482
42. Majumdar S, Saikia U, Mahanta D (2015) Polyaniline-coated filter papers: cost effective hybrid materials for adsorption of dyes. *J Chem Eng Data* 60(11):3382–3391
43. Pandiselvi K, Manikumar A, Thambidurai S (2014) Synthesis of novel polyaniline/MgO composite for enhanced adsorption of reactive dye. *J Appl Polym Sci* 131(9)
44. Saad M et al (2017) Synthesis of polyaniline nanoparticles and their application for the removal of crystal violet dye by ultrasonicated adsorption process based on response surface methodology. *Ultrason Sonochem* 34:600–608
45. Salem MA, Elsharkawy RG, Hablas MF (2016) Adsorption of brilliant green dye by polyaniline/silver nanocomposite: kinetic, equilibrium, and thermodynamic studies. *Eur Polym J* 75:577–590
46. Pandiselvi K, Thambidurai S (2016) Synthesis of adsorption cum photocatalytic nature of polyaniline-ZnO/chitosan composite for removal of textile dyes. *Desalin Water Treat* 57(18): 8343–8357
47. Bingol D et al (2012) Analysis of adsorption of reactive azo dye onto CuCl₂ doped polyaniline using Box-Behnken design approach. *Synth Metals* 162(17–18):1566–1571
48. Mahto TK et al (2015) Kinetic and thermodynamic study of polyaniline functionalized magnetic mesoporous silica for magnetic field guided dye adsorption. *Rsc Adv* 5(59):47909–47919
49. Anuradha Jabasingh S, Ravi T, Yimam A (2017) Magnetic hetero-structures as prospective sorbents to aid arsenic elimination from life water streams. *Water Sci*
50. Zhou L, He B, Huang J (2013) One-step synthesis of robust amine- and vinyl-capped magnetic iron oxide nanoparticles for polymer grafting, dye adsorption, and catalysis. *ACS Appl Mater Interf* 5(17):8678–8685
51. Chen B et al (2016) Magnetically recoverable cross-linked polyethylenimine as a novel adsorbent for removal of anionic dyes with different structures from aqueous solution. *J Taiwan Inst Chem Eng* 67:191–201
52. Beyki MH et al (2016) Green synthesized Fe₃O₄ nanoparticles as a magnetic core to prepare poly 1, 4 phenylenediamine nanocomposite: employment for fast adsorption of lead ions and azo dye. *Desalin Water Treat* 57(59):28875–28886
53. Yao T et al (2015) Investigation on efficient adsorption of cationic dyes on porous magnetic polyacrylamide microspheres. *J Hazard Mater* 292:90–97
54. Song Y-B et al (2015) Poly(4-styrenesulfonic acid-co-maleic acid)-sodium-modified magnetic reduced graphene oxide for enhanced adsorption performance toward cationic dyes. *Rsc Adv* 5(106):87030–87042
55. Mahdavinia GR, Karami S (2015) Synthesis of magnetic carboxymethyl chitosan-g-poly (acrylamide)/laponite RD nanocomposites with enhanced dye adsorption capacity. *Polym Bull* 72(9):2241–2262
56. Mu B, Wang A (2015) One-pot fabrication of multifunctional superparamagnetic attapulgite/Fe₃O₄/polyaniline nanocomposites served as an adsorbent and catalyst support. *J Mater Chem A* 3(1):281–289
57. Dong K et al (2013) Polyurethane-attapulgite porous material: preparation, characterization, and application for dye adsorption. *J Appl Polym Sci* 129(4):1697–1706
58. Zhou S et al (2015) Novel polyamidoamine dendrimer-functionalized palygorskite adsorbents with high adsorption capacity for Pb²⁺ and reactive dyes. *Appl Clay Sci* 107:220–229
59. Anirudhan TS, Suchithra PS (2009) Adsorption characteristics of humic acid-immobilized amine modified polyacrylamide/bentonite composite for cationic dyes in aqueous solutions. *J Environ Sci* 21(7):884–891
60. Ai L, Zhou Y, Jiang J (2011) Removal of methylene blue from aqueous solution by montmorillonite/CoFe₂O₄ composite with magnetic separation performance. *Desalination* 266(1):72–77

61. Dash S et al (2016) Fabrication of inexpensive polyethylenimine-functionalized fly ash for highly enhanced adsorption of both cationic and anionic toxic dyes from water. *Energy Fuels* 30(8):6646–6653
62. Gonte RR, Shelar G, Balasubramanian K (2014) Polymer-agro-waste composites for removal of Congo red dye from wastewater: adsorption isotherms and kinetics. *Desalin Water Treat* 52(40–42):7797–7811
63. Jabli M et al (2017) Almond shell waste (*Prunus dulcis*): Functionalization with dimethy-diallyl-ammonium-chloride-diallylamin-co-polymer and chitosan polymer and its investigation in dye adsorption. *J Mol Liq* 240:35–44
64. Namasivayam C, Sureshkumar MV (2006) Anionic dye adsorption characteristics of surfactant-modified coir pith, a ‘waste’ lignocellulosic polymer. *J Appl Polym Sci* 100(2): 1538–1546
65. Shabandokht M, Binaeian E, Tayebi H-A (2016) Adsorption of food dye acid red 18 onto polyaniline-modified rice husk composite: isotherm and kinetic analysis. *Desalin Water Treat* 57(57):27638–27650
66. Lu Y-S et al (2016) Direct assembly of mesoporous silica functionalized with polypeptides for efficient dye adsorption. *Chem-a Eur J* 22(3):1159–1164

Current Scenario of Nanocomposite Materials for Fuel Cell Applications



Raveendra M. Hegde, Mahaveer D. Kurkuri and Madhuprasad Kigga

List of Abbreviations

FC	Fuel cell
PEM	Proton exchange membrane
PEMFC	Proton exchange membrane fuel cell
AFC	Alkaline fuel cell
DMFC	Direct methanol fuel cell
PAFC	Phosphoric acid fuel cell
MCFC	Molten carbonate fuel cell
SOFC	Solid oxide fuel cell
MEA	Membrane electrode assembly
GDL	Gas diffusion layers
RH	Relative humidity
PEEK	Poly (ether ether ketone)
SPEEK	Sulfonated poly (ether ether ketone)
PBI	Polybenzimidazole
PVA	Polyvinyl alcohol
ORR	Oxygen reduction reaction
CV	Cyclic voltammetry
XRD	X-ray diffraction
DFT	Density functional theory
PECVD	Plasma enhanced chemical vapor deposition
CNT	Carbon nanotubes
SWCNT	Single-walled carbon nanotubes
MWCNT	Multi-walled carbon nanotubes
IEC	Ion exchange capacity

R. M. Hegde · M. D. Kurkuri (✉) · M. Kigga (✉)
Centre for Nano and Material Sciences, Jain University, Jain Global Campus,
Bengaluru 562 112, Karnataka, India
e-mail: mahaveer.kurkuri@jainuniversity.ac.in

M. Kigga
e-mail: madhuprasad@jainuniversity.ac.in

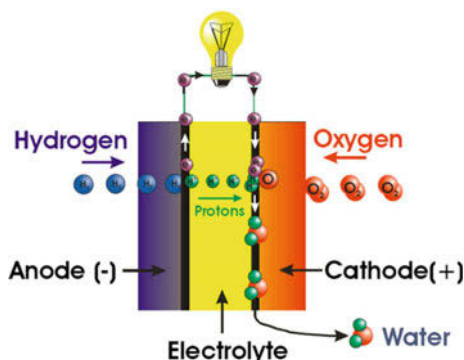
1 Introduction

The increasing population and rapid urbanization are leading to a sudden rise in the energy consumption worldwide. To fulfil this huge demand, fossil fuels have been extensively exploited as a major source of energy until date. However, this source of energy consumption is creating irreversible damage to the environment by producing huge and rapid carbon footprint and hence constant depletion of this source is eventually leading to the energy crisis in most of the countries today [1]. In addition, it has been predicted that there will be more than 50% increase in energy demand by next 25 years, which cannot be met just by relying majorly on fossil fuel source. Therefore, exploring the alternative energy sources have become inevitable in fulfilling the energy demand of future generation. Consequently, renewable energy sources, on the other hand, are promising sources of energy and are very fast developing technology as it provides the energy with significantly less pollution. Though several alternative technologies such as solar, wind, tidal, biomass have been developed, they all have been restricted for complete commercial exploitation because of their drawbacks such as storage issues, energy conversion, efficiency, transportation etc. Consequently, fuel cells (FCs) are considered to be a future source of energy to meet the rising energy demand and thus, have been attracting the wide scientific community to develop sustainable technology for efficient energy generation [2]. It is an emerging field of research in energy materials as it provides clean and green energy source with a conversion efficiency as high as 60%. Contrasting to other electrochemical sources like batteries, FCs requires the constant supply of fuel and oxygen to retain the continuous electrochemical reaction process, whereas, in a battery, the previously loaded chemicals in a batch process format attain the energy. However, FCs obtain the energy sources continuously from the exterior of the cell i.e., hydrogen from the fuel and oxygen from the environment [3]. Also, the possibilities of rapid recharging, off-grid operations, a significant reduction in weight, noise-free operations are the added advantages with FCs. More importantly, FCs reduce the greenhouse gas emission and produce only water as the main by-product. Therefore, it is significantly applied in portable energy devices, automobiles, transportation vehicles [4]. However, the conditions like high-temperature operation, availability of fuel source and infrastructures are hindering the further development of FCs and their usage in large scale.

1.1 Working Principle of FC

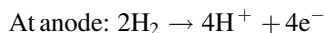
FCs are the galvanic cells, which work on the principle of oxidation and reduction reactions at the anode and cathode respectively. They use hydrogen or hydrogen-rich fuels for electrochemical reactions as hydrogen contains high energy per unit weight than any other fuels. A conventional FC is illustrated in Fig. 1

Fig. 1 Schematic representation of a conventional fuel cell. Reproduced with permission from Ref. [5], Copyright 2010, Elsevier



which consists of a sandwiched membrane between the anode, cathode, and electrolyte by forming a membrane electrode assembly (MEA) along with gas diffusion layers (GDL).

The electrochemical reactions are involving the continuous oxidation of hydrogen at anode and reduction of oxygen at the cathode. This chemical reaction produces the electrons, which are opposed by the electrolytic membrane and they move through an external circuit to produce direct current. The reactions involved in FCs are given below;



To dissociate the hydrogen fuel into constituent ions, the FCs are equipped with the catalyst at the anode. Generally, platinum is most widely used as anode catalyst as it exhibits highest electrocatalytic activities in organic fuel redox reactions. The outer layer of catalyst is constructed with GDL, which promotes the transfer of reactants into catalyst layer and helps in the removal of by-product, water. GDL is composed of a thick porous array of carbon fibers, which provides a conductive pathway for current collection. Further, GDL also helps in the electronic connection between bipolar plate and electrode through the channel of MEA. In addition, GDL enhances the mechanical strength of MEA and protects the catalyst layer from corrosion.

The amount of total current produced by the FC depends on cell size, type of the cell, operating temperature and extent of gaseous pressure applied to it. During the electrochemical reactions, FC produces only a small amount of current in the range of 0.6–0.87 V. Therefore, in order to obtain a high voltage, a parallel or series of single cells are constructed as illustrated in Fig. 2. Further, each FC in a stack is separated by a bipolar plate which assists in the uniform distribution of fuel and oxygen in MEA. Polymer-based gaskets are inserted around the edges of MEA to

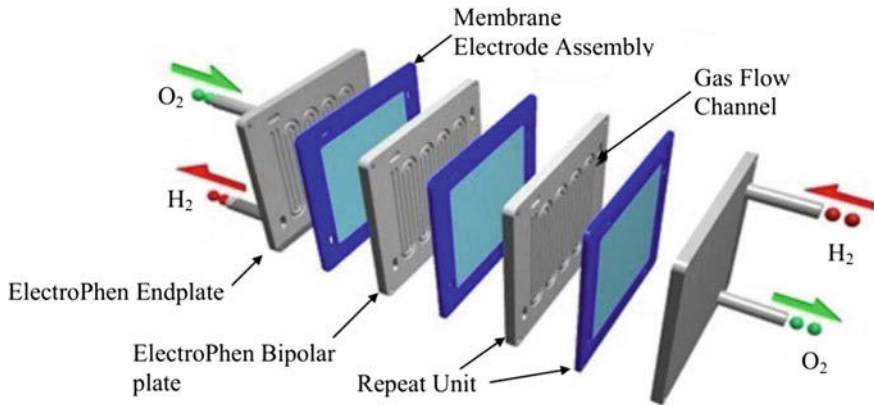


Fig. 2 Schematic representation for the construction of fuel cell stack. Reproduced from Ref. [6], Copyright 2013, Bentham Open

strengthen the FC stack as it is much effective in holding the MEA and adjusting the required pressure inside the system. The produced current is collected by a collector plate which is presented at the terminal part of MEA.

1.2 Proton Conduction Mechanism in FC

Proton conduction across the electrolyte membrane is the prime requirement to attain high current density and it is, therefore, efficiency determining a factor for the FC. This proton conduction depends on the modification made to the membrane, extent of sulfonation, relative humidity (RH), and temperature. The proton conduction phenomena generally follow either Grotthuss mechanism or Vehicle mechanism [7]. In Grotthuss mechanism, proton jumps from one ionic site to another through hydrogen bond network (Fig. 3a). For example, in Nafion[®] membranes, a proton hops from sulfonic acid (SO_3H) site to the nearby acceptor site i.e., water molecule which has potential for proton movement throughout the membrane.

On the other hand, according to the vehicle mechanism (or en masse diffusion mechanism), proton transfer takes place by the diffusion of carrier species in the form of hydrated ions in the electrolyte (Fig. 3b). Here the protons attach itself to the acceptor molecule and thus acceptor molecule moves from one end to another leading to the proton movement across the membrane. Both the above mechanisms depend on the nature and properties of nanocomposites membrane used in the FC. Moreover, the proton conductivity increases with RH of the system due to the presence of more hydrated protons in the system. Therefore, the proposed models can be used to design the suitable organic and inorganic fillers for polymeric membranes compared to pure polymer membranes [9].

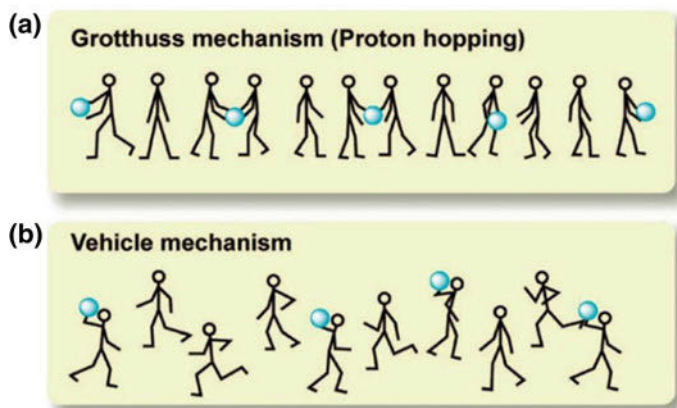


Fig. 3 Schematic representation of **a** Grotthuss mechanism and **b** Vehicle mechanism. Reproduced with permission from Ref. [8], Copyright 2008, American Chemical Society

FCs are generally classified based on the nature of electrolyte used in the cell, operating temperature and types of fuel/oxidants used. Different types of FCs with their properties, efficiency and operating temperature are listed in Table 1.

2 Nanocomposites in FC

To overcome the problems associated with low proton conduction, low current density, fuel crossover, carbon monoxide (CO) poisoning in conventional FCs, in the recent years a new variety of organic, inorganic and polymer-based nanocomposites have been developed. Nanocomposites are hybrid materials with conventional components in it [10, 11] which would be the solution for some of the challenges by providing improved water retention capacity, high energy conversion, and suppression of fuel crossover. Modification of FC composites with organic and inorganic materials is a growing technology in energy material development. Nanomaterials have been integrated with polymers to enhance their original characteristics such as thermal and chemical stabilities [12, 13]. This is attributed to the strong interfacial interaction between the polymers and inserted material. Preparation method of the nanocomposite is one of the important factors in the improvement of FCs as it alters the microstructure of the membranes [14]. Nanomaterials with conventional composite materials have specific properties such as high surface area, specific functional groups, interaction capacity [15–22] that would increase the catalytic performance of the electrodes in FC in terms of rigidity and thermal stability. On the other hand, organic nanocomposites such as sulfonated poly (ether ether ketone) (SPEEK) and polybenzimidazole (PBI) have provided the high flexibility, durability, and processability to the components of the FC [23]. The different types of potential nanocomposites and its applications in FC are described

Table 1 Types of important fuel cells and comparison of their properties

Type of fuel cell	Electrolyte	Charge carrier	Anode reaction	Cathode reaction	Overall reaction	Working temperature (°C)	Efficiency (per cell) [%]	Applications
Proton Exchange Membrane Fuel Cell (PEMFC)	Polymer membrane	H ⁺	2H ₂ → 4H ⁺ + 4e ⁻	½ O ₂ + 4H ⁺ + 4e ⁻ → 2H ₂ O	2H ₂ + ½ O ₂ → 2H ₂ O	60–120	50–70	Transportation, military
Alkaline Fuel Cell (AFC)	Aqueous alkaline solution	OH ⁻	2H ₂ + 4OH ⁻ → 4H ₂ O + 4e ⁻	O ₂ + 4e ⁻ + 2H ₂ O → 4OH ⁻	2H ₂ + O ₂ → 2H ₂ O	<80	60–70	Transportation, space
Direct Methanol Fuel Cell (DMFC)	Polymer membrane	H ⁺	CH ₃ OH + H ₂ O → CO ₂ + 6H ⁺ + 6e ⁻	3/2 O ₂ + 6H ⁺ + 6e ⁻ → 3H ₂ O	CH ₃ OH + 3/2 O ₂ → CO ₂ + 2H ₂ O	60–120	20–30	Transportation, energy storage systems
Phosphoric Acid Fuel Cell (PAFC)	Molten phosphoric acid	H ⁺	2H ₂ → 4H ⁺ + 4e ⁻	O ₂ (g) + 4H ⁺ + 4e ⁻ → 2H ₂ O	2H ₂ + O ₂ → 2H ₂ O	150–200	55	Thermal energy consuming system, air conditioning system
Molten Carbonate Fuel Cell (MCFC)	Molten alkaline carbonate	CO ₃ ²⁻	H ₂ + CO ₃ ²⁻ → H ₂ O + CO ₂ + 2e ⁻	½ O ₂ + CO ₂ + 2e ⁻ → CO ₃ ²⁻	H ₂ + ½ O ₂ + CO ₂ → H ₂ O + CO ₂	600–650	55	Combined heat and power for decentralized systems and transportation
Solid Oxide Fuel Cell (SOFC)	Solid ceramic electrolyte (Yttrium stabilized zirconia)	O ²⁻	H ₂ + O ₂ ⁻ → H ₂ O + 2e ⁻	½ O ₂ + 2e ⁻ → O ₂ ⁻	H ₂ + ½ O ₂ → 2H ₂ O	800–1000	55	Combined heat and power units, uninterruptible power systems (UPS), Primary power units

in the following section. Furthermore, the efficient working of FC by the integration of various nanocomposite materials for the anode, cathode, and hybrid membranes are summarized below.

2.1 Nafion[®] - Metal Oxide-Based Nanocomposite

Nafion[®] is a fluoropolymer which is comprised of sulfonated tetrafluoroethylene backbone and it has been extensively using in the development of FC especially the PEMFC due to its excellent proton conductivity. The proton on sulfonic acid can jump from one site to another through Grotthuss mechanism which makes them conduct protons easily and thus, prevents the electron conduction. However, the property of becoming dehydrated at high temperature, high cost and high fuel crossover of Nafion[®] made its applications in FC limited to a certain extent. Therefore, the modification of Nafion[®] with other nanomaterials to overcome these drawbacks has gained significant importance.

Recently, Nafion[®] modified with phosphonate and sulfonate silica nanoparticles (NIM_PO₃ and NIM_SO₃) for high proton conduction was reported [24]. The synthesized nanocomposite membrane (Fig. 4) revealed the excellent proton conducting property even at a low relative humidity and elevated temperature greater than 80 °C. The conductivity of sulfonate-based nanocomposites at 130 °C and 30% RH was 50 mS/cm. The NIM_SO₃ membranes also exhibited the promotion of water retention capacity by increasing the water uptake 32 (± 2) wt% and better mechanical stiffness even above the temperature of 200 °C.

Mohammadi et al. fabricated the Nafion[®] with metal oxide nanoparticles for PEMFC [25]. They recast the commercial Nafion[®] with 75 nm sized TiO₂/ZrO₂ nanoparticles by sol-gel and blending method respectively. Nafion[®]/ZrO₂ nanocomposite membrane offered good proton conduction and with an increase in the concentration of ZrO₂ and Nafion[®]/TiO₂ membrane displayed a better water retention capacity than Nafion[®] membranes modified by other conventional methods. Further, these membranes also unveiled the highest PEMFC performance

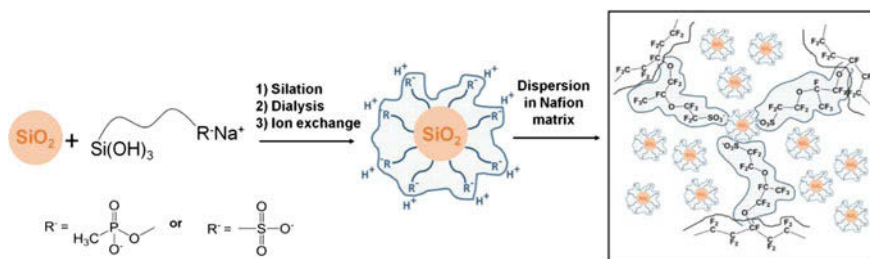


Fig. 4 Schematic representation of the synthesis of Nafion[®] membranes functionalized with phosphonate and sulfonate nanoparticles. Reproduced with permission from Ref. [24], Copyright 2016, Elsevier

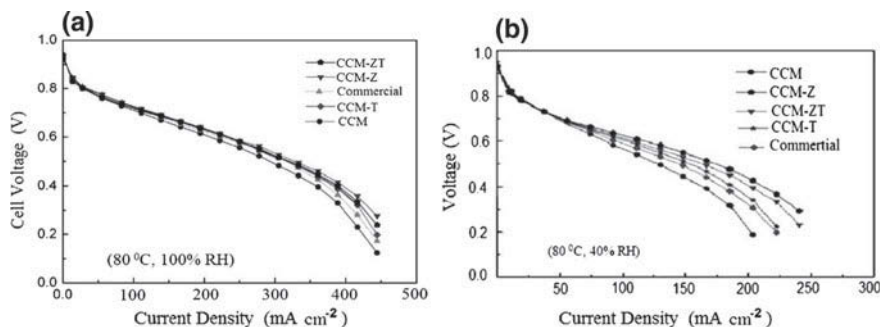


Fig. 5 Comparison of the polarization curves for modified composite membranes and Nafion[®] membranes at 110 °C, **a** 100% RH, **b** 30% RH. Reproduced with permission from Ref. [25], Copyright 2013, Elsevier

with respect to 1–5 polarization under 110 °C, 0.6 V and 30% RH at 1 atm (Fig. 5). Thus, they proved to be the best-modified membranes for PEMFC.

Integration of Fe₂TiO₅ in Nafion[®] membranes prepared in water, ethanol and water-ethanol solvent increased proton exchange capacity in FCs [26]. The comparison of the efficiency of membranes revealed that the modified membranes prepared in water solvents are superior to the membranes prepared in either of the solvents. This was due to the fact that water being a polar solvent led the nanoparticles into microscopic swelling and offered strong hydrogen bond whereas, the less polar solvent ethanol couldn't make that to happen. The proton conductivity of 226 mS/cm was obtained by the insertion of 2% Fe₂TiO₅ in commercial Nafion[®] membrane using water, ethanol and water-ethanol solvents. In addition, the membrane also showed a better water uptake capacity due to the hydrophilic nature of nanoparticles summarized (Table 2).

Table 2 Properties of solvent uptake and proton conduction in Nafion[®] and modified nanocomposite membranes at 25 °C (95% RH) and 110 °C (70% RH)

Sample code	Thickness (μm)	Solvent uptake (%)	Proton conductivity (mS/cm)	
			25 °C	110 °C
NH-2 ^a	231	33	226	240
NHE-2 ^a	226	25	87	93
NE-2 ^a	240	35	72	80
N ^a	224	22	21	24
N ^b	230	29	6	–
N ^c	238	31	1	–

Reproduced with permission from Ref. [26], Copyright 2014, Elsevier

^aMembranes stored in water solvent

^bMembranes stored in a mixture of water-ethanol solvent

^cMembranes stored in pure ethanol solvent

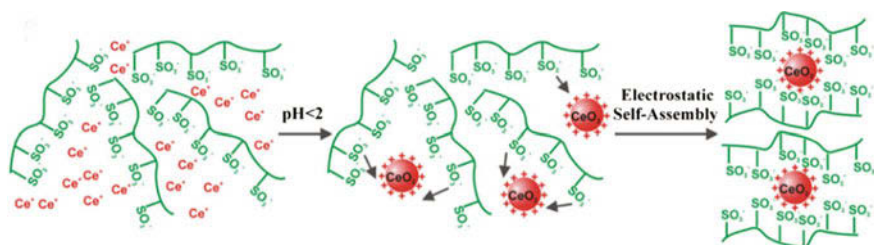


Fig. 6 Graphical representation of self-assembled Nafion[®]/CeO₂ nanocomposites. Reproduced with permission from Ref. [27], Copyright 2012, Elsevier

The Nafion[®]/CeO₂ membranes are proved to be the better nanocomposite materials for FC applications. Zhao and co-workers prepared a self-assembly of Nafion[®]/CeO₂ for electrolyte membrane between positively charged CeO₂ nanoparticle with negatively charged SO₃⁻ group of Nafion[®] as illustrated in Fig. 6 [27]. The hybrid nanocomposite membranes were displayed the superior proton exchange capacity and dimensional stability than pristine Nafion[®] membrane below the RH of 75% and low fluoride emission rate. In addition, the prepared nanocomposite membrane showed a very low fluoride emission rate of 43.05, 8.67, 6.01, and 4.47 mg/h for 1, 3, 5 and 10 wt% the CeO₂, respectively. However, the pristine Nafion[®] membrane showed 55.78 mg/h and 11.64 mg/h by the same Nafion[®] membrane synthesized by a sol-gel process. The material also exhibited the irreversible open reduction rate of 1.13×10^{-4} mV/s which was much lower than pristine Nafion[®] membrane (5.78×10^{-4} mV/s) and the Nafion[®] membrane prepared through sol-gel method (5.78×10^{-4} mV/s).

Cozzi and co-workers [28] modified the pristine Nafion[®] with propyl sulfonic acid (RSO₃H) acid on TiO₂ nanoparticles (TiO₂-RSO₃H) to achieve a higher efficiency in IEC and proton conductivity. The synthesis of TiO₂-RSO₃H is illustrated in Fig. 7. The covalently grafted hybrid materials as a nanocomposite with Nafion[®] promoted the efficiency of DMFC. The conductivity value of this material obtained was 80 mS/cm at 140 °C at the composition of 10 wt% TiO₂-RSO₃H in a single

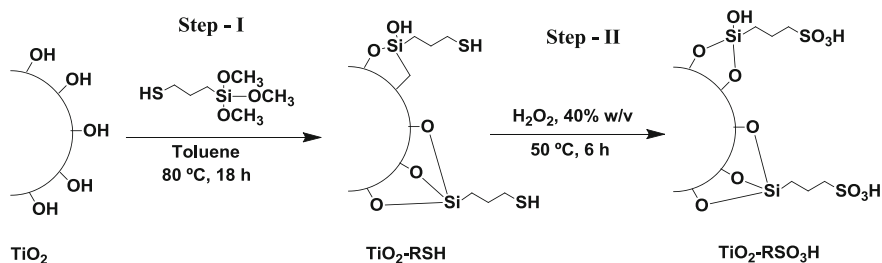


Fig. 7 Functionalization of TiO₂ nanoparticles with propyl sulfonic acid. Reproduced with permission from Ref. [28], Copyright 2014, Elsevier

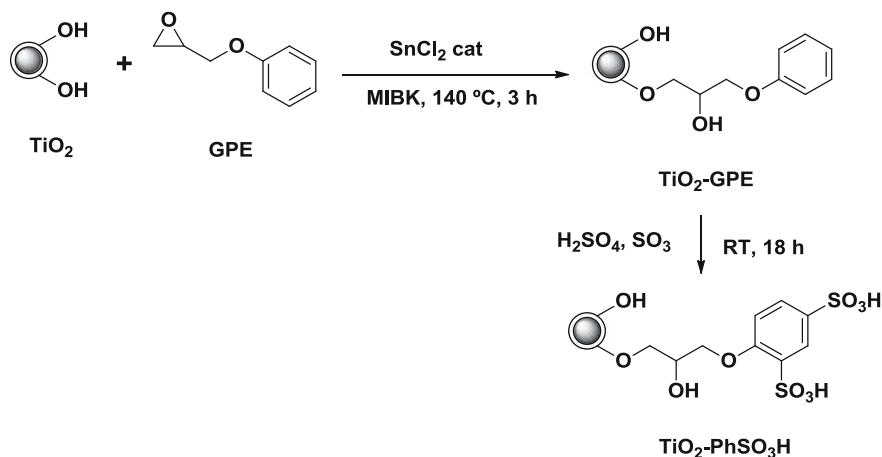


Fig. 8 Functionalization of TiO_2 nanoparticles with phenyl sulfonic acid. Reproduced with permission from Ref. [29], Copyright 2014, Elsevier

cell of DMFC. Also, they showed a supreme power density of 64 mW/cm^2 which is about 40% more than the pristine Nafion[®] composite membrane.

The organic functionalization of TiO_2 with phenyl sulfonic groups was able to overcome the less proton conduction in FC [29]. Further, the grafting of glycidyl phenyl ether group on the oxide surface was confirmed (Fig. 8) and the IEC was increased due to the covalently bound phenyl sulfonic group. The experimental observation showed that the prepared hybrid membranes reached the highest conductivity of 110 mS/cm at 140°C with the concentration of 10 wt% $\text{TiO}_2\text{-PhSO}_3\text{H}$. The material also showed the better properties such as reduced methanol crossover (up to 20%) compared to the unfilled Nafion[®] membrane.

2.2 Graphene-Based Nanocomposites

Graphene has typical properties such as high surface area, surface active sites, electrical conductivity, excellent mechanical strength, high chemical stability and low metal loading capacity. Therefore, it is used for varieties of applications such as electronic devices, energy storage [30–32], sensors and biomedical applications [33]. In addition, the graphene is being used as a supporting material due to the presence of epoxy groups and carboxylic acid groups enhances the proton conducting capacity of the material with metal electrocatalysts for oxygen reduction reaction in FCs [34]. In addition, the stability of nano-catalysts can be increased by dispersing the metal on graphene [35].

The synthetic methods for the preparation of doped graphene and graphene supported nano electrocatalysts with respect to their structure-dependent properties and

further developments were discussed by Liu et al. [36]. They have summarized the synthesis and characterization of graphene nanocomposites with various metals electrocatalysts for cathode and anode materials of FC. They elucidated the components into various types i.e. (1) graphene supported metal-free electrocatalysts for high oxygen reduction reaction (ORR) in acid and alkaline electrolytic medium. (2) graphene supported non-noble metals for efficient electrocatalysts (3) graphene-based Pt-free electrocatalysts and alloy nanomaterial for low-cost FC material (4) graphene-supported Pt-based nano-catalysts for increased ORR in electrolytes. These materials were found to participate in the electrooxidation of organic molecules at the anode of Direct Methanol Fuel Cells (DMFC) and ORR at the cathode. By the experimental observation, graphene or co-doped graphene with N, S, B, and P are found to be an excellent cost-effective cathode catalyst for FC applications.

Considering the advantages of graphene, Huang and co-workers developed a novel graphene nanoplate-Pt (GNP/Pt) composite electrocatalysts to obtain the high-performance DMFC [37]. They synthesized a series of graphene nanoplate (GNP/Pt), reduced graphene oxide nanoplate (RGO/Pt) and Vulcan XC-72 Pt (XC-72/Pt) with 0.17 mL of 0.45 M $\text{Pt}(\text{NO}_3)_2$ as demonstrated in Fig. 9. Further, its electrochemical activity was measured through cyclic voltammetry (CV) and the X-ray diffraction (XRD) patterns which revealed that the Pt was uniformly dispersed over the graphene nanoplates and confirmed the formation of an intact composite. This reduced the probable catalytic poisoning due to methanol oxidation and thus electrocatalytic activity was increased. The time required to increase the electrode potential was significantly decreased in the order of GNP/Pt (~ 130 s) followed by RGO/Pt (50 s) and XC-72/Pt (~ 30 s). Thus, they concluded that the GNP/Pt was superior for electrocatalytic activity than RGO/Pt and XC-72/Pt. Also, it is worth in mentioning that GNP can be used as the best catalyst supports for DMFC.

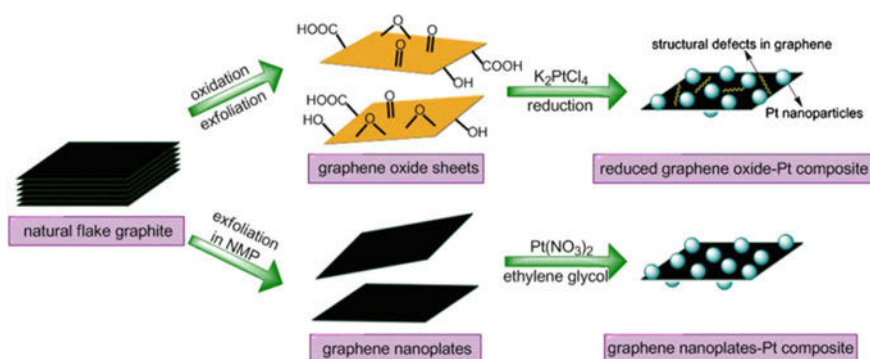
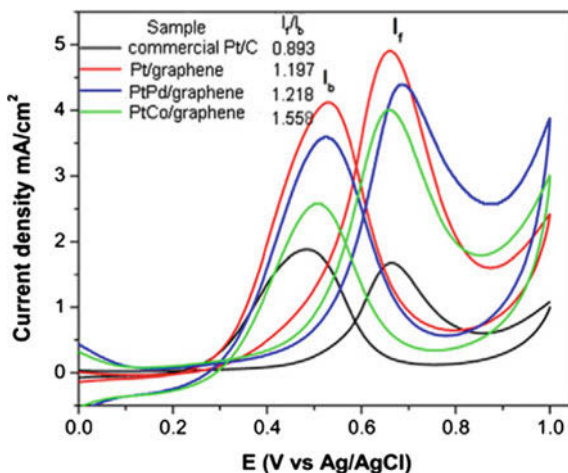


Fig. 9 Illustrations of the synthesis of reduced graphene oxide-Pt composite and graphene nanoplate-Pt composite by the traditional oxidation-reduction method and soft chemical method, respectively. Reproduced with permission from Ref. [37], Copyright 2012, Elsevier

Fig. 10 A comparison of cyclic voltammograms in 0.5 M CH₃OH/0.5 M HClO₄ electrolyte at a scanning rate of 50 mV/s displayed by modified materials to evaluate the methanol oxidation and tolerance to CO poisoning. Reproduced with permission from Ref. [38], Copyright 2013, Elsevier



The application of exfoliated graphene-supported Pt and Pt-based alloys as electrocatalysts were elucidated to enhance the performance of DMFC [38]. A low cost and environment-friendly method of “Thermal Expansion and Liquid Exfoliation Solvothermal Reaction (TELESR)” was used to hybridize the exfoliated graphene sheets to load the Pt metal and alloys such as Pt/Pd, Pt/Co nano-clusters. This method improved the methanol oxidation in FC by increasing the electrocatalytic activity. The methanol oxidation was found to be $I_f/I_b = 1.218$ and 1.558 in PtPd/graphene and PtCo/graphene respectively during an electrochemical analysis. Also, the modified material showed high conductivity and tolerant to carbon monoxide poisoning (Pt/graphene, $I_f/I_b = 1.197$) compared to commercial Pt/C catalyst ($I_f/I_b = 0.893$) as shown in Fig. 10. This was due to the interaction of graphene with Pt electronic environment occurred and graphene played a major role in controlling the electronic environment with attached Pt atom which was confirmed by Density Functional Theory (DFT) studies. Therefore, the reported process gives a novel hybridized material that could save the extensive use of expensive Pt metal as electrocatalysts in FC with the increase in performance when compared to conventional Pt/C electrocatalysts for methanol oxidation.

Recently, Nafion[®]-graphene oxide (GO-Nafion[®]) nanohybrids for the conduction of high amount protons in PEMFC were described [39]. The reaction of a chain of well-known fluoropolymer, Nafion[®] onto the GO via Atom Transfer Radical Addition (ATRA) between C-F group of Nafion[®] and C=C groups of GO presented a nanocomposite material as depicted in Fig. 11.

These nanohybrids form the proton conducting fields by the aggregation of sulfonic acid units of Nafion[®] material which increases the interfacial compatibility with Nafion[®] matrix. From the electrochemical analysis, it was evident that the developed nanohybrids showed 1.6 folds high performance in conducting the protons compared to the commercially available Nafion[®] 112 membranes which

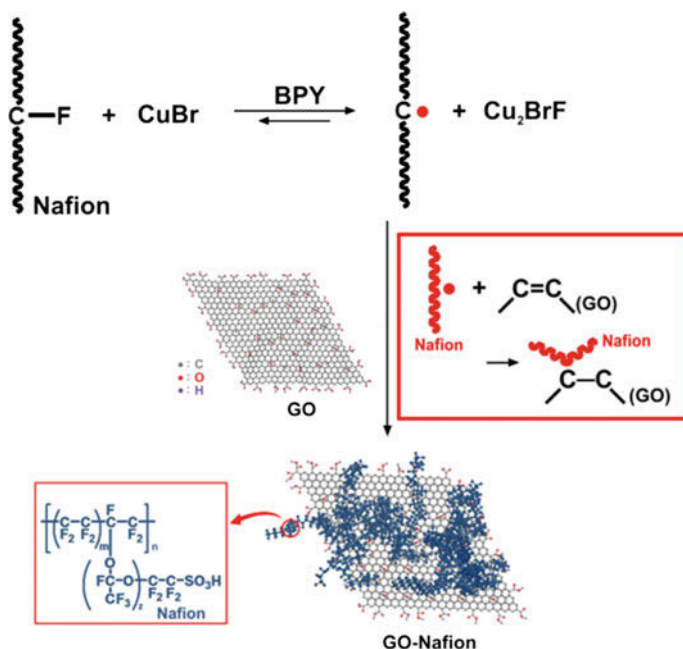


Fig. 11 Schematic representation of the reaction between Nafion[®] chains onto GO surfaces through an atom transfer radical addition reaction to prepare GO-Nafion[®] hybrid material. Reproduced with permission from Ref. [39], Copyright 2016, Elsevier

have been summarized in Table 3. Thus, a new variety of material which can be used as nano additive in the fabrication of Nafion[®] based nanocomposite for the PEM for FC was displayed.

A transition metal hierarchical porous N-doped graphene foams (HPGFs) were prepared by using silica nanoparticles as a template were reported by Zhou and co-workers [40]. The material exhibited the excellent property of ORR in 0.1 M KOH solution with high onset potential of 1.03 V and the limiting current of ~ 9 mA/cm² which was 1.7 times higher than the commercial Pt/C catalyst. Also, an excellent catalytic performance in acidic medium with an onset potential of 0.81 V and the limiting current was up to ~ 10 mA/cm² (Table 4) was observed. Further, the material also showed good methanol tolerance, long-term durability in both acidic and basic conditions. Such excellent material is a model for the development of applied energy systems such as FCs and metal-air batteries.

Nitrogen-doped graphene sheets prepared through plasma enhanced chemical vapour deposition (PECVD) method were studied as anode material for a Microbial Fuel Cell (MFC) [41]. The doping of nitrogen affected the electronic conductivity and catalytic activity due to the formation of structural defects. The material performed with excellent electrocatalytic activity towards glucose oxidation mediated via *Escherichia coli* due to the adjacent contact between microorganism and

Table 3 Proton conduction and single cell performance among various modified GO-Nafion[®] nanocomposite [39]

Membrane (with % of GO)	Proton		conductivity (mS/cm)		Single cell tests			
	20 ° C	95 ° C	H ₂ /O ₂		H ₂ /air			
			Open cell voltage (V)	Maximum power density (mW/ cm ²)	Current density at 0.6 V (mS/ cm ²)	Open cell voltage (V)	Maximum power density (mW/ cm ²)	Current density at 0.6 V (mS/ cm ²)
Recast Nafion [®]	25.8	53.3	0.97	713	1018	0.98	417	619
NM/ GO-0.05	36.7	72.4	0.98	886	1376	0.94	586	826
NM/ GO-0.10	40.8	82.3	0.98	743	1059	0.95	450	595
NM/ GO-0.15	22.3	47.5	0.96	836	1215	0.95	509	652
Nafion [®] 212	40.8	88.3	0.99	951	1347	0.98	563	740

Table 4 Electrochemical properties exhibited by HPGFs and Pt/C catalyst at different physical parameters.

Catalysts	Surface area (m ² /g)	N content (%)	Pyridinic N (%)	Graphitic N (%)	Oxidized N (%)	Onset potential (V)		Limiting current density (mA/cm ²)	
						KOH	HClO ₄	KOH	HClO ₄
HPGF-1	918.7	3.15	37.9	51.9	10.2	1.03	0.81	9.08	9.90
HPGF-2	325.9	5.49	41.9	52.0	6.1	0.99	0.81	5.87	5.05
HPGF-3	567.7	3.09	36.8	50.6	12.6	0.97	0.80	7.33	5.27
Pt/C (20 wt%)	–	–	–	–	–	1.04	1.00	5.51	5.40

Reproduced with permission from Ref. [40]. Copyright 2016, Elsevier

electrode (Fig. 12). The doped nanocomposite material showed the power density of 1008 mW/cm² at a current density of 6300 mA/m². This is a good metal free nanocomposite material which showed better performance in MFC.

2.3 Carbon Nanotubes and Its Hybrid Nanocomposites

Carbon nanotubes (CNT) are an important class of materials which significantly used in the field of material science, nanotechnology, optics, electronics, sensors, energy materials [42] due to their excellent mechanical, electrical and optical properties. Due to their light weight and high electrical conductivity, both Single-Walled Carbon Nanotubes (SWCNT) and Multi-Walled Carbon Nanotubes (MWCNT) [43] have obtained substantial consideration in FC application. They tend to increase the catalytic performance, steadiness, corrosion resistance, electron

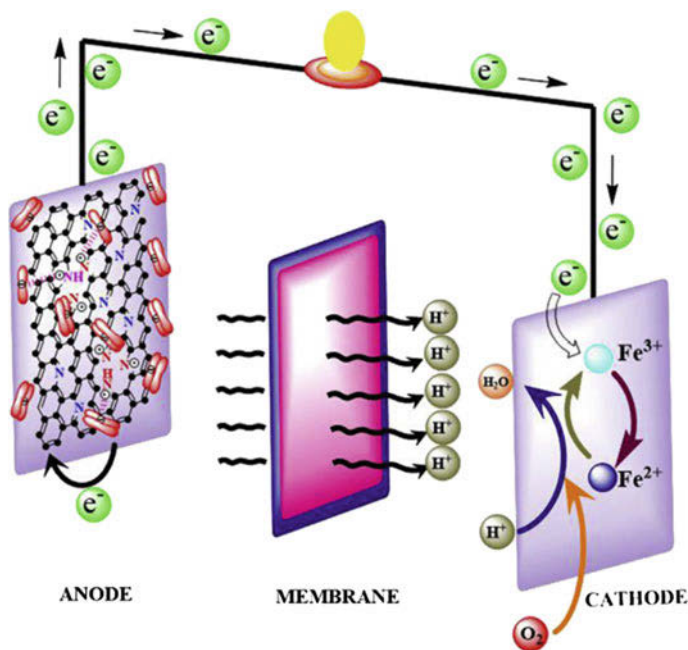


Fig. 12 Predicted mechanism involved in the electrogenic bacterial attachment to NGNS/cathode catalyst. Reproduced with permission from Ref. [41], Copyright 2015, Elsevier

transmission capacity and decreases the overall fuel cell cost [44]. Therefore, their usage as nanocomposite materials has extensively been studied in FC applications, especially in MFC.

CNT as an alternative cathode support and catalyst in MFCs was demonstrated by preparing a hybrid material containing CNT/Pt enriched with Palm Oil Mill Effluent. This material showed a better catalytic activity than undecorated Pt metal [45]. Incorporation of only 25% of Pt in the hybrid material reduced the use of precious Pt metal and thus helped in reducing the cost of FC. The material increased the MFC output voltage from 31.8 to 169.7 mW/m² at the chemical oxygen demand of 100 mg/L and 2000 mg/L, respectively which becomes a novel material as a catalyst in FC.

In 2014, Mehdinia et al. [46] compared the electrochemical performance of MFC using MWCNT-SnO₂/Glassy Carbon Electrode (GCE), MWCNT/GCE and bare GCE as anode material. From this experiment, it was concluded that the fabricated MWCNT-SnO₂/GCE (Fig. 13) produced a high electrochemical activity owing to the insertion of SnO₂ and high electron conductivity, high surface area properties of MWCNT into GCE. The power densities of MWCNT-SnO₂/(GCE), MWCNT/GCE, and bare GCE anode were found to be 1421, 699, 457 mW/m² respectively. Finally, the MWCNT-SnO₂/(GCE) nanocomposite represented as the best anode material for MFC due to its clean and green preparation and high electrochemical activity.

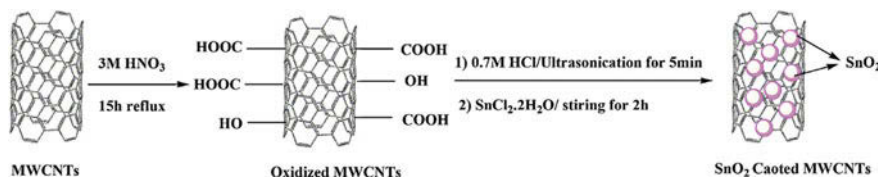


Fig. 13 Schematic representation of the synthesis of MWCNT/SnO₂ nanocomposite as an electrode material. Reproduced with permission from Ref. [46], Copyright 2014, Elsevier

A new MWCNT nanocomposite membrane modified with imidazole groups (MWCNT-Im) on Nafion[®] as proton conducting units showed the less methanol permeability, fuel crossover, and high proton conductivity in DMFC [47]. The combined interfacial attraction between the MWCNT grafted with protonated imidazole units, and a negatively charged sulfonic acid group of the Nafion[®] fluoropolymer formed a new electrostatic interaction. IEC was observed to be increased from 0.89 meq/g of Nafion[®] 117–0.92 meq/g of MWCNT-Im due to the participation of imidazole functional groups as new proton conduction sites added to the proton conduction mechanism. In addition, Nafion[®] modified with 0.5 wt% MWCNT-Im exhibited decreased methanol permeability of 1×10^{-6} cm²/s with increasing in temperature by holding methanol molecules through a formation of complex structure. Overall, compared to neat Nafion[®], the modified nanocomposite material showed excellent performance and accepted as a promising material in the application of FC.

In other work, a versatile metal-free catalyst for oxygen reduction reaction in FC was designed by Zhong et al. [48] They reformed the nitrogen, iron, and cobalt functionalized CNT (FeCoN-CNTs) with N-doped carbon foams (NCFs) with a 3D structure which provides a strong porous structure and large catalytically active sites. The composite material exhibited a synergetic effect of Fe/Co and the N species by forming the Fe/Co–N_x complex in the carbon material. In comparison with the commercial Pt/C catalyst, the newly fabricated material showed better performance in terms of resistance for fuel crossover and electrocatalysis in alkaline medium.

Recently, MWCNT functionalized with manganese oxide/polypyrrole (MWCNT-MnO₂/PPy) as an anode material in MFC was successfully demonstrated to produce the electricity from sewage water [49]. They electrochemically deposited the MWCNT-MnO₂/PPy on the surface of carbon cloth electrode as shown in Fig. 14. The fabricated electrode displayed electrical conductivity of 0.1185 S/m along with the band gap value of 0.8 eV and power density of 112.5.4 mW/m². Hence, it is a good example of MWCNT nanocomposite materials for generating the electricity from sewage source.

Mirzaei et al. [50] investigated a new catalyst support that made up of Pt/MWCNT nanocomposite for PEMFC. This hydrothermally prepared catalyst support material achieved more activity even after 4000 cycles, whereas the Pt/C catalyst showed no activity after 2000 cycles. The nanocomposite material revealed

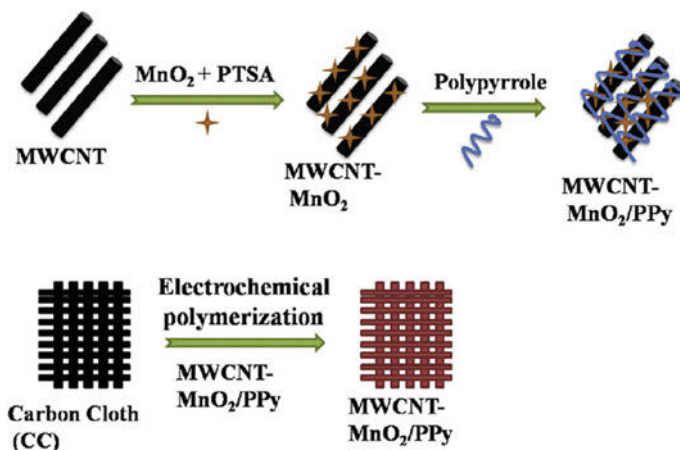


Fig. 14 Schematic representation of the synthesis of MWCNT-MnO₂/PPy and proposed electrochemical polymerization on CC. Reproduced with permission from Ref. [49], Copyright 2016, Elsevier

Table 5 Comparison of the electrochemical and physical characteristics of Pt/MWCNTs and Pt/C.

Catalyst	Q _H (μC)	Specific surface area (m ² /g)	Particle size (nm)	Specific surface area (m ² /g) after 4000 cycle	OCV (V)
Pt/MWCNTs	0.178	36.46	7	5.37	+0.9
Pt/C	0.700	52.08	3.9	0.58	+0.96

Reproduced with permission from Ref. [50], Copyright 2017, Elsevier

Electrochemical Specific Surface Areas (ECSA) were initially 52.08 m²/g was reduced to 0.58 m²/g after 4000 cycles. Also showed good catalyst stability by achieving the ECSA value from 36.46 to 5.37 m²/g (Table 5).

The HNO₃-H₂SO₄ functionalized CNT nanocomposite with MnO₂ demonstrated good catalyst for ORR in MFC maintained in neutral solution [51]. The ORR was increased by the unique interaction between MnO₂ and CNT which was fabricated through hydrothermal method. From the electrochemical measurements, it was observed that the MFC incorporated with the present material reached a power density of 520 mW/m² which is higher than the pristine CNT (275 mW/m²) and MnO₂ with HNO₃-H₂SO₄ functionalized CNT (fCNT) (440 mW/m²). Furthermore, the columbic efficiency was found to be 28.65% which was higher than the three mentioned material. Finally, it was concluded that the material is an excellent replacement for Pt/C catalyst material in MFC.

2.4 Chitosan-Based Nanocomposites

Chitosan is an environmental friendly biopolymer (polysaccharide), and hence was employed in significant applications including in the fields of biology, agriculture, industries, pharmaceutical, drug delivery system, dye removal and energy materials [52–57] due to its high molecular weight, antifungal activity, biocompatibility, gelation property, well-controlled structure and conduction capability. The usage of chitosan in FC development has received much attention in recent years owing to its extraordinary properties like that low cost, eco-friendly, hydrophilicity, low methanol permeability and ease of modifications of the polymer backbone of chitosan with other materials [58]. Chitosan can be used as an electrode and polymer electrolyte membrane in FC.

Bai et al. [59] designed a halloysite nanotube which is containing polyelectrolyte brushes (SHNTs) and it was incorporated into chitosan membrane. SHNTs generated a strong electrostatic interaction with the chitosan chain which improved the thermal and chemical properties by inhibiting the chain mobility. The nanocomposite membrane also overcome the problem of proton conduction in DMFC in an effective way by showing the highest conductivity of 18.6 mS/cm and IEC value of 0.204 mmol/g (Fig. 15) with an increase in the concentration of SHNT.

The phosphate and triphosphate salt complex membranes were inserted into chitosan membrane using chitosan hydrogel as electrode binder for increasing the proton conducting property in borohydride FCs [60]. This modified membrane was reached the highest power density of 685 mW/cm² at 60 °C which is almost 50% higher than the commercial Nafion[®] membrane. Also, the modified nanocomposite membrane showed a highest thermal stability of 200 °C as shown in Fig. 16.

A triple layer chitosan nanocomposite membrane having high efficiency in terms of power output, methanol permeability and proton exchange were demonstrated by Sadrabadi and group [61]. They coated two thin layers of chitosan on both the sides of Nafion[®] 105, chitosan acts as methanol barrier layer due to the presence of amino and hydroxyl group. Further, proton conductivity, methanol permeability, open circuit voltage measurements were proved too superior for multilayer Nafion[®] 117 membranes with the thickness of 150–170 μm. In addition, power output was found to be 68.10 mW/cm² by feeding 5 M methanol which is 72% more than that of Nafion[®] 117 membranes. Moreover, the lesser methanol crossover, ease of preparation and low cost will be the advantages to use as polyelectrolyte for DMFC (Table 6).

Chitosan was modified with polymeric reactive dyes which are containing quaternary ammonium groups (PRDQA) through blending followed by dyeing processes and studied for OH⁻ conduction in AFC [62]. The combined framework of CTS/PRDQA (1:0.5 by mass) nanocomposite membrane was exhibited an excellent OH⁻ conductivity of 8.17 mS/cm at room temperature (Table 7). The highest power density of 29.1 mW/cm² at a current density of 57.4 mA/cm² and open circuit voltage of 991.6 mV in an H₂/O₂ system was achieved which is appreciably better performance than pristine CTS membrane.

Fig. 15 A comparison of chitosan control and nanohybrid membranes at 25 °C at 100% RH in **a** IEC and **b** proton conductivity. Reproduced with permission from Ref. [59], Copyright 2014, Elsevier

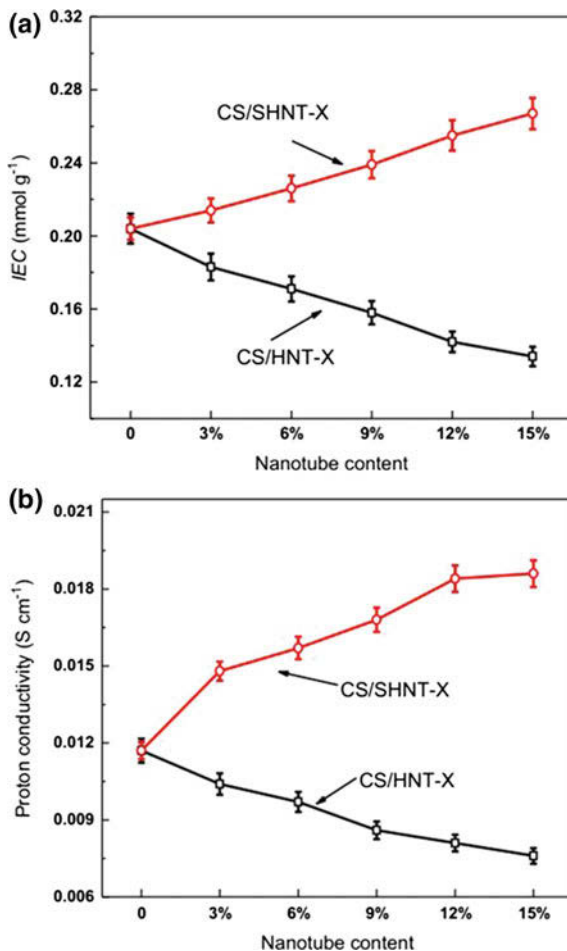


Fig. 16 TGA thermograms to demonstrate the stabilities of **a** Nafion[®], **b** pristine chitosan, **c** chitosan modified with phosphate (CsP) and **d** chitosan modified with triphosphate (CsTP) membranes. Reproduced with permission from Ref. [60], Copyright 2012, Elsevier

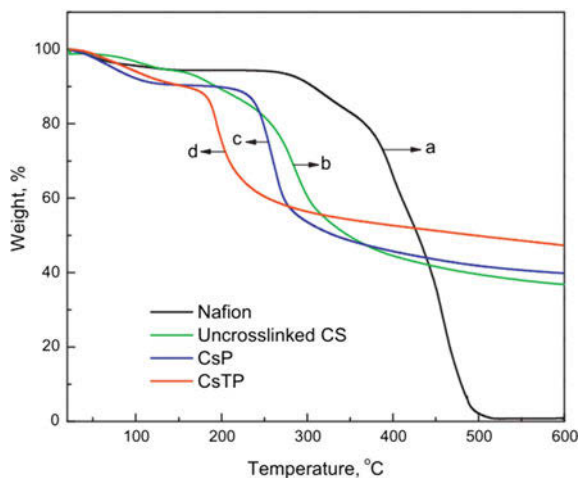


Table 6 Methanol crossover current density at open circuit condition and limiting current density of various MEAs at 1 M and 5 M methanol concentrations at 70 °C

Sample	Methanol concentration (M)	Crossover current (mA/cm ²)	Limiting current (mA/cm ²)
Nafion [®] 117	1.0	156	530
Nafion [®] 117	5.0	518	260
CGS-12	1.0	142	445
CGS-12	5.0	460	285
Multi-layer	1.0	136	575
Multi-layer	5.0	420	385

Reproduced with permission from Ref. [61], Copyright 2012, Elsevier

Table 7 Physical and chemical properties of CTS/PRDQA membrane at room temperature

CTS/PRDQA (by mass)	WU (g/g)	Σ ($\times 10^{-3}$ S/cm)	Swelling ratio		IEC (mequiv./g)
			Δ S/S (%)	Δ V/V (%)	
1:0.125	0.82	2.15	41.65	81.17	0.41
1:0.25	0.73	3.92	33.93	73.89	0.65
1:05	0.67	8.17	24.44	65.42	1.08
1:0.75	0.62	9.09	21.52	49.69	1.24

Reproduced from Ref. [62], Copyright 2016, ESG

Li et al. [63] designed a matrix by incorporating a varying amount of chitosan nanoparticles into quaternized polyvinyl alcohol (QPVA) (Fig. 17) for FC applications. The modified matrix with 10% chitosan nanoparticle showed better suppression of methanol permeability and higher ionic conductivity than pristine QPVA. Also, they have prepared glutaraldehyde cross-linked nanocomposite film which has exhibited superior peak power density of 67 mW/cm² in DMFC.

Free-standing Chitosan/Phosphotungstic acid membranes for H₂O₂ FCs were reported recently [64]. To induce the chitosan crosslinking, the membrane was prepared by using anodic alumina as a porous medium to liberate the oxo-metallate anions as illustrated in Fig. 18. The peak power density of the membrane was found to be 350 mW/cm² and polyelectrolyte conductivity was 18 mS/cm which provided the excellent properties for the development of FC.

Pt-chitosan incorporated to LaFeO₃ nanoparticles with CNT has been studied for methanol electrooxidation in DMFC [65]. They prepared a layer by layer electrode material from modified Glassy Carbon (GC) with Pt nanoparticles (PtNPs), LaFeO₃NPs, CNT and chitosan as a binder. Integration of LaFeO₃NPs and CNT material promoted the catalytic performance of the cell due to the presence of CNT decreased the dissolution of Pt. The method also reported that the methanol oxidation can be improved with the loading of a small amount of Pt.

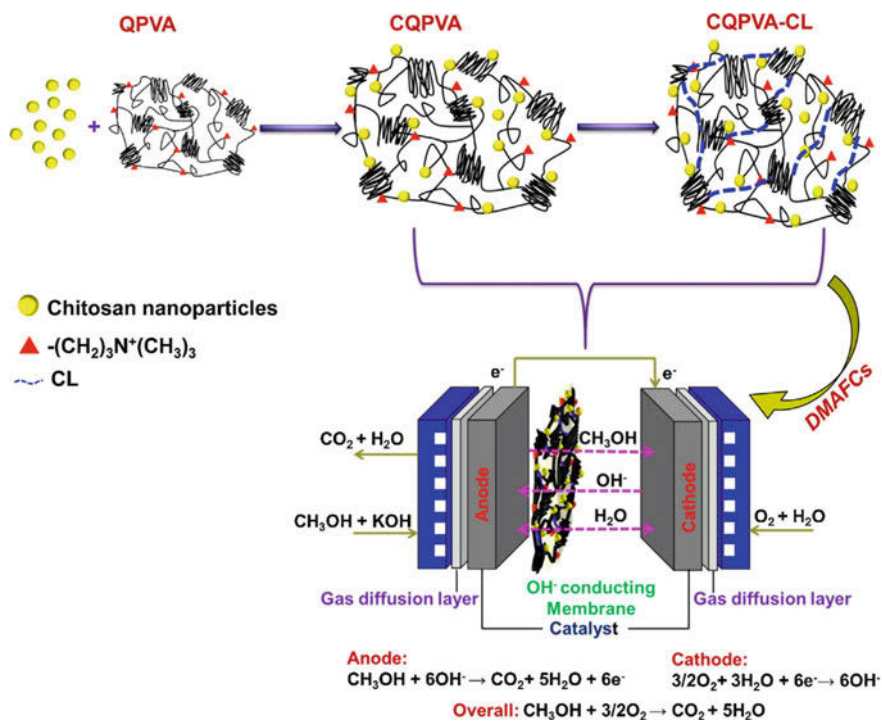


Fig. 17 Pictorial representation of glutaraldehyde cross-linked chitosan nanoparticle membrane for DMFC. Reproduced with permission from Ref. [63], Copyright 2016, Elsevier

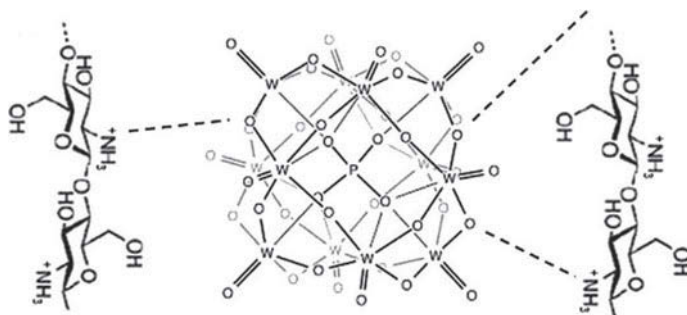


Fig. 18 Schematic representation of crosslinking the chitosan to the anionic species PTA^{3-} . Reproduced with permission from Ref. [64], Copyright 2015, Elsevier

2.5 Polybenzimidazole (PBI) Based Nanocomposite Membranes

PBI is a synthetic fiber and it has extraordinary properties such as high thermal stability, flame resistance capacity, moisture regains, retention of stiffness led to the development of high temperature operating devices. The close chain packing in PBI increases the hydrogen bonding and provides the rigidity to the materials. The use of PBI in FC has obtained utmost importance because of its high proton exchanging capacity, thermal and mechanical stabilities. PBI nanocomposite materials are excellent in proton conductivity when doped with acids like phosphoric acid because of its plasticizing property. In addition, the low gas permeability, zero water-electro osmotic drag, high CO poisoning tolerance has delivered the use of PBI units as nanocomposite membranes for high-temperature operating FCs.

Linlin et al. developed a composite material by incorporating silica in PBI to obtain high proton conductivity as well as to overcome the problem of acid leaching in acid doped PBI (dABPBI) based FCs [66]. They prepared poly (2,5-benzimidazole) (ABPBI) and embedded them on silica membrane in a methanesulfonic acid solvent to fabricate ABPBI-Si as described in Fig. 19. This modified sulfonated silica-ABPBI matrix improved the water uptake, mechanical and thermal stabilities. Similarly, the proton conductivity observed was 38 mS/cm at 140 °C and 1% RH which is a two-fold increase compared to the bare dABPBI membrane. Thus, it proved to be a promising nanocomposite membrane for FC at a higher temperature.

In a related work, Suryani and co-workers [67] incorporated silica on PBI membrane using N-(p-carboxyphenyl)maleimide (pCPM). This functionalized silica (SNP-pCPM) increased the interfacial compatibility between PBI and silica nanoparticles (SNPs) in PBI/SNP as described in Fig. 20 which created a proton conducting channel. This material was further used as nanofillers for the preparation

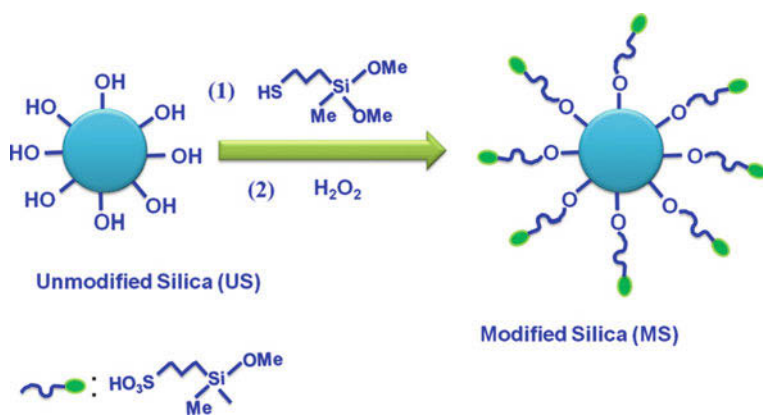


Fig. 19 Schematic representation of silica nanoparticles with methanesulfonic acid. Reproduced with permission from Ref. [66], Copyright 2012, Elsevier

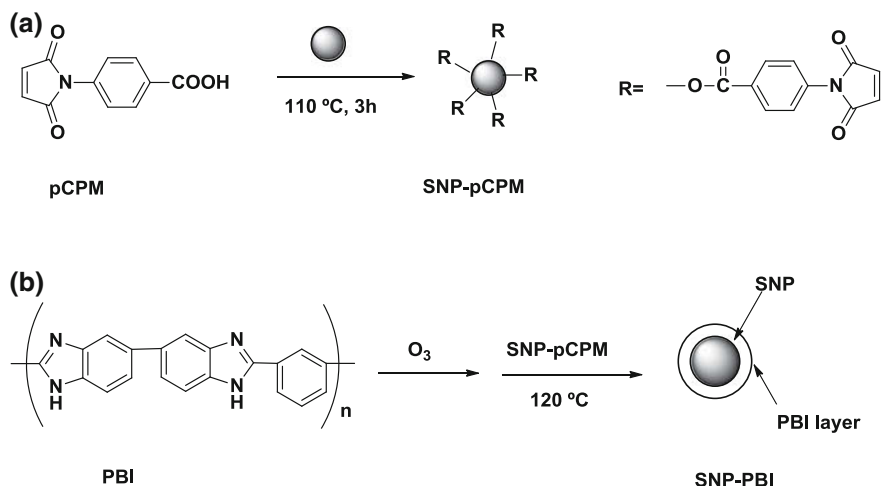


Fig. 20 a Functionalization of pCPM with silica nanoparticles b PBI functionalization with silica modified pCPM for proton conducting electrolyte membrane in FCs

of PBI/SNP-PBI membrane. With this modification, FCs displayed an excellent proton conductivity of 50 mS/cm at 160 °C by the use of 10 wt% composition of SNP-PBI. Also, a high power density of 650 mW/cm² was achieved in a single cell test which is higher than that of pristine PBI membrane.

The proton conductivity of PBI membrane was increased by functionalizing with Barium Zirconate (BaZrO₃) [68]. This modification increased the proton conduction to 125 mS/cm at 180 °C and 5% RH. At the same condition, the power density of 56 mW/cm² and a current density of 1120 mA/cm² were attained by the use of 4 wt% BaZrO₃ as nanofillers in PBI-BaZrO₃ (PBZ) membrane. This material proved to be a promising polyelectrolyte in FC membranes to improve proton conduction.

PBI/SiO₂ nanocomposite membranes were used to enhance the proton conduction membranes in PEMFC [69]. 5 wt% of SiO₂ as inorganic nanofiller was cast with PBI in dimethylacetamide solvent. The presence of SiO₂ facilitated proton conduction and acid retention properties. The nanohybrid membrane attained a conductivity of 102.7 mS/cm at 180 °C. Further, maximum cell voltage attained by this nanohybrid was found to be 0.6 V as 240 mA/cm².

A new material consisting of PBI functionalized with CNT was found to be very useful in FC applications. Wu et al. [70] doped this PBI/CNT and PBI membranes with KOH solution to make it more hydroxide conductive in ADMFC. They supplied the FC with 2 M methanol in 6 M KOH as anode fuel and humidified oxygen as oxidant at the cathode. This system attained a power density of 104.7 mW/cm² at 90 °C. In addition to this, thermal stability was enhanced and methanol permeability was reduced after the loading of 0.05–1% PBI functionalized CNT into PBI matrix. Therefore, it is considered to be a potential nanocomposite membrane for ADMFC.

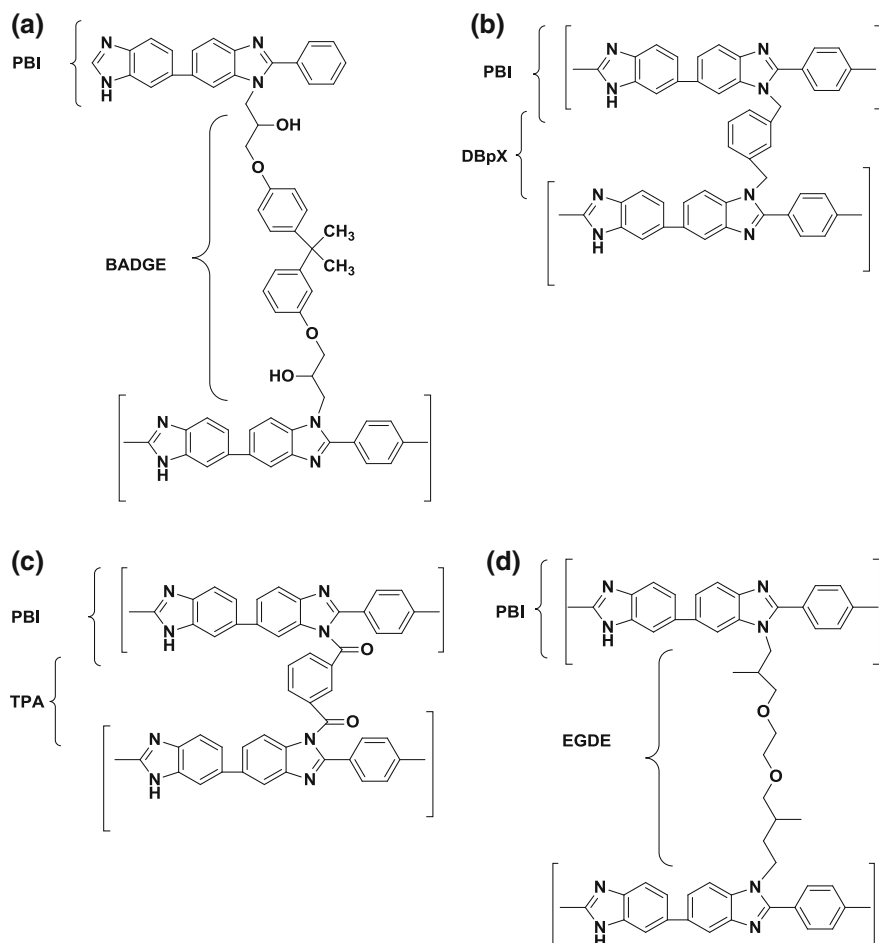


Fig. 21 Mechanism showing the crosslinking of **a** PBI/BADGE, **b** PBI/DBpX, **c** PBI/TPA and **d** PBI/EGDE. Reproduced with permission from Ref. [71], Copyright 2017 Elsevier

Recently, Özdemir et al. [71] studied the efficiency of PBI membranes fabricated with various cross-linkers for PEMFC. They cross-linked the PBI membrane with bisphenol A diglycidyl ether (BADGE), ethylene glycol diglycidyl ether (EGDE), α - α' -dibromo-*p*-xylene (DBpX) and terephthalaldehyde (TPA) as illustrated in Fig. 21. From the electrochemical analysis, it was evident that PBI/BADGE nanocomposite membrane presented the superior acid retention property, however poor proton conduction. On the other hand, PBI/DBpX membrane was reached the maximum proton conductivity of 151 mS/cm at 180 °C. Meanwhile, PBI/BADGE composite materials exhibited maximum power density of 0.123 W. Therefore, they concluded that the PBI/BADGE and PBI/DBpX nanocomposite membranes are well suited for the polyelectrolyte membranes in FCs.

2.6 Poly (ether ether ketone) Based Nanocomposite

Poly (ether ether ketone) (PEEK) are the organic thermoplastics which have been used extensively for the modification of PEM in FC due to their high thermal and mechanical stabilities. High proton conductivity was noticed when they are cast in organic solvents as they permit the direct electrophilic sulfonation [72]. There are few reports on the preparation of sulfonated PEEK (SPEEK) membrane to increase the efficiency of PEM in FC [73]. However, there are some limitations like methanol crossover and less stability in FC caused by the high sulfonation in these membranes. Therefore, the modifications of SPEEK membranes require good maintenance and skills in preparation methods.

Modified PEM was prepared by incorporating SPEEK in poly (ether sulfone) (PES) in MFC at different concentration [74]. The conductivity of PES membranes was increased with 3–5% of SPEEK addition as summarized in Table 8. At 5% of SPEEK addition, the membrane achieved a high power density of 17,000 mW/cm². Further, the conductivity was reduced from 0.000615 to 0.0693 mS/cm and capacitance was reduced from 3.0×10^{-7} to 1.56×10^{-3} F. Such performance of nanocomposite materials are due to the sulfonated groups present which enhance the hydrophilic nature of the SPEEK membrane. Eventually, the modified PES membranes were considered as the best replacing PEM material to Nafion[®] 112 and 117 for MFC applications.

Later in 2013, the functionalization of SPEEK membranes with organically functionalized GO (SSi-GO) for DMFC applications was reported [75]. The synthesized material made up of SPEEK and sulfonated GO with further oxidation was carried out as shown in Fig. 22.

Integration of this material into the membrane increased the proton conductivity and lower the methanol permeability when compared to pristine Nafion[®] 112 and Nafion[®] 115 membranes (Table 9). Similarly, the condensed matrix of SSi-GO membrane established high mechanical and chemical stabilities.

The incorporation of sulfonated GO (s-GO) in SPEEK was investigated for the efficient FC functions [76]. The embedded SPEEK/s-GO composite membrane

Table 8 The modified nanocomposites with high performance to increase the efficiency of MFC

Type of membrane	Max. power density (mW/m)	Current density (mA m ⁻²)	COD removal (%)	E _c (%)
N-112	0.003	0.124	55 ± 2	1.0 ± 0.4
N-117	3.630	9.842	60 ± 2	14.9 ± 5.5
PES	0.030	0.011	64 ± 4	0.5 ± 0.2
PES/SPEEK 3%	0.065	0.181	66 ± 6	5.4 ± 1.4
PES/SPEEK 5%	6.665	17.527	68 ± 6	26.3 ± 13.3

Reproduced with permission from Ref. [74] Copyright 2012 Elsevier

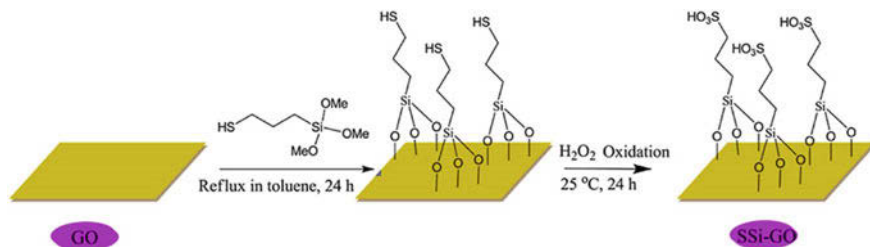


Fig. 22 Schematic illustration for the synthetic route of SSi-GO membrane. Reproduced with permission from Ref. [75], Copyright 2013, Elsevier

Table 9 Comparison of the efficiency of SPEEK membrane and modified SPEEK membranes [75]

Membrane	IEC (meq/g)	WU (%)	SW (%)	σ (mS/cm)	$P (\times 10^6 \text{ cm}^2/\text{s})$
SPEEK	1.710	40.1	15.5	88.1	1.15
SPEEK/GO (5 wt%)	1.704	33.1	13.8	98.3	0.59
SPEEK/SSi-GO (3 wt%)	1.792	38.5	16.2	146.7	0.72
SPEEK/SSi-GO (5 wt%)	1.864	49.9	17.0	160.2	0.83
SPEEK/SSi-GO (8 wt%)	1.872	50.9	18.3	162.6	1.36
Nafion [®] 112	0.941	37.1	13.9	125.4	1.53

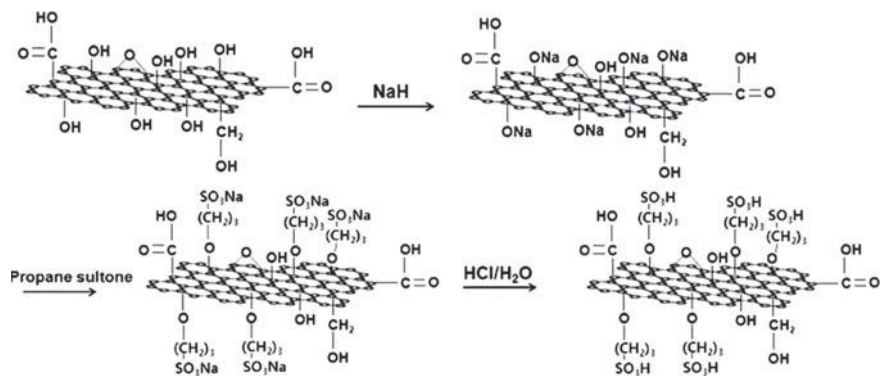


Fig. 23 A synthetic pathway for the sulfonation of GO to improve proton conduction. Reproduced with permission from Ref. [76], Copyright 2013, Elsevier

exhibited the improved proton conductivity of 8.41 mS/cm owing to the presence of high amount of sulfonic acid groups on the membrane (Fig. 23). The increased mechanical property of the membrane was attributed to the presence of strong hydrogen bonds between the s-GO and SPEEK. With the increase of GO content in the membrane, the elastic modulus and intrinsic strength were also increased. Thus,

lower methanol permeability of $2.6388 \times 10^{-7} \text{ cm}^2/\text{s}$ was attained and therefore, it is considered to be the best nanocomposite material for the applications in DMFC.

Wang et al. prepared a novel anhydrous membrane for PEM by embedding the dopamine-modified silica nanoparticles (DSiO₂) into SPEEK polymer [77]. The enhancement of thermal and mechanical stabilities are due to uniformly dispersed DSiO₂ in SPEEK which is increased interfacial electrostatic attraction. There was an occurrence of high proton conduction at the acid-base site of SPEEK/DSiO₂ via Grotthuss mechanism due to the formation of small aggregation of sulfonic acid ionic channels. By the experimentation, it was revealed that the prepared hybrid membrane with 15% DSiO₂ achieved a conductivity of 4.52 mS/cm at 120 °C under anhydrous conditions. The membrane also attained a power density of 111.7 mW/cm² and open cell potential of 0.98 V which is considered to be the superior performance in PEM under anhydrous conditions.

Incorporation of novel nanomaterial as graphitic carbon nitride (g-C₃N₄) sheets into SPEEK membrane illustrated in Fig. 24 offers the superior efficiency compared to the pristine SPEEK membrane [78]. The fabricated SPEEK membrane with 5 wt % of g-C₃N₄, proton conductivity up to 786 mS/cm at 20 °C was achieved. As previously mentioned, the Grotthuss effect played a major role in the proton conduction due to the presence of acid-base pair at the composite site. Further, it favoured the resistance of methanol crossover and maintained the power density up to 39% due to the periodic vacancies in the lattice of the g-C₃N₄ membrane. Therefore, this is accepted to be the best nanocomposite materials for FC applications.

Sulfated zirconia nanoparticles with SPEEK modified nanocomposites (Fig. 25) were found to be the best composite materials for FCs [79]. The combination of

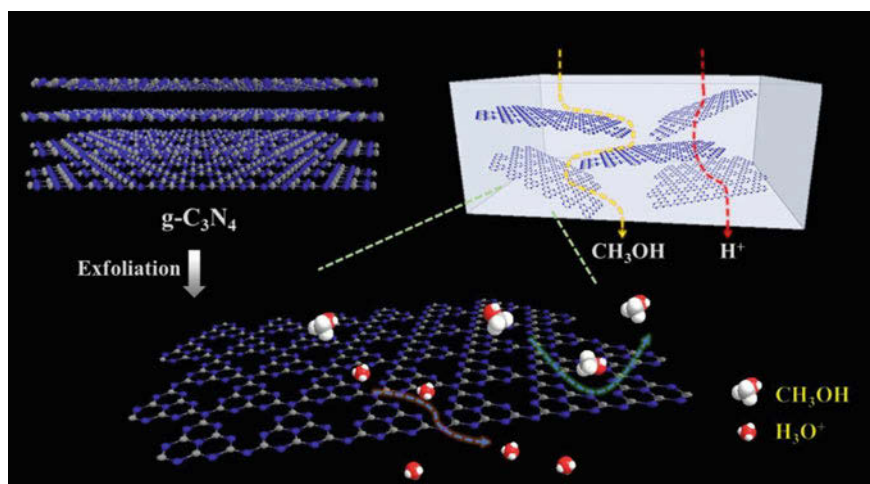


Fig. 24 Schematic illustration of the incorporation of g-C₃N₄ into SPEEK nanocomposite membrane. Reproduced with permission from Ref. [78], Copyright 2016, Elsevier

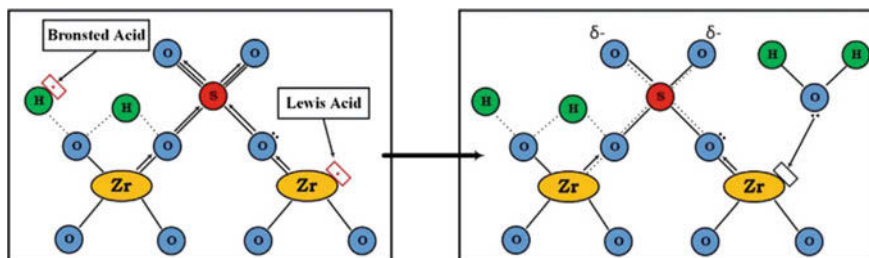


Fig. 25 Representation of the surface modification of SPEEK with sulfated zirconia nanoparticles. Reproduced with permission from Ref. [79], Copyright 2016, Elsevier

sulfonation time (6.9 h) and inorganic additives (5.94 wt%) produced the superior membranes. The proton conductivity observed was 3.88 mS/cm and oxidative stability of 102 min. In addition, the membrane also obtained the mechanical strength of 898 MPa.

SPEEK as an electrode ionomer material showed good catalytic activity for PEMFC [80]. The electrodes were prepared with 15, 25, 35 wt% of SPEEK and Pt content of 0.3, 0.4 and 0.5 mg/cm² were investigated for electrochemical reactions. The experiments demonstrated that the 25% of ionomer with 0.5 mg/cm² was found to be suitable for cathode catalyst for PEMFC.

2.7 Polyvinyl Alcohol (PVA) Based Nanocomposites

PVA is a water-soluble polymer with long chain 1, 3-diol linkages in its backbone. It has excellent film forming and emulsifying properties and hence is extensively used in membrane technology, adhesive materials development, and drug delivery etc. The flexibility, mechanical strength, thermal stability of PVA materials depends on the nature of cross-linkers used for material preparation. The excellent proton conduction capacity of organically modified PVA material attained importance in the development of nanocomposite materials in FC material applications.

The PVA modified with various poly(sulfonic acid) grafted silica nanoparticles were studied by Salarizadeh and co-workers [81]. First, they altered the surface of nanoparticles by APTES followed by preparing a nanocomposite membrane by various concentration from 0 to 20% of SNP with poly (styrene sulfonic acid) (PSSA-G-SNP), poly (2-acrylamido-2methyl-1-propane sulfonic acid) (PAMPS-g-SN) by using glutardialdehyde as a cross-linking agent as demonstrated in Fig. 26. It was observed that the membranes consisting of 5 wt% of PAMPS-g-SNP exhibited the better performance for FCs applications. This material showed the proton conductivity of 10.4 mS/cm by signifying that sulfonation of silica nanoparticles by grafting of sulfonated polyelectrolyte which increased the proton conductivity. Meanwhile, the

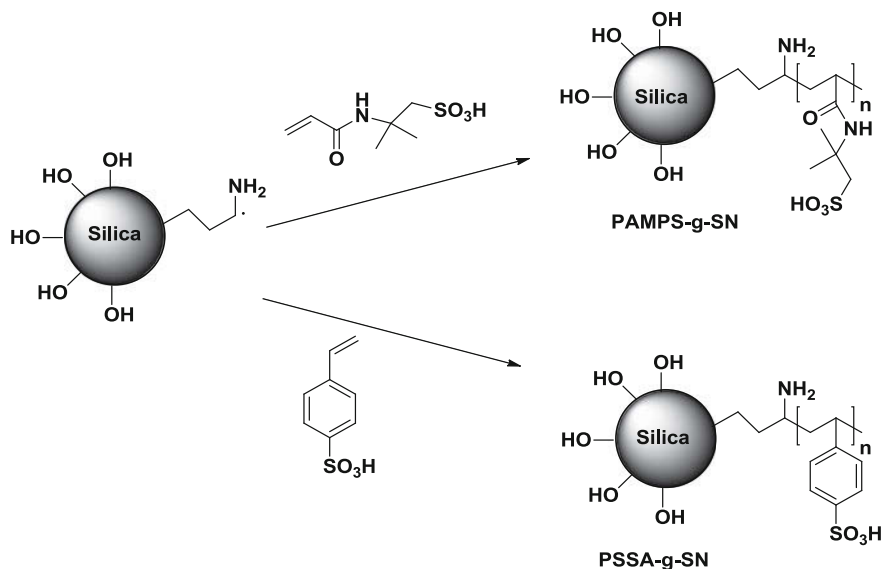


Fig. 26 Mechanism of surface-initiated free radical polymerization of AMPS and SSA onto APTES modified silica nanoparticles initiated by Ce(IV)-based redox initiation system. Reproduced with permission from Ref. [81], Copyright 2013, Elsevier

water uptake capacity was also increased for the same concentration, then diminished rapidly. Therefore, it was concluded that the prepared membrane can be effectively used for high proton conduction in FC.

A new variety of PEM for FCs prepared by PVA and the ionic liquid was reported by Liew et al. [82]. The prepared nanocomposite membrane with PVA/ammonium acetate/1-butyl-3-methylimidazolium chloride (BmImCl) reveals that increased ionic conductivity with ionic liquid mass loading. After the addition of 50 wt% of BmImCl, the PEM reached the highest ionic conductivity 5.74 ± 0.01 mS/cm. This was due to the fact that the addition of ionic liquid enhanced the plasticizing effect to the membrane. In addition, the nanocomposites also exhibited the thermal stability of up to 250 °C and achieved a maximum power density of 18 mW/cm² at room temperature with an operational current of 750 mA.

In 2014, a nanocomposite membrane was prepared by cross-linking of PVA with aryl sulfonated graphene oxide (SGO) for versatile applications in FC material [83]. The modification of the GO surface with aryl diazonium salt of the sulfanilic acid by further introducing 5 wt% SGO into PVA matrix by using glutaraldehyde as a cross-linking agent. The hybrid membrane showed high thermal stability with melting temperature of 223 °C, the tensile strength of 67.8 MPa and proton conductivity of 50 mS/cm. The increased proton conductivity owing to the interaction between—SO₃H of SGO and —OH group of GO via Grotthuss mechanism and Vehicle mechanism was explained in Fig. 27. Furthermore, the power density of 16.15 mW/cm² was attained. Overall, the modified PVA/SGO nanocomposite

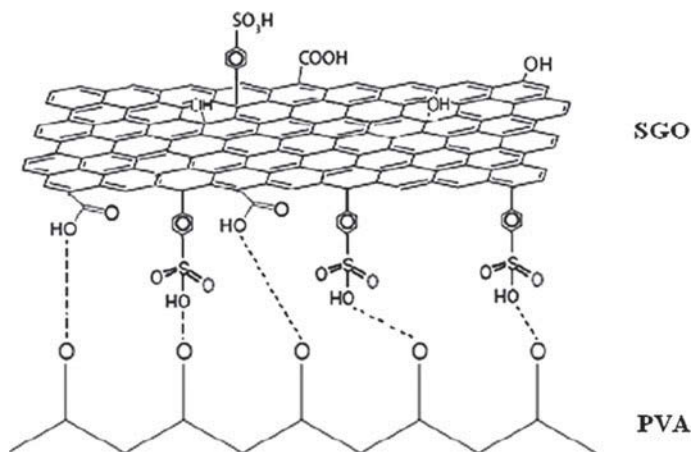


Fig. 27 Schematic representation of the reaction between PVA and SGO nanoparticles. Reproduced with permission from Copyright 2014, [83], American Chemical Society

membrane showed higher efficiency compared to unmodified GO and Nafion[®] membranes in terms of thermal stability and proton conductivity.

In other work, a novel hybrid membrane based on the infiltration of a blend of SPEEK with PVA in water and SPEEK blended with polyvinyl butyral (PVB) into electrospun nanofibres were reported [84]. A covering of hydrated SPEEK-30% PVB showed better proton conductivity. Further, the nanofibre incorporation into SPEEK-PVA matrix improved the mechanical stability, and methanol barrier capacity as explained in Table 10. Eventually, the prepared membrane was found useful for the applications in DMFC.

Yang et al. [85] prepared a blended membrane consisting of PVA and sodium alginate (PVASA) polymers of various concentration for alkaline solid PEM. This was further treated with glutaraldehyde to form a cross-linked membrane of PVASA (PVASA-GA). From the electrochemical measurements, it was observed that the ionic conductivity was found to be 91 mS/cm at 25 °C for the membrane containing 60:40 of PVA and SA. In addition, the methanol permeability was achieved in the order of 10^{-7} cm²/s. On the other hand, the membrane prepared with 80:20 of PVA and SA cross-linked with GA up to 60 min, exhibited the selectivity value of 21.50×10^3 S/cm³s⁻¹. Also, the PVASA with 80:20 composition showed a maximum power density of 20.7 mW/cm² which was achieved at $E_{p,max}$ with a peak current density of 89.20 mA/cm² at 30 °C. Therefore, the membrane was found to be extensively used in DMFC application.

Recently, the application of PVA modified with functionalized CNT (m-CNT) in ADEFC was reported [86]. Addition of m-CNT into PVA membrane increased the alkaline uptake and ionic conductivity of KOH doped electrolyte membrane. At the same time, a lower swelling ratio and ethanol permeability were suppressed in comparison with pristine PVA membrane. Also, the highest power density of 65 mW/cm² at 60 °C was achieved.

Table 10 Comparison of the performance of nanocomposite and SPEEK-35% PVA

Membrane	Crosslinking temperature (°C)	Metahmol permeability(cm^2/s)	Proton conductivity(S/cm)	Modified characteristic factor ($\text{S}^2 \text{s cm}^{-4}$)
SPEEK-35% PVA	110	$5.81 \pm 0.20 \times 10^{-6}$	$1.11 \pm 0.08 \cdot 10^{-2}$	21.2 ± 3.2
Nanocomposite	110	$4.43 \pm 0.21 \times 10^{-6}$	$1.35 \pm 0.11 \cdot 10^{-2}$	41.1 ± 5.8
SPEEK-35% PVA	120	$4.70 \pm 0.13 \times 10^{-6}$	$1.10 \pm 0.05 \cdot 10^{-2}$	25.7 ± 1.9
Nanocomposite	120	$3.82 \pm 0.18 \times 10^{-6}$	$1.03 \pm 0.08 \cdot 10^{-2}$	27.8 ± 3.6
SPEEK-35% PVA	130	$2.18 \pm 0.07 \times 10^{-6}$	$5.84 \pm 0.32 \cdot 10^{-3}$	15.6 ± 1.5
Nanocomposite	130	$2.02 \pm 0.11 \times 10^{-6}$	$2.50 \pm 0.18 \cdot 10^{-3}$	3.1 ± 0.3
SPEEK-35% PVA	140	$1.19 \pm 0.06 \times 10^{-6}$	$3.53 \pm 0.13 \cdot 10^{-3}$	10.5 ± 0.3
Nanocomposite	140	$1.34 \pm 0.09 \times 10^{-6}$	$1.63 \pm 0.10 \cdot 10^{-3}$	2.0 ± 0.1
Nafion [®] 115	–	$3.71 \pm 0.05 \times 10^{-6}$	$3.64 \pm 0.11 \cdot 10^{-2}$	357 ± 24

Reproduced with permission from Ref. [84], Copyright 2015, Elsevier

3 Conclusion

In this chapter, we summarized the current scenario of FC research and development around the world. The modification of composites with various nanomaterials is the developing technology to overcome the problems such as fuel crossover, low proton conduction, expensive raw materials, higher cost, and low membrane stability. The advantages of hybrid nanocomposites such as Nafion[®], CNT, GO, SPEEK, PBI, PVA in FCs are comprehensively discussed. A variety of improved materials as anode, cathode, and membranes are elucidated. The improved efficiency of FCs in terms of high proton conduction, better water retention, suppression of fuel crossover, high chemical and thermal stabilities are precisely explained.

Acknowledgements The authors acknowledge the financial support from DST Nanomission, India (SR/NM/NS-20/2014), DST, India (DST-TM-WTL-2K14-213) and SERB-DST, India (YSS/2015/000013) for financial support. We also thank Jain University, India for providing facilities.

References

1. Hajilary N, Shahi A, Rezakazemi M (2018) Evaluation of socio-economic factors on CO₂ emissions in Iran: factorial design and multivariable methods. *J Clean Prod* 189:108–115
2. Hashemi F, Rowshanzamir S, Rezakazemi M (2012) CFD simulation of PEM fuel cell performance: effect of straight and serpentine flow fields. *Math Comput Model* 55(3–4):1540–1557
3. Winter M, Brodd RJ (2004) What are batteries, fuel cells, and supercapacitors? *Chem Rev* 104:4245–4269
4. Lemons RA (1990) Fuel cells for transportation. *J Power Sources* 29(1–2):251–264
5. Peighambaroust S, Rowshanzamir S, Amjadi M (2010) Review of the proton exchange membranes for fuel cell applications. *Int J Hydrogen Energy* 35(17):9349–9384
6. Giorgi L, Leccese F (2013) Fuel cells: technologies and applications. *Open Fuel Cells J* 6: 1–20
7. Agmon N (1995) The grothuss mechanism. *Chem Phys Lett* 244(5):456–462
8. Ueki T, Watanabe M (2008) Macromolecules in ionic liquids: progress, challenges, and opportunities. *Macromolecules* 41(11):3739–3749
9. Rezakazemi M, Amoghini AE, Montazer Rashmati MM, Ismail AF, Matsuura T (2014) State-of-the-art membrane based CO₂ separation using mixed matrix membranes (MMMs): an overview on current status and future directions. *Prog Polym Sci* 39(5):817–861
10. Rezakazemi M, Razavi S, Mohammadi T, Nazari GA (2011) Simulation and determination of optimum conditions of pervaporative dehydration of isopropanol process using synthesized PVA–APTEOS/TEOS nanocomposite membranes by means of expert systems. *J Membr Sci* 379(1–2):224–232
11. Dashti A, Harami HR, Rezakazemi M (2018) Accurate prediction of solubility of gases within H₂-selective nanocomposite membranes using committee machine intelligent system. *Int J Hydrogen Energy* 43(13):6614–6624
12. Rezakazemi M, Vatani A, Mohammadi T (2016) Synthesis and gas transport properties of crosslinked poly(dimethylsiloxane) nanocomposite membranes using octatrimethylsiloxy POSS nanoparticles. *J Nat Gas Sci Eng* 30:10–18
13. Rezakazemi M, Vatani A, Mohammadi T (2015) Synergistic interactions between POSS and fumed silica and their effect on the properties of crosslinked PDMS nanocomposite membranes. *RSC Adv* 5(100):82460–82470
14. Rezakazemi M, Sadrzadeh M, Mohammadi T, Matsuura T (2017) Methods for the preparation of organic–inorganic nanocomposite polymer electrolyte membranes for fuel cells. In: Inamuddin D, Mohammad A, Asiri AM (eds) *Organic-inorganic composite polymer electrolyte membranes*. Springer International Publishing, Cham, pp 311–325
15. Sodeifian G, Mojtaba R, Asghari M, Rezakzemi M (2018) Polyurethane-SAPO-34 mixed matrix membrane for CO₂/CH₄ and CO₂/N₂ separation. *Chin J Chem Eng*. <https://doi.org/10.1016/j.cjche.2018.03.012>
16. Rezakazemi M, Dashti A, Asghari M, Saeed S (2017) H₂-selective mixed matrix membranes modeling using ANFIS, PSO-ANFIS GA-ANFIS. *Int J Hydrogen Energy* 42(22):15211–15225
17. Baheri B, Mahnaz S, Razakazemi M, Elahe M, Mohammadi T (2014) Performance of PVA/NaA mixed matrix membrane for removal of water from ethylene glycol solutions by pervaporation. *Chem Eng Commun* 202(3):316–321
18. Shahverdi M, Baheri B, Razakazemi M, Elahe M, Mohammadi T (2013) Pervaporation study of ethylene glycol dehydration through synthesized (PVA-4A)/polypropylene mixed matrix composite membranes. *Polym Eng Sci* 53(7):1487–1493
19. Rostamizadeh M, Rezakazemi M, Shahidi K, Mohammadi T (2013) Gas permeation through H₂-selective mixed matrix membranes: Experimental and neural network modeling. *Int J Hydrogen Energy* 38(2):1128–1135

20. Rezakazemi M, Mohammadi T (2013) Gas sorption in H₂-selective mixed matrix membranes: experimental and neural network modeling. *Int J Hydrogen Energy* 38(32):14035–14041
21. Rezakazemi M, Shahidi K, Mohammadi T (2012) Sorption properties of hydrogen-selective PDMS/zeolite 4A mixed matrix membrane. *Int J Hydrogen Energy* 37(22):17275–17284
22. Rezakazemi M, Shahidi K, Mohammadi T (2012) Hydrogen separation and purification using crosslinkable PDMS/zeolite a nanoparticles mixed matrix membranes. *Int J Hydrogen Energy* 37(19):14576–14589
23. Rezakazemi M, Sadrzadeh M, Matsuura T (2018) Thermally stable polymers for advanced high-performance gas separation membranes. *Prog Energy Combust Sci* 66:1–41
24. Boutsika LG, Enotiadis A, Nicotera I, Simari C, Charalambopoulou G, Giannelis EP, Steriotis T (2016) Nafion® nanocomposite membranes with enhanced properties at high temperature and low humidity environments. *Int J Hydrogen Energy* 41(47):22406–22414
25. Mohammadi G, Jahanshahi M, Rahimpour A (2013) Fabrication and evaluation of Nafion nanocomposite membrane based on ZrO₂-TiO₂ binary nanoparticles as fuel cell MEA. *Int J Hydrogen Energy* 38(22):9387–9394
26. Hooshyari K, Javanbakt M, Naji L, Enhessari M (2014) Nanocomposite proton exchange membranes based on Nafion containing Fe₂ TiO₅ nanoparticles in water and alcohol environments for PEMFC. *J Membr Sci* 454:74–81
27. Wang Z, Tang H, Zhang H, Lei M, Chen R, Xiao P, Pan M (2012) Synthesis of Nafion/CeO₂ hybrid for chemically durable proton exchange membrane of fuel cell. *J Membr Sci* 421: 201–210
28. Cozzi D, de Bonis C, D'Epifanio A, Mecheri B, Tavares AC, Licoccia S (2014) Organically functionalized titanium oxide/Nafion composite proton exchange membranes for fuel cells applications. *J Power Sources* 248:1127–1132
29. de Bonis C, Cozzi D, Mecheri B, D'Epifanio A, Rainer A, De Porcellenis D, Licoccia S (2014) Effect of filler surface functionalization on the performance of Nafion/Titanium oxide composite membranes. *Electrochim Acta* 147:418–425
30. Yang Y, Cuiqing H, Beibei J, James I, Chengen H, Dean S, Tao J, Zhiqun L (2016) Graphene-based materials with tailored nanostructures for energy conversion and storage. *Mater Sci Eng R Rep* 102:1–72
31. Farooqui U, Ahmad A, Hamid N (2018) Graphene oxide: a promising membrane material for fuel cells. *Renew Sust Energy Rev* 82:714–733
32. Tsang AC, Kwok HY, Leung DY (2017) The use of graphene based materials for fuel cell, photovoltaics, and supercapacitor electrode materials. *Solid State Sci* 67:A1–A14
33. Das TK, Prusty S (2013) Graphene-based polymer composites and their applications. *Polym Plast Technol Eng* 52(4):319–331
34. Zhu C, Dong S (2013) Recent progress in graphene-based nanomaterials as advanced electrocatalysts towards oxygen reduction reaction. *Nanoscale* 5(5):1753–1767
35. Fampiou I, Ramasubramaniam A (2012) Binding of Pt nanoclusters to point defects in graphene: adsorption, morphology, and electronic structure. *J Phys Chem C* 116(11): 6543–6555
36. Liu M, Zhang R, Chen W (2014) Graphene-supported nanoelectrocatalysts for fuel cells: synthesis, properties, and applications. *Chem Rev* 114(10):5117–5160
37. Huang H, Chen H, Sun D, Wang X (2012) Graphene nanoplate-Pt composite as a high performance electrocatalyst for direct methanol fuel cells. *J Power Sources* 204:46–52
38. Qian W, Hao R, Zhou J, Eastman M, Manhat BA, Sun Q, Andrea MG, Jiao J (2013) Exfoliated graphene-supported Pt and Pt-based alloys as electrocatalysts for direct methanol fuel cells. *Carbon* 52:595–604
39. Peng K-J, Lai J-Y, Liu Y-L (2016) Nanohybrids of graphene oxide chemically-bonded with Nafion: preparation and application for proton exchange membrane fuel cells. *J Membr Sci* 514:86–94
40. Zhou X, Tang S, Yin Y, Sun S, Qiao J (2016) Hierarchical porous N-doped graphene foams with superior oxygen reduction reactivity for polymer electrolyte membrane fuel cells. *Appl Energy* 175:459–467

41. Kirubakaran CJ, Santhakumar K, Gnanankumar G, Senthilkumar N, Jang J (2015) Nitrogen doped graphene sheets as metal free anode catalysts for the high performance microbial fuel cells. *Int J Hydrogen Energy* 40(38):13061–13070
42. Rezakazemi M, Zhang Z (2018) Desulfurization materials A2—Dincer, Ibrahim comprehensive energy systems. Elsevier, Oxford, pp 944–979
43. Georgakilas V, Perman JA, Tucek J, Zboril R (2015) Broad family of carbon nanoallotropes: classification, chemistry, and applications of fullerenes, carbon dots, nanotubes, graphene, nanodiamonds, and combined superstructures. *Chem Rev* 115(11):4744–4822
44. Akbari E, Buntat Z (2017) Benefits of using carbon nanotubes in fuel cells: a review. *Int J Energ Res* 41(1):92–102
45. Ghasemi M, Ismail M, Kamarudin SK, Saedfar K, Wan Daud WR, Hassan SHA, Heng LY, Alam J, Oh SE (2013) Carbon nanotube as an alternative cathode support and catalyst for microbial fuel cells. *Appl Energy* 102:1050–1056
46. Mehdinia A, Ziaei E, Jabbari A (2014) Multi-walled carbon nanotube/SnO₂ nanocomposite: a novel anode material for microbial fuel cells. *Electrochim Acta* 130:512–518
47. Tohidian M, Ghaffarian SR (2017) Polyelectrolyte nanocomposite membranes with imidazole-functionalized multi-walled carbon nanotubes for use in fuel cell applications. *J Macromol Sci B* 56(10):725–738
48. Zhang R, He S, Lu Y, Chen W (2015) Fe Co, N-functionalized carbon nanotubes in situ grown on 3D porous N-doped carbon foams as a noble metal-free catalyst for oxygen reduction. *J Mater Chem A* 3(7):3559–3567
49. Mishra P, Jain R (2016) Electrochemical deposition of MWCNT-MnO₂/PPy nano-composite application for microbial fuel cells. *Int J Hydrogen Energy* 41(47):22394–22405
50. Mirzaei F, Parnian MJ, Rowshanzamir S (2017) Durability investigation and performance study of hydrothermal synthesized platinum-multi walled carbon nanotube nanocomposite catalyst for proton exchange membrane fuel cell. *Energy* 138:696–705
51. Liew KB, Wan Daud WR, Ghasemi M, Loh KS, Ismail M, Lim SS, Leong JX (2015) Manganese oxide/functionalised carbon nanotubes nanocomposite as catalyst for oxygen reduction reaction in microbial fuel cell. *Int J Hydrogen Energy* 40(35):11625–11632
52. Mourya V, Inamdar NN, Tiwari A (2010) Carboxymethyl chitosan and its applications. *Adv Mater Lett* 1(1):11–33
53. Vakili M, Rafatullah M, Salamatinia B, Abdullah AZ, Ibrahim MH, Tan KB, Gholami Z, Amouzgar P (2014) Application of chitosan and its derivatives as adsorbents for dye removal from water and wastewater: a review. *Carbohydr Polym* 113:115–130
54. Srinivasa P, Tharanathan R (2007) Chitin/chitosan—safe, ecofriendly packaging materials with multiple potential uses. *Food Rev Int* 23(1):53–72
55. Lim S-H, Hudson SM (2003) Review of Chitosan and its derivatives as antimicrobial agents and their uses as textile chemicals. *J Macromol Sci C Polym Rev* 43(2):223–269
56. Mourya V, Inamdar NN (2009) Trimethyl chitosan and its applications in drug delivery. *J Mater Sci Mater Med* 20(5):1057
57. Ilium L (1998) Chitosan and its use as a pharmaceutical excipient. *Pharm Res* 15(9):1326–1331
58. Ma J, Sahai Y (2013) Chitosan biopolymer for fuel cell applications. *Carbohydr Polym* 92(2):955–975
59. Bai H, Zhang H, He Y, Liu J, Zhang B, Wang J (2014) Enhanced proton conduction of chitosan membrane enabled by halloysite nanotubes bearing sulfonate polyelectrolyte brushes. *J Membr Sci* 454:220–232
60. Ma J, Sahai Y, Buchheit RG (2012) Evaluation of multivalent phosphate cross-linked chitosan biopolymer membrane for direct borohydride fuel cells. *J Power Sources* 202:18–27
61. Hasani-Sadrabadi MM, Dashtimoghadam E, Mokarram N, Majedi FS, Jacob KI (2012) Triple-layer proton exchange membranes based on chitosan biopolymer with reduced methanol crossover for high-performance direct methanol fuel cells application. *Polymer* 53(13):2643–2651

62. Zhou T, He X, Song F, Xie K (2016) Chitosan modified by polymeric reactive dyes containing quaternary ammonium groups as a novel anion exchange membrane for alkaline fuel cells. *Int J Electrochem Sci* 11(1):590–608
63. Li P-C, Liao G-M, Rajeshkumar S, Shih C-M, Yang C-C, Wang D-M, Lue SJ (2016) Fabrication and characterization of chitosan nanoparticle-incorporated quaternized poly (vinyl alcohol) composite membranes as solid electrolytes for direct methanol alkaline fuel cells. *Electrochim Acta* 187:616–628
64. Santamaria M, Pecoraro CM, Di Quarto F, Bocchetta P (2015) Chitosan–phosphotungstic acid complex as membranes for low temperature H₂–O₂ fuel cell. *J Power Sources* 276: 189–194
65. Noroozifar M, Motlagh MK, Kakhki M-S, Roghayeh K-M (2014) Enhanced electrocatalytic properties of Pt–chitosan nanocomposite for direct methanol fuel cell by LaFeO₃ and carbon nanotube. *J Power Sources* 248:130–139
66. Linlin M, Mishra AK, Kim NH, Lee JH (2012) Poly (2,5-benzimidazole)–silica nanocomposite membranes for high temperature proton exchange membrane fuel cell. *J Membr Sci* 411:91–98
67. Chang Y-N, Lai J-Y, Liu Y-L (2012) Polybenzimidazole (PBI)-functionalized silica nanoparticles modified PBI nanocomposite membranes for proton exchange membranes fuel cells. *J Membr Sci* 403:1–7
68. Hooshyari K, Javanbakt M, Shabanikia A, Enhessari M (2015) Fabrication BaZrO₃/PBI-based nanocomposite as a new proton conducting membrane for high temperature proton exchange membrane fuel cells. *J Power Sources* 276:62–72
69. Devrim Y, Devrim H, Eroglu I (2016) Polybenzimidazole/SiO₂ hybrid membranes for high temperature proton exchange membrane fuel cells. *Int J Hydrogen Energy* 41(23):10044–10052
70. Wu J-F, Lo C-F, Li H-Y, Chang C-M, Liao K-S, Hu C-C, Liu Y-L, Lue S-J (2014) Thermally stable polybenzimidazole/carbon nano-tube composites for alkaline direct methanol fuel cell applications. *J Power Sources* 246:39–48
71. Özdemir Y, Özkan N, Devrim Y (2017) Fabrication and characterization of cross-linked polybenzimidazole based membranes for high temperature PEM fuel cells. *Electrochim Acta* 245:1–13
72. Hogarth WH, Da Costa JD, Lu GM (2005) Solid acid membranes for high temperature proton exchange membrane fuel cells. *J Power Sources* 142(1):223–237
73. Tripathi BP, Shahi VK (2007) SPEEK–zirconium hydrogen phosphate composite membranes with low methanol permeability prepared by electro-migration and in situ precipitation. *J Colloid Interface Sci* 316(2):612–621
74. Lim SS, Wan Daud WR, Jahim J, Ghasemi M, Chong PS, Ismail M (2012) Sulfonated poly (ether ether ketone)/poly (ether sulfone) composite membranes as an alternative proton exchange membrane in microbial fuel cells. *Int J Hydrogen Energy* 37(15):11409–11424
75. Jiang Z, Zhao X, Manthiram A (2013) Sulfonated poly (ether ether ketone) membranes with sulfonated graphene oxide fillers for direct methanol fuel cells. *Int J Hydrogen Energy* 38 (14):5875–5884
76. Heo Y, Im H, Kim J (2013) The effect of sulfonated graphene oxide on sulfonated poly (ether ether ketone) membrane for direct methanol fuel cells. *J Membr Sci* 425:11–22
77. Wang J, Bai H, Zhang H, Zhao L, Yifan Li C (2015) Anhydrous proton exchange membrane of sulfonated poly (ether ether ketone) enabled by polydopamine-modified silica nanoparticles. *Electrochim Acta* 152:443–455
78. Gang M, He G, Li Z, Cao K, Li Z, Yin Y, Wu H, Jiang Z (2016) Graphitic carbon nitride nanosheets/sulfonated poly (ether ether ketone) nanocomposite membrane for direct methanol fuel cell application. *J Membr Sci* 507:1–11
79. Mossayebi Z, Saririchi T, Rowshanzamir S, Parnian MJ (2016) Investigation and optimization of physicochemical properties of sulfated zirconia/sulfonated poly (ether ether ketone) nanocomposite membranes for medium temperature proton exchange membrane fuel cells. *Int J Hydrogen Energy* 41(28):12293–12306

80. Rahnavard A, Rowshanzamir S, Parnian MJ, Amirkhanlou GR (2015) The effect of sulfonated poly (ether ether ketone) as the electrode ionomer for self-humidifying nanocomposite proton exchange membrane fuel cells. *Energy* 82:746–757
81. Salarizadeh P, Javanbakht M, Abdollahi M, Naji L (2013) Preparation, characterization and properties of proton exchange nanocomposite membranes based on poly (vinyl alcohol) and poly (sulfonic acid)-grafted silica nanoparticles. *Int J Hydrogen Energy* 38(13):5473–5479
82. Liew C-W, Ramesh S, Arof A (2014) A novel approach on ionic liquid-based poly (vinyl alcohol) proton conductive polymer electrolytes for fuel cell applications. *Int J Hydrogen Energy* 39(6):2917–2928
83. Beydaghi H, Javanbakht M, Kowsari E (2014) Synthesis and characterization of poly (vinyl alcohol)/sulfonated graphene oxide nanocomposite membranes for use in proton exchange membrane fuel cells (PEMFCs). *Ind Eng Chem Res* 53(43):16621–16632
84. Mollá S, Compañ V (2015) Nanocomposite SPEEK-based membranes for direct methanol fuel cells at intermediate temperatures. *J Membr Sci* 492:123–136
85. Yang J-M, Wang N-C, Chiu H-C (2014) Preparation and characterization of poly (vinyl alcohol)/sodium alginate blended membrane for alkaline solid polymer electrolytes membrane. *J Membr Sci* 457:139–148
86. Huang C-Y, Lin J-S, Pan W-H, Shih C-M, Liu Y-L, Lue S-J (2016) Alkaline direct ethanol fuel cell performance using alkali-impregnated polyvinyl alcohol/functionalized carbon nano-tube solid electrolytes. *J Power Sources* 303:267–277

Rubber Clay Nanocomposites



Mariajose Cova Sanchez, Alejandro Bacigalupe, Mariano Escobar and Marcela Mansilla

List of Abbreviations

AFM	Atomic force microscopy
APTES	(3—aminopropyl) triethoxysilane
CB	Carbon black
CEC	Cation exchange capacity
CIIR	Chlorobutyl rubber
CL	Concentrated Natural Rubber Latex
Dim-Br	o-xylylenebis (triphenylphosphoniumbromide)
DMA	Dynamic mechanical analysis
DSC	Differential scanning calorimetry
DTG	Derivative thermogravimetric analysis
EDX	Electron dispersive X-ray spectroscopy
EG	Expanded graphite
EPDM	Ethylene propylene diene rubber
FL	Fresh Natural Rubber Latex
FTIR	Fourier transform infrared
Hal	Hallosyte
HDTMA ⁺	Hexadecyl trimethylammonium
IIR	Isobutylene isoprene rubber
M _H	Maximum torque
M _t	Montmorillonite
NBR	Acrylonitrile butadiene rubber

M. C. Sanchez · A. Bacigalupe

Instituto de Investigación e Ingeniería Ambiental, Universidad Nacional de San Martín (UNSAM 3iA), Francia 34, 1650 San Martín, Argentina

M. C. Sanchez · A. Bacigalupe · M. Escobar (✉) · M. Mansilla
Instituto Nacional de Tecnología Industrial (INTI), Centro de Caucho,
Av. General Paz 5445, B1650WAB San Martín, Argentina
e-mail: mescobar@inti.gob.ar

M. Escobar · M. Mansilla

Consejo Nacional de Investigaciones Científicas y Técnicas (CONICET),
Godoy Cruz 2290, C1425FQB CABA, Argentina

© Springer Nature Switzerland AG 2019

Inamuddin et al. (eds.), *Sustainable Polymer Composites and Nanocomposites*,
https://doi.org/10.1007/978-3-030-05399-4_21

NK	Nanokaolin
NR	Natural rubber
OC	Organoclay
ODTMA ⁺	Octadecyl trimethylammonium
OMt	Organommodified montmorillonite
PAS	Positron annihilation lifetime spectroscopy
PA6	Polyamide 6
phr	per hundred of rubber
PLA	Olylactide acid
SANS	Small angle neutrón scattering
SAXS	Small Angle X-Ray Scattering
SBR	Styrene Butadiene Rubber
SEM	Scanning electron microscopy
SI	Silica
tan δ	Loss tangent
t_{c90}	Cure time
TEM	Transmission electron microscopy
T_g	Glass transition temperature
TGA	Thermogravimetric analysis
t_{s2}	Scorch time
WAXS	Wide Angle X-Ray Scattering
W_c	Water content
XRD	X-ray diffraction

1 Introduction

The use of nanofillers allows the development of nanocomposites with improved properties and novel applications [1–7]. The technological goal is possible due to the new compounding method that allows a particle dispersion in the nanometer scale increasing the specific surface area [8].

This chapter focuses on explaining the role that nanoclays play as exceptional reinforcing particles in rubber matrices. The complexity of the analysis comes from the fact that it is a multicomponent system, which contains, for example, curing agents, co-agents, processing aids, reinforcements and fillers, affecting the final structure of a rubber/layered silicate nanocomposite. This was likely the reason for its late development compared to thermoplastic or thermoset clay nanocomposites.

The use of nanoclay in rubber allows to improve the mechanical properties (such as tensile strength and elastic modulus) [1, 8], barrier properties [9], thermal resistance [6] and, in some applications, antimicrobial properties [10]. Examples and cases of most used rubber matrices in the industrial field are presented. The

methods of clays incorporation into rubber matrices as well as the final properties reached are described.

2 Reinforcement Particles

A wide variety of ingredients are used in the rubber industry for various purposes, being the most important: reinforcement, fillers and process aids. The principal reinforcement effects are increase of strength, abrasion resistance, hardness and modulus. The extents to which these changes occur strongly depend on:

- (i) particle filler size
- (ii) rubber-filler interaction
- (iii) filler-filler interaction
- (iv) filler shape and structure
- (v) filler concentration
- (vi) filler dispersion in the matrix.

CB and precipitate SI, with a mean diameter of 10–30 and 30–100 nm respectively, are the conventional fillers in the rubber industry, with a content that in some compounds could reach up to 40 phr of CB. Considering compounds containing carbon black (CB) as reinforcement, it is well known the so-called *bound rubber*, which refers to a microstructure seen as a gel of reinforcement particles held together in a three-dimensional lattice by polymer molecules: the amount and morphology of the bound rubber depend on the listed variables [11]. Moreover, bound rubber type also shows a dependence on the processing conditions of the compound. Bound rubber content is measured by extracting the unbound rubber with solvent, and the result is influenced by the solvent nature and the extraction temperature.

Other nanofillers have received attention for reinforcing of rubbers like organo-clay (OC), nano silica, carbon nanotubes (CNT) and nano calcium carbonate due to the high aspect ratio and surface area as compared to conventional fillers. These characteristics are important to develop high-performance materials with low nanofiller content.

2.1 Carbon Black

CB is by far the most popular filler for rubber modification. CB is elemental carbon in the form of spherical particles that coalesced into aggregates and agglomerates, which is obtained by the combustion or thermal decomposition of hydrocarbons. The degree of aggregation is denoted by the term “structure”: a low-structure may have an average of 30 particles while a high structure may have around 200

particles per aggregate. The aggregates have a tendency to cluster together to form agglomerates due to van der Waals forces. During the mixing process, polymer free radicals are formed due to the shear forces generated and such free radicals react with CB to form bound rubber as CB acts as radical acceptors [12].

About 90% of the worldwide production of CB is used in the tire industry, in which acts as reinforcing fillers to improve tear strength, modulus, and wear characteristics. Commercially, CB fillers are available with different levels of structure, particle size, chemical reactivity and pH that lead to different levels of reinforcement.

2.2 *Silica*

SI (silicon dioxide) consists of silicon and oxygen arranged in a tetrahedral structure of a three-dimensional lattice. The use of silica as rubber reinforcement started around 1950 as an alternative to CB, shoeing sole the first applications due to the possibility of obtaining a non-black product. The incorporation of SI in heavy-service tires started in the 70's due to the improvement of cutting and chipping resistance of the compound and, also rubber adhesion to textile and metal.

The presence of hydroxyl groups in the silanol (Si-OH) on the SI results in strong filler-filler interactions and adsorption of polar materials by hydrogen bonds. Since these intermolecular bonds are very strong, the SI particles aggregate tightly, reducing the dispersion of silica in the rubber compound.

Around 1970 started the introduction of silane coupling agents such as the bis(3-(triethoxysilyl)-propyl)-tetrasulfide (TESPT) and other bifunctional silanes in order to prevent adsorption of curatives on the silica surface [13]. In these cases, the silane coupling agent reacts with the silanol on the silica surface to form a siloxane bond. The silane molecule bonded to the silica surface reacts with the rubber chain to form a crosslink between the silica and the polymer.

Silica is available as fumed SI and precipitated SI, which is obtained by coagulation of SI particles from an aqueous medium under the influence of high salt concentration or other coagulants [12, 14].

In tire treads, silica yields a lower rolling resistance at equal wear resistance and wet grip than CB [15]. Rattanasom et al. [16] analyzed the reinforcement of Natural Rubber with SI/CB hybrid filler in a total amount of 50 phr. The results reveal that the compounds with 20 and 30 phr of silica in hybrid filler exhibit the better overall mechanical properties.

2.3 *Clay*

Clays have been known for many decades as a non-black filler type for rubber compounds [4]. These fillers are inorganic in nature and therefore incompatible

with organic polymer matrices. Thus, the reinforcing effect of these fillers was lower than that of CB.

Clays have a low price and many attractive structural features such as hydroxyl groups, Lewis acidity, exchangeable interlayer cations, differences of Si–O tetrahedral sheet and Al–OH octahedral sheets [17]. Also, layered silicate nano-fillers have already been developed: the silicate layer surfaces have been effectively modified to render them organophilic so that the organically modified nano-fillers can significantly enhance the critical performance properties of polymer–clay composites. This is possible when the silicates are dispersed in nanometer- instead of micrometre-scale.

3 Layered Silicates

Galimberti et al. [18] define layered silicates as inexpensive natural mineral fillers which promote high reinforcements on the rubber matrices thanks to their high aspect ratio. They present a very thin plate-shape with low thickness (<10 nm) and width (<2 mm) [19], which permits to incorporate a relatively low amount of the filler to obtain superior mechanical properties, thermal stability, flame retardancy and gas barrier properties.

There are many works that show significant improvements in elastic modulus, tensile strength and elongation at break [8], thermal resistance [20], reduction in water/gas permeability [21] and flammability [20] for clays in their natural or modified form. The nanocomposite structure depends on the clay mineral–polymer compatibility and on processing conditions [22].

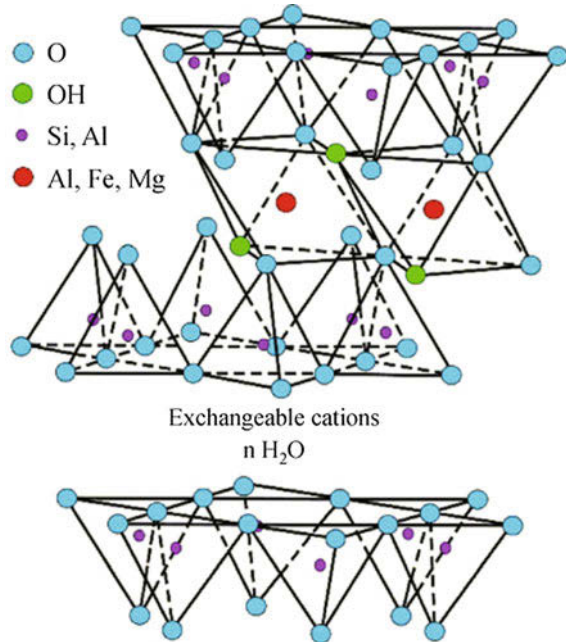
Siririttikrai et al. [19] show that clays in their natural form are easily exfoliated in aqueous suspension, which can be convenient for certain processing conditions. Depending on the compatibility with the rubber matrix, using clays in natural or pristine form can reduce the steps and cost involved.

3.1 Structure and Physical Characteristics

Figure 1 presents a typical structure of lamellar clays. Moreover, clays can be defined depending on the organization of the silicon and oxygen atoms, as well as the arrangement of the atoms within the laminar structure. The main structure consists of building blocks of tetrahedral sheets in which silicon is surrounded by four oxygen atoms and octahedral sheets in which a metal such as aluminium is between eight oxygen atoms [23, 24].

Silicate layers present oxygen atoms and hydroxide groups, giving it a hydrophilic nature. However, most rubber compounds possess a hydrophobic structure. Galimberti et al. [25] explain that, in order to achieve a compatibilization with the rubber matrix, there must be a chemical modification in the clay surface. This

Fig. 1 General layered silicate structure [24]. Reprinted from Kievani and Edrak [24]



technique consists in an exchange reaction of alkali and alkaline earth cations, which are located inside the clay galleries with different cations, modifying the clay surface polarity and increasing the interlayer distance [25]. This process of chemical modification will be described later in the chapter. Pavlidou et al. [23] define the first structure as 1:1, in which a tetrahedral sheet is fused with an octahedral sheet, whereby the oxygen atoms are shared.

The 2:1 layered silicates consists in two-dimensional layers where a central octahedral sheet of alumina is fused to two external silica tetrahedra by the tip, so the oxygen ions of the octahedral sheet also belong to the tetrahedral sheets. The layer thickness is around 1 nm and the lateral dimensions may vary from 300Å to several microns, therefore, the aspect ratio of this kind of layers (ratio length/thickness) is high, having values greater than 1000 [23]. The 2:1 structure is called pyrophyllite. Furthermore, since inside the structure, there are no substitution atoms and it has only an external surface area and no internal one, the layers do not expand in water.

When the silicon in the tetrahedral sheet is substituted with aluminium, the structure is called mica. With this type of substitution, the mineral is characterized by a negative surface charge, which is balanced by cations, such as potassium. Unlike the structure of pyrophyllite, mica does not swell in water, because due to the large size of potassium, the structure collapses and the sheets are held together only by electrostatic forces [23].

Montmorillonite (Mt) presents a structure similar to that of pyrophyllite, in which the trivalent Al-cation in the octahedral layer is partially substituted by

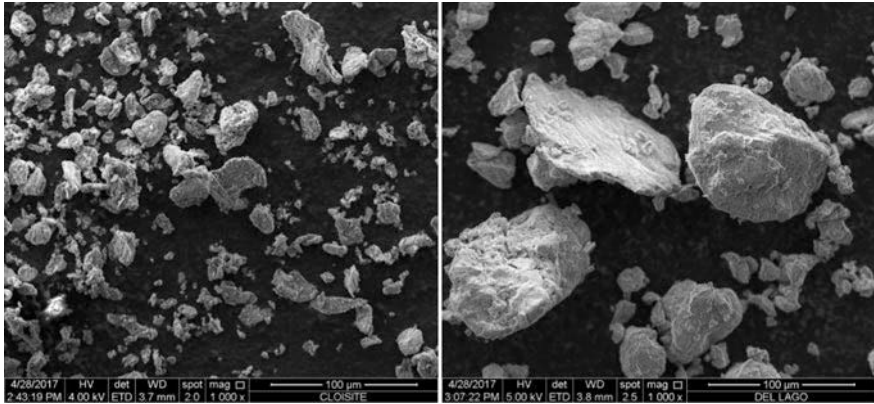


Fig. 2 SEM images of Na Mt (Left) and Raw Mt (Right)

magnesium cation. This group is called “smectites”. In addition, the overall negative charge is balanced by sodium and calcium ions, which are present in a hydrated form inside the interlayer. Since the ions are not part of the tetrahedral structure, the sheets are held together by weak interacting forces, which allow the easy entry of water molecules into the clay structure [23].

As previously mentioned, depending on the type of clay different structures can be presented, which affect the size and texture of the clay. Figure 2 compares the structural differences between two types of Mts for 1000X magnification, one Na–Mt (Left) and a Raw Mt (Right). Na–Mt clay has a smaller particle size compared to the raw Mt since it undergoes a purification process to eliminate any impurities. One of the most interchangeable cations is Na^+ , which is responsible for its swelling in presence of water. Moreover, the presence of Na^+ ions lets absorb a great number of water molecules resulting in the formation of a gel. If Ca^{+2} are the cations present in the interlayer, a lower amount of water molecule can be absorbed, so the clay is not able to swell. Depending on the cation presents in the interlayer, it will be determined the final application of the clay, as well as its compatibility with the rubber matrix.

3.2 Classification of Clays

The clays are classified according to the amount of silica present and the combination of tetrahedral and octahedral sites in the final structure. It can be separated into 5 main families:

- (a) Kaolinite
- (b) Serpentine

- (c) Smectites
- (d) Illites
- (e) Chlorites.

Mt, hectorite and saponite belong to the smectites family and are the most commonly used clay minerals for the preparation of polymer nanocomposites [22]. Hectorite is a colloidal clay widely used in the synthetic form. Dispersed in water, Hectorite forms a colloidal suspension used in many industrial and technological applications, such as rheology modifiers in several products, like paints and cosmetics. It has a very particular anisotropy due to the nanodisc shape of the particles and to the inhomogeneity of the sheet charges [26]. The Mt presents a dioctahedral structure with predominantly octahedral substitution. On the other hand, saponite presents a trioctahedral structure with the mainly isomorphous substitution of Si^{4+} by Al^{3+} in the tetrahedral sheets. This is why there are important changes in the final structure configuration; the Mt has hexagonal lamellae, while the saponite has a ribbon shape. Throughout the chapter, the discussion will focus on the use of Mt as a reinforcing, compatibilizing or property modifying agent since most of the published works use this type of clay.

- *Kaolinite*

Kaolinite is characterized by an isomorphous variation with temperature: up to 700 C, the Al^{3+} presents a tetrahedral structure (what is known as amorphous kaolin), while above this temperature has an octahedral one.

- *Montmorillonite*

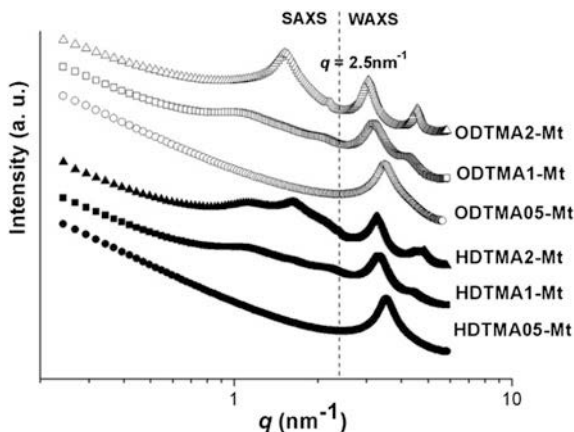
It is part of the group of smectites. Their structure consists of two silica tetrahedral sheets sandwiching an edge-shared octahedral sheet of Al or Mg hydroxide. Normally the layer thickness is around 1 nm, and the lateral dimensions may vary from 30 nm to several microns or larger. Ambre et al. [27] explain how the stacking of the clay layers leads to a van der Waals gap between the platelets called the interlayer or gallery. Also, the author described that the isomorphous substitutions within the layers generate negative charges that are counterbalanced by alkali and alkaline earth cations inside the clay galleries, and these cations are replaced by organic ones such as alkyl ammonium ions via an exchange reaction.

As it will be discussed, interlayer distance is one of the most important parameters since it defines the possibility for the polymer chains to enter inside the interlayer to effectively achieve an intercalation or exfoliation of the clay.

4 Chemical Modification of Clays

Natural clays can be well dispersed in hydrophilic polymers, such as poly (ethylene oxide) and poly(vinyl alcohol). In order to increase the compatibility with hydrophobic polymers, an ion exchange is performed with cationic-organic

Fig. 3 Variation of the interlayer distance q of Mt and OMt according to the modifier concentration, determined by SAXS and WAXS. Reprinted from Bianchi et al. [28]



surfactants. Pavlidou et al. [23] referred the alkylammonium ions as the most used, but other “onium” salts can be used, such as sulfonium and phosphonium. The objective of the modification is to decrease the surface energy of the silicate and improve wetting with the polymer matrix. The long organic chains of the surfactants are tethered to the surface of the negatively charged silicate layers, promoting an increase in the interlayer gallery and therefore favouring the entrance of polymer chain between interlayer space in order to improve the mechanical properties of the nanocomposite.

During the modification process, the excess of negative charge should be considered since it is related to the ability of clay to exchange ion, this characteristic is defined as the cation-exchange capacity (CEC), expressed in meq/100 g (milliequivalents/100grams). Pavlidou et al. [23] explain how this property is highly dependent on the nature of the isomorphous substitutions in the tetrahedral and octahedral layers.

Figure 3 shows an analysis of organo modified montmorillonite (OMt) by SAXS and WAXS. In their work, Bianchi et al. characterized a Mt two with different organic modifiers: octadecyl trimethylammonium (ODTMA⁺) and hexadecyl trimethylammonium (HDTMA⁺) in different proportions: 0.5, 1 and 2 CEC of Mt. They obtained important changes in the final interlayer distance of the clay, which determine the final interaction with a rubber or polymeric matrix [28].

4.1 Synthesis of Organoclays

Due to the hydrophobic behaviour of most elastomeric polymers, raw natural clays needs to be modified in order to use them as reinforcing materials and increase the compatibility between the matrix and the nanoparticles [29]. The most common technique is by using long tallow organic ammonium cations through ion exchange

of the interlayer cations. These new types of filler are commonly known as organoclays (OC).

OC preparation usually requires a two-step method, which includes a first step of purification, and a second step of the organic modification itself. Purification consists in the separation of impurities such as quartz, calcite, dolomite, talc and other clays [30]. Zhou et al. [31] described a method for purification and defibering of Chinese sepiolite. The technique consists of an acid treatment to decompose carbonated impurities and assisted by microwave-heating in order to improve the reaction kinetics with low energy consumption. Defibering aims to the de-agglomeration of sepiolite fiber bundles with the objective of obtaining nanoscale particles.

However, this two-step method has several disadvantages such as the consumption of large quantities of water and the energy spent on repetitive techniques. In order to avoid the drawbacks mentioned, Zhuang et al. [30] proposed a one-step method combining the purification and organic modification of sepiolite into a simple and more environmentally friendly procedure. The authors stated that organic surfactants can not only be used as an organic modifier but also as flocculants, therefore organo-sepiolite was easier to be separated from the dispersion.

Daitx et al. [29] described a method for the modification of Mt and halloysite (Hal) with (3-aminopropyl) triethoxysilane (APTES). Both OC were prepared by dispersion of the clay in an ethanol solution. In the case of Mt, the pH was adjusted to 3 with acetic acid for the protonation of the amino group and to promote the cationic exchange with Na^+ located in the interlayer space. APTES was added to the clay/ethanol suspension and stirred for 2 h and later filtered and washed with 96% ethanol. Lastly, the filtered cake was dried under vacuum at 70 °C for 8 h. In this work, the modification of the nanoparticles with aminosilane increased the interaction between clays minerals and the polymer due to the amino groups that can freely interact with the matrix.

5 Characterization of Clay Nanoparticles

The characterization of the clays is quite important to determine certain properties that are fundamental to be considered before being included into a rubber matrix. For example, mineralogical and thermal properties are important to determine the composition of the clay, particularly to know the nature of the clay (hydrophilic or hydrophobic nature). Some of the most used characterization methods include X-Ray diffraction (XRD), Infrared spectroscopy (IR), Inductively coupled plasma atomic emission spectroscopy (ICP-OES), thermal analysis (DTA, TGA), Specific surface area (SSA), CEC determination, microscopic techniques (TEM and SEM), gravimetric and grain size measurements [32–34]. In this chapter, we will show some techniques that can be useful to characterize any type of clay.

5.1 X-Ray Diffraction (XRD)

XRD is a very useful technique for the study of layered type nanoparticles. Furthermore, XRD is often used for the determination of the d_{001} plane corresponding to the basal space between the layered silicates which can be calculated by the Bragg's law:

$$\lambda = 2d \sin \theta$$

where λ is the wavelength of the incident wave, θ is the scattering angle and d is the distance between the atoms of a crystalline system.

Gamoudi and Srasra [33] studied the characterization of natural clays suitable for pharmaceutical and cosmetic applications by XRD analysis. Authors determined the presence of smectite in the composition by studying the characteristic peaks of the d_{001} reflection at 12.57 Å. Moreover, they also detected the presence of kaolinite by the $d_{001} = 7.12$ Å and $d_{002} = 3.56$ Å.

Successful organic modification of clay particles produces a shift of the d_{001} plane to lower angles values. This can be explained by taking into account the increase in the basal space due to the volume of long tallow organic molecules compared to the exchangeable cations. Ezquerro et al. [35] studied the modification of Mt with organic divalent phosphonium cations. Na-Mt showed a basal reflection at 7.78° and an interlayer spacing of 1.14 nm. The organic modification with Dim-Br (o-xylylenebis (triphenylphosphoniumbromide)) shifted the basal reflection to lower angles due to the intercalation of the surface between the layers of the OC. Moreover, an increase in the concentration of Dim-Br produced a shift to lower 2θ angles.

Alves et al. [36] studied the organic modification of Mt with ionic and non-ionic surfactants. They attributed the correct intercalation to a shift of the d_{001} to lower 2θ angles. Moreover, the basal space increase when surfactant amount increases and decreased after washed.

5.2 Microscopy

Scanning electron microscopy (SEM) and transmission electron microscopy (TEM) can provide information about the morphology of the clay platelets. Also, energy-dispersive X-Ray spectroscopy (EDX) can be used to study the composition after the modification with organic molecules.

Ezquerro et al. [35] studied the changes in the morphology of the Mt clay platelets. They claimed that pristine Mt shows soft surfaces and platelets tend to agglomerate. While surface modification of Na^+ for a phosphorous compound generates a rougher surface and breaks the agglomeration of the lamellas. Furthermore, EDX analysis was also conducted to study the yield of the organic

modification of the interlayer cation. In their studies, the Na^+ content decreases and the phosphorous content increases with the surfactant concentration.

Figure 4 presents SEM images of Mt and OMT by Bianchi et al. [28], there can be seen the morphology modifications of the Mt surface structure induced by organic modification with alkylammonium salts (ODTMA^+ and HDTMA^+), with alters the surface structure, the curvature of the plates, and the aggregate formation.

Zhuang et al. [30] studied the purification and organic modification of sepiolite by TEM analysis, which was used to detect the presence of impurities, before and after the purification, such as calcite, quartz and talc. Also, the morphology of sepiolite fibers was studied by TEM. Sepiolite fibers form crystal bundles and rods due to hydrogen bonding and van der Waals' forces between the fibers.

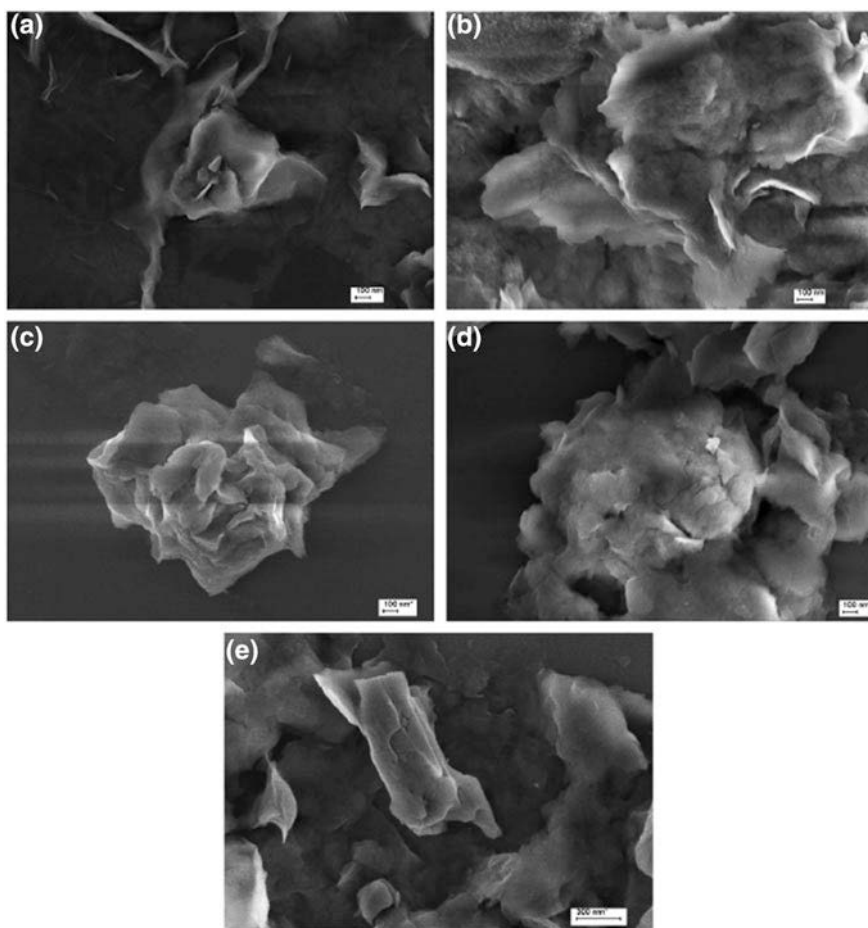


Fig. 4 SEM micrographs of Mt (A) and OMT, using as modifiers HDTMA (B and C) and ODTMA (D and F). Reprinted from Bianchi et al. [28]

5.3 *Fourier Transform Infrared Spectroscopy*

Fourier transform infrared spectroscopy (FTIR) can be used to characterize aluminium silicates materials. The most important bands present in clays are OH stretching ($3800\text{--}3200\text{ cm}^{-1}$), Si-O symmetrical and asymmetrical stretching ($1200\text{--}900\text{ cm}^{-1}$) and Al-O stretching (800 cm^{-1}). Moreover, FTIR could provide information about the substitution of cations from the interlayer space by organic molecules.

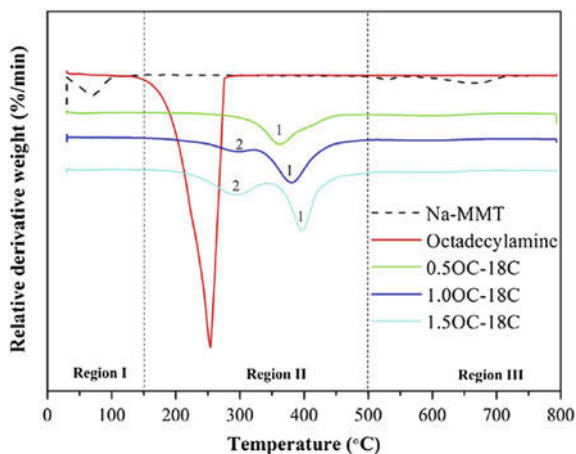
Hojiyev et al. [37] made an FTIR analysis of purified and cationic surfactant modified. They identified the bands corresponding to stretching vibrations of OH groups, Si-O groups, Al-Al-OH groups, and Al-Fe-OH groups. Moreover, Na-Mt spectra show the existence of free and interlayer water at $\sim 3400\text{ cm}^{-1}$ and adsorbed water at $\sim 1630\text{ cm}^{-1}$. In addition, the spectra of cationic modified Mt show new peaks corresponding to asymmetric stretching vibration, symmetric stretching vibration and bending stretching vibration of methylene groups (2924 , 2849 and 1469 cm^{-1} respectively). Also, the broad peak at 3404 cm^{-1} corresponding to free and interlayer water was removed upon modification due to the hydrophobic nature of the cationic surfactant.

5.4 *Thermal Properties*

Thermal analysis is also a useful tool to characterize OC due to the difference between the thermal stability of the inorganic cation and the organic surfactants. Within the thermal characterization techniques, the most commonly used ones are thermogravimetric analysis (TGA), derivative thermogravimetric analysis (DTG) and differential scanning calorimetry (DSC).

Sookyung et al. [38] quantified the modification degree of Na-Mt with octadecylamine by TGA/DTG as the ratio between the mass fraction of organic weight loss owing to alkylammonium ions, and the molecular mass of the organic cation exchanged on the clay platelets surfaces. In the TGA/DTG thermograms, three different regions can be distinguished, as is shown in Fig. 5. Region I appear below $150\text{ }^{\circ}\text{C}$ related to the loss of surface-adsorbed water and gas. Moreover, Na-Mt presents the higher weight loss in this region caused by the hydrophilic nature of sodium cation. Region II occurs in the temperature range of $150\text{--}500\text{ }^{\circ}\text{C}$ and is attributed to the decomposition of the octadecyl amine. Therefore, region II was used to the estimation of the modifying content in the OC. Finally, region III emerge at temperatures higher than $500\text{ }^{\circ}\text{C}$ as a result of the loss of structural water released by the dehydroxylation of the clays layers [38]. Also, the authors made DTG characterization for further study of OC in region II. They stated that samples with low contents of modifying agent present only one peak, while at higher CEC concentrations a second peak appears. This difference is caused by the location of the modifying agent in the OC.

Fig. 5 DTG thermograms of Na-Mt, octadecylamine and OMT with various concentrations of modifying agent: 0.5, 1.0 and 1.5 CEC times of Na-MMT. Reprinted from Sookyung et al. [38]



Soares et al. [39] analyzed the thermal behaviour of modified anionic and cationic clays with imidazolium ionic liquid by TGA. The decomposition mass below 200 °C was attributed to the absorbed water and volatile molecules. Around 320 °C, a second weight loss region appears corresponding to the decomposition of the imidazolium ionic liquid. Also, the content of the modifying agent was calculated as the difference of loss of mass between the raw clay and the organoclay.

6 Elastomeric Clay Composites

During the last 25 years, the development of nanocomposites was intensively explored by researchers, achieving remarkable improvements in mechanical, thermal and physicochemical properties compared with those of conventional composites materials. In this section, a review of some recent works with rubber as matrix reinforced with some type of clay are presented.

6.1 Natural Rubber

Natural Rubber (NR) is obtained from the sap of different trees, almost entirely from the plant *Hevea brasiliensis*, therefore is regarded as a sustainable polymer. In the latex state, NR contains approximately 30% dry rubber content. The latex is normally concentrated, mostly by centrifugation, increasing the dry rubber content approximately up to 60% before it is distributed. NR is a hydrocarbon diene monomer whose repeating unit is cis-isoprene. The outstanding strength of natural rubber has maintained its position as the preferred material in many engineering applications. It has a long fatigue life, good creep and stress relaxation resistance and low cost [40].

Clay/NR composites have been successfully prepared by several procedures: melt mixing, latex compounding and in solution.

George et al. [6] prepared NR reinforced with different organo modified Cloisite clays (10A, 15A, 25A, 30B and 93B) in a two-roll mixing mill and studied the effect of concentration (from 1 up to 15 phr), type of clay and vulcanizing systems on the mechanical properties. They concluded that the conventionally vulcanized samples exhibited higher tensile strength and elongation at break compared to efficient and peroxide vulcanized samples. The maximum tensile strength was reached by the composite containing 5 phr of nanoclay. Among the different samples, NR containing the cloisite 25A exhibited the better properties.

Carli et al. [41] prepared composites of NR with 2, 4 and 8 phr of Cloisite 15A as a substitute for conventional silica (SiO₂). Based on mechanical properties, Authors concluded that 50 phr of silica can be replaced by 4 phr of organoclay without affecting the final properties even after ageing.

Siririttikrai et al. [19] prepared compounds from fresh NR latex (FL) and from concentrated NR latex (CL) with unmodified montmorillonite, due to that mixing in the latex state before being coagulated could be advantageous and this process can be carried out at the rubber plantation or at collection points nearby. Different methods yielded different results because during centrifugation process not only water is removed, also some water-soluble materials (like proteins), therefore the chemical composition of natural latex and concentrated latex are not exactly the same, an explanation of how this could affect the material properties is proposed in the scheme shown in Fig. 6. They concluded that MMT can be used to reinforce NR effectively by using fresh latex and MMT water dispersion as the starting point.

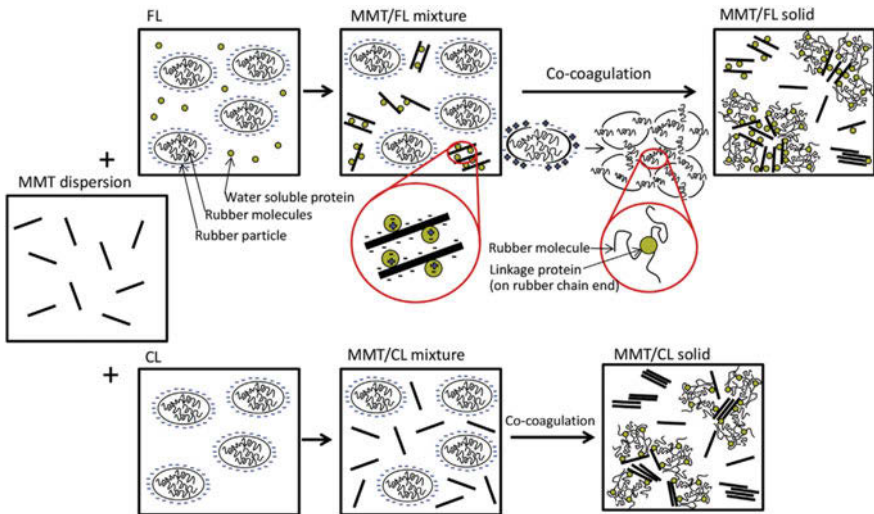


Fig. 6 Schematic illustration of Mt and rubber latex mixing and the co-coagulation processes for different types of NR latex. Reprinted from Siririttikrai et al. [19]

Sookyung et al. [38] made composites of NR with Na–Mt nanoclay modified with different concentrations of octadecylamine at 0.5, 1.0 and 1.5 times the CEC of Na–Mt, the obtained that at higher concentration value a larger *d*-spacing and a higher degree of clay dispersion in the matrix were observed. With a concentration of 1.5 times of the CEC, a faster curing reaction and a higher crosslink density were obtained and the mechanical and dynamic properties and thermal stability were enhanced.

6.2 *Styrene Butadiene Rubber*

Styrene-butadiene rubber (SBR) is an elastomeric copolymer consisting of styrene and 1,3-butadiene. Most SBR is produced by emulsion polymerization as well as by solution polymerization. SBR is characterized by a good abrasion resistance, ageing stability and low-temperature properties. The tire industry consumes approximately 70% of total SBR production. SBR formulations usually require a high amount of reinforcing filler, being CB the most used [40].

Praveen et al. [42] prepared SBR nanocomposites reinforced with a hybrid system of CB (N330) and OMT using octadecylamine as a modifier. The study included the variation of clay content (5, 10, 15 and 20 phr of OMT) in gum rubber and in rubber filled with 20 phr of CB, preparing in a two-roll mill. The presence of intercalated, aggregated and partially exfoliated structures were revealed through XDR and TEM. Samples containing 10 phr of OMT resulted in an increase of 153% in tensile strength, 157% in elongation at break and 144% of modulus 100%. The obtained results open up a new prospect in developing CB–OMT-hybrid nanocomposites, facilitating the possibility of partial replacement of CB with OMT in rubber products without affecting the critical performance properties.

Sadek et al. [43] studied SBR composites reinforced with sodium bentonite as well as modified with two types of surfactants: dodecyl benzene sulfonic acid (DBSA) and nonyl phenol ethoxylate (NPE), also a mixture of the surfactants was used: DBSA/NPE (50/50%). The clay content was 2, 4, 6, 8 and 10 phr, and the compounds were prepared in a two-roll mill. The presence of clays induces an increase in the minimum and maximum torque values, acceleration of the vulcanization process, and improved mechanical properties with organoclay content up to 6 phr. This effect was more noticeable in the presence of the treated clay with DBSA/NPE. Also, incorporation of 6 phr of DBSA/NPE-clay resulted in significant improvement of the degradation profile of the nanocomposites at 90 ± 1 °C for 4 days.

During the long period of service, most polymers (and composites) gradually lose their useful properties as a result of polymer chain degradation. The main harmful agents are oxygen, heat, and high energy radiation. The effects of these agents depend mainly upon the chemical structure of polymer chain. Youssef et al. [44] analyzed the effect of gamma radiation on the final properties of NR/Na–Mt and SBR/Na–Mt nanocomposites prepared by coagulating the mixture of rubber

latex and clay aqueous suspension. The clay concentration was varied from 2 to 10 phr and the irradiation of the samples was carried out using a cobalt-60 gamma cell source with doses of 10, 25, 50, 75, and 100 kGy at a dose rate 5 kGy h^{-1} . XRD results indicated well dispersion of rubber latex into clay stacked layers and the platelets have a preferential orientation forming exfoliated NR/Na⁺-MMT nanocomposites while SBR/Na⁺-MMT form intercalated nanocomposites. Author explains that SBR have bulky benzene groups, which partially restrict the chains to intercalate into the gallery gap of the clays. Second, NR contains a higher number of unsaturated double bonds than SBR, thus the polarity of NR is higher than SBR, as a result, NR could form exfoliated whereas SBR are intercalated. Overall irradiation dose range together with clay loading, an improve of the mechanical properties of rubber/Na-Mt nanocomposites was obtained. However, SBR nanocomposite, in particular, attains its higher value at 50 kGy, then decreases; also, the thermal stability at 50 kGy is higher than 100 kGy.

6.3 *Nitrile-Butadiene Rubber*

Nitrile-butadiene rubber (NBR) is a polar elastomer, with a carboxylic group and a double bond in the rubber backbone. The polar nature of the NBR allows a higher resistance to non-polar substances such as hydrocarbons and oils. Depending on the acrylonitrile content, important improvements in abrasion resistance are obtained, therefore it has a great performance in the seal industry. Other advantages of NBR are its low cost and good processability. However, some of the negative aspects include a low ageing resistance because of the unsaturated backbone present in the chemical structure, thus is sensitive to environmental factors [45, 46].

Costa et al. [47] explain the effect of Mt in polar rubbers as NBR. The presence of the Mt offers a crosslinking effect defined as “ion cluster”. It was demonstrated that there is a chemical interaction between the NBR chains and the clay particles, especially in cases where there are metal oxides in the rubber vulcanization formula like ZnO. This reaction can be explained taking into account the acid-base reaction, where acidic ACOOH group of the NBR reacts with the ZnO producing an ionic salt and releasing water.

De Sousa et al. [48] formulated nanocomposites of XNBR with different types of clays (Na- Mt, OMt and a natural bentonite). Using XRD and mechanical properties, they concluded that the organo-modifier agent and the molar mass of rubber had a significant influence on the dispersion of the clay after the mixing process on a two-roll mill.

Finally, Yu et al. [49] presented a very interesting work combining OMt and NBR by emulsion process. TEM images of the nanocomposites exhibited uniform dispersions of the clay sheets inside the NBR matrix. Also, the XRD patterns confirmed the intercalation of the NBR polymeric chains inside the interlayer of the OMt. The final nanocomposites showed an improvement of mechanical properties and solvent resistance comparing to pure NBR. Moreover, thermogravimetry

indicates an increase in the maximum decomposition rate of the nanocomposites in comparison with that of pure NBR were observed, indicating an enhancement of the thermal stability. There was also a faster curing rate and a higher glass transition temperature, storage modulus and loss modulus.

6.4 Ethylene-Propylene-Diene Rubbers

Ethylene propylene diene terpolymer (EPDM) is an unsaturated polyolefin rubber with wide applications. Due to its good mechanical properties, very low unsaturation and associated resistance to ageing and ozone deterioration, it has become extensively used in making automotive tire sidewalls, cover strips, wires, etc. In a non-polar rubber like EPDM, the presence of stearic acid in the formulation favours the dispersion of clays due to the chemical reactions leading to ester formation involving carbonyl groups of acid and hydroxyl group of clay [50]. The early works on preparation and characterization of EPDM nanocomposites included that of Usuki et al. [51] and Zheng et al. [52].

Liu et al. [17] analyzed the reinforcement of nano kaolin (NK) powder into four types of rubber: SBR, NR, BR and EPDM. The reinforcing effects were compared with those from precipitated silica (PS). The compounds were made in an open roll mill. The results showed that NK can greatly improve the vulcanizing process by shortening the time to optimum cure (t_{c90}) and prolonging the setting-up time (t_{10}), which improves production efficiency and operational security. The rubber composites filled with nano kaolin enhances the mechanical properties and thermal stability. The tensile strength of the rubber/NK composites is close to those of rubber/PS composites. The tear strength and modulus presented a lower performance compared with those containing precipitated silica.

Chang et al. [53] showed that the oxygen barrier properties of EPDM/OMt clay nanocomposites are better than that of pristine EPDM. The oxygen permeability of 10 phr layered clay filled EPDM nanocomposite was reduced to 60% as compared with the pristine EPDM compound. The gas permeability was ascribed due to the uniform dispersion of the impermeable clay layer with the planar orientation in the EPDM matrix.

Zhang et al. [54] synthesized an intercalation agent containing double bonds for modifying the interface of EPDM/clay nanocomposites, using a Na-Mt. In order to compare with the OMt containing double bonds (VMMT), the OMt modified with cetyl trimethyl ammonium bromide (CTAB) without double bonds was also prepared; in both cases, the content used were 0, 3, 5 and 10 phr. Authors analyzed the relaxation dynamics via broadband dielectric relaxation spectroscopy. In polymer/clay nanocomposites, the environment of the polymer chains inside the silicate gallery will greatly affect the molecular relaxation and mobility. According to the literature, two distinct types of dynamic behaviour may exist in such systems. One is the slower relaxation dynamics associated with glass-transition temperature (T_g) and is attributed to the large interlayer distance and the strong polymer-filler

interactions. In contrast, when the polymer-filler interactions are weak, the polymer segments will exhibit the faster relaxation mode, thereby leading to the depression of T_g value. According to the XRD analysis, the VMVT containing double bonds was exfoliated, and the crosslinking reaction between VMVT and EPDM chains promotes the exfoliation of the organic layered compounds. The dielectric relaxation spectra show that the segmental relaxation of EPDM shifted to higher temperature with increasing VMVT content, and a new relaxation, which was attributed to the interfacial relaxation being confined by the MMT platelets, was detected at a much higher temperature and lower frequency, whereas that did not appear when adding OMT.

6.5 Role of Nanofiller as Compatibilizer in Rubber Blends

Natural and synthetic rubbers are not used very often in an isolated form. An elastomer is mixed with another one, especially in the tire industry, for three main reasons: to improve properties of the material, to improve processing or to reduce costs. Most blends of rubbers are immiscible, which leads to a non-uniform dispersion of the components in the rubber matrix. For example, in Fig. 7 can be seen images taken by TEM of unfilled NR/SBR blend with a different ratio: on the left a compound with 25 phr of NR and 75 phr of SBR (25NR/75SBR), and on the right the complementary sample (75NR/25SBR), being SBR the dark phase and NR the clear one [55].

Nanoclay also shows preferential migration to specific rubbers when used in blends, due to organoclay is more compatible with polar rubbers. By the introduction of functional groups, the polarity can be changed so as to have better filler dispersion and hence compatibilizing action.

The different solubility of two rubber is related to different polarity and level of unsaturation in the rubber components, leading to an unequal dispersion but also to

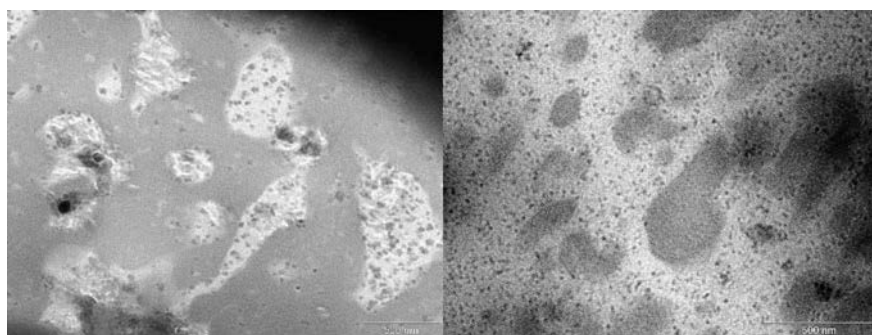


Fig. 7 TEM micrographs of vulcanized NR/SBR blends (left) 75NR/25SBR and (right) NR/SBR, being SBR the dark phase and NR the clear one

a diffusion of the components during the mixing or during the vulcanization process [56, 57], which could generate an uneven crosslinking. The presence of reinforcement particles in some cases can complicate this situation even more.

The properties of rubber blend/clay nanocomposites are strongly affected by the location and distribution of the clay in addition to the size, shape and dispersion of each rubber phase. Depending on the location of the clay in the matrix or dispersed phase, a separated or encapsulated morphology could be formed. All this can cause a narrow interphase and poor physical or chemical interactions between the two phases, influencing the mechanical properties of rubber blend.

OC particles added at a low loading level could play as interfacial compatibilizers for immiscible rubber blends reducing the domains sizes. This is due to nano level dispersion, generating a reduction of the interfacial tension between the two rubber phases [58].

Compatibilizers act through a chemical reaction (reactive compatibilization) or by its capability for interaction with blend components or by its interaction with chemicals present at the interface of blend components. Most of the interactions are intermolecular forms of attraction such as van der Waals and hydrogen bonding, based on the polarity of materials (nonreactive compatibilization). The surfactants present in organoclay also contribute to compatibilization. It is also possible that two immiscible polymer chains can intercalate the same clay platelet and play the role of a block or graft copolymer. Generally, graft or block copolymers have similar segments to blend components and hence act as compatibilizers in blends [12].

Rajasekar et al. [59] used clays as a compatibilizing agent for NR and NBR blends. They incorporated an OMt by solution mixing to promote a uniform dispersion inside the NR matrix. After that, they incorporate the first NR/OMt composite to a sulfur formulated NBR matrix, observing important changes in morphology, curing characteristics, mechanical properties, swelling and compression set. They established how the improvements in properties come from the distribution of the clay inside the rubber matrix. By their morphological studies, it was possible to determine intercalation in the whole NR/NBR composite. Also, faster scorch time and cure time, as well as an increase in maximum torque were obtained compared to the neat NBR matrix. Increases in storage modulus and lesser damping characteristics for the compounds with OMt were measured. The final reinforcing efficiency was determined comparing enhancements in mechanical properties and higher swelling resistance in oil and solvents.

7 Preparation of Nanocomposites

The incorporation process of clays into a rubber matrix influences the final properties of the nanocomposite, and the final structure depends on the nature of the rubber and the type of clay employed. Maiti et al. [4] explain the mechanism by which the nanofiller aid the rubber formulations to improve their properties [1].

The optimum improvement of the nanocomposite properties depends upon the incorporation technique, the dispersion of the clay and the concentration of the reinforcement within the rubber matrix [60].

Several techniques were used to prepare rubber/silicate nanocomposites. The most known are [1]:

- Melt mixing
- Solution blending
- Latex blending/latex compounding
- Sol-gel processing
- Emulsion polymerization.

7.1 *Melt Mixing*

The melt mixing technique is one of the most utilized to prepare elastomer/OC nanocomposites. The method involves internal mixers and open two-roll mills [4], which consists of blending the layered silicate with the polymer matrix in the molten state. The full exfoliated rubber/clay nanocomposites are difficult to obtain by this method because of the high viscosity of the rubber in the molten state but if the layer surfaces of the clay are sufficiently compatible with the constituent polymer of rubber, the polymer chains can crawl into the interlayer space and form an intercalated or an exfoliated nanocomposite (see Fig. 8b) [23].

The intercalation/exfoliation processes are governed by the modification of elastomers and also the chemistry involved in compounding and curing state to form elastomer-clay nanocomposites with improved properties [4]. Maiti et al. also explained how the temperature and shear rate are important variables to promote an intercalation/exfoliation phenomena. Ray et al. [61] discussed how the melt intercalation is highly specific to the polymer, leading to new rubber formulations that were previously inaccessible. Normally, polymers containing polar groups (capable of associative interactions, such as Lewis-acid/base interactions or hydrogen bonding) favour intercalation phenomena because the surfactant molecule in the OC has the same non-polar character as the polymer [62].

Several authors have utilized this technique to prepare nanocomposites. For example, George et al. [6] investigated the mechanical properties of natural rubber/OC systems by melt mixing using a two-roll mill. Authors have studied the effect of clay concentration, type of clay and vulcanizing systems on the mechanical properties. Their results show how the clay interlayer distance is increased in all samples after incorporation into the rubber matrix, as great improvements in tensile strength, elongation at break and modulus.

Most of the published works present the reinforcement of clay nanocomposites based on acrylonitrile butadiene rubber (NBR), ethylene propylene diene (EPDM) and NR [4]. Wang et al. [63] studied NBR/expanded graphite (EG)/CB micro and nanocomposites systems to compare with NBR/CB systems. Their results show an

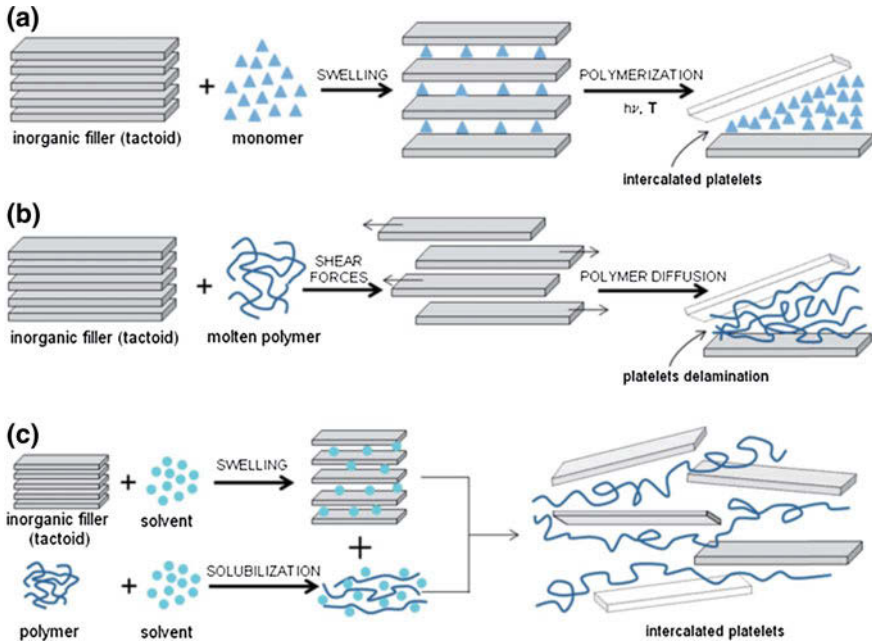


Fig. 8 Schematic representation of **a** in situ polymerization, **b** melt processing, and **c** solution casting [89]. Reprinted from Unalan et al. [90]

effect on the properties depending on the EG and CB loading content. By melt mixing, there is a better dispersion of EG, showing remarkable enhancement on tensile and dynamic mechanical properties. Przybyk et al. [63] prepared NBR reinforced with an antibacterial Mt, presenting important improvements in mechanical and thermal properties.

Melt mixing is also the preferred mode of incorporation of oxides like nano titanium dioxide, nano zinc oxide and others [4].

7.2 Solution Blending

Solution blending includes the solubilization of rubber in a proper solvent and then, the dispersion of the filler into the solution [4]. Later the solvent is evaporated after reaching a good dispersion of the nanofiller, usually, under vacuum or precipitation [4], the process is shown in Fig. 8c) and also in Fig. 9. The principal feature of this technique is that the layered silicates can be exfoliated into single layers using a solvent in which the polymer is soluble, overcoming the weak forces that stack the layers together [23]. The solvent allows the elastomer chains to be uncoiled and disentangled and easily enter between the layers of the clay or interact with the

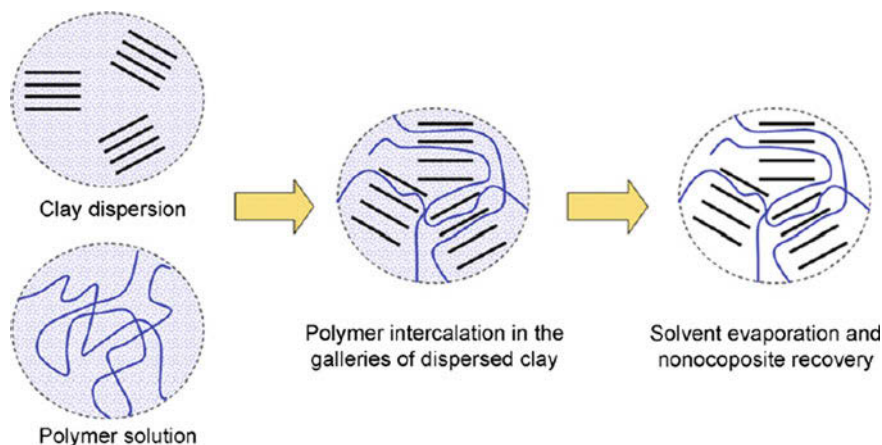


Fig. 9 Schematic representation of solution blending process. Reprinted from Pavlidou et al. [23]

particulate nanofillers [4]. In this method, the ultrasonic dispersion of clay is indispensable to increase the interfacial adhesion between clay and elastomer matrix in order to reach a high-performance rubber–clay nanocomposite. The main drawback of this method is the disposal of large quantities of solvent [23].

Usha Devi et al. [20] swelled an OMT in toluene to promote an effective method to fabricate an SBR nanocomposite, observing a complete rate of dispersion in the elastomer.

7.3 Latex Blending/Latex Compounding

The latex compounding method was developed to solve the problem of incompatibility between the rubber and fillers, improving the dispersion of fillers in the rubber matrix [3]. Latex is defined as a stable aqueous dispersion of fine rubber particles, with a particle size around 300–500 nm [1]. Most of the elastomers are available in latex form, so pristine clay can be added directly or in its aqueous dispersion (slurry). Moreover, an additional advantage is that the layered silicates can absorb water from the suspension, which aid to expand the interlayer space [4].

After the combination of latex and layered silicates, a co-coagulation process is carried out to produce a masterbatch product. This method allows the fabrication of latex film products, such as gloves, condoms, and coatings if the latex is mixed with the layered silicates and curatives in suspension [1].

If there is a good compatibility between rubber and clay, the formation of structures known as “house of cards” or “skeleton” can occur because of the presence of rubber particles that penetrate the clay interlayer gallery due to a polarity mismatch [64]. Rezende et al. [8] used the latex compounding method to

obtain an NR/clay composite obtaining improvements in mechanical properties and characterizing the nanocomposite structure by TEM and small angle neutron scattering (SANS).

7.4 Sol-Gel Processing

In this technique, rubber/clay nanocomposite is synthesized using an aqueous solution (or gel) containing the polymer and the silicate building blocks. The precursors for the reaction are clay silica sol, magnesium hydroxide sol and lithium fluoride. The polymer aids the nucleation and growth of the inorganic host crystals and gets inside the clay layers [23].

Some authors have developed sol-gel systems. Brantseva et al. [65] used clays to improve the adhesive capacity of rubber compounds showing how both structural and pressure-sensitive adhesives (PSAs) were improved. With the sol-gel method, they ensured exfoliated or at least intercalated conditions. George et al. [6] prepared SBR/NBR/OMMT composites and notice great improvements in thermal stability and swelling properties, attributed to the barrier characteristic the clays impart to the rubber matrix.

Some of the problems this method presents are [23]:

- The synthesis of clay minerals generally requires high temperatures, which can decompose the rubber chains.
- There is an aggregation tendency of the growing silicate layers.

7.5 Emulsion Polymerization

In this method, the monomers of the polymer are dispersed in water together with an emulsifying agent and the clays, as can be seen in Fig. 8a). It is beneficial to achieve a good interaction between the rubber matrix and the reinforcement, since there is a joint polymerization between the rubber chains and the clays, leaving a nanocomposite where some of the clay sheets are embedded in the rubber particles, while some polymer chains are adsorbed on the surface of the clay particles [66], due to this, a better dispersion of the reinforcement can be obtained [67].

Polymerization is promoted with temperature, and the clay swelling process occurs directly in the polymerization medium (water) and in some cases, by the low molecular weight of liquid monomers [67]. One of the drawbacks of this method is that requires a certain time period to form the nanocomposite and depends extensively on the polarity of the monomers, the type and surface of the filler and the initiation temperature of the polymerization reaction [4].

Distler et al. [68] explained a simple procedure to perform an emulsion polymerization. The base in this type of process consists of mixing: deionized water,

surfactant (for example sodium dodecyl sulfate), the reinforcement particles and the monomer. Within the process, the agitation is fundamental so that phase separation does not occur. As mentioned above, the polymerization initiator (for example sodium persulfate) is also fundamental, since the speed and the form of initiation of the process depend on it.

The polymerization system consists of a reactor with a stirrer, a reflux condenser, two lines for content the monomer emulsion and the initiator solution, and a temperature control unit which normally is rinsed with nitrogen. The reaction initiates with heat (approximately 70°C) and takes a few hours to complete. The final product is then filtered and then characterized by solid content and particle size [69].

Among the aforementioned methods, in situ polymerization and melt intercalation are considered as commercially attractive approaches for preparing polymer/clay nanocomposites [23]. In addition, the absence of a solvent makes direct melt intercalation an environmentally and an economically favourable method for industries from a waste perspective [62]. Moreover, it is compatible with the current industrial processes, such as extrusion and injection moulding. However, the dispersion of the clay in the polymer prepared by the melt mixing is not as good as that obtained by the latex compounding [69]. The main drawback is the poor dispersion within the matrix and the lack of affinity between the layered silicate and the organic polymers.

The latex compounding process is recommended when using hydrophilic clays because it occurs in an aqueous medium. While the process of melt blending is recommended when using hydrophobic clays (OMt) since with chemical modification they become more compatible with the elastomer.

8 Rubber/Clay Nanocomposites Properties

As it was mentioned above, there are numerous variables that define the final performance of a composite material, particularly when it is about a complex combination such as a vulcanized nanocomposite of rubber and clays.

The type of reinforcing the material, the shape of the particle as well as its structure, the type of rubber matrix and the preparation method play a fundamental role in the final properties of the compound. Depending on the application, it is necessary to comply with certain mechanical standards; therefore, it is necessary to consider those tests that conveniently help to determine the properties that describe how the behaviour of the material will be during its life in use.

8.1 Vulcanization Variables

The presence of nanoclay has a strong influence on the vulcanization process. The cure characterization of nanocomposites gives information about the interaction

between filler and the matrix, and also the extent of filler-filler inter aggregations. George et al. [6] investigated NR reinforced with organo modified Cloisite clay and found that the t_{c90} value decreases when the concentration of clay is higher. This indicates that organophilic clays accelerate the vulcanization process in these samples due to the formation of a transition metal complex in which sulfur and amine groups of the intercalate layers may involve [65].

Siririttikrai et al. [19] studied the cure characteristics of NR containing different amounts of Mt prepared from fresh or concentrated NR latex (FL and CL respectively). Figure 10 shows the cure curves of the compounds for different Mt content and Table 1 summarizes the characteristic cure parameters. It can be seen that, for the Mt/FL series, the maximum torque (M_H) increases with increasing Mt content. No effects were observed on scorch time (t_{s2}). The Mt/CL series displays a different behaviour: the sample made from CL with 4 phr of Mt displays the maximum value for t_{s2} and also for M_H , then these values decrease when the amount of Mt is higher. When the amount of Mt is the same, the Mt/FL compound displays slightly shorter cure times (t_{c90}) than does Mt/CL compound.

Several authors proposed that high energy ionizing radiation can be considered as a cost-effective and additive-free technique [70, 71]. Moreover, it can be carried out at room temperature, so it decreases the toxic volatile releases. Shoushtari Zadeh Naseri and Jalali-Arani [72] studied SBR/EPDM blends with and without OC vulcanized with gamma radiation. The effects of the radiation dose on the interaction between phases, crosslink density, gel content, and microstructure of the prepared OC containing samples compared to those of the unfilled blends were investigated. Authors used gel content as a criterion to estimate the crosslink density and found that the OC induces an enhancement of gel content respect to the system without reinforcement (Fig. 11), which would be related with the improvement of radical-radical interaction and formation of physical crosslinks [71]. Sookyung et al. [38] analyzed compounds of NR reinforced with 5 phr of Na-Mt modified with octadecylamine in concentration values from 0.5 up to 1.5 times

Fig. 10 Cure curves of Mt/ fresh latex (FL) and Mt/ concentrated latex (CL) compounds with the indicated amount of Mt. Reprinted from Siririttikrai et al. [19]

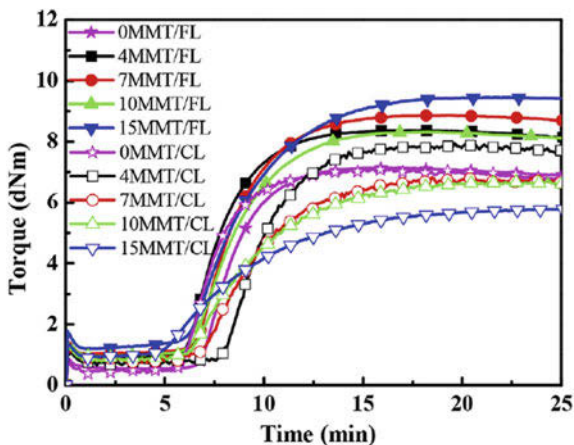
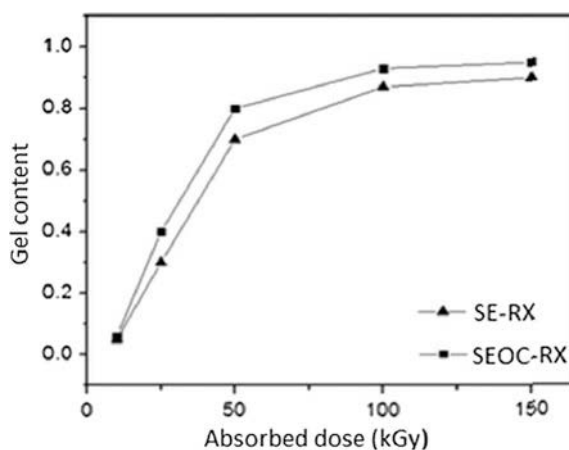


Table 1 Cure parameters of different Mt/latex compounds

Compound	M_L (dN m)	M_H (dN m)	t_{s2} (min)	t_{c90} (min)
0Mt/FL	0.54	7.15	7.60	10.88
4Mt/FL	0.91	8.37	6.83	10.65
7Mt/FL	1.04	8.86	7.33	11.67
10Mt/FL	1.00	8.32	7.32	11.93
15Mt/FL	1.20	9.42	7.15	13.21
0Mt/CL	0.44	7.08	6.65	10.15
4Mt/CL	0.71	7.94	8.79	13.10
7Mt/CL	0.78	6.72	8.18	13.86
10Mt/CL	0.83	6.76	7.75	14.82
15Mt/CL	0.94	5.79	7.43	15.09

The number in the compound indicates Mt amount in phr. Reprinted from Sirittikrai et al. [19]

Fig. 11 Gel content of unfilled SBR/EPDM (SE) and SBR/EPDM with OC (SEOC) samples as a function of absorbed dose (RX). Reprinted from Shoushtari Zadeh Naseri and Jalali-Arani [72]



the CEC value of Na-Mt. From the rheometric curves, they obtained that t_{s2} and t_{c90} decrease when the amount of the modifying agent increases. This behaviour is attributed to the effect of the ammonium groups of the octadecylamine that causes an increase of the zinc complex content, and therefore acceleration in the vulcanization reaction. Also, a higher value of M_H was obtained with a higher content of the modifying agent, which indicates a higher interaction between the clay and the rubber chains: a higher loading of the modifying agent gives a higher interlayer spacing of OC, allowing the penetration of rubber chains or their molecular segments into the silicate. This allows to explain the improvements in mechanical and thermal properties, the tensile strength and modulus at 100 and 300%; elongation and hardness of the composites were improved with the concentration of the modifying agent.

8.2 Rheological Properties

Microstructural changes of the nanocomposites can be followed by dynamic frequency sweep tests. Maroufkhani et al. [58] performed measurements within the linear viscoelastic region ($\gamma = 1$) in blends of polylactide acid (PLA) and NBR reinforced with 4 phr of Cloisite 10A (OC), prepared via melt compounding. They investigated the influence of the acrylonitrile (ACN) content of NBR on the dispersion and localization of the OC; three different ACN levels content in NBR were used: low (19%), medium (33%) and high (51%). It was found that the presence of nanoclays increases the G' values of the samples in the low-frequency region. The plateau in this region is caused by physical interactions between the nanolayers and the rubber chains. In addition, the presence of quaternary ammonium surfactants of OC promotes a good compatibility with PLA by hydrogen bonding. Finally, this phenomenon was not altered by the ACN content in the polymer blend.

Dynamic mechanical analysis (DMA) of XNBR/NR blends reinforced with nanoclays were studied by Satyanarayana et al. [73] in order to determine the T_g of the polymers. They stated that the incorporation of clays into a rubber matrix affects the rheological properties by shifting the $\tan \delta$ peak to lower temperature values [74]. As it was explained before, this effect is influenced by the filler type and load, the type of matrix and the filler-matrix interaction. Furthermore, the authors also reported that the presence of clay lowers the height of the $\tan \delta$ peak due to a reduction of the amount of rubber mobile during the dynamic transition process as consequence of the reinforcing effect of clay nanoparticles.

8.3 Mechanical Properties

Jahromi et al. [75] studied a ternary hybrid system consisting of polyamide 6 (PA6), NBR and OC. Compounds included an NBR and NBR activated with glycidyl methacrylate (GMA) groups. The Young modulus and tensile strength of the hybrid systems were improved by the increase of nanoclay content due to the effective reinforcing role of the inorganic filler [76]. However, the reinforcing effect was more effective for the nanocomposites including a reactive elastomer, which stems obviously from the better dispersion of nanoparticles along with nanoplatelet confinement in the thermoplastic phase domains.

A distinctive property to analyze the elastomer-filler interaction and filler-filler interaction is the non-linear viscoelastic response of filled systems, otherwise known as Payne effect [77]. Payne suggested that the formation of a three-dimensional structure was due to the filler incorporated in rubbers, which leads to higher modulus values at lower strains. Regarding the use of nanofiller, the surface area, surface modification and activity are some of the crucial factors that affect the non-linear viscoelastic response. A competition between filler-filler and polymer-filler interactions takes place in filled elastomers. If filler-filler interaction

predominates, the Payne effect is more pronounced. Zachariah et al. [78] evaluated the dynamic shear storage modulus and loss modulus of NR and Chlorobutyl Rubber (CIIR) containing OC. The authors studied these systems because of their application in the manufacture of automotive inner tubes and inner liners. They found that the nanoclay loading in both matrices increases the modulus values at lower strain due to the formation of filler-filler and filler-polymer networks. These networks could break at higher strains, which results in the reduction of the modulus.

8.4 Barrier Properties

Many researchers reported on the permeability behaviour of nanoclay loaded elastomeric composites proposing that this property increases due to the creation of a tortuous path in the microstructure for the transport of gas molecules [79].

Mohan et al. [80] investigated the water uptake of NR/SBR blends reinforced with OC. The water content, W_c , in the sample was measured as % weight increase in the sample. W_c was measured until the composite specimen attained equilibrium water uptake content. The following equation was used to calculate the W_c in the specimen:

$$W_c = \frac{(W_t - W_o)}{W_o} \times 100$$

where W_t is the weight of specimen at time t and W_o is the initial weight of the sample before placing in water. Figure 12 presents the water mass uptake as a function of time (in days) of all samples, the sample that containing 3 wt% nanoclay has the lower water content value. Also, static and dynamic mechanical analysis (DMA) properties were less affected in the nanoclay filled rubber than in the base rubber. Chao et al. [1] studied gas-barrier properties of IIR/clay nanocomposites obtained via the latex method. Moreover, they compared samples prepared using latex and co-coagulating methods. It is important to remark that TEM images revealed both partially exfoliated and intercalated structures for the isobutylene-isoprene rubber (IIR)/Mt nanocomposite prepared using the latex method and, on the other hand, a purely intercalated structure in the sample prepared using the co-coagulating method. It was found that the oxygen transmission of the IIR/clay nanocomposites decreases progressively as the silicate content increase. The oxygen permeability of the compound with 10 phf of clay was reduced to 60% as compared with the neat IIR. Layered silicate is composed of many monolayers that are 1 nm thick and 200–300 nm long; this aggregated platelet structure of the layered silicates in the IIR matrix could provide an excellent barrier to the diffusion of oxygen because of the increased tortuosity of the diffusing path [1].

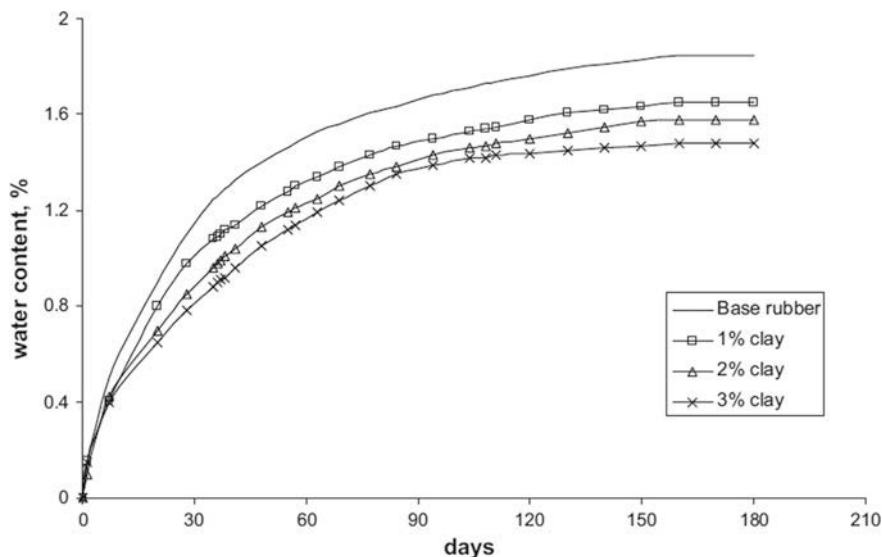


Fig. 12 Water mass uptake of rubber and rubber-nanoclay series in NR/SBR blends. Reprinted from Mohan et al. [80]

Wang et al. [81] stated through positron annihilation lifetime spectroscopy (PAS) and DSC that gas permeability in rectorite/SBR nanocomposites is mainly influenced by the free volume fraction and tortuous diffusional path effects attributed to the clay platelet-like morphology.

9 Applications

The incorporation of clays into rubber matrices comes from the need to improve the mechanical properties, such as tensile strength, elongation at break or elongation module [6, 8, 38]. There is also a need to improve vulcanization times [82, 83], as well as to extend the range of decomposition temperature [84]. There are also other properties that can be improved using rubber/clay compounds.

An important area of application of rubber/clay nanocomposites is gas and moisture barriers. The layers of clays that filled a polymer matrix serve as an impermeable medium for the gas and moisture. Although there is information about barrier properties of clay filled thermoset and thermoplastics are available in the literature, those related to barrier properties of rubber filled with clay nanoparticles are relatively few. Recently, several works were reported on the synthesis, characterization, mechanical and thermal properties.

The improvement of fatigue strength of rubber composites is also considered within automotive applications. Woo et al. [85] explain how the interest of fatigue

life evaluation for rubber components such as in engine parts was increasing according to extend the warranty period of the automotive components. In their study, they developed a rubber material environmentally friendly with superior physical properties and fatigue life using a rubber-clay nanocomposite.

Other applications include structural and pressure-sensitive adhesives (PSAs). Brantseva et al. presented a paper about the uses of clays in the adhesive industry as rheological modifiers where an enhancement of barrier properties, thermal resistance and mechanical properties were found [86–89]. For example, clays have been used to increase shear strength and heat resistance of waterborne acrylic PSAs as an environmentally friendly replacement of solvent-borne acrylic PSAs [87]. Furthermore, there are reports of the use of Na–Mt and OMt to improve rheological and mechanical properties of polyisobutylene (PIB) based adhesive [87]. Results show better compatibility between PIB/OMt systems rather than PIB/Na–Mt, which was evidenced as an increase in viscosity with a 10 wt% of OMt content. On the other hand, Na–Mt did not show significant improvement of the rheological properties.

Finally, within the most innovative applications, the use of modified clays with bactericidal agents to formulate rubber mixtures with antimicrobial properties was analyzed. Przybyłek et al. developed an elastomeric nanocomposite that exhibits antibacterial and antifungal activity for the polish company Spoiwo (Spółdzielnia Pracy Chemiczno–Wytworczej ‘Spoiwo’, Radom, Poland) [20]. They used a rubber blend matrix and modified bentonite clay (Nanobent[®] ZR2), and noticed that by adding 1–3% of bentonite nanoparticles there was an enhancement in the elongation and tensile stress at break; they also observed improvements in thermal properties. Their work resulted significantly in the medicine, biomedical engineering and in the food industry.

10 Final Remarks

In this chapter, a review of recent works including rubber/clay nanocomposites were made. This review covers the structure and physical characteristics of layered silicates used as fillers in rubber matrices as well as the chemical and physical characteristic of the type of rubber polymers, and rubber blends, which are more likely used for nanocomposites development. Moreover, it describes several techniques for organic modification of clays nanoparticles to enhance hydrophobicity and improve the compatibility by intercalation or exfoliation of the polymer chains into the clay interlaminar space. Finally, the chapter reviews the rubber/clay nanocomposites characteristics (i.e. vulcanization and rheological, mechanical and barrier properties), and the nowadays applications, like the tire, adhesive and biomedical industries.

Acknowledgements Authors wish to thank the financial support from the National Agency of Scientific and Technological Promotion (ANPCyT PICT-2015-0027) of the Minister of Science and Technology and Productive Innovation (MinCyT) of Argentina.

References

1. Chao CC, Lin GG, Tsai HC, Lee YL, Chang PH, Cheng WT, Hsiue GH (2015) Isobutylene-isoprene rubber/layered silicate nanocomposites prepared using latex method: direct casting versus melt mixing after coagulation. *J Reinf Plast Compos* 34(21):1791–1803
2. Conzatti L, Stagnaro P, Colucci G, Bongiovanni R, Priola A, Lostritto A, Galimberti M (2012) The clay mineral modifier as the key to steer the properties of rubber nanocomposites. *Appl Clay Sci* 61:14–21
3. Gui Y, Zheng J, Ye X, Han D, Xi M, Zhang L (2016) Preparation and performance of silica/SBR masterbatches with high silica loading by latex compounding method. *Compos Part B Eng* 85:130–139
4. Maiti M, Bhattacharya M, Bhowmick AK (2008) Elastomer Nanocomposites. *Rubber Chem Technol* 81(3):384–469
5. Osman AF, Abdul Hamid AR, Rakibuddin, M, Khung Weng G, Ananthkrishnan R, Ghani, SA, Mustafa Z (2017) Hybrid silicate nanofillers: impact on morphology and performance of EVA copolymer upon in vitro physiological fluid exposure. *J Appl Polym Sci* 134(12)
6. George SC, Rajan R, Aprem AS, Thomas S, Kim SS (2016) The fabrication and properties of natural rubber-clay nanocomposites. *Polym Test* 51:165–173
7. Pal K, Pal SK, Das CK, Kim JK (2010) Influence of fillers on NR/SBR/XNBR blends. Morphology and wear. *Tribol Int* 43(8):1542–1550
8. Rezende CA, Bragança FC, Doi TR, Lee LT, Galembeck F, Boué F (2010) Natural rubber-clay nanocomposites: mechanical and structural properties. *Polym (Guildf)* 51(16):3644–3652
9. Zhang Y, Liu Q, Zhang S, Zhang Y, Cheng H (2015) Gas barrier properties and mechanism of kaolin/styrene-butadiene rubber nanocomposites. *Appl Clay Sci* 111:37–43
10. Przybyłek M, Bakar M, Mendrycka M, Kosikowska U, Malm A, Worzakowska M, Szymborski T, Kędra-Królik K (2017) Rubber elastomeric nanocomposites with antimicrobial properties. *Mater Sci Eng, C* 76:269–277
11. Choi SS (2002) Difference in bound rubber formation of silica and carbon black with styrene-butadiene rubber. *Polym Adv Technol* 13(6):466–474
12. Alex R (2010) Nanofillers in rubber-rubber blends. In: Thomas S, Stephen R (eds) *Rubber nanocomposites: preparation, properties and applications*. Wiley, Chichester, UK, pp 209–234
13. Hashim AS, Azahari B, Ikeda Y, Kohjiya S (1998) The effect of bis (3-triethoxysilylpropyl) tetrasulfide on silica reinforcement of styrene-butadiene rubber. *Rubber Chem Technol* 71(2):289–299
14. Gatos KG, Karger-Kocsis J (2010) Rubber/clay nanocomposites: preparation, properties and applications. In: Thomas S, Stephen R (eds) *Rubber nanocomposites: preparation, properties and applications*. Wiley, Chichester, UK, pp 169–190
15. ten Brinke JW, Debnath SC, Reuvekamp LAEM, Noordermeer JWM (2003) Mechanistic aspects of the role of coupling agents in silica-rubber composites. *Compos Sci Technol* 63(8):1165–1174
16. Rattanasom N, Saowapark T, Deeprasertkul C (2007) Reinforcement of natural rubber with silica/carbon black hybrid filler. *Polym Test* 26(3):369–377
17. Liu Q, Zhang Y, Xu H (2008) Properties of vulcanized rubber nanocomposites filled with nanokaolin and precipitated silica. *Appl Clay Sci* 42(1–2):232–237
18. Galimberti M, Agnelli S, Cipolletti, V (2016) Hybrid filler systems in rubber nanocomposites. Elsevier Ltd

19. Siririttikrai N, Thanawan S, Suchiva K, Amornsakchai T (2017) Comparative study of natural rubber/clay nanocomposites prepared from fresh or concentrated latex. *Polym Test* 63:244–250
20. Usha Devi, KS, Ponnamma, D, Causin, V, Maria HJ, Thomas S (2015) Enhanced morphology and mechanical characteristics of clay/styrene butadiene rubber nanocomposites. *Appl Clay Sci* 114, 568–576
21. Nawani P, Burger C, Rong L, Hsiao BS, Tsou AH (2015) Structure and permeability relationships in polymer nanocomposites containing carbon black and organoclay. *Polym (United Kingdom)* 64:19–28
22. Botana A, Mollo M, Eisenberg P, Torres Sanchez RM (2010) Effect of modified montmorillonite on biodegradable PHB nanocomposites. *Appl Clay Sci* 47(3–4):263–270
23. Pavlidou S, Papaspyrides CD (2008) A review on polymer-layered silicate nanocomposites. *Prog Polym Sci* 33(12):1119–1198
24. Kievani MB, Edrak M (2015) Synthesis, characterization and assessment thermal properties of clay based nanopigments. *Front Chem Sci Eng* 9:40–45
25. Galimberti M, Senatore S, Lostritto A, Giannini L, Conzatti L, Costa G, Guerra G (2009) Reinforcement of diene elastomers by organically modified layered silicates. *E-Polymers* 57:1–16
26. Marques FADM, Angelini R, Ruocco G, Ruzicka B (2017) Isotopic effect on the gel and glass formation of a charged colloidal clay: laponite. *J Phys Chem B* 121(17):4576–4582
27. Ambre A, Jagtap R, Dewangan B (2009) ABS nanocomposites containing modified clay. *J Reinf Plast Compos* 28(3):343–352
28. Bianchi AE, Fernández M, Pantanetti M, Viña R, Torriani I, Sánchez RMT, Punte G (2013) ODTMA + and HDTMA + organo-montmorillonites characterization: new insight by WAXS, SAXS and surface charge. *Appl Clay Sci* 83–84:280–285
29. Daitx TS, Carli LN, Crespo JS, Mauler RS (2015) Effects of the organic modification of different clay minerals and their application in biodegradable polymer nanocomposites of PHBV. *Appl Clay Sci* 115:157–164
30. Zhuang G, Gao J, Chen H, Zhang, Z (2018) A new one-step method for physical purification and organic modification of sepiolite. *Appl. Clay Sci* 153(November 2017), 1–8
31. Zhou F, Yan C, Zhang Y, Tan J, Wang H, Zhou S, Pu S (2016) Purification and defibering of a Chinese sepiolite. *Appl Clay Sci* 125, 119–126
32. Milošević M, Logar M, Kaluderović L, Jelić I (2017) Characterization of clays from Slatina (Ub, Serbia) for potential uses in the ceramic industry. *Energy Proc* 125:650–655
33. Gamoudi S, Srasra E (2017) Characterization of Tunisian clay suitable for pharmaceutical and cosmetic applications. *Appl Clay Sci* 146(May):162–166
34. Payne J, Gharzouni A, Sobrados I, Rossignol S (2018) Identifying the differences between clays used in the brick industry by various methods: iron extraction and NMR spectroscopy. *Appl Clay Sci* (October 2017):0–1
35. Ezquerro CS, Ric GI, Miñana CC, Bermejo JS (2015) Characterization of montmorillonites modified with organic divalent phosphonium cations. *Appl Clay Sci* 111:1–9
36. Alves JL de T. V. e. Rosa P, Morales, AR (2017) Evaluation of organic modification of montmorillonite with ionic and nonionic surfactants. *Appl Clay Sci* 150(June):23–33
37. Hojiyev R, Ulcay Y, Çelik MS (2017) Development of a clay-polymer compatibility approach for nanocomposite applications. *Appl Clay Sci* 146(April):548–556
38. Sookyung U, Nakason C, Venneman N, Thajjaroen W (2016) Influence concentration of modifying agent on properties of natural rubber/organoclay nanocomposites. *Polym Test* 54:223–232
39. Soares BG, Ferreira SC, Livi S (2017) Modification of anionic and cationic clays by zwitterionic imidazolium ionic liquid and their effect on the epoxy-based nanocomposites. *Appl Clay Sci* 135:347–354
40. Verdejo R, Lopez-Manchado MA, Valentini L, Kenny JM (2010) Carbon nanotube reinforced rubber composites. In: Thomas S, Stephen R (eds) *Rubber nanocomposites: preparation, properties and applications*. Wiley, Chichester, UK, pp 147–162

41. Carli LN, Roncato CR, Zanchet A, Mauler RS, Giovanela M, Brandalise RN, Crespo JS (2011) Characterization of natural rubber nanocomposites filled with organoclay as a substitute for silica obtained by the conventional two-roll mill method. *Appl Clay Sci* 52(1–2):56–61
42. Praveen S, Chattopadhyay PK, Albert P, Dalvi VG, Chakraborty BC, Chattopadhyay S (2009) Synergistic effect of carbon black and nanoclay fillers in styrene butadiene rubber matrix: development of dual structure. *Compos Part A Appl Sci Manuf* 40(3):309–316
43. Sadek EM, El-Nashar DE, Ahmed SM (2015) Effect of organoclay reinforcement on the curing characteristics and technological properties of styrene-butadiene rubber. *Polym Compos* 36(7):1293–1302
44. Youssef HA, Abdel-Monem YK, Diab WW (2017) Effect of gamma irradiation on the properties of natural rubber latex and styrene-butadiene rubber latex nanocomposites. *Polym Compos* 38(2):E189–E198
45. Liu J, Li X, Xu L, Zhang P (2016) Investigation of aging behavior and mechanism of nitrile-butadiene rubber (NBR) in the accelerated thermal aging environment. *Polym Test* 54 (2016):59–66
46. Xue X, Yin Q, Jia H, Zhang X, Wen Y, Ji Q, Xu Z (2017) Enhancing mechanical and thermal properties of styrene-butadiene rubber/carboxylated acrylonitrile butadiene rubber blend by the usage of graphene oxide with diverse oxidation degrees. *Appl Surf Sci* 423:584–591
47. Costa FR, Pradhan S, Wagenknecht U, Bhowmick AK, Heinrich G (2010) XNBR/LDH nanocomposites: effect of vulcanization and organic modifier on nanofiller dispersion and strain-induced crystallization. *J Polym Sci, Part B: Polym Phys* 48(22):2302–2311
48. de Sousa F, Mantovani G, Scuracchio C (2011) Mechanical properties and morphology of NBR with different clays. *Polym Testing* 30:819–825
49. Yu Y, Gu Z, Song G, Li P, Li H, Liu W (2011) Structure and properties of organo-montmorillonite/nitrile butadiene rubber nanocomposites prepared from latex dispersions. *Appl Clay Sci* 52(4):381–385
50. Ma Y, Li Q-F, Zhang L-Q, Wu Y-P (2006) Role of stearic acid in preparing EPDM/clay nanocomposites by melt compounding. *Polym J* 39(1):48–54
51. Usuki A, Tukigase A, Kato M (2002) Preparation and properties of EPDM-clay hybrids. *J Appl Polym Sci* 43:2185–2189
52. Zheng H, Zhang Y, Peng Z, Zhang Y (2004) Influence of clay modification on the structure and mechanical properties of EPDM/montmorillonite nanocomposites. *Polym Test* 23 (2):217–223
53. Chang YW, Yang Y, Ryu S, Nah C (2002) Preparation and properties of EPDM/organomontmorillonite hybrid nanocomposites. *Polym Int* 51(4):319–324
54. Zhang F, Zhao Q, Liu T, Lei Y, Chen C (2018) Preparation and relaxation dynamics of ethylene–propylene–diene rubber/clay nanocomposites with crosslinking interfacial design. *J Appl Polym Sci* 135(1):1–8
55. Mansilla MA, Valentin JL, López-Manchado MA, González-Jiménez A, Marzocca AJ (2016) Effect of entanglements in the microstructure of cured NR/SBR blends prepared by solution and mixing in a two-roll mill. *Eur Polym J* 81:365–375
56. Hess WM, Herd CR, Vegvari PC (1993) Characterization of immiscible elastomer blends. 330–372
57. Groves S (1998) Crosslink density distributions in NR/BR blends: effect of cure temperature and time. *Rubber Chem Technol* 44:958–965
58. Maroufkhani M, Katbab AA, Zhang J (2018) Manipulation of the properties of PLA nanocomposites by controlling the distribution of nanoclay via varying the acrylonitrile content in NBR rubber. *Polym Test* 65:313–321
59. Rajasekar R, Pal K, Heinrich G, Das A, Das CK (2009) Development of nitrile butadiene rubber-nanoclay composites with epoxidized natural rubber as compatibilizer. *Mater Des* 30 (9):3839–3845

60. Kanny K, Mohan TP (2017) Rubber nanocomposites with nanoclay as the filler. In: Thomas S, Maria HJ (eds) *Progress in rubber nanocomposites*. Woodhead Publishing, Duxford, United Kingdom, pp 153–177
61. Sinha Ray S, Okamoto M (2003) Polymer/layered silicate nanocomposites: a review from preparation to processing. *Prog Polym Sci* 28(11), 1539–1641
62. Theng BKG (2012) *Polymer-clay nanocomposites*, 2nd ed., vol. 4. Elsevier B.V
63. Wang LL, Zhang LQ, Tian M (2012) Mechanical and tribological properties of acrylonitrile-butadiene rubber filled with graphite and carbon black. *Mater Des* 39:450–457
64. Varghese S, Karger-Kocsis J (2003) Natural rubber-based nanocomposites by latex compounding with layered silicates. *Polym (Guildf)* 44(17):4921–4927
65. Brantseva TV, Antonov SV, Gorbunova IY (2018) Adhesion properties of the nanocomposites filled with aluminosilicates and factors affecting them: a review. *Int J Adhes Adhes* 82:263–281
66. Fawaz J, Mittal V (2015) Synthesis of polymer nanocomposites: review of various techniques. In: Mittal V (ed) *Synthesis techniques for polymer nanocomposites*, 1st edn. Wiley-VCH, Weinheim, pp 1–30
67. Ponnamma D, Maria HJ, Chandra AK, Thomas S (2013) Rubber nanocomposites: latest trends and concepts. In: Visakh PM, Thomas S, Chandra A (ed) *Advances in elastomers II. Advanced structured materials*, vol. 12, April, Springer, Berlin, Heidelberg, pp 69–107
68. Distler D, Neto WS (2017) Machado F emulsion polymerization. In: *Reference module in materials science and materials engineering*, June, Elsevier, pp 35–56
69. Tan J, Wang X, Luo Y, Jia D (2012) Rubber clay nanocomposites by combined latex compounding. pp 825–831
70. Chaudhari CV, Dubey KA, Bhardwaj YK, Sabharwal S (2012) Radiation processed styrene-butadiene rubber/ethylene-propylene diene rubber/multiple-walled carbon nanotubes nanocomposites: effect of MWNT addition on solvent permeability behavior. *J Macromol Sci Part B Phys* 51(5):839–859
71. Dubey KA, Bhardwaj YK, Chaudhari CV, Bhattacharya S, Gupta SK, Sabharwal S (2006) Radiation effects on SBR–EPDM blends: a correlation with blend morphology. *J Polym Sci, Part B: Polym Phys* 44(12):1676–1689
72. Shoushtari Zadeh Naseri A, Jalali-Arani A (2015) A comparison between the effects of gamma radiation and sulfur cure system on the microstructure and crosslink network of (styrene butadiene rubber/ethylene propylene diene monomer) blends in presence of nanoclay. *Radiat Phys Chem* 115, 68–74
73. Satyanarayana MS, Bhowmick AK, Dinesh Kumar K (2016) Preferentially fixing nanoclays in the phases of incompatible carboxylated nitrile rubber (XNBR)-natural rubber (NR) blend using thermodynamic approach and its effect on physico mechanical properties. *Polym (United Kingdom)* 99:21–43
74. Bandyopadhyay A, Thakur V, Pradhan S, Bhowmick AK (2010) Nanoclay distribution and its influence on the mechanical properties of rubber blends. *J Appl Polym Sci* 115:1237–1246
75. Ebrahimi Jahromi A, Ebrahimi Jahromi HR, Hemmati F, Saeb MR, Goodarzi V, Formela K (2016) Morphology and mechanical properties of polyamide/clay nanocomposites toughened with NBR/NBR-g-GMA: a comparative study. *Compos Part B Eng* 90, 478–484
76. Wang C, Su JX, Li J, Yang H, Zhang Q, Du RN, Fu Q (2006) Phase morphology and toughening mechanism of polyamide 6/EPDM-g-MA blends obtained via dynamic packing injection molding. *Polym (Guildf)* 47(9):3197–3206
77. Yang R, Song Y, Zheng Q (2017) Payne effect of silica-filled styrene-butadiene rubber. *Polym (United Kingdom)* 116:304–313
78. Zachariah AK, Chandra AK, Mohammed PK, Parameswaranpillai J, Thomas S (2016) Experiments and modeling of non-linear viscoelastic responses in natural rubber and chlorobutyl rubber nanocomposites. *Appl Clay Sci* 123:1–10
79. Zachariah AK *Transport properties of polymeric membranes: gas permeability and theoretical modeling of elastomers and its nanocomposites*. Chapter 21, p 441

80. Mohan TP, Kuriakose J, Kanny K (2012) Water uptake and mechanical properties of natural rubber-styrene butadiene rubber (nr-sr)—nanoclay composites. *J Ind Eng Chem* 18(3):979–985
81. Wang ZF, Wang B, Qi N, Zhang HF, Zhang LQ (2005) *Polymer*, 46(3):719–724
82. Qureshi MN, Qammar H (2010) Mill processing and properties of rubber-clay nanocomposites. *Mater Sci Eng, C* 30(4):590–596
83. Mathew G, Rhee JM, Lee YS, Park DH, Nah C (2008) Cure kinetics of ethylene acrylate rubber/clay nanocomposites. *J Ind Eng Chem* 14(1):60–65
84. Zhang W, Ma Y, Xu Y, Wang C, Chu F (2013) Lignocellulosic ethanol residue-based lignin-phenol-formaldehyde resin adhesive. *Int J Adhes Adhes* 40(2013):11–18
85. Woo CS, Kim WD, Do Kwon J (2008) A study on the material properties and fatigue life prediction of natural rubber component 483–484(1–2) C, 376–381
86. Brantseva TV, Antonov SV, Gorbunova, IY Adhesion properties of the nanocomposites filled with aluminosilicates and factors affecting them: a review. *Int J Adhes Adhes* 82(December 2017):263–281, 2018
87. Ahsan T (2007) Composition of bulk filler and epoxy-clay nanocomposite; U.S. Patent 7163973
88. Long-acting waterborne nanometer attapulgite clay/epoxy anticorrosive coating material and preparing method thereof, Chinese patent CN 102676028A, 2012
89. Gazeley KF, Wake WC (1990) Natural rubber adhesives Handbook of adhesives 3rd ed. Skeist I (ed) Chapman & Hall, NY, pp 167–84
90. Unalan IU, Cerri Gi, Marcuzzo E, Cozzolino CA, Farris S (2014) Nanocomposite films and coatings using inorganic nanobuilding blocks (NBB): current applications and future opportunities in the food packaging sector. *RSC Adv* 4:29393

Organic/Silica Nanocomposite Membranes Applicable to Green Chemistry



Mashallah Rezakazemi, Amir Dashti, Nasibeh Hajilary
and Saeed Shirazian

1 Introduction

Organic-inorganic composites have been thoroughly used for various applications; these are referred to as nanocomposites if nano-size inorganic building blocks are used in the composite structure [1–5]. Organic-inorganic nanocomposites are commonly made of organic polymers incorporated with inorganic nanoscale building blocks such as nano silica [6–11]. They possess the beneficial features of both the inorganic substance (e.g., stiffness, thermal stability) and the organic polymer (e.g., ductility, flexibility, processability, and dielectric) [12, 13]. Furthermore, they generally include unique characteristics of fillers resulting in composites with enhanced characteristics. A primary property of nanocomposites is the tiny dimension of the nanofillers contributes to a large rise in the interfacial area in comparison to conventional composites. Also, at reduced filler content, the interfacial area growth generates a substantial increase in the volume of interfacial polymer with properties distinctive from the polymer [14].

Among the several inorganic/organic nanocomposites, polymer/Si composites are the most prevail quoted [15]. These nanocomposites have attracted considerable

M. Rezakazemi (✉)

Faculty of Chemical and Materials Engineering, Shahrood University of Technology,
Shahrood, Iran

e-mail: mashalah.rezakazemi@gmail.com

A. Dashti

Department of Chemical Engineering, Kashan University, Kashan, Iran

N. Hajilary

Department of Chemical Engineering, Golestan University, Gorgan, Iran

S. Shirazian

Department of Chemical Sciences, Bernal Institute, University of Limerick,
Limerick, Ireland

© Springer Nature Switzerland AG 2019

Inamuddin et al. (eds.), *Sustainable Polymer Composites and Nanocomposites*,

https://doi.org/10.1007/978-3-030-05399-4_22

interests recently and have been used in many different applications. Organic-inorganic nanocomposites can be fabricated by numerous synthesis techniques, showing the different strategies offered to present each phase. The organic part can be presented as (i) a precursor (oligomer or monomer), (ii) a preformed linear polymer (in emulsion, molten or solution states), or (iii) a polymer network, either chemical (e.g., elastomers, thermosets,), physical (semicrystalline linear polymer) or cross-linked [16]. The inorganic portion can be presented as (i) preformed nanoparticles or (ii) a precursor (e.g. TEOS) for further treatment. Organic or inorganic polymerization typically is required if at least one of the starting moieties is a precursor.

The addition of inorganic additives to the polymeric membranes has received the attention of numerous scientists in the recent years. Many organic-inorganic nanocomposite membranes have been studied in the literature. A number of the nanoparticles utilized in the membrane matrix contain Si [17], ZrO₂ [18], heteropolyacids [19], TiO₂ [20, 21] and carbon nanotubes [22].

Nano-si has been broadly investigated due to their reduced cost, poor electrical conductivity and enhanced water uptake characteristics compared with other nanomaterials. Phase conflict involving the organic matrix and Si was resolved using the adjustment of the Si surfaces applying various agents.

Polymer Electrolyte Membrane Fuel Cells (PEMFCs) signify an encouraging tool for the technology of power in the 21st century due to their escalated efficiency in contrast to coal combustion engines and eco-environment [23]. Among different parts within the fuel cell systems, proton exchange membranes (PEMs) are influential parts of PEMs functionality. Currently, the PEMFCs are based on per-fluoro sulfonic acid membranes like Nafion[®], and Flemion, which have particular disadvantages like huge fuel crossover and high cost. Therefore, scientists have concentrated on creating PEMs with escalated proton conductivity, longevity, thermal stability, maximum power density, minimal fuel crossover, and reduced cost.

Organic-inorganic nanocomposite PEMs consist of nanosized inorganic fillers in the polymer by the molecular level of hybridization. This structure has revealed the opportunity to integrate into an individual solid, the appealing attributes of a thermally and mechanically stable inorganic backbone and the particular chemical reactivity, dielectric, processability, ductility and flexibility of the organic polymer. The preparation, properties characterization, and polymer/Si nanocomposites applications are becoming a rapidly increasing research subject. Many publications and review articles [24, 25] have presented which are partially dedicated to the polymer/Si nanocomposites. Silicate nanoparticles were employed in various polymeric membranes applicable to PEMFCs. The aim of this account is to introduce the fabrication of silicates and nanocomposite membranes. The silicates impact on the various properties of nanocomposites such as thermal and mechanical properties, proton conductivity, water uptake and cell performance are investigated.

1.1 Challenges in Synthesizing Organic/Si Nanocomposite Membranes

PEMFCs have proved a great environmental friendly technology to satisfy the prevailing energy prerequisites of the recent years. Nafion is the extensively approved to date and has great electrochemical characteristics under 80 °C and in extreme humidity. However, a reduction in the proton conductivity of Nafion in lower humidity and over 80 °C, as well as high membrane price, has motivated the improvement of novel techniques and membranes for fuel cell applications. The incorporation of inorganic nanofillers, particularly Si-based nanofillers, into the polymeric membrane was employed, to resolve these restrictions. This is a result of availability, reduced cost, higher thermal stability and high hydrophilicity of the inorganic silicates. The addition of inorganic nanofillers into the polymeric membranes has received the attention of several research studies over the last few decades, plus lowering cost and enhanced water retention characteristics [26]. Inorganic nanofillers enhance the functioning temperature of the hybrid membranes because of their hydrophilicity [27, 28]. The polymer-nanocomposite membranes preparation for PEMFC can be achieved by using two separate approaches, namely, ex situ or in situ approach. In the ex situ method, silicate nanofiller or its precursor is dispersed in the matrix of polymer, while in situ technique includes the dispersion of nano-silicates or their precursor in the monomer followed by a polymerization step [12].

The goodness of dispersion involving the inorganic silicates and polymer matrix has important effects on enhancing the main characteristics and performance of the prepared composite membranes [4, 29, 30]. Accordingly, various methods and solvents are employed to enhance the dispersion levels of filler and the physical and chemical attributes of the nanocomposite membranes. General topics crucial to any PEMs involve: (1) elevated proton conductivity, (2) low water transportation through electro-osmosis and diffusion phenomena, (3) low fuel and oxidant permeability, (4) reduced electronic conductivity, (5) good mechanical stability in both hydrated and dry states, (6) hydrolytic and oxidative stableness, (7) low price and (8) capacity for fabrication into membrane electrode assemblies (MEAs). Because of the increased sorption of water in the membrane, mechanical properties, and water crossover emerge as critical problems. Developing proton-conducting devices with minimum or without water can be a significant challenge for novel membranes. Novel membranes with decreased methanol permeability and water transfer (by electro-osmotic drag or diffusion) in addition to appropriate conductivity and stabilities are necessary for Direct-Methanol Fuel Cells (DMFCs). Fuels diffusion from the anode to cathode sides reduces the voltage efficiency and performance of fuel cell. The intricacy and membrane resistivity were improved, with minimal energy density, by employing diluted methanol as the fuel. Conductivity and water absorption of the membrane rely upon the ionic group concentration, mostly sulphonic acids. Though, an elevated density of ionic groups motivates the increased membrane swelling that diminishes membrane durability and mechanical performance. Therefore, the

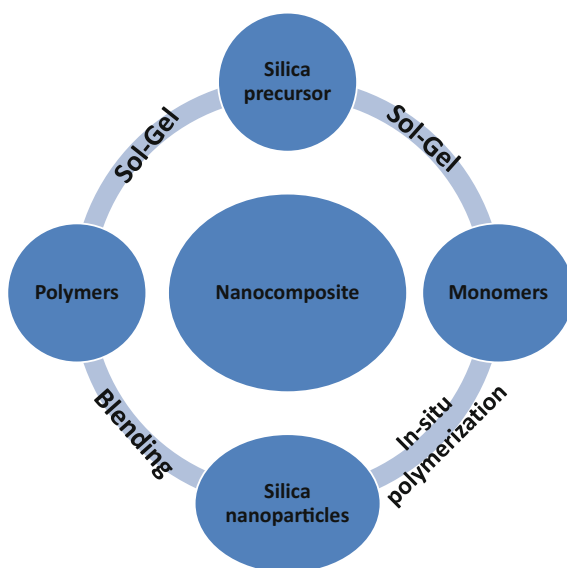
essential properties for PEMs (IEC, proton conductivity and water uptake) must be improved under the operating circumstances. The organic-inorganic nanocomposite PEMs development appears to be promising in overcoming the aforementioned operational problems.

1.2 Possible Methods to Overcome the Challenges

As exhibited in Fig. 1, showing the common preparation techniques of polymer/Si nanocomposites, generally in the blending and in situ polymerization approaches, Si nanoparticles are directly introduced into the polymer [12], while Si precursors are employed in the sol-gel processes, in which the common precursors are Tetraethyl orthosilicate (TEOS), Tetramethyl orthosilicate (TMOS) and silicon alkoxides [31]. Sometimes, alkoxy silane-containing polymers [32, 33] as Si precursors are also employed in the sol-gel method. Furthermore, in particular instances, Si in the nanocomposites is formed from precursors such as perhydropolysilazane (PHPS) [34], soluble glass [35], Na_2SiO_3 [36], silicic acid [37], etc. [38–40].

Research studies accomplished over the recent years on the subject can be split into four classes: (i) introducing inorganic proton conductors in PEMs; (ii) covalently bonded inorganic segments with a polymer; (iii) nanocomposites by sol-gel approach; and (iv) acid-based PEM nanocomposites. The fabrication of hybrid-nanocomposite membranes for PEMFC can be achieved by using two separate techniques, namely ex situ or in situ approach.

Fig. 1 The common methods to prepare polymer/Si nanocomposites



1.3 *Ex Situ Technique*

Melt blending and solution mixing, are generally accepted ways for the nanocomposites preparation through the *ex situ* approach. Melt blending is recognized as a green approach where the nanoparticles are mixed with the molten polymer. The drawbacks of the method are the raw polymers decomposition, poor filler dispersion, and the surface modifiers degradation. Therefore, the solution mixing method is the commonly accepted method, specifically for the fabrication of nanocomposites on the laboratory-scale [41, 42].

The beneficial characteristics of the solution mixing approach are the homogeneous dispersion of nanofillers in the polymer matrix. This approach consists of the nanoparticles blending (dispersed in a specific solvent) with the polymer solution, accompanied by casting and drying [42–44]. Several strategies and solvents have been chosen to improve nanoparticles dispersion in the polymer matrix and to enhance the nanocomposite membranes properties.

1.4 *In Situ Technique*

In situ techniques include the nanoparticles dispersion or their precursors in a low viscosity monomer solution. Superior dispersion, in addition to excellent physical properties, is observed in *in situ* technique. However, the intricacy of the method means that researches in this field are not enough.

Poly(styrene-co-methacrylate)-Si covalent membrane was made by blending an aqueous solution of TEOS/nitric acid with azobisisobutyronitrile (AIBN), 2-hydroxyethyl methacrylate (HEMA) and styrene (STY). At a temperature of 40 °C, the mixture was cast in a mould to start the free radical polymerization of HEMA and STY combined with the sol-gel reaction of TEOS. The produced membrane was processed at various temperatures to 150 °C. Various membranes were sulfonated via immersion in a 0.3 M solution of sulfur-chloridic acid in ethylene dichloride for 6 h [45]. In an identical experiment, the researchers used phosphotungstic acid (PWA) rather than nitric acid, and the temperature of free radical polymerization was adjusted to 55 °C [46]. In other procedure, sol 1 (including PWA or 1 N HCl and 3-methacryloxypropyl trimethoxysilane (MPS) in ethanol) and sol 2 (made up of AIBN and HEMA) were blended, cast in a mould at 60 °C, dried and post-treated at 150 °C for 24 h [26]. The post-treatment of the membranes changed the membrane colour to brown as a result of the cross-linked structure in the membrane [19, 47].

A combination of nethylimidazolium trifluoro methanesulfonate ([EIm][TfO]) (40 wt%), acrylonitrile (40 wt%), STY (20 wt%), divinylbenzene (6 wt% to the formulation, based on the monomers weight), and Si and benzoin ethyl ether as a photo initiator was mixed and ultrasonicated to acquire a homogeneous solution. At room temperature, the solution was cast onto a glass mould and using irradiation by UV light, photo cross-linked for 30 min [48]. Given that Nafion® is a commercial

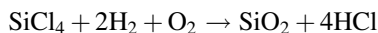
polymer, nanocomposite membranes made from it are commonly prepared by an ex situ preparation approach. Many other polymers with high performance (such as PPSU, PEEK, and PBI) require inert atmosphere and monotonous preparation process. The introduction of extremely hydrophilic nano silicate into the monomer makes the polymerization complex, leading to decreased molecular weight (M_w) and interfering crosslinking in the polymer structure. Limited selection of solvent media for the formation of nanocomposite by in situ synthesis adds further intricacy to the system. Therefore, the previous researches for the fabrication of Si-based nanocomposite using the in situ approach are scant. New synthetic procedures and proposed new types of block copolymers can be too advantageous to the aforementioned issues.

2 Si Preparation

Two types of techniques have been proposed for nano-Si preparation: the sol-gel approach and the microemulsion technique [49]. Stöber et al. [50] suggested an easy method for preparation of mono-dispersed spherical Si via hydrolysis of TEOS solution in ethanol in the acidic environment. Symmetrical amorphous Si nanoparticles were conveniently acquired by employing different reactants concentrations. Subsequently, the Stöber technique was developed by researchers and seems like the most convenient and efficient approach [51].

Osseoasare et al. [52] synthesized monodisperse nano-Si using limited TEOS hydrolysis in an inverse microemulsion. Moreover, this micro-emulsion technique is commonly employed to prepare nano-Si. These particles are now produced commercially, generally in the form of powder or colloid.

NanoSi powder is chiefly industrially synthesized using the precipitation technique and fuming approach. Fumed Si is an amorphous, fine, tasteless, white and odourless powder. This powder is prepared using a vapour process at an elevated temperature where SiCl_4 is hydrolyzed in an $\text{O}_2\text{-H}_2$ combustion process according to the following reaction [53]:



The nano-Si has a 3D structure. Siloxane and silanol groups are formed on the surface of Si, causing the nanoSi to be hydrophilic.

The Si surfaces are peculiarly ceased by three silanol species: isolated or free silanols, vicinal silanols or hydrogen-bonded and geminal silanols (Fig. 2) [51]. The silanols occupy the near molecules, in proper order, creating H_2 bonds and causing the aggregation as demonstrated in Fig. 3. The aforementioned bonds maintain single fumed Si jointly and the aggregations stay unchanged even in good blending situation if the vigorous interaction between filler and matrix does not exist [54]. Nanoparticles dispersion in the matrix of the polymer has a noticeable effect on the nanocomposites properties.

Fig. 2 Three surface silanols types

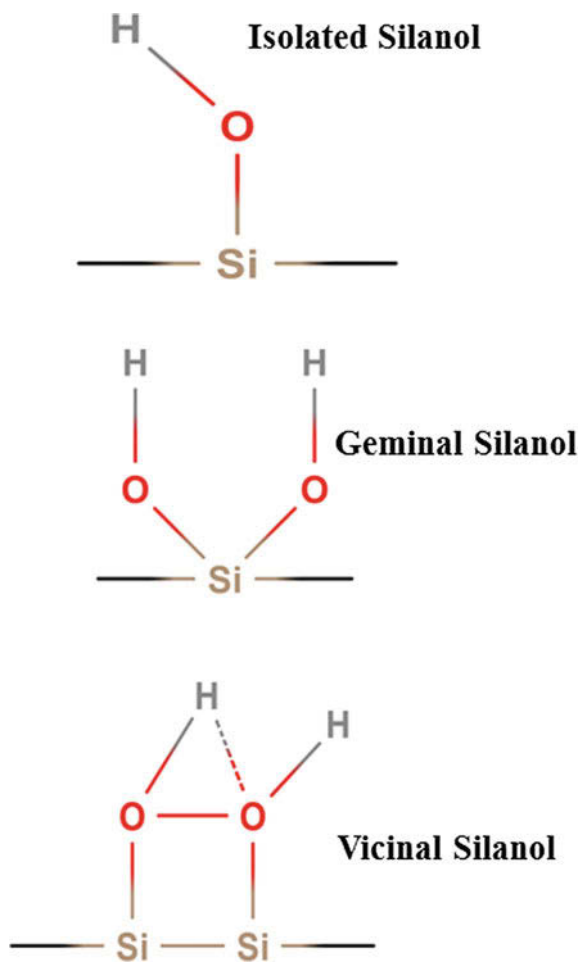
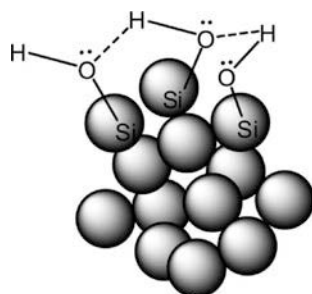


Fig. 3 Aggregate creation among adjacent molecules of fumed Si via H₂ bonding between the silanols



The proper dispersion can be obtained using a chemical modification of the surface of nanoparticles or by physical approaches like high-energy ball-milling method and ultrasonication. The considerable deviations in the Si and polymer properties may frequently result in phase separation. Hence, the surface interaction involving two phases of nanocomposites is the highly determining element influencing the resulting materials characteristics [14].

Different approaches have been applied to improve the congruity involving the polymer and Si. The widely used technique is to treat the Si nanoparticles surface (particularly for the blending and in situ approach), that in addition can enhance the dispersion of the particles in the matrix simultaneously. Generally, surface modification of Si nanoparticles can be accomplished either by physical or chemical processes [55].

3 Surface Modification of Si

3.1 Chemical Modification

A number of researches have been focused on the surface modification of the Si nanoparticles by chemical modification because it can eventuate to a vigorous interaction involving modifier agent and nano-Si. These chemical techniques can be achieved by grafting polymers or by using modifier agents. Silane coupling agents are the prevailing sort of modifiers. Their ends commonly are organofunctional and can be hydrolyzed. The structure of the silane coupling agents can be demonstrated as RSiX_3 [56], where the X shows the ends which can be hydrolyzed that can be Cl-R , $\text{CH}_3\text{CH}_2\text{O-R}$, or R-O-CH_3 groups. The R can possess different functionalities selected to satisfy the requirements of the polymer.

The hydroxyl groups on the SiO_2 surface react with functional group X, while the polymer may react with the alkyl chain in order to form, hydrophobic Si. Besides, polymer chains grafting to nano-Si is an influential approach to raise the hydrophobicity of the Si and to produce adjustable interfacial interactions.

Commonly, two principal methods of chemical joining the polymer to a surface exist: covalent attachment of end-functionalized polymers to the surface (“grafting to” method) and with polymer chains monomer growth from immobilized initiators in in situ monomer polymerization (“grafting from” method). In some respect, the polymer grafted nano-Si may be considered as polymer-nanoSi hybrid composites.

Besides the aforementioned chemical methods, polymers grafting to nanoparticles can be conceived by irradiation. The nanoparticles modification via graft polymerization is very influential in the construction of nanocomposites due to (i) a boost in particles hydrophobicity which is favourable to the nanoparticle/polymer miscibility, (ii) an enhanced interfacial interaction obtained by the molecular surrounding of the matrix polymer and the grafting polymer on the nanoparticles, and (iii) a modifiable structure-properties relationship obtained by varying the grafting monomers and the grafting conditions because different grafting polymers might provide various interfacial characteristics.

3.2 *Modification by Physical Interaction*

Tailoring the surface physically is commonly carried out utilizing adsorption of macromolecules or surfactants onto the Si particles surface. Modification based on surfactant t is based on the preferential sorption of a surfactants polar group onto the Si surface via electrostatic forces.

A surfactant decreases the interaction among the nano-Sis inside agglomerates via decreasing the physical attraction and may be combined with a polymer without any difficulty. Si was tailored with cetrimonium bromide to enhance the chemical interaction involving polymer and SiO₂ [58]; SiO₂ were treated with stearic acid to enhance the adhesion to the polymer matrix and additives [59, 60] and also improve their dispersion; Si nanoparticles were treated with oleic acid that, with a hydrogen bond, was attached to the Si surface. Polymers adsorption can also boost the Si particles surface hydrophobicity.

3.3 *Blending*

The simplest and conventional technique for fabricating polymer-Si nanocomposites is a direct blending of the Si and a polymer. The blending can typically be accomplished by solution blending or melt blending. The principal complexity of the mixing procedure is the perfect Si nanoparticles dispersion in the matrix of polymer since they usually tend to agglomerate [12].

3.3.1 *Melt Blending*

This is a most prevalent method due to its functionality, effectualness, and cleanliness. As mentioned previously, providing homogeneous nanoparticles dispersion in a polymeric matrix is a complicated task because of the powerful particles proclivity to agglomerate. Hence, the so-called nanocomposites, in certain cases, include many loosened clusters of particles (Fig. 5a) and thus demonstrate properties inferior to the usual nanoparticle/polymer systems [61]. In order to break up agglomerates of nanoparticle and to form uniform nanostructural composites, an irradiation grafting technique can be employed for the nanoparticles modification and then the grafted particles can be mixed mechanically.

By irradiation grafting polymerization, agglomerates of nanoparticles convert to a nanocomposite microstructure (Fig. 5b) that in proper order creates a powerful interfacial interaction with the encompassing, foremost polymeric matrix through the following blending process.

As various grafting polymers produce distinct filler/matrix interfacial characteristics, properties and microstructures of the final nanocomposites can be modified. It was discovered that the nanoparticles toughening and fortifying impacts on

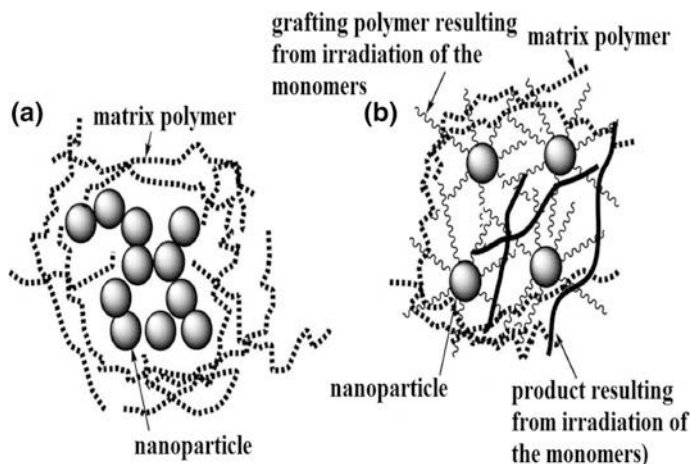


Fig. 5 **a** Schematic of an agglomerated nanoparticles dispersed in a matrix of polymer and **b** the probable structure of grafted nanoparticles dispersed in a polymer matrix [61]. Reprinted with permission from Elsevier

the matrix and could play a major role at low loadings of filler (typically lower than 3 vol.%) as compared with usual composites with larger particles. The method has several benefits, like low cost, easy to perform, easily controllable and generally practical [61]. Twice percolation of stress volumes in the vicinity of the particles and the agglomerates, that was attributed to the visibly attached shear yielded networks all over the nanocomposite, described the toughening and fortifying impacts of the processed nanoparticles [62].

An industrial-scale injection moulding machine [63] and twin-screw extruder were used instead of pilot-scale compression moulding and a screw extruder, PE [64] instead of PP, and precipitated nanoSi [65] instead of fumed nanoSi. All researchers suggested that the approach was still excellent. As grafting pre-treatment and drawing methods were integrated with melt blending to synthesize the nanocomposites, the nanoparticles separation was evoked, β -crystals in the PP matrix were generated, and the obtained PP-based nanocomposites were very stronger than the bare polymer matrix [66].

3.3.2 Solution Blending

Solution blending is a powder treatment technique in liquid-state that provides an excellent molecular size of blending and extensively is applied in material processing and preparation. Many of the restrictions of melt blending may be surmounted if the nanoparticles and polymer are dispersed or dissolved in solution but the solvent loss and its recovery must be considered [25, 55].

An approach through solution blending followed by compression moulding can also be used. Polymer-Si membranes are particularly fabricated by solution casting mixtures of Si nanoparticles and polymer. These can be employed in liquid separation like pervaporation, in gas separation like reverse-selective process, and as a PEM for PEMFC, etc. The existence of nonporous particles in usually composites significantly decreases the permeability of the polymer by decreasing the free volume for transfer and boosting the diffusion path tortuosity reachable to gas molecules [12].

3.3.3 Cryomilling Methods

Classic preparation techniques treat the materials in solution or melt and depend on surface treatment to involve particles in a matrix of polymer, but only a little progress was achieved. When the nanoparticle loading in a polymer is too much, the melt or solution methods are not applicable, as the solution is viscous or it never occurs. A solution to these issues is to treat the polymer in the solid state that hinders the thermal and solvent issues met in conventional methods but improving design and operation straightforwardness. Cryogenic ball milling (cryomilling) is a solid-state approach that efficiently enhances mixing characteristics. Poly(ethylene terephthalate) (PET)/SiO₂ nanocomposites can be synthesized using cryomilling [67]. A 3-step model (Fig. 6) to show the creation mechanism of PET-SiO₂ nanocomposite was proposed [67, 68]. The initial step was the huge decrease in nanoparticle dimension and the conversion of large PET blocks to flakes; in the meantime, the SiO₂ conglomerations were collapsed and scattered in PET flakes creating the foremost nanocomposite particle. The next step was described by the slow dispersion of nano SiO₂ to PET flakes and the creation of the second nanocomposite particle as a result of a conglomeration of the improved PET/SiO₂ initial nanocomposite particles. The next step (3) was described by the stable dimension of the second nanocomposite particles following by uniform dispersion of nano SiO₂ in the polymer. This was demonstrated that, through cryomilling around 10 h, SiO₂ were properly segregated into individual nanoparticles (approximately 30 nm) which are dispersed in polymer suitably. The originally obtained PET-SiO₂ particles formed in the shape of flake (~400 nm). These primary particles of the composite agglomerated to create second nanocomposite particles with a mean size around 7.6 μm. Well-dispersion of nano-SiO₂ in the polymer was so much higher than traditional approaches, that was attributed to solid-state treatment, the elevated mechanical energy of ball milling, and cryogenic temperature.

3.3.4 Thermal Spraying

Another superior approach to the restrictions of polymer/Si nanocomposites treatments is thermal spraying like the employment of solvent. In thermal spraying, a composite is under the heating, acceleration, and propulsion. In the propulsion procedure, a jet with a high heating rate propels a material via a restricting nozzle

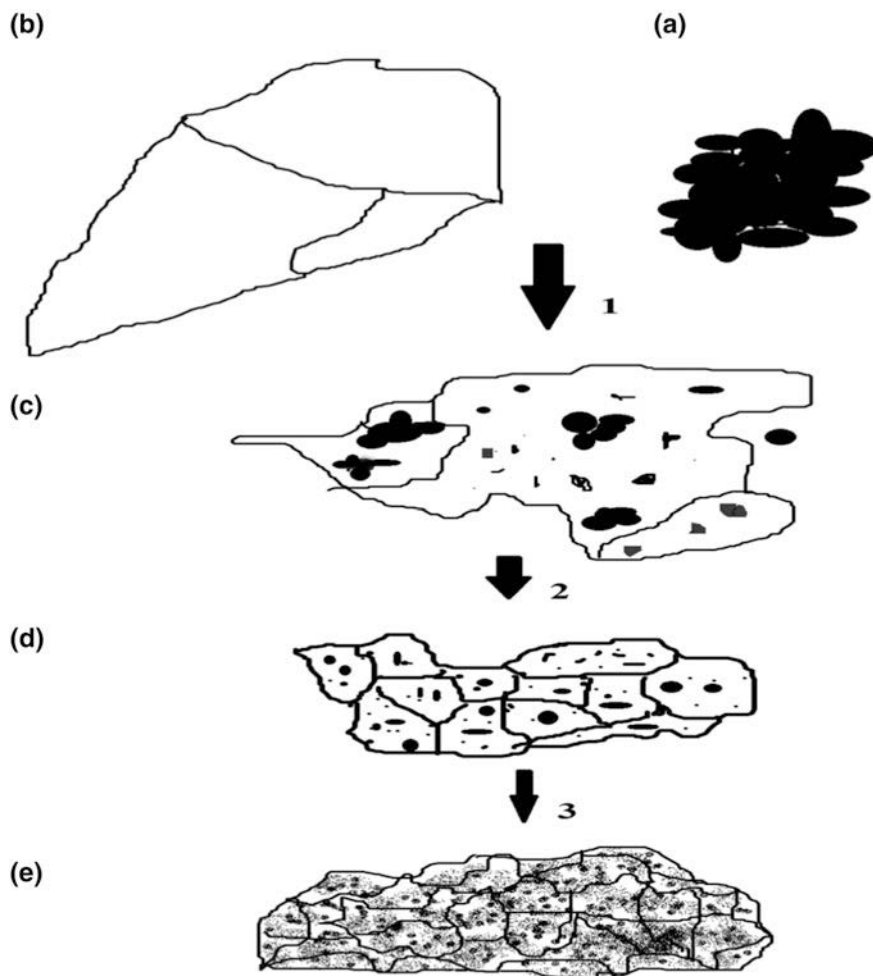


Fig. 6 Schematic of nanocomposites formation mechanism through cryo-milling, and **a** shows SiO₂ particles, **b** shows PET particles, **c** shows the initial milling step, **d** shows the secondary milling step, and **e** shows the final milling step [67]

towards a surface. The softened or single molten droplets crash, sprawl, lose heat and become solids to create uninterrupted and uniform covers. High-velocity oxy-fuel (HVOF) (Fig. 7) supplies heat given via fuels reaction with air. Petrovicova et al. [69–71] fabricated nylon 11 coatings loaded with nanoSi by the HVOF treatment. The composite powder contributed the fillers dispersion in the coating and the concurrent powder feeding into the HVOF spray jet.

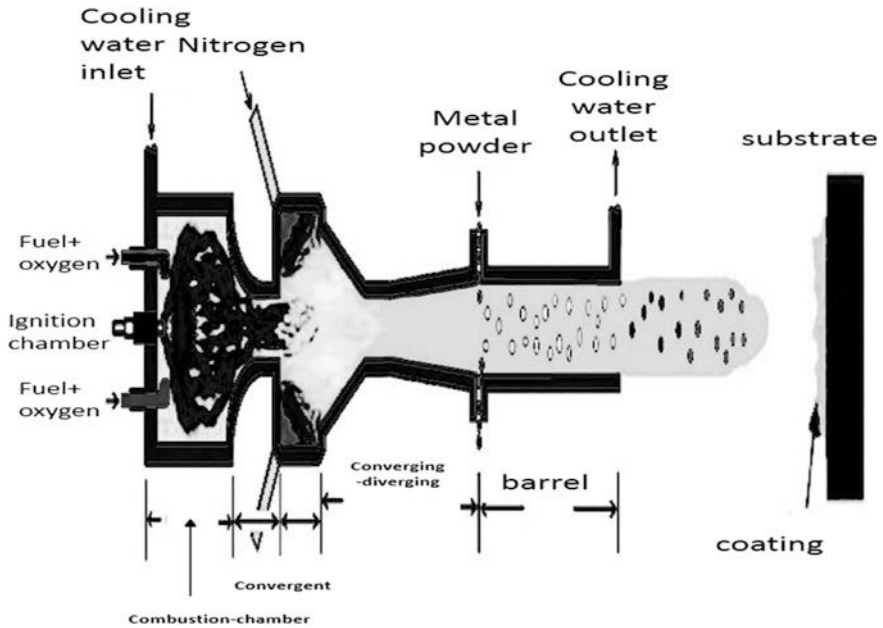


Fig. 7 Schematic of the HVOF process [72]. Reprinted with permission from Elsevier

4 Physical Properties of the Organic/Si Nanocomposite Membranes

4.1 Thermal Properties

Thermal properties can be investigated by thermal analysis methods, which include DTA, DSC, TMA, DMA/DMTA, TGA and dielectric thermal analysis, etc. DSC, TGA, and DTA are the prevailing approaches for recognizing of thermal characteristics of organic/inorganic composites. TGA exhibits the thermal stability, the degradation initiation, and the Si % present in the polymer. DSC employs to ascertain the behaviour of thermal transformation in organic/inorganic composites expeditiously. Moreover, the Coefficient of Thermal Expansion (CTE), which is used to analyze the dimensional stability of composites, is investigated by TMA. Additionally, thermal mechanical characteristics analyzed by DMA/DMTA are substantial in understanding the nanocomposites viscoelasticity. The storage and loss modulus investigate the stored energy, demonstrating the elastic share, and the energy spread as heat, demonstrating the viscous share. Moreover, the dielectric analysis is beneficial in understanding the nanocomposites viscoelasticity.

Generally, the addition of inorganic nanoparticles to the organic matrix can improve thermal stability by performing as a better insulator and mass transfer hurdle to the volatile materials formed through decomposition [73]. Moreover, this is very

impressive in reducing the CTE of the polymer. The thermal decomposition temperatures (T_d) obtained using TGA, the CTEs obtained using TMA, and the T_g obtained using DSC of PI/SiO₂ composites are shown in Table 1 [74]. Table 1 shows that the hybrid show more thermal stabilities and reduced CTEs as compared to the counterparts. Also, the T_d and T_g of a hybrid enhance with the addition of more Si.

The composite with coupling agent demonstrated increased T_g 's. Because firstly, the coupling agent reinforced the interaction between the organic polymer matrix and the inorganic mineral particles, which caused an elevated confining strength of SiO₂ on the PI molecules; second, the coupling agent reduced SiO₂ particles size and by that means highly extended the interfacial region for Si. Besides, the decreased dimension of the SiO₂, somewhat, causing a rise in the cross-linking degree. Subsequently, increased T_g and reduced CTE for the PI/SiO₂ composites with a coupling agent as compared with other composites are obtained. Sometimes, the nanocomposites thermal stability is diminished by increasing the Si content. TGA characterization of the nanocomposite of Si-PMMA demonstrated that increasing the nanoSi particles addition almost decreased the thermal stability at reduced temperatures [75].

4.2 Mechanical Properties

Given that one of the foremost justifications for incorporating inorganic materials to polymers is to enhance their mechanical properties [76, 77]. The basic prerequisite of this kind of nanocomposites is the ability to maximize the trade-off involving the stiffness and the toughness [78]. Hence, it is often essential to investigate the mechanical performance from various standpoints.

Several standards, including impact strength, tensile strength, hardness, flexural strength and fracture toughness have been employed to analyze the nanocomposites. Table 2 shows the mechanical properties of PP nanocomposites filled with SiO₂ particles grafted with different polymers at a constant SiO₂ content [61]. Although the grafting polymers monomers must have various miscibilities with PP, PEA in contrast with other grafting polymers demonstrated an intensifying impact on the tensile strength of the nanocomposites.

Table 1 Coupling agents affect the PI/SiO₂ thermal properties [74]

Run	SiO ₂ ^a (wt%)	GOTMS/TEOS	T_d^b (°C)	CTE ($\times 10^{-5}$ K ⁻¹)	T_g^c (°C)
1	0	0	561	5.41	289
2	10	0	581	4.86	294
3	20	0	588	3.45	301
4	30	0	600		310
5	10	1/10	572	2.53	298
6	20	1/10	576		309
7	30	1/10	592		316

^aCalculated Si contents in hybrid films. ^b T_d calculated via TGA in N₂, on-set. ^c T_g calculated by DSC

Table 2 Mechanical properties of PP based nanocomposites, filled with various polymer-grafted SiO₂^a, SiO₂ content = 3.31 vol.% [61]

Properties	Nanocomposites						
	PS	PBA	PVA	PEA	PMMA	PMA	Neat PP
Tensile strength (MPa)	34.1	33.3	33.0	26.8	35.2	33.9	32.0
Young's modulus (GPa)	0.92	0.86	0.81	0.88	0.89	0.85	0.75
Elongation break (%)	9.3	12.6	11.0	4.6	12.0	11.9	11.7
Area under tensile stress strain curve (MPa)	2.4	3.3	2.3	0.8	3.2	2.9	2.2
Unnotched Charpy impact strength (KJ/m ²)	19.8	19.4	22.9	14.6	20.5	4.7	8.0

^aIrradiation dose = 10 Mrad; the monomer/SiO₂ weight ratio = 20/100; the systems employed acetone as a solvent throughout the irradiation, except for methyl acrylic acid/SiO₂ system with ethanol as solvent

It was found that entanglement and inter-diffusion in contrast to the miscibility between the grafting polymer segments with the matrix, has the most contribution to the interfacial interaction. It can be inferred that high M_w PP molecules must be entangled efficaciously with the SiO₂ agglomerates, in order to create an elevated tensile strength growth.

The tensile stress-strain figure of PP and its mixed matrix nanocomposite are demonstrated in Fig. 8, showing that a toughening and reinforcing impact of the fillers on the PP were significant.

4.3 Proton Conductivity

PEMFC functionality is a result of protons transfer from the anode to the cathode via the PEM. Thus, the membranes proton conductivity is an essential factor for the efficient utilization of PEMFC. The proton conductivities of numerous membranes under various conditions are shown in Table 3.

4.4 Water Uptake

Water uptake in the PEM represents an important effect in the proton conductivity in PEMFC. The formula employed for the measurement of water uptake per cent of PEM at various temperatures is:

$$\text{Water uptake (\%)} = \frac{W_t - W_d}{W_d}$$

where W_t is the weight of the membrane following swelling at a specific temperature for 24 h and W_d is the dry weight of the membrane. The water uptakes of different polymer membranes are presented in Table 4.

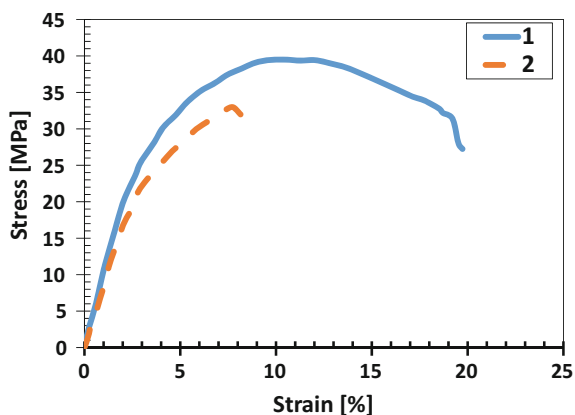


Fig. 8 Tensile stress-strain curves of (1) the neat PP matrix resin; and (2) the one filled with SiO₂-g-PS (SiO₂ content = 1.96 vol.%) [61]. Reprinted with permission from Elsevier

Table 3 Proton conductivities of different membranes

Membrane	Temp. (°C)	RH (%)	Proton conductivity (S/cm)	References
Nafion [®]	80	100	0.080	[79]
Nafion [®] -Si			0.089	
Nafion [®] -phosphonated Si			0.152	
Nafion [®]	80	50	0.008	
Nafion [®] -Si			0.014	
Nafion [®] -phosphonated Si			0.049	
Nafion [®] -117	80	100	0.120	[80]
Nafion [®] -Si (3 nm)			0.197	
Nafion [®] -Si (90 nm)			0.190	
Nafion [®] -Si(1 μm)			0.075	
Nafion [®]	60	98	0.140	[81]
Nafion [®] -sulfonated Si			0.130	
Nafion [®]	60	80	0.070	
Nafion [®] -sulfonated Si			0.080	[82]
Nafion [®] 212	80	80	0.080	
PFSA nanofiber			0.100	
PFSA/SPOSS/PAA			0.200	
Recast Nafion [®]	80	90	0.067	[18]
Nafion [®] -Si			0.068	
Nafion [®] -Si-ZrO ₂			0.100	
Nafion [®]	90	98	0.200	[83]
Nafion [®] -sulfonated MMT			0.160	

(continued)

Table 3 (continued)

Membrane	Temp. (°C)	RH (%)	Proton conductivity (S/cm)	References
Nafion [®] -protonated MMT			0.085	
Nafion [®]	95	98	0.064	[84]
Nafion [®] -unmodified Laponite			0.065	
Nafion [®] -sulfonated Laponite			0.080	
SPSU	90	100	0.170	[85]
SPSU-sulfonated Laponite			0.220	
SPAES	30	95	0.060	[86]
SPAES-SPOSS			0.150	
SPEEK	120	50	0.018	[87]
SPEEK-Si			0.019	
SPEEK-Si-HPMC			0.020	
PBI	Dry	140	0.001	[88]
PBI-Si			0.004	
PBI	120	50	0.010	[89]
PBI-SiO ₂ -Im			0.050	
PBI-SBA-15			0.070	
SiPANP	100	80	0.005	[90]
SiPANP-PWA			0.041	

4.5 Cell Performance Investigation

The ultimate utilization of the PEM in PEMFC is established employing an investigation of the PEMFC performance. In this kind of investigation, the membranes power density is determined at a specific voltage, temperature, and RH. Table 4 shows the current densities tested for various PEMs at various operational conditions.

5 Summary and Future Direction

The recent advances in the fabrication, properties, characterization, and application of polymer/Si nanocomposite are investigated. Primarily, three approaches for the polymer/Si hybrids preparation are employed: the sol-gel, blending and in situ polymerization.

All of these techniques are studied thoroughly. Apart from the properties of the single components in a nanocomposite, the interfacial interaction and nanoparticles dispersion in the matrix have significant impacts in improving or restricting the performance of the nanocomposites.

Several directions were discovered but no global trends of the polymeric nanocomposites behaviour may be inferred generally. The polymer/Si nanocomposites

Table 4 Water uptake and cell performance of different membranes

Membrane	Water uptake (%)	Temp. (°C)	Cell voltage (V)	Current density (mA/cm ²)	References
Nafion [®] -117	23.0	80	0.2	600	[80]
Nafion [®] -Si (3 nm)	28.0			1130	
Nafion [®] -Si (90 nm)	25.0			1030	
Nafion [®] -Si (1 μm)	21.0			500	
Nafion [®]	–	140	0.4	133	[91]
Nafion [®] -Si	–			225	
Nafion [®] – mesoporous Si	48	120	0.6	540	[92]
Recast Nafion [®]	13.9	60	0.4	540	[81]
Nafion [®] -sulfonated Si	24.7			1040	
Nafion [®] -Si-TBS	–	80	0.6	1600	[93]
Nafion [®] -115	32	110	0.4	95	[94]
Nafion [®] -Si	34			320	
Nafion [®] -Si-PWA	38			540	
Recast Nafion [®]	50.0	80	0.6	600	[84]
Nafion [®] -Laponite	87.0			–	
Nafion [®] -sulfonated Laponite	70.0			720	
Recast Nafion [®]	13.5	60	60	450	[83]
Nafion [®] -H + MMT	13.1	–			
Nafion [®] -sulfonated MMT	20.1			800	
SPAES	15	–	–	–	[86]
SPAES-SPOSS	21	–	–	–	
SPEEK	30.2	120	0.1	150	[87]
SPEEK-SiO ₂	38.9			250	
SPEEK-SiO ₂ -HPMC	48.5			700	
SPEEK (70°C)	100	60	0.6	80	[95]
SPEEK-Laponite clay	30			370	
PBI	16.6	–	–	–	[88]
PBI-Si	21.6	–	–	–	
PBI-sulfonated Si	23.8	–	–	–	
BIS	8.0	–	–	–	[96]
BIS-MCM	14.0	–	–	–	
BIS-sulfonated MCM	12.5	–	–	–	
SDF	100–190	93	0.3	1200	[97]
SDF-Si	187–385			1700	

properties, however, are usually better than the neat polymer matrix and microcomposites. Particularly, they generally show enhanced thermal stability and mechanical properties whatever of the preparation method. By taking advantage of this huge interfacial volume and area, distinctive combinations of polymer nanocomposites properties can be produced. Although several studies have been performed on polymer-Si nanocomposites, the extra investigation is necessary to comprehend the complicated structure-property relationships. Modifying the filler/matrix interfacial interaction contributes to an improved recognition of the relationships.

References

1. Rezakazemi M, Shahidi K, Mohammadi T (2012) Hydrogen separation and purification using crosslinkable PDMS/zeolite A nanoparticles mixed matrix membranes. *Int J Hydrogen Energy* 37:14576–14589
2. Rezakazemi M, Sadrzadeh M, Mohammadi T, Matsuura T (2017) Methods for the preparation of organic-inorganic nanocomposite polymer electrolyte membranes for fuel cells. In: Inamuddin D, Mohammad A, Asiri AM (eds) *Organic-inorganic composite polymer electrolyte membranes: preparation, properties, and fuel cell applications*. Springer International Publishing, Cham, pp 311–325
3. Baheri B, Shahverdi M, Rezakazemi M, Motaee E, Mohammadi T (2015) Performance of PVA/NaA mixed matrix membrane for removal of water from ethylene glycol solutions by pervaporation. *Chem Eng Commun* 202:316–321
4. Shahverdi M, Baheri B, Rezakazemi M, Motaee E, Mohammadi T (2013) Pervaporation study of ethylene glycol dehydration through synthesized (PVA-4A)/polypropylene mixed matrix composite membranes. *Polym Eng Sci* 53:1487–1493
5. Rezakazemi M, Ebadi Amooghin A, Montazer-Rahmati MM, Ismail AF, Matsuura T (2014) State-of-the-art membrane based CO₂ separation using mixed matrix membranes (MMMs): an overview on current status and future directions. *Prog Polym Sci* 39 817–861
6. Rostamizadeh M, Rezakazemi M, Shahidi K, Mohammadi T (2013) Gas permeation through H₂-selective mixed matrix membranes: Experimental and neural network modeling. *Int J Hydrogen Energy* 38:1128–1135
7. Rezakazemi M, Mohammadi T (2013) Gas sorption in H₂-selective mixed matrix membranes: Experimental and neural network modeling. *Int J Hydrogen Energy* 38:14035–14041
8. Rezakazemi M, Dashti A, Asghari M, Shirazian S (2017) H₂-selective mixed matrix membranes modeling using ANFIS, PSO-ANFIS, GA-ANFIS. *Int J Hydrogen Energy* 42:15211–15225
9. Rezakazemi M, Shahidi K, Mohammadi T (2012) Sorption properties of hydrogen-selective PDMS/zeolite 4A mixed matrix membrane. *Int J Hydrogen Energy* 37:17275–17284
10. Rezakazemi M, Vatani A, Mohammadi T (2015) Synergistic interactions between POSS and fumed silica and their effect on the properties of crosslinked PDMS nanocomposite membranes. *RSC Adv* 5:82460–82470
11. Rezakazemi M, Vatani A, Mohammadi T (2016) Synthesis and gas transport properties of crosslinked poly(dimethylsiloxane) nanocomposite membranes using octatrimethylsiloxy POSS nanoparticles. *J Nat Gas Sci Eng* 30:10–18
12. Zou H, Wu S, Shen J (2008) Polymer/silica nanocomposites: preparation, characterization, properties, and applications. *Chem Rev* 108:3893–3957
13. Rezakazemi M, Maghami M, Mohammadi T (2018) High loaded synthetic hazardous wastewater treatment using lab-scale submerged ceramic membrane bioreactor. *Periodica Polytech, Chem Eng* 62:299–304

14. Schadler LS, Kumar SK, Benicewicz BC, Lewis SL, Harton SE (2007) Designed interfaces in polymer nanocomposites: a fundamental viewpoint. *MRS Bull* 32:335–340
15. Rezakazemi M, Shahverdi M, Shirazian S, Mohammadi T, Pak A (2011) CFD simulation of water removal from water/ethylene glycol mixtures by pervaporation. *Chem Eng J* 168:60–67
16. Rezakazemi M, Sadrzadeh M, Matsuura T (2018) Thermally stable polymers for advanced high-performance gas separation membranes. *Prog Energy Combust Sci* 66:1–41
17. Mura F, Silva R, Pozio A (2007) Study on the conductivity of recast Nafion[®]/montmorillonite and Nafion[®]/TiO₂ composite membranes. *Electrochim Acta* 52:5824–5828
18. Park KT, Jung UH, Choi DW, Chun K, Lee HM, Kim SH (2008) ZrO₂-SiO₂/Nafion[®] composite membrane for polymer electrolyte membrane fuel cells operation at high temperature and low humidity. *J Power Sources* 177:247–253
19. Aparicio M, Mosa J, Etienne M, Durán A (2005) Proton-conducting methacrylate-silica sol-gel membranes containing tungstophosphoric acid. *J Power Sources* 145:231–236
20. Di Vona M, Sgreccia E, Donnadio A, Casciola M, Chailan J, Auer G, Knauth P (2011) Composite polymer electrolytes of sulfonated poly-ether-ether-ketone (SPEEK) with organically functionalized TiO₂. *J Membr Sci* 369:536–544
21. Zhengbang W, Tang H, Mu P (2011) Self-assembly of durable Nafion/TiO₂ nanowire electrolyte membranes for elevated-temperature PEM fuel cells. *J Membr Sci* 369:250–257
22. Rezakazemi M, Zhang Z (2018) 2.29 Desulfurization Materials A2—Dincer, Ibrahim. In: *Comprehensive energy systems*. Elsevier, Oxford, pp 944–979
23. Hashemi F, Rowshanzamir S, Rezakazemi M (2012) CFD simulation of PEM fuel cell performance: Effect of straight and serpentine flow fields. *Math Comput Model* 55:1540–1557
24. Cong H, Radosz M, Towler BF, Shen Y (2007) Polymer-inorganic nanocomposite membranes for gas separation. *Sep Purif Technol* 55:281–291
25. Ajayan PM, Schadler LS, Braun PV (2006) *Nanocomposite science and technology*. Wiley
26. Xing D, He G, Hou Z, Ming P, Song S (2011) Preparation and characterization of a modified montmorillonite/sulfonated polyphenylene ether sulfone/PTFE composite membrane. *Int J Hydrogen Energy* 36:2177–2183
27. Cho Y-H, Kim S-K, Kim T-H, Cho Y-H, Lim JW, Jung N, Yoon W-S, Lee J-C, Sung Y-E (2011) Preparation of MEA with the polybenzimidazole membrane for high temperature PEM fuel cell. *Electrochim Solid-State Lett* 14:B38–B40
28. Tago T, Kuwashiro N, Nishide H (2007) Preparation of acid-functionalized poly (phenylene oxide)s and poly (phenylene sulfone) and their proton conductivity. *Bulletin of the Chem Soc Jpn* 80:1429–1434
29. Sodeifian G, Raji M, Asghari M, Rezakazemi M, Dashti A (2018) Polyurethane-SAPO-34 mixed matrix membrane for CO₂/CH₄ and CO₂/N₂ separation. *Chin J Chem Eng*
30. Rezakazemi M, Razavi S, Mohammadi T, Nazari AG (2011) Simulation and determination of optimum conditions of pervaporative dehydration of isopropanol process using synthesized PVA-APTEOS/TEOS nanocomposite membranes by means of expert systems. *J Membr Sci* 379:224–232
31. Gómez-Romero P, Sanchez C, *Functional hybrid materials*. Wiley (2006)
32. Zhang S, Xu T, Wu C (2006) Synthesis and characterizations of novel, positively charged hybrid membranes from poly (2, 6-dimethyl-1, 4-phenylene oxide). *J Membr Sci* 269:142–151
33. Wu C, Xu T, Yang W (2005) Synthesis and characterizations of novel, positively charged poly (methyl acrylate)-SiO₂ nanocomposites. *Eur Polymer J* 41:1901–1908
34. Saito R, Kobayashi S-I, Hayashi H, Shimo T (2007) Surface hardness and transparency of poly(methyl methacrylate)-silica coat film derived from perhydropolysilazane. *J Appl Polym Sci* 104:3388–3395
35. Shen L, Du Q, Wang H, Zhong W, Yang Y (2004) In situ polymerization and characterization of polyamide-6/silica nanocomposites derived from water glass. *Polym Int* 53:1153–1160
36. Ding X, Jiang Y, Yu K, Hari B, Tao N, Zhao J, Wang Z (2004) Silicon dioxide as coating on polystyrene nanoparticles in situ emulsion polymerization. *Mater Lett* 58:1722–1725
37. Laugel N, Hemmerlé J, Porcel C, Voegel J-C, Schaaf P, Ball V (2007) Nanocomposite silica/polyamine films prepared by a reactive layer-by-layer deposition. *Langmuir* 23:3706–3711

38. Grund S, Kempe P, Baumann G, Seifert A, Spange S (2007) Nanocomposites prepared by twin polymerization of a single-source monomer. *Angew Chem Int Ed* 46:628–632
39. Sufner J, Schechner G, Sieger H, Hahn H (2007) In-situ coating of silica nanoparticles with acrylate-based polymers. *Chem Vap Deposition* 13:459–464
40. Senkevich JJ, Desu SB (1999) Near-room-temperature thermal chemical vapor deposition of poly(chloro-p-xylylene)/SiO₂ nanocomposites. *Chem Mater* 11:1814–1821
41. Mishra AK, Chattopadhyay S, Rajamohanam P, Nando GB (2011) Effect of tethering on the structure-property relationship of TPU-dual modified Laponite clay nanocomposites prepared by ex-situ and in-situ techniques. *Polymer* 52:1071–1083
42. Seo W, Sung Y, Han S, Kim Y, Ryu O, Lee H, Kim WN (2006) Synthesis and properties of polyurethane/clay nanocomposite by clay modified with polymeric methane diisocyanate. *J Appl Polym Sci* 101:2879–2883
43. Mishra AK, Rajamohanam P, Nando GB, Chattopadhyay S (2011) Structure–property of thermoplastic polyurethane–clay nanocomposite based on covalent and dual-modified Laponite. *Adv Sci Lett* 4:65–73
44. Mishra A, Nando G, Chattopadhyay S (2008) Exploring preferential association of laponite and cloisite with soft and hard segments in TPU-clay nanocomposite prepared by solution mixing technique. *J Polym Sci, Part B: Polym Phys* 46:2341–2354
45. Aparicio M, Durán A (2004) Hybrid organic/inorganic sol-gel materials for proton conducting membranes. *J Sol-Gel Sci Technol* 31:103–107
46. Aparicio M, Castro Y, Duran A (2005) Synthesis and characterisation of proton conducting styrene-co-methacrylate–silica sol–gel membranes containing tungstophosphoric acid. *Solid State Ionics* 176:333–340
47. Tillet G, Boutevin B, Ameduri B (2011) Chemical reactions of polymer crosslinking and post-crosslinking at room and medium temperature. *Prog Polym Sci* 36:191–217
48. Lin B, Cheng S, Qiu L, Yan F, Shang S, Lu J (2010) Protic ionic liquid-based hybrid proton-conducting membranes for anhydrous proton exchange membrane application. *Chem Mater* 22:1807–1813
49. Darbandi M, Thomann R, Nann T (2007) Hollow silica nanospheres: in situ, semi-in situ, and two-step synthesis. *Chem Mater* 19:1700–1703
50. Stöber W, Fink A, Bohn E (1968) Controlled growth of monodisperse silica spheres in the micron size range. *J Colloid Interface Sci* 26:62–69
51. Bronstein LM, HCD, Kim G (Ed) (2004) Dekker encyclopedia of nanoscience and nanotechnology. Taylor & Francis, New York, pp 1–10
52. Osseo-Asare K, Arriagada F (1990) Preparation of SiO₂ nanoparticles in a non-ionic reverse micellar system. *Colloids Surf* 50:321–339
53. Vassiliou AA, Papageorgiou GZ, Achilias DS, Bikiaris DN (2007) Non-Isothermal Crystallisation Kinetics of In Situ Prepared Poly (ϵ -caprolactone)/Surface-Treated SiO₂ Nanocomposites. *Macromol Chem Phys* 208:364–376
54. Jana SC, Jain S (2001) Dispersion of nanofillers in high performance polymers using reactive solvents as processing aids. *Polymer* 42:6897–6905
55. Nalwa HS (2003) Handbook of organic-inorganic hybrid materials and nanocomposites. In: Zhang MQR, MZ, Friedrich K (Ed) American Scientific Publishers, California, pp 113–150
56. Blum FD (2004) Encyclopedia of polymer science and technology, concise. In: Kroschwitz JJ (Ed) Wiley, pp 38–50
57. Gomes D, Buder I, Nunes SP (2006) Sulfonated silica-based electrolyte nanocomposite membranes. *J Polym Sci, Part B: Polym Phys* 44:2278–2298
58. Wu T-M, Chu M-S (2005) Preparation and characterization of thermoplastic vulcanizate/silica nanocomposites. *J Appl Polym Sci* 98:2058–2063
59. Ahn SH, Kim SH, Lee SG (2004) Surface-modified silica nanoparticle–reinforced poly (ethylene 2, 6-naphthalate). *J Appl Polym Sci* 94:812–818
60. Lai YH, Kuo MC, Huang JC, Chen M (2007) On the PEEK composites reinforced by surface-modified nano-silica. *Mater Sci Eng, A* 458:158–169

61. Rong MZ, Zhang MQ, Zheng YX, Zeng HM, Walter R, Friedrich K (2001) Structure–property relationships of irradiation grafted nano-inorganic particle filled polypropylene composites. *Poly* 42:167–183
62. Rong MZ, Zhang MQ, Zheng YX, Zeng HM, Friedrich K (2001) Improvement of tensile properties of nano-SiO₂/PP composites in relation to percolation mechanism. *Polymer* 42:3301–3304
63. Wu CL, Zhang MQ, Rong MZ, Friedrich K (2002) Tensile performance improvement of low nanoparticles filled-polypropylene composites. *Compos. Sci. Technol.* 62:1327–1340
64. Zhang MQ, Rong MZ, Zhang HB, Friedrich K (2003) Mechanical properties of low nano-silica filled high density polyethylene composites. *Polym Eng Sci* 43:490–500
65. Wu CL, Zhang MQ, Rong MZ, Friedrich K (2005) Silica nanoparticles filled polypropylene: effects of particle surface treatment, matrix ductility and particle species on mechanical performance of the composites. *Compos. Sci. Technol.* 65:635–645
66. Ruan WH, Huang XB, Wang XH, Rong MZ, Zhang MQ (2006) Effect of drawing induced dispersion of nano-silica on performance improvement of poly(propylene)-based nanocomposites. *Macromol Rapid Commun* 27:581–585
67. Zhu Y, Li Z, Zhang D, Tanimoto T (2006) PET/SiO₂ nanocomposites prepared by cryomilling. *J Polym Sci, Part B: Polym Phys* 44:1161–1167
68. Zhu Y-G, Li Z-Q, Zhang D, Tanimoto T (2006) Thermal behaviors of poly(ethylene terephthalate)/SiO₂ nanocomposites prepared by cryomilling. *J Polym Sci, Part B: Polym Phys* 44:1351–1356
69. Petrovicova E, Knight R, Schadler L, Twardowski T (2000) Nylon 11/silica nanocomposite coatings applied by the HVOF process. II. Mechanical and barrier properties. *J. Appl. Polym. Sci.* 78:2272–2289
70. Petrovicova E, Knight R, Schadler L, Twardowski T (2000) Nylon 11/silica nanocomposite coatings applied by the HVOF process. I. Microstructure and morphology. *J. Appl. Polym. Sci.* 77:1684–1699
71. Schadler LS, Laut KO, Smith RW, Petrovicova E (1997) Microstructure and mechanical properties of thermally sprayed silica/nylon nanocomposites. *J Therm Spray Technol* 6:475–485
72. Jafari H, Emami S, Mahmoudi Y (2017) Numerical investigation of dual-stage high velocity oxy-fuel (HVOF) thermal spray process: a study on nozzle geometrical parameters. *Appl Therm Eng* 111:745–758
73. Sinha Ray S, Okamoto M (2003) Polymer/layered silicate nanocomposites: a review from preparation to processing. *Prog. Polym. Sci.* 28:1539–1641
74. Shang X-Y, Zhu Z-K, Yin J, Ma X-D (2002) Compatibility of soluble polyimide/silica hybrids induced by a coupling agent. *Chem Mater* 14:71–77
75. Kashiwagi T, Morgan AB, Antonucci JM, VanLandingham MR, Harris RH, Awad WH, Shields JR (2003) Thermal and flammability properties of a silica–poly(methylmethacrylate) nanocomposite. *J Appl Polym Sci* 89:2072–2078
76. Crosby AJ, Lee JY (2007) Polymer Nanocomposites: the “Nano” effect on mechanical properties. *Polym Rev* 47:217–229
77. Mammeri F, Bourhis EL, Rozes L, Sanchez C (2005) Mechanical properties of hybrid organic-inorganic materials. *J Mater Chem* 15:3787–3811
78. Lach R, Kim G-M, Michler GH, Grellmann W, Albrecht K (2006) Indentation fracture mechanics for toughness assessment of PMMA/SiO₂ nanocomposites. *Macromol Mater Eng* 291:263–271
79. Joseph J, Tseng C-Y, Hwang B-J (2011) Phosphonic acid-grafted mesostructured silica/Nafion hybrid membranes for fuel cell applications. *J Power Sources* 196:7363–7371
80. Kumar GG, Kim A, Nahm KS, Elizabeth R (2009) Nafion membranes modified with silica sulfuric acid for the elevated temperature and lower humidity operation of PEMFC. *IJHE* 34:9788–9794
81. Choi Y, Kim Y, Kim HK, Lee JS (2010) Direct synthesis of sulfonated mesoporous silica as inorganic fillers of proton-conducting organic–inorganic composite membranes. *J Membr Sci* 357:199–205

82. Choi J, Wycisk R, Zhang W, Pintauro PN, Lee KM, Mather PT (2010) High Conductivity Perfluorosulfonic Acid Nanofiber Composite Fuel-Cell Membranes. *Chemsuschem* 3:1245–1248
83. Kim Y, Choi Y, Kim HK, Lee JS (2010) New sulfonic acid moiety grafted on montmorillonite as filler of organic–inorganic composite membrane for non-humidified proton-exchange membrane fuel cells. *J Power Sources* 195:4653–4659
84. Bébin P, Caravanier M, Galiano H (2006) Nafion[®]/clay-SO₃H membrane for proton exchange membrane fuel cell application. *J Membr Sci* 278:35–42
85. Buquet CL, Fatyeyeva K, Poncin-Epaillard F, Schatzel P, Dargent E, Langevin D, Nguyen QT, Marais S (2010) New hybrid membranes for fuel cells: plasma treated laponite based sulfonated polysulfone. *J Membr Sci* 351:1–10
86. Choi J, Lee KM, Wycisk R, Pintauro PN, Mather PT (2010) Sulfonated polysulfone/POSS nanofiber composite membranes for PEM fuel cells. *JEIS* 157:B914–B919
87. Zhang Y, Wang S, Xiao M, Bian S, Meng Y (2009) The silica-doped sulfonated poly (fluorenyl ether ketone) s membrane using hydroxypropyl methyl cellulose as dispersant for high temperature proton exchange membrane fuel cells. *IJHE* 34:4379–4386
88. Liu Y-L (2009) Preparation and properties of nanocomposite membranes of polybenzimidazole/sulfonated silica nanoparticles for proton exchange membranes. *J Membr Sci* 332:121–128
89. Quartarone E, Magistris A, Mustarelli P, Grandi S, Carollo A, Zukowska G, Garbarczyk J, Nowinski J, Gerbaldi C, Bodoardo S (2009) Pyridine-based PBI composite membranes for PEMFCs. *Fuel Cells* 9:349–355
90. Cui X, Zhong S, Wang H (2007) Organic–inorganic hybrid proton exchange membranes based on silicon-containing polyacrylate nanoparticles with phosphotungstic acid. *J Power Sources* 173:28–35
91. Adjemian K, Lee S, Srinivasan S, Benziger J, Bocarsly A (2002) Silicon oxide nafion composite membranes for proton-exchange membrane fuel cell operation at 80–140 C. *JEIS* 149:A256–A261
92. Pereira F, Vallé K, Belleville P, Morin A, Lambert S, Sanchez C (2008) Advanced mesostructured hybrid silica–nafion membranes for high-performance PEM fuel cell. *Chem Mater* 20:1710–1718
93. Mulmi S, Park CH, Kim HK, Lee CH, Park HB, Lee YM (2009) Surfactant-assisted polymer electrolyte nanocomposite membranes for fuel cells. *J Membr Sci* 344:288–296
94. Shao Z-G, Joghee P, Hsing I-M (2004) Preparation and characterization of hybrid Nafion–silica membrane doped with phosphotungstic acid for high temperature operation of proton exchange membrane fuel cells. *J Membr Sci* 229:43–51
95. Chang J-H, Park JH, Park G-G, Kim C-S, Park OO (2003) Proton-conducting composite membranes derived from sulfonated hydrocarbon and inorganic materials. *J Power Sources* 124:18–25
96. Wilhelm M, Jeske M, Marschall R, Cavalcanti WL, Tölle P, Köhler C, Koch D, Frauenheim T, Grathwohl G, Caro J (2008) New proton conducting hybrid membranes for HT-PEMFC systems based on polysiloxanes and SO₃H-functionalized mesoporous Si-MCM-41 particles. *J Membr Sci* 316:164–175
97. Kim YM, Choi SH, Lee HC, Hong MZ, Kim K, Lee H-I (2004) Organic–inorganic composite membranes as addition of SiO₂ for high temperature-operation in polymer electrolyte membrane fuel cells (PEMFCs). *Electrochim Acta* 49:4787–4796

Extraction of Cellulose Nanofibers and Their Eco-friendly Polymer Composites



M. Hazwan Hussin, Djalal Trache, Caryn Tan Hui Chuin,
M. R. Nurul Fazita, M. K. Mohamad Haafiz and Md. Sohrab Hossain

List of Abbreviations

%	Percentage
[BMIM]Cl	1-butyl-3-methylimidazolium chloride
[BMIM]HSO ₄	1-butyl-3-methylimidazolium hydrogen sulfate
[EMIM][OAc]	1-ethyl-3-methylimidazolium acetate
[SBMIM]HSO ₄	1-(4-sulfobutyl)-3-methylimidazolium hydrogen sulfate
AFM	Atomic force microscopy
AGU	Anhydroglucose unit
ANC	Amorphous nanocellulose
BC	Bacterial cellulose
cm	Centimeter
CNC	Cellulose nanocrystal
CNF	Cellulose nanofibrils
CNM	Cellulose nanomaterials
CNY	Cellulose nanoyarn
<i>CrI</i>	Crystallinity index
D	Apparent crystallite size
DSC	Differential scanning calorimetry
FTIR	Fourier Transform
HEBM	High-energy bead milling
kg/day	Kilogram per day

M. Hazwan Hussin (✉) · C. T. H. Chuin
Materials Technology Research Group (MaTReC), School of Chemical Sciences,
Universiti Sains Malaysia, 11800 Minden, Penang, Malaysia
e-mail: mhh@usm.my; mhh.usm@gmail.com

D. Trache
UER Procédés Energétiques, Ecole Militaire Polytechnique, BP 17,
Bordj El-Bahri, Algiers, Algeria

M. R. Nurul Fazita · M. K. Mohamad Haafiz · Md. S. Hossain
School of Industrial Technology, Universiti Sains Malaysia, 11800 Minden,
Penang, Malaysia

nm	Nanometer
PLA	Poly lactide
SEM	Scanning electron microscope
TAPPI	Technical Association of the Pulp and Paper Industry
TBAA	Tetrabutylammonium acetate
TEM	Transmission electron microscope
TEMPO	2,2,6,6-tetramethyl-1-piperidinyloxy
TGA	Thermogravimetric analysis
T _{max}	Melting point temperature
XRD	X-ray Diffraction
λ	X-ray wavelength

1 Introduction

Polymer-based materials are an important and promising area of research exhibiting strong developments [1, 2]. They play a prominent role in the modern civilization and find application in different industries related to electrical and electronic equipment, chemicals, automotive, spacecraft, energy storage in batteries and supercapacitors and medical to cite a few [3–5]. The polymeric materials have substituted the employment of metal, ceramics, and glass in various fields owing to their availability, low weight, low cost, chemical inertness, strength and ease of processing [6, 7]. However, for particular applications, some thermal, physical and mechanical properties of polymer materials appeared to be insufficient. As a way to avoid these limitations, the utilization of polymer as a matrix with along the incorporation of fibers and fillers for the creation of composites became widespread. These composite materials demonstrate interesting thermal, physicochemical, barrier and swelling properties, and mechanical features with respect to the conventional materials [8, 9]. On the other hand, rapidly depletion global petroleum resources, along with awareness of global environmental and health issues as well as the end-of-life disposal challenges, have proved the way to switch toward renewable and sustainable materials. In this regards, bio-based materials such as lignocelluloses and their derivatives can form the basis for various eco-efficient and sustainable products and can prevent the widespread dependence on fossil fuels [10–12].

Lignocelluloses are mainly composed of cellulose nano-fibrils, which can be isolated by chemical, mechanical and biological methods in order to get cellulosic nanofibers [13, 14]. Furthermore, cellulosic nanofibers can also be synthesized by the bacterial procedure. These nanofibers are an emerging class of nanomaterials with various desirable properties. These features are mainly depending on the

original source and the extraction procedure. The possibility of obtaining cellulose nanofibers with different properties remains a quite interesting topic, which can bring valorization of residual or unexplored biomass.

There are mainly two kinds of cellulose nanofibers: cellulose nanofibrils (CNF) and cellulose nanocrystal (CNC). The three-dimensional hierarchical structures that compose cellulose nanofibers at different scales, the combination of the physicochemical properties of cellulose, together with the principal advantages of nanomaterials (a high specific surface area, aspect ratio) opens new opportunities in several fields, ranging from electronics to medical applications. Cellulose nanofibers can be employed to reinforce polymers, papers, and membranes. These nanofibers have unique properties including high elastic modulus, dimensional stability, low thermal expansion coefficient, outstanding reinforcing potential and transparency [15, 16]. Figure 1 shows the comparison of specific strength and elastic modulus of various materials [11]. Furthermore, Owing to their $-OH$ side

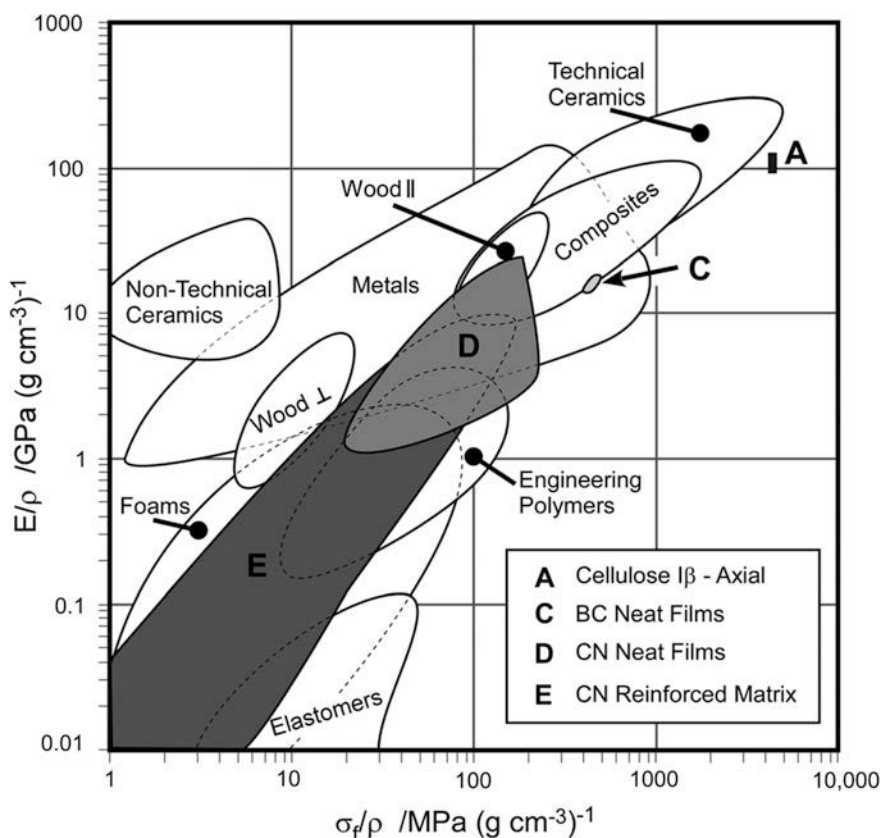


Fig. 1 Comparison of specific strength and Young's modulus of different materials. Reprinted with permission from [11], Copyright © The Royal Society of Chemistry

groups on the surface, cellulose nanofibers can be readily modified into different forms through surface functionalization allowing the tailoring of particle surface chemistry to ease self-assembly, controlled dispersion within a wide range of matrix polymers, and control of both the particle-particle and particle-matrix bond strength [17–20]. Currently, CNF and CNC have been extensively added to polymer composites as reinforcing elements. CNC have exhibited to be preferable as load-bearing component owing to their ability to enhance toughness along with strength and stiffness through the interface interaction between CNC-matrix, whereas CNF has revealed to impart greater reinforcement owing to their highly flexible fibrils and the ease of the interconnection to obtain rigid web-like fibrils networks [4, 5, 21, 22]. Thus, the extraction process of cellulose nanofibers from various sources has a particular interest in their employment as reinforcing agents.

In this review, we describe an overview on the recent research developments on principal cellulose sources followed by the principal methodologies employed for its extraction. The isolation procedures and characterization of cellulose nanofibers are considered and provided as well. In addition, the potential use of these nanofibers as reinforcing material for the development of polymer composites in various fields is discussed.

2 Overview of Cellulose Nanofibers

The emergence and development of cellulose nanofibers has attracted significant interest in recent two decades from both academic and industrial communities due to its potential for the diverse applications and many exceptional useful features, including abundance, renewability, eco-friendliness, low weight, high strength and stiffness, high surface area-to-volume ratio and low coefficient of thermal expansion. This interest is well evident from the number of scientific papers on the topic of cellulose nanofibers, which rises significantly in the last five years [13, 17, 20, 23–28]. The majority of the recently published works in this field deals with cellulose nanofibers preparation from various sources using different approaches, characterization, modification as well as their employment in a wide range of applications. Continued research works and development are looked at optimizing processes to lower costs and to improve yields, consistency, and quality. Processes are commonly multistep and tailored for the specific cellulose feedstock. One common trait among all cellulose nanofibers types is the parallel stacking of cellulose chains along the particle length. This high organization of stacking is the consequence of extensive intra- and inter-chain hydrogen bonding, generating ordered cellulose an exceptionally stable biopolymer.

2.1 Cellulose: Structure and Chemistry

Cellulose, the most abundant carbohydrate polymer in the earth, represents about fifty percent of natural biomass having a yearly fabrication estimated to be over 7.5×10^{10} tons [9, 13]. This ubiquitous renewable natural polymer is regarded as an inexhaustible source of raw materials for the increasing demand for biocompatible and environmentally friendly materials. It is present in various kinds of living species as well as wood, annual plants, tunicates, algae, fungi and some bacteria. Its empirical formula was determined since 1838 by the French chemist Anselm Payen by isolating a white powder from plant tissue [29, 30]. In 1839 he invented the term cellulose for the first time. The structure of cellulose was established late, in 1920, by Hermann Staudinger [31]. Several books [4, 17, 26, 27, 32, 33] and review papers [6, 9, 11, 13, 29, 34–36] have already summarized the state of current knowledge on this fascinating and innovative biopolymer. Hence, only some important details will be provided in the present chapter to avoid duplication. The structural levels of organization of cellulose from its source to the basic molecule are graphically depicted in Fig. 2.

Generally, cellulose is commonly produced with a desired size by the top-down enzymatic, mechanical and/or chemical treatments of cellulosic precursors, in which cotton, wood, annual plants or other agricultural residues can be utilized [9]. In contrast, cellulose can be fabricated by a bottom-up approach, where cellulose is

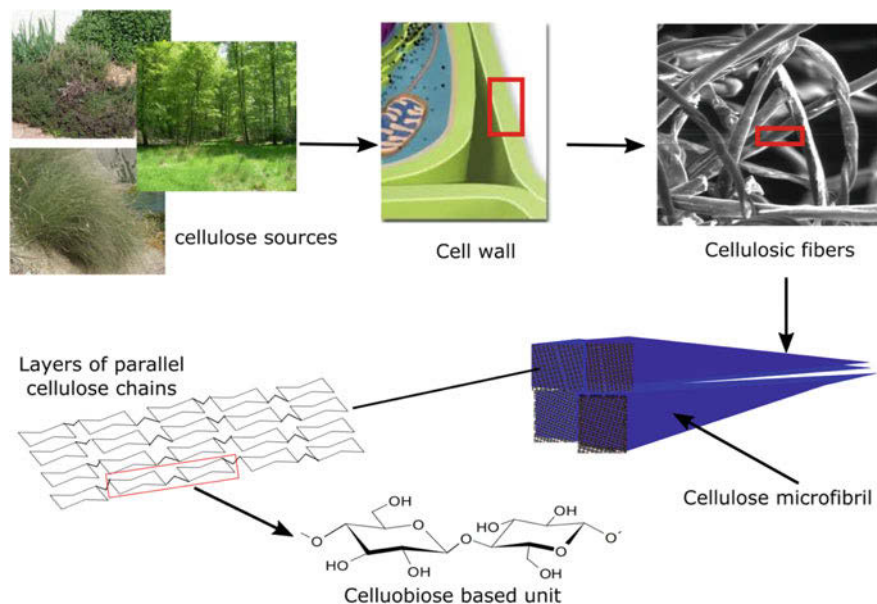


Fig. 2 Structural levels of organization of cellulose from the source to the molecule. Reprinted with permission from [9], Copyright © Elsevier Limited

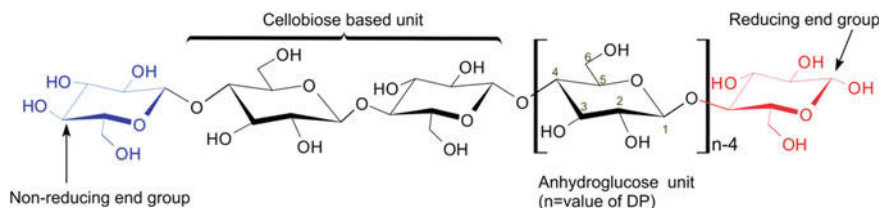


Fig. 3 Molecular structure of cellulose showing the numbering of carbon atoms, the reducing end with a hemiacetal, and the non-reducing end with a free hydroxyl at C4. Reprinted with permission from [9], Copyright © Elsevier Limited

biosynthesized from glucose using the direct action of specific bacterial strains belonging to genus such as *Alcaligenes*, *Achromobacter*, and *Gluconacetobacter* among which only *Gluconacetobacter xylinus* (*K. xylinus*) has been revealed to fabricate cellulose at commercial production levels [37]. Bacterial cellulose is typically produced in a pure form without needing intensive processing to remove unwanted impurities or contaminants [28]. It is worth noting that the quantities and the characteristics of cellulose depend closely on the isolation process, the origin and the natural source [6]. Cellulose can occur in pure form in lignocellulosic sources but it is usually accompanied by lignins, hemicelluloses, and comparably small quantities of extractives and trace elements.

Cellulose (Fig. 3) is defined as a linear polymer of repeating β (1,4)-bound D-glucopyranosyl units (anhydroglucose unit, AGU) in the 4C_1 -chain configuration, which displays the lowest energy conformation. Three reactive groups are found in each AGU within cellulose chain, a primary group at C6 and two secondary groups at C2 and C3 that are situated in the plane of the ring [38]. The monomers are related together by condensation such that glycosidic oxygen bridges link the sugar rings. In nature, cellulose chains have a degree of polymerization of roughly 15,000 glucopyranose units in native cellulose cotton and about 10,000 in wood cellulose [9]. Each polymeric chain is asymmetric, containing two different end-units; one end possesses an anomeric C atom connected by the glycosidic bonds (nonreducing end) whereas the other end has a D-glucopyranose unit in equilibrium with the aldehyde function (reducing end group). These cellulose polymer chains are biosynthesized by enzymes, placed in a continuous fashion and combined to form microfibrils, long threadlike bundles. Depending on their origin, the microfibril diameters range from about 2–20 nm for lengths that can reach several tens of microns [6]. These microfibrils highly ordered (crystalline) domains alternate with less ordered (amorphous) domains [39]. Interchain hydrogen bonds between the hydroxyl groups and oxygen atoms of neighboring ring molecules stabilize the cellulosic chains are responsible for the linear structure of the macromolecule chain.

Cellulose generally has four main polymorphs vis. cellulose I, II, III, and IV. Cellulose I, native cellulose, is the form established in nature, and it is the most crystalline type existing in two allomorphs, I_α and I_β , which are analogous to each other whereas their packing pattern in the lattice is different because of the different

extent of hydrogen bonding developed between the chains. Cellulose II, or regenerated cellulose, has an antiparallel arrangement of chains and it comes out after regeneration by solubilization and subsequent recrystallization or mercerization with aqueous sodium hydroxide. Cellulose III_I and III_{II} can be produced by ammonia treatment from either cellulose I or cellulose II, respectively. Cellulose IV₁ and cellulose IV₂ can be obtained from the corresponding form of cellulose III₁ and III₂ by heating in glycerol [38, 40].

The rigidity of chains and the existence of both polar and non-polar groups make the molecule insoluble in most common solvents. Cellulose does not melt below degradation temperature as well. This solvent resistance and thermal stability make cellulose an attractive polymer, but at the same time prevent direct application of industrial process developed for commodity polymers [41]. Furthermore, the crystallinity of cellulose makes it recalcitrant to acid and base-catalyzed hydrolysis too, thereby making the chemical processing of cellulose difficult. Because of these situations, an appropriate combination of various chemical, mechanical and enzymatic treatments of cellulose for further processing have been investigated to produce cellulose nanofibers from the early 2000s until now.

2.2 Cellulose Nanofibers

2.2.1 Types of Cellulose Nanofibers

Cellulose nanomaterials (CNM), as biopolymers, have recently gained substantial interest and have widely reported in the literature owing to their unique structural features and impressive physicochemical properties. CNM is regarded as a type of nano-objects where the term nano-object is reserved to material with one, two or three external dimensions in the nanoscale according to ISO publications [42, 43]. CNM is a term commonly used to define nanoscale of cellulosic materials, which is considered to be in the nanoscale range if the fibril particle diameters or width is between 1 and 100 nm. CNM combine crucial cellulose features—such as hydrophilicity, biodegradability, renewability, broad chemical modification capacity and the formation of versatile semicrystalline fiber morphologies as well as the specific properties of nanoscale materials, which are due to the very large specific area. Different types of CNM can be divided into various subcategories based on their preparation method, dimension, shape, function, which in turn primarily depend on the cellulosic source and processing conditions. It is worthy to note that ambiguities still exist regarding the terminology and nomenclature applied to cellulose nanomaterials [4–6, 11, 25, 30, 34, 44, 45]. More recently, the Technical Association of the Pulp and Paper Industry (TAPPI) has established a Nanotechnology Division devoted to the standardization of CNM nomenclature. A draft version of nanomaterials standard (TAPPI WI 3021: Standard Terms and Their Definition for Cellulose Nanomaterials) has been made [46], but comments on this standard are still under review. The existing literature encouraged that a

Table 1 Types of cellulose nanofibers and their particle sizes

Terminology and nomenclature of cellulose nanofibers	Width (nm)	Length (nm)	Aspect ratio (length/width)	Reference
Cellulose nanocrystals, nanocrystalline cellulose, cellulose nanocrystals	4–70	100–6000	10–100	[13]
Cellulose nanofibril, nanofibrillar cellulose, nanofibrillated cellulose	20–100	>10,000	>1000	[41]
Bacterial cellulose, microbial cellulose	10–50	>1000	100–150	[24]
Amorphous cellulose	50–120 ^a	50–120 ^a	~ 1	[4]
Cellulose nanoyarn	100–1000	>10,000	>100	[4]

^aDiameter of spherical or elliptical nanoparticles

number of terminologies have been and are currently used to refer to cellulose nanomaterials, which unfortunately reflects some misunderstanding and anomalies. Various terms have been employed to designate cellulose nanomaterial elements including nanocellulose, cellulose nanofibers, nanoscale cellulose, cellulose microfibrils, nanocellulosic fibrils, cellulose nanofibrils, cellulose nanoparticles, and nano-sized cellulose fibrils. Generally, CNM can be split up into nanostructured materials and nanofibers. The nanostructured materials are categorized into cellulose microcrystals (or microcrystalline cellulose) and cellulose microfibrils (TAPPI WI 3021), whereas, the cellulose nanofibers (Table 1) are mainly sub-grouped into two types. The first type concerned cellulose nanofibrils (CNF) with various nomenclature, including nanofibrillated cellulose, cellulosic fibrillar fines, nanofibrillar cellulose, nanoscale-fibrillated cellulose, nanofibrils, nanofibers, fibril aggregates and sometimes microfibrillated cellulose or microfibrils, while the second type involved cellulose nanocrystals (CNC) with various terminologies, comprising nanocrystalline cellulose, nanorods, cellulose whiskers, cellulose nanowhiskers, rodlike cellulose crystals, nanowires and cellulose crystallites [13]. Other families of cellulose nanofibers materials that could be considered are bacterial cellulose discussed above, amorphous nancellulose and cellulose nanoyarn [4, 47]. The nomenclature that will be utilized in the present chapter is in accordance with the TAPPI standard recommendations.

2.2.2 Feedstock

Cellulose nanofibers have exciting physicochemical and biological properties such as good stability, high strength, low degradation, and nontoxicity. Various cellulose nanofibers could be prepared, depending on the source, origin, maturity, processing procedures and reaction conditions. Broadly, cellulose nanofibers derived from lignocellulosic materials is obtained by the top-down chemical and/or mechanical treatment. In contrast, these nanofibers can be produced by biosynthesis by some

bacteria, giving rise to bacterial cellulose, which is obtained directly as a fibrous network, contains no lignin, pectin, hemicelluloses, or other biogenic products; it is very highly crystalline and possesses a high degree of polymerization (DP). Several researchers have beautifully compiled detailed studies on various sources for production/isolation of cellulose [4, 6, 13, 23, 24, 38, 40, 48–50]. Thus, only a concise overview of cellulose nanofibers sources will be displayed here.

Basically, any source of cellulose could be employed for cellulose fibers preparation. Woody and non-woody plants are considered as excellent raw materials for the production of several materials that have been demonstrated by the number of patents, peer reviewed articles and books, besides the number of products already marketed [11, 14, 16, 39, 44, 45, 51–55]. It is evident that pulps obtained from softwood and hardwood are nowadays the most important sources for cellulose nanofibers. However, agricultural residues and annual plants have recently received more attention due to costs and environmental concerns. These lignocellulose sources can be broadly classified upon the origin of the plants: (1) bast or stem, (2) seed or fruit, (3) leaf, (4) grass, and (5) straw fibers [13]. They can be defined as cellular hierarchical bio-composites naturally created in which lignin/hemicellulose/extractives and traces elements play a role of the matrix, whereas cellulose microfibrils serve as reinforcement. An effective removal process of non-cellulosic components gives rise to pure cellulose. Usually, the non-woody plants comprise less lignin than wood. Therefore, delignification and bleaching methods are less chemical and energy consuming [9]. The isolation of cellulose nanofibers from different sources is relevant since it dictates the overall properties. Cellulose nanofibers produced from various lignocellulosic sources of miscellaneous provenance employing different extraction approaches and conditions commonly vary in their degree of polymerization, geometric dimensions, morphology, surface charge, surface area, porosity, crystallinity, thermal stability, mechanical properties, etc. [4, 5, 17]. Since there are many reviews and books dealing with cellulose nanofibers from several sources, Table 2 aims to summarize the most commonly utilized feedstock for their production.

Table 2 Lignocellulosic sources for the production of cellulose nanofibers

Source group	Sources
Hardwood	Eucalyptus, Elm, Birch
Softwood	Pine, Spurge, Cedar
Annual plants/ Agricultural residues	Oil palm, Hemp, Jute, Sisal, Alfa, Kenaf, Begasse, Corn, Sunflower, Bamboo Canola, Wheat, Rice, pineapple leaf and coir, Peanut shells, Potato peel, Garlic straw residues
Animal	Tunicates
Bacteria	<i>Alcaligenes</i> , <i>Achromobacter</i> and <i>Gluconacetobacter</i>
Algae	Green, gray, red, yellow-green, brown algae

Although lignocellulosic materials are regarded as the most important sources of cellulose, other living organisms including animals (tunicates), bacteria (mainly *K. xylinus*) and some types of algae (green, gray, red, yellow-green, etc.) can be used to prepare cellulose nanofibers as well [13].

2.2.3 Preparation of Cellulose Nanofibres

Production of cellulose nanofibers (Fig. 4) has gained increasing attention during the last decades, as very recently reviewed by Trache et al. [13] and Nechyporchuk et al. [14] for CNC and CNF, respectively. The production of cellulose nanofibers is mainly a top-down process, where lignocellulosic materials are involved and are broken down into nanocellulosic materials. Broadly, these lignocellulosic sources are first submitted to different pretreatments. Here we are not going to deeply touch pulping processes for breaking lignocellulosic materials by chemical, biological, mechanical or combined methods since several books and review articles have recently treated the subject and our main concern is for extracting cellulose nanofibers [4, 5, 13, 27, 50, 56, 57]. In nature, lignocellulosic are bio-composites containing nanoscale domains of cellulose, lignin, hemicellulose, extractives, and contaminants. From a technological point of view, lignin amount is an important parameter that should be considered to correctly optimize the pretreatment procedure required to isolate a pure cellulose pulp. Indeed, lignin is regarded as the hardest chemical compound to be eliminated from lignocellulosic sources [9]. For this purpose, the dewaxing, delignification and bleaching processes have often been utilized as a pretreatment to simplify the production of CNC and CNF. On the other

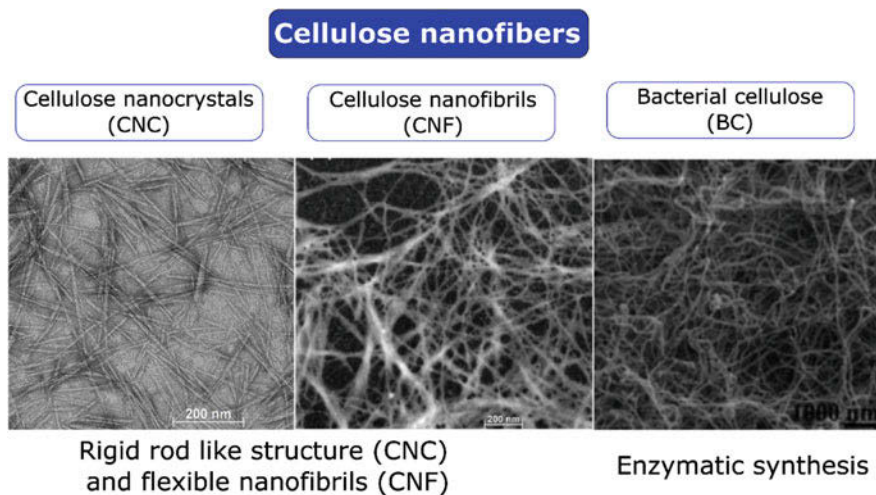


Fig. 4 Transmission electron micrographs of different cellulose nanofibers. Reprinted with permission from [98], Copyright © Elsevier Limited; [34] Copyright © WILEY-VCH

hand, bacterial cellulose production is a bottom-up process, where bacteria generate glucose, and cellulose is obtained by connecting glucose units [58–61]. This approach does not necessitate chemical or mechanical actions to remove hemicellulose and lignin, as is the case for lignocellulosic since BC is considered as a highly hydrated and pure cellulose membrane. More recently, many research works have focused on optimizing processes to lower energy consumption and other costs and to improve quality, consistency, and yields. Table 3 displays some recent examples of different cellulose nanofibers that can be obtained through the application of various methodologies for nanofibers extraction.

Table 3 Examples of cellulose nanofibers extracted by using various methodologies

Source	Form	Isolation procedure	Reference
Plum seed shells	CNC	Cellulose extraction, H ₂ SO ₄ 30% at 40 °C hydrolysis, ultrasonication, freeze drying	[99]
Waste cotton cloth	CNC	Cellulose extraction, treatment with sulfuric acid/hydrochloric acid/water mixture (3:1:11) at 55 °C assisted by ultrasonic wave, centrifugation, dialysis, freeze drying	[100]
Bleached sugarcane bagasse pulp	CNC	ultrasonic assisted TEMPO ^a /sodium bromide mediated oxidation, centrifugation, freeze drying	[101]
Bleached kraft eucalyptus dry lap pulp	CNC	Anhydrous organic acid hydrolysis at 90–120 °C, dilution, filtration, washing, centrifugation, dialysis	[65]
Commercial microcrystalline cellulose	CNC	Citric/hydrochloric acid hydrolysis	[102]
Bacterial cellulose	CNC	Washing, homogenization, drying, grinding, treatment with H ₂ SO ₄ /HCl mixture at 45 °C, dilution, centrifugation, dialysis, ultrasonication	[59]
Bleached kraft pulp	CNC	Pre-soaking in water, grinding, centrifugation, treatment with commercial enzymes or termite cellulose and incubated at intervals from 6–72 h at 35 °C, washing, lyophilization	[68]
Cotton cellulose fibers	CNC	Swelling in 1-butyl-3-methylimidazolium chloride and 1-(4-sulfobutyl)-3-methylimidazolium hydrogen sulfate followed by quenching by adding cold water, washing, centrifugation, freeze drying	[72]
Commercial microcrystalline cellulose	CNC	Water hydrolysis at 120 °C and pressure of 20.3 MPa, filtration with a Pyrex [®] Buchner funnel with glass fritted disc, dialysis, ultrasonication	[76]
Oil palm empty fruit bunch microcrystalline cellulose	CNC	Sono-assisted TEMPO-oxidation, followed by sonication, washing, centrifugation, drying	[103]

(continued)

Table 3 (continued)

Source	Form	Isolation procedure	Reference
Needle-leaf	CNF	Kraft process, refining, Extrusion (twin screw)	[104]
Softwood pulp	CNF	Sulfite process, Blending, refining, enzymatic/ carboxylation (TEMPO), grinding and/or homogenization	[105]
Hardwood pulp	CNF	Bleaching, solvent-based system (deep eutectic solvent), Homogenization (microfluidizer)	[106]
Ushar seed fiber	CNF	Cellulose isolation, TEMPO/sodium bromide/ NaClO mediated oxidation, centrifugation, homogenization, sonication	[107]
Fluff pulp	CNF	Alkaline pretreatment, high pressure homogenization, dialysis, filtration	[85]
Microalgae strains	CNF	Cellulose isolation, TEMPO/sodium bromide/ NaClO mediated oxidation, centrifugation,	[108]
Corn husks, oat hulls	CNF	Cellulose isolation, TEMPO/sodium bromide/ NaClO mediated oxidation, washing, filtration	[109]
Fluff cellulose pulp	CNF	Drying, grinding	[110]
Raft wood	CNF	Cellulose isolation, micro-fibrillation	[3]
Wood species	CNF	Cellulose isolation, defibrillation with wet disk-milling	[111]

^aTEMPO: 2,2,6,6-tetramethylpiperidine-1-oxyl

Preparation of Cellulose Nanocrystals

Cellulose nanocrystals consist of elongated, cylindrical and rod-like particles with widths and length of 4–70 nm and between 100 nm and several micrometers, respectively [24, 34, 62]. CNCs can be isolated from several feedstocks that initially require following various pretreatment processes for the complete/partial elimination of the non-cellulosic materials (hemicellulose, lignin, waxes, fats, proteins, etc.). The naturally occurring cellulose consists of highly ordered crystalline regions and amorphous domains in different proportions. A proper combination of chemical, mechanical, oxidation and/or enzymatic treatment can be applied to remove the disordered regions to recover the CNC product [4, 13, 17, 27, 33, 49]. The paracrystalline domains of cellulose act as structural defects and are responsible for the transverse cleavage of the cellulose fibers into short nanocrystals under hydrolysis process. The transformation involves the disruption of the disorder parts surrounding the microfibrils, in addition to those embedded between them leaving the crystalline parts intact. Several procedures have been developed and continue to appear in order to prepare CNC in an economic/sustainable way with desired properties [13, 21]. Until recently, the most important methods reported in the literature for the extraction of CNC are chemical acid hydrolysis (solid/liquid/gaseous/organic/inorganic acids) [17, 53, 63–67], enzymatic hydrolysis [68–70], mechanical refining [27, 68–71], ionic liquid treatment [72–75], subcritical water

hydrolysis [76, 77], oxidation method [25, 78–81] and combined processes [82–84]. The advantages and drawbacks of each procedure have been recently reviewed by Trache et al. [13]. After each process, some post-treatments of solvent elimination, washing, neutralization, centrifugation, sonication, filtration, purification, fractionation, stabilization and surface modifications are commonly required to get the final CNC product [13, 34]. It is worth noting that the acid hydrolysis treatment remains the most commonly used technique for the separation of CNC. These nanofibers may display diverse geometries, depending on their biological source; for instance, algal cellulose membrane shows a rectangular structural arrangement, whereas both bacterial and tunicate cellulose fibers present a twisted-ribbon geometry [34].

Recently, considerable research programs on the fabrication of CNC have been initiated at the industrial scale. Four commercial entities producing cellulose nanocrystals at capacities beyond pilot plant scale: CelluForce (Canada, 1000 kg/day), American process (USA, 500 kg/day), Melodea/Holmen (Sweden, 100 kg/day), and Alberta Innovates (Canada, 10 kg/day). Further research facilities are currently fabricating CNC as well [13].

Preparation of Cellulose Nanofibrils

Cellulose nanofibrils (CNF) are flexible and have entangled network structure with a diameter of approximately 1–100 nm consisting of alternating crystalline and amorphous domains [85]. This kind of cellulosic nanofibers was introduced by Turbak et al. [86] and Herrick et al. [87] who prepared cellulose in nanoscale range by passing softwood pulp aqueous suspension several times through a high-pressure mechanical homogenizer and giving rise to CNF due to high shearing forces. Depending on the preparation conditions, cellulose fibers can be disintegrated to flexible CNF with lateral dimensions starting from ca. 5 nm, demonstrating elementary fibrils, to tens of nanometers, which correspond to single microfibrils and their bundles. Production of CNF (Fig. 5) has received much attention over the past few decades, as recently reviewed by Nechyporchuk et al. [14]. CNF can be extracted by the disintegration of cellulosic fibers along their long axis. The processes include either conventional mechanical methods (e.g. homogenization, grinding) or a combination of enzymatic/chemical pretreatments with mechanical processing [5, 11, 14, 23, 57, 88].

Broadly, cellulose is present in lignocellulosic materials in combination with hemicellulose, lignin, and extractives. The latter are generally eliminated by various processes before the production of CNF. A simple mechanical disintegration includes homogenization, grinding, refining, extrusion, blending, ultrasonication, cryocrushing, steam explosion, ball milling and aqueous counter collision [5, 11, 14, 23, 57, 88, 89]. Among these processes homogenization (using homogenizers and microfluidizers), grinding and refining are the most common techniques employed in mechanical isolation of CNF. These techniques are considered more efficient for CNF extraction thanks to high shear delamination and are appropriate for scaling up. Thus, they are utilized nowadays for industrial production of CNF.

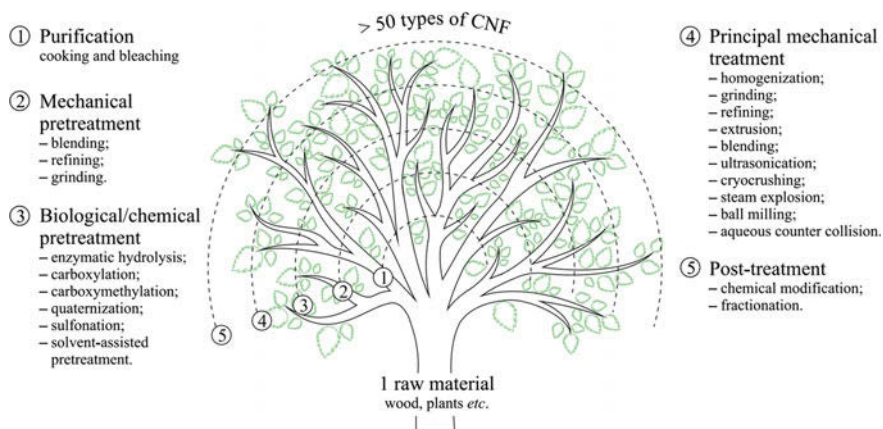


Fig. 5 Schematic diagram of CNF production “tree”. Reprinted from [14], Copyright © Elsevier Limited

However, the main drawback that should be overcome for successful commercialization of CNF is the high-energy consumption needed for mechanical disintegration involved in processing pure cellulosic fibers [90]. Therefore, chemical and/or enzymatic pretreatments have helped to decrease the energy consumption. NFC was extracted by an environmentally friendly procedure by combining enzymatic hydrolysis and mechanical shearing of lignocellulosic material pulps. Effective chemical pretreatments were also attempted prior the mechanical disintegration, by TEMPO or periodate-chlorine oxidation of cellulose, sulfonation, carboxymethylation, quaternization or solvent-assisted pretreatment [14]. After each mechanical shearing, some post-treatments such as surface chemical modification and fractionation are needed to isolate the final CNF product.

Currently, around ten companies are producing CNF at commercial/pre-commercial scale, including Forest Products Laboratory (cooperating with the University of Maine), Paperlogica, Innventia (Sweden), American Process (all USA), Borregaard (Norway), Oji Paper (both Japan), Nippon Paper, CTP/FCBA (France) and others. Moreover, several organizations have developed pilot scale production of various CNF [14].

Preparation of Other Families of Cellulose Nanofibers Materials

Bacterial cellulose (BC), known as microbial cellulose, is typically obtained from bacteria, as a separate molecule and does not necessitate processing to eliminate contaminants. In the biosynthesis of BC, the glucose chains are supplied inside the bacteria body and expelled out through minor pores existing on the cell wall. A 20–100 nm ribbon-shaped nanofibers with micrometer lengths, entangled to form stable network structures [58, 91–93].

Another category, amorphous nanocellulose (ANC), can be formed through acid hydrolysis of regenerated cellulose with subsequent ultrasound disintegration [4, 94, 95]. The obtained particles have spherical to elliptical shapes with diameters ranging from 80 to 120 nm, depending on the cellulose source, isolation procedure, and extraction conditions. Because of its amorphous structure, ANC displays specific characteristics, such as enhanced sorption, high accessibility, increased functional group content. However, this kind of nanofibers presents poor mechanical features and is unsuitable for utilization as reinforcing nanofillers. Hence, the main use of ANC as carries is for bioactive substances and thickening agent in different aqueous systems.

Cellulose nanoyarn (CNY) remains the less investigated cellulosic nanofibers. It is commonly produced by electrospinning of a solution containing cellulose or cellulose derivative [4, 49, 96]. Different parameters, such as the electric field strength, tip-to-collector distance, solution feed rate are broadly employed to control the morphological characteristics of the electrospun nanofibers [97]. The obtained electrospun nanofibers present diameters ranging from 100 to 1000 nm.

Nevertheless, these three categories of cellulose nanofibers are out of this chapter's scope.

3 Cellulose Modification

3.1 Acid Hydrolysis

Acid hydrolysis is the traditional method and widely used to manufacture micro-crystalline cellulose into nano-cellulose as this method can remove the amorphous region [68]. Ultrasonication is applied after harsh acid treatment to produce cellulose nano whiskers. The 'harsh' acid treatment usually referred to sulfuric acid which is highly acidic compared to hydrochloric acid even though it also works and the size of nano whisker reduced with the increasing of acidity. This is because during hydrochloric acid hydrolysis, there is a weaker charge density from the entire process and it leads to poorer dispersion in an organic solvent [112]. Hydrochloric acid resulted in the formation of poor nano-cellulose aqueous dispersion with the present of hydroxyl and carboxyl group [68]. While in sulfuric acid treatment, the anionic sulfonate ester group maintain resulted in the production of high crystallinity of nano whiskers that are easy to disperse in aqueous solvents [68, 112]. Also, during the process, the disordered or paracrystalline regions in cellulose are hydrolysed while the crystalline regions have higher resistance towards acid attack and remain intact [29]. Table 4 shows different types of acid used to form cellulose derivatives from various sources.

Table 4 Different types of acid used to form cellulose derivatives from various sources

Sources	Process	References
Norway spruce	H ₂ SO ₄ hydrolysis	[168]
Sisal fibres	60% H ₂ SO ₄ hydrolysis,	[170]
Pea hull	64% H ₂ SO ₄ hydrolysis	[114]
Filter paper	HCl hydrolysis	[29]
Filter paper	64–65% H ₂ SO ₄ hydrolysis	[123]
Coconut husks	64% H ₂ SO ₄ hydrolysis	[139]
Coconut husks	64% H ₂ SO ₄ hydrolysis	[170]
Sugarcane bagasse	60% H ₂ SO ₄ hydrolysis	[124]
Ethanol bio-residue	H ₂ SO ₄ hydrolysis	[155]
Bamboo fibres	64% H ₂ SO ₄ hydrolysis	[171]
Sisal fibres	64% H ₂ SO ₄ hydrolysis	[171]
Curauá fibres	64% H ₂ SO ₄ hydrolysis	[171]
Eucalyptus fibres	64% H ₂ SO ₄ hydrolysis	[171]
Cotton pulp fibres	64% H ₂ SO ₄ hydrolysis	[172]
Rice straw	64–64% H ₂ SO ₄ hydrolysis	[122]
Rice husks	H ₂ SO ₄ hydrolysis, 64% H ₂ SO ₄ hydrolysis	[126, 138]
Mengkuang leaves	60% H ₂ SO ₄ hydrolysis	[127]
Dried <i>Eucalyptus</i> pulp	H ₂ SO ₄ hydrolysis	[146]
<i>Phormium tenax</i> fibres	64% H ₂ SO ₄ hydrolysis	[173]
Raw cotton linter	60% H ₂ SO ₄ hydrolysis	[174]
Soy hulls	64% H ₂ SO ₄ hydrolysis	[141]
Pineapple leaf	64% H ₂ SO ₄ hydrolysis	[175]
Corn cob	H ₂ SO ₄ hydrolysis	[140]
Filter Paper	85% H ₃ PO ₄ hydrolysis	[176]
Coconut husks	60% H ₂ SO ₄ hydrolysis	[129]
Oil palm empty fruit bunch	64% H ₂ SO ₄ hydrolysis	[120]
Spruce bark	60% H ₂ SO ₄ hydrolysis	[177]
Hardwood pulp	H ₃ PW ₁₂ O ₄₀ hydrolysis (phosphotungstic acid)	[66]
Sugarcane bagasse	64% H ₂ SO ₄ hydrolysis	[119]
Hardwood pulp	64% H ₂ SO ₄ hydrolysis	[66]
Banana plant	H ₂ SO ₄ hydrolysis	[178]
Unripened coconut husks	30% H ₂ SO ₄ hydrolysis	[130]
<i>Posidonia oceanica</i>	H ₂ SO ₄ hydrolysis	[179]
Water hyacinth	40% H ₂ SO ₄ hydrolysis	[180]
Oil palm trunk	64% H ₂ SO ₄ hydrolysis	[131]
Recycled newspaper	65% H ₂ SO ₄ hydrolysis	[182]
Areca nut husks	CH ₃ COOH hydrolysis	[133]
<i>Eucalyptus</i> wood	60% H ₂ SO ₄ hydrolysis	[142]
Groundnut shells	65% H ₂ SO ₄ hydrolysis	[183]
Mulberry pulp	50% H ₂ SO ₄ hydrolysis	[100]

3.2 Enzyme Hydrolysis

Nano-cellulose can be also produced by enzyme hydrolysis process and the bio-masses of cellulose materials used for these enzymatic processes up to date were bacterial cellulose, cotton fibers, and crystalline cellulose powder [69]. According to Meyabadi et al. [113] and Anderson et al. [68], the evaluation of new and established methods to produce new products can be obtained through enzyme application. Enzymatic hydrolysis that produces nano-cellulose was an alternative, environmentally sustainable, and cheap method that reduced water consumption. Furthermore, the digestion of enzyme omitted the use of harsh chemicals such as sulphuric acid which must be washed and properly disposed after traditional production of nano-cellulose. The usage of energy is minimized due to less mechanical processing for fibrillation and lower temperature for heating. The amorphous region of cellulose fibres was selectively degraded by the enzyme but not the crystalline region resulted in the presence of unmodified hydroxyl group surface which is similar to hydrochloric acid digestion in the production of nano-cellulose [68]. In enzyme, there is a class which called cellulases and the sub-groups are cellobiohydrolase and endoglucose. The function of cellulases is acting as a catalyst for the hydrolysis of cellulose while for cellobiohydrolase and endogluconase are attacked in the crystalline region of cellulose and catalyzed the hydrolysis of the amorphous region in cellulose. Thus, the chain length of cellulose will decrease during the enzymatic hydrolysis in the cellulose [113]. *Aspergillus oryzae* [69], fungus *T. reesei* [125], Cellulose L from Novozyme [113] and *Aspergillus niger* [68] enzymes were used because due to low level of β -glucosidase enzyme and this condition prevent from complete hydrolysis to glucose. *Trichoderma Viride G* grows in diverse environments, safe to use as an enzyme to hydrolyze nano-cellulose due to their non-toxic nature and anti-metabolic repression ability [70].

3.3 Ionic Liquid

Another alternative nano-cellulose extraction is using ionic liquids treatment. The stabilities of ionic liquid in chemical and thermal condition, relatively low melting point, non-volatile and negligible vapour pressure proved that ionic liquid treatment has the ability to dissolve cellulose as well as allow envisaging safe and low energy consumption [72, 73, 75]. Ionic liquid has the potential at the swelling and portrays as reactants and catalysts which proved during hydrolyzing polysaccharides into nanofibers in the cellulose [74]. Apart from that, the ionic liquid is an eco-friendly solvent which can be easily recovered and maintained its activity upon reuse after the regeneration of cellulose by a simple method such as evaporation, salting out and reverse osmosis [73, 74]. According to Lazko et al. [72] considering their cost and energy, the recyclability and reuse of ionic liquid undeniable to be essential for the conception of eco-friendly and economically save to apply for extraction

nano-cellulose. The lower amount of sulfonic groups and can be cast in transparent layered films of slightly lower hydrophilicity shown ionic liquid treatment for nano-cellulose compared to the traditional method which is by concentrated sulphuric acid hydrolysis [74]. Ionic liquid that are normally used are 1-butyl-3-methylimidazolium hydrogen sulfate ([BMIM]HSO₄) [74, 73], 1-butyl-3-methylimidazolium chloride ([BMIM]Cl) [72, 75], 1-(4-sulfobutyl)-3-methylimidazolium hydrogen sulfate ([SBMIM]HSO₄) [72], 1-ethyl-3-methylimidazolium acetate ([EMIM][OAc]) [115] Tetrabutylammonium acetate (TBAA) [116]. [BMMIM]Cl treatment on cellulose gives limited impact on the length of cellulose fiber as it does not support any hydrolytic phenomena. So, this shows that [BMMIM]Cl reduces destructuring and unfolding of cellulose fibers to nano-fibrils and it maintains the crystallinity and morphology of nano-cellulose [75]. Apart from that, Tan et al. [73] revealed that [BMMIM]Cl recovery rate can be up to 99.5% by evaporating of anti-solvent and this condition showed that ionic liquid can again be desirable solvent as well as a catalyst with excellent properties. On the other hand, ([BMIM]HSO₄) treatment gives higher yields and high crystallinity of nano-cellulose from microcrystalline cellulose [73, 74].

3.4 Mechanical Treatment

To date, mechanical treatment such as microfluidization, high pressure homogenization, ultrasonication, pulp beating, cryocrushing and ball milling have been applied for the preparation of nano-cellulose. Those methods are low cost, simple and environment-friendly can be used as a part of combination of acid hydrolytic, enzymatic, and oxidative treatments [71, 117]. Ultrasonication is the application of sound energy towards chemical and physical systems. The acoustic cavitation which is the formation, growth and collapse of bubbles in a liquid form during the chemical effects of ultrasonication and the polysaccharide linkages are break down. Thus, cellulose fibers are being treated and improved on the accessibility and reactivity of cellulose [117]. High-energy bead milling (HEBM) gives better impact compared to ball milling and ultrasonication as HEBM can micronize the particles. Beads are forced to rotate around the mill when centrifugal force is generated in the mill. The centrifugal force will also goes in the opposite direction and gives advantage to the transition balls to roll over the opposite walls of the mill when the reverse rotation of disc is applied. Thus, this condition gives impact on the micronize the material in between the bead. In addition, HEBM is also cost-saving method to produce nano-cellulose effectively with great thermal stability in a bigger yield [71].

3.5 Subcritical Water

The conventional method such as acid hydrolysis method to produce nano-cellulose consume a lot of time to wash it. Thus, there is another new method which used only pressured hot water also known as subcritical water. This new method is new, greener towards the environment, and less expensive as the consumption of chemical and electrical energy is theoretically evaluated to produce nano-cellulose [77]. Hydrolyzation of amorphous and semi-crystalline region of cellulose can be enhanced by subcritical water method as it is absolutely water which act as the hydrolysing agent at higher pressurized reactor. At higher pressure in the reactor, the yield of nano-cellulose will increased linearly [76]. The opening of restrictor valve of the reactor decreased the pressure and water injection with precision pump increased the pressure inside it. Those two functions controlled the pressure inside the reactor effectively [77]. The internal pressure gives huge impact on the feasibility of the steps ad will as the hydrolyzation of cellulose which normally used in the removal of hemicellulose [76].

3.6 2,2,6,6-Tetramethyl-1-Piperidinyloxy

The 2,2,6,6-tetramethyl-1-piperidinyloxy (TEMPO) radical is a suitable solvent which is selectively oxidized the primary alcohol groups in aqueous solution [81]. 2,2,6,6-tetramethyl-1-piperidinyloxy (TEMPO) gives positive results in the fabrication of nanofibrils cellulose by stretching the stands of nanosized cellulose that consists of the amorphous and crystalline region [80].

3.7 Combined Method

Combined method is a mixed method to obtain better cellulose derivatives. Table 5 shows different types of combined method used to form cellulose derivatives from various sources.

4 Characterization of Cellulose Nanofibers

4.1 Fourier Transform Infrared

The changes in structural and chemical composition after the effect of chemical treatment is studied using infrared spectroscopy [118, 119].

Table 5 Different types of combined method used to form cellulose derivatives from various sources

Source	Combined method	References
Nordic paper	HCl hydrolysis and 2,2,6,6-tetramethylpiperidine-1-oxyl radical (TEMPO)	[184]
Oil palm empty fruit bunch	4-Acetamido-TEMPO (2,2,6,6-tetramethylpiperidin-1-oxyl) and ultrasonication	[103]
Commercial MCC	H ₂ SO ₄ hydrolysis and Subcritical water treatment	[185]
Jute	Microwave-assisted alkaline peroxide and ultrasonication	[82]
Cotton linter	HCl hydrolysis and Subcritical water treatment	[186]
Cotton linter	H ₂ SO ₄ hydrolysis and Enzymatic (<i>Cerrena sp.</i> fungus) treatment	[186]
Cotton linter	H ₂ SO ₄ hydrolysis and Enzymatic (cellulase from Fungal Bioproducts, Spain) treatment	[187]
Sugarcane Bagasse	Enzymatic (commercial enzyme extract Cellic® CTec2) treatment, purification, and H ₂ SO ₄ hydrolysis	[188]
<i>Ciona intestinalis</i>	Enzymatic treatment, TEMPO-mediated oxidation and H ₂ SO ₄ hydrolysis	[189]
Cotton fabric	H ₂ SO ₄ hydrolysis and ultrasonication	[190]
<i>Miscanthus Giganteus</i>	Acid (HCl and H ₂ SO ₄) hydrolysis and TEMPO oxidation	[191]
Cotton linter	H ₃ PW ₁₂ O ₄₀ hydrolysis (phosphotungstic acid) and ultrasonication	[192]
Wood flour	Ethanol and peroxide solvothermal and ultrasonication	[193]
Filter paper	H ₂ SO ₄ hydrolysis, Ultrasonication, and Microwave-assisted	[84]
Bamboo pulp sheet	FeCl ₃ -catalyzed hydrolysis and ultrasonication	[194]
Oil palm empty fruit bunch	H ₂ SO ₄ hydrolysis and Ultrasonication	[195]
Hardwood paper pulp	Acid (HCl and HCOOH) hydrolysis	[196]
Commercial MCC	H ₂ SO ₄ hydrolysis and Ultrasonication	[83]
Old corrugated container (OCC)	H ₃ PO ₄ hydrolysis, Enzymatic treatment, and ultrasonication	[197]
Commercial MCC	HCl hydrolysis under hydrothermal conditions	[198]

Mid-region band between 4000 and 400 cm⁻¹ in the transmittance mode has been widely used. Microcrystalline cellulose and nanowhisker cellulose have the almost identical chemical composition in Fourier Transform Infrared (FTIR) spectra. Absorption of water by cellulose appeared in the peak at 1635–1645 cm⁻¹ while the intermolecular hydrogen attraction at C₆ group happened in between 1428 and 1433 cm⁻¹ [120, 121]. There was a broad absorption band between 3000 and 3600 cm⁻¹ which proven the presence of hydroxyl groups (–OH stretching intermolecular hydrogen bonds) and absorption at 2900 cm⁻¹ was due to stretching of

–CH group from variation of biomass which were sugarcane bagasse, coconut husks, rice husks, rice straw, banana peel, cotton fabrics, mengkuang leaves, hardwood pulp, arecanut husk fibre, oil palm trunk, oil palm empty fruit bunch, pea hull, and filter paper [66, 114, 119–133].

As an example, in sugarcane bagasse and oil palm empty fruit bunch, there was a slight difference in the peak at 1105 cm^{-1} and the band between 1155 and 1167 cm^{-1} which were corresponded to C–O–C glycosidic ether band and C–C band gradually disappeared from microcrystalline cellulose to nanowhisker cellulose. The disappearance was due to the reduction in molecular weight during hydrolysis treatment [120, 124]. Same goes to nanocrystalline cellulose which was extracted from banana peel which showed that the obvious peak at 1030 cm^{-1} corresponded to C–O–C pyranose ring skeletal vibration stretching. This resulted in the presence of xylans which associated with hemicellulose [121]. The polysaccharide of glycoside bond or crystallinity band of cellulose presence at peak 896 or 897 cm^{-1} [66, 130, 133].

4.2 X-ray Diffraction Analysis

X-ray diffraction (XRD) is a fascinating instrument which used to examine the changes of crystallographic structure of the materials after hydrolysis treatment [128]. On top of that, XRD can provide the in-depth information of the crystalline solids based on their atomic-scale structure of materials [51].

The crystallinity index is calculated using the formulation reported by Segal et al. [134]:

$$\text{CrI} (\%) = \frac{(I_{002} - I_{am})}{I_{002}} \times 100$$

where CrI is percentage crystallinity index, I_{002} is the maximum intensity of the peak at 22° which is a crystalline part, and I_{am} is the intensity of diffraction of the amorphous part at 18° .

According to Chandrasaha et al. [129], acid hydrolysis treatment produced a higher degree of crystallinity index and the average size of hydrolyzed fibers will be almost 25 nm.

Scherrer equation reported by Revol et al. [135] is used to calculate the crystallite size in the following form:

$$D = \frac{k\lambda}{(\beta \cos \theta)}$$

where D is the apparent crystallite size, β is a full-width half maximum of lattice plane reflection in radian, k is Scherrer constant (0.94), λ is X-ray wavelength (0.15418 nm), and θ is corresponding Bragg angle (reflection angle).

Table 6 XRD analysis for crystallinity index (CrI) and crystallite size (L) of nano-cellulose from different biomass

Samples	Reflection at 2θ ($^{\circ}$)	CrI (%)	L (nm)	References
Coconut husks	22–24	76	N/A	[129]
Sisal fibres	18, 26	75	N/A	[169]
Pineapple leaves	20.4, 22.7	74	N/A	[137]
Coconut husks	15.6, 22.7, 34.6	66	N/A	[139]
Bioethanol-residue	14.2, 16, 22.1	77	N/A	[155]
Cotton fibres	14.7, 16.4, 22.6	86	6.3	[125]
Bamboo fibres	15, 17, 21, 22.6	87	5.7	[171]
Eucalyptus fibres	15, 17, 21, 22.6	89	6.1	[171]
Sisal fibres	15, 17, 21, 22.6	78	5.9	[171]
Curauá fibres	15, 17, 21, 22.6	87	5.0	[171]
Rice straw	14.7, 16.4, 22.6	86	7.4	[122]
Rice husks	16, 22, 35	59	N/A	[126]
Mengkuang leaves	22.6	70	N/A	[127]
Cotton fabrics	14.9, 16.5, 22.6	84	8.7	[128]
Oil palm empty fruit bunch	22.6, 15.0	88	N/A	[120]
Raw cotton linter	17.4, 19.2, 26.5	90	N/A	[174]
Soy hulls	17, 21, F 23, 34	74	2.7	[141]
Corn cob	17, 21, 23, 34	84	N/A	[140]
Sugarcane bagasse	16.5, 22.5, 34.6	73	3.5	[119]
Hardwood pulp	16.4, 22.7, 34.5	85	5.8	[66]
Unripened coconut husks	17, 19, 26, 41	82	5.0	[130]
Oil palm trunk	19, 22	70	N/A	[131]
Areca nut husk	15, 22	73	4.3	[133]
Banana peel	16, 22	64	N/A	[121]

Numerous studies reported that the crystallinity index and the sizes of nano-whisker or nanocrystalline cellulose showed the highest value compared to microcrystalline cellulose when tested under XRD with different lignocellulosic biomass (Table 6). The increase in crystallinity structure in nano-cellulose appeared after acid treatment because there was hydrolytic cleavage of glycosidic bonds which lead to rearrangement of molecules in cellulose [51, 137]. Prolonged acid treatment with the increasing of time period severe enough to destroy not only the amorphous structure but also some part of the crystalline structure in cellulose. This resulted in a slight decrease in crystallinity index [139–141].

4.3 Scanning Electron Microscope

The surface morphology is evaluated by scanning electron microscope (SEM). According to Luykx et al. [143] and Goldstein et al. [144], SEM contains a shadow-relief effect of secondary and backscattered electron contrast, produce a good image and greater view of the three-dimensional structure of the sample. The hydrolysis treatment has affected the surface morphology in terms of surface smoothness and the size of cellulose fibers [130, 131]. In Table 7, the majority of the samples have shortening in fiber and rough surface as this indicates that the cementing materials around the material of the fibre are partially removed. The cementing materials are hemicellulose, lignin, wax, and pectin [126, 136]. According to Nascimento et al. [130], bleaching process increased the surface area of the cellulose fiber.

4.4 Transmission Electron Microscope

Transmission electron microscope (TEM) is a unique and powerful nanoscale imaging with higher resolution to analyze the structure and size of nano-samples [131, 145]. The different nano-cellulose samples which stated in Table 8 shows in either rod liked the shape, needle shape or ribbon shape. Those shape formed is because of hydrolysis treatment breaks down the linkage that linked along the

Table 7 SEM analysis for surface morphology of nano-cellulose from different biomass

Samples	Surface morphology	References
Sisal fibres	Nano-ordered chain	[169]
Filter paper	Sphere-shaped structure, shortening of fibres	[123]
Pineapple leaf	Rough surface, defibrillation of fibres	[136]
Sugarcane bagasse	Refinement of fibrillar structure	[124]
Cotton pulp fibres	Rod-like shape, shortening fibres	[172]
Rice husk	Rough surface, shortening fibres, rolled shape	[126, 138]
Rice straw	Shortening fibres	[122]
Oil palm empty fruit bunch	Aggregation of fibres structure, rod-like shape, smooth surface	[120]
Raw cotton linter	Curled, soft-flat shape, rough surface with some pits	[174]
Soy hulls	Micro-sized fibres, irregular shape and size	[141]
Corn cob	Micro-sized fibres, irregular shape and size	[140]
Hardwood pulp	Porous network structure	[66]
Unripened coconut husk	Loosely fibres, rough surface	[130]
Oil palm trunk	Less irregular and impurities	[131]
Areca nut husk fibres	Defibrillation of fibres, rough surface	[133]
Banana peel	Reduced and shortening fibres	[121]

Table 8 TEM analysis for surface morphology, length and width of nano-cellulose from different biomass

Samples	Surface morphology	Length, L (nm)	Width, D (nm)	References
Norway spruce	Bundle rod-shaped whisker	200–400	<10	[168]
Pineapple leaves	Non-woven ribbon	200–300	5–25	[137]
Coconut husks	Rod-liked shape	179 ± 59	5.5 ± 1.4	[139]
Sugarcane bagasse	Rod-shaped cellulose	170	35	[124]
Bamboo fibres	Rod-liked shape with individual nanowhiskers	100 ± 28	8 ± 3	[171]
Eucalyptus	Rod-shaped in bundle form	100 ± 33	7 ± 1	[171]
Sisal fibres	Rod-shaped with individual form	119 ± 45	6 ± 1	[171]
Curauá	Rod-like shaped in bundle form	129 ± 32	5 ± 1	[171]
Rice husks	Needle-like structure	–	10–15	[126]
Rice straw	Rod-like crystal structure	50–700	10–65	[122]
Rice husks	Needle like structure	100–400	6–14	[138]
Mengkuang leaves	Rod-liked shape	200	5–25	[127]
Soy hulls	Needle-liked nanowhiskers	122.7 ± 39.4	4.43 ± 1.2	[141]
Oil palm empty fruit bunch	Rod-liked structure	>100	<10	[120]
Sugarcane bagasse	Agglomerated rod-liked nanocrystals	250–480	20–60	[119]
Hardwood pulp	Rod-liked shape	100	15–40	[66]
Unripened coconut husks	Long, disordered needles like nanowhisker	178 ± 88	8 ± 3	[130]
Oil palm trunk	Individual, needle-liked nanocrystals in fibre bundles	397.03	7.67	[131]
Arecanut husks	Long fibrils	120–150	1–10	[133]
Banana peel	Needle-liked and wire nanofibrils	263.9 ± 7.2	20 ± 5.2	[121]

microfibrils by amorphous domains. Thus, the amorphous region which portrays as structural defects and responsible for the transverse cleavage of microfibrils into nano-cellulose [139].

4.5 Atomic Force Microscopy

Similar to TEM, atomic force microscopy (AFM) is used to characterize the surface morphology, topography and measure dimensional image of different nano-samples

Table 9 AFM analysis for surface morphology, length and width of nano-cellulose from different biomass

Samples	Surface morphology	Length, L (nm)	Width, D (nm)	References
Sisal fibres	Nano-ordered chain	–	30.9 ± 12.5	[169]
Pineapple leaves	Few lateral association occur between adjacent nanofibres	–	5–15	[136]
Sugarcane bagasse	Reduced in fibres	–	70–90	[124]
Bioethanol residue	Rod-liked shape	–	10–20	[155]
Cotton fibres	Narrow and well separated distribution of nanofibrils	287.24 ± 79.75	29.69 ± 5.07	[125]
Bamboo fibres	Rod-liked nanowhiskers	–	4.5 ± 0.9	[171]
Eucalyptus	Rod-liked nanowhiskers	–	4.5 ± 1.0	[171]
Sisal fibres	Rod-liked nanowhiskers	–	3.3 ± 1.0	[171]
Curauá	Rod-liked nanowhiskers	–	4.7 ± 1.0	[171]
Rice straws	Rod-liked structure	30.7	5.95	[122]
Rice husks	Needle-liked structure	100–400	6–14	[138]
Soy hulls	Aggregation of nanocrystals	–	2.77 ± 0.67	[141]
Corn cob	Aggregation of needle-liked nanocrystal	287.3 ± 75.5	4.9 ± 1.34	[140]
Sugarcane bagasse	Rod-likes crystal fibres	250–480	20–60	[119]

which shown in Table 8 [119, 124, 141] AFM provides more precise and accurate characterization of the thickness of the individual crystallites as well as detailed structure compared to TEM [141]. Through transverse height profiles, AFM allows the discernment of individual whiskers of agglomerated structures [140, 141]. Table 9 displays about the AFM analysis for surface morphology, length and width of nano-cellulose from different biomass.

4.6 Thermal Behaviour

According to Azubuike and Okhamafe [147], thermogravimetric analysis (TGA) and differential scanning calorimetry (DSC) used to analyze the thermal and degradation properties of cellulose fibers. Information regarding on the transition phase, weight loss and decomposition pattern are provided by TGA while information on maximum temperature for sample degradation retrieved from DSC. Measurement of heat capacity needed to increase the temperature and heat energy consumed by the sample is provided by DSC. Thus, both instruments able to provide a clarification on the thermal stability and compatibility of the sample.

There are two stages in every TG curves from different biomass which indicates the weight loss of the sample. The first stage is the water removal within the cellulose in the region between 60 and 100 °C. The second stage is the degradation of hemicellulose and lignin in cellulose followed by the char residue formation in the range of 200–400 °C. Melting point temperature (T_{max}) examined by using DSC and the endothermic peak appeared which is due to volatilization of cellulose [39]. The results of TGA and DSC are constructed in Table 10. Evolution of the volatile compounds occurred when cellulose degrades while the degradation of lignin corresponds to thermal degradation properties [148].

Table 10 Comparison of thermal properties using TGA and DSC from different biomass

Samples	TG analysis						DSC analysis T_{max} (°C)	References
	Onset (°C)	Degradation temperature (°C)			Residual weight loss at 400 °C (%)	DTG peak temperature T_{max} (°C)		
		T_{10}	T_{15}	T_{20}				
Sisal fibres	190	200	280	300	30	296	347	[169]
Pea hulls	100	180	–	235	17	299	–	
Banana plant	228	300	319	328	18	–	–	[114, 118]
Filter paper	290	330	340	349	9	–	330	[123]
Coconut husks	200	240	281	300	20	160	–	[139]
Sugarcane bagasse	220	250	260	280	17	345	253	[124]
Bio-residue	215	265	275	280	35	283	–	[155]
Rice husks	215	220	230	235	38	240	–	[126]
Mengkuang leaves	261	281	310	320	18	370	–	[127]
Cotton fabric	223	256	248	256	26	281	–	[128]
<i>Phormium tenax</i> fibres	238	280	300	320	10	90	–	[173]
Oil palm empty fruit bunch	270	350	375	390	71	–	–	[120]
Raw cotton linter	201	213	230	240	42	219	–	[174]
Soy hulls	170	190	210	251	23	294	–	[141]
Coconut husks	211	240	300	310	24	319	–	[129]
Sugarcane bagasse	236	240	260	270	31	250	–	[119]
Hardwood pulp	260	330	340	348	25	–	–	[66]

(continued)

Table 10 (continued)

Samples	TG analysis						DSC analysis T _{max} (°C)	References
	Onset (°C)	Degradation temperature (°C)			Residual weight loss at 400 °C (%)	DTG peak temperature T _{max} (°C)		
		T ₁₀	T ₁₅	T ₂₀				
Unripened coconut husks	230	260	270	288	35	310	–	[130]
Oil palm empty fruit bunch	190	230	260	280	32	310	–	[132]
Areca nut husks	250	309	320	330	20	358	–	[133]
Banana peel	261	–	–	–	–	–	–	[121]

5 The Recent Development of Cellulose Nanofibre as Filler in Polymer Composite

The sustainable development of the renewable polymeric materials has received great attention in recent years, mainly due to the increasing demand for the environmentally friendly materials. Unfortunately, the thermo-mechanical properties of the natural polymer or commercially available biopolymers are often inferior when compared with the traditional petroleum-based polymer [149]. For instance, polylactide (PLA) is a commercially available biopolymer, is brittle and process at low distortion temperature [150]. Many research has been conducted to improve the mechanical and overcome the existing shortcoming of biopolymeric materials applications. Studies reported that the preparation of polymeric composite materials by combining bio-based polymers with cellulosic materials could be one of the effective solutions to match or exceed the mechanical and deterioration performance of polymeric materials with commonly used petroleum-based engineering polymers [149–151].

CNF is considered as the most promising engineering materials, which has the potentiality to be used as filler in polymeric composite because of its abundance availability, low cost, low density, renewability and biodegradability [152]. Cellulosic fibers isolated from various lignocellulosic sources such as jute, kenaf, hemp, sisal wood, flax were applied utilized as a filler in polymeric composites due to its distinct attractive properties when compared to the conventional fibers. Utilization of the CNF in polymeric composite has gained increasing attention for the last decades because of the application of CNF as filler in composite enhance mechanical, thermal and biodegradation properties [153, 154]. Although, CNF is viewed as promising engineering materials in various industrial fields, but the distinct weakness of CNF impregnated polymeric composites such as high moisture

absorption, poor wettability lack of good interfacial adhesion, low melting point and the poor compatibility between CNF and polymer matrix have limited CNF applications as a filler in polymeric composite [154–156]. These drawbacks of CNF filled polymeric composite has exhilarated researcher to focus on the modification of CNF surface to enhance the composites physicochemical and thermal properties. Generally, CNF is hydrophilic in nature, so it urges to enhance surface roughness of CNF by surface modification for the development of composites with enhanced properties. Studies reported that the exemplary stiffness and strength of CNF could be gained with a strong interface from CNF to polymeric matrix by the CNF medication [156].

The CNF has a tendency to agglomerate with a matrix to form forms larger particles [154]. Poor dispersion of the CNF as a filler into the polymer matrix affects the composite's mechanical properties [157]. Further, the $-OH$ group present on the surface of CNF form hydrogen bonding with the adjacent $-OH$ groups, results in agglomeration of the CNF. The presence of abundance $-OH$ groups on the surface of CNF attracts to scientist and engineers interest to modify the surface of CNF by targeting the $-OH$ via different chemical modifications, such as *Acetylation*, *Silylation*, *carboxylation*, *esterification* and *polymer grafting*. The purpose of chemical modification of CNF is to [158]:

- i. obtain better CNF dispersion to polymeric matrix by introducing stable electrostatic charges on the surface of CNFs; and
- ii. improve the CNF compatibility in conjunction with hydrophobic polymer matrices in composites.

The major challenge of surface modification of CNF *via* chemical functionalization to maintain the integrity of nanocellulose crystal and avoid any polymorphic conversion for preserving the original morphology CNF. Thus, the selection of the chemical functionalization methods is crucial. A brief description of some impotent chemical functionalization processes is presented below.

Acetylation is chemical functionalization process, which involves the replacement of $-OH$ group on the surface of CNF with an acetyl group (CH_3-CO-) to yield a specific ester. Wherein, acetic anhydride is most commonly utilized as acetylene agent. Generally, acetylation is a type of chemical modification, which changes the hydrophilic surface of CNF to more hydrophobic and thereby increase the CNF compatibility to be used as filler non-polar polymer matrices [158]. Ashori et al. [151] modified CNF derived from wood and noon-wood plants using acetic anhydride in presence of pyridine to change the surface properties, minimize the hydrophilic nature of CNF and enhance compatibility with non-polar polymer matrices. The study revealed that the acetylation treatment of CNF changes the surface characteristics, improve the thermal stability and enhance the crystallinity of cellulose chains [151]. However, the performance of CNF's surface modification *via* acetylation depends on susceptibility and accessibility of $-OH$ groups in the crystalline and amorphous regions within the cellulose polymer chain [158].

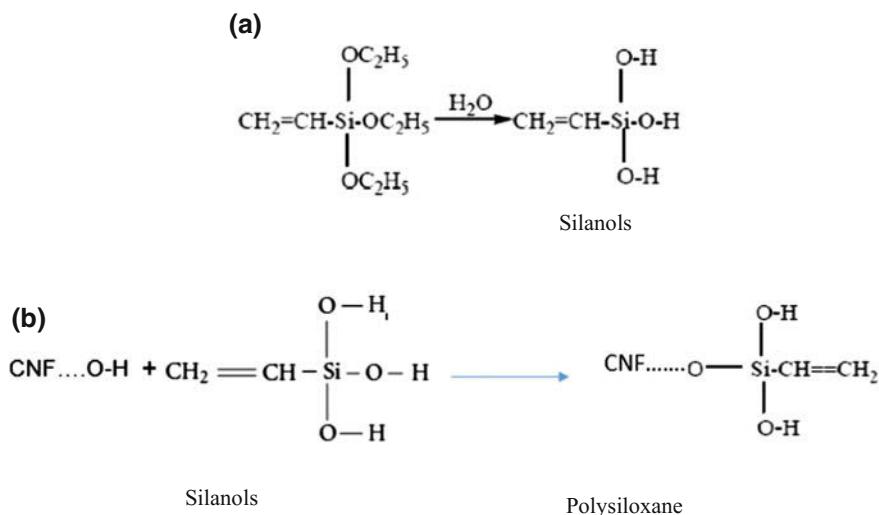


Fig. 6 a Silane hydrolysis, b Silylation of cellulosic nanofiber [160]

Silanation is an effective process for the surface modification CNF using a silane-coupling agent, generally, non-polar organic solvent. The silanation treatment improves the compatibility of CNF by eliminating surface hydroxyl groups with the non-polar organic solvent [159]. Nonetheless, the silane agent (Hydrolyzable alkoxy group) undergoes hydrolysis reaction in the presence of moisture to form silanols. Subsequently, the silanols react with the surface hydroxyl groups of CNF and forms to a Polysiloxane. The details chemical reaction of silylation process is presented in Fig. 6 [160]. Therefore, the hydrocarbon chains forms by the covalent bond of silane protect the fiber swelling by creating a crosslinked network between the matrix and the fiber [159, 161].

Carboxylation is another effective approach for the cellulosic fiber modification. In carboxylation process, TEMPO is most commonly utilized as an oxidizing agent replace surface hydroxyl groups by imparting carboxyl acid groups on the surface of CNF [162, 163]. This oxidation reaction is often performed in alkaline media in the presence of NaBr and NaOCl [163]. Figure 7 represents the TEMPO-mediated oxidation reaction for imparting carboxyl acid groups in place of the surface hydroxyl groups of CNF [164]. In carboxylation process using the TEMPO-mediated oxidizing agents involves a topologically confined reaction sequence with CNF, consequently, it forms to the 2-fold screw axis of the CNF chain. Wherein, one part of the CNF chain react with the accessible hydroxymethyl groups and the other part lies within the crystalline particle (Fig. 7). The study reported that the TEMPO-mediated oxidation maintained the CNF's initial surface morphology and morphological integrity and imparted negative charges at the CNF surface and thus induced electrostatic stabilization [164].

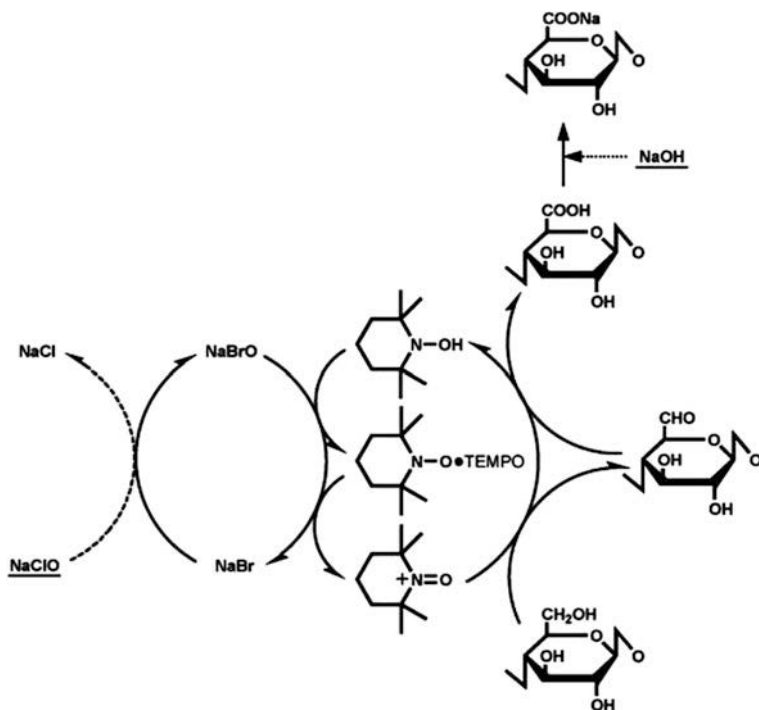


Fig. 7 TEMPO mediated oxidation for surface modification of CNF. Adapted from Missoum et al. [164]

Polymer grafting into the CNF surface is one of the research areas of development in order to fully realize the advantage of a long aliphatic chain of CNF modification for being utilized as a filler in the polymeric composite. In polymer grafting, the CNF's surface modification can be attained by covalently attaching small polymeric molecules. The main purpose of the polymer grafting is to enhance the apolar characteristics of the CNF to have better compatibility with hydrophobic polymer matrices [165]. However, the polymer chain can be covalently bounded on the surface of CNF either “grafting on” or “grafting from” approaches [166]. In the “grafting on” approach, CNF is mixing with a coupling agent or an existing polymer to assign the polymer on the surface of the CNF so that the polymer and the CNF grafting one to another one. The main advantage of the “grafting on” approach is that the molecular weight of the polymer can be determined before grafting and therefore, the grafting materials properties can be controlled. However, it is difficult to obtain high grafting from this approach because of the steric interference and high viscosity of the reaction medium due to the presence of macromolecular chains [167]. On the other hand, the “grafting from” approach, consists the cellulosic nanoparticles activation with an initiator agent and a monomer to induce polymerization of the monomer from the CNF surface.

This “grafting from” approach has been reported to be a very effective method to generate high grafting densities on the CNF surface because of steric hindrance limitation and lower viscosity. However, this process limits to a low degree of polymerization because it is unable to determine the molecular weight of the grafted polymer [164].

6 Concluding Remarks

In this chapter, a comprehensive state-of-art of several aspects of cellulose nanofibers and their importance was described. Different approaches including preparation and modification techniques were discussed in the preparation of cellulose nanofibers. Several properties of this renewable material such as chemical composition, molecular weight, crystallinity, morphology and thermal properties were also discussed. Owing to its interesting characteristics, various uses continue to be developed by scientists all around the world. With regards to cellulose nanofiber composites applications, we only report and discuss several selected examples since the number of polymers used and their applications in various fields increase continuously. However, more research should be performed, which focuses on efficient cellulose nanofiber isolation procedures, treatments, and drying. Furthermore, to date, the engineering properties and cellulose nanofiber-based composites performances are still being developed. In order to satisfy the criteria of employing cellulose nanofiber for widespread use with higher efficiency, more effort and developments are required to expand the use of cellulose nanofiber for science and technology.

Acknowledgements Authors wish to thank their parental institutes (Universiti Sains Malaysia through USM Research University Incentive, RUI Grant 1001/PKIMIA/8011077 and Short Term Grant 304/PKIMIA/6315100) for providing the necessary facility to accomplish this work.

References

1. Sadeghi A et al (2018) Predictive construction of phase diagram of ternary solutions containing polymer/solvent/nonsolvent using modified Flory-Huggins model. *J Mol Liq* 263:282–287
2. Rezakazemi M, Sadrzadeh M, Matsuura T (2018) Thermally stable polymers for advanced high-performance gas separation membranes. *Prog Energy Combust Sci* 66:1–41
3. Kumode MMN et al (2017) Microfibrillated nanocellulose from balsa tree as potential reinforcement in the preparation of ‘green’ composites with castor seed cake. *J Clean Prod* 149:1157–1163
4. Kargarzadeh H et al (2017) Handbook of nanocellulose and cellulose nanocomposites. Wiley Online Library
5. Jawaid M, Boufi S, Abdul KH et al (2017) Cellulose-reinforced nanofiber composites. Elsevier

6. Trache D (2017) Microcrystalline cellulose and related polymer somposites: synthesis, characterization and properties. In: Handbook of composites from renewable materials, Thakur VK, Kumari Thakur M, Kessler MR et al (eds). Scrivener Publishing LLC, pp 61–92
7. Kargarzadeh H et al (2017) Recent developments on nanocellulose reinforced polymer nanocomposite: A review polymer
8. Mariano M, El Kissi N, Dufresne A (2014) Cellulose nanocrystals and related nanocomposites: review of some properties and challenges. *J Polym Sci, Part B: Polym Phys* 52(12): 791–806
9. Trache D et al (2016) Microcrystalline cellulose: isolation, characterization and bio-composites application—A review. *Int J Biol Macromol* 93(Pt A):789–804
10. Satyanarayana KG, Arizaga GG, Wypych F (2009) Biodegradable composites based on lignocellulosic fibers—An overview. *Prog Polym Sci* 34(9):982–1021
11. Moon RJ et al (2011) Cellulose nanomaterials review: Structure, properties and nanocomposites. *Chem Soc Rev* 40(7):3941–3994
12. Haafiz MM et al (2015) Bionanocomposite based on cellulose nanowhisker from oil palm biomass-filled poly (lactic acid). *Polym Test* 48:133–139
13. Trache D et al (2017) Recent progress in cellulose nanocrystals: Sources and production. *Nanoscale* 9(5):1763–1786
14. Nechyporchuk O, Belgacem MN, Bras J (2016) Production of cellulose nanofibrils: a review of recent advances. *Ind Crops Prod* 93:2–25
15. Oun AA, Rhim J-W (2016) Isolation of cellulose nanocrystals from grain straws and their use for the preparation of carboxymethyl cellulose-based nanocomposite films. *Carbohydr Polym* 150:187–200
16. Chirayil CJ, Mathew L, Thomas S (2014) Review of recent research in nano cellulose preparation from different lignocellulosic fibers. *Rev Adv Mater Sci* 37:20–28
17. Thakur VK (2015) Nanocellulose polymer nanocomposites: fundamentals and applications. Wiley
18. Qin X et al (2015) Tuning glass transition in polymer nanocomposites with functionalized cellulose nanocrystals through nanoconfinement. *Nano Lett* 15(10):6738–6744
19. Boujemaoui A et al (2015) Preparation and characterization of functionalized cellulose nanocrystals. *Carbohydr Polym* 115:457–464
20. Kim J-H et al (2015) Review of nanocellulose for sustainable future materials. *Int J Prec Eng Manufact-Green Technol* 2(2):197–213
21. Ng H-M et al (2015) Extraction of cellulose nanocrystals from plant sources for application as reinforcing agent in polymers. *Compos B Eng* 75:176–200
22. Xu X et al (2014) Comparison between cellulose nanocrystal and cellulose nanofibril reinforced poly (ethylene oxide) nanofibers and their novel shish-kebab-like crystalline structures. *Macromolecules* 47(10):3409–3416
23. Singla R et al (2016) Nanocellulose and nanocomposites. In: *Nanoscale materials in targeted drug delivery, theragnosis and tissue regeneration*, Springer, pp 103–125
24. Moon RJ, Schueneman GT, Simonsen J (2016) Overview of cellulose nanomaterials, their capabilities and applications. *JOM* 68(9):2383–2394
25. Vazquez A et al (2015) Extraction and production of cellulose nanofibers. In: *Handbook of polymer nanocomposites. Processing, performance and application*. Springer, pp 81–118
26. Thakur VK (2015) Lignocellulosic polymer composites: processing, characterization, and properties. Wiley
27. Pandey J et al (2015) *Handbook of polymer nanocomposites. Processing, performance and application*. Springer
28. Lin N, Dufresne A (2014) Nanocellulose in biomedicine: current status and future prospect. *Eur Polymer J* 59:302–325
29. Habibi Y, Lucia LA, Rojas OJ (2010) Cellulose nanocrystals: chemistry, self-assembly, and applications. *Chem Rev* 110(6):3479–3500
30. Siqueira G, Bras J, Dufresne A (2010) Cellulosic bionanocomposites: a review of preparation, properties and applications. *Polym* 2(4):728–765

31. Borges J et al (2015) Cellulose-based liquid crystalline composite systems. In: Thakur VK (ed) Nanocellulose polymer nanocomposites: fundamentals and applications. Wiley-Scrivener, pp 215–235
32. Wertz J-L, Mercier JP, Bédoué O (2010) Cellulose science and technology. CRC Press, Switzerland
33. Postek MT et al (2013) Production and applications of cellulose. Tappi Press, Peachtree Corners
34. Klemm D et al (2011) Nanocelluloses: a new family of nature-based materials. *Angew Chem Int Ed* 50(24):5438–5466
35. Klemm D et al (2005) Cellulose: fascinating biopolymer and sustainable raw material. *Angew Chem Int Ed* 44(22):3358–3393
36. Eyley S, Thielemans W (2014) Surface modification of cellulose nanocrystals. *Nanoscale* 6(14):7764–7779
37. Wei H et al (2014) Environmental science and engineering applications of nanocellulose-based nanocomposites. *Environ Sci: Nano* 1(4):302–316
38. Heinze T (2016) Cellulose: structure and properties. In: Cellulose chemistry and properties: Fibers, nanocelluloses and advanced materials. Springer, pp 1–52
39. Trache D et al (2014) Physico-chemical properties and thermal stability of microcrystalline cellulose isolated from Alfa fibres. *Carbohydr Polym* 104:223–230
40. Gupta V et al (2016) Cellulose: a review as natural, modified and activated carbon adsorbent. *Biores Technol* 216:1066–1076
41. Oksman K et al (2014) Handbook of green materials: Processing technologies, properties and applications (in 4 volumes), vol 5. World Scientific
42. ISO/TS80004–1 (2010) International organization for standardization. ISO technical specification ISO/TS80004-1, Nanotechnologies—Vocabulary—Part 1: Core terms
43. ISO/TS27687 (2008) International organization for standardization. ISO technical specification ISO/TS 27687, Nanotechnologies—Terminology and definitions for nano-objects—Nanoparticle, nanofiber and nanoplate
44. Brinchi L et al (2013) Production of nanocrystalline cellulose from lignocellulosic biomass: technology and applications. *Carbohydr Polym* 94(1):154–169
45. Charreau H, Foresti ML, Vázquez A et al (2013) Nanocellulose patents trends: a comprehensive review on patents on cellulose nanocrystals, microfibrillated and bacterial cellulose. *Recent patents on nanotechnology*, 7(1), pp 56–80
46. TAPPI (2017) Standard terms and their definition for cellulose nanomaterial. WI 3021, <http://www.tappi.org/content/hidden/draft3.pdf>. Accessed 01 Dec 2017
47. Gama M, Gatenholm P, Klemm D et al (2012) Bacterial nanocellulose: a sophisticated multifunctional material. CRC Press
48. Thakur VK, Voicu SI (2016) Recent advances in cellulose and chitosan based membranes for water purification: a concise review. *Carbohydr Polym* 146:148–165
49. Dufresne A (2013) Nanocellulose: from nature to high performance tailored materials. Walter de Gruyter
50. Agbor VB et al (2011) Biomass pretreatment: fundamentals toward application. *Biotechnol Adv* 29(6):675–685
51. Trache D et al (2016) Physicochemical properties of microcrystalline nitrocellulose from Alfa grass fibres and its thermal stability. *J Therm Anal Calorim* 124(3):1485–1496
52. Ummartyotin S, Manuspiya H (2015) A critical review on cellulose: from fundamental to an approach on sensor technology. *Renew Sustain Energy Rev* 41:402–412
53. Jonoobi M et al (2015) Different preparation methods and properties of nanostructured cellulose from various natural resources and residues: a review. *Cellul* 22(2):935–969
54. Dufresne A, Belgacem MN (2013) Cellulose-reinforced composites: from micro-to nanoscale. *Polimeros* 23(3):277–286
55. Dufresne A (2013) Nanocellulose: a new ageless bionanomaterial. *Mater Today* 16(6): 220–227

56. Abdul Khalil H et al (2014) Production and modification of nanofibrillated cellulose using various mechanical processes: a review. *Carbohydr Polym* 99:649–665
57. Lavoine N et al (2012) Microfibrillated cellulose—Its barrier properties and applications in cellulosic materials: a review. *Carbohydr Polym* 90(2):735–764
58. Gama M, Dourado F, Bielecki S et al (2016) Bacterial nanocellulose: from biotechnology to bio-economy. Elsevier
59. Vasconcelos NF et al (2017) Bacterial cellulose nanocrystals produced under different hydrolysis conditions: properties and morphological features. *Carbohydr Polym* 155:425–431
60. Campano C et al (2016) Enhancement of the fermentation process and properties of bacterial cellulose: a review. *Cellul* 23(1):57–91
61. Anwar B, Bundjali B, Arcana IM (2015) Isolation of cellulose nanocrystals from bacterial cellulose produced from pineapple peel waste juice as culture medium. *Procedia Chem* 16:279–284
62. George J, Sabapathi S (2015) Cellulose nanocrystals: synthesis, functional properties, and applications. *Nanotechnol Sci Appl* 8:45
63. Kontturi E et al (2016) Degradation and crystallization of cellulose in hydrogen chloride vapor for high-yield isolation of cellulose nanocrystals. *Angew Chem Int Ed* 55(46):14455–14458
64. Du H et al (2016) Preparation and characterization of thermally stable cellulose nanocrystals via a sustainable approach of FeCl₃-catalyzed formic acid hydrolysis. *Cellulose* 1–19
65. Chen L et al (2016) Highly thermal-stable and functional cellulose nanocrystals and nanofibrils produced using fully recyclable organic acids. *Green Chem*
66. Liu Y et al (2014) A novel approach for the preparation of nanocrystalline cellulose by using phosphotungstic acid. *Carbohydr Polym* 110:415–422
67. Tang L-R et al (2011) Manufacture of cellulose nanocrystals by cation exchange resin-catalyzed hydrolysis of cellulose. *Biores Technol* 102(23):10973–10977
68. Anderson SR et al (2014) Enzymatic preparation of nanocrystalline and microcrystalline cellulose. *TAPPI J*, vol 13, pp 35–41
69. Xu Y et al (2013) Feasibility of nanocrystalline cellulose production by endoglucanase treatment of natural bast fibers. *Ind Crops Prod* 51:381–384
70. Chen X et al (2012) Controlled enzymolysis preparation of nanocrystalline cellulose from pretreated cotton fibers. *BioRes* 7(3):4237–4248
71. Amin KNM et al (2015) Production of cellulose nanocrystals via a scalable mechanical method. *RSC Adv* 5(70):57133–57140
72. Lazko J et al (2016) Acid-free extraction of cellulose type I nanocrystals using Brønsted acid-type ionic liquids. *Nanocomposites* 2(2):65–75
73. Tan XY, Hamid SBA, Lai CW (2015) Preparation of high crystallinity cellulose nanocrystals (CNCs) by ionic liquid solvolysis. *Biomass Bioenerg* 81:584–591
74. Mao J et al (2015) Cellulose nanocrystals production in near theoretical yields by 1-butyl-3-methylimidazolium hydrogen sulfate ([Bmim] HSO₄)–mediated hydrolysis. *Carbohydr Polym* 117:443–451
75. Lazko J et al (2014) Well defined thermostable cellulose nanocrystals via two-step ionic liquid swelling-hydrolysis extraction. *Cellulose* 21(6):4195–4207
76. Novo LP et al (2016) A study of the production of cellulose nanocrystals through subcritical water hydrolysis. *Indus Crops Prod*
77. Novo LP et al (2015) Subcritical water: a method for green production of cellulose nanocrystals. *ACS Sustain Chem Eng* 3(11):2839–2846
78. Miller J (2015) Cellulose nanomaterials production-state of the industry.[cited 2017 05–12-2017]; Available from <http://www.tappinano.org/media/1114/cellulose-nanomaterials-production-state-of-the-industry-dec-2015.pdf>
79. Sun B et al (2015) Sodium periodate oxidation of cellulose nanocrystal and its application as a paper wet strength additive. *Cellulose* 22(2):1135–1146

80. Visanko M et al (2014) Amphiphilic cellulose nanocrystals from acid-free oxidative treatment: Physicochemical characteristics and use as an oil—water stabilizer. *Biomacromol* 15(7):2769–2775
81. Cao X et al (2012) Cellulose nanowhiskers extracted from TEMPO-oxidized jute fibers. *Carbohydr Polym* 90(2):1075–1080
82. Chowdhury ZZ, Hamid SBA (2016) Preparation and characterization of nanocrystalline cellulose using ultrasonication combined with a microwave-assisted pretreatment process. *BioRes* 11(2):3397–3415
83. Tang Y et al (2014) Preparation and characterization of nanocrystalline cellulose via low-intensity ultrasonic-assisted sulfuric acid hydrolysis. *Cellulose* 21(1):335–346
84. Lu Z et al (2013) Preparation, characterization and optimization of nanocellulose whiskers by simultaneously ultrasonic wave and microwave assisted. *Biores Technol* 146:82–88
85. Lee H et al (2018) Improved thermal stability of cellulose nanofibrils using low-concentration alkaline pretreatment. *Carbohydr Polym* 181:506–513
86. Turbak AF, Snyder FW, Sandberg KR et al (1983) Microfibrillated cellulose, a new cellulose product: Properties, uses, and commercial potential. *J Appl Polym Sci: Appl Polym Symp (U S)*. ITT Rayonier Inc., Shelton, WA
87. Herrick FW et al (1983) Microfibrillated cellulose: Morphology and accessibility. *J Appl Polym Sci: Appl Polym Symp (U S)*. ITT Rayonier Inc., Shelton, WA
88. Osong SH, Norgren S, Engstrand P (2016) Processing of wood-based microfibrillated cellulose and nanofibrillated cellulose, and applications relating to papermaking: a review. *Cellul* 23(1):93–123
89. Lee H, Sundaram J, Mani S et al (2017) Production of cellulose nanofibrils and their application to food: a review, in *nanotechnology*. Springer, pp 1–33
90. Rol F et al (2017) Pilot-Scale twin screw extrusion and chemical pretreatment as an energy-efficient method for the production of nanofibrillated cellulose at high solid content. *ACS Sustain Chem Eng* 5(8):6524–6531
91. Yan H et al (2017) Synthesis of bacterial cellulose and bacterial cellulose nanocrystals for their applications in the stabilization of olive oil pickering emulsion. *Food Hydrocolloids* 72:127–135
92. Sacui IA et al (2014) Comparison of the properties of cellulose nanocrystals and cellulose nanofibrils isolated from bacteria, tunicate, and wood processed using acid, enzymatic, mechanical, and oxidative methods. *ACS Appl Mater Interfaces* 6(9):6127–6138
93. Keshk SM (2014) Bacterial cellulose production and its industrial applications. *J Bioprocess Biotechniques*
94. Ioelovich M (2013) Nanoparticles of amorphous cellulose and their properties. *Am J Nanosci Nanotechnol* 1(1):41–45
95. Ioelovich M (2014) Peculiarities of cellulose nanoparticles. *Tappi J* 13(5):45–51
96. Quan S-L, Kang S-G, Chin I-J (2010) Characterization of cellulose fibers electrospun using ionic liquid. *Cellulose* 17(2):223–230
97. Rebouillat S, Pla F (2013) State of the art manufacturing and engineering of nanocellulose: a review of available data and industrial applications. *J Biomater Nanobiotechnol* 4(02):165
98. Nascimento SA, Rezende CA (2018) Combined approaches to obtain cellulose nanocrystals, nanofibrils and fermentable sugars from elephant grass. *Carbohydr Polym* 180:38–45
99. Frone AN et al (2017) Isolation of cellulose nanocrystals from plum seed shells, structural and morphological characterization. *Mater Lett* 194:160–163
100. Wang Z et al (2017) Reuse of waste cotton cloth for the extraction of cellulose nanocrystals. *Carbohydr Polym* 157:945–952
101. Zhang K et al (2016) Extraction and comparison of carboxylated cellulose nanocrystals from bleached sugarcane bagasse pulp using two different oxidation methods. *Carbohydr Polym* 138:237–243
102. Yu H-Y et al (2016) New approach for single-step extraction of carboxylated cellulose nanocrystals for their use as adsorbents and flocculants. *ACS Sustain Chem. Eng* 4(5): 2632–2643

103. Rohaizu R, Wanrosli W (2017) Sono-assisted TEMPO oxidation of oil palm lignocellulosic biomass for isolation of nanocrystalline cellulose. *Ultrason Sonochem* 34:631–639
104. Ho TTT et al (2015) Nanofibrillation of pulp fibers by twin-screw extrusion. *Cellul* 22(1): 421–433
105. Nechyporchuk O, Pignon F, Belgacem MN (2015) Morphological properties of nanofibrillated cellulose produced using wet grinding as an ultimate fibrillation process. *J Mater Sci* 50(2):531–541
106. Sirviö JA, Visanko M, Liimatainen H (2015) Deep eutectic solvent system based on choline chloride-urea as a pre-treatment for nanofibrillation of wood cellulose. *Green Chem* 17(6): 3401–3406
107. Oun AA, Rhim J-W (2016) Characterization of nanocelluloses isolated from Ushar (*Calotropis procera*) seed fiber: effect of isolation method. *Mater Lett* 168:146–150
108. Lee H-R et al (2018) A new method to produce cellulose nanofibrils from microalgae and the measurement of their mechanical strength. *Carbohydr Polym* 180:276–285
109. Valdebenito F et al (2017) On the nanofibrillation of corn husks and oat hulls fibres. *Ind Crops Prod* 95:528–534
110. Lee H, Mani S (2017) Mechanical pretreatment of cellulose pulp to produce cellulose nanofibrils using a dry grinding method. *Ind Crops Prod* 104:179–187
111. Park C-W et al (2017) Preparation and characterization of cellulose nanofibrils with varying chemical compositions. *BioRes* 12(3):5031–5044
112. Eichhorn SJ (2011) Cellulose nanowhiskers: promising materials for advanced applications. *Soft Matter* 7(2):303–315
113. Meyabadi TF et al (2014) Spherical cellulose nanoparticles preparation from waste cotton using a green method. *Powder Technology*, vol 261, pp 232–240
114. Chen Y et al (2009) Bionanocomposites based on pea starch and cellulose nanowhiskers hydrolyzed from pea hull fibre: effect of hydrolysis time. *Carbohydr Polym* 76(4):607–615
115. Abushammala H, Krossing I, Laborie MP (2015) Ionic liquid-mediated technology to produce cellulose nanocrystals directly from wood. *Carbohydr Polym* 134:609–616
116. Miao J et al (2016) One-pot preparation of hydrophobic cellulose nanocrystals in an ionic liquid. *Cellulose* 23(2):1209–1219
117. Li W, Yue J, Liu S (2012) Preparation of nanocrystalline cellulose via ultrasound and its reinforcement capability for poly (vinyl alcohol) composites. *Ultrason Sonochem* 19(3): 479–485
118. Elanthikkal S et al (2010) Cellulose microfibrils produced from banana plant wastes: isolation and characterization. *Carbohydr Polym* 80(3):852–859
119. Kumar A et al (2014) Characterization of cellulose nanocrystals produced by acid-hydrolysis from sugarcane bagasse as agro-waste. *J Mater Phy Chem* 2(1):1–8
120. Haafiz MM et al (2014) Isolation and characterization of cellulose nanowhiskers from oil palm biomass microcrystalline cellulose. *Carbohydr Polym* 103:119–125
121. Khawas P, Deka SC (2016) Isolation and characterization of cellulose nanofibers from culinary banana peel using high-intensity ultrasonication combined with chemical treatment. *Carbohydr Polym* 137:608–616
122. Lu P, Hsieh YL (2012) Preparation and characterization of cellulose nanocrystals from rice straw. *Carbohydr Polym* 87(1):564–573
123. Lu P, Hsieh YL (2010) Preparation and properties of cellulose nanocrystals: rods, spheres, and network. *Carbohydr Polym* 82(2):329–336
124. Mandal A, Chakrabarty D (2011) Isolation of nanocellulose from waste sugarcane bagasse (SCB) and its characterization. *Carbohydr Polym* 86(3):1291–1299
125. Satyamurthy P et al (2011) Preparation and characterization of cellulose nanowhiskers from cotton fibres by controlled microbial hydrolysis. *Carbohydr Polym* 83(1):122–129
126. Johar N, Ahmad I, Dufresne A (2012) Extraction, preparation and characterization of cellulose fibres and nanocrystals from rice husk. *Ind Crops Prod* 37(1):93–99
127. Sheltami RM et al (2012) Extraction of cellulose nanocrystals from mengkuang leaves (*Pandanus tectorius*). *Carbohydr Polym* 88(2):772–779

128. Xiong R et al (2012) Comparing microcrystalline with spherical nanocrystalline cellulose from waste cotton fabrics. *Cellulose* 19(4):1189–1198
129. Chandrasha R, Rajamane NP, Jeyalakshmi et al (2014) Development of cellulose nanofibres from coconut husks. *Int J Emerg Technol Adv Eng* 4(4):2250–2259
130. Nascimento DM et al (2014) A novel green approach for the preparation of cellulose nanowhiskers from white coir. *Carbohyd Polym* 110:456–463
131. Lamaming J et al (2015) Cellulose nanocrystals isolated from oil palm trunk. *Carbohyd Polym* 127:202–208
132. Indarti E, Marwan, Wanrosli WD et al (2015) Thermal stability of oil palm empty fruit bunch (OPEFB) nanocrystalline cellulose: effects of post-treatment of oven drying and solvent exchange techniques. *J Phys: Conf Ser* 622(1):12–25
133. Chandra J, George N, Narayanankutty SK (2016) Isolation and characterization of cellulose nanofibrils from arecanut husk fibre. *Carbohyd Polym* 142:158–166
134. Segal LGJMA et al (1959) An empirical method for estimating the degree of crystallinity of native cellulose using the X-ray diffractometer. *Text Res J* 29(10):786–794
135. Revol JF, Dietrich A, Goring DAI (1987) Effect of mercerization on the crystallite size and crystallinity index in cellulose from different sources. *Can J Chem* 65(8):1724–1725
136. Cherian BM et al (2011) Cellulose nanocomposites with nanofibres isolated from pineapple leaf fibers for medical applications. *Carbohyd Polym* 86(4):1790–1798
137. Cherian BM et al (2010) Isolation of nanocellulose from pineapple leaf fibres by steam explosion. *Carbohyd Polym* 81(3):720–725
138. Rosa SM et al (2012) Chlorine-free extraction of cellulose from rice husk and whisker isolation. *Carbohyd Polym* 87(2):1131–1138
139. Rosa MF et al (2010) Cellulose nanowhiskers from coconut husk fibers: Effect of preparation conditions on their thermal and morphological behavior. *Carbohyd Polym* 81(1):83–92
140. Silvério HA et al (2013) Extraction and characterization of cellulose nanocrystals from corncob for application as reinforcing agent in nanocomposites. *Ind Crops Prod* 44:427–436
141. Neto WPF et al (2013) Extraction and characterization of cellulose nanocrystals from agro-industrial residue—soy hulls. *Ind Crops Prod* 42:480–488
142. Neto WPF et al (2016) Comprehensive morphological and structural investigation of cellulose I and II nanocrystals prepared by sulphuric acid hydrolysis. *RSC Adv* 6(79):76017–76027
143. Luykx DM et al (2008) A review of analytical methods for the identification and characterization of nano delivery systems in food. *J Agric Food Chem* 56(18):8231–8247
144. Goldstein J et al (2012) Scanning electron microscopy and X-ray microanalysis: a text for biologists, materials scientists, and geologists. Springer Science and Business Media, (2)
145. Wang ZL (2000) Transmission electron microscopy of shape-controlled nanocrystals and their assemblies. *J Phys Chem B* 104(6):1153–1175
146. Wang QQ et al (2012) Approaching zero cellulose loss in cellulose nanocrystal (CNC) production: recovery and characterization of cellulosic solid residues (CSR) and CNC. *Cellulose* 19(6):2033–2047
147. Azubuike CP, Okhamafe AO (2012) Physicochemical, spectroscopic and thermal properties of microcrystalline cellulose derived from corn cobs. *Inter J Recycl Org Waste Agric* 1:1–7
148. Adel AM et al (2011) Characterization of microcrystalline cellulose prepared from lignocellulosic materials. Part II: Physicochemical Properties. *Carbohyd Polym* 83:676
149. Lee KY et al (2014) On the use of nanocellulose as reinforcement in polymer matrix composites. *Compos Sci Technol* 105:15–27
150. Yang S, Bai S, Wang Q (2018) Sustainable packaging biocomposites from polylactic acid and wheat straw: enhanced physical performance by solid state shear milling process. *Compos Sci Technol* 158:34–42
151. Ashori A et al (2014) Solvent-free acetylation of cellulose nanofibers for improving compatibility and dispersion. *Carbohyd Polym* 102:369–375

152. Abdul Khalil HPS et al (2016) A review on nanocellulosic fibres as new material for sustainable packaging: process and applications. *Renew Sustain Energy Rev* 64:823–836
153. Frone AN et al (2013) Morphology and thermal properties of PLA–cellulose nanofibers composites. *Carbohyd Polym* 91(1):377–384
154. Oksman K et al (2016) Review of the recent developments in cellulose nanocomposite processing. *Compos Part A: Appl Sci Manuf* 83:2–18
155. Oksman K et al (2011) Cellulose nanowhiskers separated from a bio-residue from wood bioethanol production. *Biomass Bioenergy* 35(1):146–152
156. Lu Y et al (2017) Synthesis of new polyether titanate coupling agents with different polyethyleneglycol segment lengths and their compatibilization in calcium sulfate whisker/poly(vinyl chloride) composites. *RSC Adv* 7(50):31628–31640
157. Poveda RL, Gupta N (2016) Mechanical properties of CNF/polymer composites carbon nanofiber reinforced polymer composites. Cham: Springer, pp 27–42
158. Kobe R et al (2016) Stretchable composite hydrogels incorporating modified cellulose nanofiber with dispersibility and polymerizability: Mechanical property control and nanofiber orientation. *Polym* 97:480–486
159. Ng HM et al (2015) Extraction of cellulose nanocrystals from plant sources for application as reinforcing agent in polymers. *Composites Part B: Eng* 75:176–200
160. Kalia S et al (2011) Cellulose-Based Bio- and Nanocomposites: a review. *Int J Polym Sci*
161. Kalia S et al (2014) Nanofibrillated cellulose: Surface modification and potential applications. *Colloid Polym Sci* 292(1):5–31
162. Ishii D, Saito T, Isogai A (2011) viscoelastic evaluation of average length of cellulose nanofibers prepared by TEMPO-mediated oxidation. *Biomacromolecules* 12(3):548–550
163. Qing Y et al (2013) A comparative study of cellulose nanofibrils disintegrated via multiple processing approaches. *Carbohyd Polym* 97(1):226–234
164. Missoum K, Belgacem M, Bras J (2013) Nanofibrillated cellulose surface modification: a review. *Mater* 6(5):1745
165. Ahmadi M et al (2017) Topochemistry of cellulose nanofibers resulting from molecular and polymer grafting. *Cellulose* 24(5):2139–2152
166. Roy D et al (2009) Cellulose modification by polymer grafting: a review. *Chem Soc Rev* 38(7):2046–2064
167. Safdari F et al (2017) Enhanced properties of poly(ethylene oxide)/cellulose nanofiber biocomposites. *Cellulose* 24(2):755–767
168. Bondeson D, Mathew A, Oksman K (2006) Optimization of the isolation of nanocrystals from microcrystalline cellulose by acid hydrolysis. *Cellulose* 13(2):171–180
169. Morán JI et al (2008) Extraction of cellulose and preparation of nanocellulose from sisal fibers. *Cellulose* 15(1):149–159
170. Fahma F et al (2011) Effect of pre-acid-hydrolysis treatment on morphology and properties of cellulose nanowhiskers from coconut husk. *Cellulose* 18:443–450
171. Brito BS et al (2012) Preparation, morphology and structure of cellulose nanocrystals from bamboo fibers. *Cellulose* 19(5):1527–1536
172. Fan JS, Li YH (2012) Maximizing the yield of nanocrystalline cellulose from cotton pulp fiber. *Carbohyd Polym* 88(4):1184–1188
173. Fortunati E et al (2013) Extraction of cellulose nanocrystals from Phormium tenax fibres. *J Polym Environ* 21(2):319–328
174. Morais JPS et al (2013) Extraction and characterization of nanocellulose structures from raw cotton linter. *Carbohyd Polym* 91(1):229–235
175. Santos RMD et al (2013) Cellulose nanocrystals from pineapple leaf, a new approach for the reuse of this agro-waste. *Ind Crops Prod* 50:707–714
176. Espinosa CS et al (2013) Isolation of thermally stable cellulose nanocrystals by phosphoric acid hydrolysis. *Biomacromolecules* 14(4):1223–1230
177. Le Normand M, Moriana R, Ek M (2014) Isolation and characterization of cellulose nanocrystals from spruce bark in a biorefinery perspective. *Carbohyd Polym* 111:979–987

178. Mueller S, Weder C, Foster EJ (2014) Isolation of cellulose nanocrystals from pseudostems of banana plants. *RSC Adv* 4(2):907–915
179. Bettaieb F et al (2015) Mechanical and thermal properties of *Posidonia oceanica* cellulose nanocrystal reinforced polymer. *Carbohydr Polym* 123:99–104
180. Devi RR (2015) Fabrication of cellulose nanocrystals from agricultural compost. *Compost Sci Utilization* 23(2):104–116
181. Mohamed MA et al (2015) Physicochemical properties of “green” nanocrystalline cellulose isolated from recycled newspaper. *RSC Adv* 5(38):29842–29849
182. Dungani R et al (2016) Preparation and fundamental characterization of cellulose nanocrystal from oil palm fronds biomass. *J Poly Environ* 1:1–9
183. Salajková M, Berglund LA, Zhou Q (2012) Hydrophobic cellulose nanocrystals modified with quaternary ammonium salts. *J Mater Chem* 22(37):19798–19805
184. Pan M, Zhou X, Chen M (2013) Cellulose nanowhiskers isolation and properties from acid hydrolysis combined with high pressure homogenization. *BioRes* 8(1):933–943
185. Savadekar NR et al (2015) Preparation of cotton linter nanowhiskers by high-pressure homogenization process and its application in thermoplastic starch. *Appl Nanosci* 5(3): 281–290
186. Beltramino F et al (2015) Increasing yield of nanocrystalline cellulose preparation process by a cellulase pretreatment. *Biores technol* 192:574–581
187. Beltramino F et al (2016) Optimization of sulfuric acid hydrolysis conditions for preparation of nanocrystalline cellulose from enzymatically pretreated fibers. *Cellulose* 23(3):1777–1789
188. Camargo LA et al (2016) Feasibility of manufacturing cellulose nanocrystals from the solid residues of second-generation ethanol production from sugarcane bagasse. *BioEnergy Res* 9(3):894–906
189. Zhao Y et al (2015) Tunicate cellulose nanocrystals: preparation, neat films and nanocomposite films with glucomannans. *Carbohydr Polym* 117:286–296
190. Csiszar E et al (2016) The effect of low frequency ultrasound on the production and properties of nanocrystalline cellulose suspensions and films. *Ultrason Sonochem* 31:473–480
191. Cudjoe E et al (2017) *Miscanthus Giganteus*: a commercially viable sustainable source of cellulose nanocrystals. *Carbohydr Polym* 155:230–241
192. Hamid SBA et al (2016) Synergic effect of tungstophosphoric acid and sonication for rapid synthesis of crystalline nanocellulose. *Carbohydr Polym* 138:349–355
193. Li Y et al (2016) Facile extraction of cellulose nanocrystals from wood using ethanol and peroxide solvothermal pretreatment followed by ultrasonic nanofibrillation. *Green Chem* 18(4):1010–1018
194. Lu Q et al (2014) Preparation and characterization of cellulose nanocrystals via ultrasonication-assisted FeCl₃-catalyzed hydrolysis. *Cellulose* 21(5):3497–3506
195. Lim YH et al (2016) NanoCrystalline cellulose isolated from oil palm empty fruit bunch and its potential in cadmium metal removal. In: MATEC web of conferences, vol 59. EDP Sciences
196. Sun B et al (2016) Single-step extraction of functionalized cellulose nanocrystal and polyvinyl chloride from industrial wallpaper wastes. *Ind Crops Prod* 89:66–77
197. Tang Y et al (2015) Extraction of cellulose nano-crystals from old corrugated container fiber using phosphoric acid and enzymatic hydrolysis followed by sonication. *Carbohydr Polym* 125:360–366
198. Yu H et al (2013) Facile extraction of thermally stable cellulose nanocrystals with a high yield of 93% through hydrochloric acid hydrolysis under hydrothermal conditions. *J Mater Chem A* 1(12):3938–3944

Recyclable and Eco-friendly Single Polymer Composite



Mohd Azmuddin Abdullah, Muhammad Afzaal, Safdar Ali Mirza, Sakinatu Almustapha and Hanaa Ali Hussein

1 Introduction

Composites based on metal, ceramic and polymer matrices have ubiquitous applications in aerospace, automotive, electrical appliances, microelectronics, infrastructure and construction, medical and chemical industries [1–3]. Interest has shifted towards synthetic and biopolymers and polymer composites as replacements to conventional composite materials as they are far more economical and easier to process [3, 4]. To meet the requirements for, The polymeric material properties can be modified and tuned for specific applications using fillers and fibers [1, 2] for more well-defined physicochemical properties, enhanced mechanical strength and stiffness, with low specific gravity but high thermal and chemical resistance [5–7]. The two main constituents of a polymeric composite are the polymer matrix which is the continuous phase, and the reinforcing material which is the discontinuous or dispersed phase. The properties are governed by the properties of the matrix and the reinforcing material such as the aspect ratio, chemical nature, purity, distribution, orientation and geometry; and the amount and the interfacial adhesion between the matrix and the reinforcement material [4].

M. A. Abdullah (✉) · H. A. Hussein
Institute of Marine Biotechnology, Universiti Malaysia Terengganu,
21030, Kuala Nerus, Terengganu, Malaysia
e-mail: azmuddin@umt.edu.my; joule1602@gmail.com

M. Afzaal
Department of Sustainable Development Study Center (Environmental Sciences),
GC University, Lahore, Punjab, Pakistan

S. A. Mirza
Department of Botany, GC University, Lahore, Punjab, Pakistan

S. Almustapha
Department of Basic and Applied Sciences, Hassan Usman Katsina Polytechnic,
P.M.B 2052 Katsina State, Nigeria

The global issues of sustainability and climate change, industrial ecology, eco-efficiency, and green chemistry are the way forward to develop the new route and next generation of materials, products, and processes [8–10]. The recovery and recycling of petroleum-based plastics remain insufficient when the global plastics production has risen from 245 million tonnes in 2008 [11], to 299 million tonnes in 2013 [12]. Yet the knowledge of human and environmental hazards and risks from the chemicals associated with the diversity of plastic products is limited when most chemicals in plastic polymers production have their origin from the crude oil. Several are known to be hazardous which may be released during the production, use, and disposal of the plastic product [12], with millions of tonnes, end up in the landfills and oceans. Approximately 10–20 million tonnes of plastic end up in the oceans each year, and an estimated 5.25 trillion plastic particles weighing a total of 268,940 tons are currently floating in the world's oceans with the debris damaging the marine ecosystems [12]. Natural fibers have therefore attracted greater attention as these could be obtained from agro-wastes which are abundant, low-cost, low density, biodegradable, non-abrasive but tunable for high specific properties [3, 10, 11]. The combination of biofibers such as oil palm, kenaf, hemp, or flax, to produce composite materials with non-renewable and renewable polymer matrices are competitive with synthetic composites but may need to address the biofiber—matrix interface and novel processing routes [10].

The natural fiber—reinforced polypropylene (PP) composites or natural fiber—polyester composites have attracted attraction as this could remove some portions of the plastics from the environment [13], but these are not sufficiently eco-friendly because of the non-biodegradable nature of the polymer matrix and also the production of the synthetic polymers (like the PP or polyethylene, PE) are fossil fuel-based, and non-renewable [10, 14], which has often been singled out as the major cause of climate change and furthermore subjected to fluctuating prices and declining reserves. The natural fibers, although can be incinerated, may however not be compatible with the hydrophobic polymer matrix as they may form aggregates during processing, have poor resistance to moisture and are generally not mechanically recyclable and reused after the end-of-life [3, 14, 15]. Not all polymers, especially the thermosets, are equally easy to recycle and those composites having glass or carbon fibers can only be recycled into new fiber reinforced grades [2]. Thermoplastic composites can be re-melted and cooled to solidify for an infinite number of cycles but each melting, cooling and re-melting process necessitates high energy requirements, causing the material to eventually degrade. Composites recycling is achievable by a single polymer composite (SPC) with specific economic and ecological advantages [1, 16, 17]. SPC consists of mono-component systems or single polymer, or a minimum of different, compatible polymers [2]. This is possible by making use of the noticeable difference in melting temperature between the matrix and the reinforcement material [15]. The high-density polyethylene (HDPE—crystallized conventionally) matrix and the HDPE reinforcement (containing aligned and extended molecular chains) is an example of the SPC based on the mono-component system [15]. Also, using the natural fibers with polymers based on renewable resources, or the green bio-composites solve many

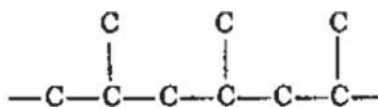
environmental issues to be solved, by embedding the biofibers with biopolymers such as cellulosic plastics, polylactides (PLA), starch plastics, polyhydroxyalkanoates (bacterial polyesters), and soy-based plastics [10]. This review article highlights the fundamental aspects of the polymer and the fibers, the production methods, different components of the SPC and the fabrication methods, and the issues and challenges in the manufacturing and the applications. The term “eco-friendly SPCs” is extended to include those chemical-based, recyclable SPCs and the natural-fibre based SPCs.

2 Recyclable Single Polymer Composite

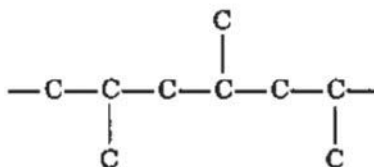
2.1 Basic Polymer Chemistry

Polymers are macromolecules joined with each other by covalent bonding along the backbone chain and lead to properties, such as the ability to form fibers and elastomers, which is not achievable with the small molecules [18]. Polymeric materials and new polymers are being discovered with unique sets of properties including from a single atom, such as sulfur, or from different building blocks arranged in a specific sequence as in proteins or nucleic acids [19]. The long chains are flexible, joined together by primary covalent bonding forces, and each chain can have side groups, branches, and copolymeric chains or blocks, through crosslinks between chains, or by van der Waals and hydrogen bonds. The linear polymers are partially crystalline or semicrystalline, composed of disordered non-crystalline (amorphous) regions and ordered crystalline regions, with the combination of folded and extended chains. Linear polymers are much easier to crystallize than the branched or cross-linked polymers [20]. Copolymerization, in which two or more homopolymers (one type of repeating unit throughout its structure) are chemically combined, disrupts the regularity of polymer chains, thus forming the non-crystalline structure. The arrangements of the side groups (X) can be in the form of atactic, isotactic, and syndiotactic (Fig. 1) [21]. The isotactic polymer is in which the pendant groups are all on the same side of the polymer backbone, as in isotactic PP. In the syndiotactic arrangement, the pendant groups are regularly spaced like the methyl groups in PP, or the HDPE (a linear polymer produced by the polymerization of ethylene in the presence of Ziegler-Natta or Phillips catalysts). The atactic arrangement is in which the side groups are randomly distributed and not packed well on each side of the chain and is normally amorphous as in the atactic PP [21]. The polymer crystallizes easily if the side groups are small like the PE ($X = H$) and the isotactic and syndiotactic arrangements are crystalline at ordinary temperatures, or even when the side groups are large because the chains are linear and are either in alternating positions or on one side of the main chain [20]. In the case of polyvinyl chloride (PVC) ($X = Cl$) and polystyrene (PS) ($X = C_6H_5$), the side groups are large and are randomly distributed along the chains (atactic) and therefore form a non-crystalline structure [20].

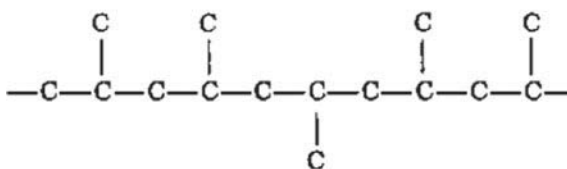
Fig. 1 Skeletal formulas of **a** isotactic, **b** syndiotactic, and **c** atactic (random) PP. (Adapted from [21])



(a) Isotactic PP



(b) Syndiotactic PP



(c) Atactic PP

The differences between all polymers including plastics, fibers, and elastomers or rubbers, are determined primarily by the intermolecular forces between the molecules and the intramolecular forces, and by the functional groups present [21]. The polymer properties are therefore controlled among others by the covalent and non-covalent intra-chain forces. Atoms in individual polymer molecules are joined to each other by strong covalent bonds with the bond energies in the order of 80–90 kcal/mol (320–370 kJ/mol) for the carbon-carbon bonds [21]. Hydrogen bonding between a positively charged hydrogen with an electronegative element nitrogen [OH \cdots N], oxygen [OH \cdots O, NH \cdots O], or fluorine [OH \cdots F] are the strongest non-covalent forces, followed by the dipole-dipole interaction, the magnitude of which depends on the electro-negativity difference of the two atoms involved in the polar bond, and the Van der Waals forces, the small attractive forces and the weakest interchain interactions between all atoms, whether with or without dipole moment, but remain important as they hold non-polar liquids and solids together [20, 21]. The thermoplastic material such as PE, PP, nylon, acetal resin, polycarbonate and polyethylene terephthalate (PET), either linear or branched structure, can be heated up, dissolved in a suitable solvent, and re-processed or remoulded when it softens or melts [22, 23]. Thermoplastics have relatively low tensile moduli, low densities and transparent which are ideal for consumer and medical products [22].

The cross-linked polymers such as phenolic resins, polyesters, and epoxy resins are thermosets, widely used in composite materials, and reinforced with stiff fibres such as fibreglass and aramids. Crosslinking stabilizes the thermoset matrix resulting in the physical properties similar to steel, but with lower densities and suffer less from fatigue and therefore ideal for lightweight structures and for safety-critical parts under regular stress [22]. Elastomers have low moduli and exhibit reversible extension when strained, valuable properties for vibration absorption and damping. Elastomers can be thermoplastic elastomers, vulcanized thermoplastic or crosslinked (as in the case of rubber tyres), and rubbers [melt-processable, natural and synthetic such as nitrile rubber, polychloroprene, polybutadiene, styrene-butadiene and fluorinated rubbers (Viton)] [22, 23].

2.2 Structural Modification

The basic building blocks of polymers are repeating monomer units, normally in covalently linked chains. By having high numbers of functional/hydrophilic groups, high surface/volume ratio, and mechanical stresses, but low molecular weight/crystallization and low or no cross-links, hydrolysis of polymers can be increased. Polymers can be formed by the addition polymerization or free radical addition, the condensation polymerization or step reaction polymerization, and the ring-opening/cyclic polymerization. Addition polymerization is rapid, with the initiated species continue to propagate until termination. It yields linear polymers and achieved by rearranging the bonds within each monomer which should have at least one double bond, for each monomer to share at least two covalent electrons with other monomers. A free radical such as benzoyl peroxide ($\text{H}_5\text{C}_6\text{COO}-\text{OCC}_6\text{H}_5$), or the cations, anions, and coordination (stereospecific) catalysts are initiators that break the double bond which can be activated by heat, ultraviolet light, and other chemicals. During propagation, the free radicals or initiators react with the monomers, and then with another monomer and continue on until termination stage where two free radicals are combined through transfer, or by disproportionate processes. Some monomers can use two or more of the initiation processes while others may use only one process [20, 21]. Addition polymers including vinyl, aldehyde, and acetylene polymers are prepared via addition polymerization reaction such as polyethers, poly(vinyl ether)s, polystyrene derivatives, polyolefins, polymethacrylate, polymethacryloylamine, and polyacetylene and [24–29]. To stiffen and retain their shape, and also make them insoluble in solvents, crosslinking agents which contain two or more double bonds per molecule can be used to produce cross-linked linear chain polymers [20].

The condensation polymerization involves two different monomer units, each containing two functional groups joining together to form a larger molecule by the elimination of a small molecule such as water [20]. While an addition polymer has the same atoms as the monomer in its repeat unit and the atoms in the polymer

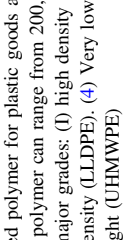
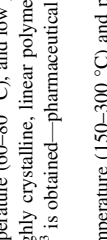
backbone are usually carbon atoms, the condensation polymers contain fewer atoms within the polymer repeat unit than the reactants because of the formation of byproducts during the polymerization process, and the polymer backbone usually contains atoms of more than one element [21]. Condensation polymerization has received considerable attention for the preparation of polymeric materials as these are used in a vast array of applications including the synthesis of chiral polymers [24, 30]. Nature uses chirality as one of the key structural factors to perform functions such as molecular recognition and catalytic activities. Optically active polymers often play important roles as key fundamental materials for well-defined polymers with specific secondary and/or tertiary structures aimed at the application in optoelectronic devices and chiral recognition materials including asymmetric catalyst, chiral stationary phase in HPLC, enantioselective permeation membrane, chiral adsorbent for separation of racemates and in liquid crystals [24]. The optically active polymers based on condensation polymers are prepared by a polycondensation reaction of chiral monomers, which is more versatile, inexpensive though generally poor in control than addition polymerization. Cross-linked gels possessing chiral cavities are prepared and their chiral recognition ability established. The synthesis of the gels is based on the molecular imprinting technique. Two distinctive methods have been developed, that is polymerizing a monomer having a removable chiral template moiety with a cross-linking agent and removing the template groups from the products; and polymerizing the monomer with the crosslinking agent in the presence of a non-polymerizable template molecule before removing the template [24, 31]. One major drawback of condensation polymerization is the tendency for the reaction to cease before the chains grow to a sufficient length due to the decreased mobility of the chains and reactant chemical species as polymerization progresses, resulting in short chains. It is possible in the case of nylon, that the chains are polymerized to a sufficiently large extent before this occurs resulting in the nylon physical properties preserved [20].

Poly(lactic glycolic acid) polymers can be obtained either by condensation from lactic acid, glycolic acid, and light condensates or by ring-opening polymerization (ROP) of the related cyclic dimers, namely, lactide and glycolide. The ROP route allows for a much higher control of the polymerization and remains by far the most widely used method for the synthesis of well-defined materials [32]. This may involve different strategies following the nature of their ancillary ligands such as the Coordination—Insertion Anionic Polymerization, Nucleophilic or Cationic Polymerization, with different catalysts or enzymes and stereoregulation of Lactide ROP [32]. For the cyclic polymerization, a variety of precisely controlled, branched and single-cyclic (ring) and multi-cyclic topologies can be realized through a bimolecular process, a unimolecular process with asymmetric telechelic, a unimolecular process with symmetric telechelic, a ring-expansion polymerization process and an electrostatic self-assembly and covalent fixation (ESA-CF) process [33]. Conventional synthetic protocol for ring polymers has been an end-to-end linking reaction using a linear polymer precursor having reactive groups, telechelic, and an

equimolar amount of a bifunctional coupling reagent [34–36]. The combination of the classical ring-expansion polymerization process, in which the initiator fragment is included within the ring polymer structure, with the end-to-end polymer cyclization process could provide a new effective means for large size ring polymers. The new ring-expansion polymerization processes make use of a metathesis catalyst having cyclic ligand, an N-heterocyclic carbene initiator, a cyclic stannate and subsequent intramolecular cross-linking. For the effective synthesis of not only cyclic but also functionalized cyclic and multicyclic polymers, the ESA-CF process has been introduced, where linear or star telechelic polymers having cyclic ammonium salt groups accompanying small or polymeric plurifunctional carboxylate counter-anions are employed as key precursors [33].

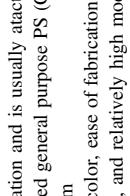
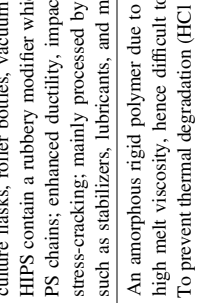
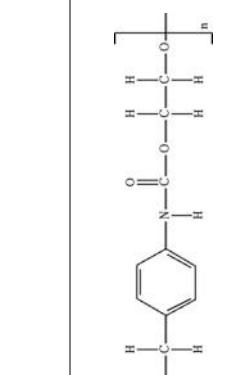
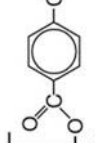
Table 1 summarizes the four most important commodity thermoplastic polymers—PP, PE, polystyrene (PS) and polyvinyl chloride (PVC); two thermosetting polymers—polyurethanes, and unsaturated polyesters; and two elastomers—rubber and acrylonitrile-butadiene-styrene (ABS); their route of polymerization and characteristics [20, 21]. The reaction temperature, pressure, and time in the presence of a catalyst(s) control the degree of polymerization, while the chemical composition and the arrangement of chains affect the physical properties such that the polymers can be tailored and tuned to meet the end user. Amorphous polymers undergo substantial changes in properties as a function of temperature. The temperature at which the transition from the glassy region where the polymer is relatively stiff to the rubbery region where it is very compliant is termed the glass transition temperature, T_g . It is the temperature at which there is a discontinuity in slope in the profile of volume change versus temperature. The melting point, T_m , is the temperature range where the total or whole polymer chain mobility occurs and the T_m is called a first-order transition temperature while the T_g is sometimes called a second-order transition temperature. The former is usually 33–100% greater than the latter and the symmetrical polymers like HDPE exhibit the greatest difference between T_m and T_g [21]. Increasing the size of the side groups in the linear polymers such as PE and cross-linking of the main chains will decrease the T_m due to the imperfect molecular packing from the steric hindrance of the side chains, resulting in a decreased mobility and reduced crystallization rate. For nylon polymer, the NH groups make hydrogen bonds with the C=O groups of another chain and each bond worth only about 15–20 kJ/mole, as compared to 300–400 kJ/mole for a covalent bond. Nevertheless, a lot of interchain hydrogen bonds add up to make the nylon polymer becoming rather stiff with a T_g of 57 °C [20]. The high melting point of nylon-66 ($T_m = 265$ °C) is, therefore, a result of the combined Van der Waals, dipole-dipole, and hydrogen bonding forces between the polyamide chains. The corresponding polyester, which cannot make hydrogen bonds, has a T_g of –40 °C [20, 21]. The dipole-dipole interactions typically only about 5 kJ/mole, which is weaker than the hydrogen bonds, can again add up so that the PVC has a T_g of 81 °C, whereas that of polyethylene is –125 °C. [20].

Table 1 Different types of polymers, structure and characteristics (Adapted from [20, 21, 152])

Types of polymer	Structure	Reaction and types
1 Thermoplastics Polyethylene (PE)		<ul style="list-style-type: none"> • The world's most commonly used polymer for plastic goods and products • Molecular weight of a linear PE polymer can range from 200,000 to 500,000 • Available commercially in five major grades: (1) high density (HDPE), (2) low density (LDPE), (3) linear low density (LLDPE), (4) Very low density (VLDPE), and (5) ultra high molecular weight (UHMWPE) • HDPE is polymerized at low temperature (60–80 °C), and low pressure (≈ 40 kg/cm²) using metal catalysts. A highly crystalline, linear polymer with a density ranging from 0.94 to 0.965 g/cm³ is obtained—pharmaceutical bottles, nonwoven fabrics, and caps • LDPE is derived from a high temperature (150–300 °C) and pressures (1000–3000 kg/cm²) using free radical initiators. A highly branched polymer with lower crystallinity and densities ranging from 0.915 to 0.935 g/cm³ is obtained—flexible container applications, nonwoven-disposable and laminated (or coextruded with paper) foil, and polymers for packaging • LLDPE (density 0.91–0.94 g/cm³) and VLDPE (density: 0.88–0.89 g/cm³), are linear polymers, polymerized under low pressures and temperatures using metal catalysts with co-monomers such as 1-butene, 1-hexene, or 1-octene to obtain the desired physical properties and density ranges. LLDPE—pouches and bags due to its excellent puncture resistance; VLDPE—extruded tubes • UHMWPE (MW $> 2 \times 10^6$ g/mol)—orthopedic implant fabrications
Polypropylene (PP)		<ul style="list-style-type: none"> • Used widely in plastic industry for its remarkable level of resistance against chemical and mechanical weathering, tear and abrasion and low thermal expansion coefficient • polymerized by a Ziegler-Natta stereo specific catalyst which controls the isotactic position of the methyl group. Thermal (<i>T_g</i>: –12 °C, <i>T_m</i>: 125–167 °C and density: 0.85–0.98 g/cm³) • Physical properties similar to PE; average molecular weight of from 2.2 to 7.0×10^5 g/mol and with wide molecular weight distribution (poly-dispersity) from 2.6 to 12 • Additives include antioxidants, light stabilizer, nucleating agents, lubricants, mold release agents; antiblock, and slip agents to improve the physical properties and processability • Exceptional high flex life and excellent environment stress cracking resistance; gas and water vapor permeability in between those of LDPE and HDPE

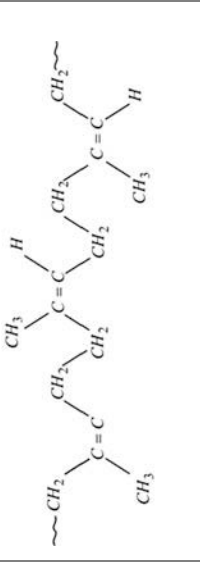
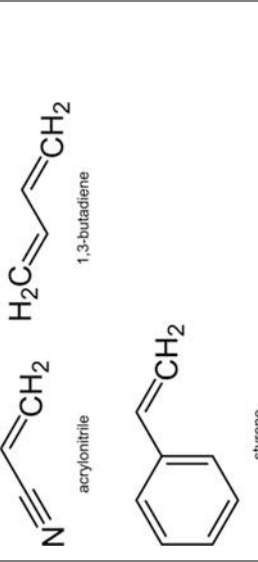
(continued)

Table 1 (continued)

Types of polymer	Structure	Reaction and types
Polystyrene (PS)		<ul style="list-style-type: none"> • Polymerized by free radical polymerization and is usually atactic • Available in three grades: (1) unmodified general purpose PS (GPPS, T: 100 °C), (2) high impact PS (HIPS), (3) PS foam • GPPS has good transparency, lack of color, ease of fabrication, thermal stability, low specific gravity (1.04–1.12 g/cm³), and relatively high modulus—tissue culture flasks, roller bottles, vacuum canisters, and filterware • HIPS contain a rubbery modifier which forms chemical bonding with the growing PS chains; enhanced ductility, impact strength and resistance to environmental stress-cracking; mainly processed by injection molding at 180–250 °C; additives such as stabilizers, lubricants, and mold releasing agents are formulated
Polyvinylchloride (PVC)		<ul style="list-style-type: none"> • An amorphous rigid polymer due to the large Cl side group; T_g of 75 to 105 °C; high melt viscosity, hence difficult to process • To prevent thermal degradation (HCl could be released), thermal stabilizers such as metallic soaps or salts are incorporated; lubricants formulated to prevent adhesion to metal surfaces and facilitate the melt flow during processing; plasticizers used at 10–100 parts per 100 parts of PVC resins to increase flexibility
2. Thermoset Polyurethanes (PU)		<ul style="list-style-type: none"> • Contain the urethane linkage • PU rubbers produced by reacting a prepared pre polymer chain with an aromatic di-isocyanate to make very long chains possessing active iso-cyanate groups for cross-linking; can be tailored for many applications by changing the chemical constituents • PU rubber is strong and has good resistance to oil and chemicals
Polyesters		<ul style="list-style-type: none"> • Polyesters such as polyethyleneterephthalate are highly crystalline; high T_m: 265 °C; hydrophobic and resistant to hydrolysis in dilute acids • Can be converted by conventional techniques into molded articles

(continued)

Table 1 (continued)

Types of polymer	Structure	Reaction and types
3. Elastomer Rubbers		<ul style="list-style-type: none"> • Silicone, natural, and synthetic rubbers have been used for the fabrication of implants • Natural rubber mostly from the latex of the <i>Hevea brasiliensis</i> tree and the chemical formula is similar to <i>cis</i>-1,4 polyisoprene; compatible with blood in its pure form that synthetic rubbers being developed to substitute the natural rubber • The Ziegler-Natta types of stereo-specific polymerization techniques made the variety possible. The synthetic rubbers rarely used to make implants; physical properties vary widely due to the wide variations in the preparation recipes
Acrylonitrile-butadiene-styrene (ABS)		<ul style="list-style-type: none"> • Produced by three monomers: acrylonitrile, butadiene, and styrene • The desired physical and chemical properties with a wide range of functional characteristics can be controlled by changing the ratio of the monomers • Resistant to the common inorganic solutions, have good surface properties, and dimensional stability

NB All chemical structures are adapted from Wikipedia

2.3 Production of Polymeric Fibers

Synthesis of SPC involves two phases—the production of polymeric fibers, and the fabrication of the fibers with the matrix. Table 2 summarizes the different techniques used for the production of different polymeric fibres and the fabrication of recyclable SPCs. In the production phase, the fibers are produced from the polymeric raw material by the spinning technique which is based upon the extrusion principle where the liquefied/molten form of the material is forced through a die to acquire desired cross sections. The different types of spinning techniques are the dry, wet, gel, melt or electrospinning method. The wet spinning technique is the oldest production method, where the polymer is dissolved in a non-volatile solvent and the fibers are extruded through a spinneret placed in a liquid filled coagulation container which contains a non-solvent for the polymer but can dissolve out the solvent used for the polymer dissolution. Once the polymer solvent and the non-solvent coagulate together, the polymer fibers are precipitated out. The polymer solvent can be recovered later which can be costly. The major drawback is that direct extrusion through a liquid phase results in larger drag force/friction which slows down the process and increasing the extrusion speed weakens the fibers by causing micro-level cavities throughout the filament. Unlike the wet method, dry spinning utilizes evaporation to extrude the fibers. The polymer is dissolved in a solvent for extrusion after which the fibers are exposed to hot air to make the solvent evaporate and to solidify the fibers. No chemical reaction or dilution involved and the evaporating solvent can be recovered via condensation without any interference to the extruded fibers [37–40].

The gel spinning/dry-wet spinning method is used when the polymeric fibers with high strength or special properties are required such as the ultra-high-molecular-weight polyethylene (UHMWPE) fibers [41]. The polymer chains, due to the close contact with each other, develop intra- and interchain linkages in a liquid crystal form, resulting in a high tensile strength fiber. After extrusion, the polymeric fibers obtained in highly oriented form with liquid crystals aligned along the length/long axis of the fibers, are immediately exposed to air and then subjected to a liquid bath for further cooling, hence the name the “dry-wet spinning”. It can be further

Table 2 Different techniques used for the production of different polymeric fibres and the fabrication of recyclable SPCs [37, 39]

Fabrication method	Polymeric materials
Wet spinning	Rayon, spandex, aramid and acrylic
Dry spinning	Spandex, vinyon, modacrylic, triacetate, acrylic and acetate
Gel spinning	Aramid and polyethylene; UHMWPE
Melt-spinning technique	Nylon, polyester, sulfar, PP, PET, PLA and PA6
Electrospinning	PE, PP, PET, PMMA and PLA
Hot compaction	PP, nylon 6, 6, PE, PMMA and crystalline polymer fibers
Film stacking method	Homocomposites of PP, PE, UHMWPE, iPP

modified into “dry-jet wet spinning” method where the polymer solution is extruded and then exposed to pressurized hot air. After heat treatment, a coagulation bath is done which is followed by further heat and drawing treatments, all under nitrogenous environment to prevent the oxidization of the extruded fibers [41–43].

Melt spinning is the most commonly used commercial process for the production of synthetic polymeric fibers and have been reported for PP, polyamides 6, and PET fibers [2], PLA [17] and isotactic PP (iPP) fibers [15, 44]. It involves direct melting of the polymeric granules and the flow of the melted polymer to the spin head, controlled through a metering pump. The polymer melt is extruded through small orifices in the spinneret and drawn into thin fibers by a uniaxial drawing process. The spinneret is submerged in the liquid coagulation bath and the emerging filaments are coagulated in a precipitating bath or a series of baths of increasing precipitant concentration or exposed to air as a cooling down step. To prevent irregularity in diameter or cross-section of the fibers, the molten polymer is passed through a filter which filters out un-melted granules. Fibers of different cross-sections can be tuned as per their applications such as round, pentagonal, trilobal, octagonal or hexagonal [39, 40, 45, 46]. Electrospinning method uses electrical charges where the extrusion material is in the form of a charged polymer solution or a polymer melt. The charged solution/melt is ejected through a nozzle onto an oppositely charged substrate (a charged metal target). In the case of polymer solution, the fibers can be spun into nonwoven structures which are porous where solvent is evaporated via hot air, and in the case of polymer melt, there is no drying step to ensure purity and mainly non-porous, with the diameter of sub-micron level or nanoscale and high surface areas [39, 47]. PE, PP, PET, poly (methyl methacrylate) (PMMA) and poly(lactic acid) (PLA) are among the polymer materials that have been successfully electrospun into fibers of different diameters [15, 48–55].

2.4 Fabrication of the Polymeric Fibres with the Matrix

The main challenge in producing an SPC is in combining the fiber and the matrix into one composite, as both may have the same chemical structure and hence the melting temperature [15]. The molecular orientation may change during spinning and drawing and from the heating and cooling processes which makes it difficult to retain the properties of the oriented polymer molecules in the final composite for enhanced mechanical properties [56]. High mechanical properties of the SPCs also require the development of high strength polymeric fibers which are recyclable, economical, have low density, and good interfacial bonding [57]. The fabrication phase involves melt or powder impregnation, hot compaction, overheating, film stacking or co-extrusion method [15, 39]. Impregnation method is a traditional method, initially developed for the fabrication of PE and PP homo composites [58, 59]. There are two types, depending on the physical state of the impregnation material, the powder impregnation and melt (solution) impregnation method. In

melt impregnation method, the fibers are impregnated with molten polymer either cross-head extruder which provides molten polymer in a die for the fibers to pass or a molten resin bath where the fibers are passed through to increase the permeability of the polymer contained in the tow. In the dry-powder impregnation method, the fibers such as the glass fibers are exposed to a dry a bed of loosely packed thermoplastic powder which is processed by heating to sinter the powder particles onto the fibers. Electrostatic attraction causes the powder particles to stick onto the fiber surface resulting in macroscopic impregnation where the fiber clusters are coated with the powder particles rather than the individual fibers [15, 39]. Impregnation is slow and not economical and more suitable for the polymers of low molecular weight. The impregnation material can be highly viscous and must fully wet the fibers, which may cause thermal degradation and loss of mechanical properties of the reinforcement material/fibers. The forces applied to the die pressure of the crosshead extruder and the partial dissolving or melting during impregnation may cause damage to the fibers' integrity [56, 60].

Hot compaction subjects the polymer fibers to a temperature range high enough to melt down the outer surface of the fiber bundle. The molten surface, upon cooling, becomes the binding phase serving as the matrix of the composite. The semi-crystalline polymers' broad melting temperature range is manipulated via prefabrication under the effect of constraints. The oriented polymer fibers are compacted to an oriented polymer sheet under suitable conditions of temperature and pressure. The major concern of this process is that the temperature should be almost 5 °C below the T_m and any overheating may result in relaxation and a loss of the fiber orientation [15]. The hot compaction method has been used to prepare the SPCs from PP [61, 62], PE [63], poly(ethylene naphthalate) (PEN) [64], and PMMA [65]. In the overheating method, the polymer fibers are embedded in a molten polymer matrix of the same grade, overheated considerably above their T_m whilst being constrained to prevent shrinkage and the loss of mechanical properties. The constraining of the fiber shifts the melting temperature to higher values to provide larger temperature window for the SPCs processing of the SPCs [2, 15].

In the film stacking technique, the reinforcement fibers are sandwiched between the films of the matrix and the composite material is produced by hot pressing. The matrix films ensure a wide temperature processing window for hot pressing, freedom to select the material with no expensive pre-production [15]. It has been applied for PP [66], PE [67], PEN [68], UHMWPE [69], PLA [17], and iPP fibers [44]. In co-extrusion technique, a multilayer web can be produced without the need for initial production of individual webs and a separate combining step. The melted polymers are fed together carefully to produce a layered melt, which is then processed in conventional ways to produce a plastic film or sheet [70]. Two different types of polymer tapes such as the random PP copolymer/PP homopolymer, each at a different melting temperature, are cold drawn to increase the mechanical properties and the reinforcement tapes are consolidated. Once oriented, the polymer tapes can be constrained by the molding pressure during consolidation to increase the melting temperature of the oriented core material, and further extend the processing window of about 20–40 °C, a high volume fraction of reinforcement (90%)

and an excellent bonding between the tapes due to the co-extrusion process [15]. All-PP tapes (PP homopolymer—core; random PP copolymer—skin) fabricated by coextrusion into tapes of different melting temperatures are superior to glass mat-reinforced thermoplastics or natural fiber mat-reinforced in terms of good mechanical properties with low density [60].

In any composite, the stress absorbed by the matrix (the weaker phase due to the weaker inter-chain interaction) is transferred to the reinforcement phase (the stronger phase) through an interphase [71]. For this reason, polymeric fibers with high performance are very important in SPC development as these high-performance polymer fibers can be designed to give SPC high mechanical features. To ensure efficient transfer of load from the matrix to the fibers, overlapping of the polymer chains is required and for this, polymers of high molecular weight with extended chains are preferred [2]. Other than strength and stiffness, the low processing cost, ease of production and recycling to meet the environmental requirements, low densities and the naturally strong interfacial bonding between the molecules of the same polymer with less requirement for surface treatments, are among major factors to be considered in the SPC development [3]. Although produced from a single type of polymer or polymers related to a single family of polymers, an SPC is still a two-phase system. Taking advantage of the high stiffness and strength, the reinforcement phase is the anisotropic semicrystalline forms of the polymers, and the matrix is either amorphous or semicrystalline but isotropic form of the same polymer [71]. Carbon and glass fibers are the common reinforcement material used in the composite materials to strengthen and enhance the efficiency of the polymer matrix. However, carbon fibre especially is wasteful to produce and both are difficult to recycle, mechanically and thermally, and for ultimate disposal, making them not environmentally-friendly [15, 60, 72]. Furthermore, the density of the polymer fibers such as PE, PP, All-PP tapes and UHMWPE is less than that of the glass and carbon fibers, and their high mechanical properties induced during drawing are major advantages in applications where a high strength-to-weight ratio is required [15]. Since the development of the first SPC based on PE [1], different matrix-fiber combinations based on PE, PET, PMMA, PLA, PEN, nylon and polyester have been reported (Table 3) [15].

The major advantage of SPCs over heterogeneous composites is the chemical compatibility for improved interfacial bonding and recyclability. PE can be classified into different categories which do not depend entirely on its density and branching, and those main forms of PE divided based on density and branching which include HDPE, High molecular weight HDPE (HMW HDPE), UHMW-HDPE, linear low-density polyethylene (LLDPE), and very low-density polyethylene (VLDPE). The most used PE grades are HDPE, low-density polyethylene (LDPE) and medium-density polyethylene (MDPE) [73]. During fabrication, the main hurdle to overcome is the small difference in T_m between the fiber and the matrix. The T_m for HDPE matrix and fibers are 132 and 139 °C, respectively [74], and for UHMWPE are in the range of 5–9 °C [75]. Under normal processing conditions of the SPCs, the PE fibers annealed at the temperature close to its T_m will have a much-reduced modulus towards that of the bulk HDPE [74].

Table 3 Matrix-fiber combinations for SPCs development (Adapted from [15])

Matrix	Fiber
HDPE	HDPE
HDPE	UHMWPE
UHMWPE	UHMWPE
LDPE	UHMWPE
PP	PP
PPE random copolymer	PP
PET	PET
PMMA	PMMA
PLA	PLA
Poly(ethylene naphthalate)	Poly(ethylene naphthalate)
Nylon 6,6	Nylon 6,6
Vectran M	Vectran HS

HDPE High density polyethylene, *UHMWPE* Ultra-high molecular weight polyethylene, *LDPE* Low density poly-ethylene, *PP* Polypropylene, *PLA* Polylactide, *PET* Polyethylene terephthalate, *PMMA* Polymethyl methacrylate and *PPE* Propylene ethylene

To enlarge the process window, the incorporation of polymers with the same chemical composition but different chemical structures have been explored such as the HDPE matrix reinforced by UHMWPE fibers [76, 77], and LDPE matrix reinforced by HDPE fibers [74] or UHMWPE fibers [77]. These composites have the manufacturability enhanced but with reduced interfacial adhesion than the original HDPE homocomposite [74, 78], a result of different molecular weight and chain configurations particularly the length of branched chains of HDPE, LDPE, and UHMWPE which affects the compatibility and miscibility [79]. The level of short chain branching (SCB) in LDPE has a strong influence on its miscibility with linear HDPE [79]. The difference between the T_m of high-performance PE fibre and LDPE matrix and the high chemical compatibility of the two components permit the use of the fibre in a composite fabrication [78]. The chemically-treated PE fibres surface substituting for the glass fibres in the PE matrix has markedly increased the adhesion but the thermal processing conditions of the composite material and the surface treatment cause a reduction in the mechanical property of the PE fibre [78]. With greater concern over climate change and sustainable development goals, the shift is now geared towards the development of SPCs from renewable and bioresources.

3 Eco-friendly Single Polymer Composites

Continuous and rapid exhaustion of natural and non-renewable resources has made it imperative for the utilization of sustainable and eco-friendly material. Regulatory and environmental authorities are making it compulsory for the manufacturers to review their processes and the impact of their products on the environment.

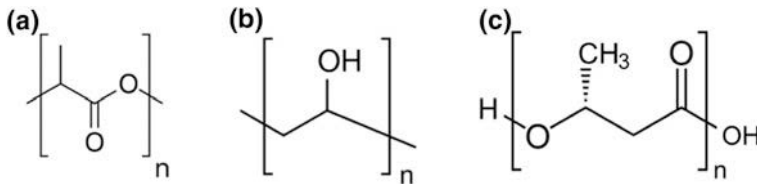


Fig. 2 Structure of **a** PLA, **b** PVA, **c** PHB. (Adapted from wikipedia)

In SPCs, the use of biopolymer matrix re-enforced with the same polymer in the reinforcement phase is the way forward for the sustainable approach as both the matrix and the fibers are from renewable resources. Despite this, the biopolymer is not the polymer of choice for SPC production due to its instability against mechanical recycling and thermal degradation during recycling process [60, 80]. Biodegradable polymers can be categorized into natural polymers (e.g. cellulose, alginate, starch), synthetic polymers [e.g. PLA, polycaprolactone, polyvinyl alcohol (PVA)], and microbial polymers [e.g. polyhydroxybutyrate (PHB) and polyhydroxybutyrate valerate (PHBV)] (Fig. 2) [81]. The two commonly reported biodegradable SPCs—PLA and PVA, are highlighted.

3.1 PLA-Based

3.1.1 PLA Synthesis

PLA is a thermoplastic, high-strength, high-modulus polymer, belonging to the family of aliphatic polyesters, and is commonly made from α -hydroxy acids which include polyglycolic acid or polymandelic acid. The basic building block for PLA is lactic acid (2-hydroxy propionic acid) which is the simplest hydroxy acid with an asymmetric carbon atom and exists in two optically active configurations. The $L(+)$ -isomer which is produced in humans and other mammals, and both the $D(-)$ - and $L(+)$ -enantiomers which are produced in the bacterial systems [82]. The basic building block for PLA is lactic acid (2-hydroxy propionic acid) which is the simplest hydroxy acid with an asymmetric carbon atom and exists in two optically active configurations—the $L(+)$ -isomer which is produced in humans and other mammals, and both the $D(-)$ - and $L(+)$ -enantiomers which are produced in the bacterial systems [82]. The commercial batch fermentation may take 3–6 days at 5–10% sugar concentrations with the production rate of $2 \text{ g L}^{-1} \text{ h}^{-1}$. The standard fermentation conditions are relatively low to neutral pH, temperatures around $40 \text{ }^\circ\text{C}$, and low oxygen concentrations and the sugars such as glucose, maltose, and dextrose can be obtained from corn or potato starch, or sucrose from cane or beet sugar, or lactose from the cheese whey. The supplements may include corn steep liquor, yeast extract, cotton seed flour, or soy flour, to provide proteins, B-vitamins, amino acids and nucleotides [83–86]. The strains that produce the $L(+)$ -isomer are *Lactobacilli*

amylophilus, *L. bavaricus*, *L. casei*, *L. maltaromicus*, and *L. salivarius* and the strains that produce the $D(-)$ -isomer or the mixtures of both are *L. delbrueckii*, *L. jensenii*, or *L. acidophilus*, with 90% yield ($1.8 \text{ mol Lactic acid mol}^{-1} \text{ glucose}$) [82, 85, 87]. Calcium hydroxide or calcium carbonate is used to neutralize the fermentation acid and give soluble calcium lactate broth which is filtered, evaporated, recrystallized, and acidified with sulphuric acid to yield the crude lactic acid. Higher purity is obtained by distillation of the acid as the methyl or ethyl ester, followed by hydrolysis back to the acid [83, 86, 84, 85] (Fig. 3).

The synthesis of lactic acid into high-molecular-weight PLA can follow two different routes of polymerization (Fig. 4). The lactic acid undergoes condensation polymerization to yield a low-molecular-weight, brittle, which can be made useful for applications if the molecular weight is increased through the use of esterification-promoting adjuvants such as bis(trichloromethyl) carbonate, dicyclohexylcarbodiimide, and carbonyl diimidazole; and chain-extending agents such as isocyanates, acid chlorides, anhydrides, epoxides, thiirane, and oxazoline [82, 87, 88]. Another route is via the ring-opening polymerization (ROP) of the lactide to yield high molecular weight PLA ($M_w = 100,000$). Lactide, the cyclic dimer of lactic acid is obtained by the depolymerization of low-molecular-weight PLA under reduced pressure to give a mixture of three stereoisomers (L, L)-lactide, (D, D)-lactide and *meso*(D, L)-lactide, the composition of which depends on the lactic acid isomer feedstock, temperature and catalyst [87]. Without racemization reactions, polymerization of (L, L)-lactide (LLA) and its enantiomer (D, D)-lactide (D-LA) give

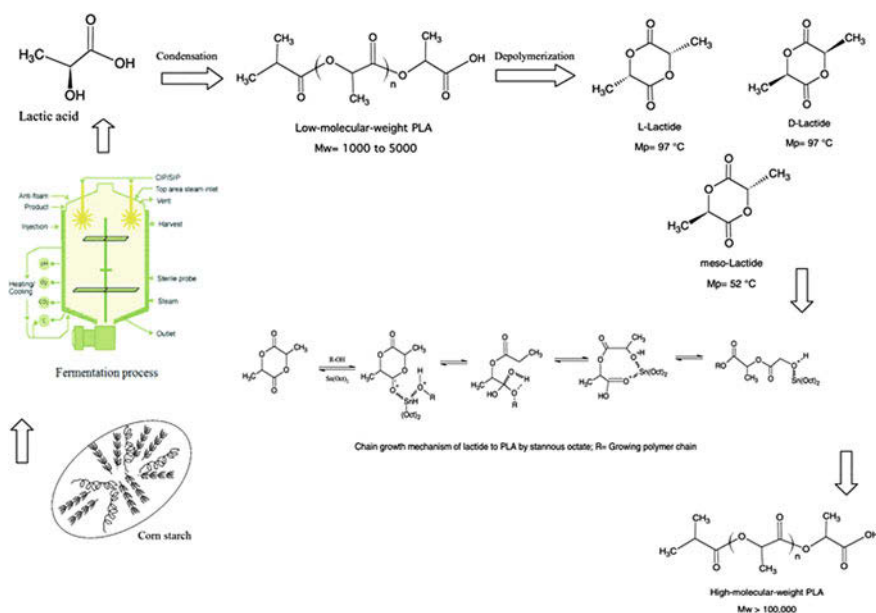


Fig. 3 Production steps for PLA. (Adapted from [153])

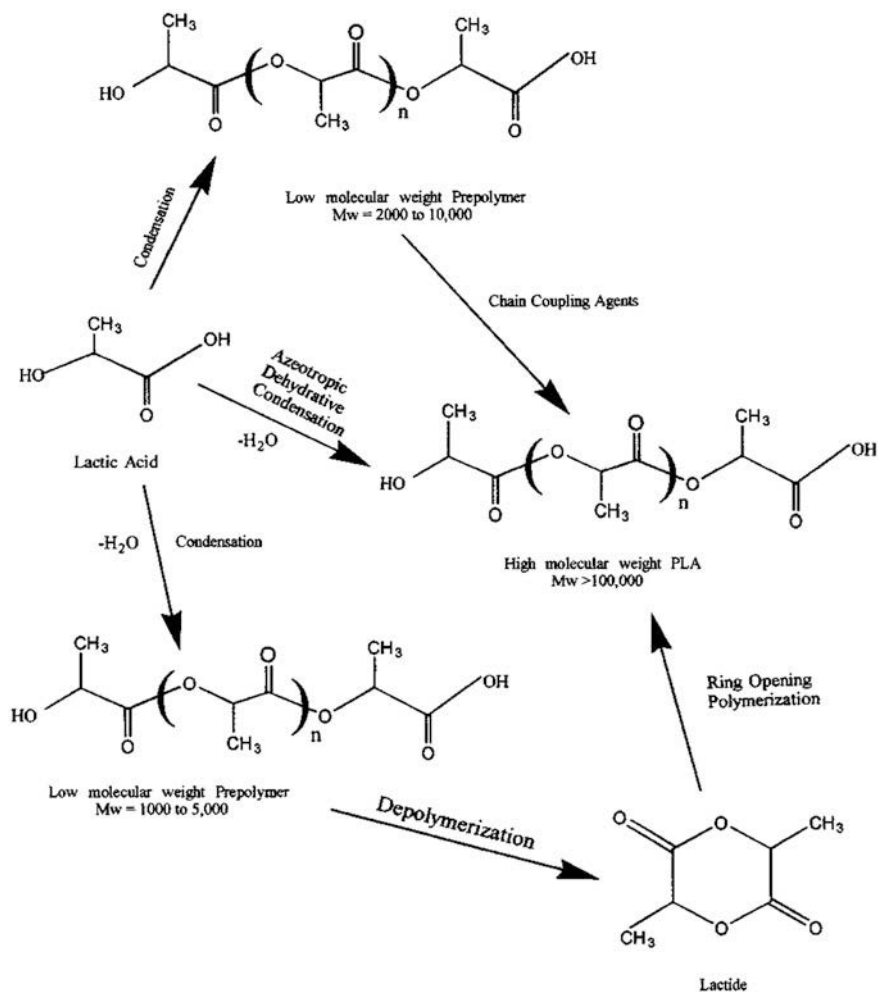


Fig. 4 Synthesis methods for high M_w PLA. (Adapted from [82])

isotactic semicrystalline polymers. The polymerization of *meso* (D, L)-lactide, or a racemic mixture of 50% of D-LA and 50% of L-LA gives an amorphous polymer, while the polymerization of optically pure monomers (L-LA or D-LA) gives a semi-crystalline polymeric material [89]. The synthesis of PLA from the lactide ring can take place via cationic ROP or anionic ROP and the D-lactide and L-lactide enantiomers can form a 1:1 racemic stereo complex (D, L-lactide), which melts at 126–127 °C [87, 90]. The cationic initiators to polymerize lactide in cationic ROP are trifluoromethane-sulfonic acid (triflic acid) and methyl trifluoromethane-sulfonic acid (methyl triflate) [91–93]. The polymerization proceeds via triflate ester end-groups at 100 °C to yield an optically active polymer without racemization. The propagation begins with the cleavage of the positively charged lactide ring at the

alkyl-oxygen bond by an S_N2 attack of the triflate anion. In another S_N2 type of attack, the triflate end-group reacts with the second molecule of the lactide to yield a positively charged lactide that is opened, and then the triflate anion again opens the charged lactide, and the polymerization proceeds [94].

The anionic lactide polymerizations proceed through the nucleophilic reaction of the anion with the carbonyl and the subsequent cleavage of the acyl-oxygen to produce an alkoxide end-group that continues to propagate [87]. For a large-scale commercial application, the use of bulk melt polymerizations with lower levels of non-toxic catalysts metal carboxylates oxides, and alkoxides are preferred. The high-molecular-weight PLA is easily polymerized in the presence of tin(II) and zinc to produce pure polymers due to their covalent metal-oxygen bonds and free *p* or *d* orbitals [95, 96] and the best results are achieved with tin oxide and octoate at 120–150 °C with 90% conversions and less than 1% racemization [97]. The tin(II) bis-2-ethyl hexanoic acid (tin or stannous octoate) is the catalyst of choice in the PLA synthesis mainly due to the FDA approval and high catalytic activity with low toxicity, and its solubility in many lactones with the ability to give high molecular-weight polymers with low racemization [82, 92, 98]. The commercial route is where the lactic acid and the catalyst are azeotropically dehydrated in a refluxing, high-boiling, aprotic solvent under reduced pressures to obtain much higher molecular weight PLA ($M_w > 300,000$) [99–102]. The azeotropic condensation polymerization utilizes reduced pressure distillation of lactic acid for 2–3 h at 130 °C to remove the majority of the condensation water and produces high-molecular-weight polymer without the use of esterification-promoting adjuvants or chain extending agents. The catalyst and diphenyl ether are added, a tube packed with 3-Å molecular sieves attached to the reaction vessel and the refluxing solvent returned to the vessel via the molecular sieves for an additional 30–40 h at 130 °C. The polymer can finally be isolated as is or dissolved and precipitated for further purification [99–104]. Though producing high molecular weight polymer, the technique may result in high catalyst impurities which can cause problems such as unwanted degradation, uncontrolled hydrolysis rates, toxicity and differing slow-release properties. The catalyst level should, therefore, be reduced to 10 ppm or less, deactivated or filtered out after the reaction [82, 87, 105].

Newly developed PLA synthesis techniques based on polycondensation and ROP on the basis of industrial technique modifications and advanced laboratory research including the various solvents, heating programs, reaction and catalyst systems have been reported. The four synthesis methods are direct polycondensation (DP), azeotropic polycondensation (AP), solid state polymerization (SSP) and ROP (Fig. 5). In the case of PLA, polycondensation of lactic acid connects carboxyl and hydroxyl groups to produce water by-product simultaneously. Due to the difficulty in removing the byproducts from the highly viscous reaction mixture, the polymer produced through DP is usually $<50,000 \text{ g}\cdot\text{mol}^{-1}$ and low quality [106]. However, with the newly developed using more efficient catalyst, solvent system, temperature, pressure, and duration have improved the polymer processing and properties, PLA with M_w of $90,000 \text{ g}\cdot\text{mol}^{-1}$ is achievable even without any catalyst, initiator or solvent. However, this may require a long heating time ($>100 \text{ h}$ at

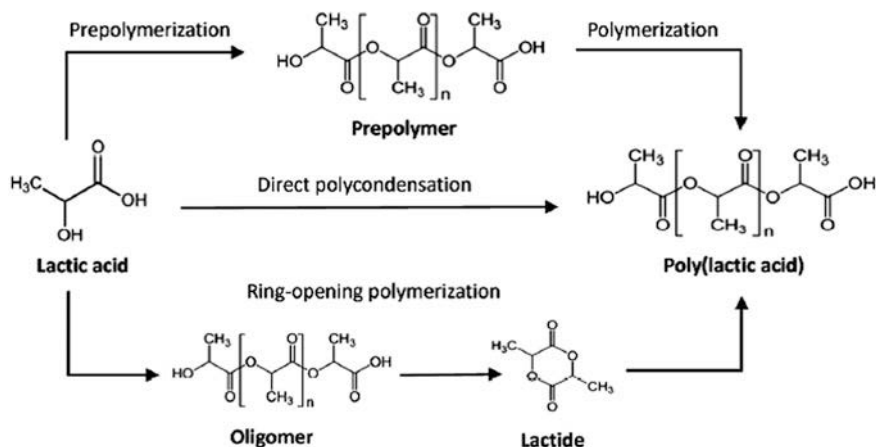


Fig. 5 Routes of PLA synthesis from lactic acid. (Adapted from [106])

200°C) resulting in high energy consumption [107]. Improved heating with microwave-assisted synthesis is more efficient with PLA (M_w 16,000 $\text{g}\cdot\text{mol}^{-1}$) produced within 30 min using the enhanced catalytic effect of binary SnCl_2 or p -TsOH catalyst [108].

For AP where the water is removed efficiently by the azeotropic solvents, the appropriate solvent is critical to the performance and polymer properties. The equilibrium between the monomer and the polymer is manipulated in the organic solvent to produce relatively high M_w polymer in one step at the temperature lower than the polymer T_m , to avoid any impurities caused by the depolymerisation and racemization [109]. Besides azeotropic solvents, a Soxhlet extractor with molecular sieve (3 Å) inside simultaneously removes trace water from the refluxed solvent to produce 33,000 $\text{g}\cdot\text{mol}^{-1}$ M_w polymer [110]. The SSP consists of the melt state to produce oligomer at high temperature (150–200 °C) and the solid state to further increase the M_w between the T_g and the T_m . In the second step before heating, the prepolymer of relatively low M_w is pulverized into semi-crystalline powder, chip, pellet or fiber of diameter less than 150 μm , and thoroughly dried for highly efficient and homogeneous heat transfer and distribution resulting in high molecular weight and improved polymer properties and purity [111]. The heating program starts at 130 °C and rises to 160 °C stepwise as the polymer T_m increases, resulting in PLA with M_w of 202,000 $\text{g}\cdot\text{mol}^{-1}$ without any catalyst and solvent used [111]. A starting mixture of L -PLA and D -PLA at 1:1 ratio in solid-state polycondensation could improve the polymer T_m from 160–170 °C to over 200 °C, suggesting reinforced thermal stability [112].

PLA leading producers, such as Cargill Dow (USA) and Shimadzu (Japan) applies ROP as the propagation process of the intermediate lactide [113–115] where the terminal end of the polymer classifies the mechanism into anionic ROP, cationic ROP and radical ROP [116]. Controlling the purity of lactide and synthesis conditions, without chain coupling agent or azeotropic system, could lead to a polymer

with specific and desirable properties such as refractive index and a wider range of molecular weight, making ROP of lactide the route to the synthesis of high molecular weight PLA [117]. A twin-screwed extruder conducts the reactive extrusion, improving the conversion yield to 99% and shortening the duration time to only 7 min, significantly improving the efficiency [118]. More hydroxyl groups as co-initiators could lead to higher M_w ($>400,000 \text{ g mol}^{-1}$) and faster polymerization ($<5 \text{ h}$), without affecting the polymer thermal properties, with M_w of $160,000 \text{ g mol}^{-1}$ at $200 \text{ }^\circ\text{C}$ for 1 h without solvent as co-initiator [119]. Solvent-free polymerization could actually achieve higher molecular weight PLA with higher efficiency [120]. PLA with high M_w ($100,000 \text{ g mol}^{-1}$) is attained at $140 \text{ }^\circ\text{C}$ for 10 h, but a longer period of preparation may be required at extremely low pressure (0.001 kPa) and dry condition [121]. The metal-free organocatalyst has also attracted increasing interest in polymerization where guanidine and amidine organocatalyst have proven highly effective towards ROP of cyclic esters such as lactide [122, 123]. The organocatalyst 1,5,7-Triazabicyclo[4.4.0]dec-5-ene (TBD) shortens the ROP reaction time of with high conversion yield of 95–99% [122]. Potent organocatalysts could contribute towards reaction efficiency improvement, ROP under atmospheric pressure at room temperature and preventing residual organometallic catalyst contamination, but the resultant polymer may be of lower M_w ($10,000\text{--}50,000 \text{ g mol}^{-1}$) and some may possess acute toxicity and high cost [123]. There is a need to develop a safe operating procedure and environmental assessment, proper catalyst recovery method and the economic flexibility for industrial application [106].

3.1.2 PLA SPCs

PLAs are biodegradable and compostable and degraded by simple hydrolysis of the ester bond without the need for enzymes but the rate of degradation is dependent on the size and shape of the article, the isomer ratio, and the temperature of hydrolysis. The current market and applications of PLA are 70% in the industrial packaging sector or the biocompatible/bioabsorbable medical device market [87, 124]. Polycondensation may produce PLA of low M_w using basic equipment and process, while ROP produces a wider range of M_w by controlling the purity of lactide and its polymerization, but the selection of the specific method should be based on its intended final application. Low M_w PLA, for example, may be suitable for drug release materials [106], so that it could be tuned for controlled-release and high M_w PLA for packaging and textile products [106]. High-molecular-weight PLA is colourless, glossy, stiff with properties similar to PS. The T_g of PLA is about $55 \text{ }^\circ\text{C}$ and the T_m is $175 \text{ }^\circ\text{C}$, and the processing temperatures should be in the excess of $185\text{--}190 \text{ }^\circ\text{C}$ [125]. PLA degrades at temperatures above $200 \text{ }^\circ\text{C}$, and can be caused by hydrolysis, lactide reformation, oxidative main chain scission, and inter- or intramolecular transesterification reactions, depending on time, temperature, low- M_w impurities, and the catalyst concentration. Catalysts and oligomers though decrease the degradation temperature may actually increase the degradation rate of

PLA, cause viscosity and rheological changes, fuming during processing, and poor mechanical properties [82, 126].

Several approaches such as copolymerization (block and stereoblock copolymers), microstructure and architecture control, and stereocomplexation, have been developed for designing new PLA-based polymers with a broad range of properties and improved processability [125]. Multiblock copolymers with alternating “soft” and “hard” segments, synthesized over a broad range of chemical compositions, show properties ranging from hard plastics to elastomers. Stereoblock copolymers with alternating amorphous and semicrystalline PLA blocks combine the advantages of PLA homopolymers (crystallinity) and random copolymers (processability). Independent control of polymer architecture and microstructure allows for the synthesis of star polymers with various arm morphologies. The stereocomplex formation between L -PLA and D -PLA, combining in situ polymerization with stereocomplexation takes advantage of the chirality of the lactide monomer, retention of configuration during polymerization, living nature of the lactide ROP in the presence of active hydrogen groups such as OH and NH_2 , and control of the level of transesterification reactions [125]. PLA homopolymers have a very narrow processing window and the most widely used method for improving PLA processability is based on T_m depression by random incorporation of small amount of D -lactide to the L -lactide to obtain PDLA, but this could lead to a significant decrease in crystallinity and crystallization rates [125]. The mixture (50/50) of preformed chains of P(L, L)LA and P(D, D)LA gives a stereocomplex with physicochemical and structural properties different from the corresponding PLA with the T_m of 230 °C, almost 50–60 °C higher than the PLA homopolymers [127, 128]. However, processing at these temperatures may lead to thermal degradation and the loss of M_w .

Compared to the bulk material, drawn fibers can exhibit a shift of the T_m and an increased enthalpy of melting. If the same grade of polymer is used for the matrix and the reinforcement, the shift in the T_m of the drawn fiber is not always sufficient enough for the production of SPCs. The concept of “overheating” is one of the methods in the manufacturing of SPCs. Both post-drawing temperature and the ultimate draw ratio have a significant influence on the degree of overheating. The enthalpy of a polymer is determined by the interaction forces between the molecular chains, while the entropy is determined by the conformation possibilities of a molecular chain. Controlled changing of either enthalpy or entropy, or both, would alter the crystalline T_m . Another way is by changing the conformation of the molecular chains and constraining the chains upon heating would shift the T_m towards higher temperatures. For the production of single fiber model composites, both ends of the polymer fibers are fixed on glass slides in order to prevent relaxation during heating. Pellets from the same polymer grade are isothermally hot pressed and the resulting thin films are placed on the same glass slide as the fiber. These stacked samples are heated in a hot-stage, melting only the matrix material but not the constrained fiber. The samples are then either air-cooled or isothermally crystallized in a hot-stage [2]. The overheating behavior of constrained fibers has resulted in the T_m shifts of about 10 °C [129–132]. Overheating of different

polymers is due to the decreased conformational entropy of constrained amorphous phase upon melting which may depend on the crystallinity level, the crystal size, and the kinetics of crystal melting and on the scan rate. A shift higher than 20 °C of the T_m has been shown with highly extended iPP (draw ratios > 14) and the 10 °C overheating observed in the ultra-drawn PE upon constraining mainly due to the change in chain mobility for PE in the hexagonal phase. iPP, and UHMWPE are apolar polymers where the interchain interactions are relatively weak which leads to a high degree of drawability [2]. The polar polymers (e.g. PET, PA) on the other hand have relative strong interchain interactions and are therefore less drawable. These are exhibited in PET and PA6 which show the draw ratios of only 4 with the temperature shifts of about 10 °C for the constrained fibers as compared to the unconstrained fibers [2]. To achieve the wide processing window, the drawing temperature should be optimized to avoid relaxation processes in the amorphous phase while at the same time induce orientation and improvement of the crystal size and perfection. The draw ratio should be above 7 to have chain unfolding and perfectly oriented especially for drawable polymers, and the chain mobility should be relative low for effective constraining. For high performance fibers and effective constraining, highly extended chains are therefore of considerable importance [2].

PLA SPCs have been prepared using PLLA fibers as reinforcement and poly (D,L-lactic acid) (PDLLA) as matrix and the PLLA SPCs prepared by partially fusing together softened PLLA fibers in the pressurized cylindrical mold [133]. PLA SPCs prepared using the same method makes use of PLA fiber for both the matrix and reinforcement such that the melt processing window is very narrow [134, 135]. The preparation of a poly(lactic acid) SPC consisting of amorphous sheets as matrix and highly crystalline fibres, yarns and fabrics have been made on the basis of PLA's slowly crystallizing characteristics. The crystallinity of the PLA sheets and fibers used are about 5 and 40%, respectively, and the T_g and T_m of the PLAs used for the sheets and the fabric are approximately 60 and 167 °C, respectively. The amorphous PLA sheets and the crystalline PLA fibers/fabrics are laminated and compression-molded to form an SPC at a processing temperature substantially lower than the PLA's T_m . The processing temperature plays a profound role in affecting the fiber–matrix bonding properties where an increase in the processing temperature results in drastic improvement in the interfacial bonding at around 135 °C, indicating the lower boundary of the process window. The compression-molded SPC exhibits enhanced mechanical properties with the tearing strength of the fabric-reinforced SPC almost an order higher than the non-reinforced PLA. The SPC with 25 wt% yarns achieves a significant improvement with Young's modulus of 3.7 GPa and the tensile strength of 58.6 MPa [17]. The amorphous PLA could be used as a matrix material but there are two competing processes for amorphous PLA, fusing and crystallizing, exist during heating. During PLA SPCs preparation, the fusion should be promoted while the crystallization in the matrix should be restricted. The amorphous PLA must therefore be rapidly heated to a suitable temperature between T_g and T_m so that it does not have time to crystallize. However, the PLA SPCs with large thickness may require a long time for thermal energy transfer from the SPC surface to its center [136] and

therefore may not be cost-effective. Highly oriented PLA tapes as the reinforcement and isotropic PLA film as matrix have also been explored to prepare the PLA SPCs. The highly oriented PLA tapes are pre-tensioned during hot-pressing to restrict the relaxation of the molecular chain so that the T_m of the PLA tape shifts to a higher temperature [137]. This widens the melt processing window of the PLA SPCs but it is difficult to prepare PLA SPCs by the normal hot-pressing device as this requires an additional constraining device [136].

Heat-bondable PLA core-shell fibre is a patented technology whereby the overlapping fibre-shells can be fused at a temperature significantly lower than the T_m of fibre-cores [138]. Mats of core-shell fibres of semi-crystalline poly(L-lactic acid) (core) and amorphous poly(D,L-lactic acid) (shell) produced through coaxial electrospinning have been used to prepare fibre reinforced SPC yarns and films [139]. The internal molecular arrangement (fine structure) within the fibres and the potential to enhance the crystallinity of the core and the heat-bond neighbouring fibres within the thermal operating window, between where the shell components fused and the T_m of the core components are established. Annealing/heat-pressing the core-shell fibres has been found to fuse the shells while enhancing the crystallinity of the cores. Heat-pressing plied fibre mats into a film has resulted in enhanced crystallinity (53%), significantly larger than the PLLA yarn (27%) although the mass component of the PLLA in the film is only 44% of that of the pure PLLA yarn. Thermal treatments therefore increase the crystallinity and the mechanical strength of the composite yarns. These core-shell fibres allow for continuous fibre reinforcement of biodegradable materials and offer a simple route to disperse nano-fibres homogeneously in a transparent matrix resin (as compared to the solvent casting impregnation methods) [139, 140]. Polylactide (PLA) SPCs have also been prepared using PLA nonwovens made of core-sheath PLA fibers as raw materials by hot-pressing. The core and sheath materials are poly(L-lactide) (PLLA) and PLA with D-lactide of about 10 mol% (PLA90), respectively. The melt processing window of PLA SPCs reaches more than 40 °C. The effects of hot-pressing temperature on the crystallinity, the crystal size distribution, the lamellar thickness and the mechanical property of PLA SPCs are more significant than the hot-pressing pressure treatment. The high mechanical properties of PLA SPCs are attributable to the strong interfacial adhesion between matrix and reinforcement. The tensile strength (σ_b), elongation at break (ϵ_b), the work of rupture (W) and impact strength (αcU) of the SPCs prepared at 130–160 °C are 47–65 MPa, 15–32%, 9–22 J, and 14.9–67.2 kJ m⁻², respectively, while those of pure PLAs prepared at 180 °C, are only 19 MPa, 1.8%, 0.15 J, and 2.8 kJ m⁻², respectively. The increase in hot-pressing temperature also reduces the σ_b , W and αcU [136].

3.2 PVA-Based

Poly(vinyl alcohol) (PVOH) is the only known water-soluble, carbon-carbon backbone polymer that is biodegradable under both aerobic and anaerobic

conditions, applicable in a wide range of applications such as films, fibres, adhesives, textile sizing, emulsifiers, paper coating [141–143]. The hydroxyl groups in its main backbone provide for the strong intra- and intermolecular hydrogen bonds, conferring high tensile strength, excellent adhesive properties, abrasion resistance, chemical resistance and gas barrier properties [144]. PVOH can be prepared by using natural gas as raw materials, and produced on an industrial scale by hydrolysis (methanolysis) of poly(vinyl acetate) through a one-pot reaction, to obtain PVOH of various grades depending upon the degree of hydrolysis [145]. Commercial production of PVOH fibres is carried out by wet spinning or dry spinning, where PVOH chips are dissolved in hot water and the solution is extruded through a spinneret. The extrudates are then coagulated to form continuous filaments and heat treated to gain adequate mechanical properties. The water resistance of the fibres can be improved by a heat treatment followed by acetalization and the thermal stability can be enhanced by plasticizers such as glycerol, ethylene glycol, amine alcohols and polyvalent hydroxyl compounds [146]. PVOH possesses excellent mechanical properties because of the high crystallinity with high tensile strength and a greater modulus of elasticity than the regular concrete, where the PVOH fibres develop a chemical bond with the cement during hydration and curing. Hence, PVOH fibres are effective in controlling the shrinkage and the fatigue cracking of the concretes [147], with wide-ranging industrial applications including as reinforcement in rubber hosing and geogrid, and in paper and non-woven applications [141].

The PVOH-based SPCs have been prepared through a melt compounding process. The PVOH chips are utilized as the matrix evaluated against three types of commercial PVOH Kuralon® fibres (WN2, WN4, WN8) as the reinforcement. The fibres are provided in the form of staples and differ in their T_m and tensile properties. PVOH fibres are dried at 60 °C for 6 h before being compounded with PVOH chips in a Thermo Haake internal mixer operating at 180 °C for 6 min. These provide good dispersion of the fibres whilst avoiding thermal degradation of the matrix. Square sheets of the composite samples with a mean thickness of about 1 mm are prepared by compression moulding the resulting materials at 180 °C for 5 min in a Carver laboratory press under a pressure of about 1 MPa. Samples are sealed in vacuum plastic bags under vacuum to prevent moisture absorption [141]. Based on the cryo-fractured surface morphology, the reinforcement structure and shape is maintained only when high fibres T_m are used. The introduction of PVOH fibres increases proportionally the stiffness, the yield properties and the Vicat softening temperature of the neat PVOH matrix with marked improvements of the viscoelastic properties of the composites. The storage modulus and the T_g of the PVOH-SPC increases with respect to the neat matrix but with progressive reduction of the elongation at break of the filled samples and strong reduction of the creep compliance values at all the tested temperatures [141].

Table 4 Ranking of different polymers based on Green design and Life-cycle assessment [154]

Material	Green design rank	LCA rank
PLA (NatureWorks)	1	6
PHA (Utilizing Stover)	2	4
PHA (General)	2	8
PLA (General)	4	9
High Density Polyethylene	5	2
Polyethylene Terephthalate	6	10
Low Density Polyethylene	7	3
Bio-polyethylene Terephthalate	8	12
Polypropylene	9	1
General Purpose Polystyrene	10	5
Polyvinyl chloride	11	7
Polycarbonate	12	11

4 Conclusion and Future Outlook

SPC preparation, morphology, and mechanical behavior based on semicrystalline polymers, amorphous—amorphous or amorphous—semicrystalline systems have been greatly developed in the past 40 years [15, 148]. The ‘toolbox’ to create SPCs include resolving the issues of matrix and reinforcement (the M_w and nucleation), tacticity (polymorphism, melting, crystallization, chain branching, copolymers, overheating), and interfacial bonding and adhesion [149]. SPCs have exhibited high levels of mechanical properties at lower densities and efficient thermal recyclability. Depending on the reinforcing component dimensions, SPC can be produced as micro- or nanocomposites. The same materials used in the SPCs matrix and the reinforcements results in enhanced interfacial adhesion and confers the composite fully recyclable by reprocessing. However, this has also led to the major issue in SPCs synthesis and fabrication which is the narrow temperature range of processing that even the slightest overheating of the fibrous material could irreversibly degrade its reinforcing properties. This can be resolved by employing the techniques of copolymerization and polymorphism of matrix and the reinforcement fibers can be improved by using nano-fillers of high aspect ratios. The SPCs are typically prepared by melt-processing techniques through the hot compaction, wherein the polymer fibers are consolidated by applying heat and pressure. A partial melting of the outer surface of the fibers allows for the matrix formation whilst the inner part remains unmelted, and highly oriented to act as reinforcement [150]. The concept of overheating of constrained fibers could resolve the problem associated with hot compaction. The key for cost-effective preparation of SPCs with optimum impregnation of the reinforcements by the matrix material of the same chemical composition can be the significant decrease of the viscosity of the matrix. This is possible when the thermoplastic matrix is obtained in situ, through polymerization of low-viscosity monomers or oligomers in the presence of the reinforcements such as the ROP [19],

where the ring-shaped monomer molecules are opened and transformed into high M_w polymers without release and accumulation of by-products [150]. Complex structures of SPCs also can be developed for more versatile applications in different fields such as for fire retardant or injection moldable grades [149, 151]. Table 4 shows that PLA attains the top spot in terms of green design ranking suggesting the bright future lies in the development of bio-based SPCs.

References

1. Capiati NJ, Porter RS (1975) The concept of one polymer composites modelled with high density polyethylene. *J Mater Sci* 10(10):1671–1677
2. Barkoula NM, Peijs T, Schimanski T, Loos J (2005) Processing of single polymer composites using the concept of constrained fibers. *Polym Compo* 26(1):114–120
3. Saheb DN, Jog JP (1999) Natural fiber polymer composites: a review. *Adv Polym Technol* 18(4):351–363
4. Herrera-Franco PJ, Valadez-Gonzalez A (2004) Mechanical properties of continuous natural fibre-reinforced polymer composites. *Compos A Appl Sci Manuf* 35(3):339–345
5. Thakur VK, Thakur MK, Raghavan P, Kessler MR (2014) Progress in green polymer composites from lignin for multifunctional applications: a review. *ACS Sustain Chem Eng* 2(5):1072–1092
6. Thakur VK, Thakur MK, Gupta RK (2014) Raw natural fiber—based polymer composites. *Int J Polym Anal Charact* 19(3):256–271
7. Klapiszewski Ł, Tomaszewska J, Skórczewska K, Jesionowski T (2017) Preparation and characterization of eco-friendly Mg (OH) 2/Lignin hybrid material and its use as a functional filler for Poly (Vinyl Chloride). *Polym* 9(7):258
8. Abdullah MA, Nazir MS, Ajab H et al (2017) Advances in eco-friendly pre-treatment methods and utilization of agro-based lignocelluloses. In: Thangadurai D, Sangeetha J (eds) *Industrial biotechnology: sustainable production and bioresource utilization*. Apple Academic Press, USA, pp 371–420
9. Nazir MS, Abdullah MA, Raza MR (2017) Polypropylene composite with oil palm fibers: method development, properties and applications. *Polypropylene-Based Biocomposites and Bionanocomposites* 287
10. Mohanty AK, Misra M, Drzal LT et al (2002) Sustainable bio-composites from renewable resources: Opportunities and challenges in the green materials world. *J Polym Environ* 10(1–2):19–26, *Environ* 10(112):19–20
11. Lithner D, Larsson Å, Dave G (2011) Environmental and health hazard ranking and assessment of plastic polymers based on chemical composition. *Sci Total Environ* 409(18):3309–3324
12. Gourmelon G (2015). Global plastic production rises, recycling lags. New Worldwatch Institute analysis explores trends in global plastic consumption and recycling. [Recuperado de http://www.worldwatch.org](http://www.worldwatch.org)
13. Abdullah MA, Nazir MS, Raza MR, Wahjoedi BA, Yussof AW (2016) Autoclave and ultra-sonication treatments of oil palm empty fruit bunch fibers for cellulose extraction and its polypropylene composite properties. *J Clean Prod* 126:686–697
14. Singh AA, Afrin S, Karim Z (2017) Green composites: versatile material for future. In *Green biocomposites*. Springer, Cham, pp 29–44
15. Matabola KP, De Vries AR, Moolman FS, Luyt AS (2009) Single polymer composites: a review. *J Mater Sci* 44(23):6213
16. Peijs T (2003) Composites for recyclability. *Mater Today* 6(4):30–35

17. Li R, Yao D (2008) Preparation of single poly (lactic acid) composites. *J Appl Polym Sci* 107(5):2909–2916
18. Huo M, Yuan J, Tao L, Wei Y (2014) Redox-responsive polymers for drug delivery: from molecular design to applications. *Polym Chem* 5(5):1519–1528
19. Sanjay MR, Madhu P, Jawaid M, Senthamaraiannan P, Senthil S, Pradeep S (2018) Characterization and properties of natural fiber polymer composites: a comprehensive review. *J Clean Prod* 172:566–581
20. Lee HB, Khang G, Lee JH (2013) Polymeric biomaterials. In: Wong JY, Bronzino JD, Peterson DR (eds) *Biomaterials: principles and practices*. CRC Press, Boca Raton. Florida, USA
21. Carraher Jr CE (2003) *Seymour/Carraher's polymer chemistry*. CRC Press
22. Shade Y (2016) *Polymer engineering*. White Word Publications, NY, USA
23. Harper CA, Petrie EM (2003) *Plastics materials and processes: a concise encyclopedia*. Wiley
24. Mallakpour S, Zadehnazari A (2011) Advances in synthetic optically active condensation polymers—a review. *Express Polym Lett* 5(2):142–181
25. Cao J, Yang NF, Wang PD, Yang LW (2008) Optically active polyethers from chiral terminal epoxides with bulky group. *Polym Int* 57(3):530–537
26. Chiellini E, Senatori L, Solaro R (1988) A new chiral poly (alkyl vinyl ether): synthesis and chiroptical properties. *Polym Bull* 20(3):215–220
27. Marvel CS, Overberger CG (1944) An optically active styrene derivative and its polymer I. *J Am Chem Soc* 66(3):475–477
28. Bailey WJ, Yates ET (1960) Polymers. III. Synthesis of optically active stereoregular polyolefins 1-3. *J Org Chem* 25(10):1800–1804
29. Pino P, Ciardelli F, Lorenzi GP, Natta G (1962) Optically active vinyl polymers. VI. Chromatographic resolution of linear polymers of (R)(S)-4-methyl-1-hexene. *J Am Chem Soc* 84(8):1487–1488
30. Rogers ME, Long TE (eds) (2003). *Synthetic methods in step-growth polymers*. Wiley
31. Nakano T (2001) Optically active synthetic polymers as chiral stationary phases in HPLC. *J Chromatogr A* 906(1–2):205–225
32. Dechy-Cabaret O, Martin-Vaca B, Bourissou D (2004) Controlled ring-opening polymerization of lactide and glycolide. *Chem Rev* 104(12):6147–6176
33. Yamamoto T, Tezuka Y (2011) Topological polymer chemistry: a cyclic approach toward novel polymer properties and functions. *Polymer Chem* 2(9):1930–1941
34. Adachi K, Tezuka Y (2009) Topological polymer chemistry in pursuit of elusive polymer ring constructions. *J Synth Org Chem Jpn* 67(11):1136–1143
35. Endo K (2008) Synthesis and properties of cyclic polymers. *New Frontiers in Polymer Synthesis*. Springer, Berlin, Heidelberg, pp 121–183
36. Yamamoto T, Tezuka Y (2012) Multicyclic polymers. In *Synthesis of polymers: new structures and methods*. Wiley-VCH, Weinheim
37. McKetta Jr JJ (1976) *Encyclopedia of chemical processing and design: volume 1-abrasives to acrylonitrile*. CRC press
38. Brody H (1994). *Synthetic fibre materials*. Longman
39. Kricheldorf HR, Nuyken O, Graham S (2005) *Handbook of polymer synthesis*. Marcel Dekker, New York
40. Zhang X (2014) *Fundamentals of fiber science*. DEStech Publications, Inc
41. <http://www.tikp.co.uk/knowledge/technology/fibre-and-filament-production/dry-jet-wet-spinning/>. Accessed 19 May 2018
42. Kristiansen M, Tervoort T, Smith P (2003) Synergistic gelation of solutions of isotactic polypropylene and bis-(3, 4-dimethyl benzylidene) sorbitol and its use in gel-processing. *Polymer* 44(19):5885–5891
43. Lemstra PJ, Kirschbaum R (1985) Speciality products based on commodity polymers. *Polymer* 26(9):1372–1384

44. Loos J, Schimanski T, Hofman J, Peijs T, Lemstra PJ (2001) Morphological investigations of polypropylene single-fibre reinforced polypropylene model composites. *Polymer* 42 (8):3827–3834
45. Takayanagi M, Imada K, Kajiyama T et al (1967) Mechanical properties and fine structure of drawn polymers. *J Polym Sci: Polym Symp* 15(1):263–281. (Wiley Subscription Services, Inc., A Wiley Company)
46. Peterlin A (1971) Molecular model of drawing polyethylene and polypropylene. *J mater sci* 6(6):490–508
47. Gupta B, Revagade N, Hilborn J (2007) Poly (lactic acid) fiber: an overview. *Prog Polym Sci* 32(4):455–482
48. Huang ZM, Zhang YZ, Kotaki M, Ramakrishna S (2003) A review on polymer nanofibers by electrospinning and their applications in nanocomposites. *Compos sci technol* 63 (15):2223–2253
49. Ma J, Zhang Q, Mayo A, Ni Z, Yi H, Chen Y, Li D (2015) Thermal conductivity of electrospun polyethylene nanofibers. *Nanoscale* 7(40):16899–16908
50. Berber E, Horzum N, Hazer B, Demir MM (2016) Solution electrospinning of polypropylene-based fibers and their application in catalysis. *Fibers Polym* 17(5):760–768
51. Biazar E, Ahmadian M, Heidari S, Gazmeh A, Mohammadi SF, Lashay A, Hashemi H (2017) Electro-spun polyethylene terephthalate (PET) mat as a keratoprosthesis skirt and its cellular study. *Fibers Polym* 18(8):1545–1553
52. Sereshti H, Amini F, Najarzadekan H (2015) Electrospun polyethylene terephthalate (PET) nanofibers as a new adsorbent for micro-solid phase extraction of chromium (VI) in environmental water samples. *RSC Adv* 5(108):89195–89203
53. Matabola KP, De Vries AR, Luyt AS, Kumar R (2011) Studies on single polymer composites of poly (methyl methacrylate) reinforced with electrospun nanofibers with a focus on their dynamic mechanical properties
54. Casasola R, Thomas NL, Trybala A, Georgiadou S (2014) Electrospun poly lactic acid (PLA) fibres: effect of different solvent systems on fibre morphology and diameter. *Polymer* 55(18):4728–4737
55. Casasola R, Thomas NL, Georgiadou S (2016) Electrospinning of poly (lactic acid): theoretical approach for the solvent selection to produce defect-free nanofibers. *J Polym Sci, Part B: Polym Phys* 54(15):1483–1498
56. Alcock B, Cabrera NO, Barkoula NM, Loos J, Peijs T (2006) The mechanical properties of unidirectional all-polypropylene composites. *Compos A Appl Sci Manuf* 37(5):716–726
57. Houshyar S, Shanks RA, Hodzic A (2005) The effect of fiber concentration on mechanical and thermal properties of fiber-reinforced polypropylene composites. *J Appl Polym Sci* 96 (6):2260–2272
58. Houshyar S, Shanks RA (2006) Mechanical and thermal properties of flexible poly (propylene) composites. *Macromol Mater Eng* 291(1):59–67
59. Lacroix FV, Lu HQ, Schulte K (1999) Wet powder impregnation for polyethylene composites: preparation and mechanical properties. *Compos A Appl Sci Manuf* 30(3):369–373
60. Cabrera N, Alcock B, Loos J, Peijs T (2004) Processing of all-polypropylene composites for ultimate recyclability. *Proc Inst Mech Eng, Part L: J Mat: Des Appl* 218(2):145–155
61. Hine PJ, Olley RH, Ward IM (2008) The use of interleaved films for optimising the production and properties of hot compacted, self reinforced polymer composites. *Compos Sci Technol* 68(6):1413–1421
62. Jordan ND, Bassett DC, Olley RH, Hine PJ, Ward IM (2003) The hot compaction behaviour of woven oriented polypropylene fibres and tapes. II. Morphology of cloths before and after compaction. *Polymer* 44(4):1133–1143
63. Shavit-Hadar L, Khalfin RL, Cohen Y, Rein DM (2005) Harnessing the melting peculiarities of ultra-high molecular weight polyethylene fibers for the processing of compacted fiber composites. *Macromol Mater Eng* 290(7):653–656

64. Hine PJ, Astruc A, Ward IM (2004) Hot compaction of polyethylene naphthalate. *J Appl Polym Sci* 93(2):796–802
65. Wright-Charlesworth DD, Lautenschlager EP, Gilbert JL (2005) Hot compaction of poly (methyl methacrylate) composites based on fiber shrinkage results. *J Mater Sci—Mater Med* 16(10):967–975
66. Wang J, Chen J, Dai P, Wang S, Chen D (2015) Properties of polypropylene single-polymer composites produced by the undercooling melt film stacking method. *Compos Sci Technol* 107:82–88
67. Lacroix FV, Loos J, Schulte K (1999) Morphological investigations of polyethylene fibre reinforced polyethylene. *Polymer* 40(4):843–847
68. Wang J, Chen J, Dai P (2014) Polyethylene naphthalate single-polymer-composites produced by the undercooling melt film stacking method. *Compos Sci Technol* 91:50–54
69. Porras A, Tellez J, Casas-Rodriguez JP (2012) Delamination toughness of ultra high molecular weight polyethylene (UHMWPE) composites. In *EPJ Web of Conferences*, vol 26, p 02016. EDP Sciences
70. Goswami TK, Mangaraj S (2011) Advances in polymeric materials for modified atmosphere packaging (MAP). In *Multifunctional and nanoreinforced polymers for food packaging*, pp 163–242
71. Karger-Kocsis J, Siengchin S (2014) Single-polymer composites: concepts, realization and outlook. *KMUTNB Int J Appl Sci Technol* 7(1):1–9
72. <https://www.theguardian.com/sustainable-business/2017/mar/22/carbon-fibre-wonder-material-dirty-secret>
73. Khanam PN, AlMaadeed MAA (2015) Processing and characterization of polyethylene-based composites. *Adv Manuf: Polym Compos Sci* 1(2):63–79
74. Mead WT, Porter RS (1978) The preparation and tensile properties of polyethylene composites. *J Appl Polym Sci* 22(11):3249–3265
75. Mosleh M, Suh NP, Arinez J (1998) Manufacture and properties of a polyethylene homocomposite. *Compos A Appl Sci Manuf* 29(5–6):611–617
76. Lacroix FV, Werwer M, Schulte K (1998) Solution impregnation of polyethylene fibre/polyethylene matrix composites. *Compos A Appl Sci Manuf* 29(4):371–376
77. Teishev A, Incardona S, Migliaresi C, Marom G (1993) Polyethylene fibers-polyethylene matrix composites: Preparation and physical properties. *J Appl Polym Sci* 50(3):503–512
78. Devaux E, Caze C (1999) Composites of ultra-high-molecular-weight polyethylene fibres in a low-density polyethylene matrix: II. Fibre/matrix adhesion. *Compos Sci Technol* 59(6):879–882
79. Hameed T, Hussein IA (2004) Effect of short chain branching of LDPE on its miscibility with linear HDPE. *Macromol Mater Eng* 289(2):198–203
80. Houshyar S, Shanks RA (2003) Morphology, thermal and mechanical properties of Poly (propylene) fibre-matrix composites. *Macromol Mater Eng* 288(8):599–606
81. Rhim JW, Park HM, Ha CS (2013) Bio-nanocomposites for food packaging applications. *Prog Polym Sci* 38(10–11):1629–1652
82. Garlotta D (2001) A literature review of poly (lactic acid). *J Polym Environ* 9(2):63–84
83. Benninga H (1990) A history of lactic acid making: a chapter in the history of biotechnology, vol 11. Springer Science & Business Media
84. Datta R, Tsai SP, Bonsignore P, Moon SH, Frank JR (1995) Technological and economic potential of poly (lactic acid) and lactic acid derivatives. *FEMS Microbiol Rev* 16(2–3):221–231
85. Kharas GB, Sanchez-Riera F, Severson DK (1994) In: Mobley DP (ed) *Plastics from microbes*. Hanser-Gardner, Munich, pp 93–137
86. Van Ness JH (1981) Kirk-Othmer encyclopedia of chemical technology. 3rd ed, vol 13. Wiley, New York, pp 80–103
87. Hartmann MH (1998) High molecular weight polylactic acid polymers. In: *Biopolymers from renewable resources*, pp 367–411. Springer, Berlin, Heidelberg
88. Buchholz B (1994) U.S. Patent No. 5,302,694. U.S. Patent and Trademark Office, Washington, DC

89. Tsuji H, Ikada Y (1999) Physical properties of polylactides. *Curr Trends Polym Sci* 4:27
90. Lunt J (1998) Large-scale production, properties and commercial applications of polylactic acid polymers. *Polym Degrad Stab* 59(1–3):145–152
91. Kricheldorf HR, Kreiser I (1987) Polylactones, 11. Cationic copolymerization of glycolide with l, l-dilactide. *Die Makromolekulare Chemie. Macromol Chem Phys* 188(8):1861–1873
92. Kricheldorf HR, Sumbel M (1989) Polylactones—18. Polymerization of l, l-lactide with Sn (II) and Sn (IV) halogenides. *Eur Polymer J* 25(6):585–591
93. Dittrich VW, Schulz RC (1971) Kinetik und Mechanismus der ringöffnenden Polymerisation von L (-)-Lactid. *Die Angewandte Makromolekulare Chemie: Applied Macromolecular Chemistry and Physics* 15(1):109–126
94. Kricheldorf HR, Dunsing R (1986) Polylactones, 8. Mechanism of the cationic polymerization of L, L-dilactide. *Die Makromolekulare Chemie. Macromol Chem Phys* 187(7):1611–1625
95. Kricheldorf HR, Kreiser-Saunders I (1990) Polylactones, 19. Anionic polymerization of L-lactide in solution. *Die Makromolekulare Chemie: Macromol Chem Phys* 191(5):1057–1066
96. Dahlmann J, Rafler G, Fechner K, Mehliß B (1990) Synthesis and properties of biodegradable aliphatic polyesters. *Polym Int* 23(3):235–240
97. Kricheldorf HR, Serra A (1985) Polylactones. *Polym Bull* 14(6):497–502
98. Kohn FE, Van Den Berg JWA, Van De Ridder G, Feijen J (1984) The ring-opening polymerization of D, L-lactide in the melt initiated with tetraphenyltin. *J Appl Polym Sci* 29(12):4265–4277
99. Enomoto K, Ajioka M, Yamaguchi A (1994) U.S. Patent No. 5,310,865. U.S. Patent and Trademark Office, Washington, DC
100. Kashima T, Kameoka T, Higuchi C, Ajioka M, Yamaguchi A (1995) U.S. Patent No. 5,428,126. U.S. Patent and Trademark Office, Washington, DC
101. Ichikawa F, Kobayashi M, Ohta M, Yoshida Y, Obuchi S, Itoh H (1995) U.S. Patent No. 5,440,008. U.S. Patent and Trademark Office, Washington, DC
102. Ohta M, Obuchi S, Yoshida Y (1995) U.S. Patent No. 5,444,143. U.S. Patent and Trademark Office, Washington, DC
103. Ajioka M, Enomoto K, Suzuki K, Yamaguchi A (1995) The basic properties of poly (lactic acid) produced by the direct condensation polymerization of lactic acid. *J Environ Polym Degradat* 3:225–234
104. Ajioka M, Enomoto K, Suzuki K, Yamaguchi A (1995) Basic properties of polylactic acid produced by the direct condensation polymerization of lactic acid. *Bull Chem Soc Jpn* 68(8):2125–2131
105. Suizu H, Takagi M, Ajioka M, Yamaguchi A (1996) U.S. Patent No. 5,496,923. U.S. Patent and Trademark Office, Washington, DC
106. Hu Y, Daoud WA, Cheuk KKL, Lin CSK (2016) Newly developed techniques on polycondensation, ring-opening polymerization and polymer modification: focus on poly (lactic acid). *Materials* 9(3):133
107. Achmad F, Yamane K, Quan S, Kokugan T (2009) Synthesis of polylactic acid by direct polycondensation under vacuum without catalysts, solvents and initiators. *Chem Eng J* 151(1–3):342–350
108. Nagahata R, Sano D, Suzuki H, Takeuchi K (2007) Microwave-assisted single-step synthesis of poly (lactic acid) by direct polycondensation of lactic acid. *Macromol Rapid Commun* 28(4):437–442
109. Gupta AP, Kumar V (2007) New emerging trends in synthetic biodegradable polymers—Polylactide: a critique. *Eur Polymer J* 43(10):4053–4074
110. Kim KW, Woo SI (2002) Synthesis of high-molecular-weight poly (L-lactic acid) by direct polycondensation. *macromolecular chemistry and physics* 203(15):2245–2250
111. Fukushima K, Kimura Y (2008) An efficient solid-state polycondensation method for synthesizing stereocomplexed poly (lactic acid) s with high molecular weight. *J Polym Sci, Part A: Polym Chem* 46(11):3714–3722

112. Fukushima K, Furuhashi Y, Sogo K, Miura S, Kimura Y (2005) Stereoblock poly (lactic acid): synthesis via solid-state polycondensation of a stereocomplexed mixture of poly (L-lactic acid) and poly (D-lactic acid). *Macromol Biosci* 5(1):21–29
113. www.jimluntllc.com/pdfs/PolylacticAcidPolymersFromCorn. Accessed 26 May 2018
114. <https://www.natureworkslc.com>. Accessed 26 May 2018
115. Oota M, Ito M (1998) U.S. Patent No. 5,821,327. U.S. Patent and Trademark Office, Washington, DC
116. Nuyken O, Pask SD (2013) Ring-opening polymerization—an introductory review. *Polymers* 5(2):361–403
117. Stridsberg KM, Ryner M, Albertsson AC (2002) Controlled ring-opening polymerization: polymers with designed macromolecular architecture. In: *Degradable aliphatic polyesters*, pp. 41–65. Springer, Berlin
118. Jacobsen S, Fritz HG, Degée P, Dubois P, Jérôme R (2000) New developments on the ring opening polymerisation of polylactide. *Ind Crops Prod* 11(2–3):265–275
119. Korhonen H, Helminen A, Seppälä JV (2001) Synthesis of poly lactides in the presence of co-initiators with different numbers of hydroxyl groups. *Polymer* 42(18):7541–7549
120. Zhong Z, Dijkstra PJ, Feijen J (2002) [(salen) Al]-mediated, controlled and stereoselective ring-opening polymerization of lactide in solution and without solvent: synthesis of highly isotactic polylactide stereocopolymers from racemic d, l-lactide. *Angew Chem Int Ed* 41(23):4510–4513
121. Kaihara S, Matsumura S, Mikos AG, Fisher JP (2007) Synthesis of poly (L-lactide) and polyglycolide by ring-opening polymerization. *Nat Protoc* 2(11):2767
122. Lohmeijer BG, Pratt RC, Leibfarth F, Logan JW, Long DA, Dove AP et al (2006). Guanidine and amidine organocatalysts for ring-opening polymerization of cyclic esters. *Macromolecules* 39(25):8574–8583
123. Kamber NE, Jeong W, Waymouth RM, Pratt RC, Lohmeijer BG, Hedrick JL (2007) Organocatalytic ring-opening polymerization. *Chem Rev* 107(12):5813–5840
124. Rusu D, Boyer SE, Lacrampe MF, Krawczak P (2001). Bioplastics and vegetal fiber reinforced bioplastics for automotive applications. In: Pilla S (ed) *Handbook of bioplastics and biocomposites engineering applications*. Scrivener Publishing, Massachusetts 2011:397–449
125. Spinu M, Jackson C, Keating MY, Gardner KH (1996) Material design in poly (lactic acid) systems: block copolymers, star homo-and copolymers, and stereocomplexes. *J Macromol Sci Part A Pure Appl Chem* 33(10):1497–1530
126. Farah S, Anderson DG, Langer R (2016) Physical and mechanical properties of PLA, and their functions in widespread applications—A comprehensive review. *Adv Drug Deliv Rev* 107:367–392
127. Ikada Y, Jamshidi K, Tsuji H, Hyon SH (1987) Stereocomplex formation between enantiomeric poly (lactides). *Macromolecules* 20(4):904–906
128. Tsuji H (2000) Stereocomplex from enantiomeric polylactides. *Res Adv Macromol* 1:25–28
129. Kirschbaum R, van Dingenen JLJ (1989) Integration of fundamental polymer science and technology, vol 3. In: Lemstra PJ, Kleintjes LA (eds) Elsevier, London, p 178
130. Bastiaansen CMW, Lemstra PJ (1989) Macromolecular chemistry. *Macromol Symp* 28: p. 73)
131. Samuels RJ (1979) High strength elastic polypropylene. *J Polym Sci, Part B: Polym Phys* 17(4):535–568
132. Tanaka H, Takagi N, Okajima S (1974) Melting behavior of highly stretched isotactic polypropylene film. *J Polym Sci, Part A: Polym Chem* 12(12):2721–2728
133. Tormala P, Rokkanen P, Laiho J, Tamminmaki M, Vainionpaa S (1988) U.S. Patent No. 4,743,257. U.S. Patent and Trademark Office, Washington, DC
134. Jia W, Gong RH, Hogg PJ (2014) Poly (lactic acid) fibre reinforced biodegradable composites. *Compos B Eng* 62:104–112
135. Wu N, Liang Y, Zhang K, Xu W, Chen L (2013) Preparation and bending properties of three dimensional braided single poly (lactic acid) composite. *Compos B Eng* 52:106–113

136. Liu Q, Zhao M, Zhou Y, Yang Q, Shen Y, Gong RH, Deng B (2018) Polylactide single-polymer composites with a wide melt-processing window based on core-sheath PLA fibers. *Mat Des* 139:36–44
137. Mai F, Tu W, Bilotti E, Peijs T (2015) Preparation and properties of self-reinforced poly (lactic acid) composites based on oriented tapes. *Compos A Appl Sci Manuf* 76:145–153
138. Barrows TH (1999) Bioabsorbable fibers and reinforced composites produced there from PCT. US 6,511,748 B1. WO99/34750
139. Kriel H, Sanderson RD, Smit E (2013) Single polymer composite yarns and films prepared from heat bondable poly (lactic acid) core-shell fibres with submicron fibre diameters. *Fibres & Textiles in Eastern Europe*
140. Chen LS, Huang ZM, Dong GH, He CL, Liu L, Hu YY, Li Y (2009) Development of a transparent PMMA composite reinforced with nanofibers. *Polym Compos* 30(3):239–247
141. Dorigato A, Pegoretti A (2012) Biodegradable single-polymer composites from polyvinyl alcohol. *Colloid Polym Sci* 290(4):359–370
142. Matsumura S, Toshima K (1996) Biodegradation of poly (vinyl alcohol) and vinyl alcohol block as biodegradable segment
143. Matsumura S, Tomizawa N, Toki A, Nishikawa K, Toshima K (1999) Novel poly (vinyl alcohol)-degrading enzyme and the degradation mechanism. *Macromolecules* 32(23):7753–7761
144. Chen N, Li L, Wang Q (2007) New technology for thermal processing of poly (vinyl alcohol). *Plast, Rubber Compos* 36(7–8):283–290
145. Chiellini E, Corti A, D'Antone S, Solaro R (2003) Biodegradation of poly (vinyl alcohol) based materials. *Progr Polym Sci* 28(6):963–1014
146. Petrusenko EF, Voskanyan PS, Pakharenko V (1988) Rheological Properties of PVA Based Compositions. *Plast Massy* 11:23–24
147. Shao Y, Shah SP (1997) Mechanical properties of PVA fiber reinforced cement composites fabricated by extrusion processing. *ACI Mater J* 94(6):555–564
148. Fakirov S (2013) Nano-and microfibrillar single-polymer composites: a review. *Macromol Mater Eng* 298(1):9–32
149. Karger-Kocsis J, Bárány T (2014) Single-polymer composites (SPCs): Status and future trends. *Compos Sci Technol* 92:77–94
150. Dencheva N, Denchev Z, Pouzada AS, Sampaio AS, Rocha AM (2013) Structure–properties relationship in single polymer composites based on polyamide 6 prepared by in-mold anionic polymerization. *J Mat Sci* 48(20):7260–7273
151. Bocz K, Toldy A, Kmetty Á, Bárány T, Igricz T, Marosi G (2012) Development of flame retarded self-reinforced composites from automotive shredder plastic waste. *Polym Degrad Stab* 97(3):221–227
152. Lukkassen D, Meidell A (2003) Advanced materials and structures and their fabrication processes. *Narrik University College, Hin*
153. Jamshidian M, Tehrani EA, Imran M, Jacquot M, Desobry S (2010) Poly-lactic acid: production, applications, nanocomposites, and release studies. *Compr Rev Food Sci Food Safety* 9(5):552–571
154. <https://www.epa.gov/greenchemistry/presidential-green-chemistry-challenge-winners>. Accessed 26th May 2018

Processing Aspects and Biomedical and Environmental Applications of Sustainable Nanocomposites Containing Nanofillers



Mohd Azmuddin Abdullah, Muhammad Shahid Nazir, Zaman Tahir, Yasir Abbas, Majid Niaz Akhtar, Muhammad Rafi Raza and Hanaa Ali Hussein

1 Introduction

Polymer matrices such as rubber, plastic, acrylic, ethylene are commonly available in the market. These materials have advantages due to their lightweight, straightforward processing, and low cost [1], with outstanding corrosion stability and ductility. The major disadvantages of the polymer components are the low thermal and environmental stability (against UV), low acid resistance, and conductivity [2]. To overcome the problems, the polymer matrices are reinforced with fillers (particles, fibers, or platelets, synthetic or natural, organic or inorganic) at macro, micro, or nanoscale [3–5]. The resultant composite materials have characteristics different from the individual constituent. The composites consisting of two or more constituents may have significantly different physical or chemical properties, but the

M. A. Abdullah (✉) · H. A. Hussein
Institute of Marine Biotechnology, Universiti Malaysia Terengganu,
21030 Kuala Nerus, Terengganu, Malaysia
e-mail: azmuddin@umt.edu.my; joule1602@gmail.com

M. S. Nazir (✉)
Department of Chemistry, COMSATS, Institute of Information Technology,
Defence Road, Off Raiwind Road, Lahore, Punjab, Pakistan
e-mail: shahid.nazir@cuilahore.edu.pk

Z. Tahir · Y. Abbas
Department of Chemical Engineering, COMSATS, Institute of Information Technology,
Defence Road, Off Raiwind Road, Lahore, Punjab, Pakistan

M. N. Akhtar
Department of Physics, Muhammad Nawaz Shareef (MNS) University of Engineering
and Technology, Multan, Punjab, Pakistan

M. R. Raza
Department of Mechanical Engineering, COMSATS, Institute of Information Technology,
Sahiwal 57000, Punjab, Pakistan

constituent components remain separate and distinct within the finished structure. The characteristics of the filler and the host material will determine the performance, although, with time, this may still deteriorate upon exposure to UV, high temperature, pH, and humidity [6].

In the petroleum industry, epoxy resins are derived products possessing superior properties, dimensional stability, and good wettability with matrices for composite fillers and structural adhesives [7]. The industries based on epoxies in 2010 have reported 2 million tonnes of production with an annual turnover of USD20 billion [8]. Approximately 90% of epoxies are produced from diglycidal ether of bisphenol A (DGEBA) [8] which is an endocrine disruptor in humans and causing morbidity, decreased fertility, and cancer [9]. Polymer composites have therefore gained prominence in sciences, technology and engineering essentially to address the issue of global sustainability and as a replacement to the conventional materials such as the epoxies, metals, and ceramics. Engineered composite materials can be found as plywood and polymer matrix composites, ceramic matrix composites, metal matrix composites and smart composite materials which require greater strength to weight ratio and cost-effectiveness. The implications are seen in industries from construction, automobiles, and furniture, to common applications such as the landfill liner which uses waste clay from boron production, wood fillers in the thermoplastic matrix, and thermal insulation of paper cups, to the more sophisticated applications in aerospace, microelectronics, biomedical and pharmaceuticals [10].

Fibre-reinforced polymers (FRPs) possess strong ecological appeal, low cost, and higher specific mechanical properties. The polymer matrix has been reinforced with synthetic or artificial fibers to improve the performance of the final products [11]. Renewable and sustainable materials from the industrial and agricultural residues and energy crops especially have bright future as reinforcement material to improve specific properties in composite or nanocomposites. The agro-based materials are attractive for sustainable technologies and safe production, whilst fulfilling the energy needs of the industries [12]. The total world biomass production of the lignocellulosic material is estimated at 10 Mg per hectare per year [13], and the total cellulose production reaches 10^{11} – 10^{12} tonnes per year [14], with the annual consumption of 7.5×10^{10} tonnes [15]. In the light of indiscriminate dumping of residual plastics which has caused serious global environmental problems, and the free availability of biomass wastes from agricultural sectors, the development of biocomposite material based on agro-residues with synthetic polymer will pave the way for enhanced waste recycling and the conversion into value-added products [16].

This review article discusses the characteristics and fabrication of nano-fillers with a special focus on cellulose, chitosan, and magnetic nanocomposites, the composites development and the preparation of nanofibers with renewable polymers. The applications in drug delivery, tissue engineering, biosensor and electrical insulation, and the catalysis and environmental remediation are highlighted.

2 Characteristics and Fabrication of Nano-fillers

The range of the host materials used in nanohybrids include the organic polymers, silica or even liquid media. A standardization committee, ISO TC229 “Nanotechnologies” in 2005 in a joint group with IEC 113 “Nanotechnology Standardization for Electrical and Electronic Products and Systems” has defined nanocomposites as those containing fillers with at least one dimension of size less than 100 nm (ISO/TS27687:2008, ISO/TS11360:2010, ISO/TS88004:2011, ISO/TS 80004-2:2015) [17]. The properties (such as mechanical, electrical, optical or thermal) of a new generation of materials can be controlled with the nano-fillers which depend upon the chemical composition, shape, size, dispersion and orientation of the nanofillers. Nanocomposites are multi-phasic materials where the matrix material incorporates units with one, two or three dimension and may contain the nanofillers up to 10% of the total mass of the matrix. The fillers and the matrix are mixed at a moderate temperature, followed by the fabrication into the desired shape, but the functionalized fillers may result in better incorporation into the composites [18]. The advantages are the integration of several component materials and their properties in a single material. The combined properties of the matrix material and the nanosized filler yield novel functional materials, which can be tailor-made for specific applications [19, 20].

The nanofillers can be divided into the one-dimensional nanoplate, two-dimensional nanofibres and three-dimensional nanoparticles (Fig. 1). The nanoplate nanofillers have a thickness in the nanometer scale, though the lateral dimension could be several hundred nanometers to microns in the range [21]. Smectite clay minerals, particularly montmorillonites (MMTs) and graphene are examples of one-dimensional nanofillers. To improve the silicate compatibility with the polymer chains, organophilic modification of the internal and external cations of the clay minerals can be carried out. Graphene is a one-atom-thick planar, single sheet of sp²-bonded carbon atoms, synthesized from graphite by micromechanical cleavage [22–24], and its one-atom thickness is advantageous for ultrafast computational and sensor applications [25]. The nanofiber nanofillers have diameters in the nanometer scale such as the carbon nanofibers (CNFs) and nanotubes (CNTs), metallic nano-rods, and whiskers. The CNFs and CNTs are the most widely used

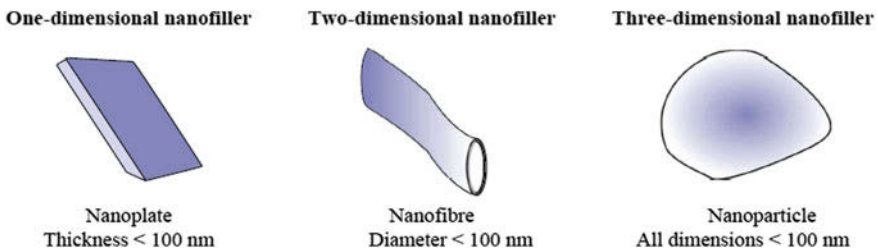


Fig. 1 Shapes of nanofillers used in the nanocomposites (adapted from [17])

nanofiber nanofillers in the polymer nanocomposites [26]. The CNTs, available in single wall or multi walls, with the lengths of tens of microns and the diversity in the synthesis routes and fabrication, may result in a different structure, diameter, aspect ratio, crystallinity, purity, and entanglement. The extraordinary properties of the CNTs such as density less than 2 g cm^{-3} with axial stiffness in the order of 1 TPa and the strength of 50 GPa [22], render the CNTs to be versatile. The nanoparticles (NPs) have the three dimensions at the nanometer scale such as the carbon black, silica, or quantum dots. The trend now is to individually disperse, control and modify the structure for enhanced properties of the composites [22].

Single biopolymer such as starch materials has poor mechanical properties and high water permeation which can be improved by reinforcing with the fibers, flakes, platelets, and particles [27–30], or the polymer matrix blending with other polymers [31]. Apart from the properties of the components, the bonding and the interfacial adhesion between the matrix and the filler also influence the final composite properties. With the nanofillers, the ratio between the area of the interface and the volume of the reinforcement is much higher than when the micro-sized or conventional reinforcements are used. NPs addition, therefore, reduces the retrogradation of the polymer matrix [32–34], as the large surface area per unit volume and the high aspect ratio of the nanofillers transfer their properties to the polymer matrix. A high fraction of the atoms in nanometric fillers is at the surface which enhances reactivity. With good dispersion, the interface region is maximized to allow the conformation of the interfacial percolation network, resulting in improved nanocomposite properties [35]. When the light reflection coefficient of the nanofiller is similar to the matrix, there will be optimal effect in terms of transparency, whereas the composites becoming opaque due to the light scattering effect of the microfillers. Nanofillers also improve the mechanical properties [29–31], as well as the electrical [36, 37] and thermal properties [36–39].

Different types of lignocellulosic fibers have been blended with biopolymers and synthetic polymers [40]. Compression and injection moulding for composites and material processing have been reported for various types of fibers and biopolymers (Table 1) [17, 41]. Compression moulding is widely used in the bakery industry, before being developed later as the processing methods in the plastics industry especially in the manufacturing of thermoset plastic parts, although also applicable to thermoplastics composite with unidirectional tapes, woven fabrics, randomly orientated fiber mat or chopped strand [42]. The raw materials, in the form of granules, putty-like masses, or preforms, are first placed in a heated mould cavity, and the pressure applied to force the material to fill up the cavity. A hydraulic ram produces sufficient force during the moulding process, and the heat and pressure are maintained until the plastic material is cured [42]. The compression moulding is low costs and low wastes, fast setup time, capable of large size parts whilst allowing intricate parts and good surface finish. Though producing fewer knit lines and less fibre-length degradation than the injection moulding, the production speed of compression moulding is lesser than the latter, and limited largely to the flat or moderately curved parts with no undercuts, and furthermore with less-than-ideal product consistency [42].

Table 1 Fabrication methods for lignocelluloses and biopolymers [41, 48]

Lignocelluloses/biopolymer		Fabrication methods
Long fibers	Jute yarn	Pultrusion and compression molding
	Flax and sisal	
	Lyocell	
	Kapok	
	Unidirectional/ multidirectional flax	
Short fibers	Cellulose filament yarn	Fabricated by single/twin screw extruder and injection molding
	Jute yarn	
	Flax yarn	
	Cellulose fiber	Fabricated hydraulic/ compression molding
	Sisal fiber	
	Kenaf fibers	
	Flax fibers	Twin screw extruder/internal mixture and injection molding
	Jute fibers	
	Vetiver grass	
Bamboo fibers		
Particulate fibers	Cellulose pulp, Sisal, Coir, Luff sponge	Screw extruder/internal mixture and compression molding
	Cellulose whiskers	
	Soft wood, Avicel fiber, Alfa	
	Pine saw dust	
	Wood fiber	
	Hemp fiber	
	Saw dust	
	Luffa fiber	
	Paper slug	
	Rice husk, wood powder	Screw extruder/internal mixing and injection molding
	Lignocel fiber	
	Hard wood dust	
	Liquefied wood mill	
	Hemp	
	Pine soft wood fiber	
Wheat straw		
Biopolymers from microorganisms	PLA Polyhydroxy alkanoates (PHB) Polyhydroxy fatty acids (PHF)	Extrusion Injection molding Injection molding

(continued)

Table 1 (continued)

Lignocelluloses/biopolymer		Fabrication methods
Biopolymers from renewable resources, biodegradable, of plant origin	Starch-based Cellulose-based Lignin-based	Extrusion and injection molding Injection molding Injection molding
Biopolymers from renewable resources, biodegradable, of animal origin	Chitin and chitosan	Dry molding
Biopolymers, biodegradable, of fossil origin	Polyester Ethanol (poly vinyl alcohol)	Extrusion

Conventional injection moulding process based on ceramic involves feedstock preparation, injection moulding, debinding process and sintering. In the case of composite granulate used as the feedstock, the key issues will be the particle sizes in microns, submicron or nano region, size distribution, shape and specific surface area and purity [43]. An optimum feedstock/thermoplastic binder content is mixed homogeneously to form a moderate viscosity mixture, free from agglomerates, with sufficient fluidity [44]. Injection moulding is used to mould the feedstock under concurrent heating and pressurization, with constant monitoring to minimize defects. This is followed by binding, where the soluble and insoluble components of the binder are removed, before sintering [43]. The use of conventional injection moulding machines on renewable and biopolymers is not easy due to a large number of products from compounds of the most varied shapes and variants. Flax fibers for example exhibit comparable elongation at break (3.3%) to the E-glass (3.4%), despite having a lower density of 1530 kg m^{-3} , E-modulus of $58 \pm 15 \text{ GPa}$ and tensile strength of $1339 \pm 486 \text{ MPa}$, than the E-glass (2550, 71 and 3400, respectively). However, the flax/lactic acid resins (70:30) fabricated by the compression moulding show higher tensile strength of 62 MPa and tensile modulus of 9 GPa, as compared to the flax/PLA fabricated by the injection moulding (40–55 and 3–6, respectively) [45–47]. The injection moulding system, especially the plasticizing unit, must be adjusted to ensure correct feeding characteristics. The special requirements are to allow gentle plastification through the customized design, using coated systems to counter abrasion and chemical resistance, and high injection rates or pressures with adequate venting [48]. In the injection moulding process, maximum possible accuracy and precision of material, machine, and the mould must be streamlined to produce very small components especially in the field of miniaturisation such as the minimal connectors for automobile engineering, ball bearing retainers in nano-mechanics or micropipettes in medical technology or biotechnology. This may necessitate appropriate know-how in the field of tool engineering with customized systems based on the standard platform to handle shot weights of a few grams, and component weights of a few tenths or even a few centigrams [48].

3 Green Nanocomposites

Nanofillers or nanomaterials are mainly classified into organic nanofillers which include cellulose, chitosan, organic clays, fullerenes or CNTs; and the inorganic nanofillers which include magnetic NPs, metals-based NPs or inorganic clays. Renewable polymers such as starch, cellulose, and chitin are biocompatible, environmentally-friendly and biodegradable. The preparation of sustainable polymer nanocomposites reinforced with cellulose, chitin, and starch is discussed in the next section.

3.1 Cellulose Nanocomposites

Cellulose ($C_6H_{10}O_5$)_n is a predominant constituent of lignocellulosic material (30%) and the most abundant biopolymer resource, employed for millennia in a wide variety of pre-industrial and industrial processes [12, 49]. It is a linear chain of a hundred to a thousand 1-4-β-d-anhydroglucose units, forming the structural component in prokaryotic and eukaryotic organisms including the green plants and several forms of algae, [12, 50]. Other natural substances in the plant fibers such as lignin, waxes, hemicelluloses and pectin are also found in large quantity [51–53]. Some bacterial species such as *Gluconacetobacter xylinum*, *Sarcina*, *Pseudomonas*, *Aerobacter*, *Alcaligenes*, *Acetobacter*, *Rhizobium*, *Achromobacter* and *Zoogloea* produce or secrete bacterial cellulose (BC) to make biofilms. Algal species such as *Pyrrophyta*, *Chrysophyceae*, *Xanthophyceae*, *Phaeophyta*, and the *Chlorophyta* have also been reported to produce cellulose [54]. Cellulose can be synthesized in vitro by using specific cellulose activator and the synthesized microfibril particles and the subfibrils are arranged and assembled [55]. Cellulose shows the phenomenon of allotropy where the allomorphs have the same chemical substances but more than one crystalline form (Table 2). The crystalline structures of native cellulose I have two phases [56], where the Cellulose phases I_a for bacteria or algae have triclinic geometry, the tunicates or animal I_a and I_β cellulose have monoclinic chains and the high plant possesses both forms of cellulose [56]. Cellulose I can be transformed into Cellulose III_I by refluxing with an ammonical solution in

Table 2 Cellulose allomorphs with crystal geometry [56]

Cellulose allomorph	Crystal geometry
Alpha cellulose (I_a)	Triclinic, one parallel chain
Beta cellulose (I_β)	Monoclinic, two parallel chains
Cellulose II	Monoclinic, two antiparallel chains
Cellulose III _I	One monoclinic, parallel chain
Cellulose III _{II}	Two monoclinic, antiparallel chains
Cellulose IV _I	Two orthorhombic, parallel chains
Cellulose IV _{II}	Two orthorhombic, antiparallel chains

ethylenediamine, and Cellulose III_I can be converted into Cellulose IV_I via glycerol refluxing or from the hydrolysis of Cellulose I_a. Cellulose II can be produced by reacting with NaOH, resulting in the monoclinic structure [56]. Prokaryotic, *Eubacteria*, and *Sarcina* synthesize Cellulose II, but the purple bacteria *Acetobacter*, *Rhizobium* and *Agrobacterium* synthesize only Cellulose I [55, 56].

The unique properties of cellulose include biodegradability, capacity for broad chemical modification, and the formation of versatile semicrystalline morphologies [57, 58]. Microcrystalline cellulose (MCC) can be prepared from various plant fibers [59–61]. Green isolation of cellulose from oil palm empty fruit bunches (OPEFB) have been reported using autoclave-based and ultrasonication pretreatments to replace non-green chlorite method [16, 62]. The ultrasonic treatment yields 49% cellulose with 91.3% α -cellulose content and 68.7% crystallinity, while the autoclave treatment produces 64% cellulose, with 93.7% α -cellulose content and 70% crystallinity. The cellulose/PP composite fabrications with 25% cellulose loading via the injection-moulding technique attains a high tensile strength of 27 MPa, without any addition of coupling agents, with high thermal stability and low water and diesel sorption [16]. High crystallinity index of 87% cellulose I MCC from OPEFB has been achieved through the use of elaborate serial bleaching of oxygen-ozone and H₂O₂, followed by acid hydrolysis [63]. Generally, an acid hydrolysis process is used to make aqueous suspensions of nano-crystallites [64]. The crystalline rod-like cellulose nanocrystals (CNC) [65, 66], can be isolated from delaminated cellulosic fibers or MCC using controlled sulfuric acid treatment to remove the amorphous material. The esterification of hydroxyl groups by sulphate ions yields a negatively charged surface to form a stable colloidal dispersion of CNC, with diameter and length less than 100 nm [67–71]. As the CNCs tend to form aggregation and agglomeration [72] the mechanical or ultrasonication treatment allows uniform aggregate dispersion for a more stable colloidal suspension [69, 73]. Two methods—acid hydrolysis and chemical-swelling method, have been compared to produce CNC from the MCC extracted from OPEFB pulp. The swelling treatment where the MCCs are swelled and partly separated to whiskers by chemical and ultrasonication treatments [74, 75] results in typical cellulose I structure, similar to the MCC, with no cellulose II. The acid hydrolysis treatment using 64% H₂SO₄ (96% purity) and strong agitation exhibits the coexistence of cellulose I and cellulose II allomorphs [71], similar to that reported for the CNC isolated from waste sugarcane bagasse [76].

The higher or lower crystallinity will determine the intended use of final composite products. The crystal size and shape are influenced by the cellulose source, the plant species and age, the local growth conditions (climate, soil) and the acid hydrolysis conditions [66, 77]. The crystallinity of CNC from acid hydrolysis of OPEFB-MCC at 84%, for example, is lower than the MCC (87%) and the CNC from the swelling-treatment (88%) [71]. The reduced crystallinity from acid hydrolysis may have been a result of the esterification of the cellulose chains [71, 78], or also possibly due to the higher surface amorphous ratio of CNC [79]. With this high aspect ratio, lightweight and better thermal properties than the MCC, the CNCs are more cost-effective and suitable as reinforcing agents in the

bio-renewable composite preparation [71]. The tensile strength of the CNC can be processed into the highest attainable composite strengths, far more than the high-volume content reinforcements [67, 80]. The CNCs from the bacterial cellulose fibrils are suitable as fillers for a transparent polymer composite due to their smaller lateral dimensions than the wavelength of the visible light [81]. The nanocomposite films of isotactic PP reinforced with CNCs dispersed with surfactant also exhibit far superior properties than the clean matrix or the composites containing other fillers [82].

3.2 Chitosan Nanocomposites

Chitosan (Cs) is the second most abundant biomaterial after cellulose. It is a naturally occurring amino polysaccharide, derived as a deacetylated form of chitin. The chemical structure of chitin and Cs is shown in Fig. 2 [83]. The primary amine group in Cs confers unique properties such as the cationic nature, anti-microbial activity, biocompatibility, and biodegradability, which are favourable in the biomedical application for controlled drug release [84]. The X-ray results of chitin and Cs show nearly similar diffraction pattern between shrimp shell (α -chitin) and anhydrous squid pen (β -chitin). The crystallographic parameters of ' α ' and ' β ' chitin exhibit two antiparallel molecules per unit cell in α -chitin, but only one

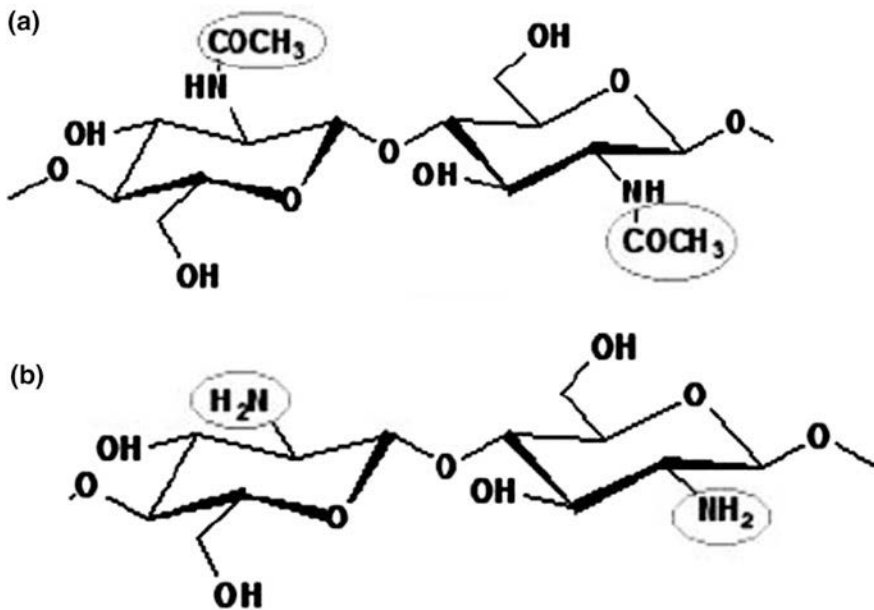


Fig. 2 Chemical structure of **a** chitin, and **b** chitosan (adapted from [84])

parallel arrangement in β -chitin. Despite this difference, it appears that *N*-acetyl glycosyl moiety is the independent crystallographic unit in both allomorphs [85, 86]. However, α -chitin samples suggest that the lobster-tendon chitin is observed at 'hkl' value of [001] [87], which is absent in the more crystalline sagitta chitin [88–90]. Further studies are needed to analyze the α -chitin crystal structure while the anhydrous β -chitin appears to be well defined and established [91, 92].

The incorporation of even 5–10% (w/w) of nanofillers into the Cs matrix could already improve the properties as compared to the 40–50% classical fillers in the conventional composites. The Cs composition in the composites can also be kept high for enhanced bioactivity and biocompatibility, thermal stability and transparency [93]. Electrospinning of Cs into nano-fibrous materials has been reported [94–98]. The high viscosity of Cs limits its spinnability and the application of an alkali treatment could hydrolyze the Cs chains and reduce its molecular weight (MW). Further treatment with aqueous 70–90% acetic acid for 48 h produces optimum nanofibers with moisture regain 74% greater than the treated and untreated chitosan powder. However, the diameter of 140 nm obtained, strongly affected by the electrospinning conditions and the solvent concentration [98], may be slightly higher than the 100 nm limit set for nanofiber [17]. Pure Cs nanofibers have been successfully produced, after the optimization of the electrospinning process parameters, from the blends of Cs and poly (ethylene oxide) (PEO) solubilized in the acetic acid. The Cs nanofibers exhibit better structural stability for at least six months in aqueous solutions (phosphate buffer (PBS) or water) [96]. Depending on the geometry and aspect ratio (particle length to thickness ratio), the Cs nanofillers can be fabricated into layer (nanoplate), rod-like (nanofiber) and spherical (nanoparticle) structure. The aspect ratio is the key factor in the enhancement of composite properties (Fig. 3) [99].

3.3 *Magnetic Nanocomposites*

Various types of magnetic particles have been combined with different materials such as gels, liquid crystals, renewable polymers, silica, carbon or metal-organic frameworks to develop novel nanocomposites. Magnetic polymer nanocomposites (MPNC) have the inorganic magnetic nanoparticles, fibers or lamellae embedded or dispersed in an organic polymer [100] which respond to external static or alternating magnetic field. The organic-inorganic synergies in MNPC possess new properties that will not be possible with single organic or individual inorganic components. The magnetic carbon nanocomposites (MCNC) use carbon as the hosting matrix, taking advantage of unique mechanical, physical and chemical properties of carbon, and diverse morphologies such as activated carbon, fullerene (C_{60}), CNFs, CNTs, expanded graphite, and graphene. Static or alternating magnetic fields as external stimulus offer relatively large penetration depth to induce

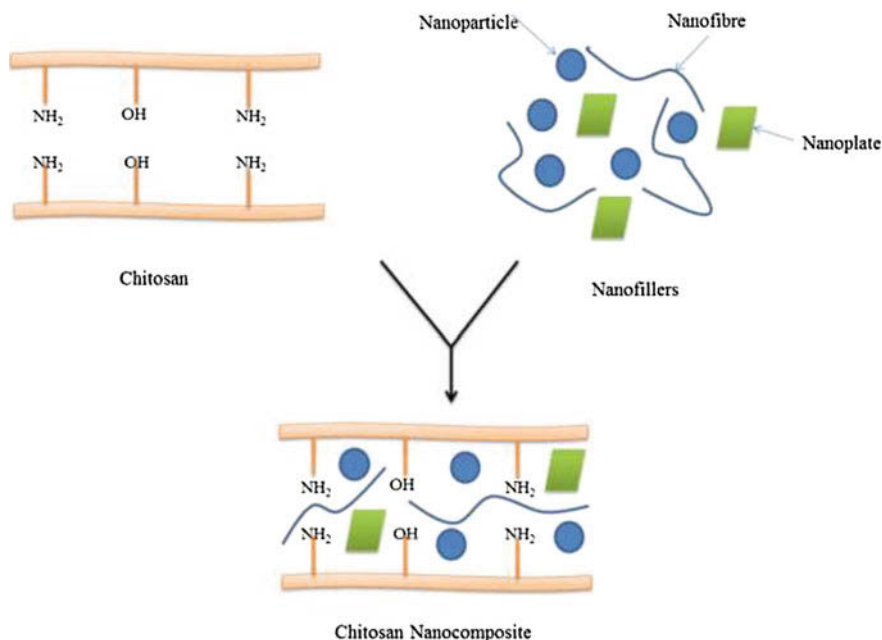


Fig. 3 Chitosan nanocomposite containing different types of nanofillers (adapted from [99])

magneto-mechanical forces, to change the shape or to move the host materials [20, 101]. These unique magnetic properties offer perspectives for fundamental understanding and applications in medical therapy and diagnosis, separations, actuation, or catalysis [101]. The common method of magnetic NPs synthesis is the co-precipitation of Fe^{2+} and Fe^{3+} ions by a base, to yield NPs of broad size distribution. To produce highly monodisperse magnetic NPs and the MPNCs with good particle distribution, thermal decomposition of metal precursors such as metal carbonyls ($\text{Co}_2(\text{CO})_8$, $\text{Fe}(\text{CO})_5$, $\text{Ni}(\text{CO})_4$) and metal oleates, should be carried out in the presence of polymers. For dispersion in PP matrix, a specific amount of metal precursor such as the liquid of $\text{Fe}(\text{CO})_5$ is injected into the dissolved PP solution, turning the transparent mixture into yellow, before gradually changing to black to indicate the NPs formation. Upon heating, $\text{Fe}(\text{CO})_5$ is decomposed into $\text{Fe}_2(\text{CO})_9$ and $\text{Fe}_3(\text{CO})_{12}$ and the $\text{Fe}_3(\text{CO})_{12}$ is then decomposed to finally form the metallic NPs [102, 103]. For raw OPEFB, cellulose and kapok fibers as base materials in the synthesis of magnetic biosorbents (MBSs), the fibers are first homogenized to the fine sizes of 0.005–0.02 mm, before mixing with the Fe_2O_3 NPs in deionized water, sonicated and shaken on an orbital shaker for the cycle of 3 times and the MBSs recovered using a permanent magnet (4000 G) [104].

4 Applications

4.1 Nano-drug Delivery

Nanomedicines confer several advantages in precision and targeted medicine such as concentrating the quantity and enhancing the absorption of chemotherapeutic agents at the specific site and tissue, increasing the retention time whilst reducing premature degradation for intracellular penetration, and improving the interaction with the biological environment to minimize their systemic distribution and reduce the adverse side effects [105–107]. Nano-vehicles/carriers including the nano-spheres/nanoshells, polymeric micelles, liposomes, polymer conjugates, dendrimers, and nucleic acid-based NPs have been the focus in the drug delivery system (DDS). The challenge is in ensuring that the encapsulating agent should not be immunogenic or at least not show any adverse immune response or react towards circulating proteins and molecules in the body. The DDS should exhibit solubility, stability *in vivo*, and bio-distribution, long circulation in the blood, passive or active targeting to the pathological or diseased sites, and responsive to the changes in the environmental conditions [105, 108]. Polymeric nano-DDS have shown potential as therapeutic carriers with remarkable results shown in preclinical studies especially for targeted delivery to tumour cells [109, 110]. Ligation of the anticancer drug to a biocompatible polymer such as hyaluronic acid (HA) could enhance drug target and controlled release [111–114]. HA is the main component of the extracellular matrix and ligand for CD44 and Receptor for Hyaluronan-Mediated Motility (RHAMM) which are over-expressed in a variety of tumour cell surfaces. HA-Cisplatin (Pt) NPs, formed through anionic polymer–metal complexation between Pt and HA, have shown no significant difference between Pt and HA-Pt cytotoxicity *in vitro* [108, 109]. The challenge, however, is that the hydrophobic drugs may be released too slowly from the DDS. To increase efficiency and efficacy, the water uptake into the NPs must be enhanced to speed up the release whilst at the same time sustain the release profile [115].

Nanofibers possess high surface to volume ratio and porosity to accommodate drug loading capacity, mass transfer and attachment to targeted cells [116]. Surface functionalization further may provide an avenue for the design of more precise drug and gene delivery [117]. However, to achieve this, the processing variables during fabrication of the nanofibers must be controlled precisely [118, 119]. Due to the unique size-dependent optical, electronic, magnetic and structural properties, NPs formulation with the therapeutic agents are being considered for target specific diagnostic applications based on imaging, diagnostics and targeted therapy to improve the anti-cancer therapeutics [120, 121]. The cellulose-based materials for example not only are biodegradable, and biocompatible, with no or low toxicity [122] but also can self-assemble or be designed into organized structures with specific properties and functions. Stimuli-responsive self-assembled cellulose materials based on temperature-, pH-, light- and redox-trigger have been developed [123]. A thermo-responsive hydroxypropyl cellulose DDS has been found to be able to self-assemble into nano-particulate systems for curcumin encapsulation with satisfactory loading. The discharge of curcumin is totally dependant on the

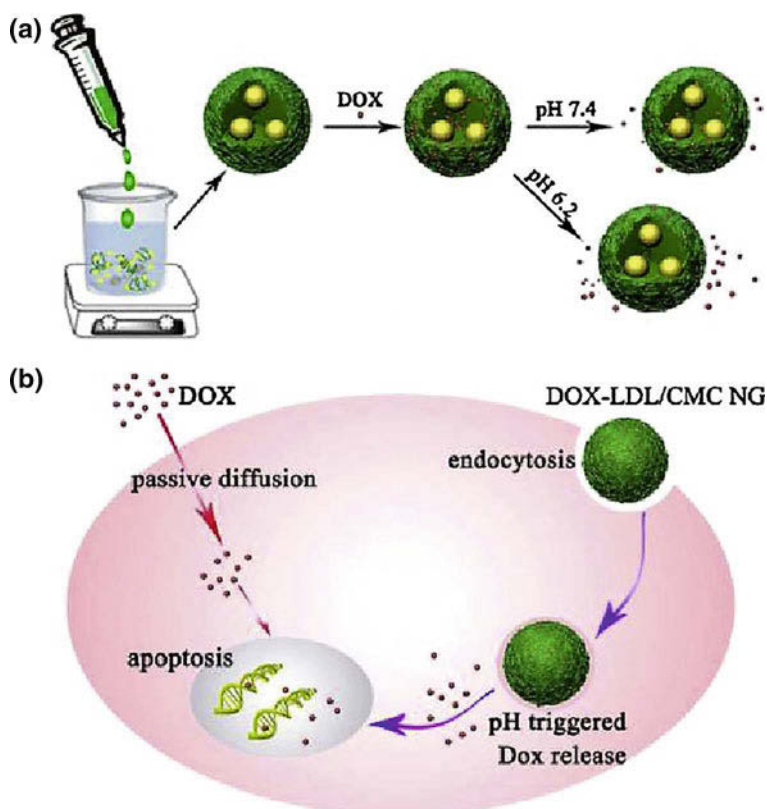


Fig. 4 **a** Illustration of the synthesis and structures of LDL/CMC nanogels, DOX loading, and pH-dependent drug release; **b** schematic diagram showing the proposed model for intracellular delivery processing of DOX-loaded LDL/CMC nanogels in tumor cells [125]

temperature in the physiologically relevant range [124]. A nano-gel obtained by the self-assembly of low-density lipoproteins (LDL) and sodium carboxymethyl cellulose (CMC) has demonstrated that the doxorubicin (DOX) release is pH-dependent, and the DOX-loaded LDL/CMC nanogels reduce endocytosis in HepG2 cells (Fig. 4) [125] has also drawn much attention due to the unique structure which leads to its application in anti-cancer drug delivery. Biodegradable CMC/Graphene oxide (GO) nanocomposite hydrogel beads, prepared via physical crosslinking with $\text{FeCl}_3 \cdot 6\text{H}_2\text{O}$ for controlled release of DOX, also exhibit faster release rate in an acidic medium which is attributable to the instability of hydrogen bonding between GO and DOX [126]. The graft copolymer hydroxypropyl methylcellulose grafted with aminated-glycidyl methacrylate-grafted cellulose-grafted polymethacrylic acid-succinyl cyclodextrin (Cell-g-(GMA/en)-PMA-SeCD) has not shown any cytotoxicity but the anticancer drug 5-fluorouracil (5-FU)-DDS exhibits significant cytotoxicity, only to a lesser extent than the naked 5-FU. The study suggests the potential of Cell-g-(GMA/en)-PMA-SeCD for drug loading and sustained release of 5-FU [127].

In an investigation on the potential use for live tumor cell imaging, the MCC-based nano-carriers developed by the self-assembly of MCC-graft-poly (p-dioxanone) copolymers (Cell-g-PPDO) in aqueous solution with fluorescent conjugated polymers (FCPs) loading have exhibited significantly stronger fluorescence in the cytoplasm of the cells treated with FCPS-loaded micelles than those treated with just FCPS in water. The FCPS-loaded micelles also exhibit lower cytotoxicity in the cell culture with improved intracellular uptake efficiency [128]. With applications in various industries such as food, biotechnology, agriculture and environmental protection [129–132], the nano-biocomposite based on Cs nanofillers are another promising materials for biomedical and pharmaceutical applications. Furthermore, the properties such as non-toxicity, biocompatibility, specificity and biodegradability of the Cs nanofillers are important to improve the biological properties of the target system or base-materials [133]. Hydroxyapatite-Cs (HAp-Cs) nanocomposite loaded with celecoxib for colon cancer therapy achieves high drug association efficiencies and sustained release profiles, but the serious side effects may hamper its application in cancer therapy [134]. Electrospinning has been used as the fabrication method for a hybrid fiber of Cs and phospholipids for transdermal drug delivery where the fibers show biocompatibility and stability [135]. The poly (lactide-co-glycolide)/poly(ethylene glycol)-g-chitosan (PLGA/PEG-g-Cs) electrospun membranes also exhibit high surface area with high release rate of ibuprofen [136]. Table 3 highlights the different nanofillers in the chitosan matrix, the drugs used for the release study, the nanocomposite types and their applications.

4.2 Tissue Engineering

In tissue engineering, the newly developed material provides scaffold for the tissue growth. The scaffold must have significant mechanical properties to bear the stresses and load, along with appropriate pore size, biocompatibility and biodegradability. BCs have high porosity which can be beneficial for medical application such as the mesoporous dressing to keep the wound moist for quick healing. *G. xylinum* secretes abundant 3D network of biocompatible fibrils which can be used to develop a scaffold for cells fabrication for artificial skin, artificial blood vessels and micro-vessels or wound dressing, or as template for cartilage regeneration. BC scaffold provides attachment as collagen type II substrate, and mechanical support for multiplication and differentiation of chondrocytes for the normal cartilage growth [56]. The properties and functionalities can be improved with the addition of NPs, nanotubes or nanofillers such as the nanocomposites BC/collagen, BC/gelatin, BC/Fibroin, BC/Chitosan [137]. Important factors to be optimized for reinforced bone scaffolds and composite dressings for dermal wounds are the surface area, porosity, density, rigidity and the morphology as thin mats or non-wovens, Pertinent among these are the safe and eco-friendly disassembly of base-materials as alternatives to acid hydrolysis, and to give higher yields and scaling-up possibilities [138]. In the electrospinning fabrication of Cs-based

Table 3 Different nanofillers in chitosan matrix, drug used for the release study, the nanocomposite type and their applications

Nanofiller	Drug used	Nanocomposite type	Applications	References
MCM-41 or MCM-41-APS	Metformin (MET) (an oral diabetes medicine)	Thin films, (Cs, polyethylene glycol)-block-poly(propylene glycol)-block-(polyethylene glycol)	Controlled DDS of MET	[166]
Fe ₃ O ₄ NPs, CdTe@ZnS QDs	Doxorubicin	Surface modified magnetic NP (MNPs) with carboxymethyl-Cs	Controlled DDS and cellular imaging	[167]
Fe and Mn magnetic nanocrystals (MNCs)	Doxorubicin	<i>N</i> -naphthyl-Odimethylmaleoyl-drug loaded magnetic NPs (NCs-DMNPs)	MIR-guided imaging for cancer therapy and pH-sensitive drug release	[168]
Fe ₃ O ₄	Curcumin	Cs, PVP, PEG nanocomposite coated with Fe ₃ O ₄ nanoparticles	pH sensitive drug delivery	[169]
Fe ₃ O ₄	Gemcitabine	Magnetite/Cs (core/shell) nanocomposite	Cancer therapy via stimuli-sensitive nanomedicine	[170]
Fe ₃ O ₄	2,7,12,18-tetramethyl-3,8-di (1-propoxyethyl)-13,17-bis-(3hydroxypropyl) porphyrin	Magnetic nanocomposite	DDS for targeting photodynamic therapy	[171]
Fe ₃ O ₄	Bacillus Calmette-Guerin	Magnetic hydrogel	Intravesical drug delivery	[172]
Iron oxide	Methotrexate, mitomycin C	Iron oxide NPs decorated with Cs and functionalized with polyethylene glycolated methotrexate and cyanine dye	Fluorescence and MRI as self-targeted therapeutic delivery device for cancer treatment	[173, 174]
Zinc oxide (ZnO)	Ibuprofen	Hydrogel beads	Controlled DDS	[175]
ZnO	Gentamicin	ZnO-Cs gel	Wound care application	[176]
Gold	5-fluorouracil	Nanocomposite	Site specific and controlled DDS	[177]
Silver	Ibuprofen	Hydrogel beads	Antibacterial DDS	[178]
Graphene oxide (GO)	Camptothecin (CPT)	Covalent functionalized GO with Cs	Delivery of water insoluble CPT and genes	[179]

(continued)

Table 3 (continued)

Nanofiller	Drug used	Nanocomposite type	Applications	References
GO	Fluorescein sodium	Cs-GO nanocomposite	Transdermal drug delivery	[180]
Montmorillonite (MMT), silicate	Ofloxacin, 5-aminosalicylic acid, Ibuprofen, vitamin B ₁₂	Hydrogel, solid-liquid interaction, nanohybrid films, nano hydrogel	Drug carrier for sustained release, electrically-induced DDS	[181–184]
MMT	5-fluorouracil	Cs coated alginate-MMT nanocomposite	Controlled release of drug to small intestine	[185]
MMT	Oxytetracycline	Nanocomposite	Enhanced drug permeation	[186]
Hydroxyapatite	Doxorubicin	Hydrogel	Drug delivery	[187]
Rectorite	Bovine serum albumin	Nanocomposite films	Controlled drug release carrier	[188]
Nanosilica	Carvedilol	Spherical nanosilica matrix	Sustained release of poor water soluble drug	[189]
Aluminosilicate	Doxorubicin	Cs-clay nanocomposite	Controlled and extended drug release	[190]

nanofibers, the spinnability and morphology are strongly dependant on the solution viscosity (in this case Cs, PEO and Triton-X) and the Cs-to-PEO ratio. The nanofibers can be designed into structures that promote the attachment of human osteoblasts and chondrocytes whilst maintaining the characteristic cell morphology and viability in tissue engineering and remodelling [94]. The PEO yields in the blend influence the degree of swelling and hydrophilicity of the films and the nanofibers. Better dispersion of the Cs in the presence of PEO will improve the mechanical properties of the composite which is when the electrospinning is performed at the optimal Cs/PEO weight ratio [139]. The composites of Cs, gelatin and polyurethane have been proposed for cardiac valves and for nerve conduits based on the fibers manufactured from the electrospun self-assembled particles. Gel drying with supercritical CO₂ leads to the structures similar to the extracellular matrix, which are of interest in orthopaedics [138].

4.3 Biosensor, Electrical Conductive Polymer and Insulator

Cellulose/HAp composites are effective for the removal of heavy metal ions from aqueous solution, taking advantage of the ion-exchange and sorption properties of the HAp with the highly accessible hydrophilic groups of the cellulose [140]. Chemically-modified carbon electrode (Cellulose-HAp-CME) composite has been successfully developed for trace Pb(II) ions detection in the physiologically relevant range of 10–60 ppb in digested and undigested blood serum (Fig. 5). This may be of great benefits for rapid environmental and clinical analyses of heavy metal ions [141]. A novel fluorescent amphiphilic cellulose nano-aggregates sensing system designed to detect the explosives in aqueous solution has shown the sensitivity significantly enhanced by up to 50-times, suggesting that the cellulose-based nano-aggregates maximize the interaction between the sensing material and the analyte [142]. A material based on cellulose acetate (CA) modified with the room temperature ionic liquid 1-butyl-3-methylimidazolium basified (trifluoro-methylsulfonyl) (BMI-N(Tf)₂) biosensor shows a wide linear range of 34.8–370.3 μM and the detection limit of 5.5 μM for the methyl dopa determination in pharmaceutical samples under optimized conditions [143].

The use of CNC fillers in the bulk cellulose improves the dielectric constant which is useful in energy storage applications [144]. Figure 6 illustrates the interaction between the CNC and the cellulose matrix and the dielectric property of cellulose and the cellulose/CNC hydrogels. The enhanced dielectric constant is attributed to the interfacial polarization effects occurring in the vicinity of the hydroxyl groups present on the CNC surface [144]. To observe a change in the dielectric properties, a polymer-filler interfacial interaction is necessary, according to the Maxwell-Wagner-Sillars (MWS) process. The large surface area of the CNCs in the cellulose reinforced matrix provides for strong interactions with the hydroxyl and carboxylic acid groups on the cellulose [145–147]. Cellulosic nanomaterials have been explored for the generation of electrically conductive materials and flexible

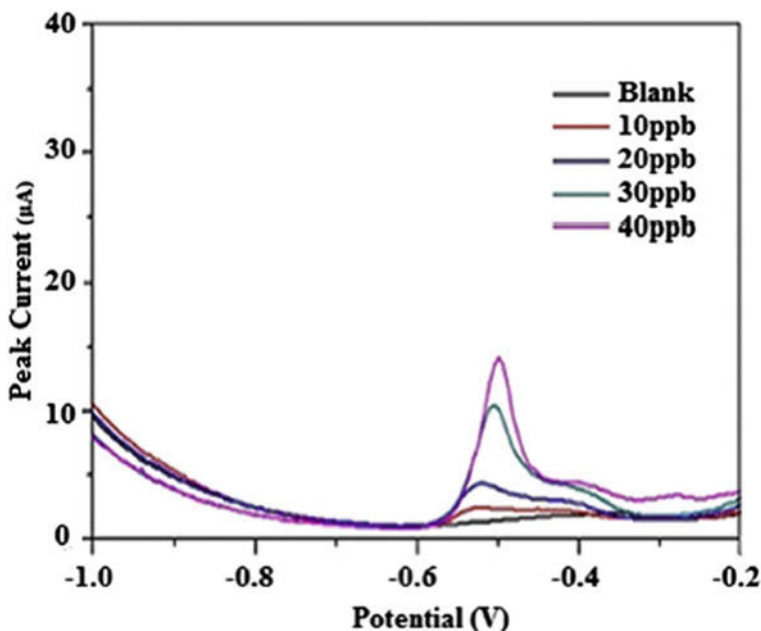


Fig. 5 Stripping voltammograms of Cellulose-HAp-CME for Pb(II) detection in undigested blood serum at pH 2, deposition potential: -1.2 V, deposition time: 240 s, frequency: 25 Hz, amplitude: 0.020 V, step potential: 0.005 V and rotation speed: 700 rpm [141]

films using polyaniline and cellulose nanofibers [148], polypyrrole and bacterial cellulose [149], single-walled CNTs with 2,2,6,6-tetramethylpiperidine-1-oxyl (TEMPO)-oxidized cellulose nanofibers [150], graphene and cellulose nanofibers [151, 152], graphene and CNCs [153], and CNCs modified with terpyridine moieties and crosslinked with Fe(II) [154]. Wood nanofibrillated cellulose (NFC) and algal *Cladophora* cellulose have potentials for electrical insulator applications [155]. The tand plots at different relative humidities (RHs) (Fig. 7) suggest that both samples exhibit a loss factor peak, where the peak is shifted to higher frequencies with increasing relative humidity (RH). These CNCs with sufficient loss factor values may be applicable in the formation of percolative composites with high dielectric constant and high dielectric loss factor for microwave receptor applications [155].

4.4 Catalysis and Environmental Remediation

There has been an increasing use of engineered magnetic nanoparticles as green catalysts and for remediation and water treatments. The cellulose-based core/shell composite with the core as catalyst solid particles have been applied for the synthesis

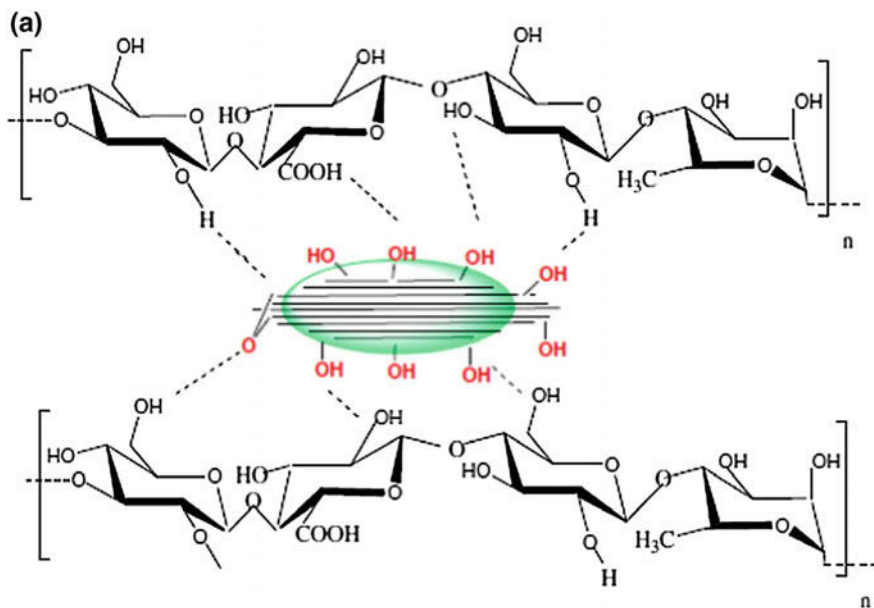


Fig. 6 a Chemical interaction between CNC and cellulose, and b dielectric property of cellulose and cellulose/CNC hydrogels [144]

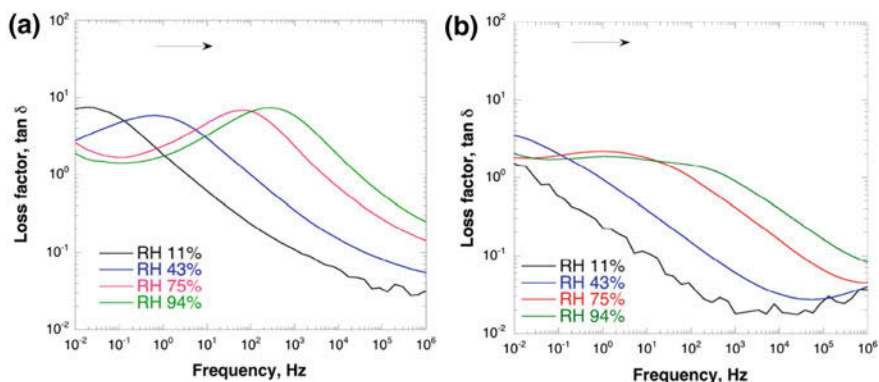


Fig. 7 Loss factor (tan δ) versus frequency for **a** *Cladophora* cellulose and **b** NFC, at different RHs [155]

of benzodiazepines [156] and multicomponent syntheses of polysubstituted tetrahydropyridines and dihydropyrimidinones [157]. A magnetic cellulose/Ag nanobiocomposite (NBC) catalyst prepared to synthesize chromene-linked nicotinitriles shows remarkable magnetic property, and can easily be separated out from the reaction mixture without considerable loss of catalytic activity [158]. Another efficient and recyclable magnetic cellulose/Ag NBC catalyst with the sizes of about 20–25 nm size has been developed for the synthesis of tetrazolo[1,5-a]pyrimidines [159]. In environmental applications, magnetic NPs focusing on zero-valent iron (ZVI), magnetite (Fe_3O_4) and maghemite ($\gamma\text{-Fe}_2\text{O}_3$) have reported the contaminant removal mechanisms where the factors affecting the efficiency include the ability for the contaminant desorption, and the recovery of the magnetic NPs (MNPs). The aggregation of MNPs, the methods to enhance the stability and the toxicological effects are important to be addressed for sustainable application [160]. Apart from reusability, the advantages of MNPs include high adsorption capacities and efficiency due to the high number of active surface sites large surface area-to-volume ratio, and low intraparticle diffusion rate [161–163]. Surface functionalized MNPs and the composite with core-shell nanostructures can make the application more economical and effective [164]. Agro-based magnetic biosorbents (AMBs), such as from *Ceiba pentandra* (Raw kapok fibres, RKF), OPEFB and celluloses (CEL), are applicable for field application not only due to the simple operation and reusability for wastewater treatment, but also because of the high capacity and selectivity from the different functional groups in the structure [104, 164, 165]. The AMBs exhibit dispersion of magnetic NPs (Fig. 8) where the regeneration is successfully performed for 5 adsorption/desorption cycles. The highest Pb(II) removal efficiency of 99.4% and 49 mg/g adsorption capacity is achieved with the kapok AMBs and the AMBs overall exhibit 10.3% higher efficiency than the raw sorbents [104].

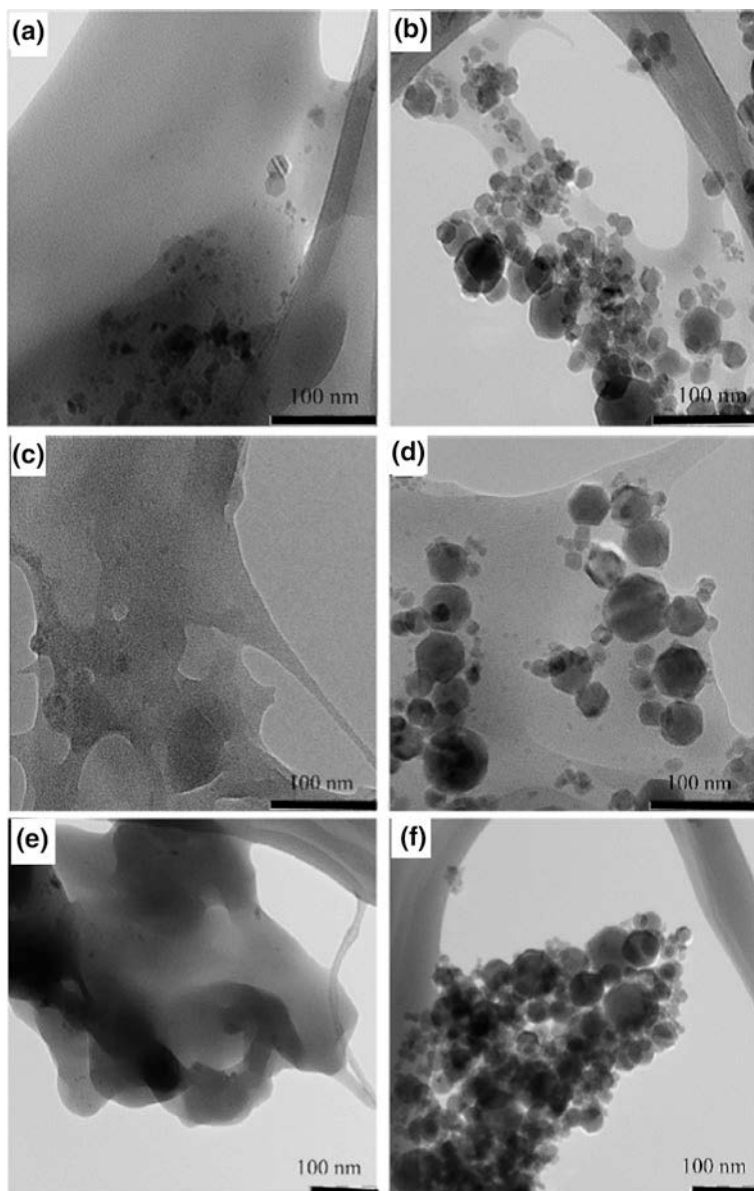


Fig. 8 TEM images of **a** raw OPEFB; **b** Fe₂O₃@EFB; **c** cellulose; **d** Fe₂O₃@CEL; **e** RKF; and **f** Fe₂O₃@RKF nanocomposites [104]

5 Conclusion and Future Outlook

Global sustainable development necessitates relooking at the whole range of input and output processes in the product manufacturing to ensure effective utilization of resources, use of eco-friendly and cleaner processes, with optimal reaction efficiency, minimal toxic reagents, or zero-wastes. Product development based on composite materials has the advantages in the integration of different component materials and their properties in a single material. The combined properties of the matrix material and the filler will result in novel functional materials, which can be tailor-made for specific applications. Composite materials based on cellulose, chitosan and magnetic nanofillers have far-reaching impacts in meeting the sustainable development goals. The unique properties of cellulose and chitosan nanofillers such as non-toxicity, biodegradability, and biocompatibility have a special place in the area of biomedical, pharmaceutical and environmental applications. The capacity for broad chemical modification and the formation of versatile semicrystalline fiber morphologies confer improved and enhanced optical, mechanical, electrical and thermal properties to the base material matrix. The magnetic nanocomposite offers unique magnetic properties for fundamental understanding and applications in medical therapy and diagnosis, separations, actuation, or catalysis, with a high number of active surface sites, and reusability for environmental remediation. The fabrication aspect should address the issue of maximum possible accuracy and precision of the material, machine and the mould that must be streamlined for miniaturisation of the end-products, with higher yields and scaling-up possibilities.

References

1. Liu Q, Paavola J (2016) Lightweight design of composite laminated structures with frequency constraint. *Compos Struct* 156:356–360
2. Azwa ZN, Yousif BF, Manalo AC, Karunasena W (2013) A review on the degradability of polymeric composites based on natural fibres. *Mater Des* 47:424–442
3. Al-Oqla FM, Sapuan SM, Anwer T, Jawaid M, Hoque ME (2015) Natural fiber reinforced conductive polymer composites as functional materials: a review. *Synth Met* 206:42–54
4. Dhand V, Mittal G, Rhee KY, Park SJ, Hui D (2015) A short review on basalt fiber reinforced polymer composites. *Compos B Eng* 73:166–180
5. Mittal G, Dhand V, Rhee KY, Park SJ, Lee WR (2015) A review on carbon nanotubes and graphene as fillers in reinforced polymer nanocomposites. *J Ind Eng Chem* 21:11–25
6. Hung PY, Lau KT, Cheng LK, Leng J, Hui D (2018) Impact response of hybrid carbon/glass fibre reinforced polymer composites designed for engineering applications. *Compos B Eng* 133:86–90
7. Pillai SK, Ray SS (2011) Epoxy-based carbon nanotubes reinforced composites. In: *Advances in nanocomposites-synthesis, characterization and industrial applications*. InTech
8. Auvergne R, Caillol S, David G, Boutevin B, Pascault JP (2013) Biobased thermosetting epoxy: present and future. *Chem Rev* 114(2):1082–1115
9. Maffini MV, Rubin BS, Sonnenschein C, Soto AM (2006) Endocrine disruptors and reproductive health: the case of bisphenol-A. *Mol Cell Endocrinol* 254:179–186

10. Poletto M, Ornaghi Júnior HL, Visakh PM, Arao Y (2016) Composites and nanocomposites based on renewable and sustainable materials. *Int J Polym Sci* 2016
11. Böer P, Holliday L, Kang THK (2014) Interaction of environmental factors on fiber-reinforced polymer composites and their inspection and maintenance: a review. *Constr Build Mater* 50:209–218
12. Abdullah MA, Nazir MS, Ajab H, Daneshfozoun S, Almustapha S (2017) Advances in eco-friendly pre-treatment methods and utilization of agro-based lignocelluloses. *Ind Biotechnol: Sustain Prod Biores Utilization* 371–419
13. Perlack RD, Wright LL, Turhollow AF, Graham RL, Stokes BJ, Erbach DC (2005) Biomass as feedstock for a bioenergy and bioproducts industry: the technical feasibility of a billion-ton annual supply. Oak Ridge National Lab, Oak Ridge
14. Yuan Z, Cheng S, Leitch M, Xu CC (2010) Hydrolytic degradation of alkaline lignin in hot-compressed water and ethanol. *Biores Technol* 101(23):9308–9313
15. Jacqueline I, Kroschwitz A (2001) *Encyclopedia of chemical technology*, vol 20. Wiley-Interscience, New York
16. Abdullah MA, Nazir MS, Raza MR, Wahjoedi BA, Yussof AW (2016) Autoclave and ultra-sonication treatments of oil palm empty fruit bunch fibers for cellulose extraction and its polypropylene composite properties. *J Clean Prod* 126:686–697
17. ISO/TS 80004-2:(2015) *Nanotechnologies—vocabulary—part 2*, no. April 2015
18. Lamouroux E, Fort Y (2016) An overview of nanocomposite nanofillers and their functionalization. In: *Spectroscopy of polymer nanocomposites*, pp 15–64
19. Schrittwieser S, Ludwig F, Dieckhoff J, Tschoepe A, Guenther A, Richter M, Schotter J et al (2014) Direct protein detection in the sample solution by monitoring rotational dynamics of nickel nanorods. *Small* 10(2):407–411
20. Roeder L, Bender P, Tschöpe A, Birringer R, Schmidt AM (2012) Shear modulus determination in model hydrogels by means of elongated magnetic nanoprobles. *J Polym Sci Part B: Polym Phys* 50(24):1772–1781
21. Okada A, Usuki A (2006) Twenty years of polymer-clay nanocomposites. *Macromol Mater Eng* 291(12):1449–1476
22. Verdejo R, Bernal MM, Romasanta LJ, Tapiador FJ, Lopez-Manchado MA (2011) Reactive nanocomposite foams. *Cell Polym* 30(2):45
23. Novoselov KS, Geim AK, Morozov SV, Jiang D, Zhang Y, Dubonos SV, Firsov AA et al (2004) Electric field effect in atomically thin carbon films. *Science* 306(5696):666–669
24. Kotov NA (2006) Materials science: carbon sheet solutions. *Nature* 442(7100):254
25. George TF, Jelski D, Letfullin RL, Zhang GP (2011) Computational studies of new materials II
26. Popov VN (2004) Carbon nanotubes: properties and application. *Mater Sci Eng R: Rep* 43(3):61–102
27. Siqueira G, Bras J, Dufresne A (2010) Cellulosic bionanocomposites: a review of preparation, properties and applications. *Polymers* 2(4):728–765
28. García NL, Ribba L, Dufresne A, Aranguren M, Goyanes S (2011) Effect of glycerol on the morphology of nanocomposites made from thermoplastic starch and starch nanocrystals. *Carbohydr Polym* 84(1):203–210
29. Famá LM, Pettarin V, Goyanes SN, Bernal CR (2011) Starch/multi-walled carbon nanotubes composites with improved mechanical properties. *Carbohydr Polym* 83(3):1226–1231
30. Famá L, Rojo PG, Bernal C, Goyanes S (2012) Biodegradable starch based nanocomposites with low water vapor permeability and high storage modulus. *Carbohydr Polym* 87(3):1989–1993
31. García NL, Ribba L, Dufresne A, Aranguren MI, Goyanes S (2009) Physico-mechanical properties of biodegradable starch nanocomposites. *Macromol Mater Eng* 294(3):169–177
32. Angellier H, Molina-Boisseau S, Dole P, Dufresne A (2006) Thermoplastic starch—waxy maize starch nanocrystals nanocomposites. *Biomacromolecules* 7(2):531–539
33. Cao X, Chen Y, Chang PR, Huneault MA (2007) Preparation and properties of plasticized starch/multiwalled carbon nanotubes composites. *J Appl Polym Sci* 106(2):1431–1437

34. Ma X, Chang PR, Yu J, Lu P (2008) Characterizations of glycerol plasticized-starch (GPS)/ carbon black (CB) membranes prepared by melt extrusion and microwave radiation. *Carbohydr Polym* 74(4):895–900
35. Qiao R, Brinson LC (2009) Simulation of interphase percolation and gradients in polymer nanocomposites. *Compos Sci Technol* 69(3–4):491–499
36. Kilbride BE, Coleman JN, Fraysse J, Fournet P, Cadek M, Drury A, Blau WJ et al (2002) Experimental observation of scaling laws for alternating current and direct current conductivity in polymer-carbon nanotube composite thin films. *J Appl Phys* 92(7):4024–4030
37. Sandler J, Kirk JE, Kinloch IA, Shaffer MSP, Windle AH (2003) Ultra-low electrical percolation threshold in carbon-nanotube-epoxy composites. *Polymer* 44(19):5893–5899
38. Biercuk MJ, Llaguno MC, Radosavljevic M, Hyun JK, Johnson AT, Fischer JE (2002) Carbon nanotube composites for thermal management. *Appl Phys Lett* 80(15):2767–2769
39. Wei C, Srivastava D, Cho K (2002) Thermal expansion and diffusion coefficients of carbon nanotube-polymer composites. *Nano Lett* 2(6):647–650
40. Yu L (2009) Biodegradable polymer blends and composites from renewable resources. Wiley
41. Malkapuram R, Kumar V, Negi YS (2009) Recent development in natural fiber reinforced polypropylene composites. *J Reinf Plast Compos* 28(10):1169–1189
42. http://www.efunda.com/processes/plastic_molding/molding_compression.cfm. Accessed 17 Apr 2018
43. Stanimirović Z, Stanimirović I (2012) Ceramic injection molding. In: Some critical issues for injection molding. InTech
44. Rak ZS (1999) New trends in powder injection moulding. *Powder Metall Met Ceram* 38(3–4): 126–132
45. Åkesson D, Skrifvars M, Seppälä J, Turunen M (2011) Thermoset lactic acid-based resin as a matrix for flax fibers. *J Appl Polym Sci* 119(5):3004–3009
46. Bax B, Müssig J (2008) Impact and tensile properties of PLA/Cordenka and PLA/flax composites. *Compos Sci Technol* 68(7–8):1601–1607
47. Zhu J, Zhu H, Njuguna J, Abhyankar H (2013) Recent development of flax fibres and their reinforced composites based on different polymeric matrices. *Materials* 6(11):5171–5198
48. (SHI) Sumitomo (2017) Demag plastics machinery GmbH. <https://www.sumitomo-shi-demag.eu/processes/biopolymers.html>. Accessed 17 Apr 2018
49. Kalia S, Dufresne A, Cherian BM, Kaith BS, Avérous L, Njuguna J, Nassiopoulou E (2011) Cellulose-based bio-and nanocomposites: a review. *Int J Polym Sci*, 2011
50. Crawford RL (1982) Lignin biodegradation and transformation. Wiley, p 118
51. Bledzki AK, Reihmane S, Gassan J (1996) Properties and modification methods for vegetable fibers for natural fiber composites. *J Appl Polym Sci* 59(8):1329–1336
52. Bismarck A, Mishra S, Lampke T (2005) Plant fibers as reinforcement for green composites. *Nat Fibers Biopolym Biocompos* 10:9780203508206
53. Satyanarayana KG, Sukumaran K, Mukherjee PS, Pavithran C, Pillai SGK (1990) Natural fibre-polymer composites. *Cement Concr Compos* 12(2):117–136
54. Perasso R, Baroin A, Qu LH, Bachelier JP, Adoutte A (1989) Origin of the algae. *Nature* 339(6220):142
55. Wertz JL, Mercier JP, Bédoué O (2010) Cellulose science and technology. CRC Press
56. Lejeune A, Deprez T (2010) Cellulose: structure and properties, derivatives and industrial uses. Nova Science Publishers
57. Zhu S, Wu Y, Chen Q, Yu Z, Wang C, Jin S, Wu G et al (2006) Dissolution of cellulose with ionic liquids and its application: a mini-review. *Green Chem* 8(4):325–327
58. Klemm D, Heublein B, Fink HP, Bohn A (2005) Cellulose: fascinating biopolymer and sustainable raw material. *Angew Chem Int Ed* 44(22):3358–3393
59. Dalvåg H, Klason C, Strömvall HE (1985) The efficiency of cellulosic fillers in common thermoplastics. Part II. Filling with processing aids and coupling agents. *Int J Polym Mater* 11(1):9–38

60. Maldas D, Kokta BV, Raj RG, Daneault C (1988) Improvement of the mechanical properties of sawdust wood fibre—polystyrene composites by chemical treatment. *Polymer* 29(7): 1255–1265
61. Zadorecki P, Michell AJ (1989) Future prospects for wood cellulose as reinforcement in organic polymer composites. *Polym Compos* 10(2):69–77
62. Nazir MS, Wahjoedi BA, Yussof AW, Abdullah MA (2013) Eco-friendly extraction and characterization of cellulose from oil palm empty fruit bunches. *BioResources* 8(2):2161–2172
63. Haafiz MM, Eichhorn SJ, Hassan A, Jawaid M (2013) Isolation and characterization of microcrystalline cellulose from oil palm biomass residue. *Carbohyd Polym* 93(2):628–634
64. Visakh PM, Thomas S (2010) Preparation of bionanomaterials and their polymer nanocomposites from waste and biomass. *Waste Biomass Valorization* 1(1):121–134
65. Bras J, Hassan ML, Bruzesse C, Hassan EA, El-Wakil NA, Dufresne A (2010) Mechanical, barrier, and biodegradability properties of bagasse cellulose whiskers reinforced natural rubber nanocomposites. *Ind Crops Prod* 32(3):627–633
66. Brito BS, Pereira FV, Putaux JL, Jean B (2012) Preparation, morphology and structure of cellulose nanocrystals from bamboo fibers. *Cellulose* 19(5):1527–1536
67. Bondeson D, Mathew A, Oksman K (2006) Optimization of the isolation of nanocrystals from microcrystalline cellulose by acid hydrolysis. *Cellulose* 13(2):171
68. Azizi Samir MAS, Alloin F, Dufresne A (2005) Review of recent research into cellulosic whiskers, their properties and their application in nanocomposite field. *Biomacromolecules* 6(2):612–626
69. Filson PB, Dawson-Andoh BE (2009) Sono-chemical preparation of cellulose nanocrystals from lignocellulose derived materials. *Biores Technol* 100(7):2259–2264
70. Petersson L, Kvien I, Oksman K (2007) Structure and thermal properties of poly (lactic acid)/cellulose whiskers nanocomposite materials. *Compos Sci Technol* 67(11–12):2535–2544
71. Haafiz MM, Hassan A, Zakaria Z, Inuwa IM (2014) Isolation and characterization of cellulose nanowhiskers from oil palm biomass microcrystalline cellulose. *Carbohyd Polym* 103:119–125
72. Liu D, Zhong T, Chang PR, Li K, Wu Q (2010) Starch composites reinforced by bamboo cellulosic crystals. *Biores Technol* 101(7):2529–2536
73. Pandey JK, Chu WS, Kim CS, Lee CS, Ahn SH (2009) Bio-nano reinforcement of environmentally degradable polymer matrix by cellulose whiskers from grass. *Compos B Eng* 40(7):676–680
74. Oksman K, Mathew AP, Bondeson D, Kvien I (2006) Manufacturing process of cellulose whiskers/poly(lactic acid) nanocomposites. *Compos Sci Technol* 66(15):2776–2784
75. Pereda M, Amica G, Rácz I, Marcovich NE (2011) Structure and properties of nanocomposite films based on sodium caseinate and nanocellulose fibers. *J Food Eng* 103(1): 76–83
76. Mandal A, Chakrabarty D (2011) Isolation of nanocellulose from waste sugarcane bagasse (SCB) and its characterization. *Carbohyd Polym* 86(3):1291–1299
77. Valentini L, Bon SB, Cardinali M, Fortunati E, Kenny JM (2014) Cellulose nanocrystals thin films as gate dielectric for flexible organic field-effect transistors. *Mater Lett* 126:55–58
78. Tang L, Huang B, Lu Q, Wang S, Ou W, Lin W, Chen X (2013) Ultrasonication-assisted manufacture of cellulose nanocrystals esterified with acetic acid. *Biores Technol* 127:100–105
79. Wang N, Ding E, Cheng R (2007) Thermal degradation behaviors of spherical cellulose nanocrystals with sulfate groups. *Polymer* 48(12):3486–3493
80. Liu H, Liu D, Yao F, Wu Q (2010) Fabrication and properties of transparent polymethylmethacrylate/cellulose nanocrystals composites. *Biores Technol* 101(14):5685–5692
81. Yano H, Sugiyama J, Nakagaito AN, Nogi M, Matsuura T, Hikita M, Handa K (2005) Optically transparent composites reinforced with networks of bacterial nanofibers. *Adv Mater* 17(2):153–155
82. Ljungberg N, Cavaillé JY, Heux L (2006) Nanocomposites of isotactic polypropylene reinforced with rod-like cellulose whiskers. *Polymer* 47(18):6285–6292

83. Bornet A, Teissedre PL (2008) Chitosan, chitin-glucan and chitin effects on minerals (iron, lead, cadmium) and organic (ochratoxin A) contaminants in wines. *Eur Food Res Technol* 226(4):681–689
84. Ali A, Ahmed S (2017) A review on chitosan and its nanocomposites in drug delivery. *Int J Biol Macromol*
85. Rinaudo M (2006) Chitin and chitosan: properties and applications. *Prog Polym Sci* 31(7):603–632
86. Gardner KH, Blackwell J (1975) Refinement of the structure of β -chitin. *Biopolymers* 14(8):1581–1595
87. Minke RAM, Blackwell J (1978) The structure of α -chitin. *J Mol Biol* 120(2):167–181
88. Saito Y, Okano T, Chanzy H, Sugiyama J (1995) Structural study of α chitin from the grasping spines of the arrow worm (*Sagitta* spp.). *J Struct Biol* 114(3):218–228
89. Chanzy H (1998) Chitin crystals. Jacques Andre, Lyon
90. Chrétiennot-Dinet MJ, Giraud-Guille MM, Vaulot D, Putaux JL, Saito Y, Chanzy H (1997) The chitinous nature of filaments ejected by Phaeocystis (Prymnesiophyceae). *J Phycol* 33(4):666–672
91. Blackwell J (1969) Structure of β -chitin or parallel chain systems of poly- β -(1 \rightarrow 4)-*N*-acetyl-D-glucosamine. *Biopolymers* 7(3):281–298
92. Gaill F, Persson J, Sugiyama J, Vuong R, Chanzy H (1992) The chitin system in the tubes of deep sea hydrothermal vent worms. *J Struct Biol* 109(2):116–128
93. Fernandes SC, Freire CS, Silvestre AJ, Neto CP, Gandini A, Berglund LA, Salmén L (2010) Transparent chitosan films reinforced with a high content of nanofibrillated cellulose. *Carbohydr Polym* 81(2):394–401
94. Bhattarai N, Edmondson D, Veisoh O, Matsen FA, Zhang M (2005) Electrospun chitosan-based nanofibers and their cellular compatibility. *Biomaterials* 26(31):6176–6184
95. Geng X, Kwon OH, Jang J (2005) Electrospinning of chitosan dissolved in concentrated acetic acid solution. *Biomaterials* 26(27):5427–5432
96. Mengistu Lemma S, Bossard F, Rinaudo M (2016) Preparation of pure and stable chitosan nanofibers by electrospinning in the presence of poly (ethylene oxide). *Int J Mol Sci* 17(11):1790
97. Ojha SS, Stevens DR, Hoffman TJ, Stano K, Klossner R, Scott MC, Gorga RE et al (2008) Fabrication and characterization of electrospun chitosan nanofibers formed via templating with polyethylene oxide. *Biomacromolecules* 9(9):2523–2529
98. Homayoni H, Ravandi SAH, Valizadeh M (2009) Electrospinning of chitosan nanofibers: processing optimization. *Carbohydr Polym* 77(3):656–661
99. Pillai SK, Ray SS (2012) Chitosan-based nanocomposites. *Nat Polym* 2:33–68
100. Mai YW, Yu ZZ (2006) Polymer nanocomposites. Woodhead publishing
101. Behrens S, Appel I (2016) Magnetic nanocomposites. *Curr Opin Biotechnol* 39:89–96
102. Zhu J, Wei S, Li Y, Sun L, Haldolaarachchige N, Young DP, Guo Z et al (2011) Surfactant-free synthesized magnetic polypropylene nanocomposites: rheological, electrical, magnetic, and thermal properties. *Macromolecules* 44(11):4382–4391
103. Smith TW, Wyckick D (1980) Colloidal iron dispersions prepared via the polymer-catalyzed decomposition of iron pentacarbonyl. *J Phys Chem* 84(12):1621–1629
104. Daneshfouzoun S, Abdullah MA, Abdullah B (2017) Preparation and characterization of magnetic biosorbent based on oil palm empty fruit bunch fibers, cellulose and *Ceiba pentandra* for heavy metal ions removal. *Ind Crops Prod* 105:93–103
105. Gul-e-Saba, Abdullah MA (2015) Polymeric nanoparticle mediated targeted drug delivery to cancer cells. In: *Biotechnology and Bioinformatics*, pp 1–34
106. Farokhzad OC, Langer R (2009) Impact of nanotechnology on drug delivery. *ACS Nano* 3(1):16–20
107. Alexis F, Pridgen E, Molnar LK, Farokhzad OC (2008) Factors affecting the clearance and biodistribution of polymeric nanoparticles. *Mol Pharm* 5(4):505–515

108. Abdullah MA, Gul-e-Saba AA (2014) Cytotoxic effects of drug-loaded hyaluronan-glutaraldehyde cross-linked nanoparticles and the release kinetics modeling. *J Adv Chem Eng* 1(104):2
109. Van Vlerken LE, Amiji MM (2006) Multi-functional polymeric nanoparticles for tumour-targeted drug delivery. *Expert Opin Drug Deliv* 3(2):205–216
110. Parveen S, Sahoo SK (2006) Nanomedicine. *Clin Pharmacokinet* 45(10):965–988
111. Gul-e-Saba, Abdah A, Abdullah MA (2010) Hyaluronan-mediated CD44 receptor cancer cells progression and the application of controlled drug delivery system. *Int J Curr Chem* 1(4):245–265
112. Jin YJ, Ubonvan T, Kim DD (2010) Hyaluronic acid in drug delivery systems. *J Pharm Invest* 40(spc):33–43
113. Jaracz S, Chen J, Kuznetsova LV, Ojima I (2005) Recent advances in tumor-targeting anticancer drug conjugates. *Bioorg Med Chem* 13(17):5043–5054
114. Akima K, Ito H, Iwata Y, Matsuo K, Watari N, Yanagi M, Tatekawa I et al (1996) Evaluation of antitumor activities of hyaluronate binding antitumor drugs: synthesis, characterization and antitumor activity. *J Drug Target* 4(1):1–8
115. Marinich JA, Ferrero C, Jiménez-Castellanos MR (2012) Graft copolymers of ethyl methacrylate on waxy maize starch derivatives as novel excipients for matrix tablets: drug release and fronts movement kinetics. *Eur J Pharm Biopharm* 80(3):674–681
116. Hu X, Liu S, Zhou G, Huang Y, Xie Z, Jing X (2014) Electrospinning of polymeric nanofibers for drug delivery applications. *J Controlled Release* 185:12–21
117. Yoo HS, Kim TG, Park TG (2009) Surface-functionalized electrospun nanofibers for tissue engineering and drug delivery. *Adv Drug Deliv Rev* 61(12):1033–1042
118. Pillay V, Dott C, Choonara YE, Tyagi C, Tomar L, Kumar P, Ndesendo VM et al (2013) A review of the effect of processing variables on the fabrication of electrospun nanofibers for drug delivery applications. *J Nanomater* 2013
119. Sridhar R, Lakshminarayanan R, Madhaiyan K, Barathi VA, Lim KHC, Ramakrishna S (2015) Electrospayed nanoparticles and electrospun nanofibers based on natural materials: applications in tissue regeneration, drug delivery and pharmaceuticals. *Chem Soc Rev* 44(3):790–814
120. Lim EK, Chung BH (2016) Preparation of pyrenyl-based multifunctional nanocomposites for biomedical applications. *Nat Protoc* 11(2):236
121. Siddiqui IA, Adhami VM, Christopher J (2012) Impact of nanotechnology in cancer: emphasis on nanochemoprevention. *Int J Nanomed* 7:591
122. Lin N, Dufresne A (2014) Nanocellulose in biomedicine: current status and future prospect. *Eur Polymer J* 59:302–325
123. Yang J, Li J (2017) Self-assembled cellulose materials for biomedicine: a review. *Carbohydr Polym*
124. Bielska D, Karewicz A, Kamiński K, Kielkiewicz I, Lachowicz T, Szczubiałka K, Nowakowska M (2013) Self-organized thermo-responsive hydroxypropyl cellulose nanoparticles for curcumin delivery. *Eur Polymer J* 49(9):2485–2494
125. He L, Liang H, Lin L, Shah BR, Li Y, Chen Y, Li B (2015) Green-step assembly of low density lipoprotein/sodium carboxymethyl cellulose nanogels for facile loading and pH-dependent release of doxorubicin. *Colloids Surf B* 126:288–296
126. Rasoulzadeh M, Namazi H (2017) Carboxymethyl cellulose/graphene oxide bio-nanocomposite hydrogel beads as anticancer drug carrier agent. *Carbohydr Polym* 168:320–326
127. Anirudhan TS, Nima J, Divya PL (2015) Synthesis, characterization and in vitro cytotoxicity analysis of a novel cellulose based drug carrier for the controlled delivery of 5-fluorouracil, an anticancer drug. *Appl Surf Sci* 355:64–73
128. Guo Y, Zhang J, Wang L, Ge W, Chen M, Wang X, Sun R (2015) Preparation of fluorescent core/shell nanoparticles from amphiphilic cellulose-based copolymers for tumor cell imaging. *J Controlled Release: Official J Controlled Release Soc* 213:e132

129. Coradin T, Allouche J, Boissière M, Livage J (2006) Sol-gel biopolymer/silica nanocomposites in biotechnology. *Curr Nanosci* 2(3):219–230
130. De Azeredo HM (2009) Nanocomposites for food packaging applications. *Food Res Int* 42(9):1240–1253
131. Liu X, Hu Q, Fang Z, Zhang X, Zhang B (2008) Magnetic chitosan nanocomposites: a useful recyclable tool for heavy metal ion removal. *Langmuir* 25(1):3–8
132. Rhim JW, Park HM, Ha CS (2013) Bio-nanocomposites for food packaging applications. *Prog Polym Sci* 38(10–11):1629–1652
133. Cheung RCF, Ng TB, Wong JH, Chan WY (2015) Chitosan: an update on potential biomedical and pharmaceutical applications. *Marine drugs* 13(8):5156–5186
134. Venkatesan P, Puvvada N, Dash R, Kumar BP, Sarkar D, Azab B, Mandal M et al (2011) The potential of celecoxib-loaded hydroxyapatite-chitosan nanocomposite for the treatment of colon cancer. *Biomaterials* 32(15):3794–3806
135. Mendes AC, Gorzelanny C, Halter N, Schneider SW, Chronakis IS (2016) Hybrid electrospun chitosan-phospholipids nanofibers for transdermal drug delivery. *Int J Pharm* 510(1):48–56
136. Jiang H, Fang D, Hsiao B, Chu B, Chen W (2004) Preparation and characterization of ibuprofen-loaded poly (lactide-co-glycolide)/poly (ethylene glycol)-g-chitosan electrospun membranes. *J Biomater Sci Polym Ed* 15(3):279–296
137. de Oliveira Barud HG, da Silva RR, da Silva Barud H, Tercjak A, Gutierrez J, Lustrri WR, Ribeiro SJ et al (2016) A multipurpose natural and renewable polymer in medical applications: bacterial cellulose. *Carbohydr Polym* 153:406–420
138. Muzzarelli RA (2011) Biomedical exploitation of chitin and chitosan via mechano-chemical disassembly, electrospinning, dissolution in imidazolium ionic liquids, and supercritical drying. *Marine Drugs* 9(9):1510–1533
139. Garcia CEG, Martinez FAS, Bossard F, Rinaudo M (2018) Biomaterials based on electrospun chitosan. Relation between processing conditions and mechanical properties. *Polymers* 10(3):257
140. Choi S, Jeong Y (2008) The removal of heavy metals in aqueous solution by hydroxyapatite/cellulose composite. *Fibers Polym* 9(3):267–270
141. Ajab H, Dennis JO, Abdullah MA (2018) Synthesis and characterization of cellulose and hydroxyapatite-carbon electrode composite for trace plumbum ions detection and its validation in blood serum. *Int J Biol Macromol* 113:376–385
142. Wang X, Guo Y, Li D, Chen H, Sun RC (2012) Fluorescent amphiphilic cellulose nanoaggregates for sensing trace explosives in aqueous solution. *Chem Commun* 48(45):5569–5571
143. Mocellini SK, Franzi AC, Vieira IC, Dupont J, Scheeren CW (2011) A novel support for laccase immobilization: cellulose acetate modified with ionic liquid and application in biosensor for methyl dopa detection. *Biosens Bioelectron* 26(8):3549–3554
144. Gao X, Sadasivuni KK, Kim HC, Min SK, Kim J (2015) Designing pH-responsive and dielectric hydrogels from cellulose nanocrystals. *J Chem Sci* 127(6):1119–1125
145. Sadasivuni KK, Ponnamma D, Thomas S, Grohens Y (2014) Evolution from graphite to graphene elastomer composites. *Prog Polym Sci* 39(4):749–780
146. Yuan JK, Yao SH, Dang ZM, Sylvestre A, Genestoux M, Bai J (2011) Giant dielectric permittivity nanocomposites: realizing true potential of pristine carbon nanotubes in polyvinylidene fluoride matrix through an enhanced interfacial interaction. *J Phys Chem C* 115(13):5515–5521
147. Ponnamma D, Sadasivuni KK, Grohens Y, Guo Q, Thomas S (2014) Carbon nanotube based elastomer composites—an approach towards multifunctional materials. *J Mater Chem C* 2(40):8446–8485
148. Mattoso LHC, Medeiros ES, Baker DA, Avloni J, Wood DF, Orts WJ (2009) Electrically conductive nanocomposites made from cellulose nanofibrils and polyaniline. *J Nanosci Nanotechnol* 9(5):2917–2922

149. Xu J, Zhu L, Bai Z, Liang G, Liu L, Fang D, Xu W (2013) Conductive polypyrrole–bacterial cellulose nanocomposite membranes as flexible supercapacitor electrode. *Org Electron* 14(12):3331–3338
150. Koga H, Saito T, Kitaoka T, Nogi M, Suganuma K, Isogai A (2013) Transparent, conductive, and printable composites consisting of TEMPO-oxidized nanocellulose and carbon nanotube. *Biomacromolecules* 14(4):1160–1165
151. Patel MU, Luong ND, Seppälä J, Tchernychova E, Dominko R (2014) Low surface area graphene/cellulose composite as a host matrix for lithium sulphur batteries. *J Power Sources* 254:55–61
152. Yan C, Wang J, Kang W, Cui M, Wang X, Foo CY, Lee PS (2014) Highly stretchable piezoresistive graphene–nanocellulose nanopaper for strain sensors. *Adv Mater* 26(13):2022–2027
153. Valentini L, Bon SB, Fortunati E, Kenny JM (2014) Preparation of transparent and conductive cellulose nanocrystals/graphene nanoplatelets films. *J Mater Sci* 49(3):1009–1013
154. Namazi H, Baghershiroudi M, Kabiri R (2017) Preparation of electrically conductive biocompatible nanocomposites of natural polymer nanocrystals with polyaniline via in situ chemical oxidative polymerization. *Polym Compos* 38(S1)
155. Le Bras D, Strømme M, Mihranyan A (2015) Characterization of dielectric properties of nanocellulose from wood and algae for electrical insulator applications. *J Phys Chem B* 119(18):5911–5917
156. Maleki A, Kamalzare M (2014) Fe₃O₄@ cellulose composite nanocatalyst: preparation, characterization and application in the synthesis of benzodiazepines. *Catal Commun* 53:67–71
157. Maleki A, Jafari AA, Yousefi S (2017) MgFe₂O₄/cellulose/SO₃H nanocomposite: a new biopolymer-based nanocatalyst for one-pot multicomponent syntheses of polysubstituted tetrahydropyridines and dihydropyrimidinones. *J Iran Chem Soc* 14(8):1801–1813
158. Maleki A, Movahed H, Ravaghi P (2017) Magnetic cellulose/Ag as a novel eco-friendly nanobiocomposite to catalyze synthesis of chromene-linked nicotinonitriles. *Carbohydr Polym* 156:259–267
159. Maleki A, Ravaghi P, Aghaei M, Movahed H (2017) A novel magnetically recyclable silver-loaded cellulose-based bionanocomposite catalyst for green synthesis of tetrazolo [1, 5-a] pyrimidines. *Res Chem Intermed* 43(10):5485–5494
160. Tang SC, Lo IM (2013) Magnetic nanoparticles: essential factors for sustainable environmental applications. *Water Res* 47(8):2613–2632
161. Nassar NN (2010) Kinetics, mechanistic, equilibrium, and thermodynamic studies on the adsorption of acid red dye from wastewater by γ -Fe₂O₃ nanoadsorbents. *Sep Sci Technol* 45(8):1092–1103
162. Tan Y, Chen M, Hao Y (2012) High efficient removal of Pb (II) by amino-functionalized Fe₃O₄ magnetic nano-particles. *Chem Eng J* 191:104–111
163. Feng Y, Gong JL, Zeng GM, Niu QY, Zhang HY, Niu CG, Yan M et al (2010) Adsorption of Cd (II) and Zn (II) from aqueous solutions using magnetic hydroxyapatite nanoparticles as adsorbents. *Chem Eng J* 162(2):487–494
164. Gómez-Pastora J, Bringas E, Ortiz I (2014) Recent progress and future challenges on the use of high performance magnetic nano-adsorbents in environmental applications. *Chem Eng J* 256:187–204
165. Nalbandian MJ, Zhang M, Sanchez J, Choa YH, Nam J, Cwiertny DM, Myung NV (2016) Synthesis and optimization of Fe₂O₃ nanofibers for chromate adsorption from contaminated water sources. *Chemosphere* 144:975–981
166. Shariatnia Z, Zahraee Z (2017) Controlled release of metformin from chitosan–based nanocomposite films containing mesoporous MCM-41 nanoparticles as novel drug delivery systems. *J Colloid Interface Sci* 501:60–76
167. Ding Y, Yin H, Shen S, Sun K, Liu F (2017) Chitosan-based magnetic/fluorescent nanocomposites for cell labelling and controlled drug release. *New J Chem* 41(4):1736–1743

168. Lim EK, Sajomsang W, Choi Y, Jang E, Lee H, Kang B, Huh YM et al (2013) Chitosan-based intelligent theragnosis nanocomposites enable pH-sensitive drug release with MR-guided imaging for cancer therapy. *Nanoscale Res Lett* 8(1):467
169. Prabha G, Raj V (2016) Preparation and characterization of polymer nanocomposites coated magnetic nanoparticles for drug delivery applications. *J Magn Magn Mater* 408:26–34
170. Arias JL, Reddy LH, Couvreur P (2012) Fe₃O₄/chitosan nanocomposite for magnetic drug targeting to cancer. *J Mater Chem* 22(15):7622–7632
171. Sun Y, Chen ZL, Yang XX, Huang P, Zhou XP, Du XX (2009) Magnetic chitosan nanoparticles as a drug delivery system for targeting photodynamic therapy. *Nanotechnology* 20(13):135102
172. Zhang D, Sun P, Li P, Xue A, Zhang X, Zhang H, Jin X (2013) A magnetic chitosan hydrogel for sustained and prolonged delivery of *Bacillus Calmette-Guérin* in the treatment of bladder cancer. *Biomaterials* 34(38):10258–10266
173. Lin J, Li Y, Li Y, Wu H, Yu F, Zhou S, Hou Z et al (2015) Drug/dye-loaded, multifunctional PEG–chitosan–iron oxide nanocomposites for methotrexate synergistically self-targeted cancer therapy and dual model imaging. *ACS Appl Mater Interfaces* 7(22):11908–11920
174. Jia M, Li Y, Yang X, Huang Y, Wu H, Huang Y, Zhang Q et al (2014) Development of both methotrexate and mitomycin C loaded PEGylated chitosan nanoparticles for targeted drug codelivery and synergistic anticancer effect. *ACS Appl Mater Interfaces* 6(14):11413–11423
175. Yadollahi M, Farhoudian S, Barkhordari S, Gholamali I, Farhadnejad H, Motasadizadeh H (2016) Facile synthesis of chitosan/ZnO bio-nanocomposite hydrogel beads as drug delivery systems. *Int J Biol Macromol* 82:273–278
176. Vasile BS, Oprea O, Voicu G, Ficai A, Andronescu E, Teodorescu A, Holban A (2014) Synthesis and characterization of a novel controlled release zinc oxide/gentamicin–chitosan composite with potential applications in wounds care. *Int J Pharm* 463(2):161–169
177. Chandran PR, Sandhyarani N (2014) An electric field responsive drug delivery system based on chitosan–gold nanocomposites for site specific and controlled delivery of 5-fluorouracil. *RSC Adv* 4(85):44922–44929
178. Yadollahi M, Farhoudian S, Namazi H (2015) One-pot synthesis of antibacterial chitosan/silver bio-nanocomposite hydrogel beads as drug delivery systems. *Int J Biol Macromol* 79:37–43
179. Bao H, Pan Y, Ping Y, Sahoo NG, Wu T, Li L, Gan LH et al (2011) Chitosan-functionalized graphene oxide as a nanocarrier for drug and gene delivery. *Small* 7(11):1569–1578
180. Justin R, Chen B (2014) Characterisation and drug release performance of biodegradable chitosan–graphene oxide nanocomposites. *Carbohydr Polym* 103:70–80
181. Depan D, Kumar AP, Singh RP (2009) Cell proliferation and controlled drug release studies of nanohybrids based on chitosan-g-lactic acid and montmorillonite. *Acta Biomater* 5(1):93–100
182. Aguzzi C, Capra P, Bonferoni C, Cerezo P, Salcedo I, Sánchez R, Viseras C et al (2010) Chitosan–silicate biocomposites to be used in modified drug release of 5-aminosalicylic acid (5-ASA). *Appl Clay Sci* 50(1):106–111
183. Hua S, Yang H, Wang W, Wang A (2010) Controlled release of ofloxacin from chitosan–montmorillonite hydrogel. *Appl Clay Sci* 50(1):112–117
184. Liu KH, Liu TY, Chen SY, Liu DM (2008) Drug release behavior of chitosan–montmorillonite nanocomposite hydrogels following electrostimulation. *Acta Biomater* 4(4): 1038–1045
185. Azhar FF, Olad A (2014) A study on sustained release formulations for oral delivery of 5-fluorouracil based on alginate–chitosan/montmorillonite nanocomposite systems. *Appl Clay Sci* 101:288–296
186. Salcedo I, Sandri G, Aguzzi C, Bonferoni C, Cerezo P, Sánchez-Espejo R, Viseras C (2014) Intestinal permeability of oxytetracycline from chitosan–montmorillonite nanocomposites. *Colloids Surf B* 117:441–448

187. Taleb MFA, Alkahtani A, Mohamed SK (2015) Radiation synthesis and characterization of sodium alginate/chitosan/hydroxyapatite nanocomposite hydrogels: a drug delivery system for liver cancer. *Polym Bull* 72(4):725–742
188. Wang X, Du Y, Luo J, Lin B, Kennedy JF (2007) Chitosan/organic rectorite nanocomposite films: structure, characteristic and drug delivery behaviour. *Carbohydr Polym* 69(1):41–49
189. Sun L, Wang Y, Jiang T, Zheng X, Zhang J, Sun J, Wang S et al (2012) Novel chitosan-functionalized spherical nanosilica matrix as an oral sustained drug delivery system for poorly water-soluble drug carvedilol. *ACS Appl Mater Interfaces* 5(1):103–113
190. Yuan Q, Shah J, Hein SRDK, Misra RDK (2010) Controlled and extended drug release behavior of chitosan-based nanoparticle carrier. *Acta Biomater* 6(3):1140–1148

Smart Materials, Magnetic Graphene Oxide-Based Nanocomposites for Sustainable Water Purification



Janardhan Reddy Koduru, Rama Rao Karri and N. M. Mubarak

1 Introduction

Water pollution is a global environmental concern [61–64, 75]. Heavy metals are one of the primary contaminants in the aqueous environment. Continuous exposure to heavy metals leads to high-risk health problems for humans. Heavy metals are naturally occurring throughout the Earth's crust [2]. Anthropogenic activities, including mining operations, industry, and the use of metals and metal-containing compounds for the domestic and agricultural purpose, are the main sources of water pollution [83]. Hence, water is one of the major routes through which heavy metals and radionuclides may enter the human body [22]. Figure 1 shows the possible sources of water pollution. The real application of frequently used conventional wastewater purification techniques is limited to the removal of heavy metals at trace levels [22]. However, the low installation cost and easy operation of adsorption technique make it one of the preferred methods for water purification [26, 40, 25, 27]. Moreover, the use of activated carbon in the adsorption process is effective, but the use of it in a real application is limited, due to the complex installation process, coupled with the high-cost operation [41]. Hence, these drawbacks have

J. R. Koduru

Department of Environmental Engineering, Kwangwoon University,
Seoul 01897, Republic of Korea
e-mail: reddyjchem@gmail.com

R. R. Karri (✉)

Petroleum and Chemical Engineering, Faculty of Engineering,
Universiti Teknologi Brunei, Gadong, Brunei Darussalam
e-mail: kramarao.iitd@gmail.com

N. M. Mubarak

Department of Chemical Engineering, Faculty of Engineering and Science,
Curtin University, 98009 Miri, Sarawak, Malaysia
e-mail: mubarak.mujawar@curtin.edu.my

necessitated the search for an alternative material that can be renewable and economic for water purification. The various potential applications of GO-based nanocomposites have been reported by different research groups [37]. Both the chemical stability of magnetic GO-based nanocomposites and literature survey, induce us to write a book chapter on magnetic GO (MGO's) based nanocomposites for the removal of heavy metals and radionuclides from water, with the purpose of reducing their environmental impact.

The numerous merits of graphene, which include high specific surface area, and thermal conductivity, high optical transmittance, and large Young's modulus have led to researchers paying great attention to it [78]. Similar to graphene, graphene-based material or graphene oxide (GO) shows the above significant properties. "However, GO is more easily dispersed than graphene, due to the presence epoxy, hydroxyl, and carboxyl functional groups, thus making its processing, synthesis, and application more convenient" (Fig. 2) [11]. Due to its imperishable hydrophilicity, GO found to be an efficient adsorbent and hence found many applications, including water purification [11]. Sreeprasad et al. [77] and Maaz et al. [47] have reported that nickel ferrite-GO composite is a better reaction media than iron ferrites, because of having higher catalytic and electron transfer efficiency through the Ni^{2+} in the nickel ferrite. Moreover, previous reports have proved the amazing removal response of magnetic nanoparticles/graphene or GO composites for pollutants like chromium [17, 67], copper [20], arsenic [105], cadmium [14], lead [100], and cobalt and an organic dye. Recently, Ligamdinne

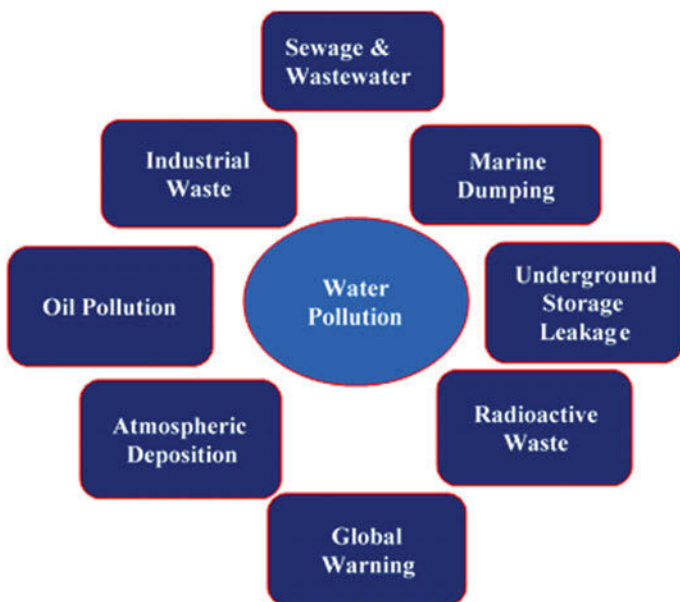


Fig. 1 Schematic of the sources of water pollution

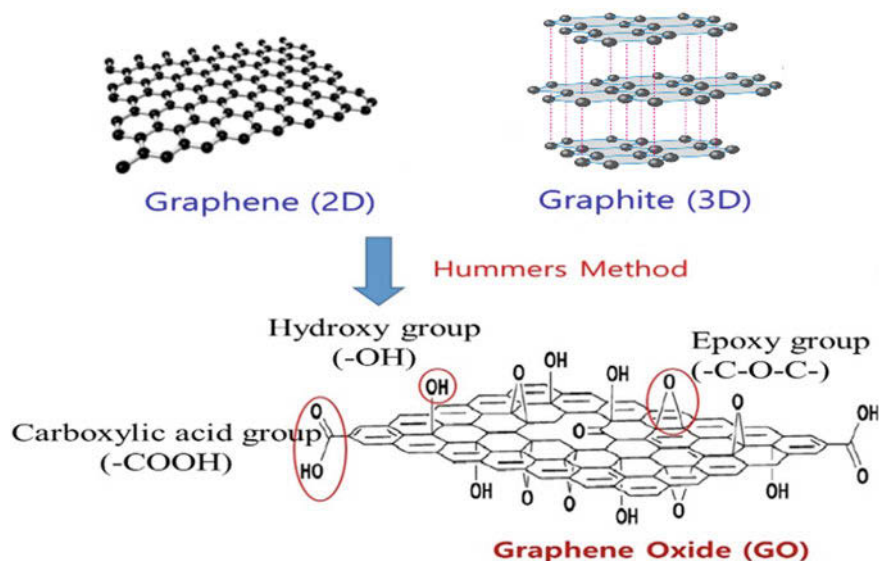


Fig. 2 Graphical representation of graphene oxide (GO) produced from graphite

et al. reported (Fig. 3) the removal of Co(II), Pb(II), Cr(III), As(III) and As(V), and radionuclides, U(VI) and Th(IV) from water, using the synthesis of “inverse spinel nickel ferrite incorporated-graphene oxide” based nanocomposites [35, 36, 39, 40]. The reported results demonstrated that the magnetic GO-based nanocomposites are promising, economic, could be separated by the external magnetic field.

Graphene can be extracted from graphite and it is merely a sheet of graphite [65]. It is defined as a single layer of sp^2 bonded carbon atoms in hexagonal lattice arrangement [97]. At the same time, graphene possesses few promising properties such as good electronic properties caused by the bonding and anti-bonding of the pi orbitals. Furthermore, graphene is clarified to be the strongest substance in terms of mechanical strength since it possesses high tensile strength and it is light in weight. For instance, it is more than 40 times stronger than diamond and more than 300 times stronger than A36 structural steel, at 130 GPa [81]. Meanwhile, for the optical properties, high absorption of white light up to 2.3% is capable to be observed from graphene.

Besides the impressive properties, appropriate method to produce graphene must be taken into consideration. There are two different type of methods to produce graphene which are exfoliation methods and direct growth of graphene layer [30]. Methods to generate graphene include “Scotch Tape Method”, dispersion of graphite, exfoliation of graphite oxide, epitaxial growth and lastly CVD [23]. However, improved Hummers method which falls under the method of dispersion of graphite is used since it is an improved method which reduces the toxic gas emission and at the same time enhances the reaction performance [50].

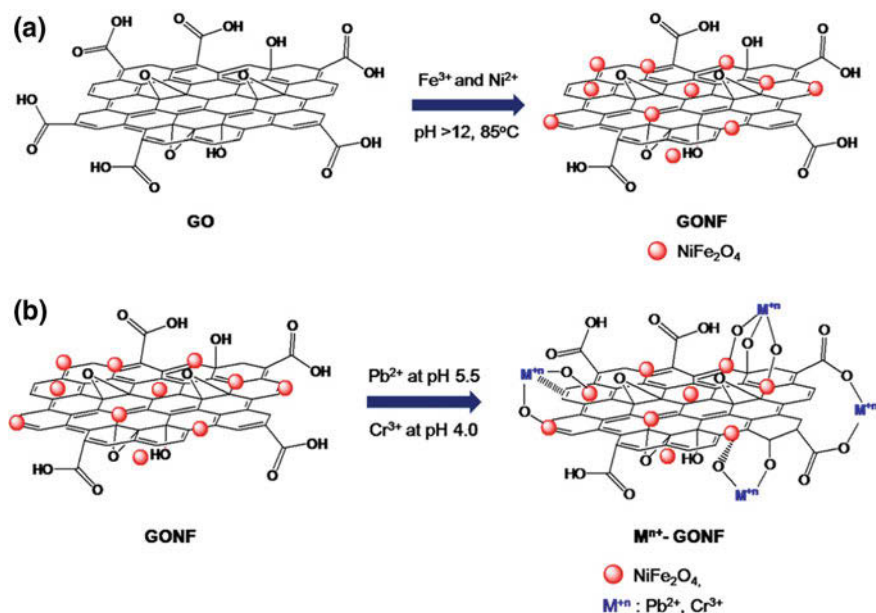


Fig. 3 Graphical representation of **a** nano-magnetic GONF composite preparation, **b** Pb(II) and Cr(III) adsorption onto GONF (reproduced from [39] with permission)

Generally, graphene generated via improved Hummers method are prepared to be further functionalized as chemical functionalization of graphene can be one of the best approaches for cadmium removal [101]. However, before functionalization takes place, the GO can be further transformed into GNs via acid treatment. Functionalization can be defined as the route where the addition of new properties, purposes, structures, or abilities to a substance via the alteration of the material in the aspect of surface chemistry. It is acknowledged that this is an essential method utilized throughout different fields such as biological engineering, chemistry, nanotechnology, materials science and the likes [93]. Functionalization can be done through the attachment of particles or nanoparticles to the surface of a substance, either via a chemical bond or via adsorption. For instance, the functionalized graphene can be produced via noncovalent and covalent alteration techniques. Both techniques share a similar process which is a superficial alteration of GO followed by reduction.

However, functionalization via ionic liquids (ILs) [48, 59] is known as a better covalent bonding technique [69]. The term of IL can be explained as poor coordination of the ions can be found in the salt below 100 °C or at room temperature. Ions in IL avoid the creation of a stable crystal lattice by having at least an ion which the charge is undergone delocalization and an organic component. Properties which include solubility of starting materials and other solvents, melting point, and viscosity are dependent on the counter ion and organic component [66]. For

instance, implementation of ILs for synthetic difficulties is common and hence ILs can be known as “designer solvents”. Furthermore, one of the promising advantages of IL is the zero presence of volatility. This condition has resulted in the solvents to have less toxicity compared to low-boiling-point solvents. For instance, by covalent bonding approach, GO obtained via modified Hummers method can be further functionalized via IL such as BF_4 [Bmim] with magnetic Fe_3O_4 nanoparticles to form core-shell structured Fe_3O_4 @GO nanospheres to perform optimal extraction of cadmium [1].

2 Properties of Graphene

2.1 Electrical and Electronic Properties

The revolution of graphene can be initiated with the electronic and electrical properties of graphene [51]. Electrical conductivities of graphene, modified graphene and modified graphene/iron pentacarbonyl porous films with composites of chitosan (5, 10, 15, and 30 wt%) are shown in Fig. 4a. It is noted from these graphene derivatives that as the chitosan composite wt% is increased, it lowered the electrical conductivity. The number of layers existing in the graphene is the major factor to affect the properties. Hence, different materials are illustrated for monolayer, bilayer, and tri-layer of graphene. Former studies on graphene have proven that probability of altering charge carriers from holes to electron has led to the possible application in transistors [52]. However, merely monolayer graphene is valid for the electron-hole dependence. Yet, the dependence will get poorer with the disturbance of electrical field transmission by other layers once the number of layers is experiencing increment. The tremendously high mobility of electron at

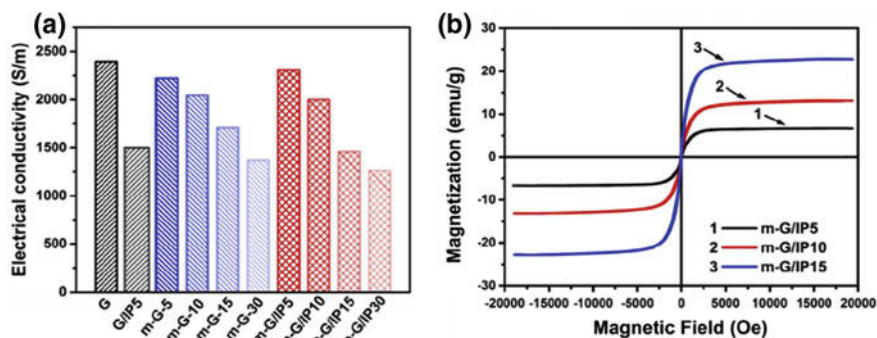


Fig. 4 **a** Electrical conductivities of graphene and its derivative films; **b** hysteresis loops of m-G/IP porous films [G—graphene; m-G—modified graphene, and m-G/IP modified graphene/iron pentacarbonyl porous films; m-GO-X, m-GO/IPX are composites of chitosan (5, 10, 15, and 30 wt%) with m-G and m-G/IP] (reproduced from [42] with permission from Elsevier)

different temperatures and exposure to magnetic fields result in the existence of quantum Hall effect in graphene for the hole and electron carriers [102]. For instance, mechanically generated graphene is found to exceed $2000 \text{ cm}^2/\text{V s}$ at room temperature. Furthermore, in graphene, it only happens at only half integers of quantum Hall effect instead of happening in the classic integer which is at $4 e^2/h$ where the electron charge represents e while Planck's constant represents h . This circumstance results from the special band structure of graphene. Besides, utilized substrate and temperature are the major components to affect the performance of electron mobility within graphene. For instance, staggering mobility of suspended and annealed graphene onto Si/SiO₂ can reach more than $200,000 \text{ cm}^2/\text{V s}$ which is considered as the highest recorded value among all the semiconductor substances [7].

2.2 *Magnetic Properties*

Magnetic properties of graphene might be affected by the presence of different types of defects [68]. The defects consist of topological defects, point defects, and extended defects. For instance, topological defects can be caused from the shapes such as heptagons and pentagons while the point defects are like adatoms, vacancies and the likes. However, extended defects include edges, voids, and cracks. Besides, defective parts like wrinkles, corrugations, and ripples can be found on the graphene surface. The defective lattice of the graphene such as voids and cracks will result in developing the local magnetic moments and forming interactions between the moments such as ferromagnetic [87]. The connection between the magnetic moments is ferromagnetic or antiferromagnetic if there is a detection of one Bohr magneton of magnetic moment formed by the vacancy or hydrogen chemisorption defects [95]. However, for the disorderly arranged graphene, induction of ferromagnetism can merely be done by monoatomic defects [94]. Furthermore, magnetism can be generated from adatoms, vacancies, and substitutional atoms [85]. In addition, induction of magnetic moment can be done by adding the monovalent and divalent adatom on graphene. The hysteresis loops of m-G/IP porous films with different chitosan composites (5, 10, and 15 wt%) is shown in Fig. 4b. Few studies also demonstrate that magnetism in graphene can be generated by zigzag edges and von Hove singularities [29]. Numerous experiments and methods have been tested regarding the magnetic properties and one of the studies states that reduced graphene oxide by using hydrazine continued by thermal treatment can form ferromagnetism in graphene [89]. Furthermore, exfoliation of graphite via ultrasonic technology in organic solvents can generate the magnetic properties in graphene nanocrystals with a minimum number of defects but no detection of ferromagnetism is observed at the temperature below than 2 K [72]. On the other hand, the presence of ferromagnetism can result from the high concentration of defects and it can be found mostly in the partly hydrogenated epitaxial graphene [91].

2.3 *Chemical Properties*

Pristine graphene sheets are regularly not reactive. Hence, graphene sheets should undergo superficial functionalization to activate its reactivity. This condition has illustrated that the domination of the surface is significant on the graphene chemistry while the graphene nanoribbons are dominated by the edges. Graphene reactivity also depends much on the thickness. As an example, monolayer graphene is found to have higher reactivity such as 10 times more than that of bilayer or multilayer graphene [73]. This statement is proved by utilizing the Raman spectroscopy in the peak measurement of relative disorder. Comparison of bulk graphene with graphene edges in terms of reactivity via spectroscopy examination is taken place and the discovery is that at least two times higher reactivity is found in the edges than that one of bulk monolayer graphene sheet [57].

2.4 *Mechanical Properties*

Performance and stability of the practical applications will be inevitably affected by the externally applied stress and unnecessary strain. The crystal-like graphene which covers an interatomic distance will eventually be affected by the externally applied stresses and hence it leads to the redistributed local charge. Indirectly, electronic transport will be varied significantly because of the developing band gap discovered in electronic structure. Anticipations from researchers can be witnessed once graphene is proven to have better performance than CNT in terms of its high stiffness and strength [12]. Hence, atomic force microscope has been utilized to make elastic properties measurement of the single layer graphene. As a result, 1 ± 0.1 TPa of Young's modulus and 130 ± 10 GPa of inherent strength are obtained [5]. Besides, measurement of strain with the applied tension and compression loads to the single layer graphene via Raman spectroscopy is recorded at the value of 1.3% for the strain and 0.7% for the compression and tension correspondingly [84]. There is a different degree of Young's modulus and fracture strength for a different layer of graphene. For instance, 1.02, 1.04 and 0.98 TPa of Young's modulus and 130, 126 and 101 GPa of fracture strength are owned by the single layer, bilayer, and tri-layer graphene correspondingly [31]. Therefore, it is obvious that increment of the layers will directly cause the increment in sliding tendency but weaken the properties. Furthermore, measurement of the alteration in 2D peaks and G with the presence of external stress can be made via Raman spectroscopy to record the measurement of the strains within the graphene sheets due to compression and tension. Potential to alter the band gap has been discovered by the introduction of measured strains because electric band structure can be varied by strain. Implementation of hydrogen plasma to carry out the reduction of graphene oxide has successfully led to the production of modified graphene with Young's modulus of 0.25 TPa [18]. Besides, the fracture toughness of pure

graphene is recorded at 4 MPa since the potential formation of agglomerates and brittle nature due to imperfect graphene are present [99]. In short, reduction of the properties is highly depending on the increment of graphene nanosheet layers.

2.5 Thermal Properties

Phonon transport is the significant variable to affect the performance of graphene in terms of thermal conductivity [106]. Phonon transport can be explained as the ballistic and diffusive conduction at low and high temperature correspondingly. Yet, transport of electronic thermal can be ignorable since the non-doped graphene possesses carrier density which is low. The inherent thermal conduction of graphene can reach to approximately the range from 2000 to 6000 W/mK for the graphene sheets to undergo suspension at room temperature [3]. However, the value of 600 W/mK is recorded for the graphene which is undergoing suspension via silicon dioxide substrate [71]. On the other hand, localization and phonon scattering can take place due to the graphene defects which include isotopic doping [24], edge scattering and sample production deposits [56]. Thus, the guaranteed high quality of graphene sheets generated via micromechanical cleavage approach results in better thermal conduction. Besides, the thermal conductivity of the mechanically exfoliated graphene was recorded within the range of 4800–5300 W/mK [4]. The thermal conductivity is clearly outstanding than that of multi-wall, natural diamond and single wall CNTs which are 3000, 2200 and 3500 W/mK respectively [57]. This has proven that the outstanding thermal conductivity of graphene is most likely to replace the usage of copper.

3 Preparation Methods of MGO Nanocomposites

Most of the MGO nanocomposites are synthesized using the hydrothermal method. Although the hydrothermal process is generally carried out at high temperatures, this technique is an eco-friendly and economically feasible method [19]. Based on the synthetic approaches of MGOs, this hydrothermal method is performed in the presence of organic molecules as precursors and in the presence of alkaline media. The hydrothermal method used to perform at a temperature between 160 and 180 °C in a Teflon-line autoclave [80], is also known as the solvothermal method. Cheng et al. [10] reported: “one-step fabrication of magnetic GO composite gel” for the efficient adsorption removal of dye. The preparation of GO magnetic gel involved the hydrothermal method in the presence of alkaline ($\text{NH}_3\text{-H}_2\text{O}$) and polymer (polyvinyl alcohol). The gel exhibited both enhanced adsorption removal capacity towards cationic and anionic dyes, and magnetic separation capability, compared with the bare GO [86]. Generally, the ultra-sonochemical method is used to prevent re-aggregation, and improve the dispersion and reduction of the size of

the material. It was used mostly before or after the synthesis of MGOs by the hydrothermal method. The main principle of the solvochemical method is the generation of ultrasound using a titanium horn that can serve to reduce the Van der Waals forces in the GO by ultra-sound irradiation of liquid [55]. Szabo et al. successfully prepared MGOs by sonication of a mixture of magnetic nanoparticles and GO solution [82].

Lately, microwave synthesis has become of great significance in the preparation of inorganic nanomaterials. In the synthesis of inorganic nanomaterials, compared to conventional heating technique, the microwave synthesis technique consumes less energy, environmentally friendly, and provides a homogeneous heating process for speedy reaction [74]. It can also offer rapid and selective heating of the reactant to a high temperature that leads to the production of “self-generated pressure in the sealed reaction vessel” [82]. Some of the previous works used the microwave synthesis method for the preparation of MGOs, including Mn_3O_4 -rGO nanocomposites [74], and GO-NiO-4ZnO-4CoO-2Fe₂O₄ nanocomposites [45].

4 Structural Characterization and Properties of MGOs

The formation and structural functionalities of the prepared GO's and MGOs can be characterized using spectroscopic techniques that include XRD, XPS and FT-IR, and RS. The surface morphology, size, porosity, and dimensions of the prepared GO's and MGOs were evaluated using microscopic techniques, including AFM, TEM, and SEM. The surface area and surface primary adsorption characteristics were evaluated using BET theory analysis. Magnetic property measurements of GO's and MGOs were performed using a magnetometer. The SEM images of GO film, modified GO film, graphene porous film, and modified graphene porous film are shown in Fig. 5 [42]. The microstructure evolution of the unmodified GO films before (Fig. 5a) and after (Fig. 5c, e) the hydrazine-induced foaming process. Clearly, the GO film with highly-oriented GO sheets is converted to porous graphene film with random porous structures due to the excessive expansion derived from the weak interlayer interactions (Fig. 5c, e). The CS modified graphene (m-G) porous film (Fig. 5d, f) has distinct and continuous porous structures inherited from its precursor (Fig. 5b), which contrasts sharply the random structures of its unmodified counterpart (Fig. 5c, e). Additionally, some small pores are observed in the porous graphene film (Fig. 5f), which are beneficial for further decreasing the density of the porous film while retaining its reasonable strength.

XRD studies are mainly used to identify the formation, structure, and crystalline nature of MGOs. The XRD 2θ strong peak in the range 8° – 12° indicates the formation of GO. By the magnetization, the crystalline property of GO is decreased by the increase of the mesoporous carbonaceous nature with alteration of the original position of the GO peak [47]. The XRD diffraction peaks are also used to identify the ferrite in MGOs. By decreasing the size of MGOs with increasing porosity, the positions of diffraction peaks shift to lower 2θ range [70].

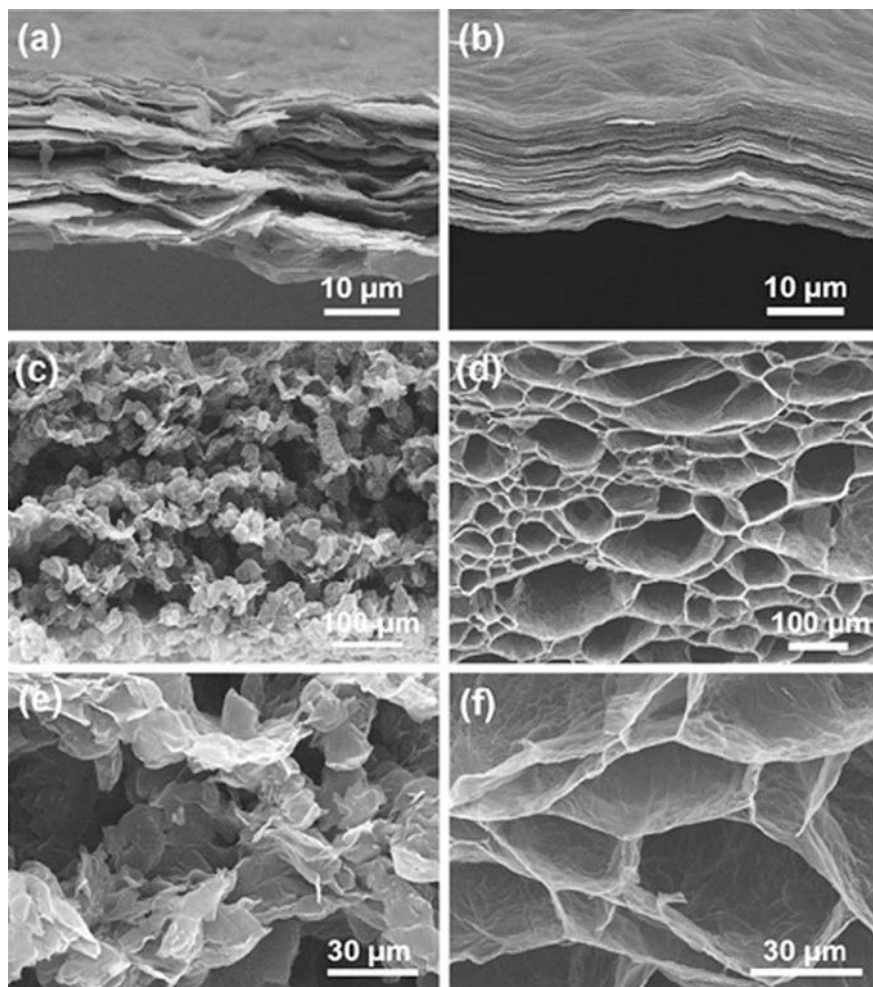


Fig. 5 SEM images of **a** GO film, **b** modified GO film, **c**, **e** graphene porous film, and **d**, **f** modified graphene porous film (reproduced from [42] with permission from Elsevier)

RS is an important technique to qualitatively identify the MGOs. As is known, the graphitic materials show two prominent Raman peaks around 1350 and 1600 cm^{-1} called the D and G bands. Here, the G band corresponds to the stretching vibrations of carbons at sp^2 hybridization, whereas the D band represents the vibrations of carbons at sp^3 hybridization, which can break the symmetry and selection rule [36]. By the magnetization of GO, these D and G bands alter their positions, based on their principal interactions. But, in the case of nickel ferrite-rGO (rGONF), both the sp^2 domain (D) and sp^3 domain (G) carbons are shifted to lower range at ~ 1303 – 1591 cm^{-1} , which indicates that both D and G band carbons are involved in the formation of reduced GO-based magnetic nanocomposite. The XPS is used to

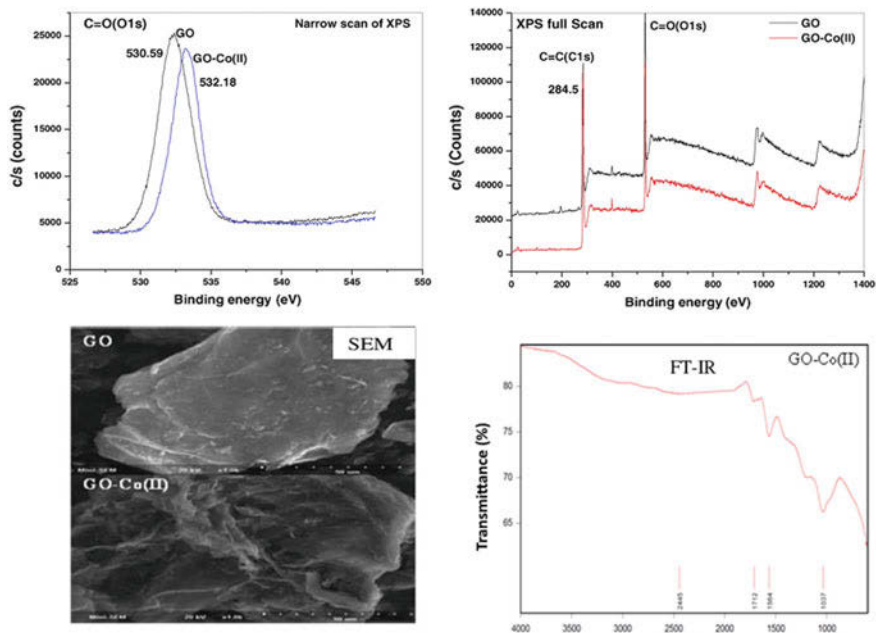


Fig. 6 XPS, SEM, FT-IR results of the Co(II)-loaded GO (reproduced from [40] with permission)

qualitative and quantitative identify the chemical composition of MGOs. The bonding energy peaks of 700–730 eV indicate the Fe peaks of magnetic materials.

The microscopic techniques, including SEM, TEM, and AFM, are used to measure the size of nanocomposites, MGOs, and their surface morphology, which is an important factor to know for the adsorption process. Their porous structure and surface area can be further evaluated by using (N₂) adsorption-desorption isotherms through BET analysis. The magnetic nature of MGOs is identified using the magnetic measurement system (MPMS). When the size of MGOs decreases to the nanoscale, it shows superparamagnetic nature. Lingamdinne et al. [36] confirmed the superparamagnetic property of magnetic nanocomposite by MT curves obtained at 1000 Oe magnetic field. They also observed the increase of superparamagnetic property by the reduction of nanocomposite [16]. The XPS, SEM, FT-IR of the Co(II)-GO were shown in Fig. 6.

5 Applications to Sustainable Water Purification

Graphene oxide is easily dispersed in water due to the plentiful hydrophilic (carboxylic, epoxide, and hydroxyl groups) groups on its surface. List of various GO based nanomaterials utilized for removal of heavy metal ions removal is given in

Table 1. Due to the hydrophilic nature of GO, it adsorbs the pollutants to stable complexes, causing difficulties for the separation and recovery of GO [96]. To overcome these difficulties of separation, magnetic functionalization of GO is an alternative solution [104]. Due to the magnetic particle has unique properties, they have been widely applied to the removal of various pollutants. Some researchers have developed magnetic graphene oxide composites for efficient applications, including water treatment, energy storage, and drug delivery [11]. Here, we review some research reports, and briefly critique the use of MGO based nanocomposites for the adsorption of heavy metals and radionuclides.

5.1 Heavy Metals Removal

Exposure to heavy metals can present serious health risks to human beings. For the purification of water, adsorption is an effective, economic, and easy operation technique, compared to conventional methods [54]. But it is limited, due to the difficulties in the filtration and regeneration of adsorbents. The use of magnetic materials for water purification can overcome the above difficulties, including the filtration and regeneration of adsorbents; therefore, many researchers have developed and widely used magnetic materials for the treatment of pollutants [60]. However, the nano metal ferrites show poor stability [47]. To overcome these difficulties, hybrid materials have been synthesized through magnetic ferrites and GO by the hydrothermal method. Due to the presence of epoxy, carboxylic, and hydroxyl functions at GO, they can enhance the adsorption of heavy metals [33]. The specific adsorption mechanisms of graphene oxide-based nanomaterials for metal ions removal are given in Table 2.

Chandra et al. [8] thru a chemical reaction developed 10 nm average size superparamagnetic magnetite reduced graphene oxide (M-RGO) composites. The M-RGO showed higher adsorption capacity over 99.9% for removal of both ionic states of Arsenic. Zhang et al. employed ferric hydroxide-GO composite for the magnificent adsorption of arsenate from water [98]. Here, high arsenate adsorption removal was observed over a pH range of 4–9 and reduced the arsenate concentration of contaminated water from 20 to 0.5 ppm. Water-soluble “magnetic graphene oxide nanocomposite” has been produced via a “copper catalyzed azide-alkyne cycloaddition”, and was utilized for the adsorption removal of Pb (II), Cd(II), and Cu(II), from aqueous solutions [100]. The results found that the nanocomposite has the higher surface area and extraordinary removal capacity for heavy metals.

RGO–MnO₂ composites showed excellent Hg(II) uptake capacity [77]. The composite shows enhanced adsorption removal capacity compared to its base material. Liu et al. [43] employed an MGO for the successful removal of Co(II). The adsorption Co(II) on MGO was the rate-limiting kinetics, with “inner-sphere surface complexation” at low pH values. Meanwhile, at higher pH values, the removal mechanism of Co(II) was associated with inner-sphere surface

Table 1 List of various graphene oxide based nanomaterials utilized for removal of heavy metal ions removal

Metal ion	Adsorbent	Max. adsorption capacity (mg/g)	Conditions	Model (adsorption isotherm; kinetics)	Remarks
Cd	GO	1792.60	303 K; pH 4.0	Langmuir and Freundlich; pseudo second-order	<ul style="list-style-type: none"> The equilibrium contact time is 120 min The graphene oxide is generated by using amorphous graphite
	PAMAMs/GO	253.81	298 K; pH 5.0	Langmuir; pseudo second-order	<ul style="list-style-type: none"> The adsorption process achieves equilibrium within 60 min The adsorbent dosage is 0.1 g
	Few-layered GO nanosheets	106.30	303 K; pH 6.0	Langmuir	<ul style="list-style-type: none"> The dosage of adsorbent is 0.1 g/L The adsorption capacity is strongly based on pH and humic acid
	GO/cellulose membranes	26.8	298 K; pH 4.5	Langmuir; pseudo second-order	<ul style="list-style-type: none"> Good adsorption and no precipitation of metal hydroxides It can be reused up to ten cycles
Pb	Few-layered GO	842.00	293 K; pH 6.0	Langmuir	<ul style="list-style-type: none"> pH value strongly affects the adsorption capacity The adsorption capacity is strongly independent of ionic strength
	Graphene nanosheet	476.19	298 K; pH 6.2	Langmuir	<ul style="list-style-type: none"> The equilibrium contact time is 35 min The dosage of adsorbent is 40 mg/L
	Ag/GO	312.57	298 K; pH 5.3	Langmuir; pseudo second-order	<ul style="list-style-type: none"> 0.05 mg of adsorbents used showed the maximum adsorption performance The equilibrium time for the lead adsorption is 50 min
Cu	Chitosan/SH/GO	425.00	293 K; pH 5.0	Freundlich; pseudo second-order	<ul style="list-style-type: none"> The dosage of adsorbents is 0.2 mg/mL The adsorption efficiency is strongly dependent on pH, temperature and adsorbent dosage
	TiO ₂ /GO	45.20	293 K; pH 6.0	Langmuir	<ul style="list-style-type: none"> The adsorption capacity is strongly based on the pH value
	GO aerogels	19.65	298 K; pH 6.2	Langmuir; pseudo second-order	<ul style="list-style-type: none"> The dosage of adsorbents is 0.6 g/L It involves ion exchange mechanism

(continued)

Table 1 (continued)

Metal ion	Adsorbent	Max. adsorption capacity (mg/g)	Conditions	Model (adsorption isotherm; kinetics)	Remarks
Cr	Chitosan/GO	310.40	318 K; pH 3.0	Redlich–Peterson/double exponential	<ul style="list-style-type: none"> • The adsorbent dosage is 0.5 g/L • Both internal and external diffusion take place effectively in the adsorption process
	Fe ₃ O ₄ /GO	32.33	293 K; pH 4.5	Langmuir; pseudo second-order	<ul style="list-style-type: none"> • pH value and ionic strength are the crucial factors to affect the adsorption capacities • The adsorbent dosage is 0.2 g/L

Adapted from [34] with permission from Elsevier

Table 2 Specific adsorption mechanisms of graphene oxide-based nanomaterials for metal ions removal

Graphene oxide-based nanomaterials	Adsorption mechanisms included for metal ions removal	Advantages	Drawbacks
Graphene oxide (GO)	<ul style="list-style-type: none"> • Electrostatic interactions • Ion exchange 	<ul style="list-style-type: none"> • Good dispersion in water • Great colloidal constancy • Contains rich oxygenated functional groups 	<ul style="list-style-type: none"> • A restricted number of sorption sites
Reduced graphene oxide (rGO)	<ul style="list-style-type: none"> • Electrostatic interactions • Lewis-base–acid mechanism 	<ul style="list-style-type: none"> • Restoration of sp² domains • Better electron-transport properties 	<ul style="list-style-type: none"> • Less oxygen-containing functional groups • Weaker colloidal stability
Magnetic graphene oxide nanocomposites	<ul style="list-style-type: none"> • Electrostatic interactions with graphene oxide • Interactions with the particles surface • Magnetic properties of the nanoparticles 	<ul style="list-style-type: none"> • Bigger surface area compared to the pure GO • Increased number of binding sites compared to pure GO • Ease the recovery process from solutions 	<ul style="list-style-type: none"> • Co-reduction of GO during the combination of the particles weakens the colloidal stability
Graphene oxide materials functionalized with organic molecules	<ul style="list-style-type: none"> • Electrostatic interactions • Complexation with organic molecules 	<ul style="list-style-type: none"> • Bigger surface area compared to pure GO • Great colloidal stability • The greater number of functional groups (–NH₂, –OH) 	<ul style="list-style-type: none"> • Large variations of the stability of the loaded molecules depending on the alteration approach physically or chemically

Reproduced from [34] with permission from Elsevier

complexation and precipitation. Co(II)-loaded MGO can be rapidly separated and recovered from aqueous solution by external magnetic field [43]. Liu et al. [44] reported a facile self-assembly of magnetic particles with GO through electrostatic interaction in the presence of 3-aminopropyltrimethoxysilane. The prepared porous MGO not only conventionally separated by a magnetic field but also enhanced the adsorption capacity of GO for Cr(VI) removal. They also concluded that the prepared MGO shows higher adsorption capacity than that of GO and Fe₃O₄. Bhunia et al. [6] developed a heterogeneous matrix of iron/iron oxide dispersed on RGO (RGO-FeO)/Fe₃O₄) that can be used for the effective adsorption of heavy metal ions, including Cr(VI), Hg(II), Pb(II), Cd(II), and As(III). Recently, Lingamdinne et al. employed porous inverse spinel composite (MGO) and porous inverse RMGO nanocomposites using nickel ferrite and GO, and applied them for the removal of Arsenic [38], Pb(II) and Cr(III) [35 36 37 39 40 41]. They also reported the as-prepared nanocomposites to show considerably enhanced adsorption capacity for Pb(II), Cr(III), As(III), and As(V), compared to that of GO. They stated that the adsorption efficiency of rMGO for As(III) and As(V) is 106.40 and 65.78 mg/g respectively was greater than that of MGO [38]. The adsorption process was thermodynamically favourable for the adsorption of Pb(II) and Cr(III) onto the nanocomposites and was spontaneous endothermic. But the As(III) and As(V) removal was enhanced with increased temperature up to 300 K, while it started decreasing with further increase of the temperature above 300 K. The unavailability of metal ions undergoing degradation process via bioprocesses and reactions chemically has led to the wider exposure to adsorption process and hence it is now considered as the most promising method to remove heavy metal ions [53].

Copper (II) ions can be removed effectively via the interaction between copper (II) ions and oxygen groups on GO which are positively charged and negatively charged respectively [92]. Besides, Pb(II), U(VI) and Co(II) ions can be adsorbed via the usage of GO as well [46]. For instance, powder X-ray diffraction (XRD), scanning electron microscopy (SEM), infrared spectroscopy (FT-IR) and X-ray photoelectron spectroscopy (XPS) are utilized to determine the adsorption characterization of GO towards copper, lead, zinc and cadmium. As a result, the largest adsorption capacities at pH 5 have been recorded as 294, 345, 530, 1119 mg/g for Cu(II), Zn(II), Cd(II) and Pb(II) respectively [76]. In addition, the adsorption capacities mentioned previously can be done in a wide range of pH values which are 3–7 for both Cu(II) and Pb(II), 4–8 for Cd(II) and 5–8 for Zn(II) [76]. It is studied that the removal of heavy metal ions via GO can be explained as the adsorption process is restricted chemically due to the participation of superficial complexity of metal ions with the presence of oxygen in the functional groups which lies on the surface of GO. As an example, cellulose hydrogel/GO possesses adsorption capacity of approximately 94 mg/g [9].

Furthermore, with the presence of metal oxides on GO and GNs, they are considered as high-performance adsorbents in the past [21]. For instance, the fabrication of GO–TiO₂ is implemented to remove Pb(II), Zn (II) and Cd(II) ions. Hence, the adsorption capacities of the GO–TiO₂ on the Pb(II), Zn (II) and Cd(II) ions at pH value of 5 are recorded at 65.8, 88.9 and 72.8 mg/g respectively [32].

The covalent bond which is securing the rGO and TiO₂ in the GO–TiO₂ has resulted in the poor electron-hole recombination and hence great amount of Cr(VI) can be reduced. Although different types of magnetic graphene composites have been utilized, to eradicate the separation difficulties, a combination of GO or GNs with magnetic materials is a good choice. The significant of the combination is to minimize the agglomeration and restacking of graphene sheets and at the same time increasing the surface area and adsorption efficiency [79].

Moreover, removal of cadmium ions and copper ions from wastewater can be done via fabrication of GNs through the method of modified Hummers [103]. For instance, at the condition of pH 6.0 ± 0.1 and temperature around 303 K, it is recorded that highest adsorption capacities of Co(II) and Cd(II) can be achieved with the value of 68.2 and 106.3 mg/g respectively. This has proven that the adsorption of heavy metal ions through GNs is depending on the ionic strength and pH. However, adsorption of chromium (VI) ions and chromium (III) ions can be done at the low range of pH levels but the adsorptions of copper (II) ions, lead (II) ions, and gold (III) ions are most likely to be occurring at higher range of pH levels [15].

Other than that, MMSP-GO to adsorb heavy metal ions such as Cd (II) and Pb(II) is worth studied as well. Once the synthesis of magnetic mesoporous silica comes with the functionalization with polyethyleneimine molecules, the conjugation of a great number of amine groups with carboxyl groups on the GO sheets could increase the affinity between the pollutants and mesoporous silica. Significant and effective data has been recorded for the MMSP-GO composites regarding its maximum adsorption capacities for Pb(II) and Cd(II) which are 333 and 167 mg/g respectively [90].

5.2 *Organic Pollutants Removal*

Presently, many process industries, including the paper, textile, paint, plastic, and leather industries, use pigments and dyes to colour their products, and excess of these colours end up in the discharge, which ultimately ends up as industrial effluent. These dyes are organic compounds, and the presence of dyes in an aquatic environment not only affects the aesthetics, it also inhibits the penetration of sunlight, and thus reduces photosynthesis for waterborne plants. Overall, the presence of dyes poses the threat of toxic materials, which are resistant to a chemical reaction in wastewaters, and which leads to cancer, mutagenesis, and other severe problems in human and aquatic creatures. The complicated chemical structures of dyes make these materials highly resistant to biodegradation [49]. Therefore, these dyes have to be removed efficiently before the effluent is discharged to the nearby aquatic environment.

In the last couple of years, magnetic nanoparticles have been extensively applied for the removal of toxic metal ions and organic pollutants. This is due to the features, like low toxicity, high chemical stability, and good magnetic properties.

Adsorbents based on magnetic nanoparticles are used in the removal of toxic dyes and heavy metals from aqueous solutions with precision and high accuracy [88]. However, the bare magnetic nanoparticles can easily be oxidized in atmospheric conditions. Therefore, to remedy these effects and increase the life of nanoparticles, researchers explored ways to coat or functionalize the magnetic nanoparticles and enhance the functional groups. In recent years, usage of GO-based magnetic nanoparticles as an adsorbent has increased. Association of graphene has resulted in high removal capacity of pollutants. Chandra et al. [8] reported that compared to free nanoparticles, RGO and GO embedded materials have shown higher binding capacity. Deng et al. [13] synthesized MGO and used it to investigate the simultaneous removal of Cd(II) and ionic dyes like orange gelb (OG) and methylene blue (MB). The maximum adsorption capacities reported for the removal of MB using graphene nanosheet/magnetite, magnetic rectorite/iron oxide, and multi-walled carbon nanotubes/Fe₂O₃, were 43.82, 31.18, and 42.30 mg/g, respectively. They also reported that the maximum sorption capacities of MGO (64.23 mg/g for MB, and 20.85 mg/g for OG) were much higher than those of “exfoliated graphene oxide” (17.3 mg/g for MB, and 5.98 for OG) used as adsorbent [58]. The maximum adsorption capacities reported for removal of dyes using bare iron oxide nanoparticles were 2.78 and 15.62 mg/g for MB and OG, respectively. Khurana et al. [28] investigated the “Eriochrome Black T” (EBT) adsorption from textile wastewater using MGO in a batch process. In this study, for the removal of toxic textile azo dye EBT, they synthesized MGO that was impregnated with α -Fe₂O₃. The maximum adsorption capacity for dye removal was reported to be 210.53 mg/g.

6 Conclusion and Future Perspective

This chapter indicates that adsorption using MGOs is becoming an alternative option to replace the conventional adsorbents used for water purification. It also shows that these MGO composites have comparable or even greater adsorption and regeneration capacity, compared to the available adsorbents and activated carbons. Moreover, the adsorbents coming out at long last with high adsorption efficiency for the handling of wastewater containing metal pollutants (heavy metals and radionuclides) and organic pollutants could be successfully implemented as beneficial to society.

The synthesis of graphene has been widely done by the latest and greatest method which is improved Hummers method. However, the experimental procedures to complete the fabrication of the graphene is time-consuming although the experimental complexity is considerably low. Therefore, replacement or removal of certain chemicals is required to be further discovered and studied to shorten the fabrication period and result in a better fabrication method.

The synthesis of graphene has been generally done by the enhanced Hummers technique. Applications are hindered due to the time-consuming methods for

fabricating the Graphene. Accordingly, appropriate techniques need to be discovered to reduce the fabrication period and thus enhance the performance of graphene obtained by these fabrications method. Another major hurdle in these applications is the scalability of these methods. Most of the recently reported studies are limited to lab scale experiments. Therefore, studies should also focus on the scalability of these applications from lab scale experiments into commercial industrial scale applications. It should also be noted that, industries which produce effluents and wastewater at a larger scale will consume higher quantities of GO's and MGO's, thus increasing the cost of operation to many folds. Therefore, the commercialized MGOS should be prepared in such a way that they can be re-used or regenerate with low operating cost.

Acknowledgments This work has been supported by the National Research Foundation (NRF) of Korea funded by the Ministry of Science, ICT & Future Planning (MSIP) (2017R1C1B5016656) of the Korea Government, Seoul, Korea.

References

1. Alvand M, Shemirani F (2016) Fabrication of Fe₃O₄@graphene oxide core-shell nanospheres for ferrofluid-based dispersive solid phase extraction as exemplified for Cd (II) as a model analyte. *Microchim Acta* 183:1749–1757. <https://doi.org/10.1007/s00604-016-1805-8>
2. Azimi A, Azari A, Rezakazemi M, Ansarpour M (2017) Removal of heavy metals from industrial wastewaters: a review. *ChemBioEng Rev* 4:37–59. <https://doi.org/10.1002/cben.201600010>
3. Balandin AA (2011) Thermal properties of graphene and nanostructured carbon materials. *Nat Mater* 10:569. <https://doi.org/10.1038/nmat3064>
4. Balandin AA, Ghosh S, Bao W, Calizo I, Teweldebrhan D, Miao F, Lau CN (2008) Superior thermal conductivity of single-layer graphene. *Nano Lett* 8:902–907
5. Berger C et al (2004) Ultrathin epitaxial graphite: 2D electron gas properties and a route toward graphene-based nanoelectronics. *J Phys Chem B* 108:19912–19916. <https://doi.org/10.1021/jp040650f>
6. Bhunia P, Kim G, Baik C, Lee H (2012) A strategically designed porous iron–iron oxide matrix on graphene for heavy metal adsorption. *Chem Commun* 48:9888
7. Bolotin KI et al (2008) Ultrahigh electron mobility in suspended graphene. *Solid State Commun* 146:351–355. <https://doi.org/10.1016/j.ssc.2008.02.024>
8. Chandra V, Park J, Chun Y, Lee JW, Hwang I-C, Kim KS (2010) Water-dispersible magnetite-reduced graphene oxide composites for arsenic removal. *ACS Nano* 4:3979–3986. <https://doi.org/10.1021/nn1008897>
9. Chen X, Zhou S, Zhang L, You T, Xu F (2016) Adsorption of heavy metals by graphene oxide/cellulose hydrogel prepared from NaOH/urea aqueous solution. *Mater* 9:582
10. Cheng Z, Liao J, He B, Zhang F, Zhang F, Huang X, Zhou L (2015) One-step fabrication of graphene oxide enhanced magnetic composite gel for highly efficient dye adsorption and catalysis. *ACS Sustain Chem Eng* 3:1677–1685
11. Chung C, Kim Y-K, Shin D, Ryoo S-R, Hong BH, Min D-H (2013) Biomedical applications of graphene and graphene oxide. *Acc Chem Res* 46:2211–2224
12. Dasari BL, Nouri JM, Brabazon D, Naher S (2017) Graphene and derivatives—synthesis techniques, properties and their energy applications. *Energy* 140:766–778. <https://doi.org/10.1016/j.energy.2017.08.048>

13. Deng J-H, Zhang X-R, Zeng G-M, Gong J-L, Niu Q-Y, Liang J (2013) Simultaneous removal of Cd (II) and ionic dyes from aqueous solution using magnetic graphene oxide nanocomposite as an adsorbent. *Chem Eng J* 226:189–200
14. Deng J-H, Zhang X-R, Zeng G-M, Gong J-L, Niu Q-Y, Liang J (2013) Simultaneous removal of Cd(II) and ionic dyes from aqueous solution using magnetic graphene oxide nanocomposite as an adsorbent. *Chem Eng J* 226:189–200
15. Duru I, Ege D, Kamali AR (2016) Graphene oxides for removal of heavy and precious metals from wastewater. *J Mater Sci* 51:6097–6116
16. Fan Z, Wang K, Wei T, Yan J, Song L, Shao B (2010) An environmentally friendly and efficient route for the reduction of graphene oxide by aluminum powder. *Carbon* 48:1686–1689
17. Gollavelli G, Chang C-C, Ling Y-C (2013) Facile synthesis of smart magnetic graphene for safe drinking water: heavy metal removal and disinfection control. *ACS Sustain Chem Eng* 1:462–472
18. Gomez-Navarro C, Burghard M, Kern K (2008) Elastic properties of chemically derived single graphene sheets. *Nano Lett* 8:2045–2049. <https://doi.org/10.1021/nl801384y>
19. Hashim N et al (2016) A brief review on recent graphene oxide-based material nanocomposites: synthesis and applications. *J Mater Environ Sci* 7:3225–3243
20. Hu X-J et al (2013) Removal of Cu(II) ions from aqueous solution using sulfonated magnetic graphene oxide composite. *Sep Purif Technol* 108:189–195
21. Hur J, Shin J, Yoo J, Seo YS (2015) Competitive adsorption of metals onto magnetic graphene oxide: comparison with other carbonaceous adsorbents. *The Sci World J* 2015:1–11. <https://doi.org/10.1155/2015/836287>
22. Abbas A, Al-Amer AM, Laoui T, Al-Marri MJ, Nasser MS, Khraisheh M, Atieh MA (2016) Heavy metal removal from aqueous solution by advanced carbon nanotubes: critical review of adsorption applications. *Sep Purif Technol* 157:141–161
23. Ionita M, Vlăsceanu GM, Watzlawek AA, Voicu SI, Burns JS, Iovu H (2017) Graphene and functionalized graphene: extraordinary prospects for nanobiocomposite materials. *Compos B Eng* 121:34–57
24. Jiang J-W, Lan J, Wang J-S, Li B (2010) Isotopic effects on the thermal conductivity of graphene nanoribbons: localization mechanism. *J Appl Phys* 107:054314. <https://doi.org/10.1063/1.3329541>
25. Karri RR, Sahu JN (2018) Modeling and optimization by particle swarm embedded neural network for adsorption of zinc (II) by palm kernel shell based activated carbon from aqueous environment. *J Environ Manage* 206:178–191
26. Karri RR, Jayakumar N, Sahu J (2017) Modelling of fluidised-bed reactor by differential evolution optimization for phenol removal using coconut shells based activated carbon. *J Mol Liq* 231:249–262
27. Karri RR, Sahu JN, Jayakumar NS (2017) Optimal isotherm parameters for phenol adsorption from aqueous solutions onto coconut shell based activated carbon: error analysis of linear and non-linear methods. *J Taiwan Inst Chem Eng* 80:472–487
28. Khurana I, Shaw AK, Bharti, Khurana JM, Rai PK (2018) Batch and dynamic adsorption of Eriochrome Black T from water on magnetic graphene oxide: experimental and theoretical studies. *J Environ Chem Eng* 6:468–477
29. Kou L, Tang C, Guo W, Chen C (2011) Tunable magnetism in strained graphene with topological line defect. *ACS Nano* 5:1012–1017. <https://doi.org/10.1021/nn1024175>
30. Krane N (2011) Selected topics in physics: physics of nanoscale carbon. Freie Universität, Berlin
31. Lee C, Wei X, Li Q, Carpick R, Kysar Jeffrey W, Hone J (2009) Elastic and frictional properties of graphene. *Physica Status Solidi (b)* 246:2562–2567. <https://doi.org/10.1002/pssb.200982329>
32. Lee Y-C, Yang J-W (2012) Self-assembled flower-like TiO₂ on exfoliated graphite oxide for heavy metal removal. *J Ind Eng Chem* 18:1178–1185

33. Li J, Guo S, Zhai Y, Wang E (2009) Nafion–graphene nanocomposite film as enhanced sensing platform for ultrasensitive determination of cadmium. *Electrochem Commun* 11:1085–1088
34. Lim JY, Mubarak NM, Abdullah EC, Nizamuddin S, Khalid M, Inamuddin (2018) Recent trends in the synthesis of graphene and graphene oxide based nanomaterials for removal of heavy metals—a review. *J Ind Eng Chem*. <https://doi.org/10.1016/j.jiec.2018.05.028>
35. Lingamdinne L, Kim I-S, Ha J-H, Chang Y-Y, Koduru J, Yang J-K (2017) Enhanced adsorption removal of Pb(II) and Cr(III) by using nickel ferrite-reduced graphene oxide nanocomposite. *Metals* 7:225
36. Lingamdinne LP, Choi Y-L, Kim I-S, Yang J-K, Koduru JR, Chang Y-Y (2017) Preparation and characterization of porous reduced graphene oxide based inverse spinel nickel ferrite nanocomposite for adsorption removal of radionuclides. *J Hazard Mater* 326:145–156
37. Lingamdinne LP, Koduru JR, Chang Y-Y, Karri RR (2018) Process optimization and adsorption modeling of Pb(II) on nickel ferrite-reduced graphene oxide nano-composite. *J Mol Liq* 250:202–211
38. Lingamdinne LP, Choi Y-L, Kim I-S, Chang Y-Y, Koduru JR, Yang J-K (2016) Porous graphene oxide based inverse spinel nickel ferrite nanocomposites for the enhanced adsorption removal of arsenic. *RSC Adv* 6(77):73776–73789
39. Lingamdinne LP, Koduru JR, Choi Y-L, Chang Y-Y, Yang J-K (2016) Studies on removal of Pb(II) and Cr(III) using graphene oxide based inverse spinel nickel ferrite nano-composite as sorbent. *Hydrometallurgy* 165:64–72
40. Lingamdinne LP, Koduru JR, Roh H, Choi Y-L, Chang Y-Y, Yang J-K (2016) Adsorption removal of Co(II) from waste-water using graphene oxide. *Hydrometallurgy* 165:90–96
41. Lingamdinne LP, Roh H, Choi Y-L, Koduru JR, Yang J-K, Chang Y-Y (2015) Influencing factors on sorption of TNT and RDX using rice husk biochar. *J Ind Eng Chem* 32:178–186
42. Liu J, Zhang H-B, Liu Y, Wang Q, Liu Z, Mai Y-W, Yu Z-Z (2017) Magnetic, electrically conductive and lightweight graphene/iron pentacarbonyl porous films enhanced with chitosan for highly efficient broadband electromagnetic interference shielding. *Compos Sci Technol* 151:71–78. <https://doi.org/10.1016/j.compscitech.2017.08.005>
43. Liu M, Chen C, Hu J, Wu X, Wang X (2011) Synthesis of magnetite/graphene oxide composite and application for cobalt(ii) removal. *J Phys Chem C* 115:25234–25240
44. Liu M, Wen T, Wu X, Chen C, Hu J, Li J, Wang X (2013) Synthesis of porous Fe₃O₄ hollow microspheres/graphene oxide composite for Cr(vi) removal. *Dalton Trans* 42:14710
45. Liu P, Yao Z, Zhou J (2015) Preparation of reduced graphene oxide/NiO-4ZnO-4CoO-2Fe₂O₄ nanocomposites and their excellent microwave absorption properties. *Ceram Int* 41:13409–13416
46. Liu, ZJ, Yang, JW, Li, CZ, Li, JX, Jiang, YJ, Dong, YH, Li, YY (2014) Adsorption of Co (II), Ni (II), Pb (II) and U (VI) from aqueous solutions using polyaniline/graphene oxide composites. *Korean Chem Eng Res* 52(6):781–788. <https://doi.org/10.9713/kcer.2014.52.6.781>
47. Maaz K, Karim S, Mumtaz A, Hasanain SK, Liu J, Duan JL (2009) Synthesis and magnetic characterization of nickel ferrite nanoparticles prepared by co-precipitation route. *J Magn Magn Mater* 321:1838–1842
48. Mesbah M, Shahsavari S, Soroush E, Rahaei N, Rezakazemi M (2018) Accurate prediction of miscibility of CO₂ and supercritical CO₂ in ionic liquids using machine learning. *J CO₂ Utilization* 25:99–107. <https://doi.org/10.1016/j.jcou.2018.03.004>
49. Mokhtari P, Ghaedi M, Dashtian K, Rahimi M, Purkait M (2016) Removal of methyl orange by copper sulfide nanoparticles loaded activated carbon: kinetic and isotherm investigation. *J Mol Liq* 219:299–305
50. Muzyka R, Kwoka M, Smeđowski Ł, Diez N, Gryglewicz G (2017) Oxidation of graphite by different modified Hummers methods. *New Carbon Mater* 32:15–20. <https://doi.org/10.1016/S1872-5805%5b17%5d60102-1>
51. Novoselov KS et al (2004) Electric field effect in atomically thin carbon films. *Science* 306:666–669

52. Novoselov KS, Jiang D, Schedin F, Booth TJ, Khotkevich VV, Morozov SV, Geim AK (2005) Two-dimensional atomic crystals. *Proc Natl Acad Sci U S A* 102:10451
53. Nupearachchi CN, Mahatantila K, Vithanage M (2017) Application of graphene for decontamination of water implications for sorptive removal. *Groundwater Sustain Dev* 5:206–215. <https://doi.org/10.1016/j.gsd.2017.06.006>
54. Oraby EA, Eksteen JJ (2015) The leaching of gold, silver and their alloys in alkaline glycine–peroxide solutions and their adsorption on carbon. *Hydrometallurgy* 152:199–203
55. Peng Y, Ji J, Chen D (2015) Ultrasound assisted synthesis of ZnO/reduced graphene oxide composites with enhanced photocatalytic activity and anti-photocorrosion. *Appl Surf Sci* 356:762–768
56. Pettes MT, Jo I, Yao Z, Shi L (2011) Influence of polymeric residue on the thermal conductivity of suspended bilayer graphene. *Nano Lett* 11:1195–1200. <https://doi.org/10.1021/nl104156y>
57. Phiri J, Gane P, Maloney TC (2017) General overview of graphene: production, properties and application in polymer composites. *Mater Sci Eng B* 215:9–28. <https://doi.org/10.1016/j.mseb.2016.10.004>
58. Ramesha G, Kumara AV, Muralidhara H, Sampath S (2011) Graphene and graphene oxide as effective adsorbents toward anionic and cationic dyes. *J Colloid Interface Sci* 361:270–277
59. Razavi SMR, Rezakazemi M, Albadarin AB, Shirazian S (2016) Simulation of CO₂ absorption by solution of ammonium ionic liquid in hollow-fiber contactors. *Chem Eng Process Process Intensification* 108:27–34. <https://doi.org/10.1016/j.cep.2016.07.001>
60. Reddy DHK, Lee S-M (2013) Application of magnetic chitosan composites for the removal of toxic metal and dyes from aqueous solutions. *Adv Coll Interface Sci* 201–202:68–93
61. Rezakazemi M, Dashti A, Riasat Harami H, Hajilari N, Inamuddin (2018) Fouling-resistant membranes for water reuse. *Environ Chem Lett* 1–49. <https://doi.org/10.1007/s10311-018-0717-8>
62. Rezakazemi M, Ghafarinazari A, Shirazian S, Khoshshima A (2013) Numerical modeling and optimization of wastewater treatment using porous polymeric membranes. *Polym Eng Sci* 53:1272–1278. <https://doi.org/10.1002/pen.23375>
63. Rezakazemi M, Khajeh A, Mesbah M (2018) Membrane filtration of wastewater from gas and oil production. *Environ Chem Lett* 16:367–388. <https://doi.org/10.1007/s10311-017-0693-4>
64. Rezakazemi M, Shirazian S, Ashrafizadeh SN (2012) Simulation of ammonia removal from industrial wastewater streams by means of a hollow-fiber membrane contactor. *Desalination* 285:383–392. <https://doi.org/10.1016/j.desal.2011.10.030>
65. Rezakazemi M, Zhang Z (2018) 2.29 Desulfurization materials A2. In: Ibrahim D (ed) *Comprehensive energy systems*. Elsevier, Oxford, pp 944–979. <https://doi.org/10.1016/B978-0-12-809597-3.00263-7>
66. Sanes J, Avilés M-D, Saurín N, Espinosa T, Carrión F-J, Bermúdez M-D (2017) Synergy between graphene and ionic liquid lubricant additives. *Tribol Int* 116:371–382. <https://doi.org/10.1016/j.triboint.2017.07.030>
67. Sari A, Tuzen M, Soylak M (2007) Adsorption of Pb(II) and Cr(III) from aqueous solution on Celtek clay. *J Hazard Mater* 144:41–46
68. Sarkar SK, Raul KK, Pradhan SS, Basu S, Nayak A (2014) Magnetic properties of graphite oxide and reduced graphene oxide. *Physica E* 64:78–82. <https://doi.org/10.1016/j.physe.2014.07.014>
69. Saurín N, Sanes J, Bermúdez M-D (2016) New graphene/ionic liquid nanolubricants. *Mater Today Proc* 3:S227–S232. <https://doi.org/10.1016/j.matpr.2016.02.038>
70. Senthilkumar B, Kalai Selvan R, Vinothbabu P, Perelshtein I, Gedanken A (2011) Structural, magnetic, electrical and electrochemical properties of NiFe₂O₄ synthesized by the molten salt technique. *Mater Chem Phys* 130:285–292
71. Seol JH et al (2010) Two-dimensional phonon transport in supported graphene. *Science* 328:213

72. Sepioni M et al (2010) Limits on intrinsic magnetism in graphene. *Phys Rev Lett* 105:207205
73. Sharma R, Baik JH, Perera CJ, Strano MS (2010) Anomalously large reactivity of single graphene layers and edges toward electron transfer chemistries. *Nano Lett* 10:398–405. <https://doi.org/10.1021/nl902741x>
74. She X, Zhang X, Liu J, Li L, Yu X, Huang Z, Shang S (2015) Microwave-assisted synthesis of Mn₃O₄ nanoparticles@reduced graphene oxide nanocomposites for high performance supercapacitors. *Mater Res Bull* 70:945–950
75. Shirazian S, Rezakazemi M, Marjani A, Moradi S (2012) Hydrodynamics and mass transfer simulation of wastewater treatment in membrane reactors. *Desalination* 286:290–295. <https://doi.org/10.1016/j.desal.2011.11.039>
76. Sitko R et al (2013) Adsorption of divalent metal ions from aqueous solutions using graphene oxide. *Dalton Trans* 42:5682–5689. <https://doi.org/10.1039/C3DT33097D>
77. Sreepasad TS, Maliyekkal SM, Lisha KP, Pradeep T (2011) Reduced graphene oxide-metal/metal oxide composites: facile synthesis and application in water purification. *J Hazard Mater* 186:921–931
78. Stankovich S et al (2006) Graphene-based composite materials. *Nature* 442:282–286
79. Sun H, Cao L, Lu L (2011) Magnetite/reduced graphene oxide nanocomposites: one step solvothermal synthesis and use as a novel platform for removal of dye pollutants. *Nano Res* 4:550–562
80. Sun L, Wang G, Hao R, Han D, Cao S (2015) Solvothermal fabrication and enhanced visible light photocatalytic activity of Cu₂O-reduced graphene oxide composite microspheres for photodegradation of Rhodamine B. *Appl Surf Sci* 358:91–99
81. Sur UK (2012) Graphene: a rising star on the horizon of materials science. *Int J Electrochem* 2012: Article ID 237689, 12 pages. <http://dx.doi.org/10.1155/2012/237689>
82. Szabo T, Nánai L, Nesztor D, Barna B, Malina O, Tombácz E (2018) A simple and scalable method for the preparation of magnetite/graphene oxide nanocomposites under mild conditions. *Adv Mater Sci Eng* 2018:1–11
83. Tangahu BV, Sheikh Abdullah SR, Basri H, Idris M, Anuar N, Mukhlisin M (2011) A review on heavy metals (As, Pb, and Hg) uptake by plants through phytoremediation. *Int J Chem Eng* 2011:1–31
84. Tsoukleri G et al (2009) Subjecting a graphene monolayer to tension and compression. *Small* 5:2397–2402. <https://doi.org/10.1002/sml.200900802>
85. Ugeda MM, Brihuega I, Guinea F, Gómez-Rodríguez JM (2010) Missing atom as a source of carbon magnetism. *Phys Rev Lett* 104:096804
86. Urbas K, Aleksandrak M, Jedrzejczak M, Jedrzejczak M, Rakoczy R, Chen X, Mijowska E (2014) Chemical and magnetic functionalization of graphene oxide as a route to enhance its biocompatibility. *Nanoscale Res Lett* 9:656
87. Vozmediano MAH, López-Sancho MP, Stauber T, Guinea F (2005) Local defects and ferromagnetism in graphene layers. *Phys Rev B* 72:155121
88. Wang H et al (2012) Fe nanoparticle-functionalized multi-walled carbon nanotubes: one-pot synthesis and their applications in magnetic removal of heavy metal ions. *J Mater Chem* 22:9230
89. Wang Y, Huang Y, Song Y, Zhang X, Ma Y, Liang J, Chen Y (2009) Room-temperature ferromagnetism of graphene. *Nano Lett* 9:220–224. <https://doi.org/10.1021/nl802810g>
90. Wang Y, Liang S, Chen B, Guo F, Yu S, Tang Y (2013) Synergistic removal of Pb (II), Cd (II) and humic acid by Fe₃O₄@ mesoporous silica-graphene oxide composites. *PLoS One* 8: e65634
91. Xie L et al (2011) Room temperature ferromagnetism in partially hydrogenated epitaxial graphene. *Appl Phys Lett* 98:193113. <https://doi.org/10.1063/1.3589970>
92. Yang S-T et al (2010) Folding/aggregation of graphene oxide and its application in Cu²⁺ removal. *J Colloid Interface Sci* 351:122–127. <https://doi.org/10.1016/j.jcis.2010.07.042>
93. Yang Y, Asiri AM, Tang Z, Du D, Lin Y (2013) Graphene based materials for biomedical applications. *Mater Today* 16:365–373. <https://doi.org/10.1016/j.mattod.2013.09.004>

94. Yazyev OV (2008) Magnetism in disordered graphene and irradiated graphite. *Phys Rev Lett* 101:037203
95. Yazyev OV, Helm L (2007) Defect-induced magnetism in graphene. *Phys Rev B* 75:125408
96. Yu S, Wang X, Tan X, Wang X (2015) Sorption of radionuclides from aqueous systems onto graphene oxide-based materials: a review. *Inorg Chem Front* 2:593–612
97. Zhang C, Shao Y, Zhu L, Wang J, Wang J, Guo Y (2017) Acute toxicity, biochemical toxicity and genotoxicity caused by 1-butyl-3-methylimidazolium chloride and 1-butyl-3-methylimidazolium tetrafluoroborate in zebrafish (*Danio rerio*) livers. *Environ Toxicol Pharmacol* 51:131–137
98. Zhang K, Dwivedi V, Chi C, Wu J (2010) Graphene oxide/ferric hydroxide composites for efficient arsenate removal from drinking water. *J Hazard Mater* 182:162–168
99. Zhang P, Ma L, Fan F, Zeng Z, Peng C, Loya PE, Liu Z, Gong Y, Zhang J, Zhang X Ajayan PM (2014) Fracture toughness of graphene. *Nat Commun* 5:3782
100. Zhang W, Shi X, Zhang Y, Gu W, Li B, Xian Y (2013) Synthesis of water-soluble magnetic graphene nanocomposites for recyclable removal of heavy metal ions. *J Mater Chem A* 1:1745–1753
101. Zhang Y-Y, Pei Q-X, Cheng Y, Zhang Y-W, Zhang X (2017) Thermal conductivity of penta-graphene: the role of chemical functionalization. *Comput Mater Sci* 137:195–200. <https://doi.org/10.1016/j.commatsci.2017.05.042>
102. Zhang Y, Small JP, Pontius WV, Kim P (2005) Fabrication and electric-field-dependent transport measurements of mesoscopic graphite devices. *Appl Phys Lett* 86:073104. <https://doi.org/10.1063/1.1862334>
103. Zhao G, Li J, Ren X, Chen C, Wang X (2011) Few-layered graphene oxide nanosheets as superior sorbents for heavy metal ion pollution management. *Environ Sci Technol* 45:10454–10462
104. Zhu J, He J, Du X, Lu R, Huang L, Ge X (2011) A facile and flexible process of β -cyclodextrin grafted on Fe_3O_4 magnetic nanoparticles and host–guest inclusion studies. *Appl Surf Sci* 257:9056–9062
105. Zhu J et al (2012) Magnetic graphene nanoplatelet composites toward arsenic removal. *ECS J Solid State Sci Technol* 1:M1–M5
106. Zhu Y, Murali S, Cai W, Li X, Suk Ji W, Potts Jeffrey R, Ruoff Rodney S (2010) Graphene and graphene oxide: synthesis, properties, and applications. *Adv Mater* 22:3906–3924. <https://doi.org/10.1002/adma.201001068>

Functionalized Carbon Nanomaterial for Artificial Bone Replacement as Filler Material



Fahad Saleem Ahmed Khan, N. M. Mubarak, Mohammad Khalid and Ezzat Chan Abdullah

1 Introduction

The human race is witnessing lots of remarkable advancement in the field of Science and Engineering. Nanotechnology is one of that remarkable advancement accomplished by mankind. According to Dr. Richard Smalley (Late), “Nanotechnology is the art and science of building stuff that does stuff at the scale of nanometer”. In general, nanotechnology is specifically an engineering of human-made structures starting from a range of 1–100 μm [1]. It is an interdisciplinary field that comprises biomedical engineering, chemical engineering, chemistry, physics, and material and particle science. At present more than 600 products available in the market globally which uses nanomaterials for their products [2]. Furthermore, United States National Institute of Health has referred the assistance of nanotechnology for systems like diagnosis, treatment, monitoring, and control of biological as nanomedicine [3]. Nanotechnology is continuously promoting positive impacts on healthcare and making life more convenient than ever imagined

F. S. A. Khan · N. M. Mubarak (✉)

Department of Chemical Engineering, Faculty of Engineering and Science,
Curtin University, 98009 Sarawak, Malaysia
e-mail: mubarak.mujaawar@curtin.edu.my

M. Khalid

Graphene & Advanced 2D Materials Research Group (GAMRG),
School of Science and Technology, Sunway University,
No. 5, Jalan Universiti, Bandar Sunway, 47500 Subang Jaya,
Selangor, Malaysia

E. C. Abdullah

Department of Chemical Process Engineering, Malaysia-Japan International
Institute of Technology (MJIT), Universiti Teknologi Malaysia (UTM),
Jalan Sultan Yahya Petra, 54100 Kuala Lumpur, Malaysia

© Springer Nature Switzerland AG 2019

Inamuddin et al. (eds.), *Sustainable Polymer Composites and Nanocomposites*,
https://doi.org/10.1007/978-3-030-05399-4_27

before. In addition, nanomaterials are significantly getting attention for the applications related to bone engineering as it holds properties that have the strength similar to natural bone. However, construction of artificial bone with uniqueness, identical properties likewise natural bone is a strenuous task. Therefore, most of the researchers rely on nanotechnology and nanomaterials when it comes to constructing artificial bone.

Carbon nanomaterial is one of the remarkable outcomes from nanotechnology. Carbon-based nanomaterial considered more accentuated and promising when it comes to the application based on the bio-medical field. Carbon nanomaterials are categorized as low-dimensional materials, having sp^2 and sp^3 carbon atoms arranged into a continuous network [4]. Since the discovery of the first well-known carbon nanomaterial i.e. fullerene, have significantly aroused the interest around the globe. Carbon nanomaterial holds tunable physical, chemical, electrical, optical, thermal, and mechanical properties, and its related composite provides remarkable usage in sensors, biomedicine, electrodes, electrocatalysis, energy storage as well as conversion. One of the main features of carbon nanomaterial i.e. biocompatibility [5] increased its demand in the field of bio-medical. Carbon nanomaterials are one of the highlighted topics when it comes to the modern medical field. Out of all carbon-based nanomaterials, carbon nanotubes (CNTs) are considered more suitable and promising for applications related to bio-medical e.g. nano-electronic bio-sensing [6], drug delivery [7], and bone tissue engineering [8].

Carbon nanomaterials are dimensionally categorized as fullerene (0-D), carbon nanotubes (1-D) and graphene (2-D). The origin of carbon nanotubes is from the synthetic carbon allotropes and categorized as sp^2 hybridized network of carbon atoms. At first, Sumio Iijima discovered the CNTs structure as helical microtubules of graphitic carbon in the year 1991 through an arc discharge process that was initially designed for fullerene production [9]. Since the discovery, significant researches took place on this extraordinary nanomaterial. Theoretically, carbon nanotubes synthesized by rolling the sheets of graphene with connecting hexagonal rings seamlessly. Vapour phase growth, corona-discharge, catalyst-supported growth, hydrocarbons pyrolysis and laser ablation are the conventional techniques for carbon nanotubes synthesis [10]. At present, plasma-enhanced chemical vapour deposition and chemical vapour deposition are the most recent synthesis methods for carbon nanotubes [11] (Fig. 1).

Carbon nanotubes are categorized generally as single-walled carbon nanotubes (SWNTs), multi-walled carbon nanotubes (MWNTs) and double-walled carbon nanotubes (DWNTs) [12]. Major making of MWNTs and DWNTs were testified via arc discharge process. And SWNTs synthesis was primarily described independently by Iijima and Ichihashi (Tokyo, Japan), and Bethune's IBM group (California, USA) in the year 1993 [13]. Furthermore, compared to all other inorganic nanoparticles in which heavy toxic metals are present, for example, quantum dots (QDs); CNTs are mainly composed of pure atoms of carbon that are relatively non-toxic [14]. Thus, carbon nanotubes direct use is restricted due to its biological toxicity in application related to bio-medical. The toxicity of carbon nanotubes are affected due to the metal impurities; shape, structure and length of the

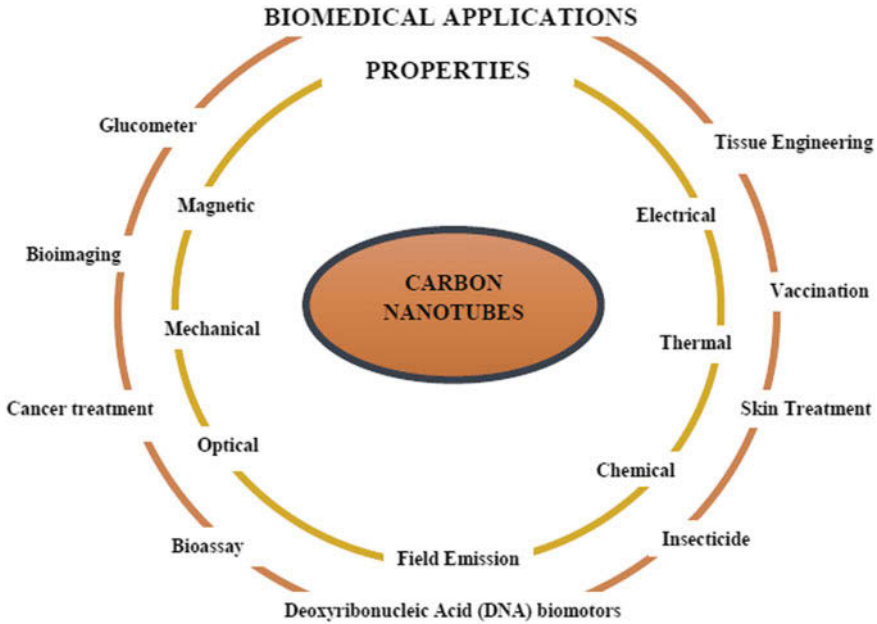


Fig. 1 Properties and biomedical applications of carbon nanotubes

tubes; layers thickness; aggregation degree; etc. Moreover, key factors for the toxicity of nanotubes include metal catalyst residual; length and hydrophobic surface of carbon nanotubes [15]. The metals catalyst (Fe, Ni etc.) containments in nanotubes support free radical generation in cells and are introduced through the process of synthesis and purification which lead to cytotoxicity [16]. In addition, experimental results as evidence clearly show that shorter length of nanotubes, i.e. less than 200 nm, compared to normal length (up to tens of micrometres) is more suitable to enter the cells [14].

Furthermore, synthesized carbon nanotubes hold hydrophobic surface, and are insoluble in many aqueous solutions. Due to the strong hydrophobic interactions, carbon nanotubes stick together and form as bundles that later make it difficult to apart. The formation of bundles trend makes the processability of carbon nanotubes complicated as well extremely difficult their integration into aqueous based biological media, which considered essential for the applications based on bio-medical [17]. Biological behaviours of the tubes precisely based on the surface chemistry. Furthermore, the experimental study proved that raw carbon nanotubes avoid the growth of ovary cells in Chinese hamster [14]. Table 1; listed the theoretical and experimentally calculated properties of carbon nanotubes.

Biomedical refers to the living system; therefore, modification of carbon-based nanomaterial is an important step, like biocompatibility and bioactivity, can be enhanced with chemically modified carbon nanotubes [18]. The modification of carbon nanomaterial includes surface modification as well as chemical alteration

Table 1 Properties of carbon nanotubes (CNTs)

Parameters	Carbon Nanotubes	References
Lattice structure	Nanotubes: ropes, tubes organized in the triangular lattice by parameters of $a = 1.7$ nm, tube-tube = 0.314	[78]
Elastic modulus	SWNTs and MWNTs ~ 1 and 1.28 terapascal (TPa), respectively	[79]
Maximum tensile strength	100 gigapascal (GPa), approximately	[79]
Specific gravity	0.8–1.8 gcc^{-1} (theoretical)	[78]
Thermal expansion	Insignificant (theoretical)	[78]
Thermal conductivity	2000 W/m/K	[79]
Oxidation in air	Greater than 700 °C	[78]

steps. Furthermore, stable dispersion helpful for biomedical use, for example, functionalized graphene make it easier for chemotherapeutics and image agent delivery [19]. At present, a countless number of natural and synthetic biopolymers and bio-ceramics are being used for designing artificial bone prosthetic but their usage remained until laboratory. Therefore, designing an artificial bone prosthetic that holds similar properties to that of human bones is a challenging task for the researchers. Furthermore, researchers keeping in mind of getting the radical benefit of nano-technology, nano-materials scaffolds and cell-based biomaterials for constructing artificial bone [20].

2 Bone Structure and Mechanics

Bone is the primary component of the skeletal structure and varies from the connective tissues due to the properties of rigidity and hardness. These properties help the skeleton to keep the shape of the body, cover the main organs, as well as transfer force of muscular contraction at the time of movement [21]. Bones are actually made of the fibrous protein collagen and soak with calcium phosphate like mineral [22]. The content of mineral serves as a reservoir for ions, more generally calcium as human body stored approximately 99% of calcium, which helps in circulating extracellular fluid composition [21]. In addition, bone contains water too, and it is very vital according to mechanical perspective. The organic matrix of the bone composed of collagen and non-collagenous proteins, 90 and 10% respectively [23]. In fact, the collagen proteins especially form-I act as storage for hydroxyapatite, and the mineral phase helps to generate the rigidity of the skeletal structure. However, according to mechanical perspective, bone is considered as an anisotropic and non-homogeneous material. Furthermore, spongy and cortical bones can be assumed as an orthotropic having 9 and 5 independent material constants, respectively. Bone

is possibly imagined as a linear elastic material with significant viscoelastic effects, in terms of the physiological range of loading [24]. Bone is stronger in compression and retaining higher Young's moduli of elasticity [25].

State to the term composite and structure of the bone; it proves that bone is a composite material. Moreover, considering bone as bio-composite, the hierarchical structure is seen at various level. For example, at microstructural level, cortical bone shows osteon (large hollow fibers with an outer diameter of 200–250 μm) fibers which are made up of concentric lamellae and pores. The fibers are comprised of hydroxyapatite mineral and collagen at nano level [26].

Bone is an internal part of the body and is surrounded by cells entire life. Because of having no-expendable nature, the process of resorption and formation for every bone take place at the surface compared to soft biological tissue which can have growth at both interstitials as well as oppositional. Bone is holding varies values of porosity and it mainly depends on bones macrostructure as it has a porous structure. However at the level of macroscopic, cortical and cancellous are two types of bone structure. Cortical bone (compact) covers 80% of the mass in a mature human and is mainly in charge of the protective function of the skeleton [27]. Osteon is a large hollow cylinder and a primary structural unit of compact bone. However, the spongy bone which is a network of narrow rods and plates of calcified bone tissue. This calcified bone tissue is known as trabeculae, covered by the bone marrow. The function of bone marrow is to provide nutrients and discard disposal for the bone cells.

In comparison with cortical bone, the content of mineralization in spongy bone is less. However, experimental studies as evidence show that spongy bone is significantly active in remodelling compared to cortical bone [28]. Furthermore, the primary cellular elements of the bone are osteoclast, osteoblast, osteocytes and bone lining [29]. Osteoblasts and osteoclasts origin are different for nurturing and categorize as temporary cells because of short life length [30].

3 History of Artificial Organ

An artificial organ is a human developed device that is an alternative to natural organ and holding bit identical but not exactly similar properties. The function of developing such devices is to make the life of patient's as convenient as possible. Referred to artificial organ definition, the device is not required to attach to any sources like filling or chemical processing units. Any kind of stationary resources, chemical refilling, exchanging of fillers, attached to the device will not categorize under the artificial organ. For example, dialysis machine, an extraordinary technology to support kidney patient's life is not an artificial organ. However, developing and installing an artificial organ is significantly expensive, and required years of experimental researches compared to the natural organ. The experiments for artificial organs mostly conduct on animals or people who are close to death. As a matter of fact, the word artificial organ rarely heard because mostly it refers to as the

replacement of human or animal bones and/or joints. At present, an immense number of artificial organs has been implanted with a high range of success. Some of the remarkable studies on different types of artificial organs have been done by scientist all around the world which include brain pacemakers, cardia, corpora cavernosa, ear (cochlear implant), eye (visual prosthetic), heart, limbs, liver, lungs, bladder, ovaries and many more [31].

The first-ever bone defect treatment was trephined prehistoric skull. However, in the year 1668, a Dutch surgeon Job van Meek'ren named himself first for operating a successful bone defect treatment. He used a dog skull to fill the defect of a soldier's cranium which was taken off after 2 years on soldier's wish. Furthermore, in the scientific era, the interest on osteogenesis and bone transplantation was begun in the year 1739 by Du Hammel. But significant numbers of patients with autogenous bone transplantation were already recorded 200 years earlier [32]. Some of the successful artificial organ transplantation is listed below (cited from 33):

- In the year 1857, Eduard Zirm conducted first successful cornea transplantation (Czech Republic).
- In the year 1954, Joseph Murray operated first successful kidney transplantation (Boston, Massachusetts).
- In the year 1966, Richard Lillehei and William Kelly named themselves first for successful pancreas transplant (Minneapolis, USA).
- In the year 1967, Christiaan Barnard operated first heart transplant successfully (Cape Town, SA).

Moreover, bone transplant referred to fix fractures and joints and to treat skeletal defects. However, there are possible side effects for the transplantation of autogenous bone material like the surgical cut on the skin, low strength bone of donors, and inclined postoperative morbidity. As a matter of fact, not only the amount of autogenous bone is limited but also bone graft has insignificant properties too, like mechanical, biological and physiological [32]. The bone transplants or implants are classified into four classes as:

- Autograft: Engraftment of organs within one individual [33].
- Isograft: Transplantation of organs between genetically similar individuals [34].
- Allograft: Engraftment of organs of genetical individuals of the same species [35]
- Xenograft: Engraftment of organs of individuals of dissimilar species [36].

For bone treatment, two well-known procedures are autograft and allografts in the field of orthopaedic. Due to the limited donors, disease transfer (hepatitis), structural problems, pain etc. [37], autograft and allograft methods are no longer preferred and replaced by artificial bone replacement. Table 2; illustrate the tensile strength, elastic modulus, and ultimate strain of the human bone tissue.

As a matter of fact, strength itself not considered enough for artificial bones to fully integrate with natural bones. In order to compete with natural bone, there are

Table 2 Human bone mechanical properties

Tissue	Tensile strength (MPa)	Elastic modulus (GPa)	Ultimate strain (%)	References
Cortical bone (longitudinally)	130	12.0	3	[80]
Cortical bone (transverse)	60	13.4	1	[80]
Cancellous bone	2	0.39	2.5	[80]

certain characteristics that an artificial bone requires which include good handling, suitable mechanical capability and excellent bio-degradability and bone-regeneration [38].

3.1 Artificial Bone Materials

Biomaterials mainly used to construct devices that are associated with the biological system to co-exist for long-lasting use with limited chance of failures. In 1981, Williams express biomaterials as “*non-viable materials with the application of making medical devices, intended to associate with the biological system*” [39]. For the past few years, the demand for biomaterials has rapidly increased. In the USA, biomaterial industry is generating more than \$300 billion annually, and it kept inclining [40]. For many years’ medical specialists have been working on finding a substitute for the treatment related to bones like bone repair or replacements. In past, a substance like leather, metals (gold, silver and platinum), bones from other species for direct transplant had utilized for bone repairing treatment. However, alternative materials for bones are categorized as natural and artificial (chemical composition) depending on the source of origin. Natural materials have some remarkable advantages, and due to that popularly used. Additionally, chitosan, collagen, fibrin, and chitin are named as natural materials [39]. And artificial materials are further divided into metal, ceramic, polymer, composites and biological origin substances [40]. Based on host reaction, biomaterials classified as:

- Bio-tolerant: It is in the body, and mainly surrounded by the fibrous membrane, for example, bone cement.
- Bio-inert: These biomaterials are not associated or interact when exposing to biological tissues, for example, titanium oxide.
- Bio-active: These biomaterials integrate with the bone, for example, hydroxyapatite.
- Bio-resorbable: These biomaterials indulge in the bone, for example, calcium.

Furthermore, features such as biocompatibility, elasticity, toughness, corrosion, fatigue resistance and allergic diathesis are vital in bone surgery [41].

4 Carbon Nanomaterials

Carbon nanomaterial is one of the remarkable outcomes from nanotechnology. Carbon nanomaterials are categorized as low-dimensional materials, having sp^2 and sp^3 carbon atoms arranged into a continuous network [4]. Since the discovery of the first well-known carbon nanomaterial in the year 1985 by Sean O'Brien, Richard Smalley, Robert Curl, Harry Kroto, and James Heath, i.e. fullerene, have significantly aroused the public's interest. Carbon nanomaterial tunable physical, chemical, electrical, optical, thermal, and mechanical properties and its related composite provide remarkable usage in sensors, biomedicine, electrodes, electrocatalysis, energy storage as well as conversion. One of the main feature of carbon nanomaterial i.e. biocompatibility [5] that increased its demand in the field of bio-medical. Out of all carbon-based nanomaterials, carbon nanotubes (CNT) consider more suitable and promising for applications related to bio-medical e.g. nano-electronic bio-sensing [6], drug delivery [7], and bone tissue engineering [8].

5 Carbon Nanotubes

1991, an exciting year for carbon science as Sumio Iijima of Nippon Electric Company (NEC) discovered a thin material identical as needle under an electron microscope while analyzing carbon nanomaterial, and named it carbon nanotubes [42]. In the same year, the scientist made the availability of fullerene as a compound too. However, fullerene was first-ever discovered in the year 1985 by researchers from the University of Houston and University of Sussex. Due to the identical shape of this element to football holding thirty-two faces, fullerene was first named as Buckminsterfullerene or Bucky-ball [43]. Carbon nanotubes display as one dimensional with the tubular structure, resemblance to rolled G nano-sheets with minute nanometer thickness. Initially, carbon nanotubes were discovered as multi-walled carbon nanotubes (MWNTs), and later as single-walled carbon nanotubes (SWNTs). Earlier applying electric discharge, laser ablation, and similar techniques used for the synthesis of fullerene but with the addition of some catalyst made the availability of carbon nanotubes in bulk form. CNTs generally have the diameter similar to fullerenes i.e. 1 nm but 1000 time longer than fullerene. These tubes even referred as macromolecules, poly disperses in size and having a molecular weight of 1,000,000 Daltons [44]. Table 3; list the discoveries and development of carbon nanomaterials, mainly carbon nanotubes:

In addition, carbon nanotubes have been studied extensively by researchers due to its promising properties [4] such as electrical, mechanical, conductivity, and chemical which help to assist in the application like bio-sensors, nano-oscillators, drug delivery systems or pure structural components in nano-devices [45].

Table 3 Discoveries and developments of carbon nanotubes (CNTs)

Year	Discovery	References
1889	Discovered carbon filaments (thermal decomposition of gaseous hydrocarbons)	[81]
1890 & 1903	Hydrocarbon (thermal decomposition), results in production of carbon-fibers	[82, 83]
1939	Transmission electron microscopy (TEM) became commercialized which help to research in-depth of carbon fibers	[83]
1952	TEM evidence was printed which display the nano sized diameter of hollow graphitic carbon fiber	[10, 84]
1958	Carbon fibers of bamboo texture were discovered with the help of electron diffraction	[83]
1976	Technique of vapor growth generated carbon fibers	[85]
1979	Arc discharge method synthesized hollow carbon fibers	[86, 87]
1987	In USA, graphitic (hollow carbon fibrils) patent were published	[83]
1991	Arc discharge synthesized carbon nanotubes, and brought into hot spot under scientific society.	[10]
1992	Discovered SWNTs	[46]
1993	Iron catalyst was used to manufacture single walled carbon nanotubes; Cobalt catalyst were used to produced SWNTs	[83]
2004	Templates were applied for carbon micro tubes synthesis	[88]
2007	Carbon nano-buds were manufactured	[83]

Carbon nanotubes properties lead them to applications related to bio-medical. SWNTs and MWNTs consider more suitable for bio-medical applications. Extensive researches have been particularly done on both SWNTs and MWNTs.

5.1 Structure and Properties of Carbon Nanotubes

5.1.1 Single-Walled Carbon Nanotubes (SWNTs)

Single-walled carbon nanotubes (SWNTs), manufactured in 1993 [46], having a diameter and length range from 1 to 7 nm and 20 to 40 nm, respectively [45]. This carbon nanotube type has generated some remarkable properties as well as the capability to apply successfully in a wide number of fields. SWNTs described as a single layer of a graphite crystal, rolled up into a continuous cylinder and capped with hemisphere (carbon rings in hexagonal and pentagonal) at both sides [46]. Since SWNTs hold some impressive properties, therefore, the synthesis of SWNTs has significantly become a matter of global studies. At present, many methods have been designed for the synthesis of SWNTs but electric arc discharge, laser ablation, and catalytic chemical vapour deposition are popular among all [47]. Catalytic chemical vapour deposition abbreviated as CCVD method generates a significant

amount of SWNTs at the economic cost compared to all other methods [46]. Moreover, in the market, the vastest method used is laser ablation for SWNTs [48].

5.1.2 Multi-walled Carbon Nanotubes (MWNTs)

In 1952, Radushkevich and Lukyanovich were the original discoverers of MWNTs. Thus, the present carbon nanotube boom in material science without any doubt was instigated by Sumio Iijima in 1991 [49]. Multi-walled carbon nanotubes (MWNTs), extended hollow cylinder, are composed of sp^2 carbon with a diameter range from 2 to 100 nm and growing length up to 10 microns as well as aspect ratio ranges from 10 to 10 million. However, the thickness of MWNTs's wall along the axis remains constant and inner channel is straight. The ends of MWNTs covered by half full-erene spheres due to the channel which is not accessible directly from the outer side but by expanding the nanotube it can be accessed, for example, oxidation, milling or ion beam treatment [50]. However, based on larger diameter and Raman spectrum of MWNTs, clearly differentiate them from SWNTs and double walled CNTs [51]. The techniques to manufacture MWNTs and SWNTs are generally same. Likewise, SWNTs synthesis, a wide variety of methods has been discovered for MWNTs synthesis but the well-known are catalytic chemical vapour deposition, arc discharge, and laser ablation. Likewise, SWNTs, catalytic chemical vapour deposition is the most efficient and most widely used process (Table 4).

Table 4 Single-walled and multi walled CNTs comparison

Single-walled carbon nanotube (SWNTs)	Multi-walled carbon nanotubes (MWNTs)	References
Mono-layer of graphene	Several layers of graphene	[89]
The catalyst is not optional for synthesis	For the synthesis catalyst not required	[79]
Appropriate control over growth as well as on atmospheric condition is compulsory for bulk synthesis	Bulk synthesis is convenient	[90]
Lack of purity	Negligible impurity	[79,90]
Chance of defect is higher at the time of functionalization	Chance of defect is limited but if occurred, it is a challenging task to improve	[90]
Convenient for characterization and evaluation	Holds a very complex structure	[79, 90]
Comparatively flexible and easy to twist	Difficult to be twisted	[90]

5.2 Synthesis of Carbon Nanotubes

Carbon nanotubes can be manufactured by a range of methods but well-known include laser ablation, arc discharge, and chemical vapour deposition. Processes like laser ablation, arc discharge and chemical vapour discharge are fallen under the category of physical and chemical processes, respectively [52]. In the process of laser ablation, high power laser is used which helps to vaporize graphite source combined with a metal catalyst. Since graphite contains carbon that transforms large numbers of single-walled carbon nanotubes (SWNTs) on the metal catalyst [53]. And in arc discharge method, high quality but limited quantities of SWNTs and MWNTs are manufactured by introducing electric discharge from the electrode (carbon-based). However, in chemical vapour deposition (CVD), carbon nanotubes are produced in a chamber by reacting hydrocarbons (for example CH₄) with an appropriate metal catalyst [48]. All of these methods come with advantages and limitations. Some of them listed in Table 5 and Fig. 2.

6 Functionalization of Carbon Nanomaterials

Carbon nanomaterials, fullerenes, graphene and carbon nanotubes (SWNTs, MWNTs & DWNTs), in organic (especially in an aqueous solvent) are poorly soluble. Like, carbon nanotubes stick together and form as bundles due to strong

Table 5 Carbon nanotubes (CNTs) synthesis method

Synthesis methods	Advantages	Disadvantages	References
Chemical-vapor deposition (CVD)	Cost-efficient; scalability; continuous operation process; low operating temperature around 500–800 °C; diameter can be adjusted	Lack of quality i.e. Wall structure contains significant defects and deposits of carbonaceous contamination; a combination of SWNTs and MWNTs	[79, 91]
Arc-discharge (AR)	Simplicity and versatility on the basis of carbon-based material and catalyst; better quality nanotubes produce; minor defects; economical process	Significant consumption of energy; lack of capability for industrial up-scaling; high temperature required (>1700 °C); shorter length of CNTs produced	[10, 73]
Laser ablation (LA)	Synthesis at room temperature; generate high purity and yield of tubes	Purification of the crude product is must; method restricts till laboratory scale; expensive process	[79, 73]

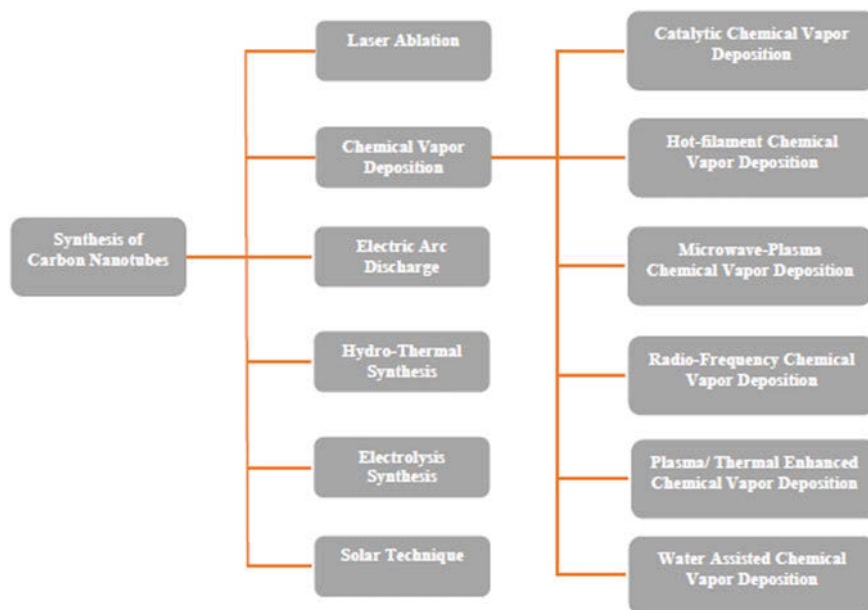


Fig. 2 Synthesis approaches of carbon nanotubes

hydrophobic interactions which later make it difficult to apart. The formation of bundles trend makes the processability of carbon nanomaterials complex and challenging their integration into aqueous based biological media, which considered essential for the applications related to bio-medical [17]. Therefore, functionalization of carbon nanomaterials is important in order to attain their remarkable strengths. As a result, a significant part of the current journals on carbon nanomaterials has an emphasis on improving their solubilization and dispersion using functionalization methods. In fact, massive range of applications in many fields has opened through functionalized carbon nanomaterials, particularly carbon nanotubes and graphene because of their extraordinary properties like lightweight, significant aspect ratio, and electrical conductivity, as well as mechanical, thermal strength. Furthermore, carbon nanomaterials uses have become applicable in many fields because of the modification of its surfaces. The exceptional physiochemical properties of functionalized carbon nanomaterials have been used for anti-viral drug development, energy, treatment for cancer, applications for biotechnological, and aerospace. Moreover, theoretical work has also been done to understand as well as optimize functionalization. On the other hand, non-functionalized carbon nanomaterials carry limitations like the capability to generate stable bundles/aggregates due to highly significant interactions, e.g. van der Waals force, strong π - π stacking. Consequences of the aggregation bring undesirable changes, like affect the aspect ratio plus declines the nanocomposites properties. Therefore, stable dispersion and functionalized role are vital in order to attain better nanomaterial support system.

The functionalization of nanomaterials with the mandatory moieties relies on the base material chemistry. And the functionalization mode on nano's surface mainly relies on the problem and proposed use of the material.

In the past, many procedures had discovered; among them, the well-known that still applies today include covalent and non-covalent functionalization. All these approaches are with organic and inorganic compounds help to attain improved solubility and dispersibility. For example, the use of pristine carbon nanotubes, particularly in living organism and cells bring toxic effects, therefore functionalization is essential to be concerned [17]. Furthermore, due to the availability of carboxylic, epoxy and hydroxyl groups, covalent functionalization is more preferable. In addition, covalent functionalization suited as better moieties for functional group conversion. Besides this, the existence of an sp^2 hybridized π network gives the chance for non-covalent interaction among host species and carbon nanomaterials [54]. Thus, modifying the surface of carbon nanomaterial in order to retain the remarkable properties is a challenging task. At present, different functionalization techniques for both covalent and non-covalent have developed for carbon nanomaterials.

6.1 Covalent Approach for CNTs

Lately, carbon nanotubes have received significant interest because of its astonishing unique electronic, optical, mechanical, thermal, and structural properties [55], especially for medical and material science fields. But the insolubility of carbon nanotubes is a chief barrier for its use in real world. The insolubility of carbon nanotubes is generally due to its hydrophobic structure, surface area, forces like Van der Waals, etc. There is only one solution for the carbon nanotubes issues (insolubility and poor dispersion) which scientist discovered, and that is a modification of the carbon nanotubes [56]. Furthermore, there are numerous approaches for covalent functionalization of carbon nanotubes among other oxidation reactions, oxidized carbon nanotubes with esterification and amidation reactions, halogenation, ozonolysis, plasma activation, electrophilic/nucleophilic additions, mechanic/electrochemical functionalization, polymer grafting, nucleophilic/radical additions, treatment with ionic liquid and oxidized carbon nanotubes with complexation reactions [57]. However, for biomedical applications, strategies developed particularly for covalent functionalization include surface oxidation of carbon nanotubes, radical additions, cycloaddition reactions and its followed functionalization with biologically related molecules [58].

6.1.1 Oxidation Treatment

Covalent modification approach with various oxidizing acids/oxidants is most common because of their capability of attaching the preferred function groups,

hydroxyl or carboxyl, on the surface of carbon nanotubes as well as tailoring the surface composition. Carbon nanotubes with the functional groups attached not only provide a positive effect for their dispersibility in different solvents but also the contact with various compounds, for example, polymers. Some of the well-known oxidizing agents for the oxidation of carbon nanotubes are sulphuric acid (H_2SO_4), nitric acid (HNO_3), tri-oxygen (O_3), hydrogen peroxide (H_2O_2) and potassium permanganate (KMnO_4). Oxidizing agents like H_2SO_4 , HNO_3 and KMnO_4 generate carboxyl groups while H_2O_2 and O_3 produce hydroxyl groups into the nanotubes [59]. However, hydrogen peroxide and tri-oxygen are categorized under mild oxidant. As an example covalent amide connection established when a mixture of single-walled carbon nanotubes (oxidized) and PEG-NH₂ sonicated for the duration of 30 min plus centrifugation to generate NH₂-PEG-modified carbon nanotubes. Moreover, oxidation of single-walled carbon nanotubes with addition covalent conjugation with amino acids shows sp³ carbon atoms [14]. However, the outcome of two oxidizing agents generates two functional groups connect concurrently on the nanotubes. Further functionalization makes these groups to be used as anchor sites either for esterification or amidation reactions which can be applicable widely for the conjugation of water-soluble organic molecules, hydrophilic polymers such as nucleic acids, peptides or polyethylene glycol, as a result, multifunctional carbon nanotubes manufactured [60]. Multifunctional carbon nanotubes possess greater chemical reactivity as well as selectivity, therefore considered better and preferable compared to other functionalized carbon nanotubes [61]. Another method for the oxidation of graphene also allowed as an alternative for the carbon nanotubes oxidation. As graphene and MWNTs both have sp²-hybridized carbons, therefore it makes them easier to oxidize. The most well-known approach for the oxidation of graphene is Hummers. As a matter of fact, various improved Hummers method has been used for unzipping carbon nanotubes with well-developed oxidation mechanisms. Consequence of mechanical mixing surely enhances the dispersion but also cause damage and length shorten of carbon nanotubes. Since, scanning electron microscope (SEM) is used for the morphology of MWNTs before and after oxidation treatment. With an outer diameter range from 10 to 20, 30 to 50, and >50 nm clearly showed varies in tube diameter as well as roughness along the walls of the tube after gone through acids treatment. In addition, MWNTs diameter slowly narrowed due the oxidation process (cited from [62]). However, treatment like ultraviolet [63], plasma [64] and microwave irradiation have been used either for incorporation of surface oxygen/for the attachment of various functional groups to the carbon nanotubes. In terms of mechanical mixing, for example, conventional reflux method is usually used at the time of oxidation. In comparison with reflux, functionalization of carbon nanotubes with ultra-sonication use may help to generate carboxyl, carbonyl and hydroxyl content greater on the MWNTs. It is because sonication method develops the greater surface area as well as defects sites for the functional group [65]. Experimental results showed that the ultra-sonication help to decrease the stacking of carbon nanotubes in bundles, and destroyed the tubes structure integrity [59].

Some of the drawbacks of oxidation treatment are that it grows defects on nanotubes surface, CNTs oxidation leading Hole doping, and introduce impurity states at the Fermi level. On the other hand, oxidation treatment helps to remove the raw materials impurities, cut/shorten the length and expand the CNTs. However, minimizing the CNTs length through oxidation treatment comprehensively based on the rate and extent of the reaction which let the rise of new length distribution. Carbon nanotubes with open and oxygenated ends are the consequences of cutting mechanism [66]. However, the oxidative stability particularly depends on diameter and production process of the carbon nanotubes.

6.1.2 Cycloaddition Reaction

Cycloaddition reaction is another well-known process that includes direct additional reaction, for example, 1, 3-Dipolar, carbene, nitrene etc. In cyclo-addition reactions, sidewalls are the primary objective where reaction occurred. The outcome of this covalent approach upgrades carbon nanotubes strength as it helps to enhance the solubility of water, different organic solvents etc. [58]. However, analogues of carbenes are nitrenes, compounds of electrophile reagents which add-up C=C bond. Thermolysis of alkyl azidoformates required for the functionalization of carbon nanotubes on the side walls through nitrenes. Development of pyrrolidine rings on the surface of carbon nanotubes with the use of 1, 3-Dipolar cycloaddition of azomethine ylides [67]. For many biomedical applications, these pyrrolidine rings can be substituted with various functional groups, for example, peptides, therapeutic agents, fluorescent molecules, etc. [58]. Like nitrenes, functionalization of carbon nanotubes using carbenes followed the same path. At first, deprotonation of imidazolium cation produced nucleophilic carbenes, and then each $-ve$ charge/moiety is replaced to the tubes, and at last carbon nanotubes functionalized [67]. Moreover, this approach sub-categorized with varies direct additional reaction, like amidation, esterification, thiolation, halogenation, and hydrogenation [68]. Like in the process of thiolation, CNTs involved with the thiol group through subsequent carboxylation sonication, reduction with the supports of NaBH_4 , and chlorination with SOCl_2 , led by thiolation with Na_2S and NaOH mixture to the CNT open end. The aftermath of cycloaddition reaction, enhance the strength of nanotubes and improve the solubility in aqueous solution, many organic solvents etc. [58].

6.1.3 Radical-Additions

Radical addition reaction falls under the category of covalent functionalization approach. A chemical agent such as aryl diazonium, sodium nitrite etc. is involved in radical addition reaction. Among these chemical agents, aryl diazonium coupling is more preferable due to its easiness and higher yield. In aryl diazonium coupling, first prepared aryl diazonium salts [58]. In 1858, Peter Griess discovered aryl diazonium compound while he was manufacturing a product. The word 'diazo'

Table 6 Surface modification approaches for carbon nanotubes using aryl diazonium salts

Approaches	Materials	Mechanism	References
Chemical	SWNTs and MWNTs	Under iso-amyl nitrite, in-situ produced aryl-diazonium salts, reaction temperature 60 °C	[70]
	Carbon nanotubes	Aryl-diazonium reduction through H ₃ PO ₂ (hypo phosphorus)	[70]
	Carbon black	In-situ produced aryl-diazonium salts in water under NaNO ₂ and excess HCl	[70, 92]
Microwave	SWNTs and MWNTs	Arene radical reaction	[70]
Thermal	SWNTs	The mechanism was not notified in the manuscript	[70, 93]

originated from French and means di-nitrogen [69]. Furthermore, Jean Pinson, the modern surface chemistry father, could be accredited for aryl diazonium salts. Since its discovering, this salt has significantly considerable for organic synthesis of a number of vital compounds, for example long known azo dyes. This salt has become an ideal diazonium salt for the illustration of proof of new concepts, for example, modification of the surface, bio-sensor, clay related nano-fillers etc. At present, commercially available aryl diazonium include 4-nitrobenzenediazonium tetra-fluoroborate, 4-bromobenzenediazonium tetra-fluoroborate, 4-formyl benzene diazonium hexafluorophosphate and 4-aminodiphenylamine diazonium sulfate. However, aryl diazonium can be prepared by the introduction of NaNO₂ aqueous solution to aromatic amine solution under additional hydrochloric acid which later cooled down below 5 °C in a water bath [70]. In addition, CNTs can be envisaged through modification with isolated aryl diazonium and in situ prepared aryl diazonium from aromatic amines under NaNO₂ (medium acidic). On the other hand, in situ prepared aryl diazonium which guarantees significant grafting density of aryl groups on CNTs through pure iso-amyl-nitrite. This alternative route generates functionalized CNTs of higher solubility and processability in organic solvents (functionalization degree of one out of twenty atoms of carbon) and polymeric blends, respectively. This approach proved to be effective due to less time for the reaction as well as less consumption of solvent. Scalable is an option under this approach therefore paving the way for its use in more application, for example, growth of structural materials. Therefore, this approach seldom considered for application related to biological [58]. Table 6; listed the approaches and reaction mechanism for the modification of carbon nanotubes using aryl diazonium salts.

6.2 *Non-covalent Approach for CNTs*

Some other advantages of using non-covalent approach include biocompatibility, stability in very biological solutions and a functional group that required additional bio-conjugation. Lately, long-range single layers graphene has been prepared using non-covalent approach (π - π stacking) for a wide range of application. Since carbon nanotubes hold significant specific area which benefits them with high loading capacity along the following molecules. Through the route of non-covalent functionalization, carbon nanotubes have been positively covered/absorbed by amphiphilic molecules such as pyrene, derivatives of naphthalene, proteins, RNA, DNA, polymers, peptides, and surfactants [71]. Carbon nanotubes dispersion generally relies on chemical characteristics, amphiphilic molecules and solvent category and concentration as well as dispersing conditions [58]. Lightweight surfactant, few organic molecules as well as amphiphilic polymers are used as agents for non-covalent approach functionalization. Molecules of surfactants for the carbon nanotubes modification react with carbon nanotubes hydrophobic side and results in replacing to hydrophilic. This interaction of surfactants with carbon nanotubes makes them soluble not only in water but also in the wide range of solvents [72]. Synthetic peptides use also another route to disperse carbon nanotubes, as they capable to cover and solubilize the tubes. Some other surfactants capable to disperse carbon nanotubes include Odium dodecyl sulfate, cetyl-trimethyl ammonium bromide, non-ionic Tween-20 [73], Gum Arabic, salmon sperm DNA, chitosan [74]. Among all carbon nanotubes types, particularly for functionalization multi-walled carbon nanotubes are considered suitable for this approach as the damage is slightly low [75].

Moreover, functionalization of carbon nanotubes through non-covalent approach using meso-porphine and 5, 15-bis-porphyrin enhance the properties of tubes like biocompatibility, solubility in aqueous solution, luminescence etc. [73]. Among all poly-ethylene-mine (a hydrophilic character with polar head) use for carbon nanotubes functionalization and improve nanotubes water solubility significantly [76].

Furthermore, aromatic molecules are more strongly absorbed on the surface of graphite compared to aliphatic because of the π - π interaction among graphite surface and amphiphilic molecules of aromatic components as well as electrostatic and van der Waals interaction involvement [77]. This effect noticed in pyrene-containing molecules which is a non-covalent modification agent. In addition, to attaining successful dispersion of carbon nanotubes, surfactants (cationic, anionic/non-ionic) have been widely used. However, hydrophobic regions length and hydrophilic structure of the surfactants are the factors on which guaranteed carbon nanotubes dispersion based. Moreover, higher critical micellar concentration, minor stability and partial interaction with cellular proteins are few limitations surfactants face in a biological environment. Several of these limitations can be avoided through the PEG-modified phospholipids [58] use which holds different functional groups that required additional functionalization with targeting and therapeutic molecules.

7 Conclusion and Perspectives

The discovery of carbon nanomaterial, particularly CNTs has aroused the attention of many researchers to study in-depth the capability of this remarkable material. In addition, functionalization approaches open completely new chapter for considering CNTs in many application where initially restricted to use. However, massive successful researches have carried out, and the outcome of these researches categorized CNTs as distinct biomaterials that hold potential to medical applications in bone engineering and orthopaedics techniques due to their outstanding capability of accelerating bone repair/restoration. Additionally, experimental results reflect that f-CNTs are capable to transmit cells without apparent cytotoxicity that eligible f-CNTs to use as a delivery vehicle for a range of biologically energetic molecules such as drugs, deoxyribonucleic/ribonucleic acid, and protein. Moreover, functionalization techniques assist in removing metallic containments and enhance the biocompatibility of CNTS, and allow them to be considered as a promising material for application related to bone tissue engineering.

In the past, CNTs were used with polymers but due to the issues like toxicity, aggregation restricted its use with polymers. Some of the experiments conducted in the past based on CNTs-polymers were MWCNT-Polycaprolactone, Polypropylene-MWCNT-nHA, Sodium hyaluronate-SWCNTs etc. However, functionalization of CNTs will certainly solve such issues and will allow its use as filler material with different polymers, and consider them appropriate for bone defects, replacement or loss.

References

1. Bawa R, Audette GF, Rubinstein I (2016) Handbook of clinical nanomedicine: nanoparticles, imaging, therapy, and clinical applications. CRC Press, Boca Raton
2. Adlakha-Hutcheon G, Khaydarov R, Korenstein R, Varma R, Vaseashta A, Stamm H et al (2009) Nanomaterials, nanotechnology. Nanomaterials: Risks and Benefits. Springer, Berlin, pp 195–207
3. Schaefer H-E (2010) Nanoscience: the science of the small in physics, engineering, chemistry, biology and medicine. Springer, Berlin Heidelberg, pp 615–735
4. Yang Y, Yang X, Yang Y, Yuan Q (2018) Aptamer-functionalized carbon nanomaterials electrochemical sensors for detecting cancer relevant biomolecules. Carbon 129:380–395
5. Liu Y, Dong X, Chen P (2012) Biological and chemical sensors based on graphene materials. Chem Soc Rev 41(6):2283–2307
6. Trung TQ, Lee NE (2016) Flexible and stretchable physical sensor integrated platforms for wearable human-activity monitoring and personal healthcare. Adv Mater 28(22):4338–4372
7. Yang W, Ratinac KR, Ringer SP, Thordarson P, Gooding JJ, Braet F (2010) Carbon nanomaterials in biosensors: should you use nanotubes or graphene? Angew Chem Int Ed 49(12):2114–2138
8. Weiss NO, Zhou H, Liao L, Liu Y, Jiang S, Huang Y et al (2012) Graphene: an emerging electronic material. Adv Mater 24(43):5782–5825

9. Backes C (2012) Introduction: noncovalent functionalization of carbon nanotubes: fundamental aspects of dispersion and separation in water. Springer, Berlin Heidelberg, pp 1–37
10. Zamolo VA, Vazquez E, Prato M (2013) Carbon nanotubes: synthesis, structure, functionalization, and characterization. In: Siegel JS, Wu Y-T (eds) *Polyarenes II*. 350, pp 65–109, Springer, Cham
11. Yadav Y, Kunduru V, Prasad S (2008) Carbon nanotubes: synthesis and characterization. In: Morris JE (ed) *Nanopackaging: nanotechnologies and electronics packaging*. Springer US, Boston, MA, pp 325–344
12. Rezakazemi M, Amooghini AE, Montazer-Rahmati MM, Ismail AF, Matsuura T (2014) State-of-the-art membrane based CO₂ separation using mixed matrix membranes (MMMs): an overview on current status and future directions. *Prog Polym Sci* 39(5):817–861
13. Kong J, Zhou C, Morpurgo A, Soh HT, Quate CF, Marcus C et al (1999) Synthesis, integration, and electrical properties of individual single-walled carbon nanotubes. *Appl Phys A* 69(3):305–308
14. Sun H, She P, Lu G, Xu K, Zhang W, Liu Z (2014) Recent advances in the development of functionalized carbon nanotubes: a versatile vector for drug delivery. *J Mater Sci* 49(20):6845–6854
15. Liu Y, Zhao Y, Sun B, Chen C (2012) Understanding the toxicity of carbon nanotubes. *Acc Chem Res* 46(3):702–713
16. Schafer FQ, Qian SY, Buettner GR (2000) Iron and free radical oxidations in cell membranes. *Cellular and molecular biology (Noisy-le-Grand, France)* 46(3):657
17. Basiuk EV, Basiuk VA (2015) Solvent-free functionalization of carbon nanomaterials. In: Basiuk VA, Basiuk EV (eds) *Green processes for nanotechnology: from inorganic to bioinspired nanomaterials*. Springer, Cham, pp 163–205
18. Krishna V, Stevens N, Koopman B, Moudgil B (2010) Optical heating and rapid transformation of functionalized fullerenes. *Nat Nanotechnol* 5(5):330
19. Bai RG, Ninan N, Muthoosamy K, Manickam S (2017) Graphene: a versatile platform for nanotheranostics and tissue engineering. *Progress in Materials Science*
20. Egli RJ, Luginbuhl R (2012) Tissue engineering-nanomaterials in the musculoskeletal system. *Swiss Med Wkly* 142:w13647
21. Cowin SC (2001) *Bone mechanics handbook*. CRC Press, Boca Roton
22. Currey J (2002) *Bones: structure and mechanics*. Princeton University Press, Princeton, NJ
23. Behari J (1991) *Solid state bone behaviour*. *Prog Biophys Mol Biol* 56(1):1–41
24. Rouhi G (2006) *Theoretical aspects of bone remodeling and resorption processes*. Ph.D. Thesis, University of Calgary
25. Bartel D, Davy D, Keaveny T (2006) *Orthopaedic biomechanics mechanics and design in musculoskeletal systems*. Pearson Education Inc., Upper Saddle River
26. Lakes R, Saha S (1979) Cement line motion in bone. *Science* 204(4392):501–503
27. van der Meulen MC (2000) Mechanics in skeletal development, adaptation and disease. *Philos Trans Royal Soc Lond A Math Phys Eng Sci* 358(1766):565–578
28. Guldberg R, Caldwell N, Guo X, Goulet R, Hollister S, Goldstein S (1997) Mechanical stimulation of tissue repair in the hydraulic bone chamber. *J Bone Miner Res* 12(8):1295–1302
29. Burger EH, Klein-Nulend J (1999) Mechanotransduction in bone—role of the lacuno-canalicular network. *FASEB J* 13(9001):S101–S112
30. Parfitt A (1995) Problems in the application of in vitro systems to the study of human bone remodeling. *Calcif Tissue Int* 56(1):S5–S7
31. Standring S (2015) *Gray's anatomy e-book: the anatomical basis of clinical practice*. Elsevier, Amsterdam
32. Patka P, Haarman HJTM, van der Elst M, Bakker FC (2000) Artificial bone. In: Wise DL, Trantolo DJ, Lewandrowski K-U, Gresser JD, Cattaneo MV, Yaszemski MJ (eds) *Biomaterials engineering and devices: human applications, vol 2, Orthopedic, Dental, and Bone Graft Applications*, pp 95–109. 2 Totowa, Humana Press, NJ

33. Autograft (2001) In: Schwab M (ed) *Encyclopedic reference of cancer*, p 83. Springer, Berlin, Heidelberg
34. Isograft (2001) In: Schwab M (ed). *Encyclopedic reference of cancer*, p 468. Springer, Berlin, Heidelberg
35. Allograft (2001) In: Schwab M (ed) *Encyclopedic reference of cancer*, p 38. Springer, Berlin Heidelberg
36. Kabbashi N, Jamal Ibrahim D, Rosli NF (2011) Statistical analysis for removal of cadmium from aqueous solution at high pH. *Aust J Basic Appl Sci* 5(6):440–446
37. Syahrom A, Kadir MRA, Abdullah J, Öchsner A (2013) Permeability studies of artificial and natural cancellous bone structures. *Med Eng Phys* 35(6):792–799
38. Saijo H, Kanno Y, Mori Y, Suzuki S, Ohkubo K, Chikazu D et al (2011) A novel method for designing and fabricating custom-made artificial bones. *Int J Oral Maxillofac Surg* 40(9):955–960
39. Kamachimudali U, Sridhar T, Raj B (2003) Corrosion of bio implants. *Sadhana* 28(3–4):601–637
40. Trebše R (2012) *Biomaterials in artificial joint replacements. Infected total joint arthroplasty*. Springer, Berlin, pp 13–21
41. Virtanen S, Milošev I, Gomez-Barrena E, Trebše R, Salo J, Kontinen Y (2008) Special modes of corrosion under physiological and simulated physiological conditions. *Acta Biomater* 4(3):468–476
42. De Volder MF, Tawfick SH, Baughman RH, Hart AJ (2013) Carbon nanotubes: present and future commercial applications. *Science* 339(6119):535–539
43. Grace T (2003) *An introduction to carbon nanotubes*. Summer, Stanford University
44. Pénicaud A (2014) Solubilization of fullerenes, carbon nanotubes, and graphene. Making and exploiting fullerenes, graphene, and carbon nanotubes. Springer, Berlin, pp 1–35
45. Rao CK, Rao L (2017) Critical velocities in fluid-conveying single-walled carbon nanotubes embedded in an elastic foundation. *J Appl Mech Tech Phys* 58(4):743–752
46. Yu O, Daoyong L, Weiran C, Shaohua S, Li C (2009) A temperature window for the synthesis of single-walled carbon nanotubes by catalytic chemical vapor deposition of CH 4 over Mo 2-Fe 10/MgO catalyst. *Nanoscale Res Lett* 4(6):574
47. Qingwen L, Hao Y, Yan C, Jin Z, Zhongfan L (2002) A scalable CVD synthesis of high-purity single-walled carbon nanotubes with porous MgO as support material. *J Mater Chem* 12(4):1179–1183
48. Ahmed W, Jackson MJ (2016) *Surgical tools and medical devices*. Springer, Berlin
49. Radushkevich L, Lukyanovich V (1952) Carbon structure formed under thermal decomposition of carbon monoxide on iron. *Zh Fiz Khim* 26(1):88–95
50. Shin Y-H, Song J-W, Lee E-S, Han C-S (2007) Imaging characterization of carbon nanotube tips modified using a focused ion beam. *Appl Surf Sci* 253(16):6872–6877
51. Vajtai R (2013) *Springer handbook of nanomaterials*. Springer Science & Business Media, Berlin
52. Huczko A (2002) Synthesis of aligned carbon nanotubes. *Appl Phys A* 74(5):617–638
53. Chauhan SK, Shukla A, Dutta S, Gangopadhyay S, Bharadwaj LM (2012) Carbon nanotubes for environmental protection. Springer, *Environmental Chemistry for a Sustainable World*, pp 83–98
54. Syrgiannis Z, Melchionna M, Prato M (2015) Covalent carbon nanotube functionalization. In: Kobayashi S, Müllen K (eds) *Encyclopedia of polymeric nanomaterials*. Springer, Berlin Heidelberg, pp 480–487
55. Yang Y, Qiu S, Xie X, Wang X, Li RKY (2010) A facile, green, and tunable method to functionalize carbon nanotubes with water-soluble azo initiators by one-step free radical addition. *Appl Surf Sci* 256(10):3286–3292
56. Mananghaya MR, Santos GN, Yu DN (2017) Solubility of amide functionalized single wall carbon nanotubes: a quantum mechanical study. *J Mol Liq* 242:1208–1214
57. Giliopoulos DJ, Triantafyllidis KS, Gournis D (2013) Chemical functionalization of carbon nanotubes for dispersion in epoxy matrices. In: Paipetis A, Kostopoulos V (eds) *Carbon*

- nanotube enhanced aerospace composite materials: a new generation of multifunctional hybrid structural composites, pp 155–183. Springer: Dordrecht, Netherlands
58. Erol O, Uyan I, Hatip M, Yilmaz C, Tekinay AB, Guler MO (2017) Recent advances in bioactive 1D and 2D carbon nanomaterials for biomedical applications. *Nanomedicine: Nanotechnology, Biology and Medicine*
 59. Liang S, Li G, Tian R (2016) Multi-walled carbon nanotubes functionalized with a ultrahigh fraction of carboxyl and hydroxyl groups by ultrasound-assisted oxidation. *J Mater Sci* 51 (7):3513–3524
 60. Battigelli A, Ménard-Moyon C, Da Ros T, Prato M, Bianco A (2013) Endowing carbon nanotubes with biological and biomedical properties by chemical modifications. *Adv Drug Deliv Rev* 65(15):1899–1920
 61. Zhao Z, Yang Z, Hu Y, Li J, Fan X (2013) Multiple functionalization of multi-walled carbon nanotubes with carboxyl and amino groups. *Appl Surf Sci* 276:476–481
 62. Khani H, Moradi O (2013) Influence of surface oxidation on the morphological and crystallographic structure of multi-walled carbon nanotubes via different oxidants. *J Nanostruct Chem* 3(1):73
 63. Martín O, Gutierrez HR, Maroto-Valiente A, Terrones M, Blanco T, Baselga J (2013) An efficient method for the carboxylation of few-wall carbon nanotubes with little damage to their sidewalls. *Mater Chem Phys* 140(2–3):499–507
 64. Zschoerper NP, Katzenmaier V, Vohrer U, Haupt M, Oehr C, Hirth T (2009) Analytical investigation of the composition of plasma-induced functional groups on carbon nanotube sheets. *Carbon* 47(9):2174–2185
 65. Saito T, Matsushige K, Tanaka K (2002) Chemical treatment and modification of multi-walled carbon nanotubes. *Physica B* 323(1–4):280–283
 66. Dillon AC, Gennett T, Jones KM, Alleman JL, Parilla PA, Heben MJ (1999) A simple and complete purification of single-walled carbon nanotube materials. *Adv Mater* 11(16):1354–1358
 67. Morelos-Gómez A, Tristán López F, Cruz-Silva R, Vega DÁ-az SM, Terrones M (2013) Modified carbon nanotubes. In: Vajtai R (ed) *Springer Handbook of Nanomaterials*, pp 189–232. Springer, Berlin Heidelberg
 68. Hirsch A, Vostrowsky O (2005) Functionalization of carbon nanotubes. *Functional molecular nanostructures*. Springer, Berlin, pp 193–237
 69. Trusova ME, Kutonova KV, Kurtukov VV, Filimonov VD, Postnikov PS (2016) Arenediazonium salts transformations in water media: coming round to origins. *Resour Efficient Technol* 2(1):36–42
 70. Mohamed AA, Salmi Z, Dahoumane SA, Mekki A, Carbonnier B, Chehimi MM (2015) Functionalization of nanomaterials with aryldiazonium salts. *Adv Coll Interface Sci* 225:16–36
 71. Backes C, Hirsch A (2010) *Noncovalent functionalization of carbon nanotubes*. Wiley, Chichester, UK, pp 1–48
 72. Composites C. Functionalization of CNTs 2018 (cited 11 Mar 2018). Available from: <https://sites.google.com/site/cntcomposites/functionalization-of-cnts>
 73. Ferreira FV, Cividanes LDS, Brito FS, de Menezes BRC, Franceschi W, Simonetti EAN et al (2016) Functionalization of carbon nanotube and applications. *Functionalizing Graphene and carbon nanotubes: A review*. Springer, Cham, pp 31–61
 74. Bianco A, Sainz R, Li S, Dumortier H, Lacerda L, Kostarelos K et al (2008) Biomedical applications of functionalised carbon nanotubes. In: Cataldo F, Da Ros T (eds) *Medicinal chemistry and pharmacological potential of fullerenes and carbon nanotubes*. Springer, Dordrecht, Netherlands, pp 23–50
 75. Kasperski A, Weibel A, Estournès C, Laurent C, Peigney A (2014) Multi-walled carbon nanotube–Al₂O₃ composites: covalent or non-covalent functionalization for mechanical reinforcement. *Scripta Mater* 75:46–49

76. Behnam B, Shier WT, Nia AH, Abnous K, Ramezani M (2013) Non-covalent functionalization of single-walled carbon nanotubes with modified polyethyleneimines for efficient gene delivery. *Int J Pharm* 454(1):204–215
77. Sanz V, Borowiak E, Lukanov P, Galibert AM, Flahaut E, Coley HM et al (2011) Optimising DNA binding to carbon nanotubes by non-covalent methods. *Carbon* 49(5):1775–1781
78. Jeon I-Y, Chang DW, Kumar NA, Baek J-B (2011) Functionalization of carbon nanotubes. *Carbon nanotubes-Polymer nanocomposites*: InTech
79. Eatemadi A, Daraee H, Karimkhanloo H, Kouhi M, Zarghami N, Akbarzadeh A et al (2014) Carbon nanotubes: properties, synthesis, purification, and medical applications. *Nanoscale Res Lett* 9(1):393
80. Pal S (2014) *Biomaterials and its characterization. Design of artificial human joints & organs*. Springer US, Boston, MA, pp 51–73
81. Tibbetts GG (2001) Vapor-grown carbon fiber research and applications: achievements and barriers. *Carbon filaments and nanotubes: common origins, differing applications?*. Springer, Berlin, pp 1–9
82. Ci L, Wei J, Wei B, Xu C, Liang J, Wu D (2000) Novel carbon filaments with carbon beads grown on their surface. *J Mater Sci Lett* 19(1):21–22
83. Ren Z, Lan Y, Wang Y (2012) *Aligned carbon nanotubes: physics, concepts, fabrication and devices*. Springer Science & Business Media, Berlin
84. Ko FK, Kuznetsov V, Flahaut E, Peigney A, Laurent C, Prinz VY, et al (2004) Formation of nanofibers and nanotubes production. *Nanoeng Nanofibrous Mater.* 169:1–129. Springer, Berlin
85. Oberlin A, Endo M, Koyama T (1976) Filamentous growth of carbon through benzene decomposition. *J Cryst Growth* 32(3):335–349
86. Demoncey N, Stephan O, Brun N, Colliex C, Loiseau A, Pascard H (1998) Filling carbon nanotubes with metals by the arc-discharge method: the key role of sulfur. *Eur Phys J B-Condens Matter Complex Syst* 4(2):147–157
87. Fonseca A, Nagy J (2001) Carbon nanotubes formation in the arc discharge process: carbon filaments and nanotubes: common origins, differing applications? p 75–84. Springer, Berlin
88. Hu J, Bando Y, Xu F, Li Y, Zhan J, Xu J et al (2004) Growth and field-emission properties of crystalline, thin-walled carbon microtubes. *Adv Mater* 16(2):153–156
89. Ren Z, Lan Y, Wang Y (2013) *Carbon nanotubes: Aligned carbon nanotubes: physics, concepts, fabrication and devices*. Springer, Berlin Heidelberg, pp 7–43
90. Iijima S, Ichihashi T (1993) Single-shell carbon nanotubes of 1-nm diameter. *Nature* 363(6430):603
91. Joselevich E, Dai H, Liu J, Hata K, Windle AH (2008) Carbon nanotube synthesis and organization. *Carbon nanotubes*. Springer, Berlin, Heidelberg, pp 101–165
92. Lyskawa J, Grondein A, Bélanger D (2010) Chemical modifications of carbon powders with aminophenyl and cyanophenyl groups and a study of their reactivity. *Carbon* 48(4): 1271–1278
93. Leinonen H, Lajunen M (2012) Direct functionalization of pristine single-walled carbon nanotubes by diazonium-based method with various five-membered S- or N-heteroaromatic amines. *J Nanopart Res* 14(9):1064

Inorganic Nanocomposite Hydrogels: Present Knowledge and Future Challenge



Nasrin Moini, Arash Jahandideh and Gary Anderson

Abbreviation

(1-ethyl-3-(3-dimethyl aminopropyl) carbodiimide	EDC
2-acrylamido-2-methylpropane sulfonic acid	AMPS
Acrylamide	AAm
Acrylic acid	AA
Carbon nanotube	CNT
Carboxy methyl cellulose	CMC
Cellulose nanocrystal	CNC
Cetyl trimethyl ammonium bromide	CTAB
Copolymer	co
Double network	DB
Ethylene glycol dimethacrylate	EGDMA
Graft	g
Graphene oxide	GO
Graphene	G
Hydroxyapatite	nHA
Hydroxyethoxyethyl metha-crylate	HEEMA
Hydroxyethyl methacrylate	HEMA
Interpenetrating polymer network	IPN
Lower critical solution temperature	LCST
Magnetic field	MF
Montmorillonite	MMT
N-(2-hydroxypropyl) methacrylamide	HPMA
N,N-dimethylacrylamide	DMA
Nanocomposite Hydrogel	NCH

N. Moini (✉) · A. Jahandideh
Adhesive and Resin Department, Iran Polymer and Petrochemical Institute (IPPI),
P.O. Box. 14975-112, Tehran, Iran
e-mail: N.Moini@ippi.ac.ir

G. Anderson
Agricultural and Biosystems Engineering Department,
South Dakota State University, Brookings, SD 57007, USA

Nanocomposite	NC
Nanoparticle	NP
N-isopropyl acrylamide	NIPAm
Poly(acrylic acid)	PAA
Poly(dimethylacrylamide)	PDMA
Poly(ethylene glycol) acrylate	PEGA
Poly(ethylene glycol) diacrylate	PEGDA
Poly(ethylene glycol) dimethacrylate	PEGDMA
Poly(ethylene glycol)	PEG
Poly(ethylene oxide)	PEO
Poly(fluorine)	PF
Poly(methacrylic acid)	PMAA
Poly(methyl methacrylate)	PMMA
Poly(N-isopropyl acrylamide)	PNIPAm
Poly(N-vinyl-2-pyrrolidone)	PVP
Polyaniline	PAN
Polycarbonate	PC
Polyvinyl alcohol	PVA
Sodium acrylate	SA
Sodium n-dodecyl sulfate	SDS
Tetraethyl orthosilicate	TEOS
Vinyl acetate	VAc

1 Introduction

Hydrogels are hydrophilic physically or chemically crosslinked polymer networks, capable of absorbing and retaining the various amount of aqueous fluids [1, 2]. This crosslinked nature affects the components rheometrical properties, and consequently, results in a non-Newtonian behavior (viscoelastic or even pure elastic) of the dissolved polymeric chains [3]. This behavior promotes swelling properties of hydrogels making it a candidate for versatile applications, including biomedicine, electronic, separation and water treatment, etc. [1]. The crosslink and charge densities of the network are of the essential factors for tailoring the hydrogels properties for a special application. Hydrogels can be articulated in a variety of physical forms, including slabs, microparticles, nanoparticles, coatings, and films [4].

Wichterlie and Lim [5] first reported the synthesis of hydrogels with controlled properties, such as swell and shrinkage, over several orders of magnitude. This initial discovery provided the foundations for a generation of the *stimuli-responsive* biocompatible systems based on glycolmethacrylate, which could be in a porous state or modified by acrylamide fibers. Great progress has been made in synthesizing and developing new types of hydrogels to meet the desired controllable

properties and overcome material deficiencies. To be highly sensitive to stimuli, such as solvent composition, the ionic strength of solutes, pH, temperature, electric field, and light could provide fabrication of various types of stimuli-responsive hydrogels [6]. Despite the great properties, these soft materials suffer from poor mechanical properties. One of the most used and efficient approach to boost the mechanical properties of hydrogels is to use inorganic nanoparticles which have great strength in the hydrogel structure [7].

In this chapter, the classification and desired properties of general hydrogels will be introduced. Various methods of nanoparticle preparation have been summarized. Different methods of nanocomposite hydrogel preparation, considering the method of nanoparticle insertion into the hydrogel structure will be presented. In addition, the application of these nanocomposite hydrogels based on the employed nanoparticles will be explained. The nanocomposite hydrogels based on organic or polymeric nanoparticles are out of the scope of this chapter.

1.1 Classification of Hydrogels

Hydrogels are classified based on different features, including the source, the network electrical charge, crosslinking type, method of preparation, polymeric composition, and the configuration of polymer networks.

Considering the source, hydrogels can be classified into natural, semi-synthetic, and synthetic polymers. While natural polymers are highly biocompatible, they lack reliability and consistency, due to the inherent inconsistencies, which stems from their natural origin. On the other hand, synthetic polymers are highly reproducible materials with tunable chemical and physical properties. However, compared to natural biopolymers, they suffer from poor biocompatibility: cytotoxic or non-biocompatible monomers and organic solvents are often required during their processing. Emission of toxic by-products, i.e. unreacted monomers or products of hydrolysis, during their lifecycle is another important issue. The choice of using natural or synthetic materials for the production of hydrogels is dependent on the aspired properties and applications [8].

Natural polymer sources consist of several minerals and animal-based or plant-based materials, and the most common examples are starch, cellulose, collagen, alginate, elastin, gelatin, lignin, chitosan, and different gum silicates.

Synthetic hydrogels are prepared from various monomers, including hydroxyethyl methacrylate (HEMA), hydroxyethoxyethyl methacrylate (HEEMA), ethylene glycol dimethacrylate (EGDMA), N-vinyl-2-pyrrolidone (NVP), N-isopropyl acrylamide (NIPAAm), vinyl acetate (VAc), acrylic acid (AA), acrylamide (AAm), N-(2-hydroxypropyl) methacrylamide (HPMA), ethylene glycol (EG), PEG acrylate (PEGA), PEG methacrylate (PEGMA), PEG diacrylate (PEGDA), and PEG dimethacrylate (PEGDMA) [9].

Three different integrated parts of the hydrogel preparation include monomers, initiators, and crosslinkers [10]. Any technique, which causes crosslinking in

polymers, can be employed to produce a hydrogel. The free-radical crosslinking polymerization/copolymerization is one of the most common techniques employed to produce hydrogels. In this technique, the network is created by the reaction of hydrophilic monomers and multifunctional crosslinkers in the presence of radical initiators [11]. Water-soluble linear polymers of both natural and synthetic origins are crosslinked to form hydrogels in several ways [10]: (a) via chemical reactions (bulk or surface crosslinking [12–16]), (b) by employing ionizing radiation to generate main-chain free radicals and recombination to form crosslink junctions, and (c) via physical interactions, such as entanglements, electrostatics, and crystallite formation. In addition, various polymerization methods, including bulk, solution, graft, or emulsion polymerization, as well as inverse suspension polymerization can be used for gel preparation [11].

1.2 Feature Characteristics of Hydrogels

The desired properties of hydrogels and their corresponding factors have been summarized in Fig. 1. The feature properties of hydrogels include aqueous solution absorption capacity, absorbency rate, the extent of soluble fraction and residual monomers, biodegradability, and biocompatibility, and mechanical strength of the swollen gel [11]. The thermodynamics of swelling can reflect the influence of

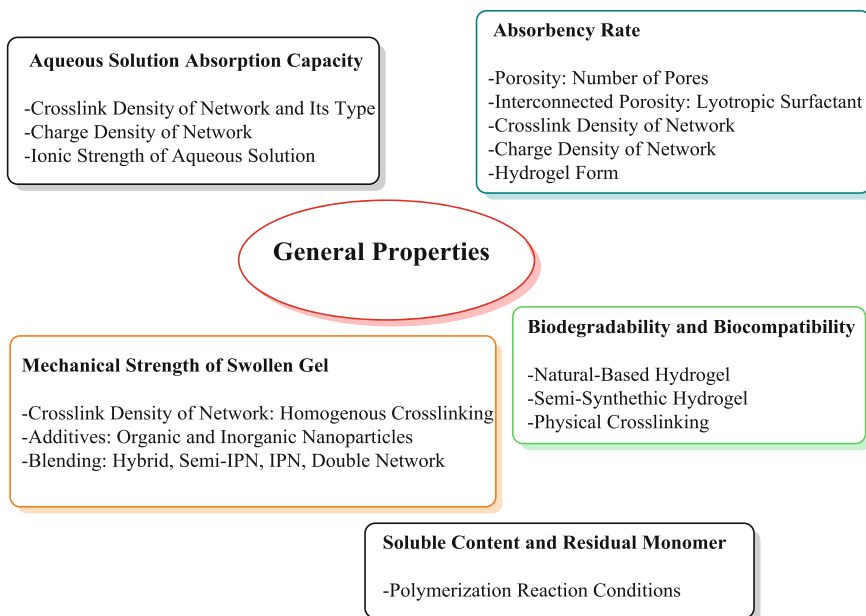


Fig. 1 Feature properties of hydrogels and their most effective parameters

crosslinking and the charge densities [17]. If the hydrogel is subjected to be used in biomedical and pharmaceutical applications, special attention must be paid to its swelling characteristics. In this case, detailed knowledge of swelling properties is essential, as the equilibrium degree of swelling affects several features of hydrogels, including its solute diffusion parameters, surface-dependent properties, optical properties as well as its mechanical properties [2].

Equilibrium swelling theory and the network characteristics of a single polymer network can be based on the contribution of mixing, network conformation (elastic), and ions. In terms of the free energy of the system, the total Gibbs free energy change (ΔG) upon swelling would be [17]:

$$\Delta G = \Delta G_{\text{elastic}} + \Delta G_{\text{mix}} + \Delta G_{\text{ion}} \quad (1)$$

Here, $\Delta G_{\text{elastic}}$ is the Gibbs free energy contribution of the elastic retractive forces (representing network crosslink density effect); ΔG_{mix} represents the thermodynamic compatibility of the polymer and the swelling agent (water), and ΔG_{ion} is the ionic contribution of poly (electrolyte) hydrogels (representing the network charge density effect) [17].

Differentiation of Eq. 1 with respect to the number of water molecules in the system, yields the chemical potential change of water, in terms of the elastic, mixing, and ion contributions during swelling of the gel [2].

$$\mu_1 - \mu_{1,0} = \Delta\mu_{\text{elastic}} + \Delta\mu_{\text{mix}} + \Delta\mu_{\text{ion}} \quad (2)$$

Here, μ_1 is the chemical potential of water within the gel and $\mu_{1,0}$ is the chemical potential of pure water. Equilibrium is reached when the chemical potentials of water inside and outside of the gel are equal. Therefore, the elastic, mixing and ion contributions to the chemical potential would balance at equilibrium. The chemical potential change upon mixing can be determined based on the Flory–Huggins theory [2, 18]. The elastic contribution of the crosslinked structure is usually described by the rubber elasticity theory and its variations [2]. The third contribution is taken as the ideal Donnan description for the ionic effect of polyelectrolytes [17]. This model has been illustrated in detail by Koetting et al. [19].

Even the *screening effect* of the ionic moieties, which is due to the high concentration of ions in an area next to the backbone that inhibits the ionization in polyelectrolytes, could influence the swelling ratio; often leads to the divergence between theory and practice [18, 20].

Swelling of polymer gels has adverse effects on its mechanical strength. Some hydrogels fracture under their own weight upon swelling. Inhomogeneity in hydrogels is often referred to as the inhomogeneous crosslinked density distribution of the gel. Inhomogeneity can decrease the hydrogels optical clarity, strength, ionization degree, electrostatic repulsion, and mobile counter ion number [21, 22].

On the other hand, several applications exist in which the hydrogels are required to sustain an external force in addition to their initial weight. *Tough hydrogels*, which reversibly deform to large extents without failure, are candidates for these

applications. The synthetic hydrogels are often brittle, while the biological tissues, such as muscles and tendons, are tough. These biological hydrogel materials offer a high swelling degree and low modulus, along with high extensibility and high toughness [23]. Recently, this combination of properties has been achieved with synthetic hydrogels [22].

Energy dissipation and high stretchability are the fundamental factors in the design of tough hydrogels [24]. So far, synthesis of different tough hydrogels have been introduced, including interpenetrating polymer network (IPN) and double network (DN) hydrogels, ionically crosslinked hydrogels, covalently and physically crosslinked nanocomposite hydrogels, slide ring hydrogels, tough tetra-PEG hydrogels, and dendritic polymer hydrogel adhesives [25].

2 Nanocomposite Hydrogels

Nanocomposite hydrogels are generally designed to promote the mechanical strength of the swollen state [7, 11]. They may also offer advanced properties such as stimuli-responsiveness [26] and self-healing [27]. Several nanoparticles have been employed in the production of nanocomposite hydrogels, including nanoparticles of inorganic ceramics, metal and metal oxides, polymer-based materials, active glass, and carbon-based nanomaterials.

2.1 Nanoparticles Preparation

Inspired by nature, the nanoscale design of polymeric materials, mainly in biomedical fields, has made great progress [28]. In this regard, nanoparticle size of compounds (0.1–100 nm), their surface area, and quantum tunnelling effects are the most important factors which confer special properties to the product [21]. Nanoparticles have been classified based on their nano dimension, source (mineral or synthetic), morphology (crystalline or amorphous), and chemistry (clays, metals, metal oxide, carbon-based, etc.). The nano-sized compartments could be arranged in one (layered, e.g. clays), two (fibrous, e.g. carbon nanotubes) or three (particulates, e.g. silica) dimensions [21].

The size of nanoparticles can strongly affect the nanocomposites properties. Moreover, the agglomeration of the nanoparticles in the suspension and their dispersion are other challenges in this field [28].

Several preparation methods have been introduced for preparation of nanoparticles: physical and chemical methods (based on chemical reaction), gas-phase, liquid-phase, and solid-phase methods (based on the state of the reaction system). Gas-phase methods include: (a) gas phase evaporation method, using heating, plasma, electron beam, and laser, (b) chemical vapour reaction, induced by heating, laser, and plasma, (c) chemical vapour condensation, and (d) sputtering methods [21].

Liquid-phase methods are the important nanoparticle preparation methods. They are based on precipitation, emulsion, hydrolysis, spray, pyrolysis, sol-gel, radiation chemical synthesis, oxidation-reduction, etc. while solid state reaction methods include milling, stripping, spark discharge, and thermal decomposition [21].

Clays, which are characterized by their crystal structure and their charge, are the most commonly used nanoparticles. The crystallinity of the clays is proportional to the composite mechanical properties. Kaolin, Serpentine, Micas ('Mica' is a generic term applied to a group of complex aluminosilicate), Chlorites and Vermiculites, Glauconite, Sepiolite, Palygorskite and Attapulgite, Bentonite, and Montmorillonite (MMT) are crystalline clays. Compared to Kaolins with uniform chemical composition, the smectites such as Bentonite and Montmorillonite have a wide range of composition and cation exchange properties [22]. Clay particles are often plate-shaped, in which the layers are *intercalated* by an intercalant (organic or inorganic material with the opposite charge of layers, e.g. onium salt), in order to induce spacing between layers (ionically induced distance is at least 1.5 nm). *Exfoliation* is another step to disperse individual platelets (an *intercalated layered*) in a polymer matrix with the distance above 8.8 nm [21].

There are some advantages and disadvantages of utilization of mineral and synthetic clays. The mineral clays are available, and can be produced by well-known technologies; whereas, the inconsistencies in composition, difficulties in the removal of amorphous clays, poor reproducibility, and the crystallographic defects which prevent total exfoliation, are of their disadvantages. On the other side, the synthetic clays, such as Laponite, would have controlled compositions and shapes, high aspect ratio, and reasonable reproducibility. The production of synthetic clays is a developing technology, resulting in a higher price for these nanoparticles than the mineral nanoparticle clays [23].

The formation of stable dispersions in the polymer matrix is even more important than the size of the nanoparticles; agglomeration of nanoparticles leads to inferior properties [29]. In order to avoid and control agglomeration in hydrogels, the in situ formation of nanoparticles (i.e. silver nanoparticles) is employed. The nanoparticles formed in this method are surrounded by the polymer matrix, and subsequently, the possibility of agglomeration is declined [30]. The in situ methods for preparation of nanoparticles, such as reduction of metal oxides, suffer from poor control over the nanoparticle properties. The risk of contamination by unconverted precursor material and/or by-products also exists in these methods [31]. Two-step preparation method has its own advantages. It is possible to optimize the synthesis conditions for each individual component (e.g. size and shape of the nanocrystals). However, the dispersion of nanoparticles by this method is a challenge and adversely affect the nanocomposite properties [31].

Modification and functionalization of nanoparticles are often employed to overcome the incompatibility of hard and soft phases of the composite hydrogels. The phase-separation is an inevitable phenomenon which occurs when compounds are incompatible. It also results in mechanical deficiency at the interfacial surface, due to the presence of losing uniform stress distribution. Therefore, various methods have been suggested to modify nanoparticles to promote the mechanical

properties. The nanoparticles could be modified by various functional groups [32, 33] such as amine [34], carboxylic acid [35], or silicone-based compounds [36].

2.2 Nanocomposite Hydrogel Preparation Methods

In general, the addition of filler compounds may be added to improve the mechanical strength of polymers. The high modulus of elasticity of the inorganic part improves the toughness of the polymer. Moreover, the nano-sized particles can significantly reform the properties, due to the scale of modification. Therefore, the combination of these two features is believed to improve mechanical properties [25] and also confer stimuli responsiveness to the hydrogels [37].

Based on the final application considered for the nanoparticle-hydrogel composite, the distribution of nanoparticles in the gels is achieved through several means, including (a) the formation of hydrogel in a nanoparticle suspension, (b) physical introduction of nanoparticles in the prepared gels, (c) in situ formation of reactive nanoparticles, (d) employing nanoparticles as the multifunctional crosslinking agents, and (e) employing nanoparticles and conductive additives along with polymeric binders [30]. Figure 2 illustrates these approaches schematically.

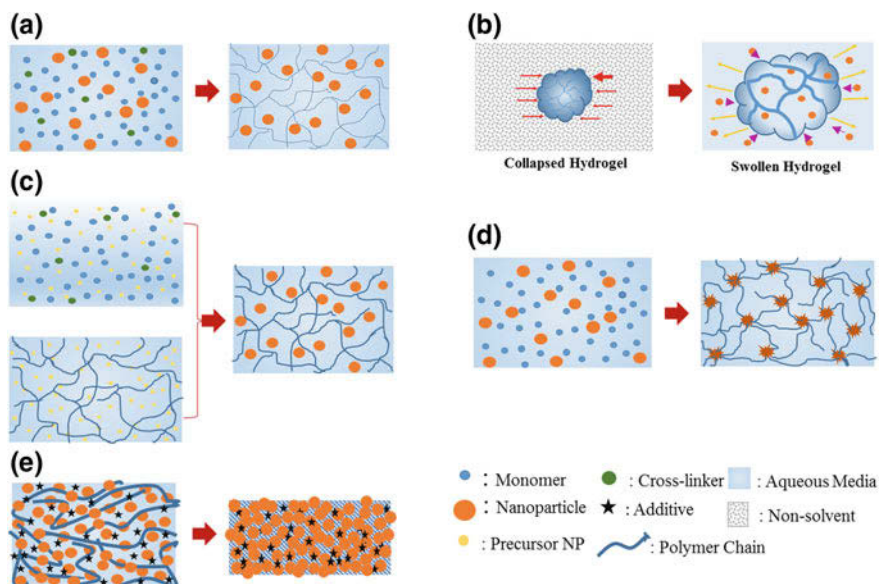


Fig. 2 Schematic representation of various methods of nanocomposite hydrogel preparation, **a** the formation of hydrogel in a nanoparticle suspension, **b** physical introduction of nanoparticles in the prepared gels, **c** in-situ formation of reactive nanoparticles, **d** employing nanoparticles as the multifunctional crosslinking agents, and **e** employing nanoparticles and conductive additives along with polymeric binders

2.2.1 Formation of a Hydrogel in a Nanoparticle Suspension

In this method, the polymerization is performed in the suspension solution of the monomers and the dispersed nanoparticles. Generally, the dispersion of nanoparticles is achieved by sonication of the suspension. In this part, the nanoparticles do not interfere with the polymerization. Ferromagnetic [38, 39] and gold nanoparticles [40] are examples of these kinds of particles. Gold nanoparticles were employed in the preparation of optically responsive hydrogel composites [41]. The weak interaction between particles and polymeric media leads to nanoparticles leaching during swelling, which is the main limitation of this method [30].

2.2.2 Physical Introduction of Nanoparticles into the Prepared Gels

Physical incorporation of nanoparticles into the gel during the polymerization, especially in non-conventional ones, is not always possible and sometimes there are obstacles to the addition of NPs during the gelation process. The electropolymerization and Au nanoparticles (Au-NP) are the best examples [30]. The Au nanoparticles cannot be used during the hydrogel preparations through electropolymerization, due to the agglomerations of Au in the electric field. To overcome this problem, the Au-NPs are doped into the hydrogel, via a “breathing in” mechanism. This mechanism consists of two steps; first, the highly aqueous swollen hydrogel is placed in an aprotic solvent (i.e. acetone) for 2 min, which is called the “breathing out” step. At the second step, the shrunk gel will be placed in an aqueous solution of citrate-stabilized Au-nanoparticles (13 nm) for 2 min (the nanoparticles have been stabilized by a chelating agent). This aqueous solution causes a swollen gel to form in the solution and the process is called “breathing in” of the suspended nanoparticles. The procedure could be repeated several times without any undesirable release of NPs during the “breathing” procedure. Since the nanoparticles have been stabilized with hydrogen bonding and physical entanglements that were induced by the chelating agent [42]. Guo et al. used the breathing mechanism for incorporation of Au-NPs into the porous anodic aluminium oxide film. For this purpose, the acrylamide gel was prepared by electropolymerization, and then, it was used as the media to absorb Au-NPs into the pores via breathing mechanism. Afterwards, the calcination is performed and the Au-NPs are trapped in the anodic aluminium oxide film [43].

2.2.3 In Situ Formation of Reactive Nanoparticles

In this approach, the nanoparticle precursors undergo a reaction to produce well-dispersed nanoparticles. It can also be called “in situ” nanoparticle formation, mostly via a reduction reaction. This method provides quite uniform distribution of metal or metal oxide NPs. In fact, the hydrogel media inhibits the aggregation of NPs during the reaction. Often, Ag-NPs are made for antibacterial purposes,

or for the addition of optical and electrical properties. Studies have shown that the size of produced Ag nanoparticles has not been varied by changing the Ag⁺ ion concentration. In addition, aggregation of particles has not been reported. Therefore, the Ag-NPs are created through in situ techniques [44–46].

The in situ reduction reaction could be performed during the polymerization or even after that. In antibacterial cryogels based on Ag NPs, the cryogel is swollen to the equilibrium state in AgNO₃ solution (for 24 h) and then the gel was added to the NaBH₄ solution to prepare in situ Ag NPs after proper preparation of the cryogel [47].

The mangogels were most of the time undergone the in situ preparation of ferromagnetic NPs. To exemplify, first, the metal ions were bounded to the gel then reaction with NaOH results in the in situ formation of magnetic NPs [48, 49].

2.2.4 Nanoparticles as the Multifunctional Crosslinking Agents

The employment of nanoparticles as multifunctional crosslinking groups, present at the nanoparticle surface, is one of the most interesting aspects in the nanocomposite hydrogel field. The clays with a hydrophilic nature have a great potential to be used as multifunctional crosslinkers. Various clays have been *organomodified* with different intercalants, to be used for the preparation of superabsorbent nanocomposite hydrogels, such as Bentonite, Montmorillonite (MMT), and Sepiolite [11]. In this method, the effective intercalant should be of opposite charge. For instance, MMT can be intercalated with cationic, low molecular weight materials or polymeric materials. Alkyl ammonium salts, such as hexadecyl ammonium chloride and (3-acrylamidopropyl) trimethyl ammonium chloride, or polymeric materials, such as chitosan and poly (dimethyldiallylammonium chloride), have been currently employed in this method [50]. During radical polymerization, the radical transfer to the surface of the NPs is an ordinary phenomenon, which may trigger the grafting at the surface of the particle. For this reason, the clays are called “radical killers” because they retard the radical polymerization and gelation [11]. In addition, ultrahigh mechanical properties of these nanocomposites (NC) hydrogels can be attributed to the multiple non-covalent effects between clay nano-sheets (Clay-NS) and the polyacrylamide chains [51].

Zhang et al. prepared a four-component semiconductor nanoparticle-based hydrogel, via self-initiated polymerization under sunlight. The system consists of four components: water, n,n-dimethylacrylamide (DMA), water-soluble semiconductor nanoparticles (NP), such as ZnO, TiO₂, and clay-nano-sheet (Clay-NS). NPs initiated the polymerization by sunlight. Since the crosslinking on the NP surfaces was insufficient to change the viscous behaviour to viscoelastic, clay-NSs were employed to achieve a three-dimensional structure [52].

Au NPs are also of biocompatible materials which have been modified to play the role of multifunctional (vinyl or carboxylate functionalized) crosslinkers [32, 53]. In an approach other than in situ formation of Au NPs the nanoparticles were functionalized by vinyl groups to design multifunctional Au NP crosslinkers.

The PNIPAm nanocomposite hydrogels have the thermos-switchable electrical properties [32].

The Au NPs could be functionalized by carboxylic acid using mercapto compounds and dispersed in collagen media. The employment of “zero-length” linkers is a recent method that chemically crosslinks collagen and Au nanoparticles. In fact, the coupling agents are capable of forming peptide bonds between the collagen molecules. EDC (1-ethyl-3-(3-dimethyl aminopropyl) carbodiimide) is one example of these coupling agents. Multiple carboxyl groups are present at the surface of Au nanoparticles which enable the nanoparticles to form multiple links with the collagen developing novel properties [53].

Silica nanoparticles have been employed as multifunctional crosslinkers that adhere to different parts of the gel [54–56]. The silica NPs solution has been used to adhere the PDMA-based hydrogel surfaces. In that study, a droplet of silica solution binds the swollen polymer network. In this case, the diameter of the employed nanoparticle must be comparable with the gel network mesh size (crosslink density). The network chains can be adsorbed on the nanoparticles surfaces binding the particles to gel pieces. Particles act as *connectors* between gel surfaces. The adsorbed chains also form bridges between particles. Particle adsorption is considered to be irreversible as the binding to the gel networks occurs through numerous attachments. Monomers have the ability to detach from a particle surface, and other repeating units (from the same or a different network strand) could be replaced. Such exchange processes allow large deformations and energy dissipation under stress [54].

2.2.5 Nanoparticles and Conductive Additives Along with Polymeric Binders

NC hydrogels of graphite and silica have been used in the production of rechargeable lithium-ion batteries. More recently, electrodes of Si nanoparticle (SiNP) slurries have received attention. In these systems, the binders are used to fix the active material to the anode. The more interactions (either hydrogen bond or ionic) between binder and SiNPs, the more efficient the batteries are. Different binders, such as PVDF, PAA, CMC, alginate and phytic acid, are present during the polymerization and formation of conductive NC hydrogels [57–60].

NC hydrogels have been used in the production of rechargeable lithium-ion batteries with different nanoparticles like graphite and silica [60]. More recently, electrodes made from Si nanoparticle (SiNP) slurries instead of graphite (traditional anode), have received attention. In these systems, the binders are used to hold the active material together in the anode. The point is that the binder concentration in the slurry is much less than the nanoparticle concentration and other additive concentrations (15 wt% binder vs. 43% Si NP and 42% C as conductive martial [58]). The binder could be a previously prepared polymer [59] or synthesized in situ during anode preparation [57]. The more interactions (either hydrogen bond or ionic) between the binder and SiNPs, the more efficiency of the batteries are owing

to less volume change (for high capacity batteries). The polymeric binders could act as dual-functional materials to improve binding and conductivity of the electrodes. The life cycle of the electrode can be extended by enhancing mechanical and electrical properties (integrity). Different binders, such as PVDF, PAA, CMC, alginate and phytic acid, are present during the polymerization and formation of conductive NC hydrogels [57–60].

2.3 How Nanoparticles Improve Mechanical Strength of Hydrogels?

Mechanisms of energy dissipations in tough hydrogels include reversible crosslinking or fracture of polymer chains, the transformation of domains in polymer chains or crosslinkers, as well as fracture and pullout of fibers or fillers. Mechanisms of maintaining elasticity in tough hydrogels can be attributed to the interpenetration of long-chain networks, hybrid physical and chemical crosslinkers, high-functionality of crosslinkers, and the presence of networks with long monodisperse polymer chains [24]. Many tough hydrogels have been produced based on these mechanisms, such as hydrogels of poly (vinyl alcohol) with crystalline domains, double-network systems, hydrogels with hybrid chemical and physical crosslinkers, hydrogels with high-functional crosslinkers, systems with transformable domains, topological hydrogels with sliding crosslinkers, and tetra-arm polymer hydrogels [25]. It is believed that employing a combination of these techniques would be a promising strategy to design next-generation tough hydrogels. For instance, a tough hydrogel may integrate fiber reinforcement at the macro-/meso-scale, high-functionality crosslinkers at the micro-scale, and hybrid crosslinkers at the nanoscale [24].

Examples of high-functional crosslinkers which are used for production of tough hydrogels include crystalline domains in polymer networks [i.e. poly(vinyl alcohol)], exfoliated nano-clays that can crosslink various polymers (i.e. polyacrylamide [61], poly(N-isopropylacrylamide [62], and poly(ethylene glycol) [63]), polyacrylamide crosslinked by chitosan nanofibers [64], and graphene oxide [65].

It is believed that nanoparticles act as multiple crosslinkers. The suggested mechanisms explaining the toughness these hydrogels exhibit will be explained in the following. Based on Flory's network theory, the number of polymer chains that can be crosslinked by a crosslinker is defined as the functionality of the crosslinker. Typically, common physical and chemical crosslinkers have functionalities less than 10; in addition, generally, a single polymer chain connects two adjacent common crosslinkers. When polymer chains are ruptured under deformation, the connections between crosslinkers are eliminated, and consequently, fracture of the network is commenced. In order to achieve high elasticity in hydrogels, large crosslinkers with very high functionality (e.g. over 100) must be incorporated into the polymer networks. In these networks, multiple polymer chains may connect two

adjacent crosslinkers; and these chains usually do not have uniform lengths. In other words, parallel to the polymerization, *grafting* happens on the surface of the nanoparticles and multiple crosslinking occurs. Therefore, as the polymer networks are deformed, relatively short chains may be ruptured or detached from the high-functionality crosslinkers, but the long chains can still maintain the elasticity of the hydrogels [24].

Depending on the employed nanoparticles, the physical adsorption and desorption of building blocks of polymer chains may increase the non-covalent and reversible interactions (which act like crosslinks). Poly(acrylamide)s and silicates show a great potential for these interactions. The shear thinning characteristics (induced by reversible interactions) of this type of hydrogel composite can expand the hydrogel composite application, especially in the biomedical field [54, 55, 66, 67].

2.4 Characterization Methods of Nanocomposites Hydrogels

Various techniques have been employed to characterize nanocomposite hydrogels structural, mechanical, thermal, electrical, and optical properties. The physico-chemical structure of these hydrogels is often studied by X-ray diffraction (XRD), transmission electron microscopy (TEM), small angle neutron scattering (SANS), and Fourier-transform infrared spectroscopy (FTIR) [11].

Based on the XRD data, the lattice related data (crystal planes, shape, and constants) can be obtained [61, 68–70]. XRD has also been used to study the extent of intercalation and exfoliation. The interlayer spacing (d) is commonly determined from the XRD patterns as the arbitrary intensity versus 2θ , based on Bragg's law [71]. To study the diffracting angles less than 0.05° , small-angle X-ray scattering (SAXS) and SANS have been employed, mainly because of their sensitivity and ability to make long-range measurements. SANS can be adopted on various types of specimens and may be assisted to probe the polymer-clay interaction, interfacial polymer conformations, phase transition, and gelation mechanism [71–73].

While the XRD/WAXS does not reveal useful information for $2\theta \cong 2$, TEM provides visual evidence of the nanoparticle distribution. TEM can also provide useful information on crystals development, morphology, and size [48]. The interactions between the clay platelets, the intercalating agent, and the polymer can be studied by FTIR techniques [74].

The thermal behaviour of the nanocomposite hydrogels can be studied by Differential Scanning Calorimetry (DCS) and Thermogravimetric analysis (TGA). Often, the mechanical properties of the nanocomposite hydrogels are investigated by dynamic mechanical analysis (DMA), oscillatory rheometry, and compression and tensile tests [11].

2.5 *Types of Nanocomposite Hydrogels and Their Applications*

2.5.1 Inorganic Ceramics and Non-metal Nanoparticles

In the last decades, inorganic ceramics mostly used as counterparts have attracted attention in hydrogel field on account of their versatility, great mechanical strength, biocompatibility and reasonable price. A range of bioactive nanoparticles has been reported to be used in various biomedical applications. These bioactive nanoparticles include hydroxyapatite (nHA), synthetic silicate nanoparticles (i.e. Laponite), bioactive glasses (SiO_2 , Na_2O , CaO , MgO , P_2O_5), silica, calcium phosphate, glass ceramic, and b-wollastonite [51].

Table 1 presents typical clay-based nanocomposite hydrogel preparations and their application. These clay-based NPs are used most in inorganic ceramics in the nanocomposite hydrogel field. They act as multifunctional crosslinkers giving great potential for functionalization and grafting. Various polymeric networks like PAA, PAAm, PEG, and chitosan have been incorporated. Based on Table 1 data, the majority of hydrogels were synthesized by aqueous solution polymerization via free radical copolymerization, which has been induced by redox initiators. Meanwhile, the inverse suspension polymerization has rarely been used to produce granular hydrogels.

The employment of the synthetic silicate nanoparticles (nanoclays) has great influence on the physical and mechanical properties of the hydrogels, which can be attributed to their anisotropic, plate-like nature, and their high aspect-ratio [56, 66]. Studies showed that the addition of silicates will improve the elongation of the polymeric hydrogels, mainly due to the formation of physically crosslinked networks [56]. The physical adsorption and desorption of building blocks of polymer chains can enhance the non-covalent and reversible interactions, which act as crosslinks. The unique bioactive properties of the synthetic silicates make it capable of being employed as an injectable tissue repair matrices, bioactive fillers, or therapeutic agents [51]. The nanoclay incorporation even renders greater mechanical properties, stretchability, and self-healing properties of the hydrogel [27].

The composite hydrogels, as drug release vehicles, may increase the biocompatibility by “hiding” the nanoparticles within the hydrogel, and also by preventing nanoparticle movement from their targeted site in vivo. This morphology of hydrogel phase (e.g. porosity) can also control the kinetics release profile and balance the burst release [4].

A class of SAPs (i.e. superporous hydrogels and SPHs) has been developed by Chen et al. [75] to be used in pharmaceutical applications. A variety of techniques have been employed to synthesis porous hydrogels, including foaming, microemulsion polymerization, porogen incorporations, freeze-drying, and phase-separation [76–78]. Typical SEM images of thermally dried particles of porous and non-porous superabsorbent hydrogels at different magnifications are displayed in Fig. 3.

Table 1 Various methods of clay preparation before nanocomposition and its incorporation in hydrogel networks

NP	NP preparation	Polymeric matrix	Polymerization method	NCH preparation	Application and feature	References
Kaolin	–	P(AAm-co-AMPS)	Thermal-induced (persulfate) aqueous solution polymerization	Method d	Super absorbency	[132]
	Suspended in SDS	PAA	Ultrasound induced (persulfate) solution polymerization	Method d	Removal of brilliant green dye from water	[83]
	–	Collagen-co-PAA-PSA	Thermal-induced (persulfate) solution graft copolymerization	Method d	Enhancement of gel strength and super absorbency	[133]
	–	Urea formaldehyde and polyphosphate potassium in core: P(AA-co-AAm) in shell	Inverse suspension polymerization	Method d	Controlled release and super absorbency by core-shell structure	[134]
	& MMT, sedimentation with water, filtered and then dried at 80 °C	P(AAm-co-AMPSNa)	Redox initiation (persulfate) and aqueous solution polymerization	Method d	Removal of Cu(II), Cd(II), and Pb(II) ions	[68]
	–	PAA	Redox initiation (persulfate) and aqueous solution polymerization	Method d	Porous, highly swelling rate and capacity	[77]
	& MMT, Mica modified and intercalated by quaternary alkylammonium-exchanged (3-acrylamidopropyl) trimethylammonium chloride)	PAA	Inverse suspension polymerization	Method d	Reactive clays, super absorbency	[135]

(continued)

Table 1 (continued)

NP	NP preparation	Polymeric matrix	Polymerization method	NCH preparation	Application and feature	References
Mica	Modified and intercalated by quaternary alkylammonium-exchanged	PAA	Inverse suspension polymerization	Method d	Reactive clays, Superabsorbency	[136]
Attapulgite	– Organification with hexadecyltrimethyl ammonium bromide (HDTMABr) – Acidified –	PAAm	Thermal-induced (persulfate) aqueous solution polymerization	Method d	Salt-resistant Super absorbency	[137]
	–	Chitosan PAA-itaconic acid (IA)	Redox initiation (Vc/Peroxide) aqueous solution polymerization	Method d	Adsorption of malachite green	[81]
	–	N-Succinylchitosan-PAAm	Inverse suspension polymerization (persulfate)	Method d	Thermal stability and superabsorbency	[138]
	–	PAA	Thermal-induced (persulfate) aqueous solution polymerization	Method d	Superabsorbency	[139]
	–	Chitosan-PAA	Aqueous solution polymerization (persulfate)	Method d	Adsorption of Hg(II) ions from aqueous solution	[91]
	–	Chitosan PAA	Redox initiation (Vc/Peroxide) aqueous solution polymerization	Method d	Adsorption of La(III) and Ce(III)	[92]
	–	PAA hydroxypropyl cellulose	Redox initiation (Fenton reagent) graft polymerization	Method d	Adsorption–desorption of the rare earth elements, La (III) and Ce(III)	[94]

(continued)

Table 1 (continued)

NP	NP preparation	Polymeric matrix	Polymerization method	NCH preparation	Application and feature	References
MMT	Dispersed in water under ultrasonication for 1 h	PAAm	Redox initiation (persulfate) and aqueous solution polymerization	Method d	Stretchability, toughness, and self-healing	[61]
		PAA	Redox initiation (persulfate) and aqueous solution polymerization	Method d	Negative impact of nanocomposite on residual monomer	[80]
	Homogenized with sodium cations	Chitosan-g-PAAm	Thermal-induced (persulfate) aqueous solution polymerization	Method d	Antibacterial and superabsorbency	[140]
	Intercalated by chitosan	PAMPS	Thermal-induced (persulfate) aqueous solution polymerization	Method d	Nontoxicity, high gel strength, superabsorbency	[141]
	Suspension modified with a sodium carbonate powder	PAA	Redox initiation (persulfate) and aqueous solution polymerization	Method d	Superabsorbency	[142]
	Ultrasonicated in water	N-isopropyl acrylamide (NIPAm) and acrylic acid (AA) onto CMC was	Thermal-induced (persulfate) graft copolymerization	Method d	Removal of Cu(II) and Pb (II) ions thermoresponsive	[62]
		Polysaccharide pullulan (PULL) with polyvinyl alcohol (PVA)	– No polymerization – Electrospinning	Method d	Superabsorbency	[143]

(continued)

Table 1 (continued)

NP	NP preparation	Polymeric matrix	Polymerization method	NCH preparation	Application and feature	References
Zeolite	& Nano Ag Ultrasound for 1 h in acetone	PAA PAAm	Redox initiation (persulfate) and aqueous solution polymerization	Method d and magnetron sputtering method	Antibacterial Removal of chemical oxygen demand (COD) wastewater	[126]
	–	CMC PAA	Thermal-induced (persulfate) graft polymerization	Method d	Controlled delivery of zinc micronutrient	[144]
	Prepared in 2,2,2-Trifluoroethanol	homo-poly (butylene succinate)	Electrospun fibers	Method d	Antimicrobial drug-delivery	[145]
Bentonite	Intercalated by the hydrochloride solution of AAm	PAA crosslinker: sugar	Thermal-induced (persulfate) solution polymerization	Method d	Superabsorbency	[146]
	–	PMAA-grafted-cellulose	Thermal-induced (persulfate) graft polymerization	Method d	Removal and recovery of thorium(IV)	[93]
Halloysite	–	Chitosan PAA	Thermal-induced (persulfate) graft polymerization	Method d	Adsorbent to remove ammonium from synthetic wastewater	[87]
Rectorite	–	Chitosan PAA	Thermal-induced (persulfate) graft polymerization	Method d	Adsorbent to remove ammonium from synthetic wastewater	[88]
Illite Smectite	Dispersed in the aqueous solution of CTAB	sodium alginate-g-P (SA-co-styrene)	Micellar solution (with SDS)	Method d	Adsorbing methylene blue	[88]

(continued)

Table 1 (continued)

NP	NP preparation	Polymeric matrix	Polymerization method	NCH preparation	Application and feature	References
Sepiolite	Dispersed in water and sonicated	kappa-carrageenan-g-PAAm	Thermal-induced (persulfate) solution polymerization	Method d	Adsorption of cationic dye	[84]
Tourmaline	–	PVA PAA	Thermal-induced (persulfate) solution polymerization	Method d	Adsorption capacity for Pb^{2+} and Cu^{2+}	[89]
Hydroxycalcite	Synthesized by urea method and intercalated by sodium methyl allyl sulfonate (SMAS)	PAA PAAm	Inverse suspension polymerization	Method d	Salt-resistance	[147]
Hydroxyapatite	Vortexing and sonication to	PEG diacrylate	Cross-linked via photopolymerization. (IRGACURE initiator)	Method d	Highly extensible, tough, and elastomeric nanocomposite	[63]
Laponite	Prepared by precipitation of disodium hydrogen phosphate and calcium chloride	Cellulose-g- polyacrylamide	Suspension polymerization (persulfate)	Method c	Removal of Cu (II)	[90]
	–	PDMA PNIPAm	Redox initiation (persulfate) and aqueous solution polymerization	Method d	Self-healable	[27]
		Telechelic dendritic macromolecule (binder) PSA	– No polymerization – Solution mixing	Method d	Self-healing and moldable for biomedical application	[148]
	Mixed with Semiconductor NP (TiO_2 , ZnO, CdTe),	PDMA	Self-initiated polymerization under sunlight	Method d	Semiconductor NP-based Hydrogels	[52]

(continued)

Table 1 (continued)

NP	NP preparation	Polymeric matrix	Polymerization method	NCH preparation	Application and feature	References
	Exfoliated	Sulfobetain polymers (poly dimethyl (acrylamidopropyl) ammonium propane & butane sulfonate)	Redox initiation (persulfate) and aqueous solution polymerization	Method d	Swelling and deswelling	[149]
	-	PEG alginate	Ionically crosslinked by Ca ions	Method d	Fabrication by 3D printing (clay provide viscosity and shear thinning ability)	[150]
	Gel/solution exfoliation method	PEO	-	Method d	Cell cultivation - Biotechnological applications such as injectable matrices, biomedical coatings, drug delivery, and regenerative medicine	[67]

These nanocomposite hydrogels prepared by in-situ formation of reactive nanoparticles (method c) and by nanoparticles with the ability of multifunctional crosslinking methods (method d)

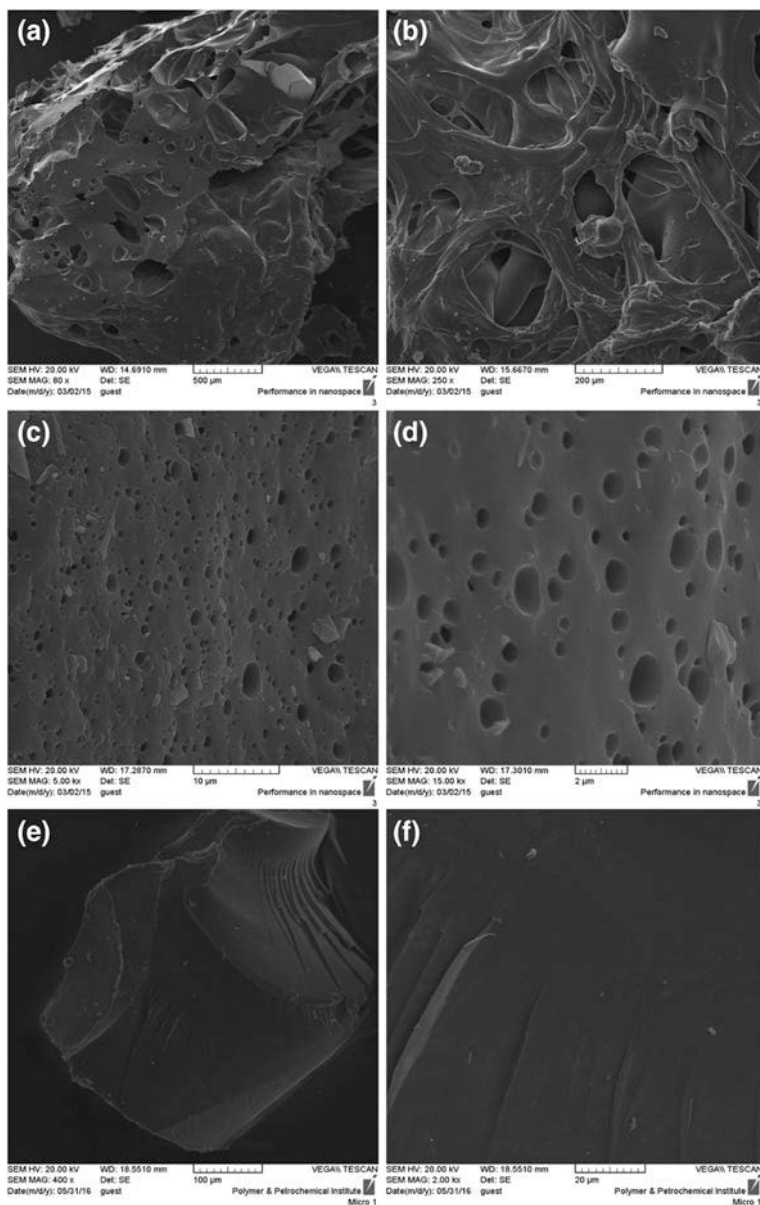


Fig. 3 Typical SEM images of porous superabsorbent hydrogel particles in **a** 500 μm magnification, **b** 200 μm magnification, **c** 10 μm magnification, **d** 2 μm magnification, and non-porous superabsorbent hydrogel particle in **e** 100 μm magnification, **f** 10 μm magnification

The SPHs were originally intended to be used in gastric retention applications. The prompt swelling of the SPHs can be attributed to the increased capillary permeability of the interconnected pore structure. The weakness in mechanical properties was mainly overcome by the development of the second-generation SPH composite (SPHCs) and the third-generation SPH hybrids [1]. Demirtas et al. [79] have synthesized and characterized polyacrylamide-based SPHCs-containing hydroxyapatite. The compressive modulus of this SPHC was 6.59 N/mm^2 , where the non-composite SPH has a compressive modulus of $\sim 0.63 \text{ N/mm}^2$.

Effects of composition and nanocomposition of superabsorbent hydrogels on their properties have also been investigated. In accordance with the other polymer composites, the presence of nanoparticles can significantly enhance the mechanical and thermal properties [11]. Besides, the optical and electrical properties of the superabsorbent hydrogels have been improved when nanoparticles have been employed [1]. However, the absorbency properties, i.e. free swelling capacity, swelling rate, reswellability, and saline sensitivity, have been pervasively influenced by the type and the content of the employed clay. Since the clays act as multifunctional crosslinkers, their hydrogels can be brittle. Moreover, in these hydrogels, employing a higher content of the clay may result in a reduction in the absorbency [11]. Composite hydrogels generally possess a slower swelling rate but exhibit a higher saline absorbency, due to the clay nature or organomodification. Moreover, the employment of the nanocomposite would have other negative impacts, such as an increase in the residual monomer content [80].

Some common inorganic components which have been used in nanocomposite hydrogels include attapulgite [81], montmorillonite [68, 82], kaolin [83], sepiolite [84], vermiculite [85], rectorite [86], halloysite [87], illite/smectite [88], tourmaline [89], and hydroxyapatite [90]. The nanocomposite superabsorbent hydrogels were also applied in water treatment and purifications processes.

These nanocomposite materials have been used for the adsorption of heavy metal ions; i.e. Pb^{2+} , Cu^{2+} [62, 68], and Hg^{2+} [91], as well as for the elimination of radioactive and rare earth elements; i.e. thorium (IV) and lanthanide (III) [92–95]. Compared to other low-cost adsorbents, fast adsorption kinetics and higher adsorption capacities are provided by the super-hydrophilic network and chelating groups of the hydrogels [49]. Other advantages of using adsorptive hydrogels include easy separation and effective desorption for the recovery and enrichment of pollutants [96]. The incorporation of the proper amount of inorganic components, not only boosts the adsorption rate but also improves the adsorption capacity [62, 68].

Efficient removal of dyes from effluents is of great importance in textile industry. Nanocomposite hydrogels are a good candidate to be tailored for this purpose. They have been tailored to be employed for separation of anionic (Silica sol) [97] and cationic dyes (Titania) [98]. Successful removal of dyes, such as malachite green (Attapulgite) [94], methylene blue (MMT) [82], methylene orange (MMT) [82], and Safranin-T (Titania) [98], has been reported using composite hydrogels. Figure 4 displays the swelling, and the methylene blue adsorption of superabsorbent polymer films, from different perspectives.

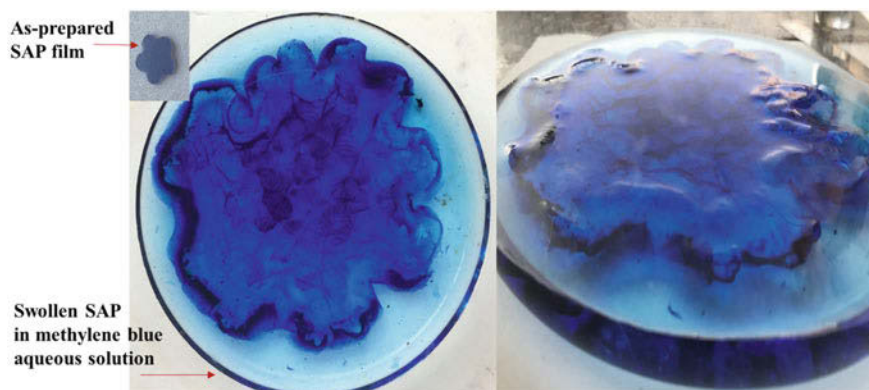


Fig. 4 Typical illustration of dye absorbency of superabsorbent hydrogels: absorption of methylene blue solution by superabsorbent polymer at different perspective

Tracking the migration of the hydrogel, which has been used as a cartilage repairing material, is a challenging task because the sensitive monitoring must be non-invasive [99]. The employment of hydrogels with desirable fluorescence properties would solve this problem. In this regard, different concepts have been employed, including polymerization of fluorescent monomers, functionalization of polymers with organic fluorophores, using fluorescent carbon dots (CDs), and semiconductor nanocrystallites [quantum dots (QDs)] [35, 99–101]. Polysaccharides are suitable candidates to be used in the synthesis of fluorescent polymeric materials. Alginate, chitosan, hyaluronic acid, dextran, and cellulose are polysaccharides commonly utilized for this purpose [99]. It has been shown that the fluorescent monomers and functionalized polymers appear to lose their luminescent properties. Therefore, the CDs are often preferred as they present high fluorescence, chemical stability, biocompatibility, and low toxicity. Recently, a novel CDs/PAM composite hydrogel with both excellent mechanical and fluorescence properties has been prepared [102].

Detection of enzymes by nanotools is of great importance; stable sensing that is very sensitive could be provided by self-assembled NPs in hydrogel media. Ruiz-Palomero et al. have reported laccase enzyme detection by immersing graphene quantum dots (GQDs) into nanocellulosic hydrogels. Noncovalent interactions between the sensor (GQDs/NC) and the analyte (laccase) have led to the stable and sensitive detection of the analyte [103].

The tracking problem can be addressed with semiconductor nanocrystals, with size-dependent emission property, can be produced in a simple synthetic process. For example, the size-dependent emission property of the CdSe nanocrystals results in blue to red emissions, with very pure colour. Chang et al. used CdSe/ZnS nanoparticles [quantum dots (QDs)] embedded in the cellulose matrices. The cellulose–QDs hydrogels displayed strong photoluminescence emission besides good compression strength [35].

2.5.2 Silicon-Based Nanoparticles

The presence and necessity of silicon in the human body are of the best reasons to use these inorganic nanoparticles for hydrogel preparation [51]. Addition of nHA and silica to the poly(ethylene glycol) (PEG) media enhanced the elasticity, mechanical strength, biological stability, and cell adhesion [63, 66]. In this case, ionic interactions could be the reason for elasticity enhancement in the gels [51]. Synthesized and modified silica nanoparticles were also used to prepare highly flexible Poly(acrylic acid)-based nanocomposite hydrogels. The silica nanoparticles were functionalized by a vinyl group, which may act as filler and multifunctional crosslinker. Entanglement trapped in the glassy polymer layers on the nanosilica leads to this flexibility [104]. The employment of sol-gel transition for preparation of silica has also been reported; this silica was further used for the preparation of a keratin-silica hydrogel, with the potential to be used for wound dressing [105].

The mesoporous silica nanoparticles (MSN), as drug vectors, have been incorporated into 3D scaffolds. The functionalized MSN has been synthesized and evaluated by different techniques: BET model for measuring the surface area, dynamic light scattering for measuring particle size, and TEM for evaluating the particle shapes. The matrix-forming self-assembling peptide, different MSNs, and precursor cells were combined to prepare injectable cell- and MSN-containing scaffolds. For this purpose, the self-assembly and coordination interactions between cells, matrices, and nanoparticles are required. Surface functionalization of MSN as well as its size, have a great impact on its nanocarrier internalization characteristics. The COOH-functionalized MSN exhibits less sensitivity to the hydrogel matrix, and in comparison with the monolayer cell culture, its internalization has been strongly enhanced in the hydrogel matrix [34].

Table 2 represents the typical silicon-based NCH preparation methods and their application. These NCHs have introduced novel properties to the hydrogel networks including toughness stretchability and self-healing which is owed to their multifunctional crosslinking role. These NPs could inherently enhance the mechanical properties of soft hydrogels. Various concepts have been explored for preparation of stretchable tough hydrogels, i.e. nanocomposition [56], micellar copolymerization [106], and hydrophobic association [107]. An example of a highly stretchable tough hydrogel under tension has been displayed in Fig. 5. The hydrogel film can be extended to desirable elongations (the displayed elongation ratio is more than 15 mm/mm).

2.5.3 Carbon-Based Nanoparticles

Carbon nanotubes (CNTs) and graphene, as the most used carbon-based nanoparticles, have attracted much attention to be used in various biomedical applications, such as actuators, conductive tapes, biosensors, tissue engineering scaffolds, etc. Table 3 summarizes typical carbon-based NCH preparation methods and their applications. In contrast to clays, the CNTs exhibit hydrophobic nature; therefore,

Table 2 Various preparation methods of silicon-based NP before nanocomposition and its incorporation into the hydrogel networks

NP	NP preparation	Polymeric matrix	Polymerization method	NCH preparation	Application and feature	References
Silica sol	–	PAAm Poly(diallyl dimethyl ammonium chloride) (DADMAC)	Thermal-induced (persulfate) aqueous solution polymerization	Method a	Removal of methyl orange from aqueous solutions	[97]
Silica CNT CNC	1-Sol-gel 2-SiO ₂ /Na ₂ O	PDMA	Thermal-induced (persulfate) aqueous solution polymerization	Method d	Adhesives for gels and biological tissues	[54]
Silica	Vinyl hybrid silica prepared by sol-gel reaction	PAAm	Thermal-induced (persulfate) aqueous solution polymerization	Method d	Highly stretchable and super tough nanocomposite	[151]
Silica	Vinyl silica prepared by methacryloxypropyl trimethoxy silane	PAA	Thermal-induced (persulfate) aqueous solution polymerization	Method d	Highly stretchable and super tough nanocomposite	[104]
Silica	Prepared by TEOS sol-gel reaction	Keratin	Siloxane network	Method d	Wound dressing	[105]
Mesoporous Silica	– Sol-gel reaction in alkaline solution (methanol and water) in the presence of CTAB – NH ₂ and COOH functionalized NPs	Peptide	–	Method d	Drug vectors into injectable 3D scaffold	[34]

(continued)

Table 2 (continued)

NP	NP preparation	Polymeric matrix	Polymerization method	NCH preparation	Application and feature	References
Sodium Silicates	–	Colloidal silica	Siloxane network	Method d	Cell encapsulation	[152]
Silica	–	PDMA	Redox initiation (persulfate) and aqueous solution polymerization	Method d	Resilient and stretchable hydrogel	[55]
Nanocrystalline silicon	Ultrasonication in presence of monomer under dry nitrogen and then degassing by freeze-pump-thaw cycles	– Ethylene glycol dimethylacrylate – 2-hydroxyethyl acrylate	Laser-induced thermal crosslinking Polymerization	Method d	Semiconductor by green process	[153]

These nanocomposite hydrogels prepared by the formation of NCH in the NPs solution (method a) and by nanoparticles with the ability of multifunctional crosslinking methods (method d)

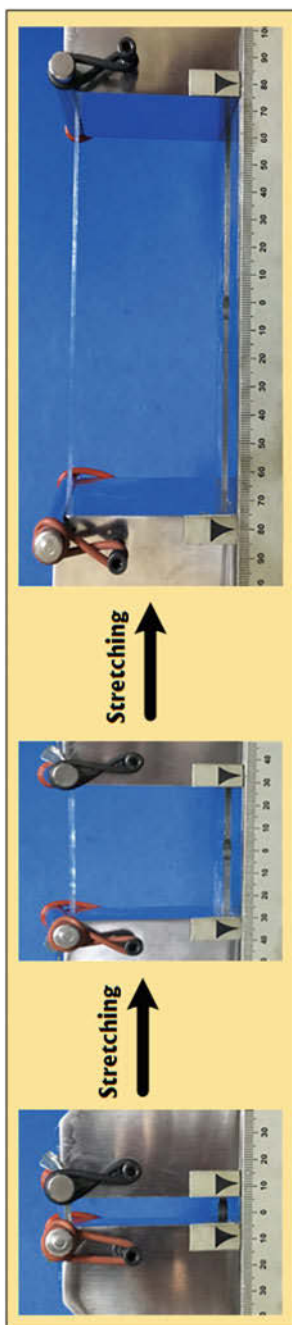


Fig. 5 Typical highly stretchable tough hydrogels under tension; the as-prepared hydrogel film (left) has been elongated to elongation ratio of ~ 15 mm/mm

Table 3 Typical carbon-based NCH preparation methods and their applications

NP	NP preparation	Polymeric matrix	Polymerization method	NCH preparation	Application and feature	References
GO	– Synthesized using Hummers' method – Sonicated	PAA	Dual ionic crosslinking Solution polymerization	Method d	Self-healable, super tough	[109]
GO	Synthesized using Hummers' method Sonicated	PNIPAm	Chemically and physically crosslinked Redox initiation (persulfate) and aqueous solution polymerization	Method d	Near-infrared light-responsive ultrahigh tensibility	[111]
Graphene nanosheets	Reduced GO to chemically converted grapheme and sonicated	Methacrylated chitosan	UV-crosslinkable conducting	Method d	3D structured biocompatible scaffold by 3D printing	[154]
Graphene	Simultaneous reduction of GO	PEGDA	UV-induced photopolymerization	Method d	Electrically conductive hydrogel	[110]
GO	Synthesized by oxidizing graphite and ultrasonication	PAAm	Redox initiation (persulfate) and aqueous solution polymerization	Method d	Tough and highly stretchable	[65]
Graphene quantum dots	Synthesis of sulfur and nitrogen codoped graphene quantum dot	Oxidize Nanocellulose (NC)	Aqueous solution in ultrasonic bath then heated with a heat gun	Method d	Eco-friendly and cost-efficient Nanotools detecting the laccase enzyme	[103]
GO	–	Poly (acryloyl-6-aminocaproic acid)	–Ca ²⁺ induces the formation of the 3D cross-linked Thermal-induced (persulfate) aqueous solution polymerization	Method d	Superior mechanical properties and self-healing Drug delivery	[155]

(continued)

Table 3 (continued)

NP	NP preparation	Polymeric matrix	Polymerization method	NCH preparation	Application and feature	References
CNT	Coating by gelatin methacrylate for better dispersion	Gelatin methacrylate	Hybrid hydrogel Photo-induced polymerization (Irgacure)	Method d, e	Cell encapsulation	[108]
CNT	CNT dispersed in PEG compounds, various surfactant and then sonicated	4-arm PEGAA PEG dithiol (linear crosslinker)	PEG remains in triethanolamine (TEA) in phosphate buffered saline for a week and then the same molar ratio of PEGAA and PEGdithiol reacted	Method a	Neural tissue engineering, sensor technology as electrode coatings, and drug delivery	[156]
CNT	Pristine CNT No surfactant	PMAA	In situ radical polymerization (aqueous dispersion)	Method a	Pulsatile drug delivery	[157]
CNT TiO ₂	First TiO ₂ dispersed and sonicated in deionized water then polymer solution and CNT solution were added	Poly (3,4-ethylenedioxythiophene (PEDOT) poly (4-styrenesulfonate) (PSS)	Radical polymerization	Method a	Flexible lithium ion battery electrodes	[158]

The NCH has been prepared by formation of hydrogel in NPs suspension (method a), in situ formation of NPs (method c), acting as multifunctional crosslinking (method d) and the polymeric network binding NPs (method e)

dispersion of CNTs in hydrogels is a potential challenge. In order to induce hydrophilicity in these systems, different approaches have been employed: modification of CNT surfaces using various polar groups, i.e. amines (NH_2), hydroxyls (OH), and carboxyls (COOH), use of single-stranded DNA (ssDNA), proteins, and surfactants, as well as by grafting hydrophilic polymer chains to the CNT surfaces. The high electrical conductivity of CNT-reinforced hydrogels makes these components ideal candidates to be engineered for various electrically conductive tissues, including cardiac tissues, nerves or muscles [51]. In hybrid nanocomposites, the slightest amount of COOH-functionalized CNTs may significantly increase the tensile strength of methacrylated gelatin hydrogels in the interconnected porous structures. The addition of CNT does not interfere in the porosity and cell-growth ability of the hydrogel. The highly aligned structure with tight intercellular junctions, along with the electrical conductivity of the CNTs results in the formation of this conductive network [108].

Graphene sheets can also provide high mechanical strength (by acting as crosslinking agents), and excellent conductivity of heat and electricity in hydrogels. In order to ensure the miscibility of the hydrophilic polymer and graphene sheets, the sheets are often treated by strong oxidizers to form graphene oxide (GO). Thus, GO can be crosslinked to the media, both physically and covalently. The GO can be employed to produce stimuli-responsive hydrogels [51]. Generally, GO is introduced into the nanocomposite hydrogels by physical mixing, in solutions, or by in situ polymerization of water-soluble monomers. The latter strategy is believed to be more efficient in terms of obtaining tough and stretchable nanocomposite hydrogels [109].

Electrically conductive hydrogels of polyethylene diacrylate, containing GO, has also been prepared by photopolymerization. In these conductive gels, the GO crosslinker has introduced electrical properties to the network [110]. The ability of GO to form crosslinks leads to the design of self-healable and tough poly (acrylic acid)-based nanocomposite hydrogels using GO and Fe^{3+} ions. Amazing dual cross-linking effects through dynamic ionic interactions has been developed: Fe^{3+} ionically crosslinked to carboxylic acid groups of the hydrogel backbone and then linking GO nanosheets to the backbone through Fe^{3+} coordination. The proposed mechanism explains the tough and self-healable behaviour of the gels based on the energy dissipation through dynamic *breakage* and *recombination* of ionic interactions. Furthermore, the GO nanosheets, coordinated on to the backbones, act as stress-transfer centres, which transfer the stress to the polymer matrix, and meanwhile, they maintain the configuration of the hydrogels [109]. These nanocomposite hydrogels can facilitate the development of soft materials to be used in various biomedical applications.

In another research, a combination of GO nanosheets and thermoresponsive poly(N-isopropylacrylamide) (PNIPAM) polymeric networks, resulted in light-responsive nanocomposite hydrogels with ultrahigh tensile strength. These novel properties which are essential for designing smart actuators, remote light-controlled devices, and artificial muscle, can be attributed to the GO nanosheets, which are physically crosslinked to the amide groups of the PNIPAM chains via hydrogen

bonds in the presence of the chemical crosslinker of N, N-methylene bis acrylamide (MBA) [111].

2.5.4 Metal and Metal Oxide Nanoparticles

Various types of nanocomposite hydrogels have been fabricated, using different metallic and metal-oxide nanoparticles, including gold, silver, copper, iron oxide (Fe_3O_4 – Fe_2O_3), ZnO, titania (TiO_2), alumina, etc. [51, 112]. In fact, the physical interactions between polymer and nanoparticles are not sufficient to provide enough mechanical strength. However, functionalization of nanoparticles will improve the mechanical strength by providing multiple crosslinking nodes in the network [51]. According to their physical, electrical, magnetic, and antimicrobial properties, various applications for imaging agents, conductive scaffolds, drug delivery systems, switchable electronics, actuators, and water treatments have the uses been developed for these hydrogels [112]. Mechanical properties also can be manipulated via magnetic field induction [26].

Thermo-responsive magnogel based on PNIPAm has been synthesized for drug delivery application; anti-cancer therapeutic drugs can be released by a magnetic field and temperature variation. In other to stabilize the Fe_2O_3 NPs, various modifications have been employed including oleic-acid, polyhedral oligomeric silsesquioxane (POSS) and nitro-dopamine PEG-dicarboxylic acid functionalization. This functionalization results in the better responsive performance of the nanocomposite hydrogel [113]. Table 4 represents the metal oxid-based NCH preparation methods especially for magnogels (ferrogels) and their applications.

Recently, ferrogels (magnetic hydrogels), which contain immobilized nanomagnetic particles (e.g. γ - Fe_2O_3 , Fe_3O_4 , Co Fe_2O_4), have attracted considerable attention. The magnetic hydrogels can quickly respond to an external magnetic field (MF), which acts as a distance-force (noncontact-or-remote force) device/system. This characteristic facilitates the incorporation of these hydrogels in various biomedical applications [38], i.e. in tissue engineering and cell/drug delivery. During the cell-growth process, limitation of available cells in the porous hydrogel is a great challenge which can be overcome by implementation of magnetic hydrogels. In fact, the required biological agents can be bound to the magnetic nanoparticles (MNPs) by applying external MF. In addition, the magnetic scaffolds can be stimulated by physical cues via interaction between MNPs and an alternating magnetic field (AMF) [37].

In order to microfabricate and 3D print hydrogels, two main strategies have been employed using microengineered hydrogels for tissue engineering including: “top-down” (hydrogel formed and cell cultivated in the fill media; for larger hydrogels) and “bottom-up” (every part of the microgels contains cells and then they are assembled into the desired shape; for microhydrogels) [114]. Magnetic microgels can be assembled in a way to form complex tissue structures in a controlled manner via MF. Several assembling techniques have been explored, including those based on microfluidics [114], nanotextured surfaces

Table 4 Typical most-used metal oxide NPs, their NCH preparation methods and their applications

NP	NP preparation	Polymeric matrix	Polymerization method	NCH preparation	Application and feature	References
ZnO	Calcination (at 850 °C) of entrapped "zinc acetate di-hydrate" in PAA gel	PAA	Thermal-induced (persulfate) aqueous solution polymerization	Method e	Biotechnology	[70]
ZnO	ZnNO ₃ hydrolyzed and then turn to ZnO crystals by heating	CMC	Crosslinked by maleic, succinic, and citric acid used as crosslinker	Method c	Antibacterial	[122]
ZnO	Synthesized by zinc acetate dihydrate and sodium hydroxide	Chitosan	NC hydrogels were lyophilized	Method b	Wound dressing	[118]
ZnO	Synthesized by zinc acetate dihydrate and sodium hydroxide	β-chitin	Freeze-dried	Method a	Wound healing	[121]
ZnO	Synthesized using zinc acetylacetonate monohydrate, oleylamine and oleic acid at 240 °C under argon flow	PNIPAm	– Linear polymer by radical polymerization – UV-induced crosslinking reaction	Method d	Hydrogel as antibacterial coating	[31]
CdSe/ZnS	COOH-functionalized Core-shell QD by octyl-amine modified PAA	Cellulose	Crosslinked by sodium hydroxid and urea ligand formation	Method d	Fluorescent semiconductors and optoelectronics	[35]
Fe ₃ O ₄ magnetic particles	Sonicated in PVA/DMSO solution	PVA	Freezing-thawing cycles	Method a	Magnetic properties for Controlled Release of Drug	[38]

(continued)

Table 4 (continued)

NP	NP preparation	Polymeric matrix	Polymerization method	NCH preparation	Application and feature	References
magnetite (Fe_3O_4) and maghemite (Fe_2O_3)	Synthesized in hydrogel network by NaOH	PAMPS	Photo-induced radical polymerization	Method c	Magnetic response hydrogels for water treatment	[49]
Ferrimagnet	Ferrofluid mixed with hydrophobic phase	Hydrophobic phase: styrene and divinyle benzene Hydrophilic phase: AAm and MBA	Anisotropic microfluidic device. – The hydrophobic monomer core with magnetic material is encapsulated by a hydrophilic monomer droplet suspended in fluorocarbon oil	Method a	Rotational control by applying an external field in biomedical application	[39]
magnetite (Fe_3O_4) and maghemite (Fe_2O_3)	In situ mineralization and coprecipitation of FeCl_2 and FeCl_3	Gelatin	Solution and physical crosslinking	Method c	Actuators	[48]
Fe_3O_4 magnetic	$\text{FeCl}_3 \cdot 6\text{H}_2\text{O}$ and sodium oleate Iron-oleate complex then it was treated by oleic acid up to 318 °C to form hydrophobic Fe_3O_4 . Their surface were treated by PEG and polyhedral oligomeric silsesquioxane	PNIPAm poly-ethylene glycol (PEG)	Redox initiation aqueous solution polymerization	Method d (functionalized NP)	Theranostic application e.g. long distance control of drug delivery by MF	[113]

(continued)

Table 4 (continued)

NP	NP preparation	Polymeric matrix	Polymerization method	NCH preparation	Application and feature	References
γ -Fe ₂ O ₃	–	Chitosan modified by catechol	Chemically and physically crosslinked by pH variation	Method d (physical crosslinking: complex)	pH and magnetic responsive Drug delivery	[159]
Fe ₃ O ₄	Coprecipitated in basic media alginate-coated in a suspension	Alginate and PAAm	Redox initiation and aqueous solution polymerization then ionically crosslinked by Fe (NO ₃) ₃	Method a	Soft robotics, clinical operations, tough, and stretchable magnogel	[160]

The NCH has been prepared by formation of hydrogel in NPs suspension (method a), in situ formation of NPs (method c), acting as multifunctional crosslinking (method d) and the polymeric network binding NPs (method e)

(micromolding) [114], acoustic and magnetic fields (photolithography) [115], and surface tension (emulsification) [39].

The magnetic gels have shown the ability of pulsatile release of drugs, through low-frequency oscillatory MFs. Recently, an intelligent Fe_3O_4 MNP-PVA hydrogel has been designed to control the drug release by “on” and “off” modes [37, 116]. When the MF was intensified, the on-off magnetization can change the volume of the ferrogels, and subsequently, affect the swelling ratio. Upon applying an MF, the nanoparticles tend to get agglomerated together [37]. The reduced porosity and volume result in “close” configuration, and subsequently, the rate of drug delivery will be minimum. On the “off” mode, the volume and swelling ratio are increased, and the drug would be delivered at its highest rate. Furthermore, the magnetic-sensitive hydrogel has shown outstanding flexibility and elasticity [38]. The magnetic-thermosensitive hydrogels have also been used for controlling the drug release rate. The AMF can adjust the hydrogels temperature. By increasing the temperature (above lower critical solution temperature (LCST)), the network will collapse and the drug diffusion would be “off”; and then, by reducing the temperature, the drug diffusion status would be “on” and the drug can be released [37]. This ability of magnetic gels to raise and control the temperature remotely has been used in cancer therapy. The concentration of Iron Oxide and the amplitude of MF are influential factors for controlling the generated heat. The local hyperthermia feature of the magnetic hydrogels makes them a promising injectable hydrogel system, especially for cancer therapy. The functionalized magnetic NPs provide better performance during swelling and deswelling phenomenon (considering no release of NPs, and subsequently less toxicity for biological application) [26].

Mechanical properties also can be manipulated via magnetic field induction [26]. Thermo-responsive magnogels based on PNIPAm have been synthesized for drug delivery application; the anti-cancer therapeutic drugs can be released by the magnetic field and temperature variation. In order to stabilize the Fe_2O_3 NPs, various modifications have been employed including oleic-acid, polyhedral oligomeric silsesquioxane (POSS) and nitro-dopamine PEG-dicarboxylic acid functionalization. This functionalization results in better responsive performance of nanocomposite hydrogel [113].

The poly(2-acrylamido-2-methyl-1-propane sulfonic acid) P(AMPS) magnetic composites have been prepared and employed for removal of toxic metals. The iron oxide can confer ferromagnetic property into the gel. These gels can be employed for absorbing toxic ions, i.e. Pb^{2+} , Cd^{2+} , Co^{2+} , Ni^{2+} , Cu^{2+} and Cr^{3+} [49].

Colonization of microorganism on the surface of the medical devices, such as implants, may result in severe infections. Therefore, the antibacterial media with the lowest cytotoxicity would be of great importance. Various metal and metal oxides nanoparticles such as silver, gold, copper, TiO_2 , and ZnO have been applied in the hydrogels to improve their antimicrobial properties [117].

Zinc oxide is the metal oxide which has been used in hygienic applications such as cosmetics. Recently, the ZnO NPs have also been used as antibacterial agents against both gram-positive [118] and gram-negative bacteria [119] and showed no cytotoxicity at concentrations of up to 10 wt% NP. Various antibacterial

mechanisms have been proposed to explain their antibacterial role, such as the formation of reactive oxygen species (ROS), and the release of Zn^{2+} ions [119, 120]. The ZnO NPs with uniform crystal structures have been successfully incorporated into poly(*N*-isopropylacrylamide) (PNIPAAm) hydrogel layers. In order to better disperse the NPs, the surfactants mediums of oleylamine and oleic acid have been employed. The antibacterial properties of these hydrogels can be altered by changing the thickness of the NP film [31]. Recently, β -chitin hydrogel/nZnO composite bandage has been fabricated and used for wound dressing applications. It has shown antibacterial effects against *E. coli* and *S. aureus*; however, the cytotoxicity of the hydrogels has been increased at elevated concentrations of ZnO NPs [121]. Furthermore, a flexible and microporous chitosan-ZnO nanocomposite hydrogel has been developed and tested for wound dressing purposes. In vivo studies revealed that this nanocomposite hydrogel has great potential to be used as a bandage for burn wounds, chronic wounds, and diabetic foot ulcers [118]. In another approach, the carboxymethyl cellulose (CMC)-based nanocomposite hydrogels were prepared by oligomeric acrylic acids, such as maleic, succinic or citric acid. The ZnO nanoparticles were synthesized in the presence of CMC to avoid agglomeration, which is known to be the main problem in zinc oxide nanocomposite hydrogel production. In fact, the polysaccharide structure, which has numerous hydrogen bonds, can effectively act as a template for nanoparticle growth. This nanocomposite hydrogel has shown a promising swelling ratio, and also great antibacterial activity against both gram positive and gram negative bacteria [122].

Metals are also used in the hydrogel network to add more functionality such as biocidal and electrical activity to the soft material. Table 5 summarizes preparation methods of the most-used metals in NCHs and their applications. Silver is the most studied antiseptic agent and has a long history in activity against gram-positive and gram-negative bacteria, fungi, protozoa, and certain viruses. Since the silver ions have shown concentration-dependent toxicity, care must be taken in the incorporation of silver in medical devices [29]. However, silver does not have the hazards associated with the accumulation of other heavy metals [29]. Factors, affecting the biocidal activity of silver nanoparticles (Ag NP) include particle size, the shape of the particle, and the dispersion status. The smaller particle size offers larger surface-to-volume ratio, which consequently enhances the antibacterial activity. In addition, the Ag NPs with triangular architecture has shown a better antibacterial effect against *E. coli* compared to the rod or spherical-shaped Ag NPs. Furthermore, for biocidal activity, the binding of Ag NPs to polymer networks is more important for effectiveness than the size of nanoparticles. The utilization of polymer supports for Ag NPs results in an increase in the stability of the particles, preserve them against aggregation, and also, increases their biocompatibility [29]. The antimicrobial activity of silver can be attributed to the strong bonding between the silver ion and the biological molecules containing sulfur, oxygen, or nitrogen. It is believed that the complex, which is formed between proteins of bacteria and the silver ion, can interfere with the metabolism and eventually, it disturbs the power functions of the bacteria. It can also prevent the cellular reproduction by interaction

Table 5 Typical most-used metals and their NCH preparation methods and applications

NP	NP preparation	Polymetric matrix	Polymerization method	NCH preparation	Application and feature	References
Ag	In situ reduction (AgNO ₃ , Acetic acid, NaBH ₄ as the Ag NP-forming agent)	Chitosan/sodium tripolyphosphate	No polymerization Ionically crosslinked by polyanions	Method c	Drug delivery Antibacterial	[69]
Ag	Reduction of Ag ions in swollen cryogel	Methacrylated carboxymethyl chitosan PEGDA	Photopolymerization on ice, and lyophilizing(cryogel)	Method c	Antibacterial tissue eng.	[47]
Ag	Reduction of Ag ions in swollen hydrogel	PVA Sodium alginate PAAm	Thermal-induced (persulfate) aqueous polymerization (IPN)	Method c	Antibacterial	[44]
Ag	Reduction of Ag ions in swollen hydrogel	PNIPAM PSA	Redox initiation (persulfate) Aqueous polymerization	Method c	Antibacterial	[45]
Ag	Maleimide-coated silver nanoparticles	Furfuryl-gelatin	Diels-Alder Cycloaddition-based cross-linking	Method d	Drug delivery systems, improved mechanical properties	[124]
Ag	Reduction of Ag ions in swollen hydrogel	poly (vinyl pyrrolidone) (PVP) PAAm	IPN redox initiation and aqueous polymerization	Method c	Antibacterial	[46]
Ag	Reduction of Ag ion	PAA	In situ polymerization and reduction of Ag ion	Method c	Conductive hydrogels	[127]
Ag	(PVP)-coated silver nanoparticles	PAAm	Redox initiation (persulfate) and aqueous polymerization	Method e	optical biosensor	[128]
Ag	Reduction by one-pot green chemistry technique using starch and glucose	PVA	Freeze-thaw	Method a	Antimicrobial dressing scaffold	[123]

(continued)

Table 5 (continued)

NP	NP preparation	Polymetric matrix	Polymerization method	NCH preparation	Application and feature	References
Ag	Reduction of Ag ions in cross-linked hydrogel	Dialdehyde hemicelluloses Chitosan	–	Method a	Antibacterial	[161]
Ag	Reduction of Ag ions in hydrogel	Chitosan (CTS) and acrylic acid (AA)	Redox initiation (fentone) and solution polymerization	Method c	Catalytic reduction of organic dyes	[129]
Ag	Using biodegradable gelatin as a stabilizing agent	Gelatin PNIPAm	Redox initiation (persulfate) and aqueous polymerization	Method c	Antibacterial thermosensitive	[125]
Au Pt	Citrate-reduced gold prepared by Frens method PVP-protected Pt NPs prepared	PAAm	No polymerization	Method b Breathing in	Dispersed metal nanoparticles in porous anodic aluminum oxide	[43]
Au	Solution	PAAm	Electropolymerization in the presence of $ZnCl_2$	Method b Breathing in	Biosensors and solvent-switchable electrical properties	[42]
Au	Tiopronin (N-(2-Mercaptopropionyl) glycine) protected gold nanoparticles	Collagen	Nanoparticles crosslinked to collagen via EDC (1-ethyl-3-(3-dimethyl aminopropyl) carbodiimide) coupling agent	Method d	Photothermal therapies, imaging, and cell targeting	[53]
Au	Reduced (by $NaBH_4$) and then functionalized (by allyl mercaptan)	PNIPAm	Thermal-induced solution polymerization (AIBN and THF)	Method d	Tunable thermo-switchable electrical properties	[32, 33]
Cu	Synthesized by reduction reaction (starch capping) and modified a silica coating by inverse emulsion	Starch	Using urea	Method c	Antibacterial	[36]

The NCH has been prepared by formation of hydrogel in NPs suspension (method a), physical incorporation of NPs into the hydrogel networks (method b), in situ formation of NPs (method c), acting as multifunctional crosslinking (method d), and the polymeric network binding NPs (method e)

with DNA [29]. The immobilization of Ag NPs has also been reported in synthetic hydrogels, such as poly(acrylic acid) and poly(methacrylate) [30]. Recently, the introduction of Ag NPs into different bio-based and biocompatible systems, such as (PVA) [123], gelatin/chondroitin sulfate [124], PVA/sodium alginate/poly(acrylamide) [44], and gelatin/N-isopropylacrylamide [125], has gained more attention.

Various studies deal with a physical dispersion of Ag NPs via in situ synthesis, in which the Ag NPs were often dispersed into the zeolite–poly (acrylamide-co-acrylic acid) hydrogels, using radical graft copolymerization and magnetron sputtering methods [126]. These antibacterial hydrogels were used for water treatment applications. Generally, the silver nanocomposite hydrogels, which have been prepared via radical graft copolymerization, display better biocidal activity. This feature is in accordance with their better dispersion which has also been confirmed by XRD result [126]. In another approach, the silver nanoparticles were synthesized in situ in the swollen hydrogel media. The superabsorbent hydrogels were based on poly(vinyl alcohol) (PVA), sodium alginate (Na–Alg), and poly (acrylamide). The Ag ion loading is proportional to the antimicrobial activity, and can be affected by the concentration of a silver ion, crosslinking density of hydrogel network, as well as the Na–Alg/PVA ratio [44]. Chitosan nanocomposite hydrogel beads have also been prepared by synthesizing Ag NPs in situ. The chitosan in these systems has been ionically crosslinked to the sodium tripolyphosphate. The amine and hydroxyl groups confer on to the chitosan the potential to interact with various metal cations, i.e. Ag^+ , Zn^{2+} ; therefore, the Ag NPs are expected to be distributed uniformly in the hydrogel beads, which is also consistent with the XRD results. Moreover, the effect of Ag NPs on the drug loading has been evaluated. It has been shown that an increase in the Ag NPs content would result in a decrease in the drug loading. It is attributed to the variation of the less porous structure of the chitosan induced by interactions between Ag ions and chitosan [69]. As it has been previously stated, the Ag NPs are incorporated into the polymer matrix physically; as a result, the continuous release of NPs to the surrounding environment is plausible. To overcome this deficiency, the Ag NPs have been covalently bonded to the furan-modified gelatin. The benzotriazole maleimide has been employed to cap the Ag NPs during in situ formation, and then, the click chemistry, Diels–Alder (DA) cycloadditions, were employed to crosslink the furan-modified gelatin to provide a mild reaction condition [124]. Multiple crosslinking effects on Ag NPs has increased the elastic modulus almost three folds. In addition to the antimicrobial applications, the Ag NPs embedded in the hybrid hydrogels, have also been employed as optoelectronic [127, 128] and catalytic materials [129]. For example, in the glucose-responsive Ag NP hydrogels, the absorbance strength of the localized surface plasmon resonance (LSPR) is decreased by an increase in the concentration of glucose. This property has been employed for the production of optical enzyme biosensors [128].

Gold is another metal element which has been used in biomedical application [30, 51, 53]. The Au NP hydrogels have been used as stimuli-responsive and switchable conductive materials. The distance variation of Au NPs during external stimulation (e.g. temperature and pH) is the main reason for the changes in its conductivity. The Au NPs have also been used for antibacterial applications, remote-controlled microfluidic valves, and surface plasmon resonance (SPR)-based sensors. However, the high-cost Au has limited incorporation of Au NPs in large-scale applications [30]. In general, the Au NPs cannot enhance the mechanical properties of the hydrogel. However, Au NPs in thiol-modified biomacromonomers can improve the gel strength. In order to hydrogel form and reform during and after printing, this nanocomposite hydrogel has been designed to represent *dynamic* crosslinking by functionalization of the Au NPs to act as multiple crosslinking agents [130].

It is believed that Au NPs are biocompatible and capable of being easily functionalized by biomolecules. The size and shape of these biocompatible NPs can be engineered; the combination of these unique features make Au NPs excellent candidates use in various applications like new contrast agents for imaging and novel photothermal therapies, biomedical applications, and drug delivery [53].

3 Summary and Outlooks

Hydrogels have tremendous potential to be tuned to obtain the desired physico-chemical properties in contact with an aqueous media. The need for engineered hydrogels with specific properties results in outstanding developments in the conventional hydrogels which often offer poorer properties. The softness of the hydrogels provides necessary and sufficient resemblance to the biological and natural systems, while this softness would defiantly affect the mechanical properties which in turn restrict the application of the gels. Inspired by nature, nano-modification can promote the properties and performance extensively. The nano-scale incorporation of minerals, as a hard component, not only confer better mechanical properties but also introduce other functionalities, such as stretchability and stimuli-responsiveness into the hydrogels. The facile techniques of nanomodification can be simply employed to shift from conventional hydrogels into smart ones.

The stimuli-responsive hydrogels trigger the idea of smart hydrogels as multi-functional materials. The nanocomposite properties can be manipulated by altering the pH and the temperature of the surrounding media. In addition, the mesh size of the nanocomposite hydrogels network can be regulated by electrical and magnetic fields. This on-off behaviour enabled the gel to change its shape, to move, and also to releases certain drugs. Quantum dot nanoparticles offer photoluminescent

properties to the nanocomposite hydrogels. The supramolecular-like behaviour and reversible crosslinking, introduced by the hydrogen bonding or ionic interactions, have resulted in self-healable hydrogels.

The engineered hydrogels have received much attention and are used in various applications, including actuators, biosensors, controllable drug delivery, artificial muscles, etc. The clinical applications of hydrogels can limit the type of hydrogels used. Various pristine and modified bio-based macromolecules have been introduced into the networks to design engineered hydrogels, which are tough, stretchable, resilient, or self-healable. Recently, click-chemistry has assisted in producing biobased hydrogels [109, 110] with various functionalities, including photopatternable, antibacterial, antifungal, and anticancer. This chemistry provides an efficient, selective, and mild situation to prepare gels with improved properties; the Au nanocomposite hydrogels with superior mechanical and electrical properties, are of examples of the employment of the click-chemistry (Diels-Alder reaction). The click-chemistry, “thiol-ene” reaction has been employed to prepare 3D structured cell capsules, using acylated-modified, sulfobetaine-derived starch, and dithiol functionalized PEG [131]. The mechanical and swelling properties, as well as gelation time, can be easily tuned in physiological condition.

Another aspect of the formation of hydrogels is the engagement of relatively simple radical polymerization. This advantage has extended hydrogel application extensively, owing to the ability to construct complicated structures precisely. Also, 3D printing is a newfound way in hydrogel fields to produce well-defined volumetric objects. The important factors in 3D printing include viscosity, gelation mechanism, and speed. The incorporation of nanoclays is an efficient way to modify the viscosity and shear-thinning effect of the hydrogel.

References

1. Zohuriaan-Mehr MJ, Omidian H, Doroudiani S, Kabiri K (2010) Advances in non-hygienic applications of superabsorbent hydrogel materials. *J Mater Sci* 45(21):5711–5735
2. Peppas NA (2012) Hydrogel. *Introd Mater Med*, pp 35–42
3. Akhtar MF, Hanif M, Ranjha NM (2016) Methods of synthesis of hydrogels... A review. *Saudi Pharm J* 24(5):554–559
4. Hoare TR, Kohane DS (2008) Hydrogels in drug delivery: progress and challenges. *Polym (Guildf)* 49(8):1993–2007
5. Wichterle O, Lim D (1960) Hydrophilic gels for biological use. *Nature* 185(4706):117–118
6. Chu L, Ju X, Xie R, Wang W (2013) Smart hydrogel functional materials
7. Schexnailder P, Schmidt G (2009) Nanocomposite polymer hydrogels. *Colloid Polym Sci* 287(1):1–11
8. Utech S, Boccaccini AR (2016) A review of hydrogel-based composites for biomedical applications: enhancement of hydrogel properties by addition of rigid inorganic fillers, vol 51, no 1. Springer US
9. Laftah WA, Hashim S, Ibrahim AN (2011) Polymer hydrogels: a review. *Polym Plast Technol Eng* 50(14):1475–1486

10. Ahmed EM (2015) Hydrogel: preparation, characterization, and applications: a review. *J Adv Res* 6(2):105–121
11. Kabiri K, Omidian H, Zohuriaan-Mehr MJ, Doroudiani S (2011) Superabsorbent hydrogel composites and nanocomposites: a review. *Polym Compos* 32(2):277–289
12. Moini N, Kabiri K (2015) Effective parameters in surface cross-linking of acrylic-based water absorbent polymer particles using bisphenol A diethylene glycidyl ether and cycloaliphatic diepoxide. *Iran Polym J* 24(11):977–987
13. Moini N, Kabiri K, Zohuriaan-Mehr MJ (2018) Surface treatment of superabsorbent. US Pat. 2018/0008960
14. Moini N, Kabiri K, Zohuriaan-Mehr MJ (2015) Practical improvement of SAP hydrogel properties via facile tunable cross-linking of the particles surface. *Polym Plast Technol Eng* 55(3):278–290
15. Moini N, Kabiri K, Zohuriaan-mehr MJ, Esmaeili N (2015) Simple and efficient approach for recycling of fine acrylic-based superabsorbent waste. *Polym Bull* 73(4):1119–1133
16. Moini N, Kabiri K, Zohuriaan-Mehr MJ, Omidian H, Esmaeili N (2017) Fine tuning of SAP properties via epoxy-silane surface modification. *Polym Adv Technol* 28(9):1132–1147
17. Buchholz FL, Graham AT (1998) Modern superabsorbent polymer technology. Wiley, Hoboken
18. Buchholz FL, Peppas NA (1994) Superabsorbent polymers. ACS, Washington DC
19. Koetting MC, Peters JT, Steichen SD, Peppas NA (2015) Stimulus-responsive hydrogels: theory, modern advances, and applications. *Mater Sci Eng R Reports* 93:1–49
20. Zeldovich KB, Khokhlov AR (1999) Osmotically active and passive counterions in inhomogeneous polymer gels. *Macromolecules* 32(10):3488–3494
21. Rutz AL, Shah RN (2016) Polymeric hydrogels as smart biomaterials
22. Naficy S, Brown HR, Razal JM, Spinks GM, Whitten PG (2011) Progress toward robust polymer hydrogels. *Aust J Chem* 64(8):1007–1025
23. Zhang YS, Khademhosseini A (2017) Advances in engineering hydrogels. *Science*, 356 (6337)
24. Zhao X (2014) Multi-scale multi-mechanism design of tough hydrogels: building dissipation into stretchy networks. *Soft Matter* 10(5):672–687
25. Peak CW, Wilker JJ, Schmidt G (2013) A review on tough and sticky hydrogels. *Colloid Polym Sci* 291(9):2031–2047
26. Ilg P (2013) Stimuli-responsive hydrogels cross-linked by magnetic nanoparticles. *Soft Matter* 9(13):3465
27. Haraguchi K, Uyama K, Tanimoto H (2011) Self-healing in nanocomposite hydrogels. *Macromol Rapid Commun* 32(16):1253–1258
28. Gupta RB, Kompella UB (2006) Nanoparticle technology for drug delivery, vol 159. New York
29. Monteiro DR, Gorup LF, Takamiya AS, Ruvollo-Filho AC, de Camargo ER, Barbosa DB (2009) The growing importance of materials that prevent microbial adhesion: antimicrobial effect of medical devices containing silver. *Int J Antimicrob Agents* 34(2):103–110
30. Thoniyot P, Tan MJ, Karim AA, Young DJ, Loh XJ (2015) Nanoparticle–hydrogel composites: concept, design, and applications of these promising, multi-functional materials. *Adv Sci* 2(1–2):1–13
31. Schwartz VB et al (2012) Antibacterial surface coatings from zinc oxide nanoparticles embedded in poly (N-isopropylacrylamide) hydrogel surface layers. *Adv Funct Mater* 22 (11):2376–2386
32. Zhao X et al (2006) A kind of smart gold nanoparticle–hydrogel composite with tunable thermo-switchable electrical properties. *New J Chem* 30(6):915–920
33. Zhao X, Ding X, Deng Z, Zheng Z, Peng Y, Long X (2005) Thermo-switchable electronic properties of a gold nanoparticle/hydrogel composite. *Macromol Rapid Commun* 26 (22):1784–1787

34. Baumann B, Wittig R, Lindén M (2017) Mesoporous silica nanoparticles in injectable hydrogels: factors influencing cellular uptake and viability. *Nanoscale* 9:12379–12390
35. Chang C, Peng J, Zhang L, Pang D-W (2009) Strongly fluorescent hydrogels with quantum dots embedded in cellulose matrices. *J Mater Chem* 19(41):7771
36. Villanueva ME et al (2016) Antimicrobial activity of starch hydrogel incorporated with copper nanoparticles. *ACS Appl Mater Interfaces* 8(25):16280–16288
37. Li Y et al (2013) Magnetic hydrogels and their potential biomedical applications. *Adv Funct Mater* 23(6):660–672
38. Liu TY, Hu SH, Liu TY, Liu DM, Chen SY (2006) Magnetic-sensitive behavior of intelligent ferrogels for controlled release of drug. *Langmuir* 22(14):5974–5978
39. Chen CH, Abate AR, Lee D, Terentjev EM, Weitz DA (2009) Microfluidic assembly of magnetic hydrogel particles with uniformly anisotropic structure. *Adv Mater* 21(31):3201–3204
40. Jayaramudu T, Raghavendra GM, Varaprasad K, Sadiku R, Raju KM (2013) Development of novel biodegradable Au nanocomposite hydrogels based on wheat: for inactivation of bacteria. *Carbohydr Polym* 92(2):2193–2200
41. Kim J-H, Lee TR (2006) Discrete thermally responsive hydrogel-coated gold nanoparticles for use as drug-delivery vehicles. *Drug Dev Res* 67:61–69
42. Pardo-Yissar V, Gabai R, Shipway AN, Bourenko T, Willner I (2001) Gold nanoparticle/hydrogel composites with solvent-switchable electronic properties. *Adv Mater* 13(17):1320–1323
43. Guo YG, Hu JS, Liang HP, Wan LJ, Bai CL (2003) Highly dispersed metal nanoparticles in porous anodic alumina films prepared by a breathing process of polyacrylamide hydrogel. *Chem Mater* 15(22):4332–4336
44. Ghazemzadeh H, Ghanaat F (2014) Antimicrobial alginate/PVA silver nanocomposite hydrogel, synthesis and characterization. *J Polym Res* 21(3):355–369
45. Mohan YM, Lee K, Premkumar T, Geckeler KE (2007) Hydrogel networks as nanoreactors: a novel approach to silver nanoparticles for antibacterial applications. *Polymer (Guildf)* 48(1):158–164
46. Murthy PSK, Mohan YM, Varaprasad K, Sreedhar B, Raju KM (2008) First successful design of semi-IPN hydrogel-silver nanocomposites: a facile approach for antibacterial application. *J Colloid Interface Sci* 318(2):217–224
47. Zou X et al (2017) Preparation of a novel antibacterial chitosan-poly(ethylene glycol) cryogel/silver nanoparticles composites. *J Biomater Sci Polym Ed* 28(13):1324–1337
48. Helminger M et al (2014) Synthesis and characterization of gelatin-based magnetic hydrogels. *Adv Funct Mater* 24(21):3187–3196
49. Ozay O, Ekici S, Baran Y, Aktas N, Sahiner N (2009) Removal of toxic metal ions with magnetic hydrogels. *Water Res* 43(17):4403–4411
50. Ullah F, Othman MBH, Javed F, Ahmad Z, Akil HM (2015) Classification, processing and application of hydrogels: a review. *Mater Sci Eng, C* 57:414–433
51. Gaharwar AK, Peppas NA, Khademhosseini A (2014) Nanocomposite hydrogels for biomedical applications. *Biotechnol Bioeng* 111(3):441–453
52. Zhang D, Yang J, Bao S, Wu Q, Wang Q (2013) Semiconductor nanoparticle-based hydrogels prepared via self-initiated polymerization under sunlight, even visible light. *Sci Rep* 3(1):1399
53. Castaneda L, Valle J, Yang N, Pluskat S, Slowinska K (2009) Collagen crosslinking with Au nanoparticles. *Biomacromolecules* 9(12):3383–3388
54. Rose S, PrevotEAU A, Elzière P, Hourdet D, Marcellan A, Leibler L (2013) Nanoparticle solutions as adhesives for gels and biological tissues. *Nature* 505(7483):382–385
55. Carlsson L, Rose S, Hourdet D, Marcellan A (2010) Nano-hybrid self-crosslinked PDMA/silica hydrogels. *Soft Matter* 6(15):3619

56. Gaharwar AK, Rivera CP, Wu CJ, Schmidt G (2011) Transparent, elastomeric and tough hydrogels from poly(ethylene glycol) and silicate nanoparticles. *Acta Biomater* 7(12):4139–4148
57. Wu H et al (2013) Stable Li-ion battery anodes by in-situ polymerization of conducting hydrogel to conformally coat silicon nanoparticles. *Nat Commun* 4:1943–1946
58. Magasinski A et al (2010) Toward efficient binders for Li-ion battery Si-based anodes: polyacrylic acid. *ACS Appl Mater Interfaces* 2(11):3004–3010
59. Liu G et al (2011) Polymers with tailored electronic structure for high capacity lithium battery electrodes. *Adv Mater* 23(40):4679–4683
60. Bridel JS, Azais T, Morcrette M, Tarascon JM, Larcher D (2010) Key parameters governing the reversibility of Si/carbon/CMC electrodes for Li-ion batteries. *Chem Mater* 22(3):1229–1241
61. Gao G, Du G, Sun Y, Fu J (2015) Self-healable, tough, and ultrastretchable nanocomposite hydrogels based on reversible polyacrylamide/montmorillonite adsorption. *ACS Appl Mater Interfaces* 7(8):5029–5037
62. Özkahraman B, Acar I, Emik S (2011) Removal of Cu 2+ and Pb 2+ ions using CMC based thermoresponsive nanocomposite hydrogel. *Clean - Soil, Air, Water* 39(7):658–664
63. Gaharwar AK, Dammu SA, Canter JM, Wu C-J, Schmidt G (2011) Highly extensible, tough, and elastomeric nanocomposite hydrogels from poly(ethylene glycol) and hydroxyapatite. *Biomacromolecules* 12:1641–1650
64. Jayakumar R, Menon D, Manzoor K, Nair SV, Tamura H (2010) Biomedical applications of chitin and chitosan based nanomaterials - a short review. *Carbohydr Polym* 82(2):227–232
65. Liu R, Liang S, Tang X-Z, Yan D, Li X, Yu Z-Z (2012) Tough and highly stretchable graphene oxide/polyacrylamide nanocomposite hydrogels. *J Mater Chem* 22(28):14160
66. Gaharwar AK et al (2013) Bioactive silicate nanoplatelets for osteogenic differentiation of human mesenchymal stem cells. *Adv Mater* 25(24):3329–3336
67. Gaharwar AK et al (2012) Physically crosslinked nanocomposites from silicate-crosslinked PEO: mechanical properties and osteogenic differentiation of human mesenchymal stem cells. *Macromol Biosci* 12(6):779–793
68. Kaşgöz H, Durmuş A, Ka A (2008) Enhanced swelling and adsorption properties of AAm-AMPSNa/clay hydrogel nanocomposites for heavy metal ion removal. *Polym Adv Technol* 19:213–220
69. Yadollahi M, Farhoudian S, Namazi H (2015) One-pot synthesis of antibacterial chitosan/silver bio-nanocomposite hydrogel beads as drug delivery systems. *Int J Biol Macromol* 79:37–43
70. Mekewi M, Shebl A, Imam AI, Amin MS, Albert T (2012) Screening the insecticidal efficacy of nano ZnO synthesized via in-situ polymerization of crosslinked polyacrylic acid as a template. *J Mater Sci Technol* 28(11):961–968
71. Utracki LA (2004) Clay-containing polymeric nanocomposites, vol 1. Shropshire, United Kingdom
72. Nelson A, Cosgrove T (2004) A small-angle neutron scattering study of adsorbed poly(ethylene oxide) on laponite. *Langmuir* 20(6):2298–2304
73. Loizou E et al (2005) Large scale structures in nanocomposite hydrogels. *Macromolecules* 38(6):2047–2049
74. Kevadiya BD, Joshi GV, Patel HA, Ingole PG, Mody HM, Bajaj HC (2010) Montmorillonite-Alginate nanocomposites as a drug delivery system: Intercalation and in vitro release of vitamin B1 and vitamin B6. *J Biomater Appl* 25(2):161–177
75. Chen J, Park H, Park K (1999) Synthesis of superporous hydrogels: hydrogels with fast swelling and superabsorbent properties. *J Biomed Mater Res - Part A* 44:53–62
76. Bao J, Chen S, Wu B, Ma M, Shi Y, Wang X (2015) A novel foaming approach to prepare porous superabsorbent poly(sodium acrylic acid) resins. *J Appl Polym Sci*, 132(3):n/a–n/a

77. Kabiri K, Zohuriaan-Mehr MJ (2004) Porous superabsorbent hydrogel composites: synthesis, morphology and swelling rate. *Macromol Mater Eng* 289(7):653–661
78. Omidian H, Rocca JG, Park K (2005) Advances in superporous hydrogels. *J Control Release* 102(1):3–12
79. Demirtaş TT, Karakeçili AG, Gümüşderelioğlu M (2008) Hydroxyapatite containing superporous hydrogel composites: synthesis and in-vitro characterization. *J Mater Sci* 19:729–735
80. Kabiri K et al (2011) Superabsorbent polymer composites: does clay always improve properties? *J Mater Sci* 46(20):6718–6725
81. Zheng Y, Zhu Y, Wang A (2014) Highly efficient and selective adsorption of malachite green onto granular composite hydrogel. *Chem Eng J* 257:66–73
82. Wang L, Zhang J, Wang A (2008) Removal of methylene blue from aqueous solution using chitosan-g-poly(acrylic acid)/montmorillonite superadsorbent nanocomposite. *Colloids Surf A Physicochem Eng Asp* 322(1–3):47–53
83. Shirsath SR, Patil AP, Patil R, Naik JB, Gogate PR, Sonawane SH (2013) Removal of brilliant green from wastewater using conventional and ultrasonically prepared poly(acrylic acid) hydrogel loaded with kaolin clay: a comparative study, vol 20, no 3. Elsevier B.V
84. Mahdavinia GR, Asgari A (2013) Synthesis of kappa-carrageenan-g-poly(acrylamide)/sepiolite nanocomposite hydrogels and adsorption of cationic dye. *Polym Bull* 70(8):2451–2470
85. Liu Y, Zheng Y, Wang A (2010) Enhanced adsorption of methylene blue from aqueous solution by chitosan-g-poly (acrylic acid)/vermiculite hydrogel composites. *J Environ Sci* 22 (4):486–493
86. Zheng Y, Wang A (2009) Evaluation of ammonium removal using a chitosan-g-poly (acrylic acid)/rectorite hydrogel composite. *J Hazard Mater* 171(1–3):671–677
87. Zheng Y, Wang A (2010) Enhanced adsorption of ammonium using hydrogel composites based on chitosan and halloysite. *J Macromol Sci Part A Pure Appl Chem* 47(1):33–38
88. Wang Y, Wang W, Wang A (2013) Efficient adsorption of methylene blue on an alginate-based nanocomposite hydrogel enhanced by organo-illite/smectite clay. *Chem Eng J* 228:132–139
89. Zheng Y, Wang A (2010) Removal of heavy metals using polyvinyl alcohol semi-IPN poly (acrylic acid)/tourmaline composite optimized with response surface methodology. *Chem Eng J* 162(1):186–193
90. Saber-Samandari S, Saber-Samandari S, Gazi M (2013) Cellulose-graft-polyacrylamide/hydroxyapatite composite hydrogel with possible application in removal of Cu(II) ions, vol 73, no 11. Elsevier Ltd
91. Wang X, Wang A (2010) Adsorption characteristics of chitosan-g-poly(acrylic acid)/attapulgite hydrogel composite for Hg(II) ions from aqueous solution. *Sep Sci Technol* 45 (14):2086–2094
92. Zhu Y, Zheng Y, Wang A (2015) Preparation of granular hydrogel composite by the redox couple for efficient and fast adsorption of La(III) and Ce(III). *J Environ Chem Eng* 3 (2):1416–1425
93. Anirudhan TS, Suchithra PS, Arauf T (2012) Kinetic and equilibrium profiles of adsorptive recovery of thorium (IV) from aqueous solutions using poly (methacrylic acid) grafted cellulose/bentonite superabsorbent composite kinetic and equilibrium profiles of adsorptive recovery of thorium (IV), no IV
94. Zhu Y, Zheng Y, Wang A (2015) A simple approach to fabricate granular adsorbent for adsorption of rare elements. *Int J Biol Macromol* 72:410–420
95. Wang M, Li X, Hua W, Shen L, Yu X, Wang X (2016) Electrospun poly(acrylic acid)/silica hydrogel nanofibers scaffold for highly efficient adsorption of lanthanide ions and its photoluminescence performance. *ACS Appl Mater Interfaces* 8(36):23995–24007
96. Zheng Y, Wang A (2015) Superadsorbent with three-dimensional networks: from bulk hydrogel to granular hydrogel. *Eur Polym J*

97. Yang X, Ni L (2012) Synthesis of hybrid hydrogel of poly(AM co DADMAC)/silica sol and removal of methyl orange from aqueous solutions. *Chem Eng J* 209:194–200
98. Dhodapkar R, Rao NN, Pande SP, Nandy T, Devotta S (2007) Adsorption of cationic dyes on Jalshakti[®], super absorbent polymer and photocatalytic regeneration of the adsorbent. *React Funct Polym* 67(6):540–548
99. Ma X, Sun X, Chen J, Lei Y (2017) Natural or natural-synthetic hybrid polymer-based fluorescent polymeric materials for bio-imaging-related applications. *Appl Biochem Biotechnol* 183(2):461–487
100. Zheng Y et al (2003) Immobilization of quantum dots in the photo-cross-linked poly (ethylene glycol)-based hydrogel, *J Phys Chem B*, pp 10464–10469
101. Cheng Z, Liu S, Beines PW, Ding N, Jakubowicz P, Knoll W (2008) Rapid and highly efficient preparation of water-soluble luminescent quantum dots via encapsulation by thermo- and redox-responsive hydrogels. *Chem Mater* 20:7215–7219
102. Wang YQ et al (2017) Nanocomposite carbon dots/PAM fluorescent hydrogels and their mechanical properties. *J Polym Res*, 24(12)
103. Ruiz-Palomero C, Benítez-Martínez S, Soriano ML, Valcárcel M (2017) Fluorescent nanocellulosic hydrogels based on graphene quantum dots for sensing laccase. *Anal Chim Acta* 974:93–99
104. Yang J, Han C-R, Duan J-F, Xu F, Sun R-C (2013) In situ grafting silica nanoparticles reinforced nanocomposite hydrogels. *Nanoscale* 5(22):10858
105. Kakkar P, Madhan B (2016) Fabrication of keratin-silica hydrogel for biomedical applications. *Mater Sci Eng, C* 66:178–184
106. Algi MP, Okay O (2014) Highly stretchable self-healing poly(N, N-dimethylacrylamide) hydrogels. *Eur Polym. J* 59:113–121
107. Haque MA, Kurokawa T, Kamita G, Gong JP (2011) Lamellar bilayers as reversible sacrificial bonds to toughen hydrogel: Hysteresis, self-recovery, fatigue resistance, and crack blunting. *Macromolecules* 44(22):8916–8924
108. Shin SR, Bae H, Cha M, Mun Y, Chen Y, Tekin H (2012) Carbon Nanotube Reinforced Hybrid Microgels as Scaffold Materials for Cell. *ACS Nano* 6(1):362–372
109. Zhong M, Liu Y-T, Xie X-M (2015) Self-healable, super tough graphene oxide–poly(acrylic acid) nanocomposite hydrogels facilitated by dual cross-linking effects through dynamic ionic interactions. *J Mater Chem B* 3(19):4001–4008
110. Fabbri P et al (2012) In-situ graphene oxide reduction during UV-photopolymerization of graphene oxide/acrylic resins mixtures. *Polym (United Kingdom)* 53(26):6039–6044
111. Shi K et al (2015) Near-infrared light-responsive poly(N-isopropylacrylamide)/graphene oxide nanocomposite hydrogels with ultrahigh tensibility. *ACS Appl Mater Interfaces* 7(49): 27289–27298
112. Schexnailder P, Schmidt G (2009) Nanocomposite polymer hydrogels. *Colloid Polym Sci* 287:1–11
113. Jaiswal MK et al (2014) Thermoresponsive magnetic hydrogels as theranostic nanoconstructs. *ACS Appl Mater Interfaces* 6(9):6237–6247
114. Khademhosseini A, Langer R (2007) Microengineered hydrogels for tissue engineering. *Biomaterials* 28(34):5087–5092
115. Gurkan UA, Tasoglu S, Kavaz D, Demirel MC, Demirci U (2012) Emerging technologies for assembly of microscale hydrogels. *Adv Healthc Mater* 1(2):149–158
116. Satarkar NS, Biswal D, Hilt JZ (2010) Hydrogel nanocomposites: a review of applications as remote controlled biomaterials. *Soft Matter* 6(11):2364
117. Jain A, Duvvuri LS, Farah S, Beyth N, Domb AJ, Khan W (2014) Antimicrobial polymers. *Adv Healthc Mater* 3(12):1969–1985
118. Sudheesh Kumar PT et al (2012) Flexible and microporous chitosan hydrogel/nano ZnO composite bandages for wound dressing: In vitro and in vivo evaluation. *ACS Appl Mater Interfaces* 4(5):2618–2629
119. Li M, Zhu L, Lin D (2011) Toxicity of ZnO nanoparticles to *Escherichia coli*: mechanism and the influence of medium components. *Environ Sci Technol* 45:1977–1983

120. Zhang L et al (2010) Mechanistic investigation into antibacterial behaviour of suspensions of ZnO nanoparticles against *E. coli*. *J Nanopart Res* 12:1625–1636
121. Sudheesh Kumar PT et al (2013) Evaluation of wound healing potential of β -chitin hydrogel/nano zinc oxide composite bandage. *Pharm Res* 30(2):523–537
122. Hashem M, Sharaf S, Abd El-Hady MM, Hebeish A (2013) Synthesis and characterization of novel carboxymethylcellulose hydrogels and carboxymethylcellulose-hydrogel-ZnO-nanocomposites. *Carbohydr Polym* 95(1):421–427
123. Bhowmick S, Koul V (2016) Assessment of PVA/silver nanocomposite hydrogel patch as antimicrobial dressing scaffold: synthesis, characterization and biological evaluation. *Mater Sci Eng, C* 59:109–119
124. García-Astrain C et al (2015) Biocompatible hydrogel nanocomposite with covalently embedded silver nanoparticles. *Biomacromolecules* 16(4):1301–1310
125. Manjula B, Varaprasad K, Sadiku R, Ramam K, Reddy GVS, Raju KM (2014) Development of microbial resistant thermosensitive Ag nanocomposite (gelatin) hydrogels via green process. *J Biomed Mater Res - Part A* 102(4):928–934
126. Zendehelel M, Zendehelel A, Hoseini F, Azarkish M (2015) Investigation of removal of chemical oxygen demand (COD) wastewater and antibacterial activity of nanosilver incorporated in poly (acrylamide-co-acrylic acid)/NaY zeolite nanocomposite. *Polym Bull* 72(6):1281–1300
127. Devaki SJ, Narayanan RK, Sarojam S (2014) Electrically conducting silver nanoparticle-polyacrylic acid hydrogel by in situ reduction and polymerization approach. *Mater Lett* 116:135–138
128. Endo T, Ikeda R, Yanagida Y, Hatsuzawa T (2008) Stimuli-responsive hydrogel-silver nanoparticles composite for development of localized surface plasmon resonance-based optical biosensor. *Anal Chim Acta* 611(2):205–211
129. Zheng Y, Wang A (2012) Ag nanoparticle-entrapped hydrogel as promising material for catalytic reduction of organic dyes. *J Mater Chem* 22(32):16552
130. Skardal A, Zhang J, McCoard L, Oottamasathien S, Prestwich GD (2010) Dynamically crosslinked gold nanoparticle-hyaluronan hydrogels. *Adv Mater* 22(42):4736–4740
131. Dong D et al (2016) In Situ 'clickable' Zwitterionic Starch-Based Hydrogel for 3D cell encapsulation. *ACS Appl Mater Interfaces* 8(7):4442–4455
132. Zhu H, Yao X (2013) Synthesis and characterization of poly(Acrylamide-co-2-Acrylamido-2-Methylpropane Sulfonic Acid)/kaolin superabsorbent composite. *J Macromol Sci Part A* 50(2):175–184
133. Pourjavadi A, Ayyari M, Amini-Fazl MS (2008) Taguchi optimized synthesis of collagen-g-poly(acrylic acid)/kaolin composite superabsorbent hydrogel. *Eur Polym J* 44(4):1209–1216
134. Liang R, Liu M, Wu L (2007) Controlled release NPK compound fertilizer with the function of water retention. *React Funct Polym* 67(9):769–779
135. Lee WF, Chen YC (2005) Preparation of reactive mineral powders used for poly(sodium acrylate) composite superabsorbents. *J Appl Polym Sci* 97(3):855–861
136. Lee WF, Chen YC (2005) Effect of intercalated reactive mica on water absorbency for poly (sodium acrylate) composite superabsorbents. *Eur Polym J* 41(7):1605–1612
137. Zhang J, Chen H, Wang A (2005) Study on superabsorbent composite. III. Swelling behaviors of polyacrylamide/attapulgitic composite based on acidified attapulgitic and organo-attapulgitic. *Eur Polym J* 41:2434–2442
138. Li P, Zhang J, Wang A (2007) A Novel N-Succinylchitosan-graft-Polyacrylamide/Attapulgitic composite hydrogel prepared through inverse suspension polymerization. *Macromol Mater Eng* 292(8):962–969
139. Li A, Wang A, Chen J (2004) Studies on Poly(acrylic acid)/Attapulgitic superabsorbent composite. I. Synthesis and characterization. *J Appl Polym* 92:1596–1603

140. Ferfera-Harrar H, Aiouaz N, Dairi N, Hadj-Hamou AS (2014) Preparation of chitosan-g-poly (acrylamide)/montmorillonite superabsorbent polymer composites: studies on swelling, thermal, and antibacterial properties. *J Appl Polym Sci* 131(1):1–14
141. Kabir K, Mirzadeh H, Zohuriaan-Mehr MJ, Daliri M (2009) Chitosan-modified nanoclay-poly(AMPS) nanocomposite hydrogels with improved gel strength. *Polym Int* 58:1252–1259
142. Li L, Liu PS, Zhou NL, Zhang J, Wei SH, Shen J (2006) Synthesis and properties of a poly (acrylic acid)/montmorillonite superabsorbent nanocomposite. *J Appl Polym Sci* 102 (6):5725–5730
143. Islam MS, Rahaman MS, Yeum JH (2015) Electrospun novel super-absorbent based on polysaccharide-polyvinyl alcohol-montmorillonite clay nanocomposites. *Carbohydr Polym* 115:69–77
144. Sarkar DJ, Singh A, Mandal P, Kumar A, Parmar BS (2015) Synthesis and characterization of poly (CMC-g-cl-PAam/Zeolite) superabsorbent composites for controlled delivery of zinc micronutrient: swelling and release behavior. *Polym Plast Technol Eng* 54(4):357–367
145. Hwang SY, Yoon WJ, Yun SH, Yoo ES, Kim TH, Im SS (2013) Fabrication of superabsorbent ultrathin nanofibers using mesoporous materials for antimicrobial drug-delivery applications. *Macromol Res* 21(11):1281–1288
146. Zhang J, Yuan K, Wang YP, Gu SJ, Zhang ST (2007) Preparation and properties of polyacrylate/bentonite superabsorbent hybrid via intercalated polymerization. *Mater Lett* 61(2):316–320
147. Zhang Y, Fan L, Zhao P, Zhang L, Chen H (2008) Preparation of nanocomposite superabsorbents based on hydrotalcite and poly(acrylic-co-acrylamide) by inverse suspension polymerization. *Compos Interfaces* 15(7–9):747–757
148. Wang Q et al (2010) High-water-content mouldable hydrogels by mixing clay and a dendritic molecular binder. *Nature* 463(7279):339–343
149. Haraguchi K, Ning J, Li G (2015) Swelling/deswelling behavior of zwitterionic nanocomposite gels consisting of sulfobetaine polymer–clay networks. *Eur Polym J* 68:630–640
150. Hong S et al (2015) 3D Printing: 3D Printing of Highly Stretchable and Tough Hydrogels into Complex, Cellularized Structures. *Adv Mater* 27(27):4034–4040
151. Shi F-K, Wang X-P, Guo R-H, Zhong M, Xie X-M (2015) Highly stretchable and super tough nanocomposite physical hydrogels facilitated by the coupling of intermolecular hydrogen bonds and analogous chemical crosslinking of nanoparticles. *J Mater Chem B* 3 (7):1187–1192
152. Ahmed NB et al (2017) The physics and chemistry of silica-in-silicates nanocomposite hydrogels and their phycocompatibility. *J Mater Chem B* 5(16):2931–2940
153. Deubel F, Steenackers M, Garrido JA, Stutzmann M, Jordan R (2013) Semiconductor/polymer nanocomposites of acrylates and nanocrystalline silicon by laser-induced thermal polymerization. *Macromol Mater Eng* 298(11):1160–1165
154. Sayyar S, Gambhir S, Chung J, Officer DL, Wallace GG (2017) 3D printable conducting hydrogels containing chemically converted graphene. *Nanoscale* 9(5):2038–2050
155. Cong H, Wang P, Yu S (2013) Stretchable and self-healing graphene oxide-polymer composite hydrogels: a dual-network design. *Chem Mater* 25:3357–3362
156. Shah K, Vasileva D, Karadaghy A, Zustiak SP (2015) Development and characterization of polyethylene glycol—carbon nanotube hydrogel. *J Mater Chem B* 3:7950–7962
157. Servant A, Methven L, Williams RP, Kostarelos K (2013) Electroresponsive polymer-carbon nanotube hydrogel hybrids for pulsatile drug delivery in vivo. *Adv Healthc Mater* 2(6):806–811
158. Chen Z et al (2014) A three-dimensionally interconnected carbon nanotube-conducting polymer hydrogel network for high-performance flexible battery electrodes. *Adv Energy Mater* 4(12):1–10

159. Ghadban A et al (2016) Bioinspired pH and magnetic responsive catechol-functionalized chitosan hydrogels with tunable elastic properties. *Chem Commun* 52(4):697–700
160. Haider H et al (2015) Exceptionally tough and notch-insensitive magnetic hydrogels. *Soft Matter* 11(42):8253–8261
161. Guan Y, Chen J, Qi X, Chen G, Peng F, Sun R (2015) Fabrication of Biopolymer Hydrogel Containing Ag Nanoparticles for Antibacterial Property. *Ind Eng Chem Res* 54(30): 7393–7400

Processing, Characterization and Application of Natural Rubber Based Environmentally Friendly Polymer Composites



Nayan Ranjan Singha, Manas Mahapatra, Mrinmoy Karmakar and Pijush Kanti Chattopadhyay

Abbreviations

BF	Bamboo fiber
CB	Carbon black
CF	Coir/coconut fiber
CV	Conventional vulcanization
DMA	Dynamic mechanical analysis
EAB	Elongation at break
EV	Efficient vulcanization
IF	Isora fiber
IPN	Interpenetrating polymer network
LW	Leather waste
MBTS	2-mercaptobenzothiazole disulfide
NC	Nanocellulose
NCP	Nanocomposite
NF	Nanofiller
NRC	Natural rubber composite
NR	Natural rubber
NW	Nanowhisker
OPF	Oil palm fiber
PC	Polymer composite
PLA	Poly(lactic acid)
PLF	Pineapple leaf fiber

N. R. Singha (✉) · M. Mahapatra · M. Karmakar
Advanced Polymer Laboratory, Department of Polymer Science and Technology,
Government College of Engineering and Leather Technology (Post-Graduate), Maulana Abul
Kalam Azad University of Technology, Salt Lake, Kolkata 700106, West Bengal, India
e-mail: drs.nrs@gmail.com

P. K. Chattopadhyay
Department of Leather Technology, Government College of Engineering and Leather
Technology (Post-Graduate), Maulana Abul Kalam Azad University of Technology,
Salt Lake, Kolkata 700106, West Bengal, India

PP	Polypropylene
RG	Rubber granulate
RRG	Recycled rubber granulate
SBR	Styrene butadiene rubber
SEV	Semi-efficient vulcanization
SF	Sisal fiber
TMTD	Tetramethyl thiuram disulfide
TSH	Toluenosulfohydrazina
TS	Tensile strength
ZMB	Zinc-2-mercaptobenzothiazole

1 Introduction

Materials, together with energy and information, are considered to be the skeleton of the world economy of the twenty-first century. Among these materials, PCs, usually constituting of a polymer and one or more solid fillers, have been widely used for several years (Fig. 1) [1–5]. Instead of having several advantages, including a combination of the main properties of the two or more solid phases, PCs suffer from several limitations, such as difficulty in reuse and recycling. In fact, once the PCs become useless, these are commonly disposed directly or incinerated. However, both of these techniques are costly as well as difficult and possess high environmental impact. Indeed, such problems have begun to be evident for the last 15 years, and hence the recent scientific research has been inclined to look for the new alternatives, such as replacement of the traditional PCs with environment friendly PCs having lower environmental impact, often referred to as ‘eco-composites’ or ‘green composites’ (Fig. 1). In fact, the ecological damage, such as global warming and plastic pollution, caused by the conventional petroleum-based polymer products has encouraged the use of renewable and biodegradable materials by both scientific and industrial communities. Moreover, replacement of orthodox microcomposites by NCP has gained high insight in the last two decades to overcome the limitations of micrometre-scale, via designing novel materials and structures with unprecedented flexibility, elevated physical properties, and considerable industrial impact [6]. Indeed, the term NCP describes a class of two-phase materials, in which one of the phases has at least one dimension lower than 100 nm (Fig. 1). Thus, green chemistry coupled with nanotechnology to produce ‘green polymeric NCP’, based on derived raw materials of natural sources of plant or animal origin and rigid nano particles are of great interest in scientific, academic, and industrial fields because of the environmental and technological concerns. Moreover, because of the high surface to volume ratio, green NCPs exhibit unique mechanical, electrical, and thermal properties along with the environmental safety. Furthermore, in recent years, extensive

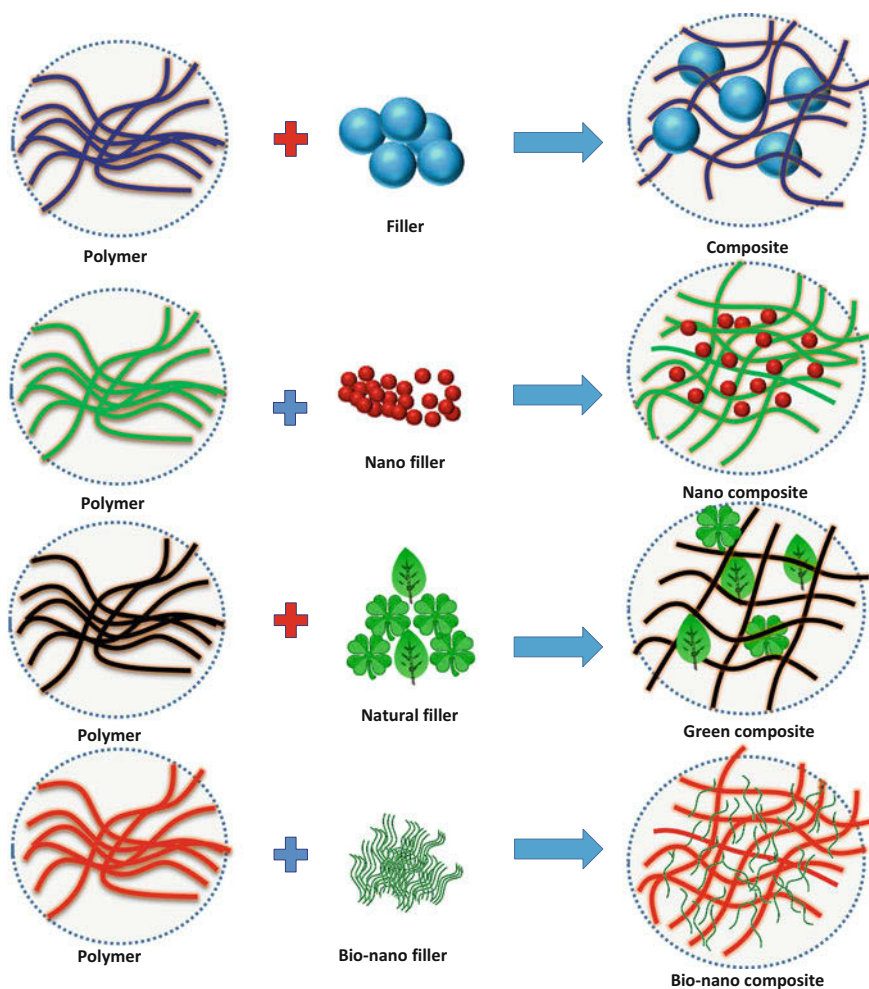


Fig. 1 Preparation of composite, NCP, green composite and bio-NCP

efforts have been devoted to develop, characterize, and utilize bio-based materials, and bio-based NCPs belonging to the new era of bio-based materials. These have attracted both industrial and academic attention because of the increasing interest in developing new sustainable, biodegradable, biocompatible, and environment-friendly nanomaterials. In fact, bio-NCPs can be considered as a subset of polymer NCPs where the NFs, the matrix or both come from bio-based renewable resources (Fig. 1). Moreover, incorporation of NFs into biopolymers provides the practical way to improve the properties of such bioplastics, to make them competitive with petroleum-derived materials.

Both natural and synthetic rubbers, essentially in vulcanized form, are used to produce different rubber products, like hoses, cushions, gloves, seals, tyres, belts, diving gear, chemical and medicinal tubing, and electrical instruments, as these vulcanized rubbers, often possess excellent flexibility, elasticity, electrical property, and resistance towards chemicals and crack propagation [7–10]. Among such rubbers, NR, a general purpose rubber, exhibits excellent physico-chemical properties, such as elasticity and flexibility, as well as magnificent formability and biodegradability. In fact, superior strength, elasticity, flexibility, resilience, and abrasion resistance makes NR as one of the most important elastomers with regards to the versatility and application volume. NR was first reported about 500 years ago, when European expeditions first experienced rubbers and latex in America. Instead of the existence of 2500 latex producing plants, the commercial production of NR is mainly produced from the *Hevea brasiliensis* tree of the Amazon rainforest. NR is a high molecular weight polymer of isoprene (2-methyl-1,3-butadiene) and is the oldest known rubber (Fig. 2). Accordingly, NR, containing long *cis* 1,4-polyisoprene chains, finds a large number of applications in the field of automotive tyres, footwears, and for manufacturing other engineering products (Fig. 3). Today, NR is used in producing 50,000 products, like adhesives, tyres, gloves, condoms, and coatings and the applications are still growing. Most of the rubbers, including NR, are available as aqueous dispersions of rubber particles, known as latex. NR is extracted as white emulsion containing *cis*-1,4-polyisoprene

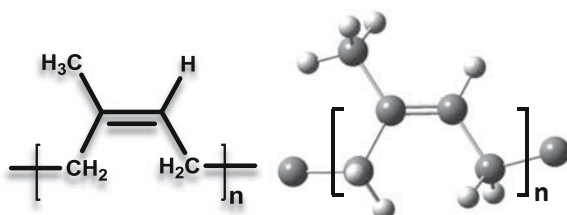


Fig. 2 2D/3D structure of NR

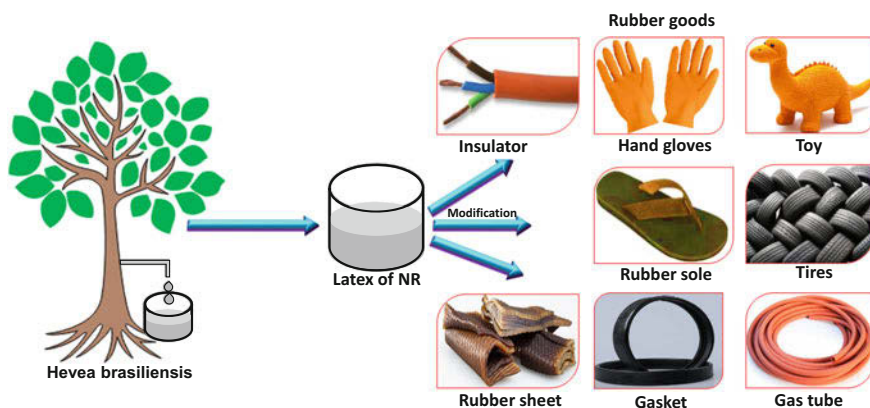


Fig. 3 Modifications and uses of NR

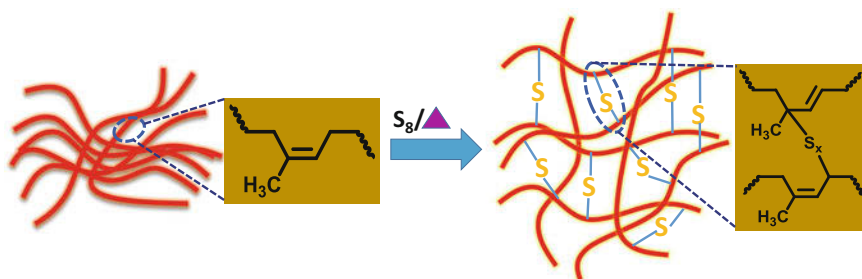


Fig. 4 Vulcanization of NR

nanoparticles, usually possessing approximately 100 nm diameter. However, sticky and inelastic uncured NR is useless. Therefore, uncured NR is vulcanized or cured to make it a more durable crosslinked material. Theoretically, vulcanization is a chemical process by which long chains of rubber molecules are crosslinked, leading to the transformation of the soft, weak plastic-like material into a strong elastic product of high and reversible deformability along with good mechanical properties because of strain-induced crystallization, low hysteresis, extraordinary dynamic properties, and fatigue resistance. During vulcanization, rubber is heated with sulfur or other equivalent curatives with/without accelerators. Such additives reinforce the polymer chains via generating crosslinks between individual polymer chains to attain improved elasticity, resilience, and enhanced mechanical properties (Fig. 4). Indeed, in the traditional vulcanization process of NR, CB is commonly employed as the reinforcing filler for achieving improved strength, weather resistance, and stiffness, leading to the production of traditional NR composites (NRC). Despite possessing several advantages, including the capability to produce reinforced NRCs, CBs are non-biodegradable petrochemical-based products, which consume a substantial amount of energy during their production. Therefore, rubber manufacturers are in search of new reinforcing fillers, which should be renewable, readily available, cheap, light-weight, and biodegradable to achieve environmentally friendly NR based PCs (Fig. 5).

Till date, rubber-based NCPs have been studied lesser than the plastic-NCPs, in which most of the research are focusing on the use of either nanoclays or carbon nanotubes as reinforcements. Over the past decade, in order to replace CB to synthesize NR composites, the use of wood, cellulosic fibers, and their derivatives as organic fillers has attracted much attention. In this context, cellulose, the most abundant natural polymer, is used to prepare high strength nanoparticles because of the outstanding properties, such as biocompatibility, required chemical stability, superior thermal stability, and environmental benignancy. In fact, cellulose nano-fibers can also be used as a matrix to form green NCPs because of the natural

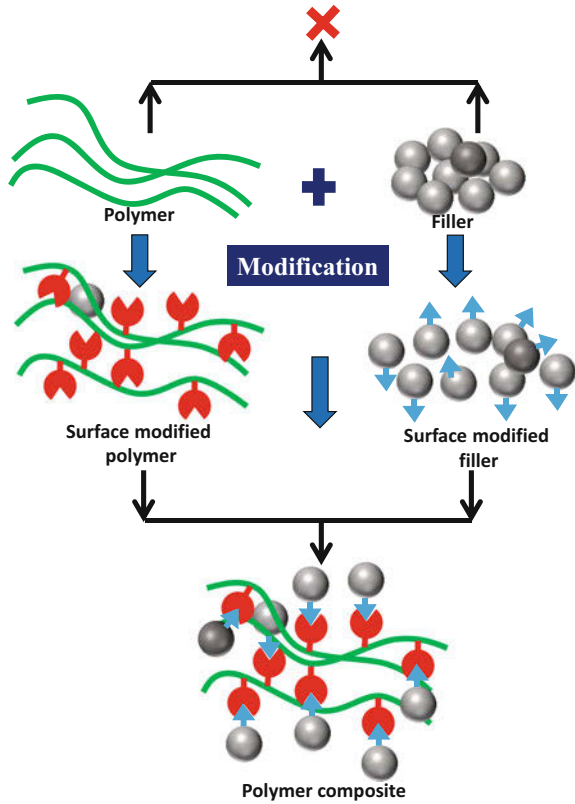


Fig. 5 Different types of fillers

abundance, renewability, and biodegradability. In this context, different workers investigated the potentials of biodegradable organic fillers, such as sisal, [11] coir, oil palm, [12] isora, BFs, starch, carrageenan, rattan, pistachio, peanut shell powder, and coconut shell powder, as the reinforcing additives in NRCs. In the recent past, the potential of NC, originated from microcrystalline cellulose, bamboo residue of newspaper production unit, [13] rachis of the date palm tree, sugar cane bagasse kraft pulp, and jute fiber, was explored as reinforcing additive in fabricating eco-friendly NR latex based NCPs. In fact, very few NR-based NCPs with bio-based nano-reinforcements, such as chitin whiskers, cellulose whiskers of *Syngonanthus nitens* (*Capim dourado*), starch nanocrystals, rachis of a palm tree, sisal, and bagasse are found in the literature. As expected, the NC not only provided the superior mechanical strength in rubber NCPs but also it increased the rate of degradation of rubber in the soil when disposed at the end of life. Thus, being a bio-based polymer, the use of bio-nano reinforcements in NR is beneficial in the development of bio-based and green NCPs.

Theoretically, in order to attain high specific strength, modulus, and dimensional stability in NRCs, the compatibility between NR and filler, and their interfacial adhesion should be sufficient enough to ensure strong interaction between filler and NR matrix. Since the surface of the added filler is often polar and hydrophilic and NR is non-polar and relatively hydrophobic, the interfacial adhesion between filler and NR can be improved by modifying the surface characteristics of both the components by physical or chemical treatment (Fig. 6). For instance, the interfacial bonding between NR and filler(s), such as rice husk, jute, sisal, and silk fiber, was improved by physical treatment, like electron beam and gamma irradiation. For instance, the hydrophobicity of NR matrix and hydrophilicity of cellulose NCPs are inherently incompatible and insufficient molecular-scale interactions can resist the

Fig. 6 Surface modification of NR/filler or both improving homogeneous dispersion and interfacial adhesion



entire activity of the material. Moreover, cellulose NCP aggregates act as stress concentrator and produce poor dispersion within the matrix to deteriorate the properties of composites. Conventionally, the chemical grafting of specific moieties on the cellulose NCP surface was used to control the interfacial adhesion and interactions. Alternatively, modification of NR chains in contact with the cellulose NCP filler could also be carried out.

Furthermore, attempts have been made to fabricate polymer-rubber composites wherein ground particles of waste tyres have effectively been utilized as potent fillers. Though waste tyres are pollutants, the ground used tyres should be treated as a source of sustainable materials, instead of a pollutant. In this regard, eight different types of NR are presently used as basic components in tyre manufacture. Therefore, a significant portion of the waste tyre should contain NR as the important constituent. Accordingly, NR based ground waste tyre can be used as an important ingredient in preparing NR based environmental friendly PCs.

2 NR Composites Filled with Plant Fibers

In the past decades, natural fiber reinforced PCs have gained substantial interest as a potential structural material and in other applications. Use of natural fiber as filler in polymeric matrix is more advantageous than the conventional inorganic fillers because of low energy the cost, positive contribution to global carbon budget, greater deformability, biodegradability, combustibility, recyclability, fair thermal and insulation properties, low density, less abrasiveness to processing equipment, environmentally friendly, inexpensive, recyclability, non-toxicity, flexibility, high specific strength, good electrical resistance, high acoustic insulation property, and universal availability. Research efforts are harnessed to develop fully biodegradable ‘green’ composites via combining natural-/bio-fibers with rubber. The major attractions for green composites are because of environment-friendly nature, degradability, and sustainability, i.e., they are truly ‘green’ in every respect. At the end of their life, they can easily be disposed of or composted without damaging the environment. In this context, different types of plant-derived natural fibers, such as OPF, CF, SF, BF, [12] IF, and PLF were employed to prepare environmentally friendly NR composites (Fig. 7).

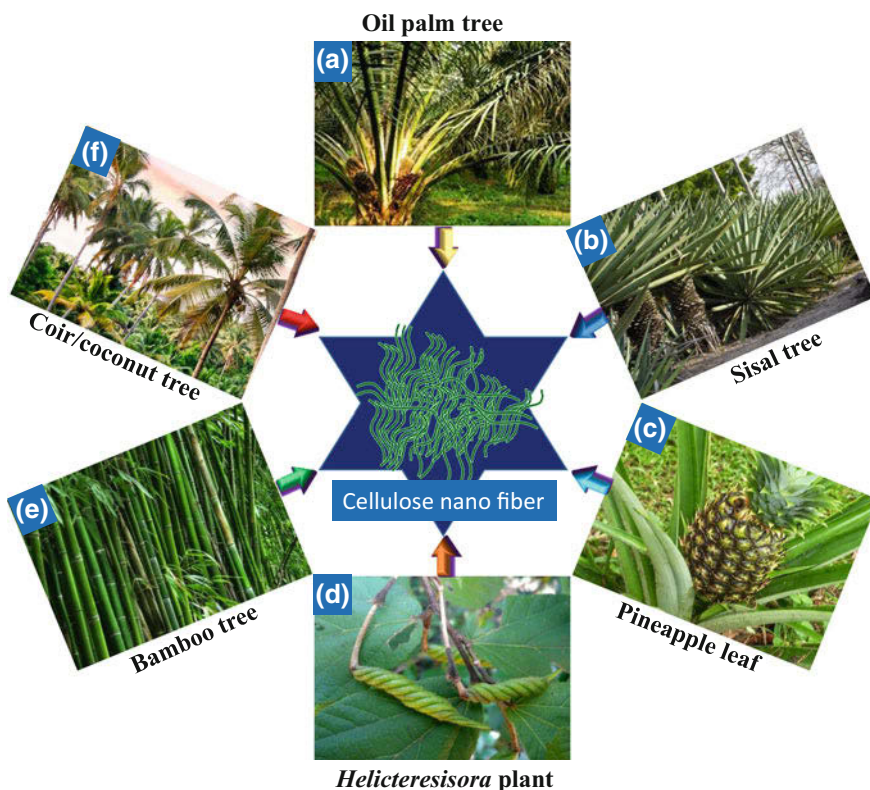


Fig. 7 Cellulose nanofibers from different plants

Natural fibers are superior to synthetic ones with regards to properties, such as biodegradability, lightweight, low toxicity, cost, and availability. In order to achieve adequate adhesion between fibers and matrix, studies were focused on the treatment of fibers to improve bonding between fiber and matrix. Various methods, such as mercerization and corona, plasma, heat, and silane treatment were reported to enhance the bonding in natural fiber composites. Moreover, various studies were conducted on hybrid NR composites filled with multiple type natural fibers derived from plant resources [11]. The main objective of fabricating a hybrid composite was to extract the combined advantages of two or more different types of fibers so that the advantages of one type of fiber could compensate the limitations of the other. As a consequence, the proper balance between performance and cost could be achieved through proper material designing. Meanwhile, the individual characteristics of plant-derived natural fibers were described one after another. In this context, physical properties and chemical constituents of different types of natural fibers are summarized in Table 1.

Table 1 Composition and properties of different natural fibers extracted from plants

Fibers	IF	CF	OPF	SF	BF	PLF
Diameter (μm)	10	100–400	150–250	103	–	55–95
Density (g cm^{-3})	1.20–1.30	1.20	0.70–1.55	1.50	0.60–1.10	0.80–1.60
TS (MPa)	500–600	175	50–400	511–635	140–230	400–627
Young modulus (GPa)	–	4.00–6.00	3.20	9.40–22.00	11.00–17.00	1.44
EAB (%)	5.0–6.0	15.0–40.0	25.0	2.0–2.5	–	14.5
Moisture content (%)	6.0–7.0	10.0–12.0	16.0	–	11.7	–
Micro fibrillar angle ($^{\circ}$)	20.00–26.00	3.49	42.00–46.00	20.00–25.00	–	–
Holocellulose (%)	–	–	68.3–86.3	–	73.3	–
Cellulose (%)	74	32–43	65	65	26–43	81
Hemicellulose (%)	–	0.15–0.25	–	12.00	30.00	–
Alpha-cellulose (%)	–	–	41.9–60.6	–	48.2	–
Lignin (%)	23.0	40.0–45.0	29.0	9.9	21.0–31.0	12.7
Fat (%)	1.09	0.30	–	–	–	–
Pentosan (%)	–	–	17.8–20.3	–	20.3	–
Waxes	–	–	–	2	–	–

3 Coir/Coconut Fiber (CF)

The lignocellulosic fiber, originated from the fibrous mesocarp of the fruit of the tropical coconut trees (*Cocos nucifera*), is called the coir. CF is more profitable than other natural fibers, including high weather resistance due to the presence of higher amount of lignin and poor water absorptivity because of the lesser cellulose content. Moreover, this fiber can be stretched beyond the elastic limit without rupture, because of the helical arrangement of micro-fibrils at 45°.

4 Oil Palm Fiber (OPF)

OPF, a waste material of oil extraction, is a lignocellulosic fiber obtained from the empty fruit and bunch fibrous mesocarp of oil palm tree (*Elaeis guineensis*). Of the different fiber sources in oil palm tree, empty fruit bunch can yield up to 73% fibers and hence, it is preferable in terms of availability and cost. Palm oil industry has to dispose of about 1.1 ton of empty fruit bunch per each ton of oil produced. In fact, retting process is utilized for extracting OPF from empty fruit bunch. Of the different commonly used retting processes, such as mechanical retting (hammering), chemical retting (boiling with chemicals), steam/vapor/dew retting and water/microbial retting, water retting is the most popular. OPFs are hard, tough, and show similarity to CFs in cellular structure. The central part of the transverse section of OPF contained a lacuna like portion surrounded by porous tubular structures. The morphology of fibrous surface, containing pores having average diameter of 0.07 μm , is essential for stronger mechanical bonding with matrix resin in composite fabrication.

5 Sisal Fiber (SF)

Sisal is an agave (*Agave sisalana*) and commercially produced in Brazil and East Africa. SF is one of the strongest fibers and can be used for several applications. SF possesses excellent ageing resistance.

6 Bamboo Fiber (BF)

Bamboo (*Bambusa Shreb.*), a perennial plant, grows up to 40 m in monsoon climates. Bamboo is most commonly used in construction, carpentry, weaving, and plaiting. Fabrication and studies on BF filled NR composites have been conducted. In fact, overall mechanical properties of BF, abundantly available in Asia, are comparable to wood.

7 Isora Fiber (IF)

For the first time, Mathew et al. investigated the applicability of the IF, extracted from the bark of the *Helicteres isora* plant by retting, as a reinforcing additive in preparing NR composites [12]. In fact, Isora shrubs grow in many parts of South India, especially in Kerala. Isora resembles jute in appearance but possesses superior strength, durability, and lustre. It has the better TS than some other natural fibers.

8 Pineapple Leaf Fiber (PLF)

Pineapple (*Ananas comosus*), a tropical plant of Brazil, is cellulose-rich, relatively inexpensive and highly abundant. PLF, the waste product of pineapple cultivation is relatively inexpensive and readily available for industrial purposes. PLF exhibits high specific strength and stiffness because of high cellulose content of 70–80% and comparatively low microfibrillar angle. However, because of the hydrophilic character of its cellulose structure and high susceptibility to water absorption, mostly at elevated temperatures, inadequate bonding between PLF and the hydrophobic matrix is the major problem associated with the application of PLF as filler in NR.

9 Processing

In general, natural fiber-filled composites are processed in an open two-roll mill. For instance, OPF filled composites were prepared in a laboratory two roll mill (150–300 mm) at a nip gap of 1.3 mm. Followed by initial mastication of NR, untreated chopped OPF is added along with other main ingredients like accelerator, activator, and vulcanizing agent. In this context, the fibers were added towards the end of the mixing process, so that to ensure minimum breakage of the fiber during mixing.

Prior to the addition of fibrous fillers, the usual practice is to execute optimal cleaning, washing, and drying of the plant fibers, followed by size reduction via chopping or any other suitable mechanical operation. However, to enhance the bonding in natural fiber composites, fibers are pre-treated before incorporating in the NR matrix. For instance, chemical treatment, such as mercerization of IF requires 3–4 h of continuous heating at 80 °C in 10% aqueous NaOH solution, followed by washing with water and drying in an air oven at 70 °C. In case of acetylation, the same fiber is initially treated by alkali and thereafter the alkali-treated fibers are soaked in glacial CH₃COOH for 1 h. Later, the material is decanted and then soaked in acetic anhydride containing two drops of concentrated

H₂SO₄ for 5 min. Finally, the acetylated fibers are filtered, washed, and dried in an air oven at 70 °C. As a consequence of chemical treatment, certain physical and microstructural changes occur on the fiber surface, such as dissolution and leaching out of fatty acids and lignin components of the fiber. For example, as a result of mercerization of IF, a considerable quantity of uranic acid, a constituent of hemi-cellulose (xylan), can be removed from the fiber. As a consequence of acetylation, substantial esterification of O–H of IF is actuated. Similarly, prior to the compounding process, raw CFs are also undergone various chemical treatments to remove coir pith and other undesirable materials, and thereby improving the binding of CF with NR.

10 Characterization

10.1 Mechanical Properties

Effect of OPF length on the mechanical properties of the NR compounds are analyzed by stress-strain measurement. Both TS and EAB are maximized when the length of OPF becomes 6 mm (Table 2). At higher fiber lengths, significant deterioration in the mechanical properties is observed because of the entangling tendency of the longer fibers. Altogether, 6 mm was found to be the optimum fiber length for OPF reinforced NR matrix. Moreover, the mechanical properties of the OPF filled NR composites in the longitudinal direction are superior to the transverse direction. However, incorporation of OPF in NR matrix decreases TS and EAB. The intrinsic high strength of NR, related to the strain-induced crystallization, is disrupted when fibers are incorporated into NR, thereby destroying the regular arrangement of rubber molecules, resulting in the deterioration of crystallization. The mechanical properties of the CF-reinforced NR composites in the longitudinal direction are superior to those in the transverse direction. However, in this case, the optimum length for CF is maintained at 10 mm for achieving good reinforcement in NR composites. Moreover, to maximize the fiber orientation and tensile properties of the CF-reinforced NR composites, CFs are immersed in 5% NaOH solution for 48 h. Similarly, NaOH and benzoyl peroxide is used to treat the surfaces of PLF. It is found that all surface modifications enhance adhesion and tensile properties of PLF-NR composites. In fact, treatment with 5% NaOH and 1% benzoyl peroxide provides the best improvement of composite strength by 28 and 57% respectively, when compared with that of untreated fiber. Similarly, the adhesion between the BF and NR can be enhanced by the use of a bonding agent, such as silane coupling agents, phenol formaldehyde, and hexamethylenetetramine, leading to improved tensile modulus and overall mechanical properties of BF-NR composites.

The influence of the ratio of two lignocelluloses fibers, i.e., sisal and oil palm on the tensile properties of NR composites have already been reported. The mechanical properties are found to be more dependent on SF than oil palm, because of the

superior tensile properties of SF than OPF (Table 1). Moreover, since the microfibrillar angle of SF is lesser (20°) than OPF (44°), the reinforcing ability of sisal is more than that of oil palm in any polymeric matrix. Furthermore, the surface area of the fiber in a unit area of the composite is higher in SF filled composite than OPF filled composite because the diameter of SF is lesser than that of OPF (Table 1). Hence, physical interaction, as well as stress transfer in the unit area, is higher for SF filled composites. Altogether, it has been noted that TS of SF-OPF-NR hybrid composite is lesser than pure gum. In this context, the mechanical properties of OPF-sisal-NR composite, studied by Jacob et al. are tabulated in Table 2.

10.2 Dynamic Mechanical Properties

Most rubber articles, such as automobile tyres, springs, and dampers, undergo cyclic loading or cyclic deformation, and hence, dynamic properties are crucial for evaluating the real-time service performance of those articles. In this context, a complete description of the viscoelastic properties is derived via dynamic experiments conducted over a range of time, temperature or frequency. It is observed that the stress relaxation rate of OPF-SF-NR hybrid composites decreases with increase in the fiber content. In fact, the relaxation of rubber molecules in the gum compound is hindered because of the influence of fiber-rubber interface formed via addition of fibers. Notably, at all temperatures, storage modulus of OPF-SF-NR composites enhances with the rise in fiber content [11]. Invariably, the unfilled NR compound, containing only rubber phase, makes the material better flexible to impart low stiffness, and thus, low storage modulus. Once the fiber was added, the stiffness of the composite increases as fibers allow greater stress transfer at the fiber-rubber interface, resulting in higher storage modulus. The loss modulus also increases with fiber loading, to reach up to 756 MPa at 50 phr fiber loading, whereas gum has loss modulus of 415 MPa. In this context, the damping factor decreases with fiber loading because of lower flexibility and lower degrees of molecular motion caused by incorporation of fibers in a rubber matrix.

Short CF reinforced NR composites with poor interfacial bonding tend to dissipate higher energy than those with fair interfacial bonding. The composite, containing fibers subjected to bleaching, exhibits very high $\tan \delta$ values in the low-temperature range but the low values at high-temperature region. This proves that such composites are good elastomeric compounds at higher temperatures. However, composites of resorcinol-formaldehyde-latex treated CFs exhibit low $\tan \delta$ values at both low and high temperatures, suggesting low damping and hence, good interfacial bonding. Moreover, with the increased fiber loading, glass transition temperature (T_g) of the composites continuously shifts towards higher temperature, because of increased immobilization of the polymer chains adhered to the treated CFs.

Table 2 Tensile properties of various polyamide-filled composites and NCPs

Composites/ nano-composites	TS (MPa)	EAB (%)	Tensile modulus or Young's modulus (Mpa)	Bending strength (Mpa)	Bending Modulus (Mpa)	Impact strength (kJ m ⁻²)	Hardness (shore A)	Abrasion resistance (mm ³ /40 m)	Hysteresis (MPa)
Non-purified NR/ silk	11.81 ± 0.31	21 ± 5	-	-	-	-	-	-	-
Purified NR/silk	8.49 ± 0.09	24 ± 5	-	-	-	-	-	-	-
Non-purified NR/ nylon	6.54 ± 0.17	76 ± 12	-	-	-	-	-	-	-
Purified NR/nylon	5.48 ± 0.16	77 ± 10	-	-	-	-	-	-	-
Silk fiber/PP:NR (50:50)	41.10	25	901.5	37.1	1413.3	23.0	93.0	-	-
Silk fiber/PP:NR (75:25)	42.40	21	955.3	39.2	1564.8	26.1	93.0	-	-
Silk fiber/PP:NR (90:10)	45.10	18	1278.8	42.9	2132.4	21.9	94.0	-	-
γ irradiated (250 krad) silk fiber/PP: NR (50:50)	46.60	-	1313.8	44.3	1620.1	-	-	-	-
γ irradiated (250 krad) silk fiber/PP: NR (75:25)	47.10	-	1410.1	46.1	2200.6	-	-	-	-
γ irradiated (250 krad) silk fiber/PP: NR (90:10)	48.30	-	1553.5	48.9	2620.8	-	-	-	-
Soy particle basic/ NR (10 phr)	21.00	550	1.9	-	-	-	-	-	-
Soy particle basic/ NR (20 phr)	21.10	510	2.4	-	-	-	-	-	-

(continued)

Table 2 (continued)

Composites/ nano-composites	TS (MPa)	EAB (%)	Tensile modulus or Young's modulus (Mpa)	Bending strength (Mpa)	Bending Modulus (Mpa)	Impact strength (kJ m ⁻²)	Hardness (shore A)	Abrasion resistance (mm ³ /40 m)	Hysteresis (MPa)
Soy particle basic/ NR (30 phr)	19.40	400	3.8	-	-	-	-	-	-
Soy particle basic/ NR (40 phr)	14.60	280	6.4	-	-	-	-	-	-
Soy particle acidic/ NR (10 phr)	20.80	550	1.9	-	-	-	-	-	-
Soy particle acidic/ NR (20 phr)	21.90	550	2.4	-	-	-	-	-	-
Soy particle acidic/ NR (30 phr)	19.80	440	4.2	-	-	-	-	-	-
Soy particle acidic/ NR (40 phr)	14.40	340	6.0	-	-	-	-	-	-
NR/CB	18.60 ± 1.10	759 ± 19	-	-	-	-	42.0 ± 1.6	77.10 ± 4.10	-
NR/CB/leather-60 phr	12.20 ± 1.10	84 ± 2	-	-	-	-	72.7 ± 0.9	213.00 ± 11.90	-
NR/CB/leather-80 phr	8.60 ± 0.80	45 ± 1	-	-	-	-	76.0 ± 1.7	178.90 ± 3.30	-
NR foam	1.38	409	0.0026	-	-	-	-	-	0.126
NR foam/leather waste-20 phr	-	395	-	-	-	-	-	-	0.206
NR foam/leather waste-40 phr	-	74	-	-	-	-	-	-	3.459
NR foam/leather waste-60 phr	2.18	58	0.1206	-	-	-	-	-	7.552
NR	4.70 ± 0.90	700 ± 65	-	-	-	-	56.6 ± 1.1	207.21 ± 33.74	-

(continued)

11 Application

Significant research is currently underway around the world to address and overcome the obstacles to developing biocomposite materials with improved performance for global applications. Interfacial adhesion between natural fibers and matrix plays the pivotal role for the overall performance, since the final properties of the composites totally depend on it. Recently, CFs bonded with NR latex are being used in seats of the Mercedes Benz A-class model.

12 NC Reinforced NR NCPs

Recently, NC based reinforcement in NCPs is gaining high insight. Besides low cost, density, and energy consumption, renewability, high specific properties, biodegradability, and relatively good surface reactivity, it shows better properties as a reinforcing phase in NCPs than micro-/macro-cellulose composites. The concept of cellulosic NF reinforced polymer materials has shown rapid advances and considerable interest in the last decade, because of their renewable character, high mechanical properties, low density, availability, and diversity of sources. Because of the perfect balance between flexibility and stiffness, NR matrix is used as a model system to study the effect of cellulose NFs reinforcement. Currently, NC reinforced NR-NCPs is one of the important categories of lignocellulosic fibers mediated rubber composite materials. In fact, the characteristics of NC depend on the origin of fibers and the isolation methods. Cellulosic nanoparticles consist of either cellulose whiskers or microfibrillated cellulose. The nanoscale dimensions of cellulose crystals enable cellulose NCPs to impart unique characteristics. The extensive research work is devoted to cellulose nanoparticles obtained by either (i) disintegration shearing for microfibrillated cellulose or (ii) chemical acid hydrolysis treatment for cellulose nanocrystals or whiskers. Cellulose of various sources has been utilized to produce such cellulosic nanoparticles. Generally, the elongated rod-like high-purity single cellulose nanocrystals are produced from different sources, whose dimensions depend on the nature of cellulose source and hydrolysis conditions. In fact, the diameter and length typically lie within 5–10 and 100–500 nm, respectively. Cellulosic nanoparticles can be classified into two main groups: (i) cellulose nanocrystals, as obtained by acid treatment and (ii) cellulose nanofibers, synthesized through mechanical disintegration (Fig. 8). Both cellulose nanocrystals and cellulose nanofibers are used for different applications depending on their properties. Indeed, nanofibrillated cellulose has been used in these NCPs, including NR based NCPs, because of typically ultra-high strength and environmental friendliness of NC.

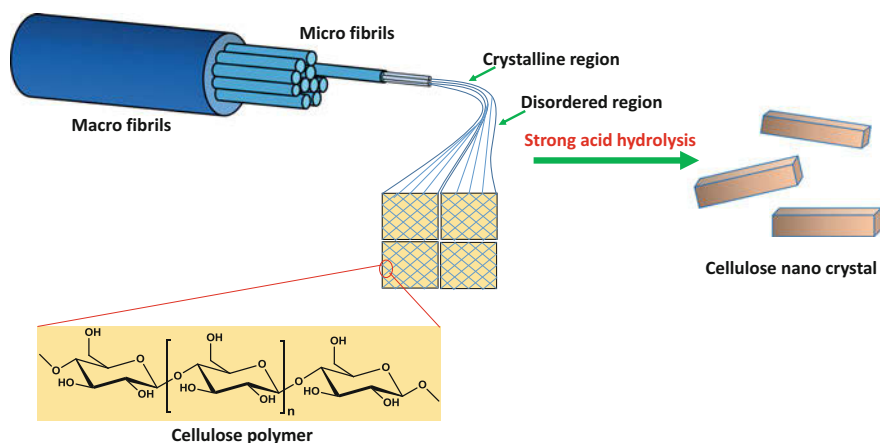


Fig. 8 Different forms of cellulose: process modification steps

13 Processing

Bio-based rubber composites are fabricated through the standard rubber processing operations, such as compression moulding, injection moulding, and extrusion. NC whisker reinforced NR-NCPs are prepared by applying the conventional rubber compounding method, after extracting cellulose NWs from bamboo pulp residue collected from newspaper production unit [13]. Initially, cellulose NWs are prepared via acid hydrolysis of the bamboo pulp and thereafter, the cellulose NW based NR NCPs have been produced via a two-step process. In the first step, a master-batch is prepared via dispersing the cellulose NWs in NR latex, followed by coagulation of the dispersion. In the next step, this coagulated master-batch is compounded with solid NR and vulcanizing agents in a two-roll mill and thereafter the NR compound is cured via compression moulding at 150 °C. Earlier, employing the similar acid hydrolysis protocol, cellulose whiskers were extracted from cellulose fibers present in cassava bagasse. Thereafter, NW-NR composites have been prepared by initial mixing of NWs into NR latex, followed by casting and evaporation. Applying the same methodology, NC-NR-NCPs are fabricated, wherein the added cellulose nanoparticles were initially extracted from soy hulls by acid hydrolysis.

NR-NCPs filled with cellulose nanoparticles, i.e. whiskers and microfibrils, are fabricated, where cellulose whiskers are extracted via bleaching the purified cell wall of the rachis of date palm tree, whereas the cellulose microfibrils are obtained through the disintegration of the bleached and purified cell wall by microfluidizer. Later, NR-NCP films have been prepared by casting/evaporation method, comprising of cellulose whiskers of 84–102 and 4–12 nm length and width, respectively. Indeed, these whiskers are initially isolated from bleached sugar cane bagasse kraft pulp. Thereafter, these purified whiskers are admixed to NR latex,

followed by casting/evaporation method for synthesizing NCPs. In an almost similar fashion, the NR-NC type composites are prepared after isolating the NC from raw jute fiber by steam explosion.

The direct extrusion method can be adopted in preparing cellulose-rubber NCPs. The lyophilized NC, produced from microcrystalline cellulose, is initially pulverized in a grinder to obtain NC powder, and then the pulverized NC powder is mixed with NR in an extruder to generate the bio-composite. While preparing bio-composite, the temperature for direct extrusion is restricted to 160 °C to avoid thermal degradation of NC whiskers. Nevertheless, such NC based NCPs are generally prepared via casting method comprising of two processing steps, in which the first step is associated with the mixing of NC suspension with rubber latex for a stipulated period (i.e. 0.5–12 h) to produce uniform NC dispersion. However, in the second step, this uniform aqueous NC dispersion is cast in a formulation mould and dried to produce NC films. In between these two steps, degassing and water evaporation should be carried out, based on the concentration and bubbles in the suspension. In addition, a combination of casting and extrusion can also be attempted, wherein the NC dispersion is cast and dried to produce NC based film and thereafter, the film is cut and extruded with NR.

Recently, attempts have been made to prepare NC-oxidized NR-NCPs via dispersing NC into oxidized NR latex, followed by usual casting and evaporation. In fact, NR latex suspensions are oxidized with a KMnO_4 solution to introduce O–H groups at the NR chains and thereby to increase the possibility of H-bonding between hydroxylated polyisoprene chains and NC. In the recent past, few publications have reported the properties of NR as a matrix to synthesize green, conductive, and flexible NCPs. Graphene sheets are introduced in water suspensions of NC prior to the reduction of the particles by adding hydrazine hydrate. The resultant hybrid suspension is mixed with NR latex and dried to form a structured conductive film. The similar strategy of coating nanoparticles may be employed to obtain polyaniline modified cellulose nanofibers, in which polyaniline is attached to the cellulose nanofiber surface by in situ polymerization, and NR-NCP is obtained by applying the casting and evaporation technique.

Recently, attempts have been made to prepare NR/Regenerated Cellulose hybrids comprising of a cellulose-rich phase and NR latex particles. Such hybrid was obtained by simply co-precipitating the mixture of NR latex and cellulose alkaline—urea—aqueous solution. As a result, honeycomb-like structural moieties of Regenerated Cellulose were noted to become homogeneously distributed in the hybrid matrix wherein Regenerated Cellulose and NR phases interlaced/interpenetrated each other to form a semi-IPN/fullIPN structure.

14 Characterization

14.1 Biodegradability

Biodegradability of the cellulose whisker filled NR-NCPs in soil was noted to become significantly enhanced as compared to that of the unfilled NR. It is well known that the NR degrades in nature by specific microorganisms, such as *Streptomyces coelicolor* 1A and *Nocardia farcinica* strain E1, in a slow process and accordingly the growth of these rubber utilizing bacteria is also slow. However, as the biodegradation of cellulose is faster than rubber, the cellulose component in the NR NCPs films is rapidly consumed by the microorganisms, producing porosity, void formation, and the loss of the integrity of the rubber matrix. Thus, the rubber matrix would be broken down into smaller particles and accordingly smaller and less organized rubber particles become more susceptible to the bacterial degradation. Similarly, jute fiber originated NC filled NR demonstrated a significantly higher level of biodegradability over the unfilled NR. As expected, the non-crosslinked NR composite showed a higher degree of biodegradation when compared with the crosslinked NR composites. In this context, a compost system of increased degradation potential, constituting of the complex biological environment having relatively higher microbial diversity, was utilized to enhance biodegradation of these composite materials. As a result of composting, quicker deterioration of the whole composite material, including the interior part of the composite, was achieved by means of rapid biodegradation of NC. Accordingly, NR-NC bio-composite envisaged lower TS retention when compared with the neat NR, as unreinforced NR showed the higher resistance to the microorganism attacks in comparison to that of the NC filled composite.

14.2 Mechanical Properties

As compared to the mere PLA materials, a strong increase in EAB is observed when 10 wt% of NR is added in PLA matrix. Such ductile behaviour and EAB of PLA-NR blend is effectively conserved in the PLA grafted NC filled PLA-NR-NC bio-NCPs, as grafted short chains of PLA on NC act as the effective compatibilizer between NC and PLA phases, even though the PLA grafted NC are preferentially located in the PLA phase (Table 3).

The stress-strain behaviour of cellulose whisker filled NR NCPs was considerably different from neat NR. In fact, a non-linear mechanical behaviour of NR-cellulose whisker NCPs is observed in the tensile test performed at room temperature. Stress-strain curves clearly demonstrate the stiffening effect of the cellulose whiskers in the NR NCPs. Both Young's modulus and TS significantly increase upon whisker addition, while the EAB decreases. Such high reinforcing effect of cellulose whisker can be assigned to the mechanical percolation

phenomenon of cellulose whiskers, which forms a stiff continuous network of cellulosic nanoparticles linked through hydrogen bonding. Such improvement in Young's modulus and TS is also explained by a mechanism based on the formation of the Zn-cellulose complex (Fig. 9). The three-dimensional network of cellulose nanofibers (cellulose-cellulose-/Zn-cellulose-network) in the NR matrix can play the pivotal role to enhance the properties of the crosslinked NCPs. In this context, relative improvements in mechanical properties, demonstrated by cellulose whiskers isolated from various sources, have been demonstrated in Table 2. Herein, the aspect ratio of different cellulose whiskers is an important factor that guides the variegated mechanical properties of NR NCPs filled with cellulose whiskers isolated from different resources. Thus, as compared to cellulose whiskers originated from starch, rachis of date palm tree and *Capim dourado*, relatively lower aspect ratio of cellulose whiskers isolated from bagasse could be the reason behind the lower TS properties of NR NCPs filled with cellulose whiskers isolated from bagasse. Similarly, mild hydrolysis is preferable in enhancing the extraction yield of NC crystals from soy hulls as well as to maintain the crystallinity of native cellulose and obtain high aspect ratio NC crystals.

Accordingly, a high reinforcing effect is observed even at low filler contents when high aspect ratio NC crystals are used to prepare NCPs with a NR matrix by casting/evaporation. For instance, by adding only 2.5 wt% NC crystals, the storage tensile modulus at 25 °C of the NCP was about 21 times higher than that of the neat NR matrix. However, it has to be kept in mind that the ultimate strength is not only dependent on the chemical interactions between the matrix and the NF but also contributed by the physical entanglements of the NC having a high aspect ratio. For this reason, the modulus of the 5% composite gives a comparative increase of fourfold with its pristine matrix. But the 10% composite showed a modulus of 9.6 MPa and the comparative increase from 5 to 10% NCP is only 2.5 fold (Table 2).

Besides, mechanical properties of NC based polymer NCPs are function of the filler dispersibility and compatibility of NC with the matrix. Moreover, because of the presence of numerous hydroxyl groups on the surface of NC, NC possesses strong tendency to form an aggregate, and hence dispersion of NC is really difficult in the nonpolar or hydrophobic polymer matrices. Improper distribution of NC may lead to the formation of NC aggregates which can act as stress concentrator, resulting in poor performance of the NCP. Thus, the formation of NC aggregates should be avoided to achieve effective reinforcement. In this regard, considerable enhancement in both TS and modulus values was observed with the increased addition of cellulose NWs, accompanied by a moderate decrease in EAB, as NCPs were devoid of any micro-scaled aggregates of cellulose NWs. Furthermore, mechanical properties of NC filled NR NCPs can be improved by enhancing the interfacial interactions between NR and NC, via introducing a limited extent of –OH groups in the NR chains via oxidation of the NR. However, uncontrolled oxidation-mediated generation of a huge number of –OH, led to severe deterioration of the mechanical properties. As discussed earlier, the percolation phenomenon of NC in NR was effectively modified by the introduction of graphene, leading to the

formation of an assembled conductive structure that played a key role to improve electrical conductivity and mechanical properties of the cellulose mediated NR/graphene composites. Such unique ‘fragile’ but effective conductive network with low percolation threshold facilitated the disconnection and reestablishment of conductive paths in presence of organic solvents. Thus, the composite, having such sensitive conductive network, can function as high-performance sensing materials with superior resistivity responses for organic liquids.

To improve the interfacial interactions and compatibility between NR and NC, attempts were made to introduce the cross-linkable mercapto-groups onto the surface of cotton originated cellulose nanocrystals by esterification [14]. In comparison to biocomposites based on NR filled with unmodified cellulose nanocrystals, the NR NCPs having modified cellulose nanocrystals showed a 2.4-fold increase in TS and 1.6-fold increase in EAB. Indeed, in the modified cellulose nanocrystals, mercaptooundecanoyl groups were introduced at the surface, leading to attachment of long hydrocarbon chain on the surface of modified cellulose nanocrystals, which reduced the hydrophilic nature of the cellulose nanocrystals and consequently improved the compatibility of the modified cellulose nanocrystals with the hydrophobic NR matrix. The cross-linking of NR with modified NC surface, through the thiol functionalities on the nanocrystal surface, increased strength and toughness of the NR/modified cellulose nanocrystal composites as summarized in Table 3. Synergistic effect of cross-linking at the filler–matrix interface together with reinforcement in NR/modified cellulose nanocrystal.

NCPs offered by the thiol-modified cellulose nanocrystals is expressed in these results. Indeed, formation of covalent thioether (C–S) bonds at the NR/modified cellulose nanocrystal composite interface was identified from the FTIR results which suggested the reaction of –SH groups of mercaptooundecanoyl group in modified cellulose nanocrystals with the double bonds of NR (Fig. 10) [14]. Likewise, both cellulose nanofibrils and polyaniline treated cellulose nanofibrils were highly effective in improving overall mechanical properties of NR NCPs (Table 3). However, both Young’s modulus and TS are lower for cellulose nanofibril/polyaniline-reinforced NCPs as compared to cellulose nanofibril reinforced NR. This result can be explained by the fact that cellulose nanofibril is more hydrophobic than cellulose nanofibril/polyaniline resulting in a higher level of adhesion with the NR matrix. Moreover, comparative reinforcing abilities of both cellulose whiskers and microfibrillated cellulose in NR composites were determined, and it was observed that the reinforcing effect was higher for NCPs filled with microfibrillated cellulose over the whisker filled NR. Again, relatively higher aspect ratio and the possible presence of entanglements in microfibrillated cellulose were the major factors behind the greater reinforcing ability of microfibrillated cellulose over the whiskers. Moreover, the presence of residual lignin, extractive substances and fatty acids at the surface of microfibrillated cellulose was also suggested to promote higher adhesion level with the NR matrix. Later, in order to investigate the role of fatty acids in enhancing the reinforcing capability, attempts were also made to achieve highly efficient reinforcement of NR with cellulose

Table 3 Tensile properties of modified and unmodified composites

Composites	TS (MPa)	Young modulus (MPa)	Work-of fracture (MJ m ⁻³)	EAB (%)	Stress at 100% (MPa)	Stress at 200% (MPa)	Crosslink density (mol L ⁻¹)
NR ^a	2.40 ± 0.40	1.01 ± 0.08	1.45 ± 0.41	910 ± 174	-	-	-
NR/CNC ^b -2	3.30 ± 0.90	1.05 ± 0.03	1.89 ± 0.67	975 ± 120	-	-	-
NR/CNC ^b -5	3.60 ± 0.40	1.10 ± 0.08	1.73 ± 0.48	960 ± 200	-	-	-
NR/CNC ^b -10	4.20 ± 0.80	1.75 ± 0.38	1.56 ± 0.32	750 ± 125	-	-	-
NR/m-CNC ^c -2	6.80 ± 1.50	1.49 ± 0.31	2.97 ± 0.39	1220 ± 30	-	-	-
NR/m-CNC ^c -5	9.60 ± 2.00	1.53 ± 0.26	4.18 ± 0.75	1270 ± 157	-	-	-
NR/m-CNC ^c -10	10.20 ± 1.30	1.86 ± 0.12	4.60 ± 0.57	1210 ± 110	-	-	-
NR ^a	3.52	-	-	860	1.90	2.05	1.39 × 10 ⁻³
1% NR ^a	3.81	-	-	750	2.20	2.30	1.61 × 10 ⁻³
nano-composite							
2% NR ^a	4.15	-	-	620	2.60	2.60	1.91 × 10 ⁻³
nano-composite							
3% NR ^a	4.25	-	-	410	3.05	3.40	2.20 × 10 ⁻³
nano-composite							
NR ^a	1.08 ± 0.18	0.65 ± 0.02	-	698 ± 45	-	-	-
NR/CNF ^d (95/05)	2.72 ± 0.21	3.12 ± 0.34	-	527 ± 28	-	-	-
NR/CNF ^d (90/10)	4.03 ± 0.30	8.15 ± 0.90	-	462 ± 14	-	-	-
NR ^a	1.72 ± 0.39	1.33 ± 0.39	-	878 ± 57	-	-	-
NRC ^e	2.08 ± 0.45	7.47 ± 1.67	-	684 ± 69	-	-	-
ONR2C ^f	2.37 ± 0.42	7.92 ± 1.02	-	703 ± 43	-	-	-
ONR3C ^f	2.18 ± 0.93	8.36 ± 0.85	-	697 ± 40	-	-	-
ONR4C ^f	0.36 ± 0.05	5.02 ± 1.13	-	570 ± 50	-	-	-
ONR5C ^f	0.11 ± 0.02	0.72 ± 0.03	-	202 ± 58	-	-	-

(continued)

Table 3 (continued)

Composites	T _S (MPa)	Young modulus (MPa)	Work-of fracture (MJ m ⁻³)	EAB (%)	Stress at 100% (MPa)	Stress at 200% (MPa)	Crosslink density (mol L ⁻¹)
NR ^a	–	0.50 ± 0.15	–	575 ± 35	0.56 ± 0.12	–	–
NR-CNW1 ^g	–	1.70 ± 0.50	–	408 ± 49	0.86 ± 0.06	–	–
NR-CNW2.5 ^g	–	2.80 ± 0.40	–	358 ± 22	1.17 ± 0.24	–	–
NR-CNW5 ^g	–	8.40 ± 1.10	–	231 ± 53	2.71 ± 0.10	–	–
NR-CNW10 ^g	–	118.00 ± 6.00	–	16 ± 3	8.93 ± 1.23	–	–
NR-CNW15 ^g	–	187.00 ± 0.50	–	14 ± 1	12.15 ± 1.48	–	–
NR-MF-1 ^h	–	1.27 ± 0.00	–	209 ± 29	0.70 ± 0.13	–	–
NR-MF-2.5 ^h	–	10.52 ± 0.66	–	15 ± 5	0.80 ± 0.26	–	–
NR-MF-5 ^h	–	35.46 ± 5.79	–	14 ± 2	2.17 ± 0.38	–	–
NR-MF-7.5 ^h	–	121.20 ± 8.80	–	8 ± 2	4.15 ± 0.71	–	–
NR-NR-MF-10 ^b	–	172.00 ± 62.00	–	7 ± 2	5.99 ± 2.56	–	–
NR-MF-15 ^h	–	233.00 ± 57.00	–	4 ± 1	6.26 ± 2.70	–	–
NR ^a	1.60 ± 0.20	1.30 ± 0.15	–	912 ± 19	–	–	–
2.5% NR ^a	5.20 ± 0.15	4.20 ± 0.25	–	576 ± 23	–	–	–
nano-composite	–	–	–	–	–	–	–
5% NR ^a	6.80 ± 0.18	6.30 ± 0.22	–	413 ± 22	–	–	–
nano-composite	–	–	–	–	–	–	–
7.5% NR ^a	9.80 ± 0.24	8.10 ± 0.35	–	275 ± 12	–	–	–
nano-composite	–	–	–	–	–	–	–
10% NR ^a	12.20 ± 0.36	9.60 ± 0.31	–	144 ± 5	–	–	–
nano-composite	–	–	–	–	–	–	–
NR ^a	0.59 ± 0.08	0.60 ± 0.10	–	611 ± 71	0.19 ± 0.04	–	–
NR1%CN ^b	0.89 ± 0.04	1.90 ± 0.30	–	396 ± 21	0.27 ± 0.01	–	–

(continued)

Table 3 (continued)

Composites	TS (MPa)	Young modulus (MPa)	Work-of fracture (MJ m^{-3})	EAB (%)	Stress at 100% (MPa)	Stress at 200% (MPa)	Crosslink density (mol L^{-1})
NR2.5%CN ^c ^b	1.11 ± 0.13	3.70 ± 0.10	–	485 ± 35	0.34 ± 0.02	–	–
NR5%CN ^c ^b	3.03 ± 0.11	18.10 ± 2.80	–	552 ± 9	0.54 ± 0.05	–	–
NR ^a	0.63 ± 0.14	0.69 ± 0.19	–	747 ± 38	–	–	–
NR/5RC ⁱ	1.36 ± 0.17	1.77 ± 0.21	–	612 ± 45	–	–	–
NR/10RC ⁱ	2.38 ± 0.19	2.63 ± 0.31	–	570 ± 32	–	–	–
NR/15RC ⁱ	4.81 ± 0.28	4.59 ± 0.45	–	505 ± 29	–	–	–
NR/20RC ⁱ	5.44 ± 0.37	11.70 ± 1.80	–	484 ± 24	–	–	–
NR/25RC ^j	5.36 ± 0.42	15.70 ± 1.70	–	370 ± 18	–	–	–
NR/30RC ⁱ	6.03 ± 0.61	20.80 ± 2.90	–	225 ± 11	–	–	–
NR ^a	1.60 ± 0.20	1.30 ± 0.15	–	912 ± 19	–	–	–
NR/2.5%NC ^j	5.20 ± 0.15	4.20 ± 0.25	–	576 ± 23	–	–	–
NR/5%NC ^j	6.80 ± 0.18	6.30 ± 0.22	–	413 ± 22	–	–	–
NR/7.5%NC ^j	9.80 ± 0.24	8.10 ± 0.35	–	275 ± 12	–	–	–
NR/10%NC ^j	12.20 ± 0.36	9.60 ± 0.31	–	144 ± 5	–	–	–
NR ^a	16.10 ± 1.40	1.70 ± 0.00	–	623 ± 14	–	–	–
NR ^a + CNF ^d 1%	20.80 ± 3.10	2.20 ± 0.10	–	658 ± 41	–	–	–
NR ^a + stCNF ^k 1%	15.20 ± 2.10	5.0 ± 0.40	–	513 ± 40	–	–	–
NR ^a + oleCNF ^l 1%	18.80 ± 1.70	5.4 ± 0.80	–	531 ± 25	–	–	–
NR ^a + CNF ^d 3%	28.40 ± 2.80	3.60 ± 0.30	–	713 ± 44	–	–	–
NR ^a + stCNF ^k 3%	22.40 ± 2.50	9.60 ± 0.80	–	537 ± 37	–	–	–
NR ^a + oleCNR ^l 3%	25.60 ± 1.00	12.70 ± 1.90	–	492 ± 12	–	–	–
NR ^a + CNF ^d 5%	30.30 ± 0.40	4.40 ± 0.10	–	718 ± 6	–	–	–

(continued)

Table 3 (continued)

Composites	TS (MPa)	Young modulus (MPa)	Work-of fracture (MJ m ⁻³)	EAB (%)	Stress at 100% (MPa)	Stress at 200% (MPa)	Crosslink density (mol L ⁻¹)
NR ^a + stCNF ^k 5%	28.90 ± 1.40	18.30 ± 1.00	–	530 ± 30	–	–	–
NR ^a + oleCNF ^l 5%	16.70 ± 2.40	27.70 ± 4.40	–	251 ± 69	–	–	–
NR ^a	9.20 ± 1.30	1.70 ± 0.20	–	554 ± 9	–	–	–
NR ^a -CNW ^g 2.5	14.00 ± 2.10	2.60 ± 0.10	–	539 ± 14	–	–	–
NR ^a -CNW ^g 5	14.50 ± 2.60	3.00 ± 0.30	–	477 ± 13	–	–	–
NR ^a -CNW ^g 10	17.30 ± 1.40	3.80 ± 0.20	–	455 ± 11	–	–	–

^aNatural rubber, ^bnatural rubber/cellulose nanocrystals, ^cnatural rubber/modified cellulose nanocrystals, ^dnatural rubber/cellulose nanofibrils, ^enatural rubber cellulose whiskers, ^fnatural rubber NCPs, ^gnatural rubber-cellulose nanowhiskers, ^hnatural rubber/regenerated cellulose, ⁱnatural rubber nano-cellulose

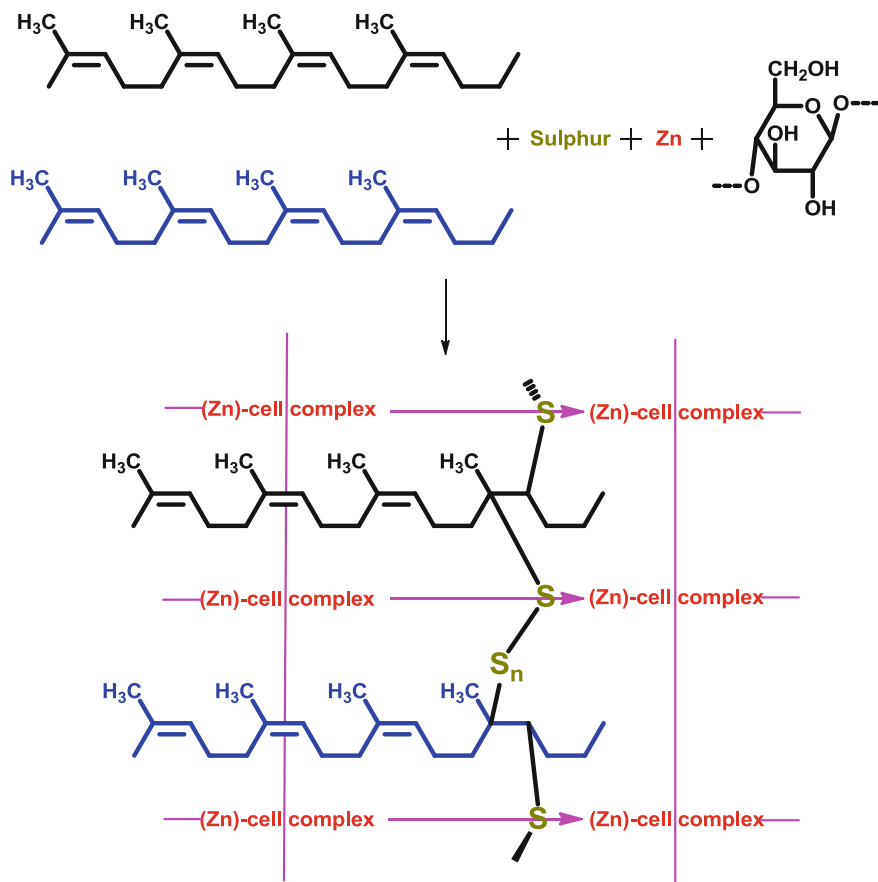


Fig. 9 Proposed mechanism for interaction of the cross linked NR/CNC composite

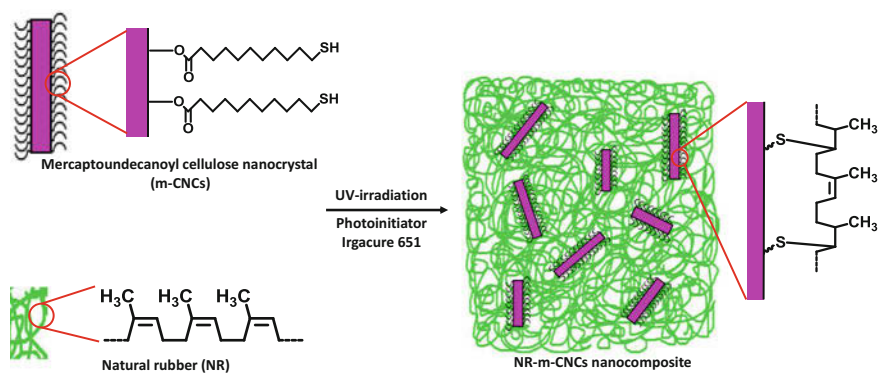
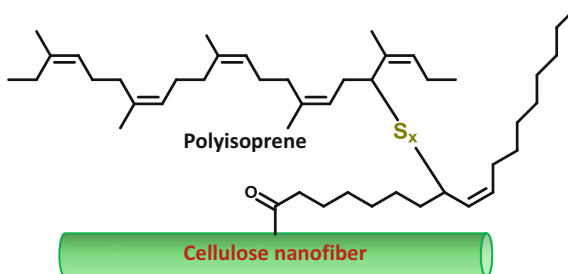


Fig. 10 Illustration of the structure for the NR-m-CNCs NCPs

Fig. 11 Diagram of sulfur vulcanization reaction between polyisoprene and CNFs incorporating unsaturated fatty acids (oleic acid)



nanofibers bearing unsaturated fatty acids, which crosslinked with sulfur using the polyisoprene double bonds (Fig. 11) [15]. In particular, the incorporation of unsaturated fatty acid groups such as oleoyl on the cellulose nanofiber surfaces was effective after sulfur vulcanization because of the creation of crosslinks with the sulfur via the polyisoprene double bonds (Table 3).

Recently, significant improvements in both Young's modulus and TS have been reported in case of semi-IPN/IPN type NR/Regenerated Cellulose hybrids having microstructures comprising of unique honeycomb-like structure that encouraged the formation of intense physical entanglements/interlocks within the matrix and thereby promoted the polymer–filler interaction (Table 3). Indeed, the stretching of NR/Regenerated Cellulose hybrids was effectively hindered because of interlocking effect imposed by the honeycomb-like structure of Regenerated Cellulose on the slippage of NR domains (Fig. 12).

14.3 Dynamic Mechanical Properties

Though the mechanical properties of cellulose whisker filled NR NCPs markedly differ from neat NR, DMA results did not exhibit any significant change in the T_g of the rubber matrix. However, above T_g , a higher increase of the storage tensile modulus is observed in NR NCPs filled with an increasingly higher amount of cellulose whiskers, which could be related to the increased whiskers/whiskers interaction probability and density of the cellulosic network. In fact, good interaction between cellulose NWs and NR chains was generally reflected in the increased storage modulus, along with the slight positive shift in $\tan \delta$ peak position of the NCP, if NCPs were devoid of any micro-scaled aggregates.

Similarly, formation of covalent thioether (C–S) bonds at the NR/modified cellulose nanocrystal composite interface in NR/modified cellulose nanocrystal composite is also responsible for the improved modulus compared to NR/cellulose nanocrystal composite in the transition region [14]. A significant reinforcing effect is observed and the rubbery modulus increased upon cellulose whiskers addition in NR.

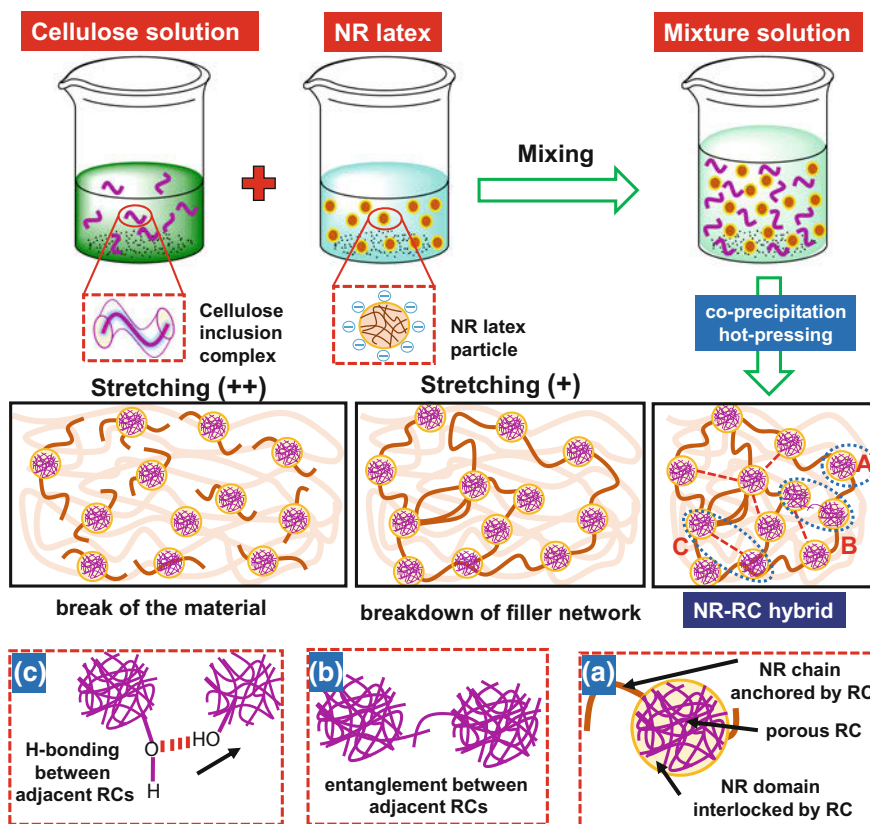


Fig. 12 Schematic illustration of NR reinforced with RC from alkaline-urea-aqueous system

15 Application

NR composites, fabricated with 3D interconnected graphene-based conductive networks, could be utilized as an eco-friendly strategy for fabrication of liquid sensors capable of sensing, discriminating, and monitoring various solvent leakage from the chemical industries.

15.1 Packaging

Because of the 100% disintegrating ability, PLA-NR-NC bio-NCPs have the potential to be utilized as biodegradable packaging materials.

16 NR Composites Based on Recycled Rubber Granulate (RRG)

With the introduction of environmentally friendlier technologies, the post-consumer tyres can be transformed into valuable raw materials, which can be used to synthesize a wide range of sustainable polymeric composites. In 1853, Charles Goodyear, the inventor of rubber vulcanization, firstly reported the use of ground rubber waste as a rubber compound filler and patented a process for moulding polymer materials obtained from RG and NR. Nowadays, dynamic increase in rubber wastes, especially as used tyres, is one of the major source for environmental pollution. Complex structure and poor recyclability of tyre materials is the potential issue for the environmental pollution. Vulcanized rubber is the major component of these used tyres, which makes up about 70–80% of the total mass of the tyres. In addition, CB and silica are present as fillers. In fact, during the manufacture of tyre materials, eight different types of NRs, thirty different high-quality synthetic rubbers, including SBR, butadiene rubber and butyl rubber, and various chemical compounds are utilized for processing as well as vulcanization of rubber matrices. Moreover, tyres also contain components, such as steel cord and fibers, made of nylon, polyester, and cellulose, which are mandatory to be isolated from rubber during recycling of waste tyre. Furthermore, because of the presence of crosslinks, the tyres are insoluble and infusible and hence, cannot be re-processed by the simple process that is generally used in manufacturing the thermoplastics. Thus, for the sustainable management of used tyres, grinding of rubber wastes, and subsequent utilization of these granulates as a component or filler can be opted to process new ‘environmentally friendly’ PCs. In this context, ground tyre rubber is usually utilized as a filler for manufacturing composites of thermosets, thermoplastics, and virgin rubber.

Continuous attempts have been made to improve the properties of RG filled NR composites. In this regard, materials containing only ground rubber wastes are developed by sintering the RGs at elevated temperature and pressure. By the application of sintering process, not only significantly higher quantity of rubber wastes can be recycled, but also no fresh rubber material is required to produce such materials. Indeed, this group of rubber materials becomes very attractive as these composites are environmentally friendlier and more economical than the composites comprising of ground rubber wastes and a newly incorporated rubber components.

17 Processing

NR-SBR based compounds have been synthesized using RRG as filler, replacing the conventionally used CB (N-220). Initially, RRGs were generated via grinding the waste tyres. Thereafter, NR based compounds are prepared in a mixer with the

rotor speed of 60 rpm at 60 °C for 6 min, followed by the addition of other ingredients in a two-roll mill. Thereafter, the compound is moulded into sheets, maintaining the vulcanizing temperature and time of 150 °C and 10 min, respectively. In an almost similar fashion, NR, RG, and various ingredients have mixed in a laboratory two-roll mill, followed by moulding at 140 °C and optimum cure time evaluated earlier by disc rheometer. Thereafter, the ageing studies of those moulded samples have also been conducted at 100 °C for 36 h in a hot air oven. In order to analyze the influence of vulcanization, three different types of NR vulcanizates have been prepared via different vulcanizing systems, viz. conventional (CV), semi-efficient (SEV) and efficient (EV) curing system. In this context, ground rubber particles are produced in the laboratory from fully cured NR vulcanizates by a mechanical crusher having rotary type cutters. Thereafter, by means of a two-roll mill, different RG particles are admixed into the NR vulcanizates produced by three different vulcanizing systems, followed by the usual molding operation in a hot press at 150 °C for a predetermined optimum curing time.

On the other hand, sintered RGs are obtained at an elevated temperature (80–240 °C) and high pressure (0.5–26.0 MPa). In fact, the RGs are press moulded at high pressure (0.5–26.0 MPa), leading to consolidated adhesion of grains and improvement in their mutual attachment. Side by side, at the elevated temperature (80–240 °C), the crosslinks in RGs are broken up and the main chains are also partially disrupted to generate radicals. Consequently, in the next stage, new bonds connecting the individual grains of granulate can be generated via rearrangement of the generated radicals, which ultimately produces a homogenous rubbery material.

18 Characterization

According to the earlier studies, properties of RGs are mostly dependent on the size-reduction methods (i.e., grinding at cryogenic or ambient-temperature grinding), grain dimension, extent of crosslinking, quantity of filler, and the type of NR that are used to produce such RGs.

18.1 Mechanical Properties

Incorporation of ground rubber tyres into NR reduces TS, EAB and tear resistance of the vulcanizates. The effect is more pronounced for composites filled with larger particles (Table 4). This is reasonable since as the particle size decreases, surface area increases, and flaw size in the matrix also decreases. However, it is found that smaller the particle, poorer is the ageing property. For example, NR mixed with ground rubber tyre of <52 mesh particles (650–450 µm) registers the retention of TS and tear strength of 71 and 78%, respectively, while the NR mixed with ground

rubber tyre of 100–150 mesh particles (150–100 μm) exhibits only 31 and 46% retention of TS and retention of tear strength, respectively. Furthermore, metals present in ground rubber tyres possess detrimental effect on the physical properties of aged vulcanizates. In fact, the occurrence of huge amounts of metals in fine-grained rubber dust is attributed to the metallic impurities generated via grinding of the residual steel wire beads present in the ground rubber tyre.

Mechanical properties and the vulcanization characteristics of rubber mixtures, obtained from NR and RGs, are dependent on the type of crosslinking agent applied at the time of their vulcanization. However, except EAB, all the properties of ground RG filled vulcanizates are adversely affected (Table 4). Notably, for NR vulcanizates prepared via SEV system, the relative decrease in TS, modulus, and tear strengths are smaller than those of NR vulcanizates fabricated by CV and EV systems. The composites containing crosslinked RGs by sulfur possess greater TS, EAB, and tear strength over the composites obtained from RGs crosslinked with a

Table 4 Tensile properties of various RRP filled NR composites and NCPs

Composites/NCPs	TS (MPa)	EAB (%)	Tensile modulus or Young's modulus (Mpa) at 100% elongation	Tear strength (kN m^{-1})
NR (unfilled)	14.00	1175.00	–	28.20
NR (unfilled and aged)	8.00	770.00	–	20.30
NR filled with 30 phr 150–100 μm RRP particles	8.00	860.00	–	21.20
NR filled with 30 phr 150–100 μm RRP particles (aged)	2.50	400.00	–	9.70
NR filled with 30 phr 650–450 μm RRP particles	2.20	430.00	–	12.40
NR filled with 30 phr 650–450 μm RRP particles (aged)	1.60	230.00	–	9.70
NR (conventional vulcanizate)	27.70	387.00	5.20	117.00
NR (conventional vulcanizate) with 50 phr RRP	17.60	368.00	2.55	73.00
NR (semi-efficient vulcanizate)	25.70	396.00	3.63	111.00
NR (semi-efficient vulcanizate) with 50 phr RRP	21.60	417.00	2.35	86.00
NR (efficient vulcanizate)	23.90	451.00	2.45	92.00
NR (efficient vulcanizate) with 50 phr RRP	15.90	461.00	1.37	61.00

peroxide. In general, it is noted that the mechanical properties significantly deteriorates with the elevated RG content of the composites. However, with the increase in the RG content, from 10 to 50 phr, EAB increases from ca 320–360 to 360–400%. Indeed, overall deterioration of mechanical properties for increasingly filled vulcanizates is closely associated with the continuous reduction of crosslink densities for vulcanizates filled with the higher amount of RGs. Moreover, significantly deteriorated mechanical properties of composites, bearing peroxide crosslinked granulate, are related to the prevalence of weaker adhesion force among fillers and the matrices. In this context, the reasonable deterioration of mechanical properties has also been noticed with the increasing particle size and extent of RGs in NR composites. However, partial replacement of CB by RRP in NR composites, amounting up to 15 wt%, cannot affect TS, EAB, and hardness of the composites. Nevertheless, the increasingly higher extent of replacement of CB by RRG adversely affects the overall mechanical properties. The EAB of RG filled NR composites increases with the increasing amount of RG.

The mechanical properties of sintered rubbers are predominantly dependent on the temperature, processing time, type of RGs and their grain size. Again, materials obtained from NR based RGs can attain TS within 3.5–6.5 MPa and EAB of 330–530%. Further improvement of these sintered materials can be possible if NR granulates are moulded for 20–30 min at 200 °C and 8.6 MPa. Moreover, the mechanical properties of sinters, based on NR granulate, can be elevated by adding organic acids of low molecular weight, such as benzoic acid, salicylic acid, maleic acid/anhydride, phthalimide, and phthalic anhydride [16]. In fact, investigation of the mechanisms of sintering and the underlying factors behind the enhancement of the properties during incorporation of additives, such as benzoic acid, salicylic acid, maleic acid/anhydride, phthalimide and phthalic anhydride, have already been reported that contains the possible way of breaking and reconstitution of crosslinks during sintering of RGs based on NR (Fig. 13). It is well-known that the mechanical properties of the rubber decrease with the increase in the formation of conjugated double (Fig. 14) bonds because of reversion. Thus, mechanical properties of sintered NR are significantly inferior to that of composites made from fresh NR. In fact, the

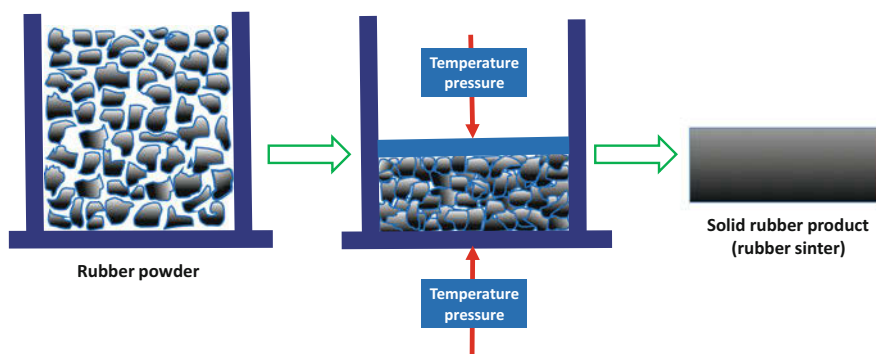


Fig. 13 Process for sintering of rubber

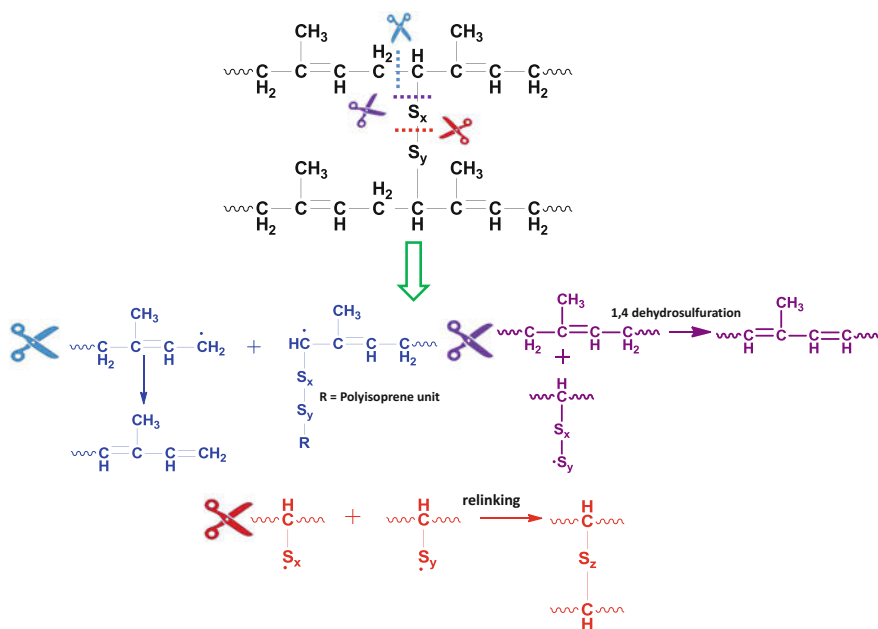


Fig. 14 Breaking of cross-link on heating

sintered rubbers have inferior mechanical properties because of the energy involved in void propagation and strain-induced crystallization. At the time of stretching, the network rubber chains demonstrate their inherent tendency to orient themselves in the stretching direction, which encourages formation of crystallites. These crystallites bind simultaneously with a multiple number of neighbouring network chains, resulting in the crosslinking network for high TS and EAB. Because of the lack of any chain entanglement, sintered rubber absorbs lesser energy to propagate a defect/void than the energy required to stretch the backbone chains to achieve strain-induced crystallization. Accordingly, the samples rupture before the commencement of strain-induced crystallization, or samples experience a marginal extent of strain-induced crystallization and therefore possess a lower strength and EAB.

The TS and EAB of these sinters increase from 0.8 to 1.3 MPa and 100 to 270%, respectively, when the moulding temperature and applied pressure are increased up to 200 °C and 6000 kg, respectively. However, as the temperature is raised beyond 200 °C, TS of the sintered NCR deteriorates considerably. At a temperature beyond 200 °C, oxidation of the sulfur from rubber may be the possible reason behind such decrease in TS. In addition, with the increase in moulding temperature, the elastic modulus of the sintered NCR decreases continuously, from 0.26 to 0.15 MPa, because of the destruction of thermolabile polysulfide linkages ($-S_x-$) in rubber with the simultaneous generation of thermally active free sulfur. The optimum parameters of sintering allowed to achieve the best mechanical properties, are 200 °C and 6000 kg.

19 Application

According to the analysis of tyre recycling market, RGs are no longer considered as a cheap filler but as a valuable component for manufacturing sustainable rubber composites. RGs are nowadays effectively utilized in widespread applications, such as molded/extruded products (wheels, gasket, sole), mulch, animal bedding, playgrounds, artificial sports surfacing, and automotive industries. However, in some applications, especially in products of higher quality and strength, e.g. in new tyres, the use of RGs are limited. Therefore, these rubber composites, obtained using RGs, are practically used to manufacture cheap articles, where strength is not important, such as floor tiles and other flooring materials, washers, windscreen wipers, tapes, cable housings, moulds, and footwear soles. Besides, sintered RGs can also be utilized in manufacturing washers, roofing materials, insulation boards, shoe soles, and solid tyres.

20 NR Composites Containing Proteins

Proteinous substances, such as silk, soy, and leather waste (LW), can be utilized as potential fillers to produce environment-friendly NR composites. The significantly huge quantity of a variety of leather solid wastes, such as buffing dust, shaving dust, and fleshings, are generated during various stages of the leather tanning process. In fact, a massive portion of these solid wastes comprise of collagenous matter and these collagenous LWs can be used as an inert filler for manufacturing environment-friendly polymeric composites. On the other hand, silk, like *Bombyx mori*, is basically a protein comprising of natural polymer fiber, used in textile production. Silk, in its natural form, is composed of a filament core protein, silk fibroin, and a glue-like coating consisting of a family of sericin proteins. Again, soy protein is a low-cost raw material, which is derived from natural resources, such as soybean.

21 Processing

Fabrication of green elastomeric composites, based on NR and silk textiles, is carried out by sandwiching a single layer of textile between layers of NR. Initially, NR samples are compressed at 70 °C for 10 min in order to obtain 1 mm thick sheets. Thereafter, silk fabric is sandwiched between two rubber sheets and the sandwich sample is compressed at 70 °C for 10 min, allowing the rubber to get impregnated with the silk fabric (Fig. 15). Earlier, silk fiber reinforced PP and NR blend composites have been prepared and characterized to monitor the environmental and gamma radiation effect on the mechanical properties of the composites comprising of NR, polypropylene, and silk. Initially, a varying amount of NR lumps are cut into small pieces and blended with PP in an extruder at 180–200 °C

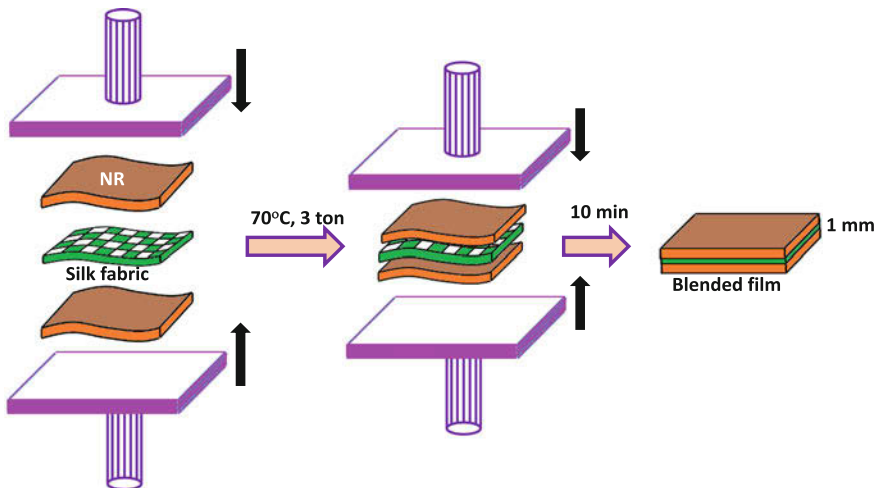


Fig. 15 Preparation of silk fabric blended NR film

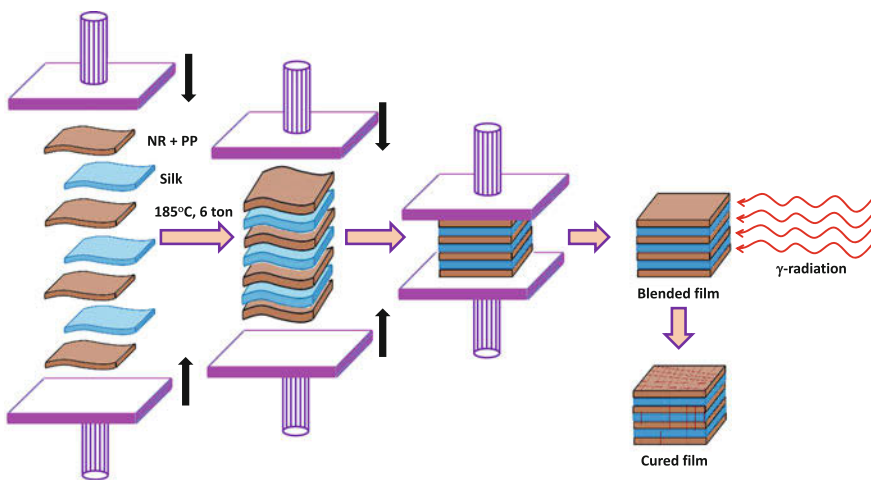


Fig. 16 Preparation of blended and cured film

to produce different compositions. Thereafter, these blends of varying compositions are cold pressed at 12-ton pressure to prepare films of desired thickness. To prepare composites, three layers of silk fibers are sandwiched among four layers of the blended films using hot pressing at 185 °C and 6 ton pressure, followed by cold pressing at 6 ton pressure (Fig. 16). Finally, in order to improve the mechanical properties, these composites are exposed to varying doses of gamma radiation.

To fabricate soy protein reinforced NR composites, initial hydrolysis of soy protein under different conditions is done, followed by microfluidization and

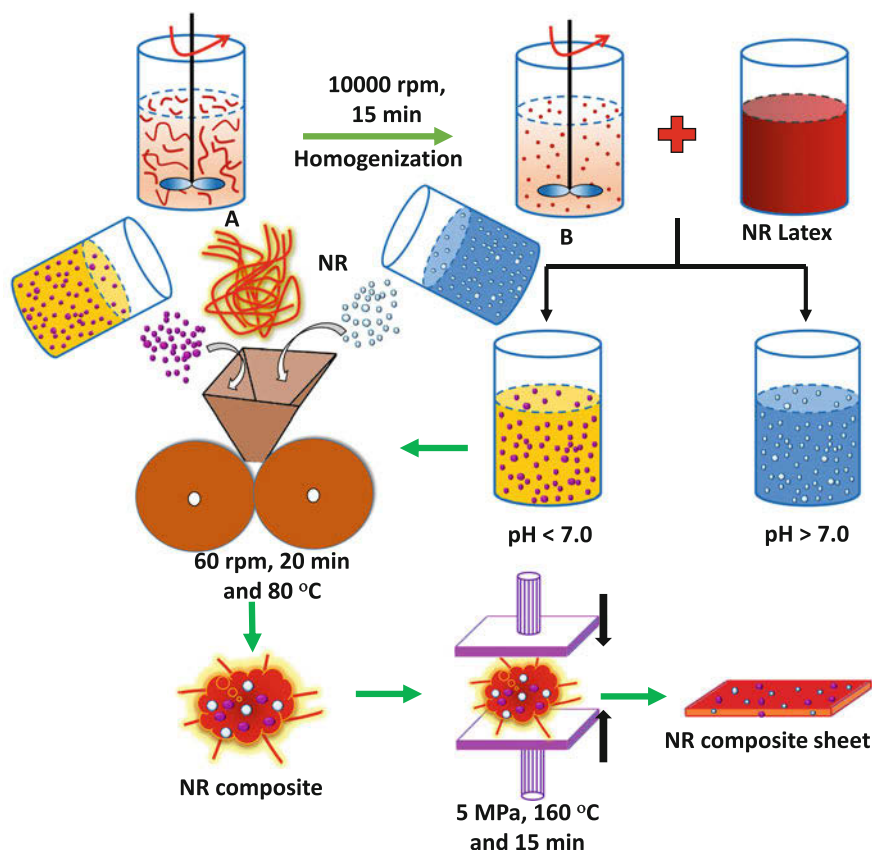


Fig. 17 Preparation of NR composite sheet

associated size reduction. Thereafter, these particles of near uniform sizes are incorporated as reinforcing additives during the preparation of NR composites in an internal mixer. In this context, initially, an alkaline dispersion of soy protein in distilled water is prepared by continuous stirring for 1 h at 60 °C. Thereafter, the dispersion is homogenized at 10,000 rpm for 15 min, followed by passing through a microfluidizer for several times (10 cycles). Later, the dispersion is admixed with NR latexes in both alkaline and acidic conditions to produce NR composite particles of varied pH (Fig. 17). In the next step, these dried composite particles, prepared under both alkaline and acidic conditions, are used as reinforcing ingredients in preparing NR composites by Brabender mixer, operated at 60 rpm for 20 min at 80 °C. Finally, the NR compounds are compression moulded in a window-type mould at 5 MPa and 160 °C for 15 min.

Processing of LW filled NR composites is performed in an open mixing mill or a rubber mixer for 20 min at 40 °C according to the ASTM D 3182 method. The composites are made of CB (60 phr), LW (60 or 80 phr), zinc oxide (5 phr),

stearic acid (3 phr), sulfur (2.5 phr), ZMB-2 (1phr), and an accelerating system consisting of MBTS (1.2 phr) and TMTD (0.4 phr). Once the mixing process is completed, the formulations are compression-moulded at 150 °C with a closing pressure of 7.5 ton in a pneumatic press for stipulated time periods determined via rheological assays.

In an almost similar fashion, fabrication of NR composite foams is carried out using LW as filler. Initially, the leather fibers are shredded to 16 mm diameter using a mill with rotating knives and a 30 mesh sliver for obtaining both short fibers and leather fiber granules. Thereafter, a two-roll mill is used to prepare the composites.

Firstly, NR is milled with leather shavings at 65 °C, maintaining the friction ratio at 1:1.25. Subsequently, stearic acid is added as a co-activator and mixed for 5 min. Later, the activity of organic accelerator was enhanced by mixing an activator, i.e., zinc oxide for 7 min. In the next step, MBTS and TMTD are added as accelerators for 3 min. Finally, sulfur is added as a vulcanizing agent and mixed for 5 min, followed by addition of a blowing agent (i.e. TSH). The compounds are vulcanized and foamed via heat transfer process in an electrically heated hydraulic press to mould into microcellular rubber foam. This process involves a simultaneous curing and foaming at 125 °C for 7 min. The foaming process occurs in NR because of the decomposition of the blowing agent (toluenesulfohydrazine) generating gases that exert pressure in the surrounding polymer network. In this context, synthesis of NR-LW composites, via employing a variegated quantity of grounded and sieved LW particles as fillers, have also been carried out. The compounding is carried out in the open two-roll mixer while various ingredients, like activator, accelerator, filler, a vulcanizing agent, are added sequentially, in addition to the polyethylene glycol 4000, which is added as an acid neutralizer or antioxidant to neutralize the acidic nature of the added LW (Fig. 18).

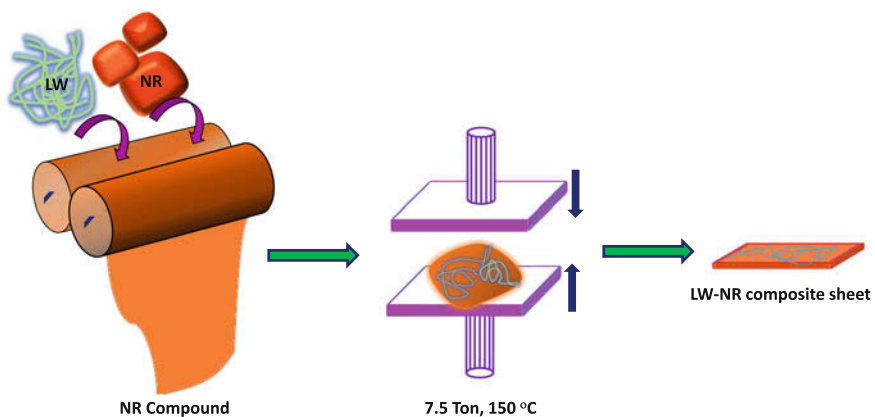


Fig. 18 Preparation of LW-NR composite

22 Characterization

22.1 Mechanical Properties

The reinforcing ability of the prepared green elastomeric composites is examined and compared with nylon textile reinforced NR composites. NR-silk composites exhibit superior mechanical properties than NR-nylon composites (Table 2). In fact, TS of nylon reinforced NRs are only 35–45% of the TS of the corresponding silk reinforced rubbers. Moreover, both nylon and silk-based non-purified NR composites exhibit significantly higher TS than the corresponding purified NR composites. Two important aspects are mainly responsible for such improvement in mechanical properties for non-purified NR based composites. First of all, better impregnation of rubber with silk results when non-purified NR is used as the matrix. In addition, protein impurities in non-purified NR increase the possibility of protein-protein interactions in NR-silk composites.

On contrary, mechanical properties of NR-PP-silk composites decrease significantly as the NR content in the matrix is increased (Table 2). However, once the composites are exposed to a certain limiting dose of gamma irradiation up to the maximum of 250 krad, both tensile and bending properties improve significantly. However, higher radiation dose, i.e. >250 krad, deteriorates the overall mechanical properties of all the composites. In fact, at higher radiation dose, bond scission occurs, which is responsible for the decreased mechanical strength of the composites. On the other hand, if the applied radiation dose is not allowed to go beyond 250 krad, the radiation-induced free radicals of silk, NR, PP might produce new bonds/crosslinks, which are responsible for the increased mechanical strength of composites.

Among the soy protein filled particulate NR composites, the less hydrolyzed soy protein particles yield NR composites with greater TS, Young's modulus, and toughness, while the highly hydrolyzed soy protein particles yield composites with greater elongation (Table 2). It is also observed that the NR composites, filled with soy-NR latex particles prepared under alkaline condition, provide greater TS, Young's modulus, and toughness, whereas NR composites, filled with soy-NR latex particles prepared under acidic condition, are of higher EAB. In this regard, when soy-NR latex particles are prepared via coagulation under acidic condition, the particle size of the filler is increased because of the enhanced aggregating tendency of soy protein particles, as soy protein particles approach to the characteristic isoelectric point at pH 4.5. Thus, the increased particle size of filler, resulting from enhanced aggregation, impairs TS, modulus of the composites filled by soy-NR latex particles coagulated under acidic condition.

Strain-strain test is also conducted for LW-NR composites. TS and EAB values of all the LW treated samples are severely reduced (Table 2), as compared to the control sample devoid of LW. Indeed, these parameters are noted to be further deteriorated with the increased addition of LW component in LW-NR composites. However, both shore A hardness and abrasion resistance of all the LW-NR

composites samples is improved substantially (Table 2), as the composite material becomes increasingly more compact with the addition of fibrous protein waste. In this context, Santosh et al. have also reported the increased level of hardness and abrasion resistance in the LW filled NR samples, along with the expected rise in TS and associated loss in EAB (Table 2).

The cyclic stress-strain compression analyses for NR composite foams, filled with LW, are also carried out in which the samples are submitted to five compression-decompression cycles. It is observed that increased proportion of LW in the polymeric matrix leads to the increased hysteresis values (Table 2), suggesting reluctance of the system to return back to the original shape. The energy dissipation during compression-decompression deteriorates the matrix. The hysteresis values are measured via estimating the area related to the cyclic compression curves, attributed to the interfacial interaction of waste with NR. This interaction decreases the effectivity of stress transfer from rubber and consequently increases the work essential to effect the deformation of the composites, resulting in the enhancement of Young's modulus (Table 2). In this context, increasing amount of LW improves the strength at rupture or TS from 1.38 for NR to 2.18 MPa for NR composite foams filled with 60 phr LW, which is attributed to the interfacial adhesion between the LW and NR, i.e. the strength is transferred from NR matrix to LW and therefore required more stress to attain the rupture. Nevertheless, the deformation at rupture decreases from NR (408.7%) to NR composite foams filled with 20 phr LW (394.9%) because of due to the reduced mobility of rubber chain. Such phenomenon is attributed to the presence of filler which enhances the rigidity of the polymer, as evidenced from the increase in respective Young's modulus from 0.0026 for NR to 0.1206 MPa for NR composite foams filled with 60 phr LW (Table 2). Accordingly, the EAB values for 40 and 60 phr LW filled NR composite foams deteriorate to 73.8 and 57.6%, respectively (Table 2).

22.2 *Dynamic Mechanical Properties*

NR-silk composites exhibit improved dynamic mechanical properties than NR-nylon composites. For the soy-NR latex particle filled composites, the experimental reinforcement factors are compared with calculated reinforcing factors, evaluated by the Einstein-Smallwood (Eq. 1) and Guth-Gold equations (Eq. 2). Almost similar reinforcing factors are obtained for the composites prepared under alkaline or acidic conditions, and are greater than the calculated reinforcing factors, as evaluated using Guth-Gold equation. In fact, composites, having 30 and 40% fillers, exhibit greater reinforcement factors than that predicted by the Guth-Gold equation, indicating greater interparticle interactions to produce stiffer filler network.

$$G' = G'_0(1 + 2.5\phi) \quad (1)$$

$$G' = G'_0(1 + 2.5\phi + 14.1\phi^2) \quad (2)$$

22.3 Biodegradability

NR-PP-silk composites become more biodegradable with the increased incorporation of NR in PP. For instance, after 24 weeks of soil burial, silk fiber reinforced PP composite loses 10.20% TS whereas silk reinforced PP and NR blend (50:50) composite loses 24.3% TS. Similarly, under the same condition, silk fiber reinforced PP composite losses 13% BS, whereas silk reinforced PP and NR blend (50:50) composite loses 29.2% BS.

23 Application

The developed green materials, such as NR-silk composites, may be suitable for applications where damping, waterproofing, or high-pressure capacities in elastomeric tubing (such as in high-end bicycle tyres), alongside high mechanical properties is desired. Because of the improved values of conductivity, LW-NR composites exhibit the potential to be used as an antistatic flooring. In this way, the development of these innovative composites based on NR, CB, and LW can be an excellent option for allocation to hazardous LW within the composites and thereby minimization of environmental impact. Again, the NR composite foams filled with LWs can be directed to diversified foam related applications and thereby the mechanical/thermal properties can be modulated by controlling the foam density and other characteristic features.

24 Conclusions

Environmentally friendly NR composites filled with natural-organic fillers induce improved environmental impact and thereby accentuate the biodegradable character of these 'green' composites. By developing such 'green' composites, the use of mineral-inorganic fillers obtained from petroleum-based non-renewable resources can be minimized or obviated. At present, many research works are concentrated upon the mechanical property enhancement of these 'green' NR composites through chemical modification of the filler, use of adhesion promoters, and additives. Improvement of interfacial adhesion between natural fibers and NR matrix will remain the key issue in terms of overall performance since it determines the

final properties of the composites. Further research is in progress to overcome the obstacles, which includes moisture absorption, inadequate toughness, and reduced long-term stability for outdoor applications. In particular, the major attention in near future would be to ensure that the different weathering conditions, such as temperature, humidity, and UV radiation, should not be able to deteriorate the service life of these environmentally friendly NRCs.

Acknowledgements The corresponding author gratefully acknowledges the Department of Science and Technology (DST), Government of India (YSS/2015/000886).

References

1. Chattopadhyay PK, Das NC, Chattopadhyay S (2011) Influence of interfacial roughness and the hybrid filler microstructures on the properties of ternary elastomeric composites. *Compos Part A-Appl Sci* 42:1049–1059
2. Chattopadhyay PK, Chattopadhyay S, Das NC et al (2011) Impact of carbon black substitution with nanoclay on microstructure and tribological properties of ternary elastomeric composites. *Mater Des* 32:4696–4704
3. Mondal M, Chattopadhyay PK, Chattopadhyay S et al (2010) Thermal and morphological analysis of thermoplastic polyurethane-clay nanocomposites: comparison of efficacy of dual modified laponite vs. commercial montmorillonites. *Thermochim Acta* 510:185–194
4. Praveen S, Chattopadhyay PK, Albert P et al (2009) Synergistic effect of carbon black and nanoclay fillers in styrene butadiene rubber matrix: development of dual structure. *Compos Part A-Appl Sci* 40:309–316
5. Singha NR, Das P, Ray SK (2013) Recovery of pyridine from water by pervaporation using filled and crosslinked EPDM membranes. *J Ind Eng Chem* 6:2034–2045
6. Yu P, He H, Luo Y et al (2017) Reinforcement of natural rubber: the use of in situ regenerated cellulose from alkaline-urea-aqueous system. *Macromolecules* 50:7211–7221
7. Karmakar M, Mahapatra M, Singha NR (2017) Separation of tetrahydrofuran using RSM optimized accelerator-sulfur-filler of rubber membranes: systematic optimization and comprehensive mechanistic study. *Korean J Chem Eng* 34:1416–1434
8. Mahapatra M, Karmakar M, Mondal B et al (2016) Role of ZDC/S ratio for pervaporative separation of organic liquids through modified EPDM membranes: rational mechanistic study of vulcanization. *RSC Adv* 6:69387–69403
9. Singha NR, Ray S, Ray SK et al (2011) Removal of pyridine from water by pervaporation using filled SBR membranes. *J Appl Polym Sci* 121:1330–1334
10. Singha NR, Ray SK (2012) Removal of pyridine from water by pervaporation using crosslinked and filled natural rubber membranes. *J Appl Polym Sci* 124:E99–E107
11. Jacob M, Francis B, Thomas S et al (2006) Dynamical mechanical analysis of sisal/oil palm hybrid fiber-reinforced natural rubber composites. *Polym Compos* 27:671–680
12. Joseph S, Joseph K, Thomas S (2006) Green composites from natural rubber and oil palm fiber: physical and mechanical properties. *Int J Polym Mater* 55:925–945
13. Visakh PM, Thomas S, Oksman K et al (2012) Crosslinked natural rubber nanocomposites reinforced with cellulose whiskers isolated from bamboo waste: processing and mechanical/thermal properties. *Compos Part A-Appl Sci* 43:735–741

14. Kanoth BP, Claudino M, Johansson M et al (2015) Biocomposites from natural rubber: synergistic effects of functionalized cellulose nanocrystals as both reinforcing and cross-linking agents via free-radical thiol-ene chemistry. *ACS Appl Mater Interfaces* 7:16303–16310
15. Kato H, Nakatsubo F, Abe K et al (2015) Crosslinking via sulfur vulcanization of natural rubber and cellulose nanofibers incorporating unsaturated fatty acids. *RSC Adv* 5:29814–29819
16. Tripathy AR, Morin JE, Williams DE et al (2002) A novel approach to improving the mechanical properties in recycled vulcanized natural rubber and its mechanism. *Macromolecules* 35:4616–4627

Electrical Properties of Sustainable Nano-Composites Containing Nano-Fillers: Dielectric Properties and Electrical Conductivity



Sabzoi Nizamuddin, Sabzoi Maryam, Humair Ahmed Baloch, M. T. H. Siddiqui, Pooja Takkalkar, N. M. Mubarak, Abdul Sattar Jatoi, Sadaf Aftab Abbasi, G. J. Griffin, Khadija Qureshi and Nhol Kao

1 Introduction

Nanocomposite materials have received much recognition in the last two decades due to their extraordinary characteristics by combining properties of different types of materials. Nanocomposites are made by mixing two or more phases such as fibers, layers, or particles, where a minimum of one phase is in the nanometer size range. The characteristics of nanocomposites are dependent on the characteristics of the nanofiller and parent material as well as upon morphological, mechanical and interfacial characteristics between the nanofillers and the parent materials [1, 2]. Nanocomposites can be utilized in a wide range of applications including aerospace, automotive, defence, energy, infrastructure, sporting goods and trans-

S. Nizamuddin · H. A. Baloch · M. T. H. Siddiqui · P. Takkalkar · S. A. Abbasi
G. J. Griffin (✉) · N. Kao
School of Engineering, RMIT University, Melbourne, VIC 3000, Australia
e-mail: gregory.griffin@rmit.edu.au

S. Maryam
Department of Electrical Engineering, Quaid-e-Awam University of Engineering,
Science, and Technology, Nawabshah, Sindh, Pakistan

N. M. Mubarak
Department of Chemical Engineering, Faculty of Engineering and Science,
Curtin University, 98009 Sarawak, Malaysia

A. S. Jatoi
Department of Chemical Engineering, Dawood University of Engineering
and Technology, Karachi, Pakistan

K. Qureshi
Department of Chemical Engineering, Mehran University of Engineering
and Technology, Jamshoro, Sindh, Pakistan

portation sectors due to their light weight, high strength, high durability, and design and process flexibility [3].

The discovery of a variety of nano-scale materials may offer a number of new composites with specific properties. Nanoparticles possess great potential to be utilized as filler materials to improve the electrical, mechanical and physical properties of nanocomposites. It is important that at least one dimension of the filler material be of nanometer order for the synthesis of nanocomposite materials but the final product can be of any size either nano, micro or macroscopic in size [2]. Carbon black, carbon fibre and carbon nanotubes have been effectively investigated as fillers to fabricate nanocomposites [4]. For example, aligned carbon nanotubes in polymeric composites result in enhanced thermal transport [5] and strong luminescence [6] favouring the direction along the nanotube axis. A number of polymer/carbon nanotubes have successfully been fabricated by incorporating carbon nanotubes in polymer matrices including polyamide, polystyrene, polycarbonate, polyethylene, polypropylene and polylactide.

Extraordinary electrical and dielectric (high dielectric constant and low dielectric loss) properties of nanosize particles with high conductivity are considered as a gateway for substituting the monolithic metals in various emerging applications such as e-paper, microelectronics, organic light emitting diodes, antistatic coatings, sensors and touch screens. The above-mentioned applications can be achieved by obtaining the maximum electrical conductivity of nanocomposites with the lowest possible filler concentration [7]. It is reported in the literature that the electric/dielectric properties of nanocomposites were greatly enhanced by incorporating nanofillers including carbon nanotubes, carbon nanofibers, metal particles and carbon black [8]. Therefore, this study mainly overviews the electrical conductivity of nanocomposites containing nanofillers. Further, dielectric properties (dielectric constant, dielectric loss and tangent loss) of nanocomposites are discussed in detail. In addition, a critical discussion on evaluation of electrical conductivity and dielectric properties of nanocomposites with nanofillers is provided. Conclusions are drawn in the light of literature; with recommendations being henceforth provided.

2 Nanocomposites with Nanofillers

Polymer nanocomposites are a branch of nanotechnology and composite science which involves the development of a new category of materials. These materials possess superior properties which improve the performance of these materials with multi-functionalities. The polymer nanocomposite is fabricated by incorporating nanofillers in a polymer matrix at different concentrations [9–13]. The addition of nanofillers helps to improve the physical, mechanical, chemical and thermal, barrier, electrical and dielectric properties of the composite [14–22]. The inherent properties of polymers like light weight, transparency and flexibility are combined in a nanocomposite with other properties.

For decades, the development of polymer composites has been one of the most important areas in materials science. When fillers are used at the nanometer scale (for the production of entities that enhance or increase polymer properties), i.e. at least one dimension is between 1 and 100 nm, it is called a nanofiller, and the composite becomes a nanocomposite [23]. In this regard, various researchers work on different nanofillers for nanocomposites fabrication [24]. Among others, the carbon nanofillers including carbon nanotubes, carbon nanofibers, and metallic nanowires get appreciable interest in the field of polymers [25]. Carbon nanotubes have a high tensile strength and are considered 100 times stronger than steel with only one-sixth of the weight, so they can be the strongest fibers and the smallest known. They also have high conductivity, high surface area, unique electronic properties and polymer adsorption potential [26]. The applications of the carbon nanotubes that are currently studied include polymeric compounds (conductive and structural fillers), electron field emitters (flat screens), electromagnetic shielding, batteries, supercapacitors, hydrogen storage and structural compounds [27].

Carbon nanotubes can be produced from different material which includes silicon and germanium, but the development and application of carbon nanotubes remains the main focus of activity [27]. Carbon nanotubes hold outstanding electronic, optical, thermal and mechanical properties [28]. Its tubular structure prevents the diffusion of cracks and dislocations, providing the carbon nanotubes with a great potential for producing materials with high Young's modulus [29]. The partial sp²-sp³ hybridization of the C-C bonds of carbon nanotubes can induce high flexibility [30]. Therefore, the potential application of carbon nanotubes has always attracted great interest. Carbon nanotubes are also excellent nanofillers for polymeric nanocomposites [31, 32]. Even if a small number of carbon nanotubes are added to the polymer, the mechanical properties can be significantly improved, and even an electrically insulating polymer can be converted into a conductive composite material by addition of carbon nanotubes as filler [33].

Nanowires can be produced from conductive (e.g. metal) or semi-conductive (e.g. carbon) materials using a variety of production techniques. They have a unique crystalline structure and typical diameter of tens of nanometers with high aspect ratio. They are used as interconnectors for the transport of electrons in nano-electronic devices. Several metals have been used to make nanowires including cobalt, gold and copper. Polymer and filler interaction can be increased through polymer grafting onto the nanofiller. For grafting, two methods are widely used for matrix preparation; the first method commonly takes place by the reaction of polymer chains with the surface of nanofiller. For example, polystyrene grafting to single-walled, oxidized carbon nanotubes and PVA grafting to multiwalled carbon nanotubes activated by carbodiimide. Other techniques include reactions with nanofillers that are oxidized by amidation or esterification, cycloaddition, nucleophilic addition, condensation and other chemical reactions. A major shortcoming of the first step is lower enthalpy density due to macromolecular steric hindrance caused by polymer chains attached to the surface of nanotubes. The second technique of grafting encompasses polymerization of the surface of the nanofillers. In this process, three-dimensional barriers are not problematic and

polymers with higher molecular weight can be prepared. However, this method requires precise control of the polymerization reaction. “Grafting” methods include radical polymerization transfer, additional separation chain transfer, free radical polymerization, ring opening polymerization, polycondensation, cationic/anionic polymerization, redox/oxidation, and metallocene and radical polymerization of nitrogen oxide. These methods of grafting are described and well explained in various outstanding reviews reported in the literature [34].

3 Dielectric Properties of Nanocomposites

Dielectric material properties define energy transmission, absorption and reflection to the electric field of electromagnetic waves. These characteristics measure the capability of materials for dissipation of electromagnetic energy as heat [35]. Dielectric characteristics are highly dependent on the nature of the materials such as structure and composition of materials, on the other hand, it is also dependent on process conditions like temperature and frequency [36]. Dielectric characteristics of different materials also depend on bulk density, moisture and association of permanent dipole moment with water and other constituent molecules [37]. An understanding of dielectric characteristics might support the design of microwave systems and predict the yield of microwave processes [38]. Knowledge of dielectric characteristics leads to applications for materials including electronic packaging and sensors [38].

The dielectric properties are dielectric loss factor, dielectric constant, tangent loss ($\tan \delta$) and penetration depth. The dielectric constant measures the dielectric's capacity for storing electrical energy. For example, the Polymer-ceramic nanocomposites hold strong potential for improving the performance in energy storage capacitors, hybrid electric vehicles and kinetic energy weapons, since they contain a high-breakdown-strength polymer matrix and high-dielectric-permittivity ceramic nanofillers and thus can reach a high level of energy-storage density as shown in Fig. 1. The loss factor estimates loss of electrical energy in dielectrics. Penetration depth is a measurement of the depth microwaves can penetrate materials at a specific frequency. The tangent loss is the determination of the capability of the materials for transforming the electromagnetic energy into internal energy at a particular temperature and frequency [39]. The tangent loss is calculated as the ratio of dielectric loss factor to dielectric constant. Penetration depth is calculated by an equation: $DP = \lambda_0 / 2\pi (\epsilon')^{0.5} [1 + (\tan \delta) / 20.5 - 1]^{-0.5}$. The relaxation time and static permittivity are calculated via the equation: $\epsilon''\tau = -(\omega\epsilon''\tau) + \epsilon s$.

The loss factor and dielectric constant depends highly on the frequency, magnitude and material's efficiency for interacting with microwaves. Therefore, the frequency is a fundamental factor for determining dielectric heating of materials [40]. The amount of moisture existing in a material strongly affects the dielectric characteristics of materials. It has been observed that the higher the moisture content the lower will be the dielectric properties [41]. The physicochemical

composition, density and temperature also have a significant influence on dielectric characteristics of materials [39].

3.1 Dielectric Constant

The dielectric constant is an important property of materials which measures their ability to store electrical energy [42]. The dielectric constant for pure polymers usually falls between 2 and 10. Generally, a high dielectric constant is required for all types of polymers except for fast static dissipation and high-speed integrated circuit applications, which requires a low dielectric constant [43]. A high dielectric constant can be achieved by reinforcing the conductive filler in the polymer matrix. For instance, graphite nanoplatelet (GNP), as shown in Fig. 2, is one promising nanofiller to fabricate polymer/GNP nanocomposites with a high dielectric constant due to strong interfacial polarization.

A number of studies have been carried out for improving the dielectric constant values of nanocomposites using suitable nanofiller. Huang et al. [44] reported the preparation of three-phase nanocomposites containing poly(vinylidene fluoride)

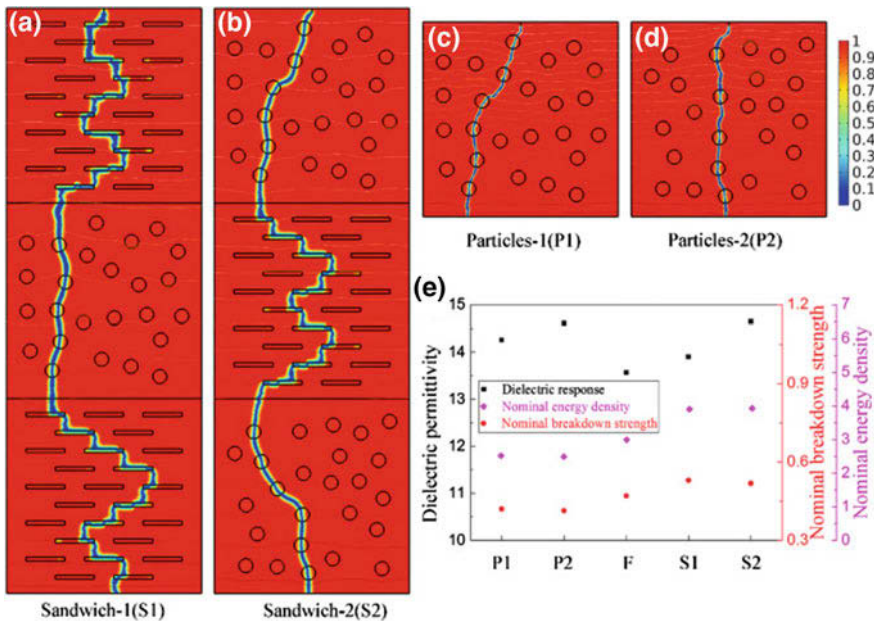


Fig. 1 The breakdown paths of nanocomposites with (a) Sandwich-1 (S1), (b) Sandwich-2 (S2), (c) Particles-1 (P1), (d) Particles-2 (P2) microstructures. (e) Dielectric permittivity, nominal breakdown strength and nominal energy density of nanocomposites with different microstructures of nanofillers [63]

(PVDF), nanoparticles of barium titanate (BT), and β -silicon carbide (β -SiC). The results showed that the three-phase nanocomposites demonstrated considerably higher dielectric constant than the two-phase PVDF/BT nanocomposites. The addition of the β -SiC whiskers caused a drastic improvement of the dielectric constant of the nanocomposite at a certain loading level. The value of dielectric constant of the three-phase system was highest (325) at a β -SiC loading of 17.5 vol.%. However, further addition of β -SiC (20 vol.%) led to a reduction in the dielectric constant of the PVDF/BT/ β -SiC composite to 253. This could possibly be due to the generation of voids and porosity in the composite [45].

He et al. [46] fabricated a novel nanocomposite with poly(vinylidene fluoride) (PVDF) as the matrix and exfoliated graphite nanoplates (xGNPs) as the conductive nanofiller. The results (refer Fig. 2.) clearly showed an increase in the dielectric constant of the PVDF/xGNP nanocomposites and this can be credited to the uniform dispersion of the xGNPs within the PVDF matrix with consequent development of micro-capacitors with the increase in xGNP concentration [47]. This network advancement was explained by three stages (I, II, and III). There is gradual increase initially in the dielectric constant of the nanocomposites when compared to the unfilled system; this is due to the initiation of the development of the micro-capacitance assemblies.

The dielectric constant continued to rise with the increasing nanofiller concentration until it reached percolation threshold. Beyond the percolation threshold, the dielectric constant continued to increase and then ultimately decreased as the loading of nanofiller reached 3.12 vol.%. The reason for this being the formation of a significant conductive network, and subsequent current leakage within the nanocomposite [48].

3.2 Dielectric Loss Factor

Dielectric properties including dielectric constant and dielectric loss factor play an important role in the simulation of propagation of electromagnetic waves in a wireless environment. The dielectric characteristics have a significant effect on the performance of the wireless system as well as in microwave heating fields [49]. The dielectric loss factor is a vital characteristic of polymer nanocomposites and is under investigation by various researchers.

Zhang et al. [50] fabricated polyamide-clay (PI) nanocomposites by adding the clay at 1, 3, 10 and 20 wt% employing an intercalation method and investigated the dielectric loss factor. Figure 3 shows the dielectric loss factor of the PI-clay nanocomposites at 1 kHz frequency and within the temperature range of -150 to 150°C . The findings of the study revealed that the dielectric loss factor of the nanocomposites increased with increase in temperature and ranged from 0.00235 to 0.0335. The decrease of dielectric loss as the temperature decreases was due to the freezing of polyamide molecules, which results in complicated segmental movements.

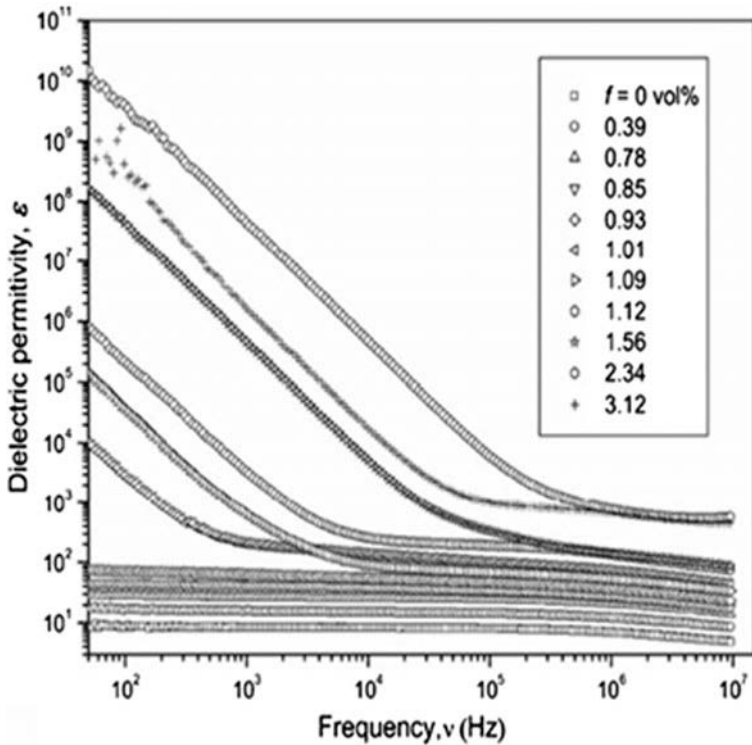


Fig. 2 The dependence of dielectric constant on frequency for PVDF/xGnP nanocomposite at room temperature [46]

The extent of adhesion and interactions at the interface between the filler and polymer play an important role in improving the dielectric properties of their nanocomposites, which include dielectric permittivity and dielectric loss. Zhang et al. [51] reported a simple method to prepare nanocomposites with $BaTi_3O_3$ (BT) nanofiber and ferroelectric polyvinylidene fluoride (PVDF) matrix. The $BaTi_3O_3$ (BT) nanofiber has the advantage of high dielectric constant. Unmodified and fluorosilane modified BT nanofibers were incorporated in PVDF matrix at different concentrations of the nanofibers. The dielectric properties of the nanocomposites were studied with respect to frequency and temperature. The dielectric loss of the nanocomposites reduced with an increase in the concentration of functionalised BT nanofibers, particularly in the frequency ranging from 102 to 107 Hz. The nanocomposite with 20 v% of modified BT exhibited the lowest dielectric loss tangent. This can be possible due to two reasons. Firstly, the surface functionalization of BT nanofiber enhances the interfacial interaction between the nanofiber and the PVDF matrix; this limits the mobility and build-up of space

charge within the nanocomposites. Secondly, as the content of nanofiber increases in the PVDF matrix, the contents of PVDF in the nanocomposite reduces and this hinders the migration of molecular chains and this leads to decrease of β -relaxation and dipole loss. The dielectric properties of the nanocomposites were studied at a fixed frequency (100 kHz) and varying the temperature as well. In this case, the dielectric loss of the nanocomposites initially decreased and then increased later as the temperature raised and finally touched the lowermost value at 60°C. At any particular temperature, the dielectric loss tends to reduce with the increasing nanofiber content. The dielectric loss of the nanocomposite with unmodified nanofiber was considerably higher as compared to the functionalised nanofiber. These trends were explained by the following: (i) at each particular temperature, there is reduction of polymer molecules, this tends to reduce molecular dipoles, and this leads to dipole loss of nanocomposites; (ii) the functionalization of the surface of the nanofiber aided in the formation of an isolating layer which limited the movement and build-up of space charge; and (iii) the formation of low molecular dipoles was likely to enhance dispersion and interfacial interaction which limits the mobility of PVDF chains within the nanocomposite [52].

3.3 *Tangent Loss*

Pradhan et al. [53] reported the frequency dependent dielectric behaviour of a polyethylene oxide based nanocomposite (PPNCE) with montmorillonite (DMMT) modified with dodecyl amine and polyethylene glycol (PEG) as the plasticizer. The PPNCE films were cast by using a tape casting technique, where the DMMT concentration was fixed at 5wt% and PEG at six different concentrations was added (0, 5, 10, 20, 30 and 50 wt%). Figure 4 shows the frequency dependency of tangent loss of PPNCE films at ambient temperature with the varying concentration of PEG.

As the PEG content increased the tangent loss peak shifts in the direction of higher frequency. The loss spectra can be related to the peak appearing at typical frequencies for PPNCE samples with and without PEG content. These peaks indicate that there are relaxing dipoles within all the nanocomposites and the strength and particular frequency of relaxation are influenced by the specific dipolar relaxation. The addition of plasticizer generally causes an increase in the amorphous content within the nanocomposite. The small and mobile PEG molecules tend to rapidly increase the segmental movement by increasing the available free volume. The reasonably fast segmental movement together with mobile ions speed up the transport properties with the addition of plasticizer. The peaks shifting towards higher frequency with an increase in plasticizer content eventually reveals that the relaxation time is decreasing.

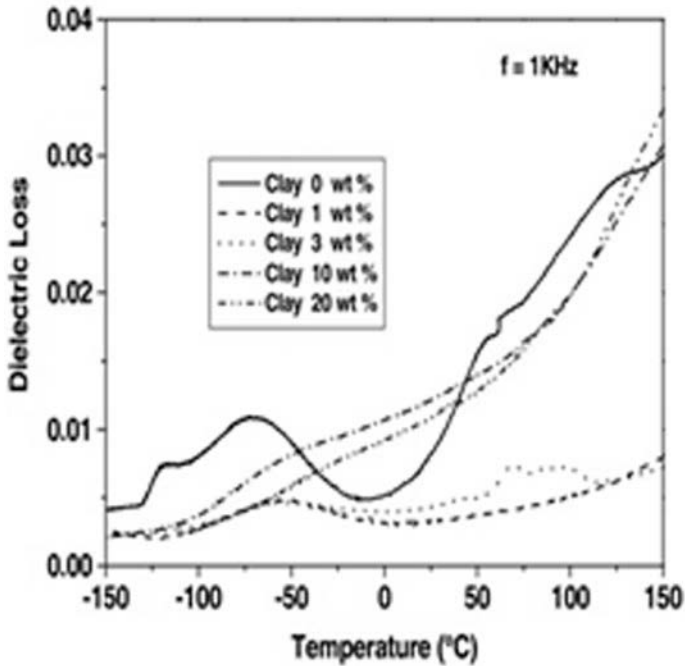


Fig. 3 Effect of temperature on dielectric loss factor of PI-clay nanocomposite at 1 kHz [50]

3.4 Static Permittivity

Static permittivity can be defined as polarization effect under dc conditions. When the sinusoidal electric field is functional, polarization and static differ under AC environments. When the sinusoidal electric field was applied, medium polarization and static are different under AC conditions. The polarization of the dielectric does not always respond in time to the changes in the applied electric field due to the thermal alterations that randomize the orientation of the dipole and the rotation of the molecule in the viscous mediums due to their interaction to neighbours. Therefore, the response of the material to the outer field is causal every time (after application of the field) and it depends on the frequency of field that can be shown through the phase difference. Therefore, the dielectric constant is commonly considered as a complex function of the frequency of the applied field.

$$D_0 e^{-j\omega t} = \epsilon(\omega) E_0 e^{-j\omega t}$$

where j is the imaginary unit, ω is electromagnetic field frequency, and 't' is time. The above equation can be rewritten as with conversion

$$\epsilon_{\tau} = \epsilon'_{\tau} - \epsilon''_{\tau}$$

For the causal and linear dielectric responses, the relationship between imaginary parts and real parts of complex permittivity is represented by the Kramers-Kronig relation [54]. Figure 5 shows the general characteristics of the dependence on frequency of real and virtual dielectric constants for four mechanisms of polarization. Although it shows the characteristics of the transitions in the characteristic peaks in ϵ' and ϵ'' , these peaks and several characteristics are usually wider in the real material [55]. Figure 5 does not denote any particular material, few materials demonstrate all mechanisms of polarization [56]. The energy loss is calculated through ϵ'' . In the engineering application of the dielectric in the capacitor, for a given ϵ' , ϵ'' is always better. The relative size of ϵ'' 'relative to ϵ' ' is defined as $\tan\delta$, which is called the loss factor [55] (Fig. 5).

3.5 Relaxation Time

Dielectric relaxation time is closely related to the electrical conductivity. In semiconductors, it is a measure of how long it takes for a conductive process to occur. This relaxation time is very small in metals and may be large in semiconductors and insulators. The relaxation time distribution was used as a rough indication of the heterogeneity of the polymer/filler interface. Maxwell-Wagner-Sillars interfacial

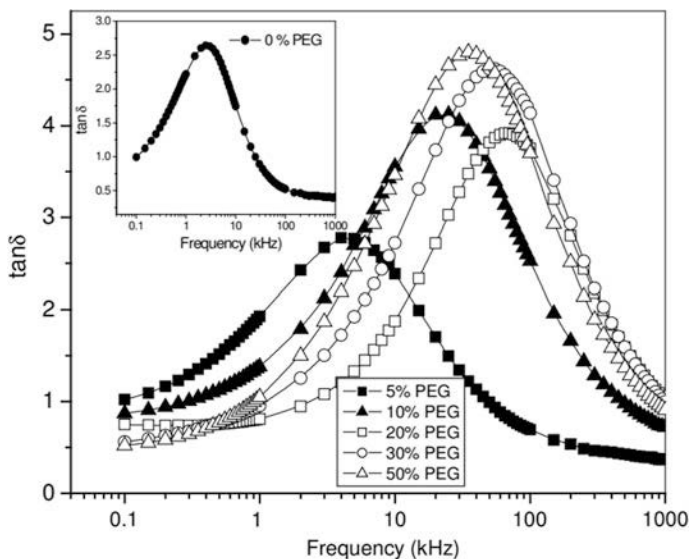


Fig. 4 Variation in Tangent loss of PPNCE thin films with respect to frequency for various concentration of PEG at the room temperature [53]

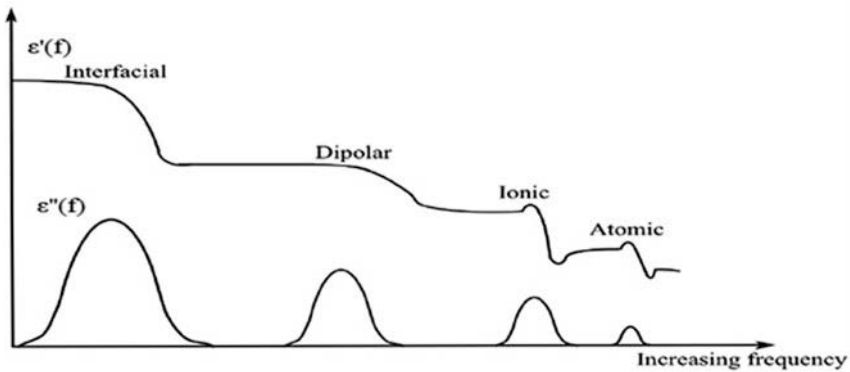


Fig. 5 Demonstration of permittivity real and imaginary dependence with the presence of orientational, ionic, electronic polarization and interfacial mechanisms [55]

polarization (MWS) can be compared with its larger dielectric strength. The presence of the filler/polymer interface increases the MWS relaxation time distribution because each interface has different interface geometry and is polarized at different time scales. However, the relaxation of the polymer melts originates from the split amorphous dynamics. The temperature shows a fairly uniform chain, much higher than the T_g value, whose nylon 12 T_g is approximately 508 °C [57].

When current flows through the biomaterial interface, the charge can accumulate at the interface between the two dielectric materials with different relaxation times ($\tau = \epsilon/\sigma$, where ϵ is the permittivity and σ is the conductivity). The nanocomposite has a large interfacial area and provides many sites for the MWS enhancement effect compared to microcomposites [58].

4 The Electrical Conductivity of Nanocomposite

Nanocomposites are materials in which at least one of the constituents has dimensions in the nanometre range (1 nm = 10^{-9} m) [59]. In the last few years, polymer nanocomposites are getting remarkable industrial and academic recognition due to their light-weight, higher mechanical and thermo-mechanical characteristics [60]. Light-weight nanocomposites can exhibit few functional characteristics including magnetic and electrical properties. Nanocomposites are electrically conductive polymers and they can offer an enormous range of electrical conductivities parallel to traditional inorganic conductors and semiconductors. These polymers can be used in a wide range of industrial applications. Nanocomposites may be distributed into two classes: one of the composites which are comprised of intrinsically conductive polymers whereas other which can be manufactured by the addition of conducting nanofillers. Composites containing

conductive polymer matrix may offer several distinct functional characteristics, for instance, their optical and electrical properties can vary to the response of external stimuli. The main disadvantage of nanocomposites with conductive polymers is their high cost and poor mechanical properties. However, the conductive composites with insulating polymer matrix are more stable and exhibit better mechanical properties. Currently, there are widespread applications of the nanocomposites with conducting polymer matrices [61].

Generally, the term electrical properties of materials refer to the response of the material under the influence of an applied electric field. Electrical conductivity is the physical quantity which characterizes how easily electric charge can flow through materials. Its values extend in a very wide range approaching 30 orders of magnitude, qualifying the electrical behaviour of materials. According to their conductivity, materials can be classified as conductors, semiconductors, and insulators (dielectrics). In nanocomposites, the matrix is considered as a continuous phase of the system and in most cases is the phase with a high volume fraction of the material. With this point of view, the nature of the matrix defines, at least at first approximation, the electrical behaviour of the composite material. Thus, metal matrix composites are obviously conductors, while polymer composites and in some cases ceramic composites are classified as insulators.

4.1 Characteristics of Electrically Respond Polymer Nanocomposites

The electrical response of any polymer matrix refers to its conductivity and dielectric behaviour. Nanocomposites have attracted the attention of researchers as an engineering material due to its thermo-mechanical performance. Work started with the manufacturing of the nanocomposites and later it expanded to its properties such as mechanical, electrical and thermal characteristics. Two were starting points of this investigation, examining the effect of nanofiller on the mechanism of polarization, molecular mobility, interfacial effect and improvement of conductivity in nanocomposites incorporating conductive inclusions. Considering the attractiveness of the nanofiller or nano-inclusions, polymer nanocomposites can be classified into two major categories: (i) the insulating matrix-dielectric reinforcing phase and (ii) the insulating matrix-conductive reinforcing phase. Conversely, the nanofiller can be ceramic, metallic as well as an allotropic type of carbon. A stimulating collection of ceramic inclusion is so-called active and functional dielectrics, for instance, pyroelectric, ferroelectric and piezoelectric elements. The existence of such type of nanofillers may provide functionality to the performance of the system. Although it is not easy to say which type of polymer nanocomposite drawn the attention of researchers from all over the world, it is recognized that several studies mentioned electrical characteristics of carbon/polymer matrix nanocomposites.

4.2 *Parameters Influencing Electrical Conductivity of Nanocomposites*

Mostly, the addition of conducting nanofiller should be as lower as possible because more filler can cause processing difficulty and also mechanical properties can be affected. But, at the same time, it should be kept in mind that the amount of filler is desired to be in acceptable quantity for getting the continuous conducting network. Therefore, it is an ideal to attain conducting composites with lower percolation threshold [62]. The electrical conductivity and percolation threshold of any conductive polymeric nanocomposite are dependent of various factors including physical properties of filler (surface properties, electrical conductivity, and aspect ratio), distribution and dispersion fillers, physical characteristics of the polymer matrix, including polarity, viscosity and crystalline and alignment and orientation of fillers. It is important to note that many of above-mentioned parameters are considerably affected by the fabrication methods of the nanocomposites.

5 Conclusion

Various nanomaterials hold tunable physical, chemical, thermal, mechanical, dielectric and electrical properties. These properties, especially dielectric and electrical properties, are important characteristics of such nanomaterials for their utilization as nanofiller for the synthesis of nanocomposite with numerous applications. This chapter deals in detail with an overview of the dielectric properties and electrical conductivity of nanocomposite synthesized by addition of different nanofillers.

References

1. Hussain F, Hojjati M, Okamoto M, Gorga RE (2006) Polymer-matrix nanocomposites, processing, manufacturing, and application: an overview. *J Compos Mater* 40:1511–1575
2. Venkatesh DN, Priya VK, Bhavitha K (2016) Polymer-matrix nanocomposites, processing, manufacturing and application: an overview
3. Choudhary V, Gupta A (2011) Polymer/carbon nanotube nanocomposites. In: *Carbon nanotubes-polymer nanocomposites*, Intech
4. Rezakazemi M, Zhang Z (2018) 2.29 Desulfurization materials. In: a2-Dincer I (ed) *Comprehensive energy systems*, Elsevier, Oxford, pp. 944–979
5. Song W-L, Wang W, Veca LM, Kong CY, Cao M-S, Wang P, Meziani MJ, Qian H, LeCroy GE, Cao L (2012) Polymer/carbon nanocomposites for enhanced thermal transport properties—carbon nanotubes versus graphene sheets as nanoscale fillers. *J Mater Chem* 22:17133–17139

6. Zhou B, Lin Y, Veca LM, Fernando KS, Harruff BA, Sun Y-P (2006) Luminescence polarization spectroscopy study of functionalized carbon nanotubes in a polymeric matrix. *J Phys Chem B* 110:3001–3006
7. Kumar V, Rawal A (2016) Tuning the electrical percolation threshold of polymer nanocomposites with rod-like nanofillers. *Polymer* 97:295–299
8. Sun L-L, Li B, Zhao Y, Zhong W-H (2010) Suppression of AC conductivity by crystalline transformation in poly (vinylidene fluoride)/carbon nanofiber composites. *Polymer* 51:3230–3237
9. Dashti A, Harami HR, Rezakazemi M (2018) Accurate prediction of solubility of gases within H₂-selective nanocomposite membranes using committee machine intelligent system. *Int J Hydrogen Energy* 43:6614–6624
10. Rezakazemi M, Sadrzadeh M, Mohammadi T, Matsuura T (2017) Methods for the preparation of organic-inorganic nanocomposite polymer electrolyte membranes for fuel cells. In: Inamuddin D, Mohammad A, Asiri AM (eds) *Organic-Inorganic composite polymer electrolyte membranes*. Springer International Publishing, Cham, pp 311–325
11. Rezakazemi M, Vatani A, Mohammadi T (2016) Synthesis and gas transport properties of crosslinked poly(dimethylsiloxane) nanocomposite membranes using octatrimethylsiloxy POSS nanoparticles. *J Nat Gas Sci Eng* 30:10–18
12. Rezakazemi M, Vatani A, Mohammadi T (2015) Synergistic interactions between POSS and fumed silica and their effect on the properties of crosslinked PDMS nanocomposite membranes. *RSC Adv* 5:82460–82470
13. Rezakazemi M, Razavi S, Mohammadi T, Nazari AG (2011) Simulation and determination of optimum conditions of pervaporative dehydration of isopropanol process using synthesized PVA–APTEOS/TEOS nanocomposite membranes by means of expert systems. *J Membr Sci* 379:224–232
14. Sodeifian G, Raji M, Asghari M, Rezakazemi M, Dashti A (2018) Polyurethane-SAPO-34 mixed matrix membrane for CO₂/CH₄ and CO₂/N₂ separation. *Chin. J. Chem. Eng*
15. Rezakazemi M, Dashti A, Asghari M, Shirazian S (2017) H₂ -selective mixed matrix membranes modeling using ANFIS, PSO-ANFIS, GA-ANFIS. *Int J Hydrogen Energy* 42:15211–15225
16. Rezakazemi M, Amooghin AE, Montazer-Rahmati MM, Ismail AF, Matsuura T (2014) State-of-the-art membrane based CO₂ separation using mixed matrix membranes (MMMs): an overview on current status and future directions. *Prog. Polym. Sci* 39(5) 817–861
17. Baheri B, Shahverdi M, Rezakazemi M, Motaee E, Mohammadi T (2014) Performance of PVA/NaA mixed matrix membrane for removal of water from ethylene glycol solutions by pervaporation. *Chem Eng Commun* 202:316–321
18. Shahverdi M, Baheri B, Rezakazemi M, Motaee E, Mohammadi T (2013) Pervaporation study of ethylene glycol dehydration through synthesized (PVA-4A)/polypropylene mixed matrix composite membranes. *Polym Eng Sci* 53:1487–1493
19. Rostamizadeh M, Rezakazemi M, Shahidi K, Mohammadi T (2013) Gas permeation through H₂-selective mixed matrix membranes: experimental and neural network modeling. *Int J Hydrogen Energy* 38:1128–1135
20. Rezakazemi M, Mohammadi T (2013) Gas sorption in H₂-selective mixed matrix membranes: experimental and neural network modeling. *Int J Hydrogen Energy* 38:14035–14041
21. Rezakazemi M, Shahidi K, Mohammadi T (2012) Sorption properties of hydrogen-selective PDMS/zeolite 4A mixed matrix membrane. *Int J Hydrogen Energy* 37:17275–17284
22. Rezakazemi M, Shahidi K, Mohammadi T (2012) Hydrogen separation and purification using crosslinkable PDMS/zeolite a nanoparticles mixed matrix membranes. *Int J Hydrogen Energy* 37:14576–14589
23. Thomas S, Rouxel D, Ponnamma D (2016) *Spectroscopy of polymer nanocomposites*, William Andrew
24. Rezakazemi M, Sadrzadeh M, Matsuura T (2018) Thermally stable polymers for advanced high-performance gas separation membranes. *Progr. Energy Combust. Sci.* 66:1–41

25. Mutiso RM, Winey KI (2015) Electrical properties of polymer nanocomposites containing rod-like nanofillers. *Prog Polym Sci* 40:63–84
26. Maynard AD, Baron PA, Foley M, Shvedova AA, Kisin ER, Castranova V (2004) Exposure to carbon nanotube material: aerosol release during the handling of unrefined single-walled carbon nanotube material. *J Toxicol Environ Health Part A* 67:87–107
27. Njuguna J, Ansari F, Sachse S, Zhu H, Rodriguez V (2014) Nanomaterials, nanofillers, and nanocomposites: types and properties. In: *Health and environmental safety of nanomaterials*, Elsevier, pp. 3–27
28. Koster LJA, Mihailtchi VD, Ramaker R, Blom PW (2005) Light intensity dependence of open-circuit voltage of polymer: fullerene solar cells. *Appl Phys Lett* 86:123509
29. Koster L, Mihailtchi V, Blom P (2006) Ultimate efficiency of polymer/fullerene bulk heterojunction solar cells. *Appl Phys Lett* 88:093511
30. Wu P-T, Ren G, Jenekhe SA (2010) Crystalline random conjugated copolymers with multiple side chains: tunable intermolecular interactions and enhanced charge transport and photovoltaic properties. *Macromolecules* 43:3306–3313
31. Lenes M, Wetzelaer GJA, Kooistra FB, Veenstra SC, Hummelen JC, Blom PW (2008) Fullerene bisadducts for enhanced open-circuit voltages and efficiencies in polymer solar cells. *Adv Mater* 20:2116–2119
32. Li G, Shrotriya V, Huang J, Yao Y, Moriarty T, Emery K, Yang Y (2005) High-efficiency solution processable polymer photovoltaic cells by self-organization of polymer blends. *Nat Mater* 4:864
33. Huang J-H, Li K-C, Chien F-C, Hsiao Y-S, Kekuda D, Chen P, Lin H-C, Ho K-C, Chu C-W (2010) Correlation between exciton lifetime distribution and morphology of bulk heterojunction films after solvent annealing. *J Phys Chem C* 114:9062–9069
34. Spitalsky Z, Tasis D, Papagelis K, Galiotis C (2010) Carbon nanotube–polymer composites: chemistry, processing, mechanical and electrical properties. *Prog Polym Sci* 35:357–401
35. Boldor D, Sanders T, Simunovic J (2004) Dielectric properties of in-shell and shelled peanuts at microwave frequencies. *Trans-Am Soc Agric Eng* 47:1159–1170
36. Sosa-Morales M, Valerio-Junco L, López-Malo A, García H (2010) Dielectric properties of foods: reported data in the 21st century and their potential applications. *LWT-Food Sci Technol* 43:1169–1179
37. Stone ML, Maness NO (2006) Plant biomass estimation using dielectric properties, ASABE paper, 15
38. Tripathi M, Sahu J, Ganesan P, Dey T (2015) Effect of temperature on dielectric properties and penetration depth of oil palm shell (OPS) and OPS char synthesized by microwave pyrolysis of OPS. *Fuel* 153:257–266
39. Motasemi F, Afzal MT, Salema AA, Mouris J, Hutcheon R (2014) Microwave dielectric characterization of switchgrass for bioenergy and biofuel. *Fuel* 124:151–157
40. Salema AA, Yeow YK, Ishaque K, Ani FN, Afzal MT, Hassan A (2013) Dielectric properties and microwave heating of oil palm biomass and biochar. *Ind Crops Prod* 50:366–374
41. Sweeney JJ, Roberts JJ, Harben PE (2007) Study of dielectric properties of dry and saturated green river oil shale. *Energy Fuels* 21:2769–2777
42. Nizamuddin S, Mubarak N, Tiripathi M, Jayakumar N, Sahu J, Ganesan P (2016) Chemical, dielectric and structural characterization of optimized hydrochar produced from hydrothermal carbonization of palm shell. *Fuel* 163:88–97
43. Li B, Zhong W-H (2011) Review on polymer/graphite nanoplatelet nanocomposites. *J Mater sci* 46:5595–5614
44. Li Y, Huang X, Hu Z, Jiang P, Li S, Tanaka T (2011) Large dielectric constant and high thermal conductivity in poly (vinylidene fluoride)/barium titanate/silicon carbide three-phase nanocomposites. *ACS Appl Mater Interfaces* 3:4396–4403
45. Calame J (2006) Finite difference simulations of permittivity and electric field statistics in ceramic-polymer composites for capacitor applications. *J Appl Phys* 99:084101
46. Herzberg M, Kang S, Elimelech M (2009) Role of extracellular polymeric substances (EPS) in biofouling of reverse osmosis membranes. *Environ Sci Technol* 43:4393–4398

47. Dang Z-M, Wu J-P, Xu H-P, Yao S-H, Jiang M-J, Bai J (2007) Dielectric properties of upright carbon fiber filled poly (vinylidene fluoride) composite with low percolation threshold and weak temperature dependence. *Appl Phys Lett* 91:072912
48. Li Y-J, Xu M, Feng J-Q, Dang Z-M (2006) Dielectric behavior of a metal-polymer composite with low percolation threshold. *Appl Phys Lett* 89:072902
49. Lee AY, Tran VN (2006) Dielectric characterisation of high loss and low loss materials at 2450 MHz. In: *Advances in microwave and radio frequency processing*, Springer, pp. 77–84
50. Zhang Y-H, Dang Z-M, Fu S-Y, Xin JH, Deng J-G, Wu J, Yang S, Li L-F, Yan Q (2005) Dielectric and dynamic mechanical properties of polyimide–clay nanocomposite films. *Chem Phys Lett* 401:553–557
51. Zhang X, Ma Y, Zhao C, Yang W (2014) High dielectric constant and low dielectric loss hybrid nanocomposites fabricated with ferroelectric polymer matrix and BaTiO₃ nanofibers modified with perfluoroalkylsilane. *Appl Surf Sci* 305:531–538
52. Yang K, Huang X, Huang Y, Xie L, Jiang P (2013) Fluoro-polymer@ BaTiO₃ hybrid nanoparticles prepared via RAFT polymerization: toward ferroelectric polymer nanocomposites with high dielectric constant and low dielectric loss for energy storage application. *Chem Mater* 25:2327–2338
53. Pradhan DK, Choudhary R, Samantaray B (2008) Studies of dielectric relaxation and AC conductivity behavior of plasticized polymer nanocomposite electrolytes. *Int J Electrochem Sci* 3:597–608
54. Balanis C (1989) In: *Advanced engineering electromechanics*, Wiley, New York
55. Kasap S (1997) *Principles of Electrical Engineering Materials*, p 184
56. Sadiku MN (2014) *Elements of electromagnetics*, Oxford university press
57. Lee YH, Bur AJ, Roth SC, Start PR, Harris RH (2005) Monitoring the relaxation behavior of nylon/clay nanocomposites in the melt with an online dielectric sensor. *Polym Adv Technol* 16:249–256
58. Yuan J-K, Yao S-H, Dang Z-M, Sylvestre A, Genestoux M, Bai J (2011) Giant dielectric permittivity nanocomposites: realizing true potential of pristine carbon nanotubes in polyvinylidene fluoride matrix through an enhanced interfacial interaction. *J Phys Chem C*, 115(13) 5515–5521
59. Paul D, Robeson LM (2008) Polymer nanotechnology: nanocomposites. *Polymer* 49:3187–3204
60. Coleman JN, Khan U, Blau WJ, Gun'ko YK (2006) Small but strong: a review of the mechanical properties of carbon nanotube–polymer composites. *Carbon* 44(9) 1624–1652
61. Lu X, Zhang W, Wang C, Wen T-C, Wei Y (2011) One-dimensional conducting polymer nanocomposites: synthesis, properties and applications. *Prog Polym Sci* 36:671–712
62. Al-Saleh MH, Sundararaj U (2009) A review of vapor grown carbon nanofiber/polymer conductive composites. *Carbon* 47:2–22
63. Cai Z, Wang X, Luo B, Hong W, Wu L, Li L (2017) Nanocomposites with enhanced dielectric permittivity and breakdown strength by microstructure design of nanofillers. *Compos Sci Technol* 151:109–114

Thermal Properties of Sustainable Thermoplastics Nanocomposites Containing Nanofillers and Its Recycling Perspective



Pooja Takkalkar, Sabzoi Nizamuddin, Gregory Griffin and Nhol Kao

1 Introduction

Commercialized fuel-based polymers have created immense adverse effects on the environment due to their non-renewable nature and emission of greenhouse gases, particularly carbon dioxide (CO₂) [1]. Pollution created by conventional polymers has risen to dangerous extents, predominantly in developing nations. These polymers, being non-biodegradable, are resistant to microbial degradation and hence they accrue in the surroundings. Furthermore, increases in oil prices have aided in stimulating interest in biodegradable polymers. Eco-friendly polymers were first introduced in the 1980s [2]. Over the past two decades, bio-based polymers have attracted considerable attention, mainly because of two major limitations with the use of conventional polymers. Firstly, the environmental pollution created by the increased reliance on fossil fuels and secondly the fact that the source of these petroleum-based polymers is limited and exhaustible [3].

Polymer nanocomposites are new engineering materials in which nanofillers [4], with at least one dimension less than 100 nm, are dispersed in a polymer to improve its properties [5–7]. Based on the appropriate application and final properties desired of the nanocomposite, the type and concentration of nanofiller can be studied. Nanocomposites possess more advanced properties than that of microcomposites as the incorporated nanofiller has a better aspect ratio and surface area. Biodegradable nanocomposites are considered more advantageous because they are light in weight, transparent, and have better mechanical, thermal and barrier properties than that of conventional composites, even at a very low concentration of nanofiller [8].

Nanocomposites have improved properties than the constituent polymers itself [9, 10]. The efficient dispersion of nanofiller in the polymer indicates that there is an

P. Takkalkar · S. Nizamuddin · G. Griffin · N. Kao (✉)
School of Engineering, RMIT University, Melbourne, Vict 3001, Australia
e-mail: nhol.kao@rmit.edu.au

increased interfacial interaction among the constituents [11]. Although the biodegradable polymers are environmentally friendly, their properties are inferior to conventional polymers; hence, nanocomposites with biodegradable polymers have been investigated to seek improved properties. The area of nanocomposites with biodegradable polymers has gained attention in the last two decades. A number of bio-based polymer matrices have been studied after incorporating organic and inorganic fillers to enhance their properties. The biodegradable polymers used as a matrix in preparation of nanocomposites are polybutyl succinate, polylactic acid, cellulose, starch, alginate, soy protein isolate, plant oil based polymers, polyhydroxy alkanolate and epoxies [12]. The properties which are aimed to be improved in these biodegradable nanocomposites include their thermal, mechanical, barrier, rheological and crystalline properties while maintaining their biodegradability. Depending on the particular application of these nanocomposites the appropriate nanofiller can be selected. The nanofillers are classified based on their source, shape, aspect ratio and crystallinity. Although the research in this area and the applications of biodegradable nanocomposites is in its infancy, it is expected to be enormous in future years.

The overall properties of the polymer nanocomposites are largely affected by-

- i. Compatibility and interactions between the polymer matrix and nanofiller
- ii. Nanofiller shape and aspect ratio
- iii. Dispersion of nanofiller within the polymer matrix
- iv. Modifications on the surface of nanofiller (if any).

This chapter provides a description of the thermal properties of sustainable thermoplastic nanocomposites; its recycling perspective is also considered.

2 Sustainable Thermoplastic Nanocomposite

Polymer scientists have shown increased interest towards developing various environmental friendly polymer nanocomposites which can potentially reduce the dependency on conventional polymers. These sustainable thermoplastic nanocomposites deserve attention as they aid in resolving concerns on issues such as the emission of greenhouse gases, depletion of fossil fuels and pollution [12]. Thermoplastic polymers are preferred over thermoset polymers due to various advantages such as low processing cost, design flexibility and easier moulding of complex parts [13]. Simple moulding techniques such as extrusion or injection moulding are widely used for fabrication of such types of composites.

The polymer matrix plays an important part for the performance of a polymer nanocomposite. In addition, the dispersion of fibers in the composite is also one of the crucial parameters for achieving the consistency of the product. Further, the properties of fibers, fibre-matrix interface and aspect ratio of fibres also govern the properties of nanocomposites [13]. The performance and properties of

thermoplastic composites are also influenced by process parameters [14]. It is reported by Takase and Shiraishi [15] that tensile strength of polypropylene/wood composite changed non-linearly with mixing temperature, mixing rate and time. The dispersion of fibers and fiber length should be optimized in order to enhance the properties of the composite. It is important that a uniform dispersion of nanomaterial within the polymer should be carried out [16]. Several dispersion methods for thermoplastic polymers have been reported in the literature, but the easiest method is blending in a minimax injection moulder's crucible [17], where the rotary cylinder is used for mixing the polymer melt with fiber addition by hand.

The concept of combining nanomaterials as filler and polymer as a matrix in order to form different forms of nanocomposites has been gaining much recognition by researchers [18–28]. Nanomaterials such as nanotubes and nanoclays provide great potential for fabrication of a variety of different forms of composites, coatings, adhesives and sealant materials with specific properties. These nanoparticles can be successfully utilized as a filler in thermoplastic polymers in order to improve the mechanical, physical and thermal properties of the polymer.

In this context, polylactide (PLA) has been leading among other thermoplastic polymers due to its inherent advantages like good mechanical strength, renewability, biocompatibility, and biodegradability. It is a versatile polymer made from agricultural raw materials, which are fermented into lactic acid. Then, this lactide acid is ring-opening polymerized through cyclic dilactone (lactide) to the desired polylactic acid. The polymer is altered through different means, which improves the thermal stability of the polymer and decreases the residual amount of monomers [29]. The thermal stability of the polylactic acid also can be improved by reinforcing it with fibers. The thermal properties are essential characteristics to understand the behaviour of the raw material and the final product [30]. Therefore, the thermal properties of various thermoplastic nanocomposites have been elaborated in detail in the following sections.

3 Thermal Properties of Sustainable Nanocomposites Based on Types of Sustainable Polymers

3.1 Polylactic Acid (PLA) Based Nanocomposites

PLA is a thermoplastic biodegradable polymer derived from corn. Although it is a biodegradable polymer, its properties need to be optimized to make it suitable for commercial packaging applications. Polylactic acid nanocomposites with improved properties by incorporation of cellulose nanofibers (CNFs) were prepared by Frone et al. [31]. CNFs were obtained using the most commonly used acid hydrolysis method. Microcrystalline cellulose (MCC) with particle size 20 μm was hydrolysed to form CNF with diameter 11–44 nm. These CNF were further surface treated to

form silanized (CNFS) after that, both the CNF and the CNFS were added in PLA at 2.5 wt% of each nanofiller were melt blended to form the nanocomposites. The effect of treated and untreated CNFs on nucleation characteristics of PLA was determined through differential scanning calorimetry (DSC) analysis. There was no substantial change in T_g , owing to the presence of nanofiller at very low concentrations. The PLA nanocomposite with CNF as nanofiller showed higher crystallinity due to the better nucleating effect created by CNF. In comparison, due to the better dispersion and adhesion of CNFS with PLA, the crystallinity was reduced as compared to CNF. Overall the degree of crystallinity was improved for PLA with both nanofillers, however, the effect was more pronounced with CNF nanofiller [31].

A similar study on cellulose nanocrystals (CNC) and silylated CNC (SCNC) in PLA was reported in the literature [32]. The authors prepared the nanocomposite with 1 and 2 wt% of each type of nanofiller through solvent casting with chloroform as a solvent. The samples with 1 and 2 wt% of CNC were labelled as PLLA-CNC-1 and PLLA-CNC-2, respectively and the samples with a similar concentration of SCNC were coded as PLLA-SCNC-1 and PLLA-SCNC-2, respectively. As expected, the bulk of the measurements showed there was no change in the melting temperature of all the nanocomposites, at around 171 °C. The degree of crystallinity (X_c) was determined using the enthalpy data from DSC. The X_c values were higher than pure PLA (14.3%) for all the nanocomposites. The X_c values were improved slightly for PLLA-CNC nanocomposites and they increased with filler loadings. Conversely, in the case of PLLA-SCNC nanocomposites, the X_c values were almost doubled, but decreased slightly with the increase in SCNC loading. The highest crystallinity was achieved for PLLA-SCNC-1 (30.4%). This was attributed to the improvement in nucleation effect triggered by homogeneous dispersion of the nanofiller within the PLLA matrix [32].

A recent study described the improvement in properties of PLA based nanocomposites with starch nanocrystals (SNC) as nanofillers at three different loadings of SNC- 1, 3 and 5 wt% [33]. The nanocomposites were prepared by solvent casting and evaporation techniques. The square-shaped SNC nanofiller used in this study was derived from acid hydrolysis of waxy maize starch, which consists of 99% amylopectin. The thermal properties of these nanocomposites were studied by means of TGA and MDSC. The TGA study revealed that all the nanocomposites were stable to process in the commercial processing range of polymers (25–240 °C). The MDSC results indicated a slightly higher degree of crystallinity for PLA-SNC-3 wt% but with further increase in the concentration of SNC, it declined. Also, a decline in the cold crystallization temperature was detected for all the nanocomposites. These changes were attributed to the enhanced nucleation effect created by crystalline SNC. Beyond the 3 wt% of SNC, the nanofillers had a tendency to aggregate and declines in thermal and rheological properties were observed. Similar results were reported for PLA and acetylated microcrystalline cellulose (Ac-MCC) based nanocomposites [34]. The optimum concentration obtained through rheological percolation threshold was at 2.5 wt% of Ac-MCC.

PLA nanocomposite with nanographite platelets (NGP) was prepared by melt blending at 180 °C [35, 36]. The concentration of NGP in PLA was varied from 1

to 10 wt%. The influence of NGP loading on thermal and crystallization properties was studied via MDSC. The NGP was unable to exhibit any nucleating effect or improve the overall crystallinity and thermal properties of the nanocomposites. However, a comparatively higher crystallinity and fusion enthalpy were noticed for nanocomposite with 5 wt% NGP. The researchers concluded that the melt compounding method alone is not sufficient to obtain a well-dispersed nanocomposite. A similar study was reported by the same group of authors [36], however, a melt intercalation and mixing technique were used to fabricate the PLA-NGP nanocomposites. In this study, the MDSC results showed that the melting temperature and glass transition temperatures were unaffected by the presence of NGPs, though the crystallisation temperature and degree of crystallinity were increased up to 5 wt% loading of NGP.

3.2 *Thermoplastic Starch (TPS)*

There is an environmental demand to create biodegradable plastics which have adequate properties and can replace commercial plastics. Nanocomposites prepared from starch as a matrix have great potential as they are available in abundance and are renewable. To overcome some of the inherent limitations of starch such as limited gas barrier properties, low heat distortion temperature and brittleness; polysaccharide nanofiller such as cellulose or starch nanocrystals can be incorporated in thermoplastic starch. The addition of biodegradable nanofiller not only improves the properties of the biodegradable polymer but maintains their biodegradability as well. Kaushik et al. [37] prepared biodegradable nanocomposites with thermoplastic starch as nanocomposite and cellulose nanofibers (CNFs) as nanofiller, at three different loadings of CNF, 5, 10 and 15 wt% by solution casting method. The CNFs reported in their study were extracted from wheat straw through a combination of steam explosion, chemical treatments (involving alkali and acid hydrolysis and bleaching) and mechanical treatments (homogenization). Morphological, structural, mechanical, thermal and moisture retention properties of the prepared nanocomposites were studied. The nano-dimensions of CNFs were measured through TEM, which showed fiber diameter in the range of 10–60 nm with a tendency to agglomerate. There was a significant improvement in the mechanical property of the nanocomposite with increase in CNF concentration; this was noted as a linear increase in tensile strength and modulus of the nanocomposite. The barrier property improved until a loading of 10 wt% and declined after a further increase in CNF concentration. This was credited to agglomeration of CNF fibers within the nanocomposite. The thermal properties of nanocomposites were studied through TGA and DSC. The thermal property study indicates the interaction between glycerol and CNF. The TGA results showed no change in onset degradation temperature until a concentration of CNF-10 wt% was reached, beyond that

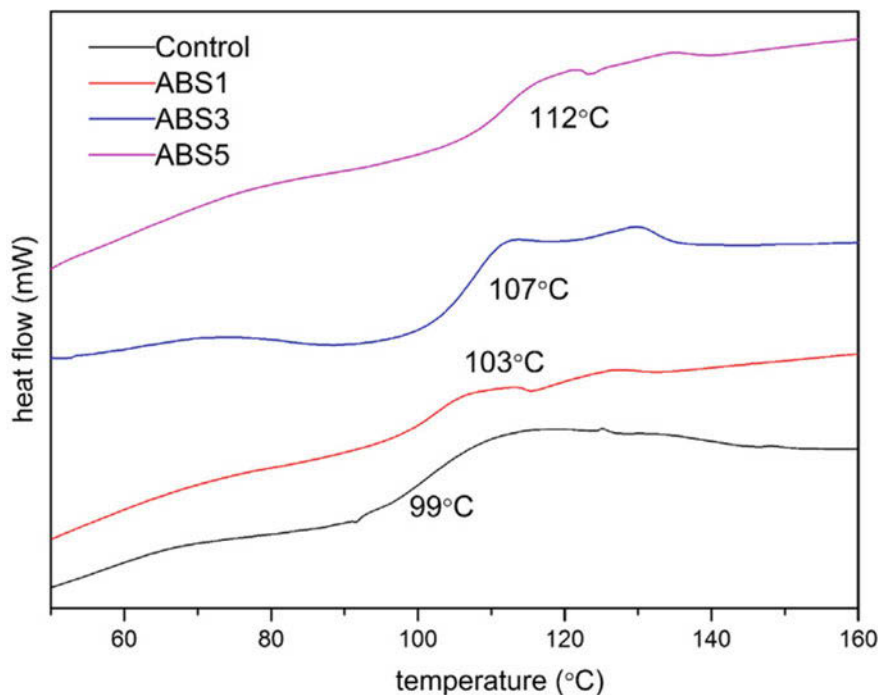


Fig. 1 DSC curves for Acrylonitrile butadiene styrene and Acrylonitrile butadiene styrene/organ-montmorillonite nanocomposite at 1, 3 and 5 wt% loading of nanofiller. Reprinted from Ref. Weng, Wang [54] with permission from Elsevier

the onset degradation temperature reduced when compared to pure starch. They presented two possible causes for this reduction- (i) the reduced flexibility of branched amylopectin hindered by nanocrystalline cellulose and (ii) accumulation of the plasticizer (glycerol) on the CNF surface [37].

Cao et al. [38] reported similar properties of solvent cast plasticized starch (PS) based nanocomposite with different concentrations of cellulose nanocrystals derived from flax fiber (FCNs). PS was reinforced with FCN at six different loadings 5, 10, 15, 20, 25, 30 wt% of FCN. The thermal properties of the prepared nanocomposites were recorded through DSC analysis. They focussed the thermal analysis on the changes in glass transition temperature (T_g). T_g was associated with two phases; T_{g1} —glycerol rich phase (-80 to -50 °C) and T_{g2} —starch-rich phase (30–60 °C). The T_{g1} remained unaffected by the presence of FCNs, however, the T_{g2} kept increasing as the FCN loadings were increased. This was ascribed to the high interaction of FCNs with PS at the interface which hinders the molecular mobility of PS chains.

3.3 Polycaprolactone (PCL)

Performance improvement of biocompatible polymers like polycaprolactone (PCL) by adding nanofillers like clay or nanocellulose is studied widely. PCL based nanocomposites were fabricated with unmodified cellulose nanowhiskers (CNWr) and poly-ester grafted cellulose nanowhiskers (CNWr-g-PCL) at three different concentrations of each nanofiller- 2, 4 and 8 wt% in PCL matrix [39]. The CNWr were obtained through alkaline and acid hydrolysis of ramie fibers. Finally, the nanocomposites were prepared by melt blending PCL and the nanofillers at 120 °C. There was no significant change in the melting and crystallisation characteristics of the nanocomposites with CNWr as nanofiller. The crystallization temperature increased slightly with the increase in the concentration of CNWr-g-PCL. The grafted nanofiller largely improved the thermo-mechanical properties of the prepared nanocomposite. A similar study of melt blended PCL nanocomposites was reported previously [40].

3.4 Polyamide/Clay Nanocomposites

In the last decade, the number of investigations about the thermal degradation of clay-based nanocomposites has increased markedly due to the importance of this property for polymers production. In particular, clay-based nanocomposites polymers have drawn more interest recently [41]. The nanofillers are added into polymers as they have a potential to improve the thermal properties, particularly increasing the flame or chemical resistance characteristics, enhance the bulk clarity and ionic conductivity as well as decrease the moisture, hydrocarbons or gases permeability [42]. However, the problem of polymers thermal degradation in nanocomposites is still an obstacle to produce anti-thermal degradation polymers. This is due to the high temperature used in the preparation process of the clay-nanocomposites. Normally, degradation of the clay-based-polymers occurs if the temperature used in the preparation is higher than the stable temperature of the organic material used to reinforce the polymer [42]. Therefore, different materials have been used to advance the thermal and the mechanical properties of polymer products. For example, clay modified with cationic surfactants, specifically quaternary ammonium-organic surfactants, dispersed at the nanoscale into the polymer to improve the mechanical compatibility and increase the interlayer spacing of the clay and, hence, decrease the forces between the single platelets and thus aid exfoliation [41].

Morgan et al. (2002) have successfully formed a clay-catalysed-carbonaceous-char and reinforced char by clay polystyrene nanocomposites. They stated that the enforcement of the char by clay has decreased the flammability of the nanocomposites of polystyrene [43]. In this case, the mass fraction of clay loading, 5%, was

the optimal percentage amount to be loaded for improving the heat release rates among the 0, 2, 5, 10% mass fractions used in this study [43].

3.5 *Polypropylene/Layered Silicates Nanocomposites*

Polymer nanocomposites, compared to traditional composites, show a dramatic transformation in various properties at low loadings of nanofillers such as graphite nanoplatelets, carbon nanotubes, and nanosilicate layers [44]. The performance of these nanofillers is highly dependent on the uniform dispersion of the nanofillers and strong interactions at the interface between the polymer matrix and nanofillers. The graphene nanosheets, which is structurally similar to silicate layers and chemically analogous to carbon nanotubes [45], are considered as the most promising nanofiller in order to improve the barrier, mechanical as well as thermal properties. In spite of great potential of graphene nanofiller, the good dispersion is still a challenge for the effective reinforcement of polymers, specifically in nonpolar polymers such as polypropylene. Trokeson et al. [45, 46] fabricated fully-exfoliated polypropylene/graphite nanocomposites through a solid-state shear pulverization method. It was noticed that 2.5 wt% loading of graphite exhibited a 100% increase in Young's modulus and around 60% improvement in yield strength compared to pure polypropylene. Miltner et al. [47] successfully incorporated carbon nanotubes in polypropylene latex by sonication for fabrication of very well-dispersed polypropylene/carbon nanotubes nanocomposites.

Graphene-based polypropylene nanocomposite with improved mechanical and thermal properties were successfully fabricated by previous researchers [44]. An eco-friendly technique was utilized for preparation of polymer nanocomposite with well-dispersed graphene sheets within the polymer matrix, through coating graphene with polypropylene latex, and then melt-blending coated graphene with polypropylene matrix. It was observed that yield strength and Young's modulus of polypropylene were improved up to 75% and 74% respectively at 0.042% loading of graphene. It was reported that the thermal properties were improved after addition of graphene. For instance, the glass transition temperature was increased by 2.5 °C at 0.041% loading of graphene. Similarly, the thermal oxidative stability was also enhanced significantly up to 26 °C at 0.42% loading of graphene. Mounir et al. [48] synthesized graphene/polypropylene nanocomposite through melt mixing and investigated the effect of graphene loading on propylene characteristics (thermal properties). It was observed that an increase in graphene loading resulted in a significant improvement of mechanical and thermal properties of polypropylene. Further, graphene showed a significant effect on thermal stability of neat polypropylene and its composite. It was reported that the thermal degradation temperature of both the neat polypropylene and polypropylene/graphene nanocomposite occurs as a single step process with maximum degradation temperature of 460 °C. An increase in thermal stability of polypropylene after graphene

loading, at initial degradation stage, was observed which was attributed to the hindered diffusion of volatile decomposition products within the nanocomposites and is highly dependent upon the interaction between chains of nanosheets and the polymer.

4 Thermal Properties of Sustainable Nanocomposites Based on Various Thermal Properties

4.1 Thermogravimetric/Differential Thermogravimetric Analysis (TGA/DTG)

TGA is an important method used to examine thermal decomposition behaviour of polymeric materials for high-temperature applications [49]. In TGA, the weight loss of a substance is monitored as a function with time or temperature. The weight loss is due to the generation of the volatile product post-degradation. The thermal properties are essential characteristics to understand the behaviour of the raw material and the final product [30]. The thermal stability of any polymer matrix can be improved by adding a small number of nano additives/nanofillers [40]. Wang et al. [50] noticed that thermal stability of Acrylonitrile butadiene styrene was improved by 5% of organ-montmorillonite.

Alemdar and Sain [51] synthesized wheat straw nanofiber/thermoplastic starch polymer nanocomposite and studied the thermal behaviour of neat polymer and nanocomposite at 5% loading of the nanofiber. It was observed that the degradation temperature for both the neat polymer matrix and nanocomposite is similar but less than that of each individual component. Similar behaviour for degradation temperature of thermoplastic starch and thermoplastic starch/lignocellulosic fiber composite was observed in the study conducted by Averous and Boquillon [52]. Yuan et al. [53] reported the effect of multiwall carbon nanotubes on thermal stability of polyamide 12. It was found that there were two stages of decomposition for neat polyamide 12 at 443 and 462 °C respectively. The addition of carbon nanotube at 1% loading stabilized the polymer matrix against first degradation stage; this is due to the carbon nanotube network capturing thermal radicals and transferring the thermal energy effectively between the polymer chains and carbon nanotube thus avoiding chemical decomposition of the polyamide 12. Similar enhancement in thermal stability of nanocomposite was detected by Weng et al. [54]. They concluded that the addition of nanofiller in the polymer increased the thermal stability by acting as a superior insulator or barrier to the volatiles produced during degradation. In addition, the onset temperature moved slightly to a higher temperature than that of pure matrix confirming that the thermal stability was improved by the reinforcement using nanofiller. Bera and Maji [55] prepared graphene oxide/polyurethane and reduced graphene oxide/polyurethane nanocomposites and measured their thermal properties with the help of TGA and DSC to

understand the effect of nanofillers on the thermal properties of end product-nanocomposite. The results suggest that both the neat polyurethane and nanocomposites represented a two-stage thermal degradation pattern which corresponds to the degradation of hard and soft segments. Further, it was reported that the neat polyurethane was thermally stable up to 300 °C and the degradation of the soft segment for raw polyurethane occurred in the range of 300–405 °C, while degradation of the hard segment took place after 405 °C. The initial degradation temperature and T_{\max} for graphene oxide/polyurethane nanocomposite at 0.10% loading of graphene oxide were increased by 6 and 8 °C; for reduced graphene oxide/polyurethane at 0.10% loading of reduced graphene oxide initial degradation temperature and T_{\max} increased by 5 and 6 °C, respectively. Based on these findings, it was concluded that the graphene oxide provides more thermal stability than reduced graphene oxide at the same loading. An increase in thermal stability by addition of graphene oxide or reduced graphene oxide nanofillers is attributed to the physicochemical interaction between nanofiller and polyurethane, which leads to restricted motion of the polyurethane chains [56]. Furthermore, the volatiles produced during decomposition also remain in the material due to the high barrier properties of nanocomposite compared to raw polyurethane. Their findings were in agreement to literature in which a similar effect of nanofiller on thermal stability of nanocomposite is reported [57].

Arrieta, Fortunati [58] studied the thermal properties of binary and ternary nanocomposite films. The binary system involved neat PLA incorporated with unmodified and surface modified CNC, coded as PLA-CNC and PLA-CNCs, respectively. The ternary system consisted of PLA-PHB-CNC (PHB refers to poly (hydroxybutyrate)) and PLA-PHB-CNCs. The key observation was that the neat PLA and PLA-CNC had a single degradation step while the PLA-CNCs had dual degradation step. The first degradation step of PLA-CNC takes place at temperatures lower than the main degradation step, which might be associated with surfactant loss.

4.2 Differential Scanning Calorimetry (DSC)

DSC provides important data such as the heat capacity (ΔC_p) assigned to the polymer matrix, heat enthalpy (ΔH_m) assigned to the nanofiller, glass transition temperature (T_g), and the melting temperature (T_m). The addition of nanofiller in polymer matrix helps to improve the DSC results. It is reported in the literature [54] that the glass transition temperature (T_g) was improved with the loading of the nanofiller. It is reported that the T_g of a neat ABS polymer was 99 °C, which increased to 103, 107 and 112 °C at 1, 3 and 5% loading of nanofiller as shown in Fig. 1. According to Yu et al. [59], the DSC results showed that the PLA used in their study had a T_g around 57.7 °C and T_m of 149.1 °C. The T_g for neat PLA was observed at 57.7 °C, with an increase in loading of starch nanocrystals (StN) to grafted PCL (StN-g-PCL) it reduced to 47.8 °C for 5 wt% filler and eventually, it disappeared for higher loadings. This was ascribed to the increased

flexibility of the PLA chains during the melting process of the PCL. The fabrication of nanocomposites, with PLA as a matrix, and 1 and 3%wt of unmodified (CNC) and surfactant-modified (s-CNC) cellulose nanocrystals as fillers, using solvent casting technique was reported by Fortunati et al. [60]. There is no significant change in the T_g as reported in the previous literature on PLA based nanocomposites. Conversely, a reduction in T_g values was detected in the PLA 1 s-CNC system (about 15 °C), though a less intense signal, which was hard to perceive, was recorded for the PLA 3 s-CNC nanocomposite. This effect may be credited to the presence of the surfactant that acts as a plasticizer of the polymer, decreasing the glass transition temperature.

The raw polyurethane did not have a sharp melting point (T_m) for the hard segment [61] due to its lower percentage i.e. 23%. Therefore, the T_m of second heating was considered as true T_m because the impurities in polymer get melted in first heating, therefore, the T_m of neat polymer or nanocomposites takes place in the second heating [55]. On the other hand, Gabr et al. [62] found that the addition of nanoclay as a nanofiller does not have any effect on T_m . They found that the T_m of both the neat polymer and nanocomposite was 165 °C as confirmed by the DSC heating curve of neat polypropylene and polypropylene/nanoclay composite as shown in Fig. 2b. Yu et al. [59] noticed that the neat PLA has a single sharp melting peak at 149.1 °C, however, dual peaks were observed for nanocomposites which were assigned to the presence of PCL. The dual peaks are indicative of the presence of interfacial layers based on the interactions between PLA, PCL, and StN. Gabr et al. [62] synthesized a polypropylene/organoclay nanocomposite up to 5% and studied the DSC analysis of both the raw polypropylene and nanocomposite as shown in Fig. 2a. The results revealed that crystallization peak temperature of neat polypropylene was 121.1 °C, which increased to 123.4 °C at 5% loading of nanoclay filler. An increase in crystallization peak temperature by the addition of organoclay is assumed to be due to the layers of organoclay acting as effective nucleating agents for crystallization of polypropylene. Due to the interaction between layers of organoclay and polypropylene, organoclay layers absorb molecule segments of polypropylene and some of the polypropylene is immobilized and

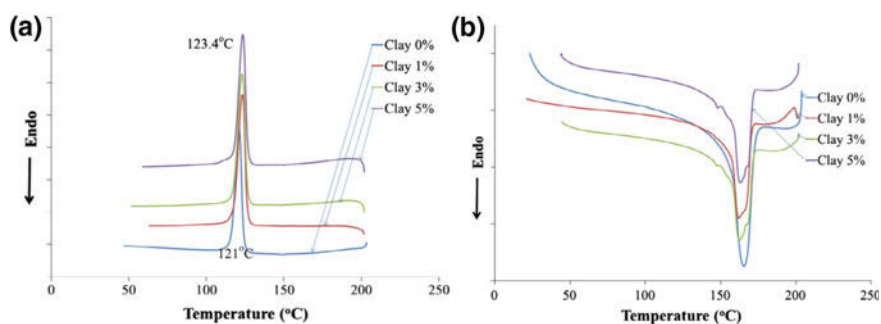


Fig. 2 a and b Cooling and heating curves for DSC of neat polypropylene and polypropylene/organoclay nanocomposite. Reprinted from Ref. Gabr, Okumura [62] with permission from Elsevier

this immobilization of polypropylene molecules helps in the crystallization of polypropylene. An increase in crystallization temperature by the addition of nanofillers in the polymer matrix was reported by Mingliang and Demin [63].

Robles, Urruzola [64] reported six different nanocomposites based on PLA and surface modified cellulose nanofibres and cellulose nanocrystals, obtained from blue agave bagasse. The nanocomposites were developed using a Haake Minilab twin-screw extruder with an L/D ratio of 24:1 at 170 °C. Two different surface modifications were done in order to modify the hydrophilic character of the nanofillers. The surface treatment was done using 3aminopropyl triethoxysilane and dodecanoyl chloride for cellulose nanofibers and cellulose nanocrystals, respectively. An improvement in crystallization of the PLA chains was noted with an increase in the loading of nanoreinforcement, without altering the overall crystallinity of the PLA matrix. The slight deviation in the T_c and the rise in the enthalpy of melting are ascribed to the good nucleation of the nanocellulose filler (fiber and crystals). This enables the PLA chains to flow freely around the crystals whilst maintaining a stable melting temperature.

4.3 Thermal Conductivity

Thermoplastic polymers have a wide range of applications to act as electrical and thermal insulators. To enhance the thermal and electrical conductivity of these polymers, it is suggested to add any nanofiller to obtain a nanocomposite, which has potential to overcome the limitations of these polymers in electrical and thermal applications [53]. Polymeric nanocomposites have the potential for utilization in a variety of thermal applications such as heat exchange and electronics thermal management. It is reported that the thermal conductivity of polymers can be enhanced significantly by reinforcement with small amounts of nanomaterials [65]. For example, single-wall carbon nanotube have thermal conductivity over 3000 W/m K; it is estimated by simulation that this value can be as high as around 6000 W/m K [66]. Another study reported that a factor of 250 enhancements in thermal conductivity was observed at 10% loading of multiwalled-carbon nanotubes [67, 68]. A number of studies have been conducted for improving the thermal conductivity of polymers by incorporating different amount of loadings of different types of nanomaterials in a polymer matrix.

Yuan et al. [53] prepared two different nanocomposites by incorporating carbon nanotube as a nanofiller in two different thermoplastic polymers i.e. polyamide 12 and polyurethane and investigated the effect of nanofiller on thermal conductivity. It was reported that the thermal conductivity was improved significantly by reinforcing 0–1% of carbon nanotube into the polymer matrix for both the polymers as shown in Fig. 3. Patton et al. [69] prepared vapour grown carbon nanofiber/epoxy nanocomposite and measured the thermal conductivity of pure resin and nanocomposite. It was found that the thermal conductivity of pure resin was 0.26 W/m K, which improved to 0.8 W/m K at 40 vol.% of carbon nanofiber. The

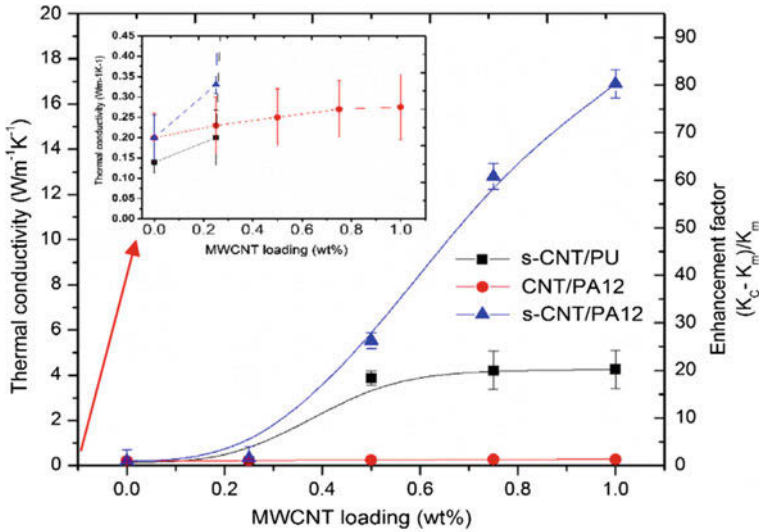


Fig. 3 Thermal conductivities of carbon nanotube/polyamide and carbon nanotube/polyurethane with 0–1% loading of carbon nanotube as a nanofiller. Reprinted from Ref. Yuan, Bai [53] with permission from Elsevier

small increment in thermal conductivity of nanocomposite was ascribed to the difficulty in transmitting thermal energy from fiber to fiber. Lafdi and Matzek produced 20% carbon nanofiber/epoxy resin and measured the thermal conductivity and observed a rise in thermal conductivity from 0.2 W/m K of neat resin to 2.8 W/m K of nanocomposite [70].

It is reported in the literature that the thermal conductivity depends on the temperature [71]. They fabricated polypropylene/single wall carbon nanotube and studied the dependence of thermal properties of both the neat polymer and nanocomposite on temperature. The research found that both the neat polypropylene and polypropylene/carbon nanotube nanocomposite showed a decreasing thermal conductivity with increasing temperature at lower temperatures but this trend reversed at higher temperatures—refer to Fig. 4. Further, the temperature dependence of thermal conductivity of both the raw polymer and nanocomposite can be modelled by bicubic regression polynomials. Also, the thermal conductivity increases with an increase in the amount of loading of nanofiller.

5 Recycling Perspective

In the past few years, considerable effort has been devoted globally to extend the applications of sustainable thermoplastic materials by conferring on them advanced properties through mixing and blending them with various nanofillers.

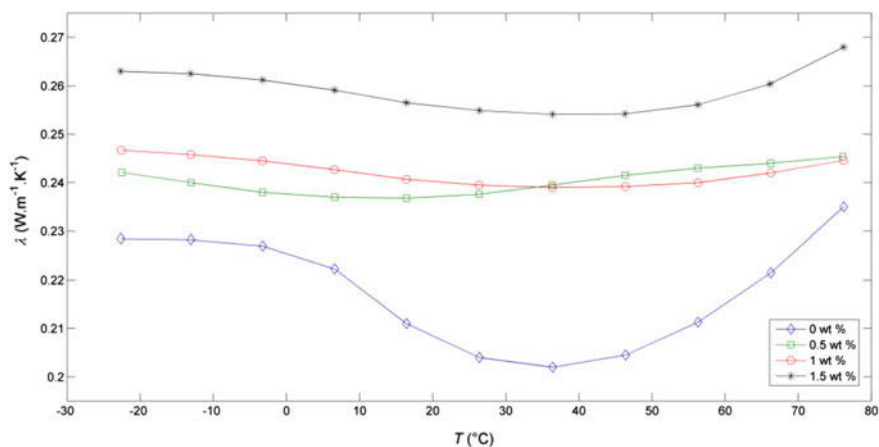


Fig. 4 Temperature dependence of thermal conductivity of pure polypropylene and nanocomposite. Reprinted from Ref. Ivan, Pavol [71] with permission from Elsevier

Thermoplastic polymers like polyolefins, polyamide, polyesters, and styrene polymers are the most representative commodity polymers for cost-efficient manufacturing techniques, outstanding thermo-mechanical properties and good compatibility with the environment, together with easy recycling. The thermal features of thermoplastics nanocomposites plays an important role in deciding its recyclability properties. Sustainable nanocomposites are considered the polymeric materials of this era and are used with organic or inorganic nanofillers with size usually of 1–100 nm. In particular, the higher surface area of the nanofillers than their counterparts allows efficient interfacial interaction with the polymer. The unique properties of the biodegradable nanofillers enhance the overall performance of the polymer matrix. These thermoplastics nanocomposites have a wide variety of applications due to their good thermal and mechanical properties as well as durability in the area of optoelectronic and chemiresistor devices, temperature sensors, linear polarizers, polymeric matrices, catalytic and other chemical sensors, functional materials, polyolefins, polyesters and polyamides. The current total production of plastics is very high and will continue to increase. Hence, due to the creation of huge quantities of plastic waste by industrial manufacturers and householders, the world is confronting a crisis in concerns to environmental, economic and petroleum affects of such production.

Old-style methods of disposal of plastics have negative influences on the environment, for instance, the combustion of unwanted polymers in the form of fumes and toxic gases as well as waste to underground water. The recycling practice is the best method to treat waste polymers and recycling commonly involves processing plastics to produce energy [72]. The overall recycling rate is 2.4 million tonnes for different polymers. Different technological processes have been reported for recycling of polymers such as chemical or feedstock recycling with energy recovery and mechanical recycling [73]. In plastic industries,

mechanical recycling is a relatively simple and common method and is also preferable for adequate quantities of homogenous and separated wastes [74]. The conventional mechanical recycling process includes the separation, grinding and producing another material without changing its chemical nature; therefore, mechanical recycling is limited. Low molecular weight materials can be produced by chemical or thermal treatment during feedstock recycling [75], which is an attractive method to substitute for mechanical recycling. The energy recovery techniques mainly applies to plastic disposal wastes via incineration, which also contains a large number of combustible solids. After melting, a stray polyvinyl chloride (PVC) bottle within 10,000 polyethylene terephthalate (PET) bottles can cause the deterioration of the whole batch of PET bottles due to separation difficulties. Therefore, the Society of plastics industry passed the numerical coding system act in the 1980s for ease of separation to determine plastic types. Therefore, these material and chemical recycling of plastic is an appropriate solution to the problems of environmental pollution from various wastes on a worldwide industry level. This can be achieved by using a wide range of different processing techniques with low-cost parameters and has gained increasing importance in the scientific and industrial communities for thermoplastics nanocomposites. Among European countries, Germany has the highest number of recyclers and is globally regarded as the most advanced country for PVC/plastic recycling. The recycling of these polymers usually requires a suitable separation method in which polymer/plastic materials in the mixed solid wastes are separated into a homogeneous stream, which allows a wide range of applications from the recycling perspective.

A simple method is a separation technique of general polymers from plastic wastes is via hand sorting. The application of low content nanofillers is one of the widest and well-known methods to add value to recycled waste plastics to produce thermoplastic nanocomposites, which enhance the thermal stability as well as mechanical properties [76]. The surface area, strength, and viscosity of polymers increase with the addition of nanofiller, which affects interfacial interactions between the polymer and filler [77] and ultimately it increases the performance. The interfacial interactions improve the tensile properties of composites. Titanium dioxide was also incorporated via solution method to improve polymer stability of recycled plastic as well as discolouration resistance [78]. The addition of small organoclays also allows a change in chemical nature of polymer to enhance the recyclability of the polymer [79]. In this way, degradation is minimized with an improvement of some properties. Thus the recycling process involves different new developments and separation techniques for waste polymers with novel energy-recovery procedures for effective cost management.

6 Conclusion

The concept of combining nanomaterials as filler with polymer as a matrix in order to form different forms of nanocomposites has been gaining much recognition these days by researchers. The nanomaterials such as nanotubes and nanoclays provide great potential for fabrication of a variety of different forms of composites, coatings, adhesives and sealant materials with specific properties. Incorporating small quantity of nano additives/nanofillers tends to affect the thermal characteristics of the polymer matrix. Both the initial degradation temperature and T_{\max} values for nanocomposites are greater than the neat polymer due to the presence of nanofiller in the nanocomposite. The thermal conductivity highly depends upon the temperature and is well-modelled by bicubic regression polynomials.

Recycling is the best way to treat and minimize waste polymer products and is achieved using various processes on plastics. Different technological processes have been reported for recycling of polymers such as chemical or feedstock recycling with energy recovery, and mechanical recycling. The recycling process involves new development and separation techniques for waste polymers with novel energy-recovery procedures for effective cost management from an economical standpoint.

References

1. Hajilary N, Shahi A, Rezakazemi M (2018) Evaluation of socio-economic factors on CO₂ emissions in Iran: factorial design and multivariable methods. *J Clean Prod* 189:108–115
2. Ghanbarzadeh B, Almasi H (2013) Biodegradable Polymers. In: *Biodegradation—Life of Science*
3. Madhavan KN, Nair NR, John RP (2010) An overview of the recent developments in polylactide (PLA) research. *Bioresour Technol* 101(22): p. 8493–501
4. Rezakazemi M, Zhang, Z (2018) 2.29 Desulfurization materials. In: a2–Dincer I (ed) *Comprehensive energy systems*. Elsevier, Oxford. p. 944–979
5. Pawelec Z, Bakar M (2013) Shaping mechanical and thermal properties of polymer nanocomposites. *Problemy Eksploatacji*
6. Rezakazemi M et al (2011) Simulation and determination of optimum conditions of pervaporative dehydration of isopropanol process using synthesized PVA–APTEOS/TEOS nanocomposite membranes by means of expert systems. *J Membr Sci* 379(1–2):224–232
7. Rezakazemi M et al (2011) CFD simulation of water removal from water/ethylene glycol mixtures by pervaporation. *Chem Eng J* 168(1):60–67
8. Bari SS, Chatterjee A, Mishra S (2016) Biodegradable polymer nanocomposites: an overview. *Polym Rev* 56(2):287–328
9. Rezakazemi M, Vatani A, Mohammadi T (2015) Synergistic interactions between POSS and fumed silica and their effect on the properties of crosslinked PDMS nanocomposite membranes. *RSC Advances* 5(100):82460–82470
10. Rezakazemi M, Vatani A, Mohammadi T (2016) Synthesis and gas transport properties of crosslinked poly(dimethylsiloxane) nanocomposite membranes using octatrimethylsiloxy POSS nanoparticles. *J Nat Gas Sci Eng* 30:10–18

11. Mittal V, Mittal V (2011) Nanocomposites with biodegradable polymers: synthesis, properties, and future perspectives. In: Mittal V Mittal V.e. (eds) Oxford, New York Oxford, Oxford University Press
12. Raquez J-M et al (2013) Polylactide (PLA)-based nanocomposites. *Prog Polym Sci* 38(10–11):1504–1542
13. Saheb DN, Jog JP (1999) Natural fiber polymer composites: a review. *Adv Polym Technol* 18 (4):351–363
14. Rezakazemi M, Shahidi K, Mohammadi T (2014) Synthetic PDMS composite membranes for pervaporation dehydration of ethanol. *Desalin Water Treat* 54(6):1–8
15. Takase S, Shiraishi N (1989) Studies on composites from wood and polypropylenes II. *J Appl Polym Sci* 37(3):645–659
16. Tibbetts GG et al (2007) A review of the fabrication and properties of vapor-grown carbon nanofiber/polymer composites. *Compos Sci Technol* 67(7–8):1709–1718
17. Tibbetts GG, McHugh JJ (1999) Mechanical properties of vapor-grown carbon fiber composites with thermoplastic matrices. *J Mater Res* 14(7):2871–2880
18. Sodeifian G et al (2018) Polyurethane-SAPO-34 mixed matrix membrane for CO₂/CH₄ and CO₂/N₂ separation. *Chin J Chem Eng*
19. Rezakazemi M et al (2017) Methods for the preparation of organic–inorganic nanocomposite polymer electrolyte membranes for fuel cells. In: Inamuddin D, Mohammad A, Asiri AM (eds) Organic-inorganic composite polymer electrolyte membranes. Springer, Cham. p. 311–325
20. Rezakazemi M et al (2014) State-of-the-art membrane based CO₂ separation using mixed matrix membranes (MMMs): an overview on current status and future directions. *Prog Polym Sci* 39(5):817–861
21. Baheri B et al (2014) Performance of PVA/NaA mixed matrix membrane for removal of water from ethylene glycol solutions by pervaporation. *Chem Eng Commun* 202(3):316–321
22. Shahverdi M et al (2013) Pervaporation study of ethylene glycol dehydration through synthesized (PVA-4A)/polypropylene mixed matrix composite membranes. *Polym Eng Sci* 53(7):1487–1493
23. Rostamizadeh M et al (2013) Gas permeation through H₂-selective mixed matrix membranes: experimental and neural network modeling. *Int J Hydrogen Energy* 38(2):1128–1135
24. Rezakazemi M, Mohammadi T (2013) Gas sorption in H₂-selective mixed matrix membranes: experimental and neural network modeling. *Int J Hydrogen Energy* 38(32):14035–14041
25. Rezakazemi M, Shahidi K, Mohammadi T (2012) Sorption properties of hydrogen-selective PDMS/zeolite 4A mixed matrix membrane. *Int J Hydrogen Energy* 37(22):17275–17284
26. Rezakazemi M, Shahidi K, Mohammadi T (2012) Hydrogen separation and purification using crosslinkable PDMS/zeolite a nanoparticles mixed matrix membranes. *Int J Hydrogen Energy* 37(19):14576–14589
27. Dashti A, Harami HR, Rezakazemi M (2018) Accurate prediction of solubility of gases within H₂-selective nanocomposite membranes using committee machine intelligent system. *Int J Hydrogen Energy* 43(13):6614–6624
28. Rezakazemi M et al (2017) H₂-selective mixed matrix membranes modeling using ANFIS, PSO-ANFIS, GA-ANFIS. *Int J Hydrogen Energy* 42(22):15211–15225
29. Oksman K, Skrifvars M, Selin J-F (2003) Natural fibres as reinforcement in polylactic acid (PLA) composites. *Compos Sci Technol* 63(9):1317–1324
30. Aji I et al (2011) Thermal property determination of hybridized kenaf/PALF reinforced HDPE composite by thermogravimetric analysis. *J Therm Anal Calorim* 109(2):893–900
31. Frone AN et al (2013) Morphology and thermal properties of PLA–cellulose nanofibers composites. *Carbohydr Polym* 91(1):377–384
32. Pei A, Zhou Q, Berglund LA (2010) Functionalized cellulose nanocrystals as biobased nucleation agents in poly(l-lactide) (PLLA)—crystallization and mechanical property effects. *Compos Sci Technol* 70(5):815–821

33. Takkalkar P et al (2018) Preparation of square-shaped starch nanocrystals/poly(lactic acid) based bio-nanocomposites: morphological, structural, thermal and rheological properties. In: Waste and biomass valorization
34. Mukherjee T et al (2013) Improved dispersion of cellulose microcrystals in poly(lactic acid) (PLA) based composites applying surface acetylation. *Chem Eng Sci* 101:655–662
35. Narimissa E et al (2012) Morphological, mechanical, and thermal characterization of biopolymer composites based on polylactide and nanographite platelets. *Polym Compos* 33 (9):1505–1515
36. Narimissa E et al (2012) Influence of nano-graphite platelet concentration on onset of crystalline degradation in polylactide composites. *Polym Degrad Stab* 97(5):829–832
37. Kaushik A, Singh M, Verma G (2010) Green nanocomposites based on thermoplastic starch and steam exploded cellulose nanofibrils from wheat straw. *Carbohydr Polym* 82(2):337–345
38. Cao X et al (2008) Starch-based nanocomposites reinforced with flax cellulose nanocrystals. *Express Polym Lett* 2(7):502–510
39. Goffin A-L et al (2011) Poly (ϵ -caprolactone) based nanocomposites reinforced by surface-grafted cellulose nanowhiskers via extrusion processing: morphology, rheology, and thermo-mechanical properties. *Polymer* 52(7):1532–1538
40. Lepoittevin B et al (2002) Poly (ϵ -caprolactone)/clay nanocomposites prepared by melt intercalation: mechanical, thermal and rheological properties. *Polymer* 43(14):4017–4023
41. Stoeffler K et al (2013) Polyamide 12 (PA12)/clay nanocomposites fabricated by conventional extrusion and water-assisted extrusion processes. *J Appl Polym Sci* 130(3):1959–1974
42. Gupta B, Lacrampe M-F, Krawczak P (2006) Polyamide-6/clay nanocomposites: a critical review. *Polym Polym Compos* 14(1):13–38
43. Morgan AB et al (2002) Flammability of polystyrene layered silicate (clay) nanocomposites: carbonaceous char formation. *Fire Mater* 26(6):247–253
44. Song P et al (2011) Fabrication of exfoliated graphene-based polypropylene nanocomposites with enhanced mechanical and thermal properties. *Polymer* 52(18):4001–4010
45. Wakabayashi K et al (2008) Polymer - Graphite Nanocomposites: Effective Dispersion and Major Property Enhancement via Solid-State Shear Pulverization. *Macromolecules* 41 (6):1905–1908
46. Wakabayashi K et al (2010) Polypropylene-graphite nanocomposites made by solid-state shear pulverization: effects of significantly exfoliated, unmodified graphite content on physical, mechanical and electrical properties. *Polymer* 51(23):5525–5531
47. Miltner HE et al (2008) Isotactic polypropylene/carbon nanotube composites prepared by latex technology. Thermal analysis of carbon nanotube-induced nucleation. *Macromolecules*. 41(15): p. 5753–5762
48. El Achaby M et al (2012) Mechanical, thermal, and rheological properties of graphene-based polypropylene nanocomposites prepared by melt mixing. *Polym Compos* 33(5):733–744
49. Agustin MB et al (2014) Bioplastic based on starch and cellulose nanocrystals from rice straw. *J Reinf Plast Compos* 33(24):2205–2213
50. Wang S et al (2002) Preparation and thermal properties of ABS/montmorillonite nanocomposite. *Polym Degrad Stab* 77(3):423–426
51. Alemdar A, Sain M (2008) Biocomposites from wheat straw nanofibers: morphology, thermal and mechanical properties. *Compos Sci Technol* 68(2):557–565
52. Averous L, Boquillon N (2004) Biocomposites based on plasticized starch: thermal and mechanical behaviours. *Carbohydr Polym* 56(2):111–122
53. Yuan S et al (2016) Highly enhanced thermal conductivity of thermoplastic nanocomposites with a low mass fraction of MWCNTs by a facilitated latex approach. *Compos A Appl Sci Manuf* 90:699–710
54. Weng Z et al (2016) Mechanical and thermal properties of ABS/montmorillonite nanocomposites for fused deposition modeling 3D printing. *Mater Des* 102:276–283
55. Bera M, Maji PK (2017) Effect of structural disparity of graphene-based materials on thermo-mechanical and surface properties of thermoplastic polyurethane nanocomposites. *Polymer* 119:118–133

56. Thakur S, Karak N (2015) A tough, smart elastomeric bio-based hyperbranched polyurethane nanocomposite. *New J Chem* 39(3):2146–2154
57. Zhang J, Zhang C, Madbouly, SA (2015) In situ polymerization of bio-based thermosetting polyurethane/graphene oxide nanocomposites. *J Appl Polym Sci* 132(13)
58. Arrieta MP et al (2014) Multifunctional PLA–PHB/cellulose nanocrystal films: processing, structural and thermal properties. *Carbohydr Polym* 107:16–24
59. Yu J et al (2008) Structure and mechanical properties of poly(lactic acid) filled with (starch nanocrystal)- graft -poly(ϵ -caprolactone). *Macromol Mater Eng* 293(9):763–770
60. Fortunati E et al (2015) Processing of PLA nanocomposites with cellulose nanocrystals extracted from *Posidonia oceanica* waste: innovative reuse of coastal plant. *Ind Crops Prod* 67:439–447
61. Sadasivuni KK et al (2014) Dielectric properties of modified graphene oxide filled polyurethane nanocomposites and its correlation with rheology. *Compos Sci Technol* 104:18–25
62. Gabr MH et al (2015) Mechanical and thermal properties of carbon fiber/polypropylene composite filled with nano-clay. *Compos B Eng* 69:94–100
63. Mingliang G, Demin J (2009) Preparation and properties of polypropylene/clay nanocomposites using an organoclay modified through solid state method. *J Reinf Plast Compos* 28(1):5–16
64. Robles E et al (2015) Surface-modified nano-cellulose as reinforcement in poly(lactic acid) to conform new composites. *Ind Crops Prod* 71:44–53
65. Gulotty R et al (2013) Effects of functionalization on thermal properties of single-wall and multi-wall carbon nanotube–polymer nanocomposites. *ACS Nano* 7(6):5114–5121
66. Kim P et al (2001) Thermal transport measurements of individual multiwalled nanotubes. *Phys Rev Lett* 87(21):215502
67. Nan C-W, Shi Z, Lin Y (2003) A simple model for thermal conductivity of carbon nanotube-based composites. *Chem Phys Lett* 375(5–6):666–669
68. Prasher RS et al (2009) Turning carbon nanotubes from exceptional heat conductors into insulators. *Phys Rev Lett* 102(10):105901
69. Patton R et al (1999) Vapor grown carbon fiber composites with epoxy and poly (phenylene sulfide) matrices. *Compos A Appl Sci Manuf* 30(9):1081–1091
70. Lafdi K, Matzek M (2003) Carbon nanofibers as a nano-reinforcement for polymeric nanocomposites. In: *SAMPE Conference Preceding Materials and Processing*
71. Ivan K et al (2016) Temperature dependence of thermal properties of thermoplastic polyurethane-based carbon nanocomposites. In: *AIP Conference Proceedings*. AIP Publishing
72. Raiisi-Nia MR, Aref-Azar A, Fasihi M (2013) Acrylonitrile–butadiene rubber functionalization for the toughening modification of recycled poly (ethylene terephthalate). *J Appl Polym Sci* 131(13)
73. Zhang Y, Broekhuis AA, Picchioni F (2009) Thermally self-healing polymeric materials: the next step to recycling thermoset polymers? *Macromolecules* 42(6):1906–1912
74. Hu X, Calo J (2006) Plastic particle separation via liquid-fluidized bed classification. *AIChE J* 52(4):1333–1342
75. Kameda T et al (2010) Chemical modification of rigid poly (vinyl chloride) by the substitution with nucleophiles. *J Appl Polym Sci* 116(1):36–44
76. Zare Y, Garmabi H (2012) Nonisothermal crystallization and melting behavior of PP/nanoclay/CaCO₃ ternary nanocomposite. *J Appl Polym Sci* 124(2):1225–1233
77. Zare Y et al (2014) An analysis of interfacial adhesion in nanocomposites from recycled polymers. *Comput Mater Sci* 81:612–616
78. Herrera-Sandoval G et al (2013) Novel EPS/TiO₂ nanocomposite prepared from recycled polystyrene. *Mater Sci Appl* 4(03):179
79. Orden MU et al (2014) Clay-induced degradation during the melt reprocessing of waste polycarbonate. *J Appl Polym Sci* 131(5)

Application of Sustainable Nanocomposites in Membrane Technology



Pravin G. Ingole

1 Introduction

Nowadays nanocomposite membrane technology is widely used in industrial application. The developments of polymer membrane using new generation materials that broaden the industrial applications of membrane processes entail an elevated level of control over a polymer base and nanoparticles addition in the support layer. Polymeric membrane-based separation processes provide a sustainable separation technique for solid/liquid/gas permeance and selectivity [32–35]. Membrane-based separation is economical and conventional base separation process. Especially the nanocomposite membrane-based separation technology is environment-friendly and economically viable. Development of nanocomposite membrane technology for diverse application is one of the best ways to resolve the current inescapable problems.

Currently, nanocomposite membrane technologies are used in gas separation, for example, functionalized TiO_2 , SiO_2 NPs incorporated thin-film nanocomposite (TFN) membranes are widely used for mixture gas separation to enhance the gas permeance and selectivity [13, 33, 34]. Also same type of nanocomposite membrane materials are used for water purification [21], wastewater treatment [61], dye separation [88] water vapour separation [5, 31, 33, 34] drug separation [91] etc. NPs incorporated membranes are mechanically strong and thermally more stable compared to without NPs incorporated membranes. Generally, two kinds of nanocomposite membranes varieties are available either it is a flat sheet or hollow fiber shape. Addition of inorganic moieties in the polymer matrix is increases the flexibility and ductility of organic polymers. Recent decade researchers found that the commercialization of nanocomposite membrane is easiest way compared with

P. G. Ingole (✉)

Chemical Engineering Group, Engineering Sciences and Technology Division,
CSIR-North East Institute of Science and Technology, Jorhat 785006, Assam, India
e-mail: ingolepravin@gmail.com

another kind of membrane over enhanced flux and selectivity. Khalid et al. suggested that PEG-CNTs nanocomposite PSU membranes are more advanced for wastewater treatment [43]. Nanocomposite membranes also provide motivation to unite the qualities of inorganic nanomaterials and polymeric matrices for exceptional nanofiltration performance [55]. Recently researchers develop the low fouling ultrathin nanocomposite membranes for efficient removal of manganese and lithium [76, 82].

To develop the nanocomposite membrane technology in large scale, early it was the main task of the researcher and now the commercial technology is available in the market. The nanocomposite membranes having mechanical, thermal and swelling properties have developed by using cellulose nanocrystals and PVA [36]. Nanocomposite membrane technology is also applicable for fuel cell applications [7, 84, 86]. Antibacterial mixed matrix nanocomposite membranes fabricated using hybrid nanostructure of silver-coated multi-walled carbon nanotubes by Aani et al. [1]. Using nanocomposite anion exchange membranes, Fernandez-Gonzalez et al. studied the valorization of desalination brines by electrodialysis with bipolar membranes [26]. Within the broad array of commercially existing nanoscale materials, TiO_2 NPs are gained special interest for water desalination [25, 73]. In membrane distillation perfluorododecyl trichlorosilane (FTCS) was employed to modify the virgin polyvinylidene fluoride electrospun nanofiber membrane (PVDF ENM) [72]. TiO_2 (P25 and ST01) deposited on porous ceramic materials for photocatalytic degradation of organic substances in water, a three-phase catalytic membrane contactor (CMC) was implemented [47, 49].

Structural modification of the polymer membrane materials improves the membrane permeability, permselectivity along with mechanical straight and thermal stability. These properties would play a very significant role in membrane science and technology. Thin film nanocomposite membranes are one of the best examples in membrane science to resolve the various issues related to water [66, 70, 78], energy [80], pharmaceuticals [39], environment [10, 33, 34] etc. Further, incorporation of nanoparticles on the thin layer while polymerization especially graphene oxide (GO) membranes offer a wide range of opportunities. Such materials can be engineered to exhibit the desired for the separation characteristics because of ultimate thinness, flexibility, chemical stability and mechanical strength. Different to glassy polymers with a rigid backbone and a high portion of free volume (PTMSP) or with highly interconnected free volume polymers of intrinsic microporosity, GO materials can achieve high-flux and high-selectivity at the same time.

Nanoparticles incorporation to a polymer matrix control the permeability [60] throughout the subsequent sound effects: (a) they work as molecular sieves and amended the permeability [95], (b) also they interrupt the polymeric structure and increase the permeability [15]. One of the examples for Global warming is the result of increasing atmospheric concentration of greenhouse gases such as carbon dioxide (CO_2), methane (CH_4), nitrous oxides (NO_2), hydrofluorocarbons (HFCs), perfluorocarbon (PFC) and sulfurhexafluoride (SF_6). These gases trap an increasing portion of terrestrial infrared radiation so, it is expected that global temperature will increase between 1.4 and 5.8 °C in 2100 if no policies on climate change are

initiated. The temperature variation causes devastating effects in large and diverse areas of the globe such as possible variations in sea levels, changes in ecosystems, biodiversity loss, reduced crop yields and changes in global precipitation patterns, among other. Different types of membrane gas absorption processes will be tested for the removal of GHGs, both solid and in liquid suspension [18, 41]. Target GHGs will be carbon dioxide, nitrous oxide and methane [46]. This elimination is performed by adsorption and/or absorption processes. The experiment will involve separation and kinetic experiments (isotherms) with nanoparticles and membranes under different conditions of concentration, both in dry or in liquid media, bottled in a small volume and operating in discontinuous (microcosm systems) and perfectly airtight. In order to think in future industrial scale implementation, special attention will be focused on the immobilization of the nanoparticles in porous supports or membranes. In this chapter, the weight has been given to nanocomposite membranes preparation and their implementation in diverse applications including gas separation, water desalination, wastewater treatment, water vapour removal, and energy generation.

Nanocomposite materials especially nanocomposite membranes are facilitating speedy improvements in structural and functional materials diagonally all industries and most of the applications. Recently developed a new method of incorporating functional nanoparticles (10–15 nm) in polymer films, which has guided to the manufacture of a new method of thin film nanocomposite (TFN) membranes technology [33]. Super-hydrophilic nanoparticles synthesis and implementation is the first invention of TFN-based membranes. Introduction studies verify that TFN membranes separate the water vapour, with significant energy savings; and it has super-hydrophilic nature. The commercialization or large-scale productions of TFN membranes using prepared nanoparticles are possible without a major change in TFC membrane process and even cost is also not much higher. It will affect only 5–7% higher cost compare with TFC but the results showed the significant effect. Figure 1 represents the types of nanocomposite used in polymer and non-polymer base materials.

2 Types of Nanoparticles

2.1 *Inorganic Metal Oxide and Hydroxide*

Along with the numerous groups of nanoparticles, inorganic metal oxide and hydroxide have been of extensive attention from both technological and scientific point of view. Compared to the untainted materials the nano size synthesized metal oxide and hydroxides show the superior properties. Nowadays metal oxides and hydroxides are incorporated into other supports, such as polymeric materials for the applications like supercapacitor electrodes [42], polymer composites for aerospace applications [65], etc. Our group have the experience to synthesize SiO₂ NPs having

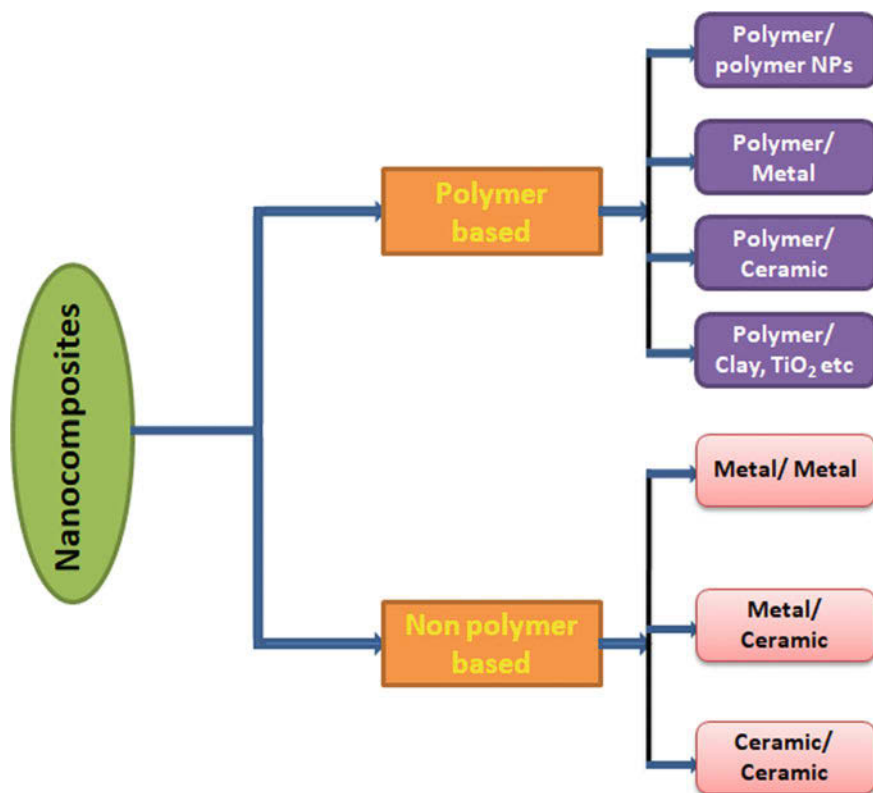


Fig. 1 Polymer and non-polymer based nanocomposite

particle size 10 to 15 nm and implemented it successfully in the nanocomposite membrane materials for diverse applications. Also, amorphous hydroxylated Silicon nanoparticles were synthesized in alcohol-based solvents to fabricate nanocomposite membranes have excellent surface hydrophilicity and roughness. After functionalization, nanoparticles showed higher cross-linking density, higher loading capacity, and high membrane performance.

Even though ceramic membranes play very imperative role in water treatment the polymer membrane technology has achieved noteworthy attention for water treatment applications because of advanced characteristics like its high flexibility, broad range of pore sizes and structures, easy developed process, low costs and easy to scale up [43, 61, 97].

2.2 Inorganic Nanoparticles to Prepare Polymeric Nanocomposite Membranes

In the polymeric composite membranes mechanical performance, lucidity, and thermal stability still remain the controlling limit for the various applications. Thus, the researchers need to develop strong, transparent and heat-resistant nanocomposite membranes for encouraging realistic outcomes. To develop the nanocomposite membrane, the main innovational target consist of concurrently obtaining high permeability and high selectivity at minimum costs, uniting reactions within the pore structures to avoid membrane fouling with avoiding further downstream unit operations, and rising membrane physical strength [50, 69, 84, 86].

Functional polymer membranes are usually premeditated and optimized with precise applications in researchers mind. Figure 2 represents the variety of nanocomposite membrane materials for diverse applications. The presence of functional groups on the surface of nanoparticles not only provides the hydrophilic nature but also reduced the Van der Waals interactive forces between nanoparticles [8]. Nanocomposite membranes, an innovative class of membranes prepared by coalescing polymeric materials with nanomaterials, are rising as a capable elucidation to resolve the various challenges. Especially several inorganic nanoparticles like zirconium phosphates, heteropolyacids, clays, ionic liquids, metal or metal oxides [4, 37, 67, 74], are of extraordinary attention for developing the composite materials. In the fuel cell application, the inorganic nanoparticles like zirconium phosphates, boron phosphate in the nanocomposite membranes do not only provide the water uptake but also provide an extra proton transport pathway [45].

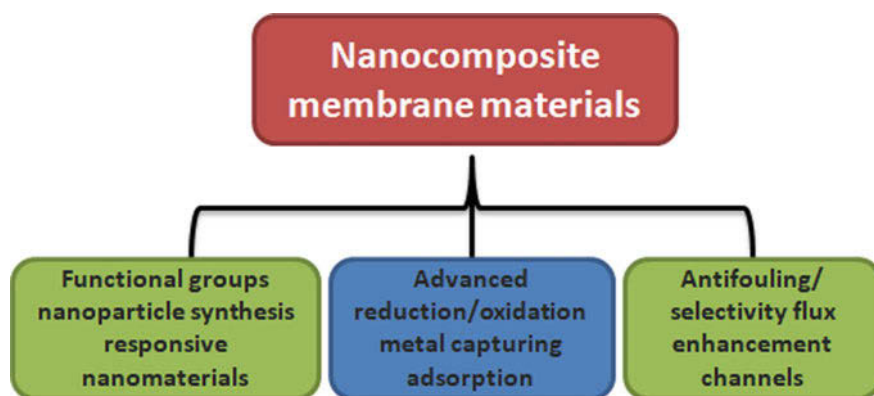


Fig. 2 Diverse nanocomposite membrane materials with various characteristic

3 Thin-Film Nanocomposite (TFN)

3.1 *Thin-Film Nanocomposite (TFN) Membranes for Water Desalination*

Many efforts have been dedicated to developing the advanced membrane technology to improve the performance of membrane in the form of flux, solute rejection and antifouling properties in the last 3 decades. Year after year research is going to progress and currently, researchers are focusing on nanocomposite membrane to improve the membrane properties. One of the attention was selected by researchers is to prepare the advance thin-film nanocomposite membrane along with support for the high flux, high rejection and antifouling property. Various conditions have been changed while interfacial polymerization (IP) to prepare TFN membranes, changing monomers, monomer concentrations, nanoparticles concentration, nanoparticles size, reaction times, applying chemical modification etc.

Nanomaterials are at present controlling the existing wave of original membrane material development because of the intrinsic explicit physicochemical features that make them apt for water treatment [97]. A number of nanoparticles like silica, graphene, zeolites, carbon nanotubes (both single and multiwalled), silver, metal-organic frameworks (MOFs), silicon and titanium dioxide are the mainly tested nanoparticles in existing and current research. The membranes prepared by using above-mentioned nanoparticles have been shows improved results in the form of permeability, rejection and antifouling properties [2, 24, 102]. Nanoporous silica incorporated membrane shown to reveal a high affinity for water and advanced hydrophilicity of TFN membrane [81]. A TiO_2 and silver nanoparticles have the main characteristic, is strong antimicrobial property so it is important material to develop the TFN membrane to resolve the biofouling issue [44, 96]. Biofouling is happened due to the formation of biofilm on membrane surface due to the intrinsic hydrophobicity of membrane materials. A metal-organic framework (MOF) is one of the best materials for water purification. Zhe et al. prepared the thin-film nanocomposite (TFN) membrane containing PSS-modified ZIF-8 nanoparticles via interfacial polymerization for the nanofiltration as shown in Fig. 3 [104]. The well TFN membrane process as shown in Figs. 3 and. 4 clearly understood that how the membrane is developed on the substrate via interfacial polymerization [94, 104]. To trounce this shortcoming, a variety of nanocomposite membranes are being modified to convey properties such as anti-fouling, hydrophilicity, self-cleaning, photocatalytic, and photodegradation using the nanoparticles (NPs) incorporated in polymeric membrane matrix or use in the interfacial polymerization process. Somehow still, it challenges the researchers to develop the cheapest nanomaterials to fabricate TFN membranes for commercial use.

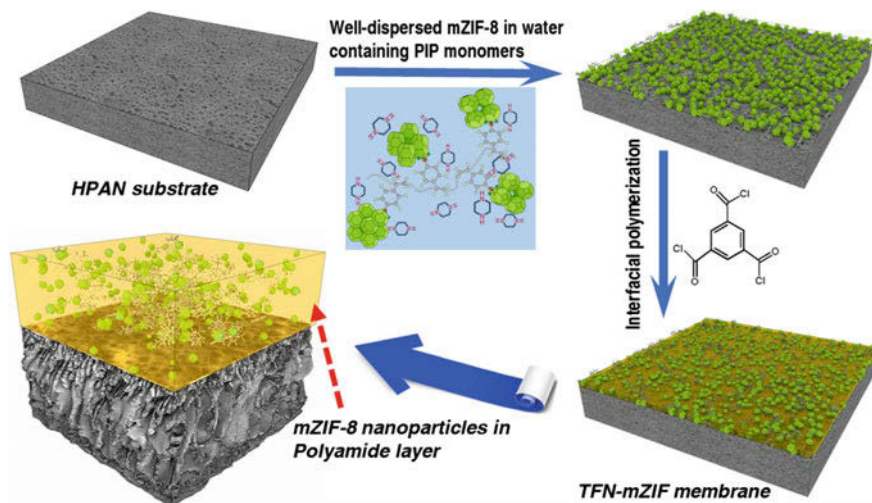


Fig. 3 Preparation process of thin-film nanocomposite (TFN) containing PSS-modified ZIF-8 nanoparticles via interfacial polymerization. Reprinted from Ref. [104], Copyright © 2017 American Chemical Society

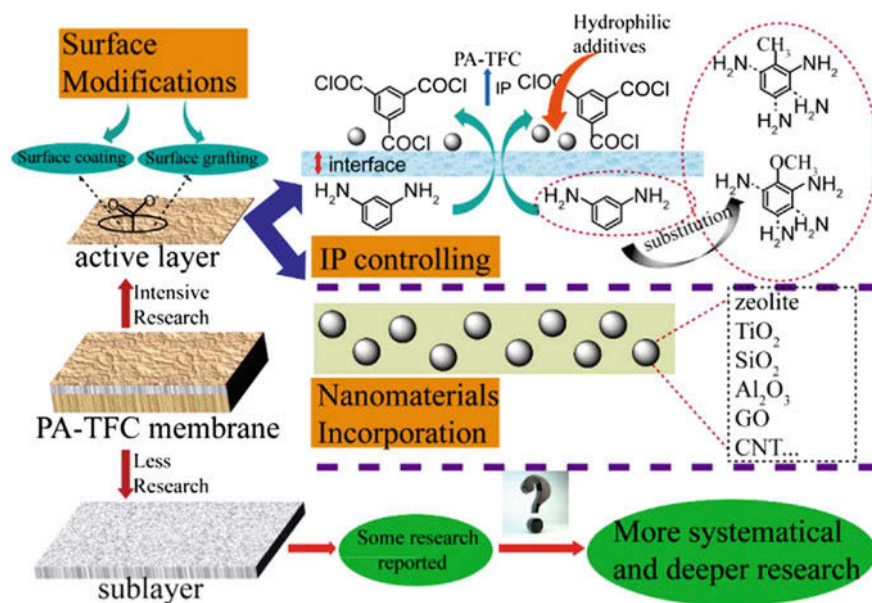


Fig. 4 Surface modification using different NPs to make nanocomposite layer. Reprinted from Ref. [94] Copyright © 2017 with permission from Elsevier

3.2 *Thin-Film Nanocomposite (TFN) Membranes for Wastewater Treatment*

In the reverse osmosis (RO) thin film composite (TFC) membranes are familiar for FO applications [14, 27, 28, 85, 87, 93, 99]. The technique used to make ultrathin polyamide (PA) selective rejection layer on the surface of porous polymer support is interfacial polymerization. Compare with market available commercial membranes (ex. Cellulose membrane) the thin film composite membranes are shown high permeability and also good resistance aligned with biodegradation [20, 103]. There are some disadvantages of TFC membranes while an operation like intrinsic internal concentration polarization (ICP), solute reverse diffusion and fouling has been found. Then researchers think there is need to develop such membranes which will resolve the above issues. So, Jeong et al. studied the concept of fabricating nanocomposite membranes and use it for RO application [38]. Furthermore, Ma et al. also develop the thin-film nanocomposite (TFN) membranes using NaY zeolite nanoparticles incorporation in the active layer while IP [57]. Later on, many research has been done by the researchers using TiO_2 , silica, SiO_2 , clay, carbon nanotubes, activated carbon, incorporated TFN membranes for wastewater treatment. The incorporation of NPs is useful for to improved surface hydrophilicity and because of it flux also enhanced drastically. In wastewater treatment researchers use functionalized MOF, CNT and other NPs like TiO_2 to improve the performance of nanocomposite membranes [56, 68, 104].

Comparative results of permeation through TFC and TFN membranes are shown in Fig. 5 on different operating pressure. Here in the TFN membranes while preparation added a different concentration of MOFs i.e. mZIFs. As a result, the water fluxes were increases sharply while increasing the operating pressure verifying a stable nanofiltration system. Based on the experimental data the water flux increases for TFC membrane $6.94 \text{ LMH bar}^{-1}$ to $14.9 \text{ LMH bar}^{-1}$ for the TFN membrane containing 0.10% w/v mZIF nanoparticles [104]. As shown in Fig. 6 Yin et al. prepared a TFN membrane containing GO nanosheets via an interfacial polymerization process. In their study, to prepare thin selective layer, aqueous *m*-phenylenediamine (MPD) and organic trimesoyl chloride (TMC)–GO mixture solutions were used [98]. A small quantity of GO addition is shown excellent results in the form of water flux and rejection as shown in Fig. 7. The GO NPs were added in thin film composite layer while IP to make TFN membranes. Increasing the concentrations of GO NPs the water fluxes were increases drastically as shown in Fig. 7.

3.3 *Thin-Film Nanocomposite (TFN) Membranes for Gas Separation*

In the gas separation, nanocomposite proposed an innovative direction to develop polymeric membrane with high performance. In gas separation, nanoporous

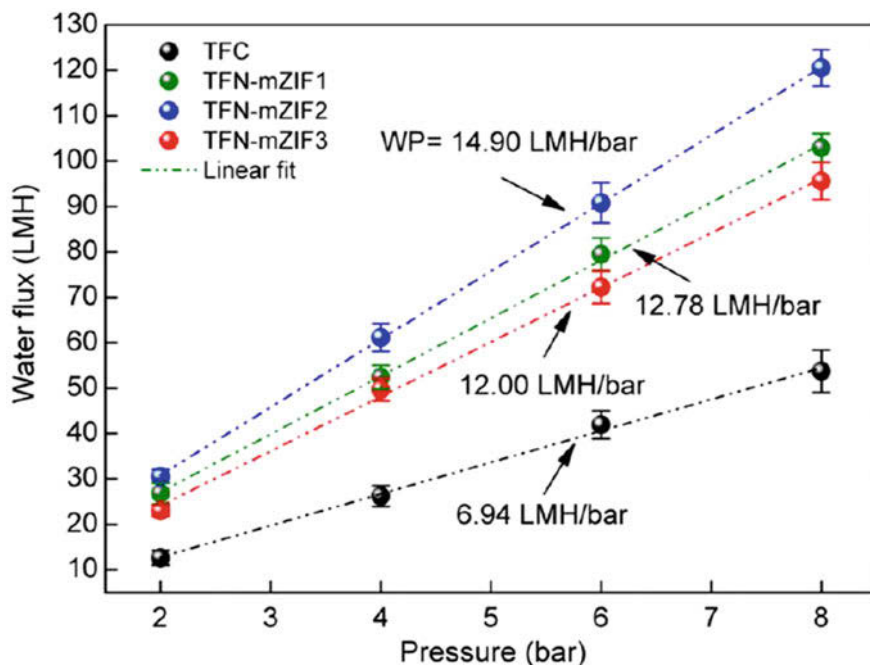


Fig. 5 Water flux of TFC, TFN-mZIF1, TFN-mZIF2, and TFNmZIF3 membranes. WP: water permeability. (Reprinted from Ref. [104] Copyright © 2017 American Chemical Society)

inorganic materials demonstrate high permeability and high selectivity because of their consistent nanopores. There are several ways to prepare the nano size, dense layer for separation after incorporating diverse NPs into polymeric materials while interfacial polymerization to improve gas permeation performance by troublesome the polymer chain packing [3, 19]. Under optimized conditions, TFN membranes performance is very high compared with TFC membranes in the gas separation due to their hydrophilic, smoother and more negatively charged nature. TFN membranes have the advantage to reduce energy consumption and make simpler operations in gas separation applications [53]. The selective TFN layer necessitates elevated selectivity and high gas permeability to reach proficient separation. As shown in Fig. 8, in mixture gas separation especially CO_2/N_2 the porous graphene (PG) nanosheets functionalized TFN shows enhanced CO_2 permeance and the CO_2/N_2 selectively compared to that of the membrane without PG separately. There are lots of literature is available on TFN membrane use in the field of water treatment but from last decades researchers started the application of gas separation using same kinds of membranes.

Figure 9 presents the permeability of O_2 on a logarithmic scale and the O_2/N_2 selectivity after adding inorganic moieties in the polymeric membranes. Wonderful enhancement in the permeability and selectivity had been achieved using diverse polymer materials. Similarly, our previous result also shows using

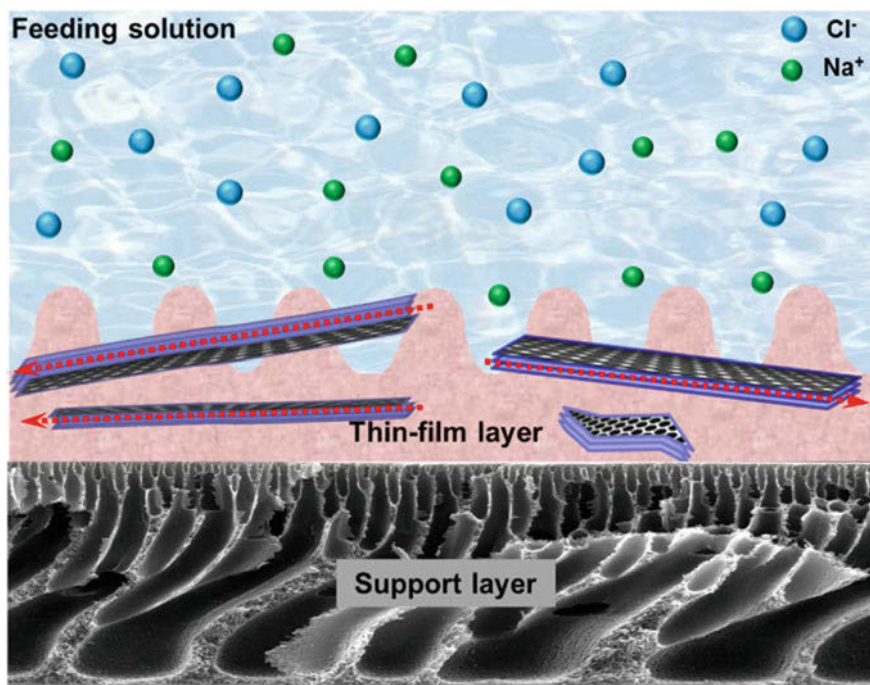


Fig. 6 Schematic illustration of the hypothesized mechanism of GO TFN membrane. Reprinted from Ref. [98] Copyright © 2016 with permission from Elsevier

PDMS CoSalen mixed matrix membrane achieved the 7.7 ideal gas selectivity and good permeance with defect-free membranes [17]. As seen in literature Ismail et al. reported an MWNTs/polymer thin film nanocomposite membranes are greatly improving the carbon capture capacity from N_2 and CH_4 [89, 90]. Xingwei et al. studies on TFN membranes have focused on using silica NPs for enhanced CO_2 separation from mixture gas separation [92]. The challenge is to develop TFN membranes with high-flux and high-selectivity is an urgent basis for cost-efficient CO_2 capture.

Thus, functional graphene oxide (GO) and/or graphene sheets contain a variety of functional groups, having excellent mechanical strength [51]. GO is a brilliant starting nanomaterial for developing size-selective, uniform and stable TFN membranes [16, 23, 40, 52, 59, 75, 77, 83]. In the TFN membrane, the GO nanoparticles are responsible for enhancing selectivity because selective pores in graphenes are allowed the separation of gas molecules.

Any TFN membranes, the NPs plays a key role in enhancing the separation performance. Most of the cases the functionalized NPs takes part in the interfacial polymerization process, also it is found that as a results chemical functionalization of the NPs pore frame could drastically improve the selectivity of mixture gases especially CO_2 over N_2 [77]. The O_2/CO_2 separation was done by using facilitated

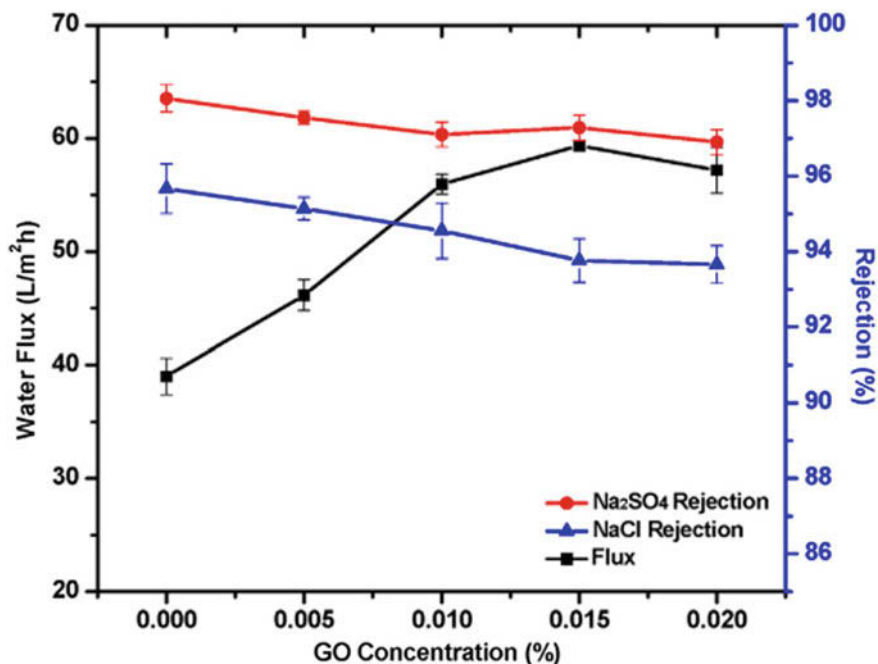


Fig. 7 Permeate flux and salt rejection of GO TFN membranes. The concentration of the salt solution is 2000 mg/L and the TMP is 300 psi. Reprinted from Ref. [98] Copyright © 2016 with permission from Elsevier

transport hollow fiber membranes. The hollow fiber membrane was coated by using poly(*n*-butyl methacrylate) and cobalt tetraphenylporphyrin complex. The prepared membrane shows 1.5 selectivity of O₂/CO₂ with a high O₂ permeance of 17 GPU at a pressure of 0.098 bar [16, 52].

3.4 Thin-Film Nanocomposite (TFN) Membranes for Fuel Cell Applications

It is well known the fuel cells are a chief technology for the nation's energy portfolio. Fuel cell contribution is a cleaner, more proficient substitute for combustion engines that exploited fossil fuels. Nanocomposite polymer electrolyte membrane (PEM) made up of nanosized inorganic building blocks in the organic polymer by the molecular level of hybridization is pertinent for fuel cell application. The researchers have selected the combined inorganic and organic solid including advance properties like mechanical and thermal stability containing inorganic backbone and specific chemical reactivity, ductility, dielectric, flexibility and processability of the organic polymer to make nanocomposites [83]. During the last ten

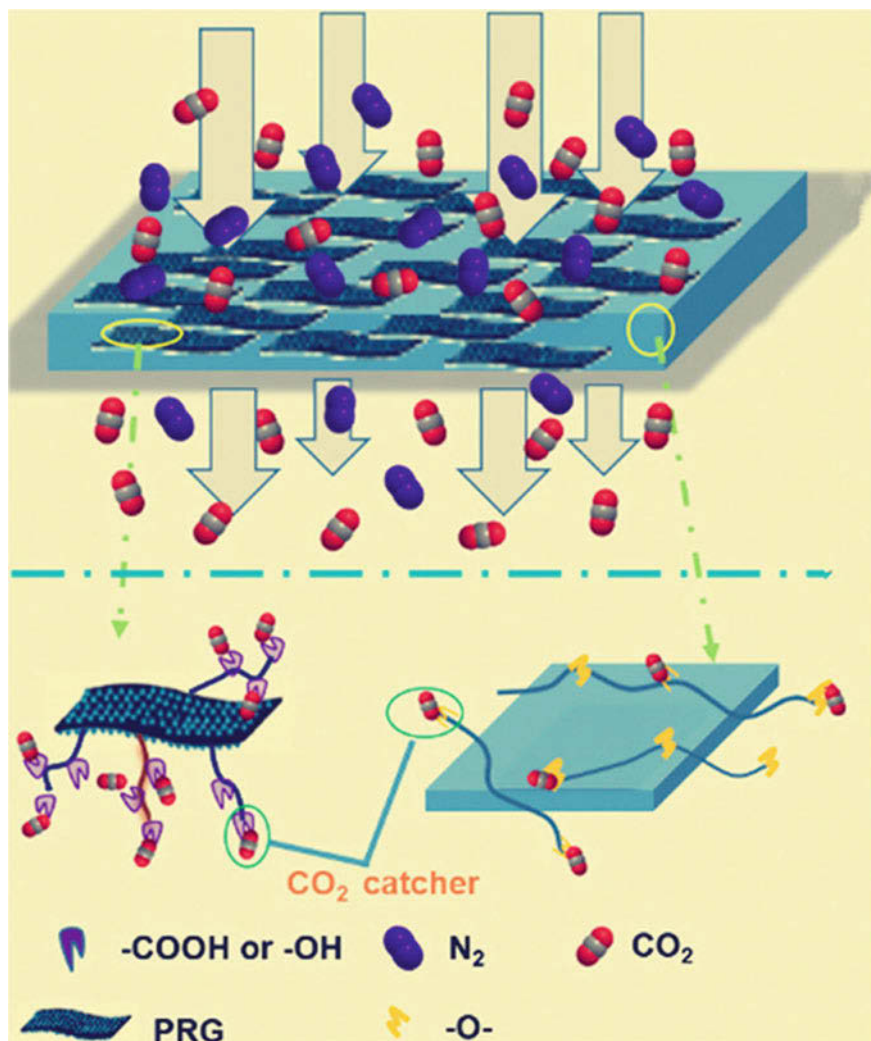


Fig. 8 Mechanism of gas molecules through PG-TFN membranes. Reprinted from Ref. [53] Copyright © 2017 with permission from Elsevier

years, zeolites have attracted a lot of attention and are more and more used in fuel cell applications [27, 28]. There are the criteria for selection of inorganic nanomaterials for fuel cell considering the hygroscopic characteristics, porosity, and pore connectivity, surface area these type of characteristics.

The important thing in the preparation of effective proton conducting nanocomposite membrane for fuel cell application is a covalent bond in between organic moieties and inorganic fillers. One more thing is required to make nanocomposite membrane for a fuel cell is the hydrolytically stable covalent bond between inorganic

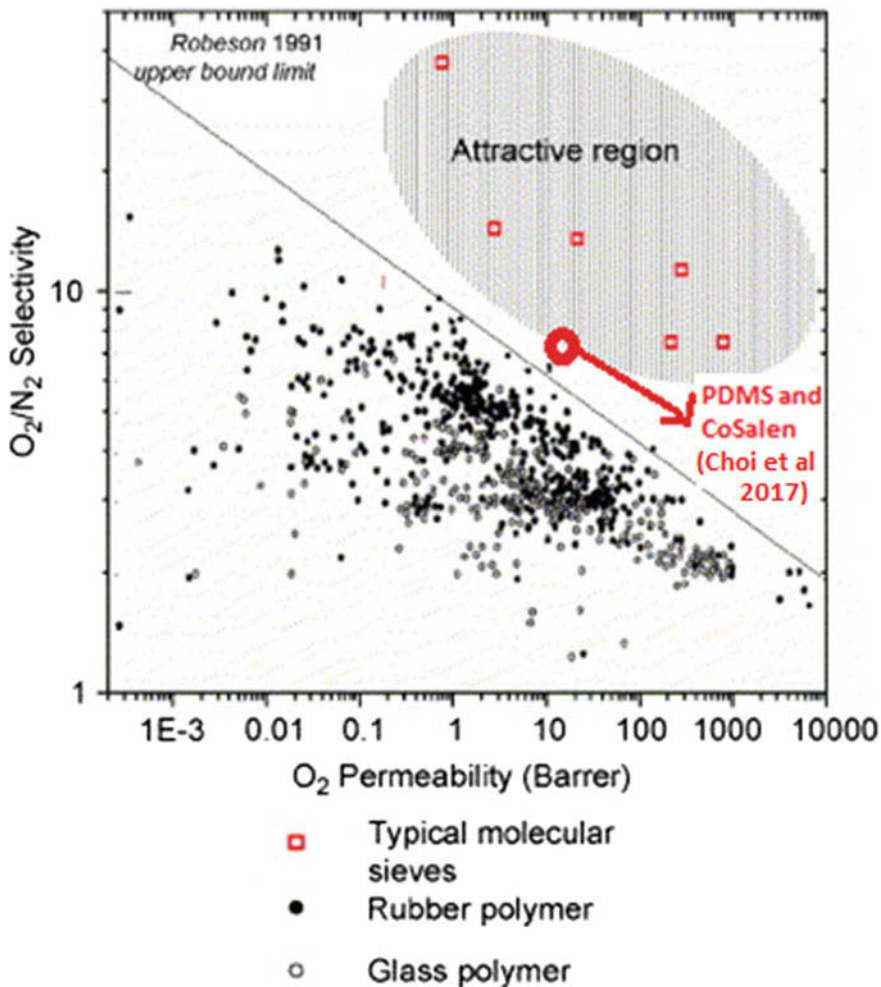


Fig. 9 Relationship between the O_2/N_2 selectivity and O_2 permeability for polymeric membranes and inorganic membranes (the dots indicate the performance of polymeric materials). Reprinted from Ref. [19] Copyright © 2007 with permission from Elsevier

and organic moieties [62]. There are several ways to modify the organic components for the formation of a stable chemical bond with inorganic components for e.g. silylation (substituted silyl group (R_3Si) to a molecule). Reinholdt et al. studied the composite membranes prepared by using synthesized silica nanoparticles and two SPEEK polymers with sulfonation degrees of 69.4 and 85.0% are characterized for their proton conductivity and water uptake properties [71].

Nafion is one of the key materials for the fuel cell application. Modification of Nafion membrane, the inorganic nanoparticles such as zirconium oxide (ZrO_2), silica, and titanium dioxide (TiO_2) have been used successfully. Modified

membrane from Nafion/ ZrO_2 is homogeneous and shows high water uptake capacity and high conductivity compare with the unmodified membrane at high temperature [64]. Sulfated zirconia (S-ZrO_2) is also used by the researchers to make the Nafion/ S-ZrO_2 nanocomposite membrane with enhanced properties [22].

In addition, the use of S-ZrO_2 nanomaterial in Nafion based nanocomposite membranes also enhanced the high-temperature response [63]. Proton conducting mixed matrix membrane (PC-MMM) is the well known an example for fuel cell applications. In PC-MMM the metal oxides (MOs) have been under scrutiny to develop polymer electrolyte membranes (PEMs) because they hold exceptional mechanical and thermal stability, outstanding hygroscopic ability and are in nature abundant [48, 54]. Figure 10 demonstrates the diverse directions used to modified/functionalized MOs for PC-MMM preparation [12]. The different types of MOs form into nanoparticles with a variety of arrangements such as nanohorns, nanorods, nanospheres, and nanotubes, in sort to augment specific surface area to volume

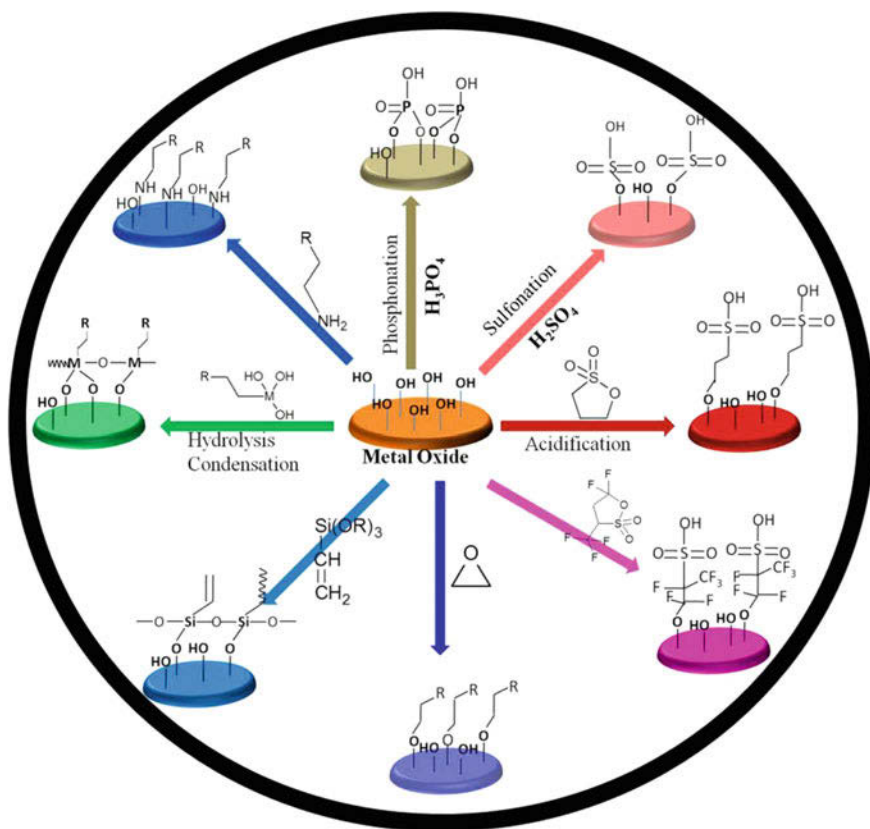


Fig. 10 Illustration of functionalization strategies used to modify metal oxides (MOs) for PC-MMM. Reprinted from Ref. [12] Copyright © 2016 adapted with permission from Elsevier Ltd

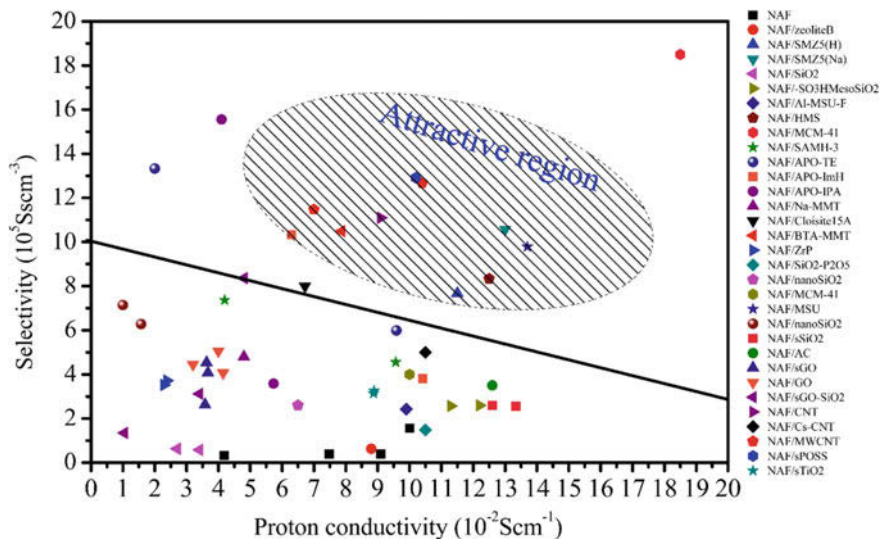


Fig. 11 Proton conductivity versus methanol crossover of PC-MMM composed with Nafion[®] matrix and inorganic particles at 30 °C and 100% relative humidity (RH). Reprinted from Ref. [12] Copyright © 2016 adapted with permission from Elsevier Ltd

ratio. Figure 11 summarizes the PC-MMM based Nafion[®] matrix and different inorganic fillers proton conductivity and methanol permeability. These types of inorganic fillers added membranes revealed advanced selectivity evaluated to pristine Nafion[®] membranes. The mesoporous fillers i.e. zeolites, aluminosilicate, MesoSiO₂, CNT that unites the benefit of porous and layered structure, was more successful in dropping the methanol permeability and rising the proton conductivity of the PC-MMM-based Nafion[®] matrix.

3.5 Thin-Film Nanocomposite (TFN) Membranes for Flue Gas Dehydration

Removal of the water vapour from the flue gas is a hard task for the researcher. Solid adsorbent materials are well known for water vapour adsorption but yet no low-cost technology is available in the market for high scale utilization. To develop the thin-film nanocomposite membranes, Ingole et al. used different types of NPs with various NPs sizes in a range of 10–100 nm in a polyamide (PA) thin film selective layer via in situ interfacial polymerization on the top of various polymer porous supports like polysulfone, polyethersulfone, polyethylene, polyetherimide etc. [29–31]. Various polymeric membrane studies for the flue gas dehydration had also been done by Metz et al. in details [58] (Fig. 12). Their studies teaches about the

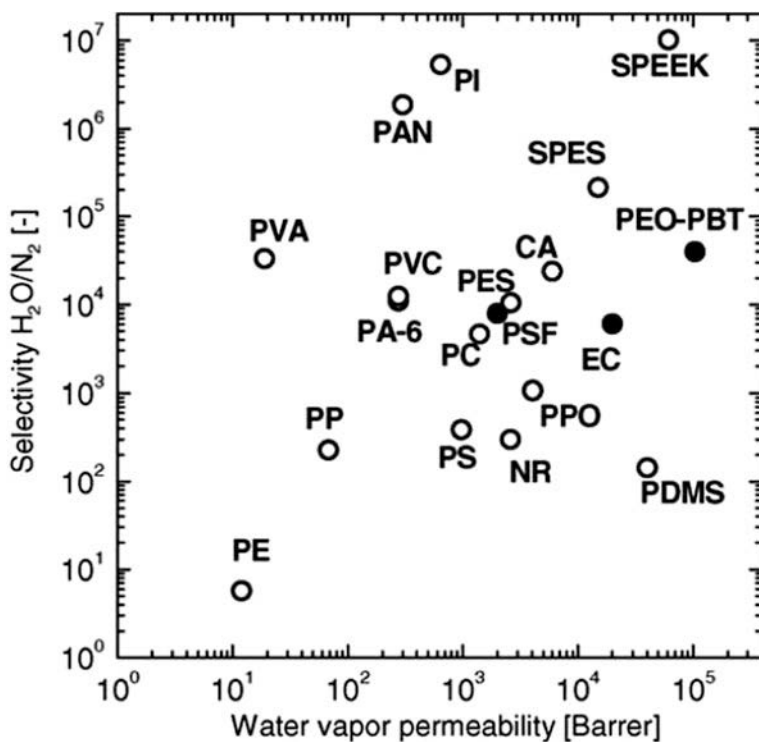


Fig. 12 Water vapour permeability and water vapour/N₂ selectivity for various polymers at 30 ° C. Reprinted from Ref. [58] Copyright © 2005 Adapted with permission from Elsevier Ltd

measurement of the permeation properties of highly permeable and highly selective polymers for water vapour/nitrogen gas mixtures, and also they reported the analysis of the mass transport of a highly permeable polymer is complicated by the presence of stagnant boundary layers at feed and permeate side. Sijbesma et al. reported that polymer membrane prepared by PEBAX[®] 1074, a block copolymer, and sulfonated poly(ether ether ketone) (SPEEK) polymers give extremely high separation factors and fluxes for the removal of water vapour from flue gasses [79]. Yun et al. also reported that hydrophilic thin film composite membranes are shown superior performances for flue gas dehydration by water vapour permeation [100, 101].

Furthermore, the flue gas dehydration using polymeric nanocomposite membranes was started by our group in detail. Thin film composite and thin film nanocomposite both types of membranes was targeted to achieve the best result. TFN membranes shows significant performance in the form of permeance and selectivity for flue gas dehydration. For the preparation of TFN membrane, Fig. 13 represented a general procedure for the interfacial polymerization to synthesize the TFN selective barrier layer. TFN membrane is more hydrophilic than TFC membrane so more water vapour has been collected on TFN layer as shown

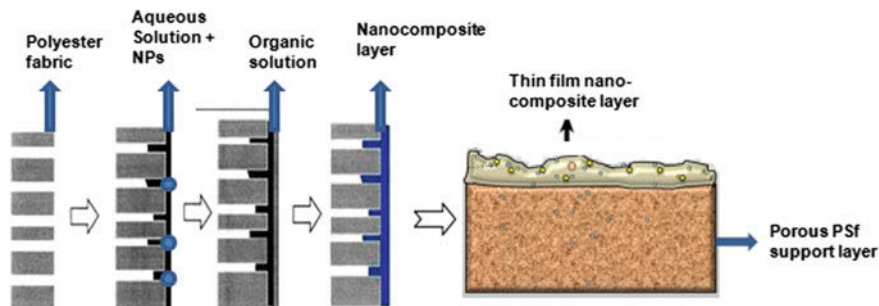


Fig. 13 Schematic illustration of the interfacial polymerization to synthesize the TFN selective barrier layer

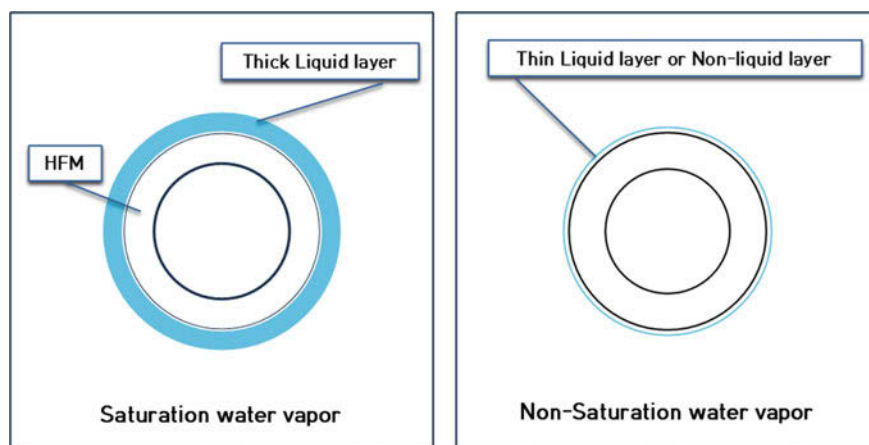


Fig. 14 The comparison, surface of the membrane in a saturated water vapour (TFN) with non-saturated water vapour (TFC)

schematically in Fig. 14. Hydrophilicity of both types of membranes was confirmed by contact angle measurement. After adding Si nanoparticles, TFN prepared from *m*-phenylenediamine and trimesoyl chloride (with 0.05% Si NPs) is more hydrophilic than TFC prepared from same monomers without Si NPs. The contact angle of TFC and TFN membranes were found 55.0° and 37.0° , respectively [9, 11].

The water vapour permeation test was conducted at 2 bar of pressure and 30°C temperature with N_2 as a carrier gas. The feed gas was fed from the shell side while the permeate side was kept under vacuum. Relative and absolute humidity was measured using the Dew Point meter (HMT 334). At first, the dry gas was passed through the fibers till the steady state of humidity was attained in the membrane. The total flow rate was kept constant at 1000 cc/min. To study the effect of water activity, the wet gas was introduced into the module by using MFC (mass flow controller). The flow rate of wet gas was increased gradually to increase the relative

Table 1 Operating conditions

Operating conditions	
Feed pressure	2 kgf/cm ²
Oven temperature	30 °C
Carrier, dilution gas	N ₂
Feed gas flow rate	1000 cc/min

Table 2 Membrane specifications

Membrane	Fiber strains	I.D. (μm)	O.D. (μm)	Area (cm ²)
PS _f TFN membrane	5	1000	1400	47.5

humidity in the feed side while keeping the total flow rate constant. Retentate and permeate flow rates were measured via bubble flow meters. The experimental operating conditions are summarized in Table 1.

The membrane specifications are mentioned in Table 2.

The calculations was done using the below equations.

Water vapour permeance was calculated by first calculating the water vapour flow rates at the feed, retentate and permeate streams by using Eq. (1).

$$Q_{vapour} = \frac{Q_{N_2} \gamma_{H_2O} V_m}{M_{W,H_2O}} \quad (1)$$

where Q_{N_2} (cm³/s) was precised by bubble flow meter following retentate and permeate streams conceded during the iced cold trap. γ_{H_2O} is the absolute humidity (g/m³) and V_m is the volume of 1 mol penetrant at standard temperature and pressure (22.4 L/mol), M_{W,H_2O} is the molecular weight of water (18 g/mol) and Q_{vapour} (cm³(STP)/s) is the water vapour flow rate at the desired stream.

The permeance of a component P_i in the mixed gas stream can be premeditated by using Eq. (2).

$$P_i = \frac{Q_P}{\Delta P_i \times A} \quad (2)$$

As results are shown in Fig. 15, the water vapour permeance and selectivity both increases until certain Si NPs concentrations but further after specific concentration of Si NPs the permeance become increases but selectivity decreases. The water vapour permeances ascended due to increased surface roughness coupled with lower contact angles contribute to excellent hydrophilic properties of TFN membranes [9, 11]. Due to more hydrophilic nature, the TFN membranes shows good water vapour permeance and selectivity until connections of Si NPS was 0.5% but furthermore, the permeance was increases but selectivity was decreased. The reason for this type of results is the agglomeration of NPs. After 0.5% NPs concentration in

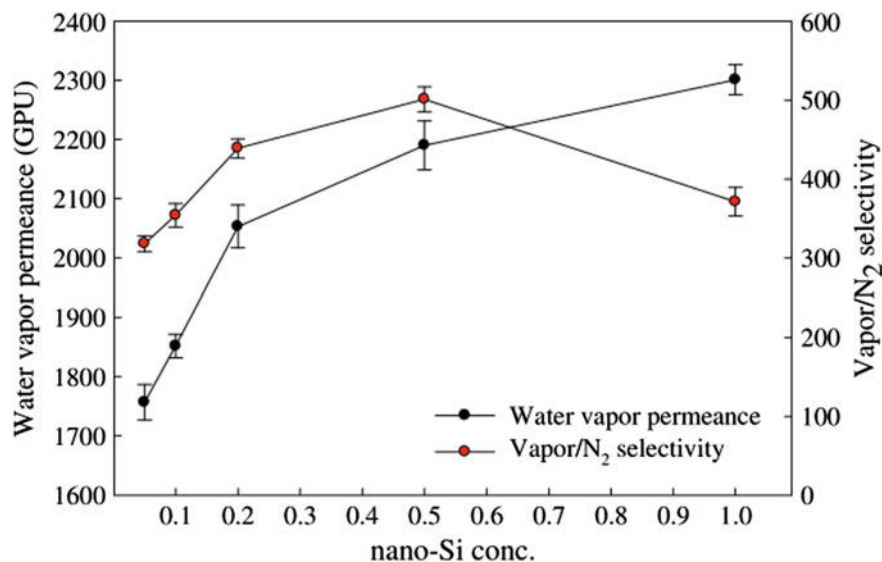


Fig. 15 Effect on the water vapour permeance and selectivity of TFN membranes at various Si nanoparticles concentration. Experimental conditions: temperature = 30 °C, operating pressure = 3 kgf/cm², feed water vapour activity = 0.7 ~ 0.8, total feed flow rate = 1000 cm³/min. Reprinted from Ref. [9, 11] Copyright © 2017 adapted with permission from Elsevier Ltd

monomer solution the NPs agglomeration started and while TFN membrane preparation its shows the disadvantageous towards selectivity because of both N₂ and water vapour permeance increases so as a side effect the selectivity decreases [6, 9, 11].

TFN membranes prepared on the inner surface of the polymeric hollow fiber are extremely terrific materials for water vapour separation from flue gas because of their advanced selectivity. The TFN membranes prepared by using MPD and TMC as monomers along with the incorporation of functionalized MOF (NH₂-MIL-125(Ti)) shows very interesting results [35]. The TFN selective layer was prepared the inner surface of the hollow fiber membrane. The schematic representations of the TFN membrane preparation on the inner surface of the PSf hollow fiber membranes are shown in Fig. 16. After incorporation of MOF (NH₂-MIL-125(Ti)) nanoparticles in the TFN layer, the performance of membranes was drastically enhanced. Results as shown in Fig. 17, the concentration of MOF (NH₂-MIL-125(Ti)) NPs increases from 0.01 to 0.1 w/w% in TFN membranes, the water vapour permeance was enhanced from TFC 785 GPU to TFN 2244 GPU, and the selectivity also jumped from 116 to 542 [35]. Furthermore, after addition of 0.1% NH₂-MIL-125(Ti) NPs, the permeance is decreased because of agglomeration of nanoparticles in the monomer solution. Because of agglomeration of NH₂-MIL-125(Ti) particles, the membrane structure become interrupted.

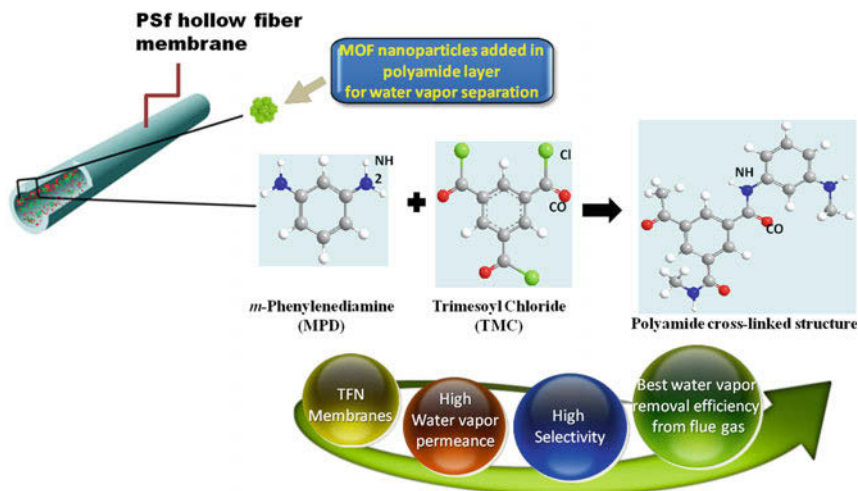


Fig. 16 Interfacial polymerization reaction between MPD (containing $\text{NH}_2\text{-MIL-125(Ti)}$ MOF nanoparticles) and TMC to form a cross-linked structure on the inner side of PSf hollow fiber membrane. Reprinted from Ref. [35] Copyright © 2018 adapted with permission from Elsevier Ltd

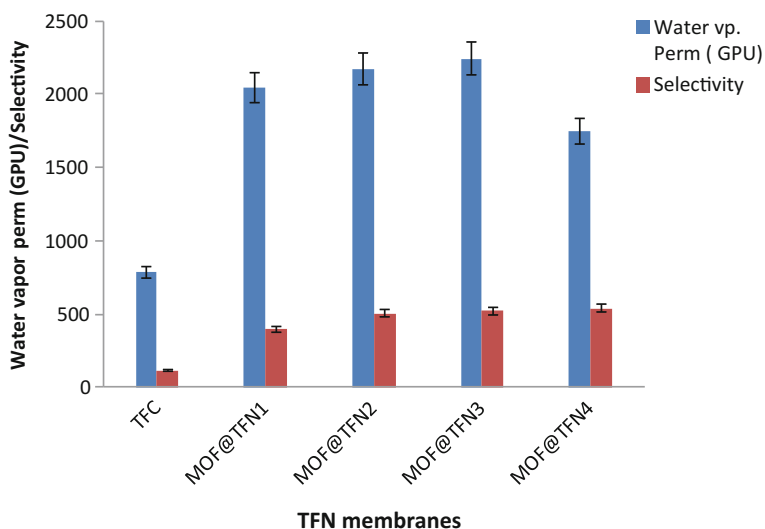


Fig. 17 Effect of $\text{NH}_2\text{-MIL-125(Ti)}$ MOF nanoparticles concentration in TFN membranes on the performance as water vapour permeance and selectivity. Experimental conditions: temperature = 30 °C, operating pressure = 3 kg-f/cm², feed water vapour activity = 0.7–0.8, total feed flow rate = 1200 cm³/min. Reprinted from Ref. [35] Copyright © 2018 adapted with permission from Elsevier Ltd

4 Conclusions

Application of sustainable nanocomposites in membrane technology is the book chapter to bring a wide study of nanocomposite membrane technology. This pioneering book chapter text offers a fluent introduction to the field as well as an inclusive overview of fundamental facets and application area of nanocomposite membrane. Approaching the subject from the materials point of view, this book chapter:

- Discusses the history, synthesis, and characterization of nanocomposite membranes.
- Examines nanocomposite membranes for water desalination, wastewater treatment, gas separation, fuel cell applications, and flue gas dehydration applications.
- Judges processing challenges, including scalability issues and real implementations.

References

1. Aani SA, Gomez V, Wright CJ, Hilal N (2017) Fabrication of antibacterial mixed matrix nanocomposite membranes using hybrid nanostructure of silver coated multi-walled carbon nanotubes. *Chem Eng J* 326:721–736
2. Aghigh A, Alizadeh V, Wong HY, Islam MS, Amin N, Zaman M (2015) Recent advances in utilization of graphene for filtration and desalination of water: a review. *Desalination* 365:389–397
3. Ahn JY, Chung WJ, Pinnau I, Guiver MD (2008) Poly sulfone/silica nanoparticle mixed matrix membranes for gas separation. *J Membr Sci* 314:123–133
4. Al-bishri HM, Abdel-Fattah TM, Mahmoud ME (2012) Immobilization of [Brim + Tf2 N] hydrophobic ionic liquid on nano-silica-amine sorbent for implementation in solid phase extraction and removal of lead. *J Ind Eng Chem* 18:1252–1257
5. An X, Ingole PG, Choi WK, Lee HK, Hong SU, Jeon JD (2017) Enhancement of water vapour separation using ETS-4 incorporated thin film nanocomposite membranes prepared by interfacial polymerization. *J Membr Sci* 531:77–85
6. An X, Ingole PG, Choi WK, Lee HK, Hong SU, Jeon JD (2018) Development of thin film nanocomposite membranes incorporated with sulfated β -cyclodextrin for water vapour/N₂ mixture gas separation. *J Ind Eng Chem* 59:259–265
7. Bae I, Oh KH, Yun M, Kang MK, Song HH, Kim H (2018) Nanostructured composite membrane with cross-linked sulfonated poly(arylene ether ketone)/silica for high-performance polymer electrolyte membrane fuel cells under low relative humidity. *J Membr Sci* 549:567–574
8. Bai L, Liang H, Crittenden J, Qu F, Ding A, Ma J, Du X, Guo S, Li G (2015) Surface modification of UF membranes with functionalized MWCNTs to control membrane fouling by NOM fractions. *J Membr Sci* 492:400–411
9. Baig MI, Ingole PG, Choi WK, Jeon JD, Jang B, Moon JH, Lee HK (2017) Synthesis and characterization of thin film nanocomposite membranes incorporated with surface functionalized Silicon nanoparticles for improved water vapour permeation performance. *Chem Eng J* 308:27–39

10. Baig MI, Ingole PG, Choi WK, Park SR, Kang EC, Lee HK (2016) Development of carboxylated TiO₂ incorporated thin film nanocomposite hollow fiber membranes for flue gas dehydration. *J Membr Sci* 514:622–635
11. Baig MI, Ingole PG, Jeon JD, Hong SU, Choi WK, Jang B, Lee HK (2019) Water vapour selective thin film nanocomposite membranes prepared by functionalized Silicon nanoparticles. *Desalination* 451:59–71
12. Bakangura E, Wu L, Ge L, Yang Z, Xu T (2016) Mixed matrix proton exchange membranes for fuel cells: state of the art and perspectives. *Prog Polym Sci* 57:103–152
13. Bhattacharya M, Mandal MK (2018) Synthesis of rice straw extracted nano-silica-composite membrane for CO₂ separation. *J Clean Prod* 186:241–252
14. Bui NN, Lind ML, Hoek EMV, McCutcheon JR (2011) Electrospun nanofiber supported thin film composite membranes for engineered osmosis. *J Membr Sci* 385–386:10–19
15. Buonomenna MG, Yave W, Golemme G (2012) Some approaches for high performance polymer based membranes for gas separation: block copolymers, carbon molecular sieves and mixed matrix membranes. *RSC Adv* 2:10745–10773
16. Choi W, Ingole PG, Li H, Kim JH, Lee HK, Baek IH (2016) Preparation of facilitated transport hollow fiber membrane for gas separation using cobalt tetraphenylporphyrin complex as a coating material. *J Cleaner Product* 133:1008–1016
17. Choi W, Ingole PG, Li H, Park SY, Kim JH, Lee HK, Baek IH (2017) Facilitated transport hollow fiber membrane prepared by t-Bu CoSalen for O₂/N₂ separation. *Microchemical J* 132:36–42
18. Choi W, Ingole PG, Park JS, Lee DW, Kim JH, Lee HK (2015) H₂/CO mixture gas separation using composite hollow fiber membranes prepared by interfacial polymerization method. *Chem Eng Res Des* 102:297–306
19. Chung TS, Jiang LY, Li Y, Kulprathipanja S (2007) Mixed matrix membranes (MMMs) comprising organic polymers with dispersed inorganic fillers for gas separation. *Prog Polym Sci* 32:483–507
20. Chung TS, Zhang S, Wang KY, Su J, Ling MM (2012) Forward osmosis processes: yesterday, today and tomorrow. *Desalination* 287:78–81
21. Dalvi V, Tang YP, Staudt C, Chung TS (2017) Influential effects of nanoparticles, solvent and surfactant treatments on thin film nanocomposite (TFN) membranes for seawater desalination. *Desalination* 420:216–225
22. D'Epifanio A, Navarra MA, Weise FC, Mecheri B, Farrington J, Licocchia S, Greenbaum S (2010) Composite Nafion/sulfated zirconia membranes: effect of the filler surface properties on proton transport characteristics. *Chem Mater* 22:813–821
23. Du H, Li J, Zhang J, Su G, Li X, Zhao Y (2014) Separation of hydrogen and nitrogen gases with porous graphene membrane. *J Phy Chem C* 115:23261–23266
24. Duan J, Pan Y, Pacheco F, Litwiller E, Lai Z, Pinnau I (2015) High-performance polyamide thin-film-nanocomposite reverse osmosis membranes containing hydrophobic zeolitic imidazolate framework-8. *J Memb Sci* 476:303–310
25. Fan Y, Chen S, Zhao H, Liu Y (2017) Distillation membrane constructed by TiO₂ nanofiber followed by fluorination for excellent water desalination performance. *Desalination* 405: 51–58
26. Fernandez-Gonzalez C, Dominguez-Ramos A, Ibañez R, Chen Y, Irabien A (2017) Valorization of desalination brines by electrodialysis with bipolar membranes using nanocomposite anion exchange membranes. *Desalination* 406:16–24
27. Han G, Zhang S, Li X, Widjojo N, Chung TS (2012) Thin film composite forward osmosis membranes based on polydopamine modified polysulfone substrates with enhancements in both water flux and salt rejection. *Chem Eng Sci* 80:219–231
28. Han W, Kwan SM, Yeung KL (2012) Zeolite applications in fuel cells: water management and proton conductivity. *Chem Eng J* 187:367–371
29. Ingole PG, Baig MI, Choi W, An X, Choi WK, Lee HK (2017) Role of functional nanoparticles to enhance the polymeric membrane performance for mixture gas separation. *J Ind Eng Chem* 48:5–15

30. Ingole PG, Baig MI, Choi W, An X, Choi WK, Jeon JD, Lee HK (2017) Synthesis of superhydrophilic Nafion based nanocomposite hollow fiber membranes for water vapour separation. *Chem Eng Res Des* 127:45–51
31. Ingole PG, Baig MI, Choi WK, Lee HK (2016) Synthesis and characterization of polyamide/polyester thin-film nanocomposite membranes achieved by functionalized TiO₂ nanoparticles for water vapour separation. *J Mat Chem A* 4:5592–5604
32. Ingole PG, Bajaj HC, Singh K (2014) Membrane separation processes: optical resolution of lysine and asparagine amino acids. *Desalination* 343:75–81
33. Ingole PG, Choi WK, Lee GB, Lee HK (2017a) Thin-film-composite hollow-fiber membranes for water vapour separation. *Desalination* 403:12–23
34. Ingole PG, Pawar RR, Baig MI, Jeon JD, Lee HK (2017b) Thin film nanocomposite (TFN) hollow fiber membranes incorporated with functionalized acid-activated bentonite (ABn-NH) clay: towards enhancement of water vapour permeance and selectivity. *J Mat Chem A* 5:20947–20958
35. Ingole PG, Sohail M, Abou-Elanwar AM, Baig MI, Jeon JD, Choi WK, Kim H, Lee HK (2018) Water vapour separation from flue gas using MOF incorporated thin film nanocomposite hollow fiber membranes. *Chem Eng J* 334:2450–2458
36. Jahan Z, Niazi MBK, Gregersen ØW (2018) Mechanical, thermal and swelling properties of cellulose nanocrystals/PVA nanocomposites membranes. *J Ind Eng Chem* 57:113–124
37. Jeon SY, Yun JM, Lee YS, Kim HI (2012) Preparation of poly (vinyl alcohol)/poly (acrylic acid)/TiO₂/carbon nanotube composite nanofibers and their photobleaching properties. *J Ind Eng Chem* 18:487–491
38. Jeong BH, Hoek EMV, Yan Y, Subramani A, Huang X, Hurwitz G, Ghosh AK, Jawor A (2007) Interfacial polymerization of thin film nanocomposites: a new concept for reverse osmosis membranes. *J Membr Sci* 294:1–7
39. Ji Y, Ke J, Duan F, Chen J (2017) Preparation and application of novel multi-walled carbon nanotubes/polysulfone nanocomposite membrane for chiral separation. *Des Wat Treat* 87:179–187
40. Jiang D, Cooper VR, Dai S (2009) Porous graphene as the ultimate membrane for gas separation. *Nano Let* 9:4019–4024
41. Jo ES, An X, Ingole PG, Choi WK, Park YS, Lee HK (2017) CO₂/CH₄ separation using inside coated thin film composite hollow fiber membranes prepared by interfacial polymerization. *Chinese J Chem Eng* 25:278–287
42. Ke Q, Wang J (2016) Graphene-based materials for supercapacitor electrodes—A review. *J Materiomics* 2:37–54
43. Khalid A, Abdel-Karim A, Atieh MA, Javed S, McKay G (2018) PEG-CNTs nanocomposite PSU membranes for wastewater treatment by membrane bioreactor. *Sep Purif Technol* 190:165–176
44. Khorshidi B, Biswas I, Ghosh T, Thundat T, Sadrzadeh M (2018) Robust fabrication of thin film polyamide-TiO₂ nanocomposite membranes with enhanced thermal stability and anti-biofouling propensity. *Sci Rep* 8:784
45. Kim DJ, Jo MJ, Nam SY (2015) A review of polymer–nanocomposite electrolyte membranes for fuel cell application. *J Ind Eng Chem* 21:36–52
46. Kim KH, Ingole PG, Kim JH, Lee HK (2013) Separation performance of PEBAX/PEI hollow fiber composite membrane for SO₂/CO₂/N₂ mixed gas. *Chem Eng J* 233:242–250
47. Kochkodan VM, Rolya EA, Goncharuk VV (2009) Photocatalytic membrane reactors for water treatment from organic pollutants. *J Wat Chem Technol* 31:227–237
48. Kreuer K (2001) On the development of proton conducting polymer membranes for hydrogen and methanol fuel cells. *J Membr Sci* 185:29–39
49. Kumakiri I, Diplas S, Simon C, Nowak P (2011) Photocatalytic membrane contactors for water treatment. *Ind Eng Chem Res* 50:6000–6008
50. Lai CY, Groth A, Gray S, Duke M (2014) Nanocomposites for improved physical durability of porous PVDF membranes. *Membranes (Basel)* 4:55–78

51. Lee C, Wei X, Kysar JW, Hone J (2008) Measurement of the elastic properties and intrinsic strength of monolayer grapheme. *Science* 321:385–388
52. Li H, Choi W, Ingole PG, Lee HK, Baek IH (2016) Oxygen separation membrane based on facilitated transport using cobalt tetraphenylporphyrin-coated hollow fiber composites. *Fuel* 185:133–141
53. Li H, Ding X, Zhang Y, Liu J (2017) Porous graphene nanosheets functionalized thin film nanocomposite membrane prepared by interfacial polymerization for CO₂/N₂ separation. *J Membr Sci* 543:58–68
54. Li Q, He R, Jensen JO, Bjerrum NJ (2003) Approaches and recent development of polymer electrolyte membranes for fuel cells operating above 100 C. *Chem Mater* 15:4896–4915
55. Lv Y, Du Y, Chen ZX, Qiu WZ, Xu ZK (2018) Nanocomposite membranes of polydopamine/electropositive nanoparticles/polyethyleneimine for nanofiltration. *J Membr Sci* 545:99–106
56. Ma L, Dong X, Chen M, Zhu L, Wang C, Yang F, Dong Y (2017) Fabrication and water treatment application of carbon nanotubes (CNTs)-based composite membranes: a Review. *Membranes (Basel)* 7:16
57. Ma N, Wei J, Liao R, Tang CY (2012) Zeolite-polyamide thin film nanocomposite membranes: towards enhanced performance for forward osmosis. *J Membr Sci* 405–406:149–157
58. Metz SJ, van de Ven WJC, Potreck J, Mulder MHV, Wessling M (2005) Transport of water vapour and inert gas mixtures through highly selective and highly permeable polymer membranes. *J Membr Sci* 251:29–41
59. Meyer JC, Geim AK, Katsnelson MI, Novoselov KS, Booth TJ, Roth S (2007) The structure of suspended graphene sheets. *Nature* 446:60–63
60. Moore TT, Mahajan R, Vu DQ, Koros WJ (2004) Hybrid membrane materials comprising organic polymers with rigid dispersed phases. *AIChE J* 50:311–321
61. Morsi RE, Alsabagh AM, Nasr SA, Zaki MM (2017) Multifunctional nanocomposites of chitosan, silver nanoparticles, copper nanoparticles and carbon nanotubes for water treatment: antimicrobial characteristics. *Int J Biol Macromol* 97:264–269
62. Nagarale RK, Shin W, Singh PK (2010) Progress in ionic organic-inorganic composite membranes for fuel cell applications. *Polym Chem* 1:388–408
63. Navarra MA, Abbati C, Scrosati B (2008) Properties and fuel cell performance of a Nafion-based, sulfated zirconia-added, composite membrane. *J Power Sources* 183:109–113
64. Navarra MA, Croce F, Scrosati B (2007) New, high temperature superacid zirconia-doped Nafion composite membranes. *J Mat Chem* 17:3210–3215
65. Njuguna J, Pielichowski K (2003) Polymer Nanocomposites for Aerospace Applications: Properties. *Adv Eng Mat* 5:769–778
66. Pandey N, Shukla SK, Singh NB (2017) Water purification by polymer nanocomposites: an overview. *Nanocomposites* 3:47–66
67. Park JT, Roh DK, Chi WS, Patel R, Kim JH (2012) Fabrication of double layer photoelectrodes using hierarchical TiO₂ nanospheres for dye-sensitized solar cells. *J Ind Eng Chem* 18:449–455
68. Pekakis PA, Xekoukoulotakis NP, Mantzavinos D (2006) Treatment of textile dyehouse wastewater by TiO₂ photocatalysis. *Water Res* 40:1276–1286
69. Pendergast MM, Hoek EMV (2011) A review of water treatment membrane nanotechnologies. *Energy Environ Sci* 4:1946–1971
70. Qu X, Alvarez PJ, Li Q (2013) Applications of nanotechnology in water and wastewater treatment. *Water Res* 47:3931–3946
71. Reinholdt MX, Kaliaguine S (2010) Proton exchange membranes for application in fuel cells: grafted silica/SPEEK nanocomposite elaboration and characterization. *Langmuir* 26:11184–11195
72. Ren LF, Xia F, Chen V, Shao J, Chen R, He Y (2017) TiO₂-FTCS modified superhydrophobic PVDF electrospun nanofibrous membrane for desalination by direct contact membrane distillation. *Desalination* 423:1–11

73. Safarpour M, Khataee A, Vatanpour V (2015) Thin film nanocomposite reverse osmosis membrane modified by reduced graphene oxide/TiO₂ with improved desalination performance. *J Membr Sci* 489:43–54
74. Saliby IE, Okour Y, Shon HK, Kandasamy J, Lee WE, Kim JH (2012) TiO₂ nanoparticles and nanofibres from TiCl₄ flocculated sludge: characterisation and photocatalytic activity. *J Ind Eng Chem* 18:1033–1038
75. Schrier J, McClain J (2012) Thermally-driven isotope separation across nanoporous graphene. *Chem Phys Lett* 521:118–124
76. Seyedpour SF, Rahimpour A, Mohsenian H, Tahezadeh MJ (2018) Low fouling ultrathin nanocomposite membranes for efficient removal of manganese. *J Membr Sci* 549:205–216
77. Shan M, Xue Q, Jing N, Ling C, Zhang T, Yan Z, Zheng J (2012) Influence of chemical functionalization on the CO₂/N₂ separation performance of porous graphene membranes. *Nanoscale* 4:5477–5482
78. Shannon MA, Bohn PW, Elimelech M, Georgiadis JG, Mariñas BJ, Mayes AM (2008) Science and technology for water purification in the coming decades. *Nature* 452:301–310
79. Sijbesma H, Nymeijer K, Marwijk RV, Heijboer R, Potreck J, Wessling M (2008) Flue gas dehydration using polymer membranes. *J Membr Sci* 313:263–276
80. Son M, Park H, Liu L, Choi H, Kim JH, Choi H (2016) Thin-film nanocomposite membrane with CNT positioning in support layer for energy harvesting from saline water. *Chem Eng J* 284:68–77
81. Su VMT, Clyne TW (2016) Hybrid filtration membranes incorporating Nanoporous silica within a nanoscale alumina fibre scaffold. *Adv Eng Mat* 18:96–104
82. Sun D, Meng M, Qiao Y, Zhao Y, Yan Y, Li C (2018) Synthesis of ion imprinted nanocomposite membranes for selective adsorption of lithium. *Sep Purif Technol* 194:64–72
83. Tripathi BP, Shahi VK (2011) Organic–inorganic nanocomposite polymer electrolyte membranes for fuel cell applications. *Prog Poly Sci* 36:945–979
84. Wang F, Wu Y, Huang Y, Liu L (2018a) Strong, transparent and flexible aramid nanofiber/POSS hybrid organic/inorganic nanocomposite membranes. *Compos Sci Technol* 156:269–275
85. Wang KY, Chung TS, Amy G (2012) Developing thin-film composite forward osmosis membranes on the PES/SPSf substrate through interfacial polymerization. *AIChE J* 58:770–781
86. Wang M, Liu G, Cui X, Feng Y, Zhang H, Wang G, Zhong S, Luo Y (2018b) Self-crosslinked organic-inorganic nanocomposite membranes with good methanol barrier for direct methanol fuel cell applications. *Solid State Ionics* 315:71–76
87. Wang R, Shi L, Tang CY, Chou S, Qiu C, Fane AG (2010) Characterization of novel forward osmosis hollow fiber membranes. *J Membr Sci* 355:158–167
88. Wang Y, Zhu J, Dong G, Zhang Y, Guo N, Liu J (2015) Sulfonated halloysite nanotubes/polyethersulfone nanocomposite membrane for efficient dye purification. *Sep Purif Technol* 150:243–251
89. Wong K, Goh P, Ismail A (2015) Gas separation performance of thin film nanocomposite membranes incorporated with polymethyl methacrylate grafted multi-walled carbon nanotubes. *Int Biodeter Biodegr* 102:339–345
90. Wong K, Goh P, Ng B, Ismail A (2015) Thin film nanocomposite embedded with polymethyl methacrylate modified multi-walled carbon nanotubes for CO₂ removal. *RSC Advances* 5:31683–31690
91. Wu X, Wu Y, Dong H, Zhao J, Wang C, Zhou S, Luc J, Yan Y, Li H (2018) Accelerating the design of molecularly imprinted nanocomposite membranes modified by Au@polyaniline for selective enrichment and separation of ibuprofen. *App Sur Sci* 428:555–565
92. Xingwei Y, Zhi W, Juan Z, Fang Y, Shichun L, Jixiao W, Shichang W (2011) An effective method to improve the performance of fixed carrier membrane via incorporation of CO₂-selective adsorptive silica nanoparticles. *Chin J Chem Eng* 19:821–832

93. Xiong S, Zuo J, Ma YG, Liu L, Wu H, Wang Y (2016) Novel thin film composite forward osmosis membrane of enhanced water flux and anti-fouling property with N-[3-(trimethoxysilyl) propyl] ethylenediamine incorporated. *J Membr Sci* 520:400–414
94. Xu GR, Xu JM, Feng HJ, Zhao HL, Wu SB (2017) Tailoring structures and performance of polyamide thin film composite (PA-TFC) desalination membranes via sublayers adjustment-a review. *Desalination* 417:19–35
95. Yang X, Fraser T, Myat D, Smart S, Zhang J, da Costa JCD, Liubinas A, Duke M (2014) A pervaporation study of ammonia solutions using molecular sieve silica membranes. *Membranes (Basel)* 4:40–54
96. Yang Z, Wu Y, Wang J, Cao B, Tang CY (2016) In Situ Reduction of Silver by Polydopamine: A novel antimicrobial modification of a thin-film composite polyamide membrane. *Environ Sci Technol* 6:9543–9550
97. Yin J, Deng B (2015) Polymer-matrix nanocomposite membranes for water treatment. *J Membr Sci* 479:256–275
98. Yin J, Zhu G, Deng B (2016) Graphene oxide (GO) enhanced polyamide (PA) thin-film nanocomposite (TFN) membrane for water purification. *Desalination* 379:93–101
99. Yip NY, Tiraferri A, Phillip WA, Schiffman JD, Elimelech M (2010) High performance thin-film composite forward osmosis membrane. *Environ Sci Technol* 44:3812–3818
100. Yun SH, Ingole PG, Kim KH, Choi WK, Kim JH, Lee HK (2014) Properties and performances of polymer composite membranes correlated with monomer and polydopamine for flue gas dehydration by water vapour permeation. *Chem Eng J* 258:348–356
101. Yun SH, Ingole PG, Kim KH, Choi WK, Lee HK (2015) Synthesis of cross-linked amides and esters as thin film composite membrane materials yields permeable and selective for water vapour/gas separation. *J Mater Chem A* 3:7888–7899
102. Zhao H, Qiu S, Wu L, Zhang L, Chen H, Gao C (2014) Improving the performance of polyamide reverse osmosis membrane by incorporation of modified multi-walled carbon nanotubes. *J Membr Sci* 450:249–256
103. Zhao S, Zou L, Tang CY, Mulcahy D (2012) Recent developments in forward osmosis: opportunities and challenges. *J Membr Sci* 396:1–21
104. Zhu J, Qin L, Uliana A, Hou J, Wang J, Zhang Y, Li X, Yuan S, Li J, Tian M, Lin J, Van der Bruggen B (2017) Elevated performance of thin film nanocomposite membranes enabled by modified hydrophilic MOFs for nanofiltration. *ACS Appl Mater Interfaces* 9:1975–1986

Reliable Natural-Fibre Augmented Biodegraded Polymer Composites



Ritu Payal

1 Introduction

Since the early 19th century investigations on natural fibre composites have been going on but get an acknowledgement in 1980s. Fibres are hair like materials which are similar to thread pieces, continuous filaments or can exist as distinct extend pieces. They may be twisted into filaments, yarn or cord, as a component of composite materials, can also be matted into sheets to yield a wide variety of products. Biodegradable polymer composites obtained by incorporating natural resources have witnessed a tremendous research interest nowadays. The biocomposite polymers are widely emergent areas in polymer science which perceived huge attention for their use in various applications such as automobiles, fossil plastic materials, building industries, railway coach interiors, packaging, storage devices and aerospace [1, 2].

Compared with traditional fibres (glass, aramid and carbon fibres), natural fibres (e.g. banana, coir, flax, hemp, henequen, kenaf, jute, sisal, kapok, and many more— Fig. 1) offers many advantages, for instance, abundance and lower cost of materials, decrease in density, biodegradability, nominal health hazards, sustainability, flexibility and less machine wear during processing, comparatively high tensile and stretch modulus, extraordinary stiffness and strength [1]. Additionally, biodegradable, eco-friendly and renewable properties of natural fibres assist their disposal by incineration or composting and alleviate the use of non-biodegradable polymers. In addition, these fibres are environmentally benign as their dimensional structure encompass confiscated atmospheric carbon dioxide and emit lower energy comparative to industrially manufactured synthetic fibres [3].

R. Payal (✉)
Department of Chemistry, Rajdhani College,
University of Delhi, Delhi 110015, India
e-mail: ritupayal.10@gmail.com

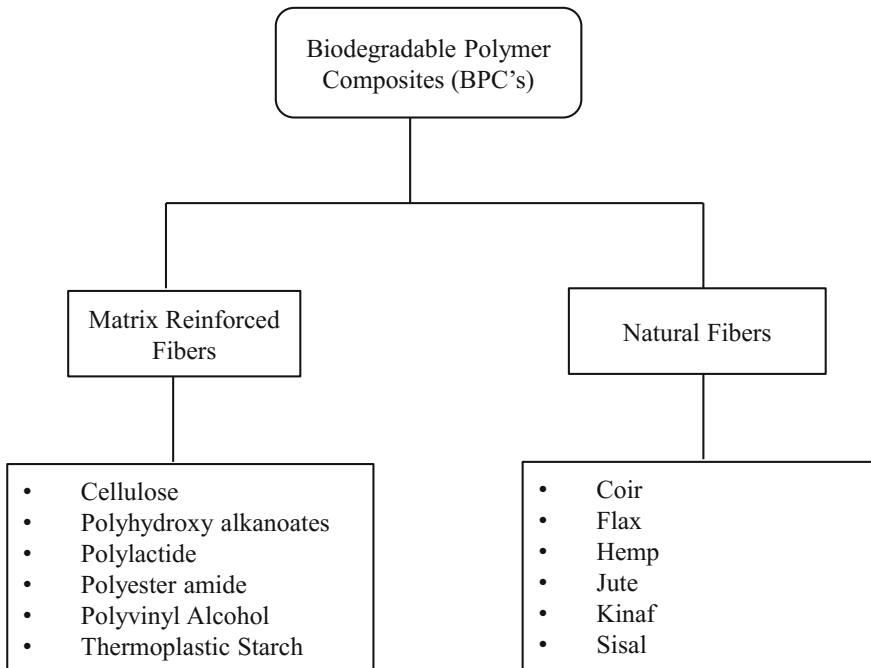


Fig. 1 Classification of biodegradable polymer composites

BPC's also showed fairly good mechanical properties, has high specific strength, and a good amount of tensile strength as an outcome of interfacial adhesion amid the matrix and fibres. Generally, the tensile strengths of BPC's increase on increasing the fibre content reached an optimum value and later a drop in value is witnessed. Also, the tensile properties of composites are prominently boosted by adding fibres to a polymer matrix as fibres have the much greater strength and stiffness relative to the matrices. Furthermore, it was established that the composites having fibres in the perpendicular direction deliver inferior tensile strength compared to the composites having fibres in the parallel direction [3–5]. Hence, it is required to alter the surface of fibre by means of chemical modifications to enhance the adhesion amid fibre and matrix by employing suitable processing methods and parameters to produce optimum composite products.

This chapter briefly deals with the reported works on the characterization of natural fibres, along with the comparative properties of natural and synthetic fibres (Table 1), advantages and disadvantages of BPC's in addition to manufacturing techniques, chemical and physical treatments and their applications in several areas.

Table 1 Properties of various natural-and synthetic fibres [1, 7–9]

Fibre	Density (g/cm ³)	Elongation	Elastic modulus (GPa)	Specific elastic modulus (GPa)	Tensile strength (MPa)
Aramid	1.4	3.3–3.7	63–67	33–36	3000–3150
Carbon	1.4	1.4–1.8	230–240	164–171	4000
Cotton	1.5–1.6	7.0–8.0	5.5–12.6	3.1–5.8	400
Coir	1.2	30	40	20.4	593
E-glass	2.5	0.5	70	28	2000–3500
S-glass	2.5	2.8	86	41.2	4570
Flax	1.5	2.7–3.2	27.6	26–46	500–1500
Hemp	1.47	2–40	70	47	690
Jute	1.3	1.5–1.8	26.5	7–21	393–773
Kenaf	1.45	1.6	53	36.5	930
Polyester	1.2–1.5	2.0–4.5	2	–	40–90
Polyhydroxy alkonates	1.1–1.4	1–6	3–6	–	35–100
Sisal	1.5	2.0–2.5	9.4–22	6.3–14.7	511–635

2 Classification of Fibres

Mostly, polymers may be categorized into two diverse classes: thermoplastics and thermosetting. Both types of materials were widely used as matrices for fabrication of bio-fibres. Polyethylene (PE), polyvinyl chloride (PVC), and polypropylene (PP) are frequently used thermoplastics; whereas epoxy, phenolic, and polyester resins are generally used thermosetting polymers for the manufacture of composites. Now a day, fibres obtained from natural sources like jute, flax, coir, hemp, kenaf, sisal etc. are extensively used in the fabrication of composites.

2.1 Drawbacks of Natural Fibres

The natural fibres suffer limitations, namely: (1) strength, (2) water absorption, (3) thermal stability

1. **Strength:** The tensile strength of BPC's formed using natural fibres is very low comparative to glass, aramid and carbon fibres. This is due to the incompatibility amid the fibre-resin matrix, which in turn reduces the wettability of the fibres and creates a challenge in their productions. Although, by comparing the specific strength of both natural and synthetic fibres, it is observed that there is barely any difference.

2. **Water absorption:** Another limiting factor for the assembly of BPC's is the absorption of water from the atmosphere or direct contact with the surroundings. The difference in the polarity of hydrophilic natural fibres and hydrophobic polymer matrix provides minimal interactions and results in the formation of aggregates. The absorption allows the distortion of surfaces of resulting composites via swelling and forming voids, thereby alleviating the interfacial adhesion and weakens the strength in addition to proliferation in the mass of composites. The wettability also permits the growth of fungi on/in the composites resulting in decay of their structure [6]. The high water absorption indicates inadequate resistant to moisture, which provides reduced tensile properties to reinforced natural fibre composites (Table 1).
3. **Thermal stability:** Natural fibres are of restricted thermal stability and lead to microcracking and, consequently, thermal degradation may possibly occur in the course of BPC's processing at an elevated temperature, specifically in the cases of hot compression and thermal extrusion processes.

2.2 *Advantages of Natural Fibres*

The biggest advantage of using natural fibres for the fabrication of BPC's is the low cost of materials, reduced density, and sustainability. Natural fibres are easy to cultivate and can be grown within few months and are cost effective. They also have the perspective as a cash crop for the agriculturalists. Natural fibres are eco-friendly, lightweight, consumes lesser energy, non-abrasive, non-carcinogens, strong, renewable, less health risk, non-irritation to the skin, recyclable and biodegradable, and have small processing time [2].

The fabrication of biocomposites uses various techniques which include: compression moulding, extrusion (extensively used for green biocomposite), filament winding, injection moulding, machine press, pultrusion, resin transfer moulding, sheet moulding compound. Thermoplastic bio-composites can be mainly processed through compounding, compression moulding, extrusion, injection, and vacuum consolidation. Alternatively, thermosetting biocomposites are manufactured by compression moulding, vacuum assisted resin transfer moulding, hand lay-up, pultrusion, resin transfer moulding, and vacuum bagging [10–12].

2.3 *Strategies for Surface Modification in Natural Fibres*

Surface modification is one of the crucial processes in the fabrication of biocomposites since natural fibres possess hydrophilic characteristic and with the aim of improving the compatibility of a hydrophobic polymer matrix with the natural fibres, this surface modification is needed. Surface modification is categorized into

types, namely chemical and physical methods. The surface modification eases fibre dispersion within polymer matrix along with enhancement in their interaction. Various techniques described in the literature surveys for altering fibre-matrix adhesion consist of acetylation [13], acrylic acid treatment [14], bleaching [15], esterification [16], grafting of monomers using maleic anhydride [17], and using bi-functional molecules [18]. The usage of coupling agents such as isocyanates [19], chitosan [20], maleated polypropylene [21], silanes [22], titanates [23], zir-conates [24], etc. have been testified in previous studies for the improvement of conventional polymer composites.

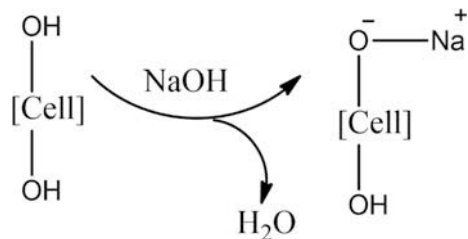
2.3.1 Chemical Techniques

A wide range of chemical techniques is reported in the literature but alkaline-, silane-, esterification-, and isocyanate treatments are some of the frequently used chemical techniques, which are described as follows:

1. **Alkaline treatment:** Alkaline treatment is a unique approach to be used as a chemical treatment of BPC's. This method is also known as mercerization and is usually used to reinforce thermoplastics and thermosets with natural fibers by removing lignin, wax and oil from the external surface of the fibers. This methodology disrupts the hydrogen bonding in the structural framework of BPC's, providing surplus positions for mechanical interlocking, henceforth support surface irregularities and boost fibre and matrix diffusion at the boundaries. In alkaline treatment, the fibres are dipped in sodium hydroxide (NaOH) solution for a fixed time period depending upon the interaction between the two. The resulting interaction facilitates the ionization of the hydroxyl group to the alkoxide group (Fig. 2), which is then stirred continuously in a binary solvent such as water-ethanol solution (80:20) for 1 h and the solution is kept undisturbed for ~3 h. Consequently, the fibers are washed repeatedly with distilled water followed by drying in a hot air oven at 80 °C for ~5 h [25, 26].

The literature surveys reported that the natural fibers such as coir, ramie, sisal, jute were utilized to fabricate BPC's using alkaline treatment and it was established that these composites possess high storage as well as significant flexural modulus [27].

Fig. 2 Ionization of the hydroxide group used in alkali treatment of the fibers



2. **Silane treatment:** Earlier silanes (with chemical formula SiH_4) were reinforced with glass fibres for the augmentation of polymer composites. Silanes reduce the prevalence of hydrogen bonding in the matrix-fiber structural complex. Presence of moisture allows hydrophilic alkoxy groups to form silanols, which in turn responds to the hydroxyl groups of the fibre and form a stable, cross-linked network due to the covalently bonded structure with the cell wall (Fig. 3a, b).

As a consequence, hydrophobic fibre surface is generated; consecutively intensify the compatibility with the polymer matrix (Fig. 3c). A significant enhancement in tensile strength was discovered as a consequence of strong interfacial bond produced by the acid and water conditions during the course of fibre pretreatment [22]. The modification of kenaf and polyester fibre composites finds mention in the literature using silane treatment method [28, 29]. The fiber modification offers higher storage modulus and lowers $\tan \delta$ values than those with untreated fiber indicating a greater interfacial interaction between the matrix resin and the fiber.

3. **Esterification:** Esterification involves the modification of the surface of fibres especially wood composites with organic acid anhydrides (Fig. 4). Acetylation

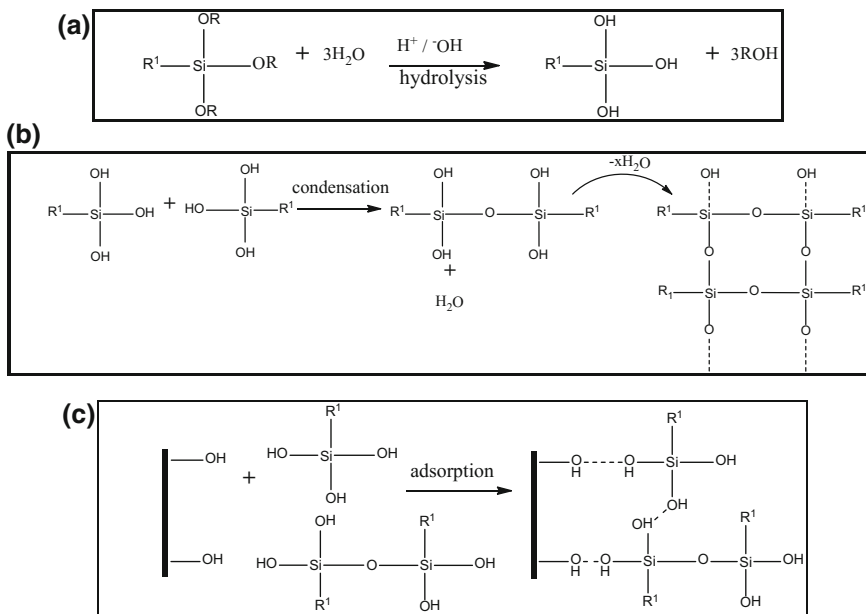


Fig. 3 Interaction of silanes with natural fibers via different processes: **a** hydrolysis, **b** condensation, **c** adsorption [30]

with acetic anhydride (non-cyclic anhydrides) and maleic anhydride (cyclic anhydrides) is broadly defined in the literature [17]. In Acetylation process, a hydroxyl group is converted into an ester group via association of the free hydroxyl groups present in wood composites with the carboxylic group of the anhydrides.

4. **Isocyanate treatment:** Isocyanates are organic compounds having isocyanate group $-N=C=O$ in their structure. These are highly reactive with polar groups such as hydroxyl ($-OH$), amino ($-NH_2$) and others (Fig. 5). Isocyanates are not considered feasible treatment method for natural fibres but testified a meek improvement in strength of polymer matrix relative to the unaided matrix.

2.3.2 Physical Techniques

Physical approaches [29, 31] mentioned in the literature involves the corona or plasma treatments for amending conventional polymers. In recent years, a “greener” alternative is available for the expansion of polymer composites, which comprises plasma treatment for reinforcement of natural fibres. Some of the chemical techniques mentioned previously proved to be harmful, e.g. isocyanates are hazardous, and as a result, such agents are not viable for the augmentation of BPC’s. Therefore, physical methods involving plasma treatment provides a better option for treating natural fibres. Plasma has the tendency to modify the properties of surface/interface of natural fibres via formation of free radicals (*for instance* electrons, ions, etc.) on their surfaces by the bombardment with high energy particles inside the stream of plasma (Fig. 6) [32].

Using physical techniques various surface properties, for example, chemistry, wettability, and surface irregularities of composites can be improved without using

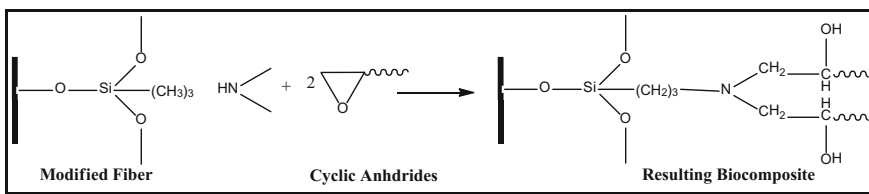


Fig. 4 Coupling reaction of modified natural fibers with anhydrides

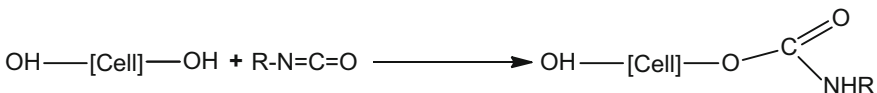


Fig. 5 Isocyanation of fibers

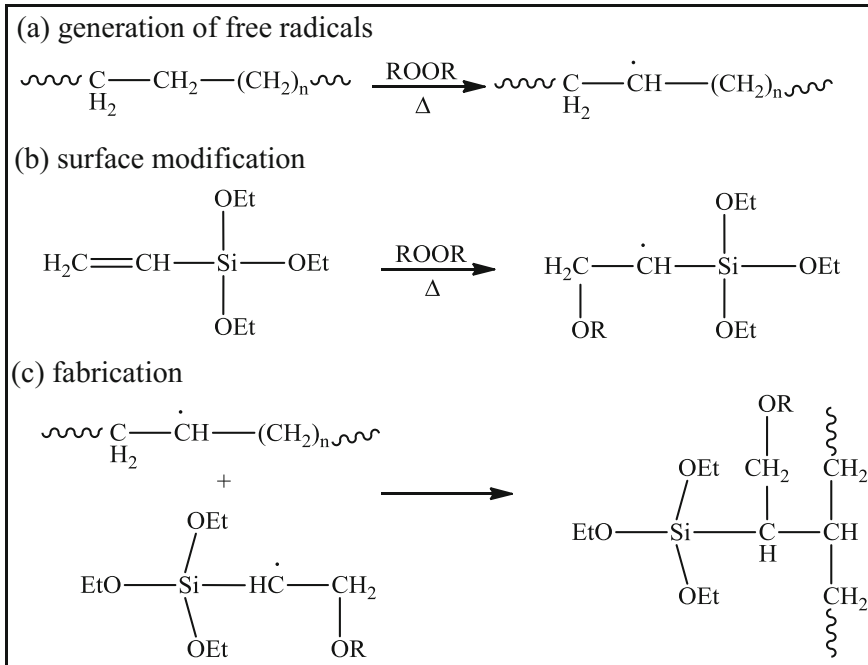


Fig. 6 Fabrication of silanes onto polymer surface by free radicals (where Et = ethyl group)

solvents or employing any other harmful materials. An alternate approach for surface modification by plasmas is to alter the carrier gas or by depositing free radicals or other reactive species on the shells of natural fibres [33]. Furthermore, this can be stimulated by embedding monomers or polymers on the surface of the reactive natural fibre, which accelerates its aptness for the polymer matrix.

3 Types of Biodegradable Polymer Composites (BPC'S)

Over the decades with the accelerated progress of biocomposites, a considerable interest has been developed for polymer matrices that are reinforced with natural fibres. Owing to difficulties in discarding the non-biodegradable polymers, researches are continuously carried out to fortified new biodegradable polymer composite materials from natural resources.

Conversely, natural fibre reinforced composites (BPC's) are manufactured from biodegradable polymers to overcome the shortcomings of non-biodegradable polymers composites. Biodegradable matrices were enclaved with natural fibres to amplify the properties of BPC's and they are scientifically sound, lightweight, high mechanical properties and cost-effective. Some of the BPC's along with their synthetic method and properties are explained as follows.

3.1 Coir Fibre Reinforced Composite

Coir is generated by the husk of coconut fruit fibre. The life expectancy of coir is more comparative to other natural fibres as a result of high lignin content. Coir fibre reinforced polyester matrix was tested for their interfacial adhesion characteristics against different ageing solutions and was found to display excellent interfacial adhesion under arid conditions [34]. Coir fibre reinforced polymer composites are developed for industrial and various household applications such as automotive interior, helmets and post boxes, packing material, paneling and roofing as building materials, mirror casing, projector cover, storage tank, paperweights, voltage stabilizer covers.

The efficiency of coir fibre fabricated epoxy composites is dependent on alkali treatment in addition length of the fibre. Coir fibres having lengths 10, 20 and 30 mm were cured with NaOH for 10 days. Fibre length was Alkali treated composite along with increased fibre had Coir fibre having length of 30 mm and 8% alkali concentrations showed better impact strength (27 kJ/m^2) [35, 36]. Pretreated coir based composite have far better mechanical and flexural properties than the untreated one. On increasing fibre content the flexural strength of composite decreases as the matrix is inadequate to shield the complete surface of the coir fibre (Fig. 7).

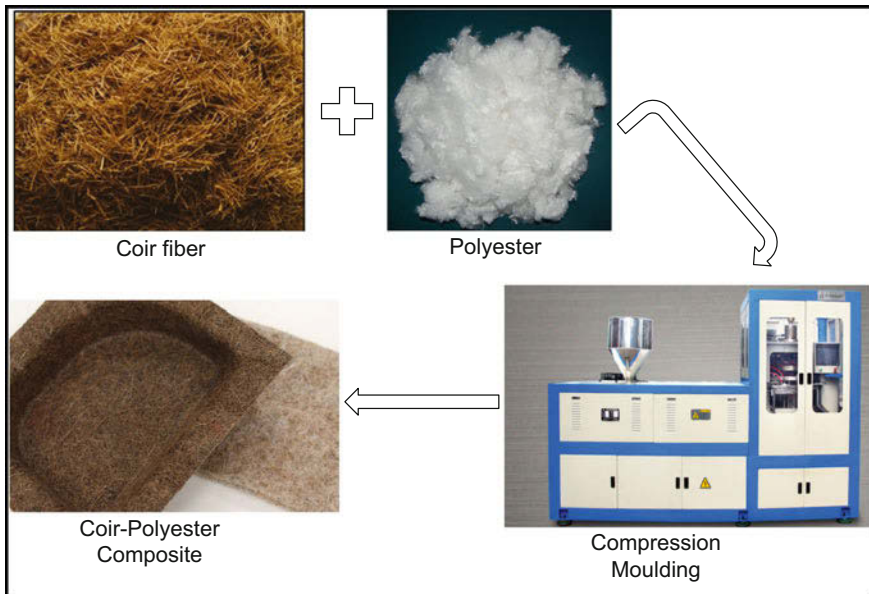


Fig. 7 Coir reinforced polyester composite formation via compression moulding

3.2 Cellulose Fibre Reinforced Composite

Cellulose and its derivatives (lignin, hemicellulose, pectin etc.) are semi-crystalline polysaccharides that impart hydrophilic nature as well as tendency to hold the fibre. These materials have found wide use in the potential matrices-composites as strong molecular interactions exist at the interface of cellulose fibres-polymer matrix composites, which in turn results in strong interfacial adhesion. The composites may be treated via blow and rotation moulding, extrusion, injection moulding, etc. to form fundamental components [18, 33].

3.3 Jute Fibre Reinforced Composite

Jute has wood like characteristics, has a high aspect ratio, good insulation properties, strength to weight ratio. In view of above-mentioned properties, jute fibre reinforced polymer composite has tested for grooved sheet, door, furniture, roofing, floor tiles, I-shaped beam, recovery of underground drain pipes, window, and water pipes [37].

The jute fibre reinforced PP composites were analyzed for their mechanical properties. The washing of fibres preceded by alkaline treatment and bleaching revealed intensification in tensile strength and tensile modulus with an increase in % weight fraction and NaOH % of fibres in the PP matrix (Fig. 8a).

Jute fibres stiffen epoxy composites were examined and results were also compared with bamboo fibre supported epoxy composites and formers were found to have a higher strength. Additionally, upon alkaline treatment jute fibre reinforced epoxy composites encompass enhanced mechanical properties of bamboo fibre reinforced epoxy composites (Fig. 8b, c).

3.4 Poly Lactide (PLA) Fibre Reinforced Composite

The blend of natural fibre and PLA bids an excellent response to preserve the viable economic and ecological development. Ochi [38] carried out a study on PLA composite and explored that PLA fabricated unidirectional biodegradable composite materials showed tensile strengths of 223 MPa. He also evaluated the biodegradability of same via composting and the conducting tests revealed a 38% decrease in composites weight after a time period of four weeks. Oksman et al. [39] reported the fabrication of PLA-Flax composites and matched them with frequently used polypropylene (PP) flax fibre composites (PP-Flax). The comparative study marked 50% higher mechanical properties of PLA-Flax fibre composites over PP-Flax fibre composites.

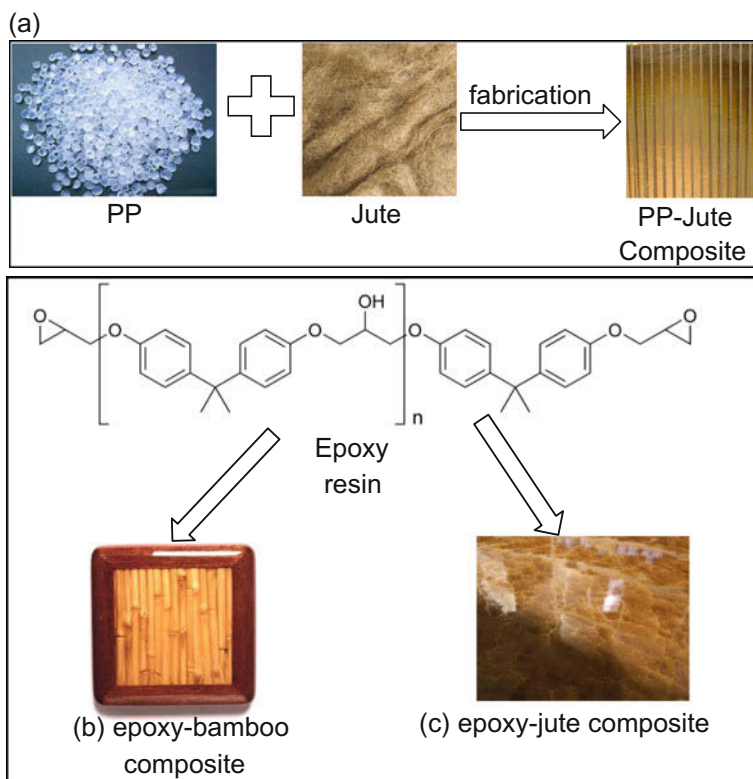


Fig. 8 **a** Jute enforced PP composites, **b** epoxy-bamboo composites, **c** epoxy-jute composite

PLA-Natural fibre composites containing >30% weight fibre showed an improved tensile modulus with lesser tensile strength on comparing with untreated PLA. This was ascribed as a result of poor interfacial interaction flanked by hydrophilic cellulose fibres and hydrophobic PLA matrix, as well as an insufficient fibre dispersion caused by the elevated amount of fibre agglomeration [40]. Hu and Lim [41] inspected that tensile properties of hemp fibre enforced PLA composite significantly improved upon alkali treatment than that of untreated composites. The composites produced using 40% treated fibre has approximately twice tensile modulus comparative to neat PLA (35 GPa). Fabrication of PLA with natural fibres is most likely done by conventional methods such as blow- and injection moulding, extrusion, as well as film-forming operations.

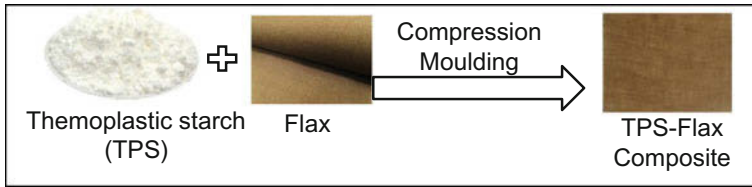


Fig. 9 Thermoplastic starch-flax composite using compression moulding

3.5 Polyhydroxyalkanoates Fibre Reinforced Composite

Polyhydroxyalkanoates (PHAs) are found to be renewable and biodegradable and represent a class of polyesters that are manufactured by bacterial action [42]. The fabrication of the green composites was carried out by Singh and Mohanty [43] by means of injection moulding succeeding the extrusion compounding of bacterial polyester (PHBV) i.e., poly(hydroxybutyrate-co-valerate) with 30–40 weight percentage of bamboo fibre. They also examined morphological, mechanical, and thermomechanical properties and corroborate that the tensile modulus and storage modulus of PHBV composites amplify progressively with increasing fibre loading. Moreover, the tensile strength of bacterial polyester was reduced by adding bamboo fibre due to insufficient interfacial interaction amid fibre and matrix.

3.6 Thermoplastic Starch (TPS)

One of the utmost popular eco-friendly biodegradable polymer-thermoplastic starch can be used as a matrix in fabricated of biocomposites [44, 45]. In the quest for improved performance of biodegradable and environmental acceptable TPS polymer, natural clays can be accumulated on to its surface to produce nanocomposites. Ecologically acceptable filler (such as clay) improve the properties of TPS so that it can be used in various applications. It has been established that the tensile strength of TPS showed an increase from 2.6 to 3.3 MPa on treatment with 5 wt% sodium montmorillonite (Fig. 9).

4 Conclusions

Natural fibre fabricated biodegradable polymer composites (BPC's) are becoming scientifically sound for a plethora of applications as they are lightweight, environmentally benign, and possess good mechanical properties. The modification of the surface of fibres is presently an area of research. The mechanical properties of biodegradable fibres such as sisal, kenaf, hemp, coir, jute, reinforced composites

have been discussed. It was established from the various studies that the tensile modulus and strength raises with an increase in fibre content. It was also accepted that the specific properties of natural fibre composites were far superior relative to synthetic fibre reinforced composites (glass, carbon and aramid). This advocates that the natural fibre composites would prove to be a potential candidate to substitute glass and alike materials in various applications. However, hydrophilic characteristics of biodegradable polymers challenge them to be a good candidate for outdoor applications due to reduced adhesion between natural fibres and matrix resins. However, BPC's are in demand these days and open their possibilities as an excellent candidate in a wide range of applications, such as an automobile, constructional and household applications.

References

1. Wambua P, Ivens J, Verpoest I (2003) Natural fibres: can they replace glass in fibre reinforced plastics. *Compos Sci Technol* 63:1259–1264
2. Malkapuram R, Kumar V, Yuvraj SN (2008) Recent development in natural fibre reinforced polypropylene composites. *J Reinf Plast Compos* 28:1169–1189
3. Li X, Tabil LG, Panigrahi S, Crerar WJ (2009) The influence of fibre content on properties of injection molded flax fibre-HDPE biocomposites. *Can Biosyst Eng* 08–148:1–10
4. Holbery J, Houston D (2006) Natural-fibre-reinforced polymer composites in automotive applications. *JOM (TMS)* 58(11):80–86
5. Ahmad I, Baharum A, Abdullah I (2006) Effect of extrusion rate and fibre loading on mechanical properties of twaron fibre-thermoplastic natural rubber (TPNR) composites. *J Reinf Plast Compos* 25:957–965
6. Pickering K (2008) *Properties and performance of natural-fibre composites*, 1st ed. Woodhead Publishing
7. Hajnalka H, Racz I, Anandjiwala RD (2008) Development of HEMP fibre reinforced polypropylene composites. *J Thermoplast Compos Mater* 21:165–174
8. Ahmad I, Baharum A, Abdullah I (2006) Effect of extrusion rate and fibre loading on mechanical properties of twaron fibre-thermoplastic natural rubber (TPNR) composites. *J Reinf Plast Compos* 25:957–965
9. Nabi SD, Jog JP (1999) Natural fibre polymer composites: a review. *Adv Polym Technol* 18:351–363
10. Pickering KL (2008) *Properties and performance of natural-fibre composites* CRC Press, Florida
11. Odian G (2004) *Principles of polymerization*, 4th edn. Wiley, New Jersey
12. Cardon LK, Ragaert KJ, Koster RP (2010) Design and fabrication of biocomposites. Woodhead Publishing, *Biomedical Composites*, pp 25–43
13. Hill CAS (2006) Chemical modification of wood (I): acetic anhydride modification 3.1. In: Cas H (ed) *Wood modification: chemical, thermal and other processes*. Wiley, New Jersey, pp 45–76
14. Li X, Panigrahi S, Tabil LG (2009) A study on flax fibre-reinforced polyethylene biocomposites. *Appl Eng Agr* 25:525–531
15. Tripathy S, Mishra S, Nayak S (1999) Novel, low-cost jute-polyester composites. Part 1: processing, mechanical properties, and SEM analysis. *Polym Compos* 20(1):62–71
16. Li X, Tabil LG, Panigrahi S (2007) Chemical treatments of natural fibre for use in natural fibre-reinforced composites: a review. *J Polym Env* 15(1):25–33

17. Panigrahy BS, Rana A, Chang P, Panigrahi S (2006) Overview of flax fibre reinforced thermoplastic composites. *Can Biosyst Eng J* 06–165:1–12
18. Belgacem MN, Gandini A (2004) The surface modification of cellulose fibres for use as reinforcing elements in composite materials. *Compos Interfaces* 12(1–2):41–75
19. Wang L, Duan Y, Zhang Y, Huang R, Dong Y, Huang C, Zhou B (2016) Surface modification of poly-(p-phenylene terephthalamide) pulp with a silane containing isocyanate group for silicone composites reinforcement 21(6):505–511
20. Shah BL, Selke SE, Walters MB, Heiden PA (2008) Effects of wood flour and chitosan on mechanical, chemical, and thermal properties of polylactide. *Polym Compos* 29(6):655–663
21. Sun-M, Lai F-CY, Yeh Wang, Hsun-C, Chan, Hsiao-F, Shen (2003) Comparative study of maleated polyolefins as compatibilizers for polyethylene/wood flour composites. *Appl Polym Sci* 87:487–496
22. Abdelmouleh M, Boufi S, Salah AB, Belgacem MN, Gandini A (2002) Interaction of silane coupling agents with cellulose. *Langmuir* 18:3203–3208
23. Gomez JA (1989) Oligomeric titanates as coupling agents for fibre-reinforced composites. Doctoral Dissertations, University of Connecticut. <http://opencommons.uconn.edu/dissertations/AAI9023893>
24. Vishnyakov LP, Moroz VP, Pisarenko VA, Samelyuk AV (2007) Composites with zirconium matrix reinforced with boron and silicon carbide fibres. *Powder Metall Metal Ceram* 46(1–2):38–42
25. Oh JT, Hong JH, Ahn Y, Kim H (2012) Reliability improvement of hemp based bio-composite by surface modification. *Fibres Polym* 13(6):735–739
26. Natrajan S, Moses JJ (2012) Surface modification of polyester fabric using polyvinyl alcohol in alkaline. *Ind J Fibre Tex Res* 37:287–291
27. Faruk Omar, Bledzki Andrzej K, Fink Hans-Peter, Sain Mohini (2012) Biocomposites reinforced with natural fibers: 2000–2010. *Prog Polym Sci* 37:1552–1596
28. Lee BH, Kim HS, Lee S, Kim HJ, Dorgan JR (2009) Bio-composites of kenaf fibers in polylactide: role of improved interfacial adhesion in the carding process. *Compos Sci Tech* 69:2573–2579
29. Pothan LA, Thomas S (2003) Polarity parameters and dynamic mechanical behavior of chemically modified banana fiber reinforced polyester composites. *Compos Sci Tech* 63:1231–1240
30. Xie Y, Hill CAS, Xiao Z, Militz H, Mai C (2010) Silane coupling agents used for natural fiber/polymer composites: a review, *compos: part A* 41:806–819
31. Dong S, Saphieha S, Schreiber HP (1992) Rheological properties of corona modified cellulose/ polyethylene composites. *Polym Eng Sci* 32(22):6
32. Lee KY, Delille A, Bismarck A (2011) Greener surface treatments of natural fibres for the production of renewable composite materials cellulose fibres: Bio- and nano-polymer composites. In: Kalia S, Kaith BS, Kaur I (eds) Springer, Berlin Heidelberg, pp 155–178
33. Nguyen MH, Kim BS, Ha JR, Song JI (2011) Effect of plasma and NaOH treatment for rice husk/PP composites. *Adv Compos Mater* 20(5):435–442
34. Yousif BF, Ku H (2012) Suitability of using coir fibre/polymeric composite for the design of liquid storage tanks. *Mater Des* 36:847–853
35. chanakan A, Charoenvaisarocha, Jongjit H, Joseph K (2009) Materials and mechanical properties of pretreated coir-based green composites. *Compos B* 40:633–637
36. Athijayamani A, Thiruchitrabalam M, Natarajan U, Pazhanivel B (2009) Effect of moisture absorption on the mechanical properties of randomly oriented natural fibres/polyester hybrid composite. *Mat Sci Eng A* 517:344–353
37. Siddiquee (2014) Investigation of an optimum method of biodegradation process for jute polymer composites. *Am J Eng Res* 3(1):200–206
38. Shinji O (2008) Shinji Ochi, Mechanical properties of kenaf fibres and kenaf/PLA composites. *Mech Mat* 40(4–5):446–452
39. Oksman K, Skrifvars M, Selin JF (2003) Natural fibres as reinforcement in polylactic acid (PLA) composites. *Comp Sci Tech* 63:1317–1324

40. Petinakis E, Yu L, Simon G, Dean K (2013) Natural fibre bio-composites incorporating poly (lactic acid). In: Masuelli MA (ed) *Fiber reinforced polymers—the technology applied for concrete repair*, Web of Science, pp 41–59
41. Hu R, Lim JK (2007) Fabrication and mechanical properties of completely biodegradable hemp fibre reinforced polylactic acid composites. *J Compos Mat* 41:1655–1669
42. Singh S, Mohanty AK, Sugie T, Takai Y, Hamada H (2008) Renewable resource based biocomposites from natural fiber and polyhydroxybutyrate-co-valerate (PHBV) bioplastic. *Comp Part A* 39(5):875–886
43. Singh S, Mohanty AK (2007) Wood fiber reinforced bacterial bioplastic composites: fabrication and performance evaluation. *Comp Sci Tech* 67:1753–1763
44. Chen B, Evans JRG (2005) Thermoplastic starch–clay nanocomposites and their characteristics. *Carbohydr Polym* 61:455–463
45. Carrado KA, Xu L, Seifert S, Csencsits R, Bloomquist CAA (2000) Polymer–clay nanocomposites derived from polymer-silicate gels. In: Pinnavaia TJ, Beall G (eds) *Polymer–clay nanocomposites*. Wiley, Chichester, pp 54–55

An Overview on Plant Fiber Technology: An Interdisciplinary Approach



Alan Miguel Brum da Silva, Sandra Maria da Luz,
Irulappasamy Siva, Jebas Thangiah Winowlin Jappes
and Sandro Campos Amico

List of Abbreviations

CML	Compound middle lamella
DP	Degree of polymerization
G	Guaiacyl (G)
GAX	Glucuronoarabinoxylans
H	p-hydroxyphenyl
HG	Homogalacturonan
L	Lumen
MET	Transmission electron microscopy
MFA	Microfibrillar angle
ML	Middle lamella
OH	Hydroxyl groups
P	Primary wall
RG-I	Rhamnogalacturonan I
RG-II	Rhamnogalacturonan II
RTM	Resin transfer molding
S	Syringyl
S1	Secondary wall 1
S2	Secondary wall 2
S3	Secondary wall 3
SMC	Sheet molding compound

A. M. B. da Silva · S. C. Amico
PPG3 M, Federal University of Rio Grande do Sul, Porto Alegre, Brazil

S. M. da Luz (✉)
Gama Campus—University of Brasília, Brasília, Federal District, Brazil
e-mail: sandra.unb@gmail.com

A. M. B. da Silva · I. Siva · J. T. W. Jappes
Centre for Composite Materials, Kalasalingam University,
Anand Nagar, Tamil Nadu, India

1 Introduction

Herbaceous plant fibers are known to humanity since pre-historic times. Evidence suggests they were being used for 34,000 years back, where flax fibers were used for fabrication of clothes, ropes, and baskets [34]. Through ages, the utilization of fibers evolved, and their use expanded for different applications. Around the third millennium BC, bricks were fabricated using wheat straw, flax and papyrus as reinforcement in a mud matrix, allowing for more resistant constructions [19, 59]. During the European expansion, beginning in the fifteenth century, hemp fibers played a critical role in the manufacturing of strong and durable sails and ropes, allowing ships to cover great distances [55].

Fiber technology continues to expand in many different applications even today. From the well known textile industry to high-performance fibers used as reinforcement in polymer composites. The latter being characteristic of our current global scenario, where economic and environmental concerns related to the exhaustive use of fossil fuels are driving a change towards a sustainable and eco-friendly replacement for the currently used synthetic fibers.

With this current research trend on plant fibers for composite materials, different areas are working together, and the literature is getting richer every day. Nevertheless, this richer literature brings some recurring problems, often including a poor understanding of subjects that do not comprise the author's background. Areas presenting this issue often include plant fiber morphology in relation to structure and composition, polysaccharide chemistry and its interactions, turning the contribution of many works restricted to very particular aspects of fiber application.

Thus, the objective of this work is to contribute to the interdisciplinary research of plant fiber for potential use as composite reinforcement. The scope of this paper will be on herbaceous plant fibers (non-wood) and will provide knowledge about morphology, chemical composition, mechanical behavior, and application. The work also aims to overcome the lack of accurate information about those types of fibers, in contrast to the well-established research of wood fibers provided by the paper and forest industry.

2 Biology of Plant Fibers

A common misunderstanding in the literature is regarding the biology of what is called fibers. As a complex organism, plants present different tissues systems. Fibers are a specific type of cells belonging to sclerenchyma tissue, possessing an elongated shape with thick cell walls, often dead at maturity, functioning as a mechanical support for the plant [40].

Botanically speaking, true plant fibers are divided into two main categories, xylary and extraxylary fibers. As the names suggest, xylary fibers are found

associated with the conductive tissue xylem; and the extraxylary fibers can be found associated with the phloem or in the cortex. The fibers of monocotyledons are classified as extraxylary whether or not associated with the vascular bundles (xylem and phloem) [20].

For sake of convenience, many fibers are classified by their location in the plant, listed as: bast fibers (jute, flax, hemp, ramie and kenaf), leaf fibers (abaca, sisal and pineapple), seed fibers (coir, cotton and kapok), core fibers (kenaf, hemp and jute), grass and reed fibers (wheat, corn and rice) and all other types (wood and roots) [21].

One should be careful when characterizing plant fibers to follow the proper scientific classification, since many apparent fibers are not fibers at all, like cotton, which are individual epidermal trichomes around the seeds of *Gossypium*, and raffia fibers, which are leaf segments of the *Raphia* palm. What is also common to find in the commercial form of monocotyledons fibers, is an aggregate of fibers and vascular bundles [20, 40].

A critical point in understanding the fiber structure is how to differentiate a single fiber cell, a fiber bundle, and yarns. The natural aggregate of fiber cells, with variable dimensions, constitutes a bundle. The bundle is the most common form of commercially extracted fibers. To become a yarn, a bundle has to be segregated mechanically, sometimes with the aid of chemicals, into single fiber cells, this cells will then be spun into a twisted aggregate, which will display other properties like twist/angle degree (Fig. 1) [42].

Plant fibers are the outer cell wall remaining of dead plant cells. They are arranged in a tube-like manner, where many elongated cells overlap and stack together to form a macroscopic “single fiber” or as explained before, a bundle (Table 1).

All properties exhibited by plant fibers are, therefore, an expression of the properties of their cell walls. So, a careful study of cell wall formation, composition, and interactions inside the fiber bundle are of higher importance.

Plant cell walls are divided into three main regions: middle lamella, primary wall, and secondary wall. Plant cells originate from specialized dividing cells grouped into regions called meristems. In this region, cells will divide to form a new cell, which will then expand until reaching its final size.

In the cytoplasm of the dividing cell, after nucleus division, an equatorial alignment of vesicles originated from the Golgi apparatus, containing hemicelluloses and pectins, will fuse together to form a cell plate, which will extend up to the point where it will connect to the cell wall, separating the cell content into two new cells [15]. Upon cytoplasm division, cellulose microfibrils are synthesized by a protein structures known as “rosettes”, which are located in plasma membrane, the newly synthesized cellulose will be deposited in the cell plate and then interact with hemicellulose (forming the cellulose/hemicellulose network) giving origin to the primary wall [7]. The innermost region of the cell plate (free of cellulose), will give origin to the middle lamella, which is pectin-rich at the growth stage.

The fiber cells will grow in the axial direction, achieving an elongated shape. When growth is complete, fiber cells will further reinforce its walls with the

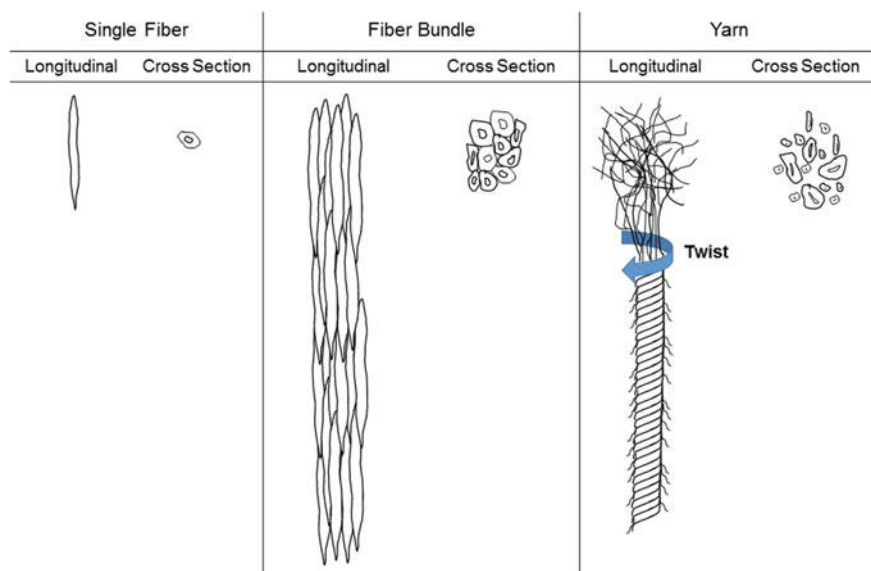


Fig. 1 Schematic of a longitudinal and cross-section view of single fibers (fiber cell), fiber bundles and yarns

Table 1 Dimensions of single fibers and fiber bundles from common herbaceous plants used for fiber extraction [42, 49]

Plant	Fiber structure	Length (mm)	Diameter (μm)
Flax	Single	9–70	5–38
	Bundle	100–1500	40–620
Hemp	Single	5–55	10–51
	Bundle	650–5000	25–500
Jute	Single	2–5	10–25
	Bundle	150–3600	25 – 200
Coir	Single	0.3–1.2	10–20
	Bundle	36–330	50–460

deposition of a secondary wall between the primary wall and the plasma membrane. The secondary wall will compress the outer primary wall to the adjacent middle lamella and reduce the cytoplasm, which at the end of wall deposition, will disappear, leaving a space called lumen. We can easily visualize the transition between the different cell wall regions in a cross-section view (Fig. 2).

Both primary and secondary cell walls present a lamellate structure consisting of progressing deposition of cellulose layers, being the layers adjacent to cytoplasm the most recent ones. Secondary walls are further differentiated in three regions, called S1 (adjacent to the primary wall), S2 and S3 (adjacent to cytoplasm). For fibers, usually, the S2 layer is the most conspicuous layer and can comprise more than 80% of the total thickness of the cell wall, thus dictating much of the fiber properties (Fig. 3).

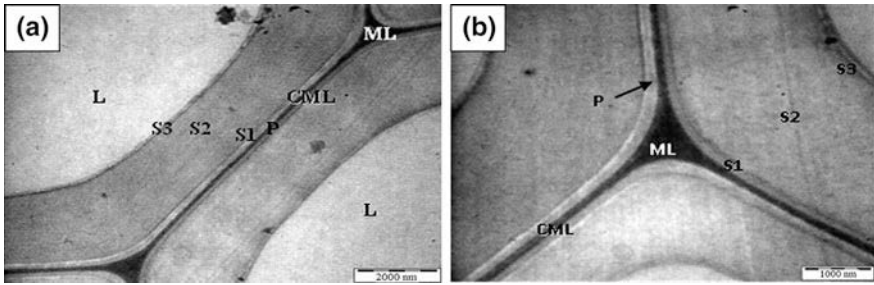


Fig. 2 Transmission electron microscope (TEM) image from an ultrathin cross section of kenaf fiber in low **a** and high **b** magnification (reprinted from industrial crops and products, 31/1, H. P. S. Abdul Khalil, A. F. Ireana Yusra, A. H. Bhat, M. Jawaid, Cell wall ultrastructure, anatomy, lignin distribution, and chemical composition of Malaysian cultivated kenaf fiber, 113–121, Copyright (2010), with permission from Elsevier). Legend: L = Lumen; ML = Middle Lamella; CML = Compound Middle Lamella; P = Primary wall; S1–3 = Secondary wall layers

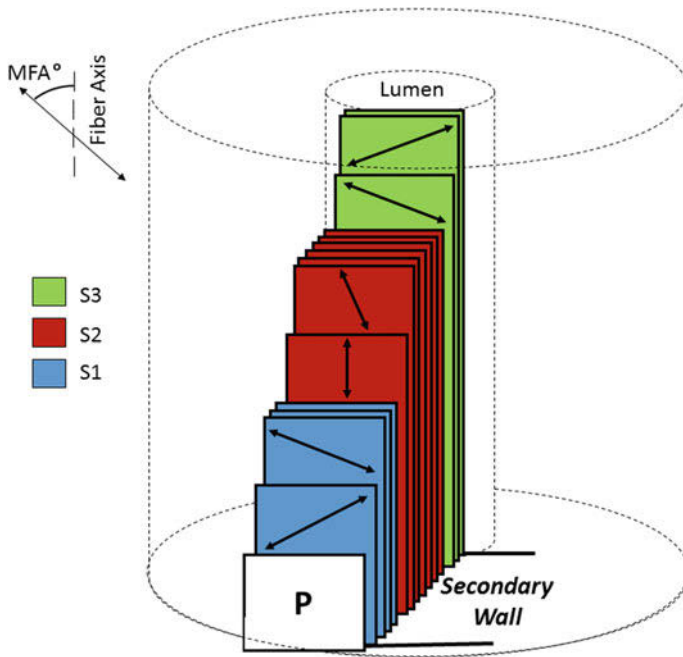


Fig. 3 Lamellar deposition of cell wall layers and average microfibrillar angle (MFA) within the secondary wall. The layers are numbered in order of deposition, being the S1 the first (in contact with the primary wall, P) and S3 the last (lumen side) [45]

During secondary wall deposition, occurs the impregnation of cell corners, middle lamella, primary wall and secondary wall by lignin, giving an extra structural stability and impermeability throughout the whole fiber structure. With lignification, the middle lamella and primary wall can be hard to distinguish, being then called as compound middle lamella (CML) [33].

2.1 Fiber Quality

Plant fibers are a result of a living organism, thus the life cycle of plants will affect how those fibers will form and which properties they will present. Plant health depends on how favourable the environment is and variables like soil composition, climate conditions, water and nutrients available will indirectly affect fiber quality [54].

For practical use of the fibers, they need to be extracted from the rest of the plant. Usually, a degrading process (retting) is used for loosening the fibers from the other plant tissues, thus facilitating fiber extraction. Retting is based on the action of microorganisms that proliferate in a moist condition and secrete specific enzymes that rot away much of plant biomass. Because fibers constitute a less susceptible tissue for degradation they will withstand the whole process. Due to this natural degradation separation, some heterogeneity is expected in the extracted fibers, besides that, climate conditions can also play a role in fiber quality if the same are subjected to field retting (dew retting), where fibers are left on the field (2–3 weeks) for retting using the moist conditions of night dew [65].

Besides field retting, water retting is another typical procedure, plant parts containing the fibers are directly immersed and kept under water, resulting in a shorter retting time (4–6 days) and in a more constant degradation, yielding fibers with more homogeneous properties. Important to notice that an extended retting time will result in damage to the fibers, so a proper retting schedule optimized for each fiber type is necessary to assure good properties [38, 39].

Further refinement of extracted bundles can be achieved by a mechanical process like scutching and combing, by chemicals like the mercerization (NaOH) or by enzymatic treatment. Those process aims to separate bigger bundles into smaller one or even to single fiber cells, depending on the final product desired. For composite applications, a higher aspect ratio (length/width) that maintain the same or better properties of the large bundle is desired to increase the relative contact area with the composite matrix [4, 42].

Fiber extraction is a crucial point in fiber quality, being the previous step to commercial availability, it dictates the final properties of the product before its use. Many drawbacks of using plant fibers for engineering applications, like in composite materials, is due to the high heterogeneity of properties presented in the fibers, thus, reliability should be pursued in areas including fiber extraction and plant cultivation, allowing plant fibers to compete in the market of custom-made synthetic fibers [23, 63].

3 Fiber Chemistry

Cellulose is the main constituent of plant cell walls, its content on fibers varies conform species and values can be found in the range of 43% (coir fibers from coconut) to 92% (cotton fibers) [6]. The presence of cellulose confers high mechanical properties to the cell walls, allowing plants to achieve impressive sizes above ground.

The improved mechanical properties of cellulose found in plant cell walls are the result of its chemical structure, where 6–10 β -(1 \rightarrow 4)-glucan chains hydrogen bond to form 2 nm diameter fibrils, this initial structure is directly correlated to the 6–10 enzymatic subunits of the rosette structure. Six of this fibrils, parallel to each other, form a 36 glucan chain microfibril, which possesses a modulus of elasticity in the axial direction of \sim 134 GPa [10]. The length of cellulose microfibrils varies in the order of few micrometres, commonly the degree of polymerization (DP) from the glucose units is used to express microfibril length. The DP found in secondary walls is in the range of 14,000 (\sim 7 μ m) while the DP in primary walls is often in the order of 8000 (\sim 4 μ m) [56] (Fig. 4).

Each glucose unit bear three reactive hydroxyl groups (–OH), which give a single cellulose chain a hydrophilic nature, in contrast, when in crystalline microfibrils, hydroxyl groups present in the interior of the structure will not be available for interaction with water molecules, thus crystalline cellulose present a more hydrophobic profile [24].

The highly ordered cellulose microfibril patterns of crystalline and non-crystalline regions are not completely understood and are thought to be either an amorphous shell surrounding a crystalline core, a crystalline and amorphous segments alternating along the axis length of the microfibril, or a combination of both [50, 51]. The amorphous cellulose region is quite similar to highly ordered linear hemicelluloses or with short side chains, probably leading to a gradual nanostructured transition between them [10].

Microfibrils can be composed of two types of cellulose, named cellulose I α and I β . I α has a single chain triclinic unit cell, whereas cellulose I β has two chains monoclinic unit cell (Fig. 5). In both forms, cellulose chains are parallel to each other but in high alkaline concentrations, cellulose fibrils can rearrange in an antiparallel alignment, called cellulose II with the respective forms II α and II β . It is reported that the ratio of cellulose α and β can be influenced by the interaction of cellulose microfibrils with hemicelluloses [29].

Microfibril cellulose is synthesized in spirals around the elongation axis of fibers cells, those spirals stag onto each other and pile up to form layers. The angle formed by those microfibrils spirals in relation to the fiber elongation axis is called microfibrillar angle (MFA) (Fig. 3). The MFA has a direct correlation with mechanical properties of the fiber cell and bundle, since cellulose is a polymer which has the strongest linkages (covalent bonds) oriented along its chain, when a load is applied in the fiber axis direction, microfibrils with lower angles, will result

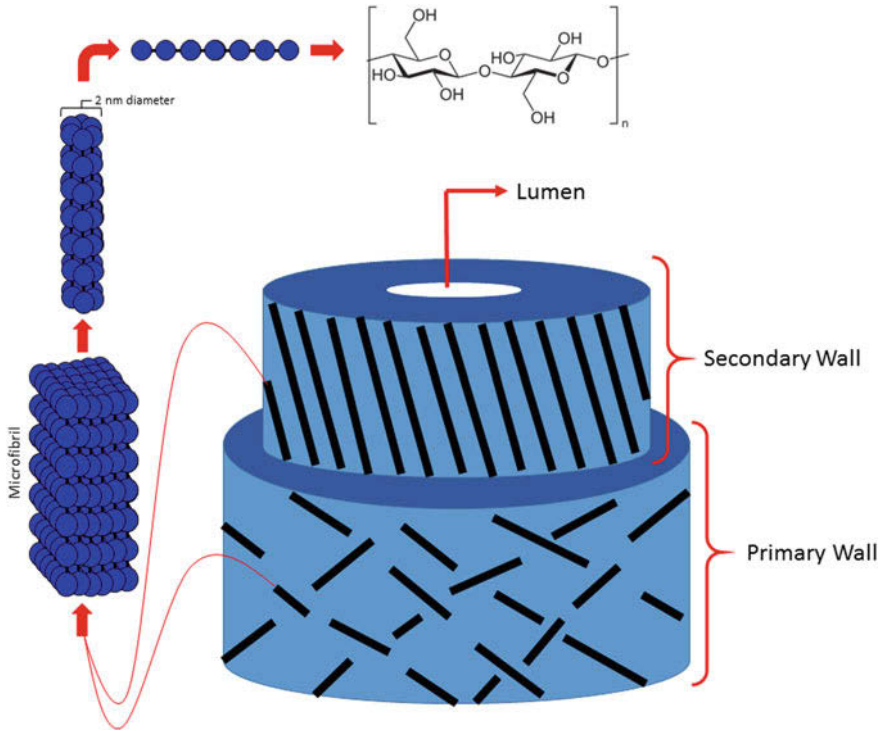


Fig. 4 Cellulose hierarchical structure in the cell wall. The micro-arrangement of cellulose chains is equal for both primary and secondary wall, but the difference in microfibril length and orientation arise at the ultrastructure level

in higher stiffness (Fig. 6). Because the S2 layer is the region with higher cellulose content and lower MFA, it will dictate the mechanical properties of the fiber [9, 10].

Closely associated with cellulose, the heterogeneous group of polysaccharides called hemicelluloses shows a branched β -(1 \rightarrow 4) linked backbone of glucose, mannose or xylose. This structure allows the non-covalent interaction by hydrogen bonding between themselves and to cellulose chains, acting as cross-linking polysaccharides [47]. The branched (amorphous) region is the main responsible for fiber moisture absorption [6].

In plant fibers, total hemicellulose content usually lies in the range of 0.25% (coir) to 30% (bamboo) [21], but lack of proper definition of its heterogeneous components is often noticed in fiber characterization works, resulting in scarce information regarding fiber cell wall composition of different species.

The essential difference between cell walls of dicotyledons and monocotyledons (grasses) plants is well known, where hemicellulose polysaccharides are markedly different (Table 2). Regarding cell wall distribution, is known that secondary wall of both monocots and dicots are more abundant in hemicelluloses than the primary wall, probably following the high concentration of cellulose [11].

Fig. 5 Cellulose I α **a** and I β **b** chain arrangement, reducing end of the chain showed in red [61]

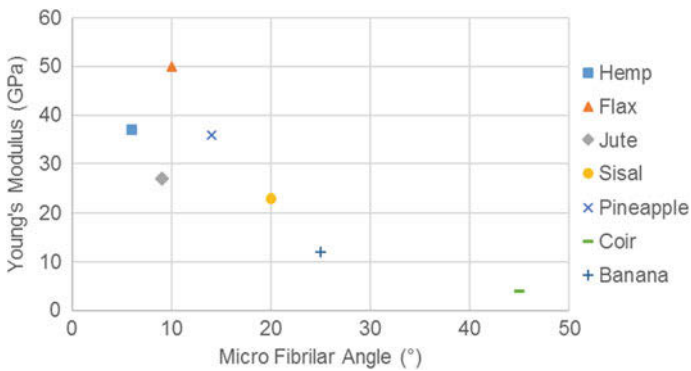
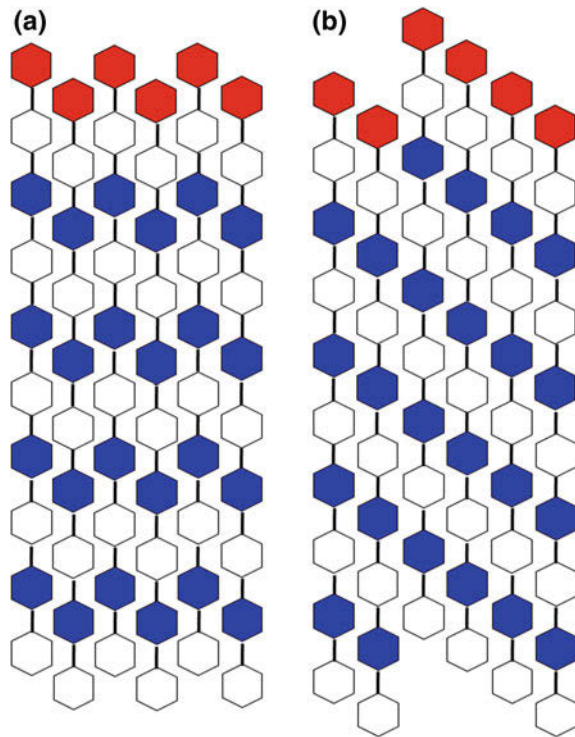


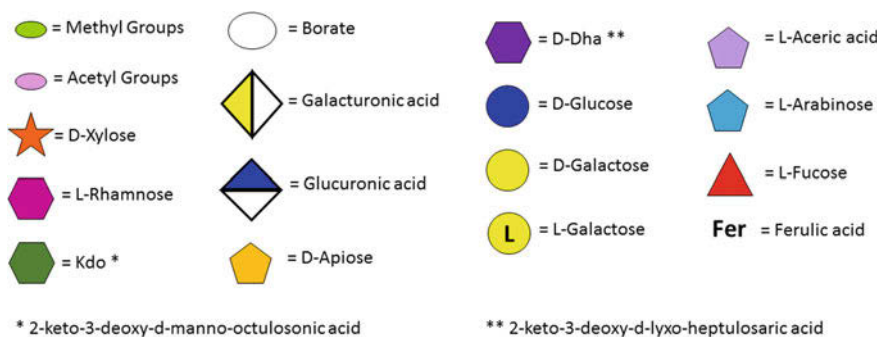
Fig. 6 The relation between MFA and elasticity modulus (values adapted from reviews of [1, 43])

The chemical structure of polysaccharides present in this work was drawn having as basis the standard provided by the Consortium for Functional Glycomics (Fig. 7), which provides a useful method for an easy visualization of polysaccharides components.

Table 2 Main hemicellulose polysaccharides found in dicot and monocot cell walls, other hemicelluloses are also present but in lower concentrations [18, 62]

Wall location	Plant type	Primary wall	Secondary wall
Dicots		Xyloglucan	Glucuronoxylan
Monocots		Glucuronoarabinoxylan	Glucuronoarabinoxylan *

*Fewer side chains

**Fig. 7** Monosaccharide symbols in part from the consortium for functional glycomics. Adapted from Varki et al. [60]

Xyloglucan found in the primary wall of dicots resembles the cellulose structure, where the same β -(1 \rightarrow 4)-glucan backbone is present, the addition of α -D-Xylose-(1 \rightarrow 6) in the glucan backbone give rise to a branching pattern that alternates with unbranched glucose. Xylose residues can be even further branched with the attachment of galactose, fucose and arabinose units (Fig. 8).

Transitioning to the secondary wall, xylose residues are now linked in a β -(1 \rightarrow 4) backbone, known as xylans. In dicots, a frequent xylan modification is an α -(1 \rightarrow 2)-linked glucuronic acid, when this is the prevalent substitution, they are known as glucuronoxylans (Fig. 9). Acetylation of glucuronoxylans at position O-3 of xylose residues is also a characteristic feature of this hemicellulose polysaccharide.

Hemicellulose of monocot plants are dominated by xylans in both primary and secondary wall, and they present substitutions with L-arabinose and glucuronic acid, being then known as glucuronoarabinoxylans (GAX) (Fig. 10). A particular feature of monocot GAX is the presence of ferulic acid attached to O-5 of some arabinose residues. They confer a significant cross-link ability between GAX molecules and between GAX and Lignin, possible by dimerization through ester and ether linkages [25, 62]. The typical properties of monocot fibers, like coarse texture and recalcitrance towards lignin extraction, is then directly correlated to feruloylation degree of GAX, which is also believed to serve as a nucleation site for lignin formation [25].

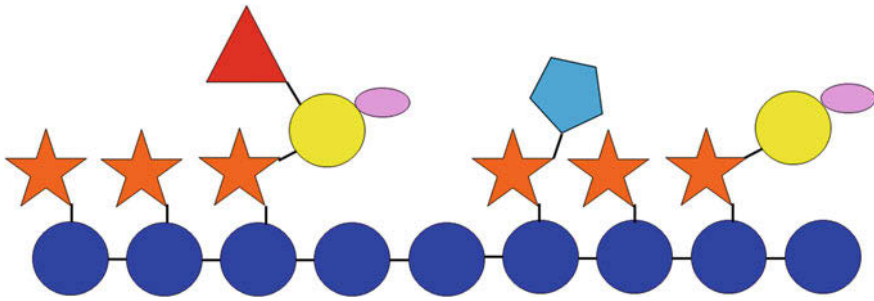


Fig. 8 Xyloglucan polysaccharide structure. A β -(1 \rightarrow 4) glucan backbone with xylose side chains

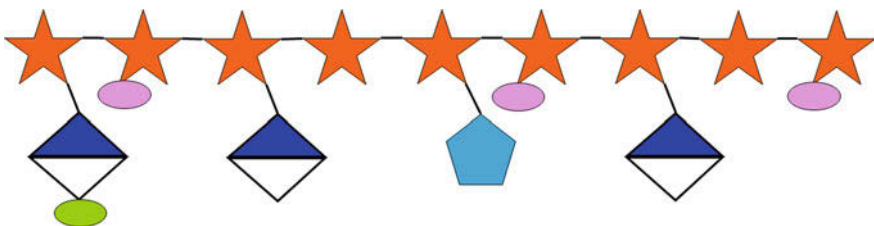


Fig. 9 Glucuronoxylan polysaccharide structure. A β -(1 \rightarrow 4) xylose backbone with predominant substitution with glucuronic acid

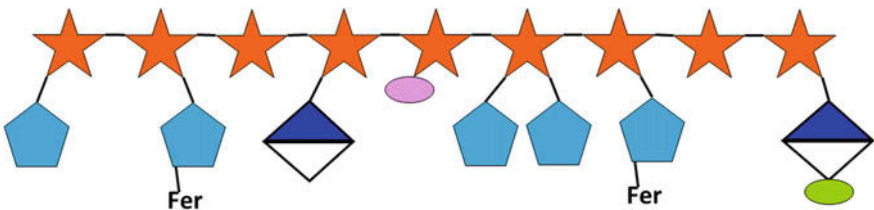


Fig. 10 Glucuronoarabinoxylan polysaccharide structure. The major hemicellulose polysaccharide structure present in monocots, with a β -(1 \rightarrow 4) xylose backbone and characteristic feruloylated arabinose side chains

There is an apparent pattern of hemicelluloses shifting from a glucan backbone in the primary wall to a xylan backbone in the secondary wall, xylan backbones found in the secondary wall are less branched, leading to a more efficient surface with cellulose chains [62].

Pectins are another polysaccharide group present in plant cell walls and are characterized by the presence of galacturonic acid units covalently linked in a repeating backbone or in a dimer repeating backbone together with rhamnose [41]. Regarding the backbone and side chains, pectic polysaccharides can be divided mainly into homogalacturonan (HG), rhamnogalacturonan I (RG-I) and rhamnogalacturonan II (RG-II) (Fig. 11).

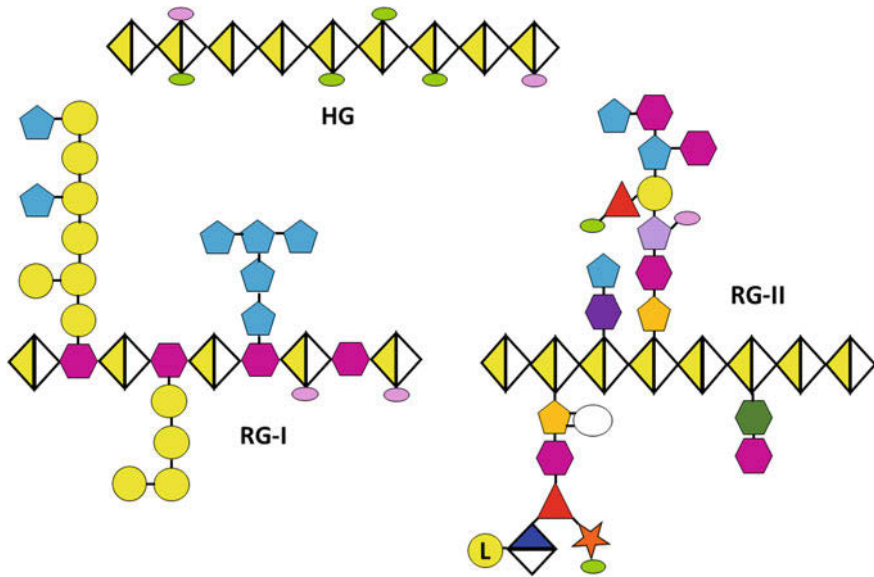


Fig. 11 Pectin major components. Homogalacturonan (HG) is the most abundant form and present a backbone of D-GalA linked in an α -1,4 configuration, is partially methyl-esterified at O-6 and acetylated at O-2 and O-3 positions. Rhamnogalacturonan I (RG-I) constitute a backbone of [4)- α -D-GalA-(1, 2)- α -L-Rha-(1,*n*] in which the GalA residues are highly acetylated at O-2 or O-3 positions. Rhamnogalacturonan II (RG-II) have an HG backbone and complex side chains, generally exist in an RG-II borate diester dimer, cross-linking HG in the wall [3]

They can be presented in a range of 0.2–6.6% [40], during fiber cell elongation, pectins are the main constituent of the middle lamella, bonding adjacent cells. It is also present in the primary wall and to a lesser extent in the secondary wall, acting as a cross-linking polymer, connecting hemicelluloses, lignin and proteins [46, 58]. At the end of cell expansion, during deposition of the secondary wall, there is usually a decline in pectin content, where the function of bonding adjacent fiber cells becomes eclipsed by the cementation and densification of middle lamella and primary wall by lignin. In most plant fibers the pectin contribution to fiber properties is not of much importance, but care should be taken in fibers with diminished lignification, like in Flax (*Linum usitatissimum*), where pectin plays a significant role in fiber cells cohesion and consecutively mechanical performance of the fiber bundle [5, 12].

When fiber cells reach their final size, the deposition of the secondary wall begins, reinforcing the current structure. At this point lignification occurs, with lignin precursors synthesized in the cytoplasm and then transported to initiation sites at middle lamella, cell corners, and cell wall, filling voids in the intercellular space and between polysaccharides [14].

The lignification of cell corners, middle lamella, and the primary wall is relatively fast, probably due to the high porosity of those regions [14]. Lignification of

the secondary wall is slower and usually completes after deposition of the S3 layer. In fiber cells, because the difference in volume between the compound middle lamella and secondary wall, around 70% of the total lignin is located in the cell wall, but not as concentrated as in the CML. The cohesion provided by lignification of fibers will enhance the load transfer capability between cellulose microfibrils by cross-linking of anchored hemicelluloses, as well as transfer load between fiber cells inside the bundle, through the CML [8].

Lignin is the second most abundant polymer found in nature, second only to cellulose, in non-wood fibers, lignin percentage is found in the range of 0.6% (Ramie) to 45% (Coir) [21] and is composed of three types of phenyl propane precursors, the so-called monolignols (hydroxycinnamyl alcohols) (Fig. 12), *p*-coumaryl (4-hydroxycinnamoyl), coniferyl (3-methoxy-4-hydroxycinnamoyl) and sinapyl (3,5-dimethoxy-4-hydroxycinnamoyl) alcohols. They differ only in the degree of substitution by methoxyl groups in the aromatic ring at C₃ and C₅ positions. Those monolignols will be initially oxidized by laccases and peroxidases to form a resonance-stabilized phenoxy radical, which will then polymerize into lignin through either a β -O-4, α -O-4, 5-5, β - β , 4-O-5, β -5 or β -1 linkage (Fig. 13) [35].

In the polymerized form, lignin assumes a very complex and branched structure without a repeating backbone like in the other polysaccharides. The aromatic constituents of the monolignols in the polymer are called *p*-hydroxyphenyl (H), guaiacyl (G) and syringyl (S) moieties [36] (Fig. 12). Generally, for herbaceous plants, all lignin moieties can be found, differently than wood lignin, which mainly consists of G/S and traces of H [13].

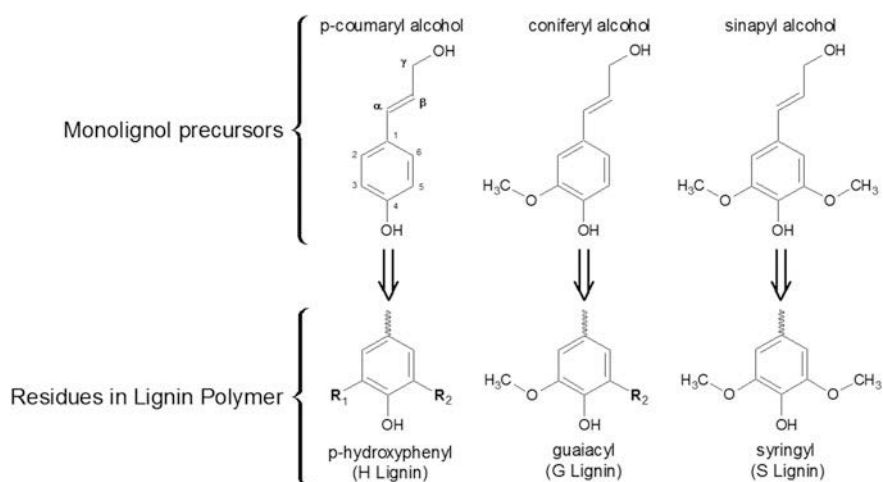


Fig. 12 Hydroxycinnamyl alcohols precursors of H, G and S lignin. R₁ and R₂ can be a hydrogen atom or another lignin molecule

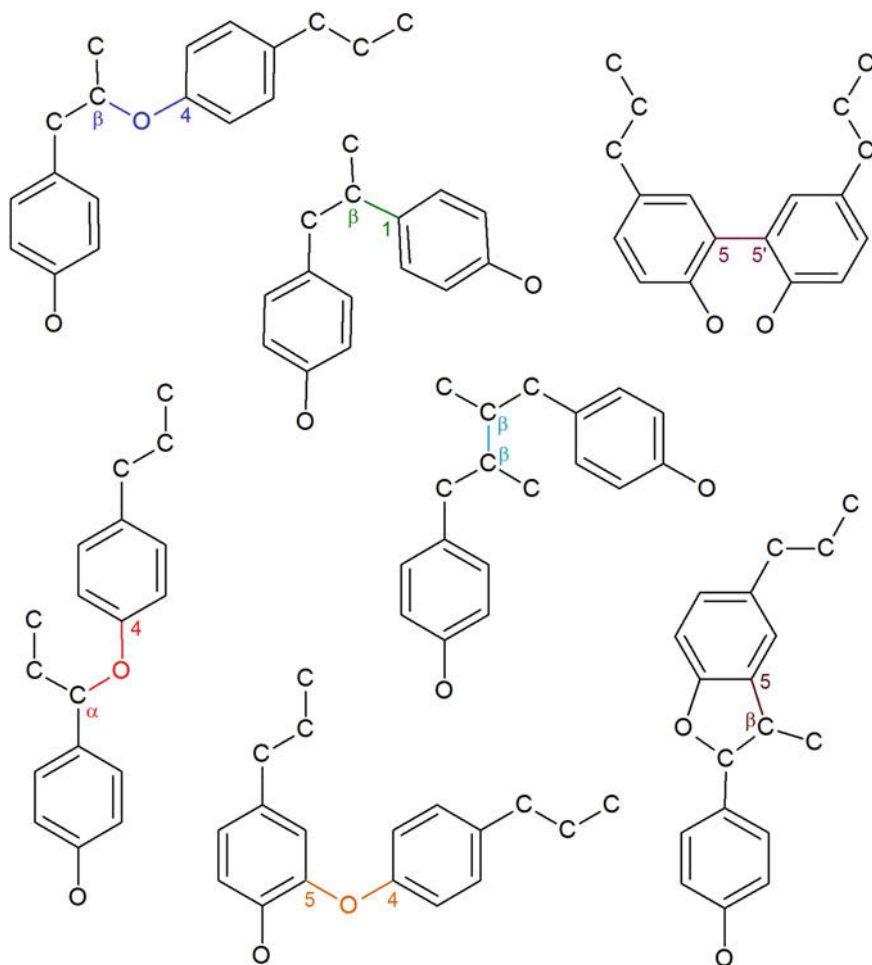


Fig. 13 Chemical bonds in lignin polymeric structure

The proportions of H/G/S moieties vary greatly by species and by region of the cell wall, for example, it is known that H lignin content is higher in the middle lamella than in the cell wall. The proportions of those moieties will determine the type of linkage and the degree of branching, which provides a valuable knowledge of the lignin reactivity [17].

The overall chemical composition of plant fibers greatly depends on the part of the plant and age, for instance, fibers extracted from the bottom of the plant will have a higher lignin content compared to fibers from the top, due to the fact that cells from the top are younger and did not have enough time to undergo lignification. This dependence and variation also influence the levels of cellulose, hemicellulose and pectin contents, contributing to fiber heterogeneity [49].

4 Engineering Aspects of Non-wood Fibers in Composite Applications

When talking about plant fibers as an engineering material, a complete knowledge of fiber biology, structure, chemistry, and physical properties is required for effective use. In the view of fibers as reinforcement in composite materials, some critical factors are oblivious for many scholars and researchers. This is often the case with cellulose crystallinity (amorphous material removal), lignin removal and defibrillation.

As mentioned before, cellulose is the main constituent of plant fibers and is arranged in a microfibril structure with crystalline domains. Those domains have excellent mechanical performance due to the extensive hydrogen bonds formed between cellulose chains [26], which suggests that increases in the crystalline content reflect on increases of the mechanical performance of the cell wall and thus the mechanical performance of the entire fiber.

Extensive works have been published in the area of fiber treatment for composite applications, most of them report effects in crystallinity of alkaline treated fibers, which can remove amorphous domains (hemicellulose and lignin), increasing the crystallinity index [53].¹

The concern is in understanding that the fiber structure behaves as a composite material by itself at two levels, at cell wall, with cellulose as reinforcement in a hemicellulose/lignin matrix, and at bundle level, with secondary cell walls acting as reinforcement in a compound middle lamella matrix (Fig. 14). Utilizing a higher crystalline fiber in a bundle format may not correspond to the total performance which one single fiber could present, due to discontinuity of cellulose-rich secondary walls [8].

To obtain higher length per diameter ratios (which provides excellent performance for fibrous reinforcement elements), a complete delignification of the compound middle lamella is required. With current methods, which involves higher alkaline concentrations at higher temperatures, there is also disruption of lignin present in the cell wall. This results in premature exposure to water sensitive regions of hydrogen bonding between cellulose and hemicellulose cross-linkages, significantly affecting the mechanical performance of the cell wall [48].

For this reason, delignification processes are limited to gentler extractions, preserving the bundle structure in the centre and defibrillating single fibers at the surface (Fig. 15), enhancing surface roughness, which promotes mechanical interlocking with the matrix in the manufactured composite material.

The challenge in the use of herbaceous plant fiber as reinforcement in polymer composites is due to its incompatibility at interface level with the matrix, this zone is where fiber and resin (matrix) are chemically and/or mechanically combined. Interfacial strength plays a significant role in mechanical properties of composites.

¹Relation between amorphous and crystalline regions, which can be calculated from x-ray diffraction analysis, most commonly by Segal's Method [52].

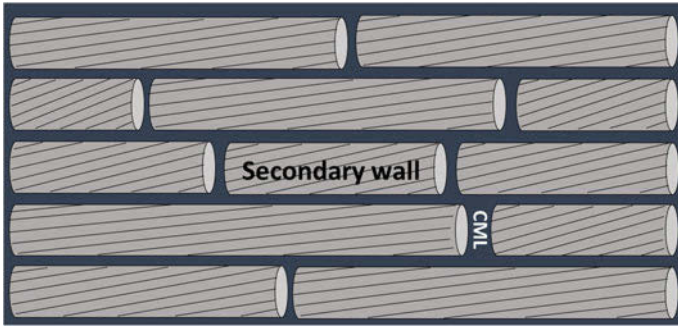


Fig. 14 Composite Bundle. The secondary wall presenting lower MFA and extensive lamella deposition assume a role of discontinuous reinforcement material due to its higher mechanical performance in relation to the compound middle lamella (CML), which acts as a continuous transferring stress matrix

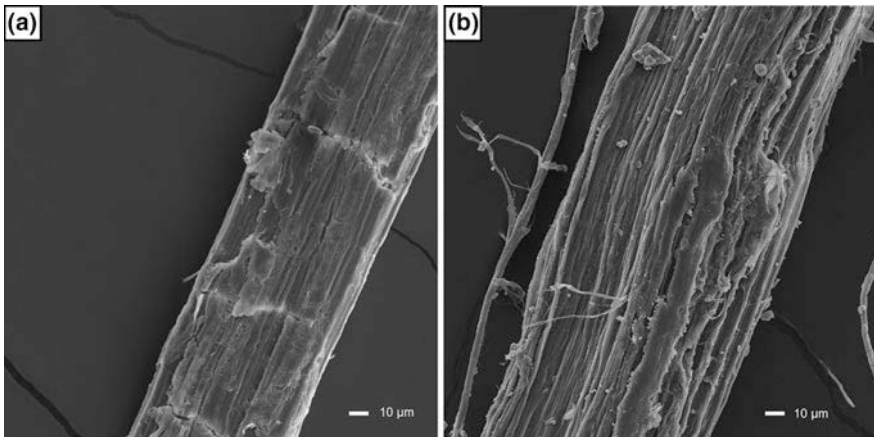


Fig. 15 Curauá (*Ananas Comosus* var. *erectifolius*) fiber bundle untreated (a) and NaOH treated (b). With the removal of lignin by NaOH, defibrillation of single fiber cells occurs at bundle surface

If the adhesion between phases is weak, then relatively weak load transfer occurs, resulting in a decrease of the mechanical properties [57].

This incompatibility arises from the hydrophilic profile of the chemical constituents of the plant fiber, which are rich in OH groups. To overcome this issue, engineering of the fiber properties can be done using chemical treatments, which can modify fiber chemistry by external agents like sodium hydroxide, acetic anhydride, silanes, etc.

The aforementioned mercerization treatment (NaOH), will interact with OH groups of the fiber through the ionization of the hydroxyl group to alkoxide. The

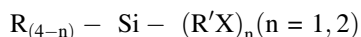
removal of those hydrophilic hydroxyl groups improves the overall moisture resistance of the fiber, but the most desired effect will be the increase in contact surface, facilitating the already mentioned mechanical interlocking with the resin [37, 44].

Similar to mercerization, is the acetylation treatment, which will provide a more extensive hydrophobization of the fiber by means of the introduction of an acetyl functional group at the free hydroxyl groups (Fig. 16), taking out existing moisture, improving compatibility with hydrophobic matrices and bringing dimensional stability to the composite [32].

Another approach for modification of plant fibers is the use of coupling agents, which can provide a bridge at the chemical level between the fiber structure and resin used in the composite, one example of those agents are the silanes.

These chemicals are hydrophilic compounds with different groups attached to silicon, presenting a bi-functional structure, where one end can react with hydroxyl groups of the fiber and the other end interact with the matrix components [30].

Chemical structure of silanes can be generalized as follows:



Where R is a group that can be hydrolyzed to form a silanol group in aqueous solution and further reacts with hydroxyl groups present in the fiber (Fig. 17), R groups can be chlorine, methoxy, ethoxy, etc. X is organofunctional that is able to react with the matrix, they can be a vinyl, γ -aminopropyl, γ -methacryloxypropyne, etc. R' is an alkyl bridge (alkyl spacer) which, depending on its length, can influence the hydrolysis of the silane [64].

During hydrolysis, the produced silanol molecules undergo a self-condensation process, where the formation of O-Si-O bonds take place, generating oligomers of increasing size depending on reaction time (ageing). This is important to get a total cell wall modification since, depending on the silanol oligomers size, the penetration in the dense cell wall can be blocked. To avoid this condition, the pH of the

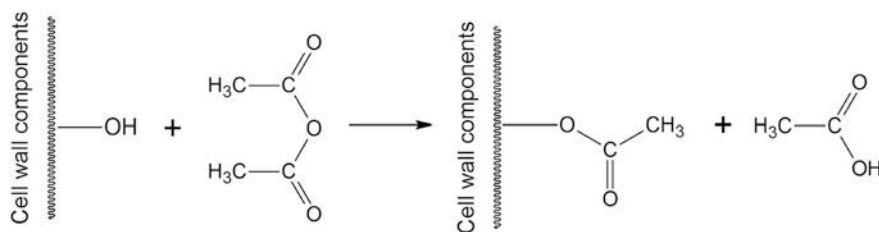


Fig. 16 The schematic reaction of acetic anhydride with hydroxyl groups present in plant fiber cell walls

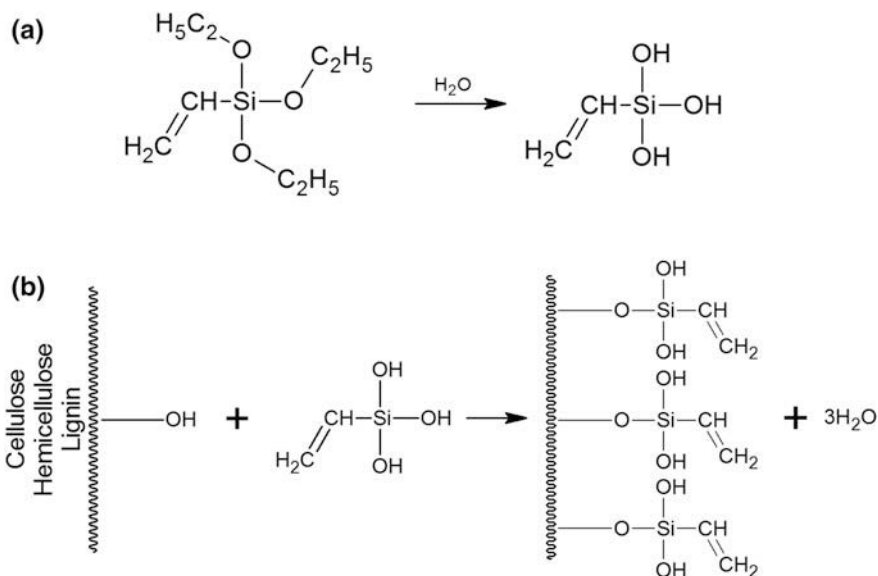


Fig. 17 Silane Modification. **a** Formation of silanol through hydrolysis. **b** The initial interaction of the silanol groups with the OH groups of fiber components is done by hydrogen bonding, but under heating conditions, the hydrogen bonds are converted into primary covalent bonds, releasing water (Grafting process)

solution can be lowered to slow down the condensation reaction, giving enough time for the solution to penetrate into the fiber [28].

Once the proper fiber modification is done, the fiber will bear matrix reactive groups linked to its components, decreasing fiber hydrophilicity, increasing dimension stability and fiber-matrix adhesion via primary covalent bonds, giving molecular continuity across the interface region of the composite [24].

Commercial application of non-wood fibers as reinforcement in polymeric composites is growing every day, notably in the automotive industry [31, 66] where concerns on weight reduction give plant fibers an edge over the more dense glass fibers. Nevertheless, when manufacturing plant fiber-reinforced composites, attention should be taken to consider the composite processing, plant and fiber format to be utilized, each of them is more appropriate for a specific use (Table 3).

Compression moulding is still the most common process method for plant fibers reinforced polymer composites due to its low cost and low requirements on fiber format, being able to use the raw fiber bundles directly after extraction [16]. Some other process like resin transfer moulding (RTM) require certain stability of fibers in a predetermined format, usually utilizing fibers yarns in a textile format (woven or non-woven) [27]. Fibers that permit the spun process to become a yarn can also be used for a continuous process, like pultrusion with thermoplastic resins [22].

Table 3 Composite processing and application of some important plant fibers utilized as reinforcement

Plant	Botanical structure	Comercial format	Composite Processing	Application
Sisal	Perivascular fibre from vascular bundle caps	Bundle, fabrics and Non-woven	Compression moulding	Semi-finished parts in automotive industry; house interior roofing
Hemp	Secondary phloem and pericyclic fibres	Bundle, fabrics and non-woven	Compression moulding	Semi-finished parts in automotive industry
		Fabrics and non-woven	SMC	Bus body component
			RTM	Signposts; furniture; automotive industry
Flax	Pericyclic fibers	Bundle, fabrics and non-woven	Compression moulding	Semi-finished parts in automotive industry
		Fabrics and non-woven	SMC	Spoilers, fenders and funnels
		Fabrics and Non-Woven	RTM	Housing for radar units; speaker boxes; automotive industry
		Yarn	Termoplastic pultrusion	Semi-structural profiles

SMC = Sheet Molding Compound; RTM = Resin Transfer Molding [2, 22, 27]

5 Conclusion

In our continuously connect society, every day more multidisciplinary groups are working on shared issues, which can only improve our complete understanding of the subject. With plant fiber technology, this kind of approach is a must and the demand for eco-friendly and renewable materials in light of climate changes and depletion of fossil fuels makes this topic a global interest.

The present work provided a broader view of the key aspects involving herbaceous plant fiber research, consolidating the biological, chemical and engineering knowledge to this interdisciplinary field of study.

Basic research is still in demand due to the not complete elucidation, especially regarding differences between herbaceous and wood fibers as well as the chemical structure of plant cell walls, which is still being updated as our current technology develops more sophisticated characterization techniques.

Acknowledgements The authors wish to thank the CNPq, Capes and FAP-DF for financial assistance during this work.

References

1. Akin DE, Eder M, Burgert I, Müssig J, Sloomaker T. (2010) What are natural fibres? In: Müssig J (ed) *Industrial applications of natural fibres*. Wiley, Chichester, UK, pp 11–48. <https://doi.org/10.1002/9780470660324.ch2>
2. Anandjiwala RD, John M (2010) Sisal—cultivation, processing and products. In: *Industrial applications of natural fibres*. Wiley, Chichester, pp 181–95. <https://doi.org/10.1002/9780470660324.ch8>
3. Atmodjo MA, Hao Z, Mohnen D (2013) Evolving views of pectin biosynthesis. *Annu Rev Plant Biol* 64:747–79. <https://doi.org/10.1146/annurev-arplant-042811-105534>
4. Baley C, Busnel F, Grohens Y, Sire O (2006) Influence of chemical treatments on surface properties and adhesion of flax fibre-polyester resin. *Compos Part A Appl Sci Manuf* 37:1626–1637. <https://doi.org/10.1016/j.compositesa.2005.10.014>
5. Beakou A, Charlet K (2013) Mechanical properties of interfaces within a flax bundle—part II: numerical analysis. *Int J Adhes Adhes* 43:54–59. <https://doi.org/10.1016/j.ijadhadh.2013.01.013>
6. Biagiotti J, Puglia D, Kenny JM (2004) A Review on natural fibre-based composites-part I: structure. *Proc Prop Vegetable Fibres J Nat Fibers* 1(2):37–41. <https://doi.org/10.1300/j395v01n02>
7. Bidlack J, Malone M, Benson R (1992) Molecular structure and components integration of secondary cell walls in plants. *ProcOklaAcadSci* 75:51–56
8. Booker RE, Sell J (1998) The nanostructure of the cell wall of softwoods and its functions in a living tree. *Eur J Wood Wood Prod* 56:1–8. <https://doi.org/10.1007/s001070050255>
9. Bourmaud A, Morvan C, Bouali A, Placet V, Perré P, Baley C (2013) Relationships between micro-fibrillar angle, mechanical properties and biochemical composition of flax fibers. *Ind Crops Prod* 44:343–351. <https://doi.org/10.1016/j.indcrop.2012.11.031>
10. Burgert I, Dunlop JWC (2011) Micromechanics of cell walls. In: Wojtaszek P (ed) *Mechanical integration of plant cells and plants*, vol 9, 1st edn. Springer, Berlin Heidelberg, pp 27–52. <https://doi.org/10.1007/978-3-642-19091-9>
11. Caffall KH, Mohnen D (2009) The structure, function, and biosynthesis of plant cell wall pectic polysaccharides. *Carbohydr Res* 344:1879–1900. <https://doi.org/10.1016/j.carres.2009.05.021>
12. Charlet K, Béakou A (2011) Mechanical properties of interfaces within a flax bundle—part I: experimental analysis. *Int J Adhes Adhes* 31:875–881. <https://doi.org/10.1016/j.ijadhadh.2011.08.008>
13. Dalimova GN, Abduazimov KA (1994) Lignins of herbaceous plants. *Chem Nat Compd* 30:146–159. <https://doi.org/10.1007/BF00629995>
14. Donaldson LA (2001) Lignification and lignin topochemistry—an ultrastructural view. *Phytochemistry* 57:859–73. [https://doi.org/10.1016/s0031-9422\(01\)00049-8](https://doi.org/10.1016/s0031-9422(01)00049-8)
15. Drakakaki G (2015) Polysaccharide deposition during cytokinesis: challenges and future perspectives. *Plant Sci* 236:177–184. <https://doi.org/10.1016/j.plantsci.2015.03.018>
16. Drieling A, Müssig J, Graupner N, Müssig J, Piotrowski S, Carus M (2010) Economic aspects. In: Müssig J (ed) *Industrial applications of natural fibres*. Wiley, Chichester, UK, pp 49–86. <https://doi.org/10.1002/9780470660324.ch3>
17. Duval A, Lawoko M (2014) A review on lignin-based polymeric, micro- and nano-structured materials. *React Funct Polym* 85:78–96. <https://doi.org/10.1016/j.reactfunctpolym.2014.09.017>
18. Ebringerova A, Hromadkova Z, Heinze T (2005) Hemicellulose. *Adv Polym Sci* 186:1–67. <https://doi.org/10.1007/b136816>
19. El-Gohary M (2012) The contrivance of new mud bricks for restoring and preserving the Edfa ancient granary—Sohag, Egypt. *Int J Conserv Sci* 3:67–78
20. Evert RF (2006) Esau's plant anatomy. <https://doi.org/10.1002/0470047380>

21. Faruk O, Bledzki AK, Fink HP, Sain M (2012) Biocomposites reinforced with natural fibers: 2000–2010. *Prog Polym Sci* 37:1552–1596. <https://doi.org/10.1016/j.progpolymsci.2012.04.003>
22. Friedrich K, Evstatiev M, Angelov I, Mennig G (2007) Pultrusion of flax-polypropylene composite profiles. In: *Handbook of engineering biopolymers*. Carl Hanser Verlag GmbH & Co. KG, München, pp 223–36. <https://doi.org/10.3139/9783446442504.007>
23. Gandini A, Belgacem MN, Barkoula N-M, Peijs T, Dufresne A, Mosiewicki MA et al (2011) *Interface engineering of natural fibre composites for maximum performance*, 1st edn. Woodhead Publishing, Cambridge
24. George J, Sreekala MS, Thomas S (2001) A review on interface modification and characterization of natural fiber reinforced plastic composites. *Polym Eng Sci* 41:1471–1485. <https://doi.org/10.1002/pen.10846>
25. Grabber JH, Ralph J, Lapierre C, Barrière Y (2004) Genetic and molecular basis of grass cell-wall degradability. I. Lignin-cell wall matrix interactions. *Comptes Rendus Biol* 327:455–65. <https://doi.org/10.1016/j.crvi.2004.02.009>
26. Haigler CH (1985) The functions and biogenesis of native cellulose. In: Nevell T, Zeronian S (ed) *Cellulose chemistry and its applications*. Ellis Horwood Ltd., Chichester, UK, pp 30–83
27. Hänninen T, Hughes M, Baur E, Otremba F, Huber T, Graupner N, et al (2010) *Composites. Industrial applications of natural fibres*. Wiley, Chichester, UK, pp 381–480. <https://doi.org/10.1002/9780470660324.ch19>
28. Hill CAS (2006) *Wood modification: chemical, thermal and other processes*. Wiley, Chichester, UK. <https://doi.org/10.1002/0470021748>
29. Jarvis MC (2000) Interconversion of the I α and I β crystalline forms of cellulose by bending. *Carbohydr Res* 325:150–154. [https://doi.org/10.1016/S0008-6215\(99\)00316-X](https://doi.org/10.1016/S0008-6215(99)00316-X)
30. John M, Anandjiwala RD (2008) Recent developments in chemical modification and characterization of natural fiber-reinforced composites. *Polym Compos* 29:187–207. <https://doi.org/10.1002/pc.20461>
31. Joshi SV, Drzal LT, Mohanty AK, Arora S (2004) Are natural fiber composites environmentally superior to glass fiber reinforced composites? *Compos Part A Appl Sci Manuf* 35:371–376. <https://doi.org/10.1016/j.compositesa.2003.09.016>
32. Kabir MM, Wang H, Aravinthan T, Cardona F, Lau K (2007) Effects of natural fibre surface on composite properties : a review. In: *eddBE2011 1st international postgraduate conference engineering design and development built environment sustain*, vol 27–29. Wellbeing, pp 94–99
33. Koch G, Schmitt U (2013) Topochemical and electron microscopic analyses on the lignification of individual cell wall layers during wood formation and secondary changes. *Plant Cell Monogr* 20:41–69. https://doi.org/10.1007/978-3-642-36491-4_2
34. Kvavadze E, Bar-Yosef O, Belfer-Cohen A, Boaretto E, Jakeli N, Matskevich Z et al (2009) 30,000-year-old wild flax fibers. *Science* 325:1359. <https://doi.org/10.1126/science.1175404>
35. Laurichesse S, Avérous L (2014) Chemical modification of lignins: towards biobased polymers. *Prog Polym Sci* 39:1266–1290. <https://doi.org/10.1016/j.progpolymsci.2013.11.004>
36. Lewis NG (1990) Lignin : occurrence, biogenesis and biodegradation
37. Li X, Tabil L, Panigrahi S (2007) Chemical treatments of natural fiber for use in natural fiber-reinforced composites: a review. *J Polym Environ* 15:25–33. <https://doi.org/10.1007/s10924-006-0042-3>
38. Liu M, Fernando D, Daniel G, Madsen B, Meyer AS, Ale MT et al (2015) Effect of harvest time and field retting duration on the chemical composition, morphology and mechanical properties of hemp fibers. *Ind Crops Prod* 69:29–39. <https://doi.org/10.1016/j.indcrop.2015.02.010>
39. Martin N, Mouret N, Davies P, Baley C (2013) Influence of the degree of retting of flax fibers on the tensile properties of single fibers and short fiber/polypropylene composites. *Ind Crops Prod* 49:755–767. <https://doi.org/10.1016/j.indcrop.2013.06.012>

40. McDougall GJ, Morrison IM, Stewart D, Weyers JDB, Hillman JR (1993) Plant fibers—botany, chemistry and processing for industrial use. *J Sci Food Agric* 62:1–20. <https://doi.org/10.1002/jsfa.2740620102>
41. Mohnen D (2008) Pectin structure and biosynthesis. *Curr Opin Plant Biol* 11:266–277. <https://doi.org/10.1016/j.pbi.2008.03.006>
42. Müssig J, Haag K (2014) The use of flax fibres as reinforcements in composites. In: *Biofiber reinforcements in composite materials*
43. Mwaikambo LY (2006) Review of the history, properties and application of plant fibres. *African J Sci Technol* 7:120–133
44. Mwaikambo LY, Tucker N, Clark AJ (2007) Mechanical properties of hemp-fibre-reinforced euphorbia composites. *Macromol Mater Eng* 292:993–1000. <https://doi.org/10.1002/mame.200700092>
45. Niklas KJ (1992) *Plant Biomechanics: an engineering approach to plant form and function*. The University of Chicago Press, Chicago and London
46. O'Neill MA, Ishii T, Albersheim P, Darvill AG (2004) Rhamnogalacturonan II: structure and function of a borate cross-linked cell wall pectic polysaccharide. *Annu Rev Plant Biol* 55:109–39. <https://doi.org/10.1146/annurev.arplant.55.031903.141750>
47. Pauly M, Gille S, Liu L, Mansoori N, de Souza A, Schultink A et al (2013) Hemicellulose biosynthesis. *Planta* 238:627–642. <https://doi.org/10.1007/s00425-013-1921-1>
48. Rowell R (2005) *Handbook of wood chemistry and wood composites*
49. Rowell RM (2008) Natural fibres: types and properties. In: *Properties and performance of natural-fibre composites*. Elsevier, pp 3–66. <https://doi.org/10.1533/9781845694593.1.3>
50. Salmén L, Bergström E (2009) Cellulose structural arrangement in relation to spectral changes in tensile loading FTIR. *Cellulose* 16:975–982. <https://doi.org/10.1007/s10570-009-9331-z>
51. Salmén L, Burgert I (2009) Cell wall features with regard to mechanical performance. A review. *Holzforschung* 63:121–129. <https://doi.org/10.1515/HF.2009.011>
52. Segal L, Creely JJ, Martin AE, Conrad CM (1959) An empirical method for estimating the degree of crystallinity of native cellulose using the X-ray diffractometer. *Text Res J* 29:786–794. <https://doi.org/10.1177/004051755902901003>
53. Ben SAEO, Chaabouni Y, Msahli S, Sakli F (2012) Morphological and crystalline characterization of NaOH and NaOCl treated *Agave americana* L. fiber. *Ind Crops Prod* 36:257–66. <https://doi.org/10.1016/j.indcrop.2011.09.012>
54. Singh SR, Kundu DK, Tripathi MK, Dey P, Saha AR, Kumar M et al (2015) Impact of balanced fertilization on nutrient acquisition, fibre yield of jute and soil quality in new gangetic alluvial soils of India. *Appl Soil Ecol* 92:24–34. <https://doi.org/10.1016/j.apsoil.2015.03.007>
55. Skoglund G, Nockert M, Holst B (2013) Viking and early middle ages northern Scandinavian textiles proven to be made with hemp. *Sci Rep* 3:2686. <https://doi.org/10.1038/srep02686>
56. Somerville C (2006) Cellulose synthesis in higher plants. *Annu Rev Cell Dev Biol* 22:53–78. <https://doi.org/10.1146/annurev.cellbio.22.022206.160206>
57. Thakur VK, Thakur MK, Gupta RK (2014) Review: raw natural fiber-based polymer composites. *Int J Polym Anal Charact* 19:256–271. <https://doi.org/10.1080/1023666X.2014.880016>
58. Thompson JE, Fry SC (2000) Evidence for covalent linkage between xyloglucan and acidic pectins in suspension-cultured rose cells. *Planta* 211:275–286. <https://doi.org/10.1007/s004250000287>
59. Unger F (1866) *Botanische Streifzüge auf dem Gebiete der Culturgeschichte—Ein Ziegel der Dashurpyramide in Ägypten nach seinem Inhalte an organischen Einschlüssen*. Sitzungsberichte der Kais. Akad. der Wissenschaften Wien Math. Klasse 54:33–62
60. Varki A, Cummings RD, Esko JD, Freeze HH, Stanley P, Marth JD et al (2009) Symbol nomenclature for glycan representation. *Proteomics* 9:5398–5399. <https://doi.org/10.1002/pmic.200900708>

61. Viëtor RJ, Mazeau K, Lakin M, Pérez S (2000) A priori crystal structure prediction of native celluloses. *Biopolymers* 54:342–354. [https://doi.org/10.1002/1097-0282\(20001015\)54:5%3c342:AID-BIP50%3e3.0.CO;2-O](https://doi.org/10.1002/1097-0282(20001015)54:5%3c342:AID-BIP50%3e3.0.CO;2-O)
62. Vogel J (2008) Unique aspects of the grass cell wall. *Curr Opin Plant Biol* 11:301–307. <https://doi.org/10.1016/j.pbi.2008.03.002>
63. Van de Weyenberg I, Ivens J, De Coster A, Kino B, Baetens E, Verpoest I (2003) Influence of processing and chemical treatment of flax fibres on their composites. *Compos Sci Technol* 63:1241–1246. [https://doi.org/10.1016/s0266-3538\(03\)00093-9](https://doi.org/10.1016/s0266-3538(03)00093-9)
64. Xie Y, Hill CAS, Xiao Z, Militz H, Mai C (2010) Silane coupling agents used for natural fiber/polymer composites: a review. *Compos Part A Appl Sci Manuf* 41:806–19. <https://doi.org/10.1016/j.compositesa.2010.03.005>
65. Yu H, Yu C (2007) Study on microbe retting of kenaf fiber. *Enzyme Microb Technol* 40:1806–1809. <https://doi.org/10.1016/j.enzmictec.2007.02.018>
66. Zah R, Hischier R, Leão AL, Braun I (2007) Curauá fibers in the automobile industry—a sustainability assessment. *J Clean Prod* 15:1032–40. <https://doi.org/10.1016/j.jclepro.2006.05.036>

Nanocellulose-Reinforced Adhesives for Wood-Based Panels



Elaine Cristina Lengowski, Eraldo Antonio Bonfatti Júnior, Marina Mieko Nishidate Kumode, Mayara Elita Carneiro and Kestur Gundappa Satyanarayana

1 Introduction

The use of wood panels is increasing in two ways. The first is by limiting the dimensions of the log diameters, by the anisotropy and other natural defects that solid wood possesses and the second by the search for greater use of the wood [93, 107]. Therefore the production of panels of reconstituted wood represents a rational use of this raw material [18].

There are several types of wood panels, which include: laminated wood panels, agglomerated wood panels or wood fiber panels [53]. It is reported that 416 million

E. C. Lengowski

Faculty of Forestry Engineering, Federal University of Mato Grosso (UFMT),
Fernando Corrêa da Costa St, 2367 - Boa Esperança, Cuiabá, MT 78068-600, Brazil
e-mail: elainelengowski@gmail.com; elainecristina@ufmt.br

E. A. Bonfatti Júnior · M. E. Carneiro

Department of Forest Engineering and Technology (DETF),
Federal University of Paraná (UFPR), Av. Pref. Lothário Meissner,
632, Jardim Botânico, Curitiba, PR 80.210-170, Brazil
e-mail: bonfattieraldo@gmail.com

M. E. Carneiro

e-mail: mayaraecarneiro@gmail.com

M. M. N. Kumode

Laboratory of Wood, Pontifical Catholic University, Curitiba, PR, Brazil
e-mail: mnishidate@gmail.com

K. G. Satyanarayana (✉)

PIPE & Department of Chemistry, Federal University of Parana,
Curitiba, Brazil
e-mail: gundsat42@hotmail.com; kgs_satya@yahoo.co.in

K. G. Satyanarayana

Poornaprajna Scientific Research Institute (PPISR), Sy. no. 167, Poornaprajnapura,
Bidalur Post, Devanahalli, Bangalore 562 110, Karnataka, India

© Springer Nature Switzerland AG 2019

Inamuddin et al. (eds.), *Sustainable Polymer Composites and Nanocomposites*,
https://doi.org/10.1007/978-3-030-05399-4_35

1001

m³ of wood panels were produced in 2016, of which 42% were wood panels and the remaining 58% were fiber based panels [35]. It is interesting to note that each panel has an application such as internal or external use, in furniture or civil construction. Depending on the environment to which the panels will be exposed, there are different types of adhesives that should be used, the most common ones being urea formaldehyde for indoor use and low moisture content, while phenol formaldehyde resin for external use [54].

Improvement of adhesive bonding is a routine process in the wood industry [29] as it is one of the key steps in the production of panels. Changes in adhesion to wood are desirable in terms of performance improvement and adhesive economy [43]. Among the several opportunities offered by nanotechnology for the forest products industry [15] the reinforcement of adhesives with nanocellulose has been already identified as an opportunity, which has been explored. This has shown improvement in both the physical and mechanical properties of the panels [43].

Obtaining nanoscale cellulose fibers and its application as reinforcement in the preparation of biodegradable composites as well as nanocomposites has attracted great attention during the last years [101, 116]. This is attributed to the unique properties of nanomaterials such as high aspect ratio, crystallinity and surface area, excellent mechanical properties combined with less weight and biodegradability [29, 76].

With this background, this chapter presents an overview of the use of nanocellulose in wood-based panels, with examples, of the use of different types of nanocelluloses as reinforcement in several types of adhesives in the production of different types of panels. This chapter also presents some important concepts and properties of all the raw materials used, viz., adhesives, wood, and nanocelluloses.

2 Wood-Based Panels

The solid wood presents some disadvantages, because it is a heterogeneous and anisotropic product, i.e., It possesses different physical properties in its tangential, longitudinal and radial axes [13, 39, 108]. It should also be taken into account that the dimensions of the wood pieces limit their use besides the natural defects, such as knots, grain inclination, the percentage of juvenile and adult wood and reaction wood, among others, all of which interfere with the rheological behaviour of the wood [54]. Also, it is reported that many times the mechanical properties of wood are unsatisfactory for certain uses [104]. Because of the above-mentioned limitations of solid wood, reconstituted wood products have been produced by gluing of veneer, boards, slabs, particles or fibers, and these elements are joined by adhesive bonds [13]; Industrial Research [78]. With the use of glue utilization of the wood has been increasing because the glue allows the use of pieces of small dimensions to obtain products with greater added value.

Reconstituted products, such as particle board, oriented strand board (OSB, also known as flakeboard) and plywood panels, among others, appear as an alternative

to solid wood, rendering improvement in the characteristics of the raw material. This is because, they allow greater homogeneity of the physicochemical properties, dimensional stability, full use of wood and residues, thus contributing to the conservation of forests [18]. However, the quality of the final product depends mainly on the adhesion technology [89].

Reconstituted wood panels can be divided into three types: laminated panels (plywood and Laminated Veneer Lumber-LVL), particle board (wafer board and OSB), and fiberboard (Medium Density Fiberboard-MDF, High-Density Fiberboard-HDF, and insulation board). The plywood panels are composed of wood overlapping and bonded with adhesives, mainly phenol-formaldehyde and urea-formaldehyde, under pressure and temperature so that they cross their fibers at an angle of 90° [54, 119]. The wood veneer can be of different thicknesses and are always in odd numbers (Finnish along the length of the part, in which the thickness of the blades should not exceed 6.4 mm—0.25 Forest Industries Federation [33]. According to the Standard Specification for Evaluation of Structural Composite Lumber Products [5], LVL can be defined as a structural compound composed by layers of thin wood assembled with adhesives with wood fibers oriented mainly in the plane of the panels. In the bonding of the LVL panels synthetic adhesives used are resistant to humidity; the most commonly used adhesive being the phenol-formaldehyde [75]. Both plywood and LVL are gaining visibility for their benefits in structural and non-structural use [10, 65, 73]. These are already used in applications typically dominated by steel and concrete [83].

Particleboard wood panels may be defined with randomly arranged small particles, agglutinated using adhesives and glued using heat and pressure [54, 87]. The most used adhesives in the production of panels of particleboard wood are the synthetic ones such as urea-formaldehyde, phenol-formaldehyde and melamine-formaldehyde [44] with phenol-formaldehyde is recommended for external use and the urea-formaldehyde recommended for internal use [44]. The waferboard used as a structural material is produced with larger wafer type particles of square or slightly rectangular shapes, glued with random particle distribution and consolidated through hot pressing [54]. While in the waferboard the particles are arranged randomly, the particles are used as layers in the OSB with perpendicular directions [87]. In view of this arrangement, the superior structural behaviour is exhibited in OSB-type panels having high dimensional stability compared to the waferboard [53, 93]. Accordingly, the OSB wood panels are used for structural applications, considering the evolution of the waferboard differs from its precursor in the direction of the particle [49].

The fiber panels are dry-fabric panels made of lignocellulosic fibers, combined with an adhesive under pressure and temperature [53, 78, 87]. In such type of panels primary adhesion occurs through the interlacing of the fibers and the adhesive properties of some chemical components of the wood [46]. When fabricated with low density, these panels can be used for insulation purposes [60], called 'insulation board', with a mean density between 0.02 and 0.40 g cm⁻³ [54]. Natural fiber insulation is known for the good thermal insulation it promotes, but this material also presents good acoustic insulation [80].

Medium density fiberboard (MDF) panels are normally bonded with urea-formaldehyde adhesive and consolidated with hot pressing [78]. Density of MDF varies from 0.50 to 0.80 g cm⁻³ [7, 54]. This is one of the most well-known wood panels, commonly used as a raw material for furniture, carpentry and building products [70]. Panels having a density varying from 0.80 to 1.10 g·cm⁻³, called as high-density fiberboard (HDF), are similar to the MDF [107]. These are used as a panel for structural purposes commonly used as a core of laminate flooring [86].

3 Adhesives and Adhesion

3.1 Adhesives

Kinloch [62] defined adhesive as any substance applied to the surface, or both surfaces, of two separate objects that bind them and offers resistance to their separation. On the hand, Peschel et al. [87] added to this concept of the condition of adhesives, these being non-metallic substances with which other materials are solidly bonded together by adhesion and cohesion.

Wood adhesives can be classified according to their origin in natural and synthetic [28, 74]. Natural adhesives can be proteins of animal or vegetable origin, while synthetic ones have the petroleum raw material and, although they resemble the natural adhesives in the physical characteristics, they can be formulated to meet specific requirements and have a higher resistance to humidity [28, 82].

Synthetic adhesives can be classified into two types: Thermoplastic adhesives and thermoset adhesives. The two types differ in their chemical structure and response to heat [81, 88]. Table 1 shows the classification of some adhesives including natural adhesives used in the wood panel industry.

Another type of classification of adhesives that can be made according to their purpose of use involving the environment to which each adhesive would be exposed. Accordingly, Table 2 shows the types of adhesives, the environment in which they are used and the name of adhesives for each of these used in the preparation of wood panels.

Thermoplastic adhesives are liquid adhesives whose aggregate state depends on temperature. The curing and melting are reversible, i.e., if heated after curing they will return to the liquid state since they are adhesives that do not form reticles (net of fibers). These adhesives may also be dissolved in a solvent and then reactivated with solvent evaporation [88]. But, the use of this type of adhesives is limited, i.e., they can only be used in non-structural applications, in low-temperature climate and are not resistant to heat or fire [81]. Of this polyvinyl acetate (PVA) adhesive is the most commonly used in wood glueing [34]. Figure 1 shows the polyvinyl acetate monomer.

PVA is a yellow-white liquid adhesive available in a ready-to-use form and which can be applied directly to the wood and cured at room temperature or through

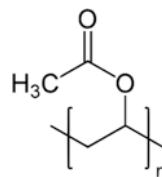
Table 1 Adhesives used in the wood panel industry

Types of adhesives	Adhesives
Natural	Animal protein derivatives (glutin, casein and albumin)
	Derivatives of vegetable origin (soybean meal)
	Derivatives of starch (wheat flour)
	Cellulose ether
	Natural rubber
Thermoplastics	Polyvinyl acetate
	Polyvinyl/acrylate
	Polyethylene
	Polystyrene
	Synthetic rubber
Thermosets	Urea formaldehyde
	Melanin-formaldehyde
	Phenol-formaldehyde
	Resorcin-formaldehyde
	Tannin-formaldehyde
	Phenol-resorcin-formaldehyde

Table 2 Classification of the use environment of the wood panels according to the type of adhesive (Adapted from [36])

Application area	Name of environment where the adhesive is used	Used adhesive
Structural	Exterior use without any restriction	Phenol-formaldehyde
		Resorcin-formaldehyde
		Phenol-resorcin-formaldehyde
		Polímeros de emulsão/ Isocianato
		Melanin-formaldehyde
	Exterior use with a restriction	Melanin-urea formaldehyde
		Isosyante
		Epoxy
	Interior	Urea-formaldehyde
Casein		
Semi-structural	Exterior use with limitations	Polyvinyl acetate “crosslinking”
		Polyurethane
		Polyvinyl acetate (PVAc)
Non structural	Interior	Construction elastomers
		Contact elastomers
		Hot-melt

Fig. 1 Polyvinyl acetate (PVA) adhesive monomer. Reproduced from [9] with the kind permission of the publishers



high frequency. After curing this adhesive exhibits high mechanical resistance; however, its use is not recommended in environments with high temperatures and high humidity [36]. Polyvinyl acetate adhesives are fixed by the loss of water mainly by diffusion of water from the adhesive in the wood [34]. This type of adhesive is used for any and all wood glueing operations. Major areas include bonding of corrugated panels, finger-jointing, laminating and assembling [48].

Unlike the thermoplastic adhesives, thermosets are plastics when cured of a soft solid or viscous liquid prepolymer results in a molecule of higher molecular weight and with higher melting point and therefore, will not have the cure reversed by heat [88, 121]. The cure of thermoset adhesives is heat induced, reaching 200 °C. These adhesives generally are stronger than the thermoplastic adhesives and more recommended for high-temperature applications [88] and are more commonly used in wood structures [121]. In spite of a large number of adhesives available for wood panels, the most used are synthetic ones, such as phenol-formaldehyde, urea-formaldehyde, resorcinol-formaldehyde and melamine-formaldehyde [54, 107]. These four adhesives make up approximately 90% of all adhesives used in wood panels and all of these are derived from fossil fuels [14].

Phenol-formaldehyde (PF), applied in a broad spectrum of engineered wood products, is very strong and resistant to dry and humid conditions and exhibits strong adhesion to wood [41, 89, 121]. Figure 2 shows part of a polymer chain of the phenol-formaldehyde adhesive.

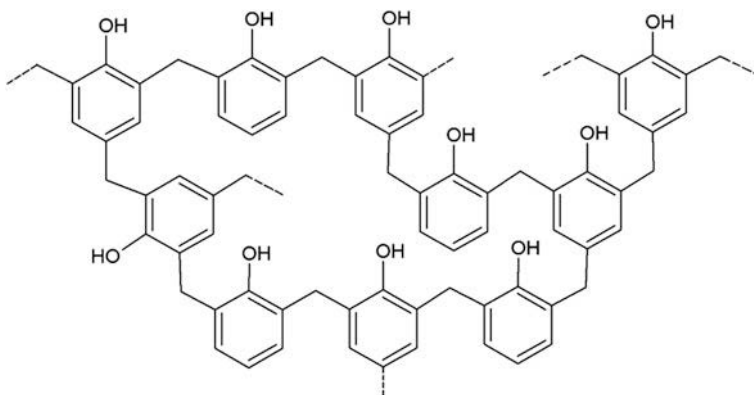


Fig. 2 The molecular structure of the polymer chain of phenol-formaldehyde. Adapted from [124] with the kind permission of the publishers

It can be cured hot or cold; however, for the cold setting process, it is necessary to reduce the pH with the addition of an acid. The PF adhesive is mainly applied to particle or fiberboard, plywood, pressed laminated wood, glued laminated wood, waferboard and OSB [54, 107].

Urea-formaldehyde (UF) is a low-cost, structural and internal-use adhesive [54, 89]. Figure 3 shows part of a polymer chain of the urea-formaldehyde adhesive.

This adhesive is fast hardening, high resistance to dry bonding and presents colourless glue joints. This adhesive can be hardened hot or cold; however, when fast hardening is desired a hardener should be applied [61]. The glue joints of this adhesive are high strength, but brittle and inelastic. Therefore, the stress of the wood, caused by changes in humidity and temperature, impairs glue joints and decreases adhesive performance [41, 121, 74].

Resorcinol-formaldehyde (RF) is a brown, cold-curing, catalyst-requiring adhesive. Figure 4 shows part of a polymer chain of the resorcinol-formaldehyde adhesive. This adhesive is much more reactive than PF [54]. Adhesive bonds of RF

Fig. 3 The molecular structure of the polymer chain of urea-formaldehyde. Adapted from [85], with the kind permission of the publishers

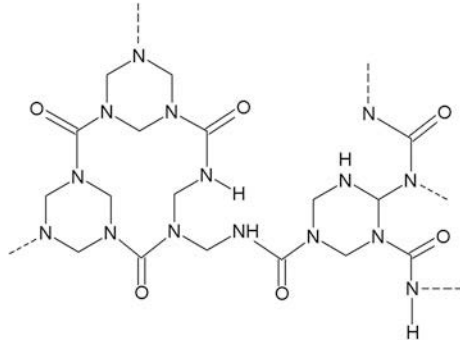
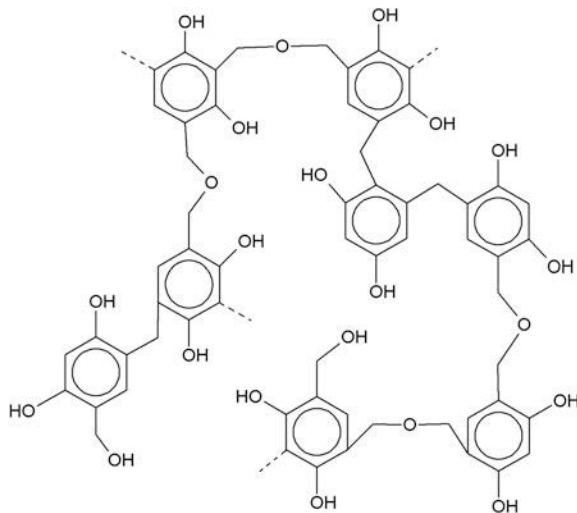


Fig. 4 The molecular structure of the resorcinol-formaldehyde polymer chain. Adapted from [47], with the kind permission of the publishers



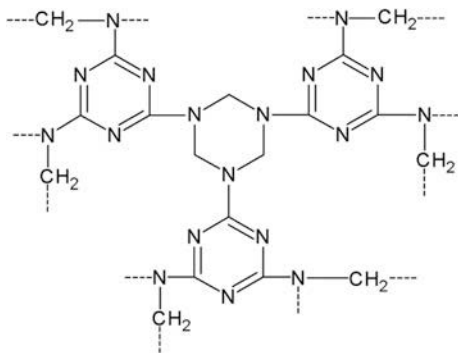
are resistant to moisture, boiling water, oil and many other solvents, i.e., an adhesive suitable for exterior use [88]. This adhesive used in the production of rolled beams, shipbuilding, and aviation. However, due to its high cost of production, it is hardly used in pure form. Therefore, it is usually mixed in the same proportion with PF [41, 54, 121].

Melamine-formaldehyde, a product between the condensation of melamine and formaldehyde, is a white-coloured adhesive classified as an intermediate between PF and UF. Figure 5 shows part of a polymer chain of the melamine-formaldehyde adhesive.

RF is a more resistant material than wood [88]. It is a hot curing around (93 °C) structural adhesive Melamine-formaldehyde has the advantages of being more resistant to moisture than UF and curing faster than PF [24, 89]. This can be used outdoors without any restriction [36]. However, its cost is higher than that of these two resins and therefore is commonly used as an additive to improve the performance of UF glue beating, even this form of use is marketed under the nomenclature melamine-urea-formaldehyde [54, 89].

Formaldehyde, present in the four synthetic adhesives mentioned above, is one of the most common chemicals in current use, with the simplest aldehyde of molecular formula H_2CO and the boiling point of $-19\text{ }^\circ\text{C}$ [97]. It is a colourless gas with pungent, inflammable and highly reactive odour [51] and highly carcinogenic [52]. The use of these resins can lead to the emission of formaldehyde into the atmosphere, generating occupational hazards to the workers involved in the manufacturing process, as well as users of the installations where these panels are used [49]. Exposure to formaldehyde may cause irritation to the mucous membranes of the eyes, nose, nasal cavity, pharynx and larynx, and may also cause drowsiness, nausea, and skin irritation through frequent contact and prolonged exposure [112]. Even coated panels can emit formaldehyde, these emissions are regulated by panel buyers countries [49]. Regulatory standards establish maximum emission limits and analytical methods for gaseous formaldehyde measurements [95].

Fig. 5 The molecular structure of the polymer chain of melamine-formaldehyde. Reproduced from [90] with the kind permission of the publishers



3.2 Adhesion

It is understood that adhesion is the force of attraction between molecules of different materials, such as the force between adhesive substance and the junction piece, and cohesion force of attraction between molecules of the same type, such as forces inside a layer of glue [87]. These authors have defined that cohesion is the force of attraction between molecules of the same type, as for example, the forces inside a layer of glue. Therefore, a good adhesive must adhere to the surface of the solid and have sufficient cohesion to ensure the bonding of the solids. According to Schultz and Nardin [100], Petrie [88] and Ebnesajjad and Landroch [27], there are six main adherence theories, viz. mechanical theory, electrical theory also known as electrostatic theory, wetting theory, theory of the diffusion of polymers, also known as diffusion theory, chemical bonding theory and weak boundary layer theory. These are explained below:

- **Mechanical theory:** According to this, the fluidity and penetration of the adhesive into porous substrates leads to the formation of hooks or a mechanical interlacing of the adhesive tightly attached to the substrate after curing and hardening of the adhesive.
- **Electrical theory (Electrostatic theory):** According to this, the forces of attraction in adhesion in terms of electrostatic effects at the interface between the adhesive/bonding system is compared to a capacitor, in which the armatures are the two electrical layers formed by the contact of the two substrates. The adhesion results from the forces of attraction developed between the two armatures.
- **Wetting theory:** According to this, adhesion results from the molecular contact between two materials that develop surface attraction forces. The process of establishing continuous contact between an adhesive and a substrate is called 'wetting', which can also be defined as the adhesion of a liquid to a solid.
- **Theory of the diffusion of polymers (diffusion theory):** According to this, adhesion occurs through the diffusion of segments of polymer chains. Adhesive forces can be visualized as those produced in mechanical adhesion but on a molecular scale. However, the applications of this theory are also limited. The mobility of long polymer chains is very restricted, severely limiting the molecular interpretation proposed in this theory.
- **Chemical bonding theory:** According to this theory, adhesion occurs through chemical bonds (covalent and metallic ionic). It is currently believed that adhesion at the interface, from the molecular point of view, is due to the action of secondary forces.
- **Weak boundary layer theory:** This theory proposes the existence of a finite boundary layer composed of absorbed molecules at the interface, which is different in their constitution from the constituent molecules of the adhesive and the adhesive.

The mechanisms related to the adhesion process and wood panels can be explained by the mechanical theories, chemical adhesion and diffusion of polymers

[37]. In the bonding of porous surfaces, such as wood, the initial process is done mechanically [37]. There is penetration of the adhesive at the cellular scale, filling void intercellular spaces, increasing the bonding durability in the wood, especially when the adhesive is diffused into cellulose and hemicellulose molecules. According to this author, deeper the penetration of the more resistant adhesive, greater is the bond, which may even exceed the resistance of the wood. According to the theory of polymer chain diffusion, adhesion occurs through ionic or covalent primary bonds, and/or by secondary intermolecular forces; however, there is no evidence that primary bonds between wood and adhesive occur [37]. After adhesive penetration into the wood, the adhesion is chemically strengthened by attractive intermolecular forces such as Van der Waal forces, dipole-dipole forces and hydrogen bonding [37]. If the polymer chain extends between the molecules of the wood, the adhesion is reinforced by the diffusion theory. Adhesion is a very complex field beyond the reach of any model or theory. In practice, several adhesion mechanisms can occur simultaneously [100].

3.2.1 Factors Influencing the Adhesion Process

The adequate bonding of wood is directly related to various physical-chemical characteristics of the adhesive. These include viscosity, gelatinization time, solids content and pH, and the intrinsic characteristics of the wood, anatomical, physical, chemical and mechanical properties.

Physico-Chemical Characteristics of the Adhesive

The viscosity is one of the most important properties of an adhesive [25], and can be defined as physical property that characterizes the resistance of a fluid to the flow, high viscosity liquids have low fluidity, such as honey, while those already having low viscosity have high fluidity, such as water. According to Peschel et al. [87], this parameter depends on the temperature, decreasing with the elevation of the temperature of the liquid. According to Iwakiri [54] and Gonçalvez and Lelis [45], when the adhesive viscosity is high, the uniform distribution of the adhesive on the wood is difficult, with insufficient penetration into the wood structure, damaging wetting and leaving a thick tail. However, adhesives with low viscosity have higher penetration and their absorption by the wood is also greater, and in extreme situations, can result in excessive absorption of adhesive by the wood [4, 45, 54, 107]. The gel time is important for the quality of the adhesive since it is related to the maximum admissible viscosity for its application. The gel time is measured in seconds, minutes or hours, and corresponds to the period from the preparation of the adhesive to the application to the hardening “point”, or gel phase,

when it reaches maximum elasticity [20]. In the industrial scope the gel time is a characteristic foundation, since, from this time on, it is no longer possible to manipulate the resin [22].

In general, the working time of the adhesives should not be very long, as it would require a longer pressing time. However, the short working time results in the difficulty of applying and spreading the adhesive in the wood, due to its rapid polymerization, causing a decrease in the strength of the glue line [22, 54]. The content of solids corresponds to the number of solids contained in the adhesive, which is composed of solid components and volatile liquids. When the panel is subjected to hot pressing, evaporation of the liquid components occurs, which is called “cure”, that is, solidification of the adhesive, forming the glue line that is responsible for the bond between the substrates [54]. The pH, hydrogen potential, of an aqueous solution is defined as the concentration of dissociated H^+ ions [97] and its determination is made by direct reading in apparatus called pH meters. In the case of bonding of wood, it is important to consider the influence pH of both wood and resin [54]. According to Wang et al. [114, 115] and Wang et al. [113] the pH of the adhesives should not exceed the range of 2.5–11, because beyond these limits the resin causes degradation of the fibers of the wood.

Intrinsic Characteristics of Wood

The anatomical structure is very diversified, especially in hardwood species, composed of cellular elements that are arranged in various ways to constitute the wood [30]. This cellular organization depends on the botanical species, the age of the plant and the environmental conditions in which it develops [17]. In addition, each cell element has a characteristic of the shape and dimensions being linked to the genotypic characteristics of the species, function of the cellular element and phylogenetic position [110]. The anatomical properties of the wood have a significant influence on the bonding, such as the variability in density and porosity that occurs in early wood (also called spring wood → less dense due to larger cells and thinner cell walls) and latewood (also called summer wood → produced in spring and later), core and sapwood, juvenile and adult wood. Also, the influence of the dimensional instability of the reaction wood, as well as the direction of the grain, in which the penetrability relates to the cutting direction [3] is highlighted.

For the production of particleboards and fiber panels, the wood density is a very important factor since it is related to the compaction ratio of the panel. The compaction ratio and indicates the degree of densification of the wood particles in the panel structure and will affect the properties and qualities of the wood [107]. According to these authors, the compaction ratio should be in the range of 1.3–1.6 so that proper densification and consolidation of the panel in the desired final thickness occurs.

According to Thoemen et al. [107], the characteristics of the growth rings, heartwood and sapwood, tree age, porosity, reaction wood and angle of inclination of the cellular elements are favourably or unfavourably involved, since they may or

may not favour the bonding process. In the process of bonding, several adhesion mechanisms occur simultaneously in the wood. The influence of the wood anatomy on the bonding process is related to its structure with respect to the differences of dimensions of the cellular elements, size, disposition, and frequency of the cellular cavities that, in turn, are related to the porosity and permeability of the wood [2]. The interaction between adhesive and substrate occurs mainly by vessels and voids, but there is an effective participation of the rays and, to a lesser extent, the axial parenchyma in this process [2, 103]. Figure 6 shows the glue line adhesive penetration of a plywood panel.

The pH of the wood varies according to the species and is around 3–6, and there may be changes of pH inside a piece of wood as a result of the migration of extractives from lower layers to superficial layers, altering the bonding conditions [54]. The capability is a characteristic of the adhesive and refers to its ability to tolerate contact with more acidic or more basic materials without altering its pH [89]. Some woods may present extractives with pH that inhibit the hardening of the adhesive, impairing the development of resistance and adequate cohesion in the glue line. While in some woods, the pH may favour the pre-hardening of the adhesive, impeding the movement and mobility functions, such as the fluidity, penetration, and wetting of the adhesive in the wood [67]. The most important physical properties of wood in terms of bonding are the density and moisture content of the wood. Antagonistic to porosity and the penetration of adhesives, the density can cause significant effects on adhesion. In low-density woods, there is greater penetration of the adhesive and may result in greater consumption of adhesive. In the case of high-density wood, there are larger dimensional changes

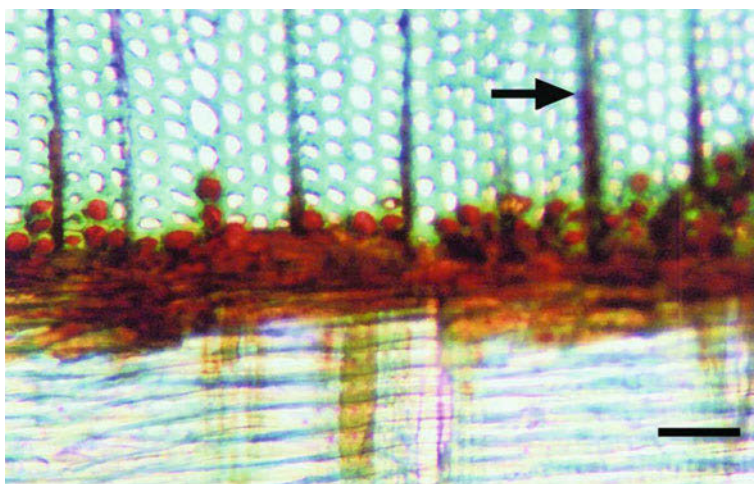


Fig. 6 Penetration of adhesives on the various types of wood cells. Reproduced from [103] with the kind permission of the publishers

resulting from variations in moisture content, generating higher glue line stresses, making the glueing process difficult [54, 77].

The influence on the moisture content of the wood in the cure of the adhesives is related to the amount and the rate of absorption of liquid adhesive by the wood, the lower the moisture content in the wood, the higher the rate of absorption, cure rate and solidification of the wood adhesive [54, 89]. According to Almeida [4], good adhesion between adhesive and wood is obtained provided the moisture content of this adhesive should not exceed 20%. In the wood/glue system, the tensions generated in the bonded product are of extreme importance in the general balance of the resistance. The greater the resistance of the glue line in relation to the strength of the wood, the greater the percentage of rupture or faults in the wood in the interface with the glue line [11]. The tension generated in the glue line is manifested by shear stresses in the plane of the adhesive bond and in the direction perpendicular to it [54].

3.3 Adhesive Additives

In the search for improvements in the adhesion process, specific properties in the panels or reduction of the cost or consumption of adhesives in the industry, additives are commonly used in the tailings formulations. Among the main additives is hardening accelerating agents one generally one comes across. Adhesive curing is influenced by the pH of the environment, in that sense pH modifiers may be employed to promote an acid or alkaline environment, depending on the type of adhesive used. Typically, with UF and melamine-urea-formaldehyde adhesives that cure in an acid environment, ammonium sulfate is used because of the fact that in addition to promoting proper pH for a cure, it leads to the formation of a less hydrolyzable microstructure [84]. For the PF adhesive, sodium hydroxide is used as a hardening accelerator because curing occurs in the basic media [32]. Types of the addition of some reagents and their effects on the final characteristics of paper are listed below:

- Paraffin emulsion: This is used to control the dimensional variation of the panels in the short term, preventing the entry of water into the liquid form by capillarity [19, 117].
- Preservatives: The insecticides and fungicides are commonly used to increase the durability of the panels. Some researchers have already employed the use of nanoparticles loaded with biocides, such as tebuconazole or chlorothalonil, aiming at the slow release of these preservatives [26, 69].
- Filler materials: These are non-stickable materials that are added to the adhesive in order to increase the total volume of the adhesive and reduce the cost without affecting the viscosity of the adhesive. These act as penetration controlling agents, avoiding excessive adhesive penetration in the case of the production of laminated panels; however excess extender may impair adhesion. Kaolin, nut shell flour, coconut husk flour are other commonly used filler materials [54].

Improvements in the rheological properties of adhesives increased mechanical and moisture resistance, reduction of formaldehyde emissions and lower production costs of wood panels are some of the goals that can be achieved with the use of additives. In this context research on the use of nanocelluloses as adhesive additives has shown promising results [6, 38, 111]. These are discussed in the next Section.

4 Nanocellulose

Nanocellulosic materials can be extracted by different methods from different plant biomasses [29, 1]. According to Fujisawa et al. [40], the nanocelluloses can be divided into three groups, viz. Nanocrystalline cellulose (CNC), microfibrillated cellulose (CMF) and nanofibrillated cellulose (CNF). The first CNC is a highly crystalline material with free of defects. This is extracted by the hydrolysis of the amorphous regions present along the axis of cellulosic fibers, by means of a chemical process of acid or enzymatic hydrolysis followed by mechanical agitation of the suspension of nanocrystals in water. The most common nanocellulose production process is by acid hydrolysis, while the most commonly used acid being sulfuric acid. Nitric acid, hydrochloric acid, phosphoric acid and hydrobromic acid can also be used in acid hydrolysis, although on a smaller scale [96, 120].

The second one CMF, obtained by a method of the mechanical disintegration of the cellulosic pulp in water. Finally, the third NCFs are extracted laterally in its nanoscale substructural units (nanofibrils) using combined processes of chemical oxidation with the reagent 2,2,6,6-tetramethylpiperidine-1-oxyl, followed of mechanical disintegration in water, or only by the method of mechanical disintegration. It may be noted that the process of obtaining CMF and CNF is similar, differing only in the final dimensions after the processing of the cellulose [99]. According to Samyn et al. [99], the CMF is commonly produced by homogenization, where the fiber shear is performed by a strong pressure drop and impact forces inside the processing chamber. A similar effect has been observed by the use of grinding processing [66], where processed suspensions generally contain a heterogeneous mixture of CMF and CNF which are characterized by different diameters and aspect ratios (length/diameter) [99]. The different aspects of the nanocelluloses described above are shown below in Fig. 7.

When isolated and prepared, CNCs have excellent physicochemical, optical, magnetic, electrical and conductimetric properties, covering a wide range of uses, different from those obtained by materials seen on a macroscopic scale. The advantages of CNC are related to its properties, such as high mechanical strength and stiffness, low density, durability, uniform size distribution, high specific surface area, low coefficient of thermal expansion, high hydrophilicity, optical transparency and self-molding that enable them to be used in a variety of uses [125, 98]. Due to its crystalline arrangement, this form of nanocellulose has a high mechanical resistance, the modulus of elasticity being estimated between 50 and 145 GPa [106, 64] and comparable to the resistance of extremely rigid materials [29] indicating its

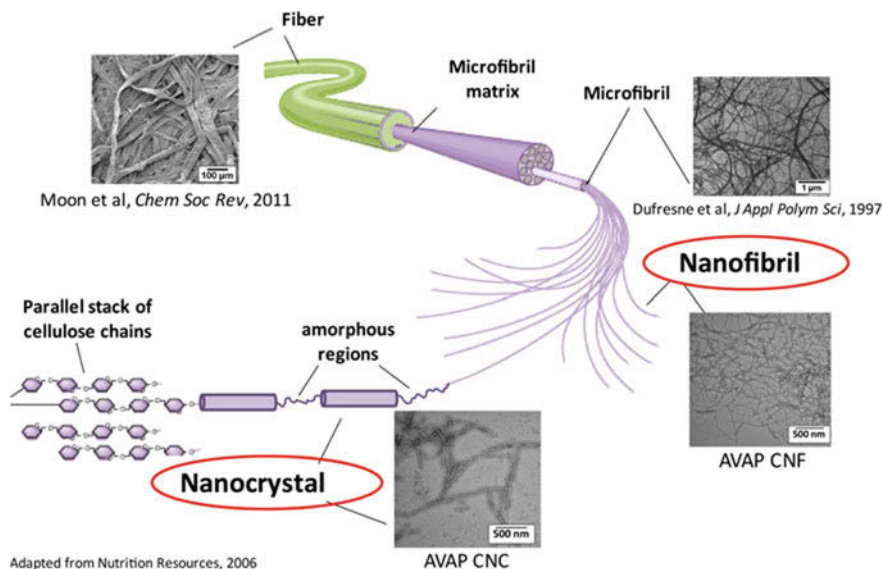


Fig. 7 The mechanism of chemical and mechanical methods for producing CNC, CMF and CNF from cellulose. Reproduced from [79] with the kind permission of the publishers

significant potential as reinforcement material, important, for example, in the automotive industry. However, herein the reported results in the literature are presented in this Chapter.

According to some researchers working on MFCs, they consist of a material obtained by the disintegration of the cellulose subjected to a mechanical process of homogenization, where it is degraded, promoting the exposure and opening of the surfaces previously located inside fibers, fibrils and microfibrils [109] cited by [63, 99, 105]. This process causes an increase in the external surface, allowing a greater area of contact and better bonding between microfibrils, increasing the resistance properties, with a value of modulus of elasticity of 145–150 GPa [55]. On drying, films with lower opacity, high density and transparency would be produced [56]. Reported definition of MFC is fibers with a diameter between 25 and 100 nm, while CNF is nanocelluloses with a diameter between 5 and 30 nm and of a variable length between 2 and 10 μm [96, 101]. Both CMF and CNF have amorphous and crystalline zones composing their structure. On the other hand, CNC refers to cellulose nanoparticles that underwent hydrolysis under controlled conditions and that lead to the formation of structures in the form of small crystalline cylinders and depending on the source of extraction has a diameter of 3–50 nm [101].

Further detailed information on the production of wood pulp and nanocellulose can be found in the following sections: 3.1 Pulping, 4: Cellulose, 5: Nanocellulose, 5.1 Method of NFC and MFC production and 5.2 Method of CNC and MFC production in the chapter on Nanocellulose in paper making in this volume.

5 Nanocellulose-Reinforced Adhesives Performance and Properties

The possibility of using nanocellulose in the adhesive formulation can be a way of promoting gains in the properties of these adhesives. This is because, the adhesion between wood components, as well as among other materials, depends on a series of parameters related to the physicochemical characteristics of the adhesive and the material to be bonded, besides the operational parameters in the bonding process, the geometric form and the size of the pieces to be bonded [29]. Although modifications in the chemistry of adhesives are a path of optimization of mechanical characteristics, the addition of filler or fibrous particles presents a possible alternative route of modification [43]. By adding fillers, the limitations imposed by polymer chemistry can be overcome, and this approach is common in high-performance adhesives, which can be reinforced with nanoparticles [122, 59, 58, 91, 92, 118].

5.1 Effects of the Addition of Nanocellulose on Adhesives

The addition of nanocellulose to the adhesives affects the physicochemical properties of the adhesives, except for the unchanged pH. In general, the percentage increase of nanocellulose in the glue causes an increase in the viscosity and the solids content. Then, the gel time is the property that varies most with this additive, since the partially acidic load in the case of CNC can delay or delay the curing, according to the type of resin to be used.

Damásio et al. [23] evaluated the addition of CNC in the glue mixture of formaldehyde urea glue observed that only the viscosity showed variation, increasing with the increasing percentage of addition in the glue mixture. A similar result has also been reported recently by Ferreira [31], who observed that the increase in the percentage of CNC added (0–8%) in the synthesis of UF adhesives provided an increase in their viscosity, solids content and gelatinization time, in comparison to the synthesis of UF without the addition of CNC. According to the author, the viscosity and solids content gains were marked with a CNC addition up to 6%, although only physical interactions were observed. That is, there was no chemical interaction of the CNC with the other elements present in the adhesive. Similar results were also reported by Liu et al. [68] while evaluating the addition of CNC in lignin PF adhesives. The author has concluded that there was no chemical reaction between the adhesive and CNC since the DSC curves presented only a similar peak at all the compositions and that the addition of the nanocellulose did not affect the energy of the adhesive. Mahrtdt et al. [72] found that the addition of CMF in the glue bead of the UF resin caused a delay in the formation of the chemical and mechanical bonding of the resin curing, in addition to increasing the viscosity of the adhesive. However, the addition of CMF allowed better distribution

of the adhesive in the wood, with less formation of clots of glue, which do not contribute to the adhesive bond, besides presenting the same penetration in the wood.

Gindl-Altmutter and Veigel [43] contend that the adhesive cure is not excessively prolonged due to the presence of nanocellulose. On the other hand, the severe increase of the viscosity caused by the addition of nanocellulose can represent a serious obstacle for resin spraying and impregnation in the wood. Cardoso et al. [16] have evaluated the addition of CNC produced without the neutralization of the surface charge on the UF glue mixture. They observed that acidic nanocellulose reduced the curing time of the UF resin. Cui et al. [21] produced CNF-reinforced particle boards in tannin-based adhesives. They observed increased gelatinization time and the viscosity of the glue mixture with the addition of CNF (1–3%).

Zhang et al. [123] modified the CNC with 3-aminopropyltriethoxysilane (APTES) and 3-methacryloxypropyltrimethoxysilane (MPS) and evaluated bond strength as well as formaldehyde emission from compensated panels. The results showed higher efficiency for modification with APTES, where 1.5% of modified CNC reduced formaldehyde emission by 53.2% and increased binding resistance by 23.6%, while for MPS modification, the results were 21.3 and 7.0%, respectively.

Ayrilmis et al. [8] used CMF produced from pine sawdust and evaluated the emission of volatile organic compounds (VOC) at different temperatures in LVL panels. The addition of CMF was efficient to reduce the emission up to 35 °C and could be used for furniture for internal use.

Hu et al. [50] have reported that hydrogen bonds between the –OH ends of nanocrystals promote an increase in the frequency and number of hydrogen bonds between UF-nanocrystalline cellulose (UF-CNC) and UF-CNC-wood. In addition, they also promote a higher frequency of the effective hydrogen bonds during the polymerization of the adhesive, allowing gains in resistance of the panels. An American patent [12] claims the use of only nanofibrillated cellulose as an adhesive for the production of particleboard panels. The advantages go beyond the non-emission of VOC, but also advantages in the carbon fixation by the trees producing cellulose used for CNF production.

5.2 Wood Composites with Nanocellulose-Reinforced Adhesives

Damásio et al. [23] have evaluated the addition of CNC in the glue mixture of formaldehyde urea glue. They have observed that the strength of the glue line of dry compaction panels increased with increasing percentage of CNC in the adhesive, where the maximum CNC addition (8%) resulted in an increase of 56% when compared to the control. This shows that the nanocrystals increase the wood-adhesive-wood bonding and interaction [50]. For wet strength, all additions increased this property in relation to the control, but the highest gain occurred with

the addition of 2% of nanocellulose. Eichhorn et al. [29] found significant gains when 5% of CNF was added to UF adhesive for the production of bonded joints. In another work, the addition of CNF from 0.5 to 5% UF resin allowed a significant gain in stress and strength until composite failure [29]. According to these authors, the UF adhesive belongs to a class of low-priced, widely used wood adhesives, which are well known for their pronounced fragility and their tendency to develop microcracks that limit their mechanical performance. In addition, the UF adhesive is less moisture-resistant due to the reduction of the molar ratio urea: formaldehyde, leaving free urea groups that bind to water molecules [42]. The addition of CNC contributed to the improvement of the two weaknesses of this type of adhesive, both the resistance of the glue line to the dry and its resistance to moisture [23].

Cardoso et al. [16] have evaluated the addition of CNC in the UF resin and observed a reduction in the swelling in thickness, compared to the panel produced with ammonium sulfate only. However, the water absorption was higher for the panels with the addition of nanocellulose.

Eichhorn et al. [29] have stated that the research group led by Wolfgang Gindl and Josef Keckes has been investigating the reinforcement of adhesives with nanocellulose. To this end, the group tested the addition of CMF and hardwood fibers as resin reinforcement. By adding 5% of untreated pulp fibers and found no significant effect on the value of shear strength of 9.9 MPa. In stark contrast, the addition of 5% nanocellulose, which resulted in a significant increase in shear strength to a value of 13.8 MPa. The researchers justify this increase in the absence of cracks commonly observed in UF glue lines. In addition, they claim that the improvement of the properties of UF resin can open doors to panels of structural uses.

The addition of 2% CNF (m/m) in tannin-based adhesives significantly have been found to improve the mechanical properties of the wood panels produced, since the water absorption did not change significantly [21]. In adhesives based on polyurethane or isocyanate, the CNF without chemical modification cannot be dispersed due to the high polarity. For addition of CNF in polyurethane-based resin Richter, et al. [94] did not find significant gains, while some others such as López-Suevos et al. [71] and Kaboorani et al. [57] have observed significantly improved binding strengths and durability of the panels by adding CNF and CNC.

In addition, the CNC increased the dry strength [57] and the CNC increased the resistance to wet and high temperature [71]. Cellulose nanofibrils obtained by high-pressure homogenizer mill added to the UF and melamine urea formaldehyde resins used in the production of agglomerate and OSB showed an increase in their mechanical properties. The improvement was significant mainly for OSB, not as pronounced for MDP [111]. However, in the case of physical properties, there was a reduction in swelling after 24 h in contact with water, and significantly increased internal bonding, flexural strength, and rupture, with the most significant results for OSB panels [111]. This result shows that the combination of larger particles with the enhanced MUF resin contributed to this significant gain. For the addition of CNC as reinforcement in lignin PF resins, Liu and collaborators [68] concluded that

the best properties of dry and wet tested glue lines occurred with the addition of 0.25–0.5% CNC.

New MDF panels produced by the addition of 1 and 3% nanocellulose produced from old MDF panels using 8 and 12% new fibers some promising results have been observed [102]. The results showed that values of the highest modulus of rupture (14.47 MPa) and modulus of elasticity (1359.09 MPa) for the panels produced with 12% of glue and 3% of nanocellulose, as well as the highest internal bond strength (0.5 MPa), the lowest swelling in thickness (4.72 and 9.86% after 2 and 24 h on water immersion) and the lowest water absorption (33.11 and 80.63% after 2 and 24 on water immersion).

In the production of particleboard panels and bonded sheet joints, Ferreira [31] has stated that due to the best adhesive and resistance properties observed in the particleboard panels prepared using 4% CNC added UF adhesive, these panels have already been used for applications in glue joints. But, the physical and mechanical results were inferior to those obtained for panels produced with commercial UF adhesive.

In addition to CNF as reinforcement in polyurethane adhesives and water-based polyvinyl acetate (PVAc) adhesives, the good rheological stability of the mixture without the CNF sedimentation after a long preparation time has been reported [94]. However, despite the increase in mechanical properties, the authors believed that new research applying the superficial chemical modification of the CNF should be performed to obtain improvements in properties and justify the industrial applications. Similarly, López-Suevos et al. [71] while producing CNF films with PVAc-latex have observed significant improvements in the storage modulus and thermal properties. Atta-Obeng [6] have found improved shear properties of MDP panels with the addition of MCC in the proportions of 0–10% in PF adhesives; however, the static bending strength was impaired. The authors believe that the presence of MCC resulted in a less pronounced spring back effect during hot-pressing. As pressure decreased, the authors have observed the spring effect occurred resulting in an increase in the thickness of the panel, less interaction of wood particles and adhesive, which resulted in the drop in static bending of the panels.

6 Final Considerations

Cellulose is considered the most abundant renewable polymer on the planet, has many advantages such as biodegradability and low cost and the products obtained from cellulose have wide application, especially in paper production. However, because it is a renewable and widely available resource, there is growing interest in the application of cellulose as an additive in activities with more advanced technologies that use nanotechnology for product development. Within the constant search for better performance of adhesives, the use of nanocelluloses appears as a viable option. The benefits of using nanocelluloses as reinforcements in adhesives

for the production of reconstituted wood panels include: the possibility of altering the properties of adhesives, gain in mechanical and physical properties of panels and reduction in formaldehyde emissions by panels using synthetic adhesives. However, despite all the advantages mentioned above, there are still some points to be considered. Therefore, it is concluded that more research needs to be done, either in the application of nanocellulose and its modification in different types of resin, as well as application technologies appropriate to the new conditions of the adhesives.

Acknowledgements At the outset, the authors express their sincere thanks to the Editors of the book (Inamuddin, Sabu Thomas, Raguendra Mishra and Abdullah M. Asiri), particularly Prof. Inamuddin for inviting us to contribute this Chapter. The authors place on record and appreciate the kind permission given by some of the authors (who have given permission to use their figures), M/s. Elsevier Inc Publishers, IN TECH d.o.o., Rijeka (Croatia), Iran Polymer and Petrochemical Institute with the scientific cooperation of Iran Polymer Society, Royal Society of Chemistry, UK, Chemical Retrieval on the Web (CROW), Springer and Wiley Publishers to reproduce some of the figures from their publications free of charges. One of the authors (KGS) would like to thank the PPIISR, Bangalore-India with whom he is associated with presently for their encouragement and interest in this collaboration.

References

1. Abdul KHPS, Tye YY, Leh CP et al (2018) Cellulose reinforced biodegradable polymer composite film for packaging applications. In: Jawaid M, Swain S (eds) *Bionanocomposites for packaging applications*. Springer, Cham, pp 49–64
2. Albino VCS, Mori FA, Mendes LM (2012) Influence of anatomical features and extractives content wood of *Eucalyptus grandis* w. hill ex maiden in quality bonding. *Cienc Florest* 22(4):803–811
3. Albuquerque CEC, Latorraca JV (2000) Anatomic features, influence in penetration and adhesion of adhesives. *Floresta Ambient* 7(1):158–166
4. Almeida VC (2009) Assessment of the potential for the use of tropical wood waste for the production of laterally glued panels—EGP. Federal University of Parana, Thesis
5. American Society for Testing and Materials (2006) ASTM D 5456: standard specification for evaluation of structural composite lumber products. ASTM, West Conshohocken
6. Atta-Obeng E (2011) Characterization of phenol formaldehyde adhesive and adhesive-wood particle composites reinforced with microcrystalline cellulose. Dissertation, Auburn University
7. Ayrimis N (2007) Effect of panel density on dimensional stability of medium and high density fiberboards. *J Mater Sci* 42:8551–8557
8. Ayrimis N, Lee Y-K, Kwon JH et al (2016) Formaldehyde Emission and VOCs from LVLs Produced with Three Grades of Urea-Formaldehyde Resin Modified with Nanocellulose. *Build Environ* 97:82–87
9. Baghersad S (2016) Coating os silk fabrics by PVA/Ciprofloxain HCl nanofibers for biomedical applications. *Iran J Polym Sci Tech* 29(2):171–184
10. Baldwin RF, Kurpiel FT, Baldwin RW (2017) Growth and reinvention 2017: a north american perspective on the global wood-based panel industry. *Forest Prod J* 67(3–4): 144–151
11. Bianche JJ (2014) Wood-adhesive interface and joints' resistance bonded with different adhesives and weight. Federal University of Viçosa, Thesis

12. Bilodeau MA, Bousfield DW (2015) Composite building products bound with cellulose nanofibers. Patent US 20,150,033,983 A1, 05 Feb 2015
13. Buligon EA (2015) Physical and mechanical properties of laminated veneer lumber reinforced gfrp. C FI 25(3):731–741
14. Campos CI (2005) Physical-mechanical properties of MDF produced with wood fibers from reforestation and alternative adhesives at different levels. University of São Paulo, Thesis
15. Candan Z, Akbulut T (2015) Physical and mechanical properties of nanoreinforced particleboard composites. *Maderas Cienc Tecnol* 17(2):319–334
16. Cardoso GV, Pereira FT, Ferreira ES et al (2016) Nanocellulose occmo urea-formaldehyde catalyst for the production of agglomerated panels of *Pinus* sp. In: Paper presented at the XV EBRAMEM—Brazilian meeting on timber and timber structures, Brazilian Institute of Wood and Wood, Curitiba, Structures, Curitiba, 9–11 Mar 2016
17. Carlquist S (2001) Comparative wood anatomy. Springer, Berlin
18. Carvalho MZ (2016) Multivariate approach to the behavior of physical-chemical properties and characterization of natural adhesives based on tannins. Federal University of Lavras, Thesis
19. Carvalho L, Martins J, Costa C (2010) Transport phenomena. In: Thoemen H, Irle M, Sernek M (eds) Wood-based panels: an introduction for specialists. Brunel University Press, London, pp 123–295
20. Costa TG (2016) Characterization of synthetic adhesives with addition of silica nanoparticles as reinforcing filler. Federal University of Lavras, Thesis
21. Cui J, Lu X, Zhou X et al (2014). Enhancement of mechanical strength of particleboard using environmentally friendly pine (*Pinus pinaster* L.) tannin adhesives with cellulose nanofibers. *Ann For Sci* 72(1):27–32
22. Cunha RCB (2016) Implementation of a method for measuring Gel Time of formaldehyde-based resins. Dissertation, Higher Institute of Engineering of Porto
23. Damásio RAP, Carvalho FJB, Carneiro ACO et al (2017) Effect of CNC interaction with urea-formaldehyde adhesive in bonded joints of *Eucalyptus* sp. *Sci For* 45(113):169–176
24. Diem H, Mathias G, Wagner RA (2012) Amino resins. Ullmann's Encyclopedia of Industrial Chemistry, Wiley-VCH, Weinheim
25. Din Z-U, Xiong H, Wang Z et al (2018) Effects of different emulsifiers on the bonding performance, freeze-thaw stability and retrogradation behavior of the resulting high amylose starch-based wood adhesive. *Colloids Surf A* 538(5):192–201
26. Ding X, Richter DL, Matuana LM et al (2011) Efficient one-pot synthesis and loading of self-assembled amphiphilic chitosan nanoparticles for low-leaching wood preservation. *Carbohydr Polym* 86:58–64
27. Ebnasajjad S, Landrock AH (2014) Adhesives technology handbook, 3rd edn. Elsevier, Amsterdã
28. Eckelman CA (1999) Brief survey of wood adhesives. Purdue University Cooperative Extension Service, West Lafayette
29. Eichhorn SJ, Dufresne A, Aranguren M et al (2010) Review: current international research into cellulose nanofibres and nanocomposites. *J Mater Sci* 45(1):1–33
30. Esteban L, Casasús AG, Oramas CP et al (2003) Wood and its anatomy. Fundación Conde de Valle de Salazar, Madrid
31. Ferreira JC (2017) Synthesis of urea-formaldehyde adhesives with the addition of kraft lignin and nanocrystalline cellulose. Federal University of Viçosa, Thesis
32. Fink J (2013) Reactive polymers Fundamentals and applications—a concise guide to industrial applications, 2nd edn. William Andrew, Norwich
33. Finnish Forest Industries Federation (2002) Handbook of finnish plywood. Kirjapaino Markprint Oy, Lahti
34. Fiorelli J (2002) Use of carbon fibers and glass fibers to reinforce wooden beams. Dissertation, São Paulo University
35. Food and Agriculture Organization (2018) Global production and trade of forest products in 2016. <http://www.fao.org/forestry/statistics/80938/en/> Accessed 12 Mar 2018

36. Forestry Products Laboratory (1999) Wood handbook—wood as an engineering material. General Technical Reports FPL-GTR-113. USDA, Forest Service, Madison
37. Forestry Products Laboratory (2010) Wood handbook—wood as an engineering material. General Technical Reports FPL-GTR-190. USDA, Forest Service, Madison
38. Forestry Products Laboratory (2012) Nanocelluloses: potential materials for advanced forest products. In: Proceedings of nanotechnology in wood composites symposium. General Technical Reports FPL-GTR-218. USDA, Forest Service, Madison
39. Fratzl P, Weinkamer R (2007) Nature's hierarchical materials. *Prog Mater Sci* 52(8):1263–1334
40. Fujisawa S, Okita Y, Fukuzumi H et al (2011) Preparation and characterization of TEMPO-oxidized cellulose nanofibrils films with free carboxyl groups. *Carbohydr Polym* 84(1):579–583
41. Gardziella A, Pilato LA, Knop A (2000) Phenolic resins: chemistry, applications, standardization, safety and ecology, 2nd edn. Springer, Heidelberg
42. Gavrilovic GI, Neskovic O, Diporovic MM et al (2010) Molar-mass distribution of urea-formaldehyde resins of different degrees of polymerisation by MALDI-TOF mass spectrometry. *J Serb Chem Soc* 75(5):689–99
43. Gindl-Altmutter W, Veigel S (2015) Nanocellulose-modified wood adhesives. In: Oksman K, Mathew AP, Bismarck A et al (eds) Handbook of green materials. World Scientific Publishing, Hackensack, pp 253–264
44. Gonçalves FG (2012) Agglomerated panels of *Acacia mangium* wood with urea-formaldehyde adhesives and powdered tannin of *Acacia mearnsii* bark. Rural Federal University of Rio de Janeiro, Thesis
45. Gonçalves FG, Leis RCC (2009) Properties of two synthetic resins after addition of Modified tannin. *Floresta Ambient* 12(2):01–07
46. Grigsby WJ, Thumm A (2012) The interactions between wax and UF resin in medium density fiberboard. *Eur J Wood Wood Prod* 70(4):507–517
47. Gupta R, Kandasubramanian B (2015) Hybrid caged nanostructure ablative composites of octaphenyl-POSS/RF as heat Shields. *RSC Adv* 5:8757–8769
48. Haubrich JL, Gonçalves C, Tonet A (2007) Vinyl adhesives present solutions for wood. *Rev Mad* 103:66–70
49. Hellmeister V (2017) OSB panel of raft wood residue (*Ochroma pyramidale*). University of São Paulo, Thesis
50. Hu K, Kulkarni DD, Choi I et al (2014) Graphene-polymer nanocomposites for structural and functional applications. *Prog Polym Sci* 39(11):1934–1972
51. International Agency for Research on Cancer (2006) Formaldehyde, 2-butoxyethanol and 1-tertbutoxypropan-2-ol. *IARC Monogr Eval Carcinog Risks Hum* 88:1–478
52. International Agency for Research on Cancer (2012) Chemical agents and related occupations: a review of human carcinogens. *IARC Monogr Eval Carcinog Risks Hum* 100:1–628
53. Irle M, Barbu C (2010) Wood-based panel technology. In: Thoemen H, Irle M, Sernek (eds) Wood-based panels: an introduction for specialists. Brunel University Press, London, pp 1–94
54. Iwakiri S (2005) Painéis de madeira reconstituída. *FUPEF, Curitiba*
55. Iwamoto S (2009) Elastic modulus of single cellulose microfibrils from tunicate measured by atomic force microscopy. *Biomacromol* 10(9):2571–2576
56. Jonoobi M, Mathew AP, Oksman K (2012) Producing low-cost cellulose nanofiber from sludge as new source of raw materials. *Ind Crops Prod* 40:232–238
57. Kaboorani A, Riedl B, Blanchet P et al (2012) Nanocrystalline cellulose (NCC): a renewable nano-material for polyvinyl acetate (PVA) adhesive. *Eur Polym J* 48(11):1829–1837
58. Khalili SMR, Jafarkarimi MH, Abdollahi MA (2009) Creep analysis of fibre reinforced adhesives in single lap joints-experimental study. *Int J Adhes Adhes* 29(6):656–661
59. Khalili SMR, Shokuhfar A, Hoseini SD et al (2008) Experimental study of the influence of adhesive reinforcement in lap joints for composite structures subjected to mechanical loads. *Int J Adhes Adhes* 28(8):436–444

60. Khedari J, Nankongnab N, Hirunlabh J et al (2004) New low-cost insulation particleboards from mixture of durian peel and coconut coir. *Build Environ* 39(1):59–65
61. Kim MG (2000) Examination of selected synthesis parameters for typical wood adhesive-type urea-formaldehyde resins by ^{13}C NMR spectroscopy. I. *J Appl Polym Sci* 75(10):1243–1254
62. Kinloch AJ (1987) *Adhesion and adhesives: science and technology*. Chapman & Hall, London
63. Kolakovic R, Peltonen L, Laaksonen T et al (2011) Spray-dried cellulose nanofibers as novel tablet excipient. *AAPS Pharm Sci Tech* 12(4):1366–1373
64. Lahiji RR, Xu X, Reifenger R, Raman A, Rudie A, Moon RJ (2010) Atomic Force Microscopy Characterization of Cellulose Nanocrystals. *Langmuir* 26(6):4480–4488
65. Lam F (2001) Modern structural wood products. *Prog Struct Eng Mat* 3(4):238–245
66. Lengowski EC (2016) Formation and characterization of films with nanocellulose. Federal University of Paraná, Thesis
67. Lima CKP, Mori FA, Mendes LM et al (2007) Anatomic and chemical characteristics of eucalyptus clones wood and its influence upon bonding. *Cerne* 13(2):123–129
68. Liu Z, Zhang Y, Wang X et al (2015) Reinforcement of lignin-based phenol-formaldehyde adhesive with nano-crystalline cellulose (NCC): curing behavior and bonding property of plywood. *Mater Sci Appl* 6:567–575
69. Liu Y, Laks P, Heiden P (2002) Controlled release of biocides in solid wood. II. Efficacy against *Trametes versicolor* and *Gloeophyllum trabeum* wood decay fungi. *J Appl Polym Sci* 86(3):608–614
70. Lubis MAR, Hong MK, Park BD (2017) Hydrolytic removal of cured urea–formaldehyde resins in medium-density fiberboard for recycling. *J Wood Chem Technol*. <https://doi.org/10.1080/02773813.2017.1316741>
71. López-Suevos F, Eyholzer C, Bordenau N et al (2010) DMA analysis and wood bonding of PVAc latex reinforced with cellulose nanofibrils. *Cellulose* 17(2):387–398
72. Mahrtdt E, Pinkl S, Schmidberger C et al (2016) Effect of addition of microfibrillated cellulose to Ureaformaldehyde on selected adhesive characteristics and distribution in particle board. *Cellulose* 23(1):571–580
73. Meng Q-X, Zhu G-Q, Yu M-M et al (2018) The effect of thickness on plywood vertical fire spread. *Procedia Eng* 211:555–564
74. Messmer A (2015) Life cycle assessment (LCA) of adhesives used in wood constructions. Master thesis (Ecological System Design), Swiss Federal Institute of Technology Zurich, Swiss, Zurich p 82
75. Molina JC, Calil Neto C, Calil Junior C et al (2013) Evaluation of the behavior of rectangular beams (LVL) with horizontal and vertical lamination. *Mad Arq Eng* 14(35):1–13
76. Mondragon G, Peña-Rodriguez C, Gonzáles A et al (2015) Bionanocomposites based on gelatin matrix and nanocellulose. *Eur Polym J* 62:1–9
77. Motta JP, Oliveira JTS, Alves RC (2012) Influence of moisture content on the adhesion properties of eucalyptus wood. *Construindo* 4(2):96–103
78. National Institute of Industrial Research (2017) *The complete technology book on wood and its derivatives*. NIIR, Delhi
79. Nelson K, Restina T, Iakovlev M et al (2016) American process: production of low cost nanocellulose for renewable, advanced materials applications. In: Madsen L, Svedberg E (eds) *Materials research for manufacturing*. Springer Series in Materials Science, vol 224. Springer, Cham
80. Nguyen DM, Grillet A-C, Diep TMH et al (2018) Influence of thermo-pressing conditions on insulation materials from bamboo fibers and proteins based bone glue. *Ind Crops Prod* 111:834–845
81. Nitthiyah A (2013) Optimization and characterization of melamine urea formaldehyde (MUF) based adhesive with waste rubber powder (WRP) as filler. University Malaysia Pahang, Thesis

82. Olorunnisola AO (2018) Design of wood connections. In: Olorunnisola AO (ed) Design of structural elements with tropical hardwoods. Springer, Berlin, pp 209–236
83. Ozarska B (1999) A review of the utilization of hardwoods for LVL. *Wood Sci Technol* 33(4):341–351
84. Park B-D, Kang E-C, Park S-B et al (2011) Empirical correlations between test methods of measuring formaldehyde emission of plywood, particleboard and medium density fiberboard. *Eur J Wood Wood Prod* 69(2):311–316
85. Périchaud AA, Isakakov RM, Kurbatov A et al (2012) Auto-repair of polyimide film coatings for aerospace applications challenges and perspectives. In: Abadie MJM (ed) High performance polymers—polyimides based—from chemistry to applications. InTech, London, pp 215–244
86. Pervan D (2018) Mechanical locking system for panels and method of installing same. US Patent 2018/0,030,738 A1, 1 Feb 2018
87. Peschel P, Hornhardy E, Nennowitz I et al (2016) Tabellenbuch Holztechnik. Europa-Lehrmittel Nourney, Vollmer GmbH & Co. KG, Haan
88. Petrie EW (2000) Handbook of adhesives and sealants, 2nd edn. McGraw-Hill, New York
89. Pizzi A (2015) Synthetic adhesives for wood panels: chemistry and technology. In: Mittal KL (ed) Progress in adhesion and adhesives. Wiley, Hoboken, pp 85–126
90. Polymer Properties Database (2015) Melamine-formaldehyde resins. <http://polymerdatabase.com/polymer%20classes/MelamineFormaldehyde%20type.html>. Accessed 30 Mar 2018
91. Prolongo SG, Gude MR, Ureña A (2009) Synthesis and characterisation of epoxy resins reinforced with carbon nanotubes and nanofibers. *J Nanosci Nanotechnol* 9(10):6181–6187
92. Prolongo SG, Gude MR, Ureña A (2010) Rheological behaviour of nanoreinforced epoxy adhesives of low electrical resistivity for joining carbon fiber/epoxy laminates. *J Adhes Sci Technol* 24(6):1097–1112
93. Ramage MH, Burrige H, Busse-Wicher M et al (2017) The wood from the trees: the use of timber in construction. *Renew Sustain Energy Rev* 68:333–359
94. Richter K, Bordeanu N, López-Suevos F et al (2009) Performance of cellulose nanofibrils in wood adhesives. In: Schindel-Bidinelli E (ed) Proceedings of the Swiss bonding. Rapperswil-Jona, Switzerland, pp 239–246
95. Risholm-Sundman M, Larsen A, Vestin E et al (2007) Formaldehyde emission—comparison of different standard methods. *Atmospheric Environ* 41(15):3193–3202
96. Rojas J, Bedoya M, Ciro Y (2015) Current trends in the production of cellulose nanoparticles and nanocomposites for biomedical applications. In: Polletto M (ed) Cellulose—fundamental aspects and current trends. InTech, Rijeka, pp 193–228
97. Rumble JR (2018) CRC handbook of chemistry and physics, 98th edn. CRC Press, Boca Raton
98. Salajková M, Berglund LA, Zhou Q (2012) Hydrophobic cellulose nanocrystals modified with quaternary ammonium salts. *J Mater Chem* 22(37):19798–19805
99. Samyn P, Barhoum A, Öhlund T et al (2018) Review: nanoparticles and nanostructured materials in papermaking. *J Mater Sci* 53(1):146–184
100. Schultz J, Nardin M (2003) Theories and mechanisms of adhesion. In: Pizzi A, Mittal KL (eds) Handbook of adhesive technology. Marcel Dekker, New York, pp 61–75
101. Sehaqui H, Allais M, Zhou Q et al (2011) Wood cellulose biocomposites with fibrous structures at micro- and nanoscale. *Compos Sci Technol* 71(3):382–387
102. Sheykhi ZH, Tabarsa T, Mashkour M (2016) Effects of nano-cellulose and resin on MDF properties produced from recycled mdf using electrolise method. *J Wood Forest Sci Technol* 23(3):271–288
103. Singh A, Dawson B, Rickard C et al (2008) Light, confocal and scanning electron microscopy of wood-adhesive interface. *Microsc Anal* 22(3):5–8
104. Song J, Chen C, Zhu S et al (2018) Processing bulk natural wood into a high-performance structural material. *Nature* 554:224–228

105. Syverud K, Chinga-Carrasco G, Toledo J et al (2011) A comparative study of *Eucalyptus* and *Pinus radiata* pulp fibres as raw materials for production of cellulose nanofibrils. *Carbohydr Polym* 84(3):1033–1038
106. Tanpichai S, Quero F, Nogi M et al (2012) Effective young's modulus of bacterial and microfibrillated cellulose fibrils in fibrous networks. *Biomacromol* 13(5):1340–1349
107. Thoemen H, Irle M, Sernek M (eds) (2010) *Wood-based panels: an introduction for specialists*. Brunel University Press, London
108. Toquarto S (2002) *Random heterogeneous materials*. Springer, Berlin
109. Turbak AF, Snyder FW, Sandberg KR (1983) Microfibrillated cellulose, a new cellulose product: Properties, uses and commercial potential. *J Appl Polym Sci: Appl Polym Symp* 37:815–827
110. Urbinati CV (2013) Influence of anatomical characteristics on cast joints of *Schizobolium parayba* var. Amazonicum (hyber ex. Ducke) barneby (Paricá). Thesis, Federal University of Lavras
111. Veigel S, Rathke J, Weigl M et al (2012) Particle board and oriented strand board prepared with nanocellulose-reinforced adhesive. *J Nanomater*. <https://doi.org/10.1155/2012/158503>
112. Veronez D, Farias ELP, Fraga R et al (2010) Potential for occupational health risk for those teachers, researchers and technical workers of anatomy who are exposed to formaldehyde. *InterfacEHS* 5(2):63–76
113. Wang XM, Casilla R, Zhang Y et al (2016) Effect of extreme pH on bond durability of selected structural wood adhesives. *Wood Fiber Sci* 48(4):1–15
114. Wang X, Huang Z, Cooper P et al (2010) The ability of wood to buffer highly acidic and alkaline adhesives. *Wood Fiber Sci* 42(3):398–405
115. Wang X, Huang Z, Cooper P et al (2013) Effects of pH on lap-shear strength for aspen veneer. *Wood Fiber Sci* 45(3):294–302
116. Wegner T, Skog KE, Ince PJ et al (2010) Uses and desirable properties of wood in the 21st century. *J Forest* 108(4):165–173
117. Xu X, Yao F, Wu Q et al (2009) The influence of wax-sizing on dimension stability and mechanical properties of bagasse particleboard. *Industrial Crops Produ* 29(1):80–85
118. Yoon SH, Kim BC, Lee KH et al (2010) Improvement of the adhesive fracture toughness of bonded aluminum joints using e-glass fibers at cryogenic temperature. *J Adhes Sci Technol* 24(2):429–444
119. Yuce B, Mastrocinque E, Packianather MS et al (2014) Neural network design and feature selection using principal component analysis and Taguchi method for identifying wood veneer defects. *Produm Manufac Res* 2(1):291–308
120. Zeni M, Favero D, Pacheci K et al (2015) Preparation of microcellulose (Mcc) and nanocellulose (Ncc) from eucalyptus kraft ssp pulp. *Polym Sci* 1:1–5
121. Zeppenfeld G, Grunwald D (2005) *Klebstoffe in der Holz-und Möbelindustrie*. DRW-Verlag, Weinbrenner
122. Zhang Y, You B, Huang H et al (2008) Preparation of nanosilica reinforced waterborne silylated polyether adhesive with high shear strength. *J Appl Polym Sci* 109(4):2434–2441
123. Zhang H, Zhang J, Song S et al (2011) Modified nanocrystalline cellulose from two kinds of modifiers used for improving formaldehyde emission and bonding strength of urea-formaldehyde resin adhesive. *BioResources* 6:4430–4438
124. Zhong Y, Jing X, Wang S et al (2016) Behavior investigation of phenolic hydroxyl groups during the pyrolysis of cured phenolic resin via molecular dynamics simulation. *Polym Degrad Stab* 125:97–104
125. Zhou J, Chen J, He M et al (2016) Cellulose acetate ultrafiltration membranes reinforced by cellulose nanocrystals: preparation and characterization. *J Appl Polym Sci* 133(39):1–7. <https://doi.org/10.1002/app.43946>

Nanocellulose in the Paper Making



**Elaine Cristina Lengowski, Eraldo Antonio Bonfatti Júnior,
Marina Mieko Nishidate Kumode, Mayara Elita Carneiro
and Kestur Gundappa Satyanarayana**

1 Introduction

Paper has been defined as a material having two dimensions, which is produced from an aqueous suspension of fibers, which in turn are ‘artificially interlaced and subsequently dewatered through mechanical and thermal processes’ [79]. It may be noted that the art of producing paper began more than two millennia ago due to the dire need felt at that time to communicate and record the discoveries in materials

E. C. Lengowski

Faculty of Forestry Engineering, Federal University of Mato Grosso (UFMT),
Fernando Corrêa da Costa St, 2367, Boa Esperança, Cuiabá, MT 78068-600, Brazil
e-mail: elainelengowski@gmail.com

E. A. Bonfatti Júnior · M. E. Carneiro

Department of Forest Engineering and Technology (DETF), Federal University
of Paraná (UFPR), Av. Prof. Lothário Meissner, 632, Jardim Botânico, Curitiba,
PR 80.210-170, Brazil
e-mail: bonfattieraldo@gmail.com

M. E. Carneiro

e-mail: mayaraecarneiro@gmail.com

M. M. N. Kumode

Laboratory of Wood, Pontifical Catholic University, Curitiba, PR, Brazil
e-mail: mnishidate@gmail.com

K. G. Satyanarayana

PIPE & Department of Chemistry, Federal University of Parana, Curitiba, Brazil

K. G. Satyanarayana (✉)

Poornaprajna Scientific Research Institute (PPISR), Sy. No. 167, Poornaprajnapura,
Bidalur Post, Devanahalli, Bangalore 562 110, Karnataka, India
e-mail: gundsat42@hotmail.com

© Springer Nature Switzerland AG 2019

Inamuddin et al. (eds.), *Sustainable Polymer Composites and Nanocomposites*,
https://doi.org/10.1007/978-3-030-05399-4_36

1027

that can be transported [53]. Of course, today the paper is being used for a lot of diverse uses, which include printing, hygiene, writing, and packaging.

In a simplified way, modern paper production can be divided into three stages: pulping, bleaching of the pulp and the production of the paper itself. It is possible to disregard the bleaching of the pulp while producing brown pulp, which will be used for papers of packaging applications. One of the earliest milestones for the industrial production of cellulosic pulp was the development of the Kraft process in 1879 [63], starting from this, the paper industry has consistently sought to improve the quality of the paper.

It is interesting to note that like in many fields, the paper industry is characterized by investing a lot in research and development. This includes research in search of new raw materials of the high industrial profile, modification and additives for the Kraft process, reduction or non-use of chlorine compounds in bleaching and, more recently, biorefinery. Van Heiningen [167] defines the term 'biorefinery' as an industry that transforms raw materials from renewable sources, such as sugarcane bagasse, wood, forest residues and black liquor into higher value-added products such as biofuels and biomaterials. In this sense obtaining nanocellulose from biomaterials for the most diverse commercial applications fits very well in this concept.

In fact, the credit goes to Wegner et al. [180], who put the use of nanotechnologies in the forest-based industry as one of the main novelties to be developed in the 21st century. Besides, they also suggested two paths for the application of nanotechnology to forest producers, viz., the first path is for nanotechnologies and nanomaterials developed in other industrial sectors to be adopted and deployed in materials, processes, and products used or produced by the forest-based industry. The second path is the development of completely new materials or product platforms using nanoscale structures and properties derived from wood. Although it was still unknown about the exact economic impacts and opportunities for wood as nanomaterials, but it was expected that all nanomaterials and nano-enabled products would grow to exceed one trillion dollars per annum as technology would be developed in the 21st century [64].

While in the last few decades, traditional uses of paper have been found to decline, other new avenues have opened up during the last decades or so. These include incorporation of nanotechnology since the 1990s into papermaking leading to lower energy costs, development of low-cost products with improved paper quality, biocompatible and flexible with sophisticated functionalities [17, 133]. It may not be exaggerating to state that the use of nanotechnology makes it possible to improve the sustainability of paper making processes for the following reasons:

- More efficient use of resources whereby more resistant papers can be formed with the smaller amount of fibers (by weight);
- Use of secondary materials such as recycled fibers or fibers with inferior properties, which can be converted into nanofibers and used as additives in papermaking, or produce high-quality papers using secondary fibers with the addition of nanofibers;

- Development of new materials such as papers with unique properties, such as films with plastic characteristics, good barrier properties for smart packaging, etc.

Considering the above and published reports on the preparation, characterization and various applications of nanomaterials in general and nanocellulose in particular and the latter's use in paper making, this Chapter will present characteristics of the most used wood in the world for pulp and paper production, main methods of obtaining cellulose in nature, process of bleaching of pulp, paper making, processes to obtain different types of nanocellulose (microfibrillar, nanofiber and cellulose nanocrystals), applications of nanocellulose in the paper making, applications of nanocellulose in paper making through coating and films as well as by nanocellulose-reinforced pulp and the resulting effects of the use of nanocellulose in paper production. The Chapter will also present marketing aspects and possible future opportunities and finally concluding remarks.

2 Wood for Pulp and Paper Production

Although a variety of woods are available, only certain types are used in the paper industry. The basic wood density is considered the most important parameter in its quality evaluation since it has a strong relationship with the other wood properties [61]. Besides, it has a strong effect on the variables of the pulping process and the characteristics of paper pulp [138]. This property is defined by the ratio of the absolute dry weight of the wood to its fully saturated volume. The ideal types of cellulosic pulps for papers for printing and writing and for absorbent papers have been distinguished [134]. According to these authors, the most required criteria for printing and writing papers are lower energy consumption in the mechanical refining, greater specific volume and greater opacity. On the other hand, high capacity for water absorption and increased softness are important in the case of manufacturing of absorbent papers. The authors further state that pulps originating from wood with lower basic densities are ideal for the production of the first type of paper since they have fibers with a smaller thickness and smaller mass per length. For the second type of paper, pulps from denser woods are suitable, because these woods possess fibers with higher thickness than the low-density woods and therefore these would present the greater potential of liquid absorption, and greater mass per length of fibers.

In hardwoods, penetration of liquids occurs rapidly through the vessels, but penetration in the transverse direction practically does not exist. This is because of the fact that the pit membranes of the punctures (Depressions in the secondary cell wall is called 'pit') prevent the passage of the cooking liquor (This is a mixture of chemical reagents- $\text{NaOH} + \text{Na}_2\text{S}$). It may be noted that in the case of softwood the penetration of the cooking liquor already occurs through the tracheids cells that, unlike the cellular elements of the hardwoods and therefore have good permeability,

even in the transverse direction [166]. Considering the dimensions of the chips, it is emphasized that the thickness should be in the range of 4–6 mm, in different sizes so that both impregnation and diffusion are compromised and, consequently, the delignification rate is decreased [103]. The wood is chemically constituted by polymers that perform the structural functions. These are cellulose, hemicelluloses, and lignins [49]. In addition to these structural components present in wood, there are other constituents, which include starches, proteins, pectins beside other substances soluble in water or other organic solvents called extractives or accidental compounds of wood. From the chemical point of view, the amount and type of lignin directly interfere with the conditions of the pulping process. In general, lignin is classified according to the relative amount of the monomers guaiacila (G), syringyl (S) and p-hydroxyphenyl (H), derived from coniferyl, synapyl and p-coumarilic alcohols respectively. Structures of these are shown in Fig. 1.

In the *Eucalyptus* wood, lignin is generally formed by the siringila and guaiacila units (SG lignin), while in conifers it is formed by units guaiacila and p-hydroxyphenyl (lignin GH) [15, 49]. The syringyl/guaiac ratio (S/G) significantly affects the degradation and solubilization of lignin from hardwoods, to the point that increasing this ratio allows the use of a lower alkali load, resulting in higher yields [60].

With fibrous structure and length between 2 and 5 mm, the cellulose originated from the conifers, such as species of the genus *Pinus*, is called ‘long fiber pulp’ and has application in the papers that demand greater resistance, as is the case of paper used in the manufacture of packaging. On the other hand, the short-fiber pulp can range from 0.5 to 2 mm and is produced from hardwoods, such as *Eucalyptus*, *Acacia*, *Propulos* and *Betula*, and is used for the production of printing and writing papers and tissue paper for sanitary purposes. Table 1 presents the technological characteristics of the main forest species planted in the world for pulp and paper production.

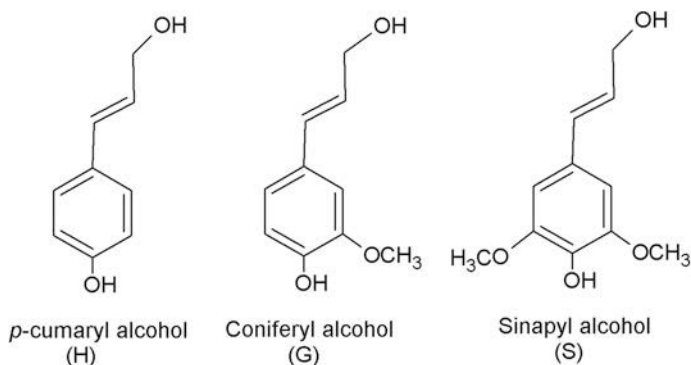


Fig. 1 Precursor alcohols of the phenylpropane units’ p-hydroxyphenyl (H), guaiacyl (G) and syringyl (S). Reproduced from Barbosa et al. [15] with the kind permission of the publishers

Table 1 Characteristics of the most used wood in the world for pulp and paper production

Type of wood	Species	Location	A	BD	TE	TL	HL
Hardwoods [137]	<i>E. grandis</i> x <i>E. urophylla</i>	Brazil	6	0.47	3.1	28.1	68.9
	<i>Eucalyptus globules</i>	Chile	12	0.63	5.6	25.9	68.5
	<i>Eucalyptus nitens</i>	Chile	12	0.52	4.5	27.1	68.4
	<i>Acacia mangiun</i>	Indonesia	6	0.52	5.2	28.0	66.8
	<i>Acacia crassicarpa</i>	Indonesia	6	0.57	4.1	29.4	66.5
	<i>Populus tremuloides</i>	Canada	55	0.37	6.9	22.1	71.0
	<i>Betula pendula</i>	Finland	67	0.50	4.8	17.4	77.8
Softwood [171]	<i>Pinus taeda</i>	Brazil	21	0.43	2.8	26.7	70.5
	<i>Pinus silvestris</i>	Finland	45	0.43	6.4	25.6	68.0

A age in years; BD basic density in $\text{g}\cdot\text{cm}^{-3}$, TE total extractives in %; TL total lignin in %; HL holocelullose content in %

3 Paper Making

3.1 Pulping

The production of cellulosic pulp can occur from processes that use different types of energies, viz., mechanical, thermal and chemical or the combination of these. Despite the great diversity of these pulping processes, the alkaline ones have become the main ones used extensively. With a well known and most used worldwide the ‘Kraft’ process, developed by the German chemist Carl F. Dahl in 1879 [63] and patented in 1884 [150], it is reported that today 90% of the whole cellulose pulp produced in the world comes from this process [111]. The Kraft process was the result of the evolution of the soda process and aimed at dissolving the middle lamella by means of the removal of lignin with consequent individualization of the wood fibers. For this purpose, the wood chips are placed in a digester that is pressurized with the alkaline cooking liquor (NaOH and Na_2S). The hegemony of its use stems from its advantages over other processes and this process is adaptable to different types of lignocellulosic materials, producing high-quality pulp and of high bleachability with high efficiency of recovery of chemical reagents and energy.

It is interesting to note that the increase in the rate of delignification and yield are opposite to each other. This is because the reagents used in the pulping processes are not specific for lignin removal; they also remove carbohydrates, which contribute to a reduction in yield [150]. Advantages, the Kraft process demands precise control of its parameters. There are several parameters that affect the delignification rate, the most important are: type of wood, chip quality, alkaline load, cooking time and temperature.

The impregnation of the cooking liquor in the chips aims to distribute the cooking liquor evenly into the wood [184]. The impregnation consists of two different phases: pore penetration and diffusion [84]. These phases are very

important for the efficiency of delignification and are directly related to the quality of wood and chip size.

In pulp obtained by chemical processes, the degree of delignification of the pulp is measured by the kappa number, which expresses the residual lignin present in the pulp after cooking [161] and is dependent on the alkaline load, cooking time and temperature. The alkaline charge is applied proportionally to the amount of wood in the digester by seeking a predetermined target kappa number. According to Almeida [7], the increase of alkaline charge leads to greater delignification with consequent reduction of the kappa number. However, greater delignification promotes the greater generation of fines, possibly resulting from the fragmentation of fibers. Time and temperature have been combined into a single control parameter called ‘H factor’, which represents the extent of the reaction [172]. Even though different temperatures can be used, delignification can be estimated accurately by ‘H factor’, provided that the other parameters of the pulping process remain constant. According to Sixta [148] the ‘H factor’ is defined as follows:

$$H = \int_{t_0}^t k_L \cdot dt$$

where k_L is the relative reaction velocity of the pulp. Assuming that the activation energy of the reaction is $134 \text{ kJ} \cdot \text{mol}^{-1}$, the H-factor can be expressed as:

$$H = \int_{t_0}^t \frac{k_{L(T)}}{k_{100^\circ\text{C}}} \cdot dt = \int_{t_0}^t \text{Exp} \cdot \left(43.19 - \frac{16113}{T} \right) \cdot dt$$

where t is time and T is temperature, the above equation is valid for temperatures above 100°C .

According to Sixta [148], the H factor is the area under the relative reaction velocity curve versus time. This parameter is designed to predict the temperature or cooking time required to reach a given kappa number. The result is valid only when the other cooking conditions, such as the effective alkali concentration and the ratio of liquor to wood, remain constant [148]. Figure 2 shows a graph of a conventional Kraft cooking having a maximum temperature of 170°C , the heating time of 80 min and time of 60 min at a constant temperature, culminating at an H factor of 1100.

H-factor is a useful process control tool for Kraft pulp industries. Even the most modern plants use this parameter to control the degree of delignification of the pulp [136].

3.2 Bleaching

This process follows the previous one. It should be noted that the pulp obtained as explained in the previous Section is so intense without the modification, which compromises the mechanical strength of the fiber. Accordingly, bleaching process,

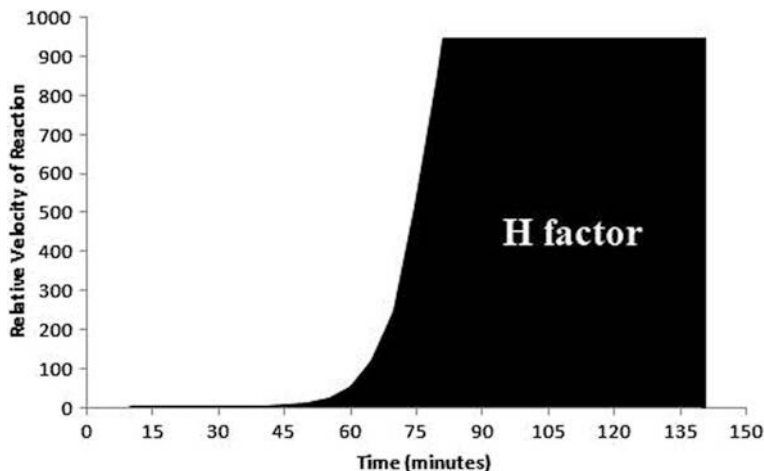


Fig. 2 H-factor plot of a conventional Kraft cooking. Eraldo Antonio Bonfatti Jr. unpublished

which is a chemical process that aims to improve the brightness and cleanliness of cellulosic pulp by removing and/or modifying chromophore and leukoprophoric groups are used [55, 72]. After the reactions with the cooking liquor, the lignin in the wood, which is almost colourless, is coloured due to the release of chromophoric groups [55, 72]. Bleaching generally occurs in stages and its progress is always followed by brightness, which is a measure of reflectance of visible blue light at the wavelength of 457 nm, of pulp sheets or paper under standard conditions [31]. The most used method to measure this process is the standard described by ISO 2470: 1999—Paper, board, and pulps. It may be noted that measurement of diffuse blue reflectance factor is expressed in % ISO, while the non-reflective material, absolute black, has a brightness of 0% and a perfect reflectance of light is considered 100%.

Over the years the bleaching chemistry has been changing rapidly, starting with the discovery of bleaching power of chlorine on vegetable fibers, being used in its elemental form (chlorination, C), as calcium hypochlorite (hypochlorination, H) and as chlorine dioxide (dioxidation, D). Table 2 shows the evolution of bleaching sequences over the years. However in the 1990s, due to environmental reasons, the industries had to develop chlorine-free bleaching sequences or sodium hypochlorite [31], as these compounds are the main contributors to the formation of chlorinated organic compounds (Absorbable Organic Halides, AOX) [22]. After this environmental concern, elemental chlorine free (ECF = elemental chlorine free) sequences were created, which is the main technology used today, and totally chlorine free (TCF) sequences, which do not use elemental chlorine or any other chemical reagent that contain chlorine in the molecule. At this stage, oxygen (oxygenation, O), caustic soda (alkaline extraction, E), hydrogen peroxide (peroxidation, P) and ozone (ozonolysis, Z) associated with chelation (Q) and acid hydrolysis (A) are the most commonly used in industries.

Table 2 Historical evolution of bleaching sequences (Prepared by authors using the information from [9, 149])

Time	With element chlorine	ECF	TCF
1880	H		
1910	HEH		
1930	CEH, CEHEH		
1950	CEHDED, CEDED		
1960	(CD)EHDED		
1970	CD(EP)HD(EP)D, OC/DEDED		
1980	O(CD)(EP)D(EP)D, OC/DEODD, OC/D (EO)DD	O/OD(EPO)D(D)	
1985	O(DC)(EO)D(EP)D	O/OD(EPO) _N D, O/OA/ D(EPO) _N D, O/ OD _{HOT} (EPO)-D _N D	
1990	O(DC)(EPO)D(EP) D	O/OA/D(EOP)DP	
1995			O/OZ/QPZ/QP, O/OQPQP, O/OQ (PAA)QP, O/OQZQP, O/ OQZQP, O/OAZPZP
2000		O/OD(EPO)D(EP)D, O/ AO/D(EPO)D	
2005		O/OZQD(EPO)D, O/AO/ D(EPO)D, O/OD(EPO)D (D)	
2010		O/OA(EOP)DP	

ECF elemental chlorine free, *TCF* totally chlorine free

The choice of the bleaching sequence will depend on the kappa number after cooking, the type of raw material used in the pulping process, the end use of the bleached pulp and the desired final brightness. As the bleached pulps present on the market have an average brightness of 90% ISO.

3.3 *Drying*

After bleaching, the cellulosic pulp will be in aqueous suspension, with a consistency of 10–12%. This needs to be transformed, into cellulose bales with final humidity of 10% for the purposes of commercialization and transportation. It may be noted that this step of drying the bleached pulp is the final stage of the manufacturing process of the bleached cellulosic pulp. The process consists of the wet process step followed by the forming step, where the cellulose sheets are formed

and finally, the dewatering step. The gradual removal of water happens through the use of force of gravity, heating, and vacuum. It should be noted that in these steps the pulp is arranged on a permeable forming screen which is also responsible for conducting the pulp along the dryer [48]. The final step of drying the pulp is the removal of the water by the compressor rolls in the pressing step, with water not being withdrawn in the forming step would be removed. Then, a stronger pulp sheet is cut, packed and finally transported.

3.4 Paper Production

3.4.1 Preparation of the Cellulosic Pulp

It may be noted that when there is the production of integrated pulp and paper, the cellulosic pulp will be transported by piping. In pulp industries, which are separate from that of paper, it is necessary to dry the cellulosic pulp to make the transport for the paper mill. Therefore, if the paper mill is integrated with the pulp mill (normally, both paper and pulp are produced using the same mill), the drying step described above does not happen. In that case, the wet cellulosic pulp is pumped through pipes until the production of paper. If there is no integration between the pulp mill and paper mill, the pulp bales will remain dry and packaged for paper production. The first stage of paper production is the mass preparation. At this stage, for non-integrated paper mills, the cellulose bales are placed in the hydropulper to be disaggregated and reduce the consistency of the mass. In the case of the integrated industries the cellulose used is already moist and are ready for the next stage, i.e., refining. This is a mechanical treatment in which cellulose pulp fibers are broken into fibrils, thus increasing the surface area and, consequently, the binding capacity between the fibers allowing the formation of a strong network [157]. In this way, the refining allows changing the structure of the fibers of the pulp, resulting in modified properties and increasing the mechanical properties of the finished paper. Figure 3 shows the scanning electron micrograph of the refined bleached cellulosic fibers obtained from *Eucalyptus* wood by one of the authors.

In addition, the energy used in refining causes changes in the fibers, leaving them more prone to collapse during the paper forming process, thereby decreasing the thickness and specific volume of formed sheet. However, refining should not be excessive as it can damage the fibers to the point of reducing the same mechanical properties that have been expected to improve the refining process. It has been recommended that when searching for high brightness pulps, it is necessary to avoid excess during the mechanical refining, as this causes a decrease in the brightness and opacity of the paper [101]. The degree of refining is measured through the Schopper-Riegler grade of drainage, which indicates the ease of the pulp in water shoring and is an important parameter for the evaluation of fiber interweaving—the greater the drainage of the pulp, the lower its capacity to drain water. The most widely used method for determining drainage is described by ISO

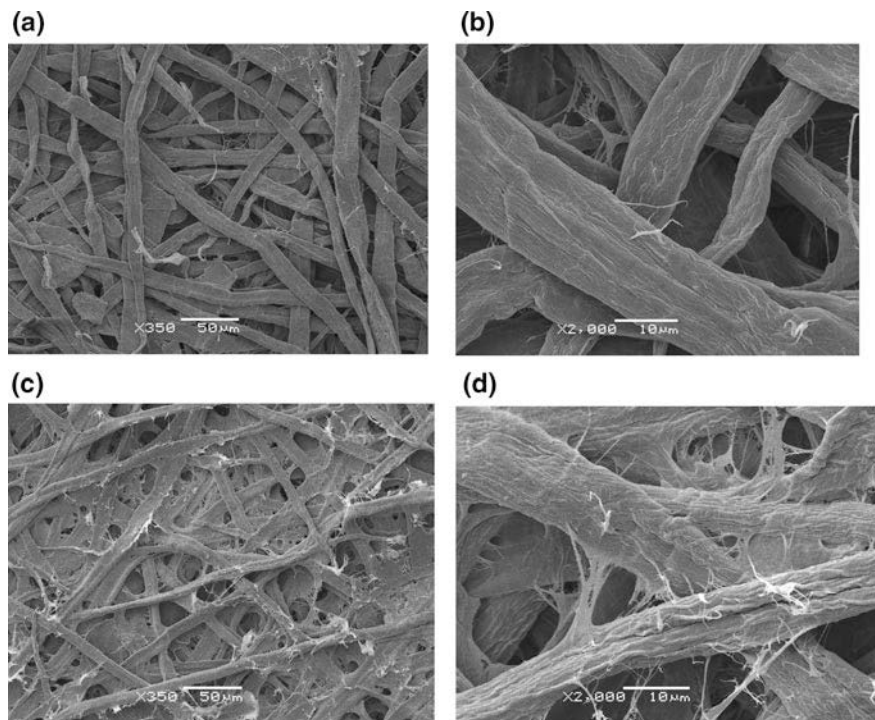


Fig. 3 Surface of a sheet formed by fibers: **a, b**—without refining at two magnifications; **c, d**—with refined fibers at two magnifications as of (**a, b**). Eraldo Antonio Bonfatti Jr—unpublished

5267-1: 1999—Pulps—Determination of drainability—Part 1: Schopper-Riegler method. In order to reach the desired degree of refining, the mass passes through the purification process. This step is aimed at reducing cellulose pulp contamination, and impurities such as plastics, metals, and sand are removed [66] followed by cleaning of pulp to prepare the dough.

In the preparation of the mass, the other components of the paper-making process are added (chemical additives) to improve the mechanical, physical and optical properties of paper as is followed normally in the paper industry [52]. Among the products that may be employed are starches, mineral compounds, vegetable gums, carboxymethylcellulose (CMC) and synthetic polymers [52, 141]. Recently nanocelluloses have also been used as additives in paper production [175].

3.4.2 The Paper Machine

A paper machine consists of different mechanical sections, each of them driven by one motor or an arrangement of one master motor and one or more helping drives, which conventionally speed or torque regulated. Typical sections are represented by

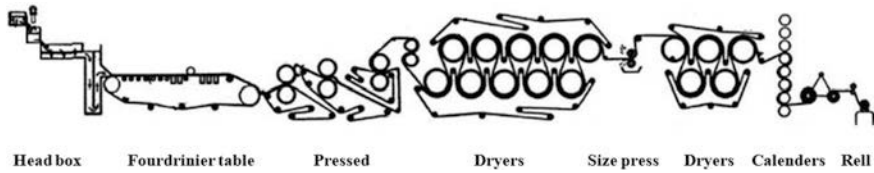


Fig. 4 A schematic drawing of a fourdrinier paper machine. Adapted from Lai [87] with the kind permission from publishers

fourdrinier, press, dryer, calender, and reel [48, 168]. A schematic drawing of a fourdrinier paper machine is shown in Fig. 4.

With the recipe of ready-made paper, the mass is transferred to the head box of the paper machine, where a uniform jet of mass is cast on a constantly moving conveyor belt forming screen flame [48]. At this stage, the first control of the paper thickness takes place; more the dough, the thicker would be the paper. The mass thrown on the mat forms a 5% layer of cellulose and additives and 95% water with water being drawn on the flat table. This stage of the process, known as ‘leaf formation’, promotes fiber entanglement and gradual water drainage, giving sufficient strength to the paper, so that it can leave the flat table and run through the various cylinders that make up the rest of the process [150].

In this part of the process, the paper passes through hydraulic presses wherein the excess water is removed, increasing the resistance and reducing the thickness of the paper [48, 150]. With the above process steps, the more resistant the paper reaches the drying step, which is promoted by a series of steam-heated cylinders; water would get evaporated from the pressed sheet, leaving it with the required moisture content for its final application [48]. Upon reaching required moisture content, the paper will receive one more layer of the surface additive according to its final use, and after another drying step, it will proceed to the calendar, which will have uniform thickness together with a better surface finish [48]. After this step, the paper is wound in smaller reels and can be commercialized, both in reels and in the form of sheets of sizes standardized for the final consumer.

4 Cellulose

Cellulose is the most abundant organic polymer on the planet and the largest component of plant biomass [89], with an estimated production of 7.5×10^{10} tons per annum [54]. It can be found in pure form, as in cotton, but is commonly found associated with hemicellulose and lignin in the cell wall [35, 89], as in wood, corresponding to approximately 40 to 45% of mass [149]. In addition to plants, it can also be synthesized by bacteria, algae, and fungi, but in lesser amounts [1]. Figure 5 depicts the main routes of obtaining cellulose in nature. Cellulose can also be obtained by synthesis in vitro and should be highlighted with important

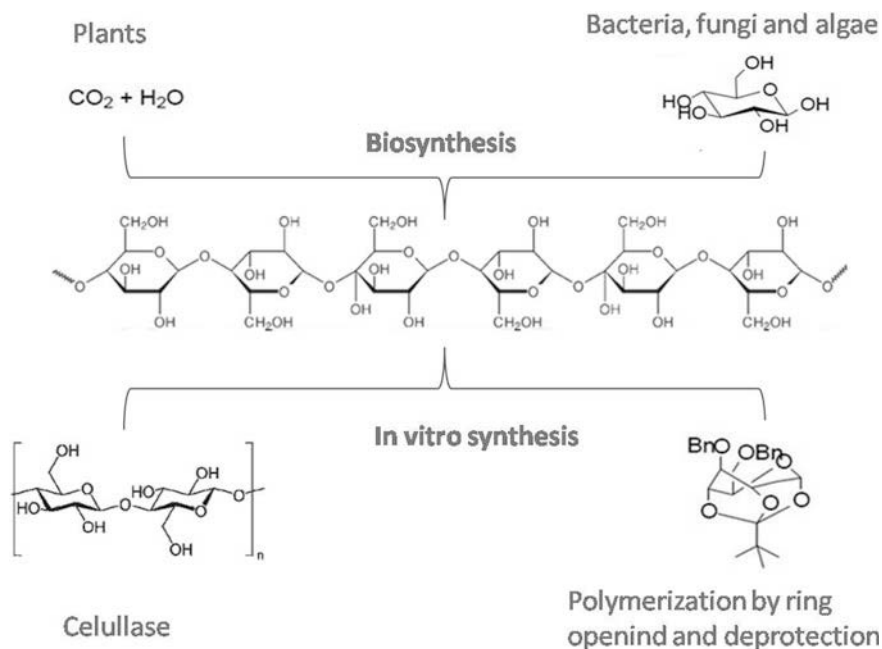


Fig. 5 Main ways of obtaining cellulose

development today [82]. The first report of cellulase-catalyzed cellulose formation was based on cellobiosyl fluoride [83] and the first chemosynthesis was performed through polymerization of substituted D-glucose and with open rings followed by deprotection [108].

Figure 6 shows schematically the ultrastructure. It can be seen from the figure that primary and secondary walls differ in the arrangement of cellulose chains. The secondary wall consists of 3 layers, S1, S2, and S3, and the S3 layer has the lowest cellulose content, being composed mainly of xylan. In the primary wall, the fibers are less ordered and essentially composed of chains in all directions within the plane of the wall. At layer S1 showing the very thin lamellae, the arrangement of the fibrils may be visible as is helical (spiral) in nature with a cross-arrangement in certain species. In layer S2 the cellulose chains are grouped in parallel microfibrils, giving a denser arrangement and aligned with the axis of the fiber. About 40–45% of the dry matter of the secondary wall is composed of cellulose [160].

Cellulose is composed of β -D-anhydroglucopyranose units which bond to each other through the carbons 1–4, forming a basic unit called ‘cellobiose’, which consists of the binding of two molecules of anhydroglucose [54, 145, 149]. The cellulose chain is linear and high molecular weight, which tends to form hydrogen bonds between the molecules [1].

The degree of polymerization (DP) is up to 20.000; however, it varies widely, and the value is around 10.000 in wood [74]. The hydroxyl groups of the cellulose

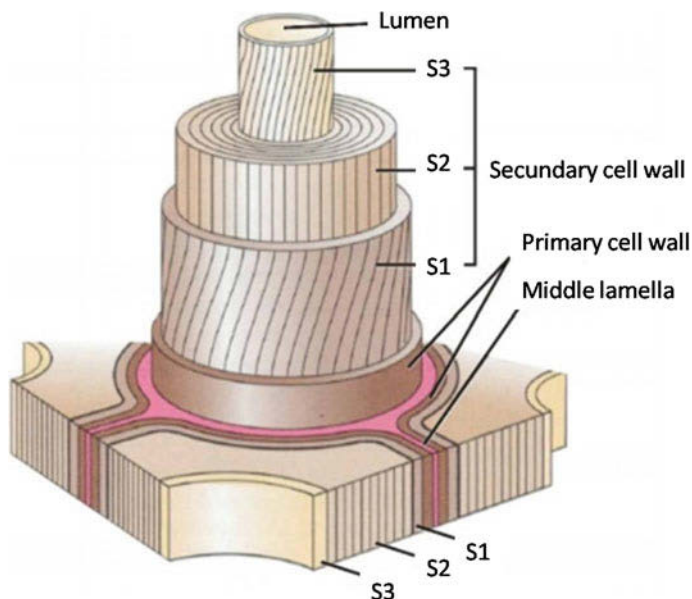


Fig. 6 Ultrastructure of wood. Reproduced from Taiz and Zeiger [160] with the kind permission of the publishers

molecules form hydrogen bonds that may be intramolecular or intermolecular. Their ability to form hydrogen bonds play a major role in leading the crystalline packing which also governs the physical properties of cellulose [74] and are these bonds that make cellulose a stable polymer and appreciated as reinforcement in composites [37, 54].

About 36 individual cellulose molecules are brought together by biomass into larger units known as elementary fibrils or microfibrils, which are packed into larger units called microfibrillated cellulose [54, 89]. The latter are in turn assembled into cellulose fibers. All these are shown in Fig. 7. The diameter of elementary fibrils is about 5 nm whereas the microfibrillated cellulose (also called nanofibrillated cellulose-NFC) has diameters ranging from 20 to 60 nm [6, 89]. The microfibrils are formed during the biosynthesis of cellulose and are several micrometres in length. This microfibrillar aggregates which allow the creation of highly ordered regions (i.e., crystalline) form the core alternate with disordered domains (i.e., amorphous) present at the surface [132]. It is these crystalline regions that are extracted, resulting in nanocrystalline cellulose (NCC). The inter- and intra-molecular interactions networks and the molecular orientations of crystalline regions can vary, giving rise to cellulose polymorphs or allomorphs [23, 89].

As mentioned earlier, the most common way to obtain pulp from wood is through the Kraft chemical pulping process [111], followed by bleaching steps to remove residual lignin on the cellulose surface. This pulp obtained in the paper industry is commonly used to obtain nanocellulose, since pulping and bleaching are

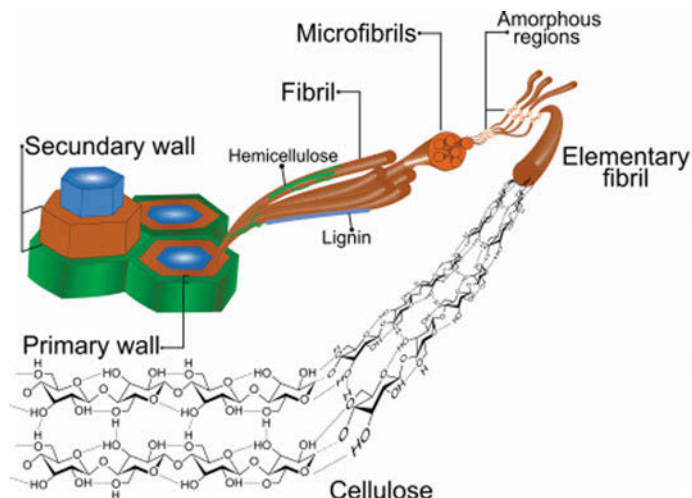


Fig. 7 Hierarchical structure of cellulose extracted from plants. Reproduced from Rojas et al. [125] with the kind permission of the publishers

characterized as pre-treatments necessary to obtain Nanocellulose, whether microfibrillated, nanofibrillated or nanocrystalline [50, 69, 91, 92, 95, 98, 109, 117, 169, 170, 185, 186].

5 Nanocellulose

The term “nanocellulose” refers to cellulosic materials having at least one of their dimensions in nanometer scale. Nanocelluloses can be produced by different methods and from various lignocellulosic sources [1].

According to Fujisawa et al. [46], so far nanocelluloses can be divided into three groups: cellulose nanocrystals (CNC), micro-fibrillated cellulose (CMF) and nano-fibrillated cellulose (CNF). While the first one (CNC) is produced by a chemical process of acid hydrolysis followed by mechanical agitation of the suspension in water, the second (CMF) is obtained by mechanical disintegration of the cellulosic pulp in water and finally third one CNF is prepared using the combination of chemical oxidation followed by mechanical disintegration in water, or only by the mechanical disintegration method. These mechanisms are shown in Fig. 8.

Reported definition of CMF is fibers with a diameter between 25 and 100 nm, while CNF are nanocelluloses with a diameter between 5 and 30 nm and a variable length between 2 and 10 μm [125, 139]. Both CMF and CNF have amorphous and crystalline zones composing their structure.

According to Samyn et al. [133], the microfibrillated nanocellulose is commonly produced by homogenization, where the fiber shear is performed by a strong

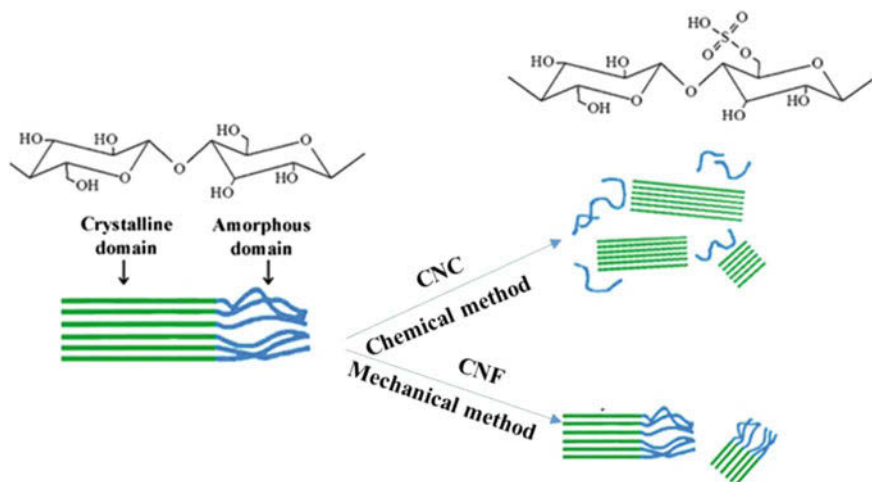


Fig. 8 The mechanism of chemical and mechanical methods for producing CNC and CNF from cellulose. Reproduced from Sofla et al. [151] with the kind permission of the publishers

pressure drop and impact forces inside the processing chamber. A similar effect is observed by the use of grinding process [91], where processed suspensions generally contain a heterogeneous mixture of CMF and CNF which are characterized by different diameters and aspect ratios (length/diameter) [133]. The CMFs are usually characterized by a smaller aspect ratio than the CNF [86, 85, 107, 177]. Depending on the number of processing steps, or passes through the mill, the geometry of the fibers in a suspension is reduced, generating more CNF, which leaves the suspension more homogeneous [91, 133]. Larger nanocellulose suspensions (CMF) present a large tendency to aggregate and flocculate microfibrils, a fact also justified by the surface charge of nanofibrils [91]. Non-uniformities in the suspending media are constructed by the high tendency of aggregation of single cell microfibrils and/or flocculation with larger fibers. According to Kumar et al. [86, 85] the CMF is generally produced by a single mechanical treatment of the cellulosic pulp, while the CNF is produced by mechanical treatment after the chemical pretreatment of the original pulp fibers [86, 85].

On the other hand, CNC refers to cellulose nanoparticles that underwent hydrolysis under controlled conditions and that lead to the formation of structures in the form of small crystalline cylinders [139]. Depending on the source of extraction, these crystallites will have a diameter of 3–50 nm. The CNFs, as well as the CMFs, exhibit zones with high fibrillation intensity due to the shear forces that the fibers undergo in the production process, whereas the nanocrystals are exclusively from the crystalline regions of the cellulose molecule. Nano-fibrillated cellulose has amorphous and crystalline regions that make up its more elongated chain in the longitudinal direction. In this way, the long length of nano-fibrillated cellulose chains associated to its surface containing a wide range of hydroxyl groups, which

Table 3 Nanocellulose derivatives and their dimensions (Reproduced from [75] with the kind permission of the Publishers)

Nanocellulose derivate	Diameter (nm)	Length (nm)	The aspect ratio (L/d)
Microcrystalline cellulose—MCC	>1000	>1000	1
Micro fibrillated cellulose—CMF	10–40	>1000	100–150
Microfibril	2–10	1000	>1000
Cellulose nano crystalline—CNC	2–20	100–600	10–100
TEMPO-oxidized nanocellulose	3–4	>1000	200–100

exposes the formation of numerous hydrogen bonds [114]. The type of processing and the raw material used results in nanocellulose with different morphologies and dimensions, as presented in Table 3.

Figure 9 shows scanning electron micrographs of cellulose microfibrils (CMFs), cellulose nanofibrils (CNFs), cellulose nanocrystals (CNCs) and others microfibrillated cellulose that can be applied in papermaking, such as MCC and microfibril.

5.1 Method of CNF and CMF Production

As a semi-crystalline polymer, cellulose allows the extraction of nanostructures with different morphological properties (length, diameter, and aspect ratio), depending on mechanical and physical, depending on the extraction method applied [125]. The methods for producing nanocelluloses can be divided into chemical, physical and biological [44]. Some forms of procurement, various types of equipment and also combinations of chemical, enzymatic and/or mechanical treatments have already been tried for the production of nanocelluloses [57, 71, 114, 130]. The nanocellulose can be produced by mechanical methods such as grinding, cryoencation with high-pressure homogenization with liquid nitrogen, steam explosion, high-intensity ultrasound etc. Some pre-treatments may be used prior to mechanical processes to promote the accessibility of the hydroxyl groups, increase the internal surface, alter the crystallinity, break the hydrogen bonds of the cellulose and thus increase the reactivity of the fibers. The pre-treatments are different chemical hydrolysis (alkali or acid) or enzymatic [125].

5.1.1 Mechanical Methods

According to Rojas et al. [125], the mechanical treatments can isolate nanofibers from the primary and secondary cell wall without severely degrading cellulose. It is reported that depending on the types of mechanical treatment and levels of mechanical force used, inter fibrillar hydrogen bonding is broken [70, 123, 131,

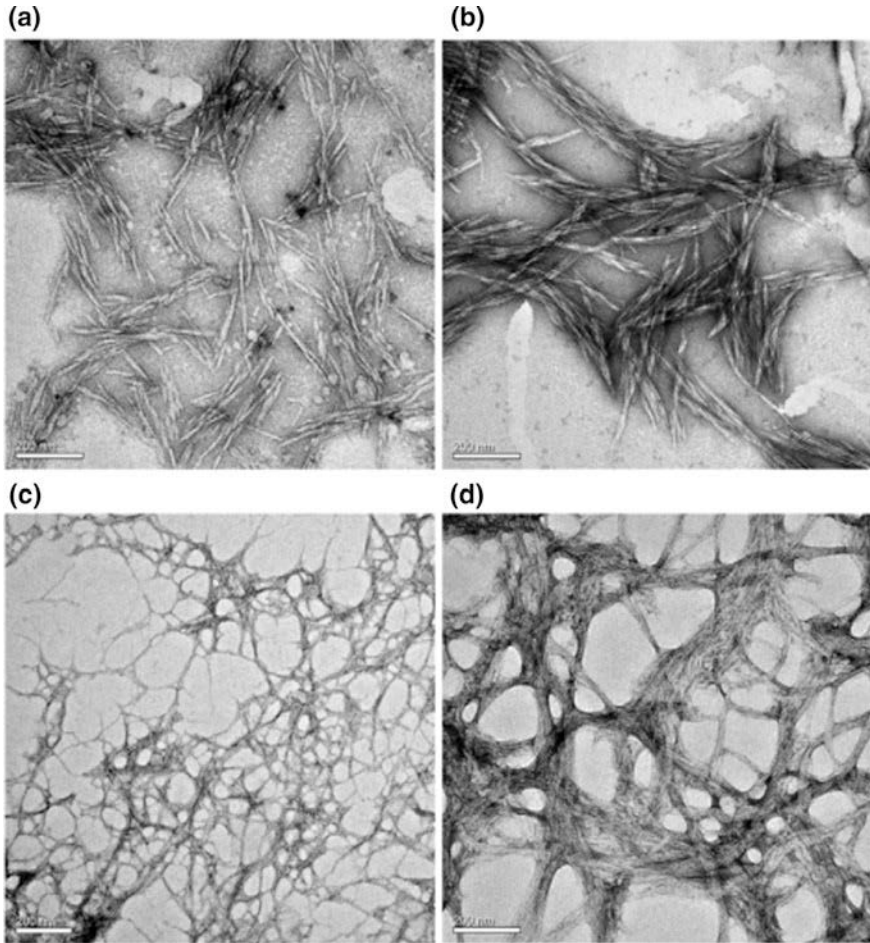


Fig. 9 TEM images of nanocelluloses extracted by: **a**—CNC prepared by sulfuric acid hydrolysis, **b**—cellulose nanocrystals isolated by formic acid hydrolysis, **c**—CNF prepared by 2,2,6,6-tetramethylpiperidine-1-oxyl (TEMPO)-mediated oxidation, and **d**—cellulose nanofibrils fabricated by pulp refining. Reproduced from Liu et al. [97] with the kind permission of the Publishers

179]. For example, microfluidization and high-intensity ultrasonic treatments produce a high shear degree, causing transverse cleavage along the longitudinal axis of the cellulose fibers. This process tends to damage the microfibrillar structure, reducing the molar mass and the degree of crystallinity of cellulose.

The mechanical methods would involve high production costs, besides they being less efficient and requiring higher energy inputs compared to that of chemical methods [96]. In view of these, it is reported that a chemical pretreatment would be necessary, which reduces energy consumption besides obtaining more hydrophobic

surface [125]. Further, the degree of polymerization (DP) is reported to get usually reduced from 1200 DP to 1400 DP between 850 and 500 by the mechanical treatment. It may be noted that a high cellulose DP is desirable because of correlation of cellulose with the tensile strength of the nanofiber, which is reported to be at least 2 GPa [26, 118].

The following are some of the mechanical methods used to produce nanocellulose:

- (i) High-Pressure Homogenization (HPH): In this process, first known quantity of the cellulose (2–7% w/v) is passed through slurry at high pressure into a vessel through very small spring-loaded valve assembly using low velocity. This is then exposed to a pressure drop to atmospheric condition with the valve opening and closing in a cyclic motion [45]. This method is reported to be an efficient method for refining of cellulosic fibers in view of its high efficiency, simplicity and without requiring any organic solvents [78]. Nanofibers having 20–100 nm of diameter and several tens of μm long are normally produced by this method. However, clogging of the homogenizer, high energy consumption, and mechanical damage of the crystalline microfibril structure are some of the limitations of this method [96, 174, 178].
- (ii) Microluidizer: This method uses the equipment, which consists of an intensifier pump and an interaction chamber. While the first is for increasing the pressure, the second is for defibrillating the fibers using two types of forces, viz., shear and impact against colliding streams and the channel walls [42]. Dimensions of CNFs produced by this process are of several μm long and less than 100 nm [125].
- (iii) Grinding: In this method mechanism involved is fibrillation of cellulose using a suitable equipment say, grinder to break the hydrogen bond and the cell wall structure of the cellulose by shearing force besides individualization of pulp to nanoscale fibers [146]. Accordingly, this method uses grinding equipment consisting of a static and rotating grindstone (1400–3000 rpm). The process involves passing of the pulp slurry between these two stones [92, 125]. Accordingly, the cell wall structure would break down by the shear and compression forces, which generate a gel due to the suspension of nanocelluloses. Therefore, a number of cycles to be passed by the pulp/fibers through a grinder or the amount of energy for processing the fibers is important parameters which affect the quality of resultant NFC produced by this method. The diameters of NFCs produced by this process range from about 5–157 nm [56, 155, 182].
- (iv) Cryocrushing: This method involves immersion of water swollen cellulosic fibers into liquid nitrogen followed by its crushing by mortar and pestle [45]. Accordingly, in this method, high impact forces would be applied in order to freeze the cellulosic fibers leading to rupture of cell wall due to the pressure exerted by ice crystals and thus, liberating nanofibers [146]. Nanofibers of soya beanstalks have been produced by this method by

- cryocrushing and high-pressure defibrillation procedures [175, 176]. Normally, this method produces CNFs with diameters from 30 to 80 nm [3].
- (v) Steam explosion: This method is a thermomechanical process. In this method, cellulose is kept at 200–270 °C is exposed to a high pressure of steam maintained between 14 and 16 bars. Then, the steam penetrates the biomass by diffusion for short periods of time between 20 s to 20 min. This is followed by applying sudden decompression (explosion), which would generate shear forces hydrolyzing the glycosidic and hydrogen bonds, between the glucose chains [77, 125]. The diameter of CNFs produced by this methods lies in the range of 10 μm –50 nm [30, 36].
 - (vi) High-intensity Ultrasonication: This method is a mechanical process wherein oscillating power is used to isolate cellulose fibrils by hydrodynamic forces of ultrasound [28]. According to Rojas et al. [125], the cavitation during the process leads to a powerful mechanical oscillating power. The gas bubbles formed would expand and explode breaking down the cellulose fibers [27]. The diameter of the nanocellulose produced by this method lies in the range of 5–35 nm [57].

It is reported that the mechanical treatment causes changes in fiber structure [32]. The author suggests following four phenomena can be observed due to the defibrillation process. First one is the internal fibrillation (IF), which is difficult to observe by microscopy techniques. Here, loosening of the fiber bundle takes place, which causes swelling and increased fiber flexibility. The swelling of the cellulose increases its accessibility to reagents, and consequently their reactivity. The second effect is the external fibrillation (EF) at the surface of the fiber. This is basically the defibrillation process of the fibrils, but without their complete removal. It may be noted that when these fibrils extend completely from the fiber there is the generation of the nanofibers (CMF), as the third phenomenon showing the structural alteration. And finally, the fourth one involves the dimensional reduction of the fiber itself by mechanical wear through fiber cutting (FC). The entire phenomenon mentioned above can be observed by microscopy techniques as is evident from Fig. 10, which is a transmission electron micrograph of nanocellulose obtained from Lengowski [91].

5.1.2 Electrospinning

This is a method to form the fibers using an electrical rather than a mechanical driving force and is termed as an ‘electromechanical’ method. Here, the cellulose dispersion is extruded and electrospun under the effect of a high electric field [43], following a 3D spiral trajectory. Once the solvent evaporates, it leaves behind randomly oriented nanofibers in the collector. The CNFs morphology produced by this technical depends on the strength of electric field, solution feed rate and the tip-to-collector distance [125].

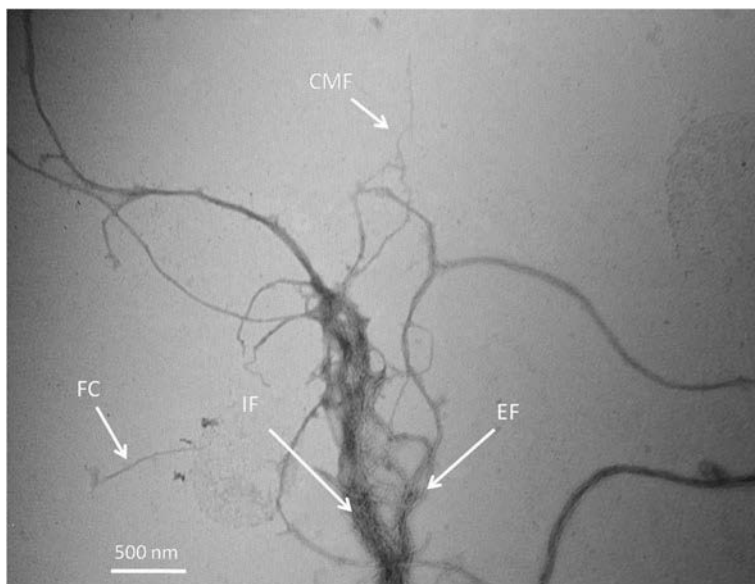


Fig. 10 Effects of refining on the production of nanofibers by the mechanical process. Reproduced from Lengowski [91]

5.2 *Methods of CNC and MCC Production*

5.2.1 Acid Hydrolysis

The mechanism for obtaining CNC by acid hydrolysis involves the removal of the amorphous regions from the cellulose elementary fibrils by hydrolysis, leaving only the crystalline regions [114]. This cellulose is obtained by cutting the elementary fibrils into small fragments followed by bleaching. Subsequently, CNC is extracted from bleached samples by strong acid hydrolysis under strictly controlled conditions of concentration, temperature, agitation, and time [125]. A typical production process involves acid hydrolysis, washing, centrifugation, dialysis, and sonication to form a suspension followed by drying by freeze-drying or heat-drying [54, 92]. CNC is also known as whiskers or cellulose nanocrystals.

The difference between the production of CNC and MCC by acid hydrolysis lies in the reaction time or in the concentration of the reagent, where less time and lower concentrations are used for MCC compared to those to produce CNC [38, 173, 185, 186]. MCC can be characterized as a white powder of fibrous particles with sizes of about 40 μm with a DP 100–200 and about 80% crystallinity, while the CNC has dimensions of 5–10 nm wide, 100–300 nm long with 90% crystallinity when made

from cotton and wood cellulose. On the other hand, other sources like bacteria, algae, and tunicin produce nanocrystals with larger size distributions and dimensions comparable to those of CMF (width: 5–60 nm, length: 100 nm to several μm) [10].

It may also be noted that CNC and MCC are similar to small cylinders or crystalline characters, isolated from acid hydrolysis of the fibers. This is illustrated in Fig. 11, which shows scanning electron micrographs of CNC obtained from Beauvalet [21] (Fig. 11a) and MCC obtained from Thoorens et al. [162] (Fig. 11b).

It may be noted that the hydrolysis processes rely on the fact that the crystalline regions are insoluble in acids under the conditions in which they are employed. This is due to their inaccessibility because of the high organization of the cellulose molecules in their nanostructure. On the other hand, the natural disorganization of the molecules in the amorphous regions favours the accessibility of the acids and consequently the hydrolysis of the cellulose chains present in these regions [132]. Sulfuric and hydrochloric acids are the most commonly used for acid hydrolysis, but phosphoric and hydrobromic acids have also been used [90].

The most commonly used method for the preparation of CNC is acid hydrolysis of cellulosic materials using sulfuric acid (64% w/w). Cellulose nanofibers have also been produced from hardwood by treatment with the 2,2,6,6-tetramethylpiperidine1-oxyl radical in combination with sodium bromide and NaClO [130].

The CNC has a high aspect ratio, a high modulus and good compatibility with matrix materials [127]. Your morphology is the elongated crystalline rodlike shape and has a limited flexibility because it has no amorphous regions. These CNCs have a degree of crystallinity (55–90%). However, it should be noted that the degree of crystallinity, aspect ratio, and morphology depends on the source of cellulosic material and preparation conditions [144]. The colloidal behaviour and superficial charge of CNCs depend on the acid used for their production [90].

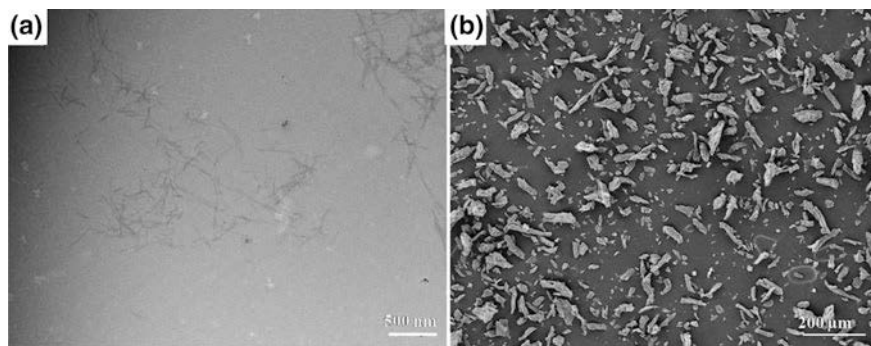


Fig. 11 **a**—Nanocrystalline cellulose morphology **b**—microcrystalline cellulose. Reproduced from Beauvalet [21] (Fig. 11a) and [162] (Fig. 11b) with the kind permission of the publishers

5.2.2 Enzymatic Hydrolysis

It is well known that enzyme is generally used to modify and/or degrade the lignin and hemicelluloses contents in biomass without altering the cellulose portion. It is known that enzyme helps in the restrictive hydrolysis of several elements or selective hydrolysis of specified components in the cellulosic fibers [71]. These enzymes are produced by cellobiohydrolases. There are two types. The first category is A- and B-type cellulases, which are capable of attacking the crystalline portion of cellulose. On the other hand, the second category is C and D type endoglucanases, which are capable of attacking the disordered structure (amorphous) of cellulose [8]. It is reported that enzymatic methods are highly expensive as these methods take long treatment time for a successful hydrolysis and also due to the isolation process of the enzymes [77]. Actually, this process can be used as a pre-treatment for production of nanocellulose by the mechanical method to reduce the energy consumption to produce CNF.

6 Applications of Nanocellulose in Paper Making

6.1 Nanocellulose-Reinforced Pulp

The development of strength in paper is influenced by several factors, viz., length and strength of fiber used, degree of adhesiveness, fiber-fiber contact area and bonding agents in the formation of dry or moist [11, 12, 81, 159]. Due to the unique properties of nanocellulose, there is a growing tendency to use it as a paper reinforcement additive [112]. Many researchers have been using nanocellulose as an additive and films in paper making, either to improve (i) strength properties, barrier properties in food packaging, paper brightness, printability [80] or (ii) to reduce paper weight without loss in mechanical properties, while improving thermal properties and to provide antimicrobial capacity in packages. The functionality of the nano paper emerges from the intrinsic properties of the nano fibrous network, the additional loading of specific nano materials or the additional deposition and modelling of thin films of nanomaterials on the paper surface [17]. According to Zimmermann et al. [187], reactive sites exposed on the surface of the cellulose micro fiber (CMF) perform the formation of a network of nanofibers due to the hydrogen bonds formed. Because of the nanometer scale, the amount of these bonds is enhanced by the larger contact surface between nano and microfibers. This increases the apparent density of the paper, making it more resistant to the passage of air and humidity besides the gain in the mechanical properties [86, 85, 106, 115].

As an additive, the nanocellulose has a similar effect to that produced by the refining of the pulp, reducing paper porosity [50, 91, 117]. This is evident from Fig. 12, which shows scanning electron micrographs of cellulose sheet with and without any additive highlighting the effect of the addition of CMF to the paper

[91]. It may be noted that Fig. 12a is micrograph of cellulose sheet without any additive, while Fig. 12b, c are micrographs of cellulose sheet with CMF additive and CMF coating. Besides, such addition of CMF to cellulose gives significant gains in the mechanical properties of the paper, whether produced by virgin fibers [117] or by secondary fibers [116]. It is also reported that wet strength is the main functionality for tissue paper, paper towels, cardboard and other papers [129]. These authors have also reported that the cationic polyelectrolyte (Poly Amideamine Epichlorohydrin—PAE) developed in the 1950s has been used as a wet strength additive in the paper making process. In order to increase the mechanical properties of the paper, the use of nanocellulose and additives such as PAE [4, 5] and amphoteric starch [93] have already been reported.

Investigations have also been carried out on the possibility of using CMF and CNF as a reinforcing and filler in a pilot experiment using different degrees of fibrillation and filler mixtures (CMF, CNF, precipitated calcium carbonate, cationic polyacrylamide and two types of starch) [164]. The author has observed that the CNF improved the resistance properties (Scott Index and tensile index) more than the CMF, and also that the CNF associated to the starch presented better resistance to traction being wet. Finally, the author has concluded that in conjunction with CMF or CNF, the filling content could be increased from 30 to 40%, which would imply a potential savings of 3–6.5% compared to conventional sheets. A dose of 6% of applied CNF has been found to promote about 40% energy savings, while the

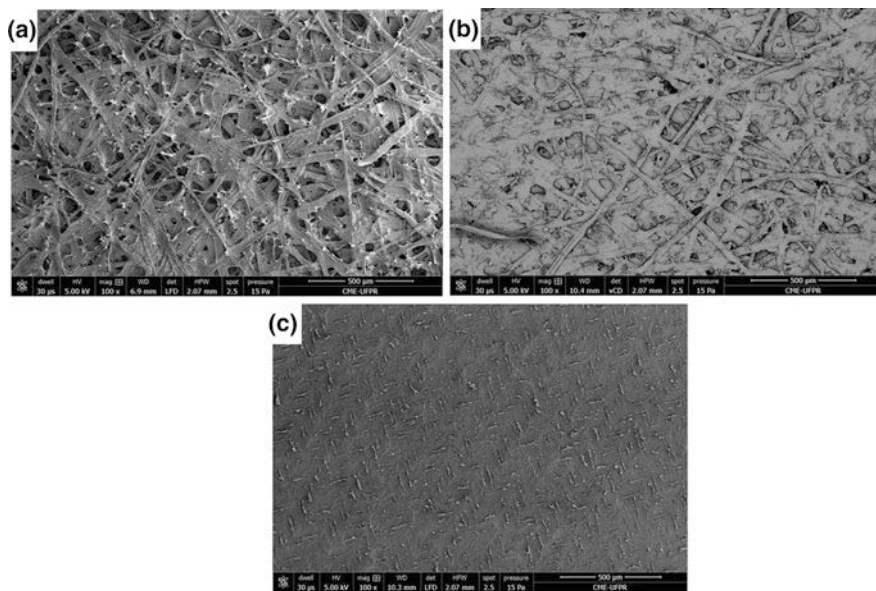


Fig. 12 Effects of nanocellulose on papermaking **a** cellulose sheet without any additive; **b** cellulose sheet with CMF such additive; **c** cellulose sheet with CMF such coating. Reproduced from Lengowski [91]

12% dose reduced energy expenditure by 85% compared to the control to produce pulps at 35 °SR [34].

Compared with micro-sized cellulose, nanocellulose is more effective as an additive for the paper industry. This is attributed to the interactions between the nanosized elements, which are connected by hydrogen bonds forming a percolated network when the nanocellulose is dispersed in the pulp [3, 73, 75, 76, 80, 183].

Another study has concluded that the drying and wetting process of paper with nanocellulose depends on the amount of added nanocellulose because thenanocellulose clogs the pores and give a greater amount of inter fibrillar connections and preventing fiber-water bonds in the rewetting [120]. It has also been pointed out that 6–12% of CMF could be used in the paper making mix [121], but indices above 5% have been reported to cause a decrease in traction and tear properties [117]. On the other hand, the use of CMF as additives to increase the resistance of thermo-mechanical pulps to produce new types of packaging has also been reported [59]. In addition to improving the mechanical properties, these authors have also observed that the addition of 6 g/m² of nanocellulose reduced the permeability and drainage of the cellulosic mass. The enzymatic pretreatment combined with mechanical shear forces at high pressure has been found to significantly improve the mechanical strength of the paper without affecting drainage [50, 51]. In another study Gonzalez et al. [50] have concluded that the porosity and mechanical properties were improved when 9% of nanocellulose was added; however the Shopper Riegler degree (This is the ‘*degree* of refining of a pulp suspension in water and expressing it in terms of the Schooper-Riegler (SR) number, and to determine the de-watering time’) was altered, which becomes a disadvantage in the drainage stage and can cause operational problems in the drying. A similar result was observed by Damásio [34] when 6 and 12% of CNF were added. A decrease in ‘freeness’ (It is ‘a measure of how quickly water is able to drain from a fiber furnish sample. In many cases there is a correlation between freeness values and either (a) a target level of refining of pulp, or (b) the ease of drainage of white water from the wet web, especially in the early sections of a Fourdrinier former’) has been observed while using nanofibers from different sources with increased fibrillation due to water imbibed in the cell cavity and also to internal fibrillation itself, which is consistent with SR behavior [86, 85]. González et al. [50] have also confirmed the tendency to increase the resistance to drainage with the increase of the addition of CNF to the pulp, mainly because of the high surface area of this material.

There are also studies which have reported about the influence of drainage by the size of fibers used, ionic strengths, type of polyelectrolyte and pH of the suspension [156, 159]. Both of the above studies have found that the higher the degree of fibrillation, or higher the concentration of CMF in the mixture, the lower the drainage. However, when the mixture of cationic polyelectrolytes and CMF are used, alteration in drainage can be observed, not to the point of damaging the drying process [159].

The addition of nanocellulose makes the sheet drainage slightly impaired. To overcome this limitation, cationic polymers, such as polyacrylamide, have been

used as a fixative for the retention of nanocellulose, as well as for better suspension drain ability [99, 181].

In all the above studies where CMF was added to the sheets, an increase in density of the paper was observed. An increase of 4–30% in density for thermo-mechanical pulp sheets containing 4% CMF and a 10% increase in density to 7% CMF in coniferous Kraft pulp leaves have been observed [39, 102].

While these authors observed a 20% increase in density with the addition of 20% CMF, Sehaqui et al. [140] have observed 30–50% increase in density with the addition of 10% homogenized CMF to softwood Kraft pulp sheets.

Optical properties have also been found to be influenced by the addition of nanocellulose [34]. The increase of nanofibers in the paper composition is reported to cause a significant reduction in the light scattering coefficient of the pulp. The opacity also has also been found to decrease in its values due to the decrease of the light scattering coefficient, with the increase of transparency.

6.2 Coating and Films

Effects of the development of nanocellulosic films and surface deposition of nanocellulose films on paper have been studied by many researchers [50, 58, 91, 122, 124, 135, 149, 153, 154, 158]. An increase in surface density, a decrease in water absorption, reduction in permeability and surface porosity has been observed by Sjöström [149] and Lengowski [91]. Increase in surface porosity has already been shown in Fig. 12. On the other hand, the increase in the surface of the fibers with the micro-fibrillation process has been found to favor a greater number of inter fiber bonds due to the greater availability of OH-groups [50], water retention capacity and increase in Schopper-Riegler grade, implying increased drying cost.

Spence et al. [153] have studied the ability of water retention in nano-cellulose films produced from bleached and unbleached pulp from hardwood and longwood. They have observed that water retention was lower for long-fiber films compared to those of short-fibers and non-bleached pulps compared to bleached pulps. They have also evaluated CMF films with different lignin contents and observed that the samples with higher lignin content had higher rates of water vapour transmission. Besides, significantly higher water retention values and larger surface area were observed by these authors in CMF prepared from unbleached hardwood in comparison to other samples. Another study has reported that the water retention for surface depositions of unbleached nanocellulose when the source of moisture was on the opposite side to that of the surface film [91]. The presence of lignin in the production of its CMF films has been found to provide longer, narrower and more connected pores, thus increasing the rate of water transmission [154]. On the other hand, larger and lignified pores have been found to increase the rate of water vapour transmission because of their lower adsorption capacity [62]. It has also been observed that the specific surface area is strongly correlated with the difficulty of removing water content for the pulps, suggesting that water diffusion is more

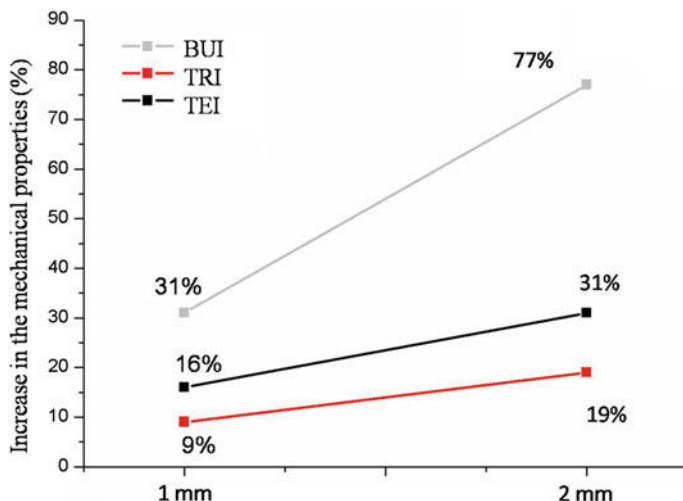


Fig. 13 Increase in the mechanical properties after superficial film deposition on the sheet in relation to a sheet without any additive. BUI = burst index; TRI = tear index; TEI = tension index. 1 mm and 2 mm = deposited moisture film thickness. Reproduced from Lengowski [91]

dependent on pore structure and surface area geometry [154]. On the other hand, Lengowski [91] found that increasing the thickness of the nanocellulosic film on paper caused an increase in mechanical strength (tension, tear and burst index). This is illustrated in Fig. 13, which shows the plots of two different thickness of moisture versus values of tension index, tear index and burst index. On the other hand, this thickness did not influence water absorption properties. While using a bleached and unbleached nano cellulose film, the author observed an increase in the tensile and burst index for bleached CMF deposition, and for the tear, the presence of lignin in CMF caused a gain in this property [91]. These are illustrated in Fig. 14, which shows the plots of mechanical properties with and without any additive on the deposition of surface film (coating) on the sheet. However, the author did not observe any influence of lignin on the thermal stability of the papers. Further, the author has also observed an increase in the mechanical properties of sheets with the addition of CMF (additive) in the production of the sheet compared to that of the sheets without additives. These results are illustrated in Fig. 15, which shows the plots of mechanical properties after surface film deposition on the sheet with and without the addition of CMF [91]. It can be seen from the figure that the gain in the tensile and tear properties are similar to the surface deposition of a nanocellulose film, while the burst index shows a reduction in resistance compared to the use of CMF as an additive. The author observed that the results of the mechanical properties of the papers are enhanced when CMF was used as a reinforcement additive as well as a coating on the paper. It can also be seen that while the values of tensile index, burst index and tear index showed a 134, 50 and 44% increase respectively compared to those values without any addition to the paper [91].

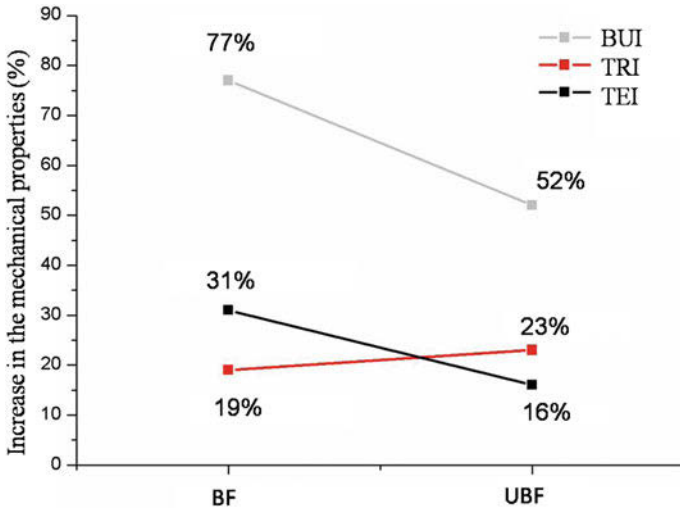


Fig. 14 Increase in the mechanical properties after superficial film deposition (coating) on the sheet in relation to a sheet without any additive. Effect of deposition of unbleached and bleached nanocellulose on mechanical properties of BUI = burst index; TRI = tear index; TEI = tension index. BF = bleached nanocellulose film; UBF = unbleached nanocellulose film. Reproduced from Lengowski [91]

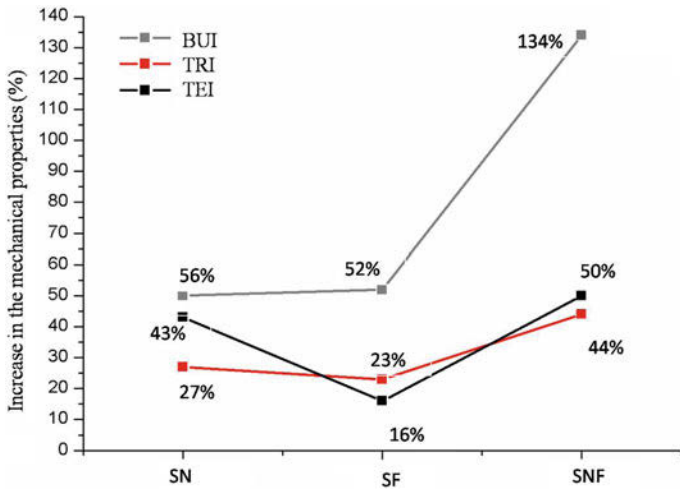


Fig. 15 Increase in the mechanical properties after superficial film deposition on the sheet in relation to a sheet without any additive. Effect of CMF addition, CMF film coating and CMF addition and coating on a paper sheet. SN = sheet with CMF addition; SF = sheet with CMF film coating; SNF = sheet with CMF film coating and addition. Reproduced from Lengowski [91]

A dense surface of the films is an important feature, as it is related to the porosity, which determines the barrier properties of the films [122]. The author has used a paper coating of nanocellulose to improve brightness properties, surface roughness, absorption, and permeability. He noticed an improvement in absorption and porosity and a very small impact on the other properties.

For CMF based films the porosity can be modified by drying from different solvents, creating an adjustable feature that provides an advantage over the melt-formed plastics. Henriksson et al. [58] were able to modify the porosity of water-dried CMF-based films from 28% to porosities of up to 40% with dry films from solvents such as methanol and acetone. In addition, when used as a coat of CMF on paper, the air permeability was found to reduce by 10% as a consequence of surface porosity [158].

Sauders et al. [135] evaluated substitution of CMF in different amounts of acetylation. It was observed that there was no improvement in the contact angle (hydrophobicity) from 15% of substitution and increased crystallinity, while there was a decrease in the rupture stress and in the stress carrying capacity of the material. These have been attributed to acetylation delaying the ability of the fibrils to form bonds during the sheet forming process. Another study has not observed any significant reduction of tensile strength and improvement in the hydrophobicity of the papers after CMF acetylation [124].

Similarly, several studies have also been carried out using CMF as a barrier to gases and liquids [13, 16, 47, 65, 91, 100, 110, 113, 147, 158]. The increase in film thickness, the amount of nanocellulose in the mass [110] reduces the permeability to oxygen, water, oils and carbon dioxide [13, 110, 158, 113] indicating that the use of larger thicknesses or greater percentages in mass, simply acts to increase the tortuous path of oxygen and an improvement of the barrier properties. It is believed that the air permeability of the films decreased due to the disconnection of the surface pores of the films [13]. However, performance is limited by its hygroscopic capacity, and its barrier properties loose efficiency at relatively high humidity [13, 113]. When nanocellulosic samples are in contact with moisture, a reduction of the inter fibrillar forces occurs, thus increasing permeability. However, many methods have been applied for nanocellulose surface modification [142], including acetylation [104], silylation, grafting, use of coupling agent for improving the hydrophobic properties [76, 88, 99], or in the presence of lignin [91]. Recognizing that porosity is an important property for printing, another study has reported that papers with greater porosity may have greater penetration of the ink and may cause printing defects [163].

Considering the applications in food packaging, studies have been reported on the CNC/CNF added to paper [119, 128]. In the study by Rampazzo et al. [119] CNC was used to form a gas barrier film for food packaging. They observed very promising results, providing oxygen and carbon dioxide permeability values hundreds of times smaller than those of equal thickness compared to common barrier synthetic polymers over a wide range of temperatures.

On the other hand, Saini et al. [128] in their study added nisin to CNF and evaluated its potential as an antimicrobial agent in food packaging. Addition of

CNF to paper sheets was done in two ways, either directly as an additive or as surface deposition such as coating. The authors found that the latter method (surface deposition) was more efficient than the former (direct addition).

Another property studied is the surface roughness of the composites of CNC-CNF. Damásio [34] produced CNF-CNC nanocomposites by the casting technique, using CNF as the dispersion polymer matrix for different CNC dosages as mechanical reinforcement. The addition of cellulose nanocrystals allowed the reduction of the surface roughness of the nanocomposites produced, increasing the mechanical properties significantly. The incorporation of CNC allowed reduction of the opacity by up to 53%, with consequent gains of transparency of the nanocomposites.

Fang et al. [41] have been reported about its modification by CNF. In this study, CNFs made from TEMPO-oxidized CNFs, where the 2,2,6,6-tetramethylpiperidine-1-oxyl (TEMPO)/NaBr/NaClO was used to modify the surface properties of the pristine wood fibers by selectively oxidizing the C6 hydroxyl groups of glucose produced transparent nanopapers. This nanopaper exhibited ultrahigh optical transparency ($\sim 96\%$) and ultrahigh haze ($\sim 60\%$), thus delivering an optimal substrate design for solar cell devices, and that may influence a new generation of environmentally.

Another field that is being explored is the use of nanocellulose together with starch in the development of biomaterials, looking for the substitution of polymers derived from petroleum. As starch presents a brittle characteristic, it is necessary to use plasticizers that improve its flexibility [14] although the mechanical and barrier properties have been compromised. Several studies have been reported on the possible applications of biofilms with starch in various sectors such as food, agricultural and pharmaceutical and also in other sectors, where biodegradability is required [18, 19, 105]. Some examples of products under study are garbage bags, films to protect food, diapers, and flexible rods; in agriculture as a film in the ground cover and containers for plants and in the production of slow release fertilizers. Also, biofilms made using starch and nanocellulose can also be used in the preparation of capsules, in the release of medicines, in the substitution of styrofoam, in the protection of equipment during transport and in several other applications [40, 126, 152, 165].

Incorporation of different types of nanocellulose (CNF, CMF, and CNC) as a reinforcing agent in starch films has been studied [29]. All the films presented excellent transparency and increased thermal stability in relation to the mechanical properties; however, the best results were for films reinforced with CMF due to the greater aspect ratio exhibited by this type of fiber. One of the main difficulties of the use of nanocelluloses is its tendency to flocculation and agglomeration in the matrix [94]. While using dispersing agents in the composition Campano et al. [24] have observed a greater homogeneity in the matrix. These authors have also evaluated different retention agents in the mixture, which allowed greater retention of the nanoparticles, causing an increase of traction with lower loads. These authors have suggested that further studies should be carried out with retention and dispersing agents with nanocelluloses in order to industrially apply such an additive. In fact,

CNC as a retention agent has already been used for fines in paper production [94]. The highly negative charge of the CNC allowed a strong interaction between cationic polyelectrolytes promoting good drainage and high retention of micro and nanoparticles.

According to Abdul Khalil et al. [2] films based on biodegradable polymer reinforced with nanocellulose present great potential and innumerable benefits for its use in packaging. However, the development of this type of biocomposites is still in the initial stage, and it is necessary to deepen the knowledge in several aspects, such as its quality, cost, and utility.

7 Market and Opportunities

The current demand for sustainability in products is driven by consumers and retailers seeking to differentiate themselves by reducing impacts of product lifecycle on the environment by reducing and minimizing the quantity of packaging and improving the sustainability of their supply chains [25]. The data indicate that this is a growing market with the development of safer and more sustainable products [67]. Also, the cellulose material being a renewable and biodegradable material having low toxicity, this new material can replace petroleum-based packaging, metal components, and other non-renewable materials, which are mostly non-biodegradable and non-renewable. In view of this, cellulose nanomaterials represent an important niche for the design and development of more sustainable products. Nano-cellulose can be used in a variety of products, among the main ones in the cement industry, automotive in the internal and external polymer structure of automobiles, packaging industry whether for food or packaging that demand high strength, waterproof papers, oils and oxygen, special papers, Tissue papers, paper cups, hygienic and absorbent products (disposable diapers), biofilms for plastic replacement, electronics, as well as acting as an excellent stabilizer for suspensions and emulsions such as paints and cosmetics and can be used as a basis for prints 3D of bones and cartilages [68, 143].

According to the “Global Nanocellulose market analysis and trends—Industry forecast to 2020” report, the global nanocellulose market is estimated to reach \$295 million by 2020, with a CAGR of 22.15 over the next 5 years due to the expansion of applications and increasing the appeal for green alternatives to oil products. According to the BCC Research Report [20], the global nanocellulose market was \$46.8 million in 2014, projected to be \$277.7 million in 2019, with a CAGR of 42.8% by 2019. Considering the types of nano-cellulose, cellulose nanofibrillation had a market of 28.2 million in 2014, it is estimated to be 158.3 million in 2019, while nanocrystalline cellulose had a market of \$18.0 million in 2014 and is expected to be 116.6 million in 2019.

According to Cowie et al. [33], the annual global market potential for high-volume applications of nanocellulose is estimated at 32.8 million metric tons, based on current markets and middle market penetration estimates. The largest uses for nanocellulose associate a paper and pulp industry are projected to be in packaging coatings (5.3 million metric tons), replacement for the plastic packaging (4.1 million metric tons), plastic film applications (3.3 million metric tons), paper filler (2.4 million metric tons), packaging filler (2.4 million metric tons) and paper coatings (2.2 million metric tons).

8 Final Considerations

The application of nanoscience is an opportunity for greater profitability and autonomy for the pulp and paper industry. This is because it is possible to produce additives and coating for papers using the same raw materials (starch, CMC, synthetic polymers, resins, alkylketene dimer emulsions, alkenyl succinic anhydride) used for paper making without needing other materials to improve the internal bonding of paper fibers, reduce porosity, whiteness, opacity, etc. This opens up possibilities for improving existing products and developing new low-cost, multi-purpose products. There are already different types of nanocellulose that can be used in paper production. However, it is necessary to know the mode of production of the paper and the routes of production of nanocellulose, since the structure or morphology of these different nanocelluloses can be altered according to the routes of and therefore can modify the final properties of the paper. The benefits of nanocellulose in pulp and paper industry products include: increased tensile and burst strengths, weight loss, improved barrier properties for oils, oxygen and moisture, better printing surface, optically transparent and/or coloured layer coatings, biodegradability, cost reduction with additives and potentially with drying. The use of nanocelluloses in papermaking presents interesting possibilities, and offers improvements in cost-benefit, energy efficiency and biocompatibility, in addition to generating new products with uses not available today.

Acknowledgements At the outset, the authors express their sincere thanks to the Editors of the book (Inamuddin, Sabu Thomas, Raguendra Mishra and Abdullah M. Asiri), particularly Prof. Inamuddin for inviting us to contribute this Chapter. The authors place on record and appreciate the kind permission given by some of the authors (who have given permission to use their figures), M/s. Elsevier Inc Publishers, Springer, Sociedade Brasileira de Química—SBQ, Brazil, www.plantphysiol.org or www.plantcell.org—“Copyright American Society of Plant Biologists.” InTech Open Publishers, IOP Publishing and the Vietnam Academy of Science and Technology (VAST) to reproduce some of the figures from their publications free of charges. One of the authors (KGS) would like to thank the PPISR, Bangalore-India with whom he is associated with presently for their encouragement and interest in this collaboration.

References

1. Abdul Khalil HPS, Davoudpour Y, Nazrul Islam MD et al (2014) Production and modification of nanofibrillated cellulose using various mechanical processes: a review. *Carbohydr Polym* 99:649–665
2. Abdul Khalil HPS, Tye YY, Leh CP, Saurabh CK et al (2018) Cellulose reinforced biodegradable polymer composite film for packaging applications. In: Jawaid M, Swain S (eds) *Bionanocomposites for packaging applications*. Springer, Cham, pp 49–64
3. Abe K, Iwamoto S, Yano H (2007) Obtaining cellulose nanofibers with a uniform width of 15 nm from wood. *Biomacromol* 8:3276–3278
4. Ahola S, Turon X, Österberg M et al (2008) Enzymatic hydrolysis of native cellulose nanofibrils and other cellulose model films: effect of surface structure. *Langmuir* 24(20):11592–11599
5. Ahola S, Salmi J, Johansson L-S et al (2008b). Model films from native cellulose nanofibrils. Preparation, swelling, and surface interactions. *Biomacromol* 9(4):1273–1282
6. Akil HM, Omar MF, Mazuki AAM et al (2011) Kenaf fiber reinforced composites: a review. *Mater Des* 32:4107–4121
7. Almeida FS (2003) Influence of alkaline load on the Lo-solids® pulping process for eucalyptus wood. Dissertation, Unisity of São Paulo
8. Anderson SR, Esposito D, Gillette W et al (2014) Enzymatic preparation of nanocrystalline and microcrystalline cellulose. *Tappi J* 13(5):35–42
9. Andrade M (2011) The fiber line of the future for eucalyptus kraft pulp. In: Paper presented at the 5 th international colloquium on eucalyptus pulp, Federal Uniuersity of Viçosa, Porto Seguro, 8–11 may 2011
10. Angles MN, Dufresne A (2000) Plasticized starch/tunicin whiskers nanocomposites. 1. Structural analysis. *Macromol* 33(22):8344–8353
11. Ankerfors M, Duker E, Lindstrom T (2013) Topo-chemical modification of fibres by grafting of carboxymethyl cellulose in pilot scale. *Nord Pulp Pap Res J* 28(1):6–14
12. Ankerfors M, Lindström T, Henriksson G (2013b) Method for the manufacture of microfibrillated cellulose. US patent 8,546,558, 8 Feb 2006,
13. Aulin C, Gallstedt M, Lindstrom T (2010) Oxygen and oil barrier properties of microfibrillated cellulose films and coatings. *Cellulose* 17:559–574
14. Azeredo HMC (2012) *Fundamentals of food stability*. EMBRAPA, Brasília
15. Barbosa LCA, Maltha CRA, Silva VL et al (2008) Determination of the sirinygl/guaiacyl ratio in eucalyptus wood by pyrolysis-gas chromatography/ mass spectrometry (PY–GC/MS) (PI-CG/EM). *Quím Nova* 31(8):2035–2041
16. Bardet R, Reverdy C, Belgacem N et al (2015) Substitution of nanoclay in high gas barrier films of cellulose nanofibrils with cellulose nanocrystals and thermal treatment. *Cellulose* 22(2):1227–1241
17. Barhoum A, Samyn P, Öhlund T et al (2017) Review of recent research on flexible multifunctional nanopapers. *Nanoscale* 9:15181–15205
18. Bastioli C (2005) *Handbook of biodegradable polymers*. Rapra Technology Limited, Shawbury
19. Batista JA, Tanada-Palmu PS, Grosso CRF (2005) The effect of addition of fatty acids on pectin films. *Ciênc Tecnol Aliment* 25:781–788
20. BCC Research (2015) ‘Biomaterial of the Future’ Nanocellulose to Send Market Booming with 42.8% CAGR. https://www.bccresearch.com/pressroom/avm/biomaterial-of-the-future-nanocellulose-to-send-market-booming-with-42.8-percent-cagr?fbclid=IwAR2AiLB_BSpIdEPCaGGHaEhupzMsL675cwpyPJZakEJGBj30UTRBMTJxnc. Accessed 9 Dec 2018.
21. Beuvalet M (2016) Application of cellulose nanomaterials in thermoplastic composites. Unisity of Waterloo, Thesis
22. Bonfatti EA Jr (2013) Oxygen delignification for kraft pulp with high kappa number. Dissertation, Unisity of São Paulo

23. Brinchi L, Cotana F, Fournunati E et al (2013) Production of nanocrystalline cellulose from lignocellulosic biomass: technology and applications. *Carbohydr Polym* 94:154–169
24. Campano C, Merayo N, Balea A et al (2017) Mechanical and chemical dispersion of nanocelluloses to improve their reinforcing effect on recycled paper. *Cellulose* 25(1):269–280
25. Carbon Disclosure Project (2012) CDP supply chain report. https://www.marriott.com/MarriottInternational/CorporateResponsibility/Performance_New_2016/SPG_PDFs/CDP-Supply-Chain-Report-2012.pdf. Accessed 6 Jun 2018
26. Chaker A, Mutjé P, Vilar MR et al (2014) Agriculture crop residues as a source for the production of nanofibrillated cellulose with low energy demand. *Cellulose* 21(6):4247–4259
27. Chen P, Yu H, Liu Y et al (2013) Concentration effects on the isolation and dynamic rheological behavior of cellulose nanofibers via ultrasonic processing. *Cellulose* 20(1):149–157
28. Cheng Q, Wang S, Rials TG (2009) Poly(vinyl alcohol) nanocomposites reinforced with cellulose fibrils isolated by high intensity ultrasonication. *Compos Part A Appl Sci Manuf* 40:218–224
29. Cheng G, Zhou M, Wei Y-J et al (2017) Comparison of mechanical reinforcement effects of cellulose nanocrystal; cellulose nanofiber; and microfibrillated cellulose in starch composites. *Polym Compos* <https://doi.org/10.1002/pc.24685>
30. Cherian BM, Leão AL, Souza SF, Thomas S, Pothan LA, Kottaisamy M (2010) Isolation of nanocellulose from pineapple leaf fibres by steam explosion. *Carbohydr Polym* 81:720–725
31. Colodette JL, Santos VLS (2015) General principles of bleaching. In: Colodette JL, Gomes FJB (eds) *Cellulose pulp bleaching*. Federal University of Viçosa, Viçosa, pp 173–202
32. Coutts RSP (2005) A review of Australian research into natural fibre cements composites. *Cem Concr Compos* 27(5):518–526
33. Cowie J, Bilek EM, Wegner T et al (2014) Market projections of cellulose nanomaterial-enabled products—part 2: volume estimates. *Tappi J* 13(6):57–69
34. Damásio RAP (2015) Characterization and nanoscale applications of nanofibrillated cellulose (NFC) and cellulose nanocrystals (CNC). Dissertation, Federal University of Viçosa
35. de Souza e Lima MM, Borsali R (2004) Rodlike cellulose microcrystals: structure, properties, and applications. *Macromol Rapid Comm* 25:771–787
36. Deep B, Abraham E, Cherian BM et al (2011) Structure, morphology and thermal characteristics of banana nano fibers obtained by steam explosion. *Bioresour Technol* 102:1988–1997
37. Dufresne A (2008) Processing of polymer nanocomposites reinforced with polysaccharide nanocrystals. *Macromolecules* 15(8):4111–4128
38. Eichhorn SJ (2011) Cellulose nanowhiskers: promising materials for advanced applications. *Soft Matter* 7(2):303–315
39. Eriksen Ø, Syverud K, Gregersen Ø (2008) The use of microfibrillated cellulose produced from kraft pulp as strength enhancer in TMP paper. *Nord Pulp Pap Res J* 23:299–304
40. Fakhouri FM, Fontes LCB, Gonçalves PVM et al (2007) Films and edible coatings based on native starches and gelatin in the conservation and sensory acceptance of Crimson grapes. *J Food Sci Technol* 27:369–375
41. Fang Z, Zhu H, Yuan Y et al (2014) Novel nanostructured paper with ultrahigh transparency and ultrahigh haze for solar cells. *Nano Lett* 14(2):765–773
42. Ferrer A, Filpponen I, Rodríguez A et al (2012) Valorization of residual empty palm fruit bunch fibers (EPFBF) by microfluidization: production of nanofibrillated cellulose and EPFBF nanopaper. *Bioresour Technol* 125:249–255
43. Frey MW (2008) Electrospinning cellulose and cellulose derivatives. *Polym Rev* 48(2): 378–391

44. Frone AN, Panaitescu DM, Donescu D (2011) Some aspects concerning the isolation of cellulose micro-and nano-fibers. *Sci Bull B Chem Mater Sci UPB* 73(2):133–152
45. Frone AN, Panaitescu DM, Donescu D et al (2011) Preparation and characterization of PVA composites with cellulose nanofibers obtained by ultrasonication. *BioResources* 6(1):487–512
46. Fujisawa S, Okita Y, Fukuzumi H et al (2011) Preparation and characterization of TEMPO-oxidized cellulose nanofibrils films with free carboxyl groups. *Carbohydr Polym* 84(1):579–583
47. Fukuzumi H, Saito T, Iwata T et al (2009) Transparent and high gas barrier films of cellulose nanofibers prepared by TEMPO-mediated oxidation. *Biomacromol* 10(1):162–165
48. Ghosh AK (2011) Fundamentals of paper drying-theory and application from industrial perspective. In: Ahasan A (ed) *Evaporation, codensation and heat transfer*. InTech, London, pp 535–541
49. Gomide JL, Gomes FJB (2015) Production and composition of unbleached pulps. In: Colodette JL, Gomes FJB (ed) *Cellulose pulp bleaching*. Federal University of Viçosa, Viçosa, Brazil. pp 59–115
50. Gonzalez I, Boufi S, Pèlach M et al (2012) Nanofibrillated cellulose as paper additive in eucalyptus pulps. *BioResources* 7(4):5167–5180
51. González I, Vilaseca F, Alcalá M et al (2013) Effect of the combination of biobeating and NFC on the physico-mechanical properties of paper. *Cellulose* 20(3):1425–1435
52. Gullichsen J, Paulapuro H (2000) *Papermaking science and technology: papermaking chemistry*. Fapet Oy, Helsinki
53. Gunaratne SA (2001) Paper, printing and the printing press: a horizontally integrative machohistory analysis. *Gazette* 63(6):459–479
54. Habibi Y, Lucia LA, Rojas OJ (2010) Cellulose nanocrystals: chemistry, self-assembly, and applications. *Chem Rev* 110(6):3479–3500
55. Hart PW, Rudie AW (2012) *The bleaching of pulp*, 5th edn. TAPPI Press, Atlanta
56. Hassan ML, Mathew AP, Hassan EA et al (2012) Nanofibers from bagasse and rice straw: process optimization and properties. *Wood Sci Technol* 46(1):193–205
57. He W, Jiang X, Sun F et al (2014) Extraction and characterization of cellulose nanofibers from *Phyllostachys nidularia* munro via a combination of acid treatment and ultrasonication. *BioResources* 9(4):6876–87
58. Henriksson M, Berglund LA, Isaksson P et al (2008) Cellulose nanopaper structures of high toughness. *Biomacromol* 9:1579–1585
59. Hii C, Gregersen ØW, Chinga-Carrasco G et al (2012) The effect of MFC on the pressability and paper properties of TMP and GCC based sheets. *Nord Pulp Pap Res J* 27(2):388–396
60. Hinche M, Bassa AGMC, Rottmann W et al (2011) Biotech enhanced levels of syringil lignin improves *Eucalyptus* pulping efficiency. In: Paper presented at the 5th international colloquium on eucalyptus pulp, Federal University of Viçosa, Porto Seguro, Brazil. 8–11 May 2011
61. Horáček P, Fajstavr M, Stojanović M (2017) The variability of wood density and compression strength of Norway spruce (*Picea abies*L./Karst.) within the stem. *Beskydy* 10(1–2):17–26
62. Hu Y, Topolkaraev V, Hitner A et al (2000) Measurement of water vapor transmission rate in highly permeable films. *J Appl Polym Sci* 81(3):1624–1633
63. Hu J, Zhang Q, Lee D-J (2018) Kraft lignin biorefinery: a proposal. *Bioresour Technol* 247:1181–1183
64. Hullmann A (2006). The economic development of nanotechnology—an indicators based analysis. European Commission, DG Research, Unit “Nano S&T—Convergent Science and Technologies”. Staff working paper. http://nanotechnology.cz/storage/nanoarticle_.pdf. Accessed 22 Feb 2018
65. Hult EL, Iotti M, Lenes M (2010) Efficient approach to high barrier packaging using microfibrillar cellulose and shellac. *Cellulose* 17(3):575–586

66. Höglund H (2009) Mechanical pulping. In: Ek M, Gellerstedt G, Henriksson G (eds) Pulp and paper chemistry and technology, vol 2. Pulping chemistry and technology. Walter de Gruyter GmbH & Co., Berlin, pp 57–89
67. Ianuzzi A (ed) (2012) Greener products: the making and marketing of sustainable brands. CRC Press, Boca Raton
68. International Organization for Standardization (2017) ISO/TC 6: paper, board and pulps
69. Ireana Yusra AF, Juahir H, Firdaus Nwana et al (2018) Controlling of Green nanocellulose fiber properties produced by chemo-mechanical treatment process via SEM, TEM, AFM and image analyzer characterization. *J Fundam Appl Sci* 10(1s):1–17
70. Isogai A (2013) Wood nanocelluloses: fundamentals and applications as new bio-based nanomaterials. *J Wood Sci* 59(6):449–459
71. Janardhanan S, Sain M (2006) Isolation of cellulose microfibrils—an enzymatic approach. *BioResources* 1:176–188
72. Jardim CM, Colodette JL (2015) Pulp chromophoric groups. In: Colodette JL, Gomes FJB (eds) Cellulose pulp bleaching. Federal University of Viçosa, Viçosa, Brazil, pp 203–215
73. Jiang F, Hsieh YL (2014) Super water absorbing and shape memory nanocellulose aerogels from TEMPO-oxidized cellulose nanofibrils via cyclic freezing-thawing. *J Mater Chem A* 2(2):350–359
74. John MJ, Thomas S (2008) Biofibres and biocomposites. *Carbohydr Polym* 71:343–364
75. Julkapli NM, Bagheri S (2016) Developments in nano-additives for paper industry. *J Wood Sci* 62:117–130
76. Kajanto I, Kosonen M (2012) The potential use of micro- and nanofibrillated cellulose as a reinforcing element in paper. *J-Fiber* 2(6):42–48
77. Kalia S, Boufi S, Celli A et al (2014) Nanofibrillated cellulose: surface modification and potential applications. *Colloid Polym Sci* 292(1):5–31
78. Keerati-u-rai M, Corredig M (2009) Effect of dynamic high pressure homogenization on the aggregation state of soy protein. *J Agric Food Chem* 57:3556–3562
79. Keller S (2013) Paper drying in the manufacturing process. In: Banik G, Brückle I (eds) Paper and water, 2nd edn. Butterworth Heinemann, Oxford, pp 173–211
80. Kim BY (2014) Investigation of coating color penetration depending on the properties of base paper. *J Korea TAPPI* 46(2):16–21
81. Klemm D, Kramer F, Moritz S et al (2011) Nanocelluloses: a new family of nature-based materials. *Angew Chem Int Ed* 50(2):5438–5466
82. Kobayashi S, Sakamoto J, Kimura S (2001) In vitro synthesis of cellulose and related polysaccharides. *Progr Polym Sci* 26(9):1525–1560
83. Kobayashi S, Uyama H, Masashi O (2001b) Enzymatic polymerization for precision polymer synthesis. *Bull Chem Soc Jpn* 74(4):635–613
84. Kolavali R (2013) Diffusion of ions in wood. Thesis, Chalmers University of Technology
85. Kumar V, Bollström R, Yang A et al (2014) Comparison of nano- and microfibrillated cellulose films. *Cellulose* 21(5):3443–3456
86. Kumar A, Singh SP, Singh AK (2014) Preparation and characterization of cellulose nanofibers from bleached pulp using a mechanical treatment method. *Tappi J* 13(5):25–31
87. Lai YZ (2012) Wood and wood products. In: Kent J (ed) Handbook of industrial chemistry and biotechnology. Springer, Boston, pp 1057–1115
88. Laine J, Lindström T, Nordmark GG et al (2002) Studies on topochemical modification of cellulosic fibres—part 2. The effect of carboxymethyl cellulose attachment on fibre swelling and paper strength. *Nord Pulp Pap Res J* 17(1):50–56
89. Lavoine N, Desloges I, Dufresne A et al (2012) Microfibrillated cellulose—its barrier properties and applications in cellulosic materials: a review. *Carbohydr Polym* 90(2):735–764
90. Lee KY, Tamelin T, Schultze K (2012) High performance cellulose nanocomposites: comparing the reinforcing ability of bacterial cellulose and nanofibrillated cellulose. *ACS Appl Mater Interfaces* 4(8):4078–86

91. Lengowski EC (2016) Formation and characterization of films with nanocellulose. Federal University of Paraná, Thesis
92. Lengowski EC, Muñiz GIB, Nisgoski S et al (2013) Cellulose acquirement evaluation methods with different degrees of crystallinity. *Sci Forest* 41(98):185–194
93. Lengowski EC, Bonfatti EA Jr (2017) Incorporation of amphoteric starch and nanocellulose in paper. In: Paper presented at the 1st semana de aperfeiçoamento em engenharia florestal, 17–24 July 2017. Federal University of Paraná, Brazil, Curitiba city
94. Lenze CJ, Peksa CA, Sun W et al (2016) Intact and broken cellulose nanocrystals as model nanoparticles to promote dewatering and fine-particle retention during papermaking. *Cellulose* 23(6):3951–3962
95. Li W, Wang R, Liu S (2011) Nanocrystalline cellulose prepared from softwood kraft pulp via ultrasonic-assisted hydrolysis. *BioResources* 6(4):4271–4281
96. Li J, Wei X, Wang Q et al (2012) Homogeneous isolation of nanocellulose from sugarcane bagasse by high pressure homogenization. *Carbohydr Polym* 90(4):1609–1613
97. Liu C, Li B, Du H et al (2016) Properties of nanocellulose isolated from corncob residue using sulfuric acid, formic acid, oxidative and mechanical methods. *Carbohydr Polym* 151:716–724
98. Liu Y, Sui Y, Liu C et al (2018) A physically crosslinked polydopamine/nanocellulose hydrogel as potential versatile vehicles for drug delivery and wound healing. *Carbohydr Polym* 188:27–36
99. Loranger E, Jradi K, Daneault C (2012) Nanocellulose production by ultrasound-assisted TEMPO oxidation of kraft pulp on laboratory and pilot scales. In: IEEE international ultrasonics symposium, IUS, Taipei, Taiwan, article number 6562112, pp 953–995
100. López-Rubio A, Lagaron JM, Ankerfors M et al (2007) Enhanced film forming and film properties of amylopectin using micro-fibrillated cellulose. *Carbohydr Polym* 68(4):718–727
101. MacDonald RG (ed) (1968) *The pulping of wood*, 2nd edn. McGraw-Hill Inc., New York
102. Manninen M, Kajanto I, Happonen J et al (2011) The effect of microfibrillated cellulose addition on drying shrinkage and dimensional stability of wood-free paper. *Nord Pulp Pap Res J* 26(3):297–305
103. Mättänen M, Tikka P (2012) Determination of phenomena involved in impregnation of softwood chips. Part 1: method for calculating the true penetration degree. *Nord Pulp Paper Res J* 27(3):550–558
104. Mertaniemi H et al (2012) Functionalized porous microparticles of nanofibrillated cellulose for biomimetic hierarchically structured superhydrophobic surfaces. *RSC Adv* 2:2882–2886
105. Missio AL, Mattos BD, Ferreira DF et al (2018) Nanocellulose-tannin films: from trees to sustainable active packaging. *J Clean Prod* 2:143–151
106. Mohanty AK, Drzal LT, Misra M (2003) Nano reinforcement of bio-based polymers—the hope and reality. *Polym Mater Sci Eng* 88:60–61
107. Moon RJ, Martini A, Naim J et al (2011) Cellulose nanomaterials review: structure, properties and nanocomposites. *Chem Soc Rev* 40:3941–3994
108. Nakatsubo F, Kamitakahara H, Hori M (1996) Cationic ring-opening polymerization of 3,6-Di-O-benzyl- α -D-glucose 1,2,4-Orthopivalate and the first chemical synthesis of cellulose. *J Am Chem Soc* 118(7):1677–1681
109. Nelson K, Retsina T (2014) Innovative nanocellulose process breaks the cost barrier. *Tappi J* 13(5):19–23
110. Nygards S (2011) *Nanocellulose in pigment coatings: aspects of barrier properties and printability in offset*. Dissertation, Linköping University
111. Oliveira RCP, Mateus M, Santos DMF (2018) Chronoamperometric and chronopotentiometric investigation of kraft black liquor. *Int J Hydrog Energy*. <https://doi.org/10.1016/j.ijhydene.2018.01.046>
112. Osong SH, Norgren S, Engstrand P (2016) Processing of wood-based microfibrillated cellulose and nanofibrillated cellulose, and applications relating to papermaking: a review. *Cellulose* 23(1):93–123

113. Österberg M, Vartiainen J, Lucenius J et al (2013) A fast method to produce strong NFC films as a platform for barrier and functional materials. *ACS Appl Mater Interfaces* 5(11): 4640–4647
114. Pääkkö M, Ankerfors M, Kosonen H et al (2007) Enzymatic hydrolysis combined with mechanical shearing and high-pressure homogenization for nanoscale cellulose fibrils and strong gels. *Biomacromol* 8(6):1934–1941
115. Podsiadlo P, Choi S-Y, Shim B et al (2005) Molecularly engineered nanocomposites: layer-by-layer assembly of cellulose nanocrystals. *Biomacromol* 6(6):2914–2918
116. Potulski DC (2016) Influence of nanocellulose on the physical and mechanical properties of primary and recycled paper of Pinus and Eucalyptus. Federal University of Paraná, Thesis
117. Potulski DC, Muñiz GIB, Klock U et al (2014) The influence of incorporation of microfibrillated cellulose on mechanical strength properties of paper. *Sci Forest* 42(103): 345–351
118. Rahimi M, Behrooz R (2011) Effect of cellulose characteristic and hydrolyze conditions on morphology and size of nanocrystal cellulose extracted from wheat straw. *Int J Polym Mater Po* 60(8):529–541
119. Rampazzo R, Alkan D, Gazzoti S et al (2017) Cellulose nanocrystals from lignocellulosic raw materials; for oxygen barrier coatings on food packaging films. *Packag Technol Sci*. <https://doi.org/10.1002/pts.2308>
120. Rantanen J, Maloney TC (2013) Press dewatering and nip rewetting of paper containing nano- and microfibril cellulose. *Nord Pulp Pap Res J* 28(4):582–587
121. Rantanen J, Pirttiniemi J, Kuosmanen P et al (2014) Development of a microfibrillated cellulose composite web forming method. In: Paper presented at TAPPI international conference on nanotechnology for renewable materials, TAPPI, Vancouver, 23–26 June 2014
122. Richmond F (2014) Cellulose nanofibers use in coated paper. University of Maine, Thesis
123. Robles NB (2014) Tailoring cellulose nanofibrils for advanced materials. KTH Royal Institute of Technology, Stockholm
124. Rodionova G, Lenes M, Eriksen Ø et al (2011) Surface chemical modification of microfibrillated cellulose: improvement of barrier properties for packaging applications. *Cellulose* 18(1):127–134
125. Rojas J, Bedoya M, Ciro Y (2015) Current trends in the production of cellulose nanoparticles and nanocomposites for biomedical applications. In: Poletto M, Ornaghi HL Jr (eds) *Cellulose—fundamental aspects and current trends*. InTech, Rijeka, pp 193–228
126. Róz ALD (2003) The future of plastics: biodegradable and photodegradable. *Polymers* 13(4):4–5
127. Sacui IA, Nieuwendaal RC, Burnett DJ et al (2014) Comparison of the properties of cellulose nanocrystals and cellulose nanofibrils isolated from bacteria, tunicate, and wood processed using acid, enzymatic, mechanical, and oxidative methods. *ACS Appl Mater Interfaces* 6(9):6127–6138
128. Saini S, Sillard C, Belgacem MN et al (2016) Nisin anchored cellulose nanofibers for long term antimicrobial active food packaging. *RSC Adv* 6:12437–12445
129. Saito T, Isogai A (2005) A novel method to improve wet strength of paper. *Tappi J* 4(3):3–8
130. Saito T, Kimura S, Nishiyama Y, Isogai A (2007) Cellulose nanofibers prepared by TEMPO-mediated oxidation of native cellulose. *Biomacromol* 8:2485–2491
131. Saito T, Nishiyama Y, Putaux J-L et al (2006) Homogeneous suspensions of individualized microfibrils from TEMPO-catalyzed oxidation of native cellulose. *Biomacromol* 7(6):1687–1691
132. Samir M, Alloin F, Dufresne A (2005) Review of recent research into cellulosic whiskers, their properties and their application in nanocomposite field. *Biomacromol* 6:612–626
133. Samyn P, Barhoum A, Öhlund T et al (2018) Review: nanoparticles and nanostructured materials in papermaking. *J Mater Sci* 53(1):146–184
134. Santos SD, Sansigolo CA (2007) Wood basic density effect of *Eucalyptus grandis* x *Eucalyptus urophylla* clones on bleached pulp quality. *Ciênc Flor* 17(1):53–63

135. Saunders RE, Pawlak JJ, Lee JM (2014) Properties of surface acetylated microfibrillated cellulose relative to intra- and inter-fibril bonding. *Cellulose* 21(3):1541–1552
136. Segura TES, Santos JRS, Sarto C et al (2016) Effect of kappa number variation on modified pulping of *Eucalyptus*. *BioResources* 11(4):9842–9855
137. Segura TES, Zanão M, Santos JRS et al (2012) Kraft pulping of the main hardwoods used around the world for pulp and paper production. In: 2012 TAPPI PEERS CONFERENCE, TAPPI Press, pp 1592–1599
138. Segura TES, Silva Júnior FG (2016) Potential of *C.citriodora* for kraft pulp production. *TAPPI J* 15(3):159–164
139. Sehaqui H, Allais M, Zhou Q et al (2011) Wood cellulose biocomposites with fibrous structures at micro- and nanoscale. *Comp Sci Technol* 71(3):382–387
140. Sehaqui H, Zhou Q, Berglund L (2013) Nanofibrillated cellulose for enhancement of strength in high-density paper structures. *Nord Pulp Pap Res J* 28(2):182–189
141. Serviço Nacional De Aprendizagem Industrial (2013) *Cellulose*. Senai, São Paulo
142. Sharma S, Zhang X, Nair SS et al (2014) Thermally enhanced high performance cellulose nano fibril barrier membranes. *RSC Adv* 4:45136–45142
143. Shatkin JA, Wegner TH, Bilek EM et al (2014) Market projections of cellulose nanomaterial-enabled products—part 1: applications. *Tappi J* 13(5):9–12
144. Sinko R, Qin X, Keten S (2015) Interfacial mechanics of cellulose nanocrystals. *MRS Bull* 40(4):340–348
145. Siqueira G, Bras J, Dufresne A (2009) Cellulose whiskers versus microfibrils: influence of the nature of the nanoparticle and its surface functionalization on the thermal and mechanical properties of nanocomposites. *Biomacromol* 10(2):425–432
146. Siró I, Plackett D (2010) Microfibrillated cellulose and new nanocomposite materials: a review. *Cellulose* 17(3):459–494
147. Siró I, Plackett D, Hedenqvist M et al (2011) Highly transparent films from carboxymethylated microfibrillated cellulose: the effect of multiple homogenization steps on key properties. *J Appl Polym Sci* 119(5):2652–2660
148. Sixta H (2006) *Handbook of pulp*. Wiley-VCH Verlag GmbH & Co, KGaA, Weinheim
149. Sjöström E (2013) *Wood chemistry fundamentals and applications*. Academic Press, New York
150. Smook G (2016) *Handbook for pulp and paper technologists*. TAPPI Press, Atlanta
151. Sofla MRK, Brown RJ, Tsuzuki T et al (2016) A comparison of cellulose nanocrystals and cellulose nanofibers extracted from bagasse using acid and ball milling methods. *Adv Nat Sci Nanosci Nanotech* 7:035004
152. Souza AC, Benze R, Ferrão ES et al (2012) Cassava starch biodegradable films: influence of glycerol and clay nanoparticles content on tensile and barrier properties and glass transition temperature. *LWT J Food Sci Technol* 46(1):110–117
153. Spence KL, Venditti RA, Rojas OJ et al (2010) The effect of chemical composition on microfibrillar cellulose films from wood pulps: water interactions and physical properties for packaging applications. *Cellulose* 17(4):835–848
154. Spence KL, Venditti RA, Rojas OJ et al (2011) A comparative study of energy consumption and physical properties of microfibrillated cellulose produced by different processing methods. *Cellulose* 18(4):1097–1111
155. Stelte W, Sanadi AR (2009) Preparation and characterization of cellulose nanofibers from two commercial hardwood and softwood pulps. *Ind Eng Chem Res* 48(24):11211–9
156. Su J, Mosse WKL, Sharman S et al (2013) Effect of tethered and free microfibrillated cellulose (MFC) on the properties of paper composites. *Cellulose* 20(4):1925–1935
157. Swinehart D (2012) *Fundamentals of refining*. MeadWestvaco Center for Packaging Innovation, Rayleigh
158. Syverud K, Stenius P (2009) Strength and barrier properties of MFC films. *Cellulose* 16: 75–85
159. Taipale T, Österberg M, Nykänen A et al (2010) Effect of microfibrillated cellulose and fines on the drainage of kraft pulp suspensions and paper strength. *Cellulose* 17(5):1005–1020

160. Taiz L, Zeiger E (2017) Plant physiology, 6th edn. Sinauer Associates, Sunderland
161. Technical Association of Pulp and Paper Industry (2013) T 236 om-13: kappa number of pulp. TAPPI Press, Atlanta
162. Thoorens G, Krier F, Leclercq B et al (2014) Microcrystalline cellulose, a direct compression binder in a quality by design environment—a review. *I J Pharm* 473(1–2):64–72
163. Tognetta L, Santos O, Dragoni O et al (2014) Paper. SENAI, São Paulo
164. Torvinen K (2014) Binding fillers for high filler content papers by using CNF/CMF. In: Paper presented at international conference on nanotechnology for renewable materials, TAPPI, Vancouver, 23–26 June 2014
165. Tuovinen L, Peltonen S, Jarvinen K (2003) Drug release from starch-acetate films. *J Control Release* 91(4):345–354
166. Usta I (2005) A review of the configuration of bordered pits to simulate the fluid flow. *Maderas Cien Tecnol* 7(2):121–132
167. Van Heiningen ARP (2006) Converting a kraft pulp mill into an integrated forest biorefinery. *Pulp Pap Canada* 107(6):38–43
168. Valenzuela A, Bentley JM, Lorenz RD (2005) Evaluation of torsional oscillations in paper machine sections. *IEEE Trans IndusAppl* 41(2):493–501
169. Viana LC, Muñoz GIB, Hein PRG et al (2016) NIR spectroscopy can evaluate the crystallinity and the tensile and burst strengths of nanocellulosic films. *Maderas Cienc Tecnol* 18(3):493–504
170. Viana LC, Muniz GIB, Magalhaes WLE (2017) Physical and mechanical properties of nano-structured films produced from the unbleached *Pinus* sp. kraft pulp. *Sci Forest* 45(116): 653–662
171. Vivian MA, Segura TES, Bonfatti Júnior EA et al (2015) Wood quality of *Pinus taeda* and *Pinus sylvestris* for kraft pulp production. *Sci Forest* 43(105):183–191
172. Vroom KE (1957) The H factor: a means of expressing cooking times and temperatures as a single variable. *Pulp Pap Canada* 58(3):228–231
173. Wang Y, Cao X, Zhang L (2006) Effects of cellulose whiskers on properties of soy protein thermoplastics. *Macromol Biosci* 6(7):524–531
174. Wang H, Li D, Zhang R (2013) Preparation of ultralong cellulose nanofibers and optically transparent nanopapers derived from waste corrugated paper pulp. *BioResources* 8:1374–1384
175. Wang B, Sain M (2007) Isolation of nanofibers from soybean source and their reinforcing capability on synthetic polymers. *Compos Sci Technol* 67(11–12):2521–2527
176. Wang B, Sain M (2007) Dispersion of soybean stock-based nanofiber in a plastic matrix. *Polym Int* 56(4):538–546
177. Wang B, Sain M, Oksman K (2007) Study of structural morphology of hemp fiber from the micro to the nanoscale. *Appl Compos Mater* 14:89–103
178. Wang Y, Wei Y, Li J et al (2013) Homogeneous isolation of nanocellulose from cotton cellulose by high pressure homogenization. *J Mater Sci Chem Eng* 1(5):49–52
179. Wang Q, Zhao X, Zhu JY (2014) Kinetics of strong acid hydrolysis of a bleached kraft pulp for producing cellulose nanocrystals (CNCs). *Ind Eng Chem Res* 53(27):11007–11014
180. Wegner T, Skog KE, Ince PJ et al (2010) Uses and desirable properties of wood in the 21st century. *J For* 108(4):165–173
181. Wågberg L, Decher G, Norgren M et al (2008) The build-up of polyelectrolyte multilayers of microfibrillated cellulose and cationic polyelectrolytes. *Langmuir* 24:784–795
182. Xie C, Liu Z-M, Wu P et al (2013) Optimization of preparation technology of alkali pretreated reed pulp nano-cellulose. *Chem Ind For Prod* 33(1):32–36
183. Xu Q, Li W, Cheng Z et al (2014) TEMPO/NaBr/NaClO-mediated surface oxidation of nanocrystalline cellulose and its microparticulate retention system with cationic polyacrylamide. *BioResources* 9(1):994–1006
184. Xu Y, Yin X, Lin T et al (2018) Silica retention by the addition of sodium metaaluminate during the impregnation stage of bamboo kraft pulping. *J Wood Chem Technol* 38(1):35–43

185. Zeni M et al (2015) Preparation of microcellulose (Mcc) and nanocellulose (Ncc) from eucalyptus kraft ssp pulp. *Polym Sci* 1:1–5
186. Zeni M, Favero D, Pacheco K et al (2015) Preparation of microcellulose (Mcc) and nanocellulose (Ncc) from Eucalyptus kraft ssp pulp. *Polym Sci* 1:1–5
187. Zimmermann T, Bordeanu N, Strub E (2010) Properties of nanofibrillated cellulose from different raw materials and its reinforcement potential. *Carbohydr Polym* 79:1086–1093

Impact of Nanoparticle Shape, Size, and Properties of Silver Nanocomposites and Their Applications



Arpita Hazra Chowdhury, Rinku Debnath, Sk. Manirul Islam and Tanima Saha

1 Introduction

The genesis of nanotechnology can be traced back to 1959 when in a meeting of the American Physical Society, Richard Feynman first introduced the branch of science [1]. One can define nanotechnology as the production and modification of structures which have at least one dimension less than 100 nm. The birth of nanoscience could be attributed to Michael Faraday as he had reported the intense red colour of stained glass, which originated from small particles of gold in 1857. He also reported that different size of gold particles gave rise to different resultant colours [2]. Recently, nanomaterials have emerged as very important materials in the scientific world as these act as a bridge between bulk materials and isolated atoms and molecules. They increase fractions of atoms at the surface due to their large surface to volume ratio. Nanomaterials have superior properties than the bulk substances due to the following attributes, like mechanical strength, thermal stability, catalytic activity, electrical conductivity, magnetic properties and optical properties etc. The applications of nanomaterials are continuously expanding and their applications in different fields are shown below (Fig. 1).

Arpita Hazra Chowdhury, Rinku Debnath—These authors contributed equally to this manuscript.

A. Hazra Chowdhury · Sk. Manirul Islam (✉)

Department of Chemistry, University of Kalyani, Kalyani, Nadia 741235,
West Bengal, India

e-mail: manir65@rediffmail.com

R. Debnath · T. Saha (✉)

Department of Molecular Biology and Biotechnology,
University of Kalyani, Kalyani, Nadia 741235, West Bengal, India

e-mail: sahatanima@klyuniv.ac.in

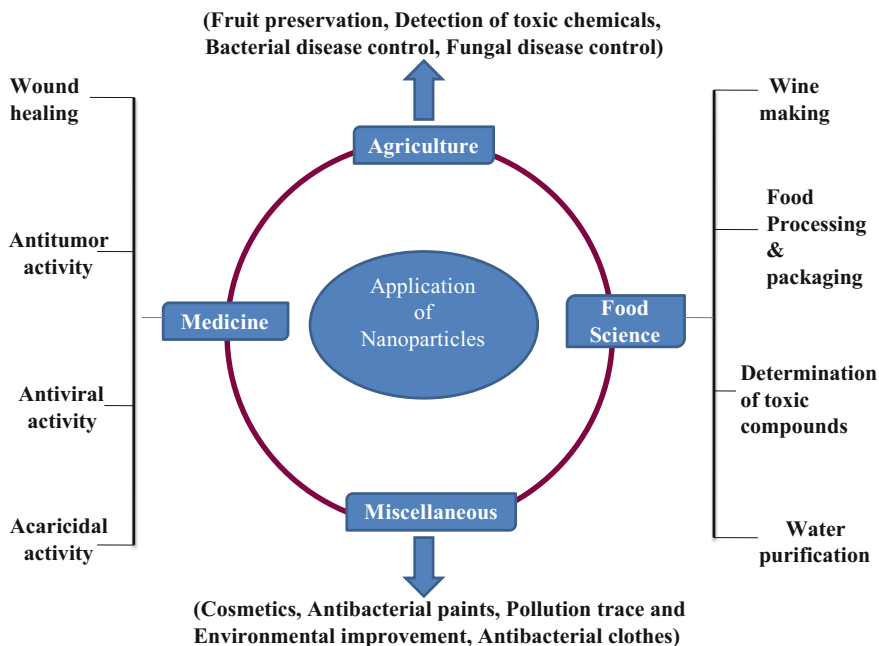


Fig. 1 Schematic illustration of different applications of nanoparticles

Researchers have growing interest in silver nanoparticles (AgNPs) as they have remarkable localized surface plasmon resonance and antimicrobial properties, which render them with unique properties for applications in broad-spectrum surface-enhanced Raman spectroscopy (SERS) [3, 4], as antimicrobial agents [5–7], biological/chemical sensors and biomedicine materials [8–10], biomarkers [11–13] and so on. Size of AgNPs usually varies within 1–100 nm. They are incorporated into industrial applications of catalysis, electronics, and photonics as they have unique electrical, optical and thermal properties. Recently, many synthetic methods and approaches for preparing AgNPs have been reported through physical, chemical, photochemical and biological routes. Every method has its own advantages and disadvantages like costs, scalability, particle sizes and size distribution and so on [14–18].

In recent years, nanocomposite (NC) materials have drawn much attention and interest at industrial and academic level due to their improved properties than single metal nanoparticles. Nanocomposite can be defined as the combination of materials to develop new properties of the materials where one of the materials has a size in the range of 1–100 nm. So, there are two parts to nanocomposite i.e. continuous phase and discontinuous reinforcing phase. Hence, nanocomposites can have a combined or have completely different electrochemical, mechanical, electrical, thermal, optical and catalytic properties of the component materials [19–23].

There can be different phases of nanocomposites such as zero-dimensional (0D) (core-shell), 1D (nanowires and nanotubes), 2D (lamellar) and 3D (metal matrix composites) [9]. Nanocomposite materials have developed as an appropriate replacement to overcome the limitations of microcomposites and monolithic while having synthetic challenges like the control of elemental composition and stoichiometry in the nanocluster phase. Nanocomposite materials have uniqueness in design and property combinations that are not observed in conventional composites and these properties establish the nanocomposites materials as the materials of the 21st century. Even though the first speculation on these properties was reported as early as 1992 [24], the general understanding of them is yet to be established.

The focus of this chapter is on silver nanocomposite systems. These NC materials have promising properties which make them suitable for wide range of structural and functional applications in various fields.

2 Different Synthesis Methods of Silver Nanoparticles

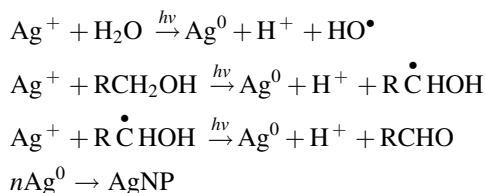
Different synthesis methods and approaches for AgNPs production have been reported by using chemical, physical, photochemical and biological routes. Each method has its own advantages and disadvantages involving costs, scalability, particle sizes and size distribution and so on [14–17, 25].

2.1 *Physical Methods*

In physical methods, metal nanoparticles are generally synthesized by evaporation-condensation, which is carried out at atmospheric pressure using a tube furnace. The source material is vaporized into a carrier gas, within a boat centred at the furnace. Different kinds of nanoparticles such as Ag, Au, PbS, and fullerene, have been produced using the evaporation/condensation technique [26–28]. Silver nanoparticles have been synthesized by laser ablation of the solution of metallic bulk materials [29, 30]. The most important advantage of laser ablation technique over another conventional method for synthesizing metal colloids is the absence of toxic chemical reagents in solutions. In summary, the physical synthesis utilizes the physical energies for preparing AgNPs with nearly narrow size distribution. The physical approach can produce large quantities of AgNPs in a single process as well as this is also the most effective method to produce AgNPs. On the other hand, primary costs for the investment of equipment have to be kept in mind before implementing such methods.

2.2 Photochemical Methods

This method is based on the light-assisted the reduction of the metal cation M^{n+} to M^0 . The mechanism of this method is based on the addition of one or more electrons to a photoexcited species. The aqueous and alcoholic solution of silver perchlorate ($AgClO_4$) was subjected to photoreduction by UV-light irradiation at 254 nm. This photochemical reaction involved electron transfer from a solvent molecule to the electronically excited state of Ag^+ to form Ag^0 . In most of the cases, UV excitation is usually required as the metal cations and/or the metal salts absorb only in this region. This method is advantageous in harsh conditions like increased temperatures can be avoidable resulting in effective control of shape and size of Silver nanoparticle (AgNP) [31].



Various photo-induced synthetic processes have been developed recently. Huang and Yang [32] synthesized AgNPs by photoreduction of $AgNO_3$ in layered inorganic clay suspensions. This suspension acts as a stabilizing agent which prevents aggregation of nanoparticles. Light irradiation leads to the disintegration of the AgNPs into a smaller size with a single mode distribution until a relatively stable size and diameter distribution were achieved [32]. However, this method requires high-end equipment and experimental environment.

2.3 Biological Methods

Lately, biosynthetic methods have emerged as a facile and simple alternative to more complex chemical synthetic methods to prepare AgNPs. In biosynthetic methods, natural reducing agents like polysaccharides, biological microorganisms like bacteria, and fungi or plant extracts, i.e. green chemistry are used. This method includes a broad range of natural resources for the synthesis of AgNPs. This method has several advantages over conventional chemical routes of synthesis and it is also an environment-friendly approach as well as a low-cost technique for nanoparticle synthesis. However, the drawback of this method is that it is not easy to synthesize a large quantity of AgNPs by using biological synthesis.

2.3.1 Microbe-Assisted Synthesis

There are two types of microbe-assisted synthesis of AgNPs:

- (a) **Bacterial Synthesis:** Bacteria can produce inorganic materials either intra- or extracellularly. Thus, they act as potential biofactories for the synthesis of nanoparticles such as gold and silver. Specifically, silver is widely known for its biological properties. AgNPs with different shapes and sizes can be effectively synthesized by varying different parameters using different bacteria such as *Klebsiella pneumoniae*, *Lactobacillus fermentum*, *Bacillus flexus*, *Escherichia coli*, and *Enterobacter cloacae* at different pH, temperatures and concentrations of AgNO₃ solutions [33–36].
- (b) **Fungal Synthesis:** Researchers have been interested in patenting their research work on the microbial synthesis of nanoparticles. One of these significant works is the synthesis of AgNPs with particle size 5–50 nm, harnessing wet biomass of *Trichoderma reesei* fungus after 120 h of continuous shaking at 28 °C [37]. When antimicrobial properties of AgNPs were tested on *Escherichia coli* and *Staphylococcus aureus*, it was found that *E. coli* was more susceptible to silver nanoparticles than *S. aureus* [38]. Extracellular nanoparticles were formed by using thermophilic fungus *Humicola* sp. which reacted with Ag(+) ions and reduced the precursor solution [39].

2.3.2 Plant-Mediated Synthesis

Microbe-mediated synthesis requires highly aseptic conditions and their maintenance which lowers the industrial feasibility of this method. Therefore, the plant extract mediated synthesis (Fig. 2) of nanoparticles is potentially advantageous

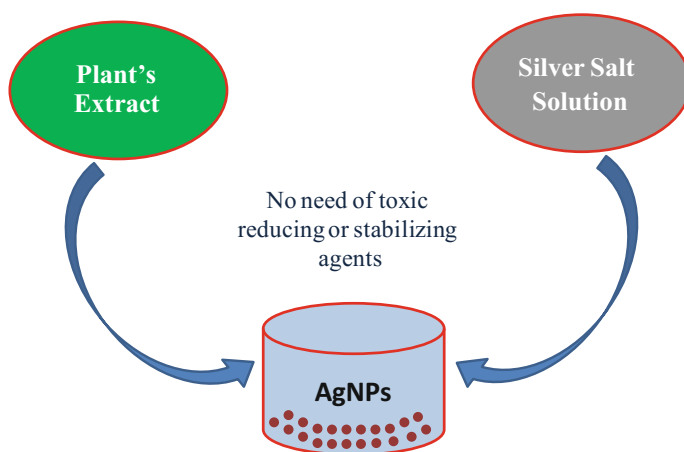


Fig. 2 Schematic diagram showing the one pot plant-mediated synthesis of silver nanoparticles

Table 1 Synthesis of silver nanoparticles using different plant extracts

Plants	Plant's part	Particle size (nm)	Particle shape	References
<i>Averrhoa carambola</i>	Fruit	12–16	Spherical	[41]
<i>Abutilon indicum</i>	Leaf	7–17	Spherical	[42]
<i>Withania somnifera</i>	Leaf	5–30	Spherical	[43]
<i>Eclipta prostrata</i>	Leaf	35–60	Triangles, pentagons, hexagons	[44]
<i>Nelumbo nucifera</i>	Leaf	25–80	Spherical, triangular	[45]
<i>Citrus sinensis</i>	Peel	10–35	Spherical	[46]
<i>Pelargonium graveolens</i>	Leaf	16–20	Spherical	[47]
<i>Tanaetum vulgare</i>	Fruit	10–40	Spherical	[48]
Tea extract	Leaf	20–90	Spherical	[49]
<i>Tribulus terrestris</i>	Fruit	16–28	Spherical	[50]

over microbe assisted synthesis due to the ease of improvement, the less biohazard and elaborate process of maintaining cell cultures [40]. It is the best way to synthesize nanoparticles without using any toxic chemical reducing and stabilizing agents as it provides natural capping agents for the stabilization of silver nanoparticles. A list of silver nanoparticles synthesis using different plant extracts is given in Table 1.

2.4 Chemical Methods

Besides all the methods described earlier, the most common method is the chemical reduction method for nanoparticle synthesis because of its convenience and simple equipment. It is required to control the growth of metal nanoparticles to prepare nanoparticles with a spherical shape and small size with a narrow particle size distribution. It is widely known that chemical reduction method can produce silver nanoparticles at low cost with high yield.

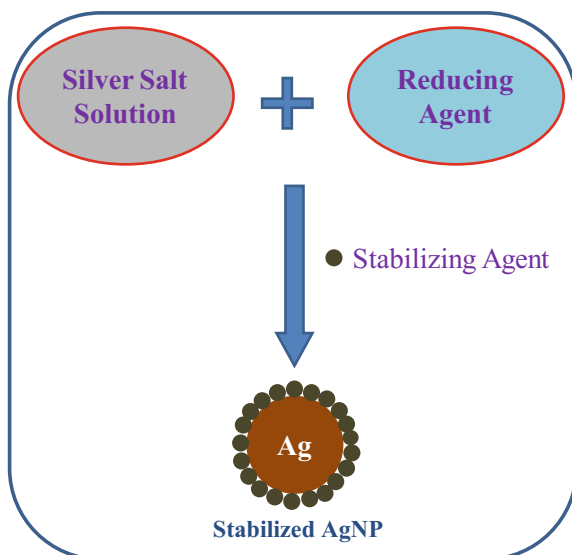
Usually, the chemical synthesis process of AgNPs in solution requires the following three main components: (1) metal precursors, (2) reducing agents and (3) stabilizing/capping agents. Generally, silver nitrate [51–54], silver acetate [55, 56], silver citrate [56–58], and silver chlorate [56, 57, 59] are the most frequently used precursors for the chemical synthesis of silver nanoparticles. Among various reducing agents, borohydride, citrate, ascorbate, and compounds with hydroxyl or carboxyl groups like aldehydes, alcohol, carbohydrates, and their derivatives

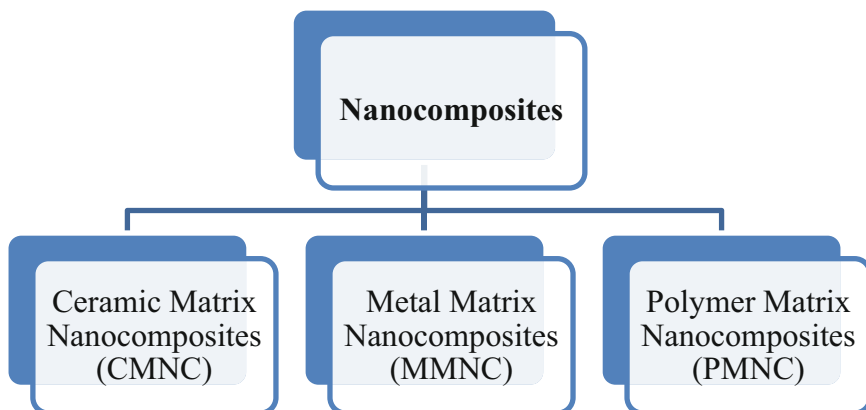
[60–63] are the most commonly used reductants. The colloidal solution formation from the reduction of silver salts involves two stages (i) nucleation and (ii) subsequent growth. It is also observed that the size and the shape of synthesized AgNPs are strongly dependent on these two stages. The two phenomenon i.e., nucleation and growth of initial nuclei can be controlled by adjusting different reaction parameters like reaction temperature, pH, precursors, reducing agents (i.e. NaBH₄, ethylene glycol, glucose) and stabilizing agents (i.e. PVA, PVP, sodium oleate) [64–66] (Fig. 3).

3 Nanocomposite Systems

Nanocomposite systems have been extensively studied since the 1990s and, it is observed that a steady and continuous increase has taken place in the number of publications on the subject, including time to time reviews. Nanocomposites can be defined as multiphase solid materials in which one of the phases has dimensions of less than 100 nm. There are two parts of NC: (i) continuous phase and (ii) discontinuous reinforcing phase. Nanocomposite materials can be classified into three different categories according to their matrix materials.

Fig. 3 Schematic diagram showing the one-pot chemical synthesis of AgNPs





Hence, nanocomposites can have a combined or have markedly different electrical, mechanical, electrochemical, thermal, catalytic and optical properties of the component materials [20–23].

3.1 Silver-Ceramic Matrix Nanocomposites

The synthesis of nanocomposites composed of noble metals (Au, Ag, Pt and Pd, as well as AuAg alloy) and ceramic matrixes such as metal oxides (ZnO, TiO₂, Cu₂O, MnO₂, Fe₂O₃, WO₃, CeO₂ etc) has received considerable attention in recent years for their applications in heterogeneous catalysis, photocatalysis, drug delivery, solar cells, surface enhanced Raman spectroscopy and many other important areas. Now-a-days, among the many nano-catalysts developed, controllable integration of different noble metals (e.g., Au, Ag, Pt, and Pd) and metal oxides (e.g., TiO₂, CeO₂, and ZrO₂) into single nanostructures has become one of the hottest research topics as they not only merge the functions of individual nanoparticles (NPs) but also show a unique combined and synergetic catalytic properties compared to the single-component materials. Generally, these composites are easily prepared by different methods like impregnation [67], co-precipitation [68], deposition-precipitation [69] and many more.

Liu et al. [70] synthesized plasmonic silver nanoparticle incorporated mesoporous metal-oxide (MMO) semiconductors to get increased photocatalysis. Different typical MMO such as TiO₂, ZnO, and CeO₂ semiconductors were synthesized by integrating evaporation-induced self-assembly and in situ pyrolysis of metal salts. Then Ag nanoparticles of different amounts were then loaded in these MMO semiconductors through an efficient photo-deposition process. The Ag nanocrystals were synthesized with sizes of 50–100 nm and then they were embedded in MMO semiconductors (Fig. 4) [70].

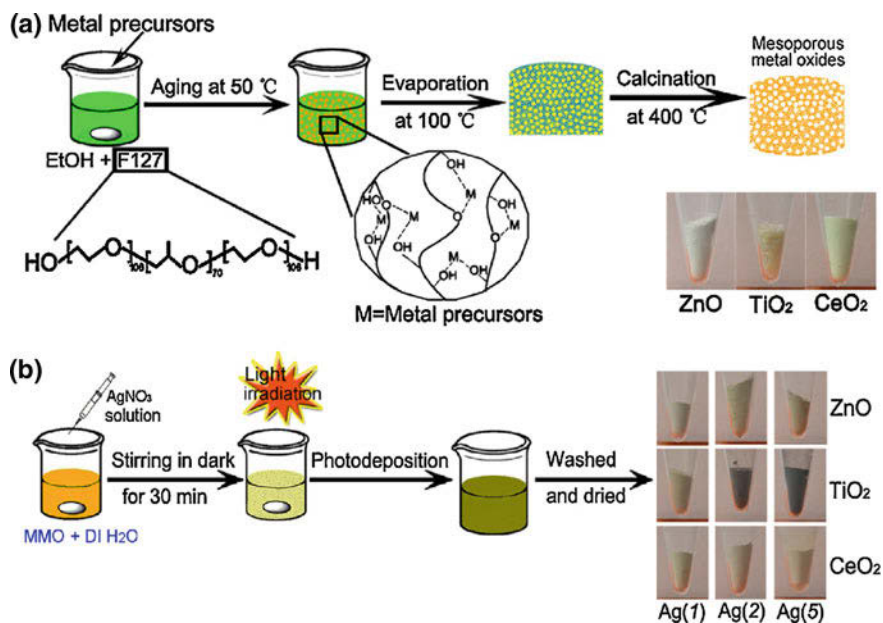


Fig. 4 Schematic diagram showing the synthesis of **a** mesoporous metal oxides (MMO) and **b** Ag/MMO nanocomposites [70]

3.2 Silver-Metal Matrix Nanocomposites

Metal matrix nanocomposites (MMNC) can be described as the materials where nanosized reinforcement material is implanted in a ductile metal or alloy matrix. Most common metal matrix nanocomposite for silver is gold-silver nanocomposite. Choudhury et al. [71, 72] synthesized Ag—Aunanocomposite substrates by a one-step galvanic replacement reaction from thin films of silver, coated on glass slides. Then there was deposition of metallic layers on the cleaned slides using a vacuum evaporation chamber under high vacuum ($<5 \times 10^{-7}$ Torr). At first, there was an adhesion layer of chromium deposited on the slides, then gold (~ 5 nm) and silver (~ 600 nm) films were deposited, without breaking vacuum [72].

3.3 Silver-Polymer Matrix Nanocomposites

Recently, researchers in various fields incorporated silver nanoparticles into the polymer matrix to enhance its performance. Polymer materials act not only as an excellent host for incorporating nanoparticles but also terminate the growth of the particles by controlling their nucleation [73]. Silver-polymer nanocomposites can be prepared by using two main approaches.

(a) Insitu Polymerization

In the in situ method, the silver nanoparticles are prepared inside a polymer by dissolving metallic precursor salt in the polymer, followed by chemical reduction of the precursor salt. The reduction of Ag^+ to Ag^0 takes place. Several reducing agents like sodium borohydride, hydrazine etc. are used in the reduction process. Curcumin-loaded chitosan-PVA silver nanoparticles film (CCPSNP) was prepared by adding AgNO_3 to chitosan solution. AgNP solution was formed, to which, poly(vinyl alcohol), glutaraldehyde (a crosslinker) and curcumin solution were added [74]. Ag-PVA film was prepared by Porel and his group by mixing an aqueous solution of AgNO_3 and poly(vinyl alcohol) (PVA) wherein the silver precursor AgNO_3 was reduced by the hydroxyl groups of the PVA macromolecule [75]. Further, Ag-polyaniline nanocomposite was prepared from a mixture of aniline and silver nitrate as precursor after well rinsing with nitric acid [76].

(b) Exsitu Polymerization

In the ex situ method, silver nanoparticles are formed first and then dispersed into a polymer matrix. The prepared nanoparticles show higher dispersibility in the polymer and get long-term stability against aggregation. Sonication provided the dispersion of nanoparticles in the polymer matrix [77]. Thin nanocomposite films of silver nanocrystal in polystyrene matrix were prepared by sonicating polystyrene and silver nanoparticles with toluene for even dispersion of the nanoparticles [78]. Silver embedded mesoporous polyaniline nanocomposite [79] and mesoporous cross-linked polymer (polyacrylic acid) (MCP-1) supported silver nanoparticles [80] were prepared by dispersing mesoporous polymers in TRIS stabilized AgNPs and then stirring it at room temperature for 1 h. At the end of the reaction, black coloured Ag-NPs containing mesoporous polymer mPANI/Ag and mesoporous polyacrylic acid/Ag nanocomposites were obtained (Fig. 5).

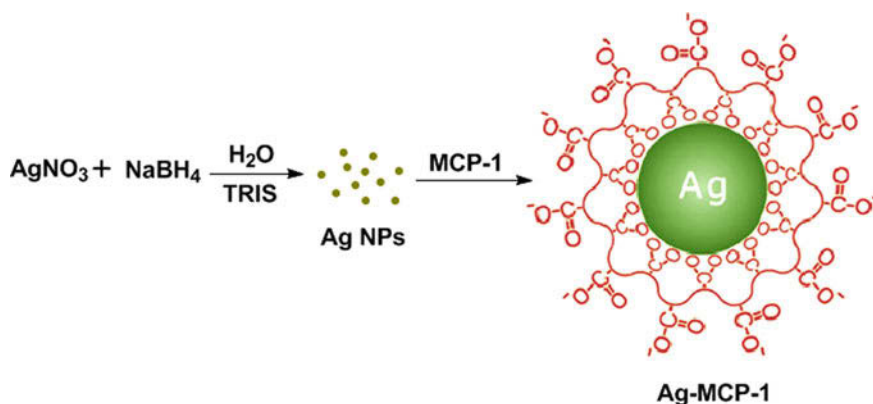


Fig. 5 Schematic diagram showing the synthesis of mesoporous polyacrylic acid/Ag nanocomposite [80]

4 Applications of Silver Nanocomposites

Recently silver nanocomposites are used extensively as anti-microbial agents in the health industry, food packaging, water treatment, agriculture, winemaking, and textile coatings. They are used as absorbents, photocatalysts, and sensors for detection and removal of environmental pollutants. Silver nanoparticles are also used in cosmetics, personal care products, and electronic devices.

4.1 Medical Field

Silver nanocomposites represent the most important polymer based functionalizing agent among the numerous nanocomposites due to their antimicrobial properties [81, 82]. Two different mechanisms are responsible for antimicrobial activity of silver nanoparticles, (a) adhesion to the cell surface, degradation of lipopolysaccharides, increasing permeability [83] and (b) penetration inside the bacterial cell, DNA damaging [84]. The silver nanoparticles release silver ions, which bind to electron donor groups in biological molecules containing sulfur, oxygen or nitrogen.

Liu et al. [85] demonstrated the doping of TiO_2 with silver that greatly improved photocatalytic bacterial inactivation. Polyethyleneglycol-polyurethane- TiO_2 silver nanocomposites showed antimicrobial activity against *E. coli* and *Bacillus subtilis* [86]. Silver nanoparticle encapsulated porous PMMA (poly methyl methacrylate) spheres have also shown good antimicrobial activity [87, 88]. Silver nanocomposites of POA (porous aluminium oxide) are effective against both Gram-negative and Gram-positive bacteria, *E. coli* and *Staphylococcus epidermidis*. Nadagouda and Varma [89] studied the applications of Ag nanocomposites with biodegradable carboxymethylcellulose in antimicrobial and antifungal coatings and biomedical devices. Zeolite is a porous crystalline material of hydrated sodium aluminosilicate. Silver can electrostatically bind to zeolite with high affinity and form silver-zeolite (SZ). Human saliva contains several kinds of cations which help in the release of silver ions from SZ and under anaerobic conditions they inhibit the growth of several oral bacteria [90]. SZ incorporated mouth rinses, acrylic resins, and tissue conditioners are used in the dental field [91]. Matsuura et al. [92] showed that tissue conditioners containing SZ exhibit the antimicrobial effect against *Candida albicans*, *Pseudomonas aeruginosa* and *Staphylococcus aureus* for a week and the use of SZ incorporated mouth rinse for 5 days showed a reduced plaque score [93].

Recently, synthesis of graphene oxide (GO) metal nanocomposites has gained attention due to excellent biocompatibility and high antibacterial activity of GO. They have possibilities to be used as an antibacterial reinforcement in biomaterials, exploration of the antiseptic properties and cytotoxic activity of GO-containing nanocomposites. Silver nanoparticles functionalized magnetic graphene oxide nanocomposites ($\text{GO}/\text{Fe}_3\text{O}_4/\text{PEI}/\text{Ag}$) were synthesized via in situ generate silver

nanoparticles on magnetic graphene oxide surface using polyethylenimine as reducing and stabilizing agent. The GO/Fe₃O₄/PEI/Ag nanocomposites highly enrich the low-abundant glycopeptides from complex biological samples. These nanocomposites might be used as low-abundant disease biomarkers. Dendritic polymer encapsulated silver nanoparticles have antimicrobial activity, besides this, they are also used as markers for cell labelling [94]. Lesniak et al. [95] demonstrated the synthesis of silver/dendrimer nanocomposites that can be used for in vitro cell labelling.

Carbohydrates such as glucose, lactose, and oligosaccharides significantly improve the cytotoxicity and cellular uptake nature of silver nanoparticles. To kill the cancerous cells in phototherapy, the carbohydrate modified silver nanoparticles can be used as a new tool [96]. Silver nanoparticles are used for the identification of calf thymus DNA (*ct*-DNA) due to their strong fluorescence signal [97]. For environmental protection and some disease detection applications such as disease diagnosis, drug screening, epidemic prevention, the oligonucleotide probe bound silver nanoparticles are used as an indicator in electrochemical DNA sensors that are able to pair with the sample DNA sequence. Based on aggregation, induced by sequence-specific hybridization, silver nanoparticles are used in the design of colourimetric assays [98]. In mouse models, silver nanoparticles exhibit anti-inflammatory property by inhibiting the interferon gamma activity and tumour necrosis factor alpha. Hence, they can play an important role in anti-inflammatory therapies [99, 100].

The emerging field of nanomedicine seeks to exploit the novel properties of engineered nanomaterials for diagnostics and therapeutic applications. The engineered nanoparticles are used to carry drug payloads, image contrast agents or gene therapeutics for diagnosing and treatment. Due to the antimicrobial activity of silver nanoparticles, they are now increasingly used in wound dressings, catheters, and various household products. The chitin-AgNP composite scaffolds have good blood clotting ability hence they are widely used in wound healing and tissue engineering applications [101]. In orthopaedic implants, prostheses, vascular grafts and wound dressings, nanosilver reinforced polymers are commonly used. Surgical instruments, contraceptive devices, creams, gels also contain nanosilver [102–104].

Cattles are affected and die by a tick *Rhipicephalus microplus* (Boophilus) leading to economic losses associated with milk, meat, and leather production [105]. Continuous use of acaricides (used for control of ticks) not only contaminates the environment and animal products but also helps in selection of chemical-resistant ticks. Bergeson [106] has reported that more than 100 silver containing pesticides are synthesized due to their antimicrobial and photocatalytic properties. Sodium dodecyl sulfate (SDS) modified photocatalytic TiO₂/Ag nanomaterial conjugated with dimethomorph (DMM) are used as nanopesticide in agriculture [107].

4.2 Food Industry

Active packaging is one type of innovative food packaging concept in which active functions like scavenging of oxygen, moisture or ethylene, emission of ethanol and flavours in addition to the antimicrobial activity are involved. Whereas in antimicrobial packaging, to reduce pathogen contamination and extend the shelf-life of food, an antimicrobial substance is included in the packaging system [108]. But the antimicrobial substances are neutralized or diffuse rapidly into the food, so their direct application has limited benefits. Incorporation of the antimicrobial substances into polymers allow their slow release in the packaging system for an extended period and prolong their effect during transport and storage of food [108]. The biopolymer-based films and coatings provide physical protection to foods, improve food quality and enhance the shelf life of food products due to their properties like - acting as barriers against moisture, oxygen, flavour, aroma, and oil [109]. Furthermore, biopolymer films act as antioxidants, antifungal agents, antimicrobials, colours, and other nutrients which are important in the food preservation [110, 111]. Due to these potential applications, biopolymer-based antimicrobial films are used in the food industry including meat, fish, poultry, cereals, cheese, fruits, and vegetables [112–114]. One of the promising candidates in this field is chitosan-based nanocomposite films. Chitosan is nontoxic, biodegradable, and biocompatible so the chitosan-based Ag nanocomposites are used in films and coatings [115, 116]. Silver nanoparticles are cost-effective and have a wide range of applicability than other antimicrobial substances. Hence, they are most commonly used polymer additive for antimicrobial food packaging [108, 117]. Besides the antimicrobial activity, they also extend the shelf life of fruits and vegetables by absorbing and decomposing ethylene from these foodstuffs [118].

Although silver releasing systems are commonly used as food additives in antimicrobial food packaging the single form of silver-releasing system is used in ion-exchange from microporous minerals sector in which silver ions partially replace the naturally occurring sodium ions in clays or other porous minerals [119]. When silver ions come in contact with moisture, they are again substituted by sodium ions present in the release environment and leached from the surface. This is practical, as the release of silver ions will depend on the amount of saline moisture, which is a crucial risk factor for the development of microbes on surfaces. A wide range of polymers and other surfaces are used to incorporate the substituted minerals. They are able to withstand any kind of plastic processing or operating temperature compared to natural antimicrobial substances for their low migration rate and high melting point [120]. Different clays like montmorillonites (MMT) [121] or tobermorites [122], silver zirconium phosphates [123] and silver zeolites [124–128] are used as minerals in this technology. These materials are generally manufactured as a 3–6 μm thick layer containing 1–5% silver content for coating on polymeric or stainless steel surfaces. The food processing equipment like cutlery, cutting boards, countertops, containers, etc. are coated with this type of layer.

Recently silver nanoparticles are marketed as nutrition supplement in form of a colloidal solution. The colloidal silver has high particle surface area for maximum effectiveness. Among the all-metal colloidal mineral supplements, the silver products are most popular [129].

In wine making SO_2 is an important antioxidant that inhibits fungal growth, effects of dissolved oxygen and endogenous enzymes of grape-polyphenoloxidase, tyrosinase and peroxidase [130]. SO_2 also improves the colour and stability of wine during ageing but it produces a negative effect on taste and odour [131–133]. Due to the antimicrobial activity of silver nanomaterials towards a wide range of Gram-negative and Gram-positive bacteria, some fungi and viruses can replace the SO_2 . It has been shown that use of colloidal silver complex (CSC) in the production of white and young red wine, displayed very similar chemical and sensory activities as that of SO_2 [134].

Electronic devices

Silver (Ag) is superior in electrical and thermal conductivities among all the noble metals. With increased surface energy, the melting point of the small-sized silver nanoparticle is drastically low which make them useful as conductive fillers in microelectronic materials [135]. The electrical loss is reduced with the lower surface roughness that gives better packing when the electrical conductors are fabricated with a thick film of silver nanoparticles [136]. Silver nanoparticles are used in electro-optical devices and sensors due to their electro reflectance (ER) effect. In this field, silver nanoparticles alter the absorption spectrum of the particle ensemble by changing the stored electronic charge on the particles with 100 times more effective than a bulk metal surface. Absorption spectroscopy directly monitors the changes in the electrostatic charge stored on small metal particles [137].

Silver nanoparticles have the ability to enhance electrical and optical properties of the polymer composites. Due to these superior properties of Ag, various conducting polymers like—polypyrrole, polythiophene, polyaniline based Ag nanocomposites are used in producing newer materials with high conductivity. Ag nanocomposites are produced in combination with silver nanowires (AgNWs) with conducting polymer matrices which are used as conductive filler and thermal interfacial material in sophisticated nanodevices [138–140]. The silver nanoparticle embedded dielectric Teflon matrix nanocomposites showed higher electrical conductivity with an increased film thickness at various silver nanoparticle concentration [141]. Multiwalled carbon nanotube (MWNTs) with high electrical and mechanical properties are used as electrodes. Silver (Ag)/polymer composites prepared by incorporating multiwalled carbon nanotubes (MWNTs) with Ag nanoparticles significantly improve the electrical conductivity [142]. To improve an optical sensor fiber, Ag-doped silica nanocomposite is coated along with bent silica on the surface of it, which is useful to trace ammonia in a gas sample [143]. Silver-poly vinyl alcohol (Ag-PVA) composites are used for light guiding and optical sensing applications [144, 145]. Silver nanoparticles rapidly trap free electrons so they are used in semiconductor applications. TiO_2 is a known photocatalyst capped with the silver nanoparticle to form TiO_2 -AgNP nanocomposites

which are used for better semiconductor efficiency [143, 146]. Conventional solar cells coated with silicon was not efficient because silicon is a poor absorber of light. To enhance the light trapping efficiency of such solar cells, undercoating silver nanoparticles along with silicon layer was performed [147]. Similarly, in ultra-thin light filters, the silver-Poly-methylmethacrylate-Poly ethylene terephthalate membrane (Ag-PMMA-PET) composite has been used. Li et al. [148] suggested that use of PVP nanofibers-silver nanoparticle composites as a thin layer in organic solar cells increase 19.44% power conversion efficiency.

Glucose oxidase (GOx) immobilized stimuli-responsive silver nanocomposites are used in optical enzyme biosensor for sugar concentration analysis. When a sugar solution like glucose is applied to the surface of optical enzyme biosensor, the interparticle distances of the silver nanoparticle present in the silver nanocomposite are increased and absorbance strength of surface Plasmon resonance is decreased [149]. In a variety of techniques like fluorescent, radiochemical, piezoelectric technology and quartz crystal microbalance, silver nanoparticle probes are also used.

4.3 Water Treatment

As silver has antimicrobial property, Ag nanoparticles and nanocomposites are used in water purification devices to retard the growth of waterborne microorganisms. The Ag-containing nanomaterials can be a more cost-effective way for water treatment than the chemical method. The stabilization and immobilization of AgNPs in polymeric ion-exchange matrices is a promising approach for water treatment processes. Porous silver nanocomposites such as cellulose/Ag nanocomposites [150], chitosan-silver nanocomposites [151], silica silver composite [152] etc., have antibacterial characteristics and are also used in water treatment system. Silver nanoparticle loaded biocompatible and biodegradable polymer, sodium carboxymethyl cellulose (CMC) is used for water treatment application [153]. Zeolite, sand, fibreglass, anion and cation resin loaded silver nanoparticles are used in groundwater purification systems as antibacterial agent [154]. Porous ceramic Ag nanocomposites and thin-film layer containing nanosilver particles are used as an antibacterial substance in water filter [155]. The silver incorporated nanocomposite ceramic membranes exhibit good salt rejection capacity and effective membrane permeability [156]. Ceramic membrane fabricated silver nanoparticles have also been used to prevent biofouling [157]. Ceramic materials, casting with nanoparticles have more nanoscale pore sizes than ceramics with conventional sintering [158]. Silver-decorated ceramic membrane removes all *E. coli* after 24 h of contact time, whereas, bacterial growth was observed on undecorated membranes [159]. Silver nanoparticles incorporated polymeric membranes are also used to mitigate the biofouling and reduce the microbial activity by releasing silver ions from the membrane. The released silver ions lyse the bacterial cell by adhering to the cell and change the permeability of the cell wall [160, 161].

Fe₃O₄-silver nanomaterial is a bifunctional composite that has the superparamagnetic and antibacterial properties against *E. coli*, *Staphylococcus epidermis*, and *B. subtilis*. This nanocomposite easily removes material from water with its superparamagnetic property. To enhance the water treatment efficiency and recyclability, mesoporous polymer nanofiber membranes can be designed with specific pore sizes and desired filtration properties. So, the nanocomposites of supermagnetic/silver nanoparticle/polymer nanofiber can be a promising water disinfectant [162, 163].

4.4 Textiles

The silver nanoparticles form bonds with the fibers of different fabrics like nylon, polyester, cotton and produce the nanoengineered fabrics. High surface area relative to the volume of particles that increases their chemical reactivity with the fibers helps the nanoparticles stick to fabrics more permanently. The silver nanoparticle coated fabrics prevent moisture, odour, dirt and have antibacterial activity. Due to these properties, they are used in medical bandages, bed linings and sports socks [164]. For prevention of foot odour, use of silver containing socks has been reported. Polymer nanofiber coated fabric materials are applied in textiles to act as a waterproof textile material. Polymer nanofiber layered fabrics with dirt-proof, stain-proof, and superhydrophobic properties are also available. Perelshteinet al. [165] prepared the silver nanocomposite coated fabric and experimented with its antibacterial activity against *E. coli* and *Staphylococcus aureus*. Silver nanocomposites of Polyvinyl alcohol (PVA) and polyvinyl pyrrolidone (PVP) are the type of polymer nanocomposites that form hydrogen bonds with polar species [166].

4.5 Nanopaints

Polymer matrices give high stability to the silver nanoparticles in polymer-silver nanocomposites. Without significant oxidation and aggregation, the polymer nanocomposites can be stable up to 200 °C. This property enables the production of silver nanoparticle embedded homogeneous paints. The nanopaint is an excellent coating material with outstanding antibacterial properties that can be applied to various surfaces including wood, glass, and polystyrene [167].

4.6 Personal Care Products

Silver nanoparticles used in cleanser soap has been found useful in treating acne due to their bactericidal and fungicidal properties [168]. Nanosilver containing hand

wash of 15 mg per litre concentration has been found highly efficient with short exposure time to prevent transmission of infectious diseases [169]. Some toothpaste and tooth creams contain silver nanoparticles which produce a natural tooth enamel like a thin layer in teeth to reduce sensitivity and pain. For imparting freshness to the skin, certain day and night creams contain silver nanoparticles [170]. Zinc oxide (ZnO) or titanium dioxide (TiO₂) effectively absorb UV light. Incorporation of silver nanoparticles in ZnO and TiO₂ make them small and transparent, enabling them to exclusively absorb UV light excluding the absorption of visible light. Silver nanoparticles are also used in face and body foams, wet wipes, deodorants, lip products etc. [171].

5 Conclusion

The present review focuses on a vivid discussion relating to various synthesis methods and applications of silver nanocomposites. This would help in our understanding and enrich our knowledge on the recent developments in the area. However, further research is needed for nanocomposite synthesis through faster, economical and cheap processes and the extension of their applicability that would result in increased specificity, competence and efficiency. Keeping in view the increasing environmental pollution due to different anthropogenic activities care should be taken to focus on green synthesis methods that would not release any harmful chemicals in the environment. Novel strategies can also be implemented towards the development of recyclable and biodegradable nanocomposite materials preventing their accumulation in the environment after disposal.

References

1. Khademhosseini A, Langer R (2006) Drug delivery and tissue engineering. *Chem Eng Prog* 102(2):38–42
2. Faraday M (1857) The bakerian lecture: experimental relations of gold (and other metals) to light. *Philos Trans R Soc Lond* 147:145
3. Konrad MP, Doherty AP, Bell SEJ (2013) Stable and uniform SERS signals from self assembled two-dimensional interfacial arrays of optically coupled Ag nanoparticles. *Anal Chem* 85:6783–6789
4. Meheretu GM, Cialla D, Popp J (2014) Surface enhanced raman spectroscopy on silver nanoparticles. *Inter J Biochemistry Biophysics* 2:63–67
5. Franci G, Falanga A, Galdiero S, Palomba L, Rai M, Morelli G, Galdiero M (2015) Silver nanoparticles as potential antibacterial agents. *Molecules* 20:8856–8874
6. Jana S, Pal T (2007) Synthesis, characterization and catalytic application of silver nanoshell coated functionalized polystyrene beads. *J Nanosci Nanotechnol* 7:2151–2156
7. Stiufiuc R, Iacovita C, Lucaciu CM, Stiufiuc G, Dutu AG, Braescu C, Leopold N (2013) SER-sactive silver colloids prepared by reduction of silver nitrate with short-chain polyethylene glycol. *Nanoscale Res Lett* 8:47

8. Evtugyn GA, Shamagsumova RV, Padnya PV, Stoikov II, Antipin IS (2014) Cholinesterase sensor based on glassy carbon electrode modified with Ag nanoparticles decorated with macrocyclic ligands. *Talanta* 127:9–17
9. Thanha NTK, Green LAW (2010) Functionalisation of nanoparticles for biomedical applications. *Nano Today* 5:213–230
10. Alon N, Miroshnikov Y, Perkas N, Nissan I, Gedanken A, Shefi (2014) Substrates coated with silver nanoparticles as a neuronal regenerative material. *Int J Nanomed* 9:23–31
11. Bu Y, Lee S (2012) Influence of dopamine concentration and surface coverage of Au shell on the optical properties of Au, Ag, and Ag@Au shell nanoparticles. *ACS Appl Mater Interfaces* 4:3923–3931
12. Luo Y, Ma L, Zhang X, Liang A, Jiang Z (2015) SERS detection of dopamine using label free acridine red as molecular probe in reduced graphene oxide/silver nanotriangle sol substrate. *Nanoscale Res Lett* 10:230
13. Rivero PJ, Urrutia A, Goicoechea J, Matias IR, Arregui FJ (2013) A lossy mode resonance optical sensor using silver nanoparticles-loaded films for monitoring human breathing. *Sens Actuators B* 187:40–44
14. El-Nour KMM, Eftaiha A, Al-Reda A, Ammar AA (2010) Synthesis and applications of silver nanoparticles. *Arabian J Chem* 3:135–140
15. Smetana AB, Klabunde KJ, Sorensen CM (2005) Synthesis of spherical silver nanoparticles by digestive ripening, stabilization with various agents, and their 3-D and 2-D superlattice formation. *J Colloid Interface Sci* 284:521–526
16. Wakuda D, Kim KS, Suganuma K (2008) Room temperature sintering of Ag nanoparticles by drying solvent. *Scrip Mater* 59:649–652
17. Lee H, Chou KS (2005) Inkjet printing of nanosized silver colloids. *Nanotechnology* 16:2436–2441
18. Anna Z, Ewa S, Adriana Z, Maria G, Jan H (2009) Preparation of silver nanoparticles with controlled particle size. *Procedia Chem* 1:1560–1566
19. Twardowski TE (2007) Introduction to nanocomposite materials: properties, processing, characterization. Destech Publications, Incorporated, Lancaster, PA
20. Pina S, Oliveira JM, Reis RL (2015) Natural-based nanocomposites for bone tissue engineering and regenerative medicine: a review. *Adv Mater* 27:1143–1169
21. Rafiee MA, Rafiee J, Wang Z, Song H, Yu Z-Z, Koratkar N (2009) Enhanced mechanical properties of nanocomposites at low graphene content. *ACS Nano* 3:3884–3890
22. Mariano M, El Kissi N, Dufresne A (2014) Cellulose nanocrystals and related nanocomposites: review of some properties and challenges. *J Polym Sci, Part B Polym Phys* 52:791–806
23. Hu H, Onyebueke L, Abatan A (2010) Characterizing and modeling mechanical properties of nanocomposites-review and evaluation. *J Miner Mater Charact Eng* 9:275
24. Gleiter H (1992) Materials with ultrafine microstructures: retrospectives and perspectives. *Nanostruct Mater* 1:1–19
25. Anna Z, Ewa S, Adriana Z, Maria G, Jan H (2009) Preparation of silver nanoparticles with controlled particle size. *ProcediaChem* 1:1560–1566
26. Gurav AS, Kodas TT, Wang LM, Kauppinen EI, Joutsensaari J (1994) Generation of nanometer-size fullerene particles via vapor condensation. *J Joutsensaari Chem Phys Lett* 218:304–308
27. Kruis F, Fissan H, Rellinghaus B (2000) Sintering and evaporation characteristics of gas-phase synthesis of size selected PbS nanoparticles. *Mater Sci Eng B* 69:329–334
28. Magnusson MH, Depfert K, Malm JO, Bovin JO, Samuelson L (1999) Gold nanoparticles: production, reshaping, and thermal charging. *J Nanoparticle Res* 1:243–251
29. Mafune F, Takeda J, Kondow T, Sawabe H (2000) Formation and size control of silver nanoparticles by laser ablation in aqueous solution. *J Phys Chem B* 104:9111–9117
30. Sylvestre JP, Kabashin AV, Sacher E, Meunier M, Luong JHT (2004) Stabilization and size control of gold nanoparticles during laser ablation in aqueous cyclodextrins. *J Am Chem* 126:7176–7177

31. Pacioni NL, Borsarelli CD, Rey V, Veglia AV (2015) Synthetic routes for the preparation of silver nanoparticles: a mechanistic perspective. In: Udekwu KI, Alarcón EL, Griffith M (eds) Silver nanoparticle applications: in the fabrication and design of medical and biosensing devices. Springer International Publishing AG, Switzerland, p 13
32. Huang H, Yang Y (2008) Preparation of silver nanoparticles in inorganic clay suspensions. *Compos Sci Technol* 68:2948–2953
33. Zhang M, Zhang K, De Gussem B, Verstraete W, Field R (2014) The antibacterial and anti-biofouling performance of biogenic silver nanoparticles by *Lactobacillus fermentum*. *Biofouling* 30:347–357
34. Priyadarshini S, Gopinath V, MeeraPriyadarshini N, MubarakAli D, Velusamy P (2013) Synthesis of anisotropic silver nanoparticles using novel strain, *Bacillus flexus* and its biomedical application. *Colloids Surf B* 102:232–237
35. Gurunathan S, Kalishwaralal K, Vaidyanathan R et al (2009) Biosynthesis, purification and characterization of silver nanoparticles using *Escherichia coli*. *Colloids Surf B Biointerfaces* 74:328–335
36. Minaeian S, Shahverdi AR, Nohi AS, Shahverdi HR (2008) Extracellular biosynthesis of silver nanoparticles by some bacteria. *J Sci (Islamic Azad University)* 17:1–4
37. Vahabi K, Ali Mansoori G, Karimi S (2011) Biosynthesis of silver nanoparticles by fungus, *Trichoderma reesei*. *Insciences J* 1:65–79
38. Ahmad T, Wani IA, Manzoor N, Ahmed J, Asiri AM (2013) Biosynthesis, structural characterization and antimicrobial activity of gold and silver nanoparticles. *Colloids Surf B* 107:227–234
39. Syed A, Saraswati S, Kundu GC, Ahmad A (2013) Biological synthesis of silver nanoparticles using the fungus *Humicola* sp. and evaluation of their cytotoxicity using normal and cancer cell lines. *Spectrochim Acta Part A Mol Biomol Spectrosc* 114:144–147
40. Kalishwaralal K, Deepak V, Pandian SRK, Kartikeyan B, Kottaisamy M, Gurunathan S (2010) Biosynthesis of silver and gold nanoparticles using *Brevibacterium casei*. *Colloids Surf B Biointerfaces* 77:257–262
41. Hazra Chowdhury I, Ghosh S, Roy M, Naskar MK (2015) Green synthesis of water-dispersible silver nanoparticles at room temperature using green carambola (star fruit) extract. *J Sol-Gel Sci Technol* 73:199–207
42. Ashokkumar S, Ravi S, Kathiravan V, Velmurugan S (2015) Synthesis of silver nanoparticles using *A. indicum* leaf extract and their antibacterial activity. *Spectrochim Acta Part A Mol Biomol Spectroscopy* 134:34–39
43. Raut RW, Mendhulkar VD, Kashid SB (2014) Photosensitized synthesis of silver nanoparticles using *Withania somnifera* leaf powder and silver nitrate. *J Photochem Photobiol, B* 132:45–55
44. Rajakumar G, Abdul Rahuman A (2011) Larvicidal activity of synthesized silver nanoparticles using *Eclipta prostrata* leaf extract against filariasis and malaria vectors. *Acta Trop* 118:196–203
45. Santhoshkumar T, Rahuman AA, Rajakumar G, Marimuthu S, Bagavan A, Jayaseelan C (2011) Synthesis of silver nanoparticles using *Nelumbo nucifera* leaf extract and its larvicidal activity against malaria and filariasis vectors. *Parasitol Res* 108:693–702
46. Kaviya S, Santhanalakshmi J, Viswanathan B, Muthumary J, Srinivasan K (2011) Biosynthesis of silver nanoparticles using *Citrus sinensis* peel extract and its antibacterial activity. *Spectrochim Acta A Mol Biomol Spectrosc* 79:594–598
47. Shankar SS, Ahmad A, Sastry M (2003) Geranium leaf assisted biosynthesis of silver nanoparticles. *Biotechnol Prog* 19:1627–1631
48. Dubey SP, Lahtinen M, Sillianpää M (2010) Tansy fruit mediated greener synthesis of silver and gold nanoparticles. *Process Biochem* 45:1065–1071
49. Suna Q, Cai X, Li J, Zheng M, Chenb Z, Yu CP (2014) Greensynthesis of silver nanoparticles using tea leaf extract and evaluation of their stability and antibacterial activity. *Colloid Surf A Physicochem Eng Aspects* 444:226–231

50. Gopinatha V, Ali MD, Priyadarshini S, Thajuddin N, MeeraPriyadharsshini N, Velusamy P (2012) Biosynthesis of silvernanoparticles from *Tribulus terrestris* and its antimicrobial activity: a novel biological approach. *Colloid Surf B Biointerface* 96:69–74
51. Tolaymat TM, El Badawy AM, Genaidy A, Scheckel KG, Luxton TP, Suidan M (2010) An evidence-based environmental perspective of manufactured silver nanoparticle in syntheses and applications: a systematic review and critical appraisal of peer-reviewed scientific papers. *Sci Total Environ* 408:999–1006
52. Creighton JA, Blatchford CG, Albrecht MG (1979) Plasma resonance enhancement of Raman scattering by pyridine adsorbed on silver or gold sol particles of size comparable to the excitation wavelength. *J Chem Soc Faraday Trans* 75:790–798
53. Sui Z, Chen X, Wang L, Chai Y, Yang C, Zhao J (2005) An improved approach for synthesis of positively charged silver nanoparticles. *ChemLett* 34:100–101
54. Shi Y, Lv L, Wang H (2009) A facile approach to synthesize silver nanorods capped with sodium triphosphosphate. *Mater Lett* 63:2698–2700
55. Horiuchi Y, Shimada M, Kamegawa T, Mori K, Yamashita H (2009) Size-controlled synthesis of silver nanoparticles on Ti-containing mesoporous silica thin film and photoluminescence enhancement of rhodamine 6G dyes by surface plasmon resonance. *J Mater Chem* 19:6745–6749
56. Zielinska A, Skwarek E, Zaleska A, Gazda M, Hupka J (2009) Preparation of silver nanoparticle. *ProcChem* 1:1560
57. Henglein A, Giersig M (1999) Formation of colloidal silver nanoparticles. Cappingaction of citrate. *J Phys Chem B* 103:9533–9539
58. Pietrobon B, Kitaev V (2008) Photochemical synthesis of monodisperse size-controlled silver decahedral nanoparticles and their remarkable optical properties. *Chem Mater* 20:5186–5190
59. Mayer AB, Hausner SH, Mark JE (2002) Colloidal silver nanoparticles generated in the presence of protective cationic polyelectrolytes. *Poly J* 32:15–22
60. Sivaraman SK, Elango I, Kumar S, Santhanam V (1997) Room-temperature synthesis of gold nanoparticles—size-control by slow addition. *CurrSci* 7:1055–1059
61. Yoosaf K, Ipe BI, Suresh CH, Thomas KG (2007) In situ synthesis of metal nanoparticles and selective naked-eye detection of lead ions from aqueous media. *J PhysChem C* 111:12839–12847
62. Chou KS, Lai YS (2004) Effect of polyvinyl pyrrolidone molecular weights on the formation of nanosized silver colloids. *Mater Chem Phys* 83:82–88
63. Chou KS, Lu YC, Lee HH (2005) Effect of alkaline ion on the mechanism and kinetics of chemical reduction of silver. *Mater Chem Phys* 94:429–433
64. Chen SF, Zhang H (2012) Aggregation kinetics of nanosilver in different watercondition. *Adv Nat Sci Nanosci Nanotechnol* 3:035006-1–035006-7
65. Dang TMD, Le TTT, Blance EF, Dang MC (2012) Influence of surfactant on the preparation of silvernanoparticles by polyol method. *Adv Nat Sci Nanosci Nanotechnol* 3:035004-1–035004-4
66. Patil RS, Kokate MR, Jambhale C, Pawar SM, Han SH, Kolekar SS (2012) One-pot synthesis of PVA-capped silvernanoparticles their characterization and biomedicalapplication. *Adv. Nat. Sci.: Nanosci Nanotechnol.* 3:015013-1–015013-7
67. Zorn K, Giorgio S, Halwax E, Henry CR, Grönbeck H, Rupprechter G (2011) CO oxidation on technological Pd–Al₂O₃ catalysts: oxidation state and activity. *J Phys Chem C* 115:1103–1111
68. Guzman J, Carrettin S, Fierro-Gonzalez JC, Hao YL, Gates BC, Corma A (2005) CO oxidation catalyzed by supported gold: cooperation between gold and nanocrystalline rare-earth supports forms reactive surface superoxide and peroxide species. *Angew Chem Int Ed* 44:4778–4781
69. Wang Y, Van de Vyver S, Sharma KK, Leshkov YR (2014) Insights into the stability of gold nanoparticles supported on metal oxides for the base-free oxidation of glucose to gluconic acid. *Green Chem* 16:719–726

70. Liu T, Li B, Hao Y, Han F, Zhang L, Hu L (2015) A general method to diverse silver/mesoporous–metal–oxidenanocomposites with plasmon-enhanced photocatalytic activity. *Appl Catal B* 165:378–388
71. Liu K, Bai Y, Zhang L, Yang Z, Fan Q, Zheng H, Yin Y, Gao C (2016) Porous Au-Ag nanospheres with high-density and highly accessible hotspots for SERS analysis 16:3675–3681
72. Dutta Choudhury S, Badugu R, Ray K, Lakowicz JR (2012) Silver–gold nanocomposite substrates for metal-enhanced fluorescence: ensemble and single-molecule spectroscopic studies. *J Phys Chem C* 116:5042–5048
73. Li HJ, Zhang AQ, Hu Y, Sui L, Qian DJ, Chen M (2012) Large-scale synthesis and self-organization of silver nanoparticles with tween 80 as a reductant and stabilizer. *Nanoscale Res Lett* 7:612
74. Vimala K, Yallapu MM, Varaprasad K, Reddy NN, Ravindra S, Naidu NS, Raju KM (2011) Fabrication of curcumin encapsulated chitosan-PVA silver nanocomposite films for improved antimicrobial activity. *J Biomater Nanobiotechnol* 2:55–64
75. Porel S, Ramakrishna D, Hariprasad E, Gupta D, Radhakrishnan P (2011) Polymer thin film with in situ synthesized silver nanoparticles as a potent reusable bactericide. *Curr Sci* 101:927–934
76. Wankhade Y, Kondawar S, Thakare S, More P (2013) Synthesis and characterization of silver nanoparticles embedded in polyaniline nanocomposite. *Adv Mater* 4:89–93
77. Guo Q, Ghadiri R, Weigel T, Aumann A, Gurevich E, Esen C, Medenbach O, Cheng W, Chichkov B, Ostendorf A (2014) Comparison of in situ and ex situ methods for synthesis of two-photon polymerization polymer nanocomposites. *Polymers* 6:2037–2050
78. Lim MH, Ast DG (2001) Free-standing thin films containing hexagonally organized silver nanocrystals in a polymer matrix. *Adv Mater* 13:718–721
79. Mandi U, Roy AS, Banerjee B, Islam SM (2014) A novel silver nanoparticle embedded mesoporous polyaniline (mPANI/Ag) nanocomposite as a recyclable catalyst in the acylation of amines and alcohols under solvent free conditions. *RSC Adv.* 4:42670–42681
80. Mandi U, Roy AS, Kundu SK, Roy S, Bhaumik A, Islam SM (2016) Mesoporous polyacrylic acid supported silver nanoparticles as an efficient catalyst for reductive coupling of nitrobenzenes and alcohols using glycerol as hydrogen source. *J Colloid Interface Sci* 472:202–209
81. Panáček A, Kvítek L, Pucek R, Kolář M, Večeřová R, Pizúrová N, Sharma VK, Nevěčná TJ, Zbořil R (2006) Silver colloid nanoparticles: synthesis, characterization, and their antibacterial activity. *J Phys Chem B* 110(33):16248–16253
82. Kvítek L, Panáček A, Soukupova J, Kolář M, Večeřová R, Pucek R, Holecova M, Zbořil R (2008) Effect of surfactants and polymers on stability and antibacterial activity of silver nanoparticles (NPs). *J Phys Chem C* 112(15):5825–5834
83. Sondi I, Salopek-Sondi B (2004) Silver nanoparticles as antimicrobial agent: a case study on *E. coli* as a model for Gram-negative bacteria. *J Colloid Interface Sci* 275(1):177–182
84. Li Q, Mahendra S, Lyon DY, Brunet L, Liga MV, Li D, Alvarez PJ (2008) Antimicrobial nanomaterials for water disinfection and microbial control: potential applications and implications. *Water Res* 42(18):4591–4602
85. Liu J, Li X, Zuo S, Yu Y (2007) Preparation and photocatalytic activity of silver and TiO₂ nanoparticles/montmorillonite composites. *Appl Clay Sci* 37(3):275–280
86. Shah MSAS, Nag M, Kalagara T, Singh S, Manorama SV (2008) Silver on PEG-PU-TiO₂ polymer nanocomposite films: an excellent system for antibacterial applications. *Chem Mater* 20(7):2455–2460
87. Kong H, Jang J (2008) Antibacterial properties of novel poly (methyl methacrylate) nanofiber containing silver nanoparticles. *Langmuir* 24(5):2051–2056
88. Lee EM, Lee HW, Park JH, Han YA, Ji BC, Oh W, Deng Y, Yeum JH (2008) Multihollow structured poly (methyl methacrylate)/silver nanocomposite microspheres prepared by suspension polymerization in the presence of dual dispersion agents. *Colloid Polymer Sci* 286(12):1379–1385

89. Nadagouda MN, Varma RS (2007) Synthesis of thermally stable carboxymethyl cellulose/metal biodegradable nanocomposites for potential biological applications. *Biomacromol* 8 (9):2762–2767
90. Kawahara K, Tsuruda K, Morishita M, Uchida M (2000) Antibacterial effect of silver-zeolite on oral bacteria under anaerobic conditions. *Dent Mater* 16(6):452–455
91. Casemiro LA, Martins CHG, Pires-de-Souza FDC, Panzeri H (2008) Antimicrobial and mechanical properties of acrylic resins with incorporated silver–zinc zeolite–part I. *Gerodontology* 25(3):187–194
92. Matsuura T, Abe Y, Sato Y, Okamoto K, Ueshige M, Akagawa Y (1997) Prolonged antimicrobial effect of tissue conditioners containing silver-zeolite. *J Dent* 25(5):373–377
93. Morishita M, Miyagi M, Yamasaki Y, Tsuruda K, Kawahara K, Iwamoto Y (1998) Pilot study on the effect of a mouthrinse containing silver zeolite on plaque formation. *J Clin Dent* 9:94–96
94. Aroca RF, Goulet PJ, dos Santos DS, Alvarez-Puebla RA, Oliveira ON (2005) Silver nanowire layer-by-layer films as substrates for surface-enhanced Raman scattering. *Anal Chem* 77(2):378–382
95. Lesniak W, Bielinska AU, Sun K, Janczak KW, Shi X, Baker JR, Balogh LP (2005) Silver/dendrimer nanocomposites as biomarkers: fabrication, characterization, in vitro toxicity, and intracellular detection. *Nano Lett* 5(11):2123–2130
96. Oh Y, Suh D, Kim Y, Lee E, Mok JS, Choi J, Baik S (2008) Silver-plated carbon nanotubes for silver/conducting polymer composites. *Nanotechnology* 19(49):495602
97. Sur I, Cam D, Kahraman M, Baysal A, Culha M (2010) Interaction of multi-functional silver nanoparticles with living cells. *Nanotechnology* 21(17):175104
98. Vilela D, González MC, Escarpa A (2012) Sensing colorimetric approaches based on gold and silver nanoparticles aggregation: chemical creativity behind the assay. A review. *Anal Chim Acta* 751:24–43
99. Shin SH, Ye MK, Kim HS, Kang HS (2007) The effects of nano-silver on the proliferation and cytokine expression by peripheral blood mononuclear cells. *Int Immunopharmacol* 7 (13):1813–1818
100. Tian J, Wong KK, Ho CM, Lok CN, Yu WY, Che CM, Chiu JF, Tam PK (2007) Topical delivery of silver nanoparticles promotes wound healing. *ChemMedChem* 2(1):129–136
101. Wu J, Balasubramanian S, Kagan D, Manesh KM, Campuzano S, Wang J (2010) Motion-based DNA detection using catalytic nanomotors. *Nat Comm* 1:36
102. Chen X, Schluesener HJ (2008) Nanosilver: a nanoparticle in medical application. *Toxicol Lett* 176(1):1–12
103. Tolaymat TM, El Badawy AM, Genaidy A, Scheckel KG, Luxton TP, Suidan M (2010) An evidence-based environmental perspective of manufactured silver nanoparticle in syntheses and applications: a systematic review and critical appraisal of peer-reviewed scientific papers. *Sci Total Environ* 408(5):999–1006
104. Gupta A, Silver S (1998) Molecular genetics: silver as a biocide: will resistance become a problem? *Nat Biotechnol* 16(10):888
105. Ghosh S, Azhahianambi P, de la Fuente J (2006) Control of ticks of ruminants, with special emphasis on livestock farming systems in India: present and future possibilities for integrated control—a review. *Exp Appl Acarol* 40(1):49–66
106. Bergeson LL (2010) Nanosilver: US EPA’s pesticide office considers how best to proceed. *Environ Qual Manage* 19(3):79–85
107. Yan J, Huang K, Wang Y, Liu S (2005) Study on anti-pollution nano-preparation of dimethomorph and its performance. *Chin Sci Bull* 50(2):108–112
108. Quintavalla S, Vicini L (2002) Antimicrobial food packaging in meat industry. *Meat Sci* 62 (3):373–380
109. Wong DW, Camirand WM, Pavlath AE (1994) Development of edible coatings for minimally processed fruits and vegetables. *Edible Coat Films Improve Food Qual* 65–88
110. Han JH (2005) New technologies in food packaging: overview. *Innov Food Packag* 3–11

111. Mei Y, Zhao Y (2003) Barrier and mechanical properties of milk protein-based edible films containing nutraceuticals. *J Agric Food Chem* 51(7):1914–1918
112. Labuza TP, Breene WM (1989) Applications of “active packaging” for improvement of shelf-life and nutritional quality of fresh and extended shelf-life foods. *J Food Process Preserv* 13(1):1–69
113. Cha DS, Chinnan MS (2004) Biopolymer-based antimicrobial packaging: a review. *Crit Rev Food Sci Nutr* 44(4):223–237
114. Cagri A, Ustunol Z, Ryser ET (2004) Antimicrobial edible films and coatings. *J Food Prot* 67(4):833–848
115. Rhim JW, Hong SI, Park HM, Ng PK (2006) Preparation and characterization of chitosan-based nanocomposite films with antimicrobial activity. *J Agric Food Chem* 54(16):5814–5822
116. Hu Z, Chan WL, Szeto YS (2008) Nanocomposite of chitosan and silver oxide and its antibacterial property. *J Appl Polym Sci* 108(1):52–56
117. Appendini P, Hotchkiss JH (2002) Review of antimicrobial food packaging. *Innov Food Sci Emerg Technol* 3(2):113–126
118. Li H, Li F, Wang L, Sheng J, Xin Z, Zhao L, Xiao H, Zheng Y, Hu Q (2009) Effect of nano-packing on preservation quality of Chinese jujube (*Ziziphus jujuba* Mill. var. *inermis* (Bunge) Rehd). *Food Chem* 114(2):547–552
119. Rai M, Yadav A, Gade A (2009) Silver nanoparticles as a new generation of antimicrobials. *Biotechnol Adv* 27(1):76–83
120. Simpson K (2003) Using silver to fight microbial attack. *Plast Addit Compd* 5(5):32–35
121. Praus P, Turicová M, Machovič V, Študentová S, Klementová M (2010) Characterization of silver nanoparticles deposited on montmorillonite. *Appl Clay Sci* 49(3):341–345
122. Coleman NJ, Bishop AH, Booth SE, Nicholson JW (2009) Ag⁺ and Zn²⁺ exchange kinetics and antimicrobial properties of 11 Å tobermorites. *J Eur Ceram Soc* 29(6):1109–1117
123. Cowan MM, Abshire KZ, Houk SL, Evans SM (2003) Antimicrobial efficacy of a silver-zeolite matrix coating on stainless steel. *J Ind Microbiol Biotechnol* 30(2):102–106
124. Galeano B, Korff E, Nicholson WL (2003) Inactivation of vegetative cells, but not spores, of *Bacillus anthracis*, *B. cereus*, and *B. subtilis* on stainless steel surfaces coated with an antimicrobial silver-and zinc-containing zeolite formulation. *Appl Environ Microbiol* 69(7):4329–4331
125. Matsumura Y, Yoshikata K, Kunisaki SI, Tsuchido T (2003) Mode of bactericidal action of silver zeolite and its comparison with that of silver nitrate. *Appl Environ Microbiol* 69(7):4278–4281
126. Nakane T, Gomyo H, Sasaki I, Kimoto Y, Hanzawa N, Teshima Y, Namba T (2006) New antiaxillary odour deodorant made with antimicrobial Ag-zeolite (silver-exchanged zeolite). *Int J Cosmet Sci* 28(4):299–309
127. Akdeniz Y, Ülkü S (2008) Thermal stability of Ag-exchanged clinoptilolite rich mineral. *J Therm Anal Calorim* 94(3):703–710
128. Gulbranson SH, Hud JA, Hansen RC (2000) Argyria following the use of dietary supplements containing colloidal silver protein. *Cutis* 66(5):373–374
129. Romano P, Suzzi G (1993) Sulfur dioxide and wine microorganisms 373–393
130. Bakker J, Bridle P, Bellworthy SJ, Garcia-Viguera C, Reader HP, Watkins SJ (1998) Effect of sulphur dioxide and must extraction on colour, phenolic composition and sensory quality of red table wine. *J Sci Food Agric* 78(3):297–307
131. Blaise A, Bertrand A (1998) Altérations organoleptiques des vins. *Oenologie. Fondements Scientifique et Technologiques* 1182–1216
132. Stratford M, Rose AH (1985) Hydrogen sulphide production from sulphite by *Saccharomyces cerevisiae*. *Microbiology* 131(6):1417–1424
133. Izquierdo-Cañas PM, García-Romero E, Huertas-Nebreda B, Gómez-Alonso S (2012) Colloidal silver complex as an alternative to sulphur dioxide in winemaking. *Food Control* 23(1):73–81

134. Umadevi M, Christy AJ (2013) Optical, structural and morphological properties of silver nanoparticles and its influence on the photocatalytic activity of TiO₂. *Spectrochim Acta Part A Mol Biomol Spectrosc* 111:80–85
135. Chen D, Qiao X, Qiu X, Chen J (2009) Synthesis and electrical properties of uniform silver nanoparticles for electronic applications. *J Mater Sci* 44(4):1076–1081
136. Jiang H, Moon KS, Li Y, Wong CP (2006) Surface functionalized silver nanoparticles for ultrahigh conductive polymer composites. *Chem Mater* 18:2969–2973
137. Alshehri AH, Jakubowska M, Młozniak A, Horaczek M, Rudka D, Free C, Carey JD (2012) Enhanced electrical conductivity of silver nanoparticles for high frequency electronic applications. *ACS Appl Mater Interfaces* 4(12):7007–7010
138. Nam S, Cho HW, Lim S, Kim D, Kim H, Sung BJ (2012) Enhancement of electrical and thermomechanical properties of silver nanowire composites by the introduction of nonconductive nanoparticles: experiment and simulation. *ACS Nano* 7(1):851–856
139. Yu YH, Ma CCM, Teng CC, Huang YL, Lee SH, Wang I, Wei MH (2012) Electrical, morphological, and electromagnetic interference shielding properties of silver nanowires and nanoparticles conductive composites. *Mater Chem Phys* 136(2):334–340
140. Lee J, Lee P, Lee HB, Hong S, Lee I, Yeo J, Lee SS, Kim TS, Lee D, Ko SH (2013) Room-temperature nanosoldering of a very long metal nanowire network by conducting-polymer-assisted joining for a flexible touch-panel application. *Adv Func Mater* 23(34):4171–4176
141. Chapman R, Mulvaney P (2001) Electro-optical shifts in silver nanoparticle films. *Chem Phys Lett* 349(5):358–362
142. Wei H, Eilers H (2008) Electrical conductivity of thin-film composites containing silver nanoparticles embedded in a dielectric fluoropolymer matrix. *Thin Solid Films* 517(2):575–581
143. Guo H, Tao S (2007) Silver nanoparticles doped silica nanocomposites coated on an optical fiber for ammonia sensing. *Sens Actuators B Chem* 123(1):578–582
144. Marques-Hueso J, Abargues R, Canet-Ferrer J, Valdes JL, Martinez-Pastor J (2010) Resist-based silver nanocomposites synthesized by lithographic methods. *Microelectron Eng* 87(5):1147–1149
145. Ananth AN, Umapathy S, Sophia J, Mathavan T, Mangalaraj D (2011) On the optical and thermal properties of in situ/ex situ reduced Ag NP's/PVA composites and its role as a simple SPR-based protein sensor. *Appl Nanosci* 1(2):87–96
146. Ghosh S, Das AP (2015) Modified titanium oxide (TiO₂) nanocomposites and its array of applications: a review. *Toxicol Environ Chem* 97(5):491–514
147. Hutter E, Fendler JH, Roy D (2001) Surface plasmon resonance studies of gold and silver nanoparticles linked to gold and silver substrates by 2-aminoethanethiol and 1, 6-hexanedithiol. *J Phys Chem B* 105(45):11159–11168
148. Li X, Choy WCH, Lu H, Sha WE, Ho AHP (2013) Efficiency enhancement of organic solar cells by using shape-dependent broadband plasmonic absorption in metallic nanoparticles. *Adv Func Mater* 23(21):2728–2735
149. Endo T, Yanagida Y, Hatsuzawa T (2008) Quantitative determination of hydrogen peroxide using polymer coated Ag nanoparticles. *Measurement* 41(9):1045–1053
150. Pinto RJ, Marques PA, Neto CP, Trindade T, Daina S, Sadocco P (2009) Antibacterial activity of nanocomposites of silver and bacterial or vegetable cellulosic fibers. *Acta Biomater* 5(6):2279–2289
151. Vimala K, Mohan YM, Sivudu KS, Varaprasad K, Ravindra S, Reddy NN, Padma Y, Sreedhar B, MohanaRaju K (2010) Fabrication of porous chitosan films impregnated with silver nanoparticles: a facile approach for superior antibacterial application. *Colloids Surf B* 76(1):248–258
152. Egger S, Lehmann RP, Height MJ, Loessner MJ, Schuppler M (2009) Antimicrobial properties of a novel silver-silica nanocomposite material. *Appl Environ Microbiol* 75(9):2973–2976

153. Hebeish A, Hashem M, El-Hady MA, Sharaf S (2013) Development of CMC hydrogels loaded with silver nano-particles for medical applications. *Carbohydr Polym* 92(1):407–413
154. Mpenyana-Monyatsi L, Mthombeni NH, Onyango MS, Momba MN (2012) Cost-effective filter materials coated with silver nanoparticles for the removal of pathogenic bacteria in groundwater. *Int J Environ Res Pub Health* 9(1):244–271
155. Kim ES, Hwang G, El-Din MG, Liu Y (2012) Development of nanosilver and multi-walled carbon nanotubes thin-film nanocomposite membrane for enhanced water treatment. *J Membr Sci* 394:37–48
156. Kim DG, Kang H, Han S, Lee JC (2012) The increase of antifouling properties of ultrafiltration membrane coated by star-shaped polymers. *J Mater Chem* 22(17):8654–8661
157. Taurozzi JS, Arul H, Bosak VZ, Burban AF, Voice TC, Bruening ML, Tarabara VV (2008) Effect of filler incorporation route on the properties of polysulfone–silver nanocomposite membranes of different porosities. *J Membr Sci* 325(1):58–68
158. Kim J, Van der Bruggen B (2010) The use of nanoparticles in polymeric and ceramic membrane structures: review of manufacturing procedures and performance improvement for water treatment. *Environ Pollut* 158(7):2335–2349
159. DiGiano FA (2008) In pursuit of innovative membrane technology. In: IWA Membrane Research Conference. University of Massachusetts
160. Lv Y, Liu H, Wang Z, Liu S, Hao L, Sang Y, Liu D, Wang J, Boughton RI (2009) Silver nanoparticle-decorated porous ceramic composite for water treatment. *J Membr Sci* 331(1):50–56
161. Banerjee M, Mallick S, Paul A, Chattopadhyay A, Ghosh SS (2010) Heightened reactive oxygen species generation in the antimicrobial activity of a three component iodinated chitosan–silver nanoparticle composite. *Langmuir* 26(8):5901–5908
162. Gong P, Li H, He X, Wang K, Hu J, Tan W, Zhang S, Yang X (2007) Preparation and antibacterial activity of Fe₃O₄@ Ag nanoparticles. *Nanotechnology* 18(28):285604
163. Jain P, Pradeep T (2005) Potential of silver nanoparticle-coated polyurethane foam as an antibacterial water filter. *Biotechnol Bioeng* 90(1):59–63
164. Czajka R (2005) Development of medical textile market. *Fibres Text Eastern Eur* 13(1):13–15
165. Perelshtein I, Applerot G, Perkas N, Guibert G, Mikhailov S, Gedanken A (2008) Sonochemical coating of silver nanoparticles on textile fabrics (nylon, polyester and cotton) and their antibacterial activity. *Nanotechnology* 19(24):245705
166. Dallas P, Sharma VK, Zboril R (2011) Silver polymeric nanocomposites as advanced antimicrobial agents: classification, synthetic paths, applications, and perspectives. *Adv Coll Interface Sci* 166(1):119–135
167. Kumar A, Vemula PK, Ajayan PM, John G (2008) Silver-nanoparticle-embedded antimicrobial paints based on vegetable oil. *Nat Mater* 7(3):236–241
168. Lohani A, Verma A, Joshi H, Yadav N, Karki N (2014) Nanotechnology-based cosmeceuticals. *ISRN Dermatol*
169. Prabhu S, Poulouse EK (2012) Silver nanoparticles: mechanism of antimicrobial action, synthesis, medical applications, and toxicity effects. *Int Nano Lett* 2(1):32
170. Gleiche M, Hoffschulz H, Lenhert S (2006) Nanotechnology in consumer products. *Nanoforum Rep* 1–30
171. Gajbhiye S, Sakharwade S (2016) Silver nanoparticles in cosmetics. *J Cosmet Dermatol Sci Appl* 6(1):48

Toxicological Evaluations of Nanocomposites with Special Reference to Cancer Therapy



Arpita Hazra Chowdhury, Arka Bagchi, Arunima Biswas
and Sk. Manirul Islam

1 Introduction

Nanotechnology is developing a new era with the development of previously unknown materials and creating possibilities having the profound impact on the economic status, environment, and society. The nanotechnology tool is allowing scientists and manufactures to fabricate materials literally molecule-by-molecule. Properties associated with matter, custom design of previously unexplored structures, devices and unique systems with remarkable properties, like considerably increased strength, significantly decreased weight, much increased electrical conductivity or having the capacity to change shape, colour could be harnessed. Their applications in the field of modern medical and biological research are immense. Though researchers have devised various techniques and well defined intricate strategies to deliver poorly-soluble drugs into the infected tissue or cells, challenges remain to design drug delivery in a target-specific manner without causing the negative impact on the normal cells and tissues. The synthesis of nanoparticles and nanocomposites covering a broad range of metal, metal-oxide, and semiconductors to fabricate nanostructures with varying morphology are now being used in various ongoing research to successfully deal with the challenges and overcome obstacles. Moreover, nanoparticles or nanofibers in fabrics enhance various physical resistance, without increasing weight, thickness or stiffness of the fabric. Water filters that are only 15–20 nm wide can sieve very small particles, including virtually all viruses and bacteria. Hence this method is presently being implemented as a cost-efficient, portable water treatment system, improving the quality of drinking

A. Hazra Chowdhury · Sk. Manirul Islam (✉)
Department of Chemistry, University of Kalyani, Kalyani Nadia, West Bengal, India
e-mail: manir65@rediffmail.com

A. Bagchi · A. Biswas (✉)
Department of Zoology, University of Kalyani, Kalyani Nadia, West Bengal, India
e-mail: arunima10@gmail.com

water in the developing countries. Not only improving the quality of life, nanoparticles like carbon nanotubes have a number of applications which includes producing strong and lightweight sports good. This proves beyond doubt that nanoparticles have an array of important usages in the modern era. But the goodness of nanoparticles and nanocomposites are not confined in the above-mentioned uses only. They are one of the main targets and hope for the betterment of human health and lifespan in future. The variety of nanotechnology-based platforms has been speculated for use in various biological purposes including improved cancer chemotherapy.

Synthesis of nanocomposites with nanoparticles and various matrix carriers improve the target specificity of the drugs along with their effectiveness in the biological system. The current problem with chemotherapeutic drugs is that they mostly affect the normal tissues along with the cancer ones. The utility of nanocomposites has the potential to address the issue of target non-specificity. Hence, they have gained importance for efficient transport of anticancer agents into the cancerous cells without affecting normal tissues or cells. Unlike the free drugs, which get neutralized in the body within the short time interval, these nanocomposites can also accumulate in the tumours, achieving a cytotoxic load, higher than the rest of the body [1, 2]. The nanocomposites increase the lifetime of a drug preventing their degradation when used in combination. The nanocomposites thus function by increasing the half-life of them in the biological system to a significant amount. Moreover, due to the process of angiogenesis, the accumulation of nanocarriers in the tumour tissues is ensured, which enhance effectivity of these carriers to significantly over free drugs [3, 4]. So, transport of these drugs through the bloodstream is facilitated by increasing half-life of nanocarriers avoiding the action of our body's first line of defence [5].

Different targeting ligands, such as monoclonal antibodies, peptides, antibody fragments, growth factors can be actually tagged to nanocarriers to achieve site-specific active targeting. Moreover, this gives an added advantage to avoid the multiple-drug resistance imparted by passive targeting [6].

But nanocarriers have few drawbacks which are responsible for its clinical failure. After entering into the tumour vasculature, the nanocarriers must reach the cancer cells by overcoming the different barriers. But the endothelial barrier adjacent to cancer cells sometimes act as a real hurdle ensuring the failure of nanocarrier functioning [7]. Moreover, the nanocarriers get attached to the first available receptor, failing to penetrate the other tumours. Also, targeting moieties increase the immunogenicity and plasma protein absorption of the nanocarriers, thereby actually minimizing their half-life in the bloodstream, which was supposed to be enhanced [7], decreasing their targeting capacity.

These shortcomings are needed to overcome to ensure the success of nanocarriers. The drawbacks and limited versatility of a single nanoparticle led to the use of nanocomposites in different fields as they exhibit cumulatively all the properties of their components, thereby increasing the versatility to a large extent. Moreover, they also show increased biocompatibility and high stability both in the environment and in biological systems. Metallic nanocomposites are useful for their

multifunctional properties and biocompatibility, keeping their own property unhampered. This is the reason why researchers are showing immense interest in the use of nanocomposites for different biomedical applications including drug delivery, imaging, MRI contrast agent, photothermal ablation agents, photoacoustic imaging contrast agents [8–10].

But the researches on the toxicological evaluation of the nanoparticles and nanocomposites are still fragmentary and even contradictory to each other. But evidence severely suggests that metal nanoparticles like gold nanoparticle are involved in showing toxic effects on cellular levels causing size, shape and surface modifications. Though a small group of scientists claimed the use of gold nanoparticles to be essentially non-toxic, various research groups demonstrated their toxicity. The size of the nanoparticles seemed associated with generating toxicity when studied in cell lines like MCF-7 in a time and dose-dependent manner. The small-sized nanoparticles showed lesser toxicity and lesser accumulation of autophagosomes. These toxic effects might be an issue for using these nanoparticles for biomedical therapies as they might affect the healthy cells along the cancerous ones. Hence researchers are in the process of synthesizing nanocomposites to decrease the toxicity associated with the metal nanoparticles.

1.1 Nanocomposite Systems

Since the 1990s, researchers are showing more interest in nanocomposite systems and as a result, the number of publications, including reviews, is continuously increasing. We can define nanocomposites (NC) as multiphase solid materials in which phases must be present with dimensions of less than 100 nm. Nanocomposite systems have two parts: (i) continuous phase and (ii) discontinuous reinforcing phase. Thus, nanocomposite systems can have a combined or have noticeably different electrical, mechanical, electrochemical, thermal, catalytic and optical properties of the component materials [11–14].

1.2 Synthesis of Nanocomposite Systems: Nanocomposite Materials Are Generally Synthesized Using One of the Two Methods

1.2.1 In Situ Method

An effective and simple way to obtain a nanocomposite is to synthesize the nanoparticle in a matrix by an in situ method. The nanocomposite can be synthesized inside the matrix material in this method, from its corresponding precursors. Therefore, this method follows one-step fabrication of nanocomposites,

where prevention of particle agglomeration as well as well spatial distribution in the matrix system both, have occurred simultaneously and these are the best advantages of this method. The disadvantage of this method is that the unreacted reagents of the in situ reaction might influence the properties of the final nanocomposite material.

1.2.2 Ex Situ Method

Ex situ method for synthesizing nanocomposites in another useful method, where the pre-made nanoparticles are directly dispersed into the matrix to form the composite. This method also has advantages and disadvantages. This method is very much advantageous for the large-scale industrial synthesis of nanocomposites than the in situ method, but the major challenge of this method is to prepare highly dispersible and stable nanoparticles. Generally, sonication method is applied to disperse the nanoparticles in the matrix.

1.3 *Synthesis of Au/Ag Supported Mesoporous Metal-Oxide Nanocomposites*

Mesoporous materials having tunable pore structure and modified framework composition, show various applications in adsorption, catalysis, separation, energy storage, conversion, biological uses etc. [15–17].

Mesoporous silicate particles have drawn a significant interest among the variety of inorganic materials as it possesses ordered porous structure, simple and cost-effective synthetic methods and wide range of applications [18–20]. Modification of mesoporous silica surface can be done by various functional groups [21–26] and various metal NPs [27–31] and these modifications made the materials potentially applicable in different biomedical fields [32–34]. It should be noted that the antibacterial activity of Ag NPs depends not only on the size of NPs [35] but also on their shape [36]. Therefore, the main reason for carrying out the antibacterial activity is to synthesize monodispersed stable Ag NPs synthesis with the similar shape of the NPs. Ghosh et al. synthesized mesoporous silica flakes (MSF) using tetraethylorthosilicate (TEOS) as a silica source and CTAB as a structure directing agent in hexane at room temperature. They modified MSF with aminopropyltriethoxyl silane (APTS). The amino group of APTS formed -NH₂CH₂OH group by reacting with formaldehyde and the resulted group acted as reducing as well as the stabilizing agent to form monodisperse Ag NPs [37]. Li et al. [38] synthesized homogeneously distributed gold nanoparticles within titania framework via a multi-component assembly approach. In this method, titania, gold building clusters, and surfactant are assembled in a single step process, that is they mixed Pluronic surfactant P123, TiCl₄, Ti(OBu)₄, and AuCl₃ in ethanol. Homogeneous mesostructured nanocomposites were obtained by casting the

mixture followed by an ageing process. The surfactant P123 was removed by calcining the sample resulting crystalline mesoporous TiO_2 networks embedding gold nanoparticles. On the other hand, the Ag/mesoporous ZnO nanocomposite was synthesized by microwave irradiation route [39]. The reaction was carried out in an argon atmosphere for 15 min with zinc (II) acetate and silver nitrate as precursor salts to synthesize ZnO and Ag NPs respectively. Briefly, zinc (II) acetate and ethylene glycol were added to the aqueous AgNO_3 solution in a round-bottomed flask, fitted to the refluxing system inside the microwave oven. The reaction was conducted for 15 min under argon atmosphere. At the end of the reaction, the powder from the liquid was separated by centrifugation with the mother liquid and then washed with water and ethanol. Then the nanocomposite product was dried overnight under vacuum. Chowdhury et al. synthesized Ag- TiO_2 nanocomposite through a green synthetic method. The mesoporous anatase TiO_2 was synthesized by a hydrothermal method where they used titanium (IV) oxysulfate (TIOS) as precursor salt, urea as reducing agent and SDS as the surfactant in aqueous solution. Then the silver nanoparticle doped TiO_2 (Ag- TiO_2) was obtained by an impregnation method. In this method, water dispersible Ag NPs were used which were obtained from green carambola extract at pH 10 [40].

Sinha et al. [41] synthesized mesoscopic manganese oxide/gold nanoparticle composites by mixing $\text{Mn}(\text{NO}_3)_2 \cdot 6\text{H}_2\text{O}$ salt solution with a solution of NaOH and an aqueous solution of CTAB at pH 8.0. The resulting gel (pH 10.5) was heated in a closed vessel. The solid product was filtered calcined at 500 °C for 4 h and then it was stirred in aqueous H_2SO_4 solution followed by filtering and washing with water, and finally dried at 105 °C to obtain mesoporous MnO_2 sheets. The Au metal was vaporized from an Au disk to create a plasma by using the second harmonic of an Nd:YAG pulsed laser with a pulse width of 7 ns and energy of 1 J pulse. The supports which were prepared as thin sheets, placed in front of the cluster beam. Then each side of the wafer was exposed to the cluster beam for the same time interval and finally, the metal content in the composite was measured by chemical analysis (inductively coupled plasma).

1.4 Synthesis of Au/Ag Supported Graphene Nanocomposites

Since the experimental existence in 2004, graphene attracts the huge attention of the scientific community in almost all fields of material science applications. This credit goes to the extraordinary properties of graphene-like its high surface area ($\sim 2600 \text{ m}^2\text{g}^{-1}$), high thermal and mechanical stability, unique electronic and charge transport properties [42, 43]. Moreover, functionalized graphene nanocomposites show a wide array of applications in different fields such as in chemical and biological sensors, charge storage devices, capacitors, nanoelectronic and nanophotonic devices etc. [44–48]. These applications of graphene like structures may vary depending upon the route of synthesis that includes micro-mechanical

exfoliation, Chemical vapour deposition (CVD), chemical reduction of graphene oxide (GO) etc. [42, 49–51]. In order to produce large-scale graphene, the chemical exfoliation of GO to produce reduced graphene oxide (RGO) is one of the most cost effective and efficient pathways [52].

The modified Hummers method is used to synthesize graphene oxide was from natural graphite. The synthesized GO was dispersed in DI water by sonication and AgNO_3 was added as the precursor salt to obtain Ag nanoparticles. Finally, the Ag/graphene composite was prepared by adding sodium borohydride (NaBH_4) as the reducing agent. The synthetic pathway of silver loaded graphene (Ag/G) is shown in Fig. 1 [53].

Wadhwa et al. demonstrated the synthesis of reduced graphene oxide silver (RGO-Ag) nanocomposite by using microwave irradiation. Modified Hummers method was also applied here to synthesize graphene oxide followed by microwave-assisted the reduction of GO and silver nitrate (AgNO_3) by hydrazine hydrate via in situ method [52].

The strong reducing agents like hydrazine and sodium borohydride can be used to synthesize metal nanoparticles very easily, but the main drawback of these reducing agents is that they are toxic and hazardous to the environment. To avoid

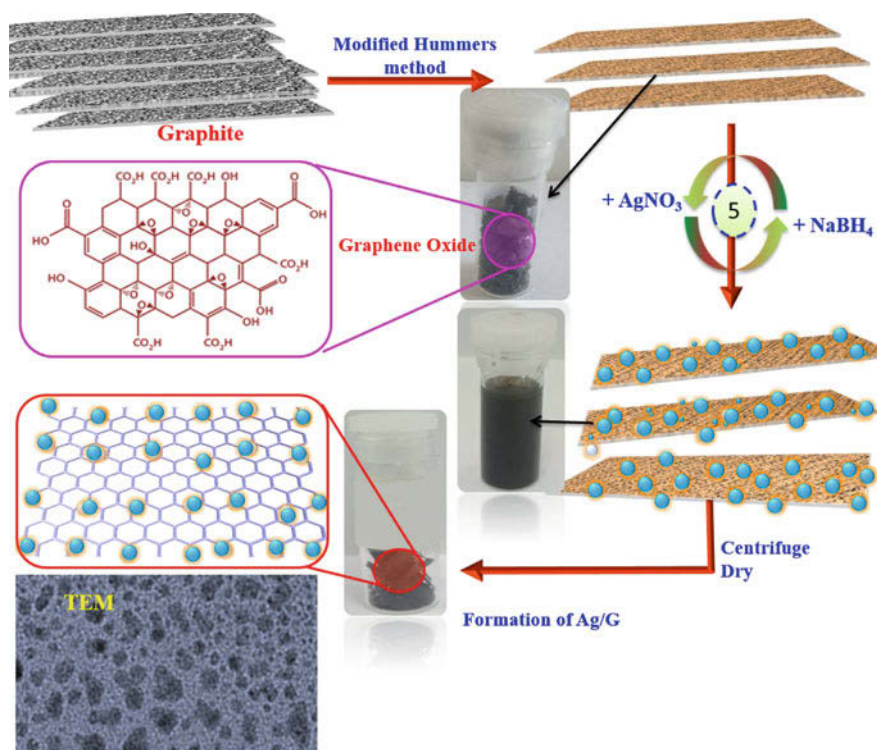


Fig. 1 Schematic representation of the synthesis of silver loaded graphene (Ag/G) composite [53]

such detrimental effects, researchers are recently using a green and inexpensive chemical synthesis approach. silver nanoparticle (AgNPs)–graphene oxide (GO) composite was also synthesized by the green synthetic approach where beta cyclodextrin used as a stabilizing agent and ascorbic acid act as reducing agent [54].

Ju and Chen demonstrated a green and simple in situ approach to synthesize Au nanoparticles on nitrogen-doped graphene quantum dots (Au NPs–N-GQDs). The composite was obtained by simple refluxing of the nitrogen-doped graphene quantum dots and $\text{HAuCl}_4 \cdot 4\text{H}_2\text{O}$ as the precursor salt of Au NPs without using any other reductant and surfactant [55].

1.5 Synthesis of Au/Ag Supported Polymer Nanocomposites

Usually, the nanoparticles tend to aggregate in the polymer matrix and thus the dispersion of nanoparticles in polymer matrices is challenging. This kind of problems of nanoparticles usually results in poor processability of composites and a high defect density [56, 57]. The composite material's physical properties are very much dependable on particle dispersion within the nanocomposite [58]. Toor and Pisano adopted ex situ approach to synthesize nanocomposite material. They prepared PVP coated gold nanoparticles in the form of a dried powder and this powder was dispersed in dimethylformamide (DMF) solvent. On the other hand, the polymer solution was prepared by them where the PVDF in pellets form was mixed with the DMF solvent at 100 °C with continuous stirring. This particle solution was mixed with the polymer solution in various concentration under sonication to prepare the nanocomposite suspension [59] (Fig. 2).

Kanahara et al. [60] prepared amino-terminated polymer particles using the SORP technique. The solution of each polymer in THF was prepared at a certain concentration. Membrane-filtered water was slowly added to the polymer solution in a glass bottle with constant stirring and the resulting mixture was then allowed to stay uncovered at ambient temperature to evaporate the THF. An opaque dispersion of polymer particles in water was obtained after complete evaporation of the THF. Then the aliquot of the aqueous dispersion of polymer particle was mixed with an

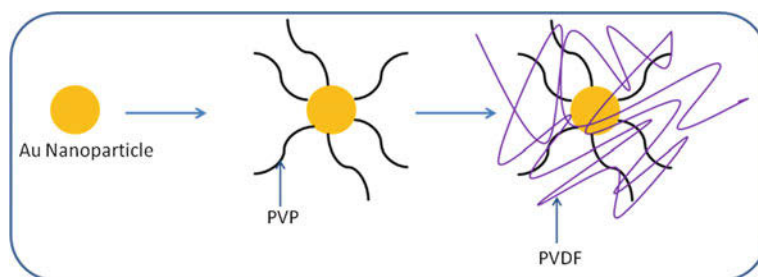


Fig. 2 PVP coated gold nanoparticles are blended with the PVDF polymer

aqueous dispersion of Au NPs and an aqueous PEG solution in a microtube, where PEG was used as a stabilizing agent that can prevent the agglomeration of polymer particles. These composite particles were then separated out by centrifugation followed by washing with water.

Cucurbit [8] uril was used to prepare a gold nanoparticle-polymer composite material, which acts as a supramolecular “handcuff” to grip together with the functionalized gold nanoparticles and acrylamide copolymer. The AuNPs must be functionalized by a water-soluble SAM yet remain accessible for CB [8] host-guest binding, as water solubility is a must for CB [8] ternary system. Water-soluble functionalized-AuNP 3 with a neutral (major) ligand tri (ethylene glycol)-1-butanethiol (EG₃-C₄-SH; 1) and a viologen-containing (minor) ligand, 1-methyl-4,40-bipyridinium-dodecanethiol bisbromide ([MV²⁺-C₁₂-SH] · 2Br⁻; 2) were prepared by a mixed self-assembled monolayer (mSAM) approach. AuNPs with a diameter of roughly 5 nm were prepared and functionalised with varying ligand mixtures of 1 and 2 leading to the AuNP 3 as depicted in Fig. 3. Another NP control was prepared in a similar manner with a SAM consisting of solely EG₃ (EG₃-AuNP 4) [61] (Fig. 4).

1.6 Synthesis of Au/Ag Supported Dendrimer Nanocomposites

Silver-dendrimer nanocomposites were synthesized by mixing dendrimers and silver nitrate solution to obtain Ag⁺/dendrimer complex at pH 7.0. Sodium

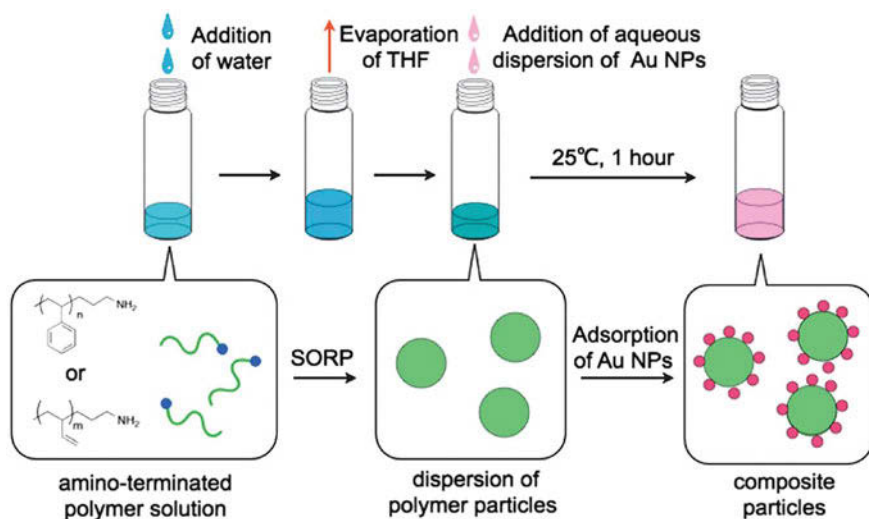


Fig. 3 Schematic illustration of the preparation of composite particles [60]

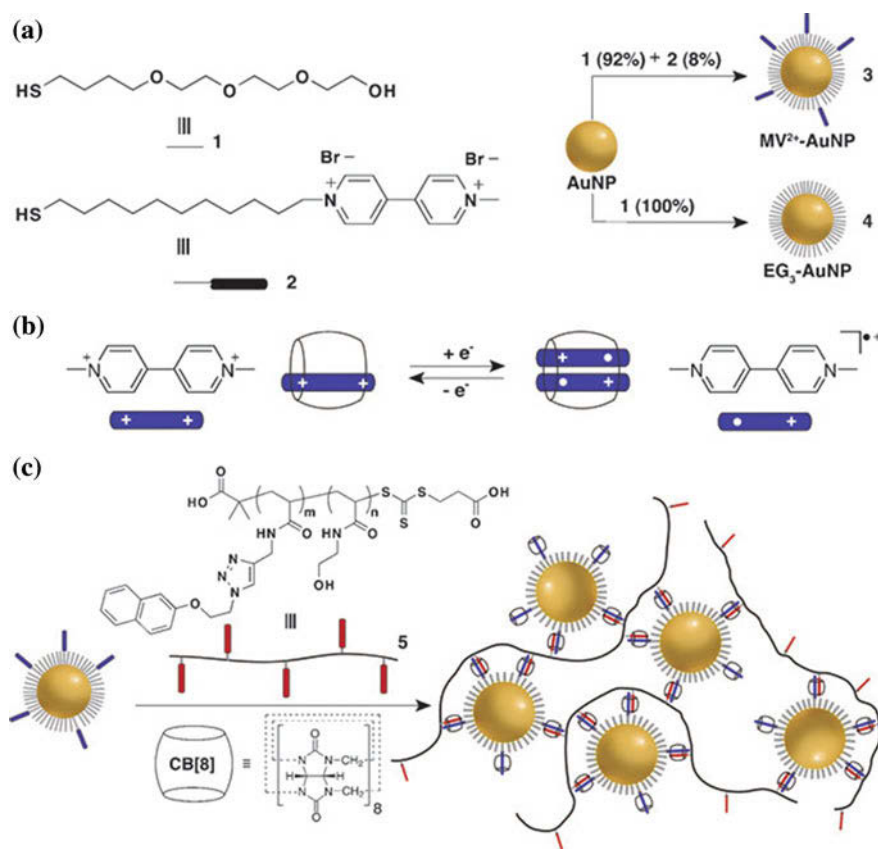


Fig. 4 Schematic representation of **a** preparation of MV²⁺-AuNP 3 and EG₃-AuNP 4, **b** formation of a 1:1 (MV⁺)₂ CB [8] inclusion complex upon reduction and **c** the noncovalent functionalization of MV²⁺-AuNP 3 with CB [8] and multivalent Np-copolymers 5 [61]

borohydride was added to the mixture as a reducing agent to reduce Ag⁺ to Ag⁰ and Silver-dendrimer nanocomposite was formed [62]. Zhang et al. showed a simple method of fabrication of thin film composite (TFC) where the silver-polyethylene glycol PEGylated dendrimer nanocomposite is used. They stirred poly (ethylene glycol) methyl ether acrylate (PEGMEA) with the AgNO₃ aqueous solution and exposed to the light for several hours to prepare the silver nanocomposite membrane [63] (Fig. 5).

Stable gold-dendrimer nanochains were synthesized in aqueous media without using any templates or organic solvents by regulating the density of dendrimers (Fig. 6). In this approach polyamidoamine (PAMAM) dendrimers self-assembled with gold nanoparticles to obtain one-dimensional nanochains [64].

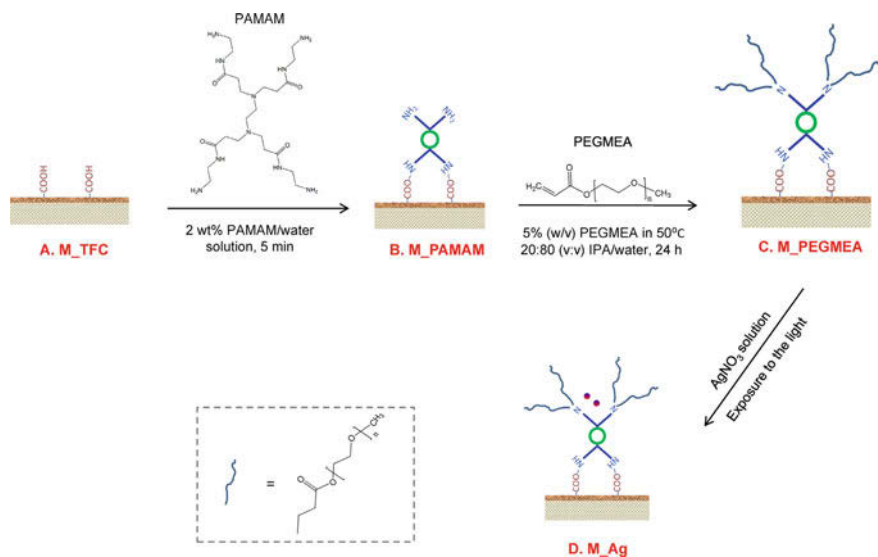


Fig. 5 Schematic diagram of the synthesis of silver-PEGylated dendrimer nanocomposite on the thin film composite membranes [63]

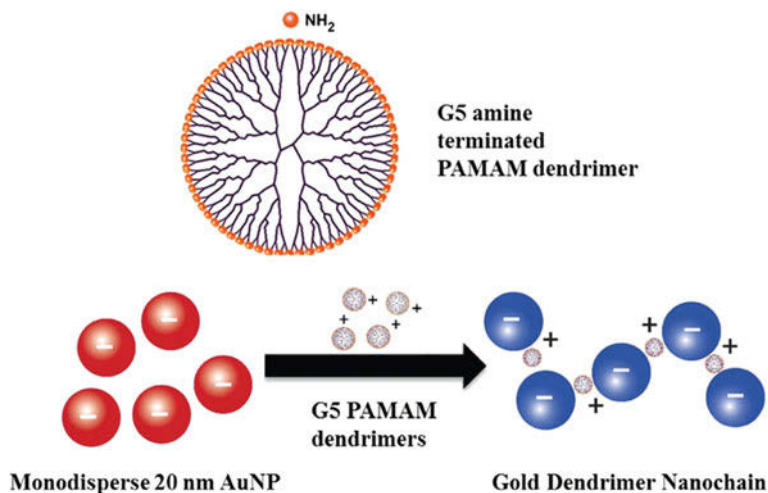


Fig. 6 Schematic representation of the chemical structure of a Generation 5 PAMAM dendrimer and the plausible mechanism of self-assembly of gold nanoparticles (20 nm) with dendrimers to produce electrostatic interactions driven one-dimensional 'nanochains' [64]

2 Applications and Toxicological Evaluations of Gold Nanocomposites

Recently, the use of gold nanoparticles to synthesize different biocompatible nanocomposites has provided various new ways of treatment of different diseases. In cancer, the use of such nanocomposites is becoming popular day by day. In present times, the use of anisotropic gold in the form of nanoparticles has generated much interest amongst scientists all over the world because of the particles' unique properties such as optical, electronic, size- and shape-dependent, and chemical properties, which are completely different from those in bulk and elemental form [65–67]. Moreover, gold nanoparticles (AuNPs) has the potential to act as a photothermal agent [68–70].

2.1 Silica-Based Gold Nanocomposite

The conventional photo-absorbing agents, which are essential for converting radiation energy to heat, have many limitations due to their lack of stability and absorption of radiation. But the use of novel nanostructures has provided the way to overcome such limitations of the conventional agents. The silica-gold-silica ($\text{SiO}_2\text{-Au-SiO}_2$) nanocomposite has demonstrated a relatively broad extinction in the NIR region, which is significant for its photothermal effect [71]. Researchers have explored its potential as a photothermal therapy material in vitro in various cell lines of mammalian origin. Researchers have also used Au– SiO_2 nanocomposites for the detection of human ovarian cancer cells (HOC) [72]. By analyzing the optical absorption spectra, it was observed that the treatment of HOC with Au– SiO_2 nanocomposites made them susceptible to change the absorption spectrum in comparison with the control cells. For these reasons, the potential of clinical applications of AuNPs is presently an intense subject for research [73]. Current researchers also indicated that mesoporous silica-coated gold nanocomposites have a strong potential to diagnose and treat breast cancer. They seemed to be potent cytotoxic agents affecting triple negative breast cancer cell line like MDA-MB-231. But toxicological implications of these composites are yet to be evaluated. Questions still remain about whether these can be used in humans with little no side effects on humans and the environment.

2.2 Lipid-Coated Gold Nanocomposite

Liposomal nanoparticles are made up of natural lipids having the potential to encapsulate both water-soluble and insoluble drugs in their core. Their design is for controlled delivery of therapeutic agents enhancing therapeutic efficacy minimizing

side effects. Encapsulation or coating of metallic nanoparticles especially Au with lipids is a useful non-covalent approach to stabilize surface chemistry and to increase the compatibility of lipid-coated nanohybrids loaded with drugs at biological level [74–79]. In a study by Kang et al. it has been shown that the administration of docetaxel (DTX) in a lipid bilayer on the nanoparticles leads to the reduction of its side effects, thereby increasing its efficacy. DTX, an anti-cancer drug showed to effectively increase its intracellular delivery and therapeutic efficacy when administered with nanoparticles [80]. The uptake of drugs by the cells was significantly enhanced by this formulation and it also enhanced cytotoxicity compared to uncoated AuNPs and the free drug. The above-mentioned effects were because of cell-cycle arrest in the G₂/M phase of skin melanoma cell line B16F10 and breast cancer cell line MCF-7 cells with the increased population of sub-G₁ phase apoptotic cells. Thus drug-encapsulated lipid-coated nanoparticles have a scope to be used as a promising nanocarrier system for significantly enhanced cancer chemotherapy.

2.3 Manganese Oxide-Based Gold Nanocomposites

Macrophages and monocytes, two of the key components of host response to tumor cells, augments cell proliferation in the tumor microenvironment and in case of infections [81], along with the hypoxic condition, which is also very essential for the survival of tumors and this hypoxic condition can be clearly noticed in case of inflammation or solid tumor formation [82]. Suppression of the hypoxic condition by modulating the signalling pathways of Hypoxia Inducing Factor (HIF) with the use of gold-manganese oxide nanocomposite induces the subset of macrophages to revert back to a cytotoxic and anti-tumorigenic form [83]. This strategy of reversing hypoxic condition of the tumour microenvironment, through their effect on Tumor-Associated Macrophages, can be utilized as a mechanism to combat cancer. Moreover, broad near-infrared absorption of porous gold nanoparticle-manganese monoxide nanocomposites effectively increase the diagnostic time and also provides deeper photoacoustic imaging depth [84], which can be used to perform more accurate MR/Photoacoustic/CT tumour imaging in the human body.

2.4 Chitosan-Based Gold Nanocomposite

A group of researchers used Chitosan, a non-toxic biopolymer, along with gold nanoparticles to develop a nanocomposite that shows properties like the high current response intensity, a high electrocatalytic tendency towards H₂O₂ reduction, high stability, and good biocompatibility. Immunosensors prepared from this gold/chitosan nanocomposite can be used for high-throughput biomedical sensing and clinical applications, such as for the detection of prostate cancer using PSA

biomarker, without any sophisticated and complicated fabrication procedure [85]. Nanocomposite, constructed with gold nanoparticles (AuNPs), Carbon nano-onions (CNOs), single-walled carbon nanotubes (SWCNTs) and chitosan (CS) (AuNPs/CNOs/SWCNTs/CS) have been used to develop high-sensitivity electrochemical immunosensor that can detect carcinoembryonic antigens (CEA), which is a clinical tumor marker [86]. Along with the high sensitivity and excellent stability in the biological system, this immunosensor also provides excellent selectivity due to the property of resistance to interference in the presence of other antigens in the serum. Moreover, this platform can be utilized to design various highly selective and sensitive immunosensors to detect important biomarkers such as ciprofloxacin and immunoglobulin A (Fig. 7).

Apart from great application benefits, this type of nanocomposites also offers some health risks. The carbon nanotubes (SWCNTs) used in the above formulation can be hazardous to the people, especially who are producing or handling such nanomaterials. Inhalation of carbon nanotubes has potential to cause inflammation and granuloma formation in the lungs as they can reach the lower respiratory tract and can persist for a year or more. They can also translocate to other organs such as lymph nodes and pleura [87].

Many studies have also shown that nanocomposites composed of gold nanoparticles encapsulated by temperature-sensitive microgel are convenient colloidal systems with trapping capabilities [88, 89]. The biocompatibility of such composites can be used as a system for drug release in low solvent pH, for example in cancer therapy.

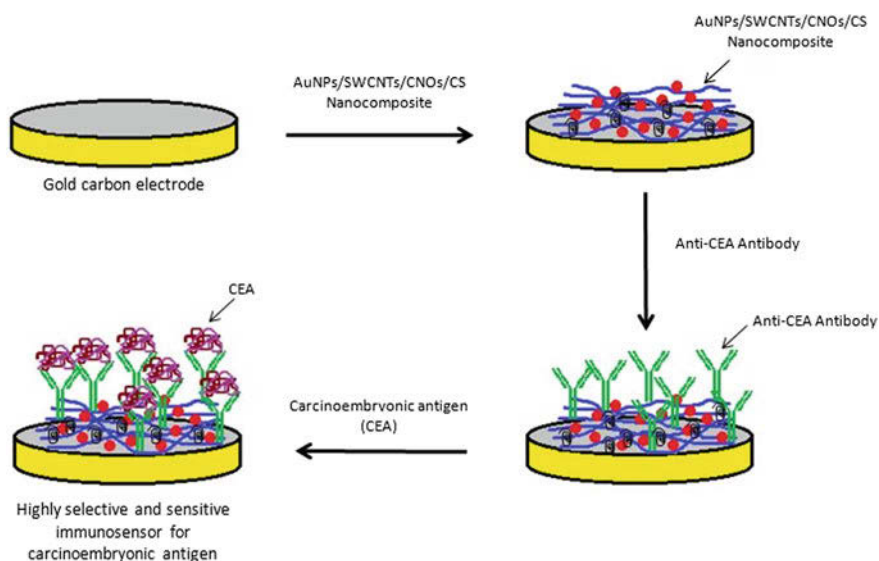


Fig. 7 Fabrication of a highly sensitive and selective immunosensor for carcinoembryonic antigen [86]

2.5 Graphene-Based Gold Nanocomposite

Not only in case of different biomarkers, but many studies have also depicted that these nanocomposites can be very efficient in determining the presence of different components in the environment, especially in the aquatic environment. Researchers have developed gold nanoparticle/Graphene nanocomposite that can be used to determine trace Chromium in water samples [90]. The hexavalent form of chromium acts as a strong oxidizing agent and shows carcinogenic and mutagenic properties, whereas the trivalent form is less toxic and studies have shown that it plays a vital role in many biological processes. So, it is of great importance to determine the level of trace hexavalent chromium in the water bodies to provide control for human and environmental concerns. The gold nanoparticle/Graphene nanocomposite sensors have been used to detect trace hexavalent chromium in the river samples of Indonesia as it shows high stability, high sensitivity, high electrocatalytic activity and low cost of analysis.

Graphene nanocomposites impart toxic effects on human erythrocytes, skin, fibroblasts and on different other cell lines. It is also extensively used in cancer research because of its unique set of characters that provide high mechanical strength and better stability preventing aggregation of the gold nanoparticles [91]. Researchers have constructed biosensors using graphene oxide based AuNP nanocomposite that can detect tumour mutations [92]. Gold nanoparticles were also added as functional agents in N₂- or S- doped graphene sheets (AuNPs-N₂-doped-GN or AuNPs-thiolated GN composite), that shows much enhanced SERS (Surface Enhanced Raman Spectroscopy) attributes on their electro-active surfaces [93, 94]. Along with these efficient diagnostic applications, these graphene oxide/gold nanocomposites have also been proven to be an efficient drug delivery system. Moreover, the whole process of drug delivery and release can be monitored by fluorescent-monitoring [95], making it a more efficient candidate for drug delivery in cancer treatments. Graphene oxide/gold nanocomposite loaded with daunorubicin enhances drug release into cancer cells by inducing morphological changes in cancer cell membrane. This also reduced P-glycoprotein expression and activated apoptosis in cancer cells in both in vitro and in vivo models [96]. Graphene nanocomposites are proposed as potent anti-cancer agents as they produce reactive oxygen species (ROS), induce cell cycle changes and might also initiate apoptosis.

In spite of these useful applications of graphene oxide as a composite with gold nanoparticles, it has some cytotoxic effects. Many in vitro studies reported that graphene oxide is cytotoxic to both normal and cancer cells when applied in high concentration and with long exposure time, though cancer cell lines showed more percentage viability may be because of its inbuilt resistance to cellular damage [97–100].

2.6 Dendrimer Stabilized Gold Nanoparticles

Multifunctional nanocomposites constructed by the researchers using gold nanoparticles stabilized by polyamidoamine (PANAM) dendrimers that can be used for combined detection of tumour cells through many processes such as flow cytometry, confocal microscopy, computed tomography, etc. [101]. These dendrimers are highly branched three-dimensional polymeric macromolecules that have highly configurable architecture. The biocompatibility and pharmacokinetics of this nanoconstruct can be adjusted by tuning the chemical synthesis of the dendrimer. Its high biocompatibility, high drug loading capacity and presence of multiple functional groups on its surface makes it a good candidate for photothermal therapy and targeted cancer therapy. Moreover, its good biodegradability and water solubility augment its use as a carrier for anticancer drugs [102–104]. It was also showed by researchers that incorporation of gold to dendrimer can actually lower the toxicity of dendrimer in a selective manner by modulating the physiochemical parameters of dendrimers.

2.7 Iron Oxide Gold Nanocomposite

Another construct with the gold nanoparticles is the Iron oxide/gold nanocomposite, which has immense importance in theranostics that is both in therapeutics and diagnostics. The flower-shaped iron oxide/gold nanocomposites possess a large number of magnetic domains, leading to enhanced magnetic properties that are helpful in magnetic resonance imaging (MRI) [105]. Not only in MRI, but this nanocomposite is also very useful in computed tomography (CT), Fluorescent optical imaging, hyperthermia and many more diagnostic processes. This nanocomposite has also been used as a carrier for drug delivery for chemotherapy such as cisplatin conjugated nanocomposite.

Several iron oxide-based nanocomposites with gold nanoparticles are under clinical trial to understand their toxicity, but only the dextran-coated superparamagnetic iron oxide is approved for human use by FDA. There are very few researches on the complete toxicological profile of the iron oxide nanocomposites and some of the researches are conflicting with each other. Moreover, some reports suggest superparamagnetic iron oxide be toxic on mouse fibroblast cells whereas reports have also shown that high concentration of this composite failed to show any toxicity.

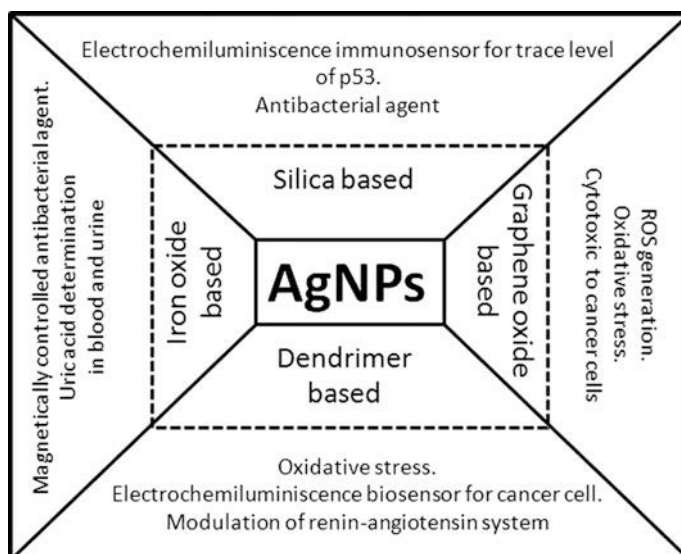
3 Applications and Toxicological Evaluations of Silver Nanocomposites

The nanoparticles and nanocomposites are popular for use in various fields for various reasons like high surface area-to-volume ratio, increased solubility of the drug and several others. But silver is definitely a suited choice for several others for

biocidal properties or microbicidal properties of silver nanoparticles (Table 1) or silver-based nanocomposites [106, 107]. Historically, before penicillin was even discovered, silver was broadly used to combat severe infections, especially for treatment of burns and chronic wounds. Even after the discovery of Penicillin, its use was revitalized in 1968 when silver nitrate was combined with sulfonamide to produce a silver sulfadiazine cream for treating burns [106]. Moreover, antibiotic resistance has imposed a major problem in using the antibiotic drugs available and very recently, silver-based nanocomposites have gained immense importance in instances of infections [108]. Presently, there are a number of medical products available, such as silver-based ointments and bandages that have been proven to be efficiently retarding and preventing bacterial infections [109]. Current researches mainly focus on the improvements in the development of novel silver nanoparticle (Table 1) and composites keeping in mind the wide use and antimicrobial properties of silver. Moreover, researchers are showing more interest towards the exploitation of silver nanoparticle to develop new biologically active materials so that the unique antibacterial properties of silver can be combined with the performance of the biomaterial [110–114]. Silver nanocomposites represent a promising strategy to fight against infections on used medical devices as a problem of proper sterilization as a major cause of hospital deaths in many places around the world. Besides having antibacterial properties, they are also antifungal and antiviral agents. Silver nanoparticles exert cytoprotective effects towards HIV-infected T cells by inhibiting the production of extracellular virions in vitro. They directly interact with the double-stranded DNA of HIV particles. But it is still not known how they affect other viruses. The effects of silver nanoparticles and nanocomposites on fungi are grossly unexplored. Though resistance to existing anti-fungal drugs are less commonly heard and it is not a menace like predominant antibacterial resistance, the long-term concern remains for different types of the antifungal agent as their options are really limited in the present world. Hence, researches are required to develop drugs with novel antifungal mechanisms. Recently, attention has focused on the potential of silver to be used as an antifungal agent, with experimental evidence that silver nanoparticles are capable of exhibiting potent antifungal effects, most likely by destroying the membrane integrity of fungal cells [115–117].

3.1 Graphene Oxide Silver Nanocomposite

The use of silver nanoparticles to develop different nanocomposites is getting very popular among scientists nowadays because of its versatility and high stability. The use of Graphene oxide/silver nanocomposite along with laser exposure (Photodynamic therapy) exhibits a synergistic effect, increasing cytotoxicity to the breast cancer cell lines [118]. This synergistic effect quickly produces reactive oxygen species such as hydroxyl radicals, superoxide ions and singlet oxygen, resulting in oxidative stress and can also include disruption of the cell membrane [119]. These properties of the graphene oxide/silver nanocomposite can be used in

Table 1 Silver nanocomposites and their biological implications

future for biomedical applications, especially in targeted cancer therapy. But it should be mentioned that researchers with two lineages of macrophages—a tumour lineage (J774) and peritoneal macrophage collected from Balb/c mouse showed that graphene oxide silver nanocomposite was toxic and induced significant ROS generation compared to silver nanoparticles, though graphene oxide/silver nanocomposites entered less inside cells. Hence the fate of the nanocomposites used should be carefully monitored and is a major concern in developing biocompatible materials.

3.2 Iron Oxide-Based Silver Nanocomposite

The magnetic iron oxide/silver nanocomposites show high anti-bacterial activity, which was tested against *E. coli*. This nanocomposite can also be used as an antibacterial agent which could be magnetically controlled in different biomedical applications. The reason behind it is the fact of the super magnetic properties of the iron oxide nanoparticles are not affected by the modulation of silver ions [120]. A group of researchers has also studied iron oxide-silver oxide quantum dots (QD) decorated cellulose nanofibres as a drug carrier for skin cancer therapy. They introduced two drugs Etoposide and Methotrexate to the melanoma cells in assistance with $\text{Fe}_3\text{O}_4\text{-Ag}_2\text{O}$ QD/cellulose nanofibre carrier and showed that the cell viability decreased [121]. This study also indicated that a high number of unloaded

nanocomposites were not cytotoxic. Iron oxide-based nanocomposites did not induce any possibility of liver or kidney toxicity. On the other hand, silver nanoparticle alone resulted in increased serum alkaline phosphatase, calcium as well as lymphocyte infiltration in liver and kidney, indicating organ toxicity. These results indicate that in vivo kinetics of nanoparticles are required to be studied to understand their hazards and also nanocomposites might be toxicologically less hazardous than the metal nanoparticle itself.

Moreover, polyaniline (PANI) supported iron oxide/silver nanocomposites is presently the composite adopted to develop a sensor for the tracing and assessing uric acid in human blood and urine sample [122]. High sensitivity, selectivity, and low detection limits augment its potential for various applications.

3.3 Dendrimer-Based Silver Nanocomposites

The silver/dendrimer nanocomposites are of great importance in modern day research. Scientists have already demonstrated several uses of this construct. Xin Jin and group have demonstrated that silver/dendrimer (PAMAM) nanocomposite labelled DNA probe shows high sensitivity and selectivity with significantly low detection limit [123].

Researchers have developed electro-chemiluminescence biosensors for HL-60 cancer cell detection from $g\text{-C}_3\text{N}_4$ nanosheets and silver-PANAM-luminol nanocomposites, which show great selectivity and low detection limit [124] and has the potential to be used as cell biomarker. 5-fluorouracil loaded silver/PAMAM nanocomposite synergistically induces oxidative stress on cancer cells which were marked by reactive oxygen species and reactive nitrogen intermediate generation, DNA condensation and cytoskeletal compaction, leading to cell blebbing and injury. This also turns on the p53 gene-mediated signalling pathway leading to apoptosis [125].

In addition to these versatile applications of dendrimer-based silver and gold nanocomposites, researchers have also demonstrated the adverse effect of different dendrimers on biological organisms. Researches indicate that the stability of some dendrimers in different physiological conditions varies considerably. In vitro studies in a fish cell line (PLHC-1) have depicted that the PAMAM dendrimer induces toxicity by the generation of reactive oxygen species, which is followed by DNA damage and cell death [126]. In vivo studies have also demonstrated that PAMAM dendrimers induce aggregation of different blood proteins and results in clots in blood vessels [127]. Administration of PAMAM dendrimer in the mouse model induce acute lung failure by modulating the renin-angiotensin system [128]. A considerable number of dendrimers have also been found to be accumulated in some other important organs of the body such as the liver, kidney, heart and in the brain of neonatal rabbit with cerebral palsy. Akhtar and group showed that PAMAM inhibits ERK1/2 and p38 MAPK phosphorylation in both the cortex and medulla region of rat kidney, modulating the MAPK signalling pathway [129].

Even the sub-lethal dose of this dendrimer effects growth and development of zebrafish adversely [130]. So, it is important to do more research on the surface modifications and drug release of such dendrimers for designing a more biocompatible dendrimer construct and make it more suitable for various biological and biomedical applications [131].

3.4 Silica-Based Silver Nanocomposite

Silica-based silver nanocomposites have been extensively used in biomedical fields, especially for developing immunosensors. Researchers have developed an electrochemiluminescence immunosensor for p53 with Ru(bpy)₃²⁺/silver nanoparticles doped silica core-shell nanocomposite (RuAg/SiO₂) that shows excellent electrochemiluminescence behaviour with wide linear range, high selectivity, stability and low detection limit [132]. It efficiently detects trace level p53, so can be a very useful tool to be used as a tumour biomarker. Moreover, Yiyang Song and the group have prepared nanocomposite of polydopamine/silver nanoparticle on mesoporous silica (SBA15) that has potential as an antimicrobial agent along with the industrial role as a catalyst [133]. This composite successfully inhibited the growth of *E.coli*, *S. aureus*, and *A. fumigatus*. Mesoporous silica/silver nanocomposite (Ag-SBA-15) also shows high Hg⁰ capture capacity with high ability of regeneration and high recyclability, therefore can be used as a catalyst to capture Hg⁰ from coal-fired power plant flue gases [134]. These depict the importance of silver/silica nanocomposites in both environmental as well as biomedical applications.

4 Conclusions

In this chapter, different synthetic methods to prepare metal nanocomposites based on recent studies are well described. There is a large scope of future research developing facile, green synthetic route to synthesize metal nanocomposites minimizing the use of hazardous chemical reagents. Synthesis of nanocomposites on a metal base can be done by two different methods: in situ method and ex situ method as described before. Mesoporous metal oxide nanocomposites, silver/gold-supported graphene nanocomposite, silver/gold supported polymer nanocomposites and silver/gold-supported dendrimer nanocomposites are a few varieties of nanocomposites whose synthesis have been discussed in this chapter keeping in mind their wide research usage in causing cell cytotoxicity, in experimental cancer therapy, in antibacterial activity and antifungal activity and in developing immunosensors to name a few. Their roles in the biological system have made it exigent to study and understand the toxicological evaluations of the same in the system as well as to the person exposed to it.

Silver, gold, graphene nanocomposites have shown promising evidence indicating their importance in cancer research and various other fields. They have promising cytotoxic effects on various cancer cells and have potent antibacterial and antifungal activities. But, in spite of their goodness in terms of human healthcare, very few of the researches are actually translating into effective market available drugs and have reached the stage of clinical trial. The reason behind the lag between innovative research to identify new nanocomposites with immense biological potency and the effective market available drug is the dearth of research studies to evaluate the toxicity generated by the composites in the cell system, in animal models and in users who are actually working with the nanocomposites.

It is important to understand the control of the concentrations in using the nanocomposites to have the beneficial effects. Though there are a large number of researches are going on in this field, a systematic in vitro–in vivo extrapolation studies after the application of the nanocomposites is necessary. There are very little information available till to date about the toxic effects of the biomarkers, such as their immunomodulatory effect or ability to alter the genetic expression. In this chapter, the synthesis of nanocomposites relevant to biological research, their wide applications and toxicological evaluations have been discussed with special reference to cancer. But more studies are required on the toxicological implications of the nanocomposites to use them as our friends and not as foes. Intensive toxicological evaluation along with the ongoing research of finding new nanocomposites are required to effectively use nanocomposites in biological systems and as a tool for cancer therapy which will lead to the innovation of modern day target-specific drugs and new arenas in chemotherapy.

References

1. Danhier F, Feron O, Préat V (2010) To exploit the tumor microenvironment: passive and active tumor targeting of nanocarriers for anti-cancer drug delivery. *J Control Release* 148:135–146
2. Northfelt DW, Martin FJ, Working P, Volberding PA, Russell J, Newman M, Amantea MA, Kaplan LD (1996) Doxorubicin encapsulated in liposomes containing surface-bound polyethylene glycol: pharmacokinetics, tumor localization and safety in patients with AIDS-related Kaposi's sarcoma. *J Clin Pharmacol* 36:55–63
3. Fang J, Nakamura H, Maeda H (2011) The EPR effect: unique features of tumor blood vessels for drug delivery, factors involved, and limitations and augmentation of the effect. *Adv Drug Deliv Rev* 63:136–151
4. Maeda H (2001) The enhanced permeability and retention (EPR) effect in tumor vasculature: the key role of tumor-selective macromolecular drug targeting. *Adv Enzyme Regul* 41: 189–207
5. Morghimi SM, Hunter AC, Murray JC (2001) Long-circulating and target-specific nanoparticles: theory to practice. *Pharmacol Rev* 53:283–318
6. Matsuo H, Wakasugi M, Takanaga H, Ohtani H, Naito M, Tsuruo T, Sawada Y (2001) Possibility of the reversal of multidrug resistance and the avoidance of side effects by liposomes modified with MRK-16, a monoclonal antibody to P-glycoprotein. *J Control Release* 77:77–86

7. Lammers T, Kiessling F, Hennink WE, Storm G (2012) Drug targeting to tumors: principles, pitfalls and (pre-) clinical progress. *J Control Release* 161:175–187
8. Mohammadreza S, Soehnen ES, Hao J et al (2010) Dual purpose prussian blue nanoparticles for cellular imaging and drug delivery: a new generation of T1-weighted MRI contrast and small molecule delivery agents. *J Mater Chem* 20(25):5251–5259
9. Liang X, Deng Z, Jing L et al (2013) Prussian blue nanoparticles operate as a contrast agent for enhanced photoacoustic imaging. *Chem Commun* 49(94):11029–11031
10. Fu G, Feng S, Liu W, Yue X (2012) Prussian blue nanoparticles operate as a new generation of photothermal ablation agents for cancer therapy. *Chem Commun* 48(94):11567–11569
11. Pina S, Oliveira JM, Reis RL (2015) Natural-based nanocomposites for bone tissue engineering and regenerative medicine: a review. *Adv Mater* 27:1143–1169
12. Rafiee MA, Rafiee J, Wang Z, Song H, Yu Z-Z, Koratkar N (2009) Enhanced mechanical properties of nanocomposites at low graphene content. *ACS Nano* 3:3884–3890
13. Mariano M, El Kissi N, Dufresne A (2014) Cellulose nanocrystals and related nanocomposites: review of some properties and challenges. *J Polym Sci, Part B Polym Phys* 52:791–806
14. Hu H, Onyebueke L, Abatan A (2010) Characterizing and modeling mechanical properties of nanocomposites-review and evaluation. *J Min Mater Charact Eng* 9:275–319
15. Beck JS, Vartuli JC (1996) Recent advances in the synthesis, characterization and applications of mesoporous molecular sieves. *Curr Opin Solid State Mater Sci* 1:76–87
16. Davis ME (2002) Ordered porous materials for emerging applications. *Nature* 417:813–821
17. Liu AM, Hidajat K, Kawi S, Zhao DY (2000) A new class of hybrid mesoporous materials with functionalized organic monolayers for selective adsorption of heavy metal ions. *Chem Commun* 1145–1146
18. Zhuang TY, Shi JY, Ma BC, Wang W (2010) Chiral norbornane-bridged periodic mesoporous organosilicas. *J Mater Chem* 20:6026–6029
19. Tsou CJ, Chu CY, Mou CY (2013) A broad range fluorescent pH sensor based on hollow mesoporous silica nanoparticles, utilising the surface curvature effect. *J Mater Chem B* 1:5557–5563
20. Heidegger S, Gößl D, Schmidt A, Niedermayer S, Argyo C, Endres S, Bein T, Bourquin C (2016) Immune response to functionalized mesoporous silica nanoparticles for targeted drug delivery. *Nanoscale* 8:938–948
21. Li Z, Barnes JC, Bosoy A, Stoddart JF, Zink JI (2012) Mesoporous silica nanoparticles in biomedical applications. *Chem Soc Rev* 41:2590–2605
22. Lin YS, Hurley KR, Haynes CL (2012) Critical considerations in the biomedical use of mesoporous silica nanoparticles. *J Phys Chem Lett* 3:364–374
23. Tao X, Liu B, Hou Q, Xu H, Chen JF (2009) Enhanced accumulation and visible light-assisted degradation of azo dyes in poly (allylamine hydrochloride)-modified mesoporous silica spheres. *Mater Res Bull* 44:306–311
24. Yuan Q, Chi Y, Yu N, Zhao N, Yan W, Li X, Dong B (2014) Amino-functionalized magnetic mesoporous microspheres with good adsorption properties. *Mater Res Bull* 49:279–284
25. Huang CH, Chang KP, Ou HD, Chiang YC, Wang CF (2011) Adsorption of cationic dyes onto mesoporous silica. *Microporous Mesoporous Mater* 141:102–109
26. Li Y, Zhaou Y, Nie W, Song L, Chen P (2015) Highly efficient methylene blue dyes removal from aqueous systems by chitosan coated magnetic mesoporous silica nanoparticles. *J Porous Mater* 22:1383–1392
27. Huang RS, Hou BF, Li HT, Fu XC, Xie CG (2015) Preparation of silver nanoparticles supported mesoporous silica microspheres with perpendicularly aligned mesopore channels and their antibacterial activities. *RSC Adv* 5:61184–61190
28. Tian Y, Qi J, Zhang W, Cai Q, Jiang X (2014) Facile, one-pot synthesis, and antibacterial activity of mesoporous silica nanoparticles decorated with well-dispersed silver nanoparticles. *ACS Appl Mater Interfaces* 6:12038–12045

29. Liong M, France B, Bradley KA, Zink JI (2009) Antimicrobial activity of silver nanocrystals encapsulated in mesoporous silica nanoparticles. *Adv Mater* 21:1684–1689
30. Song J, Kim H, Jang Y, Jang J (2013) Enhanced antibacterial activity of silver/polyrhodanine-composite-decorated silica nanoparticles. *ACS Appl Mater Interfaces* 5:11563–11568
31. Chen CC, Wu HH, Huang HY, Liu CW, Chen YN (2016) Synthesis of high valence silver-loaded mesoporous silica with strong antibacterial properties. *Int J Environ Res Pub Health* 13:99–112
32. Park JH, Gu L, Maltzahn GV, Ruoslahti E, Bhatia SN, Sailor MJ (2009) Biodegradable luminescent porous silicon nanoparticles for in vivo applications. *Nat Mater* 8:331–336
33. Tian Y, Qi J, Zhang W, Cai W, Jiang X (2014) Facile, one-pot synthesis, and antibacterial activity of mesoporous silica nanoparticles decorated with well-dispersed silver nanoparticles. *ACS Appl Mater Interfaces* 6:12038–12045
34. Soto RJ, Yang L, Schoenfish MH (2016) Functionalized mesoporous silica via an aminosilane surfactant ion exchange reaction: controlled scaffold design and nitric oxide release. *ACS Appl Mater Interfaces* 8:2220–2231
35. Agnihotri S, Mukherji S, Mukherji S (2014) Size-controlled silver nanoparticles synthesized over the range 5–100 nm using the same protocol and their antibacterial efficacy. *Rsc Adv* 4:3974–3983
36. Sadeghi B, Garmaroudi FS, Hashemi M, Nezhad HR, Nasrollahi A, Ardalan S, Ardalan S (2012) Comparison of the anti-bacterial activity on the nanosilver shapes: nanoparticles, nanorods and nanoplates. *Adv Powder Technol* 23:22–26
37. Ghosh S, Vandana V (2016) Nano-structured mesoporous silica/silver composite: synthesis, characterization and targeted application towards water purification. *Mater Res Bull* 88:291–300
38. Li H, Bian Z, Zhu J, Huo Y, Li H, Lu Y (2007) Mesoporous Au/TiO₂ nanocomposites with enhanced photocatalytic activity. *J Am Chem Soc* 129:4538–4539
39. Bhattacharyya S, Gedanken A (2008) Microwave-assisted insertion of silver nanoparticles into 3-D Mesoporous zinc oxide nanocomposites and nanorods. *J Phys Chem C* 112:659–665
40. Hazra Chowdhury I, Ghosh S, Naskar MK (2016) Aqueous-based synthesis of mesoporous TiO₂ and Ag–TiO₂ nanopowders for efficient photodegradation of methylene blue. *Ceram Int* 42:2488–2496
41. Sinha AK, Suzuki K, Takahara M, Azuma H, Nonaka T, Fukumoto K (2007) Mesoporous manganese oxide/gold nanoparticle composites for extensive air purification. *Angew Chem* 119:2949–2952
42. Allen MJ, Tung VC, Kaner RB (2010) Honeycomb carbon: a review of graphene. *Chem Rev* 110:132–145
43. Rao CNR, Sood AK, Subrahmanyam KS, Govindraj A (2009) Graphene: the new two-dimensional nanomaterial. *Angew Chem* 121:7752–7777
44. Novoselov KS, Geim AK, Morozov SV, Jiang D, Zhang Y, Dubonos SV, Grigorieva IV, Firsov AA (2004) Electric field effect in atomically thin carbon films. *Science* 306:666–669
45. Novoselov KS, Geim AK, Morozov SV, Jiang D, Katsnelson ML, Grigorieva IV, Dubonos SV, Firsov AA (2005) Two-dimensional gas of massless Dirac fermions in graphene. *Nature* 438:197–200
46. Stankovich S, Dikin DA, Dommett GHB, Kohlhaas KM, Zimney EJ, Stach EA, Piner RD, Nguyen ST, Ruoff RS (2006) Graphene-based composite materials. *Nature* 442:282–286
47. Berger C, Song Z, Li X, Wu X, Brown N, Naud C, Mayou D, Li T, Hass J, Marchenkov AN, Conrad AH, First PN, de Heer WA (2006) Electronic confinement and coherence in patterned epitaxial graphene. *Science* 312:1191–1196
48. Wu J, Pisula W, Mullen K (2007) Graphenes as potential material for electronics. *Chem Rev* 107:718–747
49. Kim KS, Zhao Y, Jang H, Lee SY, Kim JM, Kim KS, Ahn JH, Kim P, Choi JY, Hong BH (2009) Large-scale pattern growth of graphene films for stretchable transparent electrodes. *Nature* 457:706–710

50. Acik M, Chabal YJ (2013) A review on thermal exfoliation of graphene oxide. *J Mater Sci Res* 2:101–112
51. Pei S, Zhao J, Du J, Ren W, Cheng HM (2010) Direct reduction of graphene oxide films into highly conductive and flexible graphene films by hydrohalic acids. *Carbon* 48:4466–4474
52. Wadhwa H, Kumar D, Mahendia S, Kumar S (2017) Microwave assisted facile synthesis of reduced graphene oxide-silver (RGO-Ag) nanocomposite and their application as active SERS substrate. *Mater Chem Phys* 194:274–282
53. Saleh TA, Al-Shalalfeh MM, Al-Saadi AA (2018) Silver loaded graphene as a substrate for sensing 2-thiouracil using surface-enhanced Raman scattering. *Sens Actuators B* 254:1110–1117
54. Dar RA, Khare NG, Cole DP, Karna SP, Srivastava AK (2014) Green synthesis of a silver nanoparticle–graphene oxide composite and its application for As(III) detection. *RSC Adv* 4:14432–14440
55. Ju J, Chen W (2015) In situ growth of surfactant-free gold nanoparticles on nitrogen-doped graphene quantum dots for electrochemical detection of hydrogen peroxide in biological environments. *Anal Chem* 87:1903–1910
56. Kim P, Doss NM, Tillotson JP, Hotchkiss PJ, Pan MJ, Marder SR, Li J, Calame JP, Perry JW (2009) High energy density nanocomposites based on surface modified BaTiO₃ and a ferroelectric polymer. *ACS Nano* 3:2581–2592
57. Ehrhardt C, Fettkenhauer C, Glenneberg J, Münchgesang W, Pientschke C, Großmann T, Zenkner M, Wagner G, Leipner HS, Buchsteiner AS, Diestelhorst M, Lemm S, Beige H, Ebbinghaus SG (2013) BaTiO₃-P(VDF-HFP) nanocomposite dielectrics – influence of surface modification and dispersion additives. *Mater Sci Eng, B* 178:881–888
58. Wagener P, Brandes G, Schwenke A, Barcikowski S (2011) Impact of in situ polymer coating on particle dispersion into solid laser-generated nanocomposites. *Phys Chem Chem Phys* 13:5120–5126
59. Toor A, Pisano AP (2015) Gold nanoparticle/PVDF polymer composite with improved particle dispersion. In: *Proceedings of the 15th IEEE international conference on nanotechnology, Rome, Italy*
60. Kanahara M, Shimomuraa M, Yabu H (2014) Fabrication of gold nanoparticle–polymer composite particles with raspberry, core–shell and amorphous morphologies at room temperature via electrostatic interactions and diffusion. *Soft Matter* 10:275–280
61. Coulston RJ, Jones ST, Lee TC, Appel EA, Scherman EA (2011) Supramolecular gold nanoparticle–polymer composites formed in water with cucurbit[8]uril. *Chem Commun* 47:164–166
62. Jin X, Zhou L, Zhu B, Jiang X, Zhu N (2018) Silver-dendrimer nanocomposites as oligonucleotide labels for electrochemical stripping detection of DNA hybridization. *Biosens Bioelectron* 107:237–243
63. Zhang S, Qiu G, Ting YP, Chung TS (2013) Silver–PEGylated dendrimer nanocomposite coating for anti-fouling thin film composite membranes for water treatment. *Colloids Surf, A* 436:207–214
64. Ruiz-Sanchez AJ, Parolo C, Miller BS, Gray ER, Schlegel K, McKendry RA (2017) Tuneable plasmonic gold dendrimer nanochains for sensitive disease detection. *J Mater Chem B* 5:7262–7266
65. Murphy CJ, Sau TK, Gole AM et al (2005) Anisotropic metal nanoparticles: Synthesis, assembly, and optical applications. *J Phys Chem B*. 109(29):13857–13870
66. Burda C, Chen X, Narayanan R, El-Sayed MA (2005) Chemistry and properties of nanocrystals of different shapes. *Chem Rev* 105(4):1025–1102
67. Shaw CP, Fernig DG, Lévy R (2011) Gold nanoparticles as advanced building blocks for nanoscale self-assembled systems. *J Mater Chem* 21(33):12181–12187
68. Jain PK, Huang X, El-Sayed IH, El-Sayed MA (2007) Review of some interesting surface plasmon resonance-enhanced properties of noble metal nanoparticles and their applications to biosystems. *Plasmonics* 2(3):107–118

69. Huang X, Jain PK, El-Sayed IH, El-Sayed MA (2008) Plasmonic photothermal therapy (PPTT) using gold nanoparticles. *Lasers Med Sci* 23(3):217–228
70. Tong L, Wei Q, Wei A, Cheng JX (2009) Gold nanorods as contrast agents for biological imaging: optical properties, surface conjugation and photothermal effects. *PhotochemPhotobiol* 85(1):21–32
71. Liang S, Zhao Y, Xu S, Wu X, Chen J, Wu M, Zhao X (2015) A silica-gold-silica nanocomposite for photothermal therapy in near-infrared region 7(1):85–93
72. Mishra YK, Mohapatra S, Avasthi DK, Kabiraj D, Lalla NP, Pivin JC, Sharma H, Kar R, Singh N (2007) Gold–silica nanocomposites for the detection of human ovarian cancer cells: a preliminary study. *Nanotechnology* 18(34):345606
73. Boisselier E, Astruc D (2009) Gold nanoparticles in nanomedicine: preparations, imaging, diagnostics, therapies and toxicity. *ChemSoc Rev* 38(6):1759–1782
74. Rasch MR, Rossinyol E, Hueso JL, Goodfellow BW, Arbiol J, Korgel BA (2010) Hydrophobic gold nanoparticle self-assembly with phosphatidylcholine lipid: membrane-loaded and janus vesicles. *Nano Lett* 10(9):3733–3739
75. Chen Y, Bose A, Bothun GD (2010) Controlled release from bilayer-decorated magnetoliposomes via electromagnetic heating. *ACS Nano* 4(6):3215–3221
76. Ahmed S, Madathingal RR, Wunder SL, Chen Y, Bothun G (2011) Hydration repulsion effects on the formation of supported lipid bilayers. *Soft Matter* 7(5):1936–1947
77. Von White G, Chen Y, Roder-Hanna J, Bothun GD, Kitchens CL (2012) Structural and thermal analysis of lipid vesicles encapsulating hydrophobic gold nanoparticles. *ACS Nano* 6(6):4678–4685
78. Wijaya A, Hamad-Schifferli K (2007) High-density encapsulation of Fe₃O₄ nanoparticles in lipid vesicles. *Langmuir* 23(19):9546–9550
79. Xia T, Rome L, Nel A (2008) Nanobiology: particles slip cell security. *Nat Mater* 7(7):519–520
80. Kang JH, Ko YT (2015) Lipid-coated gold nanocomposites for enhanced cancer therapy. *Int J Nanomedicine* 10(Spec Iss):33–45
81. Chanmee T, Ontong P, Konno K, Itano N (2014) Tumor-associated macrophages as major players in the tumor microenvironment. *Cancer* 6(3):1670–1690
82. Lou JJ, Chua YL, Chew EH, Gao J, Bushell M, Hagen T (2010) Inhibition of hypoxia-inducible factor-1 α (HIF-1 α) protein synthesis by DNA damage inducing agents. *PLoS One* 5(5):e10522
83. Nath A, Pal R, Singh LM, Saikia H, Rahaman H, Ghosh SK, Mazumder R, Sengupta M (2018) Gold-manganese oxide nanocomposite suppresses hypoxia and augments pro-inflammatory cytokines in tumor associated macrophages. *Int Immunopharmacol* 57:157–164
84. Liu Y, Lv X, Liu H, Zhou Z, Huang J, Lei S, Cai S, Chen Z, Guo Y, Chen Z, Zhou X, Nie L (2018) Porous gold nanocluster-decorated manganese monoxide nanocomposites for microenvironment-activatable MR/photoacoustic? *CT Tumor Imag* 10(8):3631–3638
85. Suresh L, Brahman PK, Reddy KR, Bondili JS (2018) Development of an electrochemical immunosensor based on gold nanoparticles incorporated chitosan biopolymer nanocomposite film for the detection of prostate cancer using PSA as biomarker 112:43–51
86. Rizwan M, Elma S, Lim SA, Ahmed MU (2018) AuNPs/CNOs/SWCNTs/chitosan-nanocomposite modified electrochemical sensor for label-free detection of carcinoembryonic antigen 107:211–217
87. Christou A, Stec AA, Ahmed W, Aschberger K, Amentia V (2016) A review of exposure and toxicological aspects of carbon nanotubes, and as additives to fire retardants in polymers 46(1):74–95
88. Contreras-Caceres R, Sanchez-Iglesias A, Karg M, Pastoriza-Santos I, Perez-Juste J, Pacifico J, Hellweg T, Fernández-Barbero A, Liz-Marzan LM (2008) Encapsulation and growth of gold nanoparticles in thermoresponsive microgel. *Adv Mater* 20:1666–1670
89. Contreras-Caceres R, Pastoriza-Santos I, Alvarez-Puebla RA, Perez-Juste J, FernandezBarbero A, Liz-Marzan LM (2010) Growing Au/Ag nanoparticles within microgel colloids for improved SERS detection. *Chem Eur J* 16:9462–9467

90. Sari TK, Takahashi F, Jin J, Zein R, Munat E (2018) Electrochemical determination of Chromium(VI) in river water with Gold nanoparticles-Graaphene nanocomposites modified electrodes 34(2):155–160
91. Yin PT, Kim TH, Choi JW, Lee KB (2013) Prospects for graphene–nanoparticle-based hybrid sensors. *Phys Chem Chem Phys* 15:12785–12799
92. Benvidi A, Firouzabadi AD, Moshtaghiun SM, Mazloum-Ardakani M, Tezzerani MD (2015) Ultrasensitive DNA sensor based on gold nanoparticles/reduced graphene oxide/glassy carbon electrode. *Anal Biochem* 484:24–30
93. Yang G, Li L, Rana RK, Zhu JJ (2013) Assembled gold nanoparticles on nitrogen-doped graphene for ultrasensitive electrochemical detection of matrix metalloproteinase-2. *Carbon* 61:357–366
94. Ju J, Chen W (2015) In situ growth of surfactant-free gold nanoparticles on nitrogen-doped graphene quantum dots for electrochemical detection of hydrogen peroxide in biological environments. *Anal Chem* 87:1903–1910
95. Wang C, Li J, Amatore C, Chen Y, Jiang H, Wang XM (2011) Gold nanoclusters and graphene nanocomposites for drug delivery and imaging of cancer cells. *Angew Chem Int Ed* 50:11644–11648
96. Zhang G, Chang H, Amatore C, Chen Y, Jiang H, Wang X (2013) Apoptosis induction and inhibition of drug resistant tumor growth in vivo involving daunorubicin-loaded graphene–gold composites. *J Mater Chem B* 1:493–499
97. Pinto AM, Gonçalves IC, Magalhães FD (2013) Graphene-based materials biocompatibility: a review. *Colloids Surf, B* 111:188–202
98. Seabra AB, Paula AJ, de Lima R, Alves OL, Duran N (2014) Nanotoxicity of graphene and graphene oxide. *Chem Res Toxicol* 27:159–168
99. Chang Y, Yang ST, Liu JH, Dong E, Wang Y, Cao A, Liu Y, Wang H (2011) In vitro toxicity evaluation of graphene oxide on A549 cells. *Toxicol Lett* 200:201–210
100. Guo X, Mei N (2014) Assessment of the toxic potential of graphene family nanomaterials. *J Food Drug Anal* 22:105–115
101. Shi X, Wang SH, Van Antwerp ME, Chen X, Baker JR Jr (2009) Targeting and detecting cancer cells using spontaneously formed multifunctional dendrimer stabilized gold nanoparticles 134(7):1373–1379
102. Nanjwade BK, Bechra HM, Derkar GK, Manvi FV, Nanjwade VK (2009) Dendrimers: emerging polymers for drug-delivery systems. *Eur J Pharm Sci* 38:185–196
103. Cheng Y, Wang J, Rao T, He X, Xu T (2008) Pharmaceutical applications of dendrimers: promising nanocarriers for drug delivery. *Front Biosci* 13:1447–1471
104. Khan MK, Nigavekar SS, Minc LD, Kariapper MS, Nair BM, Lesniak WG, Balogh LP (2005) In vivo biodistribution of dendrimers and dendrimer nanocomposites—implications for cancer imaging and therapy. *Technol Cancer Res Treat* 4:603–613
105. Leung KC, Xuan S, Zhu X, Wang D, Chak CP, Lee SF, Ho WK, Chung BC (2012) Gold and iron oxide hybrid nanocomposite materials 41(5):1911–1928
106. Rai M, Yadav A, Gade A (2001) Silver nanoparticles as a new generation of antimicrobials. *Biotechnol Adv* 27(1):76–83
107. Grishchenko L, Medvedeva S, Aleksandrova G, Feoktistova L, Sapozhnikov A, Sukhov B, Trofimov B (2006) Redox reactions of arabinogalactan with silver ions and formation of nanocomposites. *Russian J General Chem* 76(7):1111–1116
108. Travan A, Pelillo C, Donati I, Marsich E, Benincasa M, Scarpa T, Semeraro S, Turco G, Gennaro R, Paoletti S (2009) Non-cytotoxic silver nanoparticle—polysaccharide nanocomposites with antimicrobial activity. *Biomacromol* 10(6):1429
109. Chen JP (2007) Late angiographic stent thrombosis (LAST): the cloud behind the drug—eluting stent silver lining? *J Invasive Cardiol* 19(9):395–400
110. Kuo PL, Chen WF (2003) Formation of silver nanoparticles under structured amino groups in pseudo—dendritic poly(allylamine) derivatives. *J Phys Chem B* 107(41):11267–11272
111. Huang H, Yuan Q, Yang X (2004) Preparation and characterization of metal—chitosan nanocomposites. *Colloids Surf, B* 39(1–2):31–37

112. Fu J, Ji J, Fan D, Shen J (2006) Construction of antibacterial multilayer films containing nanosilver via layer—by—layer assembly of heparin and chitosan—silver ions complex. *J Biomed Mater Res, Part A* 79(3):665–674
113. Balogh L, Swanson DR, Tomalia DA, Hagnauer GL, McManus AT (2001) Dendrimer—silver complexes and nanocomposites as antimicrobial agents 1(1):18–21
114. Sanpui P, Murugadoss A, Prasad PVD, Ghosh SS, Chattopadhyay A (2008) The antibacterial properties of a novel chitosan—Ag—nanoparticle composite. *Int J Food Microbiol* 124(2):142–146
115. Kim KJ, Sung WS, Suh BK, Moon SK, Choi JS, Kim JG, Lee DG (2009) Antifungal activity and mode of action of silver nano-particles on *Candida albicans*. *Biometals* 22(2):235–242
116. Esteban-Tejeda L, Malpartida F, Esteban-Cubillo A, Pecharroman C, Moya JS (2009) The antibacterial and antifungal activity of a soda-lime glass containing silver nanoparticles. *Nanotechnology* 20(8):85103
117. Gajbhiye MB, Kesharwani JG, Ingle AP, Gade AK, Rai MK (2009) Fungus—mediated synthesis of silver nanoparticles and their activity against pathogenic fungi in combination with fl uconazole. *Nanomedicine* 5:382–386
118. Shaheen F, Hammad Aziz M, Fakhar-E-Alam M, Atif M et al (2017) An in vitro study of the photodynamic effectiveness of GO-Ag Nanocomposites against human breast cancer cells 7(11) Pii:E401
119. Gurunathan S, Han JW, Par JH (2015) Reduced graphene oxide—silver nanoparticle nanocomposite: a potential anticancer nanotherapy. *Int J Nanomed* 10:6257–6276
120. Ghaseminezhad SM, Shojaosadati SA (2016) Evaluation of the antibacterial activity of Ag/Fe₃O₄ nanocomposites synthesized using starch 144:454–463
121. Fakhri A, Tahami S, Nejad PA (2017) Preparation and characterization of Fe₃O₄-Ag₂O quantum dots decorated cellulose nanofibers as a carrier of anticancer drugs for skin cancer 175:83–88
122. Ponnaiah SK, Periakaruppan P, Vellaichamy B (2018) New electrochemical sensor based on a silver-doped iron oxide nanocomposite coupled with polyaniline and its sensing application for picomolar level detection of uric acid in human blood and urine samples
123. Jin X, Zhou L, Zhu B, Jiang X, Zhu N (2018) Silver-dendrimer nanocomposites as oligonucleotide labels for electrochemical stripping detection of DNA hybridization 107:237–243
124. Wang YZ, Hao N, Feng QM, Shi HW, Xu JJ, Che HY (2016) A ratiometric electrochemiluminescence detection for cancer cells using g-C₃N₄ nanosheet and Ag-PANAM-luminol nanocomposites 77:76–82
125. Matai I, Sachdev A, Gopinath P (2015) Multicomponent 5-fluorouracil loaded PANAM stabilized-silver nanocomposites synergistically induce apoptosis in human cancer cells 3(3):457–68
126. Naha PC, Byrne HJ (2013) Generation of intracellular reactive oxygen species and genotoxicity effect to exposure of nanosized polyamidoamine (PAMAM) dendrimers in PLHC-1 cells in vitro. *Aquat Toxicol* 132–133:61–72
127. Jones CF, Campbell RA, Brooks AE, Assemi S, Tadjiki S, Thiagarajan G, Mulcock C, Weyrich AS, Brooks BD, Ghandehari H et al (2012) Cationic PAMAM dendrimers aggressively initiate blood clot formation. *ACS Nano* 6:9900–9910
128. Sun Y, Guo F, Zou Z, Li C, Hong X, Zhao Y, Wang C, Wang H, Liu H, Yang P et al (2015) Cationic nanoparticles directly bind angiotensin-converting enzyme 2 and induce acute lung injury in mice. *Part Fibre Toxicol* 12:4
129. Akhtar S, Al-Zaid B, El-Hashim AZ, Chandrasekhar B, Attur S, Benter IF (2016) Impact of PANAM delivery systems on signal transduction pathways in vivo: modulation of ERK1/2 and p 38 MAP kinase signaling in the normal and diabetic kidney 514(2):353–363
130. Heiden TC, Dengler E, Kao WJ, Heideman W, Peterson RE (2007) Developmental toxicity of low generation PAMAM dendrimers in zebrafish. *Toxicol Appl Pharmacol* 225:70–79

131. Naha PC, Mukherjee SP, Byrne HJ (2018) Toxicology of engineered nanoparticles: Focus on poly (amidoamine) dendriers 15(2) pii:E338
132. Wang X, Wang Y, Jiang M, Shan Y, Jin X, Gong M, Wang X (2018) Functional electrospun nanofibers-based electrochemiluminescence immunosensor for detection of the TSP53 using RuAg/SiO₂NPs as signal enhancers 548:15–22
133. Song Y, Jiang H, Wang B, Kong Y, Chen J (2018) Silver-incorporated mussel-inspired polydopamine coatings on mesoporous silica as an efficient nanocatalyst and antimicrobial agent 10(2):1792–1801
134. Cao T, Li Z, Xiong Y, Yang Y, Xu S, Bisson T, Gupta R, Xu Z (2017) Silica-silver nanocomposites as regenerable sorbents for Hg⁰ removal of flue gases 51(20):11909–11917

Synthesis, Characterization and Application of Bio-based Polyurethane Nanocomposites



Sonalee Das, Sudheer Kumar, Smita Mohanty and Sanjay Kumar Nayak

List of Abbreviations

PU _s	Polyurethane
MMT	Montmorillonite
VO _s	Vegetable oils
MDI	Methylene diisocyanate
TDI	Toluene diisocyanate
HDI	Hexamethylene diisocyanate
IPDI	Isophorone diisocyanate
JCO	Jatropha curcas oil
CO	Castor oil
PU/NS	Polyurethane/silica nanocomposites
NS	Nano silica
TGA	Thermogravimetric analysis
DTG	Derivative thermo-gravimetric
DSC	Differential scanning calorimetry
SEM	Scanning electron microscopy
TEM	Transmission electron microscopy
FTIR	Fourier transform infrared spectroscopy
E _a	Activation energy
T _m	Melting temperature
T _g	Glass transition temperature
E'	Storage modulus
E''	Loss modulus
MBPU	Modified bio-based polyurethane
MCO	Modified castor oil
HBPUS	Hyper branched polyurethane
GO	Graphene oxide

S. Das (✉) · S. Kumar · S. Mohanty · S. K. Nayak
Laboratory for Advanced Research in Polymeric Materials,
Central Institute of Plastics Engineering and Technology,
Bhubaneswar 751024, Odisha, India
e-mail: das.sonalee31@gmail.com

RGO	Reduced graphene oxide
f-RGO	Phytoextract-RGO
MWCNTs	Multiwall carbon nanotubes
XRD	X-ray diffraction
BET	Brunauer–Emmett–Teller theory
IPN	Interpenetrating polymer network
EP	Epoxy
PU/EP	Polyurethane/epoxy
DMA	Dynamic mechanical analysis
APTES	Aminopropyltriethoxy silane
WPU	Waterborne polyurethane
SMT	Silylated sodium montmorillonite
SHT	Silylated halloysite nanotubes
POBUA	Palm oil and methylene diisocyanate based polyurethane acrylate
EPOLA	Epoxidized palm oil acrylate
PCL	Poly(ϵ -caprolactone) diol
UPCEA	Poly-(urethane-esteramide)
TiO ₂	Titanium dioxide
EDX	Energy dispersive X-ray spectroscopy
WAXD	Wide-angle X-ray scattering
ECNC	<i>E. Globulus</i> derived cellulose nanocrystals

1 Introduction

Polyurethane (PU) has been one of the most attractive speciality polymers known for its excellent properties such as scratch resistance, abrasion and chemical resistance. These polymers find extensive applications in many different fields such as foams (flexible, semi-rigid and rigid), elastomers, adhesives, coatings and fibers as shown in Fig. 1.

Basically, these polymers are obtained by the polyaddition reaction of polyol and polyisocyanate as shown in Fig. 2 [1–3].

The properties of the synthesized PU depend upon the molecular weight, the degree of cross-linking, the molar ratio of NCO/OH, effective intermolecular forces and stiffness of different chain segments [4, 5]. In general, the PU chain is composed of a soft segment based on polyol and a hard segment based on diisocyanate and a chain extender [6–8]. The nature of hydrogen bonding (H-bonding) in the rigid segment leads to strong mutual attraction resulting in the formation of micro-domains which can act as physical crosslink providing elastomeric properties to the PU chain segment [7, 8]. The hard segments determine the physical properties such as rigidity, while the soft segment imparts flexibility and elasticity. Recent years have witnessed considerable research effort towards the improvement

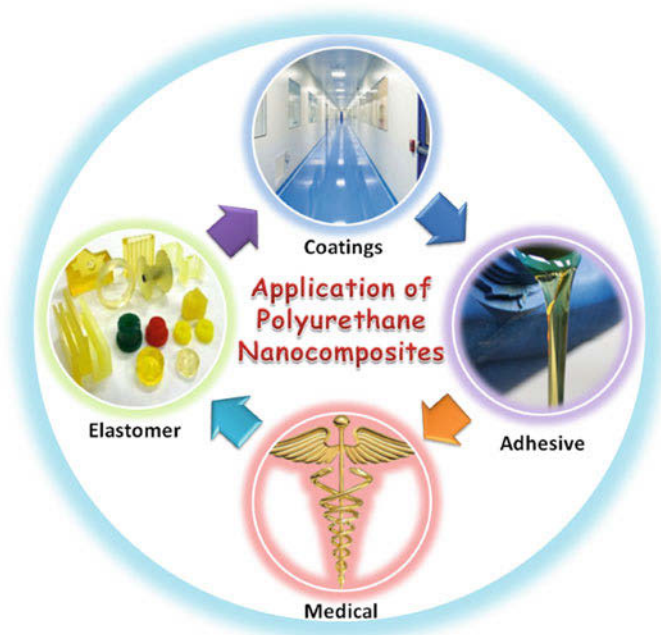


Fig. 1 Applications of polyurethane (PU) in various fields

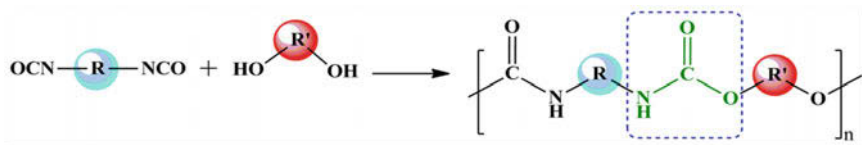


Fig. 2 Synthesis of PUs from diisocyanate and polyol

of the properties of polymer matrix i.e. PU (organic part) through the reinforcement by addition of fillers in the nanometer scale [9, 10]. Nanocomposites represent a unique class of materials that can be described by an ultrafine dispersion of nanometer size fillers in a polymer matrix [11]. The most commonly used nanofillers for PU includes nanosilica, titanium dioxide (TiO_2), organically modified montmorillonite (MMT), graphite, cellulose nanocrystals etc. [12]. The developed PU nanocomposite films using the above nanofillers exhibit good adhesion between the polymer matrix and nanofillers because of the higher surface area and surface-to-volume ratio of the nanoscale building blocks [13]. The introduction of smaller amounts of nanofillers can provide higher thermal, mechanical, optical and flame retardancy properties to the PU composite films as compared to their neat counterparts [14]. Additionally, these fillers are suitable for application in

transparent PU coatings owing to the uniform dispersion of the nanoparticles. Moreover, these uniformly dispersed particles leads to no interaction with the incident light. As a consequence, there is no turbidity in the resulting composite material.

The main ingredient for the synthesis of PUs includes the polyol and the polyisocyanate component which are based on petro-based resources. Recent decades witnessed the utilization of petro-based i.e. polyether polyol and polyester polyol as the polyol component for the synthesis of PU. However, the progressive decline in the fossil resources and the severe increase in the oil cost have led to momentous attention towards the development of green PUs based on renewable resources [14, 15]. Vegetable oils (VOs) triglyceride molecule obtained from various plant sources are gaining immense interest as a monomer in a recent decade for the synthesis of PUs and its nanocomposites [16–18]. Moreover, the feasibility of carrying out various reactions with VOs to synthesize bio-based polyol also makes it more attractive for the synthesis of PUs [19, 20]. The various VOs used in the synthesis of PUs and its nanocomposites include castor oil, palm oil, linseed oil etc. Basically VOs are a family part of chemical compounds known as lipids which are predominantly made up of triglycerides as shown in Fig. 3. The triglyceride molecule consists of three fatty acids joined at a glycerol junction. In VOs the fatty acid chain length varies from 0 to 22 carbons with 0 to 3 double bonds per fatty acid. The various fatty acids present in VOs [21].

The other main component used for the synthesis of PU is isocyanate which exists in the form of resonating structure as shown in Fig. 4 [22].

These groups are very reactive, towards nucleophilic agents due to the electron deficiency on the carbon atom and hence most of the reaction occurs across the C = N group of NCO [22, 23]. Broadly they are classified into two group i.e. (a) aromatic isocyanate and (b) aliphatic isocyanate. It has been postulated that the aromatic isocyanate is more reactive than the aliphatic ones with decreased reactivity from primary through secondary to tertiary isocyanate group unless

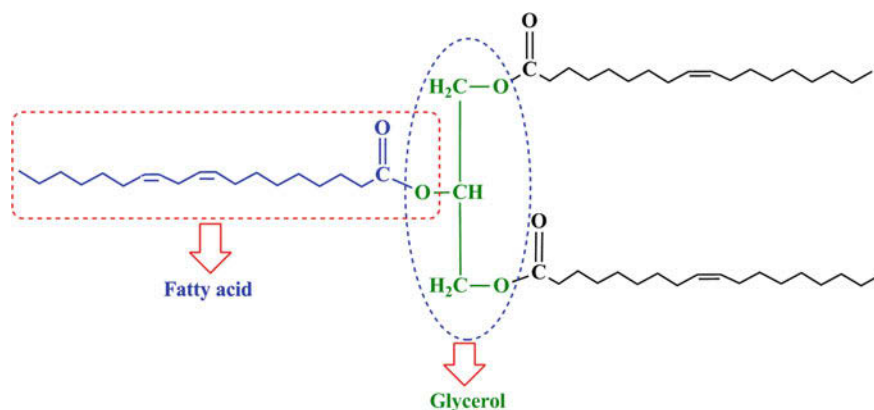


Fig. 3 Triglyceride molecule in vegetable oil

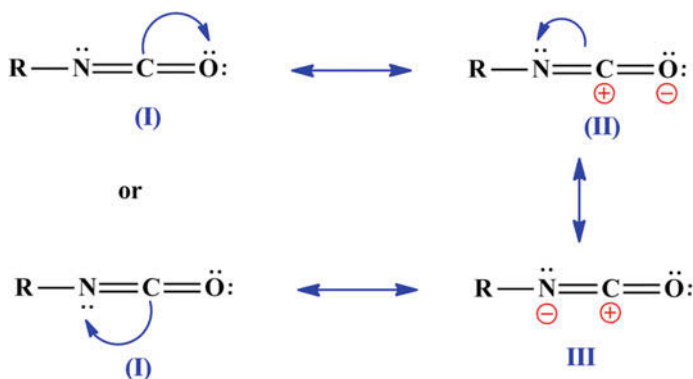


Fig. 4 Resonating structure of isocyanate group

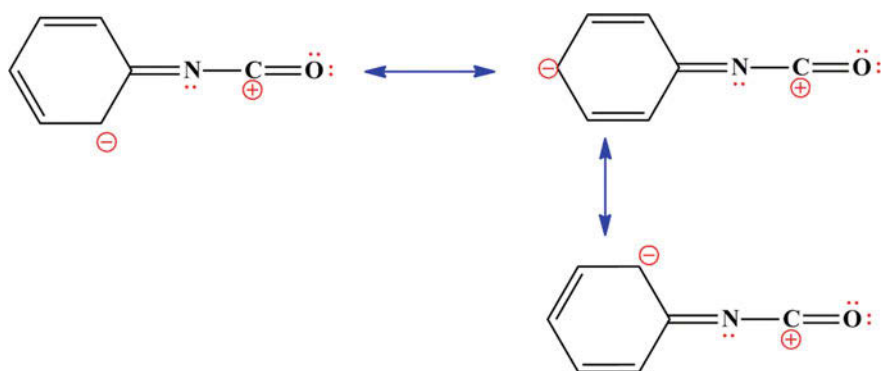


Fig. 5 Resonance in aromatic isocyanate group

catalytic or steric factors results in reversal activity [24]. This can be explained on the basis of the resonating structure wherein, the negative charge on the nitrogen atom is well distributed and stabilized throughout the benzene ring reducing the electron charge on the central carbon atom of the isocyanate when R is aromatic in nature (see Fig. 5) [25].

Thus, the formation of the mesomeric structure in Fig. 5 explains the higher reactivity of aromatic isocyanates such as methylene diisocyanate (MDI) and toluene diisocyanate (TDI) over the aliphatic isocyanate such as hexamethylene diisocyanate (HDI) and isophorone diisocyanate (IPDI). In case of an aromatic isocyanate, the nature of the substituent also determines the reactivity, i.e. electron-attracting substituent in ortho or para position increase the reactivity and electron donating substituent lower the reactivity of isocyanate group [26]. As a general rule, any electron-withdrawing group linked with R will increase the positive charge on carbon, thereby increasing the reactivity of the isocyanate group towards nucleophilic attack while electron donating groups will decrease the reactivity of isocyanate

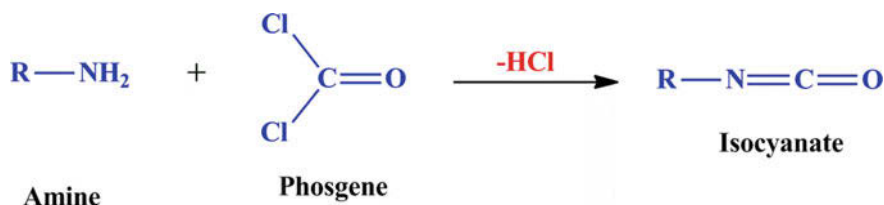


Fig. 6 Synthesis route of isocyanate

groups [22]. The basic synthesis of isocyanate is shown in Fig. 6. The synthesis starts with an amine, aliphatic or aromatic and phosgene. The synthesis route via phosgene was invented in 1884 by Hentschel in which the isocyanate is formed by the elimination of two molecules of hydrogen chloride (HCl).

However, the industrial synthesis of isocyanate through phosgene has to be minimized because of various side reactions that lead to the production of urea and salt complexes. [27]. Moreover, these diisocyanates are toxic and harmful to the environment since they are derived from phosgene and release diamines, free diisocyanate, and hydrogen cyanide on degradation [28, 29].

The diisocyanate normally used in PU synthesis are petroleum-derived as discussed in the above section, but if they are derived from VO sources then this would lead to an increased amount of renewable carbon in such materials. Moreover, the phosgenation synthesis route of isocyanate leads to the emission of carcinogenic products into the atmosphere [28, 29]. Hence, in the current scenario isocyanate based on vegetable oil would be a suitable alternative over the petro-based isocyanate to foster sustainability [30, 31]. Although, extensive research effort is being undertaken for the synthesis of isocyanate from VO precursor but only a few have been used for developing PUs [32, 33].

Thus, it is inevitable from the above discussion that PUs based on bio-based polyol and isocyanate is an essential requirement of the current scenario so as to reduce the excess usage of petro-based products and to formulate and develop environmentally benign materials. However, the PUs synthesized from VO based resources suffer from low mechanical, thermal and chemical properties hence, it is imperative to use nanoparticles for the improvement in the properties of PU matrix [34]. The following section will deal with the synthesis of PUs nanocomposite based on various VOs.

2 Synthesis of Bio-based Polyurethane Nanocomposite from Vegetable Oil

The current trend and present era are inclined towards the development of greener products. Furthermore, as discussed the depletion of fossil fuel has led to rapid research and development towards the synthesis of PUs from renewable resources.

In this concern, vegetable oil like castor oil, jatropha oil, palm oil and soybean oil etc. has led to dramatic utilization for the synthesis of PUs owing to economic, environmental and social advantages. Castor oil (CO) with 92–95% ricinoleic acid is the only commercially available natural polyol with inherent hydroxyl ($-\text{OH}$) group widely used for synthesizing PUs and its nanocomposites [35, 36]. The ricinoleic acid contains a secondary OH group at the 12th carbon position and a double bond at the 9th and 10th carbon. This structural feature distinguishes CO as a candid monomer for synthesizing of PUs amongst all other VOs [35, 36]. Jatropha curcas oil (JCO) is another one attractive VO with high unsaturated fatty acid content and good oxidation stability [37], which makes it a suitable monomer for the synthesis of non-isocyanate polyurethane for various industrial applications [38–42]. Palm oil another vital VO contains 45–60% unsaturated double bonds which can undergo epoxidation to form palm oil-based epoxides which can be used as a green polyol for synthesizing PU [39–43].

However, VO based polyol exhibits disadvantages which include inferior physical properties, poor water resistance, and low thermostability [42–44]. These disadvantages can be addressed by using nanotechnology through the incorporation of nanofillers which can be an effective method for the development of PU properties [45–50]. The following section will deal with the recent trends and development concerning the utilization of various VOs through the exploitation of their structural chemistry for synthesizing different PU nanocomposites using nano-technique.

2.1 *Castor Oil Based Polyurethane Nanocomposites*

Wang et al. [51] in a recent paper studied about the morphology, thermal and mechanical properties of castor oil-based polyurethane/silica nanocomposites (PU/NS). The NS surface was modified with 3-glycidoxypropyltrimethoxysilane and γ -methacryloxy-propyltrimethoxysilane. Thereafter PU/NS composite was prepared via in situ polymerization technique with castor oil, isophorone diisocyanate and modified NS particle. FTIR spectra indicated a successful blending of NS with silane coupling agents through the appearance of peaks at $2973\text{--}2904\text{ cm}^{-1}$ associated with the $-\text{CH}_2-$ group of 3-glycidoxypropyltrimethoxysilane, at 1636, 1718, 2953, and 2894 cm^{-1} owing to $\text{C}=\text{C}$, $\text{C}=\text{O}$ and C-H stretching vibration of 3-glycidoxypropyltrimethoxysilane group. TGA studies were carried out to investigate the thermal stability of unmodified and modified NS particles. The unmodified NS particles indicate weight loss at $180\text{ }^\circ\text{C}$. However, the modified NS particles indicated two stages of weight loss within $150\text{--}600\text{ }^\circ\text{C}$. The higher temperature of weight loss for modified NS particles indicated successful modification with silane coupling agents. Scanning electron microscopy studies indicated the uniform and homogeneous dispersion of modified NS particles within the PU matrix. However, the neat NS particles indicated aggregation with a non-homogenous surface within the PU matrix owing to hydrogen bonding and

high specific areas. Moreover, it was observed that 12% loading of modified NS particles within the PU matrix indicated homogenous morphology devoid of any aggregation. The TGA and DTG curve of PU and PU/NS composites indicate three stages of weight loss. The 1st stage was attributed to the decomposition of urethane linkage to form isocyanate, polyol, primary or secondary amine, olefin, and carbon dioxide, the 2nd stage with the decomposition of castor oil segments [52]. The incorporation of NS particles within the PU matrix led to the improvement of $T_{10\%}$ and T_{max1} as compared to neat PU. This was due to the restriction of PU chain mobility by the NS particles. Moreover, the char residue at 600 °C for PU/NS composite increased to 10.1% in comparison to neat PU. The tensile strength and Young's modulus of the PU/NS composite also increased with an increase in the loading of different NS content. As compared to neat PU, PU/NS composites with 12 wt% loading of neat SiO₂ and modified SiO₂ exhibited 222, 230, and 87% improvement in tensile strength, and 182, 182, and 88% increment in Young's modulus, respectively.

Meera et al. [53] prepared bio-based polyurethane/nanosilica (PU/NS) composite using castor oil (CO) with hexamethylene diisocyanate (HDI) at room temperature. Figure 7 shows the reaction scheme for the synthesis of PU from castor oil and HDI.

The NS particles were modified with silane surface modifiers, i.e., 3-aminopropyltrimethoxysilane for improving the dispersion, compatibility and surface activity of silica particle with PU matrix. The synthesis of PU with castor oil and modified NS particle (i.e. 0.5, 1, 3 and 5 wt%) was carried out through two-step process at 80 °C for 4 h. The prepared nanocomposite films were characterized using Fourier transform infrared spectroscopy (FTIR) to understand the chemical interaction. The thermal stability and glass transition temperature of the films were analyzed using thermogravimetric analysis (TGA) and differential scanning calorimetry (DSC). The dynamic mechanical analysis was done to study the thermo-mechanical properties of the PU nanocomposite films. The morphology of the prepared nanocomposite films was investigated using scanning electron microscopy (SEM) and transmission electron microscopy (TEM). FTIR studies indicate that with an increase in the wt% of NS particles the peak position of urethane (–NH) shifts towards higher wave number i.e. PU-0.5AMS—3332 cm⁻¹, PU-1AMS—3334 cm⁻¹, PU-3AMS—3336 cm⁻¹ and PU-5AMS—3338 cm⁻¹. This is due to the presence of strong interaction between NS particles and PU matrix. Moreover, this shift can also be related to the formation of H-bonding between NS particles and PU matrix [54]. However, the peak position of carbonyl peak (–C = O) in PU nanocomposite shifts to lower wave number with an increase in the NS content. These shift in the –NH and –C = O peak confirms the formation of the complete network structure of PU nanocomposite. Moreover, the presence of peaks at 1096 and 774 cm⁻¹ for Si–O–Si and O–Si–O also confirms the presence of NS particles within the PU matrix. Neat PU films have low thermal stability and start degrading below 250 °C owing to the presence of labile urethane linkages. On the other hand, the prepared PU nanocomposite films started degradation at around 280 °C due to the presence of NS particles. Neat PU and PU-AMS films showed

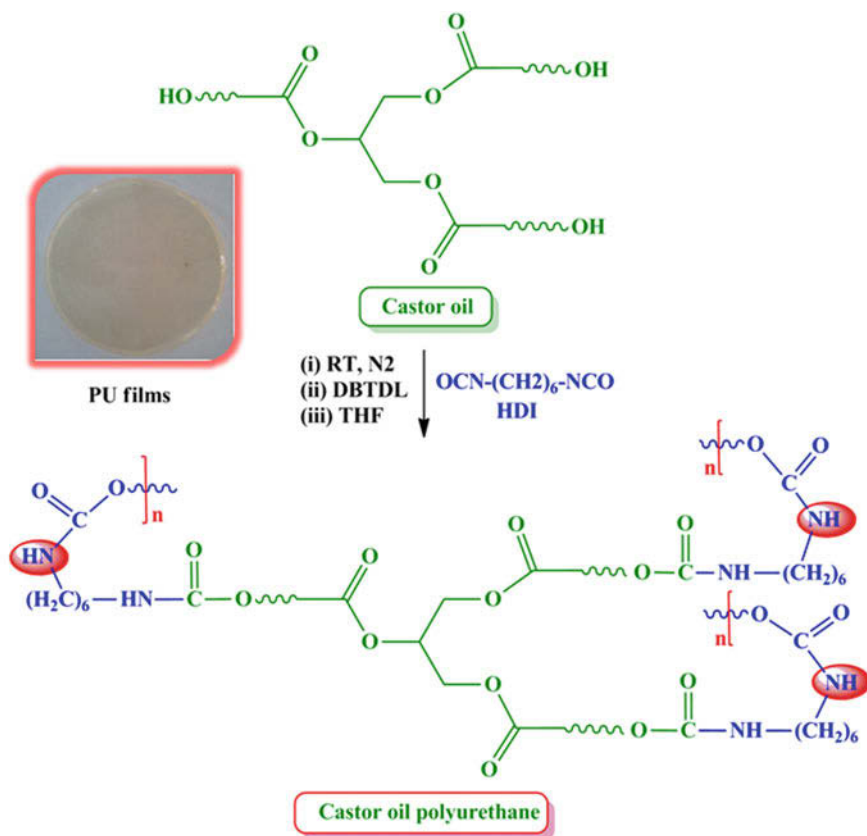


Fig. 7 Reaction scheme for the synthesis of PUs from castor oil and HDI

two-step degradation curves, wherein, the 1st stage at $350\text{ }^\circ\text{C}$ was related with the urethane degradation and the 2nd stage between 350 and $500\text{ }^\circ\text{C}$ was related with the degradation of polyol. TGA thermogram curve of PU-AMS nanocomposite film indicate improvement in thermal stability and melting temperature (T_m) owing to the presence of silica nanoparticles. It was also observed that the residual weight percentage in case of neat PU was 0.003% , whereas in case of PU-5AMS it was 8.2% . The activation energy (E_a) value of neat PU and was found to be 133 and 139 kJ mol^{-1} whereas, the E_a value of PU-5AMS was found to be between 157 and 166 kJ mol^{-1} . The presence of silica nanoparticles reinforced the PU matrix thereby improving the interfacial interaction and thermal stability of the nanocomposite film. Neat castor oil based PU indicate T_g at $-40.1\text{ }^\circ\text{C}$ corresponding to a soft segment of the polyol and T_m at $279.1\text{ }^\circ\text{C}$ corresponding to the hard segment. On the other hand, the T_g values of PU-0.5AMS, PU-1AMS, PU-3AMS and PU-5AMS was observed at 33.4 , 33.7 , 32.6 and $29.71\text{ }^\circ\text{C}$ respectively. However, the T_m value of PU nanocomposite films was unaltered. The

increment in T_g of the PU-AMS nanocomposite films was due to the good dispersion of the NS particles within the PU matrix which restricts its molecular mobility. DMA results of the PU-AMS nanocomposite film indicates an increase in storage modulus (E') and loss modulus (E'') as compared to the neat PU films which was due to the reinforcing effect and strong interfacial interaction in between PU and NS particles which restricts the segmental mobility of the PU chain as shown in Fig. 8 [55]. Optical transmittance results of the PU-AMS films decreases with an increase in the NS content owing to light scattering at the interfaces of NS and PU. Thus, the authors concluded from the above results that the modified NS particles can lead to an improvement in the properties of PU composite films.

Das et al. [56] reported about the biodegradability of modified bio-based PU (MBPU) and modified bio-based (MBPU/NS) composite synthesized from transesterified castor oil (MCO) and palm oil based isocyanate by composting technique for a duration of 90 days. The authors reported that the composting technique presents a faster and a cost-effective method for the degradation of MBPUs since the microorganism present in the compost use the ester linkage of PU as a source of carbon and nitrogen. The visual inspection results of neat MBPU and MBPU/NS after composting for 90 days indicated a color change from white to brown with pronounced surface degradation of the later sample. Bacterial and fungal colonies were also formed on the surface of the samples indicating bio-degradation. FTIR studies of MBPU and MBPU/NS composites revealed lowering of urethane carbonyl stretching peaks at 1720 cm^{-1} indicating dissociation of ester linkage thereby confirming the biodegradation of the samples [57, 58].

The probable reason behind this observation was related with the hydrolytic degradation of ester linkages as shown in Fig. 8 by extracellular enzymes secreted by the microorganism [59]. The MBPU/NS films indicated a higher decrease in the intensity of the urethane carbonyl peaks as compared to neat MBPU samples due to its higher hydrophobic behaviour and surface silanol groups that resulted in easy surface adhesion of microorganism [60]. In addition, MBPU/NS surface also indicated higher weight loss as compared to neat MBPU due to the presence of

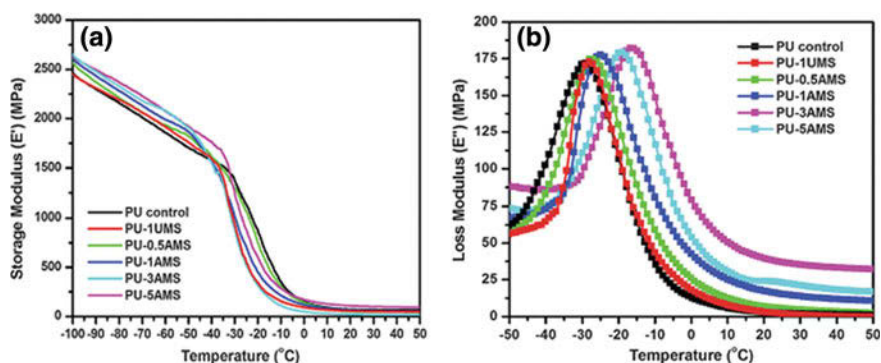


Fig. 8 Storage modulus (E') and loss modulus (E'') of PU-nanosilica composite

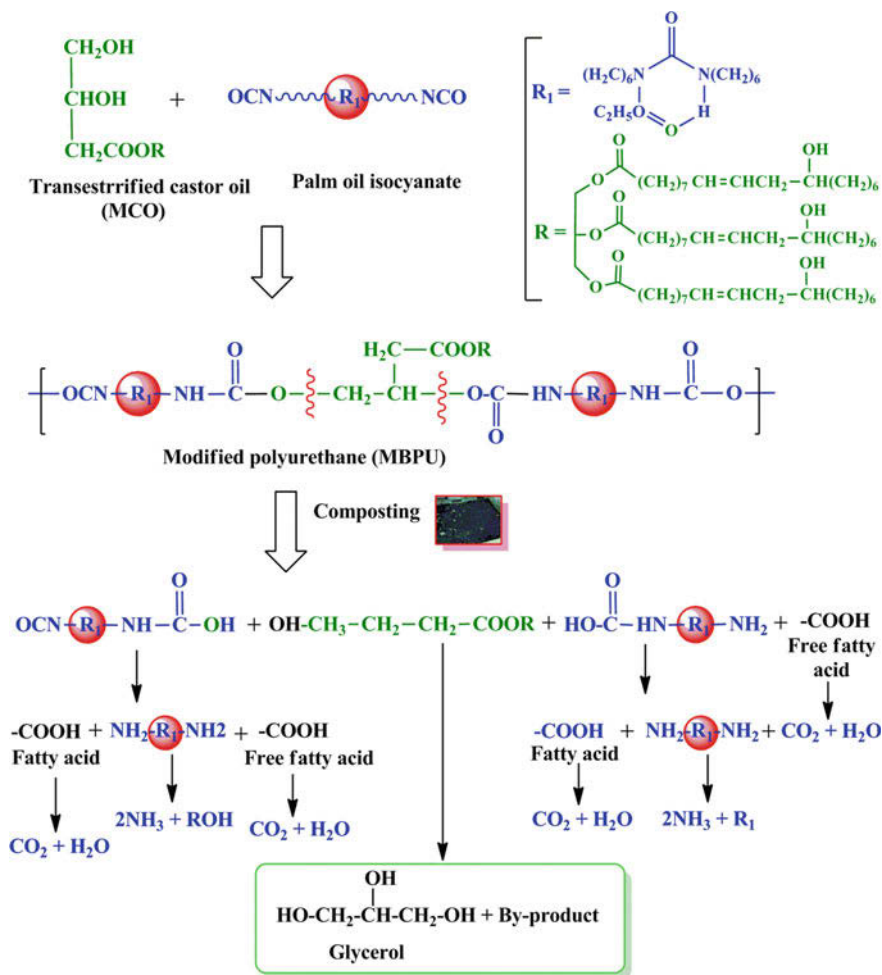


Fig. 9 Hydrolytic degradation of MBPU by extracellular enzymes in micro-organisms

hydroxyl groups on the NS surface that led to attachment of microorganism onto the former surface. SEM micrographs as shown in Figs. 10 and 11 also indicated higher surface degradation of MBPU/NS surface as compared to neat MBPU through the appearance of cracks, holes and fungal mycelia. This was again due to the reasons illustrated earlier. Thus, it can be concluded that the MBPU/NS samples can be a biodegradable as compared to neat PU on account of its structural organization and composition.

Thakur and Karak et al. [61] reported about the preparation of castor oil based-tough hyperbranched polyurethane (HPUs) nanocomposite reinforced with two different types of nanofillers, i.e., reduced graphene oxide (RGO) and phytoextract-RGO (f-RGO). f-RGO was functionalized by reacting RGO with

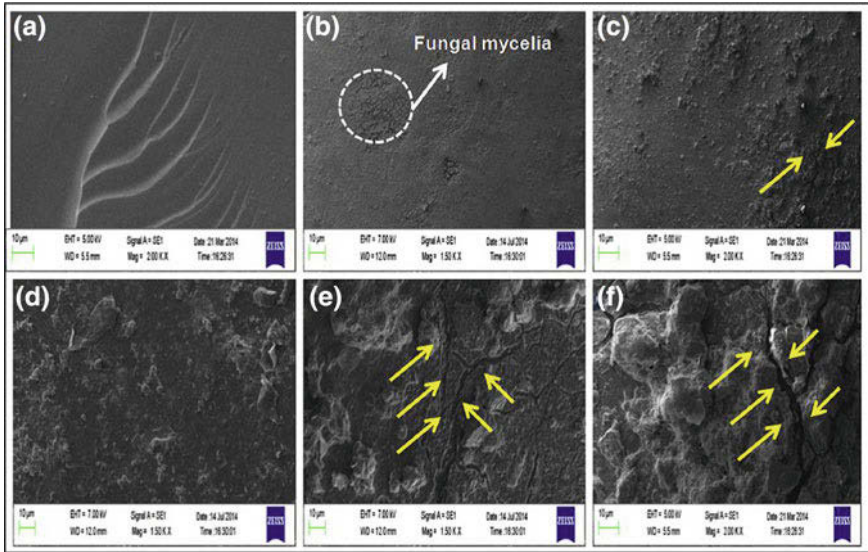


Fig. 10 SEM micrographs of neat MBPU for **a** 0 days, **b** 30 days, **c** 45 days, **d** 60 days and **e** 75 days. Reproduced from Das et al. [56]

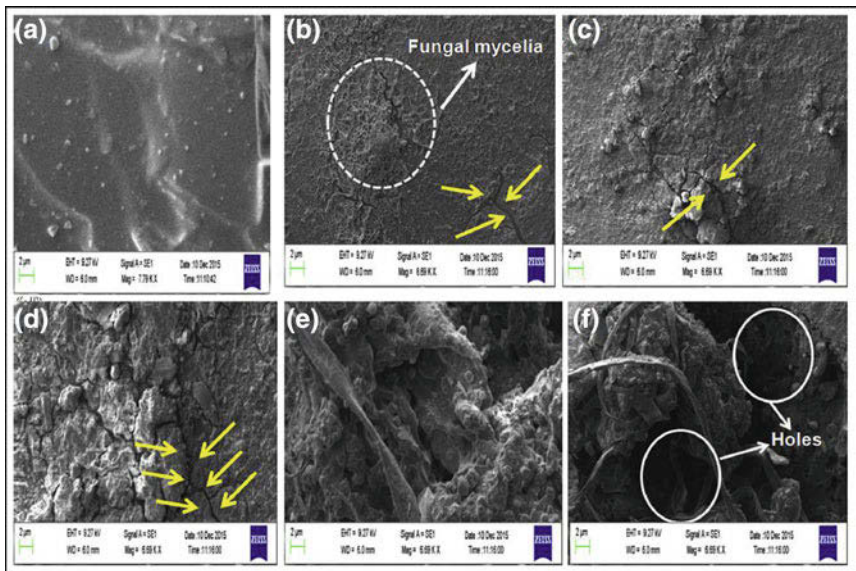


Fig. 11 SEM micrographs of neat MBPU/NS for **a** 0 days, **b** 30 days, **c** 45 days, **d** 60 days and **e** 75 days. Reproduced from Das et al. [56]

toluene diisocyanate (TDI) followed by reaction with 1, 4 butanediol (1, 4 BD). The synthesized HPU/f-RGO nanocomposite showed an improvement in tensile strength to about 525%, modulus to about 42-folds, and toughness to about 18-folds after addition of 2 wt% of f-RGO in HPUs as shown in Fig. 12. Moreover, the elongation at break for the HPU/f-RGO nanocomposite showed an increment from 71% to a maximum of 165%. HPU/f-RGO nanocomposite also exhibited better thermal stability and excellent electrical conductivity to almost 10-fold with 2 wt% loading of f-RGO. However, with the same loading RGO nanocomposites, exhibited lower mechanical, electrical and thermal properties as compared to HPU/f-RGO nanocomposites. The authors proposed that the developed HPU/f-RGO nanocomposites can be used for the development of tough, conductive nanocomposites for aerospace and tissue engineering applications.

Zhang et al. [62] reported about the preparation and characterization of in situ polymerized bio-based thermosetting polyurethane/graphene oxide (PU/GO) nanocomposites based on epoxidized soybean oil–castor oil polyol with isophorone diisocyanate (IPDI) as shown in Fig. 13. The functionalization of graphene oxide was carried out through pressure oxidation method followed by reinforcement within the PU matrix. The authors observed similar improvement in the overall properties such as mechanical, thermal and electrical conductivity as reported by Thakur and Karak et al. with a minimal loading of modified graphene oxide. This was due to the strong chemical interaction of urethane group of PU matrix with the hydroxyl (–OH) groups of modified GO.

Ali et al. [63] investigated the synthesis and characterization of polyurethane-multiwall carbon nanotube (PU/MWCNT) nanocomposites based on castor oil via in situ polymerization technique. The in situ polymerization technique led to the uniform dispersion of the nanoparticles within the PU matrix which is an important criterion in the improvement of nanocomposite properties. MWCNTs are candid and ideal reinforcing material with ordered carbon fibre imparting unique properties to the composite i.e. light weight, stiffness, superconductivity and mechanical

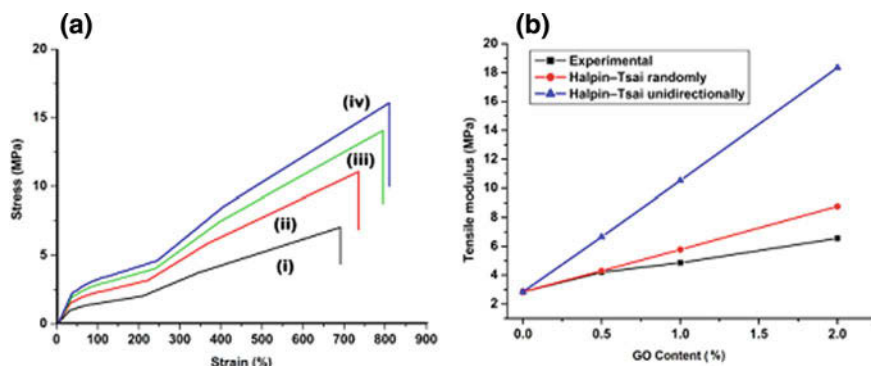


Fig. 12 Tensile test result of hyper branched polyurethane (HPUs) nanocomposite. Reproduced from Karak et al. [61]

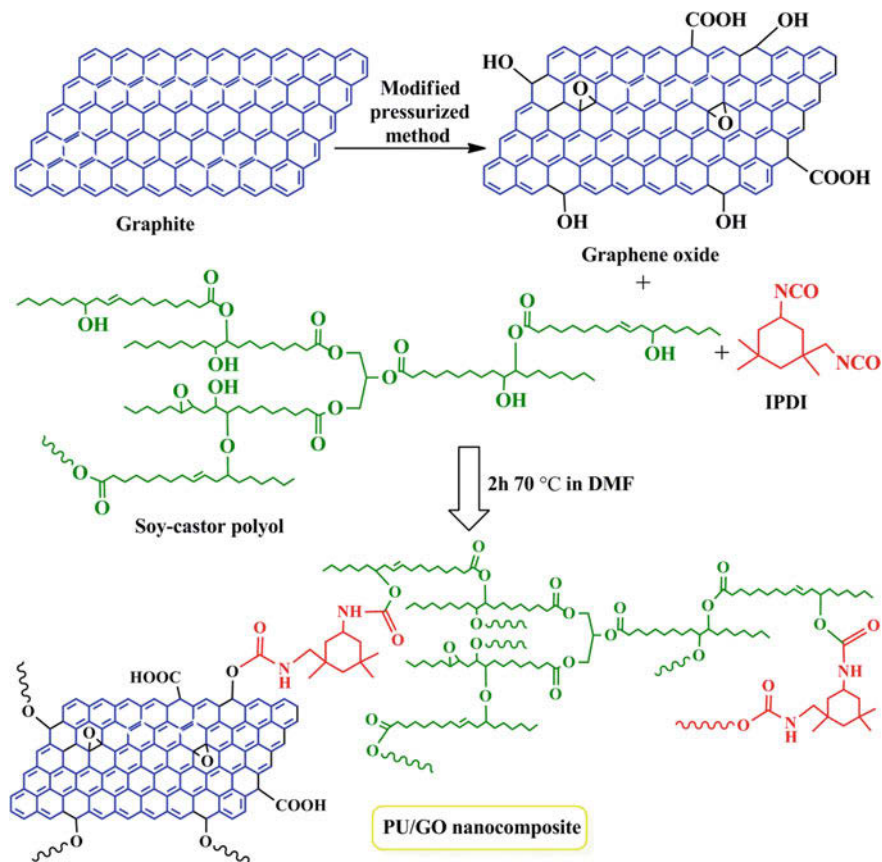


Fig. 13 Reaction scheme for the synthesis of PU/GO nanocomposite

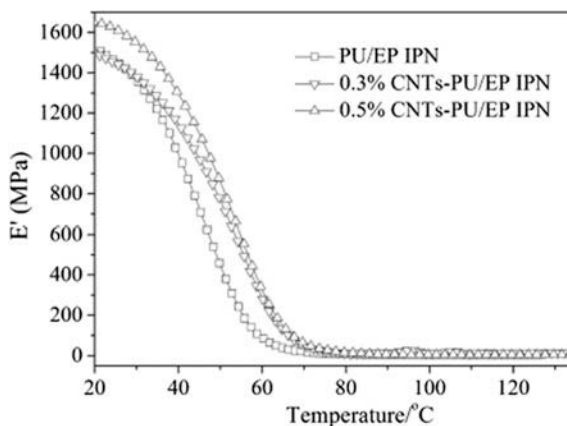
strength. The weight of MWCNTs in castor oil was varied from 0 to 1 wt%. FTIR spectra of the PU/MWCNT nanocomposite indicated broad absorption peak within the range of $1715\text{--}1725\text{ cm}^{-1}$ associated with the urethane carbonyl bond of PU. Intercalation of MWCNT within the PU matrix was observed through the lowering of carbonyl peak height and formation of hydrogen bonded carbonyl groups in the nanocomposite. X-ray diffraction (XRD) studies revealed broadening of the peak at $\theta = 21^\circ$ with reduced intensity as compared to the neat PU which was due to the strong interfacial interaction between MWCNTs and PU matrix. Scanning electron microscopy studies revealed uniform and homogeneous dispersion of MWCNTs within the PU matrix at a loading of 0.3 wt% of MWCNTs. This homogenous dispersion of MWCNT was due to the van der Waals force of attraction within MWCNT and PU matrix resulting in an improvement of the mechanical properties. In addition, the formation of H-bonds and covalent bonding between the carboxylic group in MWCNT and PU also contributed towards the observed improvement in

mechanical properties. The surface properties of the nanocomposites and neat PU was investigated using the Brunauer–Emmett–Teller (BET) theory. From the theory, it was found that the nanocomposite surface indicated the presence of few pores due to the intercalation of MWCNT within the PU matrix resulting in low permeability.

The incorporation of MWCNTs within the PU matrix had a great impact on the N_2 gas diffusion mechanism. PU/MWCNT based nanocomposites indicated a reduction in gas permeability as compared to neat PU owing to the exfoliation, compatibilization, orientation and re-aggregation of MWCNTs in the PU matrix. Thus, it could be concluded that the incorporation of MWCNTs in the PU matrix led to the improvement in the gas barrier, thermal and mechanical properties. Further, the in situ polymerization technique also led to the homogenous dispersion of MWCNT within the PU matrix resulting in an overall improvement in the properties of the nanocomposite.

Chen et al. [64] synthesized castor oil-based polyurethane/epoxy (PU/EP) interpenetrating polymer network (IPN) reinforced with MWCNTs for damping application. Damping property of a material depends upon its ability to dissipate energy which is directly proportional to the internal friction. Experimental results reveal that the damping ability of PU/EP IPN increases with a loading of 0.1 wt% of MWCNT. This was due to the presence of MWCNT that increases the friction between CNTs and PU resulting in an increment in the rate of dissipating energy. Moreover, the higher surface area and aspect ratio of MWCNT also contributes towards the overall increase in the damping property of the nanocomposites. The above results were also in line with the DMA results indicating improvement in storage modulus (E') of the nanocomposite film with the addition of MWCNTs as shown in Fig. 14. The mechanical properties of the IPN nanocomposite also increased by 30% as compared with the neat counterparts with the loading of 0.1 and 0.7 wt% of MWCNTs respectively. This was due to the strong and large interfacial area between the PU matrix and MWCNT that contributed to the effective load transfer from PU matrix to MWCNT.

Fig. 14 Variation of Storage modulus (E') in neat PU/IPN and PU/IPN-CNTs. Reproduced from Chen et al. [64]



2.2 *Jatropha Oil Based Polyurethane Nanocomposite*

Liao et al. [65] studied the surface structure and morphology of waterborne polyurethane/clay nanocomposites (WPU/Clay) prepared via in situ polymerization based on jatropha curcas oil (JCO) and isophorone diisocyanate (IPDI). The author used three different types of nanoclay (i.e. sodium montmorillonite MT, attapulgite AT and halloysite nanotubes HT) whose structures were modified using γ -aminopropyltriethoxy silane (APTES) as shown in Fig. 15.

Thereafter, WPU nanocomposite dispersion was synthesized from JCO, IPDI with three different types of nanoclay as shown in Fig. 16.

FTIR, SEM and TGA studies were carried out to investigate the degree of silylation of the nanoclays. SEM micrographs revealed that the silylated sodium montmorillonite (SMT) nanoclay had distinct and regular layered structure with tight packing. On the other hand, the silylated halloysite nanotubes (SHT) nanoclays indicated smooth surface with a cylindrical shape. FTIR spectra confirmed the successful silylation of the nanoclays with the appearance of a peak at 2930 and 1560 cm^{-1} related to the $-\text{CH}$ stretching and deformation vibration of NH_2 groups, respectively which was absent in case of unmodified nanoclays. TGA studies indicated two-stage weight losses for unmodified and modified clay respectively wherein, the modified clays indicated higher temperature weight loss as compared to the neat ones. FTIR spectra of WPU nanocomposites based on JCO indicated the appearance of $-\text{NH}$ peak at a lower wavelength at 3340 cm^{-1} due to H-bonding. SEM micrographs of the WPU nanocomposites indicated rougher surface due to the presence of clays. However, there was no aggregation of clay nanoparticles within the WPU matrix indicating good compatibility between the WPU and silylated clay nanoparticles. It was observed that WPU/SMT exhibited higher surface roughness as compared to WPU/SAT, WPU/SHT due to the layered

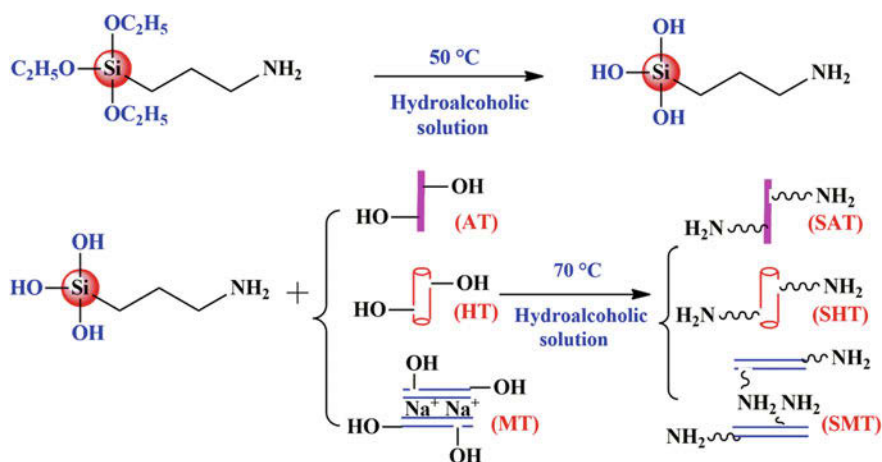


Fig. 15 Scheme showing the APTES modification of three different types of nanoclay

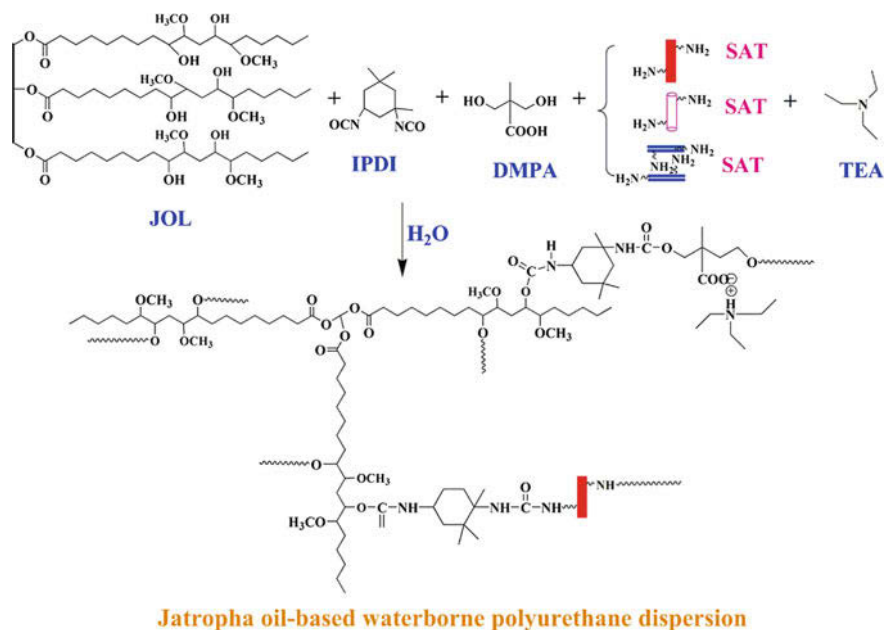


Fig. 16 Preparation of JCO based WPU nanocomposite dispersion. Reproduced from Liao et al. [65]

structure of SMT which led to the restriction of WPU molecular mobility resulting in an increase in the cross-linking density. DMA analyses result indicated strong chemical interactions between clays and WPU matrix thereby increasing the microphase separation WPU/clay nanocomposites. Out of the three nanocomposites, WPU/SHT and WPU/SAT indicated highest microphase separation degree, due to the increase in interaction between the hard segments and soft segments of WPU. The height of $\tan \delta$ peaks was also found to decrease with the incorporation of nanoclay, which was due to the increase in cross-linking density of PU matrix as shown in Fig. 17.

WPU/SMT indicated the lowest $\tan \delta$ peak value due to the layered structure of SMT which played an effective role in increasing the cross-linking density and restricting the molecular motion. Tensile test result suggested that the incorporation of nanoclay improved the tensile strength and elongation at break. WPU/SMT and WPU/SAT nanocomposite had the higher tensile strength and lower elongation at break as compared to WPU/SHT. This was due to the presence of higher $-\text{NH}_2$ groups and layered structure of SMT resulting in higher cross-linking density and restricting the molecular mobility of the WPU chain as depicted in Fig. 18. As a consequence, the tensile strength increases and the elongation at break decrease for the WPU/SMT nanocomposites. WPU/SAT indicated higher tensile strength due to the formation of more H-bonds that led to strong interfacial interaction between SAT and WPU matrix. On the other hand, reverse phenomenon was observed in

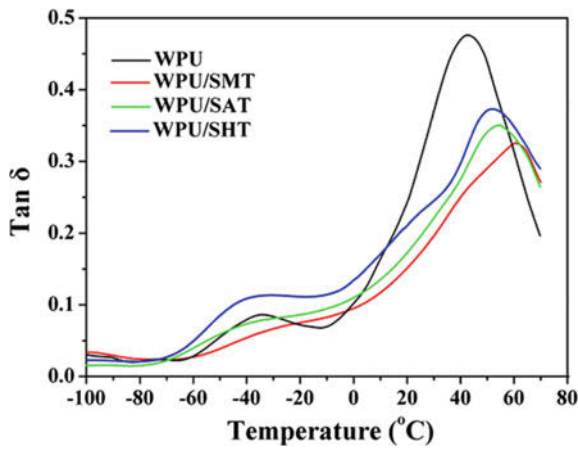


Fig. 17 Tan variation in WPU and its nanocomposite. Reproduced from Liao et al. [65]

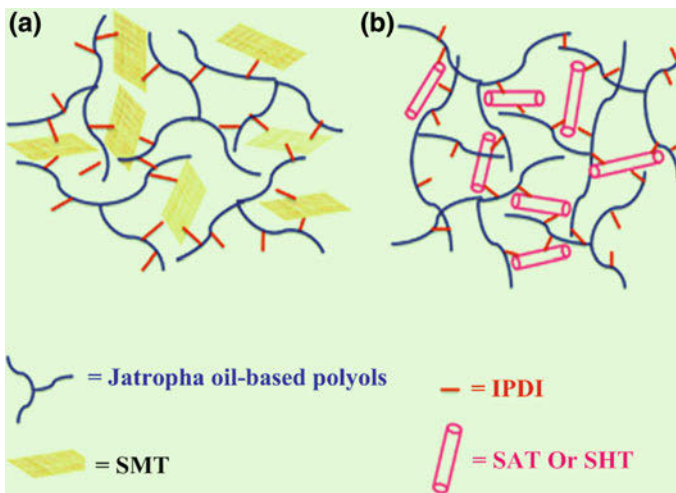


Fig. 18 Model showing the H-bonding interaction between PU and three different types of nanoclay. Reproduced from Liao et al. [65]

case of WPU/SHT which showed higher elongation at break and lower tensile strength. This was due to the higher microphase separation of WPU/SHT which made the soft segments more flexible. Thus, it can be implied from the above results that the properties of WPU/clay nanocomposites depend upon the nature, structure and type of clay.

2.3 Palm Oil-Based Polyurethane Nanocomposites

Dzulkifli et al. [66] studied the synthesis of PU foam from palm oil reinforced with diamine-modified montmorillonite (MMT) nanoclay. MMT was modified with diamino-propane and sodium carbonate and thereafter PU nanocomposite foam was prepared using palm oil, modified MMT and isophorone diisocyanate (IPDI). FTIR spectra indicate the successful modification of MMT by DAP through the appearance of peaks at 3463 cm^{-1} , indicating the successful insertion of DAP into MMT gallery. Presence of peaks at 1712 , 1509 , and 1216 cm^{-1} corresponding to the bending vibration $\text{C}=\text{O}$, N-H , and C-N , respectively, confirmed the successful synthesis of PU foam and PU/MMT foam. X-ray diffraction curves also indicated the successful modification of MMT by DAP through the shifting of the peak from 8.95° for pristine MMT towards the left side at 8.05° for the nanocomposite foam. This shift reveals the achievement of larger interlayer spacing or d-spacing in case of foam nanocomposites. SEM micrographs indicate reduced cell size and exfoliated structure for the PU/MMT composition. This was attributed to the effective dispersion of DAP-MMT within the PU foam matrix resulting in preventing coalescence, and producing smaller and fine cell structure. Thus, it was concluded that the presence of OMMT within the PU foam system led to the overall improvement in the morphology and microstructure of foam.

Adnan et al. [67] studied the development of flexible polyurethane nanostructured biocomposites foams based on palm olein-based polyol with OMMT as nanofiller. FTIR spectra of palm oil-based PU and PU nanocomposites were investigated. It was observed that there was no change in the FTIR spectra of derived PU and PU foam nanocomposites. The broad stretching peak at 3405 cm^{-1} indicates the formation of H-bonded urethane. The band at $2995\text{--}2860\text{ cm}^{-1}$ was attributed to the $-\text{CH}_2$ stretching vibration and the presence of hydrogen-bonded carbonyl groups was observed at lower wave number at $1733\text{--}1731\text{ cm}^{-1}$ for the PU foam nanocomposites. Mechanical test results indicated improvement in tensile strength and tear strength for both petro-based and palm oil-based PU with the loading of 3, 5 and 7 wt% of OMMT as compared to the neat counterparts. This increase in tensile strength and tear strength for both the petro and palm oil-based PU nanocomposites was evident for OMMT loading up to 3 and 5 wt%, beyond which there was an overall decrease in the tear and tensile strength. However, the increment in tensile strength for palm oil-based PU nanocomposites (i.e. 66%) was higher as compared to petro-based PU nanocomposites (33%). Similar result was observed in case of tear strength which increased from 13% in case of petro-based PU nanocomposites to 48% in case of palm oil based PU nanocomposites. This observation was due to the strong H-bond formation between the silicate lamellae of OMMT (mainly silanol, Si-OH and aluminol, Al-OH) with the urethane groups of PU as shown in the Fig. 19.

In addition, the intercalated quaternary ammonium salts of OMMT can act as the “bridge” connecting the MMT layers and the PU chains thereby restricting the molecular mobility [68]. SEM micrographs reveal smaller cell size for the petro and

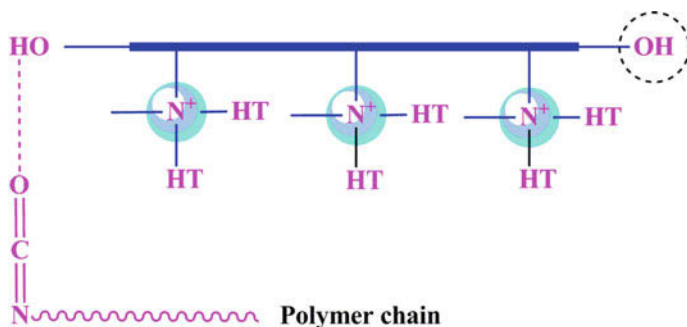


Fig. 19 Mechanism of hydrogen bonding between the PU chain and OMMT

palm oil-based PU foam nanocomposites for a loading of 3, 5 and 7 wt% of OMMT. This was due to the fact that OMMT can serve as a nucleation site for cell formation, as a result, less gas will be available for the growth of the cells. TEM micrographs indicated intercalated OMMT structure within the PU matrix with an average length of 100 nm.

Zaimahwati et al. [69] studied about the palm oil-based polyurethane nanocomposite reinforced with OMMT nanofiller. The palm oil was modified through epoxidation and hydroxylation reaction with acetic acid, hydrogen peroxide and hydrochloric acid to synthesize bio-based polyol. Thereafter PU and its nanocomposite were prepared using the polyol, IPDI and OMMT nanofiller (5 wt%). The iodine value of the palm oil decreased from 56.72 to 14.29 I₂/100 g for palm oil-based polyol after its modification indicating oxidation of double bond. FTIR spectrum of epoxidized palm oil-based polyol indicates a peak at 1050 and 1014 cm⁻¹ attributed to the C–O bond of epoxy ring confirming the successful modification of palm oil. TGA results of the synthesized PU/OMMT nanocomposites indicated higher thermal stability as compared to neat PU wherein, the weight reduction of former begins at 150–200 °C with final degradation at of 490 °C. PU/OMMT nanocoating also shows higher gloss as compared to the neat counterparts due to the ability of the OMMT coating surface to reflect light. Hence, the incorporation of OMMT led to the overall improvement of the nanocomposite films.

Salih et al. [70] investigated the thermal and mechanical properties of palm oil and methylene diisocyanate based polyurethane acrylate/clay (POBUA/OMMT) nanocomposites prepared via. in situ intercalative method and electron beam radiation technique. The in situ intercalative polymerization technique is useful for uniform dispersion of the nanofillers within the polymer matrix as shown in Fig. 20. In addition, this technique provides the possibility to polymerize various ranges of thermosets and thermoplastics.

FTIR spectra of the synthesized POBUA nanocomposites indicated the disappearance of NCO peak at 2273 cm⁻¹ indicating the complete utilization of –NCO by the –OH group of epoxidized palm oil for the synthesis of urethane linkage of

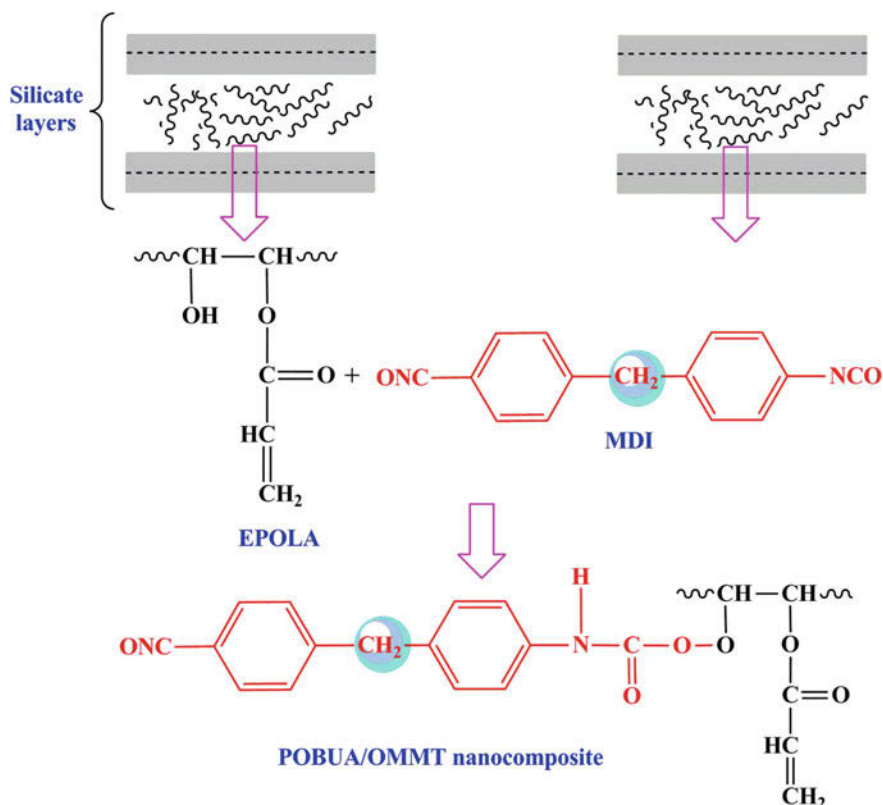


Fig. 20 Synthesis of POBUA/OMMT nanocomposite

PU at 3327 cm^{-1} . The FTIR spectra of POBUA nanocomposite also indicated the appearance of a peak at 1015 , 941 and 761 cm^{-1} related to the silicate groups in the OMMT filler indicating that the interaction of layered silicate with PU matrix. TGA thermogram of neat POBUA and its nanocomposite indicate two-stage degradation curves. The first stage of degradation was related with the decomposition of volatile products and the major decomposition which occurred in the second stage, was related to the decomposition of the organic polymer chains. TGA results of the nanocomposite indicate that improved thermostability as compared to neat POBUA due to the presence of OMMT layer creating a protective physical barrier, thereby inhibiting the heat diffusion, and delaying the degradation process. Differential scanning calorimetry (DSC) results indicate higher glass transition temperature (T_g) for the nanocomposites at $61.8\text{ }^\circ\text{C}$ as compared to neat PU at $40.5\text{ }^\circ\text{C}$. This was due to the intercalation of POBUA matrix into the silicate layers of the nanoclay that lead to the reduction of rotational and transitional mobility of the polymer chains. Tensile strength results also indicated higher modulus and strength for the POBUA nanocomposites due to the homogenous dispersion of the nanoclay within the

polymer matrix, imparting reinforcement, and restricting the molecular mobility of the PU chain resulting in higher cross-linking density in POBUA nanocomposite. TEM micrograph of POBUA nanocomposite indicates the expansion of silicate layers of OMMT revealing formation of the intercalation structure, with some separation within the silicate layers indicating exfoliation of OMMT in the POBUA matrix. SEM micrographs of POBUA nanocomposite with 3 wt% loading of OMMT indicate good dispersion, good adhesion with the PU matrix devoid of any agglomeration. It can be summarized that the inclusion of OMMT into the polyurethane acrylate system led to the improvement of thermal stability and mechanical properties.

3 Application of PU Nanocomposites

3.1 Coatings

Das et al. [33] have studied about the influence of NS inclusion on the properties of MBPU derived from transesterified castor oil and palm oil based isocyanate. The main purpose of the study was to determine the feasibility of palm oil isocyanate as an alternative to petro-based isocyanate for synthesizing MBPU/NS composite. The authors observed that MBPU/NS composite showed improved properties as compared to their neat counterparts due to better cross-linking, H-bonding and phase segregation. Moreover, the presence of polar linkages, O–Si–O bond and strong interfacial interaction led to better coating and swelling properties in synthesized MBPU nanocomposite. Further, the MBPU nanocomposite dispersion was cast onto polycarbonate substrates to determine the adhesive strength, curing properties, contact angle, gloss and abrasion resistance. The authors observed that the MBPU/NS composites derived from transesterified castor oil exhibited faster curing time owing to the presence of primary hydroxyl groups and higher hydroxyl value. The contact angle studies of MBPU/NS coatings indicated hydrophobic behaviour which was due to the H-bonding between the of O–Si–O linkage of NS with the urethane (–NHCOO) linkage of MBPU network that restricts the migration of water as shown in Fig. 21. Further, there was also an overall improvement in the abrasion resistance of the nanocoating as compared to the unreinforced ones owing to higher cross linking and effective bonding of urethane group in MBPU with NS particles. Thus, from the results obtained the authors concluded that palm oil based isocyanate can be used as an alternative to the petro-based isocyanate for the synthesis of green polyurethane nanocomposite.

Xia and Larock [71] studied about the castor oil-based waterborne PU/NS composite prepared through sol-gel process for coating application. This process involved polycondensation and hydrolysis reaction of silicon alkoxides to prepare waterborne PU/NS composite dispersion. Alkoxysilane containing PU was reacted with different weight % of aminopropyltriethoxy silane (APTES) and isocyanate to

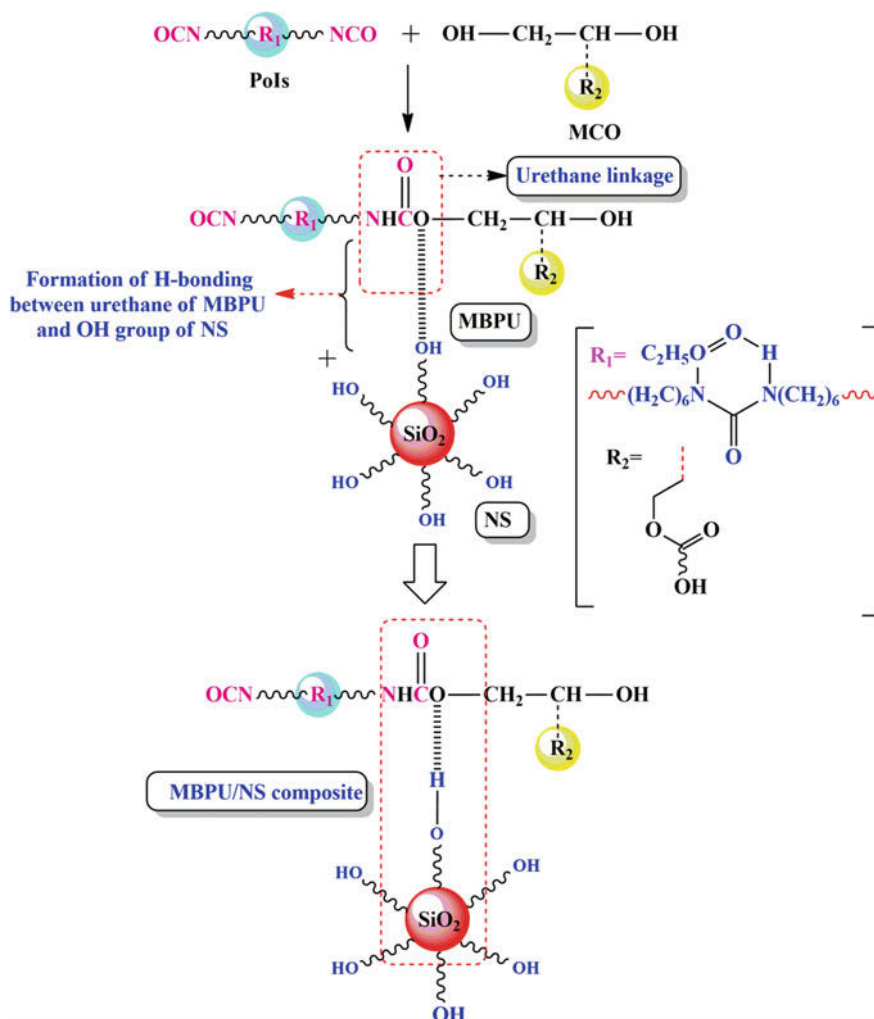


Fig. 21 Possible H-bonding interaction between MBPU and NS particle

form capped PU pre-polymer with core-shell structure as shown in Fig. 22. The sol-gel technique involved chemical cross-linking of PU with NS particle resulting in an increase in the cross-linking density of the nanocomposite films. The authors used rubber elasticity theory to calculate the crosslinking density (v_e) of the nanocomposites and they found that with an increase in NS content from 0 to 2 wt %, v_e increases from 90 to 766 mol m^{-3} . DSC studies also confirmed the increase in cross-linking density with increase in NS loading. It was observed that the PU/NS composites exhibited higher T_g from 18 to 20.9 °C with an increase in NS loading from 0 to 1.5 wt%. The TGA curves indicated three step of degradation.

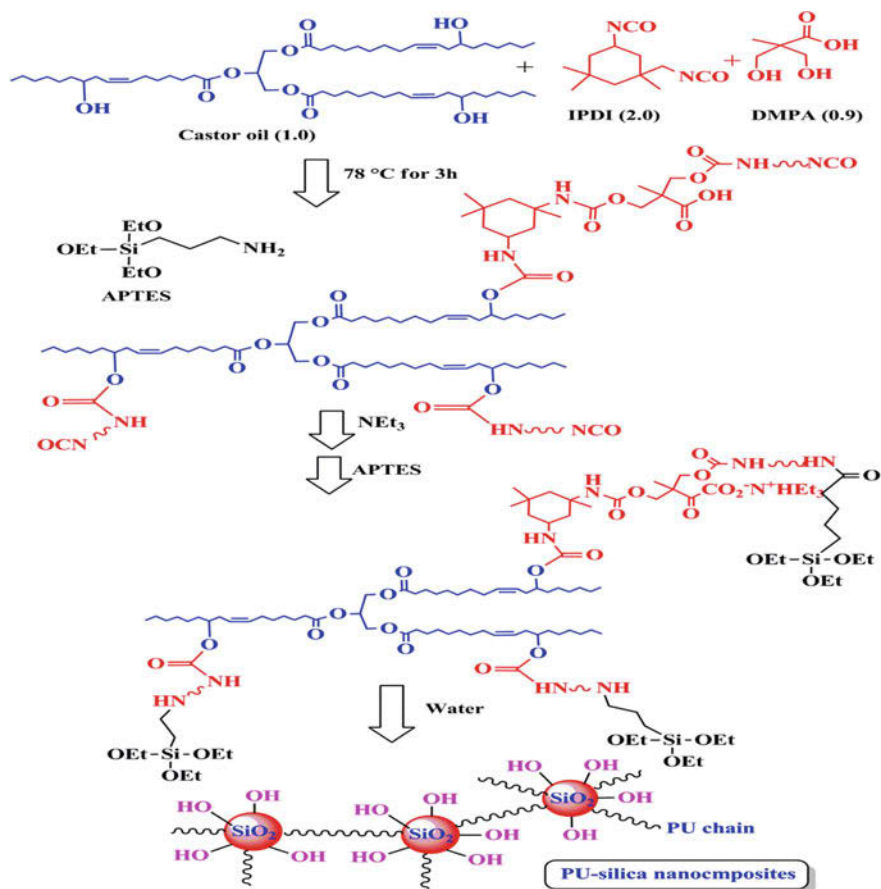


Fig. 22 Synthesis reaction scheme of PU/nanosilica composite

The 1st step of degradation occurred at 150–300 °C due to the dissociation of the urethane bonds, the 2nd step between 300 and 500 °C due to chain scission of castor oil and the last degradation step above 500 °C which was related with the thermo-oxidative degradation of the nanocomposites. With the inclusion of NS particles the temperature corresponding to T_{50} and T_{max} increases due to the increase in cross linking density as depicted in Fig. 23. The presence of NS particles within the PU matrix prohibited the heat and mass transfer thereby reducing the formation of combustible organic components. The topography of the PU-silica nanocomposite films indicated aggregation of APTES with an increase in APTES loading. The authors postulated that the presence of hydrophilic carboxylated groups on the PU chains led to the well dispersion of NS particles within the PU matrix.

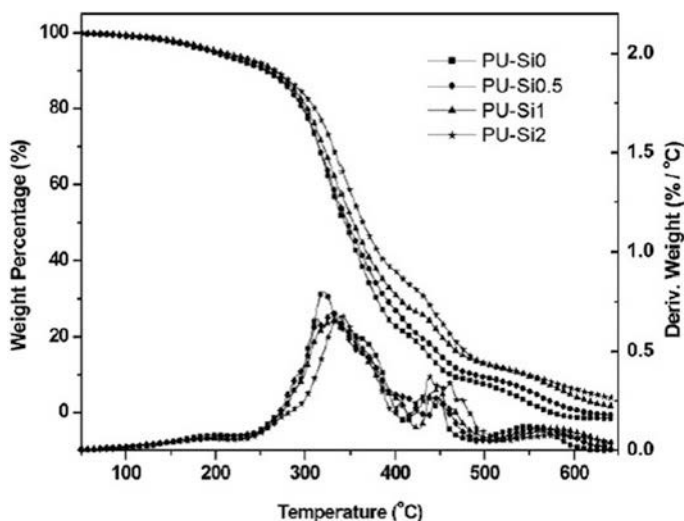


Fig. 23 DTG/TGA thermogram of PU/NS composite. Reproduced from Xia et al. [71]

3.2 Adhesives

Deka et al. [72] studied the adhesive, mechanical, and thermal properties of bio-based hyper-branched polyurethane/clay nanocomposites from nahar seed oil with toluene diisocyanate. The nanoclay (OMMT) wt% within the PU matrix was varied from 1, 2.5 and 5. The main aim of the study was to overcome the poor mechanical strength of hyperbranched polymers (HBPU) due to the absence of chain coiling and entanglement. HBPU was synthesized using PCL as macroglycol with molecular weight 3000 g mol^{-1} as the long segment with monoglyceride of *Mesua ferrea* L. seed oil. The obtained HBPU was further modified using epoxy resin and poly (amido amine) hardener to obtain modified hyperbranched polyurethane-epoxy system (MHBPU). The MHBPU was used as the matrix with OMMT as the filler. FTIR spectra of MHBPU and MHBPU/OMMT were identical indicating that OMMT doesn't influence the chemical structure of MHBPU. However, the only difference observed in the spectra of MHBPU/OMMT nanocomposite is the presence of sharp -NH vibration band at 3311 cm^{-1} . This was due to the presence of clay layers that led to restricting the interaction of hard and soft segments. The introduction of clay nanoparticles also led to the shifting of urethane carbonyl peak from 1741 to 1718 cm^{-1} indicating higher H-bonding within the PU matrix and clay in the nanocomposites. X-ray diffraction study was carried out to determine the morphology of clay nanoparticles within the PU matrix. On the basis of Bragg's equation, it was found that the d-spacing of nanocomposites increased from 2.36 (in case of OMMT) to 4.95 nm for MHBPU/OMMT. This indicates exfoliated morphology with the complete insertion of HBPU chains in the gallery spacing of the OMMT. SEM and TEM micrographs also indicate better

dispersion of OMMT particles within the MHBPU matrix. This is due to the synergistic actions of both mechanical shearing and diffusion process imparted by mechanical stirring and sonication. Lap shear test was carried out in order to investigate the adhesive strength of the MHBPU and MHBPU/OMMT using different substrates such as plywood, aluminum and polypropylene sheets. Out of all the substrates higher adhesive strength was observed for wood substrates owing to the strong polar interaction of hydroxyl, epoxy, urethane, ether of the cured MHBPU/OMMT system with the hydroxyl groups of wood substrate. Also, the adhesive strength was found to increase with an increase in loading of OMMT wt%. This was due to the exfoliation of clay layers that enhanced the interface interactions via. bridge, loop and tail linkages of PU with the OMMT layers as shown in Fig. 24. This led to the reduction in the amount of voids thereby increasing the length of crack propagation and adhesion strength. Similar observation was seen in case of aluminum substrates due to the strong interactions of polar groups present on the surface of matrix and substrate. The plastic substrates indicated lower adhesive strength owing to its low surface polarity. Thus, the authors concluded that the nanocomposites exhibited high adhesive strength, mechanical properties and thermostability.

Sahoo et al. [73] studied the shear strength of polyurethane/OMMT clay nanocomposites adhesive based on castor oil and palm oil based isocyanate. The clay % was varied from 1 to 5 wt%. The PU adhesive solution was applied onto wood substrates of 0.1 mm thickness and left overnight for curing. The lap shear strength of the neat PU and its nanocomposite was studied as per ATMD 906-82 using a universal testing machine with a loading rate of 600 lb/min. The authors observed that the shear strength values of PU adhesive increase with an increase in clay content. Out of the entire compositions PU/Clay nanocomposite with 3 wt% loading exhibited the highest adhesion strength and was chosen to be the optimized composition. However, PU/Clay nanocomposite with 5 wt% loading showed less shear strength due to the aggregation of nanoclay particles. This aggregation led to the predominance of filler-filler interaction over the polymer-filler interaction. The mode of failure of lap shear was found to be cohesive in nature. Further, a study was carried out wherein, the samples were immersed in water for 24 h. It was observed that water doesn't affect the shear strength even after 10 days of immersion. The authors concluded that the PU/clay nanocomposite exhibited higher adhesion properties due to the homogenous dispersion of the nanoparticles, intercalated structure and good chemical interaction between the clay nanoparticles and PU matrix.

3.3 *Medical*

Das et al. [74] synthesized sunflower based hyper-branched polyurethane (HBPU) reinforced with Fe_3O_4 nanoparticles via. in situ polymerization technique for designing smart antibacterial biomaterials for biomedical devices and implants.

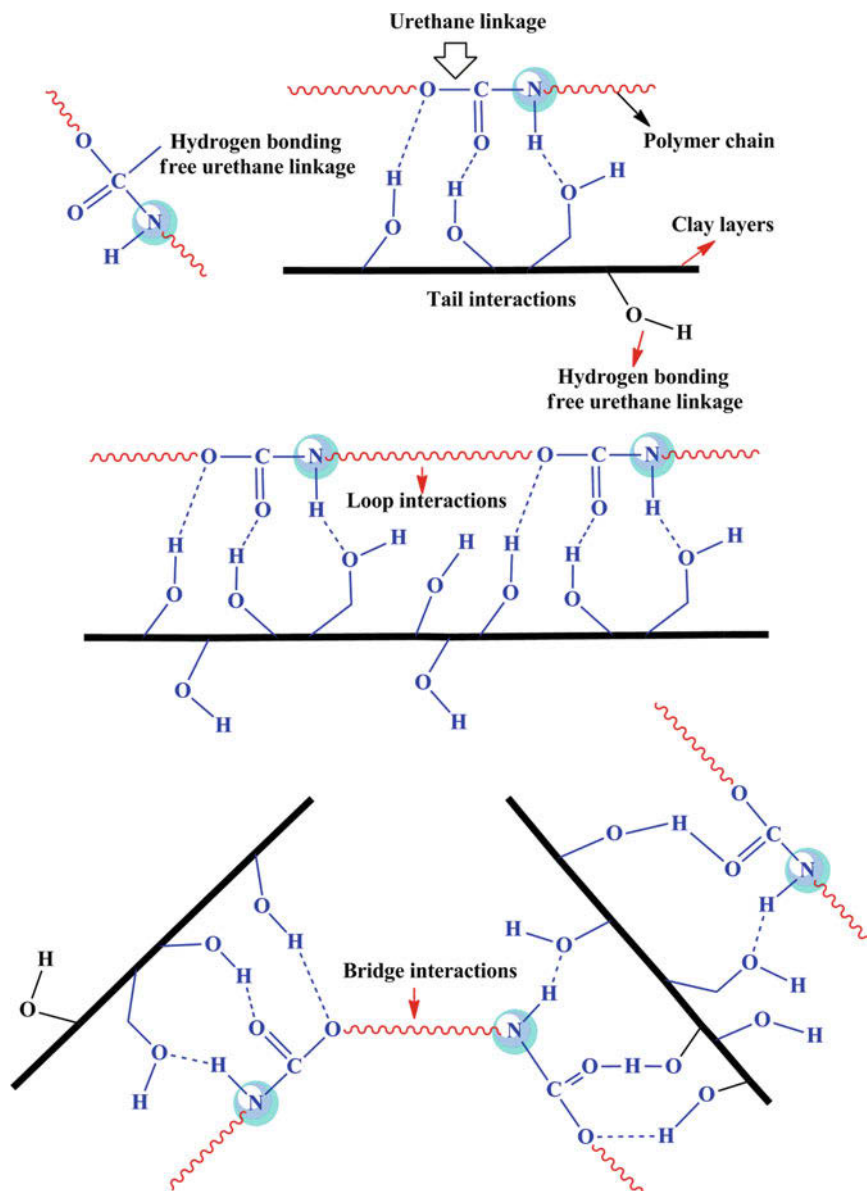


Fig. 24 Model representing the interfacial interaction between MHBPU with OMMT layers

Fe_3O_4 has various disadvantages which include poor stability, agglomeration, and low performance which can be improved through the incorporation of these nanoparticles in a suitable matrix that can provide strong structural adherence, dispersibility and stability. To overcome the above limitations the author selected

HBPU as a matrix since it provides better biocompatibility, dispersibility, low viscosity, encapsulation and good mechanical properties. The synthesized nanocomposites of Fe_3O_4 with HBPU was named as MHBPU with the loading of Fe_3O_4 of 5, 10 and 15% which can be used as smart materials, shape memory and shape recovery application since its shape can be controlled by using external stimuli such as heat energy and magnetic field, etc. The dispersion of Fe_3O_4 within the HBPU matrix was investigated using SEM and TEM. SEM micrographs indicated uniform and homogeneous dispersion of Fe_3O_4 within the HBPU matrix. A similar observation was seen for TEM image which also confirmed the uniform dispersion of the Fe_3O_4 within the HBPU matrix with an average particle size of 7.65 nm. The uniform stabilization of Fe_3O_4 is because of the chemical interaction with HBPU as shown in Fig. 25.

Mechanical properties i.e. tensile strength of the nanocomposite were also improved as compared to the neat counterparts due to the high surface area of the nanoparticles and strong chemical interaction within Fe_3O_4 and HBPU matrix, facilitating effective stress transfer. However, the elongation at break decreases for the nanocomposites owing to the restriction in HBPU chain mobility. Bio-degradation studies indicated higher degradation rate of the nanocomposites as

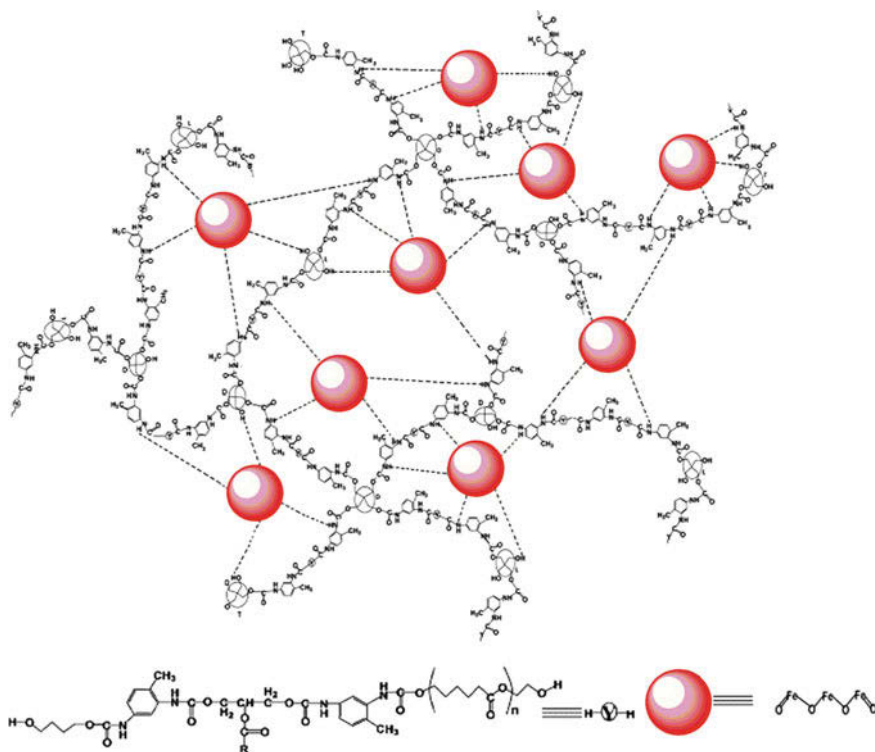


Fig. 25 Model depicting the interaction between HBPU and Fe_3O_4 nanoparticles

compared to HBPU owing to the structural feature of Fe_3O_4 nanoparticles that led to its easy leaching from the matrix surface. The nanocomposites also exhibited better shape memory behaviour owing to the increase in internally stored energy of the polymer matrix resulting in strong interactions of Fe_3O_4 with the HBPU matrix. The neat HBPU indicated no antibacterial activity whereas; Fe_3O_4 based MHBPU nanocomposites showed zones of inhibition of 13 and 11 mm against *S. aureus* and *K. pneumoniae*, bacteria respectively. The antibacterial activity of the Fe_3O_4 was due to the generation of reactive oxygen species (ROS) that led to the destruction of protein and DNA structure without harming the human cells. The biocompatibility studies using MTT assay indicated good cytocompatibility between the Fe_3O_4 and HBPU matrix. The comparatively better cytocompatibility of the prepared HBPU reinforced Fe_3O_4 nanocomposite was due to the well dispersion of the nanoparticles within the HBPU matrix which imparted better structural support and anchorage substrate to the cells.

Shaik et al. [75] synthesized castor oil based poly (urethane-esteramide) UPCEA)/ TiO_2 nanocoating with anticorrosive and antimicrobial properties. The author selected TiO_2 nanoparticles since they show excellent biocidal properties and are less volatile in nature. In this study UPCEA was synthesized by the condensation polymerization reaction of N, N-bis (2-hydroxyethyl) castor oil fatty amide with terephthalic acid which was further modified with different percentage of TDI, i.e., 7, 9, 11 and 13% respectively to obtain UPCEA-7, UPCEA-9, UPCEA-11 and UPCEA-13 as depicted in Fig. 26. Thereafter, the synthesized UPCEA was reinforced with TiO_2 nanoparticles with different concentrations, i.e., 0.1 wt%, 0.2 wt%, 0.3 wt%, 0.4 wt%, and 0.5 wt% to obtain the UPCEA/ TiO_2 nanocomposite. Out of the entire composition 0.4 wt% of TiO_2 exhibited better dispersion and excellent physicochemical properties. Hence, 0.4 wt% TiO_2 was considered to be the optimum loading and was used for synthesizing UPCEA nanocomposites i.e. UCPEA/ TiO_2 -7, UCPEA/ TiO_2 -9, UCPEA/ TiO_2 -11, and UCPEA/ TiO_2 -13.

The antibacterial and antifungal activity of UPCEA-13 with 0.4 wt% loading of TiO_2 was studied through agar disc diffusion method. The different bacterial microorganisms used for this study were, *Staphylococcus aureus*, *Escherichia coli*, and *Bacillus pasteurii*, and the different fungal strains were *Fusarium solani*, *Penicillium notatum*, and *Aspergillus niger*. The bacterial and fungal activity was investigated after 72 h of incubation at 32 °C. The antimicrobial effect of a system relies on the size of nanoparticles so as to impart better dominating attack against the microorganisms. SEM and EDX studies of the coated substrates indicated uniform coating with well trapped TiO_2 nanoparticles within the UPCEA matrix. The coating properties of the nanocomposite on mild steel indicated good adhesion; good scratch hardness with the excellent corrosion resistance properties. Regarding the antimicrobial activity, it was observed that after 48 h of incubation at 27 °C, inhibition zones of UCPEA-13 with 0.4 wt% of TiO_2 versus *Staphylococcus*, *Escherichia coli*, and *Bacillus pasteurii* were found to be 14, 25, and 16 mm in diameter, respectively. On the other hand the inhibition zone diameters of UCPEA-13 with 0.4 wt% of TiO_2 against *Fusarium solani*, *Penicillium notatum*, and *Aspergillus niger* were found to be 26, 24, and 21 mm, respectively. The above results indicated that the TiO_2 nanoparticles exhibited excellent antimicrobial activity. The TiO_2 nanoparticles could strongly adhere with the electron the donor

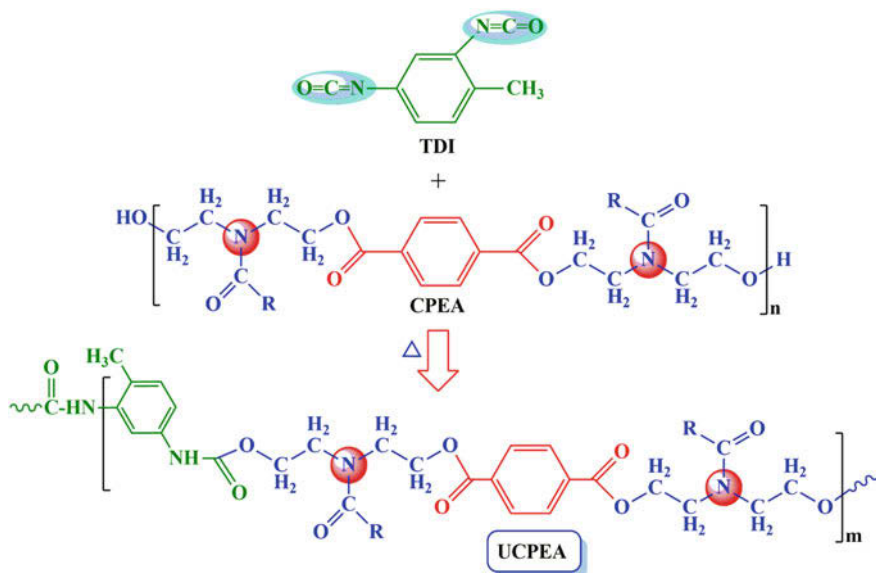


Fig. 26 Synthesis scheme for UCPEA

groups of the biological molecules containing oxygen, nitrogen, and sulphur. As a consequence, the TiO₂ nanoparticles could get uniformly distributed within the cell boundary of microorganism resulting in protection of the rigid outermost cell wall. TiO₂ nanoparticles on interaction with the electron donor groups can produce free radicals and reactive oxygen species that can permanently damage the microbes [76].

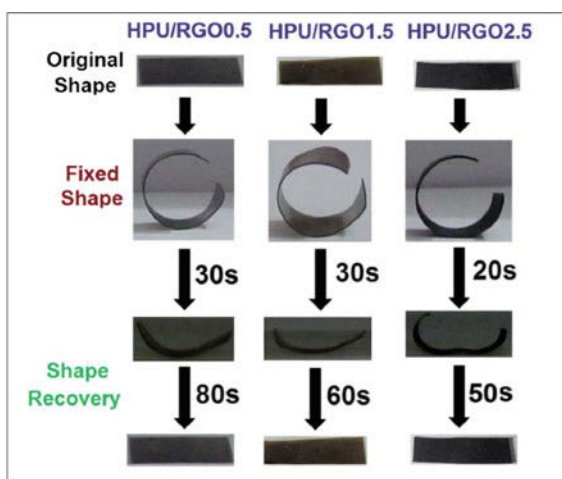
3.4 Elastomers

Thakur et al. [77] studied the synthesis and characterization of multi-stimuli responsive smart elastomeric hyperbranched polyurethane/reduced graphene oxide nanocomposites (HBPU/RGO) for shape memory application. The RGO wt% was varied from 0.5, 1.5 and 2.5 respectively. The synergistic effect of HBPU and RGO imparted several advantages which include noncontact stimuli to sunlight, eco-friendly nature and inexpensive practical stimulus. The process of reducing GO has carried out through sonochemical method a promising technology of using ultrasonic irradiation, elevated temperature, high pressure and rapid cooling rates, etc. The sonication method involves the formation of small cavities in the liquid medium. These small cavities implode rapidly generating microscopic shock waves thereby, realising the huge amount of energy in the liquid medium. Hence, the method of ultrasonication prevents the aggregation of GO thereby reducing the

reaction within the GO layers. The shape memory behaviour of the nanocomposites was investigated under sunlight, microwave and thermal condition. The shape memory activity of the nanocomposites was found to be excellent with faster shape recovery values when exposed to microwave as compared to sunlight and thermal stimulus as shown in Fig. 27. This was due to the excellent absorbance of RGO towards sunlight and microwave. Moreover, the shape recovery time decreased with an increase in the RGO content in the nanocomposite. This was due to the strong interaction of RGO with HBPU resulting in huge amount of release of elastic strain energy in nanocomposites helping faster shape recovery. The nanocomposites also had excellent thermal stability and mechanical properties with a tensile strength of 27.8 MPa, modulus of 36.3 MPa and toughness of 116 MJ m⁻³ due to the better chemical interaction of RGO with HBPU matrix. Thus, the authors concluded that the resulting nanocomposites exhibited improved thermomechanical and multi-stimuli response shape memory nature.

Ahuja et al. [78] studied the synthesis and characterization of castor oil-based polyurethane nanocomposites elastomer reinforced with organically modified clay (Cloisite 30B/C30B). The high aspect ratio of clay platelet and silicate clay offers huge potential to increase the clay/polymer interfacial area to improve properties, including flame resistance, mechanical properties, gas barrier properties, and thermal stability. Since C30B is hydrophilic in nature it was modified with hydrophobic organic polymers to impart hydrophobic character. This modification results in improving the interfacial adhesion of C30B with the hydrophobic matrix. The PU/C30 B nanocomposites were prepared through ultrasonication method using a high shear mixer with clay % varying from 0 to 5 wt%. TEM indicates the appearance of clear individual clay layers with few inseparable clay platelets and tactoids. The thickness of the platelets was found to be 1–2 nm. It was observed that beyond 3 wt % loading full exfoliated structure was not achieved. WAXD study was used to determine the morphology of the nanocomposites and to distinguish between

Fig. 27 Shape memory behaviour of synthesized nanocomposites under microwave stimulus. Reproduced from Thakur et al. [77]



ordered (intercalated) and disordered (exfoliated) states of silicates in nanocomposites. In intercalated structure, there is the finite distance within the polymer interlayer with the appearance of new basal reflection related to the interlayer height. On the other hand, in case of exfoliation, there is an increase in the interlayer distance resulting in delamination of the original silicate layers in the polymer matrix. Consequently, there is gradual disappearance of coherent X-ray diffraction from the distributed silicate layers in WAXD curve. WAXD diffraction study of C-30 B indicated a sharp peak at 4.85° corresponding to $d_{(001)}$ diffraction. However, in case of nanocomposites with loading 1 and 2 wt% there is complete absence of $d_{(001)}$ diffraction peak indicating complete exfoliation of the clay platelets. On the other hand, the nanocomposites with C30 B loading beyond 3 wt% indicates broadening of the peak at 4.85° with an increase in basal spacing which was due to the partial exfoliation of clay galleries. The broadening of peak arises due to the due to the partial disruption of parallel stacking of C 30 B. SEM micrographs reveal homogenous dispersion of C 30B within the PU matrix beyond 3 wt%. Above 3 wt% loading of C30B there was an aggregation of nanoparticles due to partial exfoliation as indicated in WAXD studies. FTIR spectra of the PU and its nanocomposite elastomers indicates similar peak confirming the PU clay nanocomposites have similar bands indicating that the PU chains have intercalated into the gallery of layered silicates. It was observed that the tensile strength and modulus increased to 4.49 and 5.88 MPa, respectively, for 4% loading of clay owing to the reinforcement imparted by the dispersed silicate layers in PU matrix. However, beyond 5 wt% of Cloisite 30B, the tensile strength of the nanocomposite decreased to 3.78 MPa due to agglomeration of the clay. In addition, the elongation at break also increases with the increase of clay content, owing to long fatty acid chains of oil, which imparted high flexibility to the elastomeric film.

Gao et al. [79] synthesized and characterized biocompatible elastomer of waterborne polyurethane (WPU) based on castor oil and polyethylene glycol reinforced with *E. globulus* derived cellulose nanocrystals (ECNc). ECNc nanoparticles obtained from acid hydrolysis of lignocelluloses' have significant properties i.e. high Young's modulus, high aspect ratio, low density, biocompatibility and biodegradability which make it candid reinforcing filler in various polymer matrices. WPU has also attracted great attention in the recent decade due to reduced volatile organic content emission and environmental safety. Castor oil and polyethylene glycol have been selected as a precursor for the synthesis of WPU's owing to their inherent properties which include bio-degradability, low cost, and easy availability. SEM micrographs of the fractured nanocomposite surface indicated a highly deflected and tortured surface with increase in the ECNc content from 0 to 5 wt%. This was due to the complicated energy dissipating mechanism between the ECNs and the WPU interface. FTIR studies were carried out to investigate the degree of H-bonding by evaluation the $-NH$ ($3400-3000\text{ cm}^{-1}$) and $-C=O$ ($1740-1720\text{ cm}^{-1}$) region of the WPU and its nanocomposites. It was observed that the $-NH$ and $-C=O$ peaks shifts towards lower wave number in case

of ECNc based WPU nanocomposites. This finding could be explained on the basis of improvement in the phase segregation degree by ECNc resulting in the micro-phase segregation of hard segment and a soft segment. As a consequence, the soft segments provide more freedom to $-\text{CO}$ and $-\text{C}-\text{O}-\text{C}$ bonds to interact with the $-\text{NH}$ of hard segments through H-bonds. The tensile strength of the WPU/ECNc nanocomposites increased from 5.43 to 12.22 MPa with an increase in the ECNc content from 0 to 1 wt%. This was due to the homogenous dispersion of the nanofillers within the WPU matrix as shown in Fig. 28. However, opposite trend was observed with increase in ECNc loading beyond 1 wt% due to the aggregation of nanoparticles. Thus, it can be concluded that ECNc based WPU nanocomposites can be interesting reinforcing material due to its rigid nature and high aspect ratio.

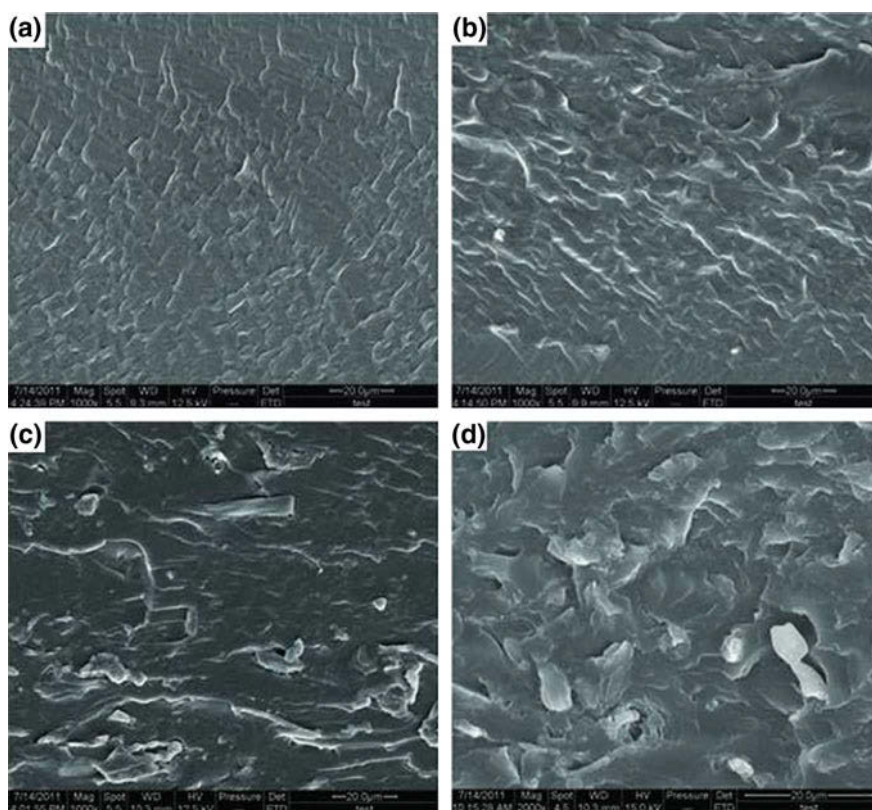


Fig. 28 SEM micrographs of waterborne polyurethane (WPU)/ECNc nanocomposite. Reproduced from Gao et al. [79]

4 Conclusion

Polyurethane nanocomposite from vegetable oil has emerged as versatile materials to overcome the limitation of neat counterparts for wide array of applications. It is imperative from the above literature findings that the properties of bio-based polyurethane nanocomposites can be tailor-made with unique blending with nanoparticles. Also, different techniques such as in situ polymerization, sol-gel technique etc. involved in the dispersion of nanofillers within the polyurethane matrix play a pivotal role in determining the overall properties of the nanocomposite. In addition, the modification of nanoparticles with different surface modifiers has also been beneficial for improving the dispersion of the nanoparticles within the PU matrix. From the above discussion and reports, it is also concluded that the developed nanocomposites possess unique shape memory ability, superhydrophobicity and excellent thermal and mechanical properties. However, much research has to be carried out in the field of polyurethane hybrid nanocomposites from vegetable oil-based polyol and isocyanate respectively.

References

1. Nohra B, Candy L, Blanco JF, Guerin C, Raoul Y, Mouloungui Z (2013) From petrochemical polyurethanes to biobased polyhydroxyurethanes. *Macromolecules* 46(10):3771–3792
2. Shen L, Haufe J, Patel MK (2009) Product overview and market projection of emerging bio-based plastics PRO-BIP. Report for European polysaccharide network of excellence (EPNOE) and European Bioplastics 243:1–245
3. Berthier JC (2009) Polyurethane PUR. *Techniques de l'ingénieur*
4. Bayer O (1947) Das di-isocyanat-polyadditionsverfahren (polyurethane). *Angew Chem* 59 (9):257–272
5. Jincheng W, Shenglin Y, Guang L, Jianming J (2003) Synthesis of a new-type carbonific and its application in intumescent flame-retardant (IFR)/polyurethane coatings. *J Fire Sci* 21 (4):245–266
6. Saunders JH, Frisch KC (1964) *Polyurethanes: Chemistry and Technology, Part II*. Technology Interscience Publishers, New York
7. Urbanski J, Czerwinski W, Janicka K, Majewska F, Zowall H (1977) *Handbook of analysis of synthetic polymers and plastics*, UK
8. Durganala S (2011) *Synthesis of non-halogenated flame retardants for polyurethane foams*. Doctoral dissertation, University of Dayton
9. Pervin F, Zhou Y, Rangari VK, Jeelani S (2005) Testing and evaluation on the thermal and mechanical properties of carbon nano fiber reinforced SC-15 epoxy. *Mater Sci Eng, A* 405(1–2):246–253
10. Thabet A, Mubarak YA, Bakry M (2011) A review of nano-fillers effects on industrial polymers and their characteristics. *J Eng Sci* 39(2):377–403
11. Peng L, Zhou L, Li Y, Pan F, Zhang S (2011) Synthesis and properties of waterborne polyurethane/attapulgit nanocomposites. *Compos Sci Technol* 71:1280–1285
12. Friedrich K, Fakirov S, Zhang Z (eds) (2005) *Polymer composites: from nano-to macro-scale*. Springer Science & Business Media
13. Pan H, Chen D (2007) Preparation and characterization of waterborne polyurethane/attapulgit nanocomposites. *Eur Polym J* 43:3766–3772

14. Chang CW, Lu KT (2012) Natural castor oil based 2-package waterborne polyurethane wood coatings. *Prog Org Coat* 75(4):435–443
15. Silva BB, Santana RM, Forte MM (2010) A solventless castor oil-based PU adhesive for wood and foam substrates. *Int J Adhes Adhes* 30(7):559–565
16. Xia Y, Larock RC (2010) Vegetable oil-based polymeric materials: synthesis, properties, and applications. *Green Chem* 12(11):1893–1909
17. Güner FS, Yağcı Y, Erciyes AT (2006) Polymers from triglyceride oils. *Prog Polym Sci* 31(7):633–670
18. Ronda JC, Lligadas G, Galià M, Cádiz V (2011) Vegetable oils as platform chemicals for polymer synthesis. *Eur J Lipid Sci Technol* 113(1):46–58
19. Rybak A, Fokou PA, Meier MA (2008) Metathesis as a versatile tool in oleochemistry. *Eur J Lipid Sci Technol* 110(9):797–804
20. Henna PH, Larock RC (2007) Rubbery thermosets by ring-opening metathesis polymerization of a functionalized castor oil and cyclooctene. *Macromol Mater Eng* 292(12):1201–1209
21. Liu K, Chapman (1997) Hall Press, New York
22. Sharmin E, Zafar F (2012) Polyurethane: an introduction. INTECH publisher, Croatia
23. Randall D, Lee S (2003) The polyurethanes book. Wiley publishers, New York
24. Szychers M, Szychers (2013) Handbook of polyurethanes. CRC Press Taylor and Francis, Florida
25. Bagdi K (2010) Role of interactions on the structure and properties of segmented polyurethane elastomers
26. Naheed S, Paridah Md, Mohammad J (2014) A review on potentiality of nano filler/natural fiber filled polymer hybrid composites. *Polymers* 6:2247–2273
27. Fink JK (2017) Reactive polymers: fundamentals and applications: a concise guide to industrial polymers. William Andrew
28. Hojabri L, Kong X, Narine SS (2010) Functional thermoplastics from linear diols and diisocyanates produced entirely from renewable lipid sources. *Biomacromol* 11(4):911–918
29. Hojabri L, Kong X, Narine SS (2010) Novel long chain unsaturated diisocyanate from fatty acid: synthesis, characterization, and application in bio-based polyurethane. *J Polym Sci, Part A: Polym Chem* 48(15):3302–3310
30. Wool RP (2014) U.S. Patent No. 8,633,257. U.S. Patent and Trademark Office, Washington, D.C
31. Kyle DR (1993) U.S. Patent No. 5,234,970. U.S. Patent and Trademark Office, Washington, D.C
32. Sahoo S, Kalita H, Mohanty S, Nayak SK (2016) Synthesis of vegetable oil-based polyurethane: a study on curing kinetics behavior. *Int J Chem Kinet* 48(10):622–634
33. Das S, Pandey P, Mohanty S, Nayak SK (2015) Influence of NCO/OH and transesterified castor oil on the structure and properties of polyurethane: synthesis and characterization. *Mater Express* 5(5):377–389
34. Kaushik A, Singh P (2005) Synthesis and characterization of castor oil/trimethylol propane polyol as raw materials for polyurethanes using time-of-flight mass spectroscopy. *Int J Polym Anal Charact* 10(5–6):373–386
35. Mutlu H, Meier MA (2010) Castor oil as a renewable resource for the chemical industry. *Eur J Lipid Sci Technol* 112(1):10–30
36. Petrović ZS (2008) Polyurethanes from vegetable oils. *Polym Rev* 48(1):109–155
37. Kumar A, Sharma S (2008) An evaluation of multipurpose oil seed crop for industrial uses (*Jatropha curcas* L.): a review. *Ind Crops Prod* 28(1):1–10
38. Segura-Campos MR, Betancur-Ancona D (2016) The promising future of *jatropha curcas*: properties and potential applications. Nova Science Publishers Incorporated, Hauppauge, NY, USA
39. Abdulla R, Chan ES, Ravindra P (2011) Biodiesel production from *jatropha curcas*: a critical review. *Crit Rev Biotechnol* 31(1):53–64

40. Chen CR, Cheng YJ, Ching YC, Hsiang D, Chang CMJ (2012) Green production of energetic jatropha oil from de-shelled jatropha curcas L. seeds using supercritical carbon dioxide extraction. *J Supercrit Fluids* 66(1):137–143
41. Hazmi ASA, Aung MM, Abdullah LC, Salleh MZ, Mahmood MH (2013) Producing jatropha oil-based polyol via epoxidation and ring opening. *Ind Crops Prod* 50:563–567
42. Lestari D, Mulder WJ, Sanders JP (2011) Jatropha seed protein functional properties for technical applications. *Biochem Eng J* 53(3):297–304
43. Pawlik H, Prociak A (2012) Influence of palm oil-based polyol on the properties of flexible polyurethane foams. *J Polym Environ* 20(2):438–445
44. Pillai PK, Li S, Bouzidi L, Narine SS (2016) Solvent-free synthesis of polyols from 1-butene metathesized palm oil for use in polyurethane foams. *J Appl Polym Sci* 133(23):1–13
45. Pillai PK, Li S, Bouzidi L, Narine SS (2016) Metathesized palm oil: fractionation strategies for improving functional properties of lipid-based polyols and derived polyurethane foams. *Ind Crops Prod* 84:273–283
46. Saalah S, Abdullah LC, Aung MM, Salleh MZ, Biak DRA, Basri M, Jusoh ER (2015) Waterborne polyurethane dispersions synthesized from jatropha oil. *Ind Crops Prod* 64:194–200
47. Aung MM, Yaakob Z, Kamarudin S, Abdullah LC (2014) Synthesis and characterization of Jatropha (*Jatropha curcas* L.) oil based polyurethane wood adhesive. *Ind Crops Prod* 60:177–185
48. Gogoi P, Boruah R, Dolui SK (2015) Jatropha curcas oil based alkyd/epoxy/graphene oxide (GO) bionanocomposites: effect of GO on curing, mechanical and thermal properties. *Prog Org Coat* 84:128–135
49. Zhang L, Zhang H, Guo J (2012) Synthesis and properties of UV curable polyester-based waterborne polyurethane/functionalized silica composites and morphology of their nanostructured films. *Ind Eng Chem Res* 51(25):8434–8441
50. Hsiao S, Ma CM, Tien H, Liao W-H, Yu-Sheng Wang, Shin-Ming Li, Sheng-Chi Yang Chih-Yu Lin, Ruey-Bin Yang (2015) Effect of covalent modification of graphene nanosheets on the electrical property and electromagnetic interference shielding performance of a water-borne polyurethane composite. *ACS Appl Mater Interfaces* 7(4):2817–2826
51. Wang C, Xu F, He M, Ding L, Li S, Wei J (2018) Castor oil-based polyurethane/silica nanocomposites: morphology, thermal and mechanical properties. *Polym Comp*. <https://doi.org/10.1002/pc.24798>
52. Chattopadhyay DK, Webster DC (2009) Thermal stability and flame retardancy of polyurethanes. *Prog Polym Sci* 34:1068–1133
53. Meera KMS, Sankar RM, Paul J, Jaisankara SN, Mandal AB (2014) The influence of applied silica nanoparticles on a bio-renewable castor oil based polyurethane nanocomposite and its physicochemical properties. *Phys Chem Chem Phys* 16(20):9276–9288
54. Liu D, Tian H, Zhang L, Chang PR (2008) Structure and properties of blended films prepared from castor oil-based polyurethane/soy protein derivative. *Ind Eng Chem Res* 47(23):9330–9336
55. Gu H, Guo J, He Q, Tadakamalla S, Zhang X, Yan X, Huang Y, Colorado HA, Wei S Guo Z (2013) Flame-retardant epoxy resin nanocomposites reinforced with polyaniline-stabilized silica nanoparticles. *Ind Eng Chem Res* 52(23):7718–7728
56. Das S, Pandey P, Mohanty S, Nayak SK (2017) Evaluation of biodegradability of green polyurethane/nanosilica composite synthesized from transesterified castor oil and palm oil based isocyanate. *Int Biodet Biodeg* 117(1):278–288
57. Filip Z, Hermann S, Demnerov (2008) FT-IR spectroscopic characteristics of differently cultivated *Escherichia coli*. *Czech J Food Sci* 26(6):458–463
58. Fukushima K, Abbate C, Tabuani D, Gennari M, Rizzarelli P, Camino G (2010) Biodegradation trend of poly(ϵ -caprolactone) and nanocomposites. *Mat Sci Eng C* 30(4):566–574

59. Kim YD, Kim SC (1998) Effect of chemical structure on the biodegradation of polyurethanes under composting conditions 62:343–352
60. Das S, Pandey P, Mohanty S, Nayak SK (2016) Effect of nanosilica on the physicochemical, morphological and curing characteristics of transesterified castor oil based polyurethane coatings. *Prog Org Coat* 97:233–243
61. Thakur S, Karak N (2013) Bio-based tough hyperbranched polyurethane–graphene oxide nanocomposites as advanced shape memory materials. *RSC Adv.* 3(24):9476–9482
62. Zhang J, Zhang C, Madbouly SA (2015) In situ polymerization of bio-based thermosetting polyurethane/graphene oxide nanocomposites. *J Appl Polym Sci* 132(13):1–8
63. Ali A, Yusoh K, Hasany SF (2014) Synthesis and physicochemical behaviour of polyurethane-multiwalled carbon nanotubes nanocomposites based on renewable castor oil polyols. *J. Nanomater* 2014, Article ID 564384, 9 pages
64. Chen S, Wang Q, Wang T (2012) Damping, thermal, and mechanical properties of carbon nanotubes modified castor oil-based polyurethane/epoxy interpenetrating polymer network composites. *Mater Des* 38:47–52
65. Liao L, Li X, Wang Y, Fu H, Li Y (2016) Effects of surface structure and morphology of nanoclays on the properties of jatropha curcas oil-based waterborne polyurethane/clay nanocomposites. *Ind Eng Chem Res* 55(45):11689–11699
66. Dzulkipli MH, Yahya MY, Majid RA (2017) Rigid palm oil-based polyurethane foam reinforced with diamine-modified montmorillonite nanoclay. *Mater Sci Eng* 204. <https://doi.org/10.1088/1757-899x/204/1/012024>
67. Adnan S, Maznee TN, Ismail T, Mohd NN, Mariam ND, Nik S, Hanzah NA, Kian YS, Hazimah AH (2016) Development of flexible polyurethane nanostructured biocomposite foams derived from palm olein-based polyol. *Adv Mater Sci Eng* 2016, Article ID 4316424, 12 pages
68. Nikolaidis AK, Achilias DS, Karayannidis GP (2012) Effect of the type of organic modifier on the polymerization kinetics and the properties of poly(methyl methacrylate)/organomodified montmorillonite nanocomposites. *Eur Polym J* 48(2):240–251
69. Zaimahwati AH, Rihayat T, Reflianto D, Gea S (2014–2015) The manufacture of palm oil-based polyurethane nanocomposite with organic montmorillonite nanoparticle as paint coatings. *Int J Chem Tech Res* 7(5):2537–2544
70. Salih AM, Ahmad MB, Ibrahim NA, Mohd Dahlan KZH, Tajau R, Mahmood MH, Wan MdZWY (2014) Thermal and mechanical properties of palm oil-based polyurethane acrylate/clay nanocomposites prepared by in-situ intercalative method and electron beam radiation. *AIP Conf Proc* 117:1584
71. Xia Y, Larock RC (2011) Preparation and properties of aqueous castor oil-based polyurethane-silica nanocomposite dispersions through a sol-gel process. *Macromol Rapid Commun* 32(17):1331–1337
72. Deka H, Niranjana K (2011) Bio-based hyperbranched polyurethane/clay nanocomposites: adhesive, mechanical, and thermal properties. *Polym Adv Technol* 22(6):973–980
73. Sahoo S, Kalita H, Mohanty S, Nayak SK (2018) Shear strength and morphological study of polyurethane-OMMT clay nanocomposite adhesive derived from vegetable oil-based constituents. *J Renew Mater* 6(1):117–125
74. Das B, Mandal M, Upadhyay A, Chattopadhyay P, Karak N (2013) Bio-based hyperbranched polyurethane/Fe₃O₄ nanocomposites: smart antibacterial biomaterials for biomedical devices and implants. *Biomed Mater* 8(3):1–12
75. Mohammed RS, Manawwer A, Naser MA (2015) Development of castor oil based poly(urethane-esteramide)/TiO₂ nanocomposites as anticorrosive and antimicrobial coatings. *J Nanomater* 2015, Article ID 745217, 10 pages. <http://dx.doi.org/10.1155/2015/745217>
76. Hajipour MJ, Fromm KM, Akbar Ashkarran A (2012) Antibacterial properties of nanoparticles. *Trends Biotechnol* 30(10):499–511

77. Thakur S, Karak N (2014) Multi-stimuli responsive smart elastomeric hyperbranched polyurethane/reduced graphene oxide nanocomposites. *Mater Chem A* 2:14867–14875
78. Ahuja D, Kaushik A (2016) Castor oil-based polyurethane nanocomposites reinforced with organically modified clay: synthesis and characterization. *J Elastomers Plast* 49(4):1–17
79. Peng Gao Z, Jun Zhong T, Sun J, Wang X, Yue C (2012) Biocompatible elastomer of waterborne polyurethane based on castor oil and polyethylene glycol with cellulose nanocrystals. *Carbohyd Polym* 87(3):2068–2075

Clay Based Biopolymer Nanocomposites and Their Applications in Environmental and Biomedical Fields



K. Sangeetha, P. Angelin Vinodhini and P. N. Sudha

1 Introduction

Clay-based biopolymer nanocomposite was an interdisciplinary subject which holds together the hands of scientists from polymer science, biology, chemistry, physics, materials and biomedical engineering. Collaborators of different discipline would always result in qualitative work and new ideologies which steps into a variety of medical and nonmedical applications. Clay is a natural material which recovers the position against synthetic materials in pharmaceutical technology as it was non-toxic and available plenty in nature. A quality research was going on at present with countless publications and innovative findings dealing with clay reinforced polymeric matrixes were available. The incorporation of nanofiller in the polymeric material will improve the mechanical, barrier and other matrix properties of nanocomposites used for biomedical and environmental applications [40]. This huge number of publications implies the importance of polymer clay nanocomposite as drug delivery system, as hemostasis, in tissue regeneration etc. In this chapter, a detailed discussion on the biomedical and environmental application of clay-polymer nanocomposite was given elaborately with recent findings.

The term clay refers to the group of materials made up of layered silicates or clay minerals with traces of metal oxides and organic matter [51]. They belong to the family of phyllosilicate or sheet silicates made of hydrated alumina–silicates. The basic building unit of clay minerals is composed of tetrahedral silicates and octahedral hydroxide sheets and they were arranged as 1:1 (e.g., kaolinite and serpentine) and 2:1 (e.g., smectite, chlorite, and vermiculite) to give rise to various

K. Sangeetha · P. Angelin Vinodhini · P. N. Sudha (✉)
Biomaterials Research Lab, D.K.M. College for Women,
Vellore 632001, Tamilnadu, India
e-mail: drparsu8@gmail.com

classes of the clay mineral. Clay minerals possess specific physicochemical characteristics such as high surface reactivity (adsorption and cation exchange capacity), colloidal and swelling capacity, optimal rheological behaviour, and high water dispersibility, which render them suitable for different biological applications including pharmaceuticals, cosmetics, veterinary medicine, biomaterials, and biosensors.

In general, clays were nanometer in size due to this it can be easily incorporated into polymer matrixes. Clay was hydrophilic in nature and it can be readily mixed with hydrophilic polymers like poly(ethylene oxide) [37] and poly(ethylene glycol) [21] to prepare polymer-clay nanocomposite. But in case of hydrophobic polymers, the preparation of nanocomposite with good miscibility was not possible by physical mixing of polymer and clay. In such cases, these clays were converted to organophilic by exchanging the cations present in the clay layer with surfactants such as quaternary alkylammonium and alkylphosphonium ions [25].

The schematic representation of various classes of clay mineral and crystal structure of some commonly used clay in the pharmaceutical application was shown in Figs. 1 and 2 respectively.

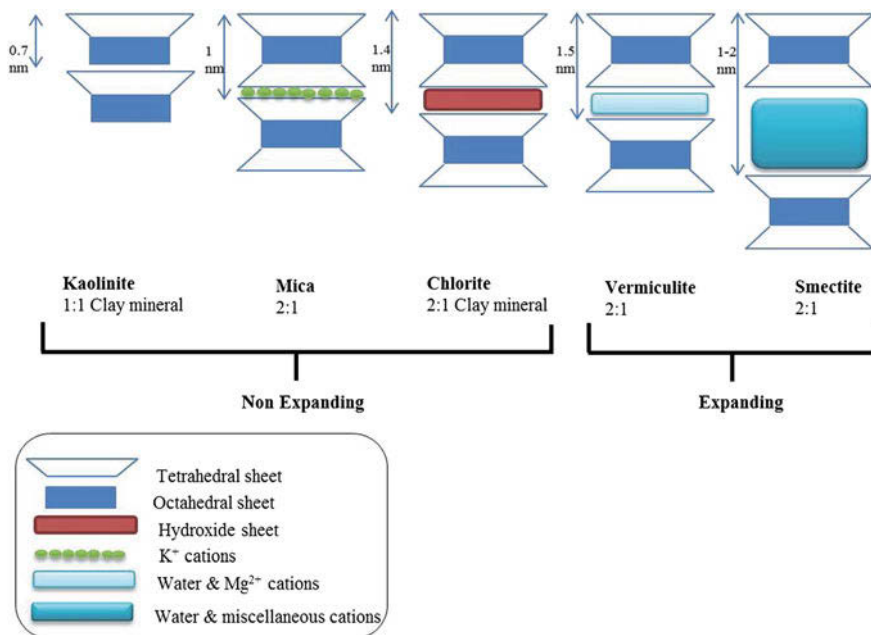


Fig. 1 Various classes of clay minerals and their arrangement [38]. Copyright (2015) Royal Society of Chemistry

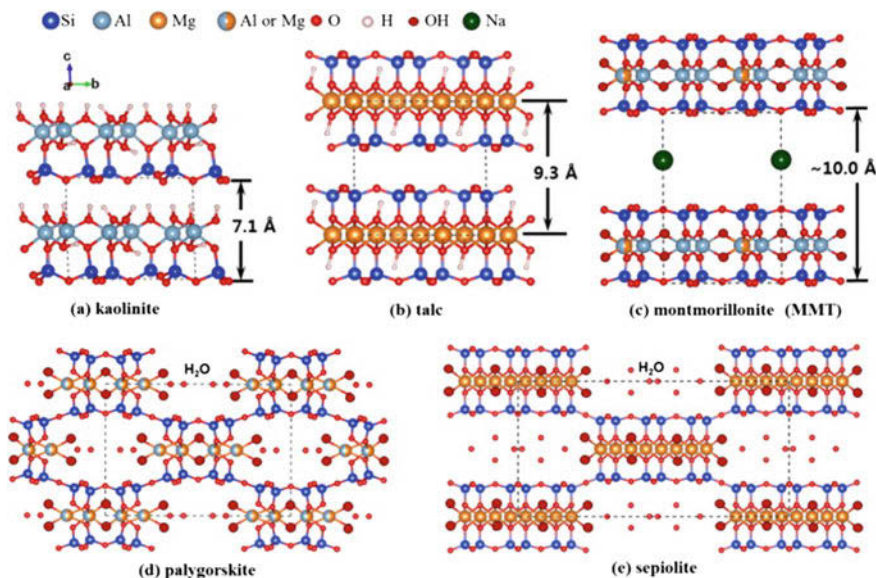


Fig. 2 Crystal structure of pharmaceutical used clays; **a** kaolinite, **b** talc, **c** montmorillonite, **d** palygorskite and **e** sepiolite, where dashed lines represent the unit cell [90]. Copyright (2016) Elsevier

2 Preparation Methods of Polymer Clay Nanocomposites

Solution intercalation, melt mixing and in situ polymerization techniques are the most commonly used methods to prepare polymeric clay nanocomposites [81]. During the preparation, the polymer was intercalated or exfoliated in layered hosts of clay with significant improvement in properties with reduction of component weight.

2.1 Solution Intercalation Method

In solution intercalation method, the polymer was dissolved in a solvent system and the silicate layer was swellable. The layered silicate is first swollen in a solvent, such as water, chloroform, or toluene. During mixing of silicate and polymeric solution, the polymer chains intercalate among themselves and the solvent was displaced within the interlayer of silicate. After the removal of solvent, the intercalated system remained with nanoscale morphology.

2.2 Melt Intercalation Method

In melt intercalation method polymer was directly mixed with clay using a twin-screw extruder or an internal mixer. When the surface layers are sufficiently compatible with the polymer matrix, the polymer will start to penetrate in between layers of clay thereby expanding gallery spacing. This driving force was called as shear force and this method was more commercial because solvents were not used in this technique. This method possesses greater advantage and it can intercalate the polymers which were not possible with other two methods of in situ intercalative polymerization and solution intercalation.

2.3 In Situ Intercalative Polymerization

In this method, the polymer and clay were intercalated by choosing suitable monomers followed by subsequent in situ polymerization. The polymerization reaction can be initiated either by heat or radiation, by the diffusion of a suitable initiator, or by an organic initiator or catalyst fixed through cation exchange inside the interlayer before the swelling step. Here the monomer was used directly as a solubilizing agent for swelling the layered silicate. Subsequent polymerization takes place after combining the silicate layers and monomer, thus allowing the formation of polymer chains between the intercalated sheets [91]. This method was widely used for thermosetting polymer-layered silicate nanocomposites.

The diagrammatic representation of exfoliation and intercalation during formation of polymer clay composite was shown in Fig. 3 and the possible interaction between the clay and polymer matrix as illustrated in Fig. 4.

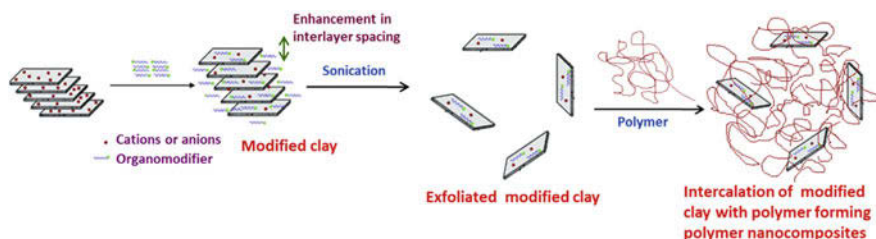


Fig. 3 Schematic diagram showing clay modification and intercalation of polymer to form polymer nanocomposites [51]. Copyright (2015) Elsevier

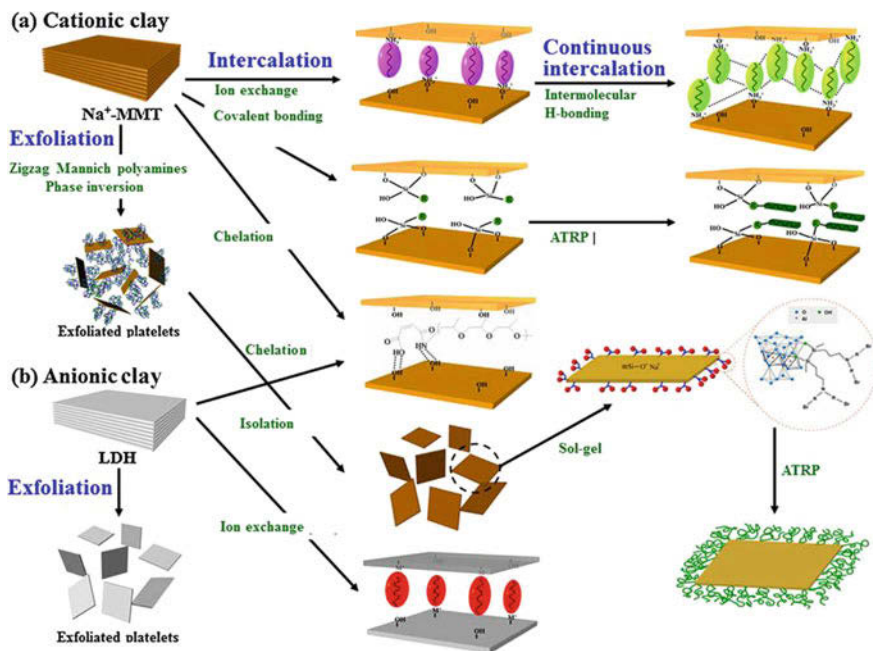


Fig. 4 Schematic representation of possible strategies for the interaction of clay mineral with the polymer [23]. Copyright (2014) Elsevier

3 Biomedical Applications of Polymeric Clay Nanocomposites

Indigenous people all around the world from ancient days have used clay both internally (geophagy) and externally (clay baths) for prevention of illness, physical healing, to improve the general health thereby prolonging their life. Clay therapy was not a new concept or modern healing technology for us, as our ancient cultures and aboriginal tribes were more familiar with clay and they have used for a variety of illness and injuries. Oral consumption of clay will cure the infection, helps in balancing pH of the body, regulate gastrointestinal problems, and counter poisoning by chelation. Some of the clay-polymer composites along with their application in the biomedical field were discussed in this section.

3.1 As Drug Delivery System

In general, usage of a single polymer or clay mineral will not meet all the necessary requirement of drug release and hence the combination of a polymeric material with clay mineral will give adequate support for effective drug delivery. Clay play a vital

role for safe drug delivery as it can act both as an excipient and active agent [3]. The addition of clay even lesser than 5% will enhance properties of mechanical strength, thixotropy, reduced gaseous permeability and heat resistance to remarkable level which was highly appreciable for adsorbing the drug and releasing them in a controlled manner [39, 69, 88]. Clay minerals such as halloysite, montmorillonite clay, bentonite were explored in a polymeric matrix as they have the ability to enhance mechanical properties as well as for their potential to act as drug delivery modifiers [61, 68]. The presence of clay mineral in nanocomposite will act as transporting vehicle to deliver drugs by modifying the rate of drug release and thereby improving the dissolution profile of drug [85]. In most of the cases, administration of the drug at a conventional dosage will result in releasing them in an uncontrolled manner and get circulated to various body organs. This drawback will be evaded in case of clay reinforced polymeric composites as colloidal clay particles and biopolymer have the possibility to release the drug in a controlled manner at a specific needed site without affecting the other portion of the organs in the body [86].

For an ideal drug delivery system, the important factor to consider was how much amount of drug was released during the process—if drug release was too high it will lead to adverse effect or harmful to the body and if it was too low will result in reduced efficiency. The optimal release of drug within required time was essential for powerful performance. The different methods adapted for drug release was shown in Fig. 5.

Kohay et al. [50] developed a novel formulation of the organic-inorganic composite in which the drug doxorubicin was incorporated in micelles (M-DOX) of polyethylene glycol-phosphatidylethanolamine (PEG-PE) adsorbed over clay layer of montmorillonite (MMT). On varying the ratio of PEG-PE/MMT, two different formulations were fabricated and named as low, high composite and it was compared with pure doxorubicin. In their work, they have used MCF-7 cells for carrying out bioassay (in vitro study) at a regular time interval of 2 and 6 h and Adriamycin resistant cell line (A2780-ADR) for evaluating cytotoxicity. They reported the following information: In low composite a single layer of polymer and for high composite two layers of polymer were intercalated between the platelets of montmorillonite clay. The release trend followed the order of high formulation > low formulation > DOX/MMT and in MCF-7 cells high formulation exhibits higher cytotoxicity whereas, for Adriamycin resistant cell line (A2780-ADR), low formulation demonstrated the highest cytotoxicity.

Sabbagh et al. [73] synthesized novel halloysite-based chitosan/oxidized starch nanocomposite hydrogel beads by incorporating clay mineral halloysite nanotubes and evaluated the changes in swelling behaviour, thermal properties as well as drug loading/releasing characteristics of hydrogel beads. The embedding of halloysite into hydrogel structure will prolong the release of drug metronidazole (MTZ) from nanocomposite hydrogel beads resulting in controlled drug release.

Lal et al. [53] examined in vitro oral delivery of insulin using montmorillonite poly lactic-co-glycolic acid nanocomposites. The prepared composite was evaluated for various parameters such as drug content, physicochemical properties,

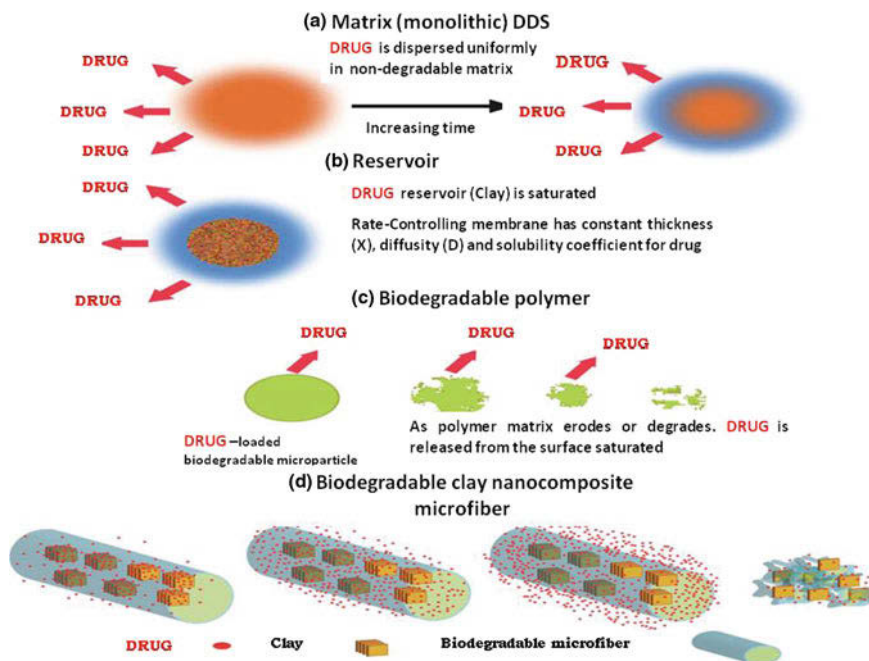


Fig. 5 Different method of drug release based on (a) monolithic, (b) reservoir, (c) degradation and (d) combined a, b and c drug delivery systems. Jafarbeglou et al. [45]. Copyright (2016) Royal Society of Chemistry

in vitro insulin release profile and cytotoxicity. The results from MMT assay reveal the nontoxicity of the formulation and this nanocomposite was effective in releasing insulin without burst effect which will definitely serve as an efficient oral drug delivery vehicle of insulin in near future. Controlled release of strontium ranelate (SRA), a drug for osteoporosis from composite scaffold polycaprolactone-laponite was reported by Nair et al. [62]. By varying Laponite-SRA complex content from 3 to 12 wt% an array of composites were prepared and evaluated in vitro using human osteosarcoma cells. They reported ratio 3 wt% laponite-SRA complex was ideal for drug release which was confirmed using ALP activity.

Khlibsuwan et al. [48] studied the drug release behaviour of spray-dried chitosan-magnesium aluminium silicate (MAS) nanocomposite microparticles, loaded with propranolol HCl. Investigation on the effect of crosslinker (sodium tripolyphosphate) and content of clay (magnesium aluminium silicate) was also reported. A sustained release of propranolol was achieved for all types of microparticles in 0.1 M HCl and phosphate buffer pH 7.4 for several hours. The drug release clearly slowed down at low and neutral pH, whereas the incorporation of 1–3% TPP caused only a slight/moderate decrease in release rate, irrespective of the type of release medium with increasing MAS content. Similarly, in another study, Fan and his coworkers [35] investigated drug release behaviour of diclofenac

sodium (DS) using novel sodium alginate/hydroxyapatite/halloysite nanocomposite hydrogel beads. The addition of hydroxyapatite and halloysite nanotube to the biopolymer sodium alginate will result in enhancing entrapment efficiency from 62.85 to 74.63% and thereby controlling the burst release of drug diclofenac sodium.

Bera et al. [10] have developed novel composite by coating montmorillonite clay on the membrane of alginate-Arabic gum (AG) gel and has been examined for intragastric flurbiprofen. The drug release rate was compared with uncoated formulation and they reported that the coated matrices (F-O, coated) depicted improved drug loading ability (DEE, $94.49 \pm 1.23\%$) and slower drug release profile (Q_{8h} , $69.24 \pm 0.65\%$) endowed with improved buoyancy and mucoadhesive suggesting them as excellent drug delivery system. Another study revealing the sustained drug release of clay composite was reported by Ji et al. [46] in which the mechanical strength of gelatin scaffold was enhanced by adding halloysite nanotube and it was loaded with the drug ibuprofen. Halloysite incorporated composite show extended drug release over 100 h compared to only 8 h when it was directly mixed with gelatin (i.e. without halloysite).

Bounabi et al. [16] have developed novel nanocomposite of poly(2-hydroxyethyl methacrylate) (HEMA) with montmorillonite clay and investigated the structural properties of nanocomposite with the addition of clay using analytical techniques of Fourier transform infrared spectroscopy (FTIR), differential scanning calorimetry (DSC) and thermogravimetric analysis (TGA). The drug release behaviour of paracetamol loaded in prepared hydrogel nanocomposite was reported with the following findings: Crosslinking of clay will reduce drug burst rate and release rate of the drug from novel composite will decrease with increase in the content of MMT loading. The composite will delay drug dissolution rate and thereby improve patient compliance through the reduction of multiple dosing.

Huang and his coworkers [43] have prepared chitosan composite hydrogels by adding halloysite nanotubes to the solution of chitosan. They have performed cytotoxicity assay using MC3T3-E1 cells and reported that the composite will support the growth of MC3T3-E1 cells indicating its biocompatibility. The composite hydrogels show a maximum drug entrapment efficiency of 45.7% for doxorubicin (DOX) which is much higher than that of pure chitosan hydrogel (27.5%) suggesting composite hydrogel shows superior drug release efficiency.

Curcumin release from composite carboxymethyl cellulose–montmorillonite clay was carried out by Madusanka and his coworkers. The sustained release rate of more than 60% was achieved from curcumin activated nanocomposite in distilled water (maintained at a pH of 5.4) at 25 °C within 2 h and 30 min. From the results, Madusanka group have reported that curcumin activated carboxymethylcellulose–montmorillonite nanocomposite is an effective curcumin carrier with enhanced solid state properties [59]. Salcedo et al. [74] prepared composites of a modified montmorillonite with chitosan by simple solid-liquid interaction and loaded with drug oxytetracycline. The penetration enhancement properties of nanocarrier towards the drug were evaluated using cell model Caco-2. Presence of clay mineral

particles in the polymer matrix resulted in effectively enhanced drug permeation and improved bioavailability in vivo after oral administration of the drug.

Kevadiya and his coworkers [47] examined drug release rate of diclofenac sodium by intercalating “in situ” the anionic drug DC into cationic polymer chitosan in montmorillonite clay. They reported the in vitro cell viability assay of the drug-loaded composite in cancer cell was less toxic than the pristine drug. They suggested applying this formulation as fruitful material in much more applications with different loaded drugs and biomolecules.

Abdeen and his coworkers [1] have prepared nanocomposite for drug carrier by intercalating chitosan into layered silicate of montmorillonite clay and the release rate of drug ibuprofen from nanocomposite was studied. The drug release of ibuprofen was affected by pH value of the medium, drug loading capacity, the percentage of chitosan in nanocomposite and its morphology. They have noted the in vitro drug release at pH of 5.4 and 7.8 which mimic the gradient of pH from the stomach to intestine. On concluding their work, the sustained-drug release was achieved and they have reported the prepared nanocomposite was effective for oral administration as it avoids the interaction between drug and gastric mucosa with prolonged duration of drug activity.

3.2 In Tissue Engineering

Tissue engineering is an emerging field widely employed to develop scaffolds for replacing the damaged tissues and organs [54]. The basic principle in tissue engineering was to fabricate scaffold which should be highly compatible with living tissues and they will help to enhance cell proliferation, adherence and differentiation thereby eventually develop regeneration or growth of new tissues in infected or defected area [5]. In order to design a composite system for replacing tissues, dispersion technology and interfacial interaction between the matrix systems was crucial to attaining. This will be effectively achieved by choosing similar molecular structures so that they will result in composites with improved properties [56].

The presence of clay in the composite will usually enhance cell adhesion and spreading. A possible reason for this increased cell attachment was due to the fact clay will create more focal adhesion sites through reactive functional groups where direct adhesion of cell attachment was taken place [36]. Another interesting reason for enhanced cell proliferation in polymeric-clay composite was due to the creation of particular hydrophobicity/hydrophilicity balance between hydrophobic polymer chains and hydrophilic clay dispersion could directly mediate cell adhesion as well as promote protein adsorption [75]. Afsar and Ghaee [2] also reported a similar result that the presence of clay will enhance cell adhesion and proliferation. Composite of chitosan/alginate/halloysite was prepared and modified with amination. The cytocompatibility was evaluated using Alamar Blue assays by culturing fibroblasts L929 on the scaffolds. They reported that the amination treatment and incorporation of clay will improve cell adherence and proliferation.

Boyer et al. [17] developed a faster gelling composite to heal articular cartilage, a connective tissue using biomaterial assisted cell therapy. Boyer and their coworkers prepared laponite silylated hydroxypropylmethyl cellulose hydrogel having the very high mechanical strength the basic criteria for healing cartilage tissues. The *in vitro* studies shows biocompatibility and nontoxic nature of composite make them a suitable material for treating cartilage defects. An interesting composite work reported more recently was Sr⁺²-modified chitosan/montmorillonite scaffold fabricated using freeze-drying method. Biocompatibility study was evaluated by employing scaffold in human osteoblasts (hOBs). Cell viability and proliferation were reported from assays of MTT (3-(4,5-dimethylthiazol-2-yl)-2,5-diphenyltetrazolium bromide) and DNA content analysis. Demir et al. [28] have concluded that the composite will possess all desirable physicochemical and biological characteristics which could mimic as an ideal biomimetic template for the repair of defective bone with osteoblasts.

A novel three-dimensional composite scaffold of chitosan/hydroxyapatite/montmorillonite clay was reported by Vyas et al. [87]. The presence of clay will reduce the swelling and degradation rate which was highly required for enhancing the mechanical strength of scaffold. Cell proliferation was tested using MG 63 cell and the cellular response show non-cytotoxic behaviour implying hemocompatibility with more favourable microenvironment for osteoblast cell proliferation. Bhowmick and his colleagues [13] reported an improved osteogenic response of osteoblast cell line MG-63 cells as a direct function of modulating organically modified montmorillonite clay content in composite chitosan/hydroxyapatite-zinc oxide (CTS/HAP-ZnO). An interesting report of a decrease in tensile strength, antibacterial effect and cytocompatibility with the MG-63 cell was observed with composite (in absence of OMMT) compared to composite with organically modified montmorillonite clay. The composite with clay will decrease swelling ability thereby increasing mechanical strength and cell proliferation of composite.

Chappidi and Mills [22] have prepared a novel composite scaffold with a unique combination of poly-glycerol sebacate (PGS), polycaprolactone (PCL) and halloysite clay nanotubes (HNTs). The presence of aluminosilicate clay nanotubes will help to enhance its structure, mechanical properties and have potential to support the development of tissues and their growth. Chitosan-agarose-gelatin nanocomposite porous scaffolds doped with halloysite was fabricated using the freeze-drying method and prepared scaffold was underwent to *in vitro*, *in vivo* studies to evaluate its biocompatibility and biodegradability. The relative number of attached cells onto chitosan-agarose-gelatin halloysite scaffold was eventually increased with halloysite content from 3 to 6 wt% which implies good cytocompatibility behavior of the scaffold. The *in vivo* study was conducted using rats with slight inflammatory effect and the reported results confirm implant was degraded without rejection and full restoration of the blood supply was achieved within six weeks [63]. Bonifacio et al. [15] prepared a novel tri-component hydrogel based on gellan gum, glycerol, halloysite and examined for different soft tissue engineering application. The *in vitro* results show a good human dermal fibroblasts biocompatibility mimicking the native microenvironment.

Huang et al. [44] prepared composite hydrogels of Sodium alginate (SA)/halloysite nanotubes and examined for tissue engineering application using pre-osteoblast (MC3T3-E1) cell line. The cell adhesion and proliferation were increased in the composite as compared to pure sodium alginate hydrogel revealing the decreased pore size due to halloysite will result in increased cell attachment and low cytotoxicity. Liu et al. [55] fabricated halloysite reinforced alginate composite scaffold by solution mixing and freeze drying. The results from analytical techniques will confirm the interfacial interactions between halloysite, alginate and also the enhancement of cell proliferation and mechanical strength was achieved due to the presence of halloysite. The reported porosity of 93–97% and pore size of around 100–200 μm , confirms the improvement in the number of sites for cell attachment. The cytotoxicity examination using mouse fibroblast cells display better attachment which in turn should be a potential member to apply in tissue engineering.

Olad and Azhar [66] reported novel three-dimensional chitosan-gelatin/nanohydroxyapatite-montmorillonite composite scaffold and examined physico-chemical properties. The addition of MMT in the composite will moderate mechanical behaviour, water absorption ability, density, biodegradation, biomineralization suggesting them to apply in bone tissue engineering application in future. A novel nanocomposite was reported by Buffa and his coworkers [19] in which they have prepared composite by loading Sr (II) on halloysite nanotube with the biopolymer matrix of (3-polyhydroxybutyrate-co-3-hydroxyvalerate). The loading of strontium and clay enhance the porosity and mechanical resistivity making them as an effective material to apply for *invitro* studies. The *invitro* study was reported by checking the compatibility of the composite in L929 fibroblast cells and the results proved that it was an effective material to apply for bone regeneration purpose.

3.3 As Regenerative Repair in Wound Healing

The largest organ in the human body was skin and it will act as a barrier to harmful mediums and prevent them to enter into the body. Sometimes skin gets wounded due to physical, chemical, mechanical and/or thermal damages. The healing of damaged skin in a natural way was more complex and it will continue for few months to years. To overcome this slow complex process, a new technique “Wound healing” was emerged and has attracted great interest to treat excessive lose of skin. A new combination of materials including natural, synthetic and even combination of both have been used for application of skin regeneration.

One such material was clay and we are familiar with clay from ancient history that our ancestors have widely used clay and clay-based products for skin ailment and for wound dressing. The usage of clay in the medical field was well documented worldwide from early days of mankind and it will continue till today. But after 19th century more scientific inquiry was emerged to analyze chemistry behind its structure, properties and the interaction/mechanism of the healing process.

The intense level of investigation and research was more concentrated in the second half of the 20th century evidencing that these clay-based products are much more compact with skin regeneration. Some of the documented research works were highlighted in the area of wound healer.

Before discussing in detail about the research works in this area, we should aware of the general term “Regenerative medicine” which comprises a broad category involving regeneration of cells, tissues, and organs in order to perform its original function. The incorporation of clay in polymers will result in enhancing mechanical properties, improve cell adhesion, proliferation, differentiation of progenitor cells and also act as biomolecule carrier [27, 36]. A simple representation of clay mineral in regenerative medicine was illustrated in Fig. 6.

An interesting study related with clay-based composite was recently reported by Kurczewska et al. [52] in which they have explained the influence of clay (halloysite nanotubes) in terms of releasing rate and biological activity of dressing material. The release rate of the drug was slowed down by halloysite as its structure allows functionalization of exterior and interior surfaces with organic ligands. This factor will result in reducing release rate as the system would act as a double barrier which in turn can be effective for long-term treatment of wounds.

Kaolin loaded polyurethane hydrogel composite was prepared using simple one-pot synthesis and hemostatic capabilities of composite were compared with commercial hemostatic dressing materials. Blood clotting index was measured using hemolysis assay and the clotting time was measured through rheology by taking Quick Clot Combat Gauze (QCCG) as a reference. Lundin and his coworkers reported that kaolin loaded polyurethane foams of 5 and 10% exhibits enhanced clotting behaviour and was highly recommended for wound dressing

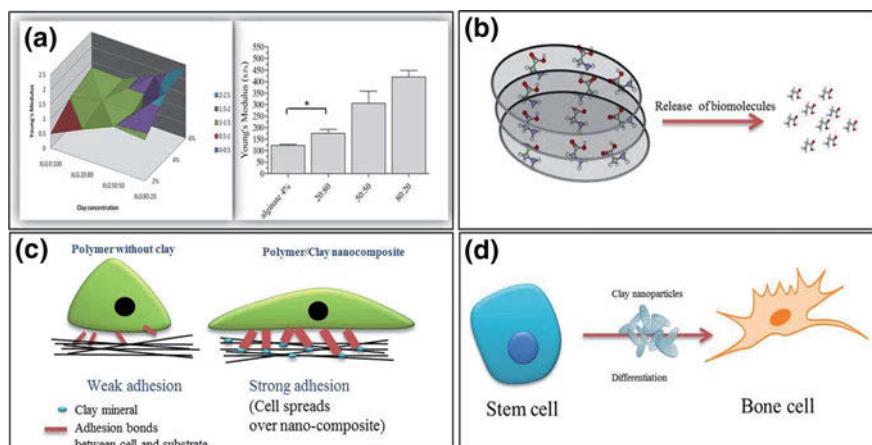


Fig. 6 Application of cationic clay minerals in regenerative medicine: enhancing the mechanical property of polymers (a), delivering biomolecules (b), improving cell adhesion (c), and facilitating the proliferation and differentiation of stem cells to bone cells (d). Ghadiri et al. [38]. Copyright (2015) Royal Society of Chemistry

[58]. Yang's research group [89] prepared nanoclay LMSH cross-linked semi-IPN silk sericin/poly(NIPAm/LMSH) nanocomposite hydrogel for wound dressing. The wounded area was treated with prepared hydrogel nanocomposite and recovery rate was monitored at regular interval of time. They reported the nanocomposite has achieved 83% of healing at 6th day followed by complete recovery within 13 days and thereby suggesting this composite as a suitable wound healer.

Solvent casting method was adapted by Devi and Dutta [29] to prepare nanocomposite films of chitosan-bentonite. The nanocomposite has good swelling and excellent antibacterial properties simultaneously, could serve as a barrier against infection, are low-antigenic, could adsorb wound exudates and show high water-vapour permeability. They reported this preliminary study was highly supported for fabricating them as wound care products. Another interesting work on wound treatment was reported by Sirousazar et al. [80]. This research group has formulated a novel wound dressing material by employing freeze-thawed and non-freeze-thawed egg white/PVA/MMT nanocomposite hydrogels. In vitro and in vivo studies were used for evaluating its cytotoxicity and rate of wound recovery. The results of in vitro study reveal the optimum level of biocompatibility was achieved and the in vivo study supports the fast closure of wound edges with the significant rate. Similar technique of freezing-thawing method was used by Noori group [65] to prepare nanocomposite hydrogels of poly (vinyl alcohol)chitosan/montmorillonite. The presence of clay will improve the mechanical properties and swelling behavior of the system. They have reported the addition of 3% of montmorillonite clay will increase tensile modulus to 35% and this enhanced mechanical property make this material highly suitable for wound dressing.

Ambrogi et al. [6] have developed a composite by intercalating chlorhexidine into the montmorillonite-chitosan film. Even though chlorhexidine is an excellent antimicrobial agent the usage of chlorhexidine was limited in wound healing because of its negative aspect of cytotoxicity towards human fibroblasts. This should be overcome on interacting with the chitosan-MMT film at a concentration of 1 and 5% of chlorhexidine resulting in sustained release of drug in long-term purpose with decreased cytotoxicity and can act as good antibiofilm and antimicrobial agents. Nistor et al. [64] have prepared crosslinked collagen/poly (N-isopropyl acrylamide) network embedded with montmorillonite clay and the prepared hybrid hydrogel was targeted for tissue engineering application to cover burned tissues and the healing of damaged skin was monitored. Pseudoplastic behaviour was attained in the hydrogel which was due to the presence of clay which makes them highly suitable for skin healing.

3.4 As Biosensors

Clay-based polymeric biosensors have been escalating as a new generation of biosensors and bioassays with ultra-low limits of detection and enhanced detection sensitivity. For sensor application, conducting polymers was an excellent choice as

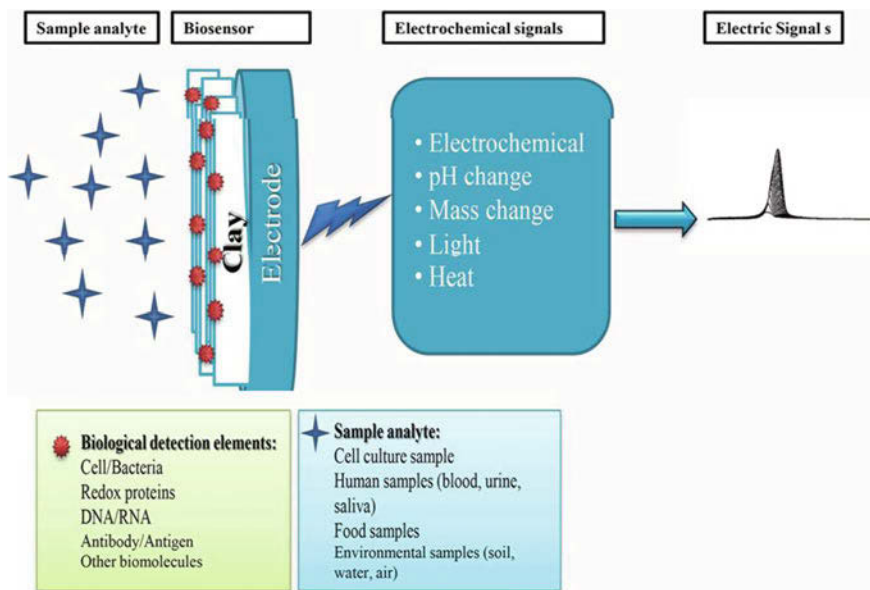


Fig. 7 Representation of a clay-based material in biosensors. Ghadiri et al. [38]. Copyright (2015) Royal Society of Chemistry

they can be easily tuned with different materials like clay to improve its surface properties and immobilization. The sensor is defined as a device that will measure analytical informative signal arises due to a chemical interaction between medium around the analyte and sensor device. If the receptor is a biological module like enzyme or antibody within the cell then the biological mechanism arises was termed as “Biosensor” Fig. 7.

Clay mineral based biosensors were prepared by depositing thin films of clay on the conductive substances [60]. Besombes et al. [11] have developed cholesterol biosensor by using Laponite- poly (amphiphilic pyrrole derivative) matrix. The incorporation of clay will enhance the sensitivity of sense, as this system does not show sensor application in the absence of clay Laponite. This finding suggests the importance of clay in sensing biological substances. Another interesting biosensor was reported by Emre et al. [33] where they developed polymer–clay nanocomposites by grafting polymethylmethacrylate (PMMA) with laponite clay and a conducting polymer; poly(BIPE) [poly(4-(2,3-dihydrothieno[3,4-*b*][1,4]dioxin-5-yl)-7-(2,3-dihydrothieno[3,4-*b*][1,4]dioxin-7-yl)-2-benzyl-1*H*- benzo [d] imidazole)] was used for detection of glucose. They reported that this system will serve as a proper immobilization platform for enzyme molecules achieving superior biosensor performance with a more proper enzyme deposition and proficient surface chemistry. By this way, an electrochemical signal for glucose detection was amplified.

Sarkar et al. [78] developed chitosan/montmorillonite nanocomposite by depositing it on indium tin oxide coated glass substrate. This fabricated enzymatic

biosensor acts as an excellent platform to detect organophosphorous (chlorpyrifos) through measuring immobilization of acetylcholine esterase. Barlas et al. [9] prepared folic acid (FA) modified poly(epsilon-caprolactone)/clay nanocomposite and have tested for selective cell adhesion and proliferation. The results suggest that this material can be adapted for various bio-applications such as 'cell culture on-chip', biosensors and design of tools for targeted diagnosis or therapy.

Advanced plastic medical devices have been prepared using clay mineral-polymeric composites. One such interesting example was the replacement of medical tubing such as catheters prepared by latex rubber and poly(vinyl chloride) was allergic to patients and this will be successfully replaced by non-allergic composite material prepared using polymer polystyrene-b-poly(ethylene-co-butylene)-b-polystyrene mixed with polyolefins and a lesser amount of filler clay mineral [82]. An interesting medical grade nanocomposite used as medical devices ranging from examination gloves and tubings to blood bags and dialysis equipment was prepared by polyvinyl chloride-montmorillonite clay [77].

4 Environmental Applications of Polymeric Clay Nanocomposites

Water, the elixir of life has now become much more important than precious metals like gold, platinum as it was depleted continuously by natural and anthropogenic activities. We may say water as a powerful indicator of sustainability, which in turn indicate the level of social development in a particular community. Water is also an issue that is linked with health, nutrition and many other factors that affect our society including the condition of nature itself! It is not an exaggeration to say that water is life. Several countries all around the world are expected to face severe water crisis by the year 2025 [18]. Contamination and degradation of the aquatic environment were considered as one of the major global concerns of our society. In particular, industrial effluents such as organic and inorganic wastes, heavy metal ions, dyes, aromatic compounds, etc. pose considerable risk to drinking water sources. Among various adsorbents used for remediating effluents, clay was considered as a suitable candidate as its layered structure has the ability to imprison water in between interlayer space resulting in heavy metal adsorption and ion exchange. Hence in this chapter, we have discussed clay based composites as a potential candidate for remediating wastes by adopting different techniques which was considered as a favorable subject for researchers.

4.1 For Heavy Metal Removal

Various scientists all around the world have conducted a huge number of studies to explore adsorptive characteristics of clay and all these experiments will result in

concluding the importance of clay as an excellent adsorbent for removing different toxic heavy metal ions from aqueous solutions. This chapter represents literature review of investigations done in the last decade with clay minerals and their modification as composites with a different polymeric combination and their positive results towards removal of heavy metals.

Edathil et al. [30] developed alginate clay composite using different clay minerals of sepiolite, montmorillonite, bentonite clays and a comparative study was reported on the adsorption performance of heavy metal chromium, total organic anions and iron. A maximum adsorption was achieved at 2.0 wt% of filler (clay) for all the combination of reported clay minerals with alginate. The sorption of the contaminant was confirmed from the results of FT-IR and Scanning electron microscopy suggesting that this composite was effective for removal of heavy metal due to the presence reinforcing material clay. Ahmad and Hasan [4] synthesized L-methionine montmorillonite encapsulated guar gum-g-polyacrylonitrile (GPCM) hybrid nanocomposite by free radical graft copolymerization. Adsorption studies were carried out for the removal of metal ions Cu (II) and Pb (II). The obtained results showed that optimum adsorption for both metal ions was achieved at pH of 5 and equilibrium time of 150 min. The adsorption kinetics of both metal ions followed pseudo-second-order model and the adsorption isotherm was well fitted by Langmuir model. The maximum adsorption capacity of the adsorbent was 125.00 mg/g for lead and 90.91 mg/g for copper.

Heydari et al. [41] have developed nanocomposite of β -Cyclodextrin polymeric bentonite clay by emulsion polymerization. The addition of clay enhances thermal stability of composite and it was confirmed by analytical techniques of DSC and TGA. The composite was employed to remove heavy metals such as copper, zinc, and cobalt from drinking water using batch adsorption method. From the calculated values of K_d and percentage of metal adsorption, the sequence followed for metal adsorption onto nanocomposites was found to be $Zn^{2+} > Cu^{2+} > Co^{2+}$. These findings suggest that maximum removal was achieved with an increase in clay content thereby reporting the composite as green absorbent and economically more effective to use on large scale for the purpose to purify drinking water.

Piri et al. [71] synthesized Polyaniline-clay nanocomposite using in situ chemical oxidative polymerization technique and this adsorbent was used to remove metal ions Pb (II) and Cd (II) from aqueous solution. Batch adsorption study was carried out by varying parameters such as pH of the solution, adsorption dose, metal ion concentration and contact time. The obtained experimental data and isothermal kinetic studies were well inserted for pseudo- second kinetic and Temkin model confirming a companionship of physical and chemical adsorption. They also reported that the preparation method "in situ chemical oxidative polymerization" was a new technique for lead removal and it was economic to employ for large-scale removal of metal ions. Onyango et al. [67] used two different techniques such as batch adsorption and fixed bed column for removal of heavy metal hexavalent chromium using polypyrrole modified montmorillonite composite. For the batch study, Langmuir model was well fitted for the composite to remove chromium with maximum adsorption capacity of 119.34 mg/g at 298 K. In fixed bed

column study process parameters such as initial Cr (VI) concentration, bed mass and flow rate were considered. Onyang and his coworkers reported maximum sorption rate was achieved at a lower flow rate and initial Cr (VI) concentration and high bed mass.

Rafei et al. [72] used the combination of polyacrylic acid-organobentonite to prepare nanocomposite by successive intercalation of cetyltrimethyl ammonium as a surfactant and it was employed to remove Pb (II) ions from aqueous solutions. The interaction of polyacrylic acid in clay was confirmed from XRD diffractogram. The sorption study was performed using batch adsorption and it was compared to untreated bentonite clay. They have reported maximum sorption of 93 mg/g was achieved which was twice as that of untreated bentonite having removal rate of 52 mg/g.

Choudhury et al. [24] synthesized nanocomposites of bentonite clay-hydroxyapatite at three different pH of 3, 7 and 10 which was further cross-linked by glutaraldehyde to increase its thermal stability. These entire composite were utilized to remove toxic lead (II) ion. The sorption capacity was analyzed by mathematical and statistical optimizing technique (response surface methodology). They reported maximum sorption was observed for composite prepared at pH of 7 by fitting Langmuir isotherm model with sorption capacity of 346 mg/g at 30 °C and the mechanism was well fitted with pseudo-second-order kinetics indicating the coexistence of both physisorption and chemisorption. Around 99% of removal was reported with this composite indicating the excellency of prepared material for lead removal.

4.2 For Dye Removal

With the fast development of industry, water pollution has become a leading global risk factor for human health [14]. The disposal of dyes without proper treatment will pollute both surface and groundwater as they are non-biodegradable and it will disrupt the growth of living organisms thereby causing illness, disease, and even human death. Some of the commonly reported dyes include methylene blue, bromophenol blue dye, congo red, methylene violet etc.

Liu et al. [57] developed a composite bead with the combination of carboxymethyl cellulose/k-carrageenan/activated montmorillonite for removing cationic methylene blue dye and reported the extent of adsorption by studying its kinetics and isotherms. The composite optimum ratio was found to be 1:1:0.4 for CMC:kC:AMMT with the removal rate of 98% of dye and follows Langmuir isotherm (R^2 0.999) fitted with pseudo-second-order kinetics. Fabryanty and his workers [34] prepared clay based composite using bentonite, alginate in three different compositions. These composites were tested for the removal of crystal violet dye using batch adsorption study. The adsorption of crystal violet dye by composite follows both Langmuir (q_{\max} 601.9339 mg/g) and Freundlich (K_f 36.3399 (mg/g)(L/mg)⁻ⁿ) model and the kinetic was well fitted with

pseudo-second-order getting higher R^2 value of 0.9916 and reported the adsorption of dye by composite was controlled by chemisorption.

A composite bead of Chitosan/KSF-montmorillonite of weight ratio 1–25% w/w was reported recently by Pereira and his coworkers [70]. The adsorption capacity of the composite was tested by evaluating removal of remazol blue dye under batch operations by varying parameters: pH (2–8), contact time (0–660 min) and dye concentration (100–1600 mg L⁻¹). The results revealed effective removal of dye onto composite by following Langmuir model suggesting monolayer adsorption of dye onto composite. Uyar et al. [84] have successfully removed methylene blue dye using a composite of alginate–clay quasi-cryogel beads. They developed this composite by following a novel technique of cryogelation by deep-freezing the alginate beads at -21 °C. The removal of dye was conducted using batch adsorption method and adsorption of methylene blue follows endothermic physical adsorption and well fitted with pseudo second-order kinetics.

Azha and his research group [8] reported industrial dye removal using composite prepared by coating commercial grade acrylic polymer emulsion (APE) and bentonite on cotton cellulosic fiber (CCF). This composite was effective to remove around 95% of cationic dye pollutant within 30 min by following pseudo-second-order kinetics. Hossein and Neda [42] developed hydrogel nanocomposite of acrylic acid and 2-acrylamido-2-methylpropane sulfonic acid monomers in presence of montmorillonite (MMT) by using ammonium persulfate as an initiator and methylene bisacrylamide as a crosslinker. The prepared composite was tested for methylene blue dye adsorption by varying the parameters of agitation time, MMT content, pH, initial dye concentration, adsorbent dose, and temperature. The sorption of dye will fit well with Redlich–Peterson model with the kinetic of pseudo-second-order.

El-Zahhar et al. [32] prepared polymeric clay nanocomposite was prepared using in situ polymerization by incorporating kaolinite clay into poly(acrylamide co-acrylic acid) with cross-linker. This composite was employed for removal of bromophenol blue (BPB) dye. The sorption study was conducted with the effect of parameters including time of contact, dye concentration and temperature. They reported that the dye removal was fitted with Lagergren (pseudo first order reaction rate) with free energy change (ΔG°) value of -110.323 kJ/mol indicating the feasibility and spontaneous nature of sorption reaction. In another study, El-Zahhar [31] reported polymeric clay nanocomposite of polyacrylonitrile (PAN)-kaolin for the removal of methylene blue dye and chromium from aqueous solution. The adsorption capacity was calculated and reported as 127 mg/g of chromium and 68 mg/g methylene blue dye.

Bhattacharyya and Ray [12] synthesized hydrogel using chitosan and the copolymer of acrylic acid and acrylamide by free radical polymerization. This prepared hydrogel was filled with micro and nano-sized bentonite clay. The removal rate of dyes malachite green and methyl violet from water was reported. The percentage of dye removal was maximum for malachite green. The adsorption data were fitted with 1st and 2nd order kinetics and the combined Langmuir–Freundlich isotherm.

Darei et al. [26] prepared novel thin film composite by coating chitosan/organoclay on commercial polyvinylidene fluoride (PVDF) microfiltration membrane. Two differently modified nanoclay (Cloisite 15A and 30B) were introduced into chitosan aqueous solution with varying content ranged between 0.5 and 2 wt% in final dope solution. The prepared membranes were evaluated for dye removal and the results reported were as follows: (a) Membrane coated with Cloisite 15A/chitosan was more efficient for methylene blue removal from water. (b) Membrane-coated with Cloisite 30B/chitosan was effective for acidic orange 7 dye at acidic pHs. Anirudhan et al. [7] removed cationic dyes such as malachite green (MG), methylene blue (MB) and crystal violet (CV) from aqueous solutions at pH of 4.8 using nanocomposite of immobilized-amine-modified bentonite–polyacrylamide (HA-Am-Bent–PAA) nanocomposite. The removal rate was reported as 98% for malachite green, 97% for methylene blue and 94% for crystal violet. Saravanan et al. [76] have synthesized blend using chitin, bentonite clay and the resulted blend was crosslinked with glutaraldehyde. The blend was employed to remove heavy metals copper and chromium from dye effluent collected from Ambur industrial, India. The adsorption of both the metal ions follow Freundlich isotherm suggesting this blend is more effective and cost-effective to apply in a large-scale application.

4.3 For General Wastewater Treatment

The disposal of untreated effluent to the environment without proper removal of waste hazardous material will result in contaminating groundwater and various open sources of water such as a lake, pond and river. This will leads to change the colour of water bodies, increase the microbial growth so that these water bodies cannot be used for drinking as well as domestic household purposes. To overcome this issue clay composite were employed and some of the studies were discussed here. Unuabonah et al. [83] have prepared chitosan modified hybrid clay composite by combining clay, chitosan, $ZnCl_2$ and commercial Alum. This composite was applied for microbial removal from contaminated water. Within reasonable time complete adsorption of bacteria was reported. Anionic micropollutants from wastewater effluent were removed by treating them with composite prepared from quarternized polyvinylpyridinium-co-styrene (QPVPcS) to montmorillonite (MMT). Diclofenac (anionic pollutant) was effectively removed by the composite and filtration process was carried out by column study. The kinetic and the adsorption at equilibrium of diclofenac to composite was calculated using Langmuir equation. The results indicate effective removal was attained by the composite [49]. A similar micropollutant removal of diazinon was demonstrated by protonated poly (4-vinyl-pyridine-co-styrene) (HPVPcoS) and montmorillonite (MMT) clay using column study. This composite was able to remove with the efficiency of 100% having values of affinity and capacity coefficients K_L 5.6×10^4 L/mol and Q_{max} of 5.8×10^{-4} mol/g respectively [79].

An interesting composite material prepared using in situ polymerization was reported by Bunhu et al. [20]. Lignocellulose-clay nanocomposites were prepared by Bunhu and his group by varying the weight ratio of montmorillonite clay to lignocellulose ranged from 1:9 to 1:1 by grafting them with a novel combination of Poly(methyl methacrylate), Polymethacryloxypropyltrimethoxysilane and Poly(methacrylic acid). All these monomers were coupled with lignocellulose and clay. The presence of clay will increase the thermal stability of composite and they suggest it was highly suitable for wastewater treatment in future studies.

5 Future Challenges

Like most of the newly emerging disciplines, the area of research dealing with polymer-clay nanocomposite also has opportunities and challenges. The most difficult task for researchers to deal with polymer clay nanocomposite was not only to prepare them with superior performance but also to check biocompatible nature of the resulting material as it should possess acceptable biological function. In general, polymer nanocomposite with nontoxic performance in vitro may not necessary to perform biocompatible in vivo. Hence on developing clay reinforced polymer composite for biomedical application includes necessary requirement to succeed both in vitro as well as in vivo. Another interesting challenge for researchers to deal with polymer-clay nanocomposite was to understand the fundamental interactions between the polymer matrix and inorganic clay filler as it plays a primary role in controlling the structure-property relationship.

6 Conclusion

We hope this chapter was informative and useful for the researchers who want to use clay minerals in combination with polymer as potential adsorbent and as effective material to apply in various biomedical applications. We have discussed more recent papers which will highlight the advancement of clay based composites in both medical and non-medical field. As stated in the introduction, these materials have likely been in use for quite some time already, but as the chemist and materials scientist become better at designing the system through fundamentals, new products and applications utilizing this technology will grow in number and capability. Though an attempt to address the health and environmental application of polymeric clay composites has been taken in this chapter, there is yet lot more to be done in this field. We address the future challenges in this chapter hence it was necessary to provide continuous effort on the theoretical as well as applied work of modified clay based polymer nanocomposites globally both in academia and industry.

References

1. Abdeen R, Salahuddin N (2013) Modified chitosan-clay nanocomposite as a drug delivery system intercalation and in vitro release of ibuprofen. *J Chem* 2013:1–9
2. Afsar HA, Ghaee A (2016) Preparation of aminated chitosan/alginate scaffold containing halloysite nanotubes with improved cell attachment. *Carbohydr Polym* 151:1120–1131
3. Aguzzi C, Cerezo P, Viseras C, Caramella C (2007) Use of clays as drug delivery systems: possibilities and limitations. *Appl Clay Sci* 36(1–3):22–36
4. Ahmad R, Hasan I (2017) L-methionine montmorillonite encapsulated guar gum-g-polyacrylonitrile copolymer hybrid nanocomposite for removal of heavy metals. *Groundwater Sustain Develop* 5:75–84
5. Ahsan SM, Thomas M, Reddy KK, Sooraparaju SG, Asthana A, Bhatnagar I (2018) Chitosan as biomaterial in drug delivery and tissue engineering. *Int J Biol Macromol* 110:97–109
6. Ambrogi V, Pietrella D, Nocchetti M, Casagrande S, Moretti V, De Marco S, Ricci M (2017) Montmorillonite-chitosan-chlorhexidine composite films with antibiofilm activity and improved cytotoxicity for wound dressing. *J Colloid Interface Sci* 491:265–272
7. Anirudhan TS, Suchithra PS, Radhakrishnan PG (2009) Synthesis and characterization of humic acid immobilized-polymer/bentonite composite and their ability to adsorb basic dyes from aqueous solutions. *Appl Clay Sci* 43:336–342
8. Azha SF, Shahadat M, Ismail S (2017) Acrylic polymer emulsion supported bentonite clay coating for the analysis of industrial dye. *Dyes Pigm* 145:550–560
9. Barlas FB, AgSelecı D, Ozkan M, Demir B, Selecı M, Aydin M, Tasdelen MA, Zareie HM, Timur S, Ozcelik S, Yagci Y (2014) Folic acid modified clay/polymer nanocomposites for selective cell adhesion. *J Mater Chem B* 2:6412–6421
10. Bera H, Reddyppaguntı S, Kumar S, Vangala P (2017) Core-shell alginate-ghatti gum modified montmorillonite composite matrices for stomach-specific flurbiprofen delivery. *Mater Sci Eng, C* 76:715–726
11. Besombes J-L, Cosnier S, Labbe P, Reverdy G (1995) Improvement of the analytical characteristics of an enzyme electrode for free and total cholesterol via laponite clay additives. *Anal Chim Acta* 317(1–3):275–280
12. Bhattacharyya R, Ray SK (2014) Micro- and nano-sized bentonite filled composite superabsorbents of chitosan and acrylic copolymer for removal of synthetic dyes from water. *Appl Clay Sci* 101:510–520
13. Bhowmick A, Banerjee SL, Pramanik N, Jana P, Gnanamani A, Das M, Paban Kundu P (2018) Organically modified clay supported chitosan/hydroxyapatite—zinc oxide nanocomposites with enhanced mechanical and biological properties for the application in bone tissue engineering. *Int J Biol Macromol* 106:11–19
14. Bolisetty S, Mezzenga R (2016) Amyloid-carbon hybrid membranes for universal water purification. *Nat Nanotechnol* 11(4):365–371
15. Bonifacio MA, Gentile P, Ferreira AM, Cometa S, De Giglio E (2017) Insight into halloysite nanotubes-loaded gellan gum hydrogels for soft tissue engineering applications. *Carbohydr Polym* 63:280–291
16. Bounabi L, Mokhnachi NB, Haddadine N, Ouazi F, Barille R (2016) Development of poly (2-hydroxyethyl methacrylate)/clay composites as drug delivery systems of paracetamol. *J Drug Deliv Sci Technol* 33:58–65
17. Boyer C, Figureiredo L, Pace R, Lesoeur J, Rouillon T, Visage CL, Tassin JF, Weiss P, Guicheux J, Rethore G (2018) Laponite nanoparticle-associated cellulose as an injectable reinforced interpenetrating network hydrogel for cartilage tissue engineering. *Acta Biomater* 65:112–122
18. Bremere I, Kennedy M, Stikker A, Schippers J (2001) Growth of 200% predicted for desalination in water scarce countries by 2025. *Int Desalination Water Reuse Q* 11(2):7–12
19. Buffa SD, Bonini M, Ridi F, Severi M, Losi P, Volp S, Al Kayal T, Soldani G, Baglioni P (2015) Design and characterization of a composite material based on Sr (II)-loaded clay nanotubes included within a biopolymer matrix. *J Colloid Interface Sci* 448:501–507

20. Bunhu T, Chaukura N, Tichagwa L (2016) Preparation and characterization of polymer-grafted montmorillonite-lignocellulose nanocomposites by in situ intercalative polymerization. *J Appl Chem* 2016:1–8
21. Chang CW, Van Spreuwel A, Zhang C, Varghese S (2010) PEG/clay nanocomposite hydrogel: a mechanically robust tissue engineering scaffold. *Soft Matter* 6(20):5157–5164
22. Chappidi DY, Mills DK (2016) Tissue engineering nanoclay composite scaffolds composed of poly-glycerol sebacate and poly-caprolactone. In: 32nd southern biomedical engineering conference
23. Chiu C-W, Huang T-K, Wang Y-C, Alamani BG, Lin J-J (2014) Intercalation strategies in clay/polymer hybrids. *Prog Polym Sci* 39:443–485
24. Choudhury PR, Mondal P, Majumdar S (2015) Synthesis of bentonite clay based hydroxyapatite nanocomposites cross-linked by glutaraldehyde and optimization by response surface methodology for lead removal from aqueous solution. *RSC Adv* 5:100838–100848
25. Chrzanowski W, Yunsun Kim S, Abou Neel EA (2013) Biomedical applications of clay. *Aust J Chem* 66:1315–1322
26. Darei P, Siavash Madeeni S, Salehi E, Ghaemi N, Ghari HS, Khadivi MA, Rostami E (2013) Novel thin film composite membrane fabricated by mixed matrix nanoclay/chitosan on PVDF microfiltration support: preparation, characterization and performance in dye removal. *J Membr Sci* 436:97–108
27. Dawson JJ, Kanczler JM, Yang XBB, Attard GS, Oreffo ROC (2011) Skeletal regeneration: application of nanotopography and biomaterials for skeletal stem cell based bone repair. *Adv Mater* 23:3304–3308
28. Demir AK, Elcin AE, Elcin YM (2018) Strontium-modified chitosan/montmorillonite composites as bone tissue engineering scaffold. *Mater Sci Eng, C* 89:8–14
29. Devi Nirmla, Dutta Joydeep (2017) Preparation and characterization of chitosan-bentonite nanocomposite films for wound healing application. *Int J Biol Macromol* 104:1897–1904
30. Edathil AA, Pal P, Banat F (2018) Alginate clay hybrid composite adsorbents for the reclamation of industrial lean methyldiethanolamine solutions. *Appl Clay Sci* 156:213–223
31. El-Zahhar AA (2015) A polymer-organoclay nanocomposite for simultaneous removal of Chromium(vi) and organic dyes. *Eur Chem Bull* 4:10–12
32. El-Zahhar AA, Awaad NS, El-Katori E (2014) Removal of bromophenol blue dye from industrial waste water by synthesizing polymer-clay composite. *J Mol Liq* 199:454–461
33. Emre FB, Kesik M, Kanik FE, Akpınar HZ, Alsan-Gurel E, Rossi RM, Toppare L (2015) A benzimidazole-based conducting polymer and a PMMA–clay nanocomposite containing biosensor platform for glucose sensing. *Synth Met* 207:102–109
34. Fabryanty R, Valencia C, Soetaredjo FE, Nyoopturo J, Santoso SP, Kumiawan A, Ju Y-H, Ismadji S (2017) Removal of crystal violet dye by adsorption using bentonite–alginate composite. *J Environ Chem Eng* 5(6):5677–5687
35. Fan L, Zhang J, Wang A (2013) In situ generation of sodium alginate/hydroxyapatite/halloysite nanotubes nanocomposite hydrogel beads as drug-controlled release matrices. *J Mater Chem B* 45:6261–6270
36. Gaharwar AK, Mihaila SM, Swami A, Patel A, Sant S, Reis RL, Marques AP, Gomes ME, Khademhosseini A (2013) Bioactive silicate nanoplatelets for osteogenic differentiation of human mesenchymal stem cells. *Adv Mater* 25(24):3329–3336
37. Gaharwar AK, Kishore V, Rivera C, Bullock W, Wu CJ, Akkus O, Schmidt G (2012) Physically crosslinked nanocomposites from silicate-crosslinked PEO: mechanical properties and osteogenic differentiation of human mesenchymal stem cells. *Macromol Biosci* 12(6):779–793
38. Ghadiri M, Chrzanowski W, Rohanizadeh R (2015) Biomedical applications of cationic clay minerals. *RSC Adv* 5:29467
39. Gunister E, Pestrel D, Unlu CH, Atici O, Gungor N (2007) Synthesis and characterization of chitosan–MMT biocomposite systems. *Carbohydr Polym* 67:358–365

40. Han C, Zhao A, Varughese E, Sahle-Demessie E (2018) Evaluating weathering of food packaging polyethylene-nano-clay composites: release of nanoparticles and their impacts. *NanoImpact* 9:61–71
41. Heydari A, Khoshnood H, Sheibani H, Doostan F (2017) Polymerization of β -cyclodextrin in the presence of bentonite clay to produce polymer nanocomposites for removal of heavy metals from drinking water. *Polym Adv Technol* 28(4):524–532
42. Hossein H, Neda K (2015) Removal of cationic dyes by poly(AA-co-AMPS)/montmorillonite nanocomposite hydrogel. *Desalination Water Treat* 1–12
43. Huang B, Liu M, Zhou C (2017) Chitosan composite hydrogels reinforced with natural clay nanotubes. *Carbohydr Polym* 175:689–698
44. Huang B, Liu M, Long Z, Shen Y, Zhou C (2017) Effects of halloysite nanotubes on physical properties and cytocompatibility of alginate composite hydrogels. *Mater Sci Eng C* 70(1):303–310
45. Jafarbeglou M, Abdouss M, Shoushtari AM, Jafarbeglou M (2016) Clay nanocomposites as engineered drug delivery systems. *RSC Adv* 6:50002–50016
46. Ji L, Qiao W, Zhang Y, Wu H, Miao S, Cheng Z, Gong Q, Liang J, Zhu A (2017) A gelatin composite scaffold strengthened by drug-loaded halloysite nanotubes. *Mater Sci Eng C* 78:362–369
47. Kevadiya BD, Rajkumar S, Bajaj H (2015) Application and evaluation of layered silicate–chitosan composites for site specific delivery of diclofenac. *Biocybernetics Biomed Eng* 35(2):120–127
48. Khilbsuwan R, Siepmann F, Siepmann J, Pongjanyakul T (2017) Chitosan-clay nanocomposite microparticles for controlled drug delivery: effects of the MAS content and TPP crosslinking. *J Drug Deliv Sci Technol* 40:1–10
49. Kohay H, Izbitski A, Mishael YG (2015) Developing polycation-clay sorbents for efficient filtration of diclofenac: effect of dissolved organic matter and comparison to activated carbon. *Environ Sci Technol* 49(15):9280–9288
50. Kohay H, Izbitski A, Mishael YG (2017) PEG-PE/clay composite carriers for doxorubicin: effect of composite structure on release, cell interaction and cytotoxicity. *Acta Biomater* 55:443–454
51. Kotal M, Bhowmick AK (2015) Polymer nanocomposites from modified clays: recent advances and challenges. *Prog Polym Sci* 51:127–187
52. Kurczewska J, Pecyna P, Ratajzak M, Gajecka M, Schroeder G (2017) Halloysite nanotubes as carriers of vancomycin in alginate-based wound dressing. *Saudi Pharm J* 25(6):911–920
53. Lal S, Perwez A, Rizvi MA, Datta M (2017) Design and development of a biocompatible montmorillonite PLGA nanocomposites to evaluate in vitro oral delivery of insulin. *Appl Clay Sci* 147:69–79
54. Langer R, Vacanti JP (1993) Tissue engineering. *Science* 260(5110):920–926
55. Liu M, Dai L, Shi H, Xiong S, Zhou C (2015) In vitro evaluation of alginate/halloysite nanotube composite scaffolds for tissue engineering. *Mater Sci Eng C* 49:700–712
56. Liu M, Zheng H, Chen J, Lim S, Huang J, Zhou C (2016) Chitosan-chitin nanocrystal composite scaffolds for tissue engineering. *Carbohydr Polym* 152:832–840
57. Liu C, Omer AM, Ouyan X (2018) Adsorptive removal of cationic methylene blue dye using carboxymethyl cellulose/k-carrageenan/activated montmorillonite composite beads: isotherm and kinetic studies. *Int J Biol Macromol* 106:823–833
58. Lundin JG, McGann CL, Daniels GC, Streifel BC, Wynne JH (2017) Hemostatic kaolin-polyurethane foam composites for multifunctional wound dressing applications. *Mater Sci Eng C* 79:702–709
59. Madusanka N, Nalin de Silva KM, Amaratunga G (2015) A curcumin activated carboxymethyl cellulose–montmorillonite clay nanocomposite having enhanced curcumin release in aqueous media. *Carbohydr Polym* 134:695–699
60. Mallouk TE, Gavin JA (1998) Molecular recognition in lamellar solids and thin-films. *Acc Chem Res* 31(5):209–217

61. Massaro M, Colletti CG, Noto R, Riela S, Poma P, Guernelli S, Parisi F, Milioto S, Lazzara G (2015) Pharmaceutical properties of supramolecular assembly of co-loaded cardanol/triazole-halloysite systems. *Int J Pharm* 478:476–485
62. Nair BP, Sindhu M, Nair PD (2016) Polycaprolactone-laponite composite scaffold releasing strontium ranelate for bone tissue engineering applications. *Colloids Surf B* 143:423–430
63. Naumenko EA, Guryanov ID, Yendluri R, Lvov YM, Fakhrollin RF (2016) Clay nanotube—biopolymer composite scaffolds for tissue engineering. *Nanoscale* 8:7257–7271
64. Nistor MT, Vasile C, Chiriac AP (2015) Hybrid collagen-based hydrogels with embedded montmorillonite nanoparticles. *Mater Sci Eng C* 53:212–221
65. Noori MK, Hassan ZM (2015) Nanoclay enhanced the mechanical properties of Poly(Vinyl Alcohol)/Chitosan/Montmorillonite nanocomposite hydrogel as wound dressing. *Procedia Mater Sci* 11:152–156
66. Olad A, Azhar FF (2014) The synergetic effect of bioactive ceramic and nanoclay on the properties of chitosan–gelatin/nanohydroxyapatite–montmorillonite scaffold for bone tissue engineering. *Ceram Int* 40(7):10061–10072
67. Onyango MS, Mbakop S, Leswif TY, Mthombeni NH, Setshedi K (2016) Application of polymer-natural clay composite in water treatment. In: *Proceedings of the 2016 annual conference on sustainable research and innovation*
68. Park JK, Choy YB, Oh JM, Kim JY, Hwang SJ, Choy JH (2008) Controlled release of donepezil intercalated in smectite clays. *Int J Pharm* 359:198–204
69. Perez CJ, Alvarez VA, Vazquez A (2008) Creep behavior of layered silicate/starch-polycaprolactone blends nanocomposites. *Mater Sci Eng A* 480:259–265
70. Pereira FAR, Sousa KS, Cavalcanti GRS, Franca DB, Quieroga LNF, Santos IMG, Fonseca MG, Jaber M (2017) Green biosorbents based on chitosan-montmorillonite beads for anionic dye removal. *J Environ Chem Eng* 5(4):3309–3318
71. Piri S, Zanjani ZA, Piri F, Zamani A, Yaftian M, Davari M (2016) Potential of polyaniline modified clay nanocomposite as a selective decontamination adsorbent for Pb(II) ions from contaminated waters; kinetics and thermodynamic study. *J Environ Health Sci Eng* 14:1–20
72. Rafiei HR, Shirvani M, Ogunseitan OA (2016) Removal of lead from aqueous solutions by a poly(acrylic acid)/bentonite nanocomposite. *Appl Water Sci* 6(4):331–338
73. Sabbagh N, Akbari A, Arsalani N, Eftekhari-Sis B, Hamishekar H (2017) Halloysite-based hybrid bionanocomposite hydrogels as potential drug delivery systems. *Appl Clay Sci* 148:48–55
74. Salcedo I, Sandri G, Aguzzi C, Bonferoni C, Cerezo P, Sanchez-Espejo P, Viseras C (2014) Intestinal permeability of oxytetracycline from chitosan-montmorillonite nanocomposites. *Colloids Surf B* 117:441–448
75. Samani F, Kokabi M, Soleimani M, Valojerdi MR (2010) Fabrication and Characterization of electrospun fibrous nanocomposite scaffolds based on poly(lactide-co-glycolide)/poly(vinyl alcohol) blends. *Polym Int* 59:901–909
76. Saravanan D, Hemalatha R, Sudha PN (2011) Synthesis and characterization of crosslinked chitin/bentonite polymer blend and adsorption studies of Cu (II) and Cr (VI) on chitin
77. Sarfraz A, Warsi MF, Sarwar MI, Ishaq M (2012) Improvement in tensile properties of PVC-montmorillonite nanocomposites through controlled uniaxial stretching. *Bull Mater Sci* 35(4):539–544
78. Sarkar T, Narayanan N, Solanki PR (2017) Polymer-clay nanocomposite-based acetylcholine esterase biosensor for organophosphorous pesticide detection. *Int J Environ Res* 11(5–6):591–601
79. Shabtai IA, Mishael YG (2017) Catalytic polymer-clay composite for enhanced removal and degradation of diazinon. *J Hazard Mater* 335:135–142
80. Sirousazar M, Jahani-Javanmardi A, Kheiri F, Hassan ZM (2016) In vitro and in vivo assays on egg white/polyvinyl alcohol/clay nanocomposite hydrogel wound dressings. *J Biomater Sci* 1–30
81. Styan KE, Martin DJ, Poole-Warren LA (2008) In vitro fibroblast response to polyurethane organosilicate nanocomposites. *J Biomed Mater Res A* 86(3):571–582

82. Tiggemann HM, Tomacheski D, Celso F, Ribeiro VF, Bachtigall SMB (2013) Use of wollastonite in a thermoplastic elastomer composition. *Polym Testing* 32(8):1373–1378
83. Unuabonah EI, Adewuyi A, Kolawole MO, Omorogie MO, Olatunde OC (2017) Disinfection of water with new chitosan-modified hybrid clay composite adsorbent. *Heliyon* 3(8):e00379
84. Uyar G, Kaygusuz H, Erim FB (2016) Methylene blue removal by alginate–clay quasi-cryogel beads. *React Funct Polym* 106:1–7
85. Viseras C, Cerezo P, Sanchez R, Salcedo I, Aguzzi C (2010) Current challenges in clay minerals for drug delivery. *Appl Clay Sci* 48:291–295
86. Viseras C, Aguzzi C, Cerezo P, Bedmar MC (2008) Biopolymer–clay nanocomposites for controlled drug delivery. *Mater Sci Technol* 24(9):1020–1026
87. Vyas V, Kaur T, Thirugnanam A (2017) Chitosan composite three dimensional macro-spheric scaffolds for bone tissue engineering. *Int J Biol Macromol* 104:1946–1954
88. Wu T-M, Wu C-Y (2006) Biodegradable poly(lactic acid)/chitosan-modified montmorillonite nanocomposites: preparation and characterization. *Polym Degrad Stab* 91:2198–2204
89. Yang C, Xue R, Zhang QS, Yang S, Liu P, Chen L, Wang K, Zhang X, Wei Y (2017) Nanoclay cross-linked semi-IPN silk sericin/poly(NIPAm/LMSH) nanocomposite hydrogel: an outstanding antibacterial wound dressing. *Mater Sci Eng C* 81:303–313
90. Yang J-H, Lee J-H, Ryu H-J, Elzatahry AA, Alothman ZA, Choy J-H (2016) Drug–clay nanohybrids as sustained delivery systems. *Appl Clay Sci* 130:20–32
91. Zanetti M, Lomakin S, Camino G (2000) Polymer layered silicate nanocomposites. *Macromol Mater Eng* 279(1):1–9

Thermal Behaviour and Crystallization of Green Biocomposites



Vasile Cristian Grigoras

List of Abbreviations

APTES	3-aminopropyltriethoxysilane
Ac-CNC	Acetate cellulose nanocrystals
ACNC	Acetylated cellulose nanocrystals
ATBC	Acetyltributyl citrate ATBC
A-sisal	Alkali treated sisal fibers
BC	Bacterial cellulose
BCN	Bacterial nanocellulose
BF	Bamboo fibers
BPU	Biobased polyurethane
CA	Citric acid CA
CE	Cellulose
CF	Cellulose fibers
ChNC	Chitin nanocrystals
CO	Cotton
CNC	Cellulose nanocrystals
CNCSD	Conventional spray dried cellulose nanocrystals
CNCFD	Freeze dried cellulose nanocrystals
C18-g-CNC	Cellulose nanocrystals grafted with long alkyl chain (C18)
CNF	Cellulose nanofibers
CNC-g-PLLA	Poly(L-lactide)-grafted-cellulose nanocrystals
CNW	Cellulose nanowhiskers
C_p	Heat capacity
ΔC_p	Heat capacity step (at glass transition)
ΔE_a	Activation energy
DDMSiCl	<i>N</i> -dodecyldimethylchlorosilane
DMA	Dynamic mechanical analysis
DSC	Differential scanning calorimetry

V. C. Grigoras (✉)

“Petru Poni” Institute of Macromolecular Chemistry, 700487 Iassy, Romania
e-mail: crgrig@icmpp.ro

DTG	Derivative thermogravimetry
DTA	Differential thermal analysis
ENR	Epoxidized natural rubber
EVA	Ethylene vinyl alcohol
GC	Green composite
GLU	Glutaraldehyde
Gly	Glycerol
GTA	Glycerol triacetate
GMA	Glycidyl methacrylate
GPS	3-glycidoxypropyltrimethoxy silane
dH/dt	Enthalpy variation in time
HAik	Alkalinized hemp fibers
HCE	Hydrolysed cellulose
HF	Hemp fibers
HW	Hard wood
ΔH	Enthalpy
ΔH_m	Melting enthalpy
ΔH_c	Crystallization enthalpy
KF	Kenaf fibers
Kraft	Bleached kraft softwood
LA-CNC	Lactate cellulose nanocrystals
LDI	Lysine-based diisocyanate
LDPE	Low density polyethylene
MA	Maleic anhydride
MBC	Modified bamboo cellulose
MC	Microcrystalline cellulose
MFC	Microfibrilated cellulose
MRSF	Modified rice straw fibers
NBSK	Black spruce and northern bleached softwood kraft
ODI	Octadecyl isocyanate
PBA	Poly(butyl acrylate)
PBAT	Poly(butylene adipate-co-terephthalate)
PBI	4-phenylbutyl isocyanate)
PBSu	Poly(butylene succinate)
PCL	Poly(ϵ -caprolactone)
PFA	Polyfurfuril alcohol
PHB	Poly(hydroxy butyrate)
PHBV	Poly(hydroxy butyrate-co-valerate)
PL	Plastified lignin
PLA	Poly(lactic acid)
PLA-g-CNC	Poly(lactic acid)-grafted-cellulose nanocrystals
PLA-g-MA	Poly(lactic acid)-grafted-maleic anhydride)
PLLA	Poly(L-lactide)
PLM	Polarizing light microscopy

PPC	Poly(propylene carbonate)
PP	Poly(propylene)
PP-g-MA	Poly(propylene-grafted-maleic anhydride)
PU	Polyurethane
PVC	Poly(vinyl chloride)
PVA	Poly(vinyl alcohol)
PVAc	Poly(vinyl acetate)
RF	Ramie fibers
RH	Rice husk
RS	Rice straw
SEBS	Styrene-ethylene-butadiene-styrene
SEBS-g-MA	Maleic anhydride-grafted-styrene-ethylene-butadiene-styrene
SCF	Standard size cellulose fibers
SPA	Anhydride plasticized soy protein
S-sisal	Sylane treated sisal fibers
SW	Softwood
TAC	Triacetate citrate TAC
TDI	Toluene isocyanate TDI
TGA	Thermogravimetric analysis
T_c	Crystallization temperature
$T_{c(\text{onset})}$	Crystallization onset temperature
T_{cc}	Cold crystallization temperature
T_g	Glass transition
T_m	Melting temperature
T_m^o	Equilibrium melting point
T_{max}	Temperature of maximum decomposition rate
TPS	Thermoplastic starch
ΔS	Entropy
U-sisal	Untreated sisal fibers
χ_c	Crystallinity index
σ_e	Fold surface free energy

1 Introduction

A general thermal behaviour of the green composites (GCs) can provide important results which if are well understood, represent the key factor in the choice of the material applications range. In this regard, speciality literature discussed most important aspects generally related to the glass transition range, melting or crystallization behaviour of the GC either to the range of temperatures that cause degradation of the organic structure of matrix or natural fillers. Reported literature results show that the temperature generally not only degrades the material structure but affects the most properties of GC, too.

Thermal properties of a GC are commonly determined by the physical and chemical characteristics of main constituents—natural fibers and polymer matrix, but interactions between them represent a decisive role. A gap between the filler and the matrix means that the heat is less conducted through the material, but a good interfacial bonding, as well as a better bonding, is related with a modification of GC thermal properties. An efficient way to improve the physical properties of GC consists in the chemical modification of natural fillers surfaces in order to facilitate interactions at the interface with the polymer matrix [1].

The most important results related to the thermal behaviour of various GCs, available by literature from last years will be reviewed in this chapter. Specifically, the literature data concerned to both on temperature range defined by thermal stability as well as in the temperature range where thermally degradation occurs will be analyzed. The main topics related to the effects of the interface between natural fillers and the polymeric matrix on the thermal behaviour will be highlighted. In this regard, the modifications induced by fillers loading on glass transition, melting and crystallization behaviour on the one hand, as well modifications induced on thermal degradation or on degradation mechanism, on the other hand, will be discussed.

2 Thermal Analysis as an Analytical Method of Green Composites Characterization

Thermal analysis unifies a lot of well-defined experimental procedures and tests; the main purpose of them consist on the qualitative and quantitative evaluation of the major changes induced on physicochemical processes and structure of the material that is subject to a temperature change. Actually, the temperature is known as fundamental state variable parameter that influences chemical reactions, physical properties or structural transformations of a material. Considering this, it can support as a general concept that any scientific and experimental method through which can be measured the effects produced by the temperature variations can be considered as thermal analysis. Thermal properties of a material can be analyzed by several methods, but in this chapter, we refer just to differential scanning calorimetry (DSC) and thermogravimetric analysis (TGA) and derivative mass loss (DTG). For a well understanding of GC thermal behaviour, a short review of these methods will precede the presentation of experimental data.

2.1 Differential Scanning Calorimetry

DSC measures the heat effects associated with phase transitions and chemical reactions function of temperature or time in a dynamic or isothermal program, respectively. In this method (Fig. 1), the heat flow difference between the sample and a reference at the same temperature is recorded as a function of temperature [2].

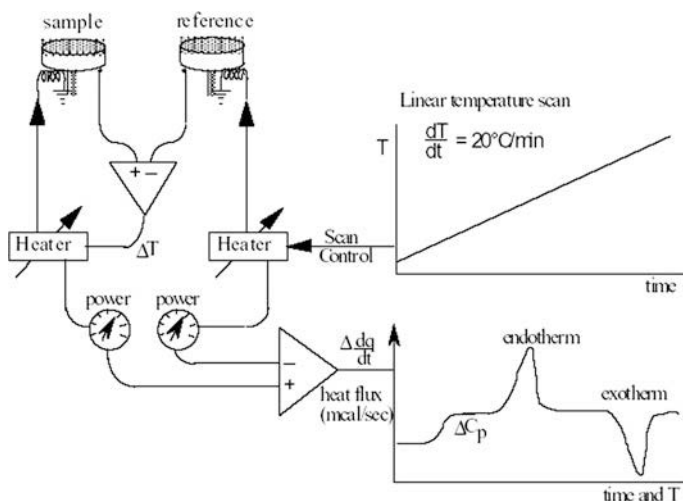


Fig. 1 Schematic representation of DSC physical principle. Adapted from Mathot [2]

The reference is an inert material such as alumina, or just an empty aluminium pan. The physical principle of this method assumes the measuring of the heat flow through material subjected on heating or cooling at a constant rate (in dynamic measurements) or at a constant temperature for a time (in isothermal measurements). In the endothermic process (e.g. most phase transitions), the heat is absorbed and normally the heat flow through the sample is higher compared with the reference: hence enthalpy variation in time (dH/dt) is accepted to have a positive value. The opposite situation happens in the exothermic process where the heat is released and dH/dt is negative as well. Reported papers from the literature that contain data provided by DSC analysis show many results, but the most relevant parameters which intensively discussed and describe a general material thermal behaviour are:

- the temperature for thermal transitions: T_g , T_c , and T_m ;
- enthalpy ΔH and entropy ΔS variation assigned to thermal transition;
- heat capacity C_p and step of the heat capacity at glass transition ΔC_p ;
- crystallinity index: χ_c (%) (assuming that ΔH_m is known);
- heat absorbed or evolved during cure reactions or decomposition process;
- sub-glass or solid state transitions (rarely, but relevant in some studies);
- crystallization kinetics (heat evolved during isothermal crystallization).

Because DSC method is intensively used in calorimetry and polymer science, a series of physical processes and chemical reaction investigated are listed in Table 1 [3].

Table 1 Physical processes in materials evaluated by the DSC method

Process/transition	Exothermal	Endothermal	Parameter
Solid solid transition	▲	▼	T
Glass transition			T, ΔC_p
Crystallization	▲		T_c , ΔH_c
Melting		▼	T_m , ΔH_m
Vaporization		▼	ΔH
Sublimation		▼	ΔH
Adsorbtion	▲		ΔH
Desorbtion		▼	ΔH
Absorbtion		▼	ΔH
Dehydration		▼	ΔH
Solid solid reaction	▲	▼	ΔH
Solid-liquid reaction	▲	▼	ΔH
Solid-gas reaction	▲	▼	ΔH
Oxidative degradation	▲		ΔH
Reduction		▼	ΔH
Oxidation	▲		ΔH
Polymerisation	▲		ΔH
Crosslinking	▲		ΔH
Catalytic reaction	▲		ΔH
Combustion	▲		ΔH

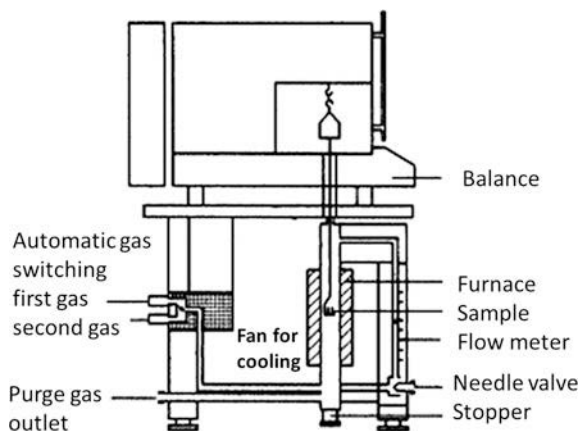
Adapted from Turi [3]

2.2 Thermogravimetric Analysis

The thermogravimetric analysis involves the heating of a sample at a constant rate up to the completed decomposition and monitoring the weight and rate of mass loss function of temperature. It is commonly used to monitor the polymer degradation reactions. TGA only requires a sensitive method for monitoring weight and the sample temperature. Ideally, the sample chamber should have a controllable environment/atmosphere to monitor the degradation process under various conditions (e.g. in the presence of oxygen or under dry nitrogen). The operation principle of TGA instrument is shown in Fig. 2 [3].

In the most accurate TGA experiments, the temperature is set to a constant value and then the sample weight has monitored the function of time. Thus, the results give quantitative information about the rate of composite degradation process at that temperature value. Repeating this experiment for several temperatures will give information about the temperature range under which this material can be used. Usually, these experiments take a long time and useful results have been obtained if the degradation occurs at a slow rate. The sample seems to resist at higher temperatures less than it would actually survive under long-term exposure at lower

Fig. 2 Schematic drawn of TGA instrument. Adapted from Turi [3]



temperatures, thus the results obtained will be very sensitive to scanning rate. The sensitivity is large because degradation rates may be slow compared to typical scanning rates such as 10–20 °C/min. By coupling the degradation products resulted from a TGA experiment to the inlet channel of the other instruments such as a mass spectrometer, infrared spectrometer or to a pyrolysis instrument, the obtained data can be useful in the study of polymer degradation mechanisms. Thus, the coupled instruments help to identify the structure of degradation products. By a combination of the structural information with those provided by kinetics analysis, a complete picture of the degradation process results.

TGA experiments provided valuable results for:

- determination of thermal stability of a composite matrix;
- the compositional analysis of composite;
- study of thermo-oxidative degradation processes;
- determination of volatile products (paraffinic, aromatic, plasticizer, solvents, moisture, cross-linking agents and unreacted accelerators) from composites;
- determination of carbon black content;
- kinetic studies used for assignment of the thermal degradation mechanism of the composite.

The poor thermal resistance of GCs shows significant disadvantages of these materials since, depending on the application, GCs must pass regulatory fire tests. For example, the thermal degradation of natural fibers begins at approximately 200 °C, what substantially limits the number of suitable polymers used as a matrix for GCs fabrication. The thermal properties of a GC are mainly governed by the characteristics of natural fibers, but they are also dependent on the matrix polymer and the interactions between these main constituents. Figure 3 shows the stages of a typical combustion in GCs.

The interface between the matrix and the reinforcement fiber in green composites is responsible not just for mechanical properties, but also for the thermal

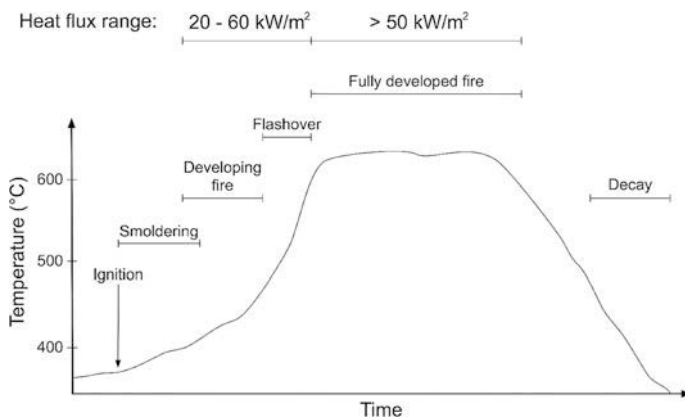


Fig. 3 Stages of combustion in green composites. Reproduced from Väisänen et al. [4]

stability of the material subjected to heat. The thermal stability of composite is enhanced by improving this interface between polymer matrix and fibers, meaning a higher energy is required to separate the constituents. Unlike to this reality, a poor interface in composite decrease the thermal resistance to heat, and finally the thermal stability is reduced [4].

An important issue on thermal degradation of a material consists of the atmosphere which influences the thermogravimetric results leading to a clearly different behaviour. Usually, the experiments can be conducted both in an inert atmosphere (helium or nitrogen) as well as in oxidative atmosphere (air or oxygen). Further, the literature recorded many works in this field that present different results from TGA analysis conducted at different flows of gases (nitrogen). By using an inert atmosphere, results of cellulose thermal degradation showed that the main degradation mechanism (a single DTG peak) was assigned to the formation of macromolecules containing rings with double bonds. When an oxidative atmosphere was used, the main peak in DTG was partially overlapped with the exothermic peak from DTA, assigned to the oxygen reaction with the cellulose. Accordingly, the main DTG peak was shifted to lower temperatures in the oxidative atmosphere as compared to the inert one [5].

3 Glass Transition and Physical Ageing of Green Biocomposites

The glass transition temperature—namely T_g represents the temperature when amorphous (noncrystalline) polymers are converted from a brittle, glass-like form to a rubbery, flexible form.

This is not a true phase transition, but one that involves a change in the local degrees of freedom, assigned to change in heat capacity (C_p) of the composite. Above the glass transition temperature, certain segmental motions of the polymer are comparatively unhindered by the interaction with neighbouring chains. Below the glass transition temperature, such motions are greatly hindered, and the relaxation times associated with these hindered motions are usually long compared to the duration of the experiment. The operative definition of glass transition temperature is that value, with a tolerance of few degrees, to which the specific heat, coefficient of thermal expansion, free volume and the dielectric constant (in the case of a polar polymer) all change rapidly. Since the mechanical behaviour of polymers markedly changes at the glass transition temperature, it is an important characteristic of every polymer. In the DSC experiment, the glass transition shows a step in the baseline, indicating a change in the heat capacity of the composite. No enthalpy is associated with this transition (reason due it is also called second-order transition); therefore, the effect in a DSC curve is slight, but observable and measurable.

A series of factors can affect the behaviour of composites in glass transition region imposed by the chemical structure of polymer matrix (main chain flexibility, stereoregularity, lateral voluminous groups, crosslinking, molecular mass) or by the effects of plasticizers or crystallinity. But a substantial number of relevant works from speciality literature contains interesting results about the interface effects between the polymer matrix and natural fillers on glass transition temperature; therefore we refer to these in the next paragraph.

Recent work recorded the effect of the interface on specific heat capacity and glass transition of poly(butylene succinate)-hemp GCs (PBS-hemp) [6]. Here is highlighted the role of specific intermolecular interactions present at the interface on the values of specific heat capacity data as resulted from DSC. The maximum of derivative of specific heat capacity signal from DSC is assigned to glass transition temperature as is known. In this study, the presence of two amorphous phases—mobile one in bulk and rigid one at interface explained the differences degree mobility of PBS amorphous segments. The rigid amorphous phase limited the relaxation of chain segments inducing a broadening of glass transition region. The effect of oil palm fibers on glass transition temperature of biocomposites was reviewed [7]. A higher content of oil palm in phenol-formaldehyde matrix increased the void formation, facilitating thus the chain mobility at lower temperatures that decreased the glass transition temperature. The opposite effect of oil palm was recorded in the polyurethane-based composites or in polyvinyl chloride (PVC)-epoxidized natural rubber composites, where the glass transition temperature increased with the fiber content. In addition, the chemical treatment (benzoylation) of fibers reduced the glass transition temperature due to a plasticization effect of fibers that diffused or dissolved into the PVC matrix.

Cuinat-Guerraz et al. [8] showed in their work that by a hydrothermal ageing treatment of the bio-epoxy/flax and the polyurethane/flax composites, the glass transition temperature was changed. There was remarked an important reduction of T_g value ($15.1 \pm 3.2\%$) for the bio-epoxy/flax, but smaller one ($10.7 \pm 5.8\%$) for the polyurethane/flax composites. This reduction was explained by authors based

on the water absorption at the interface, which acts as a plasticizer. Once again, the key role played by the interface in the polymeric biocomposites on the relaxation of polymer segments in the matrix was highlighted [9]. They showed that the chemical treatment of ramie fibers at the surface was proven to be effective for the improvement of poly(lactic acid) PLA-ramie composites. In Fig. 4, the results obtained from DSC analysis are presented.

Ramie fibers have surface chemically treated with alkali, 3-aminopropyltriethoxy silane (silane 1) and γ -glycidoxypropyltrimethoxy silane (silane 2). In this way, the interfacial adhesion with PLA matrix was enhanced, resulting in a T_g value increase such that the mechanical properties of composites were improved. In a more recent work same author assigned the decrease of glass transition temperature in PLA matrix-ramie fibers composite with the increase of chains mobility [10]. Authors found that if PLA-g-MA (poly lactic acid-g-maleic anhydride copolymer) was used as the matrix, the chain mobility of PLA molecule was improved, and accordingly, the glass transition shifted to lower temperatures (Fig. 5). More than that, the ramie fibers increased the amorphous fraction in the composite during cooling, due to a decrease of PLA chain regularity by the ramie fibers, which finally reduced crystallization ability. Restriction of PLA chain mobility was highlighted when was studied the PLA-banana fiber biocomposites [11]. Glass transition increased in these materials at lower fiber content, while the increase of fiber loading caused a poor adhesion of banana fiber on PLA matrix.

The most important issue related to the study of the GCs thermal behaviour in the glass transition region is to analyze the effect of various cellulose particles at the

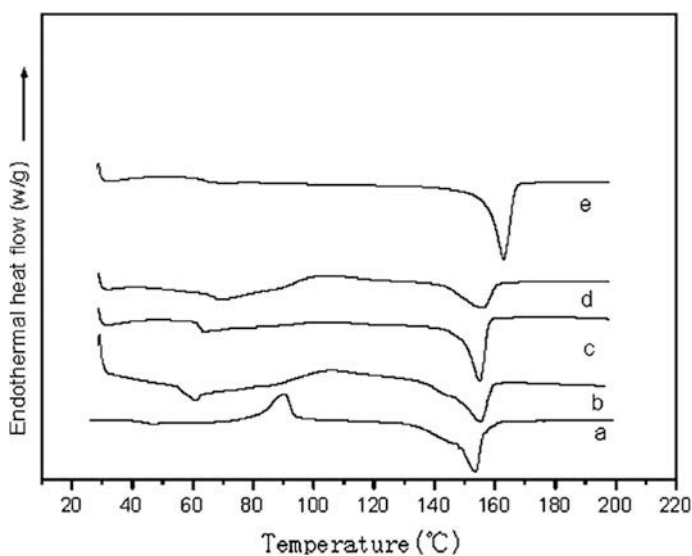


Fig. 4 DSC curves of neat PLA (a) and PLA-ramie fiber composites: untreated (b) and alkali (c), silane 1 (d) or silane 2 (e) respectively. Reproduced from Yu et al. [9]

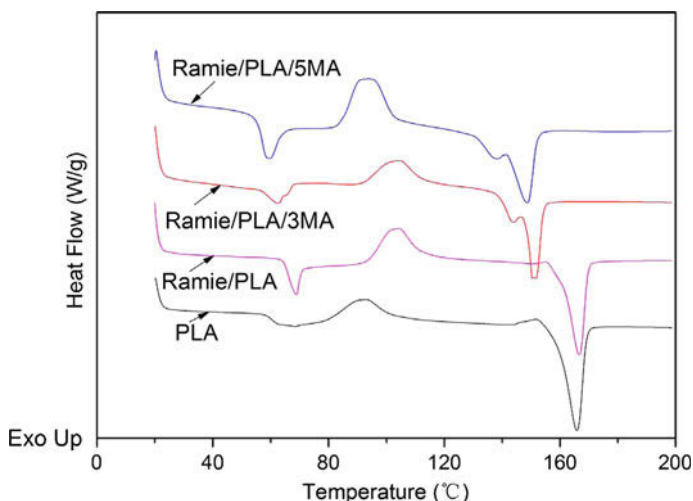


Fig. 5 DSC thermograms of neat PLA, ramie/PLA without and with different MA content. Reproduced from Yu et al. [10]

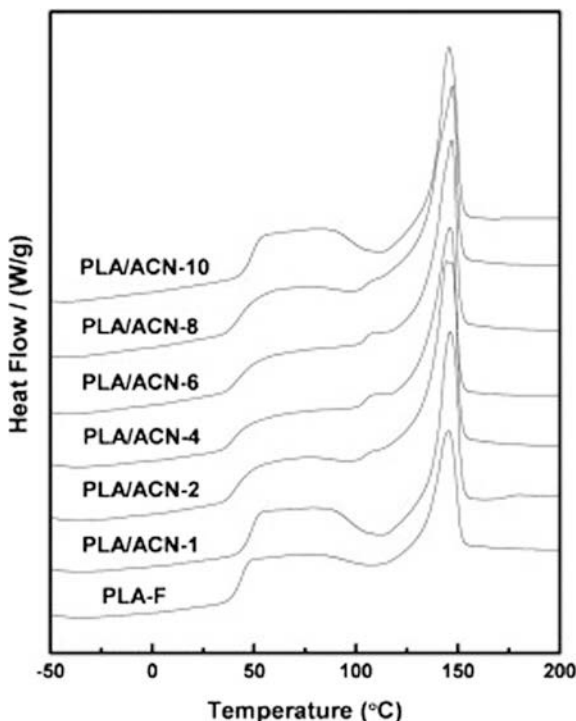
nanoscale range. Different cellulose nanoparticles as nanowhiskers, nanofibers or nanocrystals isolated from various natural fibers, showed an important effect on polymeric matrix chain mobility as literature results related. From these works, only a few most representative were reviewed in this chapter.

Thermal analysis of GCs based on cellulose nanowhiskers (CNW) using PLA as a matrix, was performed [12]. The results provided by DSC analysis showed a slight increase of T_g values for PLA-CNW-S composites (obtained by solution casting technique) compared with T_g values of neat PLA. These findings were explained by the addition of CNW-S that reduced PLA chain flexibility. In addition, the mobility restriction of PLA chains was related to the formation of hydrogen bonds between OH groups of PLA and CNW-S, which increased the energy needed for occurring of glass transition in this material.

Nanocellulose particles isolated from bagasse by acid hydrolysis were used for the preparation of nanocomposite films based both on PVA as well on crosslinked PVA (10% wt. solid PVA) with glyoxal [13]. As expected, the glass transition temperatures in nanocomposites with crosslinked PVA increased due to a restriction imposed by crosslinks of nanocellulose particles.

Cellulose nanocrystals isolated from many natural fibers were inserted into a biodegradable polymer matrix and studied by many authors. A relevant example is a work in which the cellulose nanocrystals extracted from cotton seeds were acetylated [14]. The polylactic acid was reinforced with these acetylated cellulose nanocrystals (ACN) at different contents. For lower ACN contents (up 2%), the glass transition temperature increased as Fig. 6 shown. obtained results were explained by the presence of the interactions between the acetylated surface of cellulose nanocrystals and PLA matrix, which imposed a restriction on the polymer

Fig. 6 The DSC curves of PLA and PLA-ACN nanocomposites contains ACN. Reproduced from Lin et al. [14]



chain mobility. If ACN content increases at 4–6%, a decreasing of glass transition temperatures were explained by means of a high number of interactions between crystalline and amorphous phases from nanocomposite. If a more content of ACN was added in excess (8–10%) to PLA matrix, the self-aggregation occurred between nanofillers such that restrain the PLA chain mobility in the amorphous phase, accordingly the glass transition temperature increased again in these nanocomposites. In case of CG preparation based on cellulose nanocrystals has proven to be a real success by using PLA as a matrix [15]. Here was used the neat and grafted cellulose nanocrystals onto PLLA chains to preparing PLLA-nanocomposites. Thermal behaviour of these materials studied by DSC analysis is shown in Fig. 7. The results denoted that glass transition temperature strongly was decreased (around of 5 °C) in PLLA grafted with cellulose nanocrystals (CNC-g-PLLA). The glass transition increased in PLLA matrix when it was reinforced only with neat cellulose nanocrystals, but much more when PLLA matrix is was reinforced with grafted cellulose nanocrystals. The confinement effect in nanocomposites induced by a very high number of cellulose nanocrystals surfaces was claimed by authors in this study. This effect was countered by the grafting of cellulose nanocrystals which limited the increase of glass transition temperature in PLLA matrix.

The effect of restriction imposed by the cellulose nanocrystals on chain mobility of polypropylene carbonate (PPC) matrix was demonstrated [16]. Data obtained

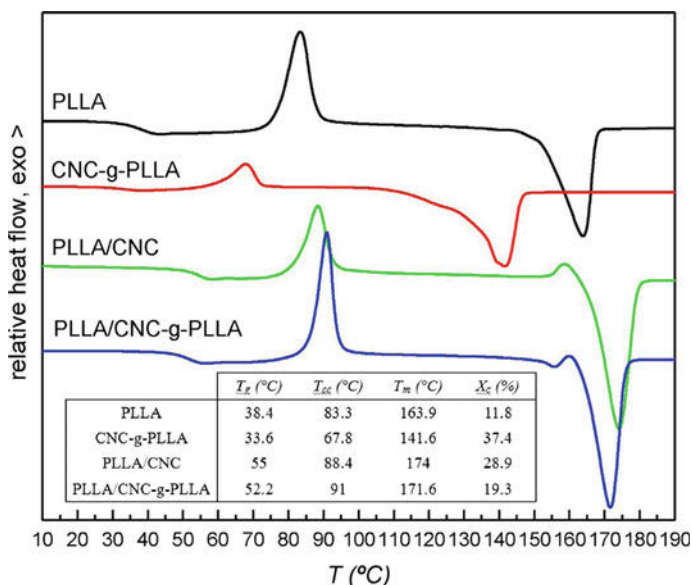


Fig. 7 DSC curves of quenched samples from the melt of PLLA, CNC-g-PLLA nanohybrid, PLLA/CNC nanocomposite and PLLA/CNC-g-PLLA nanocomposite. Reproduced from Lizundia et al. [15]

from DSC analysis and sustained by dynamic mechanical analysis (DMA) results, clearly showed an increase of the glass transition temperature with cellulose nanocrystals content. The thermoplastic and plasticized starch (with glycerol) used as a matrix in the preparation of the CG was reinforced with cellulose nanocrystals extracted from hemp fibers [17]. Heterogeneity of plasticized starch induced a separation between glycerol-rich phases and starch-rich continuous phases, hence the recording a two glass transitions by DSC analysis was expected for these materials. The low glass transition temperature corresponding to glycerol-rich phases (around of -58 °C) did not change with cellulose nanocrystals content on matrix. The intermolecular interactions between starch phases and cellulose nanocrystals limited the starch chain mobility and the glass transition temperature increased from 43.3 to 48.7 °C. Plasticized starch was used also as a matrix for incorporation of cellulose nanocrystals isolated from ramie fibers [18]. The loading of this filler produced the same effect on behaviour in glass transition of the GC: T_g values of rich starch phases increased from 26.8 to 55.7 °C. This result involved the occurrence of intermolecular interactions between starch and stiff cellulose crystallites, which reduced the molecular chains flexibility of starch matrix. In a most recent study [19], the results from thermal analysis of pectin-cellulose nanocrystals films showed that the molecular mobility of amorphous pectin chains did not change by incorporation of cellulose nanocrystals, thus the glass transition temperatures were insignificantly changed.

4 Melting and Crystallization of Green Biocomposites

The interface between natural fillers and different polymer matrix structures represent the most responsible factor in the melting and crystallization behaviour of green biocomposites. A large number of works related to this topic have been reported in the literature (maybe too exceedingly), but here just relevant results from last years were presented. However, in this chapter subsection, many results were considered pertinent for discussing this issue, so these will be presented separately as follows.

4.1 *Effects Induced by Reinforcing of Natural Fibers*

A great influence of natural fibers in the melting and crystallization behaviour of CG is attributed to the interfacial morphology, which has a direct influence on mechanical performances or wettability of the material. Numerous results provided by thermal analysis (in particularly DSC), claims the importance of this interface, confirming the changes in the melting or crystallization behaviour.

From many others natural fibers, bamboo fibers (BF) are a typical case. A comprehensive work reviewed the literature data related to composite loaded with this fiber [20]. Data resulted from DSC analysis of crystallization process in a various polymer matrix, sustained the conclusions that BF acts as nucleation agents even as a source of so call β -nucleators. After chemical treatment of these surface fibers with alkali, new bonds were generated, inducing the improved thermal properties of composites. Thus, the adhesion degree between fibers and matrix was enhanced and the crystallinity degree increase, for example. In the same work, some results were related to the crystallization behaviour: a different temperature of the crystallization peak temperature at a certain cooling rate has been found directly proportional to the content of BF loaded in GC. This remark was assigned to a heterogeneous nucleation effect of BF which increased the crystallization ability of polypropylene (PP) matrix. In the CG based on recycled PP, the melting temperature lightly decreased, but crystallization rate increased less than in neat PP composites. The crystallinity in this matrix was obtained at a lower cooling rate, thus the nucleation role played by fibers has been proved once again. Thermal behaviour of polylactic acid (PLA) and polybutylene succinate (PBSu) matrices reinforced with BF was investigated [21]. Here, the effect of lysine-based diisocyanate (LDI) used as a coupling agent in crystallization and melting of biocomposites was obvious as results presented in Table 2 are shown. Also, the influence of LDI content in composites crystallization temperature and crystallization enthalpy is relevant. Additions of LDI decreased the enthalpy of melting too, but not the melting temperature. Bamboo fibers increased the crystallization temperature meaning that the crystallization rate increased in nonisothermal processes. Actually, the urethane bonds between BF and polymer matrix promoted the

Table 2 Effect of LDI on crystallization and melting behavior of the PLA and PBS/BF (70/30) composites [21]

Sample	LDI content (%)	T_c (°C)	ΔH_c (J/g)	T_m (°C)	ΔH_m (J/g)
PLA	–	112.8	33.2	165.3	41.1
PLA/BF composite	0	115.2	23.5 (33.6)	162.3	27.4 (39.1)
	0.11	118.4	21.5 (30.7)	162.7	23.5 (33.6)
	0.33	118.7	20.2 (28.9)	161.8	23.6 (33.7)
	0.65	119.4	16.4 (23.4)	162.2	23.1 (33.0)
	1.30	120.2	14.5 (20.7)	161.6	22.8 (32.6)
PBS	–	68.1	60.1	112.1	65.3
PBS/BF composite	0	74.6	40.8 (58.2)	112.0	42.3 (60.4)
	0.11	78.0	37.8 (54.0)	112.1	35.8 (51.1)
	0.33	80.2	38.1 (54.4)	112.3	29.4 (42.0)
	0.65	82.2	37.3 (53.3)	112.9	24.5 (35.0)
	1.30	82.6	31.2 (44.6)	112.1	21.7 (31.0)

() Values divided by the weight proportion of polymers

nucleation effect. The crystallization enthalpy decrease involved the limited mobility of polymer matrix chains by LDI addition. The strong interfacial interaction between the polymer matrix and BF yielded a confinement of polymer chain orientation which explained the decrease of melting enthalpy, as authors sustained.

Interesting results were obtained by an extensive study of isothermal crystallization kinetics on bamboo cellulose/poly(ϵ -caprolactone) (MBC/PCL) composites [22]. Data were extracted from differential scanning calorimetry (DSC) study at different crystallization temperatures (T_c). For a detailed patterning of the isothermal crystallization process, it was applied the Avrami model to the data provided from DSC experiments, and parameters describing the isothermal crystallization process were computed. According to the values of these parameters, MBC reduced the crystallization half-time of composites as compared to the crystallization process of neat PCL. This work pointed out the quality of nucleating agent of the MBC fillers in PCL matrix. The *Avrami exponent n* linearly increased with crystallization temperature and recorded values in the range of 1.81–2.70 (most between 2 and 3) for all composites. Actually, these data explained a morphology evolution in these composites: gradual crystals growth from two-dimensional to a spherical three-dimensional one. Effect of the MBC loading consisted of an important increase of the crystallization kinetic constant **K** and improvement of the overall crystallization rate of PCL. These results supporting further the role played by MBC as nucleating agents. Following Hoffman–Weeks theory and after a more DSC data processing, authors of this work provided the values of equilibrium melting point (T_m^0). The results showed an increase of T_m^0 with MBC content in the composites. Based on these results, the values of the spherulite growth rate and folding-surface free energy of PCL/MBC composites have been found. Both parameters values have increased in the presence of MBC, proving the mobility constraints imposed by fibers on the PCL chains in the inter-spherulitic regions.

Thermal behaviour of GCs containing kenaf fibers (KF) was reviewed [23] and in one of the papers presented here, thermal analysis results showed wide endothermic DSC peaks present in the thermograms of the modified kenaf-PLA composites, due to the presence of moisture. Kenaf fibers were chemically treated with silanes, the most effective treatment being with 3-glycidoxypropyltrimethoxy silane (GPS). This has a great effect on the material plasticization, most of the provided data indicating the presence of moisture which reduced the mechanical performances. If observe the data from this work presented in Table 3, the crystallization process as investigated by DSC showed a strong impact of the KF on recrystallization, melting and morphology development.

Data reveal a melting temperature decrease as compared to the blend, but enthalpy values increase according to DSC results. Author remarked the modification of the onset recrystallization temperature with kenaf fiber length, highlighting the effect of fibers loading on crystallization rate increase in the polymer matrix. The non-isothermal crystallization behaviour of PHBV matrix in kenaf fiber composite model, bulk and compatible PHBV (with maleic anhydride) was investigated [24]. Data analysis resulted from DSC analysis followed the kinetic models of Avrami, Jeziorny, and Mo's analysis as well as Kissinger approach. Based on Avrami analysis, the author concluded that KF and the introduction of maleate groups onto PHBV chains did not significantly affect the crystallization kinetics of PHBV matrix in the model, bulk and compatibilized systems. Neither the processing conditions (for example different cooling rates at 20–5 °C/min), practically did not have an important influence on the crystallization process. The approximate crystallization behaviour of polymer resin in model and bulk composites could be considered as an important result in composite processing. Relevant results were obtained when the crystallization behaviour of poly(L-lactic acid) PLLA based composites prepared with KF, rice straw (RS) and two pigments was investigated [25]. This study revealed the importance of these fillers in nucleation ability of PLLA matrix in the composites. Cooling from the melt at 10 °C/min of neat PLLA induced a consistent amorphous phase. Instead, the crystallinity index increased in a composite containing KF, but much more in those containing RS in same conditions. The data resulted from analysis of the isothermal crystallization showed that all samples had a maximum rate of crystallization around of 105 °C. This rate was found about three times faster for the composite containing only KF, KF with red pigment and RS, compared with those containing neat PLLA. Both the

Table 3 DSC data for PLA-kenaf fiber composites [23]

Sample	T _g (°C)	T _m (°C)	ΔH _m (J/g)	X _c
PLA	60	160.3	–	–
PLA:Kenaf (5:5)	56.9	164.2	19.2	20.5
PLA:Kenaf (5:5) GPS (1%)	58.7	168.6	22.8	24.3
PLA:Kenaf (5:5) GPS (3%)	59.3	168.1	23.1	24.6
PLA:Kenaf (5:5) GPS (5%)	59.1	167.3	23.3	24.9

heterogeneous nucleation as well as tri-dimensional spherulitic growth rate increased the value of *Avrami exponent n* (at 3.1) for sample PLLA-RS-yellow. An interesting behaviour was observed on subsequent heating after isothermal crystallization of the samples. The analysis of melting temperatures and crystallinity as a function of T_c showed three distinct regions corresponding to the values around 90, 110 and 130 °C, respectively. There was involved a reorganization of PLLA chains during the melting process; the metastable crystals were formed in isothermal process melt and recrystallized into a more stable crystal followed by a melting of the latter. In another work, thermal behaviour of composites consisting of polylactic acid—modified rice straw fibers (PLA-MRSF) and poly-butyl acrylate (PBA) was investigated by DSC analysis [26]. Obtained results support that the presence of PBA increased the cold crystallization temperature (T_{cc}) and reduced the crystallinity in PLA matrix. In addition, the MRSF loading increased the PLA crystallinity matrix. Instead, both T_g and T_m values of composites have not changed as compared with the pure PLA. Accordingly, higher PBA content was not a suitable compatibilizer between PLA and MRSF as this work sustained.

In composites based on polycaprolactone (PCL) containing rice husk (RH), the DSC heating scans show in Fig. 8 a continuous decrease of the melting peak temperature with the increase of RH content [27]. Furthermore, the RH content decreased the crystallinity extent of PCL phase in PCL-RH eco-composites, while the results recorded lower crystallinity index values for all samples compared with the neat PCL. By RH loading in composite, the PCL chains mobility was limited and the packing affected, thus resulting in a less perfect crystalline structure

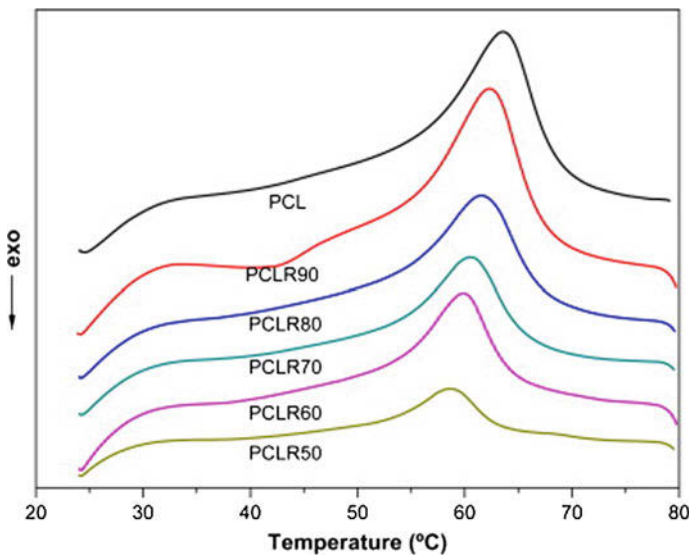


Fig. 8 DSC heating scans at 10 °C/min of PCL/RH eco-composites. Reproduced from Zhao et al. [27]

compared with neat PCL. The conclusion of this work sustained that a reducing of melting temperature and a free volume of PCL phase led to a depression in the crystallinity.

Ramie is another natural fiber used in composite manufacturing. Its content affects the thermal behaviour of melting and crystallization, too. In order to investigate the thermal and mechanical properties, the different content of poly (butylene adipate-co-terephthalate) (PBAT) was incorporated in same PLA matrix [28]. Results show in Fig. 9 a gradual decrease of T_m values and crystallinity index (χ_c) in ramie/PLA composites with PBAT content increasing. This behaviour was caused by a decrease in the PLA molecular chain regularity. In other work, the same author analyzed the effect of ramie fibers on polylactic acid-grafted-maleic anhydride/ramie (PLA-g-MA/ramie) composites [29]. Here, similar results have been obtained, but during the cooling process, the amorphous fraction in the polymer matrix seems to be changed by the ramie fibers. Once more, the decrease of the PLA-g-MA molecular chains regularity and addition of ramie fibers explained the χ_c decrease in ramie-PLA composites.

Coir used as other natural fiber, has an opposite effect in PLA based biocomposites if it is treated in alkali solution (NaOH) [30]. The number of H-bonds on fiber surface has increased by fiber treatment, inducing a better interface and the crystallinity index increased in these materials, which finally improved the mechanical properties. Coir fibers substantially decreased the cold crystallization temperature (T_{cc}) of biocomposites based on PLA matrix, confirming their nucleating agent role, which accelerated the crystallization process in PLA matrix.

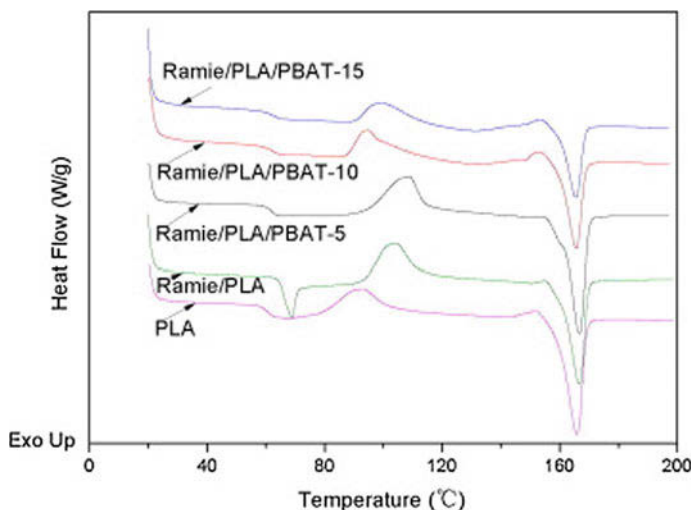


Fig. 9 DSC scans of neat PLA, ramie/PLA without and with different PBAT content. Reproduction from Yu and Li [28]

Some natural fibers like sisal, after a chemical treatment, exhibit transcrystallinity effects on PLA matrix [31]. Both untreated sisal fibers (U-sisal) as well as treated with alkali (A-sisal) and silane (S-sisal) was loaded into PLA matrix for the evaluation of crystallinity and isothermal crystallization behaviour using polarized optical microscopy. Results denoted that all type of sisal fibers had a nucleating ability, influencing transcrystallization in PLA matrix. More than, after computed the interfacial free energy functions for PLA/U-sisal, PLA/A-sisal and PLA/S-sisal composites, author supposed that the difference between these fibers has little or no influence to the nucleation ability in PLA matrix.

Natural fibers extracted from pineapple leaves have proven to be a less efficient filler when was reinforced in neat PP matrix or even in a matrix of PP grafted with maleic anhydride (PP-g-MA) [32]. Thermal analysis performed by DSC revealed a decrease of the composite melting temperature, caused by the interface between fibers and polymer matrix. Further, fibers showed a heterogeneous nucleation effect of the crystallization process, which caused the formation of small size crystals containing defects. Combined with transcrystallinity effects, this is the reason for a limited crystallinity fraction in these materials. The same behaviour was remarked after analyzing the thermal properties of LDPE based composites containing pineapple leaf fibers [33]. The DSC thermograms showed a melting enthalpy decreasing with the fibers incorporation in the LDPE matrix. Sustained by XRD data, these results could be explained by a limited molecular diffusion and finally packing of LDPE chains in the crystal growth process. The crystallinity extent in these composites increased just thanks to the nucleation effect induced by fibers. Slightly higher values of melting enthalpy were obtained for composites containing long fibers as compared with those containing short fibers. Author supposed that the effects of strong the interfacial interaction between thermoplastic matrix and long fiber that confined polymer chain orientation were involved. By comparison, this work concludes that different lengths of fibers did not have an important effect on melting and crystallization of PP matrix.

Recent work presents the behaviour of the GC containing agave fibers in poly-hydroxybutyrate (PHB) and poly-hydroxy butyrate-co-valerate (PHBV) matrix [34]. DSC results showed that the melting temperature did not modify, as well as crystallinity index had a standard deviation less than 5%. Results confirmed that the nucleation was only improved by fibers addition; in the crystallization process, the agave fibers restricted the motion of the chain which should have some effect on overall crystallinity.

Green composites based on PLA matrix filled with fibers extracted from black spruce and northern bleached softwood kraft (NBSK) was obtained through melt compounding and injection [35]. Results denoted again the role of nucleating agents played by cellulosic fibers in the PLA crystallization process.

Investigation of the nonisothermal crystallization kinetic in these composites sustained an increase of crystallization temperature and crystallinity, and a crystallization half-time decrease, as Fig. 10 is shown. Further results relieved the effect of pressurized N₂ gas during DSC analysis which affected the foaming of cellulosic fiber composites based on PLA. A further increase of crystallinity and a

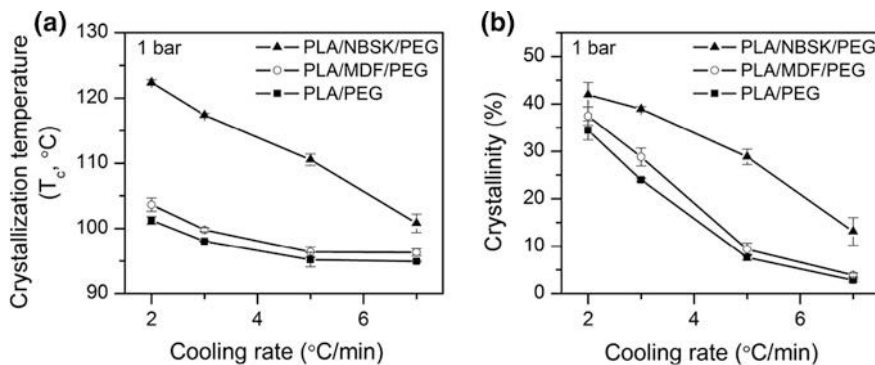


Fig. 10 **a** Crystallization temperature variation and **b** degree of crystallinity of the PLA materials measured at various cooling rates. Reproduced from Ding et al. [35]

morphology improving were observed in these composites, but the N₂ gas had not any effect on crystallization temperature or half-time crystallization.

Nowadays flax fibers are well-known as the most natural technical fibers. Chemical treatment of flax fiber surface increased the interface adhesion with the different biodegradable polymer matrix. For the first time was proceeded to the alkalization of the flax fibers, and then treated with organo silane by an optimized procedure [36]. The significant effects of treated fibers were remarked on cold crystallization process of heating: untreated flax fibers acted as nucleating agents and better promoted cold crystallization upon heating at their surface. By alkalization and organo silane treatment of flax fibers, PLA chains became entangled and covalently bonded over the fiber surface. Thus chains became less mobile to have required mobility on crystallization process, and the kinetic was reduced. The compatibilization of PP matrix by addition of grafted glycidyl methacrylate on PP (PP-g-GMA), the styrene-ethylene-butadiene-styrene block copolymer (SEBS) and SEBS-g-GMA improved the interface between hemp fibers in composites [37]. The melting and crystallization behaviour investigated by DSC analysis denoted a general decrease of PP matrix crystallization temperature with the addition of SEBS copolymers as compared to non-compatibilized PP matrix. Thanks to a poor miscibility with the polyolefin matrix, the segregation of the SEBS on the fiber surface occurred. As a result, a flexible interphase layer around the fibers has been produced, reducing thus the nucleating effect on the PP crystallization as authors sustained. On the contrary, the composite containing PP-g-GMA showed a crystallization temperature similarly to that observed in binary PP-g-GMA/Hemp composites. The interaction between fibers and polymer matrix restricted the chain mobility and a reduction of the dynamic in crystallization process was observed in case of compatibilized systems. Other fibers that do not promote the nucleation in these composites hindered the crystallization due to an induced confinement effect, according to authors.

Soy protein flour plasticized with an anhydride (SPA) was blended with polylactic acid (PLA) in order to obtain an eco-friendly composite [38]. After subjected to a biodegradation process under specific conditions, the thermal behaviour of samples was investigated by DSC analysis. The results showed a compatibilization between SPA and PLA in melt region, SPA acting as a plasticizer in this blend; both the glass transition temperatures and melting temperatures decreased with soy protein content increase. Soy protein incorporation in the blend has an important effect on acceleration of the biodegradation rate of PLA compared with pure PLA. The effect became visible with the increase of the degradation time in soil: the glass transition temperatures increased in the early stages of biodegradation and then decreased. This behaviour could be explained by the amorphous phase decrease in PLA by degradation process, resulting in a crystalline phase increase, as well as rigidity increase. When degradation process was extended for a long time, the raised depolymerisation in the blends reduced glass transition temperatures.

Known as one of the most abundant biodegradable polymer founded in many renewable resources, starch is widely used in preparing the biodegradable materials. PLA is the most efficient biodegradable polymer which can be combined with starch. The thermal behaviour of such material has been reported by a study of the isothermal crystallization kinetics in composites of thermoplastic starch/poly(lactic acid) (TPS/PLA) [39]. (DSC) provided data for samples crystallized at different temperatures (T_c). Following a kinetic-based on the Avrami theory, the process of isothermal crystallization outlined a complete imagining of the crystallization process dynamic. The obtained results from data analysis could be used to compute parameters like the spherulite growth rate, overall crystallization rate, and activation energy (ΔE_a). In case of TPS/PLA composites, the values of these parameters were really affected by the incorporation of TPS. The crystallinity in PLA-based composites was improved by TPS which acts as nucleating agent. The computed values of fold surface free energy (σ_e) according to Lauritzen-Hoffman kinetic theory for PLA blends showed a higher value in blends as compared with neat PLA. This finding was explained by a higher work of chain folding (q) needed in the crystallization process, due to a constraint imposed by TPS on the PLA chain mobility in the composite melt. Later was investigated the crystallization behaviour of thermoplastic starch/poly- ϵ -caprolactone (TPS/PCL) composites by DSC analysis [40]. The no integer values founded for *Avrami exponent* n (between 1.8 and 2.6) showed that TPS acted as a nucleating agent, and the mechanism consisted of a mix of thermal and athermal nucleation processes. However, these processes were followed by a gradual growth of crystals from two to three dimensions. As results showed, the decrease of crystallization rate from Avrami analysis has resulted in a crystallinity index reduction, effect sustained also by XRD data.

Biodegradable PCL has been used to prepare biocomposites by melt-mixing with 5 and 15 wt% of cotton (CO), cellulose (CE) and hydrolyzed-cellulose (HCE) [41]. The purpose was to study the influence of types and content of lignocellulose fillers on the morphology, crystallization behaviour and thermal properties of these biodegradable eco-composites. Obtained results have sustained the decrease of PCL crystallinity for a lower content of CO and CE matrix, while the

HCE content had no effect. By increasing the filler content, the crystallinity degree of the matrix decreased to less extent, regardless of which filler type was used. The calculated values of the theoretical melting point were clearly reduced in these biocomposites and were assigned to heterogeneous nucleation sites occurred at the lower content of CO and CE. Data resulted from crystallization kinetic investigation denoted a reduction of induction and half-crystallization times at low fillers loading, but this effect was attenuated at higher filler contents. Cellulose fibers isolated from hardwood (HW), softwood (SW), and bleached kraft softwood (Kraft) pulp was used in producing and characterization of fully biodegradable natural PLA composites [42]. Thermal behaviour of these materials on heating denoted a general increase of the cold crystallization temperatures (T_{cc}) with the pulp fibers addition as data from Table 4 show. When more fibers were loaded, T_{cc} values decreased, that was explained by the author by a heterogeneous nucleation at lower temperatures induced by pulp fibers in PLA matrix. The double melting peak present in neat PLA became more pregnant after the pulp fibers addition.

Furthermore, pulp fibers promoted the recrystallization at a higher temperature: as data from Table 4 show, the melting enthalpy for all composites increased at the higher temperature as the fiber content increased from 30 to 40% (w/w). Pulp fibers did not increase the maximum crystallinity index in composites despite the nucleation effects induced.

4.2 Effect of Micro and Nanocellulose Loading

Different procedures applied for extraction of cellulose from various natural fibers have allowed being obtained particles with different dimensions and orientation, which once they were loaded in a GC, had a significant effect on crystallization and melting behaviour.

First literature results related to the effect produced by microfibrillated cellulose (MFC) on thermal behaviour of the green composites were reported [43]. In this connection, nanocomposites based on PLA matrix and MFC were prepared in two different states (fully amorphous and crystallized) to investigate the thermal and

Table 4 DSC results of neat PLA and pulp fiber-reinforced PLA composites [42]

Sample	T_g (°C)	T_{cc} (°C)	ΔH_{cc} (J/g)	ΔH_m (J/g)	X_{sample} (%)	X_{max} (%)
PLA	60.7	125.3	35.7	37.0	1.3	39.4
PLAHW30	62.9	121.2	25.8	36.5	0.8	40.5
PLAHW40	62.9	114.0	23.0	23.9	0.9	42.5
PLASW30	62.8	119.1	27.2	27.8	0.7	42.4
PLASW40	63.1	115.5	22.1	22.8	0.8	40.6
PLAKraft30	62.9	112.2	26.1	26.6	0.5	40.5
PLAKraft40	62.8	110.0	22.3	22.7	0.4	40.4

mechanical properties. The presence of MFC accelerated the PLA matrix crystallization as DSC measurements revealed. Results confirmed that the particles of MFC clearly increased the nucleation in PLA matrix, and thus cold crystallization occurred at lower temperatures. The overall crystallinity increased in such composites improved thus their mechanical properties (storage modulus). Soon after this result, the same author prepared composites based on partially crystallized PLA matrix containing MFC, in order to reduce the manufacturing time of PLA parts [44]. Experimental data indicated that by using different annealing times (at 80 °C) has been prepared composites having different crystallinity degree. These results showing actually a possibility of replacing of fully neat crystallized PLA matrix with partially crystallized PLA. Later, MFC has been used to prepare fully biodegradable composites based on polyvinyl alcohol [45]. Thermal behaviour of these materials studied by DSC method indicated an increase of the glass transition temperature along with a reduction of melting temperature and crystallinity due to crosslinking of PVA matrix in MFC-PVA composites. Results showed also that the crystallization process in PVA matrix was prevented by nano- and micro-fibrils of MFC.

Known as efficient nanofiller used in the GCs preparation, cellulose nanowhiskers (CNW) has been isolated from oil palm and then incorporated in PLA matrix at the different content [46]. Addition of CNW in PLA matrix reduced the PLA chains mobility, consequently, glass transition temperature in these nanocomposites slightly increased, as DSC results sustain. On the other hand, CNW induced a decrease of T_{cc} values of PLA-CNW as compared to the neat PLA; this indicated a faster nucleation induced by CNW which acts as a nucleating agent for PLA. Values of melting temperatures slightly increased due to the perfection of crystalline morphology, finally leading to better mechanical performances of these materials.

The effect of cellulose fibers standard size (SF) compared with the cellulose nanofibers (CNF) induced in the crystallization process was established [47]. In this report, after studying isothermal crystallization by optical microscopy of PLA composites, authors did not observe an important effect of SF or CNF particles on crystallization process. Results sustained that spherulites developed in PLA matrix have similar sizes, concluding that CNFs doesn't have influence in the nucleation process. These findings were supported by results obtained from DSC analysis.

Using DSC results, the effect induced by interactions between the cellulose nanofibers (CNF), cellulose nanocrystals (CNC) and PU matrix based on PCL diol, both for the unfilled and filled samples was investigated [48]. Values of melting temperatures, fusion enthalpy and crystallinity index extracted for the unfilled PU film and nanocomposite materials reinforced with CNF or CNC are listed in Table 5. Nucleation effect induced by cellulose nanofillers slightly increased the crystallinity index in all nanocomposites as compared to the neat PU matrix, the effect induced by CNF being stronger. Presence of cellulosic fillers at the higher content (over 5 wt% of CNC and 7.5 wt% of CNF) imbedded the PCL crystallites growth, as result of the crystallinity index decreased in the nanocomposites.

Table 5 DSC data for PU (CNC/CNF) composites [48]

Sample	T_m (°C)	ΔH_m (J/g)	X_c (%)
PU 0%	49.4	60.4	38.5
PU/CNF 2.5%	50.1	63.1	41.7
PU/CNF 5%	52.2	65.2	44.6
PU/CNF 7.5%	50.7	59.3	45.2
PU/CNF 10%	51.0	57.5	40.0
PU/CNC 2.5%	49.0	61.8	40.7
PU/CNC 5%	48.9	64.2	42.9
PU/CNC 7.5%	49.9	57.4	40.2
PU/CNF 10%	50.1	49.8	39.7

A good dispersion and reinforcement of CNF fillers at nanoscale level improved the crystallinity levels in PCL matrix, due to a number of interactions that increased through physical bonding. The numerous hydroxyl groups (OH) on the CNF surfaces interacted with PU chains, providing a higher thermodynamic compatibility between components.

Biodegradable nanocomposites were obtained by loading polylactic acid (PLA) matrix with cellulose nanofibers (CNF) having diameters ranging from 11 to 44 nm [49]. The nanocomposites have been evaluated in detail by DSC analysis. The main purpose of this study was to investigate the influence of treated (with 3-aminopropyltriethoxysilane) and untreated nanofibers on the thermal properties of PLA matrix. Results confirmed that the addition of cellulose nanofibers shifted the cold crystallization peak at lower temperatures and broadened, as compared to the cold crystallization of neat PLA. This finding supported the nucleation role played by cellulose nanofibers (CNF) on PLA crystallization process. Furthermore, the silane treatment of nanofibers shifted to higher values and sharpened the cold crystallization peak of PLA/CNFS, as compared with the neat PLA. The CNF fillers increased the crystallinity index in PLA nanocomposites, but CNFS didn't have the same effect. Silane treatment induced a stronger adhesion between the PLA matrix and the CNFS, thus reducing the crystallization ability at fiber surface. The surface of CNF fibers has been modified by esterification to improve the dispersion and interfacial adhesion with PLA matrix in order to prepare green nanocomposites [50]. Loading of treated CNF in PLA matrix caused a slight increase in glass transition and melting temperatures. However, the nanocomposite films do not show a significant difference in thermal behaviour as compared with unfilled PLA film. Cellulose nanofibers have proven to be more effective when is dispersed in plasticized PLA matrix. Bio-nanocomposites based on CNF and PLA matrix plasticized with glycerol triacetate (GTA) recorded better thermal properties [51]. A visual monitoring of CNF diffusion in the PLA matrix using optical microscopy showed no phase separation occurred in the nanocomposites. A slight decrease in the T_m of PLA matrix, from 174.5 to 169.1 °C resulted due to the addition of 20 wt% of GTA to neat PLA. Thus, GTA plasticized the PLA matrix and increased chain mobility, accordingly the crystallinity index increased from 23 to 60%.

Results sustained that plasticizer and CNF dispersion enhanced the nucleation as well as the crystallization process of PLA matrix. DSC analysis on cooling at 20 °C/min of these nanocomposites highlighted the melt crystallization peak of PLA matrix containing CNF while melting was not visible for plasticized PLA. An opposite behaviour was observed by the further addition of 1 wt% of CNF to the plasticized PLA: crystallinity index of the PLA nanocomposite slightly dropped from approx. 60–55%. This result has been explained rather by an impingement phenomenon in the bulk crystallization process due to CNF than the induced nucleating effect. In another work, the same author prepared GCs based on plasticized PLA matrix with triacetate citrate (TAC) and reinforced with cellulose nanocrystals (CNC) or chitin nanocrystals (ChNC) [52]. The higher aspect ratio of ChNC as compared with CNC explained a high efficiency of these particles in the nucleation and crystallization processes. Accordingly, nanocomposites with better mechanical properties were obtained by using ChNC.

Cellulose nanofibers surface modified with oleic acid have been used for the preparation of nanocomposites based on PLA matrix [53]. Hydroxyl groups substituted by acyl groups on the CNFs surface, esterified CNF increasing thus the nanofibers hydrophobicity such that finally the compatibilization with PLA matrix was improved. Increasing the CNFs content (from 4 to 8%) on PLA matrix enhanced the crystallization process in nanocomposites, as DSC results sustained.

The results confirmed that more dense and perfect crystals had been developed in PLA matrix due to the ability of modified CNFs to modify PLA chain orientation. The regularity needed for crystallization process was increased, more than, a nucleation process induced by these fibers further increased the crystallinity index in these materials. These assumptions were sustained by DSC thermograms on cooling as shown in Fig. 11. The higher content (12%) of modified CNF added to PLA matrix caused fillers agglomeration and viscosity increased during nanocomposites preparation. This obstructed the crystallization process, and crystallinity index in samples decreased again.

Another strategy for preparation of PLA GCs based on nanocellulose fillers consist on the exploitation either the miscibility of the PLA matrix with a PVAc (acting as a dispersion medium for the nanocrystals) and/or the chemical modification of PLA and CNFs by radical grafting with glycidyl methacrylate (GMA) [54]. DSC analysis shows that the phase behaviour and the crystallization process of PLA in composites were clearly affected by the functionalization and the cellulose nanofibers content. The melting temperatures of the nanocomposites decreased with PVAc amount increase and the cold crystallization peak is almost not noticeable, as DSC results confirm. Functionalized CNFs cause the strong interactions at the polymer-filler interface and higher miscibility between PVAc and PLA, preventing the crystallization process in these nanocomposites. Crystallinity index in nanocomposites decreased due to hindrance caused by PVAc chains on nucleation and growth PLA crystals, despite to CNFs added to the matrix. Isothermal DSC thermograms showing a reduction of PLA overall crystallization rate from the melt in the presence of PVAc and CNC.

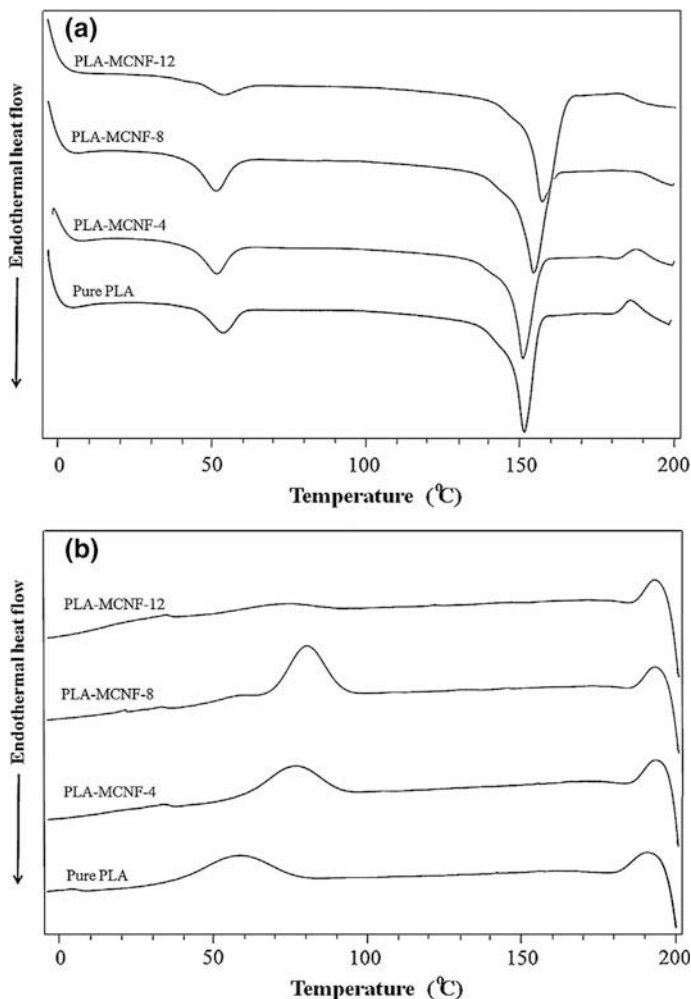


Fig. 11 DSC heating (a) and cooling (b) thermograms of the pure PLA film and PLA–MCNF nanocomposites. Reproduced from Almasi et al. [53]

The crystallization process of PLLA has a special interest in industrial processing; the using of cellulose nanocrystals (CNC) as a bio-based nucleating agent was proved an efficient way. The CNC surface was chemically treated with silane (*n*-dodecyltrimethylchlorosilane) to improve nucleation efficiency of PLLA on both nonisothermal as well as isothermal crystallization [55]. Obtained partial silanized particles (SCNC) had 15 nm width and 200–300 nm length. By addition just of 1% SCNC, the crystallization rate of PLLA was strongly increased, as compared with CNC untreated particles where did not have such strong effects. The highly dispersed treated nanocrystal phase has combined with the larger specific surface

area for crystallite nucleation in PLLA/SCNC composites as compared with PLLA/CNC. The length of cellulose nanocrystals has been reduced by silylation, thus high aspect ratio of nanocrystals has been modified, and nanospheres were obtained instead of rods. This has a real effect on composite structuration at the nanoscale level, significantly improving the crystallinity index and mechanical performances of CG. Valuable results were obtained with CNC modified with long alkyl chain grafted (C18-g-CNC) or PLA grafted with CNC (PLA-g-CNC) [56]. Crystallization behaviour of bio-nanocomposites based on PLA/natural rubber blends filled with unmodified and modified CNC was evaluated. Obtained results showed an influence of the modified CNC on crystallization process, improving the nucleation and increasing cold crystallization temperatures. Natural rubber was proven to have more affinity toward C18-g-CNC as against to PLA-g-CNC, a result which explained the reduction of nucleation efficiency in PLA matrix by C18-g-CNC. The crystals with reduced dimensions were developed, changing thus the nanocomposite morphology, and author reported good mechanical properties. Using hydrolyzed CNCs by treatment with sulfuric acid (CNC-S) and hydrochloric acid (CNC-H), a better dispersion in poly(3-hydroxybutyrate-co-3-hydroxyvalerate) (PHBV) matrix was obtained [57]. Following this way, the reinforcement at nanoscale of PHBV matrix was enhanced by the presence of both types of CNCs particles. Comparing the reinforcing effects, in Fig. 12a DSC results confirmed the stronger effect on PHBV morphology produced by the CNC-H particles, especially at higher content loading (12%). As conclusions of this study sustain, the larger aspect ratio, higher crystallinity and especially no residual acid groups exhibited by CNC-H particles have contributed to the thermal behaviour. The effect was raised by the intermolecular hydrogen bonding interactions, increased on such materials, leading to crystallite perfection, and the crystallization rate increased and finally improved the mechanical properties. Variation of T_c and $T_{c(\text{onset})}$ temperatures with both CNCs shown in Fig. 12b, sustained that in the CNC-H/PHBV nanocomposites higher T_c and the smaller $T_{c(\text{onset})} - T_c$ can be achieved, which means a stronger nucleation effect produced by CNC-H as compared to CNC-S.

Nonisothermal crystallization performed by DSC analysis and isothermal crystallization studied by PLM of PLA nanocomposites loaded with conventional spray-dried CNC (CNCS) and the freeze-dried CNC (CNCFD) were investigated [58]. A better porosity of PLA matrix was obtained by dispersion of the CNCSFD as compared with CNCFD particles. The nucleation effect induced by CNCSFD particles had strong effect on crystalline nucleation and crystallization rates of PLA. Taking into account this result, PLA based composites showing better mechanical performances were obtained if CNCSFD particles were used.

An efficient way to synthesise nanocomposites containing CNCs consisted on in situ ring-opening polymerization of L-lactide in the presence of CNC [59]. Due to the bimodal molecular weight distribution of free PLLA, the CNC-PLLA nanomaterials showed different thermal behaviour, both for glass transition as well as for cold crystallization and melting. Consequently, by blending of CNC-g-PLLA with low molecular weight and free PLLA homopolymer, resulted in a hydrophobic and homogenous material that was not able to develop any crystallinity. Blends of

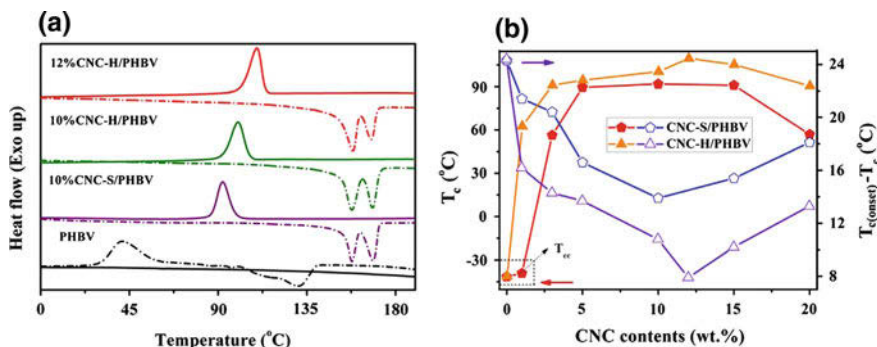


Fig. 12 DSC curves (a), the crystallization temperature (T_c) and $T_{c(\text{onset})} - T_c$ (b) for neat PHBV and the nanocomposites with various CNC contents. Reproduced from Yu et al. [57]

CNC-g-PLLA with higher molecular weights PLLA allowed the crystals growth in these nanocomposites. Thus, T_{cc} and T_m values increased with PLLA molecular weight; nanomaterial containing the highest molecular weight showed the highest crystallinity index as results confirmed.

Addition of CNC modified with surfactants (s-CNC) and silver (Ag) nanoparticles in PLA matrix denoted different thermal behaviour in the PLA-CNC films [60]. An increase in crystallinity index was recorded for nanocomposites containing a binary system of s-CNC-PLA, as thermal analysis showed. The nucleation was enhanced in these nanocomposites by a good dispersion of s-CNC in the polymer matrix as favoured by the presence of a surfactant. Instead, lower crystallinity index resulted in a binary system containing Ag nanoparticles because the nucleation was not improved. The presence of both s-CNC and Ag nanoparticles in PLA matrix didn't improve enough the crystallinity index in the nanocomposites; as expected their mechanical performances were reduced as well.

For the first time, the CNC incorporation in poly(butyleneadipate-terephthalate) pure matrix (PBAT) was studied [61]. Functionalization of CNCs with an aliphatic and aromatic isocyanate (octadecyl and 4-phenylbutyl isocyanate), and then addition to PBAT at 5 or 10% content, yielded nanocomposites having same thermal behaviour. Temperatures of crystallizations from the melt (T_c) increased with treated or untreated CNC amount. Under quiescent conditions, the CNC surfaces acted actually as nucleation centres for PBAT matrix, despite chemical treatment with isocyanates. Just a slow decrease of crystallinity index was observed on nanocomposites samples containing CNCs functionalized with 4-phenyl butyl isocyanate due only to processing technique used, as author sustained.

Interesting results reported in literature highlighted the improving crystallinity in a composite matrix through surface grafting reaction of CNCs with PHBV [62]. Toluene isocyanate (TDI) has been used as a coupling agent in grafting reaction, so by monitoring TDI/PBHV content on copolymers, the length and density of grafted

chains on CNCs surfaces were controlled. Thermal behaviour investigation of grafted CNCs by DSC analysis indicated important differences both on cooling and subsequent second heating, as a function of TDI/PBHV fractions. Results shown in Fig. 13 seem to preserve the initial morphology of PBHV in resulted copolymers.

The changes in crystallization temperatures as well in cold crystallization behaviour became visible for copolymers containing a high density of grafted PHBV chains (PHCN8 and PHCN10 from Fig. 13b). The double melting peak

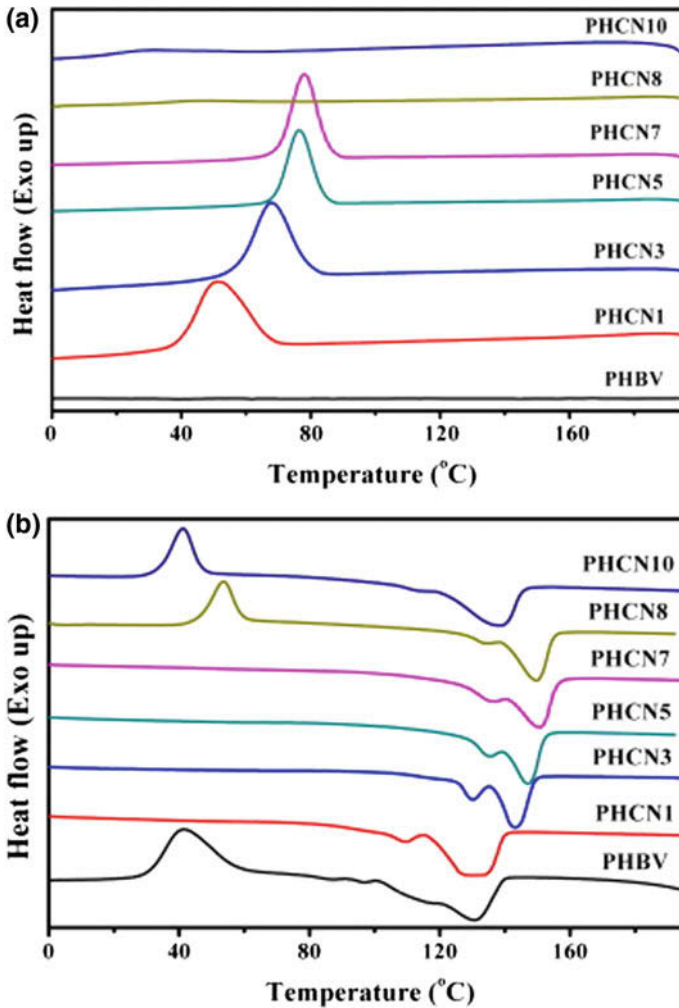


Fig. 13 DSC traces of neat PHBV and the resulting copolymers prepared under various TDI/PBHV fractions obtained during the first cooling (a) and second heating (b) scans at 10 °C/min. Reproduced from Yu and Qin [62]

observed in Fig. 13a in the second heating cycle denoted a possibility of melting transition and the crystallinity control in copolymers by modifying grafting density or side chain lengths of PHBV.

To produce electrospun bionanocomposites films, the PLA-PHB blend was plasticized with acetyltributyl citrate (ATBC) and reinforced with CNCs [63]. Due to the effect of plasticization, PLA-PHB-ATBC matrix showed increased T_{cc} and ΔH_{cc} values as the content of CNCs increased based on the rearrangement of PLA segments during crystallization. Both melting enthalpy, as well as crystallinity index, increased in a sample containing less CNC content (1%) due to a better dispersion of nanoparticles in a composite matrix, which promoted a higher nucleation effect.

Heterogeneous nucleation of CNCs on PHBV matrix changed the crystallization behaviour, implying an increase of T_c values, at lower CNC content [64]. A higher loading of CNCs amount (over 4%) limited the growth of polymer crystals due to an increase of hydrogen bonds formation, which imposed restrictions on PHBV chain mobility. Moreover, if the dispersion of CNCs on PHBV matrix was not homogenous, separate phases resulted, and lowered the composites mechanical performances as expected.

Tuning hydrogen bonds by controlling the number of hydroxyl groups of cellulose nanocrystals so-named cellulose nanocrystals citrate (CN-C) and cellulose nanocrystal formates (CN-F) were obtained [65]. Once reinforced in PBHV matrix, these nanofillers could modify the thermal behaviour of the nanocomposites. Lower values of parameter $T_{c(\text{onset})} - T_c$ extracted from DSC results for PHBV filled with untreated CNCs denoted a greater overall crystallization rate as compared with those filled with CN-C or CN-F particles. This result led to high T_c values observed in case of PHBV filled with untreated CNCs.

5 Thermal Stability and Degradation of Green Composites

Natural fillers generally were very sensitive to temperature changes; the thermal degradation is expected above 400 °C. Excepting volatile or partially stable components (e.g. pectin, waxes, water, soluble substances), for each major component of natural fibers the degradation process will proceed as follows: depending on the presence of an oxidative (air) or inert atmosphere, decomposition of cellulose involves reaction of depolymerization, thermoxidation, dehydration and glycosans formation [5]. Dehydration process occurs in a range of 210–260 °C in a non-oxidative atmosphere, or in range of 160–250 °C in presence of oxygen (or air). The depolymerization and volatilization of glucosans take place at about 310 °C in an inert atmosphere, but maximum rate increases at 350 °C (oxygen) or 375 °C (helium). The hemicellulose components decompose at relatively low temperatures (159–175 °C), this process being preceded by the cellulose

decomposition, but its effect is proportionally limited by the content in the fiber. Instead, lignin decomposition process consists on three steps: below 220–250 °C side chains are broken and split, followed by the formation of free radicals between 300 and 400 °C and a series of condensation reactions above 400 °C.

Understanding of this item has a major importance on the practical application of composites since any mechanical performance was generally altered by temperature increase. Considering that some issues related to the degradation process of natural particles, organic structures may impose limitations on different applications of material obtained. As in precedent section of this chapter, the most important results related to the thermal degradation of GCs from last years reported in the literature will be presented both for natural fibers as well as for cellulose or starch nano-particulate fillers.

5.1 Thermogravimetry of Green Composites Containing Natural Fibers

A considerable number of natural fibers have been used in composite processing, but here will be overviewed only results related to composites containing common natural fibers. For each relevant fiber type used, one paragraph will contain and discussed results provided by one or more works related to this issue.

The TG/DTG analysis of common lingo-cellulose fibers denotes similar results that could be related to the thermal decomposition of their main constituents. As thermogravimetric parameters from Table 6 suggest, the TG curve contains three stages of weight loss: the first one up to about 200 °C, is ascribed to a maximum weight loss of 10%; this step is followed by a second stage up to about 500 °C, where the loss is more than 70 wt%. In the final third stage, about 20 wt% of the mass is a loss, allowing the extending range of TG/DTG test up to 800 °C. The maximum rate of thermal decomposition was displayed in DTG curves as the main peak, while the components of the fibers could have assigned like a shoulder or tail peaks in a DTG curve. The values shown in Table 6 are similar to others reported in the literature for distinct natural fibers but may vary depending on treatments

Table 6 Thermogravimetric parameters of common natural fibers [66]

Natural fiber	1st stage weight loss (%)	1st stage DTG peak (°C)	2nd stage onset T ₀ (°C)	2nd stage weight loss (°C)	2nd stage DTG shoulder (°C)	2nd stage DTG main peak (°C)	2nd stage DTG tail (°C)	3rd stage weight loss (°C)
Jute	8	60	260	89	290	340	470	3
Sisal	9	52	250	76	275	345	465	15
Wood	2	107	290	85	270	367	400	13
Cotton	4	55	265	91	280	330	410	5

applied to the fiber. According to other results, after water loss in the first stage (DTG peak), the thermal degradation of main lignocellulose constituents of the fiber began at the onset of the second stage [66]. The cellulose decomposition was ascribed by the main DTG peak of this stage, while the hemicellulose and the end of lignin decomposition were represented by shoulder peak or by the tail peak, respectively. After the third stage, the residual weight was related to char or to other products resulted during decomposition reactions.

An important standpoint in discussions of related literature results is represented by the effect of different atmospheres on the thermogravimetric analysis of natural fibers. Actually, may be used in two distinct atmospheres, inert (helium and nitrogen) and oxidative (air and oxygen). Moreover, different flows of these gases conduct heat at different rates, such that the thermograms obtained in nitrogen may be significantly different from those obtained in helium. In an inert atmosphere, the thermal degradation of cellulose resulted in the main DTG peak associated with the formation of macromolecules containing rings bearing double bonds [5]. This peak was partially overlapped in an oxidative atmosphere due to oxygen reaction with the cellulose (exothermic peak corresponding to this reaction). Consequently, the main DTG peak was shifted to lower temperatures in that atmosphere as compared to the inert one.

Various thermal behaviours of GCs containing bamboo fibers were related to the assignment of an enhanced degree of adhesion between the matrix and bamboo fibers, because a stronger adhesion meaning a better thermal stability [20]. Biocomposites based on PLA, PBS reinforced with bamboo fiber (BF) were investigated [21]. Results of this study denoted a decrease of thermal degradation temperature of both composites as compared with those of pure polymer matrix. By using lysine-based diisocyanate (LDI) as a coupling agent between fibers and polymers matrixes, the thermal degradation temperature increased in composites. Authors sustained an increase of molecular weight due to crosslinking reactions between PLA or PBS matrix and BF, which could induce an increase of thermal degradation temperatures.

Coir fibers (CF) treated by washing with water, alkali treatment (mercerization) or bleaching filled a blended matrix consisted of starch/ethylene vinyl alcohol copolymers in order to prepare biocomposites [67]. Fibers treatments considerably affected the thermal behaviour, namely increased the thermal degradation temperatures, as TGA data sustained. These modifications were attributed to the removal of some easily hydrolyzed substances, which decomposed earlier than the major components, cellulose, and lignin. This could increase the thermal stability in the second step of degradation process as compared with composites filled with untreated fibers. Interesting results reported on thermal behaviour of PLA based biocomposites containing both untreated as well as alkali treated coir fiber were obtained [30]. By alkalization process, the number of H-bonds at surface increased, improving the adhesion at the interface between coir fibers and PLA matrix. The TGA results, consisting of both TGA and DTG curves, are shown for untreated and treated coir fibers in Figs. 14 and 15 respectively.

The chemical treatment of coir fibers seems to have a significant increase in thermal stability, increasing the maximum degradation temperatures in the composite. Removal of hemicellulose during alkali treatment could explain this finding. Nevertheless, due to the embedding of coir fibers in PLA matrix, the thermal degradation temperatures decreased and the thermal stability of biocomposites decreased irrespective of the fiber treatment as results show on Figs. 14 and 15. The author concluded that fiber loading was responsible for the composite thermal stability decrease, imposed by the lower degradation temperature of coir fibers. The effect of lignin loading in PP/CF composites both on presence as well as in absence

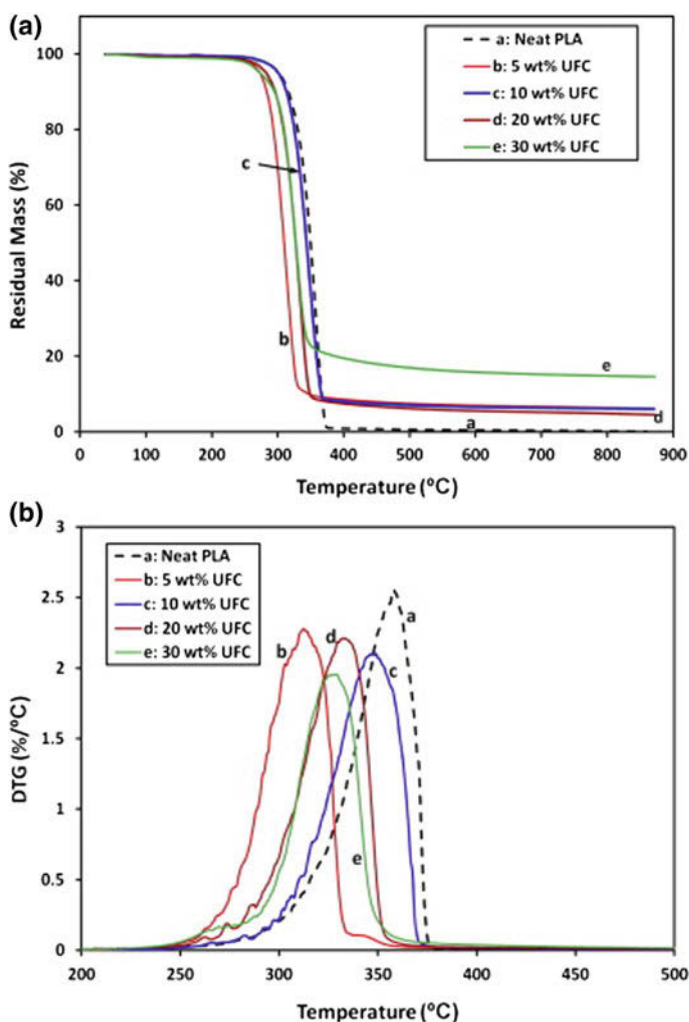


Fig. 14 TGA curves (a) and (b) DTG curves of neat PLA and PLA/UFC (untreated) coir fibre biocomposites. Reproduced from Dong et al. [30]

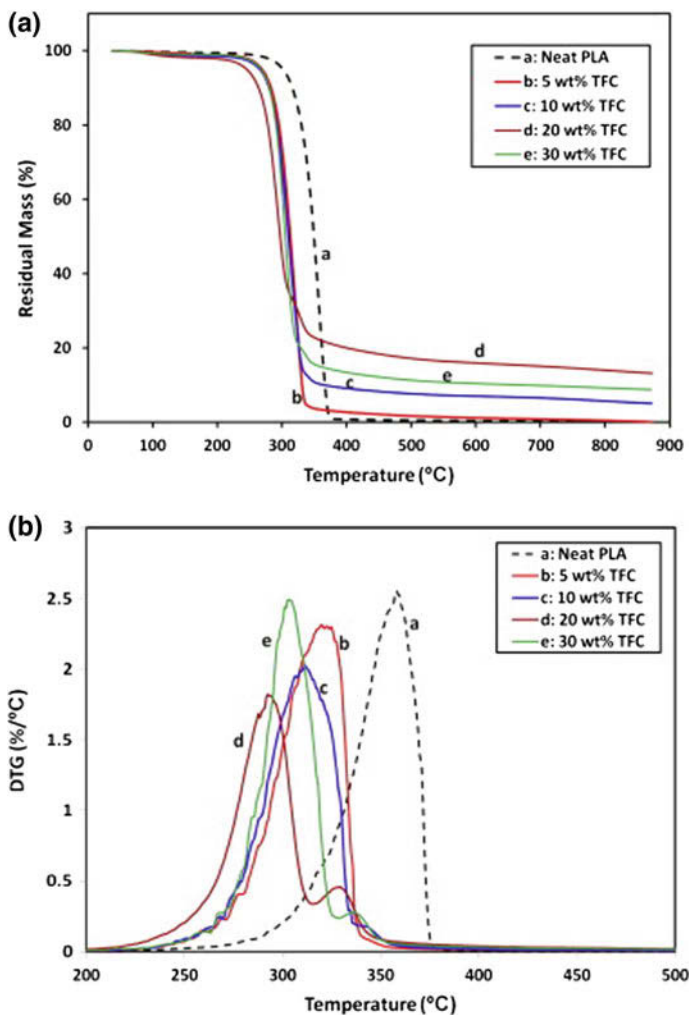


Fig. 15 TGA curves (a) and (b) DTG curves of neat PLA and PLA/TFC (treated) coir fibre biocomposites. Reproduced from Dong et al. [30]

of MA was investigated by DSC and TGA analysis [68]. The results revealed that the incorporation of lignin in composites increased the initial thermal decomposition temperatures and oxidation induction times. Two possible protections played by lignin that delayed mechanism for thermal decomposition process was involved by the author of this work: the role of antioxidant and barrier against thermal degradations.

Matrix-based on polyfurfuryl alcohol (PFA) and plastified lignin (PF) renewable from various biomasses could be an eco-friendly material having good performances for various applications [69]. These two components were blended in two

different ratios, then polymerized and investigated on their behaviour in the thermo-oxidative degradation process; results were compared to those of neat materials. As this work sustained, strong interactions between PL and PFA in the blended matrix acted as protection against chains internal scission and depolymerization during thermal degradation. The neat PL was clearly decomposed at a lower temperature than PFA/PL blend, as results from TG/DTG analysis sustained. Later, PFA bioresin was used as a matrix for preparation of fully green composite containing kenaf fibers (KF) [70]. Thermogravimetric analysis of composites showed a decrease of temperature corresponding to maximum decomposition rate T_{max} (from 466 to 458 °C) with KF content increase from 5 to 20 wt%. This behaviour was explained by increasing of thermally unstable non-cellulosic structures come from the fiber content in GCs. Retention of about 45% char residue at 800 °C was due to a higher thermostability of PFA matrix in the composite.

Thermal stability of composites containing natural fibers increases generally due to a chemical treatment applied to fibers. Waxes and non-cellulosic components were removed from surfaces, increasing thus the interaction with the polymer matrix. Thermogravimetric and pyrolysis analysis investigations bring out such results on KF/epoxy composites containing both treated as well as untreated fibers [71]. By alkalization (with NaOH) of KF, the level of moisture content with 3% decreased, which influenced the weight loss behaviour, as well as their corresponding composites. A high level of moisture content means more voids and hemicelluloses on composites, which increase thermal conductivity with thermal stability decrease. Consequently, by treated KF addition in epoxy composites, the thermal stability of composites has improved as well as its charring capability. The alkalization process reduced the char content after thermal decomposition of these KF/epoxy composites. Loading of composites based on PVC/TPU matrix with KF enhanced their thermal stability, but in composites based on the biodegradable matrix (PLA), KF induced a decrease of thermal degradation temperatures due to PLA depolymerization as in another study was showed [23]. Silanization of KF fibers induced an increase of thermal stability in these composites.

The thermal degradation of GC containing alkalized hemp fibers (HAlk) revealed different behavior when were loaded in the different matrix [72]. The degradation temperature increased from 351 °C in neat PP matrix containing 25 wt % hemp fibers, to 376 °C for PP/HAlk and up to 391 °C for PP-SEBS-g-MA/HAlk. This behavior was explained by the barrier effect induced by hemp fibers against degradation process, which increased in the ternary system due to a better adhesion of interface imposed by MA groups. A different behaviour was reported for composites based on MAPP matrix filled with silane treated hemp fibers, which denoted a decreased thermal stability as compared with those filled with untreated fibers [73]. Results obtained by thermogravimetric analysis sustained decreasing values of the temperature up to 25% at 10% weight loss (T_{10}). The weight loss was less than 2% at 240 °C, due to silane treatment of hemp fibers.

Besides the applications of natural fibers on building structures and automotive area, literature does not report too many results regarding the use of the flax fibers (FF) in GCs processing. A representative study where a green composite based on

bio-based resin reinforced with flax and basalt fibers was investigated [74]. Results from TGA analysis showed a lower thermal stability if it contained neat FF due to a higher amount of lignocellulosic content, as compared to that contained basalt fibers in addition.

Thermal behaviour of PLA composites containing ramie fibers (RF) showed increased values of thermal degradation temperatures if the RF surface was treated as compared with those which was reinforced with untreated RF [9]. Results were explained by the chemical bonds between PLA matrix and ramie fiber after treatment that could enhance the interfacial adhesion. It's worthy to note that the alkali treatment of RF induced lower thermal degradation temperature in composites as compared with the composites with silane-treated fiber. This result revealed a worsening of interface bonds between alkalized RF and PLA composites as compared with the interface of silane treated RF and PLA. Later, it was founded that in case of composites based on PLA matrix reinforced with RF compatibilized with PLA-g-MA [10] or blended with PBAT [28] thermal stability increased.

Microcrystalline cellulose (MCC) renewed from oil-palm biomass has been used as filler for PLA matrix [46]. Results based on TG/DTG data (T_{on} , T_{10} , and T_{50}) showed an improving the thermal stability of PLA/MCC composites compared to pure PLA. Due to an intrinsic flame resistant property, the higher content of cellulose I on MCC was related with the highest char residue (2.4%) displayed for the PLA/MCC 5% composites as compared to pure PLA, or composites containing 1 and 3% MCC. Data from TGA and DTG curves generally denoted a higher thermal stability for all PLA/MCC composites as compared with pure PLA, due to MCC incorporation.

Cassava and pineapple flour have been used as fillers in PLA bio-composites, improving interfacial adhesion when maleated polylactic acid (MAPLA) was added for compatibilization [75]. Both fillers have reduced the degradation temperature of PLA but de-starched cassava flour denoted higher thermal stability due to its higher lignin content compared with pineapple flour. An important result it was that the thermal degradation temperature was increased by adding MAPLA.

Effects of alkaline and silane surface treatments of wheat or rice husk on thermal degradation of PLA biocomposites was observed [76]. Both alkaline treated husks (RA and RG), as well as silane treated husks (RNA and RNG), increased thermal degradation temperatures in composites, due to an increased number of chemical bonds which enhanced interfacial adhesion. As results show in Fig. 16, the PLA biocomposites with untreated husks have lower thermal stability as compared with those filled with treated husks.

However, results from this figure denote lower thermal degradation temperature for GCs containing alkaline treated rice husks as compared with those containing silane treated husks. This study sustained that the interface bonds between alkaline treated husks and PLA were weaker than the interface bonds between silane-treated husks and PLA.

An eco-friendly polymer obtained by graft polymerization of *Hibiscus sabdariffa* fibers on poly butylacrylate (PBA) has thermal behaviour investigated by the thermogravimetric analysis (TGA) [77]. Results showed an increase of the thermal

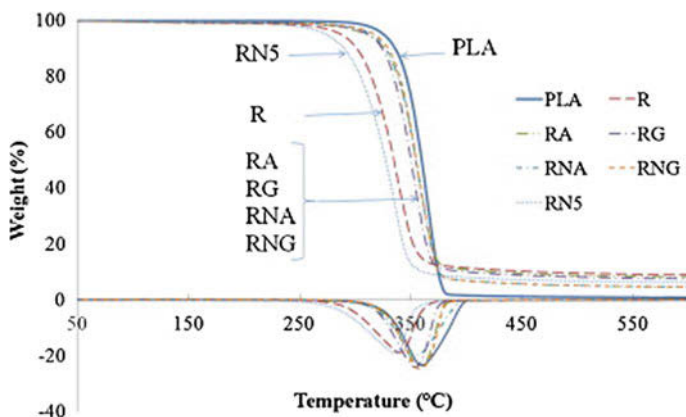


Fig. 16 Thermogravimetric curves of the neat PLA and biocomposites with untreated and treated rice husk. Reproduced from Thao Tran et al. [76]

stability in this material explained by a decay induced by the late decomposition of PBA. Generally, in the synthesis of grafted polymers crosslinked and entangled type of networks could be produced, which subjected to degradation temperatures imbedded char diffusion on the surface, and thus inhibit the degradation process.

Cellulose fiber (CF) extracted from *Grewia optiva* reinforced GC containing blend films of corn starch/poly(vinyl alcohol (St/PVA) [78]. Films were plastified with citric acid (CA) and crosslinked with glutaraldehyde (GLU). Thermogravimetric analysis of these GC films revealed that for *Grewia optiva* fibers, processes like depolymerization, dehydration and glucosan formation were occurred in the temperature range of 26.0–190 °C. The degradation temperatures of the composites fall between the degradation temperatures for the St/PVA blend films and the CF. Results indicated that CF fibers retarded the dynamic of composites degradation process. The increase of chemical bond strength at the interface between CF and matrix increased the resistance against thermal attack, improving thus thermal properties of the green composite.

5.2 Thermogravimetry of Green Composites Containing Cellulosic Nanoparticles

Thermal stability of cellulose can be differently approached if results are discussed taking in account the nanoscale dimensions of particles. A higher value of specific surface area for a cellulosic nanoparticle increase the thermal conductivity, the degradation temperatures occurring at lower values, despite to a degradation mechanism similar to hemicellulose. But, once embedded in a biodegradable polymer matrix, celluloses nanoparticles thermal degrade at higher temperatures

due to a lower thermal conductivity. Considering these aspects, a series of valuable results reported in the literature denoted various thermal degradation behaviours of composites reinforced with cellulose nanoparticles.

Thermal stability of CNCs, for example, depending on polymer matrix containing these particles. Nanofibers reinforced with CNC were used as fillers in sustainable composite materials produced via electrospinning of PVA [79]. Thermogravimetric analysis investigations revealed the effect of CNC on the thermal stability of composites and also allowed to obtain deeper insights into the interactions between the dispersed and continuous phases of nanofibers. The stability of PVA polymer was not affected by electrospinning process as TGA results sustained. Presence of CNC in electrospun nanofibers appeared as a peak in the first-order derivative curve, over the preexisting ones assigned to PVA matrix. This peak shifted to lower temperatures due to the accelerated thermal decomposition of CNCs in PVA melt, attributed to the degradation products that catalyzed the overall degradation process. Treatment of CNCs by hydrolyzation with sulfuric acid (CNC-S) and hydrochloric acid (CNC-H) promoted a better dispersion in poly(3-hydroxybutyrate-co-3-hydroxyvalerate) matrix (PHBV) [57]. Thermogravimetric analysis (TGA) of composites shown in Fig. 17 reveals a higher degradation temperature for CNC-H as compared with CNC-S where surface contained sulfated groups, which significantly lowered the degradation temperature. However, the thermal stability of both nanocomposites was higher than neat PHBV. Increased content of CNC-S in PHBV matrix resulted in a poor thermal stability of nanocomposites, an opposite effect being recorded for PBHV loaded with CNC-H where higher thermal stability was achieved. This study concluded that the number of intermolecular hydrogen bonding interactions between CNCs and PHBV (higher for CNC-H as compared with CNC-S) has a decisive role on thermal stability of composites in addition to a good reinforcement of CNC particles in the PBHV matrix.

The thermal stability of cellulose nanowhisker/bio-based polyurethane (CNW/BPU) composites were investigated indicating a clear increase in thermal degradation temperatures with CNW content [80]. The computed values of activation energies for thermal decomposition of these composites indicated that BPU matrix was decomposed more difficult due to the incorporation of CNW. The analysis of parameters following the thermal decomposition kinetics of the BPU/m-CNW composites also sustained the increasing of the thermal stability of composites due to the incorporation of CNW. Cellulose nanocrystals were modified by acid hydrolysis (HCl or H₂SO₄) and esterified using the modified Fischer method in order to obtain acetate cellulose nanocrystals (Ac-CNCs) and lactate cellulose nanocrystals (LA-CNCs) [81]. Then, these modified CNCs reinforced PLA matrices through melt blending procedure. Under the inert atmosphere, all nanocomposites showed similar thermal stability, but under oxygen, the thermal stability decrease in order: LA-CNCs > AA-CNCs > HCl-CNCs > H₂SO₄-CNCs. Improved thermal stability in nanocomposites containing LA-CNCs and AA-CNCs particles was probably caused by a good dispersion that increased compatibility with PLA matrix, as author sustained.

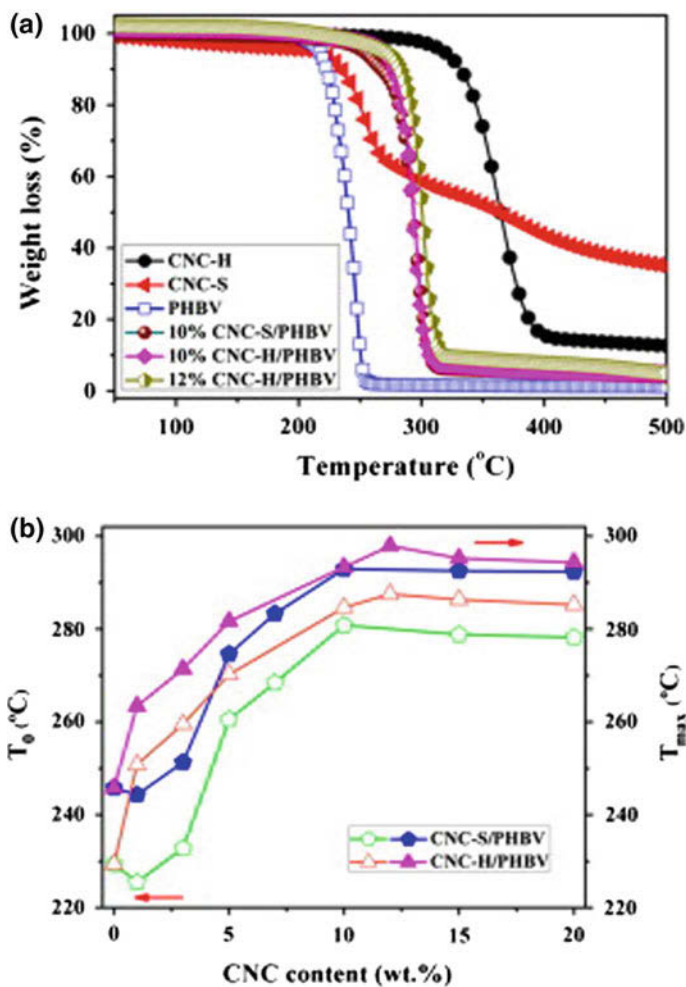


Fig. 17 TGA analysis (a), T_0 and T_{max} (b) as a function of the CNC contents of neat PHBV and the nanocomposites with CNC-S and CNC-H. Reproduced from Yu et al. [57]

Starch matrix has poor thermal stability, but if it is chemically modified following various ways this property is much improved. Thermogravimetric analysis (TGA) was performed on fully biocomposites of glycerol plasticized waxy maize starch with and without hydrolyzed starch nanocrystals [82]. The lower thermal stability reported for the biocomposite mentioned in this work was assigned by a closer association of glycerol with starch nanoparticles. Results showed that the effect of the addition of starch nanoparticles in the unplasticized matrix compared to the one induced in the glycerol plasticized material do not change the thermal stability. This work assumes a decrease of thermal degradation temperature for hydrolyzed starch nanocrystals, which act as flame retardants due to char formation.

Starches from different vegetal sources (tuber, cereal, and legume) were plasticized with glycerol and reinforced with cellulose nanocrystals [83]. In all cases, thermal degradation of TPS films filled with nanocellulose started at higher temperatures than unfilled TPS. This result showed a good thermal stability for TPS matrix containing large starch-rich domains as much as the extent of plasticization (high amylopectin starches) increased. GCs were obtained by reinforcing the glycerol plasticized corn starch matrix with cellulose nanofibrils (CNF) extracted from wheat straw (using steam explosion) [84]. The results from TGA and DSC experiments indicated an interaction between CNF and glycerol, which produced the reduction in onset of degradation temperatures as compared with the pure matrix. TGA investigations revealed that thermal stability of these GCs increased after high shear mechanical treatments. This behaviour was explained by removing of non-cellulosic material which improved crystallinity after treatments, increasing thus the thermal stability.

Bacterial cellulose (BC), when was combined with a biodegradable polymer matrix, generated a fully biodegradable composite with promising applications. The addition of low amounts (1 and 5%) of vegetal, BC fibers and glycerol (plasticizer) to the thermoplastic starch matrix (TPS) resulted in a green composite with better mechanical properties [85]. The results from TGA analysis showed that thermal stability of composites filled with vegetal cellulose and BC slightly increased (with 9 and 7 °C, respectively). The higher stability of cellulose fillers and the excellent compatibility between the two carbohydrate components of composites explained these findings. Very interesting results recently reported were related to preparing of resistant starch/pectin (RS/P) free-standing films reinforced with bacterial nanocellulose (BCN) for biomedical use [86]. Presence of BCN or CNF at 0.5% amount in nanocomposites films produced an almost similar mass loss, as resulted from TG curves. The strong interaction between matrix and both reinforcement phases (BCN or CNF) became clear at an increased concentration (from 1.0 to 3.0%), which promoted the better thermal stability in these composites. The thermal degradation process of nanocellulose (depolymerization and decomposition process of dehydrocellulose) doesn't really affect the mass loss of nanocomposite films with higher amounts of reinforcements.

6 Conclusions

Recent studies focused on the thermal behaviour of GCs presented in this chapter revealed the most important issues about glass transition, melting and crystallization on the one hand, and about thermal degradation and stability range on the other hand. Almost all reviewed works were concerned with the significance of the interface between natural fillers and various polymeric matrices because it plays the most important role in the applications area. The binding between GC components

at interface decided their thermal behaviour in any temperature range. The results have been separately presented in this chapter, for each range, in order of temperature increase.

Several studies, since 2006 have been discussed results related to glass transition range which is considered as the important parameter to define the mechanical performances of GCs. For example, when hemp was reinforced on PBSu matrix or banana fibers were reinforced on PLA matrix at any content without any chemical modification, the T_g value of resulted GCs did not show important changes, but its range was broadened. Authors remarked just a slightly decreased T_g value for CG based on phenol formaldehyde and filled with oil palm which explained a possible heterogeneity generated during processing. Decreasing of T_g value by plasticization (bio-epoxy or PU/flax) or due to some confinement effects at fiber interface with polymer matrix also were involved.

Instead, a real improvement in the mechanical performances of GCs was obtained by various chemical treatments applied to the natural fibers or fillers used as reinforcements. For example, T_g value of GC based on PLA matrix containing chemically treated ramie increased, improving thus the mechanical properties or decreased worsening the interfacial adhesion.

As a new finding in the area of GC production, CNC (or CNW) unmodified as a function of loaded content reduced the polymer matrix chains mobility at the interface (in case of PLA, PPC, TPS) and increased the T_g values, or have no any effect (case of pectin). In some situations, due to a chemical treatment (acetylation) applied to the CNC or by grafting (to PLLA) before adding to polymer matrix (PLA), T_g value increased, the effects being proportional to the modified CNC content.

From the cited literature, it seems that only a chemical treatment or any other modifications of fillers that change adhesion at the interface will have an important effect on T_g value, so it could be controlled to obtain the desired mechanical performance when GCs are prepared.

The changes in the thermal behaviour of GC were well presented also when the melting and crystallization region of polymer matrices was studied by DSC analysis. Different natural fillers isolated from various natural resources were considered in almost all presented works as nucleation agents in the crystallization process, which could change the morphology at the interface. Consequently, the resulted modifications of the T_c , T_m , ΔH_m , ΔH_c or χ_c values in polymer matrices were clearly visible in DSC analysis. The overall crystallization rate and crystallinity index value increased due to fibers loading in the follow GC: ramie, coir, rice straw—PLA, kenaf—PLLA, bamboo—PP-g-MA, bamboo—PLA/PBS or rice straw—PLLA. Instead, these values decreased in kenaf—PLA, rice husk—PC, rice straw—PLA/PBA and generally in case of chemically treated fibers. In some situations, fibers like cellulose pulp extracted, sisal, pineapple leaves or agave had reduced or had no effect on GC crystallinity. A special behaviour had TPS, which increased the crystallinity in PLA but decreased in PCL matrix.

Different ways of crystals growth and morphology development induced in polymer matrices by fillers have been determined after evaluation of the polymer

matrix crystallization kinetic using DSC method, under both isothermal as well as non-isothermal conditions. By loading of neat fibers, the crystallization kinetic was improved by the bamboo fibers in PCL matrix, kenaf fibers, and rice straw in PLLA, black spruce and northern bleached softwood kraft in PLA, but has no any effect or reduced the crystallization rate when these were chemically treated (ex. sisal—PLA).

Reduced dimensions of cellulose nanofillers extracted from various bioresources had a strong effect on crystallinity and morphology of GCs. The nucleation process was generally increased by these fillers type, and the growth of crystals was dependent on particular conditions. Thus, the crystallinity was improved in PLA based composites containing MFA, CNW or ChNC, and in the PU matrix filled with CNF. Also, in plasticized PLA or PLA/PHB blends, the crystallization was improved by CNF and CNC, respectively. Chemical treatments (hydrolyzation, esterification, and surfactant) or freeze drying applied on CNC surfaces had increased the crystallization rate in PLA matrix. Decreasing of crystallinity was reported by loading of MFA or silanized CNF in PVA, CNC-g-PLA in PVAc, CNC in PBHV, and by grafting PBHV chains onto CNC surface.

All these results mean that the GC morphology can be tuned to control crystals dimensions, obtaining thus desired mechanical properties (e.g. small crystals—good mechanical properties), as a function of the application area. To obtain GCs with good thermal and mechanical properties, at least two conditions must be satisfied to control the crystallization process: good surface treatment (fillers or/and polymer matrix) and well dispersion of fillers in the polymer matrix (to prevent heterogeneity).

In the most situations, the natural fibers improved the thermal stability of GCs, as much as fiber content increased. A better thermal stability was recorded by the bamboo fibers loaded in PLA or PBS, coir fibers reinforced in EVA/TPS blend, PLA, PP-g-MA, cassava and pineapple flour loaded in PLA or by the plasticized lignin filled with PFA. The degradation temperature was increased when the chemical treatment applied to the fibers enhanced adhesion with the polymer matrix. Thus, the scientific literature has registered results related to the alkalinized fibers as in kenaf—epoxy or PVC/TPU, hemp—PP/SEBS-g-MA and ramie—PLA-g-MA composites or to silanized (rice husk or kenaf) fibers loaded in PLA matrix. On the other hand, a decreased thermal stability was reported for kenaf (or ramie)—PLA, silanized hemp—PP-g-MA and flax (or kenaf)—PFA green composites.

Cellulose pulp fibers increased the thermal degradation temperatures in corn starch/PVA blend based composites, or in case of MCC reinforcing PLA matrix. Also, this property was enhanced in CNW—BPU and in BC—TPS (TPS/pectin blend), but a chemical treatment of cellulose nanoparticles improved thermal degradation furthermore. Thus, it was worth to notice the results that confirmed a thermal stability enhancement for alkalinized CNF—TPS, hydrolyzed CNC—PBHV (or PLA) and hydrolyzed starch nanocrystals—TPS.

Beside the interface between natural fillers (fibers or nanoparticles), a well dispersion in the processing step represent the key factors in a green composite preparation. Following these findings, the thermal properties of sustainable materials will be improved, providing thus desired and good mechanical performances.

References

1. Das O, Bhattacharyya D, Sarmah AK (2016) Sustainable ecocomposites obtained from waste derived biochar: a consideration in performance properties, production costs, and environmental impact. *J Clean Prod* 129:159–168
2. Mathot VBF (ed) (1994) *Calorimetry and thermal analysis of polymers*. Carl Hanser Verlag, München
3. Turi EA (ed) (1997) *Thermal characterization of polymeric materials*. Academic Press, New York
4. Väisänen T, Das O, Tomppo L (2017) A review on new bio-based constituents for natural fiber-polymer composites. *J Cleaner Prod* 149:582–596
5. Monteiro SN, Calado V, Rodriguez RJS et al (2012) Thermogravimetric behavior of natural fibers reinforced polymer composites—an overview. *Mat Sci Eng A* 557:17–28
6. Signori F, Pelagaggi M, Bronco S et al (2012) Amorphous/crystal and polymer/filler interphases in biocomposites from poly(butylene succinate). *Thermochim Acta* 543:74–81
7. Shinoj S, Visvanathan R, Panigrahi S et al (2011) Oil palm fiber (OPF) and its composites: a review. *Ind Crops Prod* 33:7–22
8. Cuinat-Guerraz N, Dumont M-J, Hubert P, (2016) Environmental resistance of flax/bio-based epoxy and flax/polyurethane composites manufactured by resin transfer moulding. *Compos Part A* 88:140–147
9. Yu T, Ren J, Li S et al (2010) Effect of fiber surface treatments on the properties of poly(lactic acid)/ramie composites. *Compos Part A* 41:499–505
10. Yu T, Jiang N et al (2014) Study on short ramie fiber/poly(lactic acid) composites compatibilized by maleic anhydride. *Compos Part A* 64:139–146
11. Shih YF, Huang CC (2011) Polylactic acid (PLA)/banana fiber (BF) biodegradable green composites. *J Polym Res* 18:2335–2340
12. Haafiz M, Hassan A, Khalil A et al (2016) Exploring the effect of cellulose nanowhiskers isolated from oil palm biomass on polylactic acid properties. *Int J Biol Macromol* 85:370–378
13. Mandal A, Chakrabarty D (2014) Studies on the mechanical, thermal, morphological and barrier properties of nanocomposites based on poly(vinyl alcohol) and nanocellulose from sugarcane bagasse. *J Ind Eng Chem* 20:462–473
14. Lin N, Huang J, Chang PR et al (2011) Surface acetylation of cellulose nanocrystal and its reinforcing function in poly(lactic acid). *Carbohydr Polym* 83:1834–1842
15. Lizundia E, Vilas JL, León LM (2015) Crystallization, structural relaxation and thermal degradation in poly(l-lactide)/cellulose nanocrystal renewable nanocomposites. *Carbohydr Polym* 123:256–265
16. Hu X, Xu C, Gao J et al (2013) Toward environment-friendly composites of poly(propylene carbonate) reinforced with cellulose nanocrystals. *Compos Sci Technol* 78:63–68
17. Cao X, Chen Y, Chang PR et al (2008) Green composites reinforced with hemp nanocrystals in plasticized starch. *J Appl Polym Sci* 109:3804–3810
18. Lu Y, Weng L, Cao X (2006) Morphological, thermal and mechanical properties of ramie crystallites-reinforced plasticized starch biocomposites. *Carbohydr Polym* 63:198–204
19. Chaichi M, Hashemi M, Badii F et al (2017) Preparation and characterization of a novel bionanocomposite edible film based on pectin and crystalline nanocellulose. *Carbohydr Polym* 157:167–175

20. Abdul Khalil HPS, Bhat IUH, Jawaid M et al (2012) Bamboo fibre reinforced biocomposites: a review. *Mater Des* 42:353–368
21. Lee SH, Wang S (2006) Biodegradable polymers/bamboo fiber biocomposite with bio-based coupling agent. *Compos Part A* 37:80–91
22. Liu H, Huang Y et al (2010) Isothermal crystallization kinetics of modified bamboo cellulose/PCL composites. *Carbohydr Polym* 79:513–519
23. Ramesh M (2016) Kenaf (*Hibiscus cannabinus* L.) fibre based bio-materials: a review on processing and properties. *Prog Mat Sci* 78–79:1–92
24. Buzarovska A, Bogoeva-Gaceva G, Grozdanov A et al (2007) Crystallization behavior of poly(hydroxybutyrate-co-valerate) in model and bulk PHBV/kenaf fiber composites. *J Mater Sci* 42:6501–6509
25. Dobрева T, Perena JM, Perez E et al (2010) Crystallization behavior of poly(L-lactic acid)-based ecocomposites prepared with Kenaf fiber and rice straw. *Polym Compos* 31(6):974–984
26. Qin L, Qiu J, Liu M et al (2011) Mechanical and thermal properties of poly(lactic acid) composites with rice straw fiber modified by poly(butyl acrylate). *Chem Eng J* 166:772–778
27. Zhao Q, Tao J, Yam RCM et al (2008) Biodegradation behavior of polycaprolactone/rice husk ecocomposites in simulated soil medium. *Polym Degrad Stab* 93:1571–1576
28. Yu T, Li Y (2014) Influence of poly(butylenes adipate-co-terephthalate) on the properties of the biodegradable composites based on ramie/poly(lactic acid). *Compos Part A* 58:24–29
29. Yu T, Jiang N, Li Y (2014) Study on short ramie fiber/poly(lactic acid) composites compatibilized by maleic anhydride. *Compos Part A* 64:139–146
30. Dong Y, Ghataura A, Takagi H et al (2014) Polylactic acid (PLA) biocomposites reinforced with coir fibres: evaluation of mechanical performance and multifunctional properties. *Compos Part A* 63:76–84
31. Wang Y, Tong B, Hou S et al (2011) Transcrystallization behavior at the poly(lactic acid)/sisal fibre biocomposite interface. *Compos Part A* 42:66–74
32. Biswal M, Mohanty S, Nayak SK (2009) Influence of organically modified nanoclay on the performance of pineapple leaf fiber-reinforced polypropylene nanocomposites. *J Appl Polym Sci* 114:4091–4103
33. Chollakup R, Tantatherdtam R, Ujtin S et al (2011) Pineapple leaf fiber reinforced thermoplastic composites: effects of fiber length and fiber content on their characteristics. *J Appl Polym Sci* 119:1952–1960
34. Torres-Tello EV, Robledo-Ortíz JR, González-García Y et al (2017) Effect of agave fiber content in the thermal and mechanical properties of green composites based on polyhydroxybutyrate or poly(hydroxybutyrate-co-hydroxyvalerate). *Ind Crops Prod* 99:117–125
35. Ding WD, Jahani D, Chang E et al (2016) Development of PLA/cellulosic fiber composite foams using injection molding: crystallization and foaming behaviors. *Compos Part A* 83:130–139
36. Le Moigne N, Longerey M, Taulemesse J-M et al (2014) Study of the interface in natural fibres reinforced poly(lactic acid) biocomposites modified by optimized organosilane treatments. *Ind Crops Prod* 52:481–494
37. Pracella M, Chionna D, Anguillesi I et al (2006) Functionalization, compatibilization and properties of polypropylene composites with Hemp fibres. *Compos Sci Technol* 66:2218–2230
38. Yang S, Madbouly SA, Schrader JA et al (2015) Characterization and biodegradation behavior of bio-based poly(lactic acid) and soy protein blends for sustainable horticultural applications. *Green Chem* 17:380–393
39. Cai J, Liu M, Wang L et al (2011) Isothermal crystallization kinetics of thermoplastic starch/poly(lactic acid) composites. *Carbohydr Polym* 86:941–947
40. Cai J, Xiong Z, Zhou M et al (2014) Thermal properties and crystallization behavior of thermoplastic starch/poly(ϵ -caprolactone) composites. *Carbohydr Polym* 102:746–754
41. Luduena L, Vázquez A, Alvarez V (2012) Effect of lignocellulosic filler type and content on the behavior of polycaprolactone based eco-composites for packaging applications. *Carbohydr Polym* 87:411–421

42. Du Y, Wu T, Yan N et al (2014) Fabrication and characterization of fully biodegradable natural fiber-reinforced poly(lactic acid) composites. *Compos Part B* 56:717–723
43. Suryanegara L, Nakagaito AN, Yano H (2009) The effect of crystallization of PLA on the thermal and mechanical properties of microfibrillated cellulose-reinforced PLA composites. *Compos Sci Technol* 69:1187–1192
44. Suryanegara L, Nakagaito AN, Yano H (2010) Thermo-mechanical properties of microfibrillated cellulose-reinforced partially crystallized PLA composites. *Cellulose* 17:771–778
45. Qiu K, Netravali AN (2012) Fabrication and characterization of biodegradable composites based on microfibrillated cellulose and polyvinyl alcohol. *Compos Sci Technol* 72:1588–1594
46. Haafiz MKM, Hassan A, Zakaria Z et al (2013) Properties of polylactic acid composites reinforced with oil palm biomass microcrystalline cellulose. *Carbohydr Polym* 98:139–145
47. Kowalczyk M, Piorkowska E, Kulpinski P et al (2011) Mechanical and thermal properties of PLA composites with cellulose nanofibers and standard size fibers. *Compos Part A* 42:1509–1514
48. Benhamou K, Kaddami H, Magnin A et al (2015) Bio-based polyurethane reinforced with cellulose nanofibers: a comprehensive investigation on the effect of interface. *Carbohydr Polym* 122:202–211
49. Frone AN, Berlioz S, Chailan JF et al (2013) Morphology and thermal properties of PLA—cellulose nanofibers composites. *Carbohydr Polym* 91:377–382
50. Abdulkhani A, Hosseinzadeh J, Ashori A et al (2014) Preparation and characterization of modified cellulose nanofibers reinforced polylactic acid nanocomposite. *Polym Test* 35:73–79
51. Herrera N, Mathew AP, Oksman K (2015) Plasticized polylactic acid/cellulose nanocomposites prepared using melt-extrusion and liquid feeding: mechanical, thermal and optical properties. *Compos Sci Technol* 106:149–155
52. Herrera N, Salaberria AM, Mathew AP et al (2016) Plasticized polylactic acid nanocomposite films with cellulose and chitin nanocrystals prepared using extrusion and compression molding with two cooling rates: effects on mechanical, thermal and optical properties. *Compos Part A* 83:89–97
53. Almasi H, Ghanbarzadeh B, Dehghannya J (2015) Novel nanocomposites based on fatty acid modified cellulose nanofibers/poly(lactic acid): morphological and physical properties. *Food Pack Shelf Life* 5:21–31
54. Mariano P, Minhaz-Ul H, Debora P (2014) Morphology and properties tuning of PLA/cellulose nanocrystals bionanocomposites by means of reactive functionalization and blending with PVAc. *Polymer* 55:3720–3728
55. Pei A, Zhou Q, Berglund LA (2010) Functionalized cellulose nanocrystals as biobased nucleation agents in poly(L-lactide) (PLLA)—crystallization and mechanical property effects. *Compos Sci Technol* 70:815–821
56. Bitinis N, Fortunati E, Verdejo R et al (2013) Poly(lactic acid)/natural rubber/cellulose nanocrystal bionanocomposites. Part II: properties evaluation. *Carbohydr Polym* 96:621–627
57. Yu HY, Qin ZY, Liu L et al (2013) Comparison of the reinforcing effects for cellulose nanocrystals obtained by sulfuric and hydrochloric acid hydrolysis on the mechanical and thermal properties of bacterial polyester. *Compos Sci Technol* 87:22–28
58. Kamal MR, Khoshkava V (2015) Effect of cellulose nanocrystals (CNC) on rheological and mechanical properties and crystallization behavior of PLA/CNC nanocomposites. *Carbohydr Polym* 123:105–114
59. Miao C, Hamad WY (2016) In-situ polymerized cellulose nanocrystals (CNC)-poly(L-lactide) (PLLA) nanomaterials and applications in nanocomposite processing. *Carbohydr Polym* 153:549–558
60. Fortunati E, Armentano I, Zhou Q et al (2012) Multifunctional bionanocomposite films of poly(lactic acid), cellulose nanocrystals and silver nanoparticles. *Carbohydr Polym* 87:1596–1605
61. Morelli CL, Belgacem MN, Branciforti MC et al (2016) Supramolecular aromatic interactions to enhance biodegradable film properties through incorporation of functionalized cellulose nanocrystals. *Compos Part A* 83:80–88

62. Yu HY, Qin ZY (2014) Surface grafting of cellulose nanocrystals with poly (3-hydroxybutyrate-co-3-hydroxyvalerate). *Carbohydr Polym* 101:471–478
63. Arrieta MP, López J, López D et al (2016) Biodegradable electrospun bionanocomposite fibers based on plasticized PLA–PHB blends reinforced with cellulose nanocrystals. *Ind Crops Prod* 93:290–301
64. Malmir S, Montero B, Rico M et al (2017) Morphology, thermal and barrier properties of biodegradable films of poly (3-hydroxybutyrate-co-3-hydroxyvalerate) containing cellulose nanocrystals. *Compos Part A* 93:41–48
65. Yu HY, Yao JM (2016) Reinforcing properties of bacterial polyester with different cellulose nanocrystals via modulating hydrogen bonds. *Compos Sci Technol* 136:53–60
66. Monteiro SN, Calado V, Rodriguez RJS et al (2012) Thermogravimetric stability of polymer composites reinforced with less common lignocellulosic fibers—an overview. *J Mater Res Technol* 1(2):117–126
67. Rosa MF, Chiou BS, Medeiros ES et al (2009) Effect of fiber treatments on tensile and thermal properties of starch/ethylene vinyl alcohol copolymers/coir biocomposites. *Bioresour Technol* 100:5196–5202
68. Morandim-Giannetti AA, Agnelli JAM, Lanças BZ et al (2012) Lignin as additive in polypropylene/coir composites: thermal, mechanical and morphological properties. *Carbohydr Polym* 87:2563–2568
69. Guigo N, Mija A, Vincent L et al (2010) Eco-friendly composite resins based on renewable biomass resources: polyfurfuryl alcohol/lignin thermosets. *Eur Polym J* 46:1016–1023
70. Deka H, Misra M, Mohanty A (2013) Renewable resource based “all green composites” from kenaf biofiber and poly(furfuryl alcohol) bioresin. *Ind Crops Prod* 41:94–101
71. Azwa ZN, Yousif BF (2013) Characteristics of kenaf fiber/epoxy composites subjected to thermal degradation. *Polym Degrad Stab* 98:2752–2759
72. Elkhaoulani A, Arrakhiz FZ, Benmoussa K et al (2013) Mechanical and thermal properties of polymer composite based on natural fibers: moroccan hemp fibers/polypropylene. *Mater Des* 49:203–208
73. Panaitescu DM, Vuluga Z, Ghiurea M et al (2015) Influence of compatibilizing system on morphology, thermal and mechanical properties of high flow polypropylene reinforced with short hemp fibers. *Compos Part B* 69:286–295
74. Bakare FO, Ramamoorthy SK, Åkesson D et al (2016) Thermomechanical properties of bio-based composites made from a lactic acid thermoset resin and flax and flax/basalt fibre reinforcements. *Compos Part A* 83:176–184
75. Kim KW, Lee BH, Kim HJ et al (2012) Thermal and mechanical properties of cassava and pineapple flours-filled PLA bio-composites. *J Therm Anal Calorim* 108:1131–1139
76. Thao Tran TP, Bénézet JC, Bergeret A (2014) Rice and Einkorn wheat husks reinforced poly (lactic acid) (PLA)biocomposites: effects of alkaline and silane surface treatments of husks. *Ind Crops Prod* 58:111–124
77. Thakur VJ, Thakur MT, Gupta RK (2013) Development of functionalized cellulosic biopolymers by graft copolymerization. *Int J Biol Macromol* 62:44–51
78. Priya B, Gupta VK, Pathania D (2014) Synthesis, characterization and antibacterial activity of biodegradablestarch/PVA composite films reinforced with cellulosic fiber. *Carbohydr Polym* 109:171–179
79. Peresin MS, Habibi Y, Zoppe JO et al (2010) Nanofiber composites of polyvinyl alcohol and cellulose nanocrystals: manufacture and characterization. *Biomacromolecules* 11:674–681
80. Park SH, Oh KW, Kim SH (2013) Reinforcement effect of cellulose nanowhisker on bio-based polyurethane. *Compos Sci Technol* 86:82–88
81. Spinella S, Lo Re G, Liu B et al (2015) Polylactide/cellulose nanocrystal nanocomposites: efficient routes for nanofiber modification and effects of nanofiber chemistry on PLA reinforcement. *Polymer* 65:9–17
82. Garcia NL, Ribba L, Dufresne A et al (2011) Effect of glycerol on the morphology of nanocomposites made from thermoplastic starch and starch nanocrystals. *Carbohydr Polym* 84:203–210

83. Montero B, Rico M, Rodríguez-Llamazares S et al (2017) Effect of nanocellulose as a filler on biodegradable thermoplastic starch films from tuber, cereal and legume. *Carbohydr Polym* 157:1094–1104
84. Kaushik A, Singh M, Verma G (2010) Green nanocomposites based on thermoplastic starch and steam exploded cellulose nanofibrils from wheat straw. *Carbohydr Polym* 82:337–345
85. Martins IMG, Magina SP, Oliveira L et al (2009) New biocomposites based on thermoplastic starch and bacterial cellulose. *Compos Sci Technol* 69:2163–2168
86. Meneguín AB, Cury BSF, Dos Santos AM (2017) Resistant starch/pectin free-standing films reinforced with nanocellulose intended for colonic methotrexate release. *Carbohydr Polym* 157:1013–1023

Eco-friendly Polymer Composite: State-of-Arts, Opportunities and Challenge



V. S. Aigbodion, E. G. Okonkwo and E. T. Akinlabi

1 Introduction

Polymer matrix composites (PMCs) have come a long way in becoming a key player in the world of high performing engineering materials. With a wide array of applications due to its properties, these classes of materials are becoming more popular than their metallic and ceramic counterparts and as such replacing them in various applications especially where high strength to weight ratio and low density is a priority [1]. Composites like PMCs being multiphase materials exhibit properties that are dependent on the constituents; resin and fiber/particulate (reinforcement/filler). The resin helps to re-distribute stress and holds the reinforcement together while the reinforcement (fiber/particulate) provides the necessary load carrying operation and hence the strength and stiffness of the composite. Moreover, composites can always be tailored to the choice of the producer [2]. However, most popular polymers are synthetic and coupled with decreasing petroleum resources and environmental policies, they areas such costly and non-biodegradable under standard conditions. Addition of environmental favourable and renewable source of reinforcement to these polymers have not only helped to shift the overall outlook but also give it a new and wider prospect. Aside from the ecological benefits of using these materials, overall cost implication and health problems are also eliminated [3].

As at 2016, an estimated 300 million tons of plastics were produced with the majority of it finding ways into water bodies like rivers, oceans etc. It is been

V. S. Aigbodion (✉) · E. G. Okonkwo
Department of Metallurgical and Materials Engineering,
University of Nigeria, Nsukka, Nigeria
e-mail: victor.aigbodion@unn.edu.ng

V. S. Aigbodion · E. T. Akinlabi
Department of Mechanical Engineering Science, University of Johannesburg,
P.O. BOX 524, Auckland Park, South Africa

estimated that by 2050, there will be more plastics in the ocean than fishes.¹ The menace doesn't only extend to this as poor waste management culture in most developing countries have also led to mismanagement of recyclable portion of these class of wastes. With the rising volume of plastics dumps all around the world, these properties come in handy with regard to reduction in carbon emission and greenhouse gases as is the case due to incineration or burning of these materials, and as such reclamation of lands used for landfills; environmental pollution.

The birth of eco-friendly composites can be likened to man's continual quest for newer breeds of materials crisscrossing from the time of reinforcing bricks with straw to this day where nanoscience and technology has brought in the era of nanocomposites that uses Nano-sized materials like nanoclays, nanotubes, nanofibers, and nanosheets etc. as fillers/reinforcement. This can also be associated to technological breakthroughs that have seen the significant improvement in properties of some polymers thus opening up more areas of application like in the food packaging industry that uses PLA, biomedical, agricultural, construction sector, transport and even in textiles industries [4, 5]. This quest has also led to the reinvestigation of old processes giving rise to newer products [5]. Though ecological challenges seem to be the driving point behind it, dwindling nature of other sources of materials like petroleum has also led to a turnaround in material research. Man's rate of consumption of non-renewable natural resources is ever increasing due and outways the rate at which the earth produces them [6]. Therefore the only option is the search for the sustainable and renewable source of materials and stimulates ambitious policies for a significant increase in resource efficiency, particularly through technical change and innovation. Moreover, annual quantity of agrowastes and natural fibers produces ranks in billions of tons with majority burnt on-field [7]. This can expand rural agriculture-based economics by opening up new market [8]. According to Rana S. and Fangueiro R., cultivation of one hectare of hemp on a hectare area of land causes the absorption of approximately 2.5 tons of atmospheric carbon dioxide during a vegetative season while jute absorbs 2.4 tons of carbon dioxide. On the other hand, production of one ton of polypropylene emits about 3 tons of carbon dioxide into the atmosphere [9]. Thus wastes or materials which are both biodegradables can be used to reduce the cost of production of composites without impairing their properties.

1.1 What Are Eco-friendly Composites (EFC)

According to Adeosun et al., composites that are both biodegradable and renewable are termed eco-friendly composites [10]. This is because they can be easily disposed of without harm to the environment. Asokan et al. [11] sees them as

¹FEATURE: UN's mission to keep plastics out of oceans and marine life. <https://news.un.org/en/story/2017/04/556132-feature-uns-mission-keep-plastics-out-oceans-and-marine-life>. Accessed on January 10, 2018.

biocomposites since they are manufactured from materials like natural fibers and agro-wastes. According to Mitra bio-composites covers composite materials where at least one of the component is bio-based. These include petroleum-derived polymers like epoxy, polyester etc. reinforced with natural fibres like jute, flax etc.; bio-polymer like polylactic acid (PLA) reinforced by bio-fibers like coir and bio-polymers reinforced with synthetic fibers like glass or carbon [1]. However, a composite that combines both natural fibers/particulates like agro-waste and natural resins are termed green composite because both the resin and reinforcement decompose by the action of micro-organisms. As such it is pertinent to point out that though all the aforementioned composites are friendlier to the environment than the conventional composites and as such can be termed eco-friendly, a subtle demarcation can be seen based on their constituent. Hence eco-friendly polymer matrix composites can either bio-based green since some bio-based polymer matrix composite requires the introduction of antioxidants to help facilitate degradation [12, 13] and hence are called oxo-degradable polymers [13]. Nevertheless, bio-compatible materials for the production of EPCs can either be natural or synthetic and as such can be used as either the reinforcement or matrix of a composite [14]. Synthetic degradable polymers can be divided into condensation polymers (polyesters, amides, polyureas, polyurethanes etc.), addition polymers, water-soluble polymers (polyvinyl alcohol, polyethylene glycol) and blends of natural and synthetic polymers (starch and PLA based blends). Decomposition is basically by hydrolysis, microbial action, photo or thermos-oxidation etc. [15]. Natural occurring biocompatible polymers can be divided into agro-polymers and biopolymers. Agro-polymers are polymers derived from biomass products and include polysaccharides like starch, cellulose, chitin, etc. and their respective derivatives, protein like soya protein, casein, zein, gelatin etc., lipids like triglycerides and its derivatives. Biopolymers, on the other hand, include polymers from the following sources.

- I. Synthesis of bio-derived monomers. E.g. PLA,
- II. Extraction using micro-organisms. E.g. Polyhydroxyalkanoate (PHA)
- III. Synthesis of synthetic monomers. E.g. Polycaprolactone (PCL), Polyesteramides (PEA), aliphatic copolymers like PBSA, aromatic copolymers like PBAT [5, 16].

On the other hand, most fillers used in the production of eco-friendly composites are derived from natural fibers/particulates like Nanosilica, graphene, nanoclays, carbon nanotube, nanocellulose etc. Cellulose and starch-based fibers are the quite prominent because of their availability, cost and high specific strength. Nanotechnology has also seen to the production of these fibers at the nano-sized level. For instance, nanocellulose (NC) can be categorized into three subcategories based on cellulose source and on the production methods, cellulose nanocrystals (CNC), nanofibrillated cellulose and bacterial nano-cellulose. CNCs are highly crystalline [16].

1.2 Why Eco-friendly Composites and Trends

Like earlier stated, eco-friendly Polymer composites have caught the attention of researchers due to some of their daring properties especially with regards to degradation [17]. However, the increase in the research into it can be attributed to various reasons. According to [17], the drive is because of increased drift towards maximum utilization of renewable natural resources whereas [18–20] sees it be as a result of increased environmental awareness. Ease of availability and being economical as compared to conventional composites produced wholly with synthetic material was also opinioned by [21]. Thus from the ongoing, eco-friendly composites have not only come into enhance the already existing products by emulating nature's way of producing material but also to expand on it.

One attractive feature of EPC is that it can turn what is regarded as waste to a very useful material without harm to the environment; a natural way of converting waste to wealth at little or no cost but with many benefits. For example wood flour, rice husk, egg shells and various agro and industrial wastes like sawdust [22–26] have been successfully turned into useful products with many improved properties and at no harm to the environment. Moreover, with the global demand for wood and competition from the pulp and paper industry, use of residues like stalks of cereal is no longer an option but a necessity [27]. A growing class of eco-friendly composite is the wood plastic composite. This class of composites is produced by combining thermoplastics with wood/natural fiber [28] or by melt blending polymer/wood flour or powder mix. These class of composites requires less maintenance and as such offers alternative to wood products. Moreover, they can be made into complex shapes [29]. Aigbodion and co-worker have used many natural fillers in the production of eco-composites among them are (Figs. 1 and 2):

Also, the possibility of hybridization has also increased the range of properties that can be obtained from this class of composite. According to [32] hybrid



Fig. 1 Polymer composites produced with Bagasse [30]



Fig. 2 Polymer composites produced with Breadfruit shell [31]

composites are obtained by two or more different fibers in a common matrix. Thus it allows for modifying the properties of the composite so as to meet the required need. Various works on hybrid eco-friendly polymer composites have shown improved properties. Ravindran et al. [28] used coconut shell powder and wood dust as filler for polyester resin and observed that tensile, flexural and shear strength of the hybrid composites were better than the mono-reinforced composite. The similar result has been observed in the works done by [20, 25, 33]. On the other hand, hybridization also helps in reducing the overall cost of producing a synthetic composite by balancing out some of the components with some renewable and easily available ones. Kasiviswanathan et al. [34] worked on the impact of stacking of natural fibers and a synthetic fiber as reinforcement for polyester resin. Sisal, banana, and E-glass fiber were used and the fibers were stacked alternatively. Although the presence of glass fiber improved the mechanical of the composite, that of the ones with more of sisal and banana fiber were not far off showing that they can serve as a possible replacement. Udhayasankar and Karthikeyan [35] highlighted some of the uses or applications of natural fiber composites.

Nevertheless, the developmental trend of EPCs is ever blazing. Nanoclays are known for their high aspect ratio and intercalative/exfoliation behaviour. The behaviour of nanoclay in a PMC is dependent on the type of clay, pre-treatment method, mode of dispersion of the filler and the resin itself [36]. Addition of nanoclays to EPCs not only leads to improved mechanical properties but higher thermal stability [37]. Rahmat et al. [8] from their work on the addition of nanoclay to rice husk reinforced polypropylene composite observed an improved tensile strength and modulus compared to the rice husk—polypropylene composite. Ashori A. et al. also found that introduction of nano-silica in rice husk and beach bark-Propylene composite enhanced the physical and mechanical properties like flexural strength whereas the tensile properties suffered due to the high weight fraction of the fiber incorporated [38]. Nanocellulose fibers, whiskers etc. have all led to improved optical, electrical, magnetic properties etc. of the produced EPC thus opening new grounds for engineering applications.

1.3 Properties of Eco-friendly Composites

Eco-friendly polymer composites are known to offer very enticing benefits. Besides their ability to degrade without damage to the environment, they are also known for their high strength to weight ratio, low density, excellent corrosion resistance [39]. Aside from that, its constituents are abundant, cheap and renewable [40], thus there is an assured supply means. Some of the properties of eco-friendly composites can be summarized in Table 1.

1.4 Challenges in the Processing of Eco-friendly Composites

Although eco-friendly composites posit material for the future most are lignocellulosic which are highly polar in nature. Therefore coupling with nonpolar matrix leads to poor adhesion at the interface and hence properties that are lower than expected. Addition of hydrophilic fibers to hydrophobic matrix reduces the mechanical strength of the composite formed due to incompatibility between the fiber and matrix. Likewise, nonuniform dispersion and agglomeration of nanoparticle lead to a discrepancy in result [8]. To combat this modification of the surface of the fibres have been seen to be a plausible solution. Therefore some research into biobased composite has been done with the aim of finding the right surface treatment so as to enable proper compatibility. This has been done using varied means ranging from chemical treatment (mercerization, silane treatment, acetylation etc.), physical methods (stretching, calendering, thermo treatment), electric discharge (corona treatment, cold plasma etc.) [42].

The collection, storage, transportation and economics of production is another defying factor that hinders the use of cereal by-product, straw, shell and other agricultural residues in composites [43]. However, research focused on the use of these materials have also followed a developmental market, which has led to the birth of a new market opportunity for these surplus inexpensive field crop husks.

Other challenges include the fact that most reinforcement used in producing eco-friendly polymer composites are difficult to get in the continuous fibrous state.

Table 1 Properties of eco-friendly composites [35, 41]

• Renewable source of reinforcement/matrix	• Reduced dermal and respiratory irritation
• Biodegradable	• Acoustic absorption
• Low density	• Enhanced energy recovery
• Good stiffness and strength	• Reduced tool wear
• No off-gassing of toxic compounds	• Reduced fogging behaviour
• Less spintering	• Favourable processing properties

Moreover fiber quality of plant-based fibers is dependent on many factors including, the age of the plant, retting method etc. [44–46]. The final properties of composite materials depend on fibre properties (morphology, surface chemistry, chemical composition and crystalline contents) as well as matrix properties (nature and functionality) [43]. Bledzki A. J. et al. compared the properties of by-products like barley husk, coconut shell and softwood as reinforcement for thermoplastics like polyethylene. Morphological analysis showed that coconut shell had a relatively smooth morphology. Water absorption behaviour showed that softwood absorbed the highest quantity of water in the first few days. This can be ascribed to the hemicellulose content of the fillers. Barley husk showed best tensile and impact strength whereas coconut-shell shell exhibited the best elongation at break. Addition of coupling agent (MA-PP) led to increased tensile properties and a minimal change in impact strength [43].

1.5 Opportunities

EFCs promises sets of materials with excellent environmental compatibility. Aside from serving as a possible alternative to varying already existing materials, they also provide a chance for the better utility of assumed waste. One of the class of eco-friendly composites that have been gaining relevance is the wood polymer composite which can be a good alternative to wood and as such help to relieve the pressure on the forestry industry. This class of EFC has found application as structural parts for low-cost buildings, cabinet, and upholstery etc. Incorporation of nanoclays has also led to the improved thermal stability of polymer matrix composites without affecting their ecofriendliness thus offering an opportunity for use at higher temperatures [47].

Incorporation of other nanoparticles like nanocellulose in biodegradable polymers like PLA has made it possible for applications in areas like tissue engineering, seizure for wounds etc. in food packaging industry these class of materials are of high demand due to their biodegradability, ability to form barriers to gases and repel water. Other areas of application of EFCs include as biosensors, tissue engineering etc. [48].

Likewise, polymer blend which has been identified as one of the ways to curtail the inherent poor properties of some biodegradable polymers. PLA which is a thermoplastic is known for its brittleness, poor crystallinity and poor impact strength. However blending with other polymers like PBS, rubber, Polypropylene has helped to improve its properties. Polymer blends have found application in the textile industry amongst other engineering applications.

2 Processing of Eco-friendly Composites

The trend in design and processing of polymer composites is one that has continued to evolve, the fact that can be attained to the development of new reinforcement and a better understanding of the effect of the interaction of the matrix and

reinforcement. Traditionally, polymers are classified as either thermosets or thermoplastics. Thermoplastics are known for having branched chains. Notable among them are PEEK, PP, PA-6, PPS etc. and are known for varied application in aerospace and automobile industry due to properties like high chemical resistivity, fracture toughness and crack growth resistance. Though they can be reshaped via heating and cooling, they have lower stiffness and strength compared to thermosets. Thermosets, on the other hand, are made by crosslinking or chain extension of monomer chains mostly under low heat and pressure in a processing called curing. They are characterized by rigid three-dimensional structures and high molecular weight and normally decompose before melting, unlike thermoplastic. This can be via poly-condensation, copolymerization or homo-polymerization with a catalyst as in the case of epoxy. Popular thermosets include epoxy, acrylic, polyester, polyurethanes, vinyl ester etc. and have found application as electrical insulators, waterproof coating, circuit board, car parts etc.

Most of the polymers mentioned above are synthetic polymers though when mixed with natural fibers or agro-wastes form eco-friendly composites. Nevertheless, naturally occurring polymers also can also be classified as based on the subunit (mer group) as seen in synthetic polymers. PLA is a biodegradable aliphatic thermoplastic polyester, polyhydroxyalkanoate is also a polyester. These polymers are (bio)degradable polymers due to the potentially hydrolysable ester bonds and relatively short aliphatic chains present in the macromolecules [49]. Other biopolymers include naturally produced polymers like poly-3-hydroxybutyrate (PHB), polyhydroxyvalerate (PHV) and polyhydroxyhexanoate (PHH); synthetic ones like Polybutylene succinate (PBS), polycaprolactone (PCL); Cellulose esters like cellulose acetate and nitrocellulose and their derivatives; starch and its derivatives among others. Nevertheless, the chemistry of the matrix and fiber plays an important role in the processing of composite and as such requires a quick preview.

2.1 Chemistry of Eco-friendly Composites: Matrix and Fillers for Production of EFC

Research has shown that the behaviour of composites is dependent on the integrity of the bond between the matrix and reinforcement. Eco-friendly composites are made up of materials with differing chemical make-up and hence exhibits differing behaviour. Thus for a proper understanding of this material, it is pertinent to look at the chemistry of the components which are the matrix and reinforcement. The matrix is one of the most important parts of a composite. Aside from distributing stress and acting as a bonding agent, it also shields the reinforcement from the external environment. In eco-friendly PMCs, the matrix can either be synthetic or natural polymers. Natural polymers can be derived from renewable sources or from petroleum. However, some synthetic based polymers can be derived from

renewable sources For instance polyamide can be synthesized from castor oil. One of the most widely used matrices is Poly(lactic acid (PLA). It can be produced by different methods like direct polycondensation. Other methods include azeotropic condensation polymerization, solid state polymerization, coordination-insertion mechanism which involves the use of catalysts like metallic alkoxides. PLA has high transparency and elastic modulus can be thermoplastically processed like conventional plastics and has been widely used in the development of disposable products, such as disposable cutlery, cups, and films. Its brittleness at room temperature and hydrolysability have limited its application. Another important natural occurring eco-friendly polymer used as the matrix is starch. Starch a semi-crystalline biopolymer is a branched homopolymer of glucose, with α -(1 \rightarrow 4) linear links and α -(1 \rightarrow 6) branched links and is the main carbohydrate reserve in roots, tubers, seeds, fruits, cereals etc. It is normally made up of amylose and amylopectin and depending on the source of origin, the granules can vary in size, shape, chemical composition and structure [50]. Starch in granular form has limited processability and as such is often blended with other polymers. Chitin and its derivative chitosan is another important and widely used natural polymer. This polymer is derived from the exoskeleton of insects, crustacean, insects, arthropods. Chitin has limited solubility in diluted acidic aqueous solutions unlike chitosan.

However due to its, availability, low cost, high biocompatibility, biodegradability, antimicrobial property, ease of chemical modification and excellent film-forming ability. This polymer also possesses properties, including its high viscosity, charge distribution, and release mechanisms, making it particularly suitable as a carrier this polymer has wide range application from the biomedical to industrial areas [50, 51]. Aside from cellulose, poly(hydroxyl butyrate) (PHB); a naturally occurring polyester produced by numerous bacteria in nature as an intracellular reserve of carbon or energy; guar gum, non-ionic polysaccharides another natural occurring polymer used as matrix. Just like natural occurring polymer matrices, the biodegradable polymer matrix can be derived from synthetic sources like fossil fuel via processes like polycondensation. Poly(ϵ -caprolactone) (PCL) is a biodegradable and biocompatible polymer manufactured by the ring-opening polymerization of ϵ -caprolactone (CL). PCL has a flexible chain, exhibits a high elongation at break, low modulus and the low melting point which is its major drawback. However, it is normally blended with other polymers to improve stress crack resistance, dyeability, and adhesion. Poly(butylene succinate) (PBS) is another biodegradable aliphatic thermoplastic polyester produced through the condensation polymerization. It has been blended with PLA and has found applications in the textile sector. Others include Poly[(butylene succinate)-co-adipate] (PBSA) an environmentally friendly biodegradable thermoplastic polyester made of butylene succinate adipate random copolymer, poly(butylene adipate-co-terephthalate) (PBAT), an aliphatic-aromatic liner random copolyester synthesized by polycondensation reaction of 1,4-butanediol in the presence of adipic and terephthalic acids etc. [51].

Reinforcement is generally responsible for strengthening the composite and as such to improve the mechanical properties of the composite. Thus it can be said that

composites are designed in such a way that the loads applied can be supported by the reinforcements. Reinforcements can be present in different formats e.g. spheroids, spherical, short or continuous fiber, whiskers, platelet etc. However, the most common form of reinforcements is fibers and particulates.

Fibers are classified as materials whose length is much longer than its width. They are generally known for their strength and stiffness; properties which have been taken advantage of in fiber reinforced composites. Fibers can be natural or synthetic. Synthetic fibers can be organic or inorganic based on having carbon basis. Natural fibers can be categorized based on sources: animal, plant (lignocellulosic) and mineral fiber as shown in Fig. 3.

Plant-based fibres are classified according to the part of the plant where they are obtained such as leaf, seed/fruit, stem and bast. Properties of natural fibres vary considerably depending on the fibre diameter, structure, degree of polymerization, crystal structure and source, whether the fibres are taken from the plant stem, leaf or seed, and on the growing conditions. Generally, plant fibres consist of cellulose,

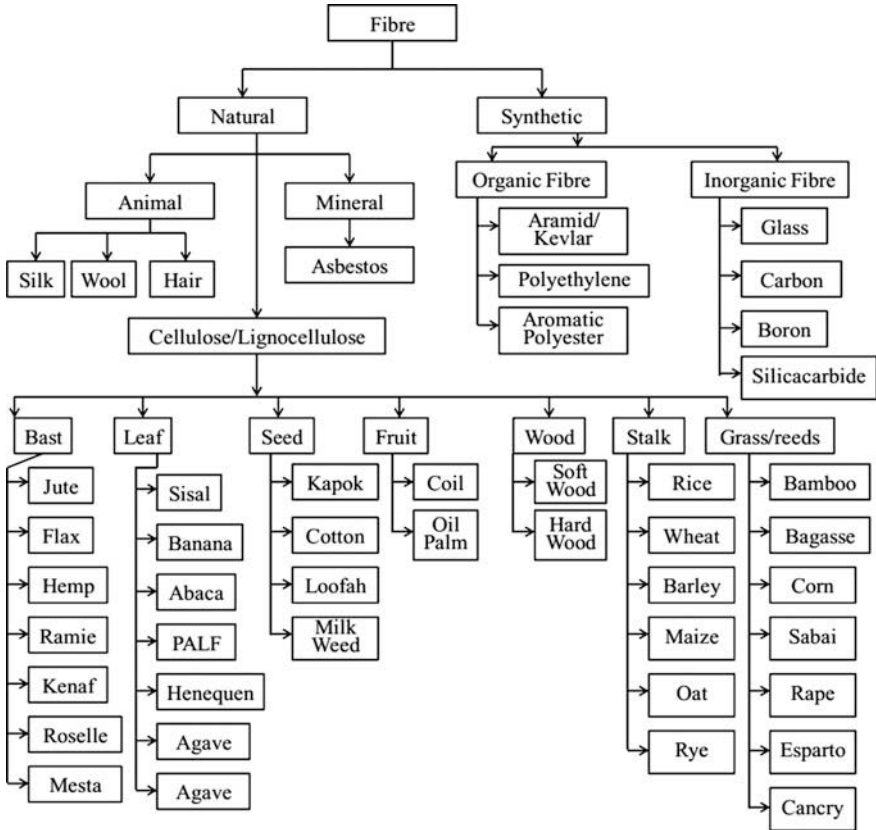


Fig. 3 Classification of fibers [52]

hemicellulose, lignin, pectin and waxes. Cellulose is a linear condensation polymer consisting of D-anhydroglucopyranose units joined together by β -1,4-glycosidic linkages. The molecular structure of cellulose, which is responsible for its supramolecular structure determines many of its chemical and physical properties. In the fully extended molecule, the adjacent chain units are oriented by their mean planes at the angle of 180° to each other. Thus, the repeating unit in cellulose is the anhydrocellulobiose unit, and the number of repeating units per molecule is half a degree of polymerization which may be as high as 14,000 in the native cellulose [53]. It provides strength, stiffness and structural stability of the fiber [54, 55]. Reinforcing efficiency of natural fiber is depends upon the nature of cellulose and its crystallinity. Depending on the type of fibre, cellulose has its own cell geometry which is responsible for the determination of mechanical properties of plant fibres [53, 56] (Fig. 4).

Hemicellulose occurs mainly in the primary cell wall and has branched polymers containing five and six carbon sugars of varied chemical structures. It differs from cellulose in three aspects firstly it contains several sugar units, exhibits a considerable degree of chain branching containing pendent side groups give rise to its ion crystalline nature and its degree of polymerization (DP). In the case of hemicelluloses it is 50–30 but in cellulose is 10–100 times more than that of hemicelluloses. Hemicellulose is very hydrophilic, soluble in alkali and easily hydrolyzed in acids [58]. Hemicellulose found in the natural fibers is believed to be a compatibilizer between cellulose and lignin [53].

Lignin is a complex hydrocarbon polymer with both aliphatic and aromatic constituents and it is totally insoluble in most of the solvents and can't be broken down into monomeric units. It is considered to be a thermoplastic polymer having a glass transition temperature of around 90°C and melting temperature of around 170°C . It is totally amorphous and hydrophobic in nature. It is not hydrolyzed by acids, but soluble in hot alkali, readily oxidized and easily condensable with phenol [55, 58] hence it often used to partially replace phenol in the phenolic and lignophenolic pre-polymers to produce composites with thermoset matrices. Lignin keeps the water in fibers, acts as a protection against biological attack and as a stiffener to give stem its resistance against gravity forces and wind [53].

Pectin is a collective name for heteropolysaccharides. They provide flexibility to plants. Pectin structure is complex and their side chains are often cross-linked with the calcium ions and arabinose sugars [58]. Pectin is soluble in water only after a

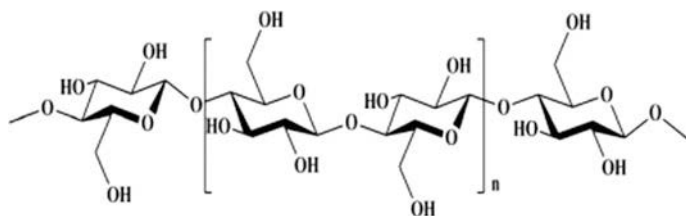


Fig. 4 Chemical structure of cellulose [57]

partial neutralization with alkali or ammonium hydroxide. Pectin is normally removed so as to separate cellulose from hemicellulose in stems. Waxes make up the last part of fibers and they consist of different types of alcohols [58]. They are insoluble in water as well as in several acids. The lignin, hemicelluloses and pectin provide the adhesive to hold the cellulose framework structure of the fiber together. Natural fibers are also composed of a small amount of organic (extractives) and inorganic (ash) components. Organic extractives are responsible for the colour, odour and decay resistance, and inorganic matters enhance abrasive nature of the fiber [55]. It is pertinent to point out that cellulose is one of most common biopolymers on earth and has found applications in various industries.

Animal-based fibers are derived from the hair, wool, and silk comprising mainly of protein and silk. Hairs and wools are made of protein and got from creatures e.g. Sheep's downy, goat hair, horse hair, alpaca hair, and so forth. Silk fiber is the filaments gathered from the dry saliva of bugs or crawling creatures cocoons. Avian strands are the fiber from fowls [59].

With regards to particulates, shells like an eggshell, periwinkle shell with calcium base are very common. Agrowastes like rice husk, bagasse ash, husks, wood dust etc. are on the side with regard to having a cellulose base. For use as particulate reinforcement is also clays. Clays are one of the most important minerals in the earth and have found varied applications in many sectors [60]. Although they are known to be hydrophilic, Nanotechnology has made it possible for a modified class of clay called nanoclay which have been found to improve quality of the product, save cost and doesn't harm the environment [61].

2.2 *Various Processing Methods*

Processing of PMCs entails a blend of both thermal and or mechanical process. However, a processing method to be used depends on the type of resin (thermoplastic or thermoset), nature of reinforcement (fiber or particulate) and even the size of the reinforcement (micro or nano-sized) [62]. In some processes, the matrix and reinforcement are combined in the mould whereas in some the reinforcement is incorporated into the matrix in a pre-moulding operation which is later used in moulding the composite part [62]. Generally, the extent of dispersion of a filler in a matrix determines the properties. Unlike in micro-sized particles where interfacial adhesion shows the extent of wettability, nano-sized particulates especially nanoclays are dependent on the extent of exfoliation and intercalation. Thus to achieve a homogenous mix, less conservative techniques have been developed. The characteristics of various processing techniques for eco-friendly composites will be highlighted and discussed here. However, the selection of the right process based on the geometry of the part, scale, cost and mechanical properties is key in achieving optimum properties from the composite.

Hand lay up

This is one of the most popular fabrication technique. Known for its low cost compared to other techniques, it involves the manual application of a laminate ply or woven fibers before the resin is poured to wet the fibers. A roller is used to ensure the uniform spread of the resin on the fibers and remove entrapped air before the composite is allowed to cure. Though it offers a cheap method of producing composites especially for academic researchers, its industrial application is minimal because of low production rate and limited volume fraction of the reinforcement that it can accommodate [63]. Also mixing of the resin is dependent on the operator's skill and this method is mostly used for resin with a low viscosity like epoxy, polyester, phenol etc. Many works on natural fiber reinforced polymer matrix composites have been done using this method.

Spray up method

In spray up method, chopped fibers and resin are made to mix at the tip of a spray nozzle before falling into an already prepared mould. Just like in hand lay-up, rollers are used to remove entrapped air. Spray up technique offers an efficient way of producing thermosetting PMC as it can accommodate more variety part sizes as well as the higher volume fraction of reinforcement compared to hand lay-up. But the skill of operator/worker plays a vital role in determining the final quality of the composite part produced [63].

Bag moulding

This involves preparing continuous prepregs which are continuous sheet of fibers already preimpregnated with a layer of the thermoset resin, staking up precuts of the prepregs in a mould, covering with a thin polymer film and curing in an autoclave or a press at a higher temperature. In this method, pressure and vacuum are used to remove excess resins, consolidate the layers of the prepregs while the resin cures. Though a slow and labour-intensive method, it is used in producing parts with accurate fiber orientation, minimal void and controlled fiber volume fraction [62].

Filament winding

Known for producing hollow structural parts using thermosetting resins, it entails pulling a band of continuous fibers through a tank filled with catalyzed resin which will be wound round a rotating mandrel. The resin-coated fiber band is also traversed back and forth along the length of the rotating mandrel to create a helical winding pattern. The winding angle can be varied by controlling the mandrel speed and the traversing rate of the fiber band. The part is cured in an oven, and the mandrel is removed to create a hollow shape. In some applications, such as oxygen tanks, the mandrel is not removed after curing, and it becomes a part of the structure. One of the primary advantages of filament winding is the ability to control resin usage and minimal fiber is used. However, the difficulty in laying fiber exactly along the length of the component and high cost of mandrels especially in producing large components makes it less economical [62, 63].

Pultrusion

This is a process of producing long, straight composite part using continuous fibers. This method of pulling continuous fibers through a tank containing already catalyzed thermosetting resin then through a heated die where the resin-coated fibers are cumulated to form the shape being produced. Curing takes place as they move along the length of the die. For industrial application, parameters like the method of preheating, die temperature, pulling speed has to be set down. Pultrusion provides a fast and economical way of impregnating and curing fibers using an enclosed impregnation area thus limiting volatile emission. On the other hand, it is limited to the production of constant or nearly constant components and cost of heating the dies cannot be overlooked. However, it can be used in producing natural fiber reinforced polymers composites [63].

Compression moulding

Here the composite materials are laid between two moulds before heat and pressure are applied for curing to take place. Varieties of this method exist including bulk moulding compound (BMC), thick moulding compound (TMC), sheet moulding compound (SMC) and wet lay-up compression; all depending on the type of moulded materials [63]. It is known for the rapid production of large quantities of complex parts, part design flexibility; however, the tooling cost is high due to high pressure involved though it can be used to produce parts with the good surface finish.

Resin transfer moulding

This is a very popular liquid composite moulding method. Here dry fiber preform is placed in the mould and thermosetting resin already mixed with a catalyst or curing agent is injected into the mould under pressure. As the prepolymer resin enters the mould, it displaces air and wets the dry fiber with curing occurring at room or elevated temperature. Compared to bag moulding and compression moulding, tooling cost is low as the resins are transferred under low pressure. However improper impregnation of parts can occur leading to increased cost due to the scrapping of the parts. A variant of this method called structural reaction injection moulding (SRIM) is used in cases of resins like polyurethanes due to the high reactivity of the chemicals used in making the matrix.

However, due to the introduction of phases with varying morphologies and at the same time need for proper dispersal, new methods have also come up. Some of these include extrusion followed by injection moulding, melt extrusion, melt compounding followed by compression moulding, direct melting, one step in situ solution polymerization, injection moulding and solution casting after gelatinization [64]. Extrusion is a process of converting a raw material into a product of uniform shape and density by forcing it through a die under controlled condition. It is basically used for thermoplastic composites. It can modify the thermal stability, mechanical strength, elongation, adhesive strength and other mechanical properties of polymers [65]. A variant of extrusion method called solid-state extrusion process

which involves solid deformation of polymers which makes it possible to highly oriented structures in quite substantial cross sections for engineering and scientific studies have been studied by [66] where a haul-off is used to pull the composite through the die. Injection moulding is one of the most widely used polymer matrix composite processing techniques. Here the filler used is either short fibers or particulates. In this method, polymer granules and reinforcement are fed into a heated rotating barrel through a hopper. Heat in the barrel melts the polymer pellets while the shearing action of the rotating barrel mixes the polymer melt and filler. The molten composite is then injected into a mould. One of the widely used types of the extruder is the twin screw extruder. However other parameters like speed, temperature etc. affect the properties of the mould. Bledzkiet al. used this method to fabricate NFC composite [43].

Intercalation method is a top-down approach that is based on the exfoliation property of layered silicates like montmorillonite, mica and other nanoclays. Here clays already modified with organic surfactants like amino acid, imidazolium, and phosphonium salts are used as inorganic fillers by intercalating an organic compound into the interlayer space of the silicate. Treatment of the silicate is done to make it be hydrophobic enough to properly mix properly with the matrix. Intercalation can be direct (mechanical technique), in situ (chemical technique) or via melt compounding [67]. Nevertheless one of the major problems with this technique is incompatibility [48]. Unlike in the normal intercalative method, In situ polymerization method or in situ intercalative polymerization method involves polymerization reaction. Here nanoparticles are mixed with a monomer or monomer solution and the polymerization reaction is allowed to take place. Proper dispersion of the particulate in the monomer is very important in this method and as such surface modification is often carried out [67]. This method allows surface modification on the nanofillers without drying. It is one of the most successful methods of producing polymer nanocomposites. Examples include Polyamide 6—clay nanocomposite [48].

Solution polymerization involves exfoliating layered nanoparticles like silicates into single layers using a solvent in which the polymer is soluble. Predispersed in a solution of the polymer, allows the fillers to be finely dispersed in the polymer matrix after which the solvents are later removed by evaporation. However certain polymers are not soluble in conventional low boiling point solvent which limits the application of this method to some polymer matrix [67]. Nevertheless, use of ultrasonic waves can be employed if there is low viscosity. Melt compounding or blending involves mixing the nanofiller with a polymer melt. Unlike solution polymerization, no solvent is required however the level of intercalation depends on the compatibility between the matrix and filler. Melt compounding depends on the shear can be less effective than in situ polymerization in producing an exfoliated nanocomposite. Thus for better exfoliation ultrasonic mixing which provides high shear force has been proposed. However, due to the weakening of this force when the viscosity is high, it would be difficult to achieve uniform dispersion of the nanofillers into the polymer melts on a large scale [67]. This is one area where solution polymerization has an upper hand [48]. Other methods include emulsion

polymerization which has the advantage of no environmental concern as in solution polymerization but involves the use of surfactant and stirring, ultrasound irradiation etc.

Although various techniques exist, new ones continue to evolve with respect to the manufacturing of composites. Tanahashi [67] developed a new method of fabricating nanocomposites that are based on the conventional simple melt compounding technique and does not require surface modification. The concept is based on the fracture strength of agglomerates of the dispersed particles and involves preparing agglomerates with a porous structure, before melt compounding. Nevertheless, the key to successful dispersion lies in having agglomerates with a low strength which can be easily broken down by shear stress induced during melt compounding. With respect to the environment, this method was seen to be environmentally friendly since it doesn't require chemicals used in the in situ and sol-gel method, is more suitable for large-scale production since its more compatible to industrial processes like extrusion and injection moulding. Moreover, it allows for the use of polymers not suitable for in situ polymerization, sol-gel and solution mixing [67]. In likewise manner new concepts like automated tape lay-up (ATL) and automated fiber placement (AFP) which entails the introduction of computer-guided robotic are also enroute. However it is pertinent to point out that each method is unique with its shortfalls and advantages, integration can also be done to achieve better results. For instance in polymer nanocomposites, better intercalation has been achieved using an extruder with the polymer in a melt. Moreover, the condition of the reinforcement (natural fibers and particulates) should always be taken into account when considering the method of choice.

2.3 Effect of Processing Technique

Literature reviews have shown that processing techniques affect the properties of the composite. Diez E. A. while using extrusion method to produce a semiconductive polymeric composite observed that extrusion temperature and screw speeds did not have a much significant effect on the electrical properties of the composite. But with respect to screw type, use of conventional screw gave better result compared to barrier screw [68]. Processing conditions like draw ratio, temperature, speed have been observed to affect the properties of composites produced by extrusion [66, 69]. Cai et al. from their work on the effect of temperature and draw ratio on the mechanical and morphological properties of a wood-polymer composite made with polypropylene and wood flour observed that density, tensile strength and tensile modulus increased with draw ratio. This was seen to be due to a high degree of orientation and morphology achieved due to use of solid state extrusion. Elongation at the break, on the other hand, decreased with increasing draw ratio which was attributed to increase in crystallinity. With regards to temperature, density and tensile modulus decreased with increasing die temperature whereas elongation at break and tensile strength increased [66].

Feldmann M. et al. studied the influence of process parameters on the mechanical properties of a bio-based polymer composed produced via extrusion. Polyamide from castor oil was used as matrix while chopped man-made cellulose was used as reinforcement. Thermogravimetric analysis shows different screw configurations and processing temperatures have an influence on the mass loss of the compounds. Also, different screw configurations and temperature settings led to minor deviations in the mechanical properties and the morphological structure of the bio-compounds [70].

Kadam and Mhaske [71] also looked at the effect of reprocessing via extrusion on the properties of nylon 6/talc nanocomposite and observed that reprocessing of the composites up to three times leads to a decrease in mechanical properties. However, with regard to the concentration of nanotalc, the mechanical properties increased showing that the decrease in mechanical properties of the composite was due to degradation of nylon 6 as was also confirmed by thermal and rheological analysis. Poletto M. looked at the effect of processing condition on cellulose fiber reinforced polystyrene composite. The result of his study showed that extruding at 400 RPM improves the mechanical and dynamic properties of a composite due to a reduction in fibre size, increasing the superficial area of the fiber and as such more contact area with matrix [72]. Reprocessing has also been observed to affect the properties of composites especially when recycling is of primary concern.

Nevertheless, the effect of processing parameters also seems to be a function of the polymer involved. Peinado V. et al. found out from their work on the mechanical and rheological properties of reinforced PLA that reprocessing and recycling via extrusion of this bio-based material doesn't have a significant effect on the mechanical properties. A number of extrusions were also seen to not have any effect on the flexural and tensile modulus of the virgin matrix and composite. Rheological studies also showed that on extrusion, the viscosity of natural PLA decreased as expected due to chain degradation especially above 190 °C. However, the composite having nanoclay showed high viscosity values [69].

Although processing parameters affects the interfacial adhesion, addition of compatibilizers do affect the end product as observed by Gunning et al. [65] who explored the effect of compatibilizer content on the mechanical properties of a bioplastic like polyhydroxybutyrate (PHB) produced via hot melt extrusion. The result showed that addition of compatibilizers to PHB resin reinforced with hemp, jute and lyocell fibres respectively increases resistance to water absorption, improves fiber dispersion, melt flow index and improved flexural modulus. Likewise some processing techniques like film stacking requires pressure, the effect of pressing parameters like pressure and pressing time have been seen to have significant effect on properties of eco-friendly composites [73] from the study on PLA/Flax fibre, PLA/Jute fibre and PLA/cotton fibre composite prepared via film stacking showed PLA/Flax fiber showed the best combination of tensile and flexural strength. All in all with higher pressure, and longer pressing time, the adhesion between the PLA and the fibers is improved which causes significant increase on the mechanical properties [74] also observed that in a polyester-kenaf fiber

composite, pressure was the only production condition that had significant impact on the mechanical and water absorption behavior of the composite.

Dispersion method has been seen to affect the mechanical behaviour of composites especially ones with nanoparticles as observed by Agubra et al. [75]. Karripal et al. [36] used ultrasonification method to disperse nanoclay particles in a hybrid composite made of epoxy, glass fibre and nanoclay. Using nanoclay ranging of 0, 2, 3, 5 and 6 wt%, they observed that tensile and flexural strength, as well as the moduli, increased up to 5 wt% fraction. This was attributed to improvement in the dispersion of nanoclay and interfacial adhesion between the matrix and nanoclay which helped in restricting chain mobility. Interlaminar shear strength (ILSS) and hardness of the composite also increased up to 5 wt% before decrease of which was attributed to lesser uniformity in the dispersion at higher weight fraction.

Morphological analysis revealed higher fiber pullout at higher weight fraction which can be due to agglomeration of the nanoclay particles and as such improper wetting. DSC scan, on the other hand, revealed a lower glass transition temperature above 2 wt% nanoclay which can be due to the alteration of chain kinetics due to interaction with the particles. Khoo et al. [16] studied the properties of poly (lactic acid) (PLA)/CNC nanocomposite prepared using solution casting technique. Cellulose nanocrystals (CNC) were synthesized by acid hydrolysis of microcrystalline cellulose (MCC) powder. Morphological analysis using Energy-filtered transmission electron microscopy (EFTEM) studies showed that the CNC exhibited needle-like structure (approximately 10–20 nm in width and 250–300 nm in length), which is a typical measurement found in wood-based nanocellulose. DSC analysis showed that CNC (up to 5 wt%) is capable of acting as nucleating agent for PLA whereas TGA analysis showed that the decomposition temperatures PLA/CNC nanocomposites were higher than that of pure PLA. Zaini A. S. S. M. et al. evaluated the effect of UV radiation on the mechanical properties of wood polymer composite produced using rice husk, waste fibre and polypropylene. The result shows that with increasing number of hours of exposure to UV radiation, the compressive strength and impact energy decreased whereas density remained barely the same [29].

3 Challenges

3.1 Drawbacks in the Processing of EFCs

The difference in hydrophilicity between polymers and reinforcement has been a core challenge in producing polymer matrix composite. This hydrophilicity results in incompatibility with the hydrophobic polymer matrix. Hydrophilicity of natural fibres indicates the high moisture absorption of the fibres which is the main reason of the weak adhesion to hydrophobic matrices and this causes the produced composites to fail in wet conditions through surface roughening by fibre swelling or

delamination. Moisture present during manufacturing will lead to poor processability and low mechanical performance of the composite. Natural fibers also have the tendency to form aggregates during processing, poor moisture resistance, inferior fire resistance, lower durability, variation in quality and price, and difficulty in using established manufacturing process. The major cause for this drawback is the presence of hydroxyl and other polar groups in natural fibres which makes them hydrophilic in nature.

Subsequent to this the majority of natural fibres have low degradation temperatures ($<200\text{ }^{\circ}\text{C}$) which are inadequate for processing with thermoplastics with processing temperatures higher than $200\text{ }^{\circ}\text{C}$. Interfacial treatments can improve this condition either through surface treatments, resins, additives, or coatings. Nourbakish et al. [38] observed that even though the eco-friendly composites showed good mechanical properties, water intake was also high which was attributed to the high content of the lignocellulosic materials present in the composite. absorbed by the cellulosic material in the composite. As mentioned, the water absorption of composites is due to the hydrogen bonding of the water molecules to the free hydroxyl groups present in the cellulosic cell wall materials and the diffusion of water molecules into the filler-matrix interface. Additionally, large numbers of porous tubular structures present in fibers accelerate the penetration of water by the capillary action [38]. Modification of the surface seems like a viable option as shown by various studies. Silane treatment is used to stabilize polymer composites reinforced with natural fibres by treating the fibres to resist water leaching. Here silicon is accumulated in the cell lumina and bordered pits of fibres thus plugging pathways for penetration of water [76].

Acrylation pretreatment of fibers provides covalent bonds across the interface. Through such treatment, the surface energy of the fibers was increased, thereby providing better wettability and high interfacial adhesion. Pretreatments with permanganate are conducted by using a different concentration of potassium permanganate (KMnO_4) solution. Plasma treatment is another effective method to modify the surface of natural polymers without changing their bulk properties. Microwave treatment, corona plasma are some of the common plasma treatment methods. The type of ionized gas and the length of exposure influenced the modification of the wood and synthetic polymer surfaces. Most of the chemical treatments have been found to decrease the fiber strength due to breakage of the bond structure, and disintegration of the noncellulosic materials but silane and acrylation treatment lead to the strong covalent bond formation and the strength was enhanced marginally.

Cruz and Figueiro [77] in his review of the effect of different modification method on the properties of eco-friendly composite showed that modification improves the properties of the composite by creating sites for proper interfacial adhesion. Chern et al. [78] in their work on the effect of addition of hydrophilic nanoclay on oil palm mesocarp fiber-reinforced polylactic acid/polycaprolactone blend observed that addition of the hydrophilic nanoclay not only led to band shift

as shown by FTIR test but improved tensile, flexural and impact strength thus suggesting that it can act as a compatibilizing agent.

Thermogravimetric analysis showed that improved thermal stability which was attributed to the ability of clay to hinder permeability of volatile degradation. Also, an improved glass transition temperature was also observed due to the incorporation of clay. However soaking time, the concentration of solution etc. helps to determine the success of this method. Longer soaking time leads to fiber degradation and as such reduction in mechanical properties of the composite. Use of compatibilizer/coupling agents has also been tried as an alternative means of improving the adhesion between the fiber and matrix [43]. Observed that addition of MA-PP to barley husk, softwood and coconut shell improved the tensile strength. Zaaba et al. [79] in their work on modification of peanut shell powder with polyvinyl alcohol showed that the modified peanut shell powder showed better interfacial adhesion to the matrix than the unmodified one.

Also, the cost of using chemicals to improve the surface of natural fibres have been highlighted as one of the shortfalls of using natural fibres. However [65] found that use of cost of using compatibilizers like is substantially when compared to the virgin matrix, but same cannot be said of another method of improving the interfacial adhesion. Lower thermal stability of most natural fibers has made processing of EFCs difficult as high processing temperature leads to fiber degradation. This is supported by morphological and thermal analysis of most EFCs. The high variability in diameter and length of fibers is another major drawback. This can be as a result of the environment where the fibre is obtained from.

3.2 Work on Eco-friendly Composites and Effect on Properties

Composites generally are materials where the addition of reinforcement to a matrix helps in bringing out a new class of material with more improved properties. In composites, PMCs have come out as the most prevalent [80] due to the ability to combine materials from different sources and morphologies i.e. particulates and fibers, natural and synthetic, micro, micron and nano to produce a more superior material. Use of different kinds of reinforcement in PMCs have been studied for decades ranging from oxides like Al_2O_3 , MgO, SiO_2 , Fe_2O_3 ; fibers like PET fibers; carbides like SiC etc. [81]. However, most of the studies started with the use of synthetic reinforcement but the incorporation of green fillers in a bid to create a more environmentally friendly material has also been seen to be able to perform comfortably well in various regards thus pushing for a total replacement of synthetic materials with green based ones. With regards to tribology, Hassan [82] showed that addition of eggshell particulates to polyester improved both the compressive strength and hardness of the composite (Figs. 5, 6 and 7).

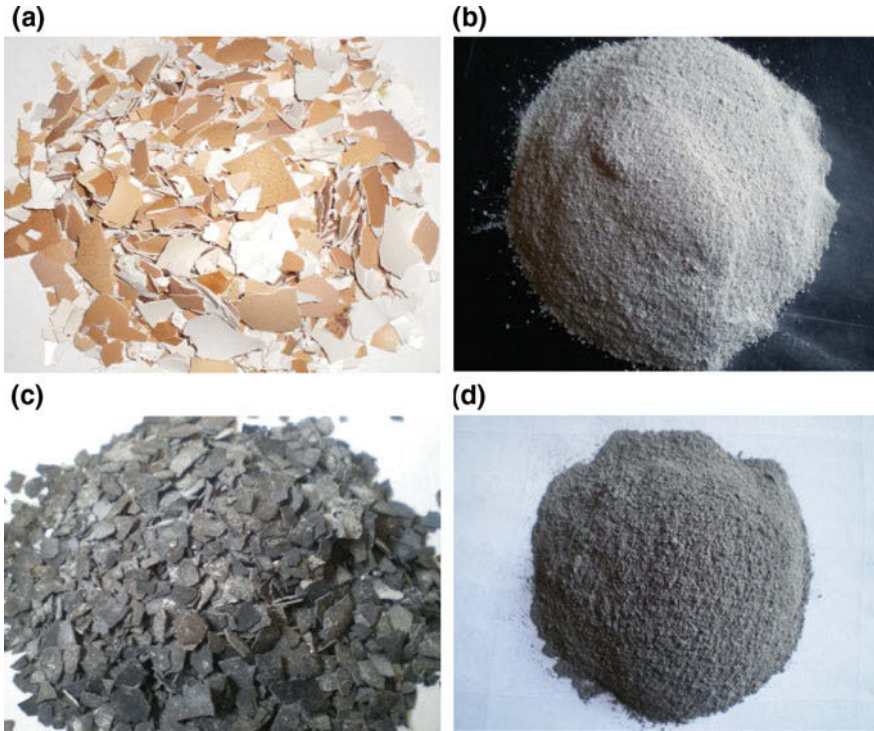


Fig. 5 Eggshell samples. **a** Uncarbonized, **b** uncarbonized (ground), **c** carbonized, **d** carbonized (ground) [82]

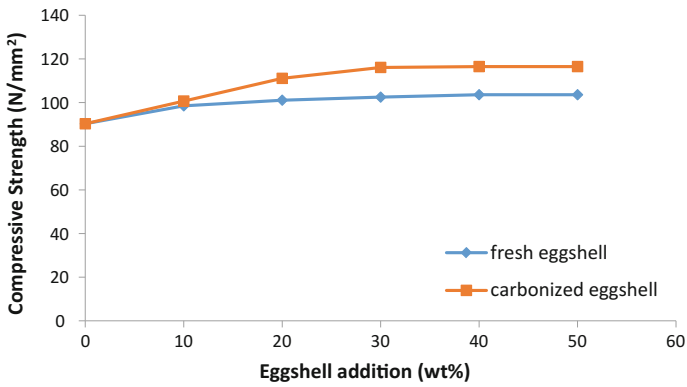


Fig. 6 Variation of compressive strength of polyester/eggshell particulate composites with wt% eggshell addition [82]

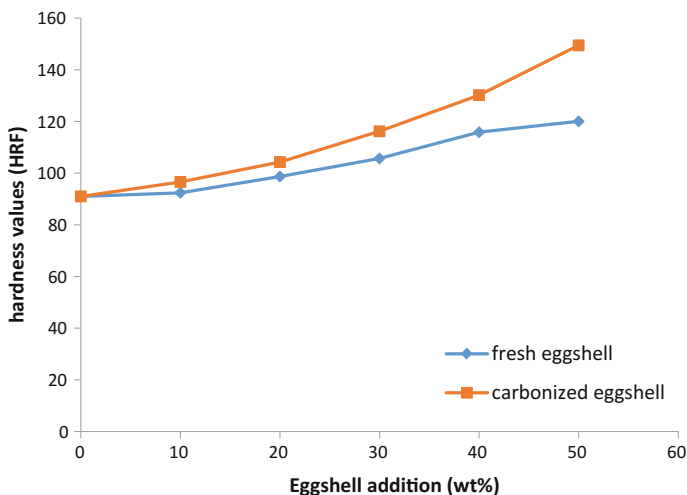


Fig. 7 Variation of hardness value of polyester/eggshell particulate composite with wt% eggshell addition [82]

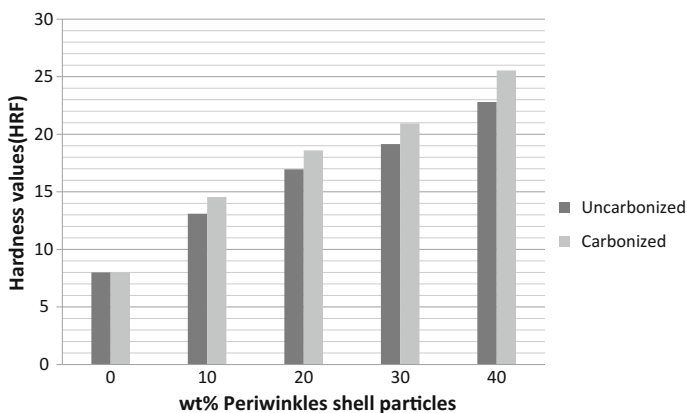


Fig. 8 Variation of hardness values of the composite with periwinkles particles addition [81]

Aigbodion et al. [30] show that incorporation of Baggase ash in recycled low-density polyethylene improved the wear resistance. Similarly, Aigbodion and Asuke observed that carbonization of agro-wastes like periwinkle shell particles before use as reinforcement also affects properties like wear resistance and hardness where the carbonized particles showed better hardness and wear resistance [81] (Figs. 8 and 9).

Likewise [83] showed that with increasing weight fraction of particulates of orange and pomegranate, the composite showcased better wear and hardness result. Atuanya et al. [84] also observed that addition of bean pod particulates to

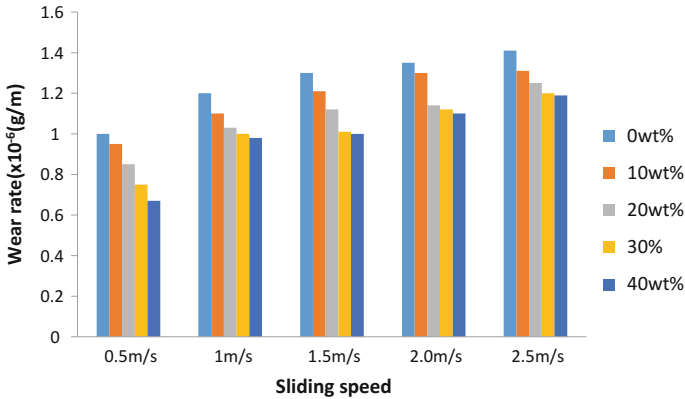


Fig. 9 Variation of wear rate with sliding speed for carbonized periwinkles shell particles [81]

low-density polyethylene led to an increased hardness, flexural and tensile strength. The similar result has also been observed by [31, 85, 86]. Other agro-wastes like a chicken feather, hooves and horns have shown improved dielectric and flame resistance in resins like polyester, and epoxy [87–89].

According to Omah et al. [90], the addition of cassava cortex to polyester improved the dielectric properties. A similar result has also been observed by Kiew et al. [88]. Use of natural fibers like jute, flax, hemp etc. has also shown the tremendous result. From the review carried out by [91, 92], the addition of these fibers have not only helped to increase the mechanical properties but also reduce cost due to the decreased wearing of tools, reduced dermal and respiratory irritation, enhanced energy recovery [93]. Mohanta N. and Acharya S. K. showed that incorporation of *Luffa Cylindrica* fibres in epoxy resin increased the tensile, flexural, impact and interlaminar shear strength of the composite [19] Sound damping properties of composites have improved due to use of natural fibres [94].

Particle size has been observed to play a major role in the properties of composites. Ameh et al. [95] studied the effect of particle size on properties of date palm seed reinforced polyester composite. Optimum tensile strength was observed at the lowest particle size whereas highest hardness was showcased by the composite with highest weight fraction and particle size. Also, water absorption behaviour was observed to decrease with decreasing particle size. Shokoufa et al. [96] worked on the effect of the addition of nanoclay to wheat stalk flour reinforced polypropylene composite. Improved flexural strength was observed and was seen to be due to the high apparent coefficient of nanoclay particles which helps to enhance the interface between the two phases. Singla et al. [97] experimented on the possibility of using lignin powder as reinforcement for producing a bio-based composite. PLA was used as matrix while the weight fraction of lignin was varied. Tensile properties were seen to increase on the addition of the lignin powders which was also supported by the SEM micrograph which showed significant interaction between the components. Impact strength decreased due to coarse and non-uniform shaped

lignin particles which cause stress concentration in the PLA matrix or because of intrinsic brittleness of PLA and rigidity of lignin particles. Nevertheless, DSC and FTIR analysis showed the existence of intermolecular interaction with the peaks of hydroxyl groups of lignin and carbonyl groups of PLA in the FTIR spectra shifting toward lower wavenumbers thus indicating the presence of hydrogen bonding interaction between them.

Natural rubber (NR) and epoxidized natural rubber (ENR) are renewable resources that exhibit a unique combination of toughness, flexibility, biocompatibility and biodegradability. Its low cost makes it was an alternative to improve the toughness of brittle thermoplastics like PLA. Pongtanayuta et al. [98] compared the morphology, crystallization behaviour, thermal stability and mechanical properties of PLA/NR blends to that of PLA/ENR blend. Morphological examinations showed a coarse structure which is due to partial compatibility between the blends. However, NR at 10% weight gave optimum property though, at a high content of NR, tensile properties did suffer. Addition of ENR led to a reduced crystallization ability, thermal resistance and tensile properties of the blend. The rubber particles behave as stress concentrators enhancing the fracture energy absorption of brittle polymers and ultimately results in a material with improved toughness. The rubber particles behave as stress concentrators enhancing the fracture energy absorption of brittle polymers and ultimately results in a material with improved toughness.

Even hybrid of these materials has not also fallen short of expected properties. Hybrid composite of coconut coir/chicken feather showed improved flexural strength [99]. Saikishore et al. [100] also observed that addition of chicken feather improves impact strength and hardness of the composite. Njoku et al. [101] showed that compatibility between sisal and periwinkle in sisal/periwinkle/E-glass fiber/polyester composite led to improved tensile strength.

Polymer blends have been seen as one of the ways of improving the properties of biodegradable composites. Blending polymer is a simple technique to enhance the property of the pure polymer. The benefits of blending include providing new materials with desired properties at low cost, quick formulation changes, plant flexibility, high productivity and reduction of the number of grades that need to be manufactured and stored [102]. Hassan et al. [103] also looked at PLA/PBS blend produced via extrusion. Thermal analysis shows that thermal stability of the blends was higher than that of pure PLA and the weight loss of PLA/PBS (40/60 wt%) was lower than neat polymers. DSC thermograms of blends indicated that the thermal properties of PLA did not change noticeably when blended with PBS. DMA analysis shows that storage modulus of the blend was lowered which indicated the increase of molecular mobility by adding PBS due to lower glass transition. Increasing PBS content led to a decrease in tensile strength because PLA has a higher tensile strength than PBS and also due to poor stress transfer across the phase of each polymer. Elongation was increased with increased PBS whereas fracture behaviour changed from brittle to ductile as PBS increased. However, the impact strength of the blends was higher than neat PLA [104]. Improvement in impact strength might be due to the high flexibility of PBS. All in all PLA and PBS have shown partial miscibility [105]. The tensile strength and modulus of blends

decreased with the increasing PBS content. But impact strength has improved about two times compared to pure PLA. Darie-Nita et al. [106] blended Poly(lactic acid) (PLA) and poly(butylene succinate) (PBS) using a twin screw extruder. Poly(butylene succinate) (PBS) is a biodegradable polymer, which derived from petroleum resources. PBS has good as well as elasticity and crystallization thus the addition of PBS could enhance the elasticity of PLA/PBS blend fibers. Tensile properties of the blend showed good tensile modulus and strength when adding PBS up to 30 wt%. it was also observed that increasing the PBS contents in the blends made it difficult for spinning Nevertheless PLA/PBS blends of 90:10 ratio could be spun and successfully collected at the take-up speed of 50 m/min and can find application in textile industry.

However, the properties of polymer blend are limited by immiscibility between neat polymers. To solve this problem, compatibilizers are often used as additives to improve the compatibility of immiscible blends. The compatibilization could achieve optimization of the interfacial tension, stabilize the morphology and enhance adhesion between the phases in the solid state [102]. The effect of polypropylene/poly(lactic acid) weight ratios on the properties of blend films compatibilized with polypropylene grafted-maleic anhydride has been investigated. FTIR spectra confirmed the interaction between compatibilizer and polymers whereas morphological analysis showed distinct phases of polypropylene and poly(lactic acid). Increasing of PLA content led to a decrease in melting temperature and crystallinity. Tensile increased with increasing PLA content, while elongation at break was drastically decreased however the blend proved to be a better barrier for oxygen than for water vapour [102].

Use of self-reinforcing polymers have also been looked at self-reinforcement is a situation whereby the same polymer is used as both matrix and reinforcement. Jia et al. [105] compared properties of PLA self-reinforced (PLA-SR) to that of PLA-PBS blend. The composites were made by film stacking and subsequent hot pressing. Tensile tests show that the tensile strength and elastic modulus of the PLA SR composite are higher than those of the PLA-PBS composite by more than 40%. This is due to the PLA film itself having better tensile properties than the PBS film and also due to the stronger interfacial adhesion between the PLA fibre and the PLA. The toughness of the PLA-PBS composite is more than three times higher than that of the PLA SR composite because matrix cracking and fibre/matrix debonding dissipate energy to give a more progressive fracture. This work goes on to show that the stiffness or toughness of a composite can be tailored to specific needs by selecting fibre and matrix constituents. Therefore if damage resistance and tolerance are required, the PLA-PBS composite is more preferable whereas, for stiffness and strength, the PLA SR composite should be offered a better option [105].

4 Current Opportunities

High demand has led to a rise in production capacity for eco-friendly polymers and its composites. The natural fibers such as flax or sisal have relatively high stiffness and are low in cost. Agrowastes like rice husk, bagasse, egg shells, coconut shells are relatively abundant. Annually, billions of tons of agro wastes and natural fibers which would have been a major source of income are burnt on the field producing all to take optimum advantage of the constituents in order to produce superior and a more economical material [7]. Similarly biodegradable polymers market is expanding year by year due to the demand from various sectors. As at 2015, the production capacity of biodegradable polymers is expected to be approximately 2.8 million ton/year [50].

4.1 Future Opportunities in EFC

The interest in biopolymers has continued to grow. In the food packaging industry, use of eco-friendly plasticizers like epoxidized soya bean oil, lactide, PLA oligomer, poly(ethylene glycol) (PEG 2000 or PEG2) poly(ethylene glycol) (PEG 4000) and for PLA films processing has been studied [106]. Wood-based fillers is another area that is bound to continue growing. Past decade has seen a rapid growth in the wood plastic industry. This is due to low cost and reinforcing capacity [107]. The main application areas of wood flour filled composites are the automotive and building industries in which they are used in structural applications as fencing, decking, outdoor furniture, window parts, roofline products, door panels, etc. There are environmental and economic reasons for replacing part of the plastics with wood but the wood could also work as reinforcement of the plastics. The elastic modulus of wood fibres is approximately 40 times higher than that of polyethylene and the strength about 20 times higher [107].

Continual improvement in the understanding of the chemistry behind the interplay between the reinforcement and matrix have continued to open more ground for an increase in the areas of application of various eco-friendly materials. However, the challenges for the future are in terms of processing, characterization and the mechanisms governing the behaviour of these advanced materials. The primary determinant of the performance of a composite material is the interface between the reinforcing fibre/particulate and matrix.

5 Conclusions

According to food and agriculture organization 2014 handbook, apart from enteric fermentation; a major contributor to greenhouse gas emission comes from rice cultivation, crop residue, manure management and burning crop residue [108].

Therefore in the bid to maintain sustainable development of environmentally compatible composites at low cost, the study of this class of materials has continued to pull in increasing research interest with amazing results recorded for various applications in many areas. Natural fibers especially the lignocellulosic ones are known for their hydrophilic. However, surface modification and blending have proved to be a way of modifying the properties. Nanotechnology has also shown to be a bright burner in the drive towards a sustainable environment by providing an avenue for environmentally friendly nanofillers to be incorporated as fillers.

All in all, EFCs promises a set of sustainable materials for the future. Though the tensile strength of composites is dependent on matrix properties whereas modulus is dependent on filler properties, use of environmentally friendly materials for both can allow for proper tailoring of the properties of the composite so as to meet both environmental policy regulation and customer satisfaction.

Our ability to solve the engineering challenges of today and tomorrow is still being driven by the cost and availability. One needs to overcome this challenge to achieve the required degrees of success. Our understanding of how materials interact, how they can be reliably integrated with combinations in functional requirements have to be explored. The challenges, as well as the opportunities, will be in the areas of **materials development, synthesis, fabrication, integration, characterization** and **validating the recycling technologies**, which of course aids capitulate a lot of potential in Innovating new ideas.

References

1. Mitra BC (2014) Environment friendly composite materials: biocomposites and green composites. *Defence Sci J* 64(3):244–261
2. Layth M, Ansari MNM, Pua G, Jawaid M, Islam MS (2015) A review on natural fiber reinforced polymer composite and its applications. *Int J Polym Sci* 1–15. <http://dx.doi.org/10.1155/2015/243947>
3. Swaroop KV, Vinod NR, Rupendra M (2017) Numerical and experimental analysis of a natural fiber reinforced composites. *Int J Mech Prod Eng* 5(11):25–27
4. Anne B (2011) Environmental-friendly biodegradable polymers and composites. In: *Integrated waste management, vol I*. <http://www.intechopen.com/books/integrated-wastemanagement-volume-i>
5. Azwa ZN, Yousif BF, Manalo AC, Karunasena W (2013) A review on the degradability of polymeric composites based on natural fibres. *Mater Des* 47:424–442
6. Material resources, productivity and the environment: key findings. www.oecd.org. Accessed 5 Feb 2018
7. Islam MS, AhmadMB Hasan M, Aziz SA, Jawaid M, Haafiz MKM, Zakaria SAH (2015) Natural fiber-reinforced hybrid polymer nanocomposites: effect of fiber mixing and nanoclay on physical, mechanical and biodegradable properties in hybrid nanocomposite. *BioResources* 10(1):1394–1407
8. Rahmat MB, Ab-Wahid WF, Ahmad M (2015) Effect of nanoclay on tensile strength of wood plastic composite made from malaysian rice husk and polypropylene. *Int J Mech Prod Eng* 3(10):61–63

9. Rana S, Fanguero R (eds) (2016) *Fibrous and textile materials for composite applications*. Springer, Berlin
10. Adeosun SO, Lawal GI, Balogun SA, Akpan EI (2012) Review of green polymer nanocomposites. *J Miner Mater Charact Eng* 11(4):385–416
11. Asokan P, Firdoos M, Sonal W (2012) Properties and potential of bio-fibres, bio-binders, and bio-composites. *Rev Adv Mater Sci* 30:254–261
12. Abilash N, Sivapragash M (2013) Environmental benefits of ecofriendly natural fiber reinforced polymeric composite materials. *Int J Appl Innov Eng Manage* 2(1):53–59
13. Vroman I, Tighzert L (2009) Biodegradable polymers. *Mater* 2:307–344. <https://doi.org/10.3390/ma2020307>
14. El-Sherbiny IM, Ali IH (2015) Eco-friendly electrospun polymeric nanofibers-based nanocomposites for wound healing and tissue engineering. In: Thakur VK, Thakur MK (eds) *Eco-friendly polymer nanocomposites processing and properties*. Springer, New Delhi, pp 399–431
15. Chen HN (2012) An overview of degradable polymers. <https://doi.org/10.1021/bk-2012-1114.pr002>
16. Khoo RZ, Ismail H, Chow WS (2016) Thermal and morphological properties of poly (lactic acid)/nanocellulose nanocomposites. *Procedia Chem* 19:788–794. <https://doi.org/10.1016/j.proche.2016.03.086>
17. Kocak D, Merdan N, Yuksek M, Sancak E (2013) Effects of chemical modification on mechanical properties of *Luffa cylindrica*. *Asian J Chem* 25(2):637–641
18. Mohanta N, Acharya SK (2013) Tensile, Flexural and interlaminar shear properties of luffa cylindrical fibre reinforced epoxy composites. *Int J Macromol Sci* 3(2):6–10
19. Pai AR, Jatap RN (2015) Surface morphology and mechanical properties of some unique natural fiber reinforced polymer composites—a review. *J Mater Environ Sci* 6(4):907–917
20. Panneerdhass R, Baskan R, Rajkumar K, Gnanavebabu A (2014) Mechanical properties of chopped randomly oriented epoxy—luffa fiber reinforced polymer composite. *Appl Mech Mater* 591:103–107
21. Gupta G, Gupta A, Dhanola A, Raturi A (2016) Mechanical behavior of glass fiber polyester hybrid composite filled with natural fibers. IOP conference series: materials science and engineering. <https://doi.org/10.1088/1757-899x/149/1/012091>
22. Hassan SB, Oghenevwea JE, Aigbodion VS (2012) Morphological and mechanical properties of carbonized waste maize stalk as reinforcement for eco-composites. *Compos B* 43:2230–2236
23. Chen RS, AhmadS, Gan S (2016) Characterization of rice husk incorporated recycled thermoplastic blend composites. *Bioresources* 11(4):8470–8482
24. Safwan MM, Lin HO, Akil HM (2013) Preparation and characterization of palm kernel shell/polypropylene biocomposite and their hybrid composite with Nanosilica. *BioResources* 8(2):1539–1550
25. Karthik R, Sathiyamurthy S, Jayabal S, Chidambaram K (2014) Tribological behaviour of rice husk and egg shell hybrid particulated coir-polyester composites. *IOSR J Mech Civil Eng* 75–80. Retrieved from <http://www.iosrjournals.org/iosr-jmce/papers/NCCAMABS/Volume-3/39.pdf>
26. Prabhu R, Amin AK, Dhyanchandra A (2015) Development and characterization of low cost polymer composites from coconut coir. *Am J Mater Sci* 5(3C):62–68
27. Ashori A, Nourbakhsh A (2010) Bio-based composites from waste agricultural residues. *Waste Manage* 30:680–684
28. Ravindran D, Sornakumar T, Prithvirajadurai DS, Varadarajan V (2015) Development of hybrid coconut shell powderwood dust polyester resin based composites. *Int J Appl Mech Prod Eng* 1(7):1–4
29. Zaini ASSM, Rus ZAM, Rahman NA, Jais FHM, Fauzan MZ, Sufian NA (2017) Mechanical properties evaluation of extruded wood polymer composites. In: 4th international conference on the advancement of materials and nanotechnology (ICAMN IV 2016), AIP conference proceedings 1877, 060005. pp 2–9. <https://doi.org/10.1063/1.4999884>

30. Aigbodion VS, Hassan SB, Agunsoye OJ (2011) Effect of bagasse ash reinforcement on dry sliding wear behaviour of polymer matrix composites. *Mater Des* 33:322–327
31. Atuanya CU, Aigbodion VS, Nwigbo SC (2014) Experimental study of the thermal and wear properties of recycled polyethylene/breadfruit seed hull ash particulate composites. *Mater Des* 53:65–73
32. Fragassa C, Santulli C, Pavlović A, Šljivić M (2015) Improving performance and applicability of green composite materials by hybridization. *Contemp Mater* 35–43. <https://doi.org/10.7251/comen1501035f>
33. Muthukumar S, Lingadurai K (2014) Investigating the mechanical behaviour of coconut shell and groundnut shell reinforced polymer composite. *Glob J Eng Sci Res* 1(3):19–23
34. Kasiviswanathan S, Santhanam K, Kumaravel A (2015) Evaluation of mechanical properties of natural hybrid fibers, reinforced polyester composite materials. *Carbon Sci Tech* 7/4:43–49 [CST-161-7-4]
35. Udhayasankar R, Karthikeyan B (2015) A review on coconut shell reinforced composites. *Int J ChemTech Res CODEN (USA): IJCRGG* 8(11):624–637
36. Karippa JJ, Murthy HNN, Rai KS, Sreejith M, Krishna M (2011) Study of mechanical properties of epoxy/glass/nanoclay hybrid composites. *J Compos Mater* 1–7
37. Meziane O, Bensedira A, Guessoum M, Haddaoui N (2016) Polypropylene-modified kaolinite composites: effect of chemical modification on mechanical, thermal and morphological properties. *J Fundam Appl Sci* 8(2):494–509
38. Nourbakhsh A, Baghlani FF, Ashori A (2011) Nano-SiO₂ filled rice husk/polypropylene composites: physico-mechanical properties. *Ind Crops Prod* 33:183–187
39. Chauhan S, Bhushan RK (2017) Study of polymer matrix composite with natural particulate/fiber in PMC: a review. *Int J Adv Res Ideas Innovations Technol* 3(3):1168–1179
40. Arpitha GR, Sanjay MR, Yogesha B (2014) Review on comparative evaluation of fiber reinforced polymer matrix composites. *Adv Eng Appl Sci Int J* 4(4):44–47
41. Chandramohan D, Marimuthu K (2011) A review on natural fibers. *IJRRAS* 8(2):194–206
42. Hashim MY, Roslan MN, Amin AM, Zaidi AMA, Ariffin S (2012) Mercerization treatment parameter effect on natural fiber reinforced polymer matrix composite: a brief review. *World Acad Sci Eng Technol* 6:1382–1388
43. Bledzki AK, Mamun AA, Volk J (2010) Barley husk and coconut shell reinforced polypropylene composites: the effect of fibre physical, chemical and surface properties. *Compos Sci Technol* 70:840–846
44. Rozyanty AR, Firdaus MYN, Liew TZ, Yunus NFM (2015) Kenaf-unsaturated polyester composite: the effect of different retting process of kenaf bast fiber on the mechanical properties. *Mater Sci Forum* 819:256–261
45. Dass PM, Akinterinwa A, Adamu JN, Abba S (2015) The influence of different retting processes on the strength of fibres obtained from *Poliostigma raticulatum*, *Grewia mollis*, *Cissus populnea* and *Hibiscus sabdariffa*. *Environ Nat Resour Res* 5(4):41–45
46. Gopu RN, Singh A, Zimmiewska M, Raghavan V (2013) Comparative evaluation of physical and structural properties of water retted and non-retted flax fibers. *Fibers* 1:59–69. <https://doi.org/10.3390/fib1030059>
47. Jawaid M, Tahir PM, Saba N (eds) (2017) Lignocellulosic fibre and biomass-based composite materials: processing, properties and applications. Woodhead Publishing, UK
48. Thakur VK, Thakur MK (eds) (2015) Eco-friendly polymer nanocomposites: chemistry and application. Springer, New Delhi
49. Rydz J, Sikorska W, Kyulavska M, Christova D (2015) Polyester-based (bio)degradable polymers as environmentally friendly materials for sustainable development. *Int J Mol Sci* 16(1):564–596
50. Ray SS (2013) Environmentally friendly polymer nanocomposites: types, processing and properties. Woodhead Publishing, New Delhi
51. Shukla SK, Mishra AK, Arotiba OA, Mamba BB (2013) Chitosan-based nanomaterials: a state-of-the-art review. *Int J Biol Macromol* 1–13. <http://dx.doi.org/10.1016/j.ijbiomac.2013.04.043>

52. Saba N, Tahir PM, Jawaid M (2014) A review on potentiality of nano filler/natural fiber filled polymer hybrid composites. *Polymers* 6(8):2247–2273. <https://doi.org/10.3390/polym6082247>
53. Thomas S, Paul SA, Pothan LA, Deepa B (2011) Natural fibres: structure, properties and applications. In: Kalia S, Kaith BS, Kaur I (eds) *Cellulose fibers: bio- and nano-polymer composites*. Springer, Berlin
54. Shehu U, Audu H, Nwamara MA, Ade-Ajayi AF, Shittu UM, Isa MT (2014) Natural fibre as reinforcement for polymers: a review. *SPJTS* 2(1):238–253
55. Kabir MM, Wang H, Aravinthan T, Cardona F, Lau KT (2011) Effects of natural fibre surface on composite properties: a review. pp 94–99
56. Kalia S, Dufresne A, Cherian BM, Kaith BS, Averous L, Njuguna J, Nassiopoulous E (2011) Cellulose-based bio- and nanocomposites: a review. *Int J Polym Sci* 1–36. <https://doi.org/10.1155/2011/837875>
57. Fan M, Dai D, Huang B (2012) Fourier transform infrared spectroscopy for natural fibres. In: Salih S (ed) *Fourier transform—materials analysis*. ISBN 978-953-51-0594-7. www.interchopen.com/books/fourier-transform-materials-analysis/Fourier-Transform-Infrared-Spectroscopy-for-natural-fibres. Accessed 5 Feb 2018
58. Kumar R, Obrai S, Sharma A (2011) Chemical modifications of natural fiber for composite material. *Der Chemica Sinica* 2(4):219–228
59. Anurag T (2016) Study of musa acuminata fibre reinforced composite—a review. *Int J Res Aeronaut Mech Eng* 4(4):29–42
60. Srinivasan R (2011) Advances in application of natural clay and its composites in removal of biological, organic, and inorganic contaminants from drinking water. *Adv Mater Sci Eng* 1–17. <https://doi.org/10.1155/2011/872531>
61. Hamid E, Raji M, Bouhfid R, Quaiss AEK (2016) Nanoclay and natural fibers based hybrid composites: mechanical, morphological, thermal and rheological properties. In: Jawaid M, Quaiss AEK, Bouhfid R (eds) *Nanoclay reinforced polymer composites, engineering materials*. Springer, Singapore
62. Mallick PK (2018) *Processing of polymermatrix composites*. CRC Press, Boca Raton
63. Zin MH, Razzi MF, Othman SLK, Abdan K, Mazlan N (2016) A review on the fabrication method of bio-sourced hybrid composites for aerospace and automotive applications. *IOP conference series: materials science and engineering*. <https://doi.org/10.1088/1757-899x/152/1/012041>
64. Dong P, Prasanth R, Xu F, Wang X, Li B, Shankar R (2015) Eco-friendly polymer nanocomposite—properties and processing. In: Thakur VK, Thakur MK (eds) *Eco-friendly polymer nanocomposites processing and properties*. Springer, New Delhi
65. Gunning M, Geever LM, Killion JA, Lyons JG, Higginbotham CL (2014) Effect of compatibilizer content on the mechanical properties of bioplastic composites via hot melt extrusion. *Polym Plast Technol Eng* 53:1223–1235
66. Cai J, Jia M, Xue P, Ding Y, Zhou X (2013) The effect of processing conditions on the mechanical properties and morphology of self-reinforced wood-polymer composite. *Polym Compos* 1567–1574. <https://doi.org/10.1002/pc.22553>
67. Tanahashi M (2010) Development of fabrication methods of filler/polymer nanocomposites: with focus on simple melt-compounding based approach without surface modification of nanofillers. *Materials* 3:1593–1619. <https://doi.org/10.3390/ma3031593>
68. Díez EA (2014) Effect of extrusion on the electrical, mechanical and rheological properties of an ethylene butylacrylate/carbon black/graphite nanoplatelets nanocomposite. Diploma work, Department of Materials and Manufacturing Technology, Chalmers University of Technology, Gothenburg, Sweden

69. Peinado V, Castell P, García L, Fernández A (2015) Effect of extrusion on the mechanical and rheological properties of a reinforced poly(lactic acid): reprocessing and recycling of biobased materials. *Materials* 8:7106–7117. <https://doi.org/10.3390/ma8105360>
70. Feldmann M, Heim HP, Zarges JC (2015) Influence of the process parameters on the mechanical properties of engineering biocomposites using a twin-screw extruder. *Compos Part A* 1–7. <http://dx.doi.org/10.1016/j.compositesa.2015.03.028>
71. Kadam PG, Mhaske ST (2014) Effect of extrusion reprocessing on the mechanical, thermal, rheological and morphological properties of nylon 6/talc nanocomposites. *J Thermoplast Compos Mater* 1–19. <https://doi.org/10.1177/0892705714551591>
72. Poletto M (2016) Polystyrene cellulose fiber composites: effect of the processing conditions on mechanical and dynamic mechanical properties. *Rev Mater* 21(3):552–559
73. Hajba S, Tábi T (2014) Development of natural fibre reinforced poly(lactic acid) biocomposites. In: ECCM16—16th European conference on composite materials, Seville, Spain, 22–26 June 2014, pp 1–8
74. Rassmann S, Reid RG, Paskaramoorthy R (2010) Effects of processing conditions on the mechanical and water absorption properties of resin transfer moulded kenaf fibre reinforced polyester composite laminates. *Compos Part A* 4(11):1612–1619
75. Agubra VA, Owuor PS, Hosur MV (2013) Influence of nanoclay dispersion methods on the mechanical behavior of E-glass/epoxy nanocomposites. *Nanomaterials* 3:550–563. <https://doi.org/10.3390/nano3030550>
76. Kalia S, Kaith BS, Kaur I (2009) Pretreatments of natural fibers and their application as reinforcing material in polymer composites—a review. *Polym Sci Eng* 49(7):1253–1272. <https://doi.org/10.1002/pen.21328>
77. Cruz J, Fanguero R (2016) Surface modification of natural fibers: a review. *Procedia Eng* 155:285–288
78. Chern CE, Nor AI, Norhazlin Z, Ariffin H, Yunus WMZW, Then YY (2014) Enhancement of mechanical and dynamic mechanical properties of hydrophilic nanoclay reinforced polylactic acid/polycaprolactone/oil palm mesocarp fiber hybrid composites. *Int J Polym Sci*. <http://dx.doi.org/10.1155/2014/715801>
79. Zaaba NF, Ismail H, Jaafar M (2014) The effects of modifying peanut shell powder with polyvinyl alcohol on the properties of recycled polypropylene and peanut shell powder composites. *BioResources* 9(2):2128–2142
80. Kumar TV, Chandrasekaran M, Padmanabhan S (2017) Characteristics and mechanical properties of reinforced polymer composites. *ARPJ Eng Appl Sci* 12(8):2450–2454
81. Asuke F, Aigbodion VS (2016) Experiment numerical study of dry sliding wear behavior of epoxy/periwinkles shell particulate composites. *J Chin Adv Mater Soc* 1–17. <https://doi.org/10.1080/22243682.2015.1124736>
82. Hassan SB, Aigbodion VS, Patrick SN (2012) Development of polyester/eggshell particulate composites. *Tribol Ind* 34(4):217–225
83. Kadhum AAU, Mohammed AA (2016) Investigation the effect of natural materials on wear and hardness properties of polymeric composite materials. *Iraqi J Mech Mater Eng* 16(4):369–372
84. Atuanya CU, Aigbodion VS, Obiorah SO (2015) Evaluation of the mechanical properties of recycled low-density polyethylene/bean pod particulate bio-composites. *J Chin Adv Mater Soc* 3(4):345–358. <https://doi.org/10.1080/22243682.2015.1081077>
85. Sarki J, Hassan SB, Aigbodion VS, Ogheneveta JE (2011) Potential of using coconut shell particle fillers in eco-composite materials. *J Alloy Compd* 509:2381–2385
86. Aigbodion VS, Atuanya CU, Igogori EA, Andlhom P (2013) Development of high-density polyethylene/orange peels particulate bio-composite. *Gazi Univ J Sci* 26(1):107–117
87. Subramani T, Krishnan S, Ganesan SK, Nagarajan G (2014) Investigation of mechanical properties in polyester and phenylester composites reinforced with chicken feather fiber. *Int J Eng Res Appl* 4(12):93–104

88. Kiew KS, Rahman MR, Hamdan S, Talibb ZA (2013) Maleic anhydride modified unsaturated polyester composites reinforced with chicken feather fiber: dielectric and morphological study. *World Appl Sci J* 25(6):899–907. <https://doi.org/10.5829/idosi.wasj.2013.25.06.1347%5b>
89. Oladele IO, Omotoyimbo JA, Ayemidejor SH (2014) Mechanical properties of chicken feather and cow hair fibre reinforced high density polyethylene composites. *Int J Sci Technol* 3(1):66–72
90. Omah AD, Okorie BA, Omah EC, Ezema C, Aigbodion VS, Orji UU (2017) Experimental correlation between varying cassava cortex and dielectric properties in epoxy/cassava cortex dielectric particulates composites. *Part Sci Technol*. <https://doi.org/10.1080/02726351.2017.1307888>
91. Tushar S, Shirish P, Vikram D, Acharya R (2015) Natural fiber reinforced polymer composite material—a review. *IOSR J Mech Civil Eng* 142–147
92. Madhusudhan T, Swaroop GK (2016) A review on mechanical properties of natural fiber reinforced hybrid composites. *Int Res J Eng Technol (IRJET)* 3(4):2247–2251
93. Nitin S, Singh VK (2013) Mechanical behaviour of walnut reinforced composite. *J Mater Environ Sci* 4(2):233–238
94. Tao Y, Li P, Cai L (2016) Effect of fiber content on sound absorption, thermal conductivity and compression strength of straw fiber filled rigid polyurethane foams. *BioResources* 11(2):4159–4167
95. Ameh AO, Isa MT, Sanusi I (2015) Effect of particle size and concentration on the mechanical properties of polyester/date palm seed particulate composites. *Leonardo Electron J Practices Technol* 26:65–78
96. Shokoufa N, Nourbakhsh A, Ashkan G, Talaeipour M, Habibollah KE (2013) Investigating the effect of nanoclay on polypropylene-made cellulose composite. *Res J Appl Sci Eng Technol* 6(21):4022–4029. <https://doi.org/10.19026/rjaset.6.3505>
97. Singla RK, Maiti SN, Ghosh AK (2016) Crystallization, morphological, and mechanical response of poly(lactic acid)/lignin-based biodegradable composites. *Polym Plast Technol Eng* 55(5):475–485. <https://doi.org/10.1080/03602559.2015.1098688>
98. Pongtanayuta K, Thongpina C, Santawiteeb O (2013) The effect of rubber on morphology, thermal properties and mechanical properties of PLA/NR and PLA/ENR blends. *Energy Procedia* 34:888–897. <https://doi.org/10.1016/j.egypro.2013.06.826>
99. Alagarsamy SV, Sagayaraj AVS, Vignesh S (2015) Investigating the mechanical behaviour of coconut coir—chicken feather reinforced hybrid composite. *Int J Sci Eng Technol Res (IJSETR)*, 4(12):4215–4221
100. Saikishore T, Rao PP, Reddy MCS (2017) Synthesis & investigation of the mechanical behaviour of luffa, groundnut shell, chicken feather and cowdung fibers reinforced epoxy composites. *IJSRD Int J Sci Res Dev* 5(4):42–46
101. Njoku RE, Obayi CS, Nnamchi PS (2011) Hybrid effect on the mechanical properties of sisal fiber and E-glass fiber reinforced polyester composites. *Niger J Technol* 30(3):97–103
102. Nalin P, Suppakula P, Atong D, Pechyen C (2014) Blend of polypropylene/poly(lactic acid) for medical packaging application: physicochemical, thermal, mechanical, and barrier properties. *Energy Procedia* 56:201–210
103. Hassan E, Wei Y, Jiao H, Muhuo Y (2013) Dynamic mechanical properties and thermal stability of poly(lactic acid) and poly(butylene succinate) blends composites. *J Fiber Bioeng Inform* 6(1):85–94. <https://doi.org/10.3993/jfbi03201308>
104. Jompanga L, Thumsorna S, Onb JW, Surinb P, Apawet C, Tirapong C, Narin K, Narongchai OC, Srisawata N (2013) Poly(lactic acid) and poly(butylene succinate) blend fibers prepared by melt spinning technique. *Energy Procedia* 34:493–499
105. Jia W, Gong RH, Soutis C, Hogg PJ (2014) Biodegradable fibre reinforced composites composed of polylactic acid and polybutylene succinate. *Plast Rubber Compos* 43(3):82–88. <https://doi.org/10.1179/1743289813Y.0000000070>

106. Darie-Nita RN, Vasile C, Irimia A, Lipsa R, Rapa M (2016) Evaluation of some eco-friendly plasticizers for PLA films processing. *J Appl Polym Sci* 1–11. <https://doi.org/10.1002/app.43223>
107. Vignesh J, Selvam CM (2015) Experimental evaluation of wood dust particulate reinforced polymer composites. *IRACST Eng Sci Technol Int J (ESTIJ)* 5(4):226–229
108. FAO Statistical Yearbook 2014 Africa: Food and Agriculture (2014) Food and agriculture organization of the United Nations Regional Office for Africa Accra

Synthesis, Characterization, and Applications of Hemicelluloses Based Eco-friendly Polymer Composites



Xinwen Peng, Fan Du and Linxin Zhong

Abbreviations

EVOH	Ethylene vinyl alcohol
PVDC	Polyvinylidene chloride
3D	Three-dimensional
AGU	Anhydroglucose units
AcGGM/GGM	<i>O</i> -acetyl galactoglucomannans
DMF	<i>N, N</i> -dimethylformamide
DMA/LiCl	<i>N, N</i> -dimethylacetamide/lithium chloride
DMSO/THF	Dimethyl sulfoxide/tetrahydrofuran
DMAP	4-dimethylamino pyridine
NBS	<i>N</i> -bromosuccinimide
TEA	Triethylamine
DS	Degree of substitution
MSA	Methane sulfonic acid
[BMIM]Cl	1-butyl-3-methylimidazolium chloride
IL	Ionic liquid
LC	Lauroyl chloride
LH	Lauroylated hemicelluloses
HFIP	Hexafluoroisopropanol/1, 1, 1, 3, 3, 3-hexafluoro-2-propanol
CDI	<i>N, N'</i> -carbonyldiimidazole
SET-LRP	Single-electron-transfer mediated living radical polymerization
AcGGM-SH	Thiolated <i>O</i> -acetyl galactoglucomannan
PEG-MA	Polyethylene glycol monomethacrylate
ETA	2, 3-epoxypropyltrimethylammonium chloride
QH	Quaternized hemicelluloses

X. Peng (✉) · F. Du · L. Zhong (✉)
State Key Laboratory of Pulp and Paper Engineering, South China
University of Technology, 381 Wushan Road, Guangzhou 510640, China
e-mail: fexwpeng@scut.edu.cn

L. Zhong
e-mail: lxzhong0611@scut.edu.cn

MMT	Montmorillonite
NaH	Sodium hydride
BnGGM	Benzyl galactoglucomannan
TBAI	Tetrabutylammonium iodide
CHMAC	3-chloro-2-hydroxypropyltrimethylammonium chloride
GTMAC	Glycidyltrimethylammonium chloride
METAC	[2-(methacryloyloxy) ethyl] trimethylammonium chloride
HPMA	2-hydroxypropyltrimethylammonium
DME	1, 2-dimethoxyethane
PHL	Pre-hydrolysis liquor
GTMAC	Glycidyltrimethylammonium chloride
METAC	[2-(methacryloyloxy) ethyl] trimethylammonium chloride
MeGlcP-Xylan	<i>O</i> -acetyl-4- <i>O</i> -methylglucuronoxylan
WH	Wood hydrolysate
AG	Arabinogalactan
EDC/NHS	<i>N</i> -ethyl- <i>N'</i> -(3-dimethylamino)propyl carbodiimide hydroxide/ <i>N</i> -hydroxysuccinimide
TA	Tyramine
HRP	260 purpurogallin unit/mg solid
DMT-MM	4-(4, 6-dimethoxy-1, 3, 5-triazin-2-yl)-4-methylmorpholinium chloride
CuAAC	Copper(I)-catalyzed azide-alkyne cycloaddition
AX	Arabinoxylan
AGX	Arabinoglucuronoxylan
[emim][Me ₂ PO ₄]	1-ethyl-3-methylimidazolium dimethyl phosphate
[DBNH][OAc]	1, 5-diazabicyclo[4.3.0]non-5-enium acetate
[Amim] ⁺ Cl ⁻	1-allyl-3-methylimidazolium chloride
XylC6N ₃	Di- <i>O</i> -(6-azidohexanoyl)-xylan
PLLA	Poly(L-lactide)
PMDETA	<i>N, N, N', N', N''</i> -pentamethyldiethylenetriamine
LLA	L-lactide
TBD	Triazabicyclodecene
PLA	Poly(lactide)
AN	Acrylonitrile
MA	Methyl acrylate
AM	Acrylamide/acrylic amide
DMC	Methacryloyloxy ethyl trimethyl ammonium chloride
APMP	Alkaline peroxide mechanical pulping
MMA	Methyl methacrylate
NIPAM	<i>N</i> -isopropyl acrylamide
GMA	Glycidyl methacrylate
GM	Galactomannan
QCM-D	Quartz crystal microbalance with dissipation
TEMPO	2, 2, 6, 6-tetramethylpiperidine-1-oxyl

Cy	Cysteine
LOD	Limit of detection
AgNPs	Silver nanoparticles
PMP	Polymeric magnetic microparticles
MP	Magnetic microparticles
CMH	Carboxymethyl functionalized hemicellulose/carboxymethyl hemicellulose
Pd NPs	Palladium nanoparticles
XH	Xylan-type hemicelluloses
CKGM	Carboxymethyl Konjac glucomannan
CS	Chitosan
BSA	Bovine serum albumin
WVP	Water vapor permeability
OP	Oxygen permeability
PVA	Polyvinyl alcohol
HPKO	Hydrogenated palm kernel oil
HLBs	Hydrophilic-lipophilic balances
LDPE	Low-density polyethylene
DMA	Dynamic mechanical analysis
NCH	Chitin nanowhiskers
BH	Bleached hemicelluloses
BAH	Acetylated bleached hemicelluloses
NCC	Nanocrystalline cellulose
CNCC	Cationically modified NCC
HC/SB	Hemicelluloses/sorbitol
GTMAC	Glycidyltrimethylammonium chloride
HL	Hemicellulose/lignin
NFC	Nanofibrillated cellulose
MFC	Microfibrillated cellulose
CNFs	Cellulose nanofibers
CNT	Carbon nanotube
κ -car/LBG	κ -carrageenan/locust bean
GA	Gum arabic
SA	Stearyl acrylate
SM	Stearyl methacrylate
EB	Electron beam
PLGA	Poly(lactic-co-glycolic acid)
TFAA	Trifluoroacetic anhydride
PET	Polyethylene terephthalate
CHPS	3-Chloro-2-hydroxypropyl sulfonic acid
SCHMAC	(S)-(-)-(3-chloro-2-hydroxypropyl)-trimethylammonium chloride
CHPMAC	3-chloro-2-hydroxypropyl-trimethylammonium chloride

Ra	Roughness value
Seq	Equilibrium swelling ratio
HEMA	2-hydroxyethyl methacrylate
HEMA-Im	2-[(1-imidazolyl)formyloxy]ethyl methacrylate
AnMan5A	Enzyme β -mannanase
M-AcGGM	Methacrylated AcGGM
CM-AcGGM	Maleic anhydride-modified M-AcGGM
AA	Acrylic acid
CA	Citric acid
SHP	Sodium hypophosphite
NIPAAm	<i>N</i> -isopropylacrylamide
MBA	<i>N</i> , <i>N'</i> -methylenebis-acrylamide
DMAP/NMP	2, 2-dimethoxy-2-phenylacetophenone/ <i>N</i> -methyl pyrrolidone
ACX	Acylated xylan
Hce-MA/AHC	Acylated hemicellulose
LCST	Lower critical solution temperature
APS/TEMEDA	Ammonium persulfate/ <i>N</i> , <i>N</i> ', <i>N'</i> , <i>N'</i> -tetramethyl-ethane-1, 2-diamine
MeDMA	[2-(methacryloyloxy) ethyl] trimethylammonium chloride
ECH	Epichlorohydrin
GDEP	Glow discharge electrolysis plasma
MFRHH	Magnetic field-responsive hemicelluloses-based hydrogel
SRs	Swelling ratios
ECH	Electrically conductive hydrogels
ECHH	Electrically conductive hemicellulose hydrogel
AP	Aniline pentamer
C-AcGGM	Carboxylated AcGGM
AT	Aniline tetramer
SRHMGs	Stimuli-responsive hemicellulose microgels
CMCH	Carboxymethyl chitosan-hemicellulose
CHNT	Carboxymethyl chitosan-hemicellulose network
SDS	Sodium dodecyl sulfate
DTPA	Diethylene triamine pentaacetic acid
DHC	Dialdehyde hemicelluloses
CNF	Cellulose nanofibrils
CNC	Nanocrystalline cellulose
NFC	Nanofibrillated cellulose
IPNs	Interpenetrating polymer networks
MA-CMC	Methacrylated carboxymethylcellulose
SWH	Softwood hemicellulose hydrolysate
kC-xylan-PVP	Kappa-carrageenan/xylan/polyvinylpyrrolidone
KPS	Sodium persulphate

PEG	Poly(ethylene glycol)
PEG-PPG-PEG	Poly(ethylene glycol)-b-poly(propylene glycol)-b-poly(ethylene glycol)
IA	Itaconic acid
PAA	Poly(amidoamine)
GO	Graphene oxide
PAM	Polymerized acrylamide
MW-CNTs	Multiwall carbon nanotube
MB	Methylene blue
PEGDE	Polyethylene glycol diglycidyl ether

1 Introduction

During the last few decades, synthetic polymers and polymer-based materials have become indispensable materials in people's lives. The polymer composites are utilized in a very wide range of applications from household to aerospace, from agriculture to medicine or pharmacy. However, due to the growing awareness on environment and human health as well as the scarcity and increase in the price of the fossil resources, tremendous attention and efforts have been given to the environmentally friendly materials. Production of environmentally friendly biomaterials from renewable biomass resources is a critical route to solve the environmental pollution and the upcoming depletion of petrochemical resources. In the past decade, various biomass resources, such as cellulose [1], lignin [2, 3], hemicelluloses [4, 5], chitosan [6, 7], starch [8, 9], psyllium [10], have been used to fabricate biomaterials and biocomposites that have potential applications in various fields. Hemicelluloses are the secondly abundant sustainable polymers on the earth which possessing 25–30% of the total weight in the wood plant, and will not compete with food supply for the production of biopolymers [5, 11–14]. Recently, the global number of trees was estimated to be ~ 3.04 trillion, and thus generating ~ 3900 million m^3 of wood per year and providing large amounts of plant materials including cellulose, hemicelluloses, and lignin [12, 13]. The hemicelluloses-based polymer can be cast into films and take a substitute to traditional non-degradable and high-cost petroleum-based products such as ethylene vinyl alcohol (EVOH) or polyvinylidene chloride (PVDC). Additionally, it also can be fabricated into three-dimensional (3D) hydrogel networks and used in adsorbing the heavy metals [15–20] and methylene blue [21, 22], drug delivery [23–26], food package [27–29] and paper surface engineering [30]. However, hemicelluloses have some inherent disadvantages, for instance, brittleness, water/moisture sensitivity, high water vapour permeability, and so on. Physical, chemical and enzymatic modifications of hemicelluloses by either bulk or surface modification are essential ways to settle these problems because of abundant free hydroxyl groups and carboxyl distributed

along the backbone and side chains of hemicelluloses [5]. Up to now, various chemical methods, such as esterification, etherification, ionization, amination, amidation, acetylation, grafting copolymerization, crosslinking, blending, have been explored to modify hemicelluloses and fabricate functional materials. This chapter gives an overview of the recent advances in the synthesis of various polymer composites based on hemicelluloses such as modified hemicellulose-based materials, hemicellulose-based particles, films, and gels, as well as their potential applications.

1.1 Occurrence of Hemicellulose

Hemicelluloses are the most abundant plant polysaccharides next to cellulose, which form the hydrophilic component of the cell wall in the wood plant. There are several methods applied to isolate hemicelluloses from the wood materials such as acid pretreatment [31], alkaline extraction [32], liquid hot-water extraction [33], steam treatment [34], ionic liquid extraction [35–37], hydrogen peroxide extraction [38], wet-oxidation [39], microwave treatment [40], and organic solvent treatment [41]. Among these methods, acid pretreatment and alkaline extraction are the most important methods for hemicelluloses isolation. However, high cost and environmental pollution make acid treatment, not a good choice. And more importantly, approximately 100% of hemicelluloses are broken down into monomeric sugars and sugar degradation products, including weak acids, furan derivatives, and phenolics during acid treatment. Therefore, alkaline extraction is extensively applied and well-studied in hemicelluloses extraction due to the integrity of extracted hemicelluloses [11, 42, 43]. Of hemicelluloses, modification of xylan draws a special attention, due to its abundance and widely available as compared with other hemicelluloses. Galactglucomannan is another important hemicellulose to develop novel hydrogel, film laminates for oxygen barriers, cationized materials, and multifunctional macroinitiator for single-electron transfer-mediated living radical polymerization [44].

1.2 Structure of Hemicellulose

Hemicelluloses are non-crystalline polysaccharides bearing different anhydroglucose units (AGU) in their chains or branches and have an average degree of polymerization ranging from 100 to 200. Figure 1 gives the structure of the most important AGU units of hemicelluloses [42, 45], to a lesser extent, 4-*O*-methyl-D-glucuronic acid, D-galacturonic acid, L-rhamnose, L-fucose, and a variety of *O*-methylated neutral sugars also exist in hemicellulose [46]. Moreover, The AGU repeating units can be *O*-acetylated at the C-2 and/or C-3 positions. It is well known that hemicelluloses belong to a highly heterogeneous group of noncellulosic

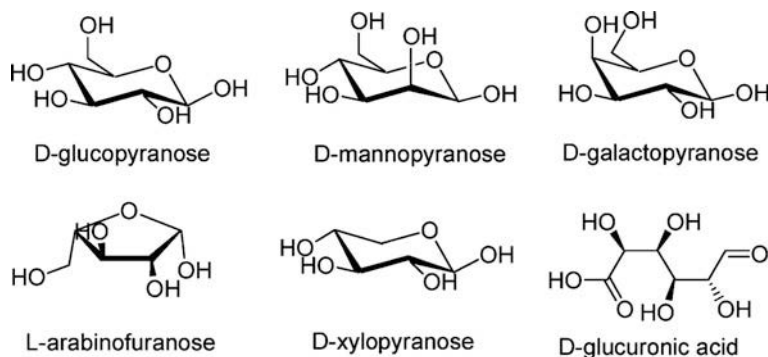


Fig. 1 The main constituents of hemicelluloses (Reproduced from [45] with permission)

polysaccharides containing xylans, mannans and glucomannans, xyloglucans, and β -(1 \rightarrow 3,1 \rightarrow 4)-glucans [12]. Additionally, hemicellulosic compositions, structures and amounts vary from different sources of different biomass resources. Xylan is the most common type of hemicelluloses in hardwood and gramineous plants. Xylan from many plant materials are heteropolysaccharides with homopolymeric backbone chains of 1, 4-linked β -D-xylopyranose units. Besides xylose, xylan may contain arabinose, glucuronic acid or its 4-*O*-methyl ether, and acetic, ferulic, and *p*-coumaric acids. The backbone consists of *O*-acetyl, α -L-arabinofuranosyl, α -1, 2-linked glucuronic or 4-*O*-methylglucuronic acid substituents. The frequency and composition of branches are dependent on the source of xylan, thus xylan can be categorized as linear homoxylan, arabinoxylan, glucuronoxylan, and glucuronoxarabinoxylan, whereas, softwood hemicelluloses contain mostly *O*-acetyl galactoglucomannans (AcGGM). AcGGM consists of a backbone chain containing β -(1 \rightarrow 4)-linked mannose and glucose units partially substituted with α -(1 \rightarrow 6)-linked galactose units [42, 47].

2 Synthesis and Characterization of Modified Hemicelluloses (Zero-Dimensional)

Hemicelluloses have an abundance of free hydroxyl groups distributed along the backbone and side chains and are, therefore, ideal candidates for chemical functionalization. Researchers have explored these options using various techniques such as esterification, etherification, ionization, amination, amidation, acetylation, fluorination, sulfation, benzylation or grafting methods [5]. Chemical modification of wood hemicelluloses offers numerous possibilities to control and tailor the properties of hemicelluloses, leading to conductive, stimuli-responsive, more elastic, and more hydrophobic or thermoplastic products [12].

2.1 Esterification

The esterification of hemicellulose is typically conducted with acid chlorides or anhydrides under solutions such as *N,N*-dimethylformamide (DMF), *N,N*-dimethylacetamide/lithium chloride (DMA/LiCl), dimethyl sulfoxide/tetrahydrofuran (DMSO/THF), or various ionic liquids and alkaline catalysts such as pyridine, 4-dimethylamino pyridine (DMAP), or *N*-bromosuccinimide (NBS) in the presence of triethylamine (TEA) to neutralize the hydrochloric acid generated during the reaction. Different types of esterification reactions (acetylation, propionylation, oleoylation, lauroylation, benzoylation, and cross-linking) have been used to tailor the potential applications of hemicelluloses, for example improving the hydrophilicity, thermal stability, thermoplastic property of hemicelluloses, as well as their solubility in organic solvents for a good use in heavy metal ions adsorption, drug delivery and food packaging [11, 12].

The esterification of hemicelluloses always happens with acid chlorides or anhydrides having short alkyl chains. In order to improve the esterification of hardwood xylan with a high degree of substitution (DS), two different approaches were investigated. The acetylation reaction of xylan-type hemicelluloses can be carried out with acetic anhydride in a homogeneous solution of DMF/LiCl in the presence of DMAP as a catalyst. This reaction can also be performed under heterogeneous conditions in the absence of organic solvent and use methane sulfonic acid (MSA) or DMAP as a catalyst. The highest DS of 1.6 and maximal yield of 85% can be achieved under the screened optimal reaction conditions. The results show that the amount of MSA has a significant influence on DS and yield. In addition, the esterification of propionic and hexanoic anhydrides was also conducted to obtain hydrophobic xylan esters with low DS values [48]. Homogeneous esterification of xylan-rich hemicelluloses with maleic anhydride in 1-butyl-3-methylimidazolium chloride ([BMIM]Cl) ionic liquid by using LiOH as a catalyst was performed by Peng et al. [49] (Fig. 2). The novel functional biopolymer has carbon-carbon double bond and carboxyl groups, and the DS values range from 0.095 to 0.75 can be achieved. The influences of the molar ratio of maleic anhydride to anhydroxylose unit in xylan-rich hemicelluloses, reaction temperature, time, and dosage of LiOH on the DS value of hemicellulosic derivatives were investigated. Most notably, the DS increased to 0.72 when 0.02 g LiOH was applied, and the thermal stability of the new polymer was lower than that of the native xylan-rich hemicelluloses.

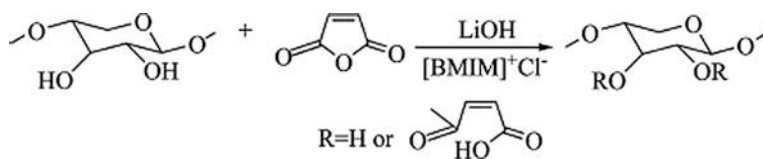


Fig. 2 Reaction scheme of homogeneous esterification of XH with MA in [BMIM]Cl ionic liquid (Reproduced from [49] with permission)

Zhang et al. [50] performed the esterification of hemicelluloses with butyryl chloride in [BMIM]Cl ionic liquid (IL) using TEA as a neutralizer, as shown in Fig. 3. The as-prepared butyrylated hemicellulose was characterized by FT-IR, TGA, ^1H , and ^{13}C NMR spectroscopies, and the results indicate that the DS of the products changed with the reaction conditions such as molar ratio of the substrates, temperature and reaction time. The highest DS of 1.89 can be obtained at the preferred reaction condition. Furthermore, the hydrophobicity and thermal stability of the butyrylated hemicelluloses increased with the increasing DS value.

Hemicelluloses modified with acid chlorides or anhydrides having long alkyl chains were also been investigated. Sun et al. [51] obtained stearylated hemicelluloses with different DS values (0.20–1.71) by a rapid reaction of wheat straw derived hemicelluloses with stearyl chloride in homogeneous DMF/LiCl system with DMAP as a catalyst and TEA as an acid acceptor. The concentrations of stearyl chloride and TEA, as well as the reaction temperature, have different effects on the DS. The results also demonstrated that TEA was better than pyridine as an acid acceptor. Under optimum conditions, the highest DS value of 1.71 can be obtained, and approximately 92% of the free hydroxyl groups in native hemicelluloses are stearylated with a minimal degradation ($\leq 8\%$). The thermal analysis shows an increase in the thermal stability of the stearylated hemicelluloses. Another ester with a low DS has been synthesized by oleoylation of sugarcane bagasse hemicelluloses using NBS as a catalyst in the DMF/LiCl system [52]. The thermal stability of the oleoylated hemicelluloses decreases slightly upon chemical modification, but no significant further decrease in thermal stability was observed for the derivatives with a $\text{DS} \geq 0.29$. Such low-DS polymers have great application in food packaging. Similarly, lauroylated hemicelluloses (LH) can be prepared in homogeneous [BMIM]Cl IL without catalyst [53]. The relationships between reaction parameters including the molar ratio of lauroyl chloride (LC) to anhydroxylose unit in hemicelluloses, reaction temperature, and reaction time with the DS value of hemicellulose are studied. The highest DS value of 1.82 can be achieved in the optimal condition. A significant degradation of the derivative occurs with the increase in molar ratio, reaction time, and temperature, and thus the thermal stability of the derivative is lower than that of the native hemicelluloses. The synthesis of poplar wood hemicellulose-based esters containing different groups (including short and long alkyl chains) are similar to Sun et al. [51]. The GPC

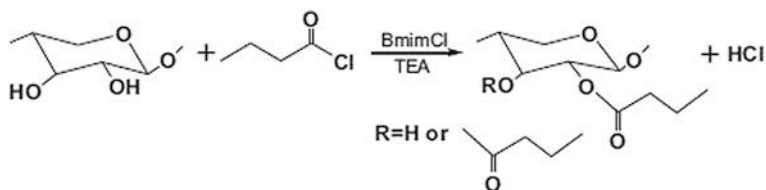


Fig. 3 Butyrylation of hemicelluloses (Reproduced from [50] with permission)

analysis reveals no significant degradation for the polymers during the reaction process [54, 55].

In some cases, xylan esters can be electrospun into nanofibers, the mechanical properties of the esters are also investigated. A series of xylan esters with varying alkyl chain lengths (C2–C12) are synthesized by heterogeneous and homogeneous reactions. The thermal stability and solubility in CHCl_3 increase after esterification. The film forming performance of the new polymers is highly dependent on the molecular weight, while the tensile strength and Young's modulus decrease with the increase of alkyl chain length and conversely in the hydrophobicity and elongation at break of the xylan esters. Especially, the high-molecular-weight xylan esters in hexafluoroisopropanol (HFIP) can be electrospun into nanofibers [56].

Hemicelluloses-based esters can be used as drug carriers. Xylan ibuprofen esters with a high drug loading were synthesized via the activation of the ibuprofen carboxylic acid with *N,N'*-carbonyldiimidazole (CDI) in DMSO [57]. For the sake of enhancing its hydrophobicity, sulfation of xylan ibuprofen esters was carried out in the SO_3/DMF system (Fig. 4). The xylan ibuprofen esters form spherical nanoparticles with a size ranging from 328 to 473 nm (PDI = 0.123–0.255) after dialyzed in DMA; the mean diameter, however, reduces from 342 to 162 nm (PDI = 1.04) after sulfation (Fig. 5). In addition, preliminary stability tests indicate that hydrolytic stability decreases with the introduction of sulfate groups.

There is an increasing need for barrier coatings in food packaging to prevent oxygen, carbon dioxide, water and toxic substances. *O*-acetyl-galactoglucomannan (GGM) is the main hemicellulose in softwoods and has been widely applied in the synthesis of biopolymers. For the environmental consideration, a way to prepare

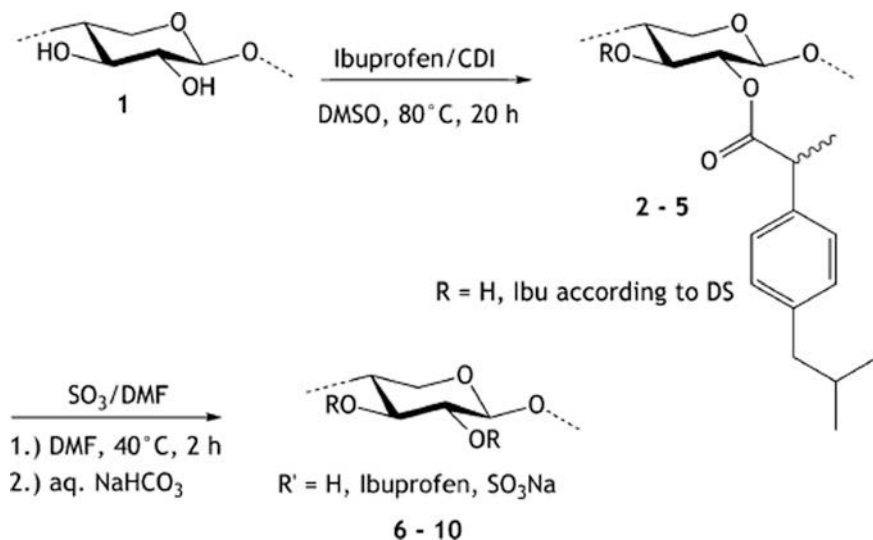


Fig. 4 Synthesis of xylan ibuprofen esters and sulfated xylan ibuprofen esters (Reproduced from [57] with permission)

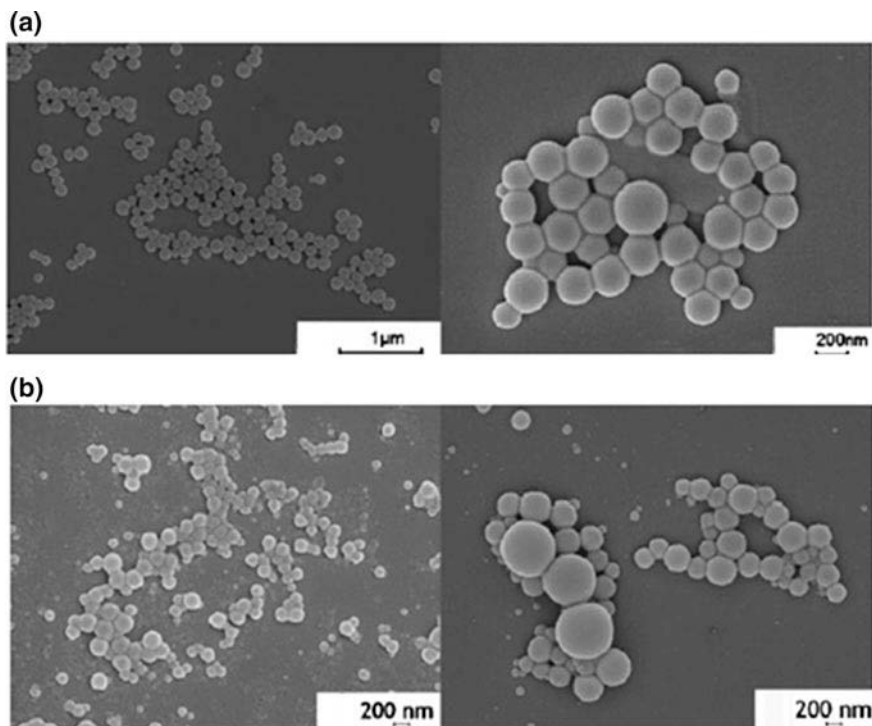


Fig. 5 SEM images of nanoparticles of xylan ibuprofen esters (upper) and sulfated xylan ibuprofen esters (beneath) prepared by dialysis: **a** $DS_{Ibu} = 0.79$, **b** $DS_{Ibu} = 1.24$ (upper); **a** $DS_{Sulfate} = 0.15$, **b** $DS_{Sulfate} = 0.25$ (beneath) (Reproduced from [57] with permission with permission)

GGM ester has been proposed by Kisonen et al. [58]. In their work, GGMs were esterified with phthalic and benzoic anhydrides, respectively. The results showed that GGM ester has a better water vapour resistance and grease barrier than native GGM when coated onto carton board with a thin coating ($1\text{--}3\text{ g/m}^2$). Penetrating 0.1% rapeseed oil with a 2.4 g/m^2 coating thickness cost up to 54 h and the lowest water vapor transmission value was $39\text{ g/m}^2/24\text{ h}$ with 9.7 g/m^2 coating, which indicates a significant decrease in grease barrier in comparison to the uncoated carton board. Moreover, the high-molar-mass GGM coating performed better than the low-molar-mass GGM coatings. To sum up, GGM and GGM esters provide a sustainable and safe conception for barrier coatings in food packaging.

Buchanan et al. [59] suggested that arabinoxylan acetate/propionate/butyrate can be rapidly prepared using MSA as a catalyst. The average molecular weight of the esters was $\sim 500,000$, and the glass transition temperatures (T_g 's) range from 61 to $138\text{ }^\circ\text{C}$ and increase with the decrease of DS, the thermal stability is enhanced in comparison to the parent arabinoxylan but undergoes a rapid degradation when the temperature was above $225\text{ }^\circ\text{C}$. Surprisingly, arabinoxylan acetate/cellulose acetate

blends can be cast into optically clear films, and the clarity of films is influenced by solvent, which provides a possibility of incorporating these arabinoxylan derivatives and other polysaccharide esters into the mixture for preparing novel composites.

Single-electron-transfer mediated living radical polymerization (SET-LRP) has appeared as an effective strategy to achieve living radical polymerization and produce graft copolymers with brush-like architecture without the use of any toxic catalyst. This method is appealing for the design of hybrid materials from macromolecules such as polymers based on sugar moieties, known as polysaccharides. An esterification between AcGGM and α -bromoisobutyric acid with the assistance of CDI yields a macroinitiator ester AcGGM-Br. The macroinitiator as a catalyst can be applied in SET-LRP of methyl acrylate (MA) with $\text{Cu}^0/\text{Me}_6\text{-TREN}$, producing hemicellulose/MA copolymer (Fig. 6) [60]. Kinetic analyses demonstrate the living property of the SET-LRP process together with a high conversion of up to 99.98%, offering a brush-like structure of the hybrid copolymers.

The synthesis of hydroxycinnamic acid xylan esters from oat spelt arabinoxylan/birchwood glucuronoxylan in the presence of LiCl/DMA and pyridine/DMAP was reported by Wrigstedt et al. [61]. Owing to the antioxidative nature of ferulic and sinapic acids, the esterified xylan polymers remained antioxidative activity and exhibited a better lipid antioxidation when comparing with the native oat spelt and birch wood xylans. Further studies show that ferulic acid glucuronoxylan esters and ferulic acid xylan esters were more efficient antioxidants than arabinoxylan and sinapic acid-modified arabinoxylan.

Thiolation is a way to form an ester bond with the hydroxyl groups in hemicelluloses. Maleki et al. [62] proposed a one-pot procedure to synthesize thiolated *O*-acetyl galactoglucomannan (AcGGM-SH) by AcGGM-mediated nucleophilic ring-opening of γ -thiobutyrolactone and the activation of the hydroxyl groups in hemicellulose (Fig. 7). ^1H , ^{13}C NMR spectroscopy and Ellman's reagent assay confirmed that the thiol groups were successfully incorporated into the backbone of hemicellulose. Interestingly, three AcGGM hydrogels were fabricated by using three different methods named thiol-ene click reaction, thiol-Michael addition and disulfide bond formation reaction, respectively. Besides, some polymers such as polyethylene glycol monomethacrylate (PEG-MA) were grafted onto AcGGM-SH by a thermally induced thiol-ene click reaction. Hence, the thiolation of AcGGM is indeed a good choice to design hemicellulose-based esters and hydrogels by employing "click" chemistry.

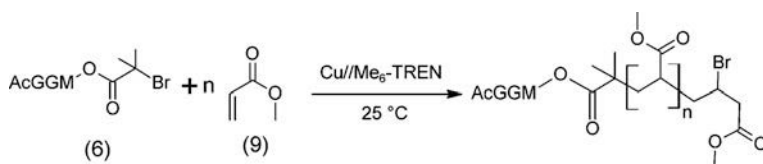


Fig. 6 The SET-LRP of MA (9) with α -Briba-AcGGM (6) as a macroinitiator (Reproduced from [60] with permission)

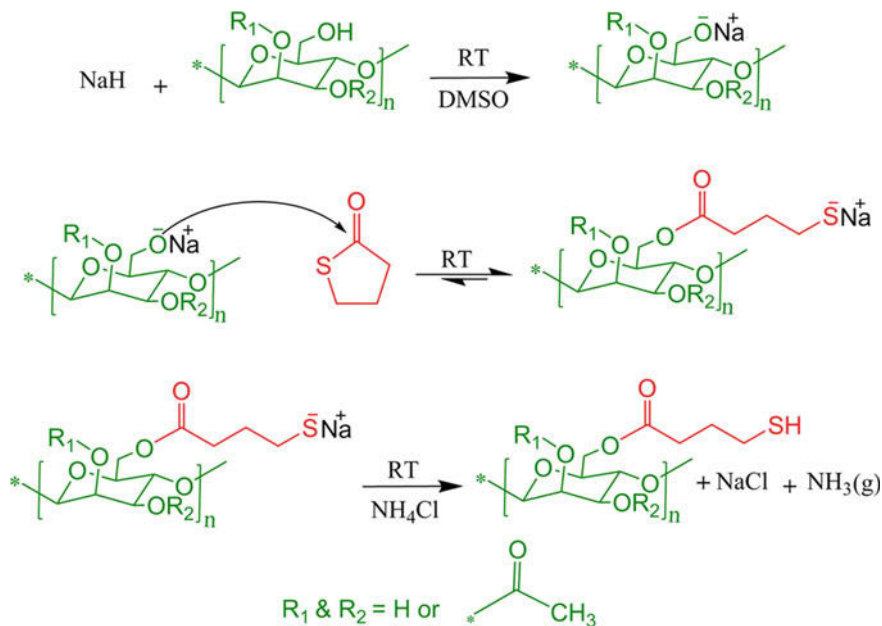


Fig. 7 One-pot thiolation of AcGGM in DMSO (Reproduced from [62] with permission)

2.2 Etherification

Etherification is extensively studied by researchers for chemical modification of hemicelluloses, and many reactions including methylation, alkylation, benzylation and cationic moieties are usually introduced by this way. This reaction occurs between hydroxyl and alkylating agent such as acrylamide, alkyl halides (chlorides, bromides, and iodides), alkyl sulfonates, and epoxides by using alkaline (e.g. sodium hydroxide) as a catalyst under the organic (e.g. DMSO, ethanol, ethanol/acetone, isopropanol, butanol, and DMF) or inorganic (e.g. water) system [5]. The ether bonds are more stable than ester bonds and not easy to be hydrolyzed in an alkaline environment. What's more, the solubility and film formability of hemicelluloses are improved through etherification. However, In order to reduce the degradation of hemicelluloses, heterogeneous reaction systems like water/organic solvents are required [12]. Ren et al. [63] synthesized novel hemicellulosic derivatives through five different heterogeneous/homogeneous systems by etherification with acrylamide in the presence of sodium hydroxide as a catalyst (Fig. 8). The as-prepared hemicellulose derivatives containing carbamoyl ethyl and carboxyethyl achieved the highest DS value of 0.58 under the optimal condition. Especially, reaction medium has a significant influence on the extent of etherification in terms of solvent polarity and stereochemistry. The reaction efficiency increased as the polarity of the solvent decreased. In addition, the thermal stability

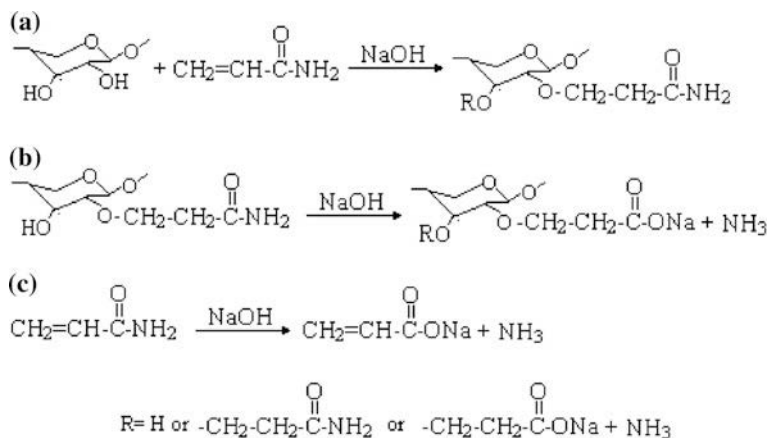


Fig. 8 Etherification of hemicelluloses with acrylamide in alkaline condition (Reproduced from [63] with permission)

decreased after etherification. According to the research described above, Peng et al. [64] synthesized identical hemicellulosic derivatives with a higher DS of 0.92 in butanol/water media. The molecular weights of the products were lower than that of the native hemicellulose due to the significant degradation of hemicellulose during alkaline activation in the etherification reaction. Furthermore, the new derivatives exhibited a less elastic behaviour as compared with the native hemicellulose due to the influences of molecular weight and the functional groups on the structure of macromolecule chains.

Etherification of hemicelluloses with 2, 3-epoxypropyltrimethylammonium chloride (ETA) can be carried out under sodium hydroxide/water media, obtaining quaternized hemicelluloses (QH). Afterwards, smooth and heat-resistant films basing on QH and montmorillonite (MMT) platelets were prepared by a vacuum-filtrated technique. It turns out to be the electrostatic and hydrogen-bonding interactions between the electropositive QH and the exfoliated anionic MMT that contribute to the film-forming process. The excellent thermal property provides a great potential application for the nanocomposite films in flame retardant [65, 66]. By using similar condition, cationic galactomannan/xylan can also be prepared (Fig. 9). The desired DS of 1.3 could be obtained with a maximal grafting rate of 48 and 64% of mass yield at the optimal condition [67]. In a similar way, Ren et al. [68] synthesized a cationic hemicellulose from sugarcane bagasse hemicellulose. ^{13}C NMR spectra justified that the etherification reaction mainly occurred to C-3 position of hemicelluloses. In addition, the molecular weight of the new products reduced sharply from 28,890 (native hemicellulose) to 15,520 g mol^{-1} (DS = 0.33), which is attributed to the degradation of hemicellulose (especially when prolonging the time of alkaline activation at higher temperature).

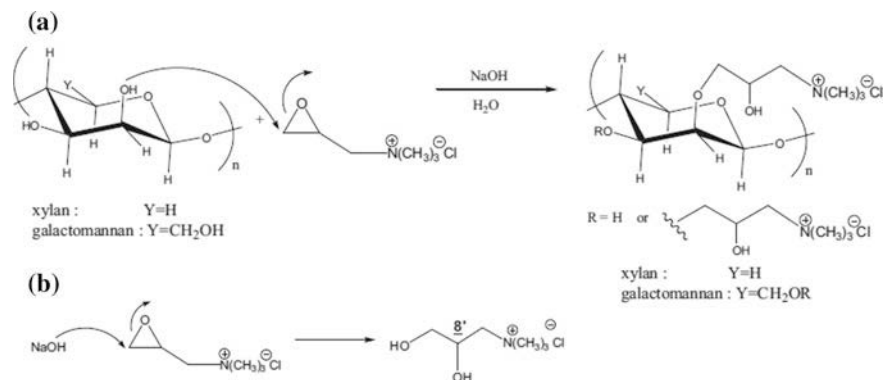


Fig. 9 **a** Cationisation of the hemicelluloses and **b** concurrent reaction forming the by-product (Reproduced from [67] with permission)

Methylation is a typical example of etherification, Fang et al. [69] prepared a methylated hemicellulose by using methyl iodide as an alkylating reagent and sodium hydride (NaH) as a catalyst in DMSO. The reaction mechanism involves methyl sulfinyl anion capturing a proton from the hemicellulose to form the polyalkoxide. The conversion of methylation was high up to 90% with a DS value of 1.7; an endothermic degradation and an obvious increase in thermal stability were observed due to the existence of methyl after methylation.

Hydroxyalkylated xylans were produced by the etherification of xylan and epoxides (propylene oxide, butyl glycidyl ether, and allyl glycidyl ethers) under an alkaline condition. The DS values of the functionalized xylans varied from 1.5 to 0.2. Moreover, the xylan derivatives exhibited a significant oxygen barrier and surface strength as well as low mineral oil migration, which indicates a promising application in barrier coatings for packaging and pigment coating binders for printing papers [28].

Williamson benzylation was used for preparing hydrophobic benzyl galactoglucomannan (BnGGM). In this research, the benzylation of AcGGM hemicellulose was carried out using benzyl chloride as a benzylation reagent and tetrabutylammonium iodide (TBAI) as a phase transfer catalyst in water/sodium hydroxide system, and then surface modification was conducted by plasma treatment followed by styrene addition or vapor-phase grafting of styrene, which was followed by lamination [70]. The vapour-phase-grafted films showed a better tolerance toward to humidity than the plasma-treated ones. The contact angle and oxygen permeability measurements indicate that the films were not only water-resistance but also had excellent oxygen barrier and moisture tolerance properties. Therefore, the surface grafting and lamination methods seem to be a good choice for obtaining good barrier properties even in high humidity environment. Another similar example about hemicelluloses benzylation is the benzylation of wheat straw hemicelluloses in an ethanol/distilled water system (Fig. 10). The low DS value ranging from 0.09 to 0.35 was dependent on the volume ratio of

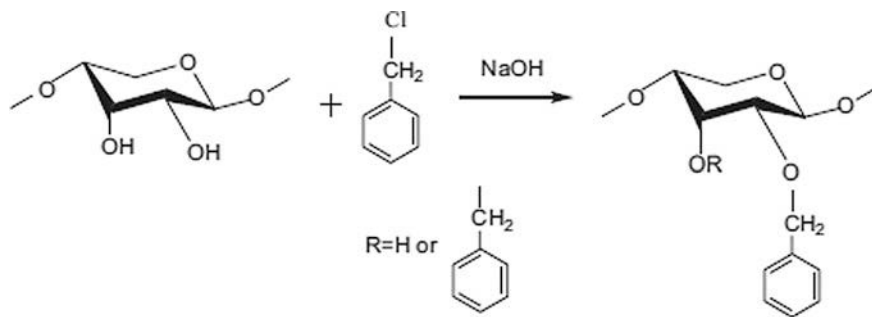


Fig. 10 Reaction scheme of benzylation of hemicelluloses with benzyl chloride (Reproduced from [71] with permission)

ethanol/water, the molar ratio of sodium hydroxide or benzyl chloride to anhydroxylose unit in hemicellulose, reaction temperature and reaction time. FT-IR and ^{13}C NMR spectra identified that benzyl groups were incorporated onto the backbone of hemicellulose, the introduction of benzyl groups increased the thermal stability as well as the hydrophobic property of the new materials [71].

Thiols are very useful groups in developing new materials and bio-inspired polymers. By combining the etherification and thiol-ene reaction, novel thioether xylans were synthesized with a protected thiol that can be stored at atmosphere. At first, allyl groups were introduced in the backbone of xylans by etherification with allyl chloride in aqueous alkaline condition at 40 °C, giving etherified xylans with a DS of up to 0.49. Afterwards, the allyl groups in xylans were reacted with different thiols via thiol-ene reaction by using potassium peroxydisulfate as a radical initiator and water as the solvent, producing novel thiol-, amine- or amino acid functionalized xylans. The thiol-functionalized xylans have broad applications such as preparing hydrogel scaffolds, cross-linking foams by a thiol-thiol oxidative coupling reaction, and modifying filter paper surface by the simple dipping method [72].

The cationization of hemicelluloses was carried out by using 3-chloro-2-hydroxypropyltrimethylammonium chloride (CHMAC), glycidyltrimethylammonium chloride (GTMAC), [2-(methacryloyloxy) ethyl] trimethylammonium chloride (METAC), or ETA as a quaternary nitrogen source in heterogeneous (e.g. H_2O) or homogeneous system (e.g. DMSO) [73]. As described in etherification [65, 67, 68], cationic 2-hydroxypropyltrimethylammonium (HPMA) xylans based on birch wood xylan and ETA were synthesized in 1, 2-dimethoxyethane (DME)/ H_2O system. In this research, adjusting the molar ratio of HPMA and anhydroxylose units of xylans led to the altering of DS in cationic xylans and the highest DS was calculated to be 1.64. Furthermore, the HPMA xylans can be cast into films and had a polyionic structure with positive charged ammonium group (Fig. 11) [74]. In a similar case, a cationic ETA-GGM polyelectrolyte was synthesized and subsequently re-acetylated to obtain enhanced thermal stability and hydrophobic property [75]. Higher reaction efficiency and lower degradation were achieved by using

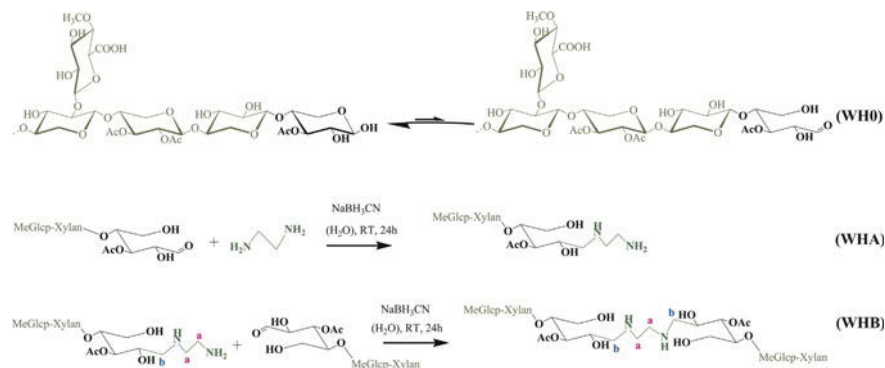


Fig. 11 (i) MeGlcP-Xylan reducing-end hemiacetal in equilibrium with the ring-opened aldehyde, (ii) MeGlcP-Xylan amine functionalization, (iii) head-to-head chain extension of MeGlcP-Xylan (Reproduced from [79] with permission)

THF/ H_2O or DMSO/ H_2O as a reaction media in comparison to that of only with plain water. As reported, the cationised GGM can be potentially utilized as polyelectrolyte layers in films and coatings.

Liu et al. exploited hemicelluloses that isolated from pre-hydrolysis liquor (PHL) to render cationic copolymers under the glycidyltrimethylammonium chloride (GTMAC)/NaOH system [73]. The cationization parameters were investigated, the result indicates the charge density and DS value of the cationic hemicelluloses increased with the increasing dosage of NaOH from 1 to 5% (wt.), but rapidly decreased when the amount of NaOH exceeded 5% (wt.). By copolymerization of xylan and [2-(methacryloyloxy) ethyl] trimethylammonium chloride (METAC) in the presence of $\text{K}_2\text{S}_2\text{O}_8$, a cationic xylan copolymer was produced. The as-prepared xylan-METAC copolymer has an application as a flocculant for dye removal from wastewater [76]. In Kong's research, a higher DS of cationic xylan was obtained by using a semi-dry process compared to that of in the wet process [77]. The GPC analysis shows a substantial degradation of the xylan copolymers occurred during the cationization under alkaline conditions. Conversely, cationic ETA-hemicellulose copolymers with low average DS value were prepared in homogeneous DMSO/ H_2O media without significant degradation in alkaline media [78].

2.3 Amination

A reductive amination is a common approach used in polysaccharide chemistry to immobilize different types of amino-functionalized moieties entities to saccharide structures by using the ring-opened aldehyde at the reducing end of the hemicellulosic chain as a reactive center for attaching amino coupling agents. This reaction

is conducted in aqueous media and under mild conditions, and thus represents a robust and highly selective method for the chemical modification of hemicellulose [12]. The hemicellulosic derivative exhibits an enhancing amphiphilic property with increasing molecular weight after reducing amination, which can be utilized as reinforce way for films and coatings. In the report by Dax et al. [79], reductive amination was conducted between native GGM and a series of amino-functional fatty acids in the presence of NaBH_3CN , yielding block-structure amphiphilic GGM derivatives which were only water-soluble [80]. In another sample, a chain-extended *O*-acetyl-4-*O*-methylglucuronoxylan-rich (MeGlcP-Xylan) wood hydrolysate (WH) was prepared through reductive amination with the assistance of NaBH_3CN (Fig. 12). Especially, the formability and mechanical performances of WH films were significantly improved after the treatment, and simultaneously reduced the need of co-components. In addition, the produced films exhibited an excellent oxygen barrier performance. Therefore, reductive amination could be applied for increasing the molar mass of a low-molecular-weight xylan with mono and bifunctional amines on its reducing end and has a potential utilization in films and coatings [81].

Ehrenfreund-Kleinman et al. [82] synthesized arabinogalactan (AG)-based sponges by reductive amination on the reducing end of the oxidized AG with different amines in the presence of NaBH_4 . The as-prepared sponges exhibited high swelling and had a possible use in cell growth in tissue engineering. Particularly,

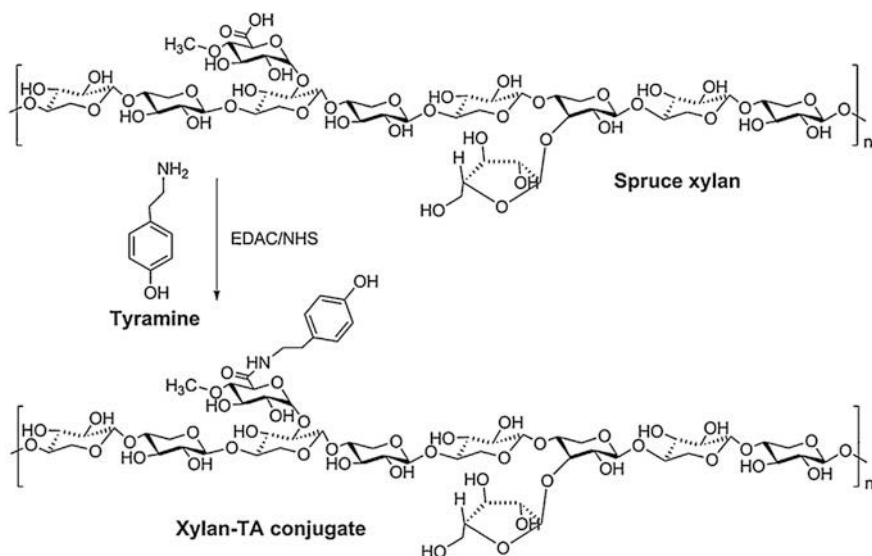


Fig. 12 Amidation of spruce xylan with tyramine (Reproduced from [84] with permission)

AG-chitosan sponges showed good biocompatibility with an inflammatory response confined to the implant site which decreased with time.

2.4 Amidation

Amidation of hemicellulose with amine-functionalized compounds can be defined as the coupling of amines to carboxylic acids through amide bonds and is commonly activated by *N*-ethyl-*N'*-(3-dimethylamino)propyl carbodiimide hydroxide/*N*-hydroxysuccinimide (EDC/NHS) (carbodiimide-mediated amidation) in aqueous media [83]. Kuzmenko et al. [84] reported the amidation of glucuronic acid groups from xylan backbone and tyramine (TA) with the activation of EDC/NHS (Fig. 13) followed by enzymatic crosslinking of the phenol-containing TA-xylan conjugate in the presence of HRP/H₂O₂, and fabricating a 3D hydrogel in a negligible time (20 ± 5 s) for cell encapsulation and vivo delivery. The spruce xylan-based hydrogel exhibits an obvious increase in the storage module and excellent swelling stability, which provides a great potential application in tissue engineering. In another case, oxidized GGM (containing uronic acid) was functionalized with arginine or 1, 6-diaminohexane by using the same carbodiimide-mediated amidation. This amidation is performed after the oxidation of hydroxyl groups in GGMs [83]. Except for EDC, 4-(4, 6-dimethoxy-1, 3, 5-triazin-2-yl)-4-methylmorpholinium chloride (DMT-MM) was also employed as a superior acid-amine coupling reagent for the amidation of an acidic xylo-oligosaccharide fragment from 4-*O*-Methylglucuronoxylan hemicellulose without the tight control of PH. As a result, amidation of C-6 acids was performed efficiently by using the coupling reagent DMT-MM and formed an amide linkage. A triazine side product which hindered C-1 amidation, however, was observed. Furthermore, the modified monomers were polymerized via copper(I)-catalyzed azide-alkyne cycloaddition (CuAAC) “click” reaction, and thus forming a soft gel. This pathway provides a rarely used system of DMT-MM with preferable performance compares to EDC under certain conditions [85].

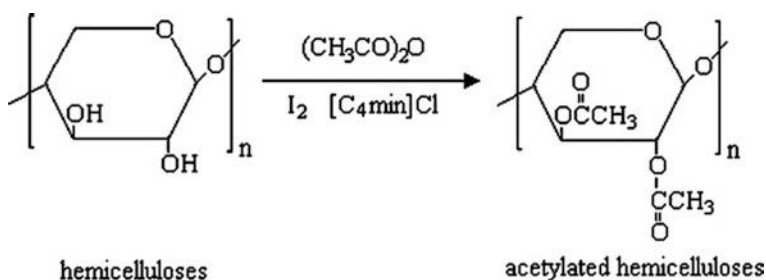


Fig. 13 Acetylation of wheat straw hemicelluloses (Reproduced from [89] with permission)

2.5 Acetylation

Hemicellulose acetylation is an important chemical modification that introduces acetyl groups to the hemicellulose chain through esterification reactions as mentioned above. This reaction was carried out in non-water medium such as ionic liquids (ILs), DMA/LiCl, DMF, in the presence of DMAP, pyridine or NBS as catalysts. The thermal stability, mechanical properties, oxygen transmittance and hydrophobicity of the acetylated hemicellulose have been investigated by altering the reaction conditions [11].

Fundador et al. [86] acetylated xylan from hardwood with acetic anhydride or propionic anhydride in homogenous DMA/LiCl system by the catalysis of pyridine, obtaining xylan acetates and xylan acetate propionates with varied DS values. The structure and DS of the modified xylyns were elucidated by ^1H , ^{13}C NMR spectroscopy, and two-dimensional (2D) NMR techniques. The results show equal reactivities at the C-2 and C-3 of xylose during the acetylation process. Moreover, the thermal stability and solubility in chloroform of xylan were improved after acetylation. In this study, xylan acetate (DS = 2.0) nanofibers with a diameter of 163–429 nm were formed by an electrospinning method and using HFIP as a solvent. Mechanical tests of xylan acetate propionate films showed that the tensile strength and elongation at break increased as the DS decreased from 1.1 to 0.6. Another acetylation of wheat straw hemicellulose was reported by Sun et al. under the same condition mentioned above, except for using DMAP as a catalyst. Both the yield and DS of the acetylated hemicellulose were increased with temperature (from 60 to 85 °C) and reaction time (from 12 to 60 h); and a high DS value of 1.49 could be obtained under the optimal condition (85 °C, 60 h) with 80% of the free hydroxyl groups being acetylated. The GPC analysis revealed a sharp decomposition when the reaction time was 72 h at 85 °C, resulting in a low molecular-average weight of 22,890 g mol⁻¹. Moreover, the chemical modification leads to a decreased thermal stability [87]. Due to the toxicity of pyridine and the high cost of DMAP, a new catalyst NBS was utilized for the acetylation of sugarcane bagasse hemicellulose with acetic anhydride under an almost solvent-free system. The overall yield varied from 66.2 to 83.5% and DS ranged from 0.27 to 1.15 by altering the reaction temperature and duration. Furthermore, the results of TG-DSC indicate that the thermal stability of the modified hemicellulose was higher than that of the native hemicellulose [88].

ILs are considered to be a green and effective solvent for the acetylation of hemicelluloses by using iodine as a catalyst (Fig. 14) [89]. The DS of acetylated hemicelluloses ranged from 0.49 to 1.53, and about 83% hydroxyl groups in the native hemicelluloses were acetylated under the optimal reaction condition. Moreover, the thermal stability was enhanced after functionalization. In order to achieve full acetylation under mild conditions, Stepan et al. [90] reacted rye arabinoxylan (AX) and spruce arabinoglucuronoxylan (AGX) with acetyl chloride and acetic anhydride in two new ILs, respectively. The first system was 1-ethyl-3-methylimidazolium dimethyl phosphate ([emim][Me₂PO₄]) with CHCl₃

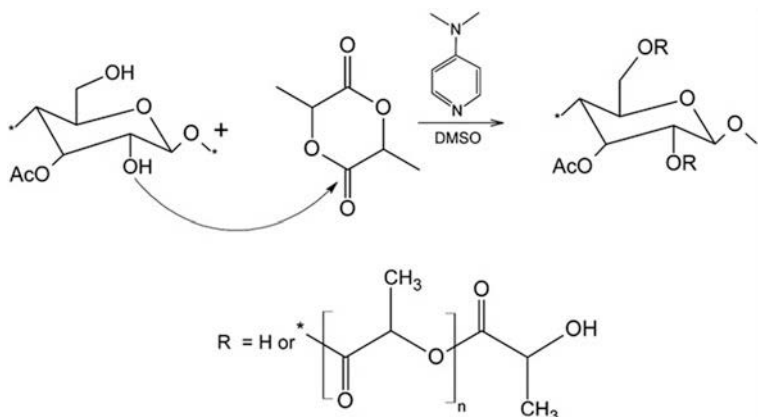


Fig. 14 Synthetic pathway for the grafting of L-lactide oligomers from the acetylated galactoglucomannan (AcGGM) backbone (Reproduced from [96] with permission)

as a co-solvent, and the other was 1, 5-diazabicyclo[4.3.0]non-5-enium acetate ([DBNH][OAc]) without co-solvent. The complete acetylation was achieved within 5 min in both reaction systems under the optimal condition. FT-IR and ^1H NMR spectroscopy confirm the full acetylation of xylan. GPC result shows no significant degradation occurred during acetylation of rye AX but a minor depolymerization took place in the case of spruce AGX. Both of the acetylated xylns maintained a relatively high molecular weight. In addition, the solubility of the new polymers in CHCl_3 and dimethyl carbonate allowing it casting into transparent films.

Acetylation has a significant influence on the solubility, water content and thermal properties of the modified hemicelluloses. The differences have been well investigated by the reaction between aspen glucuronoxylan and acetic anhydride in formamide/pyridine system [91]. For instance, the water content in humidity strongly decreased after acetylation. The fully acetylated glucuronoxylan was soluble only in aprotic solvents, such as chloroform and DMSO, while the native glucuronoxylan was partially soluble in hot water. The decomposition temperatures for a 10% weight loss were 283 and 335 $^\circ\text{C}$ for non-acetylated glucuronoxylan and the acetylated sample, indicating an improving thermal stability after acetylation. DSC analysis indicated that glucuronoxylan with a DS of 1.2 had a significant glass transition temperature during 160–200 $^\circ\text{C}$ and could form films under pressure, but not the case in non-acetylated samples.

A new method for synthesizing acetylated hemicelluloses was developed in 1-allyl-3-methylimidazolium chloride ([Amim] $^+\text{Cl}^-$) ionic liquid without using catalyst [92]. The DS ranged between 0.03 and 1.25 and increased with the reaction time and temperature. The properties of the as-prepared hemicellulosic derivative such as solubility, equilibrium water content, thermal stability were also significantly changed. In conclusion, eco-friendly ionic liquids are excellent solvents to generate value-added hemicellulose acetate with high DS and can be used in various industrial applications.

2.6 Grafting Copolymerization

Graft polymerization is an effective method to overcome the disadvantages of hemicelluloses and tailor their properties for specific end uses. Most graft copolymers are formed by free radical grafting polymerization, such as SET-LRP, which is a water-tolerating polymerization technique conductible at benign conditions with the catalysis of Cu(0). In addition, “click chemistry” offers a promising pathway for the synthesis of graft-copolymers of polysaccharides. Among the radical polymerizations of hemicelluloses, the free hydroxyl groups in hemicelluloses are used as initiator sites to perform polymerizations of a number of monomers to form grafts [5, 93–95].

Graft copolymers XylC6N₃-g-PLLAs basing on di-*O*-(6-azidohexanoyl)-xylan (XylC6N₃) and Propargyl-terminated poly(L-lactide) (PLLA) were prepared in the presence of *N, N, N', N', N''*-pentamethyldiethylenetriamine (PMDETA) and copper (I) bromide via click chemistry. The results indicate that the grafted PLLA side-chains act as an internal plasticizer for xylans [94]. Similarly, L-lactide (LLA) oligomers were functionalized with wood hydrolysate derived hemicellulose-rich fractions by ring opening graft polymerization (Fig. 15), the as-prepared copolymers can be applied as a compatibilizer for hydrolysate/PLLA film [96]. Persson et al. [97] developed biodegradable PLA-g-xylan copolymers

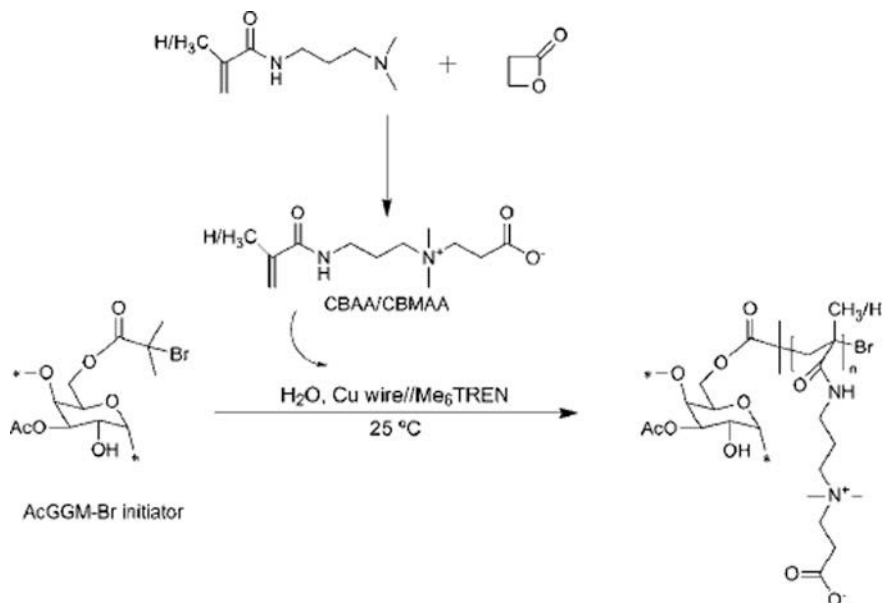


Fig. 15 Schematic outline of the pathways for grafting poly(CBAA-3) and poly(CBMAA-3) from the AcGGM-Br macroinitiator via SET-LRP under mild conditions (Reproduced from [100] with permission)

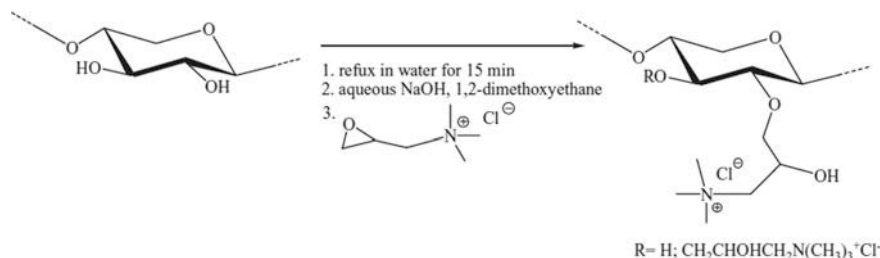


Fig. 16 Reaction scheme of the cationization of xylan with EPTA (Reproduced from [74] with permission)

with different branch length in the catalysis of triazabicyclodecene (TBD). The obtained polymers with long polylactide (PLA) branch exhibited better mechanical and thermal properties than the polymers with short PLA branch.

Acrylonitrile (AN) or methyl acrylate (MA) can be grafted onto hemicelluloses containing lignin. The graft polymerization of hemicellulose with low and high lignin content can be carried out by using ceric ammonium nitrate and FeSO₄/H₂O₂ redox system as an initiator, respectively [98]. Taking FeSO₄/H₂O₂ as an initiator, Dong et al. [93] synthesized copolymers by grafting acrylamide (AM) and methacryloyloxy ethyl trimethyl ammonium chloride (DMC) on the hemicelluloses from alkaline peroxide mechanical pulping (APMP) effluent. The resulting copolymers show enhanced physical strength and water resistance on corrugated paper, which is attributed to the functional groups (–OH and –NH₂) and the covalent bonds formed between the hemicellulose and the graft copolymer.

According to the previous description [60], a series of hemicellulose-based graft-copolymers with tunable hydrophilicity were synthesized via SET-LRP process, including methyl methacrylate (MMA)/hemicellulose, *N*-isopropyl acrylamide (NIPAM)/hemicellulose, and acrylamide (AcAm)/hemicellulose copolymers [99]. In Edlund's report, AcGGM-graft-GMA copolymers with a conversion of high up to 80% were successfully prepared by the SET-LRP procedure of AcGGM-Br and glycidyl methacrylate (GMA). A new class of zwitterionic polymers were prepared by grafting poly(carboxybetaine) onto AcGGM-Br via the same technique (Fig. 16) [100]. In another case, grafting copolymers composed of methylated xylan and polystyrene were synthesized by O'Malley's group, and the mechanism involved the reaction of "living" polystyrene with the methyl glucuronate moiety and generation of well-defined comb-like structures [101]. Therefore, SET-LRP is regarded as a powerful method for the design of new hemicellulosic copolymers.

2.7 Oxidation

Oxidation is a reaction that transforms the alcohol groups of hemicellulose to aldehydes or carboxylic acids in the presence of specific enzymes such as galactose

oxidase, catalase and horseradish peroxidase or oxidizing agents including KI/I_2 , NaClO_2 and NaIO_4 [12].

Parikka et al. [102] studied the regioselective oxidation of guar galactomannan (GM), tamarind galactoxyloglucan (XG), and spruce GGM by galactose oxidase-catalyzed reaction to form galactoaldehydes and further selectively chemical oxidation to obtain galacturonic acids with the assistance of I_2/KI or NaClO_2 (Fig. 17). Quartz crystal microbalance with dissipation (QCM-D) measurement was applied to determine the interaction of the products with cellulose, the result showed that the chemo-enzymatically oxidized galacturonic polysaccharides with an unmodified backbone had a better ability to interact with cellulose than 2, 2, 6, 6-tetramethylpiperidine-1-oxyl (TEMPO)-oxidized products. Similarly, a series of polysaccharides containing terminal galactose were oxidized by galactose oxidase, catalase and horseradish peroxidase. The oxidations result in significant changes in properties of different polysaccharides. For instance, tamarind xyloglucan formed a gel and larger particles were dispersed in the solution of spruce galactoglucomannan after oxidation [103, 104].

TEMPO oxidation can specifically convert the primary alcohols on C-6 to carboxylate groups. Song et al. [105] reported a TEMPO/ NaClO_2 oxidized β -D-glucan and the product was applied as an enhanced bonding agent for paper-making. A significant enhancement in tensile strength and folding endurance of paper could be observed when using oxidized β -D-glucan a strengthening agent. Xylan can be oxidized by NaIO_4 to introduce dialdehydes and hemiacetal bonds formed between the aldehyde groups and hydroxyl groups of the modified xylan during the freeze-casting process, obtaining cross-linking hydrogels with the reinforce of nanocrystalline cellulose [106]. The strength of the gels decreased with the increasing degree of oxidation due to the change in xylan molecular rigidity. Another aldehyde functionalized xylan MGX was prepared by the oxidation of NaIO_4 [107]. It is found that periodate oxidation is specific to vicinal diols for the formation of aldehydes at low periodate concentration and no depolymerization occurs at 0.05 NaIO_4 /xylose ratio. The effect of different oxidants on the degradation rate of oxidized arabinogalactan-chitosan sponges was proposed by Ehrenfreund-Kleinman et al. [108]. The result indicates the degradation of sponges oxidized with sodium chlorite was faster than that of the sample with sodium periodate.

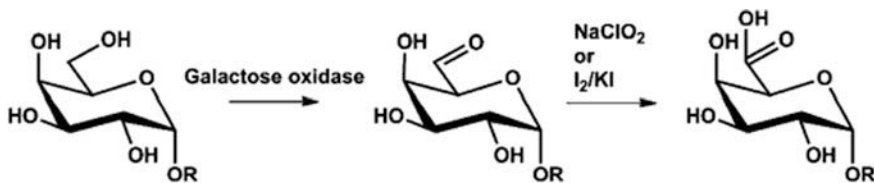


Fig. 17 Oxidation of the galactosyl units of polysaccharides to galacturonic acid ($R =$ backbone of the polysaccharide) (Reproduced from [102] with permission)

3 Hemicellulose-Based Particles (Zero-Dimensional)

Hemicelluloses possess many hydroxyl groups and reducing aldehyde groups, and exist as helical chains or random-coil chains in aqueous solution, which provides a possibility to act as a green reducing agent and stabilizing agent by capping metallic nanoparticles in the special structure [109]. In addition, hemicelluloses are widely used as a substrate or coatings for nanoparticles and have an application in target drug delivery and chemical catalysis.

By using biopolymer xylan as a stabilizing and reducing agent, Luo et al. [110] prepared highly stable xylan/Au nanoparticles (AuNPs) composites with the highly sensitive sensing of cysteine. The obtained nanoparticles could distinguish cysteine (Cy) among dozens of kinds of amino acids with a limit of detection (LOD) of 0.57 μM , exhibiting a potential application for Cys detection in real biological samples. Similarly, well-distributed spherical silver nanoparticles (AgNPs) could be rapidly synthesized by using bamboo hemicellulose as stabilizer and glucose as reducer with the assistance of microwave [111]. The effects of reaction parameters on the shape of AgNPs were investigated, the result revealed that the average particle size of AgNPs increased with AgNO_3 concentration. The coexistence of silver Ag(0) and Ag(I) was found by XPS analysis. In another case, xylan/AgNPs composites were developed via tollens reaction by reduction of $[\text{Ag}(\text{NH}_3)_2]^+$ under microwave irradiation (Fig. 18) [109]. The nanoparticles showed a high selectivity and sensitivity for Hg^{2+} detection with a low LOD of 4.6 nm, indicating a suitable detector for harmful heavy metal detection. Xylan-coated magnetic microparticles were produced by emulsification of $\text{Fe}^{2+}/\text{Fe}^{3+}$ suspension and xylan solution, followed by interfacial cross-linking in the presence of terephthaloyl chloride [112]. The obtained polymeric magnetic microparticles (PMP) can undergo not to be dissolved at gastric pH but not of that in magnetic microparticles (MP) without the xylan coating, which demonstrates the xylan coating did shield magnetite from the gastric pH.

In Wu's research, carboxymethyl functionalized hemicellulose (CMH) was used as a substrate for the deposition of palladium nanoparticles (Pd NPs) to provide a novel heterogeneous catalyst CMH-Pd(0) by using ethanol as a solvent and an in situ reducing agent. The CMH-Pd(0) was a very active and stable biobased catalyst for Heck coupling reaction and could be easily recovered and reused at least 5 times [113]. Chen et al. [114] used xylan-type hemicelluloses (XH) supported terpyridine-palladium (II) nanoparticles to catalyze Suzuki-Miyaura reaction with a high yield up to 98%. In another study by Chen et al. [115], PdNPs@XH catalyst was synthesized with the same deposition-precipitation method and showed excellent catalytic activity in the Suzuki, Heck, and Sonogashira coupling reactions. These works broaden the applications of hemicelluloses in green catalysis.

The BSA-loaded CKGM-CS nanoparticle basing on carboxymethyl Konjac glucomannan (CKGM) and chitosan (CS) was formed by electrostatic interactions and was applied for the encapsulation of bovine serum albumin (BSA). The mean

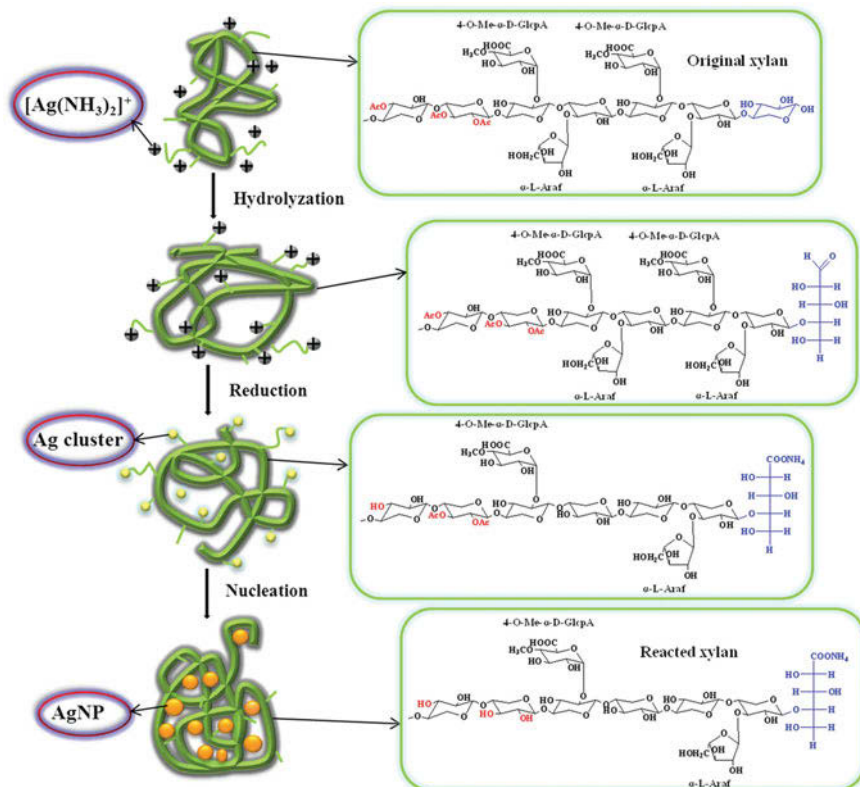


Fig. 18 The possible formation course of xylan-AgNPs composites (Reproduced from [109] with permission)

size of the nanoparticles increased with an increase in either the CKGM or CS concentration. Particularly, the concentration of CS can effectively dominant the zeta potential measurements, which was attributed to its cationic nature [116]. As observed, the nontoxic CKGM-CS nanoparticles have a promising application as green drug carriers. Xylan furoate pyroglutamate was prepared by esterification between xylan and pyroglutamic acid/furan-2-carboxylic acid in the presence of CDI [117]. Small-size spherical nanoparticles (60–85 nm) yielded by simple dialysis of the obtained esters in DMSO. Garcia et al. [118] employed an original method by neutralizing the alkaline xylan solution with HCl or acetic acid to form micro and nanoparticles. The result demonstrated that the size of xylan particles was dependent on xylan concentration and nanoparticles with 100–900 nm could be obtained in a low xylan content.

4 Hemicelluloses-Based Films and Coatings (Two-Dimensional)

Hemicelluloses have inherent properties including low oxygen permeability, water solubility, and biodegradability. The low oxygen permeability makes hemicelluloses have a promising application in barrier films and coatings, notably in food-packaging. Considering the low cost and environmental friendliness of hemicelluloses, they are good substitutions for the conventional package materials, for example, aluminium foil, EVOH or PVDC. However, the disadvantages of water/moisture sensitivity, high water vapour permeability (WVP) and brittleness hinder their better use in films and coatings. Thus, chemical or enzymatic modifications of hemicellulose are required to alter their physicochemical properties by grafting, crosslinking, blending and other methods, and finally improve the oxygen barrier, WVP and mechanical properties of native hemicelluloses for special use [12]. The oxygen barrier properties can be quantified by oxygen permeability (OP) and expressed in $\text{cm}^3 \mu\text{m}^2 \text{d kPa}$, while WVP is usually determined by the cup test in the order of $\text{g m}^{-1} \text{Pa}^{-1} \text{h}^{-1}$ or $\text{g m}^{-1} \text{Pa}^{-1} \text{s}^{-1}$.

4.1 Blending

Hemicelluloses-based films can be formed by organic and inorganic additives including emulsifiers (sucrose esters, palmitic acid, etc.) [119–121], plasticizers (glycerol, sorbitol, xylitol) [122, 123], polyvinyl alcohol (PVA) [44], MMT [27, 65, 124], chitosan [27, 125], cellulose derivatives [126–132], alginate [122], carbon nanotube [133], and other materials [134–137].

The emulsifiers have a significant effect on the stabilization for the structure of the film especially during drying, and can strongly influence the barrier and mechanical properties of films. In Phan's research, hydrogenated palm kernel oil (HPKO) and sucroesters with varied hydrophilic-lipophilic balances (HLBs) were successively added to AX/glycerol solution, and films were formed after stirring, homogenizing and drying. The film with 2.5% SP10 shows a 30% decrease in WVP value when comparing to lipid-free AX film. The presence of SP10 also improved the moisture resistance of film due to its low melting point and hydrophobic property. However, SP30, SP40, and SP70 do little effect on the water absorption rate and the contact angle of films [121]. Another two similar reports about the AX-lipid-based edible films elucidated the influences of drying temperature and lipid type on film structure and properties, [119, 120]. Increasing drying temperature induced a gain of mechanical performances (elongation) of film containing lipid and an apparent "bilayerlike" structure that led to the reduction of moisture transfer. The lowest WVP and a smallest mean diameter ($0.54 \mu\text{m}$) were observed in HPKO-AX emulsion films. Additionally, water contact angle measured on the HPOK-AX film was comparable to those observed for low-density polyethylene

(LDPE) films ($>90^\circ$). However, only triolein-AX films gained elongation after emulsification. As illuminated, HPKO is a good emulsifier to enhance water resistance of AX-based film [120].

A plasticizer was required to avoid brittleness of hemicellulosic films, and the most commonly used plasticizers are propylene glycol, glycerol, sorbitol, and xylitol. AcGGM was physically blended with alginate or carboxymethyl cellulose in the presence of plasticizer (glycerol, sorbitol or xylitol), and films were formed by solution-casting technique. All films have been evaluated by dynamic mechanical analysis (DMA) equipped with a humidity scan, Ox-Tra[®] Mocon and DSC to measure their storage modulus, oxygen permeability and thermal properties. It was found that the incorporation of plasticizer resulting in a low O_2 permeability [≤ 4.6 ($\text{cm}^3 \mu\text{m})/(\text{m}^2 \text{d kPa})$], high mechanical toughness, and flexibility within the AcGGM-based film. Therefore, AcGGM film is an excellent candidate for making new renewable barrier materials for food packaging [122]. Without alginate or carboxymethyl cellulose, corn hull arabinoxylan films with a plasticizer (glycerol, propylene glycol, or sorbitol) had lower WVPs ($0.23 \sim 0.43 \times 10^{-10} \text{ g m}^{-1} \text{ Pa}^{-1} \text{ s}^{-1}$) and may be attributed to the antiplasticization effect. Moreover, the blend films had a tensile strength of 10–61 MPa, modulus of 365–1320 MPa, and elongation ranging from 6 to 12%. Interestingly, grapes coated with arabinoxylan/sorbitol films achieved a decrease of 41% in weight loss rates after 7 days [123].

Reinforcing agents such as inorganic clays possess the flame retardant property and other superior physical properties. MMT is commonly used to incorporate with biopolymers in film casting through a green and simple paper-marking method. The heat-resistance hybrid films (Fig. 19) were prepared from QH and MMT with different ratios [65]. The film forming mechanism is the electrostatic and hydrogen-bonding interaction between QH and MMT nanoplatelets. The thermal stabilities of the hybrid films were higher than those of QH due to the addition of MMT and the proper proportion of QH and MMT. In a study by Chen et al. [124], QH/MMT/PVA or QH/MMT/chitin nanowhiskers (NCH) hybrid films with different proportions were formed by vacuum filtration. Compared with QH-MMT film, the films containing PVA or NCH exhibited an improved mechanical strength, thermal stability, and oxygen barrier property, as well as a higher optical transparency.

Chitosan (CS) is an electropositive biopolymer due to the presence of $-\text{NH}_2$ groups and could generate electrostatic interactions with anionic groups in acidic media. Together with biodegradability and biocompatibility, chitosan is an excellent film-forming candidate. When chitosan was introduced into QH/MMT matrix, producing nanocomposite films with nacre-like structure and excellent mechanical properties [27]. UV-vis test shows that the opacity was increased with the increment of MMT amount. With the addition of small amount of CS, QH-MMT-CS film showed a high tensile strength of 57.8 MPa, which was 30.2% higher than QH-MMT composite film. The new prepared films also possess a good thermal stability, lower oxygen permeability and preferable water vapour permeability. Basing on the above results, these hemicelluloses-based nanocomposite films can be good candidates for non-renewable films and have a great potential application

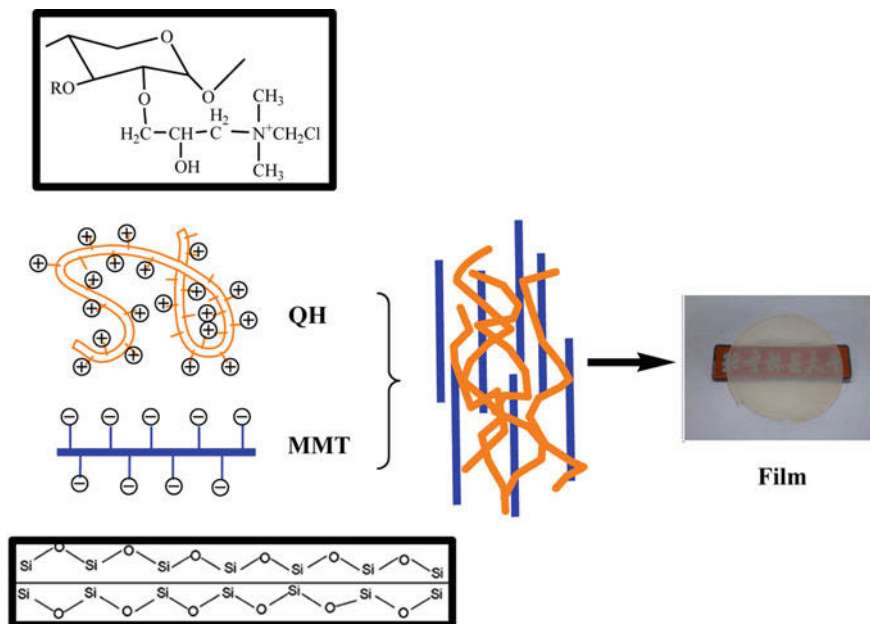


Fig. 19 The QH-MMT film forming process (Reproduced from [65] with permission)

in packaging. By introducing chitosan and glycerol, bagasse hemicelluloses films were prepared with varied hemicellulose concentrations, chitosan/glycerol amount and the drying temperature [125]. Due to the highly hydrophilic nature of glycerol, the WVP of hybrid films rose as the increasing glycerol amount and decreased by 48% as the drying temperature increased from 25 to 55 °C. Besides, the tensile strength and the elongation were changed significantly in the same range of temperature. In summary, drying temperature has a noticeable effect on the mechanical properties of these films.

In recent years, incorporation of biodegradable reinforcements such as celluloses and other polymers has been extensively used for producing composite films with enhancing mechanical performances and good barrier property. Xylan from corn cob was blended with two kinds of cellulose and elaborating two composite films by solvent casting [126]. One film was hydrophilic and fabricated from bleached hemicelluloses (BH), unmodified cellulose and glycerol (as a plasticizer). The other film was hydrophobic and composed of acetylated bleached hemicelluloses (BAH) and acetylated cellulose, as shown in Fig. 20. The hydrophobic film had a higher maximum weight loss temperature than the hydrophilic one, revealing a higher thermal stability for the hydrophobic film. In addition, hydrophobic film (a Young's modulus \sim 2300 MPa, a tensile strength of 44.1 MPa, and a strain at break of 5.7%) showed better mechanical properties than the hydrophilic films (a Young's modulus of 3 MPa, a strength of 3.3 MPa, and a strain at break of 5.3%), indicating acetylated cellulose did not alter its reinforcing potential.

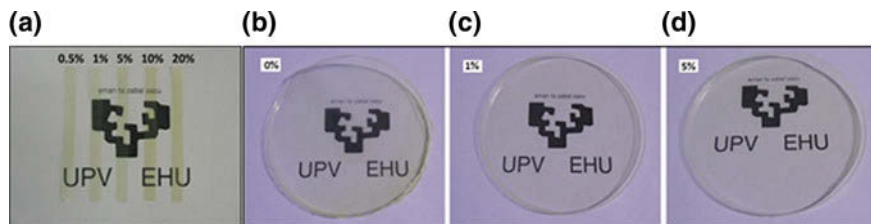


Fig. 20 Optical images of films: **a** test specimens of hydrophilic films with different percentages of nanofiber, **b** hydrophobic films without reinforcement, **c** hydrophobic films with 1% of acetylated cellulose and **d** hydrophobic films with 5% of acetylated cellulose (Reproduced from [126] with permission)

Huang et al. [128] reported a comparative study on the influence of nanocrystalline cellulose (NCC) or cationically modified NCC (CNCC) to the prepared hemicelluloses/sorbitol (HC/SB) films. NCC was cationized by glycidyltrimethylammonium chloride (GTMAC). The presence of NCC and CNCC remarkably improved the mechanical properties of HC/SB films with increased elastic modulus and higher tensile stress. Moreover, HC/SB/CNCC films exhibited better thermal stability and a relatively smooth surface as compared to that with HC/SB/NCC films. For the first time, hemicellulose/lignin (HL) film plasticized by 30% sorbitol was reinforced with different loadings of nanocelluloses (ACNF, CNC, OCNF, ACCNF). The film exhibited significant improvement in flexibility, transparency, mechanical and moisture barrier performances. For instance, the film with ACNF enhanced Young's modulus and tensile strength up to 319 MPa and 266%, respectively; while a film with CNC20 possessed a lower MVP and a less moisture content as compared to other films. This work shows a great feasibility of turning agricultural residues into high value-added film materials [127]. Kisonen et al. [129] took the good affinity between GGM and nanofibrillated cellulose (NFC) to cast films and coated with either succinic esters of GGM [GGM-Su1 (DS = 1.0) and GGM-Su2 (DS = 1.6)] or native GGM. The contact angle measurement revealed that NFC-GGM film double-coated with GGM-Su2 had better a hydrophobic characteristic than other films; the lowest OP value of 0.1 [(cm³ μm) (m² d kPa)] and an improvement in barrier property and stiffness were achieved by the addition of GGM-Su2 on NFC-GGM substrate. Furthermore, all films were demonstrated to be grease impenetrable even at high temperature. Similarly, NFC/glucomannan films could be fabricated by taking sorbitol as a plasticizer. The incorporation of NFC improved the tensile and bursting strength of the films. Notably, the films can be gravure printed with solvent-based ink using a gravure K-proofing press due to its relatively high surface energy [130]. In another case, microfibrillated cellulose (MFC) was mixed with GGM to form composite films with the addition of glycerol. The reinforcement of MFC improved the mechanical properties and decreased the moisture uptake of the films at low glycerol content (5–15%) [131]. Peng and co-workers synthesized nanocomposite films basing on xylan-rich hemicelluloses and cellulose nanofibers (CNFs) in the presence of sorbitol. The strong hydrogen

bonding between CNF and xylan allowed good interfacial adhesion between xylan matrix and CNF, which results in a high mechanical strength and increased thermal stability [132].

For the purpose of gaining conductivity of hemicelluloses, carbon nanotube (CNT) is utilized as a filler material. The prepared CNT-hemicellulose films were cast by either spinning or drop-drying method. The CNT-hemicellulose films showed excellent conductive properties with a bulk conductivity of up to 2000 S cm^{-1} [133].

Hemicelluloses also can be utilized as reinforcement. Hemicellulose from autohydrolysis process was incorporated with κ -carrageenan/locust bean (κ -car/LBG) system in the presence of 0.30% (w/w) glycerol to prepare polymer-blend films. The addition of hemicellulose resulted in a higher tensile strength and a lower moisture content but did not lead to an obvious change in WVP and elongation at break [136].

Without any addition, glucose and hemicelluloses-based films were prepared with cellulosic and hemicellulosic portions from alkaline pretreatment of cotton stalks at three different temperatures. The result showed that pretreatment temperature did significant influence on the yield of cellulose and hemicellulosic portion and the physical properties. The optimal pretreatment temperature was determined to be $60 \text{ }^\circ\text{C}$, at which could form an integrated film with a proper content of lignin, and the film had better oxygen permeability and moderate mechanical properties. Increasing pretreatment temperature to $90 \text{ }^\circ\text{C}$, however, was detrimental to the mechanical properties of the films (Fig. 21) [134]. By using autohydrolysis and alkaline extraction of hemicelluloses as mentioned above, free-standing films could be prepared from the hemicellulosic fractions with different xylan/GGM ratios. The rapeseed xylan-GGM films exhibited strain-to-break values $>60\%$ without any plasticizers [137]. Xylan could be used as an additive for production of biodegradable wheat gluten film. Mechanical properties changed not only due to the PH of suspension and drying temperature, but also were attributed to the type and composition of xylan [135]. Hemicelluloses can be applied as coating materials



Fig. 21 Films obtained from hemicelluloses isolated at the end of pretreatments conducted at 25, 60 and $90 \text{ }^\circ\text{C}$ (Reproduced from [134] with permission)

with gum arabic (GA) for food microencapsulation. The synthesis of microcapsules by encapsulating fish oil with the emulsions of GA, GA-HC and HC as the coating materials using spray dryer method was reported by Tatar et al. [29] According to SEM observation, the as-produced microcapsules were surface smooth with no cracks and splits. The viscosity increased with the addition of HC, which resulted in the coalescence of oil particles and large amounts of oil particles with the largest size. Finally, the combination of GA and HC lowered the cost of the coating material.

4.2 Cross-Linking

Cross-linking is a good way to increase the molecular weight of polymers. By using the laccase-catalyzed cross-linking method, aromatic moieties were successfully bounded to wood hemicelluloses. Subsequently, carboxymethylcellulose sodium salt and glycerol were mixed into the cross-linking hemicelluloses and cast into films. The cross-linking sample with high molecular weight (high-MW) hemicellulosic fractions formed a film that gave better mechanical properties and lowers oxygen barrier when compared with those with low-MW hemicellulosic fractions, confirming that molecular weight could significantly affect the strength and barrier properties of films [138].

4.3 Grafting

Grafting is an effective method for modifying biopolymers and their special use. Hemicellulose-lipid-based films were prepared by grafting various omega-3 fatty acids onto arabinoxylans (AXs) polymeric chains in the presence of glycerol, using cold oxygen plasma associated with electron beam (EB) irradiation treatment. Among these films, the linseed oil-based edible film had the lowest WVP ($1.09 \times 10^{-10} \text{ g m}^{-1} \text{ s}^{-1} \text{ Pa}^{-1}$), which was 50% lower than the unmodified film. Surface hydrophobicity of fish oil-based and marine oil-based films increased and were almost comparable to those of LDPE films [139]. The same technique was also applied in preparing AX-based films by grafting stearyl acrylate (SA) and stearyl methacrylate (SM). The AX-based films with functional acrylates had contact angles of superior to 110° , which was much higher than the original film (70°), indicating an improved hydrophobicity after treatment. Additionally, a decrease of 24% in the WVP occurred after modification. Combining the oxygen plasma and electron beam (EB) irradiation technique with copolymer grafting is demonstrated to be a good way to improve barrier properties of films for better use in packaging [140]. By using plasma treatment, β -(1 \rightarrow 3)-(1 \rightarrow 6)-glucan was grafted onto the poly(lactic-co-glycolic acid) (PLGA) film, resulting in an increasing hydrophobicity and inducing cell affinity onto the polymer surface. The obtained

plasma/ β -glucan PLGA film facilitated the cell proliferation procedure and was expected to be applied in skin tissue engineering [141].

4.4 Other Modifications

Modifications such as oxidation, amination, fluorination and etherification are extensively employed to obtain hemicelluloses-based films. Hydrophobic plastic films from maize bran heteroxylan were prepared by periodic oxidation with sodium periodate, followed by reductive amination with dodecylamine in the presence of sodium cyanoborohydride. The DS values ranged from 0.5 to 1.1, and a higher DS resulted in an increase in elongation and a decrease in the elastic modulus [142]. Gröndahl et al. [143] proposed a method to produce hydrophobic AX-based films by gas-phase surface fluorination with trifluoroacetic anhydride (TFAA) (Fig. 22). IR spectra confirmed the presence of fluorinated moiety only on the film surface. A hidden increase of water contact angle for AX film with 7% fluorine (70°) compared to an untreated film (30°), except that, a decrease in the equilibrium moisture content took place from 18 to 12% after the treatment. The relatively modest increase in the hydrophobicity may be attributed to a partial hydrolysis of the trifluoroacetate groups in contact with the water droplet.

In a research by Laine et al. [28], xylan extracted from bleached birch kraft pulp were hydroxyalkylated by propylene oxide or glycidyl ethers and produced barrier coatings in the presence of sorbitol/glycerol with or without citric acid. The data shows a considerable WVP and the best OP of hydroxypropylated xylan coating was nearly one-third of those for polyethylene terephthalate (PET) coating. The modified films also exhibited oil and grease resistance. Thus, the results elucidate its value-added applications in packaging and pigment coating binders for printing papers. In another case, xylan was functionalized with 3-Chloro-2-hydroxypropyl sulfonic acid (CHPS), (S)-(-)-(3-chloro-2-hydroxypropyl)-trimethylammonium chloride (SCHMAC) or 3-chloro-2-hydroxypropyl-trimethylammonium chloride (CHPMAC)/CHPS, respectively. Afterwards, these samples were applied for films casting. The products were water soluble and reproducible. Quaternized films had a

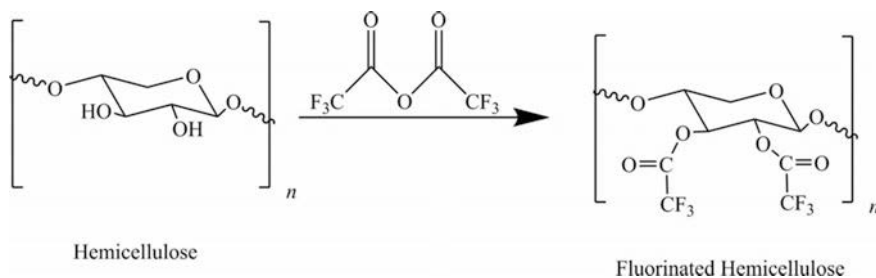


Fig. 22 Fluorination of hemicelluloses (Reproduced from [143] with permission)

supreme tensile strength (64.3 MPa) and hydroxypropyl sulfonate xylan films gained a higher Young's modulus (3350 MPa). Furthermore, the xylan-quaternized/sulfonated film was surface smooth but fractured with a higher thickness of $234 \pm 18 \mu\text{m}$ as observed by SEM. The mechanical properties gave values that are close to the average value of the two derivatives [144]. As previously described [70], the benzylated AcGGM-based film was manufactured to be a potential oxygen and moisture barrier. In order to investigate superstructural features of the hemicellulose-based film, xylan-based furan-2-carboxylic acid ester was prepared by mixing furan-2-carboxylic/CDI/DMSO solvent with xylan/DMSO solution, and the obtained xylan furoate was cast into the film. Porous structure with a macropore size of smaller than 250 nm and a meshwork-like pore-structure in the upside within the film could be observed. In addition, a roughness value (R_a) of 150 nm and a maximum height (R_{max}) of 1500 nm were determined [145]. Conclusively, research in the area of hemicellulosic films and coatings is ongoing and seems to hold great promise for future practical applications.

5 Hemicellulose-Based Hydrogels (Three-Dimensional)

Hydrogels are polymeric three-dimensional networks that have a high capacity of adsorbing a large amount of water or biological fluids and swell to many times comparing with their dry mass while maintaining structural integrity [43]. From the biocompatible and biodegradable point of view, natural polysaccharides and especially hemicelluloses are extensively used in fabricating hydrogels. Hemicellulose hydrogels, however, generally suffer from poor mechanical performances, less stretchable for special use, and thus hindering their applications. To overcome these drawbacks, the chemical modification has been made to prepare many types of highly stretchable and tough hemicellulose-based hydrogels [146]. Given to their favorable properties such as high stretchability, responsiveness, swelling/deswelling, and good mechanical performances, hemicellulose-based hydrogels have been employed in many fields such as waste treatment [15–20, 147], dye adsorption [21, 22, 148, 149], drug delivery and release [23–26, 150–152], tissue engineering [153], biodetector [154], biosensor [24, 25, 151, 155–160], conductive polymers [153, 161, 162] and so forth. The swelling ratios of the hydrogel samples are measured using a gravimetric method and defined as the equilibrium swelling ratio (Seq).

5.1 Cross-Linking Hemicellulose-Based Hydrogels

In general, hydrogels are formed either by covalently cross-linking or physically cross-linking, such as chemical treatment [163, 164], heating, or microwave irradiation. Hemicellulose-based cross-linking polymers offer resistances to thermal

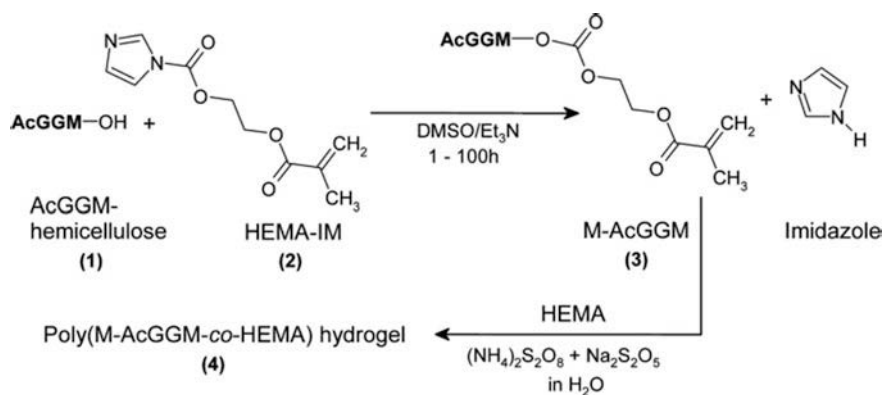


Fig. 23 Synthetical route applied for the preparation of poly(M-AcGGM-co-HEMA) hydrogels (Reproduced from [150] with permission)

degradation, cracking by liquids and other harsh environments [11]. In a research by Andersson et al. [152], AcGGM-based hydrogels were prepared by three steps. Firstly, 2-hydroxyethyl methacrylate (HEMA) was mixed with CDI in anhydrous CHCl₃ and obtained 2-[(1-imidazolyl)formyloxy]ethyl methacrylate (HEMA-Im), followed by HEMA-Im covalently coupled to AcGGM in DMSO with the catalysis of triethylamine; and finally hydrogels were synthesized by the cross-linking of HEMA with the modified AcGGM in the presence of ammonium peroxodisulphate and sodium pyrosulfite as catalysts and a simultaneous incorporation of BSA. The DS value of HEMA (DS_{HEMA}) ranged between 0.1 and 0.36, and BSA release from hydrogels was reduced with an increase of DS_{HEMA}. The addition of enzyme β -mannanase (AnMan5A) enhanced the release of BSA up to 95% within 8 h as compared with that of 60% without a catalyst. In a similar case, Voepel et al. [150] designed neutral hydrogels composed of methacrylated AcGGM (M-AcGGM) and HEMA, and ionic hydrogels basing on maleic anhydride-modified M-AcGGM (CM-AcGGM) and HEMA through radical-initiated polymerization and cross-linking method (Fig. 23). The tests elucidated the drug release rate and swelling ratio of the neutral hydrogels decreased with an increase in the degree of methacrylation. The ionic hydrogels, however, showed quicker drug release kinetics and higher swelling capabilities than the neutral gels, especially at neutral conditions. As expected, the release speed was lowered under acidic media due to the protonation of carboxylic functionalities. According to the above descriptions, these novel hemicellulose-hydrogels have future prospects in oral drug release.

Several monomers have been used to prepare hemicellulose-based hydrogels, including acrylic acid (AA), citric acid (CA), maleic acid, methacrylic acid. For example, hemicelluloses were plasticized and cross-linked by CA with or without sodium hypophosphite (SHP) as a catalyst and formed hydrogels using reactive extrusion. The highest drug release can be obtained in an alkaline medium due to a higher swelling ratio of hydrogels. Additionally, the concentration of CA and the

molecular weight of polymers can influence the degradation of hydrogels [23]. Gao et al. [24] prepared xylan-based temperature/PH sensitive hydrogels by the crosslinking copolymerization of xylan with *N*-isopropylacrylamide (NIPAAm) and AA using *N,N'*-methylenebis-acrylamide (MBA) as a cross-linker and 2,2-dimethoxy-2-phenylacetophenone/*N*-methyl pyrrolidone (DMPAP/NMP) as a UV initiating agent. The swelling ability of the hydrogel was greatly influenced by the amounts of NIPAAm, AA and MBA. A drug encapsulation efficiency of 97.60% could be achieved, and the cumulative release rates of acetylsalicylic acid were 90.12 and 26.35% in the intestinal and gastric fluids, respectively. Besides, MTT assay revealed the biocompatibility of the hydrogel with NIH3T3. Therefore, the novel hydrogels have potential applications as oral acetylsalicylic acid drug carriers for the intestinal-targeted drug delivery. Similarly, acylated xylan (ACX)-based magnetic Fe_3O_4 nanocomposite hydrogels (ACX-MNP-gels) were fabricated by copolymerization of ACX with acrylamide and NIPAAm [154], as shown in Fig. 24. Especially, the as-prepared magnetic hydrogels exhibited excellent catalytic activity and gave a sensitive response to H_2O_2 even at a concentration of $5 \times 10^{-6} \text{ mol L}^{-1}$. Therefore, the magnetic hydrogels can be utilized as a detection tool in the field of biotechnology and environmental chemistry.

By taking the UV photo-crosslinking method as described above, Yang et al. [159] synthesized honeycomb-like HC-based hydrogel by photo-cross-linking acylated hemicellulose (Hce-MA) with NIPAAm in NMP. The lower critical

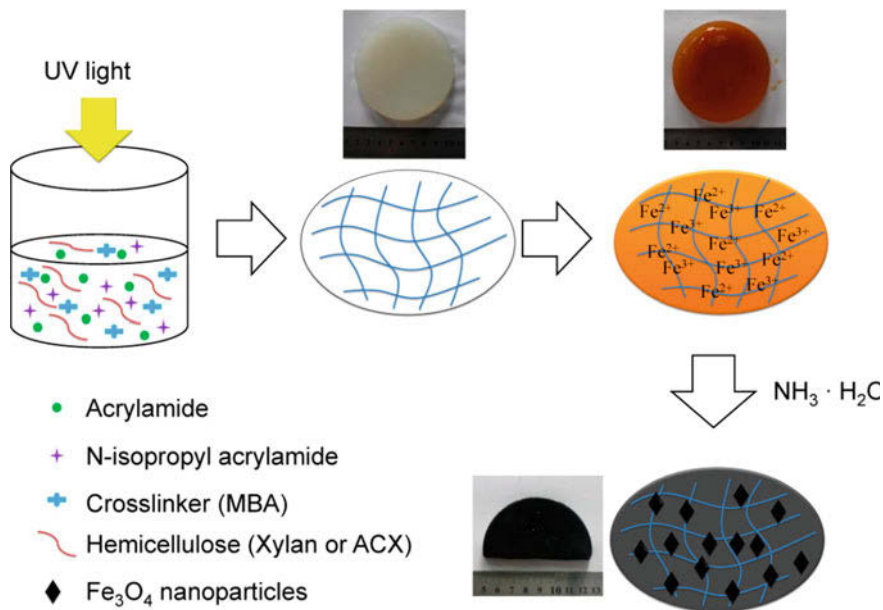


Fig. 24 Schematic process for the preparation of magnetic Fe_3O_4 nanocomposite hydrogels (Reproduced from [154] with permission)

solution temperature (LCST) of the hydrogel increased with Hce-MA and the equilibrium swelling ratio was to rest with the environment temperature, which indicated the temperature sensitivity of the hydrogels. Novel hydrogels basing on wheat straw hemicelluloses were formed by taking AA as a monomer and MBA as a cross-linker under the $K_2S_2O_8/Na_2SO_3$ system and used for acetylsalicylic acid and theophylline release. Equilibrium swelling ratio of the hydrogel can be affected by pH values [25]. Cross-linked with the same monomer AA, hemicelluloses from the spent liquor were utilized to prepare hydrogel by using ammonium persulfate/*N*, *N*, *N*', *N*'-tetramethyl-ethane-1, 2-diamine (APS/TEMEDA) as a redox initiator system. The as-prepared hydrogels gave a rapid response to pH, salt and ethanol, and showed excellent mechanical properties with the highest compressive strength of 105.1 and strain at break reach of 34.8% [155].

By graft copolymerization of AA, acrylic amide (AM) with hemicellulose in the presence of APS/ $NaHSO_3$, hydrogels with excellent water absorbency (1128 g/g) were synthesized. The results showed that the undulant surface and broad network structure were responsible for its excellent water absorbency [154]. In a research by Peng et al. [158], ionic hydrogels basing on xylan were prepared by free radical graft copolymerization of AA and xylan. The prepared ionic hydrogels exhibited different swelling degrees to pH, salt, and organic solvents, having potential applications in separation and drug release systems, as well as removing heavy metal ions [18].

Cationic hemicelluloses-based hydrogels were fabricated by Dax et al. [16]. The procedure can be concluded as: firstly, GGM was modified with GMA in the presence of DMAP and obtained GGM-MA, followed by cross-linking GGM-MA with [2-(methacryloyloxy) ethyl] trimethylammonium chloride (MeDMA) as a monomer. The resulting hydrogels can effectively remove arsenate and chromate ions from aqueous solutions. According to the previous description [26, 65, 155], CQH was synthesized by crosslinking quaternized hemicelluloses with epichlorohydrin (ECH), followed by graft copolymerization with AA and providing hemicelluloses-based hydrogels [165]. The biocompatibility test confirms the nontoxicity of the as-prepared hydrogels, which can allow cell growth and have a potential application in functional biomaterials.

By using thiol-ene click reaction with MBA, thiol-Michael addition to MBA, and disulfide bond formation, three AcGGM-hydrogels were synthesized. The as-prepared hydrogels do not dissolve in water when prolonging the immersion time over 54 h, demonstrating the successful formation of a covalently bonded three-dimensional network [62]. Glow discharge electrolysis plasma (GDEP) treatment can provide energetic species such as $HO\cdot$, $H\cdot$, and $HO_2\cdot$ to induce a chemical reaction in aqueous solution. GDEP treatment was applied for the preparation of dual sensitivity reed hemicellulose-based hydrogels. Surprisingly, all hydrogels have the same phase-transition temperatures of approximately 33 °C under different discharge voltages. However, under the discharge voltage of 600 V, the hydrogels become more sensitive to temperature and pH and thus obtaining a higher deswelling ratio [160]. By using the same technique, Zhang et al. [147] developed a hydrogel from reed hemicelluloses for the adsorption of heavy metal

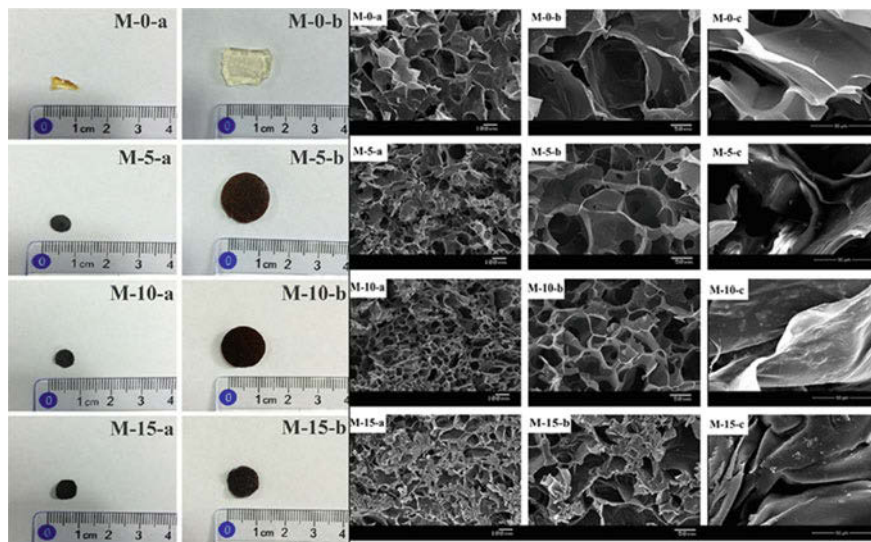


Fig. 25 Photographs of hemicellulose hydrogel (M-0) and MFRHHs (M-5, M-10, and M-15) in the dry state (M-0-a, M-5-a, M-10-a, and M-15-a) and swollen state (M-0-b, M-5-b, M-10-b, and M-15-b) (*left*). Corresponding SEM images $\times 100$ (a), $\times 300$ (b) and $\times 2000$ (c) magnification (*right*) (Reproduced from [26] with permission)

ions. The hydrogel retains high reusability for the adsorption of metal ions after 8 repeated adsorption/desorption cycles. Zhao and co-workers synthesized a magnetic field-responsive hemicelluloses-based hydrogel (MFRHH) with excellent BSA adsorption and controlled release. The fabricating process can be described as the cross-linking between AcGGM and ECH in the presence of $\text{FeCl}_3 \cdot 6\text{H}_2\text{O}$ and FeCl_2 ($\text{Fe}^{3+}:\text{Fe}^{2+} = 2:1$) under basic media. The magnetizations of the MFRHHs increased as the increasing Fe_3O_4 nanoparticles content, the equilibrium swelling ratios (SRs) were 12.1, 7.4 and 2.4 for the M-5, M-10, and M-15 hydrogels, respectively, lower than that of M-0 (hydrogel without Fe_3O_4 nanoparticles) (SR = 27.0). Therefore, the MFRHH has great potential applications in controlled drug delivery and magnetically assisted bioseparation [26]. Figure 25 shows the MFRHH in different states and the macrostructure of MFRHHs with different Fe_3O_4 nanoparticles contents.

5.2 Conductive Hemicellulose-Based Hydrogels

Conductive polymers attract much attention as humans relying on various electrical equipment such as cellphone, computer, car and daily necessities. Conductive polymers such as polyaniline, polypyrrole and polythiophene are extensively applied in the microelectronics industry, including battery technology, photovoltaic

devices, light-emitting diodes, and electrochromic displays as well as biomaterial field [161]. Electrically conductive hydrogels (ECH) combine the unique advantages of conductive polymers and hydrogels, but the non-degradability of ECH greatly limits their application. Therefore, conductive hydrogels basing on natural polymers such as hemicelluloses are synthesized to solve this problem due to the good compatibility of hemicellulose and polymers [153]. Zhao et al. [161] prepared an electrically conductive hemicellulose hydrogel (ECHH) by cross-linking AcGGM with epichlorohydrin and conductive aniline pentamer (AP) in basic media under ambient condition (Fig. 26). Increasing the AP content led to an enhancement in thermal stability of ECHH and a reduction in equilibrium swelling ratio. Simultaneously, conductivity increased from 9.05×10^{-9} to 1.58×10^{-6} S/cm. In the second study by Zhao et al. [162], free-standing ECHHs were obtained

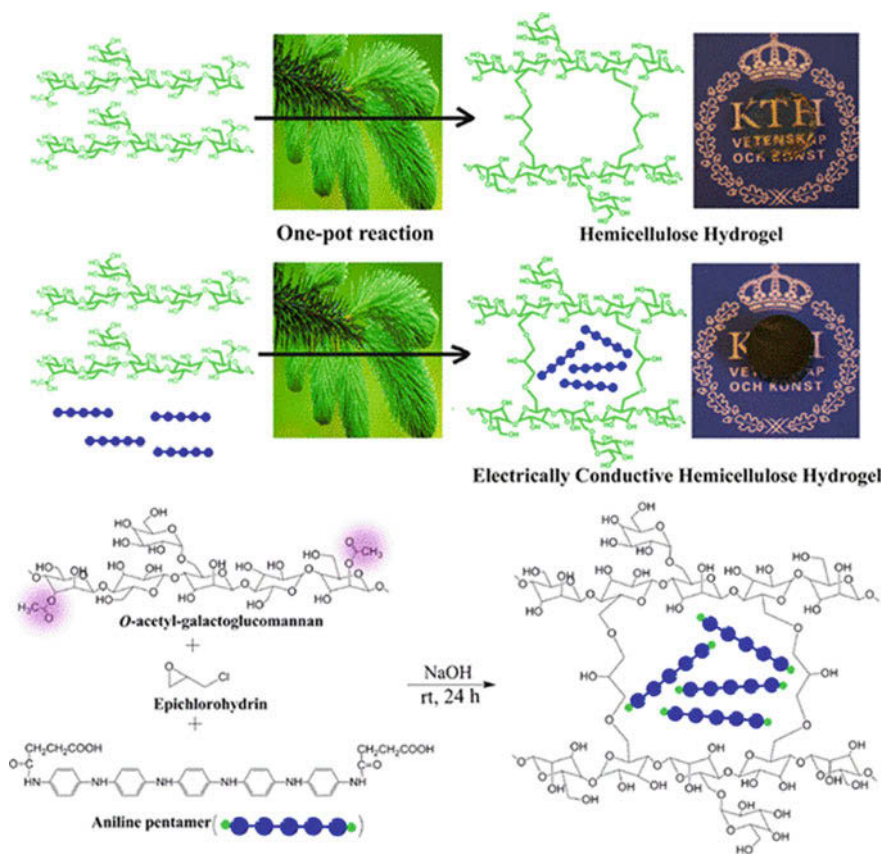


Fig. 26 Schematic synthesis of ECHHs using epichlorohydrin as a cross-linker in basic media (Reproduced from [161] with permission)

by a copolymerization of carboxylated AcGGM (C-AcGGM) with GMA and subsequently covalently coupling with aniline tetramer (AT). The swelling ratio of the hydrogels decreased with an increasing AT content; and particularly, the conductivity increased by two orders of magnitude as the AT content changed from 10 to 40% (w/w).

A series of stimuli-responsive hemicellulose microgels (SRHMGs) were reported by Zhao et al. [151]. AcGGM as a matrix was cross-linked with different functional materials (including poly(acrylic acid), AP, and iron) during spray drying, giving SRHMGs with response to pH, electrochemical stimuli, magnetic field, or dual-stimuli (Fig. 27). Comparing with single-stimuli hydrogel, the one-pot reaction products had more practical applications, such as controlled drug release, magnetic resonance imaging, biosensors, electronic devices, and tissue engineering.

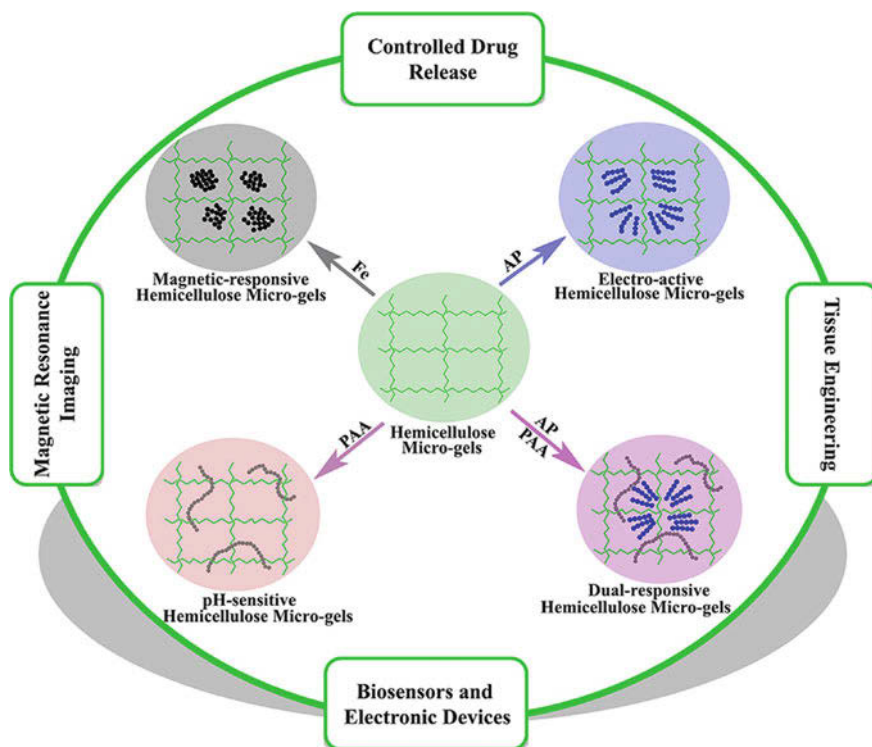


Fig. 27 Synthesis of SRHMGs and suggested application fields of these microgels (Reproduced from [151] with permission)

5.3 *Hemicellulose-Polymer Composite Gels (Hydrogels and Aerogels)*

To overcome the drawbacks of Hemicellulose hydrogels such as weak thermal stability, brittle properties and weak mechanical properties, compatible ingredients such as clay, chitosan, cellulose derivatives, carbon materials, polyvinyl alcohol and other polymers are utilized to the synthesis of composite hydrogels with enhancing functional properties [166].

Chitosan is also a renewable biopolymer possessing many functional groups such as N-acetyl groups, reactive hydroxyl and amino groups, and has been widely used to prepare natural hydrogels. Hemicellulose hydrogels can be cross-linked and/or reinforced by chitosan to improve their mechanical performances [15, 20]. In the study of Gabriellii et al. [166], xylan-containing glucuronic acid functionalities and chitosan were dissolved in acidic condition to form hydrogels. The gelation mechanism was the complexation between glucuronic acid functionalities in xylan and amino groups in chitosan. The hydrogels were sensitive to pH and responded in a reversible manner to the stimuli. In a similar way, $-\text{NH}_2$ groups in chitosan were cross-linked with carboxylic acid groups in hemicellulose derivative obtained from esterification of hemicellulose with citric acid in SHP, and producing an elastic, highly porous and durable hemicellulose citrate-chitosan hydrogel [167]. The aerogel can adsorb up to 100 g of a saline solution and 80 g of water per gram of the material, respectively, which can be used to reduce the overall salinity of the water. Wu et al. [20] demonstrated a cross-linking carboxymethyl chitosan-hemicellulose (CMCH) hydrogel with highly macroporous structure, pH-sensitivity and highly efficient adsorption with metal ions. Furthermore, CMCH could be reused without significant loss of the adsorption capacity. In another work by Wu and co-workers, TiO_2 nanoparticles were incorporated into the carboxymethyl chitosan-hemicellulose network (CHNT) with the assistance of sodium dodecyl sulfate (SDS). Due to the favourable chelating groups existing in its structure, the hydrogels not only had the capacity of removing heavy metal but also exhibited good regeneration of loaded metal ions with EDTA [19]. Since diethylene triamine pentaacetic acid (DTPA) has a high-affinity binding with hemicellulose in the catalysis of SHP, the hemicellulose-DTPA-chitosan hydrogel can be synthesized after crosslinking DTPA-hemicellulose and chitosan [15]. The resulting foam can be used for water desalination and the maximum salt uptake is nearly 0.30 g/g.

Guan et al. [168] reported a novel dialdehyde hemicelluloses (DHC)/chitosan/Ag composite hydrogel possessing antimicrobial activity against microbes. DHC was obtained by oxidation of hemicelluloses with NaIO_4 , and the hydrogel was formed by a reduction of silver ions within the cross-linked DHC/chitosan hydrogels, as shown in Fig. 28. The swelling degree of the hydrogel decreased sharply after the addition of silver ions. The composite hydrogel seems to be a potential antimicrobial material and can be used to treat accessible wounds to prevent or kill the existing infection.

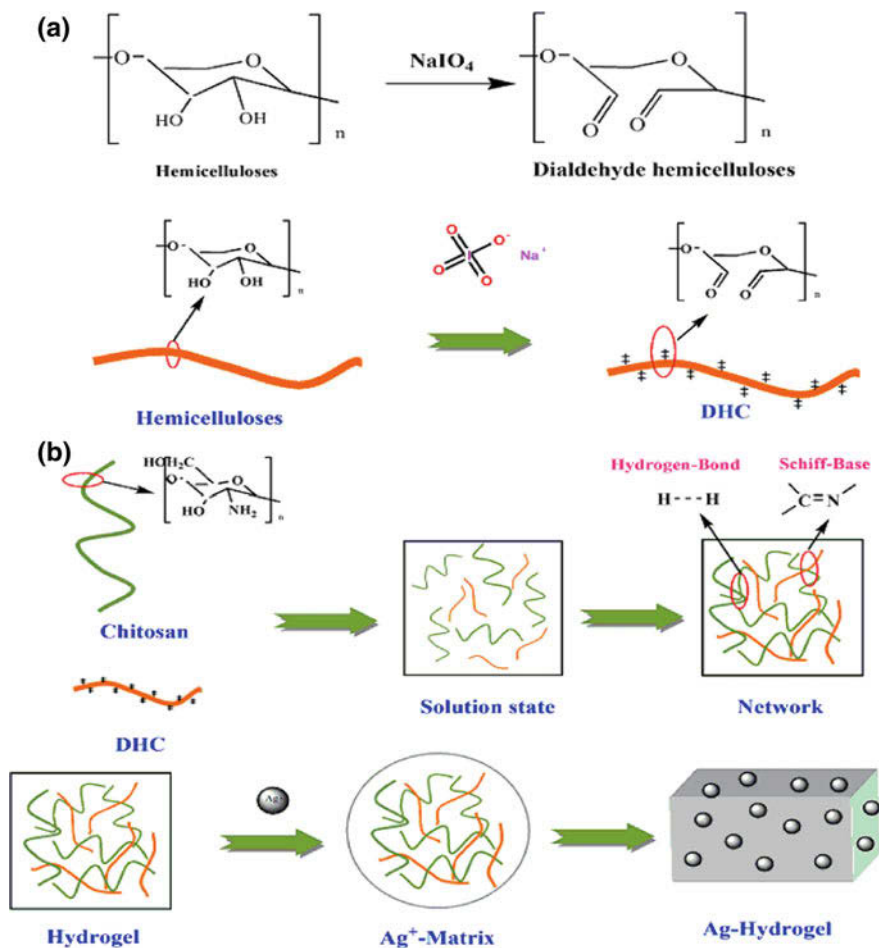


Fig. 28 The mechanism for the synthesis of (DHC)/chitosan/Ag hydrogel (Reproduced from [168] with permission)

In another work by Guan et al. [169], hemicelluloses, PVA, and chitin nano-whiskers were mixed with a mass ratio of 1:1:1 to form a hydrogel in water by using the freeze-thaw technique. FT-IR and NMR spectra confirmed that the repeated freeze-thaw cycles induced the physical crosslinking. The mechanical properties were significantly enhanced by increasing the content of chitin nano-whiskers. As a conclusion, this physical method is a good way to prepare hydrogels with good mechanical properties [169, 170]. Cellulose whiskers were coated to HEMA modified hemicellulose and formed a hydrogel by in situ radical polymerization of HEMA. The resulting hydrogels exhibited a rubber-like behaviour with enhancing toughness, increasing viscoelasticity, and improving recovery behaviour [171].

Identically, nanocellulose such as cellulose nanofibrils (CNF) and nanocrystalline cellulose (CNC) also can be applied as a reinforcing material for hemicelluloses-based gels. Cellulose nanofibrils (CNF)-GGM sponge-like aerogels was elucidated by Alakalhunmaa et al. [172], as shown in Fig. 29. The aerogels could adsorb water up to 37 times of their initial weight and possessed reversible sponge capacity, which can be used as a substitute of petroleum-based materials in food-packaging. Dax et al. [173] designed a hydrogel basing on nanofibrillated cellulose (NFC) and GGM-MA. The electrostatic attraction between the anionic charges in NFC and the quaternary ammonium groups in the polymer chains resulted in the successful connection of NFC to the polymer and thus enhancing the modulus of the hydrogel. Moreover, the hydrogels revealed a high adsorption capacity to chromate ions. Xylan/CNC hydrogels were successfully synthesized by cross-linking the oxidized xylan with CNC during freeze-casting [106]. Within this hydrogel, hemiacetal bonds formed between aldehyde groups and hydroxyl groups during solidification/sublimation process, which was determined by NMR spectra. Thus, freeze-casting/cross-linking method could enable the fabrication of nanoreinforced biopolymer-based hydrogels with tailor-made architectures.

Interpenetrating polymer networks (IPNs) are unique “alloys” of cross-linked polymers in which at least one network is synthesized and/or cross-linked in the presence of the other. IPN hydrogels are endowed with improving responsiveness and mechanical performance, as well as fast adsorption of ionic species like dyes and heavy metal ions. Lately, biopolymer-based IPN hydrogels have been widely reported, especially hemicelluloses-based IPN hydrogels [174, 175]. Malaki et al. [176] fabricated a semi-IPNs hydrogel by through cross-linking methacrylated carboxymethylcellulose (MA-CMC) with AA as co-monomer and MBA as cross-linker in the presence of softwood hemicellulose hydrolysate (SWH), as shown in Fig. 30. The semi-IPN hydrogels demonstrated a highly porous structure and appreciable mechanical performance, and the swelling ratio was similar to the single SWH network. In Malaki’s another research, full IPNs hydrogels were prepared from AcGGM via free radical polymerization and a thiol-ene click reaction. The as-prepared IPNs hydrogel showed a faster swelling rate and a higher shear storage modulus (35–40 times higher) than the corresponding single network



Fig. 29 The repeatable liquid water absorption capacity of the aerogels that maintained their structure and shape in water (Reproduced from [172] with permission)

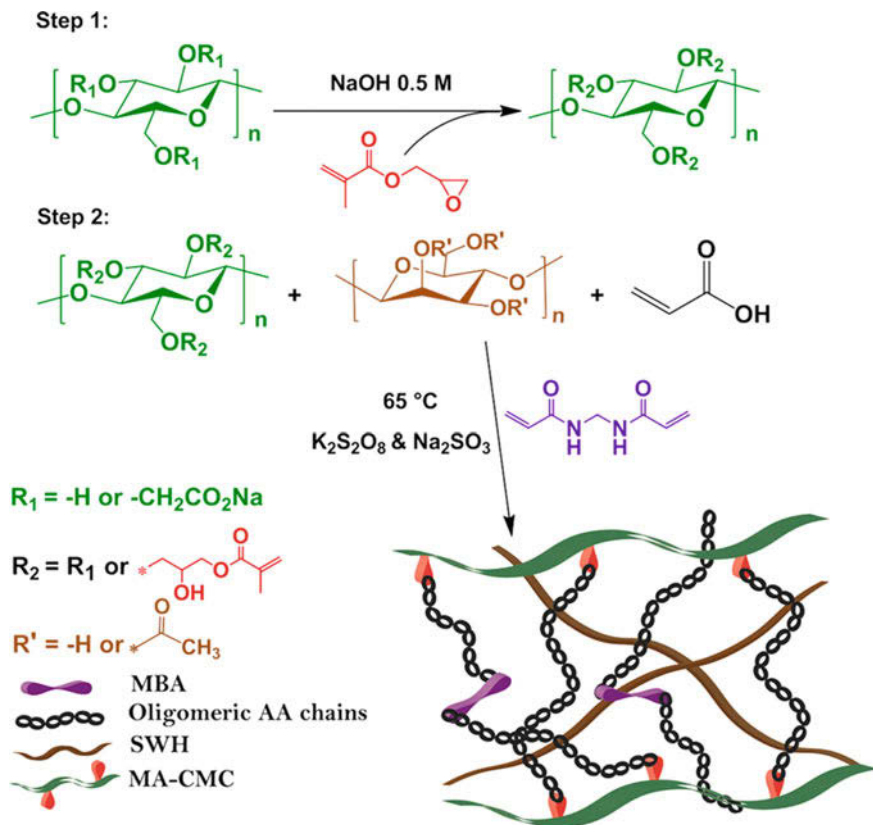


Fig. 30 Schematic outline of the synthesis of SWH-based semi-IPN hydrogels (Reproduced from [176] with permission)

of AcGGM after click reaction [177]. Meena and co-workers reported a hydrogel basing on kappa-carrageenan/xylan/polyvinylpyrrolidone (kC-xylan-PVP) blend, using sodium persulphate (KPS) as a water-soluble initiator under microwave irradiation. The resulting hydrogels also possessed a semi-IPN structure with enhancing swelling ability and water holding capacity as compared to untreated blends [178]. To sum up, the radical graft copolymerization [179] of hemicelluloses offers new opportunities to derive functional hemicellulose-based composite hydrogels; and these IPN hydrogels are preferable to serve as membranes [180], adsorbents and supports and relieve the pressure of the environment.

The fabrication of xylan (with or without acetyl moieties)/poly(HEMA)-based hydrogels is similar to the previous reports [152]. Surprisingly, the resulting hydrogels demonstrated to be stiffer and possessed a lower water swelling capacity due to the presence of acetyl moieties. Simultaneously, the drug release efficiency was enhanced and the hydrogels could act as cargo carriers to deliver an anticancer drug [181]. Basing on the studies described above [152, 181], an elastic, soft, and

water-swallowable hydrogel named as hemicellulose/HEMA and hemicellulose/poly (ethylene glycol) (PEG) was synthesized [182, 183]. The swelling behaviour of the hydrogels were comparable to the pure poly(2-hydroxyethyl methacrylate) (PHEMA) hydrogels, providing a suitable way for the preparation of novel polymeric structures. Utilizing CuAAC, thermoresponsive hydrogels basing on birchwood xylan were prepared by introducing reactive azide groups on the backbone of xylan via etherification and crosslinking the azide groups with poly(ethylene glycol)-b-poly(propylene glycol)-b-poly(ethylene glycol) (PEG-PPG-PEG) in the presence of propargyl bromide and NaH. The hydrogel showed a reversible swelling ability at low temperature and deswelling performance at high temperature. The compressive modulus of the hydrogel increased at 7 °C and its stiffness decreased at 70 °C [157]. Xylan-MA/PVA blends with different ratios of maleic anhydride (MA) and PVA were heated and then cross-linked to generate hydrogels under acidic media. Xylan-MA was the product of esterification between xylan and MA. The swelling and strength behaviours of the new hydrogel were rest with the content of PVA and MA [184]. Another PVA-enhanced temperature- and pH-sensitive hemicellulosic hydrogel was prepared by grafting MA onto hemicellulose, followed by copolymerization of the obtained acylated hemicellulose (AHC) with NIPAAm and itaconic acid (IA) and incorporated with PVA. The resulting hydrogel with enhancing compressive strength was proved to be biocompatible and the salicylic acid could release rapidly in the simulated gastric fluid at the initial time. As observed, the hydrogels have an extensive application in terms of controllable drug delivery [156]. Novel poly(amidoamine) (PAA)/hemicellulose hydrogel was prepared by graft polymerization of methacrylic acid onto the AcGGM backbone in the presence of acrylamide end-capped PAA oligomers as cross-linkers and $\text{Na}_2\text{S}_2\text{O}_5/(\text{NH}_4)_2\text{S}_2\text{O}_8$ as initiator [17]. The as-prepared hydrogel gained a high swelling degree, low storage moduli, and a high adsorption capacity of various heavy metal ions, and can be used for the treatment of highly contaminated wastewaters [185].

Graphene oxide (GO) and CNT have emerged as carbonaceous materials with the high specific surface area and excellent mechanical strength. GO and CNT is reliable and promising physical fillers for the preparation of composite hydrogels with enhanced mechanical strength [186]. Kong et al. [146] established a drawing procedure that GO was incorporated into polymerized acrylamide (PAM)/carboxymethyl hemicellulose (CMH) solution, followed by ionic crosslinking with Al^{3+} to obtain PAM/GO/Al-CMH nanocomposite hydrogel. The hydrogen bonding between GO and polymer chains and the network formed by Al^{3+} ionically cross-linking CMH led to a decrease in the swelling capacity and an enhancing mechanical property. Figure 31 shows the gelation procedure of PAM/GO/Al-CMH hydrogel and its mechanical property was depicted in Fig. 32.

Another organic-inorganic hybrid hydrogel composed of hemicellulose-g-poly (methacrylic acid) and multiwall carbon nanotube (MW-CNTs) was prepared for the removal of methylene blue. The cross-linking was initiated by $(\text{NH}_4)_2\text{S}_2\text{O}_8/\text{Na}_2\text{SO}_3$ after adding the cross-linker MBA and the monomer methacrylic acid [149]. The adsorption kinetics of methylene blue (MB) followed the

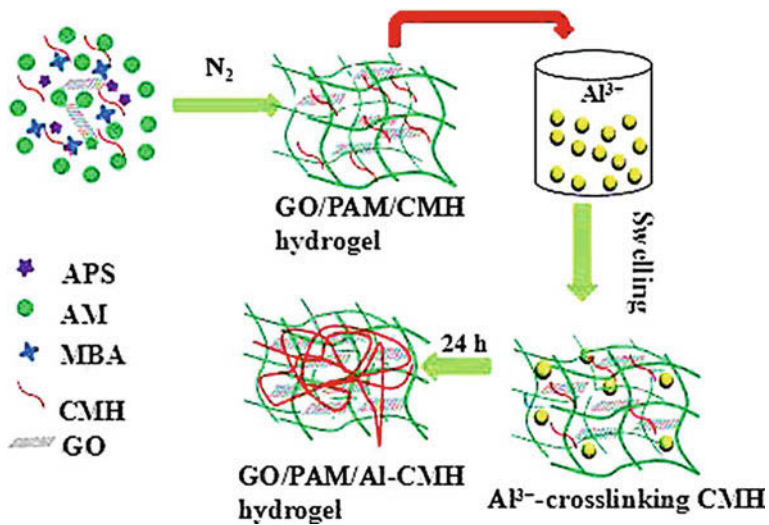


Fig. 31 Formation of GO/PAM/Al-CMH nanocomposite hydrogels (Reproduced from [146] with permission)

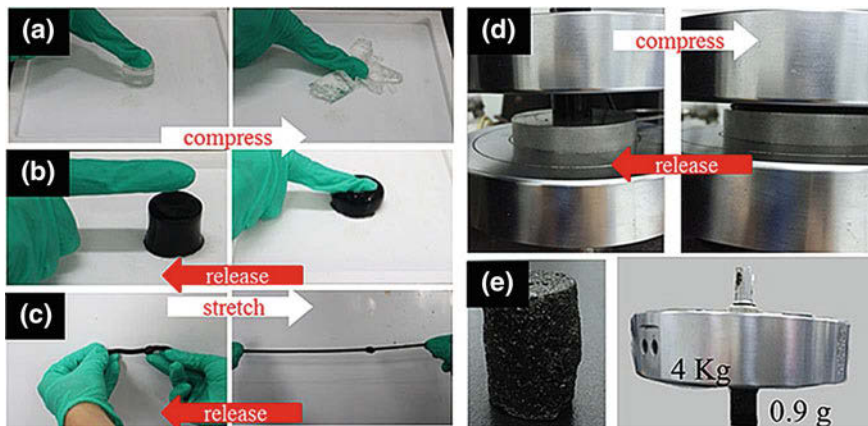


Fig. 32 Mechanical properties of the PAM hydrogel and the GO/PAM/Al-CMH hydrogels (Reproduced from [146] with permission)

pseudo-second-order kinetic model and the mechanism of adsorbing methylene blue is depicted in Fig. 33. A superabsorbent basing on MWCNT-xylan composite and poly(methacrylic acid) was synthesized by the same method described above, and also exhibited high removal rate for MB [148].

Clay can act as a physical crosslinker and provides physically crosslinking during the gelation process of hybrid hydrogels. Cheng et al. [22] developed a facial

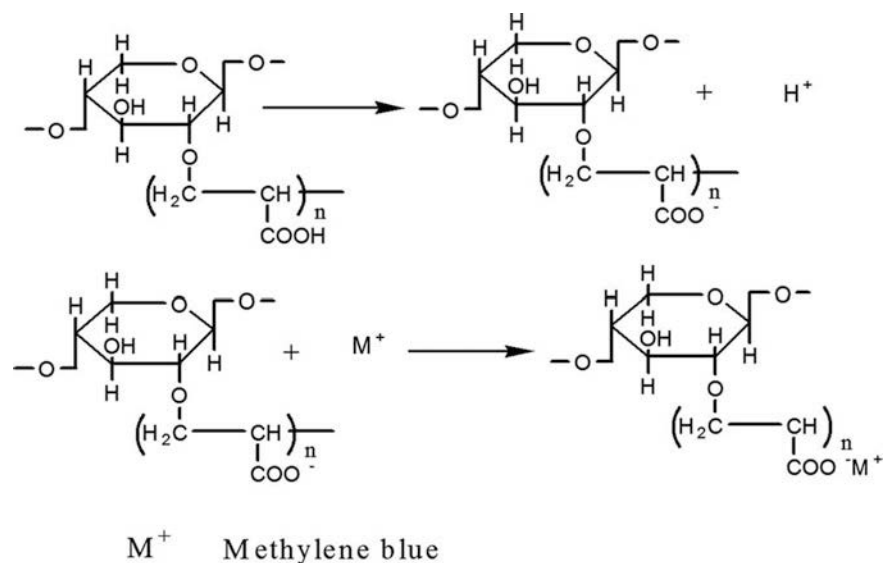


Fig. 33 The possible adsorption mechanism of methylene blue on hydrogels (Reproduced from [149] with permission)

route to prepare hemicellulose/clay hydrogels in the presence of polyethylene glycol diglycidyl ether (PEGDE). The non-covalent interactions between hemicellulose and clay hindered the penetration of water into the hydrogel network, leading to a decrease in swelling ratio. This hybrid hydrogel, however, increased the adsorption of methylene blue by approximately 50 mg/g as compared with the hydrogel without clay. In a study by Sun et al. [21], CaCO_3 was used as porogen in the fabrication of stimuli-responsive (pH/salt) porous hydrogels basing on HC and poly(sodium acrylate), the obtained HC-g-poly(sodium acrylate) hydrogels showed a high adsorption capacity of methylene blue, which is appropriate for wastewater application.

6 Summary and Outlook

Hemicelluloses as renewable resources have a lot of favourable inherent properties such as hydrophilicity, biodegradability, biocompatibility, low cost, and non-toxicity, as well as good barrier properties and mechanical properties by using appropriate chemical modification or physical treatment. Therefore, hemicelluloses-based materials hold great potentials in various applications such as packaging, water treatment, and biomedical field, which can form a viable substitute for fossil-based materials to some extent.

However, only a few applications of hemicellulose-based materials are so far explored and suggested. Societal awareness of sustainability issues is a strong driver for the implementation of such biobased materials on the market, still, commercial applicability and success depend also on the price and efficiency of extraction and production processes. There is a huge market awaiting hemicelluloses. In hence, technological breakthroughs are urgent, including the scale-up production of hemicelluloses, new fabrication methods of functional materials, unique performances and applications of various composites, and so on. These technology breakthroughs will trigger the soaring hemicellulose market in the near future.

References

1. Thakur VKT, Hakur MK (2014) Processing and characterization of natural cellulose fibers/thermoset polymer composites. *Carbohydr Polym* 109(13):102–117
2. Thakur VK, Thakur MK (2015) Recent advances in green hydrogels from lignin: a review. *Int J Biol Macromol* 72:834
3. Thakur VK, Thakur MK, Raghavan P, Kessler MR (2014) Progress in green polymer composites from lignin for multifunctional applications: a review. *ACS Sustain Chem Eng* 2(5):1072–1092
4. Mikkonen KS (2013) Recent studies on hemicellulose-based blends. *Composites and nanocomposites*. Springer, Berlin, pp 313–336
5. Hansen NM, Plackett D (2008) Sustainable films and coatings from hemicelluloses: a review. *Biomacromolecules* 9(6):1493–1505
6. Shukla SK, Mishra AK, Arotiba OA, Mamba BB (2013) Chitosan-based nanomaterials: a state-of-the-art review. *Int J Biol Macromol* 59(4):46
7. Thakur VK, Thakur MK (2014) Recent advances in graft copolymerization and applications of chitosan: a review. *ACS Sustain Chem Eng* 2(12)
8. Rahmat AR, Wan AWAR, Sin LT, Yussuf AA (2009) Approaches to improve compatibility of starch filled polymer system: a review. *Mater Sci Eng C* 29(8):2370–2377
9. Avérous L, Halley PJ (2009) Biocomposites based on plasticized starch. *Biofuels Bioprod Biorefin* 3(3):329–343
10. Thakur VK, Thakur MK (2014) Recent trends in hydrogels based on psyllium polysaccharide: a review. *J Clean Prod* 82(22):1–15
11. Farhat W, Venditti RA, Hubbe M et al (2017) A review of water-resistant hemicellulose-based materials: processing and applications. *Chemsuschem* 10(2):305–323
12. Ibn Yaich A, Edlund U, Albertsson AC (2017) Transfer of biomatrix/wood cell interactions to hemicellulose-based materials to control water interaction. *Chem Rev* 117(12):8177–8207
13. Thakur VK, Thakur MK (2015) Eco-friendly polymer nanocomposites. *Advanced structured materials*. Springer, India
14. Iwata T (2015) Biodegradable and bio-based polymers: future prospects of eco-friendly plastics. *Angew Chem Int Ed Engl* 54(11):3210–3215
15. Ayoub A, Venditti RA, Pawlak JJ, Salam A, Hubbe MA (2013) Novel hemicellulose-chitosan biosorbent for water desalination and heavy metal removal. *ACS Sustain Chem Eng* 1(9):1102–1109
16. Dax D, Chavez MS, Xu C et al (2014) Cationic hemicellulose-based hydrogels for arsenic and chromium removal from aqueous solutions. *Carbohydr Polym* 111:797–805

17. Ferrari E, Ranucci E, Edlund U, Albertsson AC (2015) Design of renewable poly (amidoamine)/hemicellulose hydrogels for heavy metal adsorption. *J Appl Polym Sci* 132 (12):41695
18. Peng XW, Zhong LX, Ren JL, Sun RC (2012) Highly effective adsorption of heavy metal ions from aqueous solutions by macroporous xylan-rich hemicelluloses-based hydrogel. *J Agric Food Chem* 60(15):3909–3916
19. Wu S, Kan J, Dai X et al (2017) Ternary carboxymethyl chitosan-hemicellulose-nanosized TiO₂ composite as effective adsorbent for removal of heavy metal contaminants from water. *Fibers Polym* 18(1):22–32
20. Wu SP, Dai XZ, Kan JR, Shilong FD, Zhu MY (2017) Fabrication of carboxymethyl chitosan–hemicellulose resin for adsorptive removal of heavy metals from wastewater. *Chin Chem Lett* 28(3):625–632
21. Sun XF, Gan Z, Jing Z et al (2015) Adsorption of methylene blue on hemicellulose-based stimuli-responsive porous hydrogel. *J Appl Polym Sci* 132(10):41606
22. Cheng HL, Feng QH, Liao CA et al (2016) Removal of methylene blue with hemicellulose/ clay hybrid hydrogels. *Chin J Polym Sci* 34(6):709–719
23. Farhat W, Venditti R, Mignard N et al (2017) Polysaccharides and lignin based hydrogels with potential pharmaceutical use as a drug delivery system produced by a reactive extrusion process. *Int J Biol Macromol* 104:564–575
24. Gao C, Ren J, Zhao C et al (2016) Xylan-based temperature/pH sensitive hydrogels for drug controlled release. *Carbohydr Polym* 151:189–197
25. Sun XF, Wang HH, Jing ZX, Mohanathas R (2013) Hemicellulose-based pH-sensitive and biodegradable hydrogel for controlled drug delivery. *Carbohydr Polym* 92(2):1357–1366
26. Zhao W, Odelius K, Edlund U, Zhao C, Albertsson AC (2015) In situ synthesis of magnetic field-responsive hemicellulose hydrogels for drug delivery. *Biomacromolecules* 16(8): 2522–2528
27. Chen GG, Qi XM, Guan Y et al (2016) High strength hemicellulose-based nanocomposite film for food packaging applications. *ACS Sustain Chem Eng* 4(4):1985–1993
28. Laine C, Harlin A, Hartman J et al (2013) Hydroxyalkylated xylans—their synthesis and application in coatings for packaging and paper. *Ind Crops Prod* 44:692–704
29. Tatar F, Tunç MT, Dervisoglu M, Cekmecelioglu D, Kahyaoglu T (2014) Evaluation of hemicellulose as a coating material with gum arabic for food microencapsulation. *Food Res Int* 57:168–175
30. Shen J, Fatehi P, Ni Y (2014) Biopolymers for surface engineering of paper-based products. *Cellulose* 21(5):3145–3160
31. Nguyen QA, Tucker MP, Keller FA, Eddy FP (2000) Two-stage dilute-acid pretreatment of softwoods. *Appl Biochem Biotechnol* 84–86(1–9):561–576
32. Egüés I, Sanchez C, Mondragon I, Labidi J (2012) Effect of alkaline and autohydrolysis processes on the purity of obtained hemicelluloses from corn stalks. *Biores Technol* 103 (1):239–248
33. Hasegawa I, Tabata K, Okuma O, Mae K (2004) New pretreatment methods combining a hot water treatment and water/acetone extraction for thermo-chemical conversion of biomass. *Energy Fuels Am Chem Soc J* 18(3):755–760
34. And MP, Zacchi G (2003) Extraction of hemicellulosic oligosaccharides from spruce using microwave oven or steam treatment. *Biomacromolecules* 4(3):617
35. Froschauer C, Hummel M, Iakovlev M et al (2013) Separation of hemicellulose and cellulose from wood pulp by means of ionic liquid/cosolvent systems. *Biomacromolecules* 14(6):1741–1750
36. Mesbah M, Shahsavari S, Soroush E, Rahaei N, Rezakazemi M (2018) Accurate prediction of miscibility of CO₂ and supercritical CO₂ in ionic liquids using machine learning. *J CO₂ Utilization* 25:99–107
37. Razavi SMR, Rezakazemi M, Albadarin AB, Shirazian S (2016) Simulation of CO₂ absorption by solution of ammonium ionic liquid in hollow-fiber contactors. *Chem Eng Process* 108:27–34

38. Gould JM (1984) Alkaline peroxide delignification of agricultural residues to enhance enzymatic saccharification. *Biotechnol Bioeng* 26(1):46–52
39. Schmidt AS, Thomsen AB (1998) Optimization of wet oxidation pretreatment of wheat straw. *Biores Technol* 64(2):139–151
40. Li H, Qu Y, Yang Y, Chang S, Xu J (2016) Microwave irradiation—a green and efficient way to pretreat biomass. *Biores Technol* 199:34–41
41. Chum HL, Johnson DK, Black S et al (1988) Organosolv pretreatment for enzymatic hydrolysis of poplars: I. Enzyme hydrolysis of cellulosic residues. *Biotechnol Bioeng* 31(7):643–649
42. Saha BC (2003) Hemicellulose bioconversion. *J Ind Microbiol Biotechnol* 30(5):279–291
43. Hu L, Du M, Zhang J (2018) Hemicellulose-Based hydrogels present status and application prospects: a brief review. *Open J Forestry* 08(01):15–28
44. Uraki Y, Koda K (2015) Utilization of wood cell wall components. *J Wood Sci* 61(5):447–454
45. Gandini A (2011) The irruption of polymers from renewable resources on the scene of macromolecular science and technology. *Green Chem* 13(5):1061
46. Cunha AG, Gandini A (2010) Turning polysaccharides into hydrophobic materials: a critical review. Part 2. Hemicelluloses, chitin/chitosan, starch, pectin and alginates. *Cellulose* 17(6):1045–1065
47. Thomas S, Visakh PM, Mathew AP (2013) Advances in natural polymers. *Advanced structured materials*, vol 18. Springer, Berlin, pp 216–217
48. Belmokaddem FZ, Pinel C, Huber P, Petit Conil M, Perez DDS (2011) Green synthesis of xylan hemicellulose esters. *Carbohydr Res* 346(18):2896–2904
49. Peng XW, Ren JL, Sun RC (2010) Homogeneous esterification of xylan-rich hemicelluloses with maleic anhydride in ionic liquid. *Biomacromolecules* 11(12):3519–3524
50. Zhang LM, Yuan TQ, Xu F, Sun RC (2013) Enhanced hydrophobicity and thermal stability of hemicelluloses by butyrylation in [BMIM]Cl ionic liquid. *Ind Crops Prod* 45:52–57
51. Sun RC, Fang JM, Tomkinson J (2000) Stearoylation of hemicelluloses from wheat straw. *Polym Degrad Stab* 67(2):345–353
52. Sun XF, Sun RC, Sun JX (2004) Oleoylation of sugarcane bagasse hemicelluloses using *N*-bromosuccinimide as a catalyst. *J Sci Food Agric* 84(8):800–810
53. Wang HT, Yuan TQ, Meng LJ et al (2012) Structural and thermal characterization of lauroylated hemicelluloses synthesized in an ionic liquid. *Polym Degrad Stab* 97(11):2323–2330
54. Sun R, Fanga JM, Tomkinson J, Hill CAS (1999) Esterification of hemicelluloses from poplar chips in homogenous solution of *N,N*-dimethylformamide/lithium chloride. *J Wood Chem Technol* 19(4):287–306
55. Sun RC, Fang JM, Tomkinson J, Geng ZC, Liu JC (2011) Fractional isolation, physico-chemical characterization and homogeneous esterification of hemicelluloses from fast-growing poplar wood. *Paper Chem* 44(1):29–39
56. Fundador NGV, Enomoto-Rogers Y, Takemura A, Iwata T (2012) Syntheses and characterization of xylan esters. *Polymer* 53(18):3885–3893
57. Daus S, Heinze T (2010) Xylan-based nanoparticles: prodrugs for ibuprofen release. *Macromol Biosci* 10(2):211–220
58. Kisonen V, Xu C, Bollström R et al (2014) *O*-acetyl galactoglucomannan esters for barrier coatings. *Cellulose* 21(6):4497–4509
59. Buchanan CM, Buchanan NL, Debenham JS et al (2003) Preparation and characterization of arabinoxylan esters and arabinoxylan ester/cellulose ester polymer blends. *Carbohydr Polym* 52(4):345–357
60. Voepel J, Edlund U, Albertsson AC, Percec V (2011) Hemicellulose-based multifunctional macroinitiator for single-electron-transfer mediated living radical polymerization. *Biomacromolecules* 12(1):253–259
61. Wrigstedt P, Kylli P, Pitkanen L et al (2010) Synthesis and antioxidant activity of hydroxycinnamic acid xylan esters. *J Agric Food Chem* 58(11):6937–6943

62. Maleki L, Edlund U, Albertsson AC (2015) Thiolated hemicellulose as a versatile platform for one-pot click-type hydrogel synthesis. *Biomacromolecules* 16(2):667–674
63. Ren JL, Peng F, Sun RC (2008) Preparation of hemicellulosic derivatives with bifunctional groups in different media. *J Agric Food Chem* 56(23):11209–11216
64. Peng X, Ren J, Sun R (2011) An efficient method for the synthesis of hemicellulosic derivatives with bifunctional groups in butanol/water medium and their rheological properties. *Carbohydr Polym* 83(4):1922–1928
65. Guan Y, Zhang B, Tan X et al (2014) Organic-inorganic composite films based on modified hemicelluloses with clay nanoplatelets. *ACS Sustain Chem Eng* 2(7):1811–1818
66. Rezakazemi M, Sadrzadeh M, Mohammadi T, Matsuura T (2017) Methods for the preparation of organic-inorganic nanocomposite polymer electrolyte membranes for fuel cells. In: Inamuddin D, Mohammad A, Asiri AM (eds) *Organic-inorganic composite polymer electrolyte membranes*. Springer International Publishing, Cham, pp 311–325
67. Bigand V, Pinel C, Da Silva Perez D et al (2011) Cationisation of galactomannan and xylan hemicelluloses. *Carbohydr Polym* 85(1):138–148
68. Ren JL, Sun RC, Liu CF (2007) Etherification of hemicelluloses from sugarcane bagasse. *J Appl Polym Sci* 105(6):3301–3308
69. Fang JM, Fowler P, Tomkinson J, Hill CAS (2002) Preparation and characterisation of methylated hemicelluloses from wheat straw. *Carbohydr Polym* 47(3):285–293
70. Hartman J, Albertsson AC, Sjöberg J (2006) Surface- and bulk-modified galactoglucomannan hemicellulose films and film laminates for versatile oxygen barriers. *Biomacromolecules* 7(6):1983
71. Ren JL, Peng XW, Zhong LX, Peng F, Sun RC (2012) Novel hydrophobic hemicelluloses: synthesis and characteristic. *Carbohydr Polym* 89(1):152–157
72. Pahimanolis N, Kilpelainen P, Master E, Ilvesniemi H, Seppala J (2015) Novel thiolamine- and amino acid functional xylan derivatives synthesized by thiolene reaction. *Carbohydr Polym* 131:392–398
73. Liu Z, Ni Y, Fatehi P, Saeed A (2011) Isolation and cationization of hemicelluloses from pre-hydrolysis liquor of kraft-based dissolving pulp production process. *Biomass Bioenerg* 35(5):1789–1796
74. Schwikal K, Heinze T, Ebringerová A, Petzold K (2005) Cationic xylan derivatives with high degree of functionalization. *Macromol Symp* 232(1):49–56
75. Kisonen V, Xu C, Eklund P et al (2014) Cationised *O*-acetyl galactoglucomannans: synthesis and characterisation. *Carbohydr Polym* 99:755–764
76. Wang S, Hou Q, Kong F, Fatehi P (2015) Production of cationic xylan-METAC copolymer as a flocculant for textile industry. *Carbohydr Polym* 124:229–236
77. Kong WQ, Ren JL, Wang S, Li MF, Sun RC (2014) A promising strategy for preparation of cationic xylan by environment-friendly semi-dry oven process. *Fibers Polym* 15(5):943–949
78. Ren JL, Peng F, Sun RC et al (2008) Synthesis of cationic hemicellulosic derivatives with a low degree of substitution in dimethyl sulfoxide media. *J Appl Polym Sci* 109(4):2711–2717
79. Ibn Yaich A, Edlund U, Albertsson AC (2015) Enhanced formability and mechanical performance of wood hydrolysate films through reductive amination chain extension. *Carbohydr Polym* 117:346–354
80. Dax D, Eklund P, Hemming J et al (2013) Amphiphilic spruce galactoglucomannan derivatives based on naturally-occurring fatty acids. *BioResources* 8(3):3771
81. Daus S, Elschner T, Heinze T (2010) Towards unnatural xylan based polysaccharides: reductive amination as a tool to access highly engineered carbohydrates. *Cellulose* 17(4):825–833
82. Ehrenfreund-Kleinman T, Gazit Z, Gazit D et al (2002) Synthesis and biodegradation of arabinogalactan sponges prepared by reductive amination. *Biomaterials* 23(23):4621–4631
83. Leppänen AS, Xu C, Eklund P et al (2014) Targeted functionalization of spruce *O*-acetyl galactoglucomannans—2,2,6,6-tetramethylpiperidin-1-oxyl-oxidation and carbodiimide-mediated amidation. *J Appl Polym Sci* 130(5):3122–3129

84. Kuzmenko V, Hagg D, Toriz G, Gatenholm P (2014) In situ forming spruce xylan-based hydrogel for cell immobilization. *Carbohydr Polym* 102:862–868
85. MacCormick B, Vuong TV, Master ER (2018) Chemo-enzymatic synthesis of clickable xylo-oligosaccharide monomers from hardwood 4-*O*-methylglucuronoxylan. *Biomacromolecules* 19(2):521–530
86. Fundador NGV, Enomoto-Rogers Y, Takemura A, Iwata T (2012) Acetylation and characterization of xylan from hardwood kraft pulp. *Carbohydr Polym* 87(1):170–176
87. Sun RC, Fang JM, Tomkinson J, Jones GL (1999) Acetylation of wheat straw hemicelluloses in *N, N*-dimethylacetamide/LiCl solvent system. *Ind Crops Prod* 10(3):209–218
88. Sun XF, Sun RC, Zhao L, Sun JX (2010) Acetylation of sugarcane bagasse hemicelluloses under mild reaction conditions by using NBS as a catalyst. *J Appl Polym Sci* 92(1):53–61
89. Ren JL, Sun RC, Liu CF, Cao ZN, Luo W (2007) Acetylation of wheat straw hemicelluloses in ionic liquid using iodine as a catalyst. *Carbohydr Polym* 70(4):406–414
90. Stepan AM, King AWT, Kakko T et al (2013) Fast and highly efficient acetylation of xylans in ionic liquid systems. *Cellulose* 20(6):2813–2824
91. Gröndahl M, Teleman A, Gatenholm P (2003) Effect of acetylation on the material properties of glucuronoxylan from aspen wood. *Carbohydr Polym* 52(4):359–366
92. Ayoub A, Venditti RA, Pawlak JJ, Sadeghifar H, Salam A (2013) Development of an acetylation reaction of switchgrass hemicellulose in ionic liquid without catalyst. *Ind Crops Prod* 44:306–314
93. Dong L, Hu H, Yang S, Cheng F (2014) Grafted copolymerization modification of hemicellulose directly in the alkaline peroxide mechanical pulping (APMP) effluent and its surface sizing effects on corrugated paper. *Ind Eng Chem Res* 53(14):6221–6229
94. Enomoto-Rogers Y, Iwata T (2012) Synthesis of xylan-graft-poly(L-lactide) copolymers via click chemistry and their thermal properties. *Carbohydr Polym* 87(3):1933–1940
95. Edlund U, Albertsson A-C (2014) A controlled radical polymerization route to polyepoxidated grafted hemicellulose materials. *Polimery* 59(01):60–65
96. Saadatmand S, Edlund U, Albertsson A-C (2011) Compatibilizers of a purposely designed graft copolymer for hydrolysate/PLLA blends. *Polymer* 52(21):4648–4655
97. Persson J, Dahlman O, Albertsson AC (2012) Birch xylan grafted with pla branches of predictable length. *Bioresources* 7(3):3640–3655
98. Fanta GF, Burr RC, Doane WM (1982) Graft polymerization of acrylonitrile and methyl acrylate onto hemicellulose. *J Appl Polym Sci* 27(11):4239–4250
99. Voepel J, Edlund U, Albertsson A-C (2011) A versatile single-electron-transfer mediated living radical polymerization route to galactoglucomannan graft-copolymers with tunable hydrophilicity. *J Polym Sci Part A Polym Chem* 49(11):2366–2372
100. Edlund U, Rodriguez-Emmenegger C, Brynda E, Albersson A-C (2012) Self-assembling zwitterionic carboxybetaine copolymers via aqueous SET-LRP from hemicellulose multi-site initiators. *Polym Chem* 3(10):2920
101. O'Malley JJ, Marchessault RH (1966) Characterization of graft copolymers of methylated xylan and polystyrene. *J Phys Chem* 70(10):3235–3240
102. Parikka K, Leppanen AS, Xu C et al (2012) Functional and anionic cellulose-interacting polymers by selective chemo-enzymatic carboxylation of galactose-containing polysaccharides. *Biomacromolecules* 13(8):2418–2428
103. Parikka K, Leppanen AS, Pitkanen L et al (2010) Oxidation of polysaccharides by galactose oxidase. *J Agric Food Chem* 58(1):262–271
104. Leppanen AS, Xu C, Parikka K et al (2014) Targeted allylation and propargylation of galactose-containing polysaccharides in water. *Carbohydr Polym* 100:46–54
105. Song X, Hubbe MA (2014) TEMPO-mediated oxidation of oat beta-D-glucan and its influences on paper properties. *Carbohydr Polym* 99:617–623
106. Kohnke T, Elder T, Theliander H, Ragauskas AJ (2014) Ice templated and cross-linked xylan/nanocrystalline cellulose hydrogels. *Carbohydr Polym* 100:24–30

107. Chemin M, Rakotoveloa A, Ham-Pichavant F et al (2016) Periodate oxidation of 4-*O*-methylglucuronoxylans: influence of the reaction conditions. *Carbohydr Polym* 142:45–50
108. Ehrenfreund-Kleinman T, Domb AJ, Golenser J (2003) Polysaccharide scaffolds prepared by crosslinking of polysaccharides with chitosan or proteins for cell growth. *J Bioact Compatible Polym* 18(5):323–338
109. Luo YQ, Shen SQ, Luo JW, Wang XY, Sun RC (2015) Green synthesis of silver nanoparticles in xylan solution via Tollens reaction and their detection for Hg²⁺. *Nanoscale* 7(2):690–700
110. Luo Y, Shen Z, Liu P, Zhao L, Wang X (2016) Facile fabrication and selective detection for cysteine of xylan/Au nanoparticles composite. *Carbohydr Polym* 140:122–128
111. Peng H, Yang A, Xiong J (2013) Green, microwave-assisted synthesis of silver nanoparticles using bamboo hemicelluloses and glucose in an aqueous medium. *Carbohydr Polym* 91(1):348–355
112. Silva AK, da Silva EL, Oliveira EE et al (2007) Synthesis and characterization of xylan-coated magnetite microparticles. *Int J Pharm* 334(1–2):42–47
113. Wu CY, Peng XW, Zhong LX, Li XH, Sun RC (2016) Green synthesis of palladium nanoparticles via branched polymers: a bio-based nanocomposite for C–C coupling reactions. *RSC Adv* 6(38):32202–32211
114. Chen W, Zhong LX, Peng XW, Lin JH, Sun RC (2013) Xylan-type hemicelluloses supported terpyridine–palladium(II) complex as an efficient and recyclable catalyst for Suzuki–Miyaura reaction. *Cellulose* 21(1):125–137
115. Chen W, Zhong LX, Peng XW et al (2014) Xylan-type hemicellulose supported palladium nanoparticles: a highly efficient and reusable catalyst for the carbon-carbon coupling reactions. *Catal Sci Technol* 4(5):1426–1435
116. Du J, Sun R, Zhang S et al (2004) Novel polyelectrolyte carboxymethyl konjac glucomannan-chitosan nanoparticles for drug delivery. *Macromol Rapid Commun* 25(9):954–958
117. Heinze T, Petzold K, Hornig S (2008) Novel nanoparticles based on xylan. *Cellul Chem Technol* 41(1):13–18
118. Garcia RB, Nagashima T Jr, Praxedes AKC et al (2001) Preparation of micro and nanoparticles from corn cobs xylan. *Polym Bull* 46(5):371–379
119. Phan The D, Debeaufort F, Péroval C et al (2002) Arabinoxylan-lipid-based edible films and coatings. 3. Influence of drying temperature on film structure and functional properties. *J Agric Food Chem* 50(8):2423–2428
120. Péroval C, Debeaufort F, Despré D, Voilley A (2002) Edible arabinoxylan-based films. 1. Effects of lipid type on water vapor permeability, film structure, and other physical characteristics. *J Agric Food Chem* 50(14):3977–3983
121. Phan TD, Péroval C, Debeaufort F et al (2002) Arabinoxylan-lipids-based edible films and coatings. 2. Influence of sucroester nature on the emulsion structure and film properties. *J Agric Food Chem* 50(2):266–272
122. Hartman J, Albertsson A-C, Lindblad MS, Sjöberg J (2006) Oxygen barrier materials from renewable sources: material properties of softwood hemicellulose-based films. *J Appl Polym Sci* 100(4): 2985–2991
123. Zhang P, Whistler RL (2004) Mechanical properties and water vapor permeability of thin film from corn hull arabinoxylan. *J Appl Polym Sci* 93(6):2896–2902
124. Chen GG, Qi XM, Li MP et al (2015) Hemicelluloses/montmorillonite hybrid films with improved mechanical and barrier properties. *Sci Rep* 5:16405
125. Liu YX, Sun B, Wang ZL, Ni YH (2016) Mechanical and water vapor barrier properties of bagasse hemicellulose-based films. *Bioresources* 11(2):4226–4236
126. Gordobil O, Egues I, Urruzola I, Labidi J (2014) Xylan-cellulose films: improvement of hydrophobicity, thermal and mechanical properties. *Carbohydr Polym* 112:56–62
127. Hu S, Gu J, Jiang F, Hsieh YL (2016) Holistic rice straw nanocellulose and hemicelluloses/lignin composite films. *ACS Sustain Chem Eng* 4(3):728–737

128. Huang B, Tang Y, Pei Q et al (2017) hemicellulose-based films reinforced with unmodified and cationically modified nanocrystalline cellulose. *J Polym Environ*
129. Kisonen V, Prakobna K, Xu C et al (2015) Composite films of nanofibrillated cellulose and *O*-acetyl galactoglucomannan (GGM) coated with succinic esters of GGM showing potential as barrier material in food packaging. *J Mater Sci* 50(8):3189–3199
130. Ma RX, Pekarovicova A, Fleming III PD, Husovska V (2017) Preparation and characterization of hemicellulose-based printable films. *Cellul Chem Technol* 51(9–10):939–948
131. Mikkonen KS, Stevanic JS, Joly C et al (2011) Composite films from spruce galactoglucomannans with microfibrillated spruce wood cellulose. *Cellulose* 18(3):713–726
132. Peng XW, Ren JL, Zhong LX, Sun RC (2011) Nanocomposite films based on xylan-rich hemicelluloses and cellulose nanofibers with enhanced mechanical properties. *Biomacromolecules* 12(9):3321–3329
133. Shao D, Yotprayoosak P, Saunajoki V et al (2018) Conduction properties of thin films from a water soluble carbon nanotube/hemicellulose complex. *Nanotechnology* 29(14):145203
134. Bahcegul E, Toraman HE, Ozkan N, Bakir U (2012) Evaluation of alkaline pretreatment temperature on a multi-product basis for the co-production of glucose and hemicellulose based films from lignocellulosic biomass. *Bioresour Technol* 103(1):440–445
135. Kayserilioğlu BŞ, Bakir U, Yilmaz L, Akkaş N (2003) Use of xylan, an agricultural by-product, in wheat gluten based biodegradable films: mechanical, solubility and water vapor transfer rate properties. *Bioresour Technol* 87(3):239–246
136. Ruiz HA, Cerqueira MA, Silva HD et al (2013) Biorefinery valorization of autohydrolysis wheat straw hemicellulose to be applied in a polymer-blend film. *Carbohydr Polym* 92(2):2154–2162
137. Svard A, Brannvall E, Edlund U (2015) Rapeseed straw as a renewable source of hemicelluloses: extraction, characterization and film formation. *Carbohydr Polym* 133: 179–186
138. Oinonen P, Areskog D, Henriksson G (2013) Enzyme catalyzed cross-linking of spruce galactoglucomannan improves its applicability in barrier films. *Carbohydr Polym* 95(2): 690–696
139. Péroval C, Debeaufort F, Seuvre A-M et al (2003) Modified arabinoxylan-based films. Part B. Grafting of omega-3 fatty acids by oxygen plasma and electron beam irradiation. *J Agric Food Chem* 51(10):3120–3126
140. Péroval C, Debeaufort F, Seuvre AM et al (2004) Modified arabinoxylan-based films grafting of functional acrylates by oxygen plasma and electron beam irradiation. *J Membr Sci* 233(1–2):129–139
141. Lee SG, An EY, Lee JB et al (2007) Enhanced cell affinity of poly(D, L-lactic-co-glycolic acid) (50/50) by plasma treatment with β -(1→3) (1→6)-glucan. *Surf Coat Technol* 201(9–11):5128–5131
142. Fredon E, Granet R, Zerrouki R et al (2002) Hydrophobic films from maize bran hemicelluloses. *Carbohydr Polym* 49(1):1–12
143. Gröndahl M, Gustafsson A, Gatenholm P (2006) Gas-phase surface fluorination of arabinoxylan films. *Macromolecules* 39(7):2718–2721
144. Šimkovic I, Gedeon O, Uhliariková I, Mendichi R, Kirschnerová S (2011) Positively and negatively charged xylan films. *Carbohydr Polym* 83(2):769–775
145. Hesse S, Liebert T, Heinze T (2005) Studies on the film formation of polysaccharide based furan-2-carboxylic acid esters. *Macromol Symp* 232(1):57–67
146. Kong W, Huang D, Xu G et al (2016) Graphene oxide/polyacrylamide/aluminum ion cross-linked carboxymethyl hemicellulose nanocomposite hydrogels with very tough and elastic properties. *Chem Asian J* 11(11):1697–1704
147. Zhang W, Liang Z, Feng Q et al (2016) Reed hemicellulose-based hydrogel prepared by glow discharge electrolysis plasma and its adsorption properties for heavy metal ions. *Fresenius Environ Bull* 25(6):1791–1798

148. Jing Z, Zhang G, Sun X-F, Shi X, Sun W (2014) Preparation and adsorption properties of a novel superabsorbent based on multiwalled carbon nanotubes-xylan composite and poly (methacrylic acid) for methylene blue from aqueous solution. *Polym Compos* 35(8):1516–1528
149. Sun XF, Ye Q, Jing Z, Li Y (2014) Preparation of hemicellulose-g-poly(methacrylic acid)/carbon nanotube composite hydrogel and adsorption properties. *Polym Compos* 35(1):45–52
150. Voepel J, Sjöberg J, Reif M et al (2009) Drug diffusion in neutral and ionic hydrogels assembled from acetylated galactoglucomannan. *J Appl Polym Sci* 112(4):2401–2412
151. Zhao W, Nugroho RW, Odelius K et al (2015) In situ cross-linking of stimuli-responsive hemicellulose microgels during spray drying. *ACS Appl Mater Interfaces* 7(7):4202–4215
152. Alexandra AR, Ulrica E, John S, Ann-Christine A, Henrik S (2008) Protein release from galactoglucomannan hydrogels: influence of substitutions and enzymatic hydrolysis by mannanase. *Biomacromolecules* 9(8):2104–2110
153. Guo B, Glavas L, Albertsson A-C (2013) Biodegradable and electrically conducting polymers for biomedical applications. *Prog Polym Sci* 38(9):1263–1286
154. Dai QQ, Ren JL, Peng F et al (2016) Synthesis of acylated xylan-based magnetic Fe₃O₄ hydrogels and their application for H₂O₂ detection. *Materials (Basel)* 9(8):3–16
155. Du J, Li B, Li C et al (2016) Tough and multi-responsive hydrogel based on the hemicellulose from the spent liquor of viscose process. *Int J Biol Macromol* 88:451–456
156. Liu S, Chen F, Song X, Wu H (2016) Preparation and characterization of temperature- and pH-sensitive hemicellulose-containing hydrogels. *Int J Polym Anal Charact* 22(3):187–201
157. Pahimanolis N, Sorvari A, Luong ND, Seppala J (2014) Thermoresponsive xylan hydrogels via copper-catalyzed azide-alkyne cycloaddition. *Carbohydr Polym* 102:637–644
158. Peng XW, Ren JL, Zhong LX, Peng F, Sun RC (2011) Xylan-rich hemicelluloses-graft-acrylic acid ionic hydrogels with rapid responses to pH, salt, and organic solvents. *J Agric Food Chem* 59(15):8208–8215
159. Yang JY, Zhou XS, Fang J (2011) Synthesis and characterization of temperature sensitive hemicellulose-based hydrogels. *Carbohydr Polym* 86(3):1113–1117
160. Zhang W, Zhu S, Bai Y et al (2015) Glow discharge electrolysis plasma initiated preparation of temperature/pH dual sensitivity reed hemicellulose-based hydrogels. *Carbohydr Polym* 122:11–17
161. Zhao W, Glavas L, Odelius K, Edlund U, Albertsson A-C (2014) Facile and green approach towards electrically conductive hemicellulose hydrogels with tunable conductivity and swelling behavior. *Chem Mater* 26(14):4265–4273
162. Zhao W, Glavas L, Odelius K, Edlund U, Albertsson A-C (2014) A robust pathway to electrically conductive hemicellulose hydrogels with high and controllable swelling behavior. *Polymer* 55(13):2967–2976
163. Rezakazemi M, Shahidi K, Mohammadi T (2012) Sorption properties of hydrogen-selective PDMS/zeolite 4A mixed matrix membrane. *Int J Hydrogen Energy* 37(22):17275–17284
164. Rezakazemi M, Shahidi K, Mohammadi T (2012) Hydrogen separation and purification using crosslinkable PDMS/zeolite A nanoparticles mixed matrix membranes. *Int J Hydrogen Energy* 37(19):14576–14589
165. Qi XM, Chen GG, Gong XD et al (2016) Enhanced mechanical performance of biocompatible hemicelluloses-based hydrogel via chain extension. *Sci Rep* 6:33603
166. Gabrieli I, Gatenholm P (2015) Preparation and properties of hydrogels based on hemicellulose. *J Appl Polym Sci* 69(8):1661–1667
167. Salam A, Venditti RA, Pawlak JJ, El-Tahlawy K (2011) Crosslinked hemicellulose citrate-chitosan aerogel foams. *Carbohydr Polym* 84(4):1221–1229
168. Guan Y, Chen J, Qi X et al (2015) Fabrication of biopolymer hydrogel containing Ag nanoparticles for antibacterial property. *Ind Eng Chem Res* 54(30):7393–7400
169. Guan Y, Bian J, Peng F, Zhang XM, Sun RC (2014) High strength of hemicelluloses based hydrogels by freeze/thaw technique. *Carbohydr Polym* 101:272–280
170. Guan Y, Zhang B, Bian J, Peng F, Sun R-C (2014) Nanoreinforced hemicellulose-based hydrogels prepared by freeze-thaw treatment. *Cellulose* 21(3):1709–1721

171. Karaaslan MA, Tshabalala MA, Yelle DJ, Buschle-Diller G (2011) Nanoreinforced biocompatible hydrogels from wood hemicelluloses and cellulose whiskers. *Carbohydr Polym* 86(1):192–201
172. Alakalhunmaa S, Parikka K, Penttilä PA et al (2016) Softwood-based sponge gels. *Cellulose* 23(5):3221–3238
173. Dax D, Bastidas MSC, Honorato C et al (2015) Tailor-made hemicellulose-based hydrogels reinforced with nanofibrillated cellulose. *Nord Pulp Pap Res J* 30(3)
174. Dragan ES (2014) Design and applications of interpenetrating polymer network hydrogels. A review. *Chem Eng J* 243:572–590
175. Myung D, Waters D, Wiseman M et al (2008) Progress in the development of interpenetrating polymer network hydrogels. *Polym Adv Technol* 19(6):647–657
176. Maleki L, Edlund U, Albertsson A-C (2016) Green semi-IPN hydrogels by direct utilization of crude wood hydrolysates. *ACS Sustain Chem Eng* 4(8):4370–4377
177. Maleki L, Edlund U, Albertsson AC (2017) Synthesis of full interpenetrating hemicellulose hydrogel networks. *Carbohydr Polym* 170:254–263
178. Meena R, Lehnen R, Saake B (2013) Microwave-assisted synthesis of kC/Xylan/PVP-based blend hydrogel materials: physicochemical and rheological studies. *Cellulose* 21(1):553–568
179. Rezakazemi M, Sadrzadeh M, Matsuura T (2018) Thermally stable polymers for advanced high-performance gas separation membranes. *Prog Energy Combust Sci* 66:1–41
180. Rezakazemi M, Ebadi Amooghin A, Montazer-Rahmati MM, Ismail AF, Matsuura T (2014) State-of-the-art membrane based CO₂ separation using mixed matrix membranes (MMMs): an overview on current status and future directions. *Prog Polym Sci* 39(5):817–861
181. Fonseca Silva TC, Habibi Y, Colodette JL, Lucia LA (2011) The influence of the chemical and structural features of xylan on the physical properties of its derived hydrogels. *Soft Matter* 7(3):1090–1099
182. Söderqvist Lindblad M, Albertsson A, Ranucci E, Laus M, Giani E (2005) Biodegradable polymers from renewable sources: rheological characterization of hemicellulose-based hydrogels. *Biomacromolecules* 6(2):684
183. Lindblad MS, Ranucci E, Albertsson AC (2001) Biodegradable polymers from renewable sources. New hemicellulose-based hydrogels. *Macromol Rapid Commun* 22(12):962–967
184. Tanodekaew S, Channasanon S, Uppanan P (2006) Xylan/polyvinyl alcohol blend and its performance as hydrogel. *J Appl Polym Sci* 100(3):1914–1918
185. Azimi A, Azari A, Rezakazemi M, Ansarpour M (2017) Removal of heavy metals from industrial wastewaters: a review. *ChemBioEng Rev* 4(1):37–59
186. Rezakazemi M, Zhang Z (2018) 2.29 desulfurization materials A2. In: Ibrahim D (ed) *Comprehensive energy systems*. Elsevier, Oxford, pp 944–979

Self-healing Bio-composites: Concepts, Developments, and Perspective



Zeinab Karami, Sara Maleki, Armaghan Moghaddam
and Arash Jahandideh

Abbreviations

BG	Bioglass
CNCs	Cellulose nanocrystals
CB	Cucurbit uril
DA	Diels-Alder
ELP	Elastin-like polypeptides
GO	Graphene oxide
MSP	Metallo-supramolecular polymer
MWCNTs	Multi-wall carbon nanotubes
NR	Natural rubber
PDAP	Polydopamine
PU	Polyurethane
PCL	Poly(ϵ -caprolactone)
Ag NWs	Silver nanowires
UV	Ultraviolet radiation
UPy	Ureidopyrimidinone

1 Introduction

As humans seek immortality, they also like their products to be able to be used infinitely, but man-made materials, such as polymer composites, are vulnerable to damage, failure, and degradation. Defects from deep within the structure, and thus, detecting such defects and repairing them is hardly feasible [1]. On the other hand, biological systems, such as muscles or bones, can be repaired after being exposed to excessive loads through complex mechanisms. Accordingly and inspired by nature,

Z. Karami (✉) · S. Maleki · A. Moghaddam · A. Jahandideh
Iran Polymer and Petrochemical Institute (IPPI), P.O. Box 14965-115, Tehran, Iran
e-mail: Z.Karami@ippi.ac.ir; Rana.Karami@gmail.com

© Springer Nature Switzerland AG 2019
Inamuddin et al. (eds.), *Sustainable Polymer Composites and Nanocomposites*,
https://doi.org/10.1007/978-3-030-05399-4_44

1323

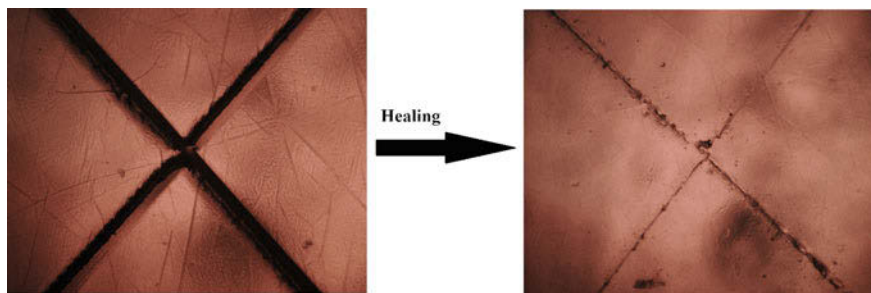


Fig. 1 Healing of a polymer coating through thermal treatment (retro diels-alder and diels-alder reactions)

synthetic healable systems have been developed. Synthetic self-healing materials are smart systems which have the ability to heal and retain the properties, similar to living organisms, after the occurrence of a damage [2].

Different types and applications of polymers including thermoplastics, thermosets, elastomers [3–8], shape memory and supramolecular polymers, coatings, and polymer composites have been reported in the field of self-healing materials, as these materials are used excessively in everyday and industrial applications [9, 10]. Figure 1 shows a healing process of a polymer coating via a thermal treatment.

In this chapter, the basics and fundamentals of healing are explored. The following sections of the chapter deal with self-healing biocomposites, and their types and applications are explained. Finally, a scope into the future of these biocomposites is discussed.

1.1 Fundamentals of Self-healing

The self-healing materials are divided into extrinsic and intrinsic systems. In extrinsic self-healing systems, healing agents such as microcapsules are embedded in the matrix, but this approach is of some drawbacks; for instance, the healing agent gets consumed during healing in the damaged region [11]. For intrinsic self-healing systems, the non-covalent or dynamic covalent chemistries control the healing process and efficiency. Unlike extrinsic healing materials, these types of healable materials can be used repeatedly in healing cycles [12].

Moreover, self-healing mechanisms based on the bonding can be categorized into two groups: covalent bonds, and non-covalent bonds. Indeed, the formation or cleavage of covalent or non-covalent bonds in the polymer materials can result in healing property in the presence or absence of an external stimulus [13]. The reactions which consequently lead to the self-healing of the polymers include covalent bonds, such as the formation of cyclic structures [14], and non-covalent bonds, meaning supramolecular chemistry (H-bonding, ionic interactions, and π - π stacking) [15, 16].

1.2 *Biocomposites: Substitutes for Fossil-Based Composites*

The ever-changing economic developments leading to increasing oil prices, global warming and endless trash being produced, have led to more light being shed on the urgency of formulating novel composites with sustainable sources, and even better, biodegradable ones [17]. Besides, with the development of polymers and composites fields and petrochemicals being the main supply for these fields, concerns about a fossil fuel-deprived future has grown. Regarding the economic and environmental issues arisen, the production of polymers derived from renewable and sustainable sources have become a necessity [18, 19]. Thus, for instance, petrochemical-based composites can be replaced with biocomposites.

A bio-based composite can consist of a bio-based reinforcing agent, matrix, both or even other ingredients in the formulation such as vegetable oils [20, 21]. Sustainable matrixes include furan derivatives, gelatin, chitin and chitosan, poly(lactic acid) (PLA), poly(lactic-co-glycolic acid) (PLGA), casein, alginate, proteins and their derivatives, reinforcing agents include cellulose and jute fibers, and other ingredients include linseed, Tung, and neem oil, to name but a few [22–32].

As mentioned earlier, based on the active agent and the degree of damage, different mechanisms and transitions can affect the healing property of the materials [33]. In following sections, the mechanisms by which the healing in biocomposites occur are discussed regarding the type of healing, more specifically, based on the bonds and transitions.

2 **Self-healing Biocomposites Based on Non-covalent Bonding (Supramolecular)**

Features including reversibility, directionality, and sensitivity make the supramolecular chemistry attractive, particularly for self-healing materials. In contrast to covalent bonding, supramolecular networks can remodel rapidly and reversibly from fluid-like to solid-like plastic networks [34, 35]. Therefore, exploiting supramolecular chemistry in biocomposite matrixes can lead to healable biocomposites. The self-healing in these biocomposites are based on hydrogen bonding, metal-ligand coordination, π - π stacking, ionic interactions and macrocyclic host-guest interactions. Table 1 summarizes the general mechanisms of self-healing for supramolecular polymers. the supramolecular self-healing biocomposites have great potentials to be used in various applications, namely fields of biomaterials, wastewater treatment, and smart materials [36–38].

Table 1 General mechanisms of self-healing for supramolecular materials

Type of interaction	Mechanism
Hydrogen bonding	It is sensitive to pH or temperature changes. For example, at ultraviolet radiation exposure, UPy motifs cleave and so the properties of these materials, such as molecular weight and viscosity, decrease and as a result, the defects heal quickly and efficiently [45]
Metal–ligand coordination	It is a temperature-sensitive complex. It has to be noted that heating leads to possible de-bonds in metal–ligand motifs, which consequently reduce the molecular weight of polymers, as well as the viscosity, and thereby, the healing of the mechanical damages would be facilitated [49]
π – π stacking interaction	It is a temperature-sensitive complex [52]
Ionic interactions	The ionic cross-links easily re-form and rearrange, which facilitate the self-healability [54]
Host–guest interactions	Macrocyclic host–guest interactions can be incorporated in a biocomposite in order to impart self-healability [56]

2.1 Self-healing of Biocomposites on the Basis of Hydrogen Bonding

Directionality and affinity features have made hydrogen bonding (H-bonding) very attractive. Besides, these features have endowed remarkable mechanical strength to the systems with hydrogen bonding. Method of selecting the hydrogen bonding motifs, such as ureidopyrimidinone (UPy, a motif with strong tendency to form H-bonds through a quadruple array of H-bonding donors and acceptors, as shown in Fig. 2), can be affected by the properties of polymers. It should be noted that these motifs are easily introduced into polymer chains either as end-groups or as pending groups [39–41]. UPy end-functionalized supramolecular polymers behave similarly to conventional polymers with an immense dependency on physical and mechanical properties to the temperature [42, 43]. UPy-monomers coupled with the thermally responsive polymer can terminate the formation of thermo-regulated self-healing

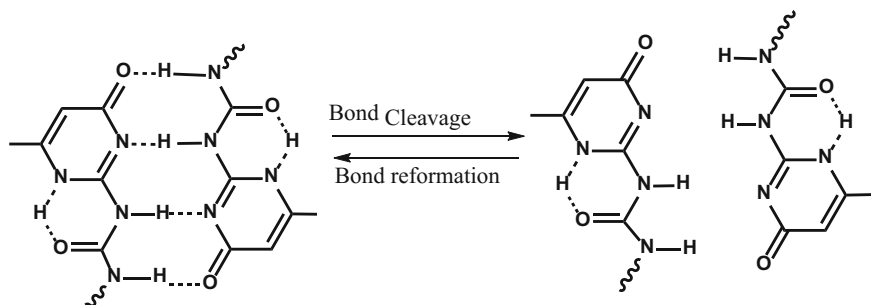


Fig. 2 Multiple H-bonds cleaving and reforming in an Upy motif as a moiety that can cause the healability [39]

polymers. In the supramolecular polymers, using materials with high segmental mobility (which act as the soft segment with low T_g), connected to the segments with the H-bonding motifs (which play the role of the hard segment with high T_g), endow a self-healing property to the system which is sensitive to the changes in temperature or pH [12]. It is also believed that the hydrophobic interactions associated with the hard segments (UPy-groups) lead to the phase separation, and therefore self-healing can be a feature in supramolecular polymers [44]. As aforementioned, H-bonding can be utilized in biocomposites to impart self-healability [45].

For example, the synthesis of light-healable nanocomposites, based on a telechelic poly(ethylene-co-butylene) (functionalized with H-bonding of UPy) and UPy-functionalized cellulose nanocrystals is reported. Under ultraviolet radiation exposure, the UPy motifs of these materials were excited by the absorbed energy that was converted into heat. This phenomenon resulted in the temporary cleavage in the H-bonding motifs, and consequently, a reversible drop in the properties of the supramolecular polymers, such as molecular weight and viscosity. As a result, defects healed quickly and efficiently, even at a filler content of up to 20 w/w%. It must be noted that healing through this method has been performed under heating, and this method is sensitive to the temperature applied [45].

2.2 Self-healing of Biocomposites on the Basis of Metal-Ligand Coordination

The optical and photochemical properties, along with reversibility and tenability (which have been achieved by incorporation of different metal ions and ligand substitutes), have made metal-ligand coordination particularly attractive. In these supramolecular polymers, incorporating ligands into metal-crosslinked polymers leads to the formation of a temperature-sensitive complex in which variations in the temperature may decouple metal ions from the ligand, resulting in bonding and de-bonding [46]. When the metallo-supramolecular polymers are exposed to the ultraviolet (UV) light, the metal-ligand motifs could be electronically excited, and the absorbed energy could be converted into heat. This, in turn, results in the de-bonding of metal-ligand motifs (Fig. 3), which consequently reduces the molecular mass of the polymers as well as the viscosity, and thereby, healing of the mechanical damages would be facilitated [47, 48].

An example for utilizing metal-ligand coordination in self-healing biocomposites discussed the synthesis of the light-healable nanocomposites, including cellulose nanocrystals (CNCs) and a metallo-supramolecular polymer (MSP) based on poly(ethylene-co-butylene) that was end-functionalized with 2,6-bis(1-methylbenzimidazolyl) pyridine ligands and Zn(NTf₂)₂. These nanocomposites were able to absorb UV radiations and convert them to heat, and thus, the metal-ligand motifs dissociated. As a result, small defects could be filled by liquefying the material. When the UV light was switched off, the MSP reassembled, and the

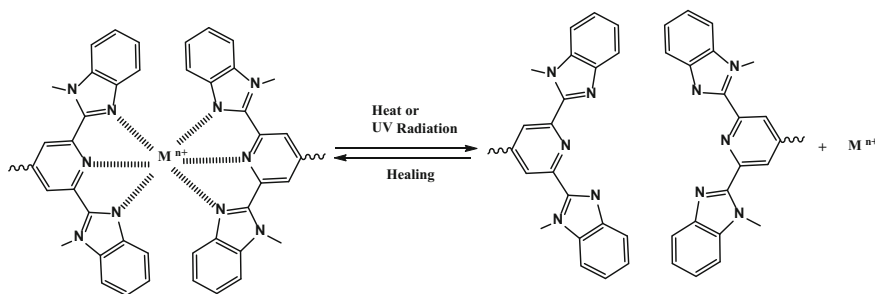


Fig. 3 A representative scheme of self-healing of MSP containing metal–ligand coordination [46]

initial properties were restored. Incorporating CNCs into the MSP matrix improved the strength and stiffness—from 52 and 1.7 MPa for the neat polymer to 135 and 5.6 MPa in 10% w/w CNCs, respectively [49].

2.3 Self-healing of Biocomposites on the Basis of π – π Stacking Interaction

When end-capped π -electron deficient groups interact with other π -electron-rich aromatic backbone molecules, stacking interactions form. In these polymers, tuning T_g facilitates the fabrication of self-healable supramolecular polymers at a wide temperature range (~ 50 – 100 °C). It has also been reported that within one supramolecular network, the intermolecular H-bonding can be combined with π – π Stacking, and consequently, thermal healable networks containing urethane and urea groups as a spacer can be achieved [50, 51].

To endow heal ability to biocomposites by π – π Stacking interactions, a supramolecular healable nanocomposite was prepared, via blending π – π interactions (between a π -electron rich pyrenyl end-capped oligomer) and a chain-folding oligomer, containing pairs of π -electron poor naphthalene-diimide units, with CNCs as the reinforcing agent. The authors prepared and studied a series of nanocomposites, employing different CNCs wt% (from 1.25 to 20.0 wt%) in the healable supramolecular polymeric matrix, via solvent casting followed by compression moulding. The authors studied the healing behaviour of nanocomposites at elevated temperatures (~ 85 °C). The results showed that the healing rate decreased by an increase in the CNC content. The best combination of healing efficiency and mechanical properties was obtained when employing 7.5 wt% CNC in the nanocomposite, which resulted in a rehealable composite (100% healability at 85 °C within 30 min). As a result, they showed enhanced mechanical properties for the supramolecular nanocomposites compared to the unreinforced polymer, while efficient thermal healing is still possible [52].

2.4 Self-healing of Biocomposites on the Basis of Ionic Interactions

In this group of supramolecular polymers and polymer composites, the formation of the ionomer leads to the formation of the final polymer network, caused by the ionic interactions. For instance, Xu et al. [53] worked on a self-healable material, exploiting the controlled peroxide-induced vulcanization to generate the physical ionic crosslinks, via polymerization of zinc dimethacrylate in natural rubber (NR). It has been noted that the rubber with covalent cross-linking has higher strengths and modulus, although these types of cross-links induce lower levels of mobility to the rubber chains. The restricted mobility of the rubber chains, in turn, hampered the healability of the system in case of the mechanical damage. On the other hand, NR chains in the ionic supramolecular network had good flexibility and mobility. The ionic cross-links easily reconstructed and rearranged, which facilitated the self-healability [53, 54].

Moreover, studied the self-assembly of chitosan chains with graphene oxide (GO) nano-sheets was studied, where GO worked as the two-dimensional cross-linker due to its multifunctional groups on both sides. The gel-formation process includes two steps: first, chitosan interacts with GO via electrostatic interactions. Due to the complex intra-/inter-molecular hydrogen bonding, the chitosan chains would be in the compressed state. After heating, the hydrogen bonding interactions (among chitosan chains) become weak and the free motion of chitosan chain and GO nano-sheets increase, resulting in the more interactions among them. As a result, the chains stretched have a higher chance to interact with other GO sheets and supramolecular hydrogels of chitosan and GO could be prepared by controlling the concentration of GO, the ratio of chitosan/GO, and the temperature. They also found that at a high GO concentration, healable hydrogels can be prepared at room temperature. However, at lower GO concentrations, the supramolecular hydrogels formed only at an elevated temperature (i.e. 95 °C) [36].

2.5 Self-healing of Biocomposites on the Basis of Macrocyclic Host–Guest Interactions

Macrocyclic host-guest interactions have been employed over the past three decades. Typically, this kind of interactions is formed where a guest molecule is locked within the cavity of the host. It should be noted that the host molecule typically owns external features (that interact with the solvent), and internal features that often cause the formation of the interaction between a ‘guest’ through either a specific shape or a favourable environment to the host molecules [55]. Macrocyclic host-guest interactions can be incorporated in a biocomposite in order to impart self-healability.

For example, a nanocomposite hydrogel was prepared from brush polymer-modified CNC, as hard domains, and ‘soft’ polymeric domains, that were bound together by cucurbit [8] uril (CB [8]) supramolecular crosslinks, which form dynamic host-guest interactions. The resulting supramolecular nanocomposite hydrogels showed three important properties: (I) high storage modulus ($G' > 10$ kPa), (II) rapid sol-gel transition (<6 s), and (III) rapid self-healing (even upon aging for several months) due to the balanced colloidal reinforcement, as well as the selectivity and dynamics of the CB [8] three-component supramolecular interactions [56].

3 Self-healing Biocomposites Based on Covalent Bonding

For self-healing biocomposite based on covalent bonds, the most important covalent bonding, which is commonly used for the preparation of the self-healing polymers and polymer composites is [2+4] cycloaddition, known as DA reaction [14]. Although this reaction was discovered in the year 1950 by Diels and Alder, just in the last decade was it employed as the cross-linking mechanism in healable polymers for healing applications [57]. DA reaction includes a cycloaddition reaction between a conjugated diene such as a furan group and a dienophile such as a maleimide group to form a substituted cyclohexene known as DA adducts [58] (Fig. 4). The formation of reversible adducts is responsible for imparting self-healability [14, 59, 60]. In *retro* DA reactions, the diene and dienophile moieties disconnect. Subsequently, at lower temperatures, the covalent bonds (DA bonds) reform, and the crack would be completely repaired [61].

Furan compounds involved in these reactions are of bio-based materials, which subsequently improve the sustainability of the final product [59]. The synthesis of partially bio-based healable composites based on DA reactions has been reported in the literature [57, 62–66].

Another kind of covalent bonding used for self-healable biocomposites is Schiff-base interaction. A Schiff-base dynamic covalent bond is formed as a result of a reaction between an aldehyde or ketone with primary amines, in which the $C=O$ group is replaced by the $C=N-R$ group, where R may be any alkyl or any aryl group. Schiff-bases which contain aryl substituents are substantially more stable

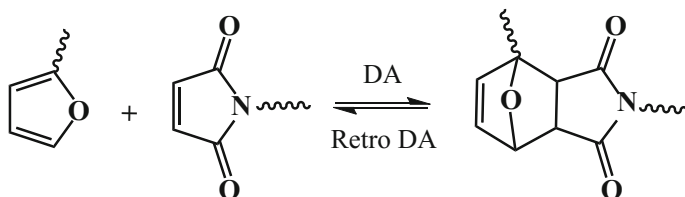


Fig. 4 A representative scheme of reversible DA reaction

and synthesized more readily, while those which contain alkyl substituents are relatively unstable. Schiff-bases of aliphatic aldehydes are relatively unstable, while those of aromatic aldehydes contain effective conjugations and are more stable [67, 68].

3.1 DA Based Self-healing Nanocomposites

Providing DA and retro DA reaction conditions for a nanocomposite matrix endow self-heal ability to the fabricated nanocomposites. These nanocomposites would have potential applications in electronics, as the conductivity of the broken electric circuit can be completely restored [64].

The first example of partially bio-based composites containing nanomaterial, based on DA chemistry was reported by Wu et al. [64], where a composite was prepared from DA polyurethane covalently connected to the functionalized graphene nano-sheets. This flexible composite displayed excellent mechanical properties in addition to its infrared (IR) laser self-healing properties. The reduced graphene oxide could absorb the IR light and convert it into heat promptly, resulting in a local increase in the temperature. The results showed that mechanical properties could be retained after healing via 1 min IR laser irradiation at 980 nm; in terms of Young's modulus, break strength, and break elongation, the healing efficiencies were 100, 96, and 97%, respectively. The healing was also visually confirmed via SEM analysis [64].

The synthesis of a healable composite, made of amino-functionalized multi-wall carbon nanotubes (MWCNTs)/epoxy, was reported based on the DA network. Crosslinking the matrix included two steps; first, the epoxy resin was reacted with furfurylamine or the amino-functionalized MWCNTs; subsequently, the substituent furan groups were reacted with bismaleimide groups through DA reaction, resulting in the formation of the DA network [69]. In this composite, the photothermal conversion of CNTs triggers both DA and retro DA reactions [70]. Both heating and IR irradiation methods can be successful in terms of healing. Nonetheless, heat-triggered self-healing procedure results in an unwanted dissociation of other parts of the specimen, which consequently results in wasting the energy and deformation of the sample [71]. For the heating method, cracks were repaired after 1 min at 120 °C and completely healed after 5 h (which is rather a long time). In irradiation method, the cracks were healed within 30 s of irradiation. It should be noted that the repairing time and efficiency (determined based on the ratio of tensile strengths of the healed and pristine sample) is adjustable by an increase of NH₂-MWCNTs content and also a reduction in the repairing time [69].

In the mobile phone industry where the devices are subjected to service for prolonged periods, healability is of great importance, especially for screens. Such screens are intended to be transparent. In this case, DA polymers, capable of self-healing, are suitable candidates to give repairable conductive screens [72].

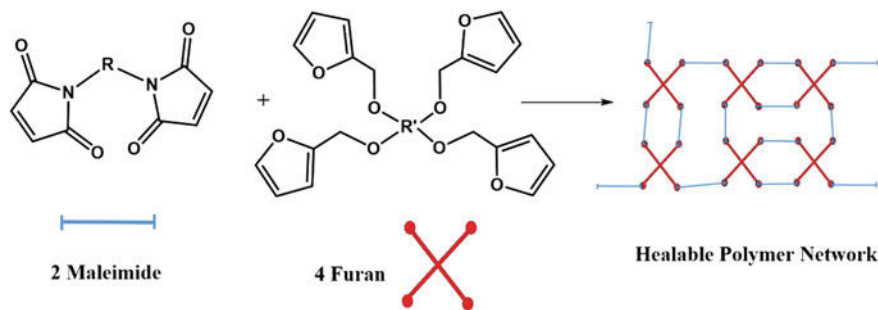


Fig. 5 Monomers and healable network used for conductive screens [65, 72]

Two studies have been reported by Pei et al. [65, 72], concerning the healable conductive screens. In these studies, the simultaneous utilization of silver nanowires (Ag NWs) network and a DA-based polymer resulted in a transparent conductor with desired mechanical properties [65]. The resulted capacitive touch screen sensors have the ability to mend their functions by being exposed to 80 °C for 30 s, which consequently provides the conditions for the efficient retro DA reaction, and thus, further healing of the surface cracks is possible [72]. Figure 5 represents the schematics of the DA healable network.

Cracks healed rapidly and efficiently due to the reformation of DA polymer matrix. In fact, reformation causes the silver nanowires to re-assemble and form an integrated network. The conductivity of the healed samples was measured and it was 97% of the pristine ones [65]. According to the SEM micrographs, the healing occurred through two pathways: (a) the DA reaction of the DA polymer network, i.e. the substrate, and (b) the reformation of the AgNW network. Healed samples possessed 86% of the mechanical strength of the pristine ones. Results also showed that the healing process can be repeatedly accomplished in the same location, without a significant decrease in the surface conductivity [65].

3.2 DA Based Self-healing Biocomposites Containing Fibers

DA reaction may be employed in fiber-reinforced composites for several reasons: (a) it can improve the adhesion of the reinforcement to the polymer matrix, (b) it facilitates the load transfer from the polymer matrix to the reinforcement material, (c) it endows healability to the composite, and (d) it extends the fatigue lifetime of the specimen [57].

Chemical sizing of reinforcements can improve the interfacial adhesion and durability of a composite [73]. One of the chemical sizing methods of fibers (in order to prepare a healable composite) can be maleimidation of fibers [57, 59].

For instance, furan-functionalized epoxy-amine thermosetting matrixes and maleimide-functionalized glass fibers were employed to fabricate a reversible DA composite by Peterson et al. [57]. The authors reported that the DA reaction occurring at room temperature resulted in DA adducts formation, which cleaved from the furan and maleimide moieties at temperatures higher than 90 °C.

Based on the results of the single-fiber micro-droplet pull-out testing, which is a common test method for investigating the mechanical properties of a single fiber [74], healing in the specimens at the interfaces was calculated to be ~41%. Herein, the system was capable of being repaired, for up to five healing cycles [57].

Similar fiber sizing method was employed for carbon fibers. After sizing carbon fibers by maleimide, the DA bonds formed at the interphase between carbon fiber surface and the epoxy matrix. These DA bonds endow an interfacial self-healing to the carbon/epoxy composite. The furan groups were dispersed in the matrix by blending the epoxy resin with furfuryl glycidyl ether as an active bio-based epoxy monomer. Both epoxies were then reacted with isophorone diamine to obtain an epoxy-amine matrix. During the healing process, the unreacted or cleaved furan groups from retro DA reaction can participate in the DA reaction with the maleimide groups to reform the fiber-matrix interphase [59].

3.3 DA Based Self-healing Biocomposites Containing Encapsulated Maleimides

Encapsulation of diene and dienophiles to prepare self-healable biocomposites has been rarely considered in the literature, probably since the repeatability is low [12]. One of the few studies in this field is presented by Prartama et al. [66]. In brief, they synthesized a self-healable epoxy-amine thermoset, via encapsulation of multimaleimides. After the rupture of the microcapsules, the multimaleimides were capable of reacting with the available furans in the matrix. According to the results of the mechanical tests, the healing extent was reported to be 71% [66].

3.4 Self-healing of Schiff-Base Biocomposites

The formation of a Schiff-base from an aldehyde or ketones is a reversible reaction, and generally takes place under acidic or basic catalysis, or upon heating [67, 68]. Schiff-base chemistry as a reversible covalent bond can be utilized to prepare self-healing biocomposites.

For example, Zhang et al. [75] prepared a magnetic self-healing hydrogel by mixing ferrofluid (chitosan-modified Fe₃O₄ nanoparticles) with telechelic difunctional poly(ethylene glycol). The hydrogel showed substantial healability potential, and in fact, healed itself automatically with no external stimulus, a sign of excellent

self-healing capability. Authors showed that by a magnet, the magnetic self-healing hydrogel can be remotely operated to pass through a narrow channel with an obstacle in the middle. They also showed that the hydrogel changed its shape and squeezed into the narrow channel, engulfed the glass obstacle in the middle of the channel, and finally, passed through the channel completely after ~ 30 min. Although the hydrogel changed its shape during this process, it still maintained its integrity. This experiment demonstrated the excellent cooperation between magnetic and self-healing features of the hydrogel, suggesting the potential drug delivery application of this novel material [75].

In another work, Zeng et al. [76] developed a novel in-situ forming organic/inorganic composite hydrogel with dynamic aldimine crosslinks (Schiff-base interactions), based on elastin-like polypeptides (ELP) and bioglass (BG). For this purpose, they first synthesized ELP containing either primary amines or carboxylic acid functional groups, and chemically modified carboxylic acids to create ELP with aldehyde functional groups. Then, the organic and inorganic components were prepared to create ELP/BG composite hydrogels. The self-healing ability of ELP/BG hydrogels was investigated and the results showed that the dynamic nature of Schiff-base reaction had endowed self-healing properties to the ELP/BG hydrogels. The authors showed that imine bonds, or more specifically, aldimine bonds are reversible, and this property makes them suitable to design self-healing hydrogel system due to constant bond association and dissociation [76–78].

4 Self-healing of Microcapsule-Based Biocomposites

One of the most common methods to endow self-healing properties to different matrixes with no intrinsic healing property is nano-/micro-capsulation. In this case, functional microcapsules (as healing agents inside the coating matrixes) are embedded in the matrix as a preventative method. For achieving self-healing through this route, microcapsules contain reactants for the polymerization of a material, usually similar to the matrix. Catalysts or monomers to carry out polymerization are also dispersed in the matrix (Fig. 6a). As soon as the matrix is damaged, the microcapsules would be ruptured, and due to the release of healing agents (Fig. 6b), the defect can be repaired locally (Fig. 6c) [79–82]. To prepare microcapsulated polymer composites, methods including interfacial, in-situ, and mini-emulsion polymerizations, solvent evaporation, and sol-gel reactions have been reported [83].

Linseed, Tung, neem, and coconut oil have been reported in different papers to be used for microcapsulation leading to the self-healing of the composites [84–87]. Namely, linseed oil was encapsulated in phenol-formaldehyde dispersed in the epoxy matrix through in-situ polymerization. Due to high unsaturated ester content of linseed oil, it tends to polymerize when exposed to oxygen, after being released from the ruptured capsules [88]. An important contributing factor in improving the self-healing of microcapsule embedded composites is the appropriate adhesion

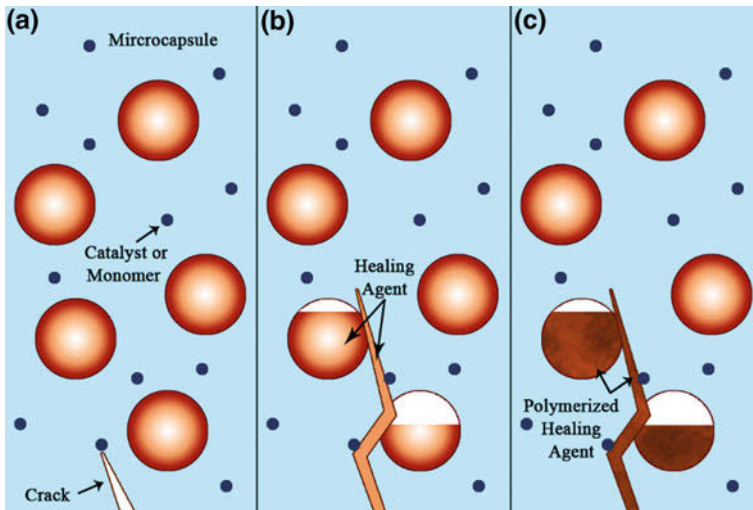


Fig. 6 Self-healing in microcapsulated materials; **a** a crack forms in the matrix, **b** microcapsules get ruptured and the healing agent is released, and **c** the polymerization is carried out to fill the crack [99]

between the microcapsules and the matrix. When the morphology of the capsules is rough, they adhere to the matrix easier through an anchoring mechanism and also break faster upon the failure of the matrix [89].

Another example for the effect of adhesion was through utilizing interfacial polymerization to prepare poly(amidoamine) embedded with linseed oil-filled polyuria microcapsules, where amino groups present on the shell of the capsules enhance the adhesion caused by the polarity [90]. Similar to linseed oil, Tung oil has been used in paints and coatings. It is primarily consisted of a glyceride of eleostearic acid, a conjugated triene, making Tung oil highly unsaturated. It can polymerize through oxidation. For instance, it was encapsulated in poly(urea-formaldehyde) in an in-situ method, and dispersed in epoxy and promoted the self-healing [31].

In another study, soy protein was reported to be encapsulated in PLGA using emulsification solvent evaporation method. For this composite, soy protein released upon the rupture of microcapsules and worked as the cross-linker for the glycolic acid present in the matrix leading to a 48% efficiency of healing [25].

Not only is the microcapsulation method used for imparting self-healing to polymer matrixes, but also as the rust formation and induction of internal stresses (which leads to the development of the cracks) are severe concerns for steel-reinforced concretes [91], embedding epoxy-coated rebar, as a physical barrier, inside the concrete matrix to prevent or delay the corrosion is a good protective method. However, the cracks may form during the transportation or handling of epoxy thermosets coatings, causing negative effects on the protective properties [92].

Due to the high reactivity of conjugated oils, self-healable epoxy coatings have also been prepared. The epoxy coatings contained 10 wt% microencapsulated Tung oil (as the healing agent) for rebar in the steel-reinforced concrete. After microcapsules rupture as a result of the scratching, the release of Tung oil would repair the crack across the damaged area. The corrosion time of surfaces coated with the healable coating was found to be three times longer than the surfaces coated with the conventional coatings. So, using healable epoxy coatings prevent the corrosion, and increase the durability of the steel, and consequently decrease the maintenance costs [93].

Microcapsulation has also been reported for renewable matrixes. For example, poly(lactic acid) was embedded with dicyclopentadiene capsules and Grubbs' 1st generation catalyst. Upon the formation of cracks, dicyclopentadiene underwent polymerization in the presence of the catalyst, leading to an 84% recovery for the composite [94]. A summary of all the results above is shown in Fig. 7.

Although microcapsulation can lead to preparing self-healable composites from different types of polymers, it suffers from different drawbacks. In case of special catalysts, microcapsulation can be costly, large microcapsules are hard to disperse in certain matrixes, small microcapsules may not rupture upon the formation of cracks in the matrix leading to the embedment of capsules to be fruitless, and also, the healing agents deplete after healing in a region, and therefore self-healing can only occur once [95, 96].

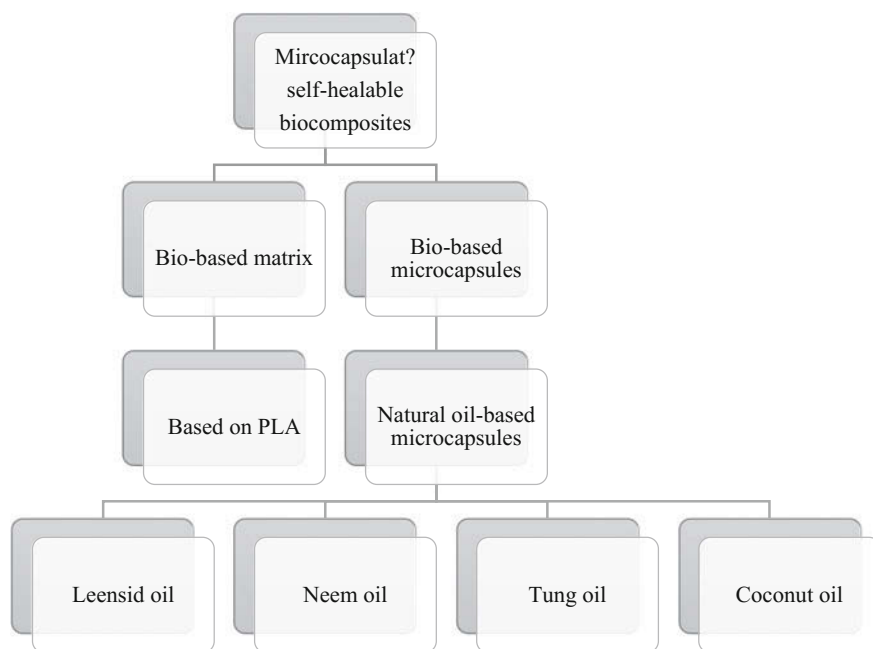


Fig. 7 Microcapsulated self-healable composites based on bio-based matrix or microcapsules [84–87, 94]

5 Self-healing of Biocomposites on the Basis of Melting-Recrystallization Cycles

In addition to physical and chemical bonding, physical transitions can result in self-healing in biocomposites. For example, in order to prepare a multifunctional composite, PDAP particles as the filler (5 wt%) and poly(ϵ -caprolactone) (PCL) as matrix were used. PCL was grafted on the PDAPs surface to ensure the fillers have strong interfaces with the matrix [97]. PDAP particles are bio-based particles obtained from animal or plant-based dopamine [98].

As heating leads to deformation in the shape of the composite, the light-induced healing of PDAP/PCL composites was used via the melting-recrystallization mechanism. This mechanism constitutes two steps: (a) melting of crystals, which happens due the presence of the hot-spots with temperatures up to melting temperature of the matrix, and subsequent diffusion of polymer chains through the cracks, and (b) recrystallization of the fused chains as a result of cooling to crystallization temperature [40]. Comparing the tensile properties of the pristine and the healed composites showed that the mechanical properties of healed composites increased slightly in terms of tensile strength and modulus, while elongation at break was decreased, suggesting that the healed composite is comparable with the pristine composite in terms of tensile properties [97].

6 Summary and Outlook

It is well known that most polymeric composites consist of petrochemical-based materials. Although the properties of synthetic materials can be more tunable, considering the declining fossil sources, global warming, and other environmental concerns, it is dire to outline a future where composites containing petrochemical- and non-sustainable-based materials consist the majority of goods. Also, inspired by nature and the mechanisms mother Erath utilizes to repair bio-based materials which can be re-used after failure, non-disposable goods are preferred at households, medical field, and industry. Accordingly, researchers have been attempting to prepare composites comprised of sustainable resources which are also self-healable. These materials can be self-healable by intrinsic or extrinsic mechanisms. The intrinsic self-healable composites can heal based on their chemistry; DA and retro DA reactions, hydrogen bonds, supramolecular polymers and non-covalent bonds can endow composites intrinsic self-healing. As for extrinsic self-healing, polymerization needs to be carried out inside the composite upon the failure; the materials needed for the polymerization are embedded in the composite using different methods, for example, microcapsulation. Upon the formation of cracks, the parcels dispersed in the matrix rupture and the materials filled in them react with materials contained in the matrix to polymerize and heal the cracks.

For future studies, researchers can look forward to improving the self-healing efficiency of composites produced, preparing composites based on intrinsic self-healing pathway consisted from other renewable polymers, increasing the healing cycles for extrinsic-based composites, and for all composites, decreasing the costs.

References

1. Yuan YC, Yin T, Rong MZ, Zhang MQ (2008) Self healing in polymers and polymer composites. Concepts, realization and outlook: a review. *Express Polym Lett* 2:238–250
2. Ghosh SK (2009) Self-healing materials: fundamentals, design strategies, and applications. In: Ghosh SK (ed) *Self-healing materials*, 1st edn. Wiley-VCH, Weinheim, pp 1–28
3. Rezakazemi M, Dashti A, Asghari M, Shirazian S (2017) H₂-selective mixed matrix membranes modeling using ANFIS, PSO-ANFIS, GA-ANFIS. *Int J Hydrogen Energy* 42:15211–15225. <https://doi.org/10.1016/j.ijhydene.2017.04.044>
4. Rezakazemi M, Shahidi K, Mohammadi T (2012) Sorption properties of hydrogen-selective PDMS/zeolite 4A mixed matrix membrane. *Int J Hydrogen Energy* 37:17275–17284. <https://doi.org/10.1016/j.ijhydene.2012.08.109>
5. Rezakazemi M, Shahidi K, Mohammadi T (2015) Synthetic PDMS composite membranes for pervaporation dehydration of ethanol. *Desalin Water Treat* 54:1542–1549. <https://doi.org/10.1080/19443994.2014.887036>
6. Rezakazemi M, Vatani A, Mohammadi T (2016) Synthesis and gas transport properties of crosslinked poly(dimethylsiloxane) nanocomposite membranes using octatrimethylsiloxy POSS nanoparticles. *J Nat Gas Sci Eng* 30:10–18. <https://doi.org/10.1016/j.jngse.2016.01.033>
7. Rezakazemi M, Vatani A, Mohammadi T (2015) Synergistic interactions between POSS and fumed silica and their effect on the properties of crosslinked PDMS nanocomposite membranes. *RSC Adv* 5:82460–82470. <https://doi.org/10.1039/C5RA13609A>
8. Rezakazemi M, Shahidi K, Mohammadi T (2012) Hydrogen separation and purification using crosslinkable PDMS/zeolite A nanoparticles mixed matrix membranes. *Int J Hydrogen Energy* 37:14576–14589. <https://doi.org/10.1016/j.ijhydene.2012.06.104>
9. Rezakazemi M, Sadrzadeh M, Matsuura T (2018) Thermally stable polymers for advanced high-performance gas separation membranes. *Prog Energy Combust Sci* 66:1–41. <https://doi.org/10.1016/j.peccs.2017.11.002>
10. Rezakazemi M, Sadrzadeh M, Mohammadi T, Matsuura T (2017) Methods for the preparation of organic-inorganic nanocomposite polymer electrolyte membranes for fuel cells
11. Thakur VK, Kessler MR (2015) Self-healing polymer nanocomposite materials: a review. *Polym (United Kingdom)* 69:369–383. <https://doi.org/10.1016/j.polymer.2015.04.086>
12. Su CC, Chen JS (2017) Self-healing polymeric materials. *Key Eng Mater* 727:482–489. <https://doi.org/10.4028/www.scientific.net/KEM.727.482>
13. Burattini S, Greenland BW, Chappell D et al (2010) Healable polymeric materials: a tutorial review. *Chem Soc Rev* 39:1973–1985. <https://doi.org/10.1039/b904502n>
14. Kloxin CJ (2013) Reversible covalent bond formation as a strategy for healable polymer networks. *Heal Polym Syst* 62–91. <https://doi.org/10.1039/9781849737470-00062>
15. Hart LR, Harries JL, Greenland BW et al (2013) Healable supramolecular polymers. *Polym Chem* 4:4860. <https://doi.org/10.1039/c3py00081h>
16. Herbst F, Döhler D, Michael P, Binder WH (2013) Self-healing polymers via supramolecular forces. *Macromol Rapid Commun* 34:203–220. <https://doi.org/10.1002/marc.201200675>
17. Mülhaupt R (2013) Green polymer chemistry and bio-based plastics: dreams and reality. *Macromol Chem Phys* 214:159–174

18. Yang Z, Hollar J, He X, Shi X (2011) A self-healing cementitious composite using oil core/silica gel shell microcapsules. *Cem Concr Compos* 33:506–512. <https://doi.org/10.1016/j.cemconcomp.2011.01.010>
19. Fornasiero P, Graziani M (2007) *Renewable resources and renewable energy: a global challenge*, 2nd edn. CRC Press, Boca Raton
20. Iqbal HMN, Kyazze G, Tron T, Keshavarz T (2014) “One-pot” synthesis and characterisation of novel P(3HB)–ethyl cellulose based graft composites through lipase catalysed esterification. *Polym Chem* 5:7004–7012. <https://doi.org/10.1039/c4py00857j>
21. Srubar WV, Pilla S, Wright ZC et al (2012) Mechanisms and impact of fiber-matrix compatibilization techniques on the material characterization of PHBV/oak wood flour engineered biobased composites. *Compos Sci Technol* 72:708–715. <https://doi.org/10.1016/j.compscitech.2012.01.021>
22. Yang B, Zhang Y, Zhang X et al (2012) Facilely prepared inexpensive and biocompatible self-healing hydrogel: a new injectable cell therapy carrier. *Polym Chem* 3:3235–3238
23. Ding F, Shi X, Wu S et al (2017) Flexible polysaccharide hydrogel with pH-regulated recovery of self-healing and mechanical properties. *Macromol Mater Eng* 302:1–9. <https://doi.org/10.1002/mame.201700221>
24. Desai KGH, Schwendeman SP (2013) Active self-healing encapsulation of vaccine antigens in PLGA microspheres. *J Control Release* 165:62–74. <https://doi.org/10.1016/j.jconrel.2012.10.012>
25. Kim JR, Netravali AN (2016) Self-healing properties of protein resin with soy protein isolate-loaded poly(d, l-lactide-co-glycolide) microcapsules. *Adv Funct Mater* 26:4786–4796. <https://doi.org/10.1002/adfm.201600465>
26. Yabuki A, Sakai M (2011) Self-healing coatings of inorganic particles using a pH-sensitive organic agent. *Corros Sci* 53:829–833. <https://doi.org/10.1016/j.corsci.2010.11.021>
27. Palin D, Wiktor V, Jonkers HM (2016) A bacteria-based bead for possible self-healing marine concrete applications. *Smart Mater Struct* 25:1–6. <https://doi.org/10.1088/0964-1726/25/8/084008>
28. Merindol R, Diabang S, Felix O et al (2015) Bio-inspired multiproperty materials: strong, self-healing, and transparent artificial wood nanostructures. *ACS Nano* 9:1127–1136. <https://doi.org/10.1021/nm504334u>
29. Abilash N, Sivapragash M (2011) Assesment of self healing property in hybrid fiber polymeric composite. *Int J Eng Sci* 3:5430–5436
30. Hatami Boura S, Peikari M, Ashrafi A, Samadzadeh M (2012) Self-healing ability and adhesion strength of capsule embedded coatings—micro and nano sized capsules containing linseed oil. *Prog Org Coatings* 75:292–300. <https://doi.org/10.1016/j.porgcoat.2012.08.006>
31. Samadzadeh M, Boura SH, Peikari M et al (2011) Tung oil: AN autonomous repairing agent for self-healing epoxy coatings. *Prog Org Coatings* 70:383–387. <https://doi.org/10.1016/j.porgcoat.2010.08.017>
32. Chaudhari AB, Tatiya PD, Hedao RK et al (2013) Polyurethane prepared from neem oil polyesteramides for self-healing anticorrosive coatings. *Ind Eng Chem Res* 52:10189–10197. <https://doi.org/10.1021/ie401237s>
33. Wu DY, Meure S, Solomon D (2008) Self-healing polymeric materials: a review of recent developments. *Prog Polym Sci* 33:479–522. <https://doi.org/10.1016/j.progpolymsci.2008.02.001>
34. Aida T, Meijer EW, Stupp SI (2012) Functional supramolecular polymers. *Science* (80-) 335:813–817
35. Schmuck C, Wienand W (2001) Self-complementary quadruple hydrogen-bonding motifs as a functional principle: from dimeric supramolecules to supramolecular Polymers. *Angew Chemie Int Ed* 40:4363–4369. [https://doi.org/10.1002/1521-3773\(20011203\)40](https://doi.org/10.1002/1521-3773(20011203)40)
36. Han D, Yan L (2014) Supramolecular hydrogel of chitosan in the presence of graphene oxide nanosheets as 2D cross-linkers. *ACS Sustain Chem Eng* 2:296–300. <https://doi.org/10.1021/sc400352a>

37. Lin L-J, Larsson M, Liu D-M (2011) A novel dual-structure, self-healable, polysaccharide based hybrid nanogel for biomedical uses. *Soft Matter* 7:5816. <https://doi.org/10.1039/c1sm05249g>
38. Wang L, Zhang X, Xiong H, Wang S (2010) A novel nitromethane biosensor based on biocompatible conductive redox graphene-chitosan/hemoglobin/graphene/room temperature ionic liquid matrix. *Biosens Bioelectron* 26:991–995. <https://doi.org/10.1016/j.bios.2010.08.027>
39. Beijer FH, Sijbesma RP, Kooijman H et al (1998) Strong dimerization of ureidopyrimidones via quadruple hydrogen bonding. *J Am Chem Soc* 120:6761–6769. <https://doi.org/10.1021/ja974112a>
40. Söntjens SHM, Sijbesma RP, Van Genderen MHP, Meijer EW (2000) Stability and lifetime of quadruply hydrogen bonded 2-Ureido-4[1H]-pyrimidinone dimers. *J Am Chem Soc* 122:7487–7493. <https://doi.org/10.1021/ja000435m>
41. Bosman AW, Sijbesma RP, Meijer EW (2004) Supramolecular polymers at work. *Mater Today* 7:34–39. [https://doi.org/10.1016/S1369-7021\(04\)00187-7](https://doi.org/10.1016/S1369-7021(04)00187-7)
42. Phadke A, Zhang C, Arman B et al (2012) Rapid self-healing hydrogels. *Proc Natl Acad Sci* 109:4383–4388. <https://doi.org/10.1073/pnas.1201122109>
43. Feldman KE, Kade MJ, De Greef TFA et al (2008) Polymers with multiple hydrogen-bonded end groups and their blends. *Macromolecules* 41:4694–4700. <https://doi.org/10.1021/ma800375r>
44. Cui J, del Campo A (2012) Multivalent H-bonds for self-healing hydrogels. *Chem Commun* 48:9302. <https://doi.org/10.1039/c2cc34701f>
45. Biyani MV, Foster EJ, Weder C (2013) Light-healable supramolecular nanocomposites based on modified cellulose nanocrystals. *ACS Macro Lett* 2:236–240
46. Schubert US, Eschbaumer C, Hien O, Andres PR (2001) 4'-Functionalized 2,2':6',2"-terpyridines as building blocks for supramolecular chemistry and nanoscience. *Tetrahedron Lett* 42:4705–4707. [https://doi.org/10.1016/S0040-4039\(01\)00796-1](https://doi.org/10.1016/S0040-4039(01)00796-1)
47. Kersey FR, Loveless DM, Craig SL (2007) A hybrid polymer gel with controlled rates of cross-link rupture and self-repair. *J R Soc Interface* 4:373–380. <https://doi.org/10.1098/rsif.2006.0187>
48. Gohy JF, Lohmeijer BGG, Schubert US (2002) Reversible metallo-supramolecular block copolymer micelles containing a soft core. *Macromol Rapid Commun* 23:555–560. [https://doi.org/10.1002/1521-3927\(20020601\)23:9<555::aid-marc555>3.0.co;2-k](https://doi.org/10.1002/1521-3927(20020601)23:9<555::aid-marc555>3.0.co;2-k)
49. Coulibaly S, Roulin A, Balog S et al (2014) Reinforcement of optically healable supramolecular polymers with cellulose nanocrystals. *Macromolecules* 47:152–160. <https://doi.org/10.1021/ma402143c>
50. Burattini S, Colquhoun HM, Fox JD et al (2009) A self-repairing, supramolecular polymer system: healability as a consequence of donor–acceptor π – π stacking interactions. *Chem Commun* 6717. <https://doi.org/10.1039/b910648k>
51. Burattini S, Greenland BW, Merino DH et al (2010) A healable supramolecular polymer blend based on aromatic π – π stacking and hydrogen-bonding interactions. *J Am Chem Soc* 132:12051–12058. <https://doi.org/10.1021/ja104446r>
52. Fox J, Wie JJ, Greenland BW et al (2012) High-strength, healable, supramolecular polymer nanocomposites. *J Am Chem Soc* 134:5362–5368. <https://doi.org/10.1021/ja300050x>
53. Xu C, Cao L, Lin B et al (2016) Design of self-healing supramolecular rubbers by introducing ionic cross-links into natural rubber via a controlled vulcanization. *ACS Appl Mater Interfaces* 8:17728–17737. <https://doi.org/10.1021/acsami.6b05941>
54. Sordo F, Mougner SJ, Loureiro N et al (2015) Design of self-healing supramolecular rubbers with a tunable number of chemical cross-links. *Macromolecules* 48:4394–4402. <https://doi.org/10.1021/acs.macromol.5b00747>
55. Cragg Peter J (2010) *Supramolecular chemistry, from biological inspiration to biomedical applications*, 1st edn. Springer, New York

56. McKee JR, Appel EA, Seitonen J et al (2014) Healable, stable and stiff hydrogels: combining conflicting properties using dynamic and selective three-component recognition with reinforcing cellulose nanorods. *Adv Funct Mater* 24:2706–2713. <https://doi.org/10.1002/adfm.201303699>
57. Peterson AM, Jensen RE, Palmese GR (2011) Thermoreversible and remendable glass-polymer interface for fiber-reinforced composites. *Compos Sci Technol* 71:586–592. <https://doi.org/10.1016/j.compscitech.2010.11.022>
58. Surajmal M (2013) Introduction to diels alder reaction, its mechanism and recent advantages: a review. *Indo Am J Pharm Res* 3:3192–3215
59. Zhang W, Duchet J, Gérard JF (2014) Self-healable interfaces based on thermo-reversible diels-alder reactions in carbon fiber reinforced composites. *J Colloid Interface Sci* 430:61–68. <https://doi.org/10.1016/j.jcis.2014.05.007>
60. Barthel MJ, Rudolph T, Crotty S et al (2012) Homo- and diblock copolymers of poly(furfuryl glycidyl ether) by living anionic polymerization: toward reversibly core-crosslinked micelles. *J Polym Sci, Part A: Polym Chem* 50:4958–4965. <https://doi.org/10.1002/pola.26327>
61. Gandini A, Hodge P (1998) Application of the diels—alder reaction to polymers bearing furan moieties. 2. Diels—alder and retro-diels—alder reactions involving furan rings in some styrene copolymers. *Macromolecules* 1:314–321
62. Wu S, Li J, Zhang G et al (2016) High mechanical strength and high dielectric graphene/polyurethane composites healed by near infrared laser. In: 2016 17th international conference on electronic packaging technology ICEPT 2016, pp 157–161. <https://doi.org/10.1109/icept.2016.7583110>
63. Li Q-T, Jiang M-J, Wu G, Chen L, Chen S-C, Cao Y-X, Wang Y-Z (2017) Photothermal conversion triggered precisely targeted healing of epoxy resin based on thermo-reversible dielsalder network and amino-functionalized carbon nanotubes. *ACS Appl Mater Interfaces* 9:20797–20807
64. Wu S, Li J, Zhang G et al (2017) Ultrafast self-healing nanocomposites via infrared laser and their application in flexible electronics. *ACS Appl Mater Interfaces* 9:3040–3049. <https://doi.org/10.1021/acsami.6b15476>
65. Gong C, Liang J, Hu W et al (2013) A healable, semitransparent silver nanowire-polymer composite conductor. *Adv Mater* 25:4186–4191. <https://doi.org/10.1002/adma.201301069>
66. Pratama PA, Sharifi M, Peterson AM, Palmese GR (2013) Room temperature self-healing thermoset based on the diels-alder reaction. *ACS Appl Mater Interfaces* 5:12425–12431. <https://doi.org/10.1021/am403459e>
67. Xavier A, Srividhya N (2014) Synthesis and study of Schiff base ligands 7:6–15
68. Hussain Z, Khalaf M, Adil H et al. Metal complexes of Schiff's bases containing sulfonamides nucleus. *Res J Pharm Biol Chem Sci* 7:1008–1025
69. Li QT, Jiang MJ, Wu G et al (2017) Photothermal conversion triggered precisely targeted healing of epoxy resin based on thermoreversible diels-alder network and amino-functionalized carbon nanotubes. *ACS Appl Mater Interfaces* 9:20797–20807. <https://doi.org/10.1021/acsami.7b01954>
70. Yang Y, Pei Z, Zhang X et al (2014) Carbon nanotube–vitrimers composite for facile and efficient photo-welding of epoxy. *Chem Sci* 5:3486–3492. <https://doi.org/10.1039/C6SC90083F>
71. Wu M, Li Y, An N, Sun J (2016) Applied voltage and near-infrared light enable healing of superhydrophobicity loss caused by severe scratches in conductive superhydrophobic films. *Adv Funct Mater* 26:6777–6784. <https://doi.org/10.1002/adfm.201601979>
72. Li J, Liang J, Li L et al (2014) Healable capacitive touch screen sensors based on transparent composite electrodes comprising silver nanowires and a Furan/Maleimide diels-alder cycloaddition polymer. *ACS Nano* 8:12874–12882
73. Wu HF, Dwight DW, Huff NT (1997) Effects of silane coupling agents on the interphase and performance of glass-fiber-reinforced polymer composites. *Compos Sci Technol* 57:975–983. [https://doi.org/10.1016/S0266-3538\(97\)00033-X](https://doi.org/10.1016/S0266-3538(97)00033-X)

74. Hodzic A, Kalyanasundaram S, Kim JK et al (2001) Application of nano-indentation, nano-scratch and single fibre tests in investigation of interphases in composite materials. *Micron* 32:765–775. [https://doi.org/10.1016/S0968-4328\(00\)00084-6](https://doi.org/10.1016/S0968-4328(00)00084-6)
75. Zhang Y, Yang B, Zhang X et al (2012) A magnetic self-healing hydrogel. *Chem Commun* 48:9305. <https://doi.org/10.1039/c2cc34745h>
76. Zeng Q, Desai MS, Jin HE et al (2016) Self-healing elastin-bioglass hydrogels. *Biomacromol* 17:2619–2625. <https://doi.org/10.1021/acs.biomac.6b00621>
77. Wei Z, Yang JH, Liu ZQ et al (2015) Novel biocompatible polysaccharide-based self-healing hydrogel. *Adv Funct Mater* 25:1352–1359. <https://doi.org/10.1002/adfm.201401502>
78. Haldar U, Bauri K, Li R et al (2015) Polyisobutylene-based pH-responsive self-healing polymeric gels. *ACS Appl Mater Interfaces* 7:8779–8788. <https://doi.org/10.1021/acsami.5b01272>
79. Yuan YC, Rong MZ, Zhang MQ et al (2008) Self-healing polymeric materials using epoxy/Mercaptan as the healant. *Macromolecules* 41:5197–5202. <https://doi.org/10.1021/ma800028d>
80. Porter R, Mile JB (1984) Extended control of marine fouling—formulation of a microencapsulated liquid organometallic biocide and vinyl rosin paint. *Appl Biochem Biotechnol* 9:439–445. <https://doi.org/10.1007/bf02798398>
81. Yeom CK, Kim YH, Lee JM (2002) Microencapsulation of water-soluble herbicide by interfacial reaction. II. Release properties of microcapsules. *J Appl Polym Sci* 84:1025–1034. <https://doi.org/10.1002/app.10383>
82. Wei H, Wang Y, Guo J et al (2015) Advanced micro/nanocapsules for self-healing smart anticorrosion coatings. *J Mater Chem A* 3:469–480. <https://doi.org/10.1039/C4TA04791E>
83. Zhu DY, Rong MZ, Zhang MQ (2015) Self-healing polymeric materials based on microencapsulated healing agents: from design to preparation. *Prog Polym Sci* 49–50:175–220. <https://doi.org/10.1016/j.progpolymsci.2015.07.002>
84. Wang H, Zhou Q (2018) Evaluation and failure analysis of linseed oil encapsulated self-healing anticorrosive coating. *Prog Org Coatings* 118:108–115. <https://doi.org/10.1016/j.porgcoat.2018.01.024>
85. Li H, Cui Y, Wang H et al (2017) Preparation and application of polysulfone microcapsules containing tung oil in self-healing and self-lubricating epoxy coating. *Colloids Surfaces A Physicochem Eng Asp* 518:181–187
86. Marathe R, Tatiya P, Chaudhari A et al (2015) Neem acetylated polyester polyol—renewable source based smart PU coatings containing quinoline (corrosion inhibitor) encapsulated polyurea microcapsules for enhance anticorrosive property. *Ind Crops Prod* 77:239–250
87. Ataei S, Khorasani SN, Torkaman R et al (2018) Self-healing performance of an epoxy coating containing microencapsulated alkyd resin based on coconut oil. *Prog Org Coatings* 120:160–166. <https://doi.org/10.1016/j.porgcoat.2018.03.024>
88. Jadhav RS, Hundiware DG, Mahulikar PP (2011) Synthesis and characterization of phenol-formaldehyde microcapsules containing linseed oil and its use in epoxy for self-healing and anticorrosive coating. *J Appl Polym Sci* 119:2911–2916. <https://doi.org/10.1002/app.33010>
89. Suryanarayana C, Rao KC, Kumar D (2008) Preparation and characterization of microcapsules containing linseed oil and its use in self-healing coatings. *Prog Org Coatings* 63:72–78. <https://doi.org/10.1016/j.porgcoat.2008.04.008>
90. Tatiya PD, Hedao RK, Mahulikar PP, Gite VV (2013) Novel polyurea microcapsules using dendritic functional monomer: synthesis, characterization, and its use in self-healing and anticorrosive polyurethane coatings. *Ind Eng Chem Res* 52:1562–1570. <https://doi.org/10.1021/ie301813a>
91. Subramanian N (2013) Understanding corrosion and cathodic protection of reinforced concrete structures
92. Lau K, Sagüés AA, Powers RG (2007) Long-term corrosion behavior of epoxy coated rebar in Florida Bridges. Houston, TX

93. Chen Y, Xia C, Shepard Z et al (2017) Self-healing coatings for steel-reinforced concrete. *ACS Sustain Chem Eng* 5:3955–3962. <https://doi.org/10.1021/acssuschemeng.6b03142>
94. Wertz JT, Mauldin TC, Boday DJ (2014) Polylactic acid with improved heat deflection temperatures and self-healing properties for durable goods applications. *ACS Appl Mater Interfaces* 6:18511–18516. <https://doi.org/10.1021/am5058713>
95. Trask RS, Williams HR, Bond IP (2007) Self-healing polymer composites: mimicking nature to enhance performance. *Bioinspiration and Biomimetics* 2. <https://doi.org/10.1088/1748-3182/2/1/p01>
96. Samadzadeh M, Boura SH, Peikari M et al (2010) A review on self-healing coatings based on micro/nanocapsules. *Prog Org Coatings* 68:159–164. <https://doi.org/10.1016/j.porgcoat.2010.01.006>
97. Xiong S, Wang Y, Zhu J et al (2016) Poly(ϵ -caprolactone)-grafted polydopamine particles for biocomposites with near-infrared light triggered self-healing ability. *Polymer (Guildf)* 84:328–335. <https://doi.org/10.1016/j.polymer.2016.01.005>
98. Ju KY, Lee Y, Lee S et al (2011) Bioinspired polymerization of dopamine to generate melanin-like nanoparticles having an excellent free-radical-scavenging property. *Biomacromol* 12:625–632. <https://doi.org/10.1021/bm101281b>
99. Coope TS, Mayer UFJ, Wass DF et al (2011) Self-healing of an epoxy resin using Scandium (III) Triflate as a catalytic curing agent, pp 4624–4631. <https://doi.org/10.1002/adfm.201101660>

Chemical Modification of Lignin and Its Environmental Application



Zhili Li, Yuanyuan Ge, Jiubing Zhang, Duo Xiao and Zijun Wu

1 Introduction

Lignin constitutes one of the main component of lignocellulosic biomass (15–30% by weight), which is second only to cellulose in mass on the earth. Lignin acts as the essential glue that gives plants their structural integrity and resistance against microbial, chemical attack and prevents other outside stresses from destroying the structure of plant cell walls [1]. Lignin is a complex and recalcitrant phenolic macromolecule composed of three phenylpropane units: p-hydroxyphenyl (H), guaiacyl (G), and syringyl (S), cross-linked by β -o-4, α -o-4, β - β , and 5-5' bonds etc. (as depicted in Fig. 1). Among them, the main linkage is the β -o-4 bond, about 40–60% of all inter-unit linkages in lignin belong to this bond [2]. The component and structural characterizations of lignin are quite different even it is separated from the same plant. It is to say, the lignin obtained from a plant is a mixture of different lignin polymers which is dependent on the source plant, species, and growing ages of the plant, such as softwood, hardwood, and grass [3].

A large quantity of technical lignin was produced as a main component in black liquor by the pulp and papering industry, which is a big threat to the environment [4]. It is estimated that the global annual production of technical lignin in pulp making is *ca.* 70 million tons, much of which is consumed as a low-value fuel. Although there are some other applications, such as a binder or dispersing agent, no large-scale application has so far been found [4]. Lignin has significant potential as a source for the production of the bio-renewable polymer [5, 6]. The main active sites of lignin are comprised of phenolic or alcoholic hydroxyl groups, which accounts for its

Z. Li (✉) · Y. Ge (✉) · J. Zhang · D. Xiao · Z. Wu
School of Chemistry and Chemical Engineering, Guangxi University,
100 Daxuedong Road, Nanning 530004, China
e-mail: lizhili@gxu.edu.cn

Y. Ge
e-mail: geyy@gxu.edu.cn

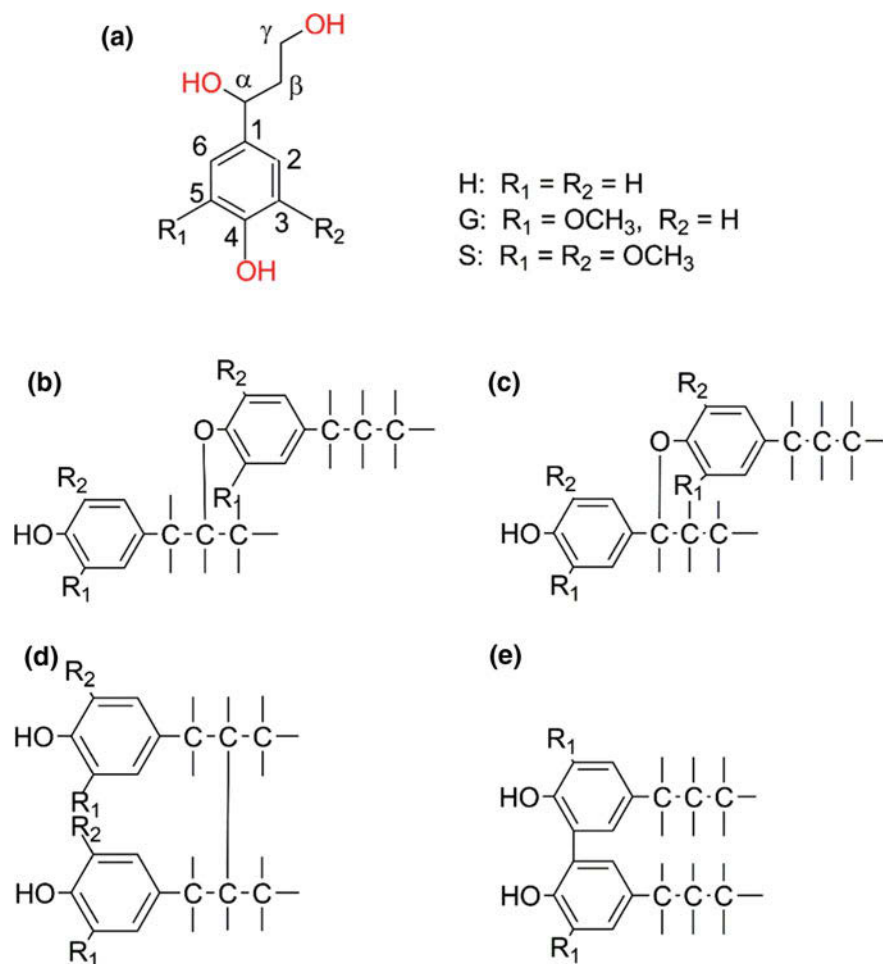


Fig. 1 a The phenylpropane type units: p-hydroxyphenyl (H), guaiacyl (G), and syringyl (S); and b β -o-4, c α -o-4, d β - β , and e 5-5' linkages in lignin

reactivity, hydrophilicity as well as other chemical and physical attributes of lignin [2]. Recently, due to the unique polyphenol structure, chemical stability and wide availability, different kinds of adsorbents, particularly for dyes and heavy metals removal from wastewater are potentially obtainable from lignin [7].

Water pollution by different kinds of contaminants is currently serious concerned [8–13]. A large amount of organic, inorganic, and biological compounds have been reported as water contaminants. For example, the dyes, particularly azo dyes are recalcitrant molecules and resistant to aerobic digestion and are also stable to oxidizing agents that makes them being hard to treat [14]. The heavy metals, lead (Pb), mercury (Hg), cadmium (Cd), chromium (Cr) and arsenic (As), etc., are

notorious with high toxicity and carcinogenicity. These toxic pollutants, even with a trace amount in water, can pollute water resources and transfer throughout the food chain to accumulate in animals and mankind, causing various diseases and disorders [15]. Therefore, the pollutants should be removed before its discharge into the environment.

Several physical and chemical treatment techniques have been reported for the removal of pollutants from wastewater, including precipitation, oxidation, biodegradation, ion exchange, adsorption [16], membrane separation [17–19], coagulation and flocculation, flotation, electrochemical methods. These methods still suffer from the limitations of low effectiveness and high cost.

Adsorption using cost-effective adsorbents is now considered as an efficient, convenient and economical method for wastewater treatment, due to the feasibility in design and operation, effectiveness in treating and the recyclability of the adsorbents [20, 21]. Activated carbon (AC) is being recognized as one of the most popular adsorbents used in the removal of contaminants from water. However, AC is of high capital cost due to the prolong production process [22]. In recent years, the development of various environmentally friendly adsorbents from biomass, biopolymers, especially the natural-occurring polymers, including cellulose, lignin, and chitosan, etc., has been intensified [23–25]. It could be seen from the literature that the adsorption of dyes and heavy metals using lignin is one of the most reported methods for the removal of contaminants from water [26–28].

Unfortunately, original lignin is less competitive in adsorption applications due to the low adsorption capability, and lignin does not own specific selectivity for a certain kind of pollutant from complex polluted water [29, 30]. The goal for the lignin modification for pollutants adsorption is to promote the adsorption capability, including adsorption capacity, stability, selectivity and recyclability [15]. The ease of separation from wastewater after the operation and the cost-effectiveness of the adsorbents should also be considered. The modification of lignin could be achieved by various methods including crosslinking, hybridization, hydrogen bonding formation, condensation, grafting and copolymerization [31]. Therefore, the main objective of this article is to collect and compile the most recent reported literature regarding the modified lignin for adsorption applications and to discuss the advantageous and disadvantageous issues of the resulting lignin as an adsorbent to remove o different environmental pollutants from the aqueous phase.

2 Modified Lignin for Dyes Adsorption

Dyes contaminated wastewater is hard to treat because of their inert properties and the residual trace amount of dyes in water. Recently, adsorption techniques using modified lignin have been widely reported in removing dyes as a promising wastewater treatment process. The dyes adsorption capacities of the modified lignin-based adsorbents are tabulated in Table 1. And the modified lignin-based materials for removing dyes will be fully discussed in the following section.

Table 1 Reported modified lignin for adsorption of dyes in water

Modified lignin	Dye	T (°C)/pH	Q _m (mg/g)	Reference
Chitosan-alkali lignin	RBBR	27/5.9	111.11	[32]
ALiCE	MB	20/7.0	36.25	[33]
Chitin/lignin hybrid	DB71	20–50/2.4–8.4	40.0	[28]
CAML	C-3R	RT/4.0–10	99.3%	[34]
	MO		67.0%	
LBF	RB	–/2.0–10	93%	[34]
MLS	MB	40/–	31.23	[35]
	RB		17.62	
Oxidized lignin	EV	30/7.0	70–80 wt%	[36]
	BB		80–95 wt%	
ALR	CV	25/3.0–12	150.4	[37]
Lignin-g-p(AM-co-NIPAM)/MMT	MB	25/1.0–11.0	9646.9	[38]
LS-g-AA	MB	30/3.0–8.0	2013	[39]
LPUF	MG	25–65/2.0–9.0	80	[40]
AAL	MB	30/5.0	63.3	[41]
Lignin sulfonate polymer	MG	30/7.0	60.2	[42]
LSMMs	MG	24/3.0–7.0	150.3	[43]
The hydrogel of acylated hemicelluloses, acrylic acid and lignosulfonate	MB	30–70/7.0–10	2691	[44]
Hydrogel of kraft lignin- <i>N</i> -isopropyl acrylamide	MB	15–45/1.0–11	–	[45]
CML-Al	PB	25/2.0	73.52	[46]
CML-Mn			55.16	
CML-Fe	BR-2	25/2.0	73.6	[47]

Nair et al. [32] reported a novel chitosan-alkali lignin composite prepared from chitosan and alkali lignin (as shown in Fig. 2). The weak interactions between β -1,4-glycosidic linkage, amide and hydroxyl groups of chitosan, and ether, an aromatic ring and hydroxyl groups of alkali lignin, impart enhanced surface and chemical properties to the composite than chitosan and alkali lignin. The composite with 50:50 chitosan: alkali lignin exhibited maximum adsorption (111.11 mg/g) of Remazol Brilliant Blue R (RBBR) compared to chitosan (76.92 mg/g), which showed that the composite exhibits 33% improvement in the maximum adsorption amount. Batch adsorption of RBBR on the composite followed the Langmuir equation, while the dynamic adsorption followed the pseudo-second-order equation. A lignin-chitosan pellet (ALiCE) was prepared for adsorption of methylene blue (MB) [33]. The results indicated the ALiCE had a maximum adsorption capacity of 36.25 mg/g for MB according to the fitting of the Langmuir equation ($R^2 = 0.997$), yielding. The adsorption kinetic data could be fitted well by the pseudo-second-order-model [33]. A chitin/lignin hybrid biosorbent was prepared

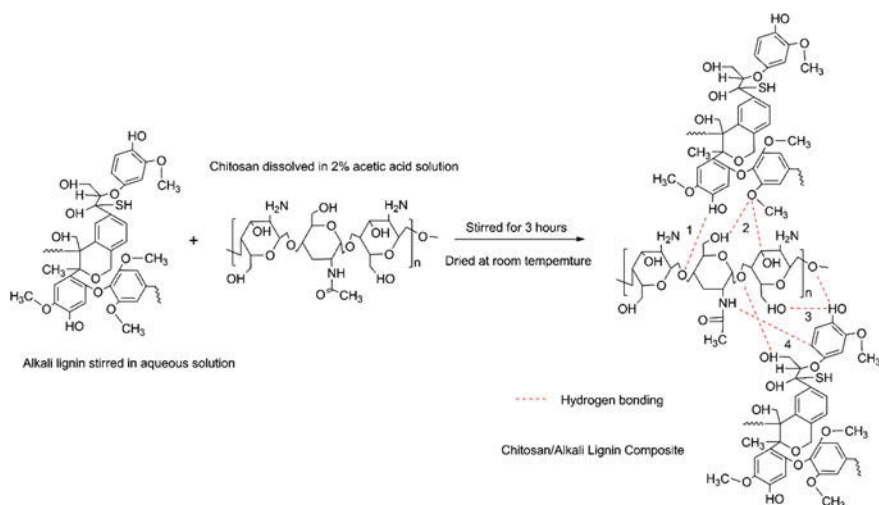


Fig. 2 An illustrative diagram of chitosan-alkali lignin composite. Reprinted with permission [32]. Copyright 2014 Elsevier

and used to adsorb C.I. Direct Blue 71 (DB71) from water [28]. The adsorption capacities of DB71 by the chitin and chitin/lignin hybrid biosorbent were 30.7 and 40 mg/g, respectively, which indicated that the hybrid chitin/lignin material has a stronger adsorptive affinity for DB 71 than the chitin. The adsorption of DB 71 onto the hybrid could be described by the Freundlich equation and the pseudo-second-order equation, respectively. The optimum solution pH for dye removal was in the range 2.4–8.4. The adsorption of DB 71 by the chitin/lignin hybrid was spontaneous and endothermic in nature [28].

Lou et al. [34] developed a ternary graft copolymer based on chitosan, acrylamide, and lignin (CAML) by a microwave-assisted method (as shown in Fig. 3). The copolymer was loosely aggregated powder with a particle size range of 1–3 μm . Adsorption experiment showed that the CAML (chitosan:acrylamide:lignin = 1:1:1) exhibited maximum removal efficiency of 99.3 and 67.0% for reactive orange C-3R and methyl orange, respectively. The CAML had a wide suitable pH range, although the removal efficiency was slightly higher under lower pH values. The removal mechanism was combined charge neutralization and bridging effects [34]. Guo et al. [48] prepared a lignin-based flocculant (LBF) via grafting

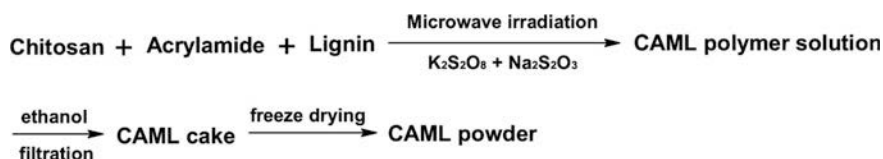


Fig. 3 Synthetic process of CAML. Reprinted with permission [34]. Copyright 2018 Elsevier

dimethyldiallylammonium chloride and acrylamide onto lignin. Adsorption results demonstrated that a high removal efficiency of 93% was achieved for the reactive dye by LBF with the addition of PAC. The high removal efficiency of dye by LBF was because of the electrostatic attraction effect and bridging action [48].

Li et al. [35] prepared magnetic lignin spheres (MLS) from different organosolv lignins with maleic anhydride and Fe_3O_4 nanoparticles. The adsorption amounts of methylene blue and Rhodamine B by the MLS from larch lignin (31.23, and 17.62 mg/g, respectively) were higher than that from poplar lignin (25.95 and 15.79 mg/g, respectively). The adsorption kinetics and isotherm were could be described by the pseudo-second-order equation and Langmuir equation, respectively. Moreover, the MLS from larch and poplar lignin had a good recyclability, after three cycles of adsorption-desorption, the removal efficiencies for the dyes still remained at 98 and 96%, respectively [35].

Couch et al. obtained [36] oxidized lignin products from softwood lignin by using HNO_3 (as shown in Fig. 4). The products were used to remove ethyl violet (EV) and basic blue (BB) dyes from simulated water. The results showed that the dyes removal efficiency was 70–80 wt% for EV and 80–95 wt% for BB within the dyes concentrations of 50 and 400 mg/L. The dye removal was pH and ionic strength dependent. Feng et al. [41] prepared a methylene blue (MB) adsorbent from acetic acid lignin (AAL) via deacetylation in NaOH aqueous solution followed by fractionation in methanol. The maximum adsorption capacity of MB reached to 63.3 mg/g by the AAL. In addition, the adsorption of MB was pH and dosage dependent.

Xu et al. [37] developed an acrylic-lignosulfonate resin (ALR) from calcium lignosulfonate and acrylic acid. The resin had a high surface area of $190.55 \text{ m}^2/\text{g}$ with a porous structure in an average pore diameter of 11.34 nm. The maximum adsorption capacity of crystal violet (CV) by the ALR was $150.40 \pm 4.80 \text{ mg/g}$ at $25 \text{ }^\circ\text{C}$. The kinetic and equilibrium data could be fitted by the pseudo-second-order equation and Freundlich equation, respectively. In addition, the calculation of thermodynamic parameters demonstrated the adsorption of CV on ALR was exothermic and spontaneous in nature.

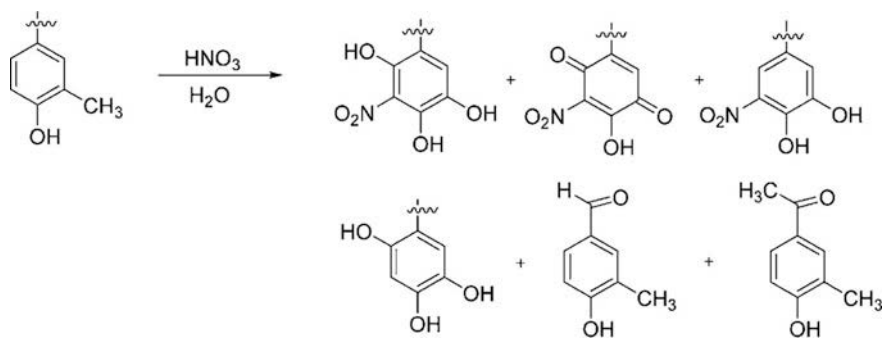


Fig. 4 Scheme of oxidized softwood lignin products. Reprinted with permission [36]. Copyright 2016 American Chemical Society

Wang et al. [38] prepared a hybrid hydrogel from lignin grafted with acrylamide and N-isopropyl acrylamide as well as montmorillonite (lignin-g-p(AM-co-NIPAM)/MMT, as shown in Fig. 5). The prepared hydrogel presented thinner pore walls, good thermal stability and strong mechanical strength due to the existence of montmorillonite. The hydrogel showed an excellent removal efficiency for methylene blue in water, as indicated by the maximum adsorption capacity of 9646.92 mg/g. The adsorption was dependent on the pH and temperature. Dynamic adsorption could be described by the pseudo-second-order equation, while both of the Langmuir and Freundlich equations could describe the equilibrium adsorption. Furthermore, the hydrogel showed an excellent reusability within five adsorption-desorption cycles.

Yu et al. [39] also prepared an LS-g-AA hydrogel by grafting of acrylic acid on lignosulfonate backbone using *N,N'*-methylene-bis-acrylamide and laccase/t-BHP (tert-butyl hydroperoxide) as cross linker and initiator respectively (Fig. 6). The successful grafting of the monomer was confirmed using FTIR. The prepared hydrogel showed a high adsorption capacity of 2013 mg/g for methylene blue (MB) dye in water. Besides, excellent reusability was shown by the LS-g-AA hydrogel with adsorption capacity of 1757 and 1681 mg/g for 3 and 4 cycles, respectively.

Kumari et al. [40] reported a pine needle lignin-based polyurethane foam (LPUF) as an adsorbent of dyes removal from water. The experiment results showed that the LPUF was effective in removing a cationic dye, malachite green (MG) with a maximum adsorption capacity of 80 mg/g, other than an anionic dye, methyl orange (MO), from the water. The adsorption kinetics and isotherms could

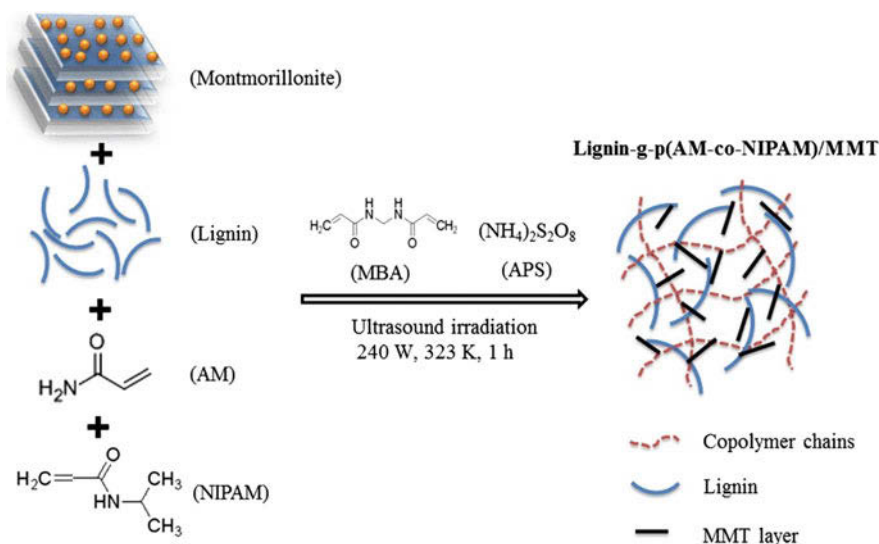


Fig. 5 Diagram of synthesis of lignin-g-p(AM-co-NIPAM)/MMT. Reprinted with permission [38]. Copyright 2017 Elsevier

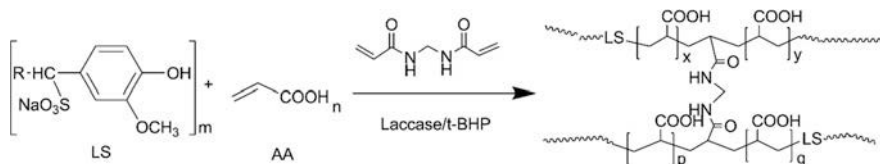


Fig. 6 Synthesis of LS-g-AA hydrogel from lignosulfonate and acrylamide catalyzed by laccase. Reprinted with permission [39]. Copyright 2016 Elsevier

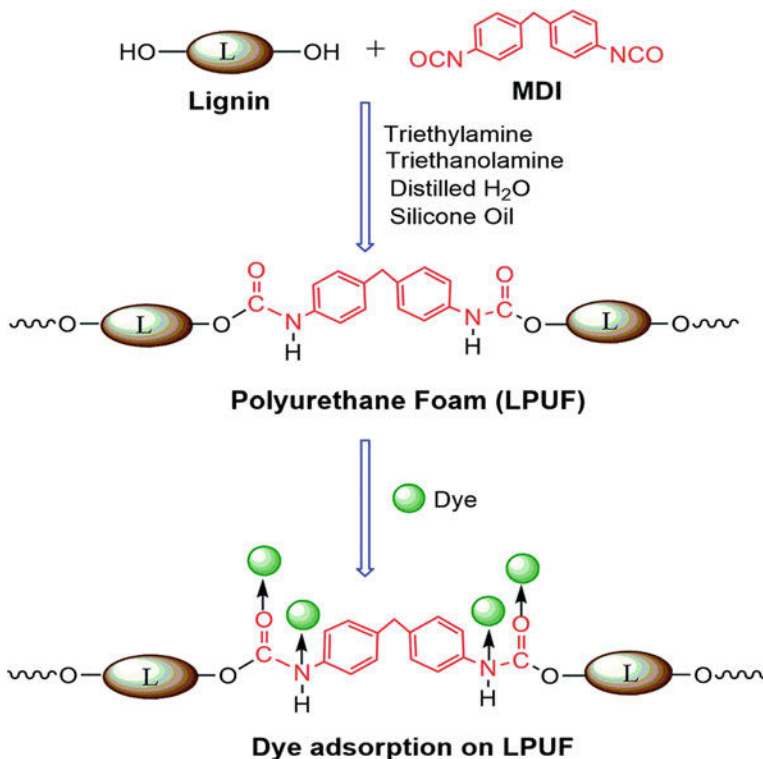


Fig. 7 Schematics of LPUF synthesis and application. Reprinted with permission [40]. Copyright 2016 Royal Society of Chemistry

be described well by the pseudo-second-order equation and Langmuir equation, respectively. Moreover, the LPUF could be used for 20 regeneration cycles with a cumulative adsorption capacity of 1.33 g/g to MG (Fig. 7).

Tang et al. [42] have reported their studies on the preparation of a lignin sulfonate polymer by a simple emulsion polymerization method and the adsorption properties of the lignin sulfonate polymer towards malachite green (MG) dyes (as shown in Fig. 8). The obtained lignin sulfonate polymer showed an effective

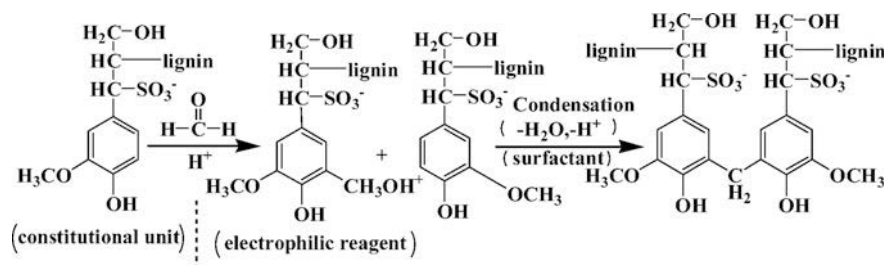


Fig. 8 Schematic diagram of the lignin sulfonate polymer. Reprinted with permission [43]. Copyright 2016 Royal Society of Chemistry

adsorption of MG with a maximum adsorption capacity of 60.2 mg/g for MG according to the Langmuir equation. A Lignosulfonate-based mesoporous material was further prepared by grafting of acrylic acid and acrylamide onto the backbone of lignosulfonate for adsorbing MG from the water. This synthesized material was mesoporous confirmed by using N₂ adsorption/desorption curve. The BET surface area was 118 m²/g and the mesopores are in an average diameter of 3.8 nm. Due to the presence of pores in the mesoporous material, it showed an enhanced adsorption capacity, 150.376 mg/g for MG.

Song et al. [44] prepared a hydrogel consisted of acylated hemicelluloses, acrylic acid, and sodium lignosulfonate by using initiator ammonium persulfate and *N,N,N',N'*-tetramethylethane-1,2-diamine. The honeycomb-like morphology was observed in the prepared hydrogel. The adsorption kinetics of methylene blue (MB) by the hydrogel was fitted well with pseudo-second-order kinetics and the isotherm was fitted well with the Langmuir isotherm model, respectively. The adsorption capacity of MG by the hydrogel could reach to 2691 mg/g. Even after a further cycle, the hydrogel exhibited an approximately 80% adsorption efficiency for MG, and accordingly, it was proposed to be a promising material for dye removal from wastewater [44].

Adebayo et al. prepared carboxyl-methyl lignin CML from the acid hydrolysis lignin from sugarcane bagasse (as shown in Fig. 9) [46]. The CMLs was further bound with Al(III) (CML-Al) and Mn(II) (CML-Mn) for the removal of Procion Blue MX-R (PB) in aqueous solutions. The experiment optimum pH and contact time were 2.0 and 5 h, respectively. The CML-Al and CML-Mn showed a

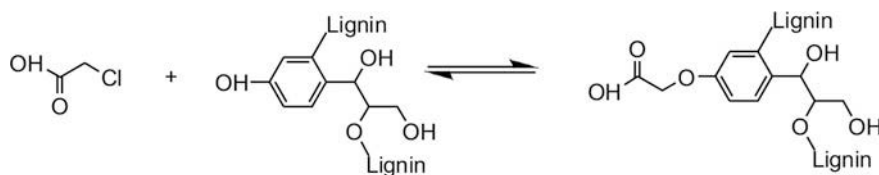


Fig. 9 Schematic of Carboxyl-methyl lignin (CML) from lignin and monochloroacetic acid. Reprinted with permission [46]. Copyright 2014 Elsevier

maximum adsorption capacity of 73.52 and 55.16 mg/g for PB at 25 °C, respectively. 98.33% of CML-Al and 98.08% of CML-Mn could be regenerated from dye-loaded adsorbents by using 50% acetone + 50% of 0.05 mol L⁻¹ NaOH. After four adsorption-desorption cycles, the removal efficiency of the dyes still remained *ca.* 93.97% and *ca.* 75.91% by the CML-Al and CML-Mn, respectively. Silva et al. [47] also reported a carboxy-methylated lignin complexed with Fe³⁺ (CML-Fe) for the adsorption of Brilliant Red 2BE (BR-2) textile dye from aqueous solutions. The maximum adsorption capacity of BR-2 was 73.6 mg/g by the CML-Fe adsorbent. Besides, the dye-loaded adsorbent could be recycled with 0.050 mol/L NaOH.

3 Modified Lignin for Heavy Metals Adsorption

Heavy metal ions are more toxic than dyes and cover a wider region of pollutants during the past decades. Modification of lignin by introducing the desired properties in physical, chemical and mechanic properties is a key issue to achieve proper characters of lignin including the hydrophilicity, hydrophobicity and adsorption ability. The most common strategies in the modification of lignin for heavy metal ion adsorption include amination, methylolation, alkylation, carboxylation, acylation, sulfonation/sulfomethylation, phosphorylation, and copolymerization etc.

Ge et al. [49] prepared an aminated lignin-based adsorbent from alkaline lignin grafted by methylamine and formaldehyde, as shown in Fig. 10. Kinetic adsorption suggested the aminated lignin could adsorb Pb(II) in water quickly and the adsorption process could be described well by a second-order model. The obtained adsorbent presented a maximum adsorption amount of 60.5 mg/g for Pb(II) that was 4.2 fold of the original alkaline lignin. Ge et al. [50] further investigated the influence of numbers of the carbon in an alkyl, from C2 (ethyl) to C18 (octadecyl), on the adsorption capacity of lignin for the lead ion. The results indicated that the carbon number had a strong influence on the adsorption of Pb(II). A suitable carbon number of alkyl (C4) helped the adsorption of Pb(II), due to the electron donating ability of the alkyl groups. Recently, Huang et al. [51] reported a modified enzymatic hydrolysis lignin-containing nitrogen and sulfur moieties, which showed a high adsorption capacity of 180 mg/g for Hg(II) at 25 °C. The adsorption kinetics

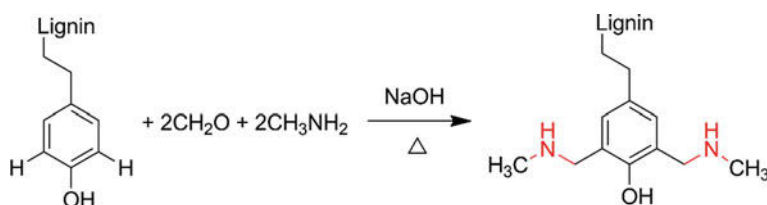


Fig. 10 Synthetic diagram of a Mannich base from lignin. Reprinted with permission [49]. Copyright 2015 Elsevier

could be fitted well with the pseudo-second-order equation, while the adsorption isotherms could be fitted well with the Freundlich equation. Besides, the increasing value of the constant (n) with temperature indicated the adsorption became more favourable at a higher temperature.

Carboxyl is a common component of lignin. The frequency of the group can be adjusted by chemical modifications as well as the hydrophilicity and polyelectrolyte characters. Quintana et al. [52] investigated the oxidized lignins from sulfuric acid pretreated cane bagasse, soda pulping bagasse, eucalypt Kraft lignin and commercial Kraft lignin. The results indicated the oxidized lignins showed higher adsorption capacities than the original lignins, due to the higher contents of carboxyl groups in the oxidized lignins. Peternele et al. [53] reported a functionalized formic lignin from sugarcane bagasse for the adsorption of Pb(II) and Cd(II). Batch adsorption equilibrium could be described well by the Langmuir equation. The oxidative modification of a wheat straw organosolv lignin has been investigated by Dizhbite et al. [54] to introducing $-\text{COOH}$ and $-\text{OH}$ groups. The oxidation was conducted under a polyoxometalate $\text{H}_3[\text{PMo}_{12}\text{O}_{40}]$ and O_2 or H_2O_2 . The oxidative modification did not damage the lignin skeleton, while the carboxyl and hydroxyl group's contents in lignin increased distinctly. As expected, the oxidized lignin showed high adsorption amounts of 35.9 and 155.4 mg/g toward Cd(II) and Pb(II), respectively, at pH 5, 20 °C.

Sulfonate functional groups can be introduced into lignin via sulfomethylation and sulfonation, which has been reported as an effective way to improve the hydrophilicity of lignin [55, 56]. Li et al. [29] prepared a modified lignin-containing both amino and sulfonic groups (as shown in Fig. 11). It was found that the modified lignin could adsorb heavy metals effectively even at low pH values. The dynamic adsorption and equilibrium adsorption could be fitted well by the pseudo-second-order equation and D-R equation, respectively. Xu et al. [57] developed a mesoporous lignin-based biosorbent (MLBB) from rice straw. The MLBB had an excellent adsorption performance for Pb(II) with a maximum capacity of 952 ± 31 mg/g at 20 °C, which was due to the large surface area (186 m²/g), plenty of mesopores ($d_p = 5.5$ nm) and high content of sulfonic groups (S: $2.51 \pm 0.01\%$).

Dithiocarbamated lignin is the most reported modified lignin due to its good adsorption ability toward heavy metal ions. Ge et al. [58] developed a lignin-based

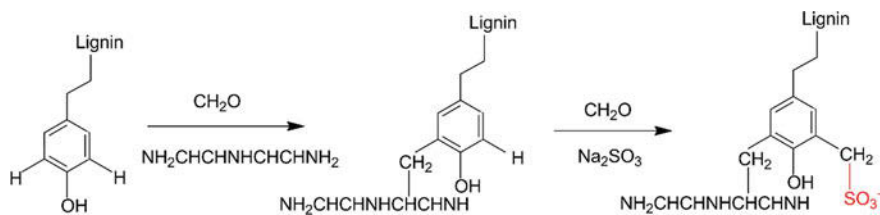


Fig. 11 Synthetic diagram of a modified lignin-containing amino and sulfonic groups. Reprinted with permission [29]. Copyright 2014 Elsevier

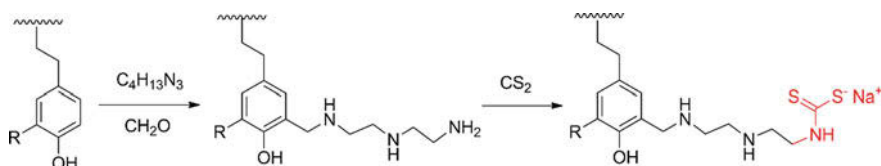


Fig. 12 Synthetic diagram of dithiocarbamated lignin. Reprinted with permission [58]. Copyright 2016 Royal Society of Chemistry

dithiocarbamate (LDTC), as shown in Fig. 12. The developed LDTC showed a high adsorption amount of 175.9 and 103.4 mg/g toward copper and lead ions, respectively. Li et al. [15] developed a porous lignin-containing a large number of mesopores and functional groups. The surface area of the modified lignin increase 11 fold of lignin to 22.3 m²/g. Accordingly, the modified lignin had a high adsorption capacity of 188 mg/g to Pb(II), 13 fold of the lignin and 7 fold of activated carbon. Ge et al. [27] further prepared a dithiocarbamate modified lignin from organosolv lignin. The modified lignin showed a high adsorption amount of 210 mg/g to Hg(II). The adsorption kinetics could be fitted well by a pseudo-second-order equation, and the adsorption equilibrium could be fitted well by the Freundlich equation. Li et al. [59] prepared a lignin xanthate resin (LXR) with xanthate functional groups ($-\text{CSS}^-$) (as shown in Fig. 13). The adsorption capacity of Pb(II) was 64.9 mg/g at pH 5.0, 30 °C.

Ge et al. [26] prepared a new kind of lignin microspheres (LMS) through an inverse suspension copolymerization method. The LMS was in diameter of 348 μm with plenty of amine groups (total N: 7.5 mmol/g). LMS showed an adsorption capacity of 33.9 mg/g for lead ions at pH 6.0, 25 °C, and the adsorption kinetics could be fitted well by the pseudo-second-order equation. Liang et al. [60] prepared a lignin-based resin (LBR) from sodium lignosulfonate and glucose. The maximum adsorption capacity of Cr(VI) by the LBR was 57.68 mg/g. The adsorption equilibrium could be fitted well by the Freundlich equation. The calculated thermodynamic parameters of the adsorption (ΔG , ΔH and ΔS) indicated that the adsorption of Cr(VI) by the LBR is a spontaneous and endothermic process. Parajuli et al. [61] developed a crosslinked lignocatechol gel from catechol and

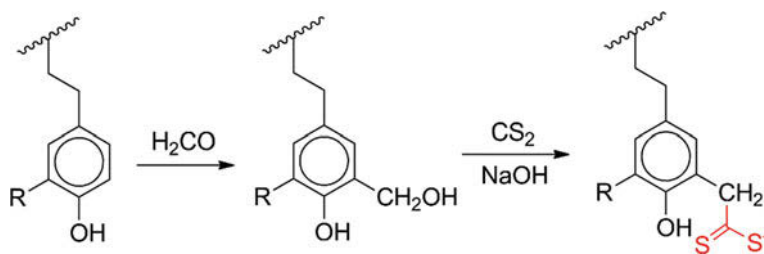


Fig. 13 Synthetic diagram of the lignin xanthate resin (LXR). Reprinted with permission [59]. Copyright 2015 Elsevier

wood lignin. The gel showed a saturated adsorption amount of 37.05 mg/g toward Pb(II) at pH 5.2. The adsorption process was mainly due to the cation exchange mechanism.

Lignin composites are now considered as a talented candidate to traditional adsorbents for cleanup of heavy metal ions in water. Qin et al. [62] synthesized a composite from poly (ethylene imine) and lignin. The composite presented a high adsorption amount of 98.0 mg/g to Cu(II), 78.0 mg/g to Zn(II) and 67.0 mg/g to Ni(II) at pH 6.0, 25 °C. In addition, the composite had good recyclability stability within 5 adsorption-desorption cycles. Klapiszewska et al. [63] prepared new TiO₂/lignin and TiO₂-SiO₂/lignin hybrids. The adsorption capacity of Pb(II) by the TiO₂/lignin and TiO₂-SiO₂/lignin was 35.7 and 59.9 mg/g, respectively, at pH 5.0, 20 °C. Kinetic analysis revealed that the adsorption followed by the pseudo-second-order equation that meant a chemical interaction occurred during the adsorption process. Equilibrium adsorption was well described well by the Langmuir equation that meant a monolayer coverage of the adsorbates on the homogeneous surface of the adsorbents. Li et al. [64] prepared a composite lignin sphere from sodium alginate and epichlorohydrin. The obtained sphere showed an excellent removal efficiency ($95.6 \pm 3.5\%$, $C_0 = 25.0$ mg/L) to Pb(II). Li et al. [65] reported a new nano-composite composed of lignin and carbon nanotubes (L-CNTs). The as-prepared nano-composite not only showed a good water-dispersibility and environmentally friendliness but also presented an excellent adsorption ability to Pb(II) with a maximum adsorption amount of 235 mg/g. The nano-composite with a lignin layer has advanced adsorption ability, low in cost and environmentally friendliness, and therefore is a talented alternative for wastewater treatment. Klapiszewski et al. [66] synthesized a 'green' adsorbent with a high surface area of 223 m²/g from the commercial silica Syloid®244 and Kraft lignin for the removal of nickel(II) and cadmium(II). The results indicated the adsorbents had maximum sorption capacities of 77.11 mg/g for Ni(II) and 84.66 mg/g for Cd(II), respectively. The kinetics adsorption data could be described well by a pseudo-second-order equation while the adsorption isotherms fitted well with Langmuir equation. Yao et al. [67] synthesized a composite composed of bentonite/sodium lignosulfonate with acrylamide and maleic anhydride (BLPAMA). Results showed that the adsorption of Pb(II) by the BLPAMA was correlated with pH values but not with the temperatures. It showed a maximum adsorption capacity of 314.8 mg/g for Pb(II) at pH 5.0, 25 °C.

The above mentioned modified lignin adsorbents for adsorption of heavy metals are tabulated in Table 2, from which it can be seen that the adsorption capacity was much dependent on the chemical methods for lignin modification and heavy metals species as well as the temperature and pH values. According to the analysis of the published literature, the research on the development of advanced lignin-based adsorbents, especially lignin-based nano-composites, is greatly needed in the coming decades.

Table 2 Comparison of adsorption capacity of heavy metals with modified lignins

Modified lignin	Heavy metal	T ($^{\circ}\text{C}$)/pH	Q_m (mg/g)	Reference
Mannich base from lignin	Pb(II)	25 \pm 1/ 6.0	60.5	[49]
EHL-NS	Hg(II)	25/6.0	180	[51]
CMLSCB	Pb(II)	30/6.0	122.9	[68]
BL	Pb(II) Cd(II)	20/5.0	35.9 155.4	[54]
ASL	Cu(II) Pb(II)	25 \pm 0.5/ 6.0	6.3 49.6	[29]
MLBB	Pb(II)	20/7.0	952 \pm 31	[57]
LDTC	Cu(II) Pb(II)	25 \pm 0.5/ 6.0	175.9 103.4	[58]
SFPL	Pb(II)	25 \pm 0.5/ 5.0	188	[15]
Dithiocarbamate functionalized organosolv lignin	Hg(II)	25 \pm 0.5/ 5.0	210	[27]
LMS	Pb(II)	25/6.0	33.9	[26]
LBR	Cr(VI)	50/2.0	57.68	[60]
Crosslinked lignocatechol gel	Pb(II)	25/5.2	37.05	[61]
Poly (ethylene imine) anchored lignin	Cu(II) Zn(II) Ni(II)	25/6.0	98.0 78.0 67.0	[62]
TiO ₂ /lignin	Pb(II)	20/5.0	35.7	[63]
TiO ₂ -SiO ₂ /lignin			59.9	
PLS	Pb(II)	30.2/5.0	31.8	[64]
Siliceous lignin	Pb(II)	70/2.0	–	[69]
L-CNT	Pb(II)	25/6.3	235	[65]
Silica/lignin	Ni(II) Cd(II)	25/3.0 9.0/–	77.11 84.66	[66]
BLPAMA	Pb(II)	25/5.5	314.8	[67]

4 Modified Lignin for Other Pollutants Adsorption

Except for the above discussed main pollutants (dyes and heavy metals), some other pollutants by lignin-based adsorbents are also reported in literature during the past decades. Although there are few papers on the topic, the removal of some other toxic and hazardous pollutants is also very important. Saad et al. [70] investigated two lignins, including alkaline lignin and organosolv lignin, for the adsorption of 2,4-dinitroanisole (DNAN) from the water. The adsorption of DNAN on both lignins could be described well with pseudo-second-order equation. The organosolv lignin showed a maximum adsorption amount of 7.5 mg/g to DNAN while the

alkaline lignin showed a maximum adsorption amount of 8.5 mg/g to DNAN. The adsorption equilibrium for either alkali or organosolv lignin could be described well by the Freundlich model.

Chen et al. [71] reported spherical lignin beads as an adsorbent to adsorb L-lysine in water. The results indicated the beads showed a maximum adsorption capacity of 67.11 mg/g to L-lysine. Dynamic adsorption was fitted well by the pseudo-first-order equation, and the adsorption of L-lysine on the beads was initially determined by film diffusion, and then by intra-particle diffusion. Adsorption equilibrium was described well with the Langmuir equation.

Żółtowska-Aksamitowska et al. [72] firstly investigated the use of chitin modified Kraft lignin as an effective sorbent of ibuprofen and acetaminophen. Batch adsorption results indicated the modified lignin showed an adsorption capacity of 400.39 $\mu\text{g/g}$ to ibuprofen and 267.07 $\mu\text{g/g}$ to acetaminophen, respectively. Adsorption isotherms data could be described with the Langmuir equation for ibuprofen, and with the Freundlich equation for acetaminophen, while the adsorption kinetics followed well to the pseudo-second-order equation for both pollutants ($R^2 = 0.999$). These results indicated that the adsorption belonged to a chemisorption. Furthermore, the used adsorbents could be easily regenerated with ethanol (yield 82.2%) in the case of ibuprofen and methanol (yield 80.8%) in the case of acetaminophen.

Application of the oxidative modification of sulfate kraft lignin with sodium periodate under mild conditions is suggested in order to obtain a sorbent for detoxication of spillage places of rocket fuels based on 1,1-dimethylhydrazine and to purify wastewaters containing this compound [73]. It was found that processing with sodium periodate at 55 °C for 20 h resulted in a more than two-fold increase in the content of carbonyl and quinone groups in lignin and a three-fold increase in the adsorption capacity for 1,1-dimethylhydrazine. The adsorbent can bind 6.7% of 1,1-dimethylhydrazine and substantially surpasses in this parameter other lignin-based adsorbents.

Table 3 listed all these reported modified lignin-based adsorbents for adsorption of some other pollutants in water. As could be seen, the adsorption capability of lignin-based adsorbents for other species is much lower than those for dyes and heavy metals. Therefore, it is in a great need of developing new lignin-based adsorbents with enhanced adsorption capability toward the emerging pollutants in the future.

Table 3 Adsorption capacity of modified lignin for other pollutants in water

Modified lignin	Species	T (°C)/pH	Q_m (mg/g)	Reference
Alkali and organosolv lignin	DNAN	25/5.7	7.5	[70]
Spherical lignin beads	L-lysine	25/9.0	67.11	[71]
Kraft lignin	Ibuprofen acetaminophen	25/6.0	0.40 0.27	[72]
Periodate oxidation of lignin	UDMH	55/5.0	67 ± 1	[73]

5 Outlook and Conclusions

With the depletion of fossil-based resources and increasing environmental concerns, the research and development of new low-cost adsorbents derived from renewable resources have received more and more attention. The utilization of aromatic lignin in replace of the fossil-based carbon will help to the establishment of the sustainable society. In this content, the adsorption of dyes, heavy metals and some other pollutants by various modified lignin materials have been collected and discussed in this study. Based on the above discussions, adsorption performance of these modified lignin materials for dyes, heavy metals, and other pollutants is expected to be amplified in the near future. It should be noted that the cost-effectiveness is firstly important because low manufacturing cost and high adsorption capability of an adsorbent is desired in practical large-scale applications. Lignin is an abundant polymer derived from plant kingdom that can provide CO₂ neutral, cost-effective, environmentally friendly and therefore can be used as building blocks to create “green” adsorbents. Secondly, although modified lignin is efficient to capture different kinds of pollutants through physical or chemical interactions, regeneration by feasible methods should be studied carefully as it is very important for the improvement of economics. The regeneration of lignin-based materials could be carried out by the most common solvent extraction method with EDTA, HCl, HNO₃, NaCl, and NaOH solutions et al. Thirdly, experiments should not only stay in the lab. As all known, the industrial wastewater always contains many kinds of contaminants. Although different kinds of modified lignin adsorbents can be obtained with good adsorption capacity and selectivity for the target contaminants, such as methylene blue (MB), toxic metals (Hg), and (Pb, Cu) et al., it is desirable in developing a multipurpose adsorbent from lignin that can be used to adsorb different kinds of contaminants simultaneously. Therefore, specific attention should be focused on the modification of lignin matrix, via hybridizing, cross-linking and grafting to develop lignin-based advanced composite, and accordingly broadening the kinds of pollutants for efficient removal and improving the reusability of the modified lignin-based composites.

Acknowledgements Financial support from the National Natural Science Foundation of China (No. 21264002, 21464002), and Guangxi Natural Science Foundation (No. 2015GXNSFBA139215, 2016GXNSFAA380329) is gratefully acknowledged.

References

1. Abe A, Dusek K, Kobayashi S (2010) Biopolymers: lignin, proteins, bioactive nanocomposites. Springer, Berlin
2. Upton BM, Kasko AM (2016) Strategies for the conversion of lignin to high-value polymeric materials: review and perspective. *Chem Rev* 116:2275–2306

3. Holladay JE, White JF, Bozell JJ, Johnson D (2007) Top value-added chemicals from biomass—volume II—results of screening for potential candidates from biorefinery lignin. In: Pacific Northwest National Laboratory (PNNL), Richland, WA (US), 2007, Medium: ED; Size: PDFN
4. Zakzeski J, Bruijninx PCA, Jongerius AL, Weckhuysen BM (2010) The catalytic valorization of lignin for the production of renewable chemicals. *Chem Rev* 110:3552–3599
5. Li Z, Zhang J, Qin L, Ge Y (2018) Enhancing antioxidant performance of lignin by enzymatic treatment with laccase. *ACS Sustain Chem Eng* 6:2591–2595
6. Calvo-Flores FG, Dobado JA (2010) Lignin as renewable raw material. *Chemsuschem* 3:1227–1235
7. Thakur VK, Thakur MK, Raghavan P, Kessler MR (2014) Progress in green polymer composites from lignin for multifunctional applications: a review. *ACS Sustain Chem Eng* 2:1072–1092
8. Rezakazemi M, Maghami M, Mohammadi T (2018) High loaded synthetic hazardous wastewater treatment using lab-scale submerged ceramic membrane bioreactor. *Periodica Polytechnica Chem Eng* 62:299–304
9. Rezakazemi M, Khajeh A, Mesbah M (2018) Membrane filtration of wastewater from gas and oil production. *Environ Chem Lett* 16:367–388
10. Rezakazemi M, Dashti A, Riasat Harami H, Hajilari N (2018) Fouling-resistant membranes for water reuse. *Environ Chem Lett* 1–49
11. Azimi A, Azari A, Rezakazemi M, Ansarpour M (2017) Removal of heavy metals from industrial wastewaters: a review. *Chem Bio Eng Rev* 4:37–59
12. Shirazian S, Rezakazemi M, Marjani A, Moradi S (2012) Hydrodynamics and mass transfer simulation of wastewater treatment in membrane reactors. *Desalination* 286:290–295
13. Rezakazemi M, Shirazian S, Ashrafizadeh SN (2012) Simulation of ammonia removal from industrial wastewater streams by means of a hollow-fiber membrane contactor. *Desalination* 285:383–392
14. Gupta VK (2009) Application of low-cost adsorbents for dye removal—a review. *J Environ Manage* 90:2313–2342
15. Li Z, Xiao D, Ge Y, Koehler S (2015) Surface-functionalized porous lignin for fast and efficient lead removal from aqueous solution. *ACS Appl Mater Interfaces* 7:15000–15009
16. Rezakazemi M, Zhang Z (2018) 2.29 desulfurization materials A2. In: Dincer I (ed) *Comprehensive energy systems*. Elsevier, Oxford, pp 944–979
17. Rezakazemi M, Sadrzadeh M, Matsuura T (2018) Thermally stable polymers for advanced high-performance gas separation membranes. *Progr Energy Combust Sci* 66:1–41
18. Rezakazemi M, Marjani A, Shirazian S (2018) Organic solvent removal by pervaporation membrane technology: experimental and simulation. *Environ Sci Poll Res*
19. Rezakazemi M, Ebadi Amooghin A, Montazer-Rahmati MM, Ismail AF, Matsuura T (2014) State-of-the-art membrane based CO₂ separation using mixed matrix membranes (MMMs): an overview on current status and future directions. *Prog Polym Sci* 39:817–861
20. Foroutan R, Esmaeili H, Abbasi M, Rezakazemi M, Mesbah M (2017) Adsorption behavior of Cu(II) and Co(II) using chemically modified marine algae. *Environ Technol* 1–9
21. Ge YY, Cui XM, Liao CL, Li ZL (2017) Facile fabrication of green geopolymer/alginate hybrid spheres for efficient removal of Cu(II) in water: batch and column studies. *Chem Eng J* 311:126–134
22. Saleh TA, Gupta VK (2014) Processing methods, characteristics and adsorption behavior of tire derived carbons: a review. *Adv Colloid Interfac* 211:93–101
23. Rafatullah M, Sulaiman O, Hashim R, Ahmad A (2010) Adsorption of methylene blue on low-cost adsorbents: a review. *J Hazard Mater* 177:70–80
24. Ahluwalia SS, Goyal D (2007) Microbial and plant derived biomass for removal of heavy metals from wastewater. *Bioresource Technol* 98:2243–2257
25. Deng S, Ting Y-P (2005) Characterization of PEI-modified biomass and biosorption of Cu(II), Pb(II) and Ni(II). *Water Res* 39:2167–2177

26. Ge YY, Qin L, Li ZL (2016) Lignin microspheres: an effective and recyclable natural polymer-based adsorbent for lead ion removal. *Mater Des* 95:141–147
27. Ge Y, Wu S, Qin L, Li Z (2016) Conversion of organosolv lignin into an efficient mercury ion adsorbent by a microwave-assisted method. *J Taiwan Inst Chem Eng* 63:500–505
28. Wawrzekiewicz M, Bartzczak P, Jesionowski T (2017) Enhanced removal of hazardous dye from aqueous solutions and real textile wastewater using bifunctional chitin/lignin biosorbent. *Int J Biol Macromol* 99:754–764
29. Ge Y, Li Z, Kong Y, Song Q, Wang K (2014) Heavy metal ions retention by bi-functionalized lignin: synthesis, applications, and adsorption mechanisms. *J Ind Eng Chem* 20:4429–4436
30. Ge Y, Li Z (2018) Application of lignin and its derivatives in adsorption of heavy metal ions in water: a review. *ACS Sustain Chem Eng* 6:7181–7192
31. Laurichesse S, Avérous L (2014) Chemical modification of lignins: towards biobased polymers. *Prog Polym Sci* 39:1266–1290
32. Nair V, Panigrahy A, Vinu R (2014) Development of novel chitosan–lignin composites for adsorption of dyes and metal ions from wastewater. *Chem Eng J* 254:491–502
33. Albadarin AB, Collins MN, Naushad M, Shirazian S, Walker G, Mangwandi C (2017) Activated lignin–chitosan extruded blends for efficient adsorption of methylene blue. *Chem Eng J* 307:264–272
34. Lou T, Cui G, Xun J, Wang X, Feng N, Zhang J (2018) Synthesis of a terpolymer based on chitosan and lignin as an effective flocculant for dye removal. *Coll Surf A* 537:149–154
35. Li YL, Wu M, Wang B, Wu YY, Ma MG, Zhang XM (2016) Synthesis of magnetic lignin-based hollow microspheres: a highly adsorptive and reusable adsorbent derived from renewable resources. *ACS Sustain Chem Eng* 4:5523–5532
36. Couch RL, Price JT, Fatehi P (2016) Production of flocculant from thermomechanical pulping lignin via nitric acid treatment. *ACS Sustain Chem Eng* 4:1954–1962
37. Xu WJ, Zhang WS, Li Y, Li W (2016) Synthesis of acrylic–lignosulfonate resin for crystal violet removal from aqueous solution. *Korean J Chem Eng* 33:2659–2667
38. Wang Y, Xiong Y, Wang J, Zhang X (2017) Ultrasonic-assisted fabrication of montmorillonite–lignin hybrid hydrogel: highly efficient swelling behaviors and super-sorbent for dye removal from wastewater. *Coll Surf A* 520:903–913
39. Yu C, Wang F, Zhang C, Fu S, Lucia LA (2016) The synthesis and absorption dynamics of a lignin-based hydrogel for remediation of cationic dye-contaminated effluent. *React Funct Polym* 106:137–142
40. Kumari S, Chauhan GS, Monga S, Kaushik A, Ahn J-H (2016) New lignin-based polyurethane foam for wastewater treatment. *RSC Adv* 6:77768–77776
41. Feng Q, Cheng H, Chen F, Zhou X, Wang P, Xie Y (2016) Investigation of cationic dye adsorption from water onto acetic acid lignin. *J Wood Chem Technol* 36:173–181
42. Tang Y, Hu T, Zeng Y, Zhou Q, Peng Y (2015) Effective adsorption of cationic dyes by lignin sulfonate polymer based on simple emulsion polymerization: isotherm and kinetic studies. *RSC Adv* 5:3757–3766
43. Tang Y, Zeng Y, Hu T, Zhou Q, Peng Y (2016) Preparation of lignin sulfonate-based mesoporous materials for adsorbing malachite green from aqueous solution. *J Environ Chem Eng* 4:2900–2910
44. Song X, Chen F, Liu S (2016) A lignin-containing hemicellulose-based hydrogel and its adsorption behavior. *BioResources* 11:6378–6392
45. Luo H, Ren S, Ma Y, Fang G, Jiang G (2015) Preparation and properties of kraft lignin–N-isopropyl acrylamide hydrogel. *BioResources* 10:3507–3519
46. Adebayo MA, Prola LDT, Lima EC, Puchana-Rosero MJ, Cataluña R, Saucier C, Umpierrez CS, Vaghetti JCP, da Silva LG, Ruggiero R (2014) Adsorption of Procion Blue MX-R dye from aqueous solutions by lignin chemically modified with aluminium and manganese. *J Haz Mater* 268:43–50
47. da Silva LG, Ruggiero R, Gontijo PdM, Pinto RB, Royer B, Lima EC, Fernandes THM, Calvete T (2011) Adsorption of Brilliant Red 2BE dye from water solutions by a chemically modified sugarcane bagasse lignin. *Chem Eng J* 168:620–628

48. Guo K, Gao B, Li R, Wang W, Yue Q, Wang Y (2018) Flocculation performance of lignin-based flocculant during reactive blue dye removal: comparison with commercial flocculants. *Environ Sci Pollut R* 25:2083–2095
49. Ge Y, Song Q, Li Z (2015) A Mannich base biosorbent derived from alkaline lignin for lead removal from aqueous solution. *J Ind Eng Chem* 23:228–234
50. Li Z, Xiao D, Kong Y, Ge Y (2015) Enhancing lead adsorption capacity by controlling the chain length of alkyl amine grafted lignin. *BioResources* 10:2425–2432
51. Huang W-X, Zhang Y-H, Ge Y-Y, Qin L, Li Z-L (2017) Soft nitrogen and sulfur incorporated into enzymatic hydrolysis lignin as an environmentally friendly antioxidant and mercury adsorbent. *BioResources* 12:7341–7348
52. Quintana GC, Rocha GJM, Goncalves AR, Velasquez JA (2008) Evaluation of heavy metal removal by oxidised lignins in acid media from various sources. *BioResources* 3:1092–1102
53. Peterlele WS, Winkler-Hechenleitner AA, Pineda EAG (1999) Adsorption of Cd(II) and Pb(II) onto functionalized formic lignin from sugar cane bagasse. *Bioresour Technol* 68:95–100
54. Dizhbite T, Jashina L, Dobele G, Andersone A, Evtuguin D, Bikovens O, Telysheva G (2013) Polyoxometalate (POM)-aided modification of lignin from wheat straw biorefinery. *Holzforschung* 67:539–547
55. Li Z, Pang Y, Ge Y, Qiu X (2011) Evaluation of steric repulsive force in the aqueous dispersion system of dimethomorph powder with lignosulfonates via X-ray photoelectron spectroscopy. *J Phys Chem C* 115:24865–24870
56. Li Z, Ge Y (2011) Extraction of lignin from sugar cane bagasse and its modification into a high performance dispersant for pesticide formulations. *J Brazil Chem Soc* 22:1866–1871
57. Xu F, Zhu TT, Rao QQ, Shui SW, Li WW, He HB, Yao RS (2017) Fabrication of mesoporous lignin-based biosorbent from rice straw and its application for heavy-metal-ion removal. *J Environ Sci* 53:132–140
58. Ge Y, Xiao D, Li Z, Cui X (2014) Dithiocarbamate functionalized lignin for efficient removal of metallic ions and the usage of the metal-loaded bio-sorbents as potential free radical scavengers. *J Mater Chem A* 2:2136–2145
59. Li Z, Kong Y, Ge Y (2015) Synthesis of porous lignin xanthate resin for Pb²⁺ removal from aqueous solution. *Chem Eng J* 270:229–234
60. Liang F-B, Song Y-L, Huang C-P, Zhang J, Chen B-H (2013) Adsorption of hexavalent chromium on a lignin-based resin: equilibrium, thermodynamics, and kinetics. *J Environ Chem Eng* 1:1301–1308
61. Parajuli D, Inoue K, Ohto K, Oshima T, Murota A, Funaoka M, Makino K (2005) Adsorption of heavy metals on crosslinked lignocatechol: a modified lignin gel. *React Funct Polym* 62:129–139
62. Qin L, Ge Y, Deng B, Li Z (2017) Poly(ethylene imine) anchored lignin composite for heavy metals capturing in water. *J Taiwan Inst Chem Eng* 71:84–90
63. Klapiszewski L, Siwinska-Stefanska K, Kolodynska D (2017) Preparation and characterization of novel TiO₂/lignin and TiO₂-SiO₂/lignin hybrids and their use as functional biosorbents for Pb(II). *Chem Eng J* 314:169–181
64. Li Z, Ge Y, Wan L (2015) Fabrication of a green porous lignin-based sphere for the removal of lead ions from aqueous media. *J Haz Mater* 285:77–83
65. Li Z, Chen J, Ge Y (2017) Removal of lead ion and oil droplet from aqueous solution by lignin-grafted carbon nanotubes. *Chem Eng J* 308:809–817
66. Klapiszewski L, Bartczak P, Wysokowski M, Jankowska M, Kabat K, Jesionowski T (2015) Silica conjugated with kraft lignin and its use as a novel ‘green’ sorbent for hazardous metal ions removal. *Chem Eng J* 260:684–693
67. Yao Q, Xie J, Liu J, Kang H, Liu Y (2014) Adsorption of lead ions using a modified lignin hydrogel. *J Polym Res* 21:465
68. Peterlele WS, Winkler-Hechenleitner AA, Gómez Pineda EA (1999) Adsorption of Cd(II) and Pb(II) onto functionalized formic lignin from sugar cane bagasse. *Bioresour Technol* 68:95–100

69. Cui J, Sun H, Wang X, Sun J, Niu M, Wen Z (2015) Preparation of siliceous lignin microparticles from wheat husks with a facile method. *Ind Crop Prod* 74:689–696
70. Saad R, Radovic-Hrapovic Z, Ahvazi B, Thiboutot S, Ampleman G, Hawari J (2012) Sorption of 2,4-dinitroanisole (DNAN) on lignin. *J Environ Sci* 24:808–813
71. Chen GF, Liu MH (2012) Adsorption of L-lysine from aqueous solution by spherical lignin beads: kinetics and equilibrium studies. *BioResources* 7:298–314
72. Żółtowska-Aksamitowska S, Bartczak P, Zembrzuska J, Jesionowski T (2018) Removal of hazardous non-steroidal anti-inflammatory drugs from aqueous solutions by biosorbent based on chitin and lignin. *Sci Total Environ* 612:1223–1233
73. Kozhevnikov AY, Ul'yanovskaya SL, Semushina MP, Pokryshkin SA, Ladesov AV, Pikovskoi II, Kosyakov DS (2017) Modification of sulfate lignin with sodium periodate to obtain sorbent of 1,1-dimethylhydrazine. *Russ J Appl Chem* + 90:516–521

Synthesis and Characterization and Application of Chitin and Chitosan-Based Eco-friendly Polymer Composites



Aneela Sabir, Faizah Altaf and Muhammad Shafiq

1 Introduction

1.1 History of Chitosan

The chitosan history begins from the 19th century, by Rouget 1859 who discussed the deacetylated parent chitin polymer (the second most plenteous carbohydrate) in nature first time. With the passage of time, a considerable amount of work has been done on chitosan especially during last 20 years, and its potential for different bio applications [1].

Chitosan is obtained from natural sources that are the external skeleton of crustaceans, fungi, and insects and has to be biocompatible and decomposable. It's being a copolymer contains *N*-acetyl-2-amino-2-deoxy-d-glucopyranose and 2-amino-2-deoxy-d-glucopyranose, the monomers are joined together by (1 → 4) glycosidic bonds. The carbon and hydrogen is a major constituent of chitosan is very alike to cellulose, in which 1,4 is linked with d-glucosamine and with varying number of *N*-acetylation, the difference is only that the hydroxyl group is replaced acetyl amino group at the C₂ position. It is a nearly synthetic derivative of aminopolysaccharide which has peculiar structures, dimensional characteristics, extremely planned practicality and a large vary of usage in medicinal speciality and alternative manufacturing areas [2]. The structure of chitosan is given in Fig. 1.

The removal of the acetyl group from chitin to produce chitosan needs a reaction with highly strong NaOH solution (water or alcohol based) with maintaining safe

A. Sabir (✉) · M. Shafiq

Department of Polymer Engineering and Technology, University of the Punjab, Lahore 54590, Pakistan

e-mail: aneela.pet.ceet@pu.edu.pk

F. Altaf

Department of Environmental Sciences, Fatima Jinnah Women University, Rawalpindi 46000, Pakistan

© Springer Nature Switzerland AG 2019

Inamuddin et al. (eds.), *Sustainable Polymer Composites and Nanocomposites*,

https://doi.org/10.1007/978-3-030-05399-4_46

1365

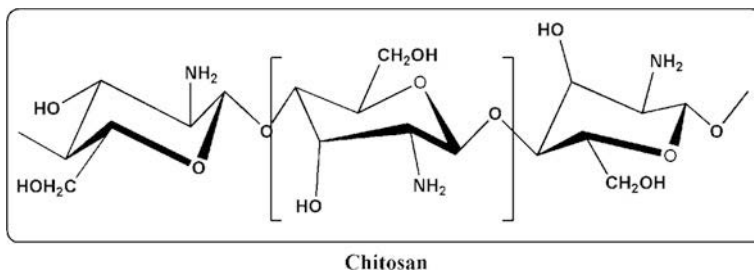


Fig. 1 Structure of chitosan

conditions that ensure the reaction mixture does not interact with oxygen and for this purpose reaction mixture is either purged with nitrogen or by adding NaBH_4 so to control unwanted depolymerization and production of reactive species. Chitosan has become attention-grabbing not solely because of its synthesis from plentiful natural resources however as a result of its highly well-matched and efficient biomaterial that is quite able to be applied. As chitin is poorly soluble in water-based and organic solvents, whereas chitosan as an anthropogenic creation of chitin is highly appropriate for the application in the biomedical field. The best features of magnificent biocompatibility and marvellous bio-decomposition that protect ecosystem protection and less poisonousness with multipurpose medical accomplishments like antibacterial activity and low immunogenicity providing plentiful openings for more development [3].

Chitosan has the most structure changes being diagrammatic by the perspective quantities of *N*-acetyl-d-glucosamine and d-glucosamine remaining, give definite chemical structure variations. This distinction within formula provides rise to many groups of chitosan that are notable. Chitosan may have various range number of deacetylation (40–98%) and molecular mass (5–104 and 2–106 Da). The degree of deacetylation and polymerization actually describe the molecular mass of the polymer. They are two necessary factors indicating the employment of chitosan for numerous solicitations. Some other parameters may alter the physical properties of CS including the order of the amino and acetamido groups and also the quality of crustacean shells (crabs, etc.) which were wastage of food industry in past but now are commercially used for chitin and CS production [4] (Fig. 2).

The purification of chitin and its method can have an effect on quality of chitosan. The crystallinity and polymorphism of chitosan are highly dependent on the beginning of the polymerization and extraction in thorough process. An aliphatic and straight chain structure having the incorporated chitosan in its blend act as a viscosity enhancing agent that work in acidic conditions and behave like false plastic material possess lower viscosity as shear rate increases. The viscosity rises by increasing the concentration of chitosan. Viscosity can have a strong effect on enhancing the biological properties like wound-recovery and osteogenesis improvement and biodegradation by lysozyme [5].

The chitosan solubilizes in solutions containing acid (below pH 6.0) because of amine groups ($\text{pK}_a = 6.3$) quaternization which enables chitosan to become

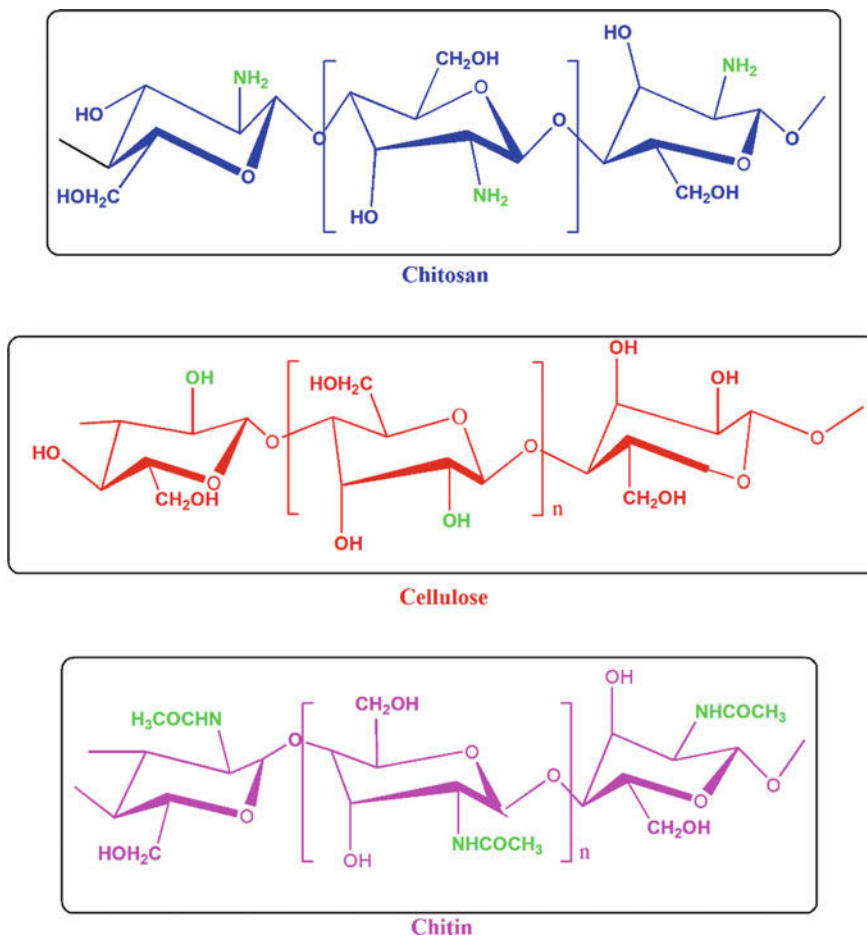


Fig. 2 The molecular structure of chitosan, cellulose and chitin

aqua-soluble. The existence of the $-\text{NH}_2$ showed that pH considerably changes the partially ionic state and characteristics of chitosan. When pH is low, protonation of amines takes place causing a positively charged species making it soluble. However at higher pH (higher than 6), chitosan's amines get deprotonated and charge loss occurs and makes insoluble ion electrolyte [6].

2 Production

Chitin is a basic precursor of chitosan production using basically two different approaches, i.e. equally distributed deacetylation and heterogeneous deacetylation. In the equally distributed deacetylation procedure, the chitin is allowed to dissolve

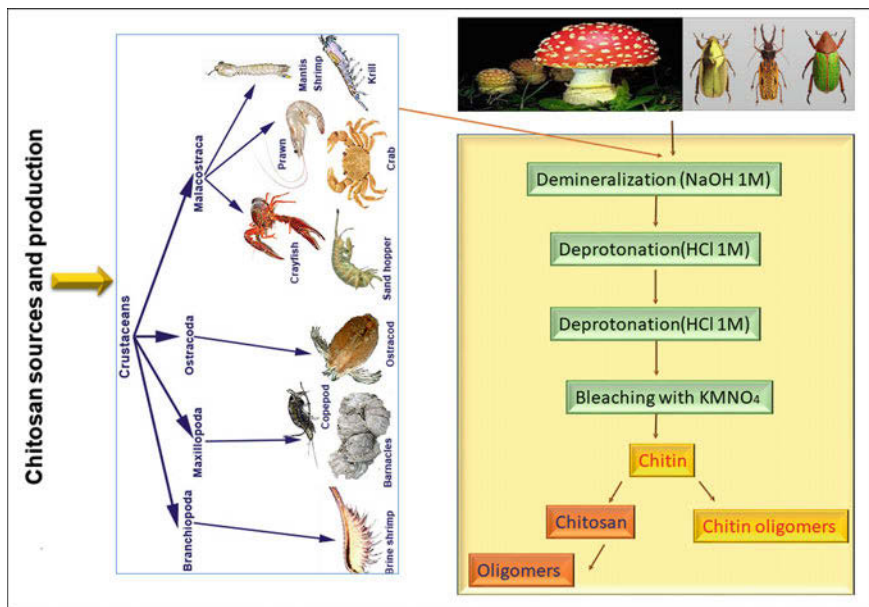


Fig. 3 Chitin, source and its application

in an alkaline solution at an appropriate temperature with vigorous stirring. While in the case of heterogeneous deacetylation process proceeds in a two-phase system, where chitin remains insoluble (hot alkali solution). Chitosan with FA (0–65%) can be synthesized by evenly deacetylation of chitin [5, 7]. The production of chitosan is given in Fig. 3.

3 Chitosan Oligomers

Owing to higher molecular mass and highly viscous nature of chitosan, it is possible to subject chitosan polymer for depolymerization (chitonolysis) results in the production of chitosan of low-molecular-weight i.e. oligomers and monomers also. These chitosan oligomers showed excellent solubility and have been used in numerous applications. There is a variety of chemical, physical and enzymatic techniques that are used to synthesize chitosan having smaller chains of repeating units (3–9) [8].

The acid hydrolysis synthesis restricts the use of chemical methods along with conventional heat procedure. It has some drawbacks including highly expensive, lower final product yield an acid residue. Degradation by acids is not a simple process; the breakage in the presence of water undergoes and results in the random generation of repeating units, D-glucosamine on increasing reaction time.

So, hydrolysis using concentrated HCl has usually been modified. First by employing 35% HCl at a temperature of 80 °C for a shorter period of time. This process produced chitosan oligomers having 1–15 and 20–40 chains. The use of nitric acid (HNO₃) for oligomer production is choosy, rapid, and easily manageable with good stoichiometric products. Hydrogen peroxide (H₂O₂) may also be convenient to breakdown chain of monomers and generate hydroxyl radicals [9].

Another process to synthesize chitosan small chains using hot H₃PO₄ has been described in the literature [10]. The obtained yields were sated as 10–20% with DP 6–8. Moreover, two kinds of chitosan oligomers (DP 7.3 and 16.8) were also produced through chitosan consistent hydrolysis using 85% H₃PO₄ at ambient temperature for four weeks. Fluoride-based hydrolysis of chitosan using dried HF appeared to be more suitable way than traditional chemical polymer breakage in term of good products yield. However, this procedure also has practical restrictions as required an additional processing for defluorination. The polymer decomposition can also be obtained effectively using microwave assisted technology supported by the adding alkali carbonates to synthesize 1-molar mass chitosan within a short period of time [11].

The production of chitosan oligomers also carried out using enzymes. Enzymatic synthesis cause chitosan depolymerized easily with a variety of hydrolase including hemicellulases, lipases, cellulases, and lysozyme, papain amylases, pectinase, pronase etc. The enzyme-based polymer degradation is favourable for the production of the chitosan. The reaction rate can be managed by means of reaction time, pH, temperature and recombinant approaches and of physical ways as sonication and electromagnetic radiation [12].

4 Modifications of Chitosan

There are a variety of materials and method that have been used to modify chitosan to enhance biofunctionality and other desired properties for utilization in different applications. Surface modification methods include blending with different other compound and derivatives such as coverings, reaction with an oxygen based compound or by employing surfactant. Moreover, the fabrication of chitosan to prepare stable, porous bioscaffold, functionalized surface, lyophilization is also carried out. Blending using numerous preservatives may change its biomedical compatibility. It is necessary to evaluate the biomedical compatibility of numerous chitosan that is considered so they can be used for wound healing and other related treatments. The other benefits associated with these include easy processability to form membranes, scaffolds, nanofibrils, gels, nanofibres, beads, nanoparticles, microparticles and sponge-like forms (Fig. 2). Due to these properties and biocompatibility, widely employed in wound healing and tissue engineering, and in drugs and gene delivery [13].

Cross-linking of chitosan is another approach to enhance the performance. In crosslinked polymeric crosslinkers interconnect the chains of polymers that in turn

help in the development of a 3D framework. The properties of crosslinked polymers depend on viscosity and molar ratio of crosslinking with a corresponding polymer chain. A precise number of crosslinks per chain is needed to allow the development of a framework. The structures of chitosan formed are: (a) self-crosslinking of chitosan; (b) composite network of polymer (c) nearly intercalating network; and (d) cationic/anionic crosslinking. Nature of crosslinking agent decides the type of bonding and interactions (whether it bond covalently or not) [14].

5 Derivatives of Chitosan

The chemical modification of chitosan can be carried out to anchor different functional groups including primary amine and primary and secondary OH groups (Fig. 4).

5.1 Quaternized Chitosan and N-Alkyl Chitosan

Quaternized chitosan can be termed as methylated chitosan. It is obtained using methyl iodide. Usually, the reaction between methyl iodide and chitosan is carried out in a basic environment, one of the most forthright way of quaternizing chitosan [15]. Proteins and peptide-based medicine are extremely adsorbed by an excellent sorbent which is chitosan. The working principle of chitosan for aiding the para-cellular transportation of water-loving drugs was recommended to be a mixture of bio adhesion and a passing broadening of the strengthen joint in the thin film mediated by H^+ functionalized chitosan in its open coiled configuration [16]. Chitosan and its metal derivatives facilitate the paracellular transportation of hydrophilic drugs by combining effect of bioadhesion and a transient broadening of the tight connections in the membrane arbitrated by protonated chitosan in its uncoiled configuration. However at 7.4 pH, chitosan and salts unable to further enhance the permeation rate because of dissolution issues. This character suggests that only chitosan can be an excellent sorbent in its original PKa which matches in the intestinal. This is the only reason that chitosan and its derivatives cannot be targeted by amino-linked protein-based drugs into the human intestine part that is jejunum to the colon [17].

N,N,N-trimethyl chitosan chloride (TMC) which is quaternarily derived are more stable in aqueous solution as compare to chitosan at higher pH. Such derivate of chitosan has used to enhance sorption for medicine. In literature tested for fluorescein-isothiocyanate dextran (FD4, MW4400) and mannitol, etc. The chitosan that is trimethylated also possesses mucous adhesive properties dependent on a number of quaternization in general mucous adhesive characteristics increases by the enhanced degree of quaternization. It is because of the enchantment of positive role of chitosan which increases its bonding with anionic mucin resulting in mucous adhesion [18].

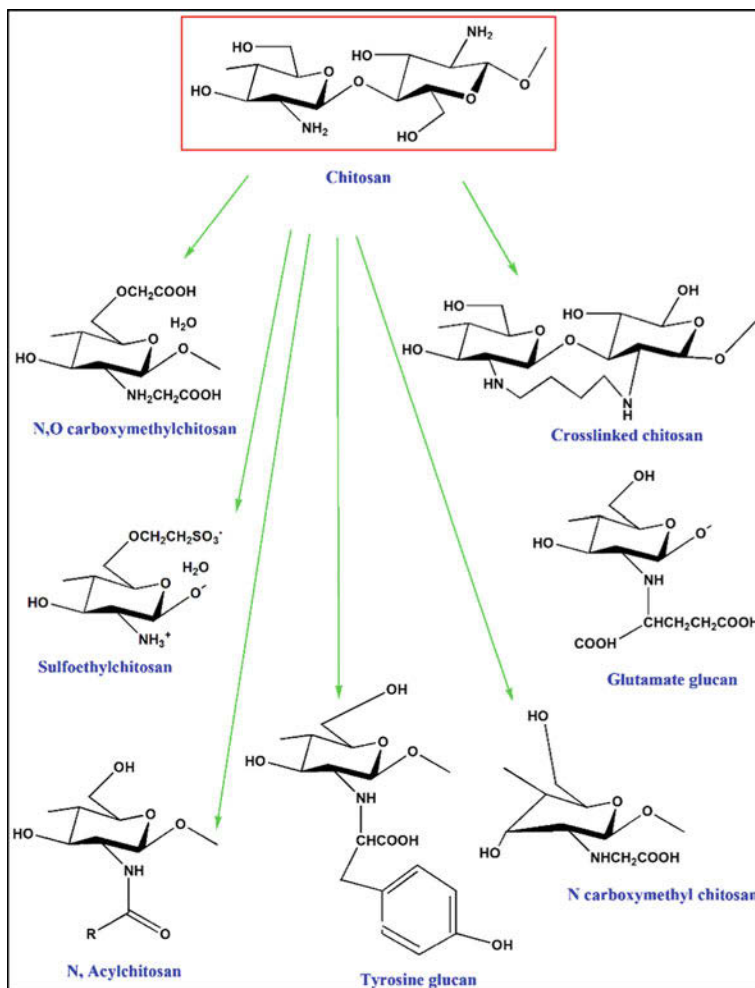


Fig. 4 Derivatives of chitosan

5.2 Hydroxyalkyl Chitosan

Hydroxyl (OH^-) functionalized chitosan is prepared by precursors such as ethylene oxide and propylene oxide (epoxide) reacting chitosan, glycidol. Basically, in an epoxide, the reaction occurred mainly at the groups like NH_2 or alcohol OH , giving *N*-hydroxyalkyl/*O*-hydroxyalkyl chitosan or maybe both. The ratio of *O*/*N*-substitution depends on types of catalyst (NaOH/HCl) used and reaction temperature. In the absence of a catalyst, *N*-hydroxypropylation is produced, while the use of acid catalysts results in predominantly *N*- but very less *O*-alkylated chitosan product. By using basic catalysts *O*-alkylation is dominant with the ability to

produce oligomers at temperature higher (above 40 °C) [19]. Peng et al. prepared hydroxypropyl chitosan and investigated it as antibacterial activity [20]. Whereas Dang et al. investigated it for its probable use as an injectable carrier (temperature sensitive) for cells [21–23].

5.3 Carboxyalkyl Chitosan

The introduction of acidic groups in polymer backbone is called as carboxyalkylation. By introducing $-\text{COOH}$ at the $-\text{NH}_2$ groups attached to chitosan, both acidic and basic mixed polyelectrolytes (that also contain both cationic and anionic) are synthesized. If the amount is changed then the exchange of the $-\text{COOH}$ containing the group, one can get a molecular chain with different charge densities which provide an easy way of controlling PKa-based behaviour. Both, *O*-carboxyalkyl and *N*-carboxyalkyl chitosan have been synthesized by employing various reacting circumstances using single halogenated carboxylic acid to obtain the *N* contrasted *O* selection [24]. *N*-Carboxymethyl chitosan possesses some peculiarities including water solubility, remarkable biological, physical and chemical characteristics (highly dense, film and aqueous dynamic volume, gelation characteristics) also, those of which enables it to be optable in food products and make-over products. CH_3COOH modified chitosan also used in preparing of various hydrogel (porous, pH-sensitive, cross-linked hydrogels) for protein drug delivery systems as *N,N*-Dicarboxymethyl chitosan exhibited excellent chelating capabilities and its chelation with calcium phosphate suitable for osteogenesis thus encouraging bone calcination. *O*- CH_3COOH chitosan also shows antimicrobial activity and adhesive properties [25].

5.4 Sugar Functionalized Chitosan

Sugar-modified chitosan was first time reported by Hall and Yalpani. They prepared chitosan that is bounded to sugar reductive *N*-alkylation with NaBH_3CN and aldehydic sugar derivative. At first, the sugar modified chitosan had been examined for rheological studies; but later on, this type of functionalization has been utilized to induce cell-specified sugars into chitosan. The synthesis of sugar bound chitosan, D- and L-fucose, and their interactions with lectin and cells was also reported [26]. Stredanska et al. prepared a chitosan derivative of lactose which is useful in the repair of articular cartilage. Kaneko et al. accomplished chemoenzymatic method for introduction of large carbohydrate as amylose on chitosan. The amylose-grafted chitosan also has been prepared it does not have a solubility in any solvent, (aqueous CH_3COOH and $\text{C}_2\text{H}_6\text{OS}$) which usually dissolve chitosan and amylose both and hence applied various specific fields [27, 28].

5.5 Cyclodextrin Linked Chitosan

Chitosan that contains cyclodextrin (CD) chains are produced with an intent to join extraordinary attributes of chitosan with the capability of cyclodextrin to shape complexes that are non-covalent in nature with various temporary particles changing their physical-chemical characteristics for the enhanced timely medicinal delivery framework, beauty care products, and systematic science and analytical chemistry. There are diverse means to connect the interface of chitosan to cyclodextrin. A researcher named Sakairi and his colleagues arranged a-CD-connected chitosan utilizing 2-*O*-formylmethyl-CD by reductive *N*-alkylation and affirmed the permanent-temporary particle complex of with $p\text{-C}_6\text{H}_5\text{NO}_2$. Another group of researchers, Auzely-Velty and Rinaudo additionally announced nearly same method of chitosan preparation containing cyclodextrin chain by amination in reducing conditions with the investigations of development of addition complexes with 4-*tert*-butyl benzoic acid [29]. The CD-chitosan derivatives arranged comparably with cyclodextrin single aldehyde has been assessed for mucous adhesion by a similar group. Chen and Wang acquired cyclodextrin linked chitosan utilizing tosylated b-cyclodextrin and further assessed the capability of b-CD for the release of I-131 in vivo and enhanced solubility [30, 31].

5.6 *N*-Acyl Chitosan

Anhydride and acyl chlorides are used to synthesize *N*-Acyl derivatives of chitosan. By and large, acylation reactions result carried out in an aqueous solution of $\text{CH}_3\text{COOH}/\text{CH}_3\text{OH}$ mediums, pyridine/chloroform, pyridine, trichloroacetic acid/dichloroethane, ethanol/methanol mixture, methanol/formamide or DMA-LiCl. Because of genuinely unique reactivity of the two groups (hydroxyl and the amino) at the monomer unit of chitosan, acylation can be carried out in control manner at the predictable sites, i.e. on either $-\text{NH}_2$, $-\text{OH}$, or on the two groups. One of the techniques for obtaining acylated chitosan derivative incorporates the solid state thermal breakdown of its acyl-ammonium derivative. This technique was utilized to obtain amides of chitosan got from acids, for example, trifluoroacetic, acrylic, acidic, methacrylic and myristic [32].

N-Acyated chitosan with long polymer chain (C6–C16) chlorides expanded its water repelling character (hydrophobic self-gathering) and caused vital improvements in its basic properties. It was shown in enhanced mechanical characteristics of drugs synthesized utilizing these subsidiaries. The discharge attributes of the drugs showed that discharge is managed by dispersion or by swelling took after by dissemination; depend upon both the acylated chain length and the level of acylation. The acylation can be accomplished region selectively at the amino site by utilizing as trityl assemble at the basic OH group. This approach was utilized to get ready *N*-haloacyl 6-*O*-triphenylmethyl chitosan which can be additionally replaced

by amines as tributylamine, pyridine, imidazole, triethylamine, *N*-chlorobetainyl chloride. The derivatives of betaine have two notable points of attention over the base chitosan: (i) their water solubility at physical pH, and (ii) they have a perpetual cationic charge on the polysaccharide backbone [33].

5.7 *O*-Acyl Chitosan

There are two main benefits of introducing of water repelling species into chitosan by ester linkage; the first one is that this water repelling species makes chitosan soluble in organic solvent and the second benefit refers to hydrolysis of ester linkage by lipase-like enzymes. Additionally, glycosidases enzyme helps in the breakdown of glycoside linkage of chitosan. Such properties make *O*-acyl derivatives of chitosan best materials for biodegradable coatings. It has been reported that *O,O*-didecanoylchitosan, *O*-succinyl chitosan was synthesized with *N*-phthaloylchitosan as an intermediate. In this procedure several steps are necessary to avoid phthaloylation of $-NH_2$ group, *O*-acylation, and at the end of the synthetic process the protected amino group is removed by N_2H_4 . In recent years, a procedure is reported in which *O*-acylation of chitosan is carried out by methyl sulfonate [32].

5.8 Thiolated Chitosan

The chitosan is modified by adding $-NH_2$ group with $-SH$ prompts the arrangement of $-SH$ functionalized chitosan are water-loving larger molecules displaying non bonded $-SH$ group clusters at the polymer spine. Up until now 4 kinds of $-SH$ functionalized chitosan have been prepared: conjugated species as chitosan-4-thiobutylamidine, chitosan-cysteine, and chitosan-thioethylamidine conjugate. Numerous characteristics of chitosan are enhanced by particular stagnancy of $-SH$ bunches assigning it to the auspicious new classification of $-SH$ monomers utilized as a part of specific for the in the spreadable organization of water loving large molecules [34].

5.8.1 Mucous Adhesion Properties

Another promising property of chitosan is mucous adhesion because of charged connections among the cationic polymeric $-NH_2$ group and adversely ionic $C_{11}H_{19}NO_9$ and $C_6H_6O_3S$ of the mucus. These mucous adhesive characteristics of chitosan can enhance by the immobilization of thiol bunch on the polymer. The improvement of mucous adhesion can be clarified by the S^{2-} bonds development with cysteine enriched subdomains of subdomains sugar bonded proteins, which are more forceful than non-covalent bonds. This hypothesis was reinforced by the

tensile strength results obtained with tablets of –SH functionalized chitosan, which exhibited a cationic connection among the level of adjustment with –SH containing moieties and the adhesive characteristics of the polymer [35].

5.8.2 Increase in Permeable Properties

The saturation of marker that is present between intestinal mucous layers of cells can be improved 1-3-fold using thiolated chitosan as compared to virgin chitosan. Chitosan has the pervasion upgrading capacities with increment in the intercellular passage of absorption, which is vital for the transportation of water-loving substances (peptides and antisense oligonucleotides used for therapy) through the membrane. The working principle beneath this diffusion upgrading impact is by all accounts in light of the cations of the polymer, which cooperate with the cell layer bringing about an auxiliary revamping of tight intersection related proteins [36].

The pervasion upgrading impact of chitosan can be emphatically enhanced by the stagnancy of –SH groups. The take-up of light named bacitracin, for example, was enhanced 1.6-fold using 0.5% of chitosan–cysteine conjugate rather than virgin chitosan. The pervasion enhancing the impact of –SH functionalized chitosan has been examined with penetration mediator glutathione which shows that chitosan–TBA/GSH is a possibly profitable instrument for repressing the ATPase action of P-gp (P-glycoprotein) in the digestive tract [35].

5.8.3 Cohesive Properties

The chitosan with reduced –SH works on the chitosan chain permit –SH modified chitosan to develop inter and intra-molecular atomic S^{2-} bonds bringing about cross-linking of the polymeric chains. Subsequently –SH modified chitosan show, other than their solid mucous adhesive and saturation improving characteristics and incredible durable quality. This quality gives a robust attachment and strength of transporting networks being founded on –SH modified chitosan and can ensure a delayed managed discharge of installed therapy agent. –SH modified chitosan present in situ gelling capabilities because of –SH groups oxidation at physiological pH-values, which bring about the development of disulfide bonds (inter and intra-molecular). To use –SH modified chitosan in nasal, buccal, vaginal, and ocular mucous treatment, it needed to be crosslinked and in situ gelling at pH ranging between 5 and 6 [37].

5.9 Sulfate Modified Chitosan

Sulfate derivatives of a chitosan exhibit quite significant group of chitosan-based materials that can show a wide range of bio-based activities. Sulfonation is carried

out using various reagents including oleum, concentrated sulfuric acid, sulfur trioxide, sulfur trioxide/trimethylamine, chlorosulfonic acid–sulfuric acid, sulfur trioxide/pyridine, sulfur trioxide/sulfur dioxide, tetrahydrofuran, and formic acid over wide ranges of temperature or with help of microwave irradiation. On chitosan, the additional sulfa group can be further substituted to form sulfanilamide derivatives of chitosan followed by the reaction among $-\text{NH}_2$ or $-\text{OH}$ (C6 position) groups [38].

Such types of chitosan sulfates possess anti-coagulant and iron agglutination control activities because of the chemical structural resemblance to heparin. In addition to that chitosan, sulfates have shown other biological activities such as antioxidant, anti-sclerotic, anti-viral, anti-HIV, anti-bacterial, and enzyme control activities. Sulfation of chitosan results in the conversion of some of the $-\text{NH}_2$ groups to negative ion centers and the polymer with improved multi electrolyte characteristics which can be used for generating potential drug transporters microcapsules or micelles form. *N*-Alkyl-*O*-sulfated chitosan show amphiphilic character as it consists alkyl substituted polymer chains having water repelling nature and SO_4^{2-} groups with water-loving nature. Both waters loving and repelling polymer converted into micelles which physically entrap drugs that are water-insoluble as taxol in substantial concentration. Another very promising quality of chitosan sulfates is sorption that is used for recovering metal ions [39].

5.10 Phosphorylated Chitosan

Phosphorous acid and formaldehyde are allowed to react with chitosan either in consecutive phases or at the same time in an acidic solution in water give condition to form a single or double bond of nitro-phosphonic-methylene chitosan. The framework of phosphorylated chitosan materials and a number of rearrangements reliant on reaction conditions, reactant ratio, and most significantly reaction time. H_3PO_4 modified chitosan is prepared in the P_2O_5 —the $\text{CH}_4\text{O}_3\text{S}$ system also. Using H_3PO_4 modified chitosan; the novel gel beads mixed with multi electrolyte have produced for ibuprofen drug as model medication by utilizing a gel that is ionotropic with P_3O_{10} for managed drug conveyance framework management during oral intake by keeping away from the medicine discharge in the exceptionally acidic gastric liquid area of the stomach. The pre-modified chitosan can likewise be stretched out with P comprising groups for instance the $-\text{COOH}$ group of CH_3COO^- chitosan created to respond with $-\text{NH}_2$ of phosphatidylethanolamine managing both acidic and basic polymer. This polymer was explored for its practicality as a conveyance transporter for the transfection of hydrophobic model drug ketoprofen by shaping dots on ionic cross-linking by sodium tripolyphosphate [40].

5.11 Enzymatic Modification of Chitosan

To modify chitosan another approach can be done by using enzymes and this method is thought-provoking because of its particularity and ecological benefits in comparison with chemo functionalization. Enzymes present the likelihood of removing the threats related to chemical substances in term of to health and safety. Enzymatic grafting of phenol species on the chitosan was first studied by Payne et al. to analyze aqueous solubility in a basic environment (Scheme 17). Quercetin and rutin quinones were effectively synthetically connected to low molecular weight chitosan. The quercetin-adjusted chitosan demonstrated an improvement of plastic, cancer prevention agent and antimicrobial properties and in addition to that also showed thermal degradability [41].

5.12 Graft Copolymers of Chitosan

Chitosan physio-chemical properties can be changed by graft copolymerization which is an attractive system for expansion of their application. The characteristics of the side chains, as well as atomic structure, length, and number comprehensively manage the attributes of the subsequent unite copolymers. Up till now, numerous research projects were carried out to study the effects of these parameters on the connecting factors and the features of polymer grafted chitosan [42].

5.12.1 Grafting Co-polymerization by Radical Production

Various types of polymeric species such as poly (vinyl and acrylic) artificial precursors are the most often grafted on polysaccharides. Radical polymerization is commonly used to prepare copolymers. In the archetypal method of free radicals production in which during first step free radical attached at backbone structure of polymeric chain followed by these free radicals react as large initiators for small repeating agents. The grafting % age and grafting efficacy are mainly achieved by initiator type precursor and initiator amount, reaction time and temperature [43].

5.12.2 Polycondensation to Form Co-polymerization

Grafting co-polymer of polysaccharides is not often prepared by condensation polymerization typically due to the vulnerability of the sugar chain backbone to elevated temperature and punitive conditions of the characteristic polycondensation reactions. The condensation polymerization process has successfully produce lactic acid, LA grafted chitosan of D, L-lactic acid in nonappearance of a catalyst which generates a pH-sensitive hydrogel. The polylactide condensation has also

been attained by application of catalyst 4-dimethylaminopyridine in which polylactide was attached through the OH^{-1} group's phthaloyl chitosan. $-\text{NH}_2$ group is linked to chitosan by condensation through carbodiimide process on the surface of PLA to increase the stickiness, strength and cell compatibility of human endothelial cells [42].

5.12.3 Coupling to Copolymerize via Oxidation

Polyaniline is polymerized on the chitosan to form conductive polymers by a well-known process called oxidative coupling. Copolymerization is not generally utilized for getting grafted copolymers of a long chain of sugar for the most part because of the vulnerability of the saccharide at elevated temperature and extreme conditions required for performing polycondensation reaction. However, the pH-sensitive hydrogel was formed by successful graft copolymerization of lactic acid (LA) over chitosan by condensation without catalyst which results in a hydrogel that is pH-sensitive. Another method is used to connect—an NH_2 group of chitosan onto the polylactic acid surface which is carbodiimide procedure to make good cell compatibility grip and bolster the expansion of human endothelial cells [44].

5.13 *Film-Forming Properties of CS*

The inherent film forming ability and antimicrobial character enable chitosan to make potential use in the packaging industry. However, chitosan forms rigid films so required plasticizers in order to lower frictional forces (hydrogen bonds or ionic forces) among polymer chains, for the enhancement of mechanical properties. The induction of polyols for the fabrication of film may overcome this problem and allows the film to be mechanically stable for the required time period. Chitosan films also offer a well-established application that is food packaging which reduces oxygen permeability and water vapour permeability that results in the increased storage of food product by giving it longer shelf life [45] (Fig. 5).

5.14 *Chitosan and Proteins*

The combination of chitosan with other hydrocolloids results in improvements of functional features of chitosan-based films. Chitosan and pectin coated membranes have been formed by the interface of the chitosan (positive ion groups) with pectin (negative ion groups). This combination results in lowering of water vapour transmission rates (WVTRs) has been observed. The physical and mechanical characteristics of these biobased membranes were improved by joining various

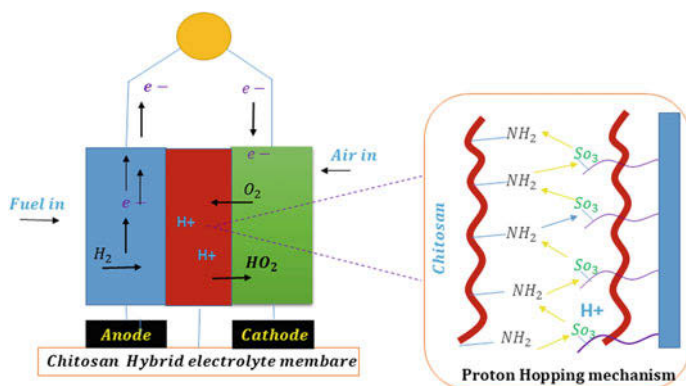


Fig. 5 Cs based membrane in fuel cell application

types of proteins including soy protein, collagen, gelatin and milk proteins with polysaccharides (e.g. alginates, chitosan, starches and cellulose) [46]. Gelatin and chitosan combination results in fabrication of homogeneous membrane because of the better miscibility among both biopolymers results into the improvement of characteristics of the thus formed mixed membranes as compared polymers films. The betterment in mechanical perspectives occurred due to development of electrostatic forces among chitosan ammonium groups and the gelatin carboxylate groups. However incomplete miscibility among polymer and protein results brittle structure as in the case of chitosan/soy protein blended membranes and phase separation occurs. The brittles are increases upon increasing protein contents. Such type of studies were aimed to develop edible films with anti-bacterial properties [47].

5.15 Chitosan and Starch Blends

Food packaging requires good mechanical properties as a basic necessity that must be edible coatings and films to enhance manual or machinery based food handling or pharmaceutical products. Tapioca and rice are two main materials that are used as starch sources that are used to form blends with chitosan and produce edible food coatings, the consequential films possess dynamic properties better than one single polymer. In South America famous crop is tapioca. The membranes produced by this food product have good physical properties like tasteless, odourless, colourless and oxygen impermeability. The only drawback associated with these membranes is brittleness that results in insufficient mechanical strength. The blending of tapioca and chitosan with the plasticizing agent of glycerol was first done by Chillo et al. During their research they investigated mechanical, dynamic mechanical and ostensible viscosity of the film-forming solution [48].

The mechanical strength is critical for eatable plastic films and covering to enhance mechanical treatment of food item or medicinal stuff. Starch from custard and rice has been combined with chitosan to utilized mix qualities than from the single polymer alone. Custard edible films show suitable physical attributes since they have no colour and taste and also impermeable to oxygen. Be that as it may, films demonstrate weakness with insufficient mechanical strength Chillo et al. have prepared (CS) and custard starch films with and glycerol (plasticizer). The mechanical properties, water vapour porousness and shade of the mix films have been examined and improvement was found [49].

The effect of biodegradable mixture of CS ratios on TS films was investigated. The results showed that improvement in TS of TS of prepared occurred by the maximum induction of chitosan was done 1:1 ratio of chitosan and starch was used. The enhancement in TS of the films upon increase of rice starch and chitosan ratios (2:1–0.5:1) is attributed to the development of hydrogen bonding between molecules of chitosan (NH_2) and the hydroxyl group of rice starch (OH). Amylopectin and amylose are attractive raw materials may use as obstacles in packaging films. They utilized for the preparation of bio-decompose able films to replace plastics partially or entirely as they are less expensive and renewable as well as better mechanical strength. To decrease the water vapour permeability of the films starch was blended with different proteins which also increases tensile strength [50].

5.16 Edible Membranes of Gelatin and Chitosan

The edible coating and membranes made up of the composite are fabricated to obtain combine benefits of every constituent. While proteins and polysaccharides are used as a strong polymer matrix, lipids give the best barrier toward vapours of water. As chitosan and gelatin both possess water loving character with better attraction as well as matching, they produce membranes of composite materials with improved characteristics. Chitosan/gelatin composite has been utilized widely for the synthesis of frameworks in biomedical applications. Rivero et al. prepare gelatin/chitosan, composite biodegradable films and investigate membrane barrier properties and structural power and to analyze their micro to the nanostructure. The composite has a showed even and regular upper layer as examined by Scanning Emission Microscopy and X-ray analysis. The influence molecular mass of chitosan along with the level of deacetylation on the physical and chemical characteristics of the prepared membrane was determined. Results exposed that bonding among chitosan and gelatin were stronger in films composed of larger molecular mass chitosan or greater level of deacetylation as compare to films made up of low molar mass or deacetylation level [51].

5.17 Composite of Chitosan, Carrageenan and Alginate

Membranes based upon alginate are impenetrable into lipids at the same time as other water-loving long chains of sugar molecules which also possess water vapour permeability. Though, a sacrificing agent used in the membrane is alginate gel film in which membrane lost its own water content prior to the loss of food water content. Polyelectrolyte produced by mixing of chitosan with both carrageenans and alginates which were utilized to get microstructure capsules of cell embodiment and gadgets for the managed arrival of medicine or different materials. It appears there is great probability to examine this collaboration to create consumable membranes from these substances which could be of implausible esteem [52].

5.18 Chitosan and Clay Natural Polymers

Natural polymers are hydrophilic in nature so they have the low mechanical strength and high moisture barrier. Many different types of methods have been discovered to improve such kind of problems associated with biodegradable packaging films made up of chitosan [53].

These may include induction of plasticizing agents (glycerol) to increase the flexibility in the final product. In other methods silicates nanoparticles (e.g. sodium montmorillonite MMT) are added into chitosan to enhance barrier and mechanical characteristics of end-user product. MMT is a layered silicate having increased thickness and surface area and thickness enables its use for strengthening uses. The literature reported the synthesis and characterization of MMT/chitosan-based composites and membranes. Chitosan and MMT interact with each other and develop homogenous film. In an ion exchange reaction of nanocomposites based upon MMT/Chitosan occur among chitosan and sodium MMT. The chitosan offered high attraction toward montmorillonite host. Powder X-ray diffraction and Thermogravimetric analysis (TGA) and analysis showed that due to electrostatic interaction among cationic chitosan molecules and anionic silicate layers the thermal stability of chitosan improved significantly. In addition to that prepared nanocomposites also showed a synergistic effect on antibacterial properties against *S. aureus* and *E. coli* certain bacterial species [54].

The antibacterial property enhances markedly on increasing amount of MMT. The biodegradation rate of nanocomposites film of chitosan/montmorillonite is also the most prevalent than that of the virgin Chitosan polymer. These results showed that MMT/CS nanocomposites have potential antimicrobial applications especially for those comprising 0.1% of MMT. Chitosan/montmorillonite bio-based composite microparticles showed more temperatures of thermal degradation as compared to pristine particles of chitosan. The glycerol and MMT were added into chitosan and the dual effect is examined by a group of researchers. The structural

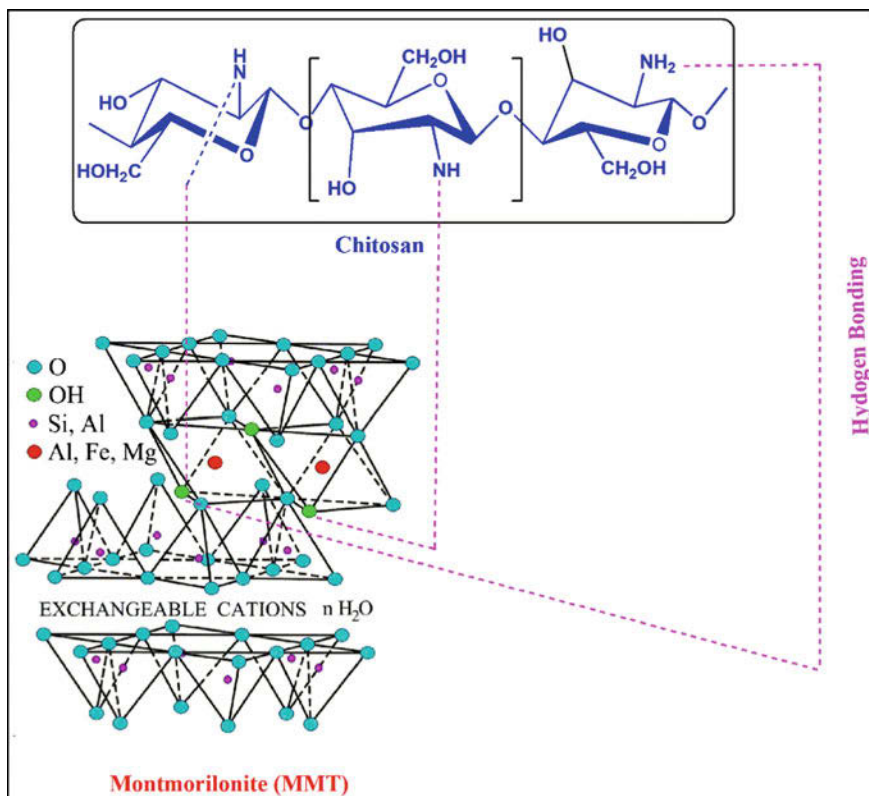


Fig. 6 CS/MMT composite membrane

strength of glycerol-based nanocomposites was increased by increasing clay loading. This is because of synergistic impacts of both plasticizing agents and clays [55] (Fig. 6).

Hydrogen bonding framework was modified by glycerol inside the material which permits the good combination of matrix with filler, which in turn simplifies strain transformation among the supporting matrix phase to enhance mechanical strength. 30% water vapour incorporation decreases by glycerol phase addition. Hydrogen bonding of montmorillonite and chitosan was significantly reduced by glycerol that blocks flocculation and breaks the montmorillonite stacks that are randomly arranged in space. The membranes of chitosan prepared without glycerol show 50% reduced permeability because of flocculation and alignment of montmorillonite stacks. Because of these frameworks material has good capability to use the membrane in the field of packaging. Glycerol adjusts the hydrogen bonding inside the substance and allows good cooperation amongst filler and matrix, subsequently encouraging the pressure to the support stage and enhancing its powerful properties [55].

5.19 Properties of Gas Permeability of Edible Coatings

The number of many eatable membrane coverings for fruits for example cellulose, zein, soy protein, chitosan and casein. They possess many required properties such as no taste and odour along with transparency. Though, oxygen permeability can be enhanced by antibacterial activity which was managed by adding potassium sorbate in starch-based membranes used for sweet potato coverings. But oxygen impermeability can better be achieved by composite membranes of chitosan and starch. 15% addition of chitosan, the starch of sweet potato source showed incredibly lower oxygen permeability. There are a few conceivable edible coatings for natural products, for example, soy protein, cellulose, casein, zein, and chitosan. These were picked since they have the attractive qualities of for the most part being transparent, odourless, and tasteless [56].

5.20 Antimicrobial Applications

Cations present in chitosan makes material an antimicrobial agent. The advances in the field of antimicrobial material need characteristics found in chitosan. It is a non-toxic polymer with dynamic antimicrobial properties that may be used as an excellent matrix for eatable coating membranes. The chitosan bonding or chelation with endotoxins related to the bacterial type of Gram-negative reduced the toxicity of such bacteria. Due to this good chelating property, EDTA like external chelating agents is not necessary. This property made chitosan good inhibitor of a wide range of microbes such as viruses, bacteria and fungi etc. [57].

5.21 Anti-inflammatory Applications

Chitosan has a range of encouraging biomedical applications and right now, is considered as another inventive material in wound healing, a hemostatic agent, antimicrobial, lipid binding effects as demonstrated by the substantial number of reports throughout the most recent couple of years. Chitosan films that are planned for wound administration may incite absence of pain by giving a good, charming and relaxing impact when connected uncovered skin or injured part. Chitosan possess fantastic agony helps when it was connected as a covering agent to open injuries, for example, burnt skin and scraped spots, skin grafted regions and skin sores [58].

Because of anti inflammatory impacts of chitosan, it provides benefits for the management of delayed swelling and sore at the injury site. Chitosan which is water solubility strangles the discharge and possession of pro-inflammatory cytokines and induction of NO₂ to prepare astrocytes which is common nerve cells in CNS and is effectively associated with inflammatory events related to the cytokine. In addition,

N-acetylglucosamine is anti-inflammatory drug and is prepared in the human body from glucose. Chito-oligosaccharides (atomic weight of 5 kDa) demonstrated preferred hostile to inflammatory specialists over nonsteroidal against swelling. Chitosan applies anti-selling impacts by restraining protein possession and weakening the pre-inflammatory cytokines [59].

5.22 Biomedical Applications of Chitosan

Chitosan is used in different health care disciplines and hygienic applications, such as carrier, wound treatment, gene distribution, and bone tissue manufacturing. Chitosan is used to prepare artificial kidney membrane, it is applied in hypocholesterolemic agents, and supports for immobilized enzymes and drug delivery systems, absorbable sutures. Chitosan has many benefits due to its nontoxicity and biodegradability without damaging the environment. It slowly breaks down to harmful products that are absorbed completely in the body as it is biocompatible [60] (Fig. 7).

5.23 Chitosan-Based Composite Scaffolds in Wound Healings

The biocompatibility of composite nanofibers of chitosan/sericin was manufactured by electrical spinning having a great texture with a small diameter between 200 and

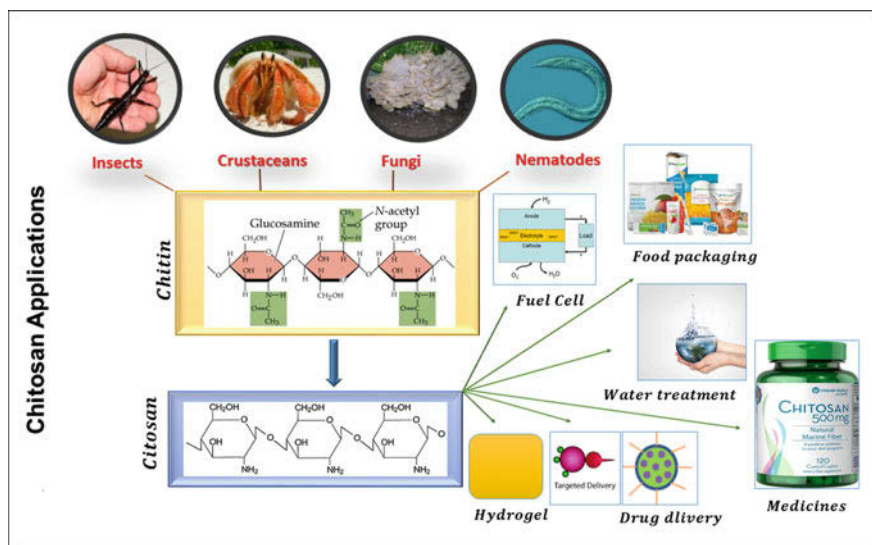


Fig. 7 Applications of chitosan

400 nm. As these composite membranes have property to block the activity of gram positive and negative bacteria so can be used as wound dressing membranes. They also have cell multiplication property so heal the wounds in short time in approximate 24 h and more than 90% at all test exhibiting the benign and biocompatible nanofibres toward cells [61].

AgS based alginate/chitosan membranes are good for wound healing as silver has sensitizing properties while chitosan and alginate heal the wound by covering. The particular sulfonation of oxide ion and additionally chitosan may create a powerful anti-retroviral agent that shows a substantially higher inhibition impact on the contamination of AIDS infection. The managed $C_{10}H_9AgN_4O_2S$ discharge was appeared with incorporated chitosan layers with water vapour vanishing, satisfactory swelling capacity, cytocompatibility and delayed antibacterial action [62].

The iron oxide, chitosan and gelatin-based nanofiber composite membranes show enhanced antibacterial properties along with the mechanical support that possesses a material with more promising wound dressing abilities. The freezing-thawing method was used to develop chitosan/PVA/chitosan/MMT nanocomposite as a biocompatible wound dressing. Enhanced mechanical characteristics, as well as other features including good swelling behavior biocompatibility and antibacterial activity, made it required a candidate for wound dressing applications [63].

The sponge-like dressings in light of glutamate chitosan (large molar mass) and sericin was produced for the cure of older skin sores. The sericin measurements improved skin healing is appropriate to apply a defensive impact on oxidative harm to human fibroblasts. In addition, the upgraded bandage can enhance fibroblast expansion, that is, to enhance injury recuperating. Several studies conducted the research utilization of $scCO_2$ as an environmentally benign media to actuate chitosan porosity frameworks. Sponges of chitosan with cross-linking stacked of anti-toxin medicines the norfloxacin were set up by dissolvable vanishing system [64].

6 Introduction to Chitin

Chitin is obtained from the exoskeleton of crustacea, creepy crawlies, and a few fungi [65]. The fundamental business wellsprings of chitin are the shrimps, krills, lobsters, and crab waste shells. On the planet, a millions of tons of chitin are reaped every year and subsequently, this biopolymer provides an inexpensive and accessible source [5, 66] (Fig. 8).

In chitin, the degree of acetylation (DA) is ordinarily 0.90 showing the occurrence of amino groups. The *N*-acetylation, i.e. the proportion of 2-acetamido-2-deoxy-d-glucopyranose to 2-amino-2-deoxy-d-glucopyranose basic units strikingly affects its solubility and structural properties [67] (Fig. 9).

The polymorphic types of chitin vary in the arrangement and polarities of neighbouring chains in progressive polymer chain [68]. For the most part, the individual chains expect a basically straight texture, which experiences one full coil

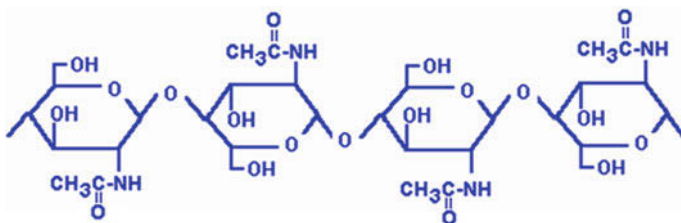


Fig. 8 The molecular structure of chitin

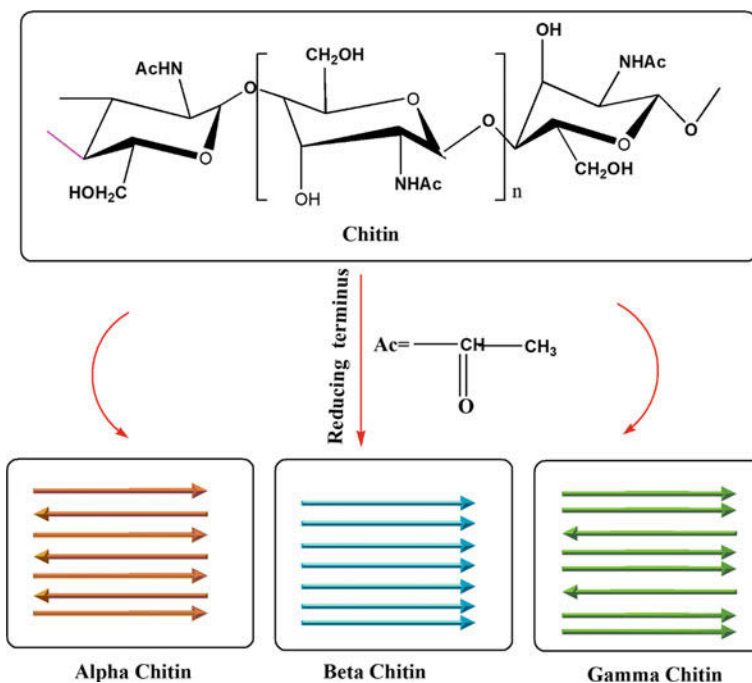


Fig. 9 The polymorphic types of chitin

each having diameter 10.0–10.49 Å along the axis of the chain. Since the chain contain chiral glycosidic units, and all units are associated by an oxygen atom that connections carbon one of one glycosidic unit to carbon four of a neighbouring unit, a particular “left” and “right” arrangement can be allotted to every polymeric chain. The most widely recognized chitin allomorph is known as A-conformation [69], where unit cell possess orthorhombic form while individual polymer chains show antiparallel design. In this manner, contiguous chains are situated in inverse ways. Another less regular allomorph termed as b-conformation relates to a

monoclinic unit cell having polymer chains arranged parallel form by weaker intermolecular bonding. A third shape, c-chitin, have two parallel chains parallel form in a relationship with chain arranged in an antiparallel way [70]. This may be reflected as a variation of a shape. XRD and NMR studies of these distinct allomorphic forms have been shown to be different [71, 72].

7 Chemical Modifications of Chitin

Chitin is a synthetic biopolymer with excellent stability. a-chitin in view of its insoluble nature it is seldom exposed to chemical reaction with the exception of the synthesis of chitosan following by deacetylation. b-Chitin has generally more reactive in nature [73]. As indicated by Noishiki et al. b-chitin can be changed into thermodynamically more stable a-chitin by treating with NaOH (20%) followed by resining with DI water. Chitin has been handled in an assortment of approaches to get altered physicochemical characteristics [74]. Vincendon prepared chitin solution in phosphoric acid (H_2SO_4) at ambient temperature, he observed that viscosity and molar mass were decreased with time but the degree of acetylation remain unchanged. The chitin is first allowed to disperse in NaOH (concentrated solution) and kept at room temperature for 3–5 h; the obtained basic chitin is then poured into ice at 0 °C. This system permitted the synthesis of chitin membrane with great mechanical strength and transparency. The prepared chitin is indistinct and by maintaining specific circumstances, it can be broken down in the presence of water. This wonder is explained by the fact of to the lowering of molecular weight under basic environment and deacetylation to some extent [75–77].

It is cleared that to obtain water dissolvable chitin, the level of deacetylation must be almost near to 50% and, likely, that the acetyl group must be consistently dispersed along the chain to keep pressing of chains causing from the interruption of the second configuration in the strong alkaline medium. The impact of this disruption was inspected and it was demonstrated that the dispersion, irregular or blockwise arrangement, is imperative in regulating structural characteristics. Deacetylation around 51%, of an exceedingly deacetylated chitin within the sight of acidic anhydride, produce a water-dissolvable derivative [78].

The chitin derivatives reported in literature are phosphoryl chitin carboxymethyl chitin [79], hydroxyalkyl chitin [13], *N*- and *O*-sulfated chitin, hydroxybutyl chitin [80], fluorinated chitin [81], (diethyl amino)ethylchitin [82], mercapto chitin and chitin carbamates [83]. Chitin can be blended with regular or manufactured polymers; and can be cross-linked using various crosslinking agents (TEO, epichlorohydrin, glutaraldehyde, and so forth.) to modify and obtain desired properties [84].

8 Chitin Fiber Formation

Chitin sutures have noteworthy characteristics over different other fibers for biomedical applications. One study showed that chitin fibers have practically identical characteristics to as those lactide and collagen fibers have. The linear chain framework of chitin is enables it to form fibers and film alike to cellulose fibers. The existence of the microfibrils in chitin that are typically engrained in a matrix of protein showed the possibility of chitin spinning into fibers. The polyamide-type structure ought to be separated to empower solubilization of chitin into a dissolvable form. This needs either softening or disintegration in apt solvents. Melting turning is discounted as chitin deteriorates before softening. Regarding this many endeavours have been carried out to control disintegration of chitin and turning of chitin and chitosan into fiber shape. The arrangement of chitin fibers for the creation of suture with absorbing capacity, dressings, and decomposable substrates for the development of human skin cells filaments has been accounted so for [85, 86] (Fig. 10).

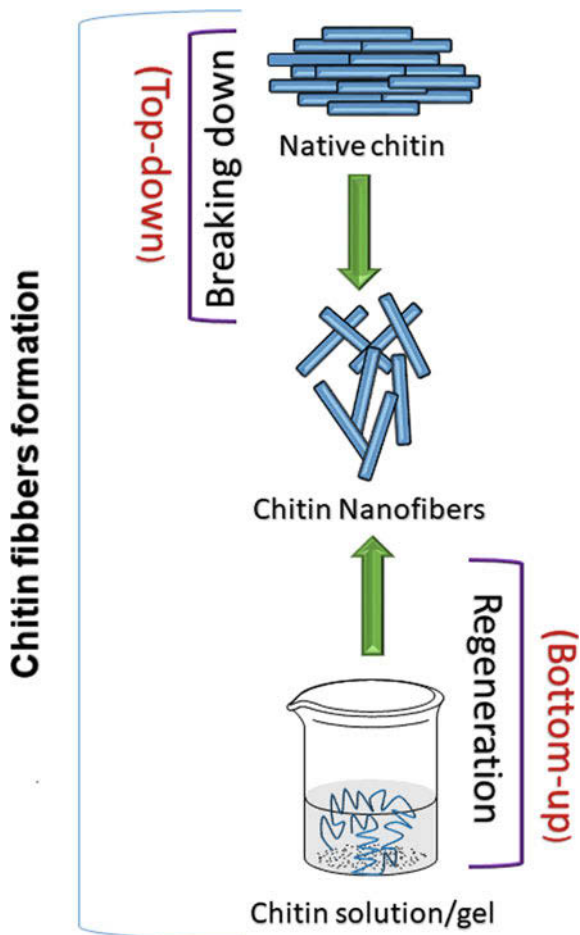
9 Preparation of Blends with Other Fibers/Polymers

The induction of chitin fibers into various synthetic polymers, composites or blend results in wide range of interesting characteristics. Young and Eichhorn discussed the process chitin fiber formation in detail. In the synthesis of blend composed of alginate and chitin, the spinning of their mixture solution was carried out by a spinneret with a coagulating bath having aqueous CaCl_2 and ethanol. The durable interface developed via the intermolecular hydrogen bonding was utilized to certify excellent miscibility. The good dry tensile strength and elongation to break were gained with 30 wt% of chitin content. While the tensile strength and elongation to break lowered by further increasing chitin content (water-soluble). Moreover, the addition of chitin into the blended fiber can enhance the water-holding characteristics of the blended fiber comparable to pristine alginate fiber [13, 87].

The treatment of chitin fibers with silver nitrate solution were results in enhancement of great antibacterial activity to *Staphylococcus aureus*. Noteworthy change in properties have been accounted for mixes of chitin/CS fibers with different natural and synthetics fibers to obtain chitin–glycosaminoglycans, chitin–silk fibroin, chitin–cellulose, chitin–cellulose–silk fibroin, and chitin–cellulose–silk fibroin, CS–tropocollagen, and chitin–natural rubber blends. The incorporation of chitin fibers in poly(lactic acid) polymer indicated reasonable mechanical properties and maintenance for settling destructive bone cracks, yet likely had lacking solidness for applications, for example, bone plates for settling cortical bone breaks [88].

Extraordinary properties could be worked by suitable compound alteration to create a progression of chemically modified fibers, for example, *N*-acylCSs,

Fig. 10 Chitin fiber formation



N-arylidene- and *N*-alkylidene CSs, *N*-acetylCS, chitin-tropocollagen and CS-transition metal complexes. The crystallinity and surface charge thickness of the deacetylated chitin can be expanded on treatment with hydrochloric acid treatment to enhance the fiber properties. It ought to be noticed that East and Qin utilized warmth treatment for getting regenerated by reaction (*N*-acetylation) between CS and acetic acid. The best properties for rigidity (4 g/d) and modulus (100 g/d) for chitin were accounted for by the blended ester of chitin or CS acetic acid derivation/format polymer [89].

The utilization of chitin whisker course might be useful getting ready high-quality fibers. A further change in fiber properties could be accomplished with the utilization of spinning fiber from lyotropic fluid crystalline solution. Fiber spinning from fluid crystalline solution has huge benefits for expanded quality and different properties. Irradiation of chitin fibre-strengthened poly (caprolactone)

composite demonstrated 45% change in rigidity and pliable modulus as for those of the untreated examples. Polymers, for example, polyvinylpyrrolidone, methylcellulose, and sulfite cellulose are accounted for to be utilized to change the properties of chitin filaments added to the spinning solution. Encourage change in fiber properties could be affected through suitable synthetic alterations [90].

10 Chitin General Characterization

The name 'chitin' is gotten from the Greek word 'chiton', which means a layer of mail [91]. The utilization of chitin was first depicted by the French scientific expert, Henri Braconnot in 1811. The structure of chitin ($C_8H_{13}O_5N$)_n shows resemblance with cellulose structure, yet with 2-acetamido-2-deoxy- β -D-glucose (NAG) monomer units, which are joined to each other by means of $\beta(1 \rightarrow 4)$ linkages. The material type of chitin is generally a white and hard nitrogenous polysaccharide which is inelastic. It has also been considered to be the main cause of beach contamination in coastal areas. The widespread presence of chitin in the biosphere and its insolubility prompted the possibility that chitin ought to survive in fossils. There have for sure been reports of fossilized chitinous materials, e.g., in Pogonophora and in insect wings preserved inside amber. The immunogenicity of chitin (disregarding nearness of nitrogen in its structure) is uncommonly low. Chitin is a very insoluble material that takes after cellulose in its low dissolvability and chemical non-reactivity.

Chitin now and then is thought to be a cellulose derivative; be that as it may, it doesn't happen in cellulose creating creatures. There is no, by and large, acknowledged classification concerning the level of *N*-deacetylation of chitin and its derivatives. Chitin has a high level of nitrogen (6.89%) contrasted with artificially substituted cellulose derivatives that must be set up with a lower nitrogen content (1.25%). The vast majority of the normally happening polysaccharides, e.g., alginic, dextran, cellulose, pectin, corrosive, agar, agarose and carrageenan are nonpartisan or acidic in nature, while chitosan is an example of a profoundly fundamental polysaccharide. Other remarkable properties of chitin composite include improvement of capacity to frame films, biocompatibility, biodegradability, non-poisonous quality, atomic adsorption properties, and so on. Despite a few reports demonstrating the synthesis of functionalized chitosan derivatives with chemical modification of the amino acid, not very many of these have worthy dissolvability by and large natural solvents, or binary dissolvable frameworks. Some synthetically adjusted chitin and chitosan derivatives having enhanced dissolvability all in all natural solvents have been accounted for.

11 Chemical Structure and Properties

The individual sugar units in chitin structure are turned 180° concerning each other, and pairs develop the disaccharide *N,N'*-diacetylchitobiose [(GlcNAc)₂] [75, 92, 93]. The single polymer chains can be depicted as helices, in which each sugar unit is transformed as for its neighbours. Such a structure prompts high strength as the inflexible strips are associated with 03-H → 05 and 06-H → 07 hydrogen bonds. Chitin additionally has three distinctive crystalline allomorphs: the α -, β - and γ -shapes depending upon the orientation of microfibrils [94].

The commonest type of chitin is α -chitin. Its unit cell is made out of two *N,N'*-diacetylchitobiose units shaping two chains in an antiparallel course of action. Along these lines, nearby polymer chains keep running in inverse ways, held together by 06-H → 06 hydrogen bonds, and the chains are held in sheets by 07 → H-N hydrogen bonds [95]. This gives a factual blend of $-\text{CH}_2\text{OH}$ orientation identical to a large portion of the oxygen molecules on every residue, having the capacity to develop intra and intramolecular hydrogen bonds. This outcome in two unique kinds of amide group; all are engaged in the development of interchain C=O → H-N bonds, while 50% of the amide group additionally fact as acceptors for 06-H → O=C intramolecular hydrogen bonds. Development of these intermolecular hydrogen bonds prompts a significant stable structure [96].

β -chitin is a less regular type of chitin, where the unit cell is a *N,N'*-diacetylchitobiose unit, giving a polymer balanced out as a rigid and inflexible ribbon, by 03 → 05 intramolecular similar as α -chitin, H-bonds [97]. The chains in this structure are joined in sheets by C=O → H-N H-bonds among the amide group and by the $-\text{CH}_2\text{OH}$ side chains, which prompts development of intersheet H-bonds to the carbonyl oxygens on the neighbouring chains (06-H → 07). This gives a structure of parallel poly-*N*-acetylglucosamine chains having no intersheet H-bonds. The parallel game plan of polymer chains in β -chitin takes into consideration more adaptability than the antiparallel gameplan found in α -chitin, yet the resultant polymer still has massive quality [98].

γ -Chitin is the third allomorph, having blended parallel and antiparallel configuration. It is found in mushrooms [99]. Chitin is constantly found to be cross-linked to other auxiliary segments except for the β -chitin found in diatoms. Chitin is discovered covalently clung to glucans in the fungal cell wall, either directly attached, as in *Candida albicans* (1) or by means of peptides. Also, in insects and other invertebrates, chitin is constantly connected with particular proteins, with both covalent and noncovalent holding. This affiliation implies it creates the observed ordered framework. There are likewise differing degrees of mineralization, for example, calcification, and sclerotization, including associations with phenolic and lipids [95]. In organisms (fungi and invertebrates) there have been studied different degrees of deacetylation, providing a continuum of structure among chitin (fully acetylated) and chitosan (fully deacetylated) [100]. Although either acids or alkalis can be utilized to deacetylate chitin, the fact that glycosidic bonds are more

vulnerable to acid which would damage the chain, the alkali deacetylation procedure is used more often [101].

N-deacetylation of chitin can be carried out by or homogeneous or heterogeneous reaction mixture [94]. The difference amongst chitin and chitosan with various degrees of deacetylation isn't strict. Setting a couple of special cases aside, chitin founds naturally related with other basic polymers like proteins or glucans, which frequently contribute over half of the mass in chitin-containing tissue [102]. Chitin can be *N*-deacetylated to such a degree, to the point that it gets noticeable solubility in dilute acidic and formic acids. The acetylated units of chitin prevail and the degree of acetylation is normally 0.90, while chitosan is a partially or fully *N*-deacetylated derivative possess a degree of deacetylation of greater than 0.65. Numerous analytical techniques have been utilized to find out degree of deacetylation such as IR spectroscopy, gel permeation chromatography, pyrolysis gas chromatography, and UV-vis spectrophotometry, solid-state NMR, H NMR spectroscopy, thermal analysis, acid hydrolysis, separation spectrometry methods, various titration schemes, HPLC and infrared spectroscopy [91].

12 Chitin Biosynthesis

The process of biosynthesis and cellular processing of chitin is very complicated, multi-faceted and interconnected sequence of occasions which begins intracellularly and ends up in inclusion of chitin in external supra-macromolecular framework such as cuticles, arthropod and fungi cell walls [103, 104].

The whole process consists of different distinct steps:

1. Successive biotransformation of sugars (specifically glucose or trehalose). This step comprises biochemical reactions such as amination, phosphorylation, and development of the enzymic substrate.
2. Chitin synthase (CS) prepares the chains. The CS enzyme is a part of a protein/carbohydrate cluster which is narrowly topologically packed molecules. Such types of organization confirm the amalgamation of nascent chitin polymers into a crystalline fibril.
3. The configuration of chitin molecules which have long chains.
4. Polymer translocation over the plasma membrane.
5. Crystallization and development of microfibrils by inter-chain hydrogen bonding.
6. Association with arthropod cuticular proteins or with other carbohydrates in fungal cell walls.

Chitosomes are cytoplasmic microvesicles. These microvesicles have been distinguished by electron microscopy utilizing fungal frameworks [105, 106]. The plenitude of chitosomes at the hyphal tip infers their critical part in CS trafficking to pre-decided areas. Chitosomes begin from organelles, for example, endoplasmic

reticulum and Golgi. Chitosomes vesicles having zymogenic chitosan bunch. After fusion of the chitosomes with the plasma membrane, the chitosan units become activated through proteolytic reactions [107].

After in the long run combination of the chitosomes with the plasma film, the chitosan units become triggered via proteolytic reactions. Chitosan addition into plasma layers includes the intervention of focusing on and recognition proteins. Chitosome-like structures likewise have been accounted for in without cell framework derived from insects [108]; be that as it may, it has not been elucidated whether they are associated with in vivo chitin development. Also, chitosome-like vesicles have not yet been depicted in intact insect epidermal cells. Diverse types of chitin are combined with the activity of the catalyst, chitin synthase UDP-*N*-acetyl-D-glucosamine [109] chitin4- β -*N*-acetylglucosaminyl-transferase. Chitin synthase utilizes UDP-*N*-acetylglucosamine (UDPGlcNAc) as the enacted sugar donor to create the chitin polymer. Candy and Kilby first proposed a chitin blend biosynthetic pathway in insects. The proposed process began with glucose and finished with UDP-GlcNAc. Jaworski et al. utilizing cell extricates from the southern armyworm *Spodoptera eridania*, at last, settled the entire pathway from UDP-GlcNAc to chitin. Results obtained from many subsequent studies conducted with synthesis from different insects reinforced the molecular mechanism of this pathway [110] (Fig. 11).

13 Industrial Processing of Chitin

The detachment of chitin from crustaceans, for example, crayfish, crab, shrimp, and different creatures such as fungi is a tedious procedure [111] It needs 17–72 h including 1–24 h of HCl treatment and NaOH processing of 16–48 h. This time taking chitin isolation process needs more energy expenditure, and consequently builds the cost of generation. Similar to crabs and shrimps, barnacles likewise have a place with the Crustacea family. Their shell structures are less crystalline and they are accounted for to contain a greater number of minerals than different individuals from the crustacean family [112]. These minerals are for the most part made up of calcite and calcium phosphate. It has been demonstrated that these two mineral materials in the carapace can be effortlessly expelled from the carapace structure by utilizing HCl. In such animals, the protein just has some bonds with the chitin so it can be expelled from effortlessly due to low-crystalline shell structure of the barnacle species. In this manner, chitin isolation from barnacle species would be a nearly speedy process. *Chelonibia patulais* (a barnacle species in the subphylum Crustacea), lives episodically on animals (turtles, crabs, whales and molluscs) or on rocks at the seashore where there is shallow water is present. In a method of the segregation of chitin from *C. spatula* shells, their demineralization is carried out in 1 M HCl for 10 min and then allowed to deproteinized in 2 M NaOH for 20 min. The finishing of the entire procedure takes just 30 min. It begins with HCl dribbling solution (1 M) over 10 g of the dust acquired from ground *C. spatula* shells along

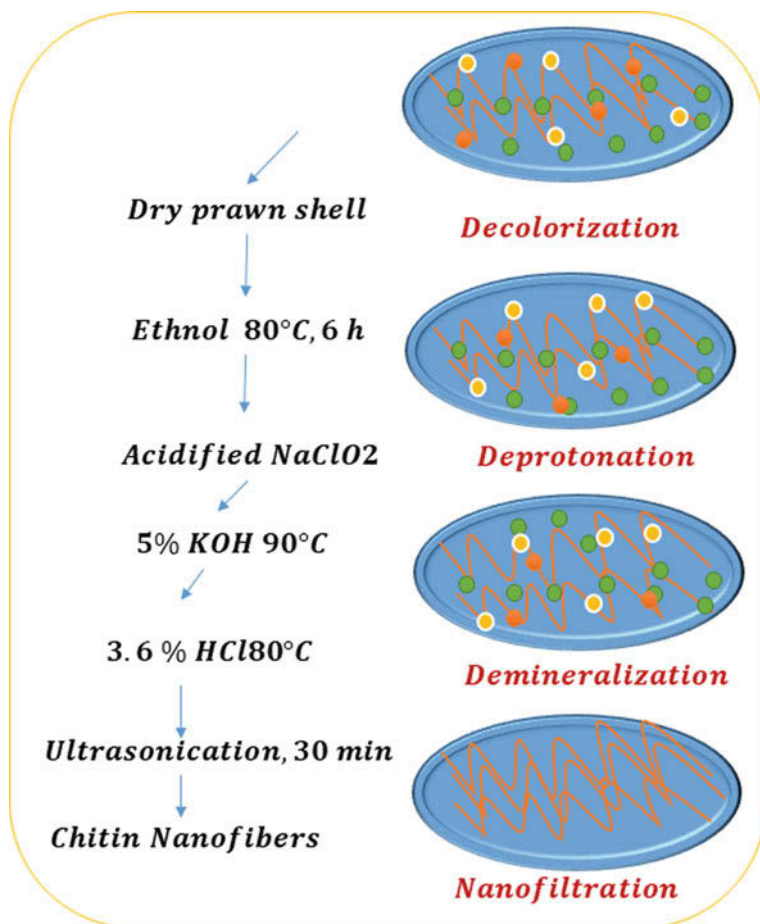


Fig. 11 Development of chitin nanofibers

and allowed to stir at room temperature for 10 min. In the event that the HCl is included too rapidly, an energetic effervescence happens that may prompt flooding. The sample at that point ought to be flushed with refined water until the point when neutral pH esteem is gotten. In an investigation, subsequent to drying the examples in an oven, 376 mg of material stayed toward the finish of the procedure. Considering that most of the first mass comprised of minerals, these have been expelled by methods of HCl.

Proteins are also present in shells and are removed by a deproteinization procedure by refluxing with a base for 20 min. This process yields 311 mg of dry chitin. Getting chitin from shrimp shells is related with food industries, for example, shrimp handling, while the creation of chitosan–glucan from parasitic mycelia is related with fermentation, for example, that such as that producing citric acid from

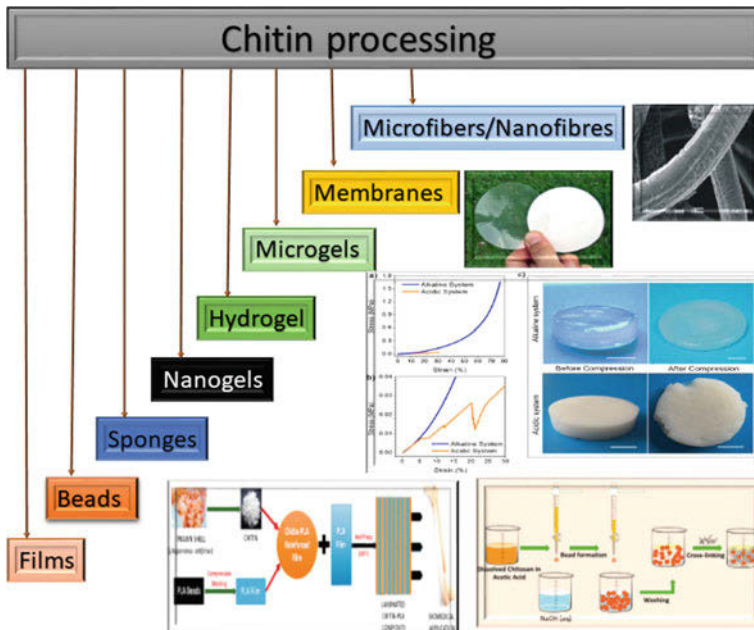


Fig. 12 Chitin processing

Aspergillus niger. For the most part, crustacean shells processing includes the expulsion of proteins and after that disintegration of calcium carbonate, which is available in the shells in a higher amount. The conventional method for obtaining chitosan from these sources additionally includes deacetylation in 40% sodium hydroxide at 120 °C for 1–3 h. This treatment gives 70% deacetylated chitosan [91] (Fig. 12).

As of late, a “green transformation” of agroindustrial waste by utilizing biological activity of Cunninghamella elegans strains and Rhizopus arrhizus has been accounted for the production of chitin and chitosan. Such industrial sources have noteworthy points of interest such as avoiding allergic reactions in individuals susceptible to shellfish antigens and reduction in time and cost of production [113].

14 Chitin Biomedical and Nanomedical Applications

14.1 Tissue Engineering

The principal motivations behind tissue building can be arranged as to repair, supplant, keep up, or upgrade the capacity of a specific tissue or organ [114]. Chitin-based materials, which can be manufactured into tubular structures, can be effectively connected in tissue designing of nerves and veins as a format for cells.

Chitin-based frameworks are flexible items and can be optimized for some, regenerative purposes [115]. Chitin has been effectively connected to create polymer platforms in tissue designing. Some fundamental prerequisites to plan polymer platforms are high porosity (with apt pore measure dispersion); biodegradability, structural integrity, being non-dangerous to cells; biocompatibility; collaborating with the cells to advance cell attachment; empowering cell work.

14.2 Wound Healing

Madhumathi et al. created α -chitin/nanosilver composite frameworks for wound healing usage. These frameworks were known to have an antibacterial movement toward *S. aureus* and *E. coli*, and also blood-clotting capacity. Such properties have made them helpful nanostructures for wound healing applications. So also, the β -chitin/nanosilver composite platforms has been created and examined for this application utilizing β -chitin hydrogel composed of silver nanoparticles. Also, these frameworks were assessed for their cell grip properties utilizing Vero cells, and the outcomes showed that nanosilver consolidated chitin platforms were perfect for wound healing applications [22] (Fig. 13).

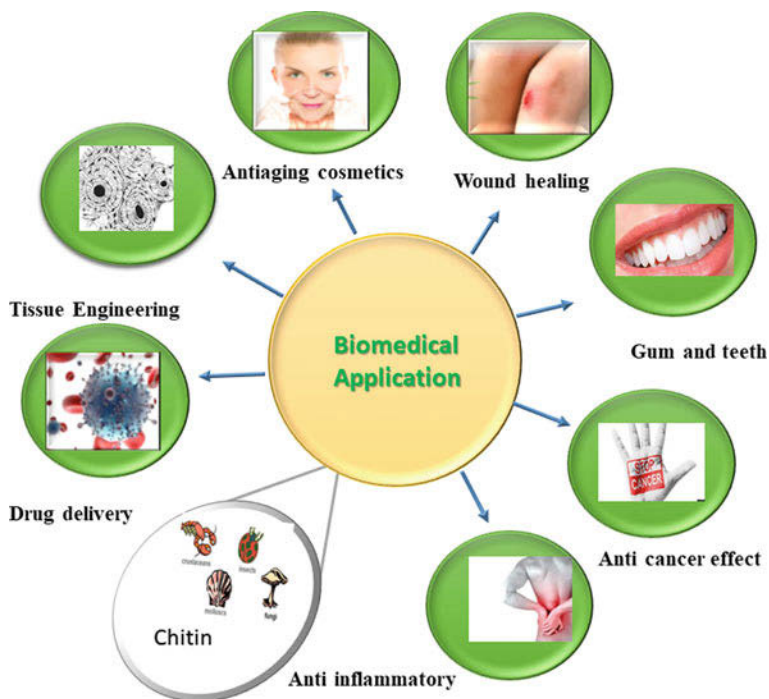


Fig. 13 Chitin applications

14.3 Drug Delivery

Carboxymethyl chitin (CMC) has been mostly used for delivery of many different kinds of drugs. CMC nanoparticles were synthesized via a cross-linking with CaCl_2 and FeCl_3 . A spherical morphology was observed in SEM images of CMC nanoparticles, with diameters ranging from 200 to 250 nm. 5-fluorouracil (5-FU) drug-loaded nanoparticles also exhibited alike morphological feature. In one study the anticancer drug 5-FU was laden into CMC nanoparticles using emulsion cross-linking technique, and these were found to have a sustained and controlled drug-release profile at pH near to neutral. An anti-HIV drug delivery application was also reported by Dev et al. [116] using poly(lactic acid) (PLA)/CS nanoparticles [116]. In addition, lamivudine (antiretroviral drug) was laden into the PLA/CS nanoparticles. In this case absorption spectrophotometry was used to evaluate the encapsulating efficiency and the in vitro drug release performance of CS nanoparticles along with drug [117, 118].

Water-dissolvable carboxymethyl chitin (CMC) was utilized to deliver drugs. CMC nanoparticles were prepared by cross-linking CaCl_2 and FeCl_3 . A circular morphology was seen in SEM photos of CMC nanoparticles, having diameter running from 200 to 250 nm. 5-fluorouracil (5-FU) loaded stacked nanoparticles likewise demonstrated comparable morphology. MTT examine comes about demonstrated that they were non-poisonous to typical fibroblast L929 mouse cells. The hydrophobic anticancer medication 5-FU was stacked into CMC nanoparticles by means of an emulsion cross-connecting strategy, and these were found to have a controlled and managed sedate discharge profile at pH-6.8. A hostile to HIV drug delivery application was likewise revealed by Dev et al. [116] utilizing poly (lactic acid) (PLA)/CS nanoparticles. What's more, lamivudine (a hydrophilic antiretroviral tranquillize) was stacked into the PLA/CS nanoparticles. For this situation absorption spectrophotometry was utilized to assess the effectiveness and the in vitro drug discharge behaviour of PLA/CS nanoparticles with loaded drugs.

14.4 Cancer Diagnosis

The new advance FA-based carboxymethyl chitosan (CMCS) facilitated to manganese doped zinc sulfide (ZnS:Mn) quantum dots (FA-CMCS- ZnS:Mn) composite nanoparticles were created by Mathew et al. [119]. This multifunctional framework could be utilized for focusing on, controlled drug release and tumour cell imaging. The chosen anticancer medication was 5-FU, which is utilized for breast tumour treatment. L929 cells were utilized to affirm the non-harmfulness of FA-CMCS- ZnS:Mn nanoparticles. Moreover, the MCF-7 breast cancer cell line was utilized to consider imaging, particularly focusing on and cytotoxicity of the drug stacked nanoparticles. The in vitro imaging of malignancy cells with the nanoparticles was examined utilizing fluorescence microscopy [120].

14.5 Chitin-Based Dressings

British Textile Technology Group (BTTG) protected a system for preparing chitin-based fibrous dressing [121]. In this strategy, the chitin/chitosan strands were acquired from microorganisms (rather than shrimp shells) and were not created by the conventional fibre-spinning method. The strategy can be outlined as follows:

1. The arrangement of mycelia of micro-fungi from *Mucor mucedo* culture developing in a supplemented medium.
2. Cleaning and deproteinizing of the mycelial matt with NaOH to chitin/chitosan precipitates.
3. Blanching and further cleaning.
4. Arrangement and scattering of the filaments utilizing the paper-production hardware.
5. Filtration and wet-laid synthesis of a fiber matt; extra mechanical quality furnished by blending with different filaments [122].

14.6 Antiaging Cosmetics

Morganti et al. prepared block copolymer nanoparticles (BPN) made out of phosphatidylcholine and linoleic acid nanocomposite along with hyaluronan and chitin nanofibrils (PHHYCN). The nanoconstructs were utilized to encapsulate items including cholesterol, melatonin, caffeine, creatine, vitamin E and C, glycine, amino acids, and arginine. The thought was to utilize these nanocarriers for skin revival, as all the individual components had demonstrated some action in such manner. The skin treated with the dynamic chitin nanofibrils with BPN was appeared to be milder softer as well as more hydrated following one month of treatment. Both fine wrinkles and wrinkle lines were diminished not long after the initial 15 days of treatment with injectable dynamic chitin nanofibril containing BPN, too less occurrence of telangiectasia, hence over-all face appearance was particularly ameliorated during the reversion period [123].

15 Conclusion

Chitosan is derivative of chitin is obtained from natural sources that are the external skeleton of crustaceans, fungi, and insects and has to be biocompatible and decomposable. The chitosan history begins in the 19th century, by Rouget 1859 who discussed the deacetylated parent chitin polymer (the second most plenteous carbohydrate) in nature first time. The surface functionalization of chitosan can be done using different enzymes so-called enzymatic modification. There is a variety

of chitosan derivatives which have been prepared and utilized in the different field of life such as quaternized chitosan and *N*-alkyl chitosan *N*-Acyl chitosan, *O*-Acyl chitosan and Thiolated chitosan which is used in edible coatings to prevent gas permeability.

The crystallinity and polymorphism of chitosan are highly dependent on the beginning of the polymerization and extraction in thorough process. The inherent film forming ability and antimicrobial character enable chitosan to make potential use in the packaging industry. Chitosan is also utilized in direct methanol fuel cell barrier of its excellent methanol permeation property.

The utilization of chitin was first depicted by the French scientific expert, Henri Braconnot in 1811. The structure of chitin ($C_8H_{13}O_5N$)_n shows resemblance with cellulose structure, yet with 2-acetamido-2-deoxy- β -D-glucose (NAG) monomer units, which are joined to each other by means of $\beta(1 \rightarrow 4)$ linkages. Chitin additionally has three distinctive crystalline allomorphs: α -, β - and γ -shapes depend upon the orientation of microfibrils. There is a variety of field where chitin is and its derivatives are being used among than most important ones are Tissue engineering and Antiaging cosmetics.

References

1. de Britto D, Celi Goy R, Campana Filho SP, Assis OB (2011) Quaternary salts of chitosan: history, antimicrobial features, and prospects. *Int J Carbohydr Chem*
2. Dash M, Chiellini F, Ottenbrite R, Chiellini E (2011) Chitosan—a versatile semi-synthetic polymer in biomedical applications. *Prog Polym Sci* 36(8):981–1014
3. Bu X, Pei J, Zhang F, Liu H, Zhou Z, Zhen X et al (2018) The hydration mechanism and hydrogen bonding structure of 6-carboxylate chitoooligosaccharides superabsorbent material prepared by laccase/TEMPO oxidation system. *Carbohydr Polym*
4. Ahmed S, Ikram S (2017) Chitosan: derivatives, composites and applications. Wiley
5. Arrouze F, Essahli M, Rhazi M, Desbrieres J, Tolaimate A (2017) Chitin and chitosan: study of the possibilities of their production by valorization of the waste of crustaceans and cephalopods rejected in Essaouira. *J Mat Environ Sci: Journal of Materials and Environmental Science* 8(7):2251–2258
6. Hattori H, Tsujimoto H, Hase K, Ishihara M (2017) Characterization of a water-soluble chitosan derivative and its potential for submucosal injection in endoscopic techniques. *Carbohydr Polym* 175:592–600
7. Hamed I, Özogul F, Regenstein JM (2016) Industrial applications of crustacean by-products (chitin, chitosan, and chitoooligosaccharides): a review. *Trends Food Sci Technol* 48:40–50
8. Feng Y, Kopplin G, Sato K, Draget KI, Vårum KM (2017) Alginate gels with a combination of calcium and chitosan oligomer mixtures as crosslinkers. *Carbohydr Polym* 156:490–497
9. Gokara M, Kimavath GB, Podile AR, Subramanyam R (2015) Differential interactions and structural stability of chitosan oligomers with human serum albumin and α -1-glycoprotein. *J Biomol Struct Dyn* 33(1):196–210
10. Ji X, Li B, Yuan B, Guo M (2017) Preparation and characterizations of a chitosan-based medium-density fiberboard adhesive with high bonding strength and water resistance. *Carbohydr Polym* 176:273–280
11. Cheon JY, Lee HM, Park WH (2018) Formation of silver nanoparticles using fluorescence properties of chitosan oligomers. *Mar Drugs* 16(1):11

12. Naqvi S, Moerschbacher BM (2017) The cell factory approach toward biotechnological production of high-value chitosan oligomers and their derivatives: an update. *Crit Rev Biotechnol* 37(1):11–25
13. Pillai C, Paul W, Sharma CP (2009) Chitin and chitosan polymers: chemistry, solubility and fiber formation. *Prog Polym Sci* 34(7):641–678
14. Ahmed S, Ikram S (2016) Chitosan based scaffolds and their applications in wound healing. *Achievements Life Sci* 10(1):27–37
15. Thanou M, Florea B, Geldof M, Junginger H, Borchard G (2002) Quaternized chitosan oligomers as novel gene delivery vectors in epithelial cell lines. *Biomaterials* 23(1):153–159
16. Liu B, Wang D, Yu G, Meng X (2013) Adsorption of heavy metal ions, dyes and proteins by chitosan composites and derivatives—a review. *J Ocean Univ China* 12(3):500–508
17. Prashanth KH, Tharanathan R (2007) Chitin/chitosan: modifications and their unlimited application potential—an overview. *Trends Food Sci Technol* 18(3):117–131
18. Polnok A, Borchard G, Verhoef J, Sarisuta N, Junginger H (2004) Influence of methylation process on the degree of quaternization of N-trimethyl chitosan chloride. *Eur J Pharm Biopharm* 57(1):77–83
19. LogithKumar R, KeshavNarayan A, Dhivya S, Chawla A, Saravanan S, Selvamurugan N (2016) A review of chitosan and its derivatives in bone tissue engineering. *Carbohydr Polym* 151:172–188
20. Peng Y, Han B, Liu W, Xu X (2005) Preparation and antimicrobial activity of hydroxypropyl chitosan. *Carbohydr Res* 340(11):1846–1851
21. Araldi SJ, Tudryn GJ, Hart CE, Carlton AJ (2017) Chemically modified mycological materials having absorbent properties: Google patents
22. Jayakumar R, Chennazhi K, Muzzarelli R, Tamura H, Nair S, Selvamurugan N (2010) Chitosan conjugated DNA nanoparticles in gene therapy. *Carbohydr Polym* 79(1):1–8
23. Krause T, Baumeister J, Weber D, Lang G, Beyer A, Florig E et al (2005) Hair treatment compositions containing N-hydroxy-alkyl-O-benzyl chitosans and methods of using same: Google patents
24. Karp J, Joshi N, He X, Bhagchandani S (2017) Self assembled gels for controlled delivery of encapsulated agents to cartilage: Google patents
25. Yin T, Zhang Y, Liu Y, Chen Q, Fu Y, Liang J, Huo M (2018) The efficiency and mechanism of N-octyl-O, N-carboxymethyl chitosan-based micelles to enhance the oral absorption of silybin. *Int J Pharm* 536(1):231–240
26. Sashiwa H, Aiba S-I (2004) Chemically modified chitin and chitosan as biomaterials. *Prog Polym Sci* 29(9):887–908
27. Chtchigrovsky M, Primo A, Gonzalez P, Molvinger K, Robitzer M, Quignard F, Taran F (2009) Functionalized chitosan as a green, recyclable, biopolymer-supported catalyst for the [3 + 2] Huisgen cycloaddition. *Angew Chem* 121(32):6030–6034
28. Srbová J, Slovákova M, Křípalová Z, Žárská M, Špačková M, Stránská D, Bílková Z (2016) Covalent biofunctionalization of chitosan nanofibers with trypsin for high enzyme stability. *React Funct Polym* 104:38–44
29. Auzély-Velty R, Rinaudo M (2002) New supramolecular assemblies of a cyclodextrin-grafted chitosan through specific complexation. *Macromolecules* 35(21):7955–7962
30. Martel B, Devassine M, Crini G, Weltrowski M, Bourdonneau M, Morcellet M (2001) Preparation and sorption properties of a β -cyclodextrin-linked chitosan derivative. *J Polym Sci Part A: Polym Chem* 39(1):169–176
31. Wang J, Chen C (2014) Chitosan-based biosorbents: modification and application for biosorption of heavy metals and radionuclides. *Biores Technol* 160:129–141
32. Badawy ME, Rabea EI, Rogge TM, Stevens CV, Smagghe G, Steurbaut W, Höfte M (2004) Synthesis and fungicidal activity of new N,O-acyl chitosan derivatives. *Biomacromolecules* 5(2):589–595
33. Sun T, Zhu Y, Xie J, Yin X (2011) Antioxidant activity of N-acyl chitosan oligosaccharide with same substituting degree. *Bioorg Med Chem Lett* 21(2):798–800

34. Zahir-Jouzani F, Mahbod M, Soleimani M, Vakhshiteh F, Arefian E, Shahosseini S, Atyabi F (2018) Chitosan and thiolated chitosan: novel therapeutic approach for preventing corneal haze after chemical injuries. *Carbohydr Polym* 179:42–49
35. Ways TM, Lau WM, Khutoryanskiy VV (2018) Chitosan and its derivatives for application in mucoadhesive drug delivery systems. *Polymers* 10(3):267
36. Chaffanel F, Charron-Bourgoin F, Soligot C, Kebouchi M, Bertin S, Payot S et al (2018) Surface proteins involved in the adhesion of *Streptococcus salivarius* to human intestinal epithelial cells. *Appl Microbiol Biotechnol*, 1–15
37. Leitner V, Marschütz M, Bernkop-Schnürch A (2003) Mucoadhesive and cohesive properties of poly (acrylic acid)-cysteine conjugates with regard to their molecular mass. *Eur J Pharm Sci* 18(1):89–96
38. Yuan N-Y, Tsai R-Y, Ho M-H, Wang D-M, Lai J-Y, Hsieh H-J (2008) Fabrication and characterization of chondroitin sulfate-modified chitosan membranes for biomedical applications. *Desalination* 234(1–3):166–174
39. Zhang C, Ping Q, Zhang H, Shen J (2003) Preparation of N-alkyl-O-sulfate chitosan derivatives and micellar solubilization of taxol. *Carbohydr Polym* 54(2):137–141
40. Shanmugam A, Kathiresan K, Nayak L (2016) Preparation, characterization and antibacterial activity of chitosan and phosphorylated chitosan from cuttlebone of *Sepia kobsiensis* (Hoyle, 1885). *Biotechnol Rep* 9:25–30
41. Karaki N, Aljawish A, Humeau C, Muniglia L, Jasniewski J (2016) Enzymatic modification of polysaccharides: mechanisms, properties, and potential applications: a review. *Enzyme Microb Technol* 90:1–18
42. Thakur VK, Thakur MK (2014) Recent advances in graft copolymerization and applications of chitosan: a review. *ACS Sustain Chem Eng* 2(12):2637–2652
43. Zhou T, Zhu Y, Li X, Liu X, Yeung KW, Wu S, Chu PK (2016) Surface functionalization of biomaterials by radical polymerization. *Prog Mater Sci* 83:191–235
44. Carreira A, Gonçalves F, Mendonça P, Gil M, Coelho J (2010) Temperature and pH responsive polymers based on chitosan: applications and new graft copolymerization strategies based on living radical polymerization. *Carbohydr Polym* 80(3):618–630
45. Kim KM, Son JH, Kim SK, Weller CL, Hanna MA (2006) Properties of chitosan films as a function of pH and solvent type. *J Food Sci* 71(3)
46. Twu Y-K, Huang H-I, Chang S-Y, Wang S-L (2003) Preparation and sorption activity of chitosan/cellulose blend beads. *Carbohydr Polym* 54(4):425–430
47. Xu Y, Du Y (2003) Effect of molecular structure of chitosan on protein delivery properties of chitosan nanoparticles. *Int J Pharm* 250(1):215–226
48. Xu Y, Kim KM, Hanna MA, Nag D (2005) Chitosan–starch composite film: preparation and characterization. *Ind Crops Prod* 21(2):185–192
49. Chillo S, Flores S, Mastromatteo M, Conte A, Gerschenson L, Del Nobile MA (2008) Influence of glycerol and chitosan on tapioca starch-based edible film properties. *J Food Eng* 88(2):159–168
50. Vázquez MB, Flores SK, Campos CA, Alvarado J, Gerschenson LN (2009) Antimicrobial activity and physical properties of chitosan–tapioca starch based edible films and coatings. *Food Res Int* 42(7):762–769
51. Nagahama H, Maeda H, Kashiki T, Jayakumar R, Furuike T, Tamura H (2009) Preparation and characterization of novel chitosan/gelatin membranes using chitosan hydrogel. *Carbohydr Polym* 76(2):255–260
52. Cheng L, Bulmer C, Margaritis A (2015) Characterization of novel composite alginate chitosan-carrageenan nanoparticles for encapsulation of BSA as a model drug delivery system. *Curr Drug Deliv* 12(3):351–357
53. Darder M, Colilla M, Ruiz-Hitzky E (2005) Chitosan–clay nanocomposites: application as electrochemical sensors. *Appl Clay Sci* 28(1–4):199–208
54. Günster E, Pestreli D, Ünlü CH, Atıcı O, Güngör N (2007) Synthesis and characterization of chitosan-MMT biocomposite systems. *Carbohydr Polym* 67(3):358–365

55. Hsu S-H, Wang M-C, Lin J-J (2012) Biocompatibility and antimicrobial evaluation of montmorillonite/chitosan nanocomposites. *Appl Clay Sci* 56:53–62
56. Mohammadi R, Mohammadifar MA, Rouhi M, Kariminejad M, Mortazavian AM, Sadeghi E, Hasanvand S (2018) Physico-mechanical and structural properties of eggshell membrane gelatin-chitosan blend edible films. *Int J Biol Macromol* 107:406–412
57. Hai TAP, Sugimoto R (2018) Surface modification of chitin and chitosan with poly (3-hexylthiophene) via oxidative polymerization. *Appl Surf Sci* 434:188–197
58. Santos-Moriano P, Fernandez-Arrojo L, Mengibar M, Belmonte-Reche E, Peñalver P, Acosta F, Fernández-Lobato M (2018) Enzymatic production of fully deacetylated chitooligosaccharides and their neuroprotective and anti-inflammatory properties. *Biocatal Biotransform* 36(1):57–67
59. Vasconcelos DP, Costa M, Neves N, Teixeira JH, Vasconcelos DM, Santos SG et al (2018) The use of chitosan porous 3D scaffolds embedded with resolvin D1 to improve in vivo bone healing. *J Biomed Mat Res Part A*
60. Singh G, Manohar M, Arya SK, Siddiqui WA, Stenström TA (2017) Potential biomedical applications of chitosan–and chitosan-based nanomaterials. *Chitosan Deriv Compos Appl*, 385–408
61. Cremar L, Gutierrez J, Martinez J, Materon L, Gilkerson R, Xu F, Lozano K (2018) Development of antimicrobial chitosan based nanofiber dressings for wound healing applications. *Nanomed J* 5(1):6–14
62. Heidari F, Bahrololoom ME, Vashae D, Tayebi L (2015) In situ preparation of iron oxide nanoparticles in natural hydroxyapatite/chitosan matrix for bone tissue engineering application. *Ceram Int* 41(2):3094–3100
63. Jayakumar R, Prabakaran M, Kumar PS, Nair S, Tamura H (2011) Biomaterials based on chitin and chitosan in wound dressing applications. *Biotechnol Adv* 29(3):322–337
64. Choi YS, Lee S, Hong SR, Lee Y, Song K, Park M (2001) Studies on gelatin-based sponges. Part III: a comparative study of cross-linked gelatin/alginate, gelatin/hyaluronate and chitosan/hyaluronate sponges and their application as a wound dressing in full-thickness skin defect of rat. *J Mat Sci: Materials in Medicine* 12(1):67–73
65. Srinivasan H, Kanayairam V, Ravichandran R (2018) Chitin and chitosan preparation from shrimp shells *Penaeus monodon* and its human ovarian cancer cell line, PA-1. *Int J Biol Macromol* 107:662–667
66. Abdelmalek BE, Sila A, Haddar A, Bougateg A, Ayadi MA (2017) β -Chitin and chitosan from squid gladius: biological activities of chitosan and its application as clarifying agent for apple juice. *Int J Biol Macromol* 104:953–962
67. Kabalak M, Aracagök YD, Torun M (2017) Extraction and physicochemical properties of chitins from four different insect species
68. Sudha PN, Saranya M, Gomathi T, Gokila S, Aisverya S, Venkatesan J, Anil S (2017) Perspectives of chitin- and chitosan-based scaffolds dressing in regenerative medicine. *Chitosan Deriv Comp Appl*, 253–269
69. Yu Z, Lau D (2017) Flexibility of backbone fibrils in α -chitin crystals with different degree of acetylation. *Carbohydr Polym* 174:941–947
70. Akpan E, Gbenebor O, Adeosun S (2018) Synthesis and characterisation of chitin from periwinkle (*Tympanotonus fusatus* (L.)) and snail (*Lissachatina fulica* (Bowdich)) shells. *Int J Biol Macromol* 106:1080–1088
71. Gbenebor OP, Akpan EI, Adeosun SO (2017) Thermal, structural and acetylation behavior of snail and periwinkle shells chitin. *Prog Biomat* 6(3):97–111
72. Kaya M, Bağrıaçık N, Seyyar O, Baran T (2015) Comparison of chitin structures derived from three common wasp species (*Vespa crabro* Linnaeus, 1758, *Vespa orientalis* Linnaeus, 1771 and *Vespa germanica* (Fabricius, 1793)). *Arch Insect Biochem Physiol* 89(4):204–217
73. Silva SS, Mano JF, Reis RL (2017) Ionic liquids in the processing and chemical modification of chitin and chitosan for biomedical applications. *Green Chem* 19(5):1208–1220

74. Isono Y, Noishiki Y (2018) Method for manufacturing water-insoluble molded article and water-insoluble molded article: Google patents
75. Roy JC, Salaün F, Giraud S, Ferri A, Chen G, Guan J (2017) Solubility of chitin: solvents, solution behaviors and their related mechanisms. Solubility of Polysaccharides, InTech
76. Tachaboonyakiat W (2017) Antimicrobial applications of chitosan. Chitosan based biomaterials, vol 2. Elsevier, pp 245–274
77. Vincendon M (1997) Regenerated chitin from phosphoric acid solutions. *Carbohydr Polym* 32(3–4):233–237
78. Jothimani B, Sureshkumar S, Venkatachalapathy B (2017) Hydrophobic structural modification of chitosan and its impact on nanoparticle synthesis—a physicochemical study. *Carbohydr Polym* 173:714–720
79. Jayakumar R, Menon D, Manzoor K, Nair S, Tamura H (2010) Biomedical applications of chitin and chitosan based nanomaterials—a short review. *Carbohydr Polym* 82(2):227–232
80. Gulati K, Meher MK, Poluri KM (2017) Glycosaminoglycan-based resorbable polymer composites in tissue refurbishment. *Regenerative Med* 12(4):431–457
81. Cao N, Lyu Q, Li J, Wang Y, Yang B, Szunerits S, Boukherroub R (2017) Facile synthesis of fluorinated polydopamine/chitosan/reduced graphene oxide composite aerogel for efficient oil/water separation. *Chem Eng J* 326:17–28
82. Yu C, Kecen X, Xiaosai Q (2018) Grafting modification of chitosan. Biopolymer grafting. Elsevier, pp 295–364
83. Badawy ME, Rabea EI (2017) Chitosan and its modifications as biologically active compounds in different applications. *Adv Physicochem Properties Biopolym (Part 2)*, 1
84. Olicón-Hernández DR, Uribe-Alvarez C, Uribe-Carvajal S, Pardo JP, Guerra-Sánchez G (2017) Response of *ustilago maydis* against the stress caused by three polycationic chitin derivatives. *Molecules* 22(12):1745
85. Swatloski RP, Barber PS, Opichka T, Bonner JR, Gurau G, Griggs CS, Rogers RD (2017) Process for electrospinning chitin fibers from chitinous biomass solution: Google patents
86. Zou H, Lin B, Xu C, Lin M, Zhan W (2018) Preparation and characterization of individual chitin nanofibers with high stability from chitin gels by low-intensity ultrasonication for antibacterial finishing. *Cellulose* 25(2):999–1010
87. Kong K, Davies RJ, McDonald MA, Young RJ, Wilding MA, Ibbett RN, Eichhorn SJ (2007) Influence of domain orientation on the mechanical properties of regenerated cellulose fibers. *Biomacromology* 8(2):624–630
88. Rinaudo M (2006) Chitin and chitosan: properties and applications. *Prog Polym Sci* 31(7):603–632
89. Khor E, Lim LY (2003) Implantable applications of chitin and chitosan. *Biomaterials* 24(13):2339–2349
90. Khor E (2014) Chitin: fulfilling a biomaterials promise. Elsevier
91. Kumar MNR (2000) A review of chitin and chitosan applications. *React Funct Polym* 46(1):1–27
92. Beier S, Bertilsson S (2013) Bacterial chitin degradation—mechanisms and ecophysiological strategies. *Front Microbiol* 4:149
93. Kumirska J, Weinhold MX, Thöming J, Stepnowski P (2011) Biomedical activity of chitin/chitosan based materials—influence of physicochemical properties apart from molecular weight and degree of N-acetylation. *Polymers* 3(4):1875–1901
94. Younes I, Rinaudo M (2015) Chitin and chitosan preparation from marine sources. Structure, properties and applications. *Mar Drugs* 13(3):1133–1174
95. Friedman AJ, Phan J, Schairer DO, Champer J, Qin M, Pirouz A, Modlin RL (2013) Antimicrobial and anti-inflammatory activity of chitosan–alginate nanoparticles: a targeted therapy for cutaneous pathogens. *J Invest Dermatol* 133(5):1231–1239
96. Gooday GW (1990) The ecology of chitin degradation. *Advances in microbial ecology*. Springer, pp 387–430
97. Badwan AA, Rashid I, Al Omari MM, Darras FH (2015) Chitin and chitosan as direct compression excipients in pharmaceutical applications. *Mar Drugs* 13(3):1519–1547

98. Yen M-T, Yang J-H, Mau J-L (2009) Physicochemical characterization of chitin and chitosan from crab shells. *Carbohydr Polym* 75(1):15–21
99. Ospina Álvarez SP, Ramírez Cadavid DA, Escobar Sierra DM, Ossa Orozco CP, Rojas Vahos DF, Zapata Ocampo P, Atehortúa L (2014) Comparison of extraction methods of chitin from *Ganoderma lucidum* mushroom obtained in submerged culture. *BioMed Res Int*
100. Yang T-L (2011) Chitin-based materials in tissue engineering: applications in soft tissue and epithelial organ. *Int J Mol Sci* 12(3):1936–1963
101. Hajji S, Younes I, Ghorbel-Bellaaj O, Hajji R, Rinaudo M, Nasri M, Jellouli K (2014) Structural differences between chitin and chitosan extracted from three different marine sources. *Int J Biol Macromol* 65:298–306
102. Xu Q, Wang C-H, Wayne Pack D (2010) Polymeric carriers for gene delivery: chitosan and poly (amidoamine) dendrimers. *Curr Pharm Des* 16(21):2350–2368
103. Chen Q, Zhang J-W, Chen L-L, Yang J, Yang X-L, Ling Y, Yang Q (2017) Design and synthesis of chitin synthase inhibitors as potent fungicides. *Chin Chem Lett* 28(6):1232–1237
104. Tang B, Yang M, Shen Q, Xu Y, Wang H, Wang S (2017) Suppressing the activity of trehalase with validamycin disrupts the trehalose and chitin biosynthesis pathways in the rice brown planthopper, *Nilaparvata lugens*. *Pestic Biochem Physiol* 137:81–90
105. Ruiz-Herrera J, Lopez-Romero E, Bartnicki-Garcia S (1977) Properties of chitin synthetase in isolated chitosomes from yeast cells of *Mucor rouxii*. *J Biol Chem* 252(10):3338–3343
106. Wang P, Bi S, Wu F, Xu P, Shen X, Zhao Q (2017) Differentially expressed genes in the head of the 2nd instar pre-molting larvae of the nm2 mutant of the silkworm, *Bombyx mori*. *PLoS One* 12(7):e0180160
107. Cohen E (2001) Chitin synthesis and inhibition: a revisit. *Pest Manag Sci* 57(10):946–950
108. Yang M, Wang Y, Jiang F, Song T, Wang H, Liu Q, Kang L (2016) miR-71 and miR-263 jointly regulate target genes chitin synthase and chitinase to control locust molting. *PLoS Genet* 12(8):e1006257
109. Bowen A, Chen-Wu J, Momany M, Young R, Szaniszlo P, Robbins P (1992) Classification of fungal chitin synthases. *Proc Natl Acad Sci* 89(2):519–523
110. Chen Q, Jin S, Zhang L, Shen Q, Wei P, Wei Z et al (2017) Regulatory functions of trehalose-6-phosphate synthase in the chitin biosynthesis pathway in *Tribolium castaneum* (Coleoptera: Tenebrionidae) revealed by RNA interference. *Bull Entomol Res*, 1–12
111. Kaya M, Sargin I, Tozak KÖ, Baran T, Erdogan S, Sezen G (2013) Chitin extraction and characterization from *Daphnia magna* resting eggs. *Int J Biol Macromol* 61:459–464
112. Kaya M, Karaarslan M, Baran T, Can E, Ekemen G, Bitim B, Duman F (2014) The quick extraction of chitin from an epizoic crustacean species (*Chelonibia patula*). *Nat Prod Res* 28(23):2186–2190
113. Philibert T, Lee BH, Fabien N (2017) Current status and new perspectives on chitin and chitosan as functional biopolymers. *Appl Biochem Biotechnol* 181(4):1314–1337
114. Jayakumar R, Nair S, Furuike T, Tamura H (2010) Perspectives of chitin and chitosan nanofibrous scaffolds in tissue engineering. *Tissue Engineering, Intech*
115. Madhally SV, Matthew HW (1999) Porous chitosan scaffolds for tissue engineering. *Biomaterials* 20(12):1133–1142
116. Dev A, Binulal N, Anitha A, Nair S, Furuike T, Tamura H, Jayakumar R (2010) Preparation of poly (lactic acid)/chitosan nanoparticles for anti-HIV drug delivery applications. *Carbohydr Polym* 80(3):833–838
117. Mourya V, Inamdar NN, Tiwari A (2010) Carboxymethyl chitosan and its applications. *Adv Mat Lett* 1(1):11–33
118. Huang Y, Yao M, Zheng X, Liang X, Su X, Zhang Y et al. (2015) Effects of chitin whiskers on physical properties and osteoblast culture of alginate based nanocomposite hydrogels. *Biomacromolecules* 16(11):3499–3507
119. Mathew ME, Mohan JC, Manzoor K, Nair S, Tamura H, Jayakumar R (2010) Folate conjugated carboxymethyl chitosan–manganese doped zinc sulphide nanoparticles for targeted drug delivery and imaging of cancer cells. *Carbohydr Polym* 80(2):442–448

120. Wu S, Huang Z, Yue J, Liu D, Wang T, Ezanno P, Pan H (2015) The efficient hemostatic effect of Antarctic krill chitosan is related to its hydration property. *Carbohydr Polym* 132:295–303
121. Komi DEA, Sharma L, Cruz CSD (2017) Chitin and its effects on inflammatory and immune responses. *Clin Rev Allergy Immunol*, 1–11
122. Elieh-Ali-Komi D, Hamblin MR (2016) Chitin and chitosan: production and application of versatile biomedical nanomaterials. *Int J Adv Res* 4(3):411
123. Morganti P, Palombo P, Palombo M, Fabrizi G, Cardillo A, Svolacchia F, Mezzana P (2012) A phosphatidylcholine hyaluronic acid chitin–nanofibrils complex for a fast skin remodeling and a rejuvenating look. *Clin Cosmet Invest Dermatol* 5:213

Nanocomposites for Environmental Pollution Remediation



Anjali Bajpai, Maya Sharma and Laxmi Gond

List of abbreviation

BENT	Bentonite
CHT	Chitosan
CNFs	Carbon nanofibers
CR	Congo red
CV	Crystal violet
DB	Disperse blue
DEA	Diethanolamine
FG	Fast green
GL	Gelatine
HAL	Halloysite
LBL	Layer by layer
MB	Methylene blue
MG	Malachite green
MMT	Montmorillonite
MO	Methyl orange
MWCNT	Multiwall carbon nanotubes
NPs	Nanoparticles
OVU	Organovermiculite
PA6	Polyamides 6
PAL	Palygorskite
PFNC	Polymer-functionalized nanocomposites
PLSN	Polymer-layered silicate nanocomposites
POPs	Persistent organic pollutants
RB	Rose Bengal

A. Bajpai (✉) · M. Sharma · L. Gond
Department of Chemistry, Government Science College,
A Centre for Excellence in Science Education, Pachpedi,
Jabalpur 482001, India
e-mail: abs_112@rediffmail.com

© Springer Nature Switzerland AG 2019
Inamuddin et al. (eds.), *Sustainable Polymer Composites and Nanocomposites*,
https://doi.org/10.1007/978-3-030-05399-4_47

1407

RhB	Rhodamine B
RR	Remazol red
SEP	Sepiolite
TEA	Triethanolamine

1 Introduction

Latter half of the past century has witnessed the great industrial revolution, which brought about significant changes in lifestyle. However, this was on the cost of anthropogenic deterioration of the environment, since several irrational industrial and agricultural activities, cause surface water quality degradation. It is the top priority in the twenty-first century to reduce/eliminate heavy metal ions and other contaminants from wastewater to improve water quality [1–3].

1.1 Heavy Metal Pollution

Among all the pollutants present in wastewater, heavy metals are most serious environmental and health threats. The industries, which contribute significantly to emanate potentially toxic metals in surface and ground waters, seriously aggravate the water pollution. The mining and metallurgical industries play a major role in the release of metals loaded effluents in the river network or indirectly by disposing of solid waste containing residual metals in the environment. These mines tailing dumps weather over time, accelerating the mobility of metal ions which are then continuously released into the surface and groundwater. The toxic heavy metal ions can migrate from sediments into the water and pose threat to flora and fauna through bioaccumulation [1–3].

Emissions from mines, metal wastes, gasoline, paints, fertilizers, manure, sewage sludge, pesticides, irrigation, coal combustion, spillage of petrochemicals, atmospheric deposition contaminate the soil with heavy metals. Heavy metals are elements with atomic number greater than 20 and density at least five times greater than that of water. Pb, Cr, As, Zn, Cd, Cu, Hg and Ni ions are commonly found as contaminants [2, 4]. Pb has raised special concerns as it adversely affects the human health and because of its frequent release in wastewaters through effluents coming from smelters and refineries, battery, steel, printing and glass industries [4].

Most of the metals do not undergo microbial or chemical decomposition; hence soil becomes their major sink [5]. However, their chemical forms change (speciation) and their bioavailability become possible. Toxic metals present in soil severely inhibit biodegradation of organic contaminants [6]. Humans and the ecosystem are at risk through direct ingestion or contact with contaminated soil/drinking

groundwater, reduction in agricultural land. The food chain is contaminated through food deteriorated by phytotoxicity. Consequently, the soil ecosystems require characterization, remediation and risk assessment for appropriate protection and restoration [7].

Techniques available for remediation of contaminated sites are immobilization, soil washing and phytoremediation [8]. Despite cost-effectiveness and eco-friendly nature, field applications of these technologies are employed in developed countries only. These techniques are not available in most of the developing countries due to inadequate awareness of inherent advantages and principles of operation. Development of technologies to remediate contaminated sites is attracting the interest of the scientific community.

1.2 Organic Pollutants

Domestic sewage, urban run-off, industrial effluents, agricultural wastewater generate organic pollution. Textile, food processing, pulp/paper making, agriculture and aquaculture industries are the sources of organic pollutants. The decomposition of organic pollutants consumes dissolved oxygen at a rate much greater than its replenishment, thus oxygen depletion adversely affects the stream biota. Organic pollutants present as suspended solids obstruct the light for photosynthesis to aquatic biota, when settled down they affect the habitat of invertebrates residing on the river bed. Common organic pollutants are pesticides, fertilizers, hydrocarbons, phenols, plasticizers, biphenyls, detergents, oils, greases, pharmaceuticals, proteins and carbohydrates. Persistent organic pollutants (POPs) are organic compounds and mixtures such as polychlorinated biphenyls, polychlorinated dibenzo-p-dioxins and dibenzofurans, organochlorine pesticides, such as hexachlorobenzene and dichloro-diphenyl-trichloroethane, dibenzo-p-dioxins and dibenzo-p-furans [9]. POPs have long-range transportability and are toxic and bioaccumulate in animals.

1.2.1 Water Pollution by Synthetic Organic Dyes

Over 100,000 dyes are commercially available and more than 7,00,000 tonnes are produced annually. Synthetic dyes are water soluble and found in trace quantities in industrial effluents. Many of them are also toxic and/or carcinogenic [10]. Inefficient processes of dyeing textile fibres can cause the colourants being released together with the effluents. The presence of dyes in very low concentrations (even 10 ppm) in water imparts a colour, making it undesirable for use [11]. The reactive dyes that are discharged into the water bodies are not biodegradable, hence, are toxic to aquatic life. Usually, removal of hazardous materials is not considered unless an environmental issue is recognized. Removal of dyes from wastewaters is difficult because of their inert properties and their low concentration in wastewater [12, 13]. These problems and their solution have been comprehensively reviewed

taking into account the advantages and disadvantages of purification techniques such as nanotechnology, ultrasound, microwave, catalysis, biosorption, enzymatic treatments, advanced oxidation processes, etc. [14].

1.3 Methods for the Remediation of Pollutants

Environmental pollution has raised worldwide concern. Remediation of natural and anthropogenic contaminants from the water and air is the need of hour especially heavy metal species which affect the health [15]. Several techniques are employed to reduce the concentration of metal ion in wastewater [2]. A brief outline of some of the methods and their salient features can be given as under:

A. Methods for physical separation from soil

The efficiency of physical separation depends on soil characteristics. Following methods have been deemed reliable in this context:

- Flotation
- Hydrodynamic classification
- Mechanical screening
- Magnetic separation
- Gravity concentration
- Attrition scrubbing
- Electrostatic separation

B. Methods of wastewater remediation

Some of the popular methods for wastewater remediation include:

i. Chemical Precipitation

- Precipitation of heavy metals as hydroxide, sulphide, carbonate and phosphate, which are insoluble
- Generation of micro fine particles
- Removal of sludge by increasing particle size by chemical precipitants, coagulants, and flocculants

ii. Coagulation and Flocculation

- Electrostatic interaction between pollutants and coagulant/flocculants
- Flocculation of discrete particles into larger ones
- Removal or separation of coagulated-flocculated particles by filtration, straining or floatation

iii. Electrochemical treatments of heavy metals

- Precipitation by forming coagulants through electrolytic oxidation
- Precipitation in a weakly acidic or neutralized catholyte as hydroxides

- Electro-deposition, electrocoagulation, electro-flotation and electro-oxidation
- Precipitation by forming coagulants through electrolytic oxidation
- Precipitation in a weakly acidic or neutralized catholyte as hydroxides
- Electro-deposition, electrocoagulation, electro-flotation and electro-oxidation

iv. Ion exchange

- Widely applicable in industries for water treatment
- Convenient operation utilizes low-cost materials
- Special ion exchanger contains cations or anions
- Synthetic organic ion exchange resins are used frequently
- Applicable only for metal ion solutions of low concentration
- pH of the aqueous phase affects the sensitivity

v. Membrane filtration

- Removal of suspended solids, organic and inorganic contaminants is dependent on the size of the particles retainable
- Various membrane filtration techniques such as ultrafiltration, nanofiltration and reverse osmosis employed for heavy metal remediation

vi. Electrodialysis

- Ionized species passed through an ion exchange membrane by application of an electric potential
- Thin sheets of plastic materials with anionic or cationic characteristics are used as membranes
- Anions and cations migrate toward the anode and the cathode respectively

vii. Biodegradation

- Microorganisms catabolise organic material with aeration and agitation and settle down solid
- Activated sludge containing bacteria is perpetually re-circulated back to the aeration tank to enhance organic decomposition
- Activated sludge, trickling filters, stabilization tanks are in wide use

viii. Adsorption

- Common mechanism applies to organic and inorganic pollutants removal
- Liquid-solid intermolecular attractive forces induce some of the solute molecules from the solution to be stuck at the solid surface when an adsorbate solution comes in contact with an adsorbent (a solid with a highly porous surface)
- All sorts of valencies/attractive forces of the constituent atoms of the adsorbate material are satisfied in the bulk. However, atoms on the surface of the adsorbent are exposed and hence attract adsorbates. The exact nature of the bonding depends on the species. Adsorption process may be physical sorption (van der Waals interactions) or chemisorption (covalent bonding). Electrostatic attraction is also possible.

Traditional methods for treatment of contaminated water include adsorption [16], chemical precipitation [17], ion-exchange [18], reverse osmosis [19], membrane technologies [20], solvent extraction [21, 22], electrochemical treatment [17], biological treatment [23, 24], phytoremediation [8] and flotation [25]. The disadvantages of these methods to restrain their application are significant capital, energy, and operational costs; the addition of chemicals, generation of hazardous wastes and poor efficiency for wastewaters with a low concentration of heavy metals [26]. Ion exchange and reverse osmosis are more attractive methods owing to the recovery of valuable pollutants, however, these are economically unfavourable due to relatively high investment and operational cost. Adsorption is of special interest due to its economy, versatility, and efficiency, especially for the remediation of trace amounts of pollutants [27].

Developing countries have high population density and poor availability of funds, hence low cost, and sustainable remedial options are required [28]. A critical review of the subject presented the best available remedial strategies for heavy metals usually found in contaminated soils along with their sources, potential biohazards, and chemistry.

2 Adsorption: An Advantageous Process for Pollution Remediation

Simplicity and cost efficiency are the attractive features of adsorption. Further, the use of eco-friendly techniques is possible, which requires minimum skill for implementation. Hence, several high-efficiency adsorbents have been developed, such as activated carbon, quartz, sand, bentonite, zeolite and oxide materials, for heavy metal ion remediation [29]. Heavy metal species emanating from industrial activities are multifarious and complex, therefore, diverse adsorbents have been explored [16, 29].

Environmentally friendly adsorbents are efficient and economic for water decontamination. Adsorbent materials, such as chitosan, clays, zeolites and activated carbons, serve as low-cost adsorbents [29]. However, they have weak affinity for metal ions. Functional groups have therefore been introduced in these materials to enhance their adsorption capacity. Still, the existing adsorbents exhibit efficiency for specific heavy metal. This limitation is attributed to hard and soft acids and bases characteristics [30].

The design of adsorbents with abundant and accessible chelating sites with high affinity is a key challenge. A host of sorbents were applied for the removal of metal ions from wastewater by covalent grafting of coordination groups on the surface of porous materials, such as silica gel and clay [31]. However, small and irregular pore structures allow only a fraction of the surface-bound ligands to bind a particular metal ion [2]. Biosorption has gained interest in recent years due to its efficiency in

extenuating heavy metals, particularly those present in low concentration. Biosorption based on biomass-derived sorbents is a cost-effective and sustainable alternative to water treatment [32, 33].

2.1 *Biosorption*

Biosorption is a potentially attractive technology for removal and/or recovery of toxic/rare heavy metals from industrial effluents by use of low-cost biosorbents in a metabolically-free manner [32, 33]. Biosorption involves complex mechanisms such as coordination, chelation, ion exchange, physical adsorption and/or ion entrapment in inter- and intra-fibrillar capillaries and spaces of the polysaccharide network, etc. [32]. The characteristics of the biosorbents, the physicochemical properties of the heavy metals and the microenvironment of the contact solution influence the operating mechanisms. Biosorption is a passive process involving the affinity between sorbate and biomass sorbent. It is advantageous because of its: (i) low cost, (ii) high efficiency, (iii) potential metal recovery, (iv) easy operation, (v) high sustainability and (vi) reduced sludge handling. Its disadvantages include: (i) limited pilot and industrial scale studies, (ii) possible increments in cost (as wastes become commodities), (iii) process mechanism of high complexity and (iv) disposal of biosorbents at the end of life [34, 35].

Biopolymers as biosorbents

Biopolymers are composed of polysaccharides, fatty acids and proteins, with a variety of abundant functional groups as active sites. Extensive research has been devoted to exuberant natural polymers or agriculture waste products to be employed as biosorbents, e.g. fungi, yeasts, bacteria, algae, chitin and chitosan. Several low-cost and renewable biological materials have been explored viz.: macroalgae, agricultural remainders, industrial waste, stuff, sludge, raw plants, etc. [36].

Biosorption experiments are typically performed by batch processing [37]. Biosorption of metal ion using agricultural or vegetable biomass, however, has been demonstrated to be amenable to continuous processing [38]. Column mode of operation is a continuous process and of greater practical importance due to its simplicity and low-cost of operation and easy scale up from laboratory to industrial scale [37].

Hydrogels have attracted wide attention as adsorbents for remediation of heavy metal ions, ammonia and dyes [39]. Polysaccharide-based hydrogels are attractive as adsorbents because they are biodegradable and biocompatible and have been successfully applied for the organic and inorganic pollutant remediation [39, 40]. A wide range of polysaccharides based hydrogels including gums, collagen, cellulose, alginate, carrageenan and chitosan have also been successfully applied for this purpose [41]. Hybrid hydrogel composite of gelatine (GL) and clinoptilolite

synthesized by free radical grafting and were utilized for metal ions remediation from the mine effluents [42].

Chitin, an acetylamino polysaccharide, the second most abundant natural resource, next to cellulose, is found in the exoskeletons of crabs, arthropods and cell walls of some fungi. Chitin and its deacetylated modification, chitosan are excellent metal ligands [43]. Chitin is amorphous and intractable, hence limits its use due to slight inertness and difficulty in processing. Cellulose/chitin beads exhibited greater adsorption capacity for heavy metals than that of pure chitin flakes [44, 45]. Thus, only some functional group content does not decide adsorption abilities of biosorbents, some other factors or their combination are decisive.

The bio-sorbents are preferred because of their unique properties such as biodegradability, low-cost and abundance [46]. However, low adsorption capacity and slow rate seriously restrict their applications. Further, being hydrophilic, they are prone to microbial attack in aqueous environments. Hence, they are being modified for improvement in their properties [47]. Some of the biosorbents are immobilized (cross-linked) in a synthetic polymer matrix [48] and/or grafted onto an inorganic support material such as silica [49] to yield particles/beads with the desired mechanical strength and chemical resistance, to ensure recyclability for subsequent cycles. Nevertheless, cross-linking decreases the adsorption efficiency of biosorbents [48, 50]. Furthermore, the cross-linking agents such as glutaric dialdehyde and ethylene glycoldiglycidyl ether are physiologically toxic and the crosslinked beads are non-biodegradable. For the development of new polymeric materials with desirable properties, polymer blending is a simple process [51]. Cellulose and clay are arousing the attention as reinforcements of various polymeric blends because they are abundant in nature, have high mechanical strength, good chemical resistance, economic and above all environmentally friendly [52, 53]. An article critically reviewed the physical and chemical treatment methods to improve the fibre-matrix adhesion and their characterization [54].

In water decontamination technology, nanostructured adsorbents are emerging as the cynosure of all eyes [55]. However, the nanoparticles suffer some drawbacks, such as a decrease in surface area due to agglomeration, difficulty in recyclability and environmental dangers caused by particle-elapsing [55]. Hybrid nanocomposites are preferred for providing high specific surface area and better adsorption properties cost-effectively by immobilizing nanoparticles onto large solid substrates [56].

3 Nanocomposites

Current research and development are being focussed on polymer matrix based nanocomposites. On nanoscale, the dimensions of the particle, platelet or fibre are in 1–100 nm. Owing to the interesting observations involving exfoliated clay, carbon nanotubes, carbon nanofibers, exfoliated graphite (graphene), nanocrystalline metals and a variety of nanoscale inorganic filler or fibre modifications,

interest in polymer matrix based nanocomposites is gaining impetus. The primary area of interest is the reinforcement aspects of nanocomposites however, barrier properties, flammability resistance, electrical/electronic properties, membrane properties, polymer blend compatibilization are important for various potential applications. An important consideration is the synergistic advantage of nanoscale dimensions relative to larger scale modification. The thickness of individual clay layers is much smaller than the wavelength of visible light, hence in well-exfoliated clay/polymer nanocomposites, optical properties of the polymer are not significantly affected rendering it optically clear. To optimize the properties of the resultant nanocomposite, it is desired to interpret the property changes as the particle (or fibre) dimensions reduce to the nanoscale level [57].

3.1 Bio-nanocomposites

Nanostructured hybrid organic-inorganic composites are invoking concern of academia and industry. Bio-nanocomposites exhibit multidimensional properties like biocompatibility, antimicrobial activity and biodegradability [58].

A review described bio-nanocomposites based on different polysaccharides functionalized by different nanofillers such as montmorillonite (MMT), Ag, SiO₂, TiO₂ and ZnO. These were used in regenerative medicine, drug delivery, tissue engineering, electronics and food packaging. The recent advancements were discussed in the light of technical and scientific issues [59].

Cellulose a hydrophilic substrate is a good choice to fabricate hybrid nanocomposites due to its origin from renewable resources and long chains capable of self-assembly [60]. The hydroxyl groups on the surface of cellulose provide numerous active sites for the proliferation of inorganic oxides. Immobilization of nano-TiO₂ onto cellulose matrix was done by various methods such as sol-gel [61], hydrothermal [62], layer by layer (LBL) assembly [63] and hydrolysis treatment [63]. Hydrothermal and hydrolysis methods require heating to attain certain temperature, microwave irradiation provides fast heating rates and molecular homogeneity, quick reaction kinetics, rapid crystallization and simplified procedure [64].

3.1.1 Bionanocomposites for Pollution Remediation

Some of the recent significant applications of bionanocomposites for metal ion remediation and adsorption of organic dyes are summarized in Tables 1 and 2, respectively.

Table 1 Bionanocomposites for metal ion remediation

Nanocomposite	Pollutant	Q _{max} ^a	Remarks	Ref.
Chitosan coated iron-oxide nanocomposites	As(III)	267.2 mg/g	Only 13% loss in initial adsorption capacity after 5 repeated adsorption cycles	[94]
Chitosan film loaded with silver nanoparticles (CS-AgNPs)	Al(III), Cd(II), Cu(II), Co(II), Fe(III), Ni(II), Pb(II), Zn(II).		Feasible material for solid-phase extraction of metal pollutants from surface waters	[95]
Chitosan-rectorite nanospheres immobilized on polystyrene fibrous mats CS-REC	Cu(II)	98.87 mg/g	The addition of REC containing Ca ²⁺ could also improve the metal adsorption because of cation exchange	[96]
Multiwalled carbon nanotubes (MWCNTs)/chitosan nanocomposite	Cu(II), Zn(II), Cd(II), Ni(II)	Cu(II)-100% Zn(II)-99% Cd(II)-98% Ni(II)-100%	Greater efficiency for the target metal ion and suitable to be used in different environmental applications	[97]
Organo vermiculite (OVU) Chitosan (CHT)	Cd(II)	10% CHT-95.9 mg/g 50% CHT-97.1% 65% CHT-141 mg/g	The adsorption capacity was increased by raising the solution pH, which most likely favours a chelation mechanism between the chitosan chains and the Cd(II) cations	[98]
Chitin/magnetite/multiwalled carbon nanotubes magnetic nanocomposite	Cr(VI)	90.7%	Potential and promising adsorbent for environmental remediation	[99]

(continued)

Table 1 (continued)

Nanocomposite	Pollutant	Q_{\max}^a	Remarks	Ref.
Chitosan and carbon nanofibers (CNFs)-supported iron (Fe)-oxide nanoparticles (NPs)	Cr(VI)	80.0 mg/g	Regenerative and reused four times efficiently	[100]
Zero-valent copper-chitosan nanocomposites	Cr(VI)	99%	Excellent adsorption behaviour	[101]
Dead yeast biomass and titania nanoparticles	Cr(VI)	162.07 mg/g	Efficiency (99.92%)	[102]
Fe ₃ O ₄ coated glycine doped polypyrrole magnetic nanocomposite (Fe ₃ O ₄ @gly-PPy NC)	Cr(VI)	238–303 mg/g	PPy moiety reduced Cr(VI) to Cr(III) Max. adsorption in 25–45 °C range and <i>pH</i> 2	[103]
Chitosan and Alginate nanocomposites	Cr(VI)	108.8 mg/g	Optimum adsorption at <i>pH</i> 5.0	[104]
Polyamides 6 (PA6)/Chitosan@Fe _x O _y composite nanofibers	Cr(VI)	64.3225 mg/g	High Cr(VI) removal efficiency of the nanofibrous membrane by electrospinning and pyrolytic reaction	[105]
Magnetic cellulose nanocomposite beads	Pb(II)	2.86 mg/g	Adsorption processes spontaneous, endothermic, controlled by chemical mechanisms and material reusable	[106]
MnO ₂ /chitosan nanocomposites	Pb(II)	Noncrosslinked-90.56%, crosslinked 59.93%	Potential adsorbent for the removal of lead ions	[107]
Nanocomposite based on nano silica filled xanthan gum grafted with polyacrylamide (XG-g-PAM/SiO ₂)	Pb(II)	537.63 mg/g	Efficient adsorbent for the treatment of battery industry wastewater due to higher	[108]

(continued)

Table 1 (continued)

Nanocomposite	Pollutant	Q_{\max}^a	Remarks	Ref.
			hydrodynamic radius/volume	
Pectin zirconium(IV) selenotungstophosphate (Pc/ZSWP)	Cu(II), Th(IV)	Cu(II) 2.48 mg/g Th(IV)-4.37 mg/g	High ion exchange capacity	[109]
Starch/SnO ₂ nanocomposite	Hg(II)	192 mg/g	Regenerative capacity (94%) was maintained till fourth cycle	[110]

^a Q_{\max} = maximum adsorption capacity

3.2 Clay-Based Nanocomposites

Clays and their minerals are abundant and cheap materials successfully used for decades as adsorbents for removing toxic heavy metals from aqueous solutions. Clays and their minerals, composed a large family of adsorbents both in natural and modified forms, effectively remove most of the chemical contaminants from aqueous solution.

Layered silicate clay minerals are extensively used nano-reinforcements due to easy availability, low cost, and environmentally benign properties. Very low levels of nanofiller (5 wt%) matches the reinforcement efficiency of conventional composites with 40–50% of classical fillers, because of the high aspect ratio and high surface area of the nanolayered clays. Extensive studies on the preparation and properties of biodegradable polymer-clay nanocomposites were conducted on polylactide, polyhydroxy butyrate, thermoplastic starch, polybutylene succinate and polycaprolactone. Clay nanoparticles enhance mechanical properties, thermal stability, barrier properties and control the biodegradation rate of the biopolymers [65].

A detailed review compiled thorough research during 2006–2016 and highlighted the key conclusions of adsorption studies which used clay minerals as adsorbents. The structure, classification, and chemical composition of various clay minerals were outlined and analysis of their adsorption behaviour was described. The author suggested the need to modify and develop a synthetic method of novel materials and for application as an adsorbent for different pollutants [66].

Halloysite (HAL) possesses disordered aluminium silicate structure, number of adsorption sites and unparalleled nanotubular morphology, which makes it a promising adsorbent. HAL is especially attractive due to its low production cost, inertness for the environment. HAL can be modified by multistep intercalation, interlayer grafting reactions or both. HAL-based hybrids can be designed with adsorption functionalities targeted towards individual contaminants (e.g., polar/apolar or positively/negatively charged) by appropriate selection of organic molecules. Matusik summarized the studies on the use of pure and modified HAL for the remediation of chosen inorganic and organic pollutants [67].

Table 2 Bionanocomposites for organic dye adsorption

Nanocomposite	Organic dye	Q_{\max}^a	Remarks	Ref.
Chitosan cenospheres (10:3) nanocomposite	Orange 25 (DO) and Disperse Blue (DB)	97.30% for DO, 94.22% for DB	Crosslinking agent glutaraldehyde	[111]
Chitosan/carbon black fiber	<i>p</i> -nitrophenol, congo red (CR) and methyl orange (MO) dyes	% reduction of CR and MO-99	Inhibited growth of <i>E. coli</i> by 47.8%	[112]
Chitosan-copper (CS-Cu) nanocomposite	Rhodamine B (RhB) and CR	Under light RhB-70% CR-93%	Excellent photocatalytic performer and antimicrobial agent	[113]
Chitosan-g-poly (acrylamide)/ZnS (ChPA/ZS) nanocomposite	MO and CR	75% of CR and 69% of MO was degraded after 4 h	MW synthesis Removal by photocatalytic degradation	[114]
Chitosan-polyvinyl alcohol (CHT-PVA) polymer matrix	Bisphenol A (BPA)	97.6%	Optimal <i>pH</i> for maximum adsorption 6.0, regenerative and reusable within five cycles	[115]
Chitosan-SnO ₂ nanocomposites	MO and RhB	Photocatalytic degradation at 365 nm	High crystallinity, high surface area, and small particle size enable superior photocatalytic degradation	[116]
Chitosan-TiO ₂ nanocomposite	RhB and CR	Photocatalytic degradation RhB-65% CR-57%	Excellent antimicrobial agent and antifungal activity	[117]
Composite of polyaniline, starch, polypyrrole, chitosan/aniline and chitosan/pyrrole using peanut waste	Crystal Violet (CV)	100.6 mg/g	Good desorption properties, recycling ability	[118]
Fe ₃ O ₄ MNPs ^b and gum xanthan based hydrogels nanocomposites	Malachite green (MG)	497.15 mg/g	Nanocomposite can be repeatedly used for the adsorption	[119]
Gelatin-Zr(IV) phosphate nanocomposite (GT/ZPNC)	Methylene blue (MB) and fast green (FG)	87.81% MB and 89.91% FG	Photocatalytical degradation of pollutants and antimicrobial efficiency against <i>E. coli</i>	[120]

(continued)

Table 2 (continued)

Nanocomposite	Organic dye	Q _{max} ^a	Remarks	Ref.
Guar gum/Al ₂ O ₃ nanocomposite	MG	~80–90% degradation of MG under solar irradiation	Effective photocatalyst	[121]
Guar gum–cerium (IV) tungstate nanocomposite (GG/CTNC)	MB		Potential adsorbent MB from aqueous system	[122]
Gum ghatti-based biodegradable hydrogel	MB and MV	98% of MB and 95% of MV from aqueous solution	Polymer degraded fully within 50 days in soil compost	[123]
Hybrid TiO ₂ /microcrystalline cellulose	MB	Photocatalytic degradation of 40–90% of MB	Catalytic adsorption of MB from aqueous solutions	[124]
MWCNTS/chitin/magnetite (MCM) nanocomposite	Rose Bengal (RB)		Adsorption of RB occurred in different steps	[125]
Gum ghatti/TiO ₂ nanoparticles-based hydrogel nanocomposite	MB	1305.5 mg/g	More efficient in adsorbing cationic dyes than anionic dyes	[126]
TiO ₂ -impregnated chitosan nano-grafts	Remazol red RB-133 (RR RB-133)	116.3 mg/g	Photoactive under sunlight-irradiation, five adsorption/sunlight-assisted self-cleaning photo regeneration cycles	[127]
Alginate/carboxymethyl cellulose TiO ₂ nanoparticles (TiO ₂ -NPs) and graphene oxide (GO)	CR	degradation efficiency 98%	Efficient visible light responsive photocatalyst, degradation efficiency retained up to seven consecutive cycles	[128]

^bMNP = magnetic nanoparticles

Clay minerals and their modified derivatives constitute a large family of adsorbents. A review presented literature on adsorption of diverse contaminants such as hydrophobic organic materials, dyes, heavy metal ions, oxyanions, radioactive nuclides, etc. Different mechanisms, such as surface adsorption, partition, ion exchange, surface precipitation and structural incorporation are involved in the uptake of these contaminants [68]. Organoclays are synthesized in the laboratory, and are smart organic-rich clay materials, for geo-environmental applications because of strong sorption affinity for nonpolar organic molecules. Organic cations

displace naturally occurring inorganic cations (e.g., Na^+ , Ca^{2+}) in the clay. By selecting a suitable organic cation that is exchanged into the clay interlayer, sorption can be managed to be linear or non-linear, competitive or non-competitive. Most commonly used clay is MMT for organoclays due to its high cation exchange capacity and quaternary ammonium cations as the organic phase. An overview of properties, synthesis, applications, synthesis techniques, modifications with several chemical compounds such as quaternary alkylammonium salts and biomolecules such as enzymes was given in a review, particularly focused on bentonite (BENT) and polymer nanocomposites [69]. Zhao et al. [70] exhaustively reviewed organoclays with reference to the fundamental behaviour and geochemical properties.

Photocatalysis emerged as an active field of research endeavour for environmental pollution abatement. This approach is more effective in combining complementary components with the inorganic semiconductor active material. Three such types of nanocomposite assemblies were discussed on the basis of combining semiconductor (usually transition metal oxides) with clays, carbon and metals [71].

3.3 *Polymer-Layered Silicate Nanocomposites (PLSN)*

Reinforcing fillers for polymer nanocomposites are layered silicates due to their economy and abundance for several years [72].

Polymer-layered silicate nanocomposites (PLSNs) are much superior to conventional micro-, macrocomposites due to unexpected properties [73]. The nanometric scale provides good reinforcement at less than 10% low filler loading as compared to conventional fillers which require more than 30% [74]. The mechanical properties, thermal resistance, solvent resistance and ionic conductivity are improved and gas permeability is reduced on reinforcement with clay [75].

Polymer-functionalized nanocomposites (PFNCs) retain the inherent remarkable surface properties of nanoparticles, functional groups provide specific bindings to target pollutants, and the polymer support materials provide high stability and processability. A review discussed synthesis, characterization and adsorption performance of PFNCs [76].

3.3.1 **Structure of PLSN**

Layered silicates are built of two structural units. In simplest 1:1 structures (e.g. kaolinite) a silica tetrahedral sheet is fused to an aluminium octahedron by sharing the oxygen atoms [77]. MMT is a smectite with 2:1 phyllosilicate structure, stacked layers made of two silica tetrahedrons fused to an edge-shared octahedral sheet of alumina (Fig. 1). The thickness of layer is ~ 1 nm and the lateral dimensions vary from 300 Å to several microns, giving an aspect ratio greater than 1000. The adjacent layers (interlayer or gallery) are held together by van der Waals forces; hence water and other polar molecules can be accommodated causing expansion of

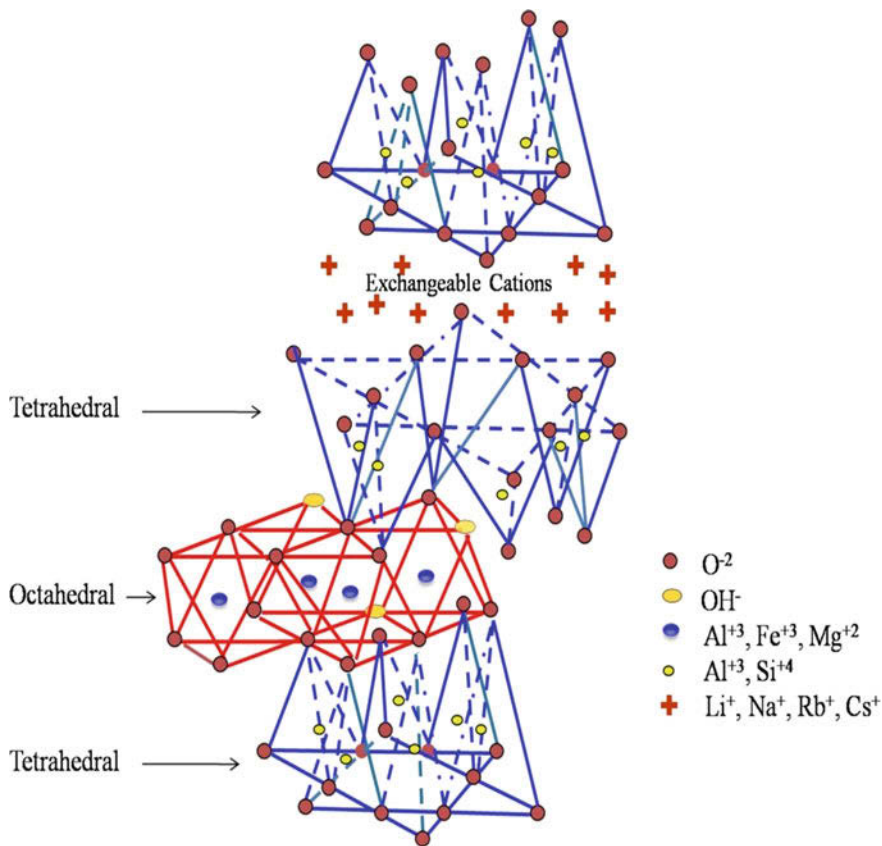


Fig. 1 The structure of 2:1 layered silicates

the lattice. Negative charges are generated by isomorphous substitution within the layers which are counter balanced by hydrated sodium or calcium ions present in the interlayer [78].

The extent of dispersion of the individual silicate platelets within the polymer matrix contributes to the enhancement of substantial properties of nanocomposites. Intercalated and exfoliated morphological structures are proposed for the layered silicate nanocomposites. The exfoliated layers impart the greatest reinforcement in nanocomposites. However, only hydrophilic polymers can be incorporated in clay. Hence, the silicate surface is modified by exchanging the interlamellar cations with organic cations to form organically modified montmorillonite. This results in better compatibility of polymer and silicate layers [79]. Organic cationic surfactants, like primary, secondary, tertiary and quaternary alkylammonium or alkylphosphonium cations are used to improve the surface properties to become compatible with the hydrophobic polymer matrix, moreover, their long aliphatic tails result in a greater interlayer spacing [80].

3.3.2 Methods of Preparation of PLSN

Clay/polymer nanocomposites [81] have been prepared by several methods, widely applied methods are described as under:

- (i) Solution method: clay and polymer components are dissolved in a polar organic solvent, where polymers remain in the extended state in the inter gallery space. An intercalated nanocomposite is formed on solvent evaporation [82].
- (ii) Interlamellar method or in situ polymerization: clay is completely dispersed in the polar monomer solution than the addition of curing agent forms an exfoliated composite.
- (iii) Melt intercalation method: molten thermoplastic is included by blending with silicate to optimize the interaction. The temperature should be kept below the decomposition temperature of the clay modifier; trial and error are practised with different compatibilizers.

Schematic presentation of various types of nanocomposites with probable polymer/layered silicate structures is shown in Fig. 2.

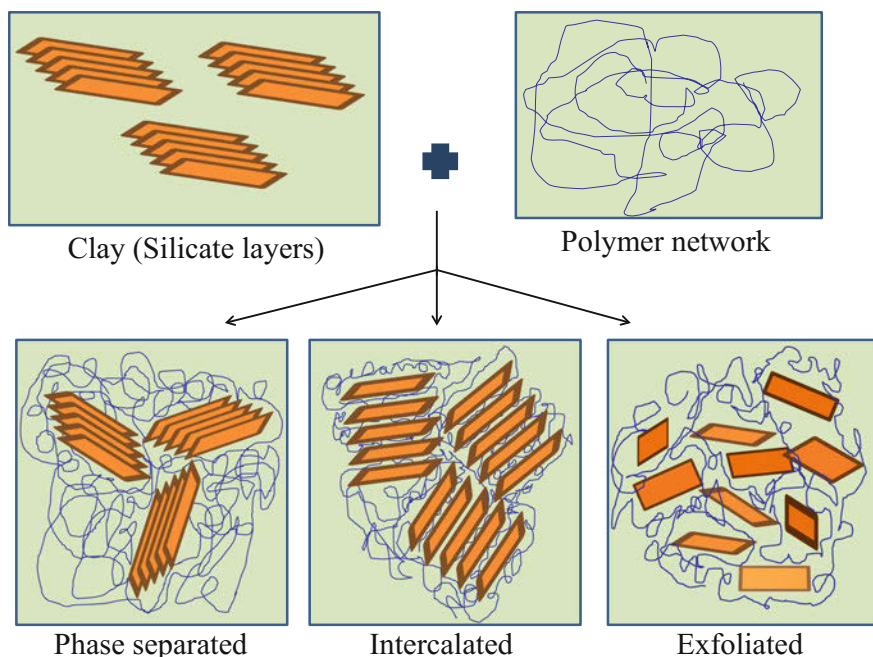


Fig. 2 Probable polymer/layered silicate structures in various types of nanocomposites

3.3.3 Challenges in Use of PLSN

Complete dispersion of the filler in the polymer matrix to prepare true nanocomposite is a scientific and technical challenge. Pandey et al. reviewed the durability of nanocomposites along with the technical problems and their feasible solutions [83]. The preparation, processing, properties, characterization, crystallization behaviours, melt rheology, and possible future applications of nanocomposites of biodegradable polymers and layered silicate have been reviewed [84, 85]. Nanotechnology increases tensile strength, flexural modulus, heat resistance and dyeability of polymeric materials [86]. Choudalakis and Gotsis reviewed the permeability and mechanisms for the transport of gas molecules and the procedures for the measurement of permeability and diffusivity in polymer nanocomposites [87].

A review examined and summarized preparation, properties, and applications of magnetic nanoparticle/clay mineral nanocomposites. Their potentials and applications in electromagnetic devices, magnetorheological fluids/ferrofluids, magnetic adsorbents, catalysts and biomaterials and the existing problems and challenges were discussed. Suggestions for future studies were given such as: to emphasize decreasing polydispersity, increasing functionalities, uncovering the preparation-modification-structure-magnetism-activity relationships and advancing the practical applications [88].

The potential toxicological effects of unmodified or modified clay minerals and their nanocomposites are gaining impetus. There is scarce information on toxicity biomarkers such as immune modulatory effects or alteration of the genetic expression, which needs systematic *in vitro*–*in vivo* extrapolation studies [89].

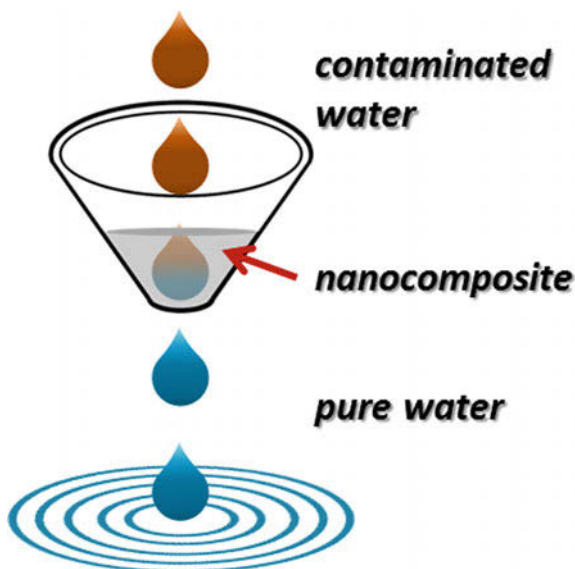
Currently, food packaging is the fast developing application utilizing clays of each phyllosilicate groups: kaolinite, MMT and sepiolite (SEP). Clays generally induce cytotoxicity with different underlying mechanisms, such as necrosis/apoptosis, oxidative stress or genotoxicity as suggested by *in vitro* studies. However, most of *in vivo* experiments performed in rodents did not show toxicity even at 5000 mg/kg doses. Pulmonary exposure is the most frequent in humans; clays are usually mixed with other minerals, which induce pneumoconiosis intrinsically. However, oral toxicity is not high; a strict control of the concentrations can provide beneficial uses (Fig. 3).

Clay minerals form highly stable suspensions in water; hence their rational use is important. The volume and treatment complexity of water contaminated with them is increased because of wide application. Current treatment techniques are either not economically viable, not environmentally friendly, or both. Flocculating agents such as polyelectrolytes have the potential to separate the above-mentioned minerals from industrial wastewater effluents [90].

3.3.4 PLSN with Bio-based Polymer Matrices

Favourable characteristics of clay nanocomposites with bio-based polymer matrices are improved *Young's modulus*, reduced gas permeability, and improved fire

Fig. 3 Schematic presentation of application of nanocomposites for water purification



retardancy. They can be applied as melt-processed thermoplastic mouldings, packaging films and coatings [91].

Different types of nanocomposites are possible depending on the inorganic filler used. In PLSN the reinforcing phase has only one nano level dimension. Intercalated nanocomposites consist of a regular array of the polymer into the clay galleries with fixed interlayer spacings, and in exfoliated nanocomposites, 1 nm thick layers are separately dispersed in the polymeric matrix to form a monolithic structure at the microscale.

MMT is most commonly employed in the synthesis of nanocomposites. It is obtained from bentonite (BENT) [92].

Structural, morphological and textural features of natural microfibrinous clay minerals Sepiolite (SEP) and palygorskite (PAL) make them useful for the preparation of nanocomposite materials. SEP- and PAL-based bionanocomposites have diverse applications as bioplastics, membranes, biomedicine, drug delivery systems and additives of vaccines, tissue engineering, sensor devices, bioreactors and as a source of supported graphene [93].

3.4 Clay-Based Nanocomposites for Pollution Remediation

Some of the recent researches involving the application of nanocomposites comprising of clay and organic components (biopolymers, organic compounds and or synthetic polymers) are summarized in Table 3.

Table 3 Clay based nanocomposites for metal ion and organic contaminant remediation

Nanocomposite	Inorganic component	Organic component	Pollutant	Q_{\max}	Comments	Ref.
Attapulgite/poly(acrylic acid-co-acrylamide)	ATP	P(AA-co-AM)	Pb(II) and Cu(II)	35.94 mg/g for Pb(II) and 30.35 mg/g for Cu (II)	Exhibit selective adsorption, adsorption-desorption process enhanced their desired reusability	[129]
Organo-bentonite/Fe ₃ O ₄ (OB-Fe ₃ O ₄ PSA)	BENT	Poly(sodium acrylate) (PSA)	Th(IV)	6.55 mmol/g	Adsorption capacity was still higher than 3.6 mmol/g after five consecutive adsorption-desorption processes	[130]
Halloysite/algininate nanocomposite beads	HAL	Alginate	Pb(II)	325 mg/g	Q_{\max} for Hal nanotubes only 84 mg/g. Nanocomposite mechanically stronger, easily separable	[131]
Nanotubularhalloysite	HAL	Amino alcohols	Pb(II), Cd(II), Zn (II), and Cu(II)	Pb(II)—64.1 (HD), 58.8 (HT); Cd(II)—41.8 (HD), 41.7 (HT); Zn(II)—52.9 (HD), 42.9 (HT); Cu (II)—64.1 (HD), 75.2 (HT) *HD is HAL grafted with diethanolamine and HT is HAL, grafted with triethanolamine	No swelling properties, diffusion of metal ion and complex binding with the grafted group. The material was non-recyclable	[132]
Polypyrrole-coated halloysite nanotube nanocomposite (PPy-HNTs NC)	HAL nanotube	PPy	Cr(VI)	149.25 mg/g	Optimum adsorption at pH 2.0 at 25 °C, some of the Cr (VI) reduced to Cr(III)	[133]

(continued)

Table 3 (continued)

Nanocomposite	Inorganic component	Organic component	Pollutant	Q_{max}	Comments	Ref.
Kaolinite supported bimetallic Fe/Ni nanoparticles (K-Fe/Ni)	Kaolinite, bimetallic Fe/Ni nanoparticles		Pb (II) and NO_3^-	86.3% of Pb(II) and 73.6% of NO_3^-	Reactivity maintained throughout 15 days and removal efficiency maintained till 3 successive cycles	[134]
Di- and triethanolamine grafted kaolinites	Kaolinites	Diethanolamine (DEA) and triethanolamine (TEA)	Cd(II), Zn(II), Pb (II) and Cu(II)		Grafted DEA or TEA donating N and O to form complexes with metals	[135]
PPy-OMMT NC	MMT	Polypyrrole	Cr(VI)	112.3, 119.34, 176.2 and 209.6 mg/g at 292, 298, 308 and 318 K, respectively	The selective adsorption of Cr(VI) was demonstrated in binary adsorption systems with co-existing ions	[136]
PPy-OMMT	MMT	Polypyrrole (ppy)	Cr(VI)	Fixed bed adsorption column studies	High bed mass, low inlet Cr (VI) concentration and flow rate enhanced removal efficiency	[137]
Fe-Ni bimetallic nanoparticles (Fe-Ni NPs) and Nanocomposites, (MMT) clay	MMT		Cr(VI)		Fe-Ni NPs exhibited a complete reduction of Cr (VI) occurs via Cr(III) to Cr (0) below pH 4 due to the generation of reactive H species	[138]
Fe_3O_4 /MMT nanocomposite (Fe_3O_4 /MMT NC)	MMT		Pb(II), Cu(II), Ni (II)	89.72% (Pb(II)), 94.89% (Cu(II)), 76.15% (Ni(II))	Response surface methodology was utilized in designing the experiment	[139]

(continued)

Table 3 (continued)

Nanocomposite	Inorganic component	Organic component	Pollutant	Q_{\max}	Comments	Ref.
Ammonium-pillared montmorillonite-CoFe ₂ O ₄	MMT	Calcium alginate beads	Cs(II)	86.46 mg/g	High selectivity for Cs ⁺ in the presence of Na ⁺ and could be rapidly separated from the mixed solution under an external magnetic field	[140]
ZnO/MMT nanocomposite	MMT		Pb(II) and Cu(II)		Stability and durability of the nanocomposite allowed it to be utilized for at least three times in adsorptive removal	[141]
Chitosan/clay nanocomposite (CCN)	Nanoclay (Cloisite 10A)	Chitosan	Cr(VI)	357.14 mg/g	Adsorption at wide pH range, pH 3 most suitable	[142]
Chitosan-nanoclay composite (CNC)	Organoclay (Cloisite 20A)	Chitosan	Cr(VI)	128.43 mg/g	Maximum adsorption at pH 2	[143]
Chitosan-palygorskite (CP) composites. Mass ratios 1:1 (CP1) 1:2 (CP2) and 2:1 (C2P)	PALY	Chitosan	Pb(II)	201.5, 154.5, 147.1, 27.7 and 9.3 mg g ⁻¹ for CP1, C2P, CP2, chitosan and palygorskite	The surface properties and specific interaction between chitosan and palygorskite in the composites-governing factors in metal ion adsorption	[144]
Polysaccharide-fibrous clay biocomposites	Sepiolite and PALY	Polysaccharide (starch, alginate or chitosan)	Heavy metal ions		Films exhibit improved mechanical properties, good water resistance, biocompatibility and biodegradability	[145]

(continued)

Table 3 (continued)

Nanocomposite	Inorganic component	Organic component	Pollutant	Q_{max}	Comments	Ref.
FeO-Fe ₃ O ₄ beads		Polyvinyl alcohol (PVA)/ sodium alginate (SA)	Cr(VI)	76.3–100%	Beads containing 0.075 wt % FeO and 0.30 wt% Fe ₃ O ₄ was mechanically stable and highly efficient in removing Cr(VI) from 99.3 to 76.3% with increasing pH from 3.0 to 11.0	[146]
Clay mineral polymer nanocomposites (CPN)	MMT	Block-(diblock or triblock) copolymers	Toluene, ethylbenzene and xylene, Cu(II), Pb(II) and Cr ₂ O ₇ ²⁻	Cu(II)-6.11 mg/g, Pb(II)-10 mg/g, Cr ₂ O ₇ ²⁻ -36.9 mg/g	Dealt with the effect on interlayer space of Mt during reaction	[147]
Xanthan gum/ Methionine-bentonite (XG/Meth-bent) nanocomposite	BENT	Xanthan gum	Congo red dye	530.549 mg/g	Desorption with regeneration (up to fifth cycle) was best observed by NaOH	[148]
Bentonite/g-C ₃ N ₄ and Ag ₃ PO ₄	BENT	Graphitic carbon nitride (g-C ₃ N ₄)	Rhodamine B	Photocatalytic degradation	The composite containing 20 wt% Ag ₃ PO ₄ exhibited the highest photocatalytic activity in decolorizing RhB	[149]
biomass-derived carbon@montmorillonite	MMT	Glucose biomass as a carbonaceous source	Methylene blue (MB)	194.2 mg/g	Carbon-clay nanocomposites could be explored as a new type of the highly efficient and green adsorbent	[150]
CdSe-MMT nanocomposites	CdSe-MMT		Indigo carmine	Photocatalytic degradation	Adsorptive removal Indigo Carmine (IC) on the composite surface occurs via photocatalytic degradation under visible light	[141]

(continued)

Table 3 (continued)

Nanocomposite	Inorganic component	Organic component	Pollutant	Q_{max}	Comments	Ref.
Arquad® 2HT-75 organobentonite	BENT	Arquad® 2HT-75 (alkyl ammonium surfactant)	Phenol and <i>p</i> -nitrophenol	Phenol-2.1 mg/g and <i>p</i> -nitrophenol-6.0 mg/g	Surface having positive zeta potential, effective against ionizable organic contaminants	[151]
Chitosan-Bentonite (Cts-Bent)	BENT	Chitosan	Highly efficient inactivation of bacteria		Ag and ZnO nanoparticles in the chitosan matrix work as a disinfectant in wastewater treatment	[152]
Copper-complexed clay/polyacrylic acid	Acid-treated BENT, natural PAL	Polyacrylic acid	NH ₃ gas	Composite with 75% clay-75.1 mg/g, with 66% clay-80.0 mg/g	Efficiently adsorbed NH ₃ gas from the contaminated air and proved to be an effective and cheaper method of air filtering	[153]
Chitosan immobilized Bentonite (CIB)	BENT	Chitosan	Remediation of distilleries (vinasse) wastewater	83% COD reduction and 78% colour removal	Immobilization of chitosan with CTAB strongly affects the sorption capacity of the clay mineral	[154]
Tubular halloysite	HAL	Organosilane and organophosphoric acid			Regulate the physical (solubility, dispersion, hydrophilicity/hydrophobicity, rheology, etc.) and the chemical (reactivity, biotoxicity, electrochemistry, etc.) controlled release and pollution remediation	[155]

(continued)

Table 3 (continued)

Nanocomposite	Inorganic component	Organic component	Pollutant	Q_{max}	Comments	Ref.
TiO ₂ - and Fe ₂ O ₃ -halloysite	HAL		Aniline, 2-chloro- and 2,6-dichloroaniline	Photocatalytic degradation	Photocatalytic active under UV radiation	[156]
MMT-CuO-Chitosan, MMT-CuO-Gum ghatti, and MMT-CuO poly lactic acid	MMT	Gum ghatti (GG), Chitosan (Ch), poly lactic acid (PLA)	Monocrotophos, and organophosphate insecticide	83.99% on MMT-CuO-PLA, 71.6% on MMT-CuO-Ch, 62.1% on MMT-CuO-GG, 40.8% on MMT-CuO		[157]
Montmorillonites intercalated with polymeric Fe/Al	MMT	Hexdecyl-trimethyl-ammonium bromide (HDTMA)	Phenol	Physical adsorption	Al/HDTMA and MMT/HDTMA possess a good affinity for phenol, in comparison to polymeric Al/Fe modified- and starting montmorillonites	[158]
Organoclay (PC-VER)	Modifying vermiculite (VER)	Phosphatidylcholine (PC)	Oxytetracycline (OTC) and ciprofloxacin (CIP)		PC-VER could serve as a low-cost, suitable and eco-friendly material for adsorption of antibiotics	[159]
Nanocomposites of ferrocenyl surfactants and clay	MMT		In situ remediations of many organic compounds in the environment		The crystal lattice iron redox reactions mechanism proposed for catalysis	[160]
TiO ₂ -sepiolite nanocomposites	SEP		β -naphthol	Photocatalytic degradation	High water vapour uptake properties and degradation ability make it a useful applicant in energy and environment	[161]

References

1. Vorosmarty CJ et al (2010) Global threats to human water security and river biodiversity. *Nature* 467:555–561. <https://doi.org/10.1038/nature09440>
2. Fu FL, Wang Q (2011) Removal of heavy metal ions from wastewaters: a review. *J Environ Manage* 92:407–418. <https://doi.org/10.1016/j.jenvman.2010.11.011>
3. Shannon MA et al (2008) Science and technology for water purification in the coming decades. *Nature* 452:301–310. <https://doi.org/10.1038/nature06599>
4. Ngah WSW, Hanafiah M (2008) Removal of heavy metal ions from wastewater by chemically modified plant wastes as adsorbents: a review. *Bioresour Technol* 99:3935–3948. <https://doi.org/10.1016/j.biortech.2007.06.011>
5. Kirpichtchikova TA et al (2006) Speciation and solubility of heavy metals in contaminated soil using X-ray microfluorescence, exafs spectroscopy, chemical extraction, and thermodynamic modeling. *Geochim Cosmochim Acta* 70:2163–2190. <https://doi.org/10.1016/j.gca.2006.02.006>
6. Maslin P, Maier RM (2000) Rhamnolipid-enhanced mineralization of phenanthrene in organic-metal co-contaminated soils. *Bioremediat J* 4:295–308. <https://doi.org/10.1080/10889860091114266>
7. Kabata-Pendias A (2017) Trace elements in soils and plants, 3rd edn. CRC Press, Boca Raton, FL, USA
8. Salt DE et al (1995) Phytoremediation—a novel strategy for the removal of toxic metals from the environment using plants. *Bio-Technology* 13:468–474. <https://doi.org/10.1038/nbt0595-468>
9. Jones KC, de Voogt P (1999) Persistent organic pollutants (pops): state of the science. *Environ Poll* 100:209–221 [https://doi.org/10.1016/s0269-7491\(99\)00098-6](https://doi.org/10.1016/s0269-7491(99)00098-6)
10. Forgacs E, Cserhati T, Oros G (2004) Removal of synthetic dyes from wastewaters: a review. *Environ Int* 30:953–971. <https://doi.org/10.1016/j.envint.2004.02.001>
11. Malik R, Ramteke DS, Wate SR (2007) Adsorption of malachite green on groundnut shell waste based powdered activated carbon. *Waste Manage* 27:1129–1138. <https://doi.org/10.1016/j.wasman.2006.06.009>
12. Salleh MAM et al (2011) Cationic and anionic dye adsorption by agricultural solid wastes: a comprehensive review. *Desalination* 280:1–13. <https://doi.org/10.1016/j.desal.2011.07.019>
13. Ngah WSW, Teong LC, Hanafiah M (2011) Adsorption of dyes and heavy metal ions by chitosan composites: a review. *Carbohydr Polym* 83:1446–1456. <https://doi.org/10.1016/j.carbpol.2010.11.004>
14. Green chemistry for dyes removal from waste water: research trends and applications (2015). Wiley, Hoboken, NJ, USA
15. Alsbaiee A et al (2016) Rapid removal of organic micropollutants from water by a porous beta-cyclodextrin polymer. *Nature* 529:U146–U190. <https://doi.org/10.1038/nature16185>
16. Crini G (2006) Non-conventional low-cost adsorbents for dye removal: a review. *Bioresour Technol* 97:1061–1085. <https://doi.org/10.1016/j.biortech.2005.05.001>
17. Ku Y, Jung IL (2001) Photocatalytic reduction of Cr(VI) in aqueous solutions by uv irradiation with the presence of titanium dioxide. *Water Res* 35:135–142. [https://doi.org/10.1016/s0043-1354\(00\)00098-1](https://doi.org/10.1016/s0043-1354(00)00098-1)
18. Luo T, Abdu S, Wessling M (2018) Selectivity of ion exchange membranes: a review. *J Membrane Sci* 555:429–454. <https://doi.org/10.1016/j.memsci.2018.03.051>
19. Missimer TM, Maliva RG (2018) Environmental issues in seawater reverse osmosis desalination: intakes and outfalls. *Desalination* 434:198–215. <https://doi.org/10.1016/j.desal.2017.07.012>
20. Alkhudhiri A, Darwish N, Hilal N (2012) Membrane distillation: a comprehensive review. *Desalination* 287:2–18. <https://doi.org/10.1016/j.desal.2011.08.027>
21. Knez Z et al (2014) Industrial applications of supercritical fluids: A review. *Energy* 77: 235–243. <https://doi.org/10.1016/j.energy.2014.07.044>

22. Djas M, Henczka M (2018) Reactive extraction of carboxylic acids using organic solvents and supercritical fluids: a review. *Sep Purif Technol* 201:106–119. <https://doi.org/10.1016/j.seppur.2018.02.010>
23. Banat IM et al (1996) Microbial decolorization of textile-dye-containing effluents: a review. *Bioresour Technol* 58:217–227. [https://doi.org/10.1016/s0960-8524\(96\)00113-7](https://doi.org/10.1016/s0960-8524(96)00113-7)
24. Aksu Z (2005) Application of biosorption for the removal of organic pollutants: a review. *Process Biochem* 40:997–1026. <https://doi.org/10.1016/j.procbio.2004.04.008>
25. Prakash R, Majumder SK, Singh A (2018) Flotation technique: its mechanisms and design parameters. *Chem Eng Process* 127:249–270. <https://doi.org/10.1016/j.ccep.2018.03.029>
26. Gundogdu A et al (2009) Biosorption of pb(ii) ions from aqueous solution by pine bark (*pinus brutia* ten.). *Chem Eng J* 153:62–69. <https://doi.org/10.1016/j.cej.2009.06.017>
27. Khan S et al (2008) Health risks of heavy metals in contaminated soils and food crops irrigated with wastewater in Beijing, China. *Environ Pollut* 152:686–692. <https://doi.org/10.1016/j.envpol.2007.06.056>
28. Li J et al (2018) Synthesis of highly porous inorganic adsorbents derived from metal-organic frameworks and their application in efficient elimination of mercury(II). *J Colloid Interface Sci* 517:61–71. <https://doi.org/10.1016/j.jcis.2018.01.112>
29. Gupta VK, Suhas (2009) Application of low-cost adsorbents for dye removal—a review. *J Environ Manage* 90:2313–2342. <https://doi.org/10.1016/j.jenvman.2008.11.017>
30. Pearson RG (1963) Hard and soft acids and bases. *J Am Chem Soc* 85:3533. <https://doi.org/10.1021/ja00905a001>
31. Mercier L, Detellier C (1995) Preparation, characterization and applications as heavy-metals sorbents of covalently grafted thiol functionalities on the interlamellar surface of montmorillonite. *Environ Sci Technol* 29:1318–1323. <https://doi.org/10.1021/es00005a026>
32. Volesky B, Holan ZR (1995) Biosorption of heavy-metals. *Biotechnol Progr* 11:235–250. <https://doi.org/10.1021/bp00033a001>
33. Wang JL, Chen C (2009) Biosorbents for heavy metals removal and their future. *Biotechnol Adv* 27:195–226. <https://doi.org/10.1016/j.biotechadv.2008.11.002>
34. Volesky B (2001) Detoxification of metal-bearing effluents: biosorption for the next century. *Hydrometallurgy* 59:203–216. [https://doi.org/10.1016/s0304-386x\(00\)00160-2](https://doi.org/10.1016/s0304-386x(00)00160-2)
35. Fomina M, Gadd GM (2014) Biosorption: current perspectives on concept, definition and application. *Bioresour Technol* 160:3–14. <https://doi.org/10.1016/j.biortech.2013.12.102>
36. Vijayaraghavan K, Balasubramanian R (2015) Is biosorption suitable for decontamination of metal-bearing wastewaters? A critical review on the state-of-the-art of biosorption processes and future directions. *J Environ Manage* 160:283–296. <https://doi.org/10.1016/j.jenvman.2015.06.030>
37. Long YC et al (2014) Packed bed column studies on lead(II) removal from industrial wastewater by modified *agaricus bisporus*. *Bioresour Technol* 152:457–463. <https://doi.org/10.1016/j.biortech.2013.11.039>
38. Ungureanu G et al (2017) Biosorption of antimony oxyanions by brown seaweeds: batch and column studies. *J Environ Chem Eng* 5:3463–3471. <https://doi.org/10.1016/j.jece.2017.07.005>
39. Zhang JP, Wang AQ (2015) Polysaccharide-based composite hydrogels for removal of pollutants from water. In: Dragan ES (ed) *Advanced separations by specialized sorbents*, vol 108. *Chromatographic science series*. CRC Press-Taylor & Francis Group, Boca Raton, pp 89–126
40. Guilherme MR et al (2015) Superabsorbent hydrogels based on polysaccharides for application in agriculture as soil conditioner and nutrient carrier: a review. *Eur Polym J* 72:365–385. <https://doi.org/10.1016/j.eurpolymj.2015.04.017>
41. Fosso-Kankeu E et al (2010) A comprehensive study of physical and physiological parameters that affect bio-sorption of metal pollutants from aqueous solutions. *Phys Chem Earth* 35:672–678. <https://doi.org/10.1016/j.pce.2010.07.008>
42. Fosso-Kankeu E et al (2017) Thermodynamic properties and adsorption behaviour of hydrogel nanocomposites for cadmium removal from mine effluents. *J Ind Eng Chem* 48:151–161. <https://doi.org/10.1016/j.jiec.2016.12.033>

43. Sag Y, Aktay Y (2000) Mass transfer and equilibrium studies for the sorption of chromium ions onto chitin. *Process Biochem* 36:157–173. [https://doi.org/10.1016/s0032-9592\(00\)00200-4](https://doi.org/10.1016/s0032-9592(00)00200-4)
44. Zhou D et al (2004) Cellulose/chitin beads for adsorption of heavy metals in aqueous solution. *Water Res* 38:2643–2650. <https://doi.org/10.1016/j.watres.2004.03.026>
45. Dao Z et al (2004) Development of a fixed-bed column with cellulose/chitin beads to remove heavy-metal ions. *J Appl Polym Sci* 94:684–691. <https://doi.org/10.1002/app.20946>
46. Morosanu I et al (2017) Biosorption of lead ions from aqueous effluents by rapeseed biomass. *N Biotechnol* 39:110–124. <https://doi.org/10.1016/j.nbt.2016.08.002>
47. Kumar DPJ, Raj V (2017) A review on the modification of polysaccharide through graft copolymerization for various potential applications. *Open Med Chem J* 11:109–126. <https://doi.org/10.2174/1874104501711010109>
48. Ngah WSW, Endud CS, Maysanar R (2002) Removal of copper(ii) ions from aqueous solution onto chitosan and cross-linked chitosan beads. *React Funct Polym* 50:181–190
49. Rangsayatorn N et al (2004) Cadmium biosorption by cells of spirulina platensis tistr 8217 immobilized in alginate and silica gel. *Environ Int* 30:57–63. [https://doi.org/10.1016/s0160-4120\(03\)00146-6](https://doi.org/10.1016/s0160-4120(03)00146-6)
50. Lee ST et al (2001) Equilibrium and kinetic studies of copper(ii) ion uptake by chitosan-tripolyphosphate chelating resin. *Polymer* 42:1879–1892. [https://doi.org/10.1016/s0032-3861\(00\)00402-x](https://doi.org/10.1016/s0032-3861(00)00402-x)
51. Sawatari C, Kondo T (1999) Interchain hydrogen bonds in blend films of poly(vinyl alcohol) and its derivatives with poly(ethylene oxide). *Macromolecules* 32:1949–1955. <https://doi.org/10.1021/ma980900o>
52. Ollier R, Perez CJ, Alvarez V (2012) Effect of relative humidity on the mechanical properties of micro and nanocomposites of polyvinyl alcohol. In: Armas AF (ed) 11th international congress on metallurgy & materials sam/conamet 2011, vol 1. *Procedia materials science*. Elsevier Science Bv, Amsterdam, pp 499–505. <https://doi.org/10.1016/j.mspro.2012.06.067>
53. Gemeiner P et al (1998) Cellulose as a (bio)affinity carrier: properties, design and applications. *J Chromatogr B-Anal Technol Biomed Life Sci* 715:245–271. [https://doi.org/10.1016/s0378-4347\(98\)00047-4](https://doi.org/10.1016/s0378-4347(98)00047-4)
54. George J, Sreekala MS, Thomas S (2001) A review on interface modification and characterization of natural fiber reinforced plastic composites. *Polym Eng Sci* 41:1471–1485. <https://doi.org/10.1002/pen.10846>
55. Zhang WX (2003) Nanoscale iron particles for environmental remediation: an overview. *J Nanopart Res* 5:323–332. <https://doi.org/10.1023/a:1025520116015>
56. Bet-moushoul E et al (2016) TiO₂ nanocomposite based polymeric membranes: a review on performance improvement for various applications in chemical engineering processes. *Chem Eng J* 283:29–46. <https://doi.org/10.1016/j.cej.2015.06.124>
57. Paul DR, Robeson LM (2008) Polymer nanotechnology: nanocomposites. *Polymer* 49:3187–3204. <https://doi.org/10.1016/j.polymer.2008.04.017>
58. Sharma M, Bajpai A (2018) Superabsorbent nanocomposite from sugarcane bagasse, chitin and clay: synthesis, characterization and swelling behaviour. *Carbohydr Polym* 193:281–288. <https://doi.org/10.1016/j.carbpol.2018.04.006>
59. Zafar R et al (2016) Polysaccharide based bionanocomposites, properties and applications: a review. *Int J Biol Macromol* 92:1012–1024. <https://doi.org/10.1016/j.ijbiomac.2016.07.102>
60. Luo Y, Huang JG (2015) Hierarchical-structured anatase-titania/cellulose composite sheet with high photocatalytic performance and antibacterial activity. *Chem Eur J* 21:2568–2575. <https://doi.org/10.1002/chem.201405066>
61. Huang JG, Kunitake T (2003) Nano-precision replication of natural cellulosic substances by metal oxides. *J Am Chem Soc* 125:11834–11835. <https://doi.org/10.1021/ja037419k>
62. Luo Y, Xu JB, Huang JG (2014) Hierarchical nanofibrous anatase-titania-cellulose composite and its photocatalytic property. *Cryst Eng Comm* 16:464–471. <https://doi.org/10.1039/c3ce41906a>

63. Li H, Fu SY, Peng LC (2013) Surface modification of cellulose fibers by layer-by-layer self-assembly of lignosulfonates and TiO₂ nanoparticles: effect on photocatalytic abilities and paper properties. *Fiber Polym* 14:1794–1802. <https://doi.org/10.1007/s12221-013-1794-8>
64. Ding KL et al (2007) Facile synthesis of high quality TiO₂ nanocrystals in ionic liquid via a microwave-assisted process. *J Am Chem Soc* 129:6362–6363. <https://doi.org/10.1021/ja070809c>
65. Nayak PL et al (2008) Nanocomposites from polycaprolactone (PCL)/soy protein isolate (SPI) blend with organoclay. *Polym Plast Technol Eng* 47:600–605. <https://doi.org/10.1080/03602550802059402>
66. Uddin MK (2017) A review on the adsorption of heavy metals by clay minerals, with special focus on the past decade. *Chem Eng J* 308:438–462. <https://doi.org/10.1016/j.cej.2016.09.029>
67. Matusik J (2016) Chapter 23–halloysite for adsorption and pollution remediation. In: Yuan P, Thill A, Bergaya F (eds) *Developments in clay science*, vol 7. Elsevier, pp 606–627. <https://doi.org/10.1016/b978-0-08-100293-3.00023-6>
68. Zhu RL et al (2016) Adsorbents based on montmorillonite for contaminant removal from water: a review. *Appl Clay Sci* 123:239–258. <https://doi.org/10.1016/j.clay.2015.12.024>
69. de Paiva LB, Morales AR, Diaz FRV (2008) Organoclays: properties, preparation and applications. *Appl Clay Sci* 42:8–24. <https://doi.org/10.1016/j.clay.2008.02.006>
70. Zhao Q et al (2017) Review of the fundamental geochemical and physical behaviors of organoclays in barrier applications. *Appl Clay Sci* 142:2–20. <https://doi.org/10.1016/j.clay.2016.11.024>
71. Rajeshwar K, Chanmanee W (2012) Bioinspired photocatalyst assemblies for environmental remediation. *Electrochim Acta* 84:96–102. <https://doi.org/10.1016/j.electacta.2012.04.072>
72. Pavlidou S, Papispyrides CD (2008) A review on polymer-layered silicate nanocomposites. *Prog Polym Sci* 33:1119–1198. <https://doi.org/10.1016/j.progpolymsci.2008.07.008>
73. Manias E et al (2001) Polypropylene/montmorillonite nanocomposites. Review of the synthetic routes and materials properties. *Chem Mater* 13:3516–3523. <https://doi.org/10.1021/cm0110627>
74. Teh PL et al (2004) On the potential of organoclay with respect to conventional fillers (carbon black, silica) for epoxidized natural rubber compatibilized natural rubber vulcanizates. *J Appl Polym Sci* 94:2438–2445. <https://doi.org/10.1002/app.21188>
75. Alexandre M, Dubois P (2000) Polymer-layered silicate nanocomposites: preparation, properties and uses of a new class of materials. *Mater Sci Eng R-Reports* 28:1–63. [https://doi.org/10.1016/s0927-796x\(00\)00012-7](https://doi.org/10.1016/s0927-796x(00)00012-7)
76. Lofrano G et al (2016) Polymer functionalized nanocomposites for metals removal from water and wastewater: an overview. *Water Res* 92:22–37. <https://doi.org/10.1016/j.watres.2016.01.033>
77. Miranda-Trevino JC, Coles CA (2003) Kaolinite properties, structure and influence of metal retention on ph. *Appl Clay Sci* 23:133–139. [https://doi.org/10.1016/s0169-1317\(03\)00095-4](https://doi.org/10.1016/s0169-1317(03)00095-4)
78. Leroux F, Besse JP (2001) Polymer interleaved layered double hydroxide: a new emerging class of nanocomposites. *Chem Mater* 13:3507–3515. <https://doi.org/10.1021/cm0110268>
79. Mousa A, Karger-Kocsis J (2001) Rheological and thermodynamical behavior of styrene/butadiene rubber-organoclay nanocomposites. *Macromol Mater Eng* 286:260–266. [https://doi.org/10.1002/1439-2054\(20010401\)286:4%3c260:aid-mame260%3e3.0.co;2-x](https://doi.org/10.1002/1439-2054(20010401)286:4%3c260:aid-mame260%3e3.0.co;2-x)
80. Kiliaris P, Papispyrides CD (2010) Polymer/layered silicate (clay) nanocomposites: an overview of flame retardancy. *Prog Polym Sci* 35:902–958. <https://doi.org/10.1016/j.progpolymsci.2010.03.001>
81. Gao FG (2004) Clay/polymer composites: the story. *Mater Today* 7:50–55. [https://doi.org/10.1016/s1369-7021\(04\)00509-7](https://doi.org/10.1016/s1369-7021(04)00509-7)
82. Deka BK, Maji TK (2011) Effect of TiO₂ and nanoclay on the properties of wood polymer nanocomposite. *Compos A* 42:2117–2125. <https://doi.org/10.1016/j.compositesa.2011.09.023>
83. Pandey JK et al (2005) An overview on the degradability of polymer nanocomposites. *Polym Degrad Stab* 88:234–250. <https://doi.org/10.1016/j.polymdegradstab.2004.09.013>

84. Ray SS, Okamoto M (2003) Polymer/layered silicate nanocomposites: a review from preparation to processing. *Prog Polym Sci* 28:1539–1641. <https://doi.org/10.1016/j.progpolymsci.2003.08.002>
85. Ray SS, Bousmina M (2005) Biodegradable polymers and their layered silicate nanocomposites: in greening the 21st century materials world. *Prog Mater Sci* 50:962–1079. <https://doi.org/10.1016/j.pmatsci.2005.05.002>
86. Ataefard M, Moradian S (2012) Investigation the effect of various loads of organically modified montmorillonite on dyeing properties of polypropylene nanocomposites. *J Appl Polym Sci* 125:E214–E223. <https://doi.org/10.1002/app.34812>
87. Choudalakis G, Gotsis AD (2009) Permeability of polymer/clay nanocomposites: a review. *Eur Polym J* 45:967–984. <https://doi.org/10.1016/j.eurpolymj.2009.01.027>
88. Chen L et al (2016) Functional magnetic nanoparticle/clay mineral nanocomposites: preparation, magnetism and versatile applications. *Appl Clay Sci* 127:143–163. <https://doi.org/10.1016/j.clay.2016.04.009>
89. Maisanaba S et al (2015) Toxicological evaluation of clay minerals and derived nanocomposites: a review. *Environ Res* 138:233–254. <https://doi.org/10.1016/j.envres.2014.12.024>
90. Shaikh SMR et al (2017) Influence of polyelectrolytes and other polymer complexes on the flocculation and rheological behaviors of clay minerals: a comprehensive review. *Sep Purif Technol* 187:137–161. <https://doi.org/10.1016/j.seppur.2017.06.050>
91. Liu AD, Berglund LA (2012) Clay nanopaper composites of nacre-like structure based on montmorillonite and cellulose nanofibers-improvements due to chitosan addition. *Carbohydr Polym* 87:53–60. <https://doi.org/10.1016/j.carbpol.2011.07.019>
92. Paranhos CM et al (2007) Microstructure and free volume evaluation of poly(vinyl alcohol) nanocomposite hydrogels. *Eur Polym J* 43:4882–4890. <https://doi.org/10.1016/j.eurpolymj.2007.10.001>
93. Ruiz-Hitzky E et al (2013) Fibrous clays based bionanocomposites. *Prog Polym Sci* 38:1392–1414. <https://doi.org/10.1016/j.progpolymsci.2013.05.004>
94. Neeraj G et al (2016) Adsorptive potential of dispersible chitosan coated iron-oxide nanocomposites toward the elimination of arsenic from aqueous solution. *Process Saf Environ Prot* 104:185–195. <https://doi.org/10.1016/j.psep.2016.09.006>
95. Djerahov L et al (2016) Chitosan film loaded with silver nanoparticles-sorbent for solid phase extraction of Al(III), Cd(II), Cu(II), Co(II), Fe(III), Ni(II), Pb(II) and Zn(II). *Carbohydr Polym* 147:45–52. <https://doi.org/10.1016/j.carbpol.2016.03.080>
96. Tu H et al (2017) Chitosan-rectorite nanospheres immobilized on polystyrene fibrous mats via alternate electrospinning/electrospraying techniques for copper ions adsorption. *Appl Surf Sci* 426:545–553. <https://doi.org/10.1016/j.apsusc.2017.07.159>
97. Salam MA, Makki MSI, Abdelaal MYA (2011) Preparation and characterization of multi-walled carbon nanotubes/chitosan nanocomposite and its application for the removal of heavy metals from aqueous solution. *J Alloys Compd* 509:2582–2587. <https://doi.org/10.1016/j.jallcom.2010.11.094>
98. Padilla-Ortega E et al (2016) Ultrasound assisted preparation of chitosan-vermiculite bionanocomposite foams for cadmium uptake. *Appl Clay Sci* 130:40–49. <https://doi.org/10.1016/j.clay.2015.11.024>
99. Salam MA (2017) Preparation and characterization of chitin/magnetite/multiwalled carbon nanotubes magnetic nanocomposite for toxic hexavalent chromium removal from solution. *J Mol Liq* 233:197–202. <https://doi.org/10.1016/j.molliq.2017.03.023>
100. Khare P et al (2016) Microchannel-embedded metal-carbon-polymer nanocomposite as a novel support for chitosan for efficient removal of hexavalent chromium from water under dynamic conditions. *Chem Eng J* 293:44–54. <https://doi.org/10.1016/j.cej.2016.02.049>
101. Wu SJ, Liou TH, Mi FL (2009) Synthesis of zero-valent copper-chitosan nanocomposites and their application for treatment of hexavalent chromium. *Bioresour Technol* 100:4348–4353. <https://doi.org/10.1016/j.biortech.2009.04.013>

102. Choudhury PR et al (2017) Removal of Cr (VI) by synthesized titania embedded dead yeast nanocomposite: optimization and modeling by response surface methodology. *J Environ Chem Eng* 5:214–221. <https://doi.org/10.1016/j.jece.2016.11.041>
103. Ballav N et al (2014) Synthesis, characterization of Fe₃O₄@glycine doped polypyrrole magnetic nanocomposites and their potential performance to remove toxic Cr(VI). *J Ind Eng Chem* 20:4085–4093. <https://doi.org/10.1016/j.jiec.2014.01.007>
104. Gokila S et al (2017) Removal of the heavy metal ion chromium(VI) using chitosan and alginate nanocomposites. *Int J Biol Macromol* 104:1459–1468. <https://doi.org/10.1016/j.ijbiomac.2017.05.117>
105. Li CJ et al (2014) Preparation of polyamides 6 (PA6)/chitosan@fexoy composite nanofibers by electrospinning and pyrolysis and their Cr(VI)-removal performance. *Catal Today* 224:94–103. <https://doi.org/10.1016/j.cattod.2013.11.034>
106. Luo XG et al (2016) Adsorptive removal of lead from water by the effective and reusable magnetic cellulose nanocomposite beads entrapping activated bentonite. *Carbohydr Polym* 151:640–648. <https://doi.org/10.1016/j.carbpol.2016.06.003>
107. Mallakpour S, Madani M (2016) Functionalized-MnO₂/chitosan nanocomposites: a promising adsorbent for the removal of lead ions. *Carbohydr Polym* 147:53–59. <https://doi.org/10.1016/j.carbpol.2016.03.076>
108. Ghorai S et al (2012) Novel biodegradable nanocomposite based on XG-g-PAM/SiO₂: application of an efficient adsorbent for Pb²⁺ ions from aqueous solution. *Bioresour Technol* 119:181–190. <https://doi.org/10.1016/j.biortech.2012.05.063>
109. Sharma G, Pathania D, Naushad M (2014) Preparation, characterization and antimicrobial activity of biopolymer based nanocomposite ion exchanger pectin zirconium(IV) selenotungstophosphate: application for removal of toxic metals. *J Ind Eng Chem* 20:4482–4490. <https://doi.org/10.1016/j.jiec.2014.02.020>
110. Naushad M et al (2016) Synthesis and characterization of a new starch/SnO₂ nanocomposite for efficient adsorption of toxic Hg²⁺ metal ion. *Chem Eng J* 300:306–316. <https://doi.org/10.1016/j.cej.2016.04.084>
111. Markandeya et al (2017) Statistical optimization of process parameters for removal of dyes from wastewater on chitosan cenospheres nanocomposite using response surface methodology. *J Clean Prod* 149:597–606. <https://doi.org/10.1016/j.jclepro.2017.02.078>
112. Ali F et al (2017) Bactericidal and catalytic performance of green nanocomposite based on chitosan/carbon black fiber supported monometallic and bimetallic nanoparticles. *Chemosphere* 188:588–598. <https://doi.org/10.1016/j.chemosphere.2017.08.118>
113. Nithya A et al (2017) A potential photocatalytic, antimicrobial and anticancer activity of chitosan-copper nanocomposite. *Int J Biol Macromol* 104:1774–1782. <https://doi.org/10.1016/j.ijbiomac.2017.03.006>
114. Pathania D et al (2016) Photocatalytic degradation of highly toxic dyes using chitosan-g-poly (acrylamide)/ZnS in presence of solar irradiation. *J Photochem Photobiol, A* 329:61–68. <https://doi.org/10.1016/j.jphotochem.2016.06.019>
115. Simsek EB et al (2017) Carbon fiber embedded chitosan/PVA composites for decontamination of endocrine disruptor bisphenol-A from water. *J Taiwan Inst Chem Eng* 70:291–301. <https://doi.org/10.1016/j.jtice.2016.11.008>
116. Gupta VK et al (2017) Degradation of azo dyes under different wavelengths of uv light with chitosan-SnO₂ nanocomposites. *J Mol Liq* 232:423–430. <https://doi.org/10.1016/j.molliq.2017.02.095>
117. Karthikeyan KT, Nithya A, Jothivenkatachalam K (2017) Photocatalytic and antimicrobial activities of chitosan-TiO₂ nanocomposite. *Int J Biol Macromol* 104:1762–1773. <https://doi.org/10.1016/j.ijbiomac.2017.03.121>
118. Tahir N et al (2017) Biopolymers composites with peanut hull waste biomass and application for crystal violet adsorption. *Int J Biol Macromol* 4:210–220. <https://doi.org/10.1016/j.ijbiomac.2016.10.013>

119. Mittal H et al (2014) Fe₃O₄ mnps and gum xanthan based hydrogels nanocomposites for the efficient capture of malachite green from aqueous solution. *Chem Eng J* 255:471–482. <https://doi.org/10.1016/j.cej.2014.04.098>
120. Thakur M et al (2017) Efficient photocatalytic degradation of toxic dyes from aqueous environment using gelatin-Zr(IV) phosphate nanocomposite and its antimicrobial activity. *Colloids Surf B: Biointerfaces* 157:456–463. <https://doi.org/10.1016/j.colsurfb.2017.06.018>
121. Pathania D et al (2016) Novel guar gum/Al₂O₃ nanocomposite as an effective photocatalyst for the degradation of malachite green dye. *Int J Biol Macromol* 87:366–374. <https://doi.org/10.1016/j.ijbiomac.2016.02.073>
122. Gupta VK et al (2014) Adsorptional removal of methylene blue by guar gum-cerium (iv) tungstate hybrid cationic exchanger. *Carbohydr Polym* 101:684–691. <https://doi.org/10.1016/j.carbpol.2013.09.092>
123. Mittal H, Maity A, Ray SS (2015) Effective removal of cationic dyes from aqueous solution using gum ghatti-based biodegradable hydrogel. *Int J Biol Macromol* 79:8–20. <https://doi.org/10.1016/j.ijbiomac.2015.04.045>
124. Virkutyte J, Jegatheesan V, Varma RS (2012) Visible light activated TiO₂/microcrystalline cellulose nanocatalyst to destroy organic contaminants in water. *Bioresour Technol* 113:288–293. <https://doi.org/10.1016/j.biortech.2011.12.090>
125. Salam MA, El-Shishtawy RM, Obaid AY (2014) Synthesis of magnetic multi-walled carbon nanotubes/magnetite/chitin magnetic nanocomposite for the removal of rose bengal from real and model solution. *J Ind Eng Chem* 20:3559–3567. <https://doi.org/10.1016/j.jiec.2013.12.049>
126. Mittal H, Ray SS (2016) A study on the adsorption of methylene blue onto gum ghatti/tio₂ nanoparticles-based hydrogel nanocomposite. *Int J Biol Macromol* 88:66–80. <https://doi.org/10.1016/j.ijbiomac.2016.03.032>
127. Essawy AA, Sayyah SM, El-Nggar AM (2017) Wastewater remediation by TiO₂-impregnated chitosan nano-grafts exhibited dual functionality: high adsorptivity and solar-assisted self cleaning. *J Photochem Photobiol B: Biol* 173:170–180. <https://doi.org/10.1016/j.jphotochem.2017.05.044>
128. Thomas M et al (2017) Self-organized graphene oxide and TiO₂ nanoparticles incorporated alginate/carboxymethyl cellulose nanocomposites with efficient photocatalytic activity under direct sunlight. *J Photochem Photobiol, A* 346:113–125. <https://doi.org/10.1016/j.jphotochem.2017.05.037>
129. Liu P et al (2015) Synthesis of covalently crosslinked attapulgite/poly (acrylic acid-co-acrylamide) nanocomposite hydrogels and their evaluation as adsorbent for heavy metal ions. *J Ind Eng Chem* 23:188–193. <https://doi.org/10.1016/j.jiec.2014.08.014>
130. Wu LS et al (2013) Organo-bentonite-Fe₃O₄ poly(sodium acrylate) magnetic superabsorbent nanocomposite: synthesis, characterization, and thorium(IV) adsorption. *Appl Clay Sci* 83–84:405–414. <https://doi.org/10.1016/j.clay.2013.07.012>
131. Chiew CSC et al (2016) Halloysite/alginate nanocomposite beads: kinetics, equilibrium and mechanism for lead adsorption. *Appl Clay Sci* 119:301–310. <https://doi.org/10.1016/j.clay.2015.10.032>
132. Matusik J, Wscislo A (2014) Enhanced heavy metal adsorption on functionalized nanotubular halloysite interlayer grafted with aminoalcohols. *Appl Clay Sci* 100:50–59. <https://doi.org/10.1016/j.clay.2014.06.034>
133. Ballav N et al (2014) Polypyrrole-coated halloysite nanotube clay nanocomposite: synthesis, characterization and Cr(VI) adsorption behaviour. *Appl Clay Sci* 102:60–70. <https://doi.org/10.1016/j.clay.2014.10.008>
134. Shi LN et al (2014) Functional kaolinite supported fe/ni nanoparticles for simultaneous catalytic remediation of mixed contaminants (lead and nitrate) from wastewater. *J Colloid Interface Sci* 428:302–307. <https://doi.org/10.1016/j.jcis.2014.04.059>
135. Koteja A, Matusik J (2015) Di- and triethanolamine grafted kaolinites of different structural order as adsorbents of heavy metals. *J Colloid Interface Sci* 455:83–92. <https://doi.org/10.1016/j.jcis.2015.05.027>

136. Setshedi KZ et al (2013) Exfoliated polypyrrole-organically modified montmorillonite clay nanocomposite as a potential adsorbent for Cr(VI) removal. *Chem Eng J* 222:186–197. <https://doi.org/10.1016/j.cej.2013.02.061>
137. Setshedi KZ et al (2014) Breakthrough studies for Cr(VI) sorption from aqueous solution using exfoliated polypyrrole-organically modified montmorillonite clay nanocomposite. *J Ind Eng Chem* 20:2208–2216. <https://doi.org/10.1016/j.jiec.2013.09.052>
138. Kadu BS et al (2011) Efficiency and recycling capability of montmorillonite supported Fe-Ni bimetallic nanocomposites towards hexavalent chromium remediation. *Appl Catal B* 104:407–414. <https://doi.org/10.1016/j.apcatb.2011.02.011>
139. Kalantari K et al (2015) Rapid and high capacity adsorption of heavy metals by Fe₃O₄/montmorillonite nanocomposite using response surface methodology: preparation, characterization, optimization, equilibrium isotherms, and adsorption kinetics study. *J Taiwan Inst Chem Eng* 49:192–198. <https://doi.org/10.1016/j.jtice.2014.10.025>
140. Zheng XM et al (2017) Ammonium-pillared montmorillonite-co-Fe₂O₄ composite caged in calcium alginate beads for the removal of Cs⁺ from wastewater. *Carbohydr Polym* 167:306–316. <https://doi.org/10.1016/j.carbpol.2017.03.059>
141. Chikate RC, Kadu BS (2014) Improved photocatalytic activity of cdse-nanocomposites: effect of montmorillonite support towards efficient removal of indigo carmine. *Spectrochim Acta A Mol Biomol Spectrosc* 124:138–147. <https://doi.org/10.1016/j.saa.2013.12.099>
142. Pandey S, Mishra SB (2011) Organic-inorganic hybrid of chitosan/organoclay bionanocomposites for hexavalent chromium uptake. *J Colloid Interface Sci* 361:509–520. <https://doi.org/10.1016/j.jcis.2011.05.031>
143. Kahraman HT (2017) Development of an adsorbent via chitosan nano-organoclay assembly to remove hexavalent chromium from wastewater. *Int J Biol Macromol* 94:202–209. <https://doi.org/10.1016/j.ijbiomac.2016.09.111>
144. Rusmin R et al (2015) Structural evolution of chitosan-palygorskite composites and removal of aqueous lead by composite beads. *Appl Surf Sci* 353:363–375. <https://doi.org/10.1016/j.apsusc.2015.06.124>
145. Alcantara ACS et al (2014) Polysaccharide-fibrous clay bionanocomposites. *Appl Clay Sci* 96:2–8. <https://doi.org/10.1016/j.clay.2014.02.018>
146. Lv XS et al (2013) Fe-0-Fe₃O₄ nanocomposites embedded polyvinyl alcohol/sodium alginate beads for chromium (vi) removal. *J Hazard Mat* 262:748–758. <https://doi.org/10.1016/j.jhazmat.2013.09.036>
147. Chen HH et al (2017) Feasible preparation and characterization of tunable novel montmorillonite/block-copolymers based composites as potential dual adsorbent candidates. *Appl Clay Sci* 137:192–202. <https://doi.org/10.1016/j.clay.2016.12.028>
148. Ahmad R, Mirza A (2017) Green synthesis of xanthan gum/methionine-bentonite nanocomposite for sequestering toxic anionic dye. *Surf Interfaces* 8:65–72. <https://doi.org/10.1016/j.surfin.2017.05.001>
149. Ma JF et al (2016) Nanocomposite of exfoliated bentonite/g-C₃N₄/Ag₃PO₄ for enhanced visible-light photocatalytic decomposition of rhodamine B. *Chemosphere* 162:269–276. <https://doi.org/10.1016/j.chemosphere.2016.07.089>
150. Ai LH, Li LL (2013) Efficient removal of organic dyes from aqueous solution with ecofriendly biomass-derived carbon@montmorillonite nanocomposites by one-step hydrothermal process. *Chem Eng J* 223:688–695. <https://doi.org/10.1016/j.cej.2013.03.015>
151. Sarkar B et al (2011) Structural characterisation of arquad (R) 2HT-75 organobentonites: surface charge characteristics and environmental application. *J Hazard Mat* 195:155–161. <https://doi.org/10.1016/j.jhazmat.2011.08.016>
152. Motshekga SC, Ray SS (2017) Highly efficient inactivation of bacteria found in drinking water using chitosan-bentonite composites: modelling and breakthrough curve analysis. *Water Res* 111:213–223. <https://doi.org/10.1016/j.watres.2017.01.003>
153. Liu EM et al (2016) Copper-complexed clay/poly-acrylic acid composites: extremely efficient adsorbents of ammonia gas. *Appl Clay Sci* 121:154–161. <https://doi.org/10.1016/j.clay.2015.12.012>

154. El-Dib FI et al (2016) Remediation of distilleries wastewater using chitosan immobilized bentonite and bentonite based organoclays. *Int J Biol Macromol* 86:750–755. <https://doi.org/10.1016/j.ijbiomac.2016.01.108>
155. Tan DYP (2016) Surface modifications of halloysite. In: Yuan P (ed) *Developments in clay science*. Elsevier, pp 167–201
156. Szczepanik B et al (2017) Synthesis, characterization and photocatalytic activity of TiO₂-halloysite and Fe₂O₃-halloysite nanocomposites for photodegradation of chloroanilines in water. *Appl Clay Sci* 149:118–126. <https://doi.org/10.1016/j.clay.2017.08.016>
157. Sahithya K, Das D, Das N (2016) Adsorptive removal of monocrotophos from aqueous solution using biopolymer modified montmorillonite-CuO composites: equilibrium, kinetic and thermodynamic studies. *Process Saf Environ Prot* 99:43–54. <https://doi.org/10.1016/j.psep.2015.10.009>
158. Jiang JQ, Cooper C, Ouki S (2002) Comparison of modified montmorillonite adsorbents—part i: preparation, characterization and phenol adsorption. *Chemosphere* 47:711–716. [https://doi.org/10.1016/s0045-6535\(02\)00011-5](https://doi.org/10.1016/s0045-6535(02)00011-5)
159. Liu S et al (2017) Preparation and characterization of organo-vermiculite based on phosphatidylcholine and adsorption of two typical antibiotics. *Appl Clay Sci* 137:160–167. <https://doi.org/10.1016/j.clay.2016.12.002>
160. Swearingen C, Macha S, Fitch A (2003) Leashed ferrocenes at clay surfaces: potential applications for environmental catalysis. *J Mol Catal A: Chem* 199:149–160. [https://doi.org/10.1016/s1381-1169\(03\)00031-1](https://doi.org/10.1016/s1381-1169(03)00031-1)
161. Karamanis D et al (2011) Water vapor adsorption and photocatalytic pollutant degradation with TiO₂-sepiolite nanocomposites. *Appl Clay Sci* 53:181–187. <https://doi.org/10.1016/j.clay.2010.12.012>

Correction to: Extraction of Nano Cellulose Fibres and Their Eco-friendly Polymer Composite



Bashiru Kayode Sodipo and Folahan Abdul Wahab Taiwo Owolabi

Correction to:
Chapter “Extraction of Nano Cellulose Fibres and Their Eco-friendly Polymer Composite” in: Inamuddin et al. (eds.), *Sustainable Polymer Composites and Nanocomposites*,
https://doi.org/10.1007/978-3-030-05399-4_8

The original version of this chapter was inadvertently published with the incorrect author sequence and corresponding author. This has now been corrected.

The updated version of this chapter can be found at
https://doi.org/10.1007/978-3-030-05399-4_8

© Springer Nature Switzerland AG 2019
Inamuddin et al. (eds.), *Sustainable Polymer Composites and Nanocomposites*,
https://doi.org/10.1007/978-3-030-05399-4_48